



Synthesis, Spectral Characterization, Structural Investigation and Antimicrobial Studies of Mononuclear Ni(II) and Cu(II) Complexes with Ketoconazole and Thiocyanate Ion as Ligands

P.Keerthika^{1*}, S.Balasubramaniyan² and R.Govindharaju³

¹Research Scholar, PG and Research Department of Chemistry, Government Arts College, Ariyalur-621713 (Affiliated to Bharathidasan University, Tiruchirappalli), Tamil Nadu, India.

²Assistant Professor, PG and Research Department of Chemistry, Government Arts College, Ariyalur-621713 (Affiliated to Bharathidasan University, Tiruchirappalli), Tamil Nadu, India.

³Assistant Professor Department of Chemistry, Thanthai Hans Roever College, Perambalur - 621 220 (Affiliated to Bharathidasan University, Tiruchirappalli), Tamil Nadu, India.

Received: 07 Feb 2023

Revised: 15 Apr 2023

Accepted: 16 May 2023

*Address for Correspondence

P.Keerthika

Research Scholar,
PG and Research Department of Chemistry,
Government Arts College, Ariyalur-621713
(Affiliated to Bharathidasan University, Tiruchirappalli),
Tamil Nadu, India.
E.Mail: lathika.ttp@gmail.com



This is an Open Access Journal / article distributed under the terms of the **Creative Commons Attribution License** (CC BY-NC-ND 3.0) which permits unrestricted use, distribution, and reproduction in any medium, provided the original work is properly cited. All rights reserved.

ABSTRACT

Transition metal complexes of Ni(II) and Cu(II) with Ketoconazole and thiocyanate ion were synthesized by using microwave irradiation. The metal complexes have been characterized by elemental analysis, molar conductance, magnetic moment, UV-Visible, FT-IR and EPR spectral studies. The antimicrobial activities of the strains *Escherichia coli* (MTCC 732) for bacteria and *Candida albicans* (MTCC 183) for fungi have been evaluated by disc diffusion method. The formulae of the complexes were derived from the percentage of the elements present in the complex and their molar conductivity. The UV-Visible and the magnetic moment indicate the geometry of the complexes is found to be octahedral. The FT-IR spectral data of the complexes were compared with those for the free ligands to confirm the entry of the ligands in to the coordination sphere. The metal ligand covalency of Cu(II) complex has been arrived at from EPR spectrum. The free radical scavenging activities of the complex and the ligand have been determined by measuring their interaction with the stable free radical DPPH. The complexes have larger antioxidant activity as compared to the ligands.

Keywords: Metal complex, Ketoconazole, thiocyanate ion, antimicrobial





Keerthika et al.,

INTRODUCTION

Ketoconazole is an effective antifungal agent[1]. It also used to treat a number of fungal infections such as tinea, cutaneous candidiasis, pityriasis versicolor, dandruff and seborrheic dermatitis. Ketoconazole is an imidazole derivative primarily used for its antifungal activity. However, in the early 1980s, the drug was also shown to have effects on steroid synthesis in humans by inhibiting cytochrome P450 enzymes and significantly reducing cortisol levels [2-7]. This drug has thus increasingly been used in the management of Cushing's disease [8]. The serious medical problem [9-11] of bacterial and fungal resistance and the rate at which it develops has led to the escalating levels of resistance to conventional antibiotics. The recognition and growth of antibacterial and antifungal drugs with inspired mechanism of action have become a critical task for communicable diseases research programs [12]. Many investigations proved that binding of a drug to a metalloelement enhances its activity and in some cases the complex possesses even more therapeutic properties than the parent drug [13]. The present study aims at the microwave assisted synthesis and spectral characterization of Ni(II) and Cu(II) complexes with Ketoconazole and thiocyanate ion as ligands. The ligands and their complexes are also focused on the biological studies.

EXPERIMENTAL METHOD

Materials

Metal nitrate, Ketoconazole and KSCN were purchased from Alfa Aaser Company and used as such. The organic solvents used, viz., DMSO, DMF, methanol and ethanol were of AnalaR grade and used as such without further purification.

Synthesis of Ni(II) complex

7.31g (13.79 mmol) of Ketoconazole in MeOH and 0.7g (7.00 mmol) of KSCN in EtOH were added to the methanolic solution of nickel nitrate 1.00g (3.40 mmol) and this was followed by microwave irradiation for few minutes after each addition by using IFB 25 BG-1S model microwave oven. The resulting precipitate was filtered off, washed with 1:1 methanol: ethanol mixture and dried under vacuum. A pale green colored complex was obtained with the yield of 52.93%.

Synthesis of Cu(II) complex

4.32g (8.32 mmol) of Ketoconazole in MeOH and 0.83g (8.40 mmol) of KSCN in EtOH were added to the methanolic solution of nickel nitrate 1.00g (4.20 mmol) and this was followed by microwave irradiation for few minutes after each addition by using IFB 25 BG-1S model microwave oven. The resulting precipitate was filtered off, washed with 1:1 methanol: ethanol mixture and dried under vacuum. A dark green colored complex was obtained with the yield of 67.69%.

Instrumentations

C,H,N elemental analyses were performed using Thermo Finnegan make, Flash EA1112 Series CHNS(O) analyzer. The molar conductivity measurements were conducted using 10^{-3} M solutions of the metal complex in acetonitrile with Systronic Conductivity Bridge (model number-304) at 30°C. The UV-Visible spectra of the complexes were recorded on Varian, Cary 5000 model UV-Vis Spectrophotometer. Infrared spectra for the complexes and the ligands were recorded on a Perkin Elmer, Spectrum RX-I, FT-IR Spectrometer in KBr discs at room temperature. The electron paramagnetic resonance spectra of the copper complex were recorded at room temperature using JES FA 200 EPR Spectrometer.

Antimicrobial activity

Antibiogram was done by disc diffusion method using free ligands and their complexes. Petri plates were prepared by pouring 30 ml of NA/PDA medium. The test organism was inoculated on solidified agar plate with the help of micropipette and spread and allowed to dry for 10 mins. The surfaces of media were inoculated with bacteria from a





Keerthika et al.,

broth culture. A sterile cotton swab is dipped into a standardized microbes test suspension and used to evenly inoculate the entire surface of the Nutrient agar /PDA plates. Briefly, inoculums containing of microbial strains were spread on Nutrient agar /PDA plates. Using sterile forceps, the sterile filter papers (6 mm diameter) containing each 50 μ l of sample, 30 μ l standard and control solution were laid down on the surface of inoculated agar plate. The plates were incubated at 37 °C for 24 h for the bacteria and 48 hr. for yeasts strains [14,15].

Antioxidant activity

Assessment of antioxidant activity stock solution (1 mg/ml) was diluted to final concentrations of 10–500 μ g/ml. Ethanolic DPPH solution (1 ml, 0.3 mmol) was added to the sample solutions in DMSO (3 ml) at different concentrations (10–500 μ g/ml) [16]. The mixture was shaken energetically and acceptable to stand at room temperature for 30 min. The absorbance was then measured at 517 nm in a UV-Vis Spectrophotometer. The lower absorbance of the reaction mixture indicates higher free radical scavenging activity. Ethanol was used as the solvent and ascorbic acid as the standard. The DPPH radical scavenging activity is designed by the following equation:

$$\text{DPPH Scavenging effect (\%)} = \frac{A_0 - A_1}{A_0} \times 100$$

where A_0 and A_1 are the absorbance of the control reaction and absorbance in the presence of the samples/standard.

RESULTS AND DISCUSSION

Elemental analysis and metal estimation

The elemental analysis and metal estimation led to the formulae of the complexes. The percentages of carbon, hydrogen and nitrogen in the complexes were found to be 44.41(44.52), 2.88(2.96), 5.09(5.18), and 47.41(41.52), 7.81(6.96), 5.87(5.01), respectively. The experimental data were in good agreement with the theoretical values [17].

Molar conductance

Molar conductance measurements of the complex, carried out using acetonitrile as the solvent at the concentration of 10^{-3} M, indicate non-electrolyte behaviour of the complexes [18,19]. Thus the complexes may be formulated as $[\text{Ni}(\text{KET})_4(\text{SCN})_2]$ and $[\text{Cu}(\text{KET})_4(\text{SCN})_2]$.

UV-Visible spectrum of complexes

The UV-Visible spectrum of Ni(II) complex shows absorption bands at 13652 cm^{-1} , 18540 cm^{-1} and 22900 cm^{-1} and their corresponding transitions, which are tentatively assigned as ${}^3\text{A}_{2g}(\text{F}) \rightarrow {}^3\text{T}_{2g}(\text{F})$ (ν_1), ${}^3\text{A}_{2g}(\text{F}) \rightarrow {}^3\text{T}_{1g}(\text{F})$ (ν_2) and ${}^3\text{A}_{2g}(\text{F}) \rightarrow {}^3\text{T}_{1g}(\text{P})$ (ν_3) respectively [20,21]. The spectrum also shows a band at 27555 cm^{-1} which may be attributed to the Ligand to metal charge transfer. The observed magnetic moment value of Ni(II) complex is 2.79 B.M. This suggests the presence of octahedral environment around Ni(II) complex. The structure is also further confirmed by the ratio $\nu_2/\nu_1 = 1.35$, which is close to the value expected for octahedral structure [22], involving d^2sp^3 hybridisation.

The electronic spectrum of Cu(II) complex exhibits three absorbance bands at 14710 cm^{-1} , 28571 cm^{-1} and 34482 cm^{-1} and their corresponding transitions are ${}^2\text{A}_{1g} \leftarrow {}^2\text{B}_{1g}$, ${}^2\text{B}_{2g} \leftarrow {}^2\text{B}_{1g}$ and ${}^2\text{E}_g \leftarrow {}^2\text{B}_{1g}$ respectively, which indicate octahedral geometry around Cu(II) metal ion. The magnetic moment value of Cu(II) complex is 1.78 B.M, that indicates further confirming hexacoordination around Cu(II) metal ion [23,24].

FT-IR Spectra of free ligands and their complexes

The FT-IR spectra of the free ligands and their complexes were recorded in the region of 4000-400 cm^{-1} . The FTIR spectrum of ketoconazole shows the presence of strong absorption at 1511 cm^{-1} and a weak at 1592 cm^{-1} which were assigned to C=N stretching vibrations. C-N exhibited stretching vibrations at 1107 cm^{-1} strongly and at 1080 cm^{-1} weakly, unique peaks at 1647 cm^{-1} (C=O stretch), 1582 cm^{-1} (C=C aromatic symmetric stretch), and 1512 cm^{-1} (C=C aromatic asymmetric stretch, In metal complexes the bands at 1511 cm^{-1} and 1107 cm^{-1} were shifted to lower





Keerthika et al.,

frequencies indicates ketoconazole coordinated to metals through the nitrogen of C=N [25,26]. The IR spectra of the complexes prepared were also compared with the spectra reported for the thiocyanato complexes. The C-N stretching frequency of N-bonded complex of thiocyanate ion was nearly 2050 cm⁻¹, It was moved by 58-23 cm⁻¹ to higher frequency range in all the complexes [27].

EPR spectrum of Cu(II) complex

The spectrum of DMSO solution of Cu(II) complex Ketoconazole and KSCN ion measured at X-band frequency at 77 K (LNT) provide useful information which is important in studying metal ion environment. The spin Hamiltonian parameters of the complex have been calculated. The Cu(II) complex in the frozen state at 77 K shows four well resolved peaks in the low field region and one intense peak in the high field region. The g-tensor value of the copper complex can be used to derive the ground state. In octahedral complexes, the unpaired electron lies in the dx²-y² orbital [28]. For this complex, the observed g-tensor values are g_{||} = 2.2460 > g_⊥ = 2.2101 > g = 2.0023 which suggest that this complex has an octahedral geometry and the ground state is ²B_{1g}. The EPR parameters of the complex coincide well with the related systems which confirm that the complex has an octahedral geometry and it is axially symmetric. In the axial spectra, the g-values are related to the exchange interaction coupling constant G by the expression [29]

$$G = g_{||} - 2.0023 / g_{\perp} - 2.0023$$

According to Hathaway [30] expression, if G value is larger than four, the exchange interaction is negligible because the local tetragonal axes are aligned parallel or slightly misaligned. If its value is less than four, the exchange interaction is considerable and the local tetragonal axes are misaligned. For the present Cu(II) complex, G is 1.172, which indicates considerable exchange interaction in the solid complex. The g_{av} and the covalent in-plane σ-bonding (α²) parameters are calculated according to the following equation [31]

$$g_{av} = 1/3[g_{||} + 2g_{\perp}]$$

$$\alpha^2 Cu = (A_{||} / 0.036) + g_{||} - 2.0023 + 3/7(g_{\perp} - 2.0023) + 0.04$$

If the α² value is 0.4221, it indicates a complete covalent bonding, and if the value is 1.0, it suggests a complete ionic bonding. Hence, it is clear that the in-plane σ-bonding parameter α²=0.4221 [32] is less than unity and this indicates the covalent character of M-L bond [33]. These data are well in accordance with the other reported values.

BIOLOGICAL ACTIVITY

Antibacterial activity

The synthesized Ni(II), Cu(II) complexes and their free ligand Ketoconazole are tested against the bacteria, *Escherichia coli* (MTCC 732) by agar-well diffusion method in *in vitro* conditions. The complexes have potential activity against the bacteria compared to free ligand Ketoconazole.

Antifungal activity

The antifungal activity of the free ligand Ketoconazole and the synthesized Ni(II) and Cu(II) complex are tested against the fungi *Candida albicans* (MTCC 183) by agar-well diffusion method. The complexes have enhanced activity against the fungi compared to free ligand Ketoconazole.

Antioxidant activity (Radical Scavenging Activity)

The antioxidant activity of the free ligand Ketoconazole and the complexes were determined by DPPH free radical scavenging method and vitamin C as standard. The reduction capability of DPPH radicals was determined by decrease in its absorbance at 517 nm induced by antioxidants [34]. The graph was plotted with percentage scavenging effects on the y-axis and concentration (µg/ml.) on the x-axis. The scavenging ability of the Ni(II) and Cu(II) complexes were compared with Vitamin C as a standard. The metal complexes showed enhance activity as a radical scavenger compared with ascorbic acid, these results were in good agreement with previous metal complexes

56802



**Keerthika et al.,**

studies where the ligand has the antioxidant activity and it is expected that the metal moiety will increase its activity [35-37]. The scavenging activities of ligand and their complex shown in Fig.8.

CONCLUSION

In the near study, our efforts was to synthesize and characterize a new Ni(II) and Cu(II) complexes with Ketoconazole and thiocyanate ion as ligands. The new complexes were synthesized using microwave irradiation. The synthesized complexes were characterized by various chemical and spectral analyses. The synthesized complexes were tested for antimicrobial activities. The metal complexes have significant antimicrobial and antioxidant activities as compared to the free ligands.

ACKNOWLEDGEMENT

The authors wish to thank the Principal for providing the infrastructural facilities in the Department of Chemistry, Government Arts College, Ariyalur, Tamil Nadu, India. They also thank the Head and Staff members of STIC, Cochin University, SAIF, IIT, Mumbai and SAIF, IIT, Chennai for providing instrumental data.

REFERENCES

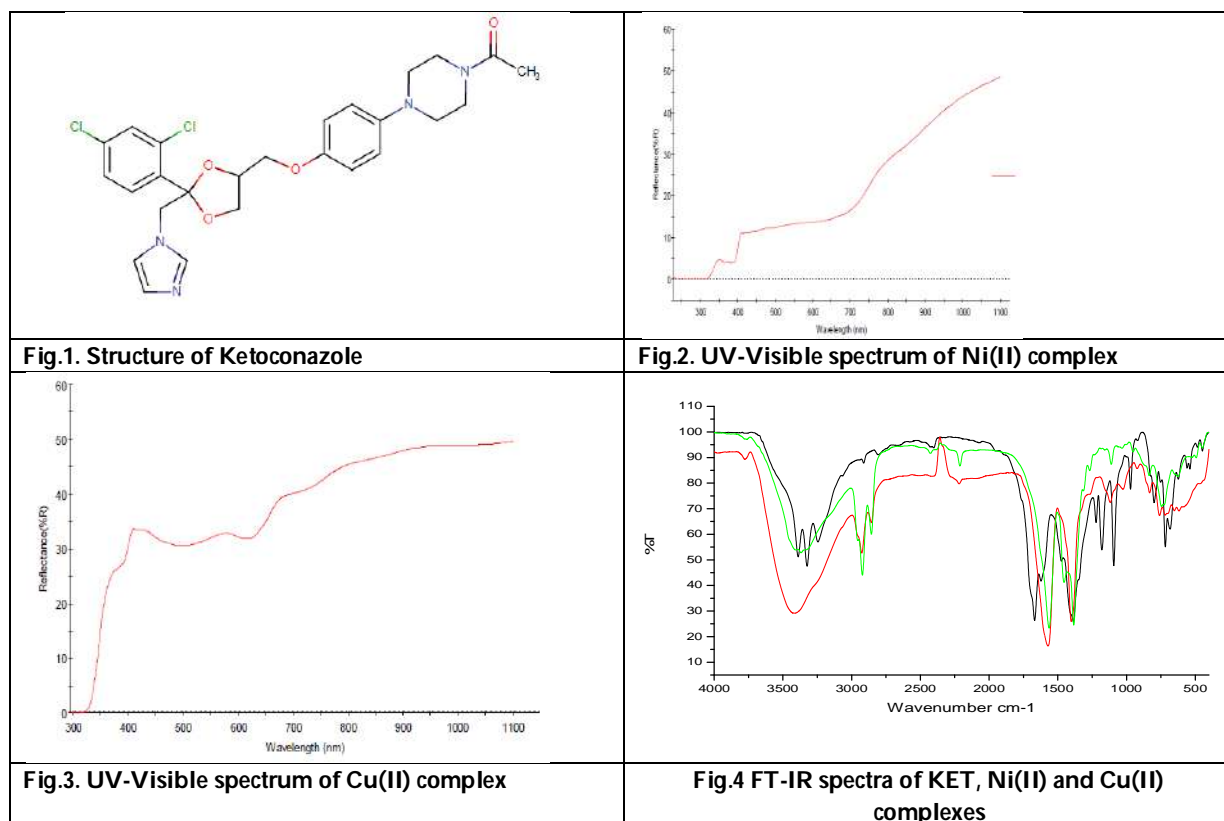
1. Graybill, J. R., and D. J. Drutz. 1980. Ketoconazole: a major innovation for treatment of fungal disease. *Ann. Znt. Med.* 93: 921-923.
2. Angeli A, Frairia R. Ketoconazole therapy in Cushing's disease. *Lancet.* 1985;1:821.
3. Bradbrook ID, Gillies HC, Morrison PJ, Robinson J, Rogers HJ, Spector RG. *Br J Clin Pharmacol.* 1985;20: 163-165.
4. Couch RM, Muller J, Perry YS, Winter JS. *J Clin Endocrinol Metab.* 1987;65:551-554.
5. Dandona P, Mohiuddin J, Prentice HG. Ketoconazole and adrenocortical secretion. *Lancet* 1985;1:227.
6. Pont A, Williams PL, Loose DS, et al. Ketoconazole blocks adrenal steroid synthesis. *Ann Intern Med.* 1982;97:370-372.
7. Feelders RA, Hofland LJ, de Herder WW. Medical treatment of Cushing's syndrome: adrenal-blocking drugs and ketaconazole. *Neuroendocrinology.* 2010;92(Suppl 1):111-115.
8. S. A. Rice, M. Givskov, P. Steinberg and S. Kjelleberg, *J. Mol. Microbiol. Biotechnol.*, 1, (1999), 23-31.
9. J. G. Lara, M. Masalha and S. J. Foster, *Drug Discov Today*, 10(9), (2005), 643-651.
10. G. D. Wright, *Chem. Biol.*, 7, (2000), R127-R132.
11. J. Travis and J. Potempa, *Biochim. Biophys. Acta.*, 14, (2000), 35-40.
12. H. J. Smith and C. Simons, *Taylor and Francis*, London, (2001).
13. S. J. Lippard and J. M. Berg, " *Principles of Bioinorganic Chemistry*", University Science Books, Mill Valley, Valley, CA, (1999).
14. Irobi O N, Moo – Young M and Anderson W A 1996 *Int . J. Pharm.* 34: 87
15. Pelczar M.J, Chan E C S and Krieg N. R (1998) *Microbiology* (New York : Blackwell Science) 5th edn.,
16. Y.Chen, M.Wong, R. H. Rosen and C. Thunb, *J. Agric. Food Chem.* 47, 2226-2228 (1999).
17. N.Raman and S.Johnson Raja, *J.Chem. Soc.*,10, 983-92 (2007).
18. Govindharaju R, Durairaj P, Maruthavanan T, Marlin Risana M, Ramachandramoorthy T. *Int. J. Pharm. Sci. Drug Res.* 2019; 11(5): 174-180.
19. R. Govindharaju, S. Balasubramanian, K. Rajasekar and T. Ramachandramoorthy, *International Journal of Development Research*, 2016, vol.6, no.4,, pp. 7459-7463.
20. M. Rajasekar, S. Sreedaran, R. Prabu, V. Narayanan, R. Jegadeesh, N. Raman and A. Kalilur Rahiman, *Journal of Coordination Chemistry*, 63(1), 136 (2009).
21. Sahbaa. A. Al-Sabaawi, *College of Basic Education Researchers Journal*, 11(3), 765 (2011).
22. Kappe CO, *Curr.Opinion.Chem.Bio.*, 2002; 6: 314.





Keerthika et al.,

23. Dandia A, Arya K, Sati M and Gautam S, *Tetrahedron*, 2004; 60: 5253.
24. A. Scozzafava and C. T. Supuran, *J. Med. Chem.*, 43, (2000), 3677.
25. R. Chadha, A. Saini, D. S. Jain, and P. Venugopalan, *Cryst. Growth Des.*, vol. 12, no. 8, pp. 4211–4224, Aug. 2012.
26. Indra Indra, Fitri Miftahul Janah and Ratih Aryani "Enhancing the Solubility of Ketoconazole via Pharmaceutical Cocrystal" 2019 *J. Phys.: Conf. Ser.* 1179 012134
27. Saeed-ur-Rehman, Muhammad Ikram, Sadia Rehman, Alia Faiz and Shahnawaz synthesis, characterization and antimicrobial studies of Transition metal complexes of imidazole derivative, *Bull. Chem. Soc. Ethiop.* 2010, 24(2), 201-207.
28. Ajaykumar D. Kulkarni, Sangamesh A. Patil and Prema S. Badami, *Int. J. Electrochem. Sci.*, 4, (2009), 717-729.
29. Raman, N, Baskaran, T, Selvan, A, Jeyamurugan, R 2008, *J. Iran. Chem. Res.* 1 pp 129–139.
30. Hathaway, B.J, Tomlinson, A.A.G 1970, *Coord. Chem. Rev.* 5 pp 1–43.
31. Tharmaraj, P, Kodimunthiri, D, Sheela, C.D, Shanmuga Priya, C.S 2009, *J. Serb. Chem. Soc.* 74 pp927–938.
32. Ei Bindary, A.A, El Sonbati, A.Z. 2000, *Pol. J. Chem.* 74 pp 615– 620
33. Raman, N, Muthuraj, V, Ravichandran, S, Kulandaisamy, A 2003, *Proc. Indian Acad. Sci. (Chem. Sci.)* 115, pp 161–167.
34. Govindharaju R, Balasubramaniyan S, Palanivelan L, Risana Marlin M and Meenakshi Mukil V: *Int J Pharm Sci & Res* 2019; 10(11): 5137-45.
35. Singh P, Goel RL and Singh BP, *J. Indian.Chem.Soc.*, 1975; 52: 958.
36. Mahindra AM, Fisher JM and Robinovitz, *Nature(London)*, 1983; 303: 64.
37. Ashry, E.S.H.El, Ramadan E, Kessem E, Kassem AA and Hager M, *Adv.Heterocycl.Chem.*, 2005; 68: 1.





Keerthika et al.,

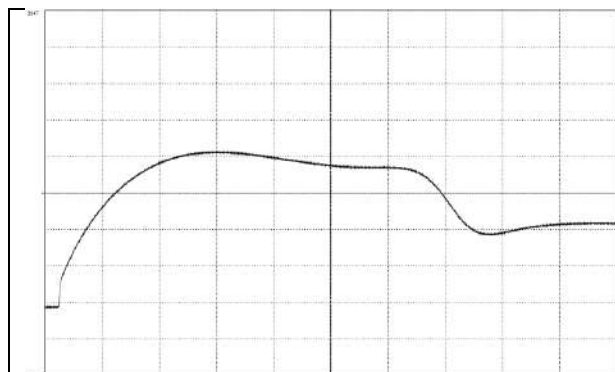


Fig.5 EPR spectrum of Cu(II) complexes



Fig.6 Antibacterial activity of Ni(II) complex against *Escherichia coli*

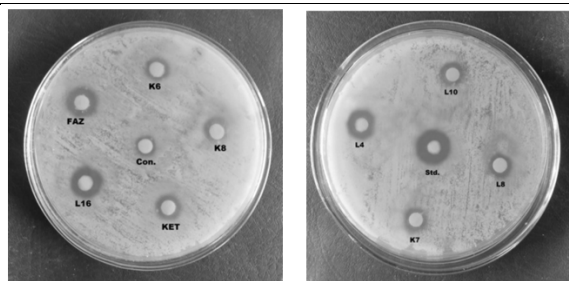


Fig.7. Antifungal activity of Cu(II) complex against *Candida albicans*

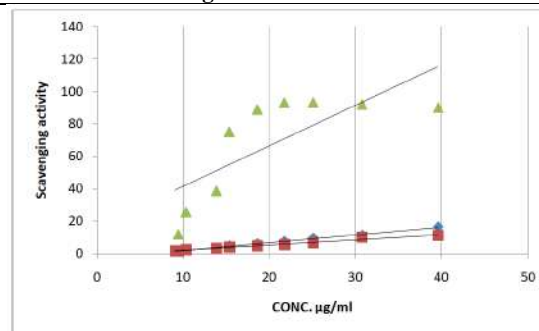


Fig.8 Antioxidant activities of free ligand and their complexes





Study on Utilization of Fiber Reinforced Polymer in the Retrofitting of Concrete Structures.

S Pooja Sri Reddy¹ and Cherupally Saikumar^{2*}

¹Professor, Department of Civil Engineering, Malla Reddy Engineering College, Secundrabad, Telangana, India.

²PG Scholar, Department of Civil Engineering, Malla Reddy Engineering College, Secundrabad, Telangana, India.

Received: 15 Feb 2023

Revised: 25 Apr 2023

Accepted: 30 May 2023

*Address for Correspondence

Cherupally Saikumar

PG Scholar,

Department of Civil Engineering,
Malla Reddy Engineering College,
Secundrabad, Telangana, India.

E.Mail: saikumar.mrec@gmail.com



This is an Open Access Journal / article distributed under the terms of the **Creative Commons Attribution License** (CC BY-NC-ND 3.0) which permits unrestricted use, distribution, and reproduction in any medium, provided the original work is properly cited. All rights reserved.

ABSTRACT

Glass fibre rebar retrofitting is a high-value-added construction breakthrough. Glass fibre rebar is a strength improvement material that has the highest potential to improve the life of public constructions where destruction can have an enormous economic and natural influence, according to super foundation providers such as the government and government funded. Structures weaken as a result of increased erosion as a result of global warming. Unlike surrenders, which may not appear at the start of a structure's administration life, but are relatively time-dependent, harm to the structure occurs. Retrofitting is any modification made to an existing structure to diminish or eliminate the risk of damage from water, disintegration, severe winds, or earthquakes. Fiberglass support material is becoming increasingly common. These serious composite materials will be able to demonstrate their traits and properties even more clearly in the future. The Flexural strength and compressive strength of M25 grade concretes are determined first, then retrofitting for similar beams with Glass fibre rebar is performed, and the compressive strength is estimated again. M25, M30, and M35 grade concretes with 4GFR bars and 6GFR bars are examined in cube specimens and beam specimens.

Keywords: Retrofitting, Glass fiber rebar, compressive strength, flexural strength,





Pooja Sri Reddy and Cherupally Saikumar

INTRODUCTION

General

Many existing structures today do not fulfill seismic strength criteria owing to material adequacy and material deterioration through time or alternative work performed over the building's service life. As a result of these factors, the building's strength deteriorates. Because the loss of most people during the collapse of a building is a major issue, it is critical to adopt a suitable planned technique to assess the structure's state before trying any repair operation. Retrofitting is a more advanced means of boosting the structural strength of concrete elements. It is the process of reinforcing the structure using standard code standards. The concrete's strength improves with the aid of retrofitting. If the cost of repair and reinforcing the building is less than 50% of the cost of construction, the retrofitting approach is used..

Glass Fibre Reinforced Polymer (GFRP)

Glass Fibre Reinforced Polymer (GFRP) materials were widely using all over the globe for retrofitting and repairing weak, ageing infrastructure, such as bridges and buildings. These constructions have lost a lot of strength and also stiffness over time due to extreme environmental conditions including humidity, salt, and alkali solutions. Advanced fibrous composite materials, such as GFRP, can protect GFRP-reinforced bars against corrosion while also greatly enhancing their strength and stiffness. Externally reinforced RC beams having GFRP plates and textiles that are exposed to extreme environmental conditions, on the other hand, the connection between the GFRP plate and the RC beam's surface has a significant influence on the external strength of reinforced RC beams. As a result, it's critical to look at the overall reaction of RC beams that have been externally reinforced with GFRP plates and textiles and subjected to various environmental conditions.

Advantages of GFRP Rebar

Rebar made of glass fibre reinforced polymer is a high-value-added building material. State run administrations and other significant foundation suppliers have now perceived that GFRP is a useful structure material with the ability to expand the existence of public offices where erosion can have a critical financial and ecological outcome.

1. GFRP is comprised of top notch erosion safe vinyl ester pitch, which expands the existence of a substantial construction.
2. A venture reinforced with GFRP rebar requires little support, permitting manufacturers to get a good deal on restoration.
3. When contrasted with standard supporting materials, GFRP rebar is multiple times lighter and has double the rigidity.

LITERATURE REVIEW

Ankit Dasgupta, et al.,(2018) This study looks at the usage of FRP in concrete structures to see whether it may help improve structural performance in terms of strength and ductility. So far, bridge culverts, slabs, beams, and columns have all been put to the test. Retrofitting using FRP looks to be a feasible alternative to traditional approaches thus far. It may be the most cost-effective (and superior) solution to a structural rehabilitation problem in many circumstances. The manufacturing procedure for FRP and its field use are both simple, with chosen experimental and analytical outcomes. In recent years, the civil engineering community has shown a strong interest in seismic retrofit using FRP materials. Chetan Yalburgimath, Akash Rathod, S Bhavanishankar, et al.,(2018)This research reports on experiments on the flexural behavior of RC beams reinforced with continuous carbon fibre reinforced polymer (CFRP) textiles. According to this article, CFRP materials are one of the most effective ways for reinforcing concrete structural reinforced components. When CFRP fabric is used to strengthen an RC beam, it improves both load bearing capacity and stiffness. Wrapping the two lateral sides as well as the soffit improves performance and serviceability. More CFRP textiles enhance the stiffness and rigidity of members, avoiding crushing or total annihilation of members without warning. These findings indicate that an employing CFRP textile whenever they



**Pooja Sri Reddy and Cherupally Saikumar**

are required, while accounting for the fabric's area, rigidity, and stiffness, boosts beam strength and provides extra support. Aleesha Alexander, Nimesh Mohan M, et al.,(2015)The impact of glass fiber reinforced polymer strips and sheets on retrofitting flexural radiates was explored in this review through a test request. There were six unmistakable wrapping techniques utilized. The quantity of FRP layers was protected as a variable in these. A sum of 26 pillars were cast and exposed to monotonic stacking tests.As per the discoveries of this review, the flexural load bearing capacity of retrofitted radiates ascends with FRP wrap when contrasted with control radiates. A definitive burden on the FRP-wrapped examples was higher. A definitive burden took care of by the examples rose when the quantity of layers of FRP was expanded.

Priyanka Sarker, Mahbuba Begum, Sabreena Nasrin, et al.,(2011)The present state of using FRP materials as a seismic retrofitting approach for structures that were not intended to resist earthquakes is discussed in this article. It describes the breadth and uses of FRP materials in RC structural seismic retrofitting, masonry seismic retrofitting, and steel seismic retrofitting schemes. The benefits of FRP applications for seismic retrofit, as well as design requirements and limits, are also discussed in the paper.According to the findings of this study, the need of restoring seismically weak structures has been clearly established in many places of the world. To promote more quick and successful uses of FRP as a seismic material, design guidelines and suggestions should be made more widely available. Despite the extensive study on their structural mechanism and performance, there is still considerable worry about early failure owing to debonding, particularly in zones of combined shear and flexural loads. To achieve a successful seismic use of FRP materials for retrofitting and rehabilitation, related staff should be appropriately educated.

Xiong et. al. (2011) The heap bearing limit and pliability of round concrete segments confined by ferrocement were researched, with steel bars (FS) being prescribed to support compressive strength and malleability. Under uniaxial pressure, the conduct of the ferrocement strengthened sections was contrasted with that of the bar mat-mortar (BS) and fiber reinforced polymer (FRP) wrapped segments. The concrete tube shaped segments had aspects of 105 mm (dia) x 450 mm and 150 mm (dia) x 450 mm. The examples were moved to a relieving chamber for 27 days after wet-restoring (24 hours). The examples with a measurement of 105 mm were contained with FS or BS, while those with a breadth of 150 mm were restricted with FRP. The compressive strength of FS segments was 30% higher than that of BS segments, as per these examples' similar appraisals. Turgay et. al. (2010) Huge scope square/rectangular segments canvassed in fiber reinforced polymer were investigated for their impact and disappointment components (FRP). The presentation of huge scope square RC segments covered in carbon fiber reinforced polymer (CFRP) sheets was examined as a feature of an exploratory examination program. Moreover, the review zeroed in on the general effect of longitudinal and cross over support, just as FRP coats, on the conduct of concentrically stacked sections. In the underlying lab, an aggregate of 20 huge scope RC segments were assembled and tried to disappointment under pivotal force Unwrapped, totally wrapped, and to some extent wrapped sections were the primary contemplations. Opened up (C1), to some degree wrapped (C2), completely wrapped (C3), to some extent wrapped with two layers (C4), and completely wrapped with two14 layers were totally tried (C5).

METHODOLOGY

The methodology of the present study is shown in the below

Testing the existing structure strength

The existing beam member was chosen at first to determine the compressive and flexural strengths of the current component. The 700mm long beam member is made up of four 12mm bars and eight 8nos stirrups. The present beam is made of concrete of the M25 grade.



**Pooja Sri Reddy and Cherupally Saikumar****Retrofitting of existing beam**

Glass fibre reinforced (GFR) rebars, which are similar to steel bars, are utilised as reinforcement in the retrofitting process. M25, M30 and M35 are the concrete grades utilised for existing beams.

Compressive strength of concrete

Steel and glass fibre reinforced bars are used to assess the compressive strength of M25 and M30 grade concrete beams after 14 and 28 days of curing, and the strength results for normal and retrofitted beams are compared.

Flexural strength of concrete

The flexural strength of concrete beams is evaluated using steel and glass fibre reinforced bars after 14 and 28 days of curing for M25 and M30 grade concrete, respectively. The steps for this test are the same as for compressive strength testing.

Rebound hammer test

According to IS: 13311, the rebound hammer test is used to assess the compressive strength of concrete (Part 2). This strength of regular and retrofitted beams in M25, M30 and M35 grade concrete mix is evaluated for the current project.

Materials used**Cement**

On the domestic market used in the investigation, ordinary cement port land of 53 grades conforming to the IS456-2000 is available. The cement is tested according to IS4031-1988 for many properties. Cement is a medium that binds. It is created by moulding, mixing and burning the raw materials in an oven at a temperature of around 1300 to 1500 degrees Celsius, depending on the pureness and composition of them.

AGGREGATES

Aggregates are a crucial part of the concrete mix. They offer a strong base for concrete, decrease shrinkage, and save money. Aggregates are inert granular materials that can be acquired from own supply sources, such as rock, sand, or broken stone. Also the raw elements that go into the making of concrete.

Steel bars

Rebar (short for building up bar) is a steel bar or lattice of steel wires used as a strain device in reinforced concrete and reinforced stone construction projects to strengthen and aid the concrete under pressure when massed as supporting steel or reinforcement steel. Concrete has a high compressive strength yet a low elasticity. The rigidity of the construction is extraordinarily expanded by rebar. To empower a superior association with the concrete and diminish the chance of slippage, rebar's surface is every now and again "disfigured" with ribs, hauls, or spaces, as shown in fig1,

Glass fiber reinforced polymer rebars

FRP rebar is acquiring fame because of its protection from destructive synthetics and capacity to keep concrete from rusting or debilitating. Glass fiber reinforced polymer rebar, or GFRP, is a sort of FRP. In the last part of the 1990s, the United States and Canada accepted progressed composite materials like FRP for primary purposes. Consumption safe rebar should be utilized to help delicate concrete designs like seawalls, dams, and power plants. Thus, fiberglass building up material is viewed as the ideal choice for fragile concrete frame works, as shown in fig1,

BASIC TESTS ON MATERIALS**Fineness of cement**

The rate of hydration and, as a result, the rate of energy improvement is affected by the fineness of the cement. The rate of hotness flow is accelerated by the fineness of the cement. Because better cement has a larger hydration surface



**Pooja Sri Reddy and Cherupally Saikumar**

area, it creates more energy in an unexpected way. As the fineness of the cement increases, concrete shrinks, resulting in approximately fractures in buildings.

Normal consistency of cement

To consider initial setting time, last setting time, soundness in cement, strength, a metric known as general consistency need to be employed. A cement paste of regular consistency lets in a Vicatplunger with a diameter of 10 mm and a size of 50 mm to penetrate from the pinnacle of the mildew to a depth of 33-35 mm.

Mix design of concrete

Concrete mix configuration is the most popular method of selecting the best concrete ingredients and determining their relative quantities in order to provide concrete with a base energy, positive utility, and durability in the most cost-effective manner possible (esteem designed). If we decide to go with a certain combination plan, we must first gather the necessary documents, as more than one plan barrier has been frozen as a result of these circumstances.

EXPERIMENTAL INVESTIGATION**COMPRESSIVE STRENGTH TEST:**

In accordance with the test procedure (IS516-1959). The compressive strength of concrete was determined using cubes of standard size 150x150x150mm. Without eccentricity, specimens of the 200T capacity CTM cube were put on its bearing surface and subjected to a consistent rate of loading up until the cube's failure. Estimated the compressive strength from the highest load.

Calculation

By dividing the most pressure utilized to the specimen all through the take a look at cross-sectional area, which is decided from the suggest dimensions of part and must be noted to the closest kilograms/cm², the specimen's compressive energy is computed.

The compressive strength of cube = (P/A) N/mm²

P is load at failure in N,

A is area of cube/contact in mm².

Rebar Hammer test Fig .5.**Procedure**

1. The tried-and-true example will be retained and repaired so that the softening and solidification of the surface caused by calcium hydroxide consumption filtration is kept at a safe distance.
2. Any residue or loose material will be removed from the example surface.
3. The example will be kept or settled such that it does not yield when sledged.
4. The sledge's plunger will always be kept on the opposite side of the surface.
5. A total of ten to twelve readings will be obtained, with their typical esteem calculated to create a hardness agent record.
6. All of the readings will be obtained with the sledge pointed in a preset direction toward the vertical and the mallet pointing in a consistent direction. The readings recorded vertically for a comparable surface will almost certainly differ from those obtained by maintaining the mallet flat.

RESULTS AND ANALYSIS**Test results on existing beam member**

The existing beam member was selected initially in order to determine the compressive strength and flexural strength of existing member. The beam member consisting of 4 bars of 12mm and stirrups of 8nos in 700mm length. The existing beam is related to M25 grade concrete mix. The results are shown in the below table 1.



**Pooja Sri Reddy and Cherupally Saikumar**

From the above table it was observed that compressive strength of concrete is 28MPa and flexural strength of concrete is 3.45MPa the values of strength are less as we compare with characteristic strength of concrete. The improvement of strength of concrete is needed for the existing members.

Retrofitting of existing beam

For the retrofitting process Glass fiber reinforced (GFR) rebars are used as the reinforcement which is same as the steel bars reinforcement. The grade of concrete for retrofitting members are used as M25, M30 grade and M35 .

Compressive strength

Compressive strength of concrete specimens are measured for M25, M30 and M35 grade concrete by using reinforcement bars as steel and glass fibers the comparison is shown in below graph 1. From the below graph1, it was observed that the value of compressive strength by providing the 4 bars as retrofitting the compressive strength averagely increased to 17% for using 4GFR bars in M25 grade concrete, 37.90% increased by using M30 grade with 4 GFR bars, 44.70% increased by using M35 grade with 4 GFR bars. From the below graph 2, by using 6 bars as retrofitting the compressive strength averagely increased to averagely increased to 19.822% for using 4GFR bars in M25 grade concrete, 40.985% increased by using M30 grade with 4 GFR bars, 45.883% increased by using M35 grade with 4 GFR bars.

Rebar hammer test The compressive strength of concrete is measured with rebar hammer at 14 days and 28 days curing. The comparison of rebar hammer value graph is shown in below . From the below graph 3 and graph 4, it was observed that the value of compressive strength is increasing for M25, M30 and M35 grade concrete with using GFR bars. When we compare with 4 bars and 6 bars the strength increases for M25, M30 and M35 grade concrete specimens. By increasing the number of bars from 4 to 6 numbers the compressive strength value increasing.

CONCLUSIONS

1. GFRP is a strengthening bar has more rigidity and higher erosion obstruction than that of the steel rebar and also, moderate in flexural strength, these properties make GFRP is acceptable option of steel in establishment of application.
2. Retrofitting is the process of increase in the strength of concrete by using extra reinforcement for existing building structural element.
3. The constituents of GFRP include great erosion safe vinyl ester tar that expands the life expectancy of a solid structure.
4. The strength values of glass fiber reinforced bars increases in case of M30 grade concrete by using glass fiber reinforced bars mix than M25 grade concrete mix.
5. GFRP rebar is non-conductive to power and warmth settling on it an ideal decision for offices like force age plants and logical establishments. The compressive strength and flexure strength is increasing by providing the 4 numbers of GFR bars in M25 grade concrete.
6. The compressive strength of concrete which is measured by using rebar hammer is also increasing by providing the GFRB for concrete beams.

REFERENCES

1. Ankit Dasgupta, et al.,(2018), "Retrofitting of Concrete Structure with Fiber Reinforced Polymer", IJIRST – International Journal for Innovative Research in Science & Technology | Volume 4 | Issue 9 | February 2018 ISSN (online): 2349-6010.
2. Priyanka Sarker, Mahbuba Begum, Sabreena Nasrin, et al.,(2011), "Fiber reinforced polymers for structural retrofitting: A review", Journal of Civil Engineering (IEB), 39 (1) (2011) 49-57.



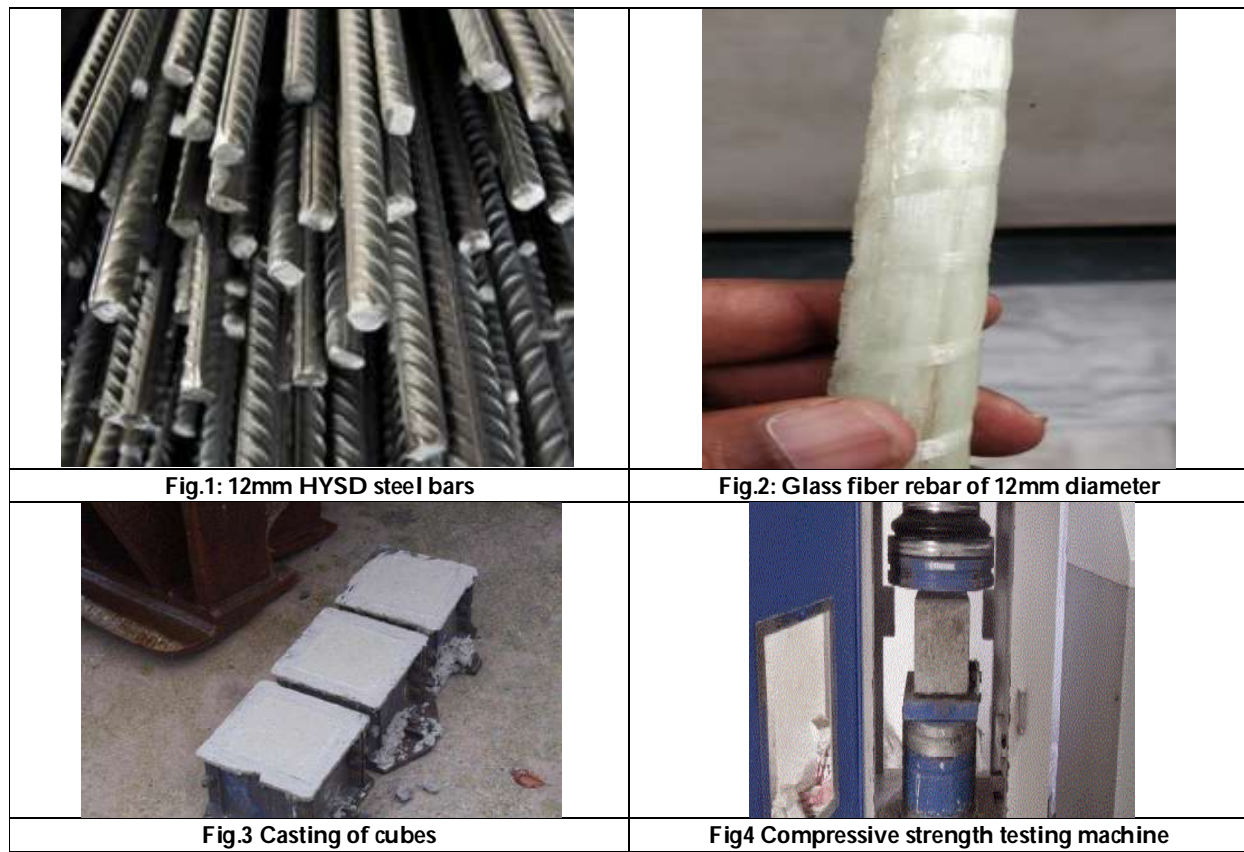


Pooja Sri Reddy and Cherupally Saikumar

3. ChetanYalburgimath, AkashRathod, S Bhavanishankar, et al.,(2018), "Retrofitting of Reinforced Concrete Beam Using Carbon Fiber Reinforced Polymer (CFRP) Fabric", International Research Journal of Engineering and Technology (IRJET) e-ISSN: 2395-0056 Volume: 05 Issue: 10 | Oct 2018.
4. Aleesha Alexander, Nimesh Mohan M, et al.,(2015), "Retrofitting of Reinforced Concrete Beam with Glass Fiber Reinforced Polymer Strips and Sheet", International Journal of Engineering Research & Technology (IJERT) ISSN: 2278-0181 Published by, www.ijert.org.
5. Pammar R. P. and Ramesh V. " Experimental study on combined effect of steel and glass fibers on compressive strength, flexural strength and durability of concrete and comparison with conventional concrete" International journal of civil and structural engineering research Vol. 3, Issue 1, pp: 146-150 2015.
6. Turgay, T., Polat, Z., Koksai, H. O., Doran, B., &Karakoç, C. (2010). Compressive behavior of large-scale square reinforced concrete columns confined with carbon fiber reinforced polymer jackets. Materials & Design, 31(1), 357-364.

Table 1: Compressive strength and flexural strength of existing beam member

S. No	Concrete Grade	Compressive strength of beam in MPa	Flexural strength of beam in MPa	Compressive strength by rebar hammer test
1	25	28	3.45	27





Pooja Sri Reddy and Cherupally Saikumar

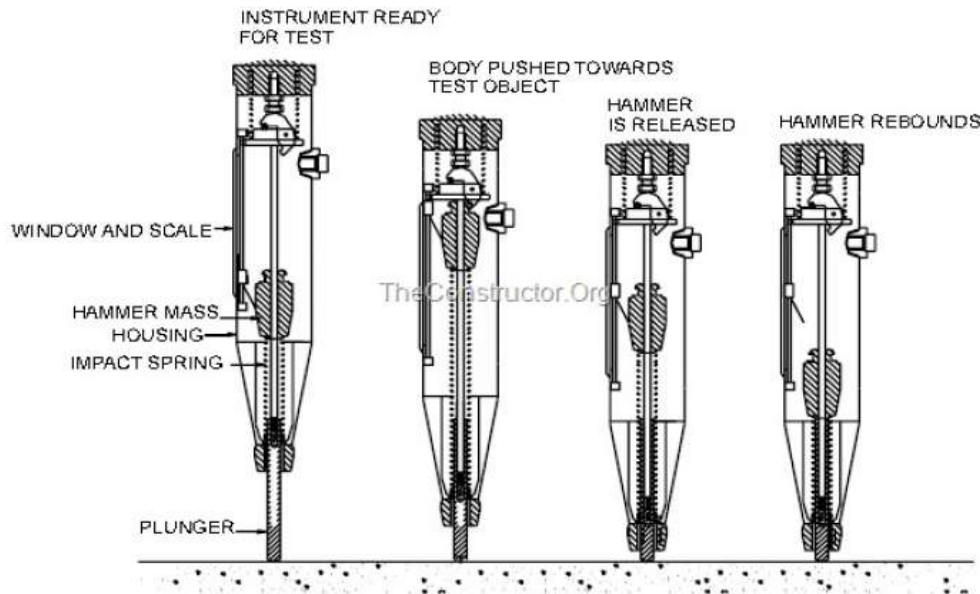
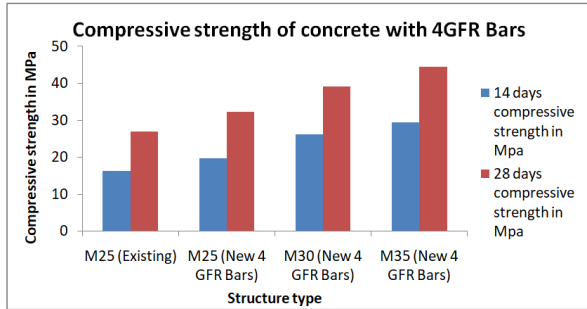
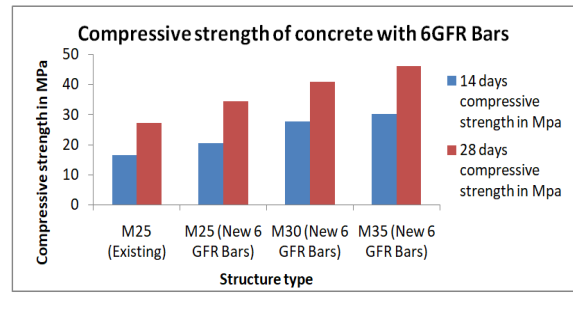


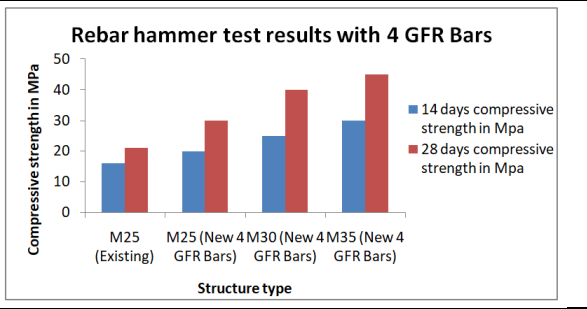
Fig. 5 Operation of the rebound hammer



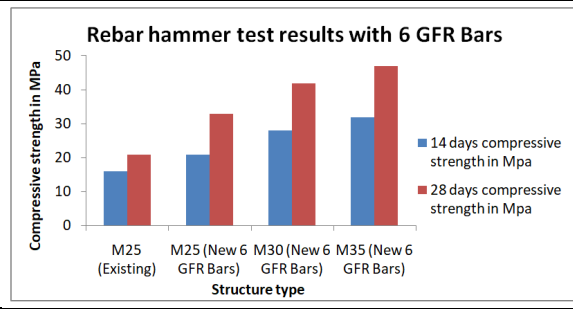
Graph 1: Compressive strength of concrete with 4GFR Bars



Graph 2: Compressive strength of concrete with 6GFR Bars



Graph 3. Rebar hammer test results with 4 GFR Bars



Graph 4. Rebar hammer test results with 6 GFR Bars





Machine Learning and Internet of Things to Improve Patient Health Monitoring Systems

Gopinath Gangadhar Patil^{1*}, B V.Febiyola Justin² and S Mohana Murali³

¹Assistant Professor, Department of Electronic Science, KRT Arts, BH Commerce and AM Science (KTHM) College, Nashik, Maharashtra, India.

²Assistant Professor, Department of Biochemistry, St. Peter's institute of Higher Education and Research, Avadi, Chennai- 600054, Tamil Nadu, India.

³Lecturer in Commerce, Govt. Degree College, Nandikotkur, Nandyal Dist. Andhra Pradesh. India.

Received: 27 Dec 2022

Revised: 23 Feb 2023

Accepted: 06 Mar 2023

*Address for Correspondence

Gopinath Gangadhar Patil

Assistant Professor,
Department of Electronic Science,
KRT Arts, BH Commerce and AM Science (KTHM) College,
Nashik, Maharashtra, India.



This is an Open Access Journal / article distributed under the terms of the **Creative Commons Attribution License** (CC BY-NC-ND 3.0) which permits unrestricted use, distribution, and reproduction in any medium, provided the original work is properly cited. All rights reserved.

ABSTRACT

Everyone's health is a key issue and a top priority in today's environment. Due to their bad lifestyle choices, humans are susceptible to a wide range of ailments. Heart attacks and low oxygen levels primarily impact people due of subpar medical care and delayed diagnosis. This effort intends to prevent such premature deaths by utilising smart health monitoring that makes use of machine learning and IoT. In case of an emergency, the suggested solution features Thing Speak cloud communication with the doctor. This system includes a blood pressure sensing module, body temperature sensor, and pulse oximeter sensor (for measuring heart rate and oxygen level). These sensors are connected to the microcontrollers Arduino Uno and Raspberry Pi. Using the Internet of Things, the obtained patient results are continuously tracked and updated on the doctor's website and LCD. After completing these processes, a trained Machine Learning model is utilised to identify the patient's disease type. This approach forecasts both healthy conditions as well as two serious diseases: lung and hypertension. We can prevent unexpected deaths in persons with heart attacks and lung conditions by implementing all these elements. In a real-world setting, this suggested strategy has an approximate 86% accuracy rate. Additionally, the approach will help clinicians in remote monitoring during epidemic conditions like covid since raw medical data can be examined quickly.

Keywords: remote health monitoring, managing epidemics, covid detection, machine learning, and Thing speak



**Gopinath Gangadhar et al.,**

INTRODUCTION

Today, a person's unhealthy lifestyle is influenced by a number of things. These elements include, among others, unsound diets, bad eating patterns, and a lack of appropriate exercise. Due to their busy schedules, people may not have enough time to concentrate on their health. There are numerous health monitoring systems available to track the health state. The majority of methods currently in use analogue devices, with the output shown in CRO. An ADC and DAC are required for this technique in order to transform the output. Using the Raspberry Pi as a minicomputer, a cost-effective small solution is created to address these issues. A single Raspberry Pi was used to collect and process various patient parameters. Many of the flaws in the current methods are resolved by the suggested methodology. The Raspberry Pi used in the proposed system controls the sensor. The Internet of Things is then used to transmit the sensor data to the doctor's website (IoT). An ML model is used in this system to forecast diseases as well. For those who require emergency services and coordination, this proposed approach might be helpful. In this technology age, some people lack access to medical facilities. They lack access to necessary medications, transportation, and hospitals. The improvement of medical facilities in and around places where people do not have appropriate access to healthcare is the main driving force behind this suggested approach.

Electronic sensors are used in the proposed system to measure patient health metrics. Health indicators including blood pressure, temperature, heart rate, and oxygen saturation are sensed when an electronic sensor is implanted in a patient's body and sent to the doctor via the cloud. The gathered data is examined using a trained Machine Learning (ML) model for disease prediction. The primary goal of the proposed work is to combine IoT and ML to create a reliable health monitoring system. The system can be used as an alternative to continuously monitoring patients. It also offers a low-cost method of increasing the accuracy of a health monitoring system. These are the significant contributions of the proposed work.

Machine learning and IoT Technology

There have been numerous literature research on patient monitoring systems. Additionally, healthcare datasets are being stored in the cloud to enhance patient and doctor communication. Artificial intelligence-based health monitoring systems that use stress and cancer detection are commonly used. The use of machine learning and IoT technology increases the accuracy of remote health monitoring. makes a suggestion for a productive health monitoring system. IoT technology is employed. The diagnosis of heart illness is the main topic. In the beginning, the clinician receives the crucial cardiac disease-related parameters through the cloud once they have been collected using biomedical sensors. The wireless sensor method was employed to gather data and conduct additional cardiovascular disease diagnosis. A suggested IoT-based clinic support system that incorporates ML and cloud computing. For the prediction and diagnosis of chronic renal disease, Particle Swarm Optimization and Deep Neural Network were utilised as classifiers experiments with real-time patient health monitoring using IoT technologies, bio, and ambient sensors. It is suggested to use a patient-centered strategy for precise health diagnosis. Furthermore, data analysis employs fuzzy logic. A prototype for a remote patient health monitoring system using the Internet of Things and Raspberry Pi and Arduino is presented. The Raspberry Pi transmits the data to the cloud server. To depict the health parameters, an Android application was created. An IoT and sensor-based solution for a behavioural monitoring system. The system recognises the elderly's fragility and mild cognitive impairment. The approach may be used as an initial screening tool for early detection of cognitive deficits. In , a health monitoring system for students is suggested in order to evaluate their vital signs and behavioural changes. Machine learning classifiers are used to analyse and categorise data obtained from biosensors. When analysing the student condition, the SVM classifier performed better than other classifiers. The method for tracking chronic disease and patient well-being is created in . Along with important parameters, their key areas of focus are diabetes, kidney disease, and heart failure. The wireless sensor mechanism used by this suggested system. A tracking system and Internet of Things monitoring of troop healthcare are being tested .



**Gopinath Gangadhar et al.,**

The suggested system Architecture makes use of GPS and biosensors to monitor the soldiers' health indicators. These data were delivered to the control room using IoT. A cardiac prediction system using IoT is suggested]. The cardiac data is analysed for this prediction, and numerous ML algorithms were utilised to increase accuracy. A method for tracking patient health reports using a wireless network and an android mobile application was proposed in [1]. It utilises real-time data and is suitable for usage in crisis situations. Both patients in hospitals and those receiving care at home will benefit from this system, which uses telemonitoring. The gathered information is kept on a server for further use. A survey was suggested in for IoT and wireless sensor-based wellness monitoring. It is an effective method with all-around monitoring. Node deployment is more challenging with this strategy than with wired networks. Proposes a real-time health monitoring system that uses cloud and IoT technologies. For elderly people and chronic sufferers, this has several advantages. Additionally, quicker ways of system implementation are also examined. In multiple bio-medical sensors were used to gather data on numerous factors, including temperature, breathing rate, heart rate, and body movement. The gathered data is processed on a raspberry pi, and the information is then saved in the cloud. Real-time patient health monitoring using a Raspberry Pi has been developed .

Biosensors were used to gather data on the patient's health indicators, and a camera was used to take pictures of the person. After data gathering, it is transmitted over IoT to the doctor's website for quicker diagnosis. In [2-3], a cheap and transportable E-health monitoring service is suggested. In order to collect information from patients and transmit it via a mobile application, several biosensors, including oximeter, pressure gauges, and temperature sensors, were attached to Raspberry Pi computers. It is found that merging IoT and machine learning speeds up diagnosis and improves reaction times when compared to current methods. This section discusses the proposed health monitoring system's system architecture, process, and steps. System Architecture, first In the system temperature sensor is connected directly to the raspberry pi controller, followed by the blood pressure sensor and the pulse oximeter sensor (which provides data on both heart rate and oxygen level). The Raspberry Pi and Arduino controller communicate serially using the I2C protocol. The results are less accurate when a pulse oximeter sensor is interfaced with a raspberry pi, which is the underlying cause. As a result, an Arduino is attached to the Raspberry Pi as a slave to interface with the pulse oximeter sensor. The biosensor values are transmitted to the doctor's website. With the use of an ML model, the generated results are used to forecast fever, hypertension, and lung illness. B. Technique The process starts with training the machine learning model. To choose the best model for a publicly accessible dataset, a comparison of four machine learning methods was conducted. There are four classes in the dataset. The classes are lung illness (class 2), hypertension (class 2), fever (class 1), and normal (class 0). (class-3). 200 samples were collected for the ML model's training. There are 48 data for class 1, 55 data for class 2, and 47 data for class 3, making up the 51 normal data. The classification process involved the use of algorithms including Decision Tree Classifier, K-Nearest Neighbour Classifier, Gaussian Naive Bayes Classifier, and Support Vector Machine. When comparing these four methods, the SVM algorithm offers the highest level of accuracy. The results are proposed system control is then handed off to the hardware component, which consists of biosensors, controllers, and the cloud, when the ML algorithm has been finished. Real-time data collection is done with the aid of biosensors. DHT11 (Temperature Sensor), BP Sensor, and Pulse Oximeter Sensor are the biosensors (used for both heartbeat rate and oxygen level measurement). The Raspberry Pi and the Arduino microcontroller are both connected to the DHT11 sensor, which is also connected to a pulse oximeter sensor. The Raspberry Pi and Arduino are then connected via serial communication. Utilizing the I2C standard, these controllers are connected to one another. Here, Raspberry Pi serves as the master while Arduino serves as the slave. These biomedical sensors capture data, which is then uploaded to the cloud. Thing Speak platform is utilised in this system as cloud storage. The Thing Speak website requires account access in order to upload data.

For consultation and medicine, the doctor is given access to the website link. Real-time forecasts are then based on the gathered data. These real-time measurements are provided to the ML model as test data. The Raspberry Pi and Arduino are then connected via serial communication. Utilizing the I2C standard, these controllers are connected to one another. Here, Raspberry Pi serves as the master while Arduino serves as the slave. These biomedical sensors capture data, which is then uploaded to the cloud. Thing Speak platform is utilised in this system as cloud storage.



**Gopinath Gangadhar et al.,**

The Thing Speak website requires account access in order to upload data. For consultation and medicine, the doctor is given access to the website link. Real-time forecasts are then based on the gathered data. These real-time measurements are provided to the ML model as test data. In order to validate the samples in real time and deliver accurate results, the trained ML model is used. The ML model is built using the SVM classifier. The system outputs normal if the data contains normal values in accordance with learned values. Medical standards state that a person's body temperature should be 36 degrees Celsius, heartbeat should be 70 to 90 beats per minute, blood pressure should be 120/80 mmHg, and blood oxygen saturation should be 90 to 100 mmHg. This proposed system also forecasts illnesses including fever, hypertension, and lung disease based on the trained data. Workflow C. The methodological following is an explanation of the steps: Start by connecting a USB cord to the Raspberry Pi and Arduino, then check sure the sensors are receiving the proper power. • Position the sensors on the patient's surface of the body. • The system displays "PLACE THE SENSORS PROPERLY" on the serial monitor if the sensor is not installed properly. • Following proper sensor placement, the vital signs (body temperature, blood oxygen saturation, and heartbeat).

These bio-medical sensors are used to gather patient data (such as heart rate and blood pressure). • The gathered data will be shown on a serial monitor and a liquid crystal display (LCD). • The doctor will receive the parameters that have been gathered via IoT utilising the Thing Speak cloud. • The gathered data was used as testing data by the support vector machine classifier. The patient is employed to provide the real-time data in this instance. The heart disease dataset from Kaggle is used to train the SVM model. This system displays the status as "NORMAL" if the person has normal values. If not, it advances to the following class. • If the patient has a high body temperature and the system outputs "FEVER."

• If the patient's pulse rate and blood pressure are high in the subsequent class, the system will indicate that they are in "Hypertension." • Hypertension occasionally just affects blood pressure readings. If the patient has low blood oxygen levels, the system indicates that they have lung disease. • The values in the dataset are used to generate the model. If the measured values differ significantly, the device displays "Consult Your Doctor" on an LCD screen shows the system's workflow.

Patient's health

The hardware design is the apparatus seen above monitors a patient's health by taking readings of their temperature, blood pressure, heart rate, and SpO2 level. For conditions like hypertension and pulmonary illness, there is an about 85% success rate between the observed and actual data. Hardware configuration and parameter measuring in AI, respectively, the results for a normal and abnormal person are displayed. Respectively, exhibit the parameters that were measured for normal and atypical people. The data that was shown in a cloud.

Protocol for Serial Communication (B)Serial connection between a raspberry pi and an Arduino microcontroller is made possible using the I2C protocol. Data is gathered by the Arduino and delivered to the Raspberry Pi. The one master, many slave idea, which allows the master controller to link with multiple slave controllers via the I2C protocol, is a key benefit of this technology. Real-time data processing is where it is most frequently used. Real-time data validation An accuracy of 86% is achieved from Table IV while validating the proposed method on real-time data. The test phase of the SVM classifier accepts the patient data that was gathered in real time as input. For the testing phase's input, 38 samples are used.33 of the 38 samples are accurately detected by the system out of the total 38 samples. Comparing the suggested method to the current health monitoring methods, it offers greater accuracy.

Applications in Intelligent Hospital Pharmacy Decision-Making System

The health of the elderly must be prioritised in a society that is getting older. Medication safety in particular is essential to the health care system as a whole. Consequently, integrating machine learning and data analysis to deliver effective services is a crucial topic. As a result, the goal of this project is to combine pharmaceutical services with information technology to create a pharmaceutical management information system for data analysis and visualization activities. Additionally, a number of smart health care management indicators are integrated, such as



**Gopinath Gangadhar et al.,**

reminders for managing medication shortages, clinical side effects and abnormal events, and patient service elements like waiting times for medications, in order to meet monitoring objectives through real-time online alerts. Making decisions is made simpler by graphical management information. Additionally, the suggested system allows access to management data on pharmaceutical events via mobile devices and real-time updates. One of the most significant patient safety objectives is to increase drug safety. Medication administration is a crucial component of the total pharmaceutical operation in hospital assessment and appraisal initiatives. Because clinical care is more convenient because to information technology, patients can get better care. The usage of decision support systems (DSSs) in the pharmaceutical or medical industries is growing. A DSS was put forth by Exarchos, Goletsis, and Fotiadis to forecast oral squamous cell cancer recurrence [3]. Based on the patient's prior data and the doctor's experience, you and your colleagues presented a medication DSS to calculate a patient's medication dosage and medication cycle [4].

Hospital Assessment

By utilising a case-based fuzzy cognitive map, Douali, Dollon, and Jaulent created a DSS for predicting gestational diabetes [5]. Sheng, Li, and Wong suggested using information from pharmacogenomics, personal genome profiles, and medication sensitivity to forecast how each patient will react to specific medications. Patients can successfully use their medication DSS to choose the appropriate prescription [6]. Critical elements of medical care include pharmaceutical services. An automated approach was created by Maniyar et al. to detect medication responses. For the purpose of arriving at an appropriate prescription decision, Hijazi, Obeid, and Sabri created logical foundations [7-9]. A drug-pregnancy alerting system was created by Wardhani, Mengko, and Setiawan to guard against medication delivery mistakes in expectant patients. Drug application safety may be guaranteed if the information system is employed for online real-time warning and tracking for reminders of medication shortage management, clinical side effects and abnormal events detection, and waiting time.

Planning and design, part two The proposed system performs three tasks: graphical management interface framework determination, smart pharmaceutical information event warning, and management indicator design and confirmation. Designing and validating management indicators. The patient service dimension and the standard tracking dimension make up the information sources needed by the graphical management interface. Patient service dimensions are used to keep track of things like patient wait times, medical side effects, and clinical anomalies. The standard tracking dimension includes information on medication management, pharmaceutical pricing adjustments, pharmacist availability, information on pharmacist-packaged medications, and other detailed data.

B. Determination of the graphical management interface framework To aid pharmaceutical management decision-making and save hospital costs, the graphic styles and content displayed on the graphic management interface are chosen and put into practise. The decision information dashboard, the normal information dashboard, and the abnormal record dashboard are the three sub-items of the graphic management interface. A selection of pertinent pharmaceutical cost control statistics, including total pharmaceutical labour costs, total drug costs, available manpower, and total hours, are displayed on the decision-making dashboard. The abnormal record dashboard gives statistics or analytical findings of abnormal record events such as clinical abnormal events, whereas the normal information dashboard displays status information such as on-duty pharmacy staff, average medication waiting time, and average medication reserve amount. C. Intelligent pharmaceutical event warning Early alerts for smart pharmaceutical information events are sent using machine learning or deep learning techniques. This makes it easier to take early warning measures in response to unusual events so that managers who make decisions can learn more in advance and lessen the chance of emergencies. Reminders for managing prescription shortages, clinical side effects events, and clinical abnormal events are the three sub-items under this future development. Machine learning is used to create reminders for managing medicine shortages. This is done by utilising historical data on the rate of drug consumption to anticipate when to remind managers to order specific medications and in what quantities. As a result, the price of medicine hoarding is decreased. Clinical side-effect events are conclusions about the likelihood of clinical side-effects based on the records of past clinical side-effects, followed by a choice on whether to give early warnings. A clinical abnormal event is defined as the estimation of the probability of clinical abnormal events based on the records of previous clinical abnormal events, followed by a choice about the issuance of early warnings.



**Gopinath Gangadhar et al.,****Smart health care**

Real-time online early warning and standard tracking are accomplished for monitoring targets in the proposed system by combining smart health care management. The system's graphical management information system facilitates decision-making. Mobile devices can access the content since real-time updates of pharmacological events and related management information are enabled.

CONCLUSION

The proposed work offers a more effective method of keeping track of the patient's medical system. It primarily focuses on using ML, IoT, and cloud services for patient monitoring. The accuracy of the decisions is increased using ML. Additionally, the system can be utilised as a sophisticated real-time patient monitoring system equipped with IOT to keep track of a patient's vital signs such as body temperature, blood pressure, heart rate, and oxygen saturation. Based on the supplied results, appropriate drugs are recommended. In the event of any abnormalities, this technology delivers the collected data to the doctor via the cloud for consultation. It reduces the expense of health monitoring and allows patients to use the existing medical resources. Additionally, the effort will make it easier for doctors to acquire patient information and can help doctors and nurses in epidemic scenarios like covid since raw medical data can be analysed in a hurry. In the future, telemedicine and wearable sensor technology may be used for remote health monitoring.

REFERENCES

1. H. Pandey and S. Prabha, "Smart Health Monitoring System using IOT and Machine Learning Techniques," 2020 Sixth International Conference on Bio Signals, Images, and Instrumentation (ICBSII), Chennai, India, 2020, pp. 1-4, doi: 10.1109/ICBSII49132.2020.9167660.
2. T. Parbat, R. S. Benhal and H. Jain, "IoT Based Health Care Data Monitoring Using Machine Learning," 2022 International Conference on Sustainable Computing and Data Communication Systems (ICSCDS), Erode, India, 2022, pp. 282-286, doi: 10.1109/ICSCDS53736.2022.9760770.
3. M. Amutha, U. Arul, G. R. Devi, J. Manikandan and R. Uma, "Machine Learning and Advanced Technology Based Patient Health Monitoring System," 2022 Sixth International Conference on I-SMAC (IoT in Social, Mobile, Analytics and Cloud) (I-SMAC), Dharan, Nepal, 2022, pp. 996-999, doi: 10.1109/I-SMAC55078.2022.9987298.
4. S. M. S, T. Sheela and T. Muthumanickam, "IoT Enabled Health Monitoring System using Machine Learning Algorithm," 2022 6th International Conference on Electronics, Communication and Aerospace Technology, Coimbatore, India, 2022, pp. 460-464, doi: 10.1109/ICECA55336.2022.10009285.
5. Q. He, A. Maag and A. Elchouemi, "Heart disease monitoring and predicting by using machine learning based on IoT technology," 2020 5th International Conference on Innovative Technologies in Intelligent Systems and Industrial Applications (CITISIA), Sydney, Australia, 2020, pp. 1-10, doi: 10.1109/CITISIA50690.2020.9371772.
6. N. Zholdas, O. Postolache and M. Mansurova, "Health Monitoring System Using Internet of Things," 2021 IEEE International Conference on Smart Information Systems and Technologies (SIST), Nur-Sultan, Kazakhstan, 2021, pp. 1-4, doi: 10.1109/SIST50301.2021.9465928.
7. S. Ahamed, P. Bhatt, S. Sultanuddin, R. Walia, M. A. Haque and S. B. InayathAhamed, "An Intelligent IoT enabled Health Care Surveillance using Machine Learning," 2022 International Conference on Advances in Computing, Communication and Applied Informatics (ACCAI), Chennai, India, 2022, pp. 1-5, doi: 10.1109/ACCAI53970.2022.9752648.
8. C. Visvesvaran, N. K. Karthikeyan, I. J. J. B. Kumar, P. Kaviya and S. Kaviya, "Advanced Patient Monitoring and Alert System with Auto Medicine Suggestion using Machine Learning," 2022 3rd International Conference on Electronics and Sustainable Communication Systems (ICESC), Coimbatore, India, 2022, pp. 829-833, doi: 10.1109/ICESC54411.2022.9885566.





Gopinath Gangadhar et al.,

9. R. S. K. Boddu, "Internet of Things (IoT): Accelerating the Digital transformation of Healthcare system," *2021 7th International Conference on Advanced Computing and Communication Systems (ICACCS)*, Coimbatore, India, 2021, pp. 1716-1720, doi: 10.1109/ICACCS51430.2021.9441876.





Recent Data Mining Technologies in Healthcare Domain

R. Kowsalya^{1*}, C. Arunpriya², V. Bharathi¹ and Bobby Lukose³

¹Assistant Professor, Department of Computer Science, PSGR Krishnammal College for Women, Coimbatore, Tamil Nadu, India

²Associate Professor, Department of Computer Science, PSG College of Arts and Science, Coimbatore, Tamil Nadu, India

³Professor, MCA, Krupanidhi Group of Institutions, Bangalore, Karnataka, India.

Received: 17 Feb 2023

Revised: 25 Mar 2023

Accepted: 28 Apr 2023

*Address for Correspondence

R. Kowsalya

Assistant Professor,
Department of Computer Science,
PSGR Krishnammal College for Women,
Coimbatore, Tamil Nadu, India.
E.Mail: kowsalya@psgrkcw.ac.in



This is an Open Access Journal / article distributed under the terms of the **Creative Commons Attribution License** (CC BY-NC-ND 3.0) which permits unrestricted use, distribution, and reproduction in any medium, provided the original work is properly cited. All rights reserved.

ABSTRACT

In today's digital environment, healthcare has turned into a data-driven industry. A common use of data in healthcare based on clinical data, domain knowledge & machine learning in order to assist doctors and medical professionals to detect any critical situation or errors during the treatment of patients as well as to improve healthcare decision. For this purpose, collection of data is very crucial with regards to healthcare data analytics. In this paper discussed about Data Mining techniques, Machine learning and deep learning techniques involved in healthcare domain, and research challenges in healthcare analysis.

Keywords: Healthcare analytics, e-health records, Machine Learning, Deep Learning, challenges

INTRODUCTION

Healthcare is a wide area that encompasses numerous practical areas, such as patient management, diagnosis of illnesses, health records tracking, telemedicine, patient engagement, and so forth. Healthcare is growing very rapidly by adopting the latest technologies and providing various healthcare services to people. The digitization of the healthcare industry provides various services and supports to physicians, clinics, laboratories, hospitals, and the major healthcare providers. In the last decade, tremendous changes have happened in the modern healthcare domain. These changes involve the advancement of the medical system and healthcare services as a result of innovative technologies [6]. The main goal of the healthcare system is to improve the patients' health and provide enhanced service to patient's satisfaction. The key objective or the most significant function in the healthcare industry is the disease diagnosis that involves the tracking of medical history, analysis of medical data and identifies

56821





Kowsalya et al.,

the presence of disease. The field of healthcare makes use of Clinical Decision Support System (CDSS) in the disease diagnosis. The healthcare data includes patient medical history, diagnoses, vital signs, billing data, and radiology images and such data are collected from various sources. Hence, the healthcare data are in different forms and voluminous in nature, which necessitates the application of data analytics in healthcare. Data analytics plays a significant role of knowledge extraction from the enormous amount of healthcare data.

The goal of improving the healthcare quality, advancing research, managing risk, or anything in between, needs access to the large volume of data. However, only having the data won't provide any useful information unless there is a systematic way to organize, analyse and interpret the data. This signifies the importance of data analytics in healthcare. The analytical techniques are not only used to make sense of the previous medical data but also predicts signs of patients' future health, for the benefit of the entire healthcare community. In the healthcare data analysis several techniques and methods are applied to extract the useful information for making clinical decisions, disease diagnosis and other medical applications.

Among the various data analytic methods available, Machine-Learning (ML) techniques are indispensable to the data analytics in healthcare organizations to improve medical data analytics. The ML algorithms have the potential to extract information from clinical notes and charts more quickly and accurately than manual review processes and become smarter as they are applied to more health records. Machine learning application in healthcare data analytics have achieved significant results in various tasks, namely disease diagnosis, chronic disease prediction, etc. Meanwhile, in the immediate past, Deep-Learning (DL) techniques (i.e., machine learning with deep neural network architecture) have seen rapid improvements in the field of healthcare. The key applications of deep learning in healthcare are medical image segmentation, signal processing, and analysing the clinical text using natural language processing.

Data Mining In Healthcare Analytics

Healthcare analytics can be defined as the collection of health data from various sources and perform analysis on these medical data that helps in decision-making. Healthcare analytics are applied to vital areas like clinical data, medical expenditure, patient behaviour, and medications on both macro and micro levels that can effectively streamline operations, enhance patient care, and reduce overall costs. The area of healthcare analytics is currently transforming from the simple descriptive analytics toward the more advanced diagnostic, predictive, and prescriptive health analytics [12]. Very shortly, healthcare industry used the primary level of healthcare analytics such as descriptive and diagnostic analytics, to perform analyses on different healthcare services data, will utilize the sophisticated level of predictive and prescriptive health analytics in the complex tasks [8]. Discovery health analytics [10], a sophisticated type of data analytics that supports to discover new scientific facts from the healthcare data. To reveal new truths, the analysis involves enormous amounts of data with full detail in order to learn new insights and relationships. Fig 1 shows the four types of analytics that are applied in the healthcare analytics.

Descriptive Analytics

Descriptive analytics uses methods such as data aggregation, data mining to get a prior knowledge of the health of the individual. The descriptive study facilitates the learning of a great deal of evidence from these health data. The most convenient basic level of data analytics is descriptive analytics that just describe the data with no further reasoning and discovery of knowledge [8]. Descriptive analytics are broadly used in making simple clinical decisions.



**Kowsalya et al.,****Diagnostic Analytics**

Diagnostic health analytics pinpoints the cause of diseases. It demands a broad study and guided analysis of the existing data to find the root causes of a problem. In addition, diagnostic analytics needs a better understanding of input factors and functional processes on performance indicators. [11].

Predictive Analytics

Predictive health analytics is than aforesaid types of analytics. It scrutinizes known readings and indicators to make predictions. The previously collected patients' data such as length of stay, whether a patient require surgery or not and the same help to predict certain changes or outcomes. [3].

Prescriptive Analytics

Prescriptive analytics in healthcare plays an important part in decision making about possible alternatives. comes into action when decisions have to be made regarding a wide range of feasible alternative. It helps the healthcare professionals to predict the problems and act in advance to handle it. The success of prescriptive analytics relies on the key elements like usage of hybrid data and situation bound adaptive [3].

Categories of E-Health Records**Electronic Health Records (EHR)**

EHR is a kind of electronic records that contains individual personhealth related information. It is responsible to store the information related tothe physicians and clinicians based on health care organization. It alsomaintains health record and share the data access in the electronic format [1]. Fig 2 shows the different types of data in HER.

Personal Health Records (PHR)

PHR is a collection of health-related information from individual patients. It isresponsible for enabling data manipulation, access and transmission in an authentic, secure and private way for customers and patients [14].

Mobile Health (MHealth)

MHealth is the emerging network topology and mobile communication used especially for healthcare systems which is shown in fig 3. It is essential to help patient health information fastly so as to reduce the additional cost by avoiding unnecessary hospital visits [4]. For quick diagnosis, the patient uses a tracking device to monitor the symptoms in real-time with the help of experts or doctors [5] [9].

Machine Learning for Healthcare Analysis

Machine learning is employed in several specialties of medicine such as radiology, cardiology, oncology, and ophthalmology [7]. Despite advancement made in healthcare Information and Communication Technologies, still there is a necessity innovation in healthcare. In healthcare, ML techniques are applied to extract the key features and learn the complex patterns from these medical data for various applications of healthcare. The major applications of machine learning in the healthcare domain are:

- Disease Diagnosis/ identification
- Personalized Treatment
- Drug Discovery
- Radiology and Medical image process
- Electronic Health Record Analysis
- Epidemic Outbreak Prediction

Deep Learning for Healthcare Analysis

Deep learning is introduced to overcome the challenges in analysis of medical images and learns the key features from the images. The Convolution Neural Network (CNN) is the popular deep neural network model for medical



**Kowsalya et al.,**

image analysis, namely segmentation of organs, image, tumor detection and image reconstruction [13]. The Recurrent Neural Network (RNN) is used to analyse the temporal data like prediction of patient readmission, activity monitoring using wearable sensors and devices [2]. Deep learning models can analyze electronic health records (EHR) that contain structured and unstructured data, including clinical notes, laboratory test results, diagnosis, and medications at exceptional speeds with the most possible accuracy. Deep learning in healthcare has a huge impact and it has enabled the sector to improve patient monitoring and diagnostics. The top pathbreaking applications of deep learning in healthcare are:

- Drug Discovery
- Medical Imaging and Diagnostics
- Simplifying Clinical Trials
- Personalized Treatment
- Improved Health Records and Patient Monitoring
- Health Insurance and Fraud Detection

Research Challenges in Healthcare Analysis

Healthcare domain industry inferred that there exists a lot of scope for further research in the area of Sentiment analysis in real-time healthcare data sets, cluster analysis of patient cohorts, development of interactive systems for appropriate survivability predictions of diseases, and classification task by using transfer learning. These investigations are carried out by adopting various techniques. These techniques and the challenges in implementing them are summarized as follows:

- Sentiment Analysis
- Cluster Analysis
- Classification and Survivability Prediction

Sentiment Analysis

The Sentiment analysis in healthcare influences text mining, and natural language processing is used to analyze the texts acquired through reviews, social media platforms, and surveys. There is a huge accessible volume of information obtained from patients online, such as social media, personal blogs, in which people exchange their views on various medical issues. The polarities in this sentiment analysis are categorized into positive, negative, or neutral and this can be achieved by opinion mining and it is a natural language processing task that employs an algorithmic methodology to detect opinionated information. The common challenges to transform the raw data into a representative numeric shape such as removing the URLs, stop words, Stemming and Lemmatizing, transform the text into numeric tensors. Due to its improved performance over conventional feature-based techniques and automatic feature extraction, deep learning algorithms have been particularly successful in doing sentiment analysis. As a result, there is possibility for research into the application of sentiment analysis techniques to gather and analyse the thoughts of billions of people on health-related issues and derive insightful conclusions. As a result, the sentiment analysis's findings must be clear-cut and useful for making decisions in the healthcare industry.

Cluster Analysis

It is usually employed as a mathematical approach that aids in the detection of hidden structures and clusters in large data sets. The K-Means clustering technique is the most suitable algorithm for cluster analysis. The benefit of using this clustering is that the results are less prone to outliers in the data. The chosen distance metric used here can evaluate incredibly large datasets. Clustering techniques have been extremely useful in the healthcare industry for the early diagnosis and prediction of diseases. It is faster, sufficient, reliable, and provides cost-effective healthcare delivery to patients. As a result, the cluster analysis is utilised to pinpoint complex patient subpopulations that could profit from specialised care management techniques.

Classification and Survivability Prediction

An enormous amount of digital medical data is available, but it is also complex in its structure using the traditional software. Several factors contribute to the inability of conventional programs in dealing with these databases,



**Kowsalya et al.,**

available in a variety of formats, which may be longitudinal, noisy, and multifaceted, including the vast diversity of standardized and unstructured data such as doctor reports, patient history, medical diagnostic images, Magnetic Resonance Imaging (MRI), Computed Tomography (CT) and RGB images.

CONCLUSION

This research work describes the various aspects of healthcare analysis system that takes the different kinds of medical data in various forms such as text, numeric, image and video data to perform analysis that can support the clinical decision in healthcare. Analysis of these complex healthcare data requires potential techniques to explore more insight into the data and learn the disease patterns and other features. It is observed from the review that Data Mining, Machine Learning, Deep learning techniques play a vital role in the classification of medical data.

REFERENCES

1. Cowie, MR, Blomster, JI, Curtis, LH, Duclaux, S, Ford, I, Fritz, F, Goldman, S, Janmohamed, S, Kreuzer, J, Leenay, M & Michel, A. Electronic health records to facilitate clinical research, *Clinical Research in Cardiology*, vol. 106, no. 1, pp. 1-9.
2. F. Ali *et al.*, "An Intelligent Healthcare Monitoring Framework Using Wearable Sensors and Social Networking Data," *Futur. Gener. Comput. Syst.*, vol. 114, pp. 23–43, 2021.
3. J. Lopes, T. Guimarães, and M. F. Santos, "Predictive and Prescriptive Analytics in Healthcare: A Survey," in *Procedia Computer Science*, Jan. 2020, vol. 170, pp. 1029–1034, doi: 10.1016/j.procs.2020.03.078.
4. Kao, CK & Liebovitz, DM 2017, 'Consumer mobile health apps: current state, barriers, and future directions', *PM&R*, vol. 9, no. 5, pp. S106-S115.
5. Kharrazi, H, Gonzalez, CP, Lowe, KB, Huerta, TR & Ford, EW 2018, 'Forecasting the maturation of electronic health record functions among US hospitals: retrospective analysis and predictive model', *Journal of Medical Internet Research*, vol. 20, no. 8, p. e10458.
6. Lashari, Saima & Ibrahim, Rosziati & Senan, Norhalina & Taujuddin, Nik. (2018). Application of Data Mining Techniques for Medical Data Classification: A Review. *MATEC Web of Conferences*. 150. 06003. 10.1051/mateconf/201815006003
7. M. Ferdous, J. Debnath, and N. R. Chakraborty, "Machine Learning Algorithms in Healthcare: A Literature Survey," in *2020 11th International Conference on 168 Computing, Communication and Networking Technologies (ICCCNT)*, 2020, pp. 1–6
8. M. Khalifa and I. Zabani, "Utilizing Health Analytics in Improving the Performance of Healthcare Services: A Case Study on A Tertiary Care Hospital," *J. Infect. Public Health*, vol. 9, no. 6, pp. 757–765, 2016.
9. Muinga, N, Magare, S, Monda, J, Kamau, O, Houston, S, Fraser, H, Powell, J, English, M & Paton, C 2018, 'Implementing an opensource electronic health record system in Kenyan health care facilities: case study', *JMIR Medical Informatics*, vol. 6, no. 2, p. e22.
10. Ray, R. (2018). *Advances in Data Mining: Healthcare Applications*. *International Research Journal of Engineering and Technology (IRJET)*, 3738 –3742.
11. S. Poornima and M. Pushpalatha, "A survey on various applications of prescriptive analytics," *Int. J. Intell. Networks*, vol. 1, pp. 76–84, 2020
12. Shan, Z., & Miao, W. (2021). COVID-19 patient diagnosis and treatment data mining algorithm based on association rules. *Expert Systems*, March, 1 –13. <https://doi.org/10.1111/exsy.12814>
13. T. G. Debelee, F. Schwenker, A. Ibenthal, and D. Yohannes, "Survey of Deep Learning in Breast Cancer Image Analysis," *Evol. Syst.*, vol. 11, no. 1, pp. 143– 163, 2020. 34
14. Woollen, J, Prey, J, Wilcox, L, Sackeim, A, Restaino, S, Raza, ST, Bakken, S, Feiner, S, Hripcsak, G & Vawdrey, D 2016, 'Patient experiences using an inpatient personal health record', *Applied Clinical Informatics*, vol. 7, no. 2, p. 446.





Kowsalya et al.,

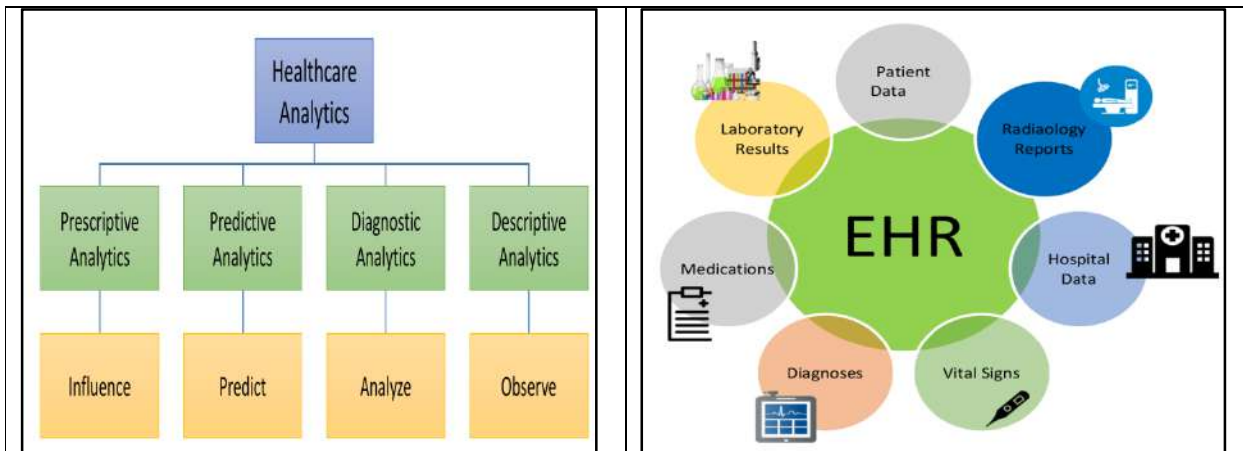


Fig. 1. Types of Analytics applied in the Healthcare domain

Fig. 2. Different kinds of Data present in EHR

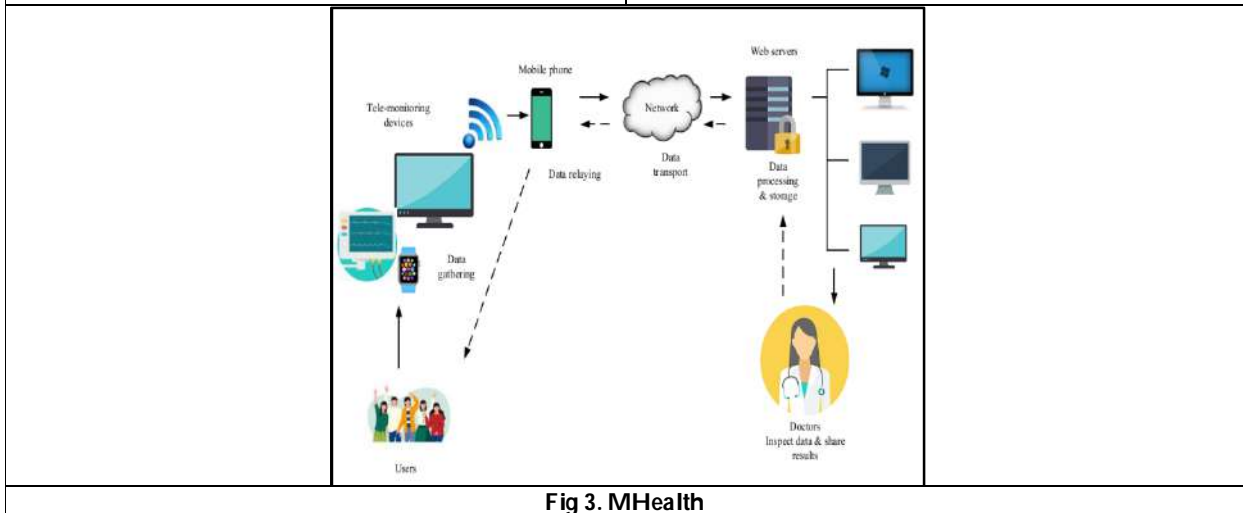


Fig 3. MHealth





A Review on the Role of Ascomycota as Potential agents for Effective Remediation of Polycyclic Aromatic Hydrocarbons

Veerasamy Veeramani¹, Arakkal Sherry Davis² and Kaliannan Thamaraiselvi^{3*}

¹Research Scholar, Department of Environmental Biotechnology, School of Environmental Sciences, Bharathidasan University, Tiruchirappalli, Tamil Nadu, India 620 024.

²Research scholar, Department of Environmental Studies, A.M. Jain college, Meenambakkam, Chennai, Tamil Nadu, India. 600 114.

³Professor and Head, Department of Environmental Biotechnology, Bharathidasan University, Tiruchirappalli, Tamil Nadu, India 620 024.

Received: 05 Mar 2023

Revised: 20 Apr 2023

Accepted: 31 May 2023

*Address for Correspondence

Kaliannan Thamaraiselvi

Professor and Head,
Department of Environmental Biotechnology,
Bharathidasan University,
Tiruchirappalli, Tamil Nadu, India 620 024.
E. Mail: thamaraiselvi@gmail.com



This is an Open Access Journal / article distributed under the terms of the **Creative Commons Attribution License** (CC BY-NC-ND 3.0) which permits unrestricted use, distribution, and reproduction in any medium, provided the original work is properly cited. All rights reserved.

ABSTRACT

Polycyclic aromatic hydrocarbons (PAHs) are the most prevalent environmental pollutants. PAHs are a large group and widely distributed organic compounds comprised of two or more fused benzene rings arranged in several configurations. These natural and anthropogenic hazardous pollutants are highly noxious to microorganism as well as to higher system including humans, moreover it may reduce the biodiversity of natural ecosystem. Among the different methods involved in the remediation of PAHs, bioremediation is a hopeful technique for treating contaminated site. A wide variety of microbial species have the potential to transform PAHs. But several studies indicated fungi can transform the structure of PAHs in the complex environment. Fungi perform a major part in the reclamation of environmental pollutant and due to their stout morphology and assorted metabolic activity. Moreover, most of the polluted environment are mainly represented by the phylum Ascomycota and are termed as a black box. They play a key role in the alteration of xenobiotic compound via intracellular enzymatic system (cytochrome P450 - CYPs).

Keywords: Polycyclic aromatic hydrocarbons (PAHs); Bioremediation; Fungi; Environmental factors; Ascomycetes





INTRODUCTION

Petroleum hydrocarbons, which comprises of both aliphatic and aromatic types, pose wide spread environmental problems. Both the forms of noxious elements are recalcitrant in nature. Although simple aliphatic hydrocarbons are transformed by microorganisms, large branched ones and polycyclic aromatic hydrocarbons are tough to remediate (Sawulski *et al.*, 2014; Al-Hawash *et al.*, 2018). Polycyclic aromatic hydrocarbons (PAHs) which are unique pollutants of the ecosystem were identified by a Physician John Hills, who reported extra ordinary occurrence of nasal cancer in tobacco users (Ghosal *et al.*, 2016). PAHs are expelled into the air due to partial burning of organic matter either naturally (e.g. forest fires) or anthropogenically (e.g. heating and incineration (Johnsen *et al.*, 2005). Health and wellbeing of many natural ecosystems have been adversely impacted as a result of anthropogenic activities. The USEPA has listed 16 priority PAHs (Xu *et al.*, 2013). PAH's are transformed to secondary pollutants (highly toxic nitrated PAH compounds) on reacting with other primary pollutants like ozone and NO_x (Park *et al.*, 2001; Zheng *et al.*, 2020). It undergoes chemical reactions like oxidation, photolysis, volatilization and adsorption once released into the environment. The carcinogenicity of PAH's increases with increase in molecular weight.

An increase in molecular weight also imparts resistance to oxidation and reduction, a decrease in acute toxicity and a decrease in vapor pressure (Akyuz and Cabuk, 2010; Kim *et al.*, 2013). Hydrophilicity of PAHs decreases with additional rings and lipophilicity increases owing to which it is highly soluble in organic solvents (Abdel-Shafy and Mansour, 2016). PAH's damage and alter the soil biota, causes infertility in wildlife, neurotoxicity and enter into food chain causing bio magnification effects (Grannas *et al.*, 2013; Zheng *et al.*, 2020; Rodrigues *et al.*, 2015; Balasubramaniyam, 2015; Collins, *et al.*, 2006; Ramesh *et al.*, 2011; Leach *et al.*, 2020). Bio amplification of PAH's through food chains damages human health and the ecosystem (Chen *et al.*, 2014). Other deleterious effects include immune toxicity (Xie *et al.*, 2017) carcinogenicity, mutagenicity and disruption in the immune defenses in organisms like *Crassostrea gigas* (Bado-Nilles *et al.*, 2008), *Pecten maximus* (Hannam *et al.*, 2010), *Haliotis diversicolor* (Gopalakrishnan *et al.*, 2011) and *Mytilus edulis* (Hoher *et al.*, 2012; Xie *et al.*, 2017). PAH's may covalently attach to DNA, RNA and proteins and the level of interaction between PAHs and DNA relates to the grade of carcinogenicity (Marston *et al.*, 2001; Santarelli *et al.*, 2008; Ghosal *et al.*, 2016). Bioremediation is a developing tool in Environmental Microbiology which can tackle this anomaly using a range of organisms from microorganisms to plants. These organisms may use individually or collectively apply various techniques like degradation, accumulation and immobilization to reduce these pollutant levels in the environment (Treu and Falandysz, 2017).

Factors affecting the biodegradation of PAHs

Several factors affect the reclamation of environmental contaminants and different studies have reported various factors which influence degradation of PAH's. The biodiversity of microbes in environment is one of the most notable factors followed by temperature, pH, oxygen, nutrient availability, bioavailability and hydrophobicity. These conditions are not the same everywhere and so there is an apparent inhibition or acceleration of biodegrading microorganisms (Al-Hawash *et al.*, 2018).

pH

pH plays a vital role in all biological processes and hence affects microbial growth and metabolism. Most microorganisms favor a neutral pH for normal activity. However the optimum pH for PAH degradation is different for each microorganism. While most microorganisms remediate in a near neutral pH condition, few can degrade at a slightly alkaline and yet some others at an acidic. But the pH of most PAH contaminated sites are far from neutral. In an abandoned gasworks site the leaching of construction material can contribute to an alkaline setting whereas in sites where there is coal the leaching can give rise to an acidic condition owed to the oxidation of sulfides. These alkaline or acidic conditions may hinder microbial proliferation and metabolic activities resulting in a decrease in biodegradation of PAH's (Ghosal *et al.*, 2016).



**Veerasamy Veeramani et al.,****Temperature**

Another crucial factor necessary for successful remediation of petroleum contaminated sites is optimum temperature. Temperature alters both the physical state of hydrocarbons as well as the metabolic activities of microbes. As temperatures increases, the solubility of the hydrophobic compounds increases, viscosity decreases, enhances dispersion and relocation of long chain n-alkanes from solid to water phase. In Polar Regions where the temperature is subzero there is a decrease in enzymatic activity of microbes an increase in the viscosity of PAH's, decrease in water solubility and reduction in the volatilization of toxic short chain alkanes (Varjani, 2017). An increase in temperature facilitates bioavailability of PAH's and increases degradation efficiency. With increasing temperatures and reduction in the oxygen levels the primary pollutants are transformed into more toxic secondary compounds which further decreases the biodegradation rates of PAH's (Al-Hawash *et al.*, 2018). Most biodegradation studies of PAH's carried out under moderate temperature conditions but there are reports of biodegradation even at very high temperatures. Higher degradation rates were observed temperature ranges of 30-40°C, 20-30°C and 15-20°C in soils, fresh water and marine environments, respectively. Photo oxidation is reported to increase the biodegradation of petroleum hydrocarbons due to their bioavailability and enhanced microbial activity (Nilanjana Das and Preethy Chandran, 2011).

Oxygen

Oxygen is another intense factor which affects o remediation of petroleum contaminated sites. It performs as a co-substrate and rate limiting factor in the degradation of PAH's. Oxygen availability in soil depends on microbial consumption rate, type of soil, water-logging capacity of soil and the presence of usable substrates. Bioconversion of organic pollutants can take place both in aerobic and anaerobic conditions, but majority of bioremediation studies have focused in aerobic conditions. Increased oxygen penetration helps speed up PAH degradation since oxygen is required to split aromatic rings (). Anaerobic conditions do support degradation of PAH's but the rates were negligible. Aerobic degradation was comparatively faster than anaerobic biodegradation (Grishchenkov *et al.*, 2000; Al-Hawash *et al.*, 2018). Aeration of soils can be attained through drainage, tilling, addition of chemicals that discharge oxygen and inoculation of air to the polluted site. *In situ* studies conducted in an aquifer polluted with phenols, BTEX compounds and PAH's used the method of circulating sodium nitrate as the oxygen source, via a series of injection and abstraction wells (Bewley and Webb, 2001; Ghosal *et al.*, 2016). Three soil scenarios are required for remediation of petroleum hydrocarbons namely, (i) consumption of oxygen (ii) penetration distance (iii) cleanup time. Abundant environmental factors such as temperature, pH, nutrient concentration, soil moisture, types of hydrocarbons, microbial densities and soil types affect consumption of oxygen by microbes during the degradation of PAH's.

Nutrients

The availability of nutrients in contaminated sites is another important factor affecting bioremediation. Bio-augmentation in nutrient deficit sites is a prerequisite to kindle microbial growth and speed up remediation of pollutants. The low level of nitrogen and phosphorus in marine environments lead to reduced biodegradation of PAH's. Nutrients fall under three categories – macro, micro and trace elements which is required for optimal metabolism and growth of microorganisms. However excess nutrient availability also inhibits bioremediation of pollutants. A study on the best nutritional composition for bioremediation of PAH contaminated soils revealed that minerals like nitrogen, phosphorus and iron are essential in a lesser quantity than carbon. Nitrates have been reported to be a basis of nitrogen for growth and bio surfactant production by microorganism (Toda and Itoh, 2012; Varjani, 2017). The petroleum polluted sites when treated with nitrogen, the growth rate of microbes and hydrocarbon degradation rate increases due to decrease in the lag phase of microbial growth and increase in microbial population. Kalantary *et al.*, (2014) reported that macronutrients like nitrogen and phosphorus constitute 14% and 3% of microbial dry weight. The optimum ratio of C: N: P which promotes microbial growth is 100:10:1. However microbial inhibition is caused by excessive nitrogen in soil. High NPK concentrations inhibit the biodegradation of hydrocarbon pollutants by inhibiting microbial growth. Nitrogen demand is comparable to biological oxygen demand and is an important parameter in the biodegradation of hydrocarbons (Zhao *et al.*, 2011; Dias *et al.*, 2013; Varjani 2017).



**Veerasamy Veeramani et al.,****Bioavailability**

Bioavailability in environmental applications denotes to the availability of organic and inorganic contaminants in soil systems of the organism for uptake. Chemical factors like hydrophobicity and volatility, soil properties, environmental conditions and biological activity affect bioavailability of pollutants (Varjani 2017). Many physico-chemical processes like sorption-desorption, diffusion and dissolution of a contaminant control the bioavailability of a contaminant. Since mass transfer is a controlling factor, improved microbial alteration capacities will not cause improve biotransformation rate. Ageing or weathering leads to reduction of bioavailability in the progress of time. The use of surfactants can be used to overcome the reduction in bioavailability of contaminants for microbial degradation (Boopathy, 2000). Many studies report less or ineffective degradation of PAHs in polluted sites owing to absorption of PAHs in black carbon and coal-tar substrate thereby decreasing its bioavailability (Hong *et al.*, 2003; Cornelissen *et al.*, 2006; Benhabib *et al.*, 2010; Rein *et al.*, 2016; Ghosal *et al.*, 2016).

The degradation of hydrocarbon pollutants by microbial cells takes place through (a) contact of microbial cells with hydrocarbons in aqueous phase (b) direct contact of cells with hydrocarbons and (c) interaction of cells with hydrocarbons droplets much smaller than cells (Kavitha *et al.*, 2014; Varjani, 2017). Organic matter in the soil greatly affects the bio availabilities and mobilities of PAHs (Godoy *et al.*, 2016). Factors like pH, microbial diversity and extent of hydrocarbon deterioration is significantly affected by limitations in the bioavailability of hydrocarbons (Al-Hawash *et al.*, 2018). As mentioned earlier the bioavailability of PAH contaminated sites is affected by sorption/desorption process. Initially sorption increases the organic concentration in micro porous regions and impermeable zones and later desorption and immobile zone diffusion occurs before biodegradation proceed. The complete rate of bioremediation can be restricted or even controlled by this mass transfer process and not by the degrading microorganism. Due to the high lipophilicity of petroleum hydrocarbons their bioavailability after ingestion and inhalation is very significant.

Electron Acceptor

Oxygen's role is as an electron acceptor which enhances the remediation mechanism and thereby improves aerobic biodegradation process (Abbasian *et al.*, 2015). But supplying sufficient oxygen to support degradation of hydrocarbon is problematic and costly (Boopathy, 2000). In oxygenase catalyzed reactions the substrate is oxygen. In anaerobic reactions alternative electron acceptors namely, sulphate, nitrate, iron (III), manganese (II) or carbon dioxide are used (Weelink *et al.*, 2009; Wilkes *et al.*, 2016; Varjani, 2017).

Broad-spectrum of Fungi

Some of the most important organisms which contribute massively to the bioremediation of PAH's belong to the kingdom fungi. The five different phyla of fungi colonies almost all ecosystems and can live even in extreme climatic conditions with wide ranges of temperature and pH, contributing to the proper functioning of the ecosystem (Rouphael *et al.*, 2015; Frac *et al.*, 2015; Frac *et al.*, 2018). *Aspergillus* (Diaz-Ramirez *et al.*, 2013) and *Candida* (Fan *et al.*, 2014; Borowik *et al.*, 2017) has been shown to effectively remove petroleum products from the soil. Fungi present in petroleum contaminated soil will aid in the degradation PAH's and are thus beneficial to the environment. Fungi on the other hand when present in petroleum tanks cause the deterioration of the product and is thus detrimental in nature (Bentoua and Gaylardeb, 2001; Borowik *et al.*, 2017). Fungi can initiate the transformation of hazardous materials in the ecosystem without the addition of nutrients and hence is a prominent bioremediation tool. They are heterotrophic in nature using one of the four modes of nutrition- saprophytic, parasitic, symbiotic and predatory. Identification of highly diverse phylotypes of fungi isolated from natural, PAH and heavy metal contaminated sites have been possible due to the employment of advanced techniques such as high throughput Next Generation Sequencing (Baldrian *et al.*, 2016; Mundra *et al.*, 2016; Schimann *et al.*, 2017; Bourceret *et al.*, 2016; Crognale *et al.*, 2017). Fungi found in the soil can be classified into three groups depending upon the role they play such as (i) Biological controllers ii) Ecosystem regulators and iii) Species participating in organic matter decomposition and compound transformation (Frac *et al.*, 2018).



**Veerasamy Veeramani et al.,****Fungal Bioremediation**

In recent years more and more researchers have started using fungi as a potential tool in bioremediation of pollutants. Fungi can catabolize diverse substrates since it is one among the primary decomposers of organics (Wisecaver *et al.*, 2014). Fungi are also excellent chemical engineers and can be used for producing metabolites like amino acids, small peptides, pigments and antibiotics, moreover intermediates can be incorporated in their growth cycles (Hoffmeister and Keller, 2007; Kohlhaw, 2003; Boonchan *et al.*, 2000; Czaplicki *et al.*, 2018). Fungal mycelium can ideally penetrate soils and access soil pore spaces. Compared to bacteria, fungi are more resistant to high concentration of toxins and can thrive in extreme climatic conditions (Gadd and Gadd, 2001; Treu and Falandysz, 2017). They proliferate through the distribution of spores in the air and also aid in preserving the stability of ecosystem. Many reports have shown the contribution of various promising enzyme systems when fungi are wide-open to demanding conditions such as extreme temperature, pH and salinity. Lade *et al.*, (2012) also reported that synergistic relationship can improve between fungal and bacterial degraders where fungi initiate degradation using their non-specific enzymatic system and bacteria carry the degradation forward. Fungi are capable to degrade wide range of pollutants including PAHs, phenols, halogenated aromatic hydrocarbons, explosives, recalcitrant dyes as well as persistent organic pollutants (Boopathy, 2000; Lewis *et al.*, 2004; Treu and Falandysz, 2017). Although recent researches stimulate the use of exogenous microorganisms for remediation purpose, autochthonous microorganisms seem to have an edge when challenging in actual situations.

Fungi belonging to Ascomycota have the capacity to resist environmental stress and are available in extreme as well as anthropogenically polluted environments (Aranda *et al.*, 2017). The ascomycetes are monokaryotic with hyphae having a thick protective wall. The hyphal tissues that form the excipulum comprise of prosenchymatous or pseudoparenchymatous tissues. The excipulum is divisible into outer ectal –and inner, medullary excipulum. The wall and the asci are jointly called ascoma. Ascomata (plural) produce the asci and also regulate the release of the ascospores. Ascomycete is the largest phylum of fungi having about 75% of all known fungi. It includes the conidial ascomycetes and the lichen forming fungi. The enormous size of the phyla makes it difficult to generalize the structure of the fungi. Advancement in molecular technologies has started to disclose that the actual players in bioremediation of polluted environments are mainly from the phylum Ascomycota, the subphylum mucoromycotina and to a lesser extent the phylum Basidiomycota (Aranda, 2016). The high variety of fungal species plays a vital role in bioremediation by improving the bioavailability and biodegradability of pollutants (Aranda, 2017).

This phylum comprises all types (parasitic, symbiotic or saprotrophic) and morphologies- unicellular (yeast), multicellular (filamentous) and dimorphic fungi (can exist as mold/hyphal/filamentous form or as yeast). They can colonize in diverse niches (Olicon-Hernandez *et al.*, 2017). Ascomycota possess certain benefits on evaluation with white-rot fungi, ie their growth is rapid at neutral pH, enzyme production does not need lignocellulose substrate and are collective inhabitants of extremely polluted areas. Recently, application of Ascomycota consortia has been assembled and promoted at an industrial level to increase the remediation of several pollutants. The degradation of PAHs by various fungal species is shown in Table. 1

Mechanism Involved In Ascomycota Remediation

Fungi have been shown to oxidize different PAHs by mechanisms similar to those observed in mammals. A variety of lignolytic and non-lignolytic fungi are capable of degrading PAHs. Fungal metabolites are classified into primary metabolites and secondary metabolites. Although the secondary metabolites are not vital for cellular life, the primary metabolites are very essential for growth and reproduction. (Demain and Fang, 2000; Keller *et al.*, 2005; Wisecaver *et al.*, 2014). Most fungi produce extracellular and intracellular enzymes. White rot fungi secrete extracellular ligninolytic enzymes such as lignin peroxidase (Lip), manganese peroxidase (MnP), and laccases. However these fungal species require ligninolytic, acidic conditions as well as lignocellulosic substrates to compete in natural environments. On account of this it is highly doubtful to assume that ligninolytic fungi aid decomposition of aromatic material under natural conditions. Many studies have emphasized on the involvement of the intracellular enzymatic system (cytochrome P450-CYPs) in PAHs transformation which is the main enzymatic step in causing genotoxicity. DNA alkylation occurs due to the enzymatic hydration of the non-K-region arene oxide via



**Veerasamy Veeramani et al.,**

hydroxyl, dihydroxy, dihydrodiol and quinone derivatives (phase I) mediated by cytochrome P450 monooxygenase to form dihydrodiol-epoxides. The cytochrome P450 monooxygenases reduce dioxygen and integrate one atom of oxygen into the hydroxyl group on the PAH and into water with the associated oxidation of NADPH (Saleha Husain, 2008). The electron needed for the insertion of one atom of oxygen into the aliphatic chain is provided by these mixed enzymes (Dacco *et al.*, 2020). The oxidized metabolites are consequently conjugated with sulfate, methyl, glucose, xylose or glucuronic acid group (Phase II) and this action is facilitated by transferases. In phase III the metabolites are transported to vacuoles, excreted or stored in organelles. Some authors suggest that once metabolites are excreted, they can be degraded by other microorganisms. A comprehensive study however is needed to assess the fate of the oxy-PAHs, methoxy-PAHs, or sulphate –PAHs when they are discharged into the environment.

CONCLUSION

Oil spillage is one of the major environmental pollution caused in recent days which needs to be addressed with all potential means. Moreover this review will be vital to derive effective *in situ* or *ex situ* methods of biotechnological remediation established on the choice of ascomycetes. This fungal species has demonstrated an effective role in the removal of broad range of xenobiotics. In addition to this several features involved in the bioremediation of PAHs contaminated soil are discussed. Each of these factors debated which may edge the usage of bioremediation in precise situations. Modification of oxygen concentration, temperature, pH, nutrient and bioavailability may upsurge PAH degradation and it also depends on the environmental condition number and type of microorganism nature and structure of chemical compound. More studies have to be initiated to understand the nature of the formed metabolites and biodegradability potential of microbes.

REFERENCES

1. Abbasian, F., Lockington, R., Mallavarapu, M., & Naidu, R. (2015). A comprehensive review of aliphatic hydrocarbon biodegradation by bacteria. *Applied biochemistry and biotechnology*, 176, 670-699.
2. Abdel-Shafy, H. I., & Mansour, M. S. (2016). A review on polycyclic aromatic hydrocarbons: source, environmental impact, effect on human health and remediation. *Egyptian journal of petroleum*, 25(1), 107-123.
3. Agrawal, N., & Shahi, S. K. (2017). Degradation of polycyclic aromatic hydrocarbon (pyrene) using novel fungal strain *Corioloropsis byrsina* strain APC5. *International Biodeterioration & Biodegradation*, 122, 69-81.
4. Akyüz, M., & Çabuk, H. (2010). Gas-particle partitioning and seasonal variation of polycyclic aromatic hydrocarbons in the atmosphere of Zonguldak, Turkey. *Science of the total environment*, 408(22), 5550-5558.
5. Al-Hawash, A. B., Dragh, M. A., Li, S., Alhujaily, A., Abbood, H. A., Zhang, X., & Ma, F. (2018). Principles of microbial degradation of petroleum hydrocarbons in the environment. *The Egyptian Journal of Aquatic Research*, 44(2), 71-76.
6. Ali, M. I., Khalil, N. M., & El-Ghany, M. N. A. (2012). Biodegradation of some polycyclic aromatic hydrocarbons by *Aspergillus terreus*. *Afr. J. Microbiol. Res*, 6(16), 3783-3790.
7. Andreolli, M., Lampis, S., Brignoli, P., & Vallini, G. (2016). *Trichoderma longibrachiatum* Evx1 is a fungal biocatalyst suitable for the remediation of soils contaminated with diesel fuel and polycyclic aromatic hydrocarbons. *Environmental Science and Pollution Research*, 23, 9134-9143.
8. Aranda, E. (2016). Promising approaches towards biotransformation of polycyclic aromatic hydrocarbons with Ascomycota fungi. *Current opinion in biotechnology*, 38, 1-8.
9. Aranda, E., Godoy, P., Reina, R., Badia-Fabregat, M., Rosell, M., Marco-Urrea, E., & García-Romera, I. (2017). Isolation of Ascomycota fungi with capability to transform PAHs: Insights into the biodegradation mechanisms of *Penicillium oxalicum*. *International Biodeterioration & Biodegradation*, 122, 141-150.
10. Bado-Nilles, A., Gagnaire, B., Thomas-Guyon, H., Le Floch, S., & Renault, T. (2008). Effects of 16 pure hydrocarbons and two oils on haemocyte and haemolymphatic parameters in the Pacific oyster, *Crassostrea gigas* (Thunberg). *Toxicology in Vitro*, 22(6), 1610-1617.



**Veerasamy Veeramani et al.,**

11. Balasubramaniyam, A. (2015). The influence of plants in the remediation of petroleum hydrocarbon-contaminated sites. *Pharm. Anal. Chem. Open Access*, 1, 1-11.
12. Baldrian, P., Zrůstová, P., Tláškal, V., Davidová, A., Merhautová, V., & Vrška, T. (2016). Fungi associated with decomposing deadwood in a natural beech-dominated forest. *Fungal Ecology*, 23, 109-122.
13. Benhabib, K., Faure, P., Sardin, M., & Simonnot, M. O. (2010). Characteristics of a solid coal tar sampled from a contaminated soil and of the organics transferred into water. *Fuel*, 89(2), 352-359.
14. Bento, F. M., & Gaylarde, C. C. (2001). Biodeterioration of stored diesel oil: studies in Brazil. *International Biodeterioration & Biodegradation*, 47(2), 107-112.
15. Bewley, R. J., & Webb, G. (2001). In situ bioremediation of groundwater contaminated with phenols, BTEX and PAHs using nitrate as electron acceptor. *Land Contamination & Reclamation*, 9(4), 335-347.
16. Boonchan, S., Britz, M. L., & Stanley, G. A. (2000). Degradation and mineralization of high-molecular-weight polycyclic aromatic hydrocarbons by defined fungal-bacterial cocultures. *Applied and environmental microbiology*, 66(3), 1007-1019.
17. Boopathy, R. (2000). Factors limiting bioremediation technologies. *Bioresource technology*, 74(1), 63-67.
18. Borowik, A., Wyszowska, J., & Oszust, K. (2017). Functional diversity of fungal communities in soil contaminated with diesel oil. *Frontiers in Microbiology*, 8, 1862.
19. Bourceret, A., Cébron, A., Tisserant, E., Poupin, P., Bauda, P., Beguiristain, T., & Leyval, C. (2016). The bacterial and fungal diversity of an aged PAH-and heavy metal-contaminated soil is affected by plant cover and edaphic parameters. *Microbial ecology*, 71, 711-724.
20. Chen, S., Yin, H., Ye, J., Peng, H., Liu, Z., Dang, Z., & Chang, J. (2014). Influence of co-existed benzo [a] pyrene and copper on the cellular characteristics of *Stenotrophomonas maltophilia* during biodegradation and transformation. *Bioresource technology*, 158, 181-187.
21. Chulalaksananukul, S., Gadd, G. M., Sangvanich, P., Sihanonth, P., Piapukiew, J., & Vangnai, A. S. (2006). Biodegradation of benzo (a) pyrene by a newly isolated *Fusarium* sp. *FEMS microbiology letters*, 262(1), 99-106.
22. Collins, C., Fryer, M., & Grosso, A. (2006). Plant uptake of non-ionic organic chemicals. *Environmental science & technology*, 40(1), 45-52.
23. Cornelissen, G., Gustafsson, Ö., Bucheli, T. D., Jonker, M. T., Koelmans, A. A., & van Noort, P. C. (2005). Extensive sorption of organic compounds to black carbon, coal, and kerogen in sediments and soils: mechanisms and consequences for distribution, bioaccumulation, and biodegradation. *Environmental science & technology*, 39(18), 6881-6895.
24. Crognale, S., D'Annibale, A., Pesciaroli, L., Stazi, S. R., & Petruccioli, M. (2017). Fungal community structure and As-resistant fungi in a decommissioned gold mine site. *Frontiers in Microbiology*, 8, 2202.
25. Czaplicki, L. M., Dharia, M., Cooper, E. M., Ferguson, P. L., & Gunsch, C. K. (2018). Evaluating the mycostimulation potential of select carbon amendments for the degradation of a model PAH by an ascomycete strain enriched from a superfund site. *Biodegradation*, 29, 463-471.
26. Daccò, C., Girometta, C., Asemoloye, M. D., Carpani, G., Picco, A. M., & Tosi, S. (2020). Key fungal degradation patterns, enzymes and their applications for the removal of aliphatic hydrocarbons in polluted soils: A review. *International Biodeterioration & Biodegradation*, 147, 104866.
27. Delsarte, I., Rafin, C., Mrad, F., & Veignie, E. (2018). Lipid metabolism and benzo [a] pyrene degradation by *Fusarium solani*: an unexplored potential. *Environmental Science and Pollution Research*, 25, 12177-12182.
28. Demain, A. L., & Fang, A. (2000). The natural functions of secondary metabolites. *History of modern biotechnology I*, 1-39.
29. Dias, R. L., Ruberto, L., Hernández, E., Vázquez, S. C., Balbo, A. L., Del Panno, M. T., & Mac Cormack, W. P. (2012). Bioremediation of an aged diesel oil-contaminated Antarctic soil: Evaluation of the "on site" biostimulation strategy using different nutrient sources. *International Biodeterioration & Biodegradation*, 75, 96-103.
30. Díaz-Ramírez, I., Escalante-Espinosa, E., Schroeder, R. A., Fócil-Monterrubio, R., & Ramírez-Saad, H. (2013). Hydrocarbon biodegradation potential of native and exogenous microbial inocula in Mexican tropical soils. *Biodegradation of hazardous and special products*, 155178.
31. Fan, M. Y., Xie, R. J., & Qin, G. (2014). Bioremediation of petroleum-contaminated soil by a combined system of biostimulation-bioaugmentation with yeast. *Environmental technology*, 35(4), 391-399.



**Veerasamy Veeramani et al.,**

32. Fraç, M., Hannula, S. E., Bełka, M., & Jędryczka, M. (2018). Fungal biodiversity and their role in soil health. *Frontiers in microbiology*, 9, 707.
33. Fraç, M., Jezierska-Tys, S., & Yaguchi, T. (2015). Occurrence, detection, and molecular and metabolic characterization of heat-resistant fungi in soils and plants and their risk to human health. *Advances in agronomy*, 132, 161-204.
34. Gadd, G. M. (2004). Mycotransformation of organic and inorganic substrates. *Mycologist*, 18(2), 60-70.
35. Ghosal, D., Ghosh, S., Dutta, T. K., & Ahn, Y. (2016). Current state of knowledge in microbial degradation of polycyclic aromatic hydrocarbons (PAHs): a review. *Frontiers in microbiology*, 1369.
36. Godoy, P., Reina, R., Calderón, A., Wittich, R. M., García-Romera, I., & Aranda, E. (2016). Exploring the potential of fungi isolated from PAH-polluted soil as a source of xenobiotics-degrading fungi. *Environmental Science and Pollution Research*, 23, 20985-20996.
37. González-Abradelo, D., Pérez-Llano, Y., Peidro-Guzmán, H., del Rayo Sánchez-Carbente, M., Folch-Mallof, J. L., Aranda, E. & Batista-García, R. A. (2019). First demonstration that ascomycetous halophilic fungi (*Aspergillus sydowii* and *Aspergillus destruens*) are useful in xenobiotic mycoremediation under high salinity conditions. *Bioresource technology*, 279, 287-296.
38. Gopalakrishnan, S., Huang, W. B., Wang, Q. W., Wu, M. L., Liu, J., & Wang, K. J. (2011). Effects of tributyltin and benzo [a] pyrene on the immune-associated activities of hemocytes and recovery responses in the gastropod abalone, *Haliotis diversicolor*. *Comparative Biochemistry and Physiology Part C: Toxicology & Pharmacology*, 154(2), 120-128.
39. Grannas, A. M., Bogdal, C., Hageman, K. J., Halsall, C., Harner, T., Hung, H., ... & Wania, F. (2013). The role of the global cryosphere in the fate of organic contaminants. *Atmospheric Chemistry and Physics*, 13(6), 3271-3305.
40. Grishchenkov, V. G., Townsend, R. T., McDonald, T. J., Autenrieth, R. L., Bonner, J. S., & Boronin, A. M. (2000). Degradation of petroleum hydrocarbons by facultative anaerobic bacteria under aerobic and anaerobic conditions. *Process Biochemistry*, 35(9), 889-896.
41. Han, M. J., Park, H. T., & Song, H. G. (2004). Degradation of phenanthrene by *Trametes versicolor* and its laccase. *Journal of Microbiology*, 42(2), 94-98.
42. Hannam, M. L., Bamber, S. D., Galloway, T. S., Moody, A. J., & Jones, M. B. (2010). Effects of the model PAH phenanthrene on immune function and oxidative stress in the temperate scallop *Pecten maximus*. *Chemosphere*, 78(7), 779-784.
43. Hoffmeister, D., & Keller, N. P. (2007). Natural products of filamentous fungi: enzymes, genes, and their regulation. *Natural product reports*, 24(2), 393-416.
44. Höher, N., Köhler, A., Strand, J., & Broeg, K. (2012). Effects of various pollutant mixtures on immune responses of the blue mussel (*Mytilus edulis*) collected at a salinity gradient in Danish coastal waters. *Marine environmental research*, 75, 35-44.
45. Hong, L., Ghosh, U., Mahajan, T., Zare, R. N., & Luthy, R. G. (2003). PAH sorption mechanism and partitioning behavior in lampblack-impacted soils from former oil-gas plant sites. *Environmental science & technology*, 37(16), 3625-3634.
46. Johnsen, A. R., Wick, L. Y., & Harms, H. (2005). Principles of microbial PAH-degradation in soil. *Environmental pollution*, 133(1), 71-84.
47. Kavitha, V., Mandal, A. B., & Gnanamani, A. (2014). Microbial biosurfactant mediated removal and/or solubilization of crude oil contamination from soil and aqueous phase: An approach with *Bacillus licheniformis* MTCC 5514. *International Biodeterioration & Biodegradation*, 94, 24-30.
48. Keller, N. P., Turner, G., & Bennett, J. W. (2005). Fungal secondary metabolism—from biochemistry to genomics. *Nature Reviews Microbiology*, 3(12), 937-947.
49. Kim, K. H., Jahan, S. A., Kabir, E., & Brown, R. J. (2013). A review of airborne polycyclic aromatic hydrocarbons (PAHs) and their human health effects. *Environment international*, 60, 71-80.
50. Kalantary, R. R., Mohseni-Bandpi, A., Esrafil, A., Nasser, S., Ashmagh, F. R., Jorfi, S., & Ja'fari, M. (2014). Effectiveness of biostimulation through nutrient content on the bioremediation of phenanthrene contaminated soil. *Journal of Environmental Health Science and Engineering*, 12, 1-9.



**Veerasamy Veeramani et al.,**

51. Kohlhaw, G. B. (2003). Leucine biosynthesis in fungi: entering metabolism through the back door. *Microbiology and Molecular Biology Reviews*, 67(1), 1-15.
52. Lade, H. S., Waghmode, T. R., Kadam, A. A., & Govindwar, S. P. (2012). Enhanced biodegradation and detoxification of disperse azo dye Rubine GFL and textile industry effluent by defined fungal-bacterial consortium. *International Biodeterioration & Biodegradation*, 72, 94-107.
53. Lange, B., Kremer, S., Sterner, O., & Anke, H. (1994). Pyrene metabolism in *Crinipellis stipitaria*: identification of trans-4, 5-dihydro-4, 5-dihydroxypyrene and 1-pyrenylsulfate in strain JK364. *Applied and Environmental Microbiology*, 60(10), 3602-3607.
54. Leech, C., Tighe, M. K., Pereg, L., Winter, G., McMillan, M., Esmaeili, A., & Wilson, S. C. (2020). Bioaccessibility constrains the co-composting bioremediation of field aged PAH contaminated soils. *International Biodeterioration & Biodegradation*, 149, 104922.
55. Lewis, T. A., Newcombe, D. A., & Crawford, R. L. (2004). Bioremediation of soils contaminated with explosives. *Journal of Environmental Management*, 70(4), 291-307.
56. Liu, S. H., Zeng, G. M., Niu, Q. Y., Liu, Y., Zhou, L., Jiang, L. H., ... & Cheng, M. (2017). Bioremediation mechanisms of combined pollution of PAHs and heavy metals by bacteria and fungi: A mini review. *Bioresourcetechnology*, 224, 25-33.
57. Marston, C. P., Pereira, C., Ferguson, J., Fischer, K., Hedstrom, O., Dashwood, W. M., & Baird, W. M. (2001). Effect of a complex environmental mixture from coal tar containing polycyclic aromatic hydrocarbons (PAH) on the tumor initiation, PAH-DNA binding and metabolic activation of carcinogenic PAH in mouse epidermis. *Carcinogenesis*, 22(7), 1077-1086.
58. Mtibaà, R., Olicón-Hernández, D. R., Pozo, C., Nasri, M., Mechichi, T., González, J., & Aranda, E. (2018). Degradation of bisphenol A and acute toxicity reduction by different thermo-tolerant ascomycete strains isolated from arid soils. *Ecotoxicology and environmental safety*, 156, 87-96.
59. Mundra, S., Halvorsen, R., Kausrud, H., Bahram, M., Tedersoo, L., Elberling, B., ... & Eidesen, P. B. (2016). Ectomycorrhizal and saprotrophic fungi respond differently to long-term experimentally increased snow depth in the High Arctic. *MicrobiologyOpen*, 5(5), 856-869.
60. Das, N., & Chandran, P. (2011). Microbial degradation of petroleum hydrocarbon contaminants: an overview. *Biotechnology research international*, 2011.
61. Olicón-Hernández, D. R., González-López, J., & Aranda, E. (2017). Overview on the biochemical potential of filamentous fungi to degrade pharmaceutical compounds. *Frontiers in microbiology*, 8, 1792.
62. Park, J. S., Wade, T. L., & Sweet, S. (2001). Atmospheric distribution of polycyclic aromatic hydrocarbons and deposition to Galveston Bay, Texas, USA. *Atmospheric Environment*, 35(19), 3241-3249.
63. Zhang, D., An, T., Qiao, M., Loganathan, B. G., Zeng, X., Sheng, G., & Fu, J. (2011). Source identification and health risk of polycyclic aromatic hydrocarbons associated with electronic dismantling in Guiyu town, South China. *Journal of Hazardous Materials*, 192(1), 1-7.
64. Rein, A., Adam, I. K., Miltner, A., Brumme, K., Kästner, M., & Trapp, S. (2016). Impact of bacterial activity on turnover of insoluble hydrophobic substrates (phenanthrene and pyrene)—model simulations for prediction of bioremediation success. *Journal of Hazardous Materials*, 306, 105-114.
65. Rodrigues, E. M., Kalks, K. H., & Tótola, M. R. (2015). Prospect, isolation, and characterization of microorganisms for potential use in cases of oil bioremediation along the coast of Trindade Island, Brazil. *Journal of Environmental Management*, 156, 15-22.
66. Roupael, Y., Franken, P., Schneider, C., Schwarz, D., Giovannetti, M., Agnolucci, M., ... & Colla, G. (2015). Arbuscular mycorrhizal fungi act as biostimulants in horticultural crops. *Scientia Horticulturae*, 196, 91-108.
67. Husain, S. (2008). Literature overview: microbial metabolism of high molecular weight polycyclic aromatic hydrocarbons. *Remediation Journal: The Journal of Environmental Cleanup Costs, Technologies & Techniques*, 18(2), 131-161.
68. Santarelli, R. L., Pierre, F., & Corpet, D. E. (2008). Processed meat and colorectal cancer: a review of epidemiologic and experimental evidence. *Nutrition and cancer*, 60(2), 131-144.





Veerasamy Veeramani et al.,

69. Sawulski, P., Clipson, N., & Doyle, E. (2014). Effects of polycyclic aromatic hydrocarbons on microbial community structure and PAH ring hydroxylating dioxygenase gene abundance in soil. *Biodegradation*, 25, 835-847.
70. Schimann, H., Bach, C., Lengelle, J., Louisanna, E., Barantal, S., Murat, C., & Buée, M. (2017). Diversity and structure of fungal communities in neotropical rainforest soils: the effect of host recurrence. *Microbial ecology*, 73, 310-320.
71. Toda, H., & Itoh, N. (2012). Isolation and characterization of styrene metabolism genes from styrene-assimilating soil bacteria *Rhodococcus* sp. ST-5 and ST-10. *Journal of bioscience and bioengineering*, 113(1), 12-19.
72. Treu, R., & Falandysz, J. (2017). Mycoremediation of hydrocarbons with basidiomycetes—a review. *Journal of Environmental Science and Health, Part B*, 52(3), 148-155.
73. Varjani, S. J. (2017). Microbial degradation of petroleum hydrocarbons. *Bioresource technology*, 223, 277-286.
74. Vasconcelos, M. R., Vieira, G. A., Otero, I. V., Bonugli-Santos, R. C., Rodrigues, M. V., Rehder, V. L., ... & Sette, L. D. (2019). Pyrene degradation by marine-derived ascomycete: process optimization, toxicity, and metabolic analyses. *Environmental Science and Pollution Research*, 26, 12412-12424.
75. Wang, S., Nomura, N., Nakajima, T., & Uchiyama, H. (2012). Case study of the relationship between fungi and bacteria associated with high-molecular-weight polycyclic aromatic hydrocarbon degradation. *Journal of bioscience and bioengineering*, 113(5), 624-630.
76. Weelink, S. A., Van Doesburg, W., Saia, F. T., Rijpstra, W. I. C., Röling, W. F., Smidt, H., & Stams, A. J. (2009). A strictly anaerobic betaproteobacterium *Georgfuchsia toluolica* gen. nov., sp. nov. degrades aromatic compounds with Fe (III), Mn (IV) or nitrate as an electron acceptor. *FEMS microbiology ecology*, 70(3), 575-585.
77. Wilkes, H., Buckel, W., Golding, B. T., & Rabus, R. (2016). Metabolism of hydrocarbons in n-alkane-utilizing anaerobic bacteria. *Microbial Physiology*, 26(1-3), 138-151.
78. Wisecaver, J. H., Slot, J. C., & Rokas, A. (2014). The evolution of fungal metabolic pathways. *PLoS genetics*, 10(12), e1004816.
79. Wunder, T., Kremer, S., Sterner, O., & Anke, H. (1994). Metabolism of the polycyclic aromatic hydrocarbon pyrene by *Aspergillus niger* SK 9317. *Applied microbiology and biotechnology*, 42, 636-641.
80. Xie, J., Zhao, C., Han, Q., Zhou, H., Li, Q., & Diao, X. (2017). Effects of pyrene exposure on immune response and oxidative stress in the pearl oyster, *Pinctada martensii*. *Fish & Shellfish Immunology*, 63, 237-244.
81. Xu, N., Bao, M., Sun, P., & Li, Y. (2013). Study on bioadsorption and biodegradation of petroleum hydrocarbons by a microbial consortium. *Bioresource technology*, 149, 22-30.
82. Zhao, D., Liu, C., Liu, L., Zhang, Y., Liu, Q., & Wu, W. M. (2011). Selection of functional consortium for crude oil-contaminated soil remediation. *International Biodeterioration & Biodegradation*, 65(8), 1244-1248.
83. Zheng, H., Kang, S., Chen, P., Li, Q., Tripathi, L., Maharjan, L., ... & Santos, E. (2020). Sources and spatio-temporal distribution of aerosol polycyclic aromatic hydrocarbons throughout the Tibetan Plateau. *Environmental Pollution*, 261, 114144.

Table. 1 Role of different Ascomycetes species in Polycyclic Aromatic Hydrocarbons Degradation

S. No	Organism	pH	Temperature (°C)	Time (Days)	Degradation (%)	Reference
1	<i>Aspergillus terreus</i>	5.8	37	10	98.5	Ali et al., 2012
2	<i>Aspergillus</i> spp.	7	30 C	10	86.3	Vasconcelos et al., 2019
3	<i>Penicillium oxalicum</i>	8	26	21	78	Aranda et al., 2017
4	<i>Tolypocladium</i> . Spp	7	28	21	94.17	Vasconcelos et al., 2019
5	<i>Aspergillus</i> spp.	8	30	60	88.9	Al-Hawash et al., 2018
6	<i>Aspergillus</i> <i>sustus</i> and <i>Trichoderma harzianum</i>	Acidic	26	21	50	Godoy et al., 2016
7	<i>Fusarium solani</i>	7	25	12	76	Delsarte et al., 2018
8	<i>Corioliopsis byrsina</i>	6	25	18	51.85	Agrawal and Shahi, 2017
9	<i>Ascomycetes</i> strain	6.5	30	28	67	Wang et al., 2012





Veerasamy Veeramani et al.,

10	<i>Trametes versicolor</i>	6	30	5	65	Han et al., 2004
11	<i>Ascomycetes strain</i>	6	35	8h	100	Mtibaa et al., 2018
12	<i>Aspergillus niger</i>	5.5	25	4		Wunder et al., 1994
13	<i>Crinipellis stipitaria</i>	4.5	21	7	40	Lange et al., 1994
14	<i>Fusarium sp.</i>		32	65-70	30	Chulalaksananukul et al., 2006
15	<i>Aspergillus sydowii</i>	8.4	28	100	15	Gonzalez-Abradelo et al., 2019
16	<i>Trichoderma longi brachiatum</i>	7	27	54	30	Andreolli et al., 2016
17	<i>Coniothyrium spp</i>	7	25	30	26.5	Liu et al., 2017
18	<i>.Fusarium spp.</i>	7	25	30	27.5	Liu et al., 2017





Determination of Living Standards of Individuals Indulged in the Non-Timber Forest Produce based Microenterprises of Raipur Division

Satya Kishan^{1*} and Kavita Silwal²

¹Assistant Professor, MSBS Department, MATS University, Raipur, Chhattisgarh, India

²Research Scholar, MSBS Department, MATS University, Raipur, Chhattisgarh, India.

Received: 20 Feb 2023

Revised: 15 Apr 2023

Accepted: 19 May 2023

*Address for Correspondence

Satya Kishan

Assistant Professor,

MSBS Department,

MATS University,

Raipur, Chhattisgarh, India

Email: imsatyakishan@gmail.com



This is an Open Access Journal / article distributed under the terms of the **Creative Commons Attribution License (CC BY-NC-ND 3.0)** which permits unrestricted use, distribution, and reproduction in any medium, provided the original work is properly cited. All rights reserved.

ABSTRACT

The research focused on determining the living conditions of the micro forest produce (MFP) or Non-Timber Forest Produce (NTFP) microenterprise workers. The NTFP microenterprise in Chhattisgarh is generally run by Self-Help Groups (SHG). Members of these groups collectively own and manage the enterprise and employ themselves as workers in the enterprise. The research own uses a novel method of assessing the living Determination of livingstandards of individuals indulged in the Non-Timber Forest Produce Based Microenterprises of Raipur Division conditions of these workers using rational dimensions of amenities, assets, and households. The research work determines that these microenterprise workers are at medium quality bracket for household and basic amenities however they do not fare well on grounds of owning asset. The analysis of the data also reveals ineffectiveness of certain government schemes aimed for betterment of those that are living in bottom of the socioeconomic pyramid.

Keywords: NTFPLiving Standards, Microenterprise,

INTRODUCTION

Chhattisgarh is a tribal state. Almost one-third of its population lives in areas that are dense forest zones. Tribals of Chhattisgarh are known for preserving their cultural values and attachment with the forest and forest produce is a part of it. Tribals of Chhattisgarh collect Tendu, Lac, Harra, Gum, Bihi,(Guava) and Imlı (Tamrind) from forest. They sell it directly to the cooperative societies for government declared minimum support price. Certain tribals sell the collected forest produce to middleman or village trader for instant cash. The entire process of selling the forest produce has been streamlined by the government in recent years. Due to this streamlining abundance of non-timber

56838



**Satya Kishan and Kavita Silwal**

forest produce was revealed. To support tribals more to improve their economic status without letting them deviate from their cultural aspect i.e., earning through forest resource. State Government with the help of European commission facilitates NTFP based microenterprises through various projects. This includes promotion of lac cultivation, herbal food processing, honey processing, mahua processing, chironjee processing etc. In Chhattisgarh at present 17196 beneficiaries are working under these microenterprises.

Objective of the Work

The present research work thus focuses on determination of living standards of individual indulged in these microenterprises. The work will thus help in accessing whether microenterprises is helpful in elevating conditions of tribals or not.

Research Hypothesis

The following null hypothesis would be tested in this research work

The living standards of individuals working in NTFP microenterprise is not optimum.

Review

(Sharma, 2019) focused on determining the livelihood security of NTFP gatherers. In their research work they focused on the Kullu circle gatherers. The research work used Gini concentration to reveal household income inequality among the gatherers. The analysis revealed that income inequality increases as literacy increases however share from NTFPs decreases with increase in literacy. (Shanley, 2015) in their research work focused on livelihood through NTFPs in 21st century. The research work stated that it has now become essential that NTFPs should enter mainstream market as their demand is now substantial and their processing and packaging is at par with other market produced goods. (Peerzada, 2022) in their research work used various rational indices other than conventional variables such as socioeconomic status to reveal that for Kashmiri Tribals NTFP holds the key of livelihood security.

METHODOLOGY

In the research work, a total of 200 respondents participated in the survey. These respondents were employed in the microenterprises indulged in processing of NTFPs in the Raipur Division of Chhattisgarh. These microenterprises are mostly run and managed by the self-help groups.

Primary data was collected from the individuals with the help of a questionnaire. The questionnaire contained three main sections. These three main sections are presented below.

The research work focuses on the progress of forest produce gatherers in terms of their quality of living after they were indulged in the microenterprises that dealt with processing of NTFPs. The research work focuses on their present quality of life through three aspects. These aspects are –

1. Their household quality
2. Their reach to the basic amenities of life
3. Assets possessed by them.

Each of these above-mentioned points contained multiple questions that would be answered using a Yes or No. A response of Yes to the question meant that a score of '1' should be assigned to the question while a No meant that a score of '0' should be assigned to the same.

The household quality index (HHQLI) was measured using the following questions.

- 1 Do you have household ownership
- 2 Is the house properly maintained
- 3 The house has a separate room for the married couple
- 4 Is the house a 'Pakka' type construction
- 5 Is the house having a toilet



**Satya Kishan and Kavita Silwal**

The basic amenity index (BAI) was measured using the following questions.

- 1 Drinking water reaches to your premises through a tap
- 2 There is no power cut in your premises
- 3 Do you have a proper bathroom (where one can take bath) facility in the household
- 4 There is proper drainage system in the household
- 5 You use LPG for cooking food
- 6 Door to Door garbage collection and street cleaning facilities are made available to you
- 7 Do you have a bank account
- 8 Kitchen in the household is separate

The asset index (AI) was measured using the following questions

- 1 Do you have a TV at your household
- 2 Do you have a mobile phone
- 3 Do you own a motor vehicle
- 4 Do you own jewelry
- 5 Your indulgence in the microenterprise lets you save comprehensively ever then before.

The overall scores for each of the index was obtained by averaging it for the total number of respondents participating in the survey.

The quality of living score was obtained using the following equation

$$QLI = (HHQLI + BAI + AI)/3$$

The QLI score determined was compared using the scale mentioned below.

Analysis

First the household quality index was determined. The responses received for the questions have been presented below.

From the table 2 presented above it is evident that –

- 1 Maximum MFP or NTP microenterprise workers do not own a house ownership
- 2 The household of maximum workers were properly maintained
- 3 The house of maximum workers has a separated room for the married couples
- 4 Maximum workers dwelled in Kaccha type of Household
- 5 All households had toilet facility.

From the table 3 presented above it is evident that –

- 1 Maximum number of respondents did not have drinking tap water facility at their household
- 2 It was noted that maximum number of households have bathroom facility but the number of households that did not have the facility was also high and cannot be ignored.
- 3 It was noted that maximum respondents cooked their foods without utilization of LPG.

From the table 4 it is evident that –

- 1 Maximum number of respondents did not own a television
- 2 Maximum number of respondents did not own a mobile phone
- 3 It was noted that maximum household own a motorcycle.

The calculation presented in the table 2, 3, and 4 was used to calculate the QLI. The average of the three index that represented QLI was determined as 0.48. Comparing this obtained value with the scale presented in table 1 reveals that the microenterprise workers were leading a medium quality of life.

Thus, it can be said that null hypothesis that the living standards of individuals working in NTFP microenterprise is not optimum cannot be rejected. As the individuals as a whole had just crossed the upper ceiling of low QLI range (0-0.4).





CONCLUSION

The research work dealt with determining the quality of life of individuals indulged in the MFP or NTFP microenterprises. The research work adopts a novel approach of determining the quality of life led by the individuals by evaluating the conditions based on their reach to the basic amenities, possession of assets, and quality of household. The method can be termed as more rational in evaluating living conditions because it does not consider conventional constraints such as occupation, education, and earnings. Microenterprise workers in general belong to tribal communities that focus more on forest and livelihood from it rather than mingling into the societal mainstream where education and occupation takes the driving seat of living standards. The research work using the analysis run over primary data concludes that –The household conditions of the workers are optimum as it is bordering the medium range presented in the table 1.

- 1 The JalJeevan Mission which focuses on delivering tap water to every household premise seems to be ineffective as maximum number of workers reported that they do not have access to the drinking tap water at their premises.
- 2 The Ujwalayojana that focuses on making available LPG to every household so that dependency on carbon fuels is reduced seems to be ineffective in case of workers involved in the NTFP microenterprises. Maximum respondent reported that they do not use LPG for cooking food. High cost of refilling and long queues might be the reason for low use of LPG for cooking food among the respondents.
- 3 Maximum respondents reported that they own a motorcycle however, an open-ended question that aimed at gauging the utility of motorcycle in the household revealed that individuals failed to explain their costly possession. Motorcycle is a depreciating asset that needs constant maintenance. Hence, possession of such asset without utility will only lead to deterioration of living conditions.
- 4 The study reveals an overall medium standard of living for the NTFP workers. This indicates that tribals have progressed slightly in terms of their living condition after associating from microenterprises. However, Government should strive and formulate policies towards improving conditions of these individuals in fields of household ownership and penetration of ICT and mobile phones. This will not help the workers to attain better living conditions but will also help them get informed towards government policies, schemes and subsidies devised with them as the primary target.

REFERENCES

1. A.K. Pandey, Y.C. Tripathi and Ashwani Kumar, 2016. Non Timber Forest Products (NTFPs) for Sustained Livelihood: Challenges and Strategies. *Research Journal of Forestry*, 10: 1-7.
2. Sharma, K. (2019). Non-Timber Forest Products (NTFPs) and Livelihood Security: An Economic Study of High Hill Temperate Zone Households of Himachal Pradesh. In *Economic Affairs* (Vol. 64, Issue 2). Agricultural Economics and Social Science Research Association (AESSRA). <https://doi.org/10.30954/0424-2513.2.2019.5>
3. Shanley, P., Pierce, A.R., Laird, S.A., Binnquist, C.L., Guariguata, M.R. (2015). From Lifelines to Livelihoods: Non-timber Forest Products into the Twenty-First Century. In: Pancel, L., Köhl, M. (eds) *Tropical Forestry Handbook*. Springer, Berlin, Heidelberg. https://doi.org/10.1007/978-3-642-41554-8_209-1
4. Peerzada, I. A., Islam, M. A., Chamberlain, J., Dhyani, S., Reddy, M., & Saha, S. (2022). Potential of NTFP Based Bioeconomy in Livelihood Security and Income Inequality Mitigation in Kashmir Himalayas. In *Sustainability* (Vol. 14, Issue 4, p. 2281). MDPI AG. <https://doi.org/10.3390/su14042281>
5. Talukdar, N. R., Choudhury, P., Barbhuiya, R. A., & Singh, B. (2021). Importance of Non-Timber Forest Products (NTFPs) in rural livelihood: A study in Patharia Hills Reserve Forest, northeast India. In *Trees, Forests and People* (Vol. 3, p. 100042). Elsevier BV. <https://doi.org/10.1016/j.tfp.2020.100042>.





Satya Kishan and Kavita Silwal

Table 1 QLI comparison Scale

QLI	Deduce
<=0.40	LOW
>0.40 - <0.60	MEDIUM
>0.60	HIGH

Table 2 Response received from the respondents for the questions belonging to HQLI

Question	Yes	% Yes	No	%NO
Do you have household ownership	97	48.5	103	51.5
Is the house properly maintained	101	50.5	99	49.5
The house has a separate room for the married couple	111	55.5	89	44.5
Is the house a 'Pakka' type construction	87	43.5	113	56.5
Is the house having a toilet	200	100	0	0
HQLI	0.596			





Comparative Study of Seismic Retrofitting Methods for Durability Gain of an Existing Old Building

Gayathri R^{1*}, Chandan N R², Putte Gowda B S³, Vatshala³ and T S Malleshiah⁴

¹Assistant Professor, Department of Civil Engineering, The Oxford College of Engineering, Bangalore, Karnataka, India.

²PG Student, Department of Civil Engineering, The Oxford College of Engineering, Bangalore, Karnataka, India.

³Associate Professor, Department of Civil Engineering, BIT College of Engineering, Bangalore, Karnataka, India.

⁴Professor and HoD, Department of Civil Engineering, The Oxford College of Engineering, Bangalore, Karnataka, India.

Received: 23 Jan 2023

Revised: 10 Apr 2023

Accepted: 16 May 2023

*Address for Correspondence

Gayathri R

Assistant Professor,
Department of Civil Engineering,
The Oxford College of Engineering,
Bangalore, Karnataka, India.



This is an Open Access Journal / article distributed under the terms of the **Creative Commons Attribution License** (CC BY-NC-ND 3.0) which permits unrestricted use, distribution, and reproduction in any medium, provided the original work is properly cited. All rights reserved.

ABSTRACT

Seismic Retrofitting of RC building is modifying or repairing the already existing building to enhance the strength and durability of buildings against earthquake forces. Karnataka located in Zone II and Zone III according to BIS 1893(2002). So, most of the buildings constructed 10 -20 years before are not designed as an Earthquake resistant Building. Building. Anepicentre of a probable 5.8 magnitude temblor could be just around 100 km away from Bengaluru, on the Ailughatta Hosakere Road near Tumakuru is predicted by a group of Scientists led by a researcher at the Indian Institute of Science using a new technique called Rupture Based Seismic Hazard Analysis. In this project we are going to retrofit and renovate the 10-year-old G+9, RC building located in Tumkur area ,as an Earthquake resistant structure, using (i)shear walls(ii)Increasing the size of column. A shear wall can resist the earthquake forces efficiently. Here the strength of the building is improvised by introducing shear walls and also increasing the size of column. Finally we will compare the results and finalise the best retrofitting method .The Structural Analysis of this building is done by Etabs.

Keywords: Seismic Retrofitting.



Gayathri *et al.*,

INTRODUCTION

Seismic retrofitting is the modification of existing structures to make them more resistance to seismic activity, ground motion or soil failure due to earthquake. The strength of the whole structure can be improved by introducing new structural elements or strengthening the existing structural elements. The retrofitting becomes necessary to improve the performance of structures, which losses strength due to deterioration or which have crossed their expected life. success of retrofitting depends on the actual cause and the measures adopted to prevent its further damage of the building.

LITERATURE REVIEW

P Anbazhagan and JS Vinod *et.al.* [1] in the year 2012 from the department of civil engineering Indian Institute of Science has worked on the seismic intensity map of south India for estimated future earthquake zone of Karnataka and has been predicted the earthquake prone areas in the next 10 years by using a modern technique called RBSHA. A Obaidat, *et al* [2] in the year 2010 examined the structurally damaged RCC beam retrofitted with CFRP laminates. The experimental results proved that the beam retrofitted with CFRP laminates are more efficient. The author concluded that the length of the CFRP sheets determines the strength of the damaged building elements. Alpa Jain *et al* [3] in the year 2008 examined the reason of major damage due to Bhuj earthquake. The negligence of engineer is the main reason for this disaster. Finally, the author concluded that the engineer should have the knowledge about the various techniques for seismic resistivity. Bhattacharya Shubhamoy *et.al* [4] in the year 2011 worked on masonry structures that are unreinforced. In Himalayan areas the masonry building without reinforcement are common. Various Retrofitting methods are applied to this type of buildings. The analysis results provide useful guidance to architects to select correct retrofitting methods. Fulin Zhou [5] in the year 1998 studied the retrofitting methods for existing structure. The design for seismic resistant is not only for new building but also to strengthen the existing structure. The author concluded that "Inelastic structural system" has limitations for application. The recent method of base isolation and energy dissipation together work well. The results are better. It is 5-20% economical than traditional methods. Iacobucci R.D, *et al* [6] in the year 2003 The retrofitting using Carbon Fibber -Reinforced Polymer(CFRP) for Concrete columns are studied here. The damaged square column is retrofitted with CFRP jackets. The prospect of strengthening damaged column is investigated here. Finally, they concluded that the installation of CFRP jacket is easy and, ductility will increase. The capacity of energy dissipation also increases.

OBJECTIVE AND METHODOLOGY

Objective

The objective of this work is to strengthen the building by

- (i)Retrofitting by increasing column size
- (ii)Retrofitting by introducing shear wall for an already existing, damaged G+9 building.

Methodology

An Existing Multistory building ,located in Tumkuru area, Bangalore is considered. By looking into the blueprint, study the architectural plan and design details of the of existed G+9 building, the column layout of the building is shown in figure

Create three model of the building in etabs with Column size as 400 X400mm.

Model 1-Existing Old Building without Retrofitting.

Model 2-Existing Old Building Retrofitted by introducing Shear Walls.

Model 3 - Existing Old Building Retrofitted by increasing the size of the column.



**Gayathri et al.,**

All the above Models, the predicted Earthquake forces are applied and analysed. From the analysis results we can detect the weak columns of the existed building which were failing due to predicted seismic forces.

Procedure Followed

Step 1: First study the architectural plan of the building and note down the complete details including loads acting on it.

Step 2: By using etabs model the existing G+9 building by utilizing the collected details of building.

Step 3: The material properties and section properties of beams, columns and slabs are defined.

Step 4: The section properties of beams, columns and slabs are assigned to the models.

Step 5: The Dead load, Live load, Earthquake loads are defined. Then the equivalent static analysis and Response spectrum also must be defined for all the three Models.

Step 6: Model 1- Existing Old Building without Retrofitting is analysed. In this Model 1, some column members got failed due to seismic effect. The damaged columns are noticed. The red mark represents the damaged columns in the existing building

Step 7: In between the failed column, Shear walls of thickness 230mm is introduced and considered as **Model 2-** Existing Old Building Retrofitted by introducing Shear Walls.

Step 8: The size of the Failed Column is increased to 500 X 500mm and considered as **Model 3 -** Existing Old Building Retrofitted by increasing the size of the column.

Step 9: Now both the Model 2 and Model 3 are analysed. The structure is Safe (i.e) It can withstand the predicted Earthquake forces.

ANALYSIS AND RESULTS

The above three models are analyzed using both the static and dynamic methods using ETABS 2016 and the results are tabulated below.

Bending Moment of the Frames

This is the graphical representation of the variation of the bending moment of the beams in the moment frame of the structural building

Shear Force of the Frames

This is the net impact of the shear force is to shear off alongside the place of beam where it is acting. The shear forces are the vertical forces acting uniformly or concentratedly on the frame of the building.

Base Shear

Base shear is the total horizontal force acting at the base of the structure that caused due to seismic force

CONCLUSIONS

In this Project, Seismic Retrofitting is done as a renovative measure. The Existing Old Building is retrofitted to counter balance the future predicted earthquake forces. So Retrofitting in renovative path can prevent Building damage and save many people life From the Analysis results we can conclude that Model 2 Retrofitted by introducing Shear Walls give better resistance to predicted Earthquake forces compared to Model 3 - Existing Old Building Retrofitted by increasing the size of the column.

REFERENCES

1. DR.T S Malleiah, R Gayathri, Harshitha, 2022, "Analysis and design of multi-storey building using etabs
2. T G Sitharam and Naveen James Indian institute of science, Bangalore 2012 "A study on seismicity and seismic hazard for Karnataka State"





Gayathri et al.,

3. PANbazhagan and JS Vinod 2012 "Seismic intensity map of south India for estimated future earthquake"
4. Fulin Zhou 1998 "Retrofitting for Existing Buildings with Seismic Control of Structure Post earthquake"
5. SivrajaSaileysh S. et al 2012 "Rehabilitation and Strengthening -Earthquake Damaged RCCStructures"
6. A Obaidat, et.al 2010 "Retrofitting of reinforced concrete beams using composite laminates"
7. Iacobucci R D et al 2003 American Concrete Institute Structural Journal, 2003 "Retrofit of Square Concrete Column with CFRP for seismic Resistance"
8. Parvez, Vaccari and Panza Geophysics Journal International, 2003 "A deterministic seismic hazard map of India and adjacent areas"
9. Mayorca Paola and Meguro Kimiro, 2004 " Proposal of an Efficient Technique for retrofitting Unreinforced Masonry Dwellings".

Table 1. Maximum Bending Moment Values Of 3 Models

Maximum Bending Moment					
Model	My		Mz		Units
	Static analysis	Response spectrum	Static analysis	Response spectrum	
Model 1	58.4	406.78	190.45	1249.313	KN-M
Model 2	62.32	999.41	195.36	2598.52	KN-M
Model 3	67.22	1495.97	242.22	4294.77	KN-M

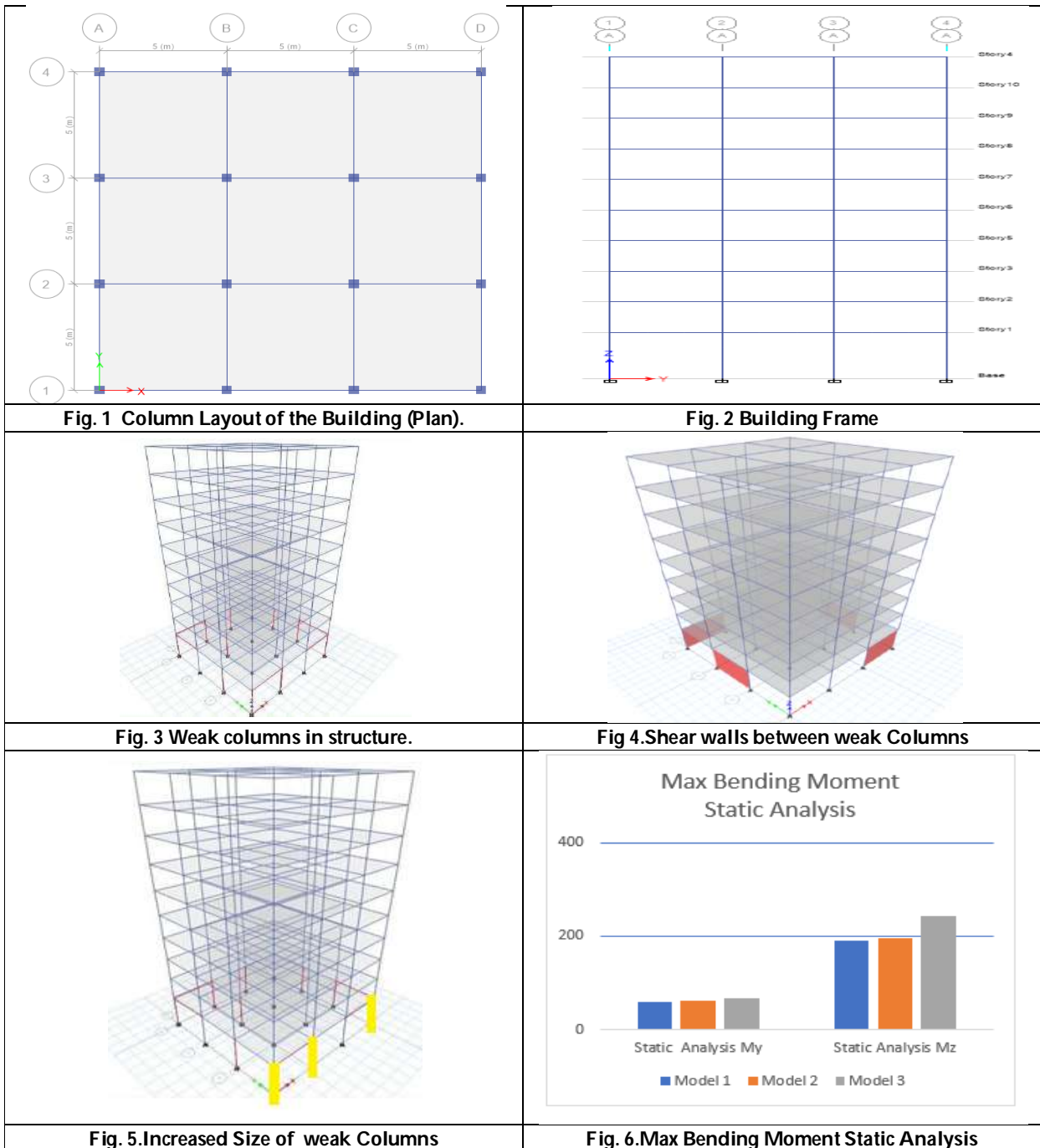
Table 2. Maximum shear values of 3 Models

Model	Maximum Shear Force		Units
	Static analysis	Response spectrum	
Model 1	88.611	734.31	KN
Model 2	146.13	1352.023	KN
Model 3	122.13	925.023	KN

Table 3. Base shear values of 3 Models

Type of Building	Equivalent Static Analysis		Response spectrum analysis	
	EQX	EQY	RSX	RSY
Model 1	0.002169	0.002169	0.003978	0.003978
Model 2	0.003159	0.003159	0.004689	0.004689
Model 3	0.002158	0.002158	0.003874	0.003874







Gayathri et al.,

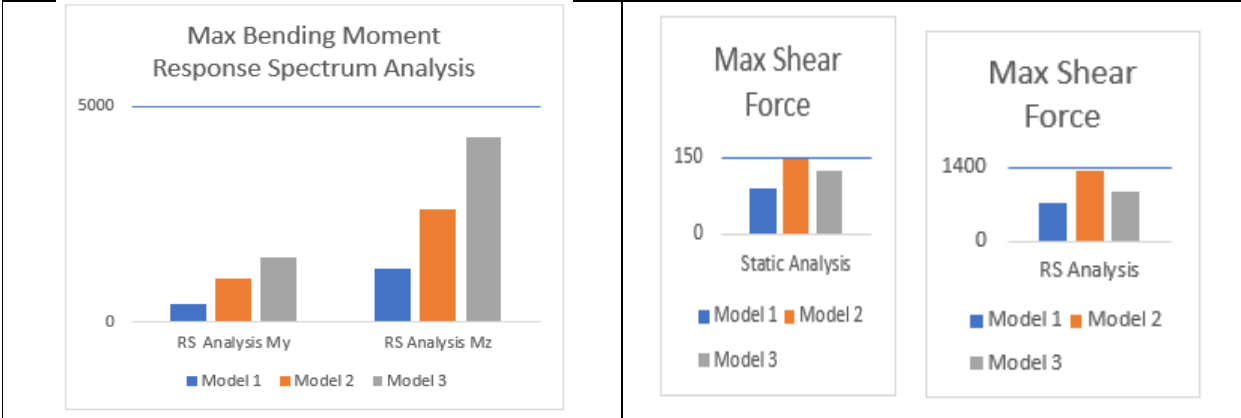


Fig. 7. Max Bending Moment RS Analysis

Fig. 8. Max Shear Force Static and RS Analysis

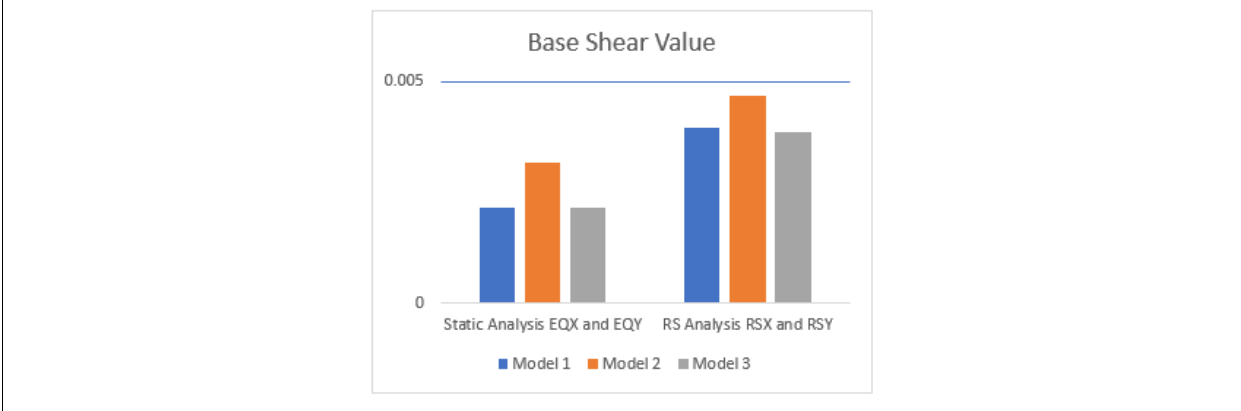


Fig. 9. Base Shear Static and RS Analysis





Social Media usage and Psychological Health of Young Adults in India

Dimple Kariya^{1*} and Geetika Tankha²

¹Ph.D Research Scholar, Department of Psychology, School of Humanities and Social Sciences, Manipal University Jaipur, Jaipur, India.

²Professor, Department of Psychology, School of Humanities and Social Sciences, Manipal University Jaipur, Jaipur, India

Received: 20 Feb 2023

Revised: 10 Apr 2023

Accepted: 15 May 2023

*Address for Correspondence

Dimple Kariya

Ph.D Research Scholar,
Department of Psychology,
School of Humanities and Social Sciences,
Manipal University Jaipur, Jaipur, India.
Email: dimple.kariya05@gmail.com



This is an Open Access Journal / article distributed under the terms of the **Creative Commons Attribution License** (CC BY-NC-ND 3.0) which permits unrestricted use, distribution, and reproduction in any medium, provided the original work is properly cited. All rights reserved.

ABSTRACT

In contemporary times, the use of social media has increased a lot across different age groups. Thus, this study aimed to explore the relationship between social media usage and psychological health among young Indians. Furthermore, the study also investigated if there were any differences in social media usage between young college-going adults and young working adults. The sample consisted of 200 college-going young adults and the other 192 young working young adults. The total sample of 392 participants was administered two psychological tests, i.e., MTUAS Scale to assess social media usage and the DASS-21 to assess mental health. The obtained data were analyzed using SPSS version 26. The bivariate correlation was applied to find out the association between media usage and the psychological health of both groups. To assess the differences, ANOVA was applied and significant differences emerged. The results revealed that females in both groups had higher social media usage. The anxiety about no technology was higher in the working population. Working males seem to be having both positive and negative attitudes toward technology.

Keywords: Social media usage, stress, anxiety, depression, young adults

INTRODUCTION

Science offers us the internet, which is indispensable in a modern environment. The internet is a scientific marvel. It enables us to get information with a click. The internet lets us share information and connect with people worldwide. It's an extensive repository of knowledge from which we may obtain various information pertaining to multiple



**Dimple Kariya and Geetika Tankha**

topics. There are positive applications for the internet as well as negative ones. It has brought the whole planet together. The term "social media" refers to a set of websites, programs, and other online platforms that let us share or generate content and allow us to engage in online social networking. In today's world, social media is a contentious issue. Nevertheless, some individuals see it as a blessing. It is a gift since it has linked us to every part of the globe. We can meet our loved ones who live far away via it, disseminate awareness about important issues, send security alerts, etc. However, overuse and addiction to social media can also result in numerous mental health issues like anxiety, depression, stress, etc. The youth of any country is the hope for the future and has the power to build or ruin our economy. The use of social media is one of the most exciting and engaging aspects of their life in modern times. The population that utilizes social networking sites most frequently is young people; social media usage (SMU) has a substantial and pervasive impact on this group. The targeted group who uses social media is also aware of the same; however, due to peer pressure or the easy accessibility, they tend to use the same and are unable to give on it. Social media is also acting as the bread and butter for many individuals as people have started to spread the word about their new endeavors, job openings, etc on the same.

A recent systematic review of the relationship between SMU and adolescents' psychological health by Keles *et al.* (2020) reported that SMU can lead to increased stress, anxiety, and depression. On the other hand, few researchers have reported mixed results on the relationship between SMU and depression (Jelenchick *et al.*, 2013; Kross *et al.*, 2013). Dempsey *et al.* (2019) found that rumination was substantially correlated with assessed FoMO, Facebook use frequency, and the severity of problematic Facebook use. Facebook use and other social media networking sites have led to a state of dependency on it, making it difficult for individuals to stay away from it. This dependency comes from parents, siblings, relatives, and peers using this specific communication mode and sharing essential moments. Therefore, that leads to the individual feeling left out from the social circuit, which is the key reason for the person to feel left out. Others have reported that SMU is associated with a reduction in subjective mood, sense of well-being, and life satisfaction, according to numerous studies (Chou & Edge, 2012; Kross *et al.*, 2013; Sagioglou & Greitemeyer, 2014)

METHODS

Sample and Procedure

The study used a survey design methodology. Purposive sampling was used for selecting the study sample. The sample consisted 200 college-going students (Males=89 and Females=111) with a mean age of 19 years and 192 young working adults (Males=85 and Females=107) with a mean age of 32 years. All the 392 participants had a minimum education of level of 10+2. Informed consent was taken from the participants. They were administered a set of standardized tools along with the general socio-demographic information.

The battery of tools consisted of the following:

1. The Media and Technology Usage and Attitudes Scale (Rosen *et al.*, 2013): This is a 60-item self-report inventory that assesses the social media usage and attitudes toward the technology of adults. It is a reliable and valid tool. Higher scores indicate higher media usage.
2. The Depression Anxiety Stress Scale (DASS-21, Lovibond & Lovibond, 1995): The DASS-21 is a widely used questionnaire. It measures mental health on three sub-scales of depression, anxiety, and stress.

Statistical Analysis

The obtained data were analyzed using descriptive (Mean, Standard deviation, Pearson correlation) and inferential statistical techniques (one-way ANOVA). The SPSS version 26 was used for analysis.

RESULTS AND DISCUSSION

The present study mainly focused on examining the relationship between SMU and the psychological health of young adults. Secondly, the study also aimed to explore if there were any differences between young college-going students and young working adults concerning media usage and attitude toward technology.



**Dimple Kariya and Geetika Tankha**

The study's findings revealed that females in both groups were more significant social media consumers. The dependency on technology was higher in the young working population than in college-going students. Working males seem to be having both positive and negative attitudes toward technology. The relationship between SMU and psychological health (i.e., depression, anxiety, and stress) was assessed for the sample of young adults. The obtained results are presented in the table 1 and 2 for the two sample groups, i.e., college-going young adults and working young adults, respectively. The results indicate that SMU is significantly and positively linked with depression ($r = .227, p < .05$). This means that media usage and depression have a linear relationship. It was observed that dependence on technology had a significant positive correlation with anxiety ($r = .234, p < .05$), and stress levels ($r = .337, p < .01$).

Table 1 further revealed that a positive attitude towards technology is positively associated with depression ($r = .240, p < .05$) only in college-going females. Dependence on technology has a significant positive association with anxiety and stress ($r = .291, p < .01$) in females and with stress in females and males, respectively. Preference for tasks shows a significant positive correlation with depression ($r = .354, p < .01$), anxiety ($r = .368, p < .01$), and stress ($r = .300, p < .01$) in college-going males. According to multiple research, excessive media use is linked to a decline in perceived mood, a feeling of welfare, and satisfaction with life. (Kross *et al.*, 2013; Chou & Edge, 2012; Sagioglou & Greitemeyer, 2014). Low subjective mood can result from a lack of social stimulation. The moment individuals meet in person, some form of social stimulation takes place and is considered healthy for human beings as the human race has belonged to social beings since the early man era when groups of people stayed together. We as individuals have evolved from the early man who would live in groups and constantly communicate and interact with those in that group. Therefore, communication that only takes place virtually might not provide the same amount of stimulation. In contrast to active conversation, passive communication through social media has been linked to loneliness and a decline in social capital for bridging and bonding (Burk & Lento, 2010). A second theory is that seeing peers' highly idealized pictures on social media makes people feel envious and makes them think that other people have more productive lives. Social media is a platform where everyone avoids putting across what they feel and puts up a mask for society and themselves to feel suitable for that particular moment. There are very few posts where individuals would post about their low times. The happy moments people keep showing on the sites make other individuals believe that to be true, and they start seeing their current misery as massive. It also showcases toxic positivity, where people on social media unconsciously don't leave any place for any negative post. Even if an individual would wish to talk about the misery they are going through, they would be discouraged to put it across on the sites thinking that others might feel low of them or that sharing negative news or misery is not allowed on the social sites. Therefore, over time, these sentiments of envy may result in despair and a sense of inferiority toward oneself. (Krasnova, 2013; Smith & Kim, 2007; Tandoc, 2015). The danger of cyber bullying, which can worsen depressive symptoms, could grow with greater social media use. (O'Keeffe, 2011; Primack, 2017). This possibly explains why college-going females experience anxiety and stress when they cannot access technology and media. The college-going males also experience stress without technology. The results also show that multi-tasking has a significant and positive relationship with mental ill-health issues in males.

Table 2 reveals an association between media usage and the mental health of young working adults. The table examination indicates that media usage has a significant positive correlation with stress in working females and not in males. A positive attitude towards technology has resulted in a positive relationship with depression ($r = .198, p < .05$) and anxiety ($r = .206, p < .05$). Dependence on technology has a significant positive correlation with anxiety ($r = .220, p < .05$). Preference for task shows a significant positive correlation with anxiety ($r = .194, p < .05$) in working females. Maintaining individual autonomy at the workplace is crucial to guaranteeing workplace satisfaction (Vos & van der Voordt, 2001). This could act as a stimulator for higher anxiety while using SM as constant fear or insecurity about accomplishing a task with success could be tedious. With social media booming everywhere, it can be a challenge sometimes to keep things extremely confidential as a threat always looms around for others to get to know what you are up to at work and to somehow either take over the same or to take credit for the same. It does become essential for every individual to concentrate on the tasks and projects to achieve the deserved credit and handle the presence on social media just so that peers don't start to question. To handle this pressure, the individual experiences



**Dimple Kariya and Geetika Tankha**

high anxiety, as they have to make sure they balance both situations. Table 2 reveals that a positive attitude towards technology shares a negative association with depression ($r=-.232$, $p<.05$) and anxiety ($r=-.343$, $p<.01$). Negative attitude shows a significant positive relationship with anxiety ($r=.273$, $p<.05$). One of the most commonly voiced worries about virtual spaces, according to Akkirman and Harris (2005), is the loss of traditional social dynamics that encourage dialogue. They studied a corporation that used various social networking techniques to keep its virtual employees in the loop. According to Nardi *et al.* (2002), contacts recurrently provide "care and feeding" after being part of a network. With media sites becoming a major source of communication or exchanging important information related to maybe jobs, careers, colleges, assignments etc, the individual might be kept aloof from all the essential information if he/she refrains from using social media. Possibly, when an activity is performed for self and leisure, it has a much more positive impact on oneself than when it is made to do out of compulsion. Therefore, we can say that even if an individual wishes to work towards their dependency or mindfully wants to work around the usage of social media they are still forced to use it to a great extent as their peers use it.

Table 3 presents the results of the one-way analysis of variance among the four groups of young adults on the SMU and 4 subscales of attitudes toward technology. The F – values indicated statistically significant differences in social media usage and attitudes toward technology across the four groups.

On the scale of social media usage, the results indicate statistically significant differences (i.e., $F(3, 296) = 9.308$, $p < .001$) along with the strength of the relationship indexed by $\eta^2 = 0.07$ (medium effect). More so, the mean scores on SMU indicated that college-going females (Group A- $M=204.24$, $SD=41.12$) and working females (Group C- $M=223.50$, $SD=44.38$) preferred SMU more than college-going males (Group B- $M=197.27$, $SD=44.94$) and working males (Group D- $M=223.91$, $SD=42.64$). The mean scores on SMU indicate that females belonging to college -going group were more inclined toward media usage than males. According to Kelly *et al.* (2019), young women were likelier than young men to use social media and report depressive symptoms. The current study showed that only college-going girls had a significant positive correlation between SMU and depressive symptoms among the four groups. Younger adults are more vulnerable to stressors, including interpersonal conflicts, marital problems, parenting, and other things (Morahan & Schumacher, 2000; Young & Rogers, 1998).

Further examination of table 3 indicates statistically significant differences (i.e., $F(3, 296) = 15.461$, $p < .001$) along with the strength of the relationship indexed by $\eta^2 = 0.11$ (medium effect) on the scale of positive attitude towards technology. More so, the mean comparisons of the four groups revealed that male working adults adopted a more positive attitude towards technology compared to the young female adults, irrespective of their employment status (Group D- $M = 4.26$; Group C- $M = 4.06$; Group A- $M = 3.93$; Group B- $M = 3.56$). Facebook and other online social networking sites influence the success of individuals at jobs. According to Abdullah & Panneerselvam (2019); North (2019), employees of an organisation utilise FB to market their business module or use to gain more recognition and execute their jobs.

On the dimension of Dependence on technology, significant differences were observed in the four groups ($F(3, 296) = 7.855$, $p < .001$) with medium effect size indexed by $\eta^2 = 0.06$. The mean scores showed that working males got triggered with anxiety when there was no technology compared to college-going males (Group D- $M = 3.71$; Group B- $M = 3.09$). More so, there was a difference in the mean scores obtained between the groups of females attending college and going to work (Group A: $M = 3.32$, $SD = 0.98$; Group C: $M = 3.57$, $SD = 0.92$). Many companies are now adopting a virtual workplace strategy (Kayworth & Leidner, 2000). It has also increased the SMU, allowing people to interact and work together formally and informally with co-workers. This could explain why both male and female working professionals have a high dependence on technology and become anxious when it is unavailable.

On the dimension of Preference of task, the findings indicated statistically significant differences among the four groups (i.e., $F(3, 296) = 7.537$, $p < .001$) followed by strength of relationship indexed by $\eta^2 = 0.06$ (medium effect size). The Preference for task sub-scale assesses Multitasking can be better explained as managing or selectively attending to more than one activity at any given point in time. Researchers (Carrier *et al.*, 2015; Dindar & Akbulut, 2016), have



**Dimple Kariya and Geetika Tankha**

reported that students misunderstand multitasking as a skill that paves the way to manage tasks effectively inside and outside of a classroom. They believe managing multiple tasks at once will save them time and help them perform tasks effectively. Individuals participate in both studying and listening to music or texting at the same time, technology encourages multitasking (Chang, 2017). The enhanced social media multitasking boosts one's self-worth and perception of their ability to successfully complete academic tasks (Boahene *et al.*, 2019). The mean scores reveal that working males (Group D- M = 3.01, SD = 0.71) preferred tasks about technology to deal with stressful situations compared to males going to college (Group B: M = 2.53, SD = 0.80). Females who were working show a marginal difference with (Group C: M=2.89, SD=0.73) those attending college (Group A: M=2.67, SD=0.75).

The only factor that indicates no statistical differences among the four groups is negative attitudes toward technology ($F(3, 296) = 0.462$). The mean scores indicated that working males (Group D: M=3.57, SD=0.81) show the highest negative attitude towards technology compared to college-going males (Group B: M=3.43, SD=0.81). There was a marginal difference in the mean scores obtained between the groups of the female who went to college (Group A: M=3.55, SD=0.87) and the working females (Group C: M=3.50, SD=0.87). With the increase in the usage of technology for personal as well as office chores, interest and curiosity got tampered. Though it positively impacts the current situation, the male working professional could have better preferred the stimulation it provided prior to the virtual world as they tend to portray both positive and negative attitudes towards technology. Thus, it can be concluded that females of the college-going age group tend to use more social media as compared to males. However, the dependence on technology is more in working adults as compared to college-going young adults. Lastly, none of the groups differ on the measure of negative attitudes towards technology.

REFERENCES

1. Abdullah, Z., & Panneerselvam, T. L. (2019). The Relationships Between Social Networking and Individual Job Performance of Law Sector in Malaysia. *Journal of Education and Social Sciences*, 12(2), 92-101.
2. https://www.jesoc.com/wp-content/uploads/2019/11/JESOC12_20-1.pdf
3. Akkirman, A. D., & Harris, D. L. (2005). Organizational communication satisfaction in the virtual workplace. *Journal of Management Development*. <https://doi.org/10.1108/02621710510598427>
4. Boahene, K. O., Fang, J., & Sampong, F. (2019). Social media usage and tertiary students' academic performance: Examining the influences of academic self-efficacy and innovation characteristics. *Sustainability*, 11(8), 2431.
5. <https://doi.org/10.3390/su11082431>
6. Burke, M., Marlow, C., & Lento, T. (2010, April). Social network activity and social well-being. In *Proceedings of the SIGCHI conference on human factors in computing systems* (pp. 1909-1912). <https://doi.org/10.1145/1753326.1753613>
7. Carrier, L., M., Rosen, L., D., Cheever, N., A., & Lim, A., F. (2015). Causes, effects, and practicalities of everyday multitasking. *Developmental Review*, 35, 64-78. <https://doi.org/10.1016/j.dr.2014.12.005>
8. Chang, Y. (2017). Why do young people multitask with multiple media? Explicating the relationships among sensation seeking, needs, and media multitasking behavior. *Media Psychology*, 20(4), 685-703.
9. <https://doi.org/10.1080/15213269.2016.1247717>
10. Chou, H. T. G., & Edge, N. (2012). "They are happier and having better lives than I am": The impact of using Facebook on perceptions of others' lives. *Cyberpsychology, Behavior, and Social Networking*, 15(2), 117-121. <https://doi.org/10.1089/cyber.2011.0324>
11. Dindar, M., & Akbulut, Y. (2016). Effects of multitasking on retention and topic interest. *Learning and Instruction*, 41, 94-105.
12. <https://doi.org/10.1016/j.learninstruc.2015.10.005>
13. Jelenchick, L. A., Eickhoff, J. C., & Moreno, M. A. (2013). "Facebook depression?" Social networking site use and depression in older adolescents. *Journal of Adolescent Health*, 52(1), 128-130. <https://doi.org/10.1016/j.jadohealth.2012.05.008>



**Dimple Kariya and Geetika Tankha**

14. Kayworth, T., & Leidner, D. (2000). The global virtual manager: A prescription for success. *European Management Journal*, 18(2), 183-194. [https://doi.org/10.1016/S0263-2373\(99\)00090-0](https://doi.org/10.1016/S0263-2373(99)00090-0)
15. Keles, B., McCrae, N., & Grealish, A. (2020). A systematic review: The influence of social media on depression, anxiety and psychological distress in adolescents. *International Journal of Adolescence and Youth*, 25(1), 79–93. <https://doi.org/10.1080/02673843.2019.1590851>
16. Kelly, Y., Zilanawala, A., Booker, C., & Sacker, A. (2019). Social Media Use and Adolescent Mental Health: Findings From the UK Millennium Cohort Study. *EClinicalMedicine*, 6, 59–68. <https://doi.org/10.1016/j.eclinm.2018.12.005>
17. Krasnova, Hanna; Wenninger, Helena; Widjaja, Thomas; and Buxmann, Peter, "Envy on Facebook: A Hidden Threat to Users' Life Satisfaction?" (2013). *Wirtschaftsinformatik Proceedings 2013*. 92. <http://aisel.aisnet.org/wi2013/92>
18. Kross, E., Verduyn, P., Demiralp, E., Park, J., Lee, D. S., Lin, N., & Ybarra, O. (2013). Facebook use predicts declines in subjective well-being in young adults. *PLoS one*, 8(8), e69841. <https://doi.org/10.1371/journal.pone.0069841>
19. Lovibond, S. H. and Lovibond, P. F. 1995. *Manual for the Depression, Anxiety and Stress Scales*, 2nd edn, Sydney, Australia: Psychology Foundation.
20. Morahan-Martin, J., & Schumacher, P. (2000). Incidence and correlates of pathological Internet use among college students. *Computers in human behavior*, 16(1), 13-29. [https://doi.org/10.1016/S0747-5632\(99\)00049-7](https://doi.org/10.1016/S0747-5632(99)00049-7)
21. Nardi, B. A., Whittaker, S., & Schwarz, H. (2002). Net WORKers and their activity in intensional networks. *Computer Supported Cooperative Work (CSCW)*, 11(1), 205-242. <https://doi.org/10.1023/A:1015241914483>
22. North, M. (2010). An evaluation of employees' attitudes toward social networking in the workplace. *Issues in Information Systems*, 11(1), 192-197. https://doi.org/10.48009/1_iis_2010_192-197
23. O'Keeffe, G. S., Clarke-Pearson, K. (2011). The impact of social media on children, adolescents, and families. *Pediatrics*, 127(4), 800-804. <https://doi.org/10.1542/peds.2011-0054>
24. Primack, B. A., & Escobar-Viera, C. G. (2017). Social media as it interfaces with psychosocial development and mental illness in transitional age youth. *Child and Adolescent Psychiatric Clinics*, 26(2), 217-233. <https://doi.org/10.1016/j.chc.2016.12.007>
25. Rosen, L. D., Whaling, K., Carrier, L. M., Cheever, N. A., & Rökkum, J. (2013). The media and technology usage and attitudes scale: An empirical investigation. *Computers in human behavior*, 29(6), 2501-2511.
26. Sagioglou, C., & Greitemeyer, T. (2014). Facebook's emotional consequences: Why Facebook causes a decrease in mood and why people still use it. *Computers in Human Behavior*, 35, 359-363. <https://doi.org/10.1016/j.chb.2014.03.003>
27. Smith, R. H., & Kim, S. H. (2007). Comprehending envy. *Psychological bulletin*, 133(1), 46. <https://psycnet.apa.org/doi/10.1037/0033-2909.133.1.46>
28. Tandoc Jr, E. C., Ferrucci, P., & Duffy, M. (2015). Facebook use, envy, and depression among college students: Is facebooking depressing?. *Computers in human behavior*, 43, 139-146. <https://doi.org/10.1016/j.chb.2014.10.053>
29. Vos, P., & Van der Voordt, T. (2001). Tomorrow's offices through today's eyes: Effects of innovation in the working environment. *Journal of Corporate Real Estate*. <https://doi.org/10.1108/14630010210811778>
30. Young, K. S., & Rogers, R. C. (1998). The relationship between depression and Internet addiction. *Cyberpsychology & behavior*, 1(1), 25-28. <https://doi.org/10.1089/cpb.1998.1.25>





Dimple Kariya and Geetika Tankha

Table 1 Correlation coefficients for SMU and Attitude towards technology for college-going adults

Variables	Depression		Anxiety		Stress	
	College-going students		College-going students		College-going students	
	Females	Males	Females	Males	Females	Males
Social media usage	0.227*	0.143	0.079	0.159	0.140	0.032
Positive attitude towards technology	0.171	0.240*	0.179	0.171	0.162	0.171
Dependence on technology	0.157	0.195	0.234*	0.197	0.337**	0.291**
Negative attitude towards technology	0.068	-0.106	0.143	-0.094	0.115	-0.023
Preference of task	0.081	0.354**	-0.013	0.368**	-0.004	0.300**

Note *p<.05.**p<.01

Table 2 Correlation coefficients for SMU and Attitude towards technology for young working adults

Variables	Depression		Anxiety		Stress	
	Working Adults		Working adults		Working adults	
	Females	Males	Females	Males	Females	Males
Social media usage	0.043	0.059	0.187	-0.028	0.201*	-0.026
Positive attitude towards technology	0.198*	-0.232*	0.206*	-0.343**	.256**	-.109
Dependence on technology	0.161	0.192	0.220*	0.125	.298**	.203
Negative attitude towards technology	0.126	0.189	0.084	0.273*	.120	.200
Preference of task	0.155	-0.006	0.194*	0.057	.169	.069

Note *p<.05;**p<.01

Table 3 Means, Standard Deviations, One-Way ANOVA across Groups of young adults on social media usage and its components

Variables	College-going students		Working young adults		F (3, 296)
	Females-Group A M(SD)	Males-Group B M(SD)	Females-Group C M(SD)	Males-Group D M(SD)	
Social media usage	204.24 (41.12)	197.27 (44.94)	223.50 (44.38)	223.91(42.64)	9.308**
Positive attitude towards technology	3.93 (0.56)	3.65 (0.74)	4.06 (0.57)	4.26 (0.58)	15.461**
Dependence on technology	3.32 (0.98)	3.09 (0.88)	3.57 (0.92)	3.71 (0.88)	7.855**
Negative attitude towards technology	3.55 (0.87)	3.43 (0.81)	3.50 (0.87)	3.57 (0.81)	0.462
Preference of task	2.67 (0.75)	2.53 (0.80)	2.89 (0.73)	3.01 (0.71)	7.537**

Note: *p<.05;**p<.01





Phytochemistry and Pharmacological Review on *Biophytum umbraculum* with a Note on its Comparison with *Biophytum sensitivum*

Raja Chandra G¹, Raunak Dhanker^{2*} and Abhijit Dey³

¹Research Scholar, Department of Basic and Applied Sciences, School of Engineering and Sciences, GD Goenka University, Haryana 122103, India.

²Assistant Professor, Department of Basic and Applied Sciences, School of Engineering and Sciences, GD Goenka University, Haryana 122103, India.

³Department of Life Sciences, Presidency University, Kolkata, India.

Received: 28 Feb 2023

Revised: 25 Apr 2023

Accepted: 31 May 2023

*Address for Correspondence

Raunak Dhanker

Assistant Professor,
Department of Basic and Applied Sciences,
School of Engineering and Sciences,
GD Goenka University, Haryana 122103, India.



This is an Open Access Journal / article distributed under the terms of the **Creative Commons Attribution License** (CC BY-NC-ND 3.0) which permits unrestricted use, distribution, and reproduction in any medium, provided the original work is properly cited. All rights reserved.

ABSTRACT

Biophytum umbraculum is a tall, annual, sessile bearing umbel herb belonging to the family Oxalidaceae found in tropics such as India, Tropical Africa, Philippines, and Vietnam. Out of nine prominently seen species in India, the *Biophytum umbraculum* is not much explored for its ethno-medical effects. In comparison to other species of *Biophytum* genus, the literature on its medical value is sparse and remains confined with the local traditional usage among certain class of people. The scientific literature on the medicinal properties of this species is not explored fully yet, as a consequence its excellent medicinal properties have ignited the interests of us to explore the hidden phytochemical properties of this unexplored species; considering this, the current review article focuses on phytochemical constituents, pharmacological activities, and future scope of *Biophytum umbraculum*. We also compared the morphological, chemical constituents and pharmacological properties of *Biophytum umbraculum* with *Biophytum sensitivum* which has been tested for its applications widely.

Keywords: *Biophytum umbraculum*; Ethno-medical effects; Phytochemical constituents; Pharmacological activities

INTRODUCTION

As a part of the Oxalidaceae family, the genus *Biophytum* is distributed in tropical Asia, Africa, America and the Philippines. "*Biophytum sensitivum*" and "*B. umbraculum*" Synonym. *Biophytum petersianum* Klotzsch are reported to

56856



**Raja Chandra et al.,**

have ethno medicinal effects such as immuno modulatory effects, anti-oxidant, anti-fungal, anti- cancer . There are nine species of Biophytum prominently present in India and three species out of them are Biophytum sensitivum DC Syn. *Oxalis sensitivum* Linn, *Biophytum reinwardtii* Edgew and *B. umbraculum*1. *B. umbraculum* is a well-known plant belonging to family Oxalidaceae found in tropics such as India, Tropical Africa, Philippines, and Vietnam. *B. umbraculum* is a tall, annual, sessile bearing umbel herb with a height of 15 cm. *B. umbraculum* is an annual plant growing 4 to 15 cm tall with an unbranched stem. The plant is sometimes wild-harvested for its local medicinal use .

Botanical Description

Taxonomy

Kingdom: Plantae

Phylum: Tracheophyta

Class: Magnoliopsida

Order: Oxalidales

Family: Oxalidaceae

Genus: Biophytum

Species: *Biophytum umbraculum* Welw

Synonyms

Biophytum apodisciaz (Turcz.) Edgew. and Hook.f.

Biophytum petersianum Klotzsch

Biophytum rotundifolium Delhaye

Oxalis petersii Edgew. and Hook. f.

Morphology

B. umbraculum is a slender perennial herb with stems up to 1 feet height and leaves in a terminal crown which are very vulnerable. Its morphological details are comprehensively explained in Kew science5.

Phyto-Constituents

Polysaccharides from *B. umbraculum* are well studied. Pectic polysaccharides have been isolated and reported as having many biological activities such as complement fixing, dendritic cell activation and immunomodulation. There are rhamnogalacturonan, xylogalacturonan, and arabinogalactan regions in these polysaccharides . Chemical constituents having low molecular weight present in the plant was not much known . It was recognized that saponins were present in the plant , but their structures remained unclear. The compounds obtained from the ethyl acetate (EtOAc) soluble fraction of the methanol (MeOH) crude extract of *B. umbraculum* were extracted by column chromatographic technique (CC). The calculated concentrations of compounds in the crude MeOH extract were 0.45 per cent (1), 0.37 per cent (2) and 0.17 per cent (3), on the basis of their weight in distilled fraction. Cassiaoccidentalin A (1), isovitexin (2) and isoorientin (3), respectively, were the compounds known . The key compound in the EtOAc extract turned out to be Cassiaoccidentalin A, and traces of it are also seen in the BuOH extract, as evidenced by NMR1. Cassiaoccidentalin A is a very rarely found flavone glycoside only described once before in Cassia occidentalis . Out of these three compounds, isoorientin exhibited strong antioxidant properties10. Cassiaoccidentalin A, isovitexin and isoorientin were first identified in the plant Cassia occidentalis (Leguminosae)11. In *Serjania marginata* (Sapindaceae) leaves, cassiaoccidentalin A was also found . These are rare compounds and are not known in any other plant as per the available literature.

Pharmacological Activities

Anticancer Property

The extract of *B. umbraculum* was found to contain number of bioactive compounds such as flavonoids (amentoflavone and cupressoflavone), saponins, phenols, polyphenols, and essential oils . Out of these biochemical constituents, several studies have shown that phenolic compounds present in the plant extracts like quercetin,



**Raja Chandra et al.,**

epigallocatechin, catechin and genistein suppresses the growth of cancer in humans . It indicates the significance of phenolic compounds as antioxidants and anti-cancerous agents¹⁴. Phenolic esters hindered carcinogenesis and decreased the formation of cancer. *B. umbraculum* extracts were tested using the 3-(4,5-dimethylthiazol-2-yl)-2,5-diphenyl tetrazolium bromide (MTS) assay for cytotoxic effects against Ralph and William's cell line (RAW) 264.7 cells. 50 µg/mL was the maximum measured concentration. Cytotoxicity was seen in the Dichloromethane (DCM) extract (37% cell viability compared to LPS control at T = 130 min). In addition, the highest concentration of EtOAc also displayed some cytotoxicity (69% cell viability at T = 130 min)².

Antioxidant Property

Many flavone compounds which were found to be responsible for antioxidant properties were found in *B. umbraculum*. They were then extracted using various solvents and studied for their various antioxidant properties¹⁰. According to Pham *et al.*, *B. umbraculum* dichloromethane (DCM) crude extract was found to be virtually inactive at the concentration greater than 167 µg/ml. DCM extract was inactive against xanthine oxidase (XO) and 15-lipoxygenase (15-LO) (enzymes that generates reactive oxygen species). The partitioning of MeOH crude extract gave a polar and a semi-polar extract which were found to have greater free radical scavenging activity and caused inhibition of 15-LO. Compared with the positive control quercetin, the extracts displayed moderate to low inhibitory activity against XO. In all three assays, the ethyl acetate extract of *B. umbraculum* has shown the highest inhibitory potential¹⁰. The DPPH scavenging activities of the extracts obtained were measured in percentage. Three determinations were taken, and an average was calculated and represented as IC₅₀ values ± SD . Antioxidant activity was measured and high free radical scavenging and high 15-lipoxygenase inhibitory effects were seen in semi-polar extracts (ethyl acetate), but less activity against XO inhibition was seen¹⁰.

Immunomodulating Property

The extracts and isolated compounds were studied in-vitro in two different subjects with regard to the potential immunomodulating activities of *B. umbraculum* ². The various parts of the innate immune system like complementary system, macrophages were more concentrated while studying the mechanism of immunomodulating activity of *B. umbraculum*². Since cerebral malaria (CM) (state of unarousable coma partnered with the presence of malaria infected red blood cells in the peripheral circulation and a lack of other potential causes of coma such as other infections or hypoglycaemia) may be associated with high complement activation and inflammation, complementary inhibitory agents and anti-inflammatory agents may be useful to treat the disease ². Semipolar extracts (ethyl acetate, butanol and methanol) of *Biophytum umbraculum* were evaluated for immunomodulating activity. They were shown to be highly active classical pathway complement inhibitors, with the most potent inhibitor being the EtOAc extract (ICH₅₀ = 5 µg/mL). The inhibitory potential which was twelve times more active than a well-known complement inhibitor Rosmarinic acid (ICH₅₀ = 64 µg/mL) .

Antifungal Property

At 20 mg/ml conc. in carbohydrate, fat and protein-enriched medium, the hexane-ethyl acetate-methanol extract of kebar grass was found to increase growth inhibition of *A. flavus* than its other extracts at different concentration. The other extracts had less than 90% growth inhibition. The findings indicate that extract of *B. petersianum* has the potential of inhibiting the growth of toxic *Aspergillus flavus* .

Antimicrobial Property

Bioactive compounds such as alkaloids, saponins, tannins, phenolics, flavonoids, triterpenoids, compounds of steroids and glycosides are found in kebar grass . Terpenoids have antibacterial activity, in addition to having other biological activities . Tannins and saponins compound classes have antimicrobial activity . Since kebar grass contains complete bioactive compounds, this plant could therefore potentially be used as an antimicrobial¹⁸. Kebar grass leaf extract has antibacterial activity against several Gram-positive bacteria like *Staphylococcus* sp, *Streptococcus* sp. and Gram-negative bacteria like *Salmonella* sp, *Escherichia. coli*¹⁸.





Antiplasmodial Activity

B. umbraculum was found to be used in the treatment of cerebral malaria (CM) by 50 per cent of the researchers². This was validated by two such in vitro studies evaluating the assays along with its antiplasmodial activity. High complement inhibition of the classical pathway and dose-dependent inhibition of nitric oxide (NO) release from activated macrophages were shown in semi-polar plant extracts². The extracts obtained from *B. umbraculum* were tested in vitro against the erythrocytic stage of *Plasmodium falciparum* (for 72 h incubation). The EtOAc extract was mildly antiplasmodial against both the chloroquine-sensitive strain *P. falciparum* NF54 and the chloroquine-resistant strain K1 .

Anthelmintic Activity

Aqueous extract of *B. umbraculum* was assessed in-vitro for its anthelmintic activity against *Haemonchus contortus* worms and concentrations were 10, 20, 40, 60, 80 and 100 mg/ml. The standard drug used was Ivermectin at a concentration of 1 mg/ml for comparison, saline was used as a control. The dead worms were subjected to sodium dodecyl sulfate polyacrylamide gel electrophoresis (SDS-PAGE) and scanning electron microscopy (SEM). The decreased number of polypeptides on treated worms indicated that this plant extract produced strong anthelmintic activity. The mortality of adult worms may be influenced by the presence of tannin in *Biophytum petersianum* crude aqueous extract (BAE). Tannin present in *Biophytum umbraculum* may respond directly to adult worms by attaching to their 'skin,' causing discomfort, or indirectly by improving protein nutrition and growing the host's immune system .

Ethno Medical Benefits

B. umbraculum (syn. *Biophytum petersianum*) is recognized as a plant historically used in medicine. It is used as a sedative in Congo and for stomach pain, wounds and urinary stones in Nigeria. It is frequently used in the treatment of cerebral malaria, fever, wounds and various kinds of skin disorders in Mali, Indonesia as a traditional medicine. Crude extracts from *B. umbraculum* have previously been reported to decrease the blood pressure and glucose concentration in rodents . The researches revealed that hormones secreted from the adrenal glands of animal models are stimulated by a 50% ethanolic extract of the aerial parts. The plant has undergone certain experiments on bioactive compounds of low molecular weight, and several flavone glycosides such as isovitexin, isoorientin, and cassiaoccidentalinalin A have been isolated. In Nigeria, *B. umbraculum* has historically been used to treat wounds, gonorrhoea, urinary stones, and stomach pain. *B. umbraculum* was used as purgative in Gabon, in Togo for hypertension, and in New Guinea the plant is believed to increase fertility³, .

Comparison of *Biophytum umbraculum* and *Biophytum sensitivum*

The species are both from the same family, i.e., Oxalidaceae, but in morphological characters, phytoconstituents, and some pharmacological results, they are somewhat different from each other. *Biophytum sensitivum* has been tested for its applications, but *Biophytum umbraculum* is in the process of being investigated. *B. umbraculum* is about 25 cm long with a slightly long stem, while *Biophytum sensitivum* with a short trunk is between 2.5-20 cm long. *B. umbraculum* mainly comprises flavonoids and pectic polysaccharides (cassiaoccidentalinalin A, isovitexin and isoorientin) and is also used predominantly as antioxidants and immunomodulators; A number of chemical constituents, such as saponins, essential oils, flavonoids, pectin and polysaccharides, are found in *Biophytum sensitivum*. Isolated from its aerial components were 2 biflavones namely cupressuflavone and amentoflavone, 3 flavonoids namely luteolin 7-methyl ether, isoorientin and 3'-methoxyluteolin 7-O-glucoside and 2 acids which are 4-caffeoylquinic acid and 5-caffeoylquinic acid . As evaluated, *B. sensitivum* has additional antipyretic and analgesic efficacy. The analgesic activity of *B. sensitivum* plant's methanolic extract was evaluated when 100-200 mg/kg dose were administered in mice by tail flick and acetic acid induced writhing procedure. In both these models, the results reported analgesic activity . *B. sensitivum* methanolic extract was found to have immunomodulating and anticancer activities, whereas ethyl acetate extract of *B. umbraculum* was found to have those activities. *B. sensitivum* extract was found to be 100 % cytotoxic. At a concentration of 0.5 mg/ml it was found to be cytotoxic to both Dalton's Lymphoma Ascites (DLA) and Ehrlich Ascites Carcinoma (EAC) cells , while *B. umbraculum* exhibited moderate cytotoxicity at higher concentrations¹³. As compared to *B. umbraculum*, *B. sensitivum* was found to be more pharmacologically active. The full potential of *B. umbraculum* is not understood due to a lack of scientific assessment and analysis. Future research



**Raja Chandra et al.,**

and assessments on it may provide a sound knowledge for its effectiveness and use and then it may be useful for some medical conditions.

Future Research and Scope

Majority of the population (>80%) in developing nations have limited economic means of consuming drugs, vaccines and medical procedures. Utilization of plants as a source of medication has been an ancient practice and is a significant part of the medical care system in India. In India, about 70% of rural population relies upon the conventional Ayurvedic system of medication. *B. umbraculum* should be researched with an emphasis on phenolic compounds and antioxidant potential, as the health benefits of antioxidants have gained substantial attention in recent years. Most of the semi polar extracts showed high antioxidant activity, and the presence of tannins and flavonoids can be attributed to this activity. Antimalarial and immunomodulatory activities have also been observed, in addition to antioxidant properties. They are derived from in vitro studies and

- 1) Need to be followed up with in vivo studies and clinical trials, although the findings are positive and can to some degree provide a justification for conventional use.
- 2) Clinical trials are necessary to evaluate the complement inhibition and reduction of macrophage activation activity due to the complex pathogenesis of cerebral malaria.
- 3) Anticancer activity requires further exploration of the chemical structure related to activity and its comprehensive mechanism of action in clinical chemotherapy.
- 4) The in vitro results showed *B. umbraculum* to have a stimulatory effect on the release of aldosterone and corticosterone, which is supposed to have an effect on the adrenal cortex.

In vivo work is needed to ensure the traditional use of the extract in the treatment of high blood pressure. Therefore, the present paper suggests relevant areas as above to work on *B. umbraculum*.

ACKNOWLEDGEMENTS

The author(s) received no financial support for the authorship, and/or publication of this article.

REFERENCES

1. Pawar, A. T., & Vyawahare, N. S. (2014). Phytochemical and pharmacological profile of *Biophytum sensitivum* (L.) DC. International Journal of Pharmacy and Pharmaceutical Sciences, 6(11), 18-22
2. Pham, A. T. (2014). Chemical, biological and ethnopharmacological studies of two Malian medicinal plants: *Terminalia macroptera* and *Biophytum umbraculum*.
3. Tropical Plants Database, Ken Fern. tropical.theferns.info. last accessed on 2021-02-18 and 2021-09-14
4. *Biophytum umbraculum* Welw. [online] India Biodiversity Portal, Species Page : {name of species field}
5. Kew science, Plants of the world online. Welwitsch, 1859
6. Inngjerdingen, M., Inngjerdingen, K. T., Patel, T. R., Allen, S., Chen, X., Rolstad, B., ... & Paulsen, B. S. (2008). Pectic polysaccharides from *Biophytum petersianum* Klotzsch, and their activation of macrophages and dendritic cells. *Glycobiology*, 18(12), 1074-1084
7. Malterud, K. E. (2017). Ethnopharmacology, chemistry and biological properties of four Malian medicinal plants. *Plants*, 6(1), 11
8. Santoso, B., Kilmaskossu, A., & Sambodo, P. (2007). Effects of saponin from *Biophytum petersianum* Klotzsch on ruminal fermentation, microbial protein synthesis and nitrogen utilization in goats. *Animal Feed Science and Technology*, 137(1-2), 58-68.
9. Hariadi, B. T., & Santoso, B. (2010). Evaluation of tropical plants containing tannin on in vitro methanogenesis and fermentation parameters using rumen fluid. *Journal of the Science of Food and Agriculture*, 90(3), 456-461.
10. Pham, A. T., Nguyen, C., Malterud, K. E., Diallo, D., & Wangensteen, H. (2013). Bioactive flavone-C-glycosides of the African medicinal plant *Biophytum umbraculum*. *Molecules*, 18(9), 10312-10319
11. Hatano, T., Mizuta, S., Ito, H., & Yoshida, T. (1999). C-Glycosidic flavonoids from *Cassia occidentalis*. *Phytochemistry*, 52(7), 1379-1383



**Raja Chandra et al.,**

12. Heredia-Vieira, S. C., Simonet, A. M., Vilegas, W., & Macias, F. A. (2015). Unusual C, O-fused glycosylapigenins from *Serjania marginata* leaves. *Journal of natural products*, 78(1), 77-84.
13. Darwati, I., Nurcahyanti, A., Trisilawati, O., Nurhayati, H., Bermawie, N., & Wink, M. (2019, June). Anticancer potential of kebar grass (*Biophytum petersianum*), an Indonesian traditional medicine. In IOP Conference Series: Earth and Environmental Science (Vol. 292, No. 1, p. 012063). IOP Publishing.
14. Abraham, N. N., Kanthimathi, M. S., & Abdul-Aziz, A. (2012). Piper betle shows
15. Antioxidant activities, inhibits MCF-7 cell proliferation and increases activities of catalase and superoxide dismutase. *BMC complementary and alternative medicine*, 12(1), 1-11.
16. Nurcahyanti, A. D., Nasser, I. J., Sporer, F., Wetterauer, B., Kadarso, I. D., Reichling, J., & Wink, M. (2018). Essential oil composition, in vivo antioxidant, and antimicrobial activities of *Pimpinella pruatjan* from West Java, Indonesia. *The Natural Products Journal*, 8(1), 61-69.
17. Grau, G. E. R., & Craig, A. G. (2012). Cerebral malaria pathogenesis: revisiting parasite and host contributions. *Future microbiology*, 7(2), 291-302
18. Sahu, A., Rawal, N., & Pangburn, M. K. (1999). Inhibition of complement by covalent attachment of rosmarinic acid to activated C3b. *Biochemical pharmacology*, 57(12), 1439-1446.
19. Lisangan, M. M., Syarif, R., Rahayu, W. P., & Dharmaputra, O. S. (2014). Antifungal activity of kebar grass leaf extracts on the growth of aflatoxigenic *Aspergillus flavus* in food model media. *International Journal of Sciences: Basic and Applied Research*, 17, 116-128.
20. Sembiring, B., & Darwati, I. (2014). Identifikasi komponen kimia aksesori rumput kebar (*Biophytum petersianum*) asal Papua dan Jawa. *Buletin Penelitian Tanaman Rempah dan Obat*, 25(1), 37-44.
21. Stephane, F. F. Y., & Juleshttps, B. K. J. (2020). Terpenoids as important bioactive constituents of essential oils. In *Essential Oils-Bioactive Compounds, New Perspectives and Applications*. IntechOpen.
22. Jaberian, H., Piri, K., & Nazari, J. (2013). Phytochemical composition and in vitro antimicrobial and antioxidant activities of some medicinal plants. *Food chemistry*, 136(1), 237-244.
23. Astarheim, I., Pham, A. T., Nguyen, C., Zou, Y. F., Diallo, D., Malterud, K. E., & Wangenstein, H. (2016). Antiplasmodial, anti-complement and anti-inflammatory in vitro effects of *Biophytum umbraculum* Welw. traditionally used against cerebral malaria in Mali. *Journal of ethnopharmacology*, 190, 159-164
24. Sambodo, P., Prastowo, J., Kurniasih, K., & Indarjulianto, S. (2018). In vitro potential anthelmintic activity of *Biophytum petersianum* on *Haemonchus contortus*. *Veterinary World*, 11 (1): 1-4. Abstract.
25. University of Oslo (UiO), Medicinal Plants Studied in Norway; *Biophytum umbraculum*[OXALIDACEAE] last modified June 20, 2013
26. Mouzou, AP, Titrikou, S., Constantin, B., Seville, S., Cognard, C., Gbeassor, M., & Raymond, G. (2010). Effects of decocté of *Biophytum petersianum* (Oxalidaceae) on the release of calcium from the sarcoplasmic reticulum of skeletal muscle cells. *Phytotherapy*, 8 (4), 231-235.
27. Lin, Y. L., & Wang, W. Y. (2003). Chemical constituents of *Biophytum sensitivum*
28. Chatterjee, T. K., Mishra, M., Pramanik, K., & Bandyopadhyay, D. (2008). Evaluation of Anti-inflammatory, Antipyretic and Analgesic properties of *Biophytum sensitivum* (L.) DC. *Indian Drugs*, 45(2), 123-131
29. Guruvayoorappan, C., & Kuttan, G. (2007). Immunomodulatory and antitumor activity of *Biophytum sensitivum* extract. *Asian Pacific Journal of cancer prevention*, 8(1), 27.
30. Pandey, M. M., Rastogi, S., & Rawat, A. K. S. (2013). Indian traditional ayurvedic system of medicine and nutritional suppleme





A Magnificent Characteristics of Sagala Noi Chooranam Revealed – A Key to Stabilize the Three Humors in Siddha System

R.N.Hema^{1*}, R.Gomathi², T.Sasi Priya³, E.Preetheeka⁴ and G.Tamilarasan⁵

¹Medical Officer, Nalam Siddha and Ayurvedic Clinic, Chrompet, Chennai – 600 044, Tamil Nadu, India.

²Medical Officer, National Institute of Siddha, Tambaram Sanatorium, Chennai – 600 047, Tamil Nadu, India.

³Lecturer, Department of Gunapadam Marunthakkaviyal, Sri Sai Ram Siddha Medical College and Research Centre, Chennai – 600 044, Tamil Nadu, India.

⁴Medical Officer, Jain Hospital, Tambaram, Chennai-600 045, Tamil Nadu, India.

⁵PG Scholar, Department of Gunapadam, Government Siddha Medical College, Arumbakkam, Chennai-600 106, Tamil Nadu, India.

Received: 26 Feb 2023

Revised: 27 Apr 2023

Accepted: 31 May 2023

*Address for Correspondence

R.N.Hema

Medical Officer,
Nalam Siddha and Ayurvedic Clinic,
Chrompet, Chennai – 600 044,
Tamil Nadu, India.
E.Mail: hema.rn91@gmail.com



This is an Open Access Journal / article distributed under the terms of the **Creative Commons Attribution License** (CC BY-NC-ND 3.0) which permits unrestricted use, distribution, and reproduction in any medium, provided the original work is properly cited. All rights reserved.

ABSTRACT

Siddha system of medicine is said to have been in existence in South India especially in Tamil Nadu from the last many centuries from the time of famous Tamil Sangam, the first. This is the primordial Indian systems of medicine. As per saint Yugi's concept, there are 4448 diseases. Diseases are caused due to the derangement of three humors: Vaatham, Pitham and Kabam. Saint Theraiyar in his text, endorse three humors being "Vaathamai padaithu", Pitha vaniyai kaathu", Sethuma seethamai thudaithu". In this vaatham analogy with developmental and growth process. Pitham equivalence to digestive fire, upholding of immunity, metabolism and energy production. Kabam maintains the body mass, shape and flexibility. Even though there are monumental medicines in siddha, Sagala noi chooranam is predominantly indicated for Manthapitham (i.e., dwindled immune response). So we choose sagala noi chooranam to equipoise the pitham humor therewise to aggrandize the immunity which leads to disease free life. This review article purvey about the ethnopharmacological and phytoconstituents of Sagala noi chooranam.

Keywords: *Sagala noi chooranam, Bramamuni Karukadai Suththiram, Siddha Medicine.*





Hema et al.,

INTRODUCTION

Siddha text book *Brammamuni Karukadai suththiram's sagala noi chooranam* is used in the treatment of kulai erivu, nenjuvali, sirasunoi, piththam, purattal, neerural, kannil neerpachchal, puzhukirumi, iduppuvali, kalladaippu, vaaikonal, vaaikularal, manthapitham, sevinoi, sevidu, umai, sethumam, pilli, vanjanai, thondaipun, kandamazhai, neerkattu. This review article deals with the phytoconstituents and pharmacological activities of sagala noi chooranam.

INGREDIENTS OF SAGALA NOI CHOORANAM

1. NARCHIRAKAM (*Cuminum cyminum* Linn.)
2. ATHIMADURAM (*Glycyrrhiza glabra* Linn.)
3. MADANAKAMAPPU (*Cycas circinalis* Linn.)
4. KARUNJCHIRAKAM (*Nigella sativa* Linn.)
5. KIRAMBU (*Syzygium aromaticum* Linn.)
6. CHATHAKUPPAI (*Anethum graveolens* Linn.)
7. KOTHTHUMALLI (*Coriandrum sativum* Linn.)

PHYTOCONSTITUENTS OF SAGALA NOI CHOORANAM

Chirakam

Alkaloid, anthraquinone, coumarin, flavonoid, glycoside, protein, resin, saponin, tannin and steroid [3].

Athimaduram

Alkaloids, glycosides, triterpenes, flavonoids, polysaccharides, pectins, simple sugars, amino acids, mineral salts, asparagins, bitters, phenolics, saponins, tannins, terpenes, anthraquinones, essential oils, fat, female hormone oestrogen, gums, mucilage, protein, resins, starches, sterols and volatile oils [4,5].

Manadakamappu

Alkaloids, Flavonoids, amino acids and triterpenoids[6].

Karunjchirakam

Alkaloids, phenols, flavonoids, glycosides, terpenoids, steroids, thymohydroquinone, p- cymene, dithymoquinone, thymoquinone, carvacrol, sesquiterpene, longifolene, pentacyclic triterpene, alpha-hederin, protein, carbohydrates, crude fibre, fat and saponin [7]

Kirambu

Clove bud contain 15-20% essential oil which is dominated by eugenol (70-80%), eugenyl acetate (15%) and β -caryophyllene (5-12%). The other essential ingredients of clove oil are vanillin, maslinic acid, kaemferol, rhamnetin, eugenitin, eugenin, gallic acid, biflorin, myricetin, campesterol, stigmasterol, oleonic acid, bicorin [8]

Chathakuppai

Tannin, Terpenoid, Saponins, cardiac glycoside, anthraquinone, essential oils, fatty oil, moisture (8.39%), proteins (15.68%), carbohydrates (36%), fiber (14.80%), ash (9.8%) and mineral elements such as calcium, potassium, magnesium, phosphorus, sodium, vitamin A and niacin. *Anethum graveolens* contain 1 - 4% essential oil comprising of major compounds: carvone (30-60%), limonene (33%), α -phellandrene (20.61%), including pinene, diterpene, dihydrocarvone, cineole, myrcene, paramyrcene, dillapiole, isomyristicin, myristicin, myristin, apiol and dillapiol. *Anethum graveolens* essential oil also contained furanocoumarin, 5-(4"-hydroxy-3"-methyl-2"-butenyloxy)-6, 7-furocoumarin, oxypeucedanin, oxypeucedanin hydrate and falcarindiol. The total phenol and total flavonoid contents of *Anethum graveolens* L. extract were 105.2 mg of gallic acid equivalents/g of the dried extract and 58.2 mg of catechin equivalents/g of the dried extract, respectively [9,10,11,12,13]





Hema et al.,

Kothumalli

Essential oils, fatty acids, carotenoids, isocoumarins, alkaloids, flavones, resins, tannins, anthraquinones, sterols, fixed oil, polyphenols, vitamins and many phytosterols. It was reported that coriander like all other green leafy vegetables is a rich source of vitamins (high amount of vitamin A/ β -carotene: 12 mg/100 g and vitamin C: 160 mg/100 g) besides minerals and iron very low in saturated fat and cholesterol and a very good source of thiamine, zinc, and dietary fiber^[14,15]

PHARMACOLOGICAL ACTIVITIES OF SAGALA NOI CHOORANAM**Chirakam (Seed of *Cuminum cyminum*)****Antimicrobial activity**

Bameri Z et al., investigated that Ethanol extracts of seed of *Cuminum cyminum* were tested for antimicrobial activity *in vitro* by the microdilution method. Ethanol extract of seed exhibited antimicrobial activity against biofilm *Escherichia coli* [16]. Leopold J et al, studied that the antimicrobial activity of the essential oil of cumin (*Cuminum cyminum*) seeds was against different strains of microorganisms. Antimicrobial testing showed high activity of the essential *Cuminum cyminum* oil against *Candida albicans*, *Aspergillus niger*, the Gram positive bacteria *Bacillus subtilis* and *Staphylococcus epidermidis* as well as the yeast (*Saccharomyces cerevisiae*)[17]. Sheikh MI et al., investigated the antibacterial activity of seed extracts of cumin (*Cuminum cyminum*) was against 10 Gram positive and Gram negative bacteria. Disc diffusion method was used to test the antibacterial activity[18].

Antidiabetic activity

Jain SC et al., studied that the orally administered seed powder (2 g/kg) lowered the blood glucose levels in hyperglycaemic rabbits [19]. Willat gamuva SA et al, examined the Antidiabetic effects of cumin seed, in streptozotocin induced diabetic rats. An eight week dietary regimen containing cumin powder (1.25%) was found to be remarkably beneficial, as indicated by reduction in hyperglycaemia and glucosuria. This was also accompanied by improvement in body weights of diabetic animals. Dietary cumin also countered other metabolic alterations as revealed by lowered blood urea level and reduced excretions of urea and creatinine by diabetic animals [20].

Anti-cancer activity

Gagandeep et al., evaluated the cancer chemo preventive potentials of different doses of a cumin seed-mixed diet against benzo(α)pyrene [B(α)P]-induced fore stomach tumorigenesis and 3-methylcholanthrene (MCA)-induced uterine cervix tumorigenesis. Results showed a significant inhibition of stomach tumor burden by cumin. Tumor burden was 7.33 ± 2.10 in the B(α)P-treated control group, whereas it reduced to 3.10 ± 0.57 ($p < 0.001$) by a 2.5% dose and 3.11 ± 0.60 ($p < 0.001$) by a 5% dose of cumin seeds [21].

Antioxidant activity

Rebey IB et al., studied that the full ripe seeds were richer on polyphenols and condensed tannin than unripe ones, and consequently exhibited higher antioxidant activities. However, the unripe seeds had a higher total flavonoid content compared to those of half ripe and full ripe ones. The comparison of two extraction methods, the soxhlet extracts contained the greatest amount of polyphenols and flavonoids, while maceration samples exhibited higher antiradical and bleaching power assay. Total phenolic contents and IC₅₀ values in cumin seed during their maturation allowed to conclude that antioxidant activity does not depend only on the high content of total phenolics but also on the phenolic composition[22].

Hypotensive activity

Kalaivani P et al., evaluated that the anti-hypertensive potential of standardized aqueous extract of *Cuminum cyminum* seeds and its role in arterial endothelial nitric oxide synthase expression, inflammation and oxidative stress in renal hypertensive rats. Renal hypertension was induced by the two-kidney one-clip (2K/1C) method in rats. The data revealed that *Cuminum cyminum* seeds augment endothelial functions and ameliorate inflammatory and oxidative stress in hypertensive rats [23].





Hema et al.,

Gastrointestinal activity

Sahoo HB et al., studied the effect of aqueous extract of *Cuminum cyminum* seeds (ACCS) against diarrhoea on albino rats. The animals were divided into five groups and the control group was given 2% acacia suspension, the standard group with loperamide (3mg/kg) or atropine sulphate (5mg/kg) and three test groups administered orally with 100, 250 and 500 mg/kg of ACCS. The ACCS showed significant ($p < 0.001$) inhibition in frequency of diarrhoea, defecation time delaying, secretion of intestinal fluid as well as intestinal propulsion as compared to control. The graded doses of the tested extract showed dose dependent protection against diarrhea [24].

Athimaduram (Root of *Glycyrrhiza glabra*)**Antimicrobial activity**

Sharma V et al, studied that each species of the genus *Glycyrrhiza* Linn is characterized by isoprenoid phenols, which have selective antimicrobial activity. Recent research has shown antibacterial effects of hydromethanolic root extract of *G. glabra* against some gram-positive and negative pathogens [25].

Antioxidant activity

Sharma V et al., studied that the Hydromethanolic root extract of *Glycyrrhiza glabra* exhibited marked antioxidant activity in a test tube system [25].

Antiulcer activity

Masoomah MJ et al., examined that the extracted glycyrrhizin, DGL (deglycyrrhizinated licorice) is generally employed for the effective treatment of ulcers. Carbenoxolone from liquorice roots produce the antiulcerogenic effect by inhibiting the secretion of gastrin [26].

Antimutagenic activity [27]

Sharma V et al., investigated that the hydromethanolic root extract of *G. glabra* also exhibited antimutagenic potential by suppressing micronucleus formation and chromosomal aberration in bone marrow cells of albino mice [27].

Karunjchirakam (Seed of *Nigella sativa*)**Neuro-pharmacological activity**

Al-Naggar TB et al., studied that the aqueous and methanol extracts of defatted *Nigella sativa* seeds were shown to possess a potent central nervous system, especially depressant action in the case of the methanolic extract [28]. Perveen T et al., studied that an anxiolytic drug acts by increasing the 5-HT and decreasing the 5-HIAA levels in brain. A long term administration of *Nigella sativa* increases 5-HT levels in brain and improves learning and memory in rats [29].

Immunomodulatory activity

Torres MP et al., investigated that immunomodulating and cytotoxic properties of volatile oil of *N. sativa* seeds was in a Long-Evans rat model designed to examine the effect of *N. sativa* seeds on selected immune components. Long-Evans rats were challenged with a specific antigen (typhoid TH) and treated with *N. sativa* seeds; Treatment with *N. sativa* oil induced about 2-fold decrease in the antibody production in response to typhoid vaccination as compared to the control rats but there was a significant decrease in splenocytes and neutrophils counts, but a rise in peripheral lymphocytes and monocytes in the these animals. These results indicated that the *N. sativa* seeds could be considered as a potential immunosuppressive cytotoxic agent [30].

Anticonvulsant activity

Raza M et al., studied the *N. sativa* seed effectively against PTZ-induced convulsions. The antiepileptic activity of the volatile oil in this model maybe attributed mainly to its content of TQ and p-cymene and to a lesser extent, α -pinene. Volatile oil and its component p-cymene effectively suppressed convulsions induced by MES [31].



**Hema et al.,****Anti-fungal activity**

Bitra A et al., investigated the methanolic extracts of *N.sativa* have the strongest antifungal effect against different strains of *Candida albicans*. Treatment of mice with the plant extract 24 h after the inoculation caused a considerable inhibitory effect on the growth of the organism in all organs studied. It was reported that the aqueous extract of *N. sativa* seeds exhibits inhibitory effect against candidiasis in mice [32].

Anti-histamine activity

Kanter M et al., suggested that the use of NS seeds and its active ingredients has a considerable effect on the histamine mediated inflammatory and gastric diseases. A low concentration of nigellone effectively inhibits histamine release from mast cells have shown that volatile oil therapy of NS and more so its constituent TQ, significantly reduced mast cell number and the gastric ulcerated lesions in ethanol treated rats[33].

Anti-microbial activity

Mahony OR et al., studied that *Nigella sativa* seed extract has been shown to possess anti-microbial activity against *Staphylococcus aureus*, *Escherichia coli*, *Proteus vulgaris*, and *Candida albicans*. In an in vitro experiment, *Nigella sativa* extract produced a 100% growth inhibition of all the *H. pylori* strains that were tested within 60 min [34].

Antioxidant activity

Al-Othman A M et al., suggested that dietary supplementation of black seeds powder inhibits the oxidative stress caused by oxidized corn oil in rats [35].

Antiparasitic activity

Bafghi AF et al., studied that alcoholic extract of *Nigella sativa* seeds was applied daily for 15 weeks to cutaneous leishmaniasis produced experimentally in mice by a subcutaneous inoculation of *Leishmania major* at the dorsal base of the tail. There was no significant difference between the average weight of mice receiving *Nigella sativa* extract ointment and controls but the lesion diameter and symptoms of inflammation were significantly lesser in the test group as compared to the controls [36].

Contraceptive and anti-fertility activity¹

Agarwal C Narula A et al., studied that the ethanolic extract of *N.sativa* seeds was found to possess an anti-fertility activity in male rats which might be due to inherent estrogenic activity of *Nigella sativa* [37].

Toxicological studies

Abou Gabal AA et al., studied that the seeds of *Nigella sativa* extract and its constituent appear to have a low level of toxicity. There is no remarkable pathological changes were recorded in bone marrow of animals treated with suspension of *Nigella sativa* in carbon tetrachloride induced bone marrow toxicity [38].

Kirambu (Bud of *Syzygium aromaticum*)**Anaesthetic activity**

Diyaware et al., demonstrated the anesthetic effect of clove seed extract on *Clarias gariepinus* under semi-arid condition[39].

Insecticidal activity

Singh et al., reported the control of bed bug (*Climex lectuarius*) by using direct contact and residual contact bioassay using different essential oil based products. Results showed that clove oil (0.3%) combined peppermint oil (1%) and sodium lauryl sulfate (1.3%) formulation caused more than 90% mortality of bed bugs nymphs in residual and direct contact assay [40].



**Hema et al.,****Chathakuppai (Seed of *Anethum graveolens*)****Anti microbial activity**

Delaquis P J et al., studied the essential oil and different extracts of *Anethum graveolens* seeds exerted antimicrobial activity against wide range of microorganisms. Many authors mentioned that the antimicrobial activities could be attributed to furano coumarin in *Anethum graveolens* [41].

Anti inflammatory activity

Valady A et al., studied that the hydro alcoholic extract of the *anethum graveolens* seed caused significant decrease in the inflammation and pain in rats[42].

Effects on gastrointestinal system

Harries N et al., studied that *A.graveolens* seed extracts possessed significant mucosal protective and anti secretory effects in the gastric mucosa lesions induced in mice by oral administration of HCl (1 N) and absolute ethanol[43]. Hosseinzadeh H et al., studied the essential oil was a mild carminative and reduced foaming *in vitro* [44].

Kothumalli (Seed of *Coriander sativum*)**Anxiolytic activity**

Emamghoreishi M et al, studied the anxiolytic effect of the aqueous extract of *Coriandrum sativum* seed and its effect on spontaneous activity and neuromuscular coordination were evaluated in mice. The anxiolytic effect of aqueous extract (10, 25, 50, 100 mg/kg, ip) was examined in male albino mice using elevated plus-maze as an animal model of anxiety. In the elevated plus-maze, 100 mg/kg of the aqueous extract showed an anxiolytic effect by increasing the time spent on open arms and the percentage of open arm entries, compared to control group. Aqueous extract at 50, 100 and 500 mg/kg significantly reduced spontaneous activity and neuromuscular coordination, compared to control group[45,46].

Antidepressant activity

Sudha K et al., studied that the diethyl ether extract of seeds of *Coriandrum sativum* showed more significant antidepressant effect than that of aqueous extract through interaction with adrenergic, dopamine-ergic and GABA-ergic system[47].

Anti-inflammatory and analgesic activity

Hashemi VH et al., studied that the anti-inflammatory and analgesic effects of *Coriandrum sativum* seeds were evaluated in animal model. Carrageenan test was used for evaluation of anti-inflammatory effect, while, writhing and formalin tests were used for evaluation of analgesic effects. The results showed that coriander had no anti-inflammatory effect in carrageenan test. In writhing test, only the essential oil (4ml/100g,) had a significant effect ($p < 0.01$). Total extract, polyphenolic extract and essential oil of coriander, had significant effect in both phases of formalin test[48].

Antidiabetic activity

Eidi M et al., investigated the ethanol extract of *Coriandrum sativum* seeds was for its effects on insulin release from the pancreatic beta cells in streptozotocin-induced diabetic rats. The results showed that administration of the ethanol extract (200 and 250 mg/kg, ip) exhibited a significant reduction in serum glucose [49].

Anticancer activity

Tang EL et al.,evaluated the anticancer activities of *Coriandrum sativum* root, leaf and stem, as well as its effect on cancer cell migration, and its protection against DNA damage, with special focus on the roots. The ethyl acetate extract of *Coriandrum sativum* roots showed the highest antiproliferative activity on MCF-7 cells ($IC_{50} = 200.0 \pm 2.6$ $\mu\text{g/ml}$), had the highest phenolic content and FRAP and DPPH scavenging activities among the extracts[50].



**Hema et al.,****Cardiovascular activity**

Medhin DG et al., studied that the aqueous extracts of coriander seeds inhibited the electrically- evoked contractions of spiral strips and tubular segments of isolated central ear artery of rabbit. The water extract of coriander seed had hypotensive effects in rats [51,52].

Hepato protective activity

Ramadan MM et al., studied the radio protective ability of *Coriandrum sativum* seeds against whole body gamma irradiation in rats. Statistical analysis indicated that rats which supplemented with aqueous extract of *Coriandrum sativum* and then administrated paracetamol showed significant improvement in all biochemical parameters, which become near to control, the results were confirmed by histopathological examination of the liver tissue of control and treated animals [53].

Detoxification activity

Velaga MK et al., studied the protective activity of the hydroalcoholic extract of *Coriandrum sativum* seed against lead-induced oxidative stress in rats. Treatment with the hydroalcoholic seed extract of *Coriandrum sativum* resulted in a tissue-specific amelioration of oxidative stress produced by lead [54].

Diuretic activity

Aissaoui A et al., evaluated the acute diuretic activity of aqueous extract of the seed of *Coriandrum sativum* in rats. The aqueous extract of coriander seed was administered by continuous intravenous infusion (120 min) at two doses (40 and 100mg/kg) to anesthetized Wistar rats. The authors concluded that the mechanism of action of the plant extract appears to be similar to that of furosemide [55].

Effect on fertility

Al-Said MS et al., studied the effect of the aqueous extract of fresh coriander (*Coriandrum sativum*) seeds on female fertility in rats including the effects on oestrus cycle, implantation, foetal loss, abortion, teratogenicity and serum progesterone levels on days 5, 12 and 20 of the pregnancy. The extracts produced a significant decrease in serum progesterone levels on day-5 of pregnancy which may be responsible for its anti-implantation effect [56].

DISCUSSION

From the features above, we are confidential with the medicines and nutriment content of herbs and their utility of Sagala noi chooranam, in providing good immunity as per Siddha system of Medicine. The individual drugs evince symbiotic action thereby contributing to the overall pre-emptive and salubrious properties of the medicine as a potent immune booster drug in Siddha. The Scientific Research Community has to explicate the above Sagala noi chooranam as a redeemed immune booster medicine.

REFERENCES

1. Brammamuni, Brammamuni karukadai Suthiram 380, page no.62.
2. C.S.Murugesu mudaliar, Gunapadam mooligai, page.no.459, 13, 726, 463, 111, 421, 389.
3. Rai N, Yadav S, Verma AK, Tiwari L and Sharma RK, A monographic profile on quality specifications for a herbal drug and spice of commerce- *Cuminum cyminum* L. International Journal of Advanced Herbal Science and Technology 2012; 1(1): 1-12.
4. Bradley PR (ed) (1992) British herbal compendium, vol 1. BHMA, Bournemouth.
5. Hoffmann D (1990) The new holistic herbal, 2nd edn. Element, Shaftesbury.
6. Senthil Kumar Babu, Vijaya kumar Jagadesan, Selvaraj Ramasamy, Panneer Selvi Gopalsam, Preliminary Phytochemical Screening Of *Cycas Circinalis* (L.) And *Ionidium Suffruticosum* (Ging.), International Journal of Pharmacy, 2013, 3(3): 510-513, ISSN 2249-1848.



**Hema et al.,**

7. Prashant Tiwari, Susmita Jena, Swaroop Satpathy, Pratap Kumar Sahu, Nigella sativa: Phytochemistry, Pharmacology and its Therapeutic Potential, 12(7), July 2019, ISSN 0974-360X.
8. Monika Mittal, Nomita Gupta, Palak Parashar, Varsha Mehra, Manisha Khatri, Phytochemical evaluation and Pharmacological activity of Syzygium aromaticum: A Comprehensive Review, International Journal of Pharmacy and Pharmaceutical Sciences, Vol 6, Issue 8, 2014, ISSN 0975-1491.
9. Ishikawa T M, Kudo M, Kitajima J. Water-soluble constituents of dill. Chem Pharm Bull 2002; 55:501-507.
10. Khafagy S M, Mnajed H K. Phytochemical investigation of the fruit of Egyptian Anethum graveolens. I. Examination of the volatile oil and isolation of dillapiole. Acta Pharmaceutica Suecica 1968; 5:155-162.
11. Stavri M, Gibbons S. The antimycobacterial constituents of Dill (Anethum graveolens). Phytoter Res 2005; 19: 938-941.
12. Radulescu V, Popescu M L, Ilies D C. Chemical composition of the volatile oil from different plant parts of Anethum graveolens L. (Umbelliferae). Farmacia 2010; 58:594-600.
13. Yazdanparast R, Bahramikia S. Evaluation of the effect of Anethum graveolens L. crude extracts on serum lipids and lipoproteins profiles in hypercholesterolaemic rats. DARU 2008; 16(2):88-94.
14. Bhat S, Kaushal P, Kaur M, Sharma HK. Coriander (Coriandrum sativum L.): Processing, nutritional and functional aspects. African Journal of Plant Science. 2014;8(1):25-33
15. Girenko MM. Initial material and basic trends inbreeding of some uncommon species of vegetables. J. Bull. VIR im. Vavilova. 1982;120:33-37
16. Bameri Z, Amini-Boroujeni N, Saeidi S and Bazi S. Antimicrobial activity of Cuminum cuminum against biofilm E. coli. International Research Journal of Applied and Basic Sciences 2013; 5 (10): 1232-1234.
17. Leopold J, Buchbauer G, Stoyanova AS, Georgiev EV and Damianova ST. Composition, quality control and antimicrobial activity of the essential oil of cumin (Cuminum cyminum L.) seeds from Bulgaria that had been stored for up to 36 years. International Journal of Food Science & Technology 2005; 40(3): 305-310.
18. Sheikh MI, Islam S, Rahman A, Rahman M, Rahim A and Alam F. Control of some human pathogenic bacteria by seed extracts of cumin (Cuminum cyminum L). Agriculturae Conspectus Scientificus 2010; 75 (1):39-44.
19. Jain SC, Purohit M and Jain R. Pharmacological evaluation of Cuminum cyminum. Fitoterapia 1992; 63(4): 291-294.
20. Willatgamuva SA, Platel K, Sarawathi G and Srinivasan K. Antidiabetic influence of dietary cumin seeds (Cuminum cyminum) in streptozotocin induced diabetic rats. Nutr Res 1998; 18:131-42.
21. Gagandeep, Dhanalakshmi S, Méndiz E, Rao AR and Kale RK. Chemopreventive effects of Cuminum cyminum in chemically induced forestomach and uterine cervix tumors in murine model systems. Nutr Cancer 2003; 47(2):171-180.
22. Rebey IB, Kefi S, Bourgou S, Ouerghemmi I, Ksouri R, Tounsi MS and Marzouk B. Ripening stage and extraction method effects on physical properties, polyphenol composition and antioxidant activities of cumin (Cuminum cyminum L.) seeds. Plant Foods Hum Nutr 2014; 69(4): 358-364.
23. Kalaivani P, Saranya RB, Ramakrishnan G, Ranju V, Sathiya S, Gayathri V, Thiyagarajan LK, Venkatesh JR, Babu CS and Thanikachalam S. Cuminum cyminum, a dietary spice, attenuates hypertension via endothelial nitric oxide synthase and NO pathway in renovascular hypertensive rats. Clin Exp Hypertens 2013; 35(7): 534-542.
24. Sahoo HB, Sahoo SK, Sarangi SP, Sagar R and Kori ML. Anti-diarrhoeal investigation from aqueous extract of Cuminum cyminum Linn seed in albino rats. Pharmacognosy Res 2014; 6(3):204-209.
25. Sharma V, Agrawal RC, Pandey S (2013) Phytochemical screening and determination of antibacterial and antioxidant potential of Glycyrrhiza glabra root extracts. J Environ Res Dev 7 (4A):1552-1558.
26. Masoomah MJ, Kiarash G (2007) In vitro susceptibility of Helicobacter pylori to licorice extract. Iran J Pharm Res 6:69-72.
27. Sharma V, Agrawal RC, Shrivastava VK (2014) Assessment of median lethal dose and antimutagenic effects of Glycyrrhiza glabra root extract against chemically induced micronucleus formation in swiss albino mice. Int J Basic Clin Pharmacol 3:292-297 35.
28. Al-Naggar TB, Gomez-Serranillos MP, Carretero ME, Villar AM. Neuropharmacological activity of Nigella sativa L. extracts. J Ethnopharmacol. 2003;88(1):63-68.



**Hema et al.,**

29. Perveen T, Abdullah A, Haider S, Sonia B, Munawar AS, Haleem DJ. Long-term administration of *Nigella sativa* effects nociception and improves learning and memory in rats. *Pak J Biochem Mol Biol.*2008; 41(3):141–14.
30. Torres MP, Ponnusamy MP, Chakraborty S, Smith LM, Das S, Arafat HA. Effects of thymoquinone in the expression of mucin 4 in pancreatic cancer cells: implications for the development of novel cancer therapies. *Mol Cancer Ther.* 2010; 9(5):1419–1431.
31. Raza M, Alghasham AA, Alorainy MS, El-Hadiyah TM. Potentiation of valproate-induced anticonvulsant response by *Nigella sativa* seed constituents: the role of GABA receptors. *Int J Health Sci (Qassim)* 2008; 2(1):15–25.
32. Bitá A, Rosu AF, Calina D, Rosu L, Zlatian O, Dindere C. An alternative treatment for *Candida* infections with *Nigella sativa* extracts. *Eur J Hosp Pharm.* 2012; 19:162.
33. Kanter M, Coskun O, Uysal, H. The antioxidative and antihistaminic effect of *Nigella sativa* and its major constituent, thymoquinone on ethanol-induced gastric mucosal damage. *Arch. Toxicol.* 2006; 80 (4), 217–224.
34. Mahony OR., Al-Khtheeri, H, Weerasekera, D, Fernando N Vaira D, Holton J, Basset C. Bactericidal and anti adhesive properties of culinary and medicinal plants against *Helicobacter pylori*. *World J. Gastroenterol.* 2005; 11 (47), 7499–7507.
35. Al-Othman A M, Ahmad F, Al-Orf S, Al-Murshed KS, Ariff Z. Effect of dietary supplementation of *Ellataria cardamun* and *Nigella sativa* on the toxicity of rancid corn oil in rats. *Int J Pharmacol.*2006; 2(1):60–65.
36. Bafghi AF, Vahidi AR, Anvari MH, Barzegar K, Ghafourzadeh M. The in vivo antileishmanial activity of alcoholic extract from *Nigella sativa* seeds. *Afr. J. Microbiol. Res.* 2011; 5 (12), 1504–1510.
37. Agarwal C Narula A, Vyas DK, Jacob D. Effect of seeds of kalaunji on fertility and sialic acid content of the reproductive organs of male rat. *Geo Bios.* 1990; 17:269–272.
38. Abou Gabal AA, Essawy AE, Abdel-Moneim AM, Hamed SS, Elzergy AA. The protective effect of black seed (*Nigella sativa*) against carbon tetrachloride-induced (2007).
39. Diyaware MY, Suleiman SB, Akinwande AA, Aliyu M. Anesthetic effects of clove (*Eugenia aromaticum*) seed extract in *Claris gariepinus* (Burchell, 1822) fingerlings under semi-arid conditions. *Journal of Agricultural Science.* 2017; 62:411-421.
40. Singh N, Wang C, Cooper R. Potential of essential oil-based pesticides and detergents for bed bug control. *Journal of Economic Entomology.* 2014; 107:2163-2170.
41. Delaquis P J, Stanich K, Girard B. Antimicrobial activity of individual and mixed fractions of dill, cilantro, coriander and eucalyptus essential oils. *Int J Food Microbiol* 2002; 74: 101-109.
42. Valady A, Nasri S, Abbasi N. Anti-inflammatory and analgesic effects of hydroalcoholic extract from the seed of *Anethum graveolens* L. *J Med Plants* 2010; 9: 130-124.
43. Harries N, James K C, Pugh W K. Antifoaming and carminative actions of volatile oils. *Journal of Clinical Pharmacology* 1978; 2:171-177.
44. Hosseinzadeh H, Karimi K R, Ameri M. Effects of *Anethum graveolens* L. seed extracts on experimental gastric irritation models in mice. *Pharmacol* 2002; 2: 21.
45. Emamghoreishi M, Khasaki M and Aazam MF. *Coriandrum sativum* has anxiolytic and potentially sedative and muscle relaxant effects. *Mol Cancer Ther* 2007; 6(3): 1013-1021.
46. Emamghoreishi M, Khasaki M and Aazam MF. *Coriandrum sativum*: evaluation of its anxiolytic effect in the elevated plus-maze. *J Ethnopharmacol* 2005; 96(3): 365-370.
47. Sudha K, Deepak G, Sushant K, Vipul P and Nilofer N. Study of antidepressant like effect of *Coriandrum sativum* and involvement of monoaminergic and Gabanergic system. *IJRAP* 2011; 2: 267-270.
48. Hashemi VH, Ghanadi A and Sharif B. Anti-inflammatory and analgesic effects of *Coriandrum sativum* L in animal models. *J Shahrekord Univ Med Sci* 2003; 5(2): 8-15.
49. Eidi M, Eidi A, Saeidi A, Molanaei S, Sadeghipour A, Bahar M and Bahar K. Effect of coriander seed (*Coriandrum sativum* L.) ethanol extract on insulin release from pancreatic beta cells in streptozotocin-induced diabetic rats. *Phytother Res* 2009; 23(3): 404-406.
50. Tang EL, Rajarajeswaran J, Fung SY and Kanthimathi MS. Antioxidant activity of *Coriandrum sativum* and protection against DNA damage and cancer cell migration. *BMC Complement Altern Med* 2013; 13:347.





Hema et al.,

51. Medhin DG, Bakos P and Hadházy P. Inhibitory effects of extracts of *Lupinus termis* and *Coriandrum sativum* on electrically induced contraction of the rabbit ear artery. *Acta Pharm Hung* 1986; 56(3): 109-113.
52. Medhin DG, Hadhazy P, Bakos P and Verzar-Petri G. Hypotensive effects of *Lupinus termis* and *Coriandrum sativum* in anesthetized rats: preliminary study. *Acta Pharmaceutica Hungarica* 1986; 56(2): 59-63.
53. Ramadan MM and Abd Algader NNE. Chemopreventive effect of *Coriandrum sativum* fruits on hepatic toxicity in male rats. *World Journal of Medical Sciences* 2013; 8 (4): 322-333.
54. Velaga MK, Yallapragada PR, Williams D, Rajanna S and Bettaiya R. Hydroalcoholic seed extract of *Coriandrum sativum* (Coriander) alleviates lead-induced oxidative stress in different regions of rat brain. *Biol Trace Elem Res* 2014; 159(1-3): 351-363.
55. Aissaoui A, El-Hilaly J, Israili ZH and Lyoussi B. Acute diuretic effect of continuous intravenous infusion of an aqueous extract of *Coriandrum sativum* L. in anesthetized rats. *J Ethnopharmacol* 2008; 115(1): 89-95.
56. Al-Said MS, Al-Khamis KI, Islam MW, Parmar NS, Tariq M and Ageel AM. Post-coital antifertility activity of the seeds of *Coriandrum sativum* in rats. *J Ethnopharmacol* 1987; 21(2):

Table 1: Herbal Ingredients of Sagala Noi Chooranam

Tamil / English Name	Botanical / Family Name	Parts used
Chirakam / Cumin seeds or fruits	<i>Cuminum cyminum</i> / Apiaceae	Seed
Athimaduram / Indian or Jamaica Liquorice	<i>Glycyrrhiza glabra</i> / Fabaceae	Root
Madanakamappu / Queen sago	<i>Cycas circinalis</i> / Cycadaceae	Flower, seed, bark
Karunjchirakam / Black cumin; Small Fennel	<i>Nigella sativa</i> / Ranunculaceae	Seed
Kirambu / Cloves	<i>Syzygium aromaticum</i> / Myrtaceae	Bud
Chathakuppai / The Dill, Gardenill, Anet	<i>Anethum graveolens</i> / Apiaceae	Leaf, flower, seed
Koththumalli / Coriander seeds	<i>Coriandrum sativum</i> / Apiaceae	Leaf, seed





Manual Therapy and Exercise Interventions for Chronic Neck Pain- A Narrative Review

Neha Mukkamala^{1*}, Dixita Sharma² and G P Kumar³

¹Associate Professor, College of Physiotherapy, Sumandeep Vidyapeeth Deemed to be University, Piparia, Waghodia road, Vadodara, Gujarat, India PIN- 391760.

²Former Post Graduate Student, College of Physiotherapy, Sumandeep Vidyapeeth Deemed to be University, Piparia, Waghodia road, Vadodara, Gujarat, India PIN- 391760.

³Dean, College of Physiotherapy, Sumandeep Vidyapeeth Deemed to be University, Piparia, Waghodia road, Vadodara, Gujarat, India PIN- 391760.

Received: 18 Jan 2023

Revised: 25 Mar 2023

Accepted: 27 Apr 2023

*Address for Correspondence

Neha Mukkamala

Associate Professor,
College of Physiotherapy,
Sumandeep Vidyapeeth Deemed to be University,
Piparia, Waghodia road, Vadodara,
Gujarat, India PIN- 391760.
Email ID: - neha.cop@sumandeepvidyapeethdu.edu.in



This is an Open Access Journal / article distributed under the terms of the **Creative Commons Attribution License** (CC BY-NC-ND 3.0) which permits unrestricted use, distribution, and reproduction in any medium, provided the original work is properly cited. All rights reserved.

ABSTRACT

Neck pain is getting more common across the world and 67% of adults will experience neck pain at some point in their lives. Physiotherapeutic intervention options for CNP include manual therapy, exercises, stretching, strengthening, relaxation techniques, craniocervical flexion training, spinal mobilization and manipulations and postural education. All these interventions effectively manage pain, improving cervical ranges, decreasing neck disability, and improving quality of life. Exercises are easily accessible, safe, low cost, and potentially effective interventions for individuals with CNP.

Keywords: Manual therapy, exercises, chronic neck pain, mobilization.

INTRODUCTION

Neck pain (NP) that persists for a duration of three months or more is defined as chronic neck pain (CNP), and it appears particularly in the neck region between C1 to C7 vertebrae [1]. Neck pain is getting more common across the





Neha Mukkamala et al.,

world and 67% of adults will experience neck pain at some point in their lives. Populations most commonly affected with neck pain are office and computer workers, manual labourers and industrial workers.[1] A vast number of physiotherapeutic intervention options for the treatment of CNP include manual therapy, range of motion exercise, stretching, strengthening exercise, relaxation techniques, craniocervical flexion training, spinal mobilization and manipulations, postural education, electrotherapy and ergonomics. These treatments are useful in reducing pain, fatigue, inflammation, and improving neuromuscular control. Studies which include all physiotherapy treatments are few. The purpose of this study is to find and review studies related to exercise therapy and manual therapy interventions used in the treatment of CNP.

METHODOLOGY

A systematic search of the literature was done using databases like Pubmed, Google Scholar, Cochrane and PEDro. Articles published between 1st January 2012 to 31st December 2021 were included. Keywords like “chronic neck pain”, “manual therapy”, “exercise therapy”, and “physiotherapy” were used. The criteria for inclusion of studies were as follows: Articles which included physiotherapy interventions for CNP like exercise therapy and manual therapy. Articles published in English language, in the last 10 years (1st January 2012 to 31st December 2021) and articles whose full text were available were included in the study. All types of studies like systematic review, meta-analysis, randomized control trials, cohort studies, case-control studies, narrative reviews were included. Articles on electrotherapy interventions and alternative therapies and articles which described operative management for neck pain were excluded.

RESULTS

After finalizing keywords, the search strategy identified numerous articles from multiple databases. Following the removal of duplicates and the screening of titles and abstracts, a total of 25 studies were included in the review.

DISCUSSION

The principle of FITT - Frequency, Intensity, Time and Type

Any workout that is given must adhere to the FITT principle, which stands for Frequency, Intensity, Time and Type. Pain and impairment can be reduced by exercising for 30 to 60 minutes three times a week at an intensity of up to 80% of maximum voluntary contraction (MVC). To promote proper muscle activation and function, resistance workouts to develop isometric strength of the deep cervical flexors are recommended.[1] Endurance exercises 2 times per week combined with gravity's resistance can improve the postural functioning of the deep cervical muscles, potentially reducing pain in people who suffer from CNP. Aerobic workouts 3 times per week can help one feel better about oneself and improve health-related quality of life.[1] Effective therapies should last 6 to 12 weeks, with encouragement to continue exercising for the rest of one's life to preserve long-term benefits and the absence of pain-related symptoms.[1] For enhancing adherence and long-term motivation, a combination of group and home-based workouts is best.[1]

Deep cervical flexor (DCF) muscle activation Exercises

The deep cervical flexors include the longus colli, rectus capitus, longus capitus, and longus cervicis. Exercise for deep cervical muscle activation includes chin tuck exercise that can be given with the help of a pressure biofeedback device. Deep cervical flexor muscle activation exercise is a low-load exercise and promotes appropriate posture and activation of deep muscles rather than superficial muscles. When compared to a neck isometric muscle retraining program, Craniocervical flexion exercise was more effective at treating or recovering cervical lordosis, deep cervical flexor muscle endurance, and active cervical range of motion in all three planes.[3] The chin tucking exercise program increased Longus Colli muscle parameters such as cross-sectional area, thickness, and width, whereas the





Neha Mukkamala et al.,

exercise program recruiting all neck flexors enhanced sternocleidomastoid (SCM) thickness. [20] Both exercise programs were equally beneficial in reducing pain and disability in those with neck pain. [20] High endurance of the deep cervical flexor muscles increased the ability to maintain an upright posture of the cervical spine. [24] As a result, DCF muscle training is suggested for the treatment of neck pain in clinical practice.[24]

Scapulothoracic and Cervical stabilization exercise

Scapular stabilization exercises helped improve pain, endurance of the neck muscles and restore the function biomechanical pattern of the neck and shoulder joint.[3] Neck stabilization exercises (NSE) limit pain,[6]maximize function and prevent further injury by which the cervical spine maintains a stable, injury-free state.[6] Cervical and scapulothoracic stabilization exercises activate the deep muscles and strengthen the whole scapulothoracic region.[17]

PRT-Progressive resistance training

A neck-specific progressive resistance training intervention enhanced neck strength and decreased patient-reported neck pain and impairment considerably.[10]Strength training possibly acts by activating arterial baroreceptors, which stimulate the endogenous opioid system, resulting in analgesic effects via the descending nociceptive inhibitory mechanism.[10]

Stretching Exercise

Stretching activities can help to relax muscles and so reduce discomfort.[4]Applying stretching exercises to the SCM muscle has a clinically significant impact on pain reduction in individuals with CNP.[4]

Endurance exercise

Endurance exercises cause an increase in motor unit recruitment and firing rate, increase the number of capillaries in the muscle, thus contribute to a reduction in muscular fatigue in individuals with persistent neck pain.[26]

Sensorimotor training

Sensorimotor training includes retraining joint position and movement sense, Oculomotor exercises, balance training and traditional exercise. Oculomotor exercises as a part of sensory-motor training as an influence on suboccipital muscles could explain the favorable effects of combined sensorimotor training and traditional exercises on joint position awareness. These muscles have a huge number of muscle spindles for controlling the head orientation in the space. As a result, exercising these muscles through sensorimotor training may help to improve muscle spindle function and awareness of neck position.[11]

Manual therapy

Manual therapy improved mobility and endurance post-intervention and at 6 months follow-up in individuals with CNP.⁵ Manual therapy has almost no adverse effects due to its application and if any they are of little clinical significance.[5] Also, it appears to be safe for treatment.[5] Hence manual therapy can be recommended for treating CNP patients.[5] Manual techniques through their neurophysiological effects produce a faster reduction in pain but may not improve disability as fast as exercises.[8] A multimodal approach including manual therapy, therapeutic exercise, and pain education may give the best results.[8]Clinical improvement could potentially be influenced by central processes.[8]Manual therapy incorporates neurophysiological mechanisms like reduction in inflammatory biomarkers, decreased spinal excitability and pain sensitivity, modification of activity in cortical areas involved in pain processing, and excitation of the sympathetic nervous system.[8] Manual therapy in the form of cervical mobilization may restore the upper cervical joint mobility and in turn, improve the recruitment of deep cervical muscles and decrease the activation of superficial muscles.[9] Following mobilization, different neurophysiological processes (peripheral, spinal, and supraspinal) have been discovered to cause hypoalgesia.[27] The release of numerous nociceptive and inflammatory mediators is frequently linked to persistent pain.[27] The release of these mediators is reduced by manual treatment.[27] The changed concentration of pain biomarkers in the blood may cause pain alleviation after mobilization.[27] Manual therapy has been shown to lower serotonin levels while

56874



**Neha Mukkamala et al.,**

increasing endorphin levels in the bloodstream.[27] The spinal cord-mediated impact of joint mobilization may also help to reduce pain.[27] The suppression of C fibers by the dorsal horn of the spinal cord, for example, has been proposed as a possible mechanism for producing hypoalgesia after spinal manipulation.[27]

Massage

Massage promotes muscle relaxation which decreases pain in turn.[4] Touch activates the pressure receptors and modifies blood flow, in turn causing psychological relaxation and decreasing pain.[4] Massage enhances blood circulation in the treatment area, thereby removing pain metabolites and decreasing pain. [2] Probable reasons for pain relief may be the Gate-control theory and an increase in neurotransmitters like serotonin that relieve pain. When applied in a downward manner on myofascial trigger points (MTrPs),[2]Thai massages may elongate and normalize the contraction knots allowing the trigger points to deactivate and break down.[2] This may release the tightness of muscle and increase the range.[2]

Connective tissue massage (CTM) is a manual reflex therapy that stretches connective tissue layers and aids in relaxing the body.[23] It increases β -endorphins in plasma.[23] Skin touch may decrease stress hormones and muscle tension, thereby increasing the pressure pain threshold.[23] The treatment is based on the induction of a reflex action on the autonomic nervous system by manipulating the fascial layers within and beneath the skin.[23] Stretching connective tissue can activate cutaneous-visceral responses by stimulating the autonomic nervous system and skin mechanoreceptors.[23] Pre- and postsynaptic inhibition may close the 'pain gate' as a result of this receptor stimulation.[23] As a result, it has been discovered to cause the release of endogenous opiates.[23] CTM reduces sympathetic activity by causing local mechanical effects on mast cells in the connective tissue, resulting in vasodilation.[23] As a result, parasympathetic activity rises, resulting in muscular relaxation and improved circulation, which aids the healing process.[23]

Myofascial Release

Myofascial release is a manual massage technique that involves stretching the fascia and releasing ties between the fascia and the skin, muscles, and bones to relieve pain, improve range of motion, and improve body balance.[28] The mechanical, neuronal facilitation, and psycho-physiological adaptability are said to be the effects of this technique.[28]

Virtual reality

For patients with CNP who are immersed in a virtual reality experience, it becomes difficult to sense stimuli outside of their range of concentration.[7] Pain can be managed by blocking sensory information with opioid analgesics or generating a diversion when treatment periods have been sustained for some time.[7] The anterior cingulate cortex, primary and secondary somatosensory cortex, insula, and thalamus all benefited from pain distraction mechanisms and reduced pain-related brain activity.[7] Furthermore, it has been proposed that VR distracting effects result from intercortical modulation of pain matrix signaling pathways via attention, emotion, memory, and other senses activated in virtual reality environments.[7]

CONCLUSION

This review highlights the interventions for chronic neck pain like exercises and manual therapy. The interventions have been found to be effective in managing pain, improving cervical ranges, decreasing neck disability, and improving quality of life. Exercises are easily accessible, safe, low cost, and potentially effective interventions for individuals with CNP. Thus there is strong evidence for use of physiotherapy interventions in CNP.





Neha Mukkamala et al.,

REFERENCES

1. O'Riordan C, Clifford A, Van De Ven P, Nelson J. Chronic neck pain and exercise interventions: frequency, intensity, time, and type principle. *Archives of physical medicine and rehabilitation*. 2014 Apr 1;95(4):770-83.
2. Buttogat V, Muenpan K, Wiriyasakunphan W, Pomsuwan S, Kluayhomthong S, Areeudomwong P. A comparative study of Thai massage and muscle energy technique for chronic neck pain: A single-blinded randomized clinical trial. *Journal of Bodywork and Movement Therapies*. 2021 Jul 1;27:647-53.
3. Ganu S, Gor U. Effects of Abdominal Control Feedback and Scapular Stabilization Exercise on Chronic Neck Pain.
4. Büyükturan B, Şaş S, Karartı C, Büyükturan Ö. The effects of combined sternocleidomastoid muscle stretching and massage on pain, disability, endurance, kinesiophobia, and range of motion in individuals with chronic neck pain: A randomized, single-blind study. *Musculoskeletal Science and Practice*. 2021 Oct 1;55:102417.
5. Díaz-Pulido B, Pérez-Martín Y, Pecos-Martín D, Rodríguez-Costa I, Pérez-Muñoz M, Calvo-Fuente V, Ortiz-Jiménez MF, Asúnsolo-del Barco Á. Efficacy of Manual Therapy and Transcutaneous Electrical Nerve Stimulation in Cervical Mobility and Endurance in Subacute and Chronic Neck Pain: A Randomized Clinical Trial. *Journal of Clinical Medicine*. 2021 Jan;10(15):3245.
6. Shin HJ, Kim SH, Hahm SC, Cho HY. Thermotherapy plus neck stabilization exercise for chronic nonspecific neck pain in elderly: a single-blinded randomized controlled trial. *International Journal of Environmental Research and Public Health*. 2020 Jan;17(15):5572.
7. Tejera DM, Beltran-Alacreu H, Cano-de-la-Cuerda R, Leon Hernández JV, Martín-Pintado-Zugasti A, Calvo-Lobo C, Gil-Martínez A, Fernández-Carnero J. Effects of virtual reality versus exercise on pain, functional, somatosensory and psychosocial outcomes in patients with non-specific chronic neck pain: A randomized clinical trial. *International Journal of Environmental Research and Public Health*. 2020 Jan;17(16):5950.
8. Bernal-Utrera C, Gonzalez-Gerez JJ, Anarte-Lazo E, Rodriguez-Blanco C. Manual therapy versus therapeutic exercise in non-specific chronic neck pain: a randomized controlled trial. *Trials*. 2020 Dec;21(1):1-0.
9. Rodríguez-Sanz J, Malo-Urriés M, Corral-de-Toro J, López-de-Celis C, Lucha-López MO, Tricás-Moreno JM, Lorente AI, Hidalgo-García C. Does the addition of manual therapy approach to a cervical exercise program improve clinical outcomes for patients with chronic neck pain in short-and mid-term? A randomized controlled trial. *International Journal of Environmental Research and Public Health*. 2020 Jan;17(18):6601.
10. Cox LG, Savur KT, De Nardis RJ, Iles RA. Progressive resistance exercise for improving pain and disability in chronic neck pain: A case series. *Physiotherapy Research International*. 2020 Oct;25(4):e1863.
11. Saadat M, Salehi R, Negahban H, Shaterzadeh MJ, Mehravar M, Hessam M. Traditional physical therapy exercises combined with sensorimotor training: The effects on clinical outcomes for chronic neck pain in a double-blind, randomized controlled trial. *Journal of Bodywork and Movement Therapies*. 2019 Oct 1;23(4):901-7.
12. de Zoete RM, Brown L, Oliveira K, Penglaze L, Rex R, Sawtell B, Sullivan T. The effectiveness of general physical exercise for individuals with chronic neck pain: a systematic review of randomised controlled trials. *European Journal of Physiotherapy*. 2020 May 3;22(3):141-7.
13. Chung S, Jeong YG. Effects of the craniocervical flexion and isometric neck exercise compared in patients with chronic neck pain: A randomized controlled trial. *Physiotherapy theory and practice*. 2018 Dec 2;34(12):916-25.
14. Iversen VM, Vasseljen O, Mork PJ, Fimland MS. Resistance training vs general physical exercise in multidisciplinary rehabilitation of chronic neck pain: A randomized controlled trial. *J Rehabil Med*. 2018 Aug 22;50(8):743-750. doi: 10.2340/16501977-2370. PMID: 30132009.
15. Domingues LA, Pimentel-Santos FM, Cruz EB, Branco JC. THU0732-HPR Individual responder analysis of the effectiveness of manual therapy and exercise versus usual care in patients with chronic nonspecific neck pain: preliminary results of a randomized controlled trial.
16. Ris I, Sogaard K, Gram B, Agerbo K, Boyle E, Juul-Kristensen B. Does a combination of physical training, specific exercises and pain education improve health-related quality of life in patients with chronic neck pain? A randomised control trial with a 4-month follow up. *Manual therapy*. 2016 Dec 1;26:132-40.





Neha Mukkamala et al.,

17. Celenay ST, Kaya DO, Akbayrak T. Cervical and scapulothoracic stabilization exercises with and without connective tissue massage for chronic mechanical neck pain: A prospective, randomised controlled trial. *Manual therapy*. 2016 Feb 1;21:144-50.
18. Blomgren J, Strandell E, Jull G, Vikman I, Røijezon U. Effects of deep cervical flexor training on impaired physiological functions associated with chronic neck pain: a systematic review. *BMC musculoskeletal disorders*. 2018 Dec;19(1):1-7.
19. Brage K, Ris I, Falla D, Sjøgaard K, Juul-Kristensen B. Pain education combined with neck-and aerobic training is more effective at relieving chronic neck pain than pain education alone—a preliminary randomized controlled trial. *Manual Therapy*. 2015 Oct 1;20(5):686-93.
20. Javanshir K, Amiri M, Mohseni Bandpei MA, Penas CF, Rezasoltani A. The effect of different exercise programs on cervical flexor muscles dimensions in patients with chronic neck pain. *Journal of back and musculoskeletal rehabilitation*. 2015 Jan 1;28(4):833-40.
21. Dunleavy K, Kava K, Goldberg A, Malek MH, Talley SA, Tutag-Lehr V, Hildreth J. Comparative effectiveness of Pilates and yoga group exercise interventions for chronic mechanical neck pain: quasi-randomised parallel controlled study. *Physiotherapy*. 2016 Sep 1;102(3):236-42.
22. Bahat HS, Takasaki H, Chen X, Bet-Or Y, Treleaven J. Cervical kinematic training with and without interactive VR training for chronic neck pain—a randomized clinical trial. *Manual therapy*. 2015 Feb 1;20(1):68-78.
23. Bakar Y, Sertel M, Öztürk A, Yümin ET, Tatarlı N, Ankaralı H. Short term effects of classic massage compared to connective tissue massage on pressure pain threshold and muscle relaxation response in women with chronic neck pain: a preliminary study. *Journal of Manipulative and Physiological Therapeutics*. 2014 Jul 1;37(6):415-21.
24. Gupta BD, Aggarwal S, Gupta B, Gupta M, Gupta N. Effect of deep cervical flexor training vs. conventional isometric training on forward head posture, pain, neck disability index in dentists suffering from chronic neck pain. *Journal of clinical and diagnostic research: JCDR*. 2013 Oct;7(10):2261.
25. Evans R, Bronfort G, Schulz C, Maiers M, Bracha Y, Svendsen K, Grimm R, Garvey T, Transfeldt E. Supervised exercise with and without spinal manipulation performs similarly and better than home exercise for chronic neck pain: a randomized controlled trial. *Spine*. 2012 May 15;37(11):903-14.
26. Visvanathan R, Paul J, Manoharlal MA, Muthuswamy S, Muthukumar N. Efficacy of Endurance Exercise on Pain and Disability in Chronic Neck Pain-A Systematic Review. *Journal of Clinical & Diagnostic Research*. 2018 Dec 1;12(12).
27. Farooq MN, Mohseni-Bandpei MA, Gilani SA, Ashfaq M, Mahmood Q. The effects of neck mobilization in patients with chronic neck pain: A randomized controlled trial. *Journal of bodywork and movement therapies*. 2018 Jan 1;22(1):24-31.
28. El-Gendy MH, Lasheen YR, Rezkalla WK. Multimodal approach of electrotherapy versus myofascial release in patients with chronic mechanical neck pain: A randomized controlled trial. *Physiotherapy Quarterly*. 2019 Oct 1;27(4):6.

Table 1: Studies related to exercise and manual therapy interventions for chronic neck pain

Author/Year	Objectives of the study	Methodology	Remarks
Buttagat et al / 2021	Comparison of Thai massage (TM) and muscle energy technique (MET) in CNP.	TM group was given gentle thumb pressing, and neck stretching. MET group was given post-isometric relaxation technique & passive stretch. Control group was given relaxation. All three groups received 8 treatment sessions for 2 weeks.	TM and MET both resulted in a significant improvement in all parameters (p <0.05) compared to control group.
Ganu et al / 2021	To see effect of addition of abdominal control feedback to scapular stabilization exercise on	Group 1 received scapular stabilization exercises including chin tucks, horizontal pull apart, serratus anterior punches, retraction plus external rotation, chest press, and	In terms of pain and endurance, there were considerable intergroup variations, with group 2





Neha Mukkamala et al.,

	pain, strength, proprioception, disability, endurance.	Scapular retraction. Group 2 received Scapular Stabilization along with Abdominal Control Feedback which included Wall presses, Knee push-ups, Wall slides.	being better.
Büyükturan et al / 2021	Effectiveness of stretching and massage applied to sternocleidomastoid muscle on ROM, endurance, pain, disability, and kinesiophobia in CNP.	The control group received slow and controlled neck flexion, extension, lateral flexion, and rotation in combination with respiration, and also posture-related exercises for 3 days a week for 5 weeks. The SCM group received additionally, massage and stretching for the sternocleidomastoid muscle.	SCM group showed superior results.
Díaz-Pulido et al / 2021 ⁵	Comparison of manual therapy (MT) and Transcutaneous Electrical Nerve Stimulation (TENS) on cervical mobility and muscle endurance in subacute and chronic mechanical neck disorders.	MT group received neuromuscular, post-isometric, spray, stretching. TENS group received high TENS. Both groups received 10 sessions for 30 min on alternate days.	MT group showed significant improvement in active mobility and endurance.
Shin et al / 2020	Comparison of thermotherapy and neck stabilization exercise in chronic nonspecific neck pain.	The intervention group received thermotherapy for 30 min twice a day for 5 days and performed neck stabilization exercise. All exercises were given for 40 min twice a day for 5 days (10 sessions). The control group performed only neck stabilization exercises.	After intervention, the pain intensity in the intervention group considerably reduced at rest ($p < 0.001$) and during movement ($p < 0.001$).
Tejera et al / 2020	Comparing effects of virtual reality (VR) versus exercise on pain intensity, in patients with NS-CNP.	The virtual reality group received craniocervical flexion with the help of virtual reality glasses. The neck exercise group received neck flexion, extension, lateral flexion, and rotation exercises. Both groups received 3 sets of 10 repetitions of each exercise.	The intra-group difference was statistically significant in the VR group ($p < 0.05$) for all the outcomes.
Bernal-Utrera et al / 2020	Comparison of Manual therapy and therapeutic exercise in patients with CNP.	The MT group received high thoracic manipulation on T4, Cervical mobilization, and Suboccipital muscle inhibition. The therapeutic exercise group received activation and recruitment of deep cervical flexors, and eccentric exercises for flexors & extensors.	MT improved perceived pain before therapeutic exercise, while therapeutic exercise reduced cervical disability before manual therapy.
Rodriguez-Sanz et al / 2020	Effectiveness of manual therapy vs cervical exercises in CNP.	Exercise groups received cervical stabilization exercises and ROM exercises. Manual Therapy + Exercise Group (MT + E) received manipulation and/or mobilization followed by exercises. Both groups received 20-min sessions once a week for 4 weeks.	No differences seen between groups ($p > 0.05$) at baseline. Significant differences in favor of the exercise group ($p < 0.05$) at 3 months follow up.
Cox et al / 2020	To see if neck-specific progressive resistance	127 participants with CNP who completed a minimum of 9 sessions of a neck-specific	Progressive resistance exercise intervention





Neha Mukkamala et al.,

	exercise leads to a change in pain and disability.	progressive resistance program.	significantly improved neck strength, and reduced patient-reported neck pain and disability.
Saadat et al / 2019	Evaluation of the sensorimotor training vs traditional physical therapy on treatment outcomes in CNP.	Traditional training group received TENS, postural re-education, scapular thoracic exercises. The combined exercise group received sensorimotor exercise including retraining joint position and movement sense, oculomotor exercises, balance training and traditional exercise. All interventions were given for 12 sessions.	Sensorimotor training combined with traditional physical therapy exercises was more effective than traditional treatments alone.
De Zoete et al / 2019	To study the effect of physical exercise compared to usual care in improving pain, disability, and quality of life in CNP.	Electronic databases MEDLINE, EMBASE, CINAHL and PEDro were searched with keywords neck pain, chronic pain, exercise, physical activity, systematic review	Physical exercise was found to be more effective than usual care therapies in six studies, and it improved pain outcomes in all of them.
Chung et al / 2018	To see if a low-load craniocervical flexion exercise (CFE) can help CNP patients in cervical lordosis, neck pain, and neck-related functions.	CFE group received craniocervical flexion exercise followed by sagittal rotation exercise. The Control group received Neck isometric exercise (NIE). Both groups received stretching of cervical muscles. Exercises were given for 30 minutes/day, 3 times a week, for 8 weeks.	Both groups showed improved pain, NDI, endurance of the cervical flexor muscles, and active cervical ROM after 8 weeks ($p < 0.001$).
Iversen et al / 2018	To compare effect of progressive resistance training (PRT) vs general physical activity (GPE) in CNP.	PRT group received exercises like stiff-legged deadlifts, flies, unilateral rows, reversed flies, lateral pulldown, unilateral shoulder abduction. GPE group received circle training, low-intensity resistance exercises, endurance training, ball games, body awareness, stretching, relaxation techniques, which lasted for 9 additional weeks.	No difference seen in NDI score between the PRT and GPE group.
Domingues et al / 2018	Effectiveness of manual therapy and exercise versus usual care (UC) on CNP	Manual therapy and exercise group received articular mobilization and exercises (coordination, strength, endurance) for 12 sessions for 6 weeks. UC group received electrotherapy, massage, and stretching exercises for 15 sessions for 6 weeks.	MET group showed a pattern of recovery over six weeks and had a higher response rate to therapy, pain intensity, and greater global perception of recovery compared to UC.
Ris et al / 2016	Comparison of combination of education, exercises, and physical activity versus pain education alone in CNP.	The Control group (education only) received 4 sessions of pain education. Experimental group received cervical ROM exercise, isometric neck exercises, endurance exercises, walking, or cycling. The exercises were given twice daily, 3 times a week for 4 months.	The exercise group found statistically significant improvement in physical HR-QoL, mental HR-QoL, depression, cervical pressure pain threshold,





Neha Mukkamala et al.,

			cervical extension movement, muscle function, and oculomotion ($p < 0.05$).
Celenay et al / 2015	Comparing cervical and scapulothoracic stabilization exercises with and without connective tissue massage (CTM) in CNP.	Group 1 received stabilization exercises with CTM and Group 2- received the same treatment without CTM. The treatment was carried out for 12 sessions, 3 days/week for 4 weeks.	A statistically significant difference was seen in all the components of group 1 ($p < 0.05$). But no statistically significant difference was seen in group 2 ($p > 0.05$). In the intergroup comparison only parameters of pain intensity at night, the pressure pain threshold, the state of anxiety, and the Mental Component ($p < 0.05$) were found to be statistically significant.
Blomgren et al / 2015	To compare deep cervical flexor (DCF) muscle exercise versus general strengthening exercise (GSE) for CNP.	DCF group received DCF activation exercises. GSE group received isometric exercise, neck stretching, and ROM exercises. Both groups received intervention for 3 times per week for 4 weeks.	In the DCF group, there was a statistical difference found in the neck-shoulder posture compared to the general strengthening exercise group after 8 weeks of intervention ($p < 0.05$).
Brage et al / 2015	To determine the effectiveness of neck/shoulder and general aerobic training combined with pain education versus pain education alone, in women with CNP.	The Control group received pain education. The intervention group received pain education, neck flexor and extensor exercises, balance/proprrioception training Aerobic training in form of walking, swimming, cycling, jogging or stick walking for 8 sessions.	Pain education and specific training reduce neck pain significantly improved compared to pain education alone.
Jayanshir et al / 2015	To analyze the effectiveness of craniocervical flexion (CCF) and cervical flexion (CF), on flexor muscles dimensions in patients with CNP.	CCF group performed Craniocervical flexion on a pressure biofeedback unit. The cervical flexion (CF) group performed Cervical flexion in supine lying.	When compared to the cervical flexion group, the craniocervical flexion group showed a substantial increase in longus Colli muscle parameters such as cross-sectional area, width, and thickness.
O'Riordan / 2014	To assess the FITT (frequency, intensity, time, and type of exercise)principle in CNP.	The articles were studied using the Allied and Complementary Medicine Database, Cumulative Index to Nursing and Allied Health, MEDLINE, SPORTDiscus, Biomedical Reference Collection, and Academic Search Premier.	3 times/ week is the ideal exercise frequency over 12 weeks. The duration of exercise should be 30 to 45 minutes.





Neha Mukkamala et al.,

Dunleavy et al / 2014	Effects of Pilates and yoga group exercise for individuals with CNP (CNP).	The Control group received education regarding body mechanics, positioning, and movement strategies. The pilates group received thoracic flexibility exercises, upper-extremity weights, increased balance challenge, and endurance exercises. The exercise group was given breathing exercises and continued with postures to address alignment, strength, and flexibility.	The Pilates and yoga groups significantly improved (P<0.05) in the outcome while there was no significant change observed in the control group.
Bahat et al / 2014	Comparison of kinematic training with or without the use of an interactive virtual reality device on patients with neck pain.	Kinematic training group received active neck movements to increase ROM, quick head movement in-between targets to facilitate quick cervical motion control, The training session lasted 30-min. The kinematic plus Virtual Reality training (KTVR) group was given 30 min of training, which included 15-20 minutes of use of VR system, followed by 10-15 minutes of kinematic instruction.	The kinematic plus Virtual Reality training (KTVR) group improved in flexion ROM and GPE after 3-months post-intervention. In the KT group, there was a statistically significant in rotation velocity and ROM.
Bakar et al / 2014	Classic massage (CM) versus connective tissue massage (CTM) on PPT and muscle relaxation in women with CNP.	CM group received Swedish technique to the upper back and neck area for 20 minutes. CTM group received over the lumbosacral area and progressed to the scapular area, the interscapular area, and the cervical-occipital area for 20 to 25 minutes.	CTM group significantly improved compared to the Classic Massage group (P< 0.05).
Gupta et al / 2013	Effectiveness of Deep cervical flexor training in dentists suffering from CNP.	The experimental group received Deep cervical flexion training. The Control group received Conventional isometrics training (CIT). for 4 weeks.	DCF training was found statistically significant compared to conventional isometrics training in improving forward head posture, reducing pain, and reducing disability.
Evans et al / 2012	Effect of supervised exercise with or without spinal manipulation and home exercise program on CNP.	Exercise Therapy (ET) group received neck and upper body strengthening exercises, dynamic neck exercises, push-ups, and dumbbell shoulder and chest exercises for 3 sets of 15 to 25 repetitions. ET with Spinal Manipulation Therapy (ET + SMT) received SMT to cervical and thoracic spines for 20 sessions. Home Exercise and Advice (HEA) group performed neck exercises, and scapular retraction for 5 to 10 repetitions, 6-8 times per day for 12 weeks.	Exercise Therapy Combined with Spinal Manipulation Therapy (ET + SMT) group was found statistically significant in CNP (P < 0.001).





Preliminary Phytochemical Screening of *Cocos nucifera* L.

Sivagamasundari U*, Esther Shobha R, Pruthvitha Prathap and Dahunlangki Swer

Department of Life Sciences, Kristu Jayanti College, Bangalore-560077, Karnataka, India.

Received: 01 Mar 2023

Revised: 20 Apr 2023

Accepted: 26 May 2023

*Address for Correspondence

Sivagamasundari. U

Department of Life Sciences,

Kristu Jayanti College,

Bangalore-560077, Karnataka, India.

E. Mail: dr.sundari@kristujayanti.com



This is an Open Access Journal / article distributed under the terms of the **Creative Commons Attribution License** (CC BY-NC-ND 3.0) which permits unrestricted use, distribution, and reproduction in any medium, provided the original work is properly cited. All rights reserved.

ABSTRACT

Plants having pharmacological actions have been discovered and in trend medicinal application since prehistoric times. Those herbs synthesize number of chemical compounds collectively called phytochemicals which play a vital role in plant defence mechanism and provide a miscellaneous nutraceuticals to humankind. However, since an individual plant have divergent phytochemicals, the practice of utilize a whole plant as medicines are unsure. Furthermore, the phytochemicals and pharmacological actions of many plants having medicinal potential remain capsulated by rigorous scientific research to define its efficacy and safety measures. *Cocos nucifera* L. from the family Arecaceae is commonly called coconut tree and cosmopolitan in distribution. It is traditionally being the main source of food supplement and also identified to have some pharmacological action on tissues. The present study was to review the preliminary screening of secondary metabolites such as alkaloids, tannins, phenols, saponins, resins, flavonoids, steroids, fats, oils and resins of coconut endosperm by using various solvents.

Keywords: *Cocos nucifera*, Phytochemicals, Endosperm

INTRODUCTION

The interest of the scientific class in the study of compounds of plant origin is increasing worldwide, especially in developing countries where the use of herbal medicines is widely used for their basic health needs [9]. Plants are the main natural source of numerous phytochemicals, although only a certain amount have been isolated and identified. Nutritional epidemiology has investigated the relation between diet and human health, reporting positive evidence on the role of phytochemicals [10]. The studies carried out to date affirm that these compounds can reduce the incidence of several chronic diseases, including cardiovascular, obesity, diabetes, and cancer diseases, as well as high blood pressure and inflammation. Vegetables, fruits, pulses, chocolate, and teas are rich sources of phytochemicals;



**Sivagamasundari et al.,**

however, the wide diversity of these compounds requires optimized extraction methodologies to further characterization [10].

Natural bioactive compounds from plants perform specific biological activities and modify different physiological functions to improve health of human being [3]. Utilization of these compounds has become widespread to minimize occurrence of common non-communicable diseases in adults. Plant-based foods contain many phytochemical compounds along with nutrients such as proteins, fats, carbohydrates, vitamins, and minerals [6]. Scientifically, research is being undertaken to bring around limelight, the therapeutic properties of the phytochemicals present in these plants and also use them as a yardstick in modern medicinal plant uses. Phytochemicals are usually commented as research compounds rather than dietary nutrients because evident of their possible health effects has not been established yet. *Cocos nucifera* (L.) (Arecaceae) is commonly called the “coconut tree” and is the most naturally widespread fruit plant on Earth. Throughout history, humans have used medicinal plants therapeutically, and minerals, plants, and animals have traditionally been the main sources of drugs. The constituents of *C. nucifera* have some biological effects, such as antihelminthic, anti-inflammatory, antinociceptive, antioxidant, antifungal, antimicrobial, and antitumor activities [2]. The aim of this study is to review the phytochemical profile of *C. nucifera*.

MATERIALS AND METHODS

Collection of Sample

The fresh nuts were procured from vegetable market of Bangalore. The collected nuts were dehusked to release the endosperm (kernel). The endosperm was washed, grated, dried (Hot air oven at 40°C) and milled for further findings.

Preparation of Extracts

The milled sample of *Cocos* endosperm was extracted with various solvents such as chloroform, methanol, ethanol and aqueous extracts prepared in 20g/200 ml. The excess solvent in the extracts was removed by distillation and concentrated on water bath. The concentrated extracts were then pooled in petridish and stored at room temperature in desiccators. These extracts were used for the detection of phytochemicals.

Preliminary Phytochemical Screening

The various solvents extracts of *Cocos nucifera* endosperm samples were subjected to preliminary phytochemical screening.

Mayer’s Test for Alkaloids

A small quantity of the extract was treated with few drops of dilute hydrochloric acid and filtered. Then it was tested with alkaloid Mayer’s reagent to observe the creamy precipitation to confirmed the presence of alkaloids.

NaOH Tests for Flavonoids

To 2-3 ml of extract, few drops of sodium hydroxide solution were added in a test tube. Deep yellow colour on addition of few drops of dilute HCl indicated the presence of flavonoids.

Phenol Test

When 0.5 ml of FeCl₃, Phytosterols solution was added to 2 ml of test solution, formation of an intense colour indicated the presence of phenols.



**Sivagamasundari et al.,****Foam Test for Saponins**

The extract was diluted with 20 ml of distilled water and it was shaken in a graduated cylinder for 15 minutes. A thin layer of foam indicated the presence of saponins.

Ferric Chloride Test for Tannins

Small quantity of extract was boiled in 20 ml of water in a test tube and then filtered. A few drop of 0.1% ferric chloride was added and observed for brownish green or blue-black coloration which indicated the presence of tannins.

Salkowski Test for Phytosterols

To 2 ml of extract, add 2ml chloroform and 2 ml concentrated H₂SO₄ was shaken well. Appearance of red and acid layers produced greenish yellow fluorescence indicated the presence of sterols.

Ninhydrin Test for Amino acids

To 5 ml of extract, 2 drops of freshly prepared 0.2 % ninhydrin reagent was added and heated. Change of blue solution indicated the presence of amino acids.

Molish's Test for Carbohydrates

With 1 ml of extract, 2 drops of Molisch's reagent was added and mixed, then 2 ml of concentrate H₂SO₄ was slowly added. Emergence of purple ring at the junction indicated the presence of carbohydrates.

Translucent Spot test for Fats and oils

The extract was rubbed between the folds of filter paper. The appearance of translucent spot confirmed the presence of fats.

Acetic anhydride test for Resins

The extract was mixed with acetic anhydride solution and 1ml of Conc. hydrochloric acid. The appearance of orange colour confirmed the presence of Resins.

RESULTS AND DISCUSSION

The preliminary phytochemical screening has been done in the various extracts of *Cocos nucifera* endosperm and the observations are tabulated. From the observation of various extracts of coconut endosperm, the chloroform extract showed the presence of alkaloids, flavonoids, tannins, carbohydrate, fats, oils and resins. It failed to confirm phenols, saponins and phytosterols. Followed by the extract from methanol confirmed the presence of alkaloids, flavonoids, phenols, carbohydrates, aminoacids, fats, oils and resins and not confirmed the other phytochemicals tested. Ethanol extract sample confirmed the presence of alkaloids, saponins, tannins, phytosterols, carbohydrate, fats, oils and resins. Aqueous extract confirmed the presence of alkaloids, saponins, tannins, phytosterols, carbohydrate, fats, oils and resins. It did not confirm the presence of compounds, flavonoids and phenols.

The findings of phytochemical analysis comprehensively substantiate the presence of therapeutically important and valuable secondary metabolites such as Alkaloids, Flavonoids, Phenols, Saponins, Tannins, Phytosterols, Amino acids, Carbohydrate, Fats, oils and Resins Medicinal plants represent the most ancient form of medication, used for thousands of years in traditional medicine in many countries around the world. The empirical knowledge about their beneficial effects was transmitted over the centuries within human communities [5]. Natural products play a pivotal role as a source of drug compounds and, currently, a number of modern drugs which are derived from traditional herbal medicine are used in modern pharmacotherapy [7]. The extraction procedure is a crucial step in the study of the bioactive molecules from plant sources. Currently, in addition to more traditional techniques, modern extraction methods are being utilized, such as ultrasound-assisted and supercritical fluid extraction methods [1]. Moreover, the development of advanced tools for the qualitative and quantitative assessment of phytochemicals, such as high-



**Sivagamasundari et al.,**

performance liquid chromatography (HPLC) and liquid chromatography/mass spectrometry (LC/MS), significantly improved phytochemical investigation [4]. On the other hand, the biological properties of many plant species traditionally utilized together with their bioactive components have been elucidated until now. The more classical bioassay-guided natural drug discovery process and the modern processes, including high-throughput screening [4], and even the new reverse Pharmacognosy approach [8], allowed the identification of a great number of bioactive phytochemicals. Nevertheless, medicinal plants still have a hopeful future, as the phytochemical composition and the potential health benefits of many species have not yet been studied or still need to be more deeply investigated [4].

CONCLUSION

Phytochemicals and their consumption strictly provides beneficial health effects. Preclinical and clinical findings recommend that phytochemicals may be effective in treating various diseases due to its antioxidant and anti-inflammatory properties. On the other side, consumption of few may led some acute and chronic toxic effects and may even cause cancer. It is obvious that the number of phytonutrients taken, the individuals age and gender, and the conditions, as well as exposure levels, is important in the occurrence of potential risks. Consumers need to know the right phytonutrients dose they should take in either foods or dietary supplements.

ACKNOWLEDGEMENT

The Authors wish to thank the Department of Life Sciences, Kristu Jayanti College (Autonomous), Bengaluru for the facilities provided in the Research Unit.

REFERENCES

1. Azwanida, N.N. A review on the extraction methods use in medicinal plants, principle, strength and limitation. *Med. Aromat. Plants* 2015, 4, 196.
2. E.B.C. Lima, C.N.S. Sousa, L.N. Meneses, N.C. Ximenes, M.A. Santos, Junior, G.S. Vasconcelos, N.B.C. Lima, M.C.A. Patrocínio, D. Macedo, and S.M.M. Vasconcelos. *Cocos nucifera* (L.) (Arecaceae): A phytochemical and pharmacological review. *Braz. J. Med. Biol. Res.* 2015 Nov; 48(11): 953–964.
3. Harvey, A.L.; Cree, I.A. High-throughput screening of natural products for cancer therapy. *Planta Medica* 2010, 76, 1080–1086.
4. Jamshidi-Kia, F.; Lorigooini, Z.; Amini-Khoei, H. Medicinal plants: Past history and future perspective. *J. Herbmed Pharmacol.* 2018, 7, 1–7.
5. Khan, H. Medicinal plants in light of history: Recognized therapeutic modality. *J. Evid. Based Integr. Med.* 2014, 19, 216–219.
6. Narzary, H., Islary., Basumatary, S., 2016. Phytochemicals and antioxidant properties of eleven wild edible plants from Assam, India. *Mediterr.J. Nutr. Metabol.* 9 (3).
7. Patwardhan, B.; Vaidya, A.; Chorghade, M.; Joshi, S. Reverse pharmacology and systems approaches for drug discovery and development. *Curr. Bioact. Compd.* 2008, 4, 201–212.
8. Takenaka, T. Classical vs reverse pharmacology in drug discovery. *BJU Int.* 2001, 88, 7–10.
9. V.K.Yadav, "Phytochemical and Pharmacognostical studies of *Blumea lacera*," *International Journal of Green Pharmacy*, vol. 12, no. 1, 2018.
10. Yolanda Aguilera and Vanesa Benitez Dietary Sources, Innovative Extraction, and Health Benefits, Institute of Food Science Research, Phytochemicals, 2021. CIAL (UAM-CSIC), 28049 Madrid, Department of Agricultural Chemistry and Food Science, Spain.



**Sivagamasundari et al.,****Table 1: Analysis of Phytochemicals in various extracts of *Cocos nucifera* endosperm**

S.No.	Phytochemicals	Chloroform Extract	Methanol Extract	Ethanol Extract	Aqueous Extract
1.	Alkaloids	+	+	+	+
2.	Flavonoids	+	+	-	-
3.	Phenols	-	+	-	-
4.	Saponins	-	-	+	+
5.	Tannins	+	-	+	+
6.	Phytosterols	-	-	+	+
7.	Amino Acids	-	+	-	+
8.	Carbohydrate	+	+	+	+
10.	Fats and Oils	+	+	+	+
11.	Resins	+	+	+	+

+ indicates presence of phytochemical, - indicates absence of phytochemical





Nano $g^\#$ -Continuous Functions in Nano Topological Space

O.Nethaji^{1*}, S.Devi², M.Rameshpandi^{3*} and R.Premkumar⁴

¹Assistant Professor, PG and Research Department of Mathematics, Kamaraj College, Thoothukudi - 628 003, Tamil Nadu, India.

²Assistant Professor, Department of Mathematics, Sri Adichunchanagairi Women's College, Kumuli Main Road, Cumbum-625 516, Tamil Nadu, India.

³Associate Professor, Department of Mathematics, P.M.T. College, Usilampatti, Madurai District, Tamil Nadu, India.

⁴Assistant Professor, Department of Mathematics, Arul Anandar College, Karumathur, Madurai - 625 514, Tamil Nadu, India.

Received: 28 Jan 2023

Revised: 20 Apr 2023

Accepted: 31 May 2023

*Address for Correspondence

O. Nethaji

Assistant Professor,
PG and Research Department of Mathematics,
Kamaraj College, Thoothukudi - 628 003,
Tamil Nadu, India.
E. Mail: jionetha@yahoo.com



This is an Open Access Journal / article distributed under the terms of the **Creative Commons Attribution License** (CC BY-NC-ND 3.0) which permits unrestricted use, distribution, and reproduction in any medium, provided the original work is properly cited. All rights reserved.

ABSTRACT

In this paper, we first study nano $g^\#$ -continuous functions and investigate their relations with various generalized nano continuous functions. We also discuss some properties of nano $g^\#$ -continuous functions. We also introduce nano $g^\#$ -irresolute functions and study some of its applications. Finally using nano $g^\#$ -continuous function we obtain a decomposition of nano continuity.

Keywords: nano $g^\#$ -continuous, nano $g_\alpha^\#$ -continuous, strongly nano $g^\#$ -continuous and nano $g^\#$ -irresolute functions

INTRODUCTION

Lellis Thivagar et al [8] introduced a nano topological space with respect to a subset X of an universe which is defined in terms of lower approximation and upper approximation and boundary region. The classical nano topological space is based on an equivalence relation on a set, but in some situation, equivalence relations are not suitable for coping with granularity, instead the classical nano topology is extended to general binary relation based covering nano topological space. In this paper, we first study nano $g^\#$ -continuous functions and investigate their relations with various generalized nano continuous functions. We also discuss some properties of nano $g^\#$ -





Nethaji et al.,

continuous functions. We also introduce nano $g^\#$ -irresolute functions and study some of its applications. Finally using nano $g^\#$ -continuous function we obtain a decomposition of nano continuity.

Preliminaries

Definition 2.1 [10] Let U be a non-empty finite set of objects called the universe and R be an equivalence relation on U named as the indiscernibility relation. Elements belonging to the same equivalence class are said to be indiscernible with one another. The pair (U, R) is said to be the approximation space. Let $X \subseteq U$.

1. The lower approximation of X with respect to R is the set of all objects, which can be for certain classified as X with respect to R and it is denoted by $L_R(X)$. That is, $L_R(X) = \bigcup_{x \in U} \{R(x) : R(x) \subseteq X\}$, where $R(x)$ denotes the equivalence class determined by x .

2. The upper approximation of X with respect to R is the set of all objects, which can be possibly classified as X with respect to R and it is denoted by $U_R(X)$. That is, $U_R(X) = \bigcup_{x \in U} \{R(x) : R(x) \cap X \neq \emptyset\}$.

3. The boundary region of X with respect to R is the set of all objects, which can be classified neither as X nor as not X with respect to R and it is denoted by $B_R(X)$. That is, $B_R(X) = U_R(X) - L_R(X)$.

Definition 2.2 [8] Let U be the universe, R be an equivalence relation on U and $\tau_R(X) = \{U, \emptyset, L_R(X), U_R(X), B_R(X)\}$ where $X \subseteq U$. Then $\tau_R(X)$ satisfies the following axioms:

1. U and $\emptyset \in \tau_R(X)$,
2. The union of the elements of any sub collection of $\tau_R(X)$ is in $\tau_R(X)$,
3. The intersection of the elements of any finite subcollection of $\tau_R(X)$ is in $\tau_R(X)$.

Thus $\tau_R(X)$ is a topology on U called the nano topology with respect to X and $(U, \tau_R(X))$ is called the nano topological space. The elements of $\tau_R(X)$ are called nano-open sets (briefly n-open sets). The complement of a n-open set is called n-closed.

In the rest of the paper, we denote a nano topological space by (U, \mathcal{N}) , where $\mathcal{N} = \tau_R(X)$. The nano-interior and nano-closure of a subset A of U are denoted by $nint(A)$ and $ncl(A)$, respectively.

Definition 2.3 A function $f: (U, \tau_R(X)) \rightarrow (V, \tau'_R(Y))$ is called:

1. nano g^* -continuous [11] if $f^{-1}(M)$ is a ng^* -closed set in U for every nano closed set M of V .
2. nano g -continuous [4] if $f^{-1}(M)$ is a ng -closed set in U for every nano closed set M of V .
3. nano αg -continuous [13] if $f^{-1}(M)$ is an $n\alpha g$ -closed set in U for every nano closed set M of V .
4. nano gs -continuous [7] if $f^{-1}(M)$ is a ngs -closed set in U for every nano closed set M of V .
5. nano gsp -continuous [5] if $f^{-1}(M)$ is a $ngsp$ -closed set in U for every nano closed set M of V .
6. nano sg -continuous [7] if $f^{-1}(M)$ is a nsg -closed set in U for every nano closed set M of V .
7. nano-semi-continuous [12] if $f^{-1}(M)$ is a nano-semi-open set in U for every nano open set M of V .
8. nano α -continuous [1] if $f^{-1}(M)$ is an $n\alpha$ -closed set in U for every nano closed set M of V .

Definition 2.4 A function $f: (U, \tau_R(X)) \rightarrow (V, \tau'_R(Y))$ is called:

1. nano αg -irresolute [13] if the inverse image of every $n\alpha g$ -closed (resp. $n\alpha g$ -open) set in V is $n\alpha g$ -closed (resp. $n\alpha g$ -open) in U .
2. nano gc -irresolute [1] if the inverse image of every ng -closed set in V is ng -closed in U .
3. nano sg -irresolute [7] if the inverse image of every nsg -closed (resp. nsg -open) set in V is nsg -closed (resp. nsg -open) in U .

Definition 2.5 [5] A function $f: (U, \tau_R(X)) \rightarrow (V, \tau'_R(Y))$ is called pre- $n\alpha g$ -closed if $f(M)$ is $n\alpha g$ -closed in V , for each $n\alpha g$ -closed set M in U .

Theorem 2.6 [6] A set A of U is $ng^\#$ -open if and only if $F \subseteq nint(A)$ whenever F is $n\alpha g$ -closed and $F \subseteq A$.

Theorem 2.7 [6] For a space U , the following properties are equivalent:

1. U is a $T_{ng^\#}$ -space.
2. Every singleton subset of U is either $n\alpha g$ -closed or nano open.





Nethaji et al.,

Nano $g^\#$ -continuous functions

We introduce the following definitions:

Definition 3.1 A function $f: (U, \tau_R(X)) \rightarrow (V, \tau'_R(Y))$ is called:

1. nano $g^\#$ -continuous if the inverse image of every nano closed set in V is $ng^\#$ -closed set in U .
2. nano $g^\#_\alpha$ -continuous if $f^{-1}(A)$ is an $ng^\#_\alpha$ -closed set in U for every nano closed set A of V .

Definition 3.2 A function $f: (U, \tau_R(X)) \rightarrow (V, \tau'_R(Y))$ is called a strongly nano $g^\#$ -continuous if the inverse image of every $ng^\#$ -open set in V is nano open in U .

Proposition 3.3 Every $ng^\#$ -continuous function is $ng^\#_\alpha$ -continuous but not conversely.

Example 3.4 Let $U = \{a_1, a_2, a_3\}$ with $U/R = \{\{a_1\}, \{a_2\}, \{a_3\}\}$ and $X = \{a_2\}$ then the sets in $\{\phi, \{a_2\}, U\}$ are called nano open and the sets in $\{\phi, \{a_1, a_3\}, U\}$ are called nano closed in U . Let $V = \{a_1, a_2, a_3\}$ with $V/R = \{\{a_1\}, \{a_2, a_3\}\}$ and $Y = \{a_2, a_3\}$. Then the sets in $\{\phi, \{a_2, a_3\}, V\}$ are called nano open and the sets in $\{\phi, \{a_1\}, V\}$ are called nano closed. We have $NG^\#C(U) = \{\phi, \{a_1, a_3\}, U\}$ and $NG^\#_\alpha C(U) = \{\phi, \{a_1\}, \{a_3\}, \{a_1, a_3\}, U\}$. Let $f: (U, \tau_R(X)) \rightarrow (V, \tau'_R(Y))$ be the identity function. Then f is $ng^\#_\alpha$ -continuous but not $ng^\#$ -continuous, since $f^{-1}(\{a_1\}) = \{a_1\}$ is not $ng^\#$ -closed in U .

Proposition 3.5 Every $ng^\#$ -continuous function is ng^* -continuous but not conversely.

Example 3.6 Let $U = \{a_1, a_2, a_3\}$ with $U/R = \{\{a_1\}, \{a_2\}, \{a_3\}\}$ and $X = \{a_1\}$. Then the sets in $\{\phi, \{a_1\}, U\}$ are called nano open and the sets in $\{\phi, \{a_2, a_3\}, U\}$ are called nano closed in U . Let $V = \{a_1, a_2, a_3\}$ with $V/R = \{\{a_1\}, \{a_2\}, \{a_3\}\}$ and $Y = \{a_3\}$. Then the sets in $\{\phi, \{a_3\}, V\}$ are called nano open and the sets in $\{\phi, \{a_1, a_2\}, V\}$ are called nano closed in V . We have $NG^\#C(U) = \{\phi, \{a_2\}, \{a_2, a_3\}, U\}$ and $NG^*C(U) = \{\phi, \{a_2\}, \{a_1, a_2\}, \{a_2, a_3\}, U\}$. Let $f: (U, \tau_R(X)) \rightarrow (V, \tau'_R(Y))$ be the identity function. Then f is ng^* -continuous but not $ng^\#$ -continuous, since $f^{-1}(\{a_1, a_2\}) = \{a_1, a_2\}$ is not $ng^\#$ -closed in U .

Proposition 3.7 Every $ng^\#$ -continuous function is ng -continuous but not conversely.

Example 3.8 Let $U = \{a_1, a_2, a_3\}$ with $U/R = \{\{a_1\}, \{a_2, a_3\}\}$ and $X = \{a_1, a_2\}$. Then the sets in $\{\phi, \{a_1\}, \{a_2, a_3\}, U\}$ are called nano open and the sets in $\{\phi, \{a_1\}, \{a_2, a_3\}, U\}$ are called nano closed in U . Let $V = \{a_1, a_2, a_3\}$ with $V/R = \{\{a_1\}, \{a_2\}, \{a_3\}\}$ and $Y = \{a_3\}$. Then the sets in $\{\phi, \{a_3\}, V\}$ are called nano open and the sets in $\{\phi, \{a_1, a_2\}, V\}$ are called nano closed in V . We have $NG^\#C(U) = \{\phi, \{a_1\}, \{a_2, a_3\}, U\}$ and $NGC(U) = \mathbb{P}(U)$. Let $f: (U, \tau_R(X)) \rightarrow (V, \tau'_R(Y))$ be the identity function. Then f is ng -continuous but not $ng^\#$ -continuous, since $f^{-1}(\{a_1, a_2\}) = \{a_1, a_2\}$ is not $ng^\#$ -closed in U .

Proposition 3.9 Every $ng^\#$ -continuous function is $n\alpha g$ -continuous but not conversely.

Example 3.10 Let $U = \{a_1, a_2, a_3\}$ with $U/R = \{\{a_1\}, \{a_2, a_3\}\}$ and $X = \{a_1, a_2\}$. Then the sets in $\{\phi, \{a_1\}, \{a_2, a_3\}, U\}$ are called nano open and the sets in $\{\phi, \{a_1\}, \{a_2, a_3\}, U\}$ are called nano closed in U . Let $V = \{a_1, a_2, a_3\}$ with $V/R = \{\{a_1\}, \{a_2\}, \{a_3\}\}$ and $Y = \{a_2\}$. Then the sets in $\{\phi, \{a_2\}, V\}$ are called nano open and the sets in $\{\phi, \{a_1, a_3\}, V\}$ are called nano closed in V . We have $NG^\#C(U) = \{\phi, \{a_1\}, \{a_2, a_3\}, U\}$ and $N\alpha GC(U) = \mathbb{P}(U)$. Let $f: (U, \tau_R(X)) \rightarrow (V, \tau'_R(Y))$ be the identity function. Then f is $n\alpha g$ -continuous but not $ng^\#$ -continuous, since $f^{-1}(\{a_1, a_3\}) = \{a_1, a_3\}$ is not $ng^\#$ -closed in U .

Proposition 3.11 Every $ng^\#$ -continuous function is ngs -continuous but not conversely.

Example 3.12 Let $U = \{a_1, a_2, a_3\}$ with $U/R = \{\{a_1\}, \{a_2\}, \{a_3\}\}$ and $X = \{a_1\}$. Then the sets in $\{\phi, \{a_1\}, U\}$ are called nano open and the sets in $\{\phi, \{a_2, a_3\}, U\}$ are called nano closed in U . Let $V = \{a_1, a_2, a_3\}$ with $V/R = \{\{a_1, a_2\}, \{a_3\}\}$ and $Y = \{a_1, a_2\}$. Then the sets in $\{\phi, \{a_1, a_2\}, V\}$ are called nano open and the sets in $\{\phi, \{a_3\}, V\}$ are called nano closed in V . We have $NG^\#C(U) = \{\phi, \{a_2, a_3\}, U\}$ and $NGSC(U) = \{\phi, \{a_2\}, \{a_3\}, \{a_1, a_2\}, \{a_1, a_3\}, \{a_2, a_3\}, U\}$. Let $f: (U, \tau_R(X)) \rightarrow (V, \tau'_R(Y))$ be the identity function. Then f is ngs -continuous but not $ng^\#$ -continuous, since $f^{-1}(\{a_3\}) = \{a_3\}$ is not $ng^\#$ -closed in U .

Proposition 3.13 Every $ng^\#$ -continuous function is $ngsp$ -continuous but not conversely.





Nethaji et al.,

Example 3.14 Let $U = \{a_1, a_2, a_3\}$ with $U/R = \{\{a_1\}, \{a_2\}, \{a_3\}\}$ and $X = \{a_2\}$. Then the sets in $\{\phi, \{a_2\}, U\}$ are called nano open and the sets in $\{\phi, \{a_1, a_3\}, U\}$ are called nano closed in U . Let $V = \{a_1, a_2, a_3\}$ with $V/R = \{\{a_1, a_2\}, \{a_3\}\}$ and $Y = \{a_1, a_2\}$. Then the sets in $\{\phi, \{1, 2\}, V\}$ are called nano open and the sets in $\{\phi, \{3\}, V\}$ are called nano closed in V . We have $\#() = \{\phi, \{1, 3\}, V\}$ and $() = \{\phi, \{a_1\}, \{a_3\}, \{a_1, a_2\}, \{a_1, a_3\}, \{a_2, a_3\}, U\}$. Let $f: (U, \tau_R(X)) \rightarrow (V, \tau'_R(Y))$ be the identity function. Then f is $ngsp$ -continuous but not $ng^\#$ -continuous, since $f^{-1}(\{a_3\}) = \{a_3\}$ is not $ng^\#$ -closed in U .

Proposition 3.15 Every $ng^\#$ -continuous function is ng -continuous but not conversely.

Example 3.16 Let $U = \{a_1, a_2, a_3\}$ with $U/R = \{\{a_1\}, \{a_2, a_3\}\}$ and $X = \{a_1, a_3\}$. Then the sets in $\{\phi, \{a_1\}, \{a_2, a_3\}, U\}$ are called nano open and the sets in $\{\phi, \{a_1\}, \{a_2, a_3\}, U\}$ are called nano closed in U . Let $V = \{a_1, a_2, a_3\}$ with $V/R = \{\{a_1, a_2\}, \{a_3\}\}$ and $Y = \{a_1, a_2\}$. Then the sets in $\{\phi, \{a_1, a_2\}, V\}$ are called nano open and the sets in $\{\phi, \{a_3\}, V\}$ are called nano closed in V . We have $NG^\#C(U) = \{\phi, \{a_1\}, \{a_2, a_3\}, U\}$ and $NSGC(U) = \mathbb{P}(U)$. Let $f: (U, \tau_R(X)) \rightarrow (V, \tau'_R(Y))$ be the identity function. Then f is ng -continuous but not $ng^\#$ -continuous, since $f^{-1}(\{a_3\}) = \{a_3\}$ is not $ng^\#$ -closed in U .

Remark 3.17 The following examples show that $ng^\#$ -continuity is independent of $n\alpha$ -continuity and nano semi continuity.

Example 3.18 Let $U = \{a_1, a_2, a_3\}$ with $U/R = \{\{a_1, a_2\}, \{a_3\}\}$ and $X = \{a_1, a_2\}$. Then the sets in $\{\phi, \{a_1, a_2\}, U\}$ are called nano open and the sets in $\{\phi, \{a_3\}, U\}$ are called nano closed in U . Let $V = \{a_1, a_2, a_3\}$ with $V/R = \{\{a_1\}, \{a_2\}, \{a_3\}\}$ and $Y = \{a_1\}$. Then the sets in $\{\phi, \{a_1\}, V\}$ are called nano open and the sets in $\{\phi, \{a_2, a_3\}, V\}$ are called nano closed in V . We have $NG^\#C(U) = \{\phi, \{a_3\}, \{a_1, a_3\}, \{a_2, a_3\}, U\}$ and $N\alpha C(U) = NSC(U) = \{\phi, \{a_3\}, U\}$. Let $f: (U, \tau_R(X)) \rightarrow (V, \tau'_R(Y))$ be the identity function. Then f is $ng^\#$ -continuous but it is neither $n\alpha$ -continuous nor nano semi continuous, since $f^{-1}(\{a_2, a_3\}) = \{a_2, a_3\}$ is neither $n\alpha$ -closed nor nano semi closed in U .

Example 3.19 In Example 3.12, we have $NG^\#C(U) = \{\phi, \{a_2, a_3\}, U\}$ and $N\alpha C(U) = NSC(U) = \{\phi, \{a_2\}, \{a_3\}, \{a_2, a_3\}, U\}$. Let $f: (U, \tau_R(X)) \rightarrow (V, \tau'_R(Y))$ be the identity function. Then f is both $n\alpha$ -continuous and nano semi continuous but it is not $ng^\#$ -continuous, since $f^{-1}(\{a_3\}) = \{a_3\}$ is not $ng^\#$ -closed in U .

Proposition 3.20 A function $f: (U, \tau_R(X)) \rightarrow (V, \tau'_R(Y))$ is $ng^\#$ -continuous if and only if $f^{-1}(A)$ is $ng^\#$ -open in U for every nano open set A in V .

Proof. Let $f: (U, \tau_R(X)) \rightarrow (V, \tau'_R(Y))$ be $ng^\#$ -continuous and A be a nano open set in V . Then A^c is nano closed in V and since f is $ng^\#$ -continuous, $f^{-1}(A^c)$ is $ng^\#$ -closed in U . But $f^{-1}(A^c) = (f^{-1}(A))^c$ and so $f^{-1}(A)$ is $ng^\#$ -open in U . Conversely, assume that $f^{-1}(A)$ is $ng^\#$ -open in U for each nano open set A in V . Let E be a nano closed set in V . Then E^c is nano open in V and by assumption, $f^{-1}(E^c)$ is $ng^\#$ -open in U . Since $f^{-1}(E^c) = (f^{-1}(E))^c$, we have $f^{-1}(E)$ is $ng^\#$ -closed in U and so f is $ng^\#$ -continuous.

Proposition 3.21 Let U and W be nano topological spaces and V be a $nT_g^\#$ -space. Then the composition $g \circ f: (U, \tau_R(X)) \rightarrow (W, \tau''_R(Z))$ of the $ng^\#$ -continuous functions $f: (U, \tau_R(X)) \rightarrow (V, \tau'_R(Y))$ and $g: (V, \tau'_R(Y)) \rightarrow (W, \tau''_R(Z))$ is $ng^\#$ -continuous.

Proof. Let E be any nano closed set of W . Then $g^{-1}(E)$ is $ng^\#$ -closed in V , since ng -continuous is $ng^\#$ -continuous. Since V is a $nT_g^\#$ -space, $g^{-1}(E)$ is nano closed in V . Since f is $ng^\#$ -continuous, $f^{-1}(g^{-1}(E))$ is $ng^\#$ -closed in U . But $f^{-1}(g^{-1}(E)) = (g \circ f)^{-1}(E)$ and so $g \circ f$ is $ng^\#$ -continuous.

Proposition 3.22 Let U and W be nano topological spaces and V be a $nT_{1/2}$ -space (resp. nT_b -space, nT_b -space). Then the composition $g \circ f: (U, \tau_R(X)) \rightarrow (W, \tau''_R(Z))$ of the $ng^\#$ -continuous function $f: (U, \tau_R(X)) \rightarrow (V, \tau'_R(Y))$ and the ng -continuous (resp. ngs -continuous, $n\alpha g$ -continuous) function $g: (V, \tau'_R(Y)) \rightarrow (W, \tau''_R(Z))$ is $ng^\#$ -continuous.

Proof. Similar to Proposition 3.21.





Nethaji et al.,

Proposition 3.23 If $f: (U, \tau_R(X)) \rightarrow (V, \tau'_R(Y))$ is $ng^\#$ -continuous and $g: (V, \tau'_R(Y)) \rightarrow (W, \tau''_R(Z))$ is nano continuous, then their composition $g \circ f: (U, \tau_R(X)) \rightarrow (W, \tau''_R(Z))$ is $ng^\#$ -continuous.

Proof. Let E be any nano closed set in $\tau''_R(Z)$. Since $g: (V, \tau'_R(Y)) \rightarrow (W, \tau''_R(Z))$ is nano continuous, $g^{-1}(E)$ is nano closed in $\tau'_R(Y)$. Since $f: (U, \tau_R(X)) \rightarrow (V, \tau'_R(Y))$ is $ng^\#$ -continuous, $f^{-1}(g^{-1}(E)) = (g \circ f)^{-1}(E)$ is $ng^\#$ -closed in $\tau_R(X)$ and so $g \circ f$ is $ng^\#$ -continuous.

Proposition 3.24 Let E be $ng^\#$ -closed in U . If $f: (U, \tau_R(X)) \rightarrow (V, \tau'_R(Y))$ is $n\alpha g$ -irresolute and nano closed, then $f(E)$ is $ng^\#$ -closed in V .

Proof. Let M be any $n\alpha g$ -open in V such that $f(E) \subseteq M$. Then $E \subseteq f^{-1}(M)$ and by hypothesis, $ncl(E) \subseteq f^{-1}(M)$. Thus $f(ncl(E)) \subseteq M$ and $f(n_\tau cl(E))$ is a nano closed set in U . Now, $n_\tau cl(f(E)) \subseteq n'_\tau cl(f(n_\tau cl(E))) = f(n_\tau cl(E)) \subseteq M$. i.e., $n'_\tau cl(f(E)) \subseteq U$ and so $f(E)$ is $ng^\#$ -closed.

Theorem 3.25 Let $f: (U, \tau_R(X)) \rightarrow (V, \tau'_R(Y))$ be a pre- $n\alpha g$ -closed and nano open bijection. If U is a $nT_{g^\#}$ -space, then V is also a $nT_{g^\#}$ -space.

Proof. Let $v \in V$. Since f is bijective, $v = f(u)$ for some $u \in U$. Since U is a $nT_{g^\#}$ -space, $\{u\}$ is $n\alpha g$ -closed or nano open in U by Theorem 2.7. If $\{u\}$ is $n\alpha g$ -closed then $\{v\} = f(\{u\})$ is $n\alpha g$ -closed, since f is pre- $n\alpha g$ -closed. Also $\{v\}$ is nano open in V if $\{u\}$ is nano open in U since f is nano open. Therefore by Theorem 2.7, V is a $nT_{g^\#}$ -space.

Theorem 3.26 If $f: (U, \tau_R(X)) \rightarrow (V, \tau'_R(Y))$ is $ng^\#$ -continuous and pre- $n\alpha g$ -closed and if K is an $ng^\#$ -open (or $ng^\#$ -closed) subset of V , then $f^{-1}(K)$ is $ng^\#$ -open (or $ng^\#$ -closed) in U .

Proof. Let K be an $ng^\#$ -open set in V and E be any $n\alpha g$ -closed set in U such that $E \subseteq f^{-1}(K)$. Then $f(E) \subseteq K$. By hypothesis, $f(E)$ is $n\alpha g$ -closed and K is $ng^\#$ -open in V . Therefore, $f(E) \subseteq n'_\tau int(K)$ by Theorem 2.6, and so $E \subseteq f^{-1}(n'_\tau int(K))$. Since f is $ng^\#$ -continuous and $n'_\tau int(K)$ is nano open in V , $f^{-1}(n'_\tau int(K))$ is $ng^\#$ -open in U . Thus $E \subseteq n_\tau int(f^{-1}(n'_\tau int(K))) \subseteq n_\tau int(f^{-1}(K))$. i.e., $E \subseteq n_\tau int(f^{-1}(K))$ and by Theorem 2.6, $f^{-1}(K)$ is $ng^\#$ -open in U . By taking complements, we can show that if K is $ng^\#$ -closed in V , $f^{-1}(K)$ is $ng^\#$ -closed in U .

Corollary 3.27 If $f: (U, \tau_R(X)) \rightarrow (V, \tau'_R(Y))$ is nano continuous and pre- $n\alpha g$ -closed and if H is a $ng^\#$ -closed (or $ng^\#$ -open) subset of V , then $f^{-1}(H)$ is $ng^\#$ -closed (or $ng^\#$ -open) in U .

Proof. Follows from Proposition 3.2, and Theorem 3.26.

Corollary 3.28 Let U, V and W be any three nano topological spaces. If $f: (U, \tau_R(X)) \rightarrow (V, \tau'_R(Y))$ is $ng^\#$ -continuous and pre- $n\alpha g$ -closed and $g: (V, \tau'_R(Y)) \rightarrow (W, \tau''_R(Z))$ is $ng^\#$ -continuous, then their composition $g \circ f: (U, \tau_R(X)) \rightarrow (W, \tau''_R(Z))$ is $ng^\#$ -continuous.

Proof. Let E be any nano closed set in $\tau''_R(Z)$. Since $g: (V, \tau'_R(Y)) \rightarrow (W, \tau''_R(Z))$ is $ng^\#$ -continuous, $g^{-1}(E)$ is $ng^\#$ -closed in V . Since $f: (U, \tau_R(X)) \rightarrow (V, \tau'_R(Y))$ is $ng^\#$ -continuous and pre- $n\alpha g$ -closed, by Theorem 3.26, $f^{-1}(g^{-1}(E)) = (g \circ f)^{-1}(E)$ is $ng^\#$ -closed in U and so $g \circ f$ is $ng^\#$ -continuous.

Nano $g^\#$ -Irresolute Functions

We introduce the following definition.

Definition 4.1 A function $f: (U, \tau_R(X)) \rightarrow (V, \tau'_R(Y))$ is called an $ng^\#$ -irresolute if the inverse image of every $ng^\#$ -closed set in V is $ng^\#$ -closed in U .

Remark 4.2 The following examples show that the notions of nsg -irresolute functions and $ng^\#$ -irresolute functions are independent.

Example 4.3 Let $U = \{a_1, a_2, a_3\}$ with $U/R = \{\{a_1, a_2\}, \{a_3\}\}$ and $X = \{a_1, a_2\}$. Then the sets in $\{\phi, \{a_1, a_2\}, U\}$ are called nano open and the sets in $\{\phi, \{a_3\}, U\}$ are called nano closed in U . Let $V = \{a_1, a_2, a_3\}$ with $V/R = \{\{a_1\}, \{a_2\}, \{a_3\}\}$ and $Y = \{a_1, a_2\}$. Then the sets in $\{\phi, \{a_1\}, \{a_2\}, \{a_1, a_2\}, V\}$ are called nano open and the sets in $\{\phi, \{a_3\}, \{a_1, a_3\}, \{a_2, a_3\}, V\}$ are





Nethaji et al.,

called nano closed in V . We have $NG^\#C(U) = \{\phi, \{a_3\}, \{a_1, a_3\}, \{a_2, a_3\}, U\}$, $NSGC(U) = \{\phi, \{a_3\}, \{a_1, a_3\}, \{a_2, a_3\}, U\}$, $NG^\#C(V) = \{\phi, \{a_3\}, \{a_1, a_3\}, \{a_2, a_3\}, V\}$ and $NSGC(V) = \{\phi, \{a_1\}, \{a_2\}, \{a_3\}, \{a_1, a_3\}, \{a_2, a_3\}, V\}$. Let $f: (U, \tau_R(X)) \rightarrow (V, \tau'_R(Y))$ be the identity function. Then f is $ng^\#$ -irresolute but it is not nsg -irresolute, since $f^{-1}(\{a_2\}) = \{a_2\}$ is not nsg -closed in U .

Example 4.4 Let $U = \{a_1, a_2, a_3\}$ with $U/R = \{\{a_1\}, \{a_2\}, \{a_3\}\}$ and $X = \{a_1, a_2\}$. Then the sets in $\{\phi, \{a_1\}, \{a_2\}, \{a_1, a_2\}, U\}$ are called nano open and the sets in $\{\phi, \{a_3\}, \{a_1, a_3\}, \{a_2, a_3\}, U\}$ are called nano closed in U . Let $V = \{a_1, a_2, a_3\}$ with $V/R = \{\{a_1\}, \{a_2, a_3\}\}$ and $Y = \{a_2, a_3\}$. Then the sets in $\{\phi, \{a_2, a_3\}, V\}$ are called nano open and the sets in $\{\phi, \{a_1\}, V\}$ are called nano closed. We have $NG^\#C(U) = \{\phi, \{a_3\}, \{a_1, a_3\}, \{a_2, a_3\}, U\}$ and $NSGC(U) = \{\phi, \{a_1\}, \{a_2\}, \{a_3\}, \{a_1, a_3\}, \{a_2, a_3\}, U\}$, $NG^\#C(V) = \{\phi, \{a_1\}, \{a_1, a_3\}, V\}$ and $NSGC(V) = \{\phi, \{a_1\}, \{a_3\}, \{a_1, a_3\}, V\}$. Let $f: (U, \tau_R(X)) \rightarrow (V, \tau'_R(Y))$ be the identity function. Then f is nsg -irresolute but it is not $ng^\#$ -irresolute, since $f^{-1}(\{a_1\}) = \{a_1\}$ is not $ng^\#$ -closed in U .

Proposition 4.5 A function $f: (U, \tau_R(X)) \rightarrow (V, \tau'_R(Y))$ is $ng^\#$ -irresolute if and only if the inverse of every $ng^\#$ -open set in V is $ng^\#$ -open in U .

Proof. Similar to Proposition 3.20.

Proposition 4.6 If a function $f: (U, \tau_R(X)) \rightarrow (V, \tau'_R(Y))$ is $ng^\#$ -irresolute then it is $ng^\#$ -continuous but not conversely.

Example 4.7 Let $U = \{a_1, a_2, a_3\}$ with $U/R = \{\{a_1\}, \{a_2\}, \{a_3\}\}$ and $X = \{a_2\}$. Then the sets in $\{\phi, \{a_2\}, U\}$ are called nano open and the sets in $\{\phi, \{a_1, a_3\}, U\}$ are called nano closed in U . Let $V = \{a_1, a_2, a_3\}$ with $V/R = \{\{a_1, a_2\}, \{a_3\}\}$ and $X = \{a_1, a_2\}$. Then the sets in $\{\phi, \{a_1, a_2\}, V\}$ are called nano open and the sets in $\{\phi, \{a_3\}, V\}$ are called nano closed. We have $NG^\#C(U) = \{\phi, \{a_1, a_3\}, U\}$ and $NG^\#C(V) = \{\phi, \{a_3\}, \{a_1, a_3\}, \{a_2, a_3\}, V\}$. Let $f: (U, \tau_R(X)) \rightarrow (V, \tau'_R(Y))$ be the identity function. Then f is $ng^\#$ -continuous but it is not $ng^\#$ -irresolute, since $f^{-1}(\{a_1\}) = \{a_1\}$ is not $ng^\#$ -open in U .

Proposition 4.8 Let U be any nano topological space, V be a $T_{ng^\#}$ -space and $f: (U, \tau_R(X)) \rightarrow (V, \tau'_R(Y))$ be a function. Then the following are equivalent:

1. f is $ng^\#$ -irresolute.
2. f is $ng^\#$ -continuous.

Proof.

(1) \Rightarrow (2) Follows from Proposition 4.6.

(2) \Rightarrow (1) Let H be a $ng^\#$ -closed set in V . Since V is a $T_{ng^\#}$ -space, H is a nano closed set in V and by hypothesis, $f^{-1}(H)$ is $ng^\#$ -closed in U . Therefore f is $ng^\#$ -irresolute.

Definition 4.9 A function $f: (U, \tau_R(X)) \rightarrow (V, \tau'_R(Y))$ is called pre- $n\alpha g$ -open if $f(K)$ is $n\alpha g$ -open in V , for each $n\alpha g$ -open set K in U .

Proposition 4.10 If $f: (U, \tau_R(X)) \rightarrow (V, \tau'_R(Y))$ is bijective pre- $n\alpha g$ -open and $ng^\#$ -continuous then f is $ng^\#$ -irresolute.

Proof. Let K be $ng^\#$ -closed set in V . Let H be any $n\alpha g$ -open set in U such that $f^{-1}(K) \subseteq H$. Then $K \subseteq f(H)$. Since K is $ng^\#$ -closed and $f(H)$ is $n\alpha g$ -open in V , $n'_\tau cl(K) \subseteq f(H)$ holds and hence $f^{-1}(n'_\tau cl(K)) \subseteq H$. Since f is $ng^\#$ -continuous and $n'_\tau cl(K)$ is nano closed in V , $f^{-1}(n'_\tau cl(K))$ is $ng^\#$ -closed and hence $n_\tau cl(f^{-1}(n'_\tau cl(K))) \subseteq H$ and so $n_\tau cl(f^{-1}(K)) \subseteq H$. Therefore, $f^{-1}(K)$ is $ng^\#$ -closed in U and hence f is $ng^\#$ -irresolute.

The following examples show that no assumption of Proposition 4.10 can be removed.

Example 4.11 The identity function defined in Example 4.7 is $ng^\#$ -continuous and bijective but not pre- $n\alpha g$ -open and so f is not $ng^\#$ -irresolute.

Example 4.12 Let $U = \{a_1, a_2, a_3\}$ with $U/R = \{\{a_1\}, \{a_2\}, \{a_3\}\}$ and $X = \{a_1, a_2\}$. Then the sets in $\{\phi, \{a_1\}, \{a_2\}, \{a_1, a_2\}, U\}$ are called nano open and the sets in $\{\phi, \{a_3\}, \{a_1, a_3\}, \{a_2, a_3\}, U\}$ are called nano closed in U . Let $V = \{a_1, a_2, a_3\}$ with $V/R = \{\{a_1\}, \{a_2, a_3\}\}$ and $Y = \{a_1, a_3\}$. Then the sets in $\{\phi, \{a_1\}, \{a_2, a_3\}, V\}$ are called nano open and the sets in $\{\phi, \{a_1\}, \{a_2, a_3\}, V\}$ are called nano closed in V . We have $NG^\#C(U) = \{\phi, \{a_3\}, \{a_1, a_3\}, \{a_2, a_3\}, U\}$ and $NSGC(U) = \{\phi, \{a_1\}, \{a_2\},$





Nethaji et al.,

$\{a_3\}, \{a_1, a_3\}, \{a_2, a_3\}, U$, $NG^\#C(V) = \{\phi, \{a_1\}, \{a_2, a_3\}, V\}$ and $NSGC(V) = \mathbb{P}(V)$. Let $f: (U, \tau_R(X)) \rightarrow (V, \tau'_R(Y))$ be the identity function. Then f is bijective and pre- αg -open but not $ng^\#$ -continuous and so f is not $ng^\#$ -irresolute, since $f^{-1}(\{a_1\}) = \{a_1\}$ is not $ng^\#$ -closed in U .

Proposition 4.13 If $f: (U, \tau_R(X)) \rightarrow (V, \tau'_R(Y))$ is bijective nano closed and αg -irresolute then the inverse function $f^{-1}: (V, \tau'_R(Y)) \rightarrow (U, \tau_R(X))$ is $ng^\#$ -irresolute.

Proof. Let K be $ng^\#$ -closed in U . Let $(f^{-1})^{-1}(K) = f(K) \subseteq H$ where H is αg -open in V . Then $K \subseteq f^{-1}(H)$ holds. Since $f^{-1}(H)$ is αg -open in U and K is $ng^\#$ -closed in U , $n_\tau cl(K) \subseteq f^{-1}(H)$ and hence $f(n_\tau cl(K)) \subseteq H$. Since f is nano closed and $n_\tau cl(K)$ is nano closed in U , $f(n_\tau cl(K))$ is nano closed in V and so $f(n_\tau cl(K))$ is $ng^\#$ -closed in V . Therefore $n'_{\tau'} cl(f(n_\tau cl(K))) \subseteq H$ and hence $n'_{\tau'} cl(f(K)) \subseteq H$. Thus $f(K)$ is $ng^\#$ -closed in V and so f^{-1} is $ng^\#$ -irresolute.

Applications

To obtain a decomposition of nano continuity, we introduce the notion of $\alpha gcl^\#$ -continuous function in nano topological spaces and prove that a function is nano continuous if and only if it is both $ng^\#$ -continuous and $\alpha gcl^\#$ -continuous.

Definition 5.1 A subset K of a nano topological space U is called $\alpha gcl^\#$ -set if $K = G \cap H$, where G is αg -open and H is nano closed in U .

The family of all $\alpha gcl^\#$ -sets in a space U is denoted by $\alpha gcl^\#(U)$.

Example 5.2 Let $U = \{a_1, a_2, a_3\}$ with $U/R = \{\{a_1\}, \{a_2\}, \{a_3\}\}$ and $X = \{a_3\}$. Then the sets in $\{\phi, \{a_3\}, U\}$ are called nano open and the sets in $\{\phi, \{a_1, a_2\}, U\}$ are called nano closed. Then $\{a_1\}$ is $\alpha gcl^\#$ -set in U .

Remark 5.3 Every nano closed set is $\alpha gcl^\#$ -set but not conversely.

Example 5.4 Let $U = \{a_1, a_2, a_3\}$ with $U/R = \{\{a_1\}, \{a_2\}, \{a_3\}\}$ and $X = \{a_1\}$. Then the sets in $\{\phi, \{a_1\}, U\}$ are called nano open and the sets in $\{\phi, \{a_2, a_3\}, U\}$ are called nano closed. Then $\{a_1, a_2\}$ is $\alpha gcl^\#$ -set but not nano closed in U .

Remark 5.5 $ng^\#$ -closed sets and $\alpha gcl^\#$ -sets are independent of each other.

Example 5.6 Let $U = \{a_1, a_2, a_3\}$ with $U/R = \{\{a_1, a_3\}, \{a_2\}\}$ and $X = \{a_1, a_3\}$. Then the sets in $\{\phi, \{a_1, a_3\}, U\}$ are called nano open and the sets in $\{\phi, \{a_2\}, U\}$ are called nano closed. Then $\{a_2, a_3\}$ is a $ng^\#$ -closed set but not $\alpha gcl^\#$ -set in U .

Example 5.7 Let $U = \{a_1, a_2, a_3\}$ with $U/R = \{\{a_1\}, \{a_2\}, \{a_3\}\}$ and $X = \{a_2\}$. Then the sets in $\{\phi, \{a_2\}, U\}$ are called nano open and the sets in $\{\phi, \{a_1, a_3\}, U\}$ are called nano closed. Then $\{a_1, a_2\}$ is an $\alpha gcl^\#$ -set but not $ng^\#$ -closed set in U .

Proposition 5.8 Let U be a nano topological space. Then a subset K of U is nano closed if and only if it is both $ng^\#$ -closed and $\alpha gcl^\#$ -set.

Proof. Necessity is trivial. To prove the sufficiency, assume that K is both $ng^\#$ -closed and $\alpha gcl^\#$ -set. Then $K = G \cap H$, where G is αg -open and H is nano closed in U . Therefore, $K \subseteq G$ and $K \subseteq H$ and so by hypothesis, $ncl(K) \subseteq G$ and $ncl(K) \subseteq H$. Thus $ncl(K) \subseteq G \cap H = K$ and hence $ncl(K) = K$ i.e., K is nano closed in U .

We introduce the following definition.

Definition 5.9 A function $f: (U, \tau_R(X)) \rightarrow (V, \tau'_R(Y))$ is said to be $\alpha gcl^\#$ -continuous if for each nano closed set M of V , $f^{-1}(M)$ is an $\alpha gcl^\#$ -set in U .

Example 5.10 Let $U = \{a_1, a_2, a_3\}$ with $U/R = \{\{a_1\}, \{a_2\}, \{a_3\}\}$ and $X = \{a_1\}$. Then the sets in $\{\phi, \{a_1\}, U\}$ are called nano open and the sets in $\{\phi, \{a_2, a_3\}, U\}$ are called nano closed in U . Let $V = \{a_1, a_2, a_3\}$ with $V/R = \{\{a_1\}, \{a_2, a_3\}\}$ and $Y =$





Nethaji et al.,

$\{a_1, a_3\}$. Then the sets in $\{\phi, \{a_1\}, \{a_2, a_3\}, V\}$ are called nano open and the sets in $\{\phi, \{a_1\}, \{a_2, a_3\}, V\}$ are called nano closed in V . Let $f: (U, \tau_R(X)) \rightarrow (V, \tau'_R(Y))$ be the identity function. Then f is $n\alpha glc^\#$ -continuous function.

Remark 5.11 From the definitions it is clear that every nano continuous function is $n\alpha glc^\#$ -continuous but not conversely.

Example 5.12 Let $U = \{a_1, a_2, a_3\}$ with $U/R = \{\{a_1\}, \{a_2\}, \{a_3\}\}$ and $X = \{a_2\}$. Then the sets in $\{\phi, \{a_2\}, U\}$ are called nano open and the sets in $\{\phi, \{a_1, a_3\}, U\}$ are called nano closed in U . Let $V = \{a_1, a_2, a_3\}$ with $V/R = \{\{a_2\}, \{a_1, a_3\}\}$ and $Y = \{a_2, a_3\}$. Then the sets in $\{\phi, \{a_2\}, \{a_1, a_3\}, V\}$ are called nano open and the sets in $\{\phi, \{a_2\}, \{a_1, a_3\}, V\}$ are called nano closed in V . Let $f: (U, \tau_R(X)) \rightarrow (V, \tau'_R(Y))$ be the identity function. Then f is $n\alpha glc^\#$ -continuous function but not nano continuous. Since for the nano closed set $\{a_2\}$ in V , $f^{-1}(\{a_2\}) = \{a_2\}$, which is not nano closed in U .

Remark 5.13 $ng^\#$ -continuity and $n\alpha glc^\#$ -continuity are independent of each other.

Example 5.14 Let $U = \{a_1, a_2, a_3\}$ with $U/R = \{\{a_1, a_2\}, \{a_3\}\}$ and $X = \{a_1, a_2\}$. Then the sets in $\{\phi, \{a_1, a_2\}, U\}$ are called nano open and the sets in $\{\phi, \{a_3\}, U\}$ are called nano closed in U . Let $V = \{a_1, a_2, a_3\}$ with $V/R = \{\{a_1\}, \{a_2\}, \{a_3\}\}$ and $Y = \{a_1\}$. Then the sets in $\{\phi, \{a_1\}, V\}$ are called nano open and the sets in $\{\phi, \{a_2, a_3\}, V\}$ are called nano closed in V . Let $f: (U, \tau_R(X)) \rightarrow (V, \tau'_R(Y))$ be the identity function. Then f is $ng^\#$ -continuous function but not $n\alpha glc^\#$ -continuous.

Example 5.15 Let $U = \{a_1, a_2, a_3\}$ with $U/R = \{\{a_1\}, \{a_2\}, \{a_3\}\}$ and $X = \{a_1\}$. Then the sets in $\{\phi, \{a_1\}, U\}$ are called nano open and the sets in $\{\phi, \{a_2, a_3\}, U\}$ are called nano closed in U . Let $V = \{a_1, a_2, a_3\}$ with $V/R = \{\{a_1\}, \{a_2, a_3\}\}$ and $Y = \{a_2, a_3\}$. Then the sets in $\{\phi, \{a_2, a_3\}, V\}$ are called nano open and the sets in $\{\phi, \{a_1\}, V\}$ are called nano closed in V . Let $f: (U, \tau_R(X)) \rightarrow (V, \tau'_R(Y))$ be the identity function. Then f is $n\alpha glc^\#$ -continuous function but not $ng^\#$ -continuous. We have the following decomposition for nano continuity.

Theorem 5.16 A function $f: (U, \tau_R(X)) \rightarrow (V, \tau'_R(Y))$ is nano continuous if and only if it is both $ng^\#$ -continuous and $n\alpha glc^\#$ -continuous.

Proof. Assume that f is nano continuous. Then by Proposition 3.2 and Remark 5.11, f is both $ng^\#$ -continuous and $n\alpha glc^\#$ -continuous.

Conversely, assume that f is both $ng^\#$ -continuous and $n\alpha glc^\#$ -continuous. Let M be a nano closed subset of V . Then $f^{-1}(M)$ is both $ng^\#$ -closed set and $n\alpha glc^\#$ -set. By Proposition 5.8, $f^{-1}(M)$ is a nano closed set in U and so f is nano continuous.

REFERENCES

1. V. Antonyamy, *An analytical study of nano topology and its implications*, (Ph.D., Thesis, Madurai Kamaraj University, (2019).
2. K. Bhuvaneshwari and K. Mythili Gnanapriya, *Nano generalised closed sets*, International Journal of Scientific and Research Publications, 4(5)(2014),1-3.
3. K. Bhuvaneshwari and K. Ezhilarasi, *On nano semi generalized and nano generalized semi-closed sets*, IJMCAR. 4(3)(2014), 117-124.
4. K. Bhuvaneshwari and K. Mythili Gnanapriya, *On nano generalized continuous function in nano topological space*, International Journal of Mathematical Archive, 6(6)(2015), 182-186.
5. P. K. Dhanasekaran, S. Brindha and P. Sathishmohan, *On almost nano pre-continuous functions in nano topological spaces*, Advances and Applications in Mathematical Sciences, 18(11)(2019), 1477-1486.
6. S. Devi, M. Rameshpandi and R.Premkumar, *Properties of nano $g^\#$ -closed set in nano topological space*, (to appear).
7. S. Jeyashri, S. Chandrasekar and G. Ramkumar, *Totally nano sg continuous functions and slightly nano sg continuous functions in nano topological spaces*, International Journal of Mathematical Archive-9(5)(2018), 13-18.
8. M. Lellis Thivagar and Carmel Richard, *On nano forms of weakly open sets*, International Journal of Mathematics and Statistics Invention,1(1)(2013), 31-37.





Nethaji et al.,

9. M. Lellis Thivagar and C. Richard, *On nano continuity*, Mathematical Theory and Modeling, 7(2013), 32-37.
10. Z. Pawlak, *Rough sets*, International Journal of Computer and Information Sciences, 11(5)(1982), 341-356.
11. V. Rajendran, P. Sathishmohan and M. Chitra, *Nano $g^* \alpha$ -continuous functions in nano topological spaces*, Turkish Online Journal of Qualitative Inquiry (TOJQI), 12(5)(2021), 1156-1164.
12. P. Sathishmohan, V. Rajendran, A. Devika and P. Vani, *On nano semi-continuity and nano pre-continuity*, International Journal of Applied Research, 3(2)(2017), 76–79.
13. R. Thanga Nachiyar and K. Bhuvaneshwari, *Nano generalized A -continuous and nano A -generalized continuous functions in nano topological spaces*, International Journal of Mathematics Trends and Technology, 14(2)(2014),79-83.





Chemistry of Schiff Base Metal Complexes and their Biological Applications

Ankit Garg, Jyoti Sharma* and Nadeem Sharma

Department of Chemistry, MMEC, Maharishi Markandeshwar (Deemed to be University) Mullana, Ambala, Haryana, India.

Received: 27 Feb 2023

Revised: 20 Apr 2023

Accepted: 26 May 2023

*Address for Correspondence

Jyoti Sharma

Department of Chemistry,
MMEC,
Maharishi Markandeshwar (Deemed to be University)
Mullana, Ambala, Haryana, India.
E. Mail: jsharma117@gmail.com



This is an Open Access Journal / article distributed under the terms of the **Creative Commons Attribution License** (CC BY-NC-ND 3.0) which permits unrestricted use, distribution, and reproduction in any medium, provided the original work is properly cited. All rights reserved.

ABSTRACT

Schiff base metal complexes are a huge group of compounds which are characterized by the double bond present between carbon and nitrogen atom. Schiff base is a flexible ligand formed by condensing primary amines with aldehyde or ketone and due to their versatile nature, there has been a tremendous interest in this area over the past few decades. Schiff base compound plays an important role in various fields like medical and pharmaceuticals such as antimicrobial, anticancer, antimalaria, analgesic, antipyretic and so many others. They have also numerous applications in polymer and dye industries, food packaging and catalytic oxidizer in synthesizing organic compounds. Schiff base moieties thus found to have an exceptional place in vitro and in vivo experiment for synthesizing drugs for various bio-entities like bacteria, fungus, cancer cells etc. In this review article our concern is to focus on Schiff base metal complexes chemistry and their applications and characterizing tools used to evaluate them.

Keywords: Metal complex; Schiff base; Magnetic Susceptibility; Anti-cancer activity; Anti-microbial activity

INTRODUCTION

Transition metals are the main group elements which occupy central part in between s and p-block elements in groups 3 – 12 of the periodic table. These are metallic in nature. Transition metals are the elements which have partly filled d – subshells in their ground state or in any of their stable oxidation state. The incompletely filled d- orbitals of these transition metals allows them to synthesize coordination complexes by accepting electrons from lewis bases. Transition metals are well known for the formation of large number of coordination complexes in which they acts as

56896



**Ankit Garg et al.,**

Lewis acid by accepting a lone pair of electrons from the Lewis base. Thus, a ligand must be a Lewis base. One such example of a conjugating ligand with transition metals is Schiff base. The Schiff base metal compounds are well known.

Schiff base are taught to be one among the main category of ligands in coordination chemistry owing to their fascinating applications, structure, geometry and interesting properties [1-7]. Numerous Schiff bases and related metal complexes have been synthesized and evaluated those which include bidentate, tridentate, tetradentate, polydentate ligands. The varying denticity among Schiff base ligands makes them capable to form stable metal complexes those with like manganese, nickel, iron, cobalt, copper, Zinc etc. The Schiff base ligand shows much better antimicrobial activities than their corresponding metal complexes [8]. The chelating properties, easiness of production, biological uses and stability of transition metal complexes makes them significantly important [9-13].

The Schiff base metal complexes having N_2O_2 donor atoms possess crucial biological properties including anticancer and herbicidal activity [14-18]. Coordination of metal ions with Schiff base ligand has also received a lot of interest because of their fascinating geometry and flexible redox activity [19,20]. Schiff base is extensively used in synthetic organic chemistry. These are basically chemical compounds which are characterized by an imine group that has a double bond between C and N. The presence of imine group in these compounds helps us in clarifying the mechanism and racemization in biological setups [21]. The Schiff base is used as ligand in synthesizing coordination compounds incorporating metal ions. While these compounds are naturally occurring, most Schiff bases are man-made. Complexes formed using Schiff base ligands has now become a separate area of research not just in chemistry but in another areas of research those of engineering Sciences, biology, materials science and physical sciences [22-24].

Schiff base coordination complexes have exceptional biological uses analgesic [25], antibacterial [26], antifungal [27], antiviral [28], antioxidant [29], anticancer [30], anti-inflammatory [31], antitumor [32], as a local pain reliever, cardiovascular [33], insecticidal, in vitro cytotoxic [34], an antipyretic agent [35] and as an antiproliferative agent [36]. Schiff base metal complexes are also effectively used as antifertility drugs [37] and food packages [38]. Thus, Schiff base metal complexes comprises of therapeutically important uses in medicinal field [39-41]. Moreover, Schiff base coordination complexes also have diverse non- biological applications in polymer chemistry and mechanochemical synthesis [42]. Schiff base Cr^{3+} complex effectively detect harmful neurotoxic organophosphates in environment [43]. Schiff bases metal complex suitably serves as a catalyst in many biosystems, polymers, pharmaceuticals and medicinal chemistry [44]. Moreover, these complex are used to synthesize organic LED's which effectively helps to save energy. These OLED'S are highly efficient due to their long life use [45]. Beside biological applications, Schiff base complexes are employed in a variety of industries including polymer stabilizers, corrosion inhibitors, analytical chemistry, agrochemical industries, ion exchange, electrical conductivity catalysis and magnetic properties [46-49].

Chemistry of Schiff Base Ligands

The main class of chelating ligands and its corresponding metal complex in coordination chemistry is of Schiff base ligands. N, O and S donor atoms are well known for their important role in bonding to metal ions in variety of ways [50]. Hugo Schiff discovered Schiff base for the first time in 1864. Schiff bases are one among the adaptable compounds in organic chemistry. These are widely prepared via primary amine condensation with carbonyl group of aldehydes and ketones forming an imine i.e., Schiff base [51]. Schiff base are prepared in different solvents by eliminating a molecule of water as shown in Figure 1. The formation of Schiff base takes place through nucleophilic addition of amine to the carbonyl group. The process by which Schiff base is formed is shown in the Figures 2 – 4 below. Firstly an unstable addition product carbinolamine is formed on reaction of amine with an aldehyde or ketone. Since carbinolamine formed is an alcohol so it loses water by acid catalyzed dehydration. Aqueous acid or base can hydrolyze several Schiff bases back to their respective aldehydes, ketones and amines[40].



**Ankit Garg et al.,**

The Schiff base are stable solid compounds, but should be purified very carefully as they can undergo degradation. Schiff base also undergoes hydrolysis so their chromatographic purification is not recommended on silica gel [52]. Schiff base is equivalent to azomethine group having general formula $RCH=N-R'$, where R and R' stands for any alkyl, aryl, cycloalkyl or heterocyclic groups. These groups can be substituted in different ways in a compound. Nitrogen atom in a azomethine group is sp^2 hybridised and contains a lone pair of electron. Nitrogen atom contains a lone pair of electron which enhances the chelating capability of the Schiff base formed when N of azomethine group bonded through different donor groups around the C=N group. This chelating capability of the Schiff bases makes them versatile and flexible ligand in the coordination chemistry [53].

Synthetic Routes used to prepare Schiff Base Metal Complexes

Schiff base ligands is the most versatile and flexible series of ligand that have ability to interact through different metal ions to form coordination compounds. Till date many Schiff base complexes have been synthesized, structurally characterized and thoroughly investigated [54, 55]. Under suitable experimental conditions, metal salts are typically treated with Schiff's base ligands to produce metal complexes of the Schiff's bases. The two general methods adopted to synthesize these complexes are well known since the past two decades [56].

Direct Method

In this method both ligand and salt of metal ion are separately dissolved in a suitable solvent in appropriate (metal:ligand) molar ratio. After dissolution salt solution of metal ion and Schiff base are mixed together for complex formation. The resultant reaction mixture is then heated by refluxing. The precipitates obtained are then filtered, washed from distilled water and finally dried under desiccator. An example that easily describes the above process [57] is shown in Figure 5.

The different Schiff bases with diverse structural features can be synthesized with ease by replacing aldehydes or amines. The prepared Schiff base can have additional donor atom linkages such as of oxygen, phosphorous, sulphur etc. which can enhance their ability towards complexation with metal ion and for their biological activity. The properties of Schiff base metal compounds can also be enhanced with insertion of suitable groups in aliphatic or aromatic systems [58].

In situ Method

In this process, metal ions and Schiff bases are synthesized in a single step reaction [59] by adding salt of metal ion in same reaction after formation of Schiff bases by constant heating with refluxing. It has been observed that in number of cases the metallic ion combines first with one constituent and then it reacts with all other constituents, to form the desired complex. This method is also called template synthesis. An example [60] that easily describes the above process is shown in Figure 6.

Characterization Techniques

There are various physico – chemical methods available to investigate complex forming reactions. These techniques include elemental analysis, analytical and spectral techniques (NMR, IR, Mass) and electronic spectral techniques (UV-Vis spectroscopy), AAS, Molar conductance and susceptibility measurements. These methods are extremely sensitive, informative and popular.

Elemental Analysis

Elemental analysis is considered as the essential part of compound characterization in coordination chemistry. This technique proves to be a powerful tool in analyzing the purity of the compound. The empirical composition of the Novel Schiff base and its corresponding metal complexes for C, H, S and N contents can be analyzed using elemental analysis technique. This technique allows us to calculate empirical formula of the compound. This formula gives elemental composition in smallest possible set integer value for the elements present in the compound by mass [61, 62]. This method is highly efficient and does not involve any manipulation as the values obtained need not to be proved using chromatographs [63].



**Ankit Garg et al.,****IR Spectroscopy**

IR spectroscopy is the most extensively used tools for the detection of functional groups in particular sample of a compound. In IR spectroscopy Nujol or KBr medium in the range $200 - 400 \text{ cm}^{-1}$ are used to record spectra of a particular sample of compound [64]. The spectra obtained help us to know the coordinating site of a ligand and strength of bonds formed during the combination of a ligand with the metal ion in a complex and to know the vibrational mode in metal compounds [65, 66]. The IR data of the complex are thus, important to know the structure of the complex.

The IR spectra of the SB ligand and its corresponding metal complex indicates that the (C=N) stretching vibration band falls in the range $1500-1700 \text{ cm}^{-1}$ shifting to lower frequencies in most of the Schiff base metal complexes as expected. However, there are various complexes in which stretching vibration bands shifts to higher frequencies indicating that the coordination of a ligand with the metal ions is with N of the azomethine group. The experimental IR bands of Schiff base metal complexes in general are in compliance with the formerly recorded results [67]. The existence of sharp bands at 819 cm^{-1} corresponds to (C=S) group indicating the presence of schiff base in thione form, its shifting to lower frequency in complexation with central metal ion to about $37-55 \text{ cm}^{-1}$ indicated its coordination through S atom in metal complexes. Hydroxyl group (-OH) shows a broad band at 3293 cm^{-1} indicating the coordination of water molecules in the complex. But it is seen that the existence of water molecules in some of the complexes misinterpret with the band of hydroxyl group present in them. This is because water molecules show a broad band at about $3100-3500 \text{ cm}^{-1}$ in most of the metal complexes [68].

The presence of stretching bands at 1514 cm^{-1} and 1200 cm^{-1} in Schiff base corresponding to phenolic and enolic (C-O) group. The phenolic (C-O) stretching band shifts to higher frequency to about $5 - 26 \text{ cm}^{-1}$ in coordination of Schiff base with metal ions [38]. Moreover, IR spectra of Schiff base exhibits bands at $1604, 3439, 820$ and 1034 cm^{-1} corresponding to stretching vibrations in (C=N), (N-H), (C=S) and alcoholic (C-O) respectively confirms its existence. The (C=N) band of Schiff base shows a negative shift cm^{-1} by $9-44 \text{ cm}^{-1}$ in complexation with metal ions. Also shifting of (C=S) stretching to lower frequency to $40-57 \text{ cm}^{-1}$ on coordination with metal ions shows the involvement of S atom in coordination [69]. Moreover, Amani *et al* have synthesized furan Schiff base [5-hydroxymethylfuran-2-yl-methyleneaminoquinolin-2-one] H- MFMAQ, whose IR spectra have shown that the bands in the range $1637-1712 \text{ cm}^{-1}$ assigned to carbonyl and azomethine stretching. These vibrations gets lowered down by $14-19 \text{ cm}^{-1}$ due to oxygen carbonyl and by $12-16 \text{ cm}^{-1}$ due to nitrogen azomethine, showing involvement of both in formation of complex. This complex shows furan ring vibration at 1618 cm^{-1} upon chelation this band shifts to lower frequency due to formation of (C-O-C) bond. In addition to these bands three new bands at $543-552, 433-438,$ and $412-416 \text{ cm}^{-1}$ are present due to the formation of M-O (carbonyl), M-O (phenol), M-N (azomethine) and (M-Cl) bands in the metal complex [70].

Molar Conductance

Molar conductance is the most useful tool used to investigate the electrolytic and non – electrolytic nature, geometry and structure of inorganic metal complexes. The Molar conductance of the schiff base metal complexes is calculated in 10^{-3} M solution at room temperature using solvents dimethylformamide (DMF) and Chloroform (CHCl_3). The results obtained can be applied to know the geometry and structure of the complexes. The complexes which shows lower value of molar conductance in the range $0.03 - 44.37 \text{ S cm}^2 \text{ mol}^{-1}$ indicates that the complex behaves as non – electrolyte. The binuclear complexes on the other hand shows higher value of molar conductance more than $50 \text{ cm}^2 \text{ mol}^{-1}$ [71].

Magnetic Susceptibility Measurements

The magnetic moment of the complex is calculated using magnetic susceptibility measurements as magnetic moment cannot be determined directly. This magnetic moment measurement values obtained are used to find molecular formulae, hybridization, shape and geometry of metal complexes. From the gram magnetic susceptibility values, the magnetic moment values are calculated in BM and the data obtained is presented in form of a table. The results obtained helps to conclude the high spin or low spin nature of M-L. Moreover, Magnetic susceptibility



**Ankit Garg et al.,**

measurements are carried out to know extend of pairing up of electrons to evaluate magnetic nature of complex i.e., whether the complex is diamagnetic or paramagnetic in nature [72]. Raman [73] et al has synthesized Schiff base metal complexes in which the value of magnetic moment for Cu (II) compound is 1.90 BM which indicates the distorted octahedral geometry of the central metal atom. Also the Co (II) and Ni (II) complexes have a magnetic moment of 4.18 BM and 2.8 BM respectively. This indicates that the intervening ligands in them are in high spin and forms six coordinated octahedral geometry around the central metal atom. The expected d^{10} configuration of Zn (II) complex shows its diamagnetic nature.

UV – Visible Spectroscopy

The UV spectroscopy is used to measure the multiple bonds or aromatic conjugation present within the molecules of compound. UV – visible spectra for the coordination compounds is taken in the range of $250-1000\text{ cm}^{-1}$. The UV visible absorption spectra and magnetic moment data works as evidence in evaluating the results obtained through other methods of structural determination. The geometry of the complex about the central metal atom is predicted on the basis of the results obtained from UV visible absorption spectra and with the data obtained from magnetic moment values. The UV- visible Spectroscopy uses d-d transitions of metal ion complexes [74]. For the Schiff base ligands and its corresponding complexes UV visible absorption spectra is recorded at RT using dimethylmethlysulphoxide (DMSO), dimethylformamide (DMF) and Chloroform (CHCl_3) as solvents [75].

Biological Applications

Antibacterial and Antifungal Activity

The properties that characterizes Schiff base metal compounds depends on the donating nature of ligands, nature of central metal atom, structure of ligand and its complex, interaction between metal atom and ligand and on the nature of solvent used [76, 77]. Schiff base based metal complexes shows excellent antimicrobial properties against many bacteria, fungi and cancer causing microbes [78, 79]. The presence of chelating donor sites such as N, O and S in Schiff base ligand enhances their antimicrobial properties in coordinating with the metal ion [80, 81]. The major factors which control the antimicrobial properties of coordination complexes are:

- Chelation
- Cell Permeability and
- Lipophilicity of cell

The bidentate and tridentate Schiff base metal complexes synthesized so far are observed to be very stable [82,83, 84, 85].The metal complex shows more antimicrobial properties than its intervening ligand [86] as because of chelation cell permeability of metal increases. Also chelation reduces polarity on metal ion thereby increasing its lipophilic nature [87, 88, 89]. The increasing lipophilicity favours cell permeability. Thus metal atoms penetrate efficiently through lipid layer of microbes and destroy them by blocking their active sites [90,91]. Thus chelation is one of the ways to improve antimicrobial activities of coordination complexes

Anticancer Activity

Cancer is lethal to life as it causes growth of uncontrolled abnormal cells in body which destroys normal body tissues. This abnormal increase in number of cells in a tissue or organ forms a cluster of proliferative cells. This excessive proliferation gives rise to a mass of cells which is initially called as tumor. Tumor can be Benign or either Malignant. Most of the benign tumors are harmless as they do not attack their nearby tissues and do not spread uncontrollably among various parts of the body. Further more Benign tumors remain localized at a specific place in body. When benign tumors locate in specific area of brain these can be life threatening but can be removed surgically and they generally never returned back. On the other hand, malignant tumors mark the beginning of cancer causing cells in the body. In malignant tumor cells become abnormal and spread throughout tissues and organs uncontrollably and keeps on re-dividing, breaks up and gets mixed up with bloodstream or lymphatic system. Once this happens, they migrate to many other sites in the body to form new tumors in all other organs as well. These cell uses oxygen and nutrients to divide and form tumors. In this condition the immune system of the body gets weaken and the body will not be able to function normally. Thus, the process in which cancer cells spread to various sites through body fluids to form secondary tumor is called metastasis [92]. Cancer can be treated using chemotherapy,



**Ankit Garg et al.,**

surgery, radiation therapy, hormone therapy, immune therapy etc. Some techniques which are used to diagnose cancer are Biopsy, Radiography, MRI etc. Many drugs have been synthesized so far to cure cancer in the pharmaceutical field.

In recent years, the advancement in the field of bio-inorganic chemistry, pharmaceutical and medicinal chemistry has enhanced the interest in biological uses of schiff base incorporating metal complexes in various fields especially in their anticancer property. The discovery of many schiff base complexes for the effectiveness against antitumor cell lines has fascinated the researchers to synthesize novel anticancer drugs having no side effects. A number of schiff base metal complexes having significant antitumor activity have been reported [93-99]. Schiff base metal complexes are used as anticancer agents due to their stability, cytological compatibility and flexibility to bind with biomolecules [100]. In the present time, the development of drugs with probable healing effect with minimum side effects has been produced. Many Schiff base metal complexes with antiproliferative action has been synthesized and examined over different cancer cell lines and investigated by MTT assay [101].

CONCLUSION

Schiff bases ligands and their corresponding transition metal complexes are a group of compounds with pharmacological potential. These are one among those molecules which have potential to cure many human diseases. In this review, we presented general mechanism used to synthesize Schiff base metal complexes and their characterization tools like elemental analysis, molar conductivity, IR Spectroscopy, Molar Susceptibility measurements, UV-Visible Spectroscopy, antimicrobial activity, anticancer activity used to evaluate them and they can be further used in pharmaceutical industry as antimicrobial and anticancer agents for mankind, after testing its toxicity to human beings.

ACKNOWLEDGMENTS

Authors are thankful to the authorities of Maharishi Markandeshwar (Deemed to be University) Mullana, Ambala, Haryana for providing the necessary support and help required to publish this article.

REFERENCES

1. Hughes MN. The Inorganic Chemistry of Biological Processes, 2nd ed. New York (Chichester): John Wiley and Sons; 1981.
2. Tarafder MH, Saravanan N, Crouse KA, Ali AM. Coordination chemistry and biological activity of Ni(II) & Cu(II) ion complexes with nitrogen-sulphur donor ligands derived from S benzyldithiocarbamate (SBDT). Transit Met Chem. 2001 Dec;26(6):613-618.
3. Yimer AM; Baraki T, Upadhyay RK; Khan MA. Spectro-magnetic and antimicrobial studies on some 3d metal complexes with ethylenediamine of ortho-hydroxyphenylglyoxal. Am J Appl Chem. 2014 March;2(1):15-18.
4. Abu-Dief AM, Mohamed IMA. A review on versatile applications of transition metal complexes incorporating Schiff bases. Beni-Suef Univ J Basic Appl Sci. 2015 June;4(2):119-133.
5. Tunde L, Yusuf Segun D, Oladipo, Zamisa S, Kumalo HM, Lawal IA, Lawal MM, Mabuba N. Design of new Schiff base copper(II) complexes: synthesis, crystal structures, DFT study, and binding potency toward cytochrome. ACS Omega. 2021 May;6(21):13704-13718.
6. Nguyen QT, Pham Thi PN, Nguyen VT. Synthesis, characterization, and in vitro cytotoxicity of unsymmetrical tetradentate Schiff base Cu(II) and Fe(III) complexes. BioinorgChemAppl. 2021 May; Article ID 6696344:1-10.
7. Borase JN, Mahale RJ, Rajput SS, Shirsath DS. Design, synthesis and biological evaluation of heterocyclic methyl substituted pyridine Schiff base transition metal complexes. SN Appl Sci. 2021 Jan [cited 25 Jan 2021]; 3(0):197.



**Ankit Garg et al.,**

8. Emriye, A.Y. Synthesis and Characterization of Schiff Base. 1-Amino-4-Methylpiperazine Derivatives. CBU J Sci. 2016 Dec;12(3):375-392.
9. Ghanghas P, Choudhary A, Kumar D, Poonia K. Coordination metal complexes with Schiff bases: useful pharmacophores with comprehensive biological applications. InorgChem Comm. 2021 May;130:article 108710:1-29.
10. Gaber M, El-Wakiel N, El-Baradie K, Hafez S. Chromone Schiff base complexes: synthesis, structural elucidation, molecular modeling, antitumor, antimicrobial, and DNA studies of Co(II), Ni(II), and Cu(II) complexes. J IranianChem Soc.2019 Sept;16:169–182.
11. BuldurunK, Turan N, Savci A, Colak N. Synthesis, structural characterization and biological activities of metal (II) complexes with Schiff bases derived from 5 bromosalicylaldehyde: Ru (II) complexes transfer hydrogenation. J Saudi Chem Soc. 2019 Feb;23(2):205–214.
12. ShayganS, Pasdar H,Foroughifar N, Davallo M, Motiee F. Cobalt (II) complexes with Schiff base ligands derived from terephthalaldehyde and ortho-substituted anilines: Synthesis, characterization and antibacterial activity. Appl Sci. 2018 March;8(3):1-12.
13. Cotton SA. Establishing coordination numbers for the lanthanides in simple complexes. C RChim. 2005 Feb;8(2):129–145.
14. Al ZoubiW. Biological activities of Schiff bases and their complexes: a review of recent works. Inter. J Org Chem. 2013 Oct;3:73–95.
15. Orojloo M, Zolgharnein P, Solimannejad M, Amani S. Synthesis and characterization of cobalt (II), nickel (II), copper (II) and zinc (II) complexes derived from two Schiff base ligands: spectroscopic, thermal, magnetic moment, electrochemical and antimicrobial studies. InorganicaChimActa. 2017 Oct;467:227–237.
16. Mohapatra RK, Sarangi AK, Azam M, El Ajaily MM, Kudrat-E-ZahanMd, Patjoshi SB, Dash DC. Synthesis, structural investigations, DFT, molecular docking and antifungal studies of transition metal complexes with benzothiazole based Schiff base ligands. J MolStruct. 2019 March;1179:65–75.
17. Wu D, Guo L, Li SJ. RETRACTED: Synthesis, structural characterization and anti-breast cancer activity evaluation of three new Schiff base metal (II) complexes and their nanoparticles. J MolStruct. 2020 Jan;1199:1-11.
18. Gandhi SR, Kumar DS, Tajudeen SS, Sheriff AKI. Studies on synthetic, structural characterization, thermal, DNA cleavage, antimicrobial and catalytic activity of tetradentate (N4) Schiff base and its transition transition metal complexes. Asian J Chem. 2017 March;29(5): 1076–1084.
19. Singh HL, Varshney AK. Synthetic structural and biochemical studies of organotin(IV) with schiff bases having nitrogen and sulfur donor ligands. BioinorgChem Appl. 2006 March;2006:1-7.
20. Arumugam AP, Guhanathan S, Elango G. Co (II), Ni (II) and Cu (II) Complexes with Schiff Base Ligand: Syntheses, Characterization, Antimicrobial Studies and Molecular Docking Studies. SOJ Mater Sci Eng. 2017 Oct;5(2):1-12.
21. Yahyazadeh, A.; Azimi, V. Synthesis of Some Unsymmetrical New Schiff Base from azo dyes. European Chemical Bulletin. 2013 March;2(7):453-455.
22. Sharma J, Dogra P, Sharma N, Ajay. Applications of coordination compounds having Schiff bases: A review. AIP Conf Proc 2019 Aug;2142:060002-1–060002-5.
23. EglofR, Piotr P, Bogumil B, Franz B. Schiff bases in biological systems. Curr Org Chem 2009 Feb;13(3):241–249.
24. Garg A, Sharma J. Copper complexes as potential catalytic, electrochemical and biochemical agents. Mat Today Proce. 2022 June;62(3):1632-1635.
25. Fareed, G.; Rizwani, G.; Ahmed, M.; Versiani, M.; Fareed, N. Schiff bases derived from 1-aminoanthraquinone: A new class of analgesic compounds. Pak J Sci Ind Res A: Phys Sci. 2017 June;60(3):122-127.
26. Malik A, Goyat G, Verma KK, Garg S. Synthesis, Spectral and Antimicrobial Studies of Some O-Vanillin-2-aminopyridine Schiff Base Complexes of OrganylTellurium(IV). ChemSci Trans. 2018;7(2):329–337.
27. Kakanejadifard, A.; Khojasteh, V.; Zabardasti, A.; Azarbani, F. New Azo-Schiff Base Ligand Capped Silver and Cadmium Sulfide Nanoparticles Preparation, Characterization, Antibacterial and Antifungal Activities. Org Chem Res. 2018 June;4(2):210-226.



**Ankit Garg et al.,**

28. Jarrahpour A, Khalili D, De Clercq E, Salmi C, Brunel JM. Synthesis, antibacterial, antifungal and antiviral activity evaluation of some new bis-Schiff bases of isatin and their derivatives. *Molecules*. 2007 Aug;12(8):1720-1730.
29. Kalaiarasi G, Dharani S, Puschmann H, Prabhakaran R. Synthesis, structural characterization, DNA/protein binding and antioxidant activities of binuclear Ni(II) complexes containing ONS chelating ligands bridged by 1,3-bis(diphenylphosphino)propane. *InorgChem Comm*. 2018 Nov;97:34-38.
30. More G, Bootwala SZ, Mascarenhas J, Aruna K. Anti-Microbial And Anti-Tubercular Activity Evaluation Of Newly Synthesized Zinc Complexes of Amino thiophene Schiff Bases. *Int J Pharm Sci Res*. 2018 July;9(7):3029-3035.
31. Hanif M, Hassan M, Rafiq M, Abbas Q, Ishaq A, Shahzadi S, Seo SY, Saleem M. Microwave-Assisted Synthesis, In Vivo Anti-Inflammatory and In Vitro Anti-Oxidant Activities, and Molecular Docking Study of New Substituted Schiff Base Derivatives. *Pharm Chem J*. 2018 Aug;52(5):424-437.
32. Luo H, Xia Y, Sun B, Huang L, Wang X, Lou H, Pan WD, Zhang XD. Synthesis and Evaluation of in Vitro Antibacterial and Antitumor Activities of Novel N,N-Disubstituted Schiff Bases. *Biochem Res Int*. 2017 June;2017:1-10.
33. Al-Shemary RK. Design, Synthesis and Biological Evaluation of Schiff Bases and Their Co(II), Cu(II), Ni(II) Chelates from Derivative Containing Indole Moiety Bearing-Triazole. *EurChem Bull*. 2017 June;10(6):433-439.
34. Bagihalli GB, Avaji PG, Patil SA, Badami PS. Synthesis, spectral characterization, in vitro antibacterial, antifungal and cytotoxic activities of Co (II), Ni (II) and Cu (II) complexes with 1, 2, 4-triazole Schiff bases. *Eur J Med Chem*. 2008 Dec;43(12):2639-2649.
35. Murtaza S, Akhtar MS, Kanwal F, Abbas A, Ashiq A, Shamim S. Synthesis and biological evaluation of schiff bases of 4-aminophenazone as an anti-inflammatory, analgesic and antipyretic agent. *J Saudi Chem Soc*. 2017 Jan;21(1):S359-S-372.
36. Catalano A, Sinicropi MS, Lacopetta D, Ceramella J, Mariconda A, Rosano C, Scali E, Saturnino C, Longo P. A Review on the Advancements in the Field of Metal Complexes with Schiff Bases as Antiproliferative Agents. *Appl Sci*. 2021 June;11(3):1-18.
37. Chaudhary A, Singh A. Synthesis, Characterization, and Evaluation of Antimicrobial and Antifertility Efficacy of Heterobimetallic Complexes of Copper (II). *J Chem*. 2017 Oct;2017:1-9.
38. Kumar A, Choudhary A, Kaur H, Mehta S, Husen A. Metal-based nanoparticles, sensors, and their multifaceted application in food packaging. *J Nanobiotech*. 2021 Aug;19(1):1-25.
39. Soroceanu A, Bargan A. Advanced and Biomedical Applications of Schiff-Base Ligands and Their Metal Complexes: A Review. *Crystals*. 2022 Oct;12(10):1-15.
40. Khan T, Zehra S, Alvi A, Fatima U, Lawrence AJ. Medicinal Utility of Some Schiff Bases and their Complexes with First transition series metals: (A-Review). *Orient J Chem*. 2021 Oct;37(5):1051-1061.
41. Chaudhary NK, Guragain B, Chaudhary SK, Mishra P. Schiff base metal complex as a potential therapeutic drug in medical science: A critical review. *BIBECHANA*. 2021 Jan;18(1):214–230.
42. Ohn N, Kim JG. Mechanochemical Post-Polymerization Modification: Solvent-Free Solid-State Synthesis of Functional Polymers. *ACS Macro Letters*. 2018 April;7(5):561-565.
43. Singh J, Kaur V, Singh R, Bhardwaj VK. Exploration of solvent responsive Cr³⁺-Schiff base conjugates for monitoring Cr³⁺ ions and organophosphates: Fabrication of spot-testing devices. *SSA*. 2018 Aug;201:46-53.
44. More MS, Joshi PG, Mishra YK, Khanna PK. Metal complexes driven from Schiff bases and semicarbazones for biomedical and allied applications: A review. *Mater Today Chem*. 2019 Dec;14:1-22.
45. Kagatkar S, Sunil D. Schiff Bases and Their Complexes in Organic Light Emitting Diode Application. *J Electron Mater*. 2021 Oct;50:1-16.
46. Arulmurugan S, Kavitha HP, Venkatraman BR. Biological Activities of Schiff Base and Its Complexes: A Review. *RJC*. 2010 March;3(3): 385-410.
47. Smirnov AS, Martins LMDRS, Nikolaev DN, Menzhos RA, Gurzhiy VV, Krivenko AG, Nikolaenko DN, Belyakov AV, Garabadzhiu AV, Devidovich PB. Structure and catalytic properties of novel copper isatin Schiff base complexes. *NJC*. 2019;43(1):188–198.
48. Tan Y, Huang J, Chi T, Lu H, Sun J. Synthesis, structure and magnetic property of a copper(II)-cobalt(II) heteronuclear complex with Schiff base ligand. *Inorg. Nano-Met. Chem*. 2019 Dec;50(3):110–113.



**Ankit Garg et al.,**

49. Boulkedid AL, Beghidja A, Beghidja C, Guari Y, Larionova J, Long, J. Synthesis, structure and magnetic properties of a series of dinuclearheteroleptic Zn^{2+}/Ln^{3+} Schiff base complexes: effect of lanthanide ions on the slow relaxation of magnetization. Dalton Trans.2019 July;48(32):11637–11641.
50. Pier GC. Metal-salenschiiff base complexes in catalysis practical aspects. Royal Soc Chem.2004 Aug;33(7):410-421.
51. Raisanen M. Schiff base complexes and their assemblies on surface. Academic Dissertation.Faculty of Science of University of Helsinki, for the public criticism in Auditorium A110 of the Department of Chemistry, A.I. VirtasenAukio, Helsinki, 13 June 2007.
52. Saqhatforoush LA,Aminkhani A, Ershad S, Karimnezhad G, Ghammamy S, Kabiri R. Preparation of zn(ii) and cadmium(ii) complexes the tetradentateschiff base ligand 2-((e)-(2-(2-(pyridinje-2-yl)-ethylthio)ethylimino)methyl)- 4-bromophenol (PytBrsalH). Molecules. 2008 Apr;13(4):804 -811.
53. Keypour H, Salehzadeh S, Parish RV. Synthesis of two potentially heptadentate (N_4O_3) schiff base ligand derived from condensation of tris-(3-amino propyl)amine and salicylaldehyde or 4-hydroxysalicylaldehyde Ni(II) and Cu(II) complexes of the former ligand. J. Molecules. 2002 Feb;7(2):140-144.
54. Kargar H, Ardakani AA, Tahir MN, Ashfaq M, Munawar KS.Synthesis, spectral characterization, crystal structure determination and antimicrobial activity of Ni(II), Cu(II) and Zn(II) complexes with the Schiff base ligand derived from 3,5-dibromosalicylaldehyde. J MolStruct.2021 Apr;1229:1-9.
55. Almasi M, Vilkova M, Bednarcik J. Synthesis, characterization and spectral properties of novel azo-azomethine-tetracarboxylic Schiff base ligand and its Co(II), Ni(II), Cu(II) and Pd(II) complexes. InorganicaChimActa.2021 Jan;555:1-22.
56. Yamada S. Recent Aspects of the Stereochemistry of Schiff-Base-Metal Complexes. S CoordChem Rev. 1966 Dec;1(4):415-420.
57. Kumar D, Chadda S, Sharma J, SurainP. Syntheses, Spectral Characterization, and Antimicrobial Studieson the Coordination Compounds of Metal Ions with Schiff BaseContaining Both Aliphatic and Aromatic Hydrazide Moieties. BioinorgChem Appl.2013 Oct;2013:1-10.
58. Kumar D, Kumar A, Sharma J. Physico-Chemical Studies on the Coordination Compounds ofThiazolidin-4-One. J Chem.2013Oct;2013:1-7.
59. Gimeno N, Vilar R. Anions as templates in coordination and supramolecular chemistry. CoordChem Rev. 2006 Dec;250(23-34):3161-3189.
60. Jacob B. Synthesis, characterization and antimicrobial studies of N, O, S containing ligands and their transition metal complexes. Academic Dissertation. Department of Chemistry Christ University Bengaluru, India, December 2016.
61. Mohammed YA. Chemical synthesis, spectral characterization and antimicrobial studies on complexes of Ni(II), Cu(II) and Zn(II) with N, N-di (o-hydroxybenzenoylemethylene) ethylenediamine. Amer J Bio Sci.2014 Nov;2(6-1):22-34.
62. Kleimark J. Mechanistic investigations of transition metal catalyzed reactions," Department of Chemistry, University of Gothenburg, 2012.
63. Kandiooller W, Theiner J, Kepplera BK, Kowol CR. Elemental analysis: an important purity control but prone to manipulations. InorgChem Frontiers. 2022 Dec;9(3):412–416.
64. Khan SA, Khan SB, Khan LU, Farooq A. Fourier Transform Infrared Spectroscopy: Fundamentals and Application in Functional Groups and Nanomaterials Characterization. In Handbook of MaterialsCharacterization, 1sted, Sharma SK, Eds, Publisher: Springer International Publishing AG, part of Springer Nature, India, 2018;1:317-344.
65. Magalhaes S,Goodfellow BJ, NunesA. FTIR spectroscopy in biomedical research: how to get the most out of its potential. ApplSpectroscRev.2021 Jul;56(8-10):869-907.
66. Dutta A. Fourier Transform Infrared Spectroscopy. In Spectroscopic Methods for Nanomaterials Characterization, Illustrated ed. Thomas S, Thomas R,Zachariah AK. Eds, Publisher: Elsevier, USA, 2017;2:73-93.
67. Raman N, Ravichandran S, Thangaraja C. Copper(II), Cobalt(II), Nickel(II) and Zinc(II) complexes of schiff base derived from benzil-2,4-dinitrophenylhydrazone with aniline. J Chemical SocInd Aca Soc.2004 Jul, 116(4), 116-215.



**Ankit Garg et al.,**

68. Mohammed YA. Synthesis, characterization and antimicrobial study on Ni(II), Cu(II) and Zn(II) Complexes with N,N-di (o-hydroxybenzenoylmethylene) ethylenediamine. IJSBAR. 2012;6(1):58-63.
69. Sharma J, Kumar D, Garg A, Sharma I, Sharma N. Synthesis, characterization and biological screening of Mn(II), Co(II), Ni(II), Cu(II) and Zn(II) ions with schiff base possessing thiosemicarbazone moiety. Rasayan J Chem. 2021;14(5):200-205.
70. Alturiqi AS, Alaghaz ANMA, Ammar RA, Zayed ME. Synthesis, Spectral Characterization, and Thermal and Cytotoxicity Studies of Cr(III), Ru(III), Mn(II), Co(II), Ni(II), Cu(II), and Zn(II) Complexes of Schiff Base Derived from 5-Hydroxymethylfuran-2-carbaldehyde. J Chem. 2018 May;2018:1-17.
71. Singh J, Kaur V, Singh R, Bhardwaj VK. Exploration of solvent responsive Cr³⁺-Schiff base conjugates for monitoring Cr³⁺ ions and organophosphates: Fabrication of spot-testing devices. Spectrochim Acta A Mol Biomol. 2018 Aug;201:46-53.
72. Al-Ahdal Z, Jadhav S, Pathrikar R, Shejul S, Rai MJ. Synthesis, Magnetic Susceptibility, Thermodynamic Study and Bio-Evaluation of Transition Metal Complexes of New Schiff Base Incorporating INH Pharmacophore Polycyclic Aromat Compds. 2021 Dec;43(1):1-15.
73. Raman N, Ravichandran S, Thangaraja C. Copper(II), cobalt(II), nickel (II) and zinc (II) complexes of schiff base derived from benzil-2,4-dinitrophenylhydrazone with aniline. J Chem Soc Indian Acad Soc. 2004 Jul;4:116- 215.
74. Forster H. UV/VIS Spectroscopy. Characterization I. Molecular Sieves – Science and Technology, 2004th ed, Karge HG, Weitkamp J, Eds; Publisher: Springer, Berlin, Heidelberg, 2004;4:337-426.
75. Naureen PB, Miana GA, Shahid K, Asghar M, Tanveer S, Sarwar. A. Iron (III) and zinc (II) monodentate Schiff base metal complexes: Synthesis, characterisation and biological activities. J Mol Struct. 2021 May;1231:1-12.
76. Nair R, Shah A, Baluja S, Chanda S. Synthesis and antibacterial activity of some Schiff base complexes. J Serb Chem Soc. 2006;71(7):733–744.
77. Ejiah FN, Fasina TM, Familoni OB, Ogunsola FT. Substituent effect on spectral and antimicrobial activity of Schiff bases derived from aminobenzoic acids. Adv Bio Chem. 2013 Sept;3(5):475-479.
78. Yamgar RS, Atram RG, Nivid Y, Nalawade S, Sawant SS. Novel Zinc(II) Complexes of Heterocyclic Ligands as Antimicrobial Agents: Synthesis, Characterization, and Antimicrobial Studies. Bio Chem Appl. 2014 Feb;2014:1-10.
79. Al-Zoubi W. Biological Activities of Schiff Bases and Their Complexes: A Review of Recent Works. Int J Org Chem. 2013 Nov;3(3A):73-95.
80. Tumer M, Ekin D, Tumer F, Bulut A. Synthesis, characterization and properties of some divalent metal(II) complexes: Their electrochemical, catalytic, thermal and antimicrobial activity studies. Spectrochim Acta Part. 2007 Jul;67(3-4):916–929.
81. Aiyelabola TO, Ojo IA, Adebajo AC, Ogunlusi GO. Synthesis, characterization and antimicrobial activities of some metal(II) amino acids complexes. Adv Bio Chem. 2012 Aug;2(3):268-273.
82. Paez PL, Albesa I, Bazan CM, Becerra MC, Bongiovanni ME, Arguello GA. Oxidative Stress and Antimicrobial Activity of Chromium(III) and Ruthenium(II) Complexes on Staphylococcus aureus and Escherichia coli. Bio Med Res Int. 2013 Sept;2013:1-7.
83. Yusuf TL, Oladipo SD, Zamisa S, Kumalo HM, Lawal, IA, Lawal MM, Mabuba N. Design of New Schiff-Base Copper(II) Complexes: Synthesis, Crystal Structures, DFT Study, and Binding Potency toward Cytochrome P450A4. ACS. 2021 May;6(21):13704–13718.
84. Anaconda JR, Santaella J, Al-Shemary RKR, Amenta J, Otero A, Ramos C, Celis F. Ceftriaxone-based Schiff base transition metal(II) complexes. Synthesis, characterization, bacterial toxicity, and DFT calculations. Enhanced antibacterial activity of a novel Zn(II) complex against S. aureus and E. coli. J Inorg Biochem. 2021 Oct;223:1-11.
85. Anaconda JR, Noriega N, Camus J. Synthesis, characterization and antibacterial activity of a tridentate Schiff base derived from cephalothin and sulfadiazine, and its transition metal complexes. Spectrochim Acta Part A: Mol Biomol Spectro. 2015 Feb;137:16-22.
86. Mobinikhaledi A, Zendejdel M, Safari P, Hamta A, Shariatzadeh SM. Synthesis and Biological Activity Evaluation of Some Binuclear Metal Complexes of Cu(II) and Zn(II) with Tridentate Schiff Base Ligands. Synthesis and Reactivity in Inorganic, Metal-Organic Nano-Metal Chem. 2012 Mar;42(2):165-170.



**Ankit Garg et al.,**

87. Chang LE, Simmers C, Knight DA. Cobalt Complexes as Antiviral and Antibacterial Agents. *Pharmaceuticals*. 2010 May;3(6):1711-1728.
88. Dhaveethu K, Ramachandramoorthy T, Thirunavukkarasu K. Microwave-assisted Synthesis of Mixed Ligand Complexes of Zn(II), Cd(II) and Hg(II) Derived from 4-aminopyridine and Nitrite Ion: Spectral, Thermal and Biological Investigations. *J Korean Chem Soc*. 2013 Jun;57(3):341-351.
89. Jigna P, Pranav I, Rathish N, Shipra B, Sumitra C. Synthesis and antibacterial activity of some Schiff bases derived from 4-aminobenzoic acid. *J Serb Chem Soc*. 2005 Oct;70(10):1155–1161.
90. Bagihalli GB, Avaji PG, Patil SA, Badami PS. Synthesis, spectral characterization, in vitro antibacterial, antifungal and cytotoxic activities of Co(II), Ni(II) and Cu(II) complexes with 1,2,4-triazole Schiff bases. *Eur J Med Chem*. 2008 Dec;43(12):2639-2649.
91. Baldaniya BB, Patel PK. Synthesis, Antibacterial and Antifungal Activities of s-Triazine Derivatives. *E-J Chem*. 2009 Feb;6(3):673-680.
92. Matela G. Schiff Bases and Complexes: A Review on Anti-Cancer Activity. *Anticancer Agents Med Chem*. 2020 Nov;20(16):1908-1917.
93. Shijua C, Arish D, Kumaresan S. Novel water soluble Schiff base metal complexes: Synthesis, characterization, antimicrobial-, DNA cleavage, and anticancer activity. *J Mol Struct*. 2020 Dec;1221:2-8.
94. Howsai HB, Basaleh AS, Abdellattif MH, Hassan WMI, Hussien MA. Synthesis, Structural Investigations, Molecular Docking, and Anticancer Activity of Some Novel Schiff Bases and Their Uranyl Complexes. *Biomolecules*. 2021 Aug;11(8):1-23.
95. Alyar S, Ozmen UO, Adem S, Alyar H, Bilen E, Kaya A. Synthesis, spectroscopic characterizations, carbonic anhydrase II inhibitory activity, anticancer activity and docking studies of new Schiff bases of sulfa drugs. *J Mol Struct*. 2020 Jan;1223:128911.
96. Ramilo Gomes F, Addis Y, Tekamo I, Cavaco I, Campos CD, Pavan FR, Gomes CSB, Brito V, Santos AO, Domingues F, Luis A, Marques MM, Pessoa JC, Ferreira S, Silvestre S, Correia I. Antimicrobial and antitumor activity of S-methyl dithiocarbamate Schiff base zinc(II) complexes. *J Inorg Biochem*. 2021 March;216:111331.
97. Wongsuwan S, Chatwichien J, Pinchaipat B, Kumphune S, Harding DJ, Harding P, Boonmak J, Youngme S, Chotima R. Synthesis, characterization and anticancer activity of Fe(II) and Fe(III) complexes containing N-(8-quinolyl)salicylaldehyde Schiff base ligands. *J Biol Inorg Chem*. 2021 Feb;26:327–339.
98. Tsakanova G, Stepanyan A, Arakelova E, Ayvazyan V, Tonoyan V, Arakelyan A, Hildebrandt G, Schultke E. The radioenhancement potential of Schiff base derived copper (II) compounds against lung carcinoma in vitro. *PLoS one*. 2021 Jun;16(6):1-28.
99. Melha KSA, Al-Hazmi GA, Althagafi I, Alharbi A, Keshk AA, Shaaban F, El-Metwaly N. Spectral, Molecular Modeling, and Biological Activity Studies on New Schiff's Base of Acenaphthaquinone Transition Metal Complexes. *Bioinorg Chem Appl*. 2021 Mar;2021:1-17.
100. Kuzmin VE, Artemenko AG, Lozytska RN, Fedtchouk AS, Lozitsky AS, Muratov EN, Mescheriakov AK. Investigation of anticancer activity of macrocyclic Schiff bases by means of 4D-QSAR based on simplex representation of molecular structure. *SAR and QSAR Environ Res*. 2005 Jan;16(3):219–230.
101. Abd El-halim HF, Omar MM, Mohamed GG. Synthesis, structural, thermal studies and biological activity of a tridentate Schiff base ligand and their transition metal complexes. *Spectrochim Acta Part A: Mol Biomol Spectro*. 2011 Jan;78(1):36–44.





Ankit Garg et al.,

<p>Where 'R' can be Hydrogen, Alkyl Group or Aryl Group</p>	
<p>Fig. 1: General Reaction Scheme for Schiff Base Formation</p>	<p>Fig. 2: General Mechanism for preparing Schiff bases</p>
<p>Ligand with a pair of lone pair + Vacant Orbital of Metal atom</p> <p>Ligand acts as Lewis Base Metal atom acts as Lewis Acid Formation of Coordinate Bond Between Ligand and Metal Atom</p>	<p>Lone Pair of Electron</p> <p>where 'L' can be Oxygen, Nitrogen or Sulphur</p>
<p>Fig. 3: Formation of Coordinate bond between Metal Atom and Ligand</p>	<p>Fig. 4: General scheme behind the preparation of Coordination Metal Transition Complexes</p>
	<p>R = Alkyl or Aryl Group M = Any Transition Metal X = Any substitution group or atom</p>
<p>Fig. 5: Synthesis of Schiff Base Complex using Direct Method</p>	<p>Fig. 6: Synthesis of Schiff Base Complex using In situ Method</p>





Smart Farming and Irrigation Automation Techniques to Improve Coconut and Palm Cultivation using IoT and Machine Learning

O. P. Uma Maheswari*

Associate Professor, Department of Computer Science, P.K.R Arts College for Women, Gobichettipalayam, Tamil Nadu, India.

Received: 26 Feb 2023

Revised: 25 Apr 2023

Accepted: 27 May 2023

*Address for Correspondence

O. P. Uma Maheswari

Associate Professor,
Department of Computer Science,
P.K.R Arts College for Women,
Gobichettipalayam. Tamilnadu, India.
Email: umapritika@gmail.com



This is an Open Access Journal / article distributed under the terms of the **Creative Commons Attribution License** (CC BY-NC-ND 3.0) which permits unrestricted use, distribution, and reproduction in any medium, provided the original work is properly cited. All rights reserved.

ABSTRACT

The irrigation efficacy of typical irrigation technologies employed in coconut and palm plantations, such as flood irrigation and basin irrigation varies from 30 to 50 percent due to significant water loss. Furthermore, the cost of inputs such as labor and energy is high when putting these systems in place. Water shortage, as well as increased labour and energy costs, hinders the adoption of traditional irrigation systems. Under these circumstances, controlled irrigation, also known as smart farming and irrigation automation, is the best irrigation method for coconut/palm. This article looks at the Internet of Things (IOT) possibilities in the coconut tree growing sector of agriculture. The traditional system is being replaced by intelligent agriculture. This study proposes a multi-model data collection system. It collects environmental data using sensors, such as the pH value and moisture content of the soil. After collecting data from the soil, the microcontroller transmits it to the data collection centre through WIFI. The collected data is fed into a proprietary classifier, which reliably identifies coconut tree deficits like Button Shedding. Excess acidity or alkalinity, insufficient drainage facilities, severe and prolonged dryness, genetic issues, insufficient nutrients, incorrect pollination, hormone deficit, insect pests, or poor management approaches may all result in premature button and nut drop. It also focuses on enhancing coconut yield by monitoring and adjusting the pH and moisture content of the soil. As a result, IoT-based smart agriculture saves time and money on soil testing in coconut tree cultivation. It also provides monthly soil health monitoring and fertilizer recommendations. It will be very beneficial to the farming community. As a result, the results of the article will be beneficial to effective coconut tree farming practices. Intelligent agriculture and automated irrigation methods enable farmers to get the most out of their land.

Keywords: Agriculture, SOIL, Coconut, IoT, ML



**Uma Maheswari**

INTRODUCTION

A major amount of Brazil's GDP is related to agriculture, which is very important to the country's economy. New methods to boost production and provide long-term solutions are only possible with irrigation, making it a crucial component of the agricultural sector. An estimated 67.2% of Brazil's freshwater consumption goes towards irrigating crops, with the country's water extraction rate. Furthermore, Brazilian farmers often experience lengthy periods of drought, making agricultural production even more difficult and expensive. As a result, cautious and planned utilization of water resources is critical [1]. Internet of Things (IoT) is a feasible solution to the problem of agricultural monitoring and control. At the same time, intelligent objects may inform harvest storage conditions [2]. Both types of information may be combined to aid in crop-related decision-making. Thus, it may advise farmers on the precise quantity of water to use in the irrigation process, preventing the waste of such a precious resource as a result of improperly conducted irrigation and a lack of control [3]. ML algorithms are also applied to anticipate weather and precipitation based on sensor data, climate history, and satellite pictures. This might save thousands of farmers from committing suicide due to agricultural losses caused by unpredictability in the weather. Precision agriculture relies heavily on intelligent animal management [4]. It facilitates the lifelong monitoring of animals' health, wellbeing, productivity, and reproduction. Sensors and cameras monitor animal health, and computer vision algorithms facilitate intelligent decision-making, such as preventing the spread of infectious illnesses [5]. Modern agricultural solutions, such as autonomous tractors and automated irrigation systems, are advantageous for farmers. Due to the availability of cutting-edge machine learning (ML) and deep learning (DL) algorithms, high-speed internet connections, and powerful computer hardware [7], precision agriculture is widely practised around the globe. The authors examine ML applications for the efficiency of sustainable agricultural supply networks (ASCs). The authors provide a novel ML-ASC framework that may aid scholars and agricultural practitioners in comprehending the role and significance of digital technology in agriculture. The authors of [8] analysed several ML applications in agriculture and the ways in which digital technology might assist the agricultural business. This article provides a comprehensive overview of the use of machine learning to precision agriculture. This research explores the acceptability of digital techniques in farm management systems by the scientific community [9-12].

Low-cost goods are required for a competitive and cost-effective IoT solution, particularly in outdoor environments like agriculture. These products are limited in processing and storage capacity, and have smaller batteries. It also entails dealing with the inaccurate or unreliable data that might be generated by sensors due to factors like environmental conditions, faulty sensors, poor connections, or background noise. One of the most popular methods for enhancing sensor accuracy, providing a comprehensive picture, and facilitating more informed decision-making is data fusion, also known as information fusion. [13-15].

BACKGROUND STUDY

Abaya, S. *et al.* [1] Self-activating irrigation might be seen as a possible route to developing intelligent agriculture. Incorporating cutting-edge tools into your planting and farming practises will help you increase your agricultural output while also reducing your impact on the Philippines' water crisis. The World Resources Institute (WRI) projects that the United States would face a "high" degree of water crisis by 2040; the proposed device exceeds conventional ways of watering in terms of both plant growth and water usage, and might be the answer.

Dahane, A., *et al.* [3] In order to maximise water resources for precision agriculture, the built smart farming system was shown to be both useful and economical. The goal of this study was to develop a unique EDGE-Fog-IoT-Cloud architecture specifically for use in smart farming. The author emphasised the significance of artificial intelligence approaches in precision agriculture by using machine learning and open-source technology. The physical characteristics of the authors' agricultural system will be gathered for use in future experiments; sensor data will be combined with weather prediction information to develop an algorithm for anticipating soil moisture in the coming days. Ghosh, S. *et al.* [5] these authors method reduces the amount of extra labor needed by the farmer for chores such as watering plants. This system uses numerous sensors, including temperature, light, humidity, and wetness,

56909





Uma Maheswari

and its parameters were decided by the data from these sensors. The farmer may control drip from any place because to Internet connectivity between client and server. Mekala, M. S., & Viswanathan, P. [7] Precision agriculture may benefit from IoT-enabled systems that enhance accuracy and efficiency. Numerous agricultural sectors, such as irrigation and power distribution, may benefit from IoT applications. Prices of water and electricity, two of agriculture's most crucial inputs, may make or break a company. A lot of water went to waste because to inadequate irrigation infrastructure, poor field application methods, and the planting of water-hungry crops in the incorrect climate. Electricity was essential for running the many pumps, boosters, lights, etc. Monitoring and adjusting water amount, position, timing, and duration of flow is made possible by IoT, leading to better water usage in agriculture. Prabha, R. et al. [9] Irrigation and fertilizer were the two most significant agricultural components. Because of its capacity to boost output while decreasing water loss, irrigation scheduling has become a major problem in agriculture. The author may reduce the quantity of fertiliser required by administering it directly to the root. This method reduces expenditures while boosting soil health. This project developed an universal IoT framework to aid farmers in appropriately scheduling irrigation and fertilization. The author created a low-cost irrigation and fertilization mechanism that delivers water and nutrients straight to the root in this research.

Terence, S., & Purushothaman, G. [11] Agriculture was the bedrock of these authors civilization. The Internet of Things (IoT) technology was being utilised in agriculture to increase agricultural efficiency. IoT approaches were used in almost every element of agriculture, including agricultural monitoring, irrigation, and insect monitoring. This study categorises and analyses current smart farming systems, concluding that researchers should concentrate on security, food supply, and food distribution. It's also worth noting that the vast majority of testing took place inside. To address more real-world difficulties, researchers should put these ideas to the test in the field. V, P. et al. [13] To help folks who don't have the resources or time to tend and seed crops manually, these writers use the internet of things to build a smart irrigation system. This automated hydroponic system saves water and provides for better water management by remotely turning on/off the motor and informing the user through the dashboard.

Because this module contains a humidity and temperature complex with a calibrated digital signal output, it is a combination module for detecting humidity and temperature with a calibrated digital output signal. DHT11 gives very precise humidity and temperature measurements while also ensuring long-term stability. This sensor combines a resistive type humidity measurement component and an NTC type temperature measurement component, as well as an integrated 8-bit microcontroller, and is available as a 4-pin single row device. The DHT11 module communicates serially, sometimes known as single-wire communication. This module sends data as a pulse train with a predefined duration. Before sending data to Arduino, it must first perform an initialization instruction with a delay.

pH Sensor

The vast majority of Si LSI-fabricated pH sensors are ISFETs or charge transfer sensors. An ISFET pH sensor with continuous operation was employed for simultaneous pH and EC measurement. A band pass filter was required to decrease crosstalk. Section 4 discusses this topic. Furthermore, the operation is easy, and miniaturisation is simple. The voltage potential of a sensor membrane in an aqueous solution conforms to the Nernst equation, given by Equation (1) with regard to H⁺/OH⁻ ions:

$$\varphi_{ch} = V_{REF} + \frac{RT}{F} \ln \alpha_H \text{ ----- (1)}$$

H represents the hydrogen to hydroxide ion activity ratio. In this context, "direct current signal" means (DC). Since the EC sensor utilises an alternating current signal of 10 kHz, this is vital for simultaneous readings (AC). Since the EC signal is masked by the flicker noise of VREF, taking simultaneous readings is a challenge. Even yet, there are ways to address this problem. Si₃N₄, Ta₂O₅, Al₂O₃, SiO₂, etc. are only some of the membrane materials that have been employed. The membrane has to be very watertight. This study used Si₃N₄ because of its impermeability and compatibility with Si LSI processes.





Uma Maheswari

Soil Moisture Sensor

Numerous studies led to the development of a method called frequency domain decomposition for determining soil water content. Soil moisture is determined by observing the frequency shift brought on by sensor alterations in the soil as a result of the resulting change in dielectric constant. The FDR is more flexible than the TDR when it comes to probe shape, length, and operating frequency. Its basic model is seen in Figure 3. The soil acts as a dielectric and the sensor's probe is like a capacitor and external oscillator, which may form a tuning circuit, all while taking measurements. The sensor's capacitance between the two levels is inversely proportional to the measured medium's dielectric constant. The equivalent capacitance of the sensor, which influences its operating frequency, will rise with increasing humidity (resonant frequency). The oscillator generates high-frequency signals in the megahertz range, and a high-frequency detecting circuit can identify the resonance frequency.

Liquid Crystal Display (LCD)

All of the pins on a parallel LCD module are the same. The eight data pins are labelled D0–D7. The 4-pin mode is used when just four pins (D4-D7) are used, whereas the 8-pin mod is used when all eight pins are used. The 4-pin method is used by engineers for obvious reasons. The LCD may be turned on and off using the dedicated EN pins. The RW pin is the default setting for read/write. The ground and +5V connections are labelled VSS and VDD. In order to pick the correct register, RS is used. For a backlight LED, there are two terminals: one for the anode and one for the cathode.

The VO pin enables a potentiometer to be used to alter the level of contrast [10]. Here is the syntax:

Liquid Crystal LCD (RS,EN,D4,D5,D6,D7); to connect to an Arduino Uno, the statement is

Liquid Crystal LCD (2,3,4,5,6,7);

Here, Arduino I/O pins 2,3,4,5,6,7 are connected to RS,EN,D4,D5,D6 and D7 respectively.

Decision Trees

There has been a lot of success in using decision trees for inductive inference because they can learn disjunctive sentences and are robust against noisy input. The nodes of a decision tree are k-arrays, and the attributes of the input feature set are tested at each node. The values of the features at each node are represented by the branches that extend from them. In addition, the test outcomes at each fork are independent. This protocol is greedy since it generates decision trees via a recursive top-down approach. The method begins with tuples representing the training set and determines which attribute will provide the most useful information for classification. This is accomplished by creating a test node and then using top-down decision tree induction to partition the current tuples according to the values of the test attributes. When all tuples in a subset are members of the same class, or when further subset separation is deemed inappropriate (because additional attribute tests yield insufficient classification-alone information), the classification-alone information-only stage of the classification process is terminated, and the classifier is no longer created. Based on these findings, it is recommended that the threshold measure be based on the IG and the Manhattan hierarchical cluster.

This study may pick out the most crucial aspects while deciding on new features using a decision tree induction method. The induction of decision trees is the process of learning decision tree classifiers, which produces a tree structure in which each internal node (but not the leaves) is an attribute test. A class prediction is represented by each outer node (leaf node). A tree's forks represent data points from several tests. Using attribute selection with Information gain, the algorithm decides which attribute is best for categorising data into separate groups at each node. The most-split IG attribute value. The IG of the attribute is expressed as

$$\text{info}(D) = -\sum_{i=1}^m P_i \log(P_i) \text{----- (2)}$$

Assume a random vector in D, and let its probability of belonging to class c_i be p_i . Bits are utilized for encoding information. Info(D) is the typical data needed to determine the labels of the vector class D. As a set of qualities, they are organized hierarchically and given a ranking by IG. The updated Manhattan distance between any two clusters of size n is as follows:

$$\text{MDist} = \sum_{i=1}^n (a_i - b_i) \text{----- (3)}$$



**Uma Maheswari**

Manhattan values are used to generate a cubic polynomial equation, and the slope of this equation is used as the threshold criteria. If the slope of an attribute is negative or zero, it is not considered useful for the classification. A random decision forest is an ensemble of trees whose training is completely random. There are numerous moving parts in the forest model. Take, for example, picking a class of split functions (in the literature, "weak learners"). In a similar vein, decide on a leaf predictor. The randomness model significantly impacts the functioning of the forest. One component at a time is covered here. In order to construct classifiers, it is required to do a random sampling of the training data with replacement, yielding a root node with a single class in its fs. When many classes of fs share the same root node, the one with the most information gain is chosen. Place D in N at the node where Disallinsces in N equal F Call Build Tree Nendif.

ID3, C4.5 produces reliable and effective decision trees. However, these trees are often too vast for human comprehension. An assortment of forks in the decision tree illustrates the training data's noise-induced anomalies. Overfitting occurs when a learning strategy repeatedly generates hypotheses to reduce errors in the training set but leads to larger errors in the test set. Overcrowding is an issue that can only be solved via extensive pruning. Pruning is essential for improving the classification accuracy and computing efficiency of a decision tree. When categorising new data, pruning may be used to reduce the size of classification trees, eliminate unnecessary complexity, and prevent overfitting. Due to overfitting, a large number of rules are created, the great majority of which have little predictive value for fresh data. Pre-pruning and post-pruning are two pruning techniques. When this occurs, it is called "back pruning." Decision trees are built to aid in the identification of unknown facts, and their unneeded branches are eliminated to improve accuracy. There are two possible approaches to this: Maintaining decision trees while replacing certain branches with leaf nodes. Firstly, this study need to transform the tree into a set of analogous rules. Next, this study have minimum error pruning, error complexity pruning, error reduction pruning, and cost based pruning.

Forward pruning is a term for this kind of tree maintenance. By creating termination criteria to determine whether it is beneficial to prematurely trim certain branches during tree development, it restricts the growth of unnecessary branches. The effectiveness of a tree construction fork may be measured in a number of ways. After a certain amount of tuples remain after splitting a node, further splitting of that subset is either halted or restarted. Trees are oversimplified when criteria are set too high, but they remain relatively unchanged when set too low. Examples of pre-pruning methods include minimum object number pruning and Chi-square pruning. Most of these pruning methods are based on the assumption that classification mistakes will be reduced if all members of the same node are assigned to their most prevalent class. A test file or statistical methods like cross-validation and bootstrapping are used to get this conclusion (Fournier & Cremilleux2000). These pruning algorithms routinely remove extraneous sub trees based on the context in which the resulting tree will be utilized as a classifier. Take a look at Figure 1.1 and focus on the offshoot that is shown there. Class D, which has two values, applies here. To find out how often a certain value of D happened, look at the node's first (or second) value. Although this subtree's leaves and root both have an error rate of 10%, it is nevertheless useful since it represents a population with a known value of D; predicting the value for the remaining population is more challenging.

DECISION TREE ALGORITHM

R. Quinlan's ID3 methodology for building decision trees is the gold standard. ID3 uses the concept of information gain, which originates in information entropy, as its criterion for evaluating the splitting characteristic. The entropy of a thermodynamic system is employed as a measure of its randomness in physics. It's used to quantify doubt in the study of information. When a system is well-organized, its information entropy decreases. On the contrary, information entropy increases when disorder increases in a system. Thus, information entropy may be seen as a quantitative index of a system's degree of organization. Let there be m groups, each containing n data points, in the sample set s. Label m distinct groups as C_i ($i = 1, 2, \dots$), where n_i is the total number of samples in group i. To effectively allocate n samples to m categories, the needed information entropy is





Uma Maheswari

$$H(S) = \sum_{i=1}^m P_i \log_2 p_i, \dots\dots (4)$$

And the probability that all of the data points in sample s belong to the class C_i is given by $p_i = n_i / n$. The sample will be broken down into subsets according to property A values if specified as the splitting attribute. The entropy of the information used to partition the sample sets into their respective groups is computed for each subset

$$H(A_j) = \sum_{i=1}^m P_i \log_2 P_i, \dots\dots (5)$$

where A_j is a subset of A 's values, and p_i is the likelihood that any random sample from A_j falls into class C_i . As a result, characteristic A , the minimum entropy of information needed to differentiate between all samples, is

$$H(A) = \sum_{v=1}^v \frac{S_v}{S} H(A_j), \dots\dots (6)$$

The importance of a given attribute value is denoted by the ratio of the number of samples with that value (S_v) to the total number of samples (S), where S_v is the number of samples within the subset of unique attribute values. Therefore, the accumulation of information is

$$\text{gain} = H(s) - H(A) \dots\dots (7)$$

The ID3 method selects the split property according to gain. According to a previous study, the character with the biggest number of attribute values gains the most from the information gain. A higher number of attribute values using the decision tree does not automatically indicate higher quality. As a result, bridging the gap between attribute and value selection is crucial.

Support Vector Machine

The support vector machine (SVM) is a powerful classification method using the idea of the lowest structural risk to guide supervised learning. This technique creates a new hyperplane for the positive/negative separation of samples at the time of training. After that, this study classify the new samples by finding where on the hyperplane each one belongs. Using a supervised learning approach, SVM examines data to find patterns that may be used for categorization. As a bonus, it may locate unique hyperplane that may amplify the distinction between two classes.

The SVM first conducts a nonlinear mapping of all input variables to a high-dimensional feature space, and then a linear classification or regression within this space. It is possible for non-linear classifications in the input space to interact with linear regression in the high-dimensional feature space. Here, the conventional SVM is being used in practice.

If the l training samples are $T = \{(x_1, y_1), \dots, (x_l, y_l)\}$, in which $x_i \in R^n, y_i \in \{1, -1\}$ (classification) or the $y_i \in R$ (regression), $i = 1, \dots, l$ The non-linear function is $k(x_i, x_j) = \phi(x_i)\theta(x_j)$ and the SVM is employed by solving the equations below (8).

$$\min_{w, \epsilon, b} \left\{ \frac{1}{2} \|w\|^2 + c \sum_i \epsilon_i \right\} \dots\dots (8)$$

$$\text{s. t. } y^i (\nabla^T(X_i)w + b) \geq 1 - \epsilon_i \forall_i = 1, \dots, n \dots\dots (9)$$

$$\epsilon_i \geq 0 \forall_i = 1, \dots, n \dots\dots (10)$$

When the Lagrangian multipliers are properly set in motion, the optimization problems may be reformulated as a dual problem that better meets their requirements (10).

$$\min_a \sum_{ij} a_i a_j y_i y_j k(x_i, y_j) - \sum_{i=1}^l a_i \dots\dots (11)$$

$$\text{s. t. } y^t a = 0 \dots\dots (12)$$

$$0 \leq a_i < C, i = 1, \dots, l \dots\dots (13)$$

The class of a sample will be decided after an optimum solution (a, b) has been found, using the subsequent decision function (3.9).

$$f(x) = \text{sgn}(\sum_{i=1}^l y_i a_i * K(x_i, x) + b *) \dots\dots (14)$$

The original data set D and the massive data set D have been broken down into smaller data sections $D1, Dn$. These nodes in the data compute nodes, and they split files using the Twister command. Job conf configures several aspects of computation, such as Map Reduce, Map tasks, Reduce tasks, and partition files. Each node in the computation





Uma Maheswari

executes these Map tasks for the Reduce jobs, while the other support vectors discovered in Map jobs are collected and delivered as feedback. This process is initiated by the Twister Driver, which uses dynamic parameters to effect the transformation.

Naive Bays

In the realm of classification, the Naive Bayes classifier is a popular option. Due to its straightforward construction and lack of requirement for sophisticated iterative parameter estimate procedures, it is easily applicable to large data sets. As a result, the classifier's classifications may be understandable by people with a lower level of technical expertise. The Naive Bayes model has several positive qualities, including its ease of use, beauty, and resiliency. One of the early categorization methods, even in its rudimentary form, is still useful today. Examples include spam filtering and textual organization. The fields of statistics, data mining, machine learning, and pattern recognition all contributed to a wide range of improvements made to increase their flexibility.

Naive Bayes is a statistical classifier that uses Bayes' theorem to assign a posterior probability to each observation in order to make a prediction about the category to which a given data set belongs. In this section, this study will look at several Naive Bayes-based algorithms:

$$q\left(\frac{d_i}{u}\right) = \frac{q\left(\frac{u}{d_i}\right)q(d_i)}{q(u)} \dots\dots\dots (15)$$

To be more precise, let's say that $u = (u_1, \dots, u_n)$ is the n-dimensional attribute vector of the document and that d_1, \dots, d_m is the m-dimensional class. However, the calculation of $P(U|d_i)$ is time-consuming and resource-intensive. A naïve conditional independence assumption of a class is established to speed up calculation time. Thus:

$$q\left(\frac{u}{d_i}\right) = \prod_{k=1}^n q\left(\frac{x_k}{d_i}\right) \dots\dots\dots (16)$$

Bayes classifiers compute the likelihood that each class in a training set will have a certain attribute value. These probabilities are used to classify recall tasks. $P(a)$ is the probability that a training pattern has an attribute array A with discrete values, where A is an array of $M > 1$ attributes A_1, A_2, \dots, A_M for the patterns in a training set. Consider the fact that the training set comprises data from classes $C_1, C_2, \dots,$ and C_m . The following probabilities are derived for a distance of one kilometre:

- i. Denoted by P , the probability that a given training pattern belongs to class $d_k (d_k)$. Predictions of class C_k are also known as the prior probability of class D_k .
- ii. The probability that a given training pattern for attribute A belongs to class k is denoted by the notation $P(d_k|A)$. Moreover, d_k . The posterior probability of d_k given A is another name for this. In other words, the values of the attributes are each discrete number.
- iii. P denotes the probability that a training pattern of class d_k has the attributes array (k) It a characterized by its distinct values.
- iv. $p(k)$ is the conditional probability density that a training pattern of class C_k contains attribute array A with continuous values for the attribute

P is the conditional probability for discrete attribute values, and p is the conditional probability for continuous attribute values.

Classifying a pattern with an attribute array A involves assigning it to the class of A to which it belongs with the highest posterior probability $P(d_k|A)$. Finally, a design is assigned to the most likely group. The pattern is thrown out if the highest posterior probabilities for three or more classes are all the same. According to Bayes' theorem of probability theory





Uma Maheswari

$$q(A|d_k) = \frac{q(d_k)q(A|d_k)}{q(A)} \dots\dots\dots (17)$$

The right side of the above equation may be optimized by maximizing $k P(D|A) \cdot P(A)$. $P(A)$, a universal constant, is included in the right-hand denominator. Since the value of $k P(D|A)$ does not have to be specified to maximize it, this is the same as maximizing $k P(D)P(A|D)$. After calculating $P(C_k)$ and k from the training set, they may be used to label a pattern with an attribute array. Considering all possible values for attributes A_1 through A_M to compute $P(k)$ would result in a training set that is too large to be feasible for most applications. There's a lot of time and effort invested in computational activities. For this reason, many people assume that the merits listed in categories A_1 through A_M are not affected by one's socioeconomic status.

$$P(A|D_k) = \prod_{i=1}^m p(A_i|D_k) \dots\dots\dots (18)$$

Assuming the above, this study call this classifier the Naive Bayes classifier (NBC), and it works by maximizing the probability that a pattern with attributes A_1 through A_M falls into one of the categories defined by $q(d_k)$ $M \leq k \leq 1$. To decrease the dangers of using the Naive Bayes classifier. Maximizing $q(A|d_k) \cdot q(d_k)$ $(i=1) \dots q(d_k)$. There are two possible values, zero and one, for a Naive Bayes binary attribute. For m classes C_1 to C_m , this study get their corresponding prior probabilities $P(C_k)$ and conditional probabilities $P(A_i|C_k)$ from the training set. Let $a_{ki} = q[(A_i=1)|d_k]$, since the binary attribute A_i can have a value of either 0 or 1

$$q[(A_i = 1)|d_k] + P[(A_i = 1)|d_k] = 1 - P[(A_i = 1)|d_k] = 1 \dots\dots\dots (19)$$

Therefore $q[(A_i = 0)|d_k] = 1 - q[(A_i = 1)|d_k] \dots\dots\dots (20)$

$$P[A_i = 0|d_k] = 1 - a_{ki} \dots\dots\dots (21)$$

Since logarithmic functions are monotonic, $\log q(D_k) + \prod_{i=1}^m \log P(A_i|D_k)$ is maximized .

The above equation is evaluated for classes $C_1, C_2 \dots C_m$ to find out for which class its value is the greatest so that the pattern is classified in that class. Thus NBC assumes that all variables (features) are conditionally independent given the class variable and thereby decomposes the posterior probability.

RESULT AND DISCUSSION

The flows for a period of 1 week with optimization based control was used to study the effectiveness of optimization based control for the three irrigation schemes. In drip irrigation method the method provided 31.2% over conventional. Figure 5 Automated versus Manual Control with sprinkler system for flow-based control. Method and a 7 percent cost savings improvement over flow-based management. Similarly, when using a solenoid valve to regulate sprinklers, costs were cut by 22%. Through modelling, this study found that optimization-based control might reduce water use by up to 30 percent compared to flow-based control. Figure 6 Automated versus Manual Control with Sprinkler System for optimization-based control.

OBSERVATIONS

1. An increase in soil moisture was shown to reduce the soil's pH.
2. The Internet of Things (IoT) and cloud connection have improved the capacity to aggregate data and display it visually.
3. Better water efficiency in agricultural systems may be achieved via the integration of Internet of Things (IoT) technologies, cloud computing, and optimization models.
4. A greater degree of controllability was achieved by the automation of the irrigation system by linking solenoid valves.





CONCLUSION

By introducing technology into the traditional and basic processes at the core of agriculture, the goal of mixing agricultural with cutting-edge technology may be realised. The Internet of Things-based approach streamlines the assessment of environmental components like climate, soil condition, and so on, while the software layer enhances the predictions of the elderly. Technology must learn from present methods and then automate vocations to make human life simpler. Because of its flexibility to field settings, this approach has the potential to be used internationally. As a consequence, by simplifying farming operations and enabling smart farming, IoT may be the saviour of a generally dying agricultural business. Apart from these advantages, smart farming offers the ability to expand a farmer's market with a single touch and no work.

REFERENCES

1. Abaya, S., De Vega, L., Garcia, J., Maniaul, M., & Redondo, C. A. (2017). A self-activating irrigation technology designed for a smart and futuristic farming. 2017 International Conference on Circuits, Devices and Systems (ICCDs). doi:10.1109/iccds.2017.8120476
2. Chetan Dwarkani M, Ganesh Ram R, Jagannathan S, & Priyatharshini, R. (2015). Smart farming system using sensors for agricultural task automation. 2015 IEEE Technological Innovation in ICT for Agriculture and Rural Development (TIAR). doi:10.1109/tiar.2015.7358530
3. Dahane, A., Benameur, R., Kechar, B., & Benyamina, A. (2020). An IoT Based Smart Farming System Using Machine Learning. 2020 International Symposium on Networks, Computers and Communications (ISNCC). doi:10.1109/isncc49221.2020.9297341
4. Dela Cruz, J. R., Baldovino, R. G., Culibrina, F. B., Bandala, A. A., & Dadios, E. P. (2017). Fuzzy-based Decision Support System for Smart Farm Water Tank Monitoring and Control. 2017 5th International Conference on Information and Communication Technology (ICoICT). doi:10.1109/icoict.2017.8074669
5. Ghosh, S., Sayyed, S., Wani, K., Mhatre, M., & Hingoliwala, H. A. (2016). Smart irrigation: A smart drip irrigation system using cloud, android and data mining. 2016 IEEE International Conference on Advances in Electronics, Communication and Computer Technology (ICAECCT). doi:10.1109/icaecct.2016.7942589
6. Maha, M. M., Bhuiyan, S., & Masduzzaman, M. (2019). Smart Board for Precision Farming Using Wireless Sensor Network. 2019 International Conference on Robotics, Electrical and Signal Processing Techniques (ICREST). doi:10.1109/icrest.2019.8644215
7. Mekala, M. S., & Viswanathan, P. (2017). A Survey: Smart agriculture IoT with cloud computing. 2017 International Conference on Microelectronic Devices, Circuits and Systems (ICMDCS). doi:10.1109/icmdcs.2017.8211551
8. P, V., Prasad, M. P. R., & C, D. (2019). Low Cost Automation for Smart Farming. 2019 Innovations in Power and Advanced Computing Technologies (i-PACT). doi:10.1109/i-pact44901.2019.8960239
9. Prabha, R., Sinitambirivoutin, E., Passelaigue, F., & Ramesh, M. V. (2018). Design and Development of an IoT Based Smart Irrigation and Fertilization System for Chilli Farming. 2018 International Conference on Wireless Communications, Signal Processing and Networking (WiSPNET). doi:10.1109/wispnet.2018.8538568
10. R. Dela Cruz, J. -A. V. Magsumbol, E. P. Dadios, R. G. Baldovino, F. B. Culibrina and L. A. Gan Lim, "Design of a fuzzy-based automated organic irrigation system for smart farm," 2017 IEEE 9th International Conference on Humanoid, Nanotechnology, Information Technology, Communication and Control, Environment and Management (HNICEM), Manila, Philippines, 2017, pp. 1-6, doi: 10.1109/HNICEM.2017.8269500.
11. Terence, S., & Purushothaman, G. (2020). Systematic review of Internet of Things in smart farming. Transactions on Emerging Telecommunications Technologies. doi:10.1002/ett.3958
12. Unal, Z. (2020). Smart farming becomes even smarter with deep learning – a bibliographical analysis. IEEE Access, 1–1. doi:10.1109/access.2020.3000175





Uma Maheswari

13. V, P. P., S M, S., & C, S. S. (2020). Robust Smart Irrigation System using Hydroponic Farming based on Data Science and IoT. 2020 IEEE Bangalore Humanitarian Technology Conference (B-HTC). doi:10.1109/b-htc50970.2020.9297842
14. Yadav, R., & Daniel, A. . (2018). Fuzzy Based Smart Farming using Wireless Sensor Network. 2018 5th IEEE Uttar Pradesh Section International Conference on Electrical, Electronics and Computer Engineering (UPCON). doi:10.1109/upcon.2018.8597086
15. Zaier, R., Zekri, S., Jayasuriya, H., Teirab, A., Hamza, N., & Al-Busaidi, H. (2015). Design and implementation of smart irrigation system for groundwater use at farm scale. 2015 7th International Conference on Modelling, Identification and Control (ICMIC). doi:10.1109/icmic.2015.7409402

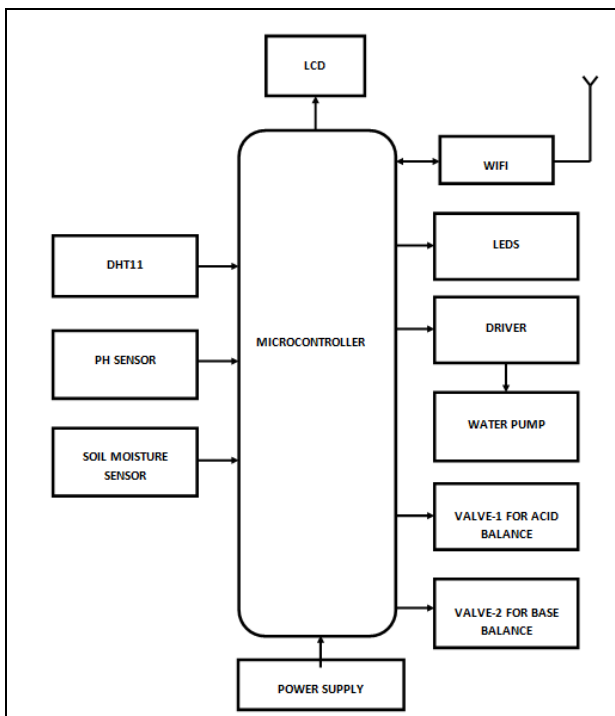


Figure 1 Block diagram

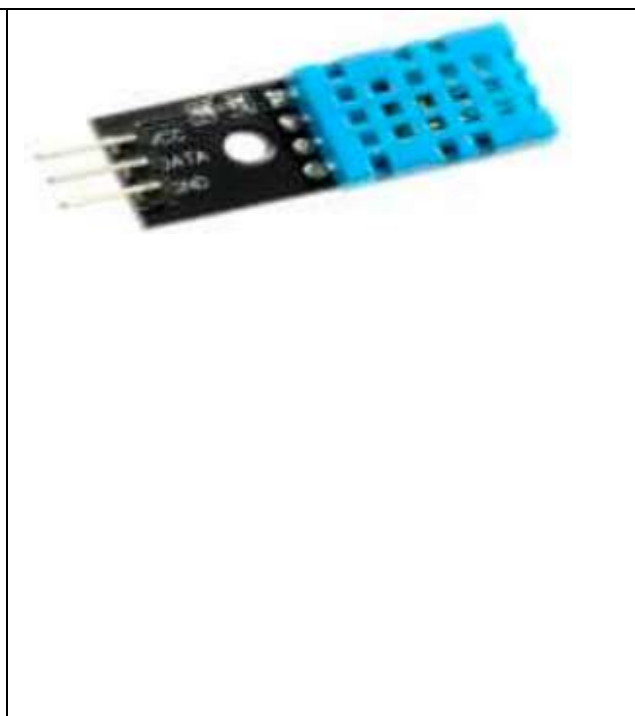


Figure 2 DHT11 Sensor

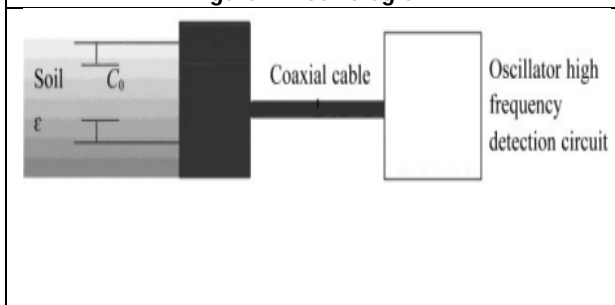


Figure 3 FDR simplified mode

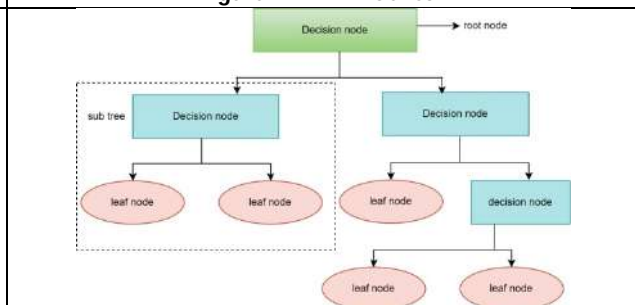


Figure 4 Bi-Valued Subtree





Uma Maheswari

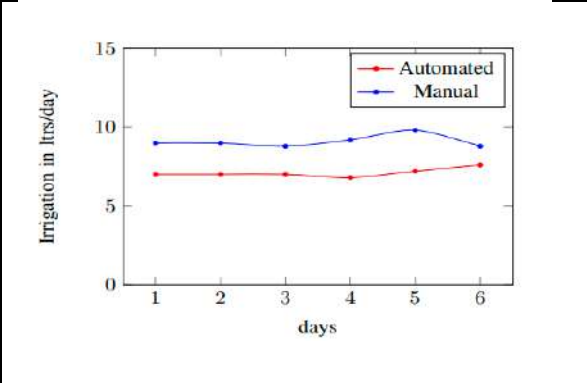


Figure 5 Automated versus Manual Control with sprinkler system for flow-based control

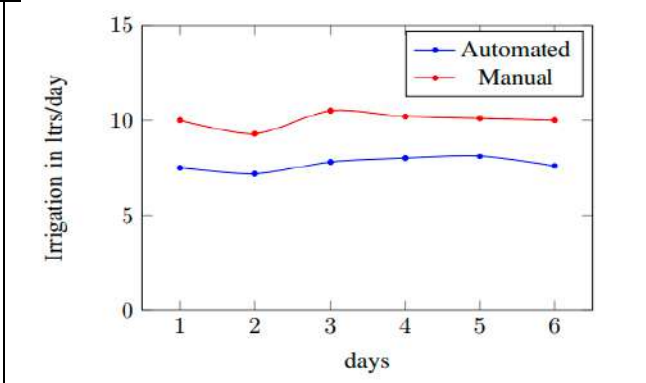


Figure 6 Automated versus Manual Control with Sprinkler System for optimization-based control





Antiretroviral : A Review on Method Development and Validation by Green Chromatography

B.Prakash Kumar^{1*}, T.Y.Pasha² and B Ramesh³

¹Assistant Professor, Department of Pharmaceutical Analysis, Sri Adichunchanagiri College of Pharmacy, Adichunchanagiri University, Mandya, Karnataka, India.

²HoD, Department of Chemistry, Sri Adichunchanagiri College of Pharmacy, Adichunchanagiri University, Mandya, Karnataka, India.

³Principal, Sri Adichunchanagiri College of Pharmacy, Adichunchanagiri University, Mandya, Karnataka, India.

Received: 13 Dec 2022

Revised: 15 Apr 2023

Accepted: 19 May 2023

*Address for Correspondence

Mr. B Prakash Kumar

Assistant Professor,

Department of Pharmaceutical Analysis,

Sri Adichunchanagiri College of Pharmacy,

Adichunchanagiri University, Mandya, Karnataka, India.

E. Mail: prakashkumar_007@yahoo.co.in



This is an Open Access Journal / article distributed under the terms of the **Creative Commons Attribution License** (CC BY-NC-ND 3.0) which permits unrestricted use, distribution, and reproduction in any medium, provided the original work is properly cited. All rights reserved.

ABSTRACT

In the current period of time the use of toxic chemicals in the analysis of various drugs are increased. In excess use of toxic organic solvents will be harmful for the environment and also the laboratory analyst, so in order to reduce the toxicity Certain Green Chromatography methods are reviewed for antiretroviral which are eco-friendly and not harmful for the analyst. The understanding of antiretroviral and green procedures can be explored by this review conducted on various green chromatographic techniques.

Keywords: Green chromatography, Anti-Retroviral Drugs, Eco-friendly, HAART, HIV.

INTRODUCTION

Since the Establishment of HIV as the causal factor of AIDS in 1983/1984, significant progress has been made in developing effective anti-retroviral medicines (ARVs). [1]HIV/AIDS is one of the deadliest and most uncontrollable chronic health crises.[2]The Retrovirus (Human immunodeficiency virus) has been one of the world's most destructive diseases, affecting both children and adults.[3]It takes lifelong therapy with significant life-saving medications.[2]The causative organism of acquired immunodeficiency syndrome is a retrovirus (AIDS).[4]The combination dosage form of cobicistat and elvitegravir is used to treat HIV infection in adults. which is an integrase inhibitor for HIV.[5]Protease is a viral growth enzyme that is necessary for viral development. The HIV protease inhibitors (PI) treatment class is an important component of current highly active antiretroviral therapy (HAART)

56919





Prakash Kumar et al.,

regimens.[4]In 1996, a big breakthrough was made when it was discovered that triple medication therapy (HAART) could effectively reduce viral replication to near-zero levels for an extended period of time. [1]Treatment for human immunodeficiency virus type 1 (HIV-1) includes dual and triple antiretroviral medication combinations. Antiretroviral medicines such as zidovudine, efavirenz, abacavir, lamivudine, emtricitabine, and tenofovir are used in dual and triple combinations to treat human immunodeficiency virus type 1 (HIV-1). Despite antiretroviral therapy's relative effectiveness, the generation of drug-resistant HIV-1 variations remain the leading cause of treatment failure.[6]In order to deliver high throughput at low cost, quality control (QC) of pharmaceutical goods necessitates rapid, sensitive, and cost-effective procedures, which are the major considerations of such economic facilities. Meanwhile, researchers must evaluate the environmental implications of research laboratories in order to reduce the risks associated with them.[7]Since Anastas introduced the notion of green chemistry in 1999.The primary themes in green analytical chemistry include the decrease (and even removal) of organic solvents and other harmful reagents in the analysis process, miniaturisation and automation of the analytical method, energy conservation, waste reduction, and solvent and material reuse.[8]Greening analytical methodologies has sparked interest in the sector of pharmaceutical analysis, with the goal of reducing environmental consequences and improving analyst health safety.[9]Faster, greener, and more cost-effective processes are in high demand across all industries, including pharmaceutical.[10]Green chromatography was recommended as a useful technology for reducing environmental issues associated with analyses during the pharmaceutical R&D phase while yet assuring that medical goods meet high-quality standards.[11]Gas chromatography utilising hydrogen as a carrier gas in the mobile phase was thought to be among the most environmentally friendly method of chromatographic analysis.[11]Traditional toxic chemicals are reduced or eliminated in chromatographic separation and sample preparation, making it a safer and more greener method of determining analytes in biological matrices.[12]

Antiretroviral

The first antiretroviral medicine, AZT (zidovudine, 3'-azido-2',3'-dideoxythymidine), was described exactly 37 years ago in October 2022.[13]Now there are seven types of antiretroviral drugs: nucleoside reverse transcriptase inhibitors (NRTIs), nucleotide reverse transcriptase inhibitors (NtRTIs), non-nucleoside reverse transcriptase inhibitors (NNRTIs), protease inhibitors (PIs), fusion inhibitors (FIs), co-receptor inhibitors (CRIs), and integrase inhibitors (INIs).[13]

HAART (Highly Active Antiretroviral Therapy)

Although the results of dual-NRTI combination therapy were far superior to those of monotherapy, their duration was still short. The effects of treatment didn't become long-lasting until triple ARV medication therapy, also known as highly active antiretroviral therapy (HAART), was released in 1996.[1]For the past 27 years, drug combination therapy, often known as HAART, has been regarded the standard treatment for patients with HIV infections, whether they are antiretroviral drug-naïve or drug-experienced. The number of conceivable medication combinations is enormous, given the number of antiretrovirals available (see above). If fixed-dose drug combinations are the only option, the number of double drug combinations is restricted to Combivir1, Epzicom1, and Truvada1, and the number of triple drug combinations is limited to Trizivir1 and Atripla1.The fixed-dose medication combinations of Truvada1 (300 mg TDF, 200 mg (-) FTC) with rilpivirine (25 mg) and Truvada1 with elvitegravir (150 mg) and GS-9350 (Cobicistat), the latter serving as a metabolic enhancer (or 'booster') of elvitegravir, is available now.[13]Antiretroviral therapy, often known as HAART, has transformed HIV disease from a nearly always fatal condition into a chronic, controllable condition[13]

The Haste to Create Antiretroviral Drugs

There were scarcely any potent antiviral medications available when AIDS initially emerged.Chain terminators of DNA synthesis, such as nucleoside and nucleotide analogues, have been proven to be some of the most effective inhibitors of HIV-1 replication.Early in 1987, ZDV entered the market after being swiftly certified by regulatory authorities.[1]Since about 15 years ago, drug combination therapy, often known as HAART, has been the accepted standard of care for people with HIV infections.[13]Despite being substantially better than those of monotherapy, the





Prakash Kumar *et al.*,

effects of dual-nrti combination therapy were nevertheless short-lived. The effects of treatment didn't become long-lasting until triple ARV medication therapy, or highly active antiretroviral therapy (HAART), was released in 1996.[1] HIV treatment is now firmly on the forefront thanks to the UNGASS commitment statement. The campaign was started by the WHO in 2003, with a goal of 3 million persons receiving ARV medication by 2005. As opposed to 9.7 million at the end of 2012 [1].

Green Chromatography

A subdivision of GAC called "green chromatography" focuses on ideas like

- o utilising direct chromatographic techniques that enable analyte detection in a sample without sample preparation or pre-treatment.
- o time and energy spent on sample preparation are reduced.
- o decrease or omission of the solvent employed in the analysis.
- o reducing interferences in the matrix.
- o lowering the need for redefinition.
- o employing hyphenated approaches to combine many steps of analytical processes into a single step.[14]
- o One of the best ways to achieve the aims of green chemistry is through the use of green chromatography, which lessens the production of organic waste during analytical or preparative separation procedures by minimising or replacing the usage of organic solvents. The chromatographic method can also be more environmentally friendly at several phases, from sample collection and preparation to separation and conclusion. Depending on the kind of chromatography, different techniques can be used to make separations more environmentally friendly.[11]

Antiretroviral: Green Chromatographic Methodologies

RP-HPLC

Adel Ehab Ibrahim *et al.*, have developed a method on Green Stability Indicating Organic Solvent-Free HPLC Determination of Remdesivir in Substances and Pharmaceutical Dosage Forms. They have studied the stability of remdesivir utilising the organic solvent-free liquid chromatographic method against various degradation routes. RP-C18 stationary phase was separated utilising a mixed-micellar mobile phase made of by adding 0.025 M Brij-35, 0.1 M sodium lauryl sulphate (SLS), and 0.02 M disodium hydrogen phosphate, with a pH of 6.0. 1 mL per minute was the mobile phase flow rate. detection was made, and carried out at a 244 nm wavelength.[15] **Yasmine Ahmed Sharaf *et al.***, have developed a two green micellar HPLC and Mathematically assisted UV spectroscopic Methods for the simultaneous Determination of Molnupiravir and Favipiravir as a Novel combined COVID-19 Antiviral Regimen. An isocratic mixed micellar mobile phase made of 0.1 M SDS, 0.01 M Brij-35, and 0.02 M monobasic potassium phosphate at 1.0 mL min⁻¹ flow rate was used to verify a green micellar HPLC technique employing an RP-C18 core-shell column (5 m, 150 4.6 mm). At 230 nm, the analytes were picked up. The chromatographic conditions were optimised, and the run duration was less than five minutes.[16]

Ibraam E Mikhail *et al.*, have worked on Green micellar solvent-free HPLC and spectrofluorimetric determination of favipiravir as one of COVID-19 antiviral regimens. In this work Based on solvent-free micellar LC and spectrofluorimetric techniques, two brand-new straightforward, sensitive, and environmentally friendly methods for FAV determination were created and validated. Numerous parameters, including solvent type, buffering, pH, and additional surfactants, were investigated in order to enhance FAV native fluorescence. In a concentration range of 20-350 ng mL⁻¹, the best sensitivity for FAV fluorescence was obtained in Britton-Robinson buffer (pH 4) at 436 nm after excitation at 323 nm. Using C18-RP (5 m, 250 4.6 mm) stationary phase and a solvent-free mobile phase made up of (0.02 M Brij-35, 0.15 M SDS, and 0.02 M disodium hydrogen phosphate, pH 5.0) isocratically eluted at a flow rate of 1 mL min⁻¹, with a detection wavelength of 323 nm, another HPLC method was verified. The LC technique was verified for various concentrations.[17]

Karthika Paul *et al.*, have worked on Development and validation of simplified RP-HPLC method for quantification of Darunavir in commercial tablets. In this study of work for quantifying DRV in the tablet dosage form, a Reverse-



**Prakash Kumar et al.,**

Phase High-Performance Liquid Chromatography (RP-HPLC) method that is accurate, precise, reproducible, easy to use, and quick was created and validated (Danavir 600). On a Phenomenex C18 analytical column with dimensions of 250 4.6 mm and 5 mm, liquid chromatography was performed using acetonitrile and water in a ratio of 30:70 v/v as the mobile phase. Using a flow rate of 1 ml/min and a 268 nm measurement, the sample was injected into a volume of 20 ml (ACN: water). Standard and sample drug retention times were discovered to be 3.16 and 3.12 min, respectively. For DRV in the concentration range of 40-200 mg/ml, the calibration curve's linearity was attained, and the regression coefficient (R²) was found to be 0.982. [18] **Hanan I. EL-Shorbagy et al.**, For the simultaneous assessment of contemporary hepatitis C antiviral medications (sofosbuvir and ledipasvir) with ribavirin as a co-administered drug in 0.1 N HCl within 10 minutes, a novel optimization by complete factorial design for a green, quick, and easy RP- HPLC-UV gradient method was created. Gradient elution was used at flow rate of 1mL min⁻¹ and injection volume of 10µl was used. Methanol and 0.005 M sodium salt of heptane-1-sulphonic acid made up the mobile phase, which was pH-adjusted with phosphoric acid to 2.5. Ribavirin, sofosbuvir, and ledipasvir had retention times of 3.700±0.005, 8.526±0.039, and 9.360±0.027 min, respectively.[19]

HPLC-UV

A C18 reversed-phase analytical column was created and validated to be used in a straightforward, quick, economical, and environmentally friendly high-performance liquid chromatographic assay for the measurement of capecitabine in human plasma. With a flow rate of 1.0 mL min⁻¹ and UV detection at 310 nm, the separation was carried out using a mobile phase made up of formic acid solution (pH = 3): ethanol (55:45). The temperature in the column was fixed at 50 °C. Protein was precipitated from the sample using a zinc sulphate-ethanol solution. This technique yields a high capecitabine recovery in human plasma of 95.98 to 102.50 percent. Over a concentration range of 0.05–10.00 g mL⁻¹, the calibration curves were linear (r² > 0.9999). The bias was within 15 percent, and the between- and between-day variability was less than 15 percent.[20]

Green-Micellar Solvent Free HPLC

A straightforward and well-established subset of high-performance liquid chromatography is micellar liquid chromatography (MLC). MLC has been used more and more frequently to identify various substances in pharmaceutical formulations, biological samples, food, and environmental materials. The MLC method has a number of advantages over other methods, including the simultaneous separation of charged and uncharged solutes, the ability to use rapid gradients, the direct injection of bodily fluids onto the column, a special separation selectivity, high reproducibility, robustness, enhanced luminescence detection, low cost, and safety.[21] This review is devoted to assessing how well MLC complies with the green chemistry concepts, which have recently become a widespread movement Based on solvent-free micellar LC and spectrofluorimetric techniques, two brand-new straightforward, sensitive, and environmentally friendly methods for FAV determination were created and validated. Several parameters, including solvent type, buffering, pH, and additional surfactants, were investigated to enhance FAV native fluorescence. After excitation at 323 nm and within a concentration range of 20-350 ng mL⁻¹, Britton-Robinson buffer (pH 4) provided the best sensitivity for FAV fluorescence. With C18-RP (5 m, 250 4.6 mm) stationary phase, 0.02 M Brij-35, 0.15 M SDS, and 0.02 M disodium hydrogen phosphate, pH 5.0) solvent-free mobile phase, isocratically eluted at a flow rate of 1 mL min⁻¹, and a detection wavelength of 323 nm, another HPLC method was verified. The proposed procedures were evaluated using two contemporary greenness metrics (GAPI and AGREE) to demonstrate their eco-friendliness because they typically use biodegradable reagents in solvent-free aqueous phases.[7]

Noha S Said et al., have reported about Assessment of the greenness of new stability indicating micellar UPLC and HPTLC methods for determination of tenofovir alafenamide in dosage forms. In this work, For the quantitative determination of tenofovir alafenamide in the presence of its degradation products in bulk powder as well as in dosage forms, green stability indicating chromatographic techniques were created and verified. The first method was micellar UPLC, in which separation was accomplished on a kinetex 1.7 m HILIC 100A, LC column using an environmentally friendly micellar mobile phase composed of 10% 1-propanol (70:30) and 0.05 M sodium dodecyl sulphate and 0.05 M sodium dihydrogen phosphate (pH 5.5) at a flow rate of 1 mL min⁻¹ with a UV detection at 210



**Prakash Kumar et al.,**

nm The second approach relied on HPTLC and was carried out on HPTLC plates that had been coated with silica gel 60 F254 beforehand. It used a mobile phase made of n-butanol and acetic acid (7:3, v/v), and 260 nm was used for detection.[22]

Juan Peris-Vicente et al., have reported about Application of micellar liquid chromatography for the determination of antitumoral and antiretroviral drugs in plasma. Here the mobile phase in micellar liquid chromatography is composed of a surfactant and eventually an alcohol. This article discusses numerous micellar liquid chromatography-based techniques for determining the plasma concentration of antitumoral and antiretroviral medications. Because proteins and other endogenous substances are solubilized in micellar medium, samples can be injected after being diluted with a micellar solution and filtered. They talk about the dilution ratio, column type, detection circumstances, and mobile phase composition that have been optimised. This article will also discuss the validation carried out in accordance with the recommendations made by the International Conference on Harmonization and the findings published in the literature that show the methods are effective for the routine analysis of plasma samples for clinical uses.[23]

Mohamed A. Abdel-Lateef et al., have reported about the Micellar spectrofluorimetric protocol for the innovative determination of HCV antiviral (daclatasvir) with enhanced sensitivity: Application to human plasma and stability study. For the determination of DAC in the presence of sofosbuvir, a sensitive, straightforward, quick, and specific fluorometric approach was created and validated. The technique relies on increasing DAC's fluorescence intensity in an aqueous solution of hexadecyl trimethyl ammonium bromide by 170% of its initial value (pH 5.5 buffer). The measurements of fluorescence intensity were carried out at 387 nm with an excitation wavelength of 328 nm. The DAC concentration and fluorescence intensity were shown to be linearly related in the 50.0-2000.0 ng ml⁻¹ range with 0.9998 and 0.9999 for the correlation and determination coefficients, respectively. The respective detection and quantitation limits were 13.4 and 40.8 ng ml⁻¹. [24]

Supercritical Fluid Chromatography (SFC)

Since its introduction in the early 1960s, supercritical fluid chromatography (SFC) has had both ups and downs. The most notable resurgence occurred at the turn of the 2000, when SFC rose to prominence in many laboratories thanks to considerable apparatus upgrades that produced great dependability and robustness. The investigation of diverse substances with varying polarities, acid-base characteristics, and molecular weights was made possible by new breakthroughs in SFC column chemistries and the ability to combine CO₂ with organic solvents. The advantages of hyphenating advanced SFC platforms with mass spectrometry (MS) are similar to those of hyphenating liquid chromatography (LC) with MS. Furthermore, chiral or unstable chemicals that are challenging to examine in LC or GC can benefit from SFC analysis. In a number of study domains, such as bioanalysis, omics sciences, plant, food, and environmental analyses, SFC-MS is primarily employed as a quick and environmentally friendly method.[25]

Louis-Felix Nothias et al., have written about Environmentally Friendly Procedure Based on Supercritical Fluid Chromatography and Tandem Mass Spectrometry Molecular Networking for the Discovery of Potent Antiviral Compounds from *Euphorbia semiperfoliata*. To examine, annotate, and separate secondary metabolites from complicated mixtures, a supercritical fluid chromatography-based targeted purification method utilising tandem mass spectrometry and molecular networking was created. combination of plant extracts. This strategy was used for the specifically separating novel antiviral diterpene esters from Whole plant extract of *Euphorbia semiperfoliata*. The evaluation of Unknown diterpene esters were discovered in bioactive fractions. Jatrophone esters and phorbol esters, among others, were detected in the specimens. The semipreparative purification process Two new jatrophone esters and one existing jatrophone ester were isolated and identified using supercritical fluid chromatography. three brand-new, as well as known, 4-deoxyphorbol esters. Compound 16's composition and exact configuration were via X-ray crystallography, verified. This substance was discovered to have antiviral properties against the Chikungunya virus (EC₅₀ = Compound 15 is 0.45 M, while compound 15 demonstrated effective and specific HIV-1 replication inhibition (EC₅₀ = 13 nM) in a recombinant viral experiment. This study shown that by focusing on molecules of interest and molecular networking, a supercritical fluid chromatography-based technique can facilitate and speed up the discovery of bioactive small compounds while using less harmful solvents.[26]



Prakash Kumar *et al.*,

Gas Chromatography (GC)

The technique of choice for the examination of semi-volatile and volatile chemicals is gas chromatography (GC). There are numerous ways to incorporate green chemistry principles into gas chromatography. As mentioned previously, it is strongly advised to reduce or completely omit the solvent during sample preparation before the final chromatographic analysis. When attempting to make GC analysis greener, the choice of carrier gas may also be taken into account. The most used carrier gas in GC is helium (He), which has the best chromatographic characteristics (high optimal linear velocity), is non-toxic, non-flammable, inert, and safe to handle.[27]

CONCLUSION

This review paper examines green chromatographic technologies that are environmentally friendly for method development for antiretroviral drug evaluation. As a result, the suggested review article introduces a green analytical chromatography approach that allows for method development and validation of antiretroviral drugs analysis without having an adverse impact on analyst health or the environment. From this review it is found that still further research and more no of method should be develop which eliminates the toxic effect on analyst and more eco friendly in nature.

REFERENCES

1. Lange JMA, Ananworanich J. The discovery and development of antiretroviral agents. *AntivirTher*2014;19:5–14. <https://doi.org/10.3851/IMP2896>.
2. Jayaseelan S, Ganesh S, Rajasekar M, Sekar V, Perumal P. A New Analytical Method Development and Validation for the Simultaneous Estimation of Lamivudine and Stavudine in Tablet Dosage Form by Rp-Hplc Method. vol. 2. n.d.
3. Joshi A, Adeyeye MC. Reversed Phase LC-UV Method Development and Validation for Simultaneous determination of three antiretrovirals: Lamivudine, Zidovudine, Nevirapine and Possible Degradants in a Fixed Dose Pharmaceutical Product. *J Pharm Technol Drug Res* 2012;1:4. <https://doi.org/10.7243/2050-120x-1-4>.
4. Nalawade D, Godge RK, Magar SD. Analytical Method Development and Validation of Ritonavir: A Review. *Research Journal of Science and Technology* 2020;12:157. <https://doi.org/10.5958/2349-2988.2020.00020.0>.
5. Kumar BMS, Rajkamal B, Bhikshapathi DVRN, Padmini T. DEVELOPMENT AND VALIDATION OF A NEW RP-HPLC METHOD FOR SIMULTANEOUS DETERMINATION OF ANTIRETROVIRAL DRUGS: COBICISTAT AND ELVITEGRAVIR. *Int J Pharm Sci Res* 2019;10:4981. [https://doi.org/10.13040/IJPSR.0975-8232.10\(11\).4981-87](https://doi.org/10.13040/IJPSR.0975-8232.10(11).4981-87).
6. Alexander AJ, Zhang L, Hooker TF, Tomasella FP. Comparison of supercritical fluid chromatography and reverse phase liquid chromatography for the impurity profiling of the antiretroviral drugs lamivudine/BMS-986001/efavirenz in a combination tablet. *J Pharm Biomed Anal* 2013;78–79:243–51. <https://doi.org/10.1016/j.jpba.2013.02.019>.
7. Mikhail IE, Elmansi H, Belal F, Ehab Ibrahim A. Green micellar solvent-free HPLC and spectrofluorimetric determination of favipiravir as one of COVID-19 antiviral regimens. *Microchemical Journal* 2021;165. <https://doi.org/10.1016/j.microc.2021.106189>.
8. Pacheco-Fernández I, Pino V. Green solvents in analytical chemistry. *Curr Opin Green Sustain Chem* 2019;18:42–50. <https://doi.org/10.1016/j.cogsc.2018.12.010>.
9. Yabré M, Ferey L, Somé IT, Gaudin K. Greening reversed-phase liquid chromatography methods using alternative solvents for pharmaceutical analysis. *Molecules* 2018;23. <https://doi.org/10.3390/molecules23051065>.
10. Orla Gaffney by, White B, Connolly D. Pharmaceutical impurity assay method development using core-shell stationary phase technology for HPLC and evaluation of stationary and mobile phases for an orthogonally selective SFC impurity assay Thesis submitted for the Degree of Master of Science Under the supervision of. 2014.



**Prakash Kumar et al.,**

11. Nguyen HA. SUSTAINABLE APPROACHES IN PHARMACEUTICAL DISCOVERY AND DEVELOPMENT OF SULFA DRUGS. 2020.
12. Iqbal M. UHPLC-MS/MS assay using environment friendly organic solvents: A green approach for fast determination of quetiapine in rat plasma. *Arabian Journal of Chemistry* 2019;12:1774–82. <https://doi.org/10.1016/j.arabjc.2014.11.039>.
13. de Clercq E. Antiretroviral drugs. *Curr Opin Pharmacol* 2010;10:507–15. <https://doi.org/10.1016/j.coph.2010.04.011>.
14. Korany MA, Mahgoub H, Haggag RS, Ragab MAA, Elmallah OA. Green chemistry: Analytical and chromatography. *J Liq Chromatogr Relat Technol* 2017;40:839–52. <https://doi.org/10.1080/10826076.2017.1373672>.
15. Ibrahim AE, elDeeb S, Abdelhalim EM, Al-Harrasi A, Sayed RA. Green stability indicating organic solvent-free hplc determination of remdesivir in substances and pharmaceutical dosage forms. *Separations* 2021;8. <https://doi.org/10.3390/separations8120243>.
16. Sharaf YA, elDeeb S, Ibrahim AE, Al-Harrasi A, Sayed RA. Two Green Micellar HPLC and Mathematically Assisted UV Spectroscopic Methods for the Simultaneous Determination of Molnupiravir and Favipiravir as a Novel Combined COVID-19 Antiviral Regimen. *Molecules* 2022;27. <https://doi.org/10.3390/molecules27072330>.
17. Mikhail IE, Elmansi H, Belal F, Ehab Ibrahim A. Green micellar solvent-free HPLC and spectrofluorimetric determination of favipiravir as one of COVID-19 antiviral regimens. *Microchemical Journal* 2021;165. <https://doi.org/10.1016/j.microc.2021.106189>.
18. Paul K, Gowda Bh J, Shankar SJ, Narasimha Reddy D. Development and validation of simplified RP-HPLC method for quantification of Darunavir in commercial tablets. *Mater Today Proc*, vol. 47, Elsevier Ltd; 2021, p. 4155–61. <https://doi.org/10.1016/j.matpr.2021.04.444>.
19. EL-Shorbagy HI, Elsebaei F, Hammad SF, El-Brashy AM. A green stability-indicating RP-HPLC-UV method using factorial design for determination of ribavirin, sofosbuvir and ledipasvir: Application to average content, acid degradation kinetics and in vitro drug interactions study. *Microchemical Journal* 2020;158. <https://doi.org/10.1016/j.microc.2020.105251>.
20. Hassanlou S, Rajabi M, Shahrasbi AA, Afshar M. Development and Validation of an Ecofriendly HPLC-UV Method for Determination of Capecitabine in Human Plasma: Application to Pharmacokinetic Studies. *South African Journal of Chemistry* 2016;69:174–9. <https://doi.org/10.17159/0379-4350/2016/v69a21>.
21. El-Shaheny RN, El-Maghrabey MH, Belal FF. Micellar liquid chromatography from green analysis perspective. *Open Chem* 2015;13:877–92. <https://doi.org/10.1515/chem-2015-0101>.
22. Assessment of the greenness of new stability indicating micellar UPLC and HPTLC methods for determination of tenofovir alafenamide in dosage forms - PubMed n.d.
23. Peris-Vicente J, Casas-Breva I, Roca-Genovés P, Esteve-Romero J. Application of micellar liquid chromatography for the determination of antitumoral and antiretroviral drugs in plasma. *Bioanalysis* 2014;6:1975–88. <https://doi.org/10.4155/bio.14.154>.
24. Abdel-Lateef MA, Omar MA, Ali R, Derayea SM. Micellar spectrofluorimetric protocol for the innovative determination of HCV antiviral (daclatasvir) with enhanced sensitivity: Application to human plasma and stability study. *Spectrochim Acta A Mol Biomol Spectrosc* 2019;206:57–64. <https://doi.org/10.1016/j.saa.2018.07.101>.
25. Pilařová V, Plachká K, Khalikova MA, Svec F, Nováková L. Recent developments in supercritical fluid chromatography – mass spectrometry: Is it a viable option for analysis of complex samples? *TrAC - Trends in Analytical Chemistry* 2019;112:212–25. <https://doi.org/10.1016/j.trac.2018.12.023>.
26. De E, Torre L. Environmentally-Friendly Workflow Based on Supercritical Fluid Chromatography and Tandem Mass Spectrometry Molecular Networking For the Discovery of Potent Anti-Viral Leads From PI 2017. <https://doi.org/10.1101/106153>.
27. Płotka J, Tobiszewski M, Sulej AM, Kupska M, Górecki T, Namieśnik J. Green chromatography. *J Chromatogr A* 2013;1307:1–20. <https://doi.org/10.1016/j.chroma.2013.07.099>.
28. Ehab Ibrahim A, Saraya RE, Saleh H, Elhenawee M. Development and validation of eco-friendly micellar-HPLC and HPTLC-densitometry methods for the simultaneous determination of paritaprevir, ritonavir and ombitasvir in pharmaceutical dosage forms. *Heliyon* 2019;5:1518. <https://doi.org/10.1016/j.heliyon.2019>.



Prakash Kumar *et al.*,

29. El-Yazbi AF, Elashkar NE, Ahmed HM, Talaat W, Abdel-Hay KM. Cost-effective green chromatographic method for the simultaneous determination of four commonly used direct-acting antiviral drugs in plasma and various pharmaceutical formulations. *Microchemical Journal* 2021;168. <https://doi.org/10.1016/j.microc.2021.106512>.

Table 1. The approved USFDA antiretrovirals 1987-2014[1]

Antiretroviral (abbreviation)	Drug class	Year of US FDA approval
Dolutegravir (DTG)	Integrase inhibitor	2013
Elvitegravir (EVT)	Integrase inhibitor	2012
Raltegravir (RAL)	Integrase inhibitor	2007
Maraviroc (MVC)	CCR5-blocker	2007
Enfuvirtide [T20 (ENF)]	Fusion inhibitor	2003
Rilpivirine (RPV)	NNRTI	2011
Etravirine (ETV)	NNRTI	2008
Efavirenz (EFV)	NNRTI	1998
Delavirdine (DLV)	NNRTI	1997
Nevirapine (NVP)	NNRTI	1996
Darunavir (DRV)	PI	2006
Tipranavir (TPV)	PI	2005
Lopinavir (LVP)	PI	2000
Fosamprenavir (fos-APV)	PI	2003
Amprenavir (APV)	PI	1999
Nelfinavir (NFV)	PI	1997
Indinavir (IDV)	PI	1996
Ritonavir (RTV or r)	PI	1996
Saquinavir (SQV)	PI	1995
Emtricitabine (FTC)	NRTI, nucleoside	2003
Tenofovir disoproxil Fumarate (TDF)	NRTI, nucleoside	2001
Abacavir (ABC)	NRTI, nucleoside	1998
Lamivudine (3TC)	NRTI, nucleoside	1995
Stavudine (d4T)	NRTI, nucleoside	1994
Zalcitabine (ddC)	NRTI, nucleoside	1992
Didanosine (ddI)	NRTI, nucleoside	1991
Zidovudine (ZDV)	NRTI, nucleoside	1987

NNRTI- non-nucleoside reverse transcriptase inhibitor
PI- protease inhibitor

NRTI- nucleoside reverse transcriptase inhibitor
US FDA- United States Food and Drug Administration



Prakash Kumar *et al.*,**Table:2: Various HPLC Methodologies**

Drug sample	Instrument utilized	Mobile phase used	Flow rate	Detector	Column Used	LOD	LOQ	References
Paritaprevir	Young line HPLC system model 9100 (Korea)	mobile phase A consisted of 0.15 M SLS, 0.01 M of sodium dihydrogen phosphate dihydrate and pH was 6.2 Mobile phase B was HPLC grade EtOH. analyses were done by isocratic elution (56:44, v/v)	1 mL/min	UV:254 nm	HPLC core-shell column Kinetix 5 mm-C18 (150*4.6 mm)	0.7 mg/mL	2.2 mg/mL	[28]
Ritonavir	Young line HPLC system model 9100 (Korea)	mobile phase A consisted of 0.15 M SLS, 0.01 M of sodium dihydrogen phosphate dihydrate and pH was 6.2 Mobile phase B was HPLC grade EtOH. analyses were done by isocratic elution (56:44, v/v)	1 mL/min	254 nm	HPLC core-shell column Kinetix 5 mm-C18 (150*4.6 mm)	0.9 mg/mL	2.6 mg/mL	[28]
Ombitasvir	Young line HPLC system model 9100 (Korea)	mobile phase A consisted of 0.15 M SLS, 0.01 M of sodium dihydrogen phosphate dihydrate and pH was 6.2 Mobile phase B was HPLC grade EtOH. analyses were done by isocratic elution (56:44, v/v)	1 mL/min	254 nm	HPLC core-shell column Kinetix 5 mm-C18 (150*4.6 mm)	0.8 mg/mL	2.4 mg/mL	[28]
Sofosbuvir (SF)	HPLC-DAD system Agilent 1200	0.1% (v/v) triethylamine acidified water with ortho-phosphoric acid (OPA) pH=2.53 and acetonitrile in the ratio (70:30 v/v).	0.8 mL.min ⁻¹	210nm	Waters XBridge BEH C18 Column (4.6 × 150 mm)	3:1	10:1	[29]
Ledipasvir (LD)	HPLC-DAD system Agilent 1200	0.1% (v/v) triethylamine acidified water with ortho-phosphoric acid (OPA) pH=2.53 and acetonitrile in the ratio (70:30 v/v).	0.8 mL.min ⁻¹	330nm	Waters XBridge BEH C18 Column (4.6 × 150 mm)	3:1	10:1	[29]



Prakash Kumar *et al.*,

Velpatas vir (VP)	HPLC-DAD system Agilent 1200	0.1% (v/v) triethylamine acidified water with ortho-phosphoric acid (OPA) pH=2.53 and acetonitrile in the ratio (70:30 v/v).	0.8 mL.min ⁻¹	210nm	Waters XBridge BEH C18 Column (4.6 × 150 mm)	3:1	10:1	[29]
Daclatas vir (DC)	HPLC-DAD system Agilent 1200	0.1% (v/v) triethylamine acidified water with ortho-phosphoric acid (OPA) pH=2.53 and acetonitrile in the ratio (70:30 v/v).	0.8 mL.min ⁻¹	300nm	Waters XBridge BEH C18 Column (4.6 × 150 mm)	3:1	10:1	[29]





Sleep and Satisfaction: An Investigation into the Connection between Professional Quality of Life and Sleep in Female Physicians

Khanna K¹, Gargi Sharma^{2*} and Dhankar C²

¹Research Scholar, Department of Psychology, Manipal University Jaipur, Rajasthan, India.

²Assistant Professor, Department of Psychology, Manipal University Jaipur, Rajasthan, India.

Received: 14 Feb 2023

Revised: 23 Apr 2023

Accepted: 26 May 2023

*Address for Correspondence

Gargi Sharma

Assistant Professor,
Department of Psychology,
Manipal University Jaipur,
Rajasthan, India.
E. Mail: gargi.sharma@jaipur.manipal.edu



This is an Open Access Journal / article distributed under the terms of the **Creative Commons Attribution License** (CC BY-NC-ND 3.0) which permits unrestricted use, distribution, and reproduction in any medium, provided the original work is properly cited. All rights reserved.

ABSTRACT

The demands of a medical career can be challenging, particularly for female physicians who often juggle demanding careers with personal responsibilities. Maintaining a balance between professional and personal life is essential for the well-being and satisfaction of individuals in this field. Recent studies have shown that poor sleep quality shows significant impact on an individual's overall wellbeing and quality of life. Additionally, professional quality of life has been linked to various factors, including job satisfaction, burnout, and work-life balance. The purpose of the present study is to examine the correlation between professional quality of life and sleep quality in female physicians, as both factors have important implications for the well-being and satisfaction of individuals in this field. In this descriptive study, self-report questionnaires were distributed to 100 female doctors working as a physician and surgeon. The survey instrument included questions about socio-demographic details, Professional quality of life (stamm, 2010), and The Pittsburgh sleep quality index (Buysee, 1988). A correlational analysis was used to analyze the associations between the variables. The results came out to highly significant, showing correlation between the variables. Female physicians show higher secondary traumatic stress.

Keywords: Professional quality of life, sleep quality, female doctors, secondary traumatic stress.

INTRODUCTION

The primary objective of health care systems across the globe is to provide high-quality, secure care. However, there is a serious hazard to both people and organizations from the rise in job-related stress. Additionally, this problem

56929



**Khanna et al.,**

may result in increased worker absenteeism and subpar performance (Almazan et al., 2019). Stress may be even more dangerous for healthcare employees because of its possible detrimental effects, despite being a substantial issue for companies. In recent years, awareness of burnout and occupational stress among healthcare professionals has increased.

This study concentrating on the relation between the aspects of professional quality of life and sleep quality of doctors. Professional quality of life (ProQOL) refers to the degree to which one's work provides satisfaction and fulfillment, and sleep quality refers to the perceived quality of one's sleep. Professionals working in the healthcare industry frequently experience sleep loss and impairments brought on by the resulting weariness (Martin AH, 2020). Female doctors, like many healthcare professionals, often experience high levels of stress and burnout, which can negatively impact their ProQOL and sleep quality. Numerous stressors have been linked to the development of sleep disorders, notably insomnia (Owens J. A., 2007). According to Somville et al. (2016), emergency physicians are more vulnerable to traumatic events at work, hectic, stressful working conditions, occupational dangers, psychological issues, a low level of support socially, somatic symptoms, subjective weariness, and conflicts with other doctors. Numerous research on workplace and organisational issues have focused on the official relationships among doctors and attendants, emergency department heads, and healthcare administrators (Doef 1999; Doef and Maes 1999). Though every ED professional is exposed to the similar organisational and work-related elements, individual attributes like personality traits might as well be extremely important in the onset of burnout (Wal et al. 2018).

The issue of sleep loss and fatigue among healthcare professionals and its negative impact on their health, job performance, and patient safety. The causes of fatigue and sleep loss, such as long working hours and shift work, are identified and the consequences, including decreased physical and cognitive function, are discussed. The study emphasizes the need for effective fatigue management strategies and specific interventions tailored to the hospital setting to address this issue. The review provides a context for improving strategies to address, recognize, and accordingly manage fatigue and sleep loss in healthcare professionals (Owens, 2007). The past literatures have shown that female doctors have lower ProQOL and worse sleep quality compared to male doctors. The factors associated with poor professional quality of life and worse sleep quality includes long working hours, work-life balance, job control, and social support. Female doctors who have more control over their schedules and who receive support from colleagues and family members have been found to have higher ProQOL and better sleep quality. There is also gender-specific factors that can impact ProQOL and sleep quality among female doctors. For example, studies have found that women who are mothers and have children at home experience additional stress and demands on their time, which can negatively impact their ProQOL and sleep quality. Additionally, gender biases and discrimination in the workplace can contribute to lower ProQOL and worse sleep quality for female doctors.

Rationale of the Study

The rationale for studying the correlation between professional quality of life that includes burnout, compassion satisfaction, and secondary traumatic stress; and sleep quality of female doctors is rooted in the importance of understanding the well-being of health care professionals. Female doctors, like other professionals in health care, often experience high levels of burnout, stress and secondary traumatic stress due to the demanding nature of their work. These factors might show a significant impact on their overall well-being and professional quality of life. Sleep quality is also a crucial aspect of overall well-being, as poor sleep can lead to decreased productivity, decreased job satisfaction, increased burnout, and decreased professional quality of life. By examining the correlation between the aspects of professional quality of life and sleep quality of female doctors, we can gain a deeper understanding of the factors that impact the well-being of female doctors and identify potential interventions to recover their life quality. In addition, it's important to consider the unique challenges faced by female doctors, such as gender bias and the demands of balancing a career and family. By doing this research, specifically in female doctors, we can gain a more comprehensive understanding of the challenges they face and develop targeted interventions to support their well-being. Overall, the rationale for studying the correlation between professional quality of life and sleep quality of



**Khanna et al.,**

female doctors is to improve our understanding of the overall well-being of doctors, with a focus on female doctors, and identify ways to support their professional and personal well-being.

METHODS

Objective

To investigate the relationship between professional quality of life and sleep quality in female doctors.

Hypotheses

1. There will be a negative relationship between compassion satisfaction and sleep quality index.
2. There will be a positive relation between burnout and sleep quality index.
3. There will be a positive relation between secondary traumatic stress and sleep quality index.

Type of the Study and Ethical Aspects

This descriptive and correlation study was performed to determine the level of compassion satisfaction, burnout, secondary traumatic stress, and sleep quality in female doctors. Confidentiality was guaranteed to all participants.

Data Collection

Descriptive study design is used in this research, the data was gathered using self-report questionnaires distributed to female doctors (physicians and surgeons). Both online survey and offline approach was followed to circulate the questionnaires among doctors, a google form was made after receiving the required approvals for the research. Google forms was shared through Whatsapp messenger, that is a social media application. Some forms was also get filled by going directly to the hospitals. There were eligible data available for 100 of the 189 questionnaires that were sent. (Response rate 52.9%; N=100/189).

The Descriptive Form

A self-made set of questions consisted of 9 items, included the questions about doctor's socio-demographic characters (gender, age, years of experience, job title, etc).

Professional Quality of Life

Professional Quality of Life Scale (ProQOL) was created to assess burnout, work satisfaction, and compassion fatigue among healthcare professionals. It is a self-report questionnaire consisting 30 items. Summing up of each subscale scores represent the component separately (stamm, 2010).

The Pittsburgh Sleep Quality Index

This 18-item questionnaire was created by Buysee *et al.* with the intention of examining the quality of sleep over the previous month. It has been claimed that this questionnaire can differentiate between poor and excellent sleep characteristics. The questionnaire has a total score that can be between 0 and 21. High scores reflect a lack of quality sleep (Buysee, 1988).

Data Analysis

The data was analysed on Microsoft excel. Descriptive statistical techniques such as frequency, mean, percentage, and SD were employed for the data analysis. Pearson correlation analysis was employed to examine the relationships between given variables.

RESULT AND DISCUSSION

Healthcare professionals run a significant risk of being exposed to trauma indirectly through their employment and may experience secondary traumatic stress symptoms (STS). Professional's secondary exposure to trauma from the

56931



**Khanna et al.,**

patient's terrible occurrences is related to the secondary traumatization. This may occur when hearing to specifics about the traumatic event while helping the patient recover from the incident (Virga, 2020; Sung Ja Kim, 2017; Sung Ja Kim, 2017). This research was done on 100 samples and secondary traumatic stress comes out to be the highest among all. Although 57% doctors show medium levels of compassion, 77% female doctors suffered from high level of secondary traumatic stress and 71% of them have medium burnout levels. Only 2% showed low level of secondary traumatic stress. 46% doctors are affected with poor sleep quality. Compassion fatigue has a component known as secondary trauma stress, which is characterised by preoccupied thinking for those one has helped. Caregivers describe feeling confined, tense, worn out, overburdened, and contaminated by the trauma of others. The inability to sleep, occasional forgetfulness of crucial details, difficulty to distinguish one's private life from that of a helper, and being affected by the trauma of a person you helped. These are all traits, goes up to the extent of getting the way out from the activities to avoid memories of the trauma. It is significant to highlight that while secondary traumatic stress disorder is uncommon, many people do experience it (stamm, 2010).

Analysis of the relationship between variables showed a significant negative relationship between compassion satisfaction and sleep quality index (Table 2). This result represents higher scores of compassion satisfaction is associated with lower scores in sleep quality index, 4 or less global sleep index shows good sleep quality. Studies have shown the similar results of negative correlations of compassion satisfaction with fatigue, anxiety, depression, and sleep disorders (Sung Ja Kim, 2017). Less relevant sleep was found in association of sleep and compassion satisfaction, although a few studies has examined this relation of former and latter in nurses. One of the studies examined sleep disturbance as facilitator of relation between health and professional quality of life in nurses. The study revealed the significantly associated relation of decreased sleep disturbance and increased compassion satisfaction (Lena J. Lee, 2021).

Table 3 shows the positive correlation between the scores of secondary traumatic stress and sleep quality index. This indicates higher secondary traumatic stress leads to poor sleep quality. Past research has been done on professional quality of life and its association with sleep quality, although limited research has been done on doctors. There is enough evidence to show the significant relation between the level of secondary traumatic stress with poor sleep quality among nurses (Davy Vancampfort, 2022).

Table 4 shows highly significant results of burnout and sleep quality index, it shows positive correlation between the scores of former and latter. The results suggest people with higher burnout tend to have poor sleep quality. The study conducted by Khamisa *et al.* (2015) provides valuable insights into the relationship between burnout, sleep disturbances, and mental and physical health in nurses. The findings suggest that burnout not only has a direct impact on mental and physical health, but also contributes to these outcomes indirectly through sleep disturbances. The research methodology used in the study appears to be appropriate, and the results are well presented and discussed in the context of previous literature. The data provide strong evidence for the hypothesis that improving compassion satisfaction and lowering burnout and secondary traumatic stress may enhance physical and mental health in nurses, especially in those with sleep problems. Overall, the study provides valuable information that can be useful for healthcare organizations, policymakers, and individual nurses in developing strategies to address burnout and promote well-being in the nursing profession. The importance of addressing burnout in healthcare providers has been widely recognized, and this study contributes to the growing body of literature in this area. In recent years, doctors have faced immense level of stress and work-load, resulting in poor mental and physical health. The present study was an attempt to understand about the contributing factors in deteriorating well-being of physicians. It is revealed that to increase the work quality, proper sleep is required, and the quality of sleep shows strong correlations with compassion satisfaction, secondary traumatic stress, and burnout.





Khanna et al.,

CONCLUSION

In conclusion, female doctors face unique challenges that can negatively impact their ProQOL and sleep quality. Addressing these challenges, such as work-life balance, job control, social support, and gender-specific factors, can help improve the well-being of female doctors and prevent burnout. A sleeping disorder, Insomnia has been defined as one of the main factors of mental health deterioration among frontline healthcare professionals. Adequate sleep must be suggested as an immense important parameter for mental health. Optimal preventive measures need to be taken care for decreasing the prevalence of high secondary traumatic stress and burnout among doctors.

Limitations of the Study

The primary limitation of this study is that it included limited data of only female doctors. Other variables resulting in the weaken professional quality of life can be studied in later studies.

REFERENCES

1. Almazan J. U., Albougami A. S., Alamri M. S. (2019). Exploring nurses' work-related stress in an acute care hospital in KSA. *Journal of Taibah University Medical Sciences*, 14(4), 376–382.
2. Almazan, J. U., Albougami, A. S., & Alamri, M. S. (2019). Exploring nurses' work-related stress in an acute care hospital in KSA. *Journal of Taibah University Medical Sciences*, 14(4), 376-382.
3. Buysse, D. J., Reynolds III, C. F., Monk, T. H., Berman, S. R., & Kupfer, D. J. (1989). The Pittsburgh Sleep Quality Index: a new instrument for psychiatric practice and research. *Psychiatry research*, 28(2), 193-213.
4. Khamisa, N., Oldenburg, B., Peltzer, K., & Ilic, D. (2015). Work related stress, burnout, job satisfaction and general health of nurses. *International Journal of Environmental Research and Public Health*, 12, 652–666. <https://doi.org/10.3390/ijerph120100652> Khormizi, H. Z., Salehinejad, M. A., Nitsche, M. A., & Nej
5. Khamisa, N., Peltzer, K., Ilic, D., & Oldenburg, B. (2017). Effect of personal and work stress on burnout, job satisfaction and general health of hospital nurses in South Africa. *health sa gesondheid*, 22, 252-258.
6. Kim, S. J., & Na, H. (2017). A study of the relationships between compassion fatigue, compassion satisfaction, depression, anxiety, and sleep disorders among oncology nurses. *Asian Oncology Nursing*, 17(2), 116-123.
7. Owens, J. A. (2007). Sleep loss and fatigue in healthcare professionals. *The Journal of perinatal & neonatal nursing*, 21(2), 92-100.
8. San Martin, A. H., Serrano, J. P., Cambriles, T. D., Arias, E. M. A., Méndez, J. M., del Yerro Álvarez, M. J., & Sánchez, M. G. (2020). Sleep characteristics in health workers exposed to the COVID-19 pandemic. *Sleep medicine*, 75, 388-394.
9. Somville, F. J., De Gucht, V., & Maes, S. (2016). The impact of occupational hazards and traumatic events among Belgian emergency physicians. *Scandinavian journal of trauma, resuscitation and emergency medicine*, 24(1), 1-10.
10. Somville, F., Van der Mieren, G., De Cauwer, H., Van Bogaert, P., & Franck, E. (2022). Burnout, stress and Type D personality amongst hospital/emergency physicians. *International Archives of Occupational and Environmental Health*, 1-10.
11. Stamm, B.H. (2010). The Concise ProQOL Manual. Pocat ello, ID: ProQOL.org.
12. Stamm, B. (2010). The concise manual for the professional quality of life scale.
13. Vancampfort, D., & Mugisha, J. (2022). Associations between compassion fatigue, burnout and secondary traumatic stress with lifestyle factors in mental health nurses: A multicenter study from Uganda. *Archives of Psychiatric Nursing*, 41, 221-226.
14. Vîrgă D.M., Baciu E.-L., Lazăr T.-A., Lupșa D. Psychological Capital Protects Social Workers from Burnout and Secondary Traumatic Stress. *Sustainability*. 2020;12:2246. doi: 10.3390/su12062246.





Khanna et al.,

Table 1. The Table Represents Mean and Standard Deviation

Variables	Mean	Standard Deviation
Compassion Satisfaction (CO)	54.47	7.49
Burnout (BO)	52.53	6.47
Secondary Traumatic Stress (STS)	63.79	8.39
Sleep Quality Index	4.62	2.79

Table 2. Correlation Compassion Satisfaction and Sleep Quality Index (SQI)

variable	Correlation coefficient	Significance level
CS and SQI	-0.465	0.01

Table 3. Correlation Sleep Quality Index and Secondary Traumatic Stress

variable	Correlation coefficient	Significance level
STS and SQI	0.429	0.01

Table 4. Correlation Burnout and Sleep Quality Index

variable	Correlation coefficient	Significance level
SQI and BO	0.337	0.01

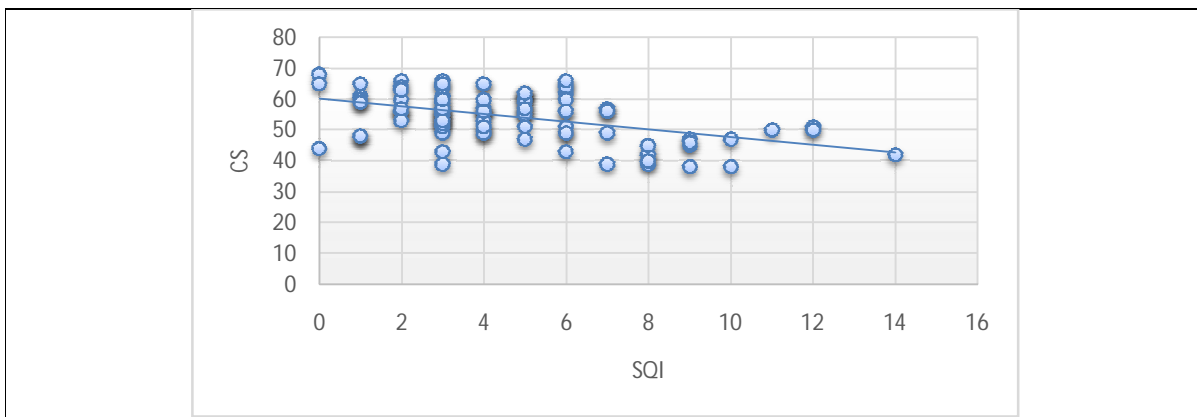


Fig. 1 Correlation Compassion Satisfaction and Sleep Quality Index (SQI)

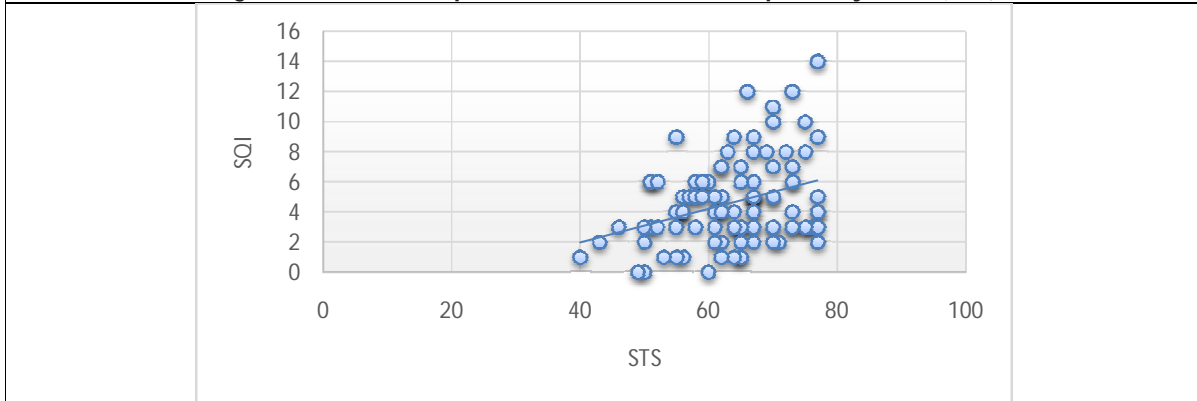


Fig.2 Correlation Sleep Quality Index and Secondary Traumatic Stress





Khanna et al.,

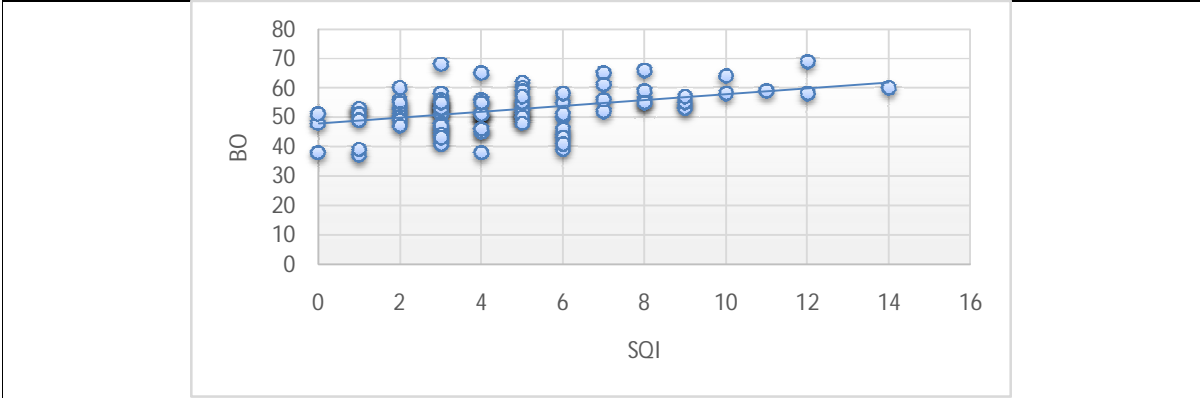


Fig.3 Correlation Burnout and Sleep Quality Index





Improved Clustering and Elliptical Curve Cryptography Based Energy Efficient Routing in WSN for Enhanced Agriculture

O.P.Uma Maheswari^{1*} and G.Dona Rashmi²

¹Associate Professor in Computer Science, P.K.R Arts College for Women, Gobichettipalayam, Tiruppur, Tamil Nadu, India.

²Assistant Professor in Computer Applications, Kongunadu Arts and Science College, Coimbatore, Tamil Nadu, India.

Received: 26 Feb 2023

Revised: 28 Apr 2023

Accepted: 31 May 2023

*Address for Correspondence

O.P.Uma Maheswari

Associate Professor in Computer Science,
P.K.R Arts College for Women,
Gobichettipalayam, Tiruppur,
Tamil Nadu, India.



This is an Open Access Journal / article distributed under the terms of the **Creative Commons Attribution License** (CC BY-NC-ND 3.0) which permits unrestricted use, distribution, and reproduction in any medium, provided the original work is properly cited. All rights reserved.

ABSTRACT

Agriculture requires tools and technologies that increase production efficiency and quality while minimizing environmental impacts on output. The agricultural wireless sensor network has the potential to greatly contribute to precision agriculture. Precision agriculture is the practice of applying the appropriate quantity of input (water, fertilizer, herbicides, etc.) at the appropriate time and location to maximize yield and quality while minimizing environmental impact. Sensors in agriculture often collect soil, weather, crop, water level, and moisture level data in order to identify and respond to unexpected behavior. A recent study titled enhanced security utilizing Rivest-Shamir-Adleman (RSA) technique presented a security system in which the key would be produced using a cryptographic approach to encrypt the data and authenticate the user. Nonetheless, the RSA technique is very slow when it comes to encrypting large amounts of data on a single system. The reliability of public keys must be certified by a third party. Intermediaries who tamper with the public key system have the ability to compromise RSA-transmitted data.

Keywords: RSA, Improved Clustering, Energy Efficient, WSN, Routing

INTRODUCTION

Modern agriculture must utilize cutting-edge technologies to increase product output, quantity, and quality. Due to advancements in microelectronics, micro electro mechanical systems, information, and sensor technologies, small, low-cost sensors have been developed to aid in the deployment phase in a wide range of scenarios, including animal

56936



**Uma Maheswari and Dona Rashmi**

tracking, forest management, crop monitoring, and yield estimation [1]. There are several benefits to using wireless sensor networks (WSNs), including its adaptability to a variety of uses, resilience in the face of adversity, closed-loop control capabilities, and the ability to cover a wider area with higher temporal and spatial accuracy. Sensor node utilization reduces labor requirements, which in turn reduces deployment, operational, and maintenance expenses. In addition, WSNs provide periodic data on parameters and the state of fields and crops in real time, enabling precision agriculture. [3]. Wireless communication decreases total network costs by roughly 80% when compared to conventional solutions. WSNs need to be simple in design, implementation, operation, and upkeep [4]. Therefore, if every node is powered by a battery, it becomes impractical to recharge or replace batteries, particularly in large-scale networks [5]. It may be difficult, if not impossible, to keep track of everything that's going on in a network under extreme circumstances because of how complex the structure becomes as a consequence of where nodes are placed. Transport, military monitoring, and surface exploration are just some of the large-scale activities that suffer [6]. There is a fundamental limitation in these scenarios, since the battery life of individual nodes is limited, and this has an effect on the efficiency of the network as a whole [7]. Therefore, further study into the difficulty of increasing the operational lifetime of wireless sensor nodes via increased energy efficiency is required. There has been research towards wireless energy transfer and energy harvesting [8].

Power is a major factor in wireless communication. Energy efficiency [9] has motivated the development of a number of communication strategies for WSN-based agricultural applications, such as data aggregation, routing, and scheduling algorithms. In this study, we go into the topic of low-power routing in wireless sensor networks. We provide a strategy for data routing that involves three steps: identifying and locating nodes, grouping them into clusters, and establishing communications between them [10]. Essential field data is quickly sent between nodes in the proposed agricultural monitoring system architecture, providing a comprehensive picture of the actual system in use. In this method, nodes are placed in a network at random [11-14]. Then, a clustering technique is used to arrange these nodes into distinct groups according to their initial energy. There are several regular nodes and one "cluster head" (CH) node in every cluster. Consequently, there are two kinds of communication topologies among the nodes that have been deployed: intercluster communication, in which nodes from different clusters exchange messages, and intracluster communication, in which nodes within the same cluster exchange messages. [15-17]. Since this is the case, the base station (BS) is responsible for collecting and transmitting all information to the network's central hub. Location, en route sensing, and data networking are only some of the additional data processing and decision making procedures that are added at this stage. When choices have been taken, they are sent to other nodes in the network. This leads to an increase in the total number of packets exchanged, which in turn increases the power requirements of the operational nodes and hence disrupts the network's energy equilibrium. [18-20].

Background Study

Ahmad, N. *et al.* [1] these authors look at how the Internet of Things (IoT) may be used to wireless sensor networks (WSNs) in precision agriculture (PA). The experimental system for self-sufficient precision agriculture was put through its paces, and real-time sensor readings were successfully sent to the server through cluster topology. After being stored in the cloud, this information was made accessible to the user using a graphical user interface. Automatic irrigation control was enabled by setting a threshold on the server. Balamurali, R., & Kathiravan, K. [3] these authors research, concluded that the Integrated MAC and Routing Algorithm was best suited for multi-hop routing in Wireless Sensor Networks for precision agriculture in terms of network lifetime (WSN). The end of the network's existence in this situation was considered to be the demise of the first WSN node. Throughput and end-to-end latency were only two of the network metrics that might be expanded upon in future development.

De la Concepcion, A. *et al.* [5] these authors research describes the process of developing and deploying a WSN for precision agriculture, with the goal of keeping tabs on various plant-based physical attributes. Dense deployment and precise monitoring were made possible by the infinite dimensions and exceptionally low power consumption. The WSN consisted of two independent networks that could switch between using various intra- and inter-subband (ISM) frequencies. Band diversity was made possible thanks to a novel dual-band reconfigurable loop antenna. The system has been acclaimed for its dependability and durability (99%), and it was now being put to the test at the





Uma Maheswari and Dona Rashmi

Boscarella vineyards in Montepulciano, Italy. This led the author to begin developing methods for including video information into the WSN infrastructure. Hu, Z. *et al.* [9] For uplink transmission in agricultural WSNs, the author used relay-aided NOMA. For a typical periodic and bursty short-range uplink broadcast, the NOMA approach may be able to handle more sensor nodes while utilising the same number of REs. When it comes to agricultural WSNs, it was recommended to utilise a hybrid transmission strategy, with conventional OMA used for downlink transmission and relay-aided NOMA used for uplink transmission from sensor nodes to sink nodes. NOMA-enabled WSNs have the potential to increase the data rate to the sink node, reduce power consumption at the sensor nodes, and increase the network's lifetime thanks to their extensive connections and high cumulative data rate. The author analysed NOMA's uplink transmission efficiency in terms of both the total data rate it could transmit and the frequency with which it experienced failures. Using relays in agricultural WSNs, numerical simulations demonstrate that NOMA was a viable solution for uplink and downlink transmission. This results in a lower chance of outages and a higher average data throughput for wireless sensor networks.

K.N., B. *et al.* [11] these authors research collects information on many soil factors, such as soil temperature, soil moisture, and air temperature, to help predict irrigation appropriateness. This method aids in the study of soil properties, which ultimately leads to a more efficient agricultural watering system. The system was totally automated thanks to the sensor data that was taught to learn using machine learning techniques. Improving crop quality while minimising the need for human labour in agriculture was a dual benefit of adopting an Internet of Things (IoT)-based smart agriculture system. The findings showed that the suggested method produced a dataset that was more suited to the Support Vector Machine (SVM) classification technique than either the KNN Classifier or the Naive Bayes Classifier, with the SVM achieving an accuracy of 87.5%. The current study explores the correlation between soil temperature and soil moisture for the purpose of categorization. Khrijji, S. *et al.* [13] The deployment of wide-area WSNs for agricultural purposes was anticipated to grow. As the number of dispersed sensor nodes grows, the need of investigating and implementing energy-efficiency techniques grows as well. It's possible that using a wireless connection uses more power than necessary. To this end, a routing system was developed that utilises both localization and clustering to cut down on the amount of power a network uses. The author presents a node location identification strategy based on RSSI localization. Next, a fuzzy-based method for uneven clustering was devised to equalise power consumption across all sensor nodes. Prakash, S. [17] According to the thorough research, wireless sensor networks play an important role in agriculture, assisting farmers in making educated crop decisions. More research was being done on predicting soil moisture. Singh, A. *et al.* [20] The agricultural sector was vital to the future of the nation. This type of cultivation requires extra care. Improved farming practises were possible with the help of the Internet of Things. IoT was used in farming to facilitate better management of time, water, crops, soil, pesticides, and other agricultural chemicals. Additionally, it helps reduce labour costs, streamlines production, and boosts yields. As an added bonus, intelligent farming may increase farmers' access to new customers with nary a fingertip.

METHODOLOGY

This section stages the proposed security enhanced precision agriculture model by elliptic curve cryptography based encryption and decryption for security and node authentication. In which nodes are clustered in an optimal way by using improved fuzzy cmeans clustering. Within these cluster members' optimal cluster heads are selected by using Hybrid cuckoo search and genetic algorithm. Agent technologies are used for packet transmission from the source to destination. Overall flow chart of the proposed model is shown in Figure 1.1.

Fuzzy C-Means Clustering Algorithm

The FCM clustering method was first introduced by Dunn, and was further refined. By minimising a weighted class sum of squared error objective function, this continuous clustering technique finds the best possible c partition.

$$J_{FCM} = \sum_{k=1}^N \sum_{i=1}^c (\mu_{ik})^q d^2(x_k, v_i) \text{ ---- (1)}$$





Uma Maheswari and Dona Rashmi

Where $X = \{x_1, x_2, x_3, \dots\} \in R^p$ the dataset occupies p dimensions, the number of data points occupies n dimensions, the number of clusters occupies n dimensions, the degree of membership in the th cluster occupies 2 dimensions, and the weighting exponent for each fuzzy membership occupies n dimensions. The prototype for a cluster's centre is its centre, which is used to calculate how far apart individual items are. An iterative process might be used to solve the object function.

Objective function algorithms are a kind of clustering method that aims to minimise a metric. C-Means, where c is the number of classes or clusters used, is a common name for algorithms that can minimise an error function, and FCM is the name given to algorithms that utilise the fuzzy method for their classes. In the FCM approach, a fuzzy membership is used to assign a degree of membership to each class. Fuzzy clustering's emphasis on membership degree is analogous to the mixture modeling's reliance on the pixel probability assumption. The primary benefit of FCM is the creation of new clusters from data points that have comparable membership values to existing groupings. The three main components of the FCM method are the membership function for fuzzy sets, the partition matrix, and the objective function.

Each vector $x_i \in R^s$ represents some aspect of x_i in terms of s real-valued measurements. Membership matrix called the Fuzzy partition matrix describes the fuzzy membership matrix. Fuzzy partition matrices $c \times n$ are defined by Eq. 2, and their set M_{fc} is denoted by the symbol.

$$M_{fc} = \{W \in R^{cn} | W_{ik} \in [0,1], \forall i, k; \dots\dots\dots (2)$$

$$\sum_{i=1}^c w_{ik} = 1, \forall k; 0 < \sum_{k=1}^n W_{ik} < n, \forall i \} \dots\dots (3)$$

Components may belong to many clusters at different levels of membership based on the criteria outlined above. Since the sum of each element's "membership" is set to 1, there is no way for all data to fit into a single cluster. The goal function (Equation 3) of the fuzzy c-means method is derived from the membership value and the Euclidean distance (Eq. 4).

$$J_m(W, P) = \sum_{\substack{1 \leq k \leq n \\ 0 \leq i < c}} (W_{ik})^m (d_{ik})^2 \dots\dots\dots (4)$$

Where

$$(d_{ik}) = ||x_k - P_i|| \dots\dots\dots (5)$$

The formed clusters are governed by the fuzziness parameter, $m \geq 1$, and the distance, in Euclidean units, from an item x_k to the cluster centre, p_i , is denoted by d_{ik} . By iteratively updating the partition matrix with Equations 5 and 6, the FCM approach minimizes the objective function J_m .

$$P_i = \frac{\sum_{k=1}^n (w_{ik})^m x_k}{\sum_{k=1}^n (w_{ik})^m} \dots\dots\dots (6)$$

Elliptic Curve Cryptography

In Verilog, the module is the basic building block of a description. The ports via which a module communicates with other modules and the design's structure or functioning are described in a module. Primitives at the switch level, the gate level, and the user-defined level are used to explain the structure of a design. Dataflow is characterised by continuously assigned variables, whereas sequential behaviour is described by procedural structures. It is possible to construct one module inside of another. A module's essential syntax looks like this.

```

module module_name (port_list);
declarations
reg, wire, parameter
input, output, inout.
Functions, tasks,
statements
initial statements
always statements,
.....
End module
    
```

The implementation in verilog HDL consists of three main modules



**Uma Maheswari and Dona Rashmi**

namely,

i) Main Controller

ii) Multiplier and

iii) Adder

The main controller

Controls the efficiency of the adder and multiplier When 0 is present on the Enable line, the multiplier building block is selected. With an elliptic curve point as an input, the multiplier performs an integer multiplication. In order to do multiplication, one must first add each of the products together in order.

Cuckoo Search Algorithm

The Cuckoo search (CS) technique is a population-based stochastic global search meta-heuristic algorithm that takes inspiration from natural systems. It's based on the Lévy flying behaviour of certain birds and fruit flies, as well as the brood-parasitism of several species of cuckoo. Species belonging to this group increase the chances of hatching their eggs by depositing them in the nests of other host birds (almost always of different species). They do this by selecting nests that have just been built and eliminating any eggs that may already be in them. However, some host birds may fight back against the parasitic behaviour of cuckoos by rejecting the foreign eggs or building a new nest elsewhere. A new optimization strategy is developed using cuckoo breeding as an example. No computer programme, no matter how simple, can accurately reflect the complexity of natural processes. Simplifying a natural system is necessary for coding it into a computer programme. The mechanism of cuckoo reproduction was simplified into three guidelines:

1. Cuckoos only lay one egg at a time, and they each deposit that egg in a different nest.
2. High-quality egg-laying lays will be passed on to subsequent generations.
3. There is a set number of host nests, therefore a host has a $p \in [0, 1]$ chance of discovering an alien egg. The parent bird will either leave the nest and abandon the egg, or the egg will hatch and the host bird will begin using it.

Applying these three guidelines yields the following cuckoo search strategy:

1. Keeping a solution in the form of an egg in a nest is a common metaphor. Only one egg at a time may be laid by the artificial cuckoo.
2. The cuckoo looks for the nicest possible nest to lay its eggs in, increasing the chance of survival for its young. In order to hatch and develop into a cuckoo, an egg must be of good quality (best solutions near to optimal value) and resemble those laid by the host bird.
3. There has been no change in the number of host nests. The host bird has a chance of $e \in [0,1]$ of either rejecting the alien egg (the worst possible outcome) or leaving the nest to start a new one somewhere else. The egg continues to grow and pass on its genetic information if this doesn't happen. Lévy goes around the current top solutions and lays fresh eggs (solutions).

Each egg represents a potential result, and the aim is to use new, maybe better solutions (cuckoos) to replace those that currently exist in the nests but are less than ideal. Each nest represents a single egg, which stands for a single cuckoo, therefore in this case the three terms are interchangeable. The Lévy flight rule governs the construction of the new nest. Birds use Lévy flight to discover their environment and forage for food.

RESULT AND DISCUSSION

Here we describe the results of our experiments with the proposed models for detecting soil fertility, fire, irrigation, and floods. For this model, we use MATLAB 2013b. Packet delivery ratio, End-to-End Delay, Average energy consumption, and Encryption time for the USGS dataset are compared among the IS-ECC, DES, and IS-RSA techniques, as well as the existing DSS, MACAG, IACOIG, and RSA methods. The data and information supplementing the journal article are presented here in a U.S. Geological Survey Data Release. Parental incubation behaviour differs between species with diverse life history breeding strategies, and this is despite the fact that nest survival is a vital demographic step in bird population dynamics. Despite studies showing an increase in nest survival rates when colonies are mixed, the behavioural processes that would account for this are mostly lacking. On



**Uma Maheswari and Dona Rashmi**

Alcatraz Island in California, researchers used video surveillance techniques to study the incubation habits of black-crowned night- herons. In terms of packet delivery ratio, the accompanying graph compares the performance of the proposed IS-ECC method with the state-of-the-art DSS and MACAG approaches. The X-Axis in the above graphic shows the total number of nodes, while the Y-Axis displays the packet delivery rates. Based on the results, it seems that the novel IS-ECC model improves upon the state-of-the-art DSS and MACAG approaches by achieving a Packet delivery ratio of 0.80 as opposed to 0.66 and 0.68, respectively. Table 1 lists the results of each PDR study side-by-side for easy comparison.

Figure 4 depicts an end-to-end delay performance comparison of the novel IS-ECC methodology with the present DSS and MACAG approaches. The manager agent gives the quickest path from the cluster to the head and from the sink to the head using the agent technology employed in the planned job, hence saving time. The X-axis in the graphic above shows the number of nodes, while the Y-axis represents the end-to-end delay values. The proposed IECC model delivers 0.4 (s) less end-to-end latency than the existing DSS and MACAG techniques, which reach 1.2 (s) and 1.1 (s), respectively. Table 2 contrasts the results for End to End Delay. In terms of energy utilisation, comparing the proposed IS-ECC approach to the present DSS and MACAG methodologies indicates the effectiveness of the IS-ECC method. Figure 3...8 depicts the total energy use in joules. The cluster heads for the network nodes in this work were chosen using a hybrid cuckoo search and genetic algorithm, in which the fitness function parameter of the cuckoo search will provide the optimised heads that will be deployed at the shortest distance between inter-clusters, thereby reducing the energy required for data transmission. The proposed IECC model uses 25(J) less energy than the present DSS and MACAG approaches, which use 39(J) and 35(J), respectively, more energy. The energy consumption of the proposed and present techniques is compared in Table 1.

In terms of encryption time, the performance of the suggested IS-ECC technique is compared to the current DES approach. In Figure 6, the X-Axis represents message size and the Y-Axis represents encryption time values. It is evident from the graphical assessment that the suggested IS-ECC model uses 8007(ms) less time for encryption than the present DES approach, which spends 9500(ms) more time for encryption (ms). Comparative Encryption Time Results for Proposed and Existing Techniques are provided in Table 4. The proposed IS-ECC technique is evaluated in comparison to the standard DSS and MACAG practises in terms of Throughput. There is a graphic representation of the throughput findings, showing that the proposed IS-ECC model produces 1665(Mbps) greater throughput than the state-of-the-art DSS and MACAG techniques, which achieve 554(Mbps) and 690(Mbps), respectively. The results of the proposed and existing methods are compared in Table 3. Figure 8 compares the proposed IS-ECC technique to the present DSS and MACAG methods for monitoring soil moisture. The x-axis of the given graph represents time, while the y-axis represents soil moisture. The graph of soil moisture measurements versus time shows that soil moisture rises overnight and declines somewhat throughout the day.

CONCLUSION

This study describes an improved WSN-based architecture for energy-aware secure communication in precision agriculture. To begin, improved fuzzy c-means is utilised to cluster the nodes in order to maximise energy efficiency. Then, a cuckoo search/genetic algorithm hybrid is used to choose the cluster leaders. Using the designated cluster head, the collected data from the clustered nodes will be sent to the sink. The key for the intrusion detection system will be generated using elliptic curve cryptography to encrypt the data and give authentication to prevent all types of attacks. The sensor nodes begin delivering encrypted data to the cluster heads with the help of the Path Finding Agent (PFA) and key authentication. Using a Query Agent (QA) as a middleman, cluster heads collect data from remote sensor nodes, encrypt it with a shared key, and transmit it to a central processing unit (CPU) for processing. The experimental findings demonstrate that the suggested method excels in packet delivery ratio, energy efficiency, and encryption time. However, this only protects against infiltration and not detection, which may be achieved in the future via machine learning.



**REFERENCES**

1. Ahmad, N., Hussain, A., Ullah, I., & Zaidi, H. (2019). IOT based Wireless Sensor Network for Precision Agriculture. 2019 7th International Electrical Engineering Congress (iEECON). doi:10.1109/ieecon45304.2019.8938854
2. Aishwarya Lakshmi, T., Hariharan, B., & Rekha, P. (2019). A Survey on Energy Efficient Routing Protocol for IoT Based Precision Agriculture. 2019 International Conference on Communication and Electronics Systems (ICCES). doi:10.1109/icces45898.2019.9002410
3. Balamurali, R., & Kathiravan, K. (2015). An analysis of various routing protocols for Precision Agriculture using Wireless Sensor Network. 2015 IEEE Technological Innovation in ICT for Agriculture and Rural Development (TIAR). doi:10.1109/tiar.2015.7358549
4. Bawage, V. P., & Mehetre, D. C. (2016). Energy efficient Secured Routing model for wireless sensor networks. 2016 International Conference on Automatic Control and Dynamic Optimization Techniques (ICACDOT). doi:10.1109/icacdot.2016.7877710
5. De la Concepcion, A. R., Stefanelli, R., & Trincherro, D. (2015). Ad-hoc multilevel wireless sensor networks for distributed microclimatic diffused monitoring in precision agriculture. 2015 IEEE Topical Conference on Wireless Sensors and Sensor Networks (WiSNet). doi:10.1109/wisnet.2015.7127408
6. Deepika, G., & Rajapirian, P. (2016). Wireless sensor network in precision agriculture: A survey. 2016 International Conference on Emerging Trends in Engineering, Technology and Science (ICETETS). doi:10.1109/icetets.2016.7603070
7. Giri, M. B., & Pippal, R. S. (2017). Use of linear interpolation for automated drip irrigation system in agriculture using wireless sensor network. 2017 International Conference on Energy, Communication, Data Analytics and Soft Computing (ICECDS). doi:10.1109/icecnds.2017.8389716
8. Haseeb, K., Islam, N., Almogren, A., Din, I. U., Almajed, H. N., & Guizani, N. (2019). Secret Sharing-based Energy-aware and Multi-hop Routing Protocol for IoT based WSNs. IEEE Access, 1–1. doi:10.1109/access.2019.2922971
9. Hu, Z., Xu, L., Cao, L., Liu, S., Luo, Z., Wang, J., ... Wang, L. (2019). Application of Non-Orthogonal Multiple Access in Wireless Sensor Networks for Smart Agriculture. IEEE Access, 1–1. doi:10.1109/access.2019.2924917
10. John, G. E. (2016). A low cost wireless sensor network for precision agriculture. 2016 Sixth International Symposium on Embedded Computing and System Design (ISED). doi:10.1109/ised.2016.7977048
11. K.N., B., H.S., M., & H.J., J. (2020). IoT based Smart System for Enhanced Irrigation in Agriculture. 2020 International Conference on Electronics and Sustainable Communication Systems (ICESC). doi:10.1109/icesc48915.2020.9156026
12. Khan, S. (2016). Wireless Sensor Network based Water Well Management System for precision agriculture. 2016 26th International Telecommunication Networks and Applications Conference (ITNAC). doi:10.1109/atnac.2016.7878780
13. Khriji, S., Houssaini, D. E., Kammoun, I., Besbes, K., & Kanoun, O. (2019). Energy-Efficient Routing Algorithm Based on Localization and Clustering Techniques for Agricultural Applications. IEEE Aerospace and Electronic Systems Magazine, 34(3), 56–66. doi:10.1109/maes.2019.2905947
14. Mat, I., Mohd Kassim, M. R., Harun, A. N., & Mat Yusoff, I. (2016). IoT in Precision Agriculture applications using Wireless Moisture Sensor Network. 2016 IEEE Conference on Open Systems (ICOS). doi:10.1109/icos.2016.7881983
15. Miglani, A., Bhatia, T., & Goel, S. (2015). TRUST based energy efficient routing in LEACH for wireless sensor network. 2015 Global Conference on Communication Technologies (GCCT). doi:10.1109/gcct.2015.7342684
16. Pascual, R. L., Sanchez, D. M. R., Naces, D. L. E., & Nunez, W. A. (2015). A Wireless Sensor Network using XBee for precision agriculture of sweet potatoes (*Ipomoea batatas*). 2015 International Conference on Humanoid, Nanotechnology, Information Technology, Communication and Control, Environment and Management (HNICEM). doi:10.1109/hnicem.2015.7393212





Uma Maheswari and Dona Rashmi

17. Prakash, S. (2020). Zigbee based Wireless Sensor Network Architecture for Agriculture Applications. 2020 Third International Conference on Smart Systems and Inventive Technology (ICSSIT). doi:10.1109/icssit48917.2020.9214086
18. Rathinam D, D. K., D, S., A, S., A, S. G., & J, S. (2019). Modern Agriculture Using Wireless Sensor Network (WSN). 2019 5th International Conference on Advanced Computing & Communication Systems (ICACCS). doi:10.1109/icaccs.2019.8728284
19. Sahitya, G., Balaji, N., Naidu, C. ., & Abinaya, S. (2017). Designing a Wireless Sensor Network for Precision Agriculture Using Zigbee. 2017 IEEE 7th International Advance Computing Conference (IACC). doi:10.1109/iacc.2017.0069
20. Singh, A., Mishra, A., & Ahmed, M. (2019). Energy Efficient Routing HART Protocol in Soil Nutrition Analysis for Agriculture. 2019 International Conference on Intelligent Computing and Control Systems (ICCS). <https://doi.org/10.1109/iccs45141.2019.9065827>

Table 1 Performance Comparison Results of Packet Delivery Ratio with Different

No. of nodes	Packet Delivery Ratio		
	DSS	MACAG	IECC
30	0.72	0.73	0.80
60	0.74	0.75	0.78
90	0.72	0.72	0.77
120	0.70	0.70	0.76
150	0.66	0.68	0.80

Table 2 Encryption Time Performance Comparison Results with Different Methods

Message size (Mega Bytes)	Encryption time (Milli Seconds)	
	DES	IECC
10	2107	1987
20	2713	2078
30	3789	3234
40	3930	2745
50	7123	6654
60	7250	6994
70	9050	8456
80	9500	8007

Table 3 Throughput Performance Comparison Results with Different Methods

No. of nodes	Throughput (Mbps)		
	DSS	MACAG	IECC
30	500	600	1000
60	550	660	1200
90	551	670	1400
120	555	690	1700
150	554	692	1665





Uma Maheswari and Dona Rashmi

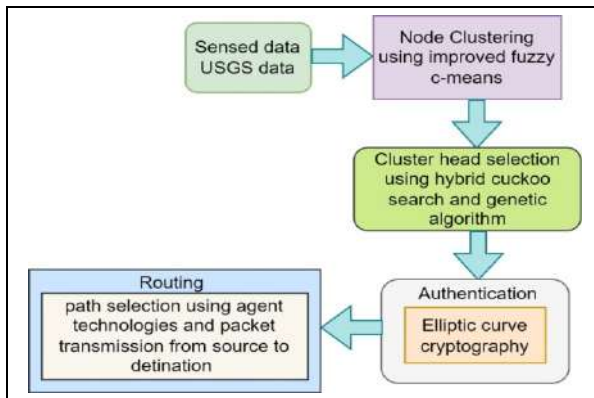


Figure 1 Overall Flow Chart of the Proposed Model

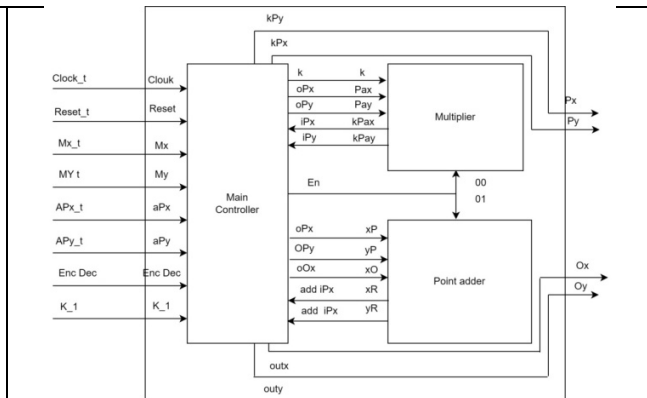


Figure 2 Main Modules in Elliptical Curve Cryptography

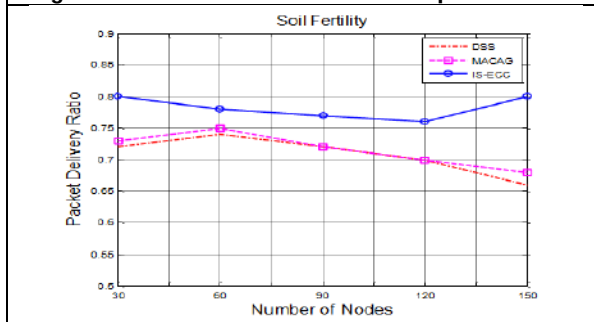


Figure 3 Packet Delivery Ratio vs Number of Nodes

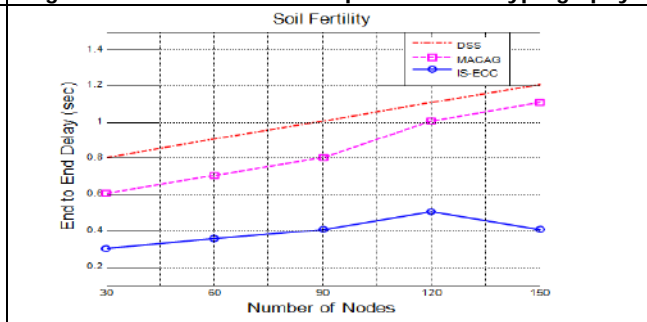


Figure 4 End to End Delay vs Number of Nodes

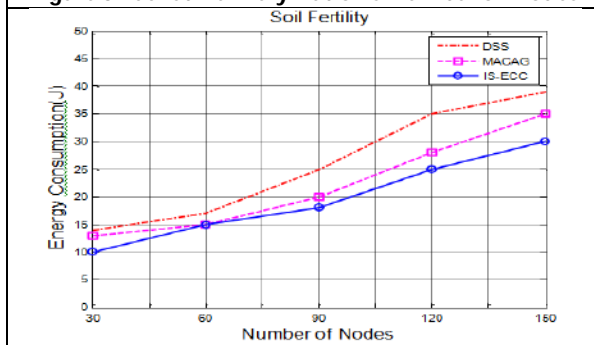


Figure 5 Energy Consumption vs Number of Nodes

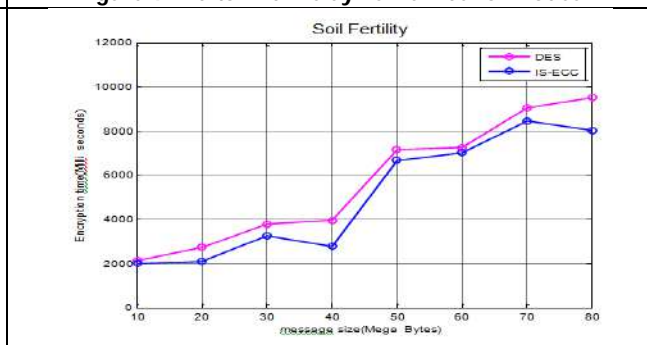


Figure 6 Encryption Time (ms) vs Message Size

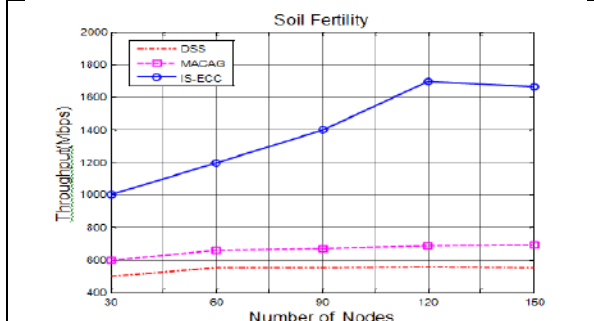


Figure 7 Throughput (Mbps) Vs Number of Nodes

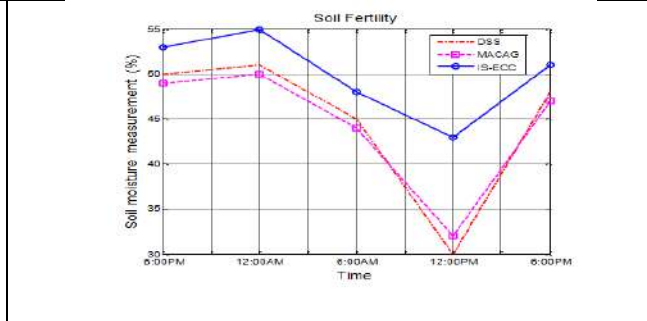


Figure 8 Soil Moisture Measurement vs Time





Assessment of Primary Healthcare in Coimbatore Region, South India using GIS

Varatharajaperumal Thangavel¹, Hema S^{2*} and Rajalakshmi S¹

¹Assistant Professor, Department of Civil Engineering, Sri Ramakrishna Engineering College, Coimbatore, Tamil Nadu, India.

²Associate Professor, Department of Civil Engineering, Sri Ramakrishna College, Coimbatore, Tamil Nadu, India.

Received: 28 Jan 2023

Revised: 20 Mar 2023

Accepted: 27 Apr 2023

*Address for Correspondence

Hema S

Associate Professor,
Department of Civil Engineering,
Sri Ramakrishna College,
Coimbatore, Tamil Nadu, India
E.Mail: hema.s@srec.ac.in.



This is an Open Access Journal / article distributed under the terms of the **Creative Commons Attribution License** (CC BY-NC-ND 3.0) which permits unrestricted use, distribution, and reproduction in any medium, provided the original work is properly cited. All rights reserved.

ABSTRACT

This study aims to analyze the proximity of all primary health centres located in the study area of Coimbatore district which could help both local people as well as the visitors during any emergency. An attempt is made to analyze the relative location of primary health centres with respect to population density and transport transits and further to develop a map that shall be utilized to locate the nearby primary health centre from any location in the study area in an emergency using GIS. Data related to health care pertaining to the study area were collected during the year 2021 and processed and analyzed in QGIS. The proximity analysis was then performed with buffer zones of 1 Km and 3 Km distance from the Road & Railway networks respectively. It aimed to identify the availability of health care facilities near by the transportation network serving the population in case of an emergency. It was inferred that the percentage of hospitals situated within 1000 m from national and state highways were 74% and 34% respectively, and 93% of the hospitals in the region are situated within 3000 m from rail lines across the study area. Notably, most of the health centres were located within the main city, and there is limited health centres in Pollachi and Tiruppur taluks which has a considerable population. Hence, proper allocation of health care facilities becomes necessary in Coimbatore. The present study proves the ability to create and share neighborhood-level spatial indicators with the help of big data for planning healthy and sustainable cities. All data were sourced through open source and relevant government geospatial resources and by using spatial query analysis; the resultant health care indicator map of Coimbatore is obtained.



**Varatharajaperumal Thangavel et al.,****Keywords:** Primary Health centre; Remote sensing & GIS; Proximity & Spatial analysis; Emergency Health care; Human life.

INTRODUCTION

Health not only refers to the physical fitness, it also imparts mental stability and happiness. A good health leads to prosperity and wealth as healthy people are more productive, save more wealth as well as live longer. And a healthy person is not only helping himself but also his family, society and in turn he helps the entire economy of the country. The definition of primary health care (PHC) has been reinterpreted repeatedly. In some contexts, primary health refers to a broad range of health care services including diagnosis, treatment and managing a long-term health care provided by medical professionals to the community. It is the first place that a person would contact in case of a health issue. Few have interpreted primary health care as a set of priority health interventions for low-income populations. The institution that offers the primary health care is generally referred as primary health centres and it could range from a local clinic or a pharmacy to a multinational hospital.

Primary healthcare, which approaches health from the perspective of the entire society, aims to achieve the highest possible distribution of health and well-being. It provides accessible and comprehensive range of services, such as health promotion, disease prevention, treatment, and rehabilitation. Primary care is crucial for integrated personal health care, public health functions, and ongoing referrals to hospital services because it serves as the first point of contact between the people and the health-care system. Not every country in the world has a proper primary healthcare system. There are many countries which do not have enough primary health services, on the other hand, countries with good health services are not accessible to the needy. One of the major problems is the uneven distribution of healthcare centres in urban regions [1]. Governments around the world, including India, have endorsed 17 Sustainable Development Goals (SDGs), the third of which, "Ensure healthy lives and promote well-being for all at all ages," specifically refers to health. 13 targets are outlined in the country for this aim, including one for establishing universal health coverage (UHC), two for environmental health, three for communicable diseases, three for non-communicable diseases, and three for addiction.

Evidence from around the world indicates that nations with sound primary health care systems have improved health outcomes and minimal healthcare expenditures. The availability and access to primary health care is a neighborhood characteristic that can directly impact health [2]. Imbalance in the spatial distribution of the health care centres can lead to inefficiency offered in the services. The physical location of health care facility and the travel time thereto influences uptake/utilization of health care services [3]. Another important factor in health care is 'treatment given on time'. Especially, in emergency scenarios like accidents, it is very important to know the availability and of easily accessible health centres. According to NCRB, there were nearly 1,81,113 deaths in India from traffic accidents in the year 2019 alone. 'Spatial accessibility' comprises two components, namely availability and proximity [4], and 'Availability' refers to the number of health care centres which needy people can choose at a specific location. Both the components have to be measured while defining spatial accessibility [5]. The National Health Policy of India from 2016, supported by the financial announcements during February 2018 declared that strengthening 150,000 sub-centers and providing increased access are the primary goals to improve the calibre of primary healthcare in India. It also emphasized universal health coverage (UHC) as a means of enacting change and ensuring that everyone in India has access to the primary healthcare, without facing financial hardship. To accomplish this objective, a thorough investigation into the factors influencing the geographic pattern of distribution of healthcare facilities is necessary. Researchers and medical practitioners around the world are recommending the utilization of GIS tools to access the health centres. GIS tool can be utilized to locate the various primary health centres ranging from a pharmacy to a hospital. Also, it is very important to consider few other factors while checking the accessibility of a health centre. High availability of services alone does not ensure proper accessibility as it depends on the proximity



**Varatharajaperumal Thangavel et al.,**

of the population to those services. Similarly, close proximity may not provide high accessibility because it depends on the size of the population for which the services are available [6].

Numerous studies make use of a number of different approaches to identify the under-served areas of these healthcare facilities and to determine how accessible they are [7]. For instance, the importance of road network in the distribution pattern of healthcare services was investigated in Kerala's capital city of Thiruvananthapuram [8] to find that medical services were dispersed unevenly, and space was not allocated consistently in the city. Consequently, not everyone has easy access to a medical centre. Another study sought to identify potential locations for healthcare facility centres and to highlight the spatial organization of current healthcare facility centres in the municipal ward of Midnapore town of West Bengal [9]. A detailed investigation included suitability analysis and mapping of slum areas, densely populated areas, health care facility and their proximity through spatial analysis. Within one kilometre of public health services, the majority of the outlying areas were determined to be underserved. Accessibility analysis of primary health care services based on population density was performed using Geospatial technique in Mysore district [10]. They noted certain accessibility issues, functional deficits, and spatial gaps in the health centres in the research region, demonstrating how inadequately the current health centres are able to serve the community and its residents.

The second-largest city in Tamil Nadu, Coimbatore, renowned for its MSME units and educational institutions is chosen as the study area. It is a significant economic hub, accounting for 7% of the state's GDP with ever-increasing population and industrial growth. In the road accident analysis report published by Tamil Nadu Transport department, Coimbatore stands second next to Chennai with highest number of accidents (2448) which includes 451 casualties [11] in the year 2020. The spatial accessibility [12] in locating the primary health centres during an emergency, thus becomes crucial in the current situation. Several studies have already reported reduced healthcare facility ratio and an improper pattern of public health facility services in India. Though, there is hardly any literature on the subject of the connection between proximity to roads and healthcare facilities during an emergency care, especially in the Coimbatore region. Hence, an analysis of proximity of health care facility during an emergency is performed using GIS techniques. Additional Factors like traffic signals, bus stations and railway stations were added with population size & location of highways for analysis in the study region. Moreover, locations of blood banks were given more importance as there is a least awareness about the whereabouts of blood banks in the society. Hence, this study focuses on the following objectives, namely, 1. To identify the locations of various primary health centres in Coimbatore district using remote sensing data; 2. To analyze the relative location of primary health centres with respect to population density and transport transits; 3. To create a map that shall be utilized to locate the nearby primary health centre from any location in the study area using GIS.

METHODOLOGY

Maps can assist local and regional planners in revealing the spatial distribution of health-promoting infrastructure and essential services inside cities as well as detect access disparities. Mapped neighborhood-level spatial indicators make it easier to show where resources are distributed and where interventions are needed, promote accountability, and provide communities the authority to demand reforms [13]. The ability to create and share neighborhood-level spatial indicators is becoming increasingly accessible with the help of big data and high-performance computers. In order to carry out this study, data were sourced through open source and relevant government geospatial resources web-portals. The flow of the work is shown in [Figure 1]. The Administrative boundary (District Boundary & Taluk Boundary) and Transportation network (Road & Railway) data were collected from Diva-GIS website (<https://www.diva-gis.org/>). The health care indicator details such as hospitals & pharmacy data were collected from open-source platform (<https://mapcruzin.com/>). The blood bank database for the study area were obtained from Open Government Data (OGD) Platform India (<https://data.gov.in/>) and all these data were processed and analyzed in QGIS - open-source GIS software. Additional inputs namely, traffic signals, bus stops, bus terminals, railway stations and population data were collected from open-source website (<https://mapcruzin.com/>). The Land Use Land



**Varatharajaperumal Thangavel et al.,**

Cover (LULC) data were obtained from Bhuvan website (https://bhuvan.nrsc.gov.in/bhuvan_links.php) and was helpful to understand the prevailing occupancy of the land in the region.

The collected data are imported into the QGIS software [14] and converted as preferable format for further GIS Analysis. The Spatial reference Coordination is World Geodetic System (WGS 1984) and projected coordination is Universal Transverse Mercator (UTM Zone 44N) assigned to all the data. The proximity analysis was then performed for the transportation networks. It was aimed to identify the number of health care facilities available near by the transportation network. Accordingly, buffer zone was created for 3Km and 5Km distance from the Road & Railway networks respectively for the analysis. All the data and outputs were integrated by overlay analysis, and using spatial & attribute query tool, and the final resultant maps were generated.

RESULTS AND DISCUSSION

Coimbatore district from Tamilnadu was taken as the study area. Coimbatore city, the headquarters of the district is the third largest city in the state and often referred as Manchester of South India. As of 2011 census, the district had a population of 3.45 million. The study area is surrounded by Tiruppur district in east and Nilgiris district in the north; Erode district in the north-east; Palakkad district, Idukki district in the west and Thrissur and Ernakulam district in the south. The district is also surrounded by the Western Ghats. The study area covers the toposheets of Survey of India, 10° 10' N to 11° 30' N and 76° 40' E to 77° 30' E. Coimbatore is one of the most industrialized regions in the country and it has nearly 25,000 small, medium and large-scale industries registered, in turn results in movement of commercialized vehicles in and out of the district. It serves as an entry and exit point for Kerala. And Coimbatore has nearly 47 tourist and pilgrimage places to visit, which attracts people from all over the country to spend their holidays. Most of the industrial as well as the tourism activities happen in the district headquarter. Apart from these activities, there are people who visit the city to take medical treatments from the reputed medical institutions in the Coimbatore city. This study aims to locate all such primary health centres located in the study area which could help both local people as well as the visitors.

Improvements to these fundamental GIS functionalities have been made in recent years, including the measurement of accessibility by employment and various modes of transportation, the inclusion of transit-based health seeking patterns in their accessibility assessment, and the introduction of a method for approximating the geographic accessibility to healthcare facilities [15]. The present study aimed to identify the proximity of hospitals, pharmacies, blood banks from any location during an emergency or any other necessary requirement for any medical assistance [16]. Coimbatore region is divided into 12 wards and there are 28 PHC's in the region. As per the data from the available sources, there are 61 hospitals, 13 pharmacies and 23 blood banks in the district [17]. Thus, all data inputs were collated and a map was created showing all the primary health centres in the study area, mapped with other spatial factors like location of highways, bus stations, traffic signals and rail lines [18]. There were 20 major bus stations, 91 bus stops, 17 railway stations and 6 traffic signals identified from the data sources.

Among all the factors, identifying the location of the health centres [19] during emergency is the lifesaving factor. In order to check the accessibility, the national and state highways, railway lines existing in the study area were identified and mapped for the analysis. Spatial queries were used to identify the health centres located near the road and railway lines [20], and maps were generated with buffer distances of 1000 m for road lines and 3000 m for rail lines. Apart from the road and rail lines, accessibility to the health centres from the bus stations were also taken for analysis. Based on the results obtained from spatial query [Table 1], it is inferred that the percentage of hospitals situated within a buffer distance of 1000 m from national and state highways were 74% and 34% respectively for providing better physical accessibility, whereas, 93% of the hospitals in the region are situated within a buffer distance of 3000 m from rail lines running across the study area [Figures 2 to 8].



**Varatharajaperumal Thangavel et al.,**

High availability of services does not always guarantee high accessibility because it also depends on the proximity of the population to those services [21]. Hence, to map the population variation in the district, the population in different taluks was considered [Figure 9]. And it is observed that most of the health centres are located within the Coimbatore city boundary, owing to the largest population prevailing in the district. However, even though Pollachi and Tiruppur taluk has a considerable population, there is a limited availability of health centres in these regions [Figure 10]. Thus, not all the people in the study region have the proper accessibility to the health centres. In addition to these, to check the proximity of the health centres, land use and land cover of the study area is also considered in the study. Population concentration will be more in the built-up area than other land cover categories. As per the data extracted from the available sources, it was found that almost all the health care facilities were located either among or very close to the built-up area, thereby providing more accessibility to the people.

CONCLUSION

This study developed accessibility status on emergency health care needs of households in the Coimbatore district to reach out the PHC. Based on QGIS tool, it was observed that most of the health centres in the district were located only within the city-centre to serve the denser population zone in the district headquarters. Also, it was found that, most of health centres in the study region are easily reachable by means of rail and road transport. The percentage of hospitals situated within 1 km were 74% and 34% respectively from the national and state highways for providing better physical accessibility and availability of blood banks within 1 km reach from national and state highways were 73% and 21% respectively. However, from the proximity analysis, it was found that people living in nearby taluks, namely, Pollachi and Tiruppur do not have adequate health care facilities proportionate to its population, and they need to travel a longer distance up to the main city for any medical assistance. Thus, the present study suggests that GIS serves as a tool to identify the spatial distribution of health centres in densely populated city or applicable to any region. Such studies may be much helpful especially in Covid-19 like pandemic situation [22]. There are technical difficulties in developing high-quality, fine-grained spatial indicators to gauge development of healthy and sustainable cities globally [23, 24]. In order to provide better services, new health centres should be planned using organised criteria, a sufficient number of staff members, and geographic considerations. Transportation is also a factor in the formation of new health centres in the future. Hence steps have to be taken to ensure a good spatial distribution of the health centres to serve a larger society, particularly in the study area of Coimbatore.

REFERENCES

1. Shaw Subhojit, Sahoo Harihar. Accessibility to Primary Health Centre in a Tribal District of Gujarat, India: application of two step floating catchment area model. *Geojournal*. 2020; 85: 505-514. <https://doi.org/10.1007/S10708-019-09977-1>.
2. Ike F, Esther N. Health-Care Facilities accessibility Analysis Using GIS: A case Study of Uyo Municipal South – Eastern Nigeria. *EJAS* [Internet]. 2022 [cited 2022 Nov.15];10(1):31-32. <https://journals.scholarpublishing.org/index.php/AIVP/article/view/11621>.
3. Tao Z, Cheng Y, Zheng Q, & Li G. Measuring spatial accessibility to healthcare services with constraint of administrative boundary: a case study of Yanqing District, Beijing, China. *International Journal for Equity in Health*. 2018; 17(1):1–12. <https://doi.org/10.1186/s12939-018-0720-5>.
4. Lawal O, Anyiam FE. Modelling geographic accessibility to Primary Health Care Facilities: Combining open data and geospatial analysis. *Geo-Spatial Information Science*. 2019; 22(3):174–184. <https://doi.org/10.1080/10095020.2019.1645508>.
5. Ajala OA, Sanni L, Adeyinka SA. Accessibility to health care facilities: A panacea for sustainable rural development in Osun State Southwestern, Nigeria. *Journal of Human Ecology*. 2017; <https://doi.org/10.1080/09709274.2005.11905819>.





Varatharajaperumal Thangavel et al.,

6. Nayak PP, Mitra S, Pai J B, et al. Mapping accessibility to oral health care in coastal India – A geospatial approach using Geographic Information System (GIS). 2022; 11:366. <https://doi.org/10.12688/f1000research.75708.2>.
7. Parvin F, Ali SA, Hashmi SNI, Khatoon A. Accessibility and site suitability for healthcare services using GIS-based hybrid decision-making approach: a study in Murshidabad, India. *Spatial Information and Research*. 2021; 29(1):1–18. <https://doi.org/10.1007/s41324-020-00330-0>.
8. Daniel CB, Mathew S, Saravanan S. Network constrained and classified spatial pattern analysis of healthcare facilities and their relationship with the road structure: a case study of Thiruvananthapuram city. *Spatial Infrastructure Research*. 2021; 29: 791–805. <https://doi.org/10.1007/s41324-021-00385-7>.
9. Dutta B, Das M, Roy U. et al. Spatial analysis and modelling for primary healthcare site selection in Midnapore town, West Bengal. *Geo Journal*. 2022; 87: 4807–4836. <https://doi.org/10.1007/s10708-021-10528-w>.
10. V Minutha. Accessibility Analysis of Primary Healthcare Services in Mysore District Using Geospatial Techniques. *International Journal of Scientific Research in Science and Technology*. 2021; 8: 62-69. <https://doi.org/10.32628/IJSRST218316>.
11. Road accident analysis in Tamil Nadu. Accessed November 2022. https://www.tnsta.gov.in/pdf/analysis_november2020.pdf.
12. Ngowi KA. Measuring Geographical Accessibility to Healthcare Facilities in Peri-Urban dwellers in Mbeya City, Tanzania. *MUST J Res Dev*. 2021;1(5):15–15.
13. Geoff Boeing, Carl Higgs, Shiqin Liu, Billie Giles-Corti, James F Sallis, et al. Using open data and open-source software to develop spatial indicators of urban design and transport features for achieving healthy and sustainable cities. *Lancet Glob Health*. 2022; 10: e907–18. <http://www.thelancet.com/lancetgh>.
14. Pramod Nayak P, Mitra S, Pai JB, Vasthare Prabhakar R, Kshetrimayum N. Mapping accessibility to oral health care in coastal India – A geospatial approach using a geographic information system (GIS). *F1000Res*. 2022 Aug 8; 11:366. doi: 10.12688/f1000research.75708.2. PMID: PMC9363979.
15. Cerin E, Sallis JF, Salvo D, et al. Determining thresholds for spatial urban design and transport features that support walking to create healthy and sustainable cities: findings from the IPEN Adult study. *Lancet Glob Health*. 2022; 10: e895–906. doi: 10.1016/S2214-109X(22)00068-7.
16. Chen T, Pan J. The Effect of Spatial Access to Primary Care on Potentially Avoidable Hospitalizations of the Elderly: Evidence from Chishui City, China. *Soc Indic Res*. 2022;160: 645–665. <https://doi.org/10.1007/s11205-020-02413-9>.
17. Coimbatore Municipal Corporation official website, <https://www.ccmc.gov.in/ccmc/index.php/cat-department/public-health>. Accessed October 2022.
18. Kaur Khakh AK, Fast V, Shahid R. Spatial accessibility to primary healthcare services by multimodal means of travel: Synthesis and case study in the city of Calgary. *International Journal of Environmental Research and Public Health*. 2019;16(2): 170. <https://doi.org/10.3390/ijerph16020170>.
19. Sumesh K. Spatial Distribution and Service Area of Primary Health Centres in Kasaragod District, Kerala. *Journal of Interdisciplinary Cycle Research*. 2020; 12(7): 308-318.
20. Lechowski Ł, Jasion A. Spatial Accessibility of Primary Health Care in Rural Areas in Poland. *Int. J. Environ. Res. Public Health*. 2021; 18: 9282. <https://doi.org/10.3390/ijerph18179282>.
21. Ajinkya Padule, Aman Patel, Aman Shaikh, Arsalan Patel, Jyoti Gavhane. A Comparative Study on Health Care using Machine Learning and Deep Learning, *International Journal of Engineering Research & Technology*. 2022;11(3):363-367. <https://www.ijert.org/a-comparative-study-on-health-care-using-machine-learning-and-deep-learning>. DOI: 10.17577/IJERTV11IS030165.
22. Alhassan GN, Adedoyin FF, Bekun FV, Agabo TJ. Does life expectancy, death rate and public health expenditure matter in sustaining economic growth under COVID-19: Empirical evidence from Nigeria? *J Public Aff*. 2021; 21(4): e2302. <https://doi.org/10.1002/pa.2302>.
23. Workman R, McPherson K. Measuring rural access for SDG 9.1.1. *Trans GIS*. 2021; 25: 721–34. doi:10.1111/tgis.12721.
24. Ahuja R, Tiwari G. Evolving term “accessibility” in spatial systems: contextual evaluation of indicators. *Transp Policy*. 2021; 113: 4–11. <https://doi.org/10.3390/land11081139>.





Varatharajaperumal Thangavel et al.,

Table 1. Health care Indicator Information using Spatial & Attribute Query

S.No	Health Care Indicator Facility		Proximity Analysis				
	Health Care Indicators	Total Count	Road way (Buffer Zone -1000 m)		Railway (Buffer Zone -3000 m)	Bus Station (Buffer Zone -1000 m)	Bus Terminal (Gandhipuram Central-Bus Stand)
			National Highway	State Highway			
1	Hospitals	61	45	21	57	15	-
2	Blood Banks	23	17	5	22	8	9

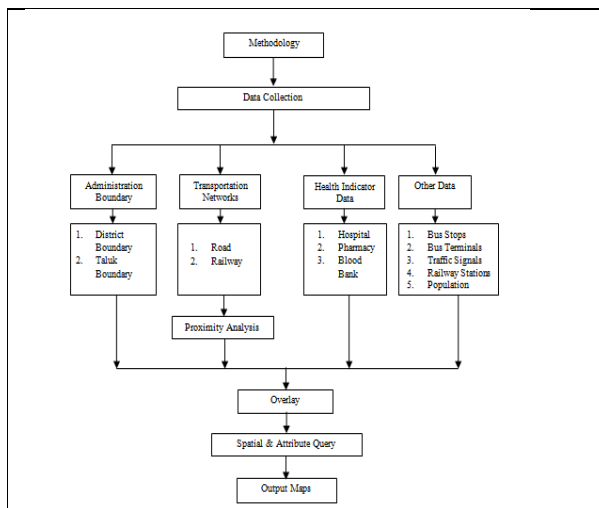


Fig. 1. Methodology Flow Chart

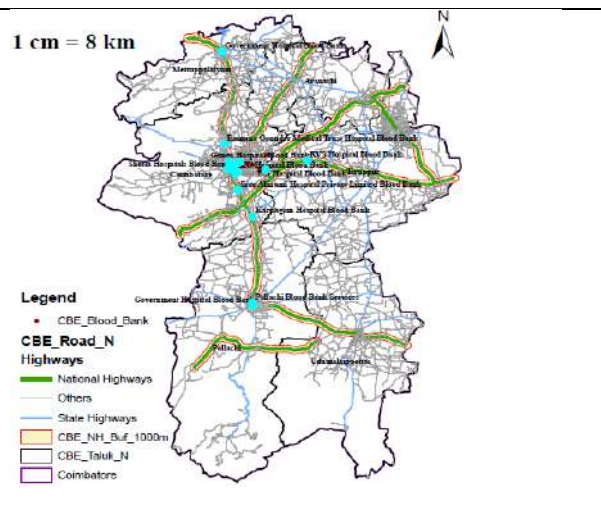


Fig. 2. Number of Hospitals Located within a buffer zone of 1000m from the National Highways

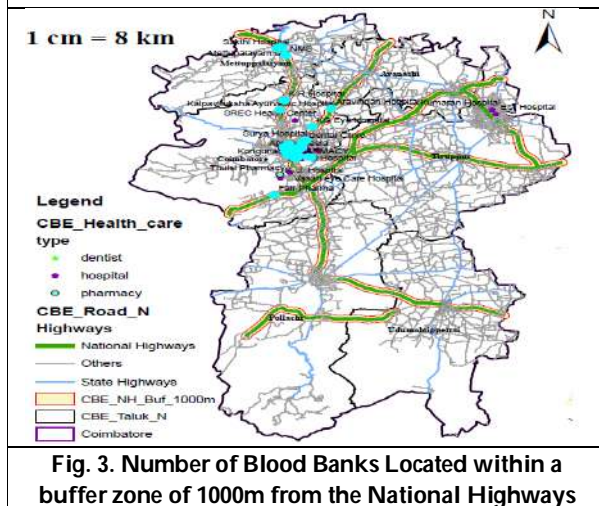


Fig. 3. Number of Blood Banks Located within a buffer zone of 1000m from the National Highways

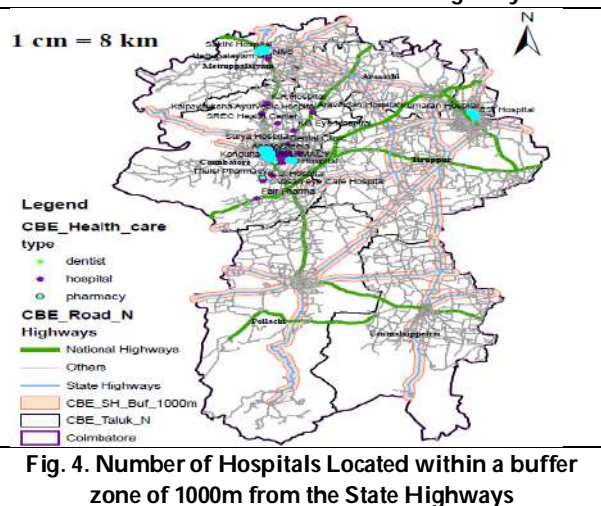
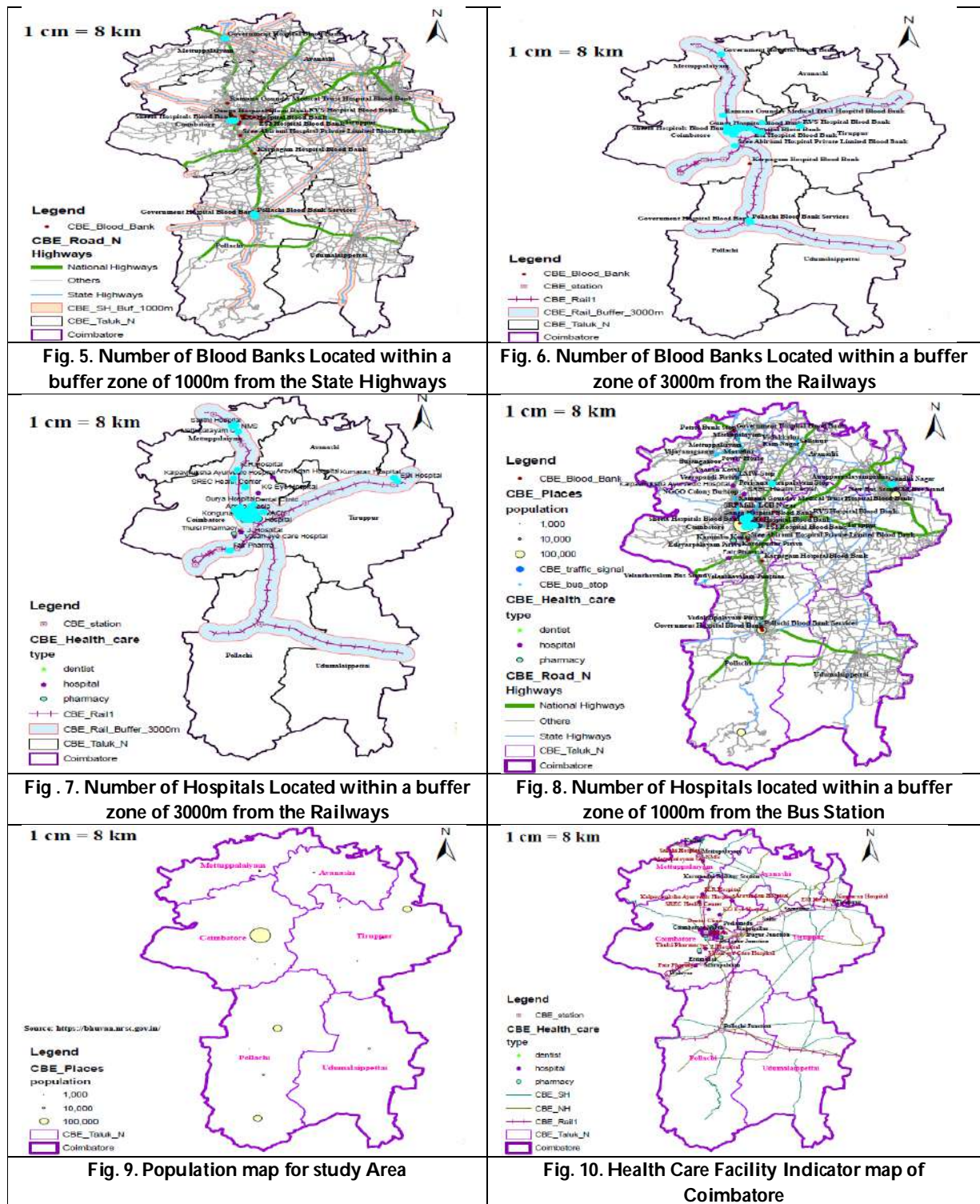


Fig. 4. Number of Hospitals Located within a buffer zone of 1000m from the State Highways





Varatharajaperumal Thangavel et al.,





Synthesis, Characterization and Biological Studies of Schiff Base Metal Complexes

R.Ezhil Arasi^{1*} and S.P.R.Kalaikathir²

¹Research Scholar (Reg.No.: 20223282032004), Department of Chemistry and Research Women's Christian College, (Affiliated to Manonmaniam Sundaranar University, Tirunelveli), Nagercoil-1, Tamil Nadu, India

²Assistant Professor, Department of Chemistry and Research, Women's Christian College, (Affiliated to Manonmaniam Sundaranar University, Tirunelveli), Nagercoil-1 Tamil Nadu, India.

Received: 20 Jan 2023

Revised: 26 Mar 2023

Accepted: 28 Apr 2023

*Address for Correspondence

R.Ezhil Arasi

Research Scholar (Reg.No.: 20223282032004),
Department of Chemistry and Research Women's Christian College,
(Affiliated to Manonmaniam Sundaranar University, Tirunelveli),
Nagercoil-1, Tamil Nadu, India.
E.Mail: arasi1920@gmail.com



This is an Open Access Journal / article distributed under the terms of the **Creative Commons Attribution License** (CC BY-NC-ND 3.0) which permits unrestricted use, distribution, and reproduction in any medium, provided the original work is properly cited. All rights reserved.

ABSTRACT

Schiff bases are considered as privileged ligand in coordination chemistry as they easily form stable complexes with most transition metal complexes. In this paper, a novel Schiff base ligand derived from Thiophene-2-carboxaldehyde (TPC) and P.Phenylene Diamine (PPD) and its transition metal complexes Cu (II), Zn (II), Co (II) and Ni (II). The structural features of the synthesized compounds were confirmed by UV visible, IR, NMR spectroscopic techniques and SEM. All the metal complexes were investigated for their anti-microbial, anti-oxidant and anti-inflammatory activity. The metal complexes were tested the larvicidal activity against *Culex quinquefasciatus*. The obtained result showed that the complexes especially Cu (II) metal complex have better active in anti-oxidant and anti-inflammatory activity

Keywords: Schiff base, Spectroscopic techniques, larvicidal activity, anticancer activity

INTRODUCTION

Coordination compounds are one of the fascinating areas of chemistry. The ever growing industrial and technological development combined with the desire for new functional generate enormous enthusiasm among scientist for novel materials. In living organisms there are a number of metal ions, which form a great variety of complexed with different species containing donor atoms ate inorganic – organic hybrid materials. These metal complexes are vitally important in enzyme actions, metabolites, vitamins etc. Schiff base and their transition metal

56953



**Ezhil Arasi and Kalaikathir**

complexes have gained much importance recently due to their chelating ability. Metal complex of Schiff bases show application as biological antimicrobial, antitumor, antifungal, antioxidant and anti-inflammatory activity. In this present work, we synthesized and characterized a novel Cu (II), Ni (II), Zn (II) and Co (II) complexes with Schiff base ligand (L) derived from Thiophene-2-carboxaldehyde (TPC) and P.Phenylene Diamine (PPD)

MATERIALS AND METHODS

All chemicals and solvent were obtained from commercial sources and were used as received without any further purification.

Synthesis of Schiff Base Ligand (L)

Ethanol solution of Thiophene-2-carboxaldehyde (TPC) and 4,4' diamino diphenyl methane (DDM) were taken in RB flask in 1:1 molar ratio and refluxed for one hour. The reaction mixture is poured into ice, a yellow compound of Schiff base ligand was obtained. The precipitate was filtered, washed with water and dried.

Synthesis of Metal Complexes (MI)

The metal complexes were prepared by adding ethanol solution of Zn(II) nitrate, Co(II) nitrate, Ni(II) nitrate and Cu(II) nitrate to the ligand in ethanol in 1:2 (metal: ligand) molar ratio and refluxed for about 12 hours at 80°C. The precipitate solid were filtered and washed with ethanol and dried.

RESULT AND DISCUSSION

All the transition metal complexes are coloured solids, stable towards air and have melting points. The complexes are insoluble in water and common organic solvent, but are soluble in DMF, $CDCl_3$ and DMSO.

UV Analysis

The electronic spectrum of Schiff base ligand (L) shows a broad band at 340nm, characteristics of $n-\pi^*$ transition of C=N chromophore. The position of the band was found to be shifted to higher wavelength on complexation suggesting coordination of azomethane nitrogen to the central metal ion. The electronic spectrum of Copper (II) complex shows an energy band at 431 and 515nm due to ${}^2B_{1g}-{}^2A_{1g}$ transition corresponding to square planar geometry. (Lever A.B.P, 1984)

IR Spectra

The infrared spectra for the Schiff base ligand (L) and its metal complexes taken in the range 4000-400 cm^{-1} help to indicate region of absorption vibrations. The ligand shows a strong band at 1627 cm^{-1} characteristics of $\nu(C=N)$ stretching vibration (Seema Varghese, 2010), this band undergoes down field shift in the complexes indicating the band at 1609, 1605, 1607 and 1608 cm^{-1} is due to azomethine nitrogen in co-ordination. (Maurya M.R)

 1H NMR Spectra

The Schiff base ligand displayed a characteristic singlet signal at 8.66 ppm could be assigned azomethine proton (Refat MS 2013), which undergoes deshielding 8.63 ppm upon coordination as observed in $[Zn(L)_2(H_2O)_2]$ conforming the coordination took place through azomethine nitrogen.

SEM Analysis

SEM picture of the ligand and metal complex show that the particles are agglomerated with controlled morphological structure and the presence of small grains in non-uniform size. The SEM images of Ligand exhibit irregular shaped grains, whereas Ni (II) complex show sharp crystalline species. The average grain size found from SEM shows that the ligand and complex are polycrystalline with micrometer sized grains.



**Ezhil Arasi and Kalaikathir****Antimicrobial Activity**

The antibacterial activity of synthesized Schiff bases and their metal (II) complexes was tested against gram positive and gram negative micro-organism using disc diffusion method. The micro-organism used in the present investigations included *Pseudomonas*, *S.Aureus* and *Klebsiella*. Amikacin was used as standard antibiotics. The antimicrobial activities of ligand and metal complexes are shown in figure.1. In *Pseudomonas* organism have highly active in L_3Cu and L_3Zn complex. In antifungal activities the microorganism used in the present investigations included *C.Albican*, *A.Niger* and *Penicillium*. In L_3Cu complex have better antifungal activity than L_2Ni and L_2Zn .

Larvicidal Activity

The Larvicidal activity of synthesized ligand (L_3) and metal complexes were tested against culex mosquito. The highest mortality values was obtained from Cu(II) complexes. The moderate mortality value was obtained in other metal complexes. The increased mortality rate observed in the Cu(II) complex can be attributed to the lipophilicity on complexation Fig.2.

Anti-Inflammatory Activity

The newly synthesized Schiff base ligand (L_3) and its Cu(II), Co(II), Ni(II) and Zn(II) The graphical representation in figure 3. Cu (II) complex is better activity than other metal complexes. The use of metal complexes in medicine, toxicity evaluation is an essential step that is needed to determine the potential pharmacological application of these metal complexes as anti-inflammatory agents. The metal complexes are approved in the clinic for the treatment of inflammatory and autoimmune diseases (Chung-Hang Leung 2014).

Anti-oxidant Activity by DPPH Radical Scavenging Assay

The antioxidant activities of ligand and metal complexes with control were assessed on the basis of the free radical scavenging effect on the stable DPPH free radical effect of the stable DPPH free radical efficiency (Breca.A2002). The examined changes in the free radical scavenging ability of the test sample on the basis of percent inhibition are presented in figure 4. In these series the results obviously showed that metal complexes are better activity than ligand. The Cu (II) metal complex exhibited best scavenging activity among the examined complexes.

CONCLUSION

Schiff base transition metal complexes Cu (II), Zn (II), Co (II) and Ni (II) were synthesized from Thiophene-2-carboxaldehyde (TPC) and P.Phenylene Diamine (PPD) and characterized on the basis of analytical and spectral data. From SEM analysis shows crystalline nature of complexes is conformed. Antimicrobial activity and larvicidal activity shows that all the metal complexes are more active than ligand. In anti-oxidant and anti-inflammatory activity Cu (II) metal complex are better active.

REFERENCES

1. Faria J.L.B, Almeida F.M, Pilla.O, Rossi.F, Saski J.M, Melo F.E.A, Mendes J.F and Freire P.T.C(2004). Raman spectra of L-histidine Hydrochloride monohydrate crystal. Journal of Raman spectroscopy 35(3), 242-248.
2. Liji John, R.SelwinJoseyphus and I.Hubert Joe (2020), Molecular docking, Photo catalytic activity and biomedical investigations of some metal complexes. Journal of bio molecular structure and Dynamics.
3. K.Singh, M.S.Barwa, P.Tyagi, Eur.J.Med.Chem.41(2006) 147.153.
4. O.M.Walsh,M.J.Meegan,R.M.Prendergast,T.Al Nakib,Eur.J.Med.Chem,31(1996) 989-999.
5. Vibi.V, Gnana Glory Kanmoni.V, C.IsacSobanaRaj,'Synthesis and charecterisation of Schiff base complexes from sulphanilamide and veratraldehyde' Infokara research, Vol 8,11,(2019) ,PP 1526-1536.
6. R.SelwinJoseyphus and M.Sivasankaranair, "Antibacterial and Antifungal studies on some Schiff base complexes of Zn(II)", My cobiology, (2008),Jun36(2),PP 93-98.
7. M.Ravanasiddappa,T. Suresh, S.Khasim, S.C.Rahavendray, C.Basavaraja and S.D.Angadi,"Transition metal

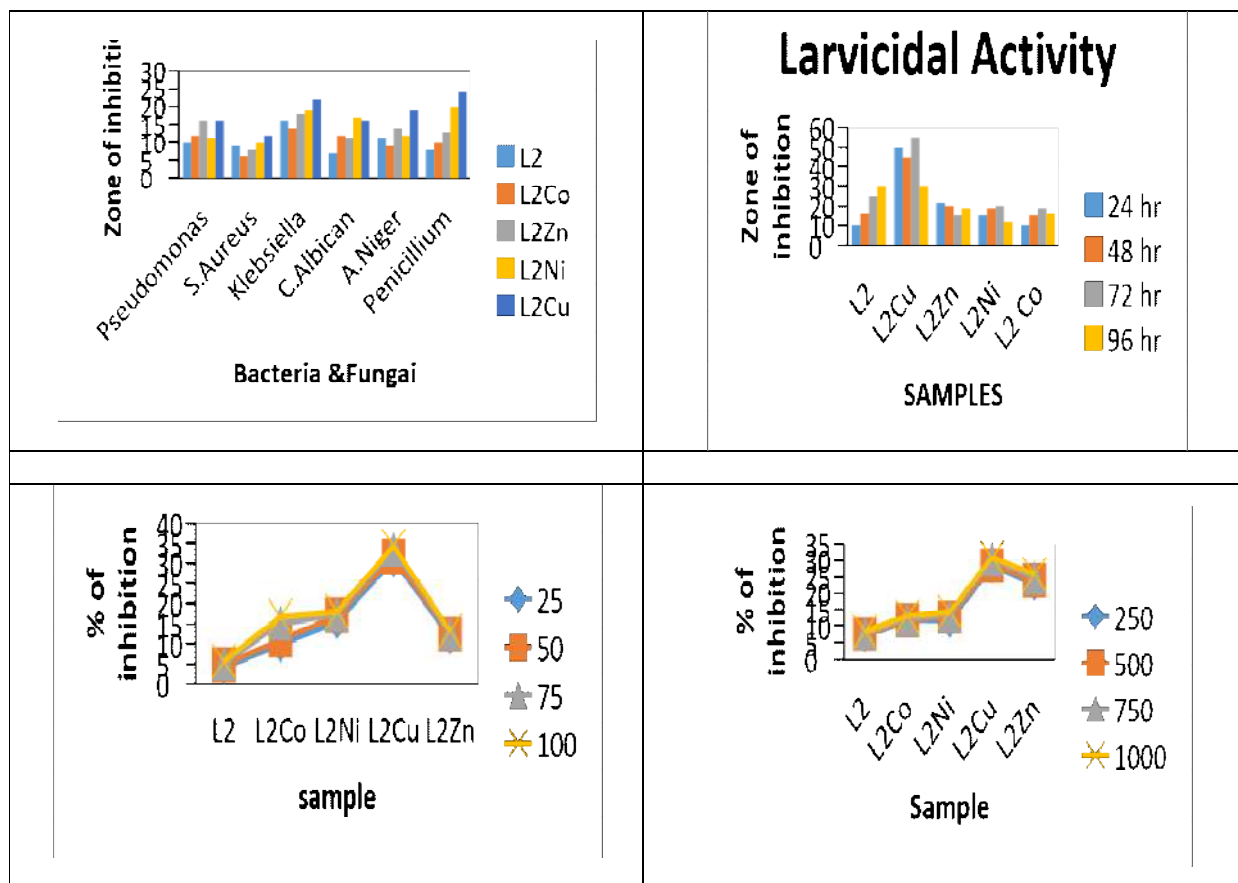




Ezhil Arasi and Kalaikathir

complexes of 1,4(2'-Hydroxy phenyl-1-yl) di-imino azine: Synthesis, Characterization and antimicrobial studies", E-Journal of chemistry, Vol.5, no.5, (2008) PP.395-403.

8. H.Naeimi and M.Moradian, "Synthesis and characterization of nitro-schiff bases derived from 5-nitro-salicylaldehyde and various diamines and their complexes of Co(II)", Journal of coordination Chemistry, Vol.63, no.1,(2010)





Deblurring of Images using Interval Valued Neutrosophic Numbers

R.Gokilamani^{1*} and A.Sahaya Sudha²

¹Associate Professor, Department of Mathematics, Sri Ramakrishna College of Arts and Science for Women, Coimbatore, Tamil Nadu, India

²Assistant Professor, Department of Mathematics, Nirmala College for Women, Coimbatore, Tamil Nadu, India

Received: 20 Feb 2023

Revised: 23 Mar 2023

Accepted: 28 Apr 2023

*Address for Correspondence

R.Gokilamani

Associate Professor,
Department of Mathematics,
Sri Ramakrishna College of Arts and Science for Women,
Coimbatore, Tamil Nadu, India
E.Mail: gokila70@gmail.com



This is an Open Access Journal / article distributed under the terms of the **Creative Commons Attribution License** (CC BY-NC-ND 3.0) which permits unrestricted use, distribution, and reproduction in any medium, provided the original work is properly cited. All rights reserved.

ABSTRACT

Interval Neutrosophic Sets (INSSs) have been proposed exactly to address issues with a set of numbers in the real unit interval. In this paper we have introduced Interval valued Double Refined Triangular Neutrosophic Numbers (IVDRTrNN) and proposed an algorithm to deblur the images by using the defined membership function. The efficacy of the algorithm is verified by using a blurred image.

Keywords: Interval Neutrosophic Set, Interval Valued Double Refined Indeterminate Neutrosophic Set , Interval Valued Double Refined Indeterminate Triangular Neutrosophic Number, Deblur.

INTRODUCTION

Interval-valued neutrosophic sets (IVNS) was introduced by Wang *et al.* [C1] as a suitable way to denote uncertain, incomplete, imprecise, and inconsistent information. Since IVNS shows greater flexibility and precision than single-valued neutrosophic sets [C2], IVNS applications became the object of interest for many researchers. The credibility of the interval-valued neutrosophic sets (IVNS) was demonstrated by [C3–C5]. Said BROUMI *et al.* [C6] implemented a variety of operations on interval valued neutrosophic matrices using a new Matlab' package. Bhimraj Basumatary and Said Broumi [C7] proposed an interval-valued triangular neutrosophic number to solve the neutrosophic linear programming problem. In [C8] [C9] Broumi *et al.* solved Shortest Path Problem using single valued and triangular and trapezoidal interval valued neutrosophic environments. Deli [C10] derived aggregation operators for interval valued generalised single valued neutrosophic trapezoidal and applied in decision-making problem. In this paper we have introduced interval valued double refined indeterminate triangular neutrosophic numbers.





Gokilamani and Sahaya Sudha

Preliminaries

Interval Valued Neutrosophic Set (IVNS)

There is space X of the certain objects where the separate generic elements $x \in X$. An interval-valued neutrosophic set (IVNS) $N \subset X$ has the form of $N = \{(x, T_N(x), I_N(x), F_N(x)) : x \in X\}$ (1) where $T_N(x) : X \rightarrow [0, 1]$, $I_N(x) : X \rightarrow [0, 1]$ and $F_N(x) : X \rightarrow [0, 1]$ with $0 \leq T_N(x) + I_N(x) + F_N(x) \leq 3$ or all $x \in X$.

The variables $T_A(x)$, $I_A(x)$ and $F_A(x)$ define truth-membership degree function, the indeterminacy-membership degree function and the falsity-membership degree function of x to N , respectively. For the case of the interval neutrosophic set, these functions must be described as $T_N(x) = [T_N^L(x), T_N^U(x)] \subseteq [0, 1]$, $I_N(x) = [I_N^L(x), I_N^U(x)] \subseteq [0, 1]$, $F_N(x) = [F_N^L(x), F_N^U(x)] \subseteq [0, 1]$ and the sum of these functions satisfy the condition $0 \leq T_N^U(x) + I_N^U(x) + F_N^U(x) \leq 3$.

Comparison of IVNS

Let $N_1 = \langle [T_{N_1}^L(x), T_{N_1}^U(x)], [I_{N_1}^L(x), I_{N_1}^U(x)], [F_{N_1}^L(x), F_{N_1}^U(x)] \rangle$ and $N_2 = \langle [T_{N_2}^L(x), T_{N_2}^U(x)], [I_{N_2}^L(x), I_{N_2}^U(x)], [F_{N_2}^L(x), F_{N_2}^U(x)] \rangle$ are two interval valued neutrosophic numbers, then N_1 is contained in N_2 , $N_1 \subseteq N_2$ iff $T_{N_1}^L(x) \leq T_{N_2}^L(x)$, $T_{N_1}^U(x) \leq T_{N_2}^U(x)$, $I_{N_1}^L(x) \geq I_{N_2}^L(x)$, $I_{N_1}^U(x) \geq I_{N_2}^U(x)$, $F_{N_1}^L(x) \geq F_{N_2}^L(x)$, $F_{N_1}^U(x) \geq F_{N_2}^U(x)$

Equality of IVNS

Two interval valued neutrosophic numbers N_1 and N_2 are equal, $N_1 = N_2$ iff $N_1 \subseteq N_2$ and $N_2 \subseteq N_1$

Interval Valued Double Refined Indeterminate Triangular Neutrosophic Numbers

Interval Valued Double Refined Indeterminate Neutrosophic Set (IVDRNS)

An interval Valued Double Refined Indeterminate Neutrosophic set is defined by

$\check{A}_{IN} = \{(x, T_{\check{A}_{IN}}(x), IT_{\check{A}_{IN}}(x), IF_{\check{A}_{IN}}(x), F_{\check{A}_{IN}}(x)) : x \in X\}$ where

$$T_{\check{A}_{IN}}(x) = [T_{\check{A}_{IN}}^L(x), T_{\check{A}_{IN}}^U(x)] \subseteq [0, 1], IT_{\check{A}_{IN}}(x) = [IT_{\check{A}_{IN}}^L(x), IT_{\check{A}_{IN}}^U(x)] \subseteq [0, 1],$$

$$IF_{\check{A}_{IN}}(x) = [IF_{\check{A}_{IN}}^L(x), IF_{\check{A}_{IN}}^U(x)] \subseteq [0, 1], F_{\check{A}_{IN}}(x) = [F_{\check{A}_{IN}}^L(x), F_{\check{A}_{IN}}^U(x)] \subseteq [0, 1]$$

$$\text{and } 0 \leq T_{\check{A}_{IN}}^U(x) + IT_{\check{A}_{IN}}^U(x) + IF_{\check{A}_{IN}}^U(x) + F_{\check{A}_{IN}}^U(x) \leq 4.$$

Where $T_{\check{A}_{IN}}(x)$, $IT_{\check{A}_{IN}}(x)$, $IF_{\check{A}_{IN}}(x)$, $F_{\check{A}_{IN}}(x)$ represents truth membership, indeterminacy leaning toward truth membership, indeterminacy leaning toward falsity membership and falsity membership respectively.

Comparison of IVDRNS

If $\check{A}_{IN} = \langle [T_{\check{A}_{IN}}^L(x), T_{\check{A}_{IN}}^U(x)], [IT_{\check{A}_{IN}}^L(x), IT_{\check{A}_{IN}}^U(x)], [IF_{\check{A}_{IN}}^L(x), IF_{\check{A}_{IN}}^U(x)], [F_{\check{A}_{IN}}^L(x), F_{\check{A}_{IN}}^U(x)] \rangle$ and

$\check{B}_{IN} = \langle [T_{\check{B}_{IN}}^L(x), T_{\check{B}_{IN}}^U(x)], [IT_{\check{B}_{IN}}^L(x), IT_{\check{B}_{IN}}^U(x)], [IF_{\check{B}_{IN}}^L(x), IF_{\check{B}_{IN}}^U(x)], [F_{\check{B}_{IN}}^L(x), F_{\check{B}_{IN}}^U(x)] \rangle$

are two interval valued double refined indeterminate neutrosophic numbers then $\check{A}_{IN} \subseteq \check{B}_{IN}$ if and only if

$$T_{\check{A}_{IN}}^L(x) \leq T_{\check{B}_{IN}}^L(x), T_{\check{A}_{IN}}^U(x) \leq T_{\check{B}_{IN}}^U(x), IT_{\check{A}_{IN}}^L(x) \leq IT_{\check{B}_{IN}}^L(x), IT_{\check{A}_{IN}}^U(x) \leq IT_{\check{B}_{IN}}^U(x), IF_{\check{A}_{IN}}^L(x) \geq IF_{\check{B}_{IN}}^L(x), IF_{\check{A}_{IN}}^U(x) \geq IF_{\check{B}_{IN}}^U(x), F_{\check{A}_{IN}}^L(x) \geq F_{\check{B}_{IN}}^L(x), F_{\check{A}_{IN}}^U(x) \geq F_{\check{B}_{IN}}^U(x)$$

Equality of two interval valued double refined indeterminate neutrosophic numbers

Two interval valued double refined indeterminate neutrosophic numbers \check{A}_{IN} and \check{B}_{IN} are equal, $\check{A}_{IN} = \check{B}_{IN}$ if and only if $\check{A}_{IN} \subseteq \check{B}_{IN}$ and $\check{B}_{IN} \subseteq \check{A}_{IN}$.

Operations on interval valued double refined indeterminate neutrosophic numbers

If $\check{A}_{IN} = \langle [T_{\check{A}_{IN}}^L(x), T_{\check{A}_{IN}}^U(x)], [IT_{\check{A}_{IN}}^L(x), IT_{\check{A}_{IN}}^U(x)], [IF_{\check{A}_{IN}}^L(x), IF_{\check{A}_{IN}}^U(x)], [F_{\check{A}_{IN}}^L(x), F_{\check{A}_{IN}}^U(x)] \rangle$ and

$$\check{B}_{IN} = \langle [T_{\check{B}_{IN}}^L(x), T_{\check{B}_{IN}}^U(x)], [IT_{\check{B}_{IN}}^L(x), IT_{\check{B}_{IN}}^U(x)], [IF_{\check{B}_{IN}}^L(x), IF_{\check{B}_{IN}}^U(x)], [F_{\check{B}_{IN}}^L(x), F_{\check{B}_{IN}}^U(x)] \rangle$$





Gokilamani and Sahaya Sudha

are two interval valued double refined indeterminate neutrosophic numbers

$$\lambda \ddot{\mathcal{A}}_{IN} = \left[1 - \left(1 - T_{\mathcal{A}_{IN}}^L(x) \right)^\lambda, 1 - \left(1 - T_{\mathcal{A}_{IN}}^U(x) \right)^\lambda \right], \left[1 - \left(1 - IT_{\mathcal{A}_{IN}}^L(x) \right)^\lambda, 1 - \left(1 - IT_{\mathcal{A}_{IN}}^U(x) \right)^\lambda \right], \left[\left(F_{\mathcal{A}_{IN}}^L(x) \right)^\lambda, \left(F_{\mathcal{A}_{IN}}^U(x) \right)^\lambda \right]$$

$$(\ddot{\mathcal{A}}_{IN})^\lambda = \left\langle \left[\left(T_{\mathcal{A}_{IN}}^L(x) \right)^\lambda, \left(T_{\mathcal{A}_{IN}}^U(x) \right)^\lambda \right], \left[\left(IT_{\mathcal{A}_{IN}}^L(x) \right)^\lambda, \left(IT_{\mathcal{A}_{IN}}^U(x) \right)^\lambda \right], \left[1 - \left(1 - IF_{\mathcal{A}_{IN}}^L(x) \right)^\lambda, 1 - \left(1 - IF_{\mathcal{A}_{IN}}^U(x) \right)^\lambda \right] \right\rangle$$

$$\ddot{\mathcal{A}}_{IN} \oplus \ddot{\mathcal{B}}_{IN} = \left\langle \left[T_{\mathcal{A}_{IN}}^L(x) + T_{\mathcal{B}_{IN}}^L(x) - T_{\mathcal{A}_{IN}}^L(x) T_{\mathcal{B}_{IN}}^L(x), T_{\mathcal{A}_{IN}}^U(x) + T_{\mathcal{B}_{IN}}^U(x) - T_{\mathcal{A}_{IN}}^U(x) T_{\mathcal{B}_{IN}}^U(x) \right], \left[IT_{\mathcal{A}_{IN}}^L(x) + IT_{\mathcal{B}_{IN}}^L(x) - IT_{\mathcal{A}_{IN}}^L(x) IT_{\mathcal{B}_{IN}}^L(x), IT_{\mathcal{A}_{IN}}^U(x) + IT_{\mathcal{B}_{IN}}^U(x) - IT_{\mathcal{A}_{IN}}^U(x) IT_{\mathcal{B}_{IN}}^U(x) \right], \left[IF_{\mathcal{A}_{IN}}^L(x) * IF_{\mathcal{B}_{IN}}^L(x), IF_{\mathcal{A}_{IN}}^U(x) * IF_{\mathcal{B}_{IN}}^U(x) \right] \right\rangle$$

$$\ddot{\mathcal{A}}_{IN} \otimes \ddot{\mathcal{B}}_{IN} = \left\langle \left[T_{\mathcal{A}_{IN}}^L(x) * T_{\mathcal{B}_{IN}}^L(x), T_{\mathcal{A}_{IN}}^U(x) * T_{\mathcal{B}_{IN}}^U(x) \right], \left[IT_{\mathcal{A}_{IN}}^L(x) * IT_{\mathcal{B}_{IN}}^L(x), IT_{\mathcal{A}_{IN}}^U(x) * IT_{\mathcal{B}_{IN}}^U(x) \right], \left[IF_{\mathcal{A}_{IN}}^L(x) + IF_{\mathcal{B}_{IN}}^L(x) - IF_{\mathcal{A}_{IN}}^L(x) IF_{\mathcal{B}_{IN}}^L(x), IF_{\mathcal{A}_{IN}}^U(x) + IF_{\mathcal{B}_{IN}}^U(x) - IF_{\mathcal{A}_{IN}}^U(x) IF_{\mathcal{B}_{IN}}^U(x) \right], \left[F_{\mathcal{A}_{IN}}^L(x) + F_{\mathcal{B}_{IN}}^L(x) - F_{\mathcal{A}_{IN}}^L(x) F_{\mathcal{B}_{IN}}^L(x), F_{\mathcal{A}_{IN}}^U(x) + F_{\mathcal{B}_{IN}}^U(x) - F_{\mathcal{A}_{IN}}^U(x) F_{\mathcal{B}_{IN}}^U(x) \right] \right\rangle$$

$$(\ddot{\mathcal{A}}_{IN})^c = \left\langle \left[F_{\mathcal{A}_{IN}}^L(x), F_{\mathcal{A}_{IN}}^U(x) \right], \left[IF_{\mathcal{A}_{IN}}^L(x), IF_{\mathcal{A}_{IN}}^U(x) \right], \left[IT_{\mathcal{A}_{IN}}^L(x), IT_{\mathcal{A}_{IN}}^U(x) \right], \left[T_{\mathcal{A}_{IN}}^L(x), T_{\mathcal{A}_{IN}}^U(x) \right] \right\rangle$$

Interval Valued Double Refined Indeterminate Triangular Neutrosophic Numbers

Interval Valued Double Refined Indeterminate Triangular Neutrosophic Numbers whose truth membership function $\mathcal{J}\zeta_{\ddot{\mathcal{A}}_{INTr}}(x)$, indeterminacy leaning towards truth membership function $\mathcal{J}\xi_{\ddot{\mathcal{A}}_{INTr}}(x)$, indeterminacy leaning towards falsity membership function $\mathcal{J}\tau_{\ddot{\mathcal{A}}_{INTr}}(x)$ and falsity membership function $\mathcal{J}\varphi_{\ddot{\mathcal{A}}_{INTr}}(x)$ are defined as follows:

$$\mathcal{J}\zeta_{\ddot{\mathcal{A}}_{INTr}}(x) = \begin{cases} \frac{(x-a)\mathcal{J}p_{\ddot{\mathcal{A}}_{INTr}}}{b-a} & a \leq x < b \\ \mathcal{J}p_{\ddot{\mathcal{A}}_{INTr}} & x = b \\ \frac{(c-x)\mathcal{J}p_{\ddot{\mathcal{A}}_{INTr}}}{c-b} & b < x \leq c \\ 0 & \text{Otherwise} \end{cases}$$

$$\mathcal{J}\xi_{\ddot{\mathcal{A}}_{INTr}}(x) = \begin{cases} \frac{(x-a)\mathcal{J}q_{\ddot{\mathcal{A}}_{INTr}}}{b-a} & a \leq x < b \\ \mathcal{J}q_{\ddot{\mathcal{A}}_{INTr}} & x = b \\ \frac{(c-x)\mathcal{J}q_{\ddot{\mathcal{A}}_{INTr}}}{c-b} & b < x \leq c \\ 0 & \text{Otherwise} \end{cases}$$

$$\mathcal{J}\tau_{\ddot{\mathcal{A}}_{INTr}}(x) = \begin{cases} \frac{b-x + \mathcal{J}r_{\ddot{\mathcal{A}}_{INTr}}(x-a)}{b-a} & a \leq x < b \\ \mathcal{J}r_{\ddot{\mathcal{A}}_{INTr}} & x = b \\ \frac{x-b + \mathcal{J}r_{\ddot{\mathcal{A}}_{INTr}}(c-x)}{c-b} & b < x \leq c \\ 1 & \text{Otherwise} \end{cases}$$

$$\mathcal{J}\varphi_{\ddot{\mathcal{A}}_{INTr}}(x) = \begin{cases} \frac{b-x + \mathcal{J}s_{\ddot{\mathcal{A}}_{INTr}}(x-a)}{b-a} & a \leq x < b \\ \mathcal{J}s_{\ddot{\mathcal{A}}_{INTr}} & x = b \\ \frac{x-b + \mathcal{J}s_{\ddot{\mathcal{A}}_{INTr}}(c-x)}{c-b} & b < x \leq c \\ 1 & \text{Otherwise} \end{cases}$$





Gokilamani and Sahaya Sudha

An interval Valued Double Refined Indeterminate Triangular Neutrosophic number can be represented by $\ddot{J}_{NT_r} = \langle (a, b, c) : Jp_{\ddot{J}_{NT_r}}, Jq_{\ddot{J}_{NT_r}}, Jr_{\ddot{J}_{NT_r}}, Js_{\ddot{J}_{NT_r}} \rangle$
 Where $Jp_{\ddot{J}_{NT_r}} = [T_{\ddot{J}_{NT_r}}^L, T_{\ddot{J}_{NT_r}}^U]$, $Jq_{\ddot{J}_{NT_r}} = [IT_{\ddot{J}_{NT_r}}^L, IT_{\ddot{J}_{NT_r}}^U]$, $Jr_{\ddot{J}_{NT_r}} = [IF_{\ddot{J}_{NT_r}}^L, IF_{\ddot{J}_{NT_r}}^U]$,
 $Js_{\ddot{J}_{NT_r}} = [F_{\ddot{J}_{NT_r}}^L, F_{\ddot{J}_{NT_r}}^U]$, $T_{\ddot{J}_{NT_r}}^L, IT_{\ddot{J}_{NT_r}}^L, IF_{\ddot{J}_{NT_r}}^L, F_{\ddot{J}_{NT_r}}^L$ being the lower bounds and $T_{\ddot{J}_{NT_r}}^U, IT_{\ddot{J}_{NT_r}}^U, IF_{\ddot{J}_{NT_r}}^U, F_{\ddot{J}_{NT_r}}^U$, the upper bounds for the truth, indeterminacy leaning toward truth membership, indeterminacy leaning toward falsity membership and falsity membership degrees.

Deblurring

Blur

Blur can be defined as unwanted transition made into the original image due to various reasons like motion between camera and an object, atmospheric turbulence, out-of-focus of the camera, taking picture in fog etc. Following are the types of blur:

Average blur

Average blur occurs on entire image. Average blur can be scattered in a vertical and horizontal direction [C11] and it can be circular averaging by radius R which can be calculated by the following formula: $R = \sqrt{g^2 + f^2}$ Where, g is the horizontal size blurring direction and f is the vertical blurring size direction and R is the radius size of the circular averaging blurring [C2].

Motion Blur

Motion blurs [C12], [C13], [C14], [C15] can be caused by relative motion between camera and scene during the exposure time. It can occur in various forms like rotation, translation, sudden change of the scale, or the combination of these [C2].

Defocus Blur

Photographical defocusing is another common type of blurring, known as defocus blur, mainly due to the finite size of the camera aperture [C16]. Defocus blur [C14], [C16], [C17], [C18] is caused by an optical imaging system. Defocus blur is employed to blur a background and “pop out” the main object using large aperture lenses.

Gaussian Blur

In this blur type, pixel weights are unequal. Gaussian blur is simulated by Gaussian function. The blur is high at the centre and decreased at the edges following bell shaped curve [C11], [C19], [C20].

Atmospheric Turbulence Blur

Blur introduced by atmospheric turbulence depends on a variety of factors such as temperature, wind speed, exposure time.

Deblurring

An image deblurring is a recovering process that recovers a sharp latent image from a blurred image, which is caused by camera shake or object motion. Image deblurring have wide applications from consumer photography, e.g., remove motion blur due to camera shake, to radar imaging and tomography. Deblurring is the process of removing blurring artifacts from images. The performance of the deblurring algorithm is evaluated using different metrics such as

- Mean – Square Error
- Peak Signal –to –Noise ratio
- Structure Similarity Index Method





Gokilamani and Sahaya Sudha

Deblurring using Interval Valued Double Refined Indeterminate Triangular Neutrosophic Number

In this section an Interval Valued Double Refined Indeterminate Neutrosophic algorithm was utilised to process images. The Interval Valued Double Refined Indeterminate Neutrosophic set split the membership into upper bound and lower bound for increase the veracity of data. The upper and lower bound values must be in between the interval (0, 1). Now we get the Truth membership, Falsity membership, indeterminate toward falsity and indeterminate towards truth membership with upper and lower bounds. Since we got upper and lower bound values using those values and following the procedure the images are processed. Images that require processing are imported into system memory and then transformed into M-N-3 matrices. On the imported image, Interval Valued Double Refined Indeterminate Neutrosophic Sets are applied. In Deblurring process of image the IVDRINSS members obtained are deconvoluted using blind deconvolution filter. Blind deconvolution filter weights were used to restore the images.

Steps involved in Deblurring

1. Importing blurred image into memory.
2. Rescaling and matrix conversion.
3. Applying Interval Valued Double Refined Indeterminate Neutrosophic set in image matrix.
4. Applying blind deconvolution in IVDRINSS applied image.
5. Finding edge location using indeterminate membership (IFL& ITL).
6. Combining edges and deconvoluted images.
7. Export deblurred images into local memory

The performance of the algorithm is evaluated by implementing the above algorithm to the blurred image.

CONCLUSION

A blur image is used to test the efficacy of the proposed algorithm. Fig 1(a) is the blurred image taken as the Input image. The image is imported in the MATLAB and output is obtained under Neutrosophic domain [Fig 1(b)], Double Refined Indeterminate Triangular Neutrosophic environment [Fig 1(c)] and in Interval Valued Double Refined Indeterminate Triangular Neutrosophic environment [Fig 1(d)]. The metric values are tabulated in table. Our proposed method generate finer result with less MSE and more PSNR and SSIM values.

REFERENCES

1. Wang, H.; Smarandache, F.; Zhang, Y.Q.; Sunderraman, R. Interval Neutrosophic Sets and Logic: Theory and Applications in Computing; Hexis: Phoenix, AZ, USA, 2005.
2. Broumi, S.; Bakali, A.; Talea, M.; Smarandache, F.; Kishore, P.K.; Sahin, R. Shortest path problem under interval valued neutrosophic setting. *Int. J. Adv. Trends Comput. Sci. Eng.* 2019, 8, 216–222.
3. Liu, P.D.; Tang, G.L. Some power generalized aggregation operators based on the interval neutrosophic numbers and their application to decision making. *J. Intell. Fuzzy. Syst.* 2015, 30, 2517–2528.
4. Pamučar, D.; Stević, Ž.; Zavadskas, E.K. Integration of interval rough AHP and interval rough MABAC methods for evaluating university web pages. *Appl. Soft Comput.* 2018, 67, 141–163.
5. Semenas, R.; Bausys, R. Modelling of Autonomous Search and Rescue Missions by Interval-Valued Neutrosophic WASPAS Framework. *Symmetry* 2020, 12, 162.
6. Broumi, S.; Bakali, A.; Talea, M. & Smarandache, F. (2017). A Matlab Toolbox For Interval Valued Neutrosophic Matrices for Computer Applications.
7. Bhimraj Basumatary and Said Broumi, "Interval-Valued Triangular Neutrosophic Linear Programming Problem", *International Journal of Neutrosophic Science (IJNS)*, Vol. 10, No. 2, PP. 105-115, 2020
8. Broumi, S, Talea, M., Bakali, A., 'Shortest path problem in fuzzy, intuitionistic fuzzy and neutrosophic environment: an overview', *Complex Intell. Syst.*, 2019, 5, pp. 371–378



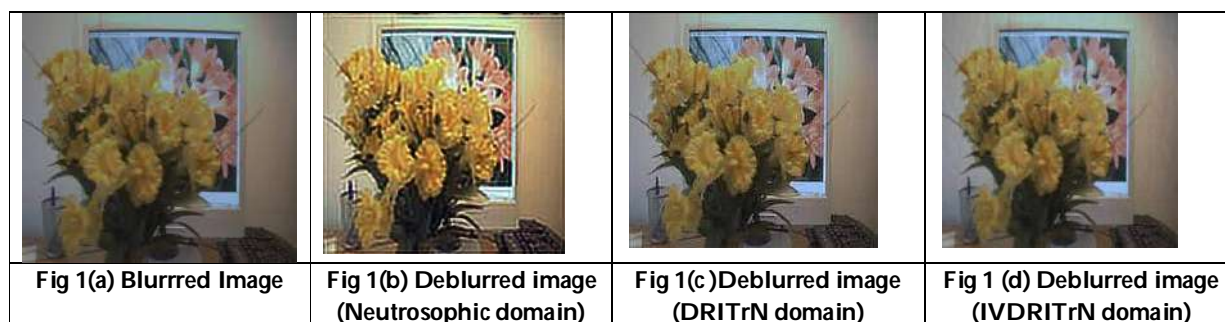


Gokilamani and Sahaya Sudha

9. Broumi,S., Nagarajan, D., Bakali, A., 'The shortest path problem in interval valued trapezoidal and triangular neutrosophic environment', *ComplexIntell. Syst.*,2019,5, pp.391–402
10. Deli, I.: 'Some operators with IVGSVTrN-numbers and their applications to multiple criteria group decision making', *Neutrosophic Sets Syst.*, 2019, 25, pp. 33–53
11. S. Yadav, C. Jain, and C. Aarti, "Evaluation of Image Deblurring Techniques," *International Journal of Computer Applications*, vol. 139, no. 12, pp. 32-36, 2016.
12. Q. Shan, J. Jia, and A. Agarwala, "High-quality Motion Deblurring from a Single Image," in *ACM Transactions on Graphics*, 2008, vol. 27, no. 3.
13. M. Tico, M. Trimeche, and M. Vehvilainen, "Motion Blur Identification Based on Differently Exposed Images," *IEEE International Conference on Image Processing*, pp. 2021-2024, 2006.
14. R. Liu, Z. Li, and J. Jia, "Image Partial Blur Detection and Classification," *IEEE international conference on computer vision and pattern recognition*, pp. 1-8, 2008.
15. B. Su, S. Lu, and C. L. Tan, "Blurred Image Region Detection and Classification," in *In proceeding of 19th ACM International Conference on Multimedia*, 2011, pp. 1397-1400.
16. G. Air, M. Indaco, D. Rolfo, L. O. Russo, P. Trotta, and P. Torino, "Evaluation of image deblurring algorithms for real-time applications," *IEEE 9th conference on Design & Technology of Integrated System*, pp. 1-6, 2014.
17. R. Wang and W. Wang, "Spatially Variant Defocus Blur Map Estimation and Deblurring from a Single Image," *Journal of Visual Communication and Image Representation*, vol. 35, pp. 257-264, 2016.
18. C. Tang, J. Wu, Y. Hou, P. Wang, and W. Li, "A Spectral and Spatial Approach of Coarse-to-Fine Blurred Image Region Detection," *IEEE Signal Proceeding Letters*, vol. 23, no. 11, pp. 1652- 1656, 2016.
19. Z. Al-ameen, G. Sulong, and G. Johar, "A Comprehensive Study on Fast image Deblurring Techniques," *International Journal of Advanced Science and Technology*, vol. 44, pp. 1-10, 2012.
20. S. Jain, A. Dubey, D. S. Chundawat, and P. K. Singh, "Image Deblurring from Blurred Images," *International Journal of Advanced Research in Computer Science & Technology*, vol. 2, no. 3, pp. 2-6, 2014.
21. Jain, Sindhu & Goswami, Sudhir. (2015). A Comparative Study of Various Image Restoration Techniques with different types of blur.

Table 1 . PSNR and SSIM

Metric	MSE	PSNR	SSIM
Neutrosophic domain	0.02042	16.9	0.6077
DRITrN domain	0.0009416	30.26	0.9369
IVDRITrN domain	0.0000697	41.57	0.9897





k-Neighbourhood Graph of a Graph

A.P.Pushpalatha¹ and K. Pitchaimani^{2*}

¹Professor, Department of Mathematics, Velammal College of Engineering and Technology, Madurai, Tamil Nadu, India.

²Assistant Professor, Department of Mathematics, Velammal College of Engineering and Technology, Madurai, Tamil Nadu, India.

Received: 15 Feb 2023

Revised: 25 Apr 2023

Accepted: 30 May 2023

*Address for Correspondence

K. Pitchaimani

Assistant Professor,
Department of Mathematics,
Velammal College of Engineering and Technology,
Madurai, Tamil Nadu, India.
E.Mail: : kpm@vcet.ac.in



This is an Open Access Journal / article distributed under the terms of the **Creative Commons Attribution License** (CC BY-NC-ND 3.0) which permits unrestricted use, distribution, and reproduction in any medium, provided the original work is properly cited. All rights reserved.

ABSTRACT

A set S of vertices in a graph $G(V, E)$ is a neighbourhood set if $G = \cup_{v \in S} \langle N[v] \rangle$, where $\langle N[v] \rangle$ is the sub graph of G induced by v and all vertices adjacent to v . Given a graph G , a new graph can be constructed by using neighbourhood sets and distance between two vertices of G . This new graph is called the k -neighbourhood graph of a graph. Such construction may also be carried out with respect to other parameter. The purpose of this paper is to introduce a new graph called k -neighbourhood graph of a graph and investigate the nature of the newly defined graph.

AMS Mathematics subject Classification (2010): 05C72

Keywords: Neighbourhood set, neighbourhood number $n_0(G)$, k -neighbourhoodset, k -neighbourhood graph of a graph.

INTRODUCTION

The representation of data can benefit greatly from the use of complicated abstractions like graphs. In actuality, graph theoretical approaches are a good way to simplify many difficulties in real world problems. We just cover a small portion of the many applications for graphs below. Protein-protein interactions graphs, transportation networks, utility graphs, social network graphs, diagrams of network packet traffic, Neural networks, the issue of signal categorization, synthetic Neural network, Airline Planning, Search engine algorithms (Page Rank algorithm), solving Sudoku puzzles (shortest path), finding directions on a map and social media marketing (Community





Pushpalatha and Pitchaimani

detection) and so on. In addition to that, John Conway, a Mathematician from Cambridge, created the Conway's game of life. When this game was mentioned in 1970 Scientific American article based on the idea of a neighbourhood, it quickly gained widespread recognition.

Unless otherwise stated all graphs $G(V, E)$ considered are connected, simple and undirected graphs. For a graph G , let $V(G)$, $E(G)$ denote its vertex set and edge set respectively. The **distance** between any two vertices $u, v \in V(G)$ is the length of shortest path joining them and it is denoted by $d(u, v)$. The **diameter** of a graph G is the maximum distance between any two vertices in $V(G)$ and it is denoted by $\text{diam}(G)$. For $v \in V(G)$, the **neighbourhood** $N(v)$ is the set of all vertices adjacent to v . $N[v] = N(v) \cup \{v\}$ is called the **closed** neighbourhood of v . A vertex $v \in V(G)$ is called the support if it is adjacent to a pendent vertex. Any undefined terms in this paper may be found in Harary [2].

Let $k \geq 1$ be a positive integer. Two vertices $u, v \in V(G)$ are said to be k -adjacent if $d(u, v) \leq k$. A graph G is said to be k -Complete if every vertex in $V(G)$ is adjacent to every other vertex in $V(G)$. The open k -neighbourhood $N_k(v)$ of a vertex v in a graph G is defined as $N_k(v) = \{u \in V(G) / d(u, v) \leq k\}$ and its closed k -neighbourhood $N_k[v]$ of a vertex v in a graph G is defined as $N_k[v] = N_k(v) \cup \{v\}$. The k -degree of a vertex v in G is denoted by $\text{deg}_k(v)$. Let $\Delta_k(G)$ and $\delta_k(G)$ denote the maximum and minimum k -degree among all the vertices of G respectively. Let $v \in V(G)$. Then $\Delta_k(G)$

$$= \max_{v \in V(G)} |N_k(v)| \text{ and } \delta_k(G) = \min_{v \in V(G)} |N_k(v)|.$$

LITERATURE REVIEW

The study of literature reveals the various concepts materializing the outcome of new dimension of graph construction. In 1958, Claude Berge introduced the domination number of a graph. A subset D of $V(G)$ is said to be a dominating set of G , if every vertex in $V-D$ is adjacent to some vertex in D . The domination number $\gamma(G)$ is the minimum cardinality of a dominating set of G . This parameter has been investigated by many authors including Berge, Cockayne, Hedetniemi and Walikar et al. The concept of γ -graph of a graph denoted by $\gamma(G)$ was introduced by Dr. N. Sridharan et al [11]. The gamma graph of a graph is denoted by $\gamma(G)$. The vertex set $V[\gamma(G)]$ is the set of all γ -sets of G and for two sets $S_i, S_j \in V[\gamma(G)]$, S_i, S_j are adjacent in $\gamma(G)$ if and only if $S_j = (S_i - \{u\}) \cup \{v\}$, where $u \in S_i, v \notin S_i, i \neq j$. In [11], Dr. N. Sridharan developed a lot of interesting results by making use of this new graph. The maximum cardinality of all maximum independent sets of G is called as an independence number of G and is denoted by $\beta_0(G)$. In [4], A.P. Pushpalatha et al introduced the concept of $\beta_0(G)$, namely β_0 -graph of a graph. The vertex set $V(\beta_0(G))$ is the set of all β_0 -sets of G and for two sets $S_i, S_j \in V(\beta_0(G))$ are adjacent in $\beta_0(G)$ if and only if $S_j = (S_i - \{u\}) \cup \{v\}$, where $u \in S_i, v \notin S_i, i \neq j$. They made a substantial contribution in this area.

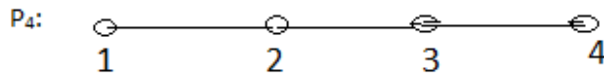
The concept of neighbourhood number of a graph has been studied by Prof. E. Sampath kumar and Prof. P.S. Neeralagi [10]. A set S of points in a graph G is a neighbourhood set if $G = \cup_{v \in S} \langle N[v] \rangle$, where $\langle N[v] \rangle$ is the sub graph of G induced by v and all vertices adjacent to v . The neighbourhood number of G denoted by $n_0(G)$ is the minimum cardinality of all neighbourhood sets of G . The neighbourhood sets of a graph may be used to create a new graph. Using those similar ideas, the concept of neighbourhood graph of a graph was introduced by G. Jothilakshmi, et al [9]. The set of all n_0 -sets of G is the vertex set of $n_0(G)$ and two n_0 -sets D_1 and D_2 are adjacent in $n_0(G)$ if and only if $|D_1 \cap D_2| = |D_1| - 1 = |D_2| - 1$. The neighbourhood graph of a graph G is denoted by $n_0(G)$. In other words, let H be the set of all neighbourhood set of G and two vertices $u, v \in H$ representing neighbourhood sets S_i, S_j respectively are adjacent if and only if $S_j = (S_i - \{u\}) \cup \{v\}$ where $u \in S_i, v \notin S_i, i \neq j$. Then H is called the **neighbourhood graph of a graph** G and is denoted by $n_0(G)$.



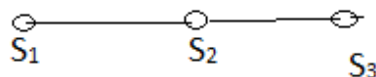


Pushpalatha and Pitchaimani

Example



The n_0 sets of P_4 are $\{1, 3\}$, $\{2, 3\}$, $\{2, 4\}$ namely S_1, S_2, S_3 respectively. The n_0 -neighbourhood graph of P_4 is as follows:
 $N_0(P_4)$:



Many type of graphs can be formed for a given graph with respect to many parameters discussed earlier. But here we construct a new graph from the given graph in a different way.

PURPOSE OF THE STUDY

The concept of the new graphs namely γ -graph, β_0 - graph and n_0 -graph inspired the researchers to introduce a new graph namely k -neighbourhood graph of a graph with a new concept. The open k -neighbourhood sets of a graph G may be used to create a new graph. The vertices of new graph are of course the vertices of the original graph and two such vertices will be adjacent if the open k -neighbourhood set of two vertices have at least one common neighbour. Acharya and Vartak seem to have introduced neighbourhood graphs earlier in [1]. In [6], Kulli has extended the idea of neighbourhood graph of a graph and looked at some of its characteristics. Additionally, the author described the graph (i) whose neighbourhood graphs are connected (ii) whose neighbourhood graphs are r -regular and (iii) whose neighbourhood graphs are Eulerian. Incorporating distance and neighbourhood sets concepts in [6], this particular graph k -neighbourhood graph of a graph is developed.

In this paper, we study the concept of k -neighbourhood graph of a graph with respect to k -neighbourhood sets of vertices. The fourth section is devoted to explore the definition of k -neighbourhood graph of a graph and example. The fifth section is dealt with the construction of k -neighbourhood graph of some standard graphs and discussed some theorems. The sixth and seventh sections discuss k -neighbourhood graph of a Barbell graph and some results and theorems on k -neighbourhood graph of a graph.

k-NEIGHBOURHOOD GRAPH OF A GRAPH

Neighbourhood graphs concept was first introduced by Acharya and Vartak in [1], where so many of its properties and characterization theorems were discussed. In [1], the open neighbourhood graph was defined as follows: the open neighbourhood graph of an undirected graph G is the graph that is defined on the same vertex set as G in which two vertices are adjacent if they have a common neighbour in G .

In this paper, we analyze the graph obtained by considering k (distance) – neighbourhood sets of vertices of G . Here we define a graph namely k -neighbourhood graph of a graph with respect to k -neighbourhood sets of G .

Definition 4.1: Let $G = (V, E)$ be a given graph and k be a positive integer. Let $u, v \in V(G)$. The open k -neighbourhood $N_k(v)$ of a vertex v in a graph G is defined as $N_k(v) = \{u \in V(G) / d(u, v) \leq k\}$ and its closed k -neighbourhood $N_k[v]$ of a vertex v in a graph G is defined as $N_k[v] = N_k(v) \cup \{v\}$.

Definition 4.2: The k -neighbourhood graph of a graph G is denoted by $NE_k(G)$ defined as follows:

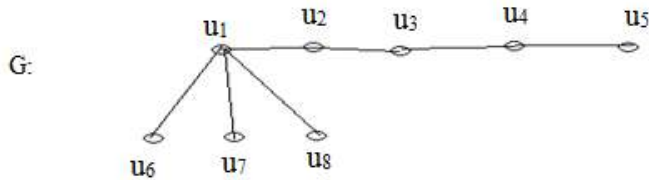
- (i) Vertex set of G is same as the vertex set of $NE_k(G)$.
- (ii) u and v are adjacent in $NE_k(G)$ iff $N_k(u)$ and $N_k(v)$ have at least one common neighbour.





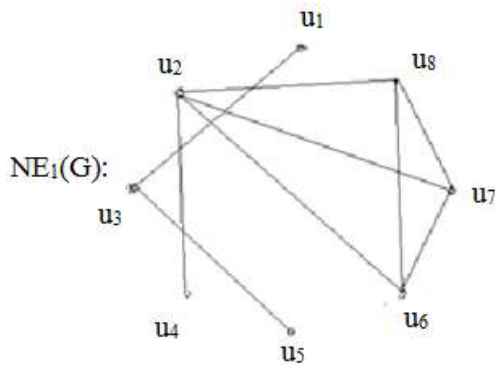
Pushpalatha and Pitchaimani

Example 4.3:



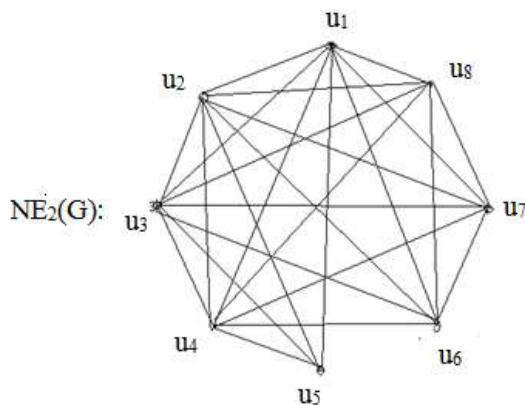
Let $k=1$

$N_1(u_1) = \{u_2, u_6, u_7, u_8\}$	$N_1(u_5) = \{u_4\}$
$N_1(u_2) = \{u_1, u_3\}$	$N_1(u_6) = \{u_1\}$
$N_1(u_3) = \{u_2, u_4\}$	$N_1(u_7) = \{u_1\}$
$N_1(u_4) = \{u_3, u_5\}$	$N_1(u_8) = \{u_1\}$



Let $k=2$

$N_2(u_1) = \{u_2, u_3, u_6, u_7, u_8\}$	$N_2(u_5) = \{u_3, u_4\}$
$N_2(u_2) = \{u_1, u_3, u_4, u_6, u_7, u_8\}$	$N_2(u_6) = \{u_1, u_2, u_7, u_8\}$
$N_2(u_3) = \{u_1, u_2, u_4, u_5\}$	$N_2(u_7) = \{u_1, u_2, u_6, u_8\}$
$N_2(u_4) = \{u_2, u_3, u_5\}$	$N_2(u_8) = \{u_1, u_2, u_6, u_7\}$





Pushpalatha and Pitchaimani

Let k=3

$$N_3(u_1) = \{u_2, u_3, u_4, u_6, u_7, u_8\}$$

$$N_3(u_5) = \{u_2, u_3, u_4\}$$

$$N_3(u_2) = \{u_1, u_3, u_4, u_5, u_6, u_7, u_8\}$$

$$N_3(u_6) = \{u_1, u_2, u_3, u_7, u_8\}$$

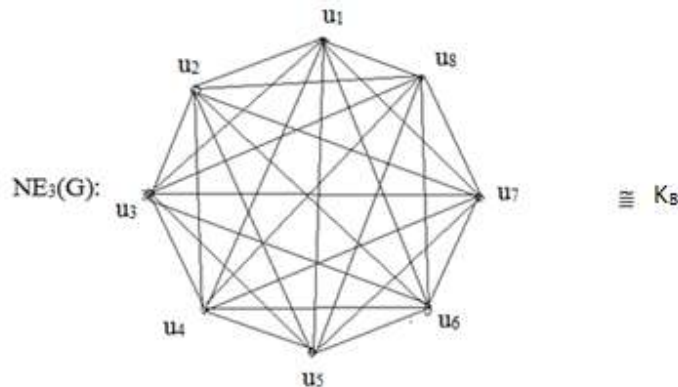
$$N_3(u_3) = \{u_1, u_2, u_4, u_5, u_6, u_7, u_8\}$$

$$N_3(u_7) = \{u_1, u_2, u_3, u_6, u_8\}$$

$$N_3(u_4) = \{u_1, u_2, u_3, u_5\}$$

$$N_3(u_8) = \{u_1, u_2, u_3, u_6, u_7\}$$

Here $N_3(u_i)$ and $N_3(u_j)$, $i \neq j$ contain at least one common neighbour. Hence $NE_3(G) \cong K_8$.



OBSERVATION 4.4: Two vertices u_i and u_j are k -adjacent in $NE_k(G)$ if $d(u_i, u_j) \leq k, i \neq j$.

OBSERVATION 4.5: For any graph G , if $k \geq \left\lceil \frac{\text{diam}(G)}{2} \right\rceil + 1$, then $NE_k(G) \cong K_n$,

where $n = |V(G)|$.

k-NEIGHBOURHOOD GRAPH OF SOME STANDARD GRAPHS

Let us discuss the k -neighbourhood graph of some standard graphs in this section.

Theorem 5.1:

For a complete bipartite graph $K_{m,n}$,

$$NE_k(K_{m,n}) = \begin{cases} K_m \cup K_n, & \text{for } k = 1 \\ K_{m+n}, & \text{for } k \geq 2 \end{cases} \quad m, n \geq 1.$$

Proof: Let $K_{m,n}$ be a complete bipartite graph with $V(K_{m,n}) = V_1 \cup V_2$, where $V_1 = \{u_1, u_2, \dots, u_m\}$ and $V_2 = \{v_1, v_2, \dots, v_n\}$

Case (i) Let $k = 1$

$$N_1(u_i) = \{v_1, v_2, \dots, v_n\}, 1 \leq i \leq m. \quad |N_1(u_1)| = |N_1(u_2)| = \dots = |N_1(u_m)| = n.$$

$$N_1(v_j) = \{u_1, u_2, \dots, u_m\}, 1 \leq j \leq n. \quad |N_1(v_1)| = |N_1(v_2)| = \dots = |N_1(v_n)| = m. \text{ In } NE_1(K_{m,n}), \text{ every vertex of } N(u_i) \text{ is adjacent to the vertices } v_1, v_2, \dots, v_n \text{ and each vertex of } N(v_j) \text{ is adjacent to the vertices } u_1, u_2, \dots, u_m.$$

Since V_1 and V_2 are disjoint sets, then $NE_1(K_{m,n})$ is a disjoint union of K_m and K_n .

Case (ii) Let $k \geq 2$.

$$N_2(u_i) = \{u_1, u_2, \dots, u_{i-1}, u_{i+1}, \dots, u_m, v_1, v_2, \dots, v_n\} \text{ and } N_2(v_j) = \{v_1, v_2, \dots, v_{j-1}, v_{j+1}, \dots, v_n, u_1, u_2, \dots, u_m\}. \text{ Any vertex of } K_{m,n} \text{ is adjacent to remaining all other vertices.}$$

Hence $NE_k(K_{m,n})$ is a complete graph of $m+n$ vertices, $k \geq 2$. Hence the theorem.

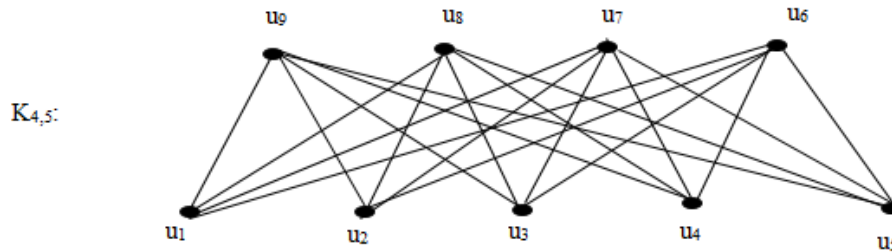
Illustration 5.2:

Consider the following graph





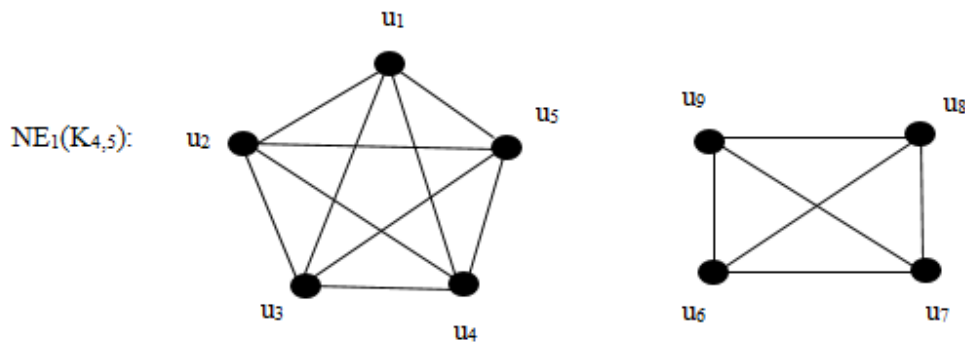
Pushpalatha and Pitchaimani



Let $k = 1$

$$N_1(u_1) = N_1(u_2) = N_1(u_3) = N_1(u_4) = N_1(u_5) = \{u_6, u_7, u_8, u_9\}$$

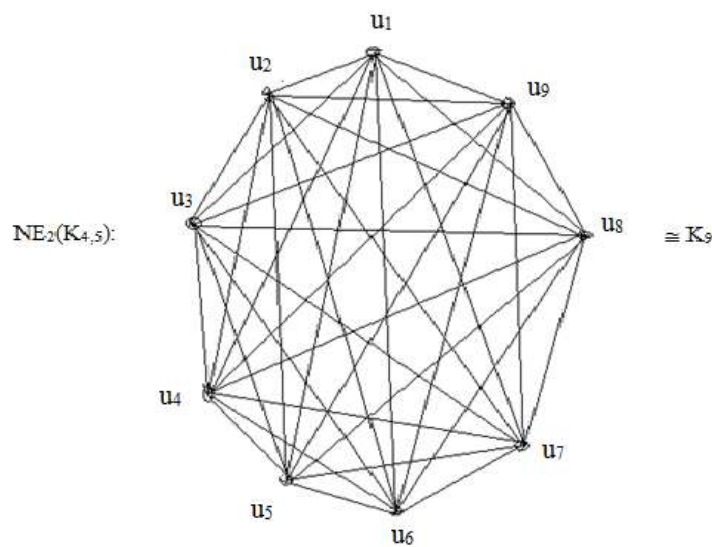
$$N_1(u_6) = N_1(u_7) = N_1(u_8) = N_1(u_9) = \{u_1, u_2, u_3, u_4, u_5\}$$



Therefore $NE_1(K_{4,5}) = K_4 \cup K_5$.

Let $k=2$

$N_2(u_i)$ is the set of all vertices $u_j, i \neq j, 1 \leq i \leq 9$ explicitly any two of $N_2(u_i)$ and $N_2(u_j) i \neq j$, contain at least one common neighbour.



Therefore $NE_2(K_{4,5}) \cong K_9$.



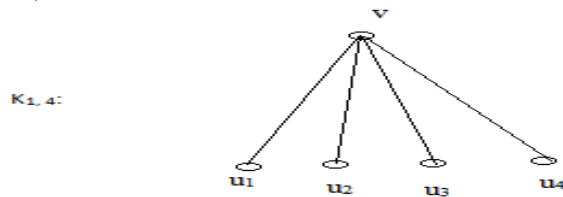


Pushpalatha and Pitchaimani

Hence $NE_k(K_{m,n}) = \begin{cases} K_m \cup K_n, & \text{for } k = 1 \\ K_{m+n}, & \text{for } k \geq 2 \end{cases} \quad m, n \geq 1.$

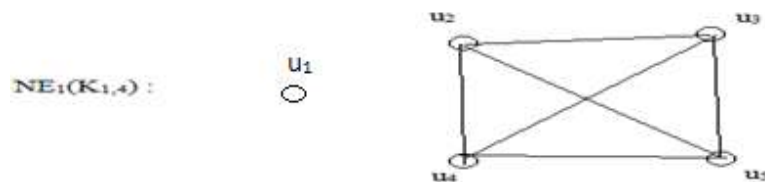
Corollary 5.3: For star graph $K_{1,n}$, $NE_k(K_{1,n}) \cong \begin{cases} K_1 \cup K_n & \text{if } k = 1 \\ K_{n+1} & \text{if } k \geq 2 \end{cases}$

For, Consider $K_{1,4}$



Case (i): Let $k = 1$

$N_1(v) = \{u_1, u_2, u_3, u_4\}$, $N_1(u_2) = N_1(u_3) = N_1(u_4) = N_1(u_1) = \{v\}$



Therefore $NE_1(K_{1,4}) = K_1 \cup K_4$.

Case (ii): Let $k = 2$

$N_2(v) = \{u_1, u_2, u_3, u_4\}$, $N_2(u_1) = \{v, u_2, u_3, u_4\}$, $N_2(u_2) = \{v, u_1, u_3, u_4\}$, $N_2(u_3) = \{v, u_1, u_2, u_4\}$, $N_2(u_4) = \{v, u_1, u_2, u_3\}$.
Hence $NE_2(K_{1,4}) = K_5$.

Definition 5.4: A double star is a graph obtained by taking two stars and joining the vertices of maximum degrees with an edge. If the stars are $K_{1,r}$ and $K_{1,s}$ then the double star is denoted by $D_{r,s}$.

Theorem 5.5: For a double star $D_{r,s}$,

$NE_k(D_{r,s}) = \begin{cases} K_{r+1} \cup K_{s+1} & \text{if } k = 1 \\ K_{r+s+2} & \text{if } k \geq 2 \end{cases} \quad r, s \geq 1.$

Proof: Let u, v be central vertices and $u_1, u_2, \dots, u_r, v_1, v_2, \dots, v_s$ be the other vertices of $D_{r,s}$.

Case (i): Let $k = 1$.

$N_1(u) = \{v, u_1, u_2, \dots, u_r\}$ and $N_1(v) = \{u, v_1, v_2, \dots, v_s\}$ have no common neighbour. Therefore u and v are non-adjacent in $NE_1(D_{r,s})$. $N_1(u_1) = N_1(u_2) = \dots = N_1(u_r) = N_1(v) = \{u\}$. Therefore u_i 's ($i = 1, 2, \dots, r$) and v are adjacent to each other in $NE_1(D_{r,s})$. Also $N_1(v_1) = N_1(v_2) = \dots = N_1(v_s) = N_1(u) = \{v\}$. Therefore v_j 's ($j = 1, 2, \dots, s$) and u are adjacent to each other in $NE_1(D_{r,s})$.

Hence $NE_1(D_{r,s}) = K_{r+1} \cup K_{s+1}$.

Case (ii): Let $k = 2$

The sets $N_2(u_i) = \{u_1, u_2, \dots, u_{i-1}, u_{i+1}, \dots, u_r, u, v\}$ ($i = 1, 2, \dots, r$), $N_2(v_j) = \{u, v, v_1, v_2, \dots, v_{j-1}, v_{j+1}, \dots, v_s\}$ ($j = 1, 2, 3, \dots, s$), have common neighbours u and v respectively and $N_2(u) = \{u_i, v, v_j\}$ ($i = 1, 2, 3, \dots, r, j = 1, 2, 3, \dots, s$) has the neighbour v , $N_2(v) = \{u, u_i, v_j\}$ ($i = 1, 2, 3, \dots, r, j = 1, 2, 3, \dots, s$) has the neighbour u . (i.e.,) every vertex of $D_{r,s}$ lies in at least one of 2-neighbourhood of every vertex of it. Therefore every vertex of $NE_2(D_{r,s})$ is adjacent to remaining all the vertices.





Pushpalatha and Pitchaimani

Hence $NE_2(D_{r,s}) = K_{r+s+2}$.

$$\text{Thus } NE_k(D_{r,s}) = \begin{cases} K_{r+1} \cup K_{s+1} & \text{if } k = 1 \\ K_{r+s+2} & \text{if } k \geq 2 \end{cases} \quad r, s \geq 1.$$

Theorem 5.6: For a Wheel graph $W_n, n \geq 4, NE_k(W_n) \cong K_n$, for all k .

Proof: The 1 – Neighbourhood of vertices of W_n are, $N_1(v_1) = \{u, v_{n-1}, v_2\}, N_1(v_2) = \{u, v_1, v_3\}, N_1(v_3) = \{u, v_2, v_4\}, \dots, N_1(v_{n-1}) = \{u, v_{n-1}, v_1\}, N_1(u) = \{v_1, v_2, \dots, v_{n-1}\}$. Since $N_1(v_i), i = 1, 2, 3, \dots, n-1$ have common neighbour u , all v_i 's, $i = 1, 2, 3, \dots, n-1$ are adjacent to each other in $NE_1(W_n)$. Also any member of $N_1(u)$ lie in at least one of $N_1(v_i), i = 1, 2, 3, \dots, n-1$. Therefore 'u' must adjacent to all v_i 's, $i = 1, 2, 3, \dots, n-1$ in $NE_1(W_n)$. That is all the vertices of W_n are adjacent to each other in $NE_1(W_n)$.

Hence $NE_1(W_n) \cong K_n, n \geq 4$.

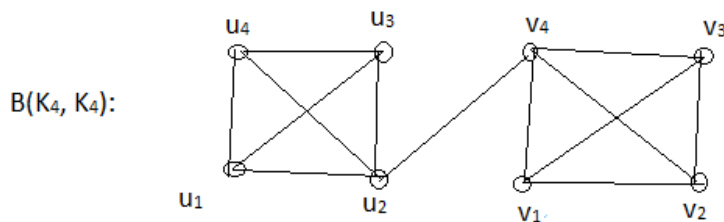
Therefore $NE_k(W_n) \cong K_n, n \geq 4$, for all k .

Barbell Graph $B(K_n, K_n)$

In [17], Dr. K. Thilagavathi & Dr. A. Sangeetha Devi introduced the concept of Barbell graph.

Definition 6.1: The **n-Barbell graph** is the simple graph obtained by connecting two vertices of a complete graph K_n by a bridge and it is denoted by $B(K_n, K_n), n \geq 3$. It has $2n$ vertices and (n^2-n+1) number of edges.

Example 6.2:



Let us find the **k-neighbourhood graph of a Barbell graph $B(K_n, K_n), n \geq 3$.**

Theorem 6.3: $NE_k(B(K_n, K_n)) \cong K_{2n}, k \geq 2$.

Proof: Let u_1, u_2, \dots, u_n and v_1, v_2, \dots, v_n are vertices of two components of K_n and K_n and let u_i and v_j be two adjacent vertices in $B(K_n, K_n)$. For $k = 1, u_1, u_2, \dots, u_n$ are adjacent to each other as each $u_i, i = 1, 2, \dots, n$ have at least one common neighbour in $NE_1(B(K_n, K_n))$. Similarly each vertex $v_i, i=1,2,\dots,n$ is adjacent to each other as they have at least one common neighbour in $NE_1(B(K_n, K_n))$ and the following adjacencies are also exist. u_i is adjacent to $v_k, k=1,2,\dots,j-1,j+1,\dots,n$, as they have v_j as common neighbour. Also v_j is adjacent to $u_k, k=1,2,\dots,i-1,i+1,\dots,n$ as they have u_i as common 1-neighbour.

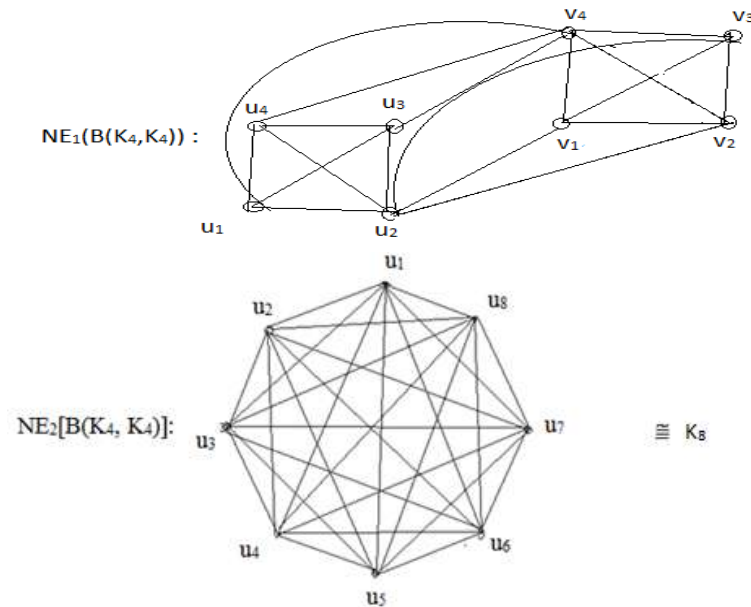
For $k = 2, NE_k(B(K_n, K_n)) \cong K_{2n}$.





Pushpalatha and Pitchaimani

Example 6.4:



RESULTS AND THEOREMS ON k-NEIGHBOURHOOD GRAPH OF A GRAPH

Theorem 7.1: $G = \overline{K_n}$ iff $NE_k(G) = G$, for all k .

Proof: Let $G = \overline{K_n}$.

The k -neighbourhood of all the isolated vertex of $\overline{K_n}$ is an empty set. Hence $NE_k(G) = G$.

Converse: Suppose $NE_k(G) = G$

To prove that $G = \overline{K_n}$

Let us assume that $e = uv$, where $u, v \in V(G)$. Then the neighbourhood of u and neighbourhood of v do not have a common neighbour, for all $u \& v \in V(G)$. This is possible only when each vertex of G is an isolated vertex. Hence $G = \overline{K_n}$.

Theorem 7.2:[2] A connected graph G is Eulerian iff every vertex of G is of even degree.

Theorem 7.3: If G is Eulerian, then $NE_k(G)$ need not be an Eulerian, if $k < \left\lceil \frac{diam(G)}{2} \right\rceil + 1$

Observation 7.4: A graph G is r -regular iff $NE_k(G)$ need not be a r -regular graph.

Result 7.5: If G is nK_2 , then $NE_1(nK_2) = (2n) K_1, (n \geq 1)$

Proof: Let $u_1, u_2; u_3, u_4; \dots; u_{n-1}, u_n$ be the (pair of) vertices of nK_2 respectively ($n \geq 1$).

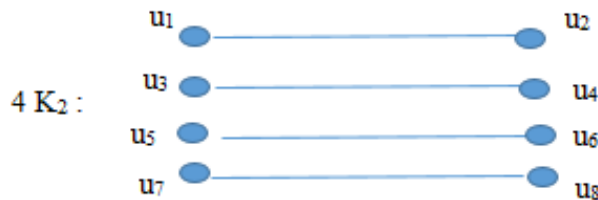
Then $N_1(u_1) = u_2$ and $N_1(u_2) = u_1$, $N_1(u_3) = u_4$ and $N_1(u_4) = u_3$, and so on. No two vertices of nK_2 have common neighbour. Therefore the vertices of $NE_1(nK_2)$, $u_1, u_2, u_3, \dots, u_n$ are not adjacent to each other. Hence $NE_1(nK_2) = (2n)K_1$





Pushpalatha and Pitchaimani

Example 7.6: Consider $4K_2$



$N_1(u_1) = \{u_2\}, N_1(u_2) = \{u_1\}, N_1(u_3) = \{u_4\}, N_1(u_4) = \{u_3\}, N_1(u_5) = \{u_6\}, N_1(u_6) = \{u_5\}, N_1(u_7) = \{u_8\}, N_1(u_8) = \{u_7\}$.
Therefore

$$NE_1(4K_2) : \overset{\circ}{u_1} \quad \overset{\circ}{u_2} \quad \overset{\circ}{u_3} \quad \overset{\circ}{u_4} \quad \overset{\circ}{u_5} \quad \overset{\circ}{u_6} \quad \overset{\circ}{u_7} \quad \overset{\circ}{u_8}$$

Hence $NE_1(nK_2) = (2n)K_1, n \geq 1$.

Result 7.7: If G is a disconnected graph, $NE_k(G), k \geq 1$ is also a disconnected graph.

Example 7.8: If $G = K_3 \cup K_2$ then $NE_1(G) = K_3 \cup 2K_2$.

Theorem 7.9: If G is a disconnected graph containing exactly two components G_1, G_2 in which each is a complete graph of size m , then $NE_k(G) = K_m \cup K_m, k \geq 1$.

Proof: Let $\{u_1, u_2, \dots, u_m\}$ and $\{v_1, v_2, \dots, v_m\}$ be the vertices of components G_1 and G_2 respectively of the graph G . Clearly $NE_1(G_1) = NE_1(G_2) = K_m$, when $k = 1$.
Therefore $NE_1(G) = NE_1(G_1) \cup NE_1(G_2) = K_m \cup K_m$.
Hence $NE_k(G) = NE_k(G_1) \cup NE_k(G_2) = K_m \cup K_m, k \geq 1$.

CONCLUSION

We conclude this section as follows;

- (i) a study of new graphs has been initiated.
- (ii) There is a good scope for further research on these graphs.
- (iii) Work on bounds, NP-completeness and characterization theorems are in progress.
- (iv) A study of this graph with some special graphs and different types of parameters are also possible
- (v) In future the combination of neighbourhood and distance concept may develop finding applicable in various fields.

REFERENCES

1. B.D. Acharya, M.N. Vartak, Open neighbourhood graphs, Technical report, Research report 7, Indian Institute of Technology, Department of Mathematics, Bombay, 1973.
2. F. Harary, Graph Theory, Addison Wesley, Reading Mass (1972).
3. S.T. Hedetniemi and R.C. Laskar, Bibliography on domination in graphs and some basic definitions of domination parameters, Discrete Math.86, (1990), pp 257-277.
4. Terasa W. Haynes, Stephen T. Hedetniemi, Peter J. Slater, Fundamentals of Domination in Graphs, Marcel Dekker Inc. (1998).



**Pushpalatha and Pitchaimani**

5. G. Jothilakshmi, A.P. Pushpalatha, S. Nasreen banu and P. Saranya, "Neighbourhood graph of a graph", JAC journal of Science, Humanities and Management, Volume 2, No.1, 2014, PP: 36-44.
6. V.R. Kulli, The neighbourhood graph of a graph, International Journal of fuzzy mathematical Archive, Vol.8, No. 2, 2015, Pp: 93-99.
7. A.P. Pushpalatha, Study of graphs with respect to the independence parameter and Forcing domination, PhD thesis, Madurai Kamaraj University, 2011.
8. A. P. Pushpalatha, G. Jothilakshmi, S. Suganthi, V. Swaminathan, and R. Sundareswaran. β_0 - graph of a graph, International Journal of Computing Technology, Vol. No. 3, March 2011.
9. A.P. Pushpalatha, G. Jothilakshmi and S. Praveena, ω -graph of a graph, Proceedings of National Conference in Recent Trends in Mathematics(NCRTM-2012), Mannar Thirumalai Nayakar College, Madurai, March 16-17, 2012.
10. A.P. Pushpalatha, G. Jothilakshmi and S. Nasreen banu, "Neighbourhood graph of strong product of some graphs", Taga journal, Volume 14, ISSN: 1748-0345, 2018, page No. 2912-2917.
11. A.P. Pushpalatha, G. Jothilakshmi and S. Nasreen banu, "Neighbourhood graph of Cartesian product for some graphs", "Mathematical Sciences International research Journal, Volume 7, Special issue 2, 2018, Pp No: 186-193.
12. E. Sampathkumar and Prabha S. Neeralagi, The neighbourhood number of a graph, Indian Journal of pure and applied Mathematics 16(2) : 126-132, February 1985.
13. N. Sridharan and K. Subramanian, γ - graph of a graph, Bulletin of Kerala Mathematics Association, Volume.5.1. (2008, June), 17-34.
14. O. Ore, Theory of Graphs, Amer.Math.Soc. Colloq. Publication, 38, Providence, (1962).
15. Robert C. Brigham, Robert D. Dutton, On neighbourhood graphs, Journal of Combinatorics information and system sciences, Vol 12, Nos. 1-2, pp 75-85 (1987).
16. D. West, Introduction to Graph Theory, II edition, Prentice Hall, Upper Saddle River, NJ, 2001.
17. K. Thilagavathi and A. Sangeetha Devi, Harmonious coloring of $C[B(K_n, K_n)]$ and $C[F_{2,k}]$, Proceedings of international conference on mathematical and computer Science. (ICMCS 2009) Department of mathematics Loyola College, Chennai. Page no. 50-52.
18. Terasa W. Haynes, Stephen T. Hedetniemi, Peter J. Slater, Domination in Graphs, Advanced topics, Marcel Dekker Inc. (1998).





Tourist Perception of the Impact of the Covid-19 Pandemic on Rajasthan Tourism before and after

Thaya Madhavi^{1*} Shivani Verma² and Sooraj. M³

¹Associate Professor, Department of Management Studies, Vivekananda Global University, Jaipur-303012, Rajasthan, India.

²MBA Scholar, School of Business and Management, Jaipur National University, Jaipur, Rajasthan, India.

³School of Business and Management, Jaipur National University, Jaipur, Rajasthan, India.

Received: 30 Jan 2023

Revised: 15 Apr 2023

Accepted: 02 May 2023

*Address for Correspondence

Thaya Madhavi

Associate Professor,
Department of Management Studies,
Vivekananda Global University,
Jaipur-303012, Rajasthan, India.
E. Mail: madhavimbabit@gmail.com



This is an Open Access Journal / article distributed under the terms of the **Creative Commons Attribution License** (CC BY-NC-ND 3.0) which permits unrestricted use, distribution, and reproduction in any medium, provided the original work is properly cited. All rights reserved.

ABSTRACT

Tourism awakens the people to strengthen the bondage of friendship, adventure and alertness among the tourists and strengthen their domestic contacts from state to state and country to country as well. Tourism is a fascinating journey which eradicates the border between two or more places and through this border between different states. With this, social, cultural and economic values of a country will raise and expand. Due to devastating scenario of Covid -19, the tourism industry has come to a grinding halt. This paper will discuss about the impact of Covid - 19 on tourism industry in Rajasthan and also draw the perception of tourists travelling in Rajasthan during Covid-19 Pandemic. It aims at defining the sustainable tourism. It also discusses about the post pandemic condition of Tourism industry in Rajasthan. The results of this study will contribute to a deeper understanding of the post-pandemic decisions and circumstances of tourists entering India.

Keywords: Tourism, Rajasthan, Perception of tourists, Covid-19, Sustainable, Post Covid.

INTRODUCTION

Tourism is not only an experience gained by the tourists but also made mandatory by imposing right schedule to make a virtual journey. Tourism is that head of a tail through which different cultural, social and economic values are witnessed as a whole. Tourism industry is an industry that brings in total understanding of the nation or a country in real terms. In light of this, studies on COVID-19 need to shift their focus from early national and industrial

56974



**Madhavi Thaya et al.,**

views to the rehabilitation of travellers' travel mentalities [1, 2, 3]. Tourism in Rajasthan would mean that tourists represent varied cultural heritages, crafts, cuisines and villages. Rajasthan gives a unique experiential tourism and alternate to the tourism to offer a break from a city life and make them know the roots of India. It has a rich tradition of handicrafts, festivals and cuisines. It promotes great marketing facilities in Jaipur, Udaipur, Jodhpur, Bikaner etc. It is not only limited to the heritage havelis but also extended to adventurous sports such as, Jeep safaris, Dirt racing, Quad biking etc. which targets the millennial and youth.

Covid-19 is a devastating pandemic whereby citizens have been forced to adopt a renewed life for their survival and livelihood. Wearing masks and maintaining social distance from each other is the order of the day as per government instructions. It is almost nine months since the people are made to work from home (Online) sanitization following all precautionary measures and taking a follow up action on safety measures the government is imposing. Citizens must understand their role and responsibility towards the nation. Researchers have discovered that travellers may defend themselves by forgoing travel or exercising caution while on their route if they consider the risk of travel due to an outbreak to be a major hazard [4]. Sustainable tourism is the order of the day as tourism industry is now more focused on preventive measures starting from entry point of the gate to the exit sanitizing, delivering hygienic services and checking the body temperatures of the people. Tourists wearing masks on their faces face little barriers while entering the borders of Rajasthan but, as required health to be treated under first priority. Tourist spots have now been reopened for the tourists in Rajasthan such as Bapu Bazaar, Amber Fort, Moti Dungri temple in Jaipur, Sawariya Seth temple in Chittorgarh, Geparnath & KST in Kota and many more. The people from various corners of the country and abroad shall be walking in and enjoy the richness of the tourism in Rajasthan, in particular.

Tourism in Rajasthan

Covid devastated normal lives of people in the month of December 2019 [5]. People somehow understood it, feared from it & took action to fight by taking safety measures with the great help of corona warriors. The foreign tourists number got reduced by -8.48% also the Indian tourists got reduced by 3.95% in the year 2019 (Fig 1). As soon as news started buzzing all around the world by March 2020, the number of foreign tourists & Indian Tourists declined by -72.19% & -71.05% respectively. There was no Movement of travelling in month April & May. From the graph we can observe that there was constant increase in the total number of visitors from 2011 but in 2020 there is a steep fall of visitors due to Covid-19 pandemic.

LITERATURE REVIEW

Covid was another pandemic that spreads rapidly through contact with a tainted individual when they sniffle [6]. The flare up of Covid – 19 was China at that point spreading to worldwide that adds to enormous number of passing's (40,598 passing's first April 2020). To stop the spreading of this pandemic, numerous nations executed lockdown strategy to halt the chain of contamination for this new sickness. The author was of opinion that lockdown strategy has disturbed the life of billions and at the same time makes financial breakdown situation. In their article [7] have studied that in pandemic situation the lockdown strategy has destroyed the tourism industry across the country. Due to Pandemic Situation employment crisis has been created in front of 38 million people associated with the industry. Even before the lockdown many airlines and Travel companies had sent more than 35percent of the employees on leave without salary. The tourism industry had suffered a lot due to this. In their article [8] have studied the Covid – 19 pandemic situation that has affected people's life in every aspect. They gave an insight that India stands in third place (33.1 lacks) of Covid cases after US and Brazil. The global economy was affected very badly with 5.2 percent in swing in global GDP and tourism industry is badly affected that has lost almost 'five to seven years' worth of growth. Studies in the sociology discipline have concentrated on the viewpoints of stakeholders like the government and relevant ministries and institutional elements, according to prior literature on the risk perception of infectious diseases [9, 10]. For getting back travel and tourism on track government has opened few states of tourists from 2nd June 2020 with new guidelines and strict protocols. In their article [11] have studied the status of Covid - 19 in Rajasthan and found the effect of the preventive measures which were taken by the



**Madhavi Thaya et al.,**

Government for tourists or people. They found that in Rajasthan there were around 7351 laboratory confirmed cases including 4061 recovered cases and 166 deaths. Although patients of all ages were affected with these disease but majority of them are in age group of 16 – 60 years. In these positive cases male predominance was also observed with M.F ratio 2.11. They also found that in Rajasthan, three districts are mostly affected by Covid – 19 in pandemic situation. The assessment of the impact of Covid – 19 pandemic in the tourism and hospitality industry which has led the global panic due to present scenario was studied by [12]. She found that present work is to analyze the future with few measures and fast recovery and regain of the tourism industry for the Indian economy, employment and business. Tourism generates various cultural, economic and social values and it is certain that tourism activity will recover but it depends on the professionals in acquiring the capacity to align themselves with this new imagination of the world transmit values of security, authenticity, trust and respect for life and planet was studied by [13]. They discussed about the current scenario in tourism industry, economic effect and scenario for economic recovery, impact of Covid – 19 on Rajasthan tourism and what the future holds.

The novel contributions of the paper are summarized as:

- The Perception of Tourists who visit Rajasthan during and after Pandemic is discussed in this study.
- The proposed Study is evaluated for outage Sustainable methods to attract tourists during Pandemic.
- The study is further evaluated in terms of the tourists view on Government measures during Covid – 19.

RESEARCH METHODOLOGY

Objectives

1. To identify the perception of Tourists regarding tourism in the State of Rajasthan.
2. To understand the tourists attitude towards Covid precautions at the time of travel
3. To assess the tourists view on Government measures during Covid 19
4. To find the impact of covid-19 on tourism industry

Hypothesis

H01: There is no significant difference in the perception of tourists in Rajasthan as regards to their demography.

H02: There is no significant difference in the perception of tourists in Rajasthan as regards to the Covid precautions to be followed at the time of travel

H03: There is no significant difference regarding tourist's perception on Government safety measures in Rajasthan during Covid 19 pandemic

RESEARCH METHODOLOGY

The present research paper is empirical. The primary data was collected through questionnaire and secondary data through journals, articles, newspapers, reports, books, and web contents. The sample size of tourists is 100. The sample consisted of both foreign and domestic tourists. Convenient sampling is the sampling technique used. The data was analyzed through SPSS version 21 software. The Cronbach's Alpha value for the eight items was 0.707 which is considered as reliable and has high internal consistency. H01 There is no significant difference in the perception of tourists in Rajasthan as regards to their demography.

The first objective is aligned with the hypothesis.

t Test

An independent sample t-test (Table 1) was conducted to examine gender differences in perception of tourists regarding tourism in Rajasthan during Covid 19 pandemic. Table 1 shows that p value is less than 0.05 for the first two question regarding tourists experience and more than 0.05 for visiting again. The assumption of homogeneity of variances was tested and satisfied via Leven's F test $F= 1.263$ $p= 0.264$, $F=14.096$, $p = 0.000$ and $F= 0.001$, $p = 0.977$. There was significant difference in mean scores of both male and female tourists regarding perception of tourists in Rajasthan $t(100) = -4.765$, $p = 0.000$, $t(100) = 4.217$, $p = 0.000$ and $t(100) = 0.000$, $p = 1.000$.



**Madhavi Thaya et al.,****ANOVA test**

Fig. 2, reveals that $p < 0.005$ for the experiences they faced during visit of Rajasthan, since p is less than 0.005 the null hypothesis is not accepted at five percent level of significance. There was significant difference in the mean scores of factors regarding perception of tourists of different age groups regarding Rajasthan tourism during Covid 19 pandemic, $F(4, 95) = 7.628$, $p = 0.000$ and $F(4, 95) = 3.771$, $p = 0.007$ regarding their experiences and $F(4, 95) = 1.468$, $p = 0.218$ regarding revisiting where p value is not significant. There was significant difference in the mean scores of factors regarding perception of tourists of different occupations regarding Rajasthan tourism during Covid 19 pandemic (Fig 3), $F(4, 95) = 4.796$, $p = 0.010$ and $F(4, 95) = 6.873$, $p = 0.002$ regarding their experiences and $F(4, 95) = 0.940$, $p = 0.394$ regarding revisiting where p value is not significant.

Regarding the perception of tourists that they disliked mostly from their last travel experience in Rajasthan was 13% of male tourists disliked putting mask and sanitization whereas 28% of female tourists disliked about the crowded shopping places. 11% of males appreciated about the hospitality which is more focused on safety measures, safe food services and work during journey also, whereas female tourists appreciated the hospitality which is more focused on sanitization and safety measures. All the tourists were eager to visit Rajasthan once again after the Pandemic. The Tables 1, 2 shows that there is a significant difference regarding the perception of tourists as regards to the demography hence the H_{01} is rejected. H_{02} There is no significant difference in the perception of tourists in Rajasthan as regards to the Covid precautions to be followed at the time of travel. The second objective is aligned with the hypothesis An independent sample t-test was conducted to examine gender differences in perception of tourists regarding Covid precautions at the time of travel in Rajasthan during Covid 19 pandemic. Table 2 shows that p value is less than 0.05 regarding source used to book tickets and more than 0.05 for Challenging while travelling. The assumption of homogeneity of variances was tested and satisfied via Leven's F test $F = 9.082$ $p = 0.00$ and $F = 4.568$, $p = 0.035$. There was significant difference in mean scores of both male and female tourists regarding perception of tourists in Rajasthan $t(100) = 2.314$, $p = 0.024$ and there was no significant difference regarding most challenging during travelling $t(100) = 0.114$ $p = 1.909$.

Table 3, reveals that $p < 0.005$ for the perception of tourists regarding Covid precautions, since p is less than 0.005 the null hypothesis is not accepted at five percent level of significance. There was significant difference in the mean scores of factors regarding perception of tourists of different age groups regarding Covid precautions in Rajasthan during Covid 19 pandemic, $F(4, 95) = 0.860$, $p = 0.491$ and $F(4, 95) = 2.707$, $p = 0.0035$. Table 4, reveals that there was significant difference in the mean scores of factors regarding perception of tourists regarding Covid precautions of different occupations in Rajasthan during Covid 19 pandemic, $F(4, 95) = 10.040$, $p = 0.000$ and $F(4, 95) = 3.678$, $p = 0.029$. It was observed that 64% of tourists preferred to book tickets through online, 43% of tourists felt challenging to put masks all the time and 78% tourists prefer to stay in hotels which are hygiene with regular sanitization. The tables 3, 4 shows that there is significant difference regarding precautionary measures taken by the tourists during Covid regarding booking hotels as well as sanitization hence H_{02} is rejected. H_{03} There is no significant difference regarding tourist's perception on Government safety measures in Rajasthan during Covid 19 pandemic. The third objective is aligned with the hypothesis

An independent sample t-test was conducted to examine gender differences in perception of tourists on Rajasthan Government measures during Covid 19 pandemic. Table 5 shows that p value is more than 0.05 for the first and third questions and more than 0.05 for second question. The assumption of homogeneity of variances was tested and satisfied via Leven's F test $F = 3.210$ $p = 0.076$, $F = 2.366$, $p = 0.127$ and $F = 0.049$, $p = 0.824$. There was significant difference in mean scores of both male and female tourists regarding perception of Government measures $t(100) = 1.110$, $p = 0.270$, $t(100) = 2.637$, $p = 0.010$ and $t(100) = 1.074$, $p = 0.285$.

ANOVA test

Fig. 4, reveals there was no significant difference in the mean scores of factors regarding perception of tourists of different age groups regarding Rajasthan Government safety measures taken during Covid 19 pandemic, $F(4, 95) = 0.435$, $p = 0.783$, regarding citizens following guidelines, $F(4, 95) = 1.468$, $p = 0.218$ regarding safety measures at

56977



**Madhavi Thaya et al.,**

tourist sites and $F(4, 95) = 0.946$, $p = 0.441$ regarding satisfaction of tourists where p value is not significant. Fig 5, reveals that there was significant difference in the mean scores of factors regarding perception of tourists of different occupations regarding Rajasthan Government safety measures taken during Covid 19 pandemic, $F(4, 95) = 8.259$, $p = 0.000$ regarding citizens following guidelines $F(4, 95) = 4.416$, $p = 0.015$ regarding safety measures at tourist sites and $F(4, 95) = 7.118$, $p = 0.001$ regarding satisfaction of tourists, where p value is significant. It was observed that 39% had neutral opinion regarding citizens following guidelines during Covid pandemic, 30% opined that proper safety measures are taking place properly at the places they visited and 34% were satisfied with the government precautionary measures. The Figures 4 and 5 shows that there is no significant difference regarding Rajasthan Government measures taken during Covid pandemic hence H_0 is accepted.

RESULTS AND DISCUSSION

Distribution sample is gender based wherein 38% of tourists are male and 62% female. Samples are also distributed according to age group wherein below 20 years of age accounted for 7%, between 20-30 years 71%, between 30-40 years 12%, and 40 to 50 years is 4% and above 50 years is 6%. Distribution of the sample as per occupation shows homemakers/students is 49%, employees is 48% and retired people is 3% [14]. As a part and parcel of the data collection the tourists have been asked certain open ended questions such as favourite places that tourists would like to visit, things liked most in Rajasthan, number of times visited the tourists places in Rajasthan. It was noticed that 40% of the tourists told that their favourite place is Kota. 13% of male and 19% of female tourists liked Jaipur, 1% of male liked to visit Udaipur, 7% of male and 15% of female liked to visit Ajmer and 1% of male and 4% of female tourists liked to visit Jodhpur. It was observed that among male tourists 7% liked handicrafts, 6% camel ride, 18% forts, 1% museum and 6% heritage about Rajasthan. Whereas, it was observed that among female tourists 15% liked handicrafts, 3% cuisines, 20% forts and 2% heritage about Rajasthan. Most of the tourists said that they have visited the place for the first time or less than three times due to pandemic.

The tourist's attitude has also changed as of the changing situations during pandemic [15]. When the tourists were asked on what basis they will select the hotel 58% of tourists preferred hygiene hotels, 32% preferred location, 7% preferred food services and 3% preferred interior. As per the current scenario 50% of tourists prefer to carry travel kit which includes sanitizer, mask, Gloves and soap, 32% prefer to carry sanitizer and mask, 17% prefer to carry sanitizer, soap, mask and PPE kit. In the prevailing situation of Covid 19 the sustainable tourism is given priority. During the pandemic period the general attitude of tourists has changed. Tourists are avoiding crowded places and are giving more priority to personal sanitation and hygiene condition [16]. The pandemic has taught that they cannot do business freely and making plans to keep focus on sustainable tourism. The hotels hither to have also to follow precautionary measures suggested by Government and adhere to Covid 19 norms which promote revival of tourism industry gradually [17]. Restaurants are offering take away orders to attract the customers. It is challenging to adopt a sustainable tourism model in tourist cities of Rajasthan to ease pressure on cities infrastructure and to provide qualitative tourism services. Some of the urban challenges faced by the heritage city Jaipur are garbage, traffic jams, dust, open urination, broken footpaths, damaged roads, stray cattle etc. In such situations for better sustenance initiatives by startups could promote qualitative tourism which will provide better chances for survival. Some of the Standard Operating procedures to be followed by hotels are to make sure that they follow hygienic conditions and ensure availability of sanitizers, non-contact thermometers, masks, gloves etc. Provide adequate isolation facilities for any tourist or staff affected by virus and also make it compulsory for staff and tourists to download the Aarogya Setu mobile app. The tourists also should provide their details, ID and self-declaration form in the reception of the hotel they stay. A rapid response team who can manage incidents effectively must be set up. The tourists also should be requested by the hotel staff to stay indoors and must observe social distancing to avoid contact [18].

In Rajasthan restaurants are offering take away food order to attract tourist's customers. Some of the challenges being faced by the heritage city like Jaipur are accumulation of garbage, often occurring traffic jam, open urination



**Madhavi Thaya et al.,**

by pedestrians, damaged foot path and roads, gathering of stray cattle in the streets. In such a situation sustainable initiatives would however help promotion of qualitative tourism [19]. Some of the standard operating procedures should be dictated to the tourist hotels so that they can follow hygienic conditions and make available sanitizers, masks, gloves and other necessities required by tourists from time to time [20]. The tourist should provide details of their selves and sign the declaration form during their entry in the reception of the hotel. During Covid 19 pandemic period the hotel staff should advice the customers to stay indoors and observe social distance and avoid physical contact. Rajasthan is one of the rich accredited tourist centres in India. It has vibrant land scape and royal heritage with historic forts, palaces and age old temples and finally famous Thar Desert. Due to Covid 19 pandemic the tourist inflow has come down deeply. Consequently, the cab drivers lost their earnings. In Rajasthan camel rides are the most attractive part of tourism that has been affected badly. The impact of Covid 19 on local folk musician and singer who entertain tourists has also affected badly. It has been estimated that due to Covid 19 impact the local business has lost its earnings by 50,000 crores during the last one year. Most of the people employed in restaurants, hotel folk artists, guides, handicraft makers, and camel owners have lost their jobs due to Covid 19 pandemic affect.

Post Covid Affect

The footfall of tourists in the state after Covid pandemic is the highest. It has also been treated as golden week in the tourism sector of Raj celebrating Christmas- New Year week and the hotels and resorts have been packed with visitors/ tourists making hospitality sector earn fabulous revenues overcoming the revenue losses last suffered during Covid 19 [21]. The Covid induced restrictions are listed and the businesses are back on track as said by people associated with tourism and hotel industry. The flow of domestic travellers is more than foreign travellers visiting some of the cities such as Jaipur, Udaipur, Jodhpur and Jaisalmer and also national parks of historical nature [22]. In Jaipur alone according to official sources, around 2.5 lakh tourists visited in a period of six days in the month of December, 2022. It has also been informed that as many as 11786 tourists visited Amber Fort and authorities earned a revenue income of thirteen lakhs so that footfall has gone high in a weeks' time as informed by officials by Archaeological Department with a large number of tourists inflow visiting walled city of Jaipur, its narrow streets are jam packed with people and vehicles. The areas having several market places, the Hawa Mahal area and Jaipur city palace areas witnessed crowds of people and traffic congestions is felt often even on normal days. Added to that on festival days with tourists inflow the situation gets more worsened. The city of lakes Udaipur is another tourist centre having high tourist footfall. In November alone more than 1.8 lakh tourists visited the city which is the record high in 12 years as stated by an official in tourism department. During the days festive New Year Udaipur witnessed mass gathering on weekends. The domestic tourist inflow is very high on these two days as informed by Deputy Director Regional tourism Office Udaipur. To obviate the heavy tourist inflow the visiting time has been extended by two hours as informed by an officer by tourism department. Night tourism is also planned in Udaipur. Events such as Sherpa meeting of G20 countries gave a boost to the city. On these days hotels, resorts and restaurants in Udaipur are packed with tourists often crowds pulling is also seen as if in temples. It has good business earnings with heavy revenues. Apart from the above tourist sites such as Pushkar and Ranthambore are often overcrowded with tourists after restrictions are lifted imposed during Covid 19 pandemic.

India should, first and foremost, resume responsible travel as many other nations open up. It is important to approach this in phases while keeping in mind thorough travel and lodging requirements. Travellers must be fully immunised to travel internationally because it has been noted that most nations have their citizens immunised at various stages. The necessity of launching rules becomes more important going forward [23]. The tourist is assured that his trip and stay will be at minimal danger levels by launching and adhering to protection regulations. The post-pandemic period will see a change in destination demand as well as the emergence of newer travel arrangements, such as closer and shorter vacations, the requirement for safe lodging, self-guided or self-drive travel campaigns, etc. Customized travel will become a more popular choice among tourists in the post-Covid era as more people will favour private travel, boutique hotels with a specific private dining menu, and avoid crowds for social distancing standards [24]. In order to arouse demand in categories that may have gone undetected in the past, tourism businesses must reorganise their current practises.



**Madhavi Thaya et al.,**

Recovery in a justifiable manner is impossible without the coordination of all the agencies involved; tourism operators, hospitality partners, local travel agencies, and local, state, and federal governments must work together to ensure a uniform evolution of the tourism sector into a post-pandemic phase. There is little doubt that the tourism sector is moving toward a "new normal" and it is obvious that the tourism sector is moving towards a "new normal," and steps to operationalize the same through more permission to the traveller and offering customised travel involvements may be the key to quicker and more reasonable retrieval. The tourist sector also has to take notice of and support newer specialty tourism opportunities and promote previously underdeveloped niches like medical and wellness tourism, spiritual tourism, etc.

Finally, new digital projects that embrace artificial intelligence, data analytics, etc. could benefit the industry significantly over a long period of time. Even when international tourism returns, domestic travel still plays a significant role in the recovery of a growing number of locations, especially those with sizable domestic markets. Close-to-home travel and domestic tourism. One of the main travel trends that will continue to influence tourism in 2022, according to experts, is domestic tourism. Close-to-home travel, open-air activities, nature-based products, and rural tourism are other major trends. Setting up and upholding safety procedures helps to reassure visitors that their travel and stay will be risk-free. In the post-pandemic era, travel demand will change, and new travel formats including shorter, speedier getaways, the need for safe lodging, self-guided or self-drive travel and accommodation, etc. will emerge. Therefore, in order to increase demand in previously underserved sectors, tourist groups must reconsider their strategic plan. Despite the global health crises, affluent earners are more likely to be concerned about health and hygiene issues, while low-income peers were heavily impacted by accessibility and discounting considerations. Normalcy is still a long way off, but as tourism slowly recovers, Indians will once again have faith and confidence to start travelling. The influence of COVID-19 has changed and will continue to change how people travel, influencing both current and upcoming travel decisions [21, 23]. The COVID-19 outbreak has given way to a new normal that will incorporate new ways of living and doing business. This pertains to travel and tourism and entails identifying and promoting fresh options for the sector, such as niche tourism, nature and wellness tourism, medical tourism, and spiritual tourism. Despite the fact that these options have always existed, it is now time for the tourism sector to use this opportunity to transform by giving a possible visitor an abundance of options. With greater three-dimensional space, fewer people, and a closer proximity to the natural environment, new destinations will be given more consideration following the COVID-19 epidemic. Locations that offer benefits like private accommodations, leisure areas, encouraging preservation and sanitation measures, and special features like natural beauty, seashore, mountain charms, or wildlife charms will draw in more visitors. To establish social distance, the destinations might also have the following regulations, including limiting size. The destination marketing Organization are now increasing tourism trends and trying to help the tour operators to revamp their tourism business to near normalcy through tourism trends which are discussed below in short.

Bleisure Travel

Bleisure Travel is getting popular among tourists wherein it promotes leisure activities by the tourists. These are business leisure trips either pre planned or it would go as job related trips through which the tourists get some experiences.

Automation- Growing trend of digitalization has led the booking of tickets online making the travelling companies to handle the same cheaper and with that the customers are enjoying all the comforts it offers.

Mobile booking- It is an important trend in digitalisation process. They are valuable to the business people for the reason of personalisation and to undertake tech-empower travels.

Sustainable tourism- With the launch of Glasgow Declaration on Climate Action in the COP 26 UN Climate Change Conference the countries participated has been urged to mobilise climate action on tourism so that sustainable tourism practices and environmental initiatives will be implemented on priority for the resilience of the sector.

Active Eco tourism- It has come up for implementation among people to increase awareness to boost sustainable and thoughtful tourism. It promotes likeness for travel with direct involvement in conservation and support to the local environment as well.





Madhavi Thaya et al.,

Transformative travel- This is a new travel trend and it make difference among travellers in their life styles in group or individually. The tour operators can make use of this trend and focus on offering usual product and services to tourists.

Experience tourism- It is on the rise now days. This trend of travel promotes emotional connection with local culture and nature. It gives a chance to tourists to interact with locals and get more closer mingle with them, and study their culture and lifestyle.

Wellness Travel-This travelling looks for enrichment in their experience for the purpose of achieving empowerment or maintaining the best health and sense of wellbeing during the travel time.

Staycation - It is another trend that gained popularity during Covid 19 pandemic. In this the tourists spend holidays in one's home. A day is spent for exploring local attraction and other activities. The tourists however feel secured and safe in their holiday environment. There will be a stream of tourist visitors during the upcoming years as expected.

CONCLUSIONS

The government should realize the difficulties of tourism agencies and take appropriate steps to bring the tourism back on rise. To implement sustainable tourism at grass root level a regulatory structure should be made compulsory. Government should encourage companies practicing sustainable tourism and help them in creating best practices. More promotion regarding use of masks, sanitization of hands and maintenance of social distancing should be strictly implemented among people at tourist spots. It is observed that awareness among the tourists and the travel agents is consistently growing emphasizing sustainable travel during Covid pandemic. Sustainable tourism to be awarded priority at grass root level and encourage the best practices i.e., use of masks, sanitization and maintain some social distance even after the post Covid 19 pandemic by all the tourists visiting the tourist areas. . Future research must be conducted by collection of available data and in consideration of other influencing factors there on. The research at present is confined to Rajasthan alone and yet many more tourist centres are to be explored in future.

REFERENCES

1. Carr, A. "COVID-19, indigenous peoples and tourism: A view from New Zealand", *Tourism Geographies*, vol.22, no.3, pp.491–502, 2020.
2. Foo, L., Chin, M., Tan, K and Phuah, K. "The impact of COVID-19 on tourism industry in Malaysia", *Current Issues in Tourism*, vol. 24, no.19, pp. 2735-2739, 2020.
3. Uğur N.G and Akbıyık A. "Impacts of COVID-19 on global tourism industry: A cross-regional comparison", *Tourism Management Perspectives*, vol.36:100744. (2020). <https://doi.org/10.1016/j.tmp.2020.100744>
4. Zheng, D., Luo, Q and Ritchie, B.W. "Afraid to travel after COVID-19? Self-protection, coping and resilience against pandemic travel fear", *Tourism Management*, Vol.83, pp.104261, 2021. <https://doi.org/10.1016/j.tourman.2020.104261>.
5. Patel, P. K; Sharma, J; Kharoliwal, S and Khemariya,P. "The Effects of Novel Corona Virus (Covid-19) in the Tourism Industry in India", *International Journal of Engineering Research & Technology (IJERT)*, vol.9, no. 05, pp.780-788, 2020 .ISSN: 2278-0181
6. Gahlot, K, L. "Impact of Covid-19 on Tourism Industry Special Reference with Rajasthan Tourism", *Journal of Information and Computational Science*, vol. 10, no. 10, pp. 318-327, 2020.ISSN: 1548 – 7741.
7. Kumar, A. "Disastrous impact of Corona virus (COVID 19) on Tourism and Hospitality Industry in India", *Journal of Xi'an University of Architecture & Technology*, vol. 12, no. 5, pp. 698-712, 2020. ISSN: 1006 – 7930.
8. Rawat, N, M and Sharma, A. "Dark Tourism in Rajasthan after Covid 19: A New Trend of Tourism in India", *International Journal of Advanced Research in Commerce, Management & Social Science*, Vol. 03, No. 03, pp. 223-233, 2020. ISSN: 2581-7930.



**Madhavi Thaya et al.,**

9. Aaltola, M. "Contagious insecurity: War, SARS and global air mobility", *Contemporary Politics*, vol. 18, no.1, pp.53–70, 2012.
10. Ratten, V. "Coronavirus (covid-19) and social value co-creation", *International Journal of Sociology and Social Policy*, Vol. 42 No. 3/4, pp. 222-231, 2022. <https://doi.org/10.1108/IJSSP-06-2020-0237>.
11. Sharma, R.P., Gupta, J., Kusum, L, G., Meena, D., Aswal, P., Sharma, K.K., Singh, R., Sharma, R and Meena, D. "COVID-19 in Rajasthan: Status and Effects of Containment Measures", *International Journal of Medicine and Public Health*, vol.10, no.4, pp.202-206, 2020.
12. Shetty, P. "The Impact of COVID-19 in the Indian Tourism and Hospitality Industry: Brief Report", *Journal of Tourism & Hospitality*, vol. 10, no.455, pp.1-7, 2020.
13. Vandana, L. "Impact of Covid 19 Pandemic on Tourism", *International Journal of Creative Research Thoughts (IJCRT)*, vol. 8, no. 6, pp. 90-93, 2020. ISSN: 2320 – 2882.
14. Rana, I.A., Bhatti, S.S., Aslam, A.B., Jamshed, A., Ahmad, J and Shah, A.A. "COVID-19 risk perception and coping mechanisms: Does gender make a difference?", *International Journal of Disaster Risk Reduction*, vol.55, pp.102096, 2021
15. Das, S.S and Tiwari, A.K. "Understanding international and domestic travel intention of Indian travellers during COVID-19 using a Bayesian approach", *Tourism Recreation Research*, vol.46, no.2 pp.228–244, 2021.
16. Reisinger, Y and Crotts, J.C. "The influence of gender on travel risk perceptions, safety, and travel intentions", *Tourism Analysis*, vol.14, no.6, pp.793–807, 2009.
17. Kulshrestha, R and Seth, K. "The effect of COVID-19 on the Indian tourism industry", *Xi'an Dianzi Keji Daxue Xuebao/Journal of Xidian University*, Vol.14, No.7, pp.1068-1077. 2020. DOI: 10.37896/jxu14.7/119.
18. Pappas, N and Glyptou, K. "Accommodation decision-making during the COVID-19 pandemic: Complexity insights from Greece", *International Journal of Hospitality Management*, Vol. 93, pp.102767, 2021.
19. Madhavi, T and Mehrotra, R. "An Effective Mapping of Competencies for Sustainable Growth", *Journal of Advanced Research in Dynamical and Control Systems*, vol. 11, 07-SI, pp. 49-56, 2019.
20. Kaushal, V and Srivastava, S. "Hospitality and tourism industry amid COVID-19 pandemic: Perspectives on challenges and learnings from India", *International Journal of Hospitality Management*, vol.92, 102707. 2021. <https://doi.org/10.1016/j.ijhm.2020.102707>
21. Vijayraj, B. V and Devi, A. J. "Restoring Tourism Industry in India after Covid-19: A Case Study", *International Journal of Case Studies in Business, IT and Education (IJCSBE)*, vol.5, no. 2, pp. 284–298, 2021. <https://doi.org/10.47992/IJCSBE.2581.6942.0134>.
21. Vachhani, A. Khatri, R. "A Descriptive Study Of The Impact Of Covid-19 On Perception And Destination Choices Of Foreign Tourists In India Post-Covid-19 Lockdown", *International Journal of Creative Research Thoughts (IJCRT)*, vol.10, no.4 , pp.975-980, 2022.
22. Singla, M. "A Case Study on Socio-cultural Impacts of Tourism in the city of Jaipur, Rajasthan: India", *Journal of Business Management & Social Sciences Research*, vol. 3, no. 2, pp. 10-23, 2014.
23. Orîndaru, A., Popescu, M.-F., Alexoaei, A.P., Căeşcu, S., -C. Florescu, M.S. and Orzan, A.-O. "Tourism in a Post-COVID-19 Era: Sustainable Strategies for Industry's Recovery", *Sustainability*, vol.13, no.6781, pp.1-22, 2021.
24. <https://doi.org/10.3390/su13126781>.
25. www.statista.com/statistics/1026993/india-tourist-arrivals-in-rajasthan-by-type/ (Accessed 12 December 2022)
26. www.rajras.in/rajasthan/tourism/policy-2020/ (Accessed 11 November 2022)
27. www.hindustantimes.com/india-news/tourism-resumes-in-rajasthan-with-over-700-visitors-entry-fee-waived-for-two-weeks/story-Qj9GJoVTkXV9cZhdceeaGP_amp.html (Accessed 4 June 2022)
28. Annual-Progress-report-2020-21 (Accessed 20 January 2022)





Madhavi Thaya et al.,

Table 1: Independent sample t-test for perception of tourists and Gender

	Gender	Mean	SD	T value	P value
Travel experience you felt uncomfortable	Male	2.11	0.981	-4.765	0.000
	Female	3.05	0.948		
Travel experience you liked	Male	2.42	1.200	4.217	0.000
	Female	1.48	0.844		
Visit Rajasthan again	Male	4.50	0.726	0.000	1.000
	Female	4.50	0.784		

(Source: Primary data based on questionnaire)

Table 2: Perception of tourists regarding Covid precautions at the time of travel

	Gender	Mean	SD	T value	P value
Source used to book tickets	Male	2.37	1.422	2.314	0.024
	Female	1.73	1.217		
Challenge faced while travelling	Male	2.24	1.076	0.114	0.909
	Female	2.21	1.269		

(Source: Primary data based on questionnaire)

Table 3 Covid precautions with reference to Age

Source used to book tickets	Age				
	Sum of Squares	df	Mean Square	F	Sig.
Between Groups	6.112	4	1.528	0.860	0.491
Within Groups	168.798	95	1.777		
Total	174.910	99			
Challenge faced while travelling					
Between Groups	14.442	4	3.610	2.707	0.035
Within Groups	126.718	95	1.334		
Total	141.160	99			

(Source: Primary data based on questionnaire)

Table 4: Covid precautions with reference to occupation

Source used to book tickets	Occupation				
	Sum of Squares	df	Mean Square	F	Sig.
Between Groups	29.998	2	14.999	10.040	0.000
Within Groups	144.912	97	1.494		
Total	174.910	99			
Challenge faced while travelling					
Between Groups	131.209	97	1.353		
Within Groups	141.160	99			
Total	29.998	2	14.999	10.040	0.000

(Source: Primary data based on questionnaire)





Madhavi Thaya et al.,

Table 5: Perception of tourists on Rajasthan Government measures during Covid

	Gender	Mean	SD	T value	P value
Citizens following guidelines given by Government	Male	3.63	1.217	1.110	0.270
	Female	3.37	1.090		
Proper safety measures at the tourist sites	Male	4.00	1.013	2.637	0.010
	Female	3.39	1.192		
Satisfaction regarding precautionary measures	Male	3.63	1.051	1.074	0.285
	Female	3.39	1.136		

(Source: Primary data based on questionnaire)



Figure 1 Number of Tourists visited Rajasthan 2011-2020 (Source: Annual Report 2019-20)

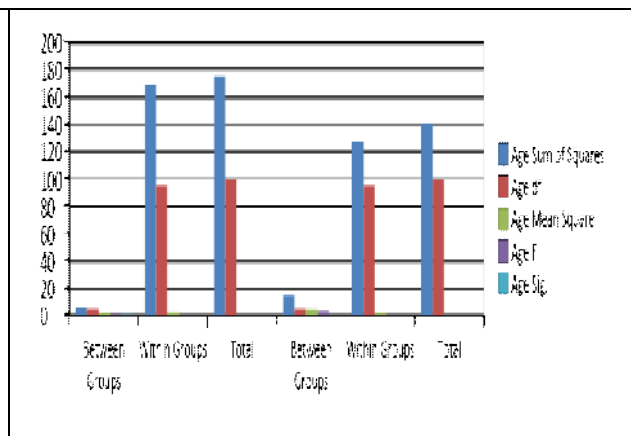


Fig 2: Perception of Tourists and Age (Source: Primary data based on questionnaire)

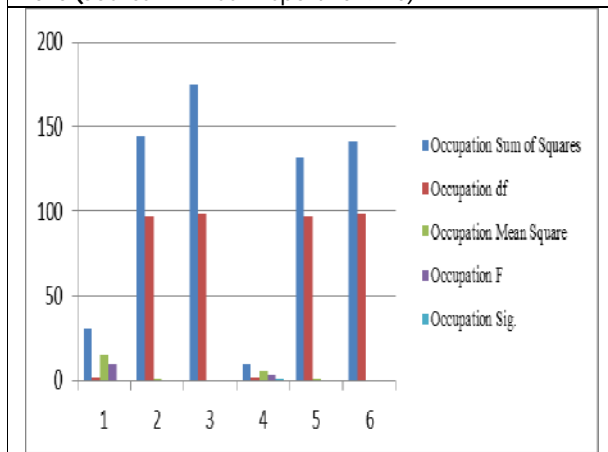


Fig 3: Perception of Tourists and Occupation (Source: Primary data based on questionnaire)

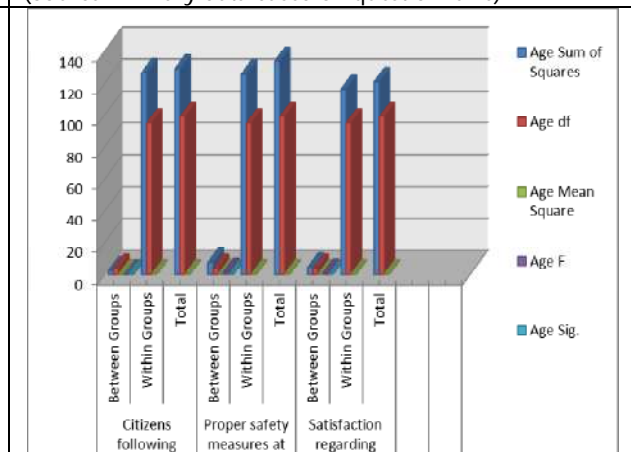


Fig 4: Perception of Tourists with reference to age on Government measures (Source: Primary data based on questionnaire)





Madhavi Thaya et al.,

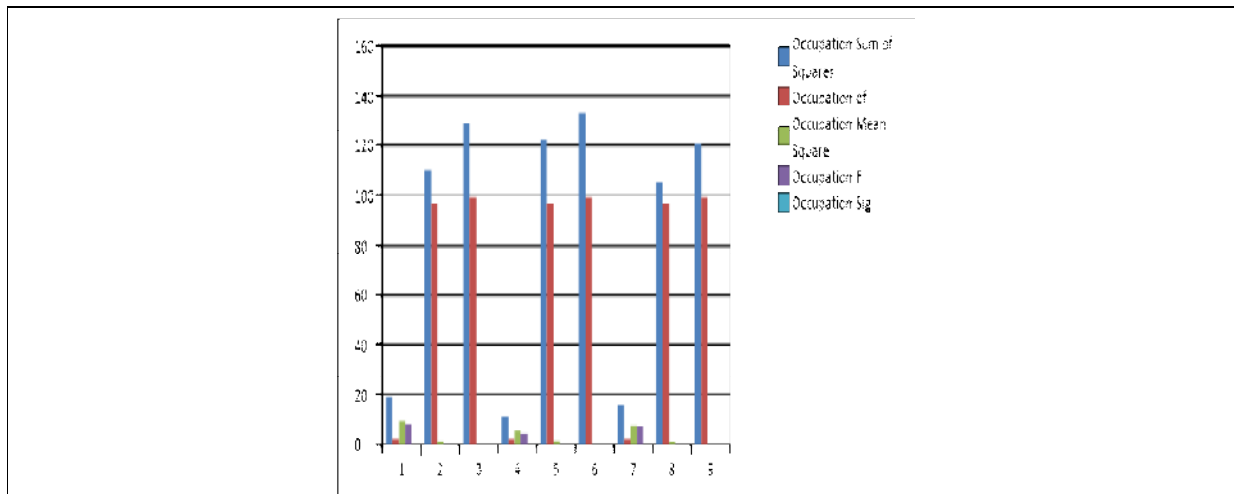


Fig 5: Perception of Tourists with reference to occupation on Government measures
(Source: Primary data based on questionnaire)





***In silico* Identification of Potential Phytocompounds from the Indian Medicinal Plants against Canine Parvovirus**

S. Shivani¹, A. Logeshwaran², A.K. Vidya³, V. Umabarathi⁴ and P. Ravikumar^{5*}

¹PG Student, Department of Biochemistry, Kongu Arts and Science College, Erode – 638 107, Tamil Nadu, India.

²Research Assistant, Iyarvi Research Center for Bioinformatics, Erode – 638 452, Tamil Nadu, India.

³Associate Professor and Head, Department of Biochemistry, Kongu Arts and Science College, Erode – 638 107, Tamil Nadu, India.

⁴Scientific Officer, Iyarvi Research Center for Bioinformatics, Erode – 638 452, Tamil Nadu, India.

⁵Senior Scientist and Head, Iyarvi Research Center for Bioinformatics, Erode – 638 452, Tamil Nadu, India.

Received: 27 Dec 2022

Revised: 23 Feb 2023

Accepted: 06 Mar 2023

***Address for Correspondence**

P. Ravikumar

Senior Scientist and Head,
Iyarvi Research Center for Bioinformatics,
Erode – 638 452, Tamil Nadu, India.
E. Mail :headircb@gmail.com



This is an Open Access Journal / article distributed under the terms of the **Creative Commons Attribution License** (CC BY-NC-ND 3.0) which permits unrestricted use, distribution, and reproduction in any medium, provided the original work is properly cited. All rights reserved.

ABSTRACT

Canine parvovirus (CPV) is a self-replicating parvovirus that causes enteritis and myocarditis in dogs. The present study was designed to find the potential phytocompounds from the Indian medicinal plants against Canine parvovirus using *in silico* studies. The 3D structure of phytocompounds was obtained using IMPPAT and PubChem database. The Lipinski rule of five for all the phytocompounds was tested using SwissADME. The sequence of the target protein was retrieved from the UniProt database and modelled using Swiss-Model. The docking studies were performed using PyRx and the results were analyzed using Discovery Studio2021. The phytocompounds N-(4-butylphenyl)-5-(ethylsulfamoyl)-2-methylbenzamide, Hispaglabridin B, Hispaglabridin A, 21alpha-Hydroxyisoglabrolide and Glabreneshowed very good binding affinity like -10.1, -9.8, -9.5, -9.5 and -9.4 Kcal/mol, respectively. Toxicity studies were done for the best-interacted phytocompounds and the results showed that the compounds had very less toxicity. The present study concludes that N-(4-butylphenyl)-5-(ethylsulfamoyl)-2-methylbenzamide, Hispaglabridin B, Hispaglabridin A, 21alpha-Hydroxyisoglabrolide and Glabrenefrom *Glycyrrhiza glabra* may have a potential effect in the treatment of infection caused by Canine parvovirus.

Keywords: Canine parvovirus, Phytocompounds, Docking, PyRx, Discovery Studio, ADMET properties.





Shivani et al.,

INTRODUCTION

One of the most important pathogenic viruses in dogs is canine parvovirus 2 (CPV-2), which causes acute haemorrhagic enteritis and myocarditis. It's an illness that's extremely contagious and often lethal. CPV-2 was initially identified in 1977, and it has since become well established as an intestinal infection in dogs all over the world, with severe morbidity (100%) and high death (up to 10%) [1,2]. The virus was given the name CPV-2 to distinguish it from a closely related canine parvovirus known as CPV-1 or minute virus of canine (MVC)[3]. In recent years, CPV-2 infections in dogs have become a global epidemic. Even in vaccinated populations, the disease has been documented in large numbers in dogs in India. The disease is very contagious and is transmitted from dog to dog through direct or indirect contact with their wastes. A number of serological and molecular diagnostic assays have been developed over the years for quick, accurate, and sensitive disease diagnosis. For the control of the disease, both inactivated and live attenuated CPV vaccines have been produced and utilised, both monovalently and in combination with vaccinations against other diseases. Vaccine failures have, nevertheless, occurred despite thorough animal vaccination [4]. Initially, enteritis and myocarditis were identified as two disease entities linked to CPV-2 infection. As a result of population immunity, the latter variety has almost vanished. Only puppies infected very close to birth, when their myocardium cells are still actively multiplying, develop parvoviral myocarditis. CPV-2 and other autonomous parvoviruses only reproduce in dividing cells[5,6,7]. In nonprotected hosts, the disease has a quick clinical course, with death occurring 2–3 days following the onset of symptoms[8,9]. It can afflict dogs of any age, although it is most frequent in pups between the ages of 6 weeks and 6 months[10]. Contact with faeces from infected dogs or contaminated surfaces is the most common way to contract the virus via the faecal-oral route. The virus primarily affects mitotically active tissues, such as lymphoid tissues, intestinal epithelium, and bone marrow, and also the heart in neonatal pups, once it enters the host [11,12].

In the Surat and Navsari districts of South Gujarat, a total of 73 samples had been received or collected. Using HA, ELISA, and PCR, 32, 33, and 35 of them were determined to be positive for CPV-2, respectively. One year later, when the fast test was included, 26/52 samples were determined to be positive in this test format. The prevalence of CPV-2 was reported to be 47.94[13] percent using PCR as the most sensitive and specific assay[14]. Anorexia, Depression, Vomiting, Profuse haemorrhagic diarrhoea, Abdominal discomfort, Cardiovascular shock, Dehydration, Pyrexia, Infection – resulting from leukopenia – or lowered white blood cell count, and destabilisation of the intestinal mucosal barrier, that enables intestinal bacteria to allow entry to systemic circulation, are all clinical signs of canine parvovirus. If myocardial injury occurs in extremely young patients, premature mortality and congestive heart failure may happen [15].

A high-throughput screening technique based on the cytopathic effect (CPE) was utilised to screen CPV inhibitors from an FDA-approved pharmacological library. 7 out of 1430 evaluated medicines were identified to have >50% CPE inhibition after two rounds of screening. Absolute PCR quantification and indirect immunofluorescence assays were used to analyse three medicines with better anti-CPV effects in F81 cells: Nitazoxanide, Closantel Sodium, and Closantel (IFA). All three medications had dose-dependent inhibitory activity[16]. The essential oil and aqueous extracts of *Mentha spicata* L. (Lamiaceae) [17] and *Isatis tinctoria* L. (Brassicaceae) [18] were found to be effective against Porcine Parvovirus (PPV). Antiviral herbs, astringent herbs, and mucosal support supplied by mucilaginous herbs may help dogs having parvoviral enteritis. When herbs are given to vomiting dogs, they must be given by enema. Canine Parvovirus proliferation was reduced *in vitro* by African plants *Bauhinia thonningii*, *Boswelliadalzielii*, *Detarium senegalensis*, and *Dichrostachys glomerata*[19]. In the present study, the Indian medicinal plants such as *Aegle marmelos*, *Aloe vera*, *Artocarpus integrifolia*, *Camellia sinensis*, *Curcuma longa*, *Cyperus rotundus*, *Euphorbia hirta*, *Glycyrrhiza glabra* [20] were taken to find the potential phytochemicals from the Indian medicinal plants for the treatment of Canine parvovirus.





MATERIALS AND METHODS

Ligand Selection

Using literature and IMPPAT database [21] around 360 phytochemical compounds were selected from the different Indian medicinal plants like *Aegle marmelos*, *Aloe vera*, *Artocarpus integrifolia*, *Camellia sinensis*, *Curcuma longa*, *Cyperus rotundus*, *Euphorbia hirta*, *Glycyrrhiza glabra* [20]. The 3D structures of these compounds were retrieved from the PubChem database [22] and using SwissADME [23] and they were subjected to test Lipinski Rule of Five. From the results, 304 compounds obeyed Lipinski Rule of Five and these compounds were taken for the study.

Target Protein Selection

The sequence of target protein Capsid protein VP2 from Canine parvovirus was taken from UniProt database [24]. It was modelled using SWISS-MODEL [25] to predict the 3D structure of target protein and the best model was taken, evaluated using SAVES online server [26] and the Ramachandran plot was taken. The modelled 3D structure of target protein Capsid protein VP2 was prepared using Discovery Studio 2021 for *in silico* docking studies.

Docking Studies

Docking studies for the target protein Capsid protein VP2 and the phytocompounds (ligands) were done using PyRx 0.8 software [27]. The target protein was further prepared for docking studies using this software. All the ligands were uploaded using Open Babel option in the PyRx 0.8. The grid was generated and the docking studies were performed using Vina wizard option in the PyRx 0.8. The values of binding affinity were saved in XL file. The results were analyzed using Discovery Studio 2021 and the 2D and 3D docked images were taken. In the results, the lowest binding affinity indicates good result.

ADMET and CYP Properties

ADMET and CYP properties were tested for all the best-interacted phytocompounds using SwissADME [23]. Lipinski, BBB (Blood - Brain Barrier), HIA (Human Intestinal Absorption), PGP (P-glycoprotein), XLogP3, TPSA (Topological Polar Surface Area), LogS, Fraction Csp3, Rotatable bonds, CYP enzyme inhibitor properties, Skin permeation and Bioavailability score were evaluated for all the best-interacted compounds.

RESULTS AND DISCUSSION

Ligand Selection

All the phytocompounds were collected from IMPPAT database and the 3D structure of ligands (phytocompounds) were retrieved from the PubChem database. Lipinski rule was checked for all the phytocompounds using SwissADME. of which, 304 compounds passed Lipinski rule of five and these compounds were taken for further study.

Target Selection

The sequence of target protein Capsid protein VP2 from Canine parvovirus was taken from the UniProt database and the UniProt ID for this target protein is P61826. Further, it was modelled using SWISS-MODEL and the best model was taken. The template for this target protein Capsid protein VP2 is 4DPV and the sequence identity is 98.29%. Moreover, the best modelled target protein was evaluated using Ramachandran plot in the SAVES online server. From the results, 87.2 % of residues were located in the most favoured regions and it confirms that the predicted model is good. The Ramachandran plot of the modelled target protein is shown in Figure 1.

Docking Studies

Docking studies were done for the phytocompounds from the different Indian medicinal plants and the target protein Capsid protein VP2 using PyRx 0.8 software to find the potential inhibitors for Canine Parvovirus. For this, 304 phytocompounds which is passed Lipinski Rule of Five were subjected to interact with the target protein. The





Shivani et al.,

results were analyzed using this software and Discovery Studio 2021 and binding affinity value was noted. In which, 10 compounds showed very binding affinity with the target protein. Further, the Synthetic drug Nitazoxanide was also taken to find the interaction with the target protein. All the docking results are shown in Table 1. The 2D and 3D interactions of phytochemicals and Synthetic drug Nitazoxanide with the target protein are shown in Figure 2-8. From the results (Table 1), among other compounds, 10 compounds showed very good results with the target protein. Of which, the phytochemical N-(4-butylphenyl)-5-(ethylsulfamoyl)-2-methylbenzamide showed very good binding affinity (-10.1 Kcal/mol) with the amino acid residue ARG 408 of the target protein Capsid protein VP2. The phytochemical Hispaglabridin B also gave very good binding affinity of -9.8 Kcal/mol with the amino acid residues ARG313, PRO289 and ILE330. The binding affinity -9.5 Kcal/mol was observed between the phytochemical Hispaglabridin A and the amino acid residues VAL316, ILE330, ILE325, PRO289, ARG313 and VAL308 of target protein. Similarly, the phytochemical 21alpha-Hydroxyisoglabrolide has binding affinity of -9.5 Kcal/mol with amino acid residues GLN365, TYR409, TRP414 and the phytochemical Glabrene has -9.4 Kcal/mol binding affinity towards the amino acid residues GLU327, PRO289, ILE325, ARG313, ARG314, VAL308 of the target protein. Besides, the binding affinity of the Synthetic drug Nitazoxanide with the target protein was -7.3 Kcal/mol and the interacted the amino acid residues were ILE330, ILE325, PRO289, PHE290, ASN292, VAL308, ARG313 and ARG314. Thus, in the results of the present study, all the phytochemicals showed very good binding affinity when compared to the Synthetic drug Nitazoxanide. Of which, the phytochemicals N-(4-butylphenyl)-5-(ethylsulfamoyl)-2-methylbenzamide, Hispaglabridin B, Hispaglabridin A, 21alpha-Hydroxyisoglabrolide and Glabrolide showed the highest binding affinity among the other phytochemicals.

Further, in the previous study, tannic acid from *Terminalia arjuna* binds to viruses with high affinity and prevents virus-host cell interaction [28]. The bark of *S. brasiliensis* shows biological activity against the influenza A virus [29]. Dengue virus serotypes 1 and 3 were resistant to the compounds astragaloside II, astragaloside III, and astragaloside IV. The selectivity index for these drugs was also found to be high, indicating that they had minimal host cell contact [30]. Aerial portions of North western Algeria *Ajuja* extract exhibited promising antiviral activity against Coxsackie virus type B-3 (CVB-3) [31]. A recent study reported that the anti-HIV and anti-herpes simplex virus properties of ajoene and allicin derived from *Allium sativum*, respectively, have been demonstrated [32]. Glycyrrhizin, derived from the *Glycyrrhiza glabra* plant, is more efficient in regulating viral replication and can be used as a prophylactic measure; it was also used to inhibit the SARS coronavirus from replicating. Gossypol, a phenolic molecule with antiviral effects against enveloped viruses such as HIV-1, HSV-2, influenza, and parainfluenza, was the main pigment in cotton seed. Casuarinin, a hydrolyzable tannin isolated from the *Terminalia arjuna* bark, has antiviral activity against herpes simplex type 2 viruses (HSV-2), and sesquiterpene cumarines isolated from the oligo-gum resin of *Ferula asafoetida* have antiviral activity against herpes simplex virus (HSV) and influenza A viruses. Similarly, in the present study, the phytochemicals N-(4-butylphenyl)-5-(ethylsulfamoyl)-2-methylbenzamide, Hispaglabridin B and Hispaglabridin A from *Glycyrrhiza glabra* showed very good binding affinity with the target protein Capsid protein VP2.

ADMET and CYP Properties

In the present study, ADMET properties were tested for the best interacted phytochemicals and Synthetic drug Nitazoxanide using SwissADME and the results were tabulated (table 2). From the results, all the best interacted phytochemicals obey Lipinski rule of five including Synthetic drug Nitazoxanide. Most of the compounds did not cross Blood – Brain Barrier (BBB) and had high Intestinal Absorption (HIA). Many phytochemicals predicted to be effluated from the CNS by P-glycoprotein. Among the 10 compounds, XLogP3 value of 5 compounds were within the range (between -0.7 and +5.0). TPSA (Topological Polar Surface Area) and Log S value of all the compounds were within the limit. And the Fraction Csp3 value of all the phytochemicals were not less than 0.25. Rotatable bonds of all the compounds were within the limit.

From the results of the Boiled Egg image of the phytochemicals (Figure 9), the compounds Shinpterocarpin (PubChem CID: 10336244), Glabrene (PubChem CID: 480774), Hispaglabridin B (PubChem CID: 15228661) and Hispaglabridin A (PubChem CID: 442774) are located in the Egg-yolk region, which means the compounds are

56989





Shivani et al.,

passively absorbed by the gastrointestinal tract and can also permeate through the blood-brain barrier. And the compounds A884715 (PubChem CID: 17751012), Glabrolide (PubChem CID: 90479675), 21alpha-Hydroxyisoglabrolide (PubChem CID: 101280184) and N-(4-butylphenyl)-5-(ethylsulfamoyl)-2-methylbenzamide (PubChem CID: 35014041) are located Egg-white region, which means they are passively absorbed by the gastrointestinal tract but cannot permeate through the blood brain barrier. Moreover, the compounds 11-Deoxoglycyrrhetic acid, Glabrolide, Hispaglabridin A and N-(4-butylphenyl)-5-(ethylsulfamoyl)-2-methylbenzamide are predicted not to be effluated from the central nervous system by the P-glycoprotein. And the compounds Shinpterocarpin, Glabrene, Hispaglabridin B, 21alpha-Hydroxyisoglabrolide and A884715 are predicted to be effluated from the central nervous system by the P-glycoprotein.

In the results of CYP properties (Table 3), the most of the compounds does not inhibit the CYP450 enzymes and does not give any adverse reactions. N-(4-butylphenyl)-5-(ethylsulfamoyl)-2-methylbenzamide, Hispaglabridin B and Glabrene inhibits all the CYP enzymes, Hispaglabridin A inhibits CYP2C19, CYP2C9 and CYP3A4. The value of log Kp (Skin Permeant) is good for all compounds and A Bioavailability Score (ABS) is good for the most of the compounds.

CONCLUSION

In the present study, the phytocompounds from different Indian medicinal plants and the target protein Capsid protein VP2 were subjected for *in silico* docking analysis to find the potential inhibitors for Canine Parvovirus. In which, 54 phytocompounds showed good results when compared to the Synthetic drug Nitazoxanide. Among them, 10 compounds showed very good binding affinity with the target protein. Of which, the phytocompounds N-(4-butylphenyl)-5-(ethylsulfamoyl)-2-methylbenzamide, Hispaglabridin B, Hispaglabridin A, 21alpha-Hydroxyisoglabrolide and Glabrene showed the highest binding affinity among the other phytocompounds. Further, toxicity studies were also done for the 10 best-interacted phytocompounds and the results showed that the compounds had very less toxicity. Hence, the present study concludes that the phytocompounds N-(4-butylphenyl)-5-(ethylsulfamoyl)-2-methylbenzamide, Hispaglabridin B, Hispaglabridin A, 21alpha-Hydroxyisoglabrolide and Glabrene from *Glycyrrhiza glabra* may give a potential effect in the treatment of infection caused by the Canine Parvovirus.

Authors' Contributions

SS and AL performed the work and wrote the manuscript. AKV and VU helped in the analysis and reviewed the work. PR designed the concept and supervised the work.

ACKNOWLEDGEMENTS

The authors would like to thank the Management and the Principal of Kongu Arts and Science College, Erode, Tamil Nadu, India for their support to complete this work successfully.

REFERENCES

1. Appel MJ, Scott FW, Carmichael LE. Isolation and immunisation studies of a canine parvo-like virus from dogs with haemorrhagic enteritis. *Vet Rec.* 1979;105(8):156-9.
2. Black JW, MA H, HS P, CS B. Parvoviral enteritis and panleukopenia in dogs. *Vet Med SmAnim Clin.*
3. Carmichael LE, Schlafer DH, Hashimoto A. Minute virus of canines (MVC, canine parvovirus type-1): pathogenicity for pups and seroprevalence estimate. *J Vet Diagn Invest.* 1994;6(2):165-74.
4. Buonavoglia C, Martella V, Pratelli A, Tempesta M, Cavalli A, Buonavoglia D, Bozzo G, Elia G, Decaro N, Carmichael L. Evidence for evolution of canine parvovirus type 2 in Italy. *J Gen Virol.* 2001;82(12):3021-5.





Shivani et al.,

5. Appel MJ, Cooper BJ, Greisen HE, Scott F, Carmichael LE. Canine viral enteritis. I. Status report on corona- and parvo-like viral enteritides. *Cornell vet.* 1979;69(3):123-33.
6. Huxtable CR, Howell JM, Robinson WR, Wilcox GE, Pass DA. Sudden death in puppies associated with a suspected viral myocarditis. *Aus Vet J.* 1979;55(1):37-8.
7. Haskins ME, Jones CL. Myocarditis of probable viral origin in pups of weaning age. *JAm Vet Med Assoc.* 1979;174(11):1204-7.
8. Carman PS, Povey RC. Pathogenesis of canine parvovirus-2 in dogs: haematology, serology and virus recovery. *Res Vet Sci.* 1985;38(2):134-40.
9. Parrish CR. 3 Pathogenesis of feline panleukopenia virus and canine parvovirus. *Bail CI Hae.* 1995;8(1):57-71.
10. Houston DM, Ribble CS, Head LL. Risk factors associated with parvovirus enteritis in dogs: 283 cases (1982-1991). *J Am Vet Med Assoc.* 1996;208(4):542-6.
11. Nelson DT, Eustis SL, McAdaragh JP, Stotz I. Lesions of spontaneous canine viral enteritis. *Vet Pathol.* 1979;16(6):680-2.
12. Hoelzer K, Shackelton LA, Holmes EC, Parrish CR. Within-host genetic diversity of endemic and emerging parvoviruses of dogs and cats. *J virol.* 2008;82(22):11096-105.
13. Sharma KK, Kalyani IH, Pandya SM, Vala JA. Diagnosis and characterization of canine parvovirus-2 affecting canines of South Gujarat, India. *Acta Vet Brno.* 2018;87(3):247-54.
14. Mochizuki M, San Gabriel MC, Nakatani H, Yoshida M, Harasawa R. Comparison of polymerase chain reaction with virus isolation and haemagglutination assays for the detection of canine parvoviruses in faecal specimens. *Res Vet Sci.* 1993;55(1):60-3.
15. Judge P. Management of the patient with canine parvovirus enteritis. *Vet Educ.* 2015;21:5-11.
16. Zhou H, Su X, Lin L, Zhang J, Qi Q, Guo F, Xu F, Yang B. Inhibitory effects of antiviral drug candidates on canine parvovirus in F81 cells. *Viruses.* 2019;11(8):742.
17. Hua Z, Baoyu Z, Guoying F. Study on inhibitive effect of Radix Astragali and Radix Isatidis in vitro on porcine parvovirus. *Journal of Northwest Sci-Tech University of Agriculture and Forestry.* 2008.
18. Han W, Cui B, Zhang H, Wang X, Xu D, Chen R. Antiviral activity of *Mentha spicata* Linn. extracts against porcine parvovirus in vitro. *Jiangsu J Agri Sci.* 2011;27(3):556-60.
19. Kudi AC, Myint SH. Antiviral activity of some Nigerian medicinal plant extracts. *Jethnopharmacol.* 1999;68(1-3):289-94.
20. Ben-Shabat S, Yarmolinsky L, Porat D, Dahan A. Antiviral effect of phytochemicals from medicinal plants: Applications and drug delivery strategies. *Drug delivtransl re.* 2020;10(2):354-67.
21. Mohanraj K, Karthikeyan BS, Vivek-Ananth RP, Chand RP, Aparna SR, Mangalapandi P, Samal A. IMPPAT: a curated database of Indian medicinal plants, phytochemistry and therapeutics. *Sci rep.* 2018;8(1):1-7.
22. PubChem (2022). <https://pubchem.ncbi.nlm.nih.gov/> Accessed on 15th May 2022.
23. Daina A, Michielin O, Zoete V. SwissADME: a free web tool to evaluate pharmacokinetics, drug-likeness and medicinal chemistry friendliness of small molecules. *Sci rep.* 2017;7(1):1-3.
24. UniProt (2022). <https://www.uniprot.org/uniprot/P61826> Accessed on 13th April 2022.
25. Waterhouse A, Bertoni M, Bienert S, Studer G, Tauriello G, Gumienny R, Heer FT, de Beer TA, Rempfer C, Bordoli L, Lepore R. SWISS-MODEL: homology modelling of protein structures and complexes. *Nucleic acids res.* 2018;46(W1):W296-303.
26. SAVES (2022). <https://saves.mbi.ucla.edu/> Accessed on 20th May 2022.
27. Trott O, Olson AJ. AutoDock Vina: improving the speed and accuracy of docking with a new scoring function, efficient optimization, and multithreading. *J comput chem.* 2010;31(2):455-61.
28. Priya S, Kumar NS, Hemalatha S. Antiviral phytochemicals target envelop protein to control Zika virus. *ComputBiol Chem.* 2018;77:402-12.
29. Sette-DE-Souza PH, Costa MJ, Araujo FA, Alencar EN, Amaral-Machado L. Two phytochemicals from *Schinopsisbrasiliensis* show promising antiviral activity with multiples targets in Influenza A virus. *An Acad Bras Cienc.* 2021;93.





Shivani et al.,

30. Indu P, Arunagirinathan N, Rameshkumar MR, Sangeetha K, Divyadarshini A, Rajarajan S. Antiviral activity of astragaloside II, astragaloside III and astragaloside IV compounds against dengue virus: computational docking and in vitro studies. *Microb Pathogenesis*. 202;152:104563.
31. Medjeldi S, Bouslama L, Benabdallah A, Essid R, Haou S, Elkahoui S. Biological activities, and phytochemicals of northwest Algeria *Ajuga reptans* (L.) extracts: Partial identification of the antibacterial fraction. *Microb pathogenesis*. 2018 Aug 1;121:173-8.
32. Perera WP, Liyanage JA, Dissanayake KG, Gunathilaka H, Weerakoon WM, Wanigasekara DN, Fernando WS, Rajapaksha RM, Liyanage RP, Perera BT. Antiviral Potential of Selected Medicinal Herbs and Their Isolated Natural Products. *BioMed Res Int*. 2021;2021.

Table 1: Interaction of phytochemicals with the target protein Capsid protein VP2

S. No.	Pub Chem (CID)	Compound Name	Plant Name	Binding Affinity (Kcal/mol)	No. of bonds	Interacting residues	Bond length (Å)
1	35014041	N-(4-butylphenyl)-5-(ethylsulfamoyl)-2-methylbenzamide	<i>Glycyrrhiza glabra</i>	-10.1	2	ARG408 ARG408	2.94 2.86
2	15228661	Hispaglabridin B	<i>Glycyrrhiza glabra</i>	-9.8	4	ARG313 ARG313 PRO289 ILE330	4.97 5.04 4.89 5.04
3	442774	Hispaglabridin A	<i>Glycyrrhiza glabra</i>	-9.5	9	VAL316 ILE330 ILE330 ILE330 ILE325 PRO289 ARG313 ARG313 VAL308	5.41 4.92 5.04 5.33 5.35 4.30 2.64 3.57 4.91
4	101280184	21alpha-Hydroxyisoglabrolide	<i>Glycyrrhiza glabra</i>	-9.5	3	GLN365 TYR409 TRP414	1.25 2.58 3.59
5	480774	Glabrene	<i>Glycyrrhiza glabra</i>	-9.4	11	GLU327 PRO289 ILE325 ARG313 ARG313 ARG313 ARG314 ARG314 ARG314 VAL308 VAL308	2.66 3.50 3.99 4.45 5.08 5.27 5.33 3.31 4.11 3.83 4.90
6	225689	beta-Amyrenol	<i>Euphorbia hirta</i>	-9.3	8	TYR451 TYR451 TYR451 PRO480 TYR338	3.51 3.82 5.10 5.28 3.74





Shivani et al.,

						TYR338 PRO356 PRO356	4.90 4.19 5.27
7	17751012	A884715	<i>Glycyrrhiza glabra</i>	-9.3	1	MET331	3.46
8	10336244	Shinpterocarpin	<i>Glycyrrhiza glabra</i>	-9.2	5	PRO289 PRO289 LEU287 ILE330 MET331	4.64 5.34 3.70 4.79 2.78
9	12305517	11-Deoxoglycyrrhetic acid	<i>Glycyrrhiza glabra</i>	-9.2	2	ARG332 THR281	2.22 2.63
10	90479675	Glabrolide	<i>Glycyrrhiza glabra</i>	-9.1	1	ARG408	2.29
Synthetic Drug							
11	41684	Nitazoxanide	—	-7.3	10	ILE330 ILE325 PRO289 PHE290 ASN292 VAL308 ARG313 ARG314 ARG314 ARG314	4.84 3.70 4.15 2.92 2.01 4.86 5.43 2.77 2.75 4.91

Table 2: ADMET Properties of Phytocompounds

S. No.	PubChem (CID)	Compound Name	Lipinski	BBB	HIA	PGP-	XLOGP3	TPSA (Å)	Log S (ESOL)	Fraction Csp3	Rotatable Bonds
1	35014041	N-(4-butylphenyl)-5-(ethylsulfamoyl)-2-methylbenzamide	Yes	No	High	Yes	4.33	83.65	-4.64	0.35	9
2	15228661	Hispaglabridin B	Yes	Yes	High	No	5.17	47.92	-5.76	0.36	1
3	442774	Hispaglabridin A	Yes	Yes	High	Yes	5.82	58.92	-6.05	0.36	3
4	101280184	21alpha-Hydroxyisoglabrolide	Yes	No	High	No	4.78	83.83	-5.86	0.87	0
5	480774	Glabrene	Yes	Yes	High	No	3.64	58.92	-4.44	0.87	0
6	225689	beta-Amyrenol	Yes	No	Low	Yes	9.15	20.23	-8.25	0.93	0
7	17751012	A884715	Yes	No	High	No	5.49	74.6	-6.15	0.87	1
8	10336244	Shinpterocarpin	Yes	Yes	High	No	3.56	47.92	-4.45	0.3	0
9	12305517	11-Deoxoglycyrrhetic acid	Yes	No	Low	Yes	7.49	57.53	-7.32	0.9	1
10	90479675	Glabrolide	Yes	No	High	Yes	5.86	63.6	-6.44	0.87	0





Shivani et al.,

Synthetic Drug											
11	41684	Nitazoxanide	Yes	No	Low	Yes	2.04	142.35	-3.02	0.08	6

Note: Obey Lipinski: Yes means 0 violation; good, BBB (Blood - Brain Barrier): Yes means good, HIA (Human Intestinal Absorption): High means good, PGP- (Molecules predicted not to be effluated from the CNS by P-glycoprotein): Yes means good, Lipophilicity: XLOGP3 value between -0.7 and +5.0 means good, Polarity: TPSA between 20 and 130 Å² means good, Solubility: Log S value not higher than 6 means good, Saturation (Fraction Csp3): Fraction of carbons in the sp³ hybridization not less than 0.25 means good, and Flexibility (Rotatable bonds): No more than 9 rotatable bonds means good.

Table 3: CYP properties of phytochemicals

S. No	Pub Chem (CID)	Compound Name	CYP1A2 inhibitor	CYP2C19 inhibitor	CYP2C9 inhibitor	CYP2D6 inhibitor	CYP3A4 inhibitor	Log K p (Skin permeation) (cm/s)	A Bioavail ability Score (ABS)
1	35014041	N-(4-butylphenyl)-5-(ethylsulfamoyl)-2-methylbenzamide	YES	YES	YES	YES	YES	-5.51	0.55
2	15228661	Hispaglabridin B	YES	YES	YES	YES	YES	-5.01	0.55
3	442774	Hispaglabridin A	NO	YES	YES	NO	YES	-4.56	0.55
4	101280184	21alpha-Hydroxyisoglabrolide	NO	NO	NO	NO	NO	-5.86	0.55
5	480774	Glabrene	YES	YES	YES	YES	YES	-5.68	0.55
6	225689	beta-Amyrenol	NO	NO	NO	NO	NO	-2.41	0.55
7	17751012	A884715	NO	NO	NO	NO	NO	-5.27	0.85
8	10336244	Shinpterocarpin	YES	YES	NO	YES	YES	-5.74	0.55
9	12305517	11-Deoxyglycyrrhetic acid	NO	NO	NO	NO	NO	-3.77	0.85
10	90479675	Glabrolide	NO	NO	NO	NO	NO	-5	0.55
Synthetic Drug									
11	41684	Nitazoxanide	NO	YES	NO	NO	NO	-6.73	0.55

Note: Yes means the compound inhibits the CYP450 enzymes and gives unanticipated adverse reactions; No means the compound does not inhibit the CYP450 enzymes and does not give any adverse reactions; The more negative the log K p, the less skin permeant is the molecule; ABS 0.55 means it passes the rule of five; 0.17 means it fails the rule of five.





Shivani et al.,

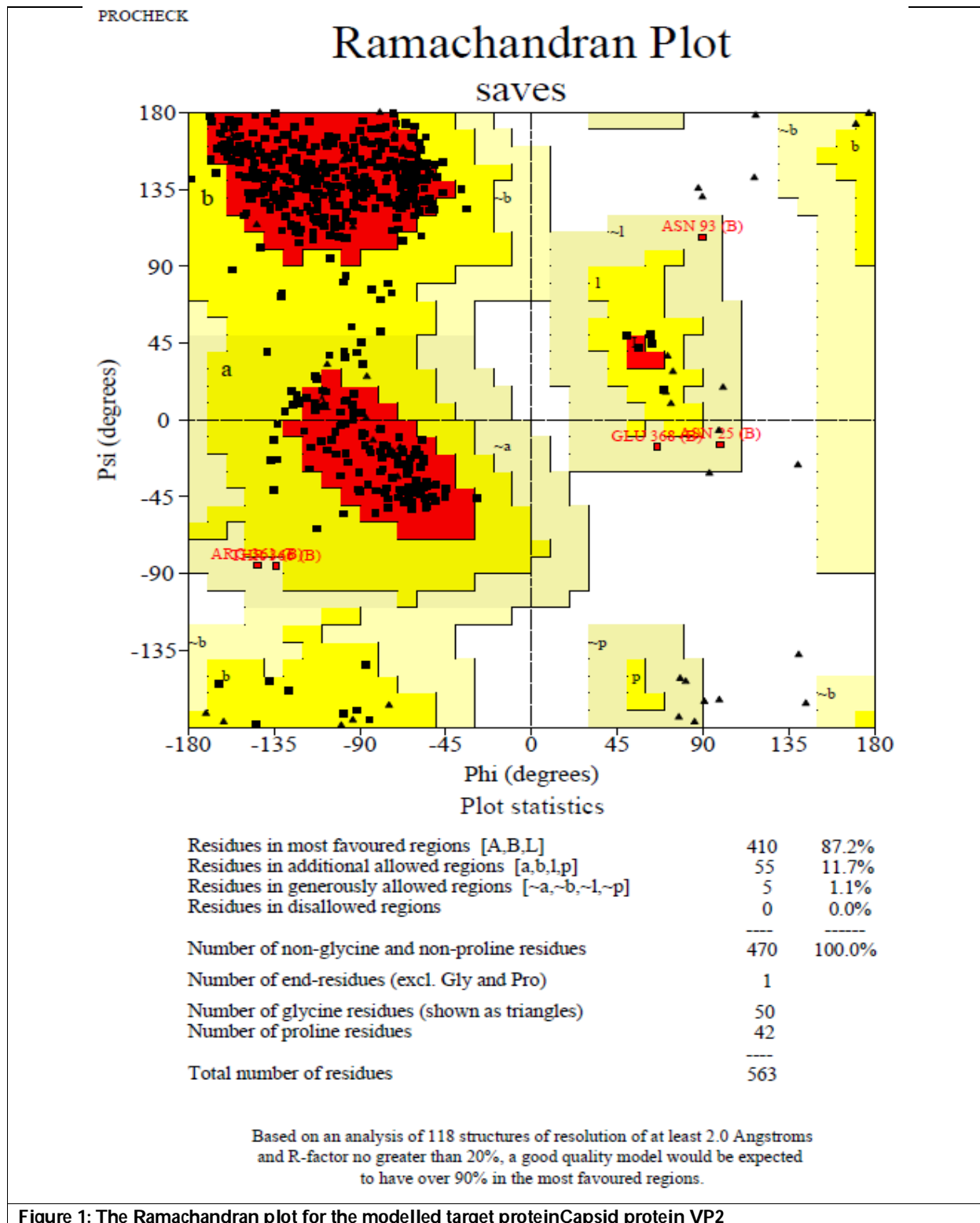


Figure 1: The Ramachandran plot for the modelled target protein Capsid protein VP2





Shivani et al.,

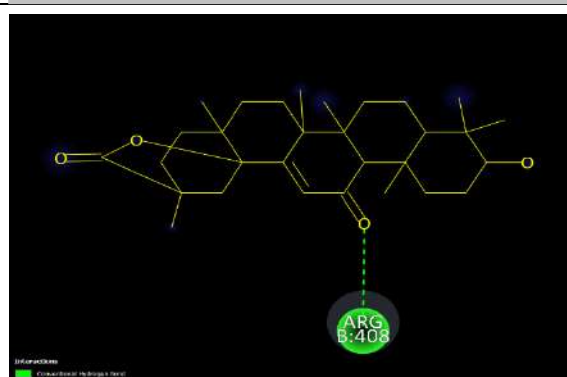


Figure 2: The 2D interaction of phytochemical N-(4-butylphenyl)-5-(ethylsulfamoyl)-2-methylbenzamide with the target protein.

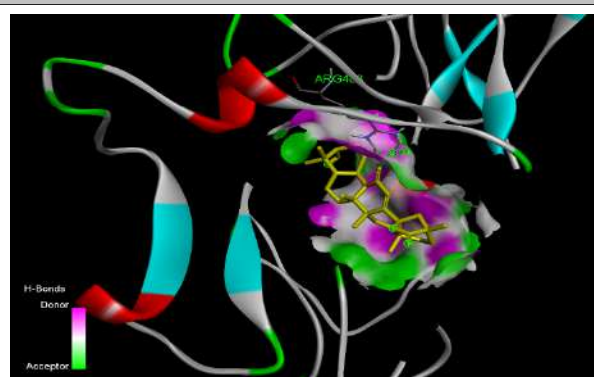


Figure 3: The 3D interaction of phytochemical N-(4-butylphenyl)-5-(ethylsulfamoyl)-2-methylbenzamide with the target protein.

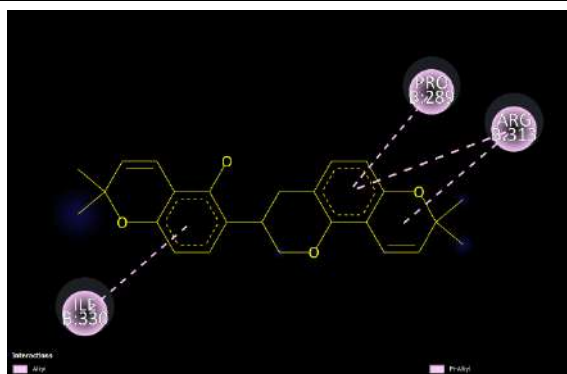


Figure 4: The 2D interaction of phytochemical Hispaglabridin B with the target protein.

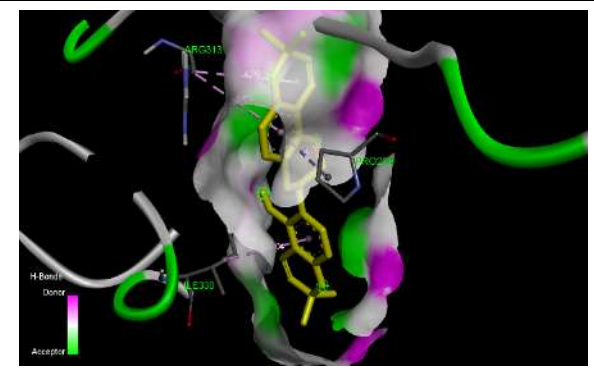


Figure 5: The 3D interaction of phytochemical Hispaglabridin B with the target protein.

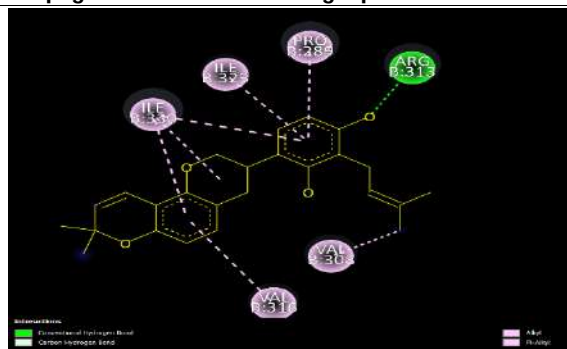


Figure 6: The 2D interaction of phytochemical Hispaglabridin A with the target protein.

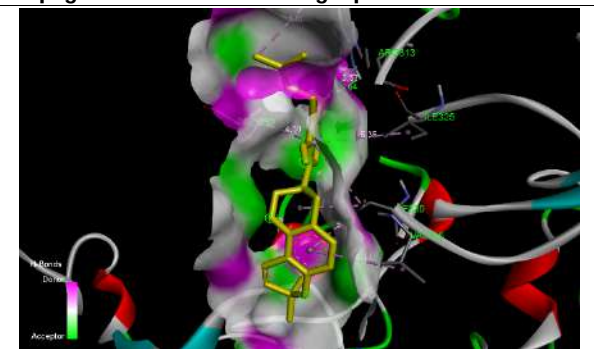


Figure 7: The 3D interaction of phytochemical Hispaglabridin A with the Target protein.



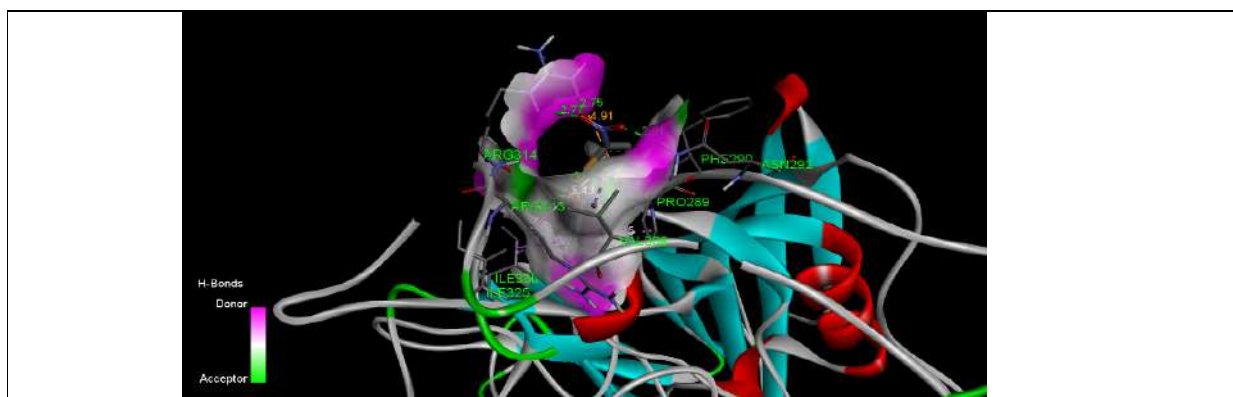


Figure 8: The 3D interaction of Synthetic drug Nitazoxanide with the target protein.

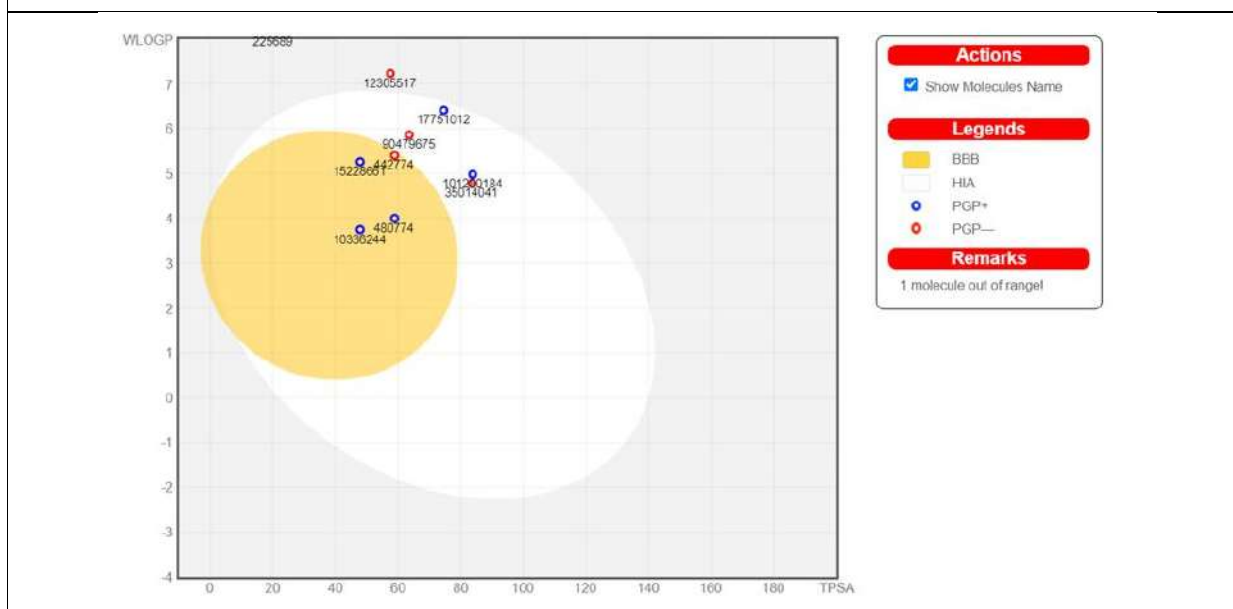


Figure 9:ADMET - Boiled Egg image of best phytochemicals

Note:

BBB: Points located in BOILED-Egg's yolk are molecules predicted to passively permeate through the blood-brain barrier.

HIA: Points located in BOILED-Egg's white are molecules predicted to be passively absorbed by the gastrointestinal tract.

PGP+: Blue dots are for molecules predicted to be effluated from the central nervous system by the P-glycoprotein.

PGP-: Red dots are for molecules predicted not to be effluated from the central nervous system by the P-glycoprotein.





A Study on Analyzing the Correlation between Economic Growth and Inflation

Venkatesh. R*

Professor, Department of MA Economics, Krupanidhi Degree College, Bangalore, Karnataka, India.

Received: 04 Jan 2023

Revised: 24 Apr 2023

Accepted: 31 May 2023

*Address for Correspondence

Venkatesh. R
Professor,
Department of MA Economics,
Krupanidhi Degree College,
Bangalore, Karnataka, India.
E. Mail: cimsvenkatesh@gmail.com



This is an Open Access Journal / article distributed under the terms of the **Creative Commons Attribution License** (CC BY-NC-ND 3.0) which permits unrestricted use, distribution, and reproduction in any medium, provided the original work is properly cited. All rights reserved.

ABSTRACT

Inflation, represented as a percentage, is the surge in the economy's average pricing levels for products and services, over a time span. It is characterized as a decrease in a currency's purchasing power. It expresses how a unit of money purchases less than in previous time periods. The economy's agents demand a constantly changing collection of commodities and services. Inflation considers the overall impact of price increase on such a heterogeneous group, allowing for a unified representation. As the value of the currency diminishes, the price shoots up, resulting in the purchase of fewer goods. Additionally, it raises the expense of living. Consequently, the economy's growth rate is slowing down. Inflation occurs when the money supply of an economy surpasses the economic growth. To address and regulate this, the monetary authorities use quantitative and qualitative measures to monitor the amount of money supply and keep inflation under control, ensuring the economy's effective functioning. India, like many other countries throughout the world, wants to maintain rapid economic growth and development while keeping inflation at minimal levels. Though, inflation and growth are believed to advance negatively, phases of trends for the same has been observed to be positive in the Indian scenario, more so in the recent times. The latter aspect being a case of stagflation. Many economists currently believe that inflation is undesired and should be avoided at all costs. They advocate for policy as well as organizational improvements ensuring meagre inflation. An approachable idea is to create autonomous centralized banking structure with an explicit objective to ensure inflation in a predetermined frame, which is commonly characterized as suitable with price stability. In this paper, an attempt has been made to investigate the connection involving inflation and growth with regards to Indian economy. Furthermore, an attempt has been made to examine the causes as to why the anomaly is occurring?

Keywords: Economic growth rate, Money Supply, Inflation, Effect, correlation.

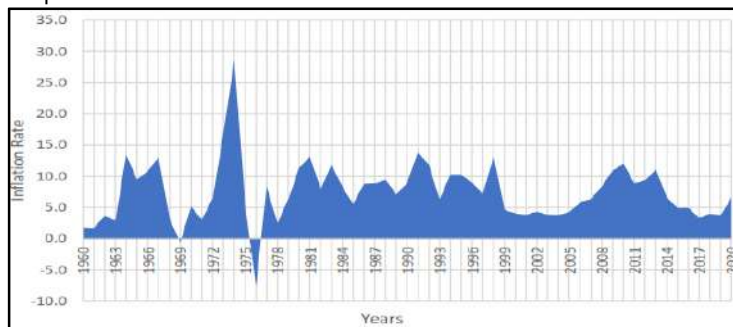




INTRODUCTION

From generations economists were trying to answer one particular question, “What causes the change in the price level, or the value of money?” in other words, they wanted to look at what caused inflation in the economy. Celebrated economists like Fisher, Marshall, Pigou, Keynes, Patinkin and Friedman believed that Quantity Theory of Money (QTM) provides explanation as to how level of price differs. There exists an inverse linkage connecting the value of money and price level. As the price level increases, the purchasing power of money, which is referred as value of money decreases and vice versa. John M. Keynes in his “A Tract on Monetary Reforms (1923)” provided that, economic agents desire to have some level of purchasing power to finance everyday transactions. Power to purchase (or the demand for money) depends partly on their taste and preferences, and partly on their wealth. People’s desire to keep money is based on these factors. Two consumption units are used to measure the money demand. A consumption unit is expressed as a basket of standard articles of consumption. When the equation is $n = pk$, K would be the amount of consumption units in the form of cash, n would be money being circulated, and p being price for units of consumption. If ‘ K ’ remains constant, an increase in ‘ n ’ will result in corresponding rise of ‘ p ’.

Stability of prices is a necessary prerequisite for both economic stability and growth. Price fluctuations, on the other hand, generate an environment of unpredictability that is not beneficial to progress. When prices grow gradually over a long period of time, national income and wealth are redistributed. As a result, the impoverished are placed in an unfavorable position, which has an impact on demand patterns. In a market economy, manufacturers carefully consider the demand for their products before making decisions. As a result, whatever pricing changes occur, they will have an impact on output. Now, we will see the Inflation trends experienced by the Indian economy from the onset of 1950s to the current time period. Since the beginning of the mid-1950s till date, there has been an unceasing upsurge in the price level in the Indian economy. The price rise has been impulsive throughout the period. As long as the rise do not create adversities, the agents in the economy are unaffected. The hassle commences when the people experience the decline in the real income along with the increasing rate of rise in the price levels.



Source: World Bank Data Base.

Analysis

Though the decade of 1950s experienced moderate levels of inflation, the price levels were a bit turbulent. But in the succeeding years, inflation started taking its toll over the economy. The standard level of inflation was about 6.2%. This was mostly as a consequence of the two wars (China-India War of 1962-67 and Indo-Pak War of 1965), two droughts, and terrible agrarian production, unimposing manufacturing improvement, static savings rate. The first three years of 1960-63 experienced a 3% level of inflation. The forthcoming years from 1964-65 to about seventeen more witnessed a general rise in price level at an average of 9.5% on a yearly basis. As in 1964-65 and 1965-66, the economy experienced 13% and 8% respectively. After the war period, it became worse as the inflation towered to about 16% in 1966-67. The four years covering the time frame of 1964-65 to 1967-68, the economy witnessed a price rise of 11% at an annual scale. Nevertheless, the next three years succeeded with a modest rise in



**Venkatesh et al.,**

the prices. In 1968-69, the economy witnessed a revival due to agricultural hike, with a -0.91% inflation. And by 1969, 14 banks were nationalized, mainly for the government funding, money supply would naturally see an enormous build in the following years, and so would inflation. Despite the fact that the decade of 1960s detected the volatile price levels, the following decennium was more unpleasant and distressing for the Indian economy. The Indian economy underwent the stage of hyper-inflation from 1971-72 to 1975-75. Adding to the woes of 1960s, the years of 1970s experienced agricultural shrink and oil shocks, this in turn raised that price levels at a startling proportion. It was disastrous and dreadful when the inflation remained static with 20%-30% from late 1973 to late 1974. This was attributed to the oil crisis of 1973 as well. At a point of time in 1974, inflation reached to an alarming level of 33.3%. Despite the average rate of inflation being 16.3% during this period, in 1974-75 the rate of price rise hit a 25.2% high. The increase in the oil prices due to the oil shocks in 1979 affixed to the already downtrodden economy, along with the severe drought, witnessing an inflation about 17.1% in 1979-80.

Then the arrival of the years of 1980s, brought along with it the inflationary pressures from 1970s. The inflation in 1980-81 was about 18.2%, this was majorly due to monetary expansion, even when the forex reserves was getting diminished due to the oil shocks, severe droughts; making the broad money grow at 18.5%. The government's fiscal deficit also was a significant reason for the rise in inflation. For about six years in 1980s the inflation rate on an average was around 7%. Only during the years of 1982-83 and 1985-86, did the inflation drop to a 5% level. This was mostly due to the agricultural production. In 1987-88, the agricultural output became sluggish due to droughts. In general, during the 1980's the economy went through an average of 8% inflation. This decade saw the vicious cycle of rising fiscal deficit, high monetary expansion and increasing inflation. During the period of 1980s, there was no respite from inflation.

The decade of 1990's in India went through a series of reforms- LPG (liberalization, privatization, and globalization). 1990-91 the inflation shot up to a double-digit mark of 10.2%, this was due to the shocks on oil and other imports goods as a result of the gulf war. In 1991, the Indian Rupee depreciated at 11%. The rate of inflation increased to a level of 13.7%. Then for the later year of 1992-93, prices increased at an average rate of 10.1%. There existed an average annual increase in prices of about 11.96% during the first three years of the post-reform period. This upswing towards a double-digit inflation which caused a grave concern was mainly due to an increase in administrative prices, and a hefty fiscal deficit. Along with that, India's trade with the rest of the world led to inflationary impacts for the initial years of 1990s. Increase in prices of food crops and oil-based commodities added to the inflation. Due to low forex reserves, imports couldn't be sought for. The first half of 1990s, experienced a distressing and frightening rise in inflation. Contrary to it, the second half of the 1990's underwent some noteworthy reversions with regards to inflation. The average level of inflation was around 5.3%. The inflation rates for the periods of 1995-96 and 1996-97 was brought down to the levels of 8% and 4.6% respectively. But again. The end of 1998 saw a rise to 8.8% owing to the steep rise in price of primary products. Surprisingly, two months later, the inflation rate underwent a decline, with it being 2.9% in the onset of 2000. Inflation decreased to a favourable rate during the years of 1996-2000. This basically happened due to the prudent monetary management of the RBI, decrease in the food inflation, world inflation started easing, and the Indian rupee depreciated at a lower rate of 4%, agricultural output was in surplus, the increase in forex reserves, the domestic supply constraint was covered by imports.

The acceptable and comfortable level of inflation initially continued on the onset of the new era as well. The average inflation of 2000-08 was 5.4%. But 2008-09 went through an upsurge due to the Global Financial Crisis (GFC). In spite of the suitable economic conditions, the rise in the administered prices of the petroleum products in 2000-01 influenced the rise in inflation of 7.27%. The inflation in the year 2001-02 was 3.6% and in the year 2002-03 was 3.6%, even though there were droughts, political tensions, international disputes, increasing oil prices. The agrarian production and output bloom helped in this aspect. But from 2003 to 2005, the inflation rose in a steady manner, due to the increasing oil prices, ores, etc.; inflating the prices of agricultural products as well. But again in 2005-06 due to the toughening and restraints of the monetary aspects by the RBI, inflation level declined to 4.4%. Again in 2006-07, due to the oil price hike, the inflation rose up. Then in 2007-08, the prices of food products increased, increasing

57000



**Venkatesh et al.,**

inflation. And in 2008-09 prices started experiencing volatility, measuring the most inflated situation of the decennium. The inflation during this period was 8.4%, which subsided with the declining commodity prices and crude oil prices from the commencement of the GFC. The average inflation of the decade of 2008-09 was 5.4%. Between 2008-13, inflation averaged 10.1% due to rise in prices of oil and so on. Drought of 2009, despite having an agricultural stock created inflation of other food items. The Government announced several stimulus packages in 2008-09, which also increased fiscal deficit, again increasing prices. The year of 2009-10 set off with a low headline inflation of 1.3% in early months of 2009, which moved to negative zone in the middle of 2009, but it increased faster in the early stages of 2010 to about 11%.

The year 2010-11 sought persistent levels of inflation of around 9.6% resulting from sharp rise in food prices from uncertain rainfall, rise in prices of non-food commodities, etc. The inflation reached to 9.7% and then came down to 6.6% in the year 2011 and 2012 respectively. Then the Indian rupee depreciated, and the prices of commodities in the world also increased. In mid of 2012, inflation reached double digits. The inflation during 2012 was 9.31%. The inflation during 2013 was 11.06%. The inflation during 2014 was 6.65%. The inflation during 2015 and 2016 was 4.91% and 4.95% respectively. The inflation during 2017, 2018 and 2019 was 3.33%, 3.95%, and 3.72% respectively. In 2017-2018 and 2018-19, the CPI based core inflation increased from 4.6% to 5.8%. From the end of 2018 to the initial phases of 2019, it decreased to 4.5%. Refined core inflation tracked core inflation closely, averaging 5.7 percent in 2018-19 compared to 4.6 percent in 2017-18 and 4.8 percent in the first half of 2019. The rate of inflation during 2020 was 6.62%. This can be attributed to the demand glut of various goods and services. And, the shrinking of the economic activity, decrease in investments, stagnation of savings, due to the unfortunate Covid-19 pandemic. The RBI, projected the inflation of India in 2021-22 to be 5.3%.

REVIEW OF LITERATURE

Stanley Fischer (1993) via the application regression of growth accounting, detected the channels by means of which economic growth is impacted by macro-economic variables. It tries to analyse the relationship between them, and also among the macroeconomic variables and changes in both the productivity, residual, or supply of factors. Utilizing the aspects of panel regressions and cross-section data, growth is depicted to be negatively associated with inflation. The recommendations that causation runs from inflation to growth is given. Capital accumulation and productivity growth are negatively related to inflation. The growth rate of the capital stock diminishes by 3.7% points when the rate of inflation upsurges by 100% points. The decrease in the rate of productivity growth of 1.8% is experienced by the escalation in inflation rate by 100%. Some few unique occurrences also suggest that for high growth there exists no necessity for minimal inflation and minute deficits, and the fact that sustained growth is not coherent with sharp inflation.

Paul S., C. Keamey and K. Chowdhury (1997) Using Granger causality, researchers examined the direction of link and causation among inflation and economic development using data from over 70 nations from 1960 to 1989. They discovered that the relationship among inflation and economic growth differed by country. 26 nations had a one-way link, 28 countries had a negligible relationship, and the remaining 16 countries were interdependent. The working group also concluded that the concept of low inflation for boosting growth was not universal, with industrial countries benefiting more than underdeveloped countries.

Veni and Choudhury (2007) From 1981-82 to 2004-05, the author looks at the link between growth (GDPFC) and inflation rate (WPI). The Granger Causality test is used to determine whether they are causally related. Co-integration between the variables is tested using the Engle Granger two-step co-integration process. During the research period, a causality test revealed that in India, growth and inflation were unrelated. The findings of the co-integration test indicated that the two variables of inflation and growth are unrelated. As a result, there is no long-term connection. It was also determined that, because economic growth is unrelated to inflation, quickening of growth should remain one of the nation's top economic priorities indefinitely. Inflation can occur as a result of





Venkatesh et al.,

both supply and demand side variables. Aside from these, monetary and foreign issues may also contribute to inflation. According to the conditions, the government must take prompt action to reduce inflation in order to maintain economic stability.

Salian and Gopakumar (2011) took the period of study for the Indian economy from 1972- 2008, using annual data. The variables taken were the Wholesale Price Index measure of inflation and the Gross Domestic Product growth rates. The paper tries to examine the relation between the inflation rates and economic growth, and the nature for the same. With the use of co-integration and Error Correction Models (ECM), the objective for short-run and long-run were found. According to the findings, there was a non-linear link between inflation and economic growth in India. They also discovered that growth's sensitivity to changes in inflation was lower than inflation's sensitivity to changes in growth. Inflationary pressures from prior eras would also cause economic development to slowdown. The policy conclusion was that the government should focus on keeping inflation low and steady rather than worrying about the threshold level.

Objectives of the Study

- To highlight different levels of inflation in the country during various years.
- To explore the nature of the association in the Indian economy between inflation and economic growth.
- To present a comprehensive study upon the rationale for a positive connection between the inflation and growth in several episodes from the period of 2001-02 to 2020-21.

Estimating the Correlation between economic growth and inflation using DCC-GARCH estimation:

Before taking up the DCC-GARCH model, at first we check for heteroscedasticity in the model to verify the suitability of applying the DCC-GARCH model for the variables considered. For this purpose, at first, an ordinary least square regression taking the form, $GWGDPSA = f(INFSA)$ is estimated. The residuals from this regression are then used to check for heteroscedasticity under the ARCH specification. The null hypothesis for the test, i.e., absence of heteroscedasticity can be rejected at 10% level of significance as the probability for both the f-test and chi-square test is 0.07.

Test for heteroscedasticity in the model

	Test Statistic	P-Value
F-Statistic	3.17	0.07
Chi-Square	3.15	0.07

Having validated the suitability of the considered variables for GARCH model, we estimate the DCC (1,1)-GARCH (1,1) model has been estimated using the quasi maximum-likelihood method. The results are presented in panel A and Panel B. At first, we note that the model is stable as $dcca1$ and $dccb2$ representing α and β in equation is positive and are less than 1. From the results we observe that $\beta = 0.85$ and hence there is persistence of time varying correlation. From the conditional variance equation, we note that variance is persistent in INFSA having both ARCH (α_1) and GARCH (β_1) coefficient closer to one. Whereas, in case on GWGDPSA, the ARCH effect is not significant.

Conditional Mean and Variance Equation

The results suggest that the dynamic conditional correlation is negative in most cases except a few episodes when the correlation was positive. Especially in the recent times since 2020 Q2 onwards when it is consistently in the positive region. Overall, the average correlation through the period is negative at around - 0.30 and is as per theoretical expectations.





Venkatesh et al.,

	GWGDPSA	INFSA
Panel A: Conditional Mean		
Constant	7.24 (23.27)	4.30 (7.13)
AR (1)	0.18 (1.22)	0.61 (8.26)
Panel B: Conditional Variance		
Constant	0.27	0.11
α (1)	1.04 (1.70)	0.18 (2.15)
β (1)	0.23 (2.05)	0.80 (12.85)
Dcca1:0.10		
Dccb1:0.85		

CONCLUSION

The world-wide accepted theory for connection amongst “economic growth and inflation” is a negative one. But transpirations of exceptions exist, wherein various studies and works have expressed contrary thoughts regarding the same. Indian economy, in the recent context, has witnessed dynamic trends of macroeconomic fundamentals, economic growth and inflation being amongst them. This study tries to evaluate the interrelation between growth and inflation in the Indian context. It analyzes the time period of 2001-02 to 2020-21, and for a finer perception it takes into account the quarterly data. To examine the relationship in the midst of growth and inflation, the Dynamic Conditional Correlation (DCC) GARCH is utilized to find the correlation. The results detect that the correlation is predominantly negative, but periods of positive bearing have also been demonstrated. And the latter correspondence has developed notably in the recent time frame. The research also tries to appraise as to why there have been instances that record such existence of positive correlation. The empirical analysis, along with the results, also accommodates collateral information entrenched via the regulatory institutional reportings and authors’ rationales providing an accessory about the auxiliary factors that determine the positive association between economic growth and inflation in the recently bygone time stretch of the Indian economy. The factors being the functioning of other macroeconomic variables of the economy such as Balance of Payments, exchange rate and policy rates. Hence, we conclude from the study that there were periods in the Indian economy where there was a positive connection amongst the “Inflation and Economic Growth”, more so in the recent time frame, and there exists rationale for such occurrence.

REFERENCES

1. Behera, J., & Mishra, A. K. (2017). The recent inflation crisis and long-run economic growth in India: An empirical survey of threshold level of inflation. *South Asian Journal of Macroeconomics and Public Finance*, 6(1), 105-132.
2. Eggoh, J. C., & Khan, M. (2014). On the nonlinear relationship between inflation and economic growth. *Research in Economics*, 68(2), 133-143.
3. Fischer, S. (1993). The role of macroeconomic factors in growth. *Journal of monetary economics*, 32(3), 485-512.
4. Jayathilake, P. M. B., & Rathnayake, R. M. K. T. (2013). Testing the link between inflation and economic growth: Evidence from Asia.
5. Sarel, M. (1996). Nonlinear effects of inflation on economic growth. *Staff Papers*, 43(1), 199-215.
6. Veni, L. K., & Choudhury, P. K. (2007). Inflation and growth dilemma: an econometric analysis of the Indian economy. *The IUP Journal of Financial Economics*, 5(1), 79-87.
7. Wai, U. T. (1959). The relation between inflation and economic development: a statistical inductive study. *Staff Papers (International Monetary Fund)*, 7(2), 302-317.





A Brief Recapitulation of Triazole Synthesis Pharmacological Activities Molecular Docking and QSAR Studies

Tejaswini R¹, Paramita Das^{2*}, Anjali Nayak², Ramya A¹ and Rashu Raju¹

¹Student, Department of Pharmaceutical Chemistry, Krupanidhi College of Pharmacy, Bengaluru – 560035, Karnataka, India

²Associate Professor, Department of Pharmaceutical Chemistry, Krupanidhi College of Pharmacy, Bengaluru – 560035, Karnataka, India

Received: 08 Feb 2023

Revised: 28 Mar 2023

Accepted: 02 May 2023

*Address for Correspondence

Paramita Das

Associate Professor,
Department of Pharmaceutical Chemistry,
Krupanidhi College of Pharmacy,
Bengaluru – 560035, Karnataka, India
E. Mail: paramitadas04@gmail.com



This is an Open Access Journal / article distributed under the terms of the **Creative Commons Attribution License** (CC BY-NC-ND 3.0) which permits unrestricted use, distribution, and reproduction in any medium, provided the original work is properly cited. All rights reserved.

ABSTRACT

Triazole also known as pyrroldiazole, a class of compound possessing a wide spectrum of various chemotherapeutic effects such as antimicrobial, anti-tubercular, antioxidant, antifungal, antimalarial and many more activities. Study reports reveal that triazole moiety acts as therapeutically promising medication candidate. Moreover, these scaffolds have different methods for their synthesis such as water based reaction, green chemistry and light induced electronic synthesis. This review mainly focuses on the research of few novel triazole derivatives synthesized and their various pharmacological activities designed in the last 10 years. It also encompasses some summarization of the *in-silico* computational studies performed for the designed triazole compounds. From all these studies it can be concluded that these moieties can serve as unique and versatile scaffolds for experimental drug design in order to design an efficient drug with best activity and less toxicity.

Keywords: Triazole, water based reaction, anti-microbial, molecular docking, QSAR.

INTRODUCTION

In the field of medicine and its chemistry, the nitrogen containing heterocyclic compounds notably the 5 membered such as triazole, oxazole, oxadiazole and so on are formidable, remarkably the triazole that is going to be embellished further [1,2]. These compounds manifest numerous pharmacological activities such as anti-inflammatory [3], antiviral [4], anticonvulsant [5], antidiabetic [6], antimicrobial [7], antitubercular [8] activities. Especially 1,2,4-triazole has been incorporated into a number of therapeutically promising medication candidates, such as antifungal



**Tejaswini et al.,**

(fluconazole), antiviral (ribavirin), anti-migraine (rizatriptan), and anti-anxiety drugs (Alprazolam). Triazole being a five membered ring is furcated under heterocyclic compound containing three nitrogen atoms with two carbon atoms adjacent or non-adjacent to each other with the molecular formula $C_2H_3N_3$ which is also known as pyrrrodiazole [9]. Triazole is generally transpired as positional isomers such as 1,2,3-triazole and 1,2,4-triazole which are also known as V – triazoles and S – triazoles respectively. The vicinal or v-triazoles, are doubly unsaturated heterocycles which consists of three sequentially arranged nitrogen atoms and two carbon atoms. This 1,2,3-triazole has one unlocated hydrogen atom which leads to two tautomeric forms. Substitution of one or more of the hydrogen atoms in these two structures leads to several different classes of v-triazole derivatives [10]. The S – triazoles or symmetrical triazole 1 and 2 N is basic in nature and 4 N is acidic while the lone pair of 4 N takes part in aromaticity. Tautomerism is due to proton present between 1 and 4 position. The aromatic stabilization energy of 1H 1,2,4 triazole is 18.01Kcal/mol and 4H 1,2,4 triazole is 12.19Kcal/mol which indicates 1H is more stable [11]. Triazoles appears as pale yellowish to white coloured crystals with extremely less odour which is soluble in water as well as in alcohol with the melting point of 120°C shown by 1,2,3-triazole and 130°C shown by 1,2,4-triazole [12,13].

Structure 01: Tautomeric isomers of 1,2,3-triazole**Structure 02: Tautomeric isomers 1,2,4-triazole**

Molecular docking is a computer assisted drug design key tool in structural molecular biology in the field of modelling the molecules. It is an approach used in prediction of the preferred orientation of a molecule to bind itself to the target [13]. The QSAR (Quantitative Structure–Activity Relationship) can be briefed as "the structure of a chemical compound that has an impact on its characteristics and bioactivity in its most basic form. QSAR is a method for developing computational or mathematical models that uses a chemometric technique to try to uncover a statistically significant association between structure and its activity [14].

Synthetic Approches of Triazole Derivatives and their Pharmacological Activities

The below table contains few novel synthesized triazole derivatives with their best synthesized derivative and its pharmacological activities.

Different Synthetic Approches of Triazole Derivatives

This current study brings two bioactive substances together, where Mostafa H *et al.* prepared a series of novel 3-(1H-pyrazol-3-yl)-4H-1,2,4-triazole derivatives and screened for anticancer activity. Out of all the compounds screened, one compound was found to possess cell growth inhibition and exhibits the highest potential to retard the proliferation of various neoplastic cells [24]. Recently Dannea AB *et al.* reported that triazoles show good anti-tubercular property and prepared futuristic triazole-incorporated di indolyl methanes (DIMs). Few compounds demonstrated potent antitubercular action against Mtb H37Ra with IC_{50} values of 2.19, 1.52, and 0.22 g/mL, respectively [25]. El-Barbary AA *et al.* synthesized few novel [1,2,4] Triazolo[3,4b][1,3,4]thiadiazolyl-isoindole-1,3-diones and screened for anti-HIV and anti-HBV activity. All of the newly synthesized compounds were evaluated for antiviral activity against HIV-1 and HBV. Some compounds demonstrated moderate antiviral activity against HBV [26]. As seen earlier, triazoles have a number of pharmacological activities among which one compound is found to possess antileishmanial activity. Researchers have reported that usage of conventional treatments or the drugs would lead to resistant development among the protozoans and is observed to exhibit least effectiveness against



Tejaswini *et al.*,

prophylactic vaccine of leishmaniasis. In this study, Suleymanoglu N *et al.* synthesised a series of 4-amino-1,2,4-triazole derivatives. The *in vitro* studies were performed using *Leishmania infantum* and reported that 4-amino-1-((4-amino-5-mercapto-4H-1,2,4-triazole-3-yl)methyl)-3-(thiophene-2-ylmethyl)-1H-1,2,4-triazole-5(4H)-one possess anti-parasitic activity. Pyrazole derivatives also possess vast variety of biological activities. With the idea of combining two different moieties - pyrazole and triazole may give rise to a better drug with potent or effective pharmacological activity, Karrouchi K *et al.* synthesized and studied a number of novel Schiff base of 4-amino-1,2,4-triazole derivatives which contains pyrazole moiety possessing analgesic and antioxidant activity. It was found that all compounds possessed significant anti-oxidant property out of which two derivatives i.e., 4-nitro and 4-fluoro derivatives found to have shown potent analgesic activity [27].

QSAR Studies of Different Triazole Derivatives and Their Molecular Docking Studies

Currently cancer has become an implacable disease throughout the world, which engulfs nine to ten million people in a year. A report says in 2020 there were 10 million deaths throughout the world due to cancer and there is a towering demand for anticancer drugs [28]. Philip S *et al.* studied the QSAR and molecular docking studies of 1,2,4-triazole derivatives and investigated to design new methionine amino peptidase 2 inhibiting agents. The CoMFA, CoMSIA, and Topomer CoMFA models performed well, with cross-validated coefficients (q^2) of 0.703, 0.704, and 0.746, respectively. These models are utilized to create novel compounds containing 1,2,4-triazoles with core substantial MetAP2 inhibitory activity. Nalidixic acid is a first synthetic quinolone derivatives possessing best antibacterial activity and is used for a broad range of infections [29]. Khaldan A *et al.* studied a total of seventeen quinolone-triazole compounds which were investigated as antibacterial agents. The CoMSIA and CoMFA models yielded high r^2 values of 0.98 for CoMFA and 0.976 for CoMSIA, with the latter displaying a high q^2 value of 0.72 and CoMFA displaying a q^2 value of 0.71 [30]. Adeniji S E *et al.* carried out studies in order to produce a replica that connects the 50 different derived compound structures to their anti-*M. tuberculosis* activity. The best replica showed an acclimated squared correlation measure (r_{adj}) of 0.91012, a squared correlation coefficient (r^2) of 0.9202 and a cross validation measure (q^2_{cv}) of 0.8954. Docking study revealed that efficient drug had docking affinity of 14.6 kcal/mol which was high amongst all and created hydrophobic interactions and hydrogen bonds with *M. tuberculosis* cytochromes amino acid residues (Mtb CYP121) [31]. Xanthine oxidoreductase, a key enzyme involved in catalysis of hypoxanthine to uric acid which in turn results in diseases like gout, hyperuricemia and cardiovascular diseases [32]. Tang HG *et al.* evaluated xanthine oxidoreductase inhibitors series. The best CoMFA model had q^2 and r^2 non-validated correlation coefficients of 0.578 and 0.988, respectively. The strongest comparative molecular similarity indices analysis (CoMSIA) model had a q^2 of 0.631 and an r^2 of 0.966. Topomer CoMFA model analysis yielded $q^2 = 0.698$ and $r^2 = 0.907$, indicating that the model has strong predictive capacity. Sodium dependent glucose co-transporter (SGLT- 2) said to be an attractive target to treat diabetes as it plays a vital role in decreasing the blood glucose level [33]. Zhi H *et al.* utilized CoMSIA and CoMFA models, to develop the 3D-QSAR of SGLT-2 inhibitors and 46 compounds were chosen with hypoglycemic activity whose r^2 value of 0.985 and a q^2 value of 0.792 were predicted by CoMFA. and r^2 value of 0.895 and a q^2 value of 0.633 were predicted by CoMSIA. Qi L *et al.* studied Six disubstituted Schiff base derivatives and the antifungal analysis indicated that 2 compounds had excellent activity for *Wheat gibberellic*, with EC_{50} values of 15.89 and 16.99 mg/L, respectively. According to molecular docking data, 2 compounds have shown lowest docking energy (-8.33, 9.00 kcal/mol) [34]. From various studies it is observed that triazoles are used in order to fight for clinical unfolding and eradicating the malaria [61]. Hmamouchi AS *et al.* Studied 3D-QSAR of a series of thirty two novel triazole attached with quinine derivatives and screened for anti-malarial activity and it showed IC_{50} ranging from 7.568 to 4.387 (IC_{50} in nM). The PLS results shows that CoMFA has high r^2 value of 0.98 and the cross validated determination coefficient q^2 was found to be 0.61.

Alzheimer's disease is an irreversible loss of memory and cognitive functions. For inhibition of alzheimer's we need to suppress the cholinergic activity at neurons which reduced disease exacerbation. Extensive research has been carried out on Alzheimer's disease. Khatbi KE *et al.* [35] worked on Alzheimer's disease and designed 1,2,3-triazole based twenty six derivatives and tested it for acetylcholinesterase inhibitory activity by 3D-QSAR studies. The study report showed $q^2=0.604$, $r^2=0.863$, $r_{ext}^2=0.701$ and CoMSIA $q^2=0.606$, $r^2=0.854$, $r_{ext}^2=0.647$. The docking scores of designed compounds showed favorable interactions with that of TYR70³⁶. Nonsteroidal anti-inflammatory



**Tejaswini et al.,**

medications (NSAIDs) act to reduce inflammation by decreasing COX-derived prostaglandin production. COX-2 being primarily responsible for inflammatory activity in the body, selective inhibition of COX-2 may lead to reduction of inflammation and pain [37], as demonstrated by El-Din GAA *et al.* Novel 1-[4-(Aminosulfonyl)phenyl]-1H-1,2,4-triazole compounds with outstanding selective COX-2 inhibition were designed and synthesized. These compounds demonstrated anti-inflammatory activity equivalent to indomethacin and celecoxib. Docking experiments depicted few compounds have lower energies of molecular docking results and high selectivity [38].

CONCLUSION

The above summarized review article mainly highlights about various research works carried out on triazole and its derivatives. As we have seen triazole, a heterocyclic compound possess adequate number of pharmacological activities, it implies that the triazole can be amplified using further studies on triazole's possible derivatives or substitutions in order to obtain a better moiety with stronger commitments. This review mainly comprises information about triazole, its various possible synthetic approaches, pharmacological activities, QSAR and molecular docking studies which was retrieved from various research works. The extensive research carried out on triazole helps us to conclude that triazole on further investigations can elevate its potency and help us bring up new pharmacological activities.

Conflict of Interest

The authors declare no conflict of interest.

ACKNOWLEDGEMENT

We would like to thank the Principal and management of Krupanidhi College of Pharmacy, Bangalore for their support and encouragement.

REFERENCES

1. Kumar S, Khokra SL, Akash Yadav A. Triazole analogues as potential pharmacological agents: a brief review. *Future J Pharma Sci.* 2021;7:106.
2. Celik F, Unver Y, Barut B, Ozel A, Sancak K. Synthesis, Characterization and Biological Activities of New Symmetric Bis-1,2,3-Triazoles with Click Chemistry. *Med Chem.* 2018;14(3):230-241.
3. Tozkoparan B, Kupeli E, Yesilada E, Ertan M. Preparation of 5-aryl-3-alkylthio-1,2,4 triazoles and corresponding sulfones with anti-inflammatory-analgesic activity. *Bioorg Med Chem* 2007;15:1808–1814.
4. Cao X, Wang W, Wang S, Bao L. Asymmetric synthesis of novel triazole derivatives and their in vitro antiviral activity and mechanism of action. *European Journal of Medicinal Chemistry.* 2017 Oct 20;139:718-25.
5. Liu, K.; Shi, W.; Cheng, P. The coordination chemistry of Zn(II), Cd(II) and Hg(II) complexes with 1,2,4-triazole derivatives. *Dalton Trans.*, 2011, 40,8475-8490.
6. Zhou, C.H.; Zhang, Y.Y.; Yan, C.Y.; Wan, K.; Gan, L.L.; Shi, Y. Recent researches in metal supramolecular complexes as anticancer agents. *Anti-Cancer Agents Med. Chem.*, 2010, 10, 371-395
7. Aggarwal N, Kumar R, Dureja P, Khurana JM. Synthesis, antimicrobial evaluation and QSAR analysis of novel nalidixic acid based 1, 2, 4-triazole derivatives. *European Journal of Medicinal Chemistry.* 2011 Sep 1;46(9):4089-99.
8. Costa MS, Boechat N, Rangel EA, Da Silva FD, De Souza AM, Rodrigues CR, Castro HC, Junior IN, Lourenço MC, Wardell SM, Ferreira VF. Synthesis, tuberculosis inhibitory activity, and SAR study of N-substituted-phenyl-1, 2, 3-triazole derivatives. *Bioorganic & Medicinal Chemistry.* 2006 Dec 15;14(24):8644-53.
9. <https://en.wikipedia.org/wiki/Triazole#:~:text=A%20triazole%20refers%20to%20any,%2C2%2C4%2DTriazoles.>
10. Benson FR, Savell WL. The chemistry of the vicinal triazoles. *Chemical Reviews.* 1950 Feb 1;46(1):1-68.





Tejaswini et al.,

11. Potts KT. The Chemistry of 1, 2, 4-Triazoles. Chemical reviews. 1961 Apr 1;61(2):87-127.
12. <https://www.slideshare.net/parth079/regioselective>
13. <https://en.wikipedia.org/wiki/1,2,4-Triazole>
14. [https://en.wikipedia.org/wiki/Docking_\(molecular\)](https://en.wikipedia.org/wiki/Docking_(molecular))
15. Shaikh MH, Subhedar DD, Akolkar SV, Nagargoje AA, Khedkar VM, Sarkar D, Shingate BB. Tetrazoloquinoline-1, 2, 3-triazole derivatives as antimicrobial agents: synthesis, biological evaluation and molecular docking study. Polycyclic Aromatic Compounds. 2022 Apr 21;42(4):1920-41.
16. El-Sayed WA, Alminderej FM, Mounier MM, Nossier ES, Saleh SM, Kassem AF. Novel 1, 2, 3-Triazole-Coumarin Hybrid Glycosides and Their Tetrazolyl Analogues: Design, Anticancer Evaluation and Molecular Docking Targeting EGFR, VEGFR-2 and CDK-2. Molecules. 2022 Mar 22;27(7):2047.
17. Irfan A, Faiz S, Rasul A, Zafar R, Zahoor AF, Kotwica-Mojzzych K, Mojzzych M. Exploring the Synergistic Anticancer Potential of Benzofuran-Oxadiazoles and Triazoles: Improved Ultrasound-and Microwave-Assisted Synthesis, Molecular Docking, Hemolytic, Thrombolytic and Anticancer Evaluation of Furan-Based Molecules. Molecules. 2022 Feb 2;27(3):1023.
18. Qi L, Li MC, Bai JC, Ren YH, Ma HX. In vitro antifungal activities, molecular docking, and DFT studies of 4-amine-3-hydrazino-5-mercapto-1, 2, 4-triazole derivatives. Bioorganic & Medicinal Chemistry letters. 2021 May 15;40:127902.
19. Chatterjee S, Kumar N, Sehrawat H, Yadav N, Mishra V. Click triazole as a linker for drug repurposing against SARs-CoV-2: A greener approach in race to find COVID-19 therapeutic. Current Research in Green and Sustainable Chemistry. 2021 Jan 1;4:100064.
20. Hmamouchi AS, Bouachrine M, Lakhilfi T. 3D-QSAR Modeling and Molecular Docking Studies of novel triazoles-quinine derivatives as antimalarial agents. Journal of Materials and Environmental Science, 2020 Feb;11(3):429-443.
21. Panigrahi, D., Mishra, A. and Sahu, S.K., 2020. Pharmacophore modelling, QSAR study, molecular docking and insilico ADME prediction of 1, 2, 3-triazole and pyrazolopyridones as DprE1 inhibitor antitubercular agents. SN Applied Sciences, 2(5), 1-28.
22. Patil PS, Kasare SL, Haval NB, Khedkar VM, Dixit PP, Rekha EM, Sriram D, Haval KP. Novel isoniazid embedded triazole derivatives: Synthesis, antitubercular and antimicrobial activity evaluation. Bioorganic & Medicinal Chemistry Letters. 2020 Oct 1;30(19):127434.
23. Verma KK, Singh UK, Jain J. Design, synthesis and biological activity of some 4, 5-disubstituted-2, 4-dihydro-3H-1, 2, 4-triazole-3-thione derivatives. Central Nervous System Agents in Medicinal Chemistry (Formerly Current Medicinal Chemistry-Central Nervous System Agents). 2019 Dec 1;19(3):197-205.
24. Tang HJ, Yang L, Li JH, Chen J. Molecular modelling studies of 3, 5-dipyridyl-1, 2, 4-triazole derivatives as xanthine oxidoreductase inhibitors using 3D-QSAR, TopomerCoMFA, molecular docking and molecular dynamic simulations. Journal of the Taiwan Institute of Chemical Engineers. 2016 Nov 1;68:64-73.
25. Danne AB, Choudhari AS, Chakraborty S, Sarkar D, Khedkar VM, Shingate BB. Triazole-diindolymethane conjugates as new antitubercular agents: synthesis, bioevaluation, and molecular docking. MedChemComm. 2018;9(7):1114-30.
26. El-Barbary AA, Abou-El-Ezz AZ, Abdel-Kader AA, El-Daly M, Nielsen C. Synthesis of some new 4-amino-1, 2, 4-triazole derivatives as potential anti-HIV and anti-HBV. Phosphorus, Sulfur, and Silicon. 2004 Aug 1;179(8):1497-508.
27. Guessas B, Othman AA, Khiati Z. Synthesis and antibacterial activity of 1, 3, 4-oxadiazole and 1, 2, 4-triazole derivatives of salicylic acid and its synthetic intermediates. South African Journal of Chemistry. 2007 Jan 1;60(1):20-4.
28. <https://www.who.int/news-room/fact-sheets/detail/cancer>
29. <https://pubchem.ncbi.nlm.nih.gov/compound/Nalidixic-acid>
30. Khaldan A. 3D QSAR Modeling and Molecular Docking Studies on a series of quinolone-triazole derivatives as antibacterial agents. RHAZES: Green and Applied Chemistry. 2019 Aug 21;6:11-26.
31. Adeniji SE, Uba S, Uzairu A. QSAR modeling and molecular docking analysis of some active compounds against mycobacterium tuberculosis receptor (Mtb CYP121). Journal of pathogens. 2018 May 10;2018.





Tejaswini et al.,

32. https://en.wikipedia.org/wiki/Xanthine_oxidase_inhibitor#:~:text=In%20humans%2C%20inhibition%20of%20xanthine,for%20management%20of%20reperfusion%20injury
33. https://en.wikipedia.org/wiki/SGLT2_inhibitor
34. <https://www.who.int/teams/global-malaria-programme/reports/world-malaria-report-2021>
35. https://en.wikipedia.org/wiki/Alzheimer%27s_disease
36. El Khatabi K, Aanouz I, El-Mernissi R, Singh AK, Ajana MA, Lakhlifi T, Kumar S, Bouachrine M. Integrated 3D-QSAR, molecular docking, and molecular dynamics simulation studies on 1, 2, 3-triazole based derivatives for designing new acetylcholinesterase inhibitors. Turkish Journal of Chemistry. 2021 Jun 30;45(3):647-60.
37. https://en.wikipedia.org/wiki/Nonsteroidal_anti-inflammatory_drug
38. Abuo-Rahma GE, Abdel-Aziz M, Farag NA, Kaoud TS. Novel 1-[4-(Aminosulfonyl) phenyl]-1H-1, 2, 4-triazole derivatives with remarkable selective COX-2 inhibition: Design, synthesis, molecular docking, anti-inflammatory and ulcerogenicity studies. European Journal of Medicinal Chemistry. 2014 Aug 18;83:398-408.

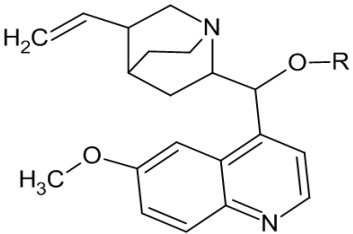
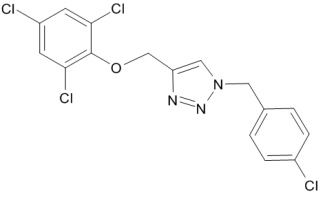
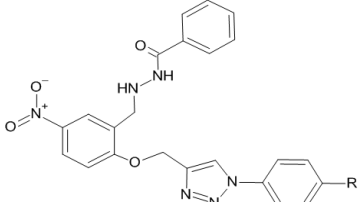
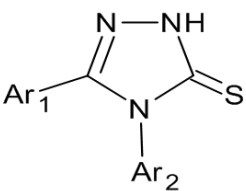
Table 01: Triazole derivatives and their pharmacological activities.

V/S-Triazole	Structure	Best Hits	Activity	Reference
V - triazole		Compound 5g – R ¹ -H R ² -CH ₃ R ³ -Cl R ⁴ -H	Antibacterial Antifungal Anti-oxidant	M.H. Shaikh et al [15].
V - triazole		Compound – 10 Glycoside- Propane-1,2-diol	Anti-cancer	El-Sayed WA. et al [16].
S - Triazole		Compound 7b - Oxane	Anticancer Hemolytic Thrombolytic	Irfan A et al [17].
S - Triazole		Compound A6 1-(3-methylphenyl)methanamine derivative	Antifungal	Qi L et al [18].
V - Triazole		3-[(1-methyl-1H-1,2,3-triazol-4-yl)methyl]-1,3-thiazolidine-2,4-dione derivative	A repurposing drug for covid-19	Chatterjee S et al [19].





Tejaswini *et al.*,

V - Triazole		R =	Anti-malarial	Hmamouchi AS <i>et al</i> [20].
V - Triazole		R = Cl	Anti-tubercular	Panigrahi D <i>et al</i> [21].
V - Triazole		Compound 5f R = Ortho Cl	Anti-tubercular Anti-microbial	Patil PS <i>et al</i> ²² .
S - Triazole		Compound 7a Ar ₁ = pyridine-3-yl Ar ₂ = 4-ClC ₆ H ₅	Anti-epileptic	Verma K Ket <i>et al</i> [23].

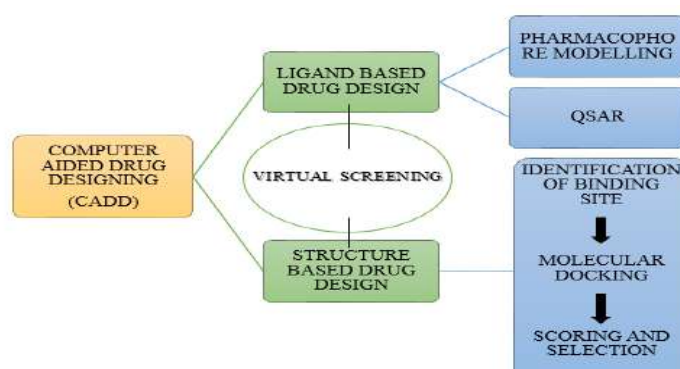


Figure 01: Flow chart of a computer aided drug designing





A Survey on Paddy Leaf Disease Detection using Machine Learning

Sreelakshmi J^{1*} and Denis.R²

¹Student, Department of Computer Science, Mount Carmel College, Bengaluru, Karnataka, India.

²Assistant Professor, Department of Computer Science, Mount Carmel College, Bengaluru, Karnataka, India.

Received: 14 Feb 2023

Revised: 23 Mar 2023

Accepted: 02 May 2023

*Address for Correspondence

Denis.R

Assistant Professor,
Department of Computer Science,
Mount Carmel College,
Bengaluru, India.
E. Mail: denisatshc@gmail.com



This is an Open Access Journal / article distributed under the terms of the **Creative Commons Attribution License** (CC BY-NC-ND 3.0) which permits unrestricted use, distribution, and reproduction in any medium, provided the original work is properly cited. All rights reserved.

ABSTRACT

The agricultural industry is vital in everyday life where paddy plays a significant role. Unfortunately, due to various diseases affecting the plant's leaves, farmers cannot produce the yield they had hoped for. As a result, quality, quantity, and production have been adversely affected. The process of identifying plant pathology by machine learning models could be automated, ensuring that diseases are identified in their early stages, allowing us to take the necessary steps to reduce the impact on yield. This can be a very effective way of ensuring that crops are healthy and thus maximize our yields. This paper briefly reviews plant leaf diseases like Brown Spot, Bacterial Leaf Blight, Leaf Smut etc, and their identification and detection.

Keywords: Convolutional Neural Network, Identification, Leaf Diseases, Machine Learning, Paddy

INTRODUCTION

The agricultural industry is crucial in delivering high-quality food and contributes most to expanding economies and populations worldwide. Plant diseases can significantly reduce food output and eliminate species variety [1]. Rice is an unavoidable food crop in the world majorly. Rice is a staple crop that many farmers rely on. Unfortunately, it is afflicted by a number of pathological causes like fungus, bacterial leaf blight, sheath blight, leaf smut, etc. The causes mentioned above affect not only the quality of the crop; but also the quantity and the overall production. Due to these conditions, farmers are unable to meet their expectations. Diagnosing the diseases is extremely difficult for farmers, leading to further problems and a decreased quality. Steps must be taken to ensure that the rice quality remains high and their expectation can be met [2]. Using precise or automatic detection methods, early identification of plant diseases can improve food quality production and reduce financial losses [1]. It is beyond dispute that,



**Sreelakshmi and Denis**

historically, farmers and plant pathologists have relied on their visual observations to identify mutations and reach conclusions based on their expertise. However, this method is often unreliable and can be biased, since symptoms appear to be the same during the preliminary stage. Furthermore, there is a need to pass this knowledge from generation to generation [3]. It is therefore essential to implement automated systems to prioritise their need and provide required support for the early detection of diseases with improved accuracy. In this process, machine learning plays a crucial role in the disease classification process [4]. Machine Learning is a subfield of Artificial Intelligence as it makes machines process similar to that of the human brain. "According to Arthur Samuel Machine Learning is defined as the field of study that gives computers the ability to learn without being explicitly programmed". Machine learning can process and deal efficiently with the data and the purpose of machine learning is to learn from the data [5]. Machine Learning depends on various methods and algorithms to find the solution. The choice of the algorithm depends on the dataset type or the problem addressed. Programmers and mathematicians heavily rely on the dataset to proceed with their work [5].

Background Study**Rice Leaf Disease Types****Brown Spot (BS)**

Leaves are affected here [6]. This disease could be identified prematurely as it develops brown oval or circular spots on the seedling leaf. The cause of this is *Bipolaris Oryzae*, a type of fungi that not only reduces the yield and can seriously affect the grain quality. It also spreads from plant to plant through the air which can destroy the entire yield [4].

Bacterial Leaf Blight (BLB)

Bacterial leaf blight is a bacteria that penetrates through hydathodes cutting wounds in the leaf tip and leading to the death of the seedling [4]. It typically affects rice plants and can be easily identified by yellow and white stripes on the leaves. The youngest leaf of an affected plant will appear pale yellow. Avoiding fertilizers with an excess of nitrogen is recommended to avoid the disease [7].

Leaf Smut

Mild rice illness in which the leaves are covered by fungus and the vertical scratches are found on the blade of the leaf with a slightly black color. This condition is called *Entyloma Oryzae*, sustainable horticulture and planting genetically modified resistant varieties could control it [4] [7].

Supervised Learning

Supervised learning plays a pivotal role in machine learning, allowing us to learn by mapping input to output with the input-output pairs. By using labeled training data, inference from training examples provides an effective way to gain insight into complex data. These need assistance or labeled datasets as they widely depend on the training set [5].

Unsupervised Learning

In unsupervised learning, there are no particular correct answers. Algorithms self-learn and there is no pre-labeled dataset. It learns from the features it exhibits. It always refers to the previously learned properties and features to understand and identify the dataset. It allows the algorithm to process as per the previously understood steps. K-means Clustering, Principal Component Analysis and Association are the categories of unsupervised learning [8] [5].

Reinforcement Learning

Reinforcement learning is an integral part of machine learning which focuses on the behavior of software agents taking actions to maximize their aggregate benefit. It is a part of the main machine learning paradigms, along with supervised learning and unsupervised learning, and is an invaluable tool for many applications. The method to be followed is decided by the reinforcement agent [5].



**Sreelakshmi and Denis****Neural Networks**

Neural networks algorithms aim to identify patterns in a given set of data, much like the way the human brain operates. They are composed of either organic or artificial neurons and can adapt to changing input, allowing them to generate good output without modifying the output criteria. Originating from artificial intelligence, it is quickly becoming popular in the advancement of trading systems [5]. Several algorithms were introduced based on these learning types. Algorithms appropriate for each process can give better accuracy performance and good results. Image Processing techniques could deploy the intention of identification and classification of the image dataset. The recent emergence of machine learning and deep learning techniques has been a game-changer in pathology. This breakthrough has enabled automatic classification and feature extraction to accurately capture the an image's intrinsic features, making the recognition process much more efficient [1]. Similarly, machine learning significantly contributes to every field like physics, healthcare, administrative data etc.

LITERATURE REVIEW

Nowadays, across the world, rice and especially in Asian countries, is considered to be a good source of food [4]. Since these crops are badly affected by the leaf disease, they are causing a significant loss in food grain productivity. Various ailments like brown spot, blast, leaf smut etc. are causing these illnesses. Deep learning techniques and ML have been a great advantage in scenarios that includes SVM, random forest, clustering, classification, CNN, ANN, pre-processing techniques etc. According to the dataset collected these supervised, unsupervised, semi-supervised and reinforcement techniques are employed to fetch the result. They tackle the leaf diseases at an earlier stage, so eradication becomes much more manageable and does not affect the productivity of the food grain [9].

The literature review summarises the prevailing research on machine-learning methodologies for paddy leaf disease diagnosis. Reviews include a narrated description of the various methods and algorithms used. Chi Yen *et al.* [10] put forth a technique using image processing to detect plant leaf diseases. Image acquisition is made in the initial stage, algorithms were made to observe the patterns, Random Forest model was constructed to learn these patterns and their results. K-means clustering was done for image segmentation [10]. The study was based on 180 images of different formats, sizes and resolutions collected from the Internet. The author has tested the images and could effectively identify and distinguish the paddy plant ailments with an overall precision of 93%.

Acharya *et al.* [11] proposed a model with an ensemble of CNN architectures including ResNet, Shuffle Net, Google Net, ResNeXt and Wide ResNet. 12 diseases in the fraction of 7:3 (training and testing) were used. The input image is pre-processed and fed to the ensemble of 5 training models. The accuracy is much higher for the four ensembles models than for single models as they reduce the bias. The author has mentioned that identification could be still improved using methods like the AdaBoost classifier. M *et al.* [12] The author used the Random Forest method because of its accuracy. The author used digital image processing with a data set containing almost 10,000 images of 5 different rice leaf diseases based on the parameters of temperature, humidity, rainfall, and pH. The author concluded that Random Forest Classifier gave higher accuracy than other algorithms like Naive Bayes, gradient boosting etc and the model also has a prediction accuracy of more than 85%. Geetharamani *et al.* [13] proposed an identification method with a plant village image set of 54,305 images of 13 different plant leaves, which were trained and tested based on deep CNN models. Different convolutions were performed with many layers of deep CNN. The comparison was made with various other models like SVM, decision tree, logistic regression and K-NN. The author concluded that the suggested model could achieve a precision of 96.4%, the max pooling method is better than average pooling and the model could perform well with the more enhanced dataset. Latif *et al.* [14] introduced a model with an upgraded VGG19-based transfer learning method, CNN with a dataset including five plant leaf diseases. The CNN models used include VGG16, DenseNet201, GoogleNet, VGG19 and Alex Net. DenseNet201 has the most accuracy compared to other CNN models [14] and obtained an average accuracy of 96.08% for the proposed modified approach. Payal *et al.* [15] introduced a hybrid machine learning alternative for paddy leaf disease identification. The author used 494 paddy leaf disease images for the training model and used RGB grey scale



**Sreelakshmi and Denis**

conversion for dimensionality reduction. TPR Loss of entropy, TNR, Accuracy Rate etc. parameters were used during the test domain. Detection and segmentation of the grey scale image were done with the K-Means clustering algorithm and PCA algorithm for feature extraction and an optimized BFO-MSVM classification method was used to classify the images. The proposed algorithm got an accuracy of 98.8% when compared to the existing Deep Learning (DL), DNN with the Jaya Optimization algorithm. The author concluded that WOLF and RCNN classifiers-hybrid approach could facilitate the faster process to minimize processing time and other factors. Harakannanavar *et al.*[16] used the plant village dataset of tomato leaf disease, proposed the model based on image processing and machine learning approach DWT+PCA+GLCM+CNN. HE and K-means clustering are employed for pre-processing, to maximize the quality and segment the leaf; features are extracted with DWT, PCA and GLCM. Classification is done with SVM, KNN and CNN and the proposed model gave higher accuracy than the other models. R.Sharma *et al.*[7] used the techniques of the CNN model for image processing, feature extraction and augmentation with three different classes of diseases and an accuracy of 90.32% was obtained in the testing phase. Hasan *et al.*[17] combined SVM classifier trained with the features extracted from the DCNN for feature extraction, transfer learning technique was used to improve the model. 1080 images were used as the dataset. The model achieved an accuracy of 95% and 94.6% using CNN-soft max software. Kamrul *et al.*[18] investigated using Inception v3, MobileNetV1 and Resnet50 Models of Convolutional Neural Network. Data augmentation and resizing were adopted in pre-processing with a dataset of 6 diseases. The model achieved a validation accuracy of 98%. A representation of the algorithms and their accuracy is presented in Table 1 Comparison of the various surveyed approaches.

CONCLUSION

Paddy is one of the major food crop in Asia. Paddy leaves getting affected by various diseases have seriously affected the yield and production of the crop. Machine learning methods could be used in the detection and identification of the disease. CNN approach has proven to give more accuracy during pre-processing as the dataset consists of images. The approaches like Random Forest, SVM also have given a higher accuracy rate in the identification process. The hybrid uses of Deep learning approaches have given more accuracy. There is a lot of scope in using these approaches combining several Deep CNN methods and they could be deployed on applications to identify diseases quickly.

REFERENCES

1. J. Andrew, J. Eunice, D. E. Popescu, M. K. Chowdary, and J. Hemanth, "Deep Learning-Based Leaf Disease Detection in Crops Using Images for Agricultural Applications," *Agronomy*, vol. 12, no. 10, Oct. 2022, doi: 10.3390/agronomy12102395.
2. V. G. Biradar, J. Shalini, R. S. Veena, and V. Prashanth, "Rice leaves disease classification using deep convolutional neural network," *Int. J. Health Sci. (Qassim)*, pp. 1218–1232, Apr. 2022, doi: 10.53730/ijhs.v6ns4.6067.
3. T. N. Pham, L. Van Tran, and S. V. T. Dao, "Early Disease Classification of Mango Leaves Using Feed-Forward Neural Network and Hybrid Metaheuristic Feature Selection," *IEEE Access*, vol. 8, pp. 189960–189973, 2020, doi: 10.1109/ACCESS.2020.3031914.
4. S. Venu Vasantha, B. Kiranmai, and S. Rama Krishna, "Techniques for Rice Leaf Disease Detection using Machine Learning Algorithms." [Online]. Available: www.ijert.org
5. M. Batta, "Machine Learning Algorithms - A Review," *Int. J. Sci. Res.*, vol. 18, no. 8, pp. 381–386, 2018, doi: 10.21275/ART20203995.
6. M. H. Tunio, L. Jianping, M. H. F. Butt, and I. Memon, "Identification and Classification of Rice Plant Disease Using Hybrid Transfer Learning," in *2021 18th International Computer Conference on Wavelet Active Media Technology and Information Processing, ICCWAMTIP 2021*, 2021, pp. 525–529. doi: 10.1109/ICCWAMTIP53232.2021.9674124.
7. R. Sharma, S. Das, M. K. Gourisaria, S. S. Rautaray, and M. Pandey, *A Model for Prediction of Paddy Crop Disease*





Sreelakshmi and Denis

- Using CNN, vol. 1119. Springer Singapore, 2020. doi: 10.1007/978-981-15-2414-1_54.
8. S. Ray, "A Quick Review of Machine Learning Algorithms," *Proc. Int. Conf. Mach. Learn. Big Data, Cloud Parallel Comput. Trends, Perspectives Prospect. Com.* 2019, pp. 35–39, 2019, doi: 10.1109/COMITCon.2019.8862451.
 9. P. Tejaswini, P. Singh, M. Ramchandani, Y. K. Rathore, and R. R. Janghel, "Rice Leaf Disease Classification Using Cnn," in *IOP Conference Series: Earth and Environmental Science*, 2022, vol. 1032, no. 1. doi: 10.1088/1755-1315/1032/1/012017.
 10. G. Chi Yen and L. Pei Ling, "Paddy Plant Disease Detection Using Image Processing," vol. 20, no. 3, pp. 13–17, 2021, [Online]. Available: www.elektrika.utm.my
 11. A. Acharya, A. Muvvala, S. Gawali, R. Dhopavkar, R. Kadam, and A. Harsola, "Plant Disease detection for paddy crop using Ensemble of CNNs," *2020 IEEE Int. Conf. Innov. Technol. INOCON 2020*, pp. 1–6, 2020, doi: 10.1109/INOCON50539.2020.9298295.
 12. S. A. M., "Rice Leaf Disease Detection and Crop Yield Prediction Using Random Forest," *Int. J. Eng. Res. Comput. Sci. Eng.*, vol. 9, no. 8, pp. 98–103, 2022, doi: 10.36647/ijercse/09.08.art018.
 13. G. Geetharamani and A. P. J., "Identification of plant leaf diseases using a nine-layer deep convolutional neural network," *Comput. Electr. Eng.*, vol. 76, pp. 323–338, Jun. 2019, doi: 10.1016/j.compeleceng.2019.04.011.
 14. G. Latif, S. E. Abdelhamid, R. E. Mallouhy, J. Alghazo, and Z. A. Kazimi, "Deep Learning Utilization in Agriculture: Detection of Rice Plant Diseases Using an Improved CNN Model," *Plants*, vol. 11, no. 17, Sep. 2022, doi: 10.3390/plants11172230.
 15. Kongunadu College of Engineering & Technology and Institute of Electrical and Electronics Engineers, *Proceedings, International Conference on Smart Electronics and Communication (ICOSEC 2020) : 10-12, September 2020*.
 16. S. S. Harakannanavar, J. M. Rudagi, V. I. Puranikmath, A. Siddiqua, and R. Pramodhini, "Plant leaf disease detection using computer vision and machine learning algorithms," *Glob. Transitions Proc.*, vol. 3, no. 1, pp. 305–310, Jun. 2022, doi: 10.1016/j.gltp.2022.03.016.
 17. M. J. Hasan, S. Mahbub, M. S. Alom, and M. Abu Nasim, "Rice Disease Identification and Classification by Integrating Support Vector Machine with Deep Convolutional Neural Network," *1st Int. Conf. Adv. Sci. Eng. Robot. Technol. 2019, ICASERT 2019*, vol. 2019, no. Icasert, pp. 1–6, 2019, doi: 10.1109/ICASERT.2019.8934568.
 18. M. H. Kamrul, P. Paul, and M. Rahman, "Machine vision based rice disease recognition by deep learning," *2019 22nd Int. Conf. Comput. Inf. Technol. ICCIT 2019*, pp. 1–6, 2019, doi: 10.1109/ICCIT48885.2019.9038350.

Table 1 Comparison of the Various Surveyed Approaches.

Author	Dataset	Algorithm	Accuracy(%)
Chi Yen et al. [10]	Internet Source(180 images)	Random Forest K-Means Clustering	93%
Acharya et al.[11]	Fr. C. Rodrigues Institute of Technology, India(dataset consisting of 1197 rice disease images)	GoogLeNet	82.95%
		ResNet18	91.16%
		Wide ResNet	91.33%
		ResNeXt	85.53%
		ShuffleNet	88.82%
	Ensemble model	95.54%	
M et al.[12]	Dataset contains almost 10,000 images of 5 different rice leaf diseases.	Random forest algorithm	85% and more





Sreelakshmi and Denis

Geetharamani et al.[13]	Plant village dataset(54,305 images of 13 different plant leaves)	Deep convolutional neural network (Deep CNN).	96.46%
Latif et al.[14]	Dataset has five rice leaf diseases.	Modified VGG19-based transfer learning method, CNN	96.08%
Payal et al.[15]	494 paddy leaves images	PCA with the BFO-MSVM classification algorithm	98.8%
Harakannanavar et al.[16]	The village database of tomato leaves with six disorders	(DWT+PCA+GLCM+CNN	99.09%
R.Sharma et al.[7]	Dataset of 3 types of disease	Convolutional Neural Network (CNN)	90.32%
Hasan et al.[17]	Images of rice plants from our research field, online sources	Support Vector Machine and deep CNN models	97.5%
Kamrul et al.[18]	BRRI Institute(600 images)	Models of CNN such as Inception -v3, MobileNet-v1, Resnet50	98%

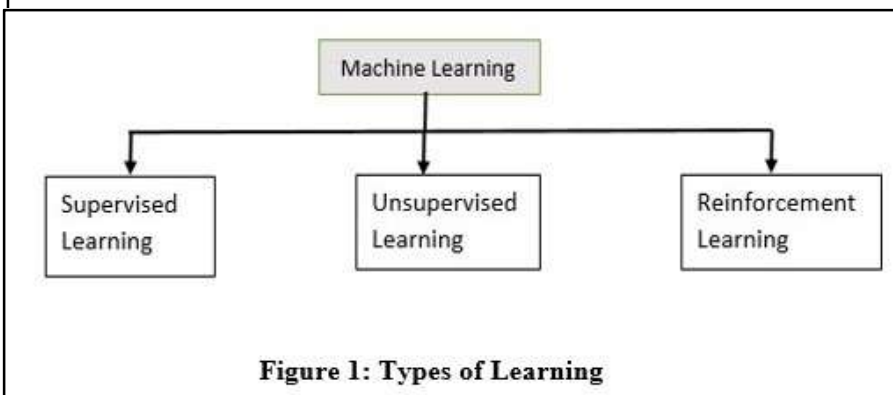


Figure 1: Types of Learning





Correlation between Palatal Rugae Pattern and Malocclusion by Employing Rugoscopy - A Retrospective Study

Lakshmi Ravi¹, Evan. A. Clement^{2*}, R.M Sushmita³, Zainab⁴, Malathi⁴ and Karthik. A⁴

¹Head of Department, Department of Orthodontics, Asan Memorial Dental College Chengalpattu, Tamil Nadu, India

²Reader, Department of Orthodontics, Asan Memorial Dental College, Chengalpattu, Tamil Nadu, India

³Tutor, Department Orthodontics, Asan Memorial Dental College Chengalpattu, Tamil Nadu, India.

⁴CRRI, Department Orthodontics, Asan Memorial Dental College Chengalpattu, Tamil Nadu, India.

Received: 16 Feb 2023

Revised: 04 Apr 2023

Accepted: 02 May 2023

*Address for Correspondence

Evan. A. Clement

Reader, Department of Orthodontics,
Asan Memorial Dental College,
Chengalpattu, Tamil Nadu, India



This is an Open Access Journal / article distributed under the terms of the **Creative Commons Attribution License** (CC BY-NC-ND 3.0) which permits unrestricted use, distribution, and reproduction in any medium, provided the original work is properly cited. All rights reserved.

ABSTRACT

The study aim to establish a relationship between palatal rugae pattern and malocclusion among population from Tamilnadu. This study involved of 140 Dental casts which were equally divided among male, female and class I and class II. Rugae was classified using Thomas and Kotze classification, variation in rugae shape is noted among different gender and malocclusion by using chi square analysis and one sample t test with help of SPSS 27 software. Angle's class I : The results of the above study suggests that wavy pattern (45%) was seen to be more common among Angle's class I population, followed by curve(23.8%) and straight(21.4%).whereas the remaining patterns of diverging converging, circular were 5.9%, 1.1%, 0.6%respectively, among which male casts revealed a majority of wavy pattern(4.6%)Angle's class II : The male patients revealed majority of wavy pattern(32.6%) followed by straight(27.3%), curve (26.5%), diverging(10.4%)and converging.(3.04)There is no circular pattern among class II male patients. . The female casts have more number of diverging rugae (17.5%) than males (10.4%).Both male and female casts revealed no circular pattern. our study reveals statistically significant variation in shape and total number of rugae between gender and malocclusion.

Keywords: Rugae, Kotze, Malocclusion, Raphae

INTRODUCTION

The irregular asymmetrical palatine folds on the anterior third of the palate are called as palatal rugae. Rugae are distributed on either side of mid palatine raphae, they extend till the first molar teeth (1). The rugae are composed of papules which are arranged in series of arrangements and is most aberrant in posterior fold. The folds are smallest where the membranes are thinnest and the largest where they are thickest. The transverse fold is the largest and lies





Lakshmi Ravi *et al.*,

between the canine teeth or between the canine or first bicuspid. The sutural rugae separate the maxillae and the pre-maxilla. Palatal rugae are irregular asymmetric rich of mucous membrane extending laterally from incisal papillae and the anterior part of mid palatine raphae (2) (3). The pattern shape and the characteristics are not affected by either eruption or loss of teeth.

As the palate grows in size, the size of rugae also increases but the shape remains same. The finger prints and dental remains are the most scientific and the most reliable method of identification, whereas the palatal rugae, bony protuberance, dental fillings are considered as second most odontogenic evidence of identification (6-8). Because the the clinicians to establish the identity through discrimination. There are several controversies that rugae shape differs between ethnic group, gender and various malocclusions. So the aim and objective of the present study is to evaluate and compare to structural morphology (number and pattern) of palatal rugae in patients with malocclusion and gender.

MATERIALS AND METHODS

This is a retrospective study conducted in the department of orthodontics and dentofacial orthopedics, ASAN MEMORIAL DENTAL COLLEGE AND HOSPITAL (AMDECH), CHENGALPET. A total of 140 dental casts above the age group of 18 were surveyed for the study. Other armentarium include color crayons and magnifying glass

Inclusion Criteria

Angle's class I and II malocclusion
Pretreatment cast from past 5 years
Permanent dentition
Above 18 years of age.

Exclusion Criteria

Primary dentition
Below 18 years of age
Angle's class III malocclusion
Patients with palatal defects

METHODOLOGY

A total of 140 casts were selected for the study. Out of which 35 were class I male, 35 were class I female, and 35 were class II male and class II female. After collecting the casts the rugae pattern were highlighted using color crayons, green for class I male, dark green for class II male, orange for class I female and red for class II female. This color coding was done for easy evaluation and identification of casts. The total number of rugae pattern were circular, Straight, diverging and converging according to THOMAS and KOTZ method of classification (1). The obtained data was tabulated and statistical analysis was done using chi square test and one sample t test with SPSS 27 software.

RESULTS

Angle's class I : The results of the above study suggests that wavy(45%) was seen to be more common among Angle's class I population, followed by curve(23.8%) and straight(21.4%).whereas the remaining patterns of diverging, converging, circular were 5.9%, 1.1%, 0.6% respectively, among which male casts revealed a majority of wavy pattern(4.6%) followed by curve, straight, diverging, converging and circular pattern, which were 24.4%, 23.5%, 3.3%, 1.4% and 0.4% respectively. whereas female casts did not shown any circular pattern of rugae, it exhibited 8.4% of diverging pattern and 1.7% of converging pattern. More than 20% was seen in straight (20.5%) and curve(24.1%) palatal rugae pattern. Similar to the male patients, female patients also revealed the highest percentage

57018





Lakshmi Ravi *et al.*,

among wavy pattern (45.08%)(Table 1&Table 2). Angle's class II: The male patients revealed majority of wavy pattern(32.6%) followed by straight(27.3%), curve (26.5%), diverging(10.4%)and converging(3.04%). There is no circular pattern among class II male patients. The female casts have more number of diverging rugae (17.5%) than males (10.4%). Both male and female casts revealed no circular pattern. A majority of wavy pattern is observed in females(36.9%) followed by straight(22.7%), curve(20.6%), diverging (17.5%) and converging(2.14%).

DISCUSSION

Palatal rugae are folds of irregular fibrous connective tissue located on anterior third of palate, and are called plica palatine. They are formed in 3rd month of intrauterine life and their orientation is formed by about 12th week of prenatal life. Palatal rugae have been shown to be highly individualized and consistent in shape throughout life. The anatomical position of rugae inside the oral cavity surrounded by cheek, lips, tongue and buccal pad of fat, also gives protection in case of trauma and inceration. It is widely acknowledged that there are limitations in identification by finger prints, dental records and DNA in forensic situations. Palatal rugae pattern of an individual maybe considered as an adjunct for identification tool(9-11).Thomas and kotz studied the rugae patterns of six South African populations to analyze the interracial difference(2). They found the rugae were unique to each ethnic group and it can be used successfully in race determination. They gave 6 patterns – curve, straight, wavy, circular, diverging and converging. Since then various studies followed Thomas and Kotz classification(1) of of palatal rugae.

Abeer*et.al* accessed palatal rugae pattern among growing individuals (6-12 yrs) of Egyptian and Saudi population(4), the results of the study suggested that among young Egyptian population curvy pattern was predominant (35%) followed by wavy (29%) and straight (20%). Whereas the Saudi growing individuals showed maximum number in wavy pattern(44.4%) followed by curve(28%) and straight (19%). The pattern of circular, crosslink and unification showed less than 5% in both the ethnic group. In another study done by S.kapali*et.al.*(5) where she compared the patterns between Aborigines and Caucasians. Both the ethnic group revealed highest phenotype of wavy pattern (40%-56.5%) followed by curve and straight pattern. The study also suggested that more than 15% Caucasians had straight type of pattern whereas aborigines revealed only 3% of straight pattern.

Kumar *et.al*, Made a study among Pondicherry population where he evaluated 100 male and 100 female(6). Where he suggested that wavy pattern was predominant among both males and females followed by curved and straight. The results of the present study is in association with the study done by kapali, Abeer and kumar *et. al.*, The above study revealed the highest percentage of palatal rugae pattern was wavy followed by curve and straight pattern. The above study also suggested that palatal rugae pattern among Angle's class I patients showed 45% of wavy pattern followed by curve and straight which was 21% to 24%. Based on gender Angle's class I males had a 4% increase in straight pattern when compared to female class I patients. Where the above study suggested that wavy pattern of 34.7% were seen predominant among angle class II patient compared to angle class I patient but straight pattern were seen more in number(25%).when compared to angle class I patient who exhibited only 2% of straight. Both malocclusions had 23% of wavy pattern.

The female patient among angles class II exhibited 17% of diverging pattern. circular rugae pattern were not seen among angles class II population as well as female part of class IKumar *et al.* Study(6) suggested that male has more number of rugae pattern when compared to female. this was not in accordance with result of above study. Females of both the class I and class II showed more number of rugae when compared to male population. The result of above study suggest that there is a significant difference among palatal rugae pattern in gender as well as the type of malocclusion





Lakshmi Ravi et al.,

CONCLUSION

Palatal rugae are considered unique for each individual. Rugoscopy can be used as a predominant tool in human investigation, on comparison of patterns of rugae wavy, curved, straight were seen more common in both the type of occlusion and male exhibited increased number of straight pattern whereas female exhibited maximum number of diverging pattern. Palatal rugae may serve as valuable indication on individual identification among various malocclusions, age, and sex determination

REFERENCES

1. Crystal Runa Sonas, Azhar Mohammed, Murali PS ,Mcqueen Mendonca, Prajwal Shetty , VartikaKumari. Morphology of palatal rugae in various sagittal skeletal malocclusion in kerala population –a retrospective study. indian journal of forensic medicine and toxicology apr 2020.
2. Thomas CJ ,Kotze TjvW.The palatal rugae pattern :a new classification .J dent AssocSouth Afr 1983 ;38:153-76.
3. Butchova,M., Ichy, F putnova, I and Misk, I :The development of paplatal rugae in the European pine vole , Microtus subterreneus (arviolic ,rodentia)V.h.valenula. J.S.P „Lopez ,Mc and Galdames,and dimensions for use in human identification int J Morphol 27:819-825 ,2009]
4. Abeer M, SalwaM,Awad and ShazaM.Hammad .Comparative study of palatal rugae shape in two samples of egyptian and saudichildren.pediatric dental journal 21(2):123-128,2011.
5. Kapali ,S.,Townsend ,G., Richards, L.and Parish ,t:palatal rugae in australian Aborigines and cacasians.Aust Dent J42:129-133,1997.
6. Kumar S, Vezhavendhan N, Shanthi V, Balaji N, Sumathi MK, VendhanP.Palatalrugoscopy among Puducherry population .J Contemp Dent Pract 2012;13(3):401-404.
7. Peavy,D.C and Kendrick ,G.S:The effects of tooth movement on the palantine rugae .JProst Dent 18:536-542,1967.
8. Limson, K.S. and Julian ,R:Computerized recording of the palatal rugae pattern and an evaluation of its application in forensic identification .JForensicOdontostomatol 22:1-4,2004.
9. KOtrashettiVS,HollikattiK,MallapurMD,HallikeremathSR,KaleAD.Determination of palatal rugae patterns among two ethnic populations of India by logistic regression analysis .JForensic Leg Med.2011;18(8):360-5.
10. Thomas CJ,KotzeTjvW.The palatal ruga pattern -II. Inter racial differences .J Dent Assoc South Afr 1983;38:166-72.
11. Thomas CJ,KotzeTjvW.The palatal ruga pattern in six southern african human populations. Part -1.A description of the population and a method for its investigation ,J Dent Assoc South Afr 1983;38:547-53.

Table 1: Mean and Standard deviation total number of rugae

	CURVED	STRAIGHT	CIRCULAR	WAVY	CONVERGING	DIVERGING	TOTAL
CLASS I	104	98	3	200	5	26	436
CLASS II	109	116	0	161	12	65	463
MEAN	106.50	107.00	1.50	180.50	8.50	45.50	449.50
SD	3.536	12.728	2.121	27.577	4.950	27.577	19.092
P-VALUE	.015	.053	.500	.069	.249	.258	.019
MALE	111	115	3	134	8	31	442
FEMALE	102	99	0	187	9	60	457
MEAN	106.50	107.00	1.50	160.50	8.50	45.50	449.50
SD	6.364	11.314	2.121	37.477	.707	20.506	10.607
P-VALUE	0.027	0.048	0.5	0.104	0.037	0.196	0.011





Lakshmi Ravi et al.,

Table 2: Mean and Standard Deviation of Rugae Pattern

INDIVIDUAL RUGAE	CHI SQUARE VALUE	P VALUE
CURVE	.000 ^a	1.000
STRAIGHT	.000 ^a	1.000
CIRCULAR	.000 ^b	1.000
WAVY	.000 ^a	1.000
CONVERGING	.000 ^a	1.000
DIVERGING	.000 ^a	1.000



Figure 1. Armentarium -Color crayons, Magnifying glass, Metal Scale and Maxilla-Dental cast





Influence of the Tool Materials on Material Removal Rate by EDM Process during Machining of SS-304

Manjeet Bohat^{1*} and Vikram²

¹Assistant Professor, Department of Mechanical Engineering, UIET, Kurukshetra University, Haryana, India.

²M.Tech Student, Department of Mechanical Engineering, UIET, Kurukshetra University, Haryana, India.

Received: 21 Feb 2023

Revised: 23 Mar 2023

Accepted: 02 May 2023

*Address for Correspondence

Manjeet Bohat

Assistant Professor,
Department of Mechanical Engineering,
UIET, Kurukshetra University,
Haryana, India.
E. Mail: msbohat2015@kuk.ac.in



This is an Open Access Journal / article distributed under the terms of the **Creative Commons Attribution License** (CC BY-NC-ND 3.0) which permits unrestricted use, distribution, and reproduction in any medium, provided the original work is properly cited. All rights reserved.

ABSTRACT

Electric Discharge Machining is based on principle of heat based erosion manufacturing and come under the non-conventional machining. Material is removed by erosion process by passing the spark between electrode and workpiece submerged under dielectric fluid. Many process parameters viz. current, sparking time, voltage etc. of EDM influence the manufacturing quality and output response viz. MRR, tool wear and surface roughness etc. In the present study three process parameter i.e. Current (I), pulse on time (T_{on}), and pulse of time (T_{off}) with one response parameter MRR. Two types of electrode made from copper and aluminium both size of 10mm diameter and 7 cm length, using SS-304 as work piece material on die sinking type EDM to prepare comparative study on MRR. Taguchi L9 orthogonal array is utilised to prepare Design of Experiments to optimize the process parameters for maximum material removal rate. 12 amp., 200 μ s and 7 μ s are the optimal process parameters values are observed current, pulse on time and pulse off time respectively. Current and pulse on time is directly proportional to higher MRR on the other hand pulse of time inversely proportional to MRR. A confirmation experiment is conducted on optimal values and noted the maximum MRR for both using copper electrode and aluminium electrode. It is calculated that MRR in case of copper is 104.54% more than in case of aluminium.

Keywords: non-Conventional machining, SS-304, EDM, Copper electrode, Aluminium electrode, Material Removal Rate, optimization.



**Manjeet Bohat and Vikram**

INTRODUCTION

From the study of past and today industrial area, it has been clear seen that industries develops various machining methods for various materials. At present manufacturing industries faces challenges related to machining of materials which has rigorous design requirements (Bending stiffness, good fatigue characteristics, noble damping capacity, high precision, small thermal expansion, and high surface quality) and the cost of machining. Industries face difficulty to machining material like ceramics, super alloys and composites due to their mechanical properties. In past recent years there is a trend to use of compact and light weight mechanical components. Due to this industries has been shows the interest in advanced materials which full fills all the requirements of design [1]. In general machining is to be carried out in two ways first one is convectional and another one is the non-convectional. In non-convectional type of machine process machining is to be done by using energy sources like as ions energy, chemical energy, electrical energy, and electrons energy the new concept for the machining [2]. Non-convectional machining process does not employ the direct contact for the material removal and one form of energy. From past study we observes that EDM was used for the machining of advanced material which require the high design accuracy, size and desired shape. In EDM machining process which electrical conductive materials are machined the help of conductive spark that occurs between the tool and work material submerged in the Dielectric fluid. It utilizes electrical energy for the machining of material has low machine-ability complicated design of irrespective hardness has been its different characteristics [3]. There is no direct contact between electrode and work material in EDM machining and controlled by servo-control mechanism. There is various type of EDM process are available but here the study is concern about the sinker type of EDM machine. Now convectional machining operations are replaced by EDM machining and it is a better machining option in machining manufacturing industries. Material properties like mechanical and physical are no barrier in EDM application make it is a popular method for machining [3]. In 1940s Sir Joseph Priestley an England scientist discover EDM technique and after that it world-wide accepted. But for their practical use in manufacturing industries it take about a century.

Two types of EDM machines are employed for machining i.e. Sinker EDM machine and Wire-Cut EDM machine. In Sinker Die Machine a periodical electric discharge flow between tool and workpiece that are immersed in insulated dielectric fluid and feed with suitable range of power supply [4]. In Die Sinking EDM Tool, made up of in desired shape, is mounted on EDM in vertical position and moves in the same direction. To maintain the suitable gap between tool and workpiece, Servo control unit is used to control the voltage gap to drive up and down the machine ram. Spark gap is the gap maintained between the tool and workpiece and its range lies from 0.01 to 0.5. During machining both tool and workpiece with constant spark gap must be immersed in dielectric fluid [5]. Kerosene provides higher dimension accuracy, better surface finish and lower tool wear so it mostly used in EDM process. Copper and brass are the materials which are commonly used as tool in the EDM process. The thermo-electrical source of energy is used for the machining of complicated intrinsic and extrinsic shape of regardless hardness and low machine-ability is its different characteristics [6]. For EDM machining both tool and workpiece are must be electrical conductive. EDM has wide no. of application in manufacturing automobile tool, forging die, press tool, plastic mould die and also has the application in aerospace and nuclear industries. In Wire-Cut EDM process, the material removal is to be carried out by the plasma channel which generated with the help of electrical spark which is generated between the two electrodes (i.e. workpiece and tool) [7]. The plasma channel is to be converted into the thermal energy of 8000°C to 12000°C range at the supply of direct current of frequency range 20000Hz to 30000 Hz. In this process both tool and workpiece are separated by a little gap and submersed into the dielectric fluid. A spark is to be produced in the gap which results to metal removal from the workpiece. For proceed this we use a 0.05 to 0.3 mm in diameter wire of copper, brass and steel is used and the resistivity is controlled by the use of de-ionized water as a dielectric medium which directly inject around it and the circulation of the dielectric is to be done with the help of pump and circulating system.



**Manjeet Bohat and Vikram****Experimental Details**

In this work SS-304, as shown in fig., 1, is used as workpiece material and two types of cylindrical shaped tool material (electrode) made from viz. copper and aluminium are used for machining as shown in fig. 2. Three input parameters i.e. pulse on (T_{on}) time, pulse off (T_{off}) time and current (I) has been adopted and material removal rate (MRR) is the response of the work. Electric Discharge Machine, Model ELEKTRA-EMS 5535 at CITCO Centre, Phase-1 Chandigarh, India is used for machining as shown in fig.3. Orthogonal array L9 of statistical approach is utilised to perform the lesser number of experiments basses of larger the better characteristics for the material removal rate for each electrode. An electrical weighing capacity of 500gm machine is used to weight the work piece after and before the experiment for calculating the MRR. After the initial trials, the value of input parameters is chosen as shown in table 1. Input parameters are optimized by Taguchi method to increase the MRR.

FINDINGS AND DISCUSSION

Table 1 shows the experimental range of three input parameters designed by the Taguchi. Weight of the work piece before machining and after machining is observed corresponding to the experimental array.

Analysis of MRR

Fig 4 and 5 shows that as the current rises the MRR also grow in both the cases of using copper electrode and using aluminium electrode respectively due to current have great impact on MRR. Graphs also reveals that the MRR is more in the case of using copper electrode as comparison to using aluminium electrode because of copper electrode properties favors effective electric mechanism between workpiece and electrode that leads higher MRR. Moreover the electrical conductivity of copper material is high as compare to the aluminium material in addition, the thermal conductivity and other properties like density, melting point, yield strength etc. are better than that of aluminium. It is calculated from the table 2 that MRR using copper electrode is averagely 104.54% more than that from the using aluminium electrode. Fig.6 also support the claim done by the fig. 4 and 5.

Analysis of Response

Delta is the Maximum value minus minimum value. Rank first, second and third is given on the basses of descending delta value, means high delta value go higher rank. Delta and rank values are 10.81, 4.43 and 0.28 and 1, 2, and 3 value for the current, pulse on time and pulse off time for copper electrode as shown in fig 4. Delta and rank values are 7.95, 4.49 and 0.32 and 1, 2, and 3 value for the current, pulse on time and pulse off time for aluminium electrode as shown in fig 5. It is observed from the table that current is on first rank for both copper electrode and aluminium electrode followed by pulse on time and further followed by pulse off time. It is concluded from the data given in table 4 and 5 MRR is directly proportional to the Current and pulse on time and inversely proportional to pulse off time.

Analysis of Variance

The analysis of variance for S/N ratio by using copper and Aluminium electrode is shown in table 6 and table 7 respectively. The P value finds out the best significant process parameters. The process parameter contains high F value gets small P value that remains less than 0.05 with 95% confidence level. Table clearly shows that the current is most significant process parameter with the P value of 0.007 which is less than 0.05 for using copper electrode as well as using aluminium electrode and on the other hand pulse off time is non-significant process parameter for maximizing material removal rate.

Main Effect Plots

The main effect plot for S/N ratio and means for the copper electrode and Aluminium electrode are shown in fig.7, 8, and 9, 10 respectively. It is summarised that MRR is increased as current and pulse on time is increased. Further could be stated that MRR is directly proportional to the current and pulse on time while machining with copper electrode as well as aluminium electrode. Graphs shows that the MRR is more in case of copper electrode because





Manjeet Bohat and Vikram

of high thermal conductivity of copper as comparison to aluminium electrode. Current and pulse on time as both increases the diameter of plasma region also grow results lot of ions from the electrodeush towards work piece and thus, the material removal from the work piece is more. Confirmation experiment is conducted with suggested optimised input parameters values by the Taguchi method as shown in table 8 and MRR is observed using copper electrode is 0.01995 and using aluminium electrode is 0.00987. In the confirmation experiment MRR using copper electrode is 102.12 % is more than that of using aluminium electrode.

CONCLUSIONS

1. Copper electrode provides more MRR averagely 104.54% as compare to an aluminium electrode.
2. Current is the significant factor tailed by pulse on time and further trailed by pulse off time for maximum MRR.
3. As both current and pulse on time upsurges, the MRR also rises i.e. MRR is directly proportional to the current and pulse on time.
4. Pulse off time has negligible effect on MRR.As the pulse off time increases, the MRR decreases i.e. MRR has inverse relation with pulse off time.

REFERENCES

1. Gupta V.K., Prasad R.B., "Optimization of MRR in Sinker EDM Process Using Generic Algorithm Technique". International Journal of Advance Engineering and Research Development, Vol.3, PP.357-362,2016.
2. Arya G., Garg S.K., "Experimental investigation to identify the parametric effect on material removal rate and electrode wear rate during PMEDM." International Journal of Engineering Technology Science and Research, Vol. 3, P.P 304-313, 2016.
3. Dhull R.S., Dhull U., "Parametric Optimization of Electric Discharge Machining of SCM 415 Alloy Steel Material using Taguchi's Technique". International Journal of Research in Advent Technology, Vol.4, PP.87-94,2016.
4. Karande P.S., Mujawar J.S., "Effect of EDM process parameter on tool wear using EN-31 Steel tool." International Journal of Innovation in Engineering Research and Technology, Vol.1,P.P972-1982,2016.
5. Mujawar J., Karande P.S., "Effect of EDM Process Parameter on Surface Roughness Using AISI D2 Material." International Journal of Innovation in Engineering, Research and Technology, Vol.2, P.P 2014-2023,2016.
6. Abrol A., Sharma S., "Effect of Chromium Powder Mixed Dielectric on Performance Characteristics of AISI D2 Die Steel Using EDM". International Journal of Research in Engineering and Technology, Vol.4, PP.232-246,2015.
7. Gudur S., Potdar V.V., "Effect of Silicon Carbide Powder Mixed EDM on Machining Characteristics of SS 316 L Material". International Journal of Innovative Research in Science, Engineering and Technology, Vol.4, PP.2003-2007,2015.
8. Ramu B., Ganesh V., Sirinivasulu K., "Experimental Investigation on Powder Mixed Electrical Discharge Machining". International Journal of Engineering Research & Technology, Vol.3, PP.102-113,2014.
9. Prajapati U., Prajapati J., Modi P., Banker K.S., "A Review of Parameter Optimization of Electro Discharge Machine by Using Taguchi Method". International Journal of Scientific Research and Development, Vol.2, PP.94-96,2014.
10. Pandey V.P., Mall R.N., "Analysis of material removal rate of AISI 304 SS in EDM process." International Journal for Scientific Research and Development, Vol. 2, PP.209-212,2014.
11. Gaikwad A., Tiwari A., Kumar A., Singh D., "Effect of EDM Parameters in Obtaining Maximum MRR and Minimum EWR By Machining SS 316 Using Copper Electrode". International Journal of Mechanical Engineering and Technology, Vol. 5, PP.101-109,2014.
12. Dhakry N.S., Prof. Bangar A., Bhaduria G., "Analysis of Electro Discharge Machining of Tungsten Carbide by Using Taguchi". International Journal of Engineering Research and Applications, Vol.4, PP.661-669,2014.
13. Ahmad S., Lajij M.A., "Electric Discharge Machining of Inconel 718 by using Copper Electrode at Higher Peak Current and Pulse Duration". International Conference on Mechanical Engineering Research, Vol.50, PP.1-7,2013.
14. Chikalthankar S.B., Nandedkar V.M., Borde S.V., "Experimental Investigations of EDM parameter". International Journal of Engineering Research and Development, Vol.7, PP.31-34,2013.





Manjeet Bohat and Vikram

15. Raghuraman S., Thirupathi K., Panneerselvam T., Santosh S., "Optimization of EDM parameters using Taguchi Method and Grey Relational Analysis for Mild Steels 2026". International Journal of Innovative Research in Science, Engineering and Technology, Vol.2, PP.3095-3104, 2013.
16. Sahoo M., Pramanik R.N., Sahoo D.R., "Experimental Investigation of Machining of Tungsten Carbide by EDM and Its Mathematical Expression". International Journal of Mechanical and Production Engineering, ISSN: 2315-4489, Vol-2, PP.1265-1276, 2013.
17. Bergaley A., Sharma N., "Optimization of Electrical and Non Electrical Factors in EDM For Machining Die Steel Using Copper Electrode by Adopting Taguchi Technique". International Journal of Innovative Technology and Exploring Engineering, Vol.3, PP.44-48, 2013.

Table 1: Parametric Setting and corresponding MRR

Run	I (amp)	T _{on} (μs)	T _{off} (μs)	Copper Electrode		Aluminium Electrode	
				Weight of work-piece before machining (g)	Weight of work-piece after machining (g)	Weight of work-piece before machining (g)	Weight of work-piece after machining (g)
1	6	100	7	265.67	265.57	276.78	276.73
2	6	150	9	265.57	265.43	276.73	276.66
3	6	200	11	265.43	265.23	276.66	276.56
4	9	100	9	265.23	265	276.56	276.44
5	9	150	11	265	264.73	276.44	276.30
6	9	200	7	264.73	264.38	276.30	276.13
7	12	100	11	264.38	264.01	276.13	275.94
8	12	150	7	264.01	263.51	275.94	275.69
9	12	200	9	263.51	262.91	275.69	275.39

Table 2: MRR for Copper and Aluminium Electrode

Run	I (amp)	T _{on} (μs)	T _{off} (μs)	MRR(g/min)		Difference of cu MRR in %age with Al MRR
				With Copper Electrode	With Aluminium Electrode	
1	6	100	7	0.00332	0.00160	107.50
2	6	150	9	0.00457	0.00225	103.11
3	6	200	11	0.00663	0.00310	113.8710
4	9	100	9	0.00757	0.00371	104.04
5	9	150	11	0.00896	0.00441	103.17
6	9	200	7	0.01137	0.00559	103.39
7	12	100	11	0.01224	0.00605	102.31
8	12	150	7	0.01666	0.00826	101.69
9	12	200	9	0.01974	0.00978	101.84
average of Copper MRR more than aluminium MRR in percentage						104.54%

Table: 4 Response table for copper electrode

Level	I	T _{on}	T _{off}
1	-46.78	-43.41	-14.34
2	-40.75	-41.11	-14.10
3	-35.97	-38.98	-14.06
Delta	10.81	4.43	0.28
Rank	1	2	3





Manjeet Bohat and Vikram

Table: 5 Response table for Aluminium electrode

Level	I	Ton	Toff
1	-50.02	-49.63	-47.54
2	-46.93	-47.24	-47.25
3	-42.07	-45.14	-47.22
Delta	7.95	4.49	0.32
Rank	1	2	3

Table:6 Analysis of Variance for S/N Ratio using Copper Electrode

Source	DF	Seq SS	AdjMS	F	P	
I	2	176.245	88.122	137.99	0.007	Significant
Ton	2	29.454	114.727	23.06	0.042	
Toff	2	0.141	0.071	0.11	0.901	Not significant
Error	2	1.277	0.639			
Total	8	207.116				

Table:7 Analysis of Variance for S/N Ratio using Aluminium Electrode

Source	DF	Seq SS	AdjMS	F	P	
I	2	180.382	90.191	133.69	0.007	Significant
T _{on}	2	30.314	15.157	22.47	0.043	
T _{off}	2	0.192	0.096	0.14	0.875	Not significant
Error	2	1.349	0.675			
Total	8	212.236				

Table: 8 Optimised input parameters values and MRR from confirmation experiment

Suggested Optimum Value			Values From Confirmation Experiment		
I (amp)	T _{on} (µs)	T _{off} (µs)	MRR(g/min)		Difference of cu MRR in %age with Al MRR
			With Copper Electrode	With Aluminium Electrode	
12	200	7	0.01995	0.00987	102.12



Fig. 1 Work Material SS-304



Fig. 2 Tool Materials

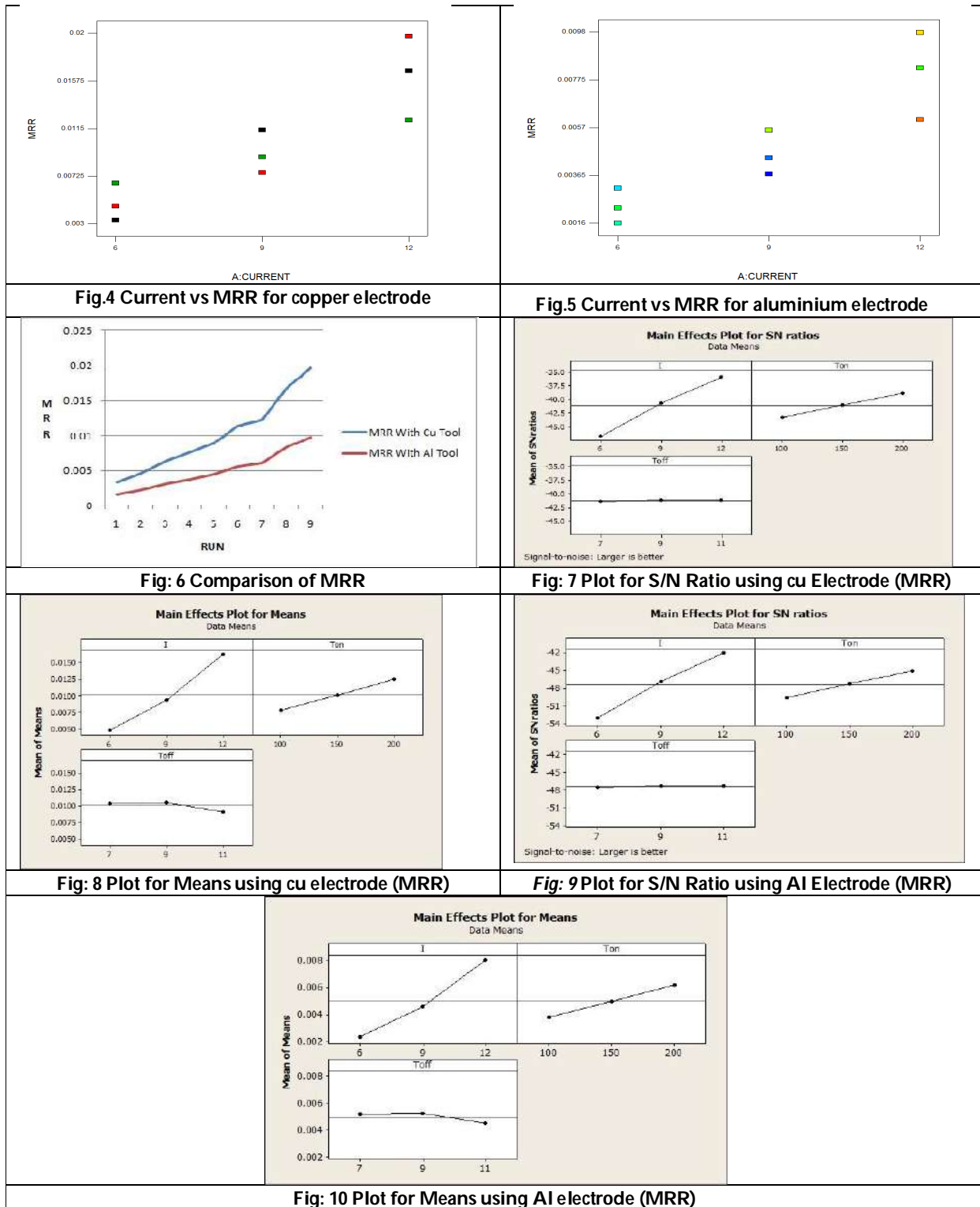


Fig.3 EDS Machine Setup





Manjeet Bohat and Vikram





New Results in Neutrosophic Soft Matrix using Multiplicative Operators

K. Lalitha^{1*}, and S. Sarguna²

¹Assistant Professor, Annamalai University, (Deputed to Thiru Kolanjiappar Government Arts College, Vriddhachalam 606 001), Tamil Nadu, India.

²Research Scholar, Department of Mathematics, Annamalai University, Chidambaram 608 002, Tamil Nadu, India

Received: 28 Dec 2022

Revised: 03 Mar 2023

Accepted: 05 May 2023

*Address for Correspondence

K.Lalitha

Assistant Professor,

Annamalai University,

(Deputed to Thiru Kolanjiappar Government Arts College, Vriddhachalam 606 001), Tamil Nadu, India.

E. Mail: sudhan_17@yahoo.com



This is an Open Access Journal / article distributed under the terms of the **Creative Commons Attribution License** (CC BY-NC-ND 3.0) which permits unrestricted use, distribution, and reproduction in any medium, provided the original work is properly cited. All rights reserved.

ABSTRACT

The Multiplicative operations over Neutrosophic Soft Matrix(NSM) have discussed in this paper. And some of the properties of X_1 and X_2 over NSM are explained. Distributive laws, max-max-min, min-min-max composition together the multiplicative operations are proved and established some concepts.

Keywords: Neutrosophic set, Neutrosophic soft set, Neutrosophic soft matrix, Multiplicative operators.

INTRODUCTION

Smarandache [8] initiated the idea of Neutrosophic fuzzy sets(NFS) which is the extension of Intuitionistic fuzzy sets. The elements of NFS are in the form of trio. Insertion of the elements lies between 0 and 3. Elements of NFS indicates accuracy, falsity and indefinite. Murugadas P, Balasubramaniyan.K, Vanmathi [6] launched the concepts, which is decomposition of Neutrosophic fuzzy Matrices. Some results associated with the max-min,max-max composition of bifuzzy matrices was explained by E.G.Emam and M.A.Fndh [4]. Intuitionistic fuzzy sets and systems was initiated by K.Atanassov [1,2]. Arithmetic operations on Intuitionistic on Mathematical sciences discussed the concepts of A.J.Boobalan and S.Sriram [3]. Many ideas about Multiplicative operators using Intuitionistic fuzzy matrices was discussed by D.Venkatesan , S.Sriram [9,10,11]. In Modern world many fields facing the problem in indeterminacy. In such types neutrosophic fuzzy sets helps to solve the indeterministic form. Application of NFS is used in many field like Medical diagnosis, Business, networking etc. In this paper we see the multiplicative operators in NFM and some properties. The Multiplicative operations over NFM have discussed in this paper. And some of the properties of X_1 and X_2 over NFM are explained. Distributive laws, max-max-min, min-min-max composition together the multiplicative operations are proved and established some concepts.





Lalitha and Sarguna

Preliminaries

Definition 2.1[6]

The Elements of Neutrosophic soft matrix (NSM) is in the form of triplets and it is defined as $\check{X} = \{ \langle \chi_{cd}^A, \chi_{cd}^I, \chi_{cd}^F \rangle \}$. whose values are non-negative real numbers and $\chi_{cd}^A, \chi_{cd}^I, \chi_{cd}^F$ are belongs to $[0,1]$. And sum of $\chi_{cd}^A, \chi_{cd}^I, \chi_{cd}^F$ lies between 0 and 3 for all c, d .

Definition 2.2[6]

For any two NSMs \check{X} and \check{L} of equal size, then

The min-min-max combination of \check{X} and \check{L} is defined by

$$\check{X} \vee \check{L} = \{ \langle \max(\chi_{cd}^A, \lambda_{cd}^A), \max(\chi_{cd}^I, \lambda_{cd}^I), \min(\chi_{cd}^F, \lambda_{cd}^F) \rangle \}$$

The max-max-min combination of \check{X} and \check{L} is defined by

$$\check{X} \wedge \check{L} = \{ \langle \min(\chi_{cd}^A, \lambda_{cd}^A), \min(\chi_{cd}^I, \lambda_{cd}^I), \max(\chi_{cd}^F, \lambda_{cd}^F) \rangle \}$$

Definition 2.3

The Zero NSM of order $c \times d$ is denoted as $O = \{ \langle 0,0,1 \rangle \}$

The universal NSM of order $c \times d$ is denoted as $J = \{ \langle 1,1,0 \rangle \}$

Definition 2.4[6]

For any two NSMs \check{X} and \check{L} of equal size. If $\check{X} \leq \check{L}$ iff $\chi_{cd}^A \leq \lambda_{cd}^A, \chi_{cd}^I \leq \lambda_{cd}^I, \chi_{cd}^F \geq \lambda_{cd}^F$. If $\check{X} = \check{L}$ iff $\chi_{cd}^A = \lambda_{cd}^A, \chi_{cd}^I = \lambda_{cd}^I, \chi_{cd}^F = \lambda_{cd}^F$

For any two NSMs \check{X} and \check{L} of equal size. If $\check{X} \geq \check{L}$ iff $\chi_{cd}^A \geq \lambda_{cd}^A, \chi_{cd}^I \geq \lambda_{cd}^I, \chi_{cd}^F \leq \lambda_{cd}^F$

Definition 2.5[6]

The Complement of any NSM is defined as $\check{X}^c = \{ \langle \chi_{cd}^F, \chi_{cd}^I, \chi_{cd}^A \rangle \}$.

Lemma 2.6

Let χ, λ and \varkappa be real numbers. The following equalities hold

- a. $\max(\chi, \min(\chi, \lambda)) = \chi$
- b. $\min(\chi, \max(\chi, \lambda)) = \chi$
- c. $\max(\chi, \max(\lambda, \varkappa)) = \max(\max(\chi, \lambda), \varkappa)$
- d. $\min(\chi, \min(\lambda, \varkappa)) = \min(\min(\chi, \lambda), \varkappa)$

Lemma 2.7

Let χ, λ and \varkappa be real numbers. Then

- a. $\max(\chi, \min(\lambda, \varkappa)) = \min(\max(\chi, \lambda), \max(\chi, \varkappa))$
- b. $\min(\chi, \max(\lambda, \varkappa)) = \max(\min(\chi, \lambda), \min(\chi, \varkappa))$
- c. $\max(\chi, \lambda) \max(\chi, \varkappa) \leq \max(\chi, \lambda \varkappa)$
- d. $\min(\chi, \lambda) \min(\chi, \varkappa) \geq \min(\chi, \lambda \varkappa)$

Main Results using X_1 and X_2

Definition 3.1

For any two NSMs \check{X} and \check{L} of equal size. Then X_1 and X_2 is defined as

- a) $\check{X} X_1 \check{L} = \{ \langle \max(\chi_{cd}^A, \lambda_{cd}^A), \max(\chi_{cd}^I, \lambda_{cd}^I), \chi_{cd}^F \lambda_{cd}^F \rangle \}$
- b) $\check{X} X_2 \check{L} = \{ \langle \chi_{cd}^A \lambda_{cd}^A, \chi_{cd}^I \lambda_{cd}^I, \max(\chi_{cd}^F, \lambda_{cd}^F) \rangle \}$

Proposition 3.2

If \check{X} and \check{L} are any two NSMs of equal size, then $\check{X} X_2 \check{L} \leq \check{X} X_1 \check{L}$.

Proof

Let $\check{X} = \{ \langle \chi_{cd}^A, \chi_{cd}^I, \chi_{cd}^F \rangle \}$,

$\check{L} = \{ \langle \lambda_{cd}^A, \lambda_{cd}^I, \lambda_{cd}^F \rangle \}$ be any two NSMs of equal size.

By definition 3.1





Lalitha and Sarguna

$$\check{X}X_1\check{L} = \{ \langle \max(\chi_{cd}^A, \lambda_{cd}^A), \max(\chi_{cd}^I, \lambda_{cd}^I), \chi_{cd}^F \lambda_{cd}^F \rangle \}$$

$$\check{X}X_2\check{L} = \{ \langle \chi_{cd}^A \lambda_{cd}^A, \chi_{cd}^I \lambda_{cd}^I, \max(\chi_{cd}^F, \lambda_{cd}^F) \rangle \}$$

Since $\chi_{cd}^A \lambda_{cd}^A \leq \max(\chi_{cd}^A, \lambda_{cd}^A)$, $\chi_{cd}^I \lambda_{cd}^I \leq \max(\chi_{cd}^I, \lambda_{cd}^I)$
 $\chi_{cd}^F \lambda_{cd}^F \leq \max(\chi_{cd}^F, \lambda_{cd}^F)$
 Therefore $\check{X}X_2\check{L} \leq \check{X}X_1\check{L}$.

Proposition 3.3

For any three NSMs \check{X} , \check{L} and \check{E} of equal size, then

- a) $\check{X}X_1\check{L} = \check{L}X_1\check{X}$
- b) $\check{X}X_2\check{L} = \check{L}X_2\check{X}$
- c) $(\check{X}X_1\check{L})X_1\check{E} = \check{X}X_1(\check{L}X_1\check{E})$
- d) $(\check{X}X_1\check{L})X_1\check{E} = \check{X}X_1(\check{L}X_1\check{E})$

Proof

a) $\check{X}X_1\check{L} = \{ \langle \max(\chi_{cd}^A, \lambda_{cd}^A), \max(\chi_{cd}^I, \lambda_{cd}^I), \chi_{cd}^F \lambda_{cd}^F \rangle \}$ (1)

$\check{L}X_1\check{X} = \{ \langle \max(\lambda_{cd}^A, \chi_{cd}^A), \max(\lambda_{cd}^I, \chi_{cd}^I), \lambda_{cd}^F \chi_{cd}^F \rangle \}$ (2)

From (1) and (2) $\check{X}X_1\check{L} = \check{L}X_1\check{X}$

Similarly, $\check{X}X_2\check{L} = \check{L}X_2\check{X}$

c) $(\check{X}X_1\check{L})X_1\check{E} = \check{X}X_1(\check{L}X_1\check{E})$

$(\check{X}X_1\check{L})X_1\check{E} = \{ \langle \max(\max(\chi_{cd}^A, \lambda_{cd}^A), \xi_{cd}^A), \max(\max(\chi_{cd}^I, \lambda_{cd}^I), \xi_{cd}^I), \chi_{cd}^F \lambda_{cd}^F \xi_{cd}^F \rangle \}$ (3)

$\check{X}X_1(\check{L}X_1\check{E}) = \{ \langle \max(\chi_{cd}^A, \max(\lambda_{cd}^A, \xi_{cd}^A)), \max(\chi_{cd}^I, \max(\lambda_{cd}^I, \xi_{cd}^I)), \chi_{cd}^F \lambda_{cd}^F \xi_{cd}^F \rangle \}$ (4)

From (3) and (4) $(\check{X}X_1\check{L})X_1\check{E} = \check{X}X_1(\check{L}X_1\check{E})$

Similarly, we can also prove (d)

Proposition 3.4

Let \check{X} be any NSM, then $\check{X}X_1\check{X} \neq \check{X}$ and $\check{X}X_2\check{X} \neq \check{X}$

Proof:

$\check{X} = \{ \langle \chi_{cd}^A, \chi_{cd}^I, \chi_{cd}^F \rangle \}$,

$\check{X}X_1\check{X} = \{ \langle \max(\chi_{cd}^A, \chi_{cd}^A), \max(\chi_{cd}^I, \chi_{cd}^I), \chi_{cd}^F \chi_{cd}^F \rangle \}$
 $\neq \{ \langle \chi_{cd}^A, \chi_{cd}^I, \chi_{cd}^F \rangle \}$

Hence $\check{X}X_1\check{X} \neq \check{X}$

And also $\check{X}X_2\check{X} \neq \check{X}$

Proposition 3.5

- a) $\check{X}X_1O = \check{X}$
- b) $\check{X}X_1J = J$
- c) $\check{X}X_1O = \check{X}$
- d) $\check{X}X_2J = \check{X}$
- e) $\check{X}X_1(\check{L}X_2\check{E}) \neq (\check{X}X_1\check{L})X_2(\check{X}X_1\check{E})$
- f) $\check{X}X_1(\check{L}X_2\check{E}) \neq (\check{X}X_1\check{L})X_2(\check{X}X_1\check{E})$
- g) $\check{X}X_1(\check{L}X_2\check{E}) \neq \check{X} : \check{X}X_2(\check{L}X_1\check{E}) \neq \check{X}$

Proof

a) $\check{X}X_1O = \{ \langle \max(\chi_{cd}^A, 0), \max(\chi_{cd}^I, 0), \chi_{cd}^F 1 \rangle \} = \check{X}$

Similarly we can prove (b),(c),(d)

e) To Prove $\check{X}X_1(\check{L}X_2\check{E}) \neq (\check{X}X_1\check{L})X_2(\check{X}X_1\check{E})$
 $(\check{L}X_2\check{E}) = \{ \langle \lambda_{cd}^A \xi_{cd}^A, \lambda_{cd}^I \xi_{cd}^I, \max(\lambda_{cd}^F, \xi_{cd}^F) \rangle \}$

$\check{X}X_1(\check{L}X_2\check{E}) = \{ \langle \max(\chi_{cd}^A, \lambda_{cd}^A \xi_{cd}^A), \max(\chi_{cd}^I, \lambda_{cd}^I \xi_{cd}^I), \chi_{cd}^F \max(\lambda_{cd}^F, \xi_{cd}^F) \rangle \}$

$(\check{X}X_1\check{L})X_2(\check{X}X_1\check{E}) = (\max(\chi_{cd}^A, \lambda_{cd}^A) \max(\chi_{cd}^I, \xi_{cd}^I), \max(\chi_{cd}^I, \lambda_{cd}^I) \max(\chi_{cd}^I, \xi_{cd}^I), \max(\chi_{cd}^F \lambda_{cd}^F, \chi_{cd}^F \xi_{cd}^F))$

Since, $\max(\chi_{cd}^A, \lambda_{cd}^A) \max(\chi_{cd}^I, \xi_{cd}^I) \leq \max(\chi_{cd}^A, \lambda_{cd}^A \xi_{cd}^A)$





Lalitha and Sarguna

$$\max(\chi_{cd}^I, \lambda_{cd}^I) \max(\chi_{cd}^I, \xi_{cd}^I) \leq \max(\chi_{cd}^I, \lambda_{cd}^I \xi_{cd}^I)$$

Therefore $\check{X}X_1(\check{A}X_2\check{E}) \neq (\check{X}X_1\check{A})X_2(\check{X}X_1\check{E})$
 Similarly, $\check{X}X_1(\check{A}X_2\check{E}) \neq (\check{X}X_1\check{A})X_2(\check{X}X_1\check{E})$
 g) To Prove $\check{X}X_2(\check{A}X_1\check{E}) \neq \check{X}$
 $(\check{A}X_1\check{E}) = (\max(\lambda_{cd}^A, \xi_{cd}^A), \max(\lambda_{cd}^I, \xi_{cd}^I), \lambda_{cd}^F \xi_{cd}^F)$ (1)
 $\check{X}X_2(\check{A}X_1\check{E}) = (\chi_{cd}^A \max(\lambda_{cd}^A, \xi_{cd}^A), \chi_{cd}^I \max(\lambda_{cd}^I, \xi_{cd}^I), \max(\chi_{cd}^F, \lambda_{cd}^F \xi_{cd}^F))$
 $\neq \{ < \chi_{cd}^A, \chi_{cd}^I, \chi_{cd}^F > \}$
 $\Rightarrow \check{X}X_2(\check{A}X_1\check{E}) \neq \check{X}$
 Similarly, $\check{X}X_1(\check{A}X_2\check{E}) \neq \check{X}$

Some Results using complement of NSM

Proposition 4.1

For any two NSMs \check{X} and \check{E} of equal size, then

- a) $(\check{X}X_1\check{E})^c \neq \check{X}^c X_2 \check{E}^c$
- b) $(\check{X}X_2\check{E})^c \neq \check{X}^c X_1 \check{E}^c$
- c) $(\check{X}X_2\check{E})^c \geq \check{X}^c X_2 \check{E}^c$
- d) $(\check{X}X_1\check{E})^c \leq \check{X}^c X_1 \check{E}^c$

Proof

$$a) (\check{X}X_1\check{E})^c = (\chi_{cd}^F \xi_{cd}^F, \max(\chi_{cd}^I, \xi_{cd}^I), \max(\chi_{cd}^A, \xi_{cd}^A))$$
 (1)

$$\check{X}^c X_2 \check{E}^c = (\chi_{cd}^F \xi_{cd}^F, \chi_{cd}^I \xi_{cd}^I, \max(\chi_{cd}^A, \xi_{cd}^A))$$
 (2)

From (1) and (2) $(\check{X}X_1\check{E})^c \neq \check{X}^c X_2 \check{E}^c$ (3)

Similarly, we can prove (b)

$$c) (\check{X}X_2\check{E})^c = (\max(\chi_{cd}^F, \xi_{cd}^F), \chi_{cd}^I \xi_{cd}^I, \chi_{cd}^A \xi_{cd}^A)$$
 (4)

$$\check{X}^c X_2 \check{E}^c = ((\chi_{cd}^F \xi_{cd}^F, \chi_{cd}^I \xi_{cd}^I, \max(\chi_{cd}^A, \xi_{cd}^A))$$
 (5)

Since, $\max(\chi_{cd}^F, \xi_{cd}^F) \geq \chi_{cd}^F \xi_{cd}^F, \chi_{cd}^A \xi_{cd}^A \leq \max(\chi_{cd}^A, \xi_{cd}^A)$

From (4) and (5) $(\check{X}X_2\check{E})^c \geq \check{X}^c X_2 \check{E}^c$

Also, we can prove (d) .

Proposition 4.2

For any NSM \check{X} , then

- a) $(\check{X}X_1\check{X}^c)^c \geq \check{X}X_2\check{X}^c$
- b) $(\check{X}X_2\check{X}^c)^c = \check{X}X_1\check{X}^c$

Proof

$$(\check{X}X_1\check{X}^c)^c = (\chi_{cd}^F \chi_{cd}^A, \max(\chi_{cd}^I, \chi_{cd}^I), \max(\chi_{cd}^A, \chi_{cd}^F))$$
 (1)

$$\check{X}X_2\check{X}^c = (\chi_{cd}^A \chi_{cd}^F, \chi_{cd}^I \chi_{cd}^I, \max(\chi_{cd}^F, \chi_{cd}^A))$$
 (2)

$(\check{X}X_1\check{X}^c)^c \geq \check{X}X_2\check{X}^c$.

Also, we can prove (b)

Proposition 4.3

For any NSM \check{X} , then

- a) $\check{X}X_1\check{X}^c \neq O$
- b) $\check{X}X_1\check{X}^c \neq J$

Proposition 4.4

For any two NSM \check{X} and \check{E} of equal size, then

- a) $(\check{X}X_1\check{X}^c)X_1(\check{X}X_1\check{X}^c) \neq (\check{X}X_1\check{X}^c)$
- b) $(\check{X}X_2\check{X}^c)X_2(\check{X}X_2\check{X}^c) \neq (\check{X}X_2\check{X}^c)$

Proof

$$a) (\check{X}X_1\check{X}^c)X_1(\check{X}X_1\check{X}^c) = (\max(\max(\chi_{cd}^A, \chi_{cd}^F), \max(\chi_{cd}^A, \chi_{cd}^F)), \max(\max(\chi_{cd}^I, \chi_{cd}^I), \max(\chi_{cd}^I, \chi_{cd}^I)), \chi_{cd}^{F^2} \chi_{cd}^{A^2})$$

$$\check{X}X_1\check{X}^c = (\max(\chi_{cd}^A, \chi_{cd}^F), \max(\chi_{cd}^I, \chi_{cd}^I), \chi_{cd}^F \chi_{cd}^A)$$

Therefore $(\check{X}X_1\check{X}^c)X_1(\check{X}X_1\check{X}^c) \neq (\check{X}X_1\check{X}^c)$

We can also prove $(\check{X}X_2\check{X}^c)X_2(\check{X}X_2\check{X}^c) \neq (\check{X}X_2\check{X}^c)$





Lalitha and Sarguna

Results on max-max-min and min-min-max using X_1 and X_2 in NSM

Proposition 5.1

Let \check{X} and \check{E} be any two NSM of equal size. Then

- a) $\check{X}X_1(\check{X}V\check{E}) \neq \check{X}$
- b) $\check{X}X_1(\check{X}\wedge\check{E}) \neq \check{X}$
- c) $\check{X}X_2(\check{X}V\check{E}) \neq \check{X}$
- d) $\check{X}X_2(\check{X}\wedge\check{E}) \neq \check{X}$

Proof

a) $(\check{X}V\check{E}) = \{ < \max(\chi_{cd}^A, \xi_{cd}^A), \max(\chi_{cd}^I, \xi_{cd}^I), \min(\chi_{cd}^F, \xi_{cd}^F) > \}$ (1)
 $\check{X}X_1(\check{X}V\check{E}) = (\max(\chi_{cd}^A, \max(\chi_{cd}^A, \xi_{cd}^A)), \max(\chi_{cd}^I, \max(\chi_{cd}^I, \xi_{cd}^I)), \chi_{cd}^F \min(\chi_{cd}^F, \xi_{cd}^F))$
 $= (\chi_{cd}^A, \chi_{cd}^I, \chi_{cd}^F \chi_{cd}^F)$
 $\neq (\chi_{cd}^A, \chi_{cd}^I, \chi_{cd}^F)$
 $\Rightarrow \check{X}X_1(\check{X}V\check{E}) \neq \check{X}$
 The proof of (b),(c),(d) are similar of (a).

Proposition 5.2

For any two \check{X} and \check{E} NSM of equal size, then

- a) $\check{X}V(\check{X}X_1\check{E}) \neq \check{X}X_1\check{E}$
- b) $\check{X}\wedge(\check{X}X_1\check{E}) = \check{X}$
- c) $\check{X}\wedge(\check{X}X_1\check{E}) \neq \check{X}X_1\check{E}$
- d) $\check{X}V(\check{X}X_1\check{E}) = \check{X}$

Proof

a) $\check{X}V(\check{X}X_1\check{E}) = (\max(\chi_{cd}^A, \max(\chi_{cd}^A, \xi_{cd}^A)), \max(\chi_{cd}^I, \max(\chi_{cd}^I, \xi_{cd}^I)), \min(\chi_{cd}^F, \chi_{cd}^F \xi_{cd}^F))$
 $\neq \check{X}X_1\check{E}$.
 b) To Prove: $\check{X}\wedge(\check{X}X_1\check{E}) = \check{X}$
 $\check{X}\wedge(\check{X}X_1\check{E}) = (\min(\chi_{cd}^A, \max(\chi_{cd}^A, \xi_{cd}^A)), \min(\chi_{cd}^I, \max(\chi_{cd}^I, \xi_{cd}^I)), \max(\chi_{cd}^F, \chi_{cd}^F \xi_{cd}^F))$
 $= (\chi_{cd}^A, \chi_{cd}^I, \chi_{cd}^F)$.
 $\Rightarrow \check{X}\wedge(\check{X}X_1\check{E}) = \check{X}$
 The proof (c) & (d) are similar of (a) and (b).

Proposition 5.3

For any three NSMs \check{X} , \check{A} and \check{E} of equal size, then

- a) $\check{X}X_1(\check{A}V\check{E}) = (\check{X}X_1\check{A})V(\check{X}X_1\check{E})$
- b) $\check{X}X_1(\check{A}\wedge\check{E}) = (\check{X}X_1\check{A})\wedge(\check{X}X_1\check{E})$
- c) $\check{X}X_2(\check{A}V\check{E}) = (\check{X}X_2\check{A})V(\check{X}X_2\check{E})$
- d) $\check{X}X_2(\check{A}\wedge\check{E}) = (\check{X}X_2\check{A})\wedge(\check{X}X_2\check{E})$

Proof

a) $\check{X}X_1(\check{A}V\check{E}) = (\max(\chi_{cd}^A, \max(\lambda_{cd}^A, \xi_{cd}^A)), \max(\chi_{cd}^I, \max(\lambda_{cd}^I, \xi_{cd}^I)), \chi_{cd}^F \min(\lambda_{cd}^F, \xi_{cd}^F))$
 $= (\max(\max(\chi_{cd}^A, \lambda_{cd}^A), \max(\chi_{cd}^A, \xi_{cd}^A)), \max(\max(\chi_{cd}^I, \lambda_{cd}^I), \max(\chi_{cd}^I, \xi_{cd}^I)), \min(\chi_{cd}^F \lambda_{cd}^F, \chi_{cd}^F \xi_{cd}^F))$
 $= (\check{X}X_1\check{A})V(\check{X}X_1\check{E})$.
 Proof of (b),(c) and (d) are similar of (a).

Proposition 5.4

For any three NSMs \check{X} , \check{A} and \check{E} of equal size, then

- a) $\check{X}V(\check{A}X_1\check{E}) \neq (\check{X}V\check{A})X_1(\check{X}V\check{E})$
- b) $\check{X}\wedge(\check{A}X_1\check{E}) \neq (\check{X}\wedge\check{A})X_1(\check{X}\wedge\check{E})$
- c) $\check{X}V(\check{A}X_2\check{E}) \neq (\check{X}V\check{A})X_2(\check{X}V\check{E})$
- d) $\check{X}\wedge(\check{A}X_2\check{E}) \neq (\check{X}\wedge\check{A})X_2(\check{X}\wedge\check{E})$

Proof

a) $\check{X}V(\check{A}X_1\check{E}) = (\max(\chi_{cd}^A, \max(\lambda_{cd}^A, \xi_{cd}^A)), \max(\chi_{cd}^I, \max(\lambda_{cd}^I, \xi_{cd}^I)), \min(\chi_{cd}^F, \lambda_{cd}^F \xi_{cd}^F))$ (1)





Lalitha and Sarguna

$$\begin{aligned}
 (\check{X}\check{V}\check{\Lambda}) &= \{ < \max(\chi_{cd}^A, \lambda_{cd}^A), \max(\chi_{cd}^I, \lambda_{cd}^I), \min(\chi_{cd}^F, \lambda_{cd}^F) > \} \\
 (\check{X}\check{V}\check{\Xi}) &= \{ < \max(\chi_{cd}^A, \xi_{cd}^A), \max(\chi_{cd}^I, \xi_{cd}^I), \min(\chi_{cd}^F, \xi_{cd}^F) > \} \\
 (\check{X}\check{V}\check{\Lambda})X_1(\check{X}\check{V}\check{\Xi}) &= (\max(\max(\chi_{cd}^A, \lambda_{cd}^A), \max(\chi_{cd}^I, \xi_{cd}^I)), \max(\max(\chi_{cd}^I, \lambda_{cd}^I), \max(\chi_{cd}^I, \xi_{cd}^I)), \\
 &\quad \min(\chi_{cd}^F, \lambda_{cd}^F) \min(\chi_{cd}^F, \xi_{cd}^F)) \dots \dots \dots (2)
 \end{aligned}$$

From (1) and (2) $\check{X}\check{V}(\check{\Lambda}X_1\check{\Xi}) \neq (\check{X}\check{V}\check{\Lambda})X_1(\check{X}\check{V}\check{\Xi})$
 We can prove (b),(c) and (d) in similar manner of (a).

Proposition 5.5

For any two \check{X} and $\check{\Xi}$ NFM of equal size, then

- a) $(\check{X}X_1\check{\Xi}) \geq \check{X}\check{\Lambda}\check{\Xi}$
- b) $(\check{X}X_2\check{\Xi}) \leq \check{X}\check{V}\check{\Xi}$
- c) $(\check{X}X_2\check{\Xi}) \neq \check{X}\check{\Lambda}\check{\Xi}$
- d) $(\check{X}X_1\check{\Xi}) \neq \check{X}\check{\Lambda}\check{\Xi}$

Proof

$$\begin{aligned}
 \text{a)} \quad (\check{X}X_1\check{\Xi}) &= \{ < \max(\chi_{cd}^A, \xi_{cd}^A), \max(\chi_{cd}^I, \xi_{cd}^I), \chi_{cd}^F \xi_{cd}^F > \} & (1) \\
 (\check{X}\check{\Lambda}\check{\Xi}) &= \{ < \min(\chi_{cd}^A, \xi_{cd}^A), \min(\chi_{cd}^I, \xi_{cd}^I), \max(\chi_{cd}^F, \xi_{cd}^F) > \} & (2) \\
 (1) &\geq (2) \\
 \Rightarrow (\check{X}X_1\check{\Xi}) &\geq \check{X}\check{\Lambda}\check{\Xi} \\
 \text{c)} \quad (\check{X}X_2\check{\Xi}) &= \{ < \chi_{cd}^A \xi_{cd}^A, \chi_{cd}^I, \xi_{cd}^I, \max(\chi_{cd}^F, \xi_{cd}^F) > \} & (3) \\
 (\check{X}\check{V}\check{\Xi}) &= \{ < \max(\chi_{cd}^A, \xi_{cd}^A), \max(\chi_{cd}^I, \xi_{cd}^I), \min(\chi_{cd}^F, \xi_{cd}^F) > \} & (4) \\
 (3) &\neq (4) \\
 \Rightarrow (\check{X}X_2\check{\Xi}) &\neq \check{X}\check{\Lambda}\check{\Xi}
 \end{aligned}$$

In similar manner of (a) & (c) we can prove (b) and (d).

Proposition 5.6

For any two \check{X} and $\check{\Xi}$ NSM of equal size, then

- a) $(\check{X}\check{\Lambda}\check{\Xi}) \wedge (\check{X}X_2\check{\Xi}) = (\check{X}X_2\check{\Xi})$
- b) $(\check{X}\check{V}\check{\Xi}) \vee (\check{X}X_1\check{\Xi}) = (\check{X}X_1\check{\Xi})$
- c) $(\check{X}\check{\Lambda}\check{\Xi})X_1(\check{X}\check{V}\check{\Xi}) = (\check{X}X_1\check{\Xi})$
- d) $(\check{X}\check{\Lambda}\check{\Xi})X_2(\check{X}\check{V}\check{\Xi}) = (\check{X}X_2\check{\Xi})$

Proof

$$\begin{aligned}
 \text{a)} \quad (\check{X}\check{\Lambda}\check{\Xi}) \wedge (\check{X}X_2\check{\Xi}) &= \\
 \min(\min(\chi_{cd}^A, \xi_{cd}^A), \chi_{cd}^A \xi_{cd}^A), \min(\min(\chi_{cd}^I, \xi_{cd}^I), \chi_{cd}^I \xi_{cd}^I), \max(\max(\chi_{cd}^F, \xi_{cd}^F), \chi_{cd}^F \xi_{cd}^F)) \\
 (\check{X}X_2\check{\Xi}) &= \{ < \chi_{cd}^A \xi_{cd}^A, \chi_{cd}^I, \xi_{cd}^I, \max(\chi_{cd}^F, \xi_{cd}^F) > \} \\
 \text{Therefore, } (\check{X}\check{\Lambda}\check{\Xi}) \wedge (\check{X}X_2\check{\Xi}) &= (\check{X}X_2\check{\Xi}) \\
 \text{c)} \quad (\check{X}\check{\Lambda}\check{\Xi})X_1(\check{X}\check{V}\check{\Xi}) &= (\max(\min(\chi_{cd}^A, \xi_{cd}^A)), \max(\chi_{cd}^A, \xi_{cd}^A), \max(\min(\chi_{cd}^I, \xi_{cd}^I), \max(\chi_{cd}^I, \xi_{cd}^I)), \\
 &\quad \max(\chi_{cd}^F, \xi_{cd}^F) \min(\chi_{cd}^F, \xi_{cd}^F)) \\
 &= \{ < \max(\chi_{cd}^A, \xi_{cd}^A), \max(\chi_{cd}^I, \xi_{cd}^I), \chi_{cd}^F \xi_{cd}^F > \} \\
 \Rightarrow (\check{X}\check{\Lambda}\check{\Xi})X_1(\check{X}\check{V}\check{\Xi}) &= (\check{X}X_1\check{\Xi})
 \end{aligned}$$

We can prove (b) & (d) in similar manner of (a) and (c)

CONCLUSION

The Multiplicative operations over NSM have discussed in this paper. And some of the properties of X_1 and X_2 over NSM are explained. Distributive laws, max-max-min, min-min-max composition together the multiplicative operations are proved and established some concepts.



**REFERENCES**

1. K.Atanassov, "Intuitionistic fuzzy sets and systems," 20(1986) 87-96.
2. K.Atanassov, E.Szmidt and J.Kacprzyk, "Intuitionistic fuzzy implications \rightarrow ," *Notes on Intuitionistic fuzzy sets*, 23(2),37-43,2017.
3. A.J.Boobalan and S.Sriram , "Arithmetic operations on Intuitionistic on Mathematical Sciences," *Sathyabama university*(2014),484-487.
4. E.G.Emam and M.A.Fndh , "Some results associated with the max-min and min-maxcomposition of bifuzzy matrices," *Journal of the Egyptian Mathematical Society*,515-521, 2016.
5. S.K.Khan and M.Pal , "Some operations on Intuitionistic Fuzzy Matrices," *Acta ciencia Indica*, XXXIIM,515-524,2006.
6. Murugadas. P, Balasubramaniyan. K, Vanmathi. N, "Decomposition of Neutrosophic Fuzzy Matrices," *Journal of Emerging Technologies and Innovative Research*, Volume 6(2019).
7. Smarandache, *Neutrosophic set of Generalization of the Intuitionistic Fuzzy Set*,2005.
8. A.K.Shyamal and M.Pal, "Two New operators on fuzzy matrices," *J.Appl Math & Computing* , 15,91-107,2004.
9. Venkatesan. D, Sriram. S, "Multiplicative operations of Intuitionistic fuzzy matrices," *Annals of pure and Applied Mathematics* ,14(1), pp.173-181,2017.
10. Venkatesan. D, Sriram. S,"Further Multiplicative operations of Intuitionistic fuzzy matrices," *Annals of pure and Applied Mathematics* ,12(2), pp.105-113, 2017.
11. Venkatesan. D, Sriram. S,"Remarks on the Multiplicative operations of Intuitionistic fuzzy matrices," *TWMS Journal of Applied and Engineering Mathematics*, pp.1116-112, 2021.
12. L.A.Zadeh, "Fuzzy Sets ," *Journal of Information and control*, 8(1965) 338-353.
13. Y.Zhang and M.Zheng, "New Operators on fuzzy matrices," *Fourth International Workshop on Advanced computation Intelligence*, Wu Han, China,(2011) 295-299.





Phenotypic and Genotypic Characterization of *Enterococcus faecium* with Multiple Drug Resistance Isolated from a Patient with Urinary Tract Infection

Nirupama Bhimani, Prachi Dave and Riteshkumar Arya*

Department of Microbiology, Mehsana Urban Institute of Sciences, Ganpat University, Mehsana, Gujarat, India.

Received: 25 Feb 2023

Revised: 06 Mar 2023

Accepted: 05 May 2023

*Address for Correspondence

Riteshkumar Arya

Department of Microbiology,
Mehsana Urban Institute of Sciences,
Ganpat University,
Mehsana, Gujarat, India.



This is an Open Access Journal / article distributed under the terms of the **Creative Commons Attribution License** (CC BY-NC-ND 3.0) which permits unrestricted use, distribution, and reproduction in any medium, provided the original work is properly cited. All rights reserved.

ABSTRACT

Several studies in the past have already highlighted the *Enterococcus* species, particularly those that are resistant to antibiotics, because *Enterococci* has the potential to develop resistance to the most classes of antibiotics that far been used for practice and it causes many types of infection and there are limited options are available for the treatment, particularly for urinary tract infection (UTI) caused by enterococci. The main aim of this study is to determine the antibiotic resistance pattern of UTI causing *Enterococcus faecium* strain to make treatment of UTI easy and also determine its phenotypic and genotypic characteristics. For this work, we collect five urine samples and isolated 16 isolates from these, one of the isolate was used for the antibiotic susceptibility test (AST), which was carried out using erythromycin(ERY), ampicillin(AM), amoxicillin(AMX) chloramphenicol(CHL), azithromycin(AZM), penicillin(P), streptomycin(S), levofloxacin(LEV) antibiotics by Kirby Bauer disk diffusion method on Muller Hinton agar plate and compare the results with MIC of antibiotics effect on particular bacteria *E. faecium* using CLSI guidelines and genome sequence of that strain also analyzed. AST depicts that all the used antibiotics do not show any effect on the *E. faecium* strain and it shows higher resistance to these antibiotics, thus these antibiotics are not used for the treatment of UTIs caused by this strain but it makes treatment of UTIs easy.

Keywords: *Enterococcus faecium*, Antibiotics resistance, and Urinary tract infection.



Nirupama Bhimani *et al.*,

INTRODUCTION

Enterococci belong to the Enterococcaceae family consisting of more than 17 species from these 17 species we are trying to study *Enterococcus faecium* strains. Enterococci are non-spore forming Gram-positive, ovoid cells arranged in single, pair, or short chains. Grow optimally at 35-37°C temperature. Many species of enterococci can grow at 42°C and 45°C and grow slowly at 10° C, thus they are resistant to drying and follow facultative anaerobic respiration. They can survive at wide pH ranges, and desiccation and also grow in the presence of 6.5% NaCl and 40% bile salt. Normal bacteriological media is required for the growth of enterococci. Amino acids, vitamin B, and purine and pyrimidine bases are core nutrition requirements for the growth of enterococci. Sodium is used as a selective agent for the isolation and enumeration of enterococci. Enterococci give regular, circular, smooth surface colonies on the agar plate. They ferment sugar by homofermentative and form L- lactic acid from glucose. The cell wall of most enterococcus species consists of Lysine-Alanine type peptidoglycan. The genome size of *E. faecium* is about 3445kb.

Habitat

Enterococci are common inhabitants of the gastrointestinal tract of humans and almost all land animals. They are core members of the human microbes but numerically minor. *E. faecalis* and *E. faecium* are found in relatively abundant amounts in humans but represent <1% of the total microbial population (Selleck *et al.*, 2019). 105 to 107 enterococcal cells are present in 1 gram of human feces (Murray and Weinstock, 1999). Some species of enterococci including *E. faecium* are also found in Poultry. Enterococci can be isolated from food, plants, soil, and water.

Infection

After *Staphylococcus aureus* and *Pseudomonas aeruginosa*, enterococci are considered as the third most common nosocomial pathogen. Overgrowth of enterococci in the colon increases the chances of dissemination of enterococci into the bloodstream and contaminated body sites and enough to establish infection. Enterococci are residential microflora of the gastrointestinal tract, when higher growth occurs of this flora in the GI tract they migrate from the GI tract to urinary tract and where cause urinary tract infections. Among enterococci, *E. faecium* and *E. faecalis* have the highest ability to hospital-acquired infection, including urinary tract infection, bacteremia, intra-abdominal infection, and endocarditis. Colonization and proliferation of lineage of enterococci adapted from hospitals are induced disruption of community structure by association with antibiotics (Selleck *et al.*, 2019).

Antibiotic Resistance

Enterococci possess a wide variety of plasmids and transposons that are responsible for the determination of antibiotic resistance and virulence factor. This plasmid is transported from donor cell to recipient cell of some enterococcal species through surface adhesion aggregation substance. Thus, transfer of antibiotic resistance genes to their lineage happens (Devriese *et al.*, 1992; Wearver, 2000, 2002). Some species of enterococci consist of transposons (jumping genes) of the Tn3 family that consist of composite and conjugative transposons. From these two, conjugative transposons encoding antibiotic resistance genes reveal a broad host range. This family also consists of genes that are vancomycin resistance. Composite transposons encode genes that are resistant to aminoglycosides, vancomycin antibiotics, and also mercury resistance genes (Tendolkar *et al.*, 2003).

Weaver *et al.*, 2002). Vancomycin resistance enterococci (VRE) are a perilous problem because it is involved in many types of infection. There are six phenotypes of Vancomycin resistance that has been narrated and characterized as VanA, VanB, VanD, VanF and VanG and are described by transposable elements. VanC phenotype is characterized by a non-transposable element that is chromosomally encoded. VanA and VanB phenotypes display higher and moderate levels of resistance to vancomycin respectively (Cetinkaya *et al.*, 2000; Mckessar *et al.*, 2000; Tendolkar *et al.*, 2003). Grossly *E. faecium* displays a higher prevalence of antibiotic resistance than *E. faecalis* and other species of enterococci.





Nirupama Bhimani *et al.*,

Treatment

Enterococcus species can carry antimicrobial resistance genes and mutation in that gene results in multiple drug resistance due to that reason treatment of infections caused by enterococci, mainly UTIs are not easy. Generally, monotherapies are preferable for uncomplicated infections but due to the multiple drug resistance ability of enterococci, treatment of enterococcal infection is not easy with using a single antibiotic. For that reason, combination agents may use to cure the enterococcal infection and that can synergistically confer an antibacterial activity (Christopher J. Kristich; 2014). In clinical practice, critically ill patients with enterococcal infections can be treated with cell wall active agents and synergistic aminoglycoside as a commixture remedy (Susan L Fraser; 2021). There is a finite course of action procurable to remediate infections caused by enterococcus species, particularly for UTIs. Therefore in this study, we check antibiotic resistance of *Enterococcus faecium* against multiple antibiotics such as erythromycin (ERY), ampicillin (AM), amoxicillin (AMX) chloramphenicol (CHL), azithromycin (AZM), penicillin (P), streptomycin (S), levofloxacin (LEV) to make possible treatment for UTI.

METHODOLOGY

Sample Collection (n=5)

There were five urine samples collected from the Supratech Pathology Laboratory in Mehsana District. About 30-100 ml of midstream urine sample was collected aseptically in a sterile screw-cap tube after the initial flow has been allowed to escape and immediately processed appropriately.

Isolation of Bacteria from UTI

Urine samples were serially diluted up to 10⁻³ in sterile distilled water tubes and 0.1ml of prepared dilution was spread on the plate containing nutrient agar by a sterile L-shaped spreader using the spread plate technique. Overnight 37°C incubation temperature was provided to the plates which were spread with the serially diluted sample. After the overnight incubation period, the distinct colonies were observed on N-agar plates, which were further sub-cultured on N-agar plates for a pure culture of each isolated colony (16) and incubated those plates for 24 hours at 37°C. The next day from those 16 isolates one isolate was checked for colonial characteristics. After note downs of colony characteristics, Gram's staining was performed of that colony, for that on a cleaned glass slide drop of sterile distilled water was placed and then one loop of isolated colony was mixed with water drop to prepare a smear and then heat-fixed the smear in medium flame then after a standard procedure of Gram's staining was followed.

Biochemical Characterization

After the process of gram staining, isolate was checked for its catalase activity, and for that catalase test was performed. A sugar fermentation test was performed for whether the isolate ferment sugar or not for that test glucose and lactose sugars were used. The standard microbiological methods for urea hydrolysis, M-R and V-P were also performed for tentative identification of bacteria using Bergey's Manual of Systematic Bacteriology (Volume 2, Parts A-C) following the methods of Rakesh Patel volume 1.

Antibiotic Susceptibility Test

A tentatively identified bacterium was checked for its antibiotic susceptibility test for whether it was resistant or susceptible to various antibiotics. The bacterial suspension was spread on a plate containing Muller Hinton media [24]. Antibiotics disks were prepared by using watchman filter paper by punching the paper and making disks and sterilized them by autoclave after that aseptically deep disks in distinct antibiotics containing solutions with different concentrations for that, antibiotics were used such as Erythromycin, azithromycin, ampicillin, amoxicillin, and levofloxacin with 50 µg/ml concentration and chloramphenicol (250µg/ml), penicillin (1U), and streptomycin (2U). Those antibiotics were placed on Muller Hinton media which were spread with bacterial culture in aseptic conditions and then provided overnight incubation at 37°C. The next day overnight culture was observed for a zone of inhibition surrounding antibiotics and measured the zone was in millimetres and finds the effectiveness of the





Nirupama Bhimani et al.,

drugs. After the completion of the antibiotic susceptibility test, antibiotics were preferred by the panels of the Clinical and Laboratory Standard Institute (CLSI) which was appropriate for particular microorganisms, these were interpreted according to the MIC of particular antibiotics selected from CLSI.

Molecular Characterization

After the completion of AST, genome sequence was analysed for identification of that isolate by the sequencing of the 16S rRNA gene using the modern Sanger sequencing method.

DNA Extraction

DNA extracted from isolated genera using overnight grown liquid culture of isolate in the nutrient broth by using the phenol-chloroform method.

Amplification of 16S rRNA Gene

By using a Thermocycler machine 16S rRNA gene was amplified following the procedure of Hi-PCR® 16S rRNA Semi-Q PCR Kit, with the help of universal primers such as forward primer and reverse primer 16S-27F (5'-AGA GTT TGA TCC TGG CTC AG- 3'), 16S-1492R (5'-ACG GCT ACC TTG TTA CGA CT-3') respectively. After the amplification process, the yield of the PCR product was used to purify.

Purification of PCR Product

By using hiPurATM PCR product purification kit, PCR amplified product purified from unincorporated primers, dNTPs, polymerase, and salts using silica binding in a micro spin format. The clean purified product was eluted in a small volume of low salt buffer.

Sequencing and Analysis

After the purification of the PCR product, it proceeded for sequencing using the modern Sanger sequencing method in that fluorescent-labelled dideoxynucleotides were used in a single tube and size separated by capillary gel electrophoresis. After the separation of sequences, each band of the capillary gel was read on a computer, to use fluorescence to identify each terminal ddNTPs. The comparison of the resulting sequence was blasted to obtain a match using the GenBank database BLAST algorithm.

RESULTS

Bacterial isolate is Gram-positive cocci, catalase-negative, homofermentative, and negative to urea hydrolysis, M-R, and V-P test which is shown in table 1 and it is resistant to all those used antibiotics shown in table 2. It is identified as *Enterococcus faecium* strain by molecular characterization.

DNA sequence of *E. faecium*

```

1 aacacttgaaacaggtgctaa taccgta taacaatcgaaccgcattggtttgattga
61 aaggcgcttccgggtgctgctga tggatggaccgcggtgattagctagttggtgaggt
121 aacggctaccaaggccacgatgcatagccgacctgagagggtgatcgccacattggga
181 ctgagacacggccaaactcctacgggaggcagcagtagggaatcttcggcaatggacga
241 aagtctgaccgagcaacgccgctgagtgaaagaaggttttcggatcgtaaaactctgtt
301 ttgagaagaacaaggatgagagtaactgttcatccttgacggta tctaaccagaaagc
361 cacggtaactacgtgccagcagcccggtaa tacgtaggtggcaagcgttgcggatt
421 tattggcgtaaaagcagcagcagcggtttcttaagtctgatgtgaaagccccggctca
481 accggggaggggtcattggaaactgggagactgagtgacagaagaggagagtggaattcca
541 tgtgtagcgggtgaaatgcgtagatatggaggaacaccagtgccgaaggcggctctctg
601 gtctgtaactgacgtgaggtcgaagcgtggggagcaaacaggga ttgataccctggt
661 agtccacgcgtaaacgatgagtgctaa gtgttgagggtttccgccttcagtctgca

```



**Nirupama Bhimani et al.,**

721 gctaacgcattaagcactccgctggggagtagcaccgcaagggtgaaactcaaaggaat
781 tgacggggcccgcaagcggtagcagtggtgtaattcgaagcaacgcaagaacc
841 ttaccaggcttgacatccttgaccactctagagatagagctcccttcgggggcaaa
901 gtgacagtggtgcatggtgtcgtcagctcgtgctgagatggtgggtaagtcccgc
961 aacgagcgcaaccctattgtagttgcatcatcagttgggcaactctagcaaagactg
1021 cccggtgacaaaccggaggaagggtgggtagcgtcaaatcatcatgcccttatgacct
1081 gggctacacagctgctacaattgggaagtacaacgagttgcgaagtcgcgaggctaagcta
1141 atctctaaagcttctcagttcggaattgcaggctgcaactcgctgcatgaagccgga
1201 atcgctagtaatcgcgatcagcagccgcgggtgaatagttcccgggcttgtaacacac
1261 cgccgctcacaccagagagttgtaacaccggaagtcggtgaggtaacctttggagcc
1321agccgcc

DISCUSSION

In the current study, we focus on the antibiotic resistance pattern of the *E. faecium* strain isolated from the UTI. Based on the MIC of antibiotics used for this study shows no effect on *E. faecium* strain. This study also includes the phenotypic and genotypic characteristics of *E. faecium*. Xuwei Zhou and his team members in the year 2020 focused on hospital-acquired vancomycin resistance *E. faecium* infections. For the control of infection, they use *E. faecium* insights for practical recombination and diagnostic purposes as well. Iain J. Abbott and his colleagues in the year 2020, also focus on the therapy of urinary tract infections caused by enterococci using a dynamic in vitro bladder infection model. Their study showed that *E. faecalis* required greater fosfomycin exposure as compared to *E. faecium*. In the year of 2019, Fakhri Haghi and her team members also studied antibiotic sensitivity pattern to malignant virulence encoding genes in enterococci selected from urine samples of hospitalised patients. They identified 69% *E. faecalis*, 21% other *Enterococcus* spp., and 10% *E. faecium*. From those isolates 93% resistance to tetracycline, ciprofloxacin, quinupristin-dalfopristin 86%, 73%, and 53% respectively. Gentamicin (50%) and streptomycin (34%) and determined genes which were shown resistance to aminoglycoside and 21% of isolates were vancomycin-resistant. Their study revealed that *E. faecium* shows a higher frequency of gentamicin and vancomycin resistance and higher heterogeneity prevalence of resistance genes and virulence.

CONCLUSION

Due to the increasing pollution, population, and climate change opportunities increase day by day of infections, in such conditions use of antibiotics gives relief against infection. But abuse of antibiotics create resistance power in bacteria. In country like India, people are very less aware about antimicrobial resistance (AMR) and resulting in abuse of antibiotics, we can create awareness and understanding in the people about AMR through effective communication and education. This study concluded that the *E. faecium* strain is resistant to all the antibiotics which are used in this study. Thus these are not used for the treatment of urinary tract infections caused by *E. faecium* but they make the treatment of UTIs easy. In the current study, we use very low concentrations (ug/ml) of antibiotics, if we take them in higher concentrations then it might influence on infection-causing bacteria and give relief to patients with UTIs. This study is one of the ways to create awareness among people about the resistance of drugs and may provide aid in many projects which are working on the identification of multiple drug resistance bacteria in India

ACKNOWLEDGEMENT

Members of this team express immense thanks to Microbiology Department, Ganpat University for furnishing needful facilities and express thanks to Supratech Pathology Laboratory, Mehsana for giving urine samples for this study and also thanks to Dr. Riteshkumar Arya for his consistent support during this study.





Nirupama Bhimani et al.,

REFERENCES

1. Revati, S., Bipin, C., Chitra, P. B., & Minakshi, B. (2015). In vitro antibacterial activity of seven Indian spices against high level gentamicin resistant strains of enterococci. Archives of medical science : AMS, 11(4), 863–868. <https://doi.org/10.5114/aoms.2015.53307>
2. Fiore, E., Van Tyne, D., & Gilmore, M. S. (2019). Pathogenicity of Enterococci. Microbiology spectrum, 7(4), 10.1128/microbiolspec.GPP3-0053-2018. <https://doi.org/10.1128/microbiolspec.GPP3-0053-2018>
3. Zhou, X., Willems, R., Friedrich, A. W., Rossen, J., & Bathoorn, E. (2020). Enterococcus faecium: from microbiological insights to practical recommendations for infection control and diagnostics. Antimicrobial resistance and infection control, 9(1), 130. <https://doi.org/10.1186/s13756-020-00770-1>
4. Hammerum A. M. (2012). Enterococci of animal origin and their significance for public health. Clinical microbiology and infection : the official publication of the European Society of Clinical Microbiology and Infectious Diseases, 18(7), 619–625. <https://doi.org/10.1111/j.1469-0691.2012.03829.x>
5. Dai, F., Xiang, X., Duan, G., Duan, B., Xiao, X., & Chang, H. (2018). Pathogenicity characteristics of Enterococcus faecium from diseased black bears. Iranian journal of veterinary research, 19(2), 82–86.
6. Trautmannsberger, I., Kolberg, L., Meyer-Buehn, M., Huebner, J., Werner, G., Weber, R., Heselich, V., Schroepfer, S., Muench, H. G., & von Both, U. (2022). Epidemiological and genetic characteristics of vancomycin-resistant Enterococcus faecium isolates in a University Children's Hospital in Germany: 2019 to 2020. Antimicrobial resistance and infection control, 11(1), 48. <https://doi.org/10.1186/s13756-022-01081-3>
7. Haghi, F., Lohrasbi, V., & Zeighami, H. (2019). High incidence of virulence determinants, aminoglycoside and vancomycin resistance in enterococci isolated from hospitalized patients in Northwest Iran. BMC infectious diseases, 19(1), 744. <https://doi.org/10.1186/s12879-019-4395-3>
8. Kristich, C. J., Rice, L. B., & Arias, C. A. (2014). Enterococcal Infection—Treatment and Antibiotic Resistance. In M. S. Gilmore (Eds.) et. al., Enterococci: From Commensals to Leading Causes of Drug Resistant Infection. Massachusetts Eye and Ear Infirmary.
9. Revati, S., Bipin, C., Chitra, P. B., & Minakshi, B. (2015). In vitro antibacterial activity of seven Indian spices against high-level gentamicin resistant strains of enterococci. Archives of medical science: AMS, 11(4), 863–868. <https://doi.org/10.5114/aoms.2015.53307>
10. Murray B. E. (2000). Vancomycin-resistant enterococcal infections. The New England journal of medicine, 342(10), 710–721. <https://doi.org/10.1056/NEJM200003093421007>
11. William B. Whitman (2009). Bergey's Manual of Systematic Bacteriology (Volume Three, Second Edition).
12. Rakesh J. Patel, Kiran R. Patel (2006). Experimental Microbiology (Volume 1, 4th Edition).

Table 1: Cultural And Bioc Characteristics Of Enterococcus Faecium.

CULTURAL CHARACTER		GRAM STAINING		
Size	Small	Gram reaction	Positive	
Shape	Round			
Margin	Entire	Size	Small	
Elevation	Convex			
Surface	Smooth	Shape	Cocci	
Opacity	Translucent			
Consistency	Moist	Arrangement	Chain, Cluster	
BIOCHEMICAL REACTION				
Urea hydrolysis test	-	Sugar fermentation test		
		Sugars	Acid	Gas
M-R test	-	Lactose	+	-





Nirupama Bhimani et al.,

V-P test	-	Glucose	+	-
Catalase test	-	- = Negative + = Positive		

Table 2: Interpretation of Antibiotic Susceptibility Test

Sr. No.	Antimicrobial agents	Disk content (µg/ml)	Zone of inhibition (mm) (follow CLSI guidelines)			Interpretational categories
			Susceptible (S)	Intermediate (I)	Resistance (R)	
1	Amoxicillin	50	80	40	20	40/I
2	Erythromycin	50	76.6	60	43.3	27/R
3	Azithromycin	50	60	51.6	43.3	21/R
4	Chloramphenicol	250	150	125	100	29/R
5	Levofloxacin	50	170	150	130	35/R
6	Ampicillin	50	85	-	80	35/R
7	Penicillin	2(U)	150	148	140	27/R
8	Streptomycin	1(U)	50	48	46	26/R

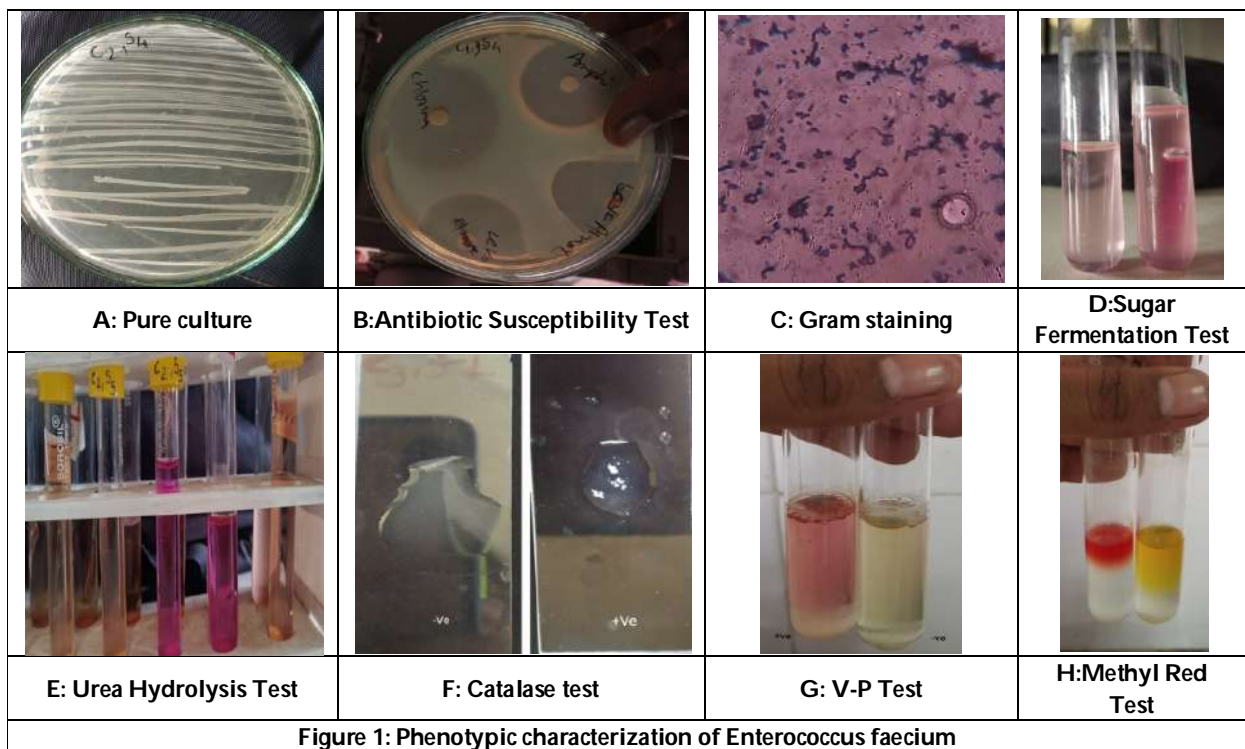


Figure 1: Phenotypic characterization of Enterococcus faecium





Classification of Alzheimer's Disease Stages using ResNet50 Architecture

Febin Antony^{1*}, Anitha H B² and Jincy A. George³

¹Ph.D. Scholar, Department of Computer Science, CHRIST (Deemed to be University), Bangalore-29, Karnataka, India.

²Associate Professor, Department of Computer Science, CHRIST (Deemed to be University), Bangalore-29, Karnataka, India.

³Ph.D. Scholar, Department of Life Sciences, CHRIST (Deemed to be University), Bangalore-29, Karnataka, India.

Received: 27 Feb 2023

Revised: 06 Apr 2023

Accepted: 08 May 2023

*Address for Correspondence

Febin Antony

Ph.D. Scholar,
Department of Computer Science,
CHRIST (Deemed to be University),
Bangalore-29, Karnataka, India.
E. Mail: febin.antony@res.christuniversity.in



This is an Open Access Journal / article distributed under the terms of the **Creative Commons Attribution License** (CC BY-NC-ND 3.0) which permits unrestricted use, distribution, and reproduction in any medium, provided the original work is properly cited. All rights reserved.

ABSTRACT

Alzheimer's disease (AD), also known as senile dementia is one of the most progressive neurological diseases which affects the memory and other important brain functions. If not detected at an early stage, Alzheimer can cause problems which increase over time. Hence it is essential to detect and diagnose this disease early. Due to its increased prominence, diagnosis of Alzheimer's disease has gained huge attention among the researchers. Several researchers have proposed different techniques for accurate detection of AD. Methods: This research proposes the classification of different stages of AD from MRI images using a Convolutional neural network (CNN) based ResNet-50 model. The MRI data for disease detection and classification is collected from the ADNI dataset with an emphasis on achieving high classification accuracy. The efficacy of the proposed approach is validated using different evaluation metrics such as accuracy, precision, recall and f1-score and support. Findings: The classification accuracy achieved by the ResNet-50 model is found to be 97.36%.

Keywords: Alzheimer's disease, Convolutional Neural Network (CNN), ResNet-50 model, Alzheimer's Disease Neuroimaging Initiative (ADNI), Deep Learning, Magnetic Resonance Images



Febin Antony *et al.*,

INTRODUCTION

Alzheimer's disease (AD) is one of the progressive diseases which can significantly harm the memory capacity and normal functioning of the brain. In the United States, addiction is the sixth prominent cause of mortality among the elderly, accounting for more than 5.5 million people. The AD's to cope with the predicted \$277 billion in AD management costs in 2018, the U.S. economy and healthcare system will be severely taxed. People with Alzheimer's disease see a steady decline in their mental faculties as the illness advances. Medically sanctioned cures are not yet available for this condition [1]. There has been a lot of interest in pre-symptomatic detection techniques in an attempt to postpone or even prevent an illness's start. Scientists have discovered early warning signs of Alzheimer's disease via the use of brain imaging techniques such as MRIs (PET). It has got more difficult to synthesize multimodal neuroimaging data as neuroimaging technology has advanced fast. As a consequence, automated techniques such as machine learning (ML) techniques are gaining significant increase in interest. Pattern analysis techniques including LDA, LPBM, logistic regression, and SVM-RFE have all been used to effectively spot early signs of Alzheimer's disease. These strategies might help in the early detection and prediction of AD[2]. Deep learning (DL) algorithms belong to the class of traditional ML algorithms which has demonstrated excellent capabilities compared to M algorithms in finding subtle patterns from complicated data pattern. The application of DL for accurate diagnosis and automatic categorization of AD has lately attracted substantial interest since fast advancement in neuroimaging methods has created huge amount of multimodal neuroimaging data.

In general, ML algorithms are employed for processing and classification applications. These applications incorporate feature extraction, feature selection, dimensionality reduction and selection methods for performing a machine learning-based classification task [3]. These sorts of tasks need a high level of competence and experience in optimization. The method's mobility is a problem for many people, not just them. Factors such as cortical thickness, build-up of amyloid in the hippocampus region, grey matter density etc. define the characteristics of AD and these factors are evaluated throughout the feature selection process (ROIs) [4].

Medical imaging analysis is rapidly turning to "on-the-fly" learning approaches like deep learning, which utilize unprocessed data for constructing the image patterns/features using "on-the-fly" learning. The phrase "on-the-fly" learning refers to the process of generating characteristics from raw neuroimaging data. Machine learning methods like convolutional neural networks (CNN) have been used to improve outcomes [5]. The main aim of this study is to detect AD in the initial stages using DL based Resnet50 model using the Alzheimer's disease Neuro imaging Initiative (ADNI) dataset. The research paper is organized with various research works based on classification and early detection of Alzheimer's Disease. The T1 weighted MRI dataset from ADNI is used for the analysis. The next sections deal with the research gap, proposed research methodology and Deep Learning classifications respectively. After the analysis, next section discusses about the results, performance evaluation and concludes the paper with experimental observations.

LITERATURE REVIEW

ADNI Dataset

Scientists began investigating imaging and blood/CSF biomarkers to expedite new therapies and confirm imaging/blood/CSF biomarkers. Research and development are conducted by several government agencies, including the National Institute on Aging, NIH, and the National Institutes of Health Foundation is a true public-private partnership [6]. ADNI was founded in response to several industry developments. Research into AD detection was started with the creation of transgenic mice with amyloid plaques growing in their brains. Because of the studies done on this animal by academic and industrial experts, new ways to eliminate amyloid have been discovered. Patients with Alzheimer's and other neurodegenerative disorders may now be diagnosed using advanced imaging techniques like MRI and PET scans. Alzheimer's disease patients' CSF and blood were shown to have amyloid peptides for the third time Clinical investigations on AD have been made possible due to the

57044



**Febin Antony et al.,**

identification of the genes responsible for the illness in the human genome. In the wake of several Alzheimer's clinical investigations, a network of AD clinical trial facilities, the Alzheimer's disease Cooperative Investigations, was established. As a sixth benefit, data may be easily transported from several places to a single data center through the Internet. Researchers in academia, the government, and the pharmaceutical industry have realized that cooperating and sharing methodologies and data would lead to speedier trials of disease-modifying drugs [7]. A clinical trial is not the goal of the ADNI research effort or any other ADNI activity. Naturalistic observation is used in this study to get a better understanding of treatment trials. The ADNI data may then be used by pharmaceutical companies and government-funded researchers to build more effective treatment trials for their patients [8].

In October 2010, first says of ADNI also known as NA-AIDI-1. During that time 821 individuals from all over the United States and Canada have joined up to participate in the past few days. Participation in the experiment was not restricted to those with Alzheimer's or moderate cognitive impairment (MCI). Researchers looked at the results of all of the individuals' physical and mental examinations as well as their structural MRI scans and blood tests throughout time. Those who had FDG-PET scans and lumbar punctures had spinal fluid biomarkers tested. The Alzheimer's Association and General Electric have expanded their financing for amyloid imaging, which resulted in the examination of 100 persons (PiB). MCI changes in an ADNI cohort of MCI patients who had gone too far in the disease process to be adequately studied thanks to a Grand Opportunities (GO) grant were examined by researchers thanks to this funding [9]. Researchers may upload MRI and PET images, as well as clinical data, to the Laboratory of Neuroimaging (LONI) database. This database, which can be accessed from anywhere in the world over the internet by academics, is accessible to them now. Anyone doing research in a relevant discipline may access ADNI data. NA-ADNI has published about 250 papers as of this writing [10]. Expanding on the NA-ADNI 2 experiment and collecting more data for pharmaceutical development was the primary purpose of this investigation, which drew on the expertise of patients with mild cognitive impairment. As in ADNI 1 and GO, 450 new volunteers will be recruited to participate in ADNI 2. These new volunteers will be distributed evenly among healthy controls, those with MCI in the late stages of the illness, and patients with AD. With the release of ADNI 2, several improvements have been made. Instead of using a 1.5-T MRI scanner, a new 3-T MRI scanner will be used, and scans will be performed every year for the first three years, then every three, six, and twelve months afterward. To see whether they can anticipate future results, scientists can keep an eye on changes in brain volume early in the study. Amyloid ligand will be AV-45 in this experiment since it is more readily accessible than PiB for use in AV-45 PET scanning. It has now been mandated that lumbar punctures be performed on all new ADNI participants due to ADNI 1. These include DTI, arterial spin labelling perfusion imaging, resting blood oxygen level-dependent imaging, and an assessment of hippocampal subfields [11].

A biomarker profile based on changes in atrophy rate and CSF biomarkers and structural MRI parameters may be created to assist predict future clinical changes in MS. both. The 11C-PiB and AV-45 results showed that MCI patients had a significant incidence of Alzheimer's disease pathology. Approximately 30% of persons in their 70s have amyloid in their brains, according to recent research. In the future, amyloid deposits have been related to cognitive decline and dementia, according to research from ADNI and other sources. The ADNI made inquiries. As a result of new research into Alzheimer's disease, moderate cognitive impairment (MCI), dementia progression from MCI, and preclinical Alzheimer's disease, organizations like the Alzheimer's Association and the National Institute on Aging have altered their diagnostic criteria [12]. There are presently ADNI initiatives throughout North America and Europe and programs in Asia and the Pacific Rim countries of Australia; Japan; Korea; China; and Brazil. It's not only the United States that ADNI plans to expand to. It has taken ADNI many years to become an international organization. All data may now be transferred across programs such as the Worldwide ADNI without any restrictions (WW-ADNI) [13].

Classification of Alzheimer's disease with and without Imagery Using Gradient Boosted Machines and ResNet-50

The paper analyzed an Open Access Series of Imaging Studies (OASIS-1) cross-sectional MRI data for detecting AD and a gradient boosted machine (GBM) was employed for predicting the disease based on different parameters such

57045



**Febin Antony et al.,**

as gender, age, education, socioeconomic status (SES), and a mini-mental state exam (MMSE). The GBM model was accompanied with another residual neural network ResNet – 50 with 50 neural layers, which predicted the presence of clinical dementia rating (CDR) and measured the intensity of MRIs. Experimental results showed that the GBM model exhibited a high mean prediction accuracy of 91.3% with a 10-fold stratified cross validation. The efficacy of the proposed approach was measured in terms of MMSE and the ResNet – 50 was trained and validated using 80% of the training data and 20% validation data respectively. The prediction accuracy of ResNet – 50 was found to be 98.99% which a near absolute multi-class prediction accuracy of 99.34%. The results of the experimental analysis prove that GBM achieves are effective in classifying the AD which is enhanced by the ResNet – 50 models which automates the detection process [14].

The potential of transfer learning (TL) algorithm for predicting AD was fine-tuned by using different network models such as VGG-19, VGG-16, Resnet-50 and Xception. Previous works have discussed the implementation of VGG-16 model for testing the AD classification based on the data collected from ADNI datasets which provided an accuracy and precision of 97% and 96% respectively. This work evaluated the classifying ability of the TL model and results show that the proposed model achieved a phenomenal accuracy of 98% in comparison to other models. It can be validated from the results that TL models achieve superior performance and hence can be helpful in detecting and predicting AD in early stages and helps to provide better treatment [15].

Different ML algorithms such as CART, Random Forest (RF), GBM, and Support Vector Machines (SVM). The MRI images of the AD was considered for the experimental analysis and the images of the full brain was collected for every 6 months. An extensive range of cognitive analysis is considered in this research for the experimental analysis with an executive function. Various researchers have proposed different techniques in this aspect and it involved the application of different progressive techniques which includes modifications and transformations in metabolic and neuroendocrine activity. Results of the experimental analysis show that the RF and GBM algorithms exhibit superior performance compared to CART and SVM. It was also observed that these algorithms showed better performance in terms of different parameters such as cognitive scores, genetic risk, accuracy, and precision etc., which are more competitive with MRI techniques. Results validate that the ML based algorithms perform better in detecting and predicting AD [16].

Role and impact of Early Detection of AD Using DL algorithm on MRI

Various researchers have examined and compared the efficacy of various DL algorithms for detecting neurological diseases with an emphasis on AD, Parkinson's disease, and schizophrenia from MRI images collected from different paradigms such as functional and structural MRI [17]. The potential detecting ability of different DL techniques was compared in terms of identifying several neurological disorders across different datasets. Results of the comparative analysis show that among different DL algorithms Convolutional Neural Network (CNN) achieves better performance by exhibiting high accuracy. The study also identified different research challenges and suggested some of the feasible future research directions. CNN was used for detecting and diagnosing of MRI in AD [18]. The neural network layers of the CNN algorithm were used for segmenting the MR images concerning patients suffering from AD. The segmentation ability of the CNN was compared with other DL algorithms such as fully CNN (FCNN) and SVM algorithms. It can be inferred from the results that the CNN algorithm achieved better segmentation performance in terms of precision, CDR score, and a lower MMSE score which is less than 0.05.

Gap Analysis

Alzheimer's disease detection, pathophysiology and its implications has gained huge significance in recent times [19]. As observed from existing literary works, computer-aided techniques have provided better results. However, in clinical point of view there are no practical diagnostic tools available. Most of the research works have focused on predicting AD using brain images [20] based on image segmentation, and drug management [21]. Recently, DL algorithms are extensively used in the classification and detection of AD due to their capacity to deal with MRI images. It is shown in several works that DL models provide accurate detection of AD compared to conventional machine learning algorithms. Despite the availability of different techniques, detection and classification of AD is



**Febin Antony et al.,**

still challenging since it requires highly discriminative feature representation for classifying distinct brain patterns from MRI images. In addition to this, there are certain prominent research gaps which needs to be addressed. Several existing AD detection techniques suffer from poor-quality of MRI images and errors in pre-processing and image segmentation. Most of the research works are conducted using a limited dataset and there is a need to investigate the performance of different techniques using a large scale datasets. In addition to this, most of the works do not address the problem of class invariance between different stages of AD, which results in inaccurate detection of AD. This research intends to address these gaps in order to detect AD with high accuracy using deep learning algorithms.

METHODOLOGY

This research present the analysis of AD using deep learning techniques. The study uses a Gradient Boosted Machine with ResNet-50 for analyzing and classifying AD from MRI data. The block diagram of the classification approach is illustrated in figure 1. The steps involved in the design of the proposed approach are listed in below steps:

Data Collection

The data for the experimental analysis is taken from the ADNI dataset. A T1 weighted MRI data from ADNI dataset is used wherein the ADNI study provides an observational analysis of the health condition of the elderly individuals with CN, MCI, or AD. An unbalanced dataset is used with 2600 MCI images, 1500 CN images and 1000 AD images. The sample MRI image data and the classification of AD, CN, and MCI from the dataset are shown in figures 2 and 4.3 respectively.

Data Pre-processing

In general, data pre-processing is performed to filter out the uncertainties from the raw input data in order to make the data suitable for classification. In this research, data pre-processing involves two stages namely skull stripping and data augmentation. Skull stripping is one of the basic and fundamental steps in pre-processing wherein it is used to identify the irregularities in the brain activity. In this process, the brain tissue is isolated from a non-brain tissue from MRI images. On the other hand, data augmentation is incorporated to maximize the amount of training data. This is done by adding additional copies or modified copies of already existing data, or by creating synthetic samples of the data which is extracted from the original data. Augmentation process increases the size of training set by 10 fold or even more and helps to train the DL algorithms in an effective manner. This process also helps to overcome the problem of over fitting while training the DL algorithms.

Classification

The images are classified using a modified ResNet-50 model which is 50 layers deep (with 48 convolutional layers with 1 MaxPool and 1 Average Pool layer). Using ResNet-50 model, CNN can go more deep into the network and can perform more complex tasks. ResNet consists of a framework which trains numerous layers (up to thousands of layers) without affecting the performance of the network. The different layers used in this research are zeropadding2D, convolutional2D, Batch Normalization, Activation, Maxpooling2D and three sets of dense layers. The robust representation capacity of the ResNet enhances the performance of DL algorithms to classify MRI images for AD detection.

Algorithms

Skull Stripping

Let the image input be i

Step 1: read image i

Step 2: Display the grayscale image i

Step 3: Denoising – Median Filter

Step 4: Binarization of the image using Otsu's Thresholding





Febin Antony et al.,

- Step 5: Cropped and resize the image to required size
- Step 6: Apply Morphological Erosion and Dilation
- Step 7: Determine the maximum perimeter of the image
- Step 8: Multiply the mask with the de-noised brain MR images
- Output i'

Image Registration

- Step 1: Read image A (Reference Image) //manually taken
- Step 2: Read image B (Floating image)
- Step 3: Transform floating image (initial parameters)
- Step 4: Geometric Transformation //displacement of the vector
- Step 5: Evaluate similarity measure of image A and B
- If Images are matched Then Registered image Else Update transformation parameter
- Output: Registered Image

Classification Model Algorithm

- Input: I , where $(i_1, \dots, i_n \in I)$
- Output : I'
- Step 1 $\forall (i_1, \dots, i_n \in I)$ apply median filter $\Rightarrow I^M$
- Step 2 $\forall (I^M)$ apply skull stripping algorithm $\Rightarrow I^{SS}$
- Step 3 Apply Image Augmentation (IA) methods
 $IA(I^{SS}) \Rightarrow I^{IA}$
- Step 4 For each image in I^{IA} apply Floating Image Registration
 $FIR(I^{IA}) \Rightarrow I^{FIR}$
- Step 5 Extract f_1, \dots, f_n features of I^{FIR} using 7x7 Convolution layer with Maxpooling and ReLU activation function for reducing time complexity
- Step 6 $\forall f_1, \dots, f_n$ apply average pooling before feeding to the dense layer
 $\Rightarrow (f_1, \dots, f_n)'$
- Step 7 Classify using the extracted features $(\forall (f_1, \dots, f_n))' \in I \Rightarrow I'$

RESULTS AND DISCUSSION

This research aims to analyze AD from MRI images using DL models. This research emphasize of GBM and ResNet-50 model for detecting different stages of AD from MRI images. The performance of the DL algorithm is analyzed in terms of different evaluation metrics such as accuracy, precision, recall, f1 score and support. These parameters are defined based on the elements of the confusion matrix namely True positives (TP), True negatives (TN), False positives (FP), False negatives (FN).

Accuracy defines the percentage of number of correctly detected Alzheimer’s stages and is calculated as shown in the below equation:

$$Accuracy = \frac{TP+TN}{TP+TN+FP+FN} \dots (1)$$

The recall score for a learning model is calculated as;

$$Recall = \frac{TP}{TP+FN} \dots (2)$$

F1 score measures the model’s accuracy and the value of this score ranges between 1 and 0. Here, 1, and 0 denotes the best and worst values respectively. The F1 score is calculated as:

$$F1\ score = \frac{2*Precision*Recall}{Precision+recall} \dots (3)$$



**Febin Antony et al.,**

Precision is defined as the number of accurate positive predictions. It is defined as:

$$\text{Precision} = \frac{TP}{TP+FP} \dots (4)$$

Support is defined as the number of actual occurrences of the class in a specific dataset. Support is used for evaluating the accuracy of the classification process. The results of the experimental analysis as obtained from the classification report is discussed in the table 1 and the graph depicting the training and validation accuracy, training and validation loss with respect to percentage on y-axis and Epochs on x-axis are shown in figures 4 and 5 respectively.

As observed from the classification report, the ResNet-50 model achieves a phenomenal test accuracy of 97.36% and a minor test loss of 0.14 with respect to Alzheimer's disease. Correspondingly, the detected AD stages are illustrated in figure 6. The classification results of the proposed ResNet-50 model are shown in figure 6. It can be inferred from the results that the proposed model is effective in classifying different stages of AD with high accuracy.

CONCLUSION

This research presents a comprehensive analysis of AD classification using deep learning models. A residual network ResNet-50 model is used for detecting and classifying different AD stages. The data for the experimental analysis was collected from the ADNI dataset and emphasized on enhancing the classification accuracy by pre-processing the MRI image data. This research also focused on the implementation of an efficient CNN based classifier and its functionality as optimizer. The performance of the ResNet-50 model was evaluated in terms of different performance measures and it was observed from the results that the model achieved a superior accuracy of 97.36% for classification. Results validate the efficacy of the proposed model as a potential classifier for MRI images. For future research, this work can implement a large scale dataset for training the classifier to improve the performance and accuracy. Ensemble learning approaches can be implemented for verifying and validating the accuracy of the AD classification process with an aim of implementing it in a real-time environment, where the data is sparse.

ACKNOWLEDGEMENT

The authors of the manuscript would like to sincerely acknowledge CHRIST (Deemed to be University), Bangalore-29, India for providing us the opportunity and necessary infrastructure towards the designing and development of this research work.

REFERENCES

1. Prince, M. J. Alzheimer's disease facts and figures. *Alzheimer's Dement.* 2018; 14(3): 367-429.
2. De Strooper, B., & Karran, E. The cellular phase of Alzheimer's disease. *Cell.* 2016; 164(4): 603-615.
3. Nath, S. S., Mishra, G., Kar, J., Chakraborty, S., & Dey, N. A survey of image classification methods and techniques. In 2014 International conference on control, instrumentation, communication and computational technologies (ICCICT). 2014; 554-557
4. Samper-González, J., Burgos, N., Bottani, S., Fontanella, S., Lu, P., Marcoux, A., & Alzheimer's Disease Neuroimaging Initiative. Reproducible evaluation of classification methods in Alzheimer's disease: Framework and application to MRI and PET data. *NeuroImage.* 2018; 183: 504-521.
5. Plis, S. M., Hjelm, D. R., Salakhutdinov, R., Allen, E. A., Bockholt, H. J., Long, J. D., ... & Calhoun, V. D. Deep learning for neuroimaging: a validation study. *Frontiers in neuroscience.* 2014; 8: 229.
6. Albert, M. S., DeKosky, S. T., Dickson, D., Dubois, B., Feldman, H. H., Fox, N. C., ... & Phelps, C. H. The diagnosis of mild cognitive impairment due to Alzheimer's disease: recommendations from the National





Febin Antony et al.,

- Institute on Aging-Alzheimer's Association workgroups on diagnostic guidelines for Alzheimer's disease. *Alzheimer's & Dementia*. 2011; 7(3): 270-279.
7. Jack Jr, C. R., Albert, M., Knopman, D. S., McKhann, G. M., Sperling, R. A., Carillo, M., ... & Phelps, C. H. Introduction to revised criteria for the diagnosis of Alzheimer's disease: National Institute on Aging and the Alzheimer Association Workgroups. *Alzheimer's & dementia: the journal of the Alzheimer's Association*. 2011; 7(3): 257.
 8. Boccardi, M., Bocchetta, M., Ganzola, R., Robitaille, N., Redolfi, A., Bartzokis, G., ... & Frisoni, G. P1-299: Estimating the impact of differences among protocols for manual hippocampal segmentation on Alzheimer's disease-related atrophy: Preparatory phase for a harmonized protocol. *Alzheimer's & Dementia*. 2011; 7: S205-S206.
 9. Sperling, R. A., Aisen, P. S., Beckett, L. A., Bennett, D. A., Craft, S., Fagan, A. M., ... & Phelps, C. H. Toward defining the preclinical stages of Alzheimer's disease: Recommendations from the National Institute on Aging-Alzheimer's Association workgroups on diagnostic guidelines for Alzheimer's disease. *Alzheimer's & Dementia*. 2011; 7(3): 280-292.
 10. Geuze, E., Vermetten, E., & Bremner, J. D. MR-based in vivo hippocampal volumetrics: 1. Review of methodologies currently employed. *Molecular psychiatry*. 2005; 10(2): 147-159.
 11. Boccardi, M., Ganzola, R., Bocchetta, M., Pievani, M., Redolfi, A., Bartzokis, G., ... & Frisoni, G. B. Survey of protocols for the manual segmentation of the hippocampus: preparatory steps towards a joint EADC-ADNI harmonized protocol. *Journal of Alzheimer's disease*. 2011; 26(s3): 61-75.
 12. Caroli, A., Prestia, A., Chen, K., Ayutyanont, N., Landau, S. M., Madison, C. M., ... & Frisoni, G. B. Summary metrics to assess Alzheimer's disease-related hypometabolic pattern with 18F-FDG PET: a head-to-head comparison. *Journal of Nuclear Medicine*. 2012; 53(4): 592-600.
 13. Frisoni, G. B., Redolfi, A., Manset, D., Rousseau, M. É., Toga, A., & Evans, A. C. Virtual imaging laboratories for marker discovery in neurodegenerative diseases. *Nature Reviews Neurology*. 2011; 7(8): 429-438.
 14. Fulton, L. V., Dolezel, D., Harrop, J., Yan, Y., & Fulton, C. P. (2019). Classification of Alzheimer's disease with and without imagery using gradient boosted machines and ResNet-50. *Brain sciences*, 9(9), 212.
 15. Rajeswari, S. S., & Nair, M. A Transfer Learning Approach for Predicting Alzheimer's Disease. In 2021 4th Biennial International Conference on Nascent Technologies in Engineering (ICNTE). 2021; 1-5.
 16. Beltran, J. F., Wahba, B. M., Hose, N., Shasha, D., Kline, R. P., & Alzheimer's Disease Neuroimaging Initiative. Inexpensive, non-invasive biomarkers predict Alzheimer transition using machine learning analysis of the Alzheimer's Disease Neuroimaging (ADNI) database. *PloS one*. 2020; 15(7): e0235663.
 17. Noor, M. B. T., Zenia, N. Z., Kaiser, M. S., Mamun, S. A., & Mahmud, M. Application of deep learning in detecting neurological disorders from magnetic resonance images: a survey on the detection of Alzheimer's disease, Parkinson's disease and schizophrenia. *Brain informatics*. 2020; 7(1): 1-21.
 18. Chen, X., Li, L., Sharma, A., Dhiman, G., & Vimal, S. The application of convolutional neural network model in diagnosis and nursing of MR imaging in Alzheimer's disease. *Interdisciplinary Sciences: Computational Life Sciences*. 2022; 14(1): 34-44.
 19. Choudhury, S., & Vellapandian, C. Alzheimer's Disease Pathophysiology and its Implications. *Research Journal of Pharmacy and Technology*. 2019; 12(4): 2045-2048.
 20. Naidu, C., Kumar, D., Maheswari, N., & Sivagami, M. Prediction of Alzheimer's Disease using Brain Images. *Research Journal of Pharmacy and Technology*. 2018; 11(12): 5365-5368.
 21. Venkatachalam, S., Jaiswal, A., De, A., & Vijayakumar, R. K. Repurposing drugs for management of Alzheimer disease. *Research Journal of Pharmacy and Technology*. 2019; 12(6): 3078-3088.

Table 1. Classification report of the proposed model

	Precision	Recall	f1-score	Support
AD	0.95	0.98	0.96	298
CN	0.97	0.95	0.96	330
MCI	0.99	0.98	0.98	661





Febin Antony et al.,

Accuracy	-	-	0.97	1289
macro avg	0.97	0.97	0.97	1289
weighted avg	0.97	0.97	0.97	1289

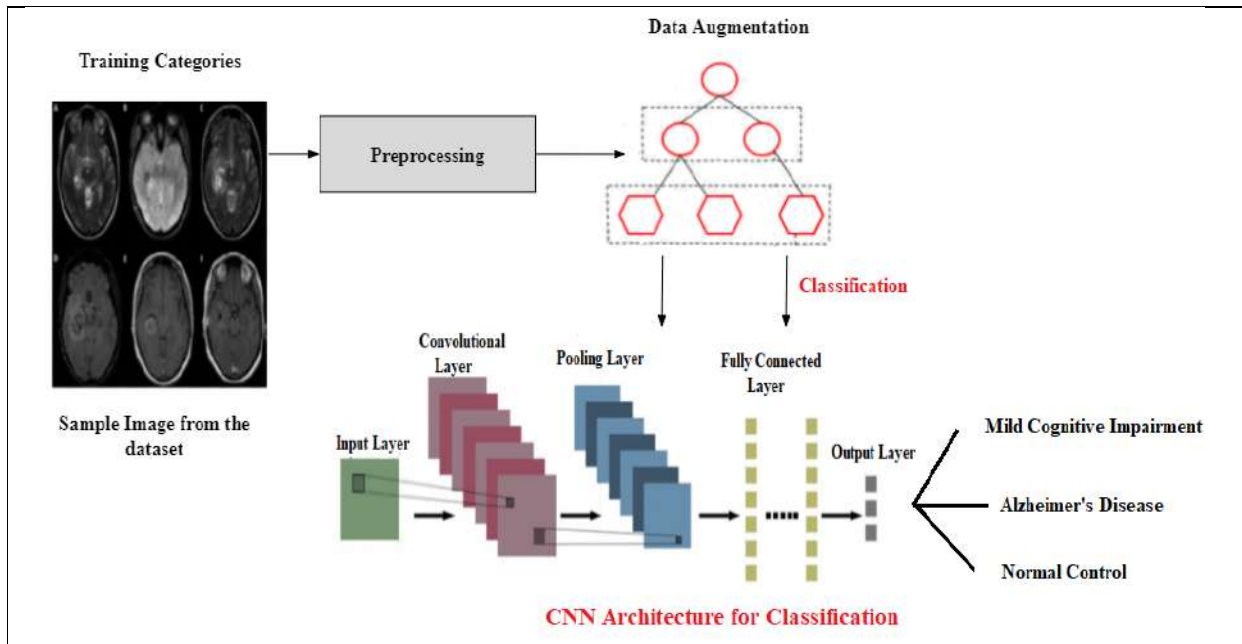


Figure 1. Block diagram of the CNN based AD classification model

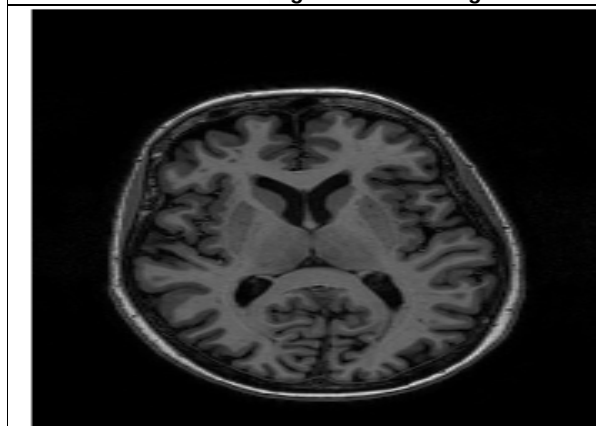


Figure 2. Sample Image from the ADNI dataset

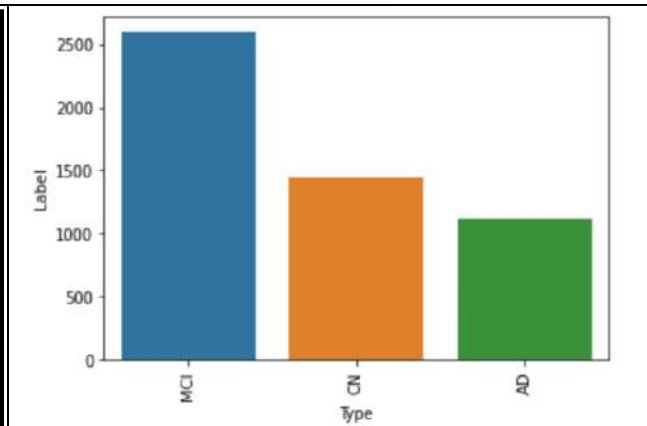


Figure 3. Classification of AD, CN, and MCI using labelled data from ADNI dataset





Febin Antony et al.,

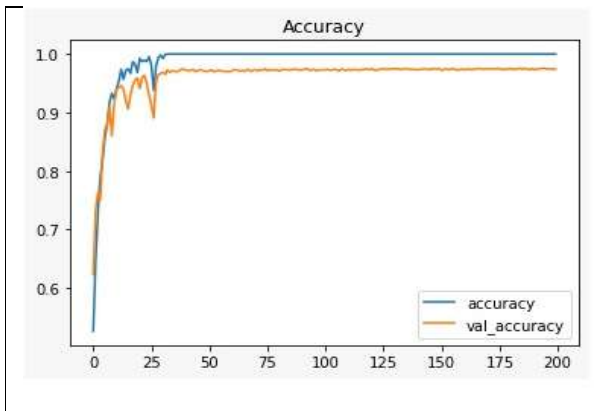


Figure 4. Training and validation accuracy of ResNet-50 model

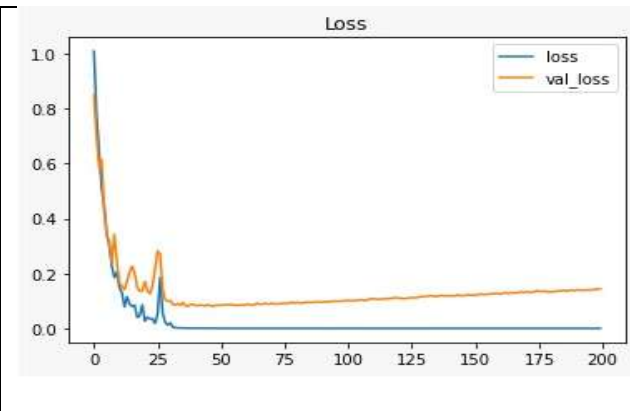


Figure 5. Training and validation loss of ResNet-50 model

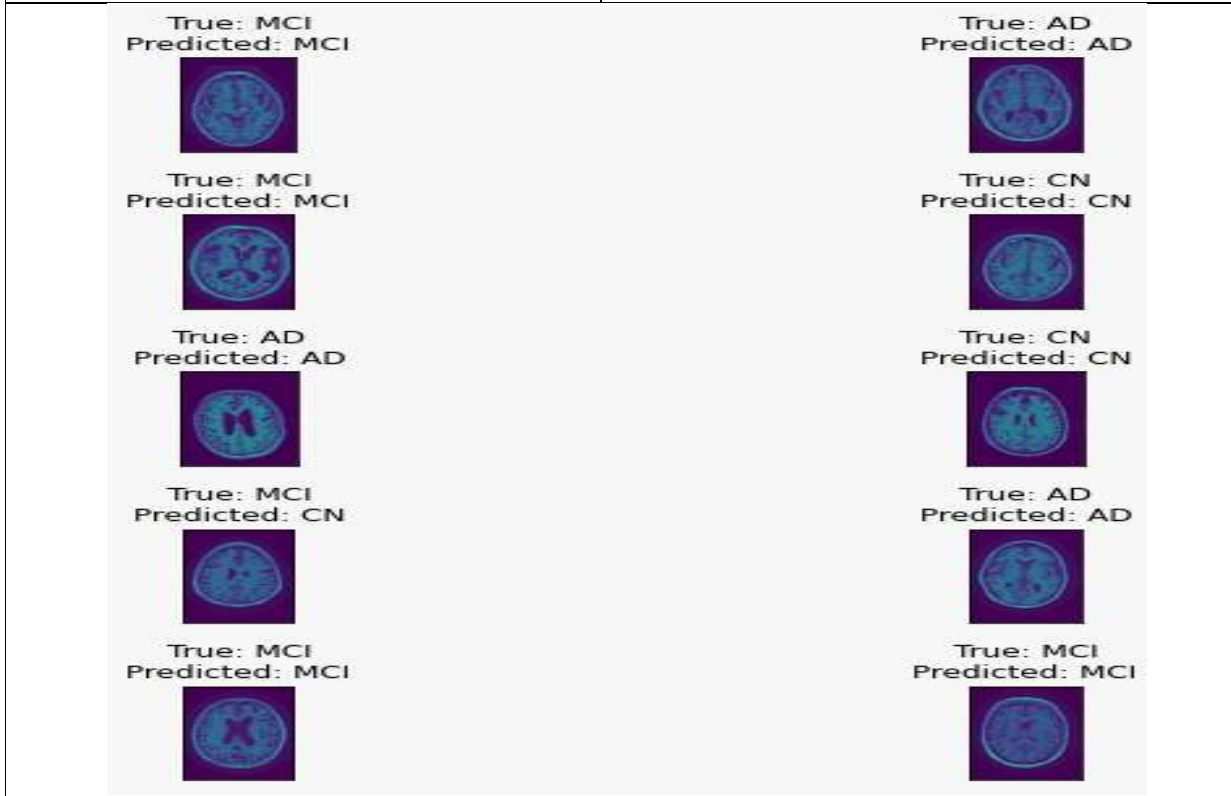


Figure 6. Validation: Detection and classification of AD stages from MRI images





A Raman and Infrared Spectroscopic Studies on Natural Quartz

Roshmi Borthakur¹, Nayan Talukdar^{2*} and Anil Kumar Goswami³

¹Research Scholar, Assam down town University, Gandhi Nagar, Panikhaiti, Guwahati-781026, Assam, India.

²Assistant Professor, Assam down town University, Gandhi Nagar, Panikhaiti, Guwahati - 781026, Assam, India.

³Professor, Assam down town University, Gandhi Nagar, Panikhaiti, Guwahati-781026, Assam, India.

Received: 24 Feb 2023

Revised: 05 Apr 2023

Accepted: 08 May 2023

*Address for Correspondence

Nayan Talukdar

Assistant Professor

Department of Physics,

Assam down town University

Gandhi Nagar, Panikhaiti,

Guwahati-781026, Assam, India.

E.Mail: ntalukdar284@gmail.com



This is an Open Access Journal / article distributed under the terms of the **Creative Commons Attribution License** (CC BY-NC-ND 3.0) which permits unrestricted use, distribution, and reproduction in any medium, provided the original work is properly cited. All rights reserved.

ABSTRACT

The present study reports a Raman and infrared spectroscopic studies on crystallinity of natural quartz procured from Assam and Arunachal Pradesh of NE region. The metamorphic pressure is correlated from infrared and Raman frequency shifts studies. The crystallinity and the peak deviations are measured by symmetry of bending and stretching vibrational modes of infrared (695 cm^{-1} and 778 cm^{-1}) and bending mode of Raman (464 cm^{-1} and 205 cm^{-1}) peaks. The purity of the sample is found from the infrared crystallinity study. The deviations of the Raman peaks associated with the temperature, pressure and frequency shift were estimated. Blue shift in Raman peaks was observed and amount of peak shift were estimated. The present study could be efficiently applied to analyze the properties of quartz samples in the study region as well as in technological and mineralogical research.

Keywords: Crystallinity, IR and Raman spectroscopy, Vibrational modes, Red and blue shift in Raman spectra.

INTRODUCTION

The rapid increased utilization of quartz for production of new materials in different industries requires high purity raw materials [1],[2],[3],[4]. Quartz is a silicate mineral (SiO_2) and one of the raw materials with less than 0.2% of total impurities. The silica forms cristobalite, tridymite and quartz all have associated derivatives and is therefore of ceramic importance. In the production of ceramic materials thermal process generates different amount of crystalline phases. The content of residual amorphous is an important for physical characterization of products [5]. Crystallinity of quartz determines the mechanical strength and physical characterization of materials in glass technology. Due to

57053



**Roshmi Borthakur et al.,**

its highly crystalline structure and availability in the earth crust its study is very important in many other fields of applications. Quartz is the mineral which crystallizes almost lastly, therefore its crystallinity can be recognized as a good indicator of minerals associated with it [6]. In geological research and mining, studies reflect the geological processes taking place in the particular regions. Extracting of silicates from rocks accomplish with crystalline silica, the over exposures of which create health hazard. Crystallinity index of silica is an important parameter for knowing the maximum permissible limit (PEL) for maintaining sustainable environment in industrial, mining, farming and agricultural sites. It was reported that the exposure limit should be less than the maximum permissible exposure limit which is 50 microgram per meter cube in average 8 hours a day [7]. Moreover the rocks and debris containing silicates minerals from cosmos brought into our by meteorites. Study helps us in understanding the origin and composition of material.

The earth crust contains 95% silicate minerals, of which 60% are feldspar and 12% quartz. Quartz minerals are available in all three types of rocks. Sedimentary rocks make up only a small volume of the earth crust so the total quartz content in sedimentary rock becomes relatively low. Metamorphic rocks are formed through heat and pressure and thus contain crystalline silica as quartz. It may be present in the original rock or it may be created during metamorphism. Thus pressure and temperature affects the crystalline structure of quartz. In the igneous rocks crystalline silica as quartz can be present in deposits of hardened, volcanic ash known as volcanic tuffs. Average quartz content of igneous rocks is only 12%. Spectroscopic study of crystallinity in metamorphic and sedimentary rock samples has been developed by many workers in view of exploration in mineral resources like mining, petroleum and also in environmental degradation [8], [9], [10], [11].

It is reported that quartz crystallinity Index (QCI) was developed more than four decades ago, it remains a relatively new tool used in environmental studies [12]. In 1976 K.J. Murata et al applied the procedure of X-ray in determining quartz crystallinity [13]. Gradually FTIR spectroscopy were found to be successful tool to study the degree of crystallinity [14],[15]. A new method has been reported in to determine crystallinity index of silicate minerals. The method is based on the measurement of intensity of the first derivative of the infrared absorption spectrum at the shoulder 1145 cm^{-1} [16]. The diffuse reflectance infrared spectroscopy has been proposed by H.Gomez et al (2004) to determine crystallinity in naturally occurring clay minerals using 800 cm^{-1} and 780 cm^{-1} band and results were correlated with X-Ray diffractometry [17]. In the field of spectroscopic study of thermal behavior of clay mixed with quartzite samples, it has been found that the structural changes were due to temperature, pressure along with hydrocarbon formation [18]. Raman spectra were used successfully in studying the degree of metamictization in zircon samples [19]. Zircon (ZrSiO_4) structure can break down to the metamict state. Metamict Zircons are characterized by poor crystallinity of the lattice. Another report was found that Raman mapping is a powerful technique for mineralogy and petrography. The small spatial of the laser beam allows detection and identification of very small phases of minerals. In near future mapping is likely to become the standard method for Raman analysis [20]. As observed from the earlier study, it is seen that spectroscopic study of metamorphic and sedimentary rock plays a prominent role in determining the crystallinity of quartz crystal and therefore, the study on crystallinity of natural quartz is still going on. In this paper we report the crystallinity measurement of natural quartz which is available in Assam and Arunachal Pradesh of NE region. The study of naturally occurring quartz of NE region will give some informative data on quartz crystallinity.

MATERIALS AND METHODS

In preparing the samples for taking IR spectra the powder sample and KBr (Potassium Bromide) are mixed and ground to reduce the particle size less than 5mm in diameter. Sample and KBr concentration ratios were taken in the range 0.2% to 1% to avoid noisy spectra. Some amount of KBr were taken out and kept in a mortar and 2% of sample were mixed and ground thoroughly to find powder to reduce distortion in absorption band and loss due to scattering. Samples were pressed at 40 Kg/cc in a hand pressed machine and were kept in desiccators. The pallets were then put in the FTIR spectrophotometer for spectra analysis. To study IR spectra, spectrum is measured as



**Roshmi Borthakur et al.,**

percentage transmission (%T) of the Infrared radiation through the sample as the function of wavelength. Occurring of dips has shown absorption at or near the frequencies of IR active vibrational modes of the sample. Raman spectra were collected using a Ar^+ excitation source (wavelength 488 nm) coupled with a Jobin-Yvon Horiba Lab Ram-HR Micro Raman spectrometer located at IIT, Guwahati. The range of the spectrometer is 100 to 4000 cm^{-1} . The formula used for calculation of crystallinity index is given by $A = \log_{10}(1/T)$. The peak height absorption ratio of 778 cm^{-1} peak and 695 cm^{-1} peak in IR spectra has determined the crystallinity index value. The relative percentage (%) of crystallinity of the samples been determined from a standard value [9].

RESULT AND DISCUSSION

Due to metamorphism of silicious biogenetic structure, initially amorphous silica was crystallized [2]. Sometimes spontaneous recrystallization also takes place due to silica bearing fluid. Quartz is an abundant mineral in earth crust and fluid are supposed to occur abundantly in depth. The interaction and inclusion of fluid with the mineral may change crystalline state of quartz [21]. It is mentioned by B. J Saikia, (2014) [22] that information about crystal growth, structural defects, and correlation between the trace oxide inclusions in quartz crystals can be obtained from spectroscopic method. Mid infrared spectra of quartz are classified in to four characteristics bands around 1080 cm^{-1} , 778 cm^{-1} , 695 cm^{-1} and 464 cm^{-1} (Fig 1). The band around 1080 cm^{-1} is assigned as Si-O asymmetrical stretching vibration. The peak around 464 cm^{-1} appears due to asymmetrical bending vibrations. The band around 778 cm^{-1} appears due to Si - O symmetrical stretching vibration. The symmetrical bending vibration at 695 cm^{-1} peak is used as an indicator for crystalline state as the Si-O symmetrical bending vibration is missing in amorphous silica [23],[9]. The absorption ratio between 778 cm^{-1} and 695 cm^{-1} can supply informative data on the degree of crystallinity of quartz [9]. The band at 695 cm^{-1} and 778 cm^{-1} arise due to symmetry of octahedral and tetrahedral site respectively. The tetrahedral site symmetry is stronger to that of octahedral site symmetry. Therefore, for any structural change due to pressure or temperature, the damage occurs first in octahedral site symmetry then in tetrahedral site symmetry. The observed variations in percent crystallinity indicate the purity of the samples (Table 1).

The vibrational energy of a metal-ligand bond is generally in the range 100 cm^{-1} to 700 cm^{-1} . These vibrations are Raman active and peaks with change in frequency are readily observed. Concerning the composition, structure and stability of mineral compounds studies are potentially very useful sources. More specifically it can be used to investigate their crystalline structure or crystallinity. Due to the presence of spatial order i.e. order in the arrangement in space and long-range translational symmetry through which phonons propagates, the solid of the same chemical composition (crystalline quartz and glass cavette) can be significantly different. The interaction of electromagnetic radiation with the phonons of the crystal lattice results the observed narrow well defined bands (Fig 2). These phonons are of very long wavelength, equal to several thousand atomic spacing. The repeating unit cells allows the propagation of lattice vibrational waves "phonons" originating in the repetitive and systematic vibrational motions of the crystal atoms (repetitive displacement) [24]. The observed characteristics Raman peaks are appeared around 128 cm^{-1} , 464 cm^{-1} , 205 cm^{-1} , 808 cm^{-1} (Fig 2). The intensities of these peaks are proportional to the square of the changes of polarizabilities. The strongest peak at 464 cm^{-1} which is due to bending mode of vibration and associated peak 205 cm^{-1} are observed in all samples [25]. In our work we consider Raman peak of 464 cm^{-1} and 205 cm^{-1} for precise calculation of amount of peak shift. The estimated peak deviation (dw) calculated from 464 cm^{-1} and 205 cm^{-1} peak difference with standard and studied samples are found to be up to 4 cm^{-1} [Table 2]. In all samples peak positions were shifted towards higher wave nos. w.r.t. standard peak positions. It is due to the pressure, cooling and crystallinity during formation. This is known as blue shift. The deviation due to the metaphoric change is already reported elsewhere [26],[27],[28],[29]. Blue shift is mainly due to compressive stress which has brought the atoms in a crystal to move closer together causing shortening of chemical bond length relative to their normal positions and lengths. As a result compressive strain produced in the crystal and the material is compressed. As Raman Effect is a quantum mechanical phenomenon, i.e. when light comes in contact with the material called phonons and if phonon gains energy the light shifted towards the higher frequency. If the tensile strain produces due to tensile stress where atoms being pulled apart or chemical bond lengthened w.r.t. their normal positions and





Roshmi Borthakur et al.,

lengths, then this is known as red shift. As the chemical bond increases and force constant remaining same the vibrational frequency must decrease causing red shift. Estimated amount of shift determine the energy of the phonon in the material. The maximum shift was found in sample Q6 with crystallinity 91.03% [Table 2].

The plot as referred to in Fig.3 shows the samples versus percent crystallinity determined from IR spectra and peak deviation (dW) estimated from 464cm^{-1} and 205cm^{-1} peak shift in Raman spectra of various samples. The estimated % crystallinity were found nearly 100% in Q3, Q4 and 97.24% in Q2 from the top. On the other hand 75.87% in Q9 and 77.9% in Q7 and Q8 from the bottom. The variations are related amongst each other.

DISCUSSION

The crystallinity of natural quartz has been studied using Raman and infrared spectroscopy. The results show that relative infrared crystallinity exhibits the purity of the samples. The strongest peak is observed at 464cm^{-1} which is due to bending mode of vibration in Raman spectra associated with 205cm^{-1} . The estimated variations in the peaks have shown that the factors causing blue shift such as pressure, cooling and crystallinity explained above associated with vibrational mode of Raman peak. The result from fig. 3 suggests that the Raman peak shift depends with degree of crystallinity along with metamorphic change. The results presented in this report indicate the utility of the quartz samples in the context of technological and mineralogical research found in NE region.

ACKNOWLEDGEMENT

No financial support has been received to carry out the present research work. The authors offer sincere acknowledgement to Central Instruments Facility (CIF), IIT Guwahati for Raman data and Department of Physics, IIT Guwahati for IR spectra. The authors wish to thank Dr. Bhaskar Jyoti Saikia Asst. professor A.D.P. College Nagaon and Dr. Sidananda Sarma, Sr. Technical officer, Physics IIT Guwahati for their technical supports.

REFERENCES

1. Balasubramanian A, Quartz group of minerals, Technical report, DOI: 10.13140. 2017.
2. Razva O, Anufrienkova A, Korovkin M, Ananieva L, Abramova, R, Calculation of quartzite crystallinity index by infrared absorption spectrum. International Scientific Symposium in Honour of Academician M.A. Usov. PGON2014 IOP Publishing IOP Conf. Series: Earth and Environmental Science 21,012006. 20143
3. Platias S, Vatalis KI, Charalampide, G, Suitability of quartz sands for different industrial application, Procedia Economics and Finance. 2014;14: 491-498.
4. Pathirage SS, Hemalal PVA, Rohotha LPS, & Ratnayake NP, Production of industry –specific quartz raw material using Sri Lankan vein quartz, Environmental Earth Sciences. 2019; 78: Article number:58.
5. Beall G, Design and properties of Glass-ceramics, Ann Rev mater Sc. 1992; 22:91-119.
6. Saikia B. J, Spectroscopic and Optical Investigation of Silicate Minerals in North Eastern Region of India, Ph.D Thesis, Dept. of Physics, Dibrugarh University, Dibrugarh. 2009; Chapter 4.
7. Matta A, Silica can be Environmental and Health Threat-Identifying Threats, 2017.
8. Stacey P, Kauffer E, Moulut J-C, Dion C, Beauparlant M, Fernandez P, Key- Schwartz R, Friede B, Wake D, An international comparison of the crystallinity of calibration material for the analysis of Respirable – Quartz using X-Ray diffraction and a comparison with results from the infrared KBr Disc method, Ann. Occup.Hyg. published by Oxford University. 2009 ;53(6): 639-649.
9. Saikia BJ, Parthasarathy G and Sarmah, NC, Fourier transform infrared spectroscopic estimation of crystallinity in SiO_2 based rocks, Bull Mater Sci . 2008 ;31: 775-779.
10. Gochmez H and Haber R A, Practical determination of α -quartz crystallinity by X-ray diffraction, Industrial ceramics. 2005;25(3) :170-172.





Roshmi Borthakur et al.,

11. Marinoni N, Broekemans MATM, Microstructure of selected aggregate quartz by XRD and a critical review of the crystallinity index, Cement and concrete research. 2013;54: 215-225.
12. Radwan OA, Humphrey JD, Al-Ramadan KA, Quartz crystallinity index of Arabian sand and sandstone, Earth and Space science. 2021;8.
13. Murata KJ and Norman MB, An index of crystallinity of quartz, American J.Sci. 1976; 276: 1120-1130.
14. Brok, BD, Mcineck J and Roller K, Fourier transform IR determination of intergranular water content in quartzites experimentally deformed with and without added water in the ductile deformation, Journal of Geophysical research. 99, 1994;19821-19829.
15. Ritz M, Vaculikova L, Plevova, E, Application of Infrared Spectroscopy and Chemometric methods to Identification of Selected Minerals, Acta Geodyn. Geometer. 2011;8: 47-582011.
16. Shoval S, Ginott Y, Nathan Y, A new method for measure crystallinity of quartz by infrared spectroscopy, Mineralogical Magazine. 1991;55: 579-582.
17. Gochmez H and Haber R A, Characterization of Quartz Crystallinity in Naturally Occurring Clay Minerals Using Diffuse Reflectance Infrared Spectroscopy, Key Engineering Materials .264-268, 2004;1601-1604.
18. Stalder R, OH, point defect in Quartz- a review, Eur. J. Minera.2021;33:145-163.
19. Nasadala L, Irmer G and Wolf D, The degree of metamictization in Zircon a Raman spectroscopic study, European Journal of Mineralogy. 1995;7: 471-478.
20. Foucher F, Guimbretiere G, Bost N and Westall F, Petrographical and Mineralogical Applications of Raman mapping , DOI:10.5772/65112. 2017.
21. Ural JL, Post J, Dijkstra I, The role of fluid-inclusion composition on dynamic recrystallization in experimentally deformed natural quartz single crystal, In press Journal of virtual Explorer. Journal of the Virtual Explorer.
22. Saikia BJ, Spectroscopic Estimation of Geometrical Structure Elucidation of natural SiO₂ crystal, Journal of materials Physics and Chemistry DOI:10.12691/jmpc-2-2-3. 2014; 2: 28-33
23. Hlavay J, Jonas K, Elek S and Inczedy J, Characterization of the particle size and the crystallinity of certain minerals by IR spectrophotometry and other instrumental methods-II. Investigations on Quartz and Feldspar. Clay and clay minerals, 1978;26: 139-143.
24. Tuschel D, Spectroscopy, 2014; 29(9): 14-21.
25. Enami M, Nishiyama T, Mouri, T, Laser Raman micro-spectrometry of metamorphic quartz: A simple method for comparison of metamorphic pressure, American Mineralogist DOI:10.2138/am.2007.2438. 2007;92(8-9): 1303-1315.
26. Nasadala L, Smith DC, Kaindl R and Emo MAZ, Raman spectroscopy: Analytical perspective in mineralogical research, Notes in Mineralogy: (2004).
27. Dean KJ, Wilkinson GR, Temperature and pressure dependence of the Raman active modes of vibration of α -quartz, Spectrochimica Acta part A Molecular Spectroscopy. 1982; 38: 1105-1108.
28. Gillet P, Lecleach A and Madon M, High- Temperature Raman-Spectroscopy of SiO₂ and GeO₂: Polymorph-Anharmonicity and Thermodynamics properties at high temperatures, Journal of Geophysical Research Atmosphere. 1990;95 :21635-21655.
29. Molen IV, Shifts of α - β transition temperature of quartz associated with the thermal expansion of granite at high pressure, Tectonophysics. 1981;73: 323-342.

Table1: Crystallinity index from IR spectra

Sample	778cm ⁻¹ peak intensity (%T)	695cm ⁻¹ peak intensity (%T)	Crystallinity Index	% crystallinity
Q1	2.5	9	1.18	81.37
Q2	3.2	8.8	1.41	97.24
Q3	9.6	19.2	1.45	100
Q4	0.8	3.6	1.45	100
Q5	0.45	1.25	1.23	84.83
Q6	7.7	14.2	1.32	91.03
Q7	0.4	0.72	1.13	77.93
Q8	0.23	0.47	1.13	77.93





Roshmi Borthakur et al.,

Q9	0.96	1.46	1.10	75.86
Q10	2.8	4.3	1.14	78.62
Q11	3.42	5.76	1.18	81.38
Q12	4.9	8.43	1.22	84.14

Table 2: Raman characteristics peak difference in observed samples

sample no.	Observed Peak(wave no.) near or at 464 cm ⁻¹	Observed Peak (wave no.) near or at 205cm ⁻¹	diff. in 464 cm ⁻¹ -205cm ⁻¹ (observed) W	diff. in 464 cm ⁻¹ -205 cm ⁻¹ (std.theoretical)w	Amount of Raman peak shift (obs.- thy.) dw(cm ⁻¹)
Q1	465	205	260	259	1
Q2	465	207	258	259	1
Q3	466	206	260	259	1
Q4	465	208	257	259	2
Q5	466	205	261	259	2
Q6	465	210	255	259	4
Q7	465	209	256	259	3
Q8	465	207	258	259	1
Q9	465	207	258	259	1
Q10	464	207	257	259	2
Q11	465	208	257	259	2
Q12	465	207	258	259	1

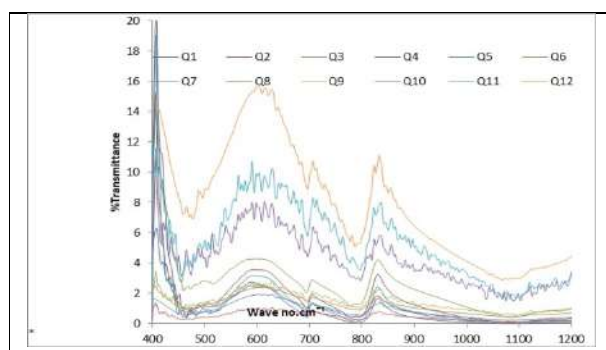


Fig. 1: Infrared spectra of the studied samples in the range 400-1200 cm⁻¹. The characteristic peaks for crystallinity are at 695 and 778 cm⁻¹

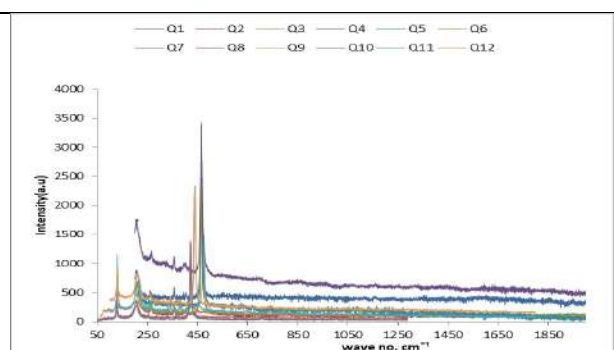


Fig. 2: Raman spectra of the studied samples

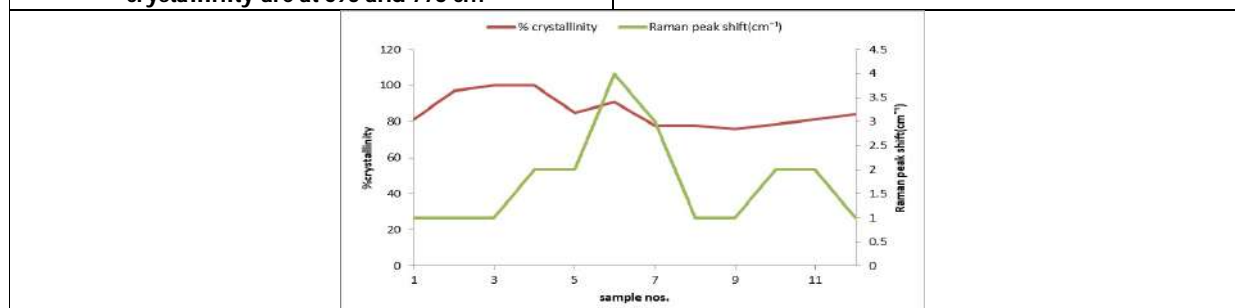


Fig. 3: Comparative variation of the crystallinity and pressure-temperature dependence peak shift of Raman spectra.





Weakly $(1,2)^*$ - \tilde{g} - Closed sets and its Continuities

O.Nethaji¹, R. Asokan² and A. Ponmalar^{3*}

¹PG and Research Department of Mathematics, Kamaraj College, Thoothukudi - 628 003, Tamil Nadu, India.

²Professor, Department of Mathematics, School of Mathematics, Madurai Kamaraj University, Madurai – 625 021, Tamil Nadu, India

³Research Scholar, Department of Mathematics, School of Mathematics, Madurai Kamaraj University, Madurai – 625 021, Tamil Nadu, India

Received: 18 Jan 2023

Revised: 04 Apr 2023

Accepted: 05 May 2023

*Address for Correspondence

A. Ponmalar

Research Scholar,
Department of Mathematics,
School of Mathematics, Madurai Kamaraj University,
Madurai – 625 021, Tamil Nadu, India
E.Mail: ponmalara76@gmail.com



This is an Open Access Journal / article distributed under the terms of the **Creative Commons Attribution License** (CC BY-NC-ND 3.0) which permits unrestricted use, distribution, and reproduction in any medium, provided the original work is properly cited. All rights reserved.

ABSTRACT

We studied new class of generalized closed sets called weakly $(1,2)^*$ - \tilde{g} -closed sets. Also, we investigate the relationships among the related generalized closed sets $(1,2)^*$ - $w\pi g$ -closed, $(1,2)^*$ - rwg -closed, and *et al* and We focused Weakly $(1,2)^*$ - \tilde{g} -continuous map.

Keywords: $(1,2)^*$ - \tilde{g} -closed set, weakly $(1,2)^*$ - \tilde{g} -closed sets., $(1,2)^*$ - $w\pi g$ -closed

INTRODUCTION

In 2012, Sanjay Mishra and Nitin Bhardwaj [4, 5] was introduced Regular generalized weakly rgw -closed sets in topological spaces, Also introduced Generalized pre regular weakly $gprw$ -closed sets in topological spaces. In 2016, R.S. Wali and Bsayya B. Mathad [9] was introduced semi regular weakly open sets in topological space and in 2020, Pre weakly generalized closed set in topological space was introduced by A.Mir and *et al* [1]. In 2021. In this paper, we introduce a new class of generalized closed sets called weakly $(1,2)^*$ - \tilde{g} -closed sets which contains the above mentioned class. Also, we investigate the relationships among the related generalized closed sets.

Preliminaries

Definition 2.1 [6] A subset A of a bitopological space (X, τ_1, τ_2) is called

1. $(1,2)^*$ - π -open set if A is the finite union of regular $(1,2)^*$ -open sets. The complement of $(1,2)^*$ - π -open sets are called $(1,2)^*$ - π -closed set.





Nethaji et al.,

2. $(1,2)^*$ - πg -closed set if $\tau_{1,2} - cl(A) \subseteq U$ whenever $A \subseteq U$ and U is $(1,2)^*$ - π -open in X . The complement of $(1,2)^*$ - πg -closed set is called $(1,2)^*$ - πg -open set.

Definition 2.2 [6] Let (X, τ_1, τ_2) and (Y, σ_1, σ_2) be two bitopological spaces. A function $f: (X, \tau_1, \tau_2) \rightarrow (Y, \sigma_1, \sigma_2)$ is called

1. completely $(1,2)^*$ -continuous (resp. $(1,2)^*$ - R -map) if $f^{-1}(V)$ is regular $(1,2)^*$ -open in X for each $\sigma_{1,2}$ -open (resp. regular $(1,2)^*$ -open) set V of Y .
2. perfectly $(1,2)^*$ -continuous if $f^{-1}(V)$ is both $\tau_{1,2}$ -open and $\tau_{1,2}$ -closed in X for each $\sigma_{1,2}$ -open set V of Y .

Definition 2.3 A subset A of a bitopological space (X, τ_1, τ_2) is called

1. weakly $(1,2)^*$ - g -closed (briefly, $(1,2)^*$ - wg -closed) set if $\tau_{1,2} - cl(\tau_{1,2} - int(A)) \subseteq U$ whenever $A \subseteq U$ and U is $\tau_{1,2}$ -open in X .
2. weakly $(1,2)^*$ - πg -closed (briefly, $(1,2)^*$ - $w\pi g$ -closed) set if $\tau_{1,2} - cl(\tau_{1,2} - int(A)) \subseteq U$ whenever $A \subseteq U$ and U is $(1,2)^*$ - π -open in X .
3. regular weakly $(1,2)^*$ -generalized closed (briefly, $(1,2)^*$ - rwg -closed) set if $\tau_{1,2} - cl(\tau_{1,2} - int(A)) \subseteq U$ whenever $A \subseteq U$ and U is regular $(1,2)^*$ -open in X .

Remark 2.4 [7] Every $\tau_{1,2}$ -open set is $(1,2)^*$ - sg -open but not conversely.

Remark 2.5 For a subset of a bitopological space, we have following implications:

regular $(1,2)^*$ -open \rightarrow $(1,2)^*$ - π -open \rightarrow $\tau_{1,2}$ -open

Definition 2.6 A subset A of a bitopological space (X, τ_1, τ_2) is said to be nowhere dense if $\tau_{1,2} - int(\tau_{1,2} - cl(A)) = \phi$.

Definition 2.7 Let $f: (X, \tau_1, \tau_2) \rightarrow (Y, \sigma_1, \sigma_2)$ be a function. Then f is said to be contra- $(1,2)^*$ - g -continuous if $f^{-1}(V)$ is $(1,2)^*$ - g -closed in X for every $\sigma_{1,2}$ -open set of Y .

3 Weakly $(1,2)^*$ - \check{g} -closed sets

Definition 3.1 A subset A of a bitopological space (X, τ_1, τ_2) is called a weakly $(1,2)^*$ - \check{g} -closed (briefly, $(1,2)^*$ - $w\check{g}$ -closed) set if $\tau_{1,2} - cl(\tau_{1,2} - int(A)) \subseteq U$ whenever $A \subseteq U$ and U is $(1,2)^*$ - sg -open.

Proposition 3.2 In a space (X, τ_1, τ_2) , every $(1,2)^*$ - \check{g} -closed set is $(1,2)^*$ - $w\check{g}$ -closed.

Remark 3.3 The converse of above Proposition 3.2 is not true as shown in the following example.

Example 3.4 Let $X = \{a, b, c\}$, $\tau_1 = \{\phi, X, \{a, b\}\}$ and $\tau_2 = \{\phi, X\}$. Then $\tau_{1,2} = \{\phi, X, \{a, b\}\}$, then the set $\{a\}$ is $(1,2)^*$ - $w\check{g}$ -closed set but not $(1,2)^*$ - \check{g} -closed.

Proposition 3.5 In a space (X, τ_1, τ_2) , every $(1,2)^*$ - $w\check{g}$ -closed set is $(1,2)^*$ - wg -closed.

proof: Let A be any $(1,2)^*$ - $w\check{g}$ -closed set and U be any $\tau_{1,2}$ -open set containing A . Then U is a $(1,2)^*$ - sg -open set containing A . We have $\tau_{1,2} - cl(\tau_{1,2} - int(A)) \subseteq U$. Thus, A is $(1,2)^*$ - wg -closed.

Remark 3.6 The converse of above Proposition 3.5 is not true as shown in the following example.

Example 3.7 Let $X = \{a, b, c\}$, $\tau_1 = \{\phi, X, \{a\}\}$ and $\tau_2 = \{\phi, X\}$. Then $\tau_{1,2} = \{\phi, X, \{a\}\}$, then the set $\{a, b\}$ is $(1,2)^*$ - wg -closed but not a $(1,2)^*$ - $w\check{g}$ -closed.

Proposition 3.8 In a space (X, τ_1, τ_2) , every $(1,2)^*$ - $w\check{g}$ -closed set is $(1,2)^*$ - $w\pi g$ -closed.

proof: Let A be any $(1,2)^*$ - $w\check{g}$ -closed set and U be any $(1,2)^*$ - π -open set containing A . Then U is a $(1,2)^*$ - sg -open set containing A . We have $\tau_{1,2} - cl(\tau_{1,2} - int(A)) \subseteq U$. Thus, A is $(1,2)^*$ - $w\pi g$ -closed.

Remark 3.9 The converse of above Proposition 3.8 is not true as shown in the following example.

Example 3.10 In Example 3.7, the subset $\{a, c\}$ is $(1,2)^*$ - $w\pi g$ -closed but it is not a $(1,2)^*$ - $w\check{g}$ -closed.

Proposition 3.11 In a space (X, τ_1, τ_2) , every $(1,2)^*$ - $w\check{g}$ -closed set is $(1,2)^*$ - rwg -closed.

proof: Let A be any $(1,2)^*$ - $w\check{g}$ -closed set and U be any regular $(1,2)^*$ -open set containing A . Then U is a $(1,2)^*$ - sg -open set containing A . We have $\tau_{1,2} - cl(\tau_{1,2} - int(A)) \subseteq U$. Thus, A is $(1,2)^*$ - rwg -closed.

Remark 3.12 The converse of above Proposition 3.11 is not true as shown in the following example.

Example 3.13 In Example 3.7, the subset $\{a\}$ is $(1,2)^*$ - rwg -closed but not $(1,2)^*$ - $w\check{g}$ -closed.

Theorem 3.14 If a subset A of a bitopological space (X, τ_1, τ_2) is both $\tau_{1,2}$ -closed and $(1,2)^*$ - αg -closed, then it is $(1,2)^*$ - $w\check{g}$ -closed in X .





Nethaji et al.,

proof: Let A be an $(1,2)^*$ - αg -closed set in (X, τ_1, τ_2) and U be any $\tau_{1,2}$ -open set containing A . Then $U \supseteq (1,2)^* - \alpha cl(A) = A \cup \tau_{1,2} - cl(\tau_{1,2} - int(\tau_{1,2} - cl(A)))$. Since A is $\tau_{1,2}$ -closed, $U \supseteq \tau_{1,2} - cl(\tau_{1,2} - int(A))$ and hence A is $(1,2)^*$ - $w\check{g}$ -closed.

Theorem 3.15 *If a subset A of a bitopological space (X, τ_1, τ_2) is both $\tau_{1,2}$ -open and $(1,2)^*$ - $w\check{g}$ -closed, then $\tau_{1,2}$ -closed.*

proof: Since A is both $\tau_{1,2}$ -open and $(1,2)^*$ - $w\check{g}$ -closed, $A \supseteq \tau_{1,2} - cl(\tau_{1,2} - int(A)) = \tau_{1,2} - cl(A)$ and hence A is $\tau_{1,2}$ -closed.

Corollary 3.16 *If a subset A of a bitopological space (X, τ_1, τ_2) is both $\tau_{1,2}$ -open and $(1,2)^*$ - $w\check{g}$ -closed, then it is both regular $(1,2)^*$ -open and regular $(1,2)^*$ -closed.*

Theorem 3.17 *Let X be a bitopological space and $A \subseteq X$ be $\tau_{1,2}$ -open. Then, A is $(1,2)^*$ - $w\check{g}$ -closed if and only if A is $(1,2)^*$ - \check{g} -closed.*

proof: Let A be $(1,2)^*$ - \check{g} -closed. By Proposition 3.2, it is $(1,2)^*$ - $w\check{g}$ -closed.

Conversely, let A be $(1,2)^*$ - $w\check{g}$ -closed. Since A is $\tau_{1,2}$ -open, by Proposition 3.5, A is $\tau_{1,2}$ -closed. Hence A is $(1,2)^*$ - \check{g} -closed.

Theorem 3.18 *If a set A is $(1,2)^*$ - $w\check{g}$ -closed then $\tau_{1,2} - cl(\tau_{1,2} - int(A))$ - A contains no non-empty $(1,2)^*$ - sg -closed set.*

proof: Let F be a $(1,2)^*$ - sg -closed set such that $F \subseteq \tau_{1,2} - cl(\tau_{1,2} - int(A)) - A$. Since F^c is $(1,2)^*$ - sg -open and $A \subseteq F^c$, from the definition of $(1,2)^*$ - $w\check{g}$ -closedness, it follows that $\tau_{1,2} - cl(\tau_{1,2} - int(A)) \subseteq F^c$. That is $F \subseteq (\tau_{1,2} - cl(\tau_{1,2} - int(A)))^c$. This implies that $F \subseteq (\tau_{1,2} - cl(\tau_{1,2} - int(A))) \cap (\tau_{1,2} - cl(\tau_{1,2} - int(A)))^c = \phi$.

Theorem 3.19 *If a subset A of a bitopological space (X, τ_1, τ_2) is nowhere dense, then it is $(1,2)^*$ - $w\check{g}$ -closed.*

proof: Since $\tau_{1,2} - int(A) \subseteq \tau_{1,2} - int(\tau_{1,2} - cl(A))$ and A is nowhere dense, $\tau_{1,2} - int(A) = \phi$. Therefore $\tau_{1,2} - cl(\tau_{1,2} - int(A)) = \phi$ and hence A is $(1,2)^*$ - $w\check{g}$ -closed in (X, τ_1, τ_2) .

The converse of Theorem 3.19 need not be true as shown in the following example.

Example 3.20 *Let $X = \{a, b, c\}$, $\tau_1 = \{\phi, X, \{a\}\}$ and $\tau_2 = \{\phi, X, \{b, c\}\}$. Then $\tau_{1,2} = \{\phi, X, \{a\}, \{b, c\}\}$. In the space (X, τ_1, τ_2) , then the subset $\{a\}$ is $(1,2)^*$ - $w\check{g}$ -closed set but not nowhere dense.*

Remark 3.21 *The following examples show that the family of $(1,2)^*$ - $w\check{g}$ -closedness and the family of $(1,2)^*$ -semi-closedness are independent.*

Example 3.22 *In Example 3.4, we have the subset $\{a, c\}$ is $(1,2)^*$ - $w\check{g}$ -closed set but not $(1,2)^*$ -semi-closed.*

Example 3.23 *Let $X = \{a, b, c\}$, $\tau_1 = \{\phi, X, \{a\}\}$ and $\tau_2 = \{\phi, X, \{b\}\}$. Then $\tau_{1,2} = \{\phi, X, \{a\}, \{b\}, \{a, b\}\}$. In the space (X, τ_1, τ_2) , then the subset $\{a\}$ is $(1,2)^*$ -semi-closed set but not $(1,2)^*$ - $w\check{g}$ -closed.*

Remark 3.24 *From the above discussions We obtain the following diagram, where $A \rightarrow B$ represents A implies B but not conversely.*

$\tau_{1,2}$ -closed \rightarrow $(1,2)^*$ - wg -closed \rightarrow $(1,2)^*$ - $w\check{g}$ -closed \downarrow
 $(1,2)^*$ - $w\pi g$ -closed \leftarrow $(1,2)^*$ - rwg -closed

Definition 3.25 *A subset A of a bitopological space (X, τ_1, τ_2) is $(1,2)^*$ - $w\check{g}$ -open set if A^c is $(1,2)^*$ - $w\check{g}$ -closed.*

Proposition 3.26 *In a space (X, τ_1, τ_2) ,*

1. any $(1,2)^*$ - \check{g} -open set is $(1,2)^*$ - $w\check{g}$ -open but not conversely.
2. any $(1,2)^*$ - \check{g} -open set is $(1,2)^*$ - $w\check{g}$ -open but not conversely.

Theorem 3.27 *A subset A of a bitopological space (X, τ_1, τ_2) is $(1,2)^*$ - $w\check{g}$ -open if $G \subseteq \tau_{1,2} - int(\tau_{1,2} - cl(A))$ whenever $G \subseteq A$ and G is $(1,2)^*$ - sg -closed.*

proof: Let A be any $(1,2)^*$ - $w\check{g}$ -open. Then A^c is $(1,2)^*$ - $w\check{g}$ -closed. Let G be a $(1,2)^*$ - sg -closed set contained in A . Then G^c is a $(1,2)^*$ - sg -open set containing A^c . Since A^c is $(1,2)^*$ - $w\check{g}$ -closed, we have $\tau_{1,2} - cl(\tau_{1,2} - int(A^c)) \subseteq G^c$. Therefore $G \subseteq \tau_{1,2} - int(\tau_{1,2} - cl(A))$.

Conversely, we suppose that $G \subseteq \tau_{1,2} - int(\tau_{1,2} - cl(A))$ whenever $G \subseteq A$ and G is $(1,2)^*$ - sg -closed. Then G^c is a $(1,2)^*$ - sg -open set containing A^c and $G^c \supseteq (\tau_{1,2} - int(\tau_{1,2} - cl(A)))^c$. It follows that $G^c \supseteq \tau_{1,2} - cl(\tau_{1,2} - int(A^c))$. Hence A^c is $(1,2)^*$ - $w\check{g}$ -closed and so A is $(1,2)^*$ - $w\check{g}$ -open.

4 Weakly $(1,2)^*$ - \check{g} -continuous map

Definition 4.1 *A map $f: (X, \tau_1, \tau_2) \rightarrow (Y, \sigma_1, \sigma_2)$ is called $((1,2)^*$ - $\check{g}, s)$ -continuous if the inverse image of each regular $(1,2)^*$ -open set of Y is $(1,2)^*$ - \check{g} -closed in X .*

Definition 4.2A *space (X, τ_1, τ_2) is called $(1,2)^*$ - \check{g} -connected if X is not the union of two disjoint nonempty $(1,2)^*$ - \check{g} -open sets.*





Nethaji et al.,

Definition 4.3 A subset of a bitopological space (X, τ_1, τ_2) is said to be

1. almost $(1,2)^*$ -connected if X cannot be written as a disjoint union of two non-empty regular $(1,2)^*$ -open sets.
2. $(1,2)^*$ -connected if X cannot be written as a disjoint union of two non-empty $\tau_{1,2}$ -open sets.

Definition 4.4 Let X and Y be two bitopological spaces. A map $f: (X, \tau_1, \tau_2) \rightarrow (Y, \sigma_1, \sigma_2)$ is called weakly $(1,2)^*$ - \check{g} -continuous (briefly $(1,2)^*$ - $w\check{g}$ -continuous) if $f^{-1}(U)$ is a $(1,2)^*$ - $w\check{g}$ -open set in X for each $\sigma_{1,2}$ -open set U of Y .

Example 4.5 Let $X = Y = \{a, b, c\}$, $\tau_1 = \{\phi, X, \{a\}\}$ and $\tau_2 = \{\phi, X, \{b, c\}\}$. Then $\tau_{1,2} = \{\phi, \{a\}, \{b, c\}, X\}$. Let $\sigma_1 = \{\phi, Y, \{a\}\}$ and $\sigma_2 = \{\phi, Y\}$. Then $\sigma_{1,2} = \{\phi, \{a\}, Y\}$. The map $f: (X, \tau_1, \tau_2) \rightarrow (Y, \sigma_1, \sigma_2)$ defined by $f(a) = b$, $f(b) = c$ and $f(c) = a$ is $(1,2)^*$ - $w\check{g}$ -continuous, because every subset of Y is $(1,2)^*$ - $w\check{g}$ -closed in X .

Proposition 4.6 Every $(1,2)^*$ - \check{g} -continuous map is $(1,2)^*$ - $w\check{g}$ -continuous.

proof: It follows from Proposition 3.26(i).

Remark 4.7 The converse of Proposition 3.33 is not true as shown in the following example.

Example 4.8 Let $X = Y = \{a, b, c\}$, $\tau_1 = \{\phi, X, \{a\}\}$ and $\tau_2 = \{\phi, X, \{b, c\}\}$. Then $\tau_{1,2} = \{\phi, \{a\}, \{b, c\}, X\}$. Let $\sigma_1 = \{\phi, Y, \{a, b\}\}$ and $\sigma_2 = \{\phi, Y\}$. Then $\sigma_{1,2} = \{\phi, \{a, b\}, Y\}$. The map $f: (X, \tau_1, \tau_2) \rightarrow (Y, \sigma_1, \sigma_2)$ be the identity map. Then f is $(1,2)^*$ - $w\check{g}$ -continuous but not $(1,2)^*$ - \check{g} -continuous.

Theorem 4.9 A map $f: (X, \tau_1, \tau_2) \rightarrow (Y, \sigma_1, \sigma_2)$ is $(1,2)^*$ - $w\check{g}$ -continuous if and only if $f^{-1}(U)$ is a $(1,2)^*$ - $w\check{g}$ -closed set in X for each $\sigma_{1,2}$ -closed set U of Y .

proof: Let U be any $\sigma_{1,2}$ -closed set of Y . According to the assumption $f^{-1}(U) = X \setminus f^{-1}(U)$ is $(1,2)^*$ - $w\check{g}$ -open in X , so $f^{-1}(U)$ is $(1,2)^*$ - $w\check{g}$ -closed in X .

The converse can be proved in a similar manner.

Theorem 4.10 Suppose that X and Y are bitopological spaces and $(1,2)^* - \check{C}(X)$ is closed under arbitrary intersections. If a map $f: (X, \tau_1, \tau_2) \rightarrow (Y, \sigma_1, \sigma_2)$ is contra $(1,2)^*$ - \check{g} -continuous and Y is $(1,2)^*$ -regular, then f is $(1,2)^*$ - \check{g} -continuous.

proof: Let x be an arbitrary point of X and V be an $\sigma_{1,2}$ -open set of Y containing $f(x)$. Since Y is $(1,2)^*$ -regular, there exists an $\sigma_{1,2}$ -open set G in Y containing $f(x)$ such that $\sigma_{1,2} - cl(G) \subseteq V$. Since f is contra $(1,2)^*$ - \check{g} -continuous, there exists $U \in (1,2)^* - \check{C}O(X)$ containing x such that $f(U) \subseteq \sigma_{1,2} - cl(G)$. Then $f(U) \subseteq \sigma_{1,2} - cl(G) \subseteq V$. Hence, f is $(1,2)^*$ - \check{g} -continuous.

Theorem 4.11 Suppose that X and Y are bitopological spaces and the family of $(1,2)^*$ - \check{g} -closed sets in X is closed under arbitrary intersections. If a map $f: (X, \tau_1, \tau_2) \rightarrow (Y, \sigma_1, \sigma_2)$ is contra $(1,2)^*$ - \check{g} -continuous and Y is $(1,2)^*$ -regular, then f is $(1,2)^*$ - $w\check{g}$ -continuous.

proof: The proof is obvious from Proposition 3.33.

Definition 4.12 A bitopological space (X, τ_1, τ_2) is said to be locally $(1,2)^*$ - \check{g} -indiscrete if every $(1,2)^*$ - \check{g} -open set of X is $\tau_{1,2}$ -closed in X .

Theorem 4.13 Let $f: (X, \tau_1, \tau_2) \rightarrow (Y, \sigma_1, \sigma_2)$ be a map. If f is $(1,2)^*$ - \check{g} -continuous and X is locally $(1,2)^*$ - \check{g} -indiscrete, then f is $(1,2)^*$ -continuous.

proof: Let V be an $\sigma_{1,2}$ -open in Y . Since f is $(1,2)^*$ - \check{g} -continuous, $f^{-1}(V)$ is $(1,2)^*$ - \check{g} -open in X . Since X is locally $(1,2)^*$ - \check{g} -indiscrete, $f^{-1}(V)$ is $\tau_{1,2}$ -closed in X . Hence f is $(1,2)^*$ -continuous.

Theorem 4.14 Let $f: (X, \tau_1, \tau_2) \rightarrow (Y, \sigma_1, \sigma_2)$ be a map. If f is contra $(1,2)^*$ - \check{g} -continuous and X is locally $(1,2)^*$ - \check{g} -indiscrete, then f is $(1,2)^*$ - $w\check{g}$ -continuous.

proof: Let $f: (X, \tau_1, \tau_2) \rightarrow (Y, \sigma_1, \sigma_2)$ be contra $(1,2)^*$ - \check{g} -continuous and X is locally $(1,2)^*$ - \check{g} -indiscrete. By Theorem 3.40, f is $(1,2)^*$ -continuous, then f is $(1,2)^*$ - $w\check{g}$ -continuous.

Corollary 4.15 Let Y be a $(1,2)^*$ -regular space and $f: (X, \tau_1, \tau_2) \rightarrow (Y, \sigma_1, \sigma_2)$ be a map. Suppose that the collection of $(1,2)^*$ - \check{g} -closed sets in X is closed under arbitrary intersections. Then if f is $((1,2)^* - \check{g}, s)$ -continuous, f is $(1,2)^*$ - $w\check{g}$ -continuous.

proof: Let f be $((1,2)^* - \check{g}, s)$ -continuous. Then f is $(1,2)^*$ - \check{g} -continuous. Thus, f is $(1,2)^*$ - $w\check{g}$ -continuous by Proposition 3.33.

Proposition 4.16 If $f: (X, \tau_1, \tau_2) \rightarrow (Y, \sigma_1, \sigma_2)$ is perfectly $(1,2)^*$ -continuous and $(1,2)^*$ - $w\check{g}$ -continuous, then it is $(1,2)^*$ - R -map.

proof: Let V be any regular $(1,2)^*$ -open subset of Y . According to the assumption, $f^{-1}(V)$ is both $\tau_{1,2}$ -open and $\tau_{1,2}$ -closed in X . Since $f^{-1}(V)$ is $\tau_{1,2}$ -closed, it is $(1,2)^*$ - $w\check{g}$ -closed. We have $f^{-1}(V)$ is both $\tau_{1,2}$ -open and $(1,2)^*$ - $w\check{g}$ -closed. Hence, by Corollary 3.40, it is regular $(1,2)^*$ -open in X , so f is $(1,2)^*$ - R -map.

Definition 4.17 A bitopological space (x, τ_1, τ_2) is called $(1,2)^*$ - \check{g} -compact (resp. $(1,2)^*$ -compact) if every cover of X by $(1,2)^*$ - \check{g} -open (resp. $\tau_{1,2}$ -open) sets has finite subcover.





Nethaji et al.,

Definition 4.18 A bitopological space (X, τ_1, τ_2) is weakly $(1,2)^*$ - \check{g} -compact (briefly, $(1,2)^*$ - $w\check{g}$ -compact) if every $(1,2)^*$ - $w\check{g}$ -open cover of X has a finite subcover.

Remark 4.19 Every $(1,2)^*$ - $w\check{g}$ -compact space is $(1,2)^*$ - \check{g} -compact.

Theorem 4.20 Let $f: (X, \tau_1, \tau_2) \rightarrow (Y, \sigma_1, \sigma_2)$ be surjective $(1,2)^*$ - $w\check{g}$ -continuous map. If X is $(1,2)^*$ - $w\check{g}$ -compact, then Y is $(1,2)^*$ -compact.

proof: Let $\{A_i; i \in I\}$ be an $\sigma_{1,2}$ -open cover of Y . Then $\{f^{-1}(A_i); i \in I\}$ is a $(1,2)^*$ - $w\check{g}$ -open cover in X . Since X is $(1,2)^*$ - $w\check{g}$ -compact, it has a finite subcover, say $\{f^{-1}(A_1), f^{-1}(A_2), \dots, f^{-1}(A_n)\}$. Since f is surjective $\{A_1, A_2, \dots, A_n\}$ is a finite subcover of Y and hence Y is $(1,2)^*$ -compact.

Definition 4.21 A bitopological space (X, τ_1, τ_2) is weakly $(1,2)^*$ - \check{g} -connected (briefly $(1,2)^*$ - $w\check{g}$ -connected) if X cannot be written as the disjoint union of two non-empty $(1,2)^*$ - $w\check{g}$ -open sets.

Theorem 4.22 If a bitopological space X is $(1,2)^*$ - $w\check{g}$ -connected, then X is almost $(1,2)^*$ -connected (resp. $(1,2)^*$ - \check{g} -connected).

proof: It follows from the fact that each regular $(1,2)^*$ -open set (resp. $(1,2)^*$ - \check{g} -open set) is $(1,2)^*$ - $w\check{g}$ -open.

Theorem 4.23 For a bitopological space X , the following properties are equivalent:

1. X is $(1,2)^*$ - $w\check{g}$ -connected.
2. The empty set ϕ and X are only subsets which are both $(1,2)^*$ - $w\check{g}$ -open and $(1,2)^*$ - $w\check{g}$ -closed.
3. Each $(1,2)^*$ - $w\check{g}$ -continuous map from X into a discrete bitopological space Y which has at least two points is a constant map.

proof: (i) \Rightarrow (ii). Let $S \subseteq X$ be any proper subset, which is both $(1,2)^*$ - $w\check{g}$ -open and $(1,2)^*$ - $w\check{g}$ -closed. Its complement $X \setminus S$ is also $(1,2)^*$ - $w\check{g}$ -open and $(1,2)^*$ - $w\check{g}$ -closed. Then $X = S \cup (X \setminus S)$ is a disjoint union of two non-empty $(1,2)^*$ - $w\check{g}$ -open sets which is a contradiction with the fact that X is $(1,2)^*$ - $w\check{g}$ -connected. Hence, $S = \phi$ or X .

(ii) \Rightarrow (i). Let $X = A \cup B$ where $A \cap B = \phi$, $A \neq \phi$, $B \neq \phi$ and A, B are $(1,2)^*$ - $w\check{g}$ -open. Since $A = X \setminus B$, A is $(1,2)^*$ - $w\check{g}$ -closed. According to the assumption $A = \phi$, which is a contradiction.

(ii) \Rightarrow (iii). Let $f: (X, \tau_1, \tau_2) \rightarrow (Y, \sigma_1, \sigma_2)$ be a $(1,2)^*$ - $w\check{g}$ -continuous map where Y is a discrete bitopological space with at least two points. Then $f^{-1}(\{y\})$ is $(1,2)^*$ - $w\check{g}$ -closed and $(1,2)^*$ - $w\check{g}$ -open for each $y \in Y$ and $X = \cup \{f^{-1}(\{y\}) | y \in Y\}$. According to the assumption, $f^{-1}(\{y\}) = \phi$ or $f^{-1}(\{y\}) = X$. If $f^{-1}(\{y\}) = \phi$ for all $y \in Y$, f will not be a map. Also there is no exist more than one $y \in Y$ such that $f^{-1}(\{y\}) = X$. Hence, there exists only one $y \in Y$ such that $f^{-1}(\{y\}) = X$ and $f^{-1}(\{y\}) = \phi$ where $y \neq y_1 \in Y$. This shows that f is a constant map.

(iii) \Rightarrow (ii). Let $S \neq \phi$ be both $(1,2)^*$ - $w\check{g}$ -open and $(1,2)^*$ - $w\check{g}$ -closed in X . Let $f: X \rightarrow Y$ be a $(1,2)^*$ - $w\check{g}$ -continuous map defined by $f(S) = \{a\}$ and $f(X \setminus S) = \{b\}$ where $a \neq b$. Since f is constant map we get $S = X$.

Theorem 4.24 Let $f: (X, \tau_1, \tau_2) \rightarrow (Y, \sigma_1, \sigma_2)$ be a $(1,2)^*$ - $w\check{g}$ -continuous surjective map. If X is $(1,2)^*$ - $w\check{g}$ -connected, then Y is $(1,2)^*$ -connected.

proof: We suppose that Y is not $(1,2)^*$ -connected. Then $Y = A \cup B$ where $A \cap B = \phi$, $A \neq \phi$, $B \neq \phi$ and A, B are $\sigma_{1,2}$ -open sets in Y . Since f is $(1,2)^*$ - $w\check{g}$ -continuous surjective map, $X = f^{-1}(A) \cup f^{-1}(B)$ are disjoint union of two non-empty $(1,2)^*$ - $w\check{g}$ -open subsets. This is contradiction with the fact that X is $(1,2)^*$ - $w\check{g}$ -connected.

5. Weakly $(1,2)^*$ - \check{g} -open and weakly $(1,2)^*$ - \check{g} -closed maps

Definition 5.1 Let (X, τ_1, τ_2) and (Y, σ_1, σ_2) be bitopological spaces. A map $f: (X, \tau_1, \tau_2) \rightarrow (Y, \sigma_1, \sigma_2)$ is called weakly $(1,2)^*$ - \check{g} -open (briefly, $(1,2)^*$ - $w\check{g}$ -open) if $f(V)$ is a $(1,2)^*$ - $w\check{g}$ -open set in Y for each $\tau_{1,2}$ -open set V of X .

Remark 5.2 Every $(1,2)^*$ - \check{g} -open map is $(1,2)^*$ - $w\check{g}$ -open but not conversely.

Example 5.3 Let $X = Y = \{a, b, c, d\}$, $\tau_1 = \{\phi, X, \{a\}\}$ and $\tau_2 = \{\phi, X, \{a, b, d\}\}$. Then $\tau_{1,2} = \{\phi, X, \{a\}, \{a, b, d\}\}$. Let $\sigma_1 = \{\phi, Y, \{a\}\}$ and $\sigma_2 = \{\phi, Y, \{b, c\}\}$. Then $\sigma_{1,2} = \{\phi, Y, \{a\}, \{b, c\}\}$. Let $f: (X, \tau_1, \tau_2) \rightarrow (Y, \sigma_1, \sigma_2)$ be the identity map. Then f is $(1,2)^*$ - $w\check{g}$ -open but not $(1,2)^*$ - \check{g} -open.

Definition 5.4 Let (X, τ_1, τ_2) and (Y, σ_1, σ_2) be bitopological spaces. A map $f: (X, \tau_1, \tau_2) \rightarrow (Y, \sigma_1, \sigma_2)$ is called weakly $(1,2)^*$ - \check{g} -closed (briefly, $(1,2)^*$ - $w\check{g}$ -closed) if $f(V)$ is a $(1,2)^*$ - $w\check{g}$ -closed set in Y for each $\tau_{1,2}$ -closed set V of X .

It is clear that an $(1,2)^*$ -open map is $(1,2)^*$ - $w\check{g}$ -open and a $(1,2)^*$ -closed map is $(1,2)^*$ - $w\check{g}$ -closed.

Theorem 5.5 Let (X, τ_1, τ_2) and (Y, σ_1, σ_2) be bitopological spaces. A map $f: (X, \tau_1, \tau_2) \rightarrow (Y, \sigma_1, \sigma_2)$ is $(1,2)^*$ - $w\check{g}$ -closed if and only if for each subset B of Y and for each $\tau_{1,2}$ -open set G containing $f^{-1}(B)$ there exists a $(1,2)^*$ - $w\check{g}$ -open set F of Y such that $B \subseteq F$ and $f^{-1}(F) \subseteq G$.

proof: Let B be any subset of Y and let G be an $\tau_{1,2}$ -open subset of X such that $f^{-1}(B) \subseteq G$. Then $F = Y \setminus f(X \setminus G)$ is $(1,2)^*$ - $w\check{g}$ -open set containing B and $f^{-1}(F) \subseteq G$.





Nethaji et al.,

Conversely, let U be any $\tau_{1,2}$ -closed subset of X . Then $f^{-1}(Y \setminus f(U)) \subseteq X \setminus U$ and $X \setminus U$ is $\tau_{1,2}$ -open. According to the assumption, there exists a $(1,2)^*$ -w \check{g} -open set F of Y such that $Y \setminus f(U) \subseteq F$ and $f^{-1}(F) \subseteq X \setminus U$. Then $U \subseteq X \setminus f^{-1}(F)$. From $Y \setminus F \subseteq f(U) \subseteq f(X \setminus f^{-1}(F)) \subseteq Y \setminus F$, it follows that $f(U) = Y \setminus F$, so $f(U)$ is $(1,2)^*$ -w \check{g} -closed in Y . Therefore f is a $(1,2)^*$ -w \check{g} -closed map.

Remark 5.6 The composition of two $(1,2)^*$ -w \check{g} -closed maps need not be a $(1,2)^*$ -w \check{g} -closed as shown in from the following example.

Example 5.7 Let $X = Y = Z = \{a, b, c\}$, $\tau_1 = \{\phi, X, \{a\}\}$ and $\tau_2 = \{\phi, X, \{a, b\}\}$. Then $\tau_{1,2} = \{\phi, X, \{a\}, \{a, b\}\}$. Let $\sigma_1 = \{\phi, Y, \{a\}\}$ and $\sigma_2 = \{\phi, Y, \{b, c\}\}$. Then $\sigma_{1,2} = \{\phi, Y, \{a\}, \{b, c\}\}$. Let $\eta_1 = \{\phi, Z, \{a, b\}\}$ and $\eta_2 = \{\phi, Z\}$. Then $\eta_{1,2} = \{\phi, Z, \{a, b\}\}$. We define $f: (X, \tau_1, \tau_2) \rightarrow (Y, \sigma_1, \sigma_2)$ by $f(a) = c, f(b) = b$ and $f(c) = a$ and let $g: (Y, \sigma_1, \sigma_2) \rightarrow (Z, \eta_1, \eta_2)$ be the identity map. Hence both f and g are $(1,2)^*$ -w \check{g} -closed maps. For a $\tau_{1,2}$ -closed set $U = \{b, c\}$, $(g \circ f)(U) = g(f(U)) = g(\{a, b\}) = \{a, b\}$ which is not $(1,2)^*$ -w \check{g} -closed in Z . Hence the composition of two $(1,2)^*$ -w \check{g} -closed maps need not be a $(1,2)^*$ -w \check{g} -closed.

Theorem 5.8 Let $(X, \tau_1, \tau_2), (Y, \sigma_1, \sigma_2)$ and (Z, η_1, η_2) be bitopological spaces. If $f: (X, \tau_1, \tau_2) \rightarrow (Y, \sigma_1, \sigma_2)$ is a $(1,2)^*$ -closed map and $g: (Y, \sigma_1, \sigma_2) \rightarrow (Z, \eta_1, \eta_2)$ is a $(1,2)^*$ -w \check{g} -closed map, then $g \circ f: (X, \tau_1, \tau_2) \rightarrow (Z, \eta_1, \eta_2)$ is a $(1,2)^*$ -w \check{g} -closed map.

Definition 5.9 A map $f: (X, \tau_1, \tau_2) \rightarrow (Y, \sigma_1, \sigma_2)$ is called a weakly $(1,2)^*$ - \check{g} -irresolute (briefly, $(1,2)^*$ -w \check{g} -irresolute) map if $f^{-1}(U)$ is a $(1,2)^*$ -w \check{g} -open set in X for each $(1,2)^*$ -w \check{g} -open set U of Y .

Example 5.10 Let $X = Y = \{a, b, c\}$, $\tau_1 = \{\phi, X, \{b\}\}$ and $\tau_2 = \{\phi, X, \{a, c\}\}$. Then $\tau_{1,2} = \{\phi, X, \{b\}, \{a, c\}\}$. Let $\sigma_1 = \{\phi, Y, \{b\}\}$ and $\sigma_2 = \{\phi, Y\}$. Then $\sigma_{1,2} = \{\phi, Y, \{b\}\}$. Let $f: (X, \tau_1, \tau_2) \rightarrow (Y, \sigma_1, \sigma_2)$ be the identity map. Then f is $(1,2)^*$ -w \check{g} -irresolute.

Remark 5.11 The concepts of $(1,2)^*$ -sg-irresoluteness and the concepts of $(1,2)^*$ -w \check{g} -irresoluteness are independent of each other.

Example 5.12 Let $X = Y = \{a, b, c\}$, $\tau_1 = \{\phi, X, \{a, b\}\}$ and $\tau_2 = \{\phi, X\}$. Then $\tau_{1,2} = \{\phi, X, \{a, b\}\}$. Let $\sigma_1 = \{\phi, Y, \{a\}\}$ and $\sigma_2 = \{\phi, Y\}$. Then $\sigma_{1,2} = \{\phi, Y, \{a\}\}$. Let $f: (X, \tau_1, \tau_2) \rightarrow (Y, \sigma_1, \sigma_2)$ be the identity map. Then f is $(1,2)^*$ -w \check{g} -continuous but not $(1,2)^*$ -sg-irresolute.

Example 5.13 Let $X = Y = \{a, b, c\}$, $\tau_1 = \{\phi, X, \{a\}\}$ and $\tau_2 = \{\phi, X, \{b\}\}$. Then $\tau_{1,2} = \{\phi, X, \{a\}, \{b\}\}$. Let $\sigma_1 = \{\phi, Y, \{a, b\}\}$ and $\sigma_2 = \{\phi, Y\}$. Then $\sigma_{1,2} = \{\phi, Y, \{a, b\}\}$. Let $f: (X, \tau_1, \tau_2) \rightarrow (Y, \sigma_1, \sigma_2)$ be the identity map. Then f is $(1,2)^*$ -sg-irresolute but not $(1,2)^*$ -w \check{g} -irresolute.

Remark 5.14 Every $(1,2)^*$ - \check{g} -irresolute map is $(1,2)^*$ -w \check{g} -continuous but not conversely. Also, the concepts of $(1,2)^*$ - \check{g} -irresoluteness and $(1,2)^*$ -w \check{g} -irresoluteness are independent of each other.

Example 5.15 Let $X = Y = \{a, b, c, d\}$, $\tau_1 = \{\phi, X, \{a\}\}$ and $\tau_2 = \{\phi, X, \{b, c\}\}$. Then $\tau_{1,2} = \{\phi, X, \{a\}, \{b, c\}\}$. Let $\sigma_1 = \{\phi, Y, \{a\}\}$ and $\sigma_2 = \{\phi, Y, \{a, b, d\}\}$. Then $\sigma_{1,2} = \{\phi, Y, \{a\}, \{a, b, d\}\}$. Let $f: (X, \tau_1, \tau_2) \rightarrow (Y, \sigma_1, \sigma_2)$ be the identity map. Then f is $(1,2)^*$ -w \check{g} -irresolute but not $(1,2)^*$ - \check{g} -irresolute.

Example 5.16 Let $X = Y = \{a, b, c\}$, $\tau_1 = \{\phi, X, \{a\}\}$ and $\tau_2 = \{\phi, X, \{b, c\}\}$. Then $\tau_{1,2} = \{\phi, X, \{a\}, \{b, c\}\}$. Let $\sigma_1 = \{\phi, Y, \{a\}\}$ and $\sigma_2 = \{\phi, Y, \{a, b\}\}$. Then $\sigma_{1,2} = \{\phi, Y, \{a\}, \{a, b\}\}$. Let $f: (X, \tau_1, \tau_2) \rightarrow (Y, \sigma_1, \sigma_2)$ be the identity map. Then f is $(1,2)^*$ -w \check{g} -irresolute but not $(1,2)^*$ - \check{g} -irresolute.

Example 5.17 In Example 3.64, then f is $(1,2)^*$ - \check{g} -irresolute but not $(1,2)^*$ -w \check{g} -irresolute.

Theorem 5.18 The composition of two $(1,2)^*$ -w \check{g} -irresolute maps is also $(1,2)^*$ -w \check{g} -irresolute.

Theorem 5.19 Let $f: (X, \tau_1, \tau_2) \rightarrow (Y, \sigma_1, \sigma_2)$ and $g: (Y, \sigma_1, \sigma_2) \rightarrow (Z, \eta_1, \eta_2)$ be maps such that $g \circ f: (X, \tau_1, \tau_2) \rightarrow (Z, \eta_1, \eta_2)$ is $(1,2)^*$ -w \check{g} -closed map. Then the following properties are true.

1. f is $(1,2)^*$ -continuous and injective g is $(1,2)^*$ -w \check{g} -closed.
2. g is $(1,2)^*$ -w \check{g} -irresolute and surjective f is $(1,2)^*$ -w \check{g} -closed.

proof: 1. Let F be a $\sigma_{1,2}$ -closed set of Y . Since $f^{-1}(F)$ is $\tau_{1,2}$ -closed in X , we can conclude that $(g \circ f)(f^{-1}(F))$ is $(1,2)^*$ -w \check{g} -closed in Z . Hence $g(F)$ is $(1,2)^*$ -w \check{g} -closed in Z . Thus g is a $(1,2)^*$ -w \check{g} -closed map.

2. It can be proved in a similar manner 1.

Theorem 5.20 If $f: (X, \tau_1, \tau_2) \rightarrow (Y, \sigma_1, \sigma_2)$ is an $(1,2)^*$ -w \check{g} -irresolute map, then it is $(1,2)^*$ -w \check{g} -continuous.

Remark 5.21 The converse of the above theorem need not be true in general. The map $f: (X, \tau_1, \tau_2) \rightarrow (Y, \sigma_1, \sigma_2)$ in the Theorem 3.71 is $(1,2)^*$ -w \check{g} -continuous but not $(1,2)^*$ -w \check{g} -irresolute.

Theorem 5.22 If $f: (X, \tau_1, \tau_2) \rightarrow (Y, \sigma_1, \sigma_2)$ is surjective $(1,2)^*$ -w \check{g} -irresolute map and X is $(1,2)^*$ -w \check{g} -compact, then Y is $(1,2)^*$ -w \check{g} -compact.

Theorem 5.23 If $f: (X, \tau_1, \tau_2) \rightarrow (Y, \sigma_1, \sigma_2)$ is surjective $(1,2)^*$ -w \check{g} -irresolute map and X is $(1,2)^*$ -w \check{g} -connected, then Y is $(1,2)^*$ -w \check{g} -connected.



**Nethaji et al.,****REFERENCES**

1. N. Bharadwaj and A. Mir, *Pre weakly generalized closed set in topological space*, Journal of Physics: Conference series, 1531 (2020), 012082.
2. J. C. Kelly, *Bitopological spaces*, Proc. London. Math Soc., 3(13) (1963), 71-89.
3. N. Levine, *Generalized closed sets in topology*, Rend. Circ. Math. Palermo., 17(2) (1970), 89-96.
4. Sanjay Mishra and Nitin Bhardwaj, *On regular generalized weakly r gw-closed sets in topological spaces*, Int. Journal of Math. Analysis., 6(39) (2012), 1939-1952.
5. Sanjay Mishra and Nitin Bhardwaj, *On generalized pre regular weakly $gprw$ -closed sets in topological spaces*, Int. Journal of Math. Analysis., 7(40) (2012), 1981-1992.
6. M. Rajakalaivanan, *Some contributions to bitopological spaces*, Ph. D Thesis, Madurai Kamaraj University, Madurai, December 2012.
7. O. Ravi and M. L. Thivagar, *A bitopological $(1,2)^*$ -semi-generalized continuous maps*, Bull. Malaysian Math. Sci. Soc., (2)(29)(1)(2006), 76-88.
8. O. Ravi and M. L. Thivagar, *Remarks on λ -irresolute functions via $(1,2)^*$ -sets*, Advances in App. Math. Analysis., 5(1) (2010), 1-15.
9. R.S. Wali and Bsayya B. Mathad, *Semi regular weakly open sets in topological space*, International Journal of Mathematics Trends and Technology, 37(1) (2016), 36-43.
10. M. K. Singal and A. R. Singal, *Almost-continuous mappings*, Yokohama Math.J., 16(1968), 63-73.
11. S. Willard, *General topology*, AdditionWesley Publishing Company, (1970).





Gas Chromatography–Mass Spectroscopy Analysis of Ethyl Acetate Extract of Aerial Parts of *Pseudomussaenda flava* Verdac

R. Murali¹, V. Perumal², M. Prabavathi², S. Sivakrishnan¹, V. Manikandan³, K. Gopalasatheeskumar⁴ and N. Srinivasan^{1*}

¹Assistant Professor, Department of Pharmacy, Faculty of Engineering and Technology, Annamalai University, Annamalai Nagar, Chidambaram, Tamil Nadu, India.

²Department of Pharmacy, Faculty of Engineering and Technology, Annamalai University, Annamalai Nagar, Chidambaram, Tamil Nadu, India.

³Assistant Professor, Department of Pharmaceutical Chemistry, Analysis, Adhiparasakthi College of Pharmacy, Melmaruvathur, Kanchipuram, Tamil Nadu, India.

⁴Research Scholar, Department of Pharmacy, Faculty of Engineering and Technology, Annamalai University, Annamalai Nagar, Chidambaram, Tamil Nadu, India.

Received: 02 Feb 2023

Revised: 04 Apr 2023

Accepted: 10 May 2023

*Address for Correspondence

N. Srinivasan*

Assistant Professor,
Department of Pharmacy,
Faculty of Engineering and Technology,
Annamalai University, Annamalai Nagar,
Chidambaram, Tamil Nadu, India.
Email: seenu301@gmail.com



This is an Open Access Journal / article distributed under the terms of the **Creative Commons Attribution License** (CC BY-NC-ND 3.0) which permits unrestricted use, distribution, and reproduction in any medium, provided the original work is properly cited. All rights reserved.

ABSTRACT

Pseudomussaenda flava Verdac., the plant species called "yellow lady's mantle," is a type of ornamental plant in the family Rubiaceae. The purpose of this study is to identify the active principles of this plant. An aerial part of *P. flava* was collected from Chidambaram, Cuddalore Dist., Tamil Nadu, India, in November 2021. The aerial parts of *P. flava* were extracted using the cold percolation method. Based on the results of the phytochemical screening, an ethyl acetate extract of *P. flava* was selected and analysed with an Agilent Model 18890 GC System with Single Quadrupole Mass Spectrometer to find the bioactive components in the aerial parts of *P. flava* Verdac. The GC–MS analysis of the ethyl acetate extract of the aerial part of *P. flava* revealed ten bioactive compounds. The compound with the highest percentage was named n- Hexadecanoic acid (14.90%), and the compound with the lowest percentage was named W-18 (1.95%). In this study, we showed that a GC-MS analysis of an ethyl acetate extract of the aerial part of *P. flava* could give scientists information that could be used to make possible phytomedicines.

Keywords: *Pseudomussaenda flava*, Ethyl acetate extract, Gas chromatography, Phytoconstituents, Secondary metabolites.





Srinivasan et al.,

INTRODUCTION

The Indian subcontinent is the largest producer of medicinal herbs in the world, and can therefore rightfully be described as the world's botanical garden. Approximately 1,500 plant species are endemic to India, making it one of the richest repositories of biodiversity on earth. Medicinal plants have been used for centuries to treat the body and mind. Several of these plants contain active components that have therapeutic properties. Medical plants provide effective treatment for a wide range of diseases, including cancer, heart disease, diabetes, and a number of others[1]. There are a number of natural products that can be derived from *Mussaenda* (Rubiaceae). It is native to West Africa, the Indian subcontinent, South-East Asia, and Southern China. There are approximately 200 types of *mussaenda*. *P. flava*, or Yellow *Mussaenda*, is an evergreen half-vine of the small shrub of the *Mussaenda* genus of the Rubiaceae. Indigenous to Eastern Sudan. Compound cymes, with pale yellow flowers blooming, only one piece of white stands out. The plant, *P. flava*, occurs in eastern Sudan. The plant grows to a height of 100–300 cm. The leaves are green and oblong or broad lanceolate in shape. A margin inflorescence is composed of compound cymes, the leaves are thin, and the phyllotaxis is opposite. The flower colour in Crown Central is yellow, dark yellow, the corolla diameter is 1-2 cm, the calyx bracts are white, round and obovate, the calyx bract length is 5 cm, the flowering period is April to November, and the fruit is berries. Applications include potted plants and gardens[2]. Chinese and Fijian traditional medicine have traditionally used some species of this plant as diuretics, antipyretics, abortifacients, expectorants, and antibiotics [3]. *Mussaenin*, an iridoid derived from *M. pubesens* that is non-glycosidic, has cytotoxic properties[4]. A GC-MS system is a hyphenated system that is a very suitable technique for the purpose of identifying and determining pharmaceutical substances. It is possible to identify unidentified biological compounds in a complex mixture by interpretation, as well as by matching their spectra with reference spectra. This study aims to examine bioactive compounds in an ethyl acetate extract of the aerial part of *P. flava* using GC-MS analysis.

MATERIALS AND METHODS

Collection and Identification of *P. flava*

The aerial plant of *P. flava* Verdc has been collected from Chidambaram, Cuddalore Dist., Tamil Nadu, India, during the month of November 2021. The plant was authenticated by Prof. Dr. Mullainathan and voucher specimen has been deposited in the Department of Botany, Annamalai University, Annamalai Nagar for future reference.

Extraction and Isolation of *P. flava*

The aerial parts of *P. flava* Verdc were dried and powdered. The plant powder materials were successfully extracted with petroleum ether (at room temperature) by the cold maceration method using an iodine flask for five days. During that time, the flask with powdered materials and the solvent was shaken, and the gas was released at regular intervals. Then this marc was dried and subjected to ethyl acetate extraction (at room temperature) for about ten days. Then the marc was dried and it was subjected to ethanol (95%) extraction (at room temperature) for about eight days. The extract was concentrated using a rotary vacuum evaporator and lyophilized in a lyophilizer until a dry powder was obtained.

Gas Chromatography–Mass Spectroscopy Analysis

GC-MS analysis was carried out in Sophisticated Analytical Instruments Facility, Indian Institute of Technology, Chennai, Tamil Nadu 600036. An Agilent Model 8890 GC System with Single Quadrupole Mass Spectrometer (5977B MSD) analyzer was used for the separation and identification of phytochemicals from an ethyl acetate extract of *P. flava* Verdc. The analysis parameters for GC-MS are as follows: Agilent 30 m x 250 μ m x 0.25 μ m column, Syringe Size: 10 μ L Injection, Volume: 1 μ L, Initial temperature: 75 °C, Pressure: 11.367 psi, Flow: 1.2 mL/min, Average Velocity: 40.402 cm/sec, Ion Source: EI Source, Temperature: 230°C, Quad Temperature: 150 °C and Fixed Electron Energy: 70 eV. NIST Library was used for matching mass spectra and identification of phytochemicals.



**Srinivasan et al.,**

GC-MS was used to identify phytochemicals based on NIST's database of over 62,000 patterns. NIST's library of known compounds was used to correlate the spectrum of the unknown compound. The components of the unknown or test substances were confirmed with respect to their structure, name, and molecular weight [5].

The GC-MS analysis of the ethyl acetate extract of the aerial part of *P. flava* revealed the presence of various compounds using the NIST library as a reference. Table 1 lists the ten most abundant compounds, along with their retention time, molecular formula, molecular weight, and peak area. Figure 1 displays the GC-MS chromatogram of the ten peaks for each compound detected. The components found in the ethyl acetate extract of aerial part of *P. flava* were 3,7,11,15-Tetra methyl-2-hexadecen-1-ol1 (3.64%), n-Hexadecanoic acid2(14.90%), Hexadecanoic acid, ethyl ester 3 (4.71%), Phytol 4 (13.86%), 1,1'-Bicyclopropyl 2-octanoic acid 2'-hexyl methyl ester5 (2.31%), Ethyl oleate 6 (5.10%), 2-Hexadecen-1-ol,3,7,11,15-tetra methyl acetate 7(2.95%), Squalene 8 (11.73%), W-189(1.95%), and 1,1,3,3,5,5,7,7,9,9,11,11,13,13,15,15-hexamethyl octa siloxane 10 (4.32%). Medicinal plants are a vast and diverse group of plants that are used to treat various health conditions. Many of these plants have active constituents that have therapeutic properties. Some of these compounds have been studied extensively for their biological activity, while others remain relatively unknown. Despite this lack of knowledge, there is evidence to suggest that many medicinal plants can be effective in treating a variety of health conditions. The GC-MS (Gas chromatography coupled with a Mass spectrometer) is a powerful tool for the analysis of plant extracts. This analytical method helps to evaluate the quality of plant extract and can provide information about the presence of key compounds, their concentrations, and any toxicants. 3,7,11,15-tetramethyl-2-hexadecen-1-ol 1 is a terpene alcohol used in cosmetic preparations as fine fragrances, shampoos, and toilet soaps as well as in non-cosmetic products such as surface cleaners and detergents[6]. Pharmaceutically used as an antimicrobial agent [7]. N-hexadecanoic acid2 has been reported to have anti-inflammatory[8]. antioxidant, hypocholesterolemic [9]. and antibacterial properties[10]. The ethyl ester of hexadecanoic acid 3 is an anti-oxidant and flavouring agent[7]. There are various biological activities associated with phytol 4, including cytotoxic, antioxidant, anti-inflammatory, and antimicrobial properties [11]. Both 1, 1'-Bicyclopropyl 2-octanoic acid 2'-hexyl methyl ester 5 and Ethyl oleate 6 are antibacterial agent[12,13]. Squalene8 is a triterpene with a broad range of biological functions including antibacterial, antioxidant, cancer preventive, immunostimulant, chemopreventive, and lipid peroxidase-inhibiting properties [14]. According to the results of the GC-MS analysis of the ethyl acetate extract of aerial parts of *P. flava*, the majority of bioactive constituents were found. The GC-MS analysis of *P. flava* identified ten bioactive compounds, many of which show potential therapeutic potential.

CONCLUSION

The presence of a variety of bioactive constituents as detected by GC-MS analysis of an ethyl acetate extract of the aerial part of *P. flava*. The aerial part of *P. flava* has been used for countless ailments in traditional medicine. It is therefore recommended as a plant with phytopharmaceutical value. Analysing the GC-MS data is the first step in understanding the nature of the active compounds in *P. flava*. A critical step in future research will be the isolation of bioactive components and study of their biological activity.

REFERENCES

1. N. Srinivasan, Medicinal plants for cancer treatment: A review approach. IntJ Biol Res2018;3:57-61.
2. N. Warinhip, B. Liawruangrath, S. Natakankitkul, T. Pojanakaron, N. Rannurags, S.G. Pyne, et al. Chemical Constituents from Leaves of *Gardenia sootepensis* and *Pseudomussaenda flava* Biological Activity and Antioxidant Activity. Chiang Mai Univ J Nat Sci 2022;21:e2022004.
3. K.S. Vidyalakshmi, S. Nagarajan, H.R. Vasanthi, V. Rajamanickam, Hepatoprotective and antioxidant activity of two iridoids from *Mussaenda 'dona aurora'*. Z Naturforsch C J Biosci 2009;64:329-334.
4. K. Vidyalakshmi, H.R. Vasanthi, G. Rajamanickam, Ethnobotany, phytochemistry and pharmacology of *Mussaenda* species (Rubiaceae). Ethnobot leafl. 2008;12: 57.

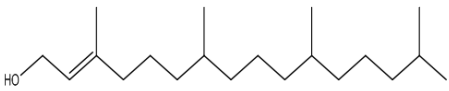
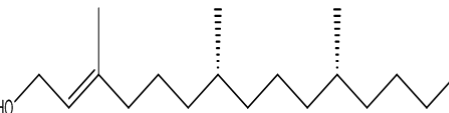




Srinivasan et al.,

5. S. Sivakrishnan, D. Pradepraj, Gas chromatography-Mass spectroscopy analysis of ethanolic extract of leaves of *Cordia obliqua* willd. Asian J Pharm Clin Res 2019;12:110-112.
6. D. McGinty, C. Letizia, A. Api, Fragrance material review on 2-hexadecen-1-ol, 3, 7, 11, 15-tetramethyl. Food Chem Toxicol 2010;48:S101-S102.
7. P.S. Selvan, S. Velavan, Analysis of bioactive compounds in methanol extract of *Cissus vitiginea* leaf using GC-MS. Rasayan J Chem 2015;8:443-447.
8. V. Aparna, K.V. Dileep, P.K. Mandal, P. Karthe, C. Sadasivan, M. Haridas, Anti-inflammatory property of n-hexadecanoic acid: structural evidence and kinetic assessment. Chem Biol Drug Des 2012;80:434-439.
9. P.P. Kumar, S. Kumaravel, C. Lalitha, Screening of antioxidant activity, total phenolics and GC-MS study of *Vitex negundo*. Afr J Biochem Res 2010;4:191-195.
10. A.A. Rahuman, G. Gopalakrishnan, B.S. Ghouse, S. Arumugam, B. Himalayan, Effect of *Feronia limonia* on mosquito larvae. Fitoterapia 2010;71:553-555.
11. M.T. Islam, E.S. Ali, S.J. Uddin, S. Shaw, M.A. Islam, M.I. Ahmed, M. Cet al. Phytol: A review of biomedical activities. Food Chem Toxicol 2018;121:82-94.
12. R. Srivastava, A. Mukerjee, A. Verma, GC-MS analysis of Phytocomponents in, pet ether fraction of *wrightia tinctoria* seed. Pharmacogn J 2015;7:249-253.
13. C. Akin-Osanaiye, A. Gabriel, R. Alebiosu, Characterization and antimicrobial screening of ethyl oleate isolated from *Phyllanthus amarus* (Schum and Thonn). Ann Biol Res 2011;2:298-305.
14. T. Sudha, S. Chidambarampillai, V. Mohan, GC-MS analysis of bioactive components of aerial parts of *Kirganelia reticulata* Poir (Euphorbiaceae). J Curr Chem Pharm Sci 2013;3:113-122.

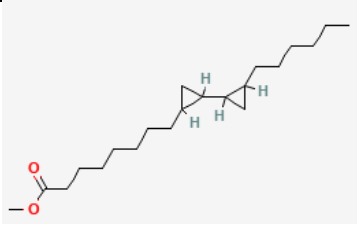
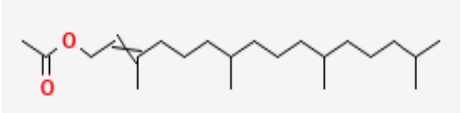
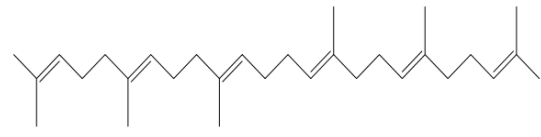
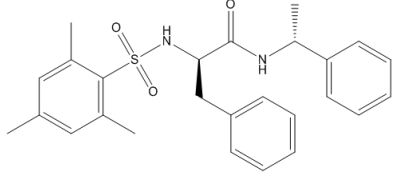
Table 1: Phytocomponents identified in ethyl acetate extract of the aerial of *Pseudomussaenda flava*

S. No	RT	Name of the compound with structure	Molecular formula	Molecular weight	Peak area %
01	23.597	3,7,11,15-Tetra methyl 2-hexadecen-1-ol 	C ₂₀ H ₄₀ O	296.5	3.64
02	27.073	n-Hexadecanoic acid 	C ₁₆ H ₃₂ O ₂	256.4	14.90
03	27.878	Hexadecanoic acid, ethyl ester 	C ₁₈ H ₃₆ O ₂	284.5	4.71
04	30.605	Phytol 	C ₂₀ H ₄₀ O	296.53	13.86
05	31.657	1,1'-Bicyclopropyl-2-octanoic acid-2'-hexyl methyl ester 	C ₂₁ H ₃₈ O ₂	322.5	2.31





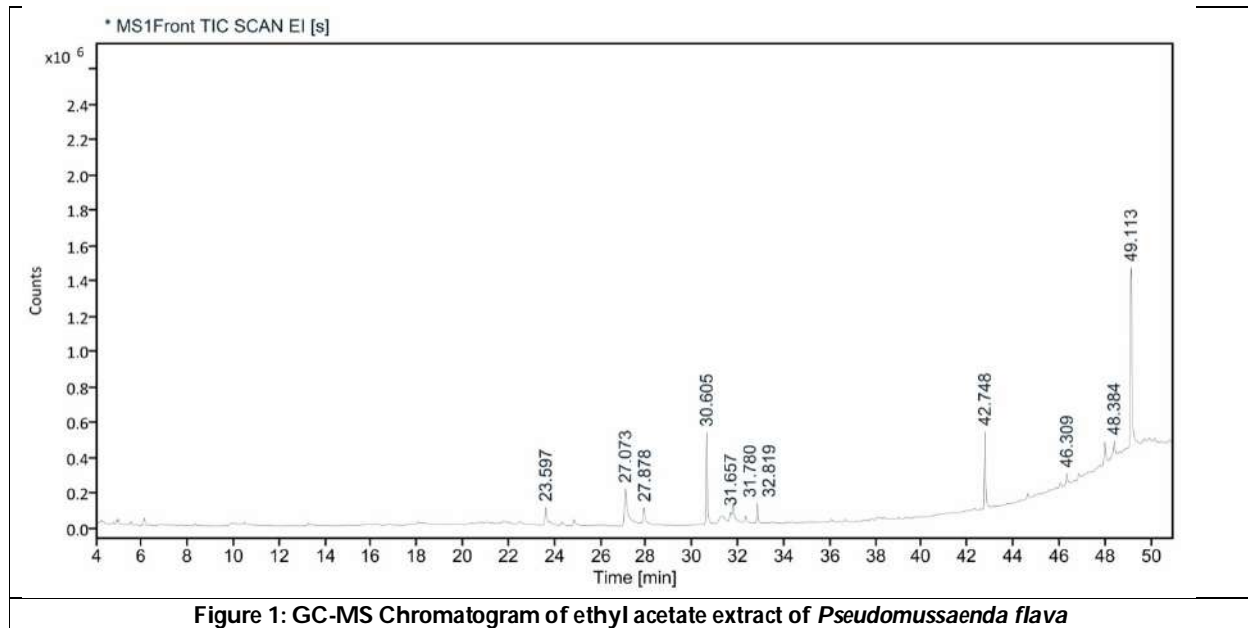
Srinivasan et al.,

					
06	31.780	Ethyl oleate 	$C_{20}H_{38}O_2$	310.5	5.10
07	32.819	2-Hexadecen-1 ol,3,7,11,15-tetra methyl acetate 	$C_{22}H_{42}O_2$	296.5	2.95
08	42.748	Squalene 	$C_{30}H_{50}$	410.7	11.73
09	46.309	W-18 	$C_{26}H_{30}N_2O_3S$	421.896	1.95
10	48.384	1,1,3,3,5,5,7,7,9,9,11,11, 13,13,15,15hexamethyloctasiloxane 	$C_{16}H_{48}O_7Si_8$	577.2	4.32





Srinivasan et al.,





An Improved Analysis of FIS through Set- Intersection Method in Association Rule Mining for Textual Dataset

Sandeep Kumar^{1*}, Rahul Kumar Mishra² and Neeraj Kumar Verma³

¹Research Scholar, School of Computer Science and Applications, IFTM University, Moradabad, Uttar Pradesh, India

²Professor, School of Computer Science and Applications, IFTM University, Moradabad, Uttar Pradesh, India.

³Assistant Professor, Department of Computer Science and Engineering, ICFAI University, Jaipur, Rajasthan, India

Received: 27 Feb 2023

Revised: 05 Apr 2023

Accepted: 08 May 2023

*Address for Correspondence

Sandeep Kumar

Research Scholar,

School of Computer Science and Applications,

IFTM University, Moradabad,

Uttar Pradesh, India.

E.Mail: shyamsandeep28@gmail.com



This is an Open Access Journal / article distributed under the terms of the **Creative Commons Attribution License** (CC BY-NC-ND 3.0) which permits unrestricted use, distribution, and reproduction in any medium, provided the original work is properly cited. All rights reserved.

ABSTRACT

This research paper presents an improved analysis of frequent item set through a set-intersection method in association rule mining (Apriori) for textual datasets. The objective of this study is to address the limitations of traditional Apriori-based association rule mining methods in handling large textual datasets. The proposed method represents textual data as sets and utilizes set-intersection to evaluate the similarity between them. The effectiveness of the proposed method is evaluated on two textual datasets, and the results demonstrate that it outperforms traditional Apriori-based association rule mining methods in terms of accuracy and efficiency. The findings of this research have significant implications for organizations that rely on association rule mining for knowledge discovery from large textual datasets. The proposed method offers a promising approach for discovering meaningful patterns from large textual data that can support decision-making processes.

Keywords: Association Rule Mining (ARM) , Data Mining , KDD, Apriori , Frequent Item Set(FIS)

INTRODUCTION

The technique of extracting patterns and information from vast volumes of data is known as data mining. To draw conclusions and generate predictions from data, statistical models and algorithms are used. The goal of data mining

57072



**Sandeep Kumar et al.,**

is to uncover hidden patterns, [1], [2] correlations, and other information that can be used to make better decisions and improve business processes. Data mining is widely used in various fields such as finance, marketing, healthcare, and more. KDD stands for Knowledge Discovery in Databases [3], which refers to the process of finding useful information and patterns in large data sets. It is a multi-disciplinary field that combines techniques from artificial intelligence, machine learning, statistics, and databases to extract insights and knowledge from data. The KDD process includes several steps such as data pre-processing, data mining, [4] pattern evaluation, and knowledge representation. The goal of KDD is to turn raw data into actionable insights that can be used to support decision-making and improve business processes. In terms of customer desire for interesting patterns among the many common patterns produced by data mining algorithms, KDD[5] is essentially more targeted. Here figure 1 illustrates the Data Mining process.

KDD is a multi-step process that includes the following steps.

- Data Selection: Selecting the relevant data from large datasets.
- Data Pre-processing: Cleaning and transforming the data to make it suitable for analysis.
- Data Transformation: Transforming the data into a suitable format for analysis.
- Data Mining: Applying algorithms and statistical models to extract insights and knowledge from the data.
- Pattern Evaluation: Evaluating the discovered patterns and knowledge to determine their usefulness and validity.
- Knowledge Representation: Representing the discovered knowledge in a meaningful and understandable format.

An example of KDD and data mining in action is a retail company using customer purchase data to identify patterns and trends in their customers' buying behavior. In this example, the company first selects relevant data from their database of customer transactions, pre-processes the data to remove errors and inconsistencies, and then transforms the data into a format suitable for analysis. Next, the company applies data mining techniques, such as association rule mining and clustering, to uncover patterns in customer behavior, such as which products are frequently purchased together. Finally, the company evaluates the discovered patterns and represents the knowledge in a useful format, such as a report or visualization, for the company to make informed business decisions based on the insights gained from the data.

LITERATURE REVIEW

Association rule mining (ARM)

ARM is a data mining technique[6] used to uncover relationships and patterns between items in large datasets. The goal of association rule mining is to find rules that describe relationships between items in a dataset, such as "if item A is purchased, item B is also likely to be purchased". These rules are represented as "if-then" statements and are used to support decision making and inform business strategies. Association rule mining algorithms typically [7], [8] use a measure of interest, such as support and confidence, to determine the significance of the discovered rules. Support is a measure of the frequency with which an item or a combination of items appear in a dataset,[9] while confidence is a measure of the reliability of the association rule. Association rules with high support and confidence values are considered to be strong and relevant, and are more likely to be useful for decision making.

Apriori Algorithm

The Apriori algorithm [7] is a classic algorithm for association rule mining, used to extract frequent item sets from large datasets. The algorithm works by iteratively scanning the dataset to identify itemsets that occur frequently together and then uses this information to generate a set of association rules.[10] The "Apriori principle," which argues that if an item set is frequent, then all of its subsets must also be frequent, is the fundamental idea underlying the Apriori algorithm. By only taking into account candidates itemsets that reach a certain support level, this approach helps to decrease the number of candidate itemsets that must be examined. The amount of itemsets and rules that are created is limited by the support threshold, which the user specifies. Apriori is a popular association





Sandeep Kumar et al.,

mining algorithm[11]It is used to first discover often occurring individual items before applying a BFS (Breadth-First Search) technique to expand those items to bigger item sets until they reach the most frequently occurring huge frequent item sets.

Algorithm: Apriori()

Define:

- $\alpha \rightarrow \{ \text{Minimum_Support}() \}$
- $CS_k \rightarrow \text{Candidate_Subset}$
- $DS_k \rightarrow \text{Discarded_Subset}$
- $FIS \rightarrow \text{Set of frequent item set}$

Input:={ $TS_j \in IS_i$ }

Output:={ FIS }

Initialize: Let $\alpha = x$;

$IS_i = \{ IS_1, IS_2, \dots, IS_n \} \parallel \forall IS_i \geq 1$
 //Set of n-Item set

$TS_j = \{ TS_1, TS_2, \dots, TS_m \} \parallel \forall TS_j \geq 1$ // Data Set of m-Transactions

$ES_i = \{ ES_1, ES_2, \dots, ES_n \} \parallel \forall ES_i \geq 1$ //Set of n^{th} -Element item set

$CS_n = \{ \}$ // Candidate Subset of n^{th} -Element item Set

$DS_n = \{ \}$ // Discarded Subset of n^{th} -Element item Set

Start

Do;

- if $\text{Minimum_Support}(ES_k) \geq x$,
- Then $\forall IS_i \parallel ES_k \in CS_k \text{ FIS} \leftarrow CS_k$
- else
- $\forall IS_i \parallel ES_k \in DS_k$
- $FIS = \{ DS_1 \cup DS_2 \cup \dots \cup DS_n \}$

End;

Example

A transaction database containing a collection of transactions serves as the input data for the Apriori algorithm. An item set constitutes each transaction. To identify the frequent things, the method begins by counting the frequency of each item in the transaction database. To create candidate itemsets of size $k + 1$, the frequent items are used. The transaction database is then used to tally the candidate itemsets in order to gauge their support. A candidate itemset is eliminated if its support falls below the required minimum. Up until no new frequent item sets can be discovered, this procedure is repeated. Association rules are generated using the final frequent item sets. Let see an illustration of the Apriori Algorithm. In this example we take 6 transactions with 5 item shown in table 1
 Let us consider the mini_supp

- $[P1^{\wedge}P4] \Rightarrow [P5]$ //confidence = $\frac{\text{sup}(P1^{\wedge}P4^{\wedge}P5)}{\text{sup}(P1^{\wedge}P4)} = \frac{2}{2} * 100 = 100\%$ //Selected
- $[P1^{\wedge}P5] \Rightarrow [P4]$ //confidence = $\frac{\text{sup}(P1^{\wedge}P4^{\wedge}P5)}{\text{sup}(P1^{\wedge}P5)} = \frac{2}{2} * 100 = 100\%$ //Selected
- $[P4^{\wedge}P5] \Rightarrow [P1]$ //confidence = $\frac{\text{sup}(P1^{\wedge}P4^{\wedge}P5)}{\text{sup}(P4^{\wedge}P5)} = \frac{2}{3} * 100 = 66.67\%$ //Selected
- $[P1] \Rightarrow [P4^{\wedge}P5]$ //confidence = $\frac{\text{sup}(P1^{\wedge}P4^{\wedge}P5)}{\text{sup}(P1)} = \frac{2}{4} * 100 = 50\%$ //Rejected
- $[P4] \Rightarrow [P1^{\wedge}P5]$ //confidence = $\frac{\text{sup}(P1^{\wedge}P4^{\wedge}P5)}{\text{sup}(P4)} = \frac{2}{3} * 100 = 66.67\%$ //Selected
- $[P5] \Rightarrow [P1^{\wedge}P4]$ //confidence = $\frac{\text{sup}(P1^{\wedge}P4^{\wedge}P5)}{\text{sup}(P5)} = \frac{2}{4} * 100 = 50\%$ //Rejected

So here for the minimum confidence >60 there are four strong result.

The Apriori algorithm has been widely used for association rule mining and has been applied in many areas, including market basket analysis, recommendation systems, and fraud detection. However, the algorithm has a high computational complexity, making it unsuitable for very large datasets. To overcome this limitation, variations of the





Sandeep Kumar et al.,

Apriori algorithm,[12] such as Partitioning Apriori and Sampling Apriori, have been developed to improve the efficiency of the algorithm.

Proposed Improved Apriori

Algorithm: Apriori()

Define:

- $\alpha \rightarrow \{ \text{Minimum_Support}() \}$
- $CS_k \rightarrow \text{Candidate Subset}$
- $DS_k \rightarrow \text{Discarded Subset}$
- $FIS \rightarrow \text{Set of frequent item set}$

Input: $\{T_j \in I_i\}$

Output: $\{FIS\}$

Initialize: Let $\alpha = x;$

- $IS_i = \{IS_1, IS_2, \dots, IS_n\} \parallel \forall IS_i \geq 1$ //Set of n-Item set
- $TS_j = \{TS_1, TS_2, \dots, TS_m\} \parallel \forall TS_j \geq 1$ // Data Set contains m-Transactions
- $ES_k = \{ES_1, ES_2, \dots, ES_n\} \parallel \forall ES_k \geq 1$ //Set of n^{th} -Element item set
- $Tn_i = \{T_1, T_2, \dots, T_m\} \parallel \forall T_i \geq 1$ // No. of Transactions involve in i^{th} element item set of CCS_i
- $CS_n = \{ \}$ // Candidate Subset of n^{th} -Element item Set
- $DS_n = \{ \}$ // Discarded Subset of n^{th} -Element item Set
- $Ln = \{ \}$ // Labeled CS with no. of transactions involve for n^{th} -Element item Set

Start

Step-1:

While;

- if $\text{Minimum_Support}(ES_k) \geq \alpha$, Then $\forall IS_i \parallel ES_k \in CS_i; CS_i \leftarrow ES_k$
- else
- $\forall IS_i \parallel ES_{n-k} \in DS_k$
- $DS_i \leftarrow ES_{n-k}$
- $i=i+1;$
- if $i > n$
- Go to Step-3

Step-2:

Do

- For $i=1;$
- $Lo \leftarrow (IS_1 \parallel \text{Support} \parallel ES_k)$ // Find Lo along with Transaction involved.
- For $i=2 \dots n;$
- $L_{i-1} \leftarrow CS_i \parallel Tn_m$ //for L_1 to L_{n-1}
- Repeat for each i
- $Tn_m \leftarrow \text{Intersection}(Lo, L_{n-1})$
- $ES_n \leftarrow Tn_m$

Step-3:

- $FIS = (CS_1, CS_2 \dots CS_n)$ // Set of all frequent items

End

For the implementation of our new Apriori algorithm, let's take 10 transactions with the data itemset from P1 to P10. Here Table 3 represent the all itemset along with the Minimum Support Value (MSV). Let us assume that the minimum support value is 3 so here in the first step we need to scan the all transaction from the transaction table to generate the first-element frequent set with the transaction's id and support value and discard those whose item which minimum support is less than minimum support value 3. Here the table 5 describe the elimination of items which are have the minimum support <3 and this table is called L_0 . In the next step algorithm will generate CS_2 for 2 elements FIS from the table 5. Here table no 6 and 7 represent 2 elements FIS. Similarly, the algorithm will generate 3 element FIS using table 7. In this example when we find 3 element FIS then all item's minimum support value is less than 3 it means all item will be discarded that is shown in table 8. Now let's discuss the comparison between traditional Apriori and proposed Apriori based upon the total number of all transactions for one to six element FIS.





Sandeep Kumar et al.,

EXPERIMENTAL AND RESULT ANALYSIS

Now, for the experimental exercise we take a dataset with 8324 transactions and divide this dataset into five groups where group G1 have 450, G2 have 910, G3 have 1342, G4 2410 and G5 3212 transactions as shown in table 10. Now we calculate the execution time for both Apriori algorithm on a uniform minimum support value 30. When we pass G1 group transaction set which have 450 transactions in traditional Apriori algorithm then the execution time is 2.8 where in new Apriori this execution time is 1.7 which is 61.9% less than the traditional Apriori. Same as for G2 transaction set new Apriori take approximate 58.4% less time and for G3 approximate 67% then the Apriori algorithm. This calculation is for uniform support. In second case we need to check the behavior of proposed new Apriori on the different support value so we take only G1 dataset with 450 transactions and check the New Apriori efficiency on the supporting value 20, 40 and 80. In the 1st case when the support value is 20 then the rate of improvement is 82.4% in comparison to traditional Apriori approach and 81.0 when the support value is 40 that is shown in table 12 and figure 4.

CONCLUSION

In this research paper we use intersection method to reduce the no of iteration for database scanning to find the FIS. When we apply this method in our proposed new Apriori then it reduces execution time approximate 61.9% in comparison to traditional approach for the smallest data set G1 and 78.3 for the largest dataset G5 for the uniform support value. After finding the effectiveness on uniform support value, we check the efficiency on various support value i.e. 20, 40 and 80. To find the effectiveness of the proposed new Apriori we calculate the time complexity on the different support value for G1 dataset and it gives us very suppressing result that shown in analysis 2 table 12. The conclusion of this Intersection approach is that proposed new algorithm give us optimize result as compare to traditional Apriori for both uniform and variable minimum support.

REFERENCES

1. R. Agrawal, A. Swami, and T. Imielinski, "Database Mining: A Performance Perspective," *IEEE Trans Knowl Data Eng*, vol. 5, no. 6, 1993, doi: 10.1109/69.250074.
2. J. Han, M. Kamber, and J. Pei, *Data Mining: Concepts and Techniques*. 2012. doi: 10.1016/C2009-0-61819-5.
3. U. Fayyad and P. Stolorz, "Data mining and KDD: Promise and challenges," *Future Generation Computer Systems*, vol. 13, no. 2–3, 1997, doi: 10.1016/s0167-739x(97)00015-0.
4. "Data Cleaning in Knowledge Discovery Database-Data Mining (KDD-DM)," *Int J Eng Adv Technol*, vol. 8, no. 6S3, 2019, doi: 10.35940/ijeat.f1100.0986s319.
5. U. Shafique and H. Qaiser, "A Comparative Study of Data Mining Process Models (KDD , CRISP-DM and SEMMA)," *International Journal of Innovation and Scientific Research*, vol. 12, no. 1, 2014.
6. S. Vijayarani and S. Sharmila, "Comparative analysis of association rule mining algorithms," in *2016 International Conference on Inventive Computation Technologies (ICICT)*, Aug. 2016, pp. 1–6. doi: 10.1109/INVENTIVE.2016.7830203.
7. C. Kaur, "Association Rule Mining using Apriori Algorithm: A Survey," *International Journal of Advanced Research in Computer Engineering & Technology (IJARCET)*, vol. 2, no. 6, 2013.
8. N. Pasquier, Y. Bastide, R. Taouil, and L. Lakhal, "Efficient mining of association rules using closed itemset lattices," *Inf Syst*, vol. 24, no. 1, 1999, doi: 10.1016/S0306-4379(99)00003-4.
9. N. K. Verma, S. Kumar, M. Kumar, and P. Saxena, "An Alternate Approach to Improve Access Time for Defining Frequent Item Set through 'A-Apriori' in Textual Data Set," in *2020 5th IEEE International Conference on Recent Advances and Innovations in Engineering, ICRAIE 2020 - Proceeding*, 2020. doi: 10.1109/ICRAIE51050.2020.9358344.





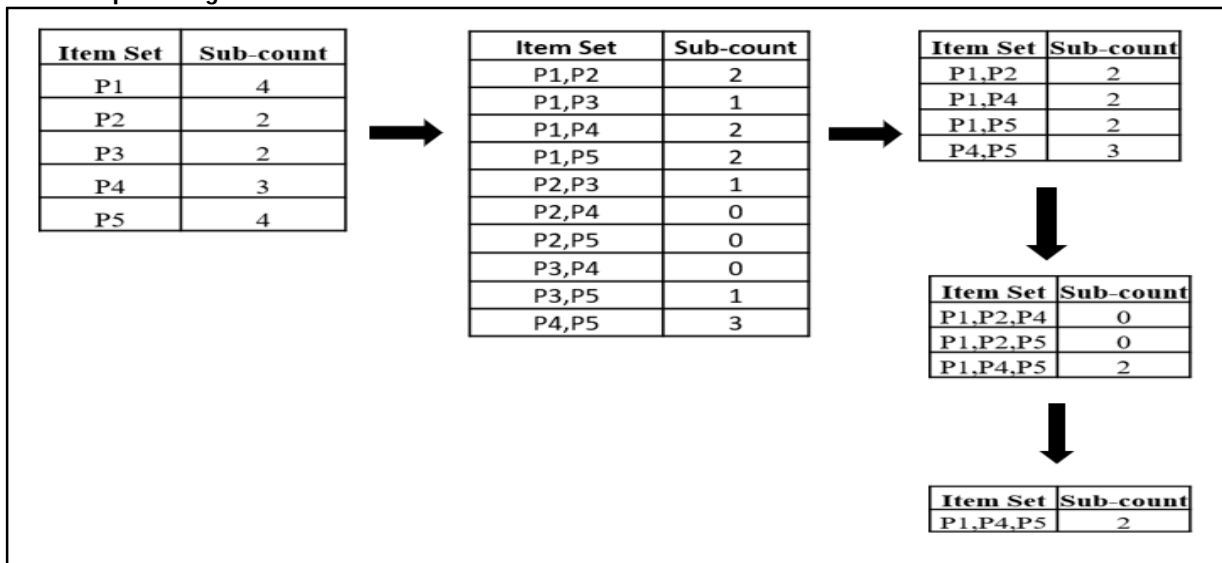
Sandeep Kumar et al.,

10. S. Rao and P. Guptha, "Implementing Improved Algorithm Over APRIORI Data Mining Association Rule Algorithm," *Ijcs*, vol. 8491, 2012.
11. R. Agrawal, T. Imieliński, and A. Swami, "Mining Association Rules Between Sets of Items in Large Databases," *ACM SIGMOD Record*, vol. 22, no. 2, 1993, doi: 10.1145/170036.170072.
12. N. K. Verma and V. Singh, "A Rational Approach to Improve Access Time of Apriori Algorithm by Applying Inner Join in a Arm to Redefining Fis in Textual Data," *ECS Trans*, vol. 107, no. 1, pp. 7749–7758, Apr. 2022, doi: 10.1149/10701.7749ecst

Table 1: Transaction Table with Item-Set

Transaction ID	Item
T1	P1,P2,P3
T2	P1,P2
T3	P1,P4,P5
T4	P4,P5
T5	P5,P3
T6	P1,P4,P5

Table 2: Apriori Algorithm Solutions





Sandeep Kumar et al.,

Table 3: Items along with Minimum Support Value (MSV)

Item	Min. Support Value
P1	4
P2	8
P3	4
P4	2
P5	6
P6	5
P7	2
P8	1
P9	2
P10	1

Item	Min. Support Value
P1	4
P2	8
P3	4
P4	2 (D)
P5	6
P6	5
P7	2(D)
P8	1(D)
P9	2(D)
P10	1(D)

Table 4 : CS₁

Item	Min. Support Value	No of Transaction									
		T1	T2	T3	T4	T5	T6	T7	T8	T9	T10
P1	4	P1	-	-	-	-	P1	-	P1	P1	-
P2	8	P2	P2	-	-	P2	P2	P2	P2	P2	P2
P3	4	-	P3	-	P3	-	-	-	-	P3	P3
P5	6	-	-	P5	P5	P5	P5	P5	-	P5	-
P6	5	-	-	P6	P6	-	P6	P6	-	-	P6

Table 5: L₀(CS₁ along with support value and transaction)

Item	Min. Support Value
P1P2	4
P1P3	1(D)
P1P5	2(D)
P1P6	1(D)
P2P3	3
P2P5	4
P2P6	3
P3P5	2(D)
P3P6	2(D)
P5P6	4

Table 6 :CS₂

Item	SPV	No of Transaction									
		T1	T2	T3	T4	T5	T6	T7	T8	T9	T10
P1P2	4	P1P2					P1P2		P1P2	P1P2	
P2P3	3		P2P3							P2P3	P2P3
P2P5	4					P2P5	P2P5	P2P5		P2P5	
P2P6	3						P2P6	P2P6			P2P6
P5P6	4			P5P6	P5P6		P5P6	P5P6			

Table 7: L₁(CS₂ along with support value and transaction)





Sandeep Kumar et al.,

Item	Min. Support Value	No of Transaction										
		T1	T2	T3	T4	T5	T6	T7	T8	T9	T10	
P1P2P3	1									P1P2P3		Discarded
P1P2P5	2						P1P2P5			P1P2P5		Discarded
P1P2P6	1						P1P2P6					Discarded
P2P3P5	1									P2P3P5		Discarded
P2P3P6	1										P2P3P6	Discarded
P3P5P6	0											Discarded

Table 8 : L₂(CS₂ along with support value and transaction)

Item-Set	Apriori	Proposed New Apriori
1 IS	60	60
2 IS	150	100
3 IS	100	60*
4 IS	60	30
5 IS	10	1
6 IS	10	0
Total	390	191

Table 9 : Transaction Comparison

Group 1	Txn ID	No. of Txn
1	Txn1	450
2	Txn2	910
3	Txn3	1342
4	Txn4	2410
5	Txn5	3212

Table 10 : Data Set of Transactions

Group	No. of Transactions	Apriori (Execution Time)	New_Apriori (Execution Time)	Time Difference (Apriori-New Apriori)	Access Time Reduction Rate (%)
G1	450	2.8	1.7	1.1	61.9
G2	910	9.3	5.1	4.2	58.4
G3	1342	7.9	3.4	4.5	67.2
G4	2410	13.1	3.6	9.5	80.1
G5	3212	84.3	20.1	64.2	78.3

Table 11 : Analysis 1: Pragmatic Analysis Of Apriori V/S A-Apriori As Per Access Time Reduction Rate (Using Uniform Support In All Transaction Sets)





Sandeep Kumar *et al.*,

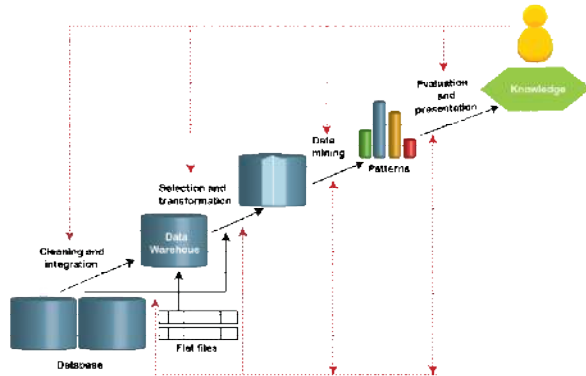


Figure 1 . Data Mining Process

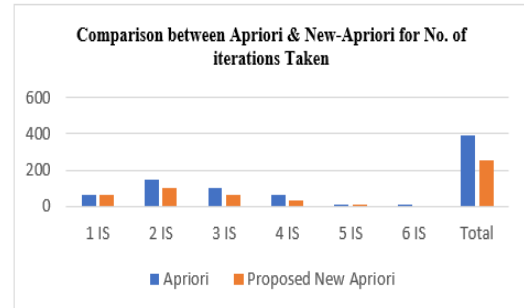


Figure 2: Transaction Comparison

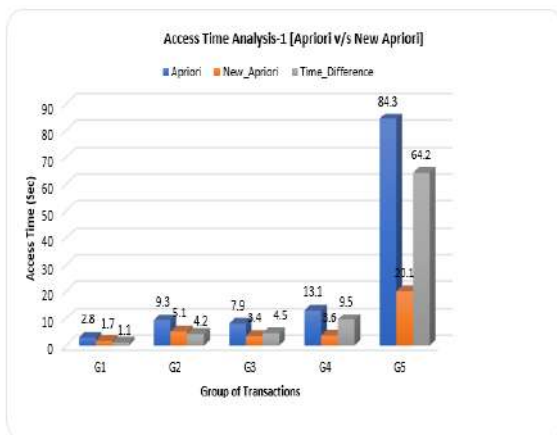


Figure 3: Comparison: Apriori v/s A-Apriori as per Table 11
 Fig.3 : Comparison : Apriori v/s A-Apriori as per Table 11

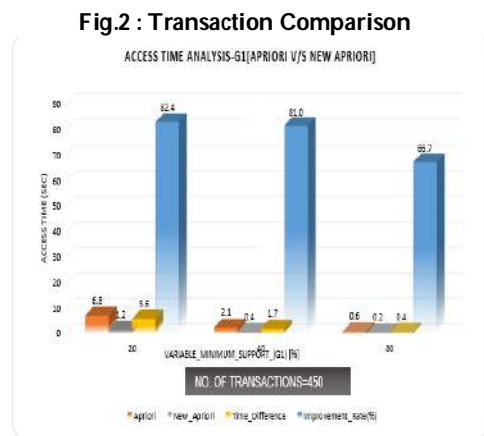


Figure 4 : Access Time Analysis-G1[Apriori v/s New Apriori] for variable support

Figure 4 : Access Time Analysis-G1 [Apriori v/s New Apriori] for variable support.





Accelerating Financial Inclusion in Rural India through the Acceptance and Diffusion of E-Wallets

Preetha Chandran¹, Gopalakrishnan Chinnasamy^{2*}, S.Vinoth³ and Pujari Sudharsana Reddy⁴

¹Professor, Welingkar Institute of Management Development and Research, Bengaluru – 560100, Karnataka, India

²Associate Professor, Faculty of Management, Jain Deemed to be University, Bengaluru - 560009, Karnataka, India.

³Professor, Faculty of Management, Jain Deemed to be University, Bengaluru – 560009, Karnataka, India.

⁴Assistant Professor, Faculty of Management, Jain Deemed to be University, Bengaluru – 560009, Karnataka, India.

Received: 04 Feb 2023

Revised: 10 Apr 2023

Accepted: 16 May 2023

*Address for Correspondence

Gopalakrishnan Chinnasamy

Associate Professor,

Faculty of Management,

Jain Deemed to be University,

Bengaluru - 560009, Karnataka, India.

Email: dr.gopalakrishnan_c@cms.ac.in.



This is an Open Access Journal / article distributed under the terms of the **Creative Commons Attribution License** (CC BY-NC-ND 3.0) which permits unrestricted use, distribution, and reproduction in any medium, provided the original work is properly cited. All rights reserved.

ABSTRACT

Recent innovations in modern payment systems have brought E wallets as top among the various digital banking channels (Anitha Kumari and Chitra Devi, 2022). E wallets was introduced as one of the payment and processing option and paved the way for diffusing the digital banking channels all over India (RBI, 2022). According to National payments corporation of India, this has been achieved by applying operational guidelines for payment and safe settlement methods. However, researches shows that the adoption of digital banking in rural India is still in the growth stage and there is a gap between urban and rural users in terms of using the digital banking channels like E-wallets (Deepesh Ranabhat *et al.*, 2022). By using both quantitative and qualitative methods of research, this study intends to identify the elements that influence rural consumers' opinions toward E-wallets and their desire to use them.

Keywords: Digital banking, E-wallets, diffusion, adoption, rural users, technology, sustainability, growth, Inclusion, Qualitative, Quantitative, Focus group.





Preetha Chandran *et al.*,

INTRODUCTION

The Digital India programme aims to use technology to better the lives of common man. In India, efforts have been made to make technology as available, affordable, and beneficial as possible. Nearly all sectors in India have embraced digital initiatives (Ligon *et al.*, 2019; Ravikumar *et al.*, 2020). The availability of technological resources and the lifestyle has brought a new platform in payment method other than cash and card payments (Seetharaman *et al.*, 2017; AnithaKumari and Chitra Devi, 2022). According to the ministry of Electronics and IT (MeitY), there are about 7422 crore digital payment transactions recorded during the financial year 2021-22 with an increase in volume by 33% by year on year in India. As per NPCI, the UPI transactions were doubled during the financial year 2021-22. The field research conducted by Deccan Herald during April 2022, the rural India lag behind on digital payments despite UPI usage doubled in the financial year 2021-22. The use of digital platform based payment apps in India has shown steady growth, especially after the pandemic but only 3 to 7 percent of rural consumers are actively using UPI to transact (Deccan Herald, April 2022). Indian union finance minister said during her Budget 2022-23 speech that in recent years, digital banking, digital payments and fintech have grown rapidly in India.

Problem Statement

The sustainability of financial services businesses is relying on the ease payment system. Electronic payments, especially e-wallets, have gained popularity due to their convenient and user-friendly features compared to any other digital payment system. The e-wallet system has gained popularity for a time, and e-commerce has expanded it all over the world. The development of any person or nation depends on an effective payment system. (Kolandaishamy *et al.*, 2020; AnithaKumari). In developing countries, account holdings tend to be lower in rural than in urban (Global Findex database 2021). However, the literatures are stating the rural customers are in the beginning phase in adopting the use of digital banking channels. Hence, it is vital to enhance the level of opportunity and the adoptability in using digital banking channels and also needs to eradicate the risks and uncertainties tied with technology based rural services. As a result, the current work aims to evaluate the elements that influence the adoption of digital banking channels, particularly the E-wallet payment method that is popular in rural Indian economy, as well as the level of diffusion among rural consumers.

Research Objectives

The study uses the below to attain the objectives of the study.

1. Identify the key elements which impact rural users' adoption of electronic e-wallet systems.
2. Ascertain issues that impede the spread of e-wallet payment systems in rural India

Theoretical underpinning framework

Innovation is the success ladder for companies to differentiate their products and services in the market for their success (KamakhyaNarain Singh and Shruti Malik, 2022). Though the technologies are beneficial, user friendly and highly secured, it has to be communicated to the end users well (Kolandaishamy *et al.*, 2020).

Diffusion of innovation (DOI)

Dissemination is the process through which invention is gradually transmitted to the broad community through a wide range of media (Rogers 1995). This was proved by Rogers in 2003 by introducing the theory of Diffusion of Innovations (DOI), which applies to various areas of management and other related areas of study. The DOI served as the theoretical basis for research on the adoption and distribution of the technology (Chinnasamy *et al.*, 2021; KamakhyaNarain Singh and Shruti Malik, 2022). Taking into account five innovation criteria that people perceive, Rogers (2003) indicated that DOIs predict the acceptability and level of acceptance of innovation. According to Rogers (2003), adoption is positively impacted by these five characteristics in addition to difficulty. The Figure 1 highlights these.





Preetha Chandran *et al.*,

Technology Readiness index (TRI)

Technology readiness is the tendency of people to understand and use new technologies to achieve their personal and professional goals. The acceptability of new technology and the desired outcomes are necessary for their survival (Wiese *et al.*, 2019; AnithaKumari and Chitra Devi. 2022). With the aid of service providers like financial institutions, payment systems have simplified numerous technological revolutions. Most studies use the Parasuraman (2000) TRI paradigm to determine a person's technical readiness. TRI measures openness to embracing new technologies and looks at traits including optimism, inventiveness, anxiety, and unpredictability. The first two attributes, which are the drivers of technology readiness, are barriers for the other two traits. Figure 2 shows the TRI theoretical underlying model of Parasuraman (2000).

E-wallet acceptance and diffusion

Mobile devices are inseparable from the everyday lives of the common man, which is the basis of all technological developments. Perceived benefit and perceived ease are the major factors that impact how people behave when using new technology, such as an e-wallet. The concepts of TAM and TRI provide a paradigm for the essential notion that users' attitudes play a crucial role in accepting and disseminating new innovation (Ajzen and Fishbein, 2011; Rose and Fogarty 2006). There are very few studies on e-wallet readiness that are focused on rural India. To evaluate the amount of adoption and penetration of developments in the field of contemporary mobile e-wallet payment systems, these two methodologies have not, however, been combined. Therefore, in order to assess the prevalence and level of acceptance of e-wallets in rural India, we will merge these models into one in this study. The theoretical basis for this investigation is displayed in Figure 3 below.

Research approach

The current study uses focus groups and interviews with structured questionnaires to examine the adoption and diffusion of e - wallets in rural India for the country's economic development. The study employed judgmental sampling to collect the primary data through structured questionnaires and it has been passed to the consumers who are coming to their bank branches/ATMs to do their banking transactions in rural district Belagavi, Karnataka. There are about 473 responses obtained from the general public. Out of 267 respondents, there are only 224 respondents only use E-wallets. The reliability also tested using Cronbach's alpha and it is observed with the acceptable value of 0.883. The SPSS (Version 27) have been used to derive the statistical results using factor analysis to identify the most influencing factors towards this subject line and the demographic analysis. The study covers five different groups of people, including groups of young people, middle-aged people, businesses, service providers, and persons in the service industry. To allow for unrestricted conversation, the group was then divided up again according to gender. There are 30 people are part of the discussion, which is a good number to set up a focus group. The researchers first conducted a pilot study in groups to ensure the credibility of the interview questions. The point of discussion was acknowledged and kept confidential by the researchers, as participants was not allowed audio / video recording capabilities and keeping the confidentiality of those involved in the data development process has been accounted. No personal name or work-related ID was created during the discussion forum. All three researchers moderated the group discussion.

Outcome of the respondents

This section discusses the result of demographic variables and the outcome from factor analysis to know the level of adoption and diffusion of E wallets in the study area. As per the demographic study, it is observed that the females (43%) are almost equal to males (57%) in terms of owning bank account. This may be reason of central government of India's financial inclusion mission achieved through Jan dhanyojana and the majority of respondents falls under the middle age (34%) category between 31 years to 50 years. The majority of the respondents are graduate with 48% and the majority are belonging to average income level of ₹10,000- ₹30,000 per month and the majority are belonging to working group either with organized or unorganized sectors. Table 3.1 represent the Kaiser-Meyer-Olkin measure of sampling adequacy which identifies the variation of the variable which may affect by unknown factors and its value varies between 0 and 1. The below table shows the score of 0.858 represents higher level of data adequacy along with the chi-square value of 0.000 with the 5% level of significance.



**Preetha Chandran et al.,**

Table 3.2 discusses that there are four components have adequate data variances and qualified for one Eigenvalue criterion and it is found that there are 64.223% of total variances observed from 4 principal components and the remaining are explained by other variables. The comparable factors like Discounts and cash back offers reduce the cost of transactions, alternative for making payments, Quality of E-wallet service providers and the interaction with mobile payment is clear and understandable are the determinant factors in adopting the E wallets. Further other three groups namely Compatibility with seven factors, Complexity & trialability together with four factors and Observability with two factors are grouped in the chronological order. So, it can be inferring that these are the influencing factors than other factors in the diffusion and adoption of E wallets in rural district Belagavi, Karnataka. Also, this outcome is supported by some research work carried by Mahmood et al (2016) in the context of Pakistan, Ligon et al (2019); *Kolandaisamy et al., (2020)*; Ashutosh Upadhyay and Kalluru Siva Reddy (2021) in the Indian and the international context.

Outcome of the focus group discussions

The focus group discussion was taken place among the people of rural district Belagavi, Karnataka. The discussion has opened up many viewpoints in terms of using the E wallet in their area. It discovers that they are the users of internet services. They are having an adequate awareness on using social media, webpage, email, newsgroup and the digital payment system i.e., E wallets. As a result, it is evident that individuals are familiar with utilising e-wallets to make purchases. It has been noted that they frequently make purchases from chain stores like Spar, D-Mart, Reliance Digital, R&B, and others as well as grocery stores and shopping malls. However, usage of this service was found to be infrequent, and no significant transactions were seen during the past six months. The discussion and conclusion of the focus group's findings regarding the characteristics of e-wallet payments are as follows in this circumstance.

Comparable gain (Relative advantages)

"It is very easy to carry mobile rather than going with cash or cards. When we are busy we tend to forget to carry these things but we never miss our mobile phones". "In our area most of the busy time the ATM's will be busy and some time may not have sufficient cash to withdraw. If I am using the E wallets will not require for me to go to ATMs and unnecessarily wasting our time". "Thanks to E wallets as it helps me to come out of pressure in paying small amounts using coins while transaction". The level of their outcome from these aspects found that the people are having high amount of confidence in using E wallets as mentioned by other researcher like Parasuraman (2000) and Rogers (2003) studies.

Compatible factors

The compatibility has been assessed in way that the E wallet payment method is suitable with the type of purchases which they made at different situations. The outcome of this discussion have brought below statements. "I would like to take up even mobile recharge or other online charges using this application only. Because it will consume my time if I go for a shop and do the transactions". "I would keep the payment through e-wallet for those expensive transactions and not keep those for buying utilities". The discussion has given an outline of using this application in terms of compatibility is found that it never minds about the nature and the volume of purchases in the most of the occasion. It was interesting to note that when the topic of how much it has been used in a week or a month came up, it was found that roughly 40% of people utilise it on a weekly or monthly basis (Michael Humbani & Melanie Wiese, 2019; Senthil Kumar and Arun Palanisamy 2019).

Complex and Uncomfortable

The complexity and discomfort have been addressed during the discussion. The following are the major outcome. "The language issues which I am facing some time while making payment. Though I am good in English language to read, write, speak, I need applications in my own language Kannada with more clear statements or translating options". "I don't know anything about the applications, downloading, installing and how to use it easily. But I am feeling that it is not too late to learn and adapt it". The above discussions have provided a broader sense of complexity & discomfort which are associated with the E wallets.





Preetha Chandran et al.,

Trial excellence and Observability

The trailability and observability is the opportunity to make the visibility and familiarity of the innovative ideas among the users of the technology. There are few observations from the group of members are: "I can switch any time from one application to another application even for minor reasons. Also I am have no problem in trying new application whether it is convenient or not". "I am so comfortable in using this application and I am not able to recall the way which I have started to use this application. I am so happy in using this application and I do not have any difficulty in using it". The above few discussions have brought some insight in terms of observability and trailability of E wallets and the intention to use them.

Optimistic and Innovative customers

The optimistic approach and innovative approach can stimulate them to move forward to other new applications whether it is convenient to use or not. These kinds of consumers can switch them at any time without any hesitation. The following are the observation obtained from the discussion forum. "No need to remember the password and other security related credentials and it is easy to do the payment processes. In payment, everything is possible without spending time". "I need the technology which saves my time and mobile phone efficiency by handling the process most quickly". As a result, we may conclude that optimism and innovation are the driving forces behind the spread and uptake of e-wallet payment systems.

Insecure

The low level of confidence in new technology creates the level of insecurity in terms of using E wallets. This was observed in the focus group discussions also. "Do the credentials shared are safe and secured. Still I am worrying about this though there is security supports embedded with the applications". "There are many private players are involving in this process and they themselves act as payment bankers. Obviously, we are in a position to share our account details with them. Is this is advisable. Still I am worrying". "Somehow, I cannot convince myself if the services offered by any banks in India are totally safe and secured". As a result, we may conclude that issues relate to insecurity have a detrimental impact on the adoption and diffusion of e-wallets in the rural district of Belagavi, Karnataka.

DISCUSSION AND CONCLUSION

The purpose of this study was to know the level of financial inclusion in a rural India through the acceptance and diffusion level of digital banking channel i.e., E wallet. To move forward as digital economy with an inclusive nature, the adoption and diffusion of digital payment channels are vital (Kuang-Hush Shih and Ching-Yi Lin, 2015; RBI, 2019). According to the outcome achieved from factor analysis, there are four major group of factors play an important role in the acceptance and diffusion of e wallets in Belagavi. These factors are comparable gains, compatibility, complexity & trailability and observability. Hence, it can be inferring that these are the influencing factors than other in the progress of diffusion and adoption of E wallets in rural district Belagavi, Karnataka. The focus group's conclusion is that these applications can be used at the user's convenience whether they are spending 100 rupees or 10,000 rupees on their purchases. It's interesting to note that about 40% of users access it on a weekly or monthly basis. This is a step in the right direction for e-wallet acceptance and dissemination in rural communities. According to quality study, the factors like insecurity, reliability, complexity in the application, and fear in operating the application are preventing bit in the progress of financial inclusion and the diffusion of digital banking channel. These results will aid the stakeholders in focusing their efforts on resolving these problems and promoting the usage of e-wallets across the country by integrating the current financial system with communications services. Applications should be compatible with high level services from all service providers in order to feel secure and comfortable using the application successfully, according to expectations from service providers. Further, there is a need to have a trust-enhancing process from the service providers in terms of providing error free or fraud free transactions. In addition to that the motivations are required to extend the process in a fast scale. These can be achieved by giving some added and additional services, cash prizes, offers and other relevant promotional factors.





Preetha Chandran et al.,

To infiltrate the habit, the government sectors bills and dues needs to be paid only through these digital banking channels. The results of this study cannot be applied to all regions of the payment system because it is qualitative and quantitative in character, provided with factor analysis, and conducted in the context of India. This study will provide information on the degree of adoption and dispersion of the digital payment channel as well as the support required to promote new applications in the transactions and payment platforms. This study can be geographically expanded and additional research methodologies, such as quantitative or time series research, can be used.

REFERENCES

1. AnithaKumari and N. Chitra Devi.(2022)'Determinants of user's behavioural intention to use blockchain technology in the digital banking services',*Int. J. Electron.Financ.* 11, 2 (2022), 159–174. <https://doi.org/10.1504/ijef.2022.122181>.
2. AshutoshUpadhyay and Kalluru Siva Reddy.(2021)'Digital financial inclusion - demand side vs. supply side approach'.*Int. J. Electron. Financ.* 10, 3 (2021), 191–210. <https://doi.org/10.1504/ijef.2021.115664>.
3. BhoomikaTrehan and Amit Kumar Sinha.(2021)'A study of confirmation bias among online investors in virtual communities'.*Int. J. Electron. Financ.* 10, 3 (2021), 159–179. <https://doi.org/10.1504/ijef.2021.115647>.
4. Calder, B. J. (1977) 'Focus groups and the nature of qualitative marketing research'. *Journal of Marketing Research*, XIV, 353-364.
5. DeepeshRanabhat, NarinderVerma, Devesh Kumar, and HotniarSiringoringo.(2022). 'The adoption of digital financial inclusion in developing countries: a systematic literature review'. *Int. J. Electron. Financ.* 11, 2 (2022), 117–142. <https://doi.org/10.1504/ijef.2022.122178>.
6. Jarvenpaa, S. L., & Lang, K. R. (2005). 'Managing the paradoxes of mobile technology. Information Systems Management.' 22(4), 7-23.
7. Kolandaisamy, Raenu&Subaramaniam, Kasthuri.(2020). 'The Impact of E-Wallets for Current Generation'.*Journal of Advanced Research in Dynamical and Control Systems*.12. 10.5373/JARDCS/V12SP1/20201126.
8. KPMG (2019). Oman banking sector demonstrates healthy growth (online). Available: <https://home.kpmg/om/en/home/media/press-releases/2019/05/oman-banking-perspectives.html>
9. Ligon E, Malick B, Sheth K, Trachtman C. (2019). 'What explains low adoption of digital payment technologies? Evidence from small-scale merchants in Jaipur, India'. *PLoS ONE* 14(7): e0219450. <https://doi.org/10.1371/journal.pone.0219450>.
10. Mallat, Niina. (2007). 'Exploring Consumer Adoption of Mobile Payments—A Qualitative Study'. *The Journal of Strategic Information Systems*. 16. 413-432. 10.1016/j.jsis.2007.08.001.
11. Manikandan, D. S. (2016). 'A Study on Awareness Level of Mobile Wallets Services among Management Students'.*International Journal of Advanced Research in Management and Social Sciences*. ISSN: 2278-6236, 10-19.
12. Pal, Abhipsa& De, Rahul &Herath, Tejaswini& Rao, H. (2019). 'A review of contextual factors affecting mobile payment adoption and use'. *Journal of Banking and Financial Technology*. 3. 10.1007/s42786-018-00005-3.
13. Parasuraman, A. (2000). 'Technology Readiness Index (TRI): A Multiple-Item Scale to Measure Readiness to Embrace New Technologies'. *Journal of Service Research*. vol. 2, no. 4, pp. 307-20.
14. Paypal.(2019). 'Privacy Statement of paypal account' (online). Available: <https://www.paypal.com/en/webapps/mpp/ua/privacy-full#2>
15. Ravikumar et al., (2020). 'Digital Payments Diffusion in Emerging and Developed Economies'.*International Journal of Innovative Technology and Exploring Engineering*, 9(4), 273–279.<https://doi.org/10.35940/ijitee.d1357.029420>.
16. Wilkinson, S. (2004). 'Focus group research'. In D. Silverman (Ed.), *Qualitative research. Theory, Method and Practice*. (2 ed.). Thousand Oaks, CA.: Sage Publications.





Preetha Chandran et al.,

Table 1. KMO and Bartlett's Test

KMO and Bartlett's Test		
Kaiser-Meyer-Olkin Measure of Sampling Adequacy.		0.858
Bartlett's Test of Sphericity	Approx. Chi-Square	1364.559
	df	153
	Sig.	0.000

Source: Survey data (2022)

Table 2.Component and Variance explained

Components	Eigenvalues	% of variances	Cumulative %
Comparable gains	6.052	33.621	33.621
Compatible	1.472	13.176	46.797
Complex & Trialexcellence	1.286	9.142	55.939
Observable	1.131	8.284	64.223

Source: Survey data (2022)

Table 3.Factors extracted using principal component analysis

	Rotated Component Matrix ^a			
	Component			
	Relative advantages	Compatibility	Complexity & trialability	Observability
Discounts and cash back offers attracts you to use these services	0.771			
Mobile wallets reduce the cost of transactions	0.757			
E-wallets serve as an appealing alternative for making payments	0.590			
Quality of E-wallet service providers	0.582			
Interaction with mobile payment is clear and understandable	0.489			
Brand Loyalty of E-wallet companies affects the usages		0.693		
Gives me greater control over my day to day transactions		0.595		
There is significant risk in Internet shopping		0.593		
Doing payments through these Electronic Wallets is convenient		0.591		
Using Mobile Wallet puts my privacy at risk		0.585		
Paying money through mobile wallets is a trust		0.555		
E-wallet services provide security to transactions		0.495		
E-wallet services provide a reduced time of transactions			0.706	
I believe that my Personal Information			0.703	





Preetha Chandran et al.,

is encrypted				
Dealing with mobile payments is a risky choice			0.697	
E-wallets system is considered as an useful payment method			0.530	
Helps me to keep track of my transaction history				0.822
Great potential to lose money if I buy goods on the Internet				0.570
Extraction Method: Principal Component Analysis. Rotation Method: Varimax with Kaiser Normalization.				
a. Rotation converged in 10 iterations.				

Source: Survey data (2022)





Introduction to Intuitionistic Generalized Fuzzy b-Metric Spaces and Fixed Point Results

M.Sornavalli^{1*} and V.Mallikadevi²

¹Assistant Professor, Department of Mathematics, Velammal College of Engineering and Technology, Madurai, Tamil Nadu, India

²Assistant Professor, Department of Mathematics, Manonmaniam Sundaranar University College, Tirunelveli, Tamil Nadu, India

Received: 05 Feb 2023

Revised: 13 Apr 2023

Accepted: 16 May 2023

*Address for Correspondence

M.Sornavalli

Assistant Professor,
Department of Mathematics,
Velammal College of Engineering and Technology,
Madurai, Tamil Nadu, India
E.Mail:sornavalliv7@gmail.com



This is an Open Access Journal / article distributed under the terms of the **Creative Commons Attribution License** (CC BY-NC-ND 3.0) which permits unrestricted use, distribution, and reproduction in any medium, provided the original work is properly cited. All rights reserved.

ABSTRACT

The main purpose of the present paper is to introduce and study the notion of intuitionistic generalized fuzzy b-metric space (Shortly IGfBMS). In this way, we generalize both the notion of intuitionistic generalized fuzzy metric space and fuzzy b-metric spaces. Further the formulation and proof of intuitionistic generalized fuzzy b-metric versions of some conventional theorems regarding fixed points via intuitionistic fuzzy sets are presented. In order to show the strength of these results, some motivating examples are established as well.

Keywords: Fuzzy b-metric spaces, intuitionistic generalized fuzzy metric space, fixed points.

Mathematics Subject Classification: 47H10; 54H25.

INTRODUCTION

Fixed point results provide tremendous circumstances in the study of mathematical analysis under which the solutions of linear and non-linear operator equations can be approximated. The theory itself is a beautiful mixture of analysis, topology, and geometry. As a result, the theory of fixed points has been revealed as a very powerful and important tool in the study of nonlinear phenomena. In particular, fixed point techniques have been applied in such diverse fields as biology, chemistry, economics, engineering, game theory, and physics. Fuzzy sets were introduced by Zadeh [15] in 1965 to represent/manipulate data and information possessing nonstatistical uncertainties. It was specifically designed to mathematically represent uncertainty and vagueness and to provide formalized tools for

57089





Sornavalli and Mallikadevi

dealing with the imprecision intrinsic to many problems. In 1975 Kramosil and Michalek [7] have introduced and studied the notion of fuzzy metric space with the help of continuous t-norm, which is modified by George and Veeramani [5].

The concept of b-metric was introduced by Bakhtin [6]. The class of b-metric spaces is larger than that of metric spaces. Shoaib et al [14] formulated and proved fixed point theorems for fuzzy mappings in a b-metric space. Kumam [8], Phiangsungnoen et al.[12] worked on fixed point theorems for fuzzy mapping in b-metric spaces. Mukheimer [9], formulated and proved some common fixed point theorems in complex valued b-metric spaces. Recently in 2016 Nădăban [10] introduced the concept of fuzzy b-metric space and agreed that the study of operators in fuzzy b-metric spaces will obtain a lot of applications both in Mathematics as well as in Engineering and Computer Science. Many wonderful and valuable fixed point results in b-metric spaces and fuzzy metric spaces have been established and proved (see [6,8-10,12,14]). In this paper we have established some conventional fixed point theorems in the setting of complete intuitionistic fuzzy b- metric spaces.

PRELIMINARIES

Definition 2.1:

Let X be an arbitrary non empty set and $s \geq 1$ be a given real number. A function $d : X \times X \rightarrow [0, \infty)$ is a *b-metric on X* if, for all $x, y, z \in X$ the following conditions are satisfied:

- (i) $d(x, y) = 0; x = y;$
- (ii) $d(x, y) = d(y, x);$
- (iii) $d(x, z) \leq s [d(x, y) + d(y, z)].$

The triple (X, d, s) will be called *b-metric space*.

Example 2.2 :

The space $l_p (0 < p < 1), l_p = \{(x_n) \subset R: \sum_{n=1}^{\infty} |x_n|^p < \infty\}$, together with a function $d : l_p \times l_p \rightarrow R$

$$d(x, y) = (\sum_{n=1}^{\infty} |x_n - y_n|^p)^{\frac{1}{p}}$$

where $x = (x_n), y = (y_n) \in l_p$ is a b-metric space. By an elementary calculation we obtain

$$\text{that } d(x, z) \leq 2^{\frac{1}{p}} [d(x, y) + d(y, z)]. \text{ Here } s = 2^{\frac{1}{p}} > 1.$$

Remark: Note that a (usual) metric space is evidently a b-metric space.

Definition 2.3 :

Let X be a nonempty set. Let $s \geq 1$ be a given real number and $*$ be a continuous t-norm. A fuzzy set M on $X \times X \times [0, \infty)$ is called *fuzzy b-metric* if,

for all $x, y, z \in X$ the following conditions hold:

- (i) $\mathcal{M}(x, y, 0) = 0;$
- (ii) $\mathcal{M}(x, y, t) = 1; \forall t \geq 0$ if and only if $x = y;$
- (iii) $\mathcal{M}(x, y, t) = \mathcal{M}(y, x, t), \forall t \geq 0$
- (iv) $\mathcal{M}(x, z, s(t + u)) \geq \mathcal{M}(x, y, t) * \mathcal{M}(y, z, u), \forall t \geq 0$
- (v) $\mathcal{M}(x, y, \cdot) : [0, \infty) \rightarrow [0, 1]$ is left continuous and $\lim_{t \rightarrow \infty} \mathcal{M}(x, y, t) = 1;$

The quadruple $(X, \mathcal{M}, *, s)$ is said to be *fuzzy b-metric space*.

Example 2.4 :

Let (X, d, s) be a b-metric space and $a * b = \min(a, b), \forall a, b \in [0, 1]$ and let M be a fuzzy set on $X \times X \times [0, \infty)$, defined as follows:





Sornavalli and Mallikadevi

$$M_d(x, y, t) = \begin{cases} \frac{t}{t+d(x,y)}, & \text{if } t > 0 \\ 0, & \text{if } t = 0 \end{cases}$$

Then $(X, M_d, *, s)$ is standard fuzzy b-metric space.

Definition 2.5 :

A 6-tuple $(X, \mathcal{M}, \mathcal{N}, *, \diamond, s)$ is said to be an *intuitionistic fuzzy b-metric space (IFbMS)*, if X is an arbitrary set, $s \geq 1$ is a given real number, $*$ is a continuous t-norm, \diamond is a continuous t-co norm, \mathcal{M} and \mathcal{N} are fuzzy sets on $X^2 \times [0, \infty)$ satisfying the following conditions: For all $x, y, z \in X$,

- (a) $\mathcal{M}(x, y, t) + \mathcal{N}(x, y, t) \leq 1$;
 - (b) $\mathcal{M}(x, y, 0) = 0$;
 - (c) $\mathcal{M}(x, y, t) = 1; \forall t > 0$ iff $x = y$;
 - (d) $\mathcal{M}(x, y, t) = \mathcal{M}(y, x, t), \forall t > 0$;
 - (e) $\mathcal{M}(x, z, s(t+u)) \geq \mathcal{M}(x, y, t) * \mathcal{M}(y, z, u); \forall t, u > 0$;
 - (f) $\mathcal{M}(x, y, \cdot) : [0, \infty) \rightarrow [0, 1]$ is left continuous and $\lim_{t \rightarrow \infty} \mathcal{M}(x, y, t) = 1$;
 - (g) $\mathcal{N}(x, y, 0) = 1$;
 - (h) $\mathcal{N}(x, y, t) = 0; \forall t > 0$ iff $x = y$;
 - (i) $\mathcal{N}(x, y, t) = \mathcal{N}(y, x, t); \forall t > 0$;
 - (j) $\mathcal{N}(x, z, s(t+u)) \leq \mathcal{N}(x, y, t) \diamond \mathcal{N}(y, z, u); \forall t, u > 0$;
 - (k) $\mathcal{N}(x, y, \cdot) : [0, \infty) \rightarrow [0, 1]$ is right continuous and $\lim_{t \rightarrow \infty} \mathcal{N}(x, y, t) = 0$.
- Here, $\mathcal{M}(x, y, t)$ and $\mathcal{N}(x, y, t)$ denote the degree of nearness and the degree of non-nearness between x and y with respect to t respectively.

Definition 2.6 :

A 6-tuple $(X, \mathcal{M}, \mathcal{N}, *, \diamond, s)$ is said to be an *intuitionistic Generalized fuzzy b-metric space (IGFbMS)*, if X is an arbitrary set, $s \geq 1$ is a given real number, $*$ is a continuous t-norm, \diamond is a continuous t-co norm, \mathcal{M} and \mathcal{N} are fuzzy sets on $X^3 \times [0, \infty)$ satisfying the following conditions: For all $x, y, z \in X$,

- (a) $\mathcal{M}(x, y, z, t) + \mathcal{N}(x, y, z, t) \leq 1$;
- (b) $\mathcal{M}(x, y, z, t) > 0$;
- (c) $\mathcal{M}(x, y, z, t) = 1; \forall t > 0$ iff $x = y = z$;
- (d) $\mathcal{M}(x, y, z, t) = \mathcal{M}(p\{x, y, z\}, t)$ where p is a permutation function,
- (e) $\mathcal{M}(x, z, s(t+u)) \geq \mathcal{M}(x, y, a, t) * \mathcal{M}(a, z, u); \forall t, u > 0$;
- (f) $\mathcal{M}(x, y, z, \cdot) : (0, \infty) \rightarrow [0, 1]$ is left continuous and $\lim_{t \rightarrow \infty} \mathcal{M}(x, y, z, t) = 1$;
- (g) $\mathcal{N}(x, y, z, t) < 1$;
- (h) $\mathcal{N}(x, y, z, t) = 0; \forall t > 0$ iff $x = y$;
- (i) $\mathcal{N}(x, y, z, t) = \mathcal{N}(p\{x, y, z\}, t)$ where p is a permutation function,
- (j) $\mathcal{N}(x, z, s(t+u)) \leq \mathcal{N}(x, y, a, t) \diamond \mathcal{N}(a, z, u); \forall t, u > 0$;
- (k) $\mathcal{N}(x, y, z, \cdot) : (0, \infty) \rightarrow [0, 1]$ is right continuous and $\lim_{t \rightarrow \infty} \mathcal{N}(x, y, z, t) = 0$.

Here, $\mathcal{M}(x, y, z, t)$ and $\mathcal{N}(x, y, z, t)$ denote the degree of nearness and the degree of non-nearness between x and y with respect to t respectively.

Example:

Let (X, d, s) be a b-metric space and $a * b = \min(a, b), a \diamond b = \max(a, b) \forall a, b \in [0, 1]$ and let $\mathcal{M}_d, \mathcal{N}_d$ be fuzzy sets on $X^3 \times (0, \infty)$, defined as follows:

$$\mathcal{M}_d(x, y, z, t) = \begin{cases} \frac{t}{t+d(x,y,z)} & \text{if } t > 0 \\ 0, & \text{if } t = 0 \end{cases} \text{ and } \mathcal{N}_d(x, y, z, t) = \begin{cases} \frac{d(x,y,z)}{t+d(x,y,z)} & \text{if } t > 0 \\ 0, & \text{if } t = 0 \end{cases}$$





Sornavalli and Mallikadevi

We check only axioms (e) and (j) of definition (2.6), because verifying the other conditions is standard. Let $x, y, z \in X$, and $t, s > 0$. Without restraining the generality we assume that

$$\mathcal{M}_d(x, y, z, t) \leq \mathcal{M}_d(y, z, z, u) \text{ and } \mathcal{N}_d(x, y, z, t) \geq \mathcal{N}_d(y, z, z, u)$$

Thus

$$\frac{t}{t+d(x,y,z)} \leq \frac{u}{u+d(x,y,z)} \text{ and } \frac{d(x,y,z)}{t+d(x,y,z)} \geq \frac{d(x,y,z)}{u+d(x,y,z)}$$

i.e., $t d(x, y, z) \leq u d(x, y, z)$. On the other hand,

$$\begin{aligned} \mathcal{M}_d(x, y, z, s(t+u)) &= \frac{s(t+u)}{s(t+u)+d(x,y,z)} \\ &\geq \frac{s(t+u)}{s(t+u) + s[d(x,y,a) + d(a,y,z)]} \\ &= \frac{t+u}{t+u + d(x,y,a) + d(a,y,z)} \end{aligned}$$

$$\begin{aligned} \text{Also, } \mathcal{N}_d(x, y, z, s(t+u)) &= \frac{d(x,y,z)}{s(t+u)+d(x,y,z)} \\ &\leq \frac{s[d(x,y,a) + d(a,y,z)]}{s(t+u) + s[d(x,y,a) + d(a,y,z)]} \\ &= \frac{[d(x,y,a) + d(a,y,z)]}{t+u + [d(x,y,a) + d(a,y,z)]} \end{aligned}$$

We will Prove that $\frac{t+u}{t+u + d(x,y,a) + d(a,y,z)} \geq \frac{t}{t+d(x,y,z)}$

$$\text{And } \frac{[d(x,y,a) + d(a,y,z)]}{t+u + [d(x,y,a) + d(a,y,z)]} \leq \frac{d(x,y,z)}{t+d(x,y,z)}$$

Hence we will obtain that

$$\mathcal{M}_d(x, y, z, s(t+u)) \geq \mathcal{M}_d(x, y, z, t) = \mathcal{M}_d(x, y, z, t) * \mathcal{M}_d(x, y, z, u)$$

$$\text{And } \mathcal{N}_d(x, y, z, s(t+u)) \geq \mathcal{N}_d(x, y, z, t) = \mathcal{N}_d(x, y, z, t) \diamond \mathcal{N}_d(x, y, z, u)$$

Hence $(X, \mathcal{M}_d, \mathcal{N}_d, *, \diamond, s)$ is (standard) intuitionistic generalized fuzzy b-metric space.

Theorem:

Let $(X, \mathcal{M}, \mathcal{N}, *, \diamond, s)$ be a complete intuitionistic generalized fuzzy b-metric space.

Let $T: X \rightarrow X$ be a mapping satisfying

$$\mathcal{M}(Tx, Ty, Ty, kt) \geq \mathcal{M}(x, y, y, t)$$

$$\mathcal{N}(Tx, Ty, Ty, kt) \leq \mathcal{N}(x, y, y, t)$$

for all $x, y \in X$ where $0 < k < 1$. Then T has a unique fixed point.

Proof:

Let $x_0 \in X$ be an arbitrary element and let $\{x_n\}$ be a sequence in X such that, $x_n = T^n x_0$ ($n \in \mathbb{N}$). Then

$$\begin{aligned} \mathcal{M}(x_n, x_{n+1}, x_{n+1}, kt) &= \mathcal{M}(T^n x_0, T^{n+1} x_0, T^{n+1} x_0, kt) \\ &\geq \mathcal{M}(T^{n-1} x_0, T^n x_0, T^n x_0, t) \\ &= \mathcal{M}(x_{n-1}, x_n, x_n, t) \\ &\geq \mathcal{M}(T^{n-2} x_0, T^{n-1} x_0, T^{n-1} x_0, \frac{t}{k}) \\ &= \mathcal{M}(x_{n-2}, x_{n-1}, x_{n-1}, \frac{t}{k}) \\ &\dots \dots \geq \mathcal{M}(x_0, x_1, x_1, \frac{t}{k^{n-1}}) \end{aligned}$$

Clearly, $1 \geq \mathcal{M}(x_n, x_{n+1}, x_{n+1}, kt) \geq \mathcal{M}(x_0, x_1, \frac{t}{k^{n-1}}) \rightarrow 1$, when $n \rightarrow \infty$.

Thus $\lim_{n \rightarrow \infty} \mathcal{M}(x_n, x_{n+1}, x_{n+1}, kt) = 1$ and

$$\begin{aligned} \mathcal{N}(x_n, x_{n+1}, x_{n+1}, kt) &= \mathcal{N}(T^n x_0, T^{n+1} x_0, T^{n+1} x_0, kt) \\ &\leq \mathcal{N}(T^{n-1} x_0, T^n x_0, T^n x_0, t) \\ &= \mathcal{N}(x_{n-1}, x_n, x_n, t) \end{aligned}$$





Sornavalli and Mallikadevi

$$\begin{aligned} &\leq \mathcal{N}(T^{n-2}x_0, T^{n-1}x_0, T^n x_0, t/k) \\ &= \mathcal{N}(x_{n-2}, x_{n-1}, x_n, t/k) \\ &\dots \leq \mathcal{N}(x_0, x_1, x_1, t/k^{n-1}) \end{aligned}$$

Clearly, $0 \leq \mathcal{N}(x_n, x_{n+1}, x_{n+1}, kt) \leq \mathcal{N}(x_0, x_1, t/k^{n-1}) \rightarrow 1$, when $n \rightarrow \infty$.

Thus $\lim_{n \rightarrow \infty} \mathcal{N}(x_n, x_{n+1}, x_{n+1}, kt) = 0$

Let $\tau_n(t) = \mathcal{M}(x_n, x_{n+1}, x_{n+1}, t)$, $\mu_n(t) = \mathcal{N}(x_n, x_{n+1}, x_{n+1}, t)$ for all $n \in \mathbb{N} \setminus \{0\}$, $t > 0$.

Next we show that the sequence $\{x_n\}$ is a Cauchy sequence. If it is not, then there exists

$0 < \varepsilon < 1$ and two sequence $p(n)$ and $q(n)$ such that for every $n \in \mathbb{N} \setminus \{0\}$, $t > 0$,

$p(n) > q(n) \geq n$,

$\mathcal{M}(x_{p(n)}, x_{q(n)}, x_{q(n)}, t) \leq 1 - \varepsilon$ and $\mathcal{N}(x_{p(n)}, x_{q(n)}, x_{q(n)}, t) \geq \varepsilon$ And

$\mathcal{M}(x_{p(n-1)}, x_{q(n-1)}, x_{q(n-1)}, t) > 1 - \varepsilon$, $\mathcal{M}(x_{p(n-1)}, x_{q(n)}, x_{q(n)}, t) > 1 - \varepsilon$ And

$\mathcal{N}(x_{p(n-1)}, x_{q(n-1)}, x_{q(n-1)}, t) < \varepsilon$, $\mathcal{N}(x_{p(n-1)}, x_{q(n)}, x_{q(n)}, t) < \varepsilon$.

Now,

$$\begin{aligned} 1 - \varepsilon &\geq \mathcal{M}(x_{p(n)}, x_{q(n)}, x_{q(n)}, t) \\ &\geq \mathcal{M}(x_{p(n-1)}, x_{q(n)}, x_{q(n)}, t/2s) * \mathcal{M}(x_{p(n-1)}, x_{q(n)}, x_{q(n)}, t/2s) \\ &> \tau_{p(n-1)}(t/2s) * (1 - \varepsilon). \end{aligned}$$

$$\begin{aligned} \varepsilon &\leq \mathcal{N}(x_{p(n)}, x_{q(n)}, x_{q(n)}, t) \\ &\leq \mathcal{N}(x_{p(n-1)}, x_{q(n)}, x_{q(n)}, t/2s) \diamond \mathcal{N}(x_{p(n-1)}, x_{q(n)}, x_{q(n)}, t/2s) \\ &< \mu_{p(n-1)}(t/2s) \diamond \varepsilon \end{aligned}$$

Since $\tau_{p(n-1)}(t/2s) \rightarrow 1$ as $n \rightarrow \infty$ and $\mu_{p(n-1)}(t/2s) \rightarrow 0$ as $n \rightarrow \infty$ for every t , therefore for

$n \rightarrow \infty$, we have $1 - \varepsilon \geq \mathcal{M}(x_{p(n)}, x_{q(n)}, x_{q(n)}, t) > 1 - \varepsilon$

$\varepsilon \leq \mathcal{N}(x_{p(n)}, x_{q(n)}, x_{q(n)}, t) < \varepsilon$

Clearly, this leads to a contradiction. Hence x_n is a Cauchy sequence in X . Since X is complete so there exist a point y in X such that $\lim_{n \rightarrow \infty} x_n = y$.

Now,

$$\begin{aligned} \mathcal{M}(y, Ty, Ty, t) &\geq \mathcal{M}(y, x_{n+1}, x_{n+1}, t/2s) * \mathcal{M}(x_{n+1}, Ty, Ty, t/2s) \\ &= \mathcal{M}(y, x_{n+1}, x_{n+1}, t/2s) * \mathcal{M}(Tx_n, Ty, Ty, t/2s) \end{aligned}$$

$$\geq \mathcal{M}(y, x_{n+1}, x_{n+1}, t/2s) * \mathcal{M}(x_n, y, y, t/2sk)$$

The case when $n \rightarrow \infty$, we have

$\mathcal{M}(y, Ty, Ty, t) \geq 1 * 1 = 1$ And

$$\begin{aligned} \mathcal{N}(y, Ty, Ty, t) &\leq \mathcal{N}(y, x_{n+1}, x_{n+1}, t/2s) \diamond \mathcal{N}(x_{n+1}, Ty, Ty, t/2s) \\ &= \mathcal{N}(y, x_{n+1}, x_{n+1}, t/2s) \diamond \mathcal{N}(Tx_n, Ty, Ty, t/2s) \end{aligned}$$

$$\leq \mathcal{N}(y, x_{n+1}, x_{n+1}, t/2s) \diamond \mathcal{N}(x_n, y, y, t/2sk)$$

The case when $n \rightarrow \infty$, we have

$$\mathcal{N}(y, Ty, Ty, t) \geq 0 \diamond 0 = 0$$

Therefore $y = Ty$.

For uniqueness of fixed point, let y, z be two fixed points of the mapping T , then $y = Ty$ and

$z = Tz$ and

$$1 \geq \mathcal{M}(y, z, z, t) = \mathcal{M}(Ty, Tz, Tz, t)$$

$$\geq \mathcal{M}(y, z, z, t/k)$$

$$= \mathcal{M}(Ty, Tz, Tz, t/k)$$

$$\geq \mathcal{M}(y, z, z, t/k^2)$$

$\geq \dots$

$$\geq \mathcal{M}(y, z, t/k^n) \rightarrow 1 \text{ as } n \rightarrow \infty.$$

Also,

$$0 \leq \mathcal{N}(y, z, z, t) = \mathcal{N}(Ty, Tz, Tz, t)$$

$$\leq \mathcal{N}(y, z, z, t/k)$$





Sornavalli and Mallikadevi

$= \mathcal{N}(Ty, Tz, Tz, t/k)$
 $\leq \mathcal{N}(y, z, z, t/k^2)$
 $\leq \dots$
 $\leq \mathcal{N}(y, z, t/k^n) \rightarrow 0$ as $n \rightarrow \infty$.
 By (c) and (h) of definition (3.1), $y = z$.

REFERENCES

1. Atanassov.K, Intuitionistic fuzzy Sets, Fuzzy sets and Systems, 20(1986), 87-96.
2. Alaca. C, On fixed point theorems in intuitionistic fuzzy metric spaces, Comm. KoreanMath. Soci., 24(4)(2009), 565-579.
3. Alaca. C., Turkoglu. D., Yildiz . C., Fixed points in intuitionistic fuzzy metric spaces,Chaos Solitons Fractals 29 (2006) 1073-1078.
4. Akbar Azam, Shazia Kanwal, Introduction to Intuitionistic Fuzzy b-metric spaces and Fixed Point Results, Thai Journal of Mathematics, 20 (2022) 141-163.
5. George A., Veeramani P., On some results in fuzzy metric spaces, fuzzy sets and systems, 64 (1994), 395-399.
6. Bakhtin I.A., The contraction mapping principle in quasi-metric spaces, Funct. AnalUnianowsk Gos. Ped. Inst. 30 (1989) 26-37.
7. Kramosil I., Michalek J., Fuzzy metric and statistical metric spaces, Kybernetica, 11(1975), 326-334.
8. Kumam. W., Sukprasert. P., Kumam. P., Shoaib. A., Shahzad. A., Mahmood. Q., Some fuzzy fixed point results for fuzzy mappings in complete b-metric spaces, Cogent Mathematics & Statistics 5 (2018) Article ID 1458933.
9. Mukheimer. A.A., Some common fixed point theorems in complex valued b-metric spaces, Sci. World J. 2014 (2014) Article ID 587825.
10. Nădăban.S., Fuzzy b-metric spaces, Int. J. Comput. Commun. Control 11 (2) (2016)273-281.
11. Park. J.H., Intuitionistic fuzzy metric spaces, Chaos, Solitons and Fractals, 22(2004),1039-1046.
12. Phiangsugnoen. S., Kumam. P., Fuzzy fixed point theorems for multivalued fuzzycontractions in b-metric spaces, J. Nonlinear Sci. Appl. 8 (2015) 55-63.
13. Sedghi .S and Shobe .N, Fixed point theorem in M-fuzzy metric spaces with property(E),Advances in Fuzzy Mathematics, Vol.1, No. 1 (2006), 55- 65.
14. Shoaib.A., Kumam. P., Shazad. A., Phiangsungnoen. Q., Mahmood. Q., Fixed point results for fuzzy mapping in a b-metric space, Fixed Point Theory Appl. 2018 (2) (2018).
15. Zadeh, L.A., Fuzzy sets, Inform. and Control, 8 (1965), 338- 353.





Comparative Critical Analysis of Modern Architectural Styles

Meeta Tandon^{1*} and Farheen Bano²

¹Associate Professor, Faculty of Architecture and Planning, Dr. A. P. J. Abdul Kalam Technical University, Lucknow (U.P.), India.

²Assistant Professor, Faculty of Architecture and Planning, Dr. A. P. J. Abdul Kalam Technical University, Lucknow (U.P.), India.

Received: 27 Dec 2022

Revised: 23 Feb 2023

Accepted: 16 May 2023

*Address for Correspondence

Meeta Tandon

Associate Professor,
Faculty of Architecture and Planning,
Dr. A. P. J. Abdul Kalam Technical University,
Lucknow (U.P.), India.
Email: meeta2012@gmail.com



This is an Open Access Journal / article distributed under the terms of the **Creative Commons Attribution License** (CC BY-NC-ND 3.0) which permits unrestricted use, distribution, and reproduction in any medium, provided the original work is properly cited. All rights reserved.

ABSTRACT

The Industrial Revolution in the 19th century marked the beginning of a new era in architecture. The invention of the new building materials, increase in the production of goods, mass production, prefabrication, the need to design for new building functions that never existed before, migration of people from the villages to the urban centers and shift from agriculture to the industry brought about a revolutionary change. New architectural styles emerged as a response to these changes. Each preceding style formed a basis for the development of a new consequent style. They were either inspired by the previous styles or developed as a reaction to the previous styles. The research paper aims to review the contemporary architecture of the western world from 19th century onwards, emphasizing the various styles of Modern architecture and their architectural characteristics.

Keywords: Contemporary, Architecture, Modernism, Functionalism

INTRODUCTION

When do you think we should start with architectural history? When actually did architecture begin? We are used to thinking of architecture as a place where we live, work and pray. But architecture seems to have been there from the very beginning, in the very arrangement of nature in the form of rivers, valleys, mountains, etc. (Kostof, 1995). Beginning from the age when the humans lived in caves and built rudimentary structures of reed, tree branches, saplings, etc., to the present day, various architectural styles emerged. The location, climate, topography, availability of building materials, technology and construction techniques were responsible for developing the style. Apart from



**Meeta Tandon and Farheen Bano**

this, various intangible attributes like the culture of the people, their belief systems, the rituals played a pivotal role in the development of the architectural styles.

EUROPEAN ARCHITECTURAL HISTORY

Starting from the Aegean civilization, the Classical styles; Greek and Roman, the Early Christian, Renaissance, Romanesque, Gothic, Baroque, Rococo, Neoclassical, Gothic Revival evolved over a period of centuries. Each of these styles had its unique architectural features; the targeted construction system and Greek orders of Classical Greek architecture, the arcuate construction system used in Classical Roman style, pendentive vault of Byzantine architecture, a cross vault of Romanesque architecture, the pinnacle, pointed arches and buttresses of Gothic architecture, geometry and simplicity of Renaissance, duality and distortion of Mannerism and high ornamentation of Baroque and Rococo. These different styles were either inspired by the previous styles or developed as a reaction to the previous styles.

Neoclassical architecture that began in the middle of the 18th century evolved as a reaction against the high ornamentation of Late Baroque and Rococo. It spread throughout Europe, but France and England were the countries that used neoclassical styles the most. The architecture of Neoclassicism emerged due to two different but related developments. Firstly, a sudden increase in the capacity of a human to exercise control over nature and secondly, the shift in the nature of human consciousness. The significant changes in society, i.e. decline in aristocracy and rise of the bourgeoisie, the changes in human consciousness to question its own identity, led to the search for an authentic style (Frampton, 1992). The thought involved was not to copy the ancient styles but to understand the principles on which their work was based. This further led to the documentation and itinerary of the existing Classical and historical structures. The Neoclassical artists emphasized logic, reason, and ideology rather than ornamentation and pleasure (Vickers, 1998). Neoclassical architecture was characterized by simplicity of forms, use of Roman or Greek details, use of columns and blank walls. The Neoclassical buildings were divided between two closely related lines of development; Structural classicism and Romantic classicism. At the same time, Structural classicism emphasized structure and concentrated on prisons, railway stations, hospitals and similar building typologies, Romantic classicism emphasized the physiognomic character of the form itself and designed more representational structures like libraries and museums.

There were three types of Neoclassical buildings: Temple style, Palladian and Classical Block or Square (Figure 1). The temple design buildings were based on the design features of ancient temples. The most famous of the neoclassical temple-style building was the Pantheon at Paris, designed by Jacques-Germain Soufflot. The palladian style was inspired from the works of Andrea Palladio and hence the name. The most famous architect of the Palladian style was Robert Adam, but the best-known examples of this style buildings are the United States Capitol and White House in America. The classical block design consists of a rectangular or square plan, with a flat, low-lying roof and classical details on the exterior façade.

MATERIALS AND METHODS

The different modern architectural styles emerged as a response to the Industrial Revolution in Europe. The paper here will discuss the various architectural styles analytically and the factors that contributed to their development.

The Industrial Revolution

The Industrial Revolution first started in England in 1780's. The cottage industries in England caused the Industrial Revolution as the machines began to replace manual labor in the 18th century in Britain. Various reasons were responsible for the Industrial Revolution to the first start in England. These included geographical, political, technological and economic factors (Curtis, 1996).



**Meeta Tandon and Farheen Bano**

1. Geographical factors: The strategic location of England played a pivotal role for the start of the Industrial Revolution in the country.
2. Political factors: The government of England provided conditions in which trade, banking, industry and farming could flourish for profit.
3. Technological factors: The improvements in the available tools, use of steam power and coal as a fuel and increased use of iron in various fields like architecture.
4. Economic factors: The high purchasing power of people and the production of cheap manufactured goods were also responsible for the Industrial Revolution to start in England.

The Industrial Revolution in the 19th century marked the beginning of a new era in architecture. What changed in the 19th century was the need to design for new building functions that never existed before throughout history. There was a need for institutions, public markets, hospitals, railway and roadway stations, housing for the working class, etc. The migration of people from the villages to the urban centers, shift from agriculture to industry, invention of new building materials like glass, wrought and cast-iron, steel, and their mass production brought about a revolutionary change (Vickers, 1998). The urban population growth inspired architects to build upward (Peel, Powell, & Garrett, 1996). The building needs that arose had never ever existed before, and it was challenging to think of these contemporary buildings in terms of the ancient examples. According to Peel, Powell & Garrett (1996), "Political reforms and the growing popularity of socialist ideas led people to question established values in every aspect of life and to look for new artistic forms that expressed the changes in human society" (p. 11).

Post Industrial Architecture

During this period, when significant changes were happening, new schools of thought emerged. The dilemma between the new inventions (materials, technological advancements, prefabrication, mass production) and the traditional style/ craftsmanship led to two different radical schools of thought: for the machine and against the machine movement. This was the period after Neoclassicism and before Modernism. The architects associated with the machine movement evolved a new style by using the new technology. The steel structure was visible and celebrated as a structural revolution. The glass was extensively used on the façade, and the design of the built form evolved through the structure. Crystal Palace, designed by Joseph Paxton in London and the Eiffel Tower by Alexander Gustave in Paris became classical examples of this movement (Figure 2). Against the machine was the movement that started as a reaction against the machine, and the machine-generated mass production in Britain. The architects associated with this movement supported the old visual styles and used hand-crafted elements and unique products that could not be mass-produced. Two different styles emerged: The art and Craft movement and Art Nouveau. While Art and Craft movement followed the traditional tools and techniques and discarded new ones, Art Nouveau used new technology, material and mixed them with their own creative expressions.

Art and Craft movement and Art Nouveau

Art and Craft movement first started in Britain and later spread to the rest of Europe and other countries and flourished between 1880's to 1920's, Art Nouveau flourished between 1880's to 1910's and started in various European countries at a similar time period (Figure 3 & 4). Peel, Powell & Garrett (1996) state, "Art Nouveau was an international reaction against the backwards-looking historicism..... and it was readily adopted in many branches of design including textiles, glassware and jewelry" (p. 12). The designs of both these movements were biomorphic, that is, inspired from nature, flora and fauna, and became more abstract in nature. The aesthetic inspirations were also taken from Baroque and Rococo. For example, Antonio Gaudi designed Casa Mila, "suggests the wave-sculpted face of a seaside cliff while, on the rooftop, the bizarrely twisted shapes of ventilator hoods stand like mysterious sentinels" (Doordan, 2001, p. 28). The two styles, i.e. Art and Craft movement and Art Nouveau though were against the machine movement but were two visually different styles and could not co-exist. A new school of thought, Modern style, emerged, which embraced the positive features of both these styles, thereby suppressing the two styles. According to Schulz (2000), "Modern architecture came into existence to help a man feel at home in a new world. To feel at home means something more than shelter, clothing, and food; primarily, it means identifying with a



**Meeta Tandon and Farheen Bano**

physical and social environment. It implies a sense of belonging and participation, that is, the possession of a known and understood world" (p. 9).

Modernism

Establishing the beginning of the period is one of the first tasks to understand the history of modern architecture. Necessary conditions appeared for modern architecture in the late 17th century. Modern architecture emerged due to cultural, territorial and technical transformations in the 18th and 19th centuries (Frampton, 1992). Modernism, the 1st phase of Contemporary architecture, started in the 1920's after the Art and Craft and Art Nouveau styles. Based on the way the styles reacted with each other, different phases emerged in Modernism. After the Industrial Revolution, the figurative expressions became more abstract in nature and moved towards geometric abstraction. The buildings designed were asymmetrical with purity in design, form, color and material and use of new materials like steel, glass and concrete.

Styles of Modernism

Modern architecture can be divided into three phases. The first phase was that of variety and emphasized 'functionalism'. Chicago school, Bauhaus movement, Prairie and Organic style, De Stijl and Art Deco gave importance to function before form and belong to phase 1 of modern architecture.

Bauhaus Style: Style of Modernism

Bauhaus is a German word and means 'house of construction'. Bauhaus movement was one of the earliest and key movement of Modernism that started in Europe. The thought process and visuals of this movement were carried forward to Late Modernism. It is based on a pure and simplified form where cuboids were combined to generate form. Pure colors like white, grey, black and primary colors were used in this style of architecture. The use of new materials and techniques in the urban and industrial context further developed a new vocabulary of aesthetics which formed a base for the later styles that developed in Europe. Walter Gropius was an important architect of this movement. The Bauhaus building (designed by Walter Gropius) and Fagus Boot Factory (designed by Walter Gropius and Adolf Meyer) are important examples of the Bauhaus movement that show how aesthetics and functionalism could be combined in a building (Figure 5). According to Gropius (1965), "the New Architecture is a bridge uniting opposite poles of thought, to relegate it to a single circumscribed province of design" (p. 23), and this became the basis of Bauhaus school of design. The international style evolved from the basic principles of the Bauhaus style since Mies van der Rohe, the last director of the Bauhaus school was also an influential architect who followed International style in his buildings with the concept of 'minimalism'.

Chicago School: Style of Modernism

Chicago school emerged parallel to the Bauhaus style in America and flourished between 1880's and 90's. It was an American style with Chicago as the center. This school of thought too supported functionalism more than aesthetics and included some ornamentation and cladding. Both these styles had a similar ideology but had different visual styles. Bauhaus style focused more on asymmetry and was closely linked with the De Stijl movement, while the Chicago style focused on symmetry and influenced Art Nouveau style in a much more simplified and geometric manner. The buildings became more vertical in character than horizontal due to the influx of people from outside and their rising demands. The development of technology like the framed steel structures also led to the construction of high rise buildings. So this style is very closely related to tall multistoried office buildings. Henry Hobson Richardson was known as the 'precursor of Chicago school of thought' and is also considered to have founded the path of American Modernism.

The pioneer architect of the Chicago school was Louis Henry Sullivan. He is known as "Father of Modernism", "Father of Skyscrapers" and gave the famous dictum "Form follows function". When rebuilding was needed after the Chicago Fire of 1871, Sullivan along with Alder were there at the right time and got the opportunity to develop the style (Frampton, 1992). His style was functional, solid and used ornamentation in the cast iron that he used in his buildings and intricate detailing in the terracotta cladding. The use of biomorphic whiplash lines was inspired from



**Meeta Tandon and Farheen Bano**

the previous Art Nouveau style. His most important work includes the Guaranty building, also known as the Prudential building in Chicago (Figure 6). The other buildings associated with this school of thought include the Auditorium building, Carson-Pirie-Scott Store designed by architects Alder and Sullivan, Reliance building with open floor plans by Daniel Burnham and Company, Chicago Savings Bank Limited William Holabird and Martin Roche. The influence of the Classical Greek Architecture was visible in the façade which was divided into three parts: Base, Shaft and the Capitol like the Greek columns. The base consisted of the ground and the first floor being most accessible accommodated the public spaces, the shaft housed the office spaces and the capital comprised of the overhanging cornice for maintenance. The 'Chicago window' became an essential characteristic of the façade with a fixed central pane and a double-hung sash window on both sides (Figure 6). The designs were functional and emphasized functionalism.

De Stijl: Style of Modernism

De Stijl, 'The Dutch Style', was another movement that started in Europe and lasted for hardly fourteen years (Frampton, 1992). It was founded in Amsterdam in 1917, with Netherland being its main center. Unlike Bauhaus, De Stijl did not follow minimalism and used assembly of different elements emphasizing aesthetics rather than function. It was predominantly an art movement and was founded by painter Theo Van Doesburg (Figure 8). The style was centered around the works of painters Theo Van Doesburg, Piet Mondrian and architect Gerrit Rietveld (Frampton, 1992). Rietveld Schroder House designed by Gerrit Rietveld in Netherlands is an example of De Stijl style in architecture (Figure 7).

Prairie Style: Style of Modernism

Prairie style emerged as a style that was original to America. The earliest styles were majorly European or inspired from Europe and Neoclassical architecture. The World's Columbian Exposition that happened in Chicago marked the 400th anniversary of the discovery of America by Christopher Columbus and depicted the city's image in front of the world. The buildings with temporary façade were also designed in European Neoclassical architecture. The American architects realized that no style could be identified as original to America (McCarter, 1997). The search for the same started, and architects looked towards nature for inspiration. The vast Prairie flatlands of America inspired the new style that came to be known as Prairie architecture. The color palette also evolved from the Prairies and was quite similar to Chicago school, emphasizing horizontality. Unlike the Chicago school, the Prairie style adopted asymmetry inspired from nature. The roofs were either sloping or were flat cantilevered with deep overhangs. The long row of casement windows too emphasized horizontality. The purity of geometry, material and texture, open floor plan were other characteristic features of Prairie style. The visual language of Prairie style was also influenced by the Art and Craft movement of England. Louis Henry Sullivan was the architect who bridged the Chicago and the Prairie style with the design of Harold C Bradley House in Wisconsin. "Sullivan built from his belief that nature could give form to architecture through a dialogue between structure and ornament" (McCarter, 1997, p. 15). The pioneer architect of the style was Frank Lloyd Wright. He also designed both inside and outside the building and used the same visual design vocabulary for furniture. Frank Lloyd Wright designed numerous buildings in the Prairie style; notable ones include the Robie House in Hyde Park (Figure 9), Ward Willits House in Oak Park, Winslow House in Illinois, etc. The horizontal lines, row windows, asymmetry, axis, balance, purity of material, cantilevered roof with emphasis on function were the architectural characteristic features of Frank Lloyd's design. According to Wright, "Taking a human height for my scale, I brought the house down to fit a normal one-5'8" tall. I broadened the mass all I could, brought it down into spaciousness... I was working towards the elimination of the wall to reach the function of a screen, as a means of opening up space."

Organic Architecture: Style of Modernism

Organic Architecture also evolved in America with Frank Lloyd Wright as the pioneer architect like Prairie style. Both the styles had the same vocabulary because both the styles emerged from the same thought process. The styles evolved from nature, nature being the context. This school of thought holds that architecture should reflect nature and exhibit the same amount of unity as prevails in nature. Organic Architecture responded to the natural surroundings. Wright defined organic architecture as "architecture that is appropriate to the time, appropriate to



**Meeta Tandon and Farheen Bano**

place, and appropriate to man" (Pfeiffer, 1997, p. 7). Wright also said, "No house should ever be 'on' any hill or 'on' anything. It should be 'of' the hill, belonging to it so that the hill and the house can live together, each the happier for the other" (2005, p. 168). Unity Temple in Oak Park, and Falling water, also known as Kaufmann House in Pennsylvania are examples of Organic architecture at their best (Figure 10). Inspiration from nature helped to derive the Hollyhock design pattern which was extensively used in the Unity temple and Hollyhock house in California. The design pattern was inspired from the hollyhock flower and transformed using geometrical shapes. Usonian houses are another example of Organic architecture. Usonian houses were a group of some sixty middle-income group affordable houses designed by Wright to depict new American style and are examples of Organic architecture. The word "Usonia" is actually an abbreviation for the United States of North America (McCarter, 1997). According to Wright, "We can never make the living room big enough, the fireplace important enough, or the sense of relationship between exterior, interior and environment close enough, or get enough of these good things I've just mentioned. A Usonian house is always hungry for the ground, lives by it, becoming an integral feature of it" (1948, p. 71). Usonian houses are small single storey houses, without a garage or large storage spaces. They have flat roofs with large cantilevered overhangs for passive heating and cooling. The houses are constructed of native materials with little or no ornamentation. Most of these houses were designed as L-shaped houses to fit around a garden terrace on cheap and odd plots and also provided a strong visual connection between the interior and exterior spaces.

Art Deco: Style of Modernism

Art Deco was another style of Modernism and came from the "International Exposition of Modern Industrial and Decorative Arts" held in 1925 in Paris. Le Corbusier used this term for the first time in his article "L'Esprit Nouveau" meaning "The New Spirit" (Tzonis, 2001). The style was influenced from Against the machine movement style that was Art Nouveau. The asymmetrical and biomorphic design of Art Nouveau was diluted and more geometrical patterns that could be machine-made were used in Art Deco movement. So the hand crafted designs were combined with machine-made technologies. The Chrysler Building designed by William Van Alen and the Empire state building by Shreve, Lamb and Harmon in Manhattan are best examples of Art Deco style (Figure 11).

International Style: Style of Modernism

The various styles that emerged in the first phase of Modernism were context-based. An international style developed as a reaction to the previous Art Deco style and a style that could be followed throughout the world irrespective of the context where it was constructed. It also opposed the previous Prairie style, which emphasized context, and the Organic style, which emphasized nature. The term International Style was coined by Henry-Russell Hitchcock and Philip Johnson, the organizers of the first International Exhibition of Modern Architecture at the Museum of Modern Art in New York in 1932. The style is characterized by 'Minimalism', 'Less is more', the concepts given by Mies van der Rohe, interpenetrating and interlocking planes, rectilinear form, visually lightweight structure and use of modern materials and techniques. The style rejected any kind of ornamentation on the façade and used steel and glass extensively. Examples of International style include Johnson House in New Canaan by Philip Johnson, German Pavilion in Barcelona and Fransworth House in Illinois by Mies van der Rohe, Villa Savoye in France by Le Corbusier (Figure 12). Villa Savoye "is a kind of belvedere, with views commanding an orchard, or, to be close to the Le Corbusier spirit, a machine for making eyes see the landscape" (Tzonis, 2001, p. 64).

RESULTS AND DISCUSSION

Modernism could be depicted as perhaps the most idealistic style in architectural history, drawing from thoughts of utopia, advancement, and the re-imagination of how people would live, work and communicate. It has been nearly a hundred years since the birth of modern architecture. In these hundred years, the design methods and aesthetic theories of modern architecture have developed from scratch and become more and more abundant. Under the guidance of these design methods and aesthetic theories, modern architects have created new forms of architecture from generation to generation, as discussed in Table 1.



**Meeta Tandon and Farheen Bano****Origin and Inspiration**

The Industrial Revolution brought about a tremendous change in various aspects of life, including architecture. The two schools of thought emerged: For the Machine movement that embraced the revolutionary changes brought due to the Industrial Revolution, the new technology and Against the Machine Movement that rejected the new inventions and laid emphasis on the traditional craftsmanship incorporating high ornamentation in their designs. Modern architecture too emerged due to cultural, territorial and technical transformations in the 18th and 19th centuries. Most of the Modern styles evolved as a reaction to their previous style and incorporated or rejected the architectural language of their previous style. Modernism itself emerged as a reaction to the previous Against the Machine Movement, i.e. Art and Craft and Art Nouveau movements, embraced the positive features of both these styles and, at the same time, suppressed the two styles. Modernism, the first phase of Contemporary architecture, started in 1920's. It is that of variety where different 'isms' evolved with different thought processes and emphasized on 'functionalism'. 'Form follows Function' was an important idiom of Phase 1 of Modernism. Bauhaus movement, Chicago school, De Stijl, Prairie style, Organic style and Art Deco gave importance to function before form and belong to phase one of modern architecture. International style, a style that could be followed throughout the world, is considered to be a style of transition from phase one to phase two of Modernism, i.e. from more to less variety in styles. So, phase two of Modern architecture is an extension of International style with less variety.

Form, proportion and scale

The modernist style prioritizes simplicity of form and design. It is based on abstraction, created by simple geometric forms, rectangular shapes, clean lines, and linear elements. This style also took advantage of the advancements in steel, glass and concrete. Proportional harmony is a core element in modern architecture's design method, emphasizing symmetry in some modern styles like Chicago school and Art Deco, while others followed the asymmetrical pattern as aesthetics in design. It's evident that the most prominent buildings of Modern Architecture, as mentioned in Table 1, are the results of developments in technologies and have developed their own specific aesthetic characteristics. Functionality being the main element of modern architecture considers humans as its prime users. Therefore, pursue scales that are compatible with human feelings.

Colour and ornamentation

Modern architecture focused on functionalism, simplicity of form and design. This led to the usage of pure material colours in the built forms. The Bauhaus style used primary colours but in a limited way. It was the De Stijl style that did use the primary colours in their interiors and forms since also gave emphasis to aesthetics. In a similar way, modernistic style because of the use of materials like steel, concrete used natural texture of the material as ornamentation. Chicago school used cladding as a means of ornamentation. The modern style buildings were therefore devoid of any ornamentation as can be seen in Table 1.

CONCLUSION

Throughout history, various architectural styles evolved from the prehistoric period influenced by the location, climate, topography, availability of building materials, technology, construction techniques, and the intangible aspects like the culture of the people, traditions, and their belief systems and rituals. The beginning of a new era in architecture started with the Industrial Revolution in the 19th century due to advancements in technology, new building materials, mass production, prefabrication, etc. As a response to these changes, new architectural styles emerged. The study reveals that Modern architecture marked a revolutionary change in the way architecture existed and led the way forward for a variety of architectural styles. Most of these styles gave emphasis to function over form, and new styles emerged in different parts of the world. With the International style, a new school of thought emerged with a single style that could be followed anywhere in the world without giving due respect to context which was followed by Post Modernism.





Meeta Tandon and Farheen Bano

REFERENCES

1. Curtis, W. J. (1996). Modern Architecture Since 1900. London: Phaidon Press.
2. Doordan, D. P. (2001). Twentieth-Century Architecture. London: Laurence King Publishing.
3. Frampton, K. (1992). Modern Architecture: A Critical History. London: Thames and Hudson Ltd.
4. Gropius, W. (1965). The New Architecture and the Bauhaus. Cambridge, Massachusetts: The MIT Press.
5. Kostof, S. (1995). A History of Architecture: Settings and Rituals. Oxford: Oxford University Press.
6. McCarter, R. (1997). Frank Lloyd Wright. London: Phaidon Press Limited.
7. Peel, L., Powell, P., & Garrett, A. (1996). An Introduction to 20th Century Architecture. London: Grange Books.
8. Pfeiffer, B. B. (1997). Frank Lloyd Wright Master Builder. London: Thames & Hudson.
9. Schulz, C. N. (2000). Principles of Modern Architecture. London: Andreas Papadakis Publisher.
10. Tzonis, A. (2001). Le Corbusier The Poetics of Machine and Metaphor. New York: Universe Publishing.
11. Vickers, G. (1998). Key Moments in Architecture The Evolution of the City. London: Hamlyn.
12. Wright, F. L. (1948, January). Frank Lloyd Wright. The Architectural Forum, 88(1).
13. Wright, F. L. (2005). Frank Lloyd Wright: An Autobiography. Portland, USA: Pomegranate.

Table 1: Styles of First Phase of Modernism

	Bauhaus movement	Chicago school	De Stijl	Prairie style	Organic architecture	Art Deco	International style
Country	Europe	America	Europe Started in Amsterdam, Netherlands main centre	America	America	Europe	America
Emphasis on	Functionalism	Functionalism	Aesthetics	Functionalism	Functionalism	Functionalism and aesthetics	Minimalism
Inspired from		Art Nouveau	Bauhaus	Nature, vast prairie lands	Nature	Art Nouveau	Bauhaus
Form	Asymmetrical, pure and simplified form	Symmetrical and vertical	Assembly of different elements	Asymmetrical and horizontal	Asymmetrical and horizontal	Symmetrical and vertical	Rectilinear form
Colour palette	Pure colours like white, grey, black and primary colours	Pure colours	Pure colours like white, grey, black and primary colours	Pure colours of the materials, brown	Pure colours of the materials, brown	Colour of the materials	Colour of the materials
Ornamentation	No ornamentation	Cladding as ornamentation	Orthogonal lines	Natural texture of the material	Natural texture of the material	Geometrical designs	No ornamentation





Meeta Tandon and Farheen Bano

Pioneer architect	Walter Gropius	Louis Henry Sullivan	Gerrit Rietveld	Frank Lloyd Wright	Frank Lloyd Wright	William Van Alen	Mies van der Rohe
Other architects	Adolf Meyer	Daniel Burnham, William Holabird and Martin Roche	Painters Theo Van Doesburg, Piet Mondrian	Louis Henry Sullivan		Shreve, Lamb and Harmon	Philip Johnson, Le Corbusier
Examples of the style	Bauhaus school, Fagus shoe factory	Prudential building, Auditorium	Rietveld Schroder House	Robie House in Hyde Park	Falling water, Usonian houses	Chrysler Building, Empire state building	Johnson House, German Pavilion, Villa Savoye



(a) Neoclassical Temple style - Pantheon, Paris designed by Jacques-Germain Soufflot

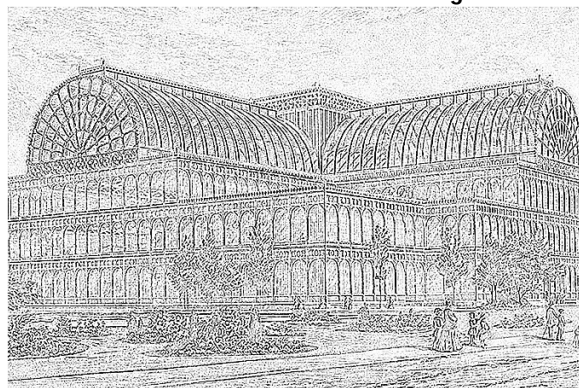


(b) Neoclassical Palladian style- Osterley Park designed by Robert Adam

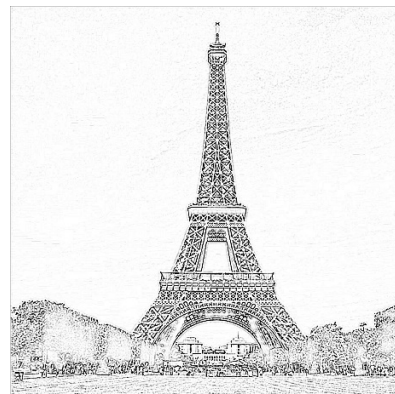


(c) Crystal Palace designed by Joseph Paxton

Figure 1: Neoclassical Architecture



(a) Crystal Palace designed by Joseph Paxton



(b) Eiffel Tower designed by Alexander Gustave

Figure 2: Impact of Industrial Revolution on Architecture





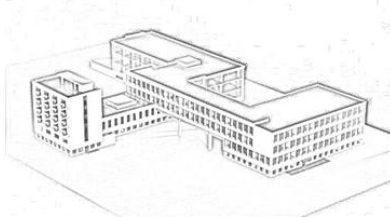
Meeta Tandon and Farheen Bano



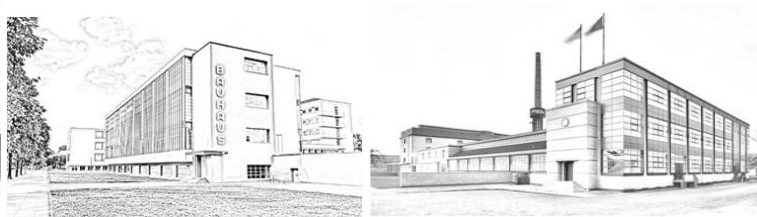
Figure 3: Art and Craft Movement (Red House designed by William Morris & Philip Webb)



Figure 4: Art Nouveau style (Casa Mila designed by Antonio Gaudi)



Bauhaus building in Dessau designed by Walter Gropius



Fagus Boot Factory designed by Walter Gropius and Adolf Meyer

Figure 5: Bauhaus style



(a) Prudential or Guaranty building designed by Louis Henry Sullivan



(b) Chicago window

Figure 6: Chicago School



Figure 7: Rietveld Schroder House designed by Gerrit Rietveld





Meeta Tandon and Farheen Bano



(a) Aubette Dance Hall by Theo Van Doesberg
Source:<https://www.hisour.com/de-stijl-28414/>



(b) Interior of Rietveld Schroder House
Source:<https://www.archdaily.com/99698/ad-classics-rietveld-schroder-house-gerrit-rietveld>

Figure 8: De Stijl

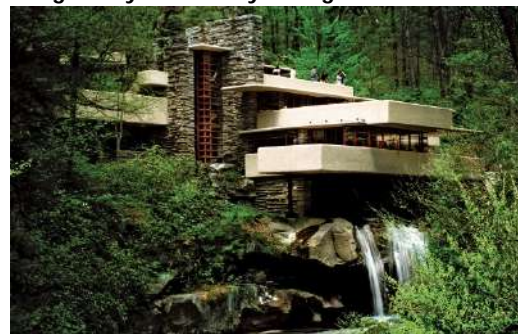


Figure 9: Prairie-style – Robie House designed by Frank Lloyd Wright



(a) Unity Temple designed by Frank Lloyd Wright

Source: <https://divisare.com/projects/396057-frank-lloyd-wright-xavier-de-jaureguiberry-unity-temple>



(b) Falling Water designed by Frank Lloyd Wright

Source:<https://www.britannica.com/place/Fallingwater>

Figure 10: Organic Architecture





Meeta Tandon and Farheen Bano



(a) Chrysler Building designed by William Van Alen



(b) Empire state building designed by Sherve, Lamb and Harmon

Figure 11: Art Deco style



(a) Johnson House designed by Philip Johnson



(b) Farnsworth House designed by Mies van der Rohe
(Source: <https://www.architecture.org/learn/resources/buildings-of-chicago/building/farnsworth-house/>)



(c) German Pavilion designed by Mies van der Rohe



(d) Villa Savoye designed by Le Corbusier

Figure 12: International style





A Few Properties of b-gs Locally Closed Sets in Binary Topological Spaces

P. Sathishmohan^{1*}, K. Lavanya², V. Rajendran³ and K. Rajalakshmi⁴

¹Assistant Professor, Department of Mathematics, Kongunadu Arts and Science College (Autonomous), Coimbatore-641 029, Tamil Nadu, India

²Research Scholar, Department of Mathematics, Kongunadu Arts and Science College (Autonomous), Coimbatore-641 029, Tamil Nadu, India

³Assistant Professor, Puratchi Thalaivi Amma Government Arts and Science College, Palladam, Coimbatore, Tamil Nadu, India

⁴Assistant Professor, Sri Krishna College of Engineering and Technology, Coimbatore, Tamil Nadu, India

Received: 20 Jan 2023

Revised: 15 Apr 2023

Accepted: 19 May 2023

*Address for Correspondence

P.Sathishmohan

Assistant Professor,
Department of Mathematics,
Kongunadu Arts and Science College (Autonomous),
Coimbatore-641 029, Tamil Nadu, India
E. Mail: iiscsathish@yahoo.co.in



This is an Open Access Journal / article distributed under the terms of the **Creative Commons Attribution License** (CC BY-NC-ND 3.0) which permits unrestricted use, distribution, and reproduction in any medium, provided the original work is properly cited. All rights reserved.

ABSTRACT

In this paper, we initiate and exploration of different binary locally closed sets such as binary generalized semi locally closed sets, bgs- LC^{*}-sets, bgs- LC^{**}-sets and furthermore the relations with different thoughts associated with the types of binary generalized semi locally closed sets are investigates. Besides, we found and explores bgs-LC-continuous, bgs- LC^{*}-continuous, bgs- LC^{**}-continuous and presents some examples to show the converses are not true.

Keywords: bgs-LC-sets, bgs- LC^{*}-sets, bgs- LC^{**}-sets, bgs-LC-continuous, bgs- LC^{*}- continuous and bgs- LC^{**}-continuous

INTRODUCTION

In 2011, Nithyanantha Jothi and Thangavelu [1] introduced binary topology from X to Y. They introduced and investigated the concepts of binary closed, binary closure, binary interior, binary continuity, base and sub base of a binary topological spaces. Nithyanantha Jothi[3] introduced binary semi open sets in binary topological spaces and obtained some basic results. Recently, Sathishmohan et.al.,[5][7] introduced and studied the concept of binary generalized semi closed sets and binary semi generalized closed sets, binary generalized semi (binary semi





generalized)-continuous functions in binary topological spaces. Consequently they[6] introduced the concept of binary generalized semi(binary semi generalized) closure and interior of a sets, in binary topological spaces. The purpose of this paper, we introduce and study a new class of binary locally closed sets such as binary generalized semi locally closed sets, bgs- LC *-sets, bgs- LC ** -sets and examine the relationships between these notions. Furthermore we initiate and study bgs-LC-continuous, bgs- LC *-continuous and bgs- LC ** -continuous and several examples are provided to illustrate the behavior of these new class of functions.

Preliminaries

Definition 2.1. Let X and Y be any two nonempty sets. A binary topology [1] from X to Y is a binary structure $\mathcal{M} \subseteq \mathcal{P}(X) \times \mathcal{P}(Y)$ that satisfies the axioms.

1. (ϕ, ϕ) and $(X, Y) \in \mathcal{M}$.
2. $(A_1 \cap A_2, B_1 \cap B_2) \in \mathcal{M}$ whenever $(A_1, B_1) \in \mathcal{M}$ and $(A_2, B_2) \in \mathcal{M}$.
3. If $\{(A_\alpha, B_\alpha) : \alpha \in \Delta\}$ is a family of members of \mathcal{M} then $(\cup_{\alpha \in \Delta} A_\alpha, \cup_{\alpha \in \Delta} B_\alpha) \in \mathcal{M}$.

Definition 2.2. [1] If \mathcal{M} is a binary topology from X to Y then the triplet (X, Y, \mathcal{M}) is called a binary topological space and the members of \mathcal{M} are called the binary open subsets of the binary topological space (X, Y, \mathcal{M}) . The elements of $X \times Y$ are called the binary points of the binary topological space (X, Y, \mathcal{M}) . If $Y=X$ then \mathcal{M} is called a binary topology on X in which case we write (X, X, \mathcal{M}) as a binary topological space.

Definition 2.3. [1] Let X and Y be any two nonempty sets and let (A, B) and $(C, D) \in \mathcal{P}(X) \times \mathcal{P}(Y)$. We say that $(A, B) \subseteq (C, D)$ if $A \subseteq C$ and $B \subseteq D$.

Definition 2.4. [1] Let (X, Y, \mathcal{M}) be a binary topological space and $A \subseteq X, B \subseteq Y$. Then (A, B) is called binary closed in (X, Y, \mathcal{M}) if $(X - A, Y - B) \in \mathcal{M}$.

Definition 2.5. [1] Let (X, Y, \mathcal{M}) be a binary topological space and $(A, B) \subseteq (X, Y)$. Let $(A, B)^{1*} = \cap \{A_\alpha : (A_\alpha, B_\alpha) \text{ is binary closed and } (A, B) \subseteq (A_\alpha, B_\alpha)\}$ and $(A, B)^{2*} = \cap \{B_\alpha : (A_\alpha, B_\alpha) \text{ is binary closed and } (A, B) \subseteq (A_\alpha, B_\alpha)\}$. Then $((A, B)^{1*}, (A, B)^{2*})$ is binary closed and $(A, B) \subseteq ((A, B)^{1*}, (A, B)^{2*})$.

Definition 2.6. [1] The ordered pair $((A, B)^{1*}, (A, B)^{2*})$ is called the binary closure of (A, B) , denoted by $b\text{-cl}(A, B)$ in the binary space (X, Y, \mathcal{M}) where $(A, B) \subseteq (X, Y)$.

Definition 2.7. [1] Let X and Y be any two nonempty sets and let (A, B) and $(C, D) \in \mathcal{P}(X) \times \mathcal{P}(Y)$. We say that $(A, B) \not\subseteq (C, D)$ if one of the following holds:

1. $A \subseteq C$ and $B \not\subseteq D$
2. $A \not\subseteq C$ and $B \subseteq D$
3. $A \not\subseteq C$ and $B \not\subseteq D$.

Definition 2.8. [1]

- (i) $(A, B)^{1^\circ} = \cup \{A_\alpha : (A_\alpha, B_\alpha) \text{ is binary open and } (A_\alpha, B_\alpha) \subseteq (A, B)\}$.
- (ii) $(A, B)^{2^\circ} = \cup \{B_\alpha : (A_\alpha, B_\alpha) \text{ is binary open and } (A_\alpha, B_\alpha) \subseteq (A, B)\}$.

Definition 2.9.

[1] Let (X, Y, \mathcal{M}) be a binary topological space and $(A, B) \subseteq (X, Y)$. The ordered pair $((A, B)^{1^\circ}, (A, B)^{2^\circ})$ is called the binary interior of (A, B) denoted by $b\text{-int}(A, B)$.

Definition 2.10.

[1] Let (X, Y, \mathcal{M}) be a binary topological space and let $(x, y) \in X \times Y$. The binary open set (A, B) is called a binary neighbourhood of (x, y) if $x \in A$ and $y \in B$.





Definition 2.11. A subset (A,B) of a binary topological space (X, Y, \mathcal{M}) is called

1. binary semi-closed [3], if $b-int(b-cl(A, B)) \subseteq (A, B)$.
2. generalized binary closed [?], if $b-cl(A, B) \subseteq (U, V)$ whenever $(A, B) \subseteq (U, V)$ and (U, V) is binary open.
3. binary b-gs(b-sg)-closed [5], if $b-scl(A) \subseteq (U, V)$ whenever $(A, B) \subseteq (U, V)$ and (U, V) is binary open (binary semi open).

Definition 2.12. Let (X, Y, \mathcal{M}) be a binary topological space and (Z, τ) be a topological space. Let $f: Z \rightarrow X \times Y$ be a function. Then f is called

1. binary continuous [2], if $f^{-1}(A, B)$ is open in Z for every binary open set (A, B) in (X, Y, \mathcal{M}) .
2. binary semi continuous [3], if $f^{-1}(A, B)$ is semi open in Z for every binary open set (A, B) in (X, Y, \mathcal{M}) .
3. generalized binary continuous [?], if $f^{-1}(A, B)$ is generalized open in Z for every binary open set (A, B) in (X, Y, \mathcal{M}) .
4. binary generalized semi continuous [7], if $f^{-1}(A, B)$ is generalized semi open in Z for every binary open set (A, B) in (X, Y, \mathcal{M}) .
5. binary semi generalized continuous [7], if $f^{-1}(A, B)$ is semi generalized open in Z for every binary open set (A, B) in (X, Y, \mathcal{M}) .

Definition 2.13. A subset (A, B) of binary space (X, Y, \mathcal{M}) is called

1. binary locally closed, if $(A, B) = (E, F) \cap (G, H)$ where $(E, F) \in \mathcal{M}$ and (G, H) is binary closed in (X, Y, \mathcal{M}) .
2. binary semi locally closed, if $(A, B) = (E, F) \cap (G, H)$ where (E, F) is binary semi open and (G, H) is binary semi closed in (X, Y, \mathcal{M}) .
3. bs-LC*, if $(A, B) = (E, F) \cap (G, H)$ where (E, F) is binary semi open and (G, H) is binary closed in (X, Y, \mathcal{M}) .
4. bs-LC**, if $(A, B) = (E, F) \cap (G, H)$ where (E, F) is binary open and (G, H) is binary semi closed in (X, Y, \mathcal{M}) .

Definition 2.14. Let (Z, τ) be a topological space and (X, Y, \mathcal{M}) be a binary topological space. Then the map $f: Z \rightarrow X \times Y$ is called

1. binary locally closed continuous (briefly, b-LC-continuous) if $f^{-1}(A, B)$ is locally closed in Z for every binary open set (A, B) in (X, Y, \mathcal{M})
2. binary semi locally closed continuous (briefly, bs-LC-continuous) if $f^{-1}(A, B)$ is semi locally closed in Z for every binary open set (A, B) in (X, Y, \mathcal{M}) .
3. bs-LC*-continuous if $f^{-1}(A, B)$ is s-LC* in Z for every binary open set (A, B) in (X, Y, \mathcal{M}) .
4. bs-LC**-continuous if $f^{-1}(A, B)$ is s-LC** in Z for every binary open set (A, B) in (X, Y, \mathcal{M}) .

Binary Generalized Semi Locally Closed Sets

In this section, we initiate a new type of sets which we call binary generalized semi locally closed sets in binary topological spaces and investigate some of their properties.

Definition 3.1. A subset (A, B) of a binary topological space (X, Y, \mathcal{M}) is called

generalized binary locally closed, if $(A, B) = (E, F) \cap (G, H)$ where (E, F) is generalized binary open and (G, H) is generalized binary closed.

gb-LC*(gb-LC**), if $(A, B) = (E, F) \cap (G, H)$ where (E, F) is generalized binary open (binary open) and (G, H) is binary closed (generalized binary closed).

binary generalized semi locally closed, if $(A, B) = (E, F) \cap (G, H)$ where (E, F) is binary generalized semi open and (G, H) is binary generalized semi closed in (X, Y, \mathcal{M}) .

bgs-LC*(bgs-LC**), if $(A, B) = (E, F) \cap (G, H)$ where (E, F) is binary generalized semi open (binary open) and (G, H) is binary closed (binary generalized semi closed) in (X, Y, \mathcal{M}) .

The class of all (binary generalized semi locally closed, binary generalized semi locally closed star and binary generalized semi locally closed star star) subsets of (X, Y, \mathcal{M}) will be denoted by (bgs-LC, bgs-LC*, bgs-LC**)





Sathishmohan et al.,

Remark 3.2. Every binary generalized semi open (resp. binary generalized semi closed) subset of (X, Y, \mathcal{M}) is binary generalized semi locally closed, converse not true.

Example 3.3. Let $X = \{a, b\}$, $Y = \{a, b, c\}$. Clearly $\mathcal{M} = \{(\phi, \phi), (\{a\}, Y), (\{b\}, \{a, b\}), (\phi, \{a, b\}), (X, Y)\}$ is a binary topology from X to Y . Then the binary generalized semi locally closed subsets are $(\phi, \phi), (\phi, \{a\}), (\phi, \{b\}), (\phi, \{c\}), (\phi, \{a, b\}), (\phi, \{a, c\}), (\phi, \{b, c\}), (\phi, Y), (\{a\}, \phi), (\{a\}, \{a\}), (\{a\}, \{b\}), (\{a\}, \{c\}), (\{a\}, \{a, b\}), (\{a\}, \{a, c\}), (\{a\}, \{b, c\}), (\{a\}, Y), (\{b\}, \phi), (\{b\}, \{a\}), (\{b\}, \{b\}), (\{b\}, \{c\}), (\{b\}, \{a, b\}), (\{b\}, \{a, c\}), (\{b\}, \{b, c\}), (\{b\}, Y), (X, \phi), (X, \{a\}), (X, \{b\}), (X, \{c\}), (X, \{a, b\}), (X, \{a, c\}), (X, \{b, c\}), (X, Y)$. Here $(\{b\}, \{b\})$ is binary generalized semi locally closed set but not binary generalized semi open (resp. binary generalized semi closed).

Theorem 3.4. A subset (A, B) of (X, Y, \mathcal{M}) is binary generalized semi locally closed if and only if $(X, Y) - (A, B)$ is the union of binary generalized semi open set and a binary generalized semi closed set.

Proof: If (A, B) is binary generalized semi locally closed then $(A, B) = (E, F) \cap (G, H)$, where (E, F) is binary generalized semi open and (G, H) is binary generalized semi closed.

Now, $(X, Y) - (A, B) = (X, Y) - ((E, F) \cap (G, H))$

$$= ((E, F) \cap (G, H))^c$$

$$= (E, F)^c \cup (G, H)^c$$

Now, $(E, F)^c$ is binary generalized semi closed and $(G, H)^c$ is binary generalized semi open.

Conversely, if $(X, Y) - (A, B) = (P, Q) \cup (R, S)$, where (P, Q) is binary generalized semi closed and (R, S) is binary generalized semi open. Then $(A, B) = (P, Q)^c \cap (R, S)^c$.

$\Rightarrow (A, B)$ is binary generalized semi locally closed.

Theorem 3.5. A subset (A, B) of (X, Y, \mathcal{M}) is binary generalized semi locally closed if and only if $(A, B) = (U, V) \cap \text{nb-cl}(A, B)$ for some binary generalized semi open set (U, V) .

Proof: Let (A, B) is binary generalized semi locally closed. Then there exists a binary generalized semi open set (U, V) and a binary generalized semi closed set (G, H) such that $(A, B) = (U, V) \cap (G, H)$. Since $(A, B) \subseteq (U, V)$ and $(A, B) \subseteq \text{b-cl}(A, B)$ we have $(A, B) \subseteq (U, V) \cap \text{nb-cl}(A, B)$.

Conversely, since $\text{b-cl}(A, B) \subseteq (G, H)$, $(U, V) \cap \text{nb-cl}(A, B) \subseteq (U, V) \cap (G, H) = (A, B)$ which implies that $(A, B) = (U, V) \cap \text{nb-cl}(A, B)$. Since (U, V) is binary open and $\text{nb-cl}(A, B)$ is binary generalized semi closed, we have $(U, V) \cap \text{nb-cl}(A, B) \in \text{b-LC}(X, Y, \mathcal{M})$.

Theorem 3.6. If $(A, B) \in \text{bgs-LC}(X, Y, \mathcal{M})$ and (C, D) is binary generalized semi open then $(A, B) \cap (C, D) \in \text{bgs-LC}(X, Y, \mathcal{M})$.

Proof: Let $(A, B) \in \text{bgs-LC}(X, Y, \mathcal{M})$. Then $(A, B) = (E, F) \cap (G, H)$ where (E, F) is binary generalized semi open and (G, H) is binary generalized semi closed. So $(A, B) \cap (C, D) = ((E, F) \cap (G, H)) \cap (C, D) = ((E, F) \cap (C, D)) \cap (G, H)$. This implies that $(A, B) \cap (C, D) \in \text{bgs-LC}(X, Y, \mathcal{M})$.

Theorem 3.7. 1. Every binary locally closed set is binary generalized semi locally closed but not conversely.

2. Every binary locally closed set is generalized binary locally closed but not conversely.

Proof: 1. Let (A, B) be a binary locally closed set in (X, Y) . Then there exists binary open set (E, F) and binary closed set (G, H) such that $(A, B) = (E, F) \cap (G, H)$. Since every binary closed set is binary generalized semi closed and its complement is binary generalized semi open. Thus (A, B) is binary generalized semi locally closed set.

2. obvious.

Example 3.8. From Example 3.3, let $(A, B) = (\{a\}, \{a, c\})$ is binary generalized semi locally closed (generalized binary locally closed) but not binary locally closed.

Remark 3.9. Let (A, B) be a subset of (X, Y, \mathcal{M}) , if (A, B) is binary locally closed then $(A, B) \in \text{bgs-LC}^*$ and $(A, B) \in \text{bgs-LC}^{**}$ but not conversely.

Example 3.11. From Example 3.3, here $(\{b\}, \{c\})$ is bgs-LC^* sets and bgs-LC^{**} sets but not binary locally closed.





Sathishmohan et al.,

Theorem 3.12. Let (A,B) be a subset of (X,Y,\mathcal{M}) , if $(A,B) \in \text{bgs-LC}^*(X,Y)$ or $(A,B) \in \text{bgs-LC}^{**}(X,Y)$ then (A,B) is $\text{bgs-LC}(X,Y)$.

Proof: It is given that $(A,B) \in \text{bgs-LC}^*(X,Y)$. Then there exists a binary generalized semi open set (E,F) and a binary generalized semi closed set (G,H) of (X,Y,\mathcal{M}) such that $(A,B) = (E,F) \cap (G,H)$. Every binary closed set is binary generalized semi closed and hence there exists a binary generalized semi open set (E,F) and a binary generalized semi closed set (G,H) of (X,Y,\mathcal{M}) such that $(A,B) = (E,F) \cap (G,H)$. Thus (A,B) is $\text{gb-LC}(X,Y)$.

Let $(A,B) \in \text{bgs-LC}^{**}(X,Y)$ then there exists a binary open set (E,F) and a binary generalized semi closed set (G,H) of (X,Y,\mathcal{M}) such that $(A,B) = (E,F) \cap (G,H)$. Since every binary open set is binary generalized semi open set. Hence there exists a binary generalized semi open set (E,F) and a binary generalized semi closed set (G,H) of (X,Y,\mathcal{M}) such that $(A,B) = (E,F) \cap (G,H)$. Hence (A,B) is $\text{bgs-LC}(X,Y)$.

Theorem 3.14. Let $(A,B) \subseteq (X,Y)$. Then $(A,B) \in \text{bgs-LC}(X,Y,\mathcal{M})$ iff there exists a binary generalized semi open set (E,F) such that $(A,B) = (E,F) \cap \text{bgscl}(A,B)$.

Proof: Necessity

Let $(A,B) \in \text{bgs-LC}(X,Y,\mathcal{M})$. Then $(A,B) = (E,F) \cap (G,H)$ where (E,F) is binary generalized semi open and (G,H) is binary generalized semi closed. As $(A,B) \subseteq (G,H)$, $\text{bgscl}(A,B) \subseteq (G,H)$ and so $(E,F) \cap \text{bgscl}(A,B) \subseteq (A,B)$. $(A,B) \subseteq (E,F)$ and $(A,B) \subseteq \text{bgscl}(A,B)$ implies $(A,B) \subseteq (E,F) \cap \text{bgscl}(A,B)$. Therefore $(A,B) = (E,F) \cap \text{bgscl}(A,B)$.

Sufficiency

Let $(A,B) = (E,F) \cap \text{bgscl}(A,B)$ where (E,F) is binary generalized semi open by definition $(A,B) \in \text{bgs-LC}(X,Y,\mathcal{M})$.

Theorem 3.16. If $(A,B) \subseteq (C,D) \subseteq (X,Y)$ and (C,D) is binary generalized semi locally closed, then there exists a binary generalized semi locally closed set (K,L) such that $(A,B) \subseteq (K,L) \subseteq (C,D)$.

Proof: As (C,D) is binary generalized semi locally closed, $(C,D) = (E,F) \cap \text{bgscl}(C,D)$ where (E,F) binary generalized semi open. As $(A,B) \subseteq (C,D)$, $(A,B) \subseteq (E,F)$. Also $(A,B) \subseteq \text{bgscl}(A,B)$. Thus $(A,B) \subseteq (E,F) \cap \text{bgscl}(A,B) = (K,L)$, (K,L) is binary generalized semi locally closed and $(A,B) \subseteq (K,L) \subseteq (C,D)$.

Theorem 3.18. For a subset (A,B) of (X,Y) , $(A,B) \in \text{bgs-LC}^*(X,Y)$ iff $(A,B) = (E,F) \cap \text{bcl}(A,B)$ for some binary generalized semi open set (E,F) in (X,Y) .

Proof: Necessity

Let $(A,B) \in \text{bgs-LC}^*(X,Y)$. Then there exists a binary generalized semi open set (E,F) and a binary closed set (G,H) in (X,Y) such that $(A,B) = (E,F) \cap (G,H)$. Since $(A,B) \subseteq (E,F)$ and $(A,B) \subseteq \text{bcl}(A,B)$, we have $(A,B) \subseteq (E,F) \cap \text{bcl}(A,B)$.

Conversely, since $\text{bcl}(A,B) \subseteq (G,H)$, $(E,F) \subseteq \text{bcl}(A,B) \subseteq (E,F) \cap (G,H) = (A,B)$. We have that $(A,B) = (E,F) \cap \text{bcl}(A,B)$.

Sufficient

Since (A,B) is binary generalized semi open and $\text{bcl}(A,B)$ is binary closed we have $(E,F) \cap \text{bcl}(A,B) \in \text{bgs-LC}^*(X,Y)$.

Theorem 3.19. For a subset (A,B) of (X,Y) , $(A,B) \in \text{bgs-LC}^{**}(X,Y)$ iff $(A,B) = (E,F) \cap \text{bgscl}(A,B)$ for some binary open set (E,F) in (X,Y) .

Proof: Necessity

Let $(A,B) \in \text{bgs-LC}^{**}(X,Y)$. Then by definition $(A,B) = (E,F) \cap (G,H)$, where (E,F) is binary open set and (G,H) is a binary generalized semi closed set containing (A,B) . Since (G,H) is a binary generalized semi closed set, we have $\text{bgscl}(A,B) \subseteq (G,H)$, which implies that $(E,F) \cap \text{bgscl}(A,B) \subseteq (E,F) \cap (G,H) = (A,B)$. Since $(A,B) \subseteq (E,F)$ and $(A,B) \subseteq \text{bgscl}(A,B)$, we have $(A,B) \subseteq (E,F) \cap \text{bgscl}(A,B)$. Therefore $(A,B) \subseteq (E,F) \cap \text{bgscl}(A,B)$, where (E,F) is a binary open.

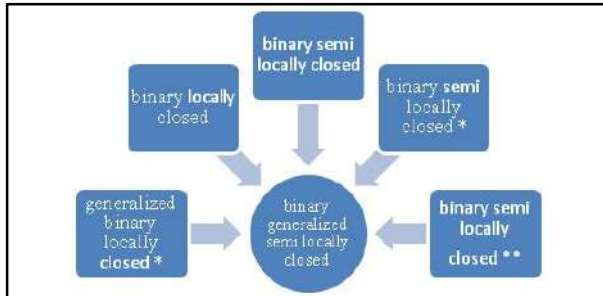
Sufficient Assume that $(A,B) = (E,F) \cap \text{bgscl}(A,B)$ for some binary open set (E,F) in (X,Y) . Since $\text{bgscl}(A,B)$ is binary generalized semi closed we have $(A,B) \in \text{bgs-LC}^{**}(X,Y)$.

Remark 2.16. The following figure shows that the relationships of binary generalized semi locally closed sets with some of the existing sets, which we have discussed in this section.





Sathishmohan et al.,



The above implications are not reversible

Binary generalized semi locally continuous functions

In this section, we initiate a new type of binary generalized semi continuous functions in binary topological spaces called binary generalized semi locally continuous functions and examine some of their characterizations.

Definition 4.1. Let (Z, τ) be a topological space and (X, Y, \mathcal{M}) be a binary topological space. Then the map $f: Z \rightarrow X \times Y$ is called

generalized binary locally closed continuous (briefly, gb-LC-continuous) if $f^{-1}(A, B)$ is generalized locally closed in Z for every binary open set (A, B) in (X, Y, \mathcal{M}) .

gb-LC*(gb-LC**)-continuous if $f^{-1}(A, B)$ is g-LC*(g-LC**) in Z for every binary open set (A, B) in (X, Y, \mathcal{M}) .

binary generalized semi locally closed continuous (briefly, bgs-LC-continuous) if $f^{-1}(A, B)$ is generalized semi locally closed in Z for every binary open set (A, B) in (X, Y, \mathcal{M}) .

bgs-LC*(bgs-LC**)-continuous if $f^{-1}(A, B)$ is gs-LC*(gs-LC**) in Z for every binary open set (A, B) in (X, Y, \mathcal{M}) .

Theorem 4.2.

Let $f: Z \rightarrow X \times Y$ be binary generalized semi continuous. Then f is bgs-LC-continuous.

Let $f: Z \rightarrow X \times Y$ be binary continuous. Then f is bgs-LC-continuous.

Let $f: Z \rightarrow X \times Y$ be binary locally continuous. Then f is bgs-LC-continuous.

Let $f: Z \rightarrow X \times Y$ be generalized binary continuous. Then f is gb-LC-continuous.

Let $f: Z \rightarrow X \times Y$ be binary continuous. Then f is gb-LC-continuous.

Let $f: Z \rightarrow X \times Y$ be binary locally continuous. Then f is gb-LC-continuous.

Proof

Let (A, B) be binary generalized semi open in (X, Y, \mathcal{M}) . Since f is binary generalized semi continuous, we have $f^{-1}(A, B)$ is generalized semi open in Z . Then $f^{-1}(A, B)$ is generalized semi locally closed in Z . Hence f is bgs-LC-continuous.

(2) to (6) Obvious.

Remark 4.3. The converse of the above theorem need not be true as seen from the subsequent example.

Example 4.7. Let $X = \{\xi, \omega\}$, $Y = \{\xi, \omega, \rho\}$ and $Z = \{a, b, c\}$. Clearly $\mathcal{M} = \{(\phi, \phi), (\phi, \{\omega\}), (\{\xi\}, \{\omega\}), (X, \{\omega\}), (\{\omega\}, \{\omega\}), (X, Y)\}$ is a binary topology from X to Y and $\tau = \{\phi, Z, \{a\}, \{a, b\}, \{a, c\}\}$ is a topology on Z . Then closed subsets in Z are $\phi, Z, \{b\}, \{c\}, \{b, c\}$ and generalized semi locally closed subsets in Z are $\phi, Z, \{a\}, \{b\}, \{c\}, \{a, b\}, \{a, c\}, \{b, c\}$. Define $f: Z \rightarrow X \times Y$ by $f(a) = (\{\xi\}, \{\omega\}) = f(b)$ and $f(c) = (\{\omega\}, \{\omega\})$. Clearly f is bgs-LC-continuous but not binary generalized semi continuous. For $f^{-1}(\phi, \phi) = \phi$, $f^{-1}(X, Y) = \{a, b, c\} = Z$ and $f^{-1}(\{\xi\}, \{\omega\}) = \{a, b\}$ which is generalized semi locally closed (generalized locally closed) in Z but not a generalized semi closed (generalized closed) set in Z .

Example 4.10. Let $X = \{\xi, \omega\}$, $Y = \{\xi, \omega, \rho\}$ and $Z = \{a, b, c\}$. Clearly $\mathcal{M} = \{(\phi, \phi), (\{\xi\}, \{\xi\}), (\{\omega\}, \{\omega\}), (X, \{\xi, \omega\}), (X, Y)\}$ is a binary topology from X to Y and $\tau = \{\phi, Z, \{a\}, \{a, b\}\}$ is a topology on Z . Then closed subsets in Z are $\phi, Z, \{c\}, \{b, c\}$ and generalized semi locally closed subsets in Z are $\phi, Z, \{a\}, \{b\}, \{c\}, \{a, b\}, \{a, c\}, \{b, c\}$. Define $f: Z \rightarrow X \times Y$ by





Sathishmohan et al.,

$f(a)=(X,\{\xi,\varpi\})=f(c)$ and $f(b)=(\{\xi\},\{\xi\})$. Clearly f is bgs-LC-continuous but not binary continuous. For $f^{-1}(\phi,\phi)=\phi$, $f^{-1}(X,Y)=\{a,b,c\}=Z$ and $f^{-1}(X,\{\xi,\varpi\})=\{a,c\}$ which is generalized semi locally closed (generalized locally closed) in Z but not a closed set (locally closed) in Z .

Theorem 4.14. If f is bgs-LC*-continuous or bgs-LC** -continuous, then it is bgs-LC - continuous.

Proof: If f is bgs-LC*-continuous or bgs-LC** -continuous. Then by definition $f^{-1}(A,B)$ is gs-LC* or gs-LC** in Z for every binary open set (A,B) in (X,Y,\mathcal{M}) by Theorem 5.8, f is bgs-LC-continuous.

Theorem 4.15. If $f: Z \rightarrow X \times Y$ be a function, if f is binary locally closed continuous, then it is bgs-LC*-continuous and bgs-LC** - continuous.

Proof: Suppose that f is binary locally closed continuous. Let (A,B) be a binary open set in (X,Y,\mathcal{M}) . Since $f^{-1}(A,B)$ is locally closed in Z by Theorem 5.6, f is bgs-LC*-continuous and bgs-LC** -continuous.

CONCLUSION

We have attempted an endeavor to concentrate about bgs-LC-sets, bgs- LC*-sets, bgs- LC** -sets. Furthermore, we initiate and study bgs-LC-continuous, bgs- LC*-continuous and bgs- LC** -continuous. In our future work, we will extended to bgs-LC-irresolute, bgs- LC*-irresolute and bgs- LC** -irresolute functions and the concept of binary locally closed set may be analyzed in semi generalized closed sets in binary topological spaces and also the decomposition of binary generalized semi closed sets and binary semi generalized closed sets may also be studied.

ACKNOWLEDGEMENT

The referees' pricey suggestions, which forced the revision of this manuscript, are acknowledged by the authors.

REFERENCES

1. Nithyanantha Jothi. S and Thangavelu. P, Topology between two sets, Journal of Mathematical Sciences and Computer Applications, 1(3), 2011, 95-107.
2. Nithyanantha Jothi. S and Thangavelu. P, On binary continuity and separation axioms, Ultra Science, 24(3)A, 2012, 121-126.
3. Nithyanantha Jothi. S, Binary Semi Open Sets in Binary Topological Spaces, International Journal of Mathematical Archive, 7(9), 2016, 73-76.
4. Nithyanantha Jothi. S, Contribution to Binary Topological Spaces, Ph.D. Thesis, Manonmaniam Sundaranar University, Tirunelveli, 2012.
5. Sathishmohan. P, Lavanya. K and Mehar sudha. U, On b-gs-closed and b-sg-closed sets in Binary Topological spaces, Strad Research, 8(3), 2021, 20-24.
6. Sathishmohan. P, Rajendran. V, Lavanya. K and Rajalakshmi. K, On b-gs(b-sg)-closure and b-gs(b-sg)-interior of a sets in Binary Topological spaces, Gedrag & Organisatie Review, 34(1), 2021, 359-366.
7. Sathishmohan. P, Lavanya. K, Rajendran. V and Rajalakshmi. K, A Few Kind of Continuous Functions in Binary Topological Spaces, Indian Journal of Natural Science, 13(75), 2022, 50193-50198.
8. Sathishmohan. P, Lavanya. K, Rajendran. V and Rajalakshmi. K, An Enlightening Perception of Operators in Binary Topological Spaces, (Communicated).





***In silico* Virtual Broadcasting of Herbal Phyto-Compounds Isolated from *Sansevieria cylindrica* and *Plumeria obtusa* as Impending Snake Venom Venin's Inhibitor**

Sunil Shewale^{1*}, Vaishali Undale², Bhagyashri Warude², Vrushali Bhalchim¹, Jay Gagare¹, Surabhi Jarare¹, Snehal Satpute¹, Sakshi Sonawane¹ and Aniket Garud³

¹Department of Pharmacology, Dr.D.Y.Patil Institute of Pharmaceutical Sciences and Research, University of Pune, Maharashtra, India.

²HoD, Department of Pharmacology, Dr.D.Y.Patil Institute of Pharmaceutical Sciences and Research, University of Pune, Maharashtra, India.

³Rasiklal M. Dhariwal College of Pharmacy, Pune, Maharashtra, India.

Received: 15 Feb 2023

Revised: 15 Apr 2023

Accepted: 19 May 2023

***Address for Correspondence**

Sunil Shewale

Department of Pharmacology,
Dr.D.Y.Patil Institute of Pharmaceutical Sciences and Research,
University of Pune, Maharashtra, India.



This is an Open Access Journal / article distributed under the terms of the **Creative Commons Attribution License** (CC BY-NC-ND 3.0) which permits unrestricted use, distribution, and reproduction in any medium, provided the original work is properly cited. All rights reserved.

ABSTRACT

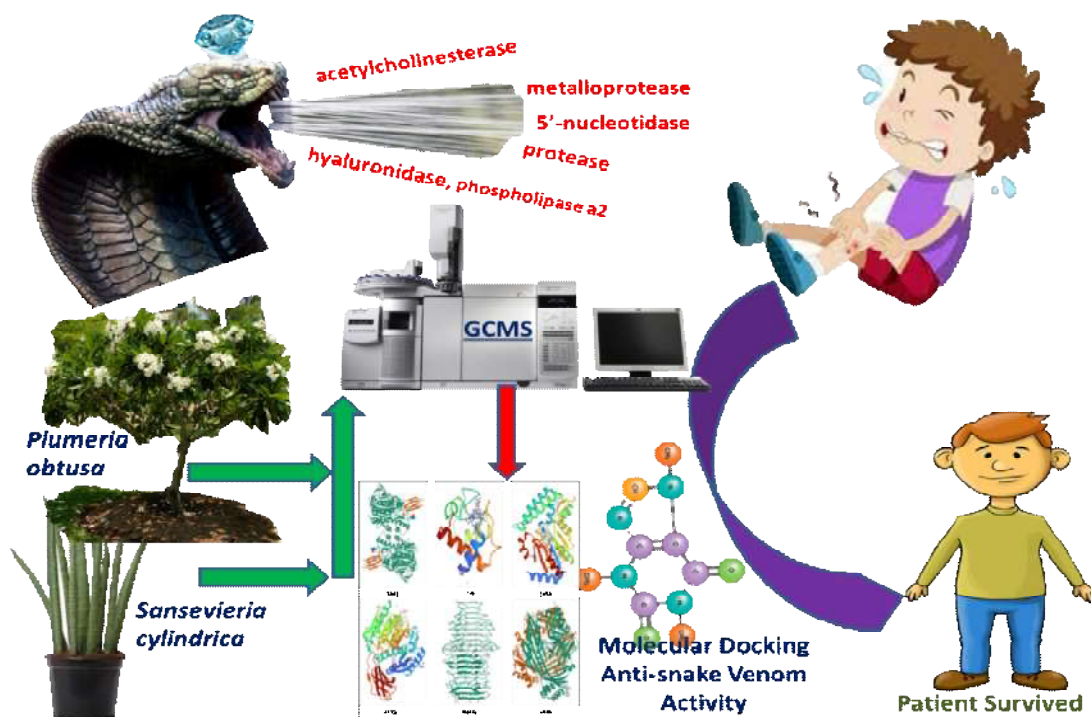
Many plants are potential birthplace of functionally bioactive compounds and vital nutrients. These compounds are obliging in treatment of different ailments. *Sansevieria cylindrica* and *Plumeria obtusa* are one of the most significant underutilized plants known for their ethnobotanical and ethnomedicinal values. Gas chromatography-mass spectrometry (GCMS) analysis of the extracts revealed the presence of five and seven bioactive compounds in *S. cylindrica* and *P. obtusa* plants in turn. Subsequently, in silico molecular docking studies of the bioactive compounds studied from published literature concluded the potential anti-snake venom chattels. The current study was aimed at verdict novel drugs like molecules derived from GCMS techniques against snake venom toxin proteins such as acetylcholinesterase, protease, hyaluronidase, phospholipase a₂, metalloprotease, 5'-nucleotidase etc. Among the twelve compounds, two from each plant were selected for 2D interactions based on the higher binding energy. The selected compounds were having not only good binding affinity but also were able to form H-bonds, alkyl, π -alkyl, Van der Waals, and π -sigma bonds with the active-site residues of toxins. Docking result interpreted the possible pharmacological activity of plant phytoconstituents against the snake-venom through inhibition of respective macromolecules.

Keywords: *Molecular docking, Plumeria obtusa, Sansevieria cylindrica, Snake venom, Enzymes.*





Sunil Shewale et al.,



INTRODUCTION

Snakebite is a major life-threatening disease of many tropical and subtropical provinces particularly; Sub-Saharan Africa, Southeast Asia, and Latin America. [1] An estimated 5.4 million cases, 2.7 million poisonous cases, and 0.08 to 1.37 million death occurs annually because of snake bites. [2] Indian cobra (*Naja naja*), Russell's viper (*Daboia russelii*), common krait (*Bungarus caeruleus*) and the saw-scaled viper (*Echis carinatus*) snakes are among the several poisonous snakes found in India and many other countries. They produce the most severe local tissue damage at the bite site. [3].

Snake venoms are complex mixes made up mostly of proteins and peptides with a wide range of biological actions. [4]. The only venom components with hemorrhagic activity are snake venom metalloproteinases (SVMPs), which are both direct and indirect mediators of local tissue damage such as bleeding, edema, myonecrosis, dermonecrosis, and inflammation after envenoming[5]. The majority of venom metalloproteinases are fibrinolytic enzymes that preferentially cleave the Achain of fibrinogen while slowly cleaving the Bchain. Casein, insulin B peptides, and intermolecularly quenched fluorogenic peptide substrates have all been used to test metalloproteinase substrate specificities. [4] Hemorrhage produced by any enzymatic toxins can subsequently lead to edema, shock, tissue necrosis, and reduced ability to regenerate muscle tissue. [6] Additionally, leakage of blood from affected vessels also helps spread other venom toxins to their target tissues. Phospholipase A2 (PLA2), Snake Venom Serine Proteases (SVSP), 5'-nucleotidase, Hyaluronidase, Acetylcholinesterase and Three Finger Toxins (3FTx) are also considered dominant protein families responsible for toxic effect in human being. Therefore, it can be hypothesized that the inhibition of these enzymes may result in a significant overall reduction in damage following envenomation. [7]





Sunil Shewale et al.,

ASV therapy is best available cure against snake envenomation, but it is expensive, not readily available and has risk of immunological reactions. [8] These factors necessitate complementary therapies to treat snakebites. The treatment of snake envenomation using plants and folk medicine is old and ancient practice in many poor communities from rural areas. [9] Moreover, many evidences support the pharmacological use of plants, its extracts and isolated compounds against snakebites as medicine [1,10]. Computational biology and bioinformatics have the potential to accelerate drug discovery and repurposing process. This involves prediction and scoring of binding free energy in between target and desired molecule by molecular docking. *In silico* approaches have paved the way for the solution of many biological problems, leading to the discovery of novel inhibitors against a variety of diseases. One way to predict the activity of drug is *In-silico* study. The present study investigates the molecular interaction between selected phytochemicals from published literature of *Plumeria obtusa* (PC) and *Sansevieria cylindrica* (SC) plants with amino acids residues of target proteins for potential snake venom enzymes inhibition.

MATERIAL AND METHODS

Protein preparation

A Protein Data Bank (PDB) was search for human acetylcholinesterase, glycosylated protein, human cytosolic phospholipase, human cytosolic 5'-nucleotidase III, Protease, and *E. coli*. Using RCSB (<https://www.rcsb.org/>) The criteria for choosing PDBs were based on highest possible resolution. The resolution ensures that the 3D structures used for docking are of high quality, and that the structure is free of mutations, as mutations can have a significant impact on the final confirmation of a protein complex with ligand. Preparation of the proteins was carried out with the Biovia Discovery Studio Visualizer (DSV) 2017 (Prepare protein protocol). Protein preparation entailed adding hydrogen atoms, defining bond orders, deleting unwanted water molecules and salts, and optimising the hydrogen bond network. As protein functions as monomer, protein chains other than standard drug interacting chains were removed. Polar hydrogens were added to optimize the hydrogen-bonding network. The proteins were minimised in terms of energy and active sites were predicted with the selection of maximized GRID parameters using DSV. Finally, the prepared structure of protein was saved in the PDB file format for docking. Details of the selected PDB are mentioned in Table 1. [11-16] Also, the cartoon ribbon model of each protein is displayed in figure 1.

Phytoconstituents and ligand structure preparation

In this study, five compounds from *Sansevieria cylindrica* and seven compounds from *Plumeria obtusa* plant were used for docking studies. These phytoconstituents were derived and identified using GCMS analytical technique. [17, 18] All phytochemical constituents and standard drugs were retrieved from PubChem database (<https://pubchem.ncbi.nlm.nih.gov/>). The list of phytoconstituents, their codes and PubChem ID is given in Table 2.

Identification of Cavity and Active Amino Acid Residues

Phytochemical constituents from *Plumeria obtusa* and *Sansevieria cylindrica* plants and proteins were imported in AutoDock Vina Wizard and macro molecules converted into PDBQT format. The three dimensional grid box for complex with standard ligand and protein (size_x = 102.708; size_y= 110.001; size_z =135.04), (size: x = 49.920; y = 14.42; z =56.75), (size: x = 32.392; y = 21.009; z =12.77), (size: x = 28.89; y = 19.48; z =5.715) (size: x = 141.220; y = 8.78; z =91.38) (size: x = 37.68; y = 71.109; z =56.63) were generated automatically for 1B41, 1CJY, 2JGA, 4TKX, 4UFQ, 5NJB respectively. Using the Toggle Selection Sphere option, the active amino acid residues were chosen to define the cavity. The grid box was aligned in a way that it occupied all of the active binding sites and essential residues. The three-dimensional grid boxes were generated. [19-20]

Docking procedure

Molecular docking of 1B41, 1CJY, 2JGA, 4TKX, 4UFQ, 5NJB with phytochemical constituents from *Plumeria obtusa* and *Sansevieria cylindrica* were subjected to docking using AutodockVina Wizard of PyRx virtual screening 0.8 version software to find the reasonable binding geometry and discover the protein ligand connections. Docking predicted non-bonded, non-covalent interactions between a receptor or active site region of a protein and a drug or





Sunil Shewale et al.,

chemical molecule forming an intermolecular complex. The final docking result includes affinity prediction (scoring) for the molecules investigated, resulting in a relative rank ordering of the docked compounds in terms of affinity, reported as kcal/mol. [21] A greater negative binding energy indicates a greater binding affinity. DSV was used to analyse binding interactions on complexes with higher docked scores.

RESULTS AND DISCUSSION

Molecular docking study of phytochemicals from *Sansevieria cylindrica* plant

Phytochemical constituent *S. cylindrica* (PC) were docked with PDB 1b41,1CYJ, 2JGA, 4TKX, 5NJB and 4UFQ in the targeted cavity. Out of the 16 molecules some other molecules show very good binding affinity as compare with standards like Phthalic acid,6 – methylhept-2-yl octyl ester – 6.6 kcal/mol with 1b41,with 2JGA -7.8 kcal/mol as compared with Vanillic acid -6.8 kcal/mol and with 5NJB -7.2 kcal/mol , 1,2 – Benzene dicarboxylic acid, bis(1-methylethyl) ester with 2JGA -6.5 kcal/mol , with 4TKX -7.0 kcal/mol as compared with Remdesivir 7.1 kcal/mol and 5NJB -7.1 kcal/mol , Diisooctyl phthalate with 5NJB -7.2 kcal/mol as compared with Batimastat -8.5 kcal/mol. Phytochemical constituents of SC interactions with active amino acid residues are shown in table 4. Docking poses of phytochemical constituents of SC with 1b41, 1CYJ, 2JGA, 4TKX, 5NJB and 4UFQ PDB in 2D-poses along with the number of hydrogen bonds involved in the interaction are shown in figure 5 respectively. The shown images focus on the interactions of functional groups on ligands with active amino acid residues in the targeted cavity. Some of the better docking poses with ligands of SC established a network of molecular interactions with anionic bonds such as H-bonds, Van der Waals [VdW], alkyl, π -alkyl, and π -sigma bonds, with the active-site residues of 1b41,1CYJ, 2JGA, 4TKX, 5NJB and 4UFQ PDB.

It established various binding interactions including conventional H bonding ARG228 (2.34 & 1.84), ARG229 (2.48 & 2.01) MET233(3.77), ASN390(2.68 & 2.91), SER669(2.43 & 3.38), ASN551(3.01) LEU202(3.02 & 3.36) THR55(2.16), HIS57(2.71), LYS53(2.7), TRP182(3.33) TYR103(2.73) ASN449(1.99 & 2.38) pi alkyl interaction with PHE395(4.62 & 4.01) VAL451 PRO52(5.04), pi-pi stack LEU178(5.38), PHE360(4.92) TRP102(4.62 & 4.38), HIS57(3.88)

Molecular docking study of phytochemicals from *Plumeria obtusa* plant

Phytochemical constituents from *Plumeria obtusa* were docked with PDB 1b41,1CYJ, 2JGA, 4TKX, 5NJB and 4UFQ in the targeted cavity. Out of the 7 molecules some of the molecules show very good binding affinity with protein such as 9,12,15-Octadecatrienoic acid, 2,3-dihydroxypropyl ester with 1b41 – 5.2 kcal/mol , 1CYJ with Undecanoic acid ethyl ester -4.7 kcal/mol, 2JGA with 9,12,15-Octadecatrienoic acid, 2,3-dihydroxypropyl ester -5.9 kcal/mol, 4TKX with 9,12,15-Octadecatrienoic acid, 2,3-dihydroxypropyl ester -5.3 kcal/mol, ligand 9,12,15-Octadecatrienoic acid,2,3-dihydroxypropyl ester with 5NJB -6.3 kcal/mol. and ligand Octaethylene glycol monododecyl ether with 4UFG -3.7 kcal/mol. The binding energy of all phytoconstituents with proteins is shown in table 5. Docking poses of phytochemical constituents of *Plumeria obtusa* with 1b41, 1CYJ, 2JGA, 4TKX, 5NJB and 4UFQ PDB in 2D-poses along with the number of hydrogen bonds involved in the interaction are shown in figure 3 and table 6. The shown images focus on the interactions of functional groups on ligands with active amino acid residues in the targeted cavity. Some of the better docking poses with ligands of PC established a network of molecular interactions with anionic bonds such as H-bonds, Van der Waals [VdW], alkyl, π -alkyl, and π -sigma bonds, with the active-site residues of 1b41,1CYJ, 2JGA, 4TKX, 5NJB and 4UFQ PDB. It established various binding interactions including conventional H-bonds Arg13, Gln250, His18, Asn23, Met 26, Lys29, Asp 227, Asp 231, Val 86, Asp 231, Ser 228, Lys 202, Asp 388, Ala43, Ala428Gla 141, Ser 53, Ser 207 Gly 192, Asn 208, Trp 204, Ile 127, pi alkyl interaction with TRP204,HIS18, TYR389, TYR102, TYR103(4.16), TRP182, TRP204 etc.

Comparison with the standard Remdisivir and phytochemical constituent 9,12-Octadecadienoic acid, ethyl ester with 4TKX shows promising interaction with ASP388, HIS 57, SER 106, TYR 103 at the active domain as Protease inhibition. Standard Vallinic acid compare with Octaethylene glycol monododecyl ether and 2JGA of human cytosolic 5'-nucleotidase III inhibition by showing similar interaction on amino acid His 57, Tyr103. 9,12,15-



**Sunil Shewale et al.,**

Octadecatrienoic acid, 2,3-dihydroxypropyl ester complex with 5NJB shows similar amino acid interaction like Val 453, His 262 compare with standard Batimastat shows Microcin-processing metalloprotease inhibition.

ADMET prediction of the phytochemical constituents of the *Sansevieria cylindrica* and *Plumeria obtusa* plants

Above data mentioned that i.e., a molecule with a molecular mass less than 500 Da, no more than 5 hydrogen bond donors, no more than 10 hydrogen bond acceptors, and an octanol–waterpartition coefficient log P not greater than 5 should be corrective measure for the better ADMET of the phytochemical constituents isolated from *Sansevieria cylindrica* and *Plumeria obtusa* plants. All phytoconstituents obey the Lipinski rule 5 (Table 7).

CONCLUSION

Docking results revealed promising pharmacological activity of anti-caseinolytic and anti-fibrinogenolytic properties against CR and NK venoms. The primary mode of action of phytochemical components will be studied further in the future using molecular simulation. Prominent scientific and technical discovery tools, widely used in applications ranging from drug discovery to materials design. The fidelity of molecular simulation predictions is determined by the dependability and precision of the force fields used. The current work is an attempt to determine anti-venom activity by PC and SC phytochemical ingredients that could be used in anti-venom medication development. The Lipinski rule 5 shows ADMET protocol of *Sansevieria cylindrica* and *Plumeria obtusa* plants. These selective phytoconstituents binding energy with the receptor quantifies the ligand-protein complex's efficiency. Taken together, we believe that the Phthalic acid, 6-methylhept-2-yl octyl ester, Diisooctyl phthalate, 1,2-Benzene dicarboxylic acid, bis(1-methylethyl) ester, 9,12,15-Octadecatrienoic acid, 2,3-dihydroxypropyl ester, Octaethylene glycol monododecyl ether and 9,12-Octadecadienoic acid, ethyl ester ligands may operate as potential inhibitors of venom activity.

ACKNOWLEDGMENTS

We are thankful to Research students of Dr. D. Y. Patil Institute of Pharmaceutical Sciences and Research, Savitribai Phule University of Pune, Maharashtra, India for their support during the collation of study data and literature search.

CONFLICT OF INTEREST

This research was conducted as part of the Dr. D. Y. Patil Institute of Pharmaceutical Sciences and Research, Savitribai Phule University of Pune, Maharashtra, India's Ph.D. programme in Pharmacology.

FUNDING

Government, business, and non-profit funding sources did not contribute to this research in any way.

REFERENCES

1. Shewale S, Undale V, Chitlange S, Sharma H. Ophidian Bite: The Balance Between Perception, Idealism and Realism. *Trop J Nat Prod Res.* 2021;5(7): 1166-1178. doi: <https://doi.org/10.26538/tjnpr/v5i7.1>
2. World Health Organization. Snakebite envenoming. Key facts. [Online]. 2021. [cited 2021 May 17]. Available from: <https://www.who.int/news-room/fact-sheets/detail/snakebite-envenoming>.
3. Pithayanukul P, Leanpolchareanchai J, Saparpakorn P. Molecular docking studies and anti-snake venom metalloproteinase activity of Thai mango seed kernel extract. *Molecules.* 2009 Aug 27;14(9):3198-213. doi: 10.3390/molecules14093198.
4. Leanpolchareanchai J, Pithayanukul P, Bavovada R, Saparpakorn P. Molecular docking studies and anti-enzymatic activities of Thai mango seed kernel extract against snake venoms. *Molecules.* 2009 Mar 31;14(4):1404-22. doi: 10.3390/molecules14041404.



**Sunil Shewale et al.,**

5. Chinnasamy S, Chinnasamy S, Nagamani S, Muthusamy K. Identification of potent inhibitors against snake venom metalloproteinase (SVMP) using molecular docking and molecular dynamics studies. *J Biomol Struct Dyn.* 2015;33(7):1516-27. doi: 10.1080/07391102.2014.963146.
6. Srinivasa V, Sundaram MS, Anusha S, Hemshekhar M, Chandra Nayaka S, Kemparaju K, Basappa, Girish KS, Rangappa KS. Novel apigenin based small molecule that targets snake venom metalloproteases. *PLoS One.* 2014 Sep 3;9(9):e106364. doi: 10.1371/journal.pone.0106364.
7. Hage-Melim LI, da Silva CH, Semighini EP, Taft CA, Sampaio SV. Computer-aided drug design of novel PLA2 inhibitor candidates for treatment of snakebite. *J Biomol Struct Dyn.* 2009 Aug;27(1):27-36. doi: 10.1080/07391102.2009.10507293.
8. World Health Organization. Guidelines for the Management of Snake-Bites [Online]. 2016. [cited 2020 Jan 28]. Available from: <https://apps.who.int/iris/handle/10665/249547>.
9. Félix-Silva J, Silva-Junior AA, Zucolotto SM, Fernandes-Pedrosa MF. Medicinal Plants for the Treatment of Local Tissue Damage Induced by Snake Venoms: An Overview from Traditional Use to Pharmacological Evidence. *Evid Based Complement Alternat Med.* 2017;2017:5748256. doi: 10.1155/2017/5748256.
10. Omara T, Kagoya S, Openy A, Omute T, Ssebulime S, Kiplagat KM, Bongomin O. Antivenin plants used for treatment of snakebites in Uganda: ethnobotanical reports and pharmacological evidences. *Trop Med Health.* 2020 Feb 11;48:6. doi: 10.1186/s41182-019-0187-0.
11. Elmaki NM, Al Sadawi IA, Hermann A, Gbaj AM. Potential molecular docking of four acetylcholinesterase inhibitors. *Drug Designing & Intellectual Properties International Journal.* 2018:191-4. doi: 10.32474/DDIPIJ.2018.02.000136.
12. Nadri MH, Salleh WM. Molecular Docking Studies of Phytochemicals from Piper Species as Potential Dual Inhibitor of Group X Secreted Phospholipase A2 (SPLA2-X) and Cyclooxygenase-2 (COX-2). *Research Journal of Pharmacy and Technology.* 2020 May 1;13(5):2181-6. doi: 10.5958/0974-360X.2020.00392.3.
13. Arafat A, Arun A, Ilamathi M, Asha J, Sivashankari PR, D'Souza CJ, Sivaramakrishnan V, Dhananjaya BL. Homology modeling, molecular dynamics and atomic level interaction study of snake venom 5' nucleotidase. *Journal of molecular modeling.* 2014 Mar;20(3):1-0. doi: <https://doi.org/10.1007/s00894-014-2156-1>.
14. Eweas AF, Alhossary AA, Abdel-Moneim AS. Molecular docking reveals ivermectin and remdesivir as potential repurposed drugs against SARS-CoV-2. *Frontiers in microbiology.* 2021:3602. doi: <https://doi.org/10.3389/fmicb.2020.592908>.
15. Mohamed EM, Hetta MH, Rateb ME, Selim MA, AboulMagd AM, Badria FA, Abdelmohsen UR, Alhadrami HA, Hassan HM. Bioassay-Guided Isolation, Metabolic Profiling, and Docking Studies of Hyaluronidase Inhibitors from *Ravenala madagascariensis*. *Molecules.* 2020 Apr 8;25(7):1714. doi: 10.3390/molecules25071714.
16. Escalante T, Franceschi A, Rucavado A, Gutiérrez JM. Effectiveness of batimastat, a synthetic inhibitor of matrix metalloproteinases, in neutralizing local tissue damage induced by BaP1, a hemorrhagic metalloproteinase from the venom of the snake *Bothrops asper*. *Biochemical pharmacology.* 2000 Jul 15;60(2):269-74. doi: [https://doi.org/10.1016/S0006-2952\(00\)00302-6](https://doi.org/10.1016/S0006-2952(00)00302-6).
17. Shewale S, Undale V, Shelar M, Bhalchim V, Kuchekar M, Warude B, Wawale V. Preliminary pharmacognostic, physicochemical and phytochemical evaluation of *Sansevieria cylindrica* leaves. *Journal of Pharmaceutical Negative Results.* 2022;13(Sp.1):1253-1271. doi: <https://doi.org/10.47750/pnr.2022.13.S01.153>
18. Shewale S, Undale V, Shelar M, Warude W, Kuchekar M, Bhalchim V, Satone S, Lembhe S, Gundecha S. Preliminary pharmacognostic, physicochemical and phytochemical evaluation of *Plumeria obtusa* seed pods. *Defence Life Sciences Journal.* (In-Press)
19. Dallakyan S, Olson AJ. Small-molecule library screening by docking with PyRx. *Methods Mol Biol.* 2015;1263:243-50. doi: 10.1007/978-1-4939-2269-7_19.
20. Trott O, Olson AJ. AutoDock Vina: improving the speed and accuracy of docking with a new scoring function, efficient optimization, and multithreading. *J Comput Chem.* 2010 Jan 30;31(2):455-61. doi: 10.1002/jcc.21334.
21. Huang SY, Grinter SZ, Zou X. Scoring functions and their evaluation methods for protein-ligand docking: recent advances and future directions. *Phys Chem Chem Phys.* 2010 Oct 28;12(40):12899-908. doi: 10.1039/c0cp00151a.





Sunil Shewale et al.,

Table 1: List of selected PDB with PDB code, ligands and resolution

S.N.	PDB Code	Target	Ligand	Resolution
1	1B41	Human acetylcholinesterase	Physostigmine	2.76 Å
2	1CJY	Human cytosolic phospholipase a2	Indomethacin	2.50 Å
3	2JGA	Crystal structure of human cytosolic 5'-nucleotidase III	Vanillic acid	3.01 Å
4	4TKX	Protease	Remdesivir	1.60 Å
5	4UFQ	Hyaluronidase	Tannic acid	1.65 Å
6	5NJB	E. Coli Microcin-processing metalloprotease	Batimastat	1.50 Å

Table 2: List of Phytoconstituents/ ligands with PubChem ID and manual code

Phytoconstituents							
<i>Sansevieria cylindrica</i>				<i>Plumeria obtusa</i>			
S. N.	Code	Ligand	Pub Chem ID	S. N.	Code	Ligand	Pub Chem ID
1.	1SC	Hexadecanoic acid, n-Octyl ester (Octyl palmitate)	85651	1.	1PO	Octaethylene glycol monododecyl ether	123921
2.	2SC	Carbonic acid,2-ethylhexyl nonyl ester	91695723	2.	2PO	Cyclopropanetetradecanoic acid, 2 octyl-methyl ester	552099
3.	3SC	Diisooctyl phthalate	33934	3.	3PO	Undecanoic acid, ethyl ester	12327
4.	4SC	Phthalic acid,6 – methylhept-2-yl octyl ester	91720824	4.	4PO	Ethyl Oleate	5363269
5.	5SC	1,2 – Benzene dicarboxylic acid, bis(1-methylethyl) ester (Diisopropyl phthalate)	11799	5.	5PO	9,12-Octadecadienoic acid, ethyl ester	12363975
				6.	6PO	9,12,15-Octadecatrienoic acid, 2,3-dihydroxypropyl ester	5367328
				7.	7PO	n-Hexadecanoic acid	985

Table 3: Binding energy of all phytoconstituents of *Sansevieria cylindrica* plant

Protein	Phytoconstituents	G score kcal/mol
1b41	Hexadecanoic acid, n-Octyl ester	-3.6
	Carbonic acid,2-ethylhexyl nonyl ester	-4.7
	Diisooctyl phthalate	-5.3
	Phthalic acid,6 – methylhept-2-yl octyl ester	-5.9
	1,2 – Benzene dicarboxylic acid, bis(1-methylethyl) ester	-6.6





Sunil Shewale et al.,

1CYJ	Hexadecanoic acid, n-Octyl ester	-3.5
	Carbonic acid,2-ethylhexyl nonyl ester	-4
	Diisooctyl phthalate	-4.5
	Phthalic acid,6 – methylhept-2-yl octyl ester	-4.7
	1,2 – Benzene dicarboxylic acid, bis(1-methylethyl) ester	-4.5
2JGA	Hexadecanoic acid, n-Octyl ester	-5.4
	Carbonic acid,2-ethylhexyl nonyl ester	-5.5
	Diisooctyl phthalate	-6.5
	Phthalic acid,6 – methylhept-2-yl octyl ester	-7.8
	1,2 – Benzene dicarboxylic acid, bis(1-methylethyl) ester	-6.5
4TKX	Hexadecanoic acid, n-Octyl ester	-5.1
	Carbonic acid,2-ethylhexyl nonyl ester	-5
	Diisooctyl phthalate	-5.7
	Phthalic acid,6 – methylhept-2-yl octyl ester	-6
	1,2 – Benzene dicarboxylic acid, bis(1-methylethyl) ester	-7
5NJB	Hexadecanoic acid, n-Octyl ester	-5.6
	Carbonic acid,2-ethylhexyl nonyl ester	-6
	Diisooctyl phthalate	-7.2
	Phthalic acid,6 – methylhept-2-yl octyl ester	-7.2
	1,2 – Benzene dicarboxylic acid, bis(1-methylethyl) ester	-7.1
4UFO	Hexadecanoic acid, n-Octyl ester	-3.9
	Carbonic acid,2-ethylhexyl nonyl ester	-3.1
	Diisooctyl phthalate	-4.3
	Phthalic acid,6 – methylhept-2-yl octyl ester	-4.1
	1,2 – Benzene dicarboxylic acid, bis(1-methylethyl) ester	-4.6

Table 4: Standard and Plant phytoconstituents interactions with amino acid residues

Protein	Phytoconstituents	Binding energy	Docking Interaction
1b41	Phthalic acid,6 – methylhept-2-yl octyl ester	-5.9	H-bond - LYS53 (3.62) Pi-Anion - GLU185 (3.99) Alkyl - LEU221 (5.14), ARG1(4.42), PRO55(4.82) Pi-Alkyl - PRO52(4.78), LEU178(5.38)
	1,2 – Benzene dicarboxylic acid, bis(1-methylethyl) ester	-6.6	H-bond - LYS53(2.7), TRP182(3.33) Pi-Anion - GLU185 (3.72) Alkyl - PRO52(4.68), PRO55(5.17) Pi-Alkyl - PRO52(5.04), LEU178(5.38)
	Physostigmine	-6.5	H bonding -ARG 245(2.32), THR 249(1.98) pi-alkyl – ARG 246(3.77)
1CYJ	Phthalic acid,6 – methylhept-2-yl octyl ester	-4.7	H-bond - LYS45(2.53), GLY42(3.45 & 3.68) Pi-Pi T-shaped - TYR51(4.76) Alkyl - ILE50(4.76) Pi-Alkyl - TYR51(5.28 & 5.99)
	1,2 – Benzene dicarboxylic acid, bis(1-methylethyl)	-4.5	H-bond - MET19(3.06) Alkyl - ARG22(3.72), PRO27(4.9), MET19(4.70)





Sunil Shewale et al.,

	ester		Pi-Alkyl - ARG22(3.67)
	Piperine	-5.4	Pi-alkyl – TYR 51(3.61) Van der waals – GLN 73(5.15)
2JGA	Phthalic acid,6 – methylhept-2-yl octyl ester	-7.8	H-bond - THR55(2.16), HIS57(2.71), TYR103(2.73) Pi-Cation - HIS57(4.26) Pi-Pi Stacked - TRP102(4.62 & 4.38), HIS57(3.88) Pi-Pi T-shaped - TYR103 (5.14) Alkyl - MET41(4.3), VAL199(4.17 & 5.13), ALA154(4.11)
	1,2 – Benzene dicarboxylic acid, bis(1-methylethyl) ester	-6.5	H-bond - LEU202(3.02 & 3.36) Pi-Sigma - LEU202(3.89 & 3.69) Alkyl - ALA215(4.64)
	Vanillic acid	-6.3	H-bonding -THR 55(2.11), ASN 58(2.53), SER 106(2.47), TYR 103(2.9) pi-pi stack HIS 57(4), TRP 102(4.52): TYR 103(5.2), TRP 102(4.52) Pi alkyl – TRP 102(4.69) Alkyl – LYS 78(4.06), LEU 74(4.7)
4TKX	Phthalic acid,6 – methylhept-2-yl octyl ester	-6	H-bond - ASN551(2.35), SER669(2.33 & 3.38) Pi-Sigma - TYR238(3.68) Pi-Alkyl - VAL641 (4.97), TYR238(5.26)
	1,2 – Benzene dicarboxylic acid, bis(1-methylethyl) ester	-7	H-bond - SER669(2.43 & 3.38), ASN551(3.01) Pi-Sigma - ASN551(3.82) Pi-Sulfur - MET594(4.72) Pi-Pi Stacked- TYR238(3.93)
	Remdesivir	-7.1	H bonding ASN 551(2.26), ASP 548(2.22), ASP548(1.82), TYR238(2.51) Pi-donor – SER549(3.44) Alkyl - ARG668(4.23)
5NJB	Diisooctyl phthalate	-7.2	H-bond - MET233(3.77), ASN390(2.68 & 2.91), ASN449(1.99 & 2.38) Pi-Alkyl - VAL451
	Phthalic acid,6 – methylhept-2-yl octyl ester	-7.2	H-bond - ARG228 (2.34 & 1.84), ARG229 (2.48 & 2.01) Pi-Anion- GLU251(4.42) Pi-Sigma- ALA249(3.97 & 3.68) Pi-Pi T-shaped - PHE360(4.92) Alkyl- ARG229(3.71), ILE402(4.14) Pi-Alkyl - PHE395(4.62 & 4.01)
	Batimastat	-8.5	H bonding - GLY394(2.33), VAL453(1.9), GLY455(2.05), GLY394(2.18), GLU263(1.82), VAL453(1.88), GLY393(3.03) Pi alkyl- TRP256(5.03), TRP256(5.12), TRP256(4.65), HIS262(4.09) Salt bridge - GLU263(2.48) Alkyl - CYS454(4.75)





Sunil Shewale et al.,

4UFQ	Diisooctyl phthalate	-4.3	H-bond - ILE177(3.22), GLY200(3.57) Pi-Alkyl - ILE177(4.68), ALA197(4.32), LEU202(5.15)
	1,2 – Benzene dicarboxylic acid, bis(1-methylethyl) ester	-4.6	H-bond - LEU202(3.03), GLY200(3.46) Pi-Sigma - LEU202(3.87 & 3.97) Pi-Alkyl - ILE177(5.19)
	Tannic acid	-5.6	H bonding –SER64(3.17)

Table 5: Binding energy of all phytoconstituents of *Plumeria obtusa* plant

Protein	Phytoconstituents	Binding energy
1b41	Octaethylene glycol monododecyl ether	-3.4
	Cyclopropanetetradecanoic acid, 2 octyl-methyl ester	-3.4
	Undecanoic acid, ethyl ester	-3.6
	Ethyl Oleate	-4.1
	9,12-Octadecadienoic acid, ethyl ester	-2.8
	9,12,15-Octadecatrienoic acid, 2,3-dihydroxypropyl ester	-5.2
	n-Hexadecanoic acid	-3.4
1CYJ	Octaethylene glycol monododecyl ether	-3.1
	Cyclopropanetetradecanoic acid, 2 octyl-methyl ester	-3.5
	Undecanoic acid, ethyl ester	-4.7
	Ethyl Oleate	-3.6
	9,12-Octadecadienoic acid, ethyl ester	-2.9
	9,12,15-Octadecatrienoic acid, 2,3-dihydroxypropyl ester	-3.7
	n-Hexadecanoic acid	-3.3
2JGA	Octaethylene glycol monododecyl ether	-5.6
	Cyclopropanetetradecanoic acid, 2 octyl-methyl ester	-3.7
	Undecanoic acid, ethyl ester	-4.3
	Ethyl Oleate	-4
	9,12-Octadecadienoic acid, ethyl ester	-5.1
	9,12,15-Octadecatrienoic acid, 2,3-dihydroxypropyl ester	-5.9
	n-Hexadecanoic acid	-3.7
4TKX	Octaethylene glycol monododecyl ether	-4.5
	Cyclopropanetetradecanoic acid, 2 octyl-methyl ester	-4
	Undecanoic acid, ethyl ester	-3.8
	Ethyl Oleate	-4.5
	9,12-Octadecadienoic acid, ethyl ester	-4.5
	9,12,15-Octadecatrienoic acid, 2,3-dihydroxypropyl ester	-5.3
	n-Hexadecanoic acid	-4.1
5NJB	Octaethylene glycol monododecyl ether	-5.9
	Cyclopropanetetradecanoic acid, 2 octyl-methyl ester	-5.5
	Undecanoic acid, ethyl ester	-5.3
	Ethyl Oleate	-5.4





Sunil Shewale et al.,

	9,12-Octadecadienoic acid, ethyl ester	-6.2
	9,12,15-Octadecatrienoic acid, 2,3-dihydroxypropyl ester	-6.3
	n-Hexadecanoic acid	-5.3
4UFQ	Octaethylene glycol monododecyl ether	-3.7
	Cyclopropanetetradecanoic acid, 2 octyl-methyl ester	-3.3
	Undecanoic acid, ethyl ester	-3.4
	Ethyl Oleate	-3.1
	9,12-Octadecadienoic acid, ethyl ester	-3.6
	9,12,15-Octadecatrienoic acid, 2,3-dihydroxypropyl ester	-3.7
	n-Hexadecanoic acid	-3.2

Table 6: Standard and Plant phytoconstituents interactions with amino acid residues

Protein	Phytoconstituents	Binding energy	Docking Interaction
1b41	Ethyl Oleate	-4.1	H-bond – ARG13(2.21) Alkyl – PRO52(4.37), LEU178(4.83), LYS53(5.47), PRO55(4.74), ARG13(4.52) Pi-Alkyl – TRP182(4.57)
	9,12,15-Octadecatrienoic acid, 2,3-dihydroxypropyl ester	-5.2	H-bond – GLN250(2.01) Alkyl – ARG245(4.24), ARG246(3.98, 4.08 & 4.58) Pi-Alkyl – HIS253(4.87)
	Physostigmine	-6.5	H-bond -ARG 245(2.32), THR 249(1.98) Pi-alkyl – ARG 246(3.77)
1CYJ	Undecanoic acid, ethyl ester	-4.7	H-bond - HIS18(2.63), ASN23(2.57) Alkyl – MET26(4.38), LYS29(4.67), LEU36(5.29), LEU40(4.2), LEU31(4.55), VAL79(4.1), LYS29(4.09) Pi-Alkyl - HIS18(4.82)
	9,12,15-Octadecatrienoic acid, 2,3-dihydroxypropyl ester	-3.7	H-bond - ASP41(2.67), SER48(3.54) Alkyl- ILE50(5.04), CD302(4.78) Pi-Alkyl - TYR51(4.73 & 5.26)
	Piperine	-5.4	Pi-alkyl – TYR 51(3.61) Van der waals – GLN 73(5.15)
2JGA	Octaethylene glycol monododecyl ether	-5.6	H-bond – ARG52(2.64) ASP252(2.94 & 3.6), ASP227(3.35), VAL86(3.65) Pi-Sigma – HIS57(3.75) TYR103(3.55) Alkyl- ALA154(5.03) Pi-Alkyl – HIS57 (4.54), TYR102(4.36,4.53,5.01 & 4.08), TYR103(4.16)
	9,12,15-Octadecatrienoic acid, 2,3-dihydroxypropyl ester	-5.9	H-bond – ASP231(2.06), SER228(2.18), LYS202(3.67) Metal Acceptor - MG1288(2.61) Alkyl – VAL199(4.81), LYS78(4.83) Pi-Alkyl – TYR82(5.45), TRP102(4.92)
	Vanillic acid	-6.3	H-bond -THR 55(2.11), ASN 58(2.53), SER 106(2.47), TYR 103(2.9) Pi-pi stack - HIS 57(4), TRP 102(4.52): TYR 103(5.2), TRP 102(4.52)





Sunil Shewale et al.,

			Pi alkyl – TRP 102(4.69) Alkyl – LYS 78(4.06), LEU 74(4.7)
4TKX	9,12-Octadecadienoic acid, ethyl ester	-4.5	H-bond – ASP388(2.21), ALA423(2.5) Alkyl- ALA387(4.38 & 5.1), ALA423(4.62 & 3.9) Pi-Alkyl – TYR389(5.39 & 4.46)
	9,12,15-Octadecatrienoic acid, 2,3-dihydroxypropyl ester	-5.3	H- bond - ALA423(2.38) Alkyl – LYS22(4.36), ALA423(3.83 & 5.23)
	Remdesivir	-7.1	H bond - ASN 551(2.26), ASP 548(2.22), ASP548(1.82), TYR238(2.51) Pi-donor – SER549(3.44) Alkyl - ARG668(4.23)
5NJB	9,12-Octadecadienoic acid, ethyl ester	-6.2	H-bond - GLN41(2.51), SER43(2.66) Alkyl – VAL162(5.33,5.39 & 5.23), PRO462(4.34 & 4.89), LEU182(5.17 & 4.03), ARG184(4.36 & 5.25)
	9,12,15-Octadecatrienoic acid, 2,3-dihydroxypropyl ester	-6.3	H-bond – ARG306(2.59) Alkyl – LEU182(5.35), PRO462(4.15), VAL162(4.21, 4.28 & 4.79) Pi-Alkyl – HIS45(4.61)
	Batimastat	-8.5	H bond - GLY394(2.33), VAL453(1.9), GLY455(2.05), GLY394(2.18), GLU263(1.82), VAL453(1.88), GLY393(3.03) Pi alkyl- TRP256(5.03), TRP256(5.12), TRP256(4.65), HIS262(4.09) Salt bridge - GLU263(2.48) Alkyl - CYS454(4.75)
4UFQ	Octaethylene glycol monododecyl ether	-3.7	H-bond – SER207(2.33,2.56 & 3.42), GLY192(2.23), ASN208(2.95), TRP204(3.42) Alkyl - LEU195(4.63 & 4.75), LEU202(5.22), ILE214(4.54 & 4.84) Pi-Alkyl – TRP204(5.14 & 4.53)
	9,12,15-Octadecatrienoic acid, 2,3-dihydroxypropyl ester	-3.7	H-bond – ILE177(2.36) Alkyl – ILE177(4.02), LEU202(4.09, 4.64 & 5.2) ALA197(4.77), ALA215(4.95)
	Tannic acid	-5.6	H bond –SER64(3.17)

Table 7: Lipinski rule of *Sansevieria cylindrica* and *Plumeria obtusa* plants

S.N.	Phytoconstituents Name	Mol. wt	Log P	HBD	HBA
Lipinski rule of <i>Sansevieria cylindrica</i>					
1	Hexadecanoic acid, n-Octyl ester	368.64	6.050	0	2
2	Carbonic acid, 2-ethylhexyl nonyl ester	300.47	6.1	0	3
3	Diisooctyl phthalate	390.6	6.43	0	4
4	Phthalic acid, 6- methylhept-2-yl octyl ester	390.6	6.57	0	4
5	1,2 -Benzene dicarboxylic acid, bis(1-methylethyl) ester	247.26	1.82	0	4
Lipinski rule of <i>Plumeria obtusa</i> plant					
1	Octaethylene glycol	538.8	4.03	1	9





Sunil Shewale et al.,

	monododecyl ether				
2	Cyclopropanetetradecanoic acid, 2 octyl-methyl ester	394.67	8.61	0	2
3	Undecanoic acid, ethyl ester	214.34	4.08	0	2
4	Ethyl Oleate	310.15	6.58	0	2
5	9,12-Octadecadienoic acid, ethyl ester	308.49	6.63	0	2
6	9,12,15-Octadecatrienoic acid, 2,3-dihydroxypropyl ester	352.5	4.47	2	4
7	n-Hexadecanoic acid	257.41	5.55	1	4

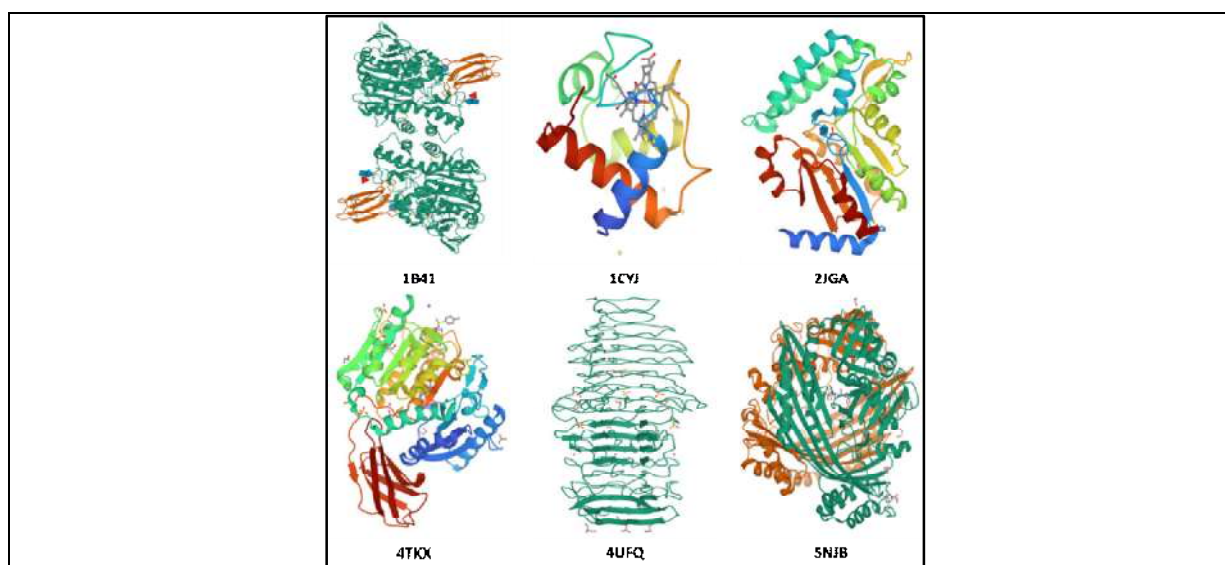
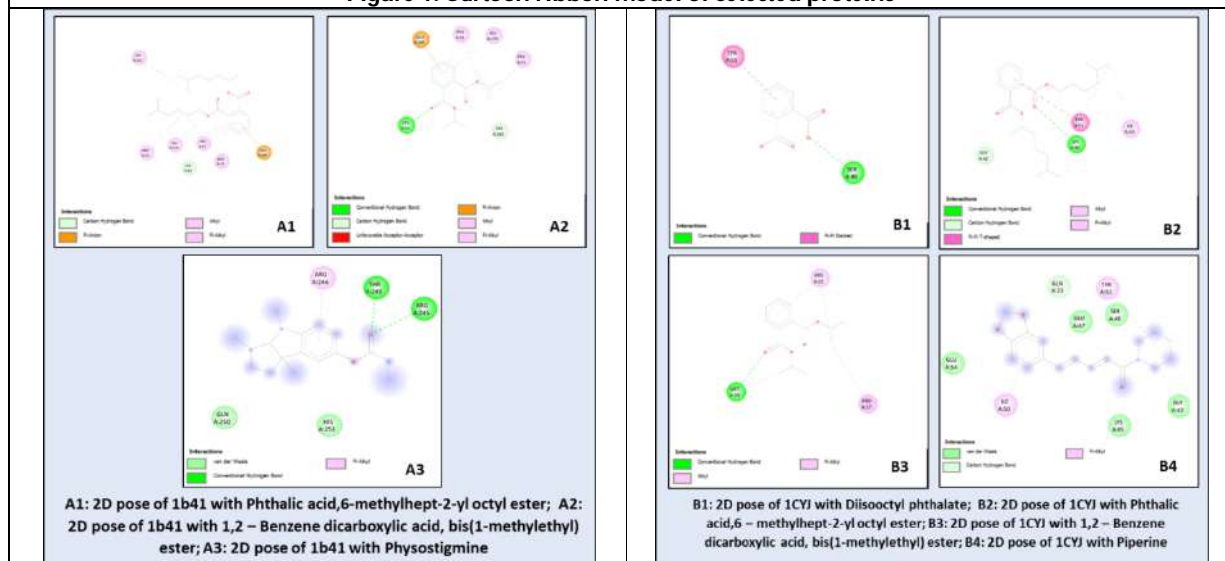


Figure 1: Cartoon ribbon model of selected proteins





Sunil Shewale et al.,

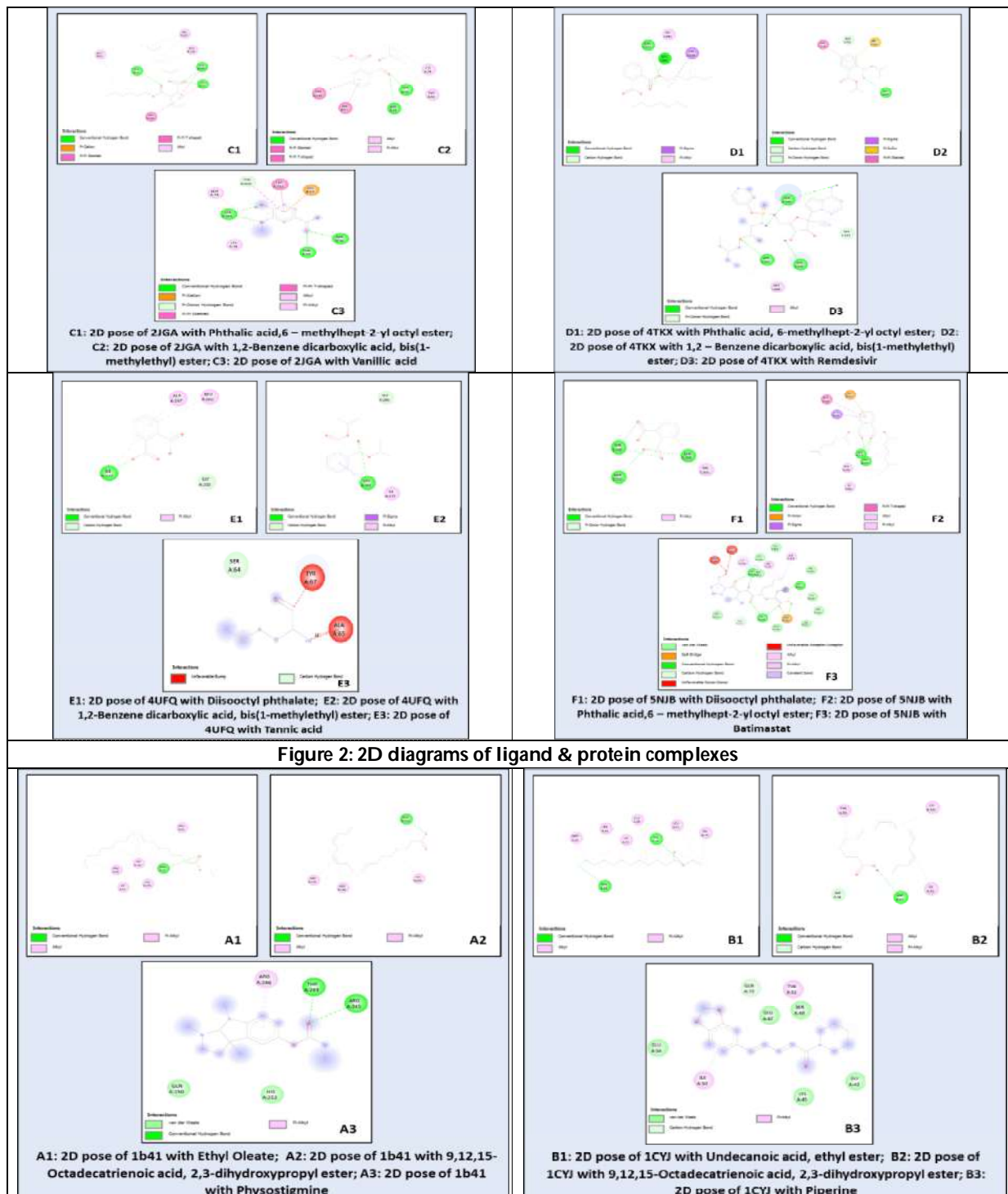


Figure 2: 2D diagrams of ligand & protein complexes





Sunil Shewale et al.,

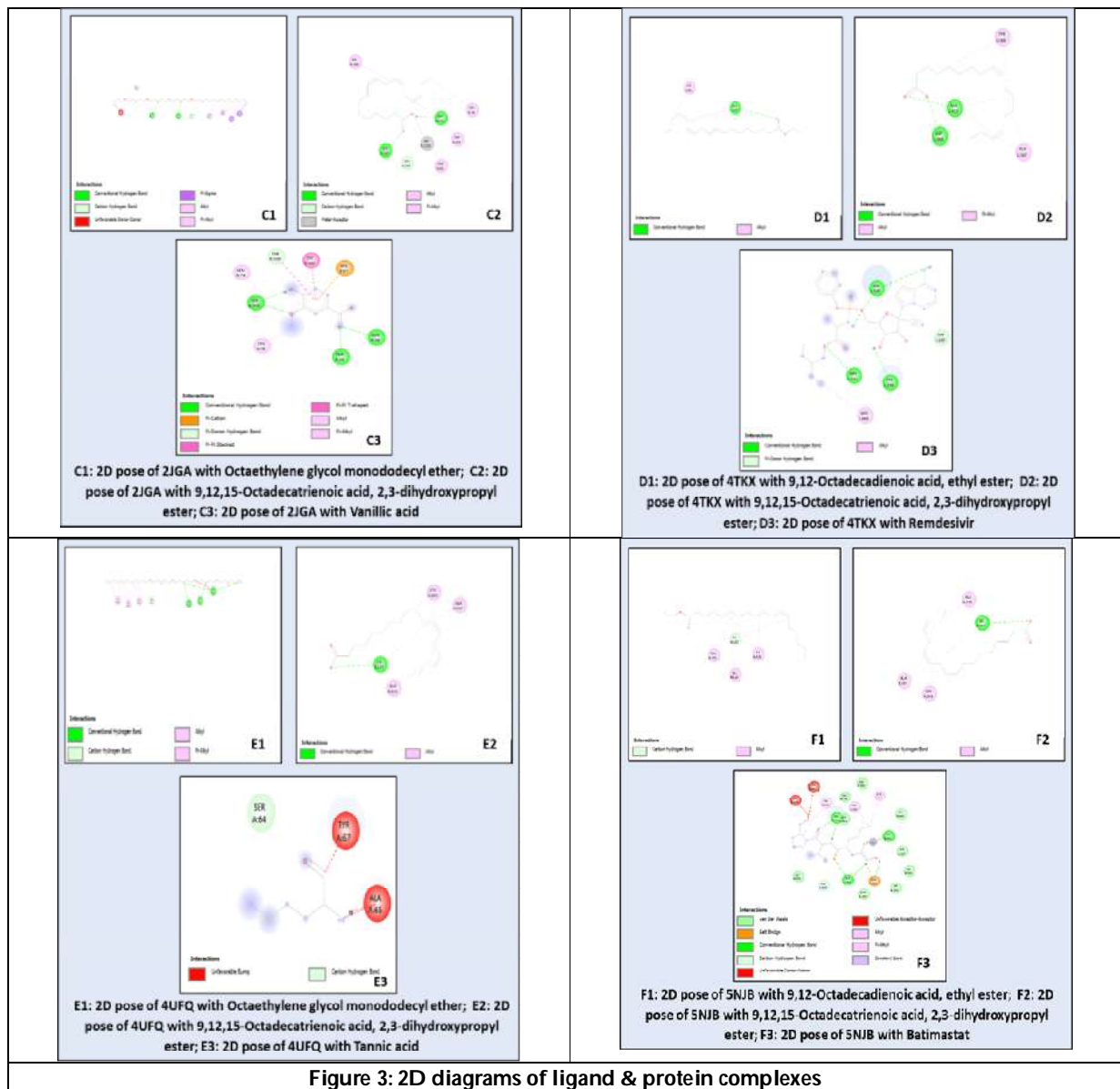


Figure 3: 2D diagrams of ligand & protein complexes





ESCE – An Optimized Load Balancing Technique to Reduce Data Center and VM Cost in Cloud Environment

N.Susitha^{1*} and G. Monika²

¹Associate Professor, Department of Computer Science, School of Arts and Science, AV Campus, Vinayaka Mission's Research Foundation (DU), OMR, Chennai, Tamil Nadu, India.

²Assistant Professor, Department of Computer Science, Jeppiar College of Arts and Science, Chennai, Tamil Nadu, India.

Received: 03 Mar 2023

Revised: 15 Apr 2023

Accepted: 19 May 2023

*Address for Correspondence

N.Susitha

Associate Professor,
Department of Computer Science,
School of Arts and Science,
Vinayaka Mission's Research Foundation (DU),
Chennai, Tamil Nadu, India.
Email: susitha.avca015@avsas.ac.in, susitha.n@gmail.com.



This is an Open Access Journal / article distributed under the terms of the **Creative Commons Attribution License** (CC BY-NC-ND 3.0) which permits unrestricted use, distribution, and reproduction in any medium, provided the original work is properly cited. All rights reserved.

ABSTRACT

Nowadays Cloud computing is becoming trending technology and used by various fields across the globe. The users access this mechanism mostly due to its fastest growth worldwide. The world gets digitalized so the cloud users are growing every day, in order to handle the workload cloud needs the load balancing strategy to reduce the overhead and to maximize the through put of cloud computing. This paper analyses three cloud algorithms namely Round Robin, Throttled, Equally Spread Current Execution Load. This study tests the three algorithms performance in terms of parameters chosen. The selected parameters in this study are, hourly data center response time, average response time and the cost of Virtual Machine (VM) etc. The cloud environment is very huge and the availability of simulation software for the research purpose is comparatively less. To simulate the cloud environment this study selects the Cloud Analyst simulator, which is best among all the available simulators in cloud environment. Simulation result demonstrates that Equally Spread Current Execution (ESCE) algorithm gives better results among these algorithms as number of user increases. Then ESCE also reduces the cost of VMs and data center cost which efficiently balances the load among the other algorithms.

Keywords: Cloud computing, cloud analyst, load balancing algorithms, Equally spread current execution load, Virtual Machine.



**Susitha and Monika**

INTRODUCTION

Cloud Computing, one of the emerging technologies, is deployed by various entrepreneurs to save their money and cost of infrastructure. Instead of buying many personal computers, processors and memory, they select cloud computing resources and pay as per the usage. The cloud services are provided by many organisations like Microsoft, Amazon, etc. These organisations provide the cloud services in form of software (SaaS), Infrastructure (IaaS) and Platforms (PaaS). The nature of user friendly, easy usage, accessibility and cost-effective business model bring lots of customers to cloud computing but this becomes a problem of balancing the load on cloud. The excess users of cloud brings the issues of load balancing in the cloud environment. There are algorithms used to sort out the problem but many researches are happening in the improvement of the load balancing algorithms [1] [2]. This paper analyses the load balancing algorithms. The cloud analyst simulator tool is used to check the act of the cloud load balancing algorithms. The algorithms used in the study are Throttled, Equally Spread current execution load and Round Robin and analyse them with respect to the parameters like VM cost and Data Center Processing Time, Response time and Data transfer cost. Then to find out how the response time is reduced to bring an efficient cloud computing services. This paper is organised on the concept of Load Balancing and its types. Then the available and frequently selected load balancing techniques are used to analyse the load balancing problem in cloud environment. The next section will have the experiment and the simulation results. The last section has the conclusion and future work of this paper.

Related Work

There are many researches happening in the cloud computing load balancing techniques, the author [1] says that the load minimizes the overhead and maximizes the through put. [2] Introduces a novel task-assignment model is proposed along with the load based task assignment algorithm and the selection processes involved. The minimum loaded virtual machine is given as task so that the resources should be efficiently used. Throttled and Equally Spread Current. To solve load balancing problem the particle swarm optimization is also simulated dynamically [3]. The author has used some performance parameter such as hourly cloud centre response, average response time etc. [4], after the analysis with cloud analyst, it was seen that Throttled is best among them and also shown that Throttled have less response time as compare to Round Robin and Active load balancing.

Methods in Load Balancing

Providing cloud to huge people becomes a problem for providers. This problem can be addressed by the load balancing methodology. This method assures that users can access maximum services from cloud with less response time. [5] In initial part in the load balancing, the overhead in cloud on virtual machines are mapped within the applications. The second step is about the host that maps the host resources and virtual resources which was easier for the cloud to allow the other applications request. [6] Then after analysis the service was shifted to the data center that was selected by the customer. Static load balancing produces fair results for standardized and steady environments. [7] In static scheduling, the complete knowledge about the tasks is already known i.e. structure of tasks, mapping of resources, estimates of execution time. It schedules the already known tasks. Dynamic method is based on current state of the decision making system.[8] In this approach task can move from highly loaded node to less loaded nodes which is one of advantage of this type of load balancing. These algorithms are changes simultaneously according to the current state of system. So that it is complex and complicated to implement dynamic load balancing but at the performance and efficiency point of view Dynamic is paramount.

The request generator creates user requests for end-user task which will execute by providing the computing resources. Task management was supervised by Data centre controller. The user's task was handled by VM and it was assigned by the load balancer. The initial level load balancer assigns the load to the physical machines which shares the work to the related virtual machines. The second level improves its service by sharing the load among



**Susitha and Monika**

various virtual machines in the different Physical Machines. Figure 2 shows the flow of the load balancing techniques.

Load Balancing Techniques**Round Robin Algorithm**

The RR algorithm is a load balancing technique which allocates the virtual machines to the client once it was requested. This algorithm selects a VM in a circular manner without any other critical process, it just chooses randomly in a circular line [8] [9]. A new algorithm based on round robin showed minimized waiting as well as turnaround time, while execution time slice is chosen to find dynamic time quantum for every service request [19]. The data centre controller informs the RR algorithm if it gets a request from client. The new virtual machines was allocated as soon as the data centre informs the RR algorithm for processing.

Algorithm:

1. Start
2. Make all virtual machines accessible in the virtual machine state list
3. Set the current state VM as -1
4. If data center controller gets a new request, increment VM and if the virtual machine corresponds to the user base that is being currently requested and the virtual machine in available, allocate the virtual machine.
5. Update the virtual machine state list
6. If machine id is greater than list size, set machine id to zero to continue in cyclic manner.
7. If request queued in data center controller, go to step iii.
8. Stop.

Throttled Algorithm

The TLB throttled load balancing algorithm checks the load on every VM. Every VM is assigned to one task at a time and next task is given if the current task was completed.] The extended version of throttle algorithm, M-throttled overweigh the load balancing capacity of shortest job first algorithm and round-robin, in terms of DC processing time and response time [20]. Optimized response time is proven while Balanced Throttled Load Balancing algorithm is simulated in cloud analyst. This method yields better response time compared to round robin algorithm, active algorithm and throttled load balancing algorithm [21].

Algorithm:

1. The TLB maintains an index with the details of all VM.
2. The request given by the client and it was handled by the data centre controller for the VM allocation.
3. TLB was sent a message to allocate a VM by data centre controller.
4. The index was scanned to find the id of the available VM. The id was returned to the data center controller.
5. Then the identified VM id was given and the index table was refreshed by mentioning the allocated VM id.
6. Finally the TLB was updated once the VM was done with the work. So the data center controller revises the table by increasing or decreasing 1 count of VM.

Equally Spread Current Execution

ESCE Algorithm gives the possible load among the virtual machines equally. This gives the VM with less load when request given by the client [9] [10]. The client request and the load is balanced similarly among the virtual machines.

Algorithm:

1. Start
2. First the table with the list of VM with status was given. The each VM is set to zero allocations The ESCE maintains a one more list with the number of allocations for the VM.
3. If a new allocation request is sent to Data center Controller, i.e. iterate through the list of virtual machines from the top and allocate the first existing virtual machine with minimum number of current allocations. Return the id of the selected machine to the data center controller.



**Susitha and Monika**

4. The Data center Controller then transfers the call to the virtual machine is recognized by that particular virtual machine id and informs the VM Load Balancer about the allocation.
5. On receiving the allocation event from the Data center Controller, update the virtual machine state list by incrementing the current allocations for the chosen machine and setting its busy status.
6. On receiving the de-allocation event from the Data center Controller, update the virtual machine state list by decrementing the current allocations for the chosen machine and setting its availability status.
7. If request queued in data center controller, go to step 3.
8. Stop

EXPERIMENTS AND RESULTS

The load balancing algorithms are analysed in this paper to obtain an effective algorithm and the parameters that affects the load balancing procedure in the cloud computing [11]. The parameters used to analyse are cost of virtual machines, data center processing time and average response time. To do simulation of cloud computing environment cloud analyst tool which is one of the effective tool among the cloud simulation tools [12]. The cloud analyst tool was setup in the Windows 7 OS and necessary setup was made to run the simulation [17]. Figure 3 gives the clear view about the configuration of cloud analyst tool. First three algorithms are simulated with different parameters. The parameters are adjusted according to the aim of the research paper [13] [14]. The number of VM, user bases and data centers are adjusted to analyse the simulation of the cloud environment. [15] [16]. The three algorithms are Round Robin Algorithm, ESCE and Throttled algorithm [18]. The following are the results received after the simulation in cloud analyst tool. In the scenario 1 and 2 number of VMs are altered and also user bases are changed in each scenario and results are listed.

This scenario 1 results having different number of virtual machines and the user bases. The numbers of virtual machines are 10 and user bases are 5. Then in the scenario 2, results having different virtual machines of 20 with this setup. The simulation was made up in the cloud environment. From the above results the scenario 1 shows that the average response time of ECSE algorithm is least and other two algorithms are high than the ECSE. So with very less response time by taking 10 VMs it was efficient to balance the load of VMs. Then in the scenario 2 also from the simulation results by setting different parameters the ECSE algorithm has the least response time and also less cost of the virtual machines. The ECSE has 282 ms in scenario 1 and 200 ms in scenario 2. The Virtual machines are increased and checked with the load balancing algorithms with different scenarios. The results shows that as we increase the sum of virtual machines in the cloud environment then with very less response time the work could be finished in the cloud environment. Figure 10, 11, and 12 shows the data transfer cost, virtual machine cost of three algorithms that is throttled, ESCE and round robin. Figure 13, 14 and 15 show the data center loading hourly basis.

CONCLUSION

In Cloud Computing environment, load balancing would be a problem which is yet to be completely solved. The load balancing is a vital challenge in the cloud computing which is essential to share the workload in an efficient and scalable way. It is a major part to find an algorithm which decreases considerably the average response time and cost of virtual machines, by analysing the three load balancing algorithms we finally choose the best load balancing algorithm in any given scenario. The highest response time was given round robin algorithm and ECSE gives the less response time. Hence ECSE results clearly states that ECSE algorithm effectively gives the less average response time which makes the load balancing smooth and fast. The ECSE was very effective by the results of the carried simulation work. The future research work is tuned to have an effective algorithm that is required to be written to solve the load balancing problems. There are also other issues in the load balancing algorithms which should also be addressed in future work.





REFERENCES

1. Mohammad Reza Mesbahi et al., "Performance Evaluation and Analysis of Load Balancing Algorithms in Cloud Computing Environments", Second International Conference on Web Research (ICWR), 2016.
2. Vishalika et al., "LD_ASG: Load Balancing Algorithm in Cloud Computing," Fifth International Conference on Parallel, Distributed and Grid Computing (PDGC), 2018, pp. 387-392, doi: 10.1109/PDGC.2018.8745948, 2018.
3. Handur, Vidya et al., Study of load balancing algorithms for Cloud Computing. 173-176. 10.1109/ICGCIoT.2018.8753091, 2018.
4. Violetta N. Volkova et al., "Load Balancing in cloud Computing" 8th Annual Ubiquitous Computing, Electronics and Mobile Communication Conference (UEMCON) IEEE, 2018.
5. Muhammad Sohaib Shakir et al., "Performance Comparison of load balancing algorithm using cloud Analyst in Cloud Computing", 8th Annual Ubiquitous Computing, Electronics and Mobile Communication Conference (UEMCON) IEEE, 2017.
6. Pawan Kumar et al., "Issues and Challenges of Load Balancing techniques in cloud Computing: A Survey", ACM Computing surveys, Vol.51, no.6, 2019.
7. Sandeep Patel et al., "Cloud Analyst: A Survey of Load Balancing Policies", International Journal of Computer Applications (0975 – 8887) Volume 117 – No. 21, May 2015.
8. Calheiros R.N. et al., "A Novel Framework for Modelling and Simulation of Cloud Computing Infrastructures and Services", Eprint: Australia, pp.9-17, 2009.
9. SimarPreet et al., "Analysis of Load Balancing Algorithms using Cloud Analyst.", Journal of Grid and Distributed Computing 9, no. 9, 11-24, 2016:
10. Kaur et al., "Load balancing in cloud computing", Proceedings of International Conference on Recent Trends in Information, Telecommunication and Computing, ITC. 2012.
11. Radojevic, B. et al., "Analysis of issues with load balancing algorithms in hosted (cloud) environments", Proc. 34th International Convention on MIPRO, IEEE, 2011.
12. Al Nuaimi, Klaitheem et al., "A survey of load balancing in cloud computing: Challenges and algorithms", Network Cloud Computing and Applications (NCCA), 2012 Second Symposium on, pp. 137-142. IEEE, 2012.
13. Neethu, M. S., "Load Balancing in Cloud Computing", International Journal of Advanced Technology in Engineering and Science, Vol. No.3, Issue 11, November 2015.
14. Randles, Martin et al., "A comparative study into distributed load balancing algorithms for cloud computing", Advanced Information Networking and Applications Workshops, IEEE 24th International Conference on, pp. 551-556. IEEE, 2010.
15. J. Sahoo et al., "Virtualization: A survey on concepts, taxonomy and associated security issues", Computer and Network Technology, IEEE, pp. 222-226. April 2010.
16. Bhaskar. R, et al., "Dynamic Allocation Method For Efficient Load Balancing In Virtual Machines for Cloud Computing Environment", Advanced Computing: An International Journal, Vol.3, No.5, September 2012.
17. SarojHiranwal et al., "Adaptive Round Robin Scheduling Using Shortest Burst Approach Based On Smart Time Slice", International Journal of Computer Science And Communication, Vol. 2, No. 2 , Pp. 319-323, July-December 2011.
18. Jasmin James et al., "Efficient VM load balancing algorithm for a cloud computing environment", International Journal on Computer Science and Engineering (IJCSE), ISSN: 0975-3397 Vol. 4 No.09, Sep 2012.
19. S. Ghosh et al., "Dynamic Time Quantum Priority Based Round Robin for Load Balancing In Cloud Environment", "Fourth International Conference on Research in Computational Intelligence and Communication Networks (ICRCICN), Kolkata, India, 2018, pp. 33-37, doi: 10.1109/ICRCICN.2018.8718694, 2018.
20. [20] Amrutanshu Panigrahi et al., "M-Throttled: Dynamic Load Balancing Algorithm for Cloud Computing", Intelligent and Cloud Computing, pp 3-10, doi: https://doi.org/10.1007/978-981-15-5971-6_1, Springer, ISBN978-981-15-5970-9, October 2020.





Susitha and Monika

21. [21] Mohamed, Shereen et al., "A Proposed Load Balancing Algorithm over Cloud Computing (Balanced Throttled)", International Journal of Recent Technology and Engineering (IJRTE), Vol. 10, doi - 10.35940/ijrte.B6101.0710221, , July,2021.

Table 1: Scenario 1

Algorithms	No. of VMs	Average response time(ms)	Parameters	
			Data Center processing time(ms)	Cost of VMs(\$)
ESCE	10	282	0.28	5.0
Throttled	10	300	0.37	5.4
Round Robin	10	300.82	0.34	5.7

Table 2: Scenario 2

Algorithms	No. of VMs	Average response time(ms)	Parameters	
			Data Center processing time(ms)	Cost of VMs(\$)
ESCE	20	200	0.20	10.5
Throttled	20	270	0.30	12.3
Round Robin	20	282.01	0.32	13.1

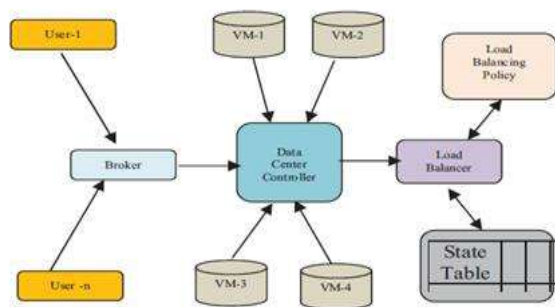


Fig 1: Structure of Load balancing

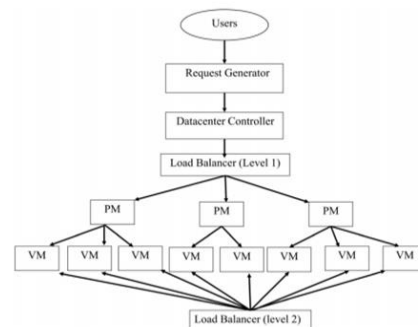


Fig 2: To understand the load balancing in cloud computing

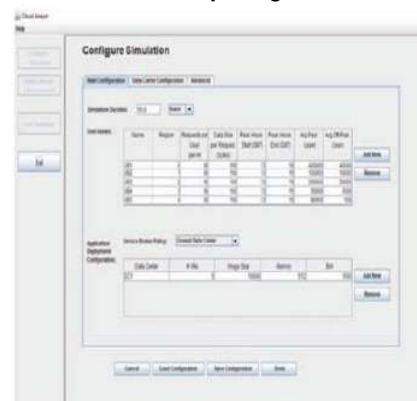
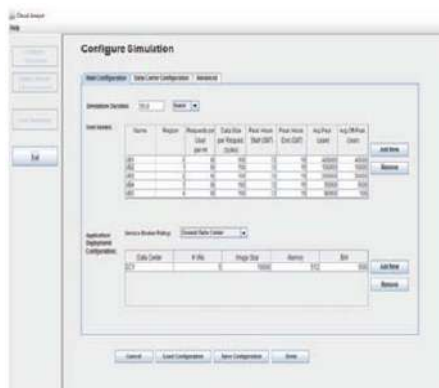


Fig 3. Configuring cloud environment parameters





Susitha and Monika

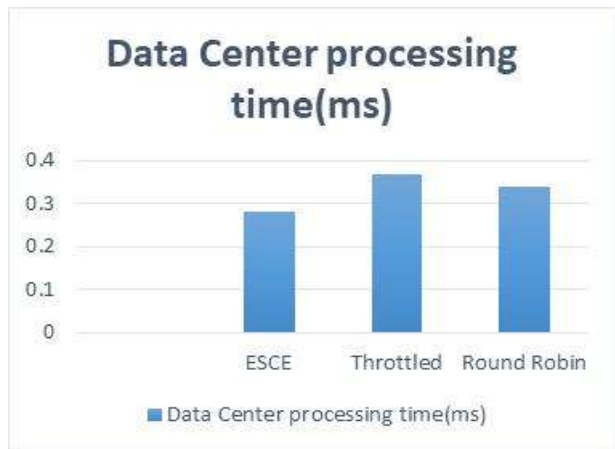


Fig 4: Datacentre processing time -10 VMs

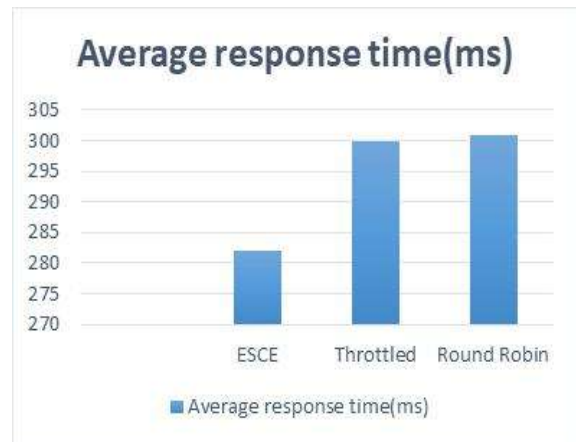


Fig 5: Average response time (ms) -10 VMs

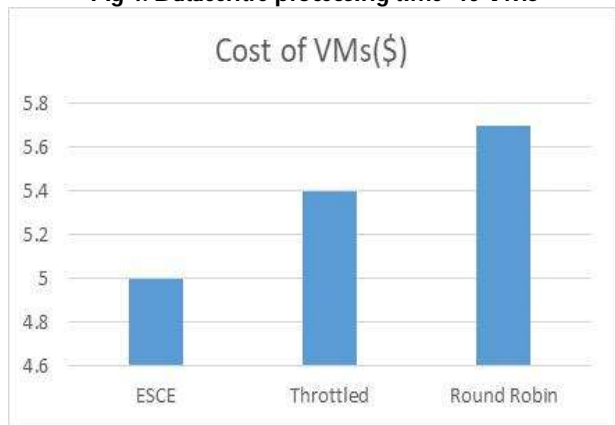


Fig 6: Cost of VMs (\$) -10 VMs

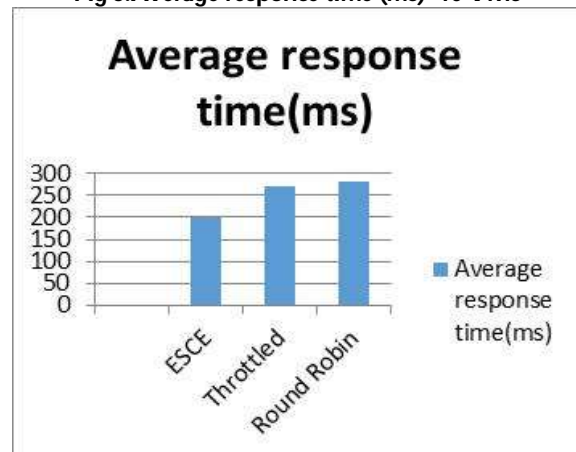


Fig 7: Average response time (ms) -20 VMs

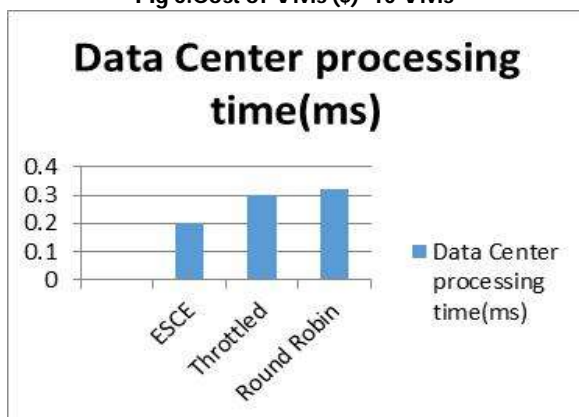


Fig 8: Datacentre processing time -20 VMs

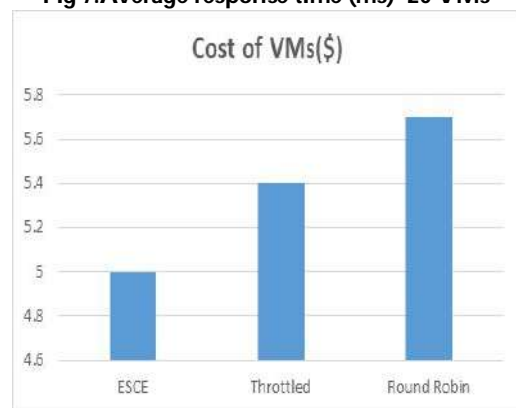


Fig 9: Cost of VMs (\$) -10 VMs





Susitha and Monika

Cost

Total Virtual Machine Cost (\$):	2.05
Total Data Transfer Cost (\$):	0.13
Grand Total: (\$)	2.16

Data Center	VM Cost \$	Data Transfer Cost \$	Total \$
DC2	0.51	0.03	0.54
DC1	0.51	0.03	0.54
DC4	0.51	0.03	0.54
DC3	0.51	0.03	0.54

Fig 10: Cost of Virtual Machines & Data transfer cost - Round robin

Cost

Total Virtual Machine Cost (\$):	5.02
Total Data Transfer Cost (\$):	0.38
Grand Total: (\$)	5.40

Data Center	VM Cost \$	Data Transfer Cost \$	Total \$
DC10	0.50	0.04	0.54
DC2	0.50	0.03	0.54

Fig 11: Cost of Virtual Machines & Data transfer cost- Throttled Algorithm

Cost

Total Virtual Machine Cost (\$):	2.51
Total Data Transfer Cost (\$):	0.32
Grand Total: (\$)	2.83

Data Center	VM Cost \$	Data Transfer Cost \$	Total \$
DC2	0.50	0.06	0.56
DC1	0.50	0.07	0.57

Fig 12: Cost of Virtual Machines & Data transfer cost-ESCE



Fig 14: Data Center - Hourly Loading-throttled

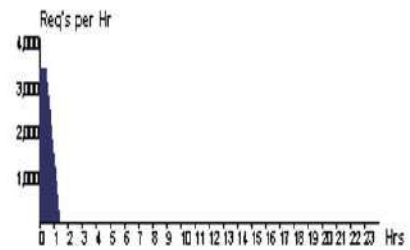


Fig 13: Data Center - Hourly Loading-RoundData Center

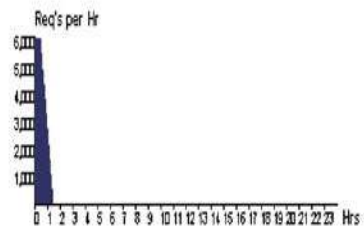


Fig 15: Data Center - Hourly Loading-ESCE





A Drug Review on Therapeutic Potency of Kaarathiri: A Siddha Formulation Indicated for Pouthiram (Fistula in ano)

Kavitha G^{1*}, Samundeswari P² and Muthukumar N J³

¹PG Scholar, Department of Pura Maruthuvam, National Institute Siddha, Chennai, Tamil Nadu, India.

²Assistant Professor, Department of Varma Maruthuvam, National Institute Siddha Chennai, Tamil Nadu, India.

³Head of the Department of Varma Maruthuvam, National Institute Siddha Chennai, Tamil Nadu, India.

Received: 07 Feb 2023

Revised: 23 Mar 2023

Accepted: 29 Apr 2023

*Address for Correspondence

Kavitha G,

PG Scholar,

Department of Pura Maruthuvam,

National Institute Siddha,

Chennai, Tamil Nadu, India.

E. Mail :thirukavig1629@gmail.com



This is an Open Access Journal / article distributed under the terms of the **Creative Commons Attribution License** (CC BY-NC-ND 3.0) which permits unrestricted use, distribution, and reproduction in any medium, provided the original work is properly cited. All rights reserved.

ABSTRACT

In *Siddha* system of medicine, According to *Siddha* classical text *Yugi Vaithiya Sinthamani*, diseases are classified into 4448s types. *Pouthiram* is classified into 8 types. *Asana Pouthiram* is one among them. It's causes, signs & symptoms may be correlated with fistula in ano in modern medicine. *Pouthiram* is a clinical condition characterized by recurrent anal abscesses, pain & swelling around the anus, pain with bowel movements, bloody or foul-smelling drainage (pus) from an opening around the anus. Patient underwent surgical treatment are more prone to reoccurrence. This is the major reason for people to switch over to traditional systems. At current scenario, *Siddha* system among Indian systems of medicine is gaining more attention globally & it serves as hope in treating this disease & preventing recurrence of fistula. Most of the *Siddha* formulations which includes herbal, mineral & herbo-mineral are proven caustic activity (*Kaaram*). *Kaarathiri* is an adjunct used for application of wound to promote healing & prevent further infection. Commonly used herbs for the preparation of *Kaarathiri* (*caustic Gauze*) are leaves of *Naayuruvi* (*Achyranthus aspera*) & *Uthamani* (*Pergularia daemia*). This review article focuses on one such polyherbal *Siddha* formulation *Kaarathiri*, mentioned in text *Sarabanthirar Vaithiya Muraigal Viranakarappan Roga Sikkichai* indicated for *Pouthiram*.

Keywords: *Kaarathiri*, *Pouthiram*, Fistula in ano, Medicated gauze, *Kaaram*





INTRODUCTION

Siddha System possess vast repository of Internal & external medicines. *Aga Marunthugal* (Internal medicine) are administered through the oral route & further classified into 32 categories based on their form, method of preparation, shelf life, etc. *Pura Marunthugal* (External medicine) includes certain forms of drugs & also certain application (such as nasal, eye & ear drops) & certain procedure (such as leech application). It is also classified into 32 categories. Among the 32 external therapies, the *Seelai* is one among them. Saint *Agathiyar, Therayar & Bogar* have described in their classical *Siddha* texts the method of preparation of *Kaaram & Kaaraseelai*. *Seelai* (Medicated gauze) is an adjunct used for application of wound to promote healing & prevent further infection. A dressing is designed to be direct conduct with the wound or abscess or fistula in ano. According to *Yugi Vaithiya Cinthamani*[1]– a classical *Siddha* text fistula in ano are classified into eight types. The pathogenesis of *Fistula* is a cryptoglandular infection in anal region that causes draining of pus & mucous discharge from external opening through fistula tract. The cardinal symptoms are recurrent anal abscesses, pain & swelling around the anus, pain with bowel movements, bloody or foul-smelling drainage (pus) from an opening around the anus.[2] A *Kaarathiri* absorbs the exudates & debris from the fistula tract (*Pauthiram*) & it may cut the tract. The major advantage of this procedure are, it will preserve the function of continence & prevents the recurrence of the condition. Even though several surgical methods are adapted & practiced in modern medicine, it is more prone to recurrence occur in *fistula*. This review article focuses on one such polyherbal *Siddha* formulation *Kaarathiri* as mentioned in text.

MATERIALS AND METHODS

Literature evidence of *Kaarathiri*

Nayuruvi Veppamuththamanimeni
Notchielainankolunthu
Thoyariththumithaiselaimertadavith
Thiriyakki Kuthu Pattu
Nooru Naal Irandu Naal Than Arinthu
Vidumerivunillathaakir
Rothirielmuththinennaippasuvinnei
Thadavidachasugamathaam [3]

Ingredients of *Kaarathiri*

Naayuiruvi tender leaves (*Achyranthes aspera*)
Uthamani tender leaves (*Pergularia daemia*)
Kuppaimeni tender leaves (*Acalypha indica*)
Vembu tender leaves (*Azadirachta indica*)
Nothchi tender leaves (*Vitex negundo*)

Purification: All tender leaves were washed with running water.

Method of Preparation

The above-mentioned tender leaves were washed & grounded with water & made in to a paste. Then it was applied over the sterilized cloth /gauze & made in to *thiri* (*Kaarathiri*)

Method of application

The medicated *thiri* before inserting into the tract dipped in castor oil & inserted. After 2 days the *Kaarathiri* was removed & then new *Kaarathiri* was inserted. This procedure was done up to cut through the tract.





Kavitha et al., .

Naayuruvi**Organoleptic Character****Bitter:** Astringent, Pungent**Potency:** Hot**Division:** Pungent**Pharmacological Activity****Antimicrobial Activity**

P.Saravanan *et al.*, (2010)[4] reported the solvent leaf extracts were tested for antibacterial & antifungal activities against *E. coli*, *P. aeruginosa*, *P. vulgaris*, *S. aureus*, *Klebsiella* species

Anti-Inflammatory Activity

T. Vetrichelvan & M. Jegadeesan (2003)[5] reported the alcoholic extracts of leaves & seeds show anti-inflammatory activity in rats using carrageenan-induced paw edema method & formalin model.

Wound Healing Activity

S. Edwin *et al.*, (2008)[6] investigated the ethanolic & aqueous of leaves of *A. aspera* for wound healing activity. The wound healing activity was studied using two wound model & incision wound model.

Analgesic Activity

The hydro alcoholic extract of the leaves & roots of *A. aspera* shows centrally acting analgesic activity in adult male albino rats using tail flick hot plate & acetic acid induced writhing method for peripherally acting analgesic activity using aspirin as standard drug (Kumar H, *et al.*,) [7]

Uthamani**Organoleptic character:****Taste:** Bitter,**Potency:** Hot**Division:** Pungent**Pharmacological Activity****Antibacterial Activity**

The antibacterial activity was observed against *Staphylococcus aureus*, *Pseudomonas aeruginosa*, *Escherichia coli*, & *Salmonella typhi* in ethyl acetate & ethanol extracts of *P.daemia* (Senthil Kumar *et al.*, 2005)[8].

Antifungal Activity

The antifungal activity of *Pergulariadaemia* was reported against keratinophilic fungi by dry weight method (Qureshi *et al.*, , 1997)[9]. *Pergulariadaemia* plant salts were used against *Aspergillus flavus*, *Cryptococcus neoformans*, & *Candida albicans*. In this study, they showed the inhibitory effect against only *Aspergillus flavus* (Suresh *et al.*, , 2010)[10]

Anti-Inflammatory, Analgesic Activity

Crude ethanol extract of *Pergularia daemia* leaves were successfully prepared by fractionating the solvents like petroleum ether, solvent ether, ethyl acetate, butanol, & butanone. The ethanolic extract & different fractions were analyzed for anti-inflammatory activities in rats. Ethanol extract & its butanol fraction showed significant results of anti-inflammatory activity when compared with other fractions (Hukkeri *et al.*, , 2001)[11]. The anti-inflammatory activity of *Pergularia daemia* extract is mainly due to the presence of steroids (Sutar *et al.*, , 2009)[12]. The analgesic effect was experimentally demonstrated by using eddy's hot plate & heat conduction method & analyzed statistically by Turkey Kramer Multiple comparison Test.

Kuppaimeni**Organoleptic character**

**Kavitha et al, .,****Taste:** Bitter, Pungent**Potency:** Hot**Division:** Pungent**Pharmacological Activity****Antibacterial Activities**

Govindarajan *et al*, ., 2008 [13] investigated the antibacterial activity of *A.indica* the shade dried coarsely powdered leaves were subjected to Soxhlet extraction using hexane, chloroform, ethyl acetate & methanol. These extracts were tested against gram positive bacteria- *Streptococcus aureus*, *Staphylococcus epidermis*, *Bacillus cereus*, *Streptococcus faecalis* & gram-negative bacteria- *Klebsiella pneumonia*, *E.coli*, *Proteus vulgaris* , *Pseudomonas aeruginosa*.

Wound Healing Activity

Vinoth raja *et al*, ., 2009[14] were evaluated the ethanolic extracts of wound healing activity in rats. The water extracts of *A. indica* showed the maximum inhibition for *Streptococcus aureus* & *Pseudomonas aeruginosa*. This screening of antibacterial activity of from costal population of medicinal plants has been highly effective to control the wound infective bacteria.

Analgesic Activity

Acalypha indica has analgesic properties as proven by conducting in vivo studies on mice (Rahaman *et al*, , 2010)[15]. They used a writhing reflex method developed by (Vogel. H, 2007)[16]to determine the analgesic activity of the *Acalypha indica* hexane extract.

Anti-Inflammatory Activity

Acalypha indica extract can behave as an anti-inflammatory medicine in the human body. Identified this activity of the *A. indica* the long even rats by using ethanolic extract. They used the anti-inflammation method with minor modifications & selected phenylbutazone as the standard drug for this activity (Rahaman *et al*, , 2010)[15]. Soruba *et al*, , 2015[17] were proven the *A. indica* plant extracts stabilized the membrane by inhibiting hypotonicity- induced lysis of San erythrocyte membrane analogous to a lysosomal membrane.

Vembu**Organoleptic character:****Taste:** Bitter**Potency:** Hot**Division:** Pungent**Pharmacological Activity****Wound Healing Effect**

Numerous plants their constituents play an important role in wound healing effect. A study was made to evaluate the wound healing activity of the extracts of leaves *A. indica* & *T. cordifolia* using excision & incision wound models in Sprague Dawley rats & results revealed that extract of both plants significantly promoted the wound healing activity in both excision& incision wound models(Barura C.C. *et al*, 2013 [18]. Furthermore, in incision wound tensile strength of the healing tissues of both plants treated groups was found to be significantly higher as compared to the control group (Ofusori D.A *et al*, 2010)[19]. Other results showed that leave extracts of *Azadirachta indica* promote wound healing activity through increased inflammatory response & neovascularization.(Osunwoke Emeka A, *et al*, 2013) [20] The aqueous extract of *Azadirachta indica* leaves exhibited antiulcer activity (Anonymous, 2004; Khare, 2007)[21, 22]

Anti-Inflammatory Activity

The aqueous extract of *A. indica* leaves exhibited anti-inflammatory activity (Anonymous 2004; Khare 2007)[21,22]



**Kavitha et al, .,**

Aqueous & petroleum ether extracts of *Azadiracta indica* leaves reduced the inflammation caused by *S. typhimurium* & its OMPs as assessed by paw flicking response. Petroleum ether *A.indica* leaf extract was found to be more effective than aqueous extract may be due to presence of steroids & triterpenoids observed in petroleum ether extract (Koul et al, 2009)[23]

Antimicrobial Activity

The organic extracts of neem (petroleum ether, chloroform, ethanol & aqueous)were screened for its antimicrobial activity against *Streptococcus mutans*, *Streptococcus salivarius* & *Fusobacterium nucleatum* strains causing dental caries method & showed that the chloroform extracts of neem has a strong antimicrobial activity(Lekshmi et al, 2012)[24]

Notchi**Organoleptic character:**

Taste: Bitter, Astringent, Pungent

Potency: Hot

Division: Pungent

Pharmacological Activities**Antibacterial Activity**

Kamruzzaman Met al, 2013[25] evaluated the antibacterial activity of *Vitex negundo* leaves extracts in water & methanol. *Vitex negundo* leaves were evaluated against enteric bacterial pathogens by using standard disc diffusion , viable bacterial cell count methods the first time we showed that methanol extract of *Vitex negundo* leaves exhibited strong bacterial activity both in vitro & vivo conditions.

Anti-Inflammatory Activity

Suganthi N et al, ., 2016[26]observed that the Carrageen in induced hind paw oedema & cotton pellet granuloma test in albino rats were used to study the potential role of *Vitex negundo Linn* leaf extract in sub effective doses as adjuvant with standard anti- inflammatory & the study proved that the sub effective doses of *Vitex negundo Linn* potentiated anti -inflammatory activity phenylbutazone & ibuprofen & can be used as adjuvant with standard anti-inflammatory.

Analgesic Activity

Anti-inflammatory drug make about half of analgesic activity, alleviate pain by reducing inflammation as opposed to opioids which affect the central nervous system. Anti-inflammatory properties of *Vitex negundo* extracts in acute & sub-acute inflammation were established by Yunos et al, . (2005) [27] & Jana et al, (1999)[28] anti-inflammatory & pain suppressing activities of fresh leaves of *V. negundo* are attributed to prostaglandin synthesis inhibition (Telang, 1999)[29], Antihistamine membrane stabilizing & antioxidant activities.(Dharmasiri, 2003)[30]

CONCLUSION

Based on the review of various *Siddha* texts, ingredients of *Kaarathiria* remedical herbs used in treating *Pouthiram* (Fistula in ano). In view of the above-mentioned pharmacological activities, most of the ingredients are found to possess Anti- inflammatory activity, Anti- microbial activity, Analgesic activity & wound healing activity which are responsible for its therapeutic indication as claimed in *Siddha* literature.

REFERENCES

1. Rajamuthaliyar T ,YugiVathiyaSithamani 800, Yelumalaipillai Publication 1890, P. no 308-312.





Kavitha et al.,

2. Saadeldin Ahmed Idris, Arafa Eltayaeb Hassan Abdalla, Aamir Abdullahi Hamza, *Medicine Journal* 2015;2(6) 99-102.
3. Venkattaraajan, S Sarabanthirar Vaithiya Muraigal ; Viranam Karappan Roga Sikkichai, Sarawathi Magalnoolagam 2007, P-101.
4. Saravanan, P., Ramasamy .V, Shivakumar. T. *Asian Journal of Chemistry*, 2008, 20(1), 823-825
5. Vetrichelvan .T & Jegadeesan. M. *Phytography Research* 2003, 17(1), 77-79.
6. Edwin .S, Jarald S, Edwin. D.L ,Jain A, Kinger .H, Dutt.K.R, Raj A.A. *Pharmacological Biology*, 2008, 46 (12), 824-828.
7. Kumar H, Singh D, Kushwaha SKS Gupta AK Comparison of leaf & root extract of *Achyranthus aspera* for its analgesic activity). *Der Pharmacia Lettre* 1(2): 193-198.
8. Senthil Kumar, M.,P. Gurumoorthi, & K. Janardhanan, *Antibacterial potential of some plants used by tribals in Maruthamalai hills, Tamil nadu Nat.Prod. Radiance*, 2005 4:27-34.
9. Quershi, S., Rai, M K., & Agarwal .S. C., 1997 . *In vitro* evaluation of inhibitory nature extracts of 18-plant species of Chindwara against 3-Keratinophilic fungi . *Hindustan Antibiotics bulletin* , 39:31-42.
10. Suresh, M., Rath , P.k., Panneerselvam A., Dhanasekaran., & Thajjudin, N., 2010., *Antifungal activity of selected Indian Echnopharmacology* ,107;164-168.
11. Hukkeri, V.I., Patil, M.B, Jabalpure , S.S., Ali, A., 2001. *Anti-inflammatory activity of a various extracts of Pergularia extensa (Asclepiadaceae)*. *Indian Journal of Pharmaceutical Sciences*, 63:429-431.
12. Sutar, N G., Sharma, Y P., Kendre, P.N Panigrahi, M. k., Deshmukh, T,A., & Jain,N.P., 2009 *Anti-inflammatory activity of whole plants from similar Biosphere reserve, Orissa. Asian Journal of plant Sciences* 7; 260-267.
13. Govindarajan M, Jebanesan A, Puspanathan T, Samidurai K, *antibacterial activity of Acalypha indica L. European review for Medical & Pharmacological Sciences*. 2008; 12: 299-302.
14. Vinoth raja A, Ramanathan T, Savitha S, *studies on wound healing property of coastal medicinal plants. Journal of Biosci. Tech.* 2009 Vol-1(1) 39-40.
15. Rahaman M.A, Bachar S.C Rahamathullah. M *Analgesic & anti-inflammatory activity of methanolic extract of Acalypha indica Linn. Pak. J. Pharm.Sci*, 2010 23:256-258.
16. Vogel H. *Drug discovery & evaluation: Pharmacological assays* Springer Science & Business Media 2007 .
17. Soruba E Sundaram V, Pathy Manian R, Kulanthai velu K, Balasundram S. *Antioxidant, Antibacterial & Anti-inflammatory activity of A.indica & Terminalia chebula: An In-vitro analysis. Research Journal of Pharmaceutical , Biological & Chemical Sciences* 2015; 6:180.
18. Barua C.C , Talukdar.A, Barua A.G, A. Chakraborty, Sarma R.K & Bora R.S, "Evaluation of the wound healing activity of methanolic extract of *Azadirachta indica* & *Tinospora cordifolia* in rats *Pharmacology online* Vol. 3, no.2, pp.142-146, 2013.
19. Ofusori .D.A, Falana B.A, Ofusori A.E Abayomi T.A, Ajayi S.A, & Ojo G.B, *Gastroprotective effect of aqueous extract of neem Azadirachta indica on induced gastric lesion in rats International Journal of Biological & Medical Research*, vol. 1, pp, 219-222, 2010.
20. Osunwoke Emeka .A, Olotu Emamoke. J . Allison Theodore & C. Onyekwere Julius, "the wound healing effects of aqueous leave extracts of *Azadirachta indica* on Westar rats " *Journal of natural Science & Research* vol.3 no.6, 2013.
21. Anonymous the wealth of India , Publication & Information Directorate CSIR, New Delhi , 2004; 1:107-111.
22. Khare C.P. *Encyclopedia of Indian medicinal plants*. Springer Berlin Heidelberg, New York. 2007, 75-76.
23. Koul A, Bharrhan S, Singh B, Rishi P. *potential of Azadirachta indica against Salmonella typhimurium induced inflammation in BALB/cmice iflammopharmacology*. 2009; 17(1):29-36.
24. Lekshmi NCJP, Sowmia N, Viveka S, Brindha JR, *against dental pathogens . Asian Journal of plant Science & Research* 2012;2(1):6-10.
25. Kamruzzaman M, Bari S.M.N & Shah M.F. *In vitro & in vivo bactericidal activity of Vitex negundo leaf extract against diverse multidrug resistant enteric bacterial pathogens. Asian pacific Journal of Tropical medicine*, 2013;325-359.
26. Suganthi N, *Phytochemical constituents & pharmacological activities of Vitexnegundo*, *Journal of chemical & pharmacological research*, 2016. 8(2) 800-807.





Kavitha et al, .,

27. YunosN.M.,Mat Ali, R., Kean O.B. & Abas R. Cytotoxicity Evaluations on *Vitex negundo* Anti-inflammatory Extracts , Malaysian Journal of Science , 2005; 24: 213-217.
28. Jana, U., Chattopadhyay, R.N. & Shaw ,B.P. Preliminary studies on anti-inflammatory activity of *Zingiber officinale*Rosc., Indian Journal of Pharmacology 1999;31:232-233.
29. Telang, R.S., Chatterjee, S. &Varshneya C. 'Studies on analgesic & anti-inflammatory activities of *Vitex negundo* Linn' Indian journal of pharmacology, 1999;31:363-366.
30. Dharmasiri, M.G., Jayakody, J.R.A.C., Galhena, G., Liyanage, S.S.P &Ratnasooriya, W.D. Anti-inflammatory & Analgesic activities of mature fresh leaves of *Vitex negundo*, Journal of Ethnopharmacology, 2003; 87: 199-206.

Table 1: Describes the ingredients of *Kaarathiri* with botanical name, English name family name & used parts of each drug.

S.No	Tamil name	English name	Botanical name	Family name	Parts used
1.	<i>Naayuiruvi</i>	Rough ghaff	<i>Achyranthes aspera</i>	Amaranthaceae	Tender leaves.
2.	<i>Uthamani</i>	Trellis vine	<i>Pergulariadaemia</i>	Apocynaceae	Tender leaves.
3.	<i>Kuppaimeni</i>	Indian Acalypha	<i>Acalypha indica</i>	Euphorbiaceae	Tender leaves.
4.	<i>Vembu</i>	Neem	<i>Azadirachta indica</i>	Meliaceae	Tender leaves.
5.	<i>Nothchi</i>	Chinese chaste tree	<i>Vitex negundo</i>	Lamiaceae	Tender leaves.

Table 2: Describes the ingredients of *Kaathiri* with chemical constituents of each drug.

S.No	Medicinal Plants	Chemical constituents
1.	<i>Naayuiruvi</i>	Achyranthine, betaine, hentriacontane, achyranthes Saponins
2.	<i>Uthamani</i>	Lupeol, alpha- sitosterol, lupeol acetate, alpha, beta- amyrrin, acetate, betaine, uscharidin, calotoxin, calotropin, calactin
3.	<i>Kuppaimeni</i>	Acalyphine, acalyphamide, amides, quinine, kaemperol, casticin, sabinene, farnesol
4.	<i>Vembu</i>	Azadirachtin, nimbolide, nimbin, nimbidin, nimbolide, gallic acid, epicatechin, margolone& catechin.
5.	<i>Nothchi</i>	flavonoids, volatile oil, triterpenes, glycosides, iridoid glycosides, sesquiterpenes, ligan, flavones glycosides & stilbene derivates





AI and Cloud based Prediction and Diagnosis of Various Heart using Data Mining Techniques with Supervised Learning Technique

S. Senthil Kumar^{1*} and C.Naveeth Babu²

¹Assistant Professor, Department of Information Technology, Sri Ramakrishna Mission Vidyalaya College of Arts and Science, Coimbatore, Tamil Nadu, India

²Assistant Professor, Department of Computer Science, Kristu Jayanti College, Bengaluru, India.

Received: 28 Feb 2023

Revised: 24 Apr 2023

Accepted: 26 May 2023

*Address for Correspondence

S. Senthil Kumar

Assistant Professor,

Department of Information Technology,

Sri Ramakrishna Mission Vidyalaya College of Arts and Science,

Coimbatore, Tamilnadu, India



This is an Open Access Journal / article distributed under the terms of the **Creative Commons Attribution License** (CC BY-NC-ND 3.0) which permits unrestricted use, distribution, and reproduction in any medium, provided the original work is properly cited. All rights reserved.

ABSTRACT

Medical care is the main application area for getting exact and furthermore taking on "haze processing" and constant outcomes for positive turns of events. The security in medical services can be expanded by presenting haze figuring through taking the assets closer to the clients fully intent on achieving the base dormancy. It brings about achieving prior results, empowering vital and speedier activities to fix basic heart patients. AI and Cloud based Prediction and Diagnosis of various heart diseases and chances of Heart attack and to prevent at early stage with affordable rate using Data Mining Techniques and Machine Learning algorithms Abstract: At this time, heart disease is considered to be one of the major causes all over the world. Because it is a complicated endeavour that necessitates knowledge as well as a significant amount of information for medical professionals to foresee, it is not something that can be simply predicted. The availability of a vast number of data is made possible by healthcare platforms that are based on the internet. On the other hand, adequate data analysis tools that can unearth buried connections and patterns in the data are in short supply. A technology that automates medical diagnosis would enhance productivity in the medical industry while also lowering costs. This web application's overarching goal is to use information gleaned from clinical research — specifically heart disease — to make educated guesses about the likelihood of a condition developing. The goal of this project is to use data mining techniques to identify patterns within the information that are important to heart illness, and then use those patterns to make predictions about the presence of heart disease in persons whose presence is measured on a scale. Predicting cardiac disease requires a huge amount of data that is both too complex and too massive to be processed and analysed using the procedures that are considered to be the industry standard. Our goal is to determine the one machine learning method that is superior to all others in terms of its ability to accurately forecast cardiac illness while simultaneously minimising the amount of computer resources required to do it.

Keywords: Heart Diagnosis, Internet of Things, AI, SVM, ESVM, Data Mining





INTRODUCTION

Cancer is the second leading cause of death in India, but heart disease remains the leading cause of death. According to the World Health Organization (WHO), heart disease is the leading cause of death, accounting for 31% of all deaths annually. As a result, it is crucial to receive an accurate diagnosis as soon as possible to lower mortality rates. In databases, data mining tools can unearth previously undisclosed information. Using the new information, those in charge of the healthcare system could attempt to enhance the service they deliver to patients. Doctors can also use this new information to reduce the amount of undesirable side effects and discover less expensive alternatives with equivalent efficacy. Predicting future patient behaviour is the most essential application of data mining techniques in healthcare administration. This is one application possibility. Providing high-quality services at cheap prices is one of the most difficult difficulties hospitals and medical centres face in the present day. To offer proper care, precise diagnoses and effective treatment approaches are required. Inadequate clinical judgement can have catastrophic results and is therefore unacceptable. The most crucial aspect is to avoid making these mistakes. The costs associated with clinical exams should be kept as low as possible by hospitals. Utilizing the necessary computer-based information and/or decision-making tools, they accomplish these objectives. In health care, there are many data. It contains information about patients, how resources are utilised, and how data is amended. Any healthcare professional must be capable of data analysis. The treatment records of millions of patients can be preserved, and data mining and other forms of computerization may provide light on some of the most serious health-care issues of the present day.

Literature Survey

Another patient checking structure was executed by Sarmah to help heart patients utilizing "Profound Learning Altered Brain Organization (DLMNN)" with IoT gadgets to analyze heart illnesses. This model purposes three stages like "(i) confirmation, (ii) encryption, and (iii) grouping." At first, the heart patient's specific clinic was validated by utilizing the SHA-512 with the replacement figure. Further, the wearable IoT sensor gadget was remembered for a "patient's body," where the sensor information was communicated simultaneously to the cloud. The High level Encryption Standard (AES) was utilized for encoding the information including "patient id, specialist id, and emergency clinic id" and "safely moved to the cloud." Then, in the wake of unscrambling the information, the DLMNN classifier was utilized to come by the grouped outcomes as unusual and ordinary classes. The recommended model has zeroed in on diagnosing the heart states of patients. The exploratory outcomes were contrasted with other ordinary procedures with get high security and furthermore accomplished less encryption and unscrambling time. The "IoT-empowered ECG checking framework" for examining the ECG signal was executed by Lakshmi and Kalaivani, where the measurable elements were extricated and dissected through the "Dish Tompkins QRS recognition" strategy to get the powerful highlights. The "dynamic and measurable highlights" were then used for the characterization phase of anticipating the cardiovascular arrhythmia illness. This model has zeroed in on examining the gamble levels of cardiovascular circumstances from ECG signals. This model was helpful for general experts to assess coronary illness precisely and without any problem.

Proposed Framework Using MI and Data Mining Techniques for Heart Disease

Many therapeutic decisions are primarily based on the attending physician's judgement and expertise, as opposed to the massive amounts of data included in databases. This technique leads to biases, errors, and rising healthcare costs, all of which diminish the quality of patient care. Wu *et al.* hypothesised that the incorporation of clinical decision support into electronic health records (EHRs) would improve medical outcomes by reducing errors, making patients safer, minimising unnecessary practise variation, and standardising care. This idea has considerable promise since it can contribute to the development of a culture that values acknowledgments, which can significantly improve the quality of treatment decisions made using data modelling and analytical approaches such as data mining. In recent years, the Internet of Things (IoT) has gained popularity as a novel concept among academics and businesses. This system, along with others, will benefit both people and the environment as a whole. This category encompasses business owners, consumers, the environment, individuals, and society at large (SHM). Structural health monitoring



**Senthil Kumar and Naveeth Babu**

(SHM) gathers data from a variety of sensors to determine the performance of a structure and how to keep it safe. The proposed system utilises Internet of Things technology to create a surveillance system that can monitor a patient in real time and from any location without requiring the nurse to be present at all times or in any location. Anywhere: The manufacturer claims that because it utilises in-house human behaviour detection and classification, this system can be used to monitor patients. This device is suitable for use by anyone and is extremely simple to operate due to its simplicity and low price. This system, which makes use of small, energyefficient devices, enables people from all over the world to communicate. Heart rate data can be extremely useful when creating a workout plan, analysing your activity or stress levels, or simply when you want your shirt to blink in time with your heartbeat. Calculating your heart rate can be challenging in some cases. While this is not always a bad thing, Pulse Sensor Amped can aid in the process.

Data Collection

Dataset having 303 total instances [Kim and Kang (2017)]. 213 samples (70%) are used for training whereas 90 samples (30%) are used for validation[7].

Data Pre-Processing

213 total patient samples are taken which further divided into 88 negative and 125 positive patient samples. It is clearly shown that 82 patient samples are estimated correctly in which no heart disease found, whereas 06 patient samples are wrongly estimated as positive in which heart disease found, but heart disease not exist. Similarly, 121 patient samples are correctly estimated as positive in which heart disease found and 04 samples are estimated wrongly in which heart disease not found, but in real heart disease exists.

Data Mining and Machine Learning Technique to Predict Heart Disease

The Support Vector Machine (SVM) is a supervised learning technique introduced first by Vapnik and has been applied in several applications recently, mainly in the area of time series prediction and classification [12]. SVM has yielded excellent generalization performance on a wide range of problems including bioinformatics, text categorization, image detection, micro-array gene expression data analysis, tone recognition, etc.SVM is called Maximum Margin Classifiers and it can be efficiently perform non-linear classification using kernel trick. An SVM model is a representation of the examples as points in space, mapped so that the examples of the separate categories are divided by a large margin gap that is as wide as possible.

An automated Machine Learning classifier for the discrimination between the person with heart disease and without heart disease has been developed using supervised learning algorithm named SVM with some modification Enhanced SVM(ESVM).As a result, this article will describe how to build an IoT-based heartbeat monitoring and alert system. Through the Internet of Things, you can monitor things like structural health using a variety of wireless technologies. As the Internet of Things gains traction, new technologies are being developed to meet community needs. Several Internet of Things (IoT) communication solutions for structural health monitoring have been proposed in recent years. These solutions establish a connection between network devices capable of detecting and collecting useful data. Chronic diseases are increasing in prevalence among the elderly, which is a major concern because there are insufficient resources and the costs of treatment are exorbitant. People who live in remote areas without access to medical facilities face an even greater risk of death as a result of late diagnosis and treatment. Diagnosis and treatment are critical to our success. Wireless communication and wearable sensors have enabled real-time healthcare monitoring systems. For people who live in remote areas, this study recommends real-time heart monitoring. System: Wearable sensors, an Android phone, and a web-based interface comprise the system. Due to the system's adaptability, it is capable of simultaneously collecting heart rate, blood pressure, and temperature readings from a large number of people. The extracted data is transmitted via Bluetooth low energy to an Android handheld device. The Android device then sends the data to a web application for further analysis. Individuals can access their medical history and personal information, such as their age, gender, address, and location, via a web interface displayed by the web application following data processing from the website. A threshold-based alarm system has been developed to alert the physician to any abnormalities such as arrhythmia, low blood pressure, high



**Senthil Kumarand Naveeth Babu**

blood pressure, fever, or hypothermia. The system monitored forty (40) heart patients who were physically separated from the web application in order to evaluate and demonstrate the system's functionality in real-world situations. The researchers determined that the data obtained via the system was statistically significant and sufficient. Additionally, Wi-Fi and 3G wireless protocols are used to validate remote monitoring by determining the time required to transmit data from the patient's interface to the doctor's interface. This is the time required to send the data. The message transmission times of both wireless protocols were found to be within the acceptable range of medical standards (4 to 6 minutes as per American Heart Association). The purpose of this research is to develop a wireless real-time monitoring system for people who live in remote areas. The built-in system is expected to alert the doctor in the event of a medical emergency. Due to the fact that 3G signals can be spotty in some remote areas, this process may take longer. Future research should consider whether to include a delayed alarm even when the optimal time window remains available. The proposed remote monitoring system will be more useful if it is implemented using wireless technology. This may become a possibility as wireless technology advances. False alarms can be caused by a variety of factors, including sensor and smartphone battery issues. Due to the battery life and false alarms, additional research can be conducted to come up with a solution.

Discovery Of Knowledge

Further, it also observed that the proposed intelligent cloud-based heart disease prediction system empowered with supervised machine learning-based system model gives 96.56% & 95.81% accuracy during training and validation respectively

CONCLUSION

Heart disease builds the death rate all over the planet. Subsequently, expectation of heart infections is fundamental, yet the distinguishing proof of heart illnesses is testing and requires both complex and expertise understanding.

REFERENCES

1. Atamanyuk, I. P.; Kondratenko, Y. P. (2015): Calculation method for a computer's diagnostics of cardiovascular diseases based on canonical decompositions of random sequences. *Information and Communication Technologies in Education, Research, and Industrial Applications*, vol. 1365, pp. 108-120.
2. Galper, S. L.; James, B. Y.; Mauch, P. M.; Strasser, J. F.; Silver, B. *et al.* (2011): Clinically significant cardiac disease in patients with Hodgkin lymphoma treated with mediastinal irradiation. *Blood*, vol. 117, no. 2, pp. 412-418.
3. Gu, K.; Wu, N.; Yin, B.; Jia, W. J. (2019): Secure data query framework for cloud and fog computing. *IEEE Transactions on Network and Service Management*.
4. Hassan, A.; Bilal, H. M.; Khan, M. A.; Khan, M. F.; Hassan, R. *et al.* (2018): Enhanced fuzzy resolution appliance for identification of heart disease in teenagers. *International Conference on Intelligent Technologies and Applications*, pp. 28-37. <http://www.who.int/mediacentre/factsheets/fs317/en/>.
5. Hussain, A.; Syed, A. H.; Abeer, F.; Shahan, Y. S.; Anwar, S. *et al.* (2020): A novel approach for thyroid disease identification empowered with fuzzy logic. *International Journal of Computer Science and Network Security*, vol. 20, no. 1, pp. 173
6. Kagadis, G.; Alexakos, C.; Papadimitroulas, P.; Papanikolaou, N.; Megalookonomou, V. *et al.* (2015): Cloud computing application for brain tumor detection. *European Congress of Radiology*, Poster C-1851, pp. 1-16.
7. Kim, J. K.; Kang, S. (2017): Neural network-based coronary heart disease risk prediction using feature correlation analysis. *Journal of Healthcare Engineering*, vol. 2017, pp. 1-13.
8. Kumar, P. J.; Chaithra, M. A. (2015): A survey on cloud computing based health care for diabetes: analysis and diagnosis. *IOSR Journal of Computer Engineering*, vol. 17, no. 4, pp. 109-117.
9. Li, H. X.; Li, W. J.; Zhang, S. G.; Wang, H. D.; Pan, Y. *et al.* (2019): Page-sharing-based virtual machine packing with multi-resource constraints to reduce network traffic in migration for clouds. *Future Generation Computer Systems*, vol. 96, pp. 462-471.





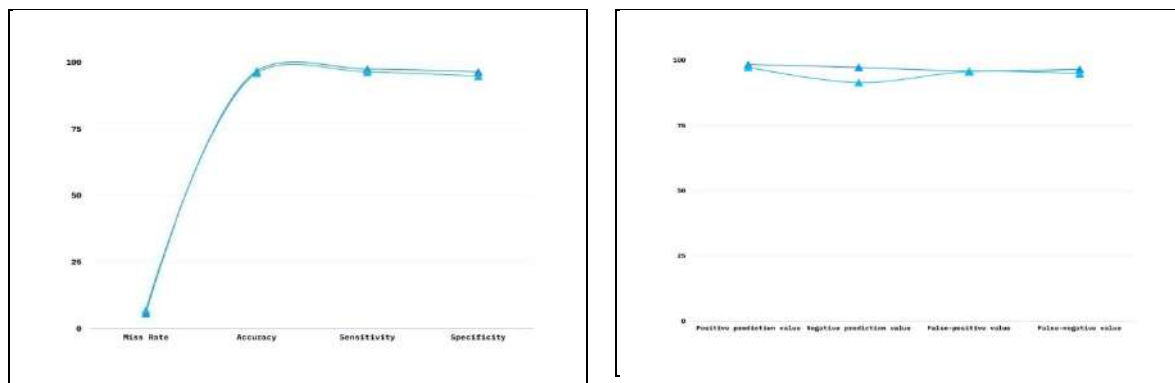
Senthil Kumar and Naveeth Babu

10. Siddiqui, S. Y.; Athar, A.; Khan, M. A.; Abbas, S.; Saeed, Y. *et al.* (2020): Modelling, simulation, and optimization of diagnosis of cardiovascular disease using computational intelligence approaches. *Journal of Medical Imaging and Health Informatics*, vol. 10, no. 5, pp. 1005-1022.
11. Wang, X.; Gui, Q.; Liu, B.; Jin, Z.; Chen, Y. *et al.* (2014): Enabling smart personalized healthcare: a hybrid mobile-cloud approach for ECG telemonitoring. *IEEE Journal of Biomedical and Health Informatics*, vol. 18, no. 3, pp. 739-745.
12. Christopher J.C. Burges. A Tutorial on Support Vector Machines for Pattern Recognition. *Data Mining and Knowledge Discovery*, Springer,2(2), PP.121-167, 1998.

Table 1. Pattern Evaluation

ML Techniques	Miss Rate	Accuracy	Sensitivity	Specificity
ESVM	5.69%	96.56%	97.35%	96.28%
SVM	6.87%	95.81%	96.29%	94.73%

ML Techniques	Positive prediction value	Negative prediction value	False-positive value	False-negative value
ESVM	98.28%	97.18%	95.78%	96.45%
SVM	97.25%	91.39%	95.59%	94.83%



Graph 1. Pattern Evaluation

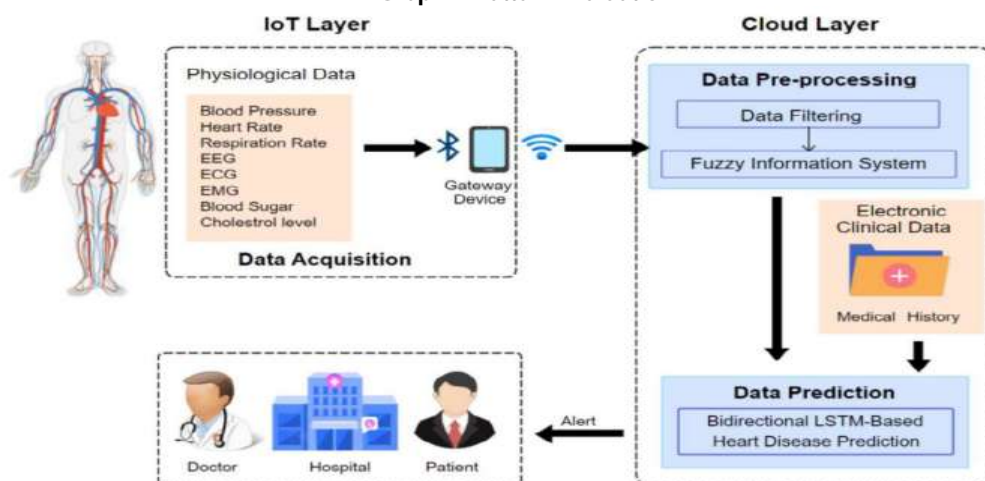


Fig (A) Smart Heart Disease Framework using IoT and Cloud





Senthil Kumar and Naveeth Babu

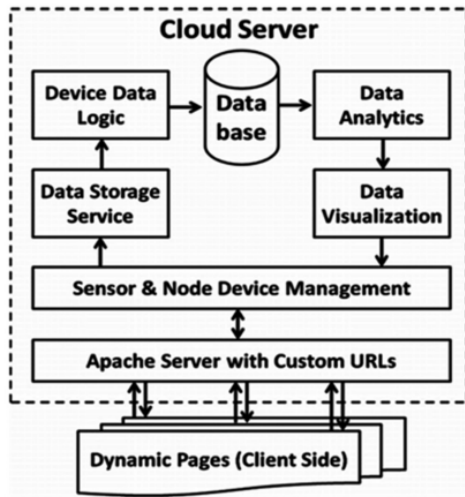


Fig (B) Cloud – How It works

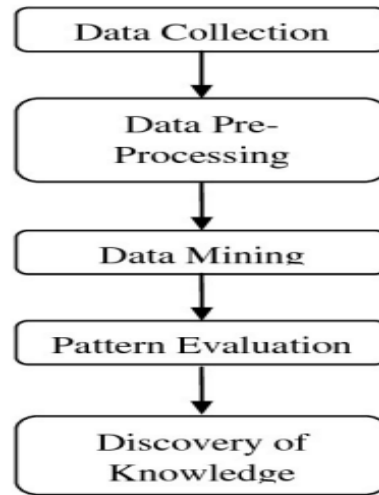


Fig (C) Proposed Heart Disease Prediction Steps





Study on Macro and Micro Nutrient Contents Present in *Padina gymnospora* and *Ulva lactuca*

N.Praba^{1*} and S. Sumaya²

¹Ph.D Research Scholar, Department of Home Science and Research Centre, Thassim Beevi Abdul Kader College for Women, Kilakarai (Autonomous), Affiliated to Alagappa University, Karaikudi, Tamil Nadu, India.

²Professor and Head, Department of Home Science and Research Centre, Thassim Beevi Abdul Kader College for Women, Kilakarai (Autonomous), Affiliated to Alagappa University, Karaikudi, Tamil Nadu, India.

Received: 28 Mar 2023

Revised: 28 Apr 2023

Accepted: 31 May 2023

*Address for Correspondence

N.Praba

Ph.D Research Scholar,
Department of Home Science and Research Centre,
Thassim Beevi Abdul Kader College for Women,
Kilakarai (Autonomous),
Affiliated to Alagappa University,
Karaikudi, Tamil Nadu, India.
E. Mail: praba2188@gmail.com



This is an Open Access Journal / article distributed under the terms of the **Creative Commons Attribution License** (CC BY-NC-ND 3.0) which permits unrestricted use, distribution, and reproduction in any medium, provided the original work is properly cited. All rights reserved.

ABSTRACT

The marine environment contains many varieties of sea animals like sea horse, sea cow, plants, corals out of these seaweeds play a major part. Seaweeds are nutrient dense compared to land plants. Seaweeds contain macro nutrients such as Carbohydrates, Proteins, Fats and Fibre and micronutrients such as Calcium, Potassium, Sodium, Magnesium, Chlorine, Iodine, Copper and Zinc. These nutrients on regular consumption which are essential for a healthy lifestyle and can eradicate many health problems. The aim of the present study was to evaluate the amount of macro and micro nutrients present in the selected seaweeds *Padina gymnospora* and *Ulva lactuca*. These two seaweeds were handpicked from Gulf of Mannar Coast. The estimation of macro and micronutrients was analyzed by standard protocols and resulted that both the seaweeds are equally nutrient dense. The result concluded that the selected seaweeds were safe for human consumption.

Keywords: *Padina gymnospora* and *Ulva lactuca*, Gulf of Mannar Coast, Macro and Micro Nutrients.





INTRODUCTION

India is a peninsular country surrounded by three segments with water. The seaweeds are present in the intertidal and tropical waters and known as the primary source of natural products. The cultivation of seaweed is the main occupation for the fisherman community in the coastal areas. Seaweeds are differentiated into green, brown and red. Seaweeds are the best sources of different nutrients which are needed for a healthy living [1]. The high amounts of fibre, complete proteins, carbohydrates, fats and minerals are found more in seaweeds compared to other plant food sources. The seaweeds are consumed either in the raw form or made into value added products to make it more palatable and delicious. Balanced nutrient food source is available more in seaweeds than other sources. The seaweeds are the excellent source of nutrients which makes a healthy food for human consumption. According to [2] dietary seaweeds provides many health benefits for the brain development. Red and brown seaweed are most commonly used for human consumption either raw or as processed foods. The following seaweed species such as *Acanthophora spicifera*, *Caulepra lentillifera*, *C. racemosa*, *Eucheuma denticulatum*, *Ulva sp.*, *Gracilaria sp.*, *Nori*, *Wakame* and *Kombu* are eaten as low calorie food, soups, salads. There are varieties of seaweeds across the world, utilised as food for human consumption, fodder for animals, fertilizers for plants and other beneficial applications in non-edible forms. Among the macro nutrients Carbohydrate helps in the metabolic changes and provides energy needed for many vital functions. The futuristic healthy food seaweeds contain cellulose and soluble fibre, which has important nutritional benefits. Seaweed contains more amino acids than the plant based foods. Seaweeds contain more amounts of fatty acids important for neural development. Seaweeds contain natural nutrients and health promoting micronutrients [3].

MATERIALS AND METHODS

Selection and Analysis of Seaweeds

The seaweeds samples for the present investigation were collected from Gulf of Mannar as it is a Marine Biosphere Reserve located along the east coast of South India from Rameswaram to Tuticorin. The samples for the study constituted *Padina gymnospora* and *Ulva lactuca* of brown and green seaweed respectively. The seaweeds were collected by handpicking at low tide Mandapam coastal area.

Processing of Seaweed Samples

The collected samples were cleaned well with seawater to remove all the extraneous matter such as epiphytes, sand particles, pebbles and shells and brought to the laboratory in plastic bags. The samples were thoroughly washed with tap water followed by pure distilled water. For drying, samples are blotted on the blotting paper and spread out in shade. Shade dried samples were grounded into fine powder using a blender. The powdered samples were stored in refrigerator for further use.

Preparation of Seaweed Extracts

15 gm powder was initially soaked in 60ml of petroleum ether in air tight conical flask for two days and then it was first filtered through double layered muslin cloth and then filtered through Whatman no 1 filter paper and filtrate was collected into sterile air tight bottle. Similar process was repeated twice with fresh petroleum ether and the filtrate was collected together. Petroleum ether was removed from the filtrate at 40°C using oven and the extract was stored in the refrigerator. The above dried residues were used for sequential extraction with acetone, ethanol, methanol and water for further studies.

Estimation of Fibre Content Present in the Selected Seaweed Samples

1. Extract 2gm of ground material with ether or petroleum ether to remove fat.
2. After extraction with ether boil 2gm of dried material with 200ml of sulphuric acid for 30minutes with bumping chips.
3. Filter through muslin and wash with boiling water until washings are no longer acidic.





Praba and Sumaya

4. Boil with 200ml of sodium hydroxide solution for 30 minutes.
5. Filter through muslin cloth again and wash with 25ml of boiling 1.25% sulphuric acid, three 50ml portions of water and 25 ml alcohol.
6. Remove the residue and transfer to ashing dish(W1).
7. Dry the residue for 2hours at $130 \pm 2^\circ\text{C}$, cool the dish in a dessicator and weigh (W2).
8. Ignite for 30minutes at $600 \pm 15^\circ\text{C}$.
9. Cool in a dessicator and reweigh (W3).

CALCULATION

$$\% \text{ dietary fibre in ground sample} = \frac{\text{loss in weight on ignition (W2-W1)-(W3-W1)}}{\text{Weight of the sample}} \times 100$$

Estimation of Carbohydrate Content Present in the Selected Seaweed Samples

Take 0.2 to 1ml of working standard solution from five different test tubes and add water to bring the volume to 1ml in each test tube, add 4ml of anthrone reagent and mix the contents as well, then cover the test tube with a bath for 10 min, then cool the test tube to room temperature and measure the optical density in a photoelectric colorimeter at 620 nm (or) by using a red filter. Prepare a blank with 1 ml of distilled water and 4 ml of anthrone reagent. Construct a calibration curve on graph paper by plotting the glucose concentration (10 to 100 mg) on the X-axis and the absorbance at 620 nm on the y-axis. Calculate the concentration of the sugar in the sample from the calibration curve and the amount of glucose present in the given sample is expressed in mg/ml.

Estimation of Protein Content Present in the Selected Seaweed Samples

1. Seaweeds powders 250 mg were taken in a test tube and 2 ml distilled water was added to it.
2. The mixtures were mixed thoroughly by shaking for 1 minute by CM 101 Cyclo mixer, REMI and 4 ml Biuret reagent (9 g of sodium potassium tartrate, 3 g of copper sulphate, 5H₂O and 5g of potassium iodide, in 400 ml of 0.2N sodium hydroxide solution and make up the volume to 1000 ml) was added to each seaweeds solution which were incubated for 30 minutes in room temperature and after incubation, mixtures were centrifuged at 4000 rpm for 10 minutes, supernatants were collected and the observance of all supernatants were taken at 540 nm with UV/Vis Spectrophotometer.
3. Bovine serum albumin (BSA) solution was used as standard. From 0-10 mg/ml of different concentration of BSA solutions was prepared and from each working standard 1 ml of solutions was taken and 4 ml Biuret reagent were added to it and incubated for 30 minutes and observance of OD value was taken at 540 nm.
4. The standard calibration curve was made by using the estimated absorbance at y axis and concentration at x axis. From this calibration standard curve protein content of seaweeds were estimated and the amount of Protein present in the given sample is expressed in mg/ml.

Estimation of Fat Content Present in the Selected Seaweed Samples

1. Approximately 10g of finely ground sample was weighed to the nearest 0.1g into the mortar and pestle and twice the weight of anhydrous sodium sulphate was added.
2. The content was ground until a free flowing powder was obtained after which it was transferred in to the extraction thimble and covered with a cotton wool.
3. The extraction thimble with the sample was placed in the soxhlet apparatus.
4. A cleaned, dried and previously weighed round bottom flask (250 ml) containing 200 ml of petroleum ether with pumice chips and a condenser was connected to the soxhlet apparatus and refluxed for 5 hours keeping the heating rate low enough to prevent solvent escaping from the top of the condenser during the refluxing.
5. After the refluxing was over, the solvent was distilled off and cooled the content with the flask and weighed.
6. The process was repeated until a constant weight was obtained. Experiment was triplicated.



**Praba and Sumaya****Calculation**

$$\text{Percentage of crude fat content of the sample} = \frac{W1 - F}{W2} \times 100$$

W1 = Weight of the flask with fat and sample. F = Weight of the flask and the sample. W2 = Weight of the sample

RESULTS AND DISCUSSION

The present study of the two selected seaweeds, *Ulva lactuca* contained higher amount of carbohydrate 12.6±0.1gm when compared to *Padina gymnospora* contained 5.0±0.4gm. [3], [4] studied that Carbohydrate is one of the most essential component for the metabolic activity and provides energy needed for respiration and other various functions [5] studied the nutritional composition of *Ulva lactuca* and found that the carbohydrate was the major component. [6] investigated the nutritional value of green alga, *Ulva lactuca* showed high content of carbohydrates. The main components of seaweeds are carbohydrates such as mucopolysaccharides, cellulose and soluble fibre, the potential nutritional benefits to develop an alternative source of a healthy food for the individual in the future [7]. The study revealed that *Ulva sp.* had high nutrient storage capacity as it can be exploited as best food source, energy resource for a healthy wellbeing [8].

The bioactive compounds of four seaweeds *Sargassum wightii*, *Padina tetrastromatica*, *Chnoospora minima* and *Hormophysa triquetra* collected from Mandapam region of Gulf of Mannar. The chemical compositions of seaweeds are good sources of proteins, lipids, carbohydrates minerals and trace elements and they have the potential for application as natural antioxidants in different food and pharmaceuticals products [9] From this study it was found that *Padina gymnospora* had high Protein content 68.5±0.1gm than green seaweed *Ulva lactuca* 26.0±0.0gm. Many scientists reported that Phaeophyta found to be rich in protein than Chlorophyta. Worldwide seaweeds have been researched that it has high nutritional value than any commonly consumed plant based local vegetables. Seaweeds are rich in various nutrients and used to develop various functional foods [10]. [11] studied on biochemical composition of marine brown algae, *Padina sp.* and the results reveal that brown seaweed contain high amount of protein and they can be used in the Food and Pharmaceutical industries for various purposes.

Seaweeds contain complete protein than the plant foods with maximum number of essential amino acids. Macro algae are called as excellent food due to its high concentration of protein. [12]. The present study also revealed significantly high quantities of protein in the selected seaweed species. The present study showed that *Padina gymnospora* has high fatty acids 15.3±0.1gm than *Ulva lactuca* 2.5±0.3gm/100gm. [13] studied the nutritional contents of brown and red seaweeds and found that brown seaweeds possess high amount of protein and fatty acids than the red. [14] studied the brown seaweeds generally have the highest lipid content followed by green and red seaweeds. [15] reported the biochemical constituents of eighteen species of marine macro algae belonging to Chlorophyta, Phaeophyta and Rhodophyta collected from Okha coast, Gulf of Kutch, India and compared their biochemical composition. The results revealed that Chlorophyta had maximum carbohydrate. *P.tetrastomatica* and *L.claviformis* were found to be rich in protein than the Chlorophyta species.

The lipids and fatty acids are present in low amounts in seaweeds compared to land vegetables and they have a significant amount of polyunsaturated fatty acids which acts as strong antioxidants such as omega 3 and omega 6 [16]. The fibre content was high in *Ulva lactuca* with 3.2±0.2gm when compared to *Padina gymnospora* with 2.9±0.4gm/100gm. Seaweeds in general contain high fibre content. The present study showed that Calcium (201.3±0.0mg), Magnesium (45.7±0.02mg), Zinc (2.7±0.32mg), Chlorine (10.3±0.05mg) and Iodine (4.1±0.21mg) are high in *Padina gymnospora* when compared to *Ulva lactuca* which contained Calcium (133.5±0.01mg), Magnesium (29.6±0.02mg), Zinc (1.0±0.1mg), Chlorine (9.6±0.12mg), and Iodine (1.0±0.1mg). [17] compared with terrestrial plants seaweeds are particularly rich in iodine, which is essential to the functioning of the thyroid and of the nervous system. The amount of Potassium (109.7±0.0mg), Sodium (137.8±0.0mg) and Copper (1.9±0.28mg) are high in green





Praba and Sumaya

algae *Ulva lactuca* than in brown algae *Padina gymnospora* which contained Potassium ($29.6\pm 0.02\text{mg}$), Sodium ($56.3\pm 0.01\text{mg}$) and Copper ($1.4\pm 0.62\text{mg}$). [18] stated that mineral content of seaweeds are considered to be a good source for minerals and trace elements which is necessary for the metabolic reactions of the human health. They are rich in vitamins, minerals, protein, polyunsaturated fatty acid and dietary fibers. Due to its high nutritional value, seaweeds can be developed as functional foods [19].

Commercially available four seaweeds such as *Marcocystis pyrifera*, *Undaria pinnatifida*, *Porphyra sp.*, *Ecklonia radiata* were tested for their nutritional composition against six wild harvested seaweed species includes *Ulva stenophylla*, *Porphyra*, *Ecklonia radiata*, *Durvillaea Antarctica*, *Hormosira banksii* and *Undaria pinnatifida*. The variation in proximate composition and mineral contents varied as they were collected at different time and between different species [20].

CONCLUSION

Seaweeds are nutrient dense staple food in many countries such as China, Indonesia, Phillipines, Japan. There are different value added food products prepared from seaweeds such as Chocolates, Salt, Snacks and Bakery products. The cultivation of seaweeds can employ coastal living people with good amount of foreign exchange earners. Large scale cultivation of commercially important seaweed species will have a profitable business. Seaweeds contain many macro and micro nutrients, phytochemicals, antioxidant rich and toxic free food. Macro algae are called as excellent food due to high concentration of protein. The fatty acids present in the seaweeds provide health benefits to human well being as they contain a huge percentage of polyunsaturated fatty acids especially omega 3 fatty acids which reduces blood pressure, strengthen the immune system and DHA improves mental health. Seaweeds contain high ash content and minerals that is required for a healthier lifestyle. The high mineral contents are found in the seaweeds than the land plants. Mineral contents of seaweeds depends on the variety of the species, geographical distribution and processing. Seaweeds are one of the most important sources of calcium when compared to other sources of calcium. Natural occurring minerals in the seaweeds play an important role in the electrolyte balance in humans. Many studies have been carried out in the mineral composition of different seaweeds and found to contain considerable amount of minerals such as copper, iron, sulphur, calcium high in *Padina gymnospora*. Seaweeds are considered safe for human population and known for their promising food from the marine ecosystem.

ACKNOWLEDGEMENT

The author expresses sincere thanks to Dr. S.Sumaya for her support in writing this manuscript.

REFERENCES

1. Tanna.B and Mishra.A (2018a). Metabolites unravel nutraceutical potential of edible seaweeds: an emerging source of functional food. *Compr. Rev. Food Sci. Food Saf.* 17, 1613–1624.
2. Cornish. M, Critchley. A.T and Mouritsen. O (2017). Consumption of seaweeds and the human brain. *J. Appl. Phycol.* 29: 2377–2398.
3. Rasyid.A (2017). Evaluation of Nutritional composition of the dried seaweed *Ulva lactuca* from Pameungpeuk Waters, Indonesia *Tropical Life Sciences Research*, 28(2), 119–125.
4. Funda Turan, Senem Ozgun, Selin Sayın, Gul Ozyilmaz (2015). Biochemical composition of some red and green seaweeds from Iskenderun Bay, the northeastern Mediterranean coast of Turkey *J. Black Sea/Mediterranean Environment*, Vol. 21, No. 3: 239-249.
5. Gokulakrishnan. S, Raja. K, Sattanathan. G and Subramania. J (2015). Proximate composition of Bio Potential Seaweeds from Mandapam, South East Coast of India, *International Letters of Natural Sciences*, 45: 49-55.
6. Saritha. K, Aswathi. E.M, Priyalaxmi. M, Jamila. P(2013). Antibacterial activity and biochemical constituents of seaweed *Ulva lactuca*. *Glob. J. Pharmacol.* 7, 276–282.





Praba and Sumaya

7. Ahmad, Faisal & Sulaiman, M.R. & Saimon, Welzan & Chye, Fook Yee & Matanjun, Patricia. (2012). Proximate compositions and total phenolic contents of selected edible seaweed from Semporna, Sabah, Malaysia. *Borneo Sci.* 31. 74-83.
8. Pirian K, Piri K, Sohrabipour J, Jahromi. S.T, Blomster.J (2016). Nutritional and phytochemical evaluation of the common green algae, *Ulva* sp. (Ulvophyceae), from the Persian Gulf *Fund Appl Limnol.*; 188:315-327.
9. Kokilam.G, Vasuki.S, Sajitha.N (2013). Biochemical composition, alginic acid yield and antioxidant activity of brown seaweeds from Mandapam region, Gulf of Mannar. *Journal of Applied Pharmaceutical Science* Vol. 3 (11), pp. 099-104.
10. Yaich. H, Garna.H., Besbes.S, Paquot.M, Blecker.C, and Attia. H.(2011). Chemical composition and functional properties of *Ulva lactuca* seaweed collected in Tunisia. *Food chemistry* 128,895-901.
11. Sethi.P (2012). Biochemical composition of marine brown algae, *Padina petrastrumatic hauck*, *Int J. of Current Pharm Res*, 4 (2): 117-118.
12. Sukalyan Chakraborty & Tanushree Bhattacharya (2012). Nutrient composition of marine benthic algae found in the Gulf of Kutch coastline, Gujarat, India. *J. Algal Biomass Utiln.* 3 (1): 32 – 38.
13. Narasimman. S and Murugaiyan. K (2012). Proximate Composition of Certain Selected Marine Macro-Algae form Mandapam Coastal Region (Gulf of Mannar), Southeast Coast of Tamil Nadu, *International Journal of Pharmaceutical & Biological Archives*; 3(4) : 918-921.
14. Gosch, Björn & Magnusson, Marie & Paul, Nicholas & de Nys, Rocky. (2012). Total lipid and fatty acid composition of seaweeds for the selection of species for oil-based biofuel and bioproducts. *GCB Bioenergy.* 4. 919-930.
15. Nirmal Kumar J.I, Megha Barot, Rita N Kumar (2017). Distribution and Biochemical constituents of different seaweeds collected from Okha Coast, Gujarat, India. *Indian Journal of Geo Marine Sciences.* Vol 46(02). Pp 349-357.
16. Mendis.E, Kim.S.K (2011). Present and future prospects of seaweeds in developing functional foods. *Adv. Food Nutr. Res.* 64, 1–15.
17. Thillaikannu Thinakaran, Mohan Balamurugan, Kathiresan Sivakumar (2012). Screening of phytochemical constituents qualitatively and quantitatively certain seaweeds from Gulf of Mannar Biosphere reserve. *International journal of Pharmacy.* vol 3(7).pp- 261-265.
18. Valentina. J, Poonguzhali. T. V, Josmin. L, Nisha.L. L, & Sumathi. E (2015). Estimation of protein, carbohydrate and mineral content in selected seaweeds. *International Journal of Current Research*, 7(1), 11329-11333.
19. Lei Liu, Michael Heinrich, Stephen Myers, Symon A. Dworjany (2012). Towards a better understanding of medicinal uses of the brown seaweed *Sargassum* in Traditional Chinese Medicine: A phytochemical and pharmacological review, *Journal of Ethnopharmacology*, Vol 142, Issue 3, Pages 591-619.
20. JL Smith, G Summers & R Wong (2010). Nutrient and heavy metal content of edible seaweeds in New Zealand, *New Zealand Journal of Crop and Horticultural Science*, 38:1, 19-28.

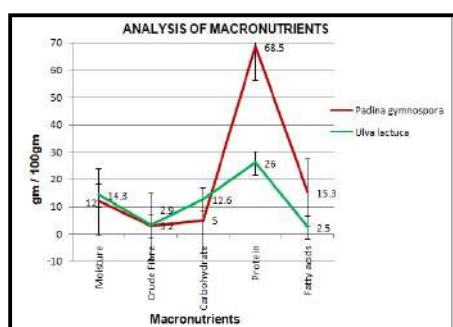


Figure 1 Analysis of Macronutrients (Mean values of the Macronutrients and the bars indicate the standard deviation)

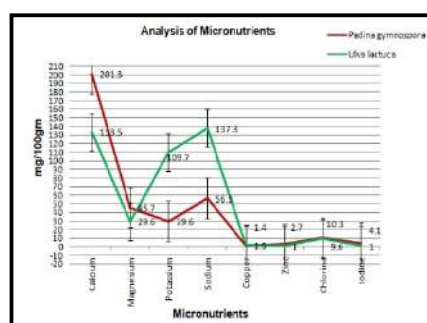


Figure 2 Analysis of Micronutrients (Mean values of the Micronutrients and the bars indicate the standard deviation)





Fungal Pulmonary Infections among Patients Suffering from Pulmonary Tuberculosis: A Cross-Sectional Study

Shushant I Jigan¹, Jyoti M Nagamoti^{2*}, Sugeerappa L Hoti³, Mahantesh B Nagamoti²

¹Research Scholar, Department of Microbiology, J. N. Medical College, KLE Academy of Higher Education and Research, Belagavi, Karnataka, IndiaPIN-590010

²Professor, Department of Microbiology, J. N. Medical College, KLE Academy of Higher Education and Research, Belagavi, Karnataka, IndiaPIN-590010

³Emeritus Scientist, ICMR-Vector Control Research Centre, Puducherry, India PIN-605006

Received: 08 Feb 2023

Revised: 26 Mar 2023

Accepted: 29 Apr 2023

*Address for Correspondence

Jyoti M Nagamoti

Professor,

Department of Microbiology,

J. N. Medical College,

KLE Academy of Higher Education and Research,

Belagavi, Karnataka, India PIN-590010.

E. Mail : jyotinagamoti@yahoo.com



This is an Open Access Journal / article distributed under the terms of the **Creative Commons Attribution License** [CC BY-NC-ND 3.0] which permits unrestricted use, distribution, and reproduction in any medium, provided the original work is properly cited. All rights reserved.

ABSTRACT

Mycobacterium tuberculosis causes pulmonary tuberculosis [TB], which is a contagious bacterial illness. The cavities in the lungs aid fungus development by supplying an abundance of oxygen and necrotic tissue debris. In TB patients, the long-term chemotherapy promotes fungal infection due to the lack of pathognomonic and radiographic characteristics. Pulmonary fungal infection is difficult to diagnose, especially in the absence of mycology laboratory testing. The aim of our study was to isolate and identify the fungi causing infection among patients with pulmonary tuberculosis using phenotypic methods and to assess the prevalence of such infection at our centre. A cross-sectional study was conducted over a period of 15 months at the Department of TB and Chest Diseases and the RNTCP laboratory at KLE'S Dr.Prabhakar Kore Charitable Hospital and medical research centre and District Hospital Belagavi, Karnataka, India. Symptomatic patients diagnosed with tuberculosis were included in the study. Sputum samples were collected and processed using standard mycological procedures. The data was analysed using SPSS version 21. Ethical clearance was obtained from the institutional ethical review committee and consent from patients was obtained. Total of 282 samples were collected and among them 128 samples grew fungi, and out of these, 80 [28.4%] were yeasts, whereas 48 [17%] were filamentous fungi. *Candida albicans* was predominant with 31 [38.8%], *Candida tropicalis* with 14 [17.5%], *Candida glabrata* and *Candida krusei* 10 [12.5%] followed by *Candida parapsilosis* 9 [11.3%] and *Cryptococcus neoformans* with 4 [5%]. Out of the 48 filamentous fungi, *Aspergillus niger* 10 [3.5%] was the predominant isolate. One sample showed



**Shushant I Jigan et al.,**

dual infection [with two different moulds in the same sample], whereas 154 [54.6%] were culture negative. The patient's situation is made more difficult by the coexistence of fungus and TB, which adds extra detrimental and fatal characteristics.

Keywords: Fungal pulmonary infection, Pulmonary Tuberculosis, Opportunistic infection, Co infection, *Candida spp.*, *Aspergillus spp.*

INTRODUCTION

Fungus-related respiratory tract infections have become more common over the past few decades, their actual impact is unknown [1]. Pulmonary tuberculosis [PTB], Human immunodeficiency virus/acquired immunodeficiency syndrome [HIV/AIDS], chronic obstructive pulmonary disease [COPD], and the widespread use of immunosuppressive medicines have all been blamed for the rise [2,3]. Globally, it is estimated that 1.2 million people have chronic pulmonary *aspergillosis* [CPA] as a result of PTB, with the largest frequency in Africa, the Western Pacific, and Southeast Asia[4]. PTB patient's immune systems were suppressed as a result of the chronic nature of the disease and extended treatment with or without corticosteroids, making them prone to fungal infection [5]. Fungi induce pulmonary fungal infection, which is an infectious condition of the lungs. The infection takes hold once fungi or their spores colonise the lungs by inhalation, reactivation of latent infection, or haematogenous spread [6]. Fungi and their spores are plentiful and may be found almost anywhere in the human environment. Colonization or infection of the lungs is unavoidable due to the pervasive nature of fungi and their spores, but methods for distinguishing fungal colonisation from fungal infection are unknown, making the issue a severe problem [7].

In this investigation, the isolation of fungus in *Mycobacterium tuberculosis* [MTB] patients was considered a possible infection. A variety of fungi have been identified as etiological agents of lung infections. In literature, species of *Aspergillus* [8], *Candida* [14], and *Cryptococcus* [9] are the most important. As a result, several mycelial fungi have arisen as etiological agents of respiratory illnesses, including *Fusarium spp.*, *Penicillium spp.*, dematiaceous filamentous fungus, zygomycetes, and yeasts. While these fungi are seldom seen in the respiratory tracts of immune-competent people, they can spread to other systemic organs and cause life-threatening invasive fungal illnesses in those who are already sick [10]. PTB is primarily a poverty-related illness, with developing nations accounting for 95% of cases and 98% of fatalities. Six nations account for 60% of the total, with India at the top of the list [11]. The high prevalence of fungal pulmonary co-infection with PTB adds to the burden of PTB in these nations, as the two illnesses are linked and cause a high rate of morbidity and death [12,13].

As a result, accurate fungal pathogen detection is crucial, particularly in PTB patients. There is a scarcity of information in north Karnataka about pulmonary fungal infections and their relationship to PTB. Moreover, pulmonary fungal infection and PTB have similar clinical and radiological presentations, distinguishing between the two illnesses is challenging. Coughing for more than three weeks is a typical sign of TB and fungal pathogen-related lung diseases[14]. Because anti-TB medications do not impact fungal pathogens, a lack of definitive diagnosis between PTB and fungal lung infection may lead to empirical treatment, where anti-TB chemotherapy is used to treat fungal infections, with subpar clinical outcomes [15]. PTB patients do not get care for the identification or treatment of pulmonary fungal infections since respiratory fungal infections are typically fatal diseases in immune-compromised people. The aim of our study was to isolate and identify the fungi causing infection among patients with PTB using phenotypic methods and to assess the prevalence of such infection at our centre.

MATERIALS AND METHODS

Study Design

It was a cross-sectional study carried out during October 2020 to December 2021.





Shushant I Jigan et al.,

Ethical Consideration

Ethical clearance was obtained from the institutional ethical review committee, consent from patients was obtained.

Study participants

Clinically, laboratory confirmed positive pulmonary tuberculosis patients; both new, old cases attending the Department of Tuberculosis [TB] Chest Diseases and the RNTCP laboratory at KLE'S Dr.Prabhakar Kore Charitable Hospital- medical research centre [MRC] and District Hospital in Belagavi were included in the research.

Sample Collection

To avoid contamination from the oral cavity, patients were encouraged to rinse their mouths with an antiseptic mouthwash containing 2% chlorhexidine. In a sterile wide mouth jar; early in the morning, a deep, productive cough sample of 5 mL was collected, sealed in a container, and labelled with sampling information [16]. The container was immediately delivered to the laboratory for additional analysis once the sample was obtained.

Isolation and Identification of Fungal isolates

Obtained sputum samples were subjected for KOH mount, Gram staining and Ziehl-Neelsen [ZN] Staining. All samples were inoculated on two sets of sabouraud's dextrose agar containing gentamicin-chloramphenicol and incubated at 25°C in the BOD incubator for the growth of filamentous fungi and at 37°C for the growth of yeasts in the general purpose incubator[19]. Within 24-48 hours, the yeasts were isolated and identified using conventional laboratory methods such as the germ tube test, corn meal agar, chrome agar, urease test, capsular stain, Sugar assimilation and fermentation[17,18]. For moulds the inoculated specimens were incubated for up to 6 weeks, during this time growths were monitored and identified using lactophenol cotton blue mounts and slide culture procedures [19, 20]. The absence of growth after 6 weeks of incubation was regarded as negative.

RESULTS

Out of 282 samples, 128 [45.4%] were positive for opportunistic fungi. out of these, 80 [28.4%] were yeasts, 48 [17%] were filamentous fungi and 154 [54.6%] were culture negative.[Graph.1]. Out of 80 yeasts isolated, *Candida albicans* were predominant 31 [38.8%] followed by *Candida tropicalis* 14 [17.5%], *Candida glabrata* 10 [12.5%], *Candida krusei* 10 [12.5%], *Candida parapsilosis* 9 [11.3%], *Cryptococcus neoformans* 4 [5%] and *Rhodotorula glutinis* 2 [2.5%] [Table-1]. Out of the 48 filamentous fungi, the predominant isolates were *Aspergillus niger* 10 [20.8%], followed by *Aspergillus fumigatus* 9 [18.8%], *Fusarium spp.* 7 [14.6%], *Penicillium spp.* 6 [12.5%], *Aspergillus flavus* 5 [10.4%], *Mucor spp.* 5 [10.4%], and *Rhizopus spp.* 5 [10.4%] and one sample showed dual infection [with two different molds, i.e., *Aspergillus niger* and *Rhizopus Spp.* in the same sample] [Table-2& Fig.2]. Direct microscopic examination revealed the budding yeast cells with pseudohyphae in 74 [26.3%] patients; the presence of septate hyphae with dichotomous branching in 20 [7.09%] patients; round or oval budding in 6 [2.1%] patients, mycelium is branched, septate, hyaline or coloured, inter- or intracellular and uninucleate to multinucleate in 7 [2.5%] patients, coenocytic hyphae in 5 [1.8%] patients, and broad hyphae, or scarcely septate with rhizoids and stolons in 5 [1.8%]. Fungal culture yielded *Aspergillus spp.* in 24 [8.5%] patients, *Candida spp.* in 83 [29.4%] patients, non-candida yeast in 6 [2.1%], *Fusarium spp.* in 7 [2.1%], *Mucor spp.* in 5 [1.8%], *Rhizopus spp.* in 5 [1.8%], and *Penicillium spp.* in 6 [2.1%]. Examination by direct microscopy failed to detect four [1.4%] samples which were later found to be culture positive for *Aspergillus*. By culture, *Candida spp.* was recovered in 83 [29.4%] patients, but in direct microscopy, budding yeast cells with pseudohyphae were seen only in 74 [7%] patients, so 9 culture positive [Candida] patients with the absence of pseudohyphae in direct microscopy were considered as commensals. Hence, the total number of candida species isolated in the present study was 74 [26.3%] only. The ages of the participants ranged from 11-80 years. The male participants were more than the female participants. In our study the age group of 21-40 years found more common for fungal pulmonary infection in both male and female participants [Table-3].





Shushant I Jigan et al.,

DISCUSSION

Pulmonary fungi are common infective processes that are becoming increasingly common in today's practise. The use of broad-spectrum antibiotics, immunosuppressive, chemotherapeutic medicines, as well as an increase in the frequency of respiratory disorders such as chronic obstructive pulmonary disease, lung cancer, and tuberculosis, has raised the likelihood of contracting these diseases. Despite the fact that therapy is challenging, the outcomes are positive. As a result, it is even more critical now to have a thorough understanding of these diseases so that we can manage them scientifically. When diseases like opportunistic fungal infections are detected early, they may be efficiently treated, preventing the disease from progressing to the fibrotic stage and lowering the number of respiratory cripples [21]. Findings from this study revealed a prevalence of fungal pulmonary infection among tuberculosis patients as 45.4%. This was strongly proved by a study conducted by Mathavi, et al.,[22] Khanna, et al.,[6] Bansal, et al., Jain, et al.,[23] Nagavane, et al.,[27] and Bansod and Rai, et al., [21] where 38%, 36%, 53%, 49%, and 46% of pulmonary tuberculosis patients were co-infected with fungal agents.

The present study shows 26.2% of pulmonary tuberculosis patients to be co-infected with *candida spp.* This is consistent with the study done by Naz SA, et al., [24] in which 15.2% of co-infection with *candida spp.* was documented. One more study was conducted by VP Baradkar, et al., [25] which showed 26% co-infection with *candida spp.* which was very much similar to our study. In our study, *C.albicans* was the most prevalent pathogen causing co-infection. *Candida albicans* accounted for 38.8 % of total *Candida* isolates. This is consistent with a research by Kalyani, et al., [26] [41.2%], Kali A, et al., [14] [50%], Khanna, et al., [6] [62%], and Nagavane, et al., [27] [34.7%], where *C.albicans* to be the most prevalent species causing co-infection in TB patients. Other than *Candida albicans*, *C.tropicalis* [17.5%], *C.glabrata*, *C.krusei* [12.5%], and *C.parapsilosis* [11.3%], these findings are in agreement with the study conducted by Chalana M, et al.,[28] and Hussein HM, et al.,[28] apart from *candida*, in our study *Cryptococcus neoformans*[5%] and *Rhodotorula glutinis* [2.5%] were isolated, which were in accordance with Shesh Rao, et al.,[29]Kalyani et al.,[26] Out of 48 filamentous fungi, the predominant isolate were *A.niger* [20.8%] followed by *A.fumigatus* [18.8%], *Fusarium Spp.*[14.6%], *Penicillium spp.*[12.5%], *A.flavus* [0.4%], *Mucor spp.*[10.4%], *Rhizopus spp.*10.4%. These findings correlate with Yahaya H, et al., and Lane et al., [20]

CONCLUSIONS

It is impossible to overstate the frequency of fungal pulmonary infection in pulmonary TB patients. Despite the effective conclusion of antituberculous medication therapy, these opportunistic fungal infections are linked to the continuation of lung symptoms. Since these opportunistic infections are linked to high rates of morbidity and death, effective precautions must be taken for their early detection and treatment.

REFERENCES

1. Fauci AS, Morens DM. The perpetual challenge of infectious diseases. New England Journal of Medicine. 2012 Feb 2; 366[5]:454-61.
2. Brown GD, Denning DW, Gow NA, Levitz SM, Netea MG, Hidden WT. Killers, Human fungal infections. SciTransl Med. 2012; 4[165]:165rv13.
3. Bongomin G. multi-national prevalence of fungal diseases-estimate precision, J. J Fungi [Basel]. [3]:57.
4. Denning DW, Pleuvry A, Cole DC. Global burden of allergic bronchopulmonary aspergillosis with asthma and its complication chronic pulmonary aspergillosis in adults. Medical mycology. 2013 May 1; 51[4]:361-70.
5. Nucci M, Marr KA. Emerging fungal diseases. Clinical Infectious Diseases. 2005 Aug 15; 41[4]:521-6.
6. Khanna BK, Nath P, Ansari AH. A study of mycotic flora of respiratory tract in pulmonary tuberculosis.
7. Roohani AH, Fatima N, Shameem M, Khan HM, Khan PA, Akhtar A. Comparing the profile of respiratory fungal pathogens amongst immunocompetent and immunocompromised hosts, their susceptibility pattern and



**Shushant I Jigan et al.,**

- correlation of various opportunistic respiratory fungal infections and their progression in relation to the CD4+ T-cell counts. Indian journal of medical microbiology. 2018 Jul 1; 36[3]:408-15.
8. Yao Z, Liao W. Fungal respiratory disease. Current opinion in pulmonary medicine. 2006 May 1;12[3]:222-7.
 9. Kronstad JW, Attarian R, Cadioux B, Choi J, D'souza CA, Griffiths EJ, Geddes JM, Hu G, Jung WH, Kretschmer M, Saikia S. Expanding fungal pathogenesis: Cryptococcus breaks out of the opportunistic box. Nature reviews Microbiology. 2011 Mar;9[3]:193-203.
 10. Elizabeth NA, Yolanda LV, Eva H, Arcadio MP, Steven M, Miguel FM, Ascencio VA, José LS, Robert L, Neil A. Clustering of Mycobacterium tuberculosis Cases in Acapulco: Spoligotyping and Risk Factors. Clinical and Developmental Immunology.;2011.
 11. Sharma SK, Mohan A. Multidrug-resistant tuberculosis. Indian Journal of Medical Research. 2004; 120[4]:354-76.
 12. Kartmann B, Stengler S, Niederweis M. Porins in the cell wall of Mycobacterium tuberculosis. Journal of Bacteriology. 1999 Oct 15; 181[20]:6543-6.
 13. Sahoo RC. Antileukotrienes in asthma and allergy. Curr Med J India. 2006; 2:48-52.
 14. Kali A, Charles MP, Noyal MJ, Sivaraman U, Kumar S, Easow JM. Prevalence of Candida co-infection in patients with pulmonary tuberculosis. The Australasian medical journal. 2013; 6[8]:387.
 15. Randhawa HS. Respiratory and systemic mycoses: an overview. The Indian Journal of Chest Diseases & Allied Sciences. 2000 Oct 1; 42[4]:207-19.
 16. USAID Report [2010]: Building Partnerships to Control Tuberculosis: United State Agency for International Development, USA.
 17. RNTCP guidelines. Diagnosis of smear positive pulmonary TB. New guidelines, effective from 1st April 2009. Available at: <http://tbcindia.nic.in/pdfs/1b%20-%20Diagnosis%20of%20smear%20positive%20pulmonary%20TB.pdf>.
 18. OcheiJ, KolhatkarA. Laboratory Techniques in Mycology. Examination of Sputum. Medical Laboratory Science, Theory and Practice. India: Tata McGraw Hill Pub Co., Ltd.; 2005. p. 105-33.
 19. Chakrabarti A, Shivaprakash MR. Venugopal PV, Venugopal TV. Medical Mycology Laboratory Procedures. In: 5. Chakrabarti A, Shivaprakash MR. Venugopal PV, Venugopal TV, eds. National Workshop in Medical Microbiology. Chennai, India: Proceedings of 29th Annual Congress of Indian Association of Medical Microbiologist; 2005: 19-20.
 20. Yahaya H, Taura DW, Aliyu IA, Bala JA, Yunusa I, Ahmad IM, Ali B. Spectrum of opportunistic mould infections in suspected pulmonary tuberculosis [TB] patients. International Journal of Microbiology and Application. 2015;2[1]:6-11.
 21. Bansod S, Rai M. Emerging of Mycotic infection in patients infected with Mycobacterium tuberculosis. W J Med Sci. 2008;3[2]:74-80
 22. Mathavi S, Shankar R, Sasikala G, Kavitha A. A study on mycotic infection among sputum positive pulmonary tuberculosis patients in Salem district. Indian journal of research. 2015 Jul;4[7]:299-302.
 23. Jain SK, Agarwal RL, Sharma DA, Agarwal M. Candida in Pulmonary Tuberculosis. Journal of Post Graduated Medicine. 1982;28:24-29.
 24. Naz SA, Tariq P. A study of the trend in prevalence of opportunistic Candidalco-infections among patients of pulmonary tuberculosis. Pak J Bot. 2004 Dec 1; 36:857-62.
 25. Baradkar VP, Mathur M, Wanjari K, Kumar S. Candida in pulmonary tuberculosis. Bombay Hosp J 2009;51:52-3
 26. Kalyani CS, Koripella RL, Madhu CH. Fungal isolates in sputum samples of multidrug-resistant tuberculosis suspects. International Journal of Scientific Study. 2016; 4[2]:164-6.
 27. Nawange M, Kavishwar A. Prevalence of opportunistic fungal infection in patients with pulmonary tuberculosis in Madhya Pradesh, Central India. J Microbiol Biomed Res. 2015 Jul 31;1:6.
 28. Hussein HM, Sekhi AA, Sekeb HS. Prevalence of fungi in clinically suspected cases of pulmonary tuberculosis In Iraq, Wasit. Systematic Reviews in Pharmacy. 2021; 12[1]:1393-6.
 29. SheshRao., et al. "Prevalence of opportunistic fungal infection in patients with pulmonary tuberculosis in Madhya Pradesh, Central India". Journal of Microbiology and Biomedical Research 1.6 [2015]: 1-6





Shushant I Jigan et al.,

Table 1: Distribution of yeasts

Isolates	Frequency	Percent (%)
<i>Candida albicans</i>	31	38.8
<i>Candida glabrata</i>	10	12.5
<i>Candida krusei</i>	10	12.5
<i>Cryptococcus neoformans</i>	4	5
<i>Candida parapsilosis</i>	9	11.3
<i>Candida tropicalis</i>	14	17.5
<i>Rhodotorulaglutinis</i>	2	2.5
Total	80	100

Table 2: Distribution of Molds

Isolates	Frequency	Percent (%)
<i>Aspergillus flavus</i>	5	10.4
<i>Aspergillus fumigatus</i>	9	18.8
<i>Aspergillus niger</i>	10	20.8
<i>Fusarium Spp.</i>	7	14.6
<i>Mucor spp.</i>	5	10.4
<i>Rhizopus spp.</i>	5	10.4
<i>Penicillium Spp.</i>	6	12.5
<i>Aspergillus niger</i> and <i>Fusarium spp.</i>	1	2.1
Total	48	100

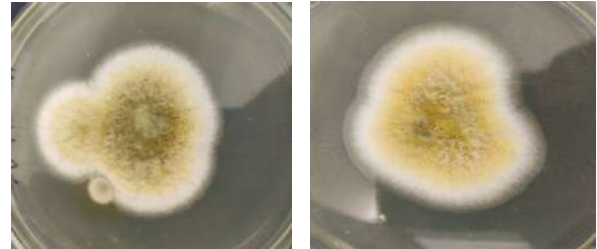
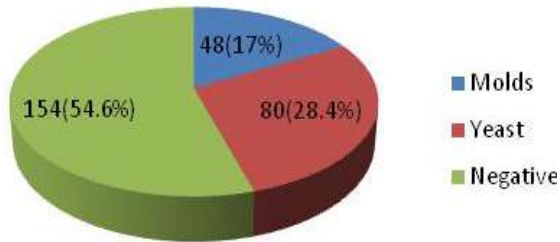
Table 3: Occurrence of pulmonary mycosis according to gender and age

Age	Molds				Yeast			
	Male		Female		Male		Female	
	Frequency	Percent %						
<=20	3	10.0	2	11.1	0	0.0	2	5.6
21-40	15	50.0	7	38.9	22	50.0	19	52.8
41-60	8	26.7	5	27.8	12	27.3	10	27.8
61-80	4	13.3	4	22.2	10	22.7	5	13.9

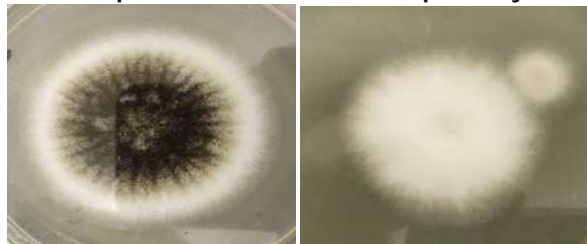




Shushant I Jigan et al.,

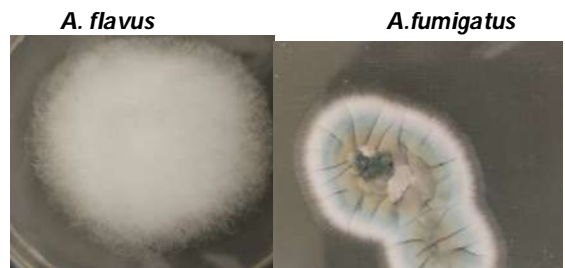


Graph 1: Distribution of culture positivity



A.niger

Fusarium spp.



A. flavus

A.fumigatus



Rhizopus spp.

Candida spp.



R.glutinis

C. neoformans





Evaluation of Heavy Metals and Microbial Contamination of Antidiabetic Herbal Medicine; A Serious Hazard to Human Health

N.Uma Maheswari* and S.Priscilla

¹Vice Principal and Head, PG and Research Department of Microbiology, STET Women's College (A) Sundarakkottai, Mannargudi, Thiruvarur, Tamil Nadu, India.

²Research Scholar, PG and Research Department of Microbiology, STET Women's College (A), Sundarakkottai, Mannargudi, Thiruvarur, Tamil Nadu, India.

Received: 01 Feb 2023

Revised: 10 Apr 2023

Accepted: 16 May 2023

*Address for Correspondence

N.Uma Maheswari

Vice Principal and Head,
PG and Research Department of Microbiology,
STET Women's College (A) Sundarakkottai,
Mannargudi, Thiruvarur, Tamil Nadu, India.
E. Mail: umasamyamf@gmail.com



This is an Open Access Journal / article distributed under the terms of the **Creative Commons Attribution License** (CC BY-NC-ND 3.0) which permits unrestricted use, distribution, and reproduction in any medium, provided the original work is properly cited. All rights reserved.

ABSTRACT

The use of commercial herbal medicine for the treatment of various ailments especially diabetes mellitus has greatly increased recently due to the approval and recommendation from regulatory bodies. The aim of the current study was to evaluate microbial contamination and heavy metals in commercial antidiabetic herbal medicines in terms of measurement of pH, limit test for radical impurities, microbial load and pathogenic bacteria in thirteen Anti Diabetic Herbal Medicines (ADHMs) collected in and around from Thiruvarur district, Tamilnadu, India. All the thirteen ADHMs had been found contaminated with different pathogenic bacteria and fungi namely *Escherichia coli*, *Pseudomonas aeruginosa*, *Staphylococcus aureus* and *Aspergillus sps*. According to the heavy metals evaluation of Pb was the highest metals present in all herbal medicine followed by Zn, Cu and Mn. The heavy metal content was analyzed by using Atomic Absorption Spectrophotometer (Zn, Cu, Mn and Pb). Microbial contaminants in these commercial herbal preparations pose a potential risk for human health and care should be taken in every step involved in the preparation of these herbal preparations to assure safety.

Keywords: Anti Diabetic Herbal Medicines, Diabetes mellitus, *Escherichia coli*, *Pseudomonas aeruginosa*, *Staphylococcus aureus*, *Aspergillus sps*.



**Uma Maheswari and Priscilla**

INTRODUCTION

Diabetes mellitus (DM) is a metabolic disorder of multiple causes characterized by chronic hyperglycemia with disturbances of carbohydrate, fat and protein metabolism resulting from defects in insulin secretion, insulin action, or both. The effects of diabetes mellitus include long-term damage, dysfunction, and failure of various organs (WHO 1999). Diabetes mellitus is divided into three main types (American Diabetes Association 2019). Diabetes is a non-communicable heterogeneous group of disorder and affects approximately 200 million individuals globally (Wild 2000). The International Diabetes Federation, in the year 2015 estimated that about 415 million of the world populace is suffering from diabetes and predicted an increase to 642 million in the year 2040. Therefore, the need to develop effective treatment methods that are safe for diabetes treatment is a necessity (Neeta et al 2017). It is estimated that approximately 80% of the population in developing countries uses traditional herbal medicines as part of their primary health care. (Umair 2017) The majority of the populations, both from developed and developing countries, use herbal preparations for primary healthcare purposes (Vaikosen 2017). The use of herbal preparations is mainly through self-medication and they are available as medicinal preparations, nutraceuticals and cosmetics (Keter 2016). Herbal medicine are nothing but the formulations used for treatment of different diseases. They are sold as tablets, capsules, powders, teas, extracts, and fresh or dried plants. People use herbal medicines to try to maintain or improve their health. The safety of herbal preparations is still a concern due to contamination by pathogenic microbes, toxic heavy metals and non-metals, agrochemical residues, mycotoxins and endotoxins. The contaminants in herbal preparations turn to be carried along from soil where the medicinal plants were grown. The microorganisms adhere to leaves, stems, flowers, seeds, and roots of the medicinal plants used to prepare the herbal product. Sources of Contaminations in Herbal Products The practices of most ethnic herbal medicine include the use crude or raw herbs that are collected from the wild or from cultivated fields and their prepared or ready-made products. Toxic contaminants may come from the processes like storage, transit, growth condition, unhygienic use of medicines by patients. The manufacturing processes when the ready-made medicinal products are produced.

MATERIALS AND METHODS

Study area and sample collection A total of 13 different antidiabetic herbal medicines were purchased randomly from the retail herbal manufactures in and around Thiruvavur district, Tamilnadu, India. Unregistered herbal drugs commonly used for the treatment diabetes mellitus were purchased. These anti-diabetic herbal drugs were selected based on the manufacturer's reputation and popularity among the general public.

Determination of pH (Munro 1970)

The pH of different herbal preparations were determined by using pH meter. For pH determination, sample solution was prepared by dissolving 12.5g in 100ml sterile distilled water with soaking to obtain homogeneous solution. The present the data was performed as the average of triplicates.

Limit Tests for Acid Radical Impurities

Limit Test for Chlorides (Kar 2005)

1 ml of herbal preparation was added 10 ml of diluted nitric acid and the solution was diluted to 50 ml with distilled water. 1 ml of silver nitrate solution (5% w/v) was added and the solution stirred immediately with the glass rod. The solution was allowed to stand for 5 minutes and thereafter the opalescence was observed. Simultaneously, the same procedure was carried out using 0.05845% w/v solution of sodium chloride as the standard solution. If opalescence produced in sample solution was less than the standard solution, the sample was considered to have passed the limit test of chlorides.

Limit Test for Sulphates (Ahmed et al 2017)

Two millilitres of dilute hydrochloric acid was added to 1 ml of herbal preparation and the solution diluted to 45 ml with distilled water. Five millilitres of barium sulphate reagent was added and the solution was allowed to stand for

57164



**Uma Maheswari and Priscilla**

5 minutes and thereafter the turbidity was observed. Simultaneously, the same procedure was carried out using 0.1089% w/v solution of potassium sulphates as the standard solution. If turbidity produced in sample solution was less than the standard solution, the sample was considered to have passed the limit test of sulphates.

Isolation of Microorganisms

The Antidiabetic Herbal Preparations were taken and subject to serial dilution followed by spread plate method.

Gram's Staining (Han's Christian Gram, 1884)

The colonies were subjected to Gram's staining in order to identify their morphology and gram's staining reaction of bacteria. A thin smear was prepared on a clean slide using the isolated individual colony. The smear was heat fixed and cooled. The dried smear was then flooded with the primary stain, Crystal Violet and allowed to stand for one minute. Then it was washed with water and flooded with gram iodine and allowed with 95% ethanol for few seconds and washed gently with running tap water. Afterwards the slide was flooded with a counter stain Safranin for one minute. After drying the stained smear was observed under microscope.

Motility Test (Bailey and Scott, 1966)

A drop of culture is placed on a concave slide that is encircled with petroleum jelly. The coverslip and drop are then inverted over the well of a depression slide. The drop hangs from the coverslip, and the petroleum jelly forms a seal that prevents evaporation. Then the slide was observed under the microscope.

Biochemical Characteristics (Cappuccino and Shermann, 1998)**Indole Test**

Sterile tryptophan broth tubes were inoculated with test organisms and incubated at 37°C for 48 hours. After incubation 0.5 ml of Kovac's reagent was added to the test tube examined the colour change of cherry red colour positive test while no such colour formation indicates negative test.

MR-VP Test

MR-VP broth was inoculated with test organisms and incubated tubes at 37°C for 48 hours. Incubation for VP test 0.6 ml of Barrit's solution A and 0.2ml of solution B was added in to each test tube and mixed well. Colour change was observed from crimson to ruby pink indicates VP positive. For MR test methyl red reagent was added and shaken gently for 30 seconds. Examined the colour change, if red colour present it indicates MR positive.

Citrate utilization Test

Citrate utilization test was performed to determine the ability of the microorganisms to utilize citrate as a source of carbon. Simmons's citrate agar medium was prepared and sterilized then a slant was prepared in a test tube. The bacterial culture was inoculated by stabbing to the base and streaking on the surface of slant and it was incubated at 37°C for 48 hours. After incubation observe the colour change. A positive test is demonstrated by growth with a color change from green to intense blue along the slant. A negative test is demonstrated by no growth and no color change, and the color of the slant remains green.

Catalase Test

Catalase test was performed to detect the ability of the organisms to produce the enzyme catalase which degrades hydrogen peroxide. Trypticase soy agar was prepared, sterilized and slants were made. They were inoculated at 37°C for 24 hours. After incubation, 3% hydrogen peroxide was added to tube. Nutrient agar medium was prepared sterilized and poured in to the petri plates. The isolated organisms were grown on the agar surface. Then 2 or 3 drops of para aminodi methyl alanine oxalate to the surface of the inoculated plates. Formation of purple indicates positive where no colour change indicates a negative result.



**Urease Test**

5ml of prepared urea agar base transferred into each test tube and sterilized by using autoclaving at 121°C for 5 minutes. Slant was made and each tube was inoculated with different bacterial culture. Later, it incubated at 37°C for 24 hours observed the colour change.

Triple Sugar iron Test

The TSI Agar slope was prepared and a loop full of colony was streaked on TSI Agar slope surface in the butt portion, incubated at 37°C for 24 hours colour change of the slant and butt or both indicates the sugar utilization.

Isolation of Fungi

About 1 ml of antidiabetic herbal sample were serially diluted up to 10⁻¹- 10⁻⁷dilution, from that 10⁻³-10⁻⁵ appropriate diluted sample was plated to Potato dextrose agar (PDA). Then plates were incubated at 37°C for 3 days. Observe the fungi under the microscope.

Identification of Fungi Wet mount Technique (During 1976)

A drop of lactophenol cotton blue place on clean glass slide using sterilized needle and a small fungus with spore bearing structure mix with the stain by using needle, and place a cover slip over the slide. Then examine under the microscope. The pure culture of fungal species was maintained in potato dextrose agar slants stored for future purpose. Identification was compared with standard lab manuals.

Lactophenol Cotton Blue Staining

Filamentous fungi and spores did not observe gram stain. The lactophenol cotton blue (LPCB) mounting used to study the fungal culture. The filamentous spores were stained and appeared as blue.

Microbial Enumeration**Determination of *Staphylococcus aureus* (Adenike et al 2007)**

10 mg of the sample was added into Tryptic soy broth and incubated at 37°C for 24 hours. The sample was then streaked on Vogel- Johnson agar and incubated at 37°C for 24 hours. A single colony on each plate was then restreaked on Mannitol salt agar and incubated at 37°C for 24 hours. After the incubation, the colonial morphology was observed.

Determination of *Escherichia coli* (Waterman 1973)

Suspended 10 gm of the specimen in lactose broth or any other broth, which has no antibacterial effect to make 100ml (may adjust PH at 7). It is called pretreatment sample, incubate 100ml of pretreatment material at 30-37°C for 2- 5 hrs. Transfer amount of above homogenized pretreatment material containing 1gm or 1ml of the material being examined to 100ml of MacConkey broth and incubate at 43-45°C for 18-24hrs. Prepared subculture on a plate with MacConkey agar and incubate at 43-45°C for 18-24hrs. The growth of red non-mucoid colonies of Gram's negative rods were surrounded by reddish zone of precipitation shows that there is possibility of presence of *Escherichia coli*.

Determination of *Pseudomonas aeruginosa* (Van Doorne 1979)

The diluted sample was streaked onto Cetrimide agar plate. After the incubation at 37°C for 24 hours, the green colonies were tested for oxidase reaction and sub cultured into Triple sugar iron medium allowed the microbe to grow and the growth of bacteria and the reaction results were observed. Total Aerobic Bacterial count and Total Coliforms (Feng et al., 2002) Total aerobic bacterial count was performed to assess the quality and shelf life of the herbal formulation. 25g of each sample was homogenized in 225mL of sterile saline water. After that, 0.1ml from twofold diluted samples was spread on a petri dish containing Trypticsoy agar and incubated at 35°C for total aerobic bacterial count (Maturin 2001). Assess the hygiene of the formulations, total coliform count was performed by spreading 0.1 ml of the sample (as used for total aerobic count) on MacConkey agar, EMB agar, Blood agar, Chocolate agar and was incubated at 42°C for 24 hours (Feng 2002).



**Disk Diffusion Method for Antibiotic Susceptibility Test****Preparation of 0.5 McFarland Standards (Dalynn Biologicals 2014)**

A 0.5 McFarland standard was prepared by adding 0.05 ml of BaCl₂.2H₂O (1.175% w/v) to 9.95 ml of H₂SO₄ (1% v/v) with constant stirring. The absorbance of prepared 0.5 McFarland standards was measured at 625 nm to verify the correct turbidity. The McFarland standard was tightly sealed in the test tube and stored in the dark at room temperature. The McFarland standard was vigorously agitated with the vortex mixer before use.

Kirby-Bauer Test Procedure (Wootton 2013)

Using a sterile inoculating loop, two isolated colonies of the organism tested was suspended in 2 ml of a sterile saline. The saline tube was vortexed to create a smooth microbial suspension and this suspension was compared with 0.5 McFarland standards and adjusted by adding more microorganisms or adding more sterile saline until both 0.5 McFarland standard and microbial suspension had the same turbidity. The plates of Mueller-Hinton agar (MHA) were inoculated by dipping the sterile swabs into the inoculum and streaking the swabs over the surface of MHA three times while rotating the plate through a 60°C angle after each application. The inoculum was left to dry for five minutes at room.

Sample Preparation and Heavy Metal analysis

Heavy metal was analysed in an element of specific hollow cathode lamp was selected and mounted on AAS (Elico 618, Biominin Laboratories, STET Women's college (Autonomous) Sundarakkottai). The flame was starts and the instrument was set at zero by using blank solution. Accurately, 25g of herbal preparation was transferred into silica crucible and kept in a muffle furnace for ash at 700°C for 1 hour. The sample was cooled down to room temperature and the heating process was repeated for three times. The ash was dissolved by adding 5-10 ml of concentrated HCl and finally, the sample was prepared for heavy metal analysis by filtering through Whatman filter paper. For heavy metal analysis, the samples were aspirated through nebulizer and measure the absorbance against a blank as a reference. Specific hollow cathode lamps were analysed copper (wavelength 324.8 nm), Manganese (wavelength 297.5 nm), Lead (wavelength 283.3 nm), Zinc (wavelength 213.9). Before analysis, the sample was diluted to appropriate factor according to the detection limit of the Atomic Absorption Spectrophotometer. Calibration curve was obtained using referent standard and all the measurements were run in triplicate for the samples and standards solutions.

Qualitative Fungi Counts (WHO 2011)

Fungi were isolated by using potato dextrose agar (PDA) after incubation at 30°C for 5 days. At the end of 5 days incubation, the fungal growth was observed under microscope (WHO, 2011). The present study was evaluated that the heavy metal and microbial contamination of Antidiabetic Herbal Medicine. The majority of the populations, both from developed and developing countries, uses herbal preparations for primary healthcare purposes. A total of thirteen herbal preparations were randomly purchased from the different areas of Thiruvavur district, Tamil Nadu, India at market price and were subjected to toxic heavy metals and microbial load analysis.

Measurement of pH

The pH analysis were performed for antidiabetic herbal medicine namely ADHM 1-13. The pH ranges of the sample 5.3±0.01, 5.8±0.02, 4.7±0.01, - 5.9±0.04, - 6.7±0.02, -4.9±0.03, 3.6±0.06, 5.39±8, 6.9±0.03, 3.9±0.06, 5.3±0.04, 4.7±0.09, 6.1±0.04 were recorded respectively.

Limit Tests for Radical Impurities

All the samples have passed the limits test for chlorides and sulphates except 5 samples (ADHM-2, ADHM- 5, ADHM-6, ADHM-9, ADHM-13) which failed the limit test for sulphates.



**Uma Maheswari and Priscilla****Isolation of Microorganism**

Nutrient agar and Potato dextrose agar were prepared. Then ADHM samples were inoculated into agar plates. The bacterial colonies were identified by Gram staining and Biochemical tests where as fungi identified by Lactophenol cotton blue mounting technique.

Morphological Characteristics of Isolated Organism

Gram positive, spherical, non motile and non sporing cocci, approximately 1µm in diameter, arranged characteristically grape like cluster showing positive results for MR and Citrate test with alkaline and acid butt formation on TSI agar identified as *S.aureus*. Gram negative and rod shaped motile organisms showed results for Indole, MR and Catalase test alkaline salt and butt formation on TSI agar identified as *E.coli* with all above results obtained this organism were confirmed according to Bergey's manual of systematic bacteriology. Gram negative, non sporing bacilli, motile approximately 1.5-3µm in diameter showed the positive results for Catalase, Oxidase and Citrate test and circular shape of formation on Triple sugar iron agar was identified as *P. aeruginosa*.

Identification of Fungi

From the Potato dextrose agar medium, the organism produced mature colonies with 2 to 6 days. The growth was initially as a yellow colony that soon developed into a black, dotted surface as conidia were produced with age colony become set black powdery where as the reverse remind butt or cream color. Microscopically this organism exhibited septate hyphae, long conidiophores that support spherical vesicles that had given rise to large metulae and smaller phialides from which long chains of brown rough walled conidia were observed. Hence the organism was identified as *Aspergillus niger*.

Pathogen Determination

Among 13 Antidiabetic herbal medicines were tested, ADHM-10, 5 and 3 had the highest level of contamination of *P.aeruginosa* followed by the presence of *E.coli* in ADHM-10 and 12. Remaining all the samples were showed the presence of pathogen. In the level of contamination of *P.aeruginosa* in ADHM 1- 6×10^2 , ADHM 2 - 12×10^2 , ADHM 3 - 13×10^2 , ADHM 4- 7×10^2 , ADHM 5- 15×10^2 , ADHM 6- 7×10^2 , ADHM 7- 5×10^2 , ADHM 8- 11×10^2 , ADHM 9- 9×10^2 , ADHM 10- 16×10^2 , ADHM 11- 8×10^2 , ADHM 12- 3×10^2 , ADHM-13- 4×10^2 . Followed by the level of contamination of *E.coli* in ADHM 1- 5×10 , ADHM 2 – Nil, ADHM 3 - 3×10 , ADHM 4- 2×10 , ADHM 5- 2×10 , ADHM 6- Nil, ADHM 7- 4×10 , ADHM 8- 1×10 , ADHM 9- Nil, ADHM 10- 7×10 , ADHM 11- 3×10 , ADHM 12- 6×10 , ADHM-13- 4×10 . (Table 1)

Total Aerobic Bacterial Count and Total Coliform Count

Total Aerobic Bacterial Count and Total coliform count was performed to assess the quality and shelf life of herbal formulation. A highest colony was counted in ADHM-11. In ADHM 9, 6, 5 were showed the highest Total aerobic Bacterial count, such as $6.0 \times 10^{-4}/g$, $5.6 \times 10^{-4}/g$, $5.0 \times 10^{-4}/g$ respectively. (Table 2)

Antibiotic Susceptibility Test

Based on the level of frequency determination of pathogen namely, *P.aeruginosa* and *E.coli* was subjected to Antibiotic susceptibility test. Antibiotic Disk namely Ampicillin, Streptomycin and Tetracyclin were used. Zone of inhibition was measured for *P.aeruginosa* and *E.coli*. For Ampicillin, *P.aeruginosa* was showed zone of inhibition as 24 ± 2.02 Next to Streptomycin, was showed zone of inhibition 17.0 ± 0.23 followed by Tetracyclin, was showed zone of inhibition 18.0 ± 6.37 . *E.coli* was showed zone of inhibition as 15.6 ± 2.06 against Ampicillin. Streptomycin and Tetracyclin was showed zone of inhibition 15 ± 5.26 and 16.4 ± 2.62 . Altogether antibiotics tested was Ampicillin showed the effective susceptibility of *P.aeruginosa* isolated from the samples namely ADHM-6 and ADHM-9.

Heavy Metal Contents

The heavy metal contents were analyzed for antidiabetic herbal medicine using Atomic Absorption Spectrometer. In the ADHM 13 showed the highest level of Zinc was 54.5 ppm than the permissible limit of WHO and US FDA. Permissible limit of Copper was 20.00 ppm, 20.00 ppm and 150.00 ppm of the regulatory bodies. Among the



**Uma Maheswari and Priscilla**

Antidiabetic Herbal Medicine tested, ADHM 4 the level of copper was 15.7 ppm exceeded permissible limits. One third of the total ADHMs (ADHM-4, ADHM-6, ADHM-8 and ADHM-13) failed to comply with the safety limit of Lead 10.00 ppm, 10.00 ppm and 20.00 ppm. Altogether tested remaining samples were showed below detection level of heavy metals ADHM- 2, ADHM-5, ADHM-8, ADHM-11. Some of the identified metals (Zn, Cu, Mn and Pb) have important biological role in the body. (Table 3)

SUMMARY AND CONCLUSION

At present, broad popularity of Herbal products has increased few folds worldwide because, they are easy to purchase in street markets. It is estimated that 80% population of the developing world depends on herbal preparations as their primary healthcare. The aim of the current study was to evaluate microbial contamination and heavy metals in commercial antidiabetic herbal medicines in terms of measurement of pH, limit test for radical impurities, microbial load and pathogenic bacteria in thirteen antidiabetic herbal Medicines (ADHMs) collected in and around from Thiruvavur district, Tamilnadu, India. All the thirteen ADHMs had been found contaminated with different pathogenic bacteria and fungi namely *Escherichia coli*, *Pseudomonas aeruginosa*, *Staphylococcus aureus* and *Aspergillus* spp. According to the heavy metals evaluation of Pb was the highest metals present in all herbal medicine followed by Zn, Cu and Mn. The heavy metal content was analyzed by using Atomic Absorption Spectrophotometer (Zn, Cu, Mn and Pb). Microbial contaminants in these commercial herbal preparations pose a potential risk for human health and care should be taken in every step involved in the preparation of these herbal preparations to assure safety. The heavy metal content particularly Lead in all ADHM samples was alarming as almost all of them failed to comply with safety limit. The study is reflect the actual situation of the herbal medicine in Thiruvavur district and will raise the herbal contamination issue with the concerned authorities. The results of this study will come up with recommendations and advice to the concerned authorities to take the necessary corrective actions.

ACKNOWLEDGEMENT

Authors are Thank full to Financial Support given by Tamilnadu State Council for Science and Technology, Chennai.

REFERENCES

1. Adenike Okunlola, Babatunde A. Adewoyin, Oluwatoyin A. Odeku 2007 Evaluation of Pharamceutical and Microbial Qualities of some Herbal Medicine products In south Western Nigeria. *Tropical Journal of Pharmaceutical research*.6(1):661-670.
2. Ahmed, H., Ehtesham, M., Rasheed, N., & Mohammad, A.S.2017. Pharmaceutical Importance and Significance of Limit Tests. *Asian Journal of Pharmaceutical Research*, 7 (1): 30– 34.
3. American Diabetes Association. 2. Classification and diagnosis of diabetes: Standards of Medical Care in Diabetes 2019. *Diabetes Care*, 42 (Suppl. 1), S13–S28.
4. Bauer R. 1998 Quality criteria and standardization of phyto pharmaceuticals: Can acceptable drugs standard be achieved? *Drugs Information J* 32:101-110.
5. Cappucino. G.C and Shermann, N.1998. Microbiology a Laboratory manual, *Pearson*, New York.
6. Dalynn Biologicals. 2014 McFarland Standard. McFarland Standards for in Vitro Use Only, 2.
7. Han's Christian, 1884. Cellular response of *B. subtilis* and *E. coli* to the Gram's stain. *J. of bacteriology* 156(2):846-858.
8. Kar, A. 2005 Pharmaceutical Drug Analysis. secondedi. New Delhi: *New Age International (P) Ltd., Publishers*.
9. Keter . L, Too .R, Mwikwabe .N, Ndwigah .S, Orwa .J, Mwamburi .E Korir.R& Mutai, C 2016 Bacteria Contaminants and their Antibiotic Sensitivity from Selected Herbal Medicinal Products from Eldoret and Mombasa, Kenya. *American Journal of Microbiology*, 7, 18–28





Uma Maheswari and Priscilla

10. Munro A. L. S, "Measurement and control of pH values," 1970 in *Methods in Microbiology*, J.R.Norris and D.W.Ribbons, Eds.,chapter3,pp.39–89, AcademicPress Cambridge.
11. Neeta, Kumar S, Purohit D, Pandey P 2017 Herbal Drugs Used in the Treatment of Diabetes: An Overview. *World J Pharm PharmSci*, (6)9:697-708
12. Umair M, Altaf M, Abbasi AM (2017)Anethnobotanical survey of indigenous medicinal plants in Hafizabad district, Punjab Pakistan. *PLOS ONE*;2.
13. Vaikosen, E. N., &Alade, G. O. 2017) Determination of heavy metals in medicinal plants from the wild and cultivated garden in Wilberforce Island, Niger Delta region, Nigeria. *Journal of Pharmacy and Pharmacognosy Research*, 5, 129– 143.
14. Van Doorne H, Claushaus EPM 1979 "The quantitative determination of Enterobacteriaceae in pharmaceutical preparations". *INT. J. Pharm.* ;4(2):119-125.
15. Waterman RF, Sumner ED, Baldwin Jn, Warren .Fw Survival 1979 of *Staphylococcus aureus* on pharmaceutical preparations. *Int.J. pharm*:4(2) 119-125.
16. Wild. S, Roglic .G, Green .A ,Sicree .R , and King .H , "Global prevalence of diabetes: estimates for the year 2000 and projections for 2030," *DiabetesCare*,vol.27,no.5,pp.1047–1053,2004.
17. World Health Organization. Definition, Diagnosis and Classification of Diabetes Mellitus and Its Complications; *Department of Noncommunicable Disease Surveillance*: Geneva, Switzerland, 1999.
18. WHO,"Determination of microorganisms," 2011 in Quality Control Methods for Herbal Materials, *World Health Organization*, Ed.,pp.75– 84, WHO Press, Geneva, Switzerland.

Table 1: Pathogen determination of ADHMs

Sample	<i>Pseudomonas aeruginosa</i> (10 ³ /gm)	<i>Escherichia coli</i> (10 ¹ /gm)
ADHM-1	6 × 10 ²	5 × 10
ADHM-2	12 × 10 ²	-
ADHM-3	13 × 10 ²	3 × 10
ADHM-4	7 × 10 ²	2 × 10
ADHM-5	15 × 10 ²	2 × 10
ADHM-6	7 × 10 ²	-
ADHM-7	5 × 10 ²	4 × 10
ADHM-8	11 × 10 ²	1 × 10
ADHM-9	9 × 10 ²	-
ADHM-10	16 × 10 ²	7 × 10
ADHM-11	8 × 10 ²	3 × 10
ADHM-12	3 × 10 ²	6 × 10
ADHM-13	4 × 10 ²	4 × 10

Table 2: Total Aerobic Bacterial Count And Total Coliforms Count

SAMPLES	Total aerobic Microbial Count
ADHM-1	2.7×10 ⁻⁴
ADHM-2	1.49×10 ⁻⁴
ADHM-3	4.8×10 ⁻⁴
ADHM-4	4.04×10 ⁻⁴
ADHM-5	5.0×10 ⁻⁴
ADHM-6	5.6×10 ⁻⁴
ADHM-7	4.9×10 ⁻⁴
ADHM-8	3.6×10 ⁻⁴
ADHM-9	6.0×10 ⁻⁴





Uma Maheswari and Priscilla

ADHM-10	3.7×10^{-4}
ADHM-11	2.6×10^{-4}
ADHM-12	5.1×10^{-4}
ADHM-13	3.6×10^{-4}

Table 3: Heavy Metal Analysis In Antidiabetic Herbal Medicine

Sample	Zn (ppm)	Cu (ppm)	Mn (ppm)	Pb (ppm)
ADHM-1	55.38	25.38	6.5	16.3 ⁺
ADHM-2	BDL	BDL	9.0	BDL
ADHM-3	58.0	30.7	6.63	27.11 [*]
ADHM-4	61.5	23.5	7.75	61.3 ^{^*}
ADHM-5	BDL	BDL	10.7	BDL
ADHM-6	53.75	21.5	8.5	53.3 ^{^*}
ADHM-7	64.9	34.7	3	33.75 ^{^*}
ADHM-8	BDL	BDL	39.5	BDL
ADHM-9	62.88	38.88	6.88	43.88
ADHM-10	77.2	27.25	8.5	29.88 ^{^*}
ADHM-11	BDL	BDL	21.8	BDL
ADHM-12	53.8	24.25	4.63	29.38 ^{^*}
ADHM-13	60.5	19.13	6	54.50 ^{^*^*}

BDL- Below detection level; ⁺exceed WHO and US FDA permission limit; ^{*}exceed HAS Singapore permission limit; [^]exceed Chines Pharmacopeia permission limit.

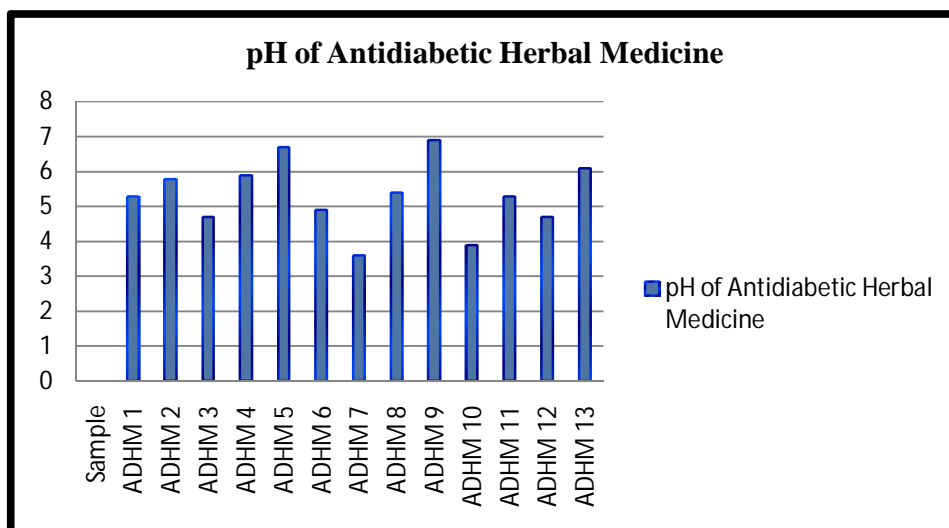


Fig.1 : pH of Antidiabetic Herbal Medicine





Levetiracetam Induced Skin Rash

Kompalli Varun¹, Sumaya Sumaya¹, M.Pratibha¹, M. Sunil¹, Rama Rao Tadikonda² and Vankadoth Sireesha^{3*}

¹Pharm.D Intern, CMR College of Pharmacy, Hyderabad, Telangana, India

²Professor and Principal, CMR College of Pharmacy, Hyderabad, Telangana, India

³Assistant professor, CMR College of Pharmacy, Hyderabad, Telangana, India

Received: 01 Feb 2023

Revised: 10 Apr 2023

Accepted: 12 May 2023

*Address for Correspondence

Vankadoth Sireesha

Assistant professor,

CMR College of Pharmacy,

Hyderabad, Telangana, India

Email: sireeshaganesh59@gmail.com



This is an Open Access Journal / article distributed under the terms of the Creative Commons Attribution License (CC BY-NC-ND 3.0) which permits unrestricted use, distribution, and reproduction in any medium, provided the original work is properly cited. All rights reserved.

ABSTRACT

Epilepsy is a chronic neurological disorder that is characterized by episodes of seizure. Levetiracetam (LEV) is a newer second-generation antiepileptic drug considered relatively safe compared with other antiepileptic drugs with multiple mechanism of action. Cutaneous side effects due to levetiracetam are rarely reported in the literature. Apart from levetiracetam inducing hyperpigmentation, on regular exposure of levetiracetam, we report a case of cutaneous reaction in young male patient who has prescribed with tablet LEV 500mg for epilepsy and the patient was shown skin reaction and treated early with a good outcome. Till date, there are only few cases reported involving skin reactions with LEV, our case is a LEV induced macula papular rash which is promptly diagnosed and successful treated in Tertiary care hospital.

Keywords: levetiracetam, maculopapular rashes, seizures, epilepsy.

INTRODUCTION

Levetiracetam is a newer second generation of anticonvulsant drug used in the treatment of Refractory partial seizures with or without secondary generalized seizures. It was introduced to the market in the year 2000. Premarketing clinical trials of the drug shows good tolerability with a wide safety margin. The FDA approved drug therapy recommended doses for adult is 500mg, Pediatric dose is 20mg given as oral Formulation (age \geq 1 month) and for intravenous use (age \geq 16) [1]. The mechanism of antiepileptic drugs is not clearly defined. Most relevant mechanism of action is modulation of synaptic Neuro transmitter release through binding to the synaptic vesicles protein SV2A in the brain(2). The Pharmacokinetic parameters of levetiracetam shows that it is absorbed very



**Kompalli Varun et al.,**

rapidly, its bioavailability is 96% peak plasma drug concentration which is achieved 1hr for oral administration and 5 to 15 min for IV administration (3). It shows <10% Protein bound. The main metabolic pathway is the enzymatic hydrolysis of the acetamide group. Metabolites have no pharmacological activity and are renally excreted (4). Approximately 34% of a levetiracetam dose is metabolised and 66% is excreted in urine unmetabolized, however, the metabolism is not hepatic but occurs primarily in blood by hydrolysis. As clearance is renal in nature it is directly dependent on creatinine clearance (6). LEV does not influence the plasma concentration of existing AEDs (phenytoin, carbamazepine, valproic acid, phenobarbital, lamotrigine, gabapentin, and primidone), and these AEDs do not influence the pharmacokinetics of LEV. The reported adverse drug reactions of LEV are somnolence, asthenia, coordination difficulties, and behavioural abnormalities. Psychosis has been reported infrequently with LEV with a reported frequency of <1%. Cutaneous side effects are rare, but drug rash with eosinophilia and systemic symptoms, reticulate drug rash, psoriasis from drug eruptions, urticarial vasculitis, angioedema, acute generalized exanthematous pustulosis, toxic epidermal necrolysis, and erythema multiforme have been reported (7). Our patient had maculopapular rash without systemic involvement, and he responded to Antihistamine drug therapy and showed complete healing by 2 weeks after drug discontinuation. Second-generation antiepileptic such as LEV has less potential for developing cutaneous side effects. Therefore, it is commonly prescribed as substitute antiepileptic in many cases of antiepileptic-related cutaneous ADR. Dermatologists should be aware of this rare cutaneous side effect of LEV for the prompt and early diagnosis

Case presentation

A 22-year-old patient was admitted to the ICU male department with chief complaints of cerebral palsy with developmental delay, high grade fever since 1month, patient had an history of face GTCs involving involuntary muscles, post ictal confusion and skin rash -95days (drug induced). On physical examination patient is conscious and cooperative, Blood pressure - 100/60mmHg, Pulse rate-90/min, CNS-no neck stiffness, CVS- S1,S2(Positive), RS -BAE (positive), Hairs and nails are normal, and scaling of skin were observed whole body. Laboratory finding of colour Doppler test reported multiple enlarged B/L cervical lymph nodes noted and increased central vascularity, Ultrasound scan of abdomen shows B/L grade 2 RPC, mild splenomegaly, mild ascites, urine examination reported significant bacteria culture, other laboratory findings are ALB-1.6g/dl(3.4-5.4g/dl), ALP-339IU/L(44-147IU/L), TSB-4.94mg/dl(0.1-1.2mg/dl) based on this evaluation the patient was diagnosed with AFI with cervical lymphadenopathy with skin rash (drug induced). The history of the patient shows scaling all over the body. 15 days before the patient had history of fever and seizures 25 days back. Patient was treated with inj. Antibiotics and midazolam, after 15 days patient was afebrile and developed seizures for which patient was given Tablet levetiracetam 500mg, 3 days later patient developed papules erythema, exfoliation all over the body. The patient also diagnosed in Dermatology DVL, on examination the patient showed diffused exfoliation all over the body as shown in the figure 1, 2, 3. So, the patient was diagnosed with Maculo papular rash secondary to tablet Levetiracetam. Treatment for this skin rash was to stop use of Tablet levetiracetam, consider alternative AED, Antihistamine like tab. CPM-4mg/OD/HS, liquid paraffin other drugs IV fluids, injection paracetamol-1gm/iv/BD, Injection Cefodoxime Proxetil.

DISCUSSION

Levetiracetam (LEV) is a novel antiepileptic drug (AED) which was discovered in early 1980s and soon, in 1999 FDA approved LEV for the management of partial onset seizure. In India, LEV tablet was approved in April 2005. (8) LEV is a novel second-generation antiepileptic drug. It is chemically unrelated to other antiepileptic drugs and is the α -ethyl analog of the nootropic agent piracetam. (9) It acts by binding to synaptic vesicle protein 2A and thereby modulation of one or more of its actions, ultimately affecting neural excitability. (10) In this case diagnosis of levetiracetam induced maculopapular rash is done when the patient developed papules, erythema and exfoliation all over the body, 3 days after the administration of levetiracetam as shown in the figure (1, 2, and 3). The patient had an episode of seizure along with fever 25 days before the administration of levetiracetam to which the physician prescribed antibiotics and inj. midazolam, 15 days later the patient had another episode of seizure without fever to which another physician prescribed levetiracetam which relieved the patient with seizures but 3 days later the patient developed papules erythema and exfoliation present all over the back, to relieve the patient from the rashes physician advised to stop taking levetiracetam and advised to apply Liquid paraffin regularly on the rash spots,



**Kompalli Varun et al.,**

Paracetamol and Monocef which led to hyperpigmentation of skin where the rashes appeared. Based on these reasons colour doppler test was performed which showed enlarged B/L cervical lymph nodes noted with increased central vascularity. Patient was then referred to dermatology on examination, diffused exfoliation was present all over the body to treat this the physician advised to stop tablet levetiracetam and consider alternative AED, Injpcpm, inj nor- adrenalinT.cpm, inj.monocef and hourly BP monitoring was prescribed by the physician. Skin exfoliation was present for a few days then the physician prescribed liqparaffn to apply on the skin. The rashes were reduced due to the drugs and liquid paraffin but the place where rashes were present hyperpigmentation had been developed.

CONCLUSION

Levetiracetam is most recommended antiepileptic drug, but in rare cases it shows its adverse drug reactions like hypersensitivity reactions like cutaneous skin rashes eg: maculopapular skin rashes, so prescriber has to stop the drug and go for other alternative therapy to the patient. Dermatologists should be aware of this rare cutaneous side effect of LEV for the prompt and early diagnosis

ABREVIATIONS

LEV-levitriacetam, FDA-food drug administratin,SVA2-synaptic vesicles protein ,AEDs-Antiepileptic drug therapy, GTCs-Generalizes tonic chlonic seizures, CNS-Central nervous system, CVS-Cardiovascular system, RS-Respiratory sysem, BAE-Bilateral air entry, RPC-Recurrent pyogenic cholangitis, ALB-Albumin, ALP-Alkaline phosphate, TSB-Total serum bilirubin, AFI-Acute febrile illness, DVL-Department Dermatology venereology and leprosy.

REFERENCES

1. Abou-Khalil, B. Levetiracetam in the treatment of epilepsy. *Neuropsychiatr. Dis. Treat.* 2008, 4, 507–523.
2. Sills GJ, Rogawski MA, Mechanisms of action of currently used antiseizure drugs. *Neuropharmacology.* 2020 May 15; PubMed PMID: 32120063
3. Simone Negrini,Sjögren's syndrome: a systemic autoimmune disease,Clinical and Experimental Medicine 2021,https://doi.org/10.1007/s10238-021-00728-6.
4. Li ZR,WangCY,ZhuX,Jiao Z, Population Pharmacokinetics of Levetiracetam: A Systematic Review. *Clinical pharmacokinetics.* 2021 Mar; PubMed PMID: 33447943.
5. Patsalos PN. Clinical pharmacokinetics of levetiracetam. *ClinPharmacokinet.* 2004;43(11):707-24. doi: 10.2165/00003088-200443110-00002. PMID: 15301575.
6. DPD Approved Drugs: Levetiracetam
7. Jones RT, Evans W, Mersfelder TL, Kavanaugh K. Rare red rashes: A case report of levetiracetam-induced cutaneous reaction and review of the literature. *Am J Ther* 2016;23:e944-6.
8. Kavita Krishna 1, Asawari L Raut, Kushal H Gohel, Priti Dave. *J Assoc Physicians India* 2011 Oct;59:656-8.
9. Lynch BA, Lambeng N, Nocka K, Kensel-Hammes P, Bajjalieh SM,Matagne A, et al. The synaptic vesicle protein SV2A is the bindingSite for the antiepileptic drug levetiracetam. *ProcNatlAcadSci U SA* 2004; 101:9861-6.
10. Rogawski MA. Brivaracetam: A rational drug discovery success story. *Br J Pharmacol* 2008; 154:1555-7.





Kompalli Varun *et al.*,



Fig.1: Describes Diffused Exfoliation on the Skin



Fig. 2: Diffused Exfoliation on the Skin





A Literature Review on the Effectiveness of Physiotherapy Approach in Postural Scoliosis among it Professionals

Seema B¹, S.Senthil Kumar² and Chandra Mohan³

¹Physiotherapy Postgraduate Student, School of Health Sciences, Department of Physiotherapy, Garden City University, Bangalore, Karnataka, India

²Professor and Research Supervisor, School of Health Sciences, Department of Physiotherapy, Garden City University, Bangalore, Karnataka, India

³Assistant Professor, School Health Sciences, Department of Physiotherapy, Garden City University, Bangalore, Karnataka, India

Received: 28 Feb 2023

Revised: 25 Apr 2023

Accepted: 08 May 2023

*Address for Correspondence

Seema B

Physiotherapy Postgraduate Student,
School of Health Sciences, Department of Physiotherapy,
Garden City University,
Bangalore, Karnataka, India.



This is an Open Access Journal / article distributed under the terms of the **Creative Commons Attribution License** (CC BY-NC-ND 3.0) which permits unrestricted use, distribution, and reproduction in any medium, provided the original work is properly cited. All rights reserved.

ABSTRACT

Scoliosis is a spinal condition that is quite prevalent worldwide, especially among adolescents, with a prevalence ranging from 0.47% to 5.2%. This complex deformity affects the spine in three dimensions, resulting in frontal curves, fixed vertebral rotations, and a flattening of the sagittal physiological curves. It can cause problems in range, including asymmetry of the body, imbalance in the muscles, reduced flexibility, back pain, and negative impacts on psychological health and quality of life. A curvature in the spine can occur at any level of the spine and is classified as thoracic, thoracolumbar, or lumbar scoliosis, depending on the vertebrae affected. To review the effectiveness of the physiotherapy approach to reduce pain and spinal deformity in postural scoliosis among IT professionals. PubMed, Google Scholar, Pedro, Sci-Hub, and Cochrane from these databases articles were searched using the keywords. 25 articles were collected from the past thirteen years. Articles stated that the application of the physiotherapy approach is found to be an effective treatment in postural scoliosis among IT professionals. The literature review analyzed the effect of the physiotherapy approach on scoliosis among IT professionals. The wide range of reviews was used to conclude that physiotherapy exercises and thermotherapy are found to be a choice of treatment for postural scoliosis among IT workers.

Keywords: Scoliosis, Postural deformity, physical therapy, Cob's angle, Exercises





INTRODUCTION

When the spine deviates from a neutral position, it can indicate poor posture. Prepubertal children who exhibit trunk symmetry and poor posture may be at risk of developing scoliosis, which is marked by uneven shoulders, spinal curvature, and uneven hips. Scoliosis can also be identified by the asymmetry in the activity of the paraspinal muscles [1]. It is a three-dimensional deformity of the spine that has no known cause. It involves a sideways deviation in the frontal plane, horizontal rotation, and an abnormal curvature in the sagittal curve reaches 50 degrees, it is typically recommended to undergo surgery since such curves pose a risk of continued progression into adulthood [2]. Moderate scoliosis is often treated with bracing, and the effectiveness of the treatment depends on where the structural curves are located. Patients often find scoliosis-specific exercise to be a favorable non-surgical option. However, using electronic devices such as cell phones, video games, and desktop computers has become more prevalent in daily life, promoting sedentary behavior linked to various health issues such as cardiovascular disorders, hypertension, diabetes, and musculoskeletal disorders [3]. The growth spurt phase during childhood and adolescence, also known as rapid growth in adolescents, may lead to postural changes such as scoliosis, which could result in uncomfortable positions for students [4].

Scoliosis is diagnosed by a standing anteroposterior radiograph that shows a Cobb angle greater than 10°. The prevalence of scoliosis worldwide ranges from 0.93% to 12% in the general population. This progressive disease impacts spinal alignment, trunk mobility, and symmetry, ultimately reducing the quality of life and potentially causing respiratory problems. Additionally, severe cases of scoliosis have been linked to psychological disturbances [5]. Scoliosis can be classified as functional or structural depending on whether the curve is fixed during bending. Functional scoliosis is a temporary curvature in the spine without rotation of the vertebrae. On the other hand, structural scoliosis is a multifactorial disorder caused by a loss of flexibility in one or more segments of the curved spinal column [6]. Adolescents with mild idiopathic scoliosis have a 10-15% risk of their curve worsening, which is believed to be related to biomechanical and morphological changes in the trunk segment and the effects of improper mechanical forces [7].

The most common conservative treatment for patients with growth potential whose Cobb angle is greater than 25° is bracing. Bracing applies an external pushing force to the trunk to straighten it and rotate the rib cage. The success of brace treatment is impacted by factors such as skeletal maturity, curve magnitude, in-brace correction, flexibility, and compliance with brace wearing [8]. However, bracing can be stressful for patients, cause a flatter back, and reduce the quality of life. Wearing braces for scoliosis during adulthood can lead to poor compliance due to discomfort, which may result in the development of various problems such as back pain, breathing dysfunction, contractures, and progressive deformity if scoliosis exceeds certain thresholds [9].

To address impairments and consequent disabilities, exercise can help. The study will involve outpatient physiotherapy with scoliosis-specific exercises, supervised by therapists for 30-minute sessions, 5 times per week for 4 weeks. After that, the subjects will continue the exercise regimen at home for another 4 weeks, under the supervision of their parents. The program includes autocorrection in three dimensions, stabilization of corrected posture, training for daily activities, and education [10]. physiotherapy scoliosis-specific exercises are given It's based on Schroth's work and a scientific approach to scoliosis exercise. Three-dimensional active correction involves fixing the curvature in the coronal, horizontal, and sagittal planes simultaneously¹¹.

METHODOLOGY

PubMed, Google Scholar, Medline, and Pedro were utilized to conduct a comprehensive literature search. It consists of keywords: postural scoliosis, physical therapy, IT professionals, and manipulative therapy. Thorough screening of articles that appeared as a result of the search was done. All potentially relevant papers were identified from the title,





Seema et al.,

abstracts, and full-text literature were assessed. Citation and references of relevant articles were also checked to find out the availability of more articles.

INCLUSION CRITERIA

Articles which are included only if are:

- Articles explaining the physiotherapy approach in postural scoliosis
- Articles published in recent years
- Full-text articles
- Articles published in English

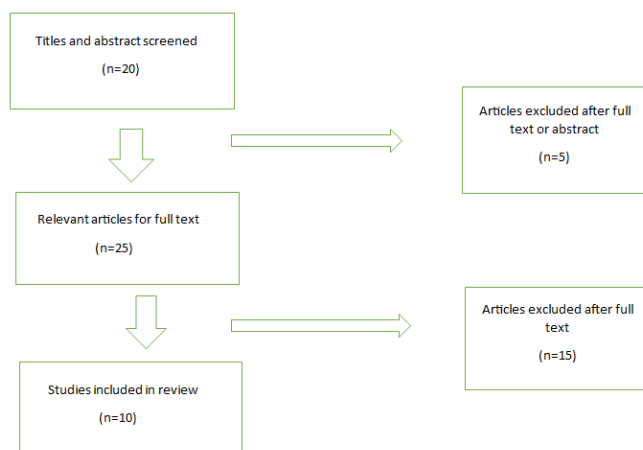
EXCLUSION CRITERIA

- Articles of past 2010
- Articles explaining surgical interventions
- Articles discussing other than physiotherapy approach in postural scoliosis are excluded

SELECTION OF INCLUSION AND EXCLUSION CRITERIA:

Based on inclusion and exclusion criteria, 7 articles were selected. The study design of all these 7 articles was systemic. Articles in the English language were selected so that proper analyses of articles can be done. English being the preferable and favorable language, the chances of occurrence of an error in analyses of these articles can be reduced. Considering articles with non-English language might have led to improper understanding, improper analyses, and gathering of inappropriate information. Hence, articles in English language and with proper analyses and appropriate interpretation, analyses of data can be done, and correct information can be stated in this review. Articles published between the years 2010 – 2022 were included in this review, so that scenario of physical therapy in postural scoliosis will be known. Articles before 2010 were excluded. Articles with full texts were selected so that thorough information from these articles can be gathered. Articles that did not contain any data regarding Participants with other symptomatic musculoskeletal diseases in the lower limbs, symptomatic central and peripheral nervous system diseases, diabetes mellitus, and rigid deformities in the feet were excluded since it is irrelevant considering the scope of this study. The scope of this study is regarding the physical therapy in postural scoliosis among IT professionals and hence articles containing no relevant information regarding the mentioned scope of the study are excluded

STUDY SELECTION STRATEGY





Seema et al.,

RESULTS

SL NO	AUTHOR	YEAR	STUDY DESIGN	SAMPLE SIZE	SUMMARY
1	Alberto Romeno et al	2022	Experimental study	20	A study was conducted on subjects with scoliosis, in which each participant received a personalized intensive daily physical activity program developed by an expert therapist. The program was implemented for a period of six months, during which pre- and post-intervention radiographs and motor functioning were examined. The study found that the intervention successfully prevented scoliosis progression in the group, and was effective for individuals with scoliosis of different ages and levels of severity.
2	Athawale V et al	2021	Experimental study	1	A 23-year-old female with a history of adolescent idiopathic scoliosis and right shoulder pain was the subject of an experimental study aimed at improving her self-image and daily activities. The subject underwent five weeks of physical therapy, which included thermotherapy, bracing, strengthening, and stretching exercises, to prevent further deformity and aggravation of symptoms. Proper follow-up was conducted to track progress, and the results showed significant improvement in muscle strength, pain relief, spinal mobility, postural control, and a decrease in further complications.
3	Xin Li et al	2020	systematic review	325	A systematic study was conducted to compare the effectiveness of core-based exercise to other nonsurgical interventions in people with scoliosis. The exercise group who performed core-based strengthening exercises had significantly lower Cobb angles and significantly better quality of life as measured by the Scoliosis Research Society-22 questionnaire than the control groups.





Seema et al.,

4	Yunli Fan et al	2020	Systematic review	494	A systematic study is conducted in which Two randomized controlled trials and two clinical controlled trials suggested that reducing Cobb angle by more than 5 degrees scoliosis-specific exercise alone and with bracing or traditional exercise had clinical significance.
5	ShkurtaRrecaj-Malaj et al	2020	Prospective research	69	During 24 weeks, patients in both the brace-wearing and non-brace-wearing groups participated in 2 periods of 2-week treatment regimens consisting of daily 60-minute exercises from the Schroth and Pilates methods. Each treatment period was followed by a 10-week home program treatment. The patients' Cobb angle (x-rays) and ATR (scoliometer) were evaluated before treatment, at 12 weeks, and 24 weeks and significant improvements were observed in both groups.
6	Jin Young Ko et al	2018	Prospective study	25	To investigate the correlation between unilateral postural instability and paraspinal muscle weakness based on curve patterns, a prospective study was carried out. Surface electromyography (sEMG) was utilized to assess the muscular activation patterns of core muscles. The most noteworthy findings from the sEMG data revealed an increase in the activities of the ipsilateral 7th thoracic erector spinae during hand-up motion, the ipsilateral 3rd lumbar erector spinae during leg-up motion, and the 12th thoracic and 3rd lumbar erector spinae during side-bridging. By using asymmetric scoliosis-specific exercises to strengthen the paraspinal muscles on the concave side, the severity of scoliosis can be improved.
7	Marc Marmarco et al	2017	Prospective study	1	A 15-year-old female with idiopathic scoliosis and a 45 degrees Cobb angle underwent a prospective case study. She was a skeletally mature adolescent female (Risser 4) who received pattern-specific scoliosis Rehabilitation (PSSR) and followed up for one year. As a result of the treatment, the patient





Seema et al.,

					achieved a 13-degree reduction in her primary thoracic cobb angle, and there was also an improvement in posture and a reduction in trunk rotation. Specifically, there was a decrease of four degrees in the thoracic spine and five degrees in the lumbar spine.
8	Josette Bettany-Saltikov et al	2017	Systematic review	181	A review study was conducted to assess the latest evidence on treating spinal deformities in both adolescents and adults, such as scoliosis and hyper kyphosis. The study found that conservative treatment using physiotherapeutic scoliosis-specific exercises (PSSE) and rigid bracing was supported by level I evidence for treating adolescent idiopathic scoliosis (AIS). Currently, there is high-quality evidence that supports the use of PSSE, particularly those involving PSSR, in conjunction with bracing for treating AIS.
9	Hans-Rudolf Weiss et al	2016	Systematic review	1	A systematic review study is conducted to evaluate the effectiveness of physical/postural reeducation/physiotherapy programs in growing scoliosis patients. These studies revealed that postural reeducation in the form of exercise rehabilitation programs may have a positive influence on scoliosis; however, the various programs were difficult to compare. There was a significant effect of Schroth scoliosis exercises in the management of AIS.
10	Sanja Schreiber et al	2015	Randomized controlled study	50	The objective of a randomized controlled trial was to assess the impact of Schroth exercises when combined with standard care on back muscle endurance and quality of life outcomes compared to standard care alone, among 50 AIS patients aged 10-18 years with curves of 10-45°, recruited from a scoliosis clinic. Participants were randomly assigned to receive standard care or supervised Schroth exercises in addition to standard care for six months. During the initial two weeks, five sessions were held to teach





Seema et al.,

					Schroth exercises. A daily home program was modified under weekly supervised sessions. After three months, the back muscle endurance (BME) improved by 32.3 seconds in the Schroth group, and by 4.8 seconds in the controlled group. The difference between the two groups was 27.5 which was statistically significant.
--	--	--	--	--	---

DISCUSSION

Body posture is defined as the ideal position adopted by human beings for their daily activities through their body structures and function to have better biomechanical efficiency with less energy expenditure. Scoliosis, which is a common spinal deformity worldwide, is often observed in adolescents of 0.47-5.2%. This condition can lead to various issues, including body asymmetry, muscle imbalance, reduced flexibility, back pain, and adverse effects on psychological well-being and overall quality of life. To prevent pain and deformity numerous treatments have emerged. Physiotherapy has been found to be the most effective treatment in scoliosis patients to reduce the deformity and severity of pain. After reviewing all the studies in which patients were treated with physiotherapeutic exercises which are done regularly with proper program period and follow up their deformity of the spine or the increased curve has shown lesser Cobb angle after the treatment. Above all articles shows the effectiveness of different physiotherapy exercise, thermotherapy, and other conventional therapy approaches in postural scoliosis. Among all of them physiotherapy approach highlights as the best treatment approach which can be given alone or with exercises compared to other treatment approaches.

CONCLUSION

The literature review analyzed the effect of the physiotherapy approach on scoliosis among IT professionals. The wide range of reviews was used to conclude that physiotherapy exercises and thermotherapy are found to be a choice of treatment for postural scoliosis among IT workers.

REFERENCES

1. Romano A, Ippolito E, Risoli C, Malerba E, Favetta M, Sancesario A, Lotan M, Moran DS. Intensive Postural and Motor Activity Program Reduces Scoliosis Progression in People with Rett Syndrome. *Journal of Clinical Medicine*. 2022 Jan 22;11(3):559.
2. Cheung MC, Yip J, Lai JS. Biofeedback posture training for adolescents with mild scoliosis. *BioMed Research International*. 2022 Jan 31;2022.
3. Wang L, Wang C, Youssef AS, Xu J, Huang X, Xia N. Physiotherapeutic scoliosis-specific exercises performed immediately after spinal manipulative therapy for the treatment of mild adolescent idiopathic scoliosis: study protocol for a randomized controlled pilot trial. *Trials*. 2021 Dec;22(1):1-2.
4. Athawale V, Phansopkar P, Darda P, Chitale N, Chinewar A. Impact of physical therapy on pain and function in a patient with scoliosis. *Cureus*. 2021 May 26;13(5).
5. Fan Y, To MK, Yeung EH, Wu J, He R, Xu Z, Zhang R, Li G, Cheung KM, Cheung JP. Does curve pattern impact on the effects of physiotherapeutic scoliosis specific exercises on Cobb angles of participants with adolescent idiopathic scoliosis: A prospective clinical trial with two years follow-up. *Plos one*. 2021 Jan 25;16(1): e0245829.
6. deAssis SJ, Sanchis GJ, de Souza CG, Roncalli AG. Influence of physical activity and postural habits in schoolchildren with scoliosis. *Archives of Public Health*. 2021 Dec;79(1):1-7.





Seema et al.,

7. Gou Y, Lei H, Zeng Y, Tao J, Kong W, Wu J. The effect of Pilates exercise training for scoliosis on improving spinal deformity and quality of life: Meta-analysis of randomized controlled trials. *Medicine*. 2021 Oct 1;100(39):e27254-.
8. Li X, Shen J, Liang J, Zhou X, Yang Y, Wang D, Wang S, Wang L, Wang H, Du Q. Effect of core-based exercise in people with scoliosis: A systematic review and meta-analysis. *Clinical rehabilitation*. 2021 May;35(5):669-80.
9. Fan Y, Ren Q, To MK, Cheung JP. Effectiveness of scoliosis-specific exercises for alleviating adolescent idiopathic scoliosis: a systematic review. *BMC musculoskeletal disorders*. 2020 Dec;21(1):1-3.
10. Rrecaj-Malaj S, Beqaj S, Krasniqi V, Qorolli M, Tufekcievski A. Outcome of 24 weeks of combined Schroth and pilates exercises on cobb angle, angle of trunk rotation, chest expansion, flexibility and quality of life in adolescents with idiopathic scoliosis. *Medical science monitors basic research*. 2020;26: e920449-1.
11. Dąbrowska A, Olszewska-Karaban MA, Permoda-Białozorczyk AK, Szalewska DA. The postural control indexes during unipodal support in patients with idiopathic scoliosis. *BioMed Research International*. 2020 Jul 4;2020.
12. Wiernicka M, Kotwicki T, Kamińska E, Łochyński D, Kozinoga M, Lewandowski J, Kocur P. Postural stability in adolescent girls with progressive idiopathic scoliosis. *BioMed Research International*. 2019 Dec 11;2019.
13. Czaprowski D, Stoliński Ł, Tyrakowski M, Kozinoga M, Kotwicki T. Non-structural misalignments of body posture in the sagittal plane. *Scoliosis and spinal disorders*. 2018 Dec;13(1):1-4.
14. Ko JY, Suh JH, Kim H, Ryu JS. Proposal of a new exercise protocol for idiopathic scoliosis: A preliminary study. *Medicine*. 2018 Dec;97(49).
15. Moramarco M, Moramarco K, Fadzani M. Suppl-9, M4: Cobb Angle Reduction in a Nearly Skeletally Mature Adolescent (Risser 4) After Pattern-Specific Scoliosis Rehabilitation (PSSR). *The Open Orthopaedics Journal*. 2017; 11:1490.
16. Bettany-Saltikov J, Turnbull D, Ng SY, Webb R. Management of spinal deformities and evidence of treatment effectiveness. *Open Orthop J*, 11: 1521–1547.
17. Weiss HR, Moramarco MM, Borysov M, Ng SY, Lee SG, Nan X, Moramarco KA. Postural rehabilitation for adolescent idiopathic scoliosis during growth. *Asian spine journal*. 2016 Jun 16;10(3):570-81.
18. Anwer S, Alghadir A, Shaphe A, Anwar D. Effects of exercise on spinal deformities and quality of life in patients with adolescent idiopathic scoliosis. *BioMed research international*. 2015 Oct 25;2015.
19. Schreiber S, Parent EC, Moez EK, Hedden DM, Hill D, Moreau MJ, Lou E, Watkins EM, Southon SC. The effect of Schroth exercises added to the standard of care on the quality of life and muscle endurance in adolescents with idiopathic scoliosis—an assessor and statistician blinded randomized controlled trial: “SOSORT 2015 Award Winner”. *Scoliosis*. 2015 Dec;10(1):1-2.
20. Romano M, Minozzi S, Bettany-Saltikov J, Zaina F, Chockalingam N, Kotwicki T, Maier-Hennes A, Negrini S. Exercises for adolescent idiopathic scoliosis. *Cochrane Database of Systematic Reviews*. 2012(8).
21. BettanySaltikov J, Parent E, Romano M, Villagrasa M, Negrini S. Physiotherapeutic scoliosis-specific exercises for adolescents with idiopathic scoliosis. *European Journal of Physical and Rehabilitation Medicine*. 2014;50(1):111-21.
22. Zapata KA, Sucato DJ, Jo CH. Physical therapy scoliosis-specific exercises may reduce curve progression in mild adolescent idiopathic scoliosis curves. *Pediatric Physical Therapy*. 2019 Jul 1;31(3):280-5.
23. Porte M, Patte K, Dupeyron A, Cottalorda J. Exercise therapy in the treatment of idiopathic adolescent scoliosis: Is it useful. *Archives de Pediatrie: Organe Officiel de la Societe Francaise de Pediatrie*. 2016 Apr 23;23(6):624-8.
24. Weiss HR. Physical therapy intervention studies on idiopathic scoliosis-review with the focus on inclusion criteria. *Scoliosis*. 2012 Dec; 7:1-2.
25. Marti CL, Glassman SD, Knott PT, Carreon LY, Hresko MT. Scoliosis Research Society members’ attitudes towards physical therapy and physiotherapeutic scoliosis-specific exercises for adolescent idiopathic scoliosis. *Scoliosis*. 2015 Dec;10(1):1-7.





A New RP-HPLC Method for the Simultaneous Determination of Sofosbuvir and Velpatasvir

Pratik Biswas^{1*}, P.D. Chaithanya Sudha², K.N.V. Chenchu Lakshmi³

¹Student, Krupanidhi College of Pharmacy, Bangaluru -560035, Karnataka, India

²Associate Professor, Krupanidhi College of Pharmacy, Bangaluru-560035, Karnataka, India.

³Associate Professor, KVSR Siddhartha College of Pharmacy, Vijayawada, Andhra Pradesh, India.

Received: 17 Jan 2023

Revised: 24 Mar 2023

Accepted: 27 Apr 2023

*Address for Correspondence

Pratik Biswas

Student,

Krupanidhi College of Pharmacy ,

Bangaluru -560035, Karnataka, India

Email: pratikbiswas710@gmail.com



This is an Open Access Journal / article distributed under the terms of the **Creative Commons Attribution License** (CC BY-NC-ND 3.0) which permits unrestricted use, distribution, and reproduction in any medium, provided the original work is properly cited. All rights reserved.

ABSTRACT

A simple, rapid and economical stability indicating RP-HPLC method has been successfully developed by applying for simultaneous determination of Sofosbuvir and Velpatasvir. The %RSD values obtained from the precision studies were also found to be less than 2, which indicate precise method. The high % recoveries indicate that the proposed method was highly accurate. The low values of LOD and LOQ indicates the high sensitivity of the proposed method. The absence of interfering peaks observed in the chromatogram of blank and placebo interference studies indicates specific method and degradants formed during stress degradation studies were also well separated and not interfere with estimation of the drugs by the proposed stability indicating RP-HPLC method.

Keywords: RP-HPLC, Degradation studies, Velpatasvir, Sofosbuvir and Validation.

INTRODUCTION

This combination is not official in any pharmacopoeia extensive literature survey results that only few analytical methods were reported like RP-HPLC and spectrophotometric methods for the determination of Sofosbuvir and Velpatasvir in alone or in combinations with the other drugs in biological fluids, bulk and pharmaceutical dosage forms but did not reveal any forced degradation studies for the fixed dose combination drug product of Velpanat. The proposed stability-indicating reversed-phase high-performance liquid chromatography method for simultaneous estimation of sofosbuvir and ledipasvir of bulk drug and formulation by using a RP-HPLC.





DRUG PROFILES

Sofosbuvir is used in prevention and treatment of viral infection. It is a nucleotide analog HCV NS5B polymerase inhibitor. It is used in a combination with Velpatasvir and is approved by USFDA. Fig. 1.1

IUPAC name: Isopropyl (2S)-2-[[[(2R,3R,4R,5R)-5-(2,4-dioxypyrimidin-1-yl)-4-fluoro-3-hydroxy-4-methyl-tetrahydrofuran-2-yl]methoxy-phenoxy-phosphoryl]amino]propanoate.

Molecular formula: C₂₂H₂₉FN₃O₉P

Molecular weight: 529.453 g/mol

Category: Anti-viral agent

Mechanism of Action: The uridine nucleotide analog sofosbuvir is a phosphoramidate prodrug that has to be triphosphorylated within the cells to produce its action. The required enzymes for its activation are present in the human hepatic cells, therefore, it is converted to its active metabolite during the first-pass metabolism, directly at the desired site of action.

Velpatasvir is a Direct-Acting Antiviral (DAA) medication used as part of combination therapy to treat chronic Hepatitis C, an infectious liver disease caused by infection with Hepatitis C Virus (HCV). Fig. 1.2

IUPAC name: Methyl ((2S,5S)-2-(9-(2-[(2S,4S)-1-((2R)-2-[(methoxy carbonyl)amino]-2-Phenylacetyl)-4-(methoxymethyl)-2-pyrrolidinyl]-1H-imidazol-4-yl)-1,11-dihydroisochromeno[4¹,3¹:6,7]naphthol[1,2-d]imidazol-2-yl)-5-methyl-1-pyrrolodiny]-3-methyl-1-oxo-2-butanyl]carbamate.

Molecular formula: C₄₉H₅₄N₈O₈

Molecular weight: 883.019 g/mol

Category: Anti-viral agent

Mechanism of Action: Velpatasvir is used in combination therapy with other antiviral medications to treat chronic hepatitis C virus (HCV) infected patients with HCV genotypes 1-6, and to treat HCV and HIV co-infected patients. This medication is a **combination** of **sofosbuvir** and **velpatasvir** and is used to treat chronic (long-lasting) hepatitis C, a viral infection of the liver. Chronic hepatitis C infection can cause serious liver problems such as scarring (cirrhosis), or liver cancer.

Experimental/Methodology

Preparation of solutions

Preparation of pH- 4.5 phosphate buffer solution

Accurately weighed 1.36gm of Potassium dihydrogen Ortho phosphate in a 1000ml of Volumetric flask add about 900ml of milli-Q water added and degas to sonicate and finally make up the volume with water then added 1ml of Triethylamine then pH adjusted to 4.5 with dil. Ortho phosphoric acid solution.

Preparation of mobile phase

Mixture of pH - 4.5 Buffer and Acetonitrile in the ratio 57.74:42.26 %V/V, filtered through 0.45 μ filter under vacuum.

Preparation of Diluent:

Mixture Water and Acetonitrile in the ratio of 50 : 50 V/V, filtered through 0.45 μ filter under vacuum.

Standard stock Preparation:

Accurately Weighed and transferred 40mg of Sofosbuvir and 10mg of Velpatasvir working Standards into a 25 ml & 25ml clean dry volumetric flasks, add 10ml of diluent, sonicated for 10 minutes and make up to the final volume with diluents.





Pratik Biswas *et al.*,

Standard working Preparation:

1ml from the above two stock solutions was taken into a 10ml volumetric flask and made up to 10ml (160µg/ml of Sofosbuvir & 40µg/ml of Velpatasvir).

Sample Preparation:

5 tablets were weighed and the average weight of each tablet was calculated, then the weight equivalent to 1 tablet was transferred into a 100 ml volumetric flask, 50ml of diluent was added and sonicated for 25 min, further the volume was made up with diluent and filtered by HPLC filters.(4000µg/ml of Sofosbuvir and 1000µg/ml of Velpatasvir).

Sample working Preparation:

0.4ml of filtered sample stock solution was transferred to 10ml volumetric flask and made up with diluent.(160µg/ml of Sofosbuvir 40µg/ml of Velpatasvir).

Method Development

To optimize chromatographic conditions, the effect of chromatographic variables such as different columns, mobile phase composition and flow rates were studied at constant conditions such as appropriate wavelength 268 nm, injection volume of 10µl and run time of about 6 minutes throughout the trials to achieve the best possible separation and resolution. The conditions which produce best resolution tailing factor, USP plate count were selected for the estimation. The resulting chromatograms were recorded and chromatographic parameters such as tailing factor, USP plate count and resolution were calculated.

Method Validation**System suitability studies**

The system stability test was carried out by injecting five replicate injections of 10µL of the standard solutions of SOF and VEL into the chromatographic system by using optimized chromatographic conditions. The system suitability parameters were evaluated for tailing factor, % relative standard deviation for retention time and peak areas, resolutions and theoretical plates were determined.

Linearity of Detector Response

The linearity of an analytical method was established by preparing a series of linearity solutions (25-150% Level) by diluting aliquots of 0.25, 0.5, 0.75, 1.0, 1.25 and 1.5 ml were taken from stock solution of concentration 40 µg/ml of Sofosbuvir and 10 µg/ml Velpatasvir and then diluted up to mark with diluent. Such that the final concentrations were in the range 40 - 240 µg/ml of Sofosbuvir and 10 - 60 µg/ml Velpatasvir. Volume of 10 µl of each sample was injected in five times for each concentration level in triplicate into the chromatographic system and the chromatographs were recorded. Calibration curve was constructed by plotting the peak area versus drug concentration. A linear relationship between peak area vs. concentration was observed in the range of study (concentration in µg/ml on X-axis and peak area response on Y-axis) from this calculate correlation coefficient, slope and intercept.

Precision**System Precision (repeatability/Intra-day precision)**

The system precision study was demonstrated by injecting 10µl solution of standard preparations six times into the chromatographic system and chromatograms were recorded. Calculated peak areas for Sofosbuvir and Velpatasvir and results were expressed as %RSD.





Method Precision

The method precision of the test method was conducted by 10 μ l solution of sample preparations six times into the chromatographic system and chromatograms were recorded. Calculated peak areas for Sofosbuvir and Velpatasvir and results were expressed as %RSD.

Intermediate/Inter-Day Precision (Ruggedness)

The intermediate precision of the method was carried out by injecting 10 μ l solution of standard preparations six times into the chromatographic system on different days and chromatograms were recorded. Calculated peak areas for Sofosbuvir and Velpatasvir and results were expressed as %RSD.

Accuracy (Recovery)

The accuracy of the method was studied by % recovery across its range by making 3 different concentrations at 50%, 100% and 150% Levels using standard addition method where sample preparations were spiked with known amount of standard and then each concentration was injected triplicate into the chromatographic system and chromatograms were recorded. The % recoveries obtained from each Level for Sofosbuvir and Velpatasvir were calculated.

Robustness

The robustness of the proposed method was determined by deliberately varying the chromatographic conditions such as mobile phase compositions, flow rate, wavelength and column temperature. The standard solutions prepared as per the test method were injected triplicate into the chromatograph at variable conditions such as flow rate at ± 0.1 ml/min, mobile organic phase composition by $\pm 10\%$, wavelength by ± 5 nm and column temperature by $\pm 5^\circ\text{C}$. System suitability parameters were evaluated from the obtained chromatograms.

Specificity (Interference Studies)

Specificity of the method for the interference of the blank and the placebo was conducted by injecting blank, placebo, standard and sample solutions in triplicate as per test method. The specificity of the proposed RP-HPLC method also assessed by comparing the chromatograms obtained from blank, placebo, standard and sample solutions.

Forced Degradation Studies

A stress study was conducted for the sample, Vonavir when exposed to the following stress conditions given in table 1. All the stressed samples were suitable diluted to required concentration with diluent and injected twice into the RP-HPLC system by using optimized chromatographic conditions and the chromatograms were recorded and evaluated for the peak purity. The % of degradation of Sofosbuvir and Velpatasvir were calculated.

Limit of Detection (LOD) and Quantification (LOQ)

The study to establish the LOD and LOQ for Sofosbuvir and Velpatasvir was conducted. A series of vary dilute LOD and LOQ solutions were prepared as per the test method and injected triplicated into the HPLC system. Chromatograms were recorded. The LOD and LOQ were established based on Signal to Noise ratio. LOD was established by identifying the concentration which gives s/n ratio of about 3 where as LOQ was established by identifying the concentration which gives s/n ratio of about 10.

Solution Stability Studies

A study to establish the stability of standard and test solutions were conducted on bench top in initial, 12 hrs, 24 hrs and 48 hrs. This was achieved by preparing standard and test preparations as per the test method and injected twice into the chromatographic system under the optimized chromatographic conditions and chromatograms were recorded. The difference in % Assay was calculated for Sofosbuvir and Velpatasvir.



Pratik Biswas *et al.*,

RESULTS AND DISCUSSION

Optimization of the method:

The optimization of the method development trials are summarized in table-2. The chromatogram of optimized chromatographic conditions are given in figure 1.3.

Validation of the Method

System Suitability Studies

System Suitability chromatography obtained is shown in fig-1.4 and results of the proposed method are presented in table-3. The % RSD were found to be less than 2%. The theoretical plates were more than 2000 for the drugs. The tailing factor was found to be less than 2.0 and resolutions between adjacent peaks were found to be more than 5.0.

Linearity of Detector response

The detector response was found to be linear in the concentration range of 40 - 240 µg/ml for Sofosbuvir and 10 - 60 µg/ml for Velpatasvir respectively. Linearity values are given in table 4.

The calibration curves of Sofosbuvir and Velpatasvir are shown in figures 1.4 & 1.5 respectively.

Precision

System Precision (Repeatability/Intra-Day precision)

The %RSD of the peak areas for Sofosbuvir and Velpatasvir are shown in table-5.

Method Precision

The %RSD of the peak areas for Sofosbuvir and Velpatasvir are shown in table-6.

Intermediate/Intra-Day Precision

The %RSD was determined for Retention time and peak areas of Sofosbuvir and Velpatasvir are shown in table-7. Hence it can be calculated that the proposed RP-HPLC method was precise.

Accuracy (Recovery)

The % recoveries obtained from each concentration level for Sofosbuvir and Velpatasvir are shown in table-8 & 9.

*mean of three determinations

The mean % recovery from spiked samples was found to be in the range of 99.06 – 100.21% for Sofosbuvir and 98.9 – 101.15 % for Velpatasvir respectively, which were within the acceptance limit.

Robustness

System suitability (Robustness) parameters from the obtained chromatograms were evaluated and are reported in tables 10 & 11. It was found that the system suitability parameters were within the limits at all variable conditions, concluding that the proposed RP-HPLC method is robust towards small variations.

Specificity (Interference studies)

The chromatograms obtained from the blank, placebo, standard and sample solutions were recorded and results of specificity studies are reported in table – 12. Chromatograms of blank and placebo solutions showed no peaks at the retention times of Sofosbuvir and Velpatasvir. So the proposed RP-HPLC method was said to be specific and free from interference due to excipients presents in the tablets.



Pratik Biswas *et al.*,

Forced Degradation Studies

From the forced degradation studies, a degradant was observed at retention time of 1.766 mins in Acid, 1.774 mins in Alkali, and 1.811 mins in Peroxide degradation studies. No significant degradant was observed under Thermal, Photolytic and Neutral degradation studies were degraded below 5% without any major degradants.

Limit of detection (LOD) And quantification(LOQ)

The LOD values were found to be 0.51 µg/ml and 0.21 µg/ml for Sofosbuvir and Velpatasvir respectively and LOQ values to found to be 1.54 µg/ml and 0.63 µg/ml Sofosbuvir and Velpatasvir respectively. These low LOD and LOQ values indicate that the proposed RP-HPLC method is sensitive.

CONCLUSION

The results of this investigation reveals that a simple, rapid and economical stability indicating RP-HPLC method for the simultaneous determination of Sofosbuvir and Velpatasvir. The %RSD values obtained from the precision studies were also found to be less than 2, which indicates precise method. The high % recoveries indicate that the proposed method was highly accurate. The low values of LOD and LOQ indicates the high sensitivity of the proposed method. The absence of interfering peaks observed in the chromatogram of blank and placebo interference studies indicates specific method and degradants formed during stress degradation studies were also well separated and not interfere with estimation of the drugs by the proposed stability indicating RP-HPLC method. From this study it is concluded that the proposed stability indicating RP-HPLC method was found to be simple, accurate, precise, rapid and useful for the routine analysis of Sofosbuvir and Velpatasvir in bulk and pharmaceutical dosage forms. The obtained results were satisfactory as per ICH guidelines.

ACKNOWLEDGEMENT

I would like to immensely express my gratitude and thankfulness to all the Corresponding Authors for their contribution towards this article work.

CONFLICT OF INTEREST

We would like to state that no conflict of interest between the authors and corresponding authors whatsoever.

REFERENCES

1. <http://www.wikipedia.com/Sofosbuvir>
2. <http://www.wikipedia.com/Velpatasvir>
3. Khalid A. M. Attiasr M. El-Abasawi; Ahmed El-Olemy; Ahmed H. Application of different Techniques for velpatasvir and sofosbuvir in the pharmaceutical preparation, Journal of liquid chromatography & Related Technologies, 41:9, 467-473.
4. Jahnavi B; Ganapaty S. Stability indicating RP-HPLC method development and validation for the simultaneous determination of Sofosbuvir and velpatasvir in tablet dosage forms, IJPBR ISSN:- 2320-9267.
5. Saroja J; P.V. Anantha L; Rammohan Y; Divya D; P Santhosh Kumar. Concurrent estimation of sofosbuvir and velpatasvir in raw and tablets using stability indicating rp-hplc method, RJC ,ISSN- 0974-1496.
6. Vanaja B; Vageesh N.M; Kistayya C; Urukundu V. Rp-hplc method development and validation for simultaneous estimation of sofosbuvir and velpatasvir in pure and pharmaceutical dosage form. IJMPs, 2018; 3(1).
7. Kalpana N; Shanmukha Kumar J V; Ramchandran D. Analytical method development and validation for the simultaneous estimation of sofosbuvir and velpatasvir drug product by reverse phase high performance liquid chromatography method, AJPCR, volume 11, issue 2, 2018.





Pratik Biswas et al.,

8. Ravikumar Vejedla, C.V.S. Subramanyam, G. Veerabhadram, Estimation and validation of Sofosbuvir in bulk and tablet dosage form by RP-HPLC, Int J Pharm, 2016; 6(2): 121-127.
9. Uppalapati.Jyothi, Parimi.Umadevi, Analytical method development and validation for the simultaneous estimation of Sofosbuvir and Velpatasvir drug product by RP-HPLC method, Indo American Journal of Pharmaceutical Research, 2017,401-409.
10. Mohamed El-Kassem M Hassouna*, Maha Mohammed Abdelrahman and Mahmoud Abdelfattah Mohamed, Assay and Dissolution Methods Development and Validation for Simultaneous Determination of Sofosbuvir and Ledipasvir by RP-HPLC Method in Tablet Dosage Forms, J Forensic Sci & Criminal Inves.1(3),2017,1-11.
11. Bakht Zaman, Faisal Siddique, Waseem Hassan, RP-HPLC Method for Simultaneous Determination of Sofosbuvir and Ledipasvir in Tablet Dosage Form and Its Application to In Vitro Dissolution Studies, December 2016, Volume 79, Issue 23–24, pp 1605–1613.
12. Ashok Chakravarty V, Sailaja B, Praveen Kumar A, Method development and validation of ultraviolet-visible spectroscopic method for the estimation of hepatitis-c drugs - Daclatasvir and Sofosbuvir in active pharmaceutical ingredient form, Asian J Pharm Clin Res, vol 9, suppl. 3, 2016, 61-66.
13. ICH Q2B, Validation of Analytical Procedures: Methodology, ICH Harmonized Tripartite Guideline, 1996,1-8.
14. A. Haritha, P. Bharath Rathna Kumar, R. Venu Priya, Journal of Global Trends in Pharmaceutical Sciences, 6(2): (2015) 2600– 2606.
15. Karthik Kandikattu, Bharath Rathna Kumar P, Devanna N., Der Pharmacia Sinica, 2014, 5(5):74-81
16. Eana Joshy, Anu Babu, Delma Cruz and Aneesh T.P Development and validation of RP-HPLC method for determination of Sofosbuvir and Daclatasvir in Pharmaceutical dosage formulation.
17. Nagaraj T, Vardhan S.V.M, Ravikumar D, and Ramachandra, A new RP-HPLC method for the Simultaneous Assay of Sofosbuvir and Ledipasvir in combined dosage form. International Journal of Chemtech Research 2017,10(7): 761-769.
18. Sarath Nalla and Seshagiri Rao J.V.L.N, A Stability indicating RP-HPLC method for simultaneous estimation of Velpatasvir and Sofosbuvir in combined tablet dosage forms, World Journal of Pharmacy and Pharmaceutical Sciences, Vol 6, Issue 9, 1596-1611.
19. Surya Prakash Y. Rai, Yural Prajapati, Pragnesh Patni, development and Validation of RP-HPLC and UV Spectroscopic methods for Simultaneous Estimation of Sofosbuvir and Ledipasvir in their combined table.

Table 1: Stress conditions for the proposed RP-HPLC method

Type of degradation	Stress condition
Control	Un degraded
Acid degradation	Refluxed with 2N HCl at 60°C for 30 mins
Alkali degradation	Refluxed with 2N NaOH at 60°C for 30 mins
Peroxide degradation	Refluxed with 20% of H ₂ O ₂ on heating mantle at 60°C for 30 mins
Photolytic (UV) degradation	Exposed to UV light at 241nm for about 3 days
Thermal degradation	Heated in an oven at 105°C for 6 hrs
Neutral degradation	Reflux on water bath 60°C for 6 hrs

Table-2.Optimized Chromatographic conditions for proposed RP-HPLC method

Instrument	Waters 2695, High performance Liquid Chromatography
Mobile phase	P ^H 4.5 phosphate buffer : Acetonitrile 57.74:42.26 %V/V
Flow rate	0.9833 ml/min
Column	Denali C ₁₈ 150 x 4.6mm, 5μ.
Detector wave length	268nm
Column temperature	30°C





Pratik Biswas et al.,

Injection volume	10.0µl
Run time	6 min
Diluent	Water : Acetonitrile (50:50)
Mode of separation	Isocratic mode

Table-3. System suitability test parameters

S.No	Name of the drug	Rt(min)	USP Resolution	USP tailing	USP plate count	%RSD
1.	SOF	2.204	-	1.29	5043	1
2.	VEL	2.893	5.1	1.11	6507	0.8

Table-4. Linearity studies of the proposed method

% Level of concentration	Sofosbuvir		Velpatasvir	
	Conc. (µg/ml)	Peak Area	Conc. (µg/ml)	Peak Area
25	40	259292	10	37601
50	80	516554	20	75330
75	120	781496	30	114973
100	160	1075515	40	151276
125	200	1313854	50	188830
150	240	1552672	60	224930

Table 5. Regression characteristics of the proposed method

Parameter	Results	
	Sofosbuvir	Velpatasvir
Linearity Range (µg/ml)	40 - 240	10 – 60
Regression equation (y=mx+b)	y = 6541.x + 687.0	y = 3761.x + 435.1
Slope(m)	6541	3761
Intercept(b)	687	435.1
Correlation Coefficient(r ²)	0.999	0.999

Table-6 .Results of Repeatability studies (Intra-Day precision)

No. of Injection	Retention time (mins)		Peak Area	
	Sofosbuvir	Velpatasvir	Sofosbuvir	Velpatasvir
1	2.199	2.891	1168835	151488
2	2.200	2.892	1130764	150949
3	2.200	2.893	1086508	151800
4	2.200	2.894	1083063	149616
5	2.202	2.895	1082279	151818
6	2.203	2.897	1102529	151335
Statistical Parameters	Mean		1108996	151168
	SD		9708.7	825.7
	%RSD		0.9	0.5



Pratik Biswas *et al.*,

Table-7.Results of Method precision Studies

No. of Injection	Retention time (mins)		Peak Area	
	Sofosbuvir	Velpatasvir	Sofosbuvir	Velpatasvir
1	2.199	2.891	1088835	151488
2	2.201	2.892	1070764	150949
3	2.200	2.893	1086508	151800
4	2.200	2.894	1083063	149616
5	2.202	2.895	1082279	151818
6	2.203	2.897	1100529	151335
Statistical Parameters	Mean		1085330	151168
	SD		9708.7	825.7
	%RSD		0.9	0.5

Table-8.Results of Intermediate (Inter-Day) precision studies

No.of injection	Peak Area(Day-1)		Peak Area(Day-2)	
	Sofosbuvir	Velpatasvir	Sofosbuvir	Velpatasvir
1	1075216	151360	1051376	150114
2	1086978	151239	1058577	150559
3	1074342	150655	1051557	150936
4	1094871	151155	1056438	149090
5	1097462	151964	1078279	148009
6	1087626	150597	1052136	150733
Mean	1088256	151162	1058061	149907
S.D	9652.3	502.9	10332.1	1138.3
%RSD	0.9	0.3	1.0	0.8

Table- 9.Data of Accuracy Studies of Sofosbuvir

S.No	% Level of test conc.	Peak Area	Amount Added (µg/ml)	Amount Recovered (µg/ml)	% Recovery	Mean % Recovery	% RSD*
1	50	1572532	80	79.36126	99.20	100.21	0.88
2	50	1580129	80	80.5227	100.65		
3	50	1580878	80	80.63721	100.80		
4	100	2104206	160	160.6445	100.40	100.1	0.19
5	100	2101429	160	160.22	100.14		
6	100	2100189	160	160.0304	100.02		
7	150	2608170	240	237.6915	99.04	99.06	0.10
8	150	2607274	240	237.5545	98.98		
9	150	2610207	240	238.0029	99.17		





Pratik Biswas et al.,

Table- 10. Data of Accuracy Studies of Velpatasvir

S.No	% Level of test conc.	Peak Area	Amount Added (µg/ml)	Amount Recovered (µg/ml)	% Recovery	Mean % Recovery	% RSD*
1	50	224864	20	19.67267	98.36	98.9	0.64
2	50	225790	20	19.91888	99.59		
3	50	225156	20	19.75031	98.75		
4	100	301708	40	40.10447	100.26	100.24	0.19
5	100	301384	40	40.01832	100.05		
6	100	301962	40	40.172	100.43		
7	150	379176	60	60.70218	101.17	101.15	0.15
8	150	379479	60	60.78274	101.30		
9	150	378769	60	60.59396	100.99		

Table-11.Data of Robustness studies of Sofosbuvir

Parameter	Optimized Condition	Used condition	Peak area	Retention Time	Plate Count	Tailing Factor
Flow rate (±0.1ml/min)	1ml/min	0.9ml/min	1089408	2.432	5698	1.3
		1ml/min	1063264	2.433	5942	1.29
		1.1ml/min	1091925	2.435	5505	1.27
Column temp. (±5°C)	30°C	25°C	1126963	2.106	4996	1.32
		30°C	1135070	2.110	5320	1.35
		35°C	1135341	2.115	5550	1.26
Mobile phase Composition (5%v/v)	40:60	35:65	1088254	2.260	6016	1.28
		40:60	1091799	2.263	5094	1.3
		45:55	1087613	2.265	5434	1.26

Table-12.Data of Robustness studies of Velpatasavir

Parameter	Optimized condition	Used condition	Peak area	Retention Time	Plate Count	Tailing Factor
Flow rate (±0.1ml/min)	1ml/min	0.9ml/min	157642	3.245	6991	1.19
		1ml/min	155840	3.246	7122	1.18
		1.1ml/min	155746	3.248	6910	1.19
Column temp. (±5°C)	30°C	25°C	162039	2.614	7010	1.23
		30°C	161645	2.629	6957	1.27
		35°C	162919	2.635	6358	1.26
Mobile phase Composition (5%v/v)	40:60	35:65	150043	3.116	7412	1.2
		40:60	150843	3.131	7018	1.19
		45:55	153182	3.132	7047	1.18

Table-13.Results of specificity studies

S.No	Solution	Sofosbuvir		Velpatasavir	
		Rt (mins)	PeakArea	Rt (mins)	PeakArea
1	Blank	-	-	-	-
2	Standard	2.197	1075216	2.891	151360
3	Placebo	-	-	-	-
4	Sample	2.201	1087626	2.892	151239





Pratik Biswas et al.,

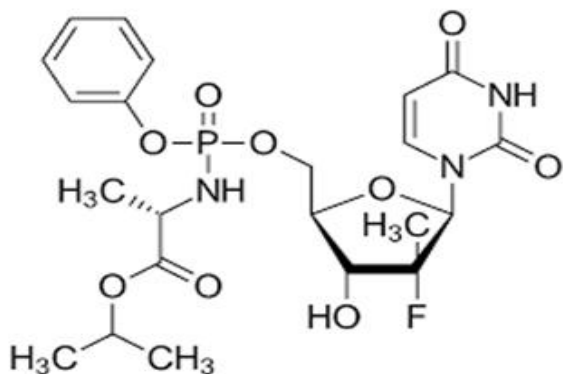


Fig. 1 Chemical structure of Velpatasvir

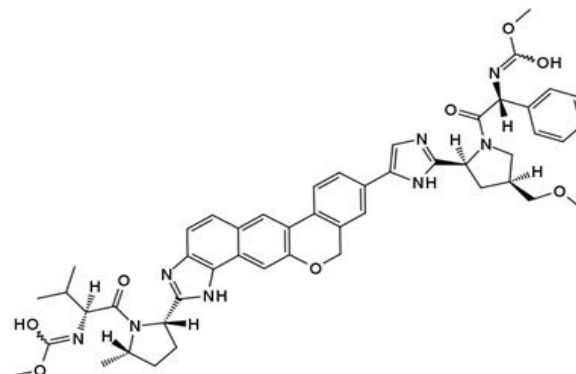


Fig.2. Chemical structure of Tenofovir Disproxil

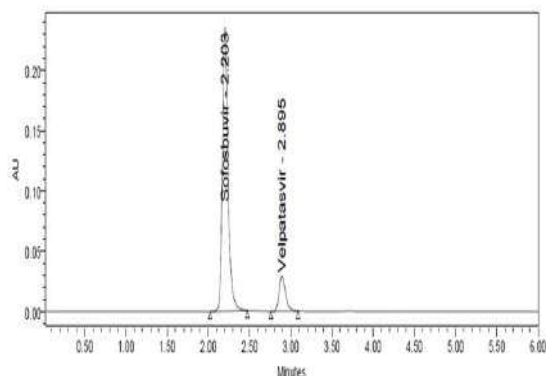


Fig. 3. Optimised conditions chromatogram

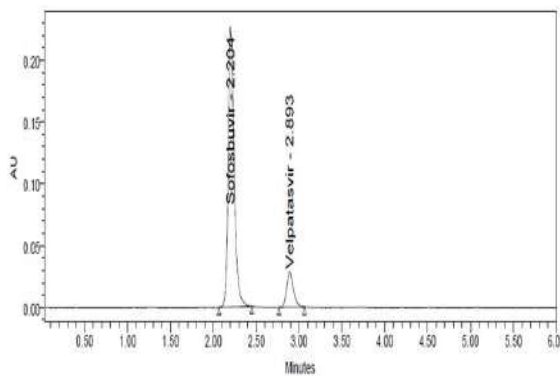


Fig. 4. Chromatogram of system suitability solution

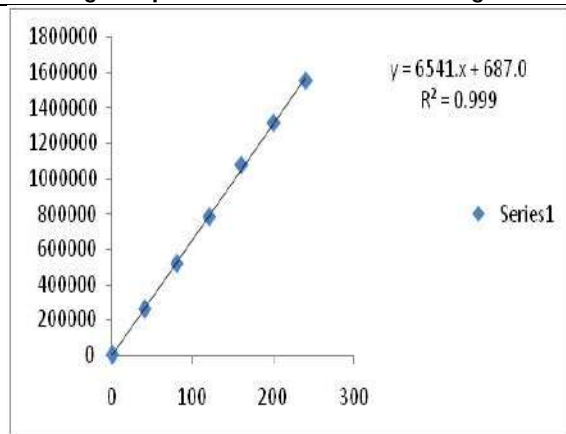


Fig. 5. Standard calibration graph of Sofosbuvir

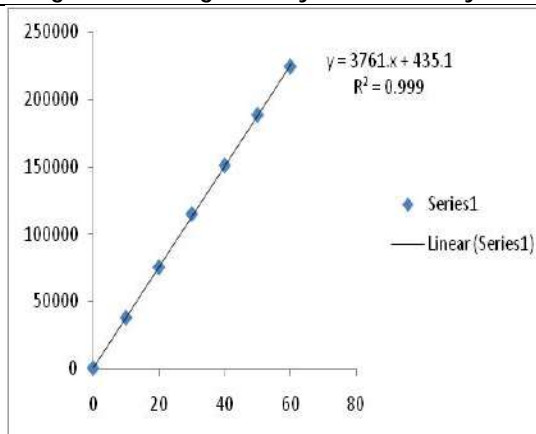


Fig. 6. Standard calibration graph of Velpatasvir





Performance and Analysis of Hybrid Electric Vehicle by using ANFIS Controller

K.Anitha Reddy^{1*}, Kurakula Vimala Kumar², S.Sunanda³ and Bolla Madhusudhana Reddy⁴

¹Assistant Professor, Department of EEE, Malla Reddy Engineering College (Autonomous), Hyderabad, Telangana, India.

²Assistant Professor, Department of EEE, JNTUK University College of Engineering, Narsaraopet, Andhra Pradesh, India

³Assistant Professor, Department of EEE, St.Martin's Engineering College, Hyderabad, Telangana, India.

⁴Associate Professor, Department of EEE, Malla Reddy Engineering College for Women, Hyderabad, Telangana, India.

Received: 28 Feb 2023

Revised: 20 Apr 2023

Accepted: 31 May 2023

*Address for Correspondence

K.Anitha Reddy

Assistant Professor,
Department of EEE,
Malla Reddy Engineering College (Autonomous),
Hyderabad, Telangana, India.



This is an Open Access Journal / article distributed under the terms of the **Creative Commons Attribution License** (CC BY-NC-ND 3.0) which permits unrestricted use, distribution, and reproduction in any medium, provided the original work is properly cited. All rights reserved.

ABSTRACT

In this study, multiple methods are used to examine coordinated plug-in hybrid electric vehicle (PHEV) charging in a grid and effective battery charge controllers. Since the transportation sector is a significant user of fossil fuel and produces a significant amount of pollution, the PHEV has gained popularity due to its lower gasoline emissions and lower fuel costs. Electric energy stored in batteries of PHEVs that could go up to 60 miles on a single charge might reduce CO₂ emissions by 50% and petroleum use by over 75%. The PHEV's ability to plug into the grid and use grid electricity to charge the battery pack is the major feature that sets it apart from Hybrid Electric Vehicles (HEV). When the PHEV motor acts as a generator, a high power bidirectional DC-DC converter is added to charge the battery. An efficient battery charge controller may shorten the time needed for charging, which lowers the PHEV demand on the grid. Effective battery charging reduces the burden on the grid, which is examined using a variety of controllers, including fuzzy logic controllers, adaptive neuro fuzzy inference systems, and a newly proposed Intelligent Controller based on Self-Computational Emotional Learning.

Keywords: SCELIC, HEV, Converters.

INTRODUCTION

A two-way power transfer from the AC to the plug-in electric car (PEV) the Vehicle to Grid (V2G) and Grid to Vehicle (G2V) functions require the electrical grid. Different power converters and controllers act as crucial mediators throughout these procedures between the electric grid and PEV. Several studies have shown how to use



**Anitha Reddy et al.,**

controllers to manage the battery power in PEVs. The typical controllers currently in use, however, have a number of technical drawbacks, including sensitivity to controller gain, correct mathematical modelling, a lack of adaptability, a slow reaction time to a rapid outburst, and slow interval execution processing. An Adaptive Neuro-Fuzzy Inference Strategy (ANFIS) to control the battery charging controller in PHEV is modelled and simulated in this work. Charging controllers are complicated, non-linear machines. These fuzzy-based systems expand a control signal that responds to the rule base firing, which is followed by the haphazardly generated prior experiences. As a result, the controller's outcomes are similarly erratic, and the best ones might not be obtained. The usage of an ANFIS controller allows for the selection of the relevant membership functions and, in turn, the selection of the suitable rule base depending on the condition. This chapter's standout result is the result of this coordinated technique for a methodology for control purposes. In the industrial sectors, power electronics-based drives can perform better thanks to artificial intelligence approaches like PI, ANN, Fuzzy Logic, hybrid networks, and more recently. The back-propagation method is used in the developed ANFIS scheme to identify a suitable rule basis using neural network techniques. The developed controller performs better thanks to this integrated approach in several areas, including reliability and cost-effectiveness.

Analysis of HEV

The purpose of this study is to model an ANFIS controller and show why it is preferable to the traditional PI controller. This study also demonstrates the ANFIS controller's advantage over the traditional controller in terms of battery characteristics. The identical power exchange scheme is carried out using two ANFIS (ANFIS1 and ANFIS2) controllers in place of the two PI controllers to demonstrate the benefits of the ANFIS controller over the PI controller. The battery power and current curves with a PI controller showed an initial surge and a continuing distortion as shown in fig.1. This distortion keeps happening as long as the battery is still being used for charging and discharging purposes. Although the bi-directional power exchange operation is not hampered by this initial surge and distortion, the battery could still be in danger.

Due to the PI controller's reliance on sensory input, the BELBIC experiences internal instability. By using a synthetically intelligent ANFIS controller as sensory input, the proposed Self Computational Emotional Learning Based Intelligent Controller (SCELIC) solves the BELBIC problem. The suggested control scheme is contrasted with controllers like PI, FLC, and ANFIS to assess SCELIC's performance in a charging controller. In contrast to statistical techniques, an artificial neural network is a nonlinear model that is simple to use and comprehend. Fuzzy logic offers good interpretability and can include the knowledge of experts. The blending of the two paradigms results in the development of learning, improved understanding, and integration of prior knowledge.

The membership values for fuzzy systems can be learned using ANN and then utilised to create IF-THEN rules. This idea of integrating a hybrid neural/fuzzy system, which delivers the benefits of both systems, is applied in this chapter's development of the ANFIS controller. The ANFIS has a fuzzy reasoning-based architecture. Fuzzy rules are used to arrange structured knowledge, but neural networks' adaptability and learning capabilities are not utilised. Results from this fuzzy logic and neural network combination are quite noteworthy. A novel technology known as neuro-fuzzy networks has been devised by combining the learning capabilities of neural networks with the knowledge representation provided by fuzzy logic. At the level of mathematics, ANN is a strong learner. Fuzzy logic can be very interpretable and can also take into account the knowledge of a skilled person. The two ideal models' ability to adapt, make accurate interpretations, and take into account existing information are forfeited in the hybridization process. Fuzzy systems' membership values can be learned using ANN, as can IF-THEN rules and decision logic. A hybrid neural/fuzzy system, which captures the advantages of both paradigms, is the real system of the two (Du & Swamy2006).

An ANFIS, as was previously noted, combines the two popular intelligent control algorithms fuzzy inference and adaptive neural networks. Combining them allows us to refer to a fuzzy inference system with its node functions, weights, and connections as a neural network while still using its semantics Fig.2. A circle node only consists of a node function; however a square node (Layer 1 and 4) signifies it has adaptive parameters (Maamounet al.2007).





Anitha Reddy et al.,

The block diagram of the developed ANFIS control scheme is shown in Fig. 3. The fuzzification unit converts crisp data into linguistic variables. The base block is ruled using these transformed data as inputs. The 25 criteria were developed based on prior information or experience. Because there are numerous rules, implementation execution times vary. In this study, a minimum of 25 principles for efficient control are selected. The neural network block is linked to the rule-based block. For neural network training, the back-propagation method is employed to choose the appropriate set of the rule basis. Training is a critical step in selecting the best rule foundation in order to develop the control signal. The control signal needed to provide the best results is generated when the appropriate rules are chosen and applied. The controller receives the input that has been fuzzy satisfied. It is suggested that an ANFIS controller create a duty ratio for a charging controller. The process of producing pulses is then contrasted with high frequency saw tooth waves. Fig.4 depicts the fundamental diagram of the ANFIS controller.

ANFIS is a Takagi-Sugeno model-based fuzzy inference system. This model creates a fuzzy inference system using a predetermined input and output data set. First and foremost, a training data set with the appropriate input/output data pairs of the target systems to be modelled is crucial for ANFIS learning. The data pairings, training data sets, checking data sets, and fuzzy inference system are the design parameters required for ANFIS training. ANFIS training begins with the selection of some epochs. After carrying out all 25 phases, which are dependent on numerous regulations, the learning results are confirmed. Here, the speed error and change in speed error serve as the modelled ANFIS's two inputs, while the reference voltage serves as the output and is utilised to regulate the inverter's output.

SIMULATION RESULTS

It is made up of a five-layer fuzzy neural network that uses the feed forward method. Each layer has an own meaning. The ANFIS controller's output, which generates pulses for the charging controller and is likened to a saw tooth, produces. Fig.6. displays the pulses generated by the ANFIS controller for the battery charging controller Fig.7. illustrates how an ANFIS-based charging controller can increase SOC with a starting SOC of 30%. Fig.7 shows the effect of the ANFIS controller, which raises SOC by 30% to 30.008 in 5 seconds. The analysis for the PI and FLC controllers was completed for 2 seconds in the previous reference. To put it into perspective, the ANFIS controller raises SOC to 30.0032% in 2 seconds. The charging controller's performance determines charging efficiency and effectively uses the energy produced quickly by the motor. Fig.8 shows a comparison of the pulses from an ANFIS, a fuzzy logic controller, and a PI controller.

The charging controller pulse width is evidently controlled by the PI, Fuzzy controller, and ANFIS, and the ANFIS controller enhances the pulse width and displays the SOC of batteries employing PI, FLC, and ANFIS-based charging controllers. Fig.9 shows that the SOC is increased by the PI-based charging controller, going from 30% to 30.0035%. In the same time frame, the FLC-based charging controller raises it to 30.0048%, while the ANFIS controller raises it to 30.0075%. It demonstrates that the battery is charged more quickly by an ANFIS-based charging controller than by a PI or FLC controller.

CONCLUSION

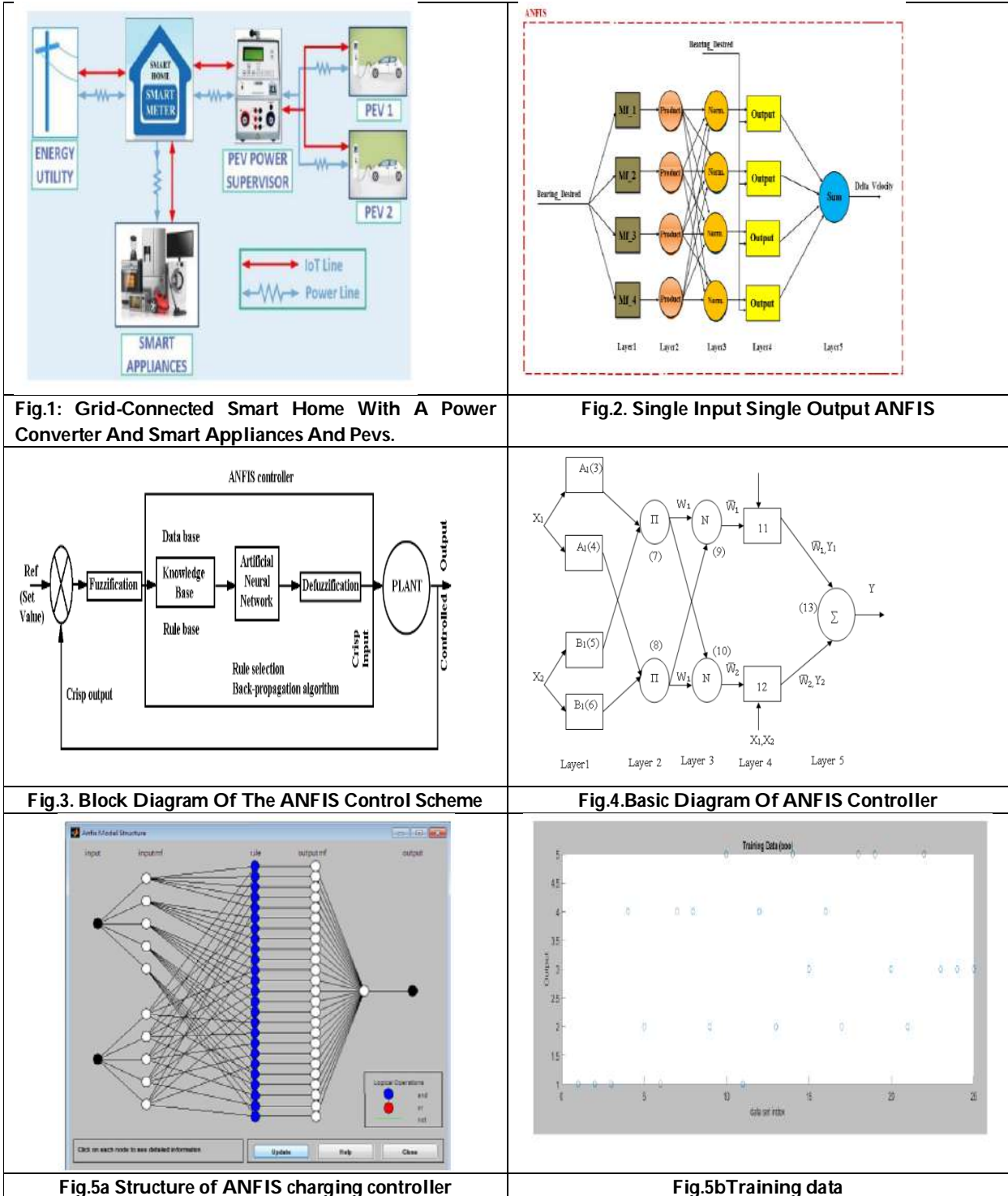
The amount of energy required to charge the battery in a PHEV impacts its efficiency and performance. When the motor in a PHEV acts as a generator, a high power bidirectional DC-DC converter is inserted to charge the battery. This form of charging lessens the amount of power drawn from the grid and eases grid issues brought on by PHEV charging. Different controllers, including PI, FLC, ANFIS, and the recently suggested innovative SCELIC, have been examined as charging controllers for effective battery charging that decreases the amount of time needed to charge the battery and lowers the burden that PHEVs place on the grid.



**Anitha Reddy et al.,****REFERENCES**

1. Bai, Ying, HanqiZhuang& Dali Wang, eds 2007, 'Advanced fuzzy logic technologies in industrial applications', Springer Science & Business Media.
2. Balcells, Josep&JosepGarcía 2010, 'Impact of plug-in electric vehicles on the supply grid', InVehicle Power and Propulsion Conference (VPPC), 2010 IEEE, pp. 1-4.
3. Beheshti, Zahra, and SitiZaitonMohdHashim 2010, 'A review of emotional learning and it's utilization in control engineering',Int. J. Adv. Soft Comput. Applvol.2, no. 2 pp. 191-208.
4. Boroogeni, Kianoosh G, HadiAmini, ShahabBahrami, M, Iyengar S, S, Arif, Sarwat&OrkunKarabasoglu 2017, 'A novel multi-time-scale modeling for electric power demand forecasting: From short-term to medium-term horizon', Electric Power Systems Researchvol.142, pp. 58-73.
1. 5.Boyali, Ali &LeventGüvenç2010, 'Real-time controller design for a parallel hybrid electric vehicle using neuro-dynamic programming method'.
2. 6.Campanari, Stefano, GiampaoloManzolini& Fernando Garcia De la Iglesia 2009, 'Energy analysis of electric vehicles using batteries or fuel cells through well-to-wheel driving cycle simulations', Journal of Power Sourcesvol.186, no. 2, pp. 464-477.
3. 7.Camus, C, CiM Silva, Farias, TL &Esteves, J 2009,'Impact of Plug-in Hybrid Electric Vehicles in the Portuguese electric utility system', InPower Engineering, Energy and Electrical Drives, POWERENG'09. International Conference on, pp. 285-290.IEEE.
4. 8. Chen, Zengshi 2012, 'PI and sliding mode control of a Cukconverter'IEEE Transactions on Power Electronicsvol.27, no. 8,pp. 3695-3703.
5. 9. Chen, Zeyu, RuiXiong&Jiayi Cao 2016,'Particle swarm optimization-based optimal power management of plug-in hybrid electric vehicles considering uncertain driving conditions', Energyvol.96, pp. 197-208.
6. 10. Chen, Zheng, Chunting Chris Mi, Jun Xu, Xianzhi Gong &Chenwen You 2014, 'Energy management for a power-split plug-in hybrid electric vehicle based on dynamic programming and neural networks',IEEE Transactions on Vehicular Technology vol.63, no. 4, pp. 1567-1580.
7. 11.Chiu, Huang-Jen & Li-Wei Lin 2006, 'A bidirectional DC–DC converter for fuel cell electric vehicle driving system',IEEE Transactions on Power Electronics vol.21, no. 4 ,pp. 950-958.
8. 12. Ciric, Rade,M, Antonio Padilla Feltrin&Luis F Ochoa 2003, 'Power flow in four-wire distribution networks-general approach',IEEE Transactions on Power Systemsvol.18, no. 4 ,pp. 1283-1290.
9. 13. Clement-Nyns, Kristien, Edwin Haesen& Johan Driesen 2010, 'The impact of charging plug-in hybrid electric vehicles on a residential distribution grid',IEEE Transactions on power systemsvol.25, no. 1,pp. 371-380.
10. 14.Cobb, Jeff 2017 'The world just bought its two-millionth plug-in car',January16 .
11. 15. Couchman, Paul, Basil Kouvaritakis, Mark Cannon & Frank Prashad 2005 'Gaming strategy for electric power with random demand',IEEE Transactions on Power Systemsvol.20, no. 3 pp. 1283-1292.
12. 16.Dabrowski, Adrian, Johanna Ullrich&EdgarRWeippl 2017, 'Grid shock: coordinated load-changing attacks on power grids',systemvol.28,p.64.
13. 17.Darabi, Zahra & Mehdi Ferdowsi2014, '1An event-based simulation framework to examine the response of power grid to the charging demand of plug-in hybrid electric vehicles',IEEE Transactions on Industrial Informaticsvol.10, no. 1 ,pp. 313-322.







Anitha Reddy et al.,

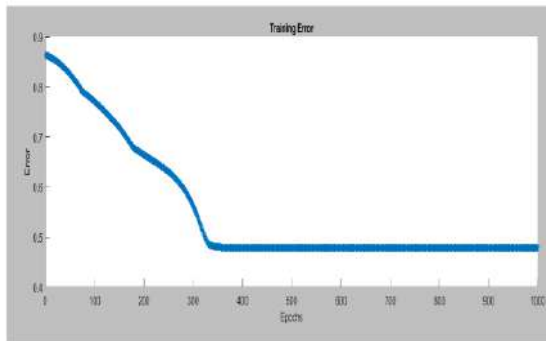


Fig.5c Training error

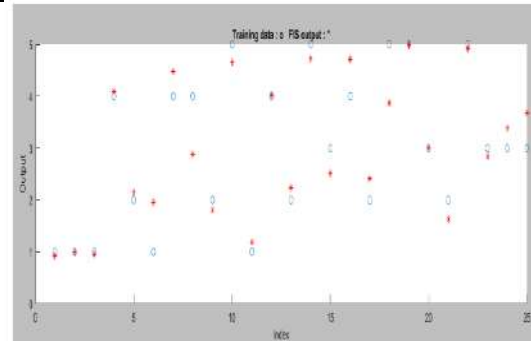


Fig.5d FIS output

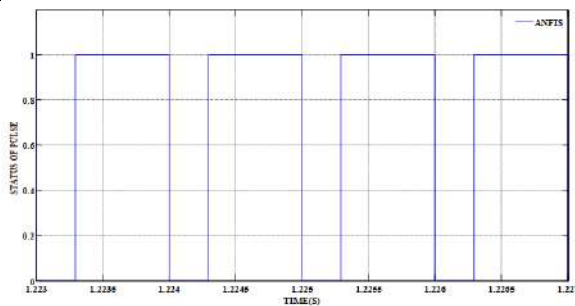


Fig.6.Triggering pulses from ANFIS controller

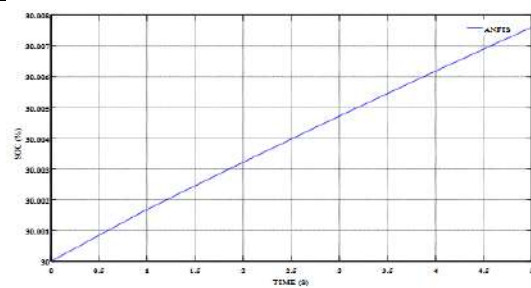


Fig.7.SOC by the Effect of ANFIS Based Charging Controller

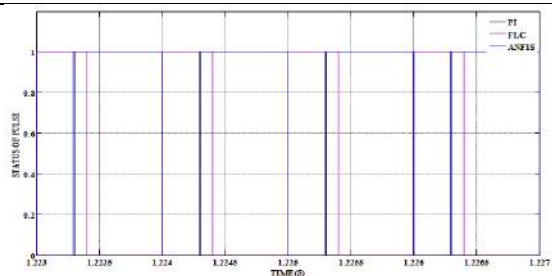


Fig.8. Comparisons of Pulses of PI Controller, FLC and ANFIS

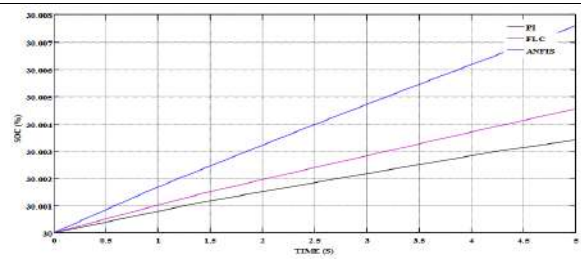


Fig.9. Comparisons of the SOC of Batteries using PI, Fuzzy Logic Controller and ANFIS





Binary γ -Continuous Function in Binary γ -Topological Space

K.Muthulakshmi¹ and M.Gilbert Rani^{2*}

¹Research Scholar, Madurai Kamaraj University, Madurai, Tamil Nadu, India.

²Assistant Professor in Mathematics, Arul Anandar College (Autonomous), Karumathur, Madurai, Tamil Nadu, India

Received: 05 Feb 2023

Revised: 27Apr 2023

Accepted: 31 May 2023

*Address for Correspondence

M.Gilbert Rani

Assistant Professor in Mathematics,
Arul Anandar College (Autonomous),
Karumathur, Madurai, Tamil Nadu, India.



This is an Open Access Journal / article distributed under the terms of the **Creative Commons Attribution License** (CC BY-NC-ND 3.0) which permits unrestricted use, distribution, and reproduction in any medium, provided the original work is properly cited. All rights reserved.

ABSTRACT

In this paper, we define binary γ -continuous function and study some new form of binary γ -continuous functions. And also we investigate the relationships between these type of binary γ -continuous functions.

Keywords: binary γ -continuity, binary γ -semi continuity, binary γ - α -continuity, binary γ -regular continuity.

INTRODUCTION

The concept of binary topology from X to Y is introduced by S. NithyananthaJothi and P. Thangavelu [12]. In the year 1979, S. Kasahara [2] imposed the operation γ of a topology τ concept. H. Ogata [19] proposed a new concept of γ -open set and he also analysed the related topological assets of the associated topology τ_γ . Jamal M. Mustafa [8] found Binary Generalized Topological Spaces. We have already presented Binary γ -open set in [7]. In this paper, we have defined and explored properties of binary γ -continuity.

Binary γ -continuous function

We follow: B_γ -TS -binary γ -topological space, b_γ -binary γ -open set, $b_\gamma O$ -binary γ -open sets, $b_\gamma C$ -binary γ -closed sets, \mathfrak{B}_γ -set of all binary γ -open sets, γ -O - gamma open set, γ -C - gamma closed set, γ -TS - γ -topological space, b_γ -continuous- binary γ -continuous, \mathfrak{B}_γ -int-binary γ -interior, \mathfrak{B}_γ -cl - binary γ -closure

Definition 2.1:

Let (ζ, η, γ) be a B_γ -TS and (W, μ) be γ -TS. A function $f: W \rightarrow \zeta \times \eta$ is called b_γ -continuous at a point $w \in W$ if for any $b_\gamma(\lambda, \aleph)$ in $(\zeta, \eta, \mathfrak{B}_\gamma)$ with $f(w) \in (\lambda, \aleph)$ there exists a γ -O H in (W, μ) such that $w \in H$ and $f(H) \subseteq (\lambda, \aleph)$. f is called b_γ -continuous if it is b_γ -continuous at each $w \in W$.





Muthulakshmi and Gilbert Rani

Theorem 2.1:

Let (ζ, η, γ) be a $B\gamma - TS$ and (W, μ) be $\gamma - TS$. A function $f: W \rightarrow \zeta \times \eta$ is $b\gamma$ -continuous iff $f^{-1}((\lambda, \kappa))$ is γ -O in (W, μ) for every $b\gamma(\lambda, \kappa)$ in $(\zeta, \eta, \mathfrak{B}\gamma)$.

Proof :

Let f be $b\gamma$ -continuous and (λ, κ) be $b\gamma$ in (ζ, η, γ) .

Now $f^{-1}((\lambda, \kappa))$ is empty, then clearly $f^{-1}((\lambda, \kappa))$ is γ -O. Suppose $f^{-1}((\lambda, \kappa))$ is non empty, then $w \in f^{-1}((\lambda, \kappa))$, $f(w) \in (\lambda, \kappa)$. Since f is $b\gamma$ -continuous at w , there exists a γ -O H in (W, μ) such that $w \in H$ and $f(H) \subseteq (\lambda, \kappa)$.

It follows that $w \in H \subseteq f^{-1}((\lambda, \kappa))$. Hence $f^{-1}((\lambda, \kappa))$ is γ -O in (W, μ) .

Conversely $f^{-1}((\lambda, \kappa))$ is γ -O in (W, μ) . Let $w \in W$ and $b\gamma(\lambda, \kappa)$ in (ζ, η, γ) and $f(w) \in (\lambda, \kappa)$. Then $f^{-1}((\lambda, \kappa))$ is γ -O in (W, μ) (our assumption) and $w \in f^{-1}((\lambda, \kappa))$ with

$$f(f^{-1}((\lambda, \kappa))) \subseteq (\lambda, \kappa)$$

Therefore, f is $b\gamma$ -continuous at $w \in W$. Hence f is $b\gamma$ -continuous.

Theorem 2.2:

Let (ζ, η, γ) be a $B\gamma - TS$ and (W, μ) be $\gamma - TS$. Let $f: W \rightarrow \zeta \times \eta$ be a function such that $(f^{-1}((\rho, \sigma)))^c = f^{-1}((\rho^c, \sigma^c))$ for all $\rho \subseteq \zeta$ and $\sigma \subseteq \eta$. Then f is $b\gamma$ -continuous iff $f^{-1}((\rho, \sigma))$ is γ -C in (w, μ) for every binary $\gamma - closed set (\rho, \sigma)$ in $(\zeta, \eta, \mathfrak{B}\gamma)$.

Proof:

Let f be $b\gamma$ -continuous and (ρ, σ) be binary $\gamma - closed set$ in $(\zeta, \eta, \mathfrak{B}\gamma)$.

Then (ρ^c, σ^c) is $b\gamma$. Since f is $b\gamma$ -continuous, $f^{-1}((\rho^c, \sigma^c))$ is γ -O in (w, μ) . Therefore $(f^{-1}((\rho, \sigma)))^c$ is γ -O. $\implies f^{-1}((\rho, \sigma))$ is γ -C in (w, μ) . Conversely, let (ρ, σ) be a $b\gamma$ in $(\zeta, \eta, \mathfrak{B}\gamma)$. Then $(\rho, \sigma)^c = (\rho^c, \sigma^c)$ is binary $\gamma - closed set$ in $(\zeta, \eta, \mathfrak{B}\gamma)$. By hypothesis, $f^{-1}((\rho^c, \sigma^c))$ is γ -C in (w, μ) . $\implies (f^{-1}((\rho, \sigma)))^c$ is γ -C in (w, μ) .

Therefore $f^{-1}((\rho, \sigma))$ is γ -O in (w, μ) . Hence f is $b\gamma$ -continuous.

Theorem 2.3:

Let (ζ, η, γ) be a $B\gamma - TS$ and (W, μ) be $\gamma - TS$ such that (ρ, σ^c) and (ρ^c, σ) are binary $\gamma - closed sets$ in $(\zeta, \eta, \mathfrak{B}\gamma)$ where (ρ, σ) is binary $\gamma - closed set$ in $(\zeta, \eta, \mathfrak{B}\gamma)$. Then $f: W \rightarrow \zeta \times \eta$ is $b\gamma$ -continuous, $f^{-1}((\rho, \sigma))$ is γ -C in (w, μ)

Proof:

Let f be a $b\gamma$ -continuous and (ρ, σ) be binary $\gamma - closed set$ in $(\zeta, \eta, \mathfrak{B}\gamma)$. Then $(\rho, \sigma)^c = (\rho^c, \sigma^c) \in \mathfrak{B}\gamma$. Since f is $b\gamma$ -continuous, $f^{-1}((\rho^c, \sigma^c))$ is γ -O in (w, μ) . Since (ρ, σ^c) and (ρ^c, σ) are $b\gamma$ O in $\mathfrak{B}\gamma$, $f^{-1}((\rho, \sigma^c))$ and $f^{-1}((\rho^c, \sigma))$ are γ -O in (w, μ) .

By [[12], lemma4.3] and above theorem, $(f^{-1}((\rho, \sigma)))^c$ is γ -O in (w, μ) . Therefore $f^{-1}((\rho, \sigma))$ is γ -C in (w, μ) .

Theorem 2.4:

$f: W \rightarrow \zeta \times \eta$ is $b\gamma$ -continuous iff for every $\rho \subseteq \zeta$ and $\sigma \subseteq \eta$,

$$f^{-1}(\mathfrak{B}\gamma - int(\rho, \sigma)) \subseteq \gamma - int(f^{-1}(\rho, \sigma)).$$

Proof:

Suppose $f: W \rightarrow \zeta \times \eta$ is $b\gamma$ -continuous. Let $\rho \subseteq \zeta$ and $\sigma \subseteq \eta$.

Then by [[7]proposition 2.1], $\mathfrak{B}\gamma - int(\rho, \sigma)$ is $b\gamma$ O in $(\zeta, \eta, \mathfrak{B}\gamma)$ and also $\mathfrak{B}\gamma - int(\rho, \sigma) \subseteq (\rho, \sigma)$. Therefore $f^{-1}(\mathfrak{B}\gamma - int(\rho, \sigma))$ is γ -O in (W, μ) .

$$\text{Now } \mathfrak{B}\gamma - int(\rho, \sigma) \subseteq (\rho, \sigma) \implies f^{-1}(\mathfrak{B}\gamma - int(\rho, \sigma)) \subseteq f^{-1}((\rho, \sigma))$$

$$\implies \gamma - int(f^{-1}(\mathfrak{B}\gamma - int(\rho, \sigma))) \subseteq \gamma - int(f^{-1}((\rho, \sigma)))$$

$$\implies f^{-1}(\mathfrak{B}\gamma - int(\rho, \sigma)) \subseteq \gamma - int(f^{-1}(\rho, \sigma))$$

Conversely, assume that $f^{-1}(\mathfrak{B}\gamma - int(\rho, \sigma)) \subseteq \gamma - int(f^{-1}((\rho, \sigma)))$, for every $\rho \subseteq \zeta$ and $\sigma \subseteq \eta$.

Let (ρ, σ) be $b\gamma$ O in $(\zeta, \eta, \mathfrak{B}\gamma)$. Then $\mathfrak{B}\gamma - int(\rho, \sigma) = (\rho, \sigma)$

$$\implies f^{-1}((\rho, \sigma)) = f^{-1}(\mathfrak{B}\gamma - int(\rho, \sigma)) \subseteq \gamma - int(f^{-1}((\rho, \sigma)))$$

$$\implies f^{-1}((\rho, \sigma)) \subseteq \gamma - int(f^{-1}((\rho, \sigma))). \text{ Therefore } f^{-1}((\rho, \sigma)) \text{ is } \gamma\text{-O in } (W, \mu). \text{ Hence } f \text{ is } b\gamma\text{-continuous.}$$





Muthulakshmi and Gilbert Rani

Definition 2.2:

A subset (ρ, σ) of $B_\gamma - TS (\zeta, \eta, \mathfrak{B}_\gamma)$ is called

1. A binary γ – semi open set if $(\rho, \sigma) \subseteq \mathfrak{B}_\gamma - cl(\mathfrak{B}_\gamma - int(\rho, \sigma))$.
2. A binary γ – preopen set if $(\rho, \sigma) \subseteq \mathfrak{B}_\gamma - int(\mathfrak{B}_\gamma - cl(\rho, \sigma))$.
3. A binary $\gamma - \alpha$ – open set if $(\rho, \sigma) \subseteq \mathfrak{B}_\gamma - int(\mathfrak{B}_\gamma - cl(\mathfrak{B}_\gamma - int(\rho, \sigma)))$.
4. A binary γ – regular open set if $(\rho, \sigma) = \mathfrak{B}_\gamma - int(\mathfrak{B}_\gamma - cl(\rho, \sigma))$.

The complement of a binary γ – semi open (resp, binary γ –pre open , binary $\gamma - \alpha$ –open, binary γ – regular open)set is called binary γ – semi closed(resp , binary γ – pre closed, binary $\gamma - \alpha$ –closed, binary γ – regular closed).

Definition 2.3:

Let (ζ, η, γ) be a $B_\gamma - TS$ and (W, μ) be a $\gamma - TS$. A function $f: W \rightarrow \zeta \times \eta$ is called

1. Binary γ – semi continuous if $f^{-1}((\rho, \sigma))$ is $\gamma - O$ in (W, μ) for every binary γ – semi open set (ρ, σ) in (ζ, η, γ) .
2. Binary γ – pre continuous if $f^{-1}((\rho, \sigma))$ is $\gamma - O$ in (W, μ) for every binary γ –pre open set (ρ, σ) in (ζ, η, γ) .
3. Binary $\gamma - \alpha$ – continuous if $f^{-1}((\rho, \sigma))$ is $\gamma - O$ in (W, μ) for every binary $\gamma - \alpha$ –open set (ρ, σ) in (ζ, η, γ) .
4. Binary γ – regular continuous if $f^{-1}((\rho, \sigma))$ is $\gamma - O$ in (W, μ) for every binary γ – regular open set (ρ, σ) in (ζ, η, γ) .

Theorem 2.5:

- (i) Every binary γ – open set is binary $\gamma - \alpha$ –open,
- (ii) Every binary $\gamma - \alpha$ –open set is binary γ –pre open.
- (iii) Every binary γ – regular open set is binary γ – open.

Proof:

(i) Let (ρ, σ) be binary γ –open set
 Then $\mathfrak{B}_\gamma - int(\rho, \sigma) = (\rho, \sigma)$
 $\mathfrak{B}_\gamma - cl(\mathfrak{B}_\gamma - int(\rho, \sigma)) = \mathfrak{B}_\gamma - cl(\rho, \sigma)$
 $(\rho, \sigma) \subseteq \mathfrak{B}_\gamma - cl(\rho, \sigma) = \mathfrak{B}_\gamma - cl(\mathfrak{B}_\gamma - int(\rho, \sigma))$
 $(\rho, \sigma) \subseteq \mathfrak{B}_\gamma - cl(\mathfrak{B}_\gamma - int(\rho, \sigma))$
 Now $\mathfrak{B}_\gamma - int(\rho, \sigma) \subseteq \mathfrak{B}_\gamma - int(\mathfrak{B}_\gamma - cl(\mathfrak{B}_\gamma - int(\rho, \sigma)))$
 $(\rho, \sigma) \subseteq \mathfrak{B}_\gamma - int(\mathfrak{B}_\gamma - cl(\mathfrak{B}_\gamma - int(\rho, \sigma)))$
 Therefore (ρ, σ) is binary $\gamma - \alpha$ – open
 (ii) Let (ρ, σ) be binary $\gamma - \alpha$ – open set.
 Then $(\rho, \sigma) \subseteq \mathfrak{B}_\gamma - int(\mathfrak{B}_\gamma - cl(\mathfrak{B}_\gamma - int(\rho, \sigma)))$
 $\Rightarrow (\rho, \sigma) \subseteq (\mathfrak{B}_\gamma - int(\mathfrak{B}_\gamma - cl(\rho, \sigma)))$.
 (iii) Using the definition 2.2(4), we get the result.

Remark 2.6:

(i) Every binary $\gamma - \alpha$ –open is not b_γ . (ii) Every binary γ –pre open is not binary $\gamma - \alpha$ –open and (iii) Every b_γ is not binary γ – regular open set.

Example 2.4:

Let $\zeta = \{a, b, c, d\}$, $\eta = \{1, 2, 3, 4, 5\}$

$\mathfrak{B} = \{(\emptyset, \emptyset), (\{a\}, \{1\}), (\{b\}, \{2\}), (\{a, b\}, \{1, 2\}), (\zeta, \eta)\}$ on $\zeta \times \eta$.

Let $\gamma: \mathfrak{B} \rightarrow \overline{2}^{\zeta} \times \overline{2}^{\eta}$ be an operation defined as follows:

For every $(\rho, \sigma) \in \mathfrak{B}$, then $\gamma((\rho, \sigma)) = \begin{cases} (\rho, \sigma) & \text{if } (\rho, \sigma) = (\{b\}, \{2\}) \\ (\rho, \sigma) \cup (\{c\}, \{2\}) & \text{if } (\rho, \sigma) \neq (\{b\}, \{2\}) \end{cases}$

Therefore, $\mathfrak{B}_\gamma = \{(\emptyset, \emptyset), (\zeta, \eta), (\{b\}, \{2\})\}$.

- (i) $(\{a, b\}, \{2\})$ is binary $\gamma - \alpha$ –open but not b_γ . (ii) $(\{a, b\}, \{4, 5\})$ is binary γ – preopen but not binary $\gamma - \alpha$ –open and
- (iii) $(\{b\}, \{2\})$ is b_γ but not binary γ – regular open set.





Muthulakshmi and Gilbert Rani

Theorem 2.7:

(ρ, σ) is binary $\gamma - \alpha$ –open set iff it is binary $\gamma -$ semi open.

Proof:

Let (ρ, σ) be binary $\gamma - \alpha$ –open set. Then $(\rho, \sigma) \subseteq \mathfrak{B}\gamma - \text{int}(\mathfrak{B}\gamma - \text{cl}(\mathfrak{B}\gamma - \text{int}(\rho, \sigma)))$.

$\mathfrak{B}\gamma - \text{cl}(\rho, \sigma) \subseteq \mathfrak{B}\gamma - \text{cl}(\mathfrak{B}\gamma - \text{int}(\mathfrak{B}\gamma - \text{cl}(\mathfrak{B}\gamma - \text{int}(\rho, \sigma))))$.

$(\rho, \sigma) \subseteq \mathfrak{B}\gamma - \text{cl}(\rho, \sigma) \subseteq (\mathfrak{B}\gamma - \text{cl}(\mathfrak{B}\gamma - \text{int}(\rho, \sigma)))$.

Therefore, $(\rho, \sigma) \subseteq (\mathfrak{B}\gamma - \text{cl}(\mathfrak{B}\gamma - \text{int}(\rho, \sigma)))$.

Conversely, assume that $(\rho, \sigma) \subseteq (\mathfrak{B}\gamma - \text{cl}(\mathfrak{B}\gamma - \text{int}(\rho, \sigma)))$, then $\mathfrak{B}\gamma - \text{int}(\rho, \sigma) \subseteq \mathfrak{B}\gamma - \text{int}(\mathfrak{B}\gamma - \text{cl}(\mathfrak{B}\gamma - \text{int}(\rho, \sigma)))$. By theorem 2.5, (ρ, σ) is binary $\gamma - \alpha$ –open set.

Result 2.1:

Every binary $\gamma -$ regular open is binary $\gamma -$ pre open, binary $\gamma -$ semi open.

Theorem 2.8:

Let (ζ, η, γ) be a $\mathfrak{B}\gamma -$ TS and (W, μ) be $\gamma -$ TS. Then $b\gamma$ -continuous function $f: W \rightarrow \zeta \times \eta$ is binary γ - regular continuous.

Proof:

Let $f: W \rightarrow \zeta \times \eta$ be a $b\gamma$ -continuous and (ρ, σ) be a binary γ -regular open in (ζ, η, γ) . Then (ρ, σ) is $b\gamma$. Since f is $b\gamma$ -continuous, $f^{-1}((\rho, \sigma))$ is γ open in (W, μ) . Therefore, f is binary γ -regular continuous.

Theorem 2.9:

Let (ζ, η, γ) be a $\mathfrak{B}\gamma -$ TS and (W, μ) be $\gamma -$ TS. Then $f: W \rightarrow \zeta \times \eta$ is binary γ -semi continuous iff it is binary $\gamma - \alpha$ -continuous.

Proof:

Let $f: W \rightarrow \zeta \times \eta$ be a binary γ -semi continuous and (ρ, σ) be a binary $\gamma - \alpha$ –open in $(\zeta, \eta, \mathfrak{B}\gamma)$. Then by the similar argument used in the proof of theorem (2.8), we get f is binary $\gamma - \alpha$ - continuous. Using the same argument, converse part is proved.

Theorem 2.10:

By using the similar argument of proof of theorem (2.8), we get the following result

(i) Every binary γ - pre continuous function is binary $\gamma - \alpha$ - continuous and binary γ - regular continuous. (ii) Every binary $\gamma - \alpha$ - continuous function is binary γ - continuous.

CONCLUSION

We have presented Binary γ -continuous function and some types of continuous functions. In future, we are going to work on continuous mapping from binary gamma topology to binary gamma topology, its quotient map .

REFERENCES

1. B. Ahmad and S. Hussain, "properties of γ - Operations on topological spaces," Aligarh Bull. Math. 22(1) (2003), 45-51.
2. S. Kasahara(1979), "Operation- compact spaces," Math.Jaon,24, 97-105.
3. G.S.S. Krishnan (2003), "A new class of semi open sets in a topological space," proceedings of NCMCM, Allied Publishers, New Delhi, 305-311.
4. G.S.S. Krishnan and K. Balachandran(2006a), "On a class of γ -pre open sets in a topological space," East Asian Math. J.,22(2),131-149
5. G.S.S. Krishnan and K. Balachandran(2006a), "On a class of γ -semiopen sets in a Topological space," Bull. Cal. Math.Soc.,98(6),517-530.



**Muthulakshmi and Gilbert Rani**

6. G.S.S. Krishnan, M. Ganster and K. Balachandran: "Operation approaches on semi-open sets and applications," Kochi. J. Math. 2, (2007), 21-33.
7. K. Muthulakshmi and M. Gilbert Rani, "Binary γ - open sets in Binary Topological Space, " Mathematical Statistician and Engineering Applications, vol. 71 No. 4(2022) , 3582-3590.
8. Jamal M. Mustafa, "On Binary Generalized Topological Spaces," Refaad General Letters in Mathematics, 2(3), 111-116, 2017.
9. F.Nakaoka and N. Oda: "Some applications of minimal open sets," International Journal of Math. Math. Sci., 27(2001), no. 8, 471-476.
10. Nazir Ahmad Ahengarand J.K. Maitra, "On g-binary continuity, "Journal of Emerging Technologies and Innovative Research, 5(7) 240-244, 2018.
11. S. NithyananthaJothi and P. Thangavelu," On binary topological spaces," Pacific- Asian journal of Mathematics 5(2), 133-138, 2011.
12. S. NithyananthaJothi and P. Thangavelu, "Topology between two sets," Journal of Mathematical Sciences & Computer Applications, 1(3) (2011), 95-107.
13. S. NithyananthaJothi and P. Thangavelu, "On binary continuity and binary separation axioms," Ultra Scientist of physical Sciences, Vol. 24(1)A, 121- 126(2012).
14. S.NithyananthaJothi and P. Thangavelu, "Binary semi open sets in binary topological spaces," IJMA-7(9), 2016,73-76.
15. S. NithyananthaJothi and P. Thangavelu, "Generalized Binary Regular Closed sets, "International Journal of Applied Sciences (ISSN 2455-4499), 4(2), 2016, 259- 263.
16. S. NithyananthaJothi, "Binary Semi Continuous functions," International Journal of Mathematics Trends and Technology -Volume 49 Number 2 September 2017.
17. O. Njastad (1965). "On some classes of nearly open sets," Pacific J. Math, 15:961-970.
18. Norman Levine, "Semi-open sets and Semi-continuity in Topological spaces," Amer. Math. Monthly. 70(1963), 36-41.
19. H. Ogata (1991), " operations on topological spaces and associated topology," Math. Japan., 36(1), 175-184.





***P*-order *e*-open sets in Cubic Topological Spaces "**

B.Vijayalakshmi¹, M.Muthukaliyammal², G.Saravanakumar^{3*} and C.Inbam⁴

¹Assistant Professor, PG and Research, Department of Mathematics, Govt. Arts College, C.Mutlur, (Affiliated to Thiruvalluvar University) Chidambaram, Tamil Nadu, India.

²Assistant Professor, Mangayarkarasi College of Arts and Science, (Affiliated to Madurai Kamaraj University), Madurai, Tamil Nadu, India.

³Assistant Professor, Vel Tech Rangarajan Dr.Sagunthala R & D Institute Science and Technology (Deemed to be University), Chennai, Tamil Nadu, India,

⁴Assistant Professor, Govt. Arts College, Melur, (Affiliated to Madurai Kamaraj University), Madurai, Tamil Nadu, India.

Received: 13 Jan 2023

Revised: 15 Mar 2023

Accepted: 27 Apr 2023

***Address for Correspondence**

G.Saravanakumar

Assistant Professor,

Vel Tech Rangarajan Dr.Sagunthala R & D Institute Science and Technology (Deemed to be University), Chennai, Tamil Nadu, India,

E.Mail: saravananguru2612@gmail.com



This is an Open Access Journal / article distributed under the terms of the **Creative Commons Attribution License** (CC BY-NC-ND 3.0) which permits unrestricted use, distribution, and reproduction in any medium, provided the original work is properly cited. All rights reserved.

ABSTRACT

In this paper, we introduce a *P*-cubic *e*-open set which is the union of *P*-cubic $\delta\mathcal{P}$ -open sets and *P*-cubic $\delta\mathcal{S}$ -open sets in *P*-cubic topological spaces. Also, we discuss about near open sets, their properties and examples of a *P*-cubic *e*-open set. Moreover, we look into some of their primary properties and examples of *P*-cubic *e*-interior and *e*-closure in a *P*-cubic topological space.

Keywords and phrases: *P*-cubic *e*-open sets, *P*-cubic *e*-closed sets, *P*-cubic $eint(\mathcal{A})$ and *P*-cubic $ecl(\mathcal{A})$.

AMS (2000) subject classification: 03E72, 54A10, 54A40.

INTRODUCTION

Fuzzy set was developed by Zadeh in 1965 [8]. After introduction of fuzzy set, The theory of fuzzy has explored in many applied branches of sciences. i.e, Information science, Decision making theory, Artificial intelligence etc. In 1975 [9], Zadeh made an extension of the concept of a fuzzy set by an interval-valued fuzzy set. Interval-valued fuzzy sets have been actually used in real-life applications. For example, Sambuc [7] in Medical diagnosis in thyroid pathology, Kohout [5] also in Medicine, Fuzzy set has many extensions i.e, Intuitionistic fuzzy set (in brief, IFS) [2],





Vijayalakshmi et al.,

Bipolar fuzzy set (in brief, BFS) [10], Cubic set(in brief,CS) [4]. Cubic set has applied to many branches of mathematics. Cubic set and operation on cubic sets was introduced by Y.B.Jun in 2012[4] and Fuzzy topological spaces was introduced by C. L. Chang in 1968 [3].

Preliminaries

The basic definitions and the properties of neutrosophic soft topological spaces are discussed in this section.

Definition 2.1 [9] A closed sub-interval of $I = [0,1]$ is called interval number. $a = [a^-, a^+]$ where $0 \leq a^- \leq a^+ \leq 1$. $[I]$ denotes the set of all interval numbers.

Definition 2.2 [9] Let X be a non-empty set. A function $A: X \rightarrow [I]$, from X to all interval number is called interval valued fuzzy set (IVFS) in X . $[I]^X$ denotes the set of all IVFS in X . $\forall A \in [I]^X$ and $x \in X$ $A(x) = [A^-(x), A^+(x)]$ is called degree of membership of x in A . individually $A^-: X \rightarrow I$ and $A^+ : X \rightarrow I$ is Fuzzy set in X . Simply A^- is called lower fuzzy set and A^+ is called upper fuzzy set.

Definition 2.3 [4] Let X be a non-empty set, Then a structure $A = \{ \langle x, \mu(x), \lambda(x) \rangle / x \in X \}$ is cubic set in X in which μ is interval valued fuzzy set (IVFS) in X and λ is fuzzy set in X . Simply a cubic set is denoted by $A = \langle \mu, \lambda \rangle$ and C^X denotes the collection of all cubic sets in X .

Definition 2.4 [4] Let $X \neq \emptyset$, Then a cubic set $A = \langle \mu, \lambda \rangle$ is said to be internal cubic set (ICS) if $\mu^-(x) \leq \lambda(x) \leq \mu^+(x) \forall x \in X$.

Definition 2.5[4] Let $X \neq \emptyset$, Then a cubic set $A = \langle \mu, \lambda \rangle$ is said to be an external cubic set (ECS) if $\lambda(x) \notin (\mu^-(x), \mu^+(x)) \forall x \in X$.

1. A cubic set $A = \langle \mu, \lambda \rangle$ in which $\mu(x) = 0$ and $\lambda(x) = 1$ (resp. $\mu(x) = 1$ and $\lambda(x) = 0$) $\forall x \in X$ is denoted by $\hat{0}$ (resp. $\hat{1}$).
 2. A cubic set $A = \langle \mu, \lambda \rangle$ in which $\mu(x) = 0$ and $\lambda(x) = 0$ (resp. $\mu(x) = 1$ and $\lambda(x) = 1 \forall x \in X$ is denoted by $\hat{0}$ (resp. $\hat{1}$).
- Let $A = \langle \mu, \lambda \rangle$ and $B = \langle \beta, \eta \rangle$ be two cubic sets in X , Then we define;

1. $A = B \Leftrightarrow \mu = \beta$ and $\lambda = \eta$
2. $A \subseteq_p B \Leftrightarrow \mu \subseteq \beta$ and $\lambda \leq \eta$
3. $A^c = \langle \mu^c, 1 - \lambda \rangle = \{ \langle x, \mu^c(x), 1 - \lambda(x) \rangle / x \in X \}$
4. $(A^c)^c = A$
5. $\hat{0}^c = \hat{1}$ and $\hat{1}^c = \hat{0}$
6. $(\cup_p A_i)^c = \cap_p A_i^c$ and $(\cap_p A_i)^c = \cup_p A_i^c$
7. P-Union $\cup_{i \in \mathbb{N}} A = \{ \langle x, (\cup_{i \in \mathbb{N}} \mu_i)(x), (\vee \lambda_i) i \in \mathbb{N}(x) / x \in X \}$
8. P-Intersection $\cap_{i \in \mathbb{N}} A = \{ \langle x, (\cap_{i \in \mathbb{N}} \mu_i)(x), i \in \mathbb{N}(\wedge \lambda_i)(x) / x \in X \}$

Definition 2.6 [1] A P- cubic topology (in brief Pct) is the family \mathcal{F}_p of cubic sets in X which satisfies the following conditions;

1. $\hat{0}, \hat{1} \in \mathcal{F}_p$.
2. Let $A_i \in \mathcal{F}_p$, Then $\cup_p A_i \in \mathcal{F}_p, i \in \mathbb{N}$
3. Let $A, B \in \mathcal{F}_p$, Then $A \cap_p B \in \mathcal{F}_p$.

The pair $(X; \mathcal{F}_p)$ is called P-cubic topological space (in brief, Pcts).

Definition 2.7 [6] A set R is said to be a P-order Cubic set (in brief, CS_p)

1. regular open set (briefly, $CS_p \delta ros$) if $R = CS_p int(CS_p cl R)$.
2. regular closed set (briefly, $CS_p \delta rcs$) if $R = CS_p cl(CS_p int R)$.

Definition 2.8 [6] A set R is said to be a CS_p





Vijayalakshmi et al.,

1. interior (resp. δ interior) of R (briefly, $CS_p\text{int}R$ (resp. $CS_p\delta\text{int}$)) is defined by $CS_p\text{int}R$ (resp. $CS_p\delta\text{int}$) = $\cup \{ \tilde{G} : \tilde{G} \subseteq R \& \tilde{G} \text{ is a } CS_p\text{os (resp. } CS_p\delta\text{os) in } X \}$.
2. closure (resp. δ closure) of R (briefly, $CS_p\text{cl}R$ (resp. $CS_p\delta\text{cl}$)) is defined by $CS_p\text{cl}R$ (resp. $CS_p\delta\text{cl}$) = $\cap \{ \tilde{G} : \tilde{G} \supseteq R \& \tilde{G} \text{ is a } CS_p\text{cs (resp. } CS_p\delta\text{cs) in } X \}$.

Definition 2.9[6] A set R is said to be a CS_p

1. β open set (briefly, $CS_p\beta\text{os}$) if $R \subseteq CS_p\text{cl}(CS_p\text{int}(CS_p\text{cl}R))$.

3 P-order e-open sets in CTSs

Definition 3.1 A set R is said to be a CS_p

1. δ -pre open set (briefly, $CS_p\delta\mathcal{P}\text{os}$) if $R \subseteq CS_p\text{int}(CS_p\delta\text{cl}R)$.
2. δ -semi open set (briefly, $CS_p\delta\mathcal{S}\text{os}$) if $R \subseteq CS_p\text{cl}(CS_p\delta\text{int}R)$.
3. e -open set (briefly, $CS_p\mathcal{E}\text{os}$) if $R \subseteq CS_p\text{cl}(CS_p\delta\text{int}R) \cup CS_p\text{int}(CS_p\delta\text{cl}R)$.
4. e^* -open set (briefly, $CS_p\mathcal{E}^*\text{os}$) if $R \subseteq CS_p\text{cl}(CS_p\text{int}(CS_p\delta\text{cl}R))$.
5. α -open set (briefly, $CS_p\mathcal{A}\text{os}$) if $R \subseteq CS_p\text{int}(CS_p\text{cl}(CS_p\delta\text{int}R))$.

The complement of a $CS_p\mathcal{E}$ -open set (resp. $CS_p\delta\text{os}$, $CS_p\delta\mathcal{P}\text{os}$, $CS_p\delta\mathcal{S}\text{os}$ & $CS_p\mathcal{E}^*\text{os}$) is called a neutrosophic soft e - (resp. δ , δ -pre, δ -semi & e^*) closed set (briefly, $CS_p\mathcal{E}\text{cs}$ (resp. $CS_p\delta\text{cs}$, $CS_p\delta\mathcal{P}\text{cs}$, $CS_p\delta\mathcal{S}\text{cs}$ & $CS_p\mathcal{E}^*\text{cs}$) in X .

The family of all $CS_p\delta\mathcal{P}\text{os}$ (resp. $CS_p\delta\mathcal{P}\text{cs}$, $CS_p\delta\mathcal{S}\text{os}$, $CS_p\delta\mathcal{S}\text{cs}$, $CS_p\mathcal{E}\text{os}$, $CS_p\mathcal{E}\text{cs}$, $CS_p\mathcal{E}^*\text{os}$ & $CS_p\mathcal{E}^*\text{cs}$) of X is denoted by $CS_p\delta\mathcal{P}\text{OS}(X)$ (resp. $CS_p\delta\mathcal{P}\text{CS}(X)$, $CS_p\delta\mathcal{S}\text{OS}(X)$, $CS_p\delta\mathcal{S}\text{CS}(X)$, $CS_p\mathcal{E}\text{OS}(X)$, $CS_p\mathcal{E}\text{CS}(X)$, $CS_p\mathcal{E}^*\text{OS}(X)$ & $CS_p\mathcal{E}^*\text{CS}(X)$).

Definition 3.2 A set R is said to be a CS_p

1. e interior (resp. δpre interior & δsemi interior) of R (briefly, $CS_p\mathcal{E}\text{int}R$ (resp. $CS_p\delta\mathcal{P}\text{int}$ & $CS_p\delta\mathcal{S}\text{int}$)) is defined by $CS_p\mathcal{E}\text{int}R$ (resp. $CS_p\delta\mathcal{P}\text{int}$ & $CS_p\delta\mathcal{S}\text{int}$) = $\cup \{ \tilde{G} : \tilde{G} \subseteq R \& \tilde{G} \text{ is a } CS_p\mathcal{E}\text{os (resp. } CS_p\delta\mathcal{P}\text{os} \& CS_p\delta\mathcal{S}\text{os) in } X \}$.
2. e closure (resp. δpre closure & δsemi closure) of R (briefly, $CS_p\mathcal{E}\text{cl}R$ (resp. $CS_p\delta\mathcal{P}\text{cl}$ & $CS_p\delta\mathcal{S}\text{cl}$)) is defined by $CS_p\mathcal{E}\text{cl}R$ (resp. $CS_p\delta\mathcal{P}\text{cl}$ & $CS_p\delta\mathcal{S}\text{cl}$) = $\cap \{ \tilde{G} : R \subseteq \tilde{G} \& R \text{ is a } CS_p\mathcal{E}\text{cs (resp. } CS_p\delta\mathcal{P}\text{cs} \& CS_p\delta\mathcal{S}\text{cs) in } X \}$.

Proposition 3.1 The statements are hold but the converse does not true.

1. Every $CS_p\delta\text{os}$ (resp. $CS_p\delta\text{cs}$) is a $CS_p\text{os}$ (resp. $CS_p\text{cs}$).
2. Every $CS_p\text{os}$ (resp. $CS_p\text{cs}$) is a $CS_p\delta\mathcal{S}\text{os}$ (resp. $CS_p\delta\mathcal{S}\text{cs}$).
3. Every $CS_p\text{os}$ (resp. $CS_p\text{cs}$) is a $CS_p\delta\mathcal{P}\text{os}$ (resp. $CS_p\delta\mathcal{P}\text{cs}$).
4. Every $CS_p\delta\mathcal{S}\text{os}$ (resp. $CS_p\delta\mathcal{S}\text{cs}$) is a $CS_p\mathcal{E}\text{os}$ (resp. $CS_p\mathcal{E}\text{cs}$).
5. Every $CS_p\delta\mathcal{P}\text{os}$ (resp. $CS_p\delta\mathcal{P}\text{cs}$) is a $CS_p\mathcal{E}\text{os}$ (resp. $CS_p\mathcal{E}\text{cs}$).
6. Every $CS_p\mathcal{E}\text{os}$ (resp. $CS_p\mathcal{E}\text{cs}$) is a $CS_p\mathcal{E}^*\text{os}$ (resp. $CS_p\mathcal{E}^*\text{cs}$).

Proof.

1. If R is a $CS_p\delta\text{os}$, then $R = CS_p\delta\text{int}R \subseteq CS_p\text{int}R$. $\therefore R$ is a $CS_p\text{os}$.
2. If R is a $CS_p\text{os}$, then $R = CS_p\text{int}R$. So, $R = CS_p\text{int}R \subseteq CS_p\text{cl}(CS_p\delta\text{int}R)$.
 $\therefore R$ is a $CS_p\delta\mathcal{S}\text{os}$.
3. If R is a $CS_p\text{os}$, then $R = CS_p\text{int}R$. So, $R = CS_p\text{int}R \subseteq CS_p\text{int}(CS_p\delta\text{cl}R)$.
 $\therefore R$ is a $CS_p\delta\mathcal{P}\text{os}$.
4. If R is a $CS_p\delta\mathcal{S}\text{os}$, then $R \subseteq CS_p\text{cl}(CS_p\delta\text{int}R) \subseteq CS_p\text{cl}(CS_p\delta\text{int}R) \cup CS_p\text{int}(CS_p\delta\text{cl}R)$.
 $\therefore R$ is a $CS_p\mathcal{E}\text{os}$.
5. If R is a $CS_p\delta\mathcal{P}\text{os}$, then $R \subseteq CS_p\text{int}(CS_p\delta\text{cl}R) \subseteq CS_p\text{cl}(CS_p\delta\text{int}R) \cup CS_p\text{int}(CS_p\delta\text{cl}R)$.
 $\therefore R$ is a $CS_p\mathcal{E}\text{os}$.
6. If R is a $CS_p\mathcal{E}\text{os}$ then $R \subseteq CS_p\text{cl}(CS_p\delta\text{int}R) \cup CS_p\text{int}(CS_p\delta\text{cl}R)$. So $R \subseteq CS_p\text{cl}(CS_p\delta\text{int}R) \cup CS_p\text{int}(CS_p\delta\text{cl}R) \subseteq CS_p\text{cl}(CS_p\text{int}(CS_p\delta\text{cl}R))$.





Vijayalakshmi et al.,

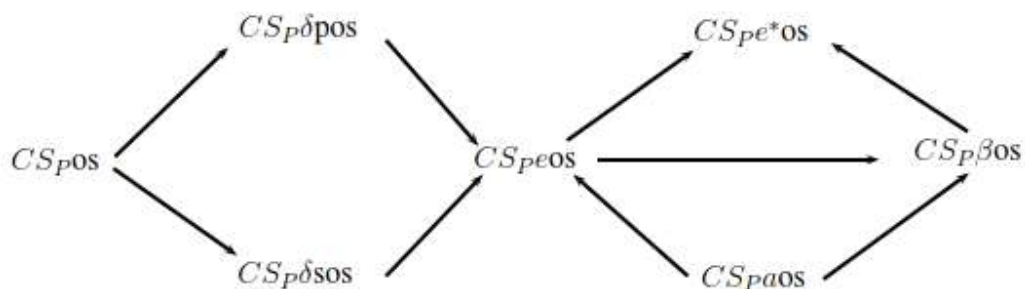
∴ R is a $CS_p e^*os$.

It is also true for their respective closed sets.

Example 3.1 Let X be a non-empty set and \mathcal{F}_p be the collection of cubic sets in X then (X, \mathcal{F}_p) be P -cubic topological space $\{\hat{0}, \hat{1}, A, B, C\}$ where $A = \langle [0.2, 0.4], 0.3 \rangle, B = \langle [0.5, 0.7], 0.6 \rangle, C = \langle [0.8, 0.9], 0.8 \rangle, D = \langle [0.3, 0.6], 0.5 \rangle, E = \langle [0.6, 0.8], 0.7 \rangle, F = \langle [0.6, 0.8], 0.7 \rangle, G = \langle [0.8, 0.9], 0.8 \rangle, H = \langle [0.1, 0.4], 0.4 \rangle, I = \langle [0.2, 0.2], 0.2 \rangle, J = \langle [0.1, 0.5], 0.4 \rangle, K = \langle [0.3, 0.4], 0.4 \rangle$, then

1. D is $CS_p \delta P os$ but not $CS_p os$
2. E is $CS_p \delta S os$ but not $CS_p os$
3. F is $CS_p eos$ but not $CS_p \delta P os$
4. G is $CS_p eos$ but not $CS_p \delta S os$
5. H is $CS_p e^*os$ but not $CS_p eos$
6. I is $CS_p e^*os$ but not
7. is but not
8. is but not
9. is but not

Remark 3.1 The diagram shows 's in' .



Theorem 3.1 The statements are true.

1. $CS_p \delta P cl R \supseteq R \cup CS_p cl(CS_p \delta int R)$.
2. $CS_p \delta P int R \subseteq R \cap CS_p int(CS_p \delta cl R)$.
3. $CS_p \delta S cl R \supseteq R \cup CS_p int(CS_p \delta cl R)$.
4. $CS_p \delta S int R \subseteq R \cap CS_p cl(CS_p \delta int R)$.

Proof. (i) Since $CS_p \delta P cl R$ is $CS_p \delta P cs$, we have

$$CS_p cl(CS_p \delta int R) \subseteq CS_p cl(CS_p \delta int(CS_p \delta P cl R)) \subseteq CS_p \delta P cl R.$$

Thus $R \cup CS_p cl(CS_p \delta int R) \subseteq CS_p \delta P cl R$.

The other cases are similar. \exists

Theorem 3.2 R is a $CS_p eos$ iff $R = CS_p \delta P int R \cup CS_p \delta S int R$.

Proof. Let R be a $CS_p eos$. Then $R \subseteq CS_p cl(CS_p \delta int R) \cup CS_p int(CS_p \delta cl R)$. By Theorem 3.1, we have

$$\begin{aligned} CS_p \delta P int R \cup CS_p \delta S int R &\subseteq R \cap (CS_p int(CS_p \delta cl R) \cup (R \cap CS_p cl(CS_p \delta int R))) \\ &= R \cap (CS_p int(CS_p \delta cl R)) \cap CS_p cl(CS_p \delta int R) \\ &= R. \end{aligned}$$

Conversely, if $R = CS_p \delta P int R \cup CS_p \delta S int R$ then, by Theorem 3.1

$$\begin{aligned} R &= CS_p \delta P int R \cup CS_p \delta S int R \\ &\subseteq (R \cap CS_p int(CS_p \delta cl R)) \cup (R \cap CS_p cl(CS_p \delta int R)) \\ &= R \cap (CS_p int(CS_p \delta cl R) \cup CS_p cl(CS_p \delta int R)) \end{aligned}$$





Vijayalakshmi et al.,

$$\subseteq CS_{pint}(CS_{p\delta cl}R) \cup CS_{pcl}(CS_{p\delta int}R)$$

and hence R is a CS_{peos} . Ξ

Theorem 3.3 The union (resp. intersection) of any family of $CS_{peOS}(X)$ (resp. $CS_{peCS_p}(X)$) is a $CS_{peOS}(X)$ (resp. $CS_{peCS_p}(X)$).

Proof. Let $\{R_a: a \in \tau\}$ be a family of CS_{peos} 's. For each $a \in \tau$, $R_a \subseteq CS_{pcl}(CS_{p\delta int}(R_a)) \cup CS_{pint}(CS_{p\delta cl}(R_a))$.

$$\begin{aligned} \bigcup_{a \in \tau} R_a &\subseteq \bigcup_{a \in \tau} CS_{pcl}(CS_{p\delta int}(R_a)) \cup CS_{pint}(CS_{p\delta cl}(R_a)) \\ &\subseteq CS_{pcl}(CS_{p\delta int}(\bigcup R_a)) \cup CS_{pint}(CS_{p\delta cl}(\bigcup R_a)) \end{aligned}$$

The other case is similar. Ξ

Remark 3.2 The intersection of two CS_{peos} 's need not be CS_{peos} .

Example 3.2 Let X be a non-empty set and \mathcal{F}_p be the collection of cubic sets in X then (X, \mathcal{F}_p) be P -cubic topological space $\{\hat{0}, \hat{1}, A, B, C\}$ where $A = \langle [0.2, 0.4], 0.3 \rangle$, $B = \langle [0.5, 0.7], 0.6 \rangle$, $C = \langle [0.8, 0.9], 0.8 \rangle$, and $D = \langle [0.1, 0.6], 0.6 \rangle$, $E = \langle [0.3, 0.5], 0.4 \rangle$, are CS_{peos} 's but $D \cap E = \langle [0.1, 0.5], 0.4 \rangle$ is not CS_{peos}

Proposition 3.2 If R is a

1. CS_{peos} and $CS_{p\delta int}R = 0_X$, then R is a $CS_{p\delta Pos}$.
2. CS_{peos} and $CS_{p\delta cl}R = 0_X$, then R is a $CS_{p\delta Sos}$.
3. CS_{peos} and $CS_{p\delta cs}$, then R is a $CS_{p\delta Sos}$.
4. $CS_{p\delta Sos}$ and $CS_{p\delta cs}$, then R is a CS_{peos} .

Proof. (i) Let R be a CS_{peos} , that is

$$R \subseteq CS_{pcl}(CS_{p\delta int}R) \cup CS_{pint}(CS_{p\delta cl}R) = 0_X \cup CS_{pint}(CS_{p\delta cl}R) = CS_{pint}(CS_{p\delta cl}R)$$

Hence R is a $CS_{p\delta Pos}$.

(ii) Let R be a CS_{peos} , that is

$$R \subseteq CS_{pcl}(CS_{p\delta int}R) \cup CS_{pint}(CS_{p\delta cl}R) = CS_{pcl}(CS_{p\delta int}R) \cup 0_X = CS_{pcl}(CS_{p\delta int}R)$$

Hence R is a $CS_{p\delta Sos}$.

(iii) Let R be a CS_{peos} and $CS_{p\delta cs}$, that is

$$R \subseteq CS_{pcl}(CS_{p\delta int}R) \cup CS_{pint}(CS_{p\delta cl}R) = CS_{pcl}(CS_{p\delta int}R).$$

Hence R is a $CS_{p\delta Sos}$.

(iv) Let R be a $CS_{p\delta Sos}$ and $CS_{p\delta cs}$, that is

$$R \subseteq CS_{pcl}(CS_{p\delta int}R) \subseteq CS_{pcl}(CS_{p\delta int}R) \cup CS_{pint}(CS_{p\delta cl}R).$$

Hence R is a CS_{peos} . Ξ

Theorem 3.4 R is a CS_{pecs} (resp. CS_{peos}) iff $R = CS_{pecl}R$ (resp. $R = CS_{peint}R$).

Proof. Suppose $R = CS_{pecl}R = \bigcap \{ \tilde{G}: R \subseteq \tilde{G} \& \tilde{G} \text{ is a } CS_{pecs} \}$. This means $R \in \bigcap \{ \tilde{G}: R \subseteq \tilde{G} \& \tilde{G} \text{ is a } CS_{pecs} \}$ and hence R is CS_{pecs} .

Conversely, suppose R be a CS_{pecs} in X . Then, we have $R \in \bigcap \{ \tilde{G}: R \subseteq \tilde{G} \& \tilde{G} \text{ is a } CS_{pecs} \}$. Hence, $R \subseteq \tilde{G}$ implies $R = \bigcap \{ \tilde{G}: R \subseteq \tilde{G} \& \tilde{G} \text{ is a } CS_{pecs} \} = CS_{pecl}R$.

Similarly $R = CS_{peint}R$. Ξ

Theorem 3.5 Let R and \tilde{G} in X , then the CS_{pecl} sets have

1. $CS_{pecl}(0_X) = 0_X$, $CS_{pecl}(1_X) = 1_X$.
2. $CS_{pecl}R$ is a CS_{pecs} in X .
3. $CS_{pecl}R \subseteq CS_{pecl}\tilde{G}$ if $R \subseteq \tilde{G}$.





Vijayalakshmi et al.,

$$4. CS_{pecl}(CS_{pecl}R) = CS_{pecl}R.$$

Proof. The proofs are directly from definitions of CS_{pecl} set. Ξ

Theorem 3.6 Let R and \tilde{G} in X , then the CS_{peint} sets have

1. $CS_{peint}(0_X) = 0_X, CS_{peint}(1_X) = 1_X.$
2. $CS_{peint}R$ is a CS_{peos} in X .
3. $CS_{peint}R \subseteq CS_{peint}\tilde{G}$ if $R \subseteq \tilde{G}.$
4. $CS_{peint}(CS_{peint}R) = CS_{peint}R.$

Proof. The proofs are directly from definitions of CS_{peint} set. Ξ

Proposition 3.3 Let R and \tilde{G} are in X , then

1. $CS_{pecl}R^c = [CS_{peint}R]^c, CS_{peint}R^c = [CS_{pecl}R]^c.$
2. $CS_{pecl}(R \cup \tilde{G}) \supseteq CS_{pecl}R \cup CS_{pecl}\tilde{G}, CS_{pecl}(R \cap \tilde{G}) \subseteq CS_{pecl}R \cap CS_{pecl}\tilde{G}.$
3. $CS_{peint}(R \cup \tilde{G}) \supseteq CS_{peint}R \cup CS_{peint}\tilde{G}, CS_{peint}(R \cap \tilde{G}) \subseteq CS_{peint}R \cap CS_{peint}\tilde{G}.$

Proof.

1. The proof is directly from definition.
2. $R \subseteq R \cup \tilde{G}$ or $\tilde{G} \subseteq R \cup \tilde{G}.$ Hence $CS_{pecl}R \subseteq CS_{pecl}(R \cup \tilde{G})$ or $CS_{pecl}\tilde{G} \subseteq CS_{pecl}(R \cup \tilde{G}).$ Therefore, $CS_{pecl}(R \cup \tilde{G}) \supseteq CS_{pecl}R \cup CS_{pecl}\tilde{G}.$ The other one is similar.
3. $R \subseteq R \cup \tilde{G}$ or $\tilde{G} \subseteq R \cup \tilde{G}.$ Hence $CS_{peint}R \subseteq CS_{peint}(R \cup \tilde{G})$ or $CS_{peint}\tilde{G} \subseteq CS_{peint}(R \cup \tilde{G}).$ Therefore, $CS_{peint}(R \cup \tilde{G}) \supseteq CS_{peint}R \cup CS_{peint}\tilde{G}.$ The other one is similar. Ξ

Proposition 3.4 If R is in X , then

1. $CS_{pecl}R \supseteq CS_{pcl}(CS_{p\delta int}R) \cap CS_{pint}(CS_{p\delta cl}R).$
2. $CS_{peint}R \subseteq CS_{pcl}(CS_{p\delta int}R) \cup CS_{pint}(CS_{p\delta cl}R).$

Proof. (i) $CS_{pecl}R$ is a CS_{pecs} and $R \subseteq CS_{pecl}R$, then

$$CS_{pecl}R \supseteq CS_{pcl}(CS_{p\delta int}(CS_{pecl}R)) \cap CS_{pint}(CS_{p\delta cl}(CS_{pecl}R)) \\ \supseteq CS_{pcl}(CS_{p\delta int}R) \cap CS_{pint}(CS_{p\delta cl}R).$$

(ii) $CS_{peint}R$ is a CS_{peos} and $R \supseteq CS_{peint}R$, then

$$CS_{peint}R \subseteq CS_{pcl}(CS_{p\delta int}(CS_{peint}R)) \cup CS_{pint}(CS_{p\delta cl}(CS_{peint}R)) \\ \subseteq CS_{pcl}(CS_{p\delta int}R) \cup CS_{pint}(CS_{p\delta cl}R).$$

Ξ

Theorem 3.7 Let R be in X , then

1. $CS_{pecl}R = CS_{p\delta Pcl}R \cap CS_{p\delta Scl}R.$
2. $CS_{peint}R = CS_{p\delta Pint}R \cap CS_{p\delta Sint}R.$

Proof. (i) It is obvious that, $CS_{pecl}R \subseteq CS_{p\delta Pcl}R \cap CS_{p\delta Scl}R.$ Conversely, from Definition 3.2, we have

$$CS_{pecl}R \supseteq CS_{pcl}(CS_{p\delta int}(CS_{pecl}R)) \cap CS_{pint}(CS_{p\delta cl}(CS_{pecl}R)) \\ \supseteq CS_{pcl}(CS_{p\delta int}R) \cap CS_{pint}(CS_{p\delta cl}R).$$

Since $CS_{pecl}R$ is CS_{pecs} , by Theorem 3.1, we have

$$CS_{p\delta Pcl}R \cap CS_{p\delta Scl}R = R \cup CS_{pcl}(CS_{p\delta int}R) \cap (R \cup CS_{pint}(CS_{p\delta cl}R)) \\ = R \cap (CS_{pcl}(CS_{p\delta int}R) \cap CS_{pint}(CS_{p\delta cl}R)) \\ = R \subseteq CS_{pecl}R.$$

Therefore, $CS_{pecl}R = CS_{p\delta Pcl}R \cap CS_{p\delta Scl}R.$

(ii) is similar from (i). Ξ





Vijayalakshmi et al.,

Theorem 3.8 Let R be in X . Then

1. $CS_{pecl}(1_X - R) = 1_X - CS_{peint}R$.
2. $CS_{peint}(1_X - R) = 1_X - CS_{pecl}R$.

Proof. (i) Let \tilde{G} be CS_{pecs} in X and R be any set in X . Then $CS_{peint}R = \cup \{1_X - \tilde{G} : 1_X - \tilde{G} \subseteq R, 1_X - \tilde{G} \text{ is a } CS_{peosin}X\} = 1_X - \cap \{\tilde{G} : \tilde{G} \supseteq 1_X - R, \tilde{G} \text{ is a } CS_{pecsin}X\} = 1_X - CS_{pecl}R$. Thus, $CS_{pecl}(1_X - R) = 1_X - CS_{peint}R$.

(ii) Let \tilde{G} be CS_{peos} in X and R be any set in X . Then $CS_{pecl}R = \cap \{1_X - \tilde{G} : 1_X - \tilde{G} \supseteq R, 1_X - \tilde{G} \text{ is a } CS_{pecsin}X\} = 1_X - \cup \{\tilde{G} : \tilde{G} \subseteq 1_X - R, \tilde{G} \text{ is a } CS_{peosin}X\} = 1_X - CS_{peint}R$. Thus, $CS_{peint}(1_X - R) = 1_X - CS_{pecl}R$. \square

CONCLUSION

We have studied about P -cubic e -open set and P -cubic e -closed set and their respective interior and closure operators in cubic topological space in this paper. Also we have studied some of their fundamental properties along with examples in CS_{pts} . Moreover, we have discussed about near open sets of P -cubic e -open set in CS_{pts} . In future, we can extend these results to P -cubic e -continuous mappings, P -cubic e -open mappings and P -cubic e -closed mappings in CS_{pts} .

REFERENCES

1. Akhter Zeb, Saleem Abdullah, Majid Khan and Abdul Majid, *Cubic Topology*, International Journal of Computer Science and Information Security, 14(8) (2016), 659-669.
2. Atanassov *Intuitionistic fuzzy sets*. Fuzzy Sets Syst 20, (1986), 87-96.
3. C. L. Chang, *Fuzzy topological spaces*, J. Math. Anal. Appl. 24 (1968)
4. Y. B. Jun, C.S.Kim, K.O.Yang, *Cubic sets and Operations on Cubic sets*. Inform.4(2012), No. 1, 83-98.
5. L. J. Kohout, W. Bandler, *Fuzzy interval inference utilizing the checklist paradigm and BK-relational products*, in: R.B. Kearfort et al. (Eds.), Applications of Interval Computations, Kluwer, Dordrecht, 1996, pp. 291-335.
6. P. Loganayagi and D. Jayanthi, *Almost continuous mappings on cubic topological spaces*, Advances in fuzzy mathematics, 15 (1) (2020), 1-12.
7. R. Sambuc, *Functions Φ -Flous, Application à laide au Diagnostic en Pathologie Thyroïdienne*, These de Doctorat en Medecine, Marseille, 1975.
8. L. A. Zadeh. *Fuzzy sets*. Inform. Control 8 (1965), 338-353.
9. L. A. Zadeh, *The concept of a linguistic variable and its application to approximate reasoning- I*, Inform. Sci. 8 (1975) 199-249.
10. W. R. Zhang *Bipolar Fuzzy Sets and Relations*, December, 1994.





Eco-Friendly Dyeing of Cotton Fabric from Aqueous Herbal Extracts and its Antibacterial Activity

D.Sowmiya^{1*}, T.Poongodi², S.Karpagam³ and R.Sowbaraniga⁴

¹Assistant Professor, Department of Botany, Nallamuthu Gounder Mahalingam College, Pollachi, Coimbatore, Tamil Nadu, India – 642001.

²Ph.D Research Scholar, Department of Botany, Nallamuthu Gounder Mahalingam College, Pollachi, Coimbatore, Tamil Nadu, India – 642001.

³M.Sc. Student, Department of Botany, Nallamuthu Gounder Mahalingam College, Pollachi, Coimbatore, Tamil Nadu, India – 642001.

⁴Assistant Professor of Biological Science, Department of Education, Avinashilingam Institute for Home Science and Higher Education for Women, Coimbatore, Tamil Nadu, India.

Received: 27 Feb 2023

Revised: 25 Apr 2023

Accepted: 31 May 2023

*Address for Correspondence

D.Sowmiya

Assistant Professor,
Department of Botany,
Nallamuthu Gounder Mahalingam College,
Pollachi, Coimbatore, Tamil Nadu, India – 642001.
E. Mail: d.sowmiya22@gmail.com



This is an Open Access Journal / article distributed under the terms of the **Creative Commons Attribution License** (CC BY-NC-ND 3.0) which permits unrestricted use, distribution, and reproduction in any medium, provided the original work is properly cited. All rights reserved.

ABSTRACT

Natural dyes are found to be environmentally friendly and possess many advantages over their synthetic counterparts. Among various clothing, cotton may act as a nutrient, becoming a suitable medium for bacterial and fungal growth. Therefore, an attempt has been made to study the dyeing capacity and antibacterial activity of some plants like *Ocimum sanctum*, *Acalypha indica*, *Phyllanthus reticulatus*, *Impatiens balsamia* and *Clitoria ternatea* and the mordant used were *Terminalia chebula* and *Acacia sinuate* on cotton fabric. The work comprises the preparation of dye and mordant from the parts of different plants by means of aqueous extraction. The dyeing ability of *A. indica*, *O. sanctum*, *P. reticulatus*, *C. Ternatea* and *I. Balsamia* showed good results when the mordant *T. chebula* was used. Among the fabricated clothes, *O. sanctum* and *A. Indica* showed good antibacterial activity with the zone of inhibition 1.00 mm, 0.5 mm respectively. It can be inferred from this study that the naturally dyed clothes showed high compatibility with the environment, softer colour shades, naturalness, cost effective and antibacterial activity.

Keywords: Dye, Mordant, Fabrication, Antibacterial, Gram positive and Gram negative





INTRODUCTION

Medicinal plants are part and parcel of human society to combat diseases, from the dawn of civilization (Chaudhary et al., 2010). Extracts of medicinal plants can be obtained from plant parts such as roots, berries, bark, leaves and wood. Many natural plant extracts have antimicrobial activity and wound healing properties. Antimicrobial agents either inhibit the growth (-static) or kill (-cidal) the microorganisms. The art of making natural dyes is one of the oldest practices and dates back to the dawn of civilization which does not cause any kind of pollution (Kannanmarikani et al., 2015). Because of the excellent antimicrobial and eco-friendly dyeing properties exhibited by the plant extracts, these are used as textile finishing agents (Sarojyadav and Neelam M Rose, 2020). In India, there are more than 450 plants that can yield dyes. Clothing is our necessary thing which should be free from microbes to avoid many life threatening diseases. Over the last few decades, considerable research effort was made to produce antibacterial coatings on the surfaces of various objects such as garments and medical devices (Danese, 2002 and Lewis et al., 2005). The current interest is to develop efficient, non-toxic, durable and cost effective antimicrobial finishing clothes with increased applications in medical, health care, hygienic products as well as protective cloth materials (Czajka, 2005 and Molloy et al., 2008).

Cotton fibres are particularly suitable for manufacturing textiles for sports, non-implantable medical products and health care/hygienic products (Czajka, 2005). However the ability of cotton fibres to absorb large amount of moisture and act as nutrient which makes them more prone to microbial attack under certain conditions of humidity and temperature. (Gao et al., 2008 and Gorenssek et al., 2007). Therefore, cotton fibres are treated with numerous chemicals to get better antimicrobial cotton textiles (Son et al, 2006 and Tarimala et al., 2006). Plant based antimicrobial compounds have great therapeutic potential as they have lesser side effects as compared with synthetic drugs and also little chance of development of resistance. Therefore, the present study has been carried out to investigate the dyeing capacity and antimicrobial activity of some medicinally important plants viz., *Ocimum sanctum*, *Acalypha indica*, *Phyllanthus reticulatus*, *Impatiens balsamina* and *Clitoria ternatea*.

MATERIALS AND METHODS

Mordant Selection and Preparation

Seeds of *Terminalia chebula* L. (Combretaceae) and *Acacia sinuate* (Lour.) Merr. (Fabaceae) (Fig.1) were selected for the present study which was used as mordant. The selected mordants were bought from herbal medicine shop in Pollachi. 50 grams of seed powder was added in 500 ml of water and allowed to boil for an hour. Then it was filtered, dried and stored for further use.

Collection of Plant Samples for Natural Dye Preparation

The leaf powder of *Ocimum santum* (Lamiaceae) and *Acalypha indica* L. (Euphorbiaceae) (Fig.2), fresh flowers of *Impatiens balsamia* L. (Balsamiaceae) and *Clitoria ternatea* (Fabaceae), fresh fruits of *Phyllanthus reticulatus* Poir. (Phyllanthaceae) were chosen for the present study due to its high dye yielding capacity and antimicrobial property.

Natural Dye Extraction

The collected leaf samples were shade dried and finely powdered using mixer grinder. 20 grams of the powdered sample was mixed with 200ml of water and boiled for an hour. The fresh flower and fruit samples were grinded by adding water in pestle and mortar and filtered using cotton cloth. The filtrates were stored for further use.

Preparation of Cotton Fabric

Pure and sterile cotton clothes (5x5cm) were used as substrate and soaked in both mordants separately for 7 hours. Dried cotton clothes were dyed with natural extract obtained from *Ocimum sanctum*, *Acalypha indica*, *Phyllanthus reticulatus*, *Impatiens balsamia* and *Clitoria ternatea*. The dye ability of soaked cloth was studied by increasing the time from 0 hour to seven hours.





Antibacterial Activity

The effectiveness of dyed clothes were tested for antibacterial activity against gram negative *Escherichia coli* and gram positive *Staphylococcus aureus*. Parallel streak method was adopted for the present study which is a qualitative test used to detect diffusible bacteriostatic activity on textile material. Muller-Hinton agar medium was used for parallel streak method.

RESULTS AND DISCUSSION

The naturally dyed cotton fabrics showed good dyeing ability at different time intervals (Fig.3). After washing the dyed fabric using mild detergent, it was subjected to antibacterial activity. A good antibacterial activity was shown by *Ocimum sanctum* dye with the zone of inhibition 1.0 mm and *Acalypha indica* dye with the zone of inhibition 0.5 mm when used *Terminalia chebula* as mordant. The flowers of *Impatiens balsamia* and *Clitoria ternatea* and fruits of *Phyllanthus reticulatus* showed less antibacterial activity (Fig.4). Hence from the present study, it is suggested that antibacterial activity was found in naturally extracted plant dyed cotton cloth. The raw materials for making this eco friendly dye are cheaper when compared to other chemicals, so the commercial production must be encouraged at industrial level. The extract of *Acalypha indica* showed good dyeing ability and exhibit effective antibacterial activity on five antibacterial pathogens (Saravanan, et al., 2013). Senthilkumar and Karthi (2018) studied the antibacterial activity on two pathogens such as *Escherichia coli* and *Staphylococcus aureus* and the zone of inhibition is 26 and 27 mm respectively. Sumithra (2017) reported the aqueous extract of *Tribulus terrestris* and *Leucas aspara* showed zero antibacterial activity. But, our present study showed antibacterial activity for *Ocimum sanctum* and *Acalypha indica* for aqueous extraction.

CONCLUSION

In the present study, Eco-friendly natural dyes were prepared from leaves of *Ocimum santum* (Lamiaceae) and *Acalypha indica* L. (Euphorbiaceae), flowers of *Impatiens balsamia* L. (Balsamiaceae) and *Clitoria ternatea* (Fabaceae), fruits of *Phyllanthus reticulatus* Poir. (Phyllanthaceae). In which, *Ocimum sanctum* dyed cotton fabrics showed high antibacterial activity when compared to dyed cotton fabrics. It can be inferred from this study that the naturally dyed clothes showed high compatibility with environment, softer color shades, naturalness, lower toxicity, cost effective and antibacterial properties.

Conflict of Interest

Authors have no conflict of interest.

ACKNOWLEDGEMENT

The authors express their sincere thanks to the Principal Dr. P.M. Palanisamy, Nallamuthu Gounder Mahalingam College, Pollachi for providing necessary facilities and infrastructure at the institution and moral support.

REFERENCES

1. Dr.Senthilkumar, B. Karthi (2018), 'To study antimicrobial effect on cotton fabric of natural dye extract of Tulsi with Myrobalan mordanting Method'. *Internal Journal of Science and Research*. 8(8), 2138-2139.
2. Sumithra. M (2017), 'Eco friendly herb extracts treated on cotton fabric using antibacterial activity'. *International Journal of Scientific Research in Engineering*. 2(1), 8-11.
3. Yuan Gao and Robin Cranston (2008), 'Recent Advances in Antibacterial Treatments of Textiles'. *Textile Research Journal* 78(1), 60-72.





Sowmiya et al.,

4. Kannanmarikani, et al, (2015), 'Assessment of Dyeing properties and quality parameters of natural dye extract from *Lawsoniainernis*'. *European Journal of Experimental Biology* 5(7), 62-70.
5. Cragg G. M, et al, (1997), 'Natural products in drug discovery and development'. *Journal of Natural Products* 60(1), 52-60.
6. Chaudhary H. J, et al, (2012), 'In vitro analysis of *Cupressempervirens* L. Plant extracts antibacterial activity. *Journal of Medicinal Plants Research* 6(2), 273-276.
7. R. Czajka, (2005), 'Development of Medical Textile Market'. *Fibre and Textiles in Eastern Europe* 13(1).
8. Kumaresan. M et al, (2012), 'Application of eco friendly natural dye on cotton using combination of mordants'. *Indian Journal of Fibre and Textile Research* 37(2), 194-198.
9. SarojYadav et al (2020), 'Assessment of wash durability of Eucalyptus Herbal extract derived Antimicrobial finish'. *Plant Archives* 20(1), 16-20.
10. Cowan M. M (1999), 'Plant Products as Antimicrobial Agents'. *Clinical Microbiology Reviews*. 12(4), 564-582.
11. GarimaBhardwaj, et al (2015) 'Antibacterial Activity in different extracts of *lantana camera* against enterpathogens' *Innovare journal of Science* 3, 4-5.
12. P. Saravanan et al,(2013) 'Extraction and Application of eco friendly Natural Dye obtained from Leaves of *Acalyphaindica* Linn on cotton fabric' *International Research Journal of Environment Science* 2(12), 1-5.
13. G. Kowsalya Devi, et al, (2020), 'Development of Natural herbs on knitted fabric to impact microbial finishing for eczema patients' *International Research finishing of Modernization in Engineering Technology and Science* 2(9), 1626-1628.

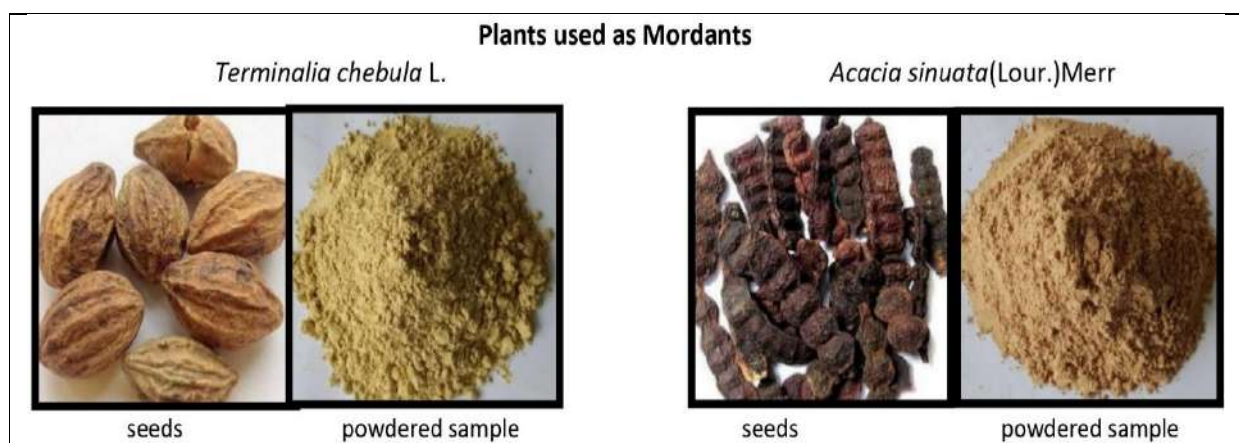


Fig. 1- Plants selected for mordant preparation

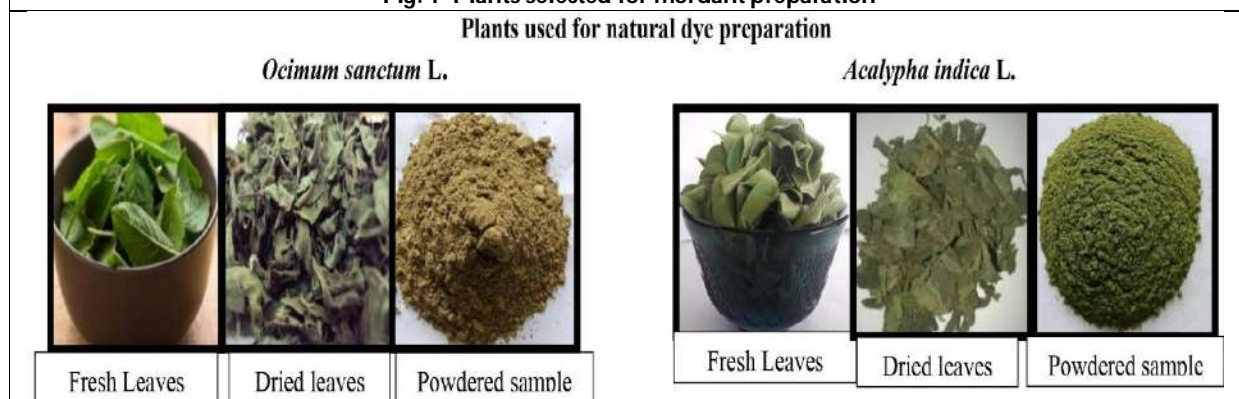


Fig. 2- Selected plants for Natural dye preparation





A Study on Antiplatelet Drug Utilization and Effectiveness of Mono and Dual Therapy in Tertiary Care Hospital

Ramya Balaprabha^{1*}, Sunil Kumar Behera², Vamshi Krishna Kandaturi², Shagupta Shalu² and T.Rama Rao³

¹Assitant Professor, CMR College of Pharmacy, Medchal, Telangana, Hyderabad, India.

²Pharm.D Intern, CMR College of Pharmacy, Medchal, Telangana, Hyderabad, India.

³Professor and Principal of CMR College of Pharmacy, Medchal, Telangana, Hyderabad, India.

Received: 13 Feb 2023

Revised: 10 Apr 2023

Accepted: 15 May 2023

*Address for Correspondence

Ramya Balaprabha

Assitant Professor,
CMR College of Pharmacy,
Medchal, Telangana,
Hyderabad, India.
Email: ramyapharmd66@gmail.com



This is an Open Access Journal / article distributed under the terms of the **Creative Commons Attribution License (CC BY-NC-ND 3.0)** which permits unrestricted use, distribution, and reproduction in any medium, provided the original work is properly cited. All rights reserved.

ABSTRACT

Antiplatelet agents reduce platelet aggregation and avoid the formation of the platelet plug. The objective of the study was to evaluate the effectiveness of the anti-platelet drug in various age groups, sex, and different social habit condition, identify the anti-platelet medication use and identify the most effective antiplatelet drug in various diseases conditions like ischemic stroke, cardiovascular disease, and other diseases. 150 patients from the Gandhi medicine department were included in this prospective observational study conducted for six months. A total of 150 cases were collected. In this, 61-70 and 71-80 age groups, patients have shown more usage of antiplatelet drugs. Out of 150 cases, female patients 66 (44%), and male patients 84 (56%). in this study, more antiplatelet therapy was used in Ischemic stroke at 36.67%. maximum number of diseases was found to be Ischemic stroke 55 (36.67%), The most commonly prescribed monotherapy antiplatelet was aspirin and dual therapy aspirin and Clopidogrel were prescribed. The male patients received more both mono and dual antiplatelet therapy as compared to female patients. Patients with both alcohol consumption and smoking habits were receive more anti-platelet therapy. According to our findings, monotherapy of aspirin was found to be the most effective treatment, followed by dual therapy of aspirin and Clopidogrel. Patients with social habits such as alcohol consumption and smoking were found to require anti-platelet therapy more than normal people.



**Ramya Balaprabha et al.,**

Timely treatment and disease counseling, as well as medication, are critical parameters for improved patient care, and disease, for better patient care.

Keywords: Antiplatelet agents, mono therapy, dual therapy, aspirin, Clopidogrel

INTRODUCTION TO ANTI-PLATELET

Anti-platelet drugs inhibit platelet accumulation and prevent platelet plug formation. The Platelet plug structures close to vascular injury to quit draining which can likewise cause neurotic atherosclerosis and apoplexy [1]. Anti-platelets are the most effective medication in blood clotting and they are known as blood thinners [2]. Anti-platelet drugs prevent the formation of secondary messenger (Cox-1 inhibitor), by interacting with intracellular signaling pathways (PDE inhibitor and PG12 analogs) and blocking membrane receptor (P2Y12 receptor antagonist and the PARI antagonist) or through inhibiting platelet aggregation (GPIIb/IIIb inhibitor) [3]. Antiplatelet agents reduced mortality and morbidity in cardiovascular disease, cerebrovascular disease, Angina (chest pain), stroke, and peripheral arterial disease [4]. Anti-platelet drugs have been shown to contribute to an increase risk of death and increase utilization of unscheduled care.

Drug Utilization and Evaluation

A drug utilization evaluation (DUE) program is defined as a structured, authorized ongoing system for improvement in the standards of drug use in healthcare [5]. According to the world health organization (WHO), DUE is a systematic program of evaluating the medicine that helps in ensuring appropriate medication use. If therapy is found to be inappropriate, interventions are necessary to optimize the therapy [6]. DUR is applicable in various settings like the hospital, other health facilities, and also community practice environments [7]. Drug utilization studies are investigative tools for determining the role of the drug in therapeutic efficacy, cost-effectiveness, and minimization of adverse effects [8]. Recently inappropriate drug use is found common and received the support of numerous studies in research to determine the safety and also the efficacy of drug use [9]. Research in drug utilization helps in managing specific drug problems and also evaluating the appropriateness of drug treatment [10].

OBJECTIVES

1. To identify the anti-platelet medication usage.
2. Effectiveness of single-agent vs dual-agent anti-platelet medication in ischemic stroke, cardiovascular disease and other diseases.
3. Effectiveness of anti-platelet drug in various age groups, sex, and co-morbidity condition.
4. To know the most common anti-platelet drug used for monotherapy and dual therapy.

METHODOLOGY

A prospective observational study was conducted by CMR College of pharmacy in association with Gandhi medical college, Secunderabad. In this study, we enrolled 150 subjects, which included 84 male patients and 66 female patients who were treated with antiplatelet therapy in the general medicine department. This study was conducted for six months, from Oct 2021 to March 2022. We obtained relevant information necessary for our project and recorded it in the patient profile forms. Then we reviewed individual case sheets and observed the frequency of antiplatelet prescriptions in the general medicine department and analyzed them as a control measure.



**Inclusion Criteria**

1. In patients of the General medicine ward.
2. Patients who are able to cooperate.
3. Patients aged above 10 years are collected.

Exclusion Criteria

Patients below 10 years of age, pregnant women and lactating women are excluded from the study. A retrospective study was conducted by CMR college of Pharmacy in association with department of General Medicine in Gandhi Medical College, Secunderabad. The study was conducted over a period of 6 months from Oct 2021 to March 2022. The databases were collected from General medicine department on daily basis after getting approval from the institutional ethics committee. Data of patients matching inclusion criteria were recorded.

RESULTS

In our study, the utilization and efficacy of anti-platelet medications were examined in a total of 150 patients who had been prescribed them based on inclusion and exclusion criteria. The male was prescribed more antiplatelet therapy than female patients shown in table 1. The majority of the patients 23.34% were 61-80 years of age shown in table 2. 55(36.67%) ischemic stroke patients took antiplatelet drugs shown in table 3. Aspirin was the most prescribed monotherapy antiplatelet drug shown in table 4. Aspirin + clopidogrel was the most prescribed dual therapy antiplatelet agent 13.33% shown in table 5. Aspirin was the most prescribed monotherapy drug highest to the patient with ischemic stroke shown in table 6. Aspirin with clopidogrel dual therapy was given more in ischemic stroke shown in table 7. Monotherapy antiplatelet is the most widely used shown in table 8. Male patients were prescribed the highest amount of monotherapy antiplatelet drug shown in table 9. Male patients were prescribed the highest amount of dual antiplatelet drug shown in table 10. 36% of patients both alcoholic and smokers were prescribed antiplatelet drugs shown in table 11.

Out of 150 patients, males were more prescribed anti-platelet therapy than females which constitute about 84 (56%) and 66 (44%). In the age group of 10-30years, we found 5 (3.33%) patients, followed by 10 (6.6%) patients at 31-40years of age, 20 (13.33%) patients at 41-50years, 25 (16.66%) patients found at 51-60years, 35 (23.34%) patients in 61-70years, 35 (23.34%) patients in 71-80years, 10 (6.67%) patients in 81-90years and 10 (6.67%) patients in 91-100 years of age used anti-platelet therapy. We found about 55 (36.67%) ischemic stroke patients took antiplatelet drugs, 25 (16.67%) patients of Altered Sensorium, ADHF patients about 23 (15.33%), then 15 (10%) Hemiparesis patients, 10 (6.66%) DCMP patients, and 22 (14.67%) MI patients have taken antiplatelet drug therapy. In our study we found that aspirin was the most used anti-platelet agent which was prescribed for 50 (33.33%) of the study population, then Clopidogrel was prescribed for 20(13.33%) of the population, and atorvastatin was prescribed for 20 (13.33%) of the study population. In our study, we found that Aspirin + clopidogrel was the most used dual anti-platelet therapy which was prescribed for about 30 (20%) of the total study population. The drug aspirin was prescribed more in monotherapy, in which it was given highest to the patients with ischemic stroke 19 (38%) followed by altered Sensorium 10(20%) and 8(16%) acute decompensated heart failure. The combination drug of aspirin with clopidogrel was prescribed more in dual therapy, in which it was given highest to the patients with ischemic stroke 12(40%) followed by altered Sensorium 7 (23.33%) and acute decompensated heart failure 6(20%). In our study, we found that 90(60%) patients were given monotherapy and 60(40%) patients were given dual therapy of the anti-platelet drug. In our study, we found that 50(55.55%) male patients and 40 (44.45%) female patients were prescribed monotherapy of anti-platelet drugs. In our study, we found that 35 (58.34%) male patients and 25 (41.66%) females were prescribed dual antiplatelet therapy.

In our study 35(23.33%) patients were found to be alcoholic, 30 (20%) patients were smokers, 54 (36%) were found to be both alcoholic & smokers and 31(20.66%) patients were both no smokers & alcoholic.



**Ramya Balaprabha et al.,**

DISCUSSION

Antiplatelets are most widely used in Acute coronary disease, ischemic stroke, coronary angioplasty, Atrioventricular valve with warfarin, peripheral arterial disease, Autism spectrum disorder for at least six months, angina pectoris, Preventing colorectal cancer, Mucocutaneous lymph node syndrome, arthritic disorder, Post heart bypass surgery, prevention of ischemic heart disease, Acute pericarditis, Atrial fibrillation, etc [11]. An observational study of six months duration was conducted at a tertiary care hospital in Secunderabad. The study was conducted to evaluate the drug utilization and effectiveness of mono and dual antiplatelet therapy. In the six-month study period, anti-platelets were most commonly prescribed for treatment as well as prophylaxis mainly on the general medicine ward. During this period 150 patients were administered different antiplatelets for many indications with diagnoses varied from Ischemic stroke, Altered Sensorium, Acute decompensated heart failure, Myocardial infarction, and Hemiparesis. In our study population of 150 patients, 84 (56%) were male and 66 (44%) were female patients prescribed antiplatelet therapy. Our study found that males are prescribed antiplatelet therapy more often than females. The study highlights the age group of 61-80 years showing the highest number of cases that received anti-platelet therapy. Kamarova M et al 2022 conducted a study and found that aspirin and clopidogrel, two antiplatelet medications, were more effective in stroke patients [11]. In our research, we also found out that ischemic stroke patients (36.67%) received more antiplatelet therapy followed by altered Sensorium (16.67%) and then acute decompensated heart failure (15.33%). Aspirin (33.33%) was found to be the most prescribed antiplatelet agent in monotherapy, followed by clopidogrel and atorvastatin. This study shows that the anti-platelet agents which are prescribed highest in dual therapy were found to be aspirin along with clopidogrel (20%), which is then followed by clopidogrel with atorvastatin. In our study, we found that patients received more monotherapy, 90 (60%) than dual therapy, 40%. In monotherapy, males were found to be prescribed more anti-platelet agents 50(55.55%) than females. In dual therapy, males 35 (58.34%) were prescribed more anti-platelet therapy compared to females. This study shows that the drug aspirin was prescribed more in monotherapy, in which it was given highest to the patients with ischemic stroke i.e (38%) followed by altered Sensorium (20%) and acute decompensated heart failure (16%). The combination drug of aspirin with clopidogrel was prescribed more in dual therapy, in which it was given highest to the patients with ischemic stroke followed by altered Sensorium and acute decompensated heart failure, and the same was also reported by Youwen Yang et al (2021) [12]. Our study shows that the social habits of both alcohol consumption and smoking were more prone to receive anti-platelet therapy dominantly than patients with only alcohol consumption or only smoking habit.

CONCLUSION

We have demonstrated from our study that monotherapy with aspirin was the most effective treatment, followed by dual therapy with aspirin and clopidogrel in cases of ischemic stroke, altered sensorium, acute heart failure, hemiparesis, dilated cardiomyopathy, and myocardial infarction. Anti-platelet therapy was required more frequently among patients with social habits like alcohol consumption and smoking. Furthermore, we found the ischemic stroke patient required more mono and dual antiplatelet therapy. As opposed to dual antiplatelet therapy, monotherapy antiplatelet drugs showed the best results.

ACKNOWLEDGEMENT

We sincerely thank CMR College of Pharmacy, Management, Principal, and staff for supporting us and helping us in publishing this project work. We express our profound gratitude to all doctors of the department of general medicine for providing their unflinching support during the collection of case and clarified various doubts regarding the cases. We would like to express our special thanks to our guidance Dr. Ramya Balaprabha for the time and effort, she





Ramya Balaprabha et al.,

provided throughout the project work. Your useful advice and suggestions were helping us during the project's completion. In this aspect, we would be externally grateful to you.

REFERENCES

1. Pramodh B, Kumar MA, Shanmugasundaram P. A prospective observational study on drug use evaluation of antiplatelet agents in tertiary care hospital. *Res J Pharm Technol.* 2017;10(12):4328-32.
2. Rajesh Hadia, Priyanshi Shah, Johny Mariam John et al. Antiplatelet Utilization Pattern and Assessment of Patients Specific Drug use Problem among Cardiac patient. *Journal of Pharmaceutical Research International.* 26 Jun 2021; 33(33B):6-12
3. Georges Jourdi, Marie Lordkipanidze, Aurelien Philippe et al. Current and Novel Antiplatelet Therapies for the Treatment of Cardiovascular Diseases. *International journal of Molecular Science.* 2021, 22,13079.
4. Pultar J, Wadowski PP, Panzer S, Gremmel T. Oral antiplatelet agents in cardiovascular disease. *Vasa.* 2019 Jul 1; 48(4):291–302.
5. P.Doherty, S. Kirska, S. Chao, David Maxwell, et al. Shpa standards of practice for drug use evaluation in Australian hospitals: shpa committee of specialty practice in drug use evaluation. *J of pharmacy practice and Research.* 2004 Sep; 43(3):220-223.
6. Management science for Health and World Health Organisation. Drug and Therapeutic Committee Training course: session 11. Drug use Evaluation (Participants Guide).
7. The Society of Hospital Pharmacists of Australia. Australian Drug Usage Evaluation Starter Kit, 1998.
8. Abrams WB (Ed.). Workshop on drug utilization review. *Clinical Pharmacology and Therapeutics* 50 (5 part-2 suppl.): 593-640, 1991.
9. Taskeen M, Anitha N, Ali SR, Bharath R, Khan AB. A study on rational drug prescribing pattern in geriatric patients in Hyderabad metropolitan. *J Drug Delivery* 2012; 2:109-13.
10. Duker MNG, World Health O. Drug utilization studies: methods and uses. World Health Organization, Regional Office for Europe Copenhagen; 1993.
11. Kamarova M, Baig S, Patel H, Monks K, Wasay M, Ali A, Redgrave J, Majid A, Bell SM. Antiplatelet Use in Ischemic Stroke. *Ann Pharmacother.* 2022 Oct;56(10):1159-1173. doi: 10.1177/10600280211073009. Epub 2022 Jan 29. PMID: 35094598; PMCID: PMC9393649.
12. Yang Y, Huang Z, Zhang X. Efficacy and safety of clopidogrel and/or aspirin for ischemic stroke/transient ischemic attack: An overview of systematic reviews and meta-analysis. *Medicine (Baltimore).* 2021 Dec 17; 100(50):e27804.

Table 1: Gender Wise Distribution

SL.NO.	Years of age	Number of cases	Percentage %
1	10-30	5	3.33%
2	31-40	10	6.66%
3	41-50	20	13.33%
4	51-60	25	16.66%
5	61-70	35	23.34%
6	71-80	35	23.34%
7	81-90	10	6.67%
8	91-100	10	6.67%





Ramya Balaprabha et al.,

Table 2: Age based Distribution

SL.NO.	Gender	No. of Cases	Percentage%
1	Male	84	56%
2	Female	66	44%
	Total	150	100 %

Table 3: Diseases Wise Dispersion

SI.No	Diseases	No. of Patients	Percentage %
1	Ischemic Stroke	55	36.67%
2	Altered Sensorium	25	16.67%
3	ADHF	23	15.33%
4	Hemiparesis	15	10%
5	DCMP	10	6.66%
6	MI	22	14.67%
	Total	150	100%

Table 4: Most Prescribed Monotherapy Anti-Platelet Agents

SI.No	Anti-platelet Agent	Frequency	Percentage (%)
1	Aspirin	50	33.33%
2	Clopidogrel	20	13.33%
3	Atorvastatin	20	13.33%

Table 5: Most Prescribed Dual Therapy Antiplatelet Agents

SL.No	Anti-platelet Agent	Frequency	Percentage %
1	Clopidogrel + Atorvastatin	20	13.33%
2	Aspirin + clopidogrel	30	20%
3	Atorvastatin + Aspirin	10	6.66%

Table 6: Monotherapy of Aspirin Distribution

Sl.No	Diseases	Comorbidity condition			Total	Percentage
		DM	HTN	BOTH		
1	Ischemic Stroke	7	6	6	19	38%
2	Altered Sensorium	4	3	3	10	20%
3	ADHF	5	1	2	8	16%
4	MI	1	3	0	4	8%
5	Hemiparesis	2	1	1	4	8%
6	DCMP	2	2	1	5	10%
	TOTAL	21	16	13	50	100%





Ramya Balaprabha et al.,

Table 7: Dualtherapy of Aspirin with Clopidogrel Distribution

SL.NO	DISEASES	COMORBIDITY CONDITION			TOTAL	PERCENTAGE
		DM	HTN	BOTH		
1	Ischemic Stroke	5	4	3	12	40%
2	Altered Sensorium	4	2	1	7	23.33%
3	ADHF	3	2	1	6	20%
4	MI	1	2	1	4	13.33%
5	Hemiparesis	0	1	0	1	3.33%
	TOTAL	13	11	6	30	100%

Table 8: Antiplatelet Drug Therapy

SL.No	Therapy	Frequency	Percentage%
1	Monotherapy	90	60%
2	Dual Therapy	60	40%
3	Total	150	100%

Table 9: Monotherapy Gender Wise Distribution

SL.No	Gender	frequency	percentage
1	Male	50	55.55%
2	Female	40	44.45%
3	Total	90	100%

Table 10: Dual Therapy Gender Wise Distribution

SL.No	Gender	Frequency	Percentage
1	Male	35	58.34
2	Female	25	41.66
3	Total	60	100%

Figure 11: Dual Therapy Gender Wise Distribution

SL.No	Social Habits	Male	Female	Total	Percentage
1	Alcoholic	25	10	35	23.33%
2	smoker	20	10	30	20%
3	Both alcoholic and smoker	39	15	54	36%
4	Non alcoholic and non smoker	0	31	31	20.66%





Ramya Balaprabha et al.,

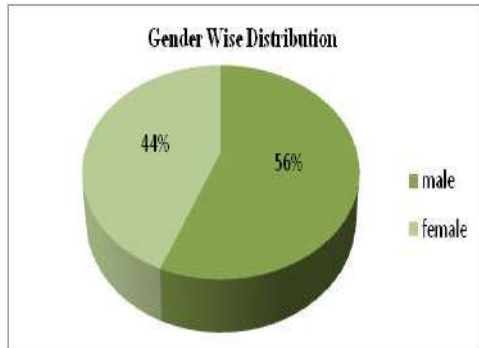


Figure 1: Gender Wise Distribution

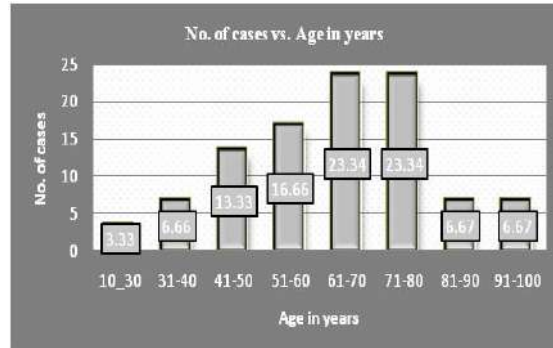


Figure 2: Age Based Distribution

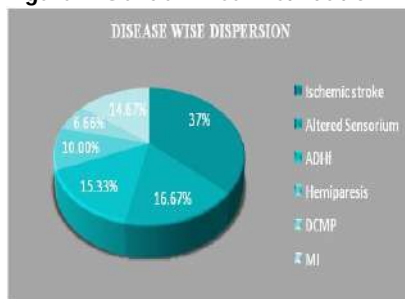


Figure 3: Disease Wise Dispersion

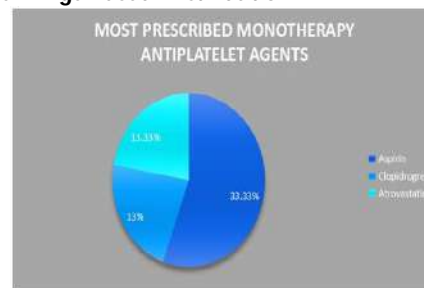


Figure 4: Most Prescribed Monotherapy Anti-Platelet Agents

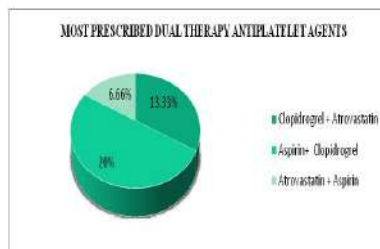


Figure 5: Most Prescribed Dual Therapy Antiplatelet Agents

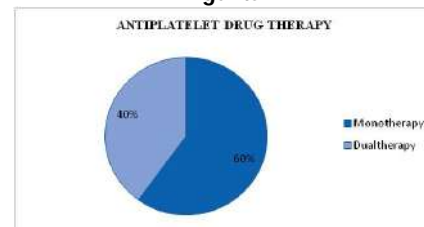


Figure 8: Antiplatelet Drug Therapy

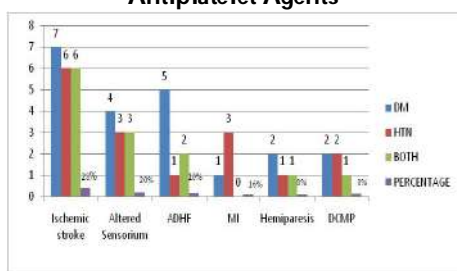


Figure 6: Monotherapy of Aspirin Distribution

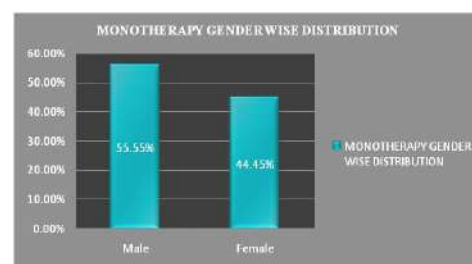


Figure 9: Monotherapy Gender Wise Distribu





Ramya Balaprabha et al.,

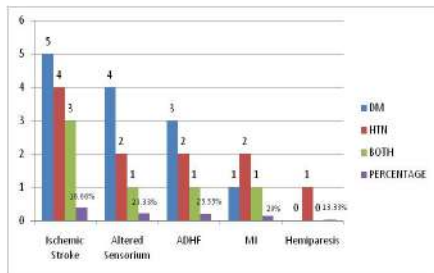


Figure 7: Dual Therapy of Aspirin with Clopidogrel Distribution



Figure 10: Dual Therapy Gender Wise Distribution

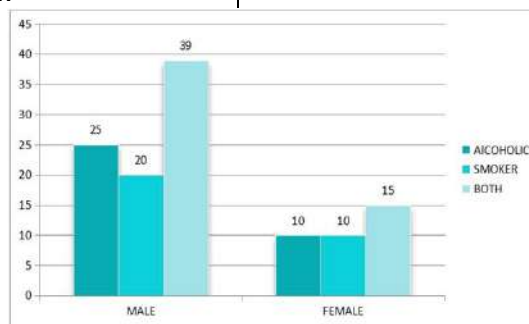


Figure 11: Distribution of Patients According to Their Social Habits





Active Polymers in Confinement

Nirmalendu Ganai*

Assistant Professor, Department of Physics, Nabadwip Vidyasagar College, Nabadwip, Nadia - 741302, West Bengal, India.

Received: 24 Feb 2023

Revised: 24 Apr 2023

Accepted: 27 May 2023

*Address for Correspondence

Nirmalendu Ganai

Assistant Professor,
Department of Physics,
Nabadwip Vidyasagar College,
Nabadwip, Nadia - 741302,
West Bengal, India.
E. Mail: nirmalendu.phy@gmail.com



This is an Open Access Journal / article distributed under the terms of the **Creative Commons Attribution License** (CC BY-NC-ND 3.0) which permits unrestricted use, distribution, and reproduction in any medium, provided the original work is properly cited. All rights reserved.

ABSTRACT

Individual chromosomes in mammalian cell nuclei between cell divisions are distributed non-randomly with respect to the nuclear centre. Their spatial organization has been argued to be a consequence of inhomogeneous transcription-linked activity, of a magnitude set by the gene densities of individual chromosomes, coupled to the confinement provided by the nuclear envelope. Simulations of model confined chromosomes support this hypothesis, but yield little intuition for the physical mechanisms underlying such segregation. To address this, we study a simplified version of our model for chromosome positioning, examining the systematics of spatial segregation in a two-component mixture of active and passive mono-disperse polymers in a confined spherical geometry. The segregation of active and passive components is clearly manifested in the centre of mass distribution. When the lengths of individual polymers are varied, keeping the overall density fixed, active and passive components are found to segregate even when the polymers are reduced in size to individual dimers. However, a mixture of active and passive monomers does not show segregation. Surprisingly, these results can be largely reproduced in *equilibrium* (i.e., purely passive) mixtures, where the active polymers are replaced by passive ones, provided we ensure that the radius of gyration we assign them is appropriate to the active component. This suggests that activity-based segregation may at least partly be understood as an entropic effect. We provide simple physical arguments justifying these results.

Keywords: active polymer; out of equilibrium; computer simulations





Nirmalendu Ganai

INTRODUCTION

Understanding the large-scale architecture of the eukaryotic cell nucleus may help us better address the influence of epigenetics, *i.e.*, transcriptional control through effects not contained in DNA sequence, on transcription programs specific to each type of cell. Chromosomes in eukaryotic cell nuclei within interphase are organised into largely non-overlapping regions, termed “chromosome territories”[1-7]. Such territories are themselves positioned probabilistically, but in a non-random manner, with chromosomes often organized radially by gene density[8]. Thus, the gene-rich chromosome 19, which contains a large number of housekeeping genes, tends to be centrally located, in contrast to the gene-poor but similarly sized chromosome 18, which is more peripheral in its positioning[9,10]. Since regions proximal to the nuclear envelope constitute a largely repressive environment, a minimal level of epigenetic control over transcription programs may simply derive from coupling between cell-type-specific transcription levels of individual chromosomes with their radial locations. Alternatively, chromosome positioning based on their size has also been suggested with the centre of mass of larger chromosome located more peripherally than shorter one[11-13] and some methods have also been developed to reproduce the positioning scheme[14-16].

Being able to quantitatively predict, from first-principles, the probabilistic “positioning code” appropriate to specific cell types appears to be a well-defined goal. In prior work, we proposed that non-random chromosome positioning was a natural consequence of combining non-equilibrium activity levels associated with individual chromosomes, together with overall confinement[15-18]. In doing so, we were largely motivated by numerical observations of segregation in mixtures of active and passive components of self-propelled particles. We were also guided by *in vivo* experiments[19], in both bacteria and eukaryotes, which indicated that local chromatin fluctuations derived overwhelmingly from non-equilibrium (ATP-dependent) effects as opposed to thermal ones. We noted that these and many similar results appeared to have been largely ignored in all previous work on higher-order chromatin structure, which either tended to proceed along the lines of studying the equilibrium problem or studied very specific model polymer systems evolving towards thermal equilibrium[20-25], such as the fractal globule state.

Although there is no natural analog of “self-propulsion” in the chromatin context, segregation based on activity appears to be generic in non-equilibrium contexts, only requiring that activity is inhomogeneous across individual components. Accordingly, in a standard coarse-grained polymer model (the SCD model[26]) for individual chromosomes, we assigned each monomer a level of activity that reflected its gene density[17]. To implement these ideas quantitatively, we argued that local transcription levels reflecting levels of activity should be directly related to gene densities, provided we averaged over a sufficiently large genomic region. Our choice of coarse-graining over 1Mb segments along the genome was consistent with the observation that genomic segments at the 1Mb scale were likely to be the fundamental building blocks of chromosome territories. Our model predictions[17] agreed very well with the experimental data. We showed that chromosomes were positioned radially according to their activity (and therefore gene density) levels, with the more active, and thus more gene dense, chromosomes positioned towards the nuclear centre. Our predictions for the radial distribution of gene-densities for chromosome pairs 18/19 as well as 12/20 agreed closely with data from 3-d FISH experiments. Further, we showed that compactness of individual chromosomes, as enforced *via* a standard random loop model for chromosomes, combined with activity-based segregation to yield a territorial organisation of chromosomes. Thus, the combination of inhomogeneous activity and confinement, as conjectured, provides a simple way of reproducing consensus features of large-scale nuclear organisation.

One drawback of very system-specific biophysical models is that it is hard to gain intuition for results which are not tied to the specific system but whose underpinnings might be more general. For example, our biophysical model for chromosomes confined to the nucleus considered 23 chromosomes (and their partners, since there are 23 pairs of chromosomes in each non-sex cell), each of a different length. Our assignment of activity to each monomer in each chromosome directly reflected the number of genes contained in each 1 Mb segment of the chromosome. Our model thus, of necessity, had to account for both substantial polydispersity as well as activity which differed from





Nirmalendu Ganai

monomer to monomer on the same chromosome, making it hard to isolate those factors responsible for activity-based segregation. Accordingly, to clarify the origins of segregation in our model system, we decided to explore simpler variants of our model in which some of these complexities could be reduced or eliminated. Our hope was that a simpler physical understanding might result from doing so. This simpler model, and the results it yields, are described in this paper. First, to eliminate possible complications due to polydispersity, we consider only mono disperse polymers. Second, we take the activity to be uniform within each polymer, (although we could allow activity to vary between different polymers), eliminating complications due to inhomogeneous activity. A final simplification comes from considering a 50:50 mixture of uniformly active and passive polymers. We confine these polymers (a total of 512 monomers, split equally among an even number of model polymers all of the same size) to a spherical geometry, ensuring that the radius of the sphere was such that the density reproduced the density in our simulations of chromosomes. We subdivide these monomers among polymers in various ways, ensuring their monodispersity and the 50-50 split of active and passive ones. Thus, we considered 2 polymers of size 256, 4 of size 128 etc, down to 256 dimers divided equally between active and inactive ones.

We use standard over-damped, Brownian dynamics simulations for our model confined polymers, measuring a variety of quantities for the active and passive components individually, including the distribution of polymer density, the distribution of polymer centres of mass, the radii of gyration, and polymer conformation. At the largest scales, active and passive polymers differ in their radius of gyration, with the active ones begin stretched more than their passive counterparts. As we describe below, we are able to recreate these patterns of active-passive segregation[27-31] in a purely equilibrium two-component system of polymers, by imposing the following constraint: we choose the radius of gyration of one component to equal the radius of gyration we calculated for the active fraction of polymers in the non-equilibrium case. We reasoned that the increased size of one component vis a vis the other, together with confinement, might lead to segregation as an entropic consequence. Our results appear consistent with this hypothesis.

MATERIALS AND METHODS

As described above, we consider a fixed total number of monomers in the system (512), initially considering 16 polymers consisting of 32 monomers each. (In the nucleus, there are 23 pairs of chromosomes, each differing in size as well as in gene content.) We fix the size of the simulated system by choosing the radius of the confining sphere R_0 so as to keep the density same as in our simulations of chromosomes. Neighbouring monomers belonging to the same polymer are connected by springs, which maintain their connectivity. The spring interaction has the form[17],

$$V_{neighbour\ monomers}(r_i, r_{i+1}) = \frac{1}{2}k(|r_i - r_{i+1}|)^2 \quad (1)$$

where, k is the spring constant.

In addition, each monomer interacts with other monomers through the Gaussian core potential, commonly used in representations of polymer brushes[32]. (In our earlier simulations, this potential represented the effects of coarse-graining microscopic chromatin configurations to the 1 Mb level.) The Gaussian core potential takes the form:

$$V_{monomer-monomer}(r_i, r_j) = V_0 \exp(-|r_i - r_j|^2 / \sigma^2) \quad (2)$$

where its strength is specified by the constant V_0 and the effective range through the parameter σ . Thus, we consider self-repelling, but not self-avoiding polymers, a choice rationalised in Ref.[17] as arising from the presence of a large number of DNA topology modulating enzymes present in the interphase nucleus. V_0 is the pair potential at zero separation between the two monomers and is chosen, as is standard for polymer brushes, to be of the order of $k_B T_{eq}$ where k_B is the Boltzmann constant and T_{eq} the equilibrium temperature, which we scale to unity. The interaction of





Nirmalendu Ganai

each monomer with the confining sphere is chosen such that it vanishes when the monomer is inside the sphere, while taking the form[17]

$$V_{wall}(r_i) = \frac{V_{conf}}{a^5} (|r_i| - R_0)^5, \quad |r_i| > R_0, \quad (3)$$

outside it. Thus, the confinement is not a “hard” confinement, but a soft one, reflecting the properties of the dense lamina network that lines the interior of the nuclear envelope. We choose $a = 0.168\sigma$ is the scale factor and $V_{conf} = k_B T_{eq}$, ensuring that all polymers are reasonably tightly confined within the sphere. We begin our simulations from random configurations of monomers across the volume of the confining sphere, but check that the same final steady-state distributions are obtained irrespective of starting configurations. We employ a standard over-damped Brownian dynamics algorithm, *via* an Euler discretization of the equation

$$\zeta \frac{dr_i}{dt} = F_i + \eta_i \quad (4)$$

where ζ represents the drag coefficient, r_i is the position of the i^{th} monomer, F_i includes all non-stochastic forces acting on the monomer i.e., forces originating from other monomers and from the wall and η_i is the stochastic forces due to the thermal fluctuations. The noise is zero-mean and Gaussian distributed, following standard procedures in Brownian dynamics. It is of the form

$$\langle \eta_i(t) \eta_j(t') \rangle = 2k_B T_i \zeta \delta_{ij} \delta(t - t') \quad (5)$$

In Eq.5, T_i represents the effective temperature associated with each monomer. In thermal equilibrium, $T_i = T_{eq}$ for all monomers, ensuring the fluctuation-dissipation relation: $D = k_B T_{eq} / \zeta$. Out of equilibrium, this relation no longer holds, and we may consider an effective temperature which depends on the monomer index and the polymer label. In our simulations of this simplified model, we choose all passive polymers to have an effective temperature T_{eq} , while varying the temperature associated with active monomers $T_{act} = \alpha T_{eq}$, with α a scale factor varying between 1 and 50. We have also tested a variant of this system in which we study a two-component system, *in equilibrium*, but in which the two components have different radii of gyration. This simulates one effect of activity - it stretches out our active polymers relative to our passive ones - and we wished to see whether a purely equilibrium system would also display similar behaviour.

Units

Our units of time are chosen in such a way that the value of $\zeta = 1.0$. We measure energies in units of $k_B T_{eq}$, taking $V_0 = 1.5k_B T_{eq}$. All length scales are set in units of σ . The radius of the confining sphere is taken to be $R_0 \simeq 8.84\sigma$ and the spring constant is measured in units of $k = 6k_B T_{eq} / l_0^2$, where $l_0 = 3.6\sigma$. When we allow this spring constant, in the fully equilibrium case, to vary across one sub-component, thus reproducing the radius of gyration in the active case, we choose $k_s = 0.1k$. We choose a time step $dt = 0.01$, testing that it leads to stable results. These parameters, apart from the choice of R_0 , follow the scalings of Ref.[17].

Analysis

Our simulations are typically run for 2.4×10^6 time steps. We do not record data for typically 0.4×10^6 time steps from the initial state, to ensure that the steady state is reached. All data are averaged over 10^4 independent configurations, taken at intervals of 2.0×10^3 time steps. We confirmed that the same steady state was obtained irrespective of initial configuration. Since the probability of finding the centre of mass of a polymer at a radial distance r from the centre of the spherical confinement is a function only of the modulus of r , i.e., $|r| \equiv r$, we compute the probability of finding this centre of mass within a fixed radial distance from the origin. We calculate a centre of mass distribution function $P_{CM}^i(r)$, equal to the probability (density) for finding the centre of mass of i^{th} polymer within a radial shell of thickness dr at a radial distance r from the centre of the sphere. This is normalized, as usual, as





Nirmalendu Ganai

$$\int dr P_{CM}^i(r) = 1 \quad (6)$$

We also measure the radius of gyration of each polymer chain of N monomers through

$$R_g^2 = \frac{1}{N} \sum_{i=1}^N \langle (R_i - R_{CM})^2 \rangle \quad (7)$$

where R_i represents the position of i^{th} monomer of a polymer and R_{CM} is the centre of mass of that polymer, given by

$$R_{CM} = \frac{1}{N} \sum_{i=1}^N R_i \quad (8)$$

The radius of gyration of each polymer is similarly averaged over 10^4 independent configurations, and then further averaged over all polymers of the same type (active/inactive).

RESULTS AND DISCUSSION

Two-Component Active-Passive Mixtures

Fig.2 exhibits plots of the centre of mass distribution $P_{CM}(r)$ of active (blue) and passive (red) polymers as a function of radial distance r . These distributions are all normalized to unity upon integration over r . In the plots shown, the temperatures assigned to the active component are varied along columns (i)-(v), for which $T_a = 1.0, 2.0, 10.0, 20.0$ & $50.0 T_{eq}$ respectively. The rows (a)-(e) show our results for varying $N = 32, 16, 8, 4$ & 2 . The total number of monomers is fixed at 512. All systems are 50:50 mixtures. Fig.2 shows that the peaks of the centre of mass distribution of active and inactive polymers, *i.e.*, the mode of the distributions, are at different positions. This reflects the spatial segregation of active and passive components with respect to their centres of mass. Our results indicate that the peak position of $P_{CM}(r)$ is more interior than the inactive one. From Fig.2, we see that spatial segregation survives to the level of dimers (Fig.2(e)(iii), (iv)&(v)) but is reduced substantially as the temperature of active polymers is decreased (see Fig.2(e)(ii)). Decreasing the number of monomers in each chain, *i.e.*, increasing the number of polymers contained within the sphere, the distribution $P_{CM}(r)$ becomes more broader while still manifesting segregation.

Fig.3 shows the density distribution of active and inactive polymers, as a function of radial distance r . In the chromosome case, this is the analog of DNA density associated with specific chromosomes, a quantity reflecting the disposition of the polymer chain about its centre of mass. Note that, as in Fig.2, there is a segregation in density between the active and passive cases, although this is less evident in the densities than in the centres of mass. Structurally, how do active polymers differ from passive ones? We extracted the radius of gyration for active and passive components, showing R_g for the active component in Fig.4(a). The radius of gyration increases with the active temperature at the same fixed number of monomers, simply reflecting the increase in the average bond length. Fig.4(a) also reflects the fact that radius of gyration increases as monomer numbers are increased. Scaling arguments suggest that the data should collapse when plotted against the combination NT which is verified in Fig.4(b).

Passive Two-Component Mixtures with Different Radii of Gyration

The difference between the radius of gyration of active and passive polymers comes from the fact that activity, which functions like an effective temperature seen by each monomer differs between active and passive polymers. We asked whether we could reproduce our results for activity-based segregation from considering a two-component system in which one component had a large radius of gyration than the other. We can vary the radius of gyration by changing the spring constant for springs connecting monomers. Using this, we study an equilibrium, two-component equal mixture of two polymer species, each with a different radius of gyration. We choose the radius of gyration of one component so as to reproduce our results for the active case, while retaining the other the same.



**Nirmalendu Ganai**

The first row of Fig.5 exhibits the effects of varying the spring constant of one species, keeping the spring strength of the other fixed ($k_s = 0.1 k$; see Units section). We observe that the spatial segregation becomes more stronger as we increase the spring strength of the harder polymer. Segregation, quantified through the separation of the two peaks, decreases as the spring constant of the softer polymer is increased while the spring strength of harder polymer is kept constant at $k_h = 100.0 k$. This is also reflected in Fig.8 where the radius of gyration decreases with increasing spring constants. Maximum segregation is seen in Fig.5(a)(v) where $k_s = 0.1 k$ and $k_h = 100.0 k$. For these values of spring constants, the difference between the radius of gyration is also maximal, as confirmed in Fig.8.

CONCLUSION

In this paper, we have shown that activity-based segregation can be reproduced and studied in a simplified model. This model eliminates much of the complexity of an earlier model constructed so as to describe gene-density-based segregation in interphase chromosomes, including eliminating effects due to polydispersity and inhomogeneous activity. This allows us to concentrate on the underlying mechanisms driving such segregation. We found that the radius of gyration of the active polymers exceeded those of the passive ones, implying that one effect of activity was to stretch out configurations of individual active polymers with respect to their passive counterparts. We then simulated 50:50 mixtures of *equilibrium* mono disperse polymers, choosing the spring constant of one component such that it reproduced the radius of gyration corresponding to the active polymers. Unusually, we found that our results for active-passive segregation could be reproduced in that case as shown in Fig.7(a) and Fig.7(b).

Phase separation in two-component equilibrium systems of different sizes is often most simply interpreted in terms of entropic effects. One such effect is the depletion interaction [33-36], operating in a system of smaller sized and larger sized particles, where the tendency of the system to maximise, its overall entropy leads to a segregation of differently sized components, and even crystallisation of one component in the presence of the other [37]. Our results on activity induced positioning of chromosomes may therefore be viewed as a special case of a depletion effect leading to spatial segregation of polymers in confinement. However, the complete picture is much more complicated. Single monomers with a size ratio equal to that of the radii of gyration of the polymers do not segregate (Fig.7(c)), showing that the polymeric nature (non-Rouse models) [38,39] plays a crucial part. Thus, both activity as well as entropic effects may play an important role in inducing segregation.

ACKNOWLEDGEMENT

My sincere thanks to Prof. Gautam I. Menon and Late Prof. Surajit Sengupta for very useful discussion.

ORCID ID:

Nirmalendu Ganai <http://orcid.org/0000-0002-8320-058X>

REFERENCES

1. Cremer, T., Cremer, M.: Chromosome territories. *Cold Spring Harbor perspectives in biology* 2(3), 003889 (2010).
2. Cremer, M., Hase, J.V., Volm, T., Brero, A., Kreth, G., Walter, J., Fischer, C., Solovei, I., Cremer, C., Cremer, T.: Non-random radial higher-order chromatin arrangements in nuclei of diploid human cells. *Chromosome Research* 9(7), 541–567 (2001).
3. Cremer, T., Cremer, C.: Chromosome territories, nuclear architecture and gene regulation in mammalian cells. *Nature Reviews Genetics* 2(4), 292–301 (2001).
4. Tanabe, H., Miller, S., Neusser, M., von Hase, J., Calcagno, E., Cremer, M., Solovei, I., Cremer, C., Cremer, T.: Evolutionary conservation of chromosome territory arrangements in cell nuclei from higher primates. *Proceedings of the National Academy of Sciences* 99(7), 4424–4429 (2002).
5. Meaburn, K.J., Misteli, T.: Chromosome territories. *Nature* 445(7126), 379–381 (2007).



**Nirmalendu Ganai**

6. Cope, N.F., Fraser, P., Eskiw, C.H.: The yin and yang of chromatin spatial organization. *Genome Biology* 11(3), 204 (2010).
7. Mayer, R., Brero, A., von Hase, J., Schroeder, T., Cremer, T., Dietzel, S.: Common themes and cell type specific variations of higher order chromatin arrangements in the mouse. *BMC Cell Biology* 6(1), 44 (2005).
8. Takizawa, T., Meaburn, K.J., Misteli, T.: The Meaning of Gene Positioning (2008).
9. Croft, J.A., Bridger, J.M., Boyle, S., Perry, P., Teague, P., Bickmore, W.A.: Differences in the Localization and Morphology of Chromosomes in the Human Nucleus. *Journal of Cell Biology* 145(6), 1119–1131 (1999).
10. Boyle, S., Gilchrist, S., Bridger, J.M., Mahy, N.L., Ellis, J.A., Bickmore, W.A.: The spatial organization of human chromosomes within the nuclei of normal and emerin-mutant cells. *Human Molecular Genetics* 10(3), 211–220 (2001).
11. Sun, H.B., Shen, J., Yokota, H.: Size-dependent positioning of human chromosomes in interphase nuclei. *Biophysical Journal* 79(1), 184–190 (2000).
12. Bolzer, A., Kreth, G., Solovei, I., Koehler, D., Saracoglu, K., Fauth, C., Müller, S., Eils, R., Cremer, C., Speicher, M.R., Cremer, T.: Three-dimensional maps of all chromosomes in human male fibroblast nuclei and prometaphase rosettes. *PLoS Biology* 3(5), 0826–0842 (2005).
13. Kölbl, A.C., Weigl, D., Mulaw, M., Thormeyer, T., Bohlander, S.K., Cremer, T., Dietzel, S.: The radial nuclear positioning of genes correlates with features of megabase-sized chromatin domains. *Chromosome Research* 20(6), 735–752 (2012).
14. Kalhor, R., Tjong, H., Jayathilaka, N., Alber, F., Chen, L.: Genome architectures revealed by tethered chromosome conformation capture and population-based modeling. *Nature Biotechnology* 30(1), 90–98 (2012).
15. Agrawal, A., Ganai, N., Sengupta, S., Menon, G.I.: Nonequilibrium bio-physical processes influence the large-scale architecture of the cell nucleus. *Biophysical Journal* 118(9), 2229–2244 (2020).
16. Ganai, N.: Size Dependent Chromosome Positioning using Gene-Density-Based Model. *Indian Journal of Natural Sciences* 12(69), 37190–37194 (2021).
17. Ganai, N., Sengupta, S., Menon, G.I.: Chromosome positioning from activity-based segregation. *Nucleic Acids Research* 42(7), 4145–4159 (2014).
18. Agrawal, A., Ganai, N., Sengupta, S., Menon, G.I.: Chromatin as active matter. *Journal of Statistical Mechanics: Theory and Experiment* 2017(1), 014001 (2017).
19. Gowrishankar, K., Ghosh, S., Saha, S., C, R., Mayor, S., Rao, M.: Active remodelling of cortical actin regulates spatiotemporal organization of cell surface molecules. *Cell* 149(6), 1353–1367 (2012).
20. Cook, P.R., Marenduzzo, D.: Entropic organization of interphase chromosomes. *Journal of Cell Biology* 186(6), 825–834 (2009).
21. Marti-Renom, M.A., Mirny, L.A.: Bridging the resolution gap in structural modeling of 3d genome organization. *PLOS Computational Biology* 7(7), 1–6 (2011).
22. Tark-Dame, M., van Driel, R., Heermann, D.W.: Chromatin folding from biology to polymer models and back. *Journal of Cell Science* 124(6), 839–845 (2011).
23. Heermann, D.W., Jerabek, H., Liu, L., Li, Y.: A model for the 3d chromatin architecture of pro and eukaryotes. *Methods* 58(3), 307–314 (2012).
24. Vasquez, P.A., Bloom, K.: Polymer models of interphase chromosomes. *Nucleus* 5(5), 376–390 (2014).
25. Imakaev, M.V., Fudenberg, G., Mirny, L.A.: Modeling chromosomes: Beyond pretty pictures. *FEBS Letters* 589(20, Part A), 3031–3036 (2015).
26. Kreth, G., Finsterle, J., von Hase, J., Cremer, M., Cremer, C.: Radial Arrangement of Chromosome Territories in Human Cell Nuclei: A Computer Model Approach Based on Gene Density Indicates a Probabilistic Global Positioning Code. *Biophysical Journal* 86(5), 2803–2812 (2004).
27. Stenhammar, J., Wittkowski, R., Marenduzzo, D., Cates, M.E.: Activity- induced phase separation and self-assembly in mixtures of active and passive particles. *Physical Review Letters* 114(1), 1–5 (2015).
28. Fily, Y., Marchetti, M.C.: Athermal phase separation of self-propelled particles with no alignment. *Physical Review Letters* 108(23), 235702 (2012).
29. Weber, S.N., Weber, C.A., Frey, E.: Binary Mixtures of Particles with Different Diffusivities Demix. *Physical Review Letters* 116(5) (2016).





Nirmalendu Ganai

30. Smrek, J., Kremer, K.: Small Activity Differences Drive Phase Separation in Active-Passive Polymer Mixtures. *Physical Review Letters* 118(9) (2017).
31. Dolai, P., Simha, A., Mishra, S.: Phase separation in binary mixtures of active and passive particles. *Soft Matter* 14, 6137–6145 (2018).
32. Stillinger, F.H.: Phase transitions in the gaussian core system. *The Journal of Chemical Physics* 65(10), 3968–3974 (1976).
33. Asakura, S., Oosawa, F.: On interaction between two bodies immersed in a solution of macromolecules. *The Journal of Chemical Physics* 22(7), 1255–1256 (1954).
34. Asakura, S., Oosawa, F.: Interaction between particles suspended in solutions of macromolecules. *Journal of Polymer Science* 33(126), 183–192 (1958)
35. Vrij, A.: Polymers at interfaces and the interactions in colloidal dispersions. *Pure and Applied Chemistry* 48(4), 471–483 (1976).
36. Mao, Y., Cates, M.E., Lekkerkerker, H.N.W.: Depletion force in colloidal systems. *Physica A: Statistical Mechanics and its Applications* 222(1), 10–24 (1995).
37. Koenderink, G.H., Vliegthart, G.A., Kluijtmans, S.G.J.M., van Blaaderen, A., Philipse, A.P., Lekkerkerker, H.N.W.: Depletion-induced crystallization in colloidal rodsphere mixtures. *Langmuir* 15(14), 4693–4696 (1999).
38. Doi, M.: *Introduction to Polymer Physics*. Clarendon Press, Oxford (1996).
39. Doi, M., Edwards, S.F.: *The Theory of Polymer Dynamics*. Clarendon Press, Oxford (1986).

TABLE(S) AND FIGURE(S)

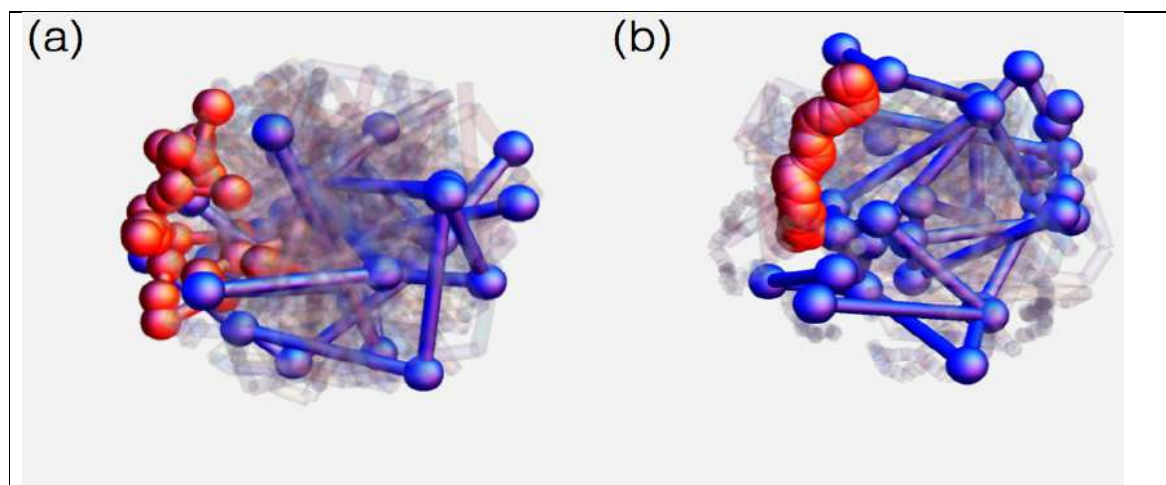


Figure 1: Snapshot configurations of 32 confined 16-mers. (a) Non-equilibrium 50:50 binary mixture where one of the constituents is at an ambient temperature $T = 1.0 T_{eq}$ while the other is in contact with a bath at $T = 50.0 T_{eq}$. For clarity, we have shown only two polymers from each constituent, red and blue respectively. (b) Snapshot of an equilibrium 50:50 mixture of 16-mers with two different values of stiffness 100 k (red) and 0.1 k (blue).





Nirmalendu Ganai

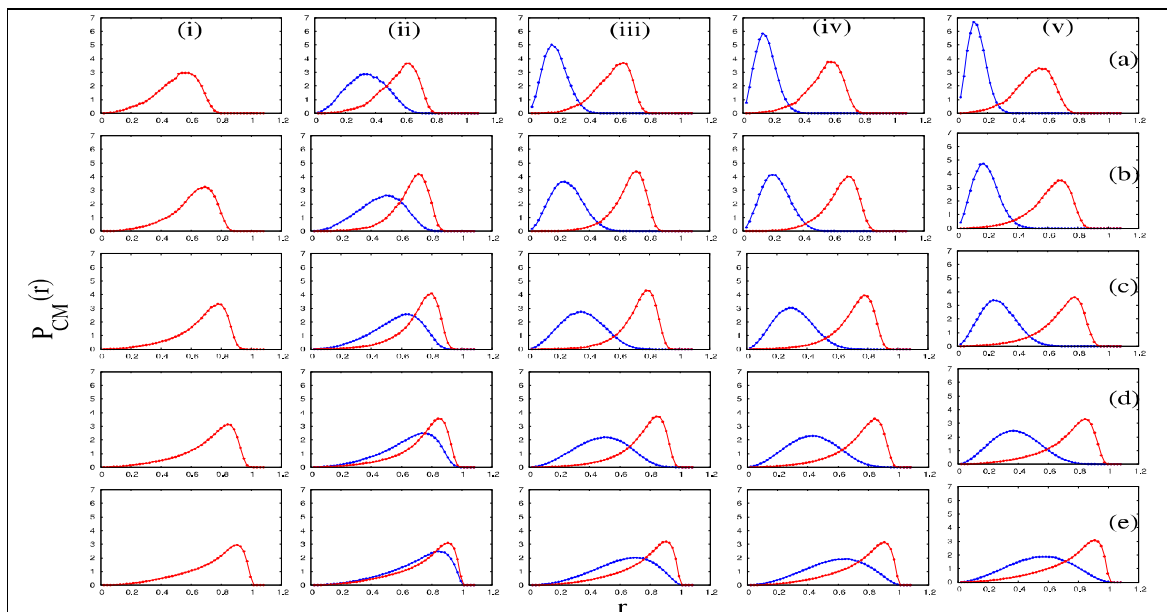


Figure 2: Plot of the centre of mass distribution $P_{CM}(r)$ of polymers as a function of radial distance r for various active temperatures along columns (i)-v) with $T_a = 1.0, 2.0, 10.0, 20.0$ & $50.0 T_{eq}$ respectively and for different $N = 32, 16, 8, 4$ & 2 along rows (a)-(e). Note that the total number of monomers is kept fixed at 512 and all systems are 50:50 mixtures. Data corresponding to active (blue line) and inactive (red line) polymers are plotted together.

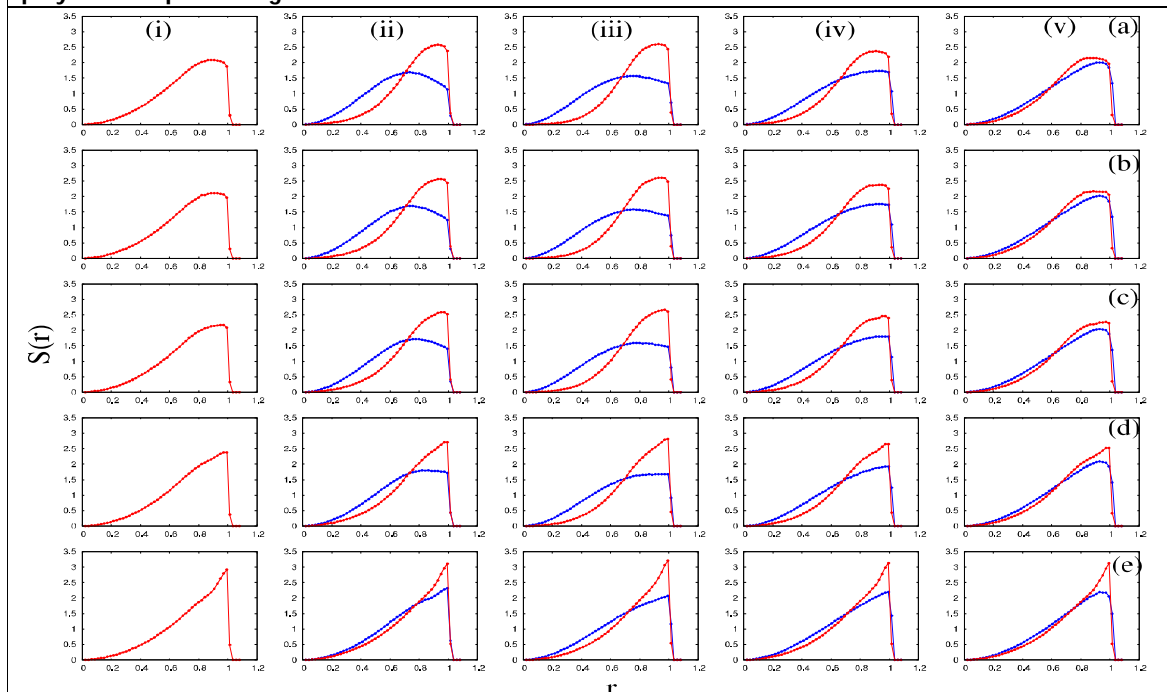


Figure 3: Probability distribution $S(r)$ of the monomer density within each spherical shell, plotted against the radial distance r from the centre of the sphere, shown for various T_a and N . The arrangement and the colour key is the same as in Fig.2.



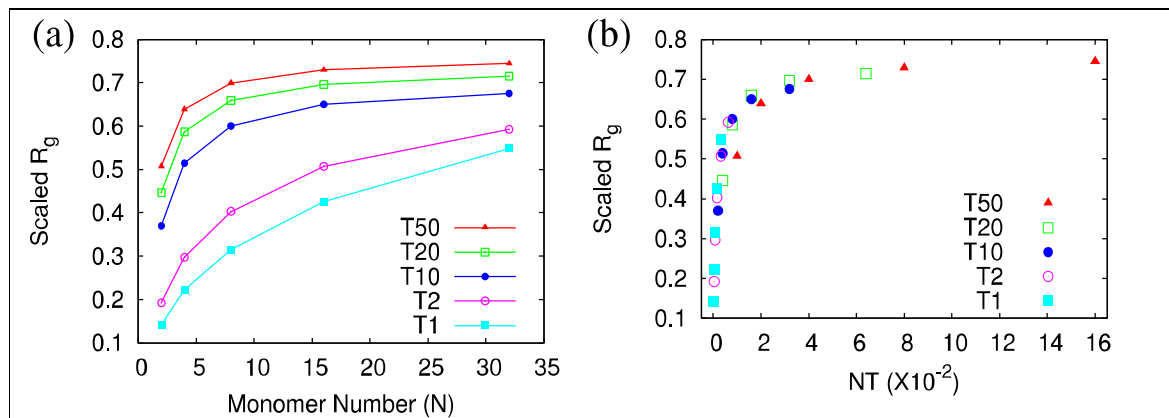


Figure 4: (a) Radius of gyration R_g of active polymers plotted against the number of monomers N for fixed active temperatures. Five plots are shown for five different active temperatures $T_a = 50.0, 20.0, 10.0, 2.0 \& 1.0 T_{eq}$. (b) Plot of R_g as a function of the combination NT .

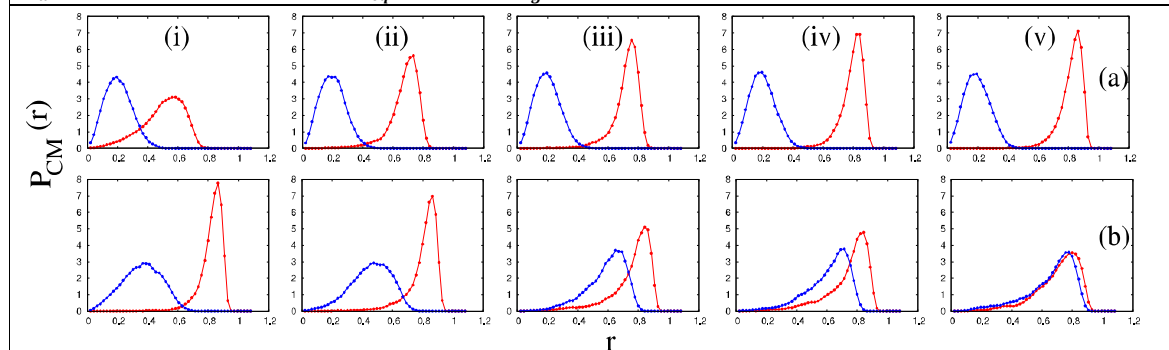


Figure 5: Plot of the centre of mass distribution $P_{CM}(r)$ of polymers as a function of radial distance r for various spring constants. Top row columns (i)-(v) show data with the harder spring constant $k_h = 1.0, 5.0, 10.0, 50.0 \& 100.0 k$ (see "Units" for the value of k) respectively keeping the softer spring constant fixed at $k_s = 0.1 k$. Bottom row $k_s = 0.5, 1.0, 5.0, 10.0 \& 50.0 k$ with k_h fixed at $100 k$. Data corresponding to the soft (blue line) and stiff (red line) polymers are plotted together. We reiterate that in all cases, 50:50 mixture of softer and harder polymers is taken and all the polymers are same in length (Number of polymer = 16 and Number of monomer in each polymer chain = 32).

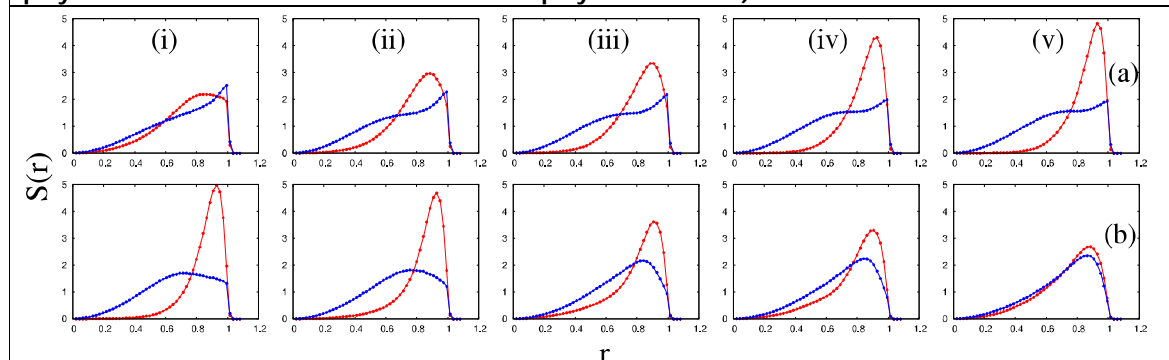


Figure 6: Probability distribution $S(r)$ of the density within each spherical shell, plotted against the radial distance r from the centre of the sphere. The arrangement and the colour key is the same as in Fig.5.





Nirmalendu Ganai

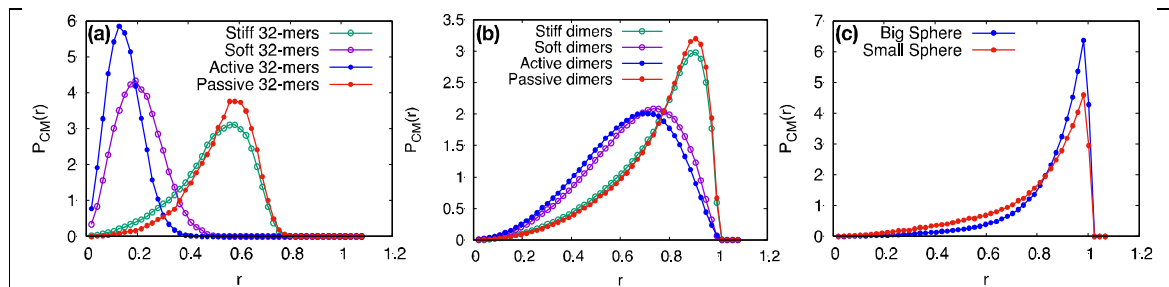


Figure 7: (a) and (b) are the comparison of the centre of mass distribution $P_{CM}(r)$ of 32-mers and dimers with radial distance r for equilibrium and non-equilibrium cases. In (a), blue and red lines with filled circle are for the non-equilibrium case where data of active (blue line - $T_a = 20.0 T_{eq}$, $R_g = 0.71 R_0$) and passive (red line - $T_a = 1.0 T_{eq}$, $R_g = 0.56 R_0$) 32-mers are plotted together while pink and green lines with open circles are the equilibrium case of 50:50 mixture of soft (pink line - $k_s = 0.1 k$, $R_g = 0.72 R_0$) and stiff (green line - $k_h = 1.0 k$, $R_g = 0.56 R_0$) 32-mers. In (b), blue and red lines with filled circle are for the non-equilibrium case where data of active (blue line - $T_a = 10.0 T_{eq}$, $R_g = 0.37 R_0$) and passive (red line - $T_a = 1.0 T_{eq}$, $R_g = 0.14 R_0$) dimers are plotted together while pink and green lines with open circles are the equilibrium case of 50:50 mixture of soft (pink line - $k_s = 0.1 k$, $R_g = 0.37 R_0$) and stiff (green line - $k_h = 1.0 k$, $R_g = 0.14 R_0$) dimers. Here, radii of gyration of active and passive polymers (32-mers and dimers) have same values as that of soft and stiff polymers (32-mers and dimers) respectively. The probability distributions of passive spheres of two different sizes are plotted against the radial distance r in (c). Radius of smaller and bigger spheres are $0.56 R_0$ and $0.72 R_0$ which are equal to the radii of gyration of passive and active polymers respectively. Data corresponding to the bigger (blue line) and smaller (red line) spheres are plotted together.

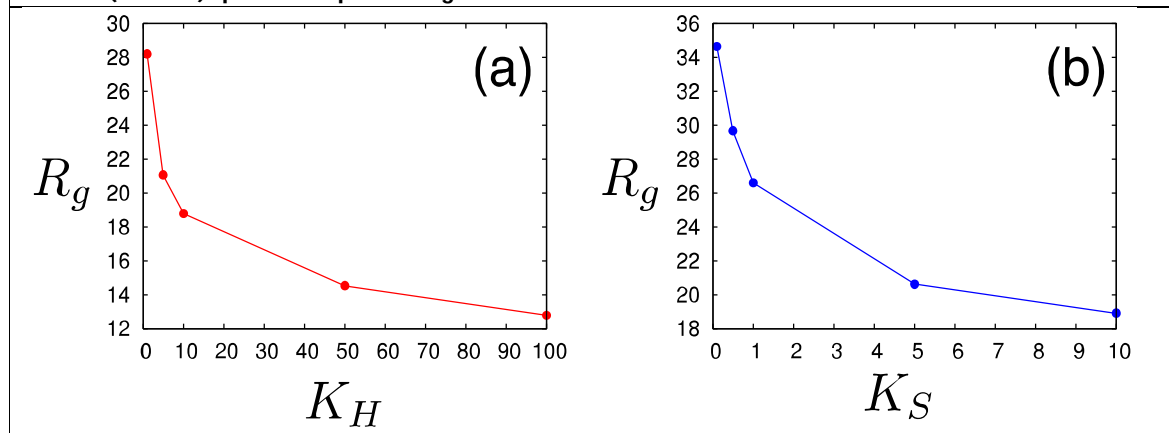


Figure 8: Variation of radius of gyration R_g with different spring constants. (a) R_g plotted against k_h with $k_s = 0.1 k$. (b) Variation of R_g with k_s while $k_h = 100.0 k$.





Vitamin D₃ Metabolite Supplementation in Layer Diet

Chromose Gene A. Pasaje^{1*} and Hershey P. Mondejar²

¹General Manager, EEJ Farms, Cebu, Philippines.

²Associate Professor V, Cebu Technological University-Barili Campus, Barili, Philippines.

Received: 15 Feb 2023

Revised: 25 Apr 2023

Accepted: 27 Apr 2023

*Address for Correspondence

Chromose Gene A. Pasaje

General Manager,

EEJ Farms, Cebu, Philippines.

E.Mail: pasaje@gmail.com



This is an Open Access Journal / article distributed under the terms of the **Creative Commons Attribution License** (CC BY-NC-ND 3.0) which permits unrestricted use, distribution, and reproduction in any medium, provided the original work is properly cited. All rights reserved.

ABSTRACT

The study is focused on the effect of vitamin D₃ metabolite 25-hydroxycholecalciferol, supplementation in the diet of 18 weeks of age commercial Lohman White® layers. The study was laid out in a Completely Randomized Design (CRD) with two treatments replicated three times with 360 birds in each treatment. The control group (T₀) used the pure layer farms' existing in-house feed formulation, while Treatment 1 utilized the in-house diet supplemented with vitamin D₃ metabolite 25-hydroxycholecalciferol at 500 grams/ton inclusion rate. Data of the layers' feed intake, final weight, number of eggs produced, egg quality through the determination of calcium and phosphorus content, and egg weight were gathered. There was no significant difference between the treatment and the control regarding the feed intake and number of eggs produced. There is, however, a highly significant difference in the final weight. The diet supplemented with vitamin D₃ metabolite also showed improvements in the egg quality, calcium and phosphorus content of the eggs.

Keywords: Vitamin D₃, metabolite, supplementation, layer diet, egg production

INTRODUCTION

A successful poultry layer operation can be attained when the three major important aspects which are production performance, immunity, and animal health, are met [1]. To attain high production performance, proper nutrition should be provided to the birds because it plays a major role in an animal's welfare [2]. The major nutrients such as proteins, fats, carbohydrates, vitamins, minerals, and water are crucial for the animal's vital functions, but vitamins have additional benefits. Adequate levels of vitamins are required to enable the animal to efficiently utilize all other nutrients in the feed [3]. The chicken needs vitamin D, a crucial fat-soluble vitamin, for appropriate calcium and phosphorus metabolism. It is important for developing and maintaining strong, healthy bones in animals. Vitamin D regulates the homeostasis of calcium (Ca) and phosphorus (P) and influences the calcification process by increasing

57238



**Chromose Gene A. Pasaje and Hershey P. Mondejar**

the uptake of minerals by the bones [4]. There are circumstances, however, when skeletal health can be a problem and vitamin D alone is not enough. Bone disorders are important welfare and economic issues in commercial layer operations. The deficiency of this vitamin in chicks causes rickets, severe weakness of the legs, causes low feathering, poor bone mineralization, and reduced structural integrity in adult chickens. Moreover, layers that are specifically caged to maximize land use will lack access to the sun, a major source of vitamin D. The birds sometimes suffer and result in poor bone mineralization and other related issues due to lack of sun exposure. Also, because eggs are laid at a very high rate, and egg formation requires calcium deposition, this will lead to the loss of bone calcium. To address these kinds of problems, supplements or alternative vitamin sources are introduced to the animals. Supplementation of an already activated form of vitamin D₃, such as one of the D₃ metabolites, has been offered to counteract such problems. The first metabolite, 25-hydroxycholecalciferol, represents the first metabolite in the cascade of vitamin D mobilization and has become commercially available to the poultry industry [4].

Vitamin D₃ (cholecalciferol) has been widely used as a feed additive to improve poultry's calcium and phosphorus metabolism and bone development [5]. It is the natural vitamin D manufactured in the skin from 7-dehydrocholesterol[6]. The active form of vitamin D is not widely distributed in nature, but vitamin D precursors are present in many vegetables. Poultry can only utilize vitamin D₃ since vitamin D₂ has no physiological value in this species. Rich sources of vitamin D₃ include the liver and viscera of fish. Vitamin D₃ metabolite, also known as 25-hydroxycholecalciferol [25-OH-D₃], provides a more bioactive form of vitamin D₃ to the animal, which was said to have advantages over vitamin D₃: improvements in weight gain, feed efficiency, and shell quality, laying persistence and reductions in bone disorders. Vitamin D₃ photo-conversion of 7-dehydrocholesterol is produced in the skin following sunlight and isomeration[7]. Aside from this, the supplemented diet represents most animals' major source of Vitamin D. Vitamin D₃ has to be first absorbed from the intestinal tract and transported to the liver to be converted to the vitamin D₃ metabolite 25-hydroxycholecalciferol. This is then transported to the kidney for conversion into several metabolites, the most important of which is 1, 25-dihydroxycholecalciferol [1, 25-(OH) 2-D₃]. A few studies focused on the effects of 25-OHD on the growth production records. Thus this study was conducted. The study aimed to show the effect of vitamin D₃ metabolite 25-hydroxycholecalciferol supplementation on commercial layers. Specifically, it aimed to determine the effects of vitamin D₃ metabolite 25-hydroxycholecalciferol supplementation in layers in terms of the following production parameters, such as feed intake, gain in weight, as well as in terms of the following egg quality parameters, such as egg weight, the calcium and phosphorus content in the eggshell.

MATERIALS AND METHODS

IACUC protocol

Before the conduct of the study, the proposal was submitted for approval of the Institutional Animal Care and Use Committee(IACUC) of Cebu Technological University.

Experimental design and treatments:

This study was laid out in a Completely Randomized Design (CRD) with two experimental treatments; the control group consists of the current farm formulation and treatment group with vitamin D₃ added to the in-house diet, replicated three times with 360 samples in replicate.

Management of experimental animals:

A total of 2160 eighteen (18) week-old Lohman White pullets were randomly allotted to two (2) dietary treatments with three (3) replicates per treatment (360 birds/replicate) raised in a three-tier cage layer house with manual chain feeders and nipple drinkers. The two dietary treatments were: (T₀), the in-house pre layer one basal diet formulation as a control group, and (T₁) pre-layer to layer one basal diet supplemented with vitamin D₃ metabolite (25-hydroxycholecalciferol) at 500 grams/ton inclusion rate added on top. The experiment duration was seventy-five (75) days which started April 2021 up to June 2021.



**Chromose Gene A. Pasaje and Hershey P. Mondejar**

The standard farm management system, feeding program, biosecurity procedure, and medication program were followed throughout the feeding trial. The corresponding diets were fed following the farm's feeding program. Drinking water was made available at all times throughout the experiment.

Data gathering procedure

The feed consumption and layer production performance was recorded daily. The body weight of the birds was recorded weekly. The average daily feed intake (ADFI) was computed by dividing the total feed intake (total FI) by the total number of feeding days and the current population. The average daily gain (ADG) was determined by dividing the weight gain by the total number of feeding days. Eggshell sampling for calcium and phosphorus content analysis was done at the end of the trial. A total of 150 grams of dried eggshell samples per replicate of the control and treatment group was subjected to laboratory analysis for calcium phosphorus content at Fast Laboratories, Mandaue City, Cebu, Philippines.

Statistical Analysis

Data gathered was analyzed using t- test and was further subjected to a Least Significant Difference (LSD) test, if found to be significant. The eggshell was analyzed for calcium and phosphorus content and results were then subjected to comparison test statistics to determine if there was a significant difference among the treatments.

RESULTS AND DISCUSSION**Effects of Vitamin D₃ metabolite 25-hydroxycholecalciferol supplementation on production parameters in layers****Feed intake of layers**

Table 1 reflects the feed intake of the layers affected by adding vitamin D₃ metabolite 25-hydroxycholecalciferol to the basal diet. Results showed no significant difference in feed consumption between the two treatments. The average feed intake for both treatment and controls is the standard feed intake of the birds. However, it is noted that the birds in treatment one consumed eight (8) kilograms less than those fed a house diet. Although there is a difference in their respective feed intake, it is notable that it is not significant enough and negligible.

Weight Gain of Layers

The effects of vitamin D₃ metabolite 25-hydroxycholecalciferol supplementation on the weight gain of layers is shown in table 2. The computed t - value (41.59) is greater than the tabulated t - value (4.604) = 0.01, and the result is highly significant. This shows that the supplementation of vitamin D₃ metabolite 25-hydroxycholecalciferol on the basal diet highly affected the weight of the layers. As shown in the feed intake data, although both treatment and control met the target feed intake, the body weight of the birds fed with a diet supplemented with vitamin D₃ metabolite was considerably higher. This seem to indicate a more efficient feed conversion performance by the treated birds and can be attributed to more efficient absorption of nutrients by the animal's body. Recently, the supplementation of 25-hydroxycholecalciferol [25-OH-D₃], a metabolite of vitamin D₃, has received more attention in the feed industry due to its higher bioavailability and potential benefit for bone mineralization in poultry. The metabolite is formulated in a stable form that is safe and approved for use in the poultry feed industry[8]. This is because 25-hydroxycholecalciferol [25-OH-D₃] bypasses the metabolic step that must be undergone by standard vitamin D₃. Furthermore, the intestinal binding proteins show a higher affinity to 25-hydroxyvitamin D₃ than to vitamin D₃, thus resulting in a more efficient and faster uptake and utilization by the birds.

The result agrees with several studies showing that 25-OH-D₃ has higher biological activity and is a more efficient source of vitamin D₃ in poultry diets than cholecalciferol. For instance, it was reported that the substitution of cholecalciferol by 25-OH-D₃ in the chickens' diet beneficially affected body weight gain and feed conversion ratio (FCR)[8]. It was also reported the beneficial influence of the partial substitution of vitamin D₃ in the chicken diet by



**Chromose Gene A. Pasaje and Hershey P. Mondejar**

25-OH-D₃ on growth performance and meat quality.[9] .It was also reported that the complete substitution of cholecalciferol by 25-OH-D₃ 154 improves FCR, increases eggshell percent, and thickens eggshells[10].

Number of eggs produced

The number of eggs produced by the layers as affected by vitamin D₃ metabolite 25-hydroxycholecalciferol supplementation are presented in Table 3. The computed t - value (0.00000019) is not equal to the tabulated z - value (4.604) @ $\alpha = 0.05$ and 0.01. The result means that there is no significant difference between the treatment and the control in terms of the volume of eggs produced. For the duration of the experiment, the expected number of eggs produced by both control and treatment 1 met the expected target set by the farm. However, the results in treatment 1 showed seventy-nine (79) more eggs were laid, which shows two percent (2%) higher egg production than the standard. Supplementation of vitamin D₃ metabolite 25-hydroxycholecalciferol somehow helped improve egg production because it is in a form that is readily available for use by the birds. This means that instead of spending more energy on converting vitamin D to its active form, the readily available vitamin D₃ metabolite lessens the birds' energy expense for maintenance; thus, it can result in a slight increase in egg production. The result is agreeable with the findings of another study with broiler breeder hens that diet supplementation with 25-OH-D₃ can improve eggshell quality without much of an influence on laying performance and egg hatchability[11].

Effects of vitamin D₃ metabolite 25-hydroxycholecalciferol supplementation on the quality of eggs

The effects of vitamin D₃ metabolite 25-hydroxycholecalciferol supplementation on the quality of the eggs are ascertained by the calcium and phosphorus content, and weight of the eggs. These aspects highly affect the eggshell strength and quality of an egg. Dried mashed eggshells were sent to a laboratory to test for calcium and phosphorus content. The egg weight was collected by getting its weight average.

Calcium content

Table 4. The calcium content of the eggs as affected by supplementing layers' basal diet with vitamin D₃ metabolite 25-hydroxycholecalciferol is presented in Table 4. The t – calculated for the calcium content of the eggs, which is reflected to be 13.22719, is greater than the tabulated t at $\alpha = 0.01$. This indicates a significant effect when supplementing vitamin D₃ metabolite 25-hydroxycholecalciferol in the calcium content. The study shows that egg quality can be improved by supplementing vitamin D₃ metabolite. In chickens, calcium is necessary for several metabolic processes and healthy eggshells [12]. The eggshell's calcium content is directly correlated to egg quality meaning the more calcium content, the higher the eggshell strength. Additionally, vitamin D₃ and phosphorus are linked to its actions. Blood calcium is quickly mobilized during eggshell production. Due to its importance in maintaining calcium homeostasis, eggshell formation, and egg production, vitamin D₃ is frequently given to layer meals [13]. The result also agreed with the findings of another study with broiler breeder hens that diet supplementation with 25-OH-D₃ can improve eggshell quality without much of an influence on laying performance and egg hatchability [11]

Phosphorus content

Like calcium, phosphorus content also correlates with egg quality. Phosphorus balances with calcium for the layers' various biological processes. The effect of vitamin D₃ metabolite 25-hydroxycholecalciferol supplement on the phosphorus content of the eggshells produced is reported in Table 5. The t – calculated for the phosphorus content of the eggs with a value of 17.5368 is greater than the tabulated t at $\alpha = 0.01$. The results suggest a highly significant effect of vitamin D₃ metabolite supplementation on the phosphorus content of eggshells. Notably, the phosphorus content is enough to confirm that the treatment has improved and is of better quality in terms of egg quality. Farm trials conducted by DSM Nutritional products have shown that optimal early frame development and proper maintenance during the production cycle are linked to improved shell quality, can help better bone growth, can support efficient calcium/phosphorus metabolism, and increases egg production percentage and lay persistence. Long-term and early supplementation of 25OHD has positive effects on egg production and egg quality [14].



**Chromose Gene A. Pasaje and Hershey P. Mondejar****Egg Weight**

Egg weight is another factor to be considered in a commercial layer farm. Though egg weight performance differs from breed to breed, there are still ways to improve egg weight performance. The effect of vitamin D₃ metabolite supplement on the weight of the eggs produced is presented in Table 6. The computed t - value (-2.439) is smaller than the tabulated t - value (4.604) @ $\alpha = 0.01$; hence the result is not significant. This means that the supplementation of vitamin D₃ metabolite 25-hydroxycholecalciferol on the basal diet did not affect the weight of eggs produced by the layers. The experiment was conducted in the early laying stages (from 19 weeks to 28 week-old layers) of the birds; it can be noted that egg weight varies depending on the birds' age. As the laying hens grow older, egg weight also increases. Both the egg weight of treatment one and control is in line with the expected egg weight average by the bird's age.

The experimental diet containing 500 grams per ton of vitamin D metabolites improved the weight of birds by 5.5 %, egg production by 2 %, and egg quality through increased calcium and phosphorus content of the eggshell. To address the vitamin D deficiency in caged commercial layers, other methods like supplementing vitamin D₃ metabolite can be practiced since sunlight exposure is inaccessible.

REFERENCES

1. Hafez HM and Attia YA. Challenges to the Poultry Industry: Current Perspectives and Strategic Future After the COVID 19 Outbreak. *Frontiers in Veterinary Science* 2020;7.
2. Fleming RH. Nutritional factors affecting poultry bone health. *Proceedings of the Nutrition Society*. 2008;67 (2).
3. DSM. Optimum vitamin nutrition of laying hens-optimum egg quality: A practical Approach. The Poultry site. 2006.
4. Weber GM. Improvement of flock productivity through supply of vitamins for higher laying performance and better egg quality. *Worlds Poultry Science Journal*. 2009;65 (3).
5. Hsiao FSH, Cheng YH, Han, JC, Chang, MH and Yu, YH. Effect of vitamin D₃ metabolites on intestinal calcium homeostasis related gene expression in broiler chickens. *Revista Brasileira de Zootecnia*. 2018;47 (0).
6. Christakos S, Dhawan P, Verstuyf A, Verlinden L and Carmeliet G. Vitamin metabolism, molecular mechanisms of action of pleiotrophic effects. *Physiological Reviews*. 2016; 96(1), 365-408.
7. Pike JW and Christakos S. Biology and mechanism of action of the vitamin D, hormone. *endocrinology and metabolism clinics of North America*. 2017;46 (4), 815-843.
8. Yarger JG, Saunders CA, McNaughton JL, Quarles C., Hollis BW and Gray RW. Comparison of dietary 25-hydroxycholecalciferol and cholecalciferol in broiler chickens. *Poult. Sci.* 1995;74:1159–1167.
9. Michalczuk M, Pietrzak D, Niemic J and Mroczek J. Effectiveness of vitamin D₃ and calcidiol (25-OH-D₃) application in feeding broiler chickens production performance and meat quality. *Polish Journal of food and Nutrition*. 2010; 60, 121-12.
10. Salvador D, Faria DED, Mazalli MR, Ito DT, Faria Filho DED, and Araujo LF. Vitamins C and for laying hens at the initial phase of egg production. *Revista Brasileira de Zootecnia*. 2009; 38:887-892.
11. Torres CA, Veira SL, Reis RN, Feireira, AK, Silva, PX and Furtado, FVF. Productive performance of broiler breeder hens fed 25-hydroxycholecalciferol. *Revista Brasileira de Zootecnia*. 2009a;38 (7), 1286-1290.
12. Berto D, Garcia E, Pelicia K, Vercese F., Molina A, Silveira A, Vieira Filho J, and Murakami E. Effects of dietary clinoptilolite and calcium levels on the performance and egg quality of commercial layer. *Revista Brasileira de ciencia Avicola*. 2013;159(3), 263-268.
13. Nascimento G, Murakami A, Guerra A, Ospinas-Rojas I, Ferreira M and Fanhani J. Effect of different vitamin D sources and calcium levels in the diet of layers in the second laying. *Revista Brasileira de ciencia Avicola*. 2014;16 (2).
14. Chen C, Turner B, Applegate TJ, Litta G and Kim, WK. Role of long term supplementation of 25-hydroxyvitamin D₃ on egg production and egg quality of laying hen. *Poultry Science*. 2020.99 (12).





Chromose Gene A. Pasaje and Hershey P. Mondejar

Table I. Feed intake of layers supplemented with Vitamin D₃ metabolite 25-hydroxycholecalciferol vs. control.

Parameters	Feed Intake (kg)			TOTAL	t _{tab}	t _{calc}
	R1	R2	R3			
Treatment	1902	1902	1901	5705	4.604	0.0000005 ^{ns}
Control	1904	1904	1905	5713		
TOTAL	2806	2806	2806	11,418		

Legend: df @ α 0.01 = 4; ** highly significant @ α 0.01 * significant @ α 0.05 ns not significant

Table II. Weight of layers supplemented with vitamin D₃ metabolite 25-hydroxycholecalciferol vs. control.

Parameters	Weight gain (g)			Total weight gain (g)	Mean	t _{tab}	t _{calc}
	R1	R2	R3				
Treatment	426	448	437	1311	437	4.604	41.59**
Control	377	425	439	1240	413		
TOTAL	803	873	876	2551	425		

Legend: df @ α 0.01 = 4; ** highly significant @ α 0.01 * significant @ α 0.05 ns not significant

Table III. Number of eggs produced with layers supplemented with Vitamin D₃ metabolite 25-hydroxycholecalciferol vs. control.

Parameters	Egg Production			TOTAL	Mean	t _{tab}	t _{calc}
	R1	R2	R3				
Treatment	4015	4004	3999	12018	4006	4.604	0.0000000519 ^{ns}
Control	3925	3927	3929	11781	3927		
TOTAL	7940	7931	7928	23799	3967		

Legend: df @ α 0.01 = 4; ** highly significant @ α 0.01 * significant @ α 0.05 ns not significant

Table IV. Calcium content of the eggs as affected by supplementing layers' basal diet with vitamin D₃ metabolite 25-hydroxycholecalciferol

Parameters	Calcium Content (%)			TOTAL	Mean	t _{tab}	t _{calc}
	R1	R2	R3				
Treatment	42.5	40.7	41.6	124.8	41.60	4.604	13.22719**
Control	41.3	40.0	41.8	123.1	41.03		
TOTAL	83.8	80.7	83.4	247.9	41.32		

Legend: df @ α 0.01 = 4; ** highly significant @ α 0.01 * significant @ α 0.05 ns not significant

Table V. Phosphorus content analysis of egg shells as affected by supplementing layers' basal diet with vitamin D₃ metabolite 25-hydroxycholecalciferol

Parameters	Phosphorus Content (%)			TOTAL	Mean	t _{tab}	t _{calc}
	R1	R2	R3				
Treatment	0.148	0.145	0.153	0.446	0.1487	-4.604	-17.5368**
Control	0.135	0.125	0.149	0.409	0.1363		
TOTAL	0.283	0.270	0.302	0.855	0.1425		

Legend: df @ α 0.01 = 4; ** highly significant @ α 0.01 * significant @ α 0.05 ns not significant





Chromose Gene A. Pasaje and Hershey P. Mondejar

Table VI. Weight of the eggs as affected by supplementing layers' basal diet with vitamin D₃ metabolite 25-hydroxycholecalciferol

Parameters	Egg weight (grams)			TOTAL	Mean	t _{tab}	t _{calc}
	R1	R2	R3				
Treatment	53.3	52.6	53.3	159.2	53.1	-4.604	-2.439 ^{ns}
Control	53.3	52.0	53.6	158.9	53.0		
TOTAL	106.6	104.6	106.9	318.1	53.05		

Legend: df @ α 0.01 = 4; ** highly significant @ α 0.01 * significant @ α 0.05 ns not significant





Effect of Early Mobilization and Chest Physiotherapy on Postoperative Pulmonary Complications in Subjects Undergoing Abdominal Surgery: A Narrative Review

Khushboo Kashodhan^{1*} and Didhiti Desai²

¹MPT Scholar, Parul Institute of Physiotherapy, Parul University, Vadodara, Gujarat, India.

²Assistant Professor, Parul Institute of Physiotherapy, Parul University, Vadodara, Gujarat, India.

Received: 17 Jan 2023

Revised: 25 Apr 2023

Accepted: 28 May 2023

*Address for Correspondence

Khushboo Kashodhan

MPT Scholar,
Parul Institute of Physiotherapy,
Parul University, Vadodara,
Gujarat, India.



This is an Open Access Journal / article distributed under the terms of the **Creative Commons Attribution License** (CC BY-NC-ND 3.0) which permits unrestricted use, distribution, and reproduction in any medium, provided the original work is properly cited. All rights reserved.

ABSTRACT

The aim of this study was to review articles, to find out effect of early mobilization and chest Physiotherapy on postoperative pulmonary complications (PPCs) in subjects undergoing abdominal surgery. A bibliographic review was performed in international databases (PubMed, google scholar, CINAHAL, MEDLINE, SCOPUS and PEDro) from 2012 to 2022. Ten clinical studies were included in this review. The evaluation of internal validity of this study was based on the PEDro scale. Results: The results showed that application of standardized early mobilization program on the day of surgery along with chest Physiotherapy can have positive effects on reducing postoperative pulmonary complications (PPCs). However, there were differences in few of the included studies regarding the implementation of early mobilization program and the technique applied for chest Physiotherapy. Postoperatively, early mobilization program along with chest Physiotherapy should be implemented from the day of surgery and must be considered one of the main factors to reduce postoperative pulmonary complications and enhance patients' recovery.

Keywords: Abdominal surgery, Early Mobilization, Postoperative complications, Pulmonary functions, Breathing exercises, Chest Physiotherapy



**Khushboo Kashodhan and Didhiti Desai**

INTRODUCTION

Indications for “abdominal surgeries” include the identification and treatment of numerous diseases, the removal of malignant tissue, the treatment of visceral tissue perforations, the removal of inflammatory bowel segments, benign growths, or vascular aneurysms, among other procedures [1]. Following abdominal procedures, it is normal to experience postoperative complications that may demand for invasive treatments such as re-exploration or intensive care management enforcing strict pre-operative and post-operative care guidelines [2]. According to AIHW report, abdominal surgery is the most frequently performed procedure in Australia and New Zealand [3]. Over 230 million major surgeries are performed annually around the world, with postoperative complications ranging from 1% to 23% in major surgeries [3][4]. Following abdominal surgery, postoperative pulmonary complications (PPCs) have been associated to higher rates of morbidity and mortality, longer hospital stays, and higher healthcare costs [1]. Following upper abdominal procedures, there is a high risk of developing PPCs that ranges from 17% to 88% and is up to 15 times more likely than following a lower abdominal incision [1][4]. A PPC is frequently referred to as “a pulmonary abnormality that produces identifiable disease or dysfunction, that is clinically significant and adversely affects the clinical course”[3]. The respiratory system is negatively impacted by abdominal surgery and general anaesthesia in a number of ways, including altered respiratory muscle drive and function, decreased lung volume, including tidal volume, total lung capacity, and vital capacity, impaired mucociliary clearance, and impaired efficiency to cough [4]. Atelectasis, hypoxemia, hypercapnia, bronchospasm, dyspnoea, pneumonia, respiratory dysfunction, and pleural effusion are examples of the frequent postoperative pulmonary issues[1][4]. Additionally, there is decrease in oxygen arterial pressure (PaO₂) and oxygen haemoglobin saturation (SPO₂) [1][4]. The “Enhanced Recovery after Surgery Society” and other perioperative care recommend and strongly advise “enforced” early mobilization (i.e., beginning out-of-bed activities from the day of surgery) as part of the fast-track approach [5][6]. Early postoperative mobilization, such as sitting, standing, and ambulation programmes, have been strongly recommended for patients after major surgery to speed up their recovery. It is claimed that these programmes improve functional capacity, lower postoperative complications, and shorten hospital stays [7]. More so than just breathing exercises, early mobilization improves pulmonary functions like forced vital capacity, maximum voluntary ventilation, and arterial oxygenation [8].

Chest Physiotherapy, which incorporates deep breathing exercises, mobilization, postural drainage, percussion, vibration, or shaking to improve bronchial drainage, as well as the use of mechanical breathing devices like the blow bottles, incentive spirometer (IS), autogenic drainage, ACBT, IPPB and CPAP plays a significant preventive role in dealing with postoperative complications [1]. It attempts to enhance the patient's breathing pattern, promote lung expansion, respiratory muscle strength, retain pulmonary function including functional residual capacity and inspiratory reserve volume, and improve oxygenation without escalating pain or leading to additional issues [1]. It reverses physiological and/or functional abnormalities that could happen in postoperative after surgery, preventing or treating PPCs [1].

So, the aim of this study was to review articles to find out the effect of early mobilization and chest Physiotherapy on postoperative pulmonary complications in subjects undergoing abdominal surgery.

MATERIALS AND METHODS

Article search process

After searching databases (PubMed, Google Scholar, CINAHAL, MEDLINE, SCOPUS, and PEDro) using the following keywords: abdominal surgery, early mobilization, postoperative problems, pulmonary functions, breathing exercises, and chest physical therapy, a review of the relevant literature was conducted in September 2022. The inclusion criteria for the articles were: (1) published material(2) studies conducted from year 2012 to 2022(3) articles related to early mobilization/ambulation and chest Physiotherapy on postoperative pulmonary complications after abdominal surgery(4) studies examining the postoperative complication rates, length of stay in hospital,

57246



**Khushboo Kashodhan and Didhiti Desai**

readmission rate, performance-based functional outcomes, patient-reported outcome measures, ABG analysis, respiratory functions, pulmonary functions, chest Physiotherapy, vital status, oxygen saturation, pain, quality of life, and patient disposition. The exclusion criteria were: (1) articles not published in English(2) systemic reviews, meta-analysis(3) articles in which mobilization programme not described or started more than postoperative day one(4) articles that did not have a comparison patient group (either a control or pre/post intervention data).

Evaluation of internal validity of articles included in this review

The PEDro scale was used as the basis for the internal validity assessment. The articles with a PEDro score of 4 or higher were considered for this review.

Search results

The search strategy generated a total 50 articles from the searches. The online searches were conducted on 16 June 2022 and 10 August 2022 respectively. All articles were collected and duplicates were removed (15 articles). 35 articles were then reviewed by reading the abstracts to determine whether they met the inclusion and exclusion criteria. Finally, from the final scanning process, 10 studies resulted, which were included in this review. The study selection process is shown in Figure 1.

RESULTS AND DISCUSSION

The following are the studies included in the review as well their main findings:

In study of Anna Svensson-Raskh et al., (2021) did a study where 214 abdominal surgery patients participated, and were randomized to one of the three groups: mobilization and standardized breathing exercises, mobilization only, or control. They reported that mobilization out of bed, with or without breathing exercises, after 2 hours of elective abdominal surgery enhanced participants' SPO₂ and PaO₂ [6]. Saba Balvardi et al., (2021) conducted a study with 100 individuals enrolled in a trial, and they were randomly assigned to receive usual care (preoperative education) or facilitated mobilization (sitting in a chair for at least two hours on the day of surgery and being active (walking and/or sitting) for at least six hours from POD 1 until discharge). The researchers observed that staff-directed facilitation of early mobilization did not result in improved postoperative pulmonary function or reduced PPCs within an enhanced recovery pathway for colorectal surgery [9].

Ajay Kumar Dhiman et al.,(2021) did a study and 52 participants were allocated into two study groups: the conventional group treatment and the ERAS (Enhanced recovery after surgery) protocol. The study demonstrated that early recovery programmes can be successfully performed with noticeably reduced hospital stays without any increase in postoperative problems in patients undergoing emergency laparotomy for abdominal trauma[10]. Md. Feroz Kabir et al., (2021) did a study with 60 participants, divided the participants into two groups: 30 in the chest physiotherapy group (control) and 30 in the chest physiotherapy along with early mobility group (experimental) and found that administering CPT along with early mobility exercise significantly decreased the length of hospital stay, increased peripheral oxygen saturation, and improved functional independence following abdominal surgeries [1]. Monika Fagevik Olsen et al., (2021) conducted a study in which 83 open pancreatic surgery patients were randomly assigned to the same-day mobilization group or the next-day mobilization group. The group that was mobilized the same day as surgery showed a larger improvement in oxygenation after mobilization, which may help to lessen complications and speed functional recovery [11].

Sana Bashir et al., (2019) concluded that in patients who have upper abdominal procedures, breathing exercises with spirometry and early post-operative mobilization prevent PPCs, improve post-operative vital status, blood gases, and QOL, and decrease post-operative pain and length of hospital stay [12]. Aml Sabra Abu Bakr et al., (2018) included 80 elderly patients and concluded that early ambulation benefited elderly patients undergoing laparotomies by decreasing postoperative RTIs (respiratory tract infections), improving respiratory parameters, and shortening hospital stays [13].



**Khushboo Kashodhan and Didhiti Desai**

AHMED M. ABD EL-RAUF et al.,(2017) did a study were 40 subjects with upper abdominal surgery and were divided into two groups: early mobilization and regular chest physiotherapy or in routine chest physiotherapy. The study demonstrated that following elective open upper abdomen surgery, early mobilization is useful in enhancing pulmonary functions (FVC, FEV 1, and PEF) [14]. SamahM. AbdElgaphar et al., (2015)conducted study with 60 upper abdominal surgery patients who were divided into two groups both received early ambulation, while those in study group received breathing exercises. According to the study, adding breathing exercises during the first few days after surgery enhances ventilatory performance, lowers pulmonary complications, and shortens postoperative hospital stays [15]. The main characteristics of the studies included in the review are presented in Table 1.

Synthesis of results included in this review

Due to the proximity of the incision close to the diaphragm and the “extensive neural-network” in the abdominal region, abdominal surgery causes more severe complications in the postoperative period [16]. According to Boden et al., (2018), the reported complication rate following major abdominal surgery which ranges from 30-60% with an astomosis leakage, bleeding and cardiovascular issues being the most common and challenging. “Early Mobilization is one of the fundamental evidence-based practices in the Fast Track Surgery (FTS)”. The total time/duration spent out of bed by subjects in the post-operative period is just as important as early mobilization, and the ERAS protocol recommends that the patient should stay out of bed for two hours on the 1stPOD and six hours per day until discharge on the subsequent days (Gustafsson et al., 2019)”. Chest Physiotherapy has been recommended as a critical element in the prevention and improvement of PPCs following abdominal surgery and has been regularly used in both preoperative and postoperative care [4]. In the early postoperative phase, breathing exercises along with early ambulation increase the dynamic ventilator parameters (FVC%/FEV1/PEF), reduce pulmonary complications, shorten postoperative hospital stays and also raises the peripheral oxygen saturation level [14]. As a result, it is recommended that “pulmonary physiotherapy” should be added to the standardized early mobilization programme as it improves pulmonary functions after upper abdominal surgery.

“The current study concluded that executing an early mobilization programme is practical, safe, and has no associated adverse consequences. However, in clinical practise, the frequency, length, and intensity of mobilization programmes vary in different settings. Additionally, it is important to research the long-term effect of early mobilization on the respiratory system”. Studies have shown that “setting-goals” for the mobilization process has a motivating effect on patient’s mobilization This was demonstrated in the study by Fadime Koyuncu et al., were patients in the intervention group were more likely to reach the established/targeted mobilization goals than those in the control group [16]. In all clinical settings, differences were found in the “definition of PPCs, the occurrence and severity of consequences (none, mild, moderate, and severe), and follow-up”. PPCs need to be measured and defined using standardized and thoroughly validated measures as 1.The European Perioperative Clinical Outcome (EPCO) taskforce or 2.The Clavien-Dindo classification of surgical complications. “Studies showed that when the therapeutic maneuvers which improve lung volume are used properly the risks, severity and frequency of postoperative complications after abdominal surgery are reduced. The results of the investigations are influenced by the lack of standardization in terms of exercise type, number of series, repetitions, intervals, frequency, and timeframes. To determine the scope of benefit and the relative efficacy of various chest physiotherapy modalities for postoperative patients, well-designed trials must be conducted”.

“Aiming to establish consensus-based, best practice guidelines on the ideal frequency, duration, and intensity of mobilization in various settings, well-designed trials and future work must concentrate on 1. clinical reasoning and 2. decision -making process in gradually mobilizing patients to maximise therapeutic response”. Following the establishment of these, compliance and result data are required to better comprehend what prescription of early mobilization should be administered in clinical practice [6]. Additionally, it has been demonstrated that getting out of bed immediately following abdominal surgery has an impact on the patient's physical and mental health [6].



**Khushboo Kashodhan and Didhiti Desai****CONCLUSION**

This narrative review summarises the key studies on a range of elective and emergency abdominal surgeries in order to reduce and avoid postoperative pulmonary complications. In accordance with the review, postoperative early mobilization along with chest physical therapy with breathing exercises shorten hospital stays, enhance pulmonary and ventilatory functions, improve peripheral and arterial oxygenation, and increase functional independence and contributes to improvement in the patient's QOL. Implementing an early mobilization protocol in accordance with ERAS recommendations minimizes the incidence of postoperative pulmonary complications, pain levels, physiotherapy inputs, and readmission rates.

ACKNOWLEDGMENTS

The authors wish to thank Dr. Bhavana Gadhavi, Principal of Parul Institute of Physiotherapy, Parul University for constant support and guidance.

CONFLICTS OF INTEREST:

None

REFERENCES

1. Kabir MF, Jahan S, Hossain MZ, Chakrovorty SK, Sarker AH, Hossain MA, Hossain KA, Kamal SM, Akter S. Effect of Chest Physiotherapy along with Early Mobility after Abdominal Surgery. *European Journal of Medical and Health Sciences*. 2021 Feb 9;3(1):150-6.
2. Saeed S, Rage KA, Memon AS, Kazi S, Samo KA, Shahid S, Ali A. Use of abdominal binders after a major abdominal surgery: a randomized controlled trial. *Cureus*. 2019 Oct 3;11(10).
3. Reeve JC, Boden I. The physiotherapy management of patients undergoing abdominal surgery. *New Zealand Journal of Physiotherapy*. 2016 Mar 1;44(1).
4. Zahari Z, Subramanian SS. The Effect of Chest Physiotherapy During Immediate Postoperative Period among Patients Underwent Abdominal Surgery. *Indian Journal of Public Health Research & Development*. 2020 May 1;11(5).
5. Fiore Jr JF, Castelino T, Pecorelli N, Niculiseanu P, Balvardi S, Hershorn O, Liberman S, Charlebois P, Stein B, Carli F, Mayo NE. Ensuring early mobilization within an enhanced recovery program for colorectal surgery: a randomized controlled trial.
6. Svensson-Raskh A, Schandl AR, Stähle A, Nygren-Bonnier M, FagevikOlsén M. Mobilization started within 2 hours after abdominal surgery improves peripheral and arterial oxygenation: a single-center randomized controlled trial. *Physical therapy*. 2021 May;101(5):pzab094.
7. Fukushima T, Adachi T, Hanada M, Tanaka T, Oikawa M, Nagura H, Eguchi S, Kozu R. Role of Early Mobilization on the Clinical Course of Patients who Underwent Pancreaticoduodenectomy: A Retrospective Cohort Study. *The Tohoku Journal of Experimental Medicine*. 2021;254(4):287-94.
8. Zafiroopoulos B, Alison JA, McCarren B. Physiological responses to the early mobilisation of the intubated, ventilated abdominal surgery patient. *Australian Journal of Physiotherapy*. 2004 Jan 1;50(2):95-100.
9. Balvardi S, Pecorelli N, Castelino T, Niculiseanu P, Alhashemi M, Liberman AS, Charlebois P, Stein B, Carli F, Mayo NE, Feldman LS, Fiore JF Jr. Impact of Facilitation of Early Mobilization on Postoperative Pulmonary Outcomes After Colorectal Surgery: A Randomized Controlled Trial. *Ann Surg*. 2021 May 1;273(5):868-875. doi: 10.1097/SLA.0000000000003919. PMID: 32324693.
10. Dhiman AK, Jagne N, Uniyal M, Kumar A, Azam Q. Enhanced recovery after surgery protocol versus conventional care in emergency abdominal trauma surgery: a prospective, randomised, controlled study. *International Surgery Journal*. 2021 Dec 28;9(1):118-23.





Khushboo Kashodhan and Didhiti Desai

11. FagevikOlsen M, Becovic S, Dean E. Short-term effects of mobilization on oxygenation in patients after open surgery for pancreatic cancer: a randomized controlled trial. BMC surgery. 2021 Dec;21(1):1-2.
12. Bashir S, Siddiqi FA, Baig M, Bashir EA, Azim ME, Tariq MI. Effect of chest physical therapy with early mobilization on post-operative pulmonary complications in upper abdominal surgeries. Rawal Medical Journal. 2019 Feb 15;44(1):99-.
13. Abu Bakr AS, Fahmy Ibrahim HD, Tohamy TA, Mohammed IR, Mohamed JA. Effect of Early Ambulation on Reducing Respiratory Tract Infection among Postoperative Elderly Patients with Abdominal Surgeries. Minia Scientific Nursing Journal. 2018 Jul 30;3(1):110-9.
14. ABD EL-RAUF AM, BORHAN WH, ABOU EL-NAGA WA, EL-ESSAWY AF. Effect of Early Mobilization on Pulmonary Functions Post Upper Abdominal Surgeries.
15. AbdElgaphar S, Soliman G. The effect of early post-anesthetic chest physiotherapy nursing intervention on patients undergoing upper abdominal surgery. IOSR Journal of Nursing And Health Science. 2015;4(4):1-7.
16. Koyuncu F, Iyigun E. The effect of mobilization protocol on mobilization start time and patient care outcomes in patients undergoing abdominal surgery. Journal of Clinical Nursing. 2022 May;31(9-10):1298-308.

Table 1: Main characteristics of included studies

AUTHOR, YEAR	STUDY DESIGN	INTERVENTION	OUTCOME MEASURE	RESULT
Anna Svensson-Raskh et al. (2021) [6]	randomized controlled trial	N= 201 Group 1 (n=68) early mobilization and breathing exercises, Group 2 (n=69) early mobilization Group 3 (n=64) no intervention	Primary: SPO ₂ , PaO ₂ Secondary: PaCO ₂ , spirometry, respiratory insufficiency, pneumonia, length of hospital stay	There were significant improvements in SPO ₂ and PaO ₂ Group 1 and 2. Secondary outcome measures did not differ between groups.
Saba Balvardi et al. (2021) [9]	randomized controlled trial	N=100 Group 1 (n=50) postoperative care, Group 2 (n=50) facilitated postoperative mobilization	FVC, FEV1 and peak cough flow	There was no between- group difference in recovery of FVC or peak cough flow.
Ajay Kumar Dhiman et al. (2021) [10]	randomized controlled trial	N=52 Group A- ERAS protocol, Group B- conventional care	Primary: length of hospital stay Secondary: complication rate, re-admission rate	Statistically significant improvement in Group A in terms of reduction in length of hospital stay and complication rate.
Md. Feroz Kabir et al. (2021) [1]	Quasi-experimental study	N=60 Group I (n=30) early mobilization along with routine CPT, Group II (n=30) received only routine CPT	Respiratory function, length of hospital stay, pain intensity, oxygen saturation, level of functional independence	Significant improvement in Group I in terms of length of hospital stay, O ₂ saturation, respiratory functions, functional independency level.
MoikaFagevik Olsen et al. (2021) [11]	randomized controlled trial	N=83 Group A- (n=42) mobilized on the same day of surgery, Group B- (n=41) mobilized on the next-day of surgery Both groups were given breathing exercises with PEP device	ABG- SaO ₂ , PaO ₂ , PaCO ₂ , PH, Spirometry- FVC, PEF and FEV1	FiO ₂ , SaO ₂ /FiO ₂ , PaO ₂ /FiO ₂ , and alveolar-arterial oxygen gradient, before and after mobilization, were superior in Group A.
Sana Bashir et al. (2019) [12]	randomized controlled trial	N= 30 Group 1 (n=15) deep breathing exercises, incentive spirometer, early mobilization, Group 2 (n=15) early mobilization	HR, RR, SPO ₂ , PH, PO ₂ , PCO ₂ , HCO ₃ , SaO ₂ , SF-36	Significant improvement (p<0.05) was observed on RR, PH, PO ₂ , pain levels, chest x-rays, auscultation prior to discharge.





Khushboo Kashodhan and Didhiti Desai

Aml Sabra Abu Bakr et al. (2018) [13]	Quasi-experimental study	N= 80 Group 1 (n =40) early ambulation, Group 2 (n =40) control group	Patient interview structured questionnaire, patient's physical and respiratory assessment, early ambulation record	Reduction in postoperative RTIs, improved respiratory parameters and decreased length of hospital stay in Group 1.
AHMED M.EL-RAUF (2017) [14]	randomized controlled trial	N=40 Group 1 (n=20) received early mobilization and routine CPT Group 2 (n=20) routine CPT	FVC, FEV1, PEF	Significant improvement in pulmonary functions measured variables FVC, FEV1 and PEF in Group 1.
Samah M.Abd Elgaphar et al. (2015) [15]	Quasi-experimental study	N=60 Group 1 (n=30) received routine physical therapy (early ambulation);Group 2 (n=30) received breathing exercises	SPO ₂ , FVC and FEV1	Significant improvement in FEV1, reduced PPCs, shorter length of hospitalization in Group 1.

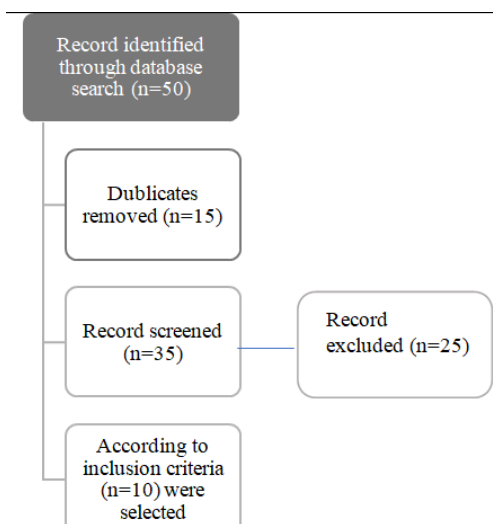


Fig 1: The study selection process flow chart





Study of Aquatic Weeds in Ponds of Mandvi Taluka, District Surat, South Gujarat, India

Choudhary Nehal L^{1*} and Jangid M.S²

¹Ph.D Student, Department of Botany, (HNGU University, Patan) Sir P.T. Science College, Modasa-383315, Gujarat, India.

²Ph.D Guide, Department of Botany, Sir P.T.Science College, Modasa-383315, Gujarat, India

Received: 28 Feb 2023

Revised: 05 Apr 2023

Accepted: 08 May 2023

*Address for Correspondence

Choudhary Nehal L

Ph.D Student,

Department of Botany, (HNGU University, Patan)

Sir P.T. Science College,

Modasa-383315, Gujarat, India.



This is an Open Access Journal / article distributed under the terms of the **Creative Commons Attribution License** (CC BY-NC-ND 3.0) which permits unrestricted use, distribution, and reproduction in any medium, provided the original work is properly cited. All rights reserved.

ABSTRACT

The present study reveals the aquatic weeds and their ecological traits of Mandvi taluka, district Surat of South Gujarat. In Mandvi taluka, natural and artificial seasonal wetlands serve as an entrance for migratory waterfowl. The recent research reports the biodiversity of wetlands viz. Maya Tadav and several ponds of Mandvi taluka during research time. In research total of 23 diverse aquatic species have been reported from the wetlands. It includes marshy, emergent, free-floating, and submerged hydrophytes. Significantly most common species belong to families like Poaceae, Araceae, Cyperaceae. Species such as *Ipomoea aquatica*, *Typha angustifolia*, *Chloris barbata*, *Hydrilla verticillata* L., and *Cyperus* are commonly occurring throughout the year in the area.

Keywords: Aquatic Weeds, Wetlands, Mandvi, South Gujarat.

INTRODUCTION

According to (Odum, E.P. (2005)), the wetland is among the center of situations inside the world. Within the aquatic plants are key modules for the well-functioning of wetland organic frameworks for natural yield and reinforce many life shapes and hence donate parcels of stuffs and comforts for the subsidiary individuals. Wetlands are vital for the conservation of biodiversity for several of the uncovered species that survive on them and for on a very basic level passing fowls. The study of Wetland are done in Gujarat by Dabgar, P.J.(2012), Deshkar S. L, (2008), Kumar *et al.*, (2006), Parmar A.J. and Patel N.K.(2010),



**Choudhary Nehal and Jangid****STUDY AREA**

Mandvi taluka is found in the Surat District of South Gujarat. Separated from the forest border of Umarpada, Mangrol, and Tapi district of Gujarat. Meadow, Wetlands, and Slopes secured most of the timberland range. Water bodies like Ambli Dam, Isar Dam, Godhdha Dam, Kevdi Dam, Kakrapad Dam, Lakhi Dam are artificial wetlands. Maya Tadav or ponds, Rataniya Tadav and Sathvav Tadav are natural damp arrive. The lake is perennial and the water level subsides altogether during summer. The bed is composed of clay and silica.

MATERIAL AND METHODS

The present work is the outcome of few years intensive survey with serious observation and collection. Bentham and Hooker system taxonomy was accepted for the current study. Moreover this survey was attempted to characterized aquatic angiosperm into emergent, submerged, marshy and free floating hydrophytes. Identification was done with help of flora. The field study were organize during year 2021-2022 every month survey carried out and collect the aquatic plants. The seasonal variation of plant species in wetland have been studied to find out the species abundance. The collected plants were identified and classified to their respective species level.

RESULTS AND DISCUSSION

The submerged aquatic plants are produce oxygen in the process of photosynthesis at the littoral zone of ponds. This oxygen is control by the dissolve oxygen in the ponds. As a result the balance of oxygen in the water and this water is suitable for pisciculture. The aquatic species found in ponds of Mandvi taluka are 22 species and 21 genera belonging to 13 angiospermic families. Floating hydrophytes habitat is dominant in the result of Table-1. Free-floating hydrophytes like *Eichhornia* and *Pistia* and Rooted with floating *Nelumbo*, *Nymphaea*, and Rooted submerged *Hydrilla*, and Rooted emergent *Typha* and *Cyperus* species found throughout the year. *Sagittaria* and *Scirpus* species are dominant during the dry season.

CONCLUSION

The current research was predictable at the identification of aquatic vegetation growing in these ponds. Wetlands are also vital for the preservation of groundwater. Also, if not suitably conserved, the catchment zone of the wetlands gets clogged upstream, causing water-logging in close inhabited and has severe economic and health problems.

REFERENCES

1. Hooker, J. D.(1872-1896). "The flora of British India". Vol I-VII Reeve 7Co.Kent England.
2. Odum, E.P. (2005). "Fundamental of Ecology". Thomson brooks/Cole.
3. Parmar A.J. and N.K. Patel (2010). Study of aquatic angiosperm plants of patan district, Gujarat.Life sciences Leaflets, 3:54-68.
4. Deshkar S.L. (2008). Avifaunal Diversity and Ecology of wetlands in semi-arid zone of central Gujarat with reference to their conservation and categorization. Ph.D.Thesis, M. S. University, Vadodara.
5. Dabgar,P.J.(2012). A Contribution to the flora of Wadhvana wetland, Dabhoi Taluka,Gujarat, India. Bioscience Discovery 3(2):218-221.
6. Kumar *et al.*,(2006). Evaluation of bio-monitoring approach to study lake contamination by accumulation of trace elements in selected aquatic macrophyte: A case study of kanewal community reserve, Gujarat, Applied Ecology and Env.,6(1):65-76.





Choudhary Nehal and Jangid

Table : 1 Aquatic weeds of Mandvi Taluka are enlisted as below.

S.R.No	Family	Scientific Name	V.Name	Habit
1	Convolvulaceae	<i>Ipomoea aquatic</i> Forssk.		Emergent
2	Hydrocharitaceae	<i>Hydrilla verticillata</i> (L.f.) Royle.		Submerged
3	Hydrocharitaceae	<i>Hydrocharis</i> L.		Floating
4	Hydrocharitaceae	<i>Vallisneria spiralis</i> L.		Submerged
5	Amaranthaceae	<i>Alternanthera pungens</i> Kuntz.		Marshy
6	Poaceae	<i>Chloris barbata</i> Sw.		Marshy
7	Poaceae	<i>Dactyloctenium aegyptium</i> (L.)		Marshy
8	Poaceae	<i>Paspalidium punctatum</i>		Marshy
9	Poaceae	<i>Hygroryza aristata</i> (Retz.) Nees ex Wight & Arn.		Emergent
10	Nymphaeaceae	<i>Nymphaea nouchali</i> Burm.F.	Poyanu	Floating
11	Nymphaeaceae	<i>Nymphaeapubescens</i> Willd.		Floating
12	Nymphaeaceae	<i>Nelumbo nucifera</i> Gaertn.	Lotus	Floating
13	Araceae	<i>Pistia stratiotes</i> L.	Jalshankhala	Floating
14	Araceae	<i>Spirodela polyrrhiza</i> (L.) Schleid.	Water velvet	Floating
15	Lemnaceae	<i>Lemna gibba</i> Linn.		Floating
16	Lemnaceae	<i>Wolffia arrhiza</i> (Linn.) Wimmer		Floating
17	Onagraceae	<i>Ludvigia octavalvis</i>		Marshy
18	Najadaceae	<i>Najas minor</i> All.		Floating
19	Scrophulariaceae	<i>Bacopa monnieri</i> (Linn.) Wettst.		Floating
20	Cyperaceae	<i>Cyperus esculentis</i>		Emergent
21	Pontederiaceae	<i>Eichhornia crassipes</i> (Mart.) Solms.	Kanphutti	Floating
22	Typhaceae	<i>Typha angustata</i> Bony. & Chaub.		Floating



Fig. 1 . Maya Tadav (Regama village) Sathvav Tadav (Sathvav village)

Fig. 2 . Isar Dam(Isar village) Kevdi Dam (Karutha village)





Fuzzy Logic Controller based 3-Phase Grid Tied Converter for Power Flow with Different Control Strategies

P. Marimuthu^{1*}, A. Naveen², Raja Reddy Duvvuru¹, M. Kondalu¹, Ch.Rami Reddy³ and T. Rajesh¹

¹Department of EEE, Malla Reddy Engineering College, Secundrabad, Telangana, India.

²PG Scholar, Department of EEE, Malla Reddy Engineering College, Secundrabad, Telangana, India.

³Department of EEE, Joginpally B. R. Engineering College, Hyderabad, Telangana, India.

Received: 31 Jan 2023

Revised: 25 Apr 2023

Accepted: 16 May 2023

*Address for Correspondence

P.Marimuthu

Professor,

Department of EEE,

Malla Reddy Engineering College,

Secundrabad, Telangana, India.

E.Mail: spm.muthu78@gmail.com



This is an Open Access Journal / article distributed under the terms of the **Creative Commons Attribution License** (CC BY-NC-ND 3.0) which permits unrestricted use, distribution, and reproduction in any medium, provided the original work is properly cited. All rights reserved.

ABSTRACT

In this work we propose fuzzy logic controller based control of bidirectional power flow in grid interfaced converters. The bidirectional power flow control feature allows in converters to charge and discharge at the same time. In addition, five charging strategies have been chosen and developed to achieve high charging efficiency while simultaneously increasing the battery's life: Charging using different methods of control strategies. To implement different methods of charging approaches, the converter employs the direct quadrature (d-q) transformation. These functions can be performed by a digital signal processor without the use of additional circuit components. This paper also examines and analyses the differences in charging power between each technique. Finally, the proposed bidirectional charger's performance and practicality are confirmed by MATLAB/SIMULINK simulation results.

Keywords : Bidirectional power flow control, Grid interfaced inverter, Digital signal processors, Fuzzy controller, Charging strategies.



Marimuthu *et al.*,

INTRODUCTION

Novel power innovations, consisting of sustainable electricity era frameworks, electric automobiles and high stage consumer hardware, have swiftly advanced in latest years to address petroleum derivative use and carbon dioxide emissions challenges [1]. In those applications, the battery module is commonly gift for energy capacity. A framework linked DC-AC converter is needed to transmit electric strength among the battery and the network, whilst the 3-stage H-span circuit might be the most often used arrangement for high-strength applications. [2]. Furthermore, the converter's bidirectional strength float regulation is a critical functionality for recognizing the battery's charging and discharging capacity [3]. Though it becomes mentioned in [4], dangle-primarily based charging/releasing is likewise a key mode. Furthermore, the bidirectional charger has turn out to be an crucial issue for electric vehicle (EV) programs [5].

Various charging strategies had been created to extend the charging execution in addition to the battery length [6]. The continuous present day constant current and voltage (CC-CV) method of charging is one of the majority customarily used method of charging. When the battery voltage falls beneath a predetermined threshold, CC charging is chosen. When the battery voltage is better than the specified esteem, CV charging might be decided on, that is uncommon. Despite the reality that CC-CV charging can take care of speedy charging, the overheating phenomenon as a result of the consistent charging modern-day should injure cathode plates and shorten the battery's lifestyles. The PRC and SRC advances have been designed in reaction to this [7]. Electron debris in the battery can be homogeneously disseminated way to the PRC and SRC's 0 charging modern-day period functions. As a end result, the charging security and battery lifestyles may be multiplied. Aside from a changed PRC price, the Reflex ideas become advanced [8]. For the Reflex TM approach, the negative charging period will be remembered in comparison to standard PRC charging. According to [9], the bad charging duration can enhance the uniform appropriation of electrolyte fixing whilst also stabilizing the battery's artificial response. Furthermore, for fixed lead-corrosive batteries in electric powered motors, Reflex TM charging becomes hired [10]. The identical bidirectional method of charging idea can also to be applied to SRC charging [11]. Control and research of the SRC and PRC charging schemes were the focal point of a few articles [12]. To begin, the SRC charging mechanism and a look at of greatest charging recurrence for Li-particle batteries were presented in [13]. The impedance of a battery checked that took into consideration of DC a part of SRC charging. A two-phase Z-source booming far off charger with line recurrence sinusoidal charging became proposed in connection with [14]. Furthermore, [15] set up a web-primarily based following computation that may be used to continually disseminate and comply with the perfect charging recurrence for normal batteries for any purpose. Furthermore, demanding situations with Li-particle battery SRC charging have been proposed in [16]. Despite the achievement of these provided tactics, the bidirectional electricity glide manage combining SRC and PRC strategies together with a three-degree converter has been ignored. A three-phase battery charger the usage of PRC and CC charging turned into presented in [17]. In any event, the SRC charging function turned into no longer considered at the same time as bidirectional charging changed into being developed/it become no longer designed to release competencies.

Test System under Implementation

The test system along with control blocks of proposed system are depicted in Fig. 1. The AC link is connected to the loads where as the DC link is associated with the batteries. To achieve better control strategies and simplified converter, directly the dq transformation method adopted hear. Hence, in this article the proposed dq controller with fuzzy implementation will provide the various control strategies for the power converters.

Proposed Controller

The proposed controller for implementation of bidirectional power flow uses dq/abc transformation. The three phase voltage signals are converted into d-axis and q-axis quantities of voltages and currents using dq transformation block. The phase locked loop fixes the voltage signals on d-axis and q-axis. The reference q-axis is set to zero for achieving unity power factor. For controlling the energy transfer among the battery and grid, the



**Marimuthu et al.,**

discharging/charging of the battery currents are regulated. This uses the fuzzy rule base (FRB) for optimal generation of the switching pulses. The FRB for this controller is presented in Table 1.

SIMULATION RESULTS

The battery voltage, current and DC link voltages with proposed controller are shown in fig's. 2, 3 and 4 respectively. For the duration of the period of charging, the converter is in AC-DC mode of operation and also the power flows in the direction to the battery from the grid. On the dissimilar, the converter is in DC-AC mode of operation during the period of discharging and the power flows to the grid from the battery. The Fig.'s 5 and 6 are depicts that the Grid current and voltage in the grid connected system. The THD of voltage and current are shown if Fig.'s 7 and 8. The THD of current and voltages by using fuzzy logic controller are shown in fig.'s 9 and 10.

CONCLUSION

In this work, we proposed a fuzzy logic controller based control of bidirectional power flow in grid interfaced converters. The converter can work in both DC-AC (PFC) and AC-DC (inverter) modes to achieve the bidirectional control to drift the regulation. The five different charging techniques have been explored and developed in order to enhance the performance of charging and battery existence. The important contribution includes the five different methods of charging and discharging techniques are incorporated with the proposed charger. These charging strategies can be completed using the proposed converter and the d-q transformation strategy. Furthermore, the charging power discrepancies among each approach are tested in element and mathematically deduced. Finally, simulation effects generated with MATLAB/SIMULINK and it exhibit the better performance and viability in terms of THD of the proposed bidirectional charger.

REFERENCES

1. K. Thirugnanam, S. K. Kerk, C. Yuen, N. Liu, and M. Zhang, "Energy management for renewable microgrid in reducing diesel generators usage with multiple types of battery", *IEEE Trans. Ind. Electron.*, vol. 65, no. 8, pp. 6772-6786, Aug. 2018.
2. P. B. L. Neto, O. R. Saavedra, and L. A. de Souza Ribeiro, "A dual-battery storage bank configuration for isolated microgrids based on renewable sources", *IEEE Trans. Sustain. Energy*, vol. 9, no. 4, pp. 1618- 1626, Oct. 2018.
3. U. Manandhar, N. R. Tummuru, S. K. Kollimalla, A. UKil, G. H. Beng, and K. Chaudhari, "Validation of faster joint control strategy for battery- and supercapacitor-based energy storage system", *IEEE Trans. Ind. Electron.*, vol. 65, no. 4, pp. 3286-3295, Apr. 2018.
4. F. Wu, X. Li, F. Feng, and H. B. Gooi, "Multi-topology-mode grid connected inverter to improve comprehensive performance of renewable energy source generation system", *IEEE Trans. Power Electron.*, vol. 32, no. 5, pp. 3623-3633, May 2017.
5. Z. Zhang, Y.-Y. Cai, Y. Zhang, D.-J. Gu, and Y.-F. Liu, "A distributed architecture based on microbank modules with self-reconfiguration control to improve the energy efficiency in the battery energy storage system", *IEEE Trans. Power Electron.*, vol. 31, no. 1, pp. 304-317, Jan. 2016.
6. S. Dey, Y. Shi, K. Smith, A. Colclasure, and X. Li, "From battery cell to electrodes: Real-time estimation of charge and health of individual battery electrodes", *IEEE Trans. Ind. Electron.*, vol. 67, no. 3, pp. 2167-2175, Mar. 2020.
7. D. Varajão, R. E. Araújo, L. M. Miranda, and J. A. P. Lopes, "Modulation strategy for a single-stage bidirectional and isolated ACDC matrix converter for energy storage systems", *IEEE Trans. Ind. Electron.*, vol. 65, no. 4, pp. 3458-3468, Apr. 2018.





Marimuthu et al.,

8. C.-Y. Tang, Y.-F. Chen, Y.-M. Chen, and Y.-R. Chang, "DC-link voltage control strategy for three-phase back-to-back active power conditioners", IEEE Trans. Ind. Electron., vol. 62, no. 10, pp. 6306-6316, Oct. 2015.
9. J. P. R. A. Mello and C. B. Jacobina, "Asymmetrical cascaded three-phase ACDC converters with injection transformers", IEEE Trans. Ind. Appl., vol. 55, no. 3, pp. 2800-2812, Jun. 2019.
10. M. M. Hasan, A. Abu-Siada, and M. S. A. Dahidah, "A three-phase symmetrical DC-link multilevel inverter with reduced number of DC sources", IEEE Trans. Power Electron., vol. 33, no. 10, pp. 8331- 8340, Oct. 2018.
11. G. Farivar, B. Hredzak, and V. G. Agelidis, "A DC-side sensor less cascaded H-bridge multilevel converter-based photovoltaic system", IEEE Trans. Ind. Electron., vol. 63, no. 7, pp. 4233-4241, Jul. 2016.
12. H. Salimian and H. Iman-Eini, "Fault-tolerant operation of three-phase cascaded H-bridge converters using an auxiliary module", IEEE Trans. Ind. Electron., vol. 64, no. 2, pp. 1018-1027, Feb. 2017.
13. B. Mangu, S. Akshatha, D. Suryanarayana, and B. G. Fernandes, "Grid connected PV-wind-battery-based multi-input transformer-coupled bidirectional DC-DC converter for household applications", IEEE J. Emerg. Sel. Topics Power Electron., vol. 4, no. 3, pp. 1086-1095, Sep. 2016.
14. R. Baranwal, K. V. Iyer, K. Basu, G. F. Castelino, and N. Mohan, "A reduced switch count single-stage three-phase bidirectional rectifier with high-frequency isolation", IEEE Trans. Power Electron., vol. 33, no. 11, pp. 9520-9541, Nov. 2018.
15. D. Sha, G. Xu, and Y. Xu, "Utility direct interfaced charger/discharger employing unified voltage balance control for cascaded H-bridge units and decentralized control for CF-DAB modules", IEEE Trans. Ind. Electron., vol. 64, no. 10, pp. 7831-7841, Oct. 2017.
16. R. Wang, Q. Sun, W. Hu, Y. Li, D. Ma, and P. Wang, "SoC-based droop coefficients stability region analysis of the battery for stand-alone supply systems with constant power loads", IEEE Trans. Power Electron., vol. 36, no. 7, pp. 7866-7879, Jul. 2021.
17. N. Tashakor, E. Farjah, and T. Ghanbari, "A bidirectional battery charger with modular integrated charge equalization circuit", IEEE Trans. Power Electron., vol. 32, no. 3, pp. 2133-2145, Mar. 2017.

Table 1: FRB for the MSVSC controller

	Error (E)					
	NB	NS	Z	PS	PB	
Change in Error (CE)	NB	NB	NS	NS	NS	Z
	NS	NB	NS	NS	Z	PS
	Z	NS	NS	Z	PS	PS
	PS	NS	Z	PS	PS	PB
	PB	Z	PS	PS	PB	PB

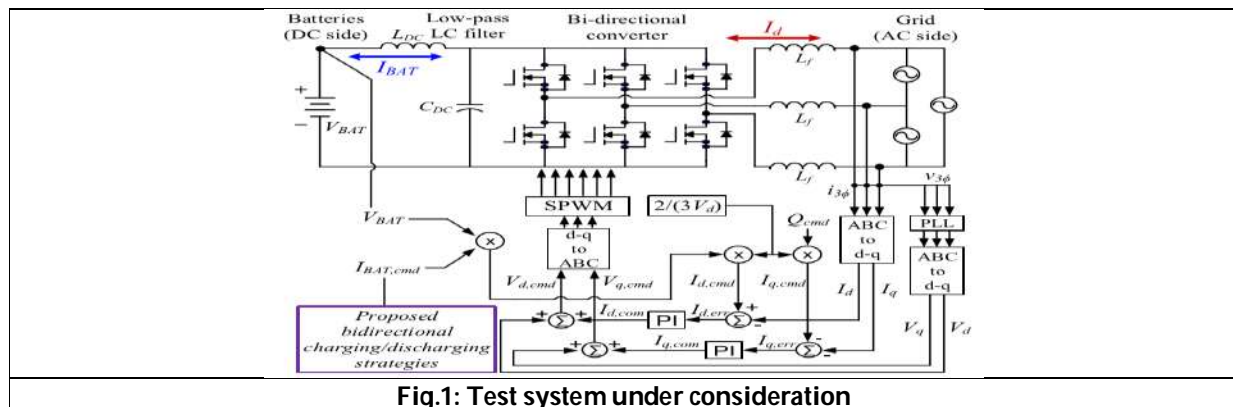


Fig.1: Test system under consideration





Marimuthu et al.,

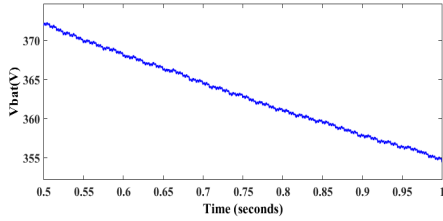


Fig.2: Battery Voltage

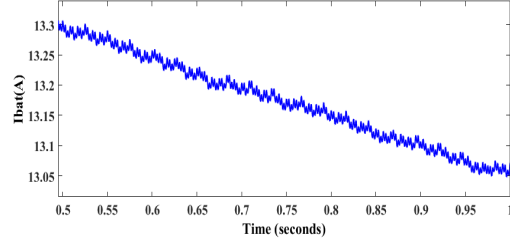


Fig. 3: Battery Current

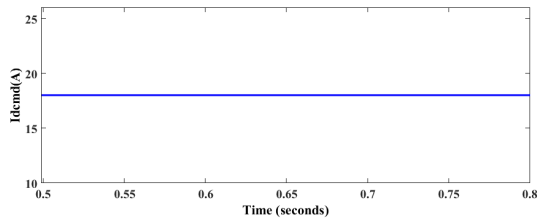


Fig. 4: DC link voltage

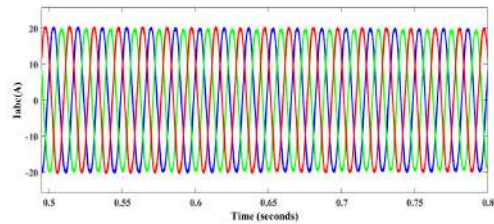


Fig. 5: Grid current

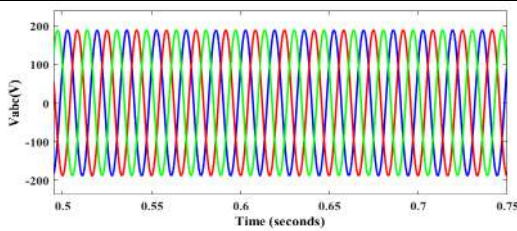


Fig.6: Grid voltage

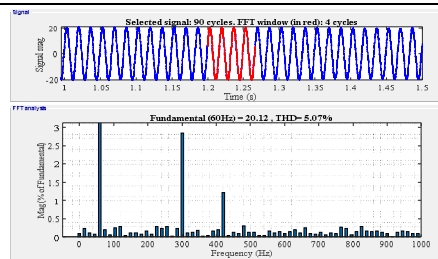


Fig.7: THD of voltage

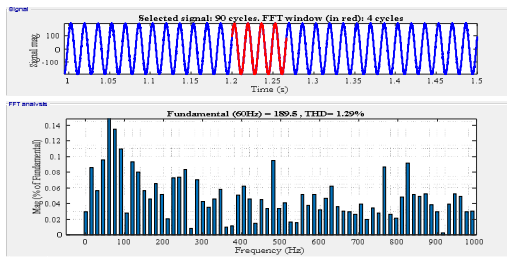


Fig.8: THD of current

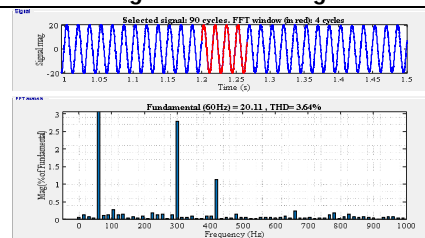


Fig.9: THD of current by using fuzzy logic controller

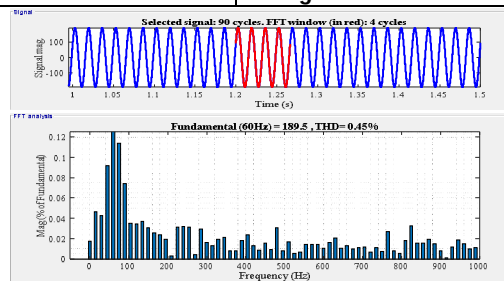


Fig.10: THD of voltage by using fuzzy logic controller





Evaluation of the Relationship between Gastrointestinal Symptoms and Liver Disease Patients: A Prospective Interventional Study

V. Karthikeyan¹, Govind K Purushothaman² and Chithira. G^{3*}

¹Professor, Department of Pharmacy Practice, Grace College of Pharmacy, Kodunthirapully, Palakkad, Kerala, India

²Surgical Gastroenterologist, Paalana Institute of Medical Sciences, Palakkad, Kerala, India.

³M.Pharm, Department of Pharmacy Practice, Grace College of Pharmacy, Kodunthirapully, Palakkad, Kerala, India.

Received: 09 Feb 2023

Revised: 25 Apr 2023

Accepted: 15 May 2023

*Address for Correspondence

Chithira. G

M.Pharm,

Department of Pharmacy Practice,

Grace College of Pharmacy,

Kodunthirapully, Palakkad, Kerala, India.

E.Mail: chithiragovindarajan@gmail.com



This is an Open Access Journal / article distributed under the terms of the **Creative Commons Attribution License** (CC BY-NC-ND 3.0) which permits unrestricted use, distribution, and reproduction in any medium, provided the original work is properly cited. All rights reserved.

ABSTRACT

Liver disease refers to any ailment that harms the liver and impairs its ability to function normally. One crucial thing to figure out is how disease patients' gastrointestinal symptoms relate to one another. To evaluate the relationship between gastrointestinal symptoms in liver disease patients. A prospective interventional study was conducted for 6 months period at a private hospital in Palakkad. The relationship between gastrointestinal symptoms was determined by the Gastrointestinal symptom rating scale (GSRs). The collected cases were entered in MS Excel 2007 & Descriptive statistics were performed. A total of 70 participants with age >18 diagnosed with liver disease were included in the study. The majority of patients (35.7%) were diagnosed with alcoholic fatty liver disease. Out of 70 patients, 28 (40%) were diagnosed with abdominal pain while it is reduced to 25(35.7) on follow-up. The average Reflux score was 1.98 on the baseline and 1.25 on the follow-up, abdominal pain was 2.49 on the baseline while 1.97 on the follow-up, indigestion score of 1.94 on the baseline while 1.51 on the follow-up, Diarrhea score of 1.14 and 1.13 and constipation score of 2.62 and 1.67 on follow-up. Except for the diarrhea domain, all the domains were found to be statistically significant. All domains of GSRs score have been found to be decreased after follow-up studies.

Keywords: NAFLD (Non- alcoholic fatty liver disease), QOL (Quality of life), CLD (Chronic liver disease), GSRs (Gastrointestinal symptom rating scale).



**Chithira et al.,**

INTRODUCTION

Protein-energy malnutrition (PEM), which is widespread in individuals with liver diseases, is due to the liver's central participation in nutritional and fuel metabolism. Moreover, this insufficiency results in poor outcomes and a reduction in living standards (QOL).[4] Worldwide, the prevalence of non-alcoholic fatty liver disease (NAFLD) has been rising. Currently, 75% of chronic cases of liver disease in the US are caused by NAFLD. Obesity, a number of metabolic disorders, and even cardiovascular problems have all been related to NAFLD. NAFLD develops without regard to weight or alcohol use. Lack of exercise and an unhealthy diet are lifestyle choices that significantly contribute to the onset of NAFLD [1].Cirrhosis is a chronic liver condition that is incurable, progresses, and is accompanied by consequences such as upper gastrointestinal hemorrhage and hepatic encephalopathy. Ascites, hepatic encephalopathy, and variceal hemorrhage are only a few of the consequences associated with chronic liver disease (CLD), which is known to cause high morbidity and death. [3] Patients with liver cirrhosis display several signs of gastrointestinal dysfunction. Such issues could affect a person's quality of life in terms of their health and nutritional state. The frequency of abdominal discomfort in liver diseases varies depending on the extent of the condition, emotional stress, and intestinal abnormalities. [10] One of the main causes of illness and death worldwide is a chronic liver disease (CLD). The most prevalent risk markers include alcohol, chronic hepatitis B and C, non-alcoholic steatohepatitis (NASH), malnutrition, toxins, and several tropical illnesses. [11]

MATERIALS AND METHOS

A prospective interventional study was conducted for 6 months period at a private hospital in Palakkad.All patients of age ≥ 18 years or older with diagnosed liver disease and Patients with or without co-morbidities were included in the study while patients who were terminally ill, hemodynamically unstable, and too ill to complete the questionnaire, patients not willing to give consent for the study and patients unable to complete the questionnaire due to severe comorbidities were excluded from the study. The study was approved by the institutional ethics committee of Grace College of Pharmacy, Palakkad. GCP/IEC/112B/2022 dated 05-07-2022. The relationship between gastrointestinal symptoms was determined by the Gastrointestinal symptom rating scale (GSRS). Signed informed consent was taken from the patient prior to the study. A pre-designed patient data collection form was used to collect the required information. The relationship between gastrointestinal symptoms in liver disease is assessed by Gastrointestinal Symptom Rating Scale (GSRS). The questionnaire contains 15 items and is rated on a seven-point Likert scale (No discomfort to very severe discomfort). Based on a factor analysis, the 15 GSRS items break down into 5 scales. Abdominal pain, reflux syndrome,Diarrhea syndrome, Indigestion syndrome, and constipation syndrome[16],[17].

STATISTICAL ANALYSIS

The collected cases were entered in MS Excel for calculating the percentage of various parameters. Descriptive statistics like frequency and percentage, Standard deviation are used to describe the demographic characteristics and determinants of liver diseases. The detection of significant differences for continuous variables between groups was performed using an unpaired t-test.

RESULTS

The study encompassed a total of 70 participants who were older than 18 and had been diagnosed with liver disease. In regards to age, table No. 1 reveals that 10 (14.2%) patients fall under the category of those who are over 65, while 30 (42.8%) patients are under 45 and an equal ratio was between 45 and 65. Demographic characteristics are presented in table no:2. The liver disease was more prevalent among male patients 46(65.7%) while only 24(34.2%) are female patients. 2(2.8%) were vegetarian whereas 68(97.14%) have a dietary habit of a mixed diet. 24 (34.2%) patients were physically active while 46 (65.7%) were not active. Based on educational qualification majority 25



**Chithira et al.,**

(35.7%) were having primary school education, 24 (34.2%) had a high school education, 11 (15.7%) had college-level education while 10 (and 14.2%) were uneducated. Most of the patients 66 (94.2%) were employed and 4 (5.7%) were unemployed. According to drinking habits, 40 (57.1%) were alcoholic while 30 (42.8%) were non-alcoholic. Of the 40 alcoholic patients, 37 (52.8%) were having an alcohol history for >5 years, 2 (2.85%) between 3-5 years, and 1 for <3 years as given in table no:3 Clinical characteristics are presented in table no:4. In terms of the etiology of liver disease, the patients with alcoholism were most prevalent 39 (55.7%) while 25 (35.7%) due to an unhealthy diet, and 3 (4.28%) each due to hereditary and other reasons. The number of patients diagnosed with alcoholic fatty liver and non-alcoholic fatty liver was almost equal to 25 (35.7%) and 23 (32.8%) respectively, while 12 (17.1%) with CLD and 10 (14.2%) with cirrhosis. The liver disease was graded the most prevalent was grade 1 with 33 (68.7%) while grade 2 with 15 (31.2%).

Out of 70 patients, 28 (40%) were diagnosed with abdominal pain while it is reduced to 25 (35.7%) on follow-up. 7 (10%) patients were having flatulence symptoms while it is reduced to 5 (7.14%) on follow-up. 8 (11.4%) patients were having constipation symptoms while it was reduced to 6 (8.57%) on follow-up. 22 (31.4%) patients had flatulence with abdominal pain while it increased to 26 (37.14%) on follow-up. 2 (2.85%) patients were having abdominal pain and constipation and it remained the same on follow-up. 5 (7.14%) had flatulence, abdominal pain, and constipation and it increased to 6 (8.57%) on follow-up as illustrated in table no: 5. Based on the GSRS score mean Reflux score was 1.98 on the baseline and 1.25 on the follow-up, abdominal pain was 2.49 on the baseline while 1.97 on the follow-up, indigestion score was 1.94 on the baseline while 1.51 on the follow-up, Diarrhea score of 1.14 and 1.23 and constipation score of 2.62 and 1.67 on follow-up when compared with baseline the Reflux score was ($p < 0.0001$), abdominal pain ($p < 0.0002$), the indigestion domain ($p < 0.0014$) and constipation domain ($p < 0.0001$) was found to be statistically significant while diarrhea domain was not statistically significant with baseline study ($p = 0.96$) is given in table no:6

DISCUSSION

In the current study patients of the male gender were mostly affected by liver diseases. The fact that there were more patients under 65 may be linked to the increasing tendency to consume processed carbs, the adoption of a sedentary lifestyle, and the expanded habit of consuming alcohol at an early age. Liver health is significantly impacted by our food. Yasutake K *et al* in a study conducted in 2014 has similar findings that support this study that, a mixed diet, which contains fat, sugar, and processed foods that promote fat buildup, raises the likelihood of developing liver disease compared to vegan diets [13]. Another intriguing discovery was that individuals with a history of alcoholism had a higher incidence of liver illness and were more numerous; this suggests that years of alcohol misuse are one of the main causes of the upsurge in liver disease. Patients who were not physically active had a heightened risk of acquiring the liver disease. Due to the lack of exposure, patients with elementary school education were more prevalent. The result revealed that alcohol consumption is the primary cause of liver disease, but it also demonstrates that genetics and other factors play a significant role in the development of liver disease. As most heavy drinkers have fatty livers, the data shows that alcoholic liver disease was the most commonly diagnosed liver disease. Wang *et al* 2022 in Beijing conducted a cross-sectional study showing similar data [14]. The modifications in lifestyle were just behind non-alcoholic fatty liver. Previous research has indicated that the duration of a person's drinking history, rather than just the typical amount taken, is virtually certainly associated with their chance of developing cirrhosis. Contrarily, some clinical evidence suggests that quitting drinking at any stage of the disease's natural history lowers the likelihood that the condition will worsen and that complications from cirrhosis will develop. The findings provide strong evidence for this theory. According to grades of liver disease, patients with fatty livers made up a larger percentage of grade 1 cases.

The current study shows that patients with liver disease were found to have increased severity of abdominal pain, flatulence, constipation, and abdominal pain with constipation, which was found to be reduced during follow-up studies. Gastrointestinal symptoms are common in liver disease, and patients exhibit several features of gut



**Chithira et al.,**

dysfunction, which may assist to induce complications. The study clearly concludes that all the GSRs average score was found to be reduced during follow-up studies

CONCLUSION

The result of the study reveals that alcohol was the major cause of liver disease and gastrointestinal symptoms play a major role in the development of liver disease. In conclusion, the severity of gastrointestinal symptoms is reduced among liver disease patients.

LIMITATIONS

This study had several limitations. This was a small study conducted at a single center. The duration of the study was done within 6 months. The follow-up period was done after 15 days.

ACKNOWLEDGEMENTS

The authors thank the doctor and all nurses and patients at Paalana institute of medical sciences for their selfless dedication and help to complete the study successfully.

CONFLICTS OF INTEREST

The authors have no conflicts of interest regarding the study

REFERENCES

1. Han AL. Association between non-alcoholic fatty liver disease and dietary habits, stress, and health-related quality of life in Korean adults. *Nutrients*. 2020 Jun;12(6)
2. Zhang X, Xi W, Liu L, Wang L. Improvement in quality of life and activities of daily living in patients with liver cirrhosis with the use of health education and patient health empowerment. *Medical science monitor: international medical journal of experimental and clinical research*. 2019; 25:4602.
3. Gao F, Gao R, Li G, Shang ZM, Hao JY. Health-related quality of life and survival in Chinese patients with chronic liver disease. *Health and Quality of Life Outcomes*. 2013 Dec;11(1):1-8.
4. Shiraki M, Nishiguchi S, Saito M, Fukuzawa Y, Mizuta T, Kaibori M, Hanai T, Nishimura K, Shimizu M, Tsurumi H, Moriwaki H. Nutritional status and quality of life in current patients with liver cirrhosis as assessed in 2007–2011. *Hepatology Research*. 2013 Feb;43(2):106-12.
5. Younossi ZM, Guyatt G, Kiwi M, Boparai N, King D. Development of a disease-specific questionnaire to measure health-related quality of life in patients with chronic liver disease. *Gut*. 1999 ;45(2):295-300.
6. Bondini S, Kallman J, Dan A, Younoszai Z, Ramsey L, Nader F, Younossi ZM. Health-related quality of life in patients with chronic hepatitis B. *Liver International*. 2007;27(8):1119-25.
7. Kanwal F, Gralnek IM, Hays RD, Zeringue A, Durazo F, Han SB, Saab S, Bolus R, Spiegel BM. Health-related quality of life predicts mortality in patients with advanced chronic liver disease. *Clinical Gastroenterology and Hepatology*. 2009 ;7(7):793-9.
8. Kim SH, Oh EG, Lee WH. Symptom experience, psychological distress, and quality of life in Korean patients with liver cirrhosis: a cross-sectional survey. *International journal of nursing studies*. 2006 ;43(8):1047-56.
9. Gazineo D, Godino L, Bui V, El Mouttaqi L, Franciosi E, Natalino A, Ceci G, Ambrosi E. Health-related quality of life in outpatients with chronic liver disease: a cross-sectional study. *BMC Gastroenterol*. 2021;21(1):318.
10. Mondal D, Das K, Chowdhury A. Epidemiology of liver diseases in India. *Clinical liver disease*, vol 19,2022:114-117.
11. Sharma, P.; Arora, A. Clinical presentation of alcoholic liver disease and non-alcoholic fatty liver disease: Spectrum and diagnosis. *Transl. Gastroenterol. Hepatol*. 2020, 5, 19.





Chithira et al.,

12. Marjot, T.; Moolla, A.; Cobbold, J.F.; Hodson, L.; Tomlinson, J.W. Nonalcoholic fatty liver disease in adults: Current concepts in etiology, outcomes, and management. *Endocr. Rev.* 2020, 41, 66–117.
13. Yasutake K, Kohjima M, Kotoh K, Nakashima M, Nakamuta M, Enjoji M. Dietary habits and behaviors associated with nonalcoholic fatty liver disease. *World Journal of Gastroenterology: WJG.* 2014 Feb 2;20(7):1756.
14. Wang H, Gao P, Chen W, Yuan Q, Lv M, Bai S, Wu J. A cross-sectional study of alcohol consumption and alcoholic liver disease in Beijing: based on 74,998 community residents. *BMC Public Health.* 2022 Apr 12;22(1):723.
15. Younossi, Z.M. Non-alcoholic fatty liver disease—A global public health perspective. *J. Hepatol.* 2019, 70, 531–544.
16. Kalaitzakis E. Gastrointestinal dysfunction in liver cirrhosis. *World J Gastroenterol.* 2014 Oct 28;20(40):14686-95.
17. Revicki DA, Wood M, Wiklund I, Crawley J. Reliability and validity of the gastrointestinal symptom rating scale in patients with gastroesophageal reflux disease. *Qual Life Res.* 1997 Jan 1;7(1):75-83.

Table no: 1. Distribution based on age. (n=70)

SI.NO	Age in years	Mean± SD	No of patients	Percentage
1	<45	35.7±0.70	30	42.8
2	45-65	49.04±0.62	30	42.8
3	>65	72±1.23	10	14.2

Table No: 2. Demographic Characteristics of Participants (N=70)

SI.NO	Characteristics	Classification	No of patients	Percentage
1	Gender	Men	46	65.7
		Women	24	34.2
2	Dietary habit	Vegetarian	2	2.8
		Both	68	97.14
4	Physical activity	Active	24	34.2
		Not-active	46	65.7
5	Level of education	Uneducated	10	14.2
		Primary school	25	35.7
		High school	24	34.2
		College	11	15.7
6	Employment	Unemployed	4	5.7
		Employed	66	94.2

Table no: 3 Drinking Habit in Patients

SI.NO	Characteristics	Classification	No of patients	Percentage
1	Drinking habit	Alcoholic	40	57.1
		Non-alcoholic	30	42.8
2	Years of alcoholism	<3	1	1.42
		3-5	2	2.85
		>5	37	52.8

Table No: 4 Clinical Characteristics of Patients(N=70)

SI NO	Characteristics	Classification	No of patients	Percentage
1	Etiology of liver disease	Hereditary	3	4.28
		Alcohol	39	55.7
		Unhealthy diet	25	35.7
		Others	3	4.28





Chithira et al.,

2	Diagnosis	Alcoholic fatty liver	25	35.7
		Non-alcoholic fatty liver	23	32.8
		Cirrhosis	10	14.2
		Chronic liver disease	12	17.1
4	Grade	Grade 1	33	68.7
		Grade 2	15	31.2
		Grade 3	0	0

Table No: 5 Overall Symptom Experience (N=70)

SI.NO	Symptoms	N (70)	(%)	N (70)	(%)
		Baseline		Follow-up	
1	Flatulence	7	10	5	7.14
2	Abdominal pain	28	40	25	35.7
3	Constipation	8	11.4	6	8.57
4	Flatulence + abdominal pain	22	31.4	26	37.14
5	Abdominal pain + constipation	2	2.85	2	2.85
6	Flatulence + abdominal pain + constipation	5	7.14	6	8.57

Table No:6 GSRS Score(N=70)

SI.NO	GSRS	Mean ± SD	Mean ± SD	p-value
		Baseline	Follow-up	
1	Reflux	1.98±0.11	1.25±0.08	<0.0001
2	Abdominal pain	2.49±0.09	1.97±0.09	0.0002
3	Indigestion	1.94±0.10	1.51±0.08	0.0014
4	Diarrhea	1.14±0.08	1.13±0.06	0.96
5	Constipation	2.62±0.13	1.67±0.11	<0.0001





An Attitude of Personality Factors among Prospective Teachers in Tamil Nadu

A.Antony Lawrence¹ and R.Jeyanthi^{2*}

¹Research Scholar, School of Education, Vels Institute of Science, Technology and Advanced Studies (VISTAS), Pallavaram, Chennai-600117, Tamil Nadu, India.

²Associate Professor, School of Education, Vels Institute of Science, Technology and Advanced Studies (VISTAS), Pallavaram, Chennai-600117, Tamil Nadu, India

Received: 13 Feb 2023

Revised: 09 Apr 2023

Accepted: 15 May 2023

*Address for Correspondence

R.Jeyanthi

Associate Professor,
School of Education,

Vels Institute of Science, Technology and Advanced Studies (VISTAS),
Pallavaram, Chennai-600117, Tamil Nadu, India.



This is an Open Access Journal / article distributed under the terms of the **Creative Commons Attribution License** (CC BY-NC-ND 3.0) which permits unrestricted use, distribution, and reproduction in any medium, provided the original work is properly cited. All rights reserved.

ABSTRACT

This cannot be achieved with intellect, but it can be achieved skillfully with character. That is the power of personality. With or without knowledge and will, we are affected and victimized by character. Teachers who work with children from infancy to adulthood have a great impact on their students at every stage. The Big Five personality factors play an important role in this process. This study used B.Ed.'s simple randomization method to examine the Big Five personalities of 1,405 prospective teachers. The statistical methods used in this study were arithmetic, mean, standard deviation, and 't-test. Here are the results of our investigation: The majority of prospective teachers had high levels of Big Five personality factors. Difference analyzes showed that male and female prospective teachers had no significant differences in the personality factors of agreeableness, conscientiousness, and emotional stability. However, there are clear differences in the personality factors extraversion and openness between male and female prospective teachers. Male trainee teachers were found to be superior to female trainee teachers in extroverted and open personality traits. Furthermore, it was shown that there were no significant differences in the personality factors of extraversion, agreeableness, conscientiousness, and openness between unmarried teachers and married teacher candidates. However, there were significant differences in emotional stability personality factors between unmarried and married teachers. Comparing mean scores for unmarried and married teacher candidates, unmarried prospective teachers performed better than married prospective teachers on the emotional stability personality trait.

Keywords: Big Five Personality Factors, Extroversion, Agreeableness, Conscientiousness, Emotional Stability, Openness



**Antony Lawrence and Jeyanthi**

INTRODUCTION

Teaching is a gift. Being a teacher is noble. Teaching is professional and rewarding in one way and demanding in another. What is gratifying in many ways and highest of these is the reputation teachers enjoy among the public and the deep sense of inner satisfaction that teachers have deep within their hearts. The dissemination of teacher knowledge brings students to life. Teachers influence their students directly and indirectly; publicly and secretly; inside the classroom and outside the classroom. Besides knowledge, skills and attitudes of teachers are the factors that shape and shape students. One of them is the personality of the teachers. This article aims to explore the Five Personality Traits of prospective teachers.

Significance of the Study

Personality is "the sum of an individual's distinct behavioural and mental characteristics. Informally, it refers to the personal qualities that make a person popular in society" ("A Dictionary of Psychology," 2008). The list of attributes, characteristics, or factors that develop a person's personality is very long. Psychologists have tried many times to enumerate these attributes meticulously and precisely. "Many contemporary personality psychologists believe that there are five basic dimensions of personality, commonly referred to as the 'Big 5' personality traits. The five major personality traits described by the theory are extraversion, agreeableness, openness, conscientiousness, and neuroticism" (Power & Pluess, 2015). Teachers and prospective teachers interact with students and their interactions greatly influence their students. Therefore, it is important to explore the personalities of these Big Five because it affects the teaching-learning process.

Research Questions

Research revolves around the problem of meaning. The beginning of a study involves defining the research problem and thus stating the research problem that gives clarity to the research. Kerlinger defines in the research context "A problem is a question or statement that asks: What relationship exists between two or more variables?" (Pandey, P. & Pandey, M. M. (2015): *Research Methodology; Tools and Techniques. Romania. Available Online at www.euacademic.org/bookupload/9.pdf, Checked on 6/25/2019., n.d.*)

- What is the level of the Five Great Personality Factors for prospective teachers?
- Are there significant differences in prospective teachers' Five Major Personality Factors for their gender and marital status?

Operational Definition of the Key Terms

Five major personality factors: It refers to five important personality traits: 1. Extraversion, 2. Pleasantness. 3. Consciousness, 4. Emotional stability and 5. Openness (Power & Pluess, 2015). In this study, the personality traits of the Five Potential Traits were measured by scores obtained in the investigator administered Five Big Group Inventory

Extroversion

This is a characteristic trait of sociability, talkativeness, assertiveness, and excellent emotional expression. People with this trait are extroverts and make new friends easily. Weak people like to be alone, difficult to talk to, and blend in with people.

Agreeableness

This is a trait characterized by trust, altruism, kindness, affection, and other social behaviours. People with this high trait tend to be more cooperative, enjoying helping and contributing to the happiness of others. Short people are less concerned with other people's problems, insult and demean others, and are more competitive.



**Antony Lawrence and Jeyanthi****Conscientiousness**

This is a hallmark of thoughtfulness, impulse control, and goal-directed behaviour. These high-trait people tend to be organized, take time to prepare, complete important tasks on time, and stick to their schedule. People who tend to dislike structure and schedules, procrastinate, and do not get things done.

Emotional Stability

This is a trait characterized by resilience and a balanced attitude. It is considered the negative of neurosis. People with this high trait tend to handle stress well, do not worry much, and are very relaxed. People who are less prone to mood swings, anxiety, irritability, and sadness.

Openness

This is a trait characterized by imagination, insight, and creativity. People with this trait tend to have many interests and are open to taking on new challenges. People who are a bit open are more traditional, do not like change, resist new ideas, and struggle with abstract thinking.

Objectives of the Study

- To find out the extent of prospective teachers' Big Five personality factors
- To find out whether there were significant differences in prospective teachers' Big Five personality factors in terms of gender and their marital status or not.

Hypotheses

- There were no significant differences in the Five Major Personality Factors of prospective teachers for gender.
- There were no significant differences in the Five Major Personality Factors of prospective teachers on marital status.

METHODOLOGY

The investigator used survey methods to study Five major personality factors of prospective teachers. Survey research is a widely used method in the social sciences. It "refers to the set of methods used to systematically collect data from a variety of individuals, organizations, or other entities of interest (*The Sage Encyclopedia of Qualitative Research Methods. 1 (2008) - Google Books, n.d.*).

Population

The study population included all prospective teachers completing a B.Ed. course at education colleges in the Cuddalore, Villupuram and Kallakurichi districts of Tamil Nadu.

Sample and Sampling Technique

The sample for this study included 442 prospective teachers from Cuddalore, 487 prospective teachers from Villupuram and 476 prospective teachers from Kallakurichidistricts. A simple random sampling technique was used to select the sample.

Tool Used

An inventory of the five major personalities developed and validated by the surveyors and documentation used for data collection. John and Srivastava's Big Five Inventory serves as the source to build the tool for the research.

Statistical Techniques Used

The enumerator used mean, standard deviation and "t" test to analyze the collected data.



**Antony Lawrence and Jeyanthi****Analysis of Data****Descriptive Analysis**

Objective 1: To find out the level of Big Five personality factors of prospective teachers

We infer from the table above that 14.7% of prospective teachers have a low degree of extroversion and 85.3% of them have a high degree of extroversion. 17.7% of prospective teachers have low agreeableness and 82.3% of them have high. 15.2% of future teachers have low cognitive level and 84.8% of them have high level. 15.9% of prospective teachers have low levels of emotional stability and 84.1% of them have high levels. 15.7% of prospective teachers have a low level of openness and 84.3% of them have a high level of openness.

Differential Analysis**Hypothesis 1**

There were no significant differences between prospective male and female teachers in their Five Major Personality Factors (1) extroversion, (2) agreeableness, (3) conscientiousness, (4) emotional stability touch, and (5) openness. From the table above, it can be deduced that the calculated "t" values of the factors of personality, consent, conscientiousness, and emotional stability (1.92, 0.73, 1.29) are lower than the values. The value in the table (1.96) is significant at the 0.05 level. Therefore, the null hypothesis regarding agreeableness, conscientiousness, and emotional stability is accepted. Therefore, the results showed that there was no significant difference between prospective male and female teachers in terms of their personality factors: agreeable, conscientious, and emotionally stable. But the calculated t-values of personality factors, extroversion, and openness (2.96, 2.91) were higher than the panel value (1.96) at the significance level of 0.05. Therefore, the null hypothesis of extroversion and openness is rejected. Therefore, the results show that there is a significant difference between prospective male and female teachers in terms of their outgoing and open personality factors. Comparing the mean scores of prospective male and female teachers, males (mean = 37.73, 30.05) outperformed females (males = 35.92, 28.35) in terms of extroversion and their opening.

Hypothesis 2

There was no significant difference between single and married prospective teachers in their Big Five Personality Factors (1) extroversion, (2) agreeableness, (3) conscientiousness, (4) emotional stability and (5) openness. From the table above, it is deduced that the calculated "t" value of the extroversion, Likeability, Dedication, and Openness personality factors (1.22, 1.59, 1.74, 1.24) is lower than the price. values in the table (1.96) at the 0.05 level of significance. Therefore, the corresponding null hypothesis is accepted. Therefore, the results show that there is no significant difference between single and married prospective teachers in terms of their personality factors of extroversion, likability, conscientiousness, and openness. But the calculated "t" value of the emotional stability level of personality factor (2.33) is larger than the panel value (1.96) at the significance level of 0.05. Therefore, the null hypothesis regarding emotional stability is rejected. Therefore, the results show that there is a significant difference between single and married prospective teachers in their emotional stability on personality factors. Comparing the mean scores of prospective single and married teachers, single prospective teachers (mean = 37.57) outperformed married prospective teachers (mean = 35.90) in terms of academic achievement. Stabilize their feelings about personality traits.

Findings

- Percentage analysis of the 5 major personality factors shows that the degree of extroversion, agreeableness, conscientiousness, emotional stability, and openness for most prospective teachers is high.
- Disparity analysis revealed no significant differences between male and female prospective teachers on their personality factors: agreeable, conscientious, and emotionally stable. But there is a significant difference between prospective male and female teachers in terms of their outgoing and open personality. Prospective male teachers were rated as better than prospective female teachers in their outgoing and outgoing personality traits.
- Disparity analysis showed no significant difference between single and married prospective teachers in terms of their personality factors of extroversion, likability, conscientiousness, and openness. But there is a significant difference between single and married prospective teachers in their emotional stability on personality factors.





Antony Lawrence and Jeyanthi

Comparing the mean scores of prospective single and married teachers, single prospective teachers (mean = 37.57) outperformed married prospective teachers (mean = 35.90) in terms of academic achievement. Stabilize their feelings about personality traits.

CONCLUSION

“Students' learning outcomes largely depend on teacher behaviour” (*The Big Five Trait Taxonomy: History, Measurement, and Theoretical Perspectives*. - PsycNET, n.d.). The behaviour of a teacher to influence and bring about change in the behaviour of students largely depends on the personality he has. The term personality is a global and inclusive term. Reducing an individual's complete personality to certain limited entities can be a halfway job. However, a variety of research efforts have demonstrated the greatest influence on personality. Since teachers engage in human interaction in a formal teaching process, they need to develop their personality. This study suggests that prospective teachers have high personality in 5 big factors, which is an encouraging sign. This shows that they could influence their students and should now be given more instruction to develop these Big Five personality traits in their students. Prospective female teachers can receive training and workshops to develop extraversion and openness traits when they appear to be inferior to their peers. Future married teachers can get advice on developing their emotional stability. Developing These Five Great Traits can contribute to helping them become better at teaching.

REFERENCES

1. A Dictionary of Psychology. (2008). *A Dictionary of Psychology*. <https://doi.org/10.1093/ACREF/9780199534067.001.0001>
2. Pandey, P. & Pandey, M. M. (2015): *Research Methodology; Tools and Techniques*. Romania. Available online at www.euacademic.org/BookUpload/9.pdf, checked on 6/25/2019. (n.d.). Retrieved December 6, 2022, from <http://www.sciepub.com/reference/384601>
3. Power, R. A., & Pluess, M. (2015). Heritability estimates of the Big Five personality traits based on common genetic variants. *Translational Psychiatry*, 5(7). <https://doi.org/10.1038/TP.2015.96>
4. *The Big Five Trait taxonomy: History, measurement, and theoretical perspectives*. - PsycNET. (n.d.). Retrieved December 6, 2022, from <https://psycnet.apa.org/record/1999-04371-004>
5. *The Sage encyclopedia of qualitative research methods. 1 (2008)* - Google Books. (n.d.). Retrieved December 6, 2022, from https://books.google.co.in/books/about/The_Sage_encyclopedia_of_qualitative_res.html?id=MqfBtQEACAAJ&redir_esc=y

Table 1: Level of Big Five personality factors of Prospective Teachers

S. No:	Personality Factors	Low		High	
		N	%	N	%
1.	Extroversion	206	14.7	1199	85.3
2.	Agreeableness	249	17.7	1156	82.3
3.	Conscientiousness	213	15.2	1192	84.8
4.	Emotional stability	223	15.9	1182	84.1
5.	Openness	221	15.7	1184	84.3





Antony Lawrence and Jeyanthi

Table 2: Difference between the Male and the Female Prospective Teachers in their Big Five Personality Factors

S. No:	Personality Factors	Gender	N	Mean	S. D	Calculated 't' Value	Remarks
1.	Extroversion	Male	317	37.73	9.501	2.96	S
		Female	1088	35.92	9.793		
2.	Agreeableness	Male	317	33.00	7.342	1.92	NS
		Female	1088	33.85	6.769		
3.	Conscientiousness	Male	317	30.74	5.985	0.73	NS
		Female	1088	30.46	5.833		
4.	Emotional Stability	Male	317	30.25	5.823	1.29	NS
		Female	1088	29.77	5.853		
5.	Openness	Male	317	30.05	6.031	2.91	S
		Female	1088	28.35	5.797		

Note: The table value of 't' is 1.96; NS= Not Significant

Table 3: Difference between the Unmarried and the Married Prospective Teachers in their Big Five Personality Factors

S. No:	Personality Factors	Marital Status	N	Mean	S. D	Calculated 't' Value	Remarks
1.	Extroversion	Unmarried	1194	32.22	5.528	1.22	NS
		Married	211	31.72	5.628		
2.	Agreeableness	Unmarried	1194	33.78	6.759	1.59	NS
		Married	211	32.96	7.684		
3.	Conscientiousness	Unmarried	1194	30.41	5.733	1.74	NS
		Married	211	31.17	6.549		
4.	Emotional Stability	Unmarried	1194	37.57	9.562	2.33	S
		Married	211	35.90	9.676		
5.	Openness	Unmarried	1194	28.57	5.878	1.24	NS
		Married	211	28.02	5.548		

Note: The table value of 't' is 1.96; NS= not significant





Screening of Secondary Metabolites by FT-IR Spectroscopy

Venci Candida X^{1*}, Tresina L², Rashmi VS², Jayashree V², Mary Ajisha S², Antony Jenisha J² and Shenkani K³

¹Assistant Professor, Department of Zoology, Holy Cross College, Nagercoil, 629004. Kanyakumari District, Tamil Nadu, India.

²Student, Department of Zoology, Holy Cross College, Nagercoil, 629004. Kanyakumari District, Tamil Nadu, India.

³Assistant Professor, Department of Zoology, JKK Nattraja college of Arts and Science, Komarapalayam, 638183. Namakkal District, Tamil Nadu, India.

Received: 15 Feb 2023

Revised: 25 Apr 2023

Accepted: 30 May 2023

*Address for Correspondence

Venci Candida X

Assistant Professor,
Department of Zoology,
Holy Cross College, Nagercoil, 629004.
Kanyakumari District, Tamil Nadu, India.
E.Mail: venciaugustine@gmail.com



This is an Open Access Journal / article distributed under the terms of the **Creative Commons Attribution License** (CC BY-NC-ND 3.0) which permits unrestricted use, distribution, and reproduction in any medium, provided the original work is properly cited. All rights reserved.

ABSTRACT

The secondary metabolites present in various vegetable products showed medicinal properties. Four common vegetable products which we often add in our diet were taken as samples for our study. The four samples Amla (*Emblica officinalis*), Drumstick leaves (*Moringa oliefera*), beetroot (*Beta vulgaris*) and turmeric (*Curcuma longa*) were selected for our study. The samples Amla and drumstick leaves were collected from local area and beetroot and turmeric were collected from the local market. The samples were cut into thin slices and shade dried for three weeks. When it is completely dried, it was ground in the mixer jar to a smooth powder. The smooth powder of the four samples were extracted with ethanol and tested for secondary metabolites by FT-IR analysis. The obtained peaks of each sample were identified using the standard IR values. From the results obtained, we could conclude that all the four samples Amla (*Emblica officinalis*), Drumstick leaves (*Moringa oliefera*), beetroot (*Beta vulgaris*) and turmeric (*Curcuma longa*) have sufficient diversity of secondary metabolites which have high medicinal properties.

Keywords : FT-IR, Phytochemicals, IR chart, Amla (*Emblica officinalis*), Drumstick leaves (*Moringa oliefera*), beetroot (*Beta vulgaris*), turmeric (*Curcuma longa*)





Venci Candida et al.,

INTRODUCTION

Traditional and folkloric remedies are significant components of global health care. Plants and their extracts are the primary source of healthcare for almost a quarter of the world's population [1]. According to the World Health Organization, 65–80% of the world's population lives in underdeveloped nations where access to modern medicine is limited and they rely primarily on natural goods for their basic healthcare [2]. One of the oldest, richest, and most varied cultural traditions involving the use of medicinal herbs is found in India. Active biocomponents are described as chemical substances that either directly or indirectly treat or prevent disease [3]. The alkaloids, tannins, flavonoids, and phenols are the most significant of these bioactive chemical components of plants. These chemical substances are employed as natural insecticides, tastes, scents, textiles, beverages, and as a precursor for a variety of therapeutic medications because of the numerous advantages they provide for people [4]. Plants have medical value because of the phytochemicals in their compounds that influence many physiological processes in the body. Thus, by phytochemical screening, one may identify the many significant bioactive chemicals of the intriguing plant that could serve as the foundation for contemporary medications to treat a variety of diseases [5].

Based on the survey recorded in the villages of Kanyakumari district, the top four vegetables often used in diet were recorded as Amla, beetroot, drumstick leaves and turmeric. These four vegetables are screened for secondary metabolites using FT-IR spectroscopy. *Phyllanthus emblica*, also known as *Emblica officinalis* Gaertn. (Family: Euphorbiaceae), is also known as "Amla" or "amlaki" in Bengali and "Indian gooseberry" in English. Amla is said to be the richest source of vitamin C and is high in iron, fibre, and carbohydrates [6]. The vegetable plant known as Shamandar, or *Beta vulgaris* L., is a member of the Amaranthaceae family. Traditional Arab medicine has long employed beet roots to treat a wide range of illnesses. Beetroot is a possible plant utilised in cardiovascular diseases because of its alleged medicinal uses, which include its anticancer, carminative, emmenagogue, hemostatic, and renal protecting characteristics [7]. In the Ayurvedic, Unani, and Siddha Herbal Systems, *Curcuma longa* is frequently employed. Additionally, it is advised for the treatment of eczema, psoriasis, wounds, jaundice, inflammation, cancerous symptoms, excessive cholesterol, diabetes, abdominal pain, monthly irregularities, and as a blood-purifying action [8]. The lack of key nutrients in food causes the vast majority of people in Asian and African nations to be malnourished. The drumstick or horseradish tree, *Moringa oleifera* Lam. (syn. *M. pterygosperma* Gaertn., 2n = 28), is a member of the family Moringaceae. It has the potential to end malnutrition because it is a cost-effective and readily available source of important critical nutrients and nutraceuticals [9].

The secondary metabolites present in the four vegetables *Phyllanthus emblica* (fruit), *Beta vulgaris* L.(tuber), *Curcuma longa* (tuber) and *Moringa oleifera* leaves were recorded and the peaks formed in FT-IR spectroscopy were analysed using standard IR spectrum chart.

MATERIALS AND METHODS

The sample vegetable products, Amla (*Emblica officinalis*), Drumstick (*Moringa oleifera*) leaves were collected from local area and beetroot (*Beta vulgaris*) and turmeric (*Curcuma longa*) were collected from the local market for the study. They were washed well in running water to remove the dust, and dried on filter papers and shade dried for three weeks. The samples were powdered using a mixer. The Amla (*Emblica officinalis*), Drumstick (*Moringa oleifera*) leaves, beetroot (*Beta vulgaris*) and turmeric (*Curcuma longa*) powders were extracted using the maceration procedure with ethanol as the solvent, yielding ethanolic extracts of each plant. For FT-IR spectroscopic analysis, these extracts were employed [10].

FT-IR Analysis

The most effective tool for determining the kinds of chemical bonds and functional groups present in compounds is an infrared spectrophotometer known as a Fourier transform infrared (FT-IR). The chemical bond's wavelength can be identified by its absorption of light. The chemical bonds of a molecule can be identified by reading the infrared

57273



**Venci Candida et al.,**

absorption spectra. The FT-IR analysis used the ethanolic extract of each plant item. The extract was dried and used for further analysis. Translucent sample discs were created by encapsulating 10 mg of the dried powder within a 100 mg KBr pellet. Each sample was placed inside an FT-IR spectroscope (Shimadzu, IR Affinity 1, Japan), which had a scan range of 400 to 4000 cm^{-1} and a resolution of 4 cm^{-1} [11].

Functional groups identification

Based on the peak values in the IR radiation region of the FTIR spectrum, the active components found in the extract were divided into functional groups. The functional groups of the constituents were divided based on the peak ratio of the extract when it was passed into the FT-IR. It is possible to identify the chemical bonds in a substance by reading its infrared absorption spectra [12].

RESULTS AND DISCUSSION

The phytochemical analysis was done for the four commonly used vegetable products such as Amla (*Emblica officinalis*), Drumstick (*Moringa oleifera*) leaves, beetroot (*Beta vulgaris*) and turmeric (*Curcuma longa*) by FT-IR analysis and the following results were obtained. When the Amla extract was subjected to FT-IR analysis, around 24 peaks were obtained ranging from the wave number 3415.93 to 626.87 as reported in Figure 1. The phytochemicals like phenols, alcohols, carboxylic acids (ascorbic acid, acetic acid, formic acid, butanic acid and propionic acid), alkaloids (alkanes, alkynes, aliphatic amines) and alkyl halides (chloromethane, bromomethane) were identified in Amla. These results coincide with the results of many researchers. Gallic acid content was suggested by the peaks 3295, 1726, 1617.96, 1538, 1239, 1107, 1059 and 864.33 cm^{-1} [13]. The researcher [14] also confirmed the aromatic stretching and bending. He also suggested the peak 1058.55 as quercetin. The presence of –OH (hydroxyl) stretch, C–O (carbonyl group) alcohol stretch, the acidic –C–O stretch, C=O stretch and =CH stretch was confirmed [15].

When the beetroot extract was subjected to FT-IR analysis, around 16 peaks were obtained ranging from wave number 3685.97 to 673.16 as explained in Figure 2. The secondary metabolites obtained were alcohol, phenol, alkaloids, aromatics, carboxylic acids and nitro compounds. The results of various scientists which coincides with our results are as follows. Additionally, the leaf of beetroot contains omega -3 such as linolenic acid [16]. In terms of phenolic acid composition, the plant's stem lacks ellagic acid but does contain gallic acid, chlorogenic acid, along with the phenolic acids and rutin combined with flavonoids found in the root [17]. When the drumstick leaves extract was subjected to FT-IR analysis, around 24 peaks were obtained ranging from the wave number 3626.17 to 526.57 as reported in Figure 3. When the leaf of drumstick is subjected to FT-IR analysis, the secondary metabolites identified were alcohol, phenol, alkaloids, carboxylic acids, cyano carbons and alkyl halides. Various scientists have reported that various parts of the *Moringa oleifera* tree have been identified as containing high levels of certain glucosinolates and flavonoids, phenolic acids, carotenoids, tocopherols, polyunsaturated fatty acids (PUFAs), highly accessible minerals, and folate [18, 19]. When the turmeric extract was subjected to FT-IR analysis, around 24 peaks were obtained ranging from 3622.32 to 522.71 as explained in Figure 4. The secondary metabolites obtained were alkyl halides, aliphatic aromatics, nitro compounds, alkaloids, phenols, flavonoids and alcohols. The existence of N-H, O-H, C=C, C-H, C-O, and CH₃ functional groups was confirmed by the findings of the FT-IR study based on the extract's peak ratio [20]. The possible phytochemicals found in Amla (*Emblica officinalis*), beetroot (*Beta vulgaris*), drumstick (*Moringa oleifera*) leaves and turmeric (*Curcuma longa*) were recorded in Table 1, Table 2, Table 3 and Table 4 respectively. The powdered samples of Amla (*Emblica officinalis*), drumstick (*Moringa oleifera*) leaves, beetroot (*Beta vulgaris*) and turmeric (*Curcuma longa*) was shown in Figure 5, Figure 6, Figure 7 and Figure 8 respectively.

CONCLUSION

The secondary metabolites found in a variety of vegetable products demonstrated therapeutic potential. For our study, four typical vegetable products namely Amla (*Emblica officinalis*), drumstick leaves (*Moringa oleifera*), beetroot (*Beta vulgaris*), and turmeric (*Curcuma longa*) were chosen. Alkaloids (alkanes, alkynes, aliphatic amines), phenols,



**Venci Candida et al.,**

alcohols, carboxylic acids (ascorbic acid, acetic acid, formic acid, butanic acid, and propionic acid), and alkyl halides (chloromethane, bromomethane) were found in Amla. Alcohol, phenol, alkaloids, aromatics, carboxylic acids, and nitro compounds were among the secondary metabolites identified in beetroot. Alkaloids, alcohol, phenol, carboxylic acids, cyano carbons, and alkyl halides were among the secondary metabolites that were reported in drumstick leaves. Alkyl halides, aliphatic aromatics, nitro compounds, alkaloids, phenols, flavonoids, and alcohols were among the secondary metabolites discovered in turmeric extract. From the above results we could conclude that all the four samples Amla (*Emblia officinalis*), Drumstick leaves (*Moringa oliefera*), beetroot (*Beta vulgaris*) and turmeric (*Curcuma longa*) could be employed frequently in our diets to boost our immunity because they include a sufficient variety of secondary metabolites with strong therapeutic capabilities.

ACKNOWLEDGEMENT

The authors thank Ms. A. Ajitha, Technical Assistant of DST- FIST sponsored Central Instrument Laboratory of Holy Cross College, Nagercoil and Dr. Sr. Francy, Assistant Professor of Chemistry, Holy Cross College, Nagercoil for helping us in doing FTIR technique and to identify the secondary metabolites.

ABBREVIATION

FT-IR - Fourier transform infrared spectroscopy

REFERENCES

1. Gabhe SY, Tatke PA, Khan TA. Evaluation of the immunomodulatory activity of the methanol extract of *Ficus benghalensis* roots in rats. Indian Journal of Pharmacology.2006;38: 271-275.
2. Singh PK, SinghJ, Medhi T, Kumar A. Phytochemical Screening, Quantification, FT-IR Analysis, and In Silico Characterization of Potential Bio-active Compounds Identified in HR-LC/MS Analysis of the Polyherbal Formulation from Northeast India. ACS Omega.2022;7:33067–33078.
3. Okigbo RN, Eme UE, Ogbogo O. Biodiversity and conservation of medicinal and aromatic plants in Africa. Biotechnology and Molecular Biology Reviews.2008;3: 127-134.
4. Sharma N, Vijayvergia R. Study of primary metabolites and antimicrobial activity of *Gomphrena celosoides* Mart. International Journal of Pharma and Bio Sciences,2013;4: 581-586.
5. SheikhN, KumarY, MishraAK, PfozeL. Phytochemical screening to validate the ethnobotanical importance of root tubers of *Dioscorea* species of Meghalaya, North East India. Journal of medical plant Studies.2013;1: 62–69.
6. SinghVK, Garg PK, Sharma, Gupta S. Wound healing activity of ethanolic extract of *Beta vulgaris*.Pharmacologyonline.2011;1:1031–1038.
7. Vali L, Stefanovits-B E,Szentmih K. Liver-protecting effects of table beet (*Beta vulgaris* var. rubra) during ischemia-reperfusion.Nutrition.2007;23(2): 172–178.
8. Sawant RS, Godghate AG. Qualitative Phytochemical Screening of Rhizomes of *Curcuma Longa* Linn. International Journal of Science, Environment and Technology. 2013;2(4): 634 – 641.
9. Kunyanga CN, Imungi, JK, Vellingiri V. Nutritional evaluation of indigenous foods with potential food-based solution to alleviate hunger and malnutrition in Kenya. J Appl Biosci. 2013;67:5277–5288. doi:10.4314/jab.v67i0.95049.
10. Geetha N,Hansiya VS, Palanisamy UM. Application of phytochemical screening and a combined FTIR spectroscopy and principal component analysis for effective discrimination of two varieties of *Eclipta alba* (L.) Hassk. International Journal of ChemTech Research. 2018;11(11): 337-347.
11. Dharmasoth RD, Ganga RB.Qualitative Phytochemical Screening and FTIR Spectroscopic Analysis of *Grewia tilifolia* (Vahl) Leaf Extracts. International Journal of Current Pharmaceutical Research.2019;11(4): 100-107.
12. Visveshwari M, Subbaiyan B, Thangapandian V. Phytochemical analysis, Antibacterial activity, FTIR and GCMS analysis of *Ceropegia juncea* Roxb. International Journal of Pharmacognosy and Phytochemical Research.2017;9(7); 914-920.
13. Nirmaladevi R, Padma PR, Kavita D. Analyzes the methanolic extract of the leaves of *Rhinacanthus nasutus*. J Med Plants Res. 2010;4:1554–1560. [[Google Scholar](#)]





Venci Candida et al.,

14. Heo BG, Park YJ, Park YS, Bae JH, Cho JY, Park K. Anticancer and antioxidant effects of extracts from different parts of *indigo* plant. *Ind. Crops Prod.* 2014;56, 9–16. 10.1016/j.indcrop.2014.02.023 [CrossRef] [Google Scholar]
15. Parveen K, KhatkarBS, Anil D. 2019. Anola phytochemicals: extraction, identification and quantification. *Journal of Food Science and Technology -Mysore.* 2019;56(2) DOI:10.1007/s13197-019-03716-7.
16. Biondo P, BoeingJ, Barizao E, Souza N, Matsushita M, Oliveira C. Boroski M, Visentainer J. Evaluation of beetroot (*Beta vulgaris* L.) leaves during its developmental stages: a chemical composition study. *Food Science and Technology.* 2014;34(1): 94-101.
17. KoubaierH, SnoussiA, Essaidil, ChaabouniM, ThonartP, Bouzouita N. Betalain and Phenolic Compositions, Antioxidant activity of Tunisian Reed Beet (*Beta vulgaris* L. Conditiva) Roots and Stems Extracts. *International Journal of Food Properties.* 2014;17: 1934-1945.
18. Amaglo NK, BennettRN, Lo Curto, RB, RosaEAS, Lo Turco V, Giuffrida A, Lo Curto A, Crea F, Timpo GM. Profiling selected phytochemicals and nutrients in different tissues of the multipurpose tree *Moringa oleifera* L., grown in Ghana. *Food Chem.* 2010;122 (4): 1047-1054.
19. Saini RK, Shetty, NP, GiridharP. Carotenoid content in vegetative and reproductive parts of commercially grown *Moringa oleifera* Lam. cultivars from India by LC–APCI–MS. *Eur Food Res Technol.* 2014c;238: 971–978.
20. Pakkirisamy M, Suresh KK, Karthikeyen R. 2017. Phytochemical Screening, GC-MS, FT-IR Analysis of Methanolic Extract of *Curcuma caesia* Roxb (Black Turmeric). *Pharmacogn J.* 2017;9(6):952-956.

Table 1: Possible phytochemicals in Amla extract

Serial Number	Wavenumber (Fastsamples)cm ⁻¹	Wave number	Functional group Assignment	Phytochemicals Identified
1.	3415.93	3500-3200	Hydrogen bonded O-H stretch	Phenols, alochols
2.	3298.28	3500-3200	Hydrogen bonded O-H stretch	Phenols, alochols
3.	3151.69	3300-2500	O-H stretch	Carboxylic acids
4.	3115.04	3300-2500	O-H stretch	Carboxylic acids
5.	2924.09	3000-2850	H-C-H Asymmetry & Symmetry Stretch	Alkanes
6.	2856.58	3000-2850	H-C-H Asymmetry & Symmetry Stretch	Alkanes
7.	2673.34	3600-3100	Hydrogen – bonded O-H Stretch	Carboxylic acid
8.	2638.62	3600-3100	Hydrogen – bonded O-H Stretch	Carboxylic acid
9.	2594.26	3600-3100	Hydrogen – bonded O-H Stretch	Carboxylic acid
10.	2547.97	3600-3100	Hydrogen – bonded O-H Stretch	Carboxylic acid
11.	2285.65	2302200	C≡N stretch	Nitriles
12.	2206.57	2260-2100	-C≡C- Stretch	Alkynes
13.	2156.42	2260-2100	-C≡C- Stretch	Alkynes
14.	1716.65	1730-1715	C=O Stretch	Alpha, Beta-unsaturated Esters
15.	1452.40	1500-1400	C-C Stretch (in ring)	Aromatics
16.	1375.25	1400-1300	N=O Bend	Nitro Compounds





Venci Candida et al.,

17.	1300.02	1360-1290	N-O Symmetrical Stretch	Nitro Compounds
18.	1226.73	1250-1020	C-N Stretch	Aliphatic amines
19.	1111.00	1250-1020	C-N Stretch	Aliphatic amines
20.	1058.92	1250-1020	C-N Stretch	Aliphatic amines
21.	925.83	950-910	O-H bend	Carboxylic acids
22.	792.74	850-550	C-Cl Stretch	Alkyl halides
23.	669.30	6700-610	-C≡C-H: C-H bend	Alkynes
24.	626.87	690-515	C-Br Stretch	Alkyl halides

Table 2: Possible phytochemicals in Beetroot extract

Serial No	Wave number (Test sample) cm ⁻¹	Wave number cm ⁻¹ Reference article	Functional group assignment	Phytochemicals identified
1.	3685.97	3700 - 3584	O-H stretch	alcohol
2.	3435.22	3500 - 3200	H-bonded	phenols
3.	3423.65	3500 - 3200	H-bonded	phenols
4.	2929.87	3000 - 2850	C-H stretch	alkanes
5.	2291.43	2250 - 2275	C≡N stretch	Nitriles
6.	2233.57	2260 - 2100	-C≡C- stretch	Alkynes
7.	2175.70	2260 - 2100	-C≡C- stretch	Alkynes
8.	1886.38	2000 - 1650	C-H bending	aromatic compound
9.	1847.81	2000 - 1650	C-H bending	aromatic compound
10.	1629.85	1680 - 1640	N-H bend	primary amines.
11.	1558.48	1560 - 1500	N-H bend	Primary amines
12.	1406.11	1500 - 1400	C-C stretch (in ring)	Aromatics
13.	1109.07	1320 - 1000	C-O stretch	Alcohols
14.	1060.85	1250 -1020	C-O stretch	Alcohols
15.	929.69	950 - 910	O-H bend	Carboxylic acid
16.	673.16	910 - 665	C-Br stretch	Alkyl halide

Table 3: Possible phytochemicals in drumstick leaf extract

Serial No	Wave Number cm ⁻¹ (Test samples)	Wave number cm ⁻¹ (Reference article)	Functional group assignment	Phyto compounds Identified
1	3626.17	3640- 3610	free hydroxyl	Phenols
2	3512.37	3550- 3200	Hydrogen bonded O-H stretch	Alcohol
3	3442.94	3500 - 3200	H bonded	Phenols
4	2922.16	3000 - 2850	C-H stretch	Alkanes
5	2854.65	3000 - 2850	C-H stretch	Alkanes
6	1807.30	2000 - 1650	C - H bending	aromatic compound
7	1624.06	1650 - 1580	N-H bend	primary amines
8	1521.84	1550 - 1475	N-O asymmetric stretch	nitro compound
9	1460.11	1470 - 1450	C-C stretch	Aromatics
10	1438.90	1500 - 1400	C-C stretch	Aromatics





Venci Candida et al.,

11	1379.10	1420 - 1330	N=O stretch	Nitro groups
12	1328.95	1335 - 1250	C-N stretch	aromatic amines
13	1265.30	1320 - 1000, 1300 - 1150	C-H wag (-CH ₂ X)	alkyl halides.
14	1155.36	1300 - 1150	C-H wag (-CH ₂ X)	alkyl halides
15	1099.43	1250 - 1020	C-N Stretch	aliphatic amines
16	1062.78	1250 - 1020	C-N Stretch	aliphatic amines
17	1028.06	1250 - 1020	C-N Stretch	aliphatic amines
18	902.69	1000 - 650	N-H wag	Primary and secondary amine
19	840.96	1000 - 650	C-Cl stretch.	alkyl halides.
20	775.38	1000 - 650 ,	C-Cl stretch.	alkyl halides.
21	719.45	1000 - 650,	C-Cl stretch.	alkyl halides.
22	678.94	1000 - 650,	C-Br stretch	alkyl halides.
23	586.36	850 - 550	C-Br stretch	alkyl halides
24	526.57	690 - 515	C-Br stretch	alkyl halides

Table 4: Possible phytochemicals in turmeric extract

S. No	Wave Number (Test Sample) cm ⁻¹	Wave Number cm ⁻¹ (Reference article)	Functional group	Phytochemicals identified
1.	3622.32	3640-3610	free hydroxyl	Phenols
2.	3560.59	3600-3100	O-H-Stretch,H-bonded	Phenols
3.	3539.38	3600-3100	O-H-Stretch,H-bonded	Phenols
4.	3518.16	3600-3100	O-H-Stretch,H-bonded	Phenols
5.	3454.51	3500-3200	O-H-Stretch,H-bonded	Phenols
6.	3437.15	3500-3200	OH-Stretch,H-bonded	Phenols
7.	3414.00	3500-3200	OH-Stretch,H-bonded	Phenols
8.	3396.64	3400-3250	N-H Stretch	Primary, Secondary amines,amides
9.	2922.16	3000-2850	CH-Stretch	Alkanes
10.	2856.58	3000-2850	CH-Stretch	Alkanes
11.	2274.07	2300-2200	C≡N stretch	Nitriles
12.	1381.03	1400-1300	N=O Bend	Nitro compounds
13.	1325.10	1335-1250	C-N Stretch	Aromatic amines
14.	1286.52	1320-1000	C-H wag (-CH ₂ x)	Alkyl halides
15.	1157.29	1250-1020	C-N Stretch	Aliphatic amines
16.	1112.93	1250-1020	C-N Stretch	Aliphatic amines
17.	1026.13	1250-1020	C-N Stretch	Aliphatic amines
18.	850.61	900-675	C-H"oop"	Aromatics
19.	806.25	910-665	C-Cl stretch	Alkyl halides
20.	761.88	910-665	C-Cl stretch	Alkyl halides
21.	709.80	910-665	C-Cl Stretch	Alkyl halides
22.	611.43	850-550	C-BrStretch	Alkyl halides
23.	574.79	690-515	C-Br Stretch	Alkyl halides
24.	522.71	690-515	C-BrStretch	Alkyl halides





Venci Candida et al.,

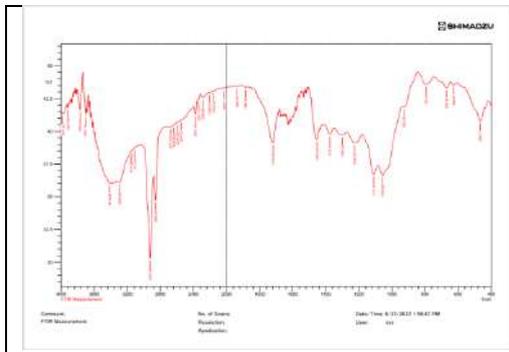


Figure 1: Peaks obtained in Amla extract by FTIR analysis

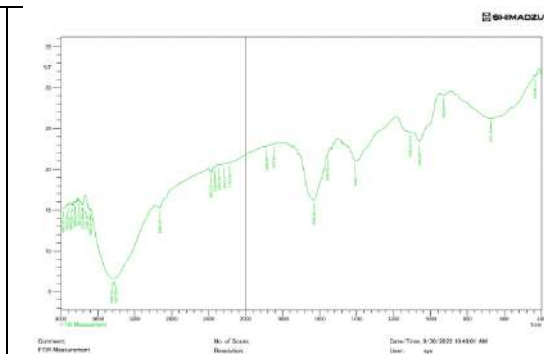


Figure 2: Peaks obtained in Beetroot extract by FTIR analysis

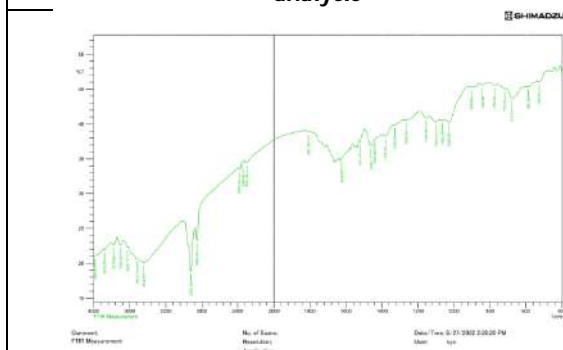


Figure 3: Peaks obtained in Drumstick leaf extract by FTIR analysis

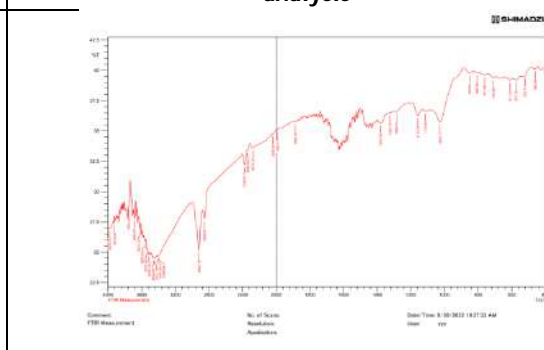


Figure 4: Peaks obtained in Turmeric extract by FTIR analysis



Figure 5: Amla powder



Figure 6: Beetroot Powder



Figure 7: Drumstick leaves Powder



Figure 8: Turmeric Powder





Qualitative Phytochemical Analysis of Some Medicinally Important Fern Species Collected from Coonoor and Udhagamandalam, Tamil Nadu, India.

Aadil Farooq Shah^{1*}, Shagufta Rashid¹, Shakoor Ahmad Mir² and Kumarasamy.D³

¹Ph.D, Research Scholar, Department of Botany, Annamalai University, Chidambaram, Tamil Nadu, India

²Ph.D, Research Scholar, Department of Botany, Jamia Hamdard University, Delhi, India.

³Professor, Department of Botany, Annamalai University, Chidambaram, Tamil Nadu, India

Received: 20 Feb 2023

Revised: 10 Apr 2023

Accepted: 16 May 2023

*Address for Correspondence

Aadil Farooq Shah

Ph.D, Research Scholar,
Department of Botany,
Annamalai University,
Chidambaram, Tamil Nadu, India.
E.Mail: shahaadil10@gmail.com



This is an Open Access Journal / article distributed under the terms of the **Creative Commons Attribution License** (CC BY-NC-ND 3.0) which permits unrestricted use, distribution, and reproduction in any medium, provided the original work is properly cited. All rights reserved.

ABSTRACT

The present report is about the study of phytochemicals of some medicinally important fern species collected from Coonoor and Udhagamandalam Tamil Nadu, India. Standard methods were used to examine the secondary metabolites like alkaloids, proteins, carbohydrates, flavonoids, terpenoids, glycosides phenolic compounds, and tannins in various plant solvent extracts. Among the forty tested extracts, twenty-seven extracts showed the presence of carbohydrates (67%) and 27 extracts showed proteins and free amino acids (67%), 27 (67%) flavonoids, 37 (92.5%) phenolic compounds and tannins, 30 (75%) glycosides, 33 (82.5%) terpenoids, 34 (85%) alkaloids. The findings reported the existence of several bioactive compounds that could be utilised for future therapeutic applications.

Key words: Extraction, Ferns, Phytochemicals, Solvent, Coonoor, Udhagamandalam

INTRODUCTION

Lycophytes and monilophytes are two plant lineages that make up the group of organisms known as pteridophytes. Both generate spores rather than seeds; the former has fronds (lycophylls) with no leaf gap in the stem stele, while the latter has fronds (stele) with a leaf gap (euphylls). The homosporous species (Lycopodiales) and the



**AadilFarooq Shahet al.,**

heterosporous species are two of the three clades of lycophytes (Isoetales and Selaginellales). In turn, monilophytes contains the species that are commonly referred to as "ferns." These two lineages have been discussed as a unit under many headings, such as "ferns and associated plant" or "pteridophytes"[1]. There are nearly 12,000 species of ferns on the planet, the majority of which are found in tropical and subtropical climates. India as a mega diversity country has a massive and rich diversity of fern and their allies represented by 1157 species [2]. Kolli hills are a part of Eastern Ghats in Tamil Nadu, India supporting large growth of diverse fern [3, 4]. About four hundred species of Pteridophytes occur in south India of which ferns are a part [5]. South Indian ferns were determined in Palani hills [6], Western Ghats [7], Nilgiri hills etc. [8]. The current study is focussed to ascertain the phytochemical constituents of *Adiantum hispidulum*, *Adiantum raddianum*, *Christella dentata*, *Cyathea crinita*, *Dryopteris redactopinnata*, *Hemionitis arifolia*, *Pellaea boivinii*, *Phlebodium aureum*, *Pteris vittata* and *Pyrossia mollis* in various solvent extracts.

MATERIALS AND METHODS

Procurement of plant materials and extraction

The study material utilized for the current study was collected from Coonoor and Udthagamandalam of Tamil Nadu, India. The identification of ferns was done with the help of an artificial key given by Manickam and Irudayaraj for South Indian fern flora. The plant materials utilized for phytochemical screening was washed thoroughly under running tap water to remove all debris and soil, and then shade dried for two weeks at room temperature. The air-dried plant material was finely crushed and stored in self-sealing, air-tight polythene bags. Using a Soxhlet apparatus, 50 g of powder was extracted sequentially with 250 mL of methanol, ethanol, acetone, and distilled water for 7 hours at 50-65 °C (not greater than the boiling point of the solvent). All of the extracts were concentrated and kept in an airtight bottle until they were needed again.

Phytochemical Screening

The tests used to screen for phytochemicals are mentioned below.

Alkaloid Test

Dragendroff's test: 2ml of Dragendroff's reagent is added to 1ml of extract. The presence of alkaloids is indicated by the formation of an orange-red precipitate.

Glycoside Test

Keller- Killiani test: 1ml of glacial acetic acid with traces of ferric chloride and 1ml of strong sulphuric acid were carefully mixed with 1ml of extract. The presence of glycosides is shown by the presence of a brown ring at the contact. Below the brown ring, a violet ring may emerge.

Carbohydrates Test

Molisch's test: A few drops of Molisch's reagent (-naphthol, 20% in ethyl alcohol) were added to 1 mL of extract. Then belatedly, 1ml of strong sulphuric acid was poured along the tube's sides. The presence of carbohydrates is indicated by the formation of a violet tint.

Proteins and free amino acids Test

Ninhydrin test: 1ml of Ninhydrin solution was added to 2ml of extract. Boil on water for some time. The presence of amino acids is indicated by the appearance of a blue to purple tint.

Phenolic compounds and tannin Test

Ferric chloride test: 1 mL ferric chloride (5%) solution (made in ethanol) was added to 1 mL extract. The colour appeared to be blue black or dark green.



**AadilFarooq Shahet al.,****Flavonoid Test**

Shinoda test: A few drops of concentrated HCl were applied to 1ml of extract. 0.5 gram of magnesium turnings were added to this solution. The presence of flavonoids was shown by the Appearance of pink colour.

Terpenoids Test

Salkowski test: 2ml of chloroform and few drops of concentrated sulphuric acid were added carefully to 1ml of extract along the Sides of test tube to form a layer. Positive results for the presence of terpenoids were shown by a reddish brown colouring of the interface.

RESULT

Each of the forty extracts of the selected fern species contains at least four secondary metabolites. Alkaloids are present in all four extracts of *Adiantum hispidulum*, *Cyathea crinita*, *Dryopteris redactopinnata*, *Phlebodium aureum*, *Pteris vittata* and *Pyrossia mollis*, three extracts of *Adiantum raddianum* and *Pellaea boivinii* and two extracts of *Christella dentata* and *Hemionitis arifolia*. Glycosides are present in methanol, ethanol, acetone and water extracts of *Christella dentata*, three extracts of *Adiantum hispidulum*, *Adiantum raddianum*, *Cyathea crinita*, *Dryopteris redactopinnata*, *Pellaea boivinii*, *Phlebodium aureum*, *Pteris vittata* and *Pyrossia mollis* and two extracts of *Hemionitis arifolia*. Free amino acids and proteins occur in all extracts of *Pellaea boivinii* and *Pyrossia mollis* except *Christella dentata* three extracts of *Adiantum hispidulum*, *Christella dentata*, *Cyathea crinita*, *Dryopteris redactopinnata*, *Phlebodium aureum* and *Pteris vittata* and one extract of *Adiantum raddianum*. Carbohydrates are present in three extracts of *Adiantum hispidulum*, *Adiantum raddianum*, *Christella dentata*, *Cyathea crinita*, *Dryopteris redactopinnata*, *Hemionitis arifolia*, *Pellaea boivinii* and *Phlebodium aureum*, two extracts of *Pyrossia mollis* and one extract of *Pteris vittata*. Flavonoids are present in all four extracts of *Pellaea boivinii* and *Pyrossia mollis* except *Christella dentata*, three extracts of *Adiantum hispidulum*, *Adiantum raddianum*, *Cyathea crinita*, *Dryopteris redactopinnata*, *Hemionitis arifolia* and *Phlebodium aureum* and one extract of *Pteris vittata*. Phenolic compounds and Tannins are present in all four extracts of *Adiantum hispidulum*, *Adiantum raddianum*, *Cyathea crinita*, *Dryopteris redactopinnata*, *Pellaea boivinii*, *Phlebodium aureum*, *Pteris vittata* and *Pyrossia mollis* and two extract of *Hemionitis arifolia*. Terpenoids are present in four extracts of *Adiantum hispidulum*, *Adiantum raddianum*, *Pellaea boivinii* and *Phlebodium aureum*, three extracts of *Christella dentata*, *Cyathea crinita*, *Dryopteris redactopinnata*, *Pteris vittata* and *Pyrossia mollis* and two extracts of *Hemionitis arifolia*.

DISCUSSION

In the current study 10 species of ferns was analyzed for the phytochemical constituents. Screening was carried out with methanol, ethanol acetone, and water extracts of the plants that form a total of 40 extracts. In this empirical study, alkaloids, carbohydrates, proteins, free amino acids and terpenoids were observed in all extracts. Out of 40 tested extracts alkaloids were present in 34 extracts (85 %), glycosides in 30 extracts (75 %), free amino acids and proteins in 27 extract (67 %), carbohydrates in 27 extracts (67 %), flavonoids in 27extracts (67 %), phenolic compounds and tannins in 37 extracts (92.5 %) and terpenoids in 33 extracts (82.5 %) respectively, the result of present study is similar to the previous studies [9]. Ethanol and methanol exhibited more phytochemicals than water and acetone among solvents. Ferns have therapeutic properties, and some have been used medicinally since ancient times. Plant parts such as stems, fronds, rhizome, and spores are used in a variety of ways by tribal people and ethnic groups all over the world to treat a variety of diseases [10]. The purpose of the current study was to use four solvent extracts to investigate the chemicals found in several Indian medicinal ferns. Antimicrobial activity can be found in alkaloids and flavonoids. Tannins could potentially be used as cytotoxic agents [11]. Tannins are anti-cancer compounds. Antimicrobial and insecticidal properties are mostly derived from phenolic chemicals. This study also leads to further research in isolating and identifying the bio-active chemicals from the selected ferns. It will also aid in the development of novel drugs with fewer side effects, lower costs, and more efficacy in the treatment of many infectious diseases in the future.





AadilFarooq Shahet al.,

Conflict of Interest Statement

We declare that we do not have any conflict of interest.

ACKNOWLEDGEMENT

The authors like to express their gratitude to the Head of Department Botany, Annamalai University Dr. K.C Ravindran for support and help of preliminary phytochemical analysis and providing all basic laboratory facilities.

REFERENCES

- Santos, M. G., Kelecom, A., Paiva, S. R., Moraes, M. G., Rocha, L., and Garrett, R. Phytochemical studies in pteridophytes growing in Brazil: A review. *American Journal of Plant Science and Biotechnology*; 2010, 4(1): 113-125.
- Fraser-Jenkins, C. R. "A revised checklist of Indian pteridophytes-I. *Indian Fern journal*; 2016,33 (1&2): 193-205.
- Vijayakanth, P S. SahayaSathish, and Mazumdar. New additions to fern flora of Tamil Nadu, India. *International Journal of Advance Research and Innovative ideas in Education*; 2017, 3 (4): 1671-1674.
- Vijayakanth, P S. SahayaSathish, Dominic Rajkumar, Irudayaraj, Kavitha R, and Mazumdar. Studies on the chromosome numbers of ferns from Kolli Hills, Eastern Ghats, Tamil Nadu, India. *Caryologia*; 2018, 4 (71): 380-396.
- Singh, BallendraPratap, and Ravi Upadhyay. Observations on some ferns of Pachmarhi Biosphere Reserve in traditional veterinary uses. *Indian fern Journal*; 2010, 27: 94-100.
- Myers N. Biodiversity revisited. *Biosciences*; 2003, 53: 916-17.
- Dudani, Sumesh N., and Mahesh M K. Conservation strategies for the hygrophilous Pteridophytes of Central Western Ghats. *International Conference on Conservation. and Managment of Wetland Ecosystems-LAKE 2012*; 2017, 6-8..
- Sonia, Abraham, Ramachandran VS, and Sofia. Potential ornamental Ferns from Nilgiris, Tamil Nadu. *Advances in Applied Science Research*; 2012, 3 (4): 2388-2391.
- Shah, A. F. Preliminary Phytochemical Studies on Some Medicinally Important Fern Species Collected from Udhagamandalam, Tamil Nadu, India. *Indian Journal of Natural Sciences*; 2022, 13 (75): 51361-51368.
- Aguinaldo A M, Espeso EI, Guevara BQ, Nonato MG. Phytochemistry. In: Guevara BQ. (ed.) A guidebook to plantscreening: *phytochemical and biological*. Manila: University of Santo Tomas; 2005, 121-125.
- Kumar, A., and Aushik P. "Antibacterial effect of *Adiantum capillsveneris* Linn. *Indian Fern J*; 1999, 16: 72-74.

Table: 1 Preliminary studies of *Adiantum hispidulum* and *Adiantum raddianum*

	<i>Adiantum hispidulum</i>				<i>Adiantum raddianum</i>			
	Ethanol	Methanol	Acetone	Water	Ethanol	Methanol	Acetone	Water
Alkaloids								
Glycosides	+	+	+	+	+	+	+	-
Flavonoids	+	+	+	-	+	+	+	-
Carbohydrates	+	+	+	-	+	+	+	-
Proteins & FAA	+	+	+	-	-	+	-	-
Flavonoids	+	+	+	-	+	+	+	-
Phenolic Compounds & Tannins	+	+	+	+	++	++	++	++
Terpenoids	++	++	+	+	++	++	++	+





AadilFarooq Shahet al.,

Table 2: Preliminary studies of *Christella dentata* and *Cyathea crinita*

<i>Christella dentata</i>					<i>Cyathea crinita</i>			
Alkaloids	Ethanol	Methanol	Acetone	Water	Ethanol	Methanol	Acetone	Water
Glycosides	+	+	-	-	+	+	+	+
Flavonoids	+	+	+	+	+	+	++	-
Carbohydrates	+	+	+	-	++	+	++	-
Proteins & FAA	+	+	+	-	+	+	+	-
Flavonoids	-	-	-	-	+	+	++	-
Phenolic Compounds & Tannins	++	+	++	-	++	+	+	+
Terpenoids	+	+	+	-	+	++	+	++

Table 3: Preliminary studies of *Dryopteris redactopinnata* and *Hemionitis arifolia*

<i>Dryopteris redactopinnata</i>					<i>Hemionitis arifolia</i>			
Alkaloids	Ethanol	Methanol	Acetone	Water	Ethanol	Methanol	Acetone	Water
Glycosides	+	+	+	+	+	+	-	-
Flavonoids	+	+	+	-	+	+	-	-
Carbohydrates	++	+	+	-	+	+	+	-
Proteins & FAA	+	+	+	-	-	-	-	-
Flavonoids	+	-	+	+	+	+	+	-
Phenolic Compounds & Tannins	++	+	+	+	+	+	-	-
Terpenoids	++	++	+	-	+	+	-	-

Table 4: Preliminary studies of *Pellaea boivinii* and *Phlebodium aureum*

<i>Pellaea boivinii</i>					<i>Phlebodium aureum</i>			
Alkaloids	Ethanol	Methanol	Acetone	Water	Ethanol	Methanol	Acetone	Water
Glycosides	+	-	+	+	+	+	+	+
Flavonoids	+	+	-	+	+	+	+	-
Carbohydrates	+	-	+	+	+	+	+	-
Proteins & FAA	+	+	+	+	+	+	+	-
Flavonoids	+	++	+	+	+	+	+	-
Phenolic Compounds & Tannins	+	+	+	+	+	+	+	+
Terpenoids	+	+	+	+	++	++	+	+



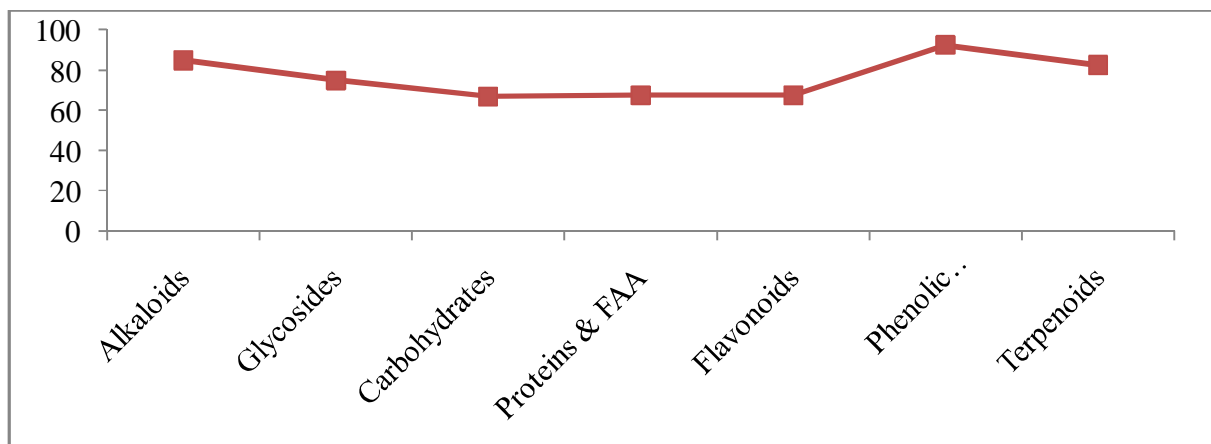


AadilFarooq Shahet al.,

Table 5: Preliminary studies of *Pteris vittata* and *Pyrossia mollis*

	<i>Pteris vittata</i>				<i>Pyrossia mollis</i>			
	Ethanol	Methanol	Acetone	Water	Ethanol	Methanol	Acetone	Water
Alkaloids								
Glycosides	+	+	+	+	+	+	+	+
Flavonoids	+	+	+	+	+	+	-	+
Carbohydrates	-	+	+	-	-	+	-	+
Proteins & FAA	+	+	+	-	+	+	+	++
Flavonoids	-	+	-	-	+	++	+	++
Phenolic Compounds & Tannins	+	+	+	+	+	+	+	++
Terpenoids	+	+	+	-	+	+	-	++

+= Present, ++ = more present , -= Absent



Graph 1. Percentage of compounds present in samples





Evaluation of *Sesamum prostratum* Retz. for Anthelmintic Activity

N.Astalakshmi¹, Gokul T^{2*}, Gowri Sankar K B², Nandhini M² and Hari Hara Sudhan M R²

¹HoD and Professor, Dept. of Pharmaceutical Chemistry, Senghundhar College of Pharmacy, Tiruchengode, Namakkal, Tamil Nadu, India.

²B.Pharm Final Year, Senghundhar College of Pharmacy, Tiruchengode, Namakkal, Tamil Nadu, India.

Received: 18 Jan2023

Revised: 20 Mar 2023

Accepted: 27 Apr 2023

*Address for Correspondence

Gokul T

B.Pharm Final Year,
Senghundhar College of Pharmacy,
Tiruchengode, Namakkal,
Tamil Nadu, India.

Mail ID:gokulmurugan855@gmail.com



This is an Open Access Journal / article distributed under the terms of the **Creative Commons Attribution License** (CC BY-NC-ND 3.0) which permits unrestricted use, distribution, and reproduction in any medium, provided the original work is properly cited. All rights reserved.

ABSTRACT

Nature is always a golden sign to show the prominent phenomena of co-existence. Natural products from plants, animals and minerals are the basis for treating human diseases. Medicinal plants are presently in demand and their acceptance is increasing progressively. Undoubtedly, plants play an important role by providing essential services in ecosystems. The pedaliaceae is one of the source of medicinal plants with 13 genus and 70 species. One of the active member among the genus is sesamum. The current study aims at exploring the anthelmintic property of the Aerial parts of *Pheritima posthuma* Retz. Anthelmintic properties of *Sesamum prostratu* material parts extracts viz., hydroalcoholic and aqueous were evaluated against *Pheritima posthuma* (Indian earthworm) at five different concentration such as 10mg/ml, 20mg/ml, 30mg/ml, 40mg/ml, and 50mg/ml. Piperazine citrate was used as the reference standard. The time consumed for paralysis and death of the *Pheritima posthuma* were calculated for all groups. The Result of current study shows the aqueous extract of *Pheritima posthuma* aerial parts possess moderate anthelmintic activity compared to hydroalcoholic extract. The anthelmintic properties of both the *Sesamum* extract are less significant as compared to the standard anthelmintic drug Piperazine citrate.

Keywords: *Sesamum prostratum*, *Pheritima posthuma*, piperazine citrate, anthelmintic.

INTRODUCTION

Helminthiasis is one of the common infection in human mankind affecting major part of the globe. Mainly in the developing countries helminthiasis pose a huge threat to public health [1]. This condition is mainly due to the



**Astalakshmi et al.,**

deficiency in sanitary facilities and lack of pure water supply associated with poverty and illiteracy [2]. Helminthiasis is seen globally among majority of population but highly common in a country like India. This problem is highly seen in rural areas and to lesser extend in urban regions. The World Health Organization reports that 35% diseases are because of roundworm, which is a typical parasitic worm. More than 1.5 billion individuals or 24% of the total population are tainted with soil transmitted helminth contaminations around the world [3]. Parasitic infections remain a major constrain to livestock production globally [4]. An anthelmintic drug will expel the parasitic worms (helminths) from the human body by stunning or killing them [5]. These gastrointestinal helminthes becomes resistant to most of the currently available anthelmintic drugs [6]. Moreover, the currently available anthelmintic drugs in the market are also at high cost [7]. These factors lead the way for bringing out novel anthelmintic agents from herbal resources.

Natural medicines including plants, animals, and minerals are the gifts of nature to humans and play an important role in fighting various diseases [8]. Plants have always been a basis for the traditional medicine systems and they have provided continuous remedies to the mankind for thousands of years [9]. The pedaliaceae (pedalium family or sesame family) is the family of flowering plant containing about 25 genus and 204 species (according to WFO plant list) distributed in tropical and southern Africa, south East Asia and tropical Australia [10]. Plants of this family are generally annual or perennial herbs and rarely shrubs. This family was reported to have medicinal values, as antimicrobial, antioxidant, anticancer, demulscent, emollient and laxative properties etc., [11] sesamum is a member of pedaliaceae family. The plant species of this genus is used to treat variety of ailments. The present study evaluates the anthelmintic potential of hydroalcoholic and aqueous extracts of *Pheritima posthuma* aerial parts against Indian earthworms (*Pheritima posthuma*).

MATERIALS AND METHODS**Plant Material Collection**

Sesamum prostratu material parts (leaves, flowers, stem) were collected and then cleaned, shade dried, mechanically grinded. The crude extracts are prepared by maceration technique. Coarsely powdered plant materials were separately soaked in extraction solvents hydroalcoholic (ethanol:water (50:50)) and aqueous followed by shaking periodically for seven days and then filtered. The extracts are then dried in hot air oven and transferred into well labeled vials and kept in a refrigerator until required for use. The resulting dry extract was weighed and provided a percentage yield of 17.86% (w/w) and 29.21% (w/w) for hydroalcoholic and aqueous extracts respectively.

PHYTOCHEMICAL SCREENING

Phytochemical screening was carried out to assess the qualitative chemical composition of crude methanolic extracts of *Sesamum prostartum*. Standard screening tests using conventional protocol, procedure, and reagents were conducted to identify the constituents as described in Trease and Evans [12] and sofowora [13].

Collection of Parasites

Earthworms shows resemblance in its anatomical and physiological nature similar to that of human intestinal roundworms [14-16]. The healthy adult earthworms were collected from muddy soil, cleaned and separated on their size and length and used for the study.

Anthelmintic Studies

Earthworms (*Pheritima posthuma*) of uniform size and length (3-5cm in length and 0.1-0.2cm width) were selected for the study. 16 Groups of 3 earthworms each were freed into 10ml of preferred solutions. Group I serves as a negative control (normal saline). Group II to VI were treated with *Pheritima posthuma* hydroalcoholic extract of 10mg/ml, 20mg/ml, 30mg/ml, 40mg/ml, 50mg/ml respectively. Group VI to XI were treated with *Pheritima posthuma* hydroalcoholic extract of 10mg/ml, 20mg/ml, 30mg/ml, 40mg/ml, 50mg/ml respectively. Whereas, Group XII to XVI



**Astalakshmi et al.,**

were treated with piperazine citrate of 10mg/ml, 20mg/ml, 30mg/ml, 40mg/ml and 50mg/ml respectively. All the groups of earthworms were kept under observation for a maximum period of 300min and the time taken by them to paralyse and death was noted. Paralysis of the earthworms was confirmed by non-revival in normal saline solution and death was confirmed by losing up of motility and fading away of their body colors [17-20].

RESULTS AND DISCUSSION

Phytochemical Screening

The preliminary phytochemical screening of the plant materials revealed the presence of flavonoids, carbohydrates, steroids, terpenoids and proteins in both hydroalcoholic and aqueous extracts (Table 1).

Anthelmintic activity

Anthelmintic properties of *Sesamum prostratum* aerial parts extracts hydroalcoholic and aqueous are evaluated against Indian earthworms *Pheritima posthuma* at 10mg/ml, 20mg/ml, 30mg/ml, 40mg/ml, 50mg/ml using piperazine citrate as standard. The study clearly reveals that *Pheritima posthuma* aqueous extract possess moderate anthelmintic properties. However, the effect of aqueous extract was found to be less significant as compared to the standard drug piperazine citrate. The result of the study are given in the table no 2.

CONCLUSION

The present study evaluates hydroalcoholic and aqueous extracts of *Sesamum prostratum* aerial parts at 10mg/ml, 20mg/ml, 30mg/ml, 40mg/ml, 50mg/ml for anthelmintic potential against the standard drug Piperazine citrate. The study concludes that the aqueous extracts possess moderate anthelmintic properties as compared then hydroalcoholic extract. The anthelmintic potential of these extracts were found to be less significant than the standard drug piperazine citrate. According to the present study the plant *Sesamum prostratum* possess significant Anthelmintic properties in both extracts. We expecting that the further investigation of various extracts of *Sesamumprostratum* may be result in high anthelmintic properties compared to standard anthelmintic drugs.

REFERENCES

1. Das S.S, Monalisha Dey, Ghosh A.K, Indian Journal of Pharmaceutical Sciences, 2011,73(1), 104-107.
2. Walter P.J, Richard K.K, Chemotherapy of parasitic infections, In; W.C. Campbell and L.S. Rew (eds), plenum, New York, 1985, 278-539.
3. Ishnava, K.B., Konar, P.S. In vitro anthelmintic activity and phytochemical characterization of *Corallocarpusepigaeus* (Rottler) Hook. F. tuber from ethyl acetate extracts. Bull Natl Res Cent.2020;44;33. <https://doi.org/10.1186/s42269-020-00286-z>.
4. SelamawitZenebe, Tekafeyera, Solomon Assefa. "In Vitro Anthelmintic Activity of Crude Extracts of Aerial Parts of *Cissusquadrangularis* L. and Leaves of *Schinusmölle* L. against *Haemonchuscontortus*", BioMed Research International, vol. 2017, Article ID 1905987, 6 pages, 2017. <https://doi.org/10.1155/2017/1905987>.
5. Temjenmongla, Yadav A, Afr. J. Trad. Cam., 2005, 2(2): 129-133.
6. MondalSubhasish, HaqueRabiul, GhoshParag, Das Debasish, International journal of drug development and research, 2010, 2(4): 826-829.
7. Nisha P.V, Shruti N, SwetaSwamy K, et. Al., International Journal of pharmaceutical sciences and drug research, 2012, 4(3): 205-208.
8. Tang C, Zhao C-C, Yi H, Geng Z-J, Wu X-Y, Zhang Y, Liu Y and Fan G. Traditional Tibetan Medicine in Cancer Therapy by Targeting Apoptosis Pathways. Front. Pharmacol. 11:976. July 7, 2020. Doi: 10.3389/fphar.2020.00976.
9. Arpita Roy, Shruti Ahuja, Navneeta Bharadvaja. A review on medicinal plants against cancer. Journal of Plant Sciences and Agricultural Research. 2017;2 (1):008.





Astalakshmi et al.,

10. Aguru, U., Okoli, B.E., Olan, J.O. Comparative Gross Morphology of Some species of Sesamum L. International Journal of Current Research in Biosciences and Plant Biology. 2016; 3: 21-32.
11. CathrineChidewe, Uvidelio F. Castillo, Daniel S. Sem. Structural Analysis and Antimicrobial Activity of Chromatographically Separated Fractions of Leaves of Sesamum angustifolium (Oliv.) Engl. TBAP. 2017; 7(6): pp 463 – 474.
12. G. E. Trease and W. C. Evans, Pharmacognosy, Bailliere Tindall, London, UK, 13th edition, 1989.
13. A. Sofowora, Medicinal Plants and Traditional Medicine in Africa, Spectrum Books Ltd, Ibadan, Nigeria, 1993.
14. Vidyarthi R.D, A Textbook of Zoology, Chand and Co. Press, New Delhi, 1977, 14th edn., 329-31.
15. Thorn G.W, Adams R.D, Braunwald E, Isselbacher K.J, Peterdrof R.G, Harrison's Principles of Internal Medicine, Mc Grew Hill, New York, 1977, 8th Edn., 1088-90.
16. Vigar Z, Atlas of Medical Parasitology. Publishing House, Singapore, 1984, 2nd Edn., 216-18.
17. Surendra Kumar M, Astalakshmi N, Mithra T, et. al., International Journal of Pharmacognosy and Phytochemical Research, 2014-15; 6(4): 778-779.
18. Astalakshmi N, Surendra Kumar M, Mithra T, et. Al., World Journal of Pharmaceutical Research, 2015; 4(6): 1029-1033.
19. Singh S, Rai A.K, Sharma P, Barshiliya Y, Asian Journal of Pharmacy and Life Science, 2011, 1(3): 211-215.
Dash G.K, Suresh P, Sahu S.K, Kar D.M, Ganapathy S, Panda A, Journal Natural Remedies, 2002; 2: 182-185.

Table No: 1 Phytochemical constituents of investigated plant extracts

S. No	Phytoconstituents	Hydroalcoholic extract	Aqueous extract
01	Alkaloids	-	+
02	Glycosides	+	+
03	Flavonoids	+	+
04	Tannins	+	+
05	Steroids	+	+
06	Carbohydrates	+	+
07	Proteins and Amino acids	+	+
08	Fats and fixed oils	-	+
09	Vitamin C	-	-

‘+’: Present, ‘-’: Absent

Table No 2: Anthelmintic activity of *Sesamum prostratum* aerial parts extract and piperazine citrate

Group	Treatment	Dose	Time taken for Paralysis in min	Time taken for Death in min
I	Control	-	-	-
II	<i>Sesamum prostratum</i> aerial parts hydroalcoholic extract	10 µg/ml	82 min	-
III		20 µg/ml	-	-
IV		30 µg/ml	-	-
V		40 µg/ml	177 min	-
VI		50 µg/ml	179 min	-
VII		<i>Sesamum prostratum</i> aerial parts aqueous extract	10 µg/ml	76 min
VIII	20 mg/ml		84 min	-
IX	30 mg/ml		93 min	-
X	40 mg/ml		108 min	-
XI	50 mg/ml		117 min	170 min
XII	10 mg/ml		86 min	105 min
XIII	20 mg/ml		33 min	48 min





Astalakshmi et al.,

XIV	Piperazine citrate	30 mg/ml	17 min	27 min
XV		40 mg/ml	11 min	25 min
XVI		50 mg/ml	6 min	9 min

*The experiment was carried out three times & average value was taken.





Optimizing Convolution Neural Networks with Genetic Algorithm for Lung Cancer Classification

Ritu Nagila^{1*} and Abhishek Kumar Mishra²

¹Research Scholar, IFTM University, Moradabad, Uttar Pradesh, India

²Associate Professor, IFTM University, Moradabad, Uttar Pradesh, India

Received: 09 Apr 2023

Revised: 29 Apr 2023

Accepted: 15 May 2023

*Address for Correspondence

Ritu Nagila

Research Scholar,
IFTM University,
Moradabad, Uttar Pradesh, India.



This is an Open Access Journal / article distributed under the terms of the **Creative Commons Attribution License** (CC BY-NC-ND 3.0) which permits unrestricted use, distribution, and reproduction in any medium, provided the original work is properly cited. All rights reserved.

ABSTRACT

One of the leading causes of cancer-related death in both men and women is lung cancer. According to the World Cancer Research Fund International, 2.2million new instances of this disease were reported in 2020. Lung nodules are essential for cancer screening, because early detection enables therapy and speeds up patient's recovery. Even though a lot of effort is being done in this area, accuracy needs to be improved in order to boost the patient persistence rate. Traditional technologies, however, fail to accurately separate cancer cells of various kinds, and no system has gained greater dependability. In this work, an efficient method is suggested to not only quickly identify lung cancer lesions but also to improve accuracy. Medical personnel are prompted to treat patients in a safer and more efficient manner by early diagnosis and classification of the disease. The development of deep learning technology has made it possible to investigate the role of specific genes in diseases like lung cancer. In order to classify a patient's lung cancer status, this study used genetic algorithm (GA) as a feature (genes) selection method for the convolutional neural network (CNN). With noteworthy predictive ability, genetic algorithm successfully discovered genes that categorise patient lung cancer status. The proposed framework has a 98.97% accuracy rate. The suggested study shows that accuracy is increased, and execution time decreases also the data is compiled utilising genetic and convolutional neural network method.

Keywords: Cancer, Big data, Cancer Detection Technique, Feature Selection, Genetic Algorithm, Convolutional Neural Network, Image segmentation, Optimization.



**Ritu Nagila and Abhishek Kumar Mishra**

INTRODUCTION

Cancer is a condition when the body's cells grow out of control. Lung cancer is a term used to describe cancer that first appears in the lungs. Lung cancer starts in the lungs and can spread to the lymph nodes or other body organs, like the brain. The lungs may potentially become infected with cancer from other organs. Metastases are the term used to describe the spread of cancer cells from one organ to another. Typically, there are two basic forms of lung cancer: small cell and non-small cell (including adenocarcinoma and squamous cell carcinoma). They develop differently and respond to treatment in different ways. The occurrence of non-small cell lung cancer exceeds that of small cell lung cancer. The type of tumour present determines how [2] lung cancer is treated. To achieve improved survival rates, it is crucial to classify distinct tumour kinds. However, it is difficult to classify lung cancers. For monitoring and making decisions regarding malignant lung growths, computed [3] tomography (CT) is the most important image mode. The early detection of lung cancer by CT allows physicians to recommend more effective therapy. For ordered and comforting treatment, estimating and healing elements for dispersed illness with definite malignancy stages are needed. The patient's continuation rate has a strong relationship to how quickly the lung cancer period ends. Clinical terminology refers to the condition as odd hyperplasia, and it affects people in ways that go well beyond the 200 types. Computer-Aided Diagnosis (CAD) technologies have become significant and indispensable in the categorization problem of lung cancer in order to simplify this diagnosis procedure and improve the odds of survival. With the use of many components like medical image processing, artificial intelligence, and computer vision, CAD is a technique that aims to lower the rate of false positive or negative diagnoses. Image pre-processing, feature extraction, and classification are the three primary processes of this technique, as shown in Figure

1. Convolutional neural networks (CNNs) are a deep learning subfield [1] that have been combined of the widely used techniques, particularly in the field of medical imaging. One of the important uses for this technology is to aid doctors in the early detection of lung cancer, which can lower mortality rates. However, a wide range of factors influence system diagnosis precision. The use of computer-aided technology for this aim has been increasingly attractive to scientists in recent years. In this study, lung cancer images are categorised using a meta-heuristic optimised CNN classifier that is applied to trained network models for visual datasets. The convolution layer in Fig. 2 analyses the output of the neurons that are input-connected to the local area. The calculation is done by multiplying the weights of each neuron by the region to which they are linked (the activation mass). The pooling layer's primary objective is to [1] subsample the input image in order to lessen the computational workload, memory requirements, and the number of parameters (over fitting). The neural network becomes less sensitive to picture displacement when the input image is smaller (independent of the position). There are, however, a variety of techniques for improving the convolutional neural network learning process, and there aren't many studies about deep learning-based neural networks and their uses. The weights and biases in the CNN models are optimised in the current work using a novel method based on the genetic algorithm. The new approach is then put to the test against 10 well-known classifiers using datasets for lung cancer, including LIDC (Lung Image Database Consortium) Database. According to experimental findings, this refined approach performs more accurately than other categorization methods.

LITERATURE REVIEW

Many research works have been conducted on different types of cancer detection and prediction. The research works applied different approaches for detecting cancer of different types. Different algorithms were developed and compared. Some of the previous research works on lung cancer detection are discussed in this section. In 2020, Long Zhang *et al* [1] proposed a method for optimizing convolution neural network with whale optimization algorithm. This approach was then put to the test against 10 well-known classifiers using two datasets for skin cancer, including Derm1 S Digital Database and Dermquest Database. According to experimental findings, this refined approach performed more accurately than other categorization methods.



**Ritu Nagila and Abhishek Kumar Mishra**

Joey Mark Diaz *et al* proposed a method [2] for in 2018. In order to classify a patient's lung cancer status, this study used genetic algorithm as a feature (genes) selection method for the support vector machine and artificial neural network. With noteworthy predictive ability, genetic algorithm (GA) successfully discovered genes that categorise patient lung cancer status. Chapala Venkatesh *et al* investigate [3] a method for optimizing neural network in 2022. In this study, a screening method that was efficient and increases accuracy was suggested for identifying lung cancer lesions. In this process, the cuckoo search algorithm was used to establish the ideal criteria for partitioning cancer nodules, and Otsu thresholding segmentation was used to achieve perfect isolation of the chosen area. The pertinent lesion features were extracted using a local binary pattern. Based on the obtained features, the CNN classifier can determine if a lung lesion is malevolent or not. The proposed framework has a 96.97% accuracy rate. The suggested study shows that accuracy is increased, and the data is compiled utilising genetic and particle swarm optimization. C Vankatesh *et al*. [4] proposed a hybrid method for classifying lung cancer in 2019. The identification of cancer in CT scans was addressed in this study using a hybrid strategy that combines a genetic optimization algorithm, SVM classification, and a unique feature selection method. With the use of this technique, clinicians can accurately identify lung nodules at an early stage. A feed-forward neural network was trained using GA by Montana *et al*. [5] in one of the earlier efforts. The authors demonstrated that by adjusting the weights during the neural network learning process, GA increased accuracy in comparison to back-propagation neural networks.

Chuang Zhu *et al* [6] proposed a categorization of breast cancer histopathology images using numerous small Convolutional Neural Networks (CNNs) in 2019. A hybrid CNN architecture with a local model branch and a global model branch was used in this study. This hybrid approach gains a stronger capacity for representation through local voting and two-branch information merging. Second, by incorporating the suggested Squeeze-Excitation-Pruning (SEP) block into this hybrid model, it was possible to learn the importance of each channel and eliminate the redundant ones. The suggested channel pruning strategy can generate improved accuracy with the same model size while lowering the danger of over fitting. In 2021 F. Taher *et al* [7] discussed the accuracy, sensitivity, and specificity of various machine learning techniques, including convolutional neural networks (CNN), support vector machines (SVM), artificial neural networks (ANN), multi-layer perceptrons (MLP), K-nearest neighbour (KNN), and the entropy degradation method (EDM). In comparison to other approaches, the CNN approach utilising a short dataset yields the greatest results (96% accuracy), whereas EDM yields the lowest accuracy (77.8%).

Samuel Zumbuka *et al* [8] showed a study in 2021. This study listed the predictive techniques and instruments for routinely detecting, predicting, contrasting, or classifying lung cancer. Thirty-four (34) papers relating to the applications of machine methods were chosen and taken into consideration using Boolean keyword searches in various journal databases and filters. The analysis's findings indicate that the majority of studied utilised combined classical models, with ANN and deep learning being used less frequently. Additionally, only a small portion of the data set—which also included personal characteristics, X-ray images, symptoms, etc.—used data sets other than CT scan images. The results of this study indicated several restrictions and future research possibilities for lung cancer and associated diseases.

METHODOLOGY

Physicians identify lung cancer after carefully analysing CT images, a process that takes a lot of time and is not always correct. Modern optimization methods and image processing techniques were necessary to produce imagery that was as accurate, functional, and efficient as feasible. The suggested technology will help physicians accurately detect lung nodules at an early stage and examine the internal structure. As a part of the contribution, certain errors with the identification of lung cancer are mentioned here. Using a cutting-edge segmentation technique called Otsu there sholding and cuckoo search optimization, the region of interest is located. With this suggested partitioning method, nodules of various sizes and shapes can be precisely separated using only a few parameters.



**Ritu Nagila and Abhishek Kumar Mishra**

Convolutional Neural Network (CNN)-Fig 3 represents a CNN architecture. CNNs frequently use pooling layers when dealing with complex layers. They are mostly employed for reducing the tensor's size and accelerating estimations. These layers are all quite basic. Therefore, the image must be divided into smaller sections in the pooling layer, with the maximum value being chosen for each portion and each piece was then completed through some technique. It is positioned appropriately in the output after being portioned. Rectified linear units, or RELUs, are a type of hidden layer. The activation function is mostly utilised in CNNs, which are neural networks.

Genetic Algorithm- Fig 4 represent the concept of Genetic Algorithm (GA). Adaptive heuristic search algorithms based on genetics and natural selection theory are known as [9] genetic algorithms (GAs). As a result, [6] they offer an innovative utilisation of a random search approach to optimization issues. GAs are not random, despite the fact that they are randomised; rather, they use previous data to focus the search on areas of the search space where it will perform the best. In particular, those who adhere to the "survival of the fittest" ideas first established by Charles Darwin, the fundamental GA techniques are created to imitate processes in natural systems necessary for evolution. After a randomly generated initial population, the method evolves through three operators in accordance with Natural Selection:

- 1.**Selection**-this corresponds to the survival of the fittest;
- 2.**Crossover**- this depicts mating between individuals;
- 3.**Mutation**- this generates random modifications.

Selection Operator

- a) **Principal concept**: prefer superior people in order to pass on their genes to the upcoming generation.
- b) Each individual's goodness is based on their level of fitness.
- c) Fitness can be assessed using a subjective evaluation or an objective function.

Crossover Operator

- a) The selection operator selects two people from the population.
- b) There is a random selection of a crossover location along the bit strings.
- c) Up until this point, the values of the two strings are switched.
If $S1=000000$ and $s2=111111$ and the crossover point is 3 then $S1'=111000$ and $s2'=000111$
- d) The two new offspring produced by this pairing are added to the population's next generation. This procedure likely results in the creation of even better people by recombining pieces of good people.

Mutation Operator

- a) With some low probability, a portion of the new individuals will have some of their bits flipped.
- b) Its goal is to prevent early convergence and preserve population variety.
- c) A random stroll through the search space is brought on by mutation alone.

Although genetic algorithms have been employed for feature selection, parameter optimization, and rule reduction, they are best for finding the best solution to a problem. But there is still a lot that can be done to enhance GAs, both generally and specifically for cancer research. In order to identify topics for future work, this section elaborates on areas that could use improvement.

Design: Combining CNN and GA

In this section, we will go through how we evolved the CNN weights for the histopathology lung image classification challenge using GA's global search feature. An effective CNN architecture for categorising binary histological lung image data is planned. The block diagram of our model is shown in Fig 6. Below is a description of the layers that the model uses.



**Ritu Nagila and Abhishek Kumar Mishra****Input Layer**

The convolutional layer receives the loaded input images from this layer and processes them. Lung images from the LIDC dataset are used as inputs in our approach.

Convolutional Layers

In order to create the feature map, convolutional layers apply the convolution operation to the input images using kernels (filters). The network has eight convolutional layers and numerous 3-by-3 filters. Each layer has eight filters for the first two levels, sixteen for the third and fourth layers, twenty-four for the following two tiers, and ultimately thirty-two for the final two layers. With either a uniform or normal distribution, these weight filters are started at random. All of the weights of the network, including the weights of the convolutional filters and fully connected layers, are stored in a matrix for subsequent computation because employing matrix form simplifies the operation of CNN. However, 1-dimensional vectors are used to hold the initial [10] population of GA.

Pooling Layer- Convolution layers stage is followed by this step. The average pooling function is used to minimise the features map dimension. The average of each filter in a convolutional layer is determined by this function.

Activation Layer

To increase the rate at which the learning process converges, all convolutional and pooling layers are subsequently followed by a activation function.

Fully-Connected Layer

Following convolution and pooling processes, a process known as flattening is used to convert the entire features matrix into a single vector. The network's fully connected layer then receives this vector as its input neurons. To put it another way, the first layer is a vector of features from the convolutional and pooling layers, and the last layer is a vector of size 2, which is equal to the number of classes in our binary classification, i.e., the Benign and Malignant classes.

Training Process

The entire system is taught following the creation of the CNN blocks. Training is the process of iteratively changing the network's weights to provide the most accurate results. Three alternative optimization methods are used in our network, and their classification accuracy is contrasted: Adam optimization, mini batch gradient descent, and GA.

Data Set-The performance of our suggested model for binary classification of lung CT images is evaluated using the LIDC dataset, a public accessible dataset. To assess the performance and demonstrate the effectiveness of their proposed classifiers, researchers need a distinctive dataset. As a result, most of the researchers used the LIDC dataset, which contains images of lung cancer, as a well-known database addressing the problem of classifying lung cancer. Examples of CT-scan images of lung cancer patients from the LIDC dataset are shown in Fig-7. To train our classifier, we employed 70% of the available images in this study, and the remaining 30% were used to test the proposed model. We did this by randomly dividing the LIDC dataset into two sets, a training set and a testing set. Both sets are Patients utilised to form the training set and the test set were divided patient-wise, therefore they are not the same patients. Additionally, we are categorising the CT-images independently of their sub-classes and magnification factors because our focus is on the binary categorization of CT images into Benign and Malignant cases.

Pseudo Code -In the following, the general pseudo code for Optimizing CNN through GA is given as follows.

Algorithm 1

Create the CNN architecture;
Generate the initial weights of the model randomly;
Store the weights of the model in a matrix;
Set the parameters of GA;
Convert the weight matrix to the vector of initial population;



**Ritu Nagila and Abhishek Kumar Mishra**

while Termination condition is not true **do**
Start the CNN process;
Predict the output using CNN;
Calculate the fitness function;
Sort individuals based on fitness value to select fitter individuals for producing the offspring of the next generation;
Applying a single-point crossover operation;
Applying mutation operation to add a random value to a randomly selected gene with probability of 0.1.

end while

The CNN using GA optimization approach is described in above Algorithm. In our implementation of the suggested GA optimizer, we make use of the following variables:

- (i) The number of solutions per population varies from 20 to 60;
- (ii) The number of generations varies from 100 to 1000;
- (iii) The mutation rate varies from 0.1 to 0.01; and
- (iv) The network weights are initially distributed using both normal and uniform distributions.

RESULTS AND DISCUSSION

Based on many measures, including classification accuracy, execution time we report the findings of the lung cancer CT image classification provided by the LIDC dataset. The binary classification of the input images is the output. Every image is sent to the network and given a Benign or Malignant case. This study combines convolutional neural network and genetic algorithm to propose an effective and automated method for detecting lung cancer. The process starts with image pre-processing, followed by image segmentation, feature extraction, and classification. The procedure is evaluated using lung CT-images. Figure 8 revealed that the proposed model is able to classify benign and malignant lung cancer patients with accuracy rates of 98.97%. Additional it also reduces the exception time which can be shown in figure 9. This result is consistent with the fact that the classification accuracy of lung cancer is frequently higher when optimising a convolution neural network with a genetic algorithm.

CONCLUSION

Because of the ability to classify data, machine learning techniques like Convolution Neural Networks (CNN) have been frequently used in CAD systems. The network weights, including the weights of all convolutional filters and the weights of connecting edges in the fully-connected layer, have a significant impact on the accuracy of extracted features in CNN. Therefore, these weights are very important for classification accuracy. In this study, we suggested employing the Genetic Algorithm (GA) to optimise the CNN weights for lung cancer classification problem. The five levels of the proposed algorithm are input layer, convolution layer, pooling layer, activation layer, fully-connected layer, and training process. The weights of these layers have a significant impact on the classification accuracy. Utilizing selection, crossover, and mutation operators, the weights are evolved. Using the LIDC dataset, we compare our suggested method with using CNN approach. To investigate metrics like accuracy, execution time, and the impact of genetic parameters on the proposed method, we carried out numerous trials with varied batch sizes and iteration counts.

REFERENCES

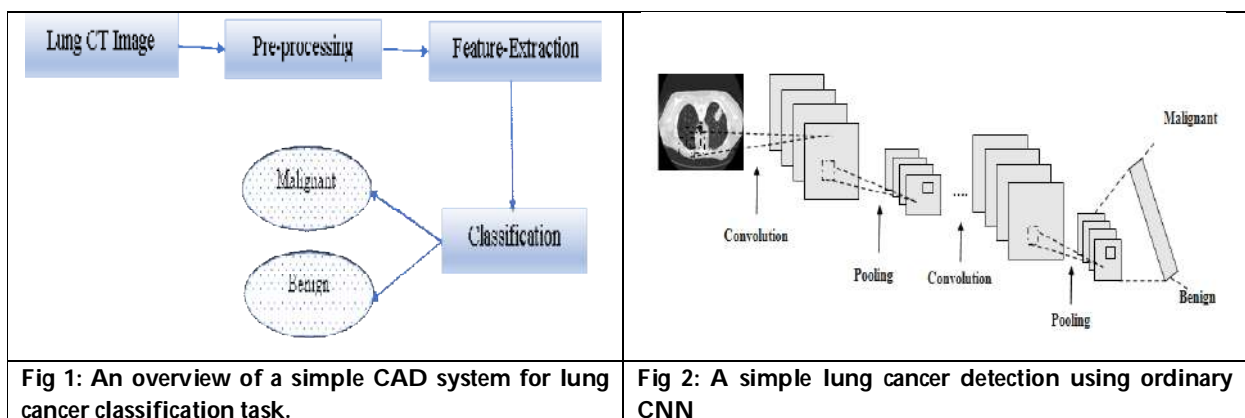
1. Long Zhang, Hong Jie Gao, Jianhua Zhang, Benjamin Badami, "Optimization of the Convolutional Neural Networks for Automatic Detection of Skin Cancer", 2020.





Ritu Nagila and Abhishek Kumar Mishra

2. Joey Mark Diaz, Raymond Christopher Pinon, Geoffrey Solano, "Lung Cancer Classification Using Genetic Algorithm to Optimize Prediction Models" ,2014.
3. Chapala Venkatesh, Kadiyala Ramana, Siva Yamini Lakkisetty, Shahab S. Band,Shweta Agarwal and Amir Mosavi, "A Neural Network and Optimization Based Lung Cancer Detection System in CT Images", Frontiers in Public Health, www.frontiersin.org, June 2022 | Volume 10 | Article 769692.
4. CVenkatesh, Polaiah Bojja, "A Novel Approach for Lung Lesion Segmentation Using Optimization Technique",Helix E-ISSN: 2319-5592; P-ISSN: 2277-3495, DOI 10.29042/2019-4832-4837.
5. D. J. Montana and L. Davis, "Training feedforward neural networks using genetic algorithms." in IJCAI, vol. 89, 1989, pp. 762–767.
6. C. Zhu, F. Song, Y. Wang, H. Dong, Y. Guo, and J. Liu, "Breast cancer histopathology image classification through assembling multiple compact CNNs,"BMC medical informatics and decision making, vol. 19, no. 1, p. 198, 2019
7. F. Taher, N. Prakash, A. Shaffie, A. Soliman, A. El-Baz, "An Overview of Lung Cancer Classification Algorithms and their Performances",IAENG International Journal of Computer Science, 48:4, IJCS_48_4_19, Volume 48, Issue 4: December 2021.
8. Samuel Zumbuka, Yusufu Gambo and O. Sarjiyus, "Application of Machine Learning in LungCancer",IJSET - International Journal of Innovative Science, Engineering & Technology, Vol. 8 Issue 9, September 2021, ISSN (Online) 2348 – 7968 | Impact Factor (2020) – 6.72.
9. Ritu Nagila, Abhishek Kumar Mishra, "A Comprehensive Analysis of Big Data Analytics Applications in Cancer Detection Methods",Industrial Engineering Journal, Volume 15 Issue 12 * December 2022, ISSN: 0970-2555.
10. Katsuo Usuda, Shun Iwai *et al*, "Novel Insights of T2-Weighted Imaging: Significance for Discriminating Lung Cancer from Benign Pulmonary Nodules and Masses", Cancers 2021, 13, 3713. <https://doi.org/10.3390/cancers13153713>.
11. Ibrahim M. Nasser, Samy S. Abu-Naser, Palestine, "Lung Cancer Detection Using Artificial Neural Network", International Journal of Engineering and Information Systems (IJEAIS), ISSN: 2000-000X ,Vol. 3 Issue 3, March – 2019, Pages: 17-23.
12. Lal Hussain *et al*, "Lung Cancer Prediction Using Robust Machine Learning and Image Enhancement Methods on Extracted Gray-Level Co-Occurrence Matrix Features",Appl. Sci. 2022, 12, 6517. <https://doi.org/10.3390/app12136517>.
13. Antony Judice A, Dr. K. Parimala Geetha, "A Novel Assessment of Various Bio-Imaging Methods for Lung Tumor Detection and Treatment by using 4-D and 2-D CT Images", International journal of Biomedical science, June 2013 Vol. 9 No. 2 Int J Biomed Sci www.ijbs.org.
14. Parthasarathy G *et al*, "PREDICTION OF LUNG CANCER USING DEEP LEARNING ALGORITHM", International Journal of Creative Research Thoughts (IJCRT), Volume 8, Issue 4 April 2020 | ISSN: 2320-2882.





Ritu Nagila and Abhishek Kumar Mishra

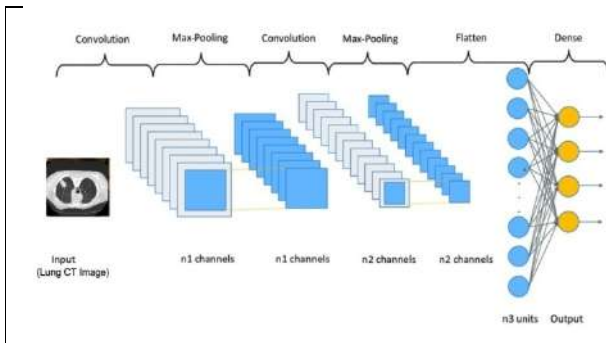


Fig.3- Architecture of CNN

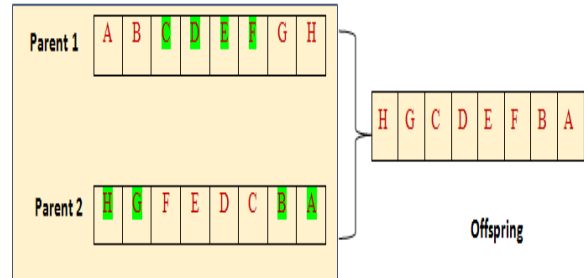


Fig.4 Concept of GA

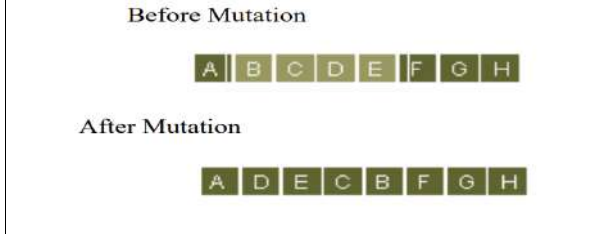


Fig.5 Before and After Mutation

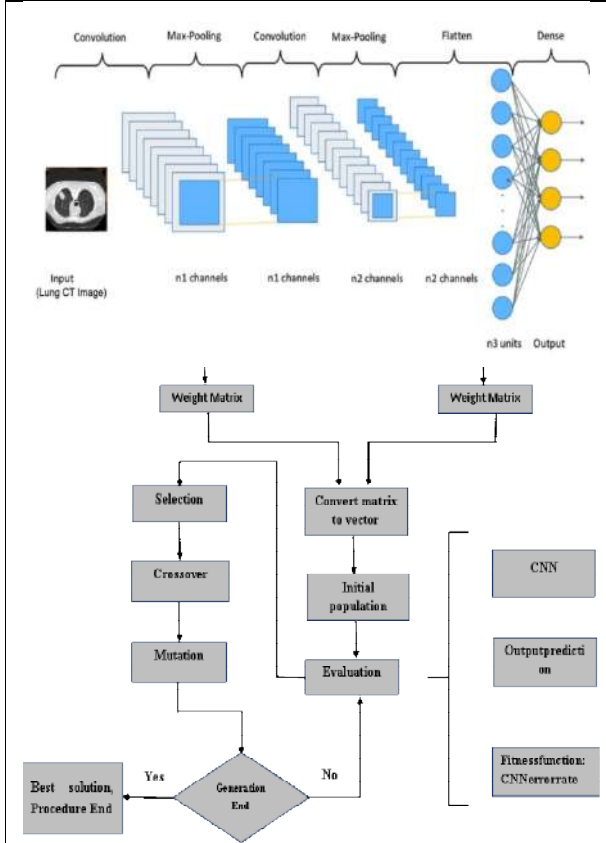


Fig. 6 Block diagram for utilising GA to optimise the CNN's parameters.

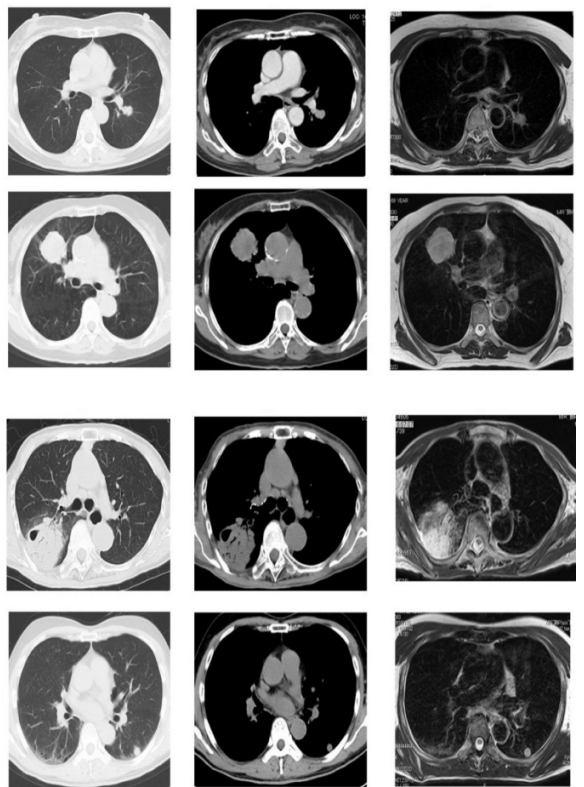


Fig.-7 CT-images of lung cancer





Ritu Nagila and Abhishek Kumar Mishra

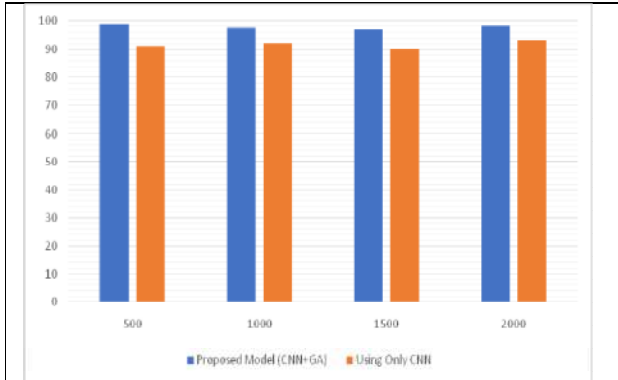


Fig.-8 Illustrates the accuracy of the proposed model and the only CNN method in percentage

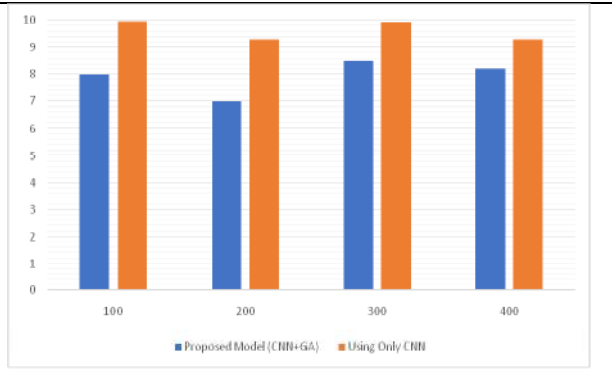


Fig.-9 Illustrates the execution time of the proposed model and the only CNN method





Health Related Quality in Pre-Diabetes Patients of Kazakhstan

Sajad Ahmad Bhat¹, AbduganiTadjibaevich Musayev², Anwar Shaikhin³, GhHussain Mir^{4*} and Aizhan Danyshbayeva⁵

¹Department of Biochemistry, International Medical School, University of International Business, Almaty, Kazakhstan.

²Department of Emergency and Urgent medical care, Kazakh National Medical University named after S.D. Asfendiyarov, Almaty Kazakhstan.

³Magistracy and doctoral programs department, West Kazakhstan Marat Ospanov Medical University, Republic of Kazakhstan.

⁴Associate Professor, Department of General Surgery, Sher-i-Kashmir Institute of Medical Sciences, Soura, Srinagar, India- 190011.

⁵Department of General Medical Practice,Asfendiyarov Kazakh National Medical University, named after S.D. Asfendiyarov, Almaty Kazakhstan.

Received: 15 Feb 2023

Revised: 25 Apr 2023

Accepted: 31 May 2023

*Address for Correspondence

GhHussain Mir

Associate Professor,
Department of General Surgery,
Sher-i-Kashmir Institute of Medical Sciences,
Soura, Srinagar, India- 190011.
E.Mail: mirhussain15.mh@gmail.com



This is an Open Access Journal / article distributed under the terms of the **Creative Commons Attribution License** (CC BY-NC-ND 3.0) which permits unrestricted use, distribution, and reproduction in any medium, provided the original work is properly cited. All rights reserved.

ABSTRACT

The level of blood glucose is more than normal but not sufficient to diagnose diabetes leads to a condition known as pre-diabetes. Globally, Pre-diabetes affects approximately 260 million people, or 6.4% of adults. According to the International Diabetes Association (ADA), diabetes prevalence will rise to 8.8% by 2035 globally. Diabetes prevalence in Kazakhstan males is 11.3 percent, and in women it is 11.7 percent, according to WHO, with a population of 17 million. According to medical experts, Kazakhstan's diabetes population would grow to a million individuals by 2030. The present study was a case control study and 82 subjects were recruited. Elevated fasting blood sugar (FBS) was defined as a plasma glucose concentration in fasting stage should be 5.6-6.9 mmol/L, and Impaired Glucose Tolerance (IGT) was defined when FBS levels should be <7.0 mmol/L and a 2 hour postprandial blood sugar (PPBS) of 7.8 mmol/L-11.0 mmol/L, with a glycosylated haemoglobin (HbA1c) value of 5.7%-6.4%. Mean±SD for BMI of all the pre-diabetic patients was 31.98 ±2.39 with p value of p<0.001. When they were separated into BMI categories, 3.3 percent were of normal weight and 96.3 percent were obese. Role physical had the lowest mean score (M= 46.48), while Social Functioning (M = 50.25) and Bodily pain (M= 50.03) had the highest



**Sajad Ahmad Bhatet al.,**

mean scores. In conclusion the data suggests that “quality of life” (QoL) in patients with pre-diabetes were at greater risk with less physical component.

Keywords: Body Mass Index, Social Functioning-36, Health Related Quality Life, Vitality

INTRODUCTION

The level of blood glucose is more than normal but not sufficient to diagnose diabetes leads to a condition known as pre-diabetes [1]. According to the ADA, conditions referred for diagnostic criteria in pre-diabetes include an increased FBS level (100 mg/dL-125 mg/dL), a glycaedhaemoglobin (HbA1c) value of 5.7%-6.4%, or an increased plasma glucose level, glucose tolerance test (140-199 mg/dL) [2,3]. Each of these diseases, whether discovered in childhood or later in life, increases the likelihood of developing T2DM. Globally, Pre-diabetes affects approximately 260 million people, or 6.4% of adults [4,5]. According to the International Diabetes Federation, diabetes prevalence will rise to 8.8% globally by 2035. According to the WHO, diabetes affects 11.3 percent of men and 11.7 percent of women in Kazakhstan, which has a population of 17 million people. According to medical experts, Kazakhstan's diabetes population would grow to a million people by 2030 [6,7]. Diabetes has an annual incidence of 187.2 19.4 per 100,000 people in Karaganda, and morbidity is 1500.7 169.2 per 100,000 people. According to data from the diabetes register, there have been 30622 diabetes patients in Karaganda over the last 15 years. Pre-diabetics are at more risk of developing diabetes and cardiovascular disease⁸. Kazakhstan has experienced fast economic expansion and urbanisation in recent decades, which has resulted in rise in the frequency of pre-diabetes and diabetes in country. The association of pre-diabetes with health-related quality of life (HRQoL) is either poorly understood or non-existent. HRQoL assessments, as measured by the SF 36, will give a useful health outcome relating to emotional, mental, social functioning, and physical. QoL can help patients understand their overall health state, the formation of health policy, the effect of treatment, and resource allocation decisions. So the aim of the present study was to see the association of HRQoL in the patients with pre-diabetes.

MATERIALS AND METHODS

The current study was a case-control study and total 82 patients were recruited in the regional clinical hospital Karaganda. In this study patients attending regional clinical hospital from 2012 to 2014 were included. Ethical clearance was obtained from the ethical committee. Written informed consents were taken from all patients in the present study.

METHOD

The diagnostic criteria for pre-diabetes were based on the American Diabetes Association (ADA), which defined Elevated fasting blood sugar (FBS) was defined as a plasma glucose concentration in fasting stage should be 5.6-6.9 mmol/L, and Impaired Glucose Tolerance (IGT) was defined when FBS levels should be <7.0 mmol/L and a 2 hour postprandial blood sugar (PPBS) of 7.8 mmol/L-11.0 mmol/L, with a glycaedhaemoglobin (HbA1c) value of 5.7%-6.4%. as well as a Patients having hypertension or a history of cardiovascular disease, dyslipidemia, psychiatric illness, or cognitive impairment such mental retardation or dementias were excluded from the study.

Quality of life (QOL) assessment

The SF-36 health survey questionnaire was used to assess HRQOL. The SF-36 questionnaire is a generalised questionnaire that is commonly used in the United States and Europe to evaluate the quality of life (QOL) of healthy persons and patients with acute and chronic illnesses. Physical functioning (PF), bodily pain (BP), role-physical (RF),



**Sajad Ahmad Bhatet *al.*,**

vitality (VT), general health (GH), social functioning (SF), mental health, and role-emotion (RE), are among the eight health categories (domains) measured (MH). The eight domains were rated on a scale of 0 to 100, with 0 indicates the poorest possible health and 100 indicates the highest possible health. The Mental Component Summary score (MCS) and Physical Component Summary score (PCS) were created from all of the scores.

Statistical analysis

All computations were performed in software SPSS.v.25. The descriptive analysis was provided as means with standard deviation (SD) and frequency for health, lifestyle factors, and socio-demographic, (percentage). Means and standard deviations were used to summarize continuous variables. The Spearman pair correlation coefficients and the Kolmogorov-Smirnov test of the sample difference criterion's expected values (R). To assess the agreement between the parameters of the physical and mental health components, the Spearman correlation coefficients (SCC) were determined.

RESULTS

This study included a total of 82 pre-diabetes patients. All of the patients were 36.8 (7.8) years old on average. There were 42 females (51%) and 40 males (48%) among the 82 participants. The SF-36 scale has been broadly used to measure QoL in people with various disorders as well as those who are disease-free. Physical functioning (PF), bodily pain (BP), role-physical (RF), vitality (VT), general health (GH), social functioning (SF), mental health, and role-emotion (RE), are among the eight health categories measured. All pre-diabetes patients had a mean (SD) BMI of 31.98 2.39 p0.001. When they were separated into BMI categories, 3.3 percent were of normal weight and 96.3 percent were obese. Role physical had the lowest mean score (M= 46.48), while Social Functioning (M = 50.25) and Bodily Pain (M = 50.03) had the highest mean scores. When compared to healthy controls, pre-diabetes had considerably worse physical functioning (47.56 2.45 vs. 51.53 3.40). When comparing pre-diabetes to controls, we found a substantial increase in mean Vitality (48.80 4.36 vs. 61.70 4.62).

DISCUSSION

Following a pre-diabetes diagnosis, it is critical to maintain a balanced diet and lifestyle. The longer a person goes without being diagnosed with diabetes, the worse their health can become. Because they view pre-diabetes to be a less serious and readily accepted condition, some people with pre-diabetes have difficulty with predictability regarding their diagnosis and its repercussions [8,9]. Pre-diabetes is frequently asymptomatic, with no serious symptoms and, in many cases, no awareness of the condition [9]. Individual HRQOL component scores revealed substantial differences between the pre-diabetes and healthy groups. The average age of pre-diabetes in this study was 36 years. According to Ibrahim et al, the average age of pre-diabetes patients in Malaysia is 52 years old [10]. Our results are consistent with those of Taylor et al, who showed similar changes in demographic profiles between pre-diabetes and healthy controls. Taylor et al [11] noted that the patients were primarily elderly (mean age 58 years which is compared to 31 years in our study), females (73.3 percent compared to 51.3 percent in our study), and had same mean BMI (31.2 6.4 kg/m² compared to 31.98 4.8 kg/m² in our study). Our results' mean BMI is likewise similar to those of the Finnish Diabetes Prevention Study (DPS) and the United States' Diabetes Prevention Program (DPP) [12,13]. In our research, we discovered that pre-diabetes adults had significantly worse mean scores on the SF-36 for role physical, role emotional mental health, vitality, and physical functioning. In our study, role physical' was shown to be impaired in the pre-diabetes group when compared to the control group (46.55 4.02 vs. 50.50 3.99), which is consistent with Ibrahim et al's findings in their literature. Overweight or obese and Pre-diabetic patients scored lower on the physical component of the SF-36 than those who were normal weight. However, in a research of 1383 persons aged 45–70 years in Western Finland, no variations in HRQOL were found (using the same questionnaire SF-36) in patients with pre-diabetes compared to healthy subjects [14]. As some of our recruited pre-diabetic patients felt difficulty in doing physical activities due to body pain, HRQOL is consistently linked to physical activity. People who are physically active reported improved HRQOL than those who are physically inactive, according to prior



**Sajad Ahmad Bhatet *al.*,**

studies. This study has some drawbacks, including a limited sample size and insufficient monitoring duration. The link between HRQOL and pre-diabetes is either poorly understood or non-existent. There have been few investigations on the relationship among HRQOL and pre-diabetes.

CONCLUSION

In conclusion the data suggests that QoL in patients with pre-diabetes were at greater risk with less physical component. Guidelines should be drawn for pre-diabetes patients according to HRQOL for lifestyle modifications related to obesity and physical inactivity.

Conflicts of Interest

None

Funding

This study is not supported by any funding agency

ACKNOWLEDGMENT

The authors would like to gratefully acknowledge the Regional clinical hospital Karaganda for providing the platform to complete this research

REFERENCES

1. American Diabetes Association: Diagnosis and classification of diabetes mellitus. *Diabetes Care* 2011, 34(Suppl 1):S62–69.
2. Morera J, Joubert M, Morello R, Rod A, Lireux B, Reznik Y. Sustained Efficacy of Insulin Pump Therapy in Type 2 Diabetes: 9-Year Follow-up in a Cohort of 161 Patients. *Diabetes care.* 2016; 39(6):e74–5. [PubMed: 27208322]
3. Picard S, Hanaire H, Baillot-Rudoni S, Gilbert-Bonnemaison E, Not D, Reznik Y, et al. Evaluation of the Adherence to Continuous Glucose Monitoring in the Management of Type 1 Diabetes Patients on Sensor-Augmented Pump Therapy: The SENLOCOR Study. *Diabetes TechnolTher.* 2016; 18(3):127–35. [PubMed: 26950530]
4. International Diabetes Federation: The global burden. *IDF Diabetes Atlas.* 5th edition. Brussels: IDF; 2011.
5. AdilSupiyev, AlibekKossumov, AliyaKassenova, TalgatNurgozhin, ZhaxybayZhumadilov, Anne Peasey, Martin Bobak. Diabetes prevalence, awareness and treatment and their correlates in older persons in urban and rural population in the Astana region, Kazakhstan. *Diabetes research and clinical practice.*2016;6-12.
6. World Health Organization. (2016) Diabetes -country profiles. [Online]. Available: <https://bit.ly/2YJwzpm>.
7. Mukasheva.A, Saparkhojayev.N, Akanov.Z, Algazieva.A. The Prevalence of Diabetes in the Republic of Kazakhstan Based on Regression Analysis Methods.*International Journal of Health and Medical Sciences.*2019;5(1):08-16.
8. L.G.Turgunova, A.R.Alina, Z.M.Bulletin of the Karaganda University.2013.
9. Tabák AG, Herder C, Rathmann W, Brunner EJ, Kivimäki M. Pre-diabetes: a high-risk state for diabetes development. *Lancet.* 2012; 379(9833):2279–90.
10. Norliza Ibrahim, Foong Ming Moy, IntanAttikahNurAwalludin, Zainudin Ali, Ikram Shah Ismail. The health-related quality of life among pre-diabetics and its association with body mass index and physical activity in a semi-urban community in Malaysia- a cross sectional study.*BMC Public Health.* 2014, 14:298.
11. Taylor LM, Spence JC, Raine K, Plotnikoff RC, Vallance JK, Sharma AM: Physical activity and health-related quality of life in individuals with prediabetes. *Diab Res and ClinPract* 2010, 90(1):15–21.





Sajad Ahmad Bhatet al.,

12. Knowler WC, Barrett-Connor E, Fowler SE, Hamman RF, Lachin JM, Walker EA, Nathan DM, Diabetes Prevention Program Research Group: Reduction in the incidence of type 2 diabetes with lifestyle intervention or metformin. *The New England J of Med* 2002, 346(6):393–403.
13. Tuomilehto J, Lindström J, Eriksson JG, Valle TT, Hämäläinen H, Ilanne-Parikka P, Keinänen-Kiukaanniemi S, Laakso M, Louheranta A, Rastas M, Salminen V, Uusitupa M, Finnish Diabetes Prevention Study Group: Prevention of type 2 diabetes by changes in lifestyle among subjects with impaired glucose tolerance. *The New England J of Med* 2001, 344:1343–1350.
14. Seppälä T, Saxen U, Kautiainen H, Järvenpää S, Korhonen PE. Impaired glucose metabolism and health related quality of life. *Prim Care Diabetes*. 2013;7(3):223–7. <https://doi.org/10.1016/j.pcd.2013.03.001>.

Table1: The difference in estimated means of HRQOL in pre-diabetes patients & controls

Group=1 DescriptiveStatistics patients					Group=2 DescriptiveStatistics Control				
	Valid N	Mean	Median	Std.Dev.		Valid N	Mean	Median	Std.Dev.
BMI	60	31,98333	32,00000	2,396973	BMI	22	30,86364	31,00000	2,376381
PF1	60	47,56667	48,00000	2,458928	PF1	22	46,86364	46,50000	2,376381
PF2	60	51,53333	52,00000	3,402226	PF2	22	46,63636	46,00000	2,479352
RP1	60	46,55000	46,00000	4,022922	RP1	22	46,31818	46,00000	2,884876
RP2	60	50,50000	50,00000	4,224625	RP2	22	46,36364	46,00000	2,735054
BP1	60	50,03333	50,00000	4,087877	BP1	22	49,63636	50,00000	3,288442
BP2	60	50,20000	51,00000	3,852360	BP2	22	49,77273	49,50000	2,266355
GH1	60	48,91667	48,00000	4,461860	GH1	22	46,72727	46,00000	3,881357
GH2	60	48,51667	48,00000	4,489127	GH2	22	47,00000	47,00000	4,220133
VT1	60	48,80000	48,00000	4,363951	VT1	22	47,36364	46,00000	4,756404
VT2	60	61,70000	62,00000	4,622348	VT2	22	46,90909	46,00000	4,729936
SF1	60	50,71667	52,00000	2,917462	SF1	22	49,00000	49,00000	3,690399
SF2	60	60,08333	60,00000	3,136940	SF2	22	48,81818	48,00000	3,417551
RE1	60	48,25000	48,00000	3,577827	RE1	22	47,59091	48,00000	3,660069
RE2	60	56,08333	56,00000	2,316424	RE2	22	46,90909	47,00000	4,799892
MH1	60	48,83333	48,00000	3,340388	MH1	22	49,00000	49,00000	2,878492
MH2	60	57,78333	58,00000	3,769151	MH2	22	49,09091	48,00000	3,190896





Immediate Effect of Intercostal Stretch on Thoracic Expansion and Pulmonary Function on Mild to Moderate COPD Subjects – A Pilot Study

Dhruvika Rathod¹ and Didhiti Desai^{2*}

¹MPT Scholar, Parul Institute of Physiotherapy, Parul University, Vadodara, Gujarat India

²Assistant Professor, Parul Institute of Physiotherapy, Parul University, Vadodara, Gujarat, India.

Received: 17 Jan2023

Revised: 20 Mar 2023

Accepted: 27 Apr 2023

*Address for Correspondence

Didhiti Desai

Assistant Professor,

Parul Institute of Physiotherapy,

Parul University, Vadodara, Gujarat, India.

Email: Didhiti.desai@paruluniversity.ac.in



This is an Open Access Journal / article distributed under the terms of the **Creative Commons Attribution License** (CC BY-NC-ND 3.0) which permits unrestricted use, distribution, and reproduction in any medium, provided the original work is properly cited. All rights reserved.

ABSTRACT

Chronic Obstructive Pulmonary Disease (COPD), a condition marked by persistent airflow obstructions, respiratory symptoms cause abnormalities in the airways and alveoli, which are typically brought on by prolonged exposure to noxious particles or gases. Aim- To determine the immediate effect of intercostal stretch along with thoracic expansion exercise on pulmonary function and thoracic expansion on mild to moderate COPD subjects. Methodology-Total 5 Subjects were selected from ParulShevashram hospital, according to inclusion and exclusion criteria. Subjects were assessed before and after the 45 minutes of intervention for pulmonary function test and chest expansion and intervention was given in the form of intercostal stretch over the second and third ribs bilaterally for 10 breaths with a minute of rest and thoracic expansion exercise. Result- The mean and SD showed statistically significant improvement of FVC pre±post (1.5800±1.5620), pre±post (.32680±.33722); FEV1 pre±post (.9520±1.1680), pre±post (.24864±.39214); FEV1/FVC pre±post (61.3740±75.1420), pre±post (14.42966±21.45409) respectively. Data was analyzed by using SPSS software 20.0 and Microsoft excel. (p<0.05) Conclusion- The study showed significant improvement on pulmonary function test and chest expansion on mild to moderate COPD patients.

Keywords: - Chest PNF, inter-costal stretch, pulmonary function, chest expansion, COPD



**Dhruvika Rathod and Didhiti Desai**

INTRODUCTION

COPD is a preventable and treatable disease characterized by airflow limitation that is not fully reversible. Chronic obstructive pulmonary disease (COPD) is a lung disease. The constraint of airflow is usually progressive and is associated with an abnormal inflammatory response of the lungs to noxious particles or gases, which is primarily caused by cigarette smoking[1]. COPD is associated with significant deaths and morbidity globally; it is the world's fifth leading cause of death in the world, with its mortality rate expected to rise by more than 30% over the next 10 years, according to the World Health Organization[2]. Chronic obstructive pulmonary disease (COPD) is a condition that affects the lungs. There are several types of COPD, each with its own set of symptoms. Some people with COPD also have asthma and emphysema[3]. COPD is a condition in which the airways become damaged and the alveolar walls are destroyed. This causes the lungs to lose their elastic recoil ability, which means that people with COPD cannot expel air very well. This can lead to air trapping and hyperinflation (an increase in air pressure)[4]. Symptoms like coughing, wheezing, shortness of breath (pulmonary edema), fatigue, chest tightness, and mood disturbances. Repeated exacerbations (episodes of worsening lung function) are a risk factor for increased mortality and contribute to the health care burden associated with COPD[5]. Patients with breathing problems may have abnormal chest biomechanics or physical changes to the chest wall, such as chest stiffness. The cloth tape measurement of the circumference of the chest wall with a cloth tape measure at three distinct levels of the rib cage was used to assess chest wall mobility, which is a simple, inexpensive, and reliable procedure in clinical practice [6]. Breathing is a physiological process that removes carbon dioxide from the body and supplies oxygen via the circulatory system. Exhalation and inhalation exercises, as well as a combination of the two, can aid to enhance pulmonary function[7]. PNF (Proprioceptive Neuromuscular Facilitation) is a type of stretching in which a muscle stretches passively and contracts alternately. The approach aims to stretch through the length of a muscle's nerve receptors. As a result, intercostal muscular tiredness is common in COPD patients [4]. So, the aim of the study is to compare the immediate effect of intercostal stretch along with thoracic expansion exercise on pulmonary function and thoracic expansion on mild to moderate COPD subjects.

METHODOLOGY

Total 5 participants were taken by convenient sampling. It is an experimental study with each patient took approximately 45 minutes. Institutional ethical committee approval was taken. Subjects were selected on the basis of the inclusion and exclusion criteria. The inclusion criteria were: (1) Both males and females of age is between 40 to 60. [4] (2) Patient with mild, moderate airway obstruction based on gold criteria: gold 1-(mild: $FEV_1 / FVC < 0.70$, $FEV_1 > 80\%$ of predicted) gold 2 -(moderate: $FEV_1 / FVC < 0.70$, $50\% < FEV_1 < 80\%$ of predicted).[4] (3) Medically diagnosed COPD patient. [2] (4) Willing to participate. [2] (5) smokers or ex-smokers of more than 10 pack-years, and symptoms suggestive of COPD.[8] The exclusion criteria were: (1) Hemodynamically unstable subjects. [1] (2) Patients with severe orthopedic problems related to spine, fracture of rib, sternum fracture, neurological deficits, affecting the respiratory muscles, unstable cardiac condition, recent myocardial infarction, intercostal muscles strain.[4] (3) Previous lung – volume reduction surgery, lung transplantation or pneumonectomy[4] (4) Patient is having history of core pulmonale[4] Study procedure: A written consent and informed consent was taken from the subjects regarding enrolling them in study and their privacy and confidentiality was maintained. Before starting the intervention, subjects were assessed for outcome measure; chest expansion and pulmonary function test before and immediately after giving chest PNF with the 10 repetitions. Materials: Measuring tape, Pen, pencil, paper, PFT machine.

Treatment protocol

Intercostal stretch: inter costal stretch along with thoracic expansion exercise: -patients were in a supine lying position. The Therapist stand behind the patient. First therapist should palpate the suprasternal notch then go downward about 5 cm to palpate the angle of Louis. Then trace the finger laterally to palpate the 2nd rib and intercostal



**Dhruvika Rathod and Didhiti Desai**

stretch was given bilaterally at 2nd and 3rd rib with the help of index finger and middle finger. The direction of stretch was downward towards the next rib in midaxillary line. The stretch was maintained as he/she continues to breathe. The stretch was applied at the end of the exhalation for 10 breaths with 1 minute rest and for 10 repetitions. Total treatment duration was 45 minutes. Thoracic expansion exercise: - Patient was seated comfortably in chair sitting position. Therapist stand in front of the patient and ask the patient to inhale slowly and deeply through the mouth and performed prolonged expiration through the mouth. Breathing with mainly expiration (15 minutes of breathing exercise after 2 minute of respiration subjects rested for 1 minute).

Outcome measure

Pulmonary function (FEV1, FVC, FEV1/FVC): The patient will be seated comfortably in front of a spirometry machine. The mouthpiece will be comfortably placed between the two lips, preventing extra air from escaping from the mouth. The patient will then be instructed to take a deep breath and exhale as much as possible through a mouthpiece for several seconds. No breathing through the nose is permitted. The following parameters will be included in the study: FEV1, FVC, and FEV1/FVC. Chest expansion (tape method): Participants will sit on a stool with their arms crossed behind their backs and their heads turned to one side. A cloth tape will be used to measure chest expansion at three different levels of the rib cage. The axillary level, nipple level, and xiphisternum level are the anatomical marks for thoracic expansion. Choosing these locations has the advantage of representing the elasticity of different lobes. The patient is then asked to breathe out through their mouth, inhale slowly through their nose, and push their chest against the tape to measure the expansion of their lungs. The patients will then be asked to exhale through their mouths. Measurements will be taken at three different levels, with the cross-hand technique being used.

Statistical Analysis

Statistical tests: Wilcoxon test were used to find the significance of parameters pre to post test. Statistical software: The Statistical software namely IBM SPSS Statistics version 20. Which were used for the analysis of the data and Microsoft word and Excel have been used to generate graphs, tables etc. Ethical clearance: Institutional ethical committee is given clearance of these study.

RESULT AND DISCUSSION

Table 1 shows the pre and post comparison of chest expansion at axillary level after 45 minutes of intervention. Pretest mean of CEAL 1.3000 with the SD .44721 when it was compared with the mean of 2.3000 after the intervention with the SD .44721 obtained "z" value was -2.236^bThis finding had showed there was significant difference in CEAL in pre and post- test. ($p < .025$)Table 2 shows the pre and post comparison of chest expansion at nipple level after 45 minutes of intervention. Pretest mean of CENL 1.7600 with the SD .33615 when it was compared with the mean of 2.8000 after the intervention with the SD .44721 obtained "z" value was -2.060^bThis finding had showed there was significant difference in CENL in pre and post- test. ($p < .039$)Table 3 shows the pre and post comparison of chest expansion at XIPHISTERNAL level after 45 minutes of intervention. Pretest mean of CEXL 2.0000 with the SD .70711 when it was compared with the mean of 3.2600 after the intervention with the SD .73348 obtained "z" value was -2.060^bThis finding had showed there was significant difference in CEXL in pre and post- test. ($p < .039$)Table 4 shows the pre and post comparison of PFT FEV1 after 45 minutes of intervention. Pretest mean of FEV1 .9520 with the SD .24864 when it was compared with the mean of FEV1 1.1680 after the intervention with the SD .39214 obtained "z" value was -1.753^b This finding had showed there was significant difference in FEV1 in pre and post- test. ($p < .080$)Table 4 shows the pre and post comparison of PFT FEV1 after 45 minutes of intervention. Pretest mean of FEV1 .9520 with the SD .24864 when it was compared with the mean of FEV1 1.1680 after the intervention with the SD .39214 obtained "z" value was -1.753^b This finding had showed there was significant difference in FEV1 in pre and post- test. ($p < .080$)Table 6 shows the pre and post comparison of PFT FEV1/FVC RATIO after 45 minutes of intervention. Pretest mean of FEV1/FVC 61.3740 with the SD 14.42966 when it was



**Dhruvika Rathod and Didhiti Desai**

compared with the mean of FEV1/FVC 75.1420 after the intervention with the SD 21.45409 obtained "z" value was -2.023^bThis finding had showed there was significant difference in FEV1/FVC in pre and post- test. (p<.043)

DISCUSSION

COPD is a lung disease characterized by persistently low airflow as a result of lung tissue breakdown and small airway dysfunction, which is usually accompanied by dyspnea, fatigue, and sputum production. Small airway abnormalities and lung parenchyma destruction contribute to the development of airflow limitation, with a consequent reduction in lung elastic recoil leading to dynamic hyperinflation and thus shortness of breath.^[1] Present study was aimed to check the immediate effect of intercostal stretch along with thoracic expansion exercise on pulmonary function and thoracic expansion on mild to moderate COPD subjects. Present study was conducted at Parulsheshram hospital, Vadodara and subjects were taken from respiratory OPD. There was a total of 10 participants screened but according to inclusion criteria and exclusion criteria only 5 participants are taken. The study is approved by the ethical committee of the institution. The age criteria are between the 40 to 60 years. The study showed mild to moderate COPD subjects were taken and they were assessed prior to the treatment and outcome measure were taken using PFT machine for pulmonary function test and measure chest expansion. As per the assessment the subjects were given intervention in the form of intercostal stretch and thoracic expansion exercise. After the 45 minutes of intervention the outcome measures (PFT, CHEST EXPANSION) were reassessed. Immediate effect of chest PNF and thoracic expansion exercise showed there was an improvement in FVC, FEV1, FEV1/FVC in table 4,5,6. And chest expansion at all 3 level in table 1,2,3.

During this study has shown in table no 4, 5 in which the improvement obtain was clinically significant but statistically it was not significant due to less sample size. Our research was supported by Puckree et al. (2002) study, "The Effect of IC Stretches on Third and the Eighth IC Space," which demonstrated a decrease in breathing frequency following the application of a stretch to these two IC spaces. The differences in respiratory rate between the groups in this study were not statistically significant. However, only the experimental group's rate of respiration was lower, demonstrating that IC stretching had an effect on respiratory rate. Localized IC stretching in the third and eighth IC spaces also demonstrated a deeper breathing pattern, greater electromyographic activity, and a decrease in breathing frequency in healthy subjects."^[4] The improvement in pulmonary function and chest expansion can be explained by a study done by DangiAshwini ET al. established that Intercostal muscles assist upward and outward movement of the rib, which can lead to increase in the anterior posterior diameter of the thoracic cavity. It is beneficial for both inspiration and forced expiration. Chest expansion decreases because of diminished chest wall mobility and lung compliance. Intercostal stretching may improve chest wall elevation and thus expand to improve intra-thoracic lung volume, which contributes to an increase in flow rate percentage. This may contribute to an increase in ventilatory capacity, such as tidal volume, minute ventilation, and oxygen status, thereby improving chest expansion, hyperinflation, and air trapping and, as a result, reducing dyspnea.^[1]

CONCLUSION

From the result we conclude that there are significant changes seen PFT and CHEST EXPANSION in patients with mild to moderate COPD by using Intercostal stretch and thoracic expansion exercise.

Conflict of interest: None





REFERENCES

1. Ashwini D, Bhagyashri S, Medha D. Comparison of Intercostal Stretch Technique Versus Diaphragmatic Breathing on Dyspnoea, Chest Expansion And Functional Capacity in Stable Copd. International Journal of Scientific and Research Publications. 2017 M5ay;7(5):256-60.
2. Jahan N. *Effectiveness of inter costal stretch techniques among copd patients at NIDCH* (Doctoral dissertation, Bangladesh Health Professions Institute, Faculty of Medicine, the University of Dhaka, Bangladesh).
3. Mohan V, Aziz KB, Kamaruddin K, Leonard JH, Das S, Jagannathan MG. Effect of intercostal stretch on pulmonary function parameters among healthy males. EXCLI journal. 2012; 11:284.
4. Hetal M Mistry, Rutuja V Kamble. Immediate effect of Chest Proprioceptive Neuromuscular Facilitation on Respiratory Rate, Chest Expansion and Peak Expiratory Flow Rate in patients with Chronic Obstructive Pulmonary Disease. Int J Physiother Res 2021;9(1):3723-3729. DOI: 10.16965/ ijpr.2020.175
5. EMCHRC P, Giri JU. Efficacy of Retraining Diaphragm by Proprioceptive Neuromuscular Facilitation versus Diaphragmatic Breathing Exercises in Reducing Dyspnoea in the Copd Patients.
6. Debouche S, Pitance L, Robert A, Liistro G, Reyhler G. Reliability and reproducibility of chest wall expansion measurement in young healthy adults. Journal of manipulative and physiological therapeutics. 2016 Jul 1;39(6):443-9.
7. Woo SD, Kim TH, Lim JY. The effects of breathing with mainly inspiration or expiration on pulmonary function and chest expansion. Journal of physical therapy science. 2016;28(3):927-31.
8. Represas-Represas C, Fernández-Villar A, Ruano-Raviña A, Priegue-Carrera A, Botana-Rial M, study group of "Validity of COPD-6 in non-specialized healthcare settings". Screening for chronic obstructive pulmonary disease: validity and reliability of a portable device in non-specialized healthcare settings. PLoS One. 2016 Jan 4;11(1): e0145571.

Table 1: Comparison of Pre and Post Data for Chest Expansion At Axillary Level

	Mean	±SD	Z- value	p-value	TEST
PRE	1.3000	.44721	-2.236	0.25	WILCOXON SIGNED RANK TEST

Table 2. Comparison of Pre and Post Data for Chest Expansion At Nipple Level

	Mean	±SD	Z- Value	P-Value	Test
PRE	1.7600	.33615	-2.060 ^b	.039	WILCOXON SIGNED RANK TEST
POST	2.8000	.44721			

Table 3 Comparison of Pre and Post Data for Chest Expansion At Xiphisternal Level

	Mean	±SD	Z- Value	P-Value	Test
PRE	2.0000	.70711	-2.060 ^b	.039	WILCOXON SIGNED RANK TEST
POST	3.2600	.73348			

Table 4 Comparison of Pre and Post Data for Pft Fev1

	Mean	±SD	Z- value	p-value	TEST
PRE	.9520	.24864	-1.753 ^b	.080	WILCOXON SIGNED RANK TEST
POST	1.1680	.39214			





Dhruvika Rathod and Didhiti Desai

Table 5 Comparison of Pre and Post Data for PftFvc

	Mean	±SD	Z- Value	P-Value	Test
PRE	1.5800	.32680	-.271 ^b	.786	WILCOXON SIGNED RANK TEST
POST	1.5620	.33722			

Table 6 Comparison of Pre and Post Data for Pft Fev1/Fvc Ratio

	Mean	±SD	Z- Value	P-Value	Test
PRE	61.3740	14.42966	-2.023 ^b	.043	WILCOXON SIGNED RANK TEST
POST	75.1420	21.45409			

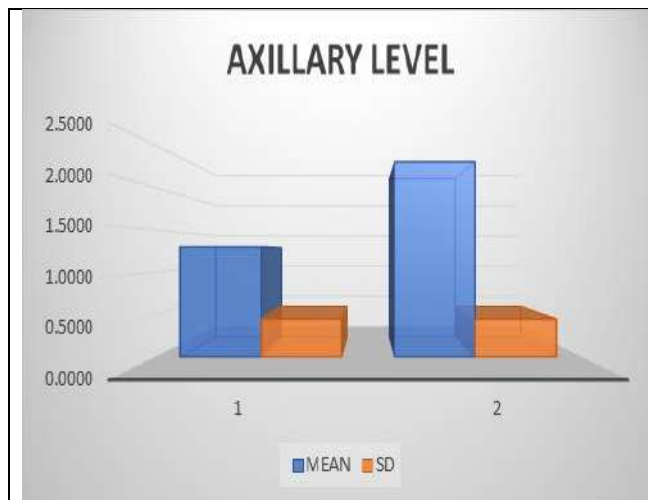


Fig.1 Axillary level

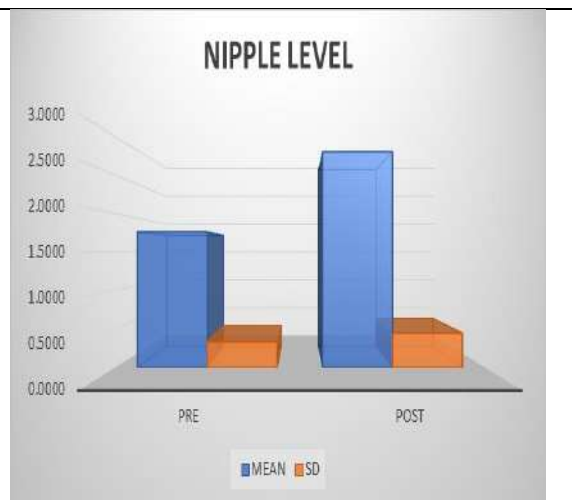
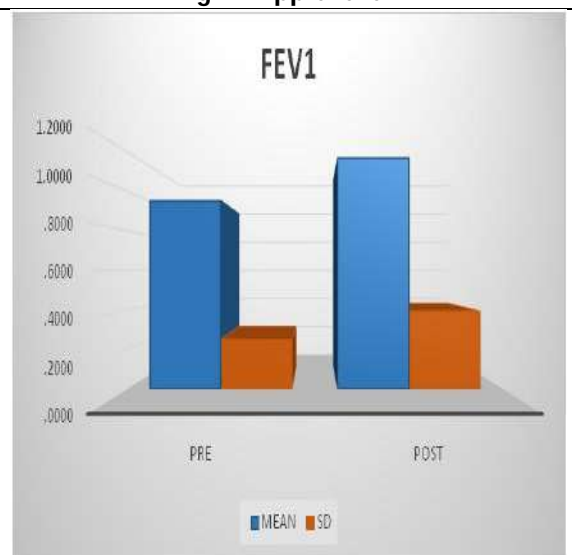
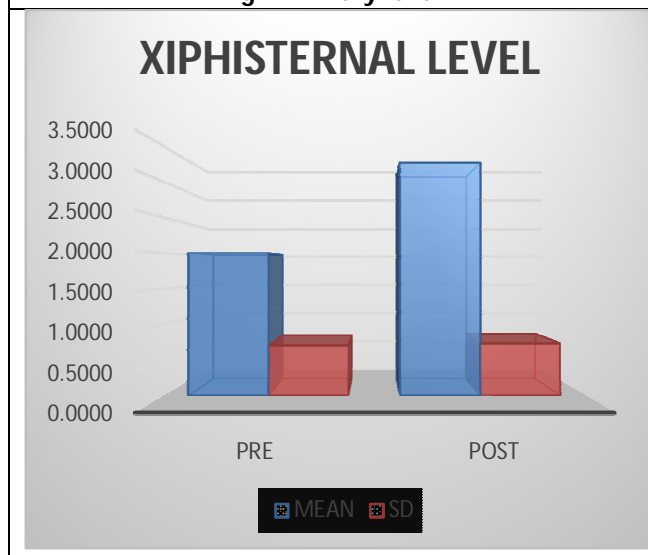


Fig.2. Nipple level





Dhruvika Rathod and Didhiti Desai

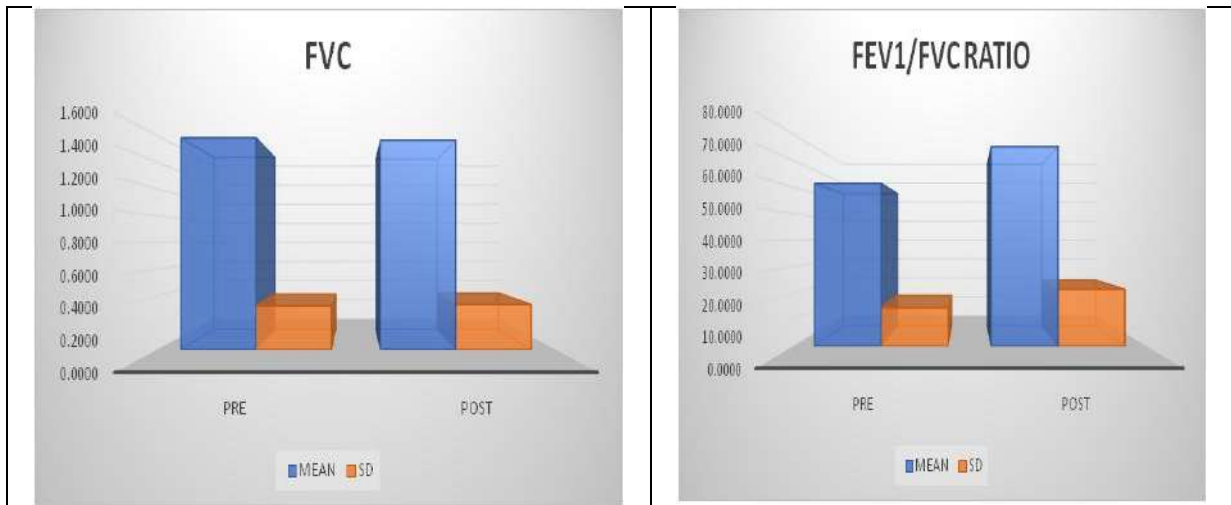


Fig.3. Xiphisternal Level





Forecasting of Milk Production in India

R.Radha^{1*} and T.Ponnarasi²

¹Ph.D Research Scholar (Agri. Business Management), Department of Agricultural Economics, Faculty of Agriculture, Annamalai University, Chidambaram, Tamil Nadu, India

²Associate Professor, Department of Agricultural Economics, Faculty of Agriculture, Annamalai University, Chidambaram, Tamil Nadu, India

Received: 10 Dec 2022

Revised: 20 Mar 2023

Accepted: 28 Apr 2023

*Address for Correspondence

R. Radha

Ph.D Research Scholar (Agri. Business Management),
Department of Agricultural Economics,
Faculty of Agriculture, Annamalai University,
Chidambaram, Tamil Nadu, India.
E.Mail: abmradha@gmail.com.



This is an Open Access Journal / article distributed under the terms of the **Creative Commons Attribution License** (CC BY-NC-ND 3.0) which permits unrestricted use, distribution, and reproduction in any medium, provided the original work is properly cited. All rights reserved.

ABSTRACT

The study has made an attempt to analyse the pattern of milk production in India. The annual compound growth rates of milk production were calculated by using time series data obtained from National Dairy Development Board. Milk Production both in Tamil Nadu and India was analyzed and it revealed that milk production growth in Tamil Nadu is comparatively less when compared to the growth of milk production in India. Similar is the situation with respect of per capita milk availability both in Tamil Nadu and India. Population census conducted indicated that number of animal category wise increased at national level. But in Tamil Nadu, the population is fluctuating between the census periods. It raises the doubt that the census is not practiced in fullest spirit and hence the supervisory mechanism needs to be intensified for getting correct data. Besides, this study has also used Coppock instability analysis to measure the instability in the milk production.

Keywords: Milk Production, Growth Pattern, Per Capita Consumption, Forecasting, Instability Index, Dairy.

INTRODUCTION

Humans have a long tradition of consuming milk produced by animals and cow's milk is the most popular milk consumed in both developed and developing nations. Milk is the single largest commodity by value contributing 5 percent to the national economy. Dairying has become an important secondary source of income for millions of rural families and has assumed the most important role in providing employment and income generation opportunities





Radha and Ponnarasi

mainly for women and marginal farmers. This has resulted in upliftment of socioeconomic aspects of rural households in the country. Major share of milk in the country is produced by small, marginal farmers and landless laborers. Small land-base encourages the farmers to practice dairying as their subsidiary. The income from agriculture is seasonal, whereas dairying provides year-round income and generates gainful employment in the rural sector (Kadirvel 2004). The drivers of demand for milk in India are population growth, urbanization, increasing per capita income and nutritional awareness. The dairy sector is therefore an important vehicle for inclusive development in the country. Top five major milk producing country in the world are India followed by USA, China, Pakistan and Brazil where other countries have only recently made it possible to produce considerable amounts of dairy. India is ranked first in milk production contributing to 23 percent (FAOSTAT) of Global milk production. Milk production in the country has grown at an annual compound growth rate of about 6.20 percent to reach 209.90 million tonnes in 2020-21 from 84.40 million tonnes in 2001-02 (NDDB). The dairy sector in India has grown substantially over the years and has emerged as a major driver of overall growth to the sector of agriculture. The all India per capita availability of milk is 427 grams per day in 2020-21. The livestock population in India has increased from 292.90 million in 1951 to 535.80 million in 2019, which includes 192.50 million Cattle (35.94 per cent), 109.85 million Buffaloes (20.45 per cent), 74.26 million Sheep (13.87 per cent), 148.88 million Goats (27.80 per cent) and about 9.06 million Pigs (1.69 per cent). Thus the overall livestock population in the country, showing an increase of 4.60 per cent over the previous census (2012) As per the 20th Livestock census, India has a vast resource of animal population totaling 536.76 million livestock, Uttar Pradesh, Rajasthan, Madhya Pradesh are the leading milk production states in the country.

In India, Tamil Nadu ranked tenth in respect of milk production during the year 2020. The production of milk has increased from 70.04 lakh tonnes in the year 2012-13 to 87.50 lakh tones during the year 2019-2020. Thus the production of milk in Tamil Nadu is attained a steady growth (NDDB2019-2020) and the per capita availability is 316 grams per day which is accounted for 74 per cent of per capita milk availability at all India level. The milk production in Tamil Nadu has increased by 4.75 per cent compared to the previous year. Tamil Nadu possesses 302.75 million total bovines including 192.52 million cattles and 109.85 million buffaloes. Population as per 20th livestock census (AHD&FD), dairy can significantly contribute to pathways out of poverty, since demand for livestock products will increase substantially in the years to come. In these circumstances, this paper has aimed at addressing how fast the growth of milk production is happening in India to address the demand for growing population and to find out the growth instability if any in milk production.

Design of the Study

The present study analyses growth rate and instability in milk production on an all India basis and the major production state as Tamil Nadu based on the data drawn from the web site of National Dairy Development Board (NDDB).

Analysis of Data

The time series data on milk production has been collected from the annual report of NDDB and analyzed for 20 years from 2001 - 2021. It has been collected and analyzed for compound mean, standard deviation (S.D.) coefficient of variation (C.V) and Compound Annual Growth Rate (CAGR).

Compound Annual Growth Rate Analysis (CAGR)

The CAGR is predicted using time series data in respect of milk Production was assessed using an exponential form of the equation and modeling the time trend used in this study.

$$Y = A (1+r)^t$$

$$\ln Y = \ln a + b t \quad [b = \ln (1+r)]$$

Growth rate was calculated by using following formula:

$$r = [\text{antilog}(b)-1] \times 100$$

Where,

Y = Milk Production in litres





Radha and Ponnarasi

a = Constant Term
b = Regression Coefficient to be estimated
r = Growth Rate of Y

Compound Growth Rate

'r' = (Antilog of B- 1) × 100

t = r / SE (r)

Where,

r = Compound Growth Rate

SE = Standard Error

Co-efficient of Variation (C.V) $C.V. = \frac{\text{Standard Deviation}}{\text{Mean}} \times 100 = \frac{\sigma}{\mu} \times 100$

Where,

X_i = Individual observations in the time series data,

X = Mean,

$(X_i - X)$ = Deviation from the mean,

n = Number of observation.

Even though Coefficient of Variation (C.V) is the simplest measure of instability, it over-estimates the level of instability in time series data which are characterized by long-term trends.

Coppock's Instability Index

Instability was also analyzed using Coppock's index which is calculated as the antilog of the square root of the logarithmic variance using the following formula (Coppock, 1962).

Coppock Instability Index = (Antilog) $\sqrt{(V \log - 1)} \times 100$

$V \log = \frac{1}{(N-1)} \sum (\log p_{t+1} - \log p_t - M)^2$

$M = \frac{1}{(N-1)} \sum (\log p_{t+1} - \log p_t)$

Where,

Xt = Area / Production / Yield

t = Number of years

m = Mean of the difference between the logs of Xt+1, Xt

Log V = Logarithmic variation of the series

Coppock instability index is a close approximation of the average year to-year percentage variation adjusted for trend and the advantage is that it measures the instability in relation to the trend in area, production and productivity. A higher numerical value for the index represents greater instability

RESULTS AND DISCUSSION

State wise Trend in Milk Production and per capita Availability of Milk

Cow's milk is the life giving food to all the living human. The Milk contains all the essential nutrients and hence it becomes friendly to everyone including the animals. Cow's milk is capable of providing 'n' number of milk based products which are dearer to the born babies and growing children. Such an important food is witnessed with increased production due to the technological innovations practiced in the dairy sector. The Table-1 is showing such increasing trend both in Tamil Nadu and in India. Milk production of the state has increased from 4.98 million tonnes in the year 2001-02 to 8.75 million tonnes in the year 2019-2020 and the growth rate during this period was found 3.18. Similar trend was witnessed at all India. level with growth rate 4.90 per cent. The average milk production in Tamil Nadu was arrived at 6.70 million tonnes. Whereas, Indian average milk production is arrived at 132.30 million tonnes. The share of Tamil Nadu to the Indian milk production is found to be 5.06 per cent. Table-1

57314





Radha and Ponnarasi

indicated that during the year 2020-21, the milk production in Tamil Nadu has come down to 8.51 million tonnes from 8.75 million tonnes during the year 2019-20. The sliding in milk production is found to be 2.74 per cent when comparing with the previous year milk production. It might be due to the failure of cattle caring, grazing and feeding to the cattle population because of the peak spread of corona in Tamil Nadu during that time. Almost from farming community to elite class in the city were totally affected in Corona would have caused such decrease in the milk production due to lesser availability of fodder and concentrates which are to be transported from different corner. But the district borders were arrested to avoid the spread of Corona. Though they have liberalized the transportation system later, the timely feeding alone could have promoted higher amount of milk production. But it has not happened.

Per Capita Availability of Milk in Tamil Nadu and India

Under this increased trend in milk production both in Tamil Nadu and India one could assume that it have promoted the per capita availability for consumption both in Tamil Nadu and India. These details are analyzed and the results are presented in Table – 2 which revealed that the per capita availability of milk in Tamil Nadu was found to be 219 grams per day. But, it was in the range of 222 grams per day in respect of India. There is no much difference in per capita availability of milk between Tamil Nadu and India. Only a marginal difference could be observed during the year 2001-02. In a decade of difference, it was rise from 219 grams to 278 grams per day. The increase was accounted to be 26.94 per cent during the year 2010 over the base year 2001. In respect of India, the increase could be 22.97 per cent during the year 2010 over the base year 2001. When one could compare the decadal difference in the increase, it is almost favor with Tamil Nadu which indicated that the milk production in Tamil Nadu is increasing and making per capita availability of milk on the higher side. When one could examine the availability in another decade of time, Tamil Nadu its per capita availability by 26.98 per cent during 2021 over the base year 2011. There is no growth in making the per capita availability between the two decades. It is almost same. When one could compare the milk production in Tamil Nadu between the decades, the milk production has grown to 36.14 per cent during 2010 over the base year 2001. But the magnitude of increase between 2011 and 2021 was found to be very less and stands at 24.60 per cent. It indicated that Tamil Nadu is not concentrating on dairy industry during the second decade of milk production considered in the study. It might be due to the alternate developments in the allied sectors like sheep and goat rearing and in the poultry sector due to the unattractive price prevailed in the market for the milk and its products. The Figure -1 has highlighted the details of per capita availability of milk During the years 2003 to 2029. The Figure -1 indicated that the per capita availability of milk in India is progressed over a period of time and at the same time Tamil Nadu also reflecting the same trend but the curve of Tamil Nadu was in the lower fringes than in India.

Animal Population in Tamil Nadu and India

In respect of India, the per capita availability of milk found to be increased to 51.96 per cent during the year 2021 over the base year 2011. When one could examine the same with Tamil Nadu, it is almost double in Indian context. It was might be due to the higher productivity of milk and the increase in the animal population. In this context, the number of animals by category is analyzed and the results are presented in Table- 3. Which outlined the status of cattle population available to mankind over a period of time to cater the milk production requirements. In Tamil Nadu, the growth of cattle and buffaloes population seems to be decreasing and stands at 7 per cent and 78 per cent respectively delineating that the buffalo population in Tamil Nadu is fast deteriorating. In this circumstance, one has to assess the reasons for such deterioration in the buffalo population and it has to be documented for taking necessary efforts to protect their population and its output which is widely preferred among the tea shops and in preparing value added milk products in the sweet stalls.

In respect of India, the cattle population is growing at the rate of 24 per cent and the buffalo population grows at 153 per cent which indicated that the buffalo rearing activity is widely popular in certain states of India particularly central and north India. In respect of Tamil Nadu, the buffalo population is accounted for 23.39 per cent to the mean cattle population and in India, the buffalo population is arrived at 40.72 per cent to the total mean cattle population available in India. The cattle population is decreasing in certain census and it is increasing in certain census which





Radha and Ponnarasi

could reveal the fact that the population census are not properly looked into for estimation in respect of Tamil Nadu. The Director, Department of Animal Husbandry who initiates such population census in every five year period should have some external forces to monitoring the conduct of population census in respect of animals which are the need of the hour. Assuming that the present trend in animal growth continues further, the animal population in Tamil Nadu and India has been projected to 2024 and 2029 to assess the extent of animal population available in India to produce the milk. These details are presented in Table - 4. Which revealed that Tamil Nadu will be holding the cattle population to the level of 9.82 million and the same will be growing to the level of 9.89 million indicated that the cattle population in Tamil Nadu is growing very slowly. In respect of India, the cattle and Buffalo population is growing almost in a stagnant manner. To be specific, it is declining marginally. However, these details are presented under the head, forecasting of milk production in Tamil Nadu and India.

Forecasting of Milk Production in Tamil Nadu and India

With this level of growth delineated in Table -5 if one could predict the milk production in Tamil Nadu and India, it is also decreasing marginally. The details of forecast are predicted and delineated in Table -5 up to 2030. Table 5 indicated that the milk production in Tamil Nadu is decreasing from 367 million tonnes during the year 2021 to 325 million tonnes during the year 2030. Similar is the situation with respect of India. It is also decreasing from 441 million tonnes to 432 million tonnes during the period indicated. The reason is the decreasing trend in the growth of animal population both cattle and Buffalo. Care has to be taken to augment the animal population and effort has to be in the direction of increasing the productivity of milk by promoting the breeds. Besides, promoting the exotic breeds, care has to be also taken to protect the native breeds so that the native animal and its advantage both in terms of milk and meat could be harnessed.

Measures of Instability Production of Milk in India

Instability analysis on production of milk for a period of 20 years was carried out. Instability measures such as coefficient of variation, Coppocks instability index were determined and presented in the Table -6. Coppock's instability analysis is used to measure the instability to the trend in milk production. A higher numerical value for the index represents greater instability in respect of number of animals and its milk production. Coppocks instability index value of production of milk in Tamil Nadu stands at 44.74 and in respect of India it was arrived at 49.53 per cent.

CONCLUSION

The study has revealed that milk production in India is increasing over a period of time. Whereas, the per capital availability of Milk in Tamil Nadu is found to be increasing but it is not up to the level witnessed in respect of India. The increased production might be due to the availability of number of animals. but the study has proved that the number of animals across different animal census is discouraging in respect of Tamil Nadu. but in India, it is increasing to the level of expectation and making a white revolution and stands number one in milk production.

Abbreviations

CV- Co-efficient of Variation, SD – Standard Deviation, CAGR-Compound Annual Growth Rate, FAOSTATE – Food and Agriculture Organization corporate Statistical database. NDDB – National Dairy Development Board. AHD&FD - Animal Husbandry, Dairying and Fisheries Department.

REFERENCES

1. (AHD&FD)Animal Husbandry, Dairying and Fisheries Department.
2. Basic Animal Husbandry Statistics 2020-21 Department of Animal Husbandry and Dairying, Ministry of Agriculture. Government of India New Delhi.
3. Coppock. J.D. 1962. International Economic Instability. McGraw-Hill, New York, pp 523-525.





Radha and Ponnarasi

4. www.fao.org.
5. Economic survey 2020-21.
6. Tulika Kumari, A.K. Chauhan, Binita Kumari and Priyanka Lal (2017) Structural Changes in Milk Production of Uttar Pradesh. International Journal of Current Microbiology and Applied Science 6(3): 2319-7706.
7. K. Kalidas, K. Mahendran¹ and K. Akila (2020) Growth, Instability and Decomposition Analysis of Coconut in India and Tamil Nadu, Western Tamil Nadu, India: A Time Series Comparative Approach Journal of Economics, Management and Trade 26(3): 59-66.
8. K.M. Singh, Nasim Ahmad, Vagish Vandana Pandey, Tulika Kumari and Ritambhara Singh (2021) Growth Performance and Profitability of Rice Production in India: An Assertive Analysis Economic Affairs, Vol. 66, No. 3, pp. 481-486,
9. M.Prabu, G. Senthil Kumar, A Serma Saravanan Pandian, K.N. Selvakumar and B.JayaVarathan (2012) Dynamics of Livestock Population - India VIS-A-VIS Tamil Nadu .Tamil Nadu J.Veterinary&Animal Sciences 8(5)266-270.
10. S. Palani and M. Sivanya (2019) An Analysis of Milk And Dairy Production In Tamil Nadu. Journal of Information and Computational Science. PP: 61-69
11. T. Nivetha and K. Uma Growth, Instability and Decomposition Analysis of Nutri Cereals in Tamil Nadu 2021 Asian Journal of Agricultural Extension, Economics & Sociology 39(12): 86-90.
12. www.nddb.org.in
13. Indiastat Report. 2021. <https://www.indiastat.com>.

Table 1: Status of Milk Production in India and Tamil Nadu

Sl. No	Milk Production (Million Tonnes)			Percentage Share of Tamil Nadu to India Total
	Year	Tamil Nadu	India	
1.	2001-02	04.98	84.40	05.90
2.	2002-03	04.62	86.20	05.36
3.	2003-04	04.75	88.10	05.39
4.	2004-05	04.78	92.50	05.17
5.	2005-06	05.47	97.10	05.63
6.	2006-07	06.27	102.60	06.11
7.	2007-08	06.54	107.90	06.06
8.	2008-09	06.65	112.20	05.92
9.	2009-10	06.78	116.40	05.83
10.	2010-11	06.83	121.80	05.60
11.	2011-12	06.96	127.90	05.45
12.	2012-13	07.00	132.40	05.23
13.	2013-14	07.04	137.70	05.12
14.	2014-15	07.13	146.30	04.89
15.	2015-16	07.24	155.50	04.65
16.	2016-17	07.55	165.40	04.45
17.	2017-18	07.74	176.30	04.41
18.	2018-19	08.36	187.70	04.46
19.	2019-20	08.75	198.40	04.42
20.	2020-21	08.51	209.60	04.06
	Total	133.95	2856.30	
	Mean	06.70	132.30	
	CV (%)	18.54	29.30	
	LONGEST	01.031	01.04	
	CAGR	03.18	04.90	

(Source: Department of Animal Husbandry, Dairying & Fisheries, Ministry of Agriculture and Farmers Welfare, Government of India)





Radha and Ponnarasi

Table 2: Per Capita Availability of Milk in Tamil Nadu and India

Year	Per Capita Availability of Milk (Grams per Day)	
	Tamil Nadu	India
2001-02	219	222
2002-03	198	224
2003-04	198	225
2004-05	204	233
2005-06	231	241
2006-07	263	251
2007-08	272	260
2008-09	274	266
2009-10	278	273
2010-11	278	281
2011-12	265	290
2012-13	280	299
2013-14	280	307
2014-15	265	322
2015-16	267	337
2016-17	277	355
2017-18	283	375
2018-19	304	394
2019-20	316	406
2020-21	353	427

(Source: Department of Animal Husbandry, Dairying & Fisheries, Ministry of Agriculture and Farmers Welfare, Government of India.)

Table 3: Animal Population in Tamil Nadu and India in Millions

year	Animal Population in Millions			
	Tamil Nadu		India	
	Cattles	Buffalos	Cattles	Buffalos
1951	10.22	02.30	155.30	43.40
1956	09.70	02.04	158.70	44.90
1961	10.83	02.59	175.60	51.20
1966	10.86	02.72	176.20	53.00
1972	10.57	02.85	178.30	57.40
1977	10.80	03.08	180.00	62.00
1982	10.37	03.21	192.50	69.80
1987	09.35	03.13	199.70	76.00
1992	09.10	02.93	204.60	84.20
1997	09.05	02.74	198.90	89.90
2003	09.14	01.66	185.20	97.90
2007	11.19	02.01	199.10	105.30
2012	08.81	00.78	190.90	108.70
2019	09.51	00.51	192.50	109.90
TOTAL	139.50	32.55	2587.50	1053.60
MEAN	09.96	02.33 (23.39)	184.82	75.26 (40.72)
SD	00.73	0.66	12.12	20.73





Radha and Ponnarasi

CV(%)	07.30	28.57	06.56	27.54
LONGEST	00.99	01.04	00.997	01.00
CAGR	(-) 00.17	(-) 02.16	00.32	01.36

(Source: Department of Animal Husbandry and Veterinary Services) (Figures in Parentheses indicate percentage to Total)

Table 4: Forecasting of Animal Population in Tamil Nadu and India

SI. No	Particulars of Population	Population in 2024 in Millions	Population in 2029 in Millions
1.	Cattle Population in Tamil Nadu	09.82	09.89
2.	Buffalo Population in Tamil Nadu	00.71	00.89
3.	Cattle Population in India	190.67	189.02
4.	Buffalo Population in India	109.62	108.87

Table 5: Forecasting of Milk Production during 2030

SI. No	Year	Tamil Nadu	India
1.	2021-22	367.054	441.152
2.	2022-23	360.783	440.141
3.	2023-24	354.990	439.139
4.	2024-25	349.641	438.147
5.	2025-26	344.701	437.164
6.	2026-27	340.139	436.189
7.	2027-28	335.926	435.223
8.	2028-29	332.035	434.266
9.	2029-30	328.442	433.317
10.	2030-31	325.124	432.377

Table 6: Measures of Instability Production of Milk

Measures of instability	Production in Tamil Nadu	Production in India
CV %	18.54	29.71
Coppock's Instability Index	44.74	49.53



Figure 1: Per Capita Availability of Milk in Tamil Nadu and India





Anti Cancerous Potential of Siddha Herbo-mineral Formulation *Rathinagara Rasa Mezhu* using MTT assay against MCF-7 (Breast Cancer Cell Line)

R.S.Parvathy^{1*} A. Mariappan² and R. Meena Kumari³

¹PG Scholar, Department of Gunapadam, National Institute of Siddha, Ministry of AYUSH, Chennai-600047, Tamil Nadu, India

²Associate Professor, Department of Gunapadam, National Institute of Siddha, Ministry of AYUSH, Chennai-600047, Tamil Nadu, India.

³Director, National Institute of Siddha, Ministry of AYUSH, Chennai-600047, Tamil Nadu, India.

Received: 06 Feb 2023

Revised: 25 Mar 2023

Accepted: 28 Apr 2023

*Address for Correspondence

R.S.Parvathy

PG Scholar,

Department of Gunapadam,

National Institute of Siddha,

Ministry of AYUSH,

Chennai-600047, Tamil Nadu, India

E.Mail : parurs94@gmail.com



This is an Open Access Journal / article distributed under the terms of the **Creative Commons Attribution License** (CC BY-NC-ND 3.0) which permits unrestricted use, distribution, and reproduction in any medium, provided the original work is properly cited. All rights reserved.

ABSTRACT

Breast cancer is the most common cancer diagnosed in women, accounting for more than 1 in 10 new cancer diagnoses each year. It is the second most common cause of death from cancer among women in the world. Available therapies for cancer & the possible side effects created an awareness to search for safe, economical alternatives for cancer therapy. Siddha system offers a lot of formulations in the management of breast cancer in a non-complicated way & many literary works support this statement. A Herbo-mineral formulation *Rathinagara rasa mezhu* is indicated for *Putrunoigal* (Cancer), *araiyappu* (adenitis), *Pun* (Ulcer), *Karunkuttam*, *Senkuttam* (leprosy), *Pilavai*(carbuncles), *Kandamalai* (Cervicaladenitis), *Puraiyodinapunkal* (deepulcers or sinus) which is mentioned in classic Siddha literature "*Anuboga vaidhaya navaneetham Part 5*. But its therapeutic use has not been scientifically validated. Therefore, the study aimed to evaluate the *In-vitro* anti-cancerous activity of *Rathinagara rasa mezhu* (RNM) in the MCF-7 cell line against breast cancer. it was determined by 3-(4,5-dimethylthiazol-2-yl)-2,5-diphenyltetrazolium bromide (MTT) assay. LD50 concentration was found at 115.97034 µg/mL. The Siddha system has provided clinically significant results in treating Breast cancer with a lot of time-tested medicines. More scientific studies has to be carried out to test the therapeutic efficacy of this medicine.





Parvathy et al.,

The long-term consumption of *Rathinagara rasa mezhugu* could be considered & promoted as adjuvant therapy for treating various malignancies.

Keywords: Breast cancer, Rathinagara rasa mezhugu, Anti-cancer activity, MTT Assay, MCF-7 Cell line.

INTRODUCTION

Breast cancer is the top-ranked cancer affecting women worldwide among other types of cancers. It has now surpassed lung cancer as the leading cause of global cancer incidence in 2020, with an estimated 2.3 million new cases, representing 11.7% of all cancer cases [1]. Epidemiological studies have shown that the global burden of BC is expected to cross almost 2 million by the year 2030 [2]. The first symptom of breast cancer is usually an area of thickened tissue in the breast or a lump in the breast or an armpit. Other symptoms include pitting, like the surface of an orange, or color changes such as redness in the skin of the breast, armpit or breast pain that does not change with the monthly cycle, a rash around or on one nipple, discharge from a nipple, which may contain blood, peeling, flaking, or scaling of the skin of the breast or nipple [3]. In modern medicine, Chemotherapy is considered to be an established & recommended treatment for cancer. Female breast cancer patients have shown higher resistance & increased vulnerability to chemotherapeutic toxicity [4]. Chemotherapeutic agents exert severe side effects, such as diarrhoea, nausea/vomiting, leukopenia, anaemia, alopecia, bone marrow depression, hyperuricemia, teratogenicity, carcinogenicity, & fertility issues in men & women [5]. So, the toxic side effects caused by chemotherapy & modern drugs increase the urgency of the demand for better therapeutics.

Every year, more breast cancer patients are turning to complementary & alternative therapies. There have been reports of patients in India benefiting from cancer treatments in traditional Indian medical systems like *Siddha*. *Siddha* system of medicine is one of the oldest Indian medicinal systems that possess shreds of evidence for both the prevention & treating various types of cancers. *Siddha* medicine has already proved that it can be useful in the management of Cancer, besides being safe, cost-effective, & non-invasive. Due to the potent anti-oxidant activity, the majority of *Siddha* medications offer nutrition & reduce the adverse effects of conventional cancer therapy [6-7]. *Rathinagararasamezhugu* (RNM) is a classical *Siddha* Herbo-mineral formulation that is mentioned in *Anuboga vaidhaya navenetham Part 5*. It has been used for the management of *Putrunoigal* (Cancer), *araiyappu* (adenitis), *Pun* (Ulcer), *Karunkuttam*, *Senkuttam* (leprosy), *Pilavai* (carbuncles), *Kandamalai* (Cervicaladenitis), *Puraiyodinapunkal* (deepulcers/sinus). Moreover the formulation consists of *ValaiRasam* (Elemental Mercury), *Gandhagam* (Sulphur), & *Serankottai* (*Semecarpus anacardium* Linn.), *Sitramanakku* (*Ricinus communis* L.) which have already been proven the tremendous potential for a cancer cure in various scientific studies [8]. The present study was designed to investigate the potential of RNM as an anticancer agent against MCF-7 breast cancer cells.

MATERIALS AND METHODS

Raw Drug Collection

Lingam (Cinnabar), *Ganthagam* (Sulphur), & *Serankottai* (*Semecarpusanacardium*) were procured from a Well reputed country shop in Parys Corner, Chennai. The Other ingredients *Sitramanakkuennai* (castor oil), *Pasunei* (ghee), & *Panaivellam* (palmjaggery) were purchased locally from the Tambaram market, Chennai.

Identification & Authentication of the Drug

The herbal ingredients were identified & authenticated by the Botany Division, National Institute of Siddha, Tambaram sanatorium. (Certificate No: NISMB4922021), The metal drugs were identified by Pharmacologist, dept. of Gunapadam, NIS, Tambaram sanatorium, Chennai. (Certificate no: Gun/Aut/026/21)





Parvathy et al.,

Preparation of Trial drug: Rathinagara rasa mezhugu

Step1: First castor oil is taken into a vessel & heated. Then Purified sulphur is powdered & mixed with the heating castor oil. When the sulphur melts, Semecarpus seeds are cut into two pieces & put in the oil. Then thailam is taken when Semecarpusseeds turn red & float. Thethailam is called *Rathinagara thailam*.

Step2: Mercury & Rathi nagara thailam are mixed & ground. When mercury is groundwell, Ghee & palm jaggery are added & ground to get *Rathi nagara rasamezhugu*.

In vitro evaluation of Anticancer Activity

Reagents

Dulbecco's Modified Eagle's Medium (DMEM), Fetal Bovine Serum (FBS), Trypsin methyl thiazolyl diphenyl-tetrazolium bromide (MTT), & Dimethyl sulfoxide (DMSO), Acridine Orange (AO) & Ethidium bromide (EB) were procured from Hi-Media Laboratories, other chemicals & reagents were obtained from Sigma Aldrich Mumbai.

Cell Line & Culture

MCF-7 (Human breast cancer) cell line was initially procured from National Centre for Cell Sciences (NCCS), Pune, India, & maintained Dulbecco's modified Eagles medium, DMEM (Sigma-Aldrich, USA). The cell line was cultured in a 25 cm² tissue culture flask with DMEM supplemented with 10% FBS, L-glutamine, sodium bicarbonate (Merck, Germany), & the antibiotic solution containing: Penicillin (100U/ml), Streptomycin (100µg/ml), & Amphotericin B (2.5µg/ml). Cultured cell lines were kept at 37°C in a humidified 5% CO₂ incubator (NBS Eppendorf, Germany). The viability of cells was evaluated by direct observation of cells by an Inverted phase contrast microscope & followed by the MTT assay method.

Cells Seeding in 96 Well Plates

Two day-olds confluent monolayer of cells were trypsinized & the cells were suspended in a 10% growth medium, 100µl cell suspension (5x10³ cells/well) was seeded in 96 well tissue culture plate & incubated at 37°C in a humidified 5% CO₂ incubator.

Preparation of Compound Stock

1mg of sample was weighed & dissolved in 1mL 0.1% DMSO using a cyclomixer. The sample solution was filtered through a 0.22 µm Millipore syringe filter to ensure sterility.

Cytotoxicity Evaluation

After 24 hours the growth medium was removed, & freshly prepared compounds in 5% DMEM were five times serially diluted by two-fold dilution (100µg, 50µg, 25µg, 12.5µg, 6.25µg in 500µl of 5% DMEM) & each concentration of 100µl were added in triplicates to the respective wells & incubated at 37°C in a humidified 5% CO₂ incubator. Non-treated control cells were also maintained.

Cytotoxicity Assay by Direct Microscopic Observation

The entire plate was observed after 24 hours of treatment in an inverted phase-contrast tissue culture microscope (Olympus CKX41 with Optika Pro5 CCD camera) & microscopic observations were recorded as images. Any detectable changes in the morphology of the cells, such as rounding or shrinking of cells, granulation, & vacuolization in the cytoplasm of the cells were considered indicators of cytotoxicity.

Cytotoxicity assay by MTT Method

Fifteen mg of MTT (Sigma, M-5655) was reconstituted in 3 ml PBS until completely dissolved & sterilized by filter sterilization. After 24 hours of the incubation period, the sample content in wells was removed & 30µl of reconstituted MTT solution was added to all test & cell control wells, the plate was gently shaken well, then incubated at 37°C in a humidified 5% CO₂ incubator for 4 hours. After the incubation period, the supernatant was

57322





Parvathy et al.,

removed & 100µl of MTT Solubilization Solution (Dimethyl sulphoxide, DMSO, Sigma Aldrich, USA) was added & the wells were mixed gently by pipetting up & down to solubilize the formazan crystals. The absorbance values were measured by using a microplate reader at a wavelength of 540 nm (Laura B. Talarico et al., 2004).

The percentage of growth inhibition was calculated using the formula:

$$\% \text{ of viability} = \frac{\text{Mean OD Samples} \times 100}{\text{Mean OD of control group}}$$

Statistical Analysis

Numerical data are expressed as mean \pm standard deviation (SD). Statistical differences were evaluated by a one-way analysis of variance (ANOVA) & Dunnett's test was performed to analyze the data. Differences were considered statistically significant if $***p < 0.001$ when compared to the control group.

RESULTS AND DISCUSSION

The study described the cytotoxic activity of *Rathinagara Rasa Mezhugu* (RNM) against the MCF-7 cell line. Using the MTT test, the experiment was screened at various concentrations to determine the LC₅₀. The O.D. of the treatment compared to the control was calculated to ascertain the percentage of cell viability. Reading optical density (OD) is performed in a spectrophotometer at a wavelength of 540 nm. Comparison values are made on a basis of 50% inhibition of growth (IC₅₀) in treated cells with specific agents. Results were tabulated in Table.2& schematically represented in Graph-1 &2. Statistics shows that there is a steady rise in the incidence rate of breast cancer among women. Chemotherapy, most intended expensive cancer treatment not only worsen side effects but also severely affects the financial security of the family. Ever since olden days, herbal based medicines are most preferred for curing various challenging ailments. [9-10].The study reveals that the drug RNM exerts cytotoxic activity against human breast cancer cell lines in dose dependent manner. The results showed the drug dose & % of Inhibition of MCF-7cells after the *Rathinagara rasa mezhugu* (RNM) extract treatment. A chart was plotted using the sample concentration on the X-axis & the percentage viability on the Y-axis. The percentage of growth inhibition was found to be increasing with increasing concentrations of the test drug RNM. Least viability was observed at the concentration of 100µg/ml showed 59.58 \pm 2.77% followed by the concentration of test sample at 50µg/ml, 25µg/ml, 12.5µg/ml showed 67.61 \pm 2.02%, 73.97 \pm 1.09%, 86.94 \pm 0.05% Similarly concentration at 6.25µg/ml showed 96.66 \pm 3.18% cell viability in the MTT assay. The LC₅₀ of the test sample in the MCF-7 cell line was found to be 115.97034 µg/mL. *Rathinagara rasa mezhugu* (RNM) at different doses (6.5-1000 µg/ml of 5% MEM) was administered for 24 hrs. It was found that the number of cells decreases as the dose increases & at approximately 145µg/ml dose of extract, 50% of the MCF-7cells were less as compared to normal control as shown in Fig.1.

The drug RNM composed of *Serankottai* (*Semecarpus anacardium* Linn.), *Sitramanaku* (*Ricinus communis* L.), *Gandhagam* (Purified Sulphur) along with *Valai Rasam* (Elemental Mercury).An earlier study on the *Rathinagara rasa mezhugu* showed the relevant anticancer activity and therapeutic potential in the treatment of cervical cancer. [11]. A previous study showed the anticancer activity of *Gowri Chinthamani Chendhuram* containing the mixture of mercury & sulphur Produce antioxidant activity via induction of metallothionein [12]. *Rasagandhi mezhugu*, a known Siddha herbo-mineral formulation which is a combination of mercury (Rasam) & sulfur (Gandhi), was clinically proved for its anticancer effect in patients with different types of cancer [13]. *Rasam* & *Gandhagam* containing medicines like *Ashta Bairava Chenduram*, *Kaalamega Narayana Chendhuram*, *Veera Rasa Padhanga* & *Panchamuga Chenduram*, *Rasa parpam* have already proven anticancerous potential in *in vitro* & *in vivo* studies [14-16]. The Sulphur compounds inhibited the production of nitricoxide (NO) & prostaglandin E₂ (PGE₂) & the expression of the pro-inflammatory cytokines tumor necrosis factor- α , interleukin-1 β , & interleukin-6 in lipopolysaccharide (LPS) –activated macrophages [17]. Mathivadhani *et al.* studied *Semecarpus anacardium* nut extract use for inhibitory effect on human breast cancer cellline (T47D). At the molecular level, these changes are accompanied by decrease in Bcl(2) & increase in Bax, cytochrome c, caspases & PARP cleavage, & ultimately by internucleosomal DNA fragmentation [18].



**Parvathy et al.,**

Srinivasan Sowmyalakshmi *et al* was tested the anti-tumor activity against twobreast cancer cell lines, MCF-7 [estrogen receptor (ER)-positive] & MDA 231(ER-negative) using cell viability & apoptosis assays. In terms of cytotoxicity as well as induction of apoptosis, then-hexane & chloroform fractions of *Semecarpus anacardium* were more significantly active against MDA 231 cells than MCF-7cells [19]. *In-vitro* anti- cancer effects of ethanolic extract of *Ricinus communis* Linn, were studied against seven human cancer cell lines. The SRB assay was used to test cytotoxic activity against all the cell line. The activity was evaluated at 100µg/ml concentration of test material [20]. From the literature it is evident that the ingredients of RNM were proved the anticancerous potential in various scientific studies. This research work denoted that the *Rathinagara rasa mezhugu* has a promising anti-cancerous effect & the evidence provides that the RNM can be used as a potential source of the drug against breast cancer.

CONCLUSION

Breast cancer develops slowly, & most cases are found through routine screenings. Siddha medicine must be chosen for the prevention as well as treatment of disease. It May be help to reduce the harmful effects of chemotherapeutic agents & improve the efficacy of supportive care. From the above results, it can be concluded that Siddha Herbo-mineral formulation *Rathinagara rasa mezhugu (RNM)* is a safe & therapeutically effective drug in treating breast cancer in the treated MCF-7 cell line. More specific experiments on animal models are required to understand the exact molecular mechanisms of action. In the future, clinical studies must be carried out to prove the efficacy of the drug.

REFERENCES

1. Sung H, Ferlay J, Siegel RL, Laversanne M, Soerjomataram I, *et al*. Global Cancer Statistics 2020: GLOBOCAN Estimates of Incidence & Mortality Worldwide for 36 Cancers in 185 Countries. *CA Cancer J Clin* 2021; 71: 209-249 [PMID: 33538338 DOI: 10.3322/caac.21660]
2. DeSantis C, Siegel R, Bandi P, Jemal A. Breast cancer statistics, 2011. *CA Cancer J Clin* 2011; 61: 409-418 [PMID: 21969133 DOI: 10.3322/caac.20134]
3. Cancer-Its various types along with causes, symptoms, treatments & stages, in: cancer info guide, 2009. <http://www.cancer-info-guide.com/> (15 Mar. 2010).
4. Jang SJ, Yang IJ, Tettey CO, Kim KM, Shin HM. In-vitro anticancer activity of green synthesized silver nanoparticles on MCF-7 human breast cancer cells. *Mater Sci Eng C* 2016; 68:430-5.
5. Ramya N, Priyadarshini XX, Prakash R, Dhivya R. Anti-cancer activity of *Trachyspermum Ammi* against MCF7 cell lines mediates by p53 & Bcl-2 mRNA levels. *J Phytopharmacol* 2017; 6:78-83.
6. Thomas M Walter, MerishS. Anticancer efficacy of a Polyherbal Siddha formulation against a 549-human lung carcinoma cells. *Asian Journal of Pharmaceutical & Clinical Research* 2017;10(2):34-5.
7. SathishkumarT .“Putrunoyum Siddha maruthuvamum”. Tamarainoolagam, Publication 292 Chennai: 106; 2006
8. Haikeem. Pa. Mu. Abdullasayub, Anuboga Vaithiya Navaneetham part V. First edition October 1995, Second edition may 2001.p.148-149.
9. Goldenberg D .Maté: a risk factor for oral & oropharyngeal cancer. *Oral Oncol* 38:2002. 646-649. [Crossref]
10. Guha N, Boffetta P, Wnsch Filho V, Eluf Neto J, Shangina O, et al. Oral health & risk of squamous cell carcinoma of the head & neck & esophagus: results of two multicentric case-control studies. *Am J Epidemiol* 166: 1159-1173. [Crossref]
11. Parvathy R. S ,Mariappan A , Meena kumariR. *In-Vitro* Anti-Cancer Activity of Rathinagara Rasa Mezhugu Against Cervical Carcinoma in Hela Cell Line. *Int J Recent Sci Res.* 13(07), pp. 1702-1706. DOI: <http://dx.doi.org/10.24327/ijrsr.2022.1307.0356>
12. Shanmugapriya P, Thamodharan S, Ramamurthy M, Mol VCJ, Nijavizhi M. Toxicological screening of ‘Gowri ChinthamaniChendooram’—A Siddha metallic preparation. *Pharma Tutor* 2014;2:119-22.
13. Guo J, Chang TY, McMichael I, Ma J, Hong JH. Light-controlled electro-optic power limiter with a Bi 12 SiO 20





Parvathy et al.,

- crystal. Opt Lett 1999;24:981-3.
14. Kaviya, V (2016) *Anti-Cancer Activity of Siddha Drug Ashta Bairava Chenduram against Oral Squamous Cell Carcinoma [OSCC] through In-Vitro Model*. Masters thesis, Government Siddha Medical College, Chennai.
 15. R Abhinaya (2018), Scientific Validation Of Anti-Oral Cancer, Anti-Tumour & Anti-Microbial Activities of Siddha Metallo mineral Formulation " Kaalamega Narayana Chendhooram " In-Vitro Studies [Masterthesis]
 16. Rajalekshmi S et al., A comparative study to evaluate the anti-cancer activity of Siddha drugs' Veerarasapadhangam' & Panchamugachendhuram, Int.J.Curr.Res.Chem.Pharm.Sci 4(12),29-33, 2017
 17. DaYeonLee et al., Anti-Inflammatory Activity of Sulfur-Containing Compounds from Garlic, Journal of Medicinal Food J Med Food 15(11) 2012, 992-999, DOI:10.1089/jmf.2012.2275
 18. Mathivadhani P, Shanthi P, Sachdanandam P. Apoptotic effect of *Semecarpus anacardium* nut extract on T47D breast cancer cell line. Cell Biol Int. 2007;31:1198-206.
 19. Sowmyalakshmi S, Nur-E-Alam M, Akbarsha MA, Thirugnanam S, Rohr J, chendil D. Investigation on *Semecarpus anacardium* L a siddha medicine for breast cancer. Planta. 2005;220(6):910-918.
 20. Sharma Poornima et al., Phytochemical Investigation & Anticancer Activity of *Ricinus communis*: A Review, Jetir May 2019, Volume 6, Issue 5

Table 1. Ingredients of Rathinagara rasa mezhugu

Sl.No	Ingredient	Botanical/EnglishName	Quantity
1	Sitramanakkennai	<i>Ricinus communis</i> L.	¼palam (8.75gm)
2	Valai Rasam	Absolutemercury	1palam (35gm)
3	Gandhakam	Purified Sulphur	1Palam (35gm)
4	Serankottai	<i>Semecarpusanacardium</i> Linn.	30
5	Pasunei	Cow'sGhee	1Palam (35gm)
6	Panaivellam	PalmJaggery	2palam(70gm)

Table 2. Cytotoxicity Assay by MTT Assay on MCF-7 Cell line.

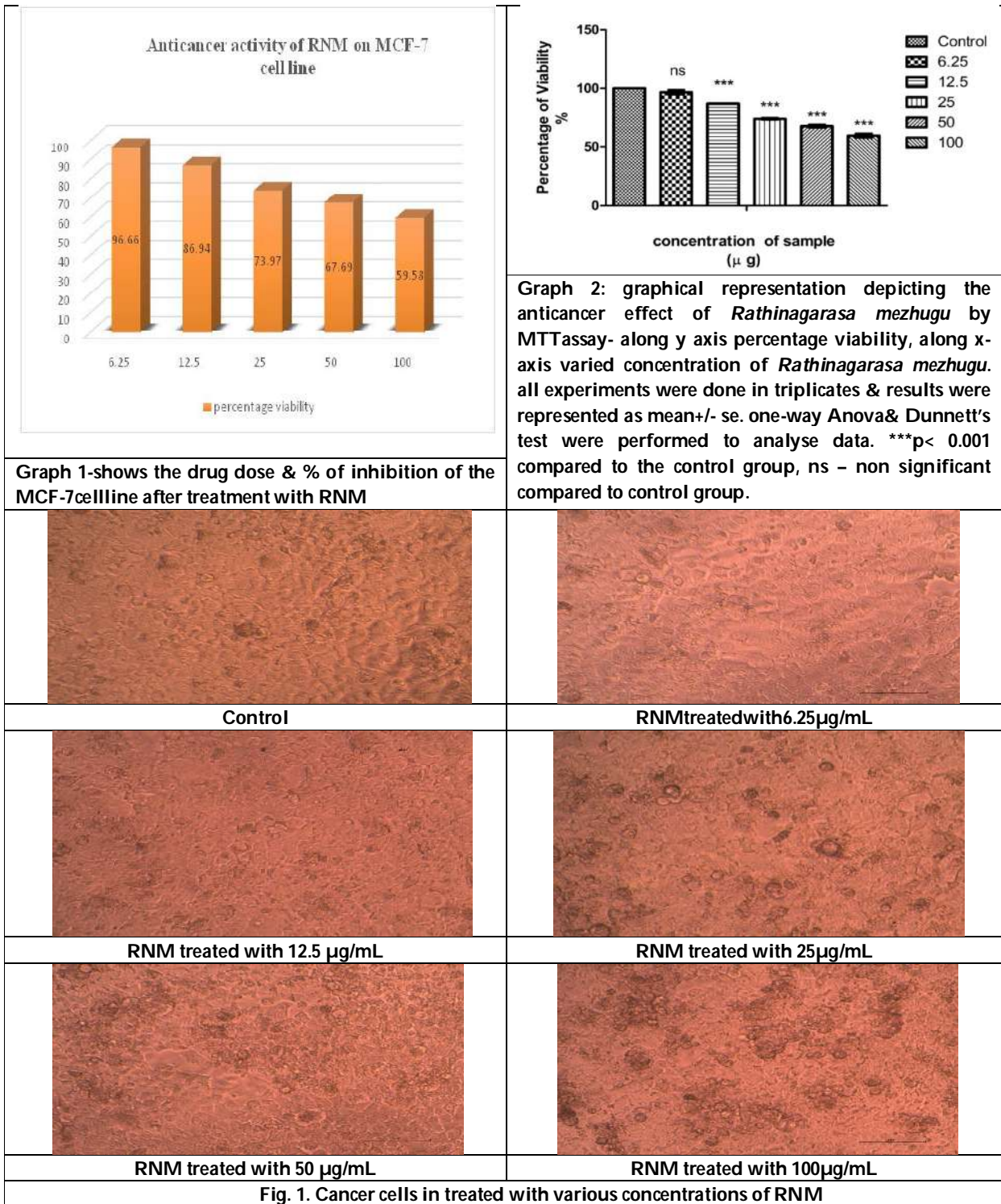
Sample Concentration (µg/mL)	OD value I	OD value II	OD value III	Average OD	Percentage Viability
Control	0.6139	0.6001	0.5813	0.5984	100.00
SAMPLE CODE-RATHINAGARASA MEZHUGU					
6.25	0.5941	0.5609	0.5803	0.5784	96.66
12.5	0.5341	0.5214	0.5053	0.5203	86.94
25	0.459	0.4463	0.4226	0.4426	73.97
50	0.4014	0.4126	0.4011	0.4050	67.61
100	0.3529	0.3518	0.3648	0.3565	59.58

LC50 Value: 115.97034 µg/MI (ED50plus software V1.0)





Parvathy et al.,





Topology Optimization and Dynamic Simulation on C- AL6061/7075 Ceramic Composite Diamond Frame Structure

M.Rajeshwaran¹, B.Shreeram^{2*}, D.Vasanth Kumar³ and G.Gokilakrishnan⁴

¹Professor, Department of Mechanical Engineering, Mother Teresa College of Engineering and Technology, Illuppur, Pudukottai, Tamil Nadu, India

²Professor, Department of Mechanical Engineering, KGISL Institute of Technology, Coimbatore, Tamil Nadu, India

³Associate Professor, Department of Mechanical Engineering, Jansons Institute of Technology, Coimbatore, Tamil Nadu, India

⁴Associate Professor, Department of Mechanical Engineering, Sri Eshwar College of Engineering, Coimbatore, India.

Received: 19 Jan 2023

Revised: 25 Apr 2023

Accepted: 12 May 2023

*Address for Correspondence

B.Shreeram

Professor,

Department of Mechanical Engineering,

KGISL Institute of Technology,

Coimbatore, Tamil Nadu, India

E.Mail: shreesotbk@gmail.com



This is an Open Access Journal / article distributed under the terms of the **Creative Commons Attribution License** (CC BY-NC-ND 3.0) which permits unrestricted use, distribution, and reproduction in any medium, provided the original work is properly cited. All rights reserved.

ABSTRACT

This article deals with the using of the Autodesk Inventor Professional software for testing and designing of a one track vehicle digital prototype. The frame design was carried out considering the ergonomics aspects in Indian Scenario. The carbon rod reinforced with AL6061, AL6061-T6 and AL7075 composite materials are evaluated for FEA analysis. The designed frame was subjected to topology optimization. The force distributions while turning, braking and combined effects of the optimized frame were performed analytically and the ENDO parameter were verified for vehicle stability. In summary, the FEA analysis of the optimized frame structure designed using AL7075 has highest rigidity suitable for a safe and ergonomically better performing one track vehicle. The findings of the tests are frequently utilised to undertake a more in-depth endurance analysis of specific building elements, model optimization, and the influence on the driver's body. This strategy enables the development of a brand new product as well as a more efficient assessment of the influence of the conditions under which it will be utilised.

Keywords: Topology Optimization, Composite, ENDO, Finite Element Analysis



**Rajeshwaran et al.,**

INTRODUCTION

Operating under strong pressure of economic process, according to reports, modern organisations are frequently required to react quickly to market demands. It should be mentioned that the planned goods must meet several precise building assessment requirements. It's very difficult to fulfil all of those requirements, which may or may not be mutually exclusive [1-3]. In terms of the current procedures for introducing new products into production, there's a relentless explore for alternative products. Virtual prototype is one in which every numerical approaches are used in this method. It is based on the building of a numerical model (usually of a machine, device, or technological process) and the subsequent execution of multi-variant simulations of the object's behaviour under various situations, with the goal of arriving at the best answer for the article's defined functions. This allows for a reduction in the value of research and, as a result, the analysis of multiple options [4-10]. This cutting-edge approach to design provides for efficient completion in the vast majority of cases-consuming and currently costly steps that, when combined, outline the procedure for making a replacement product. It should be applied to the entire structure, as well as its subgroups and individual components [11-13]. The so-called multi-body system method (MBS) is one of the most often utilised methods the term for modelling, analysis, and synthesis of real-world systems that are regarded as multi-body systems. Static analysis and optimization studies on numerous design parameters are carried out [14-17].

There are many CAD systems available and based on the level of knowledge and their widespread use in the business, this report focuses on software from intermediate organisations. This popularity stems mostly from the software's extensive capabilities, which are combined with a comparatively low cost of purchase and usage. One can create virtual models of cutting-edge mechanical structures using an intermediary system [18]. The aim of this work is to use Autodesk Inventor to create a virtual prototype of a single-track vehicle and conduct preliminary tests in a working animatronics environment, allowing for the identification of profusion and displacements at selected joints of the vehicle in doings that are more or less uneven auditorium conditions. The specific goal of these tests is to determine the possibility of using spring load regulation to delay frame deferment [4, 9, and 20]. Here the theoretical results and the virtual analysis result of the prototype is compared. Topology optimization of the diamond frame is performed using Autodesk software. The resulting frame different material conditions the stress analysis and the other stimulations are done and thus the results are taken in such a way were results can be compared and considered along with the theoretical values.

MODELING OF THE VEHICLE

In this process each components are designed using the inventor working environment and each components are then assembled as per the design requirements. The modelling of the mountain racing bicycle started with designing of the diamond frame. The dimension of the frame where selected from standard frames sizes manufactured in India (Table 1). From the table, item no 8 for average height of Indian male 5' 8" frame dimensions were considered (source: National Institute of Nutrition). The dimensions of the main frame considered are given in Table II and Figure 1. The material considered for the virtual prototype is Aluminium 7075, Aluminium 6061 and Aluminium 6061 treated to T6 condition [21]. The property of the material is listed in Table III. The frame if topology optimized and the optimized model is shown in Figure 2.

RESULTS AND DISCUSSION

Force Analysis of Bike

The virtual prototype is analysed for the theoretical analysis of forces while driving in a mountain. Under each conditions there are different external forcing acting on the vehicle and it gives different results one of them and thus under this different conditions the theoretical value is calculated and the results is observed. Different conditions on road are applied theoretically and result is observed and compared [22-26].





Rajeshwaran et al.,

A free body diagram showing the various forces involved during a. idling / freewheeling and b. during pedaling is shown in Figure 3 & 4. A graph of the force acting as a function of time. Here, X axis - the time displacement and direction of travel; y-axis – normal force (F) balancing the gravitational force (mg).

The following can be observed from the graph:

- i. *For first 15 Seconds:* The pedaling force is completely used to overcome the resistive force (mg) and hence it is negative. Resistive friction force is assumed at 15N. Hence, the graph starts at -15N.
- ii. *For next 30 seconds:* The pedaling force is used partly to overcome resistive force and partly to overcome the static friction force (Fs) in the direction of travel. As the time increases the friction force increases

proportionally the resistive force is decreased. Hence, a linear graph from -15N at 15 seconds to 540N in 45s. Considering the weight of the bicycle at 10kg and the rider at 70kg and travel velocity of the rider at 10m/s. Overall force $\bar{F} = m \cdot \bar{v} = m \cdot \Delta v = m \cdot (\bar{v}_{15s} - \bar{v}_0)$
Hence, the velocity at 15 seconds:

$$v_{15s} = v_0 + \frac{F \cdot t}{m}$$

$$v_{15s} = 10 \text{ m/s} + \frac{(-15\text{N}) \cdot (15\text{s})}{70 \text{ kg}} = 10 \text{ m/s} - 3.21 \text{ m/s} = 6.79 \text{ m/s}$$

i.e the velocity of travel of the bicycle is 6.79 m/s. As per equation 1, the impulse force is equal to momentum. The impulse force (F . Δt) can be derived from the force to time graph plotted i.e. the area under this graph for some time interval.

Area under the graph / impulsive force at 15s:

$$F \cdot \Delta t = (-15\text{N}) \cdot (15\text{s}) = -225 \text{ Ns} = -225 \text{ kg m/s}$$

Momentum at 0s:

$$m \cdot \bar{v}_0 = 70\text{kg} \cdot 10 \text{ m/s} = 700 \text{ kg m/s}$$

Momentum at 15s:

$$m \cdot \bar{v}_{15} = 700 \text{ kg m/s} - 225 \text{ kg m/s} = 475 \text{ kg m/s}$$

Velocity at 15s:

$$\bar{v}_{15} = \frac{475 \text{ kg m/s}}{70 \text{ kg}} = 6.785 \text{ m/s}$$

In order to determine the increase in velocity from 15s to 40s, the area method is employed. The area under 15s to 40s can be used to determine the increase in momentum for the next 30s (45s-15s). The area has both negative (area from 15s to 20s) and positive (area from 20s to 45s).

Negative area:

$$\text{Area of triangle} = \frac{1}{2} \cdot 5\text{s} \cdot (-15\text{N}) = -37.5 \text{ kg m/s}$$

Positive area:

$$\text{Area of triangle} = \frac{1}{2} \cdot 25\text{s} \cdot (50 \text{ N}) = 625 \text{ kg m/s}$$

$$\text{Total Area} = \text{positive area} + \text{negative area} = 625 - 37.5 = 587.5 \text{ kg m/s}$$

Momentum at 45s:

$$m \cdot \bar{v}_{45} = 587.5 \text{ kg m/s}$$

Velocity at 45s:

$$\bar{v}_{45} = \frac{\text{momentum at 15s} + \text{momentum at 45s}}{70 \text{ kg}} = \frac{475 + 587.5}{70} = 15.17 \text{ m/s}$$

General, while braking the equilibrium of the bicycle is disturbed and the load on the bicycle is transferred from the rear wheel to the front wheel gradually. But at conditions of impulsive braking, the bicycle is put to stop and the rider experiences momentum in the headed direction. Resulting in a situation called as ENDO, causing the rider to flip. ENDO cannot be totally avoided in most cases. But, the design of the vehicle can be improved by increasing the factor of safety and change in rider position [27, 28].





Rajeshwaran et al.,

The ENDO for a bicycle can be calculated considering the center of gravity location in X and Y direction. i.e. A/H = ratio of length of front wheel CG location, $L1$ / Height of CG location, H . For conditions of static equilibrium at wheel contact point O (below front wheel), if the sum of the moments at that point is zero. i.e. $\sum M_0 = (R \cdot H - mg \cdot L1) = 0$.

$$\frac{R}{mg} = \frac{L1}{H} \rightarrow (1)$$

From equation (1), it is evident that the ENDO parameter is equal to the braking force. The co-efficient of friction between the tire and the road also has an effect on braking. It has been reported that the higher the value of A/H , lesser are the chance for flipping [28]. Also, A/H value is affected by the rider's average height, mass and his riding positions. The ENDO parameter can be controlled rapidly increased to a safer level by riding at rearward position. Considering all the theoretical force analysis the ergonomically safe design is arrived at and the virtual prototype is taken for static analysis in Inventor environment.

Finite element analysis of prototype

A stress analysis can facilitate your find the most effective design alternatives for an element or assembly. The main function of the frame is to transfer the produced energy by the rider to the rear wheel. In case of bicycle differing types of loads are working on the frame, from the rider to the sphere and also the ground reaction. Static analysis evaluates structural loading conditions. The topology optimized frame is subject to finite element analysis. Mesh setting considered is presented in Table V and Figure 5. The result of Finite Element Analysis value for topology optimized frame for 3 materials is given in Table VI and Figure 6-11 [28-43].

CONCLUSION

The finite element model of a standard bike frame was modeled, topology optimized and simulated for various design parameters - 4 types of load conditions and 3 material conditions. Stress concentration areas were identified by performing dynamic simulation and correlated with the literature values. It was observed that the topology optimized diamond frame using Aluminum 7075 was found to be performing better than Aluminum 6061 and 6061 T6 for all design parameters. In order to understand the implications of safety study on how frame profile, profile thickness and load distribution between adjacent tubes affects the strength and for various road profiles.

REFERENCES

1. B. Branowski, in "Basics of machine drive design" (Wyd. PolitechnikiPoznańskiej, Poznań, 2007).
2. V. Castorani, D. LandiandM. Germani,Procedia CIRP.50 (2016) 52-57.DOI 10.1016/j.procir.2016.05.019
3. P. Nowakowski, Silesian University of Technology, Gliwice 2006.
4. A. Trąbka, in "Mechanik" (2ND Edition 2013)p.12.
5. M. Sydor, (Polish Scientific PublishersPWN,Warszawa. 2012) p.1.
6. K. Kamberov, G. Todorov, S. Stoevand B. Romanov, Proceedings in Manufacturing Systems.10 [3] (2015) 99-104.
7. M. Hirz, W. Dietrich, A.Gfrerrer, and J.Lang,(Springer-Verlag Berlin Heidelberg2013).
8. J. Rix, S. Haasand J. Teixeira,Chapman & Hall.30[3](1998) 348.DOI 10.1080/07408179808966461.
9. A.K. Matta, D. RangaRajubandK.N.S. Suman,MATER TODAY-PROC.2 [4-5] (2015) 3438-3445.
10. J. Tokarczyk,Arch. Min. Sci.60 [1] (2015) 329-340.
11. P. Dudziński, A. Kosiara and A. Konieczny.PostępyNaukiiTechniki. 14 (2012) 64-74.
12. Š. Vrtiel, Š. Hajduand M. Behúlová.IOP Conf. Series: Mat. Sci. and Eng.266 (2017) 012-015. DOI 10.1088/1757-899X/266/1/012015.
13. W.J. Hao, et al., Appl. Mech. and Mater. 365–366 (2013) 435-439.
14. K. Chadaj, P. Malczykand J. Frączek,Multibody System Dynamics39 [1-2] (2017) 51-77. DOI 10.1007/s11044-016-9531-x.
15. K. Lipińskir, Appl. Mech. and Mater, 831 (2016) 54-62. DOI 10.4028/www.scientific.net/amm.831.54





Rajeshwaran et al.,

16. W. Schiehlen, M. Valasek, in Proceedings of the lectures presented at NATO ADVANCED STUDY INSTITUTE on VIRTUAL NONLINEAR MULTIBODY SYSTEMS which was held in Prague, Czech Republic, 23-3 July 2002 (Springer Science & Business Media, 2012).
17. Z. Wang, et al., Nonlinear Dynam. 86 [3] (2016) 1571-1597. DOI 10.1007/s11071-016-2978-8
18. A. Jaskulski and Wyd. Nauk. PWN, Warszawa, 2017.
19. A. Vergnano, G. Berselli and M. Pellicciari, Int. J. Interact. Des. Manuf. 11 (2017) 331-340. DOI 10.1007/s12008-015-0295-y.
20. K. Łukaszewicz, Procedia Engineer. 182 (2017) 425-433. DOI: 10.1016/j.proeng.2017.03.127
21. W. Chia-Chin, in "Static and dynamic analyses of mountain bikes and their riders" (PhD thesis, University of Glasgow, 2013).
22. D. Arola, P.G. Reinhall, M.G. Jenkins and S.C. Iverson, IOSR-JMCE. 23 (1999) 21-24. DOI: 10.1111/j.1747-1567.1999.tb01565.x.
23. D. Covilland S. Begg, Procedia Engineer. 112 (2015) 34 – 39. DOI 10.1016/j.proeng.2015.07.172.
24. J. Enright, Industrial Project Report, Department of Mechanical Engineering, University of Glasgow, UK, 2007.
25. Weixia Dong, Yan Liang, Qifu Bao, Xingyong Gu and Jing-wei Yang, J. Ceram. Process Res. 22[3] (2021) 317-322.
26. Serkan Baslayicia, Mehmet Bugdaycib and Mahmut Ercan Acma, J. Ceram. Process Res. 22[1] (2021) 98-105.
27. B. Shreeram and I. Rajendran, Int. J. Heavy Veh. Syst. 25[3] (2017) 406-418.
28. Joo Won Lee, C.H. Lee, and H. J. Kima, J. Ceram. Process Res. 2 [3] (2001) 113-119.
29. N. Barry, D. Burton and J. Sheridan, M. Thompson and N.A.T. Brown, P. I. Mech. Eng. P-J. Spo. 229[1] (2015) 28-38.
30. H.B. Jeona, I.H. Lee, GyeSeok Ana, and Yoon-Suk Oha, J. Ceram. Process Res. 19[6] (2018) 450-454.
31. J.H. Lee, S.J. Lee, J.Y. Jeong, and S.J. Kima, J. Ceram. Process Res. 15 [6] (2014) 519-524.
32. F. Fuerle and J. Siens, Comput. Struct. 119 (2013) 48-59. DOI 10.1016/j.compstruc.2012.11.014.
33. Y.C. Lina, J. C. Hung, H.M. Chow, and A.C. Wang, J. Ceram. Process Res. 16[2] (2015) 49-257.
34. N. Pandiaraj, B. Shreeram and I. Rajendran, Int. J. of Chem. Phy. Sci. 4 (2015) 20-28.
35. A.P. Senthil Kumar, S. Yuvaraj, and S. Janak, J. Ceram. Process Res. 21[2] (2020) 217-225
36. J. Vanwallegem, W.V. Paepegem, M. Loccupier and I.D. Baere, Procedia Engineer. 112 (2015) 219-224. DOI 10.1016/j.proeng.2015.07.203
37. Remzi Gören, and Cem Özgür, J. Ceram. Process Res. 13[3] (2012) 262-266.
38. B. Shreeram and I. Rajendran, J. Inorg. Organomet. P. 28 [2] (2018) 2484-2493. DOI 10.1007/s10904-018-0920-x.
39. L. Lessard, J. Nemes and P. Lizotte, Composites. 26[1] (1995) 72-74. DOI 10.1016/0010-4361(94)P3633-C.
40. M. Levy and G.A. Smith, Sports. Engineering. 8[2] (2005) 99-106. DOI 10.1007/BF02844008
41. T. Liu and H. Wu, Mater. Design. 31[4] (2010) 1971-1980. DOI 10.1016/j.matdes.2009.10.036
42. K. Navaneetha Pandiyaraj, R.R. Deshmukh, B. Shreeram and R. Mahendiran, J. Nanosci. Nanotechnol. 2[1] (2014) 436-441.
43. S. Bakthavathsalam, R.I. Gounder and K. Muniappan, Environ. Sci. Pollut. R. 26 (2019) 24772-24794. DOI 10.1007/s11356-019-05678-x

Table 1: Standard bicycle size geometry chart (source: National Institute of Nutrition, India)

Average Height of Human	Inseam	Shoe size	Frame size cm	Top tube cm
6'1"	34.75	10.5	60	57.5
6'0"	34.25	10	59	57
5'10.75"	33.75	9.5	58	56.5
5'9.5"	33	9	57	56
5'8"	32	8.5	55	55
5'7"	31.25	8	54	54





Rajeshwaran et al.,

Table 2: Dimension of the prototype derived from Table 1 for topology optimization

Prototype dimensions	Values
Distance between handlebar to the centre axis of the front tyre	29.669"
Distance between seat to the centre axis of pedal	28.492"
Distance between the centre axis of the front tyre to the pedal	29.305"
Distance between the centre axis of the rear tyre to the centre axis of pedal	20.065"
Diameter of the tyre	31.302"
Distance between the two tyre	48.66"

Table 3: Mechanical properties of common bicycle frame materials

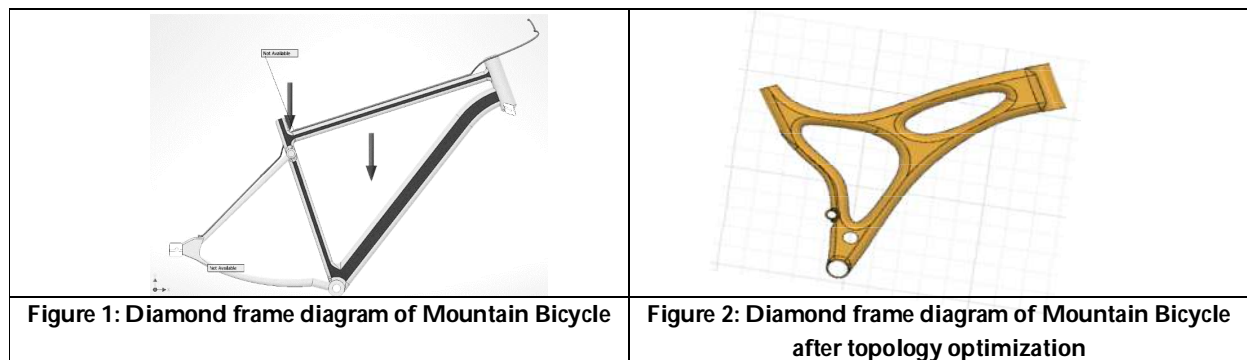
Alloy	Density (g/cc)	Modulus of Elasticity (GPa)	Poisson's Ratio	Ultimate tensile strength (MPa)	Tensile Yield Strength (MPa)
Aluminum 6061	2.7	68.9	0.33	310	275
Aluminum 6061-T6	2.7	69.0	0.33	389	369
Aluminum 7075	2.78	71.0	0.32	276	145

Table 4.Mesh settings

Element order	Parabolic
Curved mesh elements	Considered
Maximum turn angle on curves (in deg)	60
Maximum adjacent mesh size ratio	1.5
Maximum aspect ratio	10
Minimum element size (% of avg size)	20
Convergence tolerance %	20
Portion of elements refined	10

Table 5.Finite Element Analysis value for topology optimized frame for 3 materials

	Aluminum 6061	Aluminum 6061 T6	Aluminum7075
Stress (min)	3.778E-07 MPa	4.895E-07 MPa	3.778E-07 MPa
Stress (max)	0.5213 MPa	0.5215 MPa	0.5213 MPa
Displacement (min)	0 mm	0 mm	0 mm
Displacement (max)	0.002475 mm	0.07609 mm	0.002379 mm
Strain (min)	8.46E-12	3.666E-10	8.129E-12
Strain (max)	1.195E-05	3.827E-04	1.148E-05





Rajeshwaran et al.,

<p>Figure 3: Force distribution while freewheeling</p>	<p>Figure 4: Force distribution while riding</p>
<p>Figure 5: Meshed view</p>	<p>Figure 6 : Stress analysis for Aluminum 6061</p>
<p>Figure 7 : Stress analysis for Aluminum 6061 T6</p>	<p>Figure 8 : Stress analysis for Aluminum 7075</p>
<p>Figure 9 : Displacement analysis for Aluminum 6061</p>	<p>Figure 10 : Displacement analysis for Aluminum 6061 T6</p>
<p>Figure 11 : Displacement analysis for Aluminum 7075</p>	





Mobile Application for Vehicle Tracking during Lack of Internet Facility

T. Venkat Narayana Rao^{1*}, K.Siva Kumar Gowda² and Puladas Sandhya Priyanka²

¹Professor and Head, Department of CSE-IOT, Sreenidhi Institute of Science and Technology, Yamnampet, Hyderabad, Telangana, India,

²Assistant Professor, Department of C.S.E-IOT, Sreenidhi Institute of Science and Technology, Yamnampet, Hyderabad, Telangana, India.

Received: 23 Feb 2023

Revised: 10 Apr 2023

Accepted: 15 May 2023

*Address for Correspondence

T.Venkat Narayana Rao

Professor and Head,
Department of CSE-IOT,
Sreenidhi Institute of Science and Technology,
Yamnampet, Hyderabad, Telangana, India,
E. Mail: venkatnarayanaraot@sreenidhi.edu.in



This is an Open Access Journal / article distributed under the terms of the **Creative Commons Attribution License** (CC BY-NC-ND 3.0) which permits unrestricted use, distribution, and reproduction in any medium, provided the original work is properly cited. All rights reserved.

ABSTRACT

In today's fast-moving generation, with the technologies booming and high availability of services on fingertips people have become less tolerant to waiting and doing manual work. There comes the need of developing seamless services that not only fulfill the customer's needs as a service but also do them on an uninterrupted basis. Out of all the services, knowing how far your bus is from your bus bay without the use of the internet is the need of the hour. We have all faced such issues either we have lost track of our vehicle due to a fluctuating network on our side or because the driver lost his connection and the location doesn't get updated. This paper focuses on an approach of calculating the distance to be travelled or the distance that is by passed from a bus stop without using the internet. The goal is to make use of the simple speed and distance formula. Missing bus just by a few minutes will not be a problem anymore. The experiment is carried out by developing an application on android platform that will help users be aware of the location of the bus, so "that" they can plan their activities accordingly to reach the bus-bay in time. The application is planned to notify the halt at the following bus-bay in case the user misses his bus. Any changes in bus route details can be notified as and when updated. Details such as the bus number, boarding time or the bus travel route can be learned through the notifications.

Keywords: Application, MySQL, PHP, Database, Transport service.



**Venkat Narayana Rao et al.,**

INTRODUCTION

Of all transit services, bus service is the primary means of transportation for the public. Particularly in a bustling city, the bus is the simplest, convenient, and least expensive means of transport. Some of the many reasons due to which the public takes bus instead of choosing their own vehicle are traffic jam, high parking charge and unavailability of parking slots at the destination. Moreover, the service has very poor information system these days. Passengers do not know the prompt arrival time of a bus but know the estimated arriving time. Compared to other means of transportation such as the train or flight, transportation service does not have a proper system. Vehicles and their arrival time in every bus bay. These issues arrive, as the current system does not use real time tracking methodology to track. Unavailability of a proper platform to update latest vehicle traffic information to the passengers is yet another reason.

In cases where such technology is already in use, the public faces other problems. Due to rapid movement of the vehicle and unavailability of seamless network connectivity, Drivers face network fluctuations and hence their location is lost. In other scenarios, the user who is tracking the bus may lose the connection and hence has no real time estimation of his ride's arrival. Majority of the management systems are still implementing manual work which is another reason for poor service. In order to solve the above-mentioned issues and improvise the current transportation service, real time tracking system is to be inculcated and implemented. With this system, the vehicle positional data is achieved only the first time before the journey begins and is then transmitted to the central server for processing the route and extracting travel information[2][3].

A few programming languages such as PHP, java can be used in the development of the suggested system. The developed vehicle tracking system will be in a position to provide its passengers a platform to check on updated bus traffic information, for instance transport departure and arrival time. On the other hand, this system will also be able to reduce workload on the management team and provide an instantaneous platform to update latest and accurate bus information to its passengers[1]. The central server will receive the required co-ordinates from the vehicle position module. When the server receives such position data, the system will stock the information into the database tables automatically. Based on the latest position data received by the user on request, the system will exercise the information and modify the vehicle arrival time.

System Architecture

This system follows a simple architecture as depicted below. Of all the computer systems designs, object-oriented system and design methods have become the most widely used methods. They have even proven to be extremely efficient. This tracking system would require an android device, a database, and a server as depicted in figure 1. PHP is a server-side scripting language that one can use to develop applications and dynamic web pages. We only need to install PHP on the web server which will allow and host the web application and client applications can use the server resources through web browsers. MySQL and PHP are the two unique entities of the same coin. Similar to MySQL that has built in functions for data manipulations, PHP has built in functions for connecting to MySQL server and modifying the data in the backend.

Database Tier

The database level consists of two database stores as shown in figure 2. One of them is the current transport service administration database from which information about the route has been obtained. Since we are retrieving just data from this database and do not change it, the web-based information system may be used. Adding certain specialized applications, such as the list of registered application users, records of external connections to web sites, and so on is a distinct database component. This database will be used to build, read, update and delete (CRUD) activities.



**Venkat Narayana Rao et al.,****Web/Application Tier**

In this field, we create online services and mobile app admin pages. Two groups classify web services. First group consists of services which collect user's customized data from the database based on a unique user ID such as the registration number. The services do not execute any actions for creating/updating/deleting and do only read operations in the current institution database. These services provide customized data in XML/JSON format to presentation layer. The CRUD actions on the application specific data store are performed by the second group of web services as depicted in figure 2. We pass data to and from mobile applications through XML/JSON to the data storage. In this layer, web pages of admin are also developed, which the specific transport service management department may access. The administrator handles the setting of different components of the program using these pages.

Presentation Tier

We have cross-platform mobile devices at presentation level, on which apps are to be used. The layer logic of the presentation is platform-based and is written only for devices of various platforms. This logic produces the corresponding device user interface displays. In addition, this layer is used as a consumer of middle-level web services. The company records new user information and calls on the online services for passenger information. In turn, Web services communicate with the database and provide XML/JSON format for this layer. The answer is analyzed to get the information the users want to get.

Implementation

This system is built on android studio with java and XML as front end. There are three basic entities in the system. The Administrator is responsible for creating a route and allotting a driver. The driver is responsible for updating the time as and when a particular stop is reached. The user is responsible for registering and checking the notifications. All these functions have been depicted in the below algorithm[4]. For the backend, MySQL has been used. MySQL being a relational database management system allows a wide range of activities such as data warehousing, logging applications and e-commerce. Hence, a table structure drawing relation between admin, driver and the user has been created. This tightly coupled relation helps in easy retrieval of required information as and when the user requests for information. The below algorithm depicts the functionality of an administrator who has the privilege to update the time of arrival or departure of the vehicle. Similarly, a user checks include verification and authentication of his login and receiving the notification based on the vehicle location and request made[1][4][5].

Vehicle Tracking Algorithm

Step 1: Click on the respective buttons which state "Admin login" or "User Login"

Step 2: If the candidate is a new user, redirect the screen to registration page and go to Step 3 else Step 4

Step 3: Fill the details and click on register

Step 4: Enter username and password

Step 5: If credentials are authentic go to Step 4 else go to Step 3

Step 6: If the logged in candidate is an admin, update the time by clicking on the update button of a specific stop and go to Step 6 else go to Step 5

Step 7: Choose a specific stop number and click Track, a message with the details of the vehicle will be displayed

Step 8: Logout

The logic is programmed in such a way that when a candidate tries to login to the application, he is identified whether it's a new login or an old login. With that information the user is redirected to the next screen which could be registration page in case the user is new or to another screen which further depends on whether the candidate is an administrator or a passenger. In case the logged in candidate is an admin, he will be asked to click on update which will modify the time after a particular stop is reached. If the logged in candidate is a passenger, then he will be asked to select a stop from the drop down and click on track. This will fetch the details of his ride and display the appropriate message as a dialogue box pop up on the screen. For example, if the bus is at the previous stop the user



**Venkat Narayana Rao et al.,**

will be notified the calculated time to reach him. Post the requirements achieved or updates made the candidate can click on logout of the application [6][7][8].

Modules of the Application**Administrator Module**

The supervisor is in charge of registering the travelers. When a passenger submits a registration form, it is reviewed, and when the administrator approves all of the data, the student is added to the site[9]. The passwords for Event Manager are kept by the owner.

Central Server Processing Module

Before starting the route, central server receives position data from the bus position module. This module will automatically save the data to the corresponding table in the server database if the central server receives bus position data. In the system, an imaginary node and line structure is created where nodes represent the bus path. This module processes data and updates the current time for arrival in the main bus scheduled based upon the latest location data received. This automatically updated module allows bus users to get the updated information on bus traffic from the server on demand for the vehicle schedule.

Real Time Transit Arrival Tracking

This module will be created as a web page to check the time of arrival for public transport. This module retrieves the latest data from the central server periodically with AJAX technology and provides the latest and greatest time of transit arrival at each bus stop on the gadget when the user is tracked within 3 seconds.

Vehicle Status Update Module

A transport driver uses the status update module to update the vehicle status to the database when the transport is running. This is when the vehicle is busy with stop passengers and this module enables the bus driver to send an update message to the server.

RESULTS AND EXPLANATION

The major objective of this paper is to enhance the vehicle tracking system through the addition of the features required for the project such as projection of precise bus times, proper vehicle numbers and the release of network reliance. This application takes a stop number as input, showing all routes/stops data, tracking the vehicle and displaying it on the screen. There has been increasing interest in developing the Android platform throughout the previous two decades. The research of this project indicates that very few suppliers have offered automated solutions enabling the application to work without the usage of the Internet. Also, on an average, the response time of the servers on various update and retrieval operations is only a fraction of a second. Hence the passengers or users face no latency during their requests. The driver needs the use of GPS only once before he takes off his journey, as the later retrieval depends on the imaginary node line structure that gets created. Each node represents the stop of the transport where new users either get in or off the vehicle. Due to non-dependency on the internet, this method proves to be a better replacement to existing GPS navigating or tracking system. In a few thousand test cases sampled, the accuracy of the proposed system has been close to 91.4%.

The first screen that appears is the home page where either the admin or the user can login. This screen makes an important contribution to authenticating whether the candidate has the right credentials to be logged in as a user or an admin or a driver. The page mainly consists of a basic detail such as the username and password and a button to login. In case the user is new, there is another button for registration. There is also a button for Admin login which when clicked navigates to the login screen for admin.



**Venkat Narayana Rao et al.,**

Registration form is where the new passengers fill their details to register themselves. Details like name of the user, password, bus number and stop number are asked. Once the details are filled up, the user can click on submit. The admin page consists of the username and password of the driver as depicted in figure 3. If the details are filled correctly the driver is directed to the next page else displays a message asking to re-check the filled details. At the beginning of the journey, the driver has to connect to the GPS, based on the best route detected an imaginary structure like node and line network is created at the backend. With each node representing the stop and the line representing the route. The driver can now start his journey carefree of whether the internet fluctuates or is stable, as the system no longer depends on it. In the updating page, on arriving at each stop the backend recognizes as a node reached, and the driver is asked to click on the update button to store the time stamp in the database. Using the distance auto calculated at the beginning of the journey and by capturing the varying speed of the vehicle, applying speed and distance formula, the time to reach a particular stop is calculated [10]. Tracking page allows users to select the stop number and track the bus and see the message. Upon tracking, if the bus has reached the previous stop it displays the message and if not, then the message is displayed accordingly as shown in figure 4. The table 1 depicts the test scenarios and the outcomes of the application.

CONCLUSION

This application is best suitable for users who live in remote areas or locations where network connectivity is poor or fluctuates on regular intervals. There are many under-developed and developing countries that are still struggling to establish a proper nationwide network. But the public has their regular course to take care of and the need for travel is undeniable. Most importantly, not being late is many workplaces' demand. All these situations demand a service this paper talks about. This application will also prove beneficiary to all those people who cannot afford a heavy internet charge. As a future scope, since this system is based on an object-oriented design, it will be adaptable to any future enhancements including any future national security changes. Therefore, it is stated that tracking a bus or any means of transport without the use of the internet can be attained.

REFERENCES

1. Dr. Saylee Gharge, Manal Chhaya, Gaurav Chheda, Jitesh Deshpande, "Real time bus monitoring system using GPS," An International Journal of Engineering Science and Technology, Vol. 2, Issue 3, June 2012.
2. Abid Khan, Ravi Mishra, "GPS-GSM based tracking system," International Journal of Engineering Trends and Technology, Vol. 3, Issue 2, pp: 161-164, 2012.
3. S. P. Manikandan, P. Balakrishnan, "An Efficient real time query system for public transportation service using Zigbee and RFID," International Journal of Research in Communication Engineering, Vol. 2, No. 2, June 2012.
4. Swati Chandurkar, Sneha Mugade, Sanjana Sinha, Pooja Borkar, "Implementation of real time bus monitoring and passenger information system," International Journal of Scientific and Research Publications, Vol. 3, Issue 5, May 2013.
5. Pankaj Verma, J. S. Bhatia, "Design and development of GPS-GSM based tracking system with Google map based monitoring," International Journal of Computer Science, Engineering and Applications, Vol. 3, No.3, June 2013.
6. Madhu Manikya Kumar, K. Rajesekhar, K. Pavani, "Design of punctually enhanced bus transportation system using GSM and Zigbee," International Journal of Research in Computer and Communication Technology, Vol. 2, Issue 12, December 2013.
7. R. Maruthi, C. Jayakumari "SMS based Bus Tracking System using Open Source Technologies," International Journal of Computer Applications (0975 – 8887) Volume 86 – No 9, January 2014 College of Engineering, Chennai SSN College of Engineering, Chennai.
8. N. Vijayalashmy, V. Yamuna, G. Rupavani, A. Kannaki@Vasanthazhagu, "GNSS based bus monitoring and sending SMS to the passengers," International Journal of Innovative Research in Computer and Application Engineering, Vol. 2, Special Issue 1, March 2014.



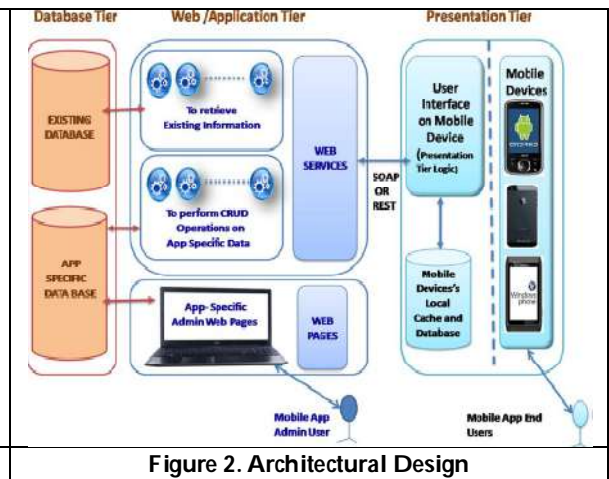
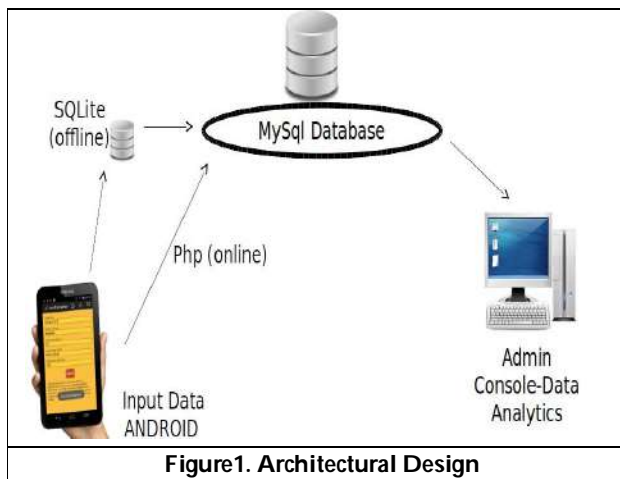


Venkat Narayana Rao et al.,

9. R. Manikandan, S. Niranjani, "Implementation on real time transportation information using GSM query response system," Contemporary Engineering Sciences, Vol. 7, No.11, pp: 509-514, 2014.
10. G. Raja, D. NaveenKumar, G. Dhanateja, G. V. Karthik, Y. Vijay Kumar, "Bus Position monitoring system to facilitate the passengers," International Journal of Engineering Science and Advanced Technology(IJESAT), Volume-3, Issue-3, pp: 132-135, 2014.

Table 1: Output of the Testing Scenarios

Test Case	Candidate	Operation	Current Bus location	Output Messages
1	Admin	Update at stop 3	3rd stop	Stop number 3 has been updated with latest time of departure
2	User	Track at stop 4	2nd stop	The bus is at stop 3, reached at 11.52.30, yet to reach your stop!
3	User	Track at stop 3	2nd stop	Your bus reached the previous stop at 12.30.12. It will reach your stop in next 15 minutes.
4	User	Track at stop 6	6th stop	Your bus has reached your stop!
5	Admin	Update at Final stop	Final stop	Your ride is complete.
6	Admin	Update at first stop	Initial stop	Your departure from the depot is noted.
7	User	Track at stop 3	4th stop	Your bus has left your stop, catch your bus at stop 5 in 10 minutes!





Venkat Narayana Rao et al.,

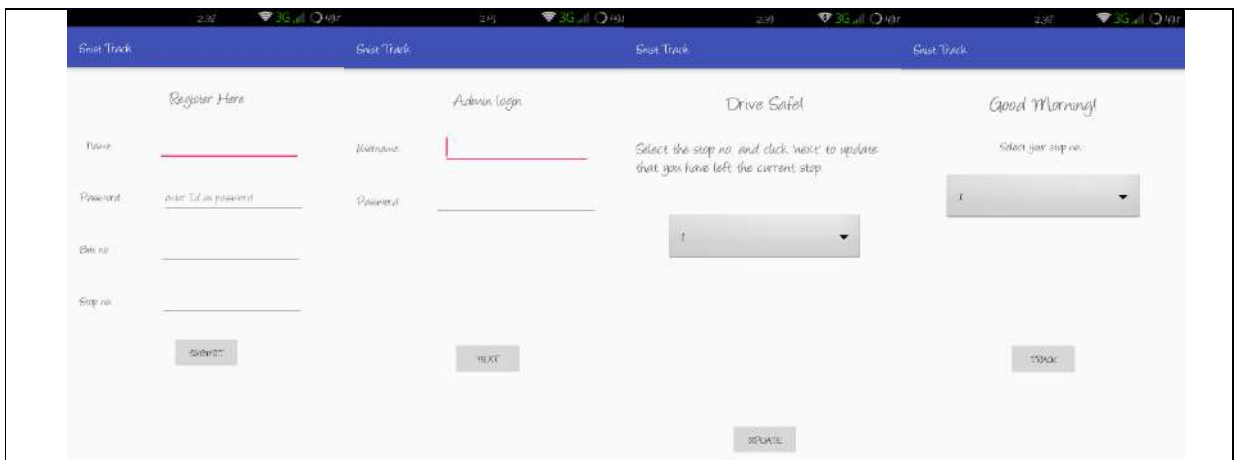


Figure 3. Registration form, admin login, updating and tracking screens

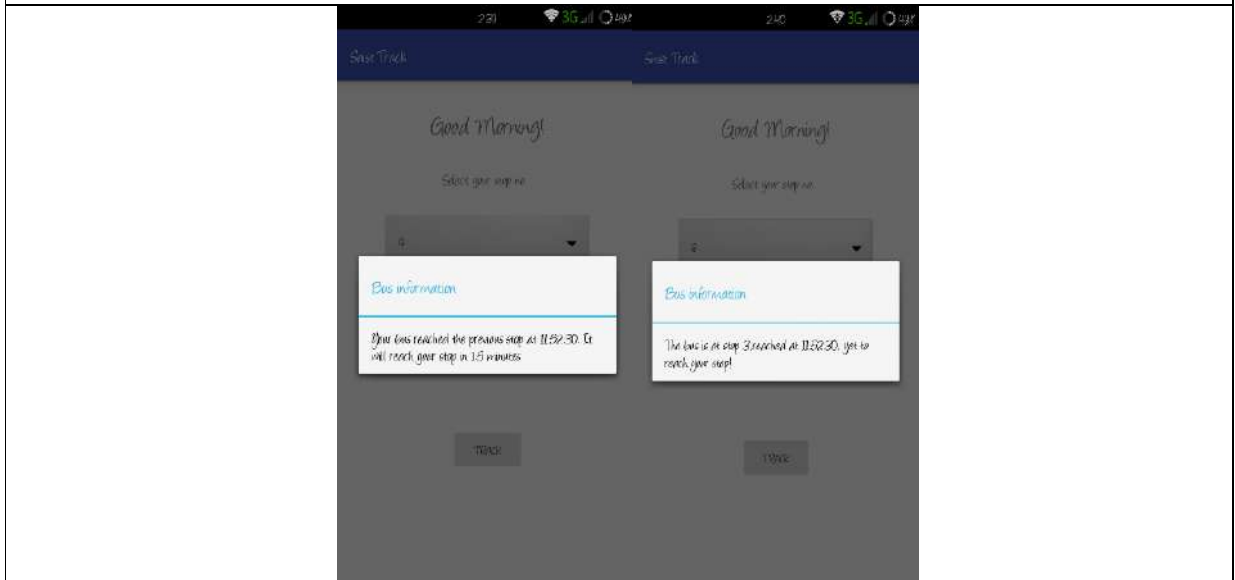


Figure 4. Screens displaying messages based on the vehicle's latest location.





Production, Purification and Characterization of Tannase from *Aspergillus niger* HP-6 using Indian Gooseberry Juice

Himani Oza¹, Dimple Pardhi¹, Vikram Raval², Rakeshkumar Panchal³ and Kiransinh Rajput^{2*}

¹Ph.D Research Scholar, Department of Microbiology and Biotechnology, Gujarat University, Ahmedabad-380009, Gujarat, India.

²Assistant Professor, Department of Microbiology and Biotechnology, Gujarat University, Ahmedabad-380009, Gujarat, India.

³Associate Professor, Department of Microbiology and Biotechnology, Gujarat University, Ahmedabad-380009, Gujarat, India.

Received: 06 Feb 2023

Revised: 10 Apr 2023

Accepted: 16 May 2023

*Address for Correspondence

Kiransinh Rajput

Assistant Professor,

Department of Microbiology and Biotechnology,

Gujarat University, Ahmedabad-380009,

Gujarat, India.

E.Mail: rajputkn@gujaratuniversity.ac.in



This is an Open Access Journal / article distributed under the terms of the **Creative Commons Attribution License** (CC BY-NC-ND 3.0) which permits unrestricted use, distribution, and reproduction in any medium, provided the original work is properly cited. All rights reserved.

ABSTRACT

Tannase (EC 3.1.1.20) is an important enzyme, which catalyze the hydrolysis of ester and despite linkages of hydrolyzable tannins like tannic acid with sugar and gallic acid production. A fungal isolate from soil, *Aspergillus niger* HP-6 was used to produce tannase with optimized production conditions. The optimum production conditions using Central Composite Design (CCD) viz., 1% (v/v) Indian gooseberry juice, 1.2% (w/v) starch, and 0.6% (w/v) peptone produced 5.01 U/ml of tannase. It was purified using ammonium sulphate precipitation and gel permeation chromatography with 52.10% and 38.49% yield. The molecular weight of partially purified tannase was found to be 50 kDa through SDS-PAGE. Furthermore, it showed optimum activity at pH 6.0 and 40°C temperature. The tannase activity was increased in the presence of Mg²⁺ and Mn²⁺, but inhibited by Ca²⁺, Fe³⁺, and Hg²⁺. Additionally, surfactants (SDS, tween 20, tween 80) and organic solvents (acetone, propanole, methanol, and formaldehyde) with 5 mM concentration were also found with considerable inhibitory effects on tannase. *Dithiothreitol* (10 mM) showed drastic inhibition of tannase activity. The K_m and V_{max} values for tannase were 0.11 μ M and 10.24 μ Mmin⁻¹, respectively. Moreover, this tannase (1 U/ml) was also used in clarification of Indian gooseberry and pomegranate juice, and effectively remove 60% of tannin which is responsible for bitterness of the juice.

Keywords: Tannase, CCD, Indian gooseberry juice, Purification, SDS-PAGE.





Himani Oza et al.,

INTRODUCTION

Tannase or tannin acyl hydrolases (EC 3.1.1.20) are well known enzymes for catalyzing the hydrolysis of ester and despite linkages in hydrolyzable tannins like tannic acid with sugar and gallic acid production. Tannase generally found in a variety of items, including instant tea, beer, wine, coffee-flavored soft drinks, and other beverages. The by product of tannase i.e., gallic acid plays an important role in food and pharmaceutical industries as an initial component for synthesizing propyl gallate and trimethoprim [1]. Typically moulds such as *Aspergillus*, *Penicillium*, *Fusaria*, and *Trichoderma* as well as yeast *Saccharomyces cerevisiae* are identified as the potential tannase producers. Several bacterial genera are also found with tannase production *Bacillus*, *Corynebacterium*, *Lactobacillus*, and *Serratia* [2]. *Aspergillus* species are mostly used to synthesize tannase at industrial levels by submerged fermentation (SmF). The SmF is widely used in the manufacture of enzymes because it provides several benefits, including homogeneous process conditions in bioreactors, such as concentration, temperature, pH, aeration, and agitation. Furthermore, the use of agricultural and industrial wastes gives alternate substrates while also reducing pollution by reducing the demand for waste disposal. The type of substrate utilised is the most important aspect in defining fermentation processes, and its selection is determined by a number of factors, the most important of which are cost and availability. As a result, screening a variety of agro-industrial leftovers may be required. The conventional method one-factor-at-a-time to optimize nutritional components is now replaced by more efficient statistical methods to get the accurate optimal production [3].

Therefore, to verify the enzyme's commercial viability, both the adjustment of growth conditions in a bioreactor and the purification of the enzyme are required. Thus, the goal of this study was to look into the bioconversion of Indian gooseberry juice for tannase synthesis, as well as the statistical optimization of fermentation processing conditions for maximal production, purifications, characterization, and probable application in juice clarification.

MATERIALS AND METHODS

Microorganism and growth conditions

The tannase producing fungal isolate HP-6 used in present study was isolated from farm soil, Ahmedabad. Morphological and microscopical studies were carried out to recognize the HP-6; furthermore 18S rRNA sequencing was done to identify the isolate. The isolate was maintained by periodic transfer on potato dextrose agar (PDA) slants supplemented with 1% (w/v) tannic acid at 4°C.

Inoculum Preparation

A young spore suspension of *A. niger* HP-6 was prepared by harvesting the 4 days sporulated culture from PDA slants using distilled water containing 0.1% (v/v) Tween 80. The suspension was vortexed and diluted appropriately to count the spores using Neuber's Chamber ($\approx 1 \times 10^8$ spores/ml). After that, the spore solution was cultivated for 1 hour at 4°C in a synchronous manner. This suspension was used as an inoculum for submerged tannase production.

Tannase assay and protein estimation

The tannase activity was measured by modified rhodanine colorimetric assay described by Sharma *et al.* [4]. This assay is based on the production of chromogen by the reaction that occurs between gallic acid and rhodanine. An appropriately diluted 0.1 ml of crude enzyme was added in 1.0 ml of 0.01 M tannic acid prepared in 0.05 M citrate buffer (pH 5.5) and incubated at 55 °C in boiling water bath for 20 min. The reaction was stopped by immediate addition of 0.2 ml of potassium hydroxide (0.5 M). After that, 0.3 ml methyl rhodanine (0.667 %, w/v) was added and mixed. Then, 4.0 ml distilled water was used to dilute the solutions color and the absorbance was measured at 520 nm. The control tube was prepared in similar manner without enzyme. The amount of gallic acid produced was estimated by performing a standard calibration curve of gallic acid (0-500 µg). One unit of enzyme is defined as the amount of enzyme required to release 1 µmol of gallic acid per minute under standard conditions. The protein



**Himani Oza et al.,**

content was determined by Folin-Lowry method[5]. Tyrosine (0-100 mg/ml) was used to prepare the standard calibration curve of protein.

Statistical optimization of tannase production

Production of tannase by optimized medium

The basal medium of 50 ml containing potato dextrose broth was inoculated with 5% (v/v) of 1×10^8 spores/ml and incubated at 30°C, 120 rpm on a rotary shaker for 48 h. After incubation, the sample was withdrawn and checked for tannase activity as mentioned in above section.

Despite the basal medium several factors like, tannic acid concentration, nitrogen source and carbon source were also optimized for tannase production. To study the effect of varied concentrations of tannic acid basal medium was supplemented with 0.25, 0.5, 0.75, 1.0, and 1.5% (w/v) tannic acid and the other production conditions were kept constant. Nitrogen sources like, peptone, yeast extract, and malt extract with 0.5% (w/v) and ammonium sulphate, and sodium nitrate with 0.3% (w/v) concentration were added in basal medium for tannase production[6]. Similarly, basal medium containing different carbon sources viz., sucrose, fructose, starch, glucose, and lactose with 0.5% (w/v) concentration were also studied to check their effect on tannase production. In contrast of these expensive components various agricultural products namely, *Phyllanthus emblica* (Indian gooseberry or Amla), *Terminalia chebula* (Harde), and *Terminalia bellirica* (Behda) juices were also used directly as the production medium without adding any other compound to produce tannase. Fifty milliliter of various juice/extract were directly inoculated with 5% (v/v) of 1×10^8 spores/ml and incubated at 30°C, 120 rpm on a rotary shaker for 48 h.

Central composite design

Central composite design (CCD) was carried out to determine the effect of different nutritional factors on tannase production by *A. niger* HP-6 after one-factor-at-a-time optimization. Three nutritional factors i.e., Indian gooseberry juice (A), starch (B), and peptone (C) were selected based on the one-factor-at-a-time study as an independent variable to study their interaction effect on tannase production (Tab 1). Other than the varying components, 0.5% (w/v) of sucrose was kept constant and the final volume of production broth was set to 100 ml with distilled water in all the experimental runs. Design-Expert Software (Version 13.0.1.0, State-Ease, Minneapolis, USA) was used to design and analyze the experiments in this study, which included a total of 20 runs.

In a 250 ml Erlenmeyer flask, 100 ml production medium (pH 6.0) supplemented with varied concentrations of Indian gooseberry juice, starch, and peptone (A, B, and C as designed by software) was prepared (Tab 2). The medium was inoculated with 3 ml of freshly prepared spore suspension (1×10^8 spore/ml) of *A. niger* HP-6 and incubated at 30 °C for 48 hours at 120 rpm. Samples were taken and centrifuged at 10,000 rpm for 10 min. The collected cell-free supernatant was used as a crude enzyme to determine the tannase production (above section). All quantitative estimate tests were carried out in triplicates ($n = 3$), and the results, together with error values, were represented as Standard Error of Mean (SEM) in GraphPad Prism 6.0 software. The two-way ANOVA approach in GraphPad Prism 6.0 was used for statistical analysis.

Validation study

Amongst the solutions provided by the Design Expert Software v. 13.0, the one with highest tannase production was performed to confirm the increased production. Hundred milliliter of sterile optimum production medium containing 1% (v/v) Indian gooseberry juice, 1.2% (w/v) starch, and 0.6% (w/v) peptone was prepared. Sucrose was kept constant with 0.5% (w/v) and the initial pH was maintained at 6.0. The production medium was inoculated with 3 ml of fresh spore suspension (1×10^8 spore/ml) and incubated at 30 °C for 48 hours at 120 rpm. Samples were taken after incubation and checked for tannase production by assay mentioned above. The experiment was predicted to produce 5.12 U/ml of tannase.



**Himani Oza et al.,****Purification of Tannase****Ammonium sulfate precipitation**

The enzyme was partially purified using ammonium sulphate precipitation. Cell-free supernatant was precipitated using solid ammonium sulfate (enzyme grade) to achieve 30% and 70 % saturation at 4°C. This mixture was gently stirred to get better dissolution of ammonium sulfate which helps the proteins in salting out. Then, the mixture was left at 4°C undisturbed for overnight in order to enhance the stabilization and precipitation of the protein. Centrifugation was carried out at 10,000 rpm for 15 minutes at 4°C to separate the precipitates obtained. The precipitates were collected in form of pellets and re-suspended in the minimal amount of citrate buffer (pH 5.5). The precipitates were further subjected for dialysis to remove the excess salt at 4°C. After dialysis, the collected dialysate was assayed for tannase activity and protein content. This partially purified enzyme was used for subsequent purification procedures [7].

Gel permeation chromatography (Sephadex G-100)

The concentrated protein by ammonium sulphate precipitation was further purified using sephadex G-100 column chromatography. Sephadex G-100 (2%, w/v) was soaked in 0.05 M citrate buffer (pH 5.5) for two days before loading in the glass column (25 × 1.2 cm). Similar buffer was used with flow rate of 2 ml/15 min. to elute the protein obtained after fractional precipitation. Tannase activity and protein content was estimated for each fraction eluted.

Characterization of partially purified tannase**SDS-PAGE**

The molecular weight and purity of tannase were determined using SDS-PAGE. Protein samples (crude enzyme, partly purified enzyme, and refined enzyme) were resolved at 80 V for 3 hours in a 13% (w/v) polyacrylamide gel with 2% (w/v) SDS. Protein samples were stained in 0.1% coomassie brilliant blue R-250 for 15 min. [8].

Determination of K_m and V_{max}

Lineweaver-Burk plot (double reciprocal plot) was used to determine the K_m and V_{max} values for tannase using various concentrations of methyl gallate (10-100 mg/ml) for 20 minutes at 55°C. The studies were done in triplicate, and the activity was evaluated using the usual tannase assay.

Effect of pH

The activity of partially purified tannase was measured at various pH values (4.0-8.0) using a 0.01 M tannic acid as a substrate dissolved in various buffers, including 0.05M citrate buffer for pH 3.0, 4.0, and 5.0; 1M phosphate buffer for pH 6.0; and 0.2M glycine-NaOH buffer for pH 7.0, and 8.0. The reaction mixture was incubated in a water bath for 20 minutes at 55°C to determine the optimal pH. Following that, the enzyme activity was determined using a conventional tannase assay.

Effect of temperature

Using 0.01 M tannic acid solution, reaction mixtures were incubated at different temperatures ranging from 30 to 70°C to investigate the effect of temperature for 20 min. on partly purified tannase. The enzyme activities were then determined as previously described assay.

Effect of metal ions

Different metal ions i.e., Mn^{+2} and Mg^{+2} in sulfide form, and Ca^{+2} , Fe^{+3} , and Hg^{+2} in chloride form were used to check the effect of metals on enzyme activity. The partially purified enzyme was pre-incubated with different metal ions (10 mM concentration) for 1 hour before adding the substrate at room temperature. Then, tannase assay was performed to measure the relative activity against the control (without metal ion exposure).



**Himani Ozaet al.,****Effect of surfactant and organic solvents**

The effect of different surfactants (tween-80, tween-20, and SDS) and organic solvents (acetone, methanol, propanol, and formaldehyde) on enzyme activity was investigated by incubating the partially purified enzyme with 5 mM concentration for 1 hour at room temperature before adding substrate. The tannase assay was performed to measure the relative activity against the control (without addition of surfactant/solvent).

Effect of inhibitors

P-chloromercuribenzoic acid (PCMB), Dithiothreitol (DTT), N-bromosuccinimide (NBS), Ethylenediaminetetraacetic acid (EDTA), and Phenylmethylsulfonyl fluoride (PMSF) were used with 10 mM concentration. The enzyme (0.1 ml) was pre-treated with inhibitors for 1 hour at room temperature, then incubated after adding the substrate. The relative tannase activity of partially purified HP-6 was measured by tannase assay (above section).

Clarification of fruit juices

The Indian gooseberry juice and pomegranate fruit juice was collected by smashing it in a blender, and followed by squeezing through clean cheesecloth. 10 ml of each fruit juice was treated with 1 U/ml of partially purified enzyme at room temperature to remove tannin. 1 ml sample was withdrawn from each fruit juice at different time intervals (2, 4, 6, 12, and 24 hours) for Folin-Denis residual tannin measurement[9].

RESULTS**Microorganism**

The potential isolate HP-6 was recognized as *Aspergillus* sp. based on its morphological and microscopical studies (figure 1). Further identification by 18S rRNA sequencing (figure 2) discovered the isolate as *Aspergillus niger* HP-6 (accession No. ON259934) with 100% similarity.

Statistical optimization of tannase production**Production of tannase by optimized media**

The basal medium showed tannase production of 4.59 U/ml, while it was slightly increased with addition of 0.75% (w/v) tannic acid i.e., 5.04 U/ml. Amongst the tested nitrogen sources 0.5% (w/v) peptone was found to be the best supporting component for tannase production with 5.99 U/ml. Furthermore, 0.5% (w/v) of sucrose also enhanced the production (2.84 U/ml). Next, amid the natural sources of tannin Indian gooseberry juice was found with enhanced tannase production of 6.0 U/ml. The other two *Terminalia chebula* (Harde) and *Terminalia bellirica* (Behda) also showed good amount of tannase activity i.e., 5.81 and 5.01 U/ml. This experiment proves that the natural tannin source like Indian gooseberry juice can support the maximum tannase production without addition of any other component, and ultimately affects the production expenses of the tannase. A comparative study was carried out to check the production ability of optimized media (10.11 U/ml) and optimized media supplemented with Indian gooseberry juice (6.98 U/ml). Both the medium have been shown closely related enzyme activity. Thus, we can replace the expensive components with such cheap and easily available products for tannase production. From the one-factor-at-a-time observations, Indian gooseberry juice, peptone, starch, and sucrose were selected as the best components and further studied for tannase production by *A. niger* HP-6.

Central composite design

The second-order polynomial equation for the response surface method (RSM) was used to determine the effect of the experimental variables (i.e., varying concentrations of Indian gooseberry juice, starch, and peptone) and their interactions on the response to tannase production by *A. niger* HP-6. The CCD of 20 randomized runs is shown in Tab 2, along with the tannase production responses. Standard run orders 10 with Indian gooseberry juice (1.30%; v/v), starch (1.1%; w/v), and peptone (0.55%; w/v) combinations produced a maximum of 5.50 units of tannase activity (Tab 2). The second order polynomial model describing the effect of independent variables on tannase activity is measured by the following formula,



**Himani Ozaet al.,**

$$\text{Tannase} = + 4.66 + 0.4595 \times A + 0.1363 \times B + 0.4483 \times C + 0.2187 \times AB - 0.2713 \times AC - 0.4963 \times BC - 0.0461 \times A^2 - 0.7514 \times B^2 - 0.2882 \times C^2$$

Where, A = Indian gooseberry juice

B = Starch

C = Peptone

Employing design expert software, the appropriate model was identified during the analysis of response data via a fit summary report (Tab 3). Fit summary plots, ANOVA, and model diagnostic plots analysis for tannase production responses from isolates *A. niger* HP-6 revealed that the quadratic model fits with each of these four responses. With a p-value of less than 0.05, the quadratic model was substantially above the >90% confidence threshold in all situations. From the ANOVA analysis, model F-value of 19.78 showed very high confidence level with the corresponding p value of < 0.0001. The experiment is showing linear effect of Indian gooseberry juice, starch, and peptone as well as the interaction effect of tannase with significance. Similarly, the quadratic model's Lack of Fit F-value was >4.0, indicating that the Lack of Fit was not significant. Furthermore, the coefficient of determination R² value of the model is 0.8989, which is near to the predicted value 0.6863. This R² value suggest that the model is able to explain 89.89% of the data variability.

Figure 3 showed 2D response surface plots of tannase production interaction to Indian gooseberry juice, starch, and peptone for *A. niger* HP-6. Each plot's highest tannase response values were tracked using axis modifications. The maximum tannase response was reported from *A. niger* HP-6 when moderate concentrations of Indian gooseberry juice (1%; v/v), starch (2%; w/v), and peptone (0.1%; w/v) were used.

The interaction effect of Indian gooseberry juice and starch indicates that higher concentrations of both Indian gooseberry juice and starch have favorable impact on tannase production (Figure 3a). Figure 3b showing the moderate effect of peptone and Indian gooseberry juice on the tannase activity; while starch (Figure 3c) showed profound interaction effect on tannase production irrespective to the peptone concentration. Overall observation revealed that Indian gooseberry juice have most significant effect on tannase production amongst the all three components varied, and the combination of starch and Indian gooseberry juice have positive interaction effect. As a result, a combination of these components can elicit the synthesis of tannase in a single setup, lowering manufacturing costs. Furthermore, the point prediction analysis was used to produce the best possible output for both.

Validation study

The optimized parameters suggested by the model i.e., 1% (v/v) Indian gooseberry juice, 1.2% (w/v) starch, and 0.6% (w/v) peptone were kept at 48 hours to validate the study. The experiment was found successful with 5.01 U/ml of tannase, which is very close to the predicted value i.e., 5.12 U/ml.

Purification of tannase

Ammonium sulphate precipitation

Optimum production of tannase by *Aspergillus niger* HP-6 was carried out as discussed earlier and the cell-free supernatant i.e., crude tannase was subjected for subsequent purification. The protein precipitates were concentrated through ammonium sulphate fractionation. The protein pellets of 0-30% and 30-70% both showed tannase activity with 9.71% and 52.10% yield, respectively (Tab 4).

Gel permeation chromatography

The next step of tannase purification by gel permeation chromatography exhibited tannase elution curve with highest peak i.e., showing maximum tannase activity in Figure 4. The active fractions (fractions no. 11-13) were mixed and dialyzed against citrate buffer. It was observed with 38.49% of yield and 7.24-fold purification (Tab 4).



**Himani Ozaet al.,**

Most tannase purification techniques include three or more stages, such as protein concentration through ammonium sulfate precipitation, dialysis, and/or gel permeation chromatography.

Characterization of partially purified tannase

SDS-PAGE

SDS-PAGE, sodium dodecyl sulfate-polyacrylamide gel electrophoresis is widely used for identification, screening and determine the homogeneity of the purified/partially purified protein fractions. The partially purified tannase from *A. niger* HP-6 showed band of protein on 13% polyacrylamide gel stained with coomassie brilliant blue R250 (Figure 5), which indicates the presence of a monomer protein with an estimated molecular mass of 50 kDa.

Determination of K_m and V_{max}

The velocity versus substrate (tannic acid) concentration from 0.05 to 0.5 mM was plotted on a double reciprocal Line weaver-Burk plot to yield the K_m and V_{max} values (Figure 6) for tannase. The K_m and V_{max} values for tannase were 0.11 μM and 10.24 μMmin^{-1} , respectively. The higher K_m value corresponds to lower affinity for the substrate and so as the reaction rate.

Effect of pH

The effect of pH value (varied from 4.0 to 8.0) on partially purified enzyme activity (Figure 7) revealed that the optimal pH value for tannase activity was 6.0 (1 M phosphate buffer) with 72.89% residual activity. The enzyme showed lowest activity in both highly acidic and moderately alkaline range i.e., pH 4.0 and pH 8.0.

Effect of temperature

The activity of the partially purified tannase increased from 30°C to 40°C and start decreasing afterwards, hence 40°C was selected as the optimal temperature for tannase activity by *A. niger* HP-6 (Figure 8). It showed that the tannase can tolerate the higher temperature, but gradually decrease the activity around 48.70% and 60.90% as the temperature increased (50-70°C).

Effect of metal ions

The effect of various metal ions on purified tannase was studied with 1.0 mM concentration for 1 hour at room temperature. The experiment showed that Mg^{2+} and Mn^{2+} supports the tannase activity while, Fe^{3+} , Ca^{2+} , and Hg^{2+} have inhibitory effect (Figure 9).

Effect of surfactants and organic solvents

The effect of surfactants like SDS (28.19 %), Tween 20 (43.23 %), and Tween 80 (65.5 %) on tannase activity was shown in Figure 10. All the surfactants have detrimental effects on the purified tannase from *A. niger* HP-6. The findings revealed that surfactants influenced the protein hydrophobic interactions and hence results in a loss of partial enzyme function. Similarly, after 60 minutes of incubation, a solvent concentration of 5 mM had a detrimental effect on tannase activity (Figure 11). The tannase activity retains at 32.78%, 45.12%, 59.34%, and 68.34% in the presence of different solvents such as propanol, methanol, formaldehyde, and acetone, respectively.

Effect of inhibitors

P-chloromercuribenzoic acid (PCMB), Dithiothreitol (DTT), N-bromosuccinimide (NBS), Ethylenediaminetetraacetic acid (EDTA), and Phenylmethylsulfonyl fluoride (PMSF) were used with 10 mM concentration. The relative tannase activity of partially purified HP-6 was inhibited drastically by dithiothreitol (approximately 70%) as shown in Figure 12. DTT, generally known for preventing the intramolecular and intermolecular disulfide bonds form between the cysteine residues of proteins. This can be correlated with the inhibitory effect of DTT on tannase, that tannase possibly contain the cysteine residues. PCMB and EDTA showed approximately equal inhibition, which is more than the NBS. In contrast of these inhibitors, PMSF supported maximum relative tannase activity with less inhibitory effect.



**Himani Ozaet al.,**

Clarification of fruit juices

Indian gooseberry and pomegranate juices were tried to be clarified by tannase and other enzymes. Tab 5 shows that after 24 hours of incubation at 37°C with 1 ml of partly purified tannase (1 U) the tannin content of both fruit juices was decreased by approximately 66.24% and 60.17%. It was observed that in the initial phase the enzyme was more active and continuously reduced the tannin content, but as time increased the enzyme got inactivated, possibly due to environmental stress and a slow-down in de-bittering. The decrease in tannin content indicates a reduction in the bitter taste of fruit juices.

DISCUSSION

The present study deals with the optimization, purification, characterization, and application of tannase produced by *Aspergillus niger* HP-6, a potential soil isolate. HP-6 isolate was determined through 18S rRNA sequencing with the closest match with *Aspergillus niger* (MK89555.1) and identified as *A. niger* HP-6. Recent studies discovered *A. niger* as the potential tannase producer [10,11]. The optimization by CCD, successfully increased the tannase production from 4.59 U/ml in basal media to 5.01 U/ml using Indian gooseberry juice as the main component. A statistical optimization of tannase by *A. niger* showed 19.7 U/ml production with 5% tannic acid in submerged production [10]. Tannase was purified using ammonium sulphate precipitation and gel permeation chromatography with 52.10% and 38.49% yield. The molecular weight of partially purified tannase was found to be 50 kDa through SDS-PAGE. Lal and Gardner [11] and Roushdy *et al.* [12], showed similar results for *A. niger* and *A. flavus* var. *columnaris* tannase, respectively. On the other hand, this finding contradicts that of Mahmoud *et al.* [13], who claimed that the migration of *Enterococcus faecalis*, *Porphyromonas verrucosum*, and *Aspergillus niger* MTCC5889 tannases on SDS-PAGE as a single band with molecular weights of 45, 81, and 89.9 kDa, respectively. Furthermore, Marco *et al.* [14] detected three bands on SDS-PAGE with molecular weights of 50, 75, and 100 kDa, but Gonçalves *et al.* [15] reported that the molecular weight of *Emericella nidulans* tannase was 302 kDa after gel filtration, with two protein bands (45.8 and 52 kDa) on SDS-PAGE.

The K_m and V_{max} values for *Aspergillus niger* HP-6 tannase were 0.11 μM and 10.24 μMmin^{-1} , respectively, while the other tannase from *A. niger* were reported with K_m values of 6.4×10^{-4} , 6.8×10^{-4} , and 6.0×10^{-4} mM; and V_{max} values were 0.84, 0.87, and 0.74 mole/min/ml respectively, during submerged, liquid-surface, and solid-state fermentation [15]. However, K_m values of 0.7×10^{-4} and 2.0×10^{-4} mM for semi-solid and submerged fermentation, were reported in another study from the same species [16]. The tannic acid K_m findings include showed 2.3×10^{-5} mM for *A. niger* GH1 [14]. Additional findings described partially purified tannase work efficiency at pH 6 and 40°C temperature. The tannase activity was enhanced by the presence of Mg^{2+} and Mn^{2+} , but other metal ions, surfactants, and solvents severely decrease the activity. The ideal pH values for tannase, according to several researchers are between 5.0 and 6.0. The optimal temperature for partially purified tannase enzymes generated by *A. tamari*, *A. nomius* GWA5, *Penicillium* sp. EZ-ZH190, *A. flavus* var. *columnaris*, and *Kluyveromyces marxianus* are substantially higher [17,18]. At a concentration of 1.0 mM, Mg^{2+} , Mn^{2+} , Ca^{2+} , Na^+ , and K^+ promoted tannase activity, but Cu^{2+} , Fe^{3+} , and Co^{2+} inhibited tannase activity from *A. awamori* MTCC 9299 [10]. According to [16], Fe^{3+} inhibited tannase from *A. niger* GH1, but Cu^{2+} and Zn^{2+} had only a minor inhibitory effect and Co^{2+} enhanced tannase activity. Mukherjee and Banerjee [19] discovered that the presence of Mg^{2+} at low concentration increased tannase activity, while tannase was maximally inhibited by Hg^{2+} followed by Fe^{3+} , Zn^{2+} , and Ba^{2+} . The study of heavy metal on tannase from *A. niger* ATCC 16620 found that the addition of metal ions such as Zn^{2+} , Mn^{2+} , Cu^{2+} , Ca^{2+} , Mg^{2+} , and Fe^{2+} inhibited the tannase activity [20]. Non-specific binding or aggregation of the tannase would be the cause of tannase activity inhibition in the presence of divalent cations.

Tween 80 fully suppressed the action of *A. foetidus* tannase [21]. The results of present study are consistent with prior research on *R. oryzae* tannase [22]. Organic solvents such as chloroform, acetic acid, isopropyl alcohol, isoamyl alcohol, and ethanol completely inhibited tannase from *A. awamori*, according to Chhokar *et al.* [18]. Butanol and benzene, on the other hand, boosted enzyme activity. After 60 minutes, tannase from the *P. variable* preserved more





Himani Oza et al.,

than 60% of its residual activity in 20% v/v of carbon tetrachloride, heptane, petroleum ether, and toluene [23]. This tannase also clarified approximately 60% of tannin content from the Indian gooseberry juice and pomegranate juices; that ultimately reduces the bitterness of the juice. Tannase from *A. carneus* URM5577 reported for clarifying 49.66% tannin content from mangaba juice [24]. Andrade *et al.* [25] efficiently reduced 70% tannin from apple juice by clarification.

CONCLUSION

The *Aspergillus niger* HP-6 produced significant tannase using the Indian gooseberry juice as the key medium ingredient and reduces the production cost. This tannase characterized as the effective enzyme and successfully clarified the Indian gooseberry and pomegranate juices. Such properties make the tannase an important candidate for industrial applications, specially in food sector.

ACKNOWLEDGMENT

All the authors kindly acknowledge the infrastructural support provided by the Department of Microbiology & Biotechnology, University School of Sciences, Gujarat University, Ahmedabad.

CONFLICT OF INTEREST STATEMENT

The authors declare that they have no conflict of interest.

COMPLIANCE WITH ETHICAL STANDARDS

This article does not contain any studies with human participants or animals performed by any of the authors.

REFERENCES

1. Govindarajan RK, Revathi S, Rameshkumar N, Krishnan M, Kayalvizhi N. Microbial tannase: Current perspectives and biotechnological advances. *Biocatal Agric Biotechnol.* 2016;6:168-175.
2. Aharwar A, Parihar DK. Tannases: production, properties, applications. *Biocatal Agric Biotechnol.* 2018;15:322-334.
3. Dhiman S, Mukherjee G, Kumar A, Mukherjee P, Verekar SA, Deshmukh SK, *et al.* Fungal tannase: recent advances and industrial applications. *Fungal Biol Rev.* 2017;295-313.
4. Sharma S, Bhat TK, Dawra RK. (2000). A spectrophotometric method for assay of tannase using rhodanine. *Anal Biochem.* 2000;279(1):85-89.
5. Lowry OH, Rosebrough NJ, Farr AL, Randall RJ. Protein measurement with the Folin phenol reagent. *J Biol Chem.* 1951;193:265–275.
6. Oza H, Pardhi D, Raval V, Panchal R, & Rajput K. Screening and Production of Tannase Using Fungal Isolates from Soil. *Biosci Biotechnol Res Commun.* 2020;Special Issue13(1);73-77.
7. Rajput KN, Patel KC, Trivedi UB. A novel cyclodextrin glucano transferase from an alkaliphile *Microbacterium terrae* KNR 9: purification and properties. *3 Biotech* 2016;6:168 DOI 10.1007/s13205-016-0495-6.
8. Prajapati J, Dudhagara P, Patel K. Production of thermal and acid-stable pectinase from *Bacillus subtilis* strain BK-3: optimization, characterization, and application for fruit juice clarification. *Biocatal Agric Biotechnol.* 2021;35:102063.
9. Rout S, Banerjee R. Production of tannase under SSF and its application in fruit juice debittering. *Indian J Biotechnol.* 2006;5(3):346-350.
10. Sharma S, Agarwal L, Saxena RK. Statistical optimization for tannase production from *Aspergillus niger* under submerged fermentation. *Indian J Microbiol.* 2007;47(2):132-138.
11. Lal D, Gardner JJ. Production, characterization, and purification of tannase from *Aspergillus niger*. *European J Exp*





Himani Ozaet al.,

- Biol. 2012;2(5):1430-1438.
12. Roushdy MM, Desouky SE, Esmael ME, El-Louboudy SS, Elshikh HH. (2014). Optimization and characterization of tannin acyl hydrolase produced by *Aspergillus flavus* var. *columnaris* using solid-state fermentation technique. N Y Sci J. 2014;7:88-98.
 13. Mahmoud AE, Fathy SA, Rashad MM, Ezz MK, Mohammed AT. Purification and characterization of a novel tannase produced by *Kluyveromyces marxianus* using olive pomace as a solid support, and its promising role in gallic acid production. Int J Biol Macromol. 2018;107:2342-2350.
 14. Marco MG, Rodríguez LV, Ramos EL, Renovato J, Cruz-Hernández MA, Rodríguez R, Aguilar CN, et al. A novel tannase from the xerophilic fungus *Aspergillus niger* GH1. J Microbiol Biotechnol, 2009;19(9):987-996.
 15. Gonçalves HB, Riul AJ, Quiapim AC, Jorge JA, Guimarães LHS. Characterization of a thermostable extracellular tannase produced under submerged fermentation by *Aspergillus ochraceus*. Electron J Biotechnol 2012;15(5):4-4.
 16. Rana NK, Bhat TK. Effect of fermentation system on the production and properties of tannase of *Aspergillus nigervan Tieghem* MTCC 2425. J Gen Appl Microbiol. 2005;51(4):203-212.
 17. Farag AM, Hassan SW, El-Says AM, & Ghanem KM. Purification, characterization, and application of tannase enzyme isolated from marine *Aspergillus nomius* GWA5. J Pure Appl Microbiol. 2018;12(4):1939.
 18. Chhokar V, Beniwal V, Salar RK, Nehra KS, Kumar A, Rana JS. Purification and characterization of extracellular tannin acyl hydrolase from *Aspergillus heteromorphus* MTCC 8818. Biotechnol Bioprocess Eng.2010;15:793-799.
 19. Mukherjee G, Banerjee R. (2006). Effects of temperature, pH, and additives on the activity of tannase produced by a co-culture of *Rhizopus oryzae* and *Aspergillus foetidus*. World J Microbiol Biotechnol. 2006;22(3):207-212.
 20. Sabu A, Shegal Kiran G, & Pandey A. Purification and characterization of tannin acyl hydrolase from *Aspergillus niger* ATCC 16620. Food Sci Biotechnol. 2005;43(2):133-138.
 21. Naidu RB, Saisubramanian N, Selvakumar D, Janardhanan S, Puvanakrishnan R. (2008). Partial purification of tannase from *Aspergillus foetidus* by aqueous two-phase extraction and its characterization. Curr Trends Biotechnol. 2008;2(1):201-207.
 22. Kar B, Banerjee R, Bhattacharyya BC. Effect of additives on the behavioral properties of tannin acyl hydrolase. Process Biochem. 2003;38(9):1285-1293.
 23. Sharma S, Agarwal L, Saxena RK. Purification, immobilization, and characterization of tannase from *Penicillium variable*. Bioresour Technol. 2008;99(7):2544-2551.
 24. Mergulhão, V., Roberta, C., Fonseca, J., Souza-Motta, C., Sena, A., and Moreira, K. Juice clarification with tannases from *Aspergillus carneus* URM5577 produced by solid-state fermentation using *Terminalia catappa* L. leaves. African J. Biotech. 2017;16:1131-1141. DOI 10.5897/AJB2017.15958
 25. Andrade, P. M. L., Baptista, L., Bezerra, C. O., Peralta, R. M., Góes-Neto, A., Uetanabaro, A. P. T., & Costa, A. M. D. Immobilization and characterization of tannase from *Penicillium rolfisii* CCMB 714 and its efficiency in apple juice clarification. Food Measure. 2021;15:1005-1013.

Table 1 Concentration levels of the variants for CCD

Name	Minimum	Low	Mean	High	Maximum
A: Indian gooseberry juice, % (v/v)	-0.20	0.1	0.55	1.0	1.31
B: Starch, % (w/v)	-0.41	0.2	1.10	2.0	2.61
C: Peptone, % (w/v)	-0.20	0.1	0.55	1.0	1.31





Himani Ozaet al.,

Table 2. CCD design for optimizing tannase production

Std.	A: Indian gooseberry juice%(v/v)	B: Starch % (w/v)	C: Peptone % (w/v)	Predicted Value Tannase (U/ml)	Actual value Tannase (U/ml)
1	0.1	0.2	0.1	1.98	2.12
2	1.0	0.2	0.1	3.01	2.88
3	0.1	2.0	0.1	2.81	3.08
4	1.0	2.0	0.1	4.71	4.92
5	0.1	0.2	1.0	4.41	4.20
6	1.0	0.2	1.0	4.35	4.08
7	0.1	2.0	1.0	3.26	3.38
8	1.0	2.0	1.0	4.07	3.93
9	-0.206807	1.1	0.55	3.76	3.57
10	1.30681	1.1	0.55	5.30	5.50
11	0.55	-0.413614	0.55	2.31	2.59
12	0.55	2.61361	0.55	2.77	2.49
13	0.55	1.1	-0.206807	3.09	2.80
14	0.55	1.1	1.30681	4.60	4.90
15	0.55	1.1	0.55	4.66	4.85
16	0.55	1.1	0.55	4.66	4.75
17	0.55	1.1	0.55	4.66	4.20
18	0.55	1.1	0.55	4.66	4.65
19	0.55	1.1	0.55	4.66	4.80
20	0.55	1.1	0.55	4.66	4.72

Table 3 ANOVA analysis for tannase production

Source	Sum of Squares	df	Mean Square	F-value	p-value	
Model	17.66	9	1.96	19.78	< 0.0001	significant
A-Indian gooseberry juice	2.88	1	2.88	29.07	0.0003	
B-Starch	0.2538	1	0.2538	2.56	0.1408	
C-Peptone	2.74	1	2.74	27.66	0.0004	
AB	0.3828	1	0.3828	3.86	0.0779	
AC	0.5886	1	0.5886	5.93	0.0351	
BC	1.97	1	1.97	19.86	0.0012	
A ²	0.0306	1	0.0306	0.3082	0.5910	
B ²	8.14	1	8.14	82.03	< 0.0001	
C ²	1.20	1	1.20	12.07	0.0060	
Residual	0.9920	10	0.0992			
Lack of Fit	0.7129	5	0.1426	2.55	0.1633	not significant
Pure Error	0.2791	5	0.0558			
Cor Total	18.65	19				





Himani Oza et al.,

Table 4. Purification of tannase

Procedure	Volume (ml)	Total activity (U)	Total Protein (mg)	Specific activity (U/mg)	Yield Enzyme (%)	Purification fold
Crude enzyme	60.0	607.2	750.60	0.808	100	1.00
Ammonium sulphate (0-30% fraction)	4.0	59.0	300.11	0.196	9.71	0.24
Ammonium sulphate (30-70% fraction)	7.0	316.36	284.72	1.111	52.10	1.37
Gel permeation chromatography	8.0	233.77	39.96	5.85	38.49	7.24

Table 5 De-bittering of natural fruit juices

Tannin(mg/ml)	0 h	2h	4h	6h	12h	24h
Indian gooseberry juice	15.91	14.95	13.56	12.55	11.04	10.54
Pomegranate juice	25.74	25.41	23.52	21.33	19.44	15.49

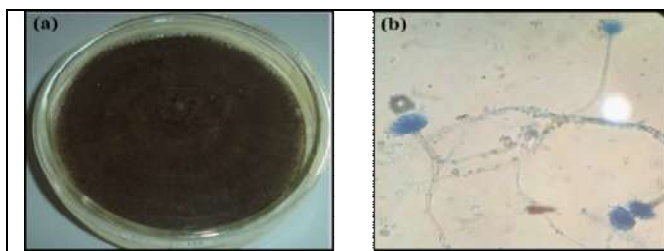


Figure 1 (a) Growth of HP-6 on PDA and (b) Microscopic view of HP-6

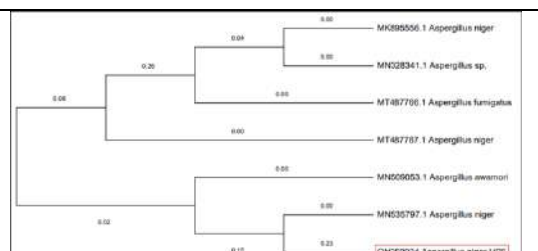


Figure 2 Phylogenetic analysis of HP-6

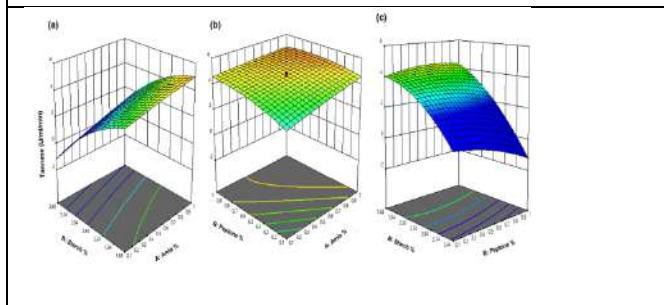


Figure 3 CCD response for variant interaction and tannase production

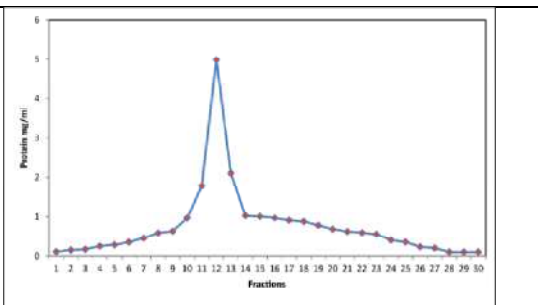


Figure 4 Tannase elution curve from gel filtration chromatography





Himani Ozaet al.,



Figure 5 SDS-PAGE of partially purified tannase: Lane 1, Markers and Lane 2, Purified tannase from ammonium sulphate precipitation

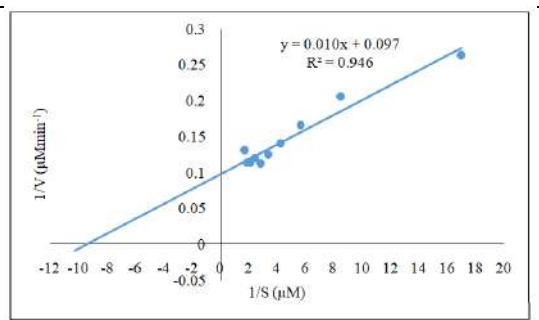


Figure 6 Lineweaver Burk plot of Tannase

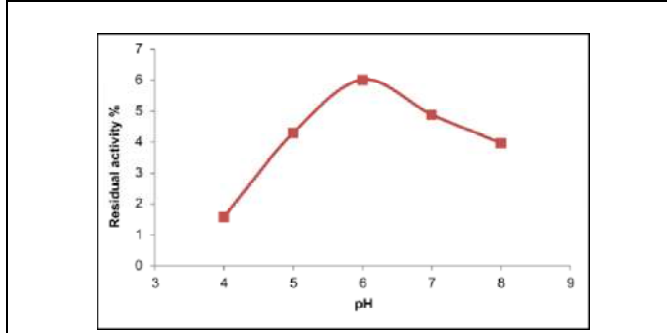


Figure 7 Effect of pH on tannase activity

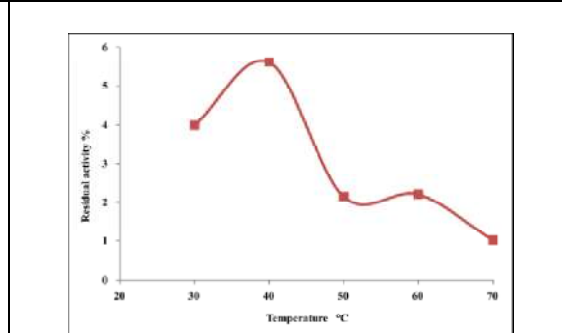


Figure 8 Effect of temperature on tannase activity

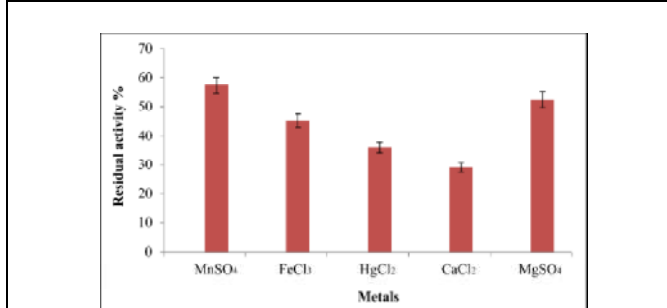


Figure 9 Effect of metal ions on tannase activity

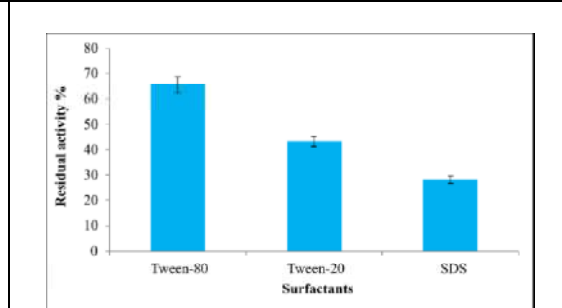


Figure 10 Effect of surfactant on tannase activity

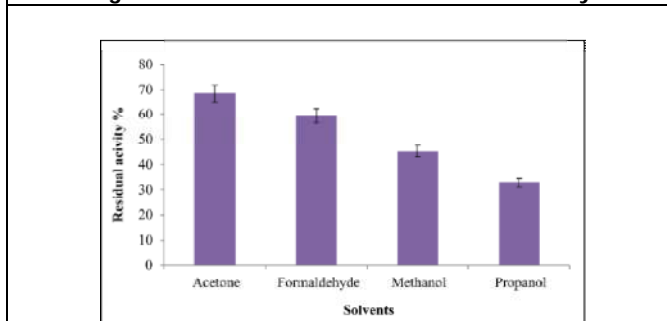


Figure 11 Effect of solvents on tannase activity

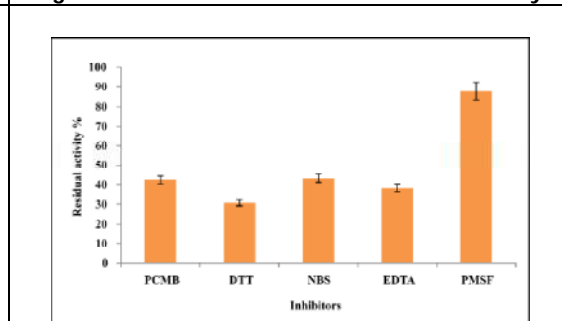


Figure 12 Effect of inhibitors on tannase activity





Palynofloristics from Bhubaneswari Colliery, Talcher Basin, Odisha, India, and its Significance to Age, Palaeovegetation and Palaeoclimate

Suryakanta Rout^{1*}, P.Madesh², Mrutyunjaya Sahoo³, Rajanikant Rout⁴ and DarshanMS¹

¹Research Scholar, Department of Studies in Earth Science, University of Mysore, Karnataka, India

²Professor, Department of Studies in Earth Science, University of Mysore, Karnataka, India

³Ph.D Scholar, Department of Geology, Ravenshaw University, Cuttack-753003, Odisha, India

⁴Research Scholar, Department of Applied Geology, Dr.Harisingh Gour Vishwavidyalaya, Madhya Pradesh, India.

Received: 27 Jan 2023

Revised: 25 Mar 2023

Accepted: 29 Apr 2023

*Address for Correspondence

Suryakanta Rout

Research Scholar,
Department of Studies in Earth Science,
University of Mysore, Karnataka, India
E.Mail: jnvsuryakanta@gmail.com



This is an Open Access Journal / article distributed under the terms of the **Creative Commons Attribution License** (CC BY-NC-ND 3.0) which permits unrestricted use, distribution, and reproduction in any medium, provided the original work is properly cited. All rights reserved.

ABSTRACT

The palynoflora recovered from the thick coal section of Bhubaneswari Colliery (N 20° 96' 20" latitude and E 85° 17' 80" longitude), Talcher Basin, Odisha, India, exhibits a distinct palynoassemblage based on the quantitative and qualitative distribution of different palynomorphs. The recovered palynoassemblage is characterised by the dominance of *Striatopodocarpites* spp. and the subdominance of *Faunipollenites* spp. The other stratigraphically significant taxa in this assemblage are *Scheuringipollenites*, *Faunipollenites*, *Striatites*, *Sulcatisporites*, *Ibisporites*, *Parasaccites*, *Lunatisporites*, *Weylandites*, *Ginkgocycadophytus*, *Densipollenites*, and *Rhizomaspora*. The studied coal section of the Bhubaneswari Colliery has been dated to the Raniganj/Lower Kamthi Formation of Late Permian (Wordian-Capitanian) affinity based on the total palynocomposition. The palynoassemblage also correlates with similar assemblages from other Indian Gondwana basins, like the Damodar, Godavari, and Son-Mahanadi basins of India. Palynofossil evidence indicates the prevalence of warm and humid conditions during the deposition. Glossopterid dominance and subdominance of conifers and cordaites indicate a freshwater depositional environment.

Keywords: Palynology, Palaeoclimate, Permian, Talcher Basin, Odisha.





INTRODUCTION

The Talcher Basin constitutes the south-easternmost part of the Mahanadi Master Gondwana Basin and spreads over Odisha's Dhenkanal, Angul and Sambalpur districts. It is occupied by the Brahmani River valley but is considered part of the Mahanadi Basin due to its geological similarities with the other sub-basins of the master basin. In India, Gondwana sequences are considered non-marine (Goswami et al., 2018; Pillai et al., 2023), however, several marine incursions have been reported from these sequences (Goswami, 2008; Jha et al., 2020; Jha and Sinha, 2022; Mishra et al., 2021; Pillai et al., 2023). The first ever palaeobotanical reports from the Talcher Basin were carried out by Blanford et al. (1859). Several palynological studies were reported from the Lower Gondwana formations of the Talcher Basin (Bhattacharya et al., 2001; Meena, 2003; Tiwari et al., 1991; Tripathi, 1993, 1996, 1997, 2001, 2009; Tripathi and Bhattacharya, 2001; Saxena et al., 2014; Sahoo et al., 2020a, b; Patel et al., 2021, 2022; Aggarwal et al., 2022 a, b; Mishra et al., 2022). The present palynological study was carried out in a coal section of the Bhubaneswari Colliery (N 20° 96' 20" latitude and E 85° 17' 80" longitude) in the Jagannath Area of Talcher Coalfield, Angul district, Odisha (Fig. 1). The colliery is managed by the public-sector company Mahanadi Coal Fields Limited (MCL), a subsidiary of the Coal India Ministry's Navratna Company Coal India Limited. The Bhubaneswari Colliery extends over 658.724 ha (6.584 sq. km.). The study aims to reconstruct the palynostratigraphy of the Lower Gondwana formations of the Talcher Basin based on palynomorphs and to decipher the age, palaeovegetation, and palaeoclimate based on palynofloral assemblages.

GEOLOGICAL SETTING

The Talcher Basin covers 1800 sq. km and is located between latitudes 20° 53' and 21° 12' and longitudes 84° 20' and 85° 23' (Fig. 2). The strike of the basin is in an E-W direction (Toposheet No. 73 H/1; RF 1:50000). It's a strike-slip basin. The Precambrian-Permian boundary in the basin is manifested by WNW-ESE trending faults in the north and an unconformity is exposed in the south (Raja Rao, 1982). The Permo-Triassic Gondwana sediments of this basin belong to the Talchir, Karharbari, Barakar, Barren Measures, Lower Kamthi/Raniganj, and Upper Kamthi formations. The stratigraphic nomenclature of the Talcher Basin is represented in Table 1 (Goswami and Singh, 2013; Sahoo et al., 2020a).

MATERIALS AND METHODS

Six samples (BA, BB, BC, BD, BE and BF) were collected from the new coal section with a total thickness of around 30 m (Fig. 3) to avoid contamination within the Bhubaneswari Colliery and carry out the palynostratigraphic studies. The samples were crushed into small pieces (between two and three millimetres in size), treated with 40% hydrofluoric acid (HF) to dissolve the siliceous components, followed by hydrochloric acid (HCl) to break down the carbonate components, and then repeatedly rinsed with water to remove acids. The resulting demineralised samples were then subjected to a three- to four-day treatment with commercial nitric acid (HNO₃), with periodic additions of fresh HNO₃ (63.09%) to aid in the digestion of humic matter. Before further processing, each sample was inspected under a microscope at each maceration stage. The samples were treated with 10–20% potassium hydroxide (KOH) after being thoroughly washed with water to get clear palynomorphs. Palynomorphs were concentrated, forming the final residue. A few drops of the final residue were used to produce slides and mounted in Canada balsam using polyvinyl alcohol (PVA). Five slides were prepared for each sample. All slides were imaged with a Zeiss Axiocam 208 camera and scanned using a Germany Zeiss Bright Light Microscope at 40X magnification. These slides were kept in the palynology laboratory of the Department of Studies in Earth Science, University of Mysore, India.





Suryakanta Rout et al.,

RESULTS AND DISCUSSION

Palynology

Out of the six collected samples, four were yielding and only two of them (BC and BD) had a countable number of palynomorphs (Fig. 3). The palynomorphs were identified based on their morphological features, and counted (around 200 specimens per sample) to calculate the respective frequency percentage. The quantitative distribution of different types of palynoflora (genus-wise) has been presented in Fig. 4. The list of recovered palynotaxa and their respective botanical affinities are presented in Table 2. Stratigraphically significant taxa of the recovered palynoassemblage are shown in Fig. 5. Based on the quantitative and qualitative distributions of various palynotaxa, one distinct palynoassemblage has been identified from the studies section of Bhubaneswari Colliery.

The palynoassemblage is characterised by the dominance of the striate bisaccate, *Striatopodocarpites multistriatus*, *S. decorus*, *S. diffuses*, *S. magnificus*, *S. subcircularis*, *S. labrus* (46.5%) and the subdominance of *Faunipollenites varius*, *F. magnus* (28.5%), along with some stratigraphically significant taxa: non-striate bisaccate: *Scheuringipollenites maximus* (11%), striate bisaccate: *Striatites tentulus*, *S. incircus* (3%), monosaccate: *Densipollenites indicus*, *D. invisus*, *D. magnicarpus* (2%), *Sulcatiporites tentulus* (1%), non-striate bisaccate: *Ibisporites diplosaccus* (1-2%), and monosaccate: *Parasaccites obscures*, *P. bilateralis*, *P. densus* (2-3%). The other recorded taxa of this palynoassemblage are taeniate *Lunatisporites* sp. (0–0.7%), striate bisaccate: *Rhizomaspota monosulcata*, *R. costa* (1–1.5%), sulcate pollen: *Weylandites lucifer* (0–0.8%) and *Ginkgocycadophytus* (0.5%). The abundance of striate bisaccates (*Striatopodocarpites* spp. and *Faunipollenites* spp.) and different stratigraphically significant taxa *Scheuringipollenites* sp., *Densipollenites* spp., *Striatites* spp., *Weylandites* sp., *Rhizomaspota* spp., and *Lunatisporites* sp. confirm its resemblance with the Raniganj palynoflora of the Late Permian.

This palynoassemblage compares well with the *Striatopodocarpites-Faunipollenites* (Zone V-A) Assemblage Zone of Tiwari and Tripathi (1992) of the Late Permian Raniganj Formation in Damodar Basin. It also compares well with Palynoassemblage-I of Kumunda, Talcher Basin (Sahoo et al., 2020a), Palynoassemblage-I of Gopalprasad, Talcher Basin (Sahoo et al., 2020b), palynoassemblage of the Ustali Area, Ib River Basin (Patel et al., 2020), Palynoassemblage-II of Brajrajnagar area, Ib River Coalfield (Meena et al., 2011), Palynozone-5 of the Lingala-Koyagudem coal belt (Aggarwal and Jha, 2013), Palynoassemblage-E of the Son Basin (Tiwari and Ram-Awatar, 1989), and Palynoassemblage-V of the Chintalapudi sub-basin of Godavari Basin (Jha et al., 2018).

Age demarcation based on palynoassemblage

The abundance of striate bisaccates *Striatopodocarpites* spp. (*S. multistriatus*, *S. decorus*, *S. diffuses*, *S. magnificus*, *S. subcircularis* and *S. labrus*) and *Faunipollenites* spp. (*F. varius* and *F. magnus*) along with the presence of stratigraphically significant taxa, namely *Scheuringipollenites* sp. (*S. maximus*), *Striatites* spp. (*S. tentulus*, *S. incircus*), *Densipollenites* spp. (*D. indicus*, *D. invisus*, *D. magnicarpus*), *Parasaccites* spp. (*P. obscures*, *P. bilateralis*, *P. densus*), *Lunatisporites* sp., *Rhizomaspota* spp. (*R. monosulcata*, *R. costa*), *Ibisporites diplosaccus* and *Weylandites lucifer* confirms its resemblance to the Raniganj palynoflora of Late Permian (Wordian-Capitanian) affinity. Lower Barakar in India contains relatively high quantities of striate bisaccates, and Raniganj/Lower Kamthi in the Late Permian continues to have striate bisaccates as its primary palynofloral component (Sahoo et al., 2020b).

Botanical affinity

The Palynocomposition retrieved from the studied samples of the Bhubaneswari Colliery section, Talcher Basin exhibits 12 genera and 22 species belonging to Glossopteridales (14 taxa: *Striatopodocarpites multistriatus*, *S. decorus*, *S. diffuses*, *S. magnificus*, *S. subcircularis*, *S. labrus*, *Faunipollenites varius*, *F. magnus*, *Scheuringipollenites maximus*, *Striatites tentulus*, *S. incircus*, *Striatites* sp., *Ibisporites diplosaccus* and *Weylandites lucifer*), Coniferales (7 taxa: *Parasaccites obscures*, *P. bilateralis*, *P. densus*, *Parasaccites* sp., *Rhizomaspota monosulcata*, *R. costa* and *Lunatisporites* sp.) and Cordaitales (4 taxa: *Densipollenites indicus*, *D. invisus*, *D. magnicarpus* and *Sulcatiporites tentulus*) (Table 2). Thus, the



**Suryakanta Routet et al.,**

coal-forming vegetation in the studied section is primarily composed of gymnosperms, represented by glossopterids, conifers and cordatites.

Palaeoclimate

Based on morphology and the cumulative abundance of palynomorphs, Tiwari and Tripathi (1987) proposed 11 climatic suits during the deposition of Lower Gondwana sediments. The present *Striatopodocarpites-Faunipollenites* palynoassemblage lies in Suite 8 of the Lower Raniganj and the lower part of the Upper Raniganj assemblages, presenting a warm and very highly humid climate. The dominance non-striated pollens over striated ones also support the aforesaid climatic condition (Tiwari and Tripathi, 1987; Pillai et al., 2023). Botanical affinities of the recovered palynoflora, with the dominance of glossopteridales, contributory presence of cordaitales and coniferales, and absence of spores, also support the warm and highly humid climatic condition and confirm a freshwater environment (Guerra-Sommer et al., 1983; Sahoo et al., 2020b).

CONCLUSIONS

- The recovered palynoflora with a *Striatopodocarpites-Faunipollenites* assemblage confirms the studied sequence to be the Lower Kamthi (Raniganj) Formation of Late Permian (Wordian-Capitanian) affinity.
- The botanical affinities of the recovered palynotaxa exhibit 12 genera and 22 species belonging to 3 different plant groups (Glossopteridales, Coniferales and Cordaitales), where Glossopteridales dominate the assemblage.
- The *Striatopodocarpites-Faunipollenites* palynoassemblage, dominance of glossopteridales and absence of spores, and dominance of non-striate over striate pollens in the sequence suggest a warm and humid climatic condition in a fresh water environment during the Late Permian in Talcher Basin, Odisha.

ACKNOWLEDGEMENTS

The authors are indebted to the Chairman of the Department of Studies in Earth Science, University of Mysore, Karnataka for providing necessary research facilities. The authors are also thankful to Mahanadi Coalfields Limited (MCL) for allowing the sample collection and providing necessary help during the field visit.

REFERENCES

1. Aggarwal, N. and Jha, N. (2013). Permian palynostratigraphy and palaeoclimate of Lingala- Koyagudem Coalbelt, Godavari Graben, Andhra Pradesh, India. *J. Asian Earth Sci.*, v. 64, pp. 38–57.
2. Aggarwal, N., Patel, R. and Goswami, S. (2022a). A study on megafloral, palynofloral, and palynofacies of Barakar sediments at and around Balaram Opencast Coal Project, Talcher Basin, Odisha, India: inferences on palaeodepositional settings, palynodiversity, palaeovegetation, and palaeoclimate. *Arab. J. Geosci.*, v. 15(3), pp. 1-10.
3. Aggarwal, N., Patel, R. and Goswami, S. (2022b). Palaeoclimate, Palaeoecology and Palaeovegetation in and around Nandira Colliery, Talcher Basin, Odisha, India during Early Permian: Inferences from Typical Karharbari Palynofloral and Palynofacies Analysis. *J. Geol. Soc. India*, v. 98(9), pp. 1244-1252.
4. Balme, B.E. (1995). Fossil in situ spores and pollen grains: An annotated catalogue. *Rev. Palaeobot. Palynol.*, v. 87, pp. 81–323.
5. Bhattacharya, A., Nandi, A. and Dutta, A. (2001). Triassic mega and micro-plant fossils from the Kamthi Formation of Talcher Coalfield, Orissa with chronological significance. In: *Proceedings of National Seminar on Recent Advances in Geology of Coal and Lignite Basins of India*, Calcutta, 1997. *Geol. Surv. India Spec. Pub.*, v. 54, pp. 123– 126.
6. Blanford, W.T. (1871). Additional note of plant bearing sandstones of Godavari Valley. *Rec. Geol. Surv. India*, v. 4(3), pp. 59-88.





Suryakanta Rout et al.,

7. Blanford, H. F., Blanford, W.T. and Theobald, W. (1859). Athagarh Sandstones, Orissa. Mem. geol. Surv. India, v. 1, pp. 68-73, 83.
8. Bharadwaj, D.C. and Srivastava, S.C. (1973). Subsurface palynological succession in Korba Coalfield, Madhya Pradesh, India. Palaeobotanist, v. 20(2), pp. 137.
9. Goswami, S. (2008). Marine influence and incursion in the Gondwana basins of Orissa, India: A review. Palaeoworld, v. 17(1), pp. 21-32.
10. Goswami, S., Das, K., Sahoo, M., Bal, S., Pradhan, S., Singh, K. J. and Saxena, A. (2018). Biostratigraphy and floristic evolution of coal swamp floras of a part of Talcher Basin, India: A window on a Permian temperate ecosystem. Arab J Geosci, 11(17), 1–14.
11. Goswami, S. and Singh K.J. (2013). Floral diversity and geology of Talcher Basin, Orissa, India during the Permian-Triassic interval. Geol. J., v. 48, pp. 39–56.
12. Guerra-Sommer, M., Marques-Toigo, M., Paim, P.S.G., Henz, G.I., Skilveira, J.B.R. and Backeuser, Y. (1983). Estudomicoflorístico e petrológico dos carvões da Mina do Faxinal, Formação Rio Bonito (Permiano), RS. Boletim IG-USP, Série Científica, v. 15, pp. 73-83.
13. Jha, N., Aggarwal, N. and Mishra, S. (2018). A review of the palynostratigraphy of Gondwana sediments from the Godavari Graben, India: Global comparison and correlation of the Permian- Triassic palynoflora. J. Asian Earth Sci., v. 163, pp. 1–21.
14. Jha, Y.N. and Sinha, H.N. (2022). Acritarchs-Palynomorphs from the Barren Measures Formation of West Bokaro Coalfield: Implications to Depositional Environment. Journal of Geosciences Research, v. 7(2), pp. 166-171.
15. Jha, Y.N., Sinha, H.N., Patel, R.C. and Chandra, K. (2020). Leiosphaeridia (Acritarchs) from Talchir Formation of West Bokaro Coalfield and its Palaeoenvironmental Significance. Journal of Geosciences Research, v. 5(2), pp. 153-160.
16. Meena, K.L. (2003). *Sporae dispersae* and correlation of Gondwana sediments of Gondwana sediments in Talcher Coalfield, Son-Mahanadi Valley, Orissa. Geophytology, v. 31(1-2), pp. 105-109.
17. Meena, K.L., Jana, B.N. and Aggarwal, N. (2011). Early and Late Permian palynoflora from Lower Gondwana sediments near Brijrajnagar area, Ib-river Coalfield, Orissa. Geophytology, v. 41(1–2), pp. 83–90.
18. Mishra, S., Aggarwal, N. and Jha, N. (2017). Palaeoenvironmental change across the Permian–Triassic boundary inferred from palynomorph assemblages (Godavari Graben, South India). Paleobiodivers Paleoenviron, v. 98(2), pp. 177–204. <https://doi.org/10.1007/s12549-017-0302-3>
19. Mishra, S., Dutta, S., Singh, V. P., Kumar, S., Mathews, R. P. and Jha, N. (2021). A new acritarch spike of Leiosphaeridia *dessicata* comb. nov. emend. from the Upper Permian and Lower Triassic sequence of India (Pranhita-Godavari Basin): its origin and palaeoecological significance. Palaeogeogr. Palaeoclimatol. Palaeoecol., v. 567, pp. 110274.
20. Mishra, D.P., Singh, V. P., Saxena, A., Uhl, D., Murthy, S., Pandey, B. and Kumar, R. (2022). Palaeoecology and depositional setting of an Early Permian (Artinskian) mire based on a multi-proxy study at the Jagannath coal mine (Talcher Coalfield), Mahanadi Basin, India. Palaeogeogr. Palaeoclimatol. Palaeoecol., v. 601, pp. 111-124.
21. Patel, R., Goswami, S., Aggarwal, N. and Mathews, R.P. (2021). Palaeofloristics of Lower Gondwana exposure in Hingula area, Talcher Basin, Odisha, India: an inclusive study on biomarkers, megafloreal and palynofloreal assemblages. Hist. Biol., pp. 1-17.
22. Patel, R., Goswami, S., Aggarwal, N. and Mathews, R.P. (2022). Lower Gondwana megaflorea, palynoflora, and biomarkers from Jagannath Colliery, Talcher Basin, Odisha, India, and its biostratigraphic significance. Geol. J., v. 57(3), pp. 986-1004.
23. Patel, R., Goswami, S., Sahoo, M., Pillai, S.S.K., Aggarwal, N., Mathews, R.P., Swain, R.R., Saxena, A. and Singh, K.J. (2020). Biodiversity of a Permian Temperate Forest: a case study from Ustali area, Ib River Basin, Odisha, India. Geol. J., v. 56(2), pp. 903-933.
24. Pillai, S. S. K., Manoj, M. C., Mathews, R. P., Murthy, S., Sahoo, M., Saxena, A. and Kumar, S. (2023). Lower Permian Gondwana sequence of Rajhara (Daltonganj Coalfield), Damodar Basin, India: floristic and geochemical records and their implications on marine incursions and depositional environment. Environ Geochem Health, pp. 1-31.



Suryakanta Routet *et al.*,

25. Raja Rao, C.S. (1982). Coalfields of India- 2.Coal Resources of Tamilnadu, AndhraPradesh, Orissa and Maharashtra. Bull.Geol. Surv. India Ser. A, v. 45, pp. 9-40.
26. Sahoo, M., Goswami, S., Aggarwal, N. and Pillai, S.S.K. (2020a). Palaeofloristics of Lower Gondwana Exposure near Kumunda Village, Angul District, Talcher Basin, Odisha, India: A comprehensive study on megafloreal and palynofloreal assemblages. J.Geol.Soc.India, v. 95(3), pp. 241–254.
27. Sahoo, M., Aggarwal, N. and Goswami, S. (2020b). Palynological investigation of the Lower Gondwana outcrop near Gopalprasad, Odisha, India: an inference on the age, palaeovegetation and palaeoclimate. J.Palaeontol.Soc. India, v. 65(1), pp. 27-35.
28. Saxena, A., Singh, K.J. and Goswami, S. (2014). Advent and decline of the genus Glossopteris Brongniart in the Talcher coalfield, Mahanadi Basin, Odisha, India. Palaeobotanist, v. 63, pp. 157- 168.
29. Tiwari, R. S. and Ram-Awatar (1989). Sporaedispersae and correlation of Gondwana sediments in Johilla Coalfield, Son Valley Graben, Madhya Pradesh. Palaeobotanist, v. 37, pp. 94–114.
30. Tiwari, R.S. and Tripathi, A. (1987). Palynological zones and their climatic inference in the coal- bearing Gondwana of peninsular India. Palaeobotanist, v. 36, pp. 87–101.
31. Tiwari, R.S. and Tripathi, A. (1992). Marker assemblage zones of spore and pollen species through Gondwana Palaeozoic-Mesozoic sequence in India. Palaeobotanist, v. 40, pp. 194–236
32. Tiwari, R.S., Tripathi, A. and Jana, B.N. (1991). Palynological evidence for Upper Permian Raniganj Coals in the western part of Talcher Coalfield, Orissa, India. Curr. Sci., v. 61, pp. 407–420.
33. Tripathi, A. (1993). Palynosequence in subsurface Permian sediments in Talcher Coalfield, Orissa, India. Geophytology, v. 23(1), pp. 99-106.
34. Tripathi, A. (1996). Early and Late Triassic palynoassemblages from subsurface Supra-Barakar sequence in Talcher Coalfield, Orissa, India. Geophytology, v. 26(1), pp. 109-118.
35. Tripathi, A. (1997). Palynostratigraphy and palynofacies analysis of subsurface Permian sediments in Talcher Coalfield, Orissa. Palaeobotanist, v. 46, pp. 79–88.
36. Tripathi, A. (2001). Palynological expression about Permian-Triassic transition in the Talcher Coalfield, Orissa, India. Palaeobotanist, v. 50, pp. 247-253.
37. Tripathi, A. (2009). Palynology of the Brahmani River Section, Talcher Coalfield, Orissa, India. J.Palaeontol.Soc. India, v. 54, pp. 179–187.
38. Tripathi, A. and Bhattacharya, D. (2001). Palynological resolution of Upper Permian sequence in Talcher Coalfield, Orissa, India. Proceedings of National Seminar on Recent Advance in Geology of Coal and Lignite Basins of India, Calcutta, 1997. Geol. Surv. India Spec. Pub.

Table 1 Stratigraphic nomenclature of Talcher Basin, Odisha (after Goswami and Singh, 2013; Sahoo *et al.*, 2020a)

Age	Formation	Lithology and fossil content	Thickness
Recent		Alluvium and laterite	
Triassic	Upper Kamthi	Upper bed (Late Triassic): Ferruginous, hard and quartzitic sandstones, bands of compact brown, grey and yellow shales and clasts of lavender and creamy white shales. Palynoassemblage includes <i>Brachysaccus</i> , <i>Rimaesporites</i> , <i>Samaropollenites</i> and <i>Callialasporites</i> .	250 + meters
		Lower bed (Early Triassic): Medium-grained, cross-bedded ferruginous yellowish white sandstones, alternating with thick bands of red and grey shales. Palynoassemblage includes <i>Striatopodocarpites</i> , <i>Satsangisaccites</i> , <i>Falcisporites</i> , <i>Weylandites</i> , <i>Muraticavea</i> , <i>Lundbladispora</i> , <i>Arcuatipollenites</i> , <i>Playfordiaspora</i> and <i>Alisporites</i>	
Late Permian	Lower Kamthi/ Raniganj	Medium to coarse grained, pebbly cross-bedded ferruginous sandstones, clasts of greenish-white and grayish-white shales, carbonaceous and grey shales, pink clays. Palynoassemblage is dominated by <i>Striatopodocarpites</i> , <i>Faunipollenites</i> and <i>Crescentipollenites</i> .	





Suryakanta Rout et al.,

Middle Permian	Barren Measures	Coarse to medium grained greenish grey feldspathic sandstones with shreds and lenses of chocolate coloured clay, micaceous siltstone, dark grey shale, carbonaceous shale, purple brown shale and clay ironstone. Palynofloral assemblage is dominated by <i>Densipollenites</i> and <i>Striatopodocarpites</i>	317+ meters
Early Permian	Barakar	Fine to coarse grained feldspathic whitish sandstones, siltstone, grey shale, sandy shale, fireclay and coal seams with polymictic conglomerate at the base. Palynoassemblage is dominated by <i>Scheuringipollenites</i> , <i>Faunipollenites</i> and <i>Striatopodocarpites</i> .	600 meters
Early Permian	Karharbari	Medium to Coarse grained whitish arkosic sandstones, carbonaceous shale, grey shale and coal seams. Palynoassemblage is dominated by <i>Parasaccites</i> , <i>Microbaculispora</i> and <i>Brevitriletes</i>	270 meters
Early Permian	Talchir	Diamictites, rhythmities, turbidites, conglomerate, fine to medium-grained greenish sandstones, olive coloured needle shales, turbidite, tillites and tilloids etc. Palynoassemblage is dominated by <i>Plicatipollenites</i> , <i>Potonieisporites</i> and <i>Caheniasaccites</i> .	170+ meters
----- Unconformity -----			
Precambrian	Granites, gneisses, amphibolites, migmatites, quartzite and pegmatites etc.		

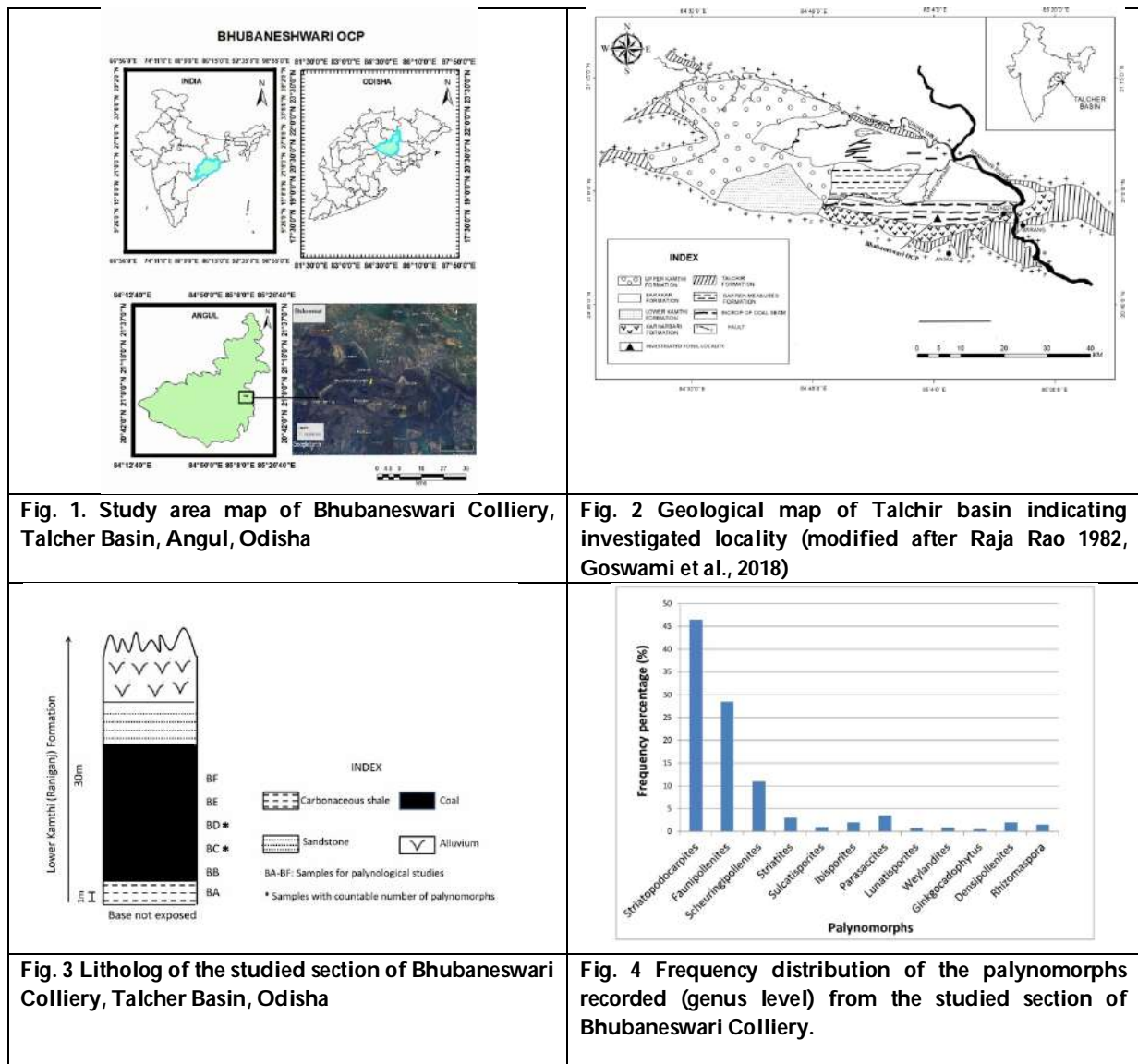
Table 2. List of palyno-taxa recorded in the Bhubaneswari Colliery section and their respective botanical affinities (Balme, 1995; Mishra et al., 2017; Sahoo et al., 2020b)

Palynotaxa	Botanical affinity
<i>Scheuringipollenites maximus</i> (Hart) Tiwari, 1973	Glossopteridales
<i>Weylanditeslucifer</i> (Bharadwaj and Salujha) Bharadwaj and Dwivedi, 1981	Glossopteridales
<i>Faunipollenites varius</i> Bharadwaj, 1962	Glossopteridales
<i>Faunipollenitesmagnus</i> (Bose and Kar) Tiwari et al. 1989	Glossopteridales
<i>Striatopodocarpites multistriatus</i> Jha, 1996	Glossopteridales
<i>Striatopodocarpites decorus</i> Bharadwaj and Salujha, 1964	Glossopteridales
<i>Striatopodocarpites diffuses</i> Bharadwaj and Salujha, 1964	Glossopteridales
<i>Striatopodocarpitesmagnificus</i> Bharadwaj and Salujha, 1964	Glossopteridales
<i>Striatopodocarpites subcircularis</i> Sinha, 1972	Glossopteridales
<i>Striatopodocarpiteslabrus</i> Tiwari, 1965	Glossopteridales
<i>Striatitestentulus</i> Tiwari, 1965	Glossopteridales
<i>Striatitesincircus</i> Maithy, 1965	Glossopteridales
<i>Striatites</i> sp.	Glossopteridales
<i>Ibisporitesdiplosaccus</i> Tiwari, 1967	Glossopteridales
<i>Parasaccites obscures</i> Tiwari, 1965	Coniferales
<i>Parasaccitesbilateralis</i> Tiwari, 1965	Coniferales
<i>Parasaccitesdensus</i> Maheshwari, 1967	Coniferales
<i>Parasaccites</i> sp.	Coniferales
<i>Rhizomaspora monosulcata</i> Tiwari, 1967	Coniferales
<i>Rhizomaspora costa</i> Wilson, 1962	Coniferales
<i>Lunatisporites</i> sp.	Coniferales
<i>Densipollenites indicus</i> Bharadwaj, 1962	Cordaitales
<i>Densipollenites invisus</i> Bharadwaj and Salujha, 1964	Cordaitales
<i>Densipollenites magnicarpus</i> Tiwari and Rana, 1981	Cordaitales
<i>Sulcatisporitestentulus</i> Tiwari, 1967	Cordaitales
<i>Ginkgocycadophytus</i> sp.	?





Suryakanta Rout et al.,





Suryakanta Rout et al.,

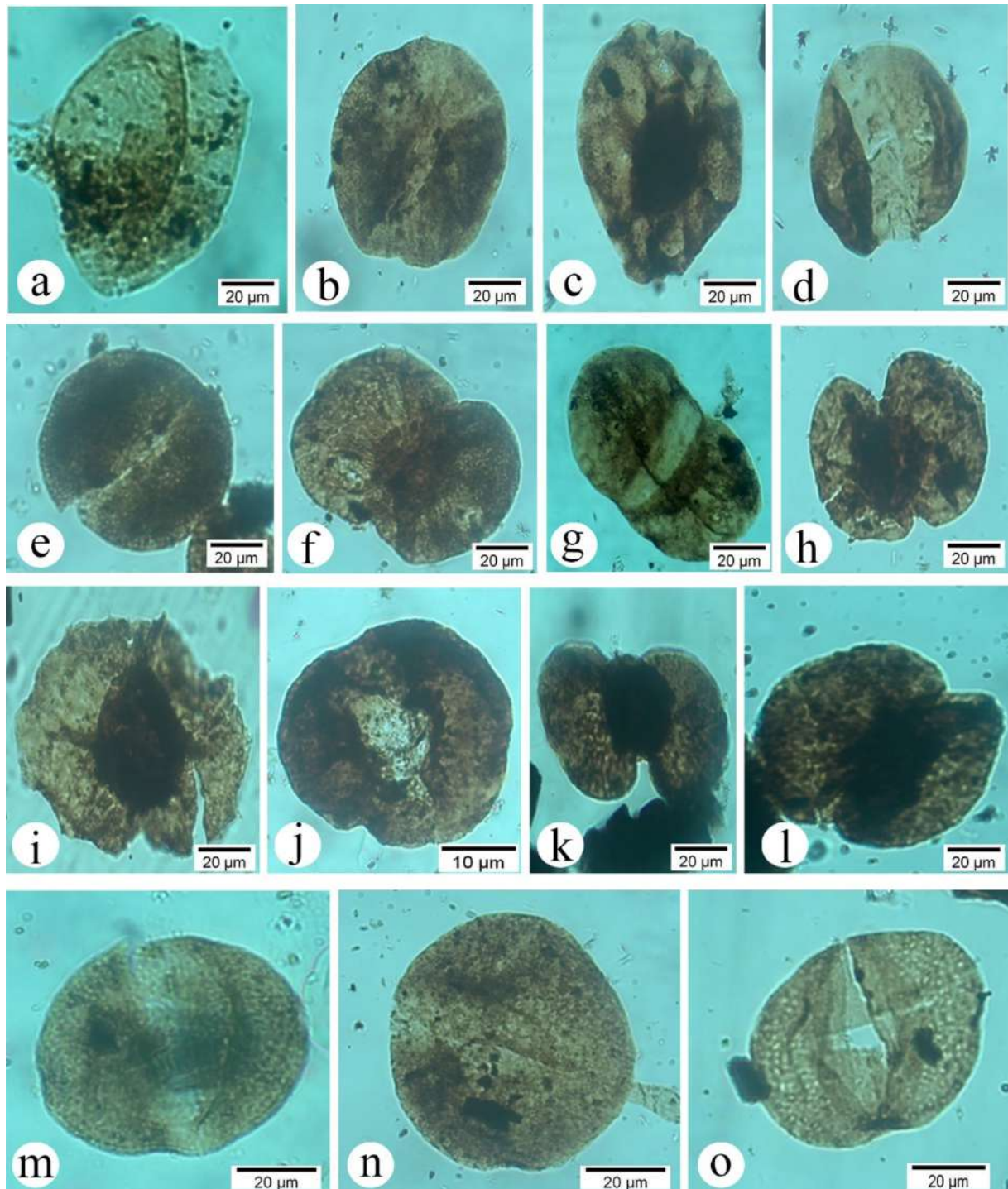


Fig. 5 a. *Ginkgocycadophytus* spp.; b. *Scheuringipollenites maximus*; c. *Rhizomasporamonosulcata*; d. *Faunipollenitesmagnus*; e. *Striatopodocarpites magnificus*; f. *Rhizomasporacosta*; g. *Striatopodocarpites* sp.; h. *Ibisporitesdiplosaccus*; i. *Parasaccitesdensus*; j. *Parasaccitesbilateralis*; k.*Striatites incircus*; l. *Striatites incircus*; m. *Striatopodocarpiteslabrus*; n. *Sulcatisporites tentulus*; o. *Lunatisporites* sp.





Rough Concept Lattice on an Information System

B.Praba* and L.P.Anto Freeda

Department of Mathematics, Sri Sivasubramaniya Nadar College of Engineering, Chennai, Tamil Nadu, India.

Received: 09 Feb 2023

Revised: 12 Apr 2023

Accepted: 16 May 2023

*Address for Correspondence

B.Praba

Department of Mathematics,
Sri Sivasubramaniya Nadar College of Engineering,
Chennai, Tamil Nadu, India.
E.Mail: prabab@ssn.edu.in



This is an Open Access Journal / article distributed under the terms of the **Creative Commons Attribution License** (CC BY-NC-ND 3.0) which permits unrestricted use, distribution, and reproduction in any medium, provided the original work is properly cited. All rights reserved.

ABSTRACT

The generalization of Pawlak's lower and upper approximation operators of rough set theory in formal concept analysis is presented in this paper. Applying the nature of formal concept analysis in rough set theory for the multi-valued attribute set of an information system $I = (U, A)$, helped to decompose the attribute set into the attribute value pair set. Using the equivalence relation on U , the rough set theoretical concepts are incorporated into the formal concept analysis to establish the rough concept lattice in an efficient way. The rough concept lattice, which is the hierarchical structure of rough concepts, represents the structural data that are derived from an information table. Filters for this rough concept lattice are also defined. All the defined concepts are illustrated with examples.

Keywords: Information system, Rough set, Formal concept analysis, Concept lattice, Filters

INTRODUCTION

Formal concept analysis is a method for modelling and manipulating the data that are incomplete and imprecise. Rough set theory and formal concept analysis are the two comparable mathematical tools for processing and analysing data. One of the primary goals of rough set theory introduced by Z. Pawlak [9] in 1982 focus on an indiscernibility relation between the set of objects with respect to the set of attributes that induces partition. The formal concepts and concept lattice are the key notions of formal concept analysis[2]. In this paper, we propose to merge these two notions into a single framework. One is to introduce the idea of concept lattice into rough set theory and the other is to introduce the approximation operators into formal concept analysis. Generally, these notions are introduced into rough set theory via formal concept analysis using approximation operators. So, a common framework used to combine these two theories is the concept lattice[6][7].





Praba and Anto Freeda

Bernhard Ganter and Rudolf Wille [2] introduced the formal concept analysis as a mathematical theory in the early 1980's, and it quickly became a popular method in information retrieval discipline. Formal concept analysis focuses on the formalization of concepts and conceptual thinking that has been used in a wide range of areas. Formal concept analysis [2] is an informal study of how objects might be hierarchically classified together based on their common attributes. Formal concept analysis and rough set theory are two similar theories for the concept analysis based on tabular data [1,3,4,8]. In this tabular data, row represent a collection of objects, column represent a collection of attributes or properties, and each cell represents the value of an object on an attribute, if not empty. A data table is a context for defining and interpreting concepts. In formal concept analysis, a table with only one value for each attribute is referred to as a one-valued formal context. When each attribute has several values, then the table is referred as many-valued context. Hence a binary relation between a set of objects and a set of attributes is easily referred as formal context.

A data table in rough set theory is defined to be an information system (U, A) consists of universe U , attributes set A , and the relation between U and A , which corresponds to the formal context in the formal concept analysis. For combining the formal concept analysis and rough set theory many efforts have been made, in which lattice for covering rough approximation [1], three-way concept lattice in social networks [4], a rough set approach on concept lattice [3] and Y.Yao [8] study on defining RS-definable concepts by incorporating ideas from formal concept analysis. In this paper, we present a rough concept lattice to incorporate the rough set theoretical idea by considering the information system [5] into a concept lattice using Indiscernibility equivalence relation. Furthermore, a new approach is initiated in defining filters in this rough concept lattice.

This paper is organized into the following sections. Preliminary definitions of rough set are provided in Section 2. An introduction to formal concept analysis and concept lattice are given in Section 3. Establishing rough set ideas in formal concept analysis is discussed in Section 4. Filters for this rough concept lattice is presented in Section 5. Conclusion is given in Section 6.

Preliminaries

In this section, preliminary knowledge about rough set is provided.

Definition 1. [5] The structure $I = (U, A)$ be an information system, where U is called the universe with the non-empty finite set of objects and A is a non-empty finite set of fuzzy attributes defined by $\mu_a: U \rightarrow [0,1]$, $a \in A$ is a fuzzy set. There is an associated equivalence relation for any subset P of A is $IND(P)$ and defined by

$$IND(P) = \{(x, y) \in U^2 \mid \forall a \in P, \mu_a(x) = \mu_a(y)\}$$

The equivalence classes obtained from the partition induced by $IND(P)$ is defined by

$$[x]_P = \{y \in U \mid (x, y) \in IND(P)\}$$

For any $X \in U$, the lower approximation space $P_-(X)$ is defined by

$$P_-(X) = \{x \in U \mid [x]_P \subseteq X\}$$

Also, the upper approximation space $P^-(X)$ is defined by

$$P^-(X) = \{x \in U \mid [x]_P \cap X \neq \emptyset\}$$

Definition 2. [5] If X is an arbitrary subset of U , then the rough set $RS(X)$ is an ordered pair $(P_-(X), P^-(X))$. The set of rough sets in U is defined by $T = \{RS(X) \mid X \subseteq U\}$.

Definition 3. [5] Let $X, Y \subseteq U$. The Praba Δ is defined as $X\Delta Y = X \cup Y$ if $I_w(X \cup Y) = I_w(X) + I_w(Y) - I_w(X \cap Y)$, where $I_w(X)$ is the number of equivalence classes in X .

Definition 4. [5] Let $X, Y \subseteq U$. The Praba ∇ of X and Y is denoted $X\nabla Y$ and defined as $X\nabla Y = \{x \mid [x]_P \subseteq X \cap Y\} \cup P_{X \cap Y}$. A pivot element $x \in P_{X \cap Y}$ such that, if $[x]_P \not\subseteq X \cap Y$, but $[x]_P \cap X \neq \emptyset$ and $[x]_P \cap Y \neq \emptyset$. Each element in $P_{X \cap Y}$ is the representative element of the particular class.





Praba and Anto Freeda

Definition 5. A non-empty subset F of a lattice, L is said to be filter if for $a \in F, b \in L, a \leq b$ implies $b \in F$, and $a \wedge b \in F$ for all $a, b \in F$.

Formal concept analysis and Concept lattice

A formal concept analysis considers the data in the form of a table with rows and columns representing the object set and attribute set respectively. A formal context which is referred as an object-attribute table in the formal concept analysis is of two types. One is the single-valued context and the other is the multi-valued context. Each attribute in the table taking one unique value is a single-valued context and on the other hand each attribute taking more than one value is a multi-valued context. The method of deriving the single-valued context from the multi-valued context is known as the conceptual scaling. Conceptual scaling is categorizing the objects (or) the process of categorizing the objects in the data table based on the common aspect (or) properties shared by the attributes. There are different types of scaling available in literature are elementary scaling, nominal scaling, ordinal scaling, inter-ordinal scaling and bi-ordinal scaling etc. The expansion of rough set theoretical concepts in the formal concept analysis in the following sections consider the nominal scaling for the conversion from the multi-valued to single-valued context.

Nominal scaling is used in the scenario when the set of attribute values exclude each other in the data table. In other words, the set of attribute values are mutually exclusive. This leads to the existence of partition in the object set as well as in the attribute set. Formal concept analysis aims at defining formal context in the form of two. One is the extension that includes all the objects in the concept and other is the intension that comprises all the attributes, that are shared by all the objects in common. These extension and intension operators in the formal concept analysis were defined using derivation operators. The extension operator in the formal concept analysis is replaced by lower and upper object approximation operator. Similarly, the intension operator is replaced by lower and upper attribute approximation operator. This replacement of operator in formal context of the formal concept analysis provides a way to the rough set theory. These operators behave much like a lower and upper approximations in the rough set theory and it helps to establish the rough set concept over the sets U and P connected by a binary relation I_a . This establishes a way to introduce the notion of rough set concepts in the formal concept analysis using approximation operators.

Information system and Formal concept analysis

In this section, an information system $I = (U, A)$ is considered to begin with the rough set notions to the formal concept analysis. An information system taken for the discourse is a multi-valued data table. A rough context (single-valued context) for this information table to be obtained is described below.

Conceptual Scaling in an Information table $I = (U, A)$

Let us consider an information table [5], where U is a non-empty with finite set of objects called the universe and A is a non-empty set with finite fuzzy attributes defined as $\mu_a: U \rightarrow [0,1]$, $a \in A$ is a fuzzy set. The association relation (or) the equivalence relation known as Indiscernibility of P , for $P \subseteq A$ induces partition in the object set U .

The conceptual scaling method introduced by Ganter and Wille [2] is the technique used for constructing formal context from the many-valued context. For each attribute $a \in A$, the value set $V = \cup \{V_a | a \in A\}$ where $V_a = \{\mu_a(x) | \mu_a(x) = x_a, x_a \in [0,1]\}$. The attribute value pair (a, x_a) for $a \in A, x_a \in V$ satisfies $\mu_a(x) = x_a$. This means that the value x_a is satisfying the attribute value pair (or) x_a is the value of x on a . The set of all attribute value pairs in an information table is denoted by $AVP(A)$ and defined by $AVP(A) = \{(a, x_a) | a \in A, x_a \in V\}$. For each attribute value pair in $AVP(A)$, the mapping θ is defined by $\theta: 2^{AVP(A)} \rightarrow 2^U$ such that $\theta((a, x_a)) = X \subseteq U$. Then the family of attribute value pair is the set defined by $W = \{p \subseteq AVP(A) | \theta(p) \subseteq U\} \subseteq 2^{AVP(A)}$.

Hence the conversion from multi-valued to single-valued context is attained by taking the attribute set A as the attribute value pair set W . It is given in the form (U, W, R_c) , where R_c is the binary relation between the object set





Praba and Anto Freeda

U and the attribute value pair set W . For any set P of W , the binary relation $R_c(P) = \{(x, p) \in U \times W \mid \forall p \in P, R_{c_p}(x) = 1\}$.

This derived rough context (U, W, R_c) with the binary relation R_c between U and W is represented by a value 1 in the cell, if the relation exists and empty, if there is no relation. This will lead to the new formulation of defining rough concepts.

Definition 6. A single-valued context (U, W, R_c) is the rough context derived from an information table with the identical object set. A binary relation R_c for $x \in U$ and $p \in W$ is given by $(x, p) \in R_c$ if and only if $R_{c_p}(x) = 1$.

For an element $x \in U$, the attribute value pair set obtained under R_c is

$$xR_c = \{p \in W \mid (x, p) \in R_c\} \subseteq W$$

And for an element $p \in W$, the object set obtained under R_c is

$$R_cp = \{x \in U \mid (x, p) \in R_c\} \subseteq U$$

Therefore, the partition in the object set and attribute value pair set is given by

$$[p]_c = xR_c = \{p \in W \mid \forall x \in X, (x, p) \in R_c\} \subseteq W$$

$$[x]_c = R_cp = \{x \in U \mid \forall p \in P, (x, p) \in R_c\} \subseteq U$$

Note 1: For the rough context (U, W, R_c) , the partition in the attribute value pair set W exists because by the indiscernibility equivalence relation defined on U .

Definition 7. Let (U, W, R_c) be the rough context of an information system $I = (U, A)$. For any $X \subseteq U$, the mapping of lower and upper object approximation of X is $X_-, X^- : 2^U \rightarrow 2^W$ and defined by

$$X_- = \{p \in W \mid \forall x \in U, R_cp \subseteq X\} = \{p \in W \mid [x]_c \subseteq X\}$$

$$X^- = \{p \in W \mid \exists x \in U, R_cp \cap X \neq \emptyset\} = \{p \in W \mid [x]_c \cap X \neq \emptyset\}$$

and for $P \subseteq W$, the mapping of lower and upper attribute approximation of P is $P_-, P^- : 2^W \rightarrow 2^U$ and defined by

$$P_- = \{x \in U \mid \forall p \in W, xR_c \subseteq P\} = \{x \in U \mid [p]_c \subseteq P\}$$

$$P^- = \{x \in U \mid \exists p \in W, xR_c \cap P \neq \emptyset\} = \{x \in U \mid [p]_c \cap P \neq \emptyset\}$$

Construction of rough concepts

For the subsets $X \subseteq U$ and $P \subseteq W$, their corresponding lower and upper object approximation of X and the lower and upper attribute approximation of P are used to define the rough concepts. The possible pairs made out of these lower and upper approximation operators of object and attribute sets are (X_-, X^-) , (P_-, P^-) , (X_-, P_-) , (X^-, P^-) , (X_-, P^-) and (X^-, P_-) . First, we consider the pairs (X_-, X^-) and (P_-, P^-) . The pair (X_-, X^-) produce the same lattice structure as of T in [5], the structure obtained for the set rough sets of ordered by the partial ordering relation. But the pair (X_-, X^-) produce the subsets of the attribute value pair set of W for the X considered. On the other hand, the pair (P_-, P^-) produce the same lattice T itself in terms of the subsets of U . Hence these pairs do not provide the desired results related to rough sets in formal concept analysis.

Now, consider the pairs (X_-, P_-) , (X^-, P^-) , (X_-, P^-) and (X^-, P_-) . For the arbitrary choice of subsets of object set U and the attribute value pair set W do not provide two-way deduction, but some. In other words, for the pair (X_-, P^-) . X_- is the collection of $p \in W$, such that all x related to p must be the subset of X and P^- is the collection of $x \in U$, such that there exists some p related to x must have non-empty intersection with P . So, for any pair (X, P) , $X_- = P$ and $P^- = X$ is the condition to be verified, where the derivation operator in formal concept analysis is replaced by object and attribute approximation operators. This is the two-way deduction for the subsets of U and W . This method is applicable to the remaining three pairs as well. This gives rise to defining the rough concept in the formal concept analysis for the rough context. The next level of constructing rough concept lattice will include the pair (X_-, P^-) in the discussion. The remaining pairs and their operators are discussed in examples.





Praba and Anto Freeda

Definition 8.(Rough Concept) Let (U, W, R_c) be a rough context. For $X \subseteq U$ and $P \subseteq W$, a rough concept is a pair (X, P) such that $P = X_-$ and $X = P^-$.

Definition 9. (Partial order relation) The set of all rough concepts in the rough context (U, W, R_c) is denoted by $\widetilde{(U, A)}$. For any two rough concepts $(X, P), (Y, Q)$ in $\widetilde{(U, A)}$, the partial ordering relation $\tilde{c}over(\widetilde{(U, A)})$ is given by $\tilde{c} = \{(X, P), (Y, Q) | X \subseteq Y \ \& \ P \subseteq Q\}$.

Theorem 1. \tilde{c} is a partial ordering relation on $\widetilde{(U, A)}$.

Proof. Proof is straight forward.

Theorem 2. $(X \Delta Y, P \cup Q)$ is the least upper bound of (X, P) and (Y, Q) in \tilde{c} .

Proof. First to check $(X \Delta Y, P \cup Q)$ is a rough concept. That is $(X \Delta Y)_- = P \cup Q$ and $(P \cup Q)^- = X \Delta Y$. Claim $(X \Delta Y)_- = P \cup Q$. Let $p \in (X \Delta Y)_-$

$$\begin{aligned} &\Rightarrow [x]_c \subseteq X \Delta Y \\ &\Rightarrow [x]_c \subseteq X \cup Y \\ &\Rightarrow [x]_c \subseteq X \text{ (or) } [x]_c \subseteq Y \\ &\Rightarrow p \in X_- \text{ (or) } p \in Y_- \\ &\Rightarrow p \in P \text{ (or) } p \in Q \text{ } (\because X_- = P \ \& \ Y_- = Q) \\ &\Rightarrow p \in P \cup Q \\ &(X \Delta Y)_- \subseteq P \cup Q \end{aligned}$$

Let $p \in P \cup Q$

$$\begin{aligned} &\Rightarrow p \in P \text{ (or) } p \in Q \\ &\Rightarrow p \in X_- \text{ (or) } p \in Y_- \text{ } (\because X_- = P \ \& \ Y_- = Q) \\ &\Rightarrow [x]_c \subseteq X \text{ (or) } [x]_c \subseteq Y \\ &\Rightarrow [x]_c \subseteq X \cup Y \\ &\Rightarrow [x]_c \subseteq X \Delta Y \\ &\Rightarrow p \in (X \Delta Y)_- \\ &P \cup Q \subseteq (X \Delta Y)_- \end{aligned}$$

Therefore, $(X \Delta Y)_- = P \cup Q$. Now claim $(P \cup Q)^- = X \Delta Y$. Let $x \in (P \cup Q)^-$

$$\begin{aligned} &\Rightarrow [p]_c \cap (P \cup Q) \neq \emptyset \\ &\Rightarrow [p]_c \cap P \neq \emptyset \text{ (or) } [p]_c \cap Q \neq \emptyset \\ &\Rightarrow x \in P^- \text{ (or) } x \in Q^- \\ &\Rightarrow x \in X \text{ (or) } x \in Y \text{ } (\because P^- = X \ \& \ Q^- = Y) \\ &\Rightarrow x \in X \cup Y \\ &\Rightarrow x \in X \Delta Y \\ &(P \cup Q)^- \subseteq X \Delta Y \end{aligned}$$

Let $x \in X \Delta Y$

$$\begin{aligned} &\Rightarrow x \in X \cup Y \\ &\Rightarrow x \in X \text{ (or) } x \in Y \\ &\Rightarrow x \in P^- \text{ (or) } x \in Q^- \text{ } (\because P^- = X \ \& \ Q^- = Y) \\ &\Rightarrow [p]_c \cap P \neq \emptyset \text{ (or) } [p]_c \cap Q \neq \emptyset \\ &\Rightarrow [p]_c \cap (P \cup Q) \neq \emptyset \\ &\Rightarrow x \in (P \cup Q)^- \\ &X \Delta Y \subseteq (P \cup Q)^- \end{aligned}$$

Therefore, $(P \cup Q)^- = X \Delta Y$. Hence $(X \Delta Y, P \cup Q)$ is a rough concept. To show $(X \Delta Y, P \cup Q)$ is the least upper bound of (X, P) and (Y, Q) , it requires to show first that $(X \Delta Y, P \cup Q)$ is the upper bound of (X, P) and (Y, Q) .

To prove $(X, P) \subseteq (X \Delta Y, P \cup Q)$ and $(Y, Q) \subseteq (X \Delta Y, P \cup Q)$.

Consider $(X, P) \subseteq (X \Delta Y, P \cup Q)$, it is equivalent to prove $X_- \subseteq (X \Delta Y)_-$ and $P^- \subseteq (P \cup Q)^-$. Claim $X_- \subseteq (X \Delta Y)_-$

Let $p \in X_-$

$$\begin{aligned} &\Rightarrow [x]_c \subseteq X \\ &\Rightarrow [x]_c \subseteq X \cup Y \text{ } (\because X \subseteq X \cup Y) \\ &\Rightarrow [x]_c \subseteq X \Delta Y \\ &\Rightarrow p \in (X \Delta Y)_- \end{aligned}$$





Praba and Anto Freeda

$X_- \subseteq (X\Delta Y)_-$
Let $x \in P^-$

$$\begin{aligned} &\Rightarrow [p]_c \cap P \neq \emptyset \\ \Rightarrow [p]_c \cap (P \cup Q) \neq \emptyset & (\because P \subseteq P \cup Q) \\ &\Rightarrow x \in (P \cup Q)^- \\ &P^- \subseteq (P \cup Q)^- \end{aligned}$$

Therefore $(X, P) \subseteq (X\Delta Y, P \cup Q)$. Similarly, it can be proved that $(Y, Q) \subseteq (X\Delta Y, P \cup Q)$. Hence $(X\Delta Y, P \cup Q)$ is the upper bound of (X, P) and (Y, Q) .

Now to prove $(X\Delta Y, P \cup Q)$ is the least upper bound. Suppose (K, S) is the upper bound of (X, P) and (Y, Q) , then $(X, P) \subseteq (K, S)$ and $(Y, Q) \subseteq (K, S)$. To prove now $(X\Delta Y, P \cup Q) \subseteq (K, S)$, it is required to show $(X\Delta Y)_- \subseteq K_-$ and $(P \cup Q)^- \subseteq S^-$. Let $p \in (X\Delta Y)_-$

$$\begin{aligned} &\Rightarrow [x]_c \subseteq X\Delta Y \\ &\Rightarrow [x]_c \subseteq X \cup Y \\ \Rightarrow [x]_c \subseteq X & \text{ (or) } [x]_c \subseteq Y \\ \Rightarrow p \in X_- & \text{ (or) } p \in Y_- \\ \Rightarrow p \in K_- & (\because X_- \subseteq K_- \& Y_- \subseteq K_-) \\ &(X\Delta Y)_- \subseteq K_- \end{aligned}$$

Let $x \in (P \cup Q)^-$

$$\begin{aligned} &\Rightarrow [p]_c \cap (P \cup Q) \neq \emptyset \\ \Rightarrow [p]_c \cap P \neq \emptyset & \text{ (or) } [p]_c \cap Q \neq \emptyset \\ \Rightarrow x \in P^- & \text{ (or) } x \in Q^- \\ \Rightarrow x \in S^- & (\because P^- \subseteq S^- \& Q^- \subseteq S^-) \\ &(P \cup Q)^- \subseteq S^- \end{aligned}$$

Hence $(X\Delta Y, P \cup Q)$ is the least upper bound of (X, P) and (Y, Q) .

Theorem 3. $(X\forall Y, P \cap Q)$ is the greatest lower bound of (X, P) and (Y, Q) in \tilde{c} .

Proof. Proved like Theorem 1 using the definitions of \forall and \cap .

Definition 10. (Rough concept lattice) The set of rough concepts denoted by $(\widetilde{U}, \widetilde{A})$ and ordered by the partial order relation \tilde{c} , then $((\widetilde{U}, \widetilde{A}), \tilde{c})$ is called a rough concept lattice.

Theorem 4. $(\widetilde{U}, \widetilde{A}) = \{(X, P) | X \subseteq U \& P \subseteq W\}$ is a rough concept lattice.

Proof. Proof is the immediate consequence from Theorem 1, 2 and 3.

Example 1. [5] Let us consider the information table as in Table 1

Where, $U = \{x_1, x_2, x_3, x_4, x_5, x_6\}$ is the object set and $A = \{a_1, a_2, a_3, a_4\}$ is the fuzzy attribute set whose membership values are given in the table. The relation $IND(P)$ induces the equivalence classes $X_1 = \{x_1, x_3\}$, $X_2 = \{x_2, x_4, x_6\}$ and $X_3 = \{x_5\}$.

The value set of A from the table is

$$V = \{0, 0.1, 0.2, 0.3, 0.4, 0.5, 0.6, 0.7, 0.9, 1\}$$

The collection of attribute value pair is

$$AVP(A) = \{(a_1, 0), (a_1, 1), (a_1, 0.8), (a_2, 0.1), (a_2, 0.6), (a_2, 0.5), (a_3, 0.3), (a_3, 0.7), (a_3, 0.2), (a_4, 0.2), (a_4, 0.3), (a_4, 0.4)\}$$

The family of attribute value pair set is given by

$$W = \{p_1, \dots, p_{45}\} \subseteq 2^{AVP(A)}$$

$$\begin{aligned} p_1 &= \{(a_1, 0)\}, p_2 = \{(a_1, 1)\}, p_3 = \{(a_1, 0.8)\}, p_4 = \{(a_2, 0.1)\}, p_5 = \{(a_2, 0.6)\}, \\ p_6 &= \{(a_2, 0.5)\}, p_7 = \{(a_3, 0.3)\}, p_8 = \{(a_3, 0.7)\}, p_9 = \{(a_3, 0.2)\}, p_{10} = \{(a_4, 0.2)\}, \\ p_{11} &= \{(a_4, 0.3)\}, p_{12} = \{(a_4, 0.4)\}, p_{13} = \{(a_1, 0)(a_2, 0.1)\}, p_{14} = \{(a_1, 0)(a_3, 0.3)\}, \\ p_{15} &= \{(a_1, 0)(a_4, 0.2)\}, p_{16} = \{(a_1, 1)(a_2, 0.6)\}, p_{17} = \{(a_1, 1)(a_3, 0.7)\}, \\ p_{18} &= \{(a_1, 1)(a_4, 0.3)\}, p_{19} = \{(a_1, 1)(a_2, 0.5)\}, p_{20} = \{(a_1, 0.8)(a_3, 0.2)\}, \end{aligned}$$





Praba and Anto Freeda

$$\begin{aligned}
 p_{21} &= \{(a_1, 0.8)(a_4, 0.4)\}, p_{22} = \{(a_2, 0.1)(a_3, 0.3)\}, p_{23} = \{(a_2, 0.1)(a_4, 0.2)\}, \\
 p_{24} &= \{(a_2, 0.6)(a_3, 0.7)\}, p_{25} = \{(a_2, 0.6)(a_4, 0.3)\}, p_{26} = \{(a_2, 0.5)(a_3, 0.2)\}, \\
 p_{27} &= \{(a_2, 0.5)(a_4, 0.4)\}, p_{28} = \{(a_3, 0.3)(a_4, 0.2)\}, p_{29} = \{(a_3, 0.7)(a_4, 0.3)\}, \\
 p_{30} &= \{(a_3, 0.2)(a_4, 0.4)\}, p_{31} = \{(a_1, 0)(a_2, 0.1)(a_3, 0.3)\}, p_{32} = \{(a_1, 0)(a_2, 0.1)(a_4, 0.2)\}, \\
 p_{33} &= \{(a_1, 1)(a_2, 0.6)(a_3, 0.7)\}, p_{34} = \{(a_1, 1)(a_2, 0.6)(a_4, 0.3)\}, \\
 p_{35} &= \{(a_1, 0.8)(a_2, 0.5)(a_3, 0.2)\}, p_{36} = \{(a_1, 0.8)(a_2, 0.5)(a_4, 0.4)\} \\
 p_{37} &= \{(a_1, 0)(a_3, 0.3)(a_4, 0.2)\}, p_{38} = \{(a_1, 1)(a_3, 0.7)(a_4, 0.3)\}, \\
 p_{39} &= \{(a_1, 0.8)(a_3, 0.2)(a_4, 0.4)\}, p_{40} = \{(a_2, 0.1)(a_3, 0.3)(a_4, 0.2)\} \\
 p_{41} &= \{(a_2, 0.6)(a_3, 0.7)(a_4, 0.3)\}, p_{42} = \{(a_2, 0.5)(a_3, 0.2)(a_4, 0.4)\} \\
 p_{43} &= \{(a_1, 0)(a_2, 0.1)(a_3, 0.3)(a_4, 0.2)\}, p_{44} = \{(a_1, 1)(a_2, 0.6)(a_3, 0.7)(a_4, 0.3)\} \\
 p_{45} &= \{(a_1, 0.8)(a_2, 0.5)(a_3, 0.2)(a_4, 0.4)\}
 \end{aligned}$$

Now the object set of the attribute value pair set is given,

$$\begin{aligned}
 \theta(p_1) &= \theta((a_1, 0)) = \{x_1, x_3\} = X_1, \\
 \theta(p_2) &= \theta((a_1, 1)) = \{x_2, x_4, x_6\} = X_2, \\
 \theta(p_3) &= \theta((a_1, 0.8)) = \{x_5\} = X_3, \dots, \\
 \theta(p_{13}) &= \theta((a_1, 0)) \wedge \theta((a_2, 0.1)) = \{x_1, x_3\} \wedge \{x_1, x_3\} = \{x_1, x_3\} = X_1, \dots, \\
 \theta(p_{33}) &= \theta((a_1, 1)) \wedge \theta((a_2, 0.6)) \wedge \theta((a_3, 0.7)) = \{x_2, x_4, x_6\} = X_2, \dots, \\
 \theta(p_{45}) &= \theta((a_1, 0.8)) \wedge \theta((a_2, 0.5)) \wedge \theta((a_3, 0.2)) \wedge \theta((a_4, 0.4)) = \{x_5\} = X_3
 \end{aligned}$$

and its object table is of the form

Thus, the considered information table is converted into a single-valued rough context (U, W, R_c) and the partition in the object set obtained using the relation R_c is

$$\begin{aligned}
 X_1 &= [x_1]_c = R_c P = \{x_1, x_3\} \\
 X_2 &= [x_2]_c = R_c P = \{x_2, x_4, x_6\} \\
 X_3 &= [x_5]_c = R_c P = \{x_5\}
 \end{aligned}$$

and the partition in the attribute set W obtained using the relation R_c is

$$\begin{aligned}
 P_1 &= [p_1]_c = X R_c = \{p_1, p_4, p_7, p_{10}, p_{13}, p_{14}, p_{15}, p_{22}, p_{23}, p_{28}, p_{31}, p_{32}, p_{37}, p_{40}, p_{43}\} \\
 P_2 &= [p_2]_c = X R_c = \{p_2, p_5, p_8, p_{11}, p_{16}, p_{17}, p_{18}, p_{24}, p_{25}, p_{29}, p_{33}, p_{34}, p_{38}, p_{41}, p_{44}\} \\
 P_3 &= [p_3]_c = X R_c = \{p_3, p_6, p_9, p_{12}, p_{19}, p_{20}, p_{21}, p_{26}, p_{27}, p_{30}, p_{35}, p_{36}, p_{39}, p_{42}, p_{45}\}
 \end{aligned}$$

Using these partitions, the rough concepts for the single-valued rough context (U, W, R_c) is obtained. For the subsets $X \subseteq U$ and $P \subseteq W$, their lower object approximation and upper attribute approximation are as follows,

$$1. X = \emptyset \text{ and } P = \emptyset$$

$$X_- = P \Leftrightarrow \emptyset_- = \emptyset \text{ and } P^- = X \Leftrightarrow \emptyset^- = \emptyset$$

(\emptyset, \emptyset) is a rough set concept.

$$2. X = \{x_1, x_3\} \text{ and } P = P_1$$

$$(\{x_1, x_3\})_- = P_1 \text{ and } P_1^- = \{x_1, x_3\} = X_1$$

(X_1, P_1) is a rough set concept.

$$3. X = \{x_2, x_4, x_6\} \text{ and } P = P_2$$

$$(\{x_2, x_4, x_6\})_- = P_2 \text{ and } P_2^- = \{x_2, x_4, x_6\} = X_2$$





Praba and Anto Freeda

(X_2, P_2) is a rough set concept

4. $X = \{x_5\}$ and $P = P_3$

$(\{x_5\})_- = P_3$ and $P_3^- = \{x_5\} = X_3$

(X_3, P_3) is a rough set concept

5. $X = X_1X_2$ and $P = P_1P_2$

$(X_1X_2)_- = P_1P_2$ and $(P_1P_2)^- = X_1X_2$

(X_1X_2, P_1P_2) is a rough set concept

6. $X = X_1X_3$ and $P = P_1P_3$

$(X_1X_3)_- = P_1P_3$ and $(P_1P_3)^- = X_1X_3$

(X_1X_3, P_1P_3) is a rough set concept

7. $X = X_2X_3$ and $P = P_2P_3$

$(X_2X_3)_- = P_2P_3$ and $(P_2P_3)^- = X_2X_3$

(X_2X_3, P_2P_3) is a rough set concept

8. $X = U$ and $P = W$

$(U)_- = W$ and $W^- = U$

(U, W) is a rough set concept.

Thus, the set of all rough concepts for the rough context is obtained to be

$$(\overline{U, A}) = \{(X, P) | X_- = P \ \& \ P^- = X\}$$

$$(\overline{U, A}) = \{(\emptyset, \emptyset), (X_1, P_1), (X_2, P_2), (X_3, P_3), (X_1X_2, P_1P_2), (X_1X_3, P_1P_3), (X_2X_3, P_2P_3), (U, W)\}$$

Hence the rough concept lattice obtained is given by

This is the rough concept lattice structure obtained from the derived single-valued rough context.

Remark 1:

From Example-1, the collection of pairs obtained for the lower and upper attribute approximation of X for the pair (X_-, X^-) is

$$\{(\emptyset, \emptyset), (\emptyset, P_1), (\emptyset, P_2), (P_1, P_1), (P_2, P_2), (P_3, P_3), (\emptyset, P_1 \cup P_2), (P_2, P_1 \cup P_2), (P_1, P_1 \cup P_2), (P_3, P_1 \cup P_3), (P_3, P_2 \cup P_3), (P_1 \cup P_2, P_1 \cup P_2), (P_2 \cup P_3, P_2 \cup P_3), (P_1 \cup P_3, P_1 \cup P_3), (P_3, W), (P_1 \cup P_3, W), (P_2 \cup P_3, W), (W, W)\}$$

Introducing the partial order relation between the elements of (X_-, X^-) gives the lattice structure of the form in **Figure 2**.

Similarly, the collection of pairs obtained for the lower and upper object approximation for the pair (P_-, P^-) is

$$\{(\emptyset, \emptyset), (\emptyset, X_1), (\emptyset, X_2), (X_1, X_1), (X_2, X_2), (X_3, X_3), (\emptyset, X_1 \cup X_2), (X_2, X_1 \cup X_2), (X_1, X_1 \cup X_2), (X_3, X_1 \cup X_3), (X_3, X_2 \cup X_3), (X_1 \cup X_2, X_1 \cup X_2), (X_2 \cup X_3, X_2 \cup X_3), (X_1 \cup X_3, X_1 \cup X_3), (X_3, U), (X_1 \cup X_3, U), (X_2 \cup X_3, U), (U, U)\}$$

Introducing partial order relation between the elements of (P_-, P^-) gives the lattice structure of the form in **Figure 3**.

Figure 2: (X_-, X^-) **Figure 3:** (P_-, P^-)

Note 2. Both the pairs (X_-, X^-) and (P_-, P^-) produce similar lattice structure with the object approximation and attribute approximation operators.

Example 2. From example-1, for the object set $U = \{x_1, x_2, x_3, x_4, x_5, x_6\}$ and attribute value pair set $W =$





Praba and Anto Freeda

$\{p_1, \dots, p_{45}\}$, the pairs that satisfies the condition of rough concept are given in Table 5

Note 3. The pairs that satisfy the conditions of rough concept in Example-2 produce the similar rough concept lattice structure as in Figure 1.

Remark 2. This is one kind of rough concept lattice structure obtained for the partition on U induced by the indiscernibility relation. In this example, we have $n = 3$ and $m = 2$, where n is the number of the equivalence classes in U and m is the number of equivalence classes whose cardinality is greater than 1. There are variety of rough concept lattice structures obtained for the same object set U and attribute set A in an information system, by introducing various partition between the elements of U by the choice of membership values.

Note 4. A similar rough concept lattice structure in Figure-1, is obtained for $n = 3, m = 3$ and $n = 3, m = 1$ for $I = (U, A)$ in Example-1. But the partition here is done with the various choices of membership values.

Example 3. From Example-1, for $n = 2$ and $m = 2$ and $n = 2, m = 1$ the set of rough set concepts is

$$(\overline{U}, \overline{A}) = \{(\emptyset, \emptyset), (X_1, P_1), (X_2, P_2), (U, W)\}$$

and its rough concept lattice obtained is given in Figure 4,

Also, for $n = 4, m = 2$ and $n = 4, m = 1$ the set of rough concepts obtained is

$$\begin{aligned} (\overline{U}, \overline{A}) = \{ & (\emptyset, \emptyset), (X_1, P_1), (X_2, P_2), (X_3, P_3), (X_4, P_4), (X_1X_2, P_1P_2), (X_1X_3, P_1P_3), \\ & (X_1X_4, P_1P_4), (X_2X_3, P_2P_3), (X_2X_4, P_2P_4), (X_3X_4, P_3P_4), (X_1X_2X_3, P_1P_2P_3), (X_1X_2X_4, P_1P_2P_4), \\ & (X_1X_3X_4, P_1P_3P_4), (X_2X_3X_4, P_2P_3P_4), (U, W)\} \end{aligned}$$

and its rough concept lattice structure is given in Figure 5,

Remark 3. Thus, defining partition in the object set provides the better scaling of obtaining single valued rough context from the multi-valued context. It reduces complexity in the structure of rough concept lattice unlike other relation used between the elements of object set in the data table. This rough concept lattice structure is found to be the refinement of the structure in comparison with the lattice structure T . This motivates us to define filters on this rough concept lattice.

Filters in Rough concept lattice

In this section, a rough concept lattice structure $((\overline{U}, \overline{A}), \tilde{c})$ is considered to define filters in it.

Definition 11. Let $((\overline{U}, \overline{A}), \tilde{c})$ be a rough concept lattice. For any subset $X \subseteq U$ and $P \subseteq W$, a non-empty subset $F_{(X,P)}((\overline{U}, \overline{A}))$ of $(\overline{U}, \overline{A})$ is said to be filter if

1. $(X, P) \wedge (Y, Q) \in F_{(X,P)}((\overline{U}, \overline{A}))$ for $(X, P), (Y, Q) \in F_{(X,P)}((\overline{U}, \overline{A}))$
2. If $(X, P) \in F_{(X,P)}((\overline{U}, \overline{A}))$ and $(X, P) \leq (Y, Q)$ then $(Y, Q) \in F_{(X,P)}((\overline{U}, \overline{A}))$

Definition 12. Let $((\overline{U}, \overline{A}), \tilde{c})$ be a rough concept lattice, where $(\overline{U}, \overline{A})$ is the set of rough concepts. Then the rough concept upset of an element (X, P) in $(\overline{U}, \overline{A})$ is defined by $RCupset((X, P)) = \{(Y, Q) \in (\overline{U}, \overline{A}) | (X, P) \leq (Y, Q)\}$

Theorem 5. $RCupset((X, P))$ is a filter.

Proof. (i) Let $(Y_1, Q_1), (Y_2, Q_2) \in RCupset((X, P))$. Then by the definition of $RCupset$

$$\begin{aligned} (X, P) & \leq (Y_1, Q_1) \quad (1) \\ (X, P) & \leq (Y_2, Q_2) \quad (2) \end{aligned}$$

From (1) and (2),

$$\begin{aligned} (X, P) \wedge (X, P) & \leq (Y_1, Q_1) \wedge (Y_2, Q_2) \\ \Rightarrow (X, P) & \leq (Y_1, Q_1) \wedge (Y_2, Q_2) \end{aligned}$$

$\Rightarrow (Y_1, Q_1) \wedge (Y_2, Q_2) \in RCupset((X, P))$





Praba and Anto Freeda

Therefore, RCupset $((X, P))$ is closed under \wedge .

(ii) Consider $(Y, Q) \in \text{RCupset}((X, P))$

$$\Rightarrow (X, P) \leq (Y, Q)$$

There exists $(Z, S) \in (\overline{U, A})$ and $(Y, Q) \leq (Z, S)$, then $(Y, Q) \leq (Y \Delta Z, Q \cup S)$

$$\Rightarrow (X, P) \leq (Y \Delta Z, Q \cup S)$$

$\Rightarrow (Y \Delta Z, Q \cup S) \in \text{RCupset}((X, P))$

$\Rightarrow (Z, S) \in \text{RCupset}((X, P))$

Hence $\text{RCupset}((X, P))$ is a filter.

Theorem 6.

$F_{(X,P)}(\overline{U, A}) = \{(Y, Q) \in (\overline{U, A}) \mid (Y, Q) = (X, P) \vee N, N \in (P(E_U \setminus E_X), P(E_W \setminus E_P))\}$ is the $\text{RCupset}((X, P))$.

Proof. To prove $F_{(X,P)}(\overline{U, A}) = \text{RCupset}((X, P))$

Claim: $F_{(X,P)}(\overline{U, A}) \subseteq \text{RCupset}((X, P))$

Let $(Y, Q) \in F_{(X,P)}(\overline{U, A})$

$\Rightarrow (Y, Q) = (X, P) \vee N$ for $N \in (P(E_U \setminus E_X), P(E_W \setminus E_P))$

To prove $(Y, Q) \in \text{RCupset}((X, P))$, it is enough to prove $(X, P) \leq (Y, Q)$. Since by assumption $(Y, Q) = (X, P) \vee N$, then $(X, P) \leq (X, P) \vee N$

$$\Rightarrow (X, P) \leq (Y, Q)$$

$\Rightarrow (Y, Q) \in \text{RCupset}((X, P))$

$F_{(X,P)}(\overline{U, A}) \subseteq \text{RCupset}((X, P))$ (3)

Now claim: $\text{RCupset}((X, P)) \subseteq F_{(X,P)}(\overline{U, A})$

Let $(Y, Q) \in \text{RCupset}((X, P))$

$$\Rightarrow (X, P) \leq (Y, Q)$$

To prove $(Y, Q) \in F_{(X,P)}(\overline{U, A})$ it is enough to prove $(Y, Q) = (X, P) \vee N$, for $N \in (P(E_U \setminus E_X), P(E_W \setminus E_P))$. Since $(X, P) \leq (Y, Q)$

$$\begin{aligned} (X, P) \vee (Y, Q) &= (Y, Q) = (X, P) \vee N \\ \Rightarrow (Y, Q) &= (X, P) \vee (E_Y \setminus E_X \cap E_Y, E_Q \setminus E_P \cap E_Q) \\ &\Rightarrow (Y, Q) \in F_{(X,P)}(\overline{U, A}) \end{aligned}$$

$\text{RCupset}((X, P)) \subseteq F_{(X,P)}(\overline{U, A})$ (4)

From (3) and (4), $F_{(X,P)}(\overline{U, A})$ is the $\text{RCupset}((X, P))$.

Note 5. In theorem 6, E_U, E_X, E_W and E_P stands for the union of equivalence classes in U, X, W and P respectively.

Example 4. From Example-1, the set of rough concepts obtained for an information system $I = (U, A)$ is

$$(\overline{U, A}) = \{(\emptyset, \emptyset), (X_1, P_1), (X_2, P_2), (X_3, P_3), (X_1X_2, P_1P_2), (X_1X_3, P_1P_3), (X_2X_3, P_2P_3), (U, W)\}$$

The $\text{RCupset}((X_2, P_2))$ is

$$\begin{aligned} \text{RCupset}((X_2, P_2)) &= F_{(X_2,P_2)}(\overline{U, A}) \\ &= \{(X_2, P_2), (X_1X_2, P_1P_2), (X_2X_3, P_2P_3), (U, W)\} \end{aligned}$$

The filter conditions for the $\text{RCupset}((X_2, P_2))$ is verified in Table 6 and 7,

Example 5. From Example-1, for the rough context the set of rough concepts obtained is given to be

$$(\overline{U, A}) = \{(\emptyset, \emptyset), (X_1, P_1), (X_2, P_2), (X_3, P_3), (X_1X_2, P_1P_2), (X_1X_3, P_1P_3), (X_2X_3, P_2P_3), (U, W)\}$$

The set of filters obtained for the rough concepts of $(\overline{U, A})$ is

$$\begin{aligned} \text{Rupset}((\emptyset, \emptyset)) &= F_{((\emptyset, \emptyset))}(\overline{U, A}) = (\overline{U, A}) \\ \text{Rupset}((X_1, P_1)) &= F_{((X_1,P_1))}(\overline{U, A}) = \{(X_1, P_1), (X_1X_2, P_1P_2), (X_1X_3, P_1P_3), (U, W)\} \\ \text{Rupset}((X_2, P_2)) &= F_{((X_2,P_2))}(\overline{U, A}) = \{(X_2, P_2), (X_1X_2, P_1P_2), (X_2X_3, P_2P_3), (U, W)\} \\ \text{Rupset}((X_3, P_3)) &= F_{((X_3,P_3))}(\overline{U, A}) = \{(X_3, P_3), (X_1X_3, P_1P_3), (X_2X_3, P_2P_3), (U, W)\} \end{aligned}$$





Praba and Anto Freeda

$$\begin{aligned} \text{Rupset}((X_1X_2, P_1P_2)) &= F_{((X_1X_2, P_1P_2))}(\overline{(U, A)}) = \{(X_1X_2, P_1P_2), (U, W)\} \\ \text{Rupset}((X_1X_3, P_1P_3)) &= F_{((X_1X_3, P_1P_3))}(\overline{(U, A)}) = \{(X_1X_3, P_1P_3), (U, W)\} \\ \text{Rupset}((X_2X_3, P_2P_3)) &= F_{((X_2X_3, P_2P_3))}(\overline{(U, A)}) = \{(X_2X_3, P_2P_3), (U, W)\} \\ \text{Rupset}((U, W)) &= F_{((U, W))}(\overline{(U, A)}) = \{(U, W)\} \end{aligned}$$

CONCLUSION

In this paper, a framework that exhibits the interpretation of analyzing rough concepts by combining ideas from formal concept analysis is given. This is accomplished via conceptual scaling, to obtain the single-valued rough context from an information system $I = (U, A)$. So, by integrating the rough concepts from the formal concept analysis, a refined rough concept lattice structure is obtained. This refinement in the structure helped to define filters in this rough concept lattice. Filters defined on this rough concept lattice is the unified iterative search of an information in information retrieval, data analysis etc. for the data table considered. The results provided in this work gives the systematic understanding of constructing rough concept lattice and defining filters on it, through an information system $I = (U, A)$.

ACKNOWLEDGMENT

The authors thank the Management and the Principal, SSN College of Engineering for providing the necessary facilities to carry out this work.

DECLARATIONS

The authors declare no conflict of interest.

REFERENCES

1. Anhui Tan, Jinjin Li, and Guoping Lin. "Connections between covering-based rough sets and concept lattices." *International journal of approximate reasoning* 56 (2015): 43-58.
2. Bernhard Ganter, and Rudolf Wille. "Formal concept analysis: mathematical foundations". Springer Science & Business Media, 2012.
3. Dipankar Rana, and Sankar Kumar Roy. "Rough set approach on lattice." *Journal of Uncertain Systems* 5, no. 1 (2011): 72-80.
4. Fei Hao, Yixuan Yang, Geyong Min, and Vincenzo Loia. "Incremental construction of three-way concept lattice for knowledge discovery in social networks." *Information Sciences* 578 (2021): 257-280.
5. Praba, B., and R. Mohan. "Rough lattice." *International Journal of Fuzzy Mathematics and System* 3, no. 2 (2013): 135-151.
6. Xia Wu, Jialu Zhang, and Jiaming Zhong. "Layered concept lattice model and its application to build rapidly concept lattice." *Computational Intelligence and Neuroscience* 2020 (2020).
7. Xuerong Zhao, Duoqian Miao, and Bao Qing Hu. "On relationship between three-way concept lattices." *Information Sciences* 538 (2020): 396-414.
8. Yiyu Yao. "Rough-set concept analysis: interpreting RS-definable concepts based on ideas from formal concept analysis." *Information Sciences* 346 (2016): 442-462.
9. Zdzislaw Pawlak. "Rough sets." *International journal of computer & information sciences* 11, no. 5 (1982): 341-356.





Praba and Anto Freeda

Table 1: Information table

A/U	a ₁	a ₂	a ₃	a ₄
x ₁	0	0.1	0.3	0.2
x ₂	1	0.6	0.7	0.3
x ₃	0	0.1	0.3	0.2
x ₄	1	0.6	0.7	0.3
x ₅	0.8	0.5	0.2	0.4
x ₆	1	0.6	0.7	0.3

Table 2: Object table

W	p ₁	p ₂	p ₃	p ₄	p ₅	p ₆	p ₇	p ₈	p ₉	p ₁₀	p ₁₁	p ₁₂	p ₁₃	p ₁₄	p ₁₅	p ₁₆	p ₁₇	p ₁₈	p ₁₉	p ₂₀	p ₂₁	p ₂₂	
θ	X ₁	X ₂	X ₃	X ₁	X ₂	X ₃	X ₁	X ₂	X ₃	X ₁	X ₂	X ₃	X ₁	X ₁	X ₁	X ₂	X ₂	X ₂	X ₃	X ₃	X ₃	X ₃	X ₁

Table 3: Object table

W	p ₂₃	p ₂₄	p ₂₅	p ₂₆	p ₂₇	p ₂₈	p ₂₉	p ₃₀	p ₃₁	p ₃₂	p ₃₃	p ₃₄	p ₃₅	p ₃₆	p ₃₇	p ₃₈	p ₃₉	p ₄₀	p ₄₁	p ₄₂	p ₄₃	p ₄₄	p ₄₅
θ	X ₁	X ₂	X ₂	X ₃	X ₃	X ₁	X ₂	X ₃	X ₁	X ₁	X ₂	X ₂	X ₃	X ₃	X ₁	X ₂	X ₃	X ₁	X ₂	X ₃	X ₁	X ₂	X ₃

Table 4: Rough context table

W	p ₁	p ₂	p ₃	p ₄	p ₅	p ₆	p ₇	p ₈	p ₉	p ₁₀	p ₁₁	p ₁₂	p ₁₃	p ₁₄	p ₁₅	p ₁₆	p ₁₇	p ₁₈	p ₁₉	p ₂₀	p ₂₁	p ₂₂	
x ₁	1			1			1			1			1	1	1								1
x ₂		1			1			1			1					1	1	1					
x ₃	1			1			1			1			1	1	1								1
x ₄		1			1			1			1					1	1	1					
x ₅			1			1			1			1								1	1	1	
x ₆		1			1			1			1					1	1	1					

	p ₂₃	p ₂₄	p ₂₅	p ₂₆	p ₂₇	p ₂₈	p ₂₉	p ₃₀	p ₃₁	p ₃₂	p ₃₃	p ₃₄	p ₃₅	p ₃₆	p ₃₇	p ₃₈	p ₃₉	p ₄₀	p ₄₁	p ₄₂	p ₄₃	p ₄₄	p ₄₅
	1					1			1	1					1			1			1		
		1	1				1				1	1				1			1			1	
					1			1		1					1			1				1	
			1	1			1						1	1			1			1			1
		1	1				1				1	1				1			1			1	

Table 5:

$X \subseteq U$ and $P \subseteq W$	(X_-, P_-)	(X^-, P^-)	(X^-, P_-)
$X = \emptyset$ and $P = \emptyset$	(\emptyset, \emptyset)	(\emptyset, \emptyset)	(\emptyset, \emptyset)
$X = \{x_1, x_3\}$ and $P = P_1$	$(\{x_1, x_3\}, P_1)$	$(\{x_1, x_3\}, P_1)$	$(\{x_1, x_3\}, P_1)$
$X = \{x_2, x_4, x_6\}$ and $P = P_2$	$(\{x_2, x_4, x_6\}, P_2)$	$(\{x_2, x_4, x_6\}, P_2)$	$(\{x_2, x_4, x_6\}, P_2)$
$X = x_5$ and $P = P_3$	$(\{x_5\}, P_3)$	$(\{x_5\}, P_3)$	$(\{x_5\}, P_3)$
$X = U$ and $P = W$	(U, W)	(U, W)	(U, W)





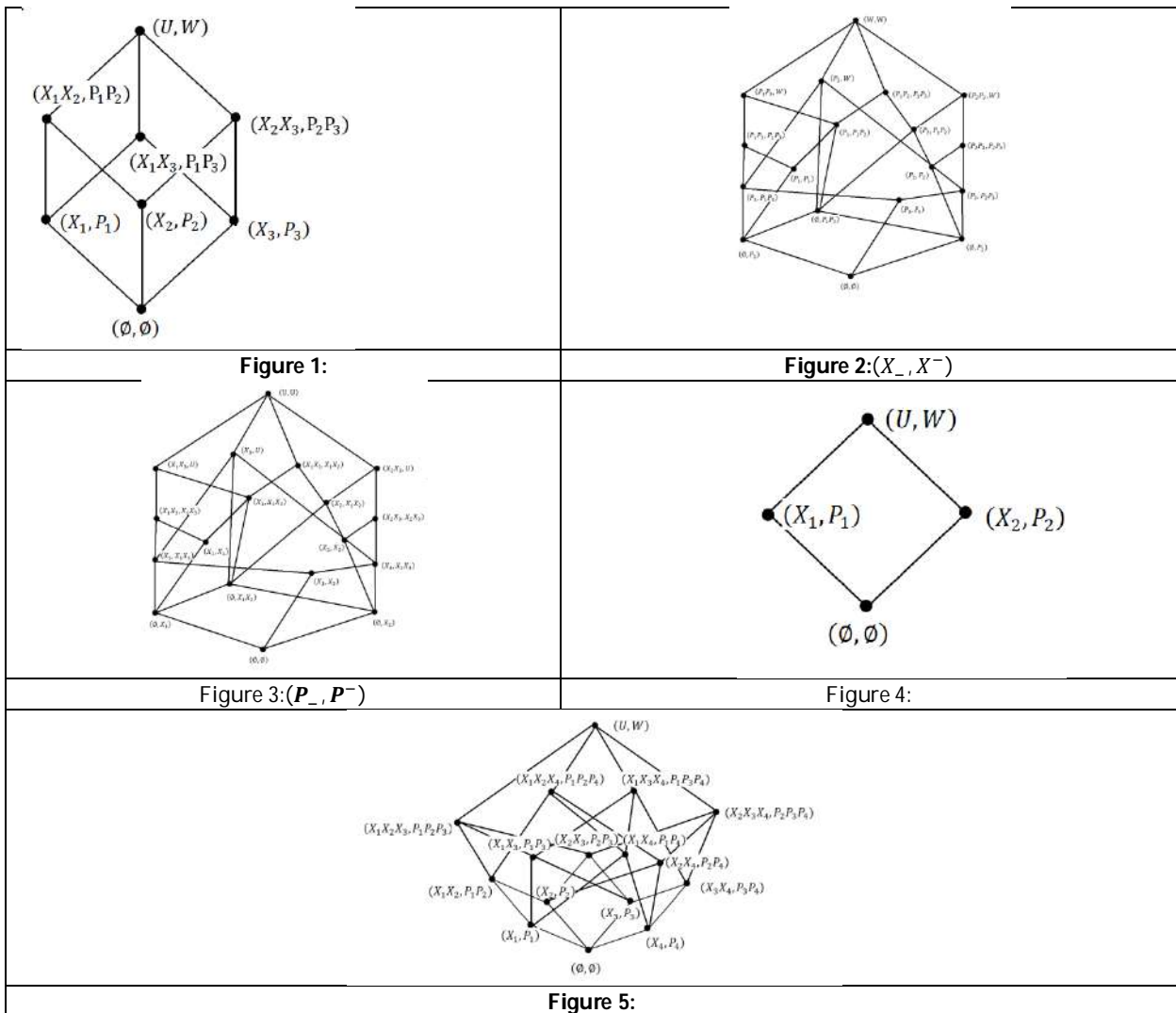
Praba and Anto Freeda

Table 6: $F_{(X_2, P_2)}(\overline{(U, A)})$ is closed under \wedge

\wedge	(X_2, P_2)	(X_1X_2, P_1P_2)	(X_2X_3, P_2P_3)	(U, W)
(X_2, P_2)	(X_2, P_2)	(X_2, P_2)	(X_2, P_2)	(X_2, P_2)
(X_1X_2, P_1P_2)	(X_2, P_2)	(X_1X_2, P_1P_2)	(X_2, P_2)	(X_1X_2, P_1P_2)
(X_2X_3, P_2P_3)	(X_2, P_2)	(X_2, P_2)	(X_2X_3, P_2P_3)	(X_2X_3, P_2P_3)
(U, W)	(X_2, P_2)	(X_1X_2, P_1P_2)	(X_2X_3, P_2P_3)	(U, W)

Table 7:

\vee	(\emptyset, \emptyset)	(X_1, P_1)	(X_2, P_2)	(X_1X_2, P_1P_2)	(X_2X_3, P_2P_3)	(U, W)
(X_2, P_2)	(X_2, P_2)	(X_1X_2, P_1P_2)	(X_2, P_2)	(X_1X_2, P_1P_2)	(X_2X_3, P_2P_3)	(U, W)
(X_1X_2, P_1P_2)	(X_1X_2, P_1P_2)	(X_1X_2, P_1P_2)	(X_1X_2, P_1P_2)	(X_1X_2, P_1P_2)	(U, W)	(U, W)
(X_2X_3, P_2P_3)	(X_2X_3, P_2P_3)	(U, W)	(X_2X_3, P_2P_3)	(U, W)	(X_2X_3, P_2P_3)	(U, W)
(U, W)	(U, W)	(U, W)	(U, W)	(U, W)	(U, W)	(U, W)





Analysis of Applications for Mobile Banking using UPI - Security Analysis and Advancements

M.Padmapriya^{1*} and V.Sripriya²

¹Assistant Professor, Management Studies, PSG College of Arts and Science, Tamil Nadu, India.

²Head and Professor, Management Studies, College of Arts and Science, Tamil Nadu, India

Received: 15 Feb 2023

Revised: 25 Apr 2023

Accepted: 16 May 2023

*Address for Correspondence

M.Padmapriya

Assistant Professor,
Management Studies,
PSG College of Arts and Science,
Tamil Nadu, India.



This is an Open Access Journal / article distributed under the terms of the **Creative Commons Attribution License** (CC BY-NC-ND 3.0) which permits unrestricted use, distribution, and reproduction in any medium, provided the original work is properly cited. All rights reserved.

ABSTRACT

As a result of technological improvements, everyone can now afford a mobile device and a broadband connection. Parallel to this, the number of mobile applications is growing, offering quick, simple door-step solutions to one's professional and personal needs. Mobile-based app solutions provide a wide range of banking financial services (pay/collect money, etc.) and non-financial services in the present trend of the digital and cashless economy (cheque request, account balance, view transaction history etc.). The explosion of mobile apps is also accompanied by numerous known and unidentified security threats. UPI (Unified Payment Interface) based apps are among the more user-friendly, dependable, centrally certified (by NPCI [National Payment Corporation of India]), and secure mobile banking applications. Studying UPI apps indicated the potential for additional security improvements using technology breakthroughs to stop fraud and cybercrimes in mobile transactions. This paper examines information security improvement recommendations with regard to authentication and authorisation, as well as UPI-based mobile apps (architecture, transactions, functionality and security challenges).

Keywords: Security; UPI; USSD; Authentication; Authorization; Encryption; Financial Service; Application Security; Information Security; Mobile Banking;

INTRODUCTION

With the help of a handheld mobile device, the end user can do remote banking operations (both financial and non-financial) at any time and from any location. There are many different technology-specific mobile banking solutions available, including IMPS (Immediate Payment Service), USSD (Unstructured Supplementary Service Data), SMS





Padmapriya and Sripriya

(Short Messaging Service), and UPI (Unified Payment Interface) [1] based app solutions (like BHIM (Bharat Interface for Money), GooglePay (Tez), PhonePe, and Bank-specific apps like SBI Pay, Axis Pay, i Mobile, Mobile Money, etc.). Every programme offers different functionality and security levels depending on the mobile device's capabilities, operating system, and internet connectivity. Banking activities based on USSD and SMS are appropriate for low-end non-smart phones without an internet connection. In collaboration with Mobile Network Operators (MNOs), USSD service is provided. Even though there are a few security issues with mobile banking apps, everyone still prefers them because of their well-known benefits like being quick, simple to use, useful for paying bills, portable, available, etc. Even banks support mobile banking [2] because it increases consumer capacity while lowering operational costs without sacrificing service quality. To promote mobile banking, banks often provide discounts, prizes, etc.

The terminologies frequently used in mobile payment kinds are listed below. Virtual Private Address: VPA An address with the @upi [6] format that is used to send money via UPI Apps. A user may create several VPAs. VPA is used internally by UPI-based fund transfers to look up account numbers. Indian Financial System Code (IFSC) The eleven-digit code on the back of a check is used to identify the financial institutions that are involved in money transfers. Mobile Money Identifier, or MMID, a special seven-digit code given to clients when they register to use the IMPS service as a beneficiary. The paper's content is divided into seven sections, including Section 2 on the evolution of financial and payment solutions, Section 3 on UPI-based mobile banking, Section 4 on security enhancement suggestions, Section 5 on UPI vs. other parallel systems, Section 6 on conclusions, and Section 7 on the paper's future work scope.

Evolution of financial and payment solutions

Over the years, coins have given way to paper and plastic money as part of the evolution of money, which began with the barter system (i.e., the reciprocal exchange of goods and services) (i.e. cards). The below depicts the changes in the development of money. In the twenty-first century, currency-free money transfers are now possible through mobile payments and virtual currencies. NEFT (National Electronic Fund Transfer), RTGS (Real Time Gross Settlement), IMPS (Immediate Payments Service), UPI, USSD, and mobile wallets are just a few of the many alternatives available to users for mobile-based payments. The many mobile payment methods available. Portable Payment Methods. Methods of Mobile Payment Below is a list of mobile payment options. NEFT: A method of transferring money between accounts. RTGS: A system for immediate 30-minute money transfers [3]. Unlike NEFT, RTGS immediately and without delay executes the instructions. IMPS: An immediate payment mechanism that enables mobile money transfers between accounts. It is an NPCI initiative. UPI: The upgraded version of IMPS is UPI. A single VPA can be used to manage several mobile accounts in this mobile-based payment modality. Enables merchant payment and fund routing. UPI PIN is used to verify UPI fund transfers.

It is based on the IMPS network. Using *99#service codes, USSD is a method of making mobile banking transactions. A safe approach to save credit/debit card information is in a mobile wallet. Enables mobile payment at retail locations. The availability of multiple payment methods enables the user to select the most appropriate method in accordance with the capabilities of his or her device (smart/GSM phone), internet connectivity (online/offline), known/available confidential information (i.e. Account Number/IFSC/MMID code/Mobile number/VPA and MPIN), fund transaction details including amount, day and time (i.e. weekday/weekend, and time of day), and known/available confidential information (i.e. B. An evaluation of mobile payment options

The comparison of different mobile payment solutions. Users prefer to use their bank account data in net banking on a PC rather than a mobile device because NEFT/RTGS/IMPS require them. Depending on an affordable transfer time, one may select NEFT or RTGS for transactions of 2 lakhs within banking hours (i.e. within 30 minutes or more but on same day). NEFT is the only option for offline/online transactions over \$2 lakh, but for transactions under \$5,000, one may pick between NEFT (only on business days), UPI, and USSD (any day any time). UPI is the sole option for big amounts (up to 1 lakh) to be transferred quickly, easily, and securely online or offline without the need for private information (such as a bank account number or an IFSC code).





Padmapriya and Sripriya

The only choice on low-end non-smart phone devices is USSD. To sum up, every new payment method overcomes the drawbacks of its prior iteration and offers more capabilities, allowing the user to select one in accordance with his needs and resources.

Mobile Banking Based On UPI

The IMPS infrastructure is used in the backend by UPI, which is an immediate payment system. The mobile financial revolution's push towards a cashless [4] economy has resulted in UPI. UPI Goals, These are its main goals, according to its design. A one-click, two-factor authentication-based payment system with a simple, secure interface. Should be able to send and receive protected payments without revealing any private information about the user, such as their bank account number. Utilize the cutting-edge capabilities of mobile devices to offer a creative solution with excellent security. Offer a streamlined payment method. Must be able to integrate with third-party security measures to add extra protection.

Architecture by UPI. The UPI's architecture is provided. A common collection of UPI APIs [9,10,11,13] and an architecture make up the Unified Payment Interface, which is used to carry out transactions (credit/debit). The following parties are involved in UPI payment transactions. The UPI Architecture PSPs: Refers to Banks' UPI apps that are used to offer payment services to end users. Banks: Customer's bank Provides the UPI interface is NPCI.

A. Types of Transactions

Both financial and non-financial transactions are supported by UPI. Financial Exchanges: Pay Request: A PUSH transaction that the customer started to transfer money to the beneficiary account using the beneficiary's account number, IFSC code, mobile number, MMID, Aadhaar number, etc. Collect Request: The customer uses his VPA to obtain the monies from the remitter. Transactions That Are Not Financial: Mobile Banking Sign-Up OTP Generation Update PIN Set Status Check Transaction

B. Flow of Transactions

A UPI transaction includes three phases: push/pull transaction, one-time customer registration [5], and bank account registration. To register a customer, download and install the UPI app. Create and send a [2,3,4] SMS with a PKI encrypted device fingerprint (i.e. about mobile number is bound with other device identities namely Device Id, App Id, IMEI number etc. [5]). Create a VPA (a unique identifier with the @ sign that is used internally during transactions to map to the bank account number). Registering a bank account Create bank accounts in the app. Create an MPIN using an OTP; after it is authenticated with the user's debit card's last six digits and expiration date, the app registers the user's MPIN with the bank.

The transaction flow of a pull request is called a push/pull transaction. UPI Pull Transaction, Push can be done with a VPA, IFSC, or Aadhaar number. Pull is carried out by starting a collect request with the payer's VPA as the input, and after authorization by the remitters PSP and MPIN authentication by the payee, the money is sent to the beneficiary's account.

C. Permission

UPI utilizes the following 2F authentication method. 1F - Device finger prints after a mobile number transaction that the PSP has allowed. 2F - UIDAI-authenticated PIN/Biometrics (Unique Identification Authority of India).

D. Benefits

Simple and convenient to use Multifactor Authentication that is Easy and Secure (as it uses only VPA). Gives users unified access to many accounts with a single VPA. UPI APIs make it easier to design apps quickly and incrementally. PSP application innovation and exponential growth are facilitated by straightforward, compact, and feature-specific UPI APIs. resolves all issues that other Non-UPI applications are now experiencing. PSPs are periodically audited and approved by NPCI as secure and authentic UPI Apps. No beneficiary information is required to send funds. Based on the device's capabilities, security can be either biometric or non-biometric. uses the



**Padmapriya and Sripriya**

third-party programme UIDAI to provide biometric authentication using the finger and IRIS (Unique Identity Aadhaar to all residents of India). Multiple identifiers, including VPA, Aadhaar Number, Account number and IFSC, Mobile number and MMID, and QR Scancode, can be used to make payments according to RBI norms, payments can be combined with security apps and technologies from other parties. Infrastructure prerequisites can function both with and without internet access.

4. Proposals for Security Improvement

The security risks and improvement suggestions for UPI-based apps. Discreet MPIN Update security. Currently, MPIN operation just employs the last six digits of the credit card number and the expiration date for authentication; however, this will need to be improved because it is easy for anyone to remember and abuse. Instead, you might read the user's responses to a few pre-registered queries (let this be a subset of randomly selected queries from a primary set that have been registered upon Bank registration) and then compare them. Update the MPIN only when all prompted questions have 100% matching answers; else, stop. Limit the amount of invalid MPIN update transactions to 3 as well. Excessive retries need to prevent the VPA. MPIN updates fraud. Currently, information is stored in the transaction log in the event of MPIN failure. In some bank applications, frequent MPIN update errors cause the UPI app to lock, requiring the user to go to the bank branch. In circumstances when a stolen phone is used inappropriately, MPIN failures may occur, and if an email address is registered, the user may be alerted. Account Improve the present UPI app so that it can record unsuccessful MPIN update attempts with information. An email alert can be sent to a registered email address in the event that a UPI transaction is not authenticated. For additional security improvements, it may also be investigated to leverage optional requirements outlined in RBI recommendations for UPI Apps, behavioural features, and artificial intelligence.

Other Parallel Systems vs. UPI

The mobile wallet is another parallel method for UPI [6]. Mobile wallet apps are less secure than UPI but are technologically more advanced and have an intuitive user experience. UPI is also more secure and runs on the tried-and-true IMPS technology. Mobile wallet providers are growing their customer base through marketing campaigns and clever alliances with particular businesses. Mobile wallets are adapting their business models to meet shifting market demands and technological advancements. Additionally, they have started working with particular banks (For eg Freecharge with Axis, SBI etc). Therefore, in the future, wallets and UPI will coexist and compete with one another. The architecture of UPI-based apps, their transactional flow, their authentication method, and its USP in comparison to alternative mobile banking payment systems have all been covered in this article. We have found a few security problems and suggested security improvement measures to address them (MPIN update transaction security issues and detection of fraud transactions related to MPIN update and UPI financial transactions). It has been noted that adding email notifications and more fields to MPIN authentication will strengthen the security of the current UPI application. Additionally, there is potential to include AI and behavioural characteristics to improve security.

Projective Area of Work

The next phase is to design, execute, and evaluate the suggested solutions once specific UPI difficulties have been discovered and their associated solutions have been outlined in outline form in this work. It is necessary to investigate the optional RBI rules related to security for the inclusion and usage of behavioural features and artificial intelligence for authentication during UPI transactions in order to make further security upgrades.

Utilizing Online Banking

We have examined a pilot case of victimisation in Sangli City in order to understand the functioning on the area of preventative and remedial legal actions in cases involving digital identity theft (Maharashtra, India). The investigation demonstrates how customers who conduct online banking might become easy targets for cybercriminals due to banking sectors' violations of precautionary legislation and how victims' legal remedies sometimes fail to help them. Since IT has proven to be a boon for industries around the world, every nation, including India, is now making efforts to recognise the legality of consumer online transactions, providing the



**Padmapriya and Sripriya**

necessary infrastructure, and creating a variety of other favourable legal conditions for the expansion of the IT industry. However, given the increasing prevalence of online identity theft around the world, these developmental goals shouldn't take precedence over the interests of particular consumers. In order to protect them against victimisation, it is essential to implement the appropriate preventive and corrective legal measures as well as strong law enforcement. The paper will aid in understanding the issues at hand and potential remedies for successful application of pertinent legislation connected to Identity Theft.

Findings from the research

From the foregoing considerations, it can be concluded that the government agencies in India support the development of information technology in order to advance the economic interests of the nation. Giving legal status to every transaction carried out electronically or online was one of the goals for passing the Information Technology Act. By providing the necessary facilities and infrastructure, the government is also attempting to create an environment that is appropriate for the goal. The regulatory agencies are also establishing standards and guidelines that must be followed by banks and other service providers in order to promote customer confidence in online transactions. However, as was already mentioned, the scenario on the field is entirely different.

The government and its law enforcement organisations are least concerned with protecting the interests of consumers in the industrial sector (banking, telecommunications, and other corporate bodies). Few banking and telecommunications businesses are breaking the preventive regulatory standards, and police personnel lack the skills necessary to look into crimes that hide behind complicated procedures and technicalities. Between investigative officers from state police departments across the nation, there is a lack of coordination. The victims are not aware of the legal options they have. As a result, our legal system encounters a number of obstacles while attempting to apply the pertinent law for the interests of consumers. As a result, it can be said that India's legal framework and general strategies for addressing the issue of digital identity theft are development-oriented rather than consumer- or victim-oriented.

Artificial Machine Intelligence Language for Chatbot Conversational Banking Automation

The subject of artificial machine intelligence is quite complex. It entails building tools with the ability to simulate knowledge. This essay looks at some of the most recent AI behaviours and trends before offering an alternative idea for how some of the most widely held beliefs of the day might evolve. System-Chatbots are created based on fundamental A.I. (Artificial Intelligence) structuring and working for this (or chatter bots). The study demonstrates how AI is always evolving. There is currently a lack of knowledge regarding artificial intelligence, but this study introduces a novel idea that discusses machine intelligence and highlights the possibilities of intelligent systems. The latest disruptive force that has altered how customers connect is the growth of chatbots in the finance industry. Artificial intelligence has transformed the way that banks communicate with their consumers in the banking sector by enabling chatbots. Any nation's development depends heavily on the banking industry. It also investigates the chatbot's current usability to determine whether it can satisfy customers' fluctuating needs.

CONCLUSION AND FUTURE WORK,

This article discusses ontology-based dialogue management techniques for the banking and financial industry. Although this work has not yet undergone comprehensive testing, the existing successes are promising. The framework must be finished, and a chatbot must be developed, among other tasks [24]. The future system would serve as a first step in the development of an intelligent question management programme that is capable of not only responding to queries but also self-improving in subsequent stages. This would improve user service while also lessening the burden on human workers, boosting productivity, and, of course, increasing the number of satisfied users. In the rapidly expanding field of artificial intelligence, consumers receive technical support in every part of their life.

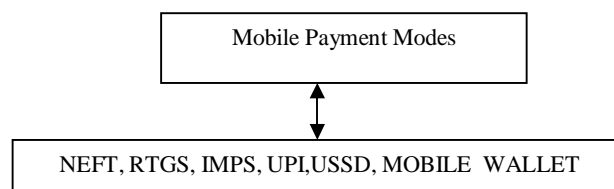


**Padmapriya and Sripriya**

The internet offers a variety of information-gathering options and has fundamentally altered how we communicate. Innovation has improved our lives by giving us more opportunities, and things are now very straightforward for us. Everyone enjoys working together and anticipates quick responses. For a variety of reasons, you can frequently contact with others using websites or online networking networks. A chatbot is a programme or service that connects with you simply and assists you in finding answers to your questions. A chatbot can offer a wide range of resources, from monitoring the weather to ordering a new pair of shoes to sending crucial life-saving safety alerts. When dealing with a chatbot, you should feel as though you are speaking to a real person. Additionally, the domain's growth is necessary. Intelligent responses are generated by including not only the most recent FAQ list but also numerous additional sources, including servers, twitter, and other data sources. Presenting solutions for a conclusion. Imaginative answer image and links. Combining cosine similarity with linguistic similarity. Information pertaining to the reporting account using the Bank's integrated system.

REFERENCES

1. Ozili, P.K. Decentralized finance research and developments around the world. *J BANK FINANC TECHNOL*6, 117–133 (2022). <https://doi.org/10.1007/s42786-022-00044-x>
2. Bandara, E., Shetty, S., Mukkamala, R. *et al.* Casper: a blockchain-based system for efficient and secure customer credential verification. *J BANK FINANC TECHNOL*6, 43–62 (2022). <https://doi.org/10.1007/s42786-021-00036-3>
3. Ioannou, I., Demirel, G. Blockchain and supply chain finance: a critical literature review at the intersection of operations, finance and law. *J BANK FINANC TECHNOL*6, 83–107 (2022). <https://doi.org/10.1007/s42786-022-00040-1>
4. Oyeboode, O., Orji, R. A hybrid recommender system for product sales in a banking environment. *J BANK FINANC TECHNOL*4, 15–25 (2020). <https://doi.org/10.1007/s42786-019-00014-w>
5. Patki, A., Sople, V. Indian banking sector: blockchain implementation, challenges and way forward. *J BANK FINANC TECHNOL*4, 65–73 (2020). <https://doi.org/10.1007/s42786-020-00019-w>
6. Kaul, S.D., Hatzinakos, D. Intelligent RFID biometric enabled dual security lock in the banking environment. *J BANK FINANC TECHNOL*4, 159–173 (2020). <https://doi.org/10.1007/s42786-020-00022-1>

**Fig. 1. Application of Mobile Payment Modes**



An Analytical Study on Union Budget and its Impact on the Infrastructure Sector Index of India

Syed Tabassum Sultana*

Professor, Matrusri Engineering College, 16-1-486, Saidabad, Hyderabad, India.

Received: 24 Feb 2023

Revised: 20 Apr 2023

Accepted: 26 May 2023

*Address for Correspondence

Syed Tabassum Sultana

Professor,

Matrusri Engineering College,

16-1-486, Saidabad,

Hyderabad, India.

E. Mail: s.tabassumsultana@gmail.com



This is an Open Access Journal / article distributed under the terms of the **Creative Commons Attribution License** (CC BY-NC-ND 3.0) which permits unrestricted use, distribution, and reproduction in any medium, provided the original work is properly cited. All rights reserved.

ABSTRACT

The rationale of the current research is to analyse the allocation of funds to infrastructure sector in the Union budget and explore the relationship between union budget and infrastructure sector index. The study has focused on the Union budget funds allocation to the infrastructure sector. The budget allocation to infrastructure is crucial to the Indian economy because this will create the new metro lines, roads railways that increases the movement of goods and also expedites the growth of the economy. The current study considers secondary data from 2007-08 to 2019-20 that is 13 years annual data. Auto regressive Distribution Lag and Ordinary least square method were applied to analyse the data. The study concludes that every year in the union budget is increasing the proportion of allocation funds to the infrastructure sector. The current study confirms that there is a long run and positive relationship between Union budget and infrastructure sector stock prices. Allocation of funds in the budget is significantly affecting the infrastructure sector stocks and infrastructure stock prices. The current study aids the policy makers in allocating union budget funds to infrastructure sector.

Keywords: Union Budget, Fund allocation, Impact, Infrastructure Sector index.

INTRODUCTION

A Union budget is defined as an official document approved by the legislature and accepted by the President. The two fundamental elements of any budget are the revenues and expenses. Union Budget is intended for best possible allocation of scarce financial resources taking into consideration economical and socio-political. Union Budget is an estimation of expenditure and receipts with the help of past performance for plans of the future government for various Departments. The budget is the financial manifestation of what the government proposes to do. The vital

57382



**Syed Tabassum Sultana**

feature of allocating funds in the budget is to choose or prefer which of the activities to be approved on and to what level, with the limited financial resources available. The dilemma is not only how to maximize the benefits of the budget but also who will get the benefits and to what extent. The ultimate objective is optimal utilization of financial resources in terms social benefit.

The principal goal of a budget is economic growth which leads to improvement of living standards of the people along with balanced economic growth. The primary objective of the budget is to attain higher economic growth, price stability and full employment. Budget plays a crucial role in the pooling of capital in public and private sector, mobilizing financial resources for projects related to infrastructure and reduce the imbalance is the dispersal of wealth and income in the hands of the people of the country. Budget impact all the sectors greatly in India. Industries performance depends on the overall policy and guidelines laid by the government. The union budget by the central government issues the extensive guidelines for all the major sectors of the country. Infrastructure sector refers to power, bridges, dams, roads, and urban infrastructure. Infrastructure sector is attributed as a most important facilitator of economic growth of a country. It creates a multiplier effect, which ushers the development cycle through diverse industries such as Construction, Steel, Power, Cement, etc. These sectors in turn boost employment and improve efficiency of supply chain while developing infrastructure sector.

REVIEW OF LITERATURE

Thomas, Susan and Shah (2002), viewed that the union budget is the most awaited and viewed event from the perspective of economic policy of India. According to their observation that the maximum number of trade transactions on NSE were 1.4 million transactions on 28th February 2001 on the budget day. In their paper, they discussed the relationship between the Union Budget and the Indian stock market in the certain areas. At the end they concluded that the Indian stock market index is important for the Union budget in influencing prices and volatility. Kaur (2004), explored month effect on Indian stock market. January month has influence on Indian stock market is not significant; however February & December gave considerable positive returns. Sensex and Nifty were found to be more volatile in the month of February when compared to March and April. The returns in the month of March and September were significantly low.

Gupta and Kundu (2006), evaluated the Budget influence on stock markets of India, taking into consideration the sensex returns and volatility of BSE Sensex. The study confirms that the budget has highest impact on post short term budget phase, however during post medium and long term the average returns and instability of Sensex is not much. Soni (2010), analysed the budget influence based on the logarithmic daily returns starting from 2000 to 2009. Budget announcement before and after 3 days, 15 days and 30 days returns were analysed and the results confirm that there is no long run impact of budget on Indian stock markets and during short term there was positive and negative impact on the Sensex. Singhvi (2014), has analysed the influence of Union budget announcement on Nifty from the perspective of Post and pre budget announcement. The time period considered is 3, 15 and 30 trading days. The study confirmed that the day on which budget announcement is made the returns were high compared to previous 3, 15 and 30 trading days return. However, it is found that there is no significant change in the average returns of Nifty..

Asish (2016), study focused on union budget impact on Indian stock market that has considered data between a period of 2012 to 2016. Their analysis of the study has confirmed that during the month of February the index was found to be highly volatile. Gakhar (2016), their research paper evaluated the impact of Union budget on NIFTY. Five budget periods starting from 2011 to 2015 is considered, to study impact on daily average returns and volatility over a period of 3, 10 and 30 trading days in before and after budget period. Paired T-test was used to analyse the average returns and F-test was applied to analyse the variance of the Nifty. Their study has confirmed that there was a maximum impact of budget during short term, less impact during medium term and no impact during long term.



**Syed Tabassum Sultana**

Gayathiri & Ganesamoorthy (2018), they have analysed the impact of 2018 budget on Sensex. They have analysed by using Returns, Average Abnormal Returns and Cumulative Average Abnormal Returns of Sensex. Results of their study confirmed that there is no significant impact of union budget 2018 on the Sensex, however the Cumulative Average Abnormal Returns one day pre and post announcement of budget had a insignificant negative effect on Sensex. Joshi & Mehta (2018), The study analysed the indices of BSE such as BSE Sensex, BSE 500, BSE Auto, BSE Bankex, BSE IT and BSE finance. It has explored from the perspective of how the stock market reacts during the budget announcement and the closing values of the indices. Statistical techniques such as F-test and T-test were used for the analysis. The results of their study confirm there is a considerable impact of budget on these indices.

Based on past literature it can be substantiated that many researchers have explored the influence of Union budget on Indian stock market. The focus of extant literature was more on impact of union budget on short term or medium term returns on the Indian stock market and stock market volatility. Past impact studies related to budget were based on event study method. None of the past studies in the literature have explored the effect of union budget on infrastructure sector. The current study fills the research gap by focusing on long-term impact of budget on infrastructure sector. The current study is based on the empirical data collected over a period of time.

Objectives of the Study

- To analyse Union Budget from the perspective of allocation of funds to infrastructure sector.
- To analyse the trend of infrastructure Index.
- To investigate the association between Union Budget and Infrastructure Sector.
- To evaluate the impact of Union Budget on Infrastructure sector Index.

RESEARCH METHODOLOGY

The present study considers 13 years annual data starting from 2007-08 to 2019-20. The data prior to 2007 could not be considered due to the limitation of data i.e., non availability of CNX Infra, as NSE Infra started in the year 2007.

Data Analysis

The Table 2 presents the figures related Union budget, allocation of funds to infrastructure and percentage of funds allocated to infrastructure sector. Based on the figures presented in Table 2, it can be inferred that there is constant increase in Budget Allocation to Infrastructure Sector during the period 2007-08 to 2019-20. In the year 2018-19 Government allocated the highest 24% of the total Budget towards infrastructure development which shows that the Government is focusing on infrastructure and its development by allocating more funds to infrastructure sector.

Infrastructure Index CNX Infra

Infrastructure Index is designed to measure the performance of the Indian Companies involved in Infrastructure. NIFTY Infrastructure Index comprised of stocks associated to Telecom, Power, Port, Roads, Shipping, and other Utility Service providers. The Index CNX Infra includes 30 companies listed on the National Stock Exchange of India. The table 3 show the weightage of sectors and stocks under the Infrastructure Index. The table 3 presents the list of Sectors and their respective weight in the infrastructure index CNX Infra. Oil & Gas is given 32.36 weights, Cement & Cement products is 17.67, Construction sector is 15.19, Telecom sector is 10.67 and power sector is 9.63. The other sectors such as Services, Automobile, Healthcare services and Industrial Manufacturing is 5.89, 4.48, 2.88 and 1.23 respectively.

Table 4 presents the list of top companies that constituent the CNX Infra and their weightage. Reliance Industries Limited is the Company with highest weightage of 19.10 percent in the CNX Infra followed by Larsen & Toubro Limited with 13.71 percent; Bharati Airtel Limited is 9.40 percent. Top 3 companies stocks have more than 42% of weightage in the CNX Infra Index. Table 5 presents annualized returns of Infrastructure Index CNX Infra during the period 2007 to 2020. Data for the current study is considered from 2007 as Index was launched on August 07, 2007.



**Syed Tabassum Sultana**

Infrastructure Index was trading at 2388 points on December 2008 and it is closed at 3650 on December 2020. In the past 13 years CNX Infra gave 1.07% of average annual returns. Index gave highest return of 50.83% in the period of 2009 and the lowest return of 5.22 in the year 2019. During the year 2008 the CNX Infra has seen maximum fall to an extent of 61.55%. The average annual positive returns of the index during 2007 to 2020 is 21.94% and average annual negative returns is -23.27%.

Table 6 presents the performance of CNX Infra with reference to Nifty. CNX Infra index has given price returns of 8.83 since inception. The standard deviation, Beta with Nifty 50, Correlation with Nifty 50 is 26.51, 1.05 and .90 respectively. Based on the correlation figure it can be concluded that there is a perfect correlation between Nifty 50 and CNX Infra. The beta value is 1.05 indicating that 1 percent rise Nifty 50 will lead to 1.05 percent rise in the CNX Infra. As the beta value of CNX Infra is greater than 1 hence it can be concluded that the CNX Infra is more volatile than Nifty 50. As the data used for the analysis is time series data. Stationarity of the data series is checked by applying Augmented Dickey Fuller (ADF) unit root test. Both variables are found to be stationary at 1st lag. The results of the same are presented in the table 7.

After confirming stationarity, the next step was to investigate the relationship between Union Budget and Infrastructure sector, for which Auto regressive Distribution Lag (ARDL) and Bound Test is applied and the results of the same is presented.

The Figure 2 shows that ARDL(1,1) is considered to have an optimal lag order selection by the study, which implies that the dependent variable (Infrastructure Sector) fits at lag 1, while the independent variable (Union Budget) fits at lag 1. ARDL(1,1) is therefore used to determine the ARDL model with respect to Infrastructure Sector. Auto regressive Distribution Lag (ARDL) represents the long run association between the independent variable and the dependent variable and the results of the same is presented in Table 8. Here, Infrastructure Sector is considered as Dependent variable and Union Budget is considered as Independent variable. To estimate the association between them and study considered period from 2007-08 to 2019-20. The coefficient value of the Infrastructure Sector is found to be positively associated with the independent variable Union Budget. The ARDL model have identified that coefficient value is positive that is 0.016656 between the infrastructure sector and union budget. In order to check the significance of the model, Persaran Bound test has been applied and results are presented in Table 9.

Table 9 shows the results of the Bound Test. From Bound test or Persaran test indicates that, f-statistic calculated values is lies above the persaran critical value at 5% significant level, implies there is Long run association between the Infrastructure Sector index and Union Budget. To evaluate the impact of Union Budget on Infrastructure Sector, Ordinary Least Square method is applied, the results of the same is presented in Table 10. Ordinary Least Square shows the influence of Independent Variable on Dependent variable. Here, Dependent variable is considered as Infrastructure Sector and Independent variable is considered as Union Budget. Table 10 shows that the coefficient value of Infrastructure Sector is positive which indicates that Union Budget is found to have a positive impact on Infrastructure Sector. It also represent that the Probability value is less that 0.0(<0.05). Hence, it is concluded that union budget is significantly influencing the infrastructure index. As the amount of allocation of funds to infrastructure increases the infrastructure index returns also increases.

CONCLUSION

Infrastructure sector is considered as the backbone of any country. Roads, railways, power, telecommunication etc are the pillars on which the economy of any country stands and grows. Infrastructure sector is a key factor of the economy of any country as it propels the countries' economy as a whole. Government policies and initiatives are directed towards creation of top notch infrastructure in India. A country which has robust infrastructure will grow and prosper. The current study has focused on the Union budget funds allocation to the infrastructure sector and analyse the relationship between union budget and infrastructure sector. The study has considered the secondary





Syed Tabassum Sultana

data and the period of study is 13 years annual data starting from 2007-08 to 2019-20. Auto regressive Distribution Lag and Ordinary least square method were used to analyse the data. The study concludes that every year in the union budget vast amount of funds is allocated to the infrastructure sector. The current study confirms that there is a long run and positive relationship between Union budget and infrastructure sector. In long run the union budget is positively affecting the infrastructure sector so the policy makers has to see to it that expenditure on infrastructure has to be still considered as paramount objective while allocating funds in union budget.

REFERENCES

1. Gayathiri & Ganesamoorthy (2018), A study on the impact of union budget 2018 on Indian Stock Market with reference to BSE, International Journal of Research in Humanities, Arts and Literature, 6(6), 129-138.
2. Gupta and Kundu (2006), A Study of the Impact of Union Budgets on Stock Prices in India, The ICFAI Journal of Applied Finance, 12(10), 65-76.
3. Joshi, M. C., & Mehta, R. D. (2018). Impact of Union Budget on Stock Market. In P. C. J. Patel, Mrunal C. (Ed.), Contemporary Issues in Marketing and Finance (First ed., pp. 29-45). Jaipur: Prism Books (India).
4. Kaur (2004). Stock Market Volatility in India. The Indian Journal of Commerce, Volume 57, 4, 55-70.
5. Kutchu, Vishal (2012). Testing Semi-Strong Efficiency of Indian Stock Market - A Study on Effect of Union Budget 2012 on Six Select Sectoral Stocks. International Refereed Research Journal, 3(2), 74.
6. Singhvi, Abha (2014). Impact of Union Budget on NIFTY. Pacific Business Review International, 6(12).
7. Soni (2010), Reaction of stock market to Union Budget and Monetary Policy Announcements, Asia Pacific Journal of Research in Business Management, 1(2), 155-175
8. Thomas, Susan, and Shah, Ajay (2002). Stock Market Response to Union Budget. Economic and Political Weekly, February, 455-458.

Table 1: Sources of data

S. No.	Type of Variable	Variable Name	Proxy	Source of data
1	Independent Variable	Union Budget	Budget Allocation Amount	https://www.indiabudget.gov.in/
2	Dependent Variable	Infrastructure Sector	Returns of Infrastructure Index NSE: CNXINFRA	https://www.nseindia.com/

Source: Compiled by the author

Table 2: Budget Allocation to Infrastructure Sector from 2007-08 to 2019-20

Years	Total Budget (Cr)	Allocation to Infrastructure Sector (Cr)	Percentage of Budget allocated to Infrastructure
2007-08	2,05,000	12,864	6.28%
2008-09	7,50,884	26,832	3.57%
2009-10	10,20,838	32,660	3.20%
2010-11	11,08,749	1,73,552	15.65%
2011-12	12,57,729	2,14,000	17.01%
2012-13	14,909,25	1,94,360	13.04%
2013-14	16,65,297	1,66,756	10.01%
2014-15	17,94,892	1,81,134	10.09%
2015-16	17,77,477	2,51,134	14.13%





Syed Tabassum Sultana

2016-17	19,78,000	2,21,246	11.19%
2017-18	21,47,000	3,96,000	18.44%
2018-19	24,42,213	5,97,000	24.45%
2019-20	27,86,349	4,56,000	16.37%

Source: <https://www.indiabudget.gov.in/>

Table 3 : List of Sectors and their respective weight in the Infrastructure Index (CNX Infra)

Sector	Weight (%)
Oil & Gas	32.36
Cement & Cement Products	17.67
Construction	15.19
Telecom	10.67
Power	9.63
Services	5.89
Automobile	4.48
Healthcare Services	2.88
Industrial Manufacturing	1.23

Source: nseindia.com

Table 4: List of top companies that constituent the CNX Infra and their weightage

Company's Name	Weight (%)
Reliance Industries Ltd.	19.10
Larsen & Toubro Ltd.	13.71
Bharti Airtel Ltd.	9.40
Ultratech Cement Ltd.	6.23
Grasim Industries Ltd.	4.20
Power Grid Corporation of India Ltd.	4.15
NTPC Ltd.	3.98
Adani Ports and SEZ Ltd.	3.51
Oil & Natural Gas Corporation Ltd	2.98
Bharat Petroleum Corporation Ltd.	2.95

Source: nseindia.com

Table 5: Infrastructure Index- Annualized Returns & Growth Rate.

Year	Infrastructure Index	Growth Rate
2007	6210.95	-
2008	2388.1	-61.55%
2009	3602.05	50.83%
2010	3457.6	-4.01%
2011	2124.9	-38.54%
2012	2648.5	24.64%
2013	2389.8	-9.76%
2014	2985.8	24.93%
2015	2631.85	-11.85%





Syed Tabassum Sultana

2016	2712.25	3.05%
2017	3637.5	34.11%
2018	3130.65	-13.93%
2019	3294.25	5.22%
2020	3650.95	10.82%

Source: nseindia.com

Table 6: Performance of CNX Infra with reference to Nifty 50 as on July 2021.

	1 Year	5 Years	Since Inception (2007)
Index Price Returns	40.56	8.36	8.83
Standard Deviation	17.87	19.78	26.51
Beta with Nifty 50	0.95	0.95	1.05
Correlation with Nifty 50	0.87	0.87	0.90

Source: nseindia.com

Table 7: Augmented Dickey Fuller (ADF) Unit Root Test Results of the two Variables.

Variables	1 st Lag	
	t-statistic	Prob.
Budget	-3.610425	0.0074
Infrastructure Index	-4.883909	0.0036

Table 8: ARDL Long Run Form.

Dependent Variable: D(INFRASTRUCTURESECTOR)

Selected Model: ARDL(1, 1)

Case 2: Restricted Constant and No Trend

Sample: 2007 2019

Included observations: 11

Conditional Error Correction Regression

Variable	Coefficient	Std. Error	t-Statistic	Prob.
C	758176.7	677090.2	1.119757	0.2998
INFRASTRUCTURESECTOR(-1)*	-1.108047	0.372961	-2.970944	0.0208
DUNIONBUDGET(-1)	0.016656	1.513888	0.011002	0.9915
D(DUNIONBUDGET)	0.004452	0.888654	0.005010	0.9961

* p-value incompatible with t-Bounds distribution.

Levels Equation

Case 2: Restricted Constant and No Trend

Variable	Coefficient	Std. Error	t-Statistic	Prob.
DUNIONBUDGET	0.015032	1.366436	0.011001	0.9915
C	684245.7	565975.7	1.208967	0.2659

EC = INFRASTRUCTURESECTOR - (0.0150*DUNIONBUDGET + 684245.6586)

Source: eviews output





Syed Tabassum Sultana

Table 9: Bound test				
F-Bounds Test		Null Hypothesis: No levels relationship		
Test Statistic	Value	Signif.	I(0)	I(1)
			Asymptotic: n=1000	
F-statistic	2.947615	10%	3.02	3.51
k	1	5%	3.62	4.16
		2.5%	4.18	4.79
		1%	4.94	5.58
Actual Sample Size	11		Finite Sample: n=35	
		10%	3.223	3.757
		5%	3.957	4.53
		1%	5.763	6.48
			Finite Sample: n=30	
		10%	3.303	3.797
		5%	4.09	4.663
		1%	6.027	6.76

Source: eviews output

Table 10: Results of Ordinary Least Squares Method.				
Squares Dependent Variable INFRASTRUCTURE SECTOR				
Method: Least Squares				
Sample (adjusted): 2008 2019				
Included observations: 12 after adjustments				
Variable	Coefficient	Std. Error	t-Statistic	Prob.
C	225179.6	220693.6	1.020327	0.0024
DUNIONBUDGET	0.163412	0.2414620	0.160012	0.0013
R-squared	0.600372	Mean dependent var		230998.7
Adjusted R-squared	-0.699591	S.D. dependent var		657473.8
S.E. of regression	689436.0	Akaike info criterion		29.87615
Sum squared resid	4.75E+12	Schwarz criterion		29.95696
Log likelihood	-177.2569	Hannan-Quinn criter.		29.84623
F-statistic	4.003723	Durbin-Watson stat		2.898860
Prob(F-statistic)	0.000549			

Source: eviews output

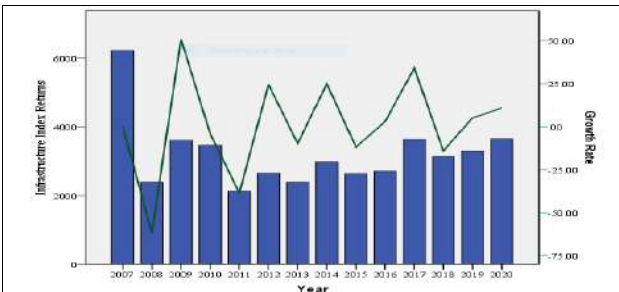


Figure 1: Infrastructure Index- Annualized Returns & Growth Rate

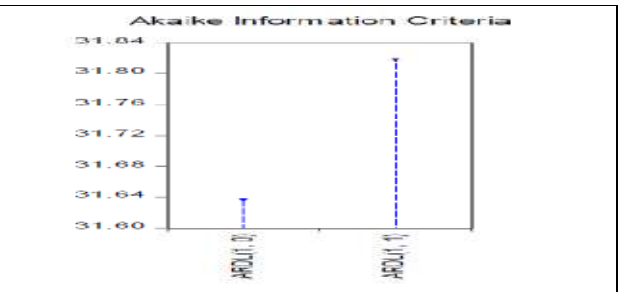


Figure 2: Graph showing ARDL (1, 1)





Effect of Ethanolic Extract of *Achyranthes aspera* Leaves on Polycystic Ovarian Syndrome

M. Ramayyappa¹, K. Srikanth Kumar^{2*}, G. Premi³, G. Raveendra Babu⁴, Ch. Devadasu⁵, M. Jalaiah⁶, K. Sri Ramakrishna⁷, B. Sasidhar⁸, D. Dhachinamoorthi⁹

¹Associate Professor, Dept. of Pharmaceutical Analysis, Shri Vishnu College of Pharmacy, Bhimavaram, AP, India.

²Professor, Dept. of Pharmaceutical Chemistry, QIS College of Pharmacy, Ongole, AP, India.

³Assistant Professor, Dept. of Pharmacology, Shri Vishnu College of Pharmacy, Bhimavaram, AP, India.

⁴Professor, Dept. of Pharmaceutical Analysis, QIS College of Pharmacy, Ongole, AP, India.

⁵Associate Professor, Dept. of Pharmaceutical Analysis, QIS College of Pharmacy, Ongole, AP, India.

⁶Associate Professor, Dept. of Pharmacology, QIS College of Pharmacy, Ongole, AP, India.

⁷Associate Professor, Dept. of Pharmacognosy, QIS College of Pharmacy, Ongole, AP, India.

⁸Associate Professor, Dept. of Pharmaceutical Biotechnology, QIS College of Pharmacy, Ongole, AP, India.

⁹Principal & Professor, Dept. of Pharmaceutics, QIS College of Pharmacy, Ongole, AP, India.

Received: 20 Feb 2023

Revised: 23 Apr 2023

Accepted: 27 May 2023

*Address for Correspondence

K. Srikanth Kumar

Professor,

Department of Pharmaceutical Chemistry,

QIS College of Pharmacy, Ongole-523272,

Andhra Pradesh, India.

Email: drsrikanth@gmail.com



This is an Open Access Journal / article distributed under the terms of the **Creative Commons Attribution License** (CC BY-NC-ND 3.0) which permits unrestricted use, distribution, and reproduction in any medium, provided the original work is properly cited. All rights reserved.

ABSTRACT

Effect of ethanolic extract of *Achyranthes aspera* leaves on polycystic ovarian syndrome (PCOS) was studied. PCOS was induced by administration of Letrozole orally. Estimated the levels of blood glucose, total cholesterol, triglycerides and hormonal changes like increase in level of testosterone, estrogen and decreased levels of progesterone with menstrual irregularity confirmed by vaginal smears and histopathological changes in the ovary of polycystic ovarian disease control. The various treatment groups of *Achyranthes aspera* exhibited significant reduction in blood glucose levels, total cholesterol and testosterone levels have a most prominent action. Identified the presence of phytoconstituents like glycosides, carbohydrates, alkaloids, saponins, terpinoids, proteins, steroids and phenolic compounds. Administration of *Achyranthes aspera* was reduce the blood glucose levels, decrease of androgen production and it showed beneficial effect on anovulation and menstrual irregularity. Also analysed the level of SGOT, SGPT found that significantly reverted in all the treatments. All the treatment groups

57390



**Ramayyappaet al.,**

indicate reduction in Serum urea and creatinine levels weight of these organs, which are related to the endocrine functions. Histopathological study of PCOS control showed more number of developed cyst and theca lutein cells. Various treatment groups showed significant reduction of number of cysts as compared to PCOS control rats.

Keywords: Ethanolic extract, *Achyranthes aspera*, Letrazole, Histopathological studies, blood glucose, menstrual cycle, biochemical estimation, hormonal analysis, follicular cyst.

INTRODUCTION

Polycystic ovary syndrome (PCOS) is one of the most common endocrine disorder frequently characterised by the accumulation of numerous cysts (fluid- filled sacs) on the ovaries associated with high male hormone levels (hyperandrogenism), ovulatory dysfunction, abdominal obesity, and other metabolic disturbances. The reproductive features of Polycystic ovary syndrome (PCOS) include the increased production of androgen and disordered gonadotropin secretion leading to the menstrual irregularity, hirsutism, and infertility [1,2]. PCOS is characterized by hyperandrogenism, elevated androgen levels, acne, acanthosis nigricans, insulin insensitivity, and chronic anovulation [3-6]. The aetiology of PCOS is not clearly understood, but lipid imbalance, oxidative stress, insulin resistance and genetics are some of the contributing factors [7-9]. The association with insulin resistance leads to increased production of androgen in theca cell by leutinizing hormone was increased and also the inhibition of hepatic synthesis of SHBG synthesis in liver cell. It prevents the normal follicular development in granulose cell by decrease in the level of follicular stimulating hormones which leads to follicular arrest [10].The treatment options in this case contribute to be more natural. Patients may be influenced to avoid dairy while also being prescribed supplements such as Iodine, Vitamin D, Magnesium, and Zinc, along with herbal formulas to reduce testosterone. Natural progesterone may also be prescribed in order to improve the hormonal imbalance and induce ovulation [11-15].In the United States, polycystic ovarian syndrome (PCOS) is one of the most common endocrine disorders of reproductive-age women, with a prevalence of 4-12%. Up to 10% of women are diagnosed with PCOS during gynecologic visits. In some European studies, the prevalence of PCOS has been reported to be 6.5-8%. Ranging from 2.2% to as high as 26%. As a result, the levels of estrogen, progesterone, LH, and FSH become imbalanced. Androgens are normally produced by the ovaries and the adrenal glands[16-18].Androgens may become increased in women with PCOS because of the high levels of LH but also because of high levels of insulin that are usually seen with PCOS [19, 20].In the present study is to evaluate the *in-vivo* polycystic ovarian syndrome of ethanolic leaves extract of *Achyranthes aspera*.The main objective of this study is to evaluate theeffectiveness of *Achyranthes aspera*on PCOS through blood glucose levels estimation, identification of irregularity in menstrual cycle, biochemical estimation, hormonal analysis, follicular cyst developments in Letrozole induced PCOS in rats.

Plant Profile

Achyranthes aspera belongs to Amaranthaceae, six species of *Achyranthes* occur in warm temperate and tropical regions of the world. The root, seeds and leaves of *Apamarga* is used in the form of juice and powder to treat excessive hunger, piles, visucika, sidhma, calculi and stone, wounds, difficult labour, sin, accidental wounds, eye disease, ear disease, head disease, dog-bite, abdominal pain, jaundice, insomnia and pain in vagina [21,22].

MATERIALS AND METHODS

Preparation of Stock Solutions

1mg/ml solution was prepared by using carboxy methylcellulose as a diluting solvent.



**Ramayyappaet al.,****Preparation of Test Dose**

From the above prepared 1mg/ml solution 200, 400,600 mg/ml solution were prepared. Doses were given to animals according to body weight.

Preparation of Standard Dose

1mg/ml solution of Clomiphene citrate was prepared by using carboxy methylcellulose as a diluting solvent. Doses were given to animals according to body weight.

Authentication of Plant

The fresh plant of *Achyranthes aspera* was collected from Nallajerla, West Godavari Andhra Pradesh. The plant was identified and authenticated by Dr. Ramadevi, Associate Professor of Dr. Y.S.R Horticulture University, Venkatramanna Gudem.

Drying

After collection of leaves they were washed; left for shade dry for 10 days.

Soxhlet Extraction Procedure

After drying, plant leaves were size reduced by grinder. The dried powdered material was weighed and subjected to extraction by soxhlet apparatus. The apparatus was ran at a speed of 3 cycles/1hr. This process was continued for 16 hrs. Finally solvent was recovered by simple distillation. Crude drug obtained from above procedure was stored carefully at room temperature. Phytochemical investigation was done to this crude material to identify secondary metabolites or constituents of plant. This crude material was used as a drug in the treatment of our present *in-vivo* screening [23].

Phytochemical Screening**Animal Study**

The Wister albino female rats weighing 180-220g were obtained from Sai Agencies Secunrabad all animals were kept under 27± 2°C, 80±10% humidity and a 12 hr light/ 12hr dark cycle. The animals were provided with free access to water and they were fed with standard rat diet. Each case contained 3 rats with bedding of husk. Animals were acclimatized 7 days prior to initiation of experiment. Polycystic ovary was induced in female rats by giving an oral administration of Letrozole once daily at the concentration of 1.0mg/kg dissolved in 0.25% carboxymethylcellulose (2ml/kg body weight vehicle) For 21 days. After 21 days (i.e. 22 day) PCOS control group animals were anesthetised by diethyl ether and retro orbital puncturing was done to determine blood glucose, estrogen, progesterone and total cholesterol. Then animals were sacrificed to determine the weight of uterus, ovaries, kidneys liver and heart. The treatment group animals were treated with different doses of plant extract and standard group animals were treated with Clomiphene citrate for a period of 15 days. On 36th day animals were anesthetised by diethyl ether and retro orbital puncturing was done to determine blood glucose, estrogen, progesterone and total cholesterol then animals were sacrificed according to the protocol to determine the weight of uterus, ovaries kidneys, liver and heart [24-26].

Vaginal Smear Preparation Procedure

The value of the vagina smear method for the study of ovarian function is based upon the response of the vaginal epithelium to the hormones of the ovary. Smears were taken every day on 10am. Female animals were anesthetised according to procedure by diethyl ether then animals were positioned in ventral side. A piece of cotton ear swab was taken and wetted by normal saline. Inserted the swab into vagina of the rat to certain depth and then rotated the swab gently in a clock wise direction. Then slowly removed the swab out of the vagina, and then rolled the swab on microscopic glass slide. The glass slide was stained by crystal violet or methylene blue then dried. Glass slide was gently washed by water again dried for one minute. Then cells were observed by light microscope by 10X [27].





Ramayyappaet al.,

Biochemical Parameters Determination

On 22nd day (only PCOS induced group) and 36th day (remaining all groups) of the study, the animals were anesthetized with diethyl ether. The blood was drawn through retro orbital plexus and the serum was separated after centrifugation of total blood without anticoagulants, at 3000rp, for 10 min. The analysis of blood glucose, Total cholesterol, Triglycerides, serum glutamic-oxaloacetic transaminase (SGOT), serum glutamic pyruvic transaminase (SGPT), urea, creatinine were estimated in serum by standard laboratory technique [28-30].

Hormonal Determination

The Serum testosterone, estrogen and progesterone were measured using an enzyme immunoassay kits by standard laboratory techniques [31].

Body Weight Observation

Body weights of the animals were monitored every day morning by using weighing balance till the end of the experiment [32].

Histopathology

After Scarification of animals ovaries were dissected immediately without any delay. After that they were placed in a formalin containing container for fixation for a period of 16hrs. After fixation samples were subjected to dehydration by immersing them in a series of alcoholic solutions of increasing order normally 70%, 90%, 100% alcohol for a period of each 15mins respectively. Later samples were immersed in a clearing solution like xylene for 20min. then samples were placed in a tissue embedding cassette and pour molten pure paraffin wax on cassette then they were kept at 20°C for 20min. Finally they were sectioned at a thickness down to at least 2µm and sections were observed by using microscope [33].

RESULTS AND DISCUSSION

Polycystic ovarian syndrome was induced by oral administration of Letrozole 1mg/kg body weight of female rats at single dose. This causes the animals to produce irregular estrus cycle, anovulation and hormonal imbalance, abnormal follicular development hyperlipidemia and hyperglycemia. Hormonal evaluation showed that Letrozole induced PCOS rats were shown significant increase in serum Estrogen, Testosterone levels and decreased Progesterone levels as compare to PCOS control group. Letrozole administration increased sensitivity of the pituitary to GnRH results an increase in leutinizing hormone (LH) and increased insulin levels mainly amplify the intrinsic abnormality of their steroidogenesis. Excess androgen activity leads to hyperandrogenism. *Achyranthes aspera* changed these levels to almost normal. The present study total cholesterol and triglycerides levels were increased to high level in Letrozole induced PCOS rats these high levels might cause obesity and cardiovascular diseases. *Achyranthes aspera* significantly decrease the levels of cholesterol and triglycerides in all treatment groups (Group-III, IV, V, VI) as compared to letrozole induced PCOS control.

Vaginal Smears

Total 36 days smears were taken to all animals. Every day at 10am smears were taken.

Biochemical Parameters

The above Values are expressed as Mean±SEM, n=6. used one way ANOVA to calculate statistical significance of various groups at *P<0.05, **P<0.01, ***P<0.001 by using Dunnette multiple comparison test. The above Values are expressed as Mean±SEM, n=6 used. one way ANOVA to calculate statistical significance of various groups at *P<0.05, **P<0.01, ***P<0.001 by using Dunnette multiple comparison test. The above Values are expressed as Mean±SEM, n=6. used one way ANOVA to calculate statistical significance of various groups at *P<0.05, **P<0.01, ***P<0.001 by using Dunnette multiple comparison test.





Ramayappa et al.,

CONCLUSION

The present study polycystic ovarian disease was induced by administration of Letrozole orally. It confirmed that elevated levels of blood glucose, total cholesterol, triglycerides and hormonal changes like increase in level of testosterone, estrogen and decreased levels of progesterone with menstrual irregularity confirmed by vaginal smears and histopathological changes in the ovary of polycystic ovarian disease control. In this study, SGOT, SGPT level was significantly increased in PCOS control group as compared to the normal control. It indicate that the impairment of hepatic function in PCOS group. The elevated level of SGOT, SGPT and ALP was significantly reverted in all the treatments. Serum Urea and Creatinine levels were increased in Letrozole induced PCOS rats it might be the causes of renal dysfunction the earliest stages of atherogenesis is endothelial cell dysfunction. Result of this study suggests the *Achyranthes aspera* treatment prevent the impairment of renal functions evident by a decrease in serum urea and creatinine. The increase in liver and ovary weight are related to inhibit the hepatic synthesis, and increases the immature development of follicles in ovary and increase androgen secretions in Letrozole induced PCOS rat. Histopathological study of PCOS control showed more number of developed cyst and theca lutein cells. Various treatment groups showed significant reduction of number of cysts as compared to PCOS control rats.

REFERENCES

1. Angela hywood ND and Kerry bone. Phytotherapy for polycystic ovarian syndrome. Medi Herb A phytotherapists perspective 2004; 1: 46.
2. Daljit Singh Arora and Henna Sood. In vitro antimicrobial potential of extracts and phytoconstituents from *Gymnema sylvestre* R.Br. leaves and their biosafety evaluation. AMB Express 2017; 7: 115.
3. Monica Robinson Green, Uche Anadu Ndefo, Angie Eaton. Polycystic Ovary Syndrome: A Review of Treatment Options with a Focus on Pharmacological Approaches. Pharmacology & Toxicology 2013; 38(6): 336-338, 348, 355
4. Sushma P Reddy, Nazia Begum, Sumith Mutha, Vasudha Bakshi. Beneficial effect of Curcumin in Letrozole induced polycystic ovary syndrome. Asian Pacific Journal of Reproduction 2016; 5(2): 116-122.
5. Polikistik over sendromu olusturmak için kullanılan deneysel modeller Mehmet CİNar, Özlem GuN EryİlMaz. Experimental models of polycystic ovary syndrome Medeniyet Medical Journal 2016; 31(1): 53-57.
6. Radha Maharjan, Padamnabhi S. Nagar, Laxmipriya Nampootheri. Effect of Aloe barbadensis Mill. formulation on Letrozole induced polycystic ovarian syndrome rat model. Journal of Ayurveda and Integrative Medicine 2015; 1(4): 273-279.
7. Sudhakar Pachiappan, Suganeswari Matheswaran, Poorana Pushkalai Saravanan and Gayathiri Muthusamy. Medicinal plants for polycystic ovary syndrome: A review of phytomedicine research. International Journal of Herbal Medicine 2017; 5(2): 78-80.
8. Susan M, Sirmans and Kristen A Pate. Epidemiology, diagnosis, and management of polycystic ovary syndrome. Clin Epidemiol 2014; 6: 1-13.
9. Susan Sam, MD Obesity and Polycystic Ovary Syndrome. Obes Manag 2007; 3(2): 69-73.
10. Srinath Reddy T, Arafath S, Saba Shafeen, Hima Bindu R, Adithya N, Nagarjuna S. In Vitro Evaluation of Anthelmintic Activity of *Gymnema sylvestre* leaves against *Pheretima posthuma*. Pharmacognosy Res 2011; 3(2): 140-142.
11. Chinenye Jane Ugwah-Oguejiofor, Shaibu Oricha Bello Ramyond U Okolo, Emmanuel U Etuk, Michael oguejiofor ugwah Vincent ugochukwu Igbokwe, Mohammed Umar. Effect of aqueous extract of *Ficus platyphylla* on female wistar rats with estradiol valerate-induced polycystic ovarian syndrome. International journal of Phytomedicine 2014; 6 (3): 405-411.
12. Doss.A and Anand S.P. Antihyperglycemic activity of methanol and aqueous extracts of *Pergularia daemia*. African Journal of Biotechnology 2013; 13(1): 170-174.
13. Srividya AR, Varma SK, Dhanapal SP, Vadivelan R, and Vijayan P. In vitro and in vivo evaluation of hepatoprotective activity of *Gymnema sylvestre*. International Journal of Pharmaceutical Sciences and Nanotechnology 2010; 2: 768-773.





Ramayappaet al.,

14. Adegoke AA, Iberi PA, Akinpelu DA, Aiyegoro OA, Mboto CI. Studies on phytochemical screening and antimicrobial potentials of *Phyllanthus amarus* against multiple antibiotic resistant bacteria. *International Journal of Applied Research in Natural Products* 2010; 3 (3): 6-12.
15. Ahmed M Kabel Polycystic Ovarian Syndrome: Insights into Pathogenesis, Diagnosis, Prognosis, Pharmacological and Non-Pharmacological Treatment. *Journal of Pharmacological Report* 2016; 27: 347-352.
16. Akah PA, Uzodinma SU, Okolo CE. Antidiabetic activity of aqueous and methanol extract and fractions of *Gongronema latifolium* leaves in Alloxan Diabetic Rats. *J. Appl. Pharm. Sci* 2011; 1(09): 99-102.
17. Alexandra Danesa, Cristina Cucolas, Lavinia Manuela Ienghel, Diana Oleteanh Remus, Orasan and Gabriela a Filp. *Society for Reproduction and Fertility* 2016; 151: 401-409.
18. Ali Noorafshan, Mayam Ahmadi, Seyed-Fakhroddin Mesbah, Saied Karbalay- Doust. Sterological study of the effects of letrozole and estradiol valerate treatment on the ovary of rats. *Clin Exp Reprod Med* 2013; 40(3): 115-121.
19. Aliyah M, Sowjanya M. A Review on Polycystic Ovarian Syndrome *RRJPA* 2016; 5(2): 9-14.
20. Anbu J, Sukanya K, Santhosh Kumar S, Ramya PS Reddy, Vani B Nandihalli. Effect of *sargassum ilicifolium* on ovogenesis in polycystic ovary syndrome- induced rats. *Asian J Pharm Clin Res* 2016; 9(6): 127-13.
21. Barua CC, Archana Talukdar, Begum SA, Pathak DC, Sarma DK, Borah RS, Asheesh Gupta, 2012. In vivo wound-healing efficacy and antioxidant activity of *Achyranthes aspera* in experimental burns. *Pharmaceutical Biology*, 50(7):892-899.
22. Hopwood D. Fixation and fixatives. In Bancroft J and Stevens A eds. *Theory and practice of histological techniques*. New York: Churchill Livingstone, 1996.
23. Badawy A, Mosbah A, Shady M. Anastrozole or letrozole for ovulation induction in clomiphene-resistant women with polycystic ovarian syndrome: A prospective randomized trial. *Fertil Steril* 2008; 89 (5): 1209–1212.
24. Radha Maharajan, Padamnabhi S. Nagar, Laxmipriya Nampoothiri. Effect of *Aloe barbadensis* Mill. Formulation on Letrozole induced PCOS rat model. *JAIM* 2010; 1(4): 273-279.
25. Farquhar C, Brown J, Marjoribanks J. Laparoscopic drilling by diathermy or laser for ovulation induction in anovulatory polycystic ovary syndrome. *Cochrane Database Syst Rev* 2012; 13(6): CD001122.
26. Foltyn W, Strzelczyk J, Marek B, Kajdaniuk D, Sieminska L, Zemczak A, Blicharz-Dorniak J, Kos-Kudła B. Selected markers of endothelial dysfunction in women with polycystic ovary syndrome. *Endokrynol Pol* 2011; 62(3): 243-248.
27. Gambineri A, Patton L, Vaccina A, Cacciari M, Morselli Labate AM, Cavazza. Treatment with flutamide, metformin, and their combination added to a hypocaloric diet in overweight obese women with polycystic ovary syndrome: a randomized, 12-month, placebo controlled study. *J Clin Endocrinol Metab* 2006; 91(10): 3970-3980.
28. Habibeh Ghafurniyan, Mahnaz Azarnia, Mohammad Nabiuni, and Latifeh Karimzadeh. The Effect of Green Tea Extract on Reproductive Improvement in Estradiol Valerate-Induced Polycystic Ovarian Syndrome in Rat. *Iran J Pharm Res* 2015; 14(4): 1215–1233.
29. <http://www.planetayurveda.com>.
30. R.Vidya Bharathi, S.Swetha, J.Neeraja, J.Varsha Madhavi, D MoorthyJanani, S.N.Rekha, S. Ramya, B.Usha. An epidemiological survey: Effect of predisposing factors for PCOS in Indian urban and rural population. *Middle East Fertility Society Journal*, 2017; 22(4): 313-316.
31. Selma Feldman Witchel, Sharon E Oberfield, and Alexia S Peña. Polycystic Ovary Syndrome: Pathophysiology, Presentation, and Treatment with Emphasis on Adolescent Girls. *J Endocr Soc*. 2019; 3(8): 1545–1573.
32. P. Sushma Reddy, Nazia Begum, Sumith Mutha Vasudha Bakshi. Beneficial effect of Curcumin in Letrozole induced polycystic ovary syndrome. *Asian Pacific Journal of Reproduction*. 2016; 5(2): 116-112.
33. M. Sasikala, P. Parthiban, S. Vijay Kumar. A comprehensive review on polycystic ovary syndrome and its therapeutic management for ovulation induction in infertile women. *International Journal of Advances in Case Reports*, 2014;





Ramayappa et al.,

Table-1: Phytochemical investigation of *Achyranthes Aspera*

S.No	Phytochemicals	Presence
1	Alkaloids	+
2	Carbohydrates	+
3	Glycosides	+
4	Tannins or Phenolic Compounds	+
5	Phytosterols and Triterpenoids	+
6	Flavonoids	+
7	Proteins	+
8	Saponins	+

Table-2: Protocol for evaluation of efficacy

Animal model	Female Albino wistar rats
Weight of animals	Between 170-180g
No of dose groups	10
Animal per group	6
Dose of Letrozole	1.0mg/kg body weight
Route of administration	P.O.(oral administration)
Vehicle for administration	0.25%carboxymethylcellulose
Volume of vehicle	2.0ml/kg body weight
Test sample	Leaves of <i>Achyranthes aspera</i>
Standard sample	Clomiphene citrate
Dose of standard	1.0mg/kg body weight
Dose volume for evaluation	Testosterone, Estrogen, Progesterone; cholesterol and triglycerides; Histopathological evolution of ovary

Table-3: Animal groups design

Group-I	Normal control	Received 2ml distilled water orally chow diet
Group-II	Letrozole control	Scarified on day 22
Group-III	Letrozole+clomiphene citrate	Received 1.0mg/kg body weight dose of clomiphene citrate (for 15days post letrozole induction)
Group-IV	Letrozole+ <i>Achyranthes aspera</i> (Treatment-1)	Received 200mg/kg body weight dose of clomiphene citrate (for 15days post letrozole induction)
Group-V	Letrozole + <i>Achyranthes aspera</i> (Treatment-2)	Received 400mg/kg body weight dose of Clomiphene citrate (for 15days post letrozole induction)
Group-VI	Letrozole + <i>Achyranthes aspera</i> (Treatment-3)	Received 600mg/kg body weight dose of Clomiphene citrate (for 15days post letrozole induction)
Group-VII	Vehicle control	CMC 0.25%
Group-VIII	Natural recovery	After induction was over only chow diet and water was given





Ramayyappaet al.,

Table-6: Effect of various treatments on Hormones in Letrozole induced PCOS rats

Name of the Group	Estrogen	Progesterone	Testosterone
Group-1 (Normal control)	6.042±0.1586	30.39±1.30	7.01±0.1647
Group-2(Letrozole control)	21.45±0.6357	21±1.289	15.87±1.045
Group-3 (Letrozole+ Clomiphene citrate)	11.42±0.6401***	29.80±2.84**	10.42±0.6140***
Group-4(Treatment-1) Letrozole+A.aspera extract 200mg/kg	13.19±0.7151***	30.12±0.87**	11.30±0.9081***
Group-5(Treatment-2) Letrozole+A.aspera extract 400mg/kg	11.30±0.4928***	39.62±1.924***	9.46±0.7446**
Group-6(Treatment-3) Letrozole+A.aspera extract 600mg/kg	9.075±0.2253	42.47±1.904*	6.36±0.5181***
Group-7 (Natural recovery)	20.72±0.6079	18.55±0.690	15.13±0.5213
Group-8(Vehicle control)	6.573±0.2005**	32.50±1.318***	7.35±0.2078**

Table-8: Effect of various treatments on cholesterol and triglycerides in Letrozole induced PCOS rats

Name of the group	Cholesterol	Triglycerides
Group-1 (Normal control)	170.8±2.120	148.7±2.539
Group-2(Letrozole control)	228.5±15.62	183.7±5.308
Group-3 (Letrozole+ Clomiphene citrate)	186.7±9.528*	167.5±1.455*
Group-4(Treatment-1) Letrozole+A.aspera extract 200mg/kg	180.7±3.78*	163.8 ±2.404**
Group-5(Treatment-2) Letrozole+A.aspera extract 400mg/kg	171.3±8.999**	152.7±0.097**
Group-6(Treatment-3) Letrozole+A.aspera extract 600mg/kg	164.3±1.687***	134.3±2.431***
Group-7 (Natural recovery)	215.2±13.58	177.3±4.558
Group-8(Vehicle control)	169.5±2.01***	1445.8±3.487

Table-9: Effect of various treatments on SGOT and SGPT levels in Letrozole induced PCOS rats

Name of the group	SGPT	SGOT
Group-1 (Normal control)	36.50±1.057	31.00±0.856
Group-2(Letrozole control)	56.35±6.869	56.17±4.468
Group-3 (Letrozole+ Clomiphene citrate)	36.50±2.141*	44.50±4.559*
Group-4(Treatment-1) Letrozole+A.aspera extract 200mg/kg	35.17 ±.167***	36.50±1.784*
Group-5(Treatment-2) Letrozole+A.aspera extract 400mg/kg	29.83±1.108***	33.67±1.08*
Group-6(Treatment-3) Letrozole+A.aspera extract 600mg/kg	28.00±0.930**	36.33±1.382***
Group-7 (Natural recovery)	52.50±5.772	52.00±3.967
Group-8(Vehicle control)	35.83±1.195***	31.50±0.896





Ramayappa et al.,

Table-10: Effect of various treatments on Creatinine and Urea in Letrozole induced PCOS rats

Name of the group	Creatinine	Urea
Group-1 (Normal control)	0.983±0.033	26.83±1.138
Group-2(Letrozole control)	2.100±0.344	4.17±5.510
Group-3 (Letrozole+Clomiphene citrate)	1.233±0.067*	31.50±0.9220**
Group-4(Treatment-1) Letrozole+A.aspera extract 200mg/kg	1.233±0.070*	32.83±1.641**
Group-5(Treatment-2) Letrozole+A.aspera extract 400mg/kg	1.117±0.080**	33.83±0.703*
Group-6(Treatment-3) Letrozole+A.aspera extract 600mg/kg	1.050±0.080**	26.33±0.881***
Group-7 (Natural recovery)	2.167±0.373	41.33±3.756
Group-8(Vehicle control)	1.067±0.030	27.33±0.802

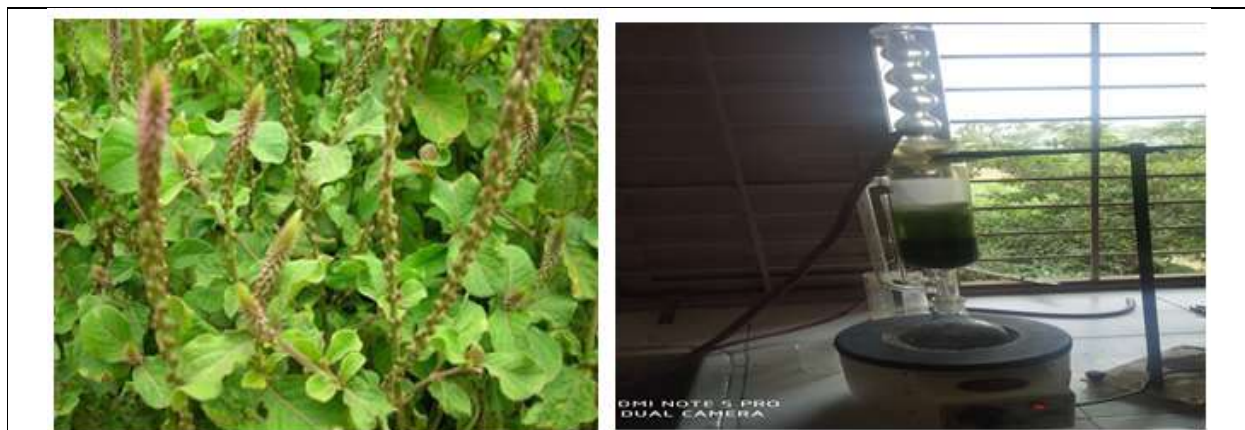


Fig-1: Achyranthes aspera plant & Soxhlet process for extraction of plant constituents

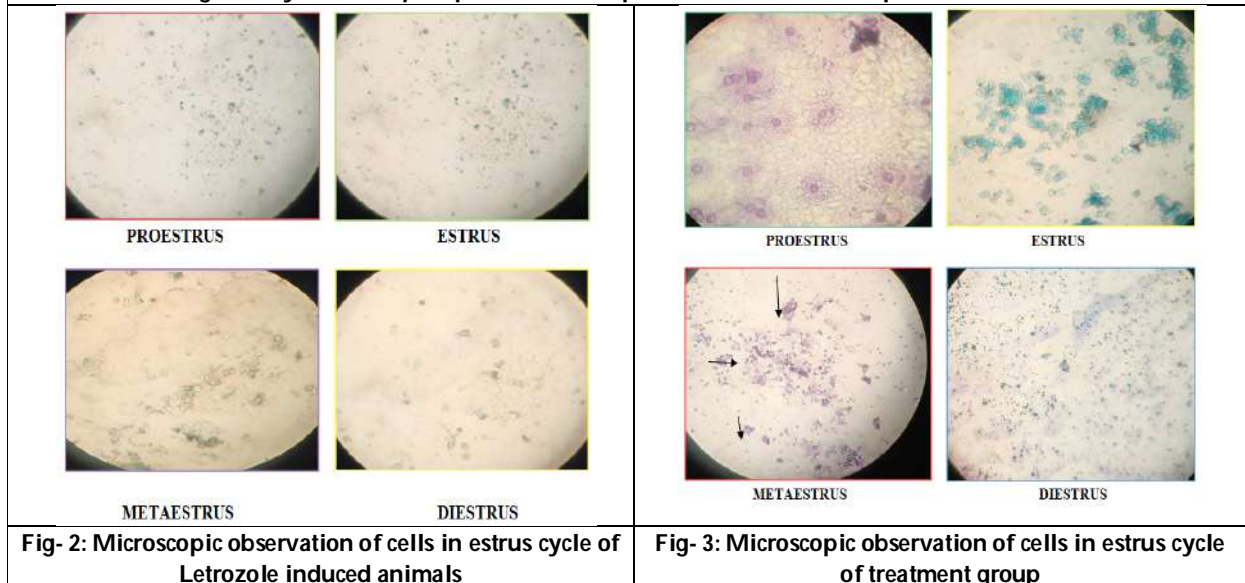


Fig- 2: Microscopic observation of cells in estrus cycle of Letrozole induced animals

Fig- 3: Microscopic observation of cells in estrus cycle of treatment group





Ramayyapaet al.,

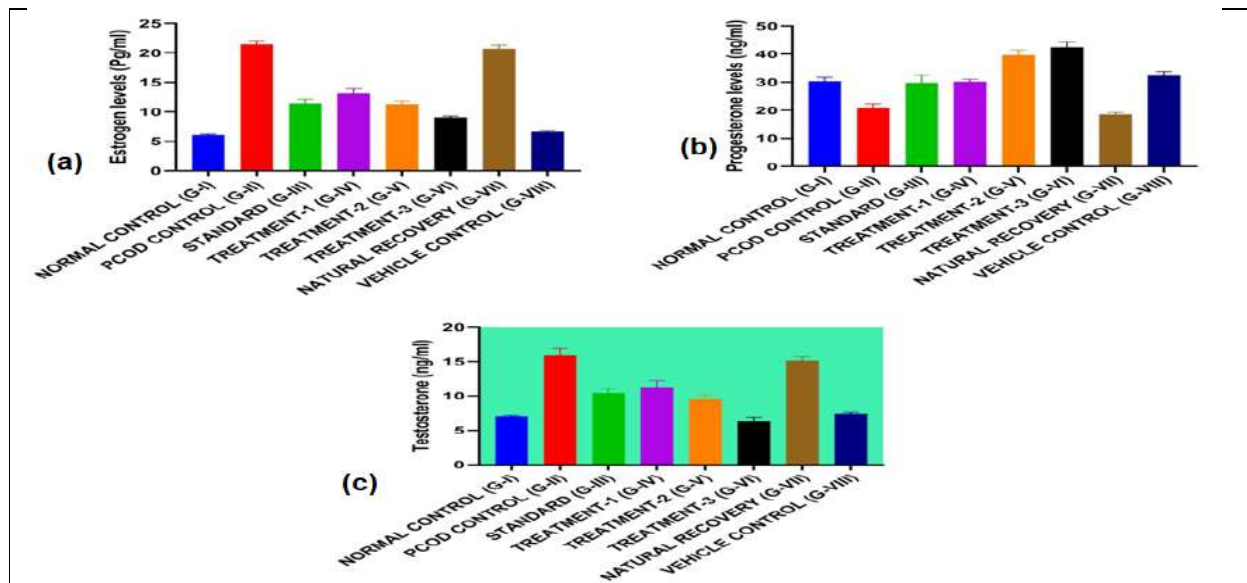


Fig- 4. Effect of *A.aspera* on Estrogen (a), Progesterone (b) and testosterone (c) levels in PCOS induced rat

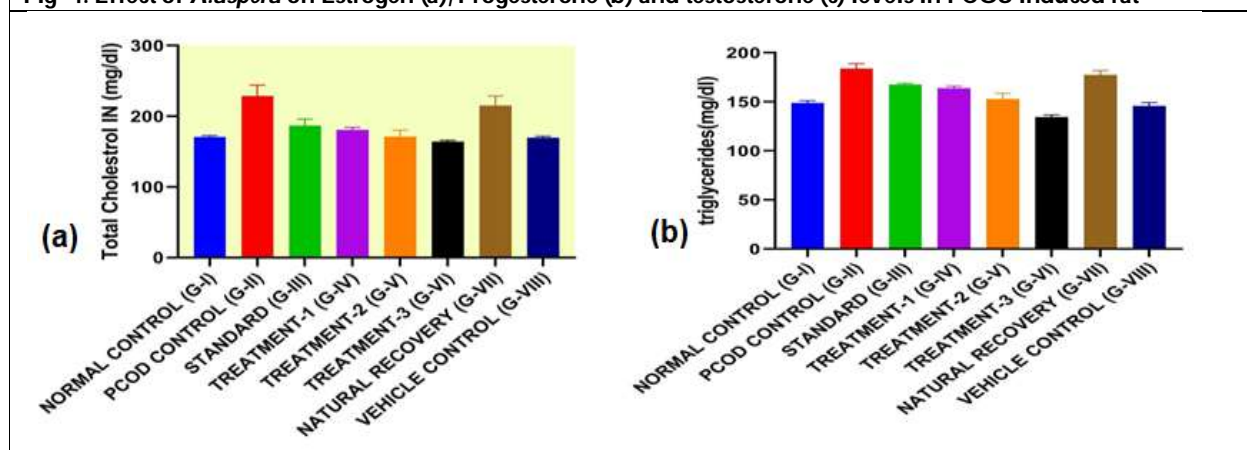


Fig- 5.:Effect of *A.aspera* on total cholesterol (a) and triglycerides (b) in PCOS induced rats

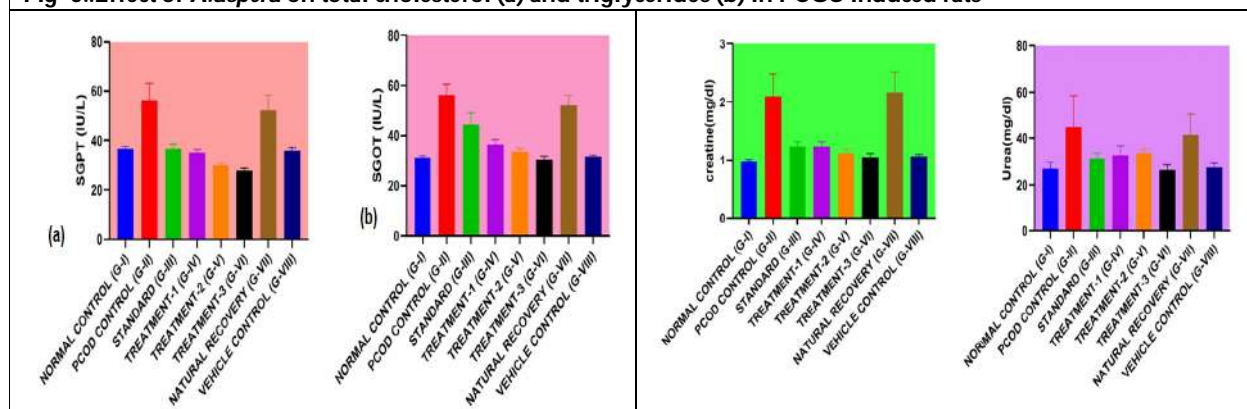


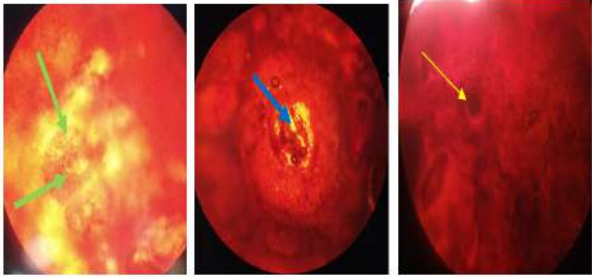
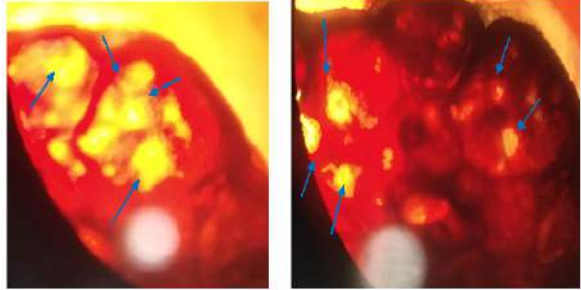
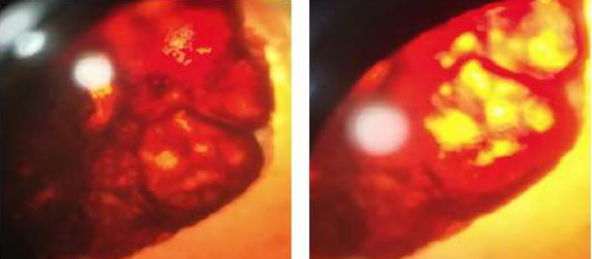
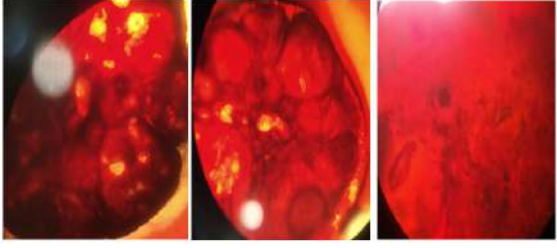
Fig- 6: Effect of *A.aspera* on SGPT& SGOT levels in PCOS induced rats

Fig- 7: Effect of *A.aspera* on Creatinine and Urea levels in PCOS induced rats





Ramayyappaet al.,

 <p>GRAAFIANFOLLICLE CORPUSLUTEUM OVUM</p>	
<p>Fig -8: Histopathology observation of ovaries of Normal control (Group-1)</p>	<p>Fig-9: Histopathology observation of ovaries of Letrozole induced animals (Group-2)</p>
	 <p>Treatment-1 (200mg/ml) Treatment-2 (400mg/ml) Treatment-3 (600mg/ml)</p>
<p>Fig- 10: Histopathology observation of ovaries of animals treated with standard Group-3 & natural recovery</p>	<p>Fig- 11: Histopathology of ovaries treated with Treatment-1, Treatment-2 and Treatment-3</p>





Evaluation of New Herbicides for Weed Management in Irrigated Blackgram (*Vigna mungo* L.)

K. Sharmitha¹, K. Arivukkarasu^{2*}, A. Sundari³ and N. Muthukumaran⁴

¹Research Scholar, Department of Agronomy, Faculty of Agriculture, Annamalai University, Annamalai Nagar – 608002, Tamil Nadu, India.

²Assistant Professor, Department of Agronomy, Faculty of Agriculture, Annamalai University, Annamalai Nagar – 608002, Tamil Nadu, India.

³Professor, Department of Agronomy, Faculty of Agriculture, Annamalai University, Annamalai Nagar – 608002, Tamil Nadu, India.

⁴Assistant Professor, Department of Entomology, Faculty of Agriculture, Annamalai University, Annamalai Nagar – 608002, Tamil Nadu, India.

Received: 30 Aug 2022

Revised: 25 Apr 2023

Accepted: 31 May 2023

*Address for Correspondence

K. Arivukkarasu

Assistant Professor,
Department of Agronomy,
Faculty of Agriculture,
Annamalai University,
Annamalai Nagar – 608002,
Tamil Nadu, India.
E.Mail: arivuagron@gmail.com



This is an Open Access Journal / article distributed under the terms of the **Creative Commons Attribution License** (CC BY-NC-ND 3.0) which permits unrestricted use, distribution, and reproduction in any medium, provided the original work is properly cited. All rights reserved.

ABSTRACT

A field experiment was conducted at Musiri (Taluk), Trichy (District), Tamil Nadu during August- October 2021 to study the effect of weed management practices on the weed parameters, yield and economics irrigated blackgram. The treatment comprises of Unweeded control (T_1), Hand weeding twice on 15 and 30 DAS (T_2), Pendimethalin @ 750 g ha⁻¹ (T_3), Imazethapyr @ 90 g ha⁻¹ (T_4), Quizalofop-p-ethyl @ 50 g ha⁻¹ (T_5), Sodium acifluorfen + clodinafoppropargyl @ 306.2 g ha⁻¹ (T_6), Flumioxazin @ 125 g ha⁻¹ (T_7). All the treatments significantly influenced the weed biometrics, growth, yield components and yield of blackgram. Among the treatments compared hand weeding twice on 15 and 30 DAS (T_2) recorded the least weed dry matter production (DMP) with highest weed control index, higher grain and haulm yield. This was followed by sodium acifluorfen + clodinafoppropargyl @ 306.2 g ha⁻¹. However, sodium acifluorfen + clodinafoppropargyl @ 306.2 g ha⁻¹ (T_6) was recorded the higher net return and highest benefit cost ratio of (2.43). The least gross return, net return and benefit cost ratio was recorded in unweeded control (T_1).



**Sharmitha et al.,**

Keywords: Blackgram, Hand weeding, Weed control index, Sodium acifluorfen + clodinafoppropargyl, Yield, Economic.

INTRODUCTION

Pulses are a source of supplementary protein to daily diet based on cereals and starch food for a predominantly vegetarian population. Blackgram [*Vigna mungo* (L.) Hepper] is called as king of pulses and it is one of the most important pulse crop cultivated in tropical and sub-tropical region. Blackgram is native of India and it is originated from its wild progenitor *Phaseolous sublobatus*. Along with biological nitrogen fixation, it helps in the reduction of greenhouse gases emission by 5-7 times as compared to other crops [1]. Weeds results in a drastic decline of 66.67 per cent yield in blackgram if grown uncontrolled [5]. Weed control plays a key role in increasing the productivity of blackgram. Removal of weeds at appropriate time using a suitable weed control practices is essential to obtain higher yield of blackgram. Various herbicides are effective against the weeds of blackgram and other pulse crops and the best alternative to mitigate crop-weed competition at different stages of the crop is either by the use of pre-emergence or early post-emergence herbicides were to be studied for better weed management in blackgram. Keeping the above facts the present study, the effect of weed management on the weed parameters, yield and economics of blackgram.

MATERIALS AND METHODS

The field experiment was conducted at Musiri of Trichy district during August – October 2021 and was laid out in a Randomized block design with seven treatments and replicated thrice viz., Unweeded control (T₁), Hand weeding twice on 15 and 30 DAS (T₂), Pendimethalin @ 750 g ha⁻¹ (T₃), Imazethapyr @ 90 g ha⁻¹ (T₄), Quizalofop-p-ethyl @ 50 g ha⁻¹ (T₅), Sodium acifluorfen + clodinafop propargyl @ 306.2 g ha⁻¹ (T₆), Flumioxazin @ 125 g ha⁻¹ (T₇) with 3 replications. The blackgram variety VBN – 5 was raised under optimum conditions of agronomic practices and plant protection measures in the field. The soil was Sandy clay loam in texture having pH 7.7, EC 0.42 dsm⁻¹ with low in available nitrogen N (115.59 kg ha⁻¹), medium in available phosphorous P (21.61 kg ha⁻¹) and high in available potassium K (432.25 kg ha⁻¹). Observation on weed dry matter production was taken at 30 and 45 DAS and also the yield was taken at the time of harvesting.

RESULTS AND DISCUSSION

The predominant weed flora found in the experimental mainly consists of *Cynodon dactylon* and *Brachiaria reptans* under grass, *Cyperus rotundus* under sedge, *Cleome viscosa* and *Trichodesma indicum* under broad leaved weeds.

Weed dry matter production

Weed dry matter production reflects the growth potential of the weeds and is a better indicator of its competitive ability with the crop plants. All the treatments significantly influenced the weed DMP. Among the weed control measures compared, hand weeding twice on 15 and 30 DAS (T₂) performed better in control of weeds throughout the cropping period and is superior to other treatments that removed all types of weeds effectively in the critical stages and also due to restriction of the emergence of fresh weeds in the later stages of crop growth [3]. This was followed by early post emergence application of sodium acifluorfen + clodinafop propargyl @ 306.2 g ha⁻¹ (T₆). Lesser weed DMP in this treatment was due to better control of weeds especially in the early stages of crop growth. Further,

57402





the lower dry matter production of weeds might be due broad spectrum herbicidal activity contributing to weed free conditions during crop weed competition period [4]. The highest weed dry matter production was recorded in unweeded control (T₁) due to uncontrolled weed growth.

Weed control index

Weed control index (WCI) is a measure of yield loss caused due to varying degrees of weed competition compared to relatively weed free conditions throughout the crop period leading to higher productivity. In the present study, hand weeding twice on 15 and 30 DAS (T₂) (Table 1) was found to be superior that resulted in highest weed control index. It was followed by early post emergence application of sodium acifluorfen + clodinafop propargyl @ 306.2 g ha⁻¹ (T₆) was found to be next in order. This was due to greater reduction in weed dry matter in this treatment which might have increased the weed control index [5], [6].

Grain and Haulm yield

Results of the study revealed that all the weed control treatments have a salutary effect on yield of blackgram over unweeded control. Among the different treatments compared, hand weeding twice on 15 and 30 DAS registered the maximum seed and haulm yields was 910 and 1528 kg ha⁻¹ higher over control (T₁) (Table 1). This might be due to better control of all categories of weeds which reduced the crop weed competition by providing no weed situation in blackgram field. Thus, the crop plants being vigorous by efficient utilization of nutrients, moisture, sunlight with space gave better yield [6]. Further, the treatment with sodium acifluorfen + clodinafop propargyl @ 306.2 g ha⁻¹ (T₆) was found to be next in order. This might be due to the lower crop-weed competition, weed population and weed dry weight, enabling the crop to establish and to grow vigorously resulting in better growth and development of the crop [7]. Unweeded control recorded significantly lower seed yield and haulm yield compared to other treatments due to narrow spectrum of weed control and higher crop weed competition [8], [5] and [9].

Economics

Economic efficiency and viability of crop cultivation are the main criteria for successful crop production. In general, higher crop productivity resulted in better economic parameters like net income and benefit cost ratio (Table 2). Among the treatments compared, early post emergence application of sodium acifluorfen + clodinafop propargyl @ 306.2 g ha⁻¹ (T₆) recorded highest with a BCR of 2.43 and highest net return of Rs.46450 ha⁻¹. This might be due to the less cost of cultivation compared to other treatments. The treatment with hand weeding twice at 15 and 30 DAS (T₂) was found to be next in order. The lowest net income and benefit cost ratio invested were recorded in unweeded control treatment, due to the weed competition throughout the cropping period [10], [11].

CONCLUSION

From the present study, it could be concluded that hand weeding twice on 15 and 30 DAS (T₂) significantly recorded the least weed dry matter production, higher weed control index and favouring higher grain yield and haulm yield in irrigated blackgram compared to other treatments. However, sodium acifluorfen + clodinafop propargyl @ 306.2 g ha⁻¹ (T₆) recorded the higher values with respect to net income and highest benefit cost ratio compared to hand weeding twice at 15 and 30 DAS. Thus, sodium acifluorfen + clodinafop propargyl @ 306.2 g ha⁻¹ (T₆) was found to be economically viable chemical weed management option for better weed management and thereby enhancing the growth and yield of irrigated blackgram in situation with higher labour cost incurred for hand weeding.





REFERENCES

1. Stagnari, F., A. Maggio, A. Galieni and M. Pisante. 2017. Multiple benefits of legumes for agriculture sustainability: an overview. Chemical and Biological Technologies in Agriculture 4: 1-13
2. Mansoori, N., N. Bahaduria and R.L. Rajput. 2015. Effect of weed control practices on weeds and yield of blackgram (*Vigna mungo*). Leg Res., 38: 855-857.
3. Khot, D.B., S.D. Munde, and R.D. Pagar. 2012. Evaluation of new herbicides for weed management in summer blackgram (*Vigna mungo* L.). Crop Res., 44(3): 326-330.
4. Patel, K.R., B.D. Patel, R.B. Patel, V.J. Patel and V.B. Darji. 2015. Bio efficacy of herbicides against weeds in blackgram. Indian J. Weed Sci., 47(1): 78-81.
5. Harithavardhini, J., K. Jayalalitha, Y. Ashoka Rani and B. Krishnaveni. 2016. Efficacy of post-emergence herbicides on weed control efficiency, partitioning of dry matter and yield of blackgram (*Vigna mungo* (L) Hepper). Int. J. Food, Agric. Vet Sci., 6(2): 39-44. ISSN: 2277-2079.
6. Elankavi, S., S. Raman, G. Baradhan and S.M. Suresh Kumar. 2019. Effect of new generation herbicides on weed parameters of Blackgram. Plant Archi., 19(1): 421-424.
7. Susmitha, M., U. V. B. Reddy, P. V. R. Babu and M. S. Reddy. 2019. Efficacy of different herbicides on weed dynamics and yield attributes in kharif blackgram [*Vigna mungo* (L.) Hepper]. Int. J. Curr. Microbial. App. Sci., 8(6): 2026- 2031.
8. Kumar, S., M. S. Bhatto, S. S. Punia and R. Punia. 2015. Bioefficacy of herbicides in blackgram and their residual effect on succeeding mustard. Indian J. Weed Sci., 47(2): 211-213.
9. Tarun Suryavanshi, M.L. Kewet, Shyam Lal and S.S. Porte. 2018. Weed indices as Influenced by Propaquizafop and Imazethapyr Mixture in Blackgram. Int. J. Curr. Microbiol. App. Sci., 7: 738-744.
10. Naidu, K.R.K., A.V. Ramana, R. Veeraraghavaiah and Y. Ashoka Rani. 2011. Effect of pre and post emergence herbicides to the control of *Vicia sativa* in rice - fallow blackgram [*Vigna mungo* (L)]. The Andhra Agric. J., 58(1): 5-8.
11. Sakthi, J. and A. Velayutham. 2018. Economics of herbicides against weeds of blackgram (*Vigna mungo* (L.) Hepper) under irrigated condition. Int. J. Advances in Agric. Sci. and Tech., 5(7): 133-143.

Table 1: Effect of weed management on weed dry matter production of weed, weed control control (WCI), grain yield and haulm yield of blackgram.

Treatments	Dry matter production at 45 DAS (kg ha ⁻¹)	WCI (%) at 45 DAS	Grain yield (kg ha ⁻¹)	Haulm yield (kg ha ⁻¹)
T ₁ – Unweeded Control	942.61	-	426	803
T ₂ – Hand Weeding twice on 15 and 30 DAS	152.84	83.78	910	1528
T ₃ – Pendimethalin @ 750 g ha ⁻¹	443.09	52.99	778	1164
T ₄ – Imazethapyr @ 90 g ha ⁻¹	324.10	65.61	826	1359
T ₅ – Quizalofop-p-ethyl @ 50 g ha ⁻¹	336.71	64.30	819	1344
T ₆ – Sodium acifluorfen + Clodinafop propargyl @ 306.2 g ha ⁻¹	281.69	70.11	868	1463
T ₇ – Flumioxazin @ 125 g ha ⁻¹	468.86	50.26	771	1156
SEm±	13.13	-	12.37	38.19
CD (P= 0.05)	40.91	-	37.12	121.23





Sharmitha et al.,

Table 2: Economics of irrigated blackgram as influenced by weed management practices

Treatments	Cost of cultivation (Rs ha ⁻¹)	Gross income (Rs ha ⁻¹)	Net income (Rs ha ⁻¹)	Benefit cost ratio (BCR)
T ₁ – Unweeded Control	28722	38751	10029	1.34
T ₂ – Hand Weeding twice on 15 and 30 DAS	34699	82664	47965	2.38
T ₃ – Pendimethalin @ 750 g ha ⁻¹	31626	70602	38976	2.23
T ₄ – Imazethapyr @ 90 g ha ⁻¹	31983	75019	43036	2.34
T ₅ – Quizalofop-p-ethyl @ 50 g ha ⁻¹	31934	74382	42448	2.32
T ₆ – Sodium acifluorfen + Clodinafop propargyl @ 306.2 g ha ⁻¹	32401	78851	46450	2.43
T ₇ – Flumioxazin @ 125 g ha ⁻¹	32889	69968	37079	2.12





L (2, 1) Labeling of Barbell Graph by using Python

R.Ramalakshmi^{1*}, B.Rajapandian² and R. Siluvaidasan³

¹Assistant Professor, Department of Mathematics, Velammal College of Engineering and Technology, Madurai, Tamil Nadu, India

²Associate Professor, Sri Sairam Engineering College, Chennai, Tamil Nadu, India.

³Assistant Professor, Rajalakshmi Engineering College, Chennai, , Tamil Nadu, India.

Received: 23 Feb 2023

Revised: 20 Apr 2023

Accepted: 31 May 2023

*Address for Correspondence

R.Ramalakshmi

Assistant Professor,
Department of Mathematics,
Velammal College of Engineering and Technology,
Madurai, Tamil Nadu, India.
E.Mail: rlr@vcet.ac.in



This is an Open Access Journal / article distributed under the terms of the **Creative Commons Attribution License** (CC BY-NC-ND 3.0) which permits unrestricted use, distribution, and reproduction in any medium, provided the original work is properly cited. All rights reserved.

ABSTRACT

An L(2,1)- labeling of a graph G is a function f from the vertex set V(G) to the set of all non-negative integers such that $|f(x) - f(y)| \geq 2$ if $d(x,y)=1$ and $|f(x) - f(y)| \geq 1$ if $d(x,y)=2$, where $d(x,y)$ denotes the distance between x and y number. The L(2,1) – labeling number $\lambda(G)$ of G is the smallest number k such that G has an L(2,1)- labeling with $\max\{f(v) : v \in V(G)\} = k$. In this paper we obtain the L(2,1) number for some special graphs in terms of the number of vertices(n) and finding L(2,1) number by using Python Program. Finally, we got interesting result.

Keywords: labeling, number, paper

INTRODUCTION

The assignment of FM frequencies to stations became a problem as technology advanced in the early 20th century. As more and more stations requested frequencies, it became difficult to assign frequencies without having new stations interfere with the broadcast of other stations nearby. The channel assignment problem is an engineering problem in which the task is to assign a channel (non-negative integer) to each FM radio station in a set of given stations such that there is no interference between stations and the span of the assigned channels is minimized. The level of interference between any two FM radio stations correlates with the geographic locations of the stations. Closer stations have a stronger interference, and thus there must be a greater difference between their assigned channels. In 1980, Hale introduced a graph theory model of the channel assignment problem where it was

57406





Ramalakshmi et al.,

represented as a vertex coloring problem [3]. Vertices on the graph correspond to the radio stations and the edges show the proximity of the stations. In 1991, Roberts proposed a variation of the channel assignment problem in which the FM radio stations were considered either "close" or "very close." "Close" stations were vertices of distance two apart on the graph and were assigned channels that differed by two; stations that were considered "very close" were adjacent vertices on the graph and were assigned distinct channels [6].

More precisely, Griggs and Yeh defined the $L(2, 1)$ -labeling of a graph $G = (V, E)$ as a function f which assigns every x, y in V a label from the set of positive integers such that $|f(x) - f(y)| \geq 2$ if $d(x, y) = 1$ and $|f(x) - f(y)| \geq 1$ if $d(x, y) = 2$ [2]. $L(2, 1)$ -labeling has been widely studied in recent years.

Definitions and Notation

Definition 1. Let $G = (V, E)$ be a graph and f be a mapping $f: V \rightarrow \mathbb{N}$. f is an $L(2, 1)$ -labeling of G if, for all $x, y \in V$,

$$|f(x) - f(y)| \geq \begin{cases} 1 & \text{if } d(x, y) = 2 \\ 2 & \text{if } d(x, y) = 1 \end{cases}$$

Definition 2. The $L(2, 1)$ -number, $\lambda(G)$, of a graph G is the smallest natural number λ such that G has an $L(2, 1)$ -labeling with λ as the maximum label. An $L(2, 1)$ -labeling of a graph G is called a *minimal $L(2, 1)$ -labeling* of G if, under the labeling, the highest label of any vertex is $\lambda(G)$.

Note. If 1 is not used as a vertex label in an $L(2, 1)$ -labeling of a graph, then every vertex label can be decreased by one to obtain another $L(2, 1)$ -labeling of the graph. Therefore in a minimal $L(2, 1)$ -labeling 1 will necessarily appear as a vertex label.

Definition 3. Let $G = (V, E)$ be a graph. G is called a *complete graph* on n vertices, K_n , if for all vertices $x, y \in V$, $(x, y) \in E$.

Definition 4:

Barbell graph is a simple graph obtained by connecting two copies of a complete graph K_n by a bridge and it is denoted by $B(K_n, K_n)$.

Analysis:

1. Total number of nodes (In n -barbell graph):

The Total number of Nodes = $2 \cdot N$

2. Total number of edges (In n -barbell graph):

Total number of edges = $2 \cdot$ number of edges in complete graph + 1
 $= 2 \cdot (n \cdot (n-1) / 2) + 1 = n \cdot (n-1) + 1$

Properties:

1. The barbell graph contains cycles in it.
2. The barbell graph is connected every two nodes have a path between them.
3. It has a bridge between 2 complete graphs.
4. Bridge may and may not have nodes in it.





Ramalakshmi et al.,

Theorem:

The L (2, 1) number of a Barbell graph is 2n.

$$\lambda(B(K_n, K_n)) = 2n.$$

Proof:

Let G= (V, E) be a Barbell graph $B(K_n, K_n)$ with the vertex set $V = \{u_1, u_2, u_3, \dots, u_n, v_1, v_2, v_3, \dots, v_n\}$ and the edge set $E = \{u_i u_j; 1 \leq i \leq n; 1 \leq j \leq n\} \cup \{u_i v_n\} \cup \{v_i v_j; 1 \leq i \leq n; 1 \leq j \leq n\}$.

Let f be a minimal L (2, 1) labeling of the Barbell graph $B(K_n, K_n)$. We have $d(u_i, u_j) = 1$ for all $1 \leq i \leq n$ and $d(u_1, v_n) = 1$ for $i=1, j=n$ and $d(v_i, v_j) = 1$ for all $1 \leq i \leq n; 1 \leq j \leq n$ and $d(u_i, v_j) = 2$ $i \neq 1$ and $j \neq n$

Since f is minimal, any one of the vertices of G should have label 1.

Let $f(u_1) = 1$

$$\text{Define, } f(u_i) = \begin{cases} 1 & , i = 1 \\ 2i - 1 & , 2 \leq i \leq n \end{cases} \text{----- (1)}$$

$$f(v_j) = \begin{cases} 2 & , j = n \\ 2(j + 1) & , 1 \leq i \leq n - 1 \end{cases} \text{----- (2)}$$

Case 1:

For all $u_i, u_k \in V$

By (1)

$$\begin{aligned} |f(u_i) - f(u_k)| &\geq |2i - 1 - (2k - 1)| \\ &\geq |2i - 1 - 2k + 1| \\ &\geq |2i - 2k| \\ &\geq 2|i - k| \\ &\geq 2 \end{aligned}$$

Therefore f is an L(2,1) labelling.

Case 2:

For all $v_j, v_m \in V$, $j \neq n$

By (2)

$$\begin{aligned} |f(v_j) - f(v_m)| &\geq |2(j + 1) - 2(m + 1)| \\ &\geq |2j + 2 - 2m - 2| \\ &\geq |2j - 2m| \\ &\geq 2|j - m| \\ &\geq 2 \end{aligned}$$

Therefore f is an L(2,1) labelling.

Case 3:

For u_j, v_j , $j = n$





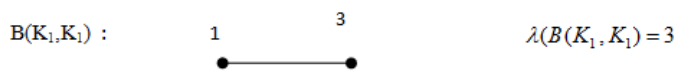
By (1) and (2)

$$\begin{aligned}
 |f(u_n) - f(v_n)| &\geq |2n - 1 - 2| \\
 &\geq |2n - 3| \\
 &\geq 1
 \end{aligned}$$

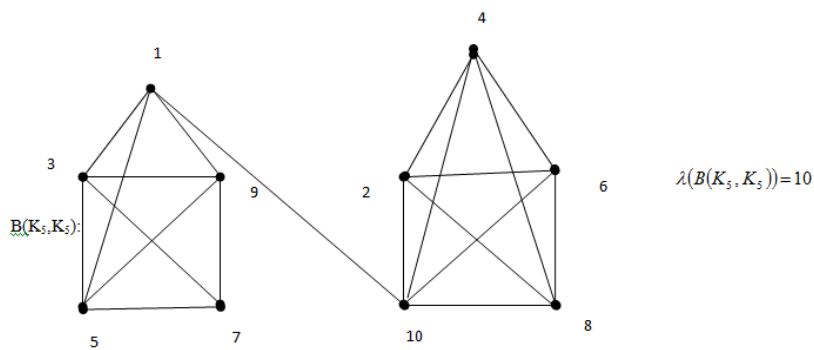
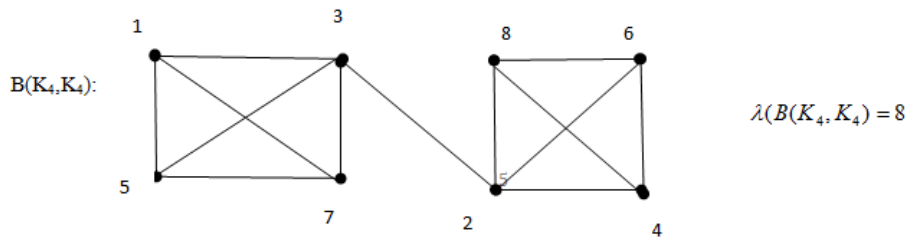
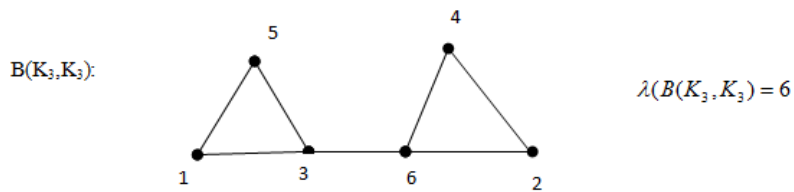
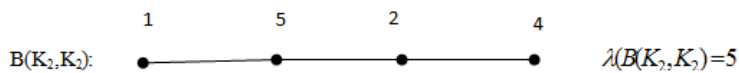
Therefore f is an L (2, 1) labelling.

Therefore the labeling pattern $\{1, 3, 5, \dots, 2n-1, 4, 6, \dots, 2(n-1+1)\} = \{1, 3, 5, \dots, 2n-1, 4, 6, \dots, 2n\}$ shows that $\lambda(B(K_n, K_n)) = 2n$.

Example:



|





Ramalakshmi et al.,

Python Program For L(2,1) Labeling of Barbell Graph

Python Program For L(2,1) Labeling of Barbell Graph

```
import networkx as nx
import matplotlib.pyplot as plt
import numpy as np

def get_points(vals):
    points = []
    for a in range(len(vals)):
        for b in range(a+1, len(vals)):
            points.append((vals[a], vals[b]))
    return points

while True:
    try:
        n = int(input("Enter n value (greater than 1):"))
        if n > 1:
            break
        else:
            print("n value should be greater than 1.")
    except:
        print("Invalid Entry. Please enter an integer greater than 1.")

u_values = [1] + [2 * i - 1 for i in range(2,n+1)]
v_values = [2 * (j+1) for j in range(1,n)] + [2]

print("u-values:", u_values)
print("v-values:", v_values)

points1 = get_points(v_values)
points2 = get_points(u_values)
print(f"L(2,1) number of B(k{n}, k{n}) = {max(v_values)}")
G1 = nx.Graph()
G1.add_edges_from(points1)

G2 = nx.Graph()
G2.add_edges_from(points2)

G_connector = nx.from_edgelist([(points1[0][0], points2[-1][1])])
G = nx.compose_all([G1, G2, G_connector])

seed = np.random.seed(31)
pos = nx.spring_layout(G, seed=seed)
plt.figure(figsize=(10,6))
nx.draw(G, pos=pos, with_labels=True, node_size = 1000, node_color = 'skyblue')
plt.show()
```





Output

```
Enter n value (greater than 1): 4
u-values: [1, 3, 5, 7]
v-values: [4, 6, 8, 2]
L(2,1) number of B(k4,k4) = 8
```

REFERENCES

1. G. Chartrand, D. Erwin, F. Harary, and P. Zhang, Radio labeling of graphs, Bull. Inst. Combin. Appl., 33(2001), 77-85.
2. J. R. Griggs and R. K. Yeh, Labeling graphs with a condition at distance two, J SIAM. Discrete Math., 5(1992) 586-5995.
3. W. K. Hale, Frequency assignment: theory and application, Proc. IEEE, 68 (1980), 1497-1514.





Effectiveness of task Oriented Sitting Training with Functional Electrical Stimulation on Balance and Postural Control in Subacute Stroke Patients : An Experimental Study

Mahima Y. Tailor¹, Vivek H. Ramanandi^{2*}, Jenny D. Chaudhari¹, Priyanshi R.Patel

¹Consultant Physiotherapist, Surat, Gujarat, India.

²Associate Professor, SPB Physiotherapy College, Surat, Gujarat, India

Received: 27 Dec 2022

Revised: 23 Feb 2023

Accepted: 06 Mar 2023

*Address for Correspondence

Vivek H. Ramanandi

Associate Professor,
SPB Physiotherapy College,
Surat, Gujarat, India.
Email: vivekramanandi@gmail.com



This is an Open Access Journal / article distributed under the terms of the **Creative Commons Attribution License (CC BY-NC-ND 3.0)** which permits unrestricted use, distribution, and reproduction in any medium, provided the original work is properly cited. All rights reserved.

ABSTRACT

According to World Health Organization (WHO), balance and postural impairments are commonest and affects approximately 50% of stroke survivors. This study intends to determine 4-week task oriented sitting training given in conjunction with functional electrical stimulation on balance, postural control and functional activity. 54 subjects with subacute stroke were invited and screened for participation in this experimental study following the selection criteria, through purposive sampling method. Total 32 patients were included in the study, out of which withdrew due to time limitation and health issues. Participants were involved in task oriented sitting training in conjunction with FES intervention, which was given 20 minutes daily, 5 days per week, 4 weeks in addition to 20 minutes conventional physiotherapy. Data of total 29 participants were analyzed and showed significant improvement in balance, postural control and functional activities ($p < 0.001$). This study shows that 4-week task oriented sitting training in conjunction with FES is effective in improving balance, postural control and functional activities in subacute stroke patients.

Keywords: Balance, functional electrical stimulation, functional independence, subacute stroke, task oriented sitting training, trunk control.

INTRODUCTION

According to the World Health Organization (WHO), cerebrovascular stroke or accident (CVA) is the third most common cause of chronic disability in developing countries [1]. Globally, there is a huge burden of stroke with 10.3 million new stroke and 113 million disability adjusted life years (DALY) per year [2]. Clinically, a variety of focal deficits shows changes in level of consciousness, motor, cognitive, impairments of sensory, perceptual and language function [3]. Stroke survivors shows chronic disabilities related to impairments in body structure and function, such





Mahima Y. Tailor et al.,

as changes in motor function, limitations in certain activities, changes in mobility, increased risk of falling during functional activities, and restriction of participation[4]. Balance and postural disorders among the most prevalent consequences, affecting 50%of post-stroke patients. 83% of stroke patients experienced difficulty in executing successful balance and postural control [5].Post stroke mechanisms of balance disorders are diverse and in stroke patient imbalance is due to postural sway, asymmetrical weight shifting, asymmetrical weight distribution [6]. Causes of postural imbalance include muscle weakness, spasticity, delayed activity of the trunk muscles, perceptual deficits [7]. Trunk Control is an important predictor of recovery and along with the sitting balance it is significantly correlated with other functional abilities related to balance[7].

Recently, physiotherapy interventions have focused on 'Task Oriented Training (TOT)' approach which is based on behavioral neuroscience as well as recent models of motor control and motor learning. It includes a repetitive training of functional task or an element of a single functional task that is carried out in an open environment to acquire efficient and effective motor skill [8].Literature has demonstrated the efficacy of a task specific sitting training protocol for improving loading on affected lower extremity; enhanced ability to reach further and faster; sitting ability, sitting quality and standing up early; balance and functional independence in individuals who had suffered stroke [8-12].Functional Electrical Stimulation (FES)is widely researched for rehabilitation of lower extremity function after stroke. It is commonly used to initiate and facilitate the voluntary contraction of paretic or paralyzed muscles to produce functional movement; and augment repetitive task-specific practice, thereby improving motor control [13,14].There is Unavailability of literature suggesting that both of this intervention can be used in conjunction to show their effects on balance and postural control in subacute stroke patients. This study intends to assess the combined effects of these interventions and also inspect its clinical implications using an experimental study design.

METHODS

This study was conducted at the Department of Neurological Physiotherapy,S.P.B. Physiotherapy College, Surat between April-2021 to May-2022. After receiving ethical approval from the Institutional Ethical committee, total 54 patients were screened on the basis of inclusion and exclusion criteria following purposive sampling method.Inclusion criteria were: both male and female patients having stroke between 4 weeks -6 months; first episode of stroke diagnosed by CT or MRI or diagnostic medical reports by an europhysician; mini mental scale score>24; Brunnstorm voluntary control grade 3 or more; and participant who was able to sit for 20 minutes and reach forward and 45 degrees across the body onbothsides.Exclusion criteria included: any visual, neurological, musculoskeletal or motor planning deficit affecting patient's ability to participate in the study. After receiving informed consent from patients, 32 eligible subjects were subjected to intervention. 3 subjects withdrew their participation, 2 from group A and 1 from group B, during the period of intervention (i.e., 1- time limitation, 2- worsening of health condition).Total 29 sub-acute stroke patients' data were used for final analyses (Figure 1). Participants performed a standardized training program which involved 10 daily practice sessions of reaching beyond arm's length for 20 minutes for 4 weeks in conjunction with FES applied as shown in figure-2 and additionally a 20 minutes' session of the conventional physiotherapy. Conventional physiotherapy treatment included exercises for reduction of tone, gait and balance training, strengthening, stretching, co-ordination exercises, etc.

The subjects used their unaffected hand for reaching, picking up and drink water from a glass from 3 reach direction conditions: (a) Forward, (b) 45° towards the unaffected side and (c) 45° across the body towards affected side. Subject practiced reaching while sitting on the height adjustable stool while feet were resting completely on floor. Height of the seat was adjusted to 100% of lower leg length. The glass was kept at height adjusted to 75% of shoulder height. The progression in training was done by increasing number of repetitions and complexity of task over 4 weeks' period. Each participant performed 250-350 reaches per session and average 3000 reaches over 4 weeks [8].





Mahima Y. Tailor et al.,

The FES was applied simultaneously using Walker 3035 channel FES2' (Figure 3) through self-adhesive rubber electrodes which was be positioned: one over the motor point of the tibialis anterior (TA) muscle and one immediately below the belly of the muscle. Active FES was conducted for maximum up to 20 minutes with a pulse width of 250 μ s, modulated at a frequency of 50 Hz and stimulation cycles of 1:2 (Time on: Time off = 6 sec: 12 sec) associated with active contraction of the TA muscle [15].

In this study, berg balance scale for balance (BBS) [16] and performance-oriented mobility assessment (POMA) [17] for postural control during mobility were used as primary outcomes. As a secondary outcome, Indian stroke scale (ISS) [18] was used for assessing functional activity in daily life. All outcome measures were recorded at the starting and at the end of 4-week training period. Statistical analysis for demographic details, BBS scores, POMA scores and ISS scores was done using SPSS version 20.00 Software. Microsoft Office Excel for Windows was used for creating graphs and tables.

RESULTS AND DISCUSSION

Total 29 participants with mean age 53.96 + 7.68 years participated out of which majority, i.e., 65.52% were male and only 34.48% were female. Most of the participants had ischemic stroke (55.17%) and only 44.83% were hemorrhagic. Age group wise distribution showed that majority of the patients belonged to the age group 56-60 years (31.03%) followed by 61-65 years (20.69%) and least were from younger age group of 35-40 years (3.45%). As shown in table 1, the mean difference of BBS values was 3.62 \pm 1.56. The pre-post difference of means for BBS scores were compared using parametric paired t-test. The comparison results indicate statistically highly significant ($p < 0.05$) improvement on balance of subacute stroke patients. A previous experimental study from India which assessed effect of task-oriented training on in balance and self-efficacy reported findings same as the present study by showing statistically significant improvements in Berg balance scale, timed up and go test, activity specific balance confidence scale and Barthel index scores [19]. Non-parametric Wilcoxon Signed rank test was used to compare pre- and post- intervention differences of means for POMA and ISS scores. The mean difference for ISS and POMA was, 2.79 \pm 0.94 and 2.93 \pm 1.43 respectively. These findings are also indicative of statistically significant ($p < 0.05$) improvement on postural control and functional status of subacute stroke patients. The findings of this study are in coherence with previous studies which concluded that balance and functional independence measured by BBS and Barthel index scores show significant improvements after task oriented sitting training [8,10].

The mean difference values for pre- and post- intervention scores of BBS (3.62), POMA (2.93) and ISS (2.79) suggest that out of three outcome measures BBS shows more significant change in comparison with POMA and ISS scores after 4-weeks of intervention. In previous studies, it was concluded that the task-oriented training approach showed more changes in specific tasks like 'standing feet together unsupported' 'picking up an object from the ground', 'turning 360 degrees', 'placing alternate foot on step or stool', 'tandem standing' and 'standing on one leg' [20-22]. In this study, individual components of BBS or POMA were not scored separately and only total scoring was considered which can be considered for future study where we can analyze which components are more affected by seated reaching. Study by Dean M. et al (1997) provides strong evidence of the efficacy of task-related motor training in improving the ability to balance during seated reaching activities after stroke [11].

The findings of Kang et. Al. (2020) illustrate the role of the lower limbs in balancing the body in sitting during reaching tasks. Peak vertical ground reaction force (GRF) through the feet occurs normally around the end of the reach. At this time, force through the feet acts to break the forward momentum of the body mass and to prevent a fall forward. Additional force enables the return of the upper body to the upright position. After training, stroke subjects had improved the timing of peak vertical GRF to normal and were able to activate anterior tibial and soleus muscles in the affected leg more consistently. Activation of these muscles, which link the shank to the foot, assists in balancing the body mass during distant reaches both in sitting [13]. Almost all the functional activities require postural control including trunk in erect position and as the seated reaching works through activation of trunk





Mahima Y. Tailor et al.,

muscles and anterior tibial group muscles, it may be helpful in improving the functional independence. Improvements in functional activity measured by ISS scores are indirect reflection of improvement in specific components such as 'standing up from an armchair', 'moving around inside home', 'getting dressed', and 'standing without support for 5 min'. Jung-Hyun Kim et.al. (2011) concluded that in their study when FES was applied to the tibialis anterior (TA) and gluteus Medius (GM) muscles it produced significant improvement of the spatiotemporal parameters of gait in individuals with a hemiparetic stroke. They compared the groups of patients who received FES for TA only and FES for TA+GM with the group of patients who did not receive FES. In comparison to the TA only and non-FES conditions, the GM + TA group showed significantly higher gait speed, cadence, and stride length. In the TA only condition versus the non-FES condition, the gait speed, cadence, and stride length were all significantly increased[23]. In present study also, there is application of FES for TA, resulting in improvement in both postural control and gait functions measured by BBS and POMA.

The study has implications for rehabilitation, demonstrating that the performance of subacute stroke patients can be improved in functions of daily living by inclusion of short task related seated reach training along with FES that takes into account normative biomechanics related to trunk and lower limb function. It can be included in treatment intervention at an early stage of rehabilitation when there is greatest potential for neuroplasticity. As for all studies this study has its limitations, which include: (a). a smaller sample, (b). lack of long-term follow ups to confirm persistence of interventional gains, (c). exclusion of subjects who were not able to sit and reach, (d). lack of training for seated reach training on dynamic surface. Future studies may be undertaken with larger sample and shall consider long term follow up of the outcomes while also including training on dynamic surfaces.

CONCLUSION

As per result present study supports use of task-oriented approach using task oriented sitting training along with functional electrical stimulation for improving balance and postural control leading to increased functional independence in subacute patients with stroke.

REFERENCES

1. Fruhauf AMA, Politti F, Dal Corso S, Costa GC, Teodósio ADC, Silva SM, Corrêa JCF, Corrêa FI. Immediate Effect Of transcranial direct current stimulation combined with functional electrical stimulation on activity of the tibialis anterior muscle and balance of individuals with hemiparesis stemming from a stroke. *JPhysTherSci*. 2017Dec;29(12):2138-2146. doi: 10.1589/jpts.29.2138. Epub 2017 Dec 7. PMID: 29643591;PMCID:PMC5890217.beq
2. Pandian JD, Gall SL, Kate MP, Silva GS, Akinyemi RO, Ovbiagele BI, Lavados PM, Gandhi DB, Thrift AG. Prevention of stroke: a global perspective. *The Lancet*. 2018 Oct 6;392(10154):1269-78.
3. O'Sullivan SB, Schmitz TJ, Fulk G. *Physical rehabilitation*. FA Davis; 2019 Jan 25.
4. In T, Jin Y, Jung K, Cho HY. Treadmill training with Thera-Band improves motor function, gait and balance in stroke patients. *NeuroRehabilitation*. 2017;40(1):109-114. doi: 10.3233/NRE-161395. PMID: 27814306.
5. Bae S, Lee J, Lee BH. Effect of an EMG-FES Interface on Ankle Joint Training Combined with Real-Time Feedback on Balance and Gait in Patients with Stroke Hemiparesis. *Healthcare (Basel)*. 2020 Aug 24;8(3):292. doi: 10.3390/healthcare8030292. PMID: 32846971; PMCID: PMC7551751.
6. Cho KH, Lee KJ, Song CH. Virtual-reality balance training with a video-game system improves dynamic balance in chronic stroke patients. *TohokuJExpMed*. 2012Sep;228(1):69-74. doi:10.1620/tjem.228.69. PMID: 22976384.
7. Van Criekinge T, Truijien S, Schröder J, Maebe Z, Blanckaert K, van der Waal C, Vink M, Saeys W. The effectiveness of trunk training on trunk control, sitting and standing balance and mobility post-stroke: a systematic review and meta-analysis. *Clinical rehabilitation*. 2019 Jun;33(6):992-1002.





Mahima Y. Tailor et al.,

8. Ramanandi VH, Shukla YU. Effects of Task Related Sitting Training on Balance and Functional Independence in Subacute Stroke Patients with Hemiplegia: A Randomized Sham Controlled Study. Indian Journal of Natural Sciences. 2022; 13(71):40303-40308.
9. Khallaf ME. Effect of Task-Specific Training on Trunk Control and Balance in Patients with Subacute Stroke. Neurology research international. 2020 Nov 17; 2020.
10. Ramanandi VH. Effects of task related sitting training on balance in hemiplegic patients. SRJI. 2013; 2(4): 1-9
11. Dean CM, Channon EF, Hall JM. Sitting training early after stroke improves sitting ability and quality and carries over to standing up but not to walking: a randomized controlled trial. Australian Journal of Physiotherapy. 2007; 53: 97-102.
12. Cho G, Lee S & Woo Y. The effects of task related circuit program on functional improvements in stroke patients. KAUTPT vol.11 no.3, 2004.
13. Kang N, Lee RD, Lee JH, Hwang MH. Functional Balance and Postural Control Improvements in Patients with Stroke After Non-invasive Brain Stimulation: A Meta-analysis. Arch Phys Med Rehabil. 2020 Jan; 101(1):141-153. doi:10.1016/j.apmr.2019.09.003. Epub 2019 Sep 27. PMID: 31568760.
14. Howlett OA, Lannin NA, Ada L, McKinstry C. Functional electrical stimulation improves activity after stroke: a systematic review with meta-analysis. Arch Phys Med Rehabil. 2015 May; 96(5):934-43. doi:10.1016/j.apmr.2015.01.013. Epub 2015 Jan 26. PMID: 25634620.
15. Robinson BS, Williamson EM, Cook JL, Harrison KS, Lord EM. Examination of the use of a dual-channel functional electrical stimulation system on gait, balance and balance confidence of an adult with spastic diplegic cerebral palsy. Physiotherapy Theory Pract. 2015 Mar; 31(3):214-20. doi:10.3109/09593985.2014.982774. Epub 2014 Nov 21. PMID: 25412562.
16. Berg KO, Wood-Dauphinee SL, Williams JI, Maki B. Measuring balance in the elderly: validation of an instrument. Canadian journal of public health = Revue canadienne de sante publique. 1992 Jul 1; 83:S7-11.
17. Tinetti ME, Williams TF, Mayewski R. Fall Risk Index for elderly patients based on number of chronic disabilities. Am J Med 1986; 80:429-434
18. Prakash V, Ganesan M. The Indian Stroke Scale: Development and validation of a scale to measure participation in daily activities among patients with stroke in India. Int J Stroke. 2021 Oct; 16(7):840-848. doi: 10.1177/1747493020979361.
19. Katerawala S, Shah R, Sarvanan M. Effect of Task Oriented Activity Training on Improving Balance and Self Efficacy in Sub Acute Stroke. Website: www.ijpot.com. 2019 Oct; 13(4):4104.
20. Rowe VT, Neville M. Task oriented training and evaluation at home. OTJR: occupation, participation and health. 2018 Jan; 38(1):46-55.
21. Lee HY, Kim YL, Lee SM. Effects of virtual reality-based training and task-oriented training on balance performance in stroke patients. Journal of physical therapy science. 2015; 27(6):1883-8.
22. Ogwumike OO, Badaru UM, Adeniyi AF. Effect of task-oriented training on balance and motor function of ambulant children with cerebral palsy. Rehabilitation (Madr). 2019 Oct- Dec; 53(4):276-283. doi:10.1016/j.rh.2019.07.003. Epub 2019 Nov 19. PMID: 31813423.
23. Kim JH, Chung Y, Kim Y, Hwang S. Functional electrical stimulation applied to gluteus medius and tibialis anterior corresponding gait cycle for stroke. Gait & posture. 2012 May 1; 36(1):65-7.

Table 1: Pre- and post-intervention within group comparison of means (n=29)

OUTCOME MEASURES	PRE-SCORE		POST-SCORE		TEST APPLIED	P -VALUE
	Mean	SD	Mean	SD		
BBS Scores	46.10	2.65	49.55	2.81	Paired t- test	<u><0.05</u>
POMA Scores	22.11	3.02	25.06	2.81	Wilcoxon signed rank test	<u><0.05</u>
ISS Scores	70.13	3.52	72.89	9.37		<u><0.05</u>

Note: Here, Underlined values of 'p' shows statistically significant difference at < 0.05 levels.



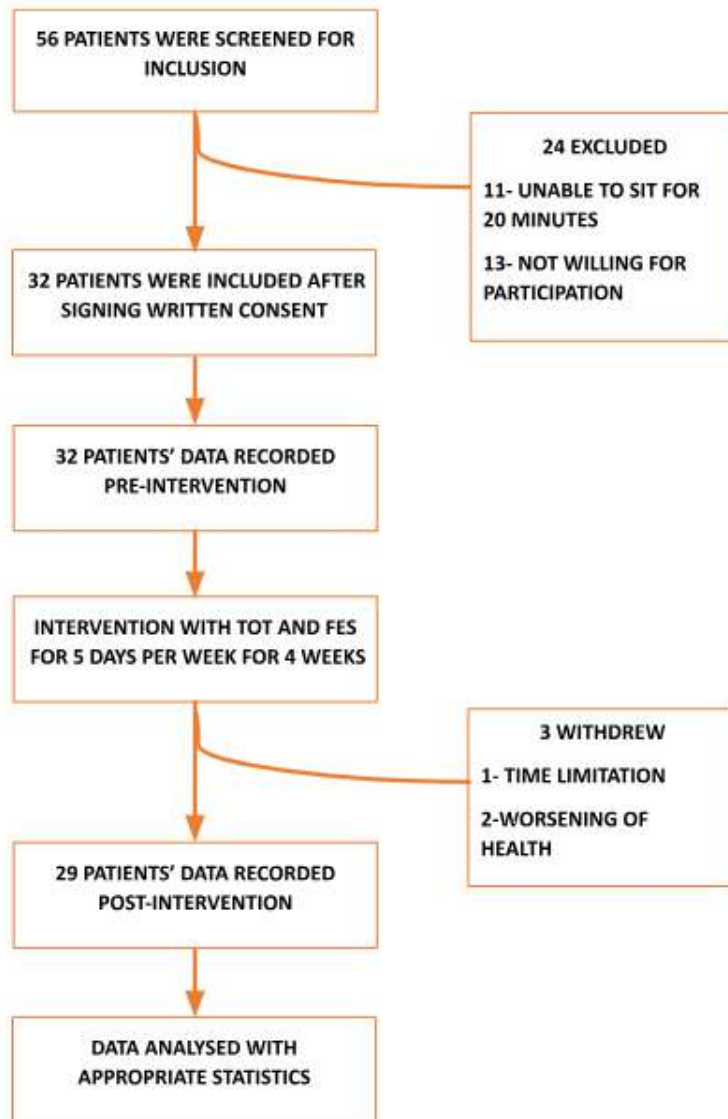


Figure 1: Participant Flow





Figure 2: Setup for Task Oriented Sitting Training with FES for Tibialis Anterior



Figure 3: Parts of 'Walkex 3035 channel FES2' System





Agriculture Product Farming: An Empirical Study on Perception and Satisfaction of Farmers

G.R.Rajalakshmi¹, D.Priya^{2*}, B.Navaneetha³ and G.Rajamani⁴

¹Assistant Professor, Department of Commerce with CA, PSG College of Arts and Science, Coimbatore, Tamil Nadu, India.

²Assistant Professor, Department of B.Voc (Banking Stock and Insurance), PSG College of Arts and Science, Coimbatore, Tamil Nadu, India.

³Assistant Professor, Department of B.Com (CA), PSG College of Arts and Science, Coimbatore, Tamil Nadu, India.

⁴Assistant Professor, Department of B.Com (A and F), Sri Ramakrishna College of Arts and Science, Coimbatore, Tamil Nadu, India.

Received: 25 Jan 2023

Revised: 23 Apr 2023

Accepted: 31 May 2023

*Address for Correspondence

D.Priya

Assistant Professor,
Department of B.Voc (Banking Stock and Insurance),
PSG College of Arts and Science,
Coimbatore, Tamil Nadu, India.



This is an Open Access Journal / article distributed under the terms of the **Creative Commons Attribution License** (CC BY-NC-ND 3.0) which permits unrestricted use, distribution, and reproduction in any medium, provided the original work is properly cited. All rights reserved.

ABSTRACT

Agriculture is the backbone of the Indian economy and it remains for a long time. Agricultural productivity mainly depends on various factors like availability and quality of agricultural inputs such as land, water, seeds and fertilizers, assurance of remunerative prices for agricultural produce, crop insurance and storage and marketing infrastructure etc. Indian agriculture is largely depended by agro-ecological diversities in soil, rainfall, temperature, and cropping system. A proper harvesting and proficient utilization of water is of great importance. Besides, major commodities imported to India are pulses, edible oils, fresh fruits and cashew nuts. Major agriculture produce are exported by India such as rice, spices, cotton, meat and its preparations, sugar, etc. The main objectives of the study are to know the demographic profile of the farmers and their retention of customers towards market produce, to identify the labour shortage after implementation of lockdown during COVID-19 and to examine the satisfaction level of the farmers towards the Marketing of Agricultural Produce after implementing Plans and policies during COVID Crisis. A sample of 150 farmers has been taken for the study. A purposive sampling technique has been adopted to collect the data from farmers. A tool such as Percentage analysis, Chi-square, ANOVA and T-test has been applied to analyze the data. The study reveals that Indian farmers should expand their cropping pattern from cereals to high-value crops. This will increase revenue and reduce environmental degradation simultaneously. It is concluded that marketing

57419



**Rajalakshmi et al.,**

before and after covid-19 have a significant association with retention of the customer, the marketing before covid-19 of the respondents have a significant association with labour shortage after implementation of lockdown. The respondents have been varied significantly in the satisfaction score for marketing of agricultural produce during covid crisis when they are classified based on age groups, gender, marital status, educational qualification, monthly income, problem faced on exporting and future farming.

Keywords: Agriculture productivity, Agro-ecological, Harvesting, Commodities and Lockdown during COVID-19

INTRODUCTION

India is an agriculture country where two-thirds of its population is involved in agricultural production activity. Agriculture is the pillar of Indian economy, as it contributes 4 per cent of global gross domestic product (GDP) and in developing countries; it contributes more than 25 per cent of GDP as reported by World Bank. It is a primary activity, whose source of income for about 58 per cent of total India's population. It employs nearly half of the country workforce. India's food grains production is increasing every year and India is among one of the top producers of various crops such as rice, wheat, pulses, sugarcane etc. India becomes the highest producer of milk followed by fruits and vegetables. In 2013, India contributed 25 per cent to the world's pulses production, 22 per cent to rice production and 13 per cent to the wheat production. Agriculture refers to the act of growing crops and raising livestock for human consumption. It consists of two types of agriculture namely industrialized agriculture and subsistence agriculture. Industrialized agriculture is a type of agriculture where huge numbers of crops and livestock are produced for massive consumption and the products were exported to different countries. This type of agriculture increases the crop yield by implementing the large irrigation system and also by chemical fertilizers & pesticides. Another method of industrialized agriculture is monocultures, where single crop is planted on large scale in order to acquire high yield. Subsistence agriculture is based on small farming and the farmer produces enough food for own personal consumption. The main goal of subsistence agriculture is to produce sufficient food to ensure the survival of individual family. If there is any excess in food production, it may cater the needs of the local families. Instead of using chemical pesticides, subsistence farmers used only natural predators of pests to control the pest population. Polyculture is another method of subsistence agriculture, where different types of crops are planted in a single area to get the most crop yield out of a small area of land.

STATEMENT OF THE PROBLEM

India is the second major producer of rice, wheat, cotton, sugarcane, fruits & vegetables and groundnuts. As of last decade, it also produced 25 per cent of the world's pulses until 2019. India is one among the top 15 exporters of agricultural products in the world. Agricultural export from India reached US\$ 38.54 billion (FY19) and US\$ 35.09 billion (FY20). High percentage of agriculture land, diverse agro-climatic situations encourages farming of different crops. Due to increase in population and rising urban & rural income is driving the demand. Demand for agriculture contributions such as hybrid seeds and fertilizers and associated services like warehousing and cold storages are increasing pace in India. In India, consumer spending is in growth during 2021 post the pandemic-led contraction, expanding by as much as 6.6 per cent.

REVIEW OF LITERATURE

David Harris and Dorian Q Fuller (2014) have made a study on the topic "Agriculture: Definition and Overview". This study mainly focused on the evolutionary model involving pre-domestication cultivation and post-domestication cultivation evolution syndrome. This study reveals the various indicators like cultivation, domestication, mixed crop-livestock farming, pastoralism, horticulture, arboriculture and vegeculture.



**Rajalakshmi et al.,**

Chandra Shekara, Ajit Kumar, Balasubramani et al (2016) have made a study on “Basic Agriculture”. The study focused on the important extension sources to farmers, input dealers, Cooperative Society, ATMA, Kissan Call Center, KrishiVigyan Kendra, Agricultural Universities, ICAR Institutions, Commodity Boards, National Institutes, International Institutes and Agricultural Magazines. This study concludes that the important sources of finance to farmers are banks, cooperatives and SHGs. Kissan Credit Cards provides adequate and timely financial support from the banking system to the farmers. Non loanee farmers are advised to take the benefits of agricultural insurance coverage by paying nominal premium, maintain close liaison with extension. William R. Cline (2008) has conducted a study on the topic “Global warming and agriculture”. This study focused on the effect on agriculture due to climatic changes, impact on crop yields and technological rescue. The researcher applies the ricardian model in the study. The study reveals that developing countries get affected due to the effects of global warming on agriculture and green revolution has been slow down the global warming. This study specifies the importance of coordinated international action to limit the carbon dioxide emissions.

OBJECTIVES OF THE STUDY

1. To know the demographic profile of the farmers and their retention of customers towards market products.
2. To identify the labour shortage after implementation of lockdown during COVID-19.
3. To examine the satisfaction level of the farmers towards the Marketing of Agricultural Products after implementing Plans and Policies during COVID Crisis.

RESEARCH METHODOLOGY

A sample of 150 respondents has been chosen for the study by adopting purposive sampling techniques. Structural questionnaire is used to collect the data from the farmers. Secondary data such as newspaper, magazine, journals, articles etc., have been taken for the study. Tools such as Percentage analysis, Chi-square, ANOVA and T-test have been applied to analyze the data.

Analysis and Interpretation

With respect to market before covid-19 of the respondents, it is clear that out of 150 respondents, 78 respondents belong to directly selling the products in market before covid-19. Among them, most (28.6 per cent) of the respondents has gained the customer. It is observed from the above table that 48 per cent of the respondents are in the age group of 40 to 60 years, 67.3 per cent of the respondents are male, 65.3 per cent of the respondents are married, 38 per cent of the respondents are graduate, 38 per cent of the respondents have a monthly income of Rs.25,000 to Rs.50,000 and 42 per cent of the respondents are undertaking farm up to 5 years. 23.3 per cent of the respondents has neither gained nor lost the customer with respect to market after covid-19. The chi-square result have shown that the marketing before covid-19 of the respondents ($\chi^2=20.655$, $P > .05$) have a significant association with retention of the customer at 1 per cent level. Hence, the null hypothesis has been rejected with respect to marketing of the respondents before covid-19 whereas the null hypothesis has been rejected with respect to marketing of the respondents after covid-19 at 5% level of significance.

With respect to market before covid-19 of the respondents, it is clear that out of 150 respondents, 78 respondents belong to directly selling the products in market before covid-19. Among them, most (46 per cent) of the respondents has labour shortage before COVID 19. Among 64 respondents, 32 per cent of the respondents have labour shortage after COVID 19. The chi-square result have shown that the marketing before covid-19 of the respondents ($\chi^2=20.655$, $P > .05$) have a significant association with labour shortage after implementation of lockdown at 5 per cent level. Hence, the null hypothesis has been rejected with respect to labour shortage after implementation of lockdown before covid-19. The null hypothesis has been accepted with respect to market after covid-19.



**Rajalakshmi et al.,****ANOVA****Satisfaction vs. Socio-economic profile and study factors**

ANOVA and t-test have been used to test whether the 'Satisfaction' mean score has differed significantly among the respondents classified based on 'socio- economic profile ' and study profile with the following null hypothesis.

H₀: "The mean score of satisfaction does not have significant difference with Socio- economic Profile and study profile of the respondents".

The null hypothesis has been tested for each of the Socio- Economic Profile factors and study factors separately and the results are presented in the following table. It is inferred from the above table that the respondents whose age belong to below 20 years (3.7353) have been highly satisfied the Marketing of Agricultural Produce after implementing Plans and policies during COVID Crisis and the respondents whose age above 60 years (2.0556) have been highly dissatisfied the marketing of agricultural produce during COVID Crisis. Female respondents are highly satisfied when compared to male respondents towards Marketing of Agricultural Produce after implementing Plans and policies during COVID Crisis. Graduates are highly satisfied when compared to others with respect to Marketing of Agricultural Produce after implementing Plans and policies during COVID Crisis. Most of the respondents (4.25) who have a monthly income of above Rs.1,00,000 have a highest satisfaction score. Most of the respondents do not face any problems on exporting agriculture produce since, it has highest mean score. Most of the respondents wish to continue their farming business.

However, with the F-ratio value / T-value, it is revealed that the respondents have been varied significantly in the satisfaction mean score for marketing of agricultural produce during covid crisis when they are classified based on age groups, gender, marital status, educational qualification, monthly income, problem faced on exporting and future farming. Therefore, the null hypothesis has been rejected at 1 per cent level and 5 per cent level with respect to Marketing of Agricultural Produce after implementing Plans and policies during COVID Crisis.

SUGGESTIONS

1. Marketing of agricultural produce gets affected after COVID-19. Farmers should compare the gross margins of different crops and the production techniques, helps to make decisions on using the land to maximize revenue. The retention of the customers is necessary in order to increase the sale of agriculture produce. Therefore farmers should retain their customers by fixing affordable price, discounting the agriculture produce and providing hospitality to their customers.
2. The farmers are facing the labour shortage after implementation of lockdown. Hence, the labour productivity helps to identify the crops and techniques that make best use of labour (family or wage labour). It also indicates if it is profitable to work on your own farm. In order to reduce the labour shortage, farmers should adopt various measures such as providing mask, sanitizer and adequate labour wage to work effectively.
3. The farmers in the age group of above 60 years are dissatisfied with the Marketing of agricultural produce. Therefore government should take appropriate steps to sell the agriculture produce by procuring goods directly from the senior citizens.
4. The farmers who have completed their primary education have less satisfaction score on Marketing of agricultural produce. So, the government should provide various awareness programs and skill enhancement programs to market the agriculture produce.
5. Farmer should analyze the capital productivity indicates which crops or production techniques make best use of money invested.

CONCLUSION

Agriculture sector is expected to grow in India in next few years due to increased investment in infrastructure facilities like irrigation facilities, warehousing and cold storage. Nowadays genetically modified crops has been





Rajalakshmi et al.,

increased the yield for Indian farmers. After globalization (1990), the India farmers have faced various challenges. Although being significant producer of rice, spices, cotton, rubber, tea, coffee and jute our agricultural products are unable to contest with the developed countries due to highly subsidized agriculture in those countries. In order to make the agriculture successful and profitable, it is necessary to improve the condition of marginal and small farmers. The study has been concluded that the marketing before and after covid-19 have a significant association with retention of the customer, the marketing before covid-19 of the respondents have a significant association with labour shortage after implementation of lockdown. The respondents have been varied significantly in the satisfaction score for marketing of agricultural produce during covid crisis when they are classified based on age groups, gender, marital status, educational qualification, monthly income, problem faced on exporting and future farming. Therefore, the null hypothesis has been rejected at 1 per cent level and 5 per cent level with respect to Marketing of Agricultural Produce after implementing Plans and policies during covid crisis.

REFERENCES

1. David R. Harris and Dorian Q Fuller , "Agriculture: Definition and Overview", 2014, Encyclopedia of Global Archaeology (Claire Smith, Ed.), New York, pp 104-113, <https://www.researchgate.net/publication/301345493>.
2. Chandra Shekara, Ajit Kumar, Balasubramani et al, "Farmer's Handbook on Basic Agriculture", 2016, pp 1-154, <https://www.manage.gov.in/publications/farmerbook.pdf>.
3. William R. Cline, Finance & Development, March 2008, pp 1-5, <https://www.imf.org/external/pubs/ft/fandd/2008/03/pdf/cline.pdf>
4. <https://study.com/academy/lesson/types-of-agriculture-industrialized-and-subsistence-agriculture.html>
5. <file:///C:/Users/user/Downloads/HarrisFullerms.pdf>
6. [http://cbseacademic.nic.in/web_material/Curriculum/Vocational/2018/Basic%20Agriculture%20X%20\(408\).pdf](http://cbseacademic.nic.in/web_material/Curriculum/Vocational/2018/Basic%20Agriculture%20X%20(408).pdf)
7. https://prsindia.org/files/policy/policy_analytical_reports/State%20of%20Agriculture%20in%20India.pdf
8. <https://www.worldbank.org/en/topic/agriculture/overview#1>
9. <https://www.ibef.org/industry/agriculture-india.aspx>
10. <https://ncert.nic.in/ncerts/l/jess104.pdf>

Table-1 Demographic Factors

Demographic Factors	Categories	Frequency	Per cent
Age	Below 20	17	11.3
	20 – 40	52	34.7
	40 -60	72	48.0
	Above 60	9	6.0
Gender	Male	101	67.3
	Female	49	32.7
Marital Status	Married	98	65.3
	Unmarried	46	30.7
	Widowed	6	4.0
Educational Qualification	No formal education	17	11.3
	Primary education	15	10.0
	Secondary education	40	26.7
	Graduate	57	38.0
	Post graduate	12	8.0
	Others	9	6.0





Rajalakshmi et al.,

Monthly Income of the family	Below 25000	47	31.3
	25000 – 50000	57	38.0
	50000 – 75000	27	18.0
	75000 – 100000	14	9.3
	Above 100000	5	3.3
Years of farming	Under 5 years	63	42
	5 to 15 years	46	30.7
	More than 15 years	41	27.3

Table-2 Chi square–Retention of the customer before and after COVID 19

	Groups	Retention before and after COVID 19						Total		Sig
		Customer Lost		Neither gained nor lost		Customer Gained		No.	%	
		No.	%	No.	%	No.	%			
Market before COVID 19	Direct	10	6.7	25	16.7	43	28.6	78	100	**
	Through middle men	11	7.3	37	24.7	8	5.3	56	100	
	Through agencies	7	4.7	5	3.3	4	2.7	16	100	
Market after COVID 19	Direct	18	12.0	26	17.3	10	6.7	54	100	*
	Through middle men	21	14	35	23.3	8	5.3	64	100	
	Through agencies	22	14.7	6	4.0	4	2.7	32	100	

(Source: Computed Ns- Not Significant **- Significant at 1% level *- Significant at 5% level)

Table-3 Chi square - Labour Shortage after Implementation of Lockdown

	Groups	Labour shortage after Implementation of Lockdown				Total		Sig
		Yes		No		No.	%	
		No.	%	No.	%			
Market before COVID 19	Direct	69	46.0	9	6	78	100	*
	Through middle men	40	26.7	16	10.7	56	100	
	Through agencies	10	6.7	6	4.0	16	100	
Market after COVID 19	Direct	44	29.3	10	6.7	54	100	NS
	Through middle men	48	32	16	10.7	64	100	
	Through agencies	27	18	5	3.3	32	100	

(Source: Computed Ns- Not Significant **- Significant at 1% level *- Significant at 5% level)

Table-4 Satisfaction Vs. Socio-economic profile factors and study factors

Marketing strategies	Groups	N	Mean	S.D	F-value/ T-value	Sig.
Age	Below 20	17	3.7353	.93320	10.056	**
	20 – 40	52	3.5240	.93444		
	40 -60	72	2.9792	.94361		
	Above 60	9	2.0556	.54167		





Rajalakshmi et al.,

Marketing strategies	Groups	N	Mean	S.D	F-value/ T-value	Sig.
Gender	Male	101	3.0668	1.01544	-2.342	*
	Female	49	3.4694	.92651		
Marital Status	Married	98	3.0230	.96062	10.737	**
	Unmarried	46	3.6902	.92524		
	Widowed	6	2.2917	.71443		
Educational Qualification	No formal education	17	3.1471	1.00023	7.180	**
	Primary education	15	2.5667	.94239		
	Secondary education	40	2.6875	.89470		
	Graduate	57	3.5746	.96010		
	Post graduate	12	3.4375	.65821		
	Others	9	3.9167	.68465		
Monthly income of the family	Below 25000	47	3.2819	.94928	4.187	*
	25000 – 50000	57	2.9386	1.01141		
	50000 – 75000	27	3.0833	.90671		
	75000 – 100000	14	3.8214	1.00684		
	Above 100000	5	4.2500	.46771		
Faced problems on exporting agricultural produce	Strongly agree	43	3.2907	1.09236	7.308	**
	Agree somewhat	63	2.7619	.91077		
	Neither agree nor disagree	24	3.6979	.65100		
	Disagree	12	3.8333	.77850		
	Strongly disagree	8	3.6875	.97055		
Future of farming in upcoming years	Continue farming business as usual	52	3.5240	.92257	8.016	**
	Continue and expand farming business	44	3.4148	.87095		
	Will allow family	21	2.9524	1.06835		
	Will rent it	17	2.9118	1.04561		
	Will discontinue from farming	16	2.1719	.64368		

(Source: computed)(Ns – Not significant, ** - significant at 1 per cent level, * - significant at 5 per cent level)





Modelling of Dynamically Graded Plates with a Four-Variable Power Law for use in Aircraft

GulshanTaj MNA¹, Nandipati Govind², M.Siva³, K.Mohan Das^{4*} and JagadishShrisaila Haranatti⁵

¹Assistant Professor, Department of Civil Engineering, Sona College of Technology, Salem, Tamil Nadu, India.

²Associate Professor, Department of Mechanical Engineering, RVR and JC college of Engineering, Guntur, Andhra Pradesh, India.

³Professor, Department of Civil Engineering, Easwari Engineering College, Chennai, Tamil Nadu, India.

⁴Professor, Department of Civil Engineering, CMR College of Engineering and Technology, Telangana, India.

⁵Assistant Professor, Department of Civil Engineering, KG Reddy College of Engineering and Technology, Hyderabad, Telangana, India.

Received: 17 Feb 2023

Revised: 25 Apr 2023

Accepted: 31 May 2023

*Address for Correspondence

K.Mohan Das

Professor,

Department of Civil Engineering,

CMR College of Engineering and Technology,

Telangana, India.

E. Mail: kmohandas11780@gmail.com



This is an Open Access Journal / article distributed under the terms of the **Creative Commons Attribution License** (CC BY-NC-ND 3.0) which permits unrestricted use, distribution, and reproduction in any medium, provided the original work is properly cited. All rights reserved.

ABSTRACT

The prior literature has a sizable amount of data and conclusions relevant to analysis of advanced composite materials dubbed as functionally graded material plates/shells. Due to their functional characteristics along the desired direction, reliable micromechanical modelling of such parts is essential to forecast their reaction under various operating situations. Most investigations use a generalized single parameter dependent power law to evaluate the constituents' real mechanical properties at any generic position, often along the thickness direction. Such a strategy results in the plate/shell arrangement, where the bottom surface is occupied by a metal segment and the top surface is dominated by a ceramic component. However, the designer or analyst must produce a model that takes into account every conceivable combination of the constituents at the upper and lower levels in order to satisfy the practical requirements. To address this issue and facilitate accurate computation, the authors conducted the





GulshanTajet *et al.*

current investigation on functionally graded plates using the finite element approach. The generalized four-parameter rule is utilized in this study to determine the material profile and account for different profiles in combination. An aluminum or zirconia plate will be used for the study under various support arrangements. It is thought that plates having symmetric properties in reference to the neutral plane produce better results. Various ramifications of the study are examined in depth. Performance in comparison to any other combination of profiles.

Keywords: Functionally graded plate, four-parameter power law, finite element method, higher order shear deformation theory, bending analysis.

INTRODUCTION

Numerous articles [1-3] provide clear justifications for choosing FGM constructions over more traditional forms of structures (isotropic or laminated composites). Regarding this, numerous traditional and contemporary approaches have been developed, including diverse solution methodologies, for the analysis of such structures under varied loading circumstances. A few of the most often used solution tools by many scholars working in this field are the mesh-free collocation radial basis techniques [12], the differential quadrature method (DQM) [11], and the finite element method (FEM) [10]. The main results drawn from such methodologies on the reaction of FGM structures follow a similar route, despite the fact that each method has its own channel for handling the problem of interest. On the classical plate theory, many branches of kinematics are In order to combine transverse and normal deformation modes for extension-bending coupling, the total response of the plate is established. The finite element method is used to implement Reddy's higher order theory, which requires no shear factor. To solve for an unidentified higher order component present in the displacement fields, no stress boundary conditions are applied at the upper and lower profile. As a result, second order terms in the relevant strain field components result from the first order transverse displacement components existing in the in-plane and transverse displacement field. The aforementioned circumstance prompted the formulation of the C1 continuity problem; it is generally recognized that this problem presents a number of challenges. Additionally, C0 elements are preferred over C1 elements in most real-world situations.

Problem Description and Finite Element Formulation

The discrepancy in volume fraction over the thickness direction for various numbers of a , b , and c is shown in Figure 1. Having a thorough understanding of profiles enables one to select the best top and bottom profiles. It is required to depict the displacement field, which includes membrane and flexure components in in-plane and transverse fields as well, in order to accurately predict the configuration's overall response. A kinematics field that includes normal and transverse cross-sectional deformation modes is taken into consideration in order to solve the problem. In the current study, transverse fields use the second degree of thickness term, whereas in-plane fields incorporate the third degree of thickness term. At points $P(x, y, \text{ and } z)$ in the current investigation, the in-plane (u and v) and transverse displacement (w) fields are incorporated in the following manner.

$$\begin{aligned} u(x, y, z) &= u_o(x, y, z) + z\theta_x(x, y, z) + z^2\xi_x(x, y, z) + z^3\rho_x(x, y, z) \\ v(x, y, z) &= v_o(x, y, z) + z\theta_y(x, y, z) + z^2\xi_y(x, y, z) + z^3\rho_y(x, y, z) \\ w(x, y, z) &= w_o(x, y, z) + z\zeta_z(x, y, z) + z^2\xi_z(x, y, z) \end{aligned} \quad (1)$$

Here, the u_0 , v_0 , and w_0 values in the x , y , and z directions, respectively, stand in for the displacement components at the reference plane ($z = 0$). Q_x and Q_y , respectively, stand for the bending rotations of normal components about the reference plane or the centre plane around the y and x axes. Taylor's higher terms are polynomial functions that include the cubic and quadratic terms in the in-plane and transverse field and take into account the shear





GulshanTajet et al.,

deformation modes in the z-direction. No stress boundary condition is employed at the upper and lower portion of the plate (i.e., $xz = xz = 0 = h/2$) to resolve higher order polynomial equations. The following expression for in-plane fields is produced by making the following assumption and appropriately substituting the variables:

$$\begin{aligned}
 u(x, y, z) &= u_o + \left(z - \frac{4z^3}{3h^2} \right) \theta_x - \frac{z^2}{2} \frac{\partial \zeta_z}{\partial x} - \frac{4z^3}{3h^2} \frac{\partial w_0}{\partial x} - \frac{z^3}{3} \frac{\partial \xi_z}{\partial x} \\
 v(x, y, z) &= v_o + \left(z - \frac{4z^3}{3h^2} \right) \theta_y - \frac{z^2}{2} \frac{\partial \zeta_z}{\partial y} - \frac{4z^3}{3h^2} \frac{\partial w_0}{\partial y} - \frac{z^3}{3} \frac{\partial \xi_z}{\partial y}
 \end{aligned}
 \tag{2}$$

Here, the displacement components at the reference plane ($z = 0$) are represented by the values u_0 , v_0 , and w_0 in the x , y , and z directions, respectively. The normal component bending rotations around the reference plane or the centre plane around the y and x axes are denoted by the letters θ_x and θ_y , respectively. Taylor's higher terms are polynomial functions that take into consideration the shear deformation modes in the z -direction as well as the cubic and quadratic terms in the in-plane and transverse fields. In order to solve higher-order polynomial equations, no stress boundary condition is used at the upper and lower parts of the plate (i.e., $xz = xz = 0 = h/2$). By assuming the following assumption and properly inserting the, the following formula for in-plane fields is derived.

$$\alpha_x - \frac{\partial \zeta_z}{\partial x} = 0; \beta_x - \frac{\partial w_0}{\partial x} = 0; \psi_x - \frac{\partial \xi_z}{\partial x} = 0; \alpha_y - \frac{\partial \zeta_z}{\partial y} = 0; \beta_y - \frac{\partial w_0}{\partial y} = 0; \psi_y - \frac{\partial \xi_z}{\partial y} = 0$$

Thus the final manifestation for kinematics formula (u, v and w) incorporating C_0 variables turns into

$$\begin{aligned}
 u(x, y, z) &= u_o + \left(z - \frac{4z^3}{3h^2} \right) \theta_x - \frac{z^2}{2} \alpha_x - \frac{4z^3}{3h^2} \beta_x - \frac{z^3}{3} \psi_x \\
 v(x, y, z) &= v_o + \left(z - \frac{4z^3}{3h^2} \right) \theta_y - \frac{z^2}{2} \alpha_y - \frac{4z^3}{3h^2} \beta_y - \frac{z^3}{3} \psi_y
 \end{aligned}
 \tag{3}$$

$$w(x, y, z) = w_o + z \zeta_z + z^2 \xi_z$$

The displacement vector thus can be represented with thirteen unknowns as $\{d\} = [u_0, v_0, w_0, \theta_x, \theta_y, \zeta_z, \alpha_x, \alpha_y, \xi_z, \beta_x, \beta_y, \psi_x, \psi_y]^T$ for each node. Proposed plate geometry is configured with Lagrangian element having nine nodes thus contributing a total of 117 nodal unknowns for each element. The present element is not subjected to any locking issue and any other false modes. Shape functions N_i which are related with natural co-ordinates (ξ and η) are written below for further analysis.

For corner nodes:

$$N_1 = \frac{1}{4}(\xi - 1)(\eta - 1)\xi\eta, N_3 = \frac{1}{4}(\xi + 1)(\eta - 1)\xi\eta, N_7 = \frac{1}{4}(\xi - 1)(\eta + 1)\xi\eta, N_9 = \frac{1}{4}(\xi + 1)(\eta + 1)\xi\eta$$

For mid nodes:

$$N_2 = \frac{1}{2}(1 - \xi^2)(\eta^2 - \eta), N_4 = \frac{1}{2}(\xi^2 - \xi)(1 - \eta^2), N_6 = \frac{1}{2}(\xi^2 + \xi)(1 - \eta^2), N_8 = \frac{1}{2}(1 - \xi^2)(\eta^2 + \eta)$$

For center node:

$$N_5 = (1 - \xi^2)(1 - \eta^2)$$

In addition, the nodal unknowns within the FGM plate could accommodate terms for N along with the vector to represent nodal displacement.

Linear strain-displacement expression for the proposed element based on the assumed displacement field could be expressed as





GulshanTajet al.,

$$\begin{aligned} \varepsilon_{xx} &= \frac{\partial u}{\partial x}; \varepsilon_{yy} = \frac{\partial v}{\partial y}; \varepsilon_{zz} = \frac{\partial w}{\partial z} \\ \gamma_{xy} &= \frac{\partial u}{\partial y} + \frac{\partial v}{\partial x}; \gamma_{xz} = \frac{\partial u}{\partial z} + \frac{\partial w}{\partial x}; \gamma_{yz} = \frac{\partial v}{\partial z} + \frac{\partial w}{\partial y} \end{aligned} \quad (4)$$

Here, the variables u_0 , v_0 , and w_0 in the x , y , and z directions, respectively, represent the displacement components at the reference plane ($z = 0$). The letters Q_x and Q_y , respectively, stand for the normal component bending rotations about the reference plane or the centre plane around the y and x axes. Taylor's higher terms are polynomial functions that include the cubic and quadratic terms in the in-plane and transverse fields as well as the shear deformation modes in the z -direction. No stress boundary condition is employed at the upper and lower portions of the plate (i.e., $xz = xz = 0 = h/2$) in order to solve higher-order polynomial equations. The following formula can be obtained by making the following.

Investigation on Numerical Problems

The inquiry uses MATLAB (R2013b) to create an effective C0 finite element formulation that includes shear and deformation in the transverse and normal axes. An aluminium/zirconia profile is used to construct a plate model that uses a generalised four-parameter-based law to determine the material variation in the z direction. Only the specific situations (classical, symmetric, and asymmetric) are taken into account to conduct the numerical part in order to offer succinct and relevant results. It should be noted that each case is a subset of a generalised power law function that was generated by carefully choosing the material profile parameters. The isotropic and composite examples of plate shape were represented by the material gradient index (n), and its impact on bending response was demonstrated. The current FE-based formulation is validated using the remaining literature data for numerous FGM skew plate or shell situations under static, buckling, and dynamic analysis. For more information on the convergence and validation sections, see [25–26]. To create a particular FGM model in the current work, five different combinations of material parameters are taken into account. Here, the displacement components at the reference plane ($z = 0$) are represented by the variables u_0 , v_0 , and w_0 in the x , y , and z directions, respectively. The normal component bending rotations around the reference plane or the centre plane around the y and x axes are denoted by the letters Q_x and Q_y , respectively. Polynomial functions that incorporate cubic and quadratic components in the in-plane form of Taylor's higher terms and transverse fields, as well as the shear deformation modes in the z -direction. No stress boundary condition is employed at the upper and lower portions of the plate (i.e., $xz = xz = 0 = h/2$) in order to solve higher-order polynomial equations. The following formula can be obtained by making the following assumption and appropriately inputting it (Table 1).

A variety of mixtures of material parameters are chosen as shown in Figure 1 to demonstrate the impact of parameter values (a , b , and c) on the volume fraction distribution of ceramic V_c . The parameters were selected so that the picture could include even the most basic configurations. The volumetric relationship between ceramic and metal ($V_m + V_c = 1.0$) must be met for each set of combinations when setting the material parameters, though. In order to clarify the distribution range of each component (ceramic and metal) in the material, the value of the material gradient index n was set between 0.2 and 50. To help visualise and interpret the relevance of the current generalised four-parameter power law-based FGM model in relation to the traditional kind, the classical profile has been introduced as a special case for each numerical example. The distribution is linear for homogeneous cases, or when $n = 0.2$ and 50 (representing a high volume fraction with respect to isotropic material), among the various presented profiles. Further values in between, however, reflect a non-linear distribution, and this non-linearity gradually decreases when entering an isotropic zone (either ceramic or metal). If the volumetric relationship has been considered during the parameter selection, profiles different from those in Figure 1 are likely.

In the group with material gradient index, the plate with all of the edges clamped exhibits the least amount of deflection, as anticipated (Figure 2). For lower numerical values of the material index ($n = 0, 0.5, 1.0, \text{ and } 5.0$), several



**GulshanTajet al.,**

FGM models show the same magnitude of deflection. Beyond $n = 50.0$, an increase in the value of n causes the deflection to climb gradually and enter an unstable state. The fact is that as n increases, the gradation property slowly decreases, meaning that a large proportion of the material in the plate is isotropic. Furthermore, it is demonstrated that, among the numerous profiles displayed, symmetric profiles, which guarantee a minimal deflection component, are preferable to conventional and asymmetric natured profiles. All of the selected models, with the exception of the FGM2 model, exhibit no discernible behavioural divergence, and this trend is particularly apparent when n is between 5 and 50. Three profiles (FGM1, FGM2, and FGM3) are assumed with various ranges of material gradient index ($n = 0$ to 100) in order to illustrate the impact of side-thickness (a/h) ratio on the reaction of deflection (Figure 3).

When the thickness range came into the thick category, no appreciable improvement in deflection was seen. This finding holds true for all FGM models being considered for thin models, where there is a discernible variance in deflection. Symmetric profiles, which show little deflection, come after asymmetric and conventional profiles. Additionally, parametric study involving various material gradient indices was conducted for deflection vs aspect ratio (a/b) (Figure 4). The parameter b was left untouched, even though the value of a was modified from 0.5 to 5.0. The graphs depicting various material gradient indices show an increased trend with aspect ratios greater than 0.5 and no variation in deflection response for aspect ratios lower than that. When the length of the plate increased to three times its breadth, asymptotic reactions were seen. A plate with a lower volume proportion of ceramic or metal does not clearly react to changes in a or b , with the exception of the FGM1 type. A FGM model with a high value of n ($n = 100.0$) produces the highest deflection because, in all three of the circumstances (Figures 4(a) to 4(c)), the corresponding plate offers less stiffness.

Having performed the brief parametric study with regard to the bending response of FGM plates incorporating different profiles, in what follows, the z -distribution of the in-plane axial, shear, and transverse shear components of stress was exploited. Linear stress distribution is discerned for in-plane stress (xx) through the z -direction (Figure 5), and the trend transforms when $n > 5.0$. Non-linear variation of compressive and tensile stresses was noticed for $n = 10.0$, but stresses are lower in magnitude. This implies the presence of a significant percentage of ceramic and metal components in comparison with other material index options. However, the value of the volume fraction of a particular constituent in the lateral direction depends on the type of FGM model under consideration. Under different categories, the FGM5 model records the maximum tensile nature and compressive nature of stresses at upper and lower levels, respectively, with different material gradient indexes.

Figure 6 shows the same types of stresses that Figure 5 showed, with the exception that the isotropic plate hides any differences in stresses in a linear sense. For isotropic plates, large compressive stresses are seen at the bottom zone. When $n = 10.0$, there is a significant departure from the stresses displayed by isotropic and graded plates at the top segment of the plate. For all FGM models, graded plates record the lowest compressive stresses, on par with isotropic plates. In light of the types of strains that have been generated at the top and lower regions of the plate, exemption is seen. The variation of transverse shear stress (yz) is shown in order to demonstrate the precision of the current formulation in forecasting the transverse shear mode. Stresses are shown for three ranges of material gradient index ($n=0, 0.5$ and 1.0) and symmetric profile shows minimum stresses (compression and tension) like other cases.

CONCLUSION

A nine-node Lagrangian element is used in this research to create a 2D FE model that includes $C0$ continuity. The fluctuation profile in thickness is defined by a generalized power law distribution with four variables known as material gradient parameters. By altering the values of the parameters in the specified power-based law equation, a suitable selection of four parameters was used to execute the numerical component. The success of the investigation is assessed by comparing the bending analysis results to conventional profiles. Below is a summary of the main conclusions drawn from the current inquiry.





GulshanTajet al.,

- The key findings from the investigation are summarized here.
- By using the right selection of material gradient parameters, the generalized power law distribution described in the literature leads to various combinations of FGM constituents.
- For $n > 5$, many FGM models with various boundary conditions exhibit noticeable bending responses. Furthermore, when n exceeds 50, an asymptotic response is guaranteed.
- It is demonstrated that, for symmetric profiles, lower values of the material gradient index have no bearing on how the deflection parameter changes as the aspect ratio changes.
- For isotropic and graded plates, linear axial stress change in the x-direction is observed, but the trend is not immediately apparent when n is set to 10.0. The neutral plane shift is another one towards the bottom when $n = 10.0$ and remains unchanged for any other values.
- When axial load varied in the y direction, there was a noticeable response between isotropic and graded plates, and this response was strong at the bottom segment.
- The response on graded plates is comparable to that on isotropic plates. For isotropic plates, the magnitudes of the tensile and compressive stresses are equal; however, this is not the case for graded plates (see Figures 6 and 7).
- In every instance, it was found that symmetric profiles were superior to other profiles in terms of minimizing plate deflection.
- The four-parameter generalized power law for static modelling of FGM plates gives the designer a versatile tool for multi-functional requirements after establishing the various outcomes.

REFERENCES

1. G. N. Praveen and J. N. Reddy, "Non linear transient thermo elastic analysis of functionally graded ceramic-metal plates", *Int J Solids Struct*, 1998, 35, 4457-4476.
2. J. N. Reddy, "Analysis of functionally graded plate", *Int J Numer Meth Eng*, 2000, 47, 663-684.
3. S. S. Vel and R. C. Batra, "Exact solution for thermo elastic deformation of functionally graded thick rectangular plates", *J Amer Ins Aero Astro*, 2002, 40, 20-24.
4. T. E. Tay, F. Shen and K. H. Lee et al., "Mesh design in finite element analysis of post-buckled delamination in composite laminates", *Compos Struct*, 1999, 47, 603-611.
5. Francesco Tornabene, "Free vibration analysis of functionally graded conical, cylindrical shell and annular plate structures with a four-parameter power-law distribution", *Comp Meth App Mech Eng*, 2009, 198, 2911-2935.
6. G. R. Liu and J. G. Wang, "A point interpolation meshless methods based on radial basis functions", *Int J Numer Meth Eng*, 2002, 54, 1623-1648.
7. J. M. Ferreira, "A formulation of the multi-quadratic radial basis function method for the analysis of laminated composite plates", *Compos Struct*, 2003, 59, 385-392.
8. J. M. Ferreira, "Thick composite beam analysis using a global meshless approximation based on radial basis function", *Mech Adv Mater Struct*, 2003, 10, 271-284.
9. J. M. Ferreira, C. M. C. Rouque and P. A. L. S. Martins, "Analysis of composite plates using higher order shear deformation theory and a finite point formulation based on the multi-quadratic radial basis function method", *Compos Part B*, 2003, 34, 627-636.
10. M. A. Neves, A. J. M. Ferreira and E. Carrera, "Static analysis of functionally graded sandwich plates according to a hyperbolic theory considering Zig-Zag and warping effects", *Advances Eng Soft*, 2012, 52, 30-43.
11. M. A. Neves, A. J. M. Ferreira and E. Carrera, "A quasi 3d sinusoidal shear deformation theory for the static and free vibration analysis of functionally graded plates", *Compos Part B*, 2012, 43, 711-725.
12. M. A. Neves, A. J. M. Ferreira and E. Carrera, "Static, free vibration and buckling analysis of isotropic and sandwich functionally graded plates using a quasi-3D higher-order shear deformation theory and a meshless technique", *Compos Part B*, 2013, 44, 657-674.
13. E. Carrera, S. Brischetto, M. Cinefra et al., "Effects of thickness stretching in functionally graded plates and shells", *Comp Part B*, 2009, 42, 123-133.





GulshanTajet al.,

14. Rychter, "Generalized displacements and the accuracy of classical plate theory", *Int J Solids Struct*, 1993, 30, 129-136.
15. K. Yu and Volokh, "On the classical theory of plates", *J App Math Mech*, 1994, 58, 1101-1110.
16. FarzadEbrahimiand Abbas Rastgo, "An analytical study on the free vibration of smart circular thin FGM plate based on classical plate theory", *Thin Walled Struct*, 2008, 46, 1402-1408.
17. MetinAydogdu, "Conditions for functionally graded plates to remain flat under in-plane loads by classical plate theory", *Compos Struct*, 2008, 82, 155-157.
18. J. N. Reddy, "Nonlocal nonlinear formulations for bending of classical and shear deformation theories of beams and plates", *J EngSci*, 2010, 48, 1507-1518.
19. Z. Q. Cheng and R. C. Batra, "Deflection relationships between the homogeneous Kirchhoff plate theory and different functionally graded plate theories", *Arch Mech*, 2000, 52, 143-158.
20. L. F. Qian, R. C. Batra and L. M. Chen, "Elasto static deformations of a thick plate by using a higher-order shear and normal deformable plate theory and two meshless local Petrov-Galerkin (MLPG) Methods", *Comp Model EngSci*, 2003, 4, 161-176.
21. L. F. Qian, R. C. Batra and L. M. Chen, "Free and forced vibrations of thick rectangular plates by using higher-order shear and normal deformable plate theory and meshless local Petrov-Galerkin (MLPG) Method", *Comp Model Eng Sci*, 2003, 4, 519-534.
22. T. M. Liu, L. N. Thach and T. H. Quoc, "Finite element modeling for bending and vibration analysis of laminated and sandwich composite plates based on higher order theory", *Comput Mat Sci*, 2010, 49, 390-394.
23. M. Cinefra, E. Carrera and S. Brischetto et al., "Thermo-Mechanical analysis of functionally graded shells", *J Ther Stress*, 2010, 33, 942-963.
24. J. N. Reddy, "A generalization of two dimensional theories of laminated composite plates", *Commun App Numer Methods*, 1987, 3, 173-180.

Table 1. Selection range of material parameters and distribution

Type	Parameters	Profile	Distribution
FGM ₁	a=1.0, b=c=0	Classical	Metal at upper and ceramic at lower part
FGM ₂	a=1.0, b=1.0, c=2.0	Symmetric	Ceramic at upper and lower part
FGM ₃	a=1.0, b=1.0, c=4.0	Asymmetric	Ceramic at upper and lower part
FGM ₄	a=1.0, b=0.5, c=2.0	Asymmetric	Ceramic at upper/lower and mixture of metal and ceramic at upper/lower
FGM ₅	a=0.8, b=0.2, c=3.0	Asymmetric	Ceramic at upper/lower and mixture of metal and ceramic at upper/lower





GulshanTajet al.,

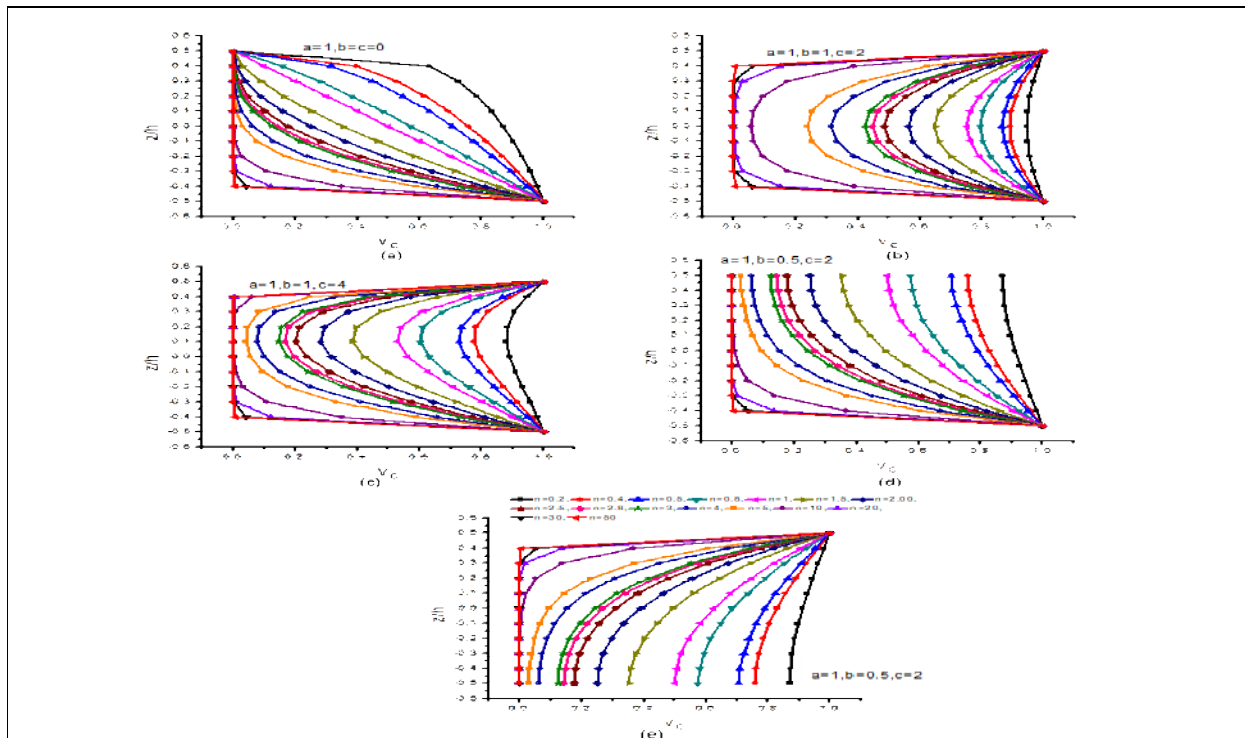


Figure 1. Graphical representation of volume fraction variation of ceramic (V_c) for Al/Zr₀₂ plate for different ranges of material parameters.

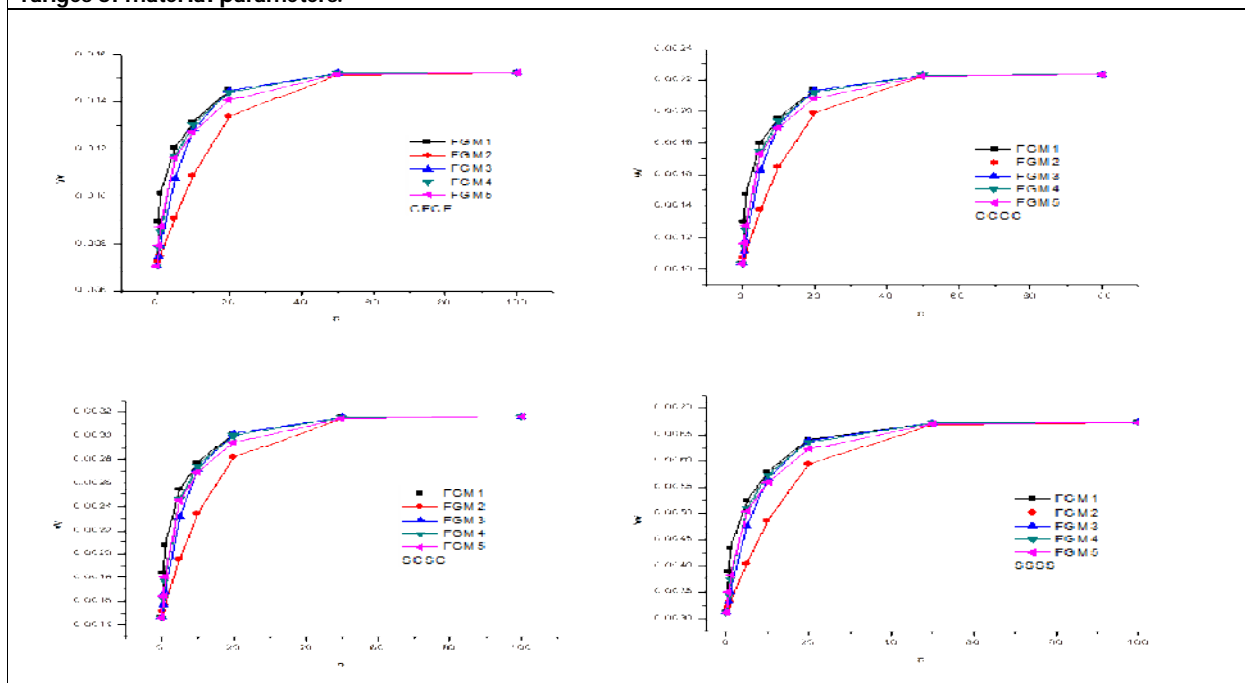


Figure 2. Variation of transverse displacement with material gradient index for different types of support conditions.





GulshanTajet *al.*,

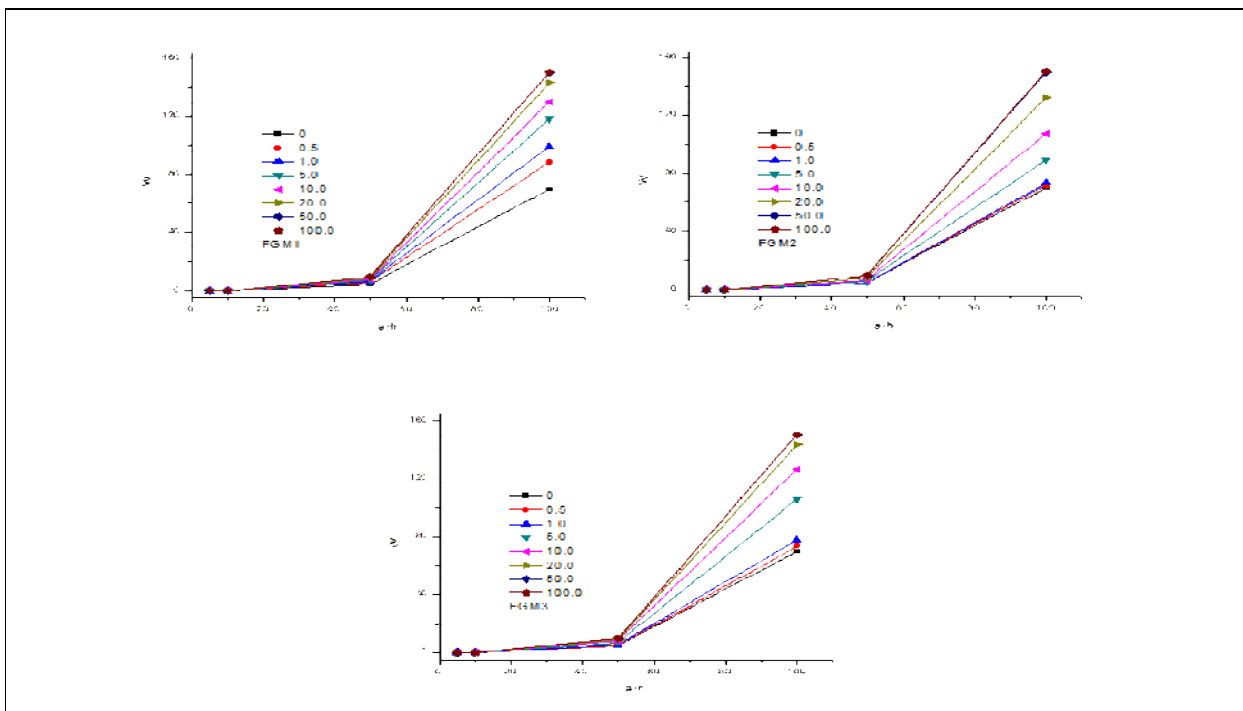


Figure 3. Variation of transverse displacement for diverse types of FGM models.

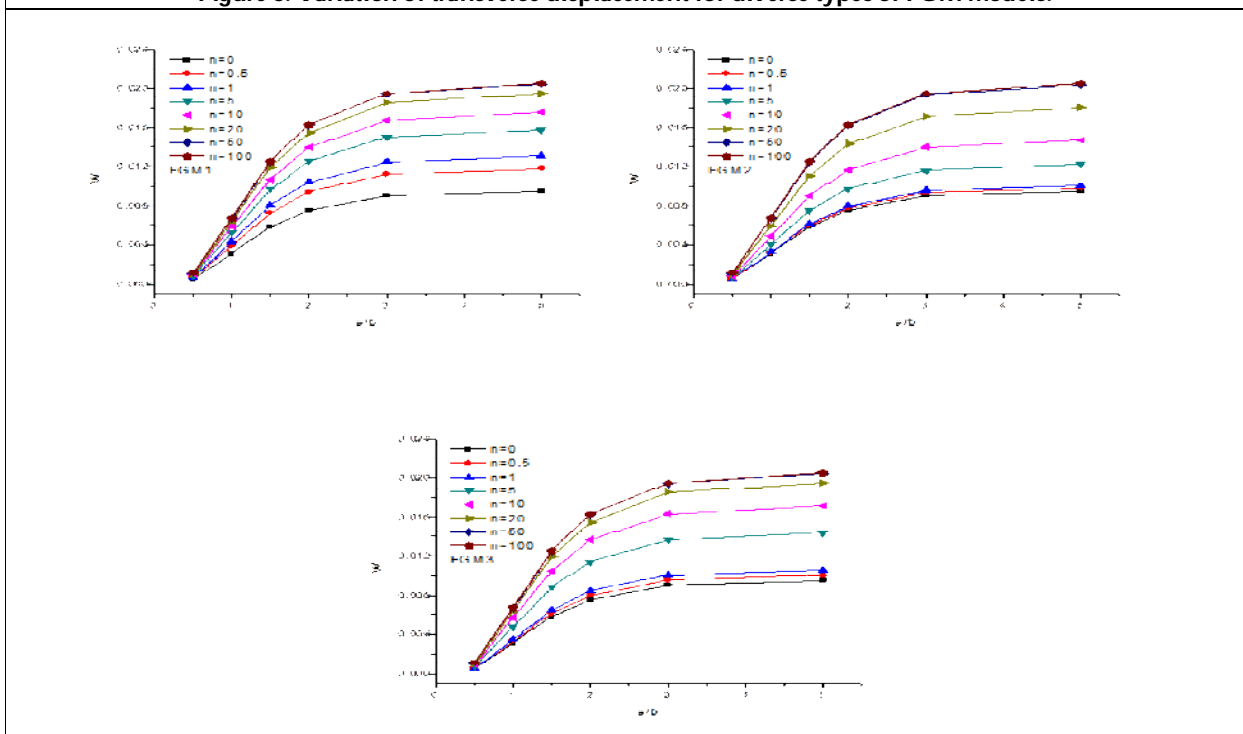


Figure 4. Variation of transverse displacement with aspect ratio (a/b) for diverse kind of FGM models.





GulshanTajet al.,

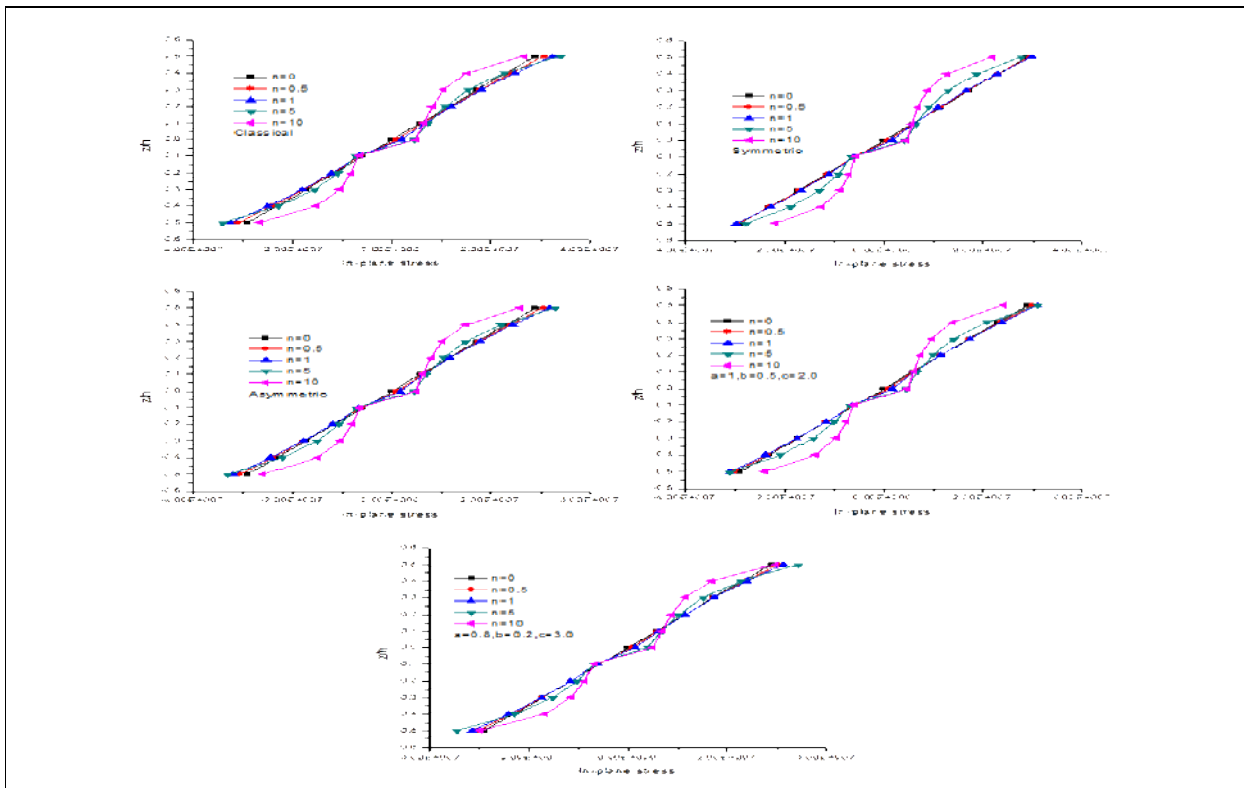


Figure 5. Variation of in-plane normal stress (σ_{xx}) in z-direction

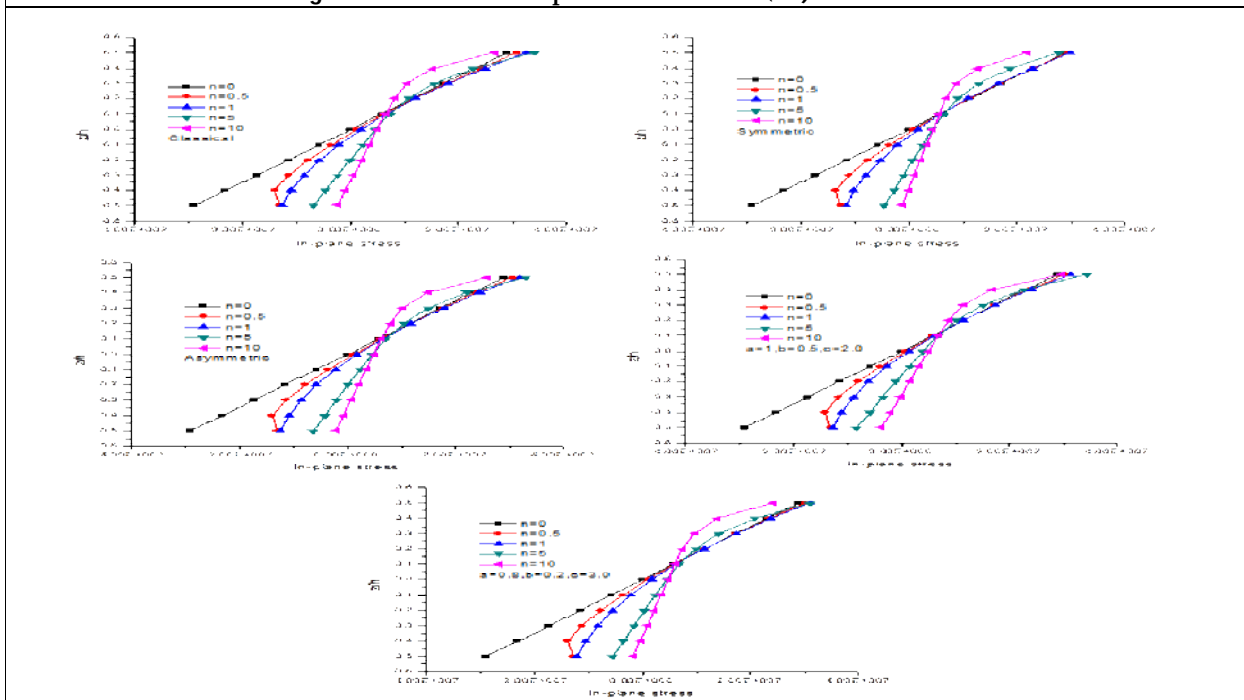


Figure 6. Variation of in-plane normal stress (σ_{yy}) in z-direction.





GulshanTajet al.,

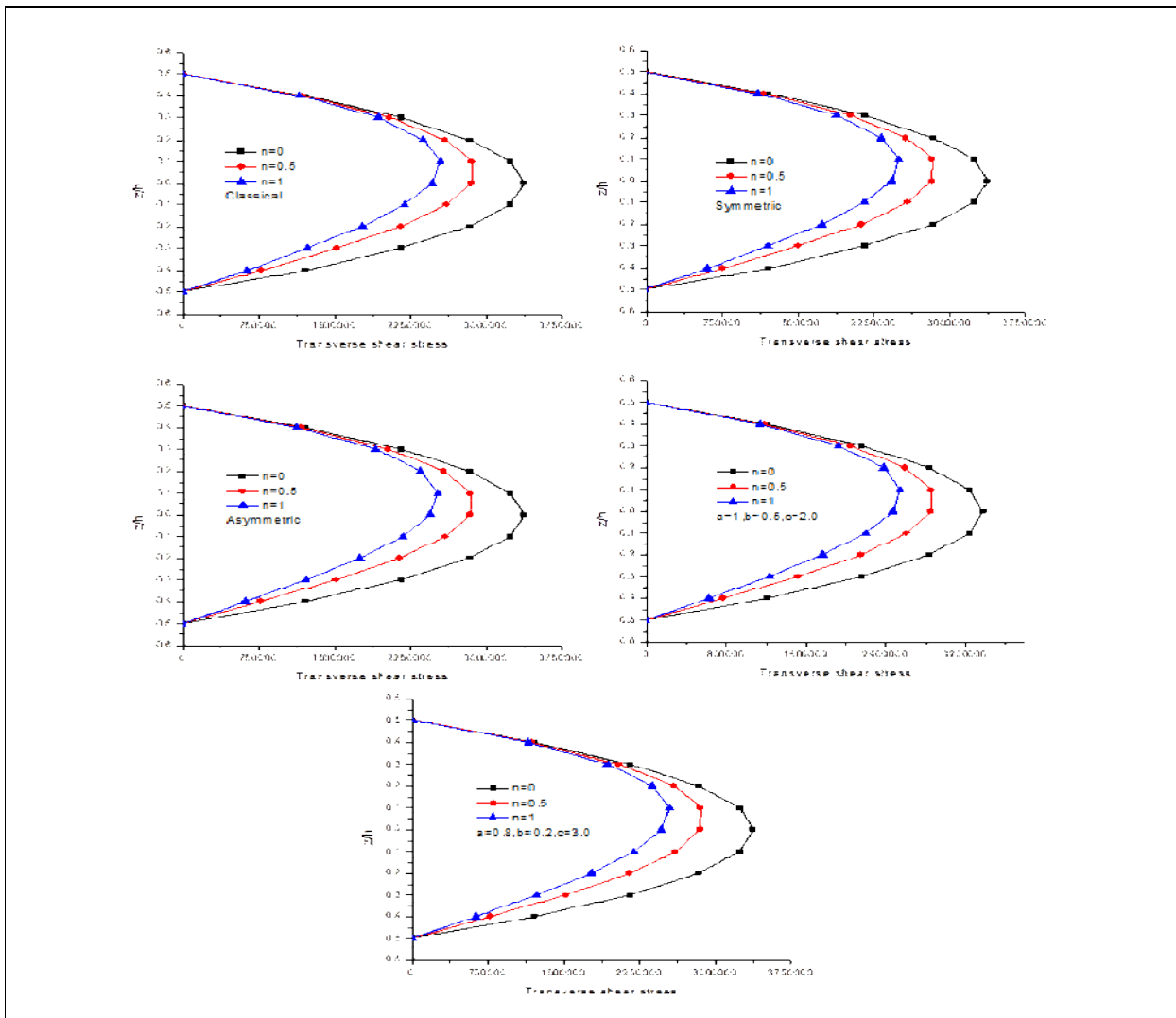


Figure 7. Variation of transverse shear stress (τ_{yz}) in z-direction.





Effect of Heavy Metals on *In vitro* Pollen Germination and Pollen Tube Length of *Catharanthus roseus*

Lavanya Giridhar¹ and Chetan H.C² and Haseena Rafath^{3*}

¹Research Scholar, Department of Botany, Annamalai University, Chidambaram, Tamil Nadu, India.

²Centre for Conservation of Natural Resources, The University of Trans-Disciplinary Health Sciences and Technology, yelhanka, Bengaluru, Karnataka, India

³Assistant Professor, Department of Botany, Annamalai University, Chidambaram, Tamil Nadu, India.

Received: 09 Feb 2023

Revised: 25 Apr 2023

Accepted: 03 May 2023

*Address for Correspondence

Haseena Rafath

Assistant Professor,
Department of Botany,
Annamalai University,
Chidambaram, Tamil Nadu, India.
E.Mail: rahamtullah1967@gmail.com



This is an Open Access Journal / article distributed under the terms of the **Creative Commons Attribution License** (CC BY-NC-ND 3.0) which permits unrestricted use, distribution, and reproduction in any medium, provided the original work is properly cited. All rights reserved.

ABSTRACT

Different concentrations of metals and heavy metals affect development of pollen grain, which is an essential aspect of plant reproduction. In this study of pollen development in *Catharanthus roseus*, percentage of pollen germination and length of pollen tube were taken as parameters. Heavy metals Hg, Cu, Al and Cr were used in different concentrations. With the change in metal concentration both pollen germination and pollen tube length were inhibited. Percentage of pollen germination and length of pollen tube was $\geq 95\%$ and $1111.23\mu\text{m}$ respectively in the control. In this study Hg was the most toxic element followed by Cu. Al and Cr showed toxicity in higher concentrations. Pollen germination was reduced to less than 10% at $40\mu\text{M}$ concentration of Hg, $100\mu\text{M}$ of Cu, $200\mu\text{M}$ of Al and $200\mu\text{M}$ of Cr. Pollen tube length also showed significant reduction with increase in metal concentration with exception at low concentration of Al. Pollen tube length was reduced by 92% at $40\mu\text{M}$ of Hg and $100\mu\text{M}$ of Cu, and 84% at $200\mu\text{M}$ of Al and 83% at $200\mu\text{M}$ of Cr. Pollen tube length showed increase by 10% at low concentration of $20\mu\text{M}$ of Al.

Keywords: Heavy metals, Mercury, Copper, Aluminium, Chromium, *Catharanthus*, Pollen tube length, Pollen germination





Lavanya Giridharet al.,

INTRODUCTION

Usage of metals especially heavy metals is essential in various industrial processes which is required for economic growth and development of a region. In recent years, alongwith rapid growth in industrialization, environmental pollution is also increasing in the ecosystem[1]. Environmental pollution by heavy metals is a cause of damage to both animal and plant life. Damages can be physiological or morphological which have to be detected experimentally to prevent damage to the ecosystem. The source of heavy metals to living organisms can be by air, water or soil. Rock mineralization processes can release heavy metals in the ecosystem, but the main source of pollution are anthropogenic activities, such as metallurgic industries, waste incinerators, urban traffic, phosphate fertilizers, and fungicides[2].

Effects of pollution can be seen in the vegetative parts of a plant, but pollen germination and tube growth are found to be more sensitive to atmospheric pollution[3,4]. Various *in vitro* studies have been made to study the effect of different heavy metals on pollen tube growth and pollen germination. The effects of mercury, copper, aluminium and chromium ions have been studied in pollen of *Lilium longiflorum*[5], tobacco (*Nicotiana tabacum* L.) [3], cherry (*Cerasus avium* L.) and apricot (*Armenica vulgaris* Lam.)[6], *Jatropha curcas* [7], sweet cherry [8] and date palm (*Phoenix dactylifera* L.), [2]. In the present study pollen grains of *Catharanthus roseus* were used for *in vitro* studies on percentage of pollen germination and pollen tube length. *Catharanthus roseus* (L.) G. Don, is an important medicinal plant belonging to the Apocynaceae family. *Catharanthus* is commonly called periwinkle, and flower throughout the year. Though flowers are bisexual, studies suggest that automatic self-pollination does not occur in periwinkle. Many flowers are produced on a single day, due to which pollinators cause geitonogamous self-pollination.[9]. According to other studies reproduction in *Catharanthus* is mostly dependent on pollinators which are agricultural pests [10].

MATERIALS AND METHODS

Pollen studies were done on pollen obtained from freshly bloomed flowers of *Catharanthus* from a healthy plant. The flowers were collected and their pollen was dusted on the experimental medium at 8am for *in vitro* germination studies. For *in vitro* germination, a solution containing 10% sucrose, 300mg/L of calcium nitrate, 100mg/L of boric acid, 100mg/L of potassium nitrate, and 200mg/L of magnesium sulphate, known as the standard Brewbaker and Kwack's medium, was used[11]. For heavy metal Hg and Cu treatments, concentrations of 20, 40, 60, 80 and 100µM were used and for Cr and Al concentrations taken were 20, 50, 100, 150 and 200µM. Salts taken were mercury (II) chloride, copper(II) sulphate, aluminium sulphate and potassium dichromate. Control contained only the germination medium. The medium was solidified with 1% agar. Pollen was spread onto petri plates and incubated at 26±2°C for 6 hours. Under a light microscope, pollen germination and pollen tube length were analysed. For percentage of pollen germination six observations were recorded. Pollen was considered germinated if pollen tube length was equal to or longer than the diameter of the pollen grain. Pollen tube length was recorded with an ocular micrometer and stage micrometer for 40 pollen tubes selected randomly. Statistical analysis was done by calculating mean, standard deviation and one-way analysis of variance (ANOVA). To establish significance between different concentrations of metals, Tukey's test was applied.

RESULTS

The effects of Hg, Cu, Al and Cr on percentage of pollen germination and pollen tube length of *Catharanthus* are summarised in Table 1. Pollen germination and pollen tube length showed decrease with increase in concentrations of heavy metals. The study showed Hg to be a very toxic metal. The percentage of pollen germination was ≥95.66% and pollen tube length was 1111.23µm in the control. But at 20µM and 40µM concentration of Hg percentage of pollen germination was 34.46% and 7.43% and pollen tube length was 252.17µm and 88.77µm respectively. The next toxic metal was Cu with percentage of pollen germination 74.37%, 34.47%, 29.72%, 21.17% and 8.89% and pollen tube

57438



**Lavanya Giridharet al.,**

length 679.71 μ m, 250.36 μ m, 140.94 μ m, 129.71 μ m and 90.22 μ m in 20 μ M, 40 μ M, 60 μ M, 80 μ M and 100 μ M concentration respectively. Al and Cr were less toxic compared to Hg and Cu. Results of Al and Cr were similar at concentrations \geq 50 μ M. The decrease in both the parameters was gradual. Drastic inhibition was seen at higher concentrations of greater than 100 μ M. In Al percentage of pollen germination was 95.13%, 83.01%, 61.97%, 38.13%, 31.05% and 10.83% and pollen tube length 1108.70 μ m, 1219.57 μ m, 797.83 μ m, 530.80 μ m, 432.25 μ m and 179.71 μ m in control, 20 μ M, 50 μ M, 100 μ M, 150 μ M and 200 μ M concentration respectively. Al was the only metal which increased pollen tube length at low concentration. For Cr percentage of pollen germination was 95.13%, 83.01%, 61.25%, 37.24%, 31.05% and 9.38% and pollen tube length 1108.70 μ m, 1061.96 μ m, 800.72 μ m, 531.16 μ m, 431.16 μ m and 183.33 μ m in control, 20 μ M, 50 μ M, 100 μ M, 150 μ M and 200 μ M concentration respectively.

The comparison of percentage of pollen germination and pollen tube length of Cu and Hg is shown in Figure 1 and Figure 3 respectively; and the comparison of percentage of pollen germination and pollen tube length of Al and Cr is shown in Figure 2 and Figure 4 respectively. Pollen germination was less than 10% and pollen tube length was reduced by 92% at 40 μ M concentration of Hg. 100 μ M of Cu, reduced pollen germination to less than 10% and pollen tube length by 92%. Pollen tube length did not show significant difference at 60 and 80 μ M concentration of Cu. Pollen germination was reduced to less than 10% at 200 μ M of Al and 200 μ M of Cr. Pollen tube length was reduced by 84% at 200 μ M of Al and 83% at 200 μ M of Cr. Pollen tube length showed increase by 10% at low concentration of 20 μ M of Al. But pollen germination always decreased with increase in concentration of metal ions. At higher concentrations of Hg and Cu both pollen tube length and germination reduced significantly whereas in Al and Cr at higher concentrations pollen germination was inhibited but pollen tube grew to a considerable length. At higher concentrations bursting of pollen grains was also observed. Analysis of variance of data demonstrated significant differences for percentage of pollen germination and pollen tube length among treatments of different concentrations.

DISCUSSION

Mercury is a hazardous heavy metal pollutant and India is a major emitter of mercury [12]. Coal burning, nonferrous metal production, cement production and ASGM (artisanal and small-scale gold mining) are some activities which contribute to emission of mercury in India. Mercury is also emitted in the waste of electronic and healthcare products [13]. Both plant and animal life are affected by mercury pollution and to study this various *in vitro* experiments have been done on pollen germination. Cu and Hg greatly inhibited pollen tube growth and pollen germination in *Lilium* [5]. Similarly in tobacco, Cu and Hg showed maximum toxicity as compared to Al, Ni, Fe, Pb, Co, Cd and Zn [3]. In *Jatropha curcas* Hg, Pb, Cd and Cr proved to be most toxic whereas Cu and Zn affected the least [7]. In the present *in vitro* study too mercury was found to be the most toxic metal. Mercury caused anomalies in the morphology of pollen tube in *Lilium* [14]. According to the studies in *Lilium* pollen, the tips of pollen tubes developed anomalous cell wall. The tip contained a large number of organelles and secretory vesicles were reduced. This in turn reduced cytoplasmic movement integrity and cytosol streaming due to which pollen tubes did not grow [14].

In the present work copper was also found to inhibit pollen germination but was not as toxic as mercury. Copper has redox properties and hence is an essential metal for plants. Copper is used as an antifungal agent in agriculture and in industries for electroplating and smelting operations. The main effect of copper was abnormal cell wall organization at the tip of the pollen tube due to which normal growth of the tube is inhibited [5]. Aluminium is abundantly found in soil and is increasing due to industrial pollution. High concentration of aluminium has negative effect on growth of crops. Nevertheless, in low concentrations it has been considered as a beneficial element. In the present study too, pollen tube growth was enhanced at low concentration of aluminium. The influences of low concentration of AlCl₃ and its possible cytological mechanism on the pollen tube growth have been studied in apple (*Malus domestica*) [15]. The results pollen of apple have shown that 20 μ M AlCl₃ promoted pollen tube elongation by enhancing Ca²⁺ influx and by decreasing acid pectins in pollen tubes but increasing esterified pectins and arabinan pectins in pollen tubes. At higher concentrations aluminium has similar effect as copper, it interfered with



**Lavanya Giridharet al.,**

pectin–calcium binding sites, caused thickening of cell wall at tip of pollen tubes, decrease in calcium influx and caused accumulation of callose, acid pectins, esterified pectins, and arabinogalactan proteins [16, 17, 18]. Chromium is used in different industries like metallurgy, electroplating, paint production, tanning, chemical, pulp and paper production [19]. Chromium ($\text{Cr}^{3+}/\text{Cr}^{6+}$) is highly toxic and a very common environmental pollutant due to its extensive use in industries especially tanneries [20]. In the present study potassium dichromate was used which contains hexavalent chromium. Studies on effect of chromium on pollen grains of kiwifruit have shown that plasma membrane remained undamaged in most of the treated pollen grains, but chromium caused ultrastructural alterations, chromatin condensation, and swelling of mitochondria, cytoplasmic vacuolization, and change in arrangement of endoplasmic reticulum cisternae [21].

All studies indicate various physiological and morphological changes in the pollen grain which results in inhibition of pollen germination or bursting of pollen grains. Cell wall of pollen tubes contain large amount of pectin, which is stabilised by calcium but increase in heavy metal concentrations may cause decrease in cell wall elasticity by interfering with the pectin-calcium binding sites, in turn hampering the growth of pollen tube [5]. Heavy metals also interfere in the uptake and regulation of essential ions like calcium and boron for metabolic activity in the pollen grains and thus inhibit pollen germination [22]. With this research we conclude that heavy metals have a negative impact on the pollen grains of plants and thus can influence reproduction in them. The studies show that toxic effects of heavy metals are not the same for all plants and hence the growth of a plant in a polluted area will depend on its tolerance to the metal found in that area. However, both in vitro and in vivo studies are required to analyse the actual effect of a heavy metal on the reproduction of a plant.

REFERENCES

1. Jayakumar, K., Jaleel, C. A., & Vijayarengan, P. (2007). Changes in growth, biochemical constituents, and antioxidant potentials in radish (*Raphanus sativus* L.) under cobalt stress. *Turkish Journal of Biology*, 31(3), 127-136.
2. Mohammed Mesnoua, Messaoud Roumani, Ouahiba Mizab and Reguia Zeguerrou, (2020) 'Heavy metals differentially affect date palm pollen germination and tube elongation', *Italus Hortus*, Vol. 27, Pages 64-71 doi: 10.26353/j.itahort/2020.3.6471
3. TUNA, A. L., BÜRÜN, B., YOKAŞ, İ., & Coban, E. (2002). The effects of heavy metals on pollen germination and pollen tube length in the tobacco plant. *Turkish Journal of Biology*, 26(2), 109-113.
4. Xiong, Z. T., & Peng, Y. H. (2001). Response of pollen germination and tube growth to cadmium with special reference to low concentration exposure. *Ecotoxicology and Environmental Safety*, 48(1), 51-55.
5. Sawidis, T., & Reiss, H. D. (1995). Effects of heavy metals on pollen tube growth and ultrastructure. *Protoplasma*, 185, 113-122.
6. Gür, N., & Topdemir, A. (2008). Effects of some heavy metals on in vitro pollen germination and tube growth of apricot (*Armenica vulgaris* Lam.) and cherry (*Cerasus avium* L.). *World Applied Sciences Journal*, 4(2), 195-198.
7. Acharya, S., Sharma, D. K., Joshi, H. C., & Chakraborti, M. (2011). Effects of some heavy metals on in vitro pollen germination and pollen tube growth of *Jatropha curcas*. *Range Management and Agroforestry*, 32(1), 52-55.
8. Sharafi, Y., Talebi, S. F., & Talei, D. (2017). Effects of heavy metals on male gametes of sweet cherry. *Caryologia*, 70(2), 166-173.
9. Sreevalli, Y., Baskaran, K., Kulkarni, R. N., & Sushil, K. (2000). Further evidence for the absence of automatic and intra-flower self-pollination in periwinkle. *Current Science*, 79(12), 1648-1649.
10. D. Miyajima (2004) Pollination and seed set in vinca [*Catharanthus roseus* (L.) G. Don], *The Journal of Horticultural Science and Biotechnology*, 79:5, 771-775, DOI: 10.1080/14620316.2004.11511841
11. Brewbaker, J.L. and Kwack, B.H. (1963) The Essential Role of Calcium Ion in Pollen Germination and Pollen Tube Growth. *American Journal of Botany*, 50, 859-865. <https://doi.org/10.1002/j.1537-2197.1963.tb06564.x>
12. Burger Chakraborty, L., Qureshi, A., Vadenbo, C., & Hellweg, S. (2013). Anthropogenic mercury flows in India and impacts of emission controls. *Environmental science & technology*, 47(15), 8105-8113.





Lavanya Giridharet al.,

13. Sharma, B. M., Bharat, G. K., Šebková, K., & Scheringer, M. (2019). Implementation of the Minamata Convention to manage mercury pollution in India: challenges and opportunities. *Environmental Sciences Europe*, 31(1), 1-12.
14. Sawidis, T., Baycu, G., Cevahir-Öz, G., & Weryszko-Chmielewska, E. (2018). Effect of mercury on pollen germination and tube growth in *Lilium longiflorum*. *Protoplasma*, 255, 819-828.
15. Zhang, C., Xie, P., Zhang, Q., Xing, Y., Cao, Q., Qin, L., & Fang, K. (2022). Low Concentration of Aluminum-Stimulated Pollen Tube Growth of Apples (*Malus domestica*). *Plants*, 11(13), 1705.
16. Zhang, W. H., Rengel, Z., Kuo, J., & Yan, G. (1999). Aluminium effects on pollen germination and tube growth of *Chamelaucium uncinatum*. A comparison with other Ca²⁺ antagonists. *Annals of Botany*, 84(4), 559-564.
17. Konishi, S., & Miyamoto, S. (1983). Alleviation of aluminum stress and stimulation of tea pollen tube growth by fluorine. *Plant and cell physiology*, 24(5), 857-862.
18. Fang, K., Xie, P., Zhang, Q., Xing, Y., Cao, Q., & Qin, L. (2020). Aluminum toxicity-induced pollen tube growth inhibition in apple (*Malus domestica*) is mediated by interrupting calcium dynamics and modification of cell wall components. *Environmental and Experimental Botany*, 171, 103928.
19. Dotaniya, M. L., Thakur, J. K., Meena, V. D., Jajoria, D. K., & Rathor, G. (2014). Chromium pollution: a threat to environment-a review. *Agricultural Reviews*, 35(2), 153-157.
20. Pushkar, B., Sevak, P., Parab, S., & Nilkanth, N. (2021). Chromium pollution and its bioremediation mechanisms in bacteria: A review. *Journal of Environmental Management*, 287, 112279.
21. Speranza, A., Ferri, P., Battistelli, M., Falcieri, E., Crinelli, R., & Scoccianti, V. (2007). Both trivalent and hexavalent chromium strongly alter in vitro germination and ultrastructure of kiwifruit pollen. *Chemosphere*, 66(7), 1165-1174.
22. Wang, X., Gao, Y., Feng, Y., Li, X., Wei, Q., & Sheng, X. (2014). Cadmium stress disrupts the endomembrane organelles and endocytosis during *Piceawilsonii* pollen germination and tube growth. *PLoS One*, 9(4), e94721.

Table 1: Effect of Hg, Cu, Al and Cr on Pollen Germination and Length of Pollen Tube in *Catharanthus*

CONCENTRATION (µM)	MERCURY		COPPER	
	PERCENTAGE OF POLLEN GERMINATION (%)	LENGTH OF POLLEN TUBE (µm)	PERCENTAGE OF POLLEN GERMINATION (%)	LENGTH OF POLLEN TUBE (µm)
0 (CONTROL)	95.66 ± 0.04 ^a	1111.23 ± 30.68 ^a	95.66 ± 0.04 ^a	1111.23 ± 30.68 ^a
20	34.46 ± 0.07 ^b	252.17 ± 16.34 ^b	74.37 ± 0.04 ^b	679.71 ± 24.95 ^b
40	7.43 ± 0.03 ^c	88.77 ± 10.98 ^c	34.47 ± 0.07 ^c	250.36 ± 16.41 ^c
60	0	0	29.72 ± 0.06 ^{cd}	140.94 ± 11.83 ^d
80	0	0	21.17 ± 0.04 ^d	129.71 ± 11.81 ^d
100	0	0	8.89 ± 0.04 ^e	90.22 ± 10.11 ^e
CONCENTRATION (µM)	ALUMINIUM		CHROMIUM	
	PERCENTAGE OF POLLEN GERMINATION (%)	LENGTH OF POLLEN TUBE (µm)	PERCENTAGE OF POLLEN GERMINATION (%)	LENGTH OF POLLEN TUBE (µm)
0 (CONTROL)	95.13 ± 0.02 ^a	1108.70 ± 29.54 ^b	95.13 ± 0.02 ^a	1108.70 ± 29.54 ^a
20	83.01 ± 0.02 ^b	1219.57 ± 30.53 ^a	83.01 ± 0.02 ^b	1061.96 ± 23.66 ^b
50	61.97 ± 0.06 ^c	797.83 ± 20.74 ^c	61.25 ± 0.05 ^c	800.72 ± 22.20 ^c
100	38.13 ± 0.08 ^d	530.80 ± 22.43 ^d	37.24 ± 0.06 ^d	531.16 ± 21.41 ^d
150	31.05 ± 0.07 ^d	432.25 ± 20.99 ^e	31.05 ± 0.07 ^d	431.16 ± 20.95 ^e
200	10.83 ± 0.03 ^e	179.71 ± 13.85 ^f	9.38 ± 0.03 ^e	183.33 ± 29.75 ^f

Table 1 shows the means and standard deviations of pollen germination and pollen tube length in different concentrations of mercury, copper, aluminium and chromium. Different letters in superscript indicate statistically significant differences (Tukey's test, $p \leq 0.05$).





Lavanya Giridharet al.,

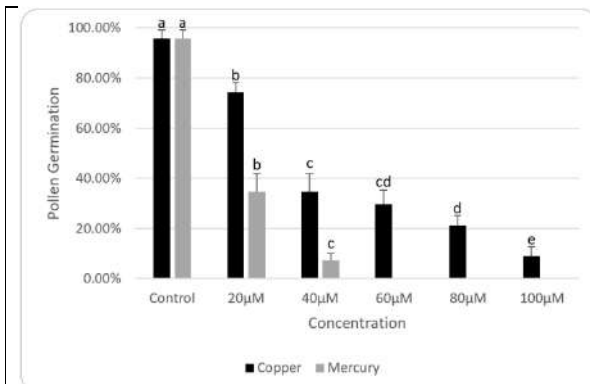


Figure 1: Effect of Copper and Mercury on Pollen Germination at various concentrations

Percentage of pollen germination of *Catharanthus* pollen treated with different concentrations of $CuSO_4$ (black) and $HgCl_2$ (grey) for 6 hours. Each value represents the mean \pm SD and the letters indicate statistically significant differences (Tukey's test, $p \leq 0.05$).

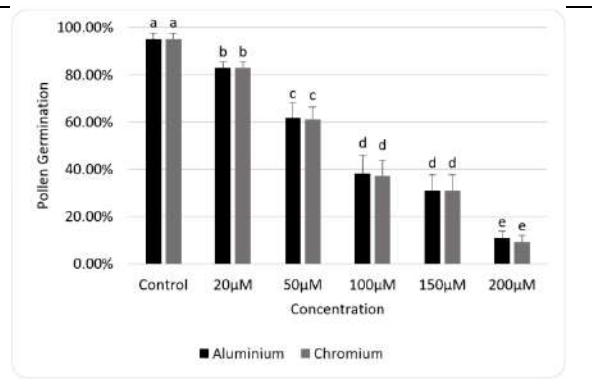


Figure 2: Effect of Aluminium and Chromium on Pollen Germination at various concentrations

Percentage of pollen germination of *Catharanthus* pollen treated with different concentrations of $Al_2(SO_4)_3$ (black) and $K_2Cr_2O_7$ (grey) for 6 hours. Each value represents the mean \pm SD and the letters indicate statistically significant differences (Tukey's test, $p \leq 0.05$).

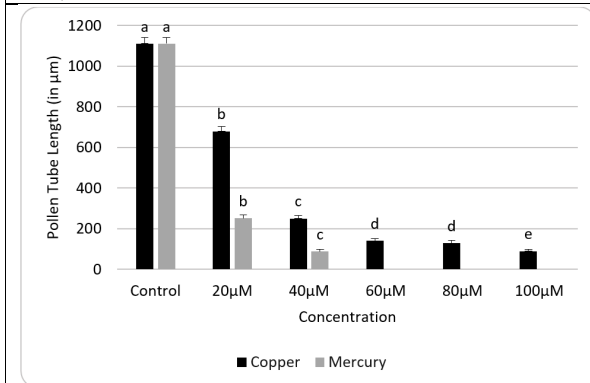


Figure 3: Effect of Copper and Mercury on Pollen Tube Length at various concentrations

Length of pollen tube of *Catharanthus* pollen treated with different concentrations of $CuSO_4$ (black) and $HgCl_2$ (grey) for 6 hours. Each value represents the mean \pm SD and the letters indicate statistically significant differences (Tukey's test, $p \leq 0.05$).

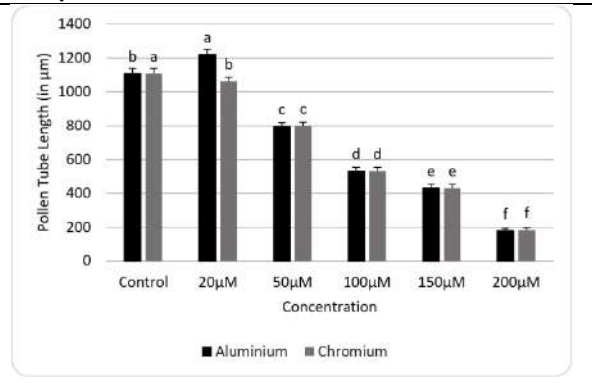


Figure 4: Effect of Aluminium and Chromium on Pollen Tube Length at various concentrations

Length of pollen tube of *Catharanthus* pollen treated with different concentrations of $Al_2(SO_4)_3$ (black) and $K_2Cr_2O_7$ (grey) for 6 hours. Each value represents the mean \pm SD and the letters indicate statistically significant differences (Tukey's test, $p \leq 0.05$).





Synthesis and Characterization Studies of SnO₂ for Gas Sensing Application

V.Vidhya^{1*}, P.Anbarasu² and D.Geetha³

¹Assistant Professor, Department of Electronics, GAC, Affiliated to Bharathidasan University, Trichy, Tamil Nadu, India.

²Associate Professor, Department of Electronics, DKGAC, Kulithalai- 639120, Karur, Affiliated to Bharathidasan University, Trichy, Tamil Nadu, India.

³Associate Professor, Department of Physics, Annamalai University, Annamalai Nagar, Chidambaram – 608002, Tamil Nadu, India.

Received: 28 Feb2023

Revised: 20 Apr 2023

Accepted: 31 May 2023

*Address for Correspondence

V.Vidhya

Assistant Professor,
Department of Electronics,
GAC, Affiliated to Bharathidasan University,
Trichy, Tamil Nadu, India.
E. Mail: vinoth31vid@gmail.com



This is an Open Access Journal / article distributed under the terms of the **Creative Commons Attribution License** (CC BY-NC-ND 3.0) which permits unrestricted use, distribution, and reproduction in any medium, provided the original work is properly cited. All rights reserved.

ABSTRACT

In recent years, a significant amount of garbage from industries and people has been released into the atmosphere due to growing concerns about global environmental degradation. Gas sensors play a vital role in pollution prevention efforts. In this paper, we describe the hydrothermal combined with co-precipitation synthesis of SnO₂ nanopowder using Stannic chloride as a precursor. The crystallization, morphology, element composition, identification of functional groups, and structure of the resulting nanopowders were studied using X-ray diffract tograms (XRD), scanning electron microscopy (SEM), FTIR, and UV-DRS spectroscopy. The doctor blade method was used to powder coat the final sample on a glass plate. a gas sensor designed to detect gas molecules present in the atmosphere. The sensor device made from the films is more sensitive to the reducing group of acetone gas, which accepts electrons during the reaction with surface oxygen species.

Keywords: Co precipitate method, Gas sensor, Hydrothermal method, SnO₂, thick-film.

INTRODUCTION

In our global environment, gas sensors play a vital role in many aspects of technology, in fields such as environmental monitoring, air quality assurance, industrial processes, and automotive technologies, to name just a

57443





Vidhyaet al.,

few, and are increasingly important [1]. The gas sensing layer is the most important element in gas sensor devices, as it can be used to sense gases of various concentrations and generate changes in electrical resistance [2]. The gas sensing layer is basically a chemiresistor, which changes its resistance value according to the concentration of particular gases in the environment [3]. So whenever toxic gases are detected, the current flow through them varies because the resistance of the element changes, which represents the change in concentration of the gases.

Several advantages like fabrication method, cost effectiveness, stability, durability, miniaturization, and low detection limit are satisfied by semiconducting-based metal oxide-based gas sensors [SMOS]. There are two types of SMOS. (i) P-type CuO, NiO, and Cr₂O₃; (ii) N-type SnO₂, TiO₂, and ZnO. Among these, SnO₂ is the most suitable material for gas sensing because of its good sensing behaviour towards various gases. SnO₂ shows high sensitivity at high temperatures [4 - 6], but it has the disadvantage of low sensitivity and selectivity at low temperatures. Li, R., Chen *et al.* prepared porous SnO₂ nanowires (PNWs), which were used to create high-performance gas sensors, using a controlled two-step process that included electrospinning and hydrothermal etching with Na₂S solution to detect ethanol [7]. Metal tin (Sn) powders were evaporated at 800 °C to create mass-produced SnO₂ nanowhiskers. The ethanol gas sensitivity of the SnO₂ nanowhiskers ranged from 23 to 50 ppm at 300 °C. Ying *et al.* showed that SnO₂ nanowhiskers have a prospective use in the construction of gas sensors [8]. This report describes the synthesis of SnO₂ at various temperatures in order to improve the selectivity and sensitivity of gas sensors at low temperatures. SnO₂ nanostructures are synthesised using a simple hydrothermal with co-precipitation route that controls the material size [9]. Three different samples were taken at different temperatures to optimise the sensing material and determine the best sensing performance. The aim of this work is to investigate the effect of temperature on the reduced gas sensing performance of SnO₂. As expected, the SnO₂ nanostructure shows excellent selectivity to acetone at room temperature.

Experimental Procedure

Synthesis process of S1, S2 and S3 nanostructures

Stannic chloride (SnCl₄·5H₂O), ethanol, and deionized water were purchased from Sigma Aldrich. Stannic chloride was placed in a conical flask after it had been cleaned and dried. The sample was then dissolved in de-ionized water and stirred for 60 minutes before being transferred to a Teflon-lined autoclave, sealed, and kept at 120 °C for 6 hours. After that, the samples were filtered, washed, and dried at 80 °C for 6 hours in the hotter oven. The sample was divided into three boats, named S1, S2, and S3, and kept in a tubular furnace maintained at three different temperatures (500 °C, 600 °C, and 700 °C) for three hours each. The final samples were grind into a fine powder using a mortar and then collected in a separate vile. S1, S2 are black in colour and S3 is in semi white colour.

RESULT AND DISCUSSION

Crystal Structure Analysis (XRD)

The diffraction patterns were studied with the help of X'Pert-PRO using Cu K α radiation. X-ray diffractometer scanned at a rate of 1° between the range 20°–80° (2 θ) at room temperature. The XRD patterns of the S1, S2 and S3 nanostructures are shown in Figure 1. The diffracted peaks of S1 can be pointed as 2 θ value positioned at 29.9, 33.9, 50.7, 51.8, and 57.4 corresponding to the (001), (110), (112), (021), and (003) of Bragg reflection planes. S2 peaks can be indexed peaks at 30.4, 33.4, 37.2, 48.0, 50.9, and 57.5 corresponding to the (001), (110), (002), (112), and (121) miller indices value. S3 samples peaked at 26.4, 33.7, 37.7, 51.7 and the corresponding hkl values are (110), (011), (020), and (121). The SnO tetragonal nanostructure (JCPDS card no. 00-6052) and its estimated crystal sizes of 36.9 and 24.1 nm are represented by the S1 and S2 samples. The S3 sample indicates a SnO₂ tetragonal nanostructure (JCPDS: 10 - 7228) [8], and its average crystalline size is estimated at 21.1 nm. The average crystalline structure was estimated by Bragg's equation

$$D = \frac{0.9\lambda}{\cos\theta}$$

Cos θ



**Vidhya et al.,**

Where ' β ' is FWHM (in radians), ' D ' is the estimated average crystalline size ' θ ' the angle of reflection and ' λ ' the wavelength of X-ray radiation used.

Structural Analysis (FTIR)

Fourier transform infrared spectroscopy (Perkin Elmer) was used to identify the presence of functional groups in nanostructures, which ranged from 400 to 4000 cm^{-1} . Figure 2 shows FTIR spectra of S1, S2 and S3 nanostructures. According to O-H stretching and bending vibrations of the absorbed water surface, the large absorption bands at 3455 and 1660 cm^{-1} are caused by these wavelengths. C=C stretching is the cause of the sharp band absorption at 1384 cm^{-1} and 613 cm^{-1} . The appearance of large number of IR bending modes for particles indicating the homogeneous formations of particles.

Morphological Analysis (SEM)

The surface morphology of S1, S2 and S3 were shown in Figure 4. It is clearly shows that S1 nanostructure are spherical in shape, and flake like structure was formed for S2. S3 microstructure exhibits sphere like morphology with pores was visible on the surface of the nanostructure.

Fabrication and Measurement set-up

The following is the gas sensing film fabrication method: (i) The nanostructure sensor materials were mixed with ethanol for binding in a 4:1 ratio to form slurry; (ii) the slurry was coated on a glass substrate; (iii) the glass substrate was then dried and kept in an oven at 100° C for 1 hr. A gas sensor is placed inside the gas measurement setup chamber, which consists of a gas inlet and outlet path. The inlet gas path is connected to a gas mixer that controls the mass flow and ppm level of the gas. Silver leads are connected to the gas sensing film. These leads are connected to the reaction chamber and Keithley source meter. The reaction chamber is kept at room temperature, and a Keithley meter measures the variation in resistance of the gas sensor.

Gas Sensing Studies

The performance of gas sensors is typically described in terms of a number of variables, including sensor response, sensitivity, selectivity, stability, response time, and recovery time.

Selectivity

By monitoring the change in resistance of S1, S2 and S3 at room temperature for 50 ppm of gas concentration. The gas sensing capabilities of S1, S2 are very low nearly negligible value from 50 ppm to 150 ppm. Hence S3 deposited film are investigated by examining the change in electrical resistance of the thick sensor films at room temperature when there are at 50 ppm of various gases, such as ethanol ($\text{C}_2\text{H}_5\text{OH}$), acetone (CH_3COCH_3), toluene ($\text{C}_6\text{H}_5\text{CH}_3$), and formaldehyde (HCHO) and trichloroethylene (C_2HCl_3). Figure 4a clearly shows that S3 sample have good sensing capability towards acetone.

Sensitivity

As the acetone concentration increases from 50 to 150 ppm, the reaction rises linearly as shown in Figure 4b. Due to response saturation, the slope of each graph reduced as concentration increased. There was less surface reaction when a tiny concentration of gas was exposed on a fixed surface area of a sample because there were few gaseous molecules covering the surface. Due to greater surface coverage, an increase in vapour concentration accelerates the surface reaction [10]. When the saturation point on molecule coverage was reached, we found continuous response above a particular concentration, and the rise in surface reaction will only occur gradually after that point.

Response Time and Recovery Time

The response time is the period in which the sensor resistance change reaches 90% of the steady value. The recovery time is defined as the time for the resistance to recover 90% of the total variation when the test gas was removed.





Vidhyaet al.,

Sensing Mechanism

From the results, the resistance changing behaviors may be attributed to the adsorption and desorption of Acetone molecules on the SnO₂ coated sensing film. The SnO₂-based sensors gas sensing method is of the surface-controlled variety, and the resistance changes as a result of the adsorption of oxygen and test gases and the subsequent interaction between them [11]. When oxygen species are chemisorbed onto the surface of tin oxide when there is an air atmosphere present, the resistance of SnO₂ will rise as a result of the removal of electrons from the conduction band [12 -14]. The surface of the SnO₂ adsorbs oxygen from the atmosphere onto the film surface when sensors are exposed to air. As it absorbs electrons from the SnO₂ conduction band, absorbed oxygen transforms into oxygen ions (O⁻ or O₂⁻) [15]. Here is the reaction mechanism

1. O₂ (ads) + e⁻ O₂⁻ (ads), which causes the formation of depletion layers on the interface of the sensing film and causes the sensor's high resistance in air when exposed to Acetone vapour [16, 17], will react with oxygen species as follows:
(2) CH₃COCH₃ + 8 O⁻ → 3CO₂ + 3H₂O + 8 e⁻

As CO₂ and H₂O are the reaction's byproducts, it is simple to desorption them from surfaces and quickly establish reproducible response-recovery properties [18].

CONCLUSION

In summary, S1, S2 and S3 have been successfully prepared by the simple hydro thermal method associated with Co-precipitation method and systematically characterized for acetone sensing at room temperature. The crystalline structure of SnO and SnO₂ were identified and particle size were calculated by XRD, functional groups were analyzed by FTIR, and Sphere and flake like structured were identified by morphological studies. As seen from the gas-sensing results, S3 coated sensor demonstrated a rapid decrease of resistance upon exposure to Acetone and fully recovered to its baseline values in air with good repeatability. The S3 gas sensor exhibited ultrahigh selectivity toward Acetone against various volatile organic compounds (VOCs) and environmental gases at room temperature with no effect of humidity in the range 18% RH.

ACKNOWLEDGEMENT

We would like to thank Prof. Dr. K.Jeyadheepan, School of Electrical and Electronics Engineering, SASTRA Deemed to be University, Thanjavur 613401, for providing instrument to study gas sensing characterization.

REFERENCES

1. Javaid, M., Haleem, A., Singh, R. P., Rab, S., & Suman, R. (2021). Significance of sensors for industry 4.0: Roles, capabilities, and applications. *Sensors International*, 2, 100110.
2. Mirzaei, A., Hashemi, B., & Janghorban, K. (2016). α-Fe₂O₃ based nanomaterials as gas sensors. *Journal of Materials Science: Materials in Electronics*, 27, 3109-3144.
3. Padvi, M. N., Moholkar, A. V., Prasad, S. R., & Prasad, N. R. (2021). A critical review on design and development of gas sensing materials. *Engineered Science*, 15, 20-37.
4. Kumar, A., Shringi, A. K., & Kumar, M. (2022). RF sputtered CuO anchored SnO₂ for H₂S gas sensor. *Sensors and Actuators B: Chemical*, 370, 132417.
5. Keshtkar, S., Rashidi, A., Kooti, M., Askarieh, M., Pourhashem, S., Ghasemy, E., & Izadi, N. (2018). A novel highly sensitive and selective H₂S gas sensor at low temperatures based on SnO₂ quantum dots-C60 nanohybrid: Experimental and theory study. *Talanta*, 188, 531-539.
6. Manjula, P., Arunkumar, S., & Manorama, S. V. (2011). Au/SnO₂ an excellent material for room temperature carbon monoxide sensing. *Sensors and Actuators B: Chemical*, 152(2), 168-175.
7. Li, R., Chen, S., Lou, Z., Li, L., Huang, T., Song, Y., ... & Shen, G. (2017). Fabrication of porous SnO₂ nanowires gas sensors with enhanced sensitivity. *Sensors and Actuators B: Chemical*, 252, 79-85.





Vidhyaet al.,

8. Ying, Z., Wan, Q., Song, Z. T., &Feng, S. L. (2004). SnO₂ nanowhiskers and their ethanol sensing characteristics. *Nanotechnology*, 15(11), 1682.
9. Leangtanom, P., Wisitsoraat, A., Chanlek, N., Phanichphant, S., &Kruefu, V. (2020). Highly sensitive and selective ethylene gas sensors based on CeOx-SnO₂ nanocomposites prepared by a Co-precipitation method. *Materials Chemistry and Physics*, 254, 123540.
10. Basu, S., & Bhattacharyya, P. (2012). Recent developments on graphene and graphene oxide based solid state gas sensors. *Sensors and Actuators B: Chemical*, 173, 1-21.
11. Debataraja, A., Zulhendri, D. W., Yuliarto, B., &Sunendar, B. (2017). Investigation of nanostructured SnO₂ synthesized with polyol technique for CO gas sensor applications. *Procedia engineering*, 170, 60-64.
12. Marikutsa, A. V., Rummyantseva, M. N., Gaskov, A. M., &Samoylov, A. M. (2015). Nanocrystalline tin dioxide: Basics in relation with gas sensing phenomena. Part I. Physical and chemical properties and sensor signal formation. *Inorganic Materials*, 51, 1329-1347.
13. Shankar, P., &Rayappan, J. B. B. (2015). Gas sensing mechanism of metal oxides: The role of ambient atmosphere, type of semiconductor and gases-A review. *Sci. Lett. J*, 4(4), 126.
14. Ng, S., Prášek, J., Zazpe, R., Pytlíček, Z., Spatz, Z., Pereira, J. R., ...&Macák, J. M. (2020). Atomic layer deposition of SnO₂-coated anodic one-dimensional TiO₂ nanotube layers for low concentration NO₂ sensing. *ACS applied materials & interfaces*, 12(29), 33386-33396.
15. Sopiha, K. V., Malyi, O. I., Persson, C., & Wu, P. (2021). Chemistry of oxygen ionosorption on SnO₂ surfaces. *ACS Applied Materials & Interfaces*, 13(28), 33664-33676.
16. Salehi, S., Nikan, E., Khodadadi, A. A., &Mortazavi, Y. (2014). Highly sensitive carbon nanotubes-SnO₂ nanocomposite sensor for acetone detection in diabetes mellitus breath. *Sensors and Actuators B: Chemical*, 205, 261-267.
17. Sharma, B., Sharma, A., &Myung, J. H. (2021). Highly selective detection of acetone by TiO₂-SnO₂ heterostructures for environmental biomarkers of diabetes. *Sensors and Actuators B: Chemical*, 349, 130733.
18. Wadkar, P., Bauskar, D., &Patil, P. (2013). High performance H₂ sensor based on ZnSnO₃ cubic crystallites synthesized by a hydrothermal method. *Talanta*, 105, 327-332.

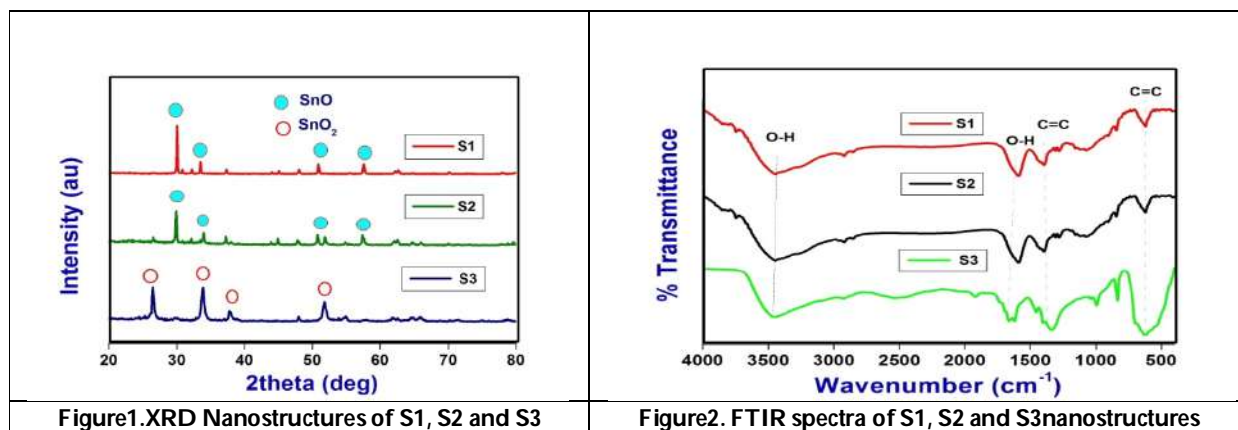


Figure1.XRD Nanostructures of S1, S2 and S3

Figure2. FTIR spectra of S1, S2 and S3 nanostructures





Vidhya et al.,

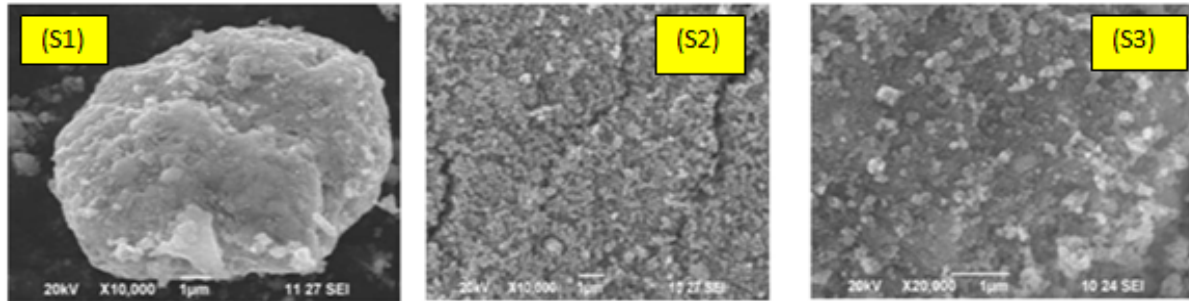


Figure 3. SEM of S1, S2 and S3 nanostructures

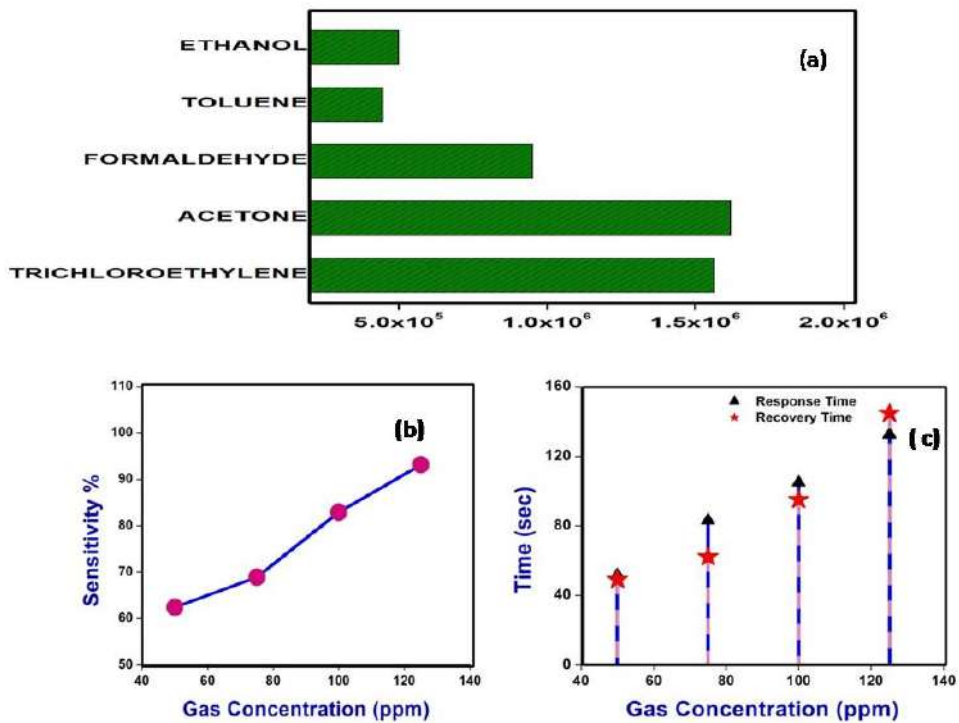


Figure 4. (a). Selectivity (b). Sensitivity and (c). Response time and Recovery Time of S3





e-Card for Futuristic Indian Education System

Rajendra Kumar^{1*}, Aman Anand¹, Praveen Pachauri², Devanshi Singh³ and Khursheed Alam⁴

¹School of Engineering and Technology, Sharda University, Greater Noida, U.P., India.

²Uttar Pradesh Institute of Design, Noida, U.P., India.

³School of ICT, Gautam Buddha University, Greater Noida, U.P., India.

⁴The A. H. Siddiqi Centre for Advanced Research in Applied Mathematics & Physics, Sharda University, Greater Noida, U.P., India.

Received: 06 Apr 2023

Revised: 10 May 2023

Accepted: 31 May 2023

*Address for Correspondence

Rajendra Kumar

School of Engineering and Technology,

Sharda University,

Greater Noida

E. Mail: rajendra04@gmail.com



This is an Open Access Journal / article distributed under the terms of the **Creative Commons Attribution License** (CC BY-NC-ND 3.0) which permits unrestricted use, distribution, and reproduction in any medium, provided the original work is properly cited. All rights reserved.

ABSTRACT

In India, there are several identification mechanisms for individual in place. But none of the existing identification system provides the information about individual's up to date verified educational qualification details. This paper presents the concept and framework to design an e-Card (education card) which will carry all the educational details along with necessary personal details of an individual. The card will reduce the huge amount of data entry and data replication. It will facilitate quick response (QR) code and smart card through which anyone can access the educational and other necessary personal details such as address, mail id, phone number, experience etc. of an individual. It will also give permission to employment sectors to access and verify educational and personal data of candidate or employee. The e-Card will carry a unique identification number (issued by Ministry of Education) for each educated individual in India. As the individual accelerates towards the higher education, it is just a matter of updating the details of the same in the particular identification number. The e-Card can be made mandatory everywhere in rural/urban which will not only reduce the burden of carrying important certificates or marks cards but also will give the advantage of using it anywhere and anytime whenever required encouraging paperless and faster communication.

Keywords: e-Card, Unique Identification Number, Centralized System, QR Code and Smart Card.



**Aashish Jain et al.,**

INTRODUCTION

The strength of information technology infrastructure of a country is evaluated by its governance. The term governance implies the structure and processes designed for ensuring the accountability, transparency, responsiveness, protocols, permanence measures, fairness, and fullness, enabling, and broad-based participation. *e*-governance is a framework to organize public management for increasing efficiency, transparency, convenience, and responsiveness to citizens by applying the intensive and strategic use of regional and cumulative data with communication technologies for intra and inter-governmental relations. *e*-governance helps in daily life relations and long-term plans with citizens and users of public services offered by the government. *e*-governance is powered by the ICT-tools for achieving fast and reliable analysis of data [1]. Digital India, the initiative of present government of India (GOI) is a program for transforming India into a digitally empowered society for preparing it for fast and corruption free transactions in future ahead [2].

Following are some of the agenda points for digital India mission:

- The GOI should establish state-of-the-art ICT infrastructure for ministries/departments/states fully leveraged with the most common services. Deity would also evolve or laydown the standards and policies providing technical supports, undertaking capacity building, and many more.
- The current ongoing *e*-Governance initiatives should be revamped to align them with the focused principles of Digital India under sustainable development goals (SDGs). Scope enrichment, process re-engineering, integrated and inter-operable systems, implementing emerging technologies like IoT, blockchain [3, 4], cloud computing [5], artificial intelligence [6], etc. would be undertaken for enhancing the delivery of government services to the public.
- Different states should be given flexible scope for identifying the state-specific projects in public welfare as per current socio-economic demands.
- The *e*-Governance should be encouraged as a centralized initiative to necessary extent for ensuring the citizen-oriented services, interoperations of various *e*-governance apps and optimum use of ICT infrastructure and resources to adopt a decentralized model to implement.
- The successes of *e*-Governance should be evaluated under standard operating procedures (SOPs) and their reproduction should be promoted in proactive manner with the required production and customization wherever and wherever required.
- The public and private collaborations should be chosen wherever there is feasibility of implementing *e*-Governance projects with ample management and strategic controls.
- The 100% implementation of unique-ID (UID) should be promoted for facilitating identification, authentication, and delivery of government schemes to the unprivileged people.
- Doing restructuring of national informatics centers (NICs) should be for strengthening the information technology support to all the government departments at all levels.

Identification system is a mapping from a known quantity to an unknown entity, the known quantity is called the identifier and the unknown entity is what needs to be identified. It is the process to find, retrieve, modify, delete/report specific data without ambiguity from data storage. In India, several government ID systems exist such as Passport, Voter Card, DL, PAN, AADHAAR, etc. But none of these provides the educational qualification details of any individual. Beside these, an individual also needs governmental identification proof issued by government during his/her study period (primary, secondary, higher secondary and university education). Any individual is eligible to apply any identity proof after attaining age 18. The *e*-Card will be an identification proof of a student issued by government which will carry all the educational details along with other necessary personal details such as address, phone number, mail id, experience etc. The *e*-Card will also allow individual to pay course fee and examination fee through online using its smart card feature. So, he/she can avoid visiting brick 'n' mortar and standing in a queue to pay in cash or to make demand draft or bankers' cheque [7, 8].



**Aashish Jain et al.,**

The e-Card will allow the students or professionals to carry all the educational details starting from the day of their education. As the student proceeds towards higher education the concerned institution is assigned to update the details. The proposed e-Card is supposed to have the following information along with other specified details:

- Name of the Institution and the Board from which he has passed his/her 10th standard.
- The marks and percentage he/she got in class 10th examination.
- Conduct and school leaving certificate
- Extra-curricular activity details such as sports, cultural, NCC, Scout or NSS

The e-Card information can easily be used to take admission in new school or in university for higher education subject to eligibility required. So, it is just a matter of swapping the card (using QR Code facility) or verifying with unique ID. Now it is new school/university responsibility to update the details further degree a student earns. The e-Card will facilitate online payment using smart card technology. The e-Card is equipped with different smart card technology such as Chameleon card with Tokenization Process [9]. The Chameleon Card is a programmable card, represents each of the owner's credit, debit, and customer cards which avoids unnecessarily carrying all of the aforementioned. The tokenization is the process to replace the sensitive information with unique identifiable symbols to retain all the essential information without security breach.

When a candidate proceeds towards other higher education, he/she can pay the course fee and examination fee through e-Card which facilitates electronic wallet feature. The smart card number of e-Card is equivalent to the E-ID of e-Card. Based on the smart card number, an individual will be eligible to open an account in any bank. After opening the account, he/she can do transaction based on his/her smart card number given in e-Card which will be remain same for all banks. It means bank will create separate account for everyone based on the unique smart card number for their official usage. When an individual swipes the card for any transaction, the smart card number will refer in an encrypted way to the corresponding bank's account number and transaction will be made for him/her. The e-Card also facilitates QR code feature where it scans the code and to get all the required information such as personal, name of the college / board / council / University / year-of-appearing-examination / percentage scored / co-curricular and extra-curricular achievement/ project details/workshop or conference or webinar attended and also presented any research article. Therefore, if e-Card is made mandatory everywhere in rural and urban it will not only reduce the burden of carrying important certificates or marks cards but also will give the advantage of using it anywhere, anytime whenever required encouraging paperless and faster communication. An individual can also avail the learning material and resources from different learning center such as INFLIBNET, British library.

The technology integration model in education will enable the use of e-Card to be carried by a student for many purposes. A major role of IoT, blockchain, cryptography, etc. will be there.

CENTRALIZED DATABASE FRAMEWORK

The centralized database is to be created and maintained by Government or Ministry of Education (formerly Ministry of Human Resource Development or MHRD) for e-Cards. Since citizens of India are its most valuable resources, therefore the nation needs the nurturing and caring in terms of free basic education for achieving a better-quality life. For a better e-governance the main objectives to be fulfilled by Ministry of Education (MoE) are:

- To coordinate with all institutions for issuing new e-Card and updating existing if new certificate is earned.
- The institutions are supposed to update the student's data in centralized database with proper authentication.
- To plan the development, including expanding access and improving the quality of education sector by enhancing infrastructure, teachers' training, etc. throughout the country. Also, it needs to pay special consideration to the underprivileged communities like the economical backward, females and the minorities.
- To provide financial favor in terms of the scholarships, free-ships, loan subsidies, etc. to the deserving scholars from underprivileged sections of the communities.
- To encourage the international collaborations in education, including working closely with foreign countries' universities for enhancing the educational opportunities in our country.



**Aashish Jain et al.,**

Currently, the MoE (GOI) is working through two departments:

Department of School Education and Literacy. It has set the universalization of education which makes our students better citizens through global exposure. It also deals with primary, secondary/higher secondary education, adult education, literacy, and many more [10].

Department of Higher Education. It is responsible for bringing world class opportunities in higher education and research to the students so that Indian students are not lagging behind when presenting themselves at an international platform. Department of Higher Education deals with university education, technical education, certification courses, trainings, etc. It also deals with scholarship, free-ship, loan subsidy, etc. to deserving students [11].

ROLE OF E-GOVERNANCE AND MoE

The MoE should create a centralized database which will store the educational details of the students offered by different institutions [12]. The MoE will also design the e-Card which will carry the information of a student such as Name, Fathers' Name, Mothers' Name, Date of Birth, Sex, Nationality, E-ID (Permanent id for an individual), biometrics of the student, Quick Response Code (QR Code) facility and Smart Card facility and a permanent smart card number which is based on E-ID of e-Card. Anyone can access students' details from the database through the E-ID or QR Code.

MoE will generate the E-ID for each student which is based on country code, state code, birthplace pin code and ten-digit unique codes. The MoE will also generate unique authentication id for Primary Institution, Secondary Education and Tertiary Education institution to upload and update educational and curricular and extra and co-curricular information. It will be mandatory to all the institutions to upload all education related data in different stage of education by different institution. This needs to be further verified by Secondary board, Higher Secondary council or University. The MoE will also generate unique authentication id to student to upload and update their personal information such as address, mail id, phone number etc. The student can also borrow various library resources from reputed libraries. The MoE will also generate unique authentication id to secondary board, higher secondary council or university to verify whether different primary education, secondary education and tertiary education institutions are uploading correct educational information and curricular and extra-curricular information for each individual or not. If they get any mismatch information, they will send a reminder to make a correction.

In rural and tribal areas, the MoE can establish nodal center with the help of state government where all nearby educational institute can come and upload and update the educational details of a student. It will also give permission to governmental and corporate employment sectors to access and verify educational and personal data of candidate for preparing the merit list to conduct campus recruitment process and internship process or of employee for appointing in different task. The government can also identify list of eligible students to disburse scholarship and free ship where the amount can be disbursed in the different categories such as SC, ST, OBC, minorities and other economically backward class according to the deserving candidates. It can identify the dropout rate of students, especially girls. The government can generate the annual report on literacy rate. The Government can also identify list of eligible students for government jobs and intimate them through given mail id and phone number which is uploaded by student in their personal information. The MoE can tie up with different banking sector to generate the permanent smart card number for each candidate using their E-ID. The candidate can use e-Card as an electronic wallet to pay course fee and exam fee. Whenever the candidate will open account in any bank, the same smart card number will be used to create an account and will be carried further.

The entire online bank transaction can be done using smart card technology. The smart card will hold all information about the candidate and the bank and account details. The institutions will make a mandatory clause to pay different fees through online which can be possible through the e-Card. He/she can increase the debit limit by using e-Card as electronic wallet.



**Aashish Jain et al.,**

In the beginning of the academic year, the MoE will send circular to different institution and university to upload the educational, co-curricular and extra-curricular information of students in the centralized database. The database admin will maintain the data as well as the security of all data at institution level.

Role of secondary board, higher secondary council and Universities

The unique id and password will be generated and given by MoE admin to all boards of secondary education, council of higher secondary education and universities of different states in India. The boards and councils will verify all data and result details from the centralized database uploaded by different primary institution, Secondary and higher secondary institution respectively. If there is any data mismatch, then they must send the reminder to those institutions to rectify the mistake within the time limit. It also ensures that there will not be any data redundancy and duplicity done by any institution. Similarly, University will also get unique id and password from admin of the database created by MoE. Through the id, the University can check the result from the database uploaded by tertiary educational institution.

Role of Primary, Secondary and Tertiary Educational Institutions

The unique id will be also given to different primary, secondary, higher secondary and tertiary educational institution. Through the id, each institution can upload their institutional admission details, students' caste wise details, gender wise details etc. and result of each individual student in the database either annually or semester wise. They can also upload students' curricular and co-curricular activities details in the database created by MoE for e-Card. They include students' participation in different wings of NCC, NSS or Scout. They also upload and update participation and achievement of different level of State and National level Sports and Cultural participation [13].

Education e-Cards

The proposed e-Card model is targeted that MoE will collaborate with education institutions for issuing e-Card. Students have to provide all necessary information to the school authority at the time of admission. Then the school authority will submit that relevant information in the database created by MoE. Once it is submitted the student will receive the permanent e-Card from MoE [13]. Following are concerns of e-card:

- *e-Card Contents* - The card will provide all the relevant information of student such as Name, Father Name, Mother Name, Date of Birth, sex (male or female), Student's E-ID and bio metrics of the student. This permanent E-ID will be based on country code, birthplace pin code, and ten-digit id code.
- *Validity of e-Card* - The E-ID will remain same for lifetime.
- *Identification Proof* - The student can use the e-card as an identification proof, and it is helpful to apply for other nationalized documents like passport and driving license, etc.
- *Verification e-Card* - Through the E-ID, anyone can access the educational details and personal information of a student. Also, scanning QR code, anyone can get that information in detail. Using the E-ID and smart card number, banking sectors can create bank account and provide electronic payment option using smart card technology.
- *Issuing of e-Card* - Through the id and password generated for the student, the student can update his/her personal details such as address, e-mail id, phone number, add-on course details, certification course details and all other necessary information with time changes. He/she can also update his/her areas of interest and employment details like year of experience and details of different employers. The student can create electronic wallet using smart card feature of e-card.
- *As an electronic wallet* - The student can pay his/her course fee and other study related fee to the institutions using e-card which facilitates the electronic payment option.
- *Job Alerts* - By entering the card details the student can login in mobile app targeted for jobs. The students can receive intimation from Government and corporate organization regarding job vacancies on his/her mobile.
- *Employment Sector* - The government and corporate employment sector can also use centralized database created by MoE. They can access the database and collect information of a particular student according to the criteria.



**Aashish Jain et al.,**

They can also prepare a list of students in general, SC, ST category for interview process, inform them about schedule of interview through mail id. Based on the merit list, employment sectors can organize campus recruitment process or inform candidates about current vacancies. They can verify the educational details and personal information details of a student from the database. Using blockchain, the organization can easily identify the fake candidates as well as the forge information submitted by candidates. The organization can upload previous experience of employee and insist the employee to update his/her newly assigned task and details which can be further verified by the authority of employment sector. The organization can also prepare a list of students for internship program according to the merit list. The database will be maintained by the system admin appointed by MoE. The system admin will take care of the security of the database.

- *e-Card for Banking Sector* - Candidate can create the bank account in different banks using the E-ID and permanent smart card number given by MoE. All information related to candidate, bank and account can be created and updated with the help of smart card technology. Whenever any device will read the smart card, a report of all necessary information will be generated. It means bank will utilize the smart card number to create its own account number. The smart card number will remain same for other banks also. It means if candidate will open another account in a different bank, the same smart card number will be utilized. When system reads the smart card number, it will encrypt that number to bank's own account number given to the candidate in a secure way. So, the candidate can do transaction without having separate account and separate debit card. Using the *e-Card*, which facilitates electronic wallet feature, an individual can do different transaction. And any bank can avoid generating different passbook, debit card, ATM card etc. Further banks can add credit facility to *e-Card* where candidate can use the same smart card number and create credit account for him/her.
- *Transaction Alerts* – The single mobile app will provide all kinds of alerts. The students can receive intimation from banking sectors regarding different transaction made by students with the help of *e-Card* through their given email id and phone number.

As shown in figure 1, the student provides his/her personal details, and the school/institute/university uploads his/her details along with the certificate/degree completed in the centralized server secured with blockchain by government. The *e-Card* data is accessed by the *e-Card* production unit and the produced cards are sent to the concerned school/institute/university.

Quick Response Code

Quick response (QR) code is a two-dimensional matrix code representing coded information about something. A QR code is a machine-readable optical label which consists of information about the item to which it is associated. By scanning the QR code on *e-Card* will provide all the details of the card holder like personal details, educational qualification but the sensitive details like banking and other things will be protected. The scanning of QR code will permit the entry to a student in exams as the admit card can be linked with the smart *e-Card*. QR Code for an individual personal information which provides individuals name, fathers' name, mother's name, date of birth, sex, E-ID number, and necessary information which is uploaded by individual. It also provides an individuals' achievement and participation in different level of co-curricular and extra-curricular activities and details of different certifications and add-on program attended by individual, details of science model or project designed by individual, research projects, etc.

QR Code for schooling details which provides when and where an individual started his/her studies. It also provides information about the school, location of the school and other schools (If individual completed his schooling in different schools). QR Code for secondary examination details which provides the information about result of the candidate appearing in secondary examination, school where he/she has appeared exam, percentage and CGPA of his/her secondary examination. QR Code for higher secondary examination details which provides the information about result of the candidate appearing in higher secondary examination, school or college where he/she has appeared exam, percentage and CGPA of his/her higher secondary examination. QR Code for undergraduate examination details which provides the information about result of the candidate appearing in semester or annual university examination, college where he/she has appeared exam, percentage and CGPA of his/her university



**Aashish Jain et al.,**

examination. QR Code post graduate examination details which provides the information about result of the candidate appearing in semester university examination, college where he has appeared exam, percentage and CGPA of his/her university examination.

Smart Card Technology

Card enabled for transactions using integrated circuit (or a chip) is most common now a days for secure payments [14]. It is fabricated using microprocessor under a gold contact pad. Smart cards can provide user identification, authentication, data storage, security code, application processing mechanism, etc. Smart cards are equipped with high security authentication.

The e-Card facilitates all the smart card feature. The smart card is having permanent number which holds several information of an individual such as candidates' name, address, bank account number, location of bank and date of issuing the account etc. Candidate can create the bank account in different banks using the E-ID and permanent smart card number given by MoE. Whenever any device or system will read the smart card, a report of all necessary information will be generated. It means bank will utilize the smart card number to create its own account number.

The smart card number will remain same for other banks also. It means if candidate will open another account in a different bank, the same smart card number will be utilized. Using the e-Card, which facilitates electronic wallet feature, an individual can do different transaction. And any bank can avoid generating different passbook, debit card, ATM card etc. Further banks can add credit facility to e-Card where candidate can use the same smart card number and create credit account number for him/her. The figure 2 shows the proposed contents on e-Card along with QR code.

Benefits of Using E-Card

The e-Card can hold all necessary information of a candidate along with educational, co-curricular, extra-curricular and personal information. The e-Card can be used as identity proof and as most valuable documents to apply other nationalized documents such as passport and driving license. It can also be used to borrow learning resources from different repositories. The e-Card can be used as electronic wallet to pay various fees during studies and further payments also. It can be used as debit as well as credit card. The e-Card holds E-ID, through which anyone can access the details of educational, co-curricular, extra-curricular and personal information. It also facilitates smart card technology through which electronic payment option can be generated to pay several fees during studies and so on. Having this, any candidate can apply different competitive examination, government and corporate job. Using this, a candidate receives different applicable financial support from different government agencies without applying. The e-Card can be used anywhere and anytime which encourages paperless and faster communication.

CONCLUSION

Implementation of e-Card can bring revolutionary changes in education system in India. It can serve as a strong identification proof for educational details of a student. Validation and verification process is ensured using blockchain at various level of education system guarantees the authenticity of information. Addition of QR Code facilitates the freedom to anybody to use the card to collect and verify an individual's details. Additionally, the smart card technology facilitates the freedom to the students to use card for paying different fees in a secure way which cannot be possible with any other identity proof. In this case, the e-card system is proposed, and the benefits are analyzed. If the Government takes up this initiative in a serious note, then the destination is not so far to reach.

REFERENCES

1. <http://www.digitalindia.gov.in/>
2. <https://india.gov.in/e-governance/national-e-governance-plan>





Aashish Jain et al.,

3. Kumar, R., Singh, R. C., Khokher, R., 2022. Framework for Modelling, Procuring, Building Systems for Smart City Scenarios using Blockchain Technology and IoT, Book chapter in *The Data-Driven Blockchain Ecosystem: Fundamentals, Applications and Emerging Technologies* (Book chapter), CRC Press, ISBN: 9781003269281
4. Kumar, R., Kapil, A. K., Athavale, V., Leong W. Y., Touzene A., 2023. Catalyst for Clean and Green Energy Using Blockchain Technology, Book chapter in *Modeling for Sustainable Development - Multidisciplinary Approach*, Nova Science Publisher (in press).
5. Namasudra S., Roy P., Balusamy B., 2017. Cloud Computing: Fundamentals and Research Issues, *Second International Conference on Recent Trends and Challenges in Computational Models (ICRTCCM)*, 2017, pp. 7-12.
6. Huang-Fu C. -Y., Liao C. -H., Wu J. -Y. 2021. Comparing the performance of machine learning and deep learning algorithms classifying messages in Facebook learning group, *International Conference on Advanced Learning Technologies (ICALT)*, 2021, pp. 347-349
7. Gronlund Ake, Horan Thomas, Orebo 2004. Introducing E-Gov: History, Definitions and Issues, *Communications of the Association for Information Systems*, Volume 15, pp. 713-729.
8. Evers David, Routray Ramani, Zhang Rui, Will Douglas cocks and Pietzuch Peter, 2011. Configuring large-scale storage using a middleware with machine learning, concurrency and computation: practice and experience, pp. 1-15.
9. Varsha K., Aneena M., Dhaniya Abdul Nazar, Jameema Mol K., Jithin T. P., 2018. RFID Based Chameleon Card for Tribals, *International Conference on Emerging Trends and Innovations in Engineering and Technological Research (ICETIETR)*, pp. 1-4,
10. <https://www.education.gov.in/en/school-education>
11. https://www.education.gov.in/en/higher_education
12. Ministry of Human Resource Development (MHRD): www.mhrd.gov.in
13. Identity, privacy and Information Technology: <http://net.educause.edu/ir/library/pdf/erm0267.pdf>
14. Smart card technology details: www.searchsecurity.techtarget.com/definition/smar-card.

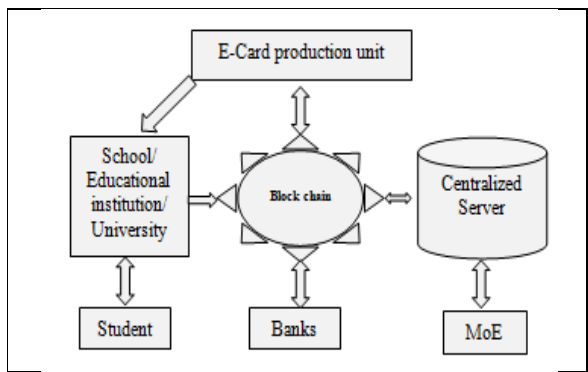


Figure 1: The e-Card management



Fig 2: Facing side of e-Card





A Study on Climate Conditions of Various Geographical Territories in the World through Machine Learning Techniques

Deepthi Gupta^{1*}, Rudra Pratap Jena² and Soumya Sucharita Patel³

¹Patna College, Patna, Bihar, India

²Rajdhani Engineering College, Bhubaneswar, Odisha, India

³OUTR, Bhubaneswar, Odisha, India.

Received: 10 Apr 2023

Revised: 16 May 2023

Accepted: 31 May 2023

*Address for Correspondence

Deepthi Gupta

Patna College,

Patna, Bihar, India

E. Mail: dg.gupta399@gmail.com



This is an Open Access Journal / article distributed under the terms of the **Creative Commons Attribution License** (CC BY-NC-ND 3.0) which permits unrestricted use, distribution, and reproduction in any medium, provided the original work is properly cited. All rights reserved.

ABSTRACT

Global climate change has already had observable effects on the environment. Glaciers have shrunk, ice on rivers and lakes is breaking up earlier, plant and animal ranges have shifted and trees are flowering sooner, frequent wildfires, longer periods of drought in some regions and an increase in the number, duration and intensity of tropical storms. The number of climate-related disasters has tripled in the last 30 years. Between 2006 and 2016, the rate of global sea-level rise was 2.5 times faster than it was for almost all of the 20th century. In this paper, presents the trend analysis of temperature which is being calculated using the machine learning technique such as Gradient Descent Algorithm, Linear Regression with Multiple Variables, Polynomial Regression using gradient descent. The overall purpose of this study is to investigate the possible trend of temperature variation as well as the effect of climate change in the world.

Keywords: Global climate, Gradient Descent Algorithm, Linear Regression with Multiple Variables, Polynomial Regression.

INTRODUCTION

Machine Learning (ML) is an important aspect of modern business and research. It uses algorithms and neural network models to assist computer systems in progressively improving their performance. Machine Learning algorithms automatically build a mathematical model using sample data – also known as “training data” – to make decisions without being specifically programmed to make those decisions. Machine learning is a method of data analysis that automates analytical model building. It is a branch of artificial intelligence based on the idea that systems can learn from data, identify patterns and make decisions with minimal human intervention. Because of new



**Deepti Gupta et al.,**

computing technologies, machine learning today is not like machine learning of the past. It was born from pattern recognition and the theory that computers can learn without being programmed to perform specific tasks; researchers interested in artificial intelligence wanted to see if computers could learn from data. The iterative aspect of machine learning is important because as models are exposed to new data, they are able to independently adapt. They learn from previous computations to produce reliable, repeatable decisions and results. It's a science that's not new – but one that has gained fresh momentum.

Numerous foundational ideas in machine learning come from probability theory and statistics, and they have their roots in the 18th century. The English statistician Thomas Bayes developed a mathematical theorem for probability in 1763. This theorem became known as the Bayes Theorem and is still a key idea in several contemporary methods of machine learning. The Dartmouth Workshop, usually regarded as the event that gave rise to the science of artificial intelligence, gave rise to the phrase "artificial intelligence" in 1956. Mathematicians and scientists from several fields attended the six to eight-week long workshop, including computer scientist John McCarthy, Marvin Minsky, Nathaniel Rochester, and Claude Shannon. To aid in making predictions from unlabelled data sets, future research will focus more on enhancing unsupervised machine learning systems. This function will be more and more crucial as computers are able to find intriguing hidden patterns or groupings in data sets, which will aid organisations in better understanding their market or clients.

Temperature, measure of hotness or coldness expressed in terms of any of several arbitrary scales and indicating the direction in which heat energy will spontaneously flow—i.e., from a hotter body (one at a higher temperature) to a colder body (one at a lower temperature). The world is getting warmer. Thermometer readings around the world have been rising since the Industrial Revolution, and the causes are a blend of human activity and some natural variability—with the prevalence of evidence saying humans are mostly responsible. According to an ongoing temperature analysis conducted by scientists at NASA's Goddard Institute for Space Studies (GISS), the average global temperature on Earth has increased by a little more than 1° Celsius (2° Fahrenheit) since 1880. Two-thirds of the warming has occurred since 1975, at a rate of roughly 0.15-0.20°C per decade. December's combined global land and ocean surface temperature departure from average for 2019 was also second highest in the 140-year record. For 2019, the average temperature across global land and ocean surfaces was 1.71°F (0.95°C) above the 20th century average. This was the second highest among all years in the 1880–2019 record and just 0.07°F (0.04°C) less than the record value set in 2016. 2019 marks the 43rd consecutive year (since 1977) with global land and ocean temperatures, at least nominally, above the 20th century average. The five warmest years have occurred since 2015; nine of the 10 warmest years have occurred since 2005. The year 1998 is the only 20th century year among the 10 warmest years on record. The annual global land and ocean temperature has increased at an average rate of +0.13°F (+0.07°C) per decade since 1880; however, since 1981 the average rate of increase is more than twice that rate (+0.32°F / +0.18°C). For the 21-year span that is considered a reasonable surrogate for pre-industrial conditions (1880–1900), the 2019 global land and ocean temperature was 2.07°F (1.15°C) above the average. Without human intervention, climate change has occurred on Earth in the past. Because of the traces left behind in tree rings, glacier ice sheets, ocean sediments, coral reefs, and sedimentary rock strata, we are able to reconstruct former temperatures. For instance, air bubbles trapped in glacier ice allow scientists to study minute samples of the Earth's atmosphere that date back more than 800,000 years.

The average global temperature can be inferred from the chemical composition of the ice. With the use of this historical data, scientists have created a record of former climates on Earth, or "paleoclimates." Past ice ages and times significantly warmer than the present are shown by the paleoclimate record and global models. However, the paleoclimate record also demonstrates that the present-day rate of climatic warming is far higher than that of earlier warming episodes. Over the past million years, as the Earth emerged from ice periods, the average global temperature increased by 4 to 7 degrees Celsius over a period of around 5,000 years. The temperature has risen 0.7 degrees Celsius in just the last century, approximately ten times faster than the usual warming pace associated with ice ages. In the coming century, models project that the Earth will warm by 2 to 6 degrees Celsius. It has taken the globe roughly 5,000 years to warm by 5 degrees when global warming has occurred many times during the past two



**Deepti Gupta et al.,**

million years. In the coming century, warming is expected to occur at a rate that is at least 20 times quicker. Extremely unusually, this rate of change. As of 1981 [Hansen et al., 1981], GISS analyses of changes in the earth's surface temperature have been ongoing since the late 1970s. The goal was to determine an estimate of global temperature change that could be compared to projected global climate change in response to known or suspected climate forcing mechanisms, such as atmospheric carbon dioxide, volcanic activity, and variations in solar irradiance.

Prior studies on temperature change have been conducted, as noted by Jones et al. [1982] and summarised by the Intergovernmental Panel on Climate Change (IPCC) [2007], with the majority of the research focusing on sizable but not entirely global regions. Because the methodology solely considers temperature change, it does not yield estimates of absolute temperature. With a degree of Celsius of uncertainty, we calculated the worldwide mean surface air temperature for the period 1951–1980 to be 14°C. In order to fill in temperatures at grid points without observations, that value was produced using a global climate model [Hansen et al., 2007], however it is compatible with findings from Jones et al. [1999] based on observational data. There are maps of absolute temperature in the review paper by Jones et al. (1999), as well as a wealth of background data on investigations of absolute temperature and surface temperature change. Hansen and Lebedeff [1987] used the correlation of temperature anomaly time series as a function of station spacing for various latitude bands.

METHODS AND CALCULATION**Data Explanation**

Statistics on mean surface temperature change by nation are made available in the FAOSTAT Temperature Change domain, with yearly updates. The era covered by the current circulation is 1961 to 2019. Anomalies in monthly, seasonal, and yearly mean temperatures, or changes in temperature relative to a reference climatology covering the years 1951–1980, are quantified statistically. Additionally included is the baseline methodology's standard deviation for temperature change. The National Aeronautics and Space Administration Goddard Institute for Space Studies (NASA-GISS) distributes the Global Surface Temperature Change data, or GISTEMP, which is publicly available.

Environment Temperature Change Data given in the following table:

CONCLUSION

From the above results we concluded that the world temperature is going to increase rapidly in the near future, and the temperature is to be doubled almost at the end of 2049 as of now, so we need more precaution and we should give more attention to the problem of temperature change in the near future.

REFERENCES

1. Brohan, P., Kennedy J.J., Harris J., Tett S.F.B., Jones P.D., 2006: Uncertainty estimates in regional and global observed temperature changes: A new data set from 1850. *Geophys. J. R.*, 111.D12106, doi:10.1029/2005JD006548, Access at:05/05/2021
2. Cavalieri, D. J., Parkinson C.L., Gloersen P., Comiso J.C., Zwally H.J., 1999: Deriving long-term time series of sea ice cover from satellite passive-microwave multisensor data sets. *J. Geophys. Res.*, 104, 15803–15814, Access at:07/05/2021
3. Folland, C. K., Coauthors, 2001: Global temperature change and its uncertainties since 1861. *Geophys. Res. Lett.*, 28, 2621–2624, Access at:01/05/2021
4. Global Greenhouse Gas Reference Network. (n.d.). Retrieved from Earth System Research Laboratory Global Monitoring Division website: <https://www.esrl.noaa.gov/gmd/ccgg/trends/global.html> Access at:06/05/2021
5. Global Weather Data for SWAT. (n.d.). Retrieved from Global Weather Data for SWAT website: <https://globalweather.tamu.edu/>, Access at:07/05/2021





Deepti Gupta et al.,

6. Hansen J., Ruedy R., Stao M., Imhoff M., Lawrence W., Easterling D., Peterson T., Karl T., 2001: A closer look at United States and global surface temperature change. *J. Geophys. Res.*, 106, 23947–23963, Access at:10/05/2021
7. Jin, M., 2004: Analysis of land skin temperature using AVHRR observations. *Bull. Amer. Meteor. Soc.*, 85, 587–600. Access at:08/05/2021
8. Jones P. D., Moberg A., 2003: Hemispheric and large-scale surface air temperature variations: An extensive revision and an update to 2001. *J. Climate*, 16, 206–223, Access at:11/05/2021
9. Kaplan A., Cane M.A., Kushnir Y., Clement A.C., Blumenthal M.B., Rajagopalan B., 1998: Analyses of global sea surface temperature 1856–1991. *J. Geophys. Res.*, 103, 18567–18589, Access at:03/05/2021

Table1 : Temperature Change Data

	Area code	Area	Months Code	Months	Element Code	Elements	Unit	Y1961	Y1962	...	Y2017	Y2018	Y2019
0	2	Afghanistan	7001	January	7271	Temperature change	°C	0.777	0.062		1.201	1.996	2.951
1	2	Afghanistan	7001	January	6078	Standard Deviation	°C	1.950	1.950		1.950	1.950	1.950
2	2	Afghanistan	7002	February	7271	Temperature change	°C	-1.743	2.465		-0.323	2.705	0.086
3	2	Afghanistan	7002	February	6078	Standard Deviation	°C	2.597	2.597		2.597	2.597	2.597
4	2	Afghanistan	7003	March	7271	Temperature change	°C	0.516	1.336		0.834	4.418	0.234
5	2	Afghanistan	7003	March	6078	Standard Deviation	°C	1.512	1.512		1.512	1.512	1.512
6	2	Afghanistan	7004	April	7271	Temperature change	°C	-1.709	0.117		1.252	1.442	0.899
7	2	Afghanistan	7004	April	6078	Standard Deviation	°C	1.406	1.406		1.406	1.406	1.406
8	2	Afghanistan	7005	May	7271	Temperature change	°C	1.412	-0.092		3.280	0.855	0.647
9	2	Afghanistan	7005	May	6078	Standard Deviation	°C	1.230	1.230		1.230	1.230	1.230
10	2	Afghanistan	7006	June	7271	Temperature change	°C	-0.058	1.061		2.002	1.786	-0.289
11	2	Afghanistan	7006	June	6078	Standard Deviation	°C	0.930	0.930		0.930	0.930	0.930
12	2	Afghanistan	7007	July	7271	Temperature change	°C	0.884	0.884		0.901	1.815	1.885
13	2	Afghanistan	7007	July	6078	Standard Deviation	°C	0.585	0.585		0.585	0.585	0.585
14	2	Afghanistan	7008	August	7271	Temperature change	°C	0.391	0.391		0.102	0.982	0.773
15	2	Afghanistan	7008	August	6078	Standard Deviation	°C	0.773	0.773		0.773	0.773	0.773
16	2	Afghanistan	7009	September	7271	Temperature change	°C	1.445	1.445		0.930	1.063	2.004
17	2	Afghanistan	7009	September	6078	Standard Deviation	°C	0.832	0.832		0.832	0.832	0.832
18	2	Afghanistan	7010	October	7271	Temperature change	°C	-1.102	0.968		2.092	-0.103	1.264
...





Deepti Gupta et al.,

9655	5873	OECD	7019	Sep&Oct & Nov	7271	Temperature change	°C	0.378	0.378	0.378	0.378	0.378
9656	5873	OECD	7020	Meteorological year	6078	Standard Deviation	°C	0.165	-0.009	1.349	1.088	1.297
9657	5873	OECD	7020	Meteorological year	7271	Temperature change	°C	0.260	0.260	0.260	0.260	0.260

Table 2 : Inputs

	ds	y
0	1961	1.43032
1	1962	-0.028398
2	1963	-0.026297
3	1964	-0.122865
4	1965	-0.224154
5	1966	0.095070
6	1967	-0.131975
7	1968	-0.167841
8	1969	0.105694
9	1970	0.072189
10	1971	-0.177649
11	1972	-0.049936
12	1973	0.199149
13	1974	-0.128841
14	1975	-0.030398
15	1976	-0.210907
16	1977	0.185724
17	1978	0.053986
18	1979	0.230299
19	2039	1.764388
20	2040	1.790991
21	2041	1.817595
22	2042	1.844199
...
55	2016	1.440185
56	2017	1.299112
57	2018	1.310459
58	2019	1.464899

Table 2 gives the temperature of 59 years i.e from 1961 to 2019. We will use this data to forecast the future world temperature.





Deepti Gupta et al.,

Table 3: In Forecast

	ds	y
0	2005	0.757588
1	2006	0.779762
2	2007	0.801935
3	2008	0.824109
4	2009	0.846283
5	2010	0.868457
6	2011	0.890630
7	2012	0.912804
8	2013	0.934978
9	2014	0.957151
10	2015	0.979325
11	2016	1.001499
12	2017	1.023673
13	2018	1.045846
14	2019	1.068020

Table 3 describes the forecasting data from 2005 to 2009 after applying the forecasting algorithm which says that our forecasting temperature with 0.1760 absolute mean error, as compared to the given data.

Table 4 : Out Forecast

	y	yhat
0	2020	1.258916
1	2021	1.285520
2	2022	1.312124
3	2023	1.338727
4	2024	1.365331
5	2025	1.391935
6	2026	1.418539
7	2027	1.445142
8	2028	1.471746
...
20	2040	1.790991
21	2041	1.817595
22	2042	1.844199
23	2043	1.870803
24	2044	1.897407
25	2045	1.924010
26	2046	1.950614
27	2047	1.97218
28	2048	2.003822
29	2049	2.030425





Deepti Gupta et al.,

Table 4 describes the output i.e. the forecasting temperature of the year 2020-2049.

```

In [1]: import numpy as np
import pandas as pd
from matplotlib import pyplot as plt
import seaborn as sns
import plotly.express as px
from sklearn.linear_model import LinearRegression
from sklearn.model_selection import train_test_split
from sklearn.preprocessing import PolynomialFeatures
from sklearn.pipeline import Pipeline
from sklearn import metrics
from fbprophet import Prophet

In [2]: Etemp_path='B:\python\Environment_Temperature_change_E_All_Data_WOFLAG.csv'
Code_path='B:\python\FAOSTAT_data_11-24-2020.csv'

data1 = pd.read_csv(Etemp_path, encoding='latin-1')
data2 = pd.read_csv(Code_path)

data1
    
```

	Area Code	Area	Months Code	Months	Element Code	Element	Unit	Y1961	Y1962	Y1963	...	Y2010	Y2011	Y2012	Y2013	Y2014	Y2015	Y2016	Y2017	Y2018	Y2019
0	2	Afghanistan	7001	January	7271	Temperature change	°C	0.777	0.062	2.744	...	3.601	1.179	-0.583	1.233	1.755	1.943	3.416	1.201	1.996	2.951
1	2	Afghanistan	7001	January	6078	Standard Deviation	°C	1.950	1.950	1.950	...	1.950	1.950	1.950	1.950	1.950	1.950	1.950	1.950	1.950	1.950
2	2	Afghanistan	7002	February	7271	Temperature change	°C	-1.743	2.465	3.919	...	1.212	0.321	-3.201	1.454	-3.107	2.699	2.251	-0.323	2.705	0.086
3	2	Afghanistan	7002	February	6078	Standard Deviation	°C	2.597	2.597	2.597	...	2.597	2.597	2.597	2.597	2.597	2.597	2.597	2.597	2.597	2.597
4	2	Afghanistan	7003	March	7271	Temperature change	°C	0.516	1.336	0.403	...	3.390	0.748	-0.527	2.246	-0.076	-0.497	2.296	0.824	4.418	0.234
...
9651	5873	OECD	7016	JunJulAug	6078	Standard Deviation	°C	0.247	0.247	0.247	...	0.247	0.247	0.247	0.247	0.247	0.247	0.247	0.247	0.247	0.247
9652	5873	OECD	7019	SepOctNov	7271	Temperature change	°C	0.036	0.461	0.665	...	0.938	1.106	0.885	1.041	0.999	1.670	1.535	1.194	0.581	1.233
9653	5873	OECD	7019	SepOctNov	6078	Standard Deviation	°C	0.378	0.378	0.378	...	0.378	0.378	0.378	0.378	0.378	0.378	0.378	0.378	0.378	0.378
9654	5873	OECD	7020	Meteorological year	7271	Temperature change	°C	0.165	-0.009	0.134	...	1.246	0.805	1.274	0.991	0.811	1.282	1.830	1.349	1.088	1.297
9655	5873	OECD	7020	Meteorological year	6078	Standard Deviation	°C	0.260	0.260	0.260	...	0.260	0.260	0.260	0.260	0.260	0.260	0.260	0.260	0.260	0.260

9656 rows x 26 columns

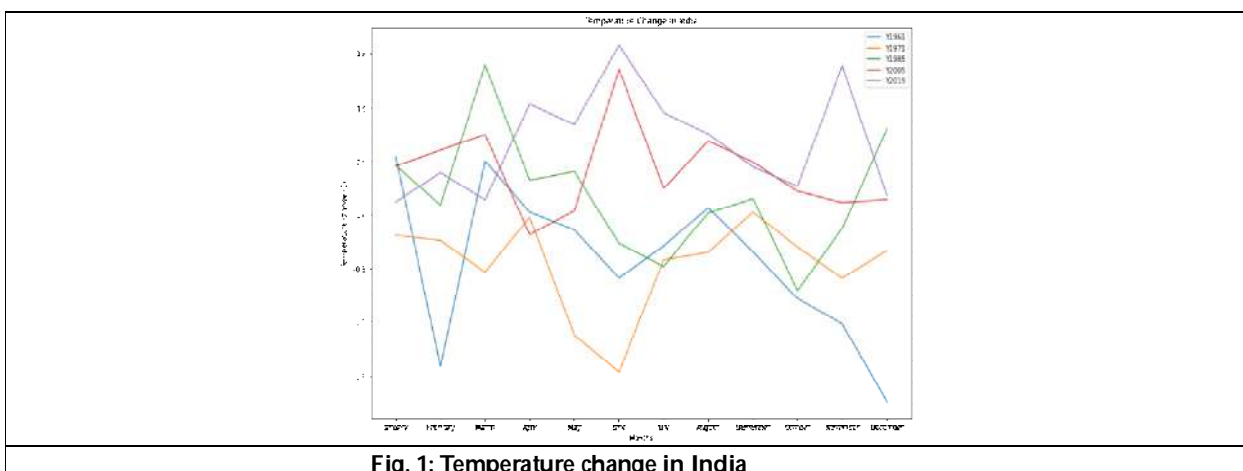


Fig. 1: Temperature change in India





Deepti Gupta et al.,

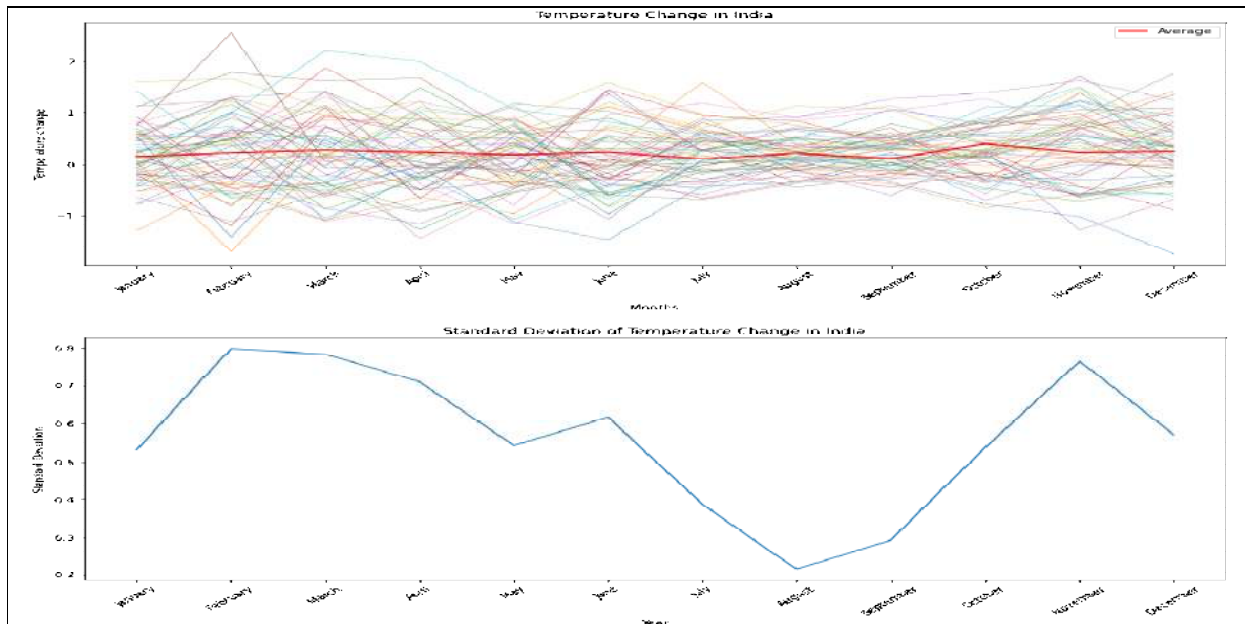


Fig. 2: (a) Temperature Change in India (b) Standard Deviation of Temperature Change in India

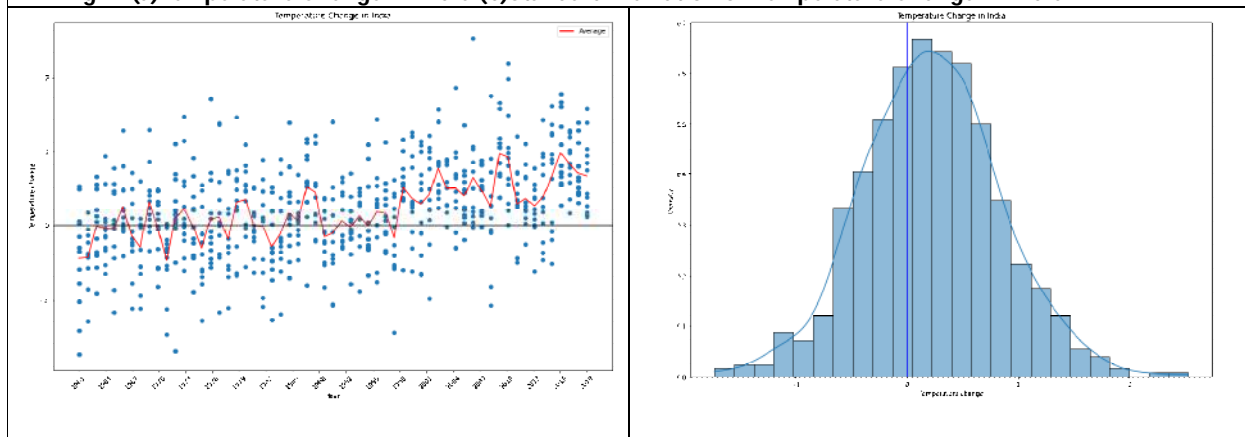


Fig. 3 : Temperature Change of the India

Fig. 4: Temperature Change of the India

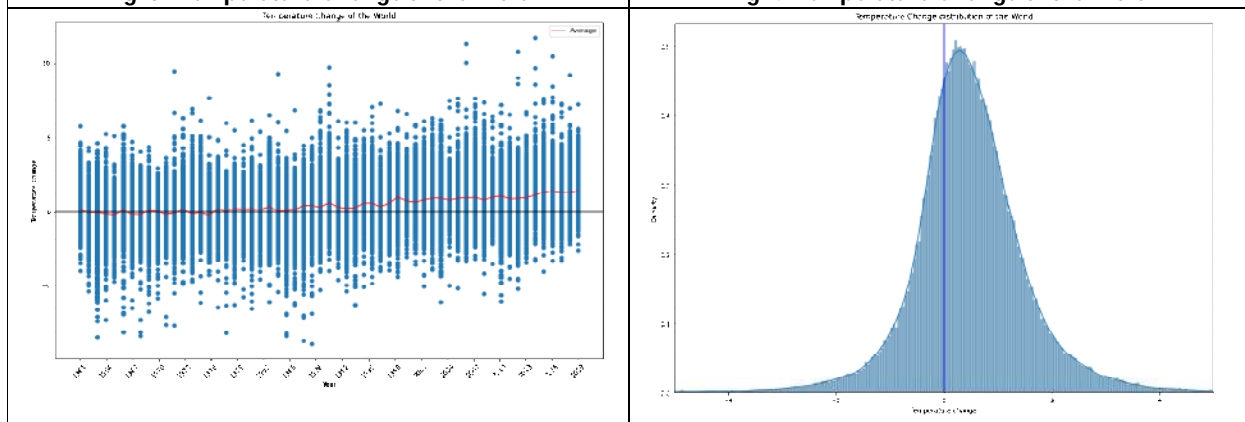


Fig. 5: Temperature Change of the World

Fig. 6: Temperature Change of the World





Deepti Gupta et al.,

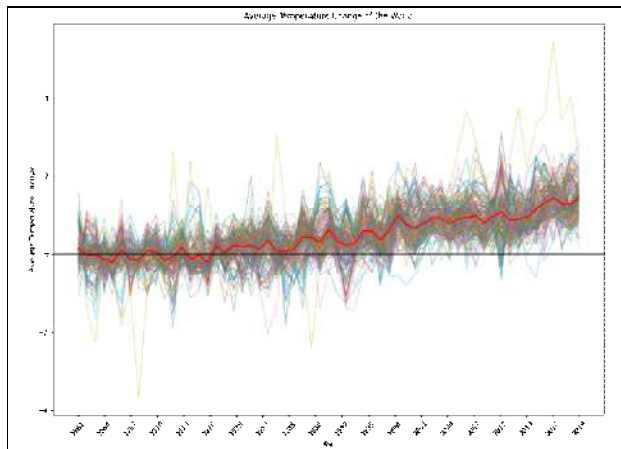


Fig. 7: Average Temperature of the World(1961-2019)

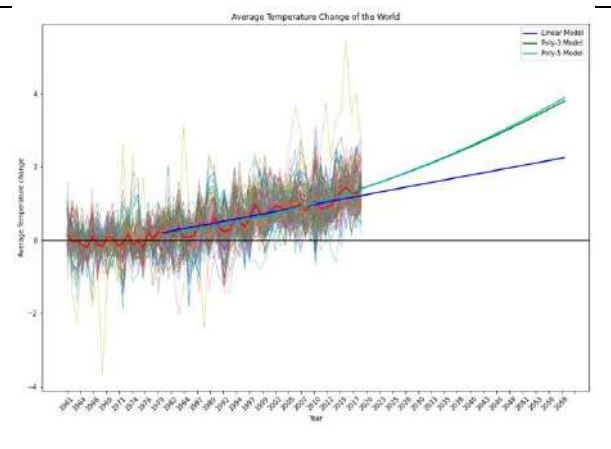


Fig. 8: Average Temperature of the World in Future Years





Partnership to Achieve Goal: To Protect Aquatic Life

Iftikhar Haider^{1*}, Chosching Lazés², Santosh Kumar² and Sakshi Pathak²

¹Department of Mathematics and IT, Center for Preparatory Studies, Sultan Qaboos University, Muscat, Sultanate of Oman.

²The A.H. Siddiqi Centre for Advanced Research in Applied Mathematics & Physics (CARAMP) Sharda University, Greater Noida-201306 UP, India.

Received: 06 Apr 2023

Revised: 10 May 2023

Accepted: 31 May 2023

*Address for Correspondence

Iftikhar Haider

Department of Mathematics and IT,
Center for Preparatory Studies,
Sultan Qaboos University,
Muscat, Sultanate of Oman.
E. Mail: haider@squ.edu.om



This is an Open Access Journal / article distributed under the terms of the **Creative Commons Attribution License** (CC BY-NC-ND 3.0) which permits unrestricted use, distribution, and reproduction in any medium, provided the original work is properly cited. All rights reserved.

ABSTRACT

Sustainable development goals (SDGs) are one of the best ways to improve the world for a better future and to make an easy lifestyle for every global living organism. To achieve these global goals, every individual on earth can take responsible by obeying the laws and holding hands as a family towards the goals. One people or two people's hard work will not reach these global goals. About 75% of the earth's surface is covered by water bodies. Our aquatic wildlife is an important source of food, energy, jobs, atmosphere oxygen, and buffer against new diseases, pests, and predators. According to researchers, more than 3 billion people depend on aquatic organisms. But due to over consumption of seafood, pollution, and human activities most aquatic species are extinct and the rest of the aquatic life is in danger, as they live in a hazardous environment. To solve their problem everyone on the earth especially water users, from small communities to every country should participate as a partner. The partnership is very important because they provide an opportunity to build a network across the world through different sectors. Here partnership to achieve the goal is to help efficiently implement SDGs and complete it in a given duration. Moreover, partnerships play a vital role when it comes to the conservation and production of things. As conservation and production will be more successful when participations are more defined as partners. Our research is mainly focused on the issue of life below water. This research going to focus on the research area, and research question which leads to implement of SDGs. Some SDG-related questions were asked to the public and sought to mobilize action to achieve a global SDG goal. This research has been limited to a few important subtopics mainly why partnership is important, consumption of seafood, new production to implement and maintain the lifestyle of life below water, and conservation of aquatic ecosystem.



**Iftikhar Haider et al.,****Keywords:**Sustainable Development, Aquatic Ecosystem, Partnership, Seafood, Consumption, Production, and Conservation.

INTRODUCTION

United nation operates sustainable development goals (2015-2030) consisting of 17 goals, one of the best ways to improve the world for a better future, to make an easy lifestyle for every global living organism, and to make this earth safer[1]. Partnership to achieve is one of the best goals to fulfill other goals. The partnership includes financing development, connecting people through information technology networks, and international trade flows, and strengthening data collection and analysis. A stronger partnership or collaboration will contribute to environmental protection and sustainable development by mobilizing resources, sharing knowledge, promoting the creation and transfer of environmentally sound technology, building capacity, and mobilizing financial from multiple sources[2]. Aquatic ecosystems are water-dependent living organisms like plants, animal, microbes, and plankton and their livelihood [3]. The fact you should know is the first life originated in the water and the first organisms were also aquatic organisms. As the ocean covered the maximum area of water bodies, the ocean has the maximum number of varieties of living organisms[4]. In an ocean, coral reefs host a maximum of aquatic living organisms. Human activities and climate change have left coral bleached and rise in extinction rates of species which leads to a decrease in biodiversity. Of coral reefs, 88% of them are threatened by excessive carbon dioxide (CO₂) emissions. These reefs are among the most important stores of biodiversity on the planet. It takes around 10,000 years for a reef to form from coral polyps, and up to 30 million years for a reef to fully mature, hosting an estimated 25% of all marine life[5]. And yet, around the world, coral reefs are dying, as warming temperatures and stressful conditions bleach the corals white as they are forced to expel color depending on their survival[6].

The total consumption of seafood in the world has consistently increased[7]. Where different methods are used to catch the sea animals. But due to wrong methods of catching, many species are in danger[8]. Overfishing has caused fish stocks to plummet. Coastal economies often rely on fishing and tourism. To maintain and sustain our livelihood and aquatic livelihood we should come up with less consumption of seafood, new products should be innovating mainly focus on limiting the damage caused to the aquatic ecosystem and conservation of the aquatic ecosystem should be done to preserve threatened aquatic life[9]. The main threats in oceans include species loss, habitat degradation, and changes in ecosystem function. Conservation is one of the sustainable methods to maintain our resource and living organisms to pass it to future generations[10].

Why Partnership?

As different partners bring specific expertise from their perspectives and they can work together and which adds to each of the partner's knowledge which builds the capacity to achieve the goals easily. So, getting every people to take part in the SDGs is the best method to create something productive & make it sustainable, as their involvement ensures long-term engagement and guarantees that, no ideas and knowledge are left behind to create a better world. Countries should come up with common issues at the global level so that researchers and experts will be identifying the problems, emerge the issues, and come up with the solution and recommend it to other countries too. We will have to use the existing and additional resources, technology development, and financial resources. If the world needs new products, they should be created in such a manner that it should be essential and it should be advancing models for better versions and long-lasting. The government of every country should come up with the best decision and laws to develop their own country and also to develop this earth. Government should protect its citizen from their difficulties. Government should provide basic needs and well-being for every citizen, especially in remote places. Government should inspect and facilitate the hospital, old-age, and orphan homes and institutions. NGOs were also acting a huge role to make this earth a better place, especially for needy ones. Members of every NGO should work actively and also think out of the box to connect with the government and other NGOs to solve larger problems and global problems. As this world is all about business from our food, shelter, clothes, medication, and education, through this they fulfilled and solved every essential problem. Businessmen and entrepreneurs give



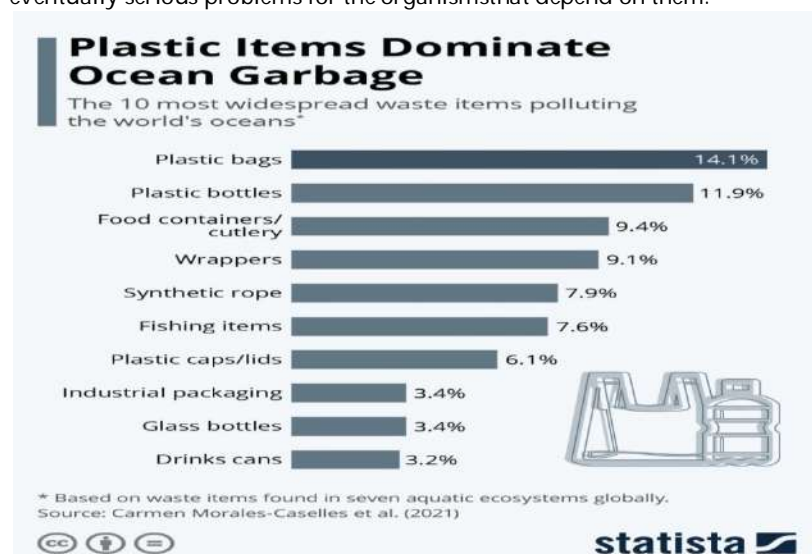


Iftikhar Haider et al.,

different directions for our lives. They can make our life easy in large quantities. Therefore, they should have invested the money in new ideas and new technology. Every citizen of the earth should take care of this earth as their home and caring others as their family. We are interdependent on this earth so every species and every particle play role in our lives, but humans play a vital role on this earth as we can think and act. So, every human on earth should be united and make this earth worth living for all beings. We should conserve the planet Earth. Being a student as a partner, study and understand the field in such a way that you can apply today's knowledge to upcoming issues. As children are future generation people and educating the children is the pillar of society. We have to think about what kind of environment we want in our future and we have to act according to it, as every matter will impact the future.

Some simple things that you should do as a partner to conserve the aquatic ecosystem.

- Consumption of water should be used as per necessity. This will not only save you money but will reduce excess runoff, containing pollutant waste, into water bodies.
- Use less energy in your day-to-day life. Higher temperatures can cause the death of corals, rising sea levels and flooding, and more extreme weather which can damage aquatic ecosystems. Many aquatic species also rely on specific temperatures to determine what sex they develop into (i.e. they have temperature-dependent sex determination), and so by changing the temperature, we can throw the entire population out of balance.
- Consumption of less seafood or not at all if you can.
- Reducing your use of plastics is also essential. Ingestion of microplastic (bits of plastics that are less than 5 mm across) can lead to bio-accumulation. This is where harmful substances build up in a harmful chain and eventually serious problems for the organisms that depend on them.



Consumption of Seafood

Seafood is a natural source of vitamins and other nutrients. This is a healthy option with low fat and cholesterol. Seafood is also rich in vitamin D, calcium, vitamin A, vitamin B, and B-complex vitamins. Seafood is good for your energy production, concentration, metabolism, and even beauty. Omega-3 is very nutritious and present in seafood. As omega-3 plays a critical role in our body improving the immune system, and is good for the skin, and the health of those that suffer from allergies.

The world's appetite for seafood and seafood products shows increasing day by day. This also shows the growing role of fisheries and aquaculture in providing food, nutrition, and employment.

The main reason to increase in consumption of seafood

- Cheapness is an important factor.





Iftikhar Haideret al.,

- Showing tasty advertisements by the company to consume seafood on social media platforms, people were more and more desired to consume seafood.
- Good nutrition and a healthy diet.

Due to pollution in the oceans, seafood is often contaminated. It could cause mild to severe poisoning. Seafood has high levels of mercury which leads to different sorts of diseases. So when you consume seafood, you should be very careful where to buy and where to eat seafood. Be sure that seafood is coming fresh from the water as farm seafood is a high chance of contamination and is dangerous to people's health. Get tested that whether you are allergic to seafood or not, allergic reaction is also dangerous, the person could stop breathing and die. Be sure what kind of seafood you are consuming as some fish like tilapia do not have omega-3 rather it is rich in fat.

Corona virus Impact

The COVID-19 pandemic affected most countries in the world, with a severe impact on the global economy and the food production and distribution sector, including fisheries and aquaculture. According to an addendum, global fishing activity may have declined by about 6.5% as a result of restrictions and labor shortages due to the health emergency. At the same time, the FAO said the disruption of international transport has particularly affected aquaculture production for export, while greatly reduced tourism and restaurant closure have dramatically impacted distribution channels for many fish types, although retail sales have remained stable or increased for frozen, canned, marinated, and smoked fish with long shelf life.

It was arguably one of humanity's finest moments — the whole planet signed up. But after the pandemic, it is our duty to make these look for what we had signed on to make Earth a better place to live in and make it better for the future so that everyone can enjoy its beauty. As of now, we are in a different place right now, as we have seen a pandemic rise to fall and we can give our future generation an education about responsible consumption and production so that no one would end their life in misery. Our planet is One big family, so we must care for and share this world.



Top 10 States in Total Fish Production in India (2016-17) in '000 Tons

Production Should be Need to Improve Lifestyle

Keeping in mind that maintaining and restoring the healthy ecosystem, we have to develop our country to the next level. If a country is developed make sure that the country is well implemented, if the country is undeveloped make it developed and smart. To make it developed and digital, we have to work on new knowledge and inspire a young innovator to make it sustainable and updated. And multi-stakeholders should give a chance for new innovators and entrepreneurs, where new plan and ideology is much needed to achieve the goals. Entrepreneurs should innovate in such a way that where huge and wide problems were solved in an easy way within a short period. Government should help by giving loans and investing in budding companies and entrepreneurs.



**Iftikhar Haideret al.,**

Most of the coastal people are dependent on the ocean and other water bodies like fishermen, collecting shells, octopus harvesting, and seaweed farming, and all this contributes to their livelihood. Over the year, aquaculture become an essential and sustainable source of income and food for local communities[11].

After research, in aquaculture seaweed farming is one of the eco-friendly aquatic farming, even though they can't harm them as aquatic life play an important role in their farming. In an environment where there is natural flora and fauna, seagrasses, and microalgae, seaweed grows much better than it is grown in white sand. If we do not conserve the aquatic plant, we will also end up planting seaweed in the sand, then production may go down. The main threat to seaweed farming is climate change. During the climate is very hot, it affects the seaweed growth. Water temperature is increasing over the year; the farmer has to farm much below the water as it is cooler. Still, farmers need new technology and innovation to farm seaweed. Seaweed is used to make different products like medicinal and pharmaceutical products and also used in making beauty products and food products[13].

When human interacts with the marine environment through demersal fishing like

1. trawling: where a net is dragged along the bottom of the ocean and destroys the seafloor which often contains ecologically important plant and coral species.
2. Active pelagic fishing techniques, where a net is dragged through the open ocean as it's indiscriminate, meaning that the nets will catch anything in their way, regardless of whether or not the fisherman is looking for it. This often leads to protected animals like dolphins and turtles being injured or even killed. From research: for every 1kg of prawns, 9kg of other sea animals are caught bycatch, and then injured or killed, and then thrown away.
3. A catch that is not the species we're targeting is called by-catch. Fishers sometimes bring by-catch back to land, to eat or sell.

Discards

Fishers often throw these unwanted fish back into the water. The animals they throw back are called discards. Discards can be dead or alive, but the survival rate is very low. Some hardy shellfish might survive, but most discarded are dead. There are various reasons why fishers might not want these fish. They might be too small, inedible, damaged, or not even give them a good return in the market. Fishers might also have strict quota restrictions on how much they can bring back each day. If they're over the limit they will have to throw some fish back. Discards bring a negative impact on aquatic ecosystems. First killing for no reason or threatening their environment. Second, most of the discards are not reported. After landing unwanted fish, fishers can give that unwanted fish to a production company as they produce fish meal and fish body oil. To reduce the destruction caused by different fishing techniques, either by reducing how often they are allowed to be used or by making the less destructive. Also, innovation has to be done to fulfill both aquatic and human goals. For example: By using specific fishing hooks that are less likely to catch unwanted species. Solving these sorts of problems does take a lot of hard work, but that doesn't mean there is nothing you can do even though you are not a conservationist. Fishers can also catch fish as given by the law and never overfish, as they were discarded.

Conservation of Aquatic Ecosystem

With half of the world's coral reefs having perished in the previous 30 years, oceans are today more endangered than ever. Therefore, it is crucial that you practice aquatic conservation in order to protect threatened species and ecosystems and to lessen the damage that various fishing methods do, either by limiting their usage or by developing less damaging alternatives. Different species in an environment depend on one another for survival. If one species is threatened, a chain reaction occurs and finally the entire ecosystem is in danger. To keep up with these developments, sustainable aquaculture development and efficient fisheries management are essential. There is mounting evidence for fisheries showing, when they are managed properly, stocks are constantly above target level or are rebuilding. Most importantly, we had less food, fewer money, and less life on our world without aquatic life. The status of fish stocks is poor and deteriorating in areas where fisheries management is absent or inefficient. Therefore, water bodies must be clean and healthy and must be protected before we begin to conserve it. The Indian government devises various programmes to clean up water bodies.

Hypothesis 1: **National mission for clean Ganga project (June 2014)**

Partnership: Department of Water Resources, River Development and Ganga Rejuvenation, Ministry of Jal Shakti.



**Iftikhar Haider et al.,**

Aim is to reduce pollution and conserve & rejuvenate Ganga. However, the pollution in the Ganga has remained mostly consistent because there is no sewage treatment facility. The local government has set up water monitoring stations and waste treatment facilities, but these plans have generally failed to raise the water quality to a level that is suitable for residential use, not even for bathing. After all, treatment plants were inoperable due to lack of funding and skilled workers [14].

Hypothesis 2: Sagar Mala Project, also known as the Blue Revolution (till 2025)

Partnership: Ministry of Ports and Shipping Waterways: Its aim is port modernization, port connectivity, port-led industrialization and coastal community development. This project is under process. This is specially developed to increase Indian economic through trade of export and import.

Hypothesis 3: Clean Yamuna Project (2021-2023): The main component was upgradation of sewage treatment plants (STPs), connecting every household to the sewage system and in-situ treatment of untreated water. This project is under process.

Hypothesis 4: Water Quality Guideline: A water quality guideline is a recommended numerical (narrative or descriptive) concentration level of variables such as contaminants or nutrients, or dissolved oxygen in a specified aquatic system, that will result in negligible risk to the ecosystem and ensure that the designated use of the specified aquatic system is supported and maintained. A number of developed countries have national water quality guidelines or criteria or standards (goals) to protect aquatic life in fresh and marine water [12].

Hypothesis 5: Marine Protected Areas: Marine life will live in a much safer habitat, free from the effects of overfishing, ship noise pollution, and other human activities. Biodiversity has been found to increase by 21% within marine reserves like these, which leads to positive results.

Hypothesis 6: Artificial Reefs: These artificial structures were created to support marine life and the development of fresh coral. Artificial reefs have been shown to be effective in restoring damaged ecosystems, providing a habitat for imperiled creatures, and regenerating priceless biodiversity within reef ecosystems.

CONCLUSION

Things were different back in 2015 when the United Nations adopted 17 Sustainable Development Goals (SDGs) to improve people's lives and the natural world by 2030. As the world is trying to overcome this pandemic and seeks to restore global prosperity, the focus must be on addressing underlying factors through the Sustainable Development Goals. Sustainable development cannot be without humans: it happens with the coexistence of biodiversity conservation and development of the human society by meeting various equity needs. All of us must work together to protect the oceans, seas, inland waters, and marine resources and ensure sustainable livelihoods, diets, and development for the future. Due to the pollution of water, many aquatic life is threatened and endangered and some species may be about to extinct. To solve any kind of problem, we need experts to come up with solutions and the rest should work on their expertise. As a partner, we all come together and we will make our problem diminished. To date, most of the country's governments try to improve the aquatic ecosystem and some NGOs work on it.

Alongside the Environmental Protection Act, the protection of aquatic ecosystems is provided by several legal institutions, such as the Nature Conservation Act, the Water Management Act and their implementing decrees, domestic environmental policy documents, and international conventions by introducing restrictions, prohibitions, and licensing procedures. The Hungarian regulation follows and enforces the implementation of the goals set in the field of environmental protection and nature protection, the maintenance and increase of the level of protection, although there are still some obstacles and shortcomings that have to be solved. In this research, we make it easy to understand people about why partnership is important in our life as well as to improve aquatic life, and also explain about aquatic ecosystems play a vital role on the earth. Moreover, aquaculture should be improved to reduce our health issues and save aquatic life from extinct and maintain their species which leads improve government economics. In 2030 when the sustainable development goal comes to an end and the problem may diminish, we should continue the sustainable development goal as our routine for a better lifestyle for every living being on this earth.





Iftikhar Haideret al.,

REFERENCES

1. Kumar, S., Kumar, N. and Vivekadhish, S., 2016. Millennium development goals (MDGs) to sustainable development goals (SDGs): Addressing unfinished agenda and strengthening sustainable development and partnership. *Indian Journal of community medicine: official publication of Indian Association of Preventive & Social Medicine*, 41(1), p.1.
2. Agboola, J. I., and A. K. Braimoh. "Strategic partnership for sustainable management of aquatic resources." *Water resources management* 23 (2009): 2761-2775.
3. Häder, D-P., H. D. Kumar, R. C. Smith, and R. C. Worrest. "Effects on aquatic ecosystems." *Journal of Photochemistry and photobiology B: Biology* 46, no. 1-3 (1998): 53-68.
4. Qadri, R. and Faiq, M.A., 2020. Freshwater pollution: effects on aquatic life and human health. In *Fresh water pollution dynamics and remediation* (pp. 15-26). Springer, Singapore.
5. Collier, K.J., Probert, P.K. and Jeffries, M., 2016. Conservation of aquatic invertebrates: concerns, challenges and conundrums. *Aquatic Conservation: Marine and Freshwater Ecosystems*, 26(5), pp.817-837.
6. Abelson, A., 2006. Artificial reefs vs coral transplantation as restoration tools for mitigating coral reef deterioration: benefits, concerns, and proposed guidelines. *Bulletin of Marine Science*, 78(1), pp.151-159
7. Kris-Etherton, P.M., Harris, W.S. and Appel, L.J., 2002. Fish consumption, fish oil, omega-3 fatty acids, and cardiovascular disease. *circulation*, 106(21), pp.2747-2757.
8. Minahal, Q., Munir, S., Kumal, W., Fatima, S., Liaqat, R. and Shehdzadi, I., 2020. Global impact of COVID-19 on aquaculture and fisheries: a review. *Int. J. Fish. Aquat. Stud*, 8, pp.42-48
9. Satir, T. and Doğan-Sağlamtimur, N., 2018. The protection of marine aquatic life: Green Port (EcoPort) model inspired by the Green Port concept in selected ports from Turkey, Europe and the USA. *Periodicals of Engineering and Natural Sciences (PEN)*, 6(1), pp.120-129.
10. Kim, J.K., Yarish, C., Hwang, E.K., Park, M., Kim, Y., Kim, J.K., Yarish, C., Hwang, E.K., Park, M. and Kim, Y., 2017. Seaweed aquaculture: cultivation technologies, challenges and its ecosystem services. *Algae*, 32(1), pp.1-13.
11. Naylor, R.L., Goldburg, R.J., Primavera, J.H., Kautsky, N., Beveridge, M., Clay, J., Folke, C., Lubchenco, J., Mooney, H. and Troell, M., 2000. Effect of aquaculture on world fish supplies. *Nature*, 405(6790), pp.1017-1024.
12. Casillas-García, L.F., de Anda, J., Yebra-Montes, C., Shear, H., Díaz-Vázquez, D. and Gradilla-Hernández, M.S., 2021. Development of a specific water quality index for the protection of aquatic life of a highly polluted urban river. *Ecological Indicators*, 129, p.107899.
13. Ferraz, J.B.S. and de Felício, P.E., 2010. Production systems—An example from Brazil. *Meat Science*, 84(2), pp.238-243.
14. Alley, K.D., Barr, J. and Mehta, T., 2018. Infrastructure disarray in the Clean Ganga and clean India campaigns. *Wiley Interdisciplinary Reviews: Water*, 5(6), p.e1310.





Multimodal Brain Tumor Segmentation using 3D-U-Net

Novsheena Rasool^{1*} and Javaid Iqbal Bhat²

¹Islamic University of Science and Technology (IUST), Kashmir, India.

²Associate Prdofessor, Dept. of Computer Science, Islamic University of Science and Technology (IUST), Kashmir, India.

Received: 11 Apr 2023

Revised: 13 May 2023

Accepted: 31 May 2023

*Address for Correspondence

Novsheena Rasool

Islamic University of Science & Technology (IUST),
Kashmir, India.

E. Mail: novsheena.rasool@iust.ac.in



This is an Open Access Journal / article distributed under the terms of the **Creative Commons Attribution License** (CC BY-NC-ND 3.0) which permits unrestricted use, distribution, and reproduction in any medium, provided the original work is properly cited. All rights reserved.

ABSTRACT

Brain tumours are the tenth biggest cause of mortality in the world, killing thousands of people each year. Gliomas are the most frequent and severe kind of brain tumour, having a relatively short life expectancy. Thus, treatment planning is essential for improving the quality of life. Magnetic resonance imaging (MRI) is a frequent imaging modality for evaluating these tumours; however, the volume of data generated by MRI prevents manual segmentation in an acceptable amount of time. This demands the employment of automatic segmentation techniques; however, automatic segmentation is difficult due to the great spatial and structural heterogeneity among brain tumours. In this paper, we propose a 3D U-Net deep learning architecture for the semantic segmentation of gliomas. We train our model twice: the first time, we use the bias correction procedure and the minmax scaler normalization in the pre-processing stage, and the second time, we skip the bias field correction technique. Without using bias correction techniques, we found that we still obtained outstanding results. The precision, sensitivity, specificity, dice score, and accuracy metrics are used to evaluate the quality of the segmentation results. We trained and tested our model using the High-Grade Glioma (HGG) of the BRATs 2018 dataset. Our model achieved a maximum Dice score metric of 0.89 for the whole tumour, 0.95 for the core tumour, and 0.90 for the enhancing tumour, with a 98% accuracy rate.

Keywords: Brain Tumor; Segmentation; MRI; Deep Learning; Medical Image Analysis.

INTRODUCTION

Medical imaging is an umbrella term for a variety of non-invasive methods used to view inside the human body without causing any harm. It creates images of internal body organs by using various medical imaging procedures such as MRI, CT scan, ultrasound, and others [18] for diagnostic and treatment purposes and is essential for making proper decisions that will enhance health of millions of people. medical image segmentation plays a crucial role in

57473



**Novsheena Rasool and Javaid Iqbal Bhat**

processing medical images, Manual segmentation is not effective in removing brain tumours without harming neighboring healthy brain tissue. However Deep Learning in Healthcare [16] particularly, automatic segmentation can be used Automated segmentation can be used to quickly and accurately detect brain tumours[14], which is helpful for making treatment decisions and exact measurements.

Brain tumours are one of the global diseases[17] that must be detected early to save person's life. They are classified as benign and malignant. A benign brain tumour is a collection of cells that grows very slowly in the brain. Malignant brain tumours start in the brain, grow quickly, and aggressively penetrate the surrounding tissues. It can also spread to other parts of the brain and disrupt the central nervous system [14]. Magnetic resonance imaging (MRI) is a popular imaging technique that use radio waves, a computer, and a magnetic field to produce complete, detailed images of organs, soft tissues, bones, and other bodily components [20] and is regarded as one of the best imaging technique for identifying, size, location and shape of brain tumours [19]. It allows medical practitioners to analyze the interior anatomy of the brain and identify specific parts of the brain that are responsible for certain critical activities. T1-weighted MRI, T1-weighted contrast enhancement, T2-weighted, and fluid-attenuated inversion recovery as shown in Fig. 3 are combined to generate a multimodal image with details that can be used for tumour segmentation resulting in significant performance improvement .This is due to the challenge of detecting irregularly shaped tumours using only one MRI modality [15].

Gliomas are the most common type of tumour and are composed of three regions: the core, the enhancing region and the edema. It is difficult to accurately diagnose this form of tumour due to the fact that the cells in different sections of the tumour are not all of the same type[1]. Also, these tumours can form in any section of the brain, and borders between surrounding tissues are fuzzy due to smooth intensity changes, bias field artifacts, and partial volume effects, making tumour volume difficult to determine. Early diagnosis of brain tumours is essential for improving treatment options and survival. However, manual tumour segmentation is a complex, time-consuming, and laborious job due to the large volume of MRI images generated in medical practice [15]. Additionally, soft tissue boundaries of tumours, particularly in gliomas, can make them difficult to distinguish, making it challenging to acquire accurate boundaries tumour regions of the human brain. The remaining portion of this paper is organized as follows: Section 2 highlights previous research, section 3 explains proposed approach, Section 4 provides dataset description and experiment findings, Section 5 provides conclusion and future scope.

RELATED WORK

Dongjin Kwon *et al.* in 2014 [1] proposed a semi-automatic generative technique for multifocal segmentation and registration of glioma brain tumors. Using the brats2013 dataset, dice scores of 0.86, 0.79, and 0.59 were achieved for the complete tumour, core tumour, and enhancing tumour sub region. A semi-automatic Generative system (tumour cut method) for segmenting t1ce brain MRI images was proposed by Andac Hamamci *et al.* in 2012[2] in order to standardize the region of interest and seed selection, the authors used a seeded tumour segmentation approach on t1ce MRI pictures. The proposed technique revealed how the iterative CA architecture or framework, which connects CA (cellular automata)-based segmentation to graph-theoretic techniques, overcomes the shortest path problem. To determine the actual shortest path, authors modify the CA's state transition approach. Additionally, they used a sensitivity variable to address the difficulty of segmenting non-homogeneous tumours, and to impose spatial flatness, they established an inferred level set exterior on a tumour likelihood map derived from CA state data. To begin the procedure, information is obtained from the user simply by drawing a line on the maximum diameter of the tumour. Additionally, a technique based on CA is provided for distinguishing the tissue composition of enhancing and necrotic or core tumours, which is essential for a thorough investigation for response to radiation therapy.

Mostefa *et al.* in 2020[3] introduced a new Deep Convolutional Neural Network architecture to automatically segment glioblastomas (high and low grade) tumours. To improve the quality of the MRI images, smaller portions of lesser than 110 pixels were removed and the CNN model was used to extract more meaningful patterns. The



**Novsheena Rasool and Javaid Iqbal Bhat**

proposed approach was tested using the BRATS 2018 dataset, which produced results with median dice scores of 0.83 for enhancing tumour sub regions, 0.90 for the whole tumour, and 0.83 for the core tumour. The outcomes of the research showed that the segmentation results were accurate and reliable for classifying different types of tissue in brain MRI images. Mohammad havaei *et al.* in 2016 [4] proposed a novel CNN model to segment glioblastomas autonomously in MR images. The authors employed a two-phase training strategy to address the imbalance in tumour labelling. The proposed method extracts both local and global contextual characteristics simultaneously. The output of an initial Convolutional Neural Network acts as a secondary source of data or information for the subsequent CNN in the proposed cascaded system. Experimental results on brats 2018 dataset showed that the proposed technique achieved dice score outcomes of 0.85 for the whole tumour, 0.78 for the Core tumour, and 0.73 for the enhancing tumour sub region.

R. Pitchai *et al.* in 2021[5] presented an automated brain tumour segmentation system using a combination of the fuzzy K-means approach and an artificial neural network (ANN). The Wiener filter, followed by ANN, was used to reduce noise and classify brain MRI images into healthy and diseased classes. And finally, a fuzzy K-means algorithm was used to locate the tumour from abnormal images. On the BRATS dataset, performance was evaluated using accuracy, sensitivity, and specificity, authors obtained 99% specificity, 94% accuracy, and 98% sensitivity. Dvorak *et al.* in 2015 [6] developed a technique for 3D segmentation of multimodal brain tumour MRIs that relies on local structure prediction utilizing a convolutional neural network model. The provided technique outperformed conventional techniques in predicting voxel-wise labels. The authors tested their approaches using the BRATS2014 dataset, which is openly available, and obtained cutting-edge findings in less than 13 seconds of processing time per volume.

Andriy Myronenko *et al.* in 2015[7] proposed a semantic segmentation network of brain tumours in MRI images using an encoder-decoder architecture to identify tumour subregions from 3-d MRI images. The authors used a vibrational auto-encoder branch to standardize the common decoder and apply extra restrictions to its neural layers. Because of the short training dataset, they employed a vibrational auto-encoder branch to recreate the original input image and increased the number of filters or network width, resulting in consistently better outcomes. The results obtained for enhancing core tumour had an average dice score of 0.7664, the whole tumour had 0.8839 and 0.8154 for core tumor. The proposed technique won first place in the BraTS 2018 competition. GuotaiWang *et al.* in 2017[8] developed a cascaded anisotropic convolutional neural network for automated brain MRI segmentation into three hierarchical regions: whole tumour, core tumour, and enhancing core tumour. In the first phase, the authors segmented the whole tumour; in the second phase, the tumour core was segmented using the result of the first phase's bounding box. To reduce false positives, proposed networks incorporate layers of dilated and anisotropic convolution filters with multi-view fusion and residual connections and multiple-scale predictions to improve segmentation performance. The technique enhanced the enhancing tumour, whole tumour and tumour core, with average Dice values of 0.7859, 0.9050, and 0.8378 on the BraTS 2017 dataset.

METHODOLOGY

Bias Field Correction

Due to the irregularities in the magnetic fields of the MRI machine. The bias field, a low-frequency unwanted signal that affects pixel intensity values and reduces the effectiveness of processing models, has a negative impact on MRI images. It is critical to eliminate bias or variable frequency from MRI images during the pre-processing step in order to increase algorithm performance. We use the N41TK approach [11] to correct the bias in the BRATS2018 dataset. N41TK was created by merging the strong B-spline approximation method with a new optimization approach called nonparametric non uniform normalization (N3).





Novsheena Rasool and Javid Iqbal Bhat

Normalization

Normalization is the process of converting data such that all characteristics are on an equivalent scale, typically between 0 to 1. It is helpful for training the model since it equalizes all features, which helps to stabilize the gradient descent.

$$X_{scaled} = \frac{X - X_{min}}{X_{max} - X_{min}} \quad (1)$$

3D-UNet Architecture for Segmentation

In this paper, we aim to address the issue of brain tumour segmentation by putting forth a novel network architecture based on U-Net [9]. The UNet deep learning architecture is the most popular architecture for segmenting biomedical images. It is composed of a contracting or down sampling path and expanding or up-sampling path. In the down sampling path, we create a convolution block that captures an increasing number of high-level, abstract features related to the context of the MRI images. Next, we use the Max Pooling operation with a 2 stride to reduce the resolution by two. The convolution block consists of two consecutive 3x3x3 filters, each accompanied by "Selu" nonlinearity and a Lecun Normal kernel initializer. At a certain level, the total number of kernels are constant, but double what it was at the previous level. The up-sampling path employs deconvolution layers to simultaneously learn parameters for transforming a low-resolution image into a high-resolution one, while also retaining enough feature mappings to provide high resolution segmentations with sufficient context information. Furthermore, feature maps from the encoder path are concatenated with feature maps of the decoder path at the same level to keep track of crucial information encoded by the encoder, assisting in precise localization and accurate bounds. In our model, a multi-channel feature map is represented by each blue box. On top of the box, the channel count is shown. At the lower left corner of the box, the x-y size is displayed. Copied feature maps are represented by white boxes and the various operations are shown by the arrows (see Fig. 4).

Training

We first divided the High-Grade Glioma (HGG) MRIs in the ratio of 80:20 (or 80% for training and 20% for testing). Then we combine each MRI's three input modalities, such as T2, T1ce, and FLAIR, and we crop the centre 128x128x128 blocks of combined images to reduce unnecessary background areas surrounding the essential volume. We load and process the multimodal MRIs using a customised data generator while maintaining a small batch size to lower the generalisation error and speed up model learning (see Fig 6). The network receives blocks of size 128x128x128x3 as inputs and generates Soft Max of size 128x128x128x4. We trained the network by utilizing the fit function and reduced the cost function in terms of its parameters using the adaptive moment estimator (Adam). Adam typically uses the first and second gradient moments to update and modify the moving average of the existing gradients. The learning rate, which regulates how frequently we want to update our weights, is one of our Adam optimizer's parameters. If we choose a high learning rate, our model may not identify the optimum solution, and if we choose a low learning rate, the best results will most likely need too many iterations. As a consequence, we determined that the learning rate should be set at 0.0001. Furthermore, we set the number of epochs to 250 (see Fig 2) and use the dropout approach to reduce over fitting in our model. As a result, we use the dice coefficient [10,12], which balances the four classes better than the quadratic or cost function cross-entropy function [15], and evaluate the segmentation for each tumoural by using the DSC (Dice Similarity Coefficient).

$$DSC = \frac{2TP}{(TP + FP) + (TP + FN)} \quad (2)$$

where TP, FN, and FP represent true positive, false negative, and false positive measures, respectively. To ascertain the model's actual performance.

DATASET DESCRIPTION

The main focus of the BraTS 2018 Dataset is the segmentation of intrinsically heterogeneous brain tumours, specifically gliomas, using pre-operative 3D-MRI data from several institutions. BraTS 2018 dataset consists of four



**Novsheena Rasool and Javaid Iqbal Bhat**

distinct types of magnetic resonance imaging (MR) sequences: T1-weighted images (T1), T2 weighted images (T2), post-contrast T1-weighted images (T1ce), and fluid attenuated inversion recovery (FLAIR). Each of them has 240 x 240 x 155 volumes. Labels for tumour segmentation include necrotic (label 1), edema (label 2), background (label 0), and enhancing tumour (label 4). The dataset includes 210 High Grade Glioma (HGG) patient cases and 75 Low Grade Glioma (LGG) patient cases[13]. we exclusively used HGG images. We divided the HGG dataset into two sections, employing 168 images for training and 42 for testing. Performance on the testing set is measured mostly by segmentation accuracy. The accuracy of the segmentation is assessed using the dice score metrics. The workflow diagram of proposed model is shown in Fig.5.

CONCLUSION AND FUTURE SCOPE

Medical image segmentation divides healthcare images into only the necessary regions, and thus allows more accurate anatomical examination. The most often used imaging technology for segmenting brain tumours is MRI, which produces more detailed pictures [17], and the majority of researchers are employing this method when detecting and segmenting brain tumours. In this paper, we first preprocess HGG of BRATS 2018 datasets using N41TK bias field correction [11] and Min Max scaler normalization techniques, and then we create a 3d-unet model for distinguishing brain tumour pixels from healthy pixels or for segmentation purpose. Even without post-processing, our method reliably predicts tumour cells. Furthermore, we observe that our model produces better results without the bias correction procedure. We evaluated our model based on dice score, accuracy, sensitivity, specificity, and precision, and we obtained extremely good results by training and testing on the NVIDIA Tesla V100 32 GB GPU. Using the Bias Field Correction technique in preprocessing, our model produced dice scores of 0.86,0.83,0.78 for the whole, core, and enhancing tumours respectively, additionally, our model achieved 99% specificity, 98% sensitivity, 98% accuracy, and 98% precision. Contrarily, when we exclude the bias correction procedure from our model, we get results that are more accurate, such as dice scores of 0.89 for the whole tumour, 0.95 for the core tumour, and 0.90 for the enhancing tumour. Additionally, without bias correction, the proposed model generated accuracy, sensitivity, specificity, and precision values of 98%,98%, 99%, and 98% respectively. In the future, we'll attempt new things to see if we can further enhance the dice score, including changing the model architecture or using post-processing techniques Table I & II.

REFERENCES

1. Kwon, D., Shinohara, R. T., Akbari, H., & Davatzikos, C. (2014, September). Combining generative models for multifocal glioma segmentation and registration. In International conference on medical image computing and computer-assisted intervention (pp. 763-770). Springer, Cham.
2. Hamamci, A., Kucuk, N., Karaman, K., Engin, K., & Unal, G. (2011). Tumor-cut: segmentation of brain tumors on contrast enhanced MR images for radiosurgery applications. IEEE transactions on medical imaging, 31(3), 790-804.
3. Akil, M., Saouli, R., & Kachouri, R. (2020). Fully automatic brain tumor segmentation with deep learning-based selective attention using overlapping patches and multi-class weighted cross-entropy. Medical image analysis, 63, 101692.
4. Havaei, M., Davy, A., Warde-Farley, D., Biard, A., Courville, A., Bengio, Y., ... & Larochelle, H. (2017). Brain tumor segmentation with deep neural networks. Medical image analysis, 35, 18-31.
5. R. Nicole, " Title of paper with only first word capitalized," J. Name Stand. Abbrev., in press.
6. Dvořák, P., & Menze, B. (2015, October). Local structure prediction with convolutional neural networks for multimodal brain tumor segmentation. In International MICCAI workshop on medical computer vision (pp. 59-71). Springer, Cham.
7. Myronenko, A. (2018, September). 3D MRI brain tumor segmentation using autoencoder regularization. In International MICCAI Brainlesion Workshop (pp. 311-320). Springer, Cham.





Novsheena Rasool and Javaid Iqbal Bhat

8. Wang, G., Li, W., Ourselin, S., & Vercauteren, T. (2017, September). Automatic brain tumor segmentation using cascaded anisotropic convolutional neural networks. In International MICCAI brainlesion workshop (pp. 178-190). Springer, Cham.
9. Ronneberger, O., Fischer, P., & Brox, T. (2015). U-net: Convolutional networks for biomedical image segmentation. In Medical Image Computing and Computer-Assisted Intervention–MICCAI 2015: 18th International Conference, Munich, Germany, October 5-9, 2015, Proceedings, Part III 18 (pp. 234-241). Springer International Publishing.
10. Isensee, F., Kickingereder, P., Wick, W., Bendszus, M., & Maier-Hein, K. H. (2018). Brain tumor segmentation and radiomics survival prediction: Contribution to the brats 2017 challenge. In Brainlesion: Glioma, Multiple Sclerosis, Stroke and Traumatic Brain Injuries: Third International Workshop, BrainLes 2017, Held in Conjunction with MICCAI 2017, Quebec City, QC, Canada, September 14, 2017, Revised Selected Papers 3 (pp. 287-297). Springer International Publishing.
11. 'https://simpleitk.readthedocs.io/en/v1.2.3/Examples/N4BiasFieldCorrection/Documentation.html'
12. Kermi, A., Mahmoudi, I., & Khadir, M. T. (2019). Deep convolutional neural networks using U-Net for automatic brain tumor segmentation in multimodal MRI volumes. In Brainlesion: Glioma, Multiple Sclerosis, Stroke and Traumatic Brain Injuries: 4th International Workshop, BrainLes 2018, Held in Conjunction with MICCAI 2018, Granada, Spain, September 16, 2018, Revised Selected Papers, Part II 4 (pp. 37-48). Springer International Publishing.
13. Saeed, M. U., Ali, G., Bin, W., Almotiri, S. H., AlGhamdi, M. A., Nagra, A. A., ... & Amin, R. U. (2021). RMU-net: a novel residual mobile U-net model for brain tumor segmentation from MR images. *Electronics*, 10(16),1962.
14. Hossain, T., Shishir, F. S., Ashraf, M., Al Nasim, M. A., & Shah, F. M. (2019, May). Brain tumor detection using convolutional neural network. In *2019 1st international conference on advances in science, engineering and robotics technology (ICASERT)* (pp. 1-6). IEEE.
15. Cherguif, H., Riffi, J., Mahraz, M. A., Yahyaouy, A., & Tairi, H. (2019, December). Brain tumor segmentation based on deep learning. In *2019 International Conference on Intelligent Systems and Advanced Computing Sciences (ISACS)* (pp. 1-8). IEEE.
16. Malik, M., Singh, Y., Garg, P., & Gupta, S. (2020). Deep learning in healthcare system. *International Journal of Grid and Distributed Computing*, 13(2), 469-468.
17. 'https://www.cancer.net/cancer-types/brain-tumor/diagnosis#:~:text=MRIs%20create%20more%20detailed%20pictures,are%20different%20types%20of%20MRI.'
18. Iniewski, K. (Ed.). (2009). *Medical imaging: principles, detectors, and electronics*. John Wiley & Sons.
19. Rasool, N., & Bhat, J. I. (2023, March). Glioma Brain Tumor Segmentation using Deep Learning: A Review. In *2023 10th International Conference on Computing for Sustainable Global Development (INDIACom)* (pp. 484-489). IEEE.
20. Sajid, S., Hussain, S., & Sarwar, A. (2019). Brain tumor detection and segmentation in MR images using deep learning. *Arabian Journal for Science and Engineering*, 44(11), 9249-9261.
21. Zhao, X., Wu, Y., Song, G., Li, Z., Zhang, Y., & Fan, Y. (2018). 3D brain tumor segmentation through integrating multiple 2D FCNNs. In Brainlesion: Glioma, Multiple Sclerosis, Stroke and Traumatic Brain Injuries: Third International Workshop, BrainLes 2017, Held in Conjunction with MICCAI 2017, Quebec City, QC, Canada, September 14, 2017, Revised Selected Papers 3 (pp. 191-203). Springer International Publishing.
22. Zhao, B., Ren, Y., Yu, Z., Yu, J., Peng, T., & Zhang, X. Y. (2021). AUCseg: An Automatically Unsupervised Clustering Toolbox for 3D-Segmentation of High-Grade Gliomas in Multi-Parametric MR Images. *Frontiers in Oncology*, 11, 679952.

Table I. Comparison on the HGG Brats 2018 dataset

Ref.	Grade	Method	Data set	Dice Similarity Coefficient		
				WT	CT	ET
[9]	HGG	Shallow U-Net	BRATS 2018	0.467	0.703	0.584
[10]	HGG	U-Net(axial)+3D CRF	BRATS 2018	0.811	0.750	0.754
[18]	HGG	3D-unsupervised method	BRATS 2018	0.8209	0.7089	0.7254





Novsheena Rasool and Javaid Iqbal Bhat

[10]	HGG	FCNNs (coronal, sagittal, axial)	BRATS 2018	0.696	0.800	0.730
[10]	HGG	Fusing (FCNNs+3D CRF) +post-process	BRATS 2018	0.873	0.868	0.828
Proposed Method	HGG	3D-UNet	BRATS 2018	0.876	0.962	0.918

Table II. Results of Our Experiments On Brats 2018 Model Using Proposed Method

Results	Dice Loss	Dice-Coefficient	Accuracy	Sensitivity	Specificity	Precision	Dice Similarity Coefficient		
							WT	CT	ET
Training (without bias field correction)	0.0348	0.9652	0.9943	0.9941	0.9982	0.9945	0.960	0.964	0.932
Testing (without bias field correction)	0.0731	0.9269	0.9889	0.9887	0.9964	0.9892	0.899	0.955	0.903
Training (with bias field correction)	0.0612	0.9362	0.9914	0.9913	0.9972	0.9917	0.893	0.949	0.906
Testing (with bias field correction)	0.1908	0.8103	0.9802	0.9807	0.9937	0.9812	0.869	0.837	0.786

Table III. Proposed Model Parameter

Total Number of Parameters	Number of Trainable Parameters	Number of Non-Trainable Parameters
90,448,356	90,448,356	0

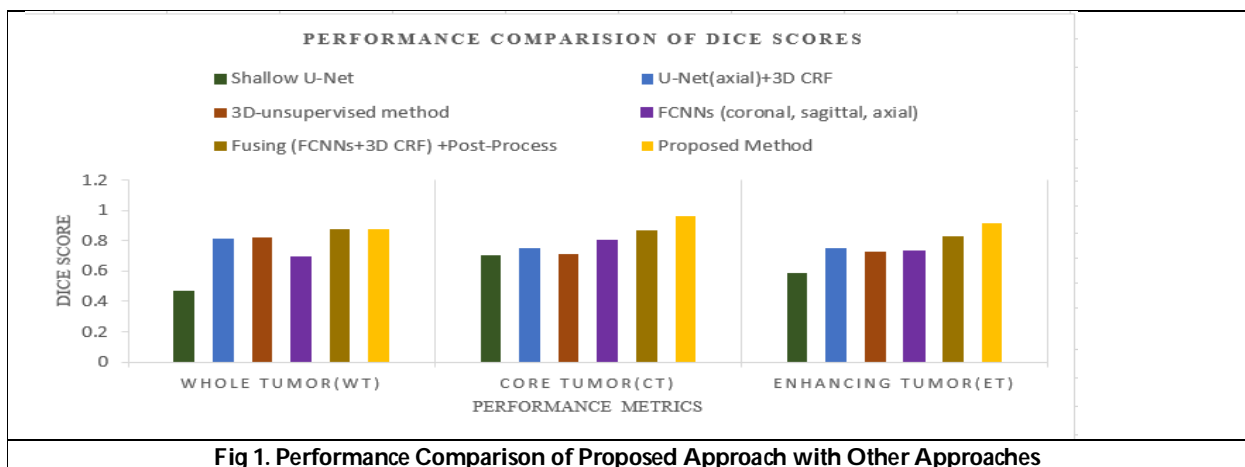
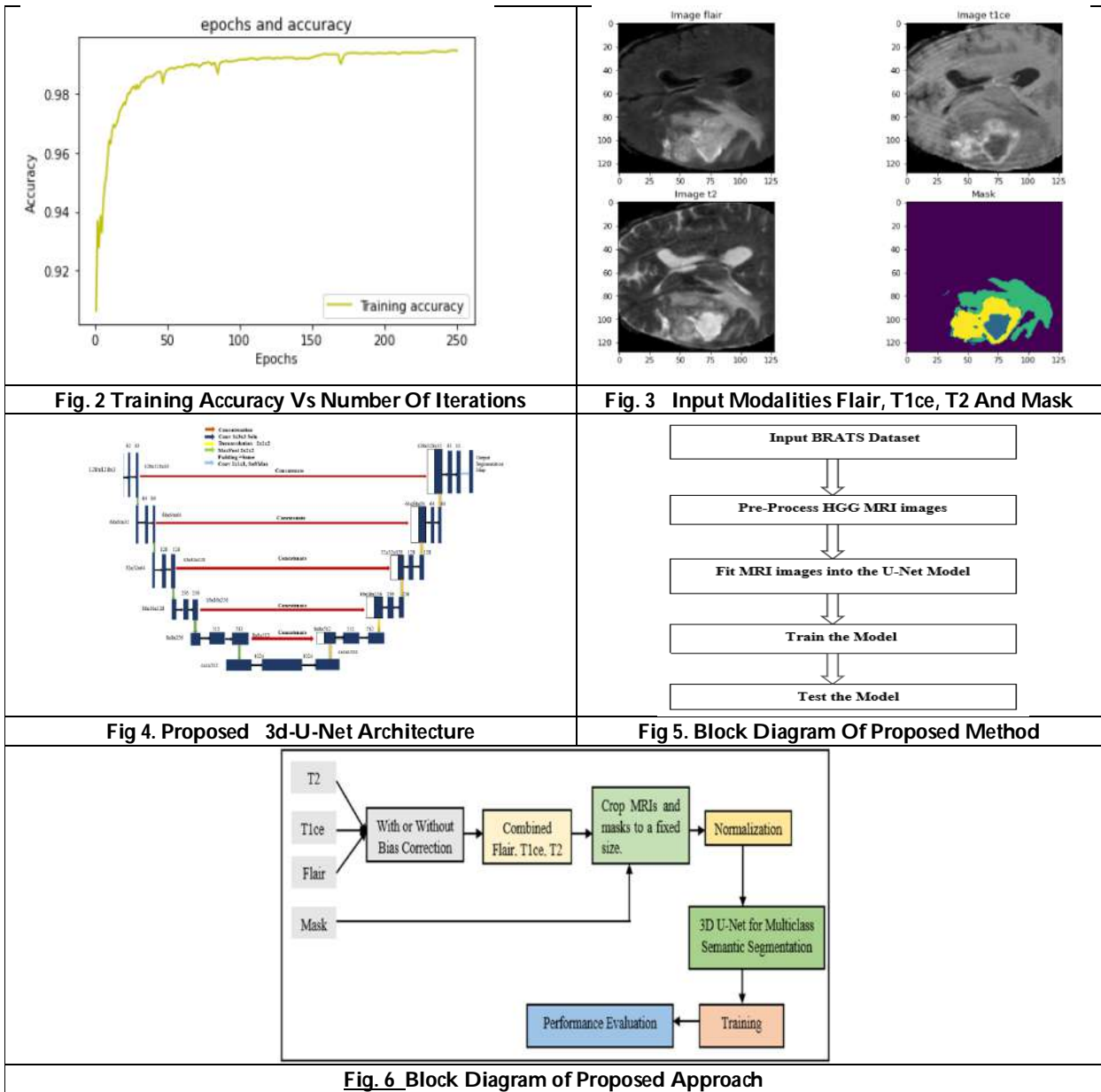


Fig 1. Performance Comparison of Proposed Approach with Other Approaches





Novsheena Rasool and Javaid Iqbal Bhat





A Practical Approach to Solving Differential Equation with MATLAB Simulink for Solar PV Panel

Chosching Lazes, Isaac TC Vanlalhruaizela and Khursheed Alam*

The A.H. Siddiqi Centre for Advanced Research in Applied Mathematics & Physics (CARAMP), Sharda University, Greater Noida, Uttar Pradesh, India.

Received: 06 Apr 2023

Revised: 13 May 2023

Accepted: 31 May 2023

*Address for Correspondence

Khursheed Alam

The A.H. Siddiqi Centre for Advanced Research in Applied Mathematics & Physics (CARAMP)
Sharda University,
Greater Noida, India
E. Mail: khursheed.alam@sharda.ac.in



This is an Open Access Journal / article distributed under the terms of the **Creative Commons Attribution License** (CC BY-NC-ND 3.0) which permits unrestricted use, distribution, and reproduction in any medium, provided the original work is properly cited. All rights reserved.

ABSTRACT

Differential equations have numerous applications in solving problem in the real world. Differential equation is applied to predict future time and at an unidentified location. In this paper, differential equations are used in circuit analysis to describe the behaviour of electric systems. MATLAB is a widely used software tool in studies of engineering and provides a practical approach to solving differential equation in circuit analysis and then demonstrate how to use MATLAB to solve these equations.

Keywords: Differential equation, circuit analysis, MATLAB Simulink, PV panel and MPPT

INTRODUCTION

The differential equations have coefficients. Differential equations that involve only derivatives with respect to one variable are known as ordinary differential equations, whereas partial differential equations involve partial derivatives with respect to many independent variables. Electricity is crucial for our daily lives, powering both lighting at night and appliances during the day. It flows through circuits as either direct current (DC) or alternating current (AC). A basic circuit consists of wire, a battery, and an appliance. In our project, we focused on simulating an RLC circuit using MATLAB SIMULINK, analysing the output graphs for different resistances. Solar energy, generated by the sun, can produce heat, trigger reactions, and generate electricity. It surpasses our energy needs and should be harnessed through solar PV panels as a renewable resource.

This project emphasizes photovoltaic panel modelling method, and a simulation is presented. The suggested model resembles a single-diode model that includes a series resistance. The parameters used in the proposed model are derived solely from datasheet measurements under Standard Test Conditions and do not require iterative routines to determine the I-V characteristics. This makes the model suitable for use in MATLAB/Simulink when creating MPPT

57481





Chosching Lazeset *al.*,

(Maximum Power Point Tracking) algorithms. This project also provides Simulink modelling of the photovoltaic model performance, and the graphs obtained with various irradiances with current, voltage, and power sources are compared, and the results are discussed.

The Purpose and Objectives

The practical approach to first-order differential equations in electric circuits involves understanding their applications, utilizing MATLAB and Simulink for circuit analysis, building and simulating circuits, and exploring specific applications such as MPPT for PV panels. This approach helps gain a deeper understanding of electric circuits and their behaviour.

Brief Theoretical Part

First-order differential equations are essential for describing electric circuits, representing the relationship between voltage and current for circuit components like resistors, capacitors, and inductors. Solving these equations reveals the circuit's time response, allowing us to understand its behaviour under different conditions. Similarly, a first-order differential equation can model the current flow in a solar PV panel, considering factors such as generated current, panel resistance, and connected load. By solving this equation, we can determine the current as a function of time, aiding in the analysis and optimization of solar PV panel performance.

Electric Circuit Theory

Electrical circuit theory studies interconnected circuits with nodes and edges. Charge accumulation (q) at nodes and current flow (I) between nodes are related by the differential equation $I = dq/dt$.

$$I = \frac{dq}{dt} \quad (1)$$

Electric currents are created by the differences in the energy levels expressed in the voltage measurements. Voltage (V) is determined by the change in electromagnetic energy (dE/dt) divided by current (I), which represents the power (P) per unit time flowing through the circuit.

$$V = \frac{dE/dt}{I} = \frac{P}{I} \quad (2)$$

This is equivalent to the amount of power (P) per unit time that flows through the edge.

A List of Circuit Elements

Resistor: A resistor is an electronic device that hinders the flow of current and reduces the potential by using a poorly conductive material connected by conducting wires at both ends.

The resistance R ,

$$R = \frac{V}{I} \quad (3)$$

where V is the voltage drop across the resistance and I is the current flowing through the resistor

Power dissipation is formulated as follows:

$$P = VI \quad (4)$$

Inductor: An inductor, which is a passive electronic component, stores energy in the form of a magnetic field, and generally includes a conductor coil that provides resistance to the applied voltage.

The stored energy is formulated as follows:

$$E = LI^2 \quad (5)$$

where L denotes the inductance of a circuit measured by Henries, and I represent the current passing through it.

Capacitor: A capacitor is a passive electronic component that stores the electrical charge and exhibits reactance to the current flow. The quantity of stored charge is defined by

$$Q = CV \quad (6)$$

where C is the capacitive reactance and V is the applied voltage. In addition, the current flowing through a capacitor is expressed as

$$I = C dV/dt \quad (7)$$





Chosching Lazeset al.,

Kirchhoff's Laws To analyze complex circuits like bridges, Ohm's Law is insufficient. Kirchhoff's Circuit Laws, including Kirchhoff's Current Law (KCL) and Kirchhoff's Voltage Law (KVL), are essential. KCL deals with current flow around a closed circuit, while KVL focuses on voltage sources within a closed circuit.

Kirchhoff's Current Law or KCL, Kirchhoff's Current Law or KCL is a principle that states that the sum of all currents flowing into and out of a node must be zero. This is known as the Conservation of Charge, which ensures that the total charge entering a node equals the charge leaving that node.

Kirchhoff's Voltage Law or KVL states that "in any closed-loop network, the total voltage around the loop is equal to the sum of all the voltage drops within the same loop, which is also equal to zero (**Conservation of Energy**).

Applications of first order differential equations in Electric Circuit

In an RL series circuit with a constant-voltage source and a closed switch, the current does not immediately reach its maximum value due to the self-induced emf in the inductor. After a certain time, the current becomes constant as the voltage source neutralizes the self-induced emf. Kirchhoff's Voltage Law (KVL) can be used to determine voltage drops and express the current flow. Kirchhoff's voltage law gives us

$$\mathbf{V(t) = V_R + V_L = 0} \tag{8}$$

The voltage drop across the resistor R is IR (Ohm's law):

$$\mathbf{V_R = IR} \tag{9}$$

The voltage drops across the inductor, L is

$$\mathbf{L = \frac{di}{dt}} \tag{10}$$

The final expression for the individual voltage drops around the RL series circuit can then be expressed as

$$\mathbf{V = RI + L \frac{di}{dt}} \tag{11}$$

Mathematics Involved

We start with:

$$Ri + L \frac{di}{dt} = V$$

Subtracting Ri from sides:

$$L \frac{di}{dt} = V - Ri$$

Divide both sides by L:

$$\frac{di}{dt} = \frac{V - Ri}{L}$$

Multiply both sides by dt and divide both by (V-Ri):

$$\frac{di}{V - Ri} = \frac{dt}{L}$$

$$\int \frac{di}{V - Ri} = \int \frac{dt}{L}$$

$$-\frac{\ln(V - Ri)}{R} = \frac{1}{L}t + K$$

Now, since i = 0 when t=0, we have:

$$K = -\frac{\ln V}{R}$$

Substituting K back into our expression:

$$-\frac{\ln(V - Ri)}{R} = \frac{1}{L}t - \frac{\ln V}{R}$$

Rearranging:

$$\frac{\ln V}{R} - \frac{\ln(V - Ri)}{R} = \frac{1}{L}t$$

Multiplying throughout by -R:

$$-\ln V + \ln(V - Ri) = -\frac{R}{L}t$$

Collecting the logarithm parts together:

$$\ln\left(\frac{V - Ri}{V}\right) = -\frac{R}{L}t$$

Taking "e" to both sides" $\frac{V - Ri}{V} = e^{-\frac{R}{L}t}$

$$1 - \frac{Ri}{V} = e^{-\frac{R}{L}t} \tag{12}$$





Chosching Lazaset al.,

Subtracting 1 from both sides :

$$-\frac{Ri}{V} = 1 + e^{-\frac{R}{L}t}$$

Multiplying both sides by $-\frac{V}{R}$

$$I = \frac{V}{R}(1 - e^{-\frac{R}{L}t}) \quad (13)$$

Example: The RL circuit has an emf of 5 V, a resistance of 50 Ω , an inductance of 1 H, and no initial current. Find the current in the circuit at time t . Distinguishing between the transient and steady-state currents.

Method 1 - Solving the differential Equation

The formula is: $Ri + L\frac{di}{dt} = V$

After substituting: $50i + \frac{di}{dt} = 5$

We rearrange to obtain: $\frac{di}{dt} + 50i = 5$

This is a first-order linear differential equation.

We must apply the formula to solve a first-order differential equation for these variables:

$$i e^{Pdt} = \int (Qe^{Pdt}) dt$$

We have $P=50$ and $Q=5$.

We found the following integrating factor:

$$I.F. = e^{50dt} = e^{50t}$$

Therefore, after substituting into the formula, we have

$$(e^{50t}) = \int (5)e^{50t} dt = \frac{5}{50}e^{50t} + K = \frac{1}{10}e^{50t} + K$$

When $t=0$, $i=0$, $K = -\frac{1}{10} = -0.1$.

This gives us: $i = 0.1(1 - e^{-50t})$

The transient current is $i=0.1(1 - e^{-50t})$ A.

The steady-state current was $i=0.1$ A.

Method 2: Using the Formula

The general formula is as follows:

$$i = \frac{V}{R}(1 - e^{-(R/L)t})$$

So in this case:

$$i = \frac{5}{50}(1 - e^{-50t}) = 0.1(1 - e^{-50t})$$

In this example, the time constant is

$$\tau = \frac{L}{R} = \frac{1}{50} = 0.02$$

Therefore, we see that the current reached a steady state at $t = 0.02 \times 5 = 0.1$ s.

SIMULINK and MATLAB

Simulation: This imitates the operation of a real-world process or system over time. The act of simulating something first requires that a model be developed that represents the key characteristics or behaviours of the selected physical or abstract system or process.

Using Maximum Power Point Tracking Coding

MPPT is a technique used by charge controllers to maximize power output from PV modules. It adjusts operating conditions based on factors like solar radiation and temperature to achieve peak power. When measured at a cell temperature of 25°C, the maximum power voltage of a typical PV module is approximately 17 V; however, on extremely hot or extremely cold days, the value can fluctuate between 15 and 18 V.

I-V and P-V Curves of solar cells The output voltage drops sharply as temperature rises, while the current at the output terminal increases slightly. This results in an overall decrease in power. Conversely, increasing irradiance





Chosching Lazeset *al.*,

leads to a significant rise in output current and ultimately an increase in output power. Figure 6.3 shows that solar irradiation has a significant impact on the output current of the PV array. To simulate the PV module at various irradiance levels, the proposed model is employed, and the resulting I(V) characteristics are presented by varying the irradiance from 500 W/m² to 1000 W/m². Using MATLAB Simulink To get PV and VI characteristics for solar cell for different radiation in MATLAB

CONCLUSION

First-order differential equations are a powerful tool to analyze the time-dependent behavior of electrical systems in circuits. They help understand capacitor charging, inductor current flow, and resistor behavior. By applying these equations, engineers can design and optimize circuits for improved performance, efficiency, and stability. The application of first-order differential equations has greatly contributed to the advancement of modern electronics. Simulink has built-in scopes that make it possible to see the results of simulations, and it also lets you export data for more in-depth study. These statistics and visualisations can be used to compare various solar cell arrangements, assess the effects of various radiation intensities, and make system design and deployment decisions. In conclusion, the application of first order differential equations in the study of solar PV panels has been a vital tool in advancing the field of renewable energy and promoting the widespread adoption of solar power.

Future scope and further enhancement of the project

- Further improvement of the proposed model: To improve the performance of solar PV panels, incorporate complex elements like temperature and shading impacts.
- Implementation of advanced algorithms: Increase solar PV panel performance and efficiency by using modern MPPT (maximum power point tracking) algorithms.
- Integration with energy storage systems: For increased energy efficiency and a dependable power source, combine solar PV panels with energy storage devices (such batteries).
- Experimentation and validation of the model: Validate the suggested model through experiments to determine its accuracy and dependability in forecasting the behaviour of solar PV panels under various circumstances.
- Application in real-world scenarios: Apply the model to create and optimise solar PV systems for a variety of uses to promote renewable energy and reduce dependency on traditional energy sources.

REFERENCES

1. SHAQIRI, Mirlinda, Lazim KAMBERI, Merita BAJRAMI, and Besim BERISHA. "IMPLEMENTATIONS OF FIRST-ORDER DIFFERENTIAL EQUATIONS." *Journal of Natural Sciences and Mathematics of UT7*, no. 13-14 (2022): 143-145. Publishing, 2019.
2. Rawat, Tarun Kumar, and Harish Parthasarathy. "Modeling of an RC circuit using a stochastic differential equation." *Science & Technology Asia* (2008): 40-47.
3. Bebikhov, Yu V., A. S. Semenov, I. A. Yakushev, N. N. Kugusheva, S. N. Pavlova, and M. A. Glazun. "The application of mathematical simulation for solution of linear algebraic and ordinary differential equations in electrical engineering." In *IOP conference series: materials science and engineering*, vol. 643, no. 1, p. 012067. IOP
4. Bellia, Habbati, Ramdani Youcef, and Moulay Fatima. "A detailed modeling of photovoltaic module using MATLAB." *NRIAG journal of astronomy and geophysics* 3, no. 1 (2014): 53-61
5. Salmi, Tarak, Mounir Bouzguenda, Adel Gastli, and Ahmed Masmoudi. "Matlab/simulink based modeling of photovoltaic cell." *International journal of renewable energy research* 2, no. 2 (2012): 213-218.
6. Sumathi S. (2015). Solar PV and Wind energy conversion systems, Green Energy and Technology (Springer International Publishing, Switzerland)
7. Walker, Geoff Evaluating MPPT converter topologies using a MATLAB PV model *Aust. J. Electr. Electron. Eng.*, 21 (1) 2001





Chosching Lazeset *al.*

8. Bryan F., 1999, Simulation of grid-tied building integrated photovoltaic systems. MS thesis. Solar Energy Laboratory, University of Wisconsin, Madison.
9. A. Chouder, L. Rahmani, N. Sadaoui, S. Silvestre Modeling and simulation of a grid connected PV system based on the evaluation of main PV module parameters Simul. Model. Pract. Theory, 20 (2012)
10. T. Esmar and P. L. Chapman, "Comparison of photovoltaic array maximum power point tracking techniques," IEEE Trans. Energy Convers., vol. 22, no. 2, pp. 439–449, Jun. 2007
11. W. De Soto, S.A. Klein, and W. A. Beckman, "Improvement and validation of a model for photovoltaic array performance," Solar Energy, vol. 80, no. 1, pp. 78–88, Jan. 2006.
12. T. Esmar and P. L. Chapman, "Comparison of photovoltaic array maximum power point tracking techniques," IEEE Trans. Energy Convers., vol. 22, no. 2, pp. 439–449, Jun.
13. C. Qi, and Z. Ming, "Photovoltaic Module Simulink Model for a Stand-alone PV System," 2012 International Conference on Applied Physics and Industrial Engineering, Physics Procedia 24 (2012) 94 – 100.

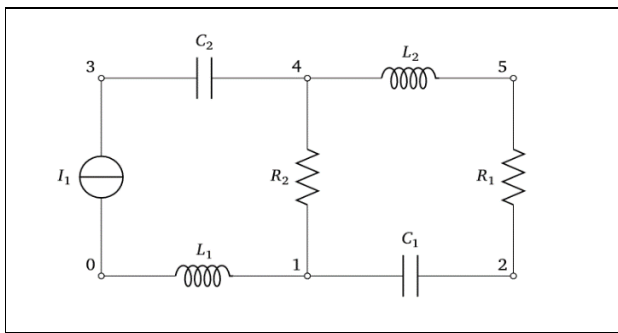


Fig.1 RLC Circuit diagram

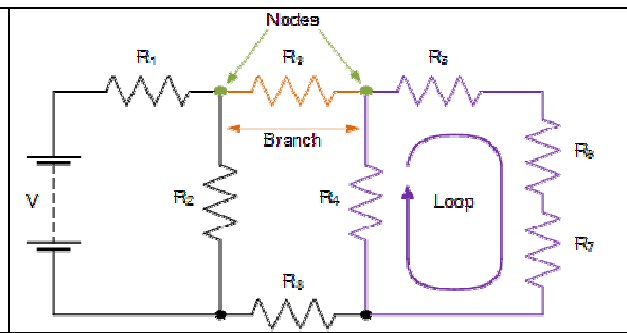


Fig.2: circuit diagram of Kirchoff's bridge

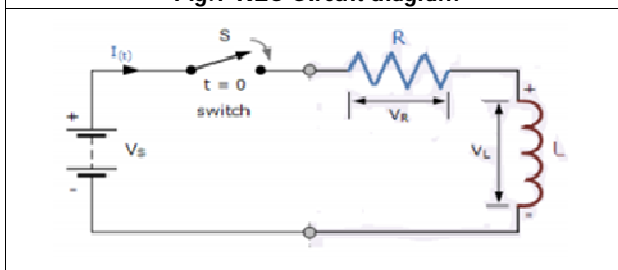


Fig.3: RL circuit

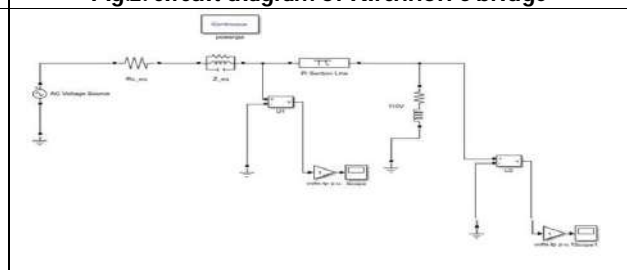


Fig.4: RL Circuit using MATLAB Simulink

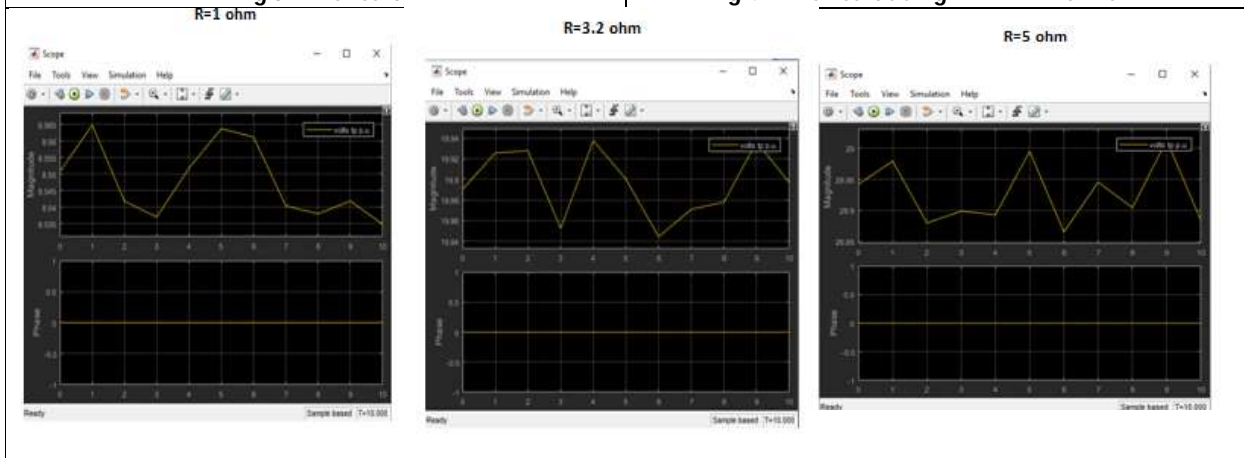


Fig.5: Output of simulation for different resistance values and at constant phase





Chosching Lazeset al.,

```

Command Window
>> %Declaring variables
T=302;
Tr=298;
Trl=40;
ki=0.00023;
Iscr=3.75;
Irr= 0.000021;
A=2.15;
Eg0=1.66;
alpha=0.473;
beta=636;
s= [100 80 60 40 20];
k=1.38065*10^(-23);
q=1.6022*10^(-19);
Eg=Eg0 - (alpha*T*T) / (T+beta)*q;
Np=4;
Ns=60;
VO= [0:1:300];
for i=1:5
    Iph=(Iscr+ki*(T-Tr))*((s(i))/100); %phase current
    Irs=Irr* ((T/Tr)^3)*exp(q*Eg/(k*A)*((1/Tr)-(1/T))); %current through shunt resistor
    IO=Np*Iph-Np*Irs*(exp(q/(k*T*A)*VO./Ns)-1); %output current
    PO=VO.*IO; %output power
    figure(1)%voltage vs current plot
    plot(VO,IO);
    axis([0 50 0 20]);
    xlabel('voltage in volts');
    ylabel('current in amps');
    hold on;
    figure(2)%voltage vs power plot
    plot(VO,PO);
    axis([0 50 0 400]);
    xlabel('voltage in volts');
    ylabel('power in watts');
    hold on;
    figure(3) %current vs power plot
    plot(IO,PO);
    axis([0 20 0 400]);
    xlabel('current in amps');
    ylabel('power in watts');
    hold on;
end
    
```

Fig.6: MATLAB coding for MPPT

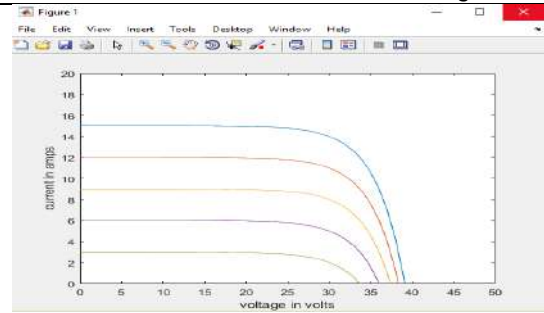
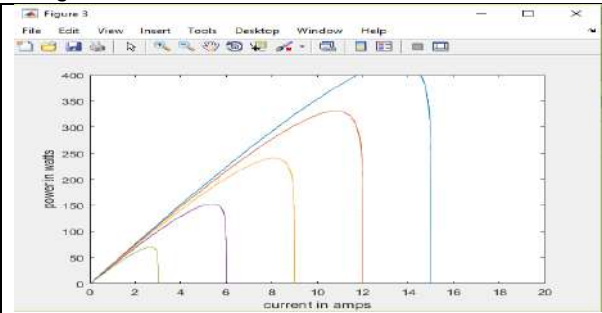


Fig.7.1: Graph showing voltage vs current plot



7.2: Graph showing current vs power plot





Chosching Lazeset al.,

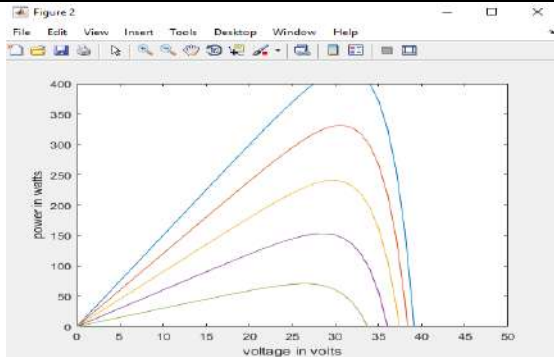


Fig.7.3: Graph showing voltage vs power plot

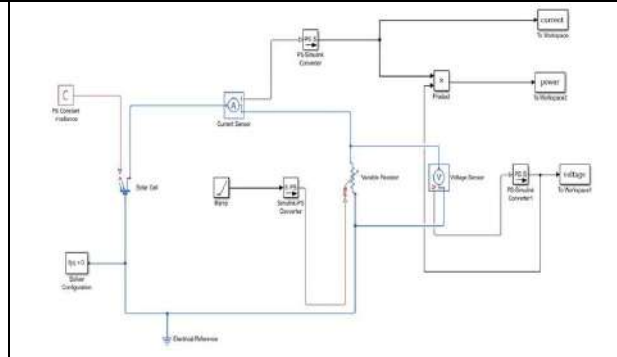


Fig.8: Input Simulink model in MATLAB

```

>> plot(voltage,current,voltage1,current1,voltage2,current2,voltage3,current3,voltage4,current4,voltage5,current5)
>> xlabel('voltage')
>> ylabel('current')
>> title('V-I CURVE FOR SOLAR CELL')
>>
>> plot(voltage,power1,voltage1,power1,voltage2,power2,voltage3,power3,voltage4,power4,voltage5,power5)
>> xlabel('voltage')
>> ylabel('power')
>> title('P-V CURVE FOR SOLAR CELL')
>>
>> plot(current,power,current1,power1,current2,power2,current3,power3,current4,power4,current5,power5)
>> xlabel('current')
>> ylabel('power')
>> title('I-P CURVE FOR SOLAR CELL')
>>
    
```

Fig.9: Input MATLAB coding for MPPT in solar cell

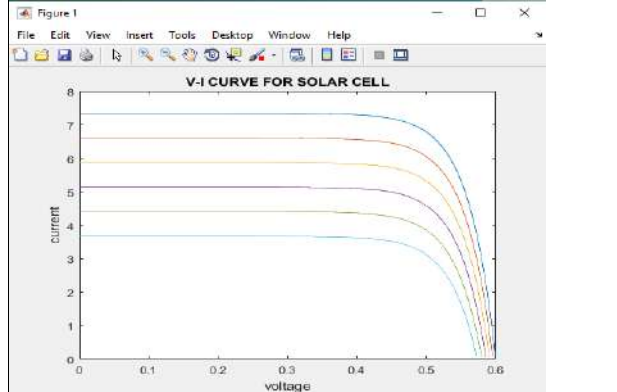


Fig.10.1: Graph showing voltage versus current plot

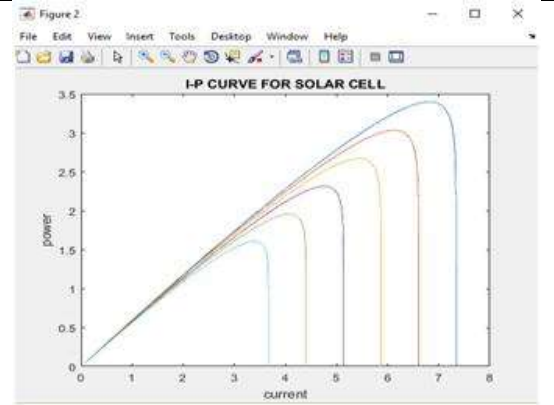


Fig. 10.2 Graph showing current versus power plot

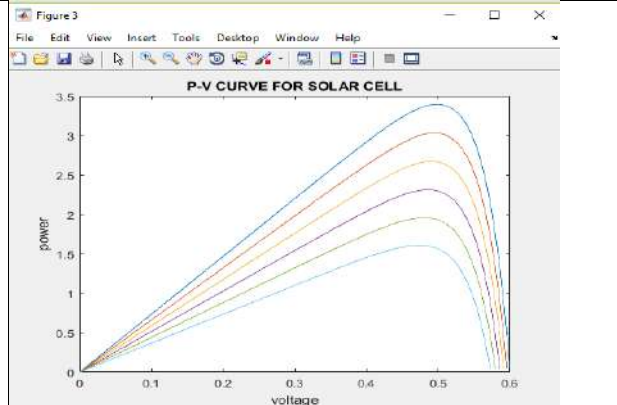


Fig.10.3: Graph showing voltage versus power plot





A Partially Backlogged Inventory Model for Deteriorating Items with Ramp-Type Demand, Time-Dependent Holding Cost and Salvage Value

Ekta Chauhan^{1*}, R. K .Srivastav¹ and Sangeeta Gupta²

¹Department of Mathematics, Agra College, Agra, Dr. Bhimrao Ambedkar University, Agra, U.P., India

²The A.H. Siddiqi Centre for Advanced Research in Applied Mathematics and Physics, Sharda University, Greater Noida, U.P., India

Received: 06 Apr 2023

Revised: 14 May 2023

Accepted: 31 May 2023

*Address for Correspondence

Ekta Chauhan

Department of Mathematics,
Agra College, Agra,
Dr. Bhimrao Ambedkar University,
Agra, U.P., India.
E. Mail: ekta.chauhan0562@gmail.com



This is an Open Access Journal / article distributed under the terms of the **Creative Commons Attribution License** (CC BY-NC-ND 3.0) which permits unrestricted use, distribution, and reproduction in any medium, provided the original work is properly cited. All rights reserved.

ABSTRACT

In this paper, we have developed an inventory model for deteriorating items. The demand for the items is assumed to be ramp-type in this case. Holding cost is time-dependent, and the Salvage value is associated with the deteriorated items. This model is considered here to allow for shortages and partial backlogging. The results are shown using numerical examples, and a sensitivity analysis of the model with regard to various parameters for an optimal solution is also conducted.

Keywords: Ramp-type demand rate, Deterioration rate, Partial Backlogging, Salvage value

INTRODUCTION

Inventory is characterised as a stock of items that a company keeps on hand in preparation for potential future demand. The amount that inventories must drop to in order to indicate that a replenishment order needs to be made for a certain item. In a lot of inventory systems, the impact of deterioration is crucial. Deterioration is described as decay or deterioration that prevents an item from being utilized for its intended purpose. Commonly used things like fruits, vegetables, meat, meals, etc. are examples of objects exhibiting this type of degradation. The majority of physical products become obsolete over time. Highly volatile liquids like petrol, alcohol, and fragrances, among others, deteriorate physically over time due to evaporation. Electronic items, radioactive materials, photographic films, etc. eventually degrade within their typical storage time. Within [17] first considered inventory in decaying products. He investigated the fashion goods that were deteriorating at the end of the shortage period. Most of the researchers have taken an interest in developing inventory models with constant and time-proportional



**Ekta Chauhan et al.,**

deterioration. Ghare and Schrader [3] were the first to develop an inventory model with an exponential deterioration rate. Mishra and Singh [9] discussed an inventory model for ramp-type demand, time dependent deteriorating items with salvage value and shortages. An inventory system's main component is demand. Demand is the rate at which customers wish to purchase a product. According to economic theory, demand is made up of two elements, including consumer preference and the ability to purchase. The market price affects the consumer preference and the ability to purchase products both demand factors. A product will have low demand if its market price for a product is high. Demand is high when the market prices for products are low. Many customers will be able to get a product at extremely low prices. The majority of researchers have focused their studies on a demand function that changes over time. Normally, a constant demand rate shouldn't be taken as a factor for all kinds of products, including trendy clothing, computer equipment, etc. Because the demand function for these kinds of products is completely dependent on time. Hill [5] was the first to discuss inventory modelling with ramp-type demand. Mandal and Pal [7] proposed on his approach by using ramp-type demand and shortages. Aggrawal and Singh [1] gave an EOQ Model with Ramp-type Demand Rate, Time-Dependent Deterioration Rate, and Shortages. Shi. et al. [14] have studied Optimal ordering policies for a single deteriorating item with a ramp-type demand rate under permissible delay in payments. Saha *et al.* [12] discussed an inventory model with Ramp-Type Demand and Price Discount on Back Order for Deteriorating Items under Partial Backlogging.

The holding cost plays a significant role in determining the total cost of inventory planning as well as the total profit. Depending on the time parameter, the holding cost's nature may be linear or nonlinear. Many researchers have thought about expanding their work on inventory planning for time-dependent variable holding costs. First, Goh [4] thought about a stock-dependent demand model with variable holding costs, assuming that the unit holding cost was a nonlinear continuous function of time. A few inventory models, such as those by Sahoo and Tripathy [13] found an EOQ Model for Quadratic Demand Rate, Parabolic Deterioration, Time Dependent Holding Cost with Partial Backlogging. Salvage value is the estimated resale worth of any asset after its economic life has expired with a specific owner. Its importance stems from the requirement for asset evaluation because understanding the idea of salvage value needs to understand what depreciation requires. Every asset object has a different economic worth depending on how long it has been used, how well it is maintained, and how valuable it is to resell. Real-world examples of marketplaces for used goods include vehicles, buildings, production equipment, aircraft, and ships, which demonstrate the importance of the phenomenon of reusing durable real assets.

Jaggi and Aggarwal [6] proposed an EOQ model for deteriorating items with salvage values. Mohan [11] studied Quadratic demand, Variable holding cost with Time Dependent Deterioration without Shortages, and Salvage Value. Mishra [10] introduced an inventory model for time-dependent holding cost and deterioration with salvage value and shortages. Venkateswarlu and Mohan [15] investigated an inventory model for deteriorating items with Time-dependent Quadratic demand and Salvage value. Chang and Dye [2] explained an EOQ model for deteriorating items with time varying demand and partial backlogging. Mishra *et al.* [8] worked on a deteriorating inventory model with time-dependent demand and partial backlogging. Wee [16] emphasized economic production lot size model for deteriorating items with partial back ordering. In this research paper, we introduced an inventory model for deteriorating item. Here, we consider the demand for this item to be ramp type and time dependent holding cost. The Deterioration rate taken in this paper is constant and consider salvage value. Shortages are allowed with partially backlogging. We solved this model to minimize the total inventory cost. A numerical example is examined to determine the model's validity. Sensitivity analysis is shown graphically for certain parameters.

Assumptions and Notations

The following assumptions are considered in this paper to formulate the proposed mathematical model of the inventory system.

Assumptions

- Demand is taken as Ramp type.
- Deterioration rate is constant.





Ekta Chauhan et al.,

- Holding cost is time dependent.
- Shortage are allowed with partially backlogging.
- Replenishment rate is infinite.
- Salvage value is associated with deterioration items

Notations

- The demand rate $R(t)$ is assumed to be a ramp-type demand function of time

$$R(t) = D_0 \left[(t - (t - \mu)) H(t - \mu) \right] D_0 > 0$$
 Where $H(t - \mu)$ is known as Heaviside's unit function.

$$H(t - \mu) = \begin{cases} 1 & t_1 \geq \mu \\ 0 & t_1 < \mu \end{cases}$$
- The inventory level at time t is denoted by $I(t)$.
- The rate of deterioration is taken as θ , where θ is constant
- Holding cost HC per item per unit time is time dependent and is assumed to be $H(t) = h_1 + h_2t$, where $h_1 > 0, 0 < h_2 < 1$.
- The cost for every order for ordering is A .
- A_1 is the deterioration cost per unit.
- A_2 is the shortage cost per unit.
- A_3 is the opportunity cost per unit.
- t_1 is the time when shortages begin.
- The length of each ordering cycle is T .
- For each ordering cycle, I_0 is the maximum inventory level.
- I_B is the maximum quantity of backlogged demand for each ordering cycle.
- For each ordering cycle, the economic order quantity is S .
- The variable backlogging rate is based on how long it will be before the next replenishment when the shortage period starts. The backlog rate decreases as waiting times increase. thus, the number of consumers ready to accept the backlog at time t decreases with the waiting time $(T-t)$ until the next replenishment. To avoid this problem, we defined $\frac{1}{1+\alpha(T-t)}$ as the backlogging rate when inventory is negative during the time period (t_1, T) with constant positive backlogging parameter α .

Mathematical Model

The inventory level of the system at time t over the period $[0, T]$ can be given as

$$\frac{dI(t)}{dt} + \theta I(t) = -D(t), \quad 0 \leq t \leq t_1 \quad \dots (1)$$

In this Model

$$\frac{dI(t)}{dt} + \theta I(t) = -D_0 t, \quad 0 < t < \mu \quad \dots (2)$$

$$\frac{dI(t)}{dt} + \theta I(t) = -D_0 \mu, \quad \mu < t < t_1 \quad \dots (3)$$

With $I(0) = I_0$

Solutions to the Equations (2) and (3) are

$$I(t) = \left[I_0(1 - \theta t) - \frac{D_0}{2} \left(t^2 - \frac{\theta t^3}{3} \right) \right] 0 < t < \mu \quad \dots (4)$$

$$I(t) = \left[I_0(1 - \theta t) + D_0 \mu \left(\frac{\theta t^2}{2} - \frac{\theta \mu t}{2} - t + \frac{\theta \mu^2}{6} + \frac{\mu}{2} \right) \right] \mu < t < t_1 \quad \dots (5)$$

When $I(t_1) = 0$, we obtain the value of I_0 from Equation (5) while ignoring higher-order variables of θ

$$I_0 = D_0 \mu \left(\frac{\theta t_1^2}{2} + t_1 - \frac{\theta \mu^2}{6} - \frac{\mu}{2} \right) \quad \dots (6)$$

At the time t , the demand is partially backlogged at the fraction $\frac{1}{1+\alpha(T-t)}$ during the period of shortage $[t_1, T]$.

Consequently, the differential equation controlling how much demand is backlogged is

$$\frac{dI(t)}{dt} = -\frac{D_0 \mu}{1+\alpha(T-t)}, \quad t_1 < t < T \quad \dots (7)$$

When the boundary condition $I(t_1) = 0$. Eq. (7) has the following solution:





Ekta Chauhan et al.,

$$I(t) = - \int \frac{D_0\mu}{1+\alpha(T-t)} dt$$

After solving this equation, we get

$$I(t) = \frac{D_0\mu}{\alpha} [\log(1 + \alpha(T - t)) - \log(1 + \alpha(T - t_1))] \dots(8)$$

By taking t = T in equation (8) to get the maximum amount of demand backlogged every cycle is

$$I_B = -I(t) = \frac{D_0\mu}{\alpha} [\log(1 + \alpha(T - t_1))] \dots(9)$$

Economic Order Quantity per cycle

$$S = I_0 + I_B$$

$$S = D_0\mu \left(\frac{\theta t_1^2}{2} + t_1 - \frac{\theta\mu^2}{6} - \frac{\mu}{2} \right) + \frac{D_0\mu}{\alpha} [\log(1 + \alpha(T - t_1))] \dots(10)$$

The cost of holding inventories per cycle is

$$HC = \int_0^{t_1} H(t)I(t)dt$$

$$HC = h_1 \left[I_0 \left(t_1 - \frac{\theta t_1^2}{2} \right) + D_0 \left(-\frac{\mu^3}{6} - \frac{\theta\mu^4}{24} + \frac{\theta\mu t_1^3}{6} - \frac{\theta\mu^2 t_1^2}{4} - \frac{\mu t_1^2}{2} + \frac{\theta\mu^3 t_1}{6} + \frac{\mu^2 t_1}{2} \right) \right] + h_2 \left[I_0 \left(\frac{t_1^2}{2} - \frac{\theta t_1^3}{3} \right) + D_0 \left(-\frac{\mu^4}{24} - \frac{\theta\mu^5}{120} + \frac{\theta\mu t_1^4}{8} - \frac{\theta\mu^2 t_1^3}{6} - \frac{\mu t_1^3}{3} + \frac{\theta\mu^3 t_1^2}{4} + \frac{\mu^2 t_1^2}{4} \right) \right] \dots(11)$$

The Deterioration cost per cycle is

$$DC = \int_0^{t_1} R(t)dt$$

$$DC = A_1 \left[I_A - \left\{ \int_0^{\mu} I(t) dt + \int_{\mu}^{t_1} I(t) dt \right\} \right]$$

$$DC = \frac{A_1 D_0 \theta \mu}{2} \left(t_1^2 - \frac{\mu^2}{3} \right) \dots(12)$$

The Shortage cost per cycle is

$$SC = A_2 \left[- \int_{t_1}^T I(t) dt \right]$$

$$SC = \frac{A_2 D_0 \mu}{\alpha} \left[T - t_1 - \frac{1}{\alpha} \log(1 + \alpha(T - t_1)) \right] \dots(13)$$

The Opportunity cost due to lost sales per cycle is

$$OC = A_3 \left[\int_{t_1}^T D_0 \mu \left(1 - \frac{1}{1 + \alpha(T - t)} \right) dt \right]$$

$$OC = A_3 D_0 \mu \left[T - t_1 - \frac{1}{\alpha} \log(1 + \alpha(T - t_1)) \right] \dots(14)$$

Salvage value of deteriorated items is

$$SV = \gamma \frac{A_1 D_0 \theta \mu}{2} \left(t_1^2 - \frac{\mu^2}{3} \right) \dots(15)$$

Thus, C (t₁, T) represents the Total average cost per unit time during the cycle.

$$C(t_1, T) = \frac{1}{T} (A + HC + DC + CS + OC - SV)$$

$$TC = \frac{1}{T} \left[A + h_1 \left[I_0 \left(t_1 - \frac{\theta t_1^2}{2} \right) + D_0 \left(-\frac{\mu^3}{6} - \frac{\theta\mu^4}{24} + \frac{\theta\mu t_1^3}{6} - \frac{\theta\mu^2 t_1^2}{4} - \frac{\mu t_1^2}{2} + \frac{\theta\mu^3 t_1}{6} + \frac{\mu^2 t_1}{2} \right) \right] + h_2 \left[I_0 \left(\frac{t_1^2}{2} - \frac{\theta t_1^3}{3} \right) + D_0 \left(-\frac{\mu^4}{24} - \frac{\theta\mu^5}{120} + \frac{\theta\mu t_1^4}{8} - \frac{\theta\mu^2 t_1^3}{6} - \frac{\mu t_1^3}{3} + \frac{\theta\mu^3 t_1^2}{4} + \frac{\mu^2 t_1^2}{4} \right) \right] + \frac{A_1 D_0 \theta \mu}{2} \left(t_1^2 - \frac{\mu^2}{3} \right) + \frac{(A_2 + \alpha A_3) D_0 \mu (T - t_1)}{\alpha} - \frac{(A_2 + \alpha A_3) D_0 \mu}{\alpha^2} \log(1 + \alpha(T - t_1)) - \gamma \frac{A_1 D_0 \theta \mu}{2} \left(t_1^2 - \frac{\mu^2}{3} \right) \right] \dots(16)$$

Put the value of I₀ in Eq.(16), then

$$TC = \frac{1}{T} \left[A + \frac{h_1 D_0 \mu}{24} (12t_1^2 - 4\mu^2 - \theta\mu^3 + 4\theta t_1^3) + \frac{h_2 D_0 \mu}{120} (20t_1^3 + 30\theta t_1^4 + 20\theta\mu^2 t_1^2 - 5\mu^3 - \theta\mu^4) + \frac{A_1 D_0 \theta \mu}{2} \left(t_1^2 - \frac{\mu^3}{3} \right) + \frac{(A_2 + \alpha A_3) D_0 \mu (T - t_1)}{\alpha} - \frac{(A_2 + \alpha A_3) D_0 \mu \log(1 + \alpha(T - t_1))}{\alpha^2} - \gamma \frac{A_1 D_0 \theta \mu}{2} \left(t_1^2 - \frac{\mu^3}{3} \right) \right] \dots(17)$$

Our objective is to identify the optimal values of t₁ and T in order to reduce total average cost C(t₁, T) per unit time.

The solution to the equations is the optimal values of t and T for the minimal average cost C(t₁, T).

$$\frac{\partial C(t_1, T)}{\partial t_1} = 0 \text{ and } \frac{\partial^2 C(t_1, T)}{\partial t_1^2} > 0$$

By satisfying the sufficient condition Eq. (17) written as





Ekta Chauhan et al.,

$$\frac{\partial C(t_1, T)}{\partial t_1} = \frac{1}{T} \left[\frac{h_1 D_0 \mu}{2} (2t_1 + \theta t_1^2) + \frac{h_2 D_0 \mu}{6} (3t_1^2 + 6\theta t_1^3 + 2\theta \mu^2 t_1) + A_1 D_0 \theta \mu t_1 - \frac{(A_2 + \alpha A_3) D_0 \mu}{\alpha} + \frac{(A_2 + \alpha A_3) D_0 \mu}{\alpha(1 + \alpha(T - t_1))} - \gamma A_1 D_0 \theta \mu t_1 \right] = 0 \dots(18)$$

Again Differentiating Eq. (18)

$$\frac{\partial^2 C(t_1, T)}{\partial t_1^2} > 0$$

$$\frac{\partial^2 C(t_1, T)}{\partial t_1^2} = \frac{1}{T} \left[h_1 D_0 \mu (1 + \theta t_1) + \frac{h_2 D_0 \mu}{3} (3t_1 + 9\theta t_1^2 + \theta \mu^2) + A_1 D_0 \theta \mu + \frac{(A_2 + \alpha A_3) D_0 \mu}{(1 + \alpha(T - t_1))^2} - \gamma A_1 D_0 \theta \mu \right] \dots(19)$$

Numerical Examples

We have given numerical example to determine the validity of the model, A=300, A₁=3, A₂=10, A₃=15, h₁=4, h₂=0.4, α=0.8, T=1year, γ=0.4, D₀=100, θ=0.02, μ=0.12

Applying the solution procedure described above the optimal values obtained is as follows

t₁ = **299.06days** and the Total Inventory Cost= ₹**320.61**.

CONCLUSION

The goal of this paperto develop an inventory model for deterioration items with ramp type demand.Holding cost is time dependent. Shortages are allowed with partially backlogging. This model determine the effect of cost per unit time for variation of different parameters. It has been determined from the model's research that

- When the salvage value (γ) and deterioration rate (θ) increase the total cost increase marginally.
- When the deterioration rate (θ) increase, the total cost increase marginally.
- When the demand rate (μ) increase, the total cost increase significantly.
- When the deterioration cost (A₁) increase,the total cost increase marginally.
- When the shortage cost (A₂) increase, the total cost increase significantly.
- When the opportunity cost (A₃) increase, the total cost increase significantly.
- When the salvage value (γ) increase,the total cost decrease marginally.
- When the partially backlogging parameter increase the total cost increase significantly.

REFERENCES

1. Aggrawal, P. and Singh, T.J. (2017). An EOQ Model with Ramp Type Demand Rate, Time Dependent Deterioration Rate and Shortages, *Global Journal of Pure and Applied Mathematics*, 13(7) ,3381-3393.
2. Chang H. J. and Dye C. Y. (1999).An EOQ model for deteriorating items with time varying demand and partial backlogging. *Journal of the Operational Research Society*, (50),1176-1182.
3. Ghare P.M. and Schraderb G.F. (1963). A model for exponentially decaying inventories. *Journal of Industrial Engineering*, (14), 238-243.
4. Goh M. (1994). EOQ models with general demand and holding costs functions. *European Journal of Operational Research*, 73, 50–54.
5. Hill, R. M. (1995). Inventory models for increasing demand followed by level demand. *Journal of the Operational Research Society*, 46(10), 1250-1259.
6. Jaggi C.K. and Aggarwal S. P. (1996). EOQ model for deteriorating items with salvage values. *Bulletin of Pure and Applied Science*, 15E(1),67–71.
7. Mandal B., Pal A. K. (1998).Order level inventory system with ramp type demand rate for deteriorating items. *Journal of Interdisciplinary Mathematics*, (1), 49-66.
8. Mishra V.K. and Singh L.S. (2010). Deteriorating inventory model with time dependent demand and partial backlogging. *Applied Mathematical Science*, 4(72), 3611–3619.
9. Mishra V.K., Singh L.S. (2011). Inventory model for ramp type demand, time dependent deteriorating items with salvage value and shortages. *International Journal of Applied Mathematics Statistics*, 23(11), 84–91.





Ekta Chauhan et al.,

10. Mishra V.K. (2012). Inventory Model for Time-Dependent Holding Cost and Deterioration with Salvage Value and Shortages. *The Journal of Mathematics and Computer Science*, 4 (1),37 – 47.
11. Mohan R., (2017). Quadratic demand, Variable holding cost with Time Dependent Deterioration without Shortages and Salvage Value. *IOSR Journal of Mathematics*, 13(2), 59-66.
12. Saha S., Sen N., and Nath B.K. (2018). Inventory Model with Ramp-type Demand and Price Discount on Back Order for Deteriorating Items under Partial Backlogging. *Applications and Applied Mathematics*, 1(1), 472 – 483.
13. Sahoo N.K.and Tripathy P.K.(2018). An EOQ Model for Quadratic Demand Rate, Parabolic Deterioration, Time Dependent Holding Cost with Partial Backlogging, *International. Journal of Mathematics and its Applications*, 6(1), 325–332.
14. Shi Y., Zhang Z, Zhou F. andShi Y.(2019). Optimal ordering policies for a single deteriorating item with ramp-type demand rate under permissible delay in payments. *Journal of the Operational Research Society*, 70(10),1848–1868.
15. Venkateswarlu R. and Mohan R. (2011). Inventory model for deteriorating items Time Dependent Quadratic Demand and Salvage value. *International Journal of Applied Mathematical Sciences*, 5(1), 11-18.
16. Wee HM. (1993).Economic production lot size model for deteriorating items with partial back ordering. *Computer and Industrial Engineering*, 24(3),.449-458.
17. Whitin TM. (1957). Theory of inventory management. Princeton University Press, Princeton, NJ.62-72.

Table (1): Effect of θ and γ

$\theta \backslash \gamma$	0.01	0.015	0.02	0.025	0.03
0.2	TC=320.52	TC=320.59	TC=320.66	TC=320.73	TC=320.81
0.3	TC=320.50	TC=320.57	TC=320.64	TC=320.70	TC=320.77
0.4	TC=320.49	TC=320.55	TC=320.61	TC=320.67	TC=320.74
0.5	TC=320.48	TC=320.53	TC=320.59	TC=320.64	TC=320.70
0.6	TC=320.47	TC=320.52	TC=320.57	TC=320.61	TC=320.66

Table (2): Variation in system parameter

Parameters	% Change	-50%	-25%	0%	+25%	+50%
θ	TC	320.49	320.55	320.61	320.67	320.74
A_1	TC	320.54	320.58	320.61	320.65	320.69
A_2	TC	319.50	320.12	320.61	321.02	321.36
A_3	TC	319.21	320.01	320.61	321.09	321.48
γ	TC	320.66	320.64	320.61	320.59	320.57
D_0	TC	310.31	315.46	320.61	325.46	330.92
α	TC	309.74	310.05	320.61	310.51	310.68
μ	TC	310.35	315.58	320.61	325.69	330.70





Ekta Chauhan et al.,

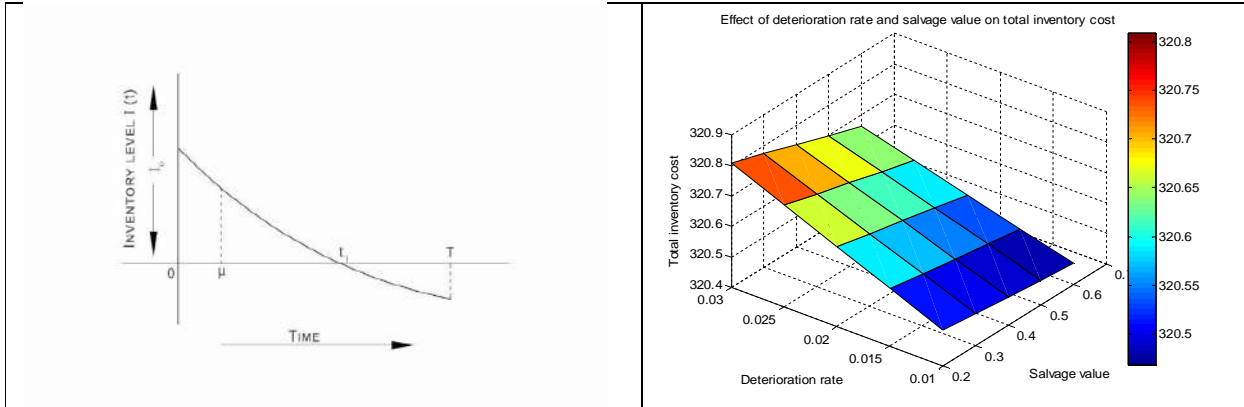


Figure:1 of Mathematical Model

Figure:2 of Effect of Deterioration rate and Salvage value on Total inventory cost for Table (1)

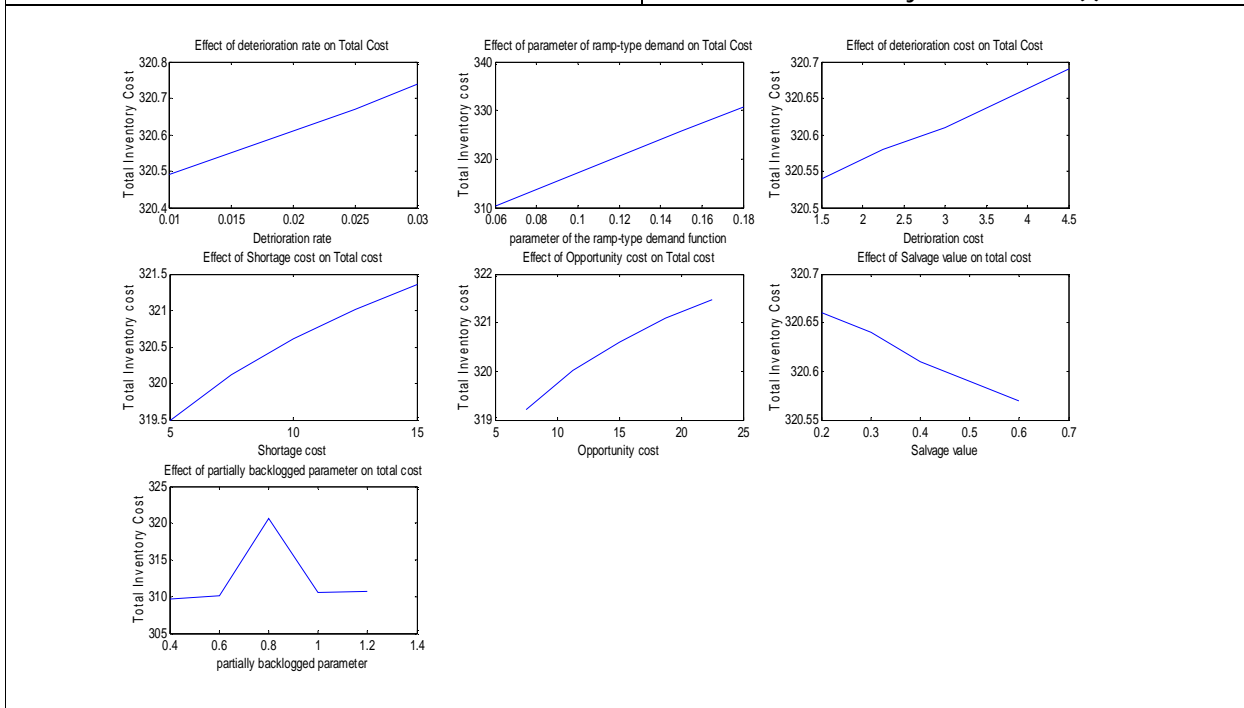


Figure:3 of Sensitive Analysis for Table (2)





Cordial Labeling in Context of Some New Graphs

SlashiLeel^{1*}, Sweta Srivastav² and Sangeeta Gupta¹

¹Department of Mathematics, Sharda University, Greater Noida, Uttar Pradesh 201310, India

²The A.H.Siddiqi Centre for Advanced Research in Applied Mathematics and Physics, Sharda University, Greater Noida, Uttar Pradesh, India.

Received: 10 Apr 2023

Revised: 15 May 2023

Accepted: 31 May 2023

*Address for Correspondence

SlashiLeel

Department of Mathematics,
Sharda University,
Greater Noida,
Uttar Pradesh 201310, India.

E. Mail: 2022301198.slashi@dr.sharda.ac.in



This is an Open Access Journal / article distributed under the terms of the **Creative Commons Attribution License** (CC BY-NC-ND 3.0) which permits unrestricted use, distribution, and reproduction in any medium, provided the original work is properly cited. All rights reserved.

ABSTRACT

In this paper we investigate cordial labeling for some different types of graphs. A labeling of the graph is the mapping that carries the graph elements to the set of numbers, usually to the set of non-negative or positive numbers. Graph labeling allows us to assign integers to the edges or vertices of the graph. We have investigated cordial labeling for H graph $H_n \odot K_1$, Shell graph $S_n \odot K_1$ and Cycle graph $C_n \odot K_{1,n}$. The concept of graph labeling is widely used in radar systems, circuit plans, communication systems etc. Labeled graphs can also be used in astronomy, contact systems, crystallography, Ad hoc networks.

Keywords: Graph labeling, Cordial labeling, H-graph, Shell graph, Cycle graph, Complete bipartite graph

INTRODUCTION

This study includes finite, connected and undirected graphs. Graph $G=(V,E)$ having a set of vertices as $V(G)$ and a set of edges as $E(G)$ respectively. Labeling involves the assignment of integers to either the vertices or edges, or even both, based on specific conditions. The idea of graph labeling was discussed by Kalabet *al.* [5] and product cordial labeling of some cycle related graphs was discussed by Barasaraet *al.* [2]. Motivated by their ideas we have discussed cordial labeling related to some new graphs.

A graph $G(A,B)$ where A represents a vertex set and B represents Edge set is cordial if there exists a function $g: A(G) \rightarrow \{0,1\}$ then the induced labeling defined as $g^*: B(G) \rightarrow \{0,1\}$ and $g^*(xy) = |g(x)-g(y)|$, where $xy \in B(G)$ and also holds inequalities like $|A_g(0)-A_g(1)| \leq 1$ and $|B_g(0)-B_g(1)| \leq 1$ where $g(u)$ is the label of vertex u of G under g . Also $A_g(0)$ denotes the number of vertices with label 0 under g and $A_g(1)$ denotes the number of vertices with label 1

57496





SlashiLeelet al.,

under g . We have investigated cordial labeling for H graph $H_n \odot K_1$, Shell graph $S_n \odot K_1$ and Cycle graph $C_n \odot K_{1,n}$.

Definition 1.1: Graph labeling involves the process of assigning values to the vertices of a graph while adhering to specific conditions.

Graph labeling problems exhibit three typical characteristics:

1. A collection of numbers used for assigning labels to vertices.
2. A rule that assigns a label to each edge in the graph.
3. Certain condition(s) that these assigned labels must adhere to.

Definition 1.2: A graph $G(V,E)$ where V represents a vertex set and E represents Edge set is cordial if there exists a function $f: V(G) \rightarrow \{0,1\}$ then the induced labeling defined as $f^*: E(G) \rightarrow \{0,1\}$ defined as $f^*(xy) = |f(x)-f(y)|$, where $xy \in E(G)$ and also holds inequalities like $|V_f(0)-V_f(1)| \leq 1$ and $|E_f(0)-E_f(1)| \leq 1$ where $f(u)$ is the label of vertex u of G under f . Also $V_f(0)$ denotes the number of vertices with label 0 under f and $V_f(1)$ denotes the number of vertices with label 1 under f .

Definition 1.3: The H -graph of path P_n is the graph obtained from two copies of P_n with the vertices $v_1, v_2, v_3, v_4, \dots, v_n$ and $u_1, u_2, u_3, u_4, \dots, u_n$ by joining the vertices $v_{(n+1)/2}$ and $u_{(n+1)/2}$ if n is odd and $v_{n/2+1}$ and $u_{n/2+1}$ if n is even.

Definition 1.4: The H - graph ($H_n \odot K_1$) is obtained by joining a pendant edge to each vertex of H_n .

Definition 1.5: A shell graph, denoted as $C_{(n,n-3)}$, is a cycle C_n with $(n-3)$ chords that share a common endpoint known as the apex. Additionally, a shell S_n is often referred to as a fan f_{n-1} .

Definition 1.6: A shell graph ($S_n \odot K_1$) is obtained by joining a pendant edge to each vertex of S_n .

Definition 1.7: A cycle graph, also known as a circular graph, is a type of graph comprising a single cycle or a closed chain of connected vertices, with a minimum of three vertices. The cycle graph with n vertices is commonly referred to as C_n .

Definition 1.8: A cycle graph ($C_n \odot K_{1,n}$) is obtained by joining $K_{1,n}$ with any one vertex of C_n .

MAIN RESULTS

Theorem 2.1: The graph $H_n \odot K_1$ follows cordial labeling for all n .

Proof: Let G be $H_n \odot K_1$ graph and let $v_1, v_2, v_3, v_4, \dots, v_n$ be the successive vertices of H -graph and $p_1, p_2, p_3, p_4, \dots, p_n$ are the pendant vertices of $H_n \odot K_1$.

Such that there exists a function $f, f: V(H_n \odot K_1) \rightarrow \{0,1\}$ as follows:

Case (i) $n \equiv 0 \pmod 4$

$$f(v_i) = \begin{cases} 1 & \{i \equiv 0, 1 \pmod 4\} \\ 0 & \{i \equiv 2, 3 \pmod 4\}, 1 \leq i \leq n \end{cases}$$

$$f(p_i) = \begin{cases} 1 & \{i \equiv 1, 2 \pmod 4\} \\ 0 & \{i \equiv 0, 3 \pmod 4\}, 1 \leq i \leq n \end{cases}$$

Case (ii) $n \equiv 1 \pmod 4$

$$v_1 = 1 \text{ and } p_1 = 1 \text{ and } p_2 = 0$$

$$f(v_i) = \begin{cases} 1 & \{i \equiv 0, 1 \pmod 4\} \\ 0 & \{i \equiv 2, 3 \pmod 4\}, 2 \leq i \leq n \end{cases}$$

$$f(p_i) = \begin{cases} 1 & \{i \equiv 0, 3 \pmod 4\} \\ 0 & \{i \equiv 1, 2 \pmod 4\}, 3 \leq i \leq n \end{cases}$$





SlashiLeelet al.,

Case(iii) $n \equiv 2 \pmod 4$

$$f(v_i) = \begin{cases} 1 & \{i \equiv 1, 2 \pmod 4\} \\ 0 & \{i \equiv 0, 3 \pmod 4\}, 1 \leq i \leq n \end{cases}$$

$$f(p_i) = \begin{cases} 1 & \{i \equiv 0, 1 \pmod 4\} \\ 0 & \{i \equiv 2, 3 \pmod 4\}, 1 \leq i \leq n \end{cases}$$

Case(iv) $n \equiv 3 \pmod 4$

$$v_1 = 0$$

$$f(v_i) = \begin{cases} 1 & \{i \equiv 1, 2 \pmod 4\} \\ 0 & \{i \equiv 0, 3 \pmod 4\}, 2 \leq i \leq n \end{cases}$$

$$f(p_i) = \begin{cases} 1 & \{i \equiv 0, 2 \pmod 4\} \\ 0 & \{i \equiv 1, 3 \pmod 4\}, 1 \leq i \leq n \end{cases}$$

In each case, the graph G under consideration satisfies the conditions $|v_r(0)-v_r(1)| \leq 1$ and $|e_r(0)-e_r(1)| \leq 1$. Thus, G possesses a cordial labeling.

Example: $H_7 \odot K_1$ is cordial.

In the above graph $V_r(0)=14, V_r(1)=14$ and $E_r(0)=14, E_r(1)=13$

$H_7 \odot K_1$ satisfies the condition of $|V_r(0)-V_r(1)| \leq 1$ and $|E_r(0)-E_r(1)| \leq 1$. Hence $H_7 \odot K_1$ satisfies cordial labeling.

Theorem 2.2: The graph $S_n \odot K_1$ follows cordial labeling for all n.

Proof: Let G be $S_n \odot K_1$ graph and let $v_1, v_2, v_3, v_4, \dots, v_n$ be the successive vertices of shell graph and $p_1, p_2, p_3, p_4, \dots, p_n$ are the pendant vertices of $S_n \odot K_1$.

Such that there exists a function $f: V(S_n \odot K_1) \rightarrow \{0,1\}$ as follows:

Case(i) $n \equiv 0 \pmod 4$

$$f(v_i) = \begin{cases} 1 & \{i \equiv 1, 3 \pmod 4\} \\ 0 & \{i \equiv 0, 2 \pmod 4\}, 1 \leq i \leq n \end{cases}$$

$$f(p_i) = \begin{cases} 1 & \{i \equiv 1, 3 \pmod 4\} \\ 0 & \{i \equiv 0, 2 \pmod 4\}, 1 \leq i \leq n \end{cases}$$

Case(ii) $n \equiv 1 \pmod 4$

$$f(v_i) = \begin{cases} 1 & \{i \equiv 0, 1 \pmod 4\} \\ 0 & \{i \equiv 2, 3 \pmod 4\}, 1 \leq i \leq n \end{cases}$$

$$f(p_i) = \begin{cases} 1 & \{i \equiv 0, 2 \pmod 4\} \\ 0 & \{i \equiv 1, 3 \pmod 4\}, 1 \leq i \leq n \end{cases}$$

Case(iii) $n \equiv 2 \pmod 4$

$$f(v_i) = \begin{cases} 1 & \{i \equiv 2, 3 \pmod 4\} \\ 0 & \{i \equiv 0, 1 \pmod 4\}, 1 \leq i \leq n \end{cases}$$

$$f(p_i) = \begin{cases} 1 & \{i \equiv 0, 2 \pmod 4\} \\ 0 & \{i \equiv 1, 3 \pmod 4\}, 1 \leq i \leq n \end{cases}$$

Case(iv) $n \equiv 3 \pmod 4$

$$f(v_i) = \begin{cases} 1 & \{i \equiv 0, 1 \pmod 4\} \\ 0 & \{i \equiv 2, 3 \pmod 4\}, 1 \leq i \leq n \end{cases}$$

$$f(p_i) = \begin{cases} 1 & \{i \equiv 1, 3 \pmod 4\} \\ 0 & \{i \equiv 0, 2 \pmod 4\}, 1 \leq i \leq n \end{cases}$$

In each case the graph G under consideration satisfies the conditions $|v_r(0)-v_r(1)| \leq 1$ and $|e_r(0)-e_r(1)| \leq 1$. Thus, G possesses a cordial labeling.

Example: $S_9 \odot K_1$ is cordial.

In the above graph $V_r(0)=9, V_r(1)=9$ and $E_r(0)=12, E_r(1)=12$

$S_9 \odot K_1$ satisfies the condition of $|V_r(0)-V_r(1)| \leq 1$ and $|E_r(0)-E_r(1)| \leq 1$. Hence, $S_9 \odot K_1$ satisfies cordial labeling.





SlashiLeelet al.,

Theorem 2.3: The graph $C_n \odot K_{1,n}$ follows cordial labeling for all n .

Proof: Let G be the cycle graph with $K_{1,n}$. Let $V(G) = V_1 \cup V_2$, where $V_1 = \{u_1, u_2, u_3, u_4, \dots, u_n\}$ be the vertex set of C_n and $V_2 = \{v_1, v_2, v_3, v_4, \dots, v_n\}$ be the vertex set of $K_{1,n}$.

Here, $v_1, v_2, v_3, v_4, \dots, v_n$ are pendant vertices. Also $|V(G)| = |E(G)| = 2n$.

We define labeling $f: V(G) \rightarrow \{0, 1\}$ as follows.

Case (i) $n \equiv 0, 2 \pmod{4}$

$$f(u_i) = 1, 1 \leq i \leq n$$

$$f(v_j) = 0, 1 \leq j \leq n$$

Case (ii) $n \equiv 1 \pmod{4}$

$$f(u_i) = 1 \{i \equiv 1, 2 \pmod{4}\}$$

$$0 \{i \equiv 0, 3 \pmod{4}\}, 1 \leq i \leq n$$

$$f(v_j) = 1 \{j \equiv 0, 2 \pmod{4}\}$$

$$0 \{j \equiv 1, 3 \pmod{4}\}, 1 \leq j \leq n$$

Case (iii) $n \equiv 3 \pmod{4}$

$$f(u_i) = 1 \{i \equiv 0, 1 \pmod{4}\}$$

$$0 \{i \equiv 2, 3 \pmod{4}\}, 1 \leq i \leq n$$

$$f(v_j) = 1 \{j \equiv 1, 3 \pmod{4}\}$$

$$0 \{j \equiv 0, 2 \pmod{4}\}, 1 \leq j \leq n$$

In each case the graph G under consideration satisfies the conditions $|v_i(0) - v_i(1)| \leq 1$ and $|e_i(0) - e_i(1)| \leq 1$. Thus, G possesses a cordial labeling.

Example: $C_6 \odot K_{1,6}$ is cordial.

In the above graph $V_i(0)=6, V_i(1)=6$ and $E_i(0)=6, E_i(1)=6$

$C_6 \odot K_{1,6}$ satisfies the condition of $|V_i(0) - V_i(1)| \leq 1$ and $|E_i(0) - E_i(1)| \leq 1$. Hence, $C_6 \odot K_{1,6}$ satisfies cordial labeling.

CONCLUDING REMARKS

We have proved that the H graph $H_n \odot K_1$, Shell graph $S_n \odot K_1$ and Cycle graph $C_n \odot K_{1,n}$ follows cordial labeling. Similarly, this process can be applied to duplicate, merge, or reconstruct graphs. In the future, this approach can be utilized for the reconstruction of various graph operations. Improving the comparability of outcomes across diverse graphs remains an active area of research.

ACKNOWLEDGEMENT

I extend my sincere appreciation to all individuals who contributed to the completion of this research paper. Your support, guidance, and valuable insights have been instrumental in shaping the outcomes of this study.

REFERENCES

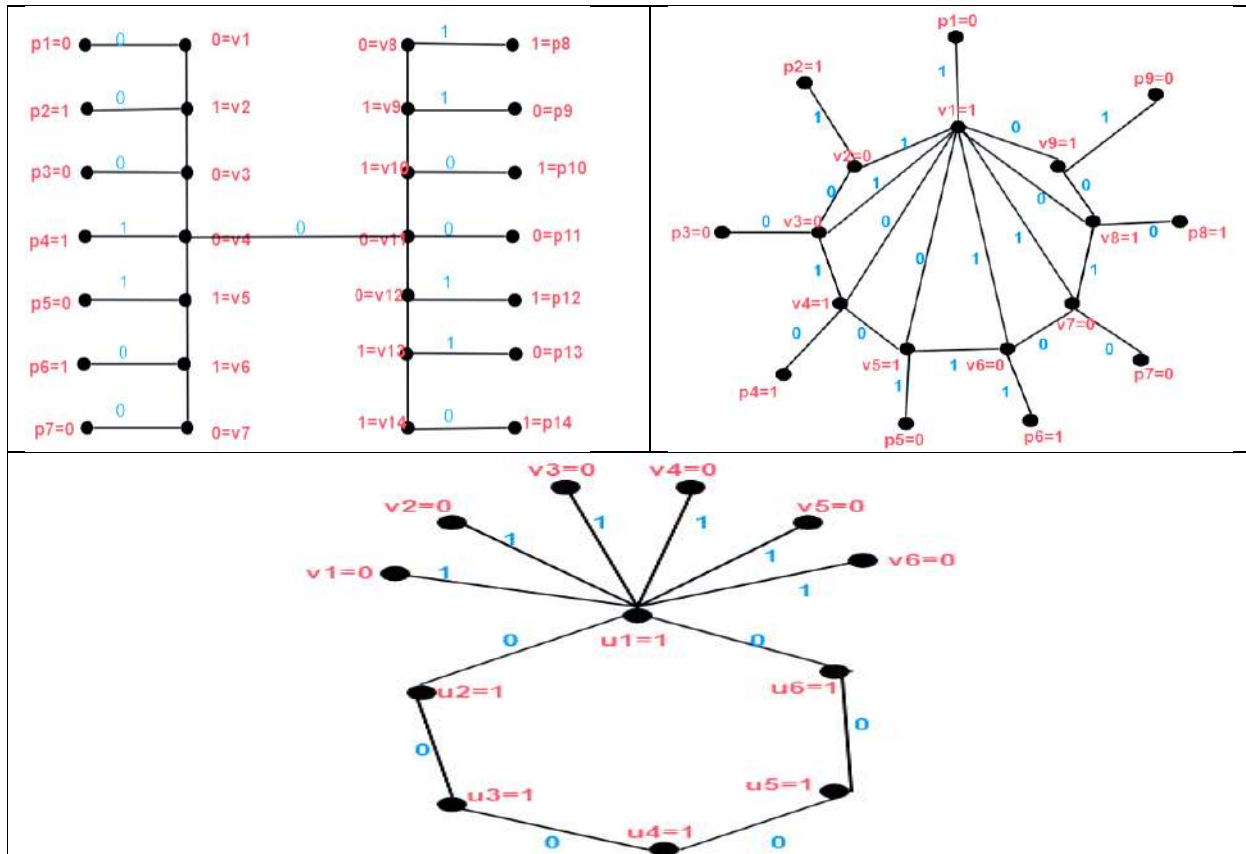
1. Barasara, C.M. and Prajapati, P.J. (2022) 'Prime cordial labeling for some path, cycle and wheel related graphs', *Advances and Applications in Discrete Mathematics*, 30, pp. 35–58.
2. Barasara, C.M. and Ghodasara, G. V. and Rokad, A.H. (2015) 'Product Cordial Labeling of Some Cycle Related Graphs', *International Journal of Innovative Research in Science, Engineering and Technology*, 4(11), pp. 11590-11594
3. Barasara, C. M. and Vaidya, S. K. (2012) 'Edge product cordial labeling of graphs,' *Journal of Mathematical and Computational Science*, 2(5), pp. 1436–1450.
4. Barasara, C.M. and Vaidya, S. K. (2011) 'Product Cordial Labeling for Some New Graphs', *Journal of Mathematics Research*, 3(2), pp. 206-2011





SlashiLeelet al.,

5. Kalab, R., Narayanana, S. and Ponraja, R. (2015) 'Radio mean labeling of a graph', *AKCE International Journal of Graphs and Combinatorics*, pp. 224–228.
6. Kumari, G. (2020), 'Graph labeling in graph theory', *Malaya Journal of Matematik*, 5(2), pp. 3943-3946
7. Revathi, N.(2013), 'Mean Labeling of Some Graphs', *International Journal of Science and Research*, pp. 2319-7064
8. Vaidya, S. K., & Barasara, C. M. (2012), 'Further results on product cordial labeling', *Mathematical Combinatorics*, 3, 64-71.





IoT Based Real-Time Water Level Monitoring and Early Warning cum Alert System for Dams

Ramesh Kumar Sah¹, Suman Lata^{2*}, Soma Deb² and Kalpana Sagar³

¹ARC Auto Tech Pvt Ltd. Noida, Uttar Pradesh, India 201310

²Department of Electrical Electronics and Communication Engineering, Sharda School of Engineering and Technology, Sharda University, Uttar Pradesh, 201301, India

³KIET Group of Institutions, AKTU, Ghaziabad, Uttar Pradesh, 201206, India

Received: 17 Apr 2023

Revised: 19 May 2023

Accepted: 31 May 2023

*Address for Correspondence

Suman Lata

Department of Electrical Electronics and Communication Engineering,
Sharda School of Engineering and Technology,
Sharda University, Uttar Pradesh, 201301, India
E. Mail: suman.lata@sharda.ac.in



This is an Open Access Journal / article distributed under the terms of the **Creative Commons Attribution License** (CC BY-NC-ND 3.0) which permits unrestricted use, distribution, and reproduction in any medium, provided the original work is properly cited. All rights reserved.

ABSTRACT

Flooding occurs due to heavy rainfall, heavy downpour or sudden release of water from dam. It may cause huge structural and human loss. Therefore, developing a reliable real-time water level monitoring as well as an early alert system becomes essential. This paper presents design and implementation of a real-time early warning cum alert system for monitoring of water level in a dam using IoT. It consists of alert devices (RTUs) at different locations and a water level sensor for level sensing. Siemens PLC is used as core controller. It processes the acquired data and transmits it over internet via 4G GSM/GPRS modem. Received data is compared with the reference threshold. In case water level is beyond threshold alert signals from RTUs activate strobe light, hooter and PA System according to preprogrammed sequences. For remote monitoring Node-Red GUI is used to display real time water level and status of alert systems.

Keywords: IoT, Dam, Water Level Monitoring, Water level Sensor, Early-Warning, GSM/GPRS Modem, PLC

INTRODUCTION

Dams/Water reservoirs are the main sources of water that are being used by Industries, Farmer's irrigation/farming, Livestock, hydroelectric power stations for generating electricity and so on. It also acts as a barrier/blockade that limits the unnecessary flow of water that may cause flooding resulting the damage of physical structures of bridges, flooding of cultivable fields/crops, lives and property of nearby areas. The variable hydrological conditions as well as



**Ramesh Kumar Sahet al.,**

seasonal changes call for storage and management of dams/reservoirs. This is required as the level of water may increase beyond the safe limits especially in Monsoon season [1]. Still conventional methods for controlling the dams and measuring the level of water are prevalent except for a few dams where monitoring of water level is automatized [2]. Such traditional way of monitoring of water level/flood is not fast, reliable and safe for the workers working at such vulnerable areas so that during emergency, fast, accurate and timely information can be delivered to the concerned authorities and the people living nearby to take the preventive actions on time. Therefore, there is a need of an early-warning cum alert system that accurately monitors and informs about the status of increasing water level or release of water from the dam in real-time so that the downriver natives can communicate to the safe zone. This can be achieved by the use of the latest and widely used technology, which is Internet of things (IoT). IoT is a collection of physical devices, like sensors, actuators etc. that are networked together in such a way which enables these devices to connect and exchange data over internet. Therefore, IoT can be implemented for monitoring of water level in dams and send the control command to the remote terminal unit RTUs installed at different remote locations to control the alert systems wirelessly from the central control station so that advance warning of flooding can be issued promptly and more efficiently. In the literature it has been found that many authors have focused on various applications based on IoT based monitoring. Authors Rapalir Shevale *et.al.* has presented and designed continuous monitoring system for smart cities using IoT. In this work authors focused on real-time monitoring water level and flow, temperature and water quality for making a city a smart city. Different sensors have been used for data collection and have been accessed through the website. It uses raspberry PI as a microcontroller for processing of signals collected from sensors and the data storage is done wirelessly using a Wi-Fi on cloud to prevent data loss and to ensure data security and safety [3]. Authors Tibin Mathew Thekkil *et.al.* implemented a WSN based flood detection system. For data collection CMOS image sensors has been used. Data transmission for remote monitoring is achieved using a Zigbee and GSM network. The data processing is done at the control station by analyzing and comparing the received data with reference data and generating alerts/warnings for clients using internet, email or SMS. Authors concluded that this system has overcome the shortcomings like poor network connection and high cost of traditional manual monitoring by the use of Zigbee which has low cost with better network connectivity [4]. Authors Devaraj Sheshu E *et.al.* developed a flood warning system using IoT.

For the measurement of flow rate IR sensor has been considered in this work. Also, for level measurement of water ultrasonic sensor has been used. Acquired data collected from these sensors is sent to the main controller using Wi-Fi technology for processing and is then transmits the obtained value of water level and flow rate to the NodeMCU. These values are compared with reference values. In case the sensed values are beyond the threshold, then an alert via SMS to the mobile phone of the concerned authority and/ or buzzer/alarm goes on. It also updates the same in the webpage in the form of graphs providing information in real-time [5]. Periodic flood monitoring system has been proposed by M.S. Baharum *et.al.* considering the increase or decrease in level of water and sending alert notifications to the users via GSM cellular network. [6]. Authors Anand Dersing reported a flood warning system using mobile and computer. Parameters of interest, namely, quantity of rainfall, water level and image have been collected periodically using an embedded data acquisition module. Through cellular data, the acquired information is sent to a server for storage [7]. A disaster alert as well as notification system using an android mobile phone has been proposed by S. Sarah *et.al.* Main component of the system was disaster management server (DMS) that contains the details of disaster prone areas. Present location of the user is provided by GPS provider and is transmitted to the server. Proposed android applications in phone determine the state of disaster exposed zone. Audio and visual means have been considered for notifying the shelter or the safe zone [8]. Authors R. Jayaramachandran *et.al.* focused on design and implementation of wireless rapid flood detection and warning system. It consists of electronic components assembled and programmed in such a way to monitor the increase/decrease of water level in remote locations or residential areas. The system has subunits, namely, water sensing unit and data display unit. The system uses arduino Uno AT mega 328 as a microcontroller to which all the low power consumption electronics peripherals are connected and communication takes place between them wirelessly via GSM module. Messages can be communicated to concerned people about the status of water level [9]. Author Uyipghosa B. Iyekiempo *et.al.* proposed and implemented flood monitoring system. Authors have used a wireless sensor network for it. The wireless sensor network consists of two nodes. The nodes consisted of a rain sensor module and water level



**Ramesh Kumar Sahet al.,**

sensors. The system uses Wemos D1 microcontroller to control each node along with additional components like GPS and memory. For testing validation various flood conditions have been simulated [10]. In paper [11] the early flood warning system has been powered by solar energy. The warning station has been integrated with the water level sensor and a precipitation sensor. A memory card has been used for storage of the data from and a GPRS system has been used for transmission of data to central monitoring station [11]. Authors Kavitha.R *et.al.* designed the application system with integration of Internet of Things for alert about the occurrence of flood due to rise in the water level in reservoirs/dams. The proposed system consists of Node MCU microcontroller, ultrasonic sensor to collect and transfer sensor data to cloud (Thing Speak) via Esp8266 Wi-Fi module. The cloud based database technique is used that supports the periodic monitoring of water level. It has been found that by using this technique the level of accuracy is increased as compared with ordinary method of monitoring and alerting system [12].

This paper mainly focuses on water level monitoring and early warning/alert system so as to monitor real-time water level status in a fast, accurate and more efficient way and alert the communities and local authorities in advance by early warning system in the form of siren sound, pre-recorded audio voice and beacon light using PLC. Section 2 of the paper is focused on system architecture and section 3 covers the wiring diagram. Section 4 is dedicated to software part and section 5 for implementation. Section 6 is covering the results and discussions and conclusions have been presented in section 7.

System Architecture**Block Diagram**

The proposed system design of a real-time monitoring of water level as well as early warning cum alert system for a dam using internet of things is given below in Fig.1. The system mainly, consists of

- a) Water level sensor
- b) Core controller (PLC)
- c) An alert system (Hooter, Strobe light, PA system with speaker)
- d) Control room
- e) Accessories

For data communication between the remote locations and control station a wireless GSM network (Via 4G GSM/GPRS Modem) has been used and 4G router with Static IP is connected to the host PC at control station in which the remote server (OpenVPN server) software is running continuously. The same PC is used to monitor the status of water level and control the alert system via node-red GUI, based on the wireless communication as shown in Fig 1. In order to measure the level of water, radar type water level sensor is used in the Barrage/Dam along with the remote terminal unit (RTU) which is connected to pre-warning/alert system. The level sensor senses the level of water, gathers data and sends it to the core microcontroller for further processing. It also analyzes and compares the processed data with the reference values to determine the water level and hence the flood danger status. If the water level increases beyond the safe threshold limit, the warning signal is generated, this in turn activates the alert system (Hooter, Strobe light, PA system) as per the pre-programmed sequence of the controller and repeats until the release of water is completed. Also, to monitor the status of water level and to remotely control the alert system in case of emergency from the central control station that is located far away from the remote locations, the data from RTUs (from remote locations) is wirelessly transmitted over the Internet via GSM/GPRS network using 4G cellular modem and it is received at the defined port (say port 1194) of Server having static IP that is connected through router via Ethernet to the server PC. The data collected by router is transmitted serially to the data processing software (Node-red) for the purpose of monitor, storage and display. The software also records the logs, generates trends and alarms. The control command is also sent from the application software via Router with static IP over GSM/GPRS network to control the alert systems at remote locations.





Ramesh Kumar Sahet *et al.*,

The hardware description along with specifications

Sensor for water level measurement

The radar type water level sensor sensor VEGAPLUS WL 61 is an economical solution through versatile and simple mountings and is ideal sensor for continuous water level measurement related applications. It can measure with high accuracy being unaffected by pressure, temperature, steam and fog. During Operation, the antenna system of the radar sensor emits the extremely short duration (approx. 1 ns) microwave impulses (radar pulses) in the direction of the product to be measured. The reflected pulses from surface are received as echoes by the radar sensor of antenna system that is converted into an appropriate output signal. The measuring range of this sensors is upto 15m with deviation of ± 2 mm. The operating voltage of it is 9.6 to 36 V DC. [13] [14];

Programmable Logic Controller (PLC)

To meet the requirement of the Hydropower Dam/ Reservoir water level monitoring and hence the early warning cum alert system before the release of water, SIEMENS SIMATIC S7-1200 PLC has been selected to function as the remote terminal unit installed at three different remote locations at site. It has Number of Integrated Digital Outputs (DO) and Digital Inputs (DI) Channels are 10 and 14, respectively, whereas Number of Integrated Analog Inputs (AI) Channels are 2. The detailed technical Specification of the PLC is given below [15] [16];

Alert System

The Alert System consists of, Hooter, PA system and Strobe Light. The details of each have been given below.

Electronic Hooter

An electronic hooter of Model No. HDT-325 of Kheraj make has been used in this work. It is used to produce the loud range audible sound so that it reaches to the several kilometers distance to alert the people/ communities [17]. It can be used as horizontal mounting and is audible upto 3.25Km.

Strobe Light (Aviation Lamp)

A surface mount type red-colored strobe light of high intensity has been installed at the different remote locations as an emergency/alert conditions. The model number of the selected strobe is BL-24-AM-SN and is made by Winpow Tech. The strobe light is connected to the RTUs and can be controlled both automatically or through the application software. The light intensity produced by it is 1000 Lumens (+/- 5%), and requires an operating voltage of 24V DC and operating temperature of 20°C to 80°C. The body material of this strobe light is Aluminium [18].

Pre-announcement) System

The Pre-announcement (PA) System which is basically an electronic sound amplification and distribution system consisting of microphone, amplifiers, loudspeakers/horn etc has been used as a common system to address the public or community at a distance. To alert the public before the release of water from the dam pre-announcements through the speakers have been used. The power requirements of it are 220-240V AC, 50/60Hz|DC 12V and frequency specifications are 50-15000 Hz +/- 3Db [19].

Loud Speaker (Horn)

The Kheraj make Loud-Speaker of Model PUH 60 XT has been used in this work. It is also used in the form of alert as sounds is loud enough to be audible at a distance. Multiple (2 Nos.) loud speaker is connected to the pre-announcement system and installed at each remote locations to play the pre-recorded voice announcement before the water is released from the dam/reservoir upstream. The frequency range supported by it is 180Hz -7000Hz [20].

Control Room

Main parts of control have been described in following section.

3G/4G Modem with Antenna and SIM Card

LTE & WCDMA 4G router manufactured by San Telequip (P) Ltd. has been used in this research work as it supports data transmission through public LTE-FDD network. It has been selected as it is widely used in machine to machine

57504



**Ramesh Kumar Sahet al.,**

fields. It has Industrial 32-bits CPU with embedded real-time operating system. For wired communication it has an ethernet port and supports RS232, RS485/RS422 protocols. For optimizing the power, it can be adopt three modes of operation, namely, sleep mode, scheduled online/offline mode, scheduled power-on/power-off modes. The entire housing is made up of Iron with IP30 protection. It enters into communication state automatically when it is powered by 5-36V DC supply. The device has management software for remote management/maintenance and configuration according to the user requirement [21].

Server PC

An Industrial 32-bits CPU with flash memory of 16MB (Extendable upto 64MB) and DDR2 memory of 128MB (Extendable to 256 MB) has been used in control room.

4G LTE Router

To collect the data wirelessly from RTUs deployed at different remote locations, and to send the control command to the RTUs, the 4G LTE Router with Static (Fixed) IP address SIM card is used. The data transmitted wirelessly over the GPRS network to the Control station is received at that fixed IP without any loss of data. It acts as a gateway between the GPRS network and the Server PC. The gateway also functions as a data collector that continuously collects data wirelessly from remote RTUs at its Specific Open port say 1194 and send the collected data using to the PC for further display, processing and storage. There is a wired connection (cat6 UTP Ethernet Cable) between gateway and CPU of PC for the serial data transfer. The real-time data collected at the open port of the router is further processed using Node-red software running on the PC and can be visualized in Node-red GUI dashboard. The TP Link Archer MR 200 AC750 Wireless Dual Band 4G LTE Router is used in our application [22].

LTE supports 150Mbps+ downloading speed and 50 Mbps uploading speed.

Other important specifications are listed below.

Wireless: 300 Mbps on 2.4GHz + 433 Mbps on 5GHz

Antennas: 2 Detachable External 4G LTE Antennas

Ports: 1 10/100Mbps LAN/WAN+ 3 10/100 Mbps LANs

Misellaneous**UPS (Uninterruptible Power Supply)**

For the continuous power supply without interruption in case of main supply failure, the RTUs and Modems at all the remote locations are connected with the External UPS having 2 hours battery backup. In Control station, the Server PC is also connected with the UPS Power backup. In present work, the Liebert.GXTMT+Cx UPS manufactured by Emerson Power Network has been used. Detailed specification sheets can be checked from [23].

Ethernet Cable

The D-link Cat-6, 24AWG UTP cable used in the work to communicate between PLC and the 3G/4G Modem or between Server PC and router/Gateway. It is the most-suited pair cables for transmitting data over LANs at 100 Mbps (approx. 1 GB per second) with a frequency of 250 MHz. It is also suitable for 10 BASE-T, fast Ethernet and Gigabit Ethernet as these cables reduce the cross talk and system-noise [24].

SMPS (Switched Mode Power Supply)

Conversion of AC/DC input voltage to a regulated DC output voltage is done using SMPS. In this work, Delta make SMPS of Model PMC-24V036W1AA has been considered to convert 230V AC supply into 24V DC supply to operate the PLC, Emergency button and the Modem used at different remote locations [25].

Emergency Push Button

It is a special type of fail-safe control switch or circuit that performs the emergency shutdown operation of the associated equipment/electrical systems. It is used manually in emergency condition when automatic fails to stop the main supply of the RTU panel.





Ramesh Kumar Sahet *al.*,

Wiring connections (Connection diagram for I/O Allocation)

Connection of DI, DO Terminal Block is shown in Fig 2 below.

Software Description

Siemens Totally Integrated Automation (TIA) Portal V15.0 has been used in this work to create the blocks of programs by using Ladder instructions and also used to upload/ download program to the siemens s7- 1200 PLC [26]. The PLC is programmed in such a way that the Dam control system generates an alarm when the predefined abnormal condition is sensed by the radar type water level sensor installed at barrage site.

Based upon this input, it will activate all the local stations. Immediately upon activation, the strobe light will turn on along with the Public Announcement (PA) system at all the local locations giving out the pre-recorded "ALARM" message in form of voice in their local languages and this will continue for the first 3 minutes. After 3 minutes, the PA system stops and siren (Hooter) will start sounding and will continue for next 5 minutes along with the strobe light. Again after 5 minutes, the siren stops and the PA system will resume giving out "ALARM" message i.e. pre-recorded voice for next 3 minutes. This sequence is repeated till the alarm conditions return to normal i.e. till the water is being released from the dam or until the process is stopped manually from the Barrage control room.

Node-Red Programming

Node-Red developed by IBM is a GUI based programming tool which is an Open Source software. It is used for integrating hardware components, Application Programming Interfaces and as well as various online services. It has a flexible and powerful library of tools enabling wiring of wide range of nodes in the palette for development of prototypes. It helps in creating the interactive Graphical User Interface /Dashboards. The Node-Red dashboard acts as an output window for displaying the real time status of all the connected devices and provides access to control the devices. [27] [28]. The Node-Red flows used in this work is shown in Fig.3 below.

OpenVPN Setup, Installation and Configuration

OpenVPN is an Open Source Virtual Private network (VPN) System which has been used to create secure site-to-site connections. OpenVPN tunnel has been established between server and client and Multiple OpenVPN clients have been connected to the same OpenVPN server. OpenVPN Configuration involves two Steps. First one is building a separate-certificate and private keys for the server and each client and second one is configuring server and clients. For building certificates and private keys for OpenVPN server and multiple clients, vars.bat.sample file is suitably modified and saved. To build certificate and key, build-ca command has been used. To build a certificate and private key for server, build-key-server server has been used. To build Diffie Hellman key/parameters, the command is build-dh. To build a certificate and private key for client1, type build-key client1 [29]. To build a certificate and private key for client2, type build-key client2. Same steps have been repeated for client3, client4 etc. To build ta.key, type command as openvpn --genkey --secret keys/ta.key. In order to configure OpenVPN as a server, go to C:\OpenVPN\sample-config folder, open server.opvn file and modify and save it.

Configuration of GSF 8372 as OpenVPN Client

To configure GSF 8372 as OpenVPN client, from the web browser settings of GSF 8372 have been opened by using default IP address mentioned on the GSF 8372 and using default username and password to login. After that, security settings like setting in APN Name and disable firewall have been considered. After that settings like, OpenVPN client settings, public static IP, Port number and set other settings have been initiated as shown in Fig. 5 below. In next step, ca.crt, client1.crt, and client1.key files from 'begin certificate' to 'end certificate' in the certificate section are copied and saved. OpenVPN client gets connected to the OpenVPN server. Same procedure is repeated for the client2 and client3 to configure so as to connect them to the same OpenVPN server. After the connection has been established, OpenVPN server having IP 192.168.105.24 will be able to ping GSF 8372 client 1 having IP 1192.168.105.21, client2 (192.168.105.31) and client3 (192.168.105.41) [30].



**Ramesh Kumar Sahet al.,****Implementation**

The designed system for early warning cum alert system before release of water has been implemented using Radar type ultrasonic water-level sensor, PLC, GSM/GPRS Modem, Hooter, PA-System with loud-speakers, Strobe light, along with Node-red Server at Barrage of HPPCL (Himachal Pradesh Power Corporation limited), sawda-kuddu, Hatkoti, Dist. Shimla, India. The alert system has been installed at 3 different locations

At the very first stage of implementation, it involves determination of water level in dam by using Radar type ultrasonic water level sensor mounted on the top of a dam at a distance of 10 meters surface of water, which is used for calculating the distance between the sensor and surface of water. If distance goes below the defined point, it indicates that the level of water in the dam has exceeded to the optimal level and vice-versa. The water level sensor is interfaced with the PLC. It is programmed in such a way that it acquires the data of water level at the interval of every 3 seconds and it wirelessly delivers the acquired data using GSM/GPRS telemetry via modem to the Dam control room server PC connected to Router having Static Ip Sim Card for data processing, display and data storage. The data acquired by the server PC is Displayed on the Node-Red GUI so that the operators at the control room can take decision to open /close gate of dam when water is required to release from dam. Since, the communication between different locations to the control room uses GSM/GPRS Telemetry, it can be controlled/monitored as per requirements from anywhere in the world where network connectivity is present. The control signals can also be sent manually through the dashboard to the controller to turn PA system, Hooter, strobe light ON and OFF before the release of water from the dam or during the emergency situations.

RESULTS AND DISCUSSION

The results obtained by the system implementation, we can see that as the Dam is fully empty, the sensor senses minimum level i.e zero level and it is displayed on Gauge on Node-red GUI. This condition shows normal therefore all the status of Alert/warning system is at normal state as shown in Fig.7a). As the Dam starts to store the water, the water level sensor senses the real-time values of water level and is displayed on gauge on Node-red GUI as shown in Fig.7b). The status of strobe light, PA system, Hooter, Emergency press for all the remote locations are displayed on the node-red GUI as shown in Fig.7c).

CONCLUSIONS AND FUTURE WORK

This Paper Successfully implemented & Tested IoT based early warning system with alert status and remote water level monitoring system dam. This designed system is more flexible, easily configurable, cheap and fast. The designed system automatically issues/generate a warning/alert by sounding hooters, PA-Systems or through Strobe-light to alert the peoples living around the dam side areas and prevents from disasters. Therefore, it solved the issues related to manual monitoring and control. As the system uses GSM/GPRS Cellular networks for communication, the system can be monitored /controlled from anywhere in the world. As the designed system is capable of incorporating more remote locations, we can add sms alert features and CCTV footage to the data to send the information about the downstream surroundings of the dam before the release of water. In future, mobile apps can be developed to find the spots where the flood may occurs. We can also extend the system to a complete disaster management system by taking into account all the major natural disaster like landslide, earthquakes etc.

ACKNOWLEDGMENTS

Authors would like to acknowledge the support extended by M/s Telecon Systems, Noida, Uttar Pradesh, India and its IT and an Automation Team for providing the constant encouragement and guidance for the successful completion of the project and using the data for publication. Authors will also like to thank Shrada University for providing the laboratory support for carrying out this work.





Ramesh Kumar Sahet *al.*,

REFERENCES

1. Monjardin, F.Cris Edward.Uy, A. Francis Aldrine. Tan, J. Fibor Cruz, G.FebusReidj, " Automated Real-time Monitoring System (ARMS) of Hydrological Parameters for Ambuklao, Binga and San Roque Dams Cascade in Luzon Island, Philippines," IEEE Conference on Technologies for Sustainability (Sus Tech), 2017.
2. Sai SreekarSiddula, P. Jain and Madhur Deo Upadhayay, "Real Time Monitoring and ontrolling of Water Level in Dams using IoT," 8th International Advance omputingonference (IACC),
3. ShevaleRupalir, Karad Shweta, Merchant Maryam, Kardile Ashwini and Vijeyata Mishra, " IOT Based Real time water Monitoring System for Smart City," International Journal of Innovative Science and Research Technology, Vol 3, Issue 4, 2018.
4. Tibin Mathew Thekkil and N.Prabakaran,"Real-time WSN Based Early Flood Detection and Control Monitoring System," IEEE International Conference on Intelligent Computing, Instrumentation and Control Technologies (ICICT), 2017.
5. E.DevarajSheshu, N.Manjunath, S.Karthik and U.Akash, " Implementation of Flood Warning System using IoT," IEEE Second International Conference on Green Computing and Internet of Things (ICGCIOT), 2018.
6. M.S.Baharum, R. A. Awang and N.H.Baba, " Flood Monitoring System 2011," IEEE International Conference on System Engineering and Technologies (ICSET).
7. Anand Dersingh, Department of Computer Engineering , Assumption University, Bangkok, Thailand, "Design and Development of a Flood Warning System viaMobile and Computer Networks".
8. S.Sarah, M.Dilip and R.RahulAravindh, Disaster Alert amd Notification System Via Android Mobile Phone by Using Google Map," International Research Journal of Engineering and Technology (IRJET) 2395-0072, Volume 03, Issue 04, April 2016.
9. R.Jayaramachandran, S.Lingamoorthy and S.Ohmshankar, "Wireless Based Rapid Flood Detection and Warning System 2017," International Conference on Innovative Trends In Engineering And Technology (ICITET).
10. UyipghosaB.lyekekepolo, Francis E. Idachaba and Segun I.Popoola, "Early Flood Detection and Monitoring System Based on Wireless Sensor Network," IEEE Proceedings of the International Conference on Industrial Engineering and Operations Management, Washington DC,USA, September 27-29, 2018.
11. Hung Ngoc Do, Minh-Thanh, Van-Su, Phuoc Vo Tan and Cuong Viet Trinh, "An Early Flood Detection System Using Mobile Networks," IEEE International Conference on Advanced Technologies for Communications (ATC), 2015.
12. R.Kavitha, R.Kavitha, C.Jayalakshmi and k.Senthil Kumar, "Dam Water Level Monitoring and Alerting System using IOT," International Journal of Electronics and Communication Engineering (SSRG-IJECE), Volume 5, Issue 6, June 2018.
13. VEGAPLUS WL 61 4.20 MA/HART two-wire Specification sheet
14. VEGAPLUS WL 61 4.20 MA/HART two-wire Operating Instruction User Manual
15. SIMATIC S7-1200 " Siemens AG 2010"
16. SIEMENS Data Sheet 6ES7214-1AG40-0XB0
17. Kheraj Sierens Product Catalog
18. Winpow Aviation Lamp Model BL-24-AM-SN "Product catalogue"
19. Mega Denson 80U P.A. "User Manual"
20. Kheraj PUH 60 XT Horn Product Catalogue
21. San Telequip LTE & WCDMA ROUTER, Model 8372 product Specification
22. TP Link Archer MR200, "User Guide"
23. Liebert GXT MT+ CX,"User Manual- 1000-3000VA"
24. D-Link CAT-6-UTP-Cable, "User Manual"
25. Delta Electronics SMPS installation Manual
26. SIMATIC TIA Portal STEP 7 Basic V15, " User Manual





Ramesh Kumar Sahet al.,

27. Gaurav A. Bedge and Vijay M.Purohit, "IoT Based Weather Monitoring System using Mqtt," International Conference on Smart Systems (ICSS-2018), School of Engineering, Ajeenkya DY Patil University, Pune, India, September, 2018.
28. M.Pongothai, A.L.Karupaiya and R.Priyadarshini, "Implementation of IoT Based Smart Laboratory," International Journal of Computer Applications (0975-8887), Volume 182-No.15, September 2018.
29. Robustel Application Note v.1.0.0 openVPN Client with x.509 certificates.
30. San Telequip OpenVPN testing, "User Guide"

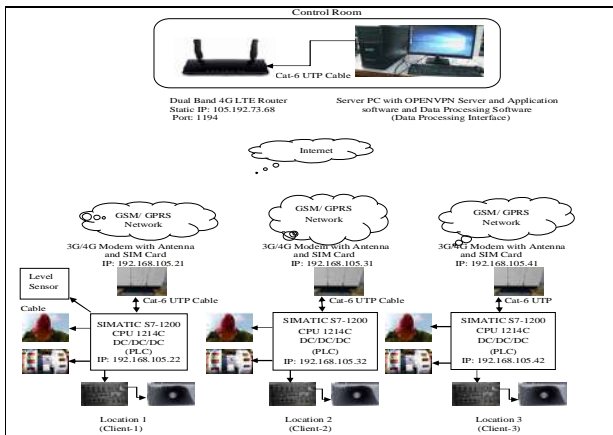


Fig.1. Architecture of the IoT based real-time water level monitoring and early warning system

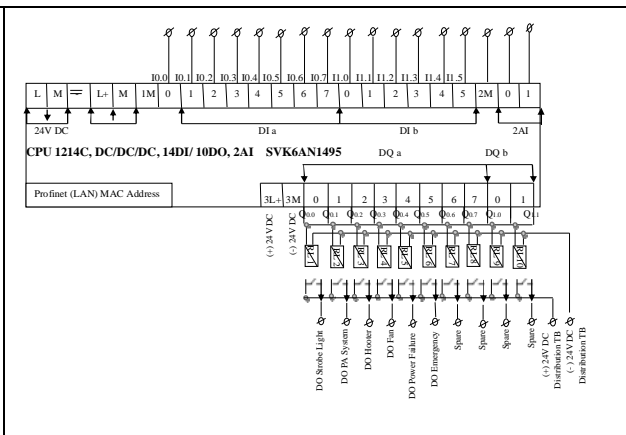


Fig. 2. Wiring diagram of S7-1200 PLC for I/O allocations

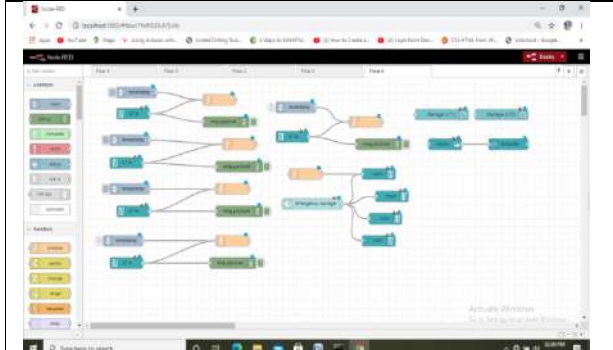


Fig. 3. Node-red flows used in the work

```

Administrator: Command Prompt
Using configuration from openssl-1.0.0.cnf
Check that the request matches the signature
Signature ok
The Subject's Distinguished Name is as follows
countryName      : PRINTABLE: 'IN'
stateOrProvinceName : PRINTABLE: 'MP'
localityName     : PRINTABLE: 'sausa-kaddu'
organizationName : PRINTABLE: 'HPSL'
organizationalUnitName: PRINTABLE: 'client1'
commonName       : PRINTABLE: 'Tel'
emailAddress     : PRINTABLE: 'automation@telcelon-systems.com'
Certificate is to be certified until Feb 21 06:10:42 2031 GMT (3650 days)
Can the certificate be certified? [y/n]y

1 out of 1 certificate requests certified, commit? [y/n]y
Write out database with 1 new entries
Data Base Updated

C:\OpenVPN\easy-rsa>
    
```

Fig. 4. CA Certificate for Client1



Fig. 5. GSF 8372 modem configuration as OpenVPN Client1





Ramesh Kumar Sahet *et al.*,

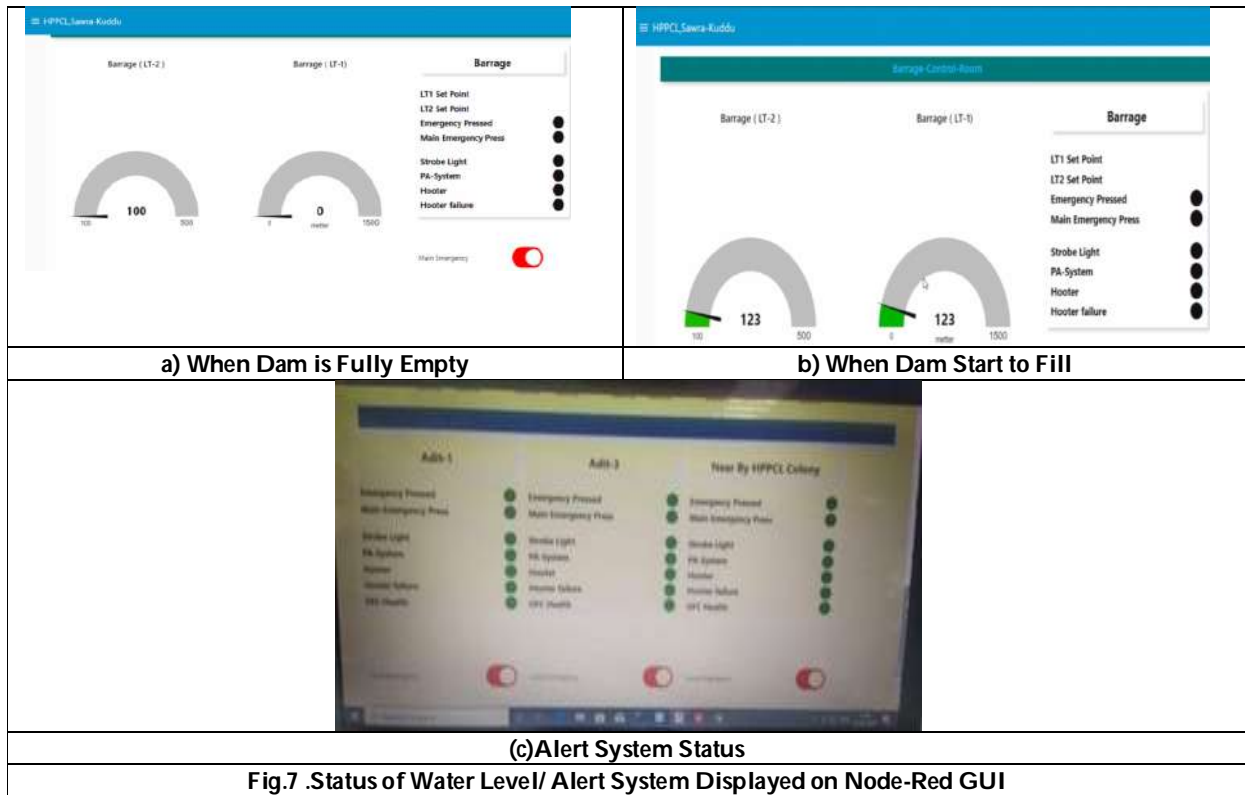


Fig.7 .Status of Water Level/ Alert System Displayed on Node-Red GUI





Few Summation Theorems for Appell's Function F_2 of Second kind having different Arguments

Bhawna Gupta^{1*}, M.S.Baboo¹ and Ashfaq Ahmad²

¹School of Basic Sciences and Research, Sharda University, Greater Noida, Uttar Pradesh, 201306, India

²Department of Applied Sciences and Humanities, Faculty of Engineering and Technology, Jamia Millia Islamia, New Delhi-110025, India.

Received: 17 Apr 2023

Revised: 14 May 2023

Accepted: 31 May 2023

*Address for Correspondence

Bhawna Gupta

School of Basic Sciences and Research,

Sharda University,

Greater Noida,

Uttar Pradesh, 201306, India.

E. Mail: 2022302257.bhawna@dr.sharda.ac.in



This is an Open Access Journal / article distributed under the terms of the **Creative Commons Attribution License** (CC BY-NC-ND 3.0) which permits unrestricted use, distribution, and reproduction in any medium, provided the original work is properly cited. All rights reserved.

ABSTRACT

The aim of this paper is to finding the closed forms of several reduction formulas for "Appell's" double hypergeometric function of second kind $F_2[A; B; C; B, D; x, y]$ with suitable adjustment of parameters and convergent conditions, where y takes the form $\frac{(1-x)}{2}, \frac{8(1-x)}{9}, \frac{1-x}{4}, \frac{1-x}{9}, \frac{x-1}{3}, \frac{x-1}{8}, \frac{3(1-x)}{4}, \frac{(\sqrt{2}-1)(1-x)}{(\sqrt{2}+1)}$ and more rational functions of x .

Keywords: Generalized hypergeometric function, Appell functions of Second kind, Generalized Kummer's First, Second and third summation theorem.

INTRODUCTION, DEFINITIONS AND PRELIMINARIES

Let \mathfrak{R} and \mathbb{C} represent the sets of real and complex numbers, respectively, in the standard notation.

$N_0 := N \cup \{0\}$, $N = \{1, 2, 3, \dots\} = N_0 \setminus \{0\}$,

$Z_0^- := \{0, -1, -2, -3, \dots\} = Z^- = \{-1, -2, -3, \dots\}$

and $Z_0^- \cup N$ consisting of sets of integers.





Bhawna Gupta et al.,

“ KUMMER’S SECOND SUMMATION THEOREM”:is given by, (see [7, p.134])

$${}_2F_1 \left[\begin{matrix} a, b; \\ 1+a+b; \end{matrix} \frac{1}{2} \right] = \frac{\Gamma(\frac{1}{2})\Gamma(\frac{1+a+b}{2})}{\Gamma(\frac{a+1}{2})\Gamma(\frac{b+1}{2})}; \quad \left(\frac{1+a+b}{2} \in \mathbb{C} \setminus \mathbb{Z}_0^- \right) \tag{1.1}$$

“ KUMMER’S THIRD SUMMATION THEOREM”: is given by, (see [7, p.134])

$${}_2F_1 \left[\begin{matrix} a, 1-a; \\ c; \end{matrix} \frac{1}{2} \right] = \frac{2^{1-c} \sqrt{\pi} \Gamma(c)}{\Gamma(\frac{c+a}{2})\Gamma(\frac{c+1-a}{2})} = \frac{\Gamma(\frac{c}{2})\Gamma(\frac{c+1}{2})}{\Gamma(\frac{c+a}{2})\Gamma(\frac{c+1-a}{2})}; \quad (c \in \mathbb{C} \setminus \mathbb{Z}_0^-). \tag{1.2}$$

“ APPELL’S FUNCTION OF SECOND KIND ” :

In the year 1880 Appell’s defined the following double hypergeometric series (see [3, p.73, Equation 4] see also[14, p.211. Equation 8.1.6])

$$F_2[A, B, C, D, G; x, y] = \sum_{s=0}^{\infty} \frac{(A)_s (C)_s y^s}{(G)_s s!} {}_2F_1 \left[\begin{matrix} A + S, B; \\ D; \end{matrix} x \right] \tag{1.3}$$

“ CONVERGENCE CONDITIONS OF APPELL’S DOUBLE SERIES F_2 ”

The series F_2 of Appell’s is convergent when $|x| + |y| < 1; A, B, C, D, G \in \mathbb{C} \setminus \mathbb{Z}_0^-$.

The series F_2 of Appell’s is absolutely convergent when $|x| + |y| = 1; x \neq 0, y \neq 0; A, B, C, D, G \in \mathbb{C} \setminus \mathbb{Z}_0^-$ and $R(A + B + C - D - G) < 0$.

When A is a negative integer, then Appell’s series F_2 will be a polynomial $B, C, D, G \in \mathbb{C} \setminus \mathbb{Z}_0^-$.

When B, C are negative integers, then Appell’s series F_2 will be a polynomial $A, D, G \in \mathbb{C} \setminus \mathbb{Z}_0^-$.

Now the “absolutely” and “conditionally” convergence of Appell’s series F_2 see [5] .

APPLICATION OF $F_2[A; B, C; B, D; x, y]$ IN REDUCTION FORMULAS

The second kind of Appell’s function is explain as equation (1.3) can also be written as

$$F_2[A; B, C; B, D; x, y] = (1-x)^{-A} {}_2F_1 \left[\begin{matrix} A, C; \\ D; \end{matrix} \frac{y}{(1-x)} \right], \tag{2.1}$$

$$(|x| + |y| < 1, |x| < 1, \left| \frac{y}{1-x} \right| < 1; D \in \mathbb{C} \setminus \mathbb{Z}_0^-)$$

Putting the values "A = a, B = b, C = c, D = $\frac{1+a+c}{2}$ and $y = \frac{1-x}{2}$ ", in above equation (2.1) and use the Kummer’s second summation theorem’, we get

$$F_2 \left[a; b, c; b; \frac{1+a+c}{2}; x, \frac{1-x}{2} \right] = \frac{\Gamma(\frac{1}{2})\Gamma(\frac{1+a+c}{2})}{(1-x)^a \Gamma(\frac{1+a}{2})\Gamma(\frac{1+c}{2})} \tag{2.2}$$

$$(|x| + \left| \frac{1-x}{2} \right| < 1; \frac{-1}{3} < R(x) < 1, \text{ when } \text{Im}(x) = 0; \frac{1+a+c}{2} \in \mathbb{C} \setminus \mathbb{Z}_0^-)$$

Putting the values "A = a, B = b, C = c, D = $\frac{1+a+c-m}{2}$ and $y = \frac{1-x}{2}$ ", in above equation (2.1) and use the Kummer’s second summation theorem’ [10, p.491, Entry (7.3.7.2)], we get

$$F_2 \left[a; b, c; b; \left(\frac{1+a+c-m}{2} \right); x, \frac{1-x}{2} \right] = \frac{2^{c-1} \Gamma\left(\frac{a+c+1-m}{2}\right)}{(1-x)^a \Gamma(c)} \sum_{r=0}^m \left\{ \binom{m}{r} \frac{\Gamma\left(\frac{c+r}{2}\right)}{\Gamma\left(\frac{a+1+r-m}{2}\right)} \right\} \tag{2.3}$$

$$\left(|x| + \left| \frac{1-x}{2} \right| < 1; \frac{-1}{3} < R(x) < 1, \text{ when } \text{Im}(x) = 0; c, \frac{1+a+c-m}{2} \in \mathbb{C} \setminus \mathbb{Z}_0^-, m \in \mathbb{N}_0 \right),$$





Bhawna Gupta et al.,

Putting the values "A = a, B = b, C = c, D = $\frac{1+a+c-m}{2}$ and y = $\frac{1-x}{2}$ ", in above equation (2.1) and use the Kummer's second summation theorem' [13, p.827, Theorems (1)], we get

$$F_2 \left[a, b, c, b, \left(\frac{1+a+c-m}{2} \right); x, \frac{1-x}{2} \right] = \frac{2^{c-1} \Gamma \left(\frac{a+c+1-m}{2} \right)}{(1-x)^a \Gamma(c)} \sum_{r=0}^m \left\{ \binom{m}{r} \frac{\Gamma \left(\frac{c+r}{2} \right)}{\Gamma \left(\frac{a+1+r-m}{2} \right)} \right\} \tag{2.4}$$

$$\left(|x| + \left| \frac{1-x}{2} \right| < 1; \frac{-1}{3} < R(x) < 1, \text{ when } \text{Im}(x) = 0; c, \frac{a+c+1-m}{2}, \frac{a-c+1-m}{2} \in \mathbb{C} \setminus \mathbb{Z}_0^-, m \in N_0 \right)$$

Putting the values "A = a, B = b, C = c, D = $\frac{a+c-m}{2}$ and y = $\frac{1-x}{2}$ ", in above equation (2.1) and use the Kummer's second summation theorem' [11, p.48, Equation (3.1)], we get

$$F_2 \left[a, b, c, b, \left(\frac{a+c-m}{2} \right); x, \frac{1-x}{2} \right] = \frac{2^{a-1} \Gamma \left(\frac{a+c-m}{2} \right)}{(1-x)^a \Gamma(a)} \sum_{r=0}^m \left\{ \binom{m}{r} \left[\frac{\Gamma \left(\frac{r+a}{2} \right)}{\Gamma \left(\frac{c+r-m}{2} \right)} + \frac{\Gamma \left(\frac{r+a+1}{2} \right)}{\Gamma \left(\frac{c+r-m+1}{2} \right)} \right] \right\} \tag{2.5}$$

$$\left(|x| + \left| \frac{1-x}{2} \right| < 1; \frac{-1}{3} < R(x) < 1, \text{ when } \text{Im}(x) = 0; a, \frac{a+c-m}{2} \in \mathbb{C} \setminus \mathbb{Z}_0^-, m \in N_0 \right)$$

Putting the values "A = a, B = b, C = c, D = $\frac{a+c-m}{2}$ and y = $\frac{1-x}{2}$ ", in above equation (2.1) and use the Kummer's second summation theorem' [11, p.48, Equation (3.3)], we get

$$F_2 \left[a, b, c, b, \left(\frac{a+c+m}{2} \right); x, \frac{1-x}{2} \right] = \frac{2^{a-1} \Gamma \left(\frac{a+c+m}{2} \right) \Gamma \left(\frac{c-a-m}{2} \right)}{(1-x)^a \Gamma(a) \Gamma \left(\frac{c-a+m}{2} \right)} \sum_{r=0}^m \left\{ \binom{m}{r} \left[\frac{(-1)^r \Gamma \left(\frac{r+a}{2} \right)}{\Gamma \left(\frac{c+r-m}{2} \right)} + \frac{(-1)^r \Gamma \left(\frac{r+a+1}{2} \right)}{\Gamma \left(\frac{c+r-m+1}{2} \right)} \right] \right\} \tag{2.6}$$

$$\left(|x| + \left| \frac{1-x}{2} \right| < 1; \frac{-1}{3} < R(x) < 1, \text{ when } \text{Im}(x) = 0; a, \frac{a+c+m}{2}, \frac{c-a-m}{2} \in \mathbb{C} \setminus \mathbb{Z}_0^-, m \in N_0 \right)$$

Putting the values "A = a, B = b, C = 1 - a, D = d and y = $\frac{1-x}{2}$ ", in above equation (2.1) and use the Kummer's second summation theorem', we get

$$F_2 \left[a; b, 1-a; b, d; x, \frac{1-x}{2} \right] = \frac{\Gamma \left(\frac{d}{2} \right) \Gamma \left(\frac{d+1}{2} \right)}{(1-x)^a \Gamma \left(\frac{d+a}{2} \right) \Gamma \left(\frac{d+1-a}{2} \right)} \tag{2.7}$$

$$\left(|x| + \left| \frac{1-x}{2} \right| < 1; \frac{-1}{3} < R(x) < 1, \text{ when } \text{Im}(x) = 0; d \in \mathbb{C} \setminus \mathbb{Z}_0^- \right)$$





Bhawna Gupta et al.,

Putting the values "A = a, B = b, C = 1 – a – m, D = dandy = $\frac{1-x}{2}$ ", in above equation (2.1) and use the Kummer's second summation theorem' [13, p.828, Theorem (6)], we get

$$F_2 \left[a, b, 1-a-m, b, d; x, \frac{1-x}{2} \right] = \frac{2^{1-m-d} \Gamma\left(\frac{1}{2}\right) \Gamma(d)}{(1-x)^a \Gamma\left(\frac{d-a}{2}\right) \Gamma\left(\frac{d-a+1}{2}\right)} \sum_{r=0}^m \left\{ \binom{m}{r} \left[\frac{\Gamma\left(\frac{d-a+r}{2}\right)}{\Gamma\left(\frac{d+a+r}{2}\right)} \right] \right\} \tag{2.8}$$

$\left(|x| + \left| \frac{1-x}{2} \right| < 1; \text{ when } \text{Im}(x) = 0; d, d-a \in \mathbb{C} \setminus \mathbb{Z}_0^- \right)$

Putting the values "A = a, B = b, C = 1 – a + m, D = dandy = $\frac{1-x}{2}$ ", in above equation (2.1) and use the Kummer's second summation theorem' [13, p.828, Theorem (5)], we get

$$F_2 \left[a, b, 1-a+m, b, d; x, \frac{1-x}{2} \right] = \frac{2^{1+m-d} \Gamma\left(\frac{1}{2}\right) \Gamma(d) \Gamma(a-m)}{(1-x)^a \Gamma(a) \Gamma\left(\frac{d-a}{2}\right) \Gamma\left(\frac{d-a+1}{2}\right)} \sum_{r=0}^m \left\{ \binom{m}{r} \frac{(-1)^r \Gamma\left(\frac{d-a+r}{2}\right)}{\Gamma\left(\frac{d+a+r}{2}-m\right)} \right\} \tag{2.9}$$

$\left(|x| + \left| \frac{1-x}{2} \right| < 1; \frac{-1}{3} < R(x) < 1, \text{ when } \text{Im}(x) = 0; d, a, a-m, d-a \in \mathbb{C} \setminus \mathbb{Z}_0^- \right)$

Putting the values "A = a, B = b, C = –a – m, D = dandy = $\frac{1-x}{2}$ ", in above equation (2.1) and use the Kummer's second summation theorem' [12, Equation (3.3)], we get

$$F_2 \left[a, b, -a-m, b, d; x, \frac{1-x}{2} \right] = \frac{2^{-a-m-1} \Gamma(d)}{(1-x)^a \Gamma(d-a)} \sum_{r=0}^m \left\{ \binom{m}{r} \left[\frac{\Gamma\left(\frac{d-a+r}{2}\right)}{\Gamma\left(\frac{d+a+r}{2}\right)} + \frac{\Gamma\left(\frac{d-a+r+1}{2}\right)}{\Gamma\left(\frac{d+a+r+1}{2}\right)} \right] \right\} \tag{2.10}$$

$\left(|x| + \left| \frac{1-x}{2} \right| < 1; \frac{-1}{3} < R(x) < 1, \text{ when } \text{Im}(x) = 0; d, d-a \in \mathbb{C} \setminus \mathbb{Z}_0^- \right)$

Putting the values "A = a, B = b, C = c, D = –a + m, D = dandy = $\frac{1-x}{2}$ ", in above equation (2.1) and use the second Kummer's summation theorem' [12, Equation (3.5)], we get

$$F_2 \left[a; b, -a+m; b, d; x, \frac{1-x}{2} \right] = \frac{2^{-a+m-1} \Gamma(d) \Gamma(a-m)}{\Gamma(a) \Gamma(d-a)} \times \sum_{r=0}^m \left\{ \binom{m}{r} (-1)^r \left[\frac{\Gamma\left(\frac{d-a+r}{2}\right)}{\Gamma\left(\frac{d+a+r-2m}{2}\right)} + \frac{\Gamma\left(\frac{d-a+r+1}{2}\right)}{\Gamma\left(\frac{d+a+r+1-2m}{2}\right)} \right] \right\} \tag{2.11}$$





Bhawna Gupta et al.,

$(|x| + \left| \frac{1-x}{2} \right| < 1; \frac{-1}{3} < R(x) < 1, \text{ when } \text{Im}(x) = 0; a, d, a - m, d - a \in \mathbb{C} \setminus \mathbb{Z}_0^-; m \in \mathbb{N}_0)$

Putting the values " $A = \frac{b}{2}, B = b, C = \frac{b+1}{2}, D = \frac{2b+2}{3}$ and $y = \frac{8(1-x)}{9}$ " in above equation (2.1) and use the Kummer's second summation theorem' ([2, p.131, Entry (3.1.20)]; [7, p.136, Article 25(6)]), we get

$$F_2 \left[\frac{b}{2}; b, \frac{b+1}{2}; b, \frac{2b+2}{3}; x, \frac{8(1-x)}{9} \right] = \left(\frac{3}{2} \right)^b \frac{\Gamma(\pi) \Gamma(\frac{2b+2}{3})}{(1-x)^{\frac{b}{2}} \Gamma(\frac{b+4}{6}) \Gamma(\frac{b+1}{2})} \tag{2.12}$$

$(|x| + \left| \frac{8(1-x)}{9} \right| < 1; \frac{-1}{17} < R(x) < 1, \text{ when } \text{Im}(x) = 0; \frac{2b+2}{3} \in \mathbb{C} \setminus \mathbb{Z}_0^-)$

Putting the values " $A = \frac{b}{2}, B = b, C = \frac{b+1}{2}, D = \frac{2b+5}{6}$ and $y = \frac{(1-x)}{9}$ " in above equation (2.1) and use the Kummer's second summation theorem' ([2, p.131, Entry (3.1.17)]; [1, p.557, Entry (15.1.30)]; [7, p.135, Article 25(4)]; [6, p.330, Equation (1.1)]), we get

$$F_2 \left[\frac{b}{2}; b, \frac{b+1}{2}; b, \frac{2b+5}{3}; x, \frac{(1-x)}{9} \right] = \left(\frac{3}{4} \right)^b \frac{\Gamma(\pi) \Gamma(\frac{2b+2}{3})}{(1-x)^{\frac{b}{2}} \Gamma(\frac{b+4}{6}) \Gamma(\frac{b+1}{2})} \tag{2.13}$$

$(|x| + \left| \frac{(1-x)}{9} \right| < 1; \frac{-4}{5} < R(x) < 1, \text{ when } \text{Im}(x) = 0; \frac{2b+5}{6} \in \mathbb{C} \setminus \mathbb{Z}_0^-)$

Putting the values " $A = \frac{b}{2}, B = b, C = \frac{2-b}{6}, D = \frac{2b+5}{6}$ and $y = \frac{(x-1)}{8}$ " in above equation (2.1) and use the Kummer's second summation theorem' [2, p.177, Question 3(a)], we get

$$F_2 \left[\frac{b}{2}; b, \frac{2-b}{2}; b, \frac{2b+5}{3}; x, \frac{(x-1)}{8} \right] = \frac{\Gamma(\pi) \Gamma(\frac{2b+2}{3})}{2^{\frac{b}{2}} (1-x)^{\frac{b}{2}} \Gamma(\frac{b+4}{6}) \Gamma(\frac{b+1}{2})} \tag{2.14}$$

$(|x| + \left| \frac{(x-1)}{8} \right| < 1; \frac{-7}{9} < R(x) < 1, \text{ when } \text{Im}(x) = 0; \frac{2b+5}{6} \in \mathbb{C} \setminus \mathbb{Z}_0^-)$

Putting the values " $A = 2a, B = b, C = a + \frac{1}{4}, D = a + \frac{3}{4}$ and $y = \left(\frac{\sqrt{2}-1(1-x)}{\sqrt{2}+1} \right)$ " in above equation (2.1) and use the second Kummer's summation theorem' [2, p.177, Question 3(b)], we get

$$F_2 \left[2a; b, a + \frac{1}{4}; b, a + \frac{3}{4}; x, \left(\frac{\sqrt{2}-1(1-x)}{\sqrt{2}+1} \right) \right] = \frac{\Gamma(\pi) \Gamma(a + \frac{3}{4})}{(1-x)^{2a} (4-2\sqrt{2})^{2a} \Gamma(\frac{2a+3}{4}) \Gamma(\frac{a+1}{2})} \tag{2.15}$$

$(|x| + \left| \frac{(\sqrt{2}-1)(1-x)}{\sqrt{2}+1} \right| < 1; \frac{-1}{2} < R(x) < 1, \text{ when } \text{Im}(x) = 0; a + \frac{3}{4} \in \mathbb{C} \setminus \mathbb{Z}_0^-)$

Putting the values " $A = \frac{1}{2}, B = b, C = 1 - b, D = 2b + \frac{1}{2}$ and $y = \left(\frac{1-x}{4} \right)$ " in above equation (2.1) use the second Kummer's summation theorem' ([15, p.894]; [9, p.273, Equation 6.8(20)]), we get

$$F_2 \left[\frac{1}{2}; b, 1 - b, b, 2b + \frac{1}{2}; x, \left(\frac{1-x}{4} \right) \right] = \frac{2\Gamma(b) \Gamma(2b + \frac{1}{2})}{3(1-x)^{\frac{1}{2}} \Gamma(2b) \Gamma(b + \frac{1}{2})} \tag{2.16}$$

$(|x| + \left| \frac{(1-x)}{4} \right| < 1; \frac{-3}{5} < R(x) < 1, \text{ when } \text{Im}(x) = 0; b, 2b + \frac{1}{2} \in \mathbb{C} \setminus \mathbb{Z}_0^-)$

Putting the values " $A = a, B = b, C = a + \frac{1}{2}, D = -2a + \frac{3}{2}$ and $y = \left(\frac{x-1}{3} \right)$ " in above equation (2.1) and use the Kummer's second summation theorem' ([1, p.557, Entry (15.1.29)]; [4, p.104, Entry (2.8.53)]; [6, p.334, Equation (2.12)]), we get

$$F_2 \left[a; b, a + \frac{1}{2}; b, -2a + \frac{3}{2}; x, \left(\frac{x-1}{3} \right) \right] = \left(\frac{9}{8} \right)^{2a} \frac{\Gamma(\frac{4}{3}) \Gamma(-2a + \frac{3}{2})}{(1-x)^a \Gamma(\frac{2}{3}) \Gamma(-2a + \frac{1}{2})} \tag{2.17}$$

$(|x| + \left| \frac{(x-1)}{3} \right| < 1; \frac{-1}{2} < R(x) < 1, \text{ when } \text{Im}(x) = 0; b, -2a + \frac{3}{2} \in \mathbb{C} \setminus \mathbb{Z}_0^-)$

Putting the values " $A = a, B = b, C = a + \frac{1}{3}, D = -a + \frac{4}{3}$ and $y = \left(\frac{x-1}{8} \right)$ " in above equation (2.1) and use the Kummer's second summation theorem' [8, p.45, Equation (8)], we get





Bhawna Gupta et al.,

$$F_2 \left[a; b, a + \frac{1}{3}; b, -a + \frac{4}{3}; x, \left(\frac{x-1}{8} \right) \right] = \left(\frac{2}{3} \right)^{3a} \frac{\Gamma(\frac{2}{3}-a)\Gamma(\frac{4}{3}-a)}{(1-x)^a \Gamma(\frac{2}{3})\Gamma(\frac{4}{3}-2a)}, \tag{2.18}$$

$$\left(|x| + \left| \frac{x-1}{8} \right| \right) < 1; \frac{-7}{9} < R(x) < 1, \text{ when } \text{Im}(x) = 0; -a + \frac{4}{3}, -a + \frac{2}{3} \in \mathbb{C} \setminus \mathbb{Z}_0^-$$

Putting the values "A = 2a, B = b, C = 1/2 - a, D = a + 5/6 and y = (1-x)/9" in above equation (2.1) use the second summation theorem' [6, p.330, Equation (1.2)], we get

$$F_2 \left[2a; b, \frac{1}{2} - a; b, a + \frac{5}{6}; x, \left(\frac{1-x}{9} \right) \right] = \frac{3^a \Gamma(a + \frac{5}{6}) \Gamma(\frac{2}{3})}{4^a (1-x)^{2a} \Gamma(a + \frac{2}{3}) \Gamma(\frac{2}{6})} \tag{2.19}$$

$$\left(|x| + \left| \frac{1-x}{9} \right| \right) < 1; \frac{-4}{5} < R(x) < 1, \text{ when } \text{Im}(x) = 0; a + \frac{5}{6} \in \mathbb{C} \setminus \mathbb{Z}_0^-$$

Putting the values "A = 2a, B = b, C = 1 - a, D = a + 2/3 and y = (1-x)/9" in above equation (2.1) use the second Kummer's summation theorem' [6, p.330, Equation (1.3)], we get

$$F_2 \left[2a; b, 1 - a; b, a + \frac{2}{3}; x, \left(\frac{1-x}{9} \right) \right] = \frac{3^a \Gamma(a + \frac{2}{3}) \Gamma(\frac{1}{3})}{4^a (1-x)^{2a} \Gamma(a + \frac{1}{2}) \Gamma(\frac{2}{3})} \tag{2.20}$$

$$\left(|x| + \left| \frac{1-x}{9} \right| \right) < 1; \frac{-4}{5} < R(x) < 1, \text{ when } \text{Im}(x) = 0; a + \frac{2}{3} \in \mathbb{C} \setminus \mathbb{Z}_0^-$$

Putting the values "A = 2a + 1, B = b, C = -a, D = 2/3 and y = 8(1-x)/9" in above equation (2.1) and use the second Kummer's summation theorem' [6, p.335, Equation (3.2)], we get

$$F_2 \left[2a + 1; b, -a; b, \frac{2}{3}; x, \left(\frac{8(1-x)}{9} \right) \right] = \frac{2 \times 3^a \sin(\pi a + \frac{5\pi}{6})}{(1-x)^{2a-1}} \tag{2.21}$$

$$\left(|x| + \left| \frac{8(1-x)}{9} \right| \right) < 1; \frac{-1}{17} < R(x) < 1, \text{ when } \text{Im}(x) = 0$$

Putting the values "A = 2a + 2, B = b, C = -a, D = 1/3 and y = 8(1-x)/9" in above equation (2.1) and use the second Kummer's summation theorem' [6, p.335, Equation (3.3)], we get

$$F_2 \left[2a + 2; b, -a; b, \frac{4}{3}; x, \left(\frac{8(1-x)}{9} \right) \right] = \frac{3^a \Gamma(\frac{2}{3}) \Gamma(\frac{1}{6}) \sin(\pi a + \frac{5\pi}{6})}{(1-x)^{2a-2} \Gamma(\frac{1}{6}-a) \Gamma(a + \frac{2}{3})} \tag{2.22}$$

$$\left(|x| + \left| \frac{8(1-x)}{9} \right| \right) < 1; \frac{-1}{17} < R(x) < 1, \text{ when } \text{Im}(x) = 0$$

Putting the values "A = -a, B = b, C = 1/4 - a, D = 2a + 5/4 and y = (1-x)/9" in above equation (2.1) and use the second Kummer's summation theorem' [6, p.330, Equation (1.4)], we get

$$F_2 \left[-a; b, \frac{1}{4} - a; b, 2a + \frac{5}{4}; x, \left(\frac{1-x}{9} \right) \right] = \frac{2^{6a} (1-x)^a \Gamma(\frac{2}{3}) \Gamma(\frac{13}{12})}{(3)^{5a} \Gamma(a + \frac{2}{3}) \Gamma(a + \frac{13}{12}) \Gamma(\frac{5}{4})} \tag{2.23}$$

$$\left(|x| + \left| \frac{1-x}{9} \right| \right) < 1; \frac{-4}{5} < R(x) < 1, \text{ when } \text{Im}(x) = 0; 2a + \frac{5}{4} \in \mathbb{C} \setminus \mathbb{Z}_0^-$$

Putting the values "A = -a, B = b, C = 1/4 - a, D = 2a + 9/4 and y = (1-x)/9" in above equation (2.1) and use the second Kummer's summation theorem' [6, p.330, Equation (1.5)], we get

$$F_2 \left[-a; b, \frac{1}{4} - a; b, 2a + \frac{9}{4}; x, \left(\frac{1-x}{9} \right) \right] = \frac{2^{6a} (1-x)^a \Gamma(2a + \frac{9}{4}) \Gamma(\frac{4}{3}) \Gamma(\frac{17}{12})}{(3)^{5a} \Gamma(a + \frac{4}{3}) \Gamma(a + \frac{17}{12}) \Gamma(\frac{9}{4})} \tag{2.24}$$

$$\left(|x| + \left| \frac{1-x}{9} \right| \right) < 1; \frac{-4}{5} < R(x) < 1, \text{ when } \text{Im}(x) = 0; 2a + \frac{5}{4} \in \mathbb{C} \setminus \mathbb{Z}_0^-$$

Putting the values "A = 3a, B = b, C = 3a + 1/4, D = 4a + 1/3 and y = 8(1-x)/9" in above equation (2.1) and use the second Kummer's summation theorem' [6, p.335, Equation (3.4)], we get





Bhawna Gupta et al.,

$$F_2 \left[3a; b, 3a + \frac{1}{4}; b, 4a + \frac{1}{3}; x, \left(\frac{8(1-x)}{9} \right) \right] = \frac{108^a \Gamma(a + \frac{7}{12}) \Gamma(a + \frac{5}{6}) \Gamma(\frac{3}{4}) \Gamma(\frac{2}{3})}{(1-x)^{3a} \Gamma(a + \frac{3}{4}) \Gamma(a + \frac{2}{3}) \Gamma(\frac{7}{12}) \Gamma(\frac{5}{6})} \tag{2.25}$$

$$\left(|x| + \left| \frac{(1-x)}{9} \right| \right) < 1; \frac{-1}{17} < R(x) < 1, \text{ when } \text{Im}(x) = 0; 4a + \frac{1}{3}, a + \frac{7}{12}, a + \frac{5}{6} \in \mathbb{C} \setminus \mathbb{Z}_0^-$$

Putting the values "A = 3a, B = b, C = 3a - 1/4, D = 4a + 1/3 and y = 8(1-x)/9" in above equation (2.1) and use the second Kummer's summation theorem' [6, p.335, Equation (3.5)], we get

$$F_2 \left[3a; b, 3a - \frac{1}{4}; b, 4a + \frac{1}{3}; x, \left(\frac{8(1-x)}{9} \right) \right] = \frac{108^a \Gamma(a + \frac{1}{12}) \Gamma(a + \frac{5}{6}) \Gamma(\frac{1}{4}) \Gamma(\frac{2}{3})}{(1-x)^{3a} \Gamma(a + \frac{1}{4}) \Gamma(a + \frac{2}{3}) \Gamma(\frac{1}{12}) \Gamma(\frac{5}{6})} \tag{2.26}$$

$$\left(|x| + \left| \frac{8(1-x)}{9} \right| \right) < 1; \frac{-1}{17} < R(x) < 1, \text{ when } \text{Im}(x) = 0; 4a + \frac{1}{3}, a + \frac{1}{12}, a + \frac{5}{6} \in \mathbb{C} \setminus \mathbb{Z}_0^-$$

Putting the values "A = 3a, B = b, C = 3a + 1/2, D = 4a + 2/3 and y = 8(1-x)/9" in above equation (2.1) and use the second Kummer's summation theorem' ([7, p.136, Article 25(6)]; [6, p.335, Equation (3.1)]), we get

$$F_2 \left[3a; b, 3a + \frac{1}{2}; b, 4a + \frac{2}{3}; x, \left(\frac{8(1-x)}{9} \right) \right] = \frac{(27)^a \Gamma(2a + \frac{5}{6}) \Gamma(\frac{1}{2})}{(1-x)^{3a} \Gamma(a + \frac{5}{6}) \Gamma(a + \frac{1}{2})} \tag{2.27}$$

$$\left(|x| + \left| \frac{8(1-x)}{9} \right| \right) < 1; \frac{-1}{17} < R(x) < 1, \text{ when } \text{Im}(x) = 0; 4a + \frac{2}{3}, 2a + \frac{5}{6} \in \mathbb{C} \setminus \mathbb{Z}_0^-$$

In equation (2.1) put "A = a, B = b, C = 1/2, D = 3a and y = 3(1-x)/4" and use the second Kummer's summation theorem' [9, p.273, Equation 6.8(18)], we get

$$F_2 \left[a; b, \frac{1}{2}; b, 3a; x, \left(\frac{3(1-x)}{4} \right) \right] = \left(\frac{16}{27} \right)^a \frac{\Gamma(a) \Gamma(3a)}{(1-x)^a (\Gamma(2a))^2} \tag{2.28}$$

$$\left(|x| + \left| \frac{3(1-x)}{4} \right| \right) < 1; \frac{-1}{17} < R(x) < 1, \text{ when } \text{Im}(x) = 0; a \in \mathbb{C} \setminus \mathbb{Z}_0^-$$

CONCLUSION

By acknowledging that other fascinating reduction formulas for Appell functions of the second kind may be constructed in a comparable method, we draw a conclusion to our current investigation. Additionally, the formulas offered should be helpful to anyone with an interest in applied physics and mathematics.

ACKNOWLEDGEMENT

The authors are very appreciative of the referee anonymous for their insightful criticism.

REFERENCES

1. Abramowitz, M., Stegun, I. A., & Romer, R. H. Handbook of mathematical functions with formulas, graphs, and mathematical tables 1988.
2. Beukers, F. Special functions (Encyclopedia of Mathematics and its Applications 71) by George e. Andrews, Richard askey and Ranjan roy: 664 pp., £ 55.00 (US \$85.00), ISBN 0-521-62321-9 (Cambridge University Press, 1999). *Bulletin of the London Mathematical Society*, 33(1), 116-127, 2001.
3. Bailey, W. N. Generalized hypergeometric series, Cambridge Math 1935.
4. Erdélyi, A. Higher transcendental functions. *Higher transcendental functions*, 59, (1953).
5. Háï, N., Marichev, O. I., & Srivastava, H. M. A note on the convergence of certain families of multiple hypergeometric series. *Journal of mathematical analysis and applications*, 164(1), 104-115, (1992).
6. Karlsson, P. W. On two hypergeometric summation formulas conjectured by Gosper. *Simon Stevin*, 60(4), 329-337 (1986).



**Bhawna Gupta et al.,**

7. Kummer, E. E. Über die hypergeometrische Reihe. *J. Reine Angew. Math* 15 (1836), 39–83 and 127–172; see also *Collected papers, II: Function Theory, Geometry and Miscellaneous* (Edited and with a Foreword by Andre Weil), Springer-Verlag, Berlin, Heidelberg and New York, 1975.
8. Lavoie, J. L., & Trottier, G. On the sum of certain Appell's series. *Ganita*, 20(1), 31-32, 1969.
9. Luke, Y. L. *Mathematical functions and their approximations*. Academic Press, 2014.
10. Prudnikov, A. P., Brychkov, Y. A., Marichev, O. I. *Integrals and series III*, 1990.
11. Qureshi, M. I., & Baboo, M. S. Some Unified and Generalized Kummer's Second Summation Theorems with Applications in Laplace Transform Technique. *International Journal of Mathematics and its Applications*, 4(1-C), 45-52, 2016.
12. Qureshi, M. I., & Baboo, M. S. Some Unified and Generalized Kummer's Second Summation Theorems with Applications in Laplace Transform Technique. *International Journal of Mathematics and its Applications*, 4(1-C), 45-52, 2016.
13. Rakha, M. A., & Rathie, A. K. Generalizations of classical summation theorems for the series ${}_2F_1$ and ${}_3F_2$ with applications. *Integral Transforms and Special Functions*, 22(11), 823-840, 2011.
14. Kerimov, M. K. *Generalized hypergeometric functions*: LJ Slater. London, Cambridge Univ. Press, 1970, XIII+ 273 pp., 1966.
15. Spiegel, M. R. Some interesting special cases of the hypergeometric series. *The American Mathematical Monthly*, 69(9), 894-896, 1962.





Design and Development of IoT based PV Monitoring System

S.Wend_Kuuni Boris Jean Armand, Suman Lata*, Mohammad. Hassan and Shubham Kumar

Department of Electrical Electronics and Communication Engineering, Sharda School of Engineering and Technology, Sharda University, U.P. India 201310

Received: 06 Apr 2023

Revised: 10 May 2023

Accepted: 31 May 2023

*Address for Correspondence

Suman Lata

Department of Electrical Electronics and Communication Engineering,
Sharda School of Engineering and Technology,
Sharda University, U.P.India 201310
E. Mail: suman.lata@sharada.ac.in



This is an Open Access Journal / article distributed under the terms of the **Creative Commons Attribution License** (CC BY-NC-ND 3.0) which permits unrestricted use, distribution, and reproduction in any medium, provided the original work is properly cited. All rights reserved.

ABSTRACT

In this paper IoT based Surveillance and control system for PV modules, has been proposed. Input parameters which impact the performance of photovoltaic modules considered are atmospheric temperature, humidity, dust and luminosity. For the calculation of the power output the current and voltage of photovoltaic module is considered. For measurement of temperature and humidity a dual sensor DHT11 sensor has been used. A dust detecting sensor (GP2Y1010AU0F) which is an optical sensor and a photo diode for measuring the irradiance level has been considered in this work. An impedance divider sensor has been used to measure the output voltage of PV modules. ACS712, a current sensor, has been used to detect the current. These sensors are integrated with a microcontroller Arduino. ESP8266 a Wi-Fi module has been used to upload all the solar sensing parameters on Thing speak Server. The data acquisition has been done under uncontrolled as well as controlled conditions. Automation for water tank for cleaning based on atmospheric dust level and fan on the basis of temperature has been incorporated. The acquired data under various conditions using physical meters as well as the data using Arduino which at the end was available on IoT server are in close agreement. In future a network of developed prototype may be implemented for solar farms and hybrid PV systems. The collected data may be used for prediction using AI and Machine Learning.

Keywords: Energy, Internet of Things, PV Module, Power, Sensors

INTRODUCTION

IoT solutions are made up of a variety of components, including physical devices like sensors, actuators, and interactive gadgets, as well as a network connecting them all. These components collect and analyze the data they acquire by sending commands to their actuators, which improves the monitoring system. Photovoltaic (PV)



**Wend_Kuuni Boris Jean Armandet *al.*,**

monitoring is crucial for ensuring the optimal performance and efficiency of a solar energy system. Monitoring of PV is important because of following reasons. a) Detecting Issues: PV monitoring systems can detect issues with the solar panels, before they lead to a significant loss in energy production. This can help prevent expensive repairs and downtime. b) Maximizing Energy Production: By monitoring the performance of individual solar panels and the system as a whole, PV monitoring can help identify areas where improvements can be made to maximize energy production. This can include optimizing panel placement and adjusting the angle of the panels to capture more sunlight. c) Improvement Efficiency: PV monitoring systems can identify areas where the system is not operating efficiently, such as when there is a mismatch between the output of the solar panels and the inverter. Utilizing this knowledge will increase system effectiveness and cut down on wasted energy. d) Preventing Maintenance Needs: By monitoring the performance of the solar energy system over time, PV monitoring can help predict when maintenance is needed, such as when panels need to be cleaned or replaced. This can help reduce the cost and frequency of maintenance.

As government is providing subsidy for installation of solar panels in the houses for promoting solar energy as alternate energy source. The concept of using the IoT was to replace the traditional method of measuring current and voltage through the multi-Meters which is a time taking process. The IoT based system does not require any manual intervention. All the data is stored but in this we can store the data for the future reference. In order to monitor, the health and solar energy generation of PV panels, an IoT based monitoring system may be a good option because of many advantages of using the Internet of Things (IoT) for monitoring. Major key benefits are a) Real-time monitoring: IoT devices can collect data and transmit it in real-time, providing up-to the minute information about a wide range of variables such as temperature, humidity, and motion b) Improved efficiency: By collecting data automatically, IoT monitoring system can reduce the need for manual data collection, saving time and resources. c) Predictive maintenance: IoT sensors can detect when equipment is starting to show signs of wear and tear, allowing maintenance teams to perform repairs before any failure occurs d) Cost savings: IoT monitoring can help reduce the costs by minimizing the need for manual labor, reducing downtime due to equipment failures, and optimizing energy consumption e) Enhanced safety: IoT sensors can be used to monitor potentially hazardous environments, such as factories or mines, keeping workers safe by detecting and responding to dangerous situations.

LITERATURE REVIEW

This section presents a brief about IoT based solutions for PV monitoring. Tellawar, M. and Chamat, N reported a IoT based home monitoring system. Authors used ESP32 a microcontroller-based data logger for storing the chosen monitoring parameters in a micro-SD card. For data display blynk App has been used in this work. The captured data can be downloaded directly from the web page for analysis and verification. Authors did not focus on real time data acquisition [1]. For the acquisition and analysis of solar energy parameters authors, Kavidha, V and Malathi, V designed a IoT system. The reported work's primary objective is to forecast PV performance, so as to ensure a stable power generation. Different parameters have been displayed on different graphs [2]. Kekre, A and Gawre, S.K reported an IoT based embedded monitoring system which gives real time information of PV system. In this work a GPRS module has been used by authors to publish the data on the internet [3]. Priharti, W *et al.* reported an IoT-based solar PV monitoring system. Smart phone has been used for displaying data. Authors concluded that the transmission time is more and may be reduced in future. [4]. Gupta, S reported IoT based solar power monitoring system. The main focus was to monitor sun tracking system. Main components used in this work are ESP32 board, MPPT circuit, a shunt resistor lithium battery, active Wi-Fi network, a temperature sensor, and a voltage divider circuit. Authors have considered the impact of only one parameter, namely, temperature in this work [5]. Cheragee S H *et al.* reported an Internet of Things-based real-time solar power monitoring system. The developed system has been used to collect real-time environmental conditions of a PV panel and continuously monitor the output power generated by it. The sampling time used in this work is one day. [6]. Saraswat S *et al.* reported real time monitoring of solar PV parameter using IoT. The important thing in this report is the app which will collect the data has been built by the person in which the programming can be done either in java, C or C++ etc. [7]. Hardas V *et al.* reported solar panel monitoring system using IoT to predict failure [8].



**Wend_Kuuni Boris Jean Armandet al.,**

Pereira R.I.S et al. reported the primary goal of in order to design and install an IoT monitoring system to measure the temperature at the center and edge of the PV Module grid, comparative research of photovoltaic modules' center and edge temperatures utilizing embedded IoT systems was conducted.[9]. Abou Saltouh Tarek M.E et al. reported an experimental study employing Utilizing an advanced virtual RISC (AVR) AT mega microprocessor, it was implemented experimentally. [10]. Basir Khan M. Reyasudin *et al.* reported system for monitoring the performance of wireless PV modules. This system's primary goal is to identify the PV modules that run in less-than-ideal circumstances that may be brought on by PV module temperature rises, mitigation of PV module performance, and Maximum Power Point Tracker (MPPT) performance.[11]. The project is built on designs for microcontroller boards that are produced by multiple manufacturers utilizing a variety of microcontrollers. [12]. Katiyar.D *et al* explains a way to monitor dust buildup on solar panels so that you can collect the most electricity possible for practical usage. To increase the efficiency of solar panels. Systems consist of controllers incorporated with node MCU, LDR sensor [13]. SapuanI, Abudullah N Reported in their paper that the design of a standalone Building a solar photovoltaic (PV) monitoring system and a solar PV system for the fertigation system.[14]. Njoka.F, Thimo.L reported inpaper that they Analyze the capabilities and corresponding O&M cost savings of the IOT platforms that are most frequently used.[15]. Ganga, Renuka Samreen *et al.*, Madadi.S ed discussed about Internet of A framework with help from the Internet of Things (IOT) is intended to maximize the power production of the solar panels. Using this IOT technology, the various solar panel parameters, including temperature, current, and voltage, are presented on the LCD. [16,17] S.S.S Ranjit *et al* In this study work, the for the purpose of keeping track of the condition of solar photovoltaic panels, the author presented the integration of an IoT-based system. The four thermocouple K-type sensors in the suggested system are each connected to a thermocouple amplifier made by Adafruit, model MAX31855. Also included are a Raspberry Pi Zero Wireless, an Adafruit MAX31855 thermocouple amplifier, and an INA219 voltage/current sensor. [18].

System Design and Implementation

The suggested Internet of Things-based solar panel monitoring system is shown in Figure 1. It will be measuring the input parameters, viz, temperature, humidity, luminosity, and dust in the environment to which the PV panel is subjected to as well as the voltage and current which are the output parameters. Also, control of the water tank and fan which have been used to remove the dust of the PV system and reduce the temperature to set value has been added in the proposed system. As soon as the amount of dust exceeds a preset limit in the atmosphere, a command will be issued to the pumping system of the tank. Similarly, if the temperature goes beyond a limit, the fan control is initiated. The next sections provide information on the software and hardware required for implementing the suggested IoT-based solar PV surveillance system. Figure 2 depicts the suggested system's hardware configuration wiring. The key elements that have been employed for the proposed system's implementation are covered in the subsections that follow.

Solar Sensing Parameter Module

The sensors that have been taken into consideration in this research effort are a combined humidity and temperature sensing module (DHT11), an optical sensor for dust detection (GP2Y1010AU0F), and a photo diode for irradiance level measurement. Since DHT11 has superior precision than DHT22, it been employed to measure both humidity and temperature of the room. An impedance divider sensor is also used to separate the input voltage from the PV module and measure the solar panel's output voltage. The current was measured using a current sensor, model number ACS712. Depending on the range of current to be sensed, there are three sorts of current sensors. The sensor has the ability to find the circuit's AC and DC currents. These sensors have an Arduino microcontroller and an ESP8266 incorporated into them. The ESP8266, after connecting to the Wi-Fi network, uploads the settings for solar sensing to the Thing speak server.

ESP8266-based Node MCU controller

It has a Wi-Fi module and a 32-bit microcontroller. It is the central controlling module of the proposed system. For creating IoT based application framework, an open-source firmware, and a development kit called Node MCU is used in this work. Use of Node MCU results in simplifying the application programming requirement for input-output (IO) devices. The time and the effort required for configuring and modifying hardware devices gets





Wend_Kuuni Boris Jean Armandet al.,

decreased with the aid of APIs. The main advantage of selecting Node MCU in this work is that it can be programmed using an integrated development environment (IDE) that is open source using a variety of programming dialects. The code can be simply The Arduino IDE was used to upload data to the node MCU device. This work also makes use of the ESP8266, an integrated Wi-Fi device.

Solar Panel Details

In this work, 35W mono crystalline solar panel has been considered in this work. The other details of solar panel are in Table 1 below.

Software Layout

Thing Speak is an analytics platform for the Internet of Things that has been used to visualize and examine real-time data gathered from several sensors in the cloud. The platform, which consists of three fields—a position field, a data ground, and a status field—is the brains of the Thing Speak system. The real-time data collection, location of the data obtained geographically, data processing, and visualization characteristics of Thing Spaaak are some of its important features.

METHODOLOGY

In uncontrolled conditions the solar panel has been subjected to normal environmental conditions. And for the controlled conditions the solarpanel has been kept inside a glass house of 1.20(L) x 0.90(W) x 0.90(H). It has been subjected to different conditions of temperature, luminosity and dust and corresponding changes in output current and voltage have been measured with the help of multimeter as well as the Arduino and Node MCU controller. The data is acquired under following conditions.

- a) Ambient conditions: In this condition the PV panel have been kept in natural environment and not in the laboratory conditions.
- b) Controlled conditions: The solar panel has been subjected to following conditions.
 - i) Variable temperature conditions: Under these conditions the temperature of the of the environment has been varied by keeping a heater near the PV panel but luminosity, humidity and dust are kept unaltered.
 - ii) Variable luminosity conditions: Artificial lighting has been used to vary the luminosity levels to which the PV panel is being subjected. However, temperature, humidity, and level of dust are being kept constant.
 - iii) Variable dust level: Dust has been sprayed in the environment of the PV panel. However, temperature, humidity, and luminosity level are kept unaltered.

RESULTS AND DISCUSSIONS

The results under different types of conditions are discussed and deliberated in following sections.

A) Under ambient conditions

Output values of the current and voltage as well as the input parameters temperature, humidity, luminosity, and dust level have been measured using Arduino as well as Node MCU, simultaneously Table 2 lists the output current of a PV module in mA that was obtained using a physical multimeter reading of the real current value, expressed in mA, along with an online monitoring system. Every circumstance has a calculated difference between the actual current and the current that is being watched online. The data was gathered at a sample rate of once every minute.

Table 3 shows the voltage that the online monitoring system acquired from the PV panel as well as the real voltage value. The current sampling rate has been maintained constant.

Power can be calculated based on the values of voltage and current using the formula $P = V I$ and the unit of Watt. A single pane displays the online acquired current, voltage, and associated estimated power PV Panel. Also, the





Wend_Kuuni Boris Jean Armandet *al.*,

temperature and humidity measured both by online system as well as with reference sensors are in agreement with each other. The online measured values for these two parameters are given in Figure 4. Same observation is for luminosity and dust level.

B) Under Variable Conditions

Variables conditions have been created within the glass house in the laboratory setup. The laboratory set up is as shown in Figure 6.

i) Variables temperature conditions

The temperature was varied from 28° C to 35° C and corresponding values of current and voltage have been acquired with Arduino and then transmitted through Wi-Fi module to Thing speak platform. There is a transmission delay approximately of 15 seconds in communicating the data to online mode. As the temperature is varied, accordingly the currents and voltages are varying and as the temperature is increased beyond 28° C power output, starts decreasing. At 35° C the control action has been initiated and fan is turned on. The laboratory set

ii) Variable luminosity conditions

In first instant the PV module was covered with an opaque cover and the readings of the current and voltage acquired with the developed online system was 0.04 A and 0.07 and the output power was 0mW. The calculations in the programming have been truncated to two decimal places. Also, artificial lighting was created using LED light. Correspondingly out-put lux readings of photodiode sensor increased which resulted in increase in power.

iii) Variable dust level

Initially within the glass model the dust reading from the sensor was 0.70ppm and power output was 8.92 mW. Using a dust gun, dust was sprayed inside the chamber. It increased and started settling on the PV module and at 0.72 ppm the control signal was generated by Arduino and the water tank was activated.

CONCLUSION

In this paper IoT-based PV monitoring system under consideration has been successfully implemented. The datavarious sensor, namely, temperature and humidity sensor, luminosity sensor and dust sensor have been acquired using Arduino microcontroller. It has been sent to Thing speak app using wi-fi module. There is a delay between the acquired data and displayed data on the Thing speak without any data corruption. Additionally, physical meters have been used to measure the current, voltage, and power calculations in ambient as well as changeable environmental circumstances. It has been observed by authors that there is a strong agreement between the online data and data measured using physical meters. Thus, it can be concluded that online monitoring techniques, using IoT platforms are beneficial and technically sound to monitor data, and can also sense and signal possible uncertainties based on the PV outputs. It also minimizes human-induced errors making the entire architecture optimal, cost-effective, and automated. In the future, this work can be extended to hybrid PV systems and PV farms for monitoring and control of solar panel voltage, current, temperature, and humidity in addition to defect finding. Also, collected data may be used for prediction using AI and Machine Learning.

REFERENCES

1. Kekre, Ankit &Gawre, Suresh. (2017). Solar photovoltaic remote monitoring system using IOT. 619-623. 10.1109/RISE.2017.8378227.
2. Priharti, Wahmisari&Rosmawati, A &Wibawa, I. (2019). IoT based photovoltaic monitoring system application. Journal of Physics: Conference Series. 1367. 012069. 10.1088/1742-6596/1367/1/012069.
3. Abdullah, B.U.D. and Lata, S., 2022, November. IoT-Based Solar Monitor System. In 2022 International Conference on Computing, Communication, and Intelligent Systems (ICCCIS) (pp. 997-1002). IEEE.





Wend_Kuuni Boris Jean Armandet al.,

4. Gupta, A.K., Chauhan, Y.K. and Maity, T., 2018. Experimental investigations and comparison of various MPPT techniques for photovoltaic system. *Sādhanā*, 43, pp.1-15.
5. Cheragee, S.H., Hassan, N., Ahammed, S. and Islam, A.Z.M.T., 2021. A Study OF IOT BASED REAL-TIME SOLAR POWER REMOTE MONITORING SYSTEM. *Int. J. Amb. Syst. Appl.*, 9(2), pp.27-36.
6. Sahu, D. and Brahmin, A., 2021. A Review on Solar Monitoring System. *International Research Journal of Engineering and Technology*, 8.
7. Pereira, R.I.S., Jucá, S.C.S., Carvalho, P.C.M.D. and Fernández Ramírez, L.M., 2019. Comparative analysis of photovoltaic modules center and edge temperature using IoT embedded system.
8. Abou Saltouha, T.M., Nafeha, A.E.S.A., Fahmya, F.H. and Yousefb, H.K., 2018. Microcontroller-based sun tracking system for PV module. *International Journal of Smart Grid and Clean Energy*, 7(4), pp.286-296.
9. Mule, S., Hardas, R. and Kulkarni, N.R., 2016, March. P&O, IncCon and Fuzzy Logic implemented MPPT scheme for PV systems using PIC18F452. In 2016 international conference on wireless communications, signal processing and networking (WiSPNET) (pp. 1320-1325). IEEE.
10. Karthik, S., Mahalakshmi, M., Mahitha, R. and Meena, S., 2019. IoT based solar panel fault monitoring and control. *International Journal of Information and Computing Science*, 6(3), pp.238-243.
11. Mangore, A., Chougale, S., Palekar, M., Bhosale, K., Kadam, S., Kshirsagar, K. and Bagwan, M.S., 2022. IOT BASED SOLAR POWER MONITORING SYSTEM. *Open Access Repository*, 9(7), pp.35-46.
12. Abdullah, M.N. and Sapuan, I., 2020. Stand-alone Solar Monitoring System using Internet of Things for Fertigation System. *Evolution in Electrical and Electronic Engineering*, 1(1), pp.106-115.
13. Njoka, F., Thimo, L. and Agarwal, A., 2022. Evaluation of IoT-based remote monitoring systems for stand-alone solar PV installations in Kenya. *Journal of Reliable Intelligent Environments*, pp.1-13.
14. Kumar, P., Nigam, G.K., Sinha, M.K. and Singh, A. eds., 2022. *Water Resources Management and Sustainability*. Springer Singapore.
15. Madadi, S., 2021. A Study of Solar Power Monitoring System Using Internet of Things (IOT). *International Journal of Innovative Science and Research Technology*, 6(5)
16. Ranjit, S.S.S. and Abbod, M., 2018. Research and integration of IoT based solar photovoltaic panel health monitoring system.
17. Samuel, J. and Rajagopal, B., 2021. IoT Based Solar Panel Monitoring and Control. *NVEO-NATURAL VOLATILES & ESSENTIAL OILS Journal| NVEO*, pp.7609-7618.
18. Srinivasan, K.G., Vimaladevi, K. and Chakravarthi, S., 2019. Solar energy monitoring system by IOT. *Special Issue Published in Int J Adv Network Appl (IJANA)*.

Table No 1. Details of Solar Panel

Parameter	Value
Temperature (T)	25 degrees
Open Circuit Voltage (VOC)	12 V
Short Circuit Current Isc	3.8 A

Table. 2. Actual offline Current along with Online

S.NO	IOT online Monitored Current(A)	Actual PV current (A)	Error(%)
1	0.14	0.1509	0.0109
2	0.52	0.5421	0.0221
3	0.88	0.882	0
4	1.44	1.495	-3.36
5	1.97	2.0247	-2.48
6	3.67	3.8454	-4.43





Wend_Kuuni Boris Jean Armandet al.,

Table. 3. Actual offline Voltage along with Online

S.NO	IOT online Monitored Voltage(V)	Actual PV Voltage (V)	Error (%)
1	23.73	22.7947	-0.9353
2	23.27	22.4069	-0.8631
3	22.15	22.0649	-0.0851
4	21.95	21.4643	-0.4857
5	21.24	20.9409	-0.2991
6	18.51	18.6221	0.1121

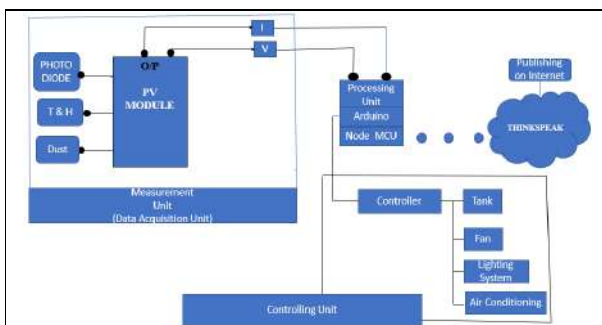


Fig.1 System Design

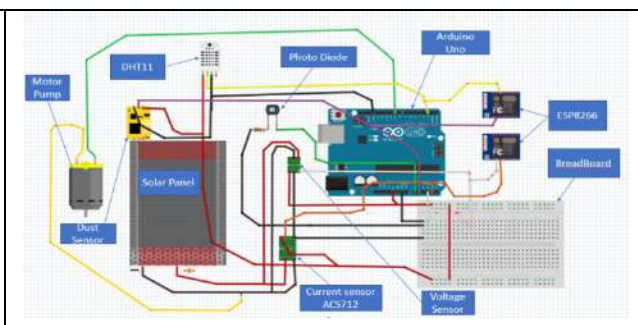


Fig.2. The proposed system's hardware implementation

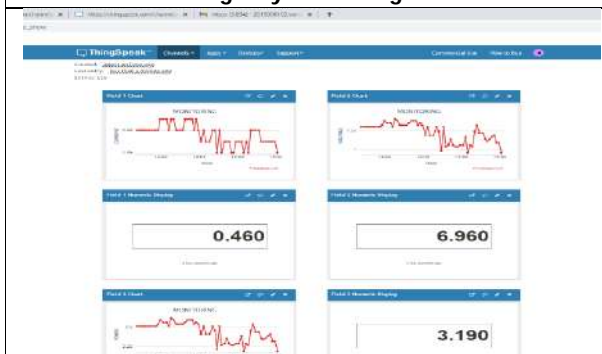


Fig. 3 Online acquired current, voltage and calculated power of PV Panel in single frame in Thing Speak server

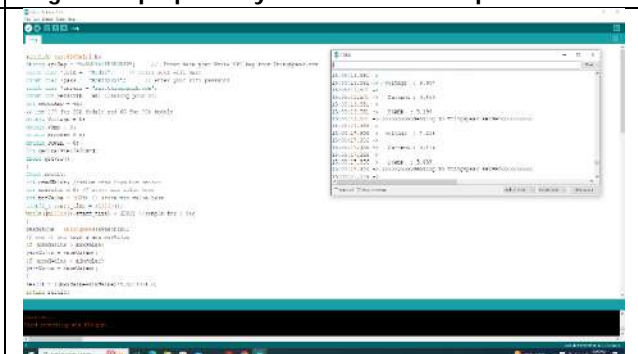


Fig. 4 Online acquired current, voltage and calculated power of PV Panel in single frame in Arduino Software



Fig.5. Online acquired Temperature and Humidity of PV Panel

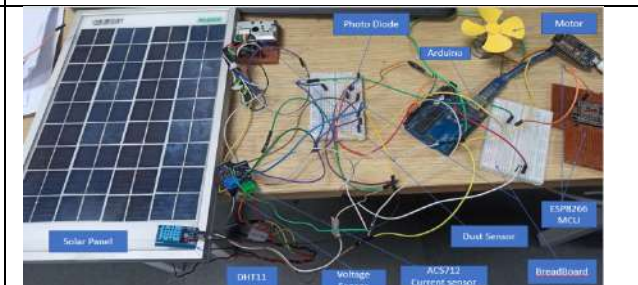


Fig.6. Hardware Implementation in laboratory setup





Product Cordial Labeling in Context of Some New Graphs

Varsha Rathi^{1*}, Sweta Srivastav² and Sangeeta Gupta¹

¹Department of Mathematics, Sharda University, Greater Noida, Uttar Pradesh 201310, India.

²The A.H. Siddiqi Centre for Advanced Research in Applied Mathematics and Physics, Sharda University, Greater Noida, Uttar Pradesh, India.

Received: 10 Apr 2023

Revised: 15 May 2023

Accepted: 31 May 2023

*Address for Correspondence

Varsha Rathi

Department of Mathematics,
Sharda University,
Greater Noida,
Uttar Pradesh 201310, India.
E. Mail: 2022401996.varsha@dr.sharda.ac.in



This is an Open Access Journal / article distributed under the terms of the **Creative Commons Attribution License** (CC BY-NC-ND 3.0) which permits unrestricted use, distribution, and reproduction in any medium, provided the original work is properly cited. All rights reserved.

ABSTRACT

A binary vertex labeling $f : V(G) \rightarrow \{0,1\}$ of graph G with induced edge labeling $f^* : E(G) \rightarrow \{0,1\}$ defined by $f^*(uv) = f(u)f(v)$ is called a product cordial labeling if $|v_f(0) - v_f(1)| \leq 1$ and $|e_f(0) - e_f(1)| \leq 1$, where $v_f(0), v_f(1)$ denote the number of vertices of G having labels 0, 1 respectively under f and $e_f(0), e_f(1)$ denote the number of edges of G having labels 0, 1 by respectively under f^* . A graph G is product cordial if it admits product cordial labeling. In this investigation the helm graph and sunlet graph are product cordial graph.

Keywords: Graph Theory, Cordial Graph, Product Cordial Graph, Helm Graph, Sunlet Graph.

INTRODUCTION

We begin with simple, finite, connected and undirected graph $G = (V(G), E(G))$ with order p and size q . Graph labeling is the process of assigning values to a graph vertices based on a condition or conditions. If the vertices are assigned values subject to certain condition then it is known as *graph labeling*. A mapping $f : V(G) \rightarrow \{0,1\}$ is called *binary vertex labelling* of G and $f(v)$ is called the *label* of vertex v of G under f . Gallian [2] is a good resource for a thorough overview of graph labeling and bibliographic references. The graph formed by the union of the two graphs G_1 and G_2 has the properties $V(G_1 \cup G_2) = V(G_1) \cup V(G_2)$ and $E(G_1 \cup G_2) = E(G_1) \cup E(G_2)$. Graph labelling involves assigning integers to the vertices, edges, or both. Motivated by the idea of cordial labelling, Sundaram *et al.* [3] have introduced a label that flavour like cordial labelling but the product of vertex labels replaces the absolute difference in vertex labels. Astronomy, coding theory, x-ray crystallography, radar, circuit design, communication network addressing, database management, secret sharing methods, and models for constraint programming over finite domains are just a few of the scientific disciplines where graph labelling is significant. The cordial labeling of

57526





Varsha Rathiet al.,

graphs was first presented by cahit [1]. In this paper, we look at different graphs for labelling sunlet graph and helm graph. Introduced labeling in some new graphs of product cordial graph.

Definition 1.1 : A graph labeling is an assignment of integers to the vertices or edges or both subject to certain condition(s). If the domain of the mapping is the set of vertices (or edges) then the labeling is called a vertex labeling (or an edge labeling).

Definition 1.2 : A mapping $f : V(G) \rightarrow \{0, 1\}$ is called binary vertex labeling of G and $f(v)$ is called the label of the vertex v of G under f . The induced edge labeling $f^* : E(G) \rightarrow \{0, 1\}$ is given by $f^*(e = uv) = |f(u) - f(v)|$. Let us denote

$vf(0) = \text{number of vertices of } G \text{ having label } 0 \text{ under } f$

$vf(1) = \text{number of vertices of } G \text{ having label } 1 \text{ under } f$

$ef(0) = \text{number of edges of } G \text{ having label } 0 \text{ under } f^*$

$ef(1) = \text{number of edges of } G \text{ having label } 1 \text{ under } f^*$

Definition 1.3 : If the vertices of the graph are assigned values subject to certain conditions is known as graph labeling.

Definition 1.4 : A product cordial labeling of graph G with vertex set V is a function $f : V \rightarrow \{0, 1\}$ such that each edge uv is assigned the label $f(u)f(v)$, the number of vertices with label 0 and the number of vertices with label 1 differ by at most 1 and the number of edge with label 0 and the number of edge with label 1 differ by at most 1. A graph which admits product cordial labeling is called a product cordial.

Definition 1.5 : A binary vertex labeling of graph G with induced edge labeling $f^* : E(G) \rightarrow \{0, 1\}$ defined by $f^*(e = uv) = f(u)f(v)$ is called a product cordial labeling. If $|v_f(0) - v_f(1)| \leq 1$ and $|ef(0) - ef(1)| \leq 1$.

Definition 1.6 : The graph that is produced from the wheel W_n by adding a pendant edge to each rim vertex is known as the helm H_n . It has an apex of *degree*, n vertices of *degree* 4 and n pendant vertices.

Definition 1.7 : The subdivision of graph G on the edge is denoted by $SG(E_k)$ is the graph obtain from graph G by adding K new vertices w_1, w_2, \dots, w_k and w_{k+1} new edges b/w every pair of vertices.

Definition 1.8 : The helm H_n is the graph obtained from a Wheel W_n by attaching a pendant edge to each of the rim vertices.

Definition 1.9 : The sunlet graph is the graph attained by attaching pendant edges to m cyclic graph and denoted as S_n .

MAIN RESULTS

Theorem 2.1: The helm graph H_n , for all n is product cordial.

Proof : Let $G = (V, E)$ be the graph with the vertex set. Let v_0 be the apex vertex, $\{v_1, v_2, \dots, v_k\}$ be the vertex of inner cycle attached with apex vertex and $\{v_{k+1}, \dots, v_n\}$ be the vertices of outer cycle and edge set $\{E = e_1, e_2, \dots, e_k\}$. We consider the following function for labeling helm graph:

For $n \equiv 0, 1, 2, 3 \pmod{4}$

$f(v_i) = 0, 1 \leq i \leq k,$

$f(v_i) = 1, \quad k + 1 \leq i \leq n$

The apex vertex v_0 labeled as $f(v_0) = 1$.





Varsha Rathiet al.,

In view of the above pattern we have $\{v_f(0) = v_f(1) + 1\}$ and $\{e_f(0) = e_f(1)\}$.
Therefore, clearly $\{|v_f(0) - v_f(1)| \leq 1\}$ and $\{|e_f(0) - e_f(1)| \leq 1\}$. Thus, G admits product cordial labeling.
The labeling satisfy the condition as shown below:

Example 2.1 For better understanding of above define labeling pattern we consider the example for H_9 , i.e. $n \equiv 1(mod 4)$.

In the above graph $|v_f(0)|=9, |v_f(1)|=10,$ and $|e_f(0)| = 18, |e_f(1)| = 18$ thus $|v_f(0) - v_f(1)| \leq 1$ and $e_f(0) = e_f(1) \leq 1$.

Theorem 2.2 : The subdivision of the circuit of helm graph $SG(H_n)$ is product cordial.

Proof : Let $G = (V, E)$ be the helm graph with the vertices $\{v_1, v_2, \dots, v_n\}$. The graph obtained by adding a vertex between every pair of vertices in the cycle or circuit of the helm graph is subdivision of the cycle of helm graph denoted by $SG(H_n)$. $\{v_1, v_2, \dots, v_k\}$ are vertices of inner cycle of the helm graph and $\{v_{k+1}, \dots, v_n\}$ are vertices of outer cycle of the helm graph. So, the joined vertex set by apex. after subdivision will be $\{v_1, v_2, \dots, v_{2k}\}$ are the vertices of inner cycle and $\{v_{k+1}, \dots, v_{2n}\}$ are the vertices of outer cycle.

We consider the following function for label the subdivision of helm graph.

$$f(v_i) = 0, 1 \leq i \leq 2_k$$

$$f(v_i) = 1, 2_{k+1} \leq i \leq 2_n$$

The apex vertex v_0 labeled as $f(v_0) = 1$. In view of the above pattern we have, $\{v_f(0) = v_f(1) + 1\}$ and $\{e_f(0) = e_f(1)\}$.

Therefore, Clearly $\{|v_f(0) - v_f(1)| \leq 1\}$ and $\{|e_f(0) - e_f(1)| \leq 1\}$. Thus, G admits product cordial graph.

Example 2.2 For better understanding of above define labeling pattern we consider the example for $SG(H_{12})$, i.e. $n \equiv 0(mod 4)$.

In the above graph $|v_f(0)|=12, |v_f(1)|=13,$ and $|e_f(0)| = 24, |e_f(1)| = 24$ thus $|v_f(0) - v_f(1)| \leq 1$ and $|e_f(0) - e_f(1)| \leq 1$.

Theorem 2.3 : The sunlet graph S_n , for all n is product cordial.

Proof : Let G be the sunlet graph S_n , $|V(S_n)| = 2_n$ and $|E(S_n)| = 2_n$. The vertex set is $\{V(S_n) = v_1, v_2, \dots, v_n; v'_1, v'_2, \dots, v'_n\}$ and edge set is $\{E(S_n) = \{v_i v_i / 1 \leq i \leq n\} \cup \{v_i v_{i+1} / 1 \leq i \leq n - 1\} \cup \{v_1 v_n\}\}$. Where n is both even and odd. To define binary vertex labeling.

$$f(v_1) = 1, 1 \leq i \leq n$$

$$f(v_i) = 0, 1 \leq i \leq n$$

Thus, Labeling of every vertex and edges satisfy the condition

$\{|v_f(0) - v_f(1)| \leq 1\}, \{|e_f(0) - e_f(1)| \leq 1\}$ respectively, Thus G admits product cordial labeling. Hence, sunlet graph is product cordial graph. The labeling satisfy the condition as shown below:

Example 2.3 For better understanding of above define labeling pattern we consider the example for S_{15} , i.e. $n \equiv 3(mod 4)$.

In the above graph $|v_f(0)|=15, |v_f(1)|=15,$ and $|e_f(0)| = 15, |e_f(1)| = 15$ thus $|v_f(0) - v_f(1)| \leq 1$ and $|e_f(0) - e_f(1)| \leq 1$.

CONCLUDING REMARKS

Here we have demonstrated the product cordial labeling for some new graph. Likewise this can be operate on duplication, fusion or some reconstruction of graphs. In future this work can be done for reconstruction some graph operation of the graphs. To enhance comparable outcomes for many different graphs is an open research area.





Varsha Rathiet al.,

REFERENCES

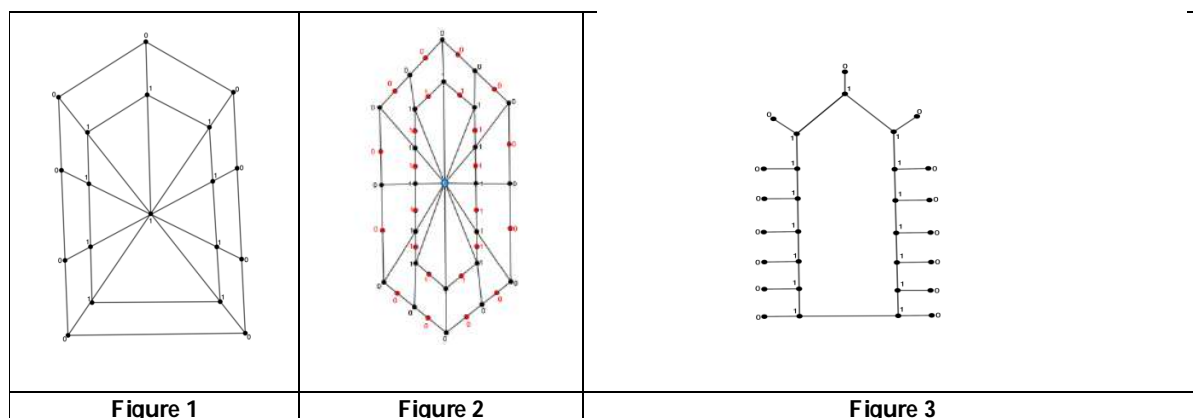
1. Cahit, I. (1987). Cordial graphs-a weaker version of graceful and harmonious graphs. *Ars combinatoria*, 23, 201-207.
2. Gallian, J. A. (2018). A dynamic survey of graph labeling. *Electronic Journal of combinatorics*, 1(DynamicSurveys), DS6.
3. Sundaram, M., Ponraj, R., & Somasundaram, S. (2004). Product cordial labeling of graphs. *Bulletin of Pure and Applied Sciences E*, 23, 155-163.
4. Prajapati, U. M., & Raval, K. K. (2017). Some graphs in the context of product cordial labeling. *Math. Today*, 33, 58-66.
5. Prajapati, U. M., & Patel, N. B. (2016). Edge product cordial labeling of some cycle related graphs. *Open Journal of Discrete Mathematics*, 6(4), 268-278.
6. Prajapati, U. M., & Raval, K. K. (2016). Product Cordial Graph in the Context of Some Graph Operations on Gear Graph. *Open Journal of Discrete Mathematics*, 6(04), 259.
7. Rokad, A. H. (2019). Product cordial labeling of double wheel and double fan related graphs. *Kragujevac Journal of Mathematics*, 43(1), 7-13.
8. Vaidya, S. K., & Barasara, C. M. (2013). Some new families of edge product cordial graphs. *Advanced Modeling and Optimization*, 15(1), 103-111.
9. Vaidya, S. K., & Barasara, C. M. (2012). Further results on product cordial labeling. *Mathematical Combinatorics*, 3, 64-71.
10. Vaidya, S. K., & Barasara, C. M. (2011). Product cordial labeling for some new graphs. *Journal of mathematics Research*, 3(2), 206-211.
11. Vaidya, S. K., & Barasara, C. M. (2011). Product cordial graphs in the context of some graph operations. *International Journal of Mathematics and Scientific Computing*, 1(2), 1-6.

Table 2.1

$f(0), f(1)$	$f(v_1) = f(v_0) + 1$	$f(e_1) = f(e_0)$
--------------	-----------------------	-------------------

Table 2.2

$f(0), f(1)$	$f(v_1) = f(v_0)$	$f(e_1) = f(e_0)$
--------------	-------------------	-------------------





A Non-Destructive Deep Learning Technique for Fresh and Rotten Fruits Classification

Surya Kant Pal^{1*}, Suyog Khanal¹, Prem Shankar Jha² and Rita Roy³

¹Department of Mathematics, Sharda School of Basic Sciences and Research, Sharda University, Greater Noida-201306, India.

²Department of Statistics, Patna College, Patna University, Bihar, India-800005.

³Department of Computer Science and Engineering, GITAM Institute of Technology, GITAM, Visakhapatnam, A.P., India.

Received: 06 Apr 2023

Revised: 20 May 2023

Accepted: 31 May 2023

*Address for Correspondence

Surya Kant Pal

Department of Mathematics,
Sharda School of Basic Sciences and Research,
Sharda University,
Greater Noida-201306, India.
E. Mail: suryakantpal6676@gmail.com



This is an Open Access Journal / article distributed under the terms of the **Creative Commons Attribution License** (CC BY-NC-ND 3.0) which permits unrestricted use, distribution, and reproduction in any medium, provided the original work is properly cited. All rights reserved.

ABSTRACT

Considering the significance of fruit status in everyone's lives, the need for effective fruit freshness grading is acknowledged. There must be an end-to-end system for fruit freshness detection either at the farm or industrial levels. In this project work, transfer learning algorithms were used to build the fruit image classification model to classify fresh and rotten fruit. As our Model_O was poorly generalized, we tried to implement transfer learning architecture with parameters of our choice. We then did hyperparameter tuning in the best-performing transfer learning architecture. The architectures used were, Model_O (which is our own designed architecture), NasNet Mobile, InceptionV3, Inception ResNet V2, ResNet50V2, MobileNetV2, VGG16, DenseNet 121 and finally Xception. A detailed comparison was made between these nine architectures, and we found that fitting the Xception model into the training set resulted in vast improvement compared to other models. After running it for 15 epochs, we found our training accuracy to be 0.9882 and our training loss to be 0.0386. The model was then checked for test data, and we got a testing accuracy of 0.9804 and a testing loss of 0.0679. This was the best-generalized model we could ever get.

Keywords: Fruit; Fruit freshness detection; Rotten fruit; Xception model; Accuracy.



**Surya Kant Palet *et al.*,**

INTRODUCTION

India is ranked second in the world as the largest fruit-producing country after China. With 31,504 metric tons, India became the leading producer of bananas worldwide in 2020 [1]. Alongside these fruit-producing agricultural industries, India is also home to some of the largest juice beverage industries. As of the fiscal year 2020, the Indian juice beverage market had a size of approximately INR 270 billion, this paper projected the market size to reach INR 405 billion by the end of the fiscal year 2025. Due to the nutritious nature of fruit and its processed juice, people have included it in their everyday diet. Fruit surpassing that specific span is not edible, and consumption of such fruit will lead to critical illness as the nutrient contained in it will have lost their nature [2]. Nowadays also, there is a supply of such degraded quality fruits in the fruit industry due to improper packaging during the fruit transportation process from the area of plantation to the fruit industry [3]. As of now, we know the vast supply and demand of fruits and their products in India. The volume and variety at which the fruits enter the industry and market are immeasurable. Sorting out fresh fruits and discarding degraded fruits from such huge volumes is time-consuming and requires many human sources [4].

Considering the significance of fruit status in everyone's lives, the need for effective fruit freshness grading is acknowledged [5], [6]. There must be an end-to-end system for fruit freshness detection either at the farm or industrial levels. The typical way of determining fruit quality is done visually; however, performing such a task with a machine is difficult [7], [8]. Through computer vision technology, the system can identify the various characteristics of fruit, such as its shape, color, and texture [9]. A single image can contain thousands of pixels, and as already discussed, each pixel value is essential, and slight ups and downs can impact the model as a whole [10]. This paper discusses the detailed comparison of our own built deep Convolutional Neural Network (CNN) model with eight different transfer learning models, which are stunned by the hyperparameters of our choice on a publicly available dataset. This paper discusses the end-to-end implementation of deep learning models integrated with a mobile app.

LITERATURE REVIEW

They even discussed how agriculture would progress shortly when it was introduced with deep learning. They found that deep learning can easily outperform existing image processing technologies in agriculture [11], [12]. The technology around us has progressed significantly as deep learning made significant breakthroughs [13]. It was more accurate and powerful to work with noises in colors. Support Vector Machine (SVM) was used as a robust algorithm. Convolutional Neural Network (CNN) to classify defected and non-defected mangosteen fruits. This paper uses k-folds cross-validation with setting $K = 4$ for data validation [14]. This method depicted the proper non-destructive and online detection of the quality of fruits [4]. Artificial intelligence to count pineapples from drones which produced aerial pictures of the land of the plantation [7]. They used Keras-RetinaNet for AI training models. They finally came up with a web-based AI application [15]. It was a good use of deep learning in agriculture and plantations, which classified fruit into 81 different classes, considering computer vision-based approach and algorithms have experienced tremendous usage growth in recent decades [16]. Their PCNN model had a 98.88% classification accuracy. They employed Global Average Pooling (GAP) to build a well-generalized model [17], [18]. A new deep convolutional neural network architecture, Xception, inspired by Inception architecture. Still, this Xception outperformed Inception V3 to all extent on the dataset they were trained on. Xception also had equal numbers of parameters as Inception, but the significant difference was that more efficient model parameters were used in Xception architecture [19], [20]. It was fast and small in size, and it used residual learning for more rapid convergence of gradient descent. It was also well generalized and matched the accuracy of image recognition compared to other huge models. It was 88.4% smaller and 23.86% faster while training. A residual learning framework which made the training process easy as deeper neural networks were not easy to train [21].



Surya Kant Palet *et al.*

RESEARCH METHODOLOGY

Data Acquisition and Pre-processing

The dataset obtained for this study was obtained from Kaggle. Apples, oranges, and bananas are among the three different fruit varieties in the dataset. Each fruit was further sub-grouped into fresh and rotten fruits. This means we had altogether of 6 other classes. The six classes were Rotten Apple, Fresh Apple, Rotten Orange, Fresh Orange, Rotten Banana, and Fresh Banana. ImageDataGenerator was used to separate the images in the training, validation and testing set after applying the proper data augmentation technique. Rescaling of the painting was done. Thus, the pixel values in the image lay between 0 to 1 after getting divided by 255 pixels. The validation split value was set to 0.2. The target_size for the train, test and validation set was (224,224) with three color channels. The batch_size value was set to 12 for each train, test and validation set.

Implementation of Convolutional neural networks

Deep learning, an ongoing hot subfield in machine learning, is preferred when handling big unstructured data. For image classification, Convolutional Neural Network works fascinatingly well. We use pixel representation to represent images on the computer. Different pixels combination means different patterns in an image, such as edge, shadow and many more. Convolutional operations are the most effective way to detect these patterns. A matrix known as; a filter is made to perform these convolutional operations. The values in the filter depend upon the design we want to find. The filter is moved across the image pixel matrix, and either multiplication, averaging or min-max operation is performed. The ratio with which it moves is dependent upon the value of stride. The output after this operation is shared with the next layer. The next layer, i.e., the pooling layer, tries to generalize the model by decreasing the output size. Then, it is again passed to a fully connected layer, which will be the last. Before taking the input, this fully connected layer converts the matrix into a column vector using the Flatten () function. To normalize the values in the vector, we use the Batch Normalization () process and reduce computational efficiency; we use the Dropout () function. The dropout () function's parameter represents the probability of each neuron turning on or off. Figure 2 CNNs, or CNNs are frequently employed. This deep learning architecture is arguably the most well-known. The huge success and popularity of convolutional networks are to credit for the recent surge in interest in deep learning. AlexNet first introduced CNN in 2012, and its popularity has since significantly increased. Researchers progressed from 8-layer AlexNet to 152-layer ResNet in just three years.

Proposed CNN models and recommended Transfer learning architectures for fruit freshness classification

On the verge of solving the problem of detection between fresh and rotten fruits., we proposed a convolutional neural network model of our own, named; Model_O. The creation of this Model_O had some prerequisites. This tensor was then processed through BatchNormalization () function to normalize the pixel values. Then we applied MaxPooling2D on the next layer so that the size of the tensor was reduced to (111,111,32). After this, the Dropout () function was implied to drop the neurons at the probability of 0.25. Here, the Conv2D () function was applied for the last time so that we get a tensor of size; (52,52,128), which was passed through BatchNormalization () and then the MaxPooling2D () function, and we got a tensor of much-reduced size; (26,26,128). This resulted in 512 neurons in the network later. After this, Batch Normalization () and Dropout () with a probability of 0.4 was applied for the last time. The formula for Rectified Linear Unit (ReLU) activation function is:

$$f(x) = \max(0, x) \quad (1)$$

A Flutter based Mobile App

For the large-scale implementation of this project, we thought deploying a deep learning model on a mobile app would be easy to use afterwards. The dependencies for the mobile app were tflite and image_picker. The mobile application development field continues to advance and astound the world.





Transfer Learning

In a transfer learning scenario, several models were trained on image classification data using a batch size specified as a ratio of the training and validation set sizes. Each model was trained for 15 epochs with the number of training steps in each epoch set according to the ratio of the training set size and batch size, and the number of validation steps set according to the ratio of the validation set size and batch size. To achieve maximum accuracy, we applied the following transfer learning algorithms:

NasNet Mobile.

NasNet Mobile is a deep learning architecture for image classification, part of the NAS family, optimized for resource-constrained environments such as mobile devices. It utilizes depth wise separable convolutions and inverted residual blocks to reduce the number of parameters and computational cost while still achieving high accuracy. NasNet Mobile is a cutting-edge and efficient architecture for image classification on mobile and resource-constrained devices.

InceptionV3. InceptionV3 is a well-known CNN architecture for image classification that uses multi-scale Inception modules to capture information from an input image at different levels of abstraction. It has a deep network architecture with about 300 layers and uses the PReLU activation function. InceptionV3 is widely used as a benchmark for comparing the performance of other deep learning models.

PReLU activation function is given in the equation (2) as:

$$f(y_i) = y_i, \text{ if } y_i > 0 \text{ else } a_i y_i \quad (2)$$

The InceptionV3 model was trained for 15 epochs on image classification data and achieved a training accuracy of '0.9568' and training loss of '0.1394'. However, when evaluated on test data, the model showed lower performance with a testing accuracy of '0.9607' and testing loss of '0.1250', not meeting expectations. To address this, the model was replaced with Inception ResNet V2.

Inception ResNet V2. Inception ResNet V2 is an image classification architecture that combines elements of the InceptionV3 and ResNet models. It uses multi-scale Inception modules and residual connections to capture information from an input image at different levels of abstraction and learn complex representations of the data. Inception ResNet V2 is a deeper network than InceptionV3 with around 550 layers and uses the PReLU activation function. It is considered an improvement over InceptionV3 and has been used in several state-of-the-art image classification models. An Inception ResNet V2 deep learning architecture was trained on image classification data for 15 epochs, resulting in a training accuracy of 96.50% and a training loss of '0.0974'. The performance of the model was evaluated on test data, yielding a testing accuracy of 96.26% and a testing loss of '0.1015'. Despite these results, the performance was still lower than desired, leading to the replacement of the model with a ResNet50V2 architecture.

ResNet50V2. ResNet50V2 is a 50-layer CNN architecture for image classification, featuring skip connections and updated batch normalization. It is an improvement over the original ResNet50, with changes such as the use of the swish activation function and a modified version of batch normalization. ResNet50V2 is a well-established and commonly used model in the field of deep learning for image classification. The ResNet50V2 model was trained for 15 epochs on image classification data and achieved a training accuracy of '0.9723' and training loss of '0.0878'. However, when evaluated on test data, the model showed lower performance with a testing accuracy of '0.9644' and a testing loss of '0.1493', not meeting expectations. To address this, the model was replaced with MobileNetV2.

MobileNetV2. MobileNetV2 is a fast and efficient neural network architecture for on-device image classification, designed for low computational cost and high accuracy. It uses depth wise separable convolutions and inverted residual blocks with linear bottlenecks to reduce parameters and computation, while increasing the number of filters efficiently. MobileNetV2 achieves state-of-the-art performance on image classification benchmarks. The model performed 15 iterations of training, with an accuracy of '0.9775' and a loss of 0.0628 during training, and '0.9759' and





Surya Kant Palet *et al.*,

a loss of '0.0715' during testing. However, these results were lower than the expected outcome, so another architecture (VGG16) was tested.

VGG16. The Visual Geometry Group at the University of Oxford introduced the VGG16 deep learning neural network architecture in 2014. It is a 16-layer architecture with a focus on depth, using multiple consecutive convolutional and max pooling layers to extract features from images, followed by fully connected layers for classification. VGG16 is known for its good performance on image recognition benchmarks and remains a widely used architecture in computer vision and deep learning. The model trained for 15 epochs with a training accuracy of '0.9764' and a training loss of '0.0651'.

DenseNet 121. DenseNet 121 is a convolutional neural network architecture for image classification, characterized by its dense connectivity between all layers in the network. The architecture uses dense blocks and transition layers to efficiently extract features from input images and improve performance on image recognition tasks. DenseNet121 has shown strong performance on benchmark datasets. The model was trained for 15 epochs and achieved a training accuracy of '0.9828' and a training loss of '0.0493'. When evaluated on the test data, it had a testing accuracy of '0.9796' and a testing loss of '0.0654'. Although these results were an improvement from previous models, they were still lower than the expected outcome, so the team moved on to another architecture, Xception.

Xception. Fitting the Xception model into the training set resulted in vast improvement compared to other models. Xception is a deep learning neural network architecture designed for efficient and effective image classification. The architecture also uses residual connections to improve the flow of information through the network, leading to better feature representation and improved performance on image classification tasks. Xception has been trained on large datasets and achieved state-of-the-art performance on various benchmarks, making it a popular choice for computer vision and deep learning tasks. After running it for 15 epochs, we found our training accuracy to be '0.9882' and our training loss to be '0.0386'. The model was then checked for test data, and we got a testing accuracy of '0.9804' and a testing loss of '0.0679'. This was the best-generalized model we could ever get.

RESULTS AND INTERPRETATION

The comparison of accuracy and loss of both training and test set for all the architecture is shown below in the figure 4 and figure 5. The best performing model was Xception, hence the epoch wise accuracy and loss depiction for both training and testing set is given in Figure 6. And 7. Respectively According to how much the forecast deviates from the actual number, Figure 3 demonstrates how a loss function—often referred to as a cost function—takes into consideration the estimate's probabilities, or uncertainty. This helps us understand the model's performance in greater depth. Accuracy is one way to evaluate a classification model's performance. A percentage is a common way to express it [22]. The accuracy for a given sample is defined as the proportion of predictions when the predicted value matches the actual value [23]. In figure 4, ensure that your test set meets the following two conditions, is big enough to produce statistically significant outcomes, and is a good representation of the entire data set. The visual representation of how the model predicted a real-world object with the help of mobile app is shown above in Figure 8. The image was taken from the web and was not part of the training or testing dataset [24]. The tabular comparison of our work with previous work is shown below in the Table (1).

CONCLUSION

Proper classification of fruit freshness is necessary as it is directly related to human health. In this project work, we created our own Model_O and compared it with other transfer learning algorithms to classify fresh and rotten fruit. As our Model_O was poorly generalized, we tried to implement transfer learning architecture with parameters of our choice. We then did hyperparameter tuning in the best-performing transfer learning architecture. The





Surya Kant Palet *et al.*,

architectures used were, Model_O (which is our own designed architecture), NasNet Mobile, InceptionV3, Inception ResNet V2, ResNet50V2, MobileNetV2, VGG16, DenseNet 121 and finally Xception. A detailed comparison was made between these nine architectures, and we found that fitting the Xception model into the training set resulted in vast improvement compared to other models. The Xception model showed significant improvement over other models for the training set, with a training accuracy of '0.9882' and a training loss of '0.0386' after 15 epochs. The model also performed well on test data with a testing accuracy of '0.9804' and a testing loss of '0.0679', making it the best-generalized model for this particular dataset.

Future Scope and Recommendation

More varieties of fruits can be included in the training and testing set so that this process of fruit freshness detection can work in any part of the world in any climatic condition. This system can even be implemented in the fruit and juice industry conveyor belts so that rotten fruits can be automatically removed before the fruit processing. The mobile app can be published in Google Playstore or Apple Store so that many farmers can be benefited.

REFERENCES

1. R. Verma and A. K. Verma, "Fruit Classification Using Deep Convolutional Neural Network and Transfer Learning," *Communications in Computer and Information Science*, vol. 1591 CCIS, pp. 290–301, 2022, doi: 10.1007/978-3-031-07012-9_26/COVER.
2. H. H. C. Nguyen, A. T. Luong, T. H. Trinh, P. H. Ho, P. Meesad, and T. T. Nguyen, "Intelligent Fruit Recognition System Using Deep Learning," *Lecture Notes in Networks and Systems*, vol. 251, pp. 13–22, 2021, doi: 10.1007/978-3-030-79757-7_2/COVER.
3. R. Roy, K. Chekuri, G. Sandhya, S. K. Pal, S. Mukherjee, and N. Marada, "Exploring the blockchain for sustainable food supply chain," *Journal of Information and Optimization Sciences*, vol. 43, no. 7, pp. 1835–1847, Oct. 2022, doi: 10.1080/02522667.2022.2128535.
4. Koirala, K. B. Walsh, Z. Wang, and C. McCarthy, "Deep learning – Method overview and review of use for fruit detection and yield estimation," *Comput Electron Agric*, vol. 162, pp. 219–234, Jul. 2019, doi: 10.1016/J.COMPAG.2019.04.017.
5. Bhargava and A. Bansal, "Classification and Grading of Multiple Varieties of Apple Fruit," *Food Anal Methods*, vol. 14, no. 7, pp. 1359–1368, Feb. 2021, doi: 10.1007/S12161-021-01970-0/FIGURES/8.
6. R. Roy, M. D. Babakerkhell, S. Mukherjee, D. Pal, and S. Funiilkul, "Evaluating the Intention for the Adoption of Artificial Intelligence-Based Robots in the University to Educate the Students," *IEEE Access*, vol. 10, pp. 125666–125678, 2022, doi: 10.1109/ACCESS.2022.3225555.
7. D. I. Patrício and R. Rieder, "Computer vision and artificial intelligence in precision agriculture for grain crops: A systematic review," *Comput Electron Agric*, vol. 153, pp. 69–81, Oct. 2018, doi: 10.1016/J.COMPAG.2018.08.001.
8. S. Mukherjee et al., "Blockchain-based circular economy for achieving environmental sustainability in the Indian electronic MSMEs," *Management of Environmental Quality: An International Journal*, vol. ahead-of-print, no. ahead-of-print, Oct. 2022, doi: 10.1108/MEQ-03-2022-0045.
9. K. Roy, S. S. Chaudhuri, and S. Pramanik, "Deep learning based real-time Industrial framework for rotten and fresh fruit detection using semantic segmentation," *Microsystem Technologies*, vol. 27, no. 9, pp. 3365–3375, Sep. 2021, doi: 10.1007/S00542-020-05123-X/FIGURES/9.
10. J. Kang and J. Gwak, "Ensemble of multi-task deep convolutional neural networks using transfer learning for fruit freshness classification," *Multimed Tools Appl*, vol. 81, no. 16, pp. 22355–22377, Jul. 2022, doi: 10.1007/S11042-021-11282-4/TABLES/5.
11. Bhargava and A. Bansal, "Automatic Detection and Grading of Multiple Fruits by Machine Learning," *Food Anal Methods*, vol. 13, no. 3, pp. 751–761, Mar. 2020, doi: 10.1007/S12161-019-01690-6/TABLES/6.
12. S. Mukherjee, M. M. Baral, S. K. Pal, V. Chittipaka, R. Roy, and K. Alam, "Humanoid robot in healthcare: A Systematic Review and Future Research Directions," *2022 International Conference on Machine Learning, Big Data*,



Surya Kant Palet *et al.*,

- Cloud and Parallel Computing (COM-IT-CON), pp. 822–826, May 2022, doi: 10.1109/COM-IT-CON54601.2022.9850577.
13. J. Gené-Mola *et al.*, "Fruit detection and 3D location using instance segmentation neural networks and structure-from-motion photogrammetry," *Comput Electron Agric*, vol. 169, p. 105165, Feb. 2020, doi: 10.1016/J.COMPAG.2019.105165.
 14. J. Li, Y. Tang, X. Zou, G. Lin, and H. Wang, "Detection of Fruit-Bearing Branches and Localization of Lit-chi Clusters for Vision-Based Harvesting Robots," *IEEE Access*, vol. 8, pp. 117746–117758, 2020, doi: 10.1109/ACCESS.2020.3005386.
 15. S. Chakraborty, F. M. J. M. Shamrat, M. M. Billah, M. al Jubair, M. Alauddin, and R. Ranjan, "Implementation of Deep Learning Methods to Identify Rotten Fruits," *Proceedings of the 5th International Conference on Trends in Electronics and Informatics, ICOEI 2021*, pp. 1207–1212, Jun. 2021, doi: 10.1109/ICOEI51242.2021.9453004.
 16. Kamilaris and F. X. Prenafeta-Boldú, "Deep learning in agriculture: A survey," *Comput Electron Agric*, vol. 147, pp. 70–90, Apr. 2018, doi: 10.1016/J.COMPAG.2018.02.016.
 17. J. Chen, J. Chen, D. Zhang, Y. Sun, and Y. A. Nanekaran, "Using deep transfer learning for image-based plant disease identification," *Comput Electron Agric*, vol. 173, p. 105393, Jun. 2020, doi: 10.1016/J.COMPAG.2020.105393.
 18. R. Roy, M. M. Baral, S. K. Pal, S. Kumar, S. Mukherjee, and B. Jana, "Discussing the present, past, and future of Machine learning techniques in livestock farming: A systematic literature review," *2022 International Conference on Machine Learning, Big Data, Cloud and Parallel Computing (COM-IT-CON)*, pp. 179–183, May 2022, doi: 10.1109/COM-IT-CON54601.2022.9850749.
 19. J. G. A. Barbedo, "Factors influencing the use of deep learning for plant disease recognition," *Biosyst Eng*, vol. 172, pp. 84–91, Aug. 2018, doi: 10.1016/J.BIOSYSTEMSENG.2018.05.013.
 20. S. Mukherjee and V. Chittipaka, "Analysing the Adoption of Intelligent Agent Technology in Food Supply Chain Management: An Empirical Evidence," *FIIB Business Review*, p. 231971452110592, Nov. 2021, doi: 10.1177/23197145211059243.
 21. M. Weiss, F. Jacob, and G. Duveiller, "Remote sensing for agricultural applications: A meta-review," *Remote Sens Environ*, vol. 236, p. 111402, Jan. 2020, doi: 10.1016/J.RSE.2019.111402.
 22. D. Caceres-Hernandez *et al.*, "Recent advances in automatic feature detection and classification of fruits including with a special emphasis on Watermelon (*Citrillus lanatus*): A review," *Neurocomputing*, vol. 526, pp. 62–79, Mar. 2023, doi: 10.1016/J.NEUCOM.2023.01.005.
 23. J. F. Dou *et al.*, "Recent advances and development of postharvest management research for fresh jujube fruit: A review," *Sci Hortic*, vol. 310, p. 111769, Feb. 2023, doi: 10.1016/J.SCIENTA.2022.111769.
 24. E. Karadağ and A. Kılıç, "Non-destructive robotic sorting of cracked pistachio using deep learning," *Postharvest Biol Technol*, vol. 198, p. 112229, Apr. 2023, doi: 10.1016/J.POSTHARVBIO.2022.112229.
 25. Karakaya, D., Ulucan, O., & Turkan, M. (2019, October). A comparative analysis on fruit freshness classification. In *2019 Innovations in Intelligent Systems and Applications Conference (ASYU)* (pp. 1-4). IEEE.
 26. Fu, Y. (2020). Fruit freshness grading using deep learning (Doctoral dissertation, Auckland University of Technology).
 27. Pathak, R., & Makwana, H. (2021). Classification of fruits using convolutional neural network and transfer learning models. *Journal of Management Information and Decision Sciences*, 24, 1-12.
 28. Miah, M. S., Tasnuva, T., Islam, M., Keya, M., Rahman, M. R., & Hossain, S. A. (2021, July). An Advanced Method of Identification Fresh and Rotten Fruits using Different Convolutional Neural Networks. In *2021 12th International Conference on Computing Communication and Networking Technologies (ICCCNT)* (pp. 1-7). IEEE.

Table 1. Comparison with previous work.

Karakaya <i>et. al</i> , 2019	97.61
Yuhang Fu, 2020	92.37
Pathak, R. and Makwana, H., 2021	98.23
M. S. Miah <i>et. al</i> , 2021	97.34
Our work	98.82





Surya Kant Palet *et al.*,

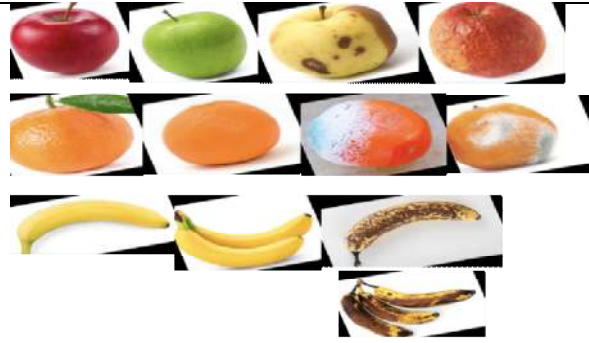


Fig. 1. Samples of Images from our dataset belonging to 6 different classes

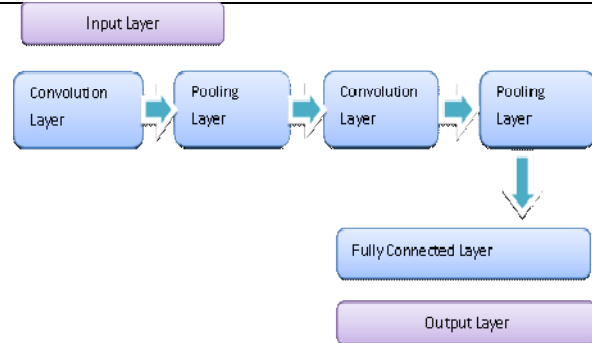


Fig. 2. Basic Architecture of CNN Model used for Multiclass Classification

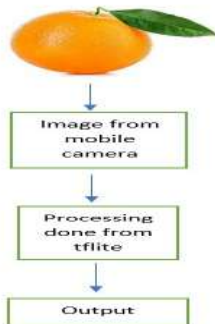


Fig 3. Representation of working of mobile app.

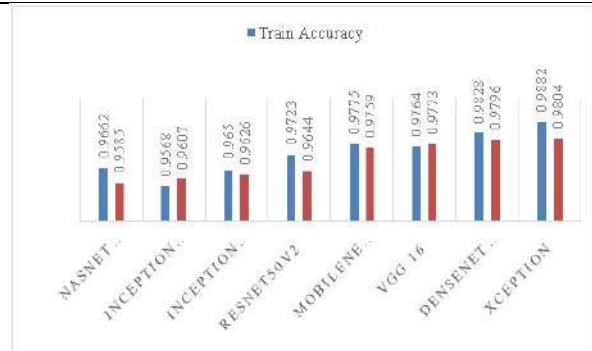


Fig. 4. Loss comparison of all the architectures.

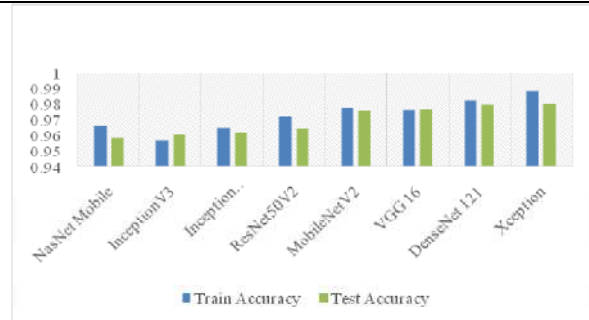


Fig. 5. Accuracy comparison of all the architectures.

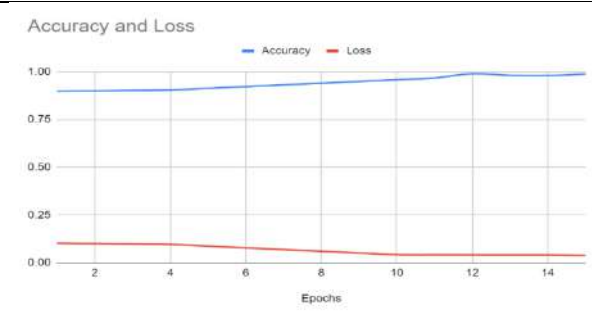


Fig. 6. Training Set Result

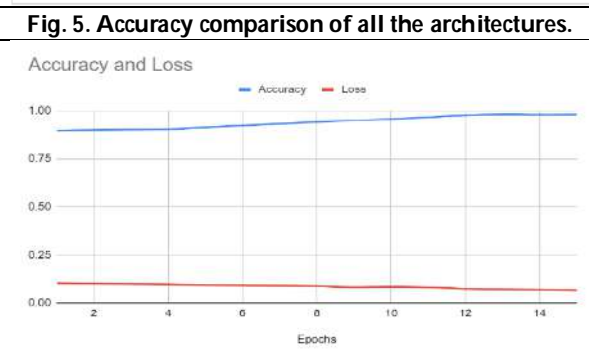


Fig. 7. Testing Set Result

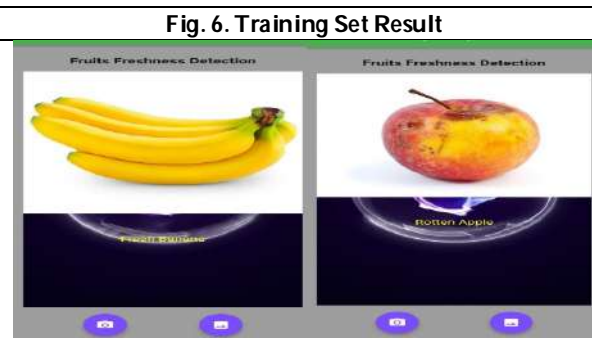


Fig. 8. A visual overview of mobile app.





Retinal Fundus Multi-Disease Classification using Machine Learning and Computer Vision Techniques

Aparna Chaudhary* and H.D.Arora

Department of Mathematics, Amity Institute of Applied Sciences, Amity University Uttar Pradesh, Noida-201303.

Received: 06 Apr 2023

Revised: 15 May 2023

Accepted: 31 May 2023

*Address for Correspondence

Aparna Chaudhary

Department of Mathematics,
Amity Institute of Applied Sciences,
Amity University Uttar Pradesh,
Noida-201303
E. Mail: aparna.chaudhary@s.amity.edu



This is an Open Access Journal / article distributed under the terms of the **Creative Commons Attribution License** (CC BY-NC-ND 3.0) which permits unrestricted use, distribution, and reproduction in any medium, provided the original work is properly cited. All rights reserved.

ABSTRACT

Eye screening along with prompt diagnosis and care is a widely accepted approach to prevent vision loss and harm to other body parts. Models based on deep learning have been created in this research work to classify the retinal fundus images into healthy and unhealthy retinas and further classifying them into 45 categories of ocular abnormalities. The suggested models are developed on the architecture of the VGG-16 deep learning model. The research has been compared with cutting-edge models for diagnosing retinal diseases. It has been properly statistically evaluated in terms of characteristics such as performance, accuracy, specificity, sensitivity, AUC, F1-score, etc. The results demonstrated that, in comparison to the latest techniques, the suggested transfer learning models perform better for the automatic diagnosis of retinal disorders. The efficiency of both models is statistically assessed and compared with other deep learning models and results shows that the suggested VGG-16 based models outperforms the existing deep learning models.

Keywords: Artificial intelligence; Image processing; Retinal fundus images; Neural networks; VGG-16 architecture

INTRODUCTION

The WHO's 2019 World Report on Vision estimates that there are 2.2 billion visually impaired persons globally, of which at least 1 billion instances might have been avoided or still need to be handled [1]. A unique option for non-interfering examining human retinal vascular microcirculation is provided by eye screening using colour fundus pictures to show retinal blood flow. The identification of early warning signs for a wide range of chronic conditions

57538





Aparna Chaudhary and Arora

has been made possible by a thorough clinical analysis of recognisable retinal fundus characteristics [2,3,4]. As a result, the retina could operate as a substitute organ whose testing is essential for determining the wellbeing of the eye as well as any underlying systemic problems. Thus, eye screening along with prompt diagnosis and care is a widely accepted approach to prevent vision loss and harm to other body parts. Visual impairment could be prevented by Early ocular disease identification and diagnosis are essential for effective treatment. Therefore, creating an autonomous disease detection system is essential to reducing the financial consequences associated with eyesight loss.

Data Description

The Retinal fundus multi-disease image dataset (RFMiD) is a brand-new, freely accessible dataset of 3200 retinal pictures that includes specialist remarks split into 2 categories.

- Sorting retinal images into categories for normal and pathological conditions.
- The categorization of retinal images into 45 varied disease classes.

Training set which consists of 1920 images i.e 60% of the dataset, evaluation set with 640 images (20%), and test set with 640 images(20%) are three subsets that make up the dataset. In the training, assessment, and test sets, the disease-wise stratification is typically $60 \pm 7\%$, $20 \pm 7\%$ and $20 \pm 5\%$, respectively. This dataset's main goal is to give a variety of disorders that frequently arise in clinical settings. The CSV files, namely, *Train_Label.csv*, *Valid_Label.csv*, and *Test_Label.csv*, contain the labels. Figure.1 displays the data from the CSV file:

Experimental Procedures

Data Acquisition

Three distinct digital fundus cameras—the Kowa VX-10 α , TOPCON TRC-NW300, and TOPCON 3D OCT-2000—all with their focus set on the optic disc—were used to capture the retinal images. These images have been captured of patients who went to an eye clinic concerning their eye health.

Preparation of Samples

Prior to image capture, the majority of the patients had their pupils dilated with a small amount of tropicamide with a dosage of 0.5%. The fundus images were taken using a non-invasive fundus camera while the patient was seated upright, with lenses spaced 39 millimeters (Kowa VX-10 α) and 40.7 millimeters (TOPCON 3D OCT-2000) apart.

Data Quality

From the thousands of examinations conducted between 2009 and 2020, 3200 photos were extracted to create the dataset. To make the dataset difficult, all high and low-resolution images were used.

Model Approach

VGG16: Concept and Architecture

One of the most substantial computer vision models accessible at present is the CNN variant called VGG16. The VGG model stands for the Visual Geometry Group. Karen Simonyan and Andrew Zisserman [5] from the Visual Geometry Group Lab at Oxford University proposed VGG 16 in the work "VERY DEEP CONVOLUTIONAL NETWORKS FOR LARGE-SCALE IMAGE RECOGNITION" published in 2014. VGG16 is a feature recognition and categorization algorithm which was once applied to classify one thousand images into thousand different categories, achieved an accuracy rate of 92.7%. It is a well-known approach for categorising photos and is convenient for transfer learning.

1. VGG16 has 16 layers with weights. 13 convolutional layers, five Max Pooling layers, and three dense layers make up VGG16's total of 21 layers, although only sixteen of those layers are weight layers, also known as learnable parameters layers.
2. The input tensor for VGG16 has three RGB channels and is 224×224 in size.
3. VGG16's strongest defining characteristic is that it prioritised convolution layers of a 3×3 filter with stride 1 rather than a large number of hyper-parameters and consistently employed the same padding and maxpool layer of a 2×2 filter with stride 2.



**Aparna Chaudhary and Arora**

4. Max pool and convolution layers are uniformly arranged during the entire design.
5. The Conv-1 Layer contains 64 filters, the Conv-2 Layer 128 filters, the Conv-3 layer 256 filters and the Conv-4 and Conv-5 Layers 512 filters.
6. 3 fully connected layers are inserted after a set of convolutional layers, each of the first 2 having 4096 channels, and the third having 1000 channels (one for each class). The soft-max layer is the last one.

Fine-tuning

Fine-tuning is a transfer learning technique used in machine learning where pre-trained model weights are trained on data that is unfamiliar [6]. The layers that are not getting fine-tuned are "frozen" (not modified during the backpropagation step) when fine-tuning is performed on the neural network as a whole or on a subset of its layers.

- After the fifth block of VGG16, we modified the model by adding 3 dense layers and 2 dropout layers. $250 \times 400 \times 3$ is the size of our input dimension of the first convolutional layer.
- There are 2 convolutional layers in the initial block, each with 64 channels, using the same padding and a 3×3 kernel size. a Maxpooling layer of size 2×2 with a stride of 2×2 is then added. The second block follows the first with a Maxpooling layer of stride 2×2 and 2 convolution layers with 128 channels each having a kernel size of 3×3 .
- Three convolutional layers are found in the final three blocks, which are followed by a Maxpooling layer. Blocks 3, 4, and 5 with three convolutional layers all have a 3×3 kernel size and have channel sizes of 256, 512, and 512, respectively.
- A flatten layer was introduced to create a 1×43088 feature vector. Three dense layers were also inserted along with two dropout layers. The classification vector is normalised at the end using a Sigmoid activation function.

Data preprocessing

Data preprocessing, considered an important aspect of data preparation, refers to any sort of processing done on raw data to get it ready for more data processing. The data is transformed into a format that can be processed more quickly and efficiently in applications of data science such as machine learning, data mining, and others.

The steps involved in the preprocessing of the sample data are as follows:

Formation of Input Image

After investigating a batch of images from each class, it was discovered that the training dataset's shape of images exists in a variety of sizes. So, the same shape of 300×450 was created by synthesizing all the photos. Our model will be less prone to errors as a result.

Image Rescaling

Across training, validation, and test datasets, all data images' pixels are rescaled into the range of (0–1) with a rescaling factor of $1./255$.

Data Augmentation

The image augmentation process is applied to the training dataset, increasing the size of the training set and improving the model's ability to handle images on different axes. Since contrast in retinal images taken with a fundus camera is highest in the center of the image and gradually decreases as one moves away from the center, contrast enhancement is crucial. Image scaling and various augmentations employing methods like rotation, flipping, and zooming are additional frequent preprocessing operations. Images are enhanced in the manner described below:

Contrast = 1.35

Random Left-Right (horizontally) flip

Random Up-Down (vertically) flip





Model training

For this project two models have been created, one to classify between healthy and unhealthy state of retinas and another one for classifying among 45 states of retinal pathologies present in the dataset. We will discuss the training procedure for each of the model in detail.

Model for classifying between healthy and unhealthy retinas

The dataset that was used for this study had already been split into subsets for training, validation and testing. The division is carried out separately at the level of the candidate, which means that every individual image of a certain set is included in the corresponding subset of the dataset. Retinal disease detection method is performed on dataset of two classes that represent the images with healthy retinas and the images with diseases present in retinas.

The parameters of the VGG-16-based model that was trained for this project (using pre-trained weights from ImageNet) were enhanced and shaped using the training and validation dataset, respectively. Table .1 provides a summary of the various additional parameters used in this innovative work's model training.

Model for multi-disease classification

Using the training as well as validation dataset, respectively, the parameters of the VGG-16-based model that was developed for identifying 45 retinal states/pathologies (using pre-trained weights from ImageNet) were optimized and shaped. Table .2 provides a summary of the various additional parameters used in this innovative work's model training.

Performance Evaluation

The effectiveness of the suggested models has been calculated using the various performance measures. For the binary classification model which detects the healthy and unhealthy retinas, precision, accuracy, recall and F1-score have been calculated using classification report and confusion matrix. The following metrics have been calculated for the multi-disease classification model: area under the curve (AUC), sensitivity, receiver operating characteristics (ROC) graph, specificity, and accuracy.

Performance of model classifying healthy and unhealthy retinal fundus

The proposed model, built using VGG-16 architecture and transfer learning, achieved an accuracy of 97.18% during performance evaluation of binary classification of healthy and unhealthy states of retina. According to the classification report, the model has achieved a precision of 0.962, recall of 0.9417 and F1-score of 0.951.

The confusion matrix for the model is represented in Fig. 2.

When comparing performance on training data to performance on a test (or validation) set, overfitting is identified if there is a significant discrepancy. It follows that when the two curves are close together, as they are in our instance, there is slightly overfitting. As you can see, training accuracy eventually surpasses validation accuracy by a small margin, but since there's not much gap between train accuracy and validation accuracy it represents good fit.

Below is a display of the output plot:

Fig. 3. represents the loss graph. Almost always, the training dataset's model loss will be lower than that of the validation dataset. As a result, there will probably be a difference between the validation loss learning curve and the train learning curve. This discrepancy is known as the "generalization gap." As can be seen in Fig. 4 instruction and approval A good match is when the loss lowers to the point of stability with just a slight variance between the both final loss figures.

Performance of model classifying 45 states of retina (multi-disease classification)

The suggested model constructed using VGG-16 model employing obtained an accuracy of 95.17% during the multiclass comparison among the specified retinal disorders. The stated values for sensitivity and specificity are 90.85% and 92.50%, respectively. The model evaluation likewise reports a high AUC value of 0.9155. Table 3. represents the performance metrics of the proposed multi-disease classification model.

Fig. 6. represents the accuracy graph. As can be seen in the graph, there is a tiny overfitting when the two curves are close together. Training accuracy eventually outperforms validation accuracy by a slight margin, but since there isn't



**Aparna Chaudhary and Arora**

much of a difference between the two, this is still a fairly good fit. The loss graph is shown in Fig. 7. Almost always, the training dataset's model loss will be lower than that of the validation dataset. As a result, there may probably be a difference between the training loss learning curve and the validation learning curve. As demonstrated in Fig. 8, A training and validation loss which reduces to a point of consistency with little difference between the two final loss values indicates a successful match.

Comparative analysis

In this section the suggested model which is built-up on VGG-16 deep learning architecture is being compared to different deep learning models: ResNet50, InceptionV3 and DenseNet-121. Now we will briefly take a look over the architecture of these models and how they are used for retinal fundus multi-disease classification.

Comparative study of model classifying healthy and unhealthy retinal fundus

Based on the accuracy, precision, recall and F1-score listed in Table 5, these trained models are scrutinised. With a classification accuracy of 97.18%, the proposed model performed well. InceptionV3 came in second with a 95.15% accuracy followed by ResNet50 and DenseNet121 with accuracy of 94.68% and 91.40% respectively. A better F1-score of 0.951 is achieved by the proposed model followed by other models. Also, in terms of sensitivity and specificity the proposed model performed better than other models. Table 6. contrasts the computing times required for training and testing by each model. It can be seen that the proposed model was the fastest during training (462 minutes) and testing (3 minutes) with the best accuracy.

Comparative study of model classifying 45 states of retina (multi-disease classification)

Based on the accuracy, sensitivity, specificity and AUC values listed in Table 6, we compared these pre-trained models. With a classification accuracy of 95.17%, the proposed model performed well. ResNet50 came in second with a 90.85% accuracy followed by InceptionV3 and DenseNet121 with accuracy of 89.32% and 85% respectively. A better value of AUC (0.9155) is achieved by the proposed model followed by other models. Also, in terms of sensitivity and specificity the proposed model performed better than other models. Table 7 contrasts the computing times required for training and testing by each model. It can be observed that the suggested model was the fastest during training (383 minutes) and testing (3 minutes) with the best accuracy.

For each modified model, the loss values during the training and validation processes are displayed in Fig. 9 –12. While analysing the number of epochs needed for each model to attain the minimal validation loss, we observed that DenseNet121 and InceptionV3 used merely 3 and 4 epochs, respectively, to achieve the minimum validation loss. This demonstrates how rapidly these algorithms can pick up on the differences between various retinal pathologies. The accuracy of training is most prominent for VGG16 based proposed model along with ResNet50, although the proposed model has the least training loss when accuracy and loss are taken into account. Therefore, based on this information, it can be concluded that, out of the four models, the proposed model performs better in terms of training and validation.

CONCLUSION

Models based on deep learning have been created in this research work to classify the retinal fundus images into healthy and unhealthy retinas and further classifying them into 45 categories of ocular abnormalities. The suggested models are developed on the architecture of the VGG-16 deep learning model. The growing application of retinal scan imaging methods and CAD in the detection of medical diseases served as the inspiration for this work. To train, validate, and test the models over the dataset of retinal fundus images dataset (using pre-trained weights from the ImageNet dataset) transfer learning has been used. The research has been compared with cutting-edge models for diagnosing retinal diseases. It has been properly statistically evaluated in terms of characteristics such as performance, accuracy, specificity, sensitivity, AUC, F1-score, etc. The results demonstrated that, in comparison to the latest techniques, the suggested transfer learning models perform better for the automatic diagnosis of retinal





Aparna Chaudhary and Arora

disorders. The proposed binary classification model can distinguish between the healthy and unhealthy classes and obtained an accuracy of 97.18%. According to the classification report, the model has achieved outstanding precision (0.962), recall (0.9417) and F1-score (0.951). Furthermore, the other proposed multi-disease classification model can distinguish between the 45 states of the retina with a notable accuracy (95.17%), sensitivity (90.85%), specificity (92.50%), and AUC (0.9155). The efficiency of both models is statistically assessed and compared with other deep learning models and results shows that the suggested VGG-16 based models outperforms the existing deep learning models. It is widely understood that ophthalmologists are unable to independently examine a significant number of retinal images due to the lack of knowledge required to provide a manual classification of retinal illnesses. The suggested DL strategy based on transfer learning integrates automated classification of eye diseases in its entirety and outperformed the conventional approaches.

Future Scope

Deep learning needs a lot of data to perform well and prevent overfitting. In general practice, obtaining diagnostic data is difficult, on concerning impairments with low prevalence. Future projects will concentrate on evaluating the models using larger dataset. Due to variations in the retinal appearance, ophthalmologists can utilise more advanced learning algorithms in the years to come to improve diagnosis accuracy. By creating a special model for identification of objects and boosting the proposed models' functioning by integrating additional layers, we might eventually be able to detect the retinal diseases more precisely. After testing and adjusting the datasets with an improved consistent distribution, the system might function even better.

REFERENCES

1. Who Launches First World Report on Vision. Available online: https://www.who.int/blindness/Vision2020_report.pdf (accessed on 29 January 2021).
2. Chang, Y.S.; Weng, S.F.; Chang, C.; Wang, J.J.; Tseng, S.H.; Wang, J.Y.; Jan, R.L. Risk of retinal vein occlusion following end-stage renal disease. *Medicine* 2016, 95, e3474.
3. MacGillivray, T.; Trucco, E.; Cameron, J.; Dhillon, B.; Houston, J.; Van Beek, E. Retinal imaging as a source of biomarkers for diagnosis, characterization and prognosis of chronic illness or long-term conditions. *Br. J. Radiol.* 2014, 87, 20130832.
4. Goller C, Kuchler A. Learning task-dependent distributed representations by backpropagation through structure. In: Proceedings of international conference on neural networks (ICNN'96), vol 1. IEEE; 1996. p. 347–52.
5. <https://doi.org/10.48550/arXiv.1409.1556>
6. Quinn, Joanne (2020). *Dive into deep learning: tools for engagement*. Thousand Oaks, California. p. 551. ISBN 978-1-5443-6137-6. Archived from the original on January 10, 2023. Retrieved January 10, 2023.

Table 1. Experimental parameters and their specific values in model training for healthy vs unhealthy retinal fundus classification

EXPERIMENTAL PARAMETERS	SPECIFIC VALUES
Initialized Weights	ImageNet Dataset
Training set	1920 images
Training set (after oversampling)	3123 images
Validation set	640 images
Test set	640 images
Input image size	300 x 450
Model Output	Sigmoid activation for 2 classes; healthy and unhealthy retinas
Model Training steps per epoch	Approx. 25 steps per epoch





Aparna Chaudhary and Arora

Table 2. Experimental parameters and their specific values in model training for multi-disease classification

EXPERIMENTAL PARAMETERS	SPECIFIC VALUES
Initialized Weights	ImageNet Dataset
Input image size	300 x 450
Model Output	Sigmoid activation for 45 different retinal states
Model Training steps per epoch	30 steps per epoch

Table 3. Performance metrics of binary classification model

Accuracy	Precision	Recall	F1-score
97.18%	0.962	0.9417	0.951

Table 4. Performance metrics of multi-disease classification model

Accuracy	Sensitivity	Specificity	AUC value
95.17%	90.85%	92.50%	0.9155

Table 5. Performance evaluation of binary classification model and its comparative analysis with different deep learning models.

Parameters	ResNet50	InceptionV3	DenseNet121	Proposed Model
Accuracy	94.68%	95.15%	91.40%	97.18%
Precision	0.947	0.958	0.916	0.962
Recall	0.866	0.902	0.830	0.9417
F1-score	0.904	0.929	0.871	0.951
Training Time (mins)	468	471	473	462
Testing Time (mins)	3	4	5	3

Table 6. Performance of multi-disease classification model and comparative analysis with different deep learning models.

Parameters	ResNet50	InceptionV3	DenseNet121	Proposed Model
Accuracy	90.85%	89.32%	85.00%	95.17%
Sensitivity	89.77%	84.15%	85.22%	90.85%
Specificity	90.00%	85.70%	84.19%	92.50%
AUC	0.8950	0.8455	0.8577	0.9155
Training Time (mins)	391	403	415	383
Testing Time (mins)	3	4	5	3

	A	B	C	D	E	F	G	H	I	J	AU
1	ID	Disease_Risk	DR	ARM	MH	DN	MYA	BRVO	TSLN	CL
2	1	1	1	1	0	0	1	0	0		0
3	2	1	0	0	0	0	0	1	0		0
4	3	1	1	0	1	1	0	0	1		0
5	4	1	0	0	0	0	0	0	0		1
6	5	0	0	0	0	0	0	0	0		0

Fig. 1 An example of CSV files





Aparna Chaudhary and Arora

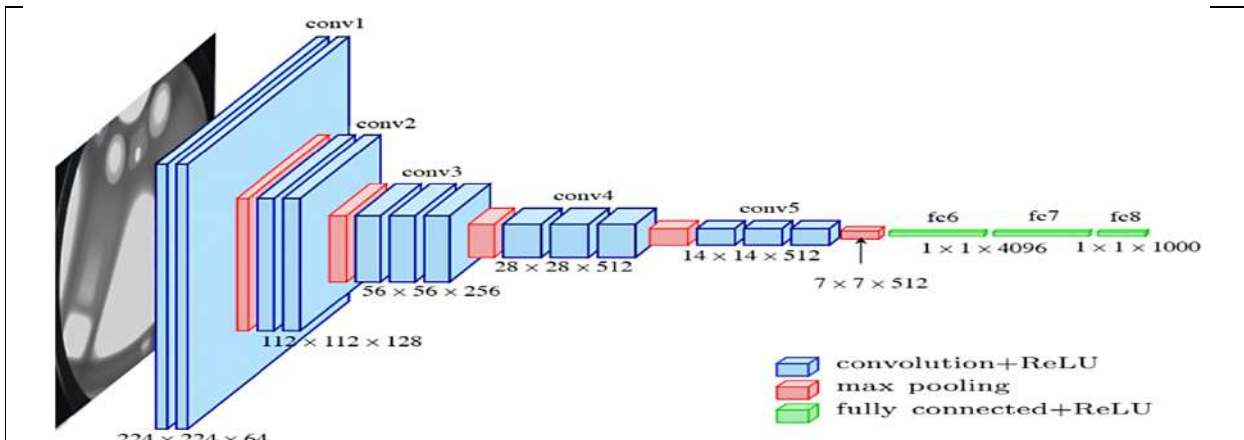


Fig. 2.VGG-16 architecture



Fig. 3.Random image sample before and after data augmentation

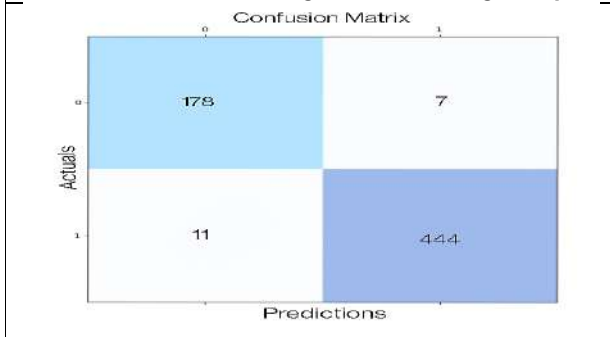


Fig. 4.Confusion matrix for the suggested model

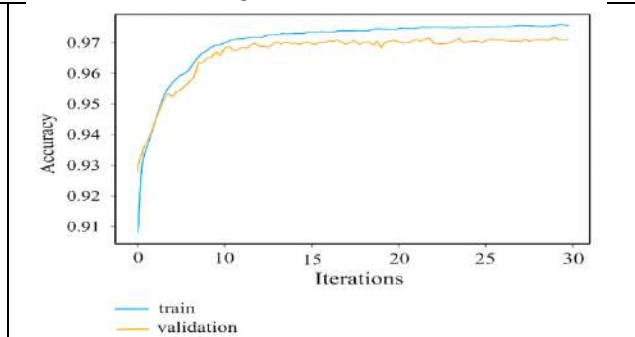


Fig. 5.Accuracy graph of binary classification model

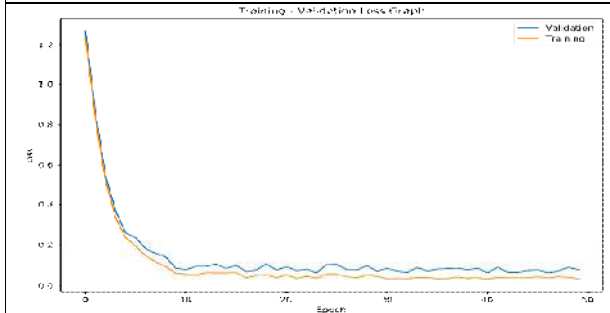


Fig. 6.Loss graph of binary classification model

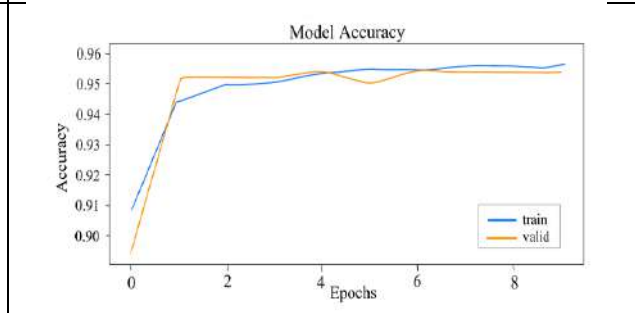


Fig. 7.Accuracy graph of multi-disease classification model





Aparna Chaudhary and Arora

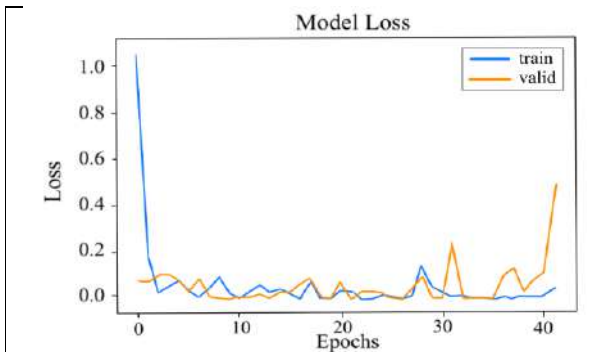


Fig. 8. Loss graph of multi-disease classification model

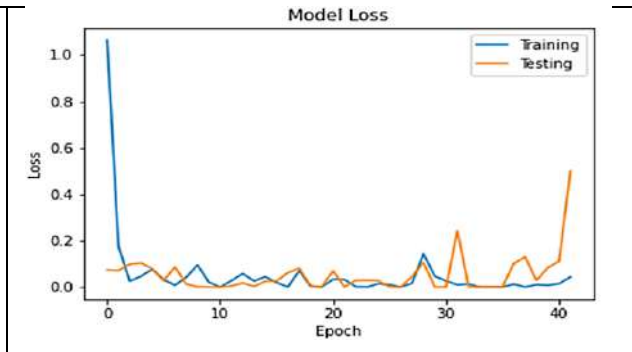


Fig. 9. VGG16 based proposed model loss graph

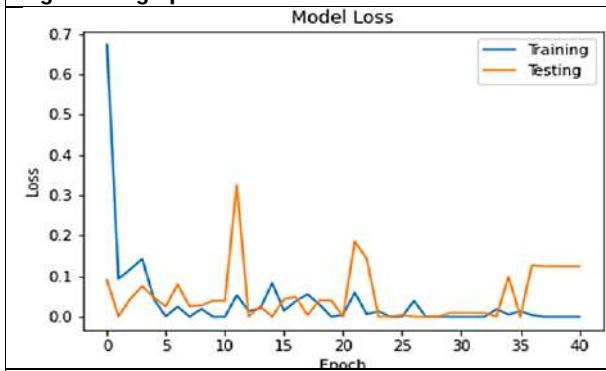


Fig. 10. ResNet50 model loss graph

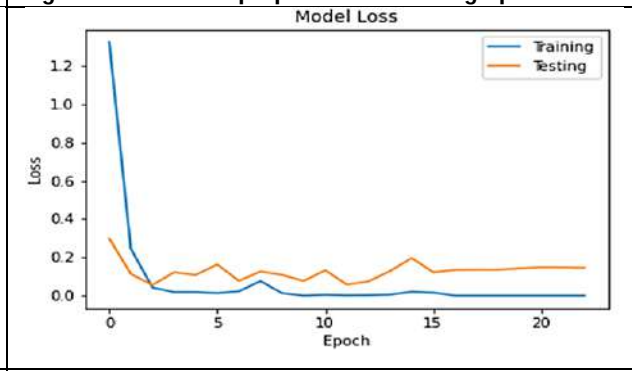


Fig. 11. InceptionV3 model loss graph

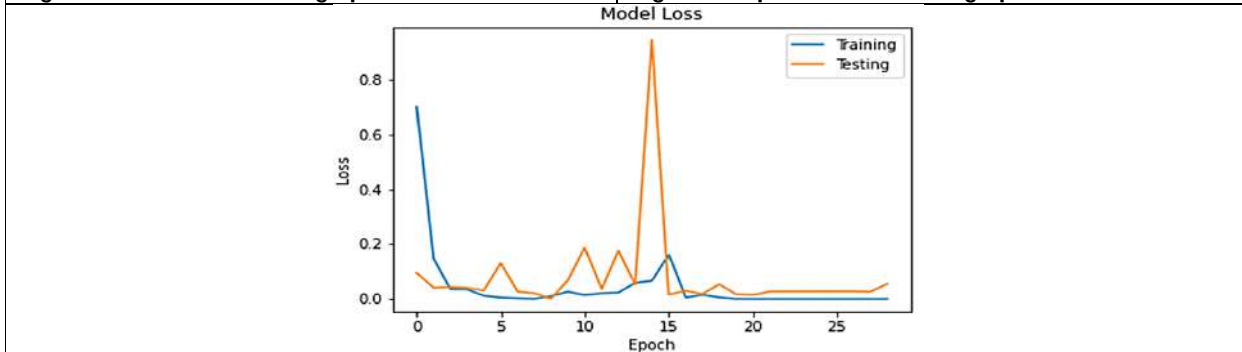


Fig. 12. DenseNet121 model loss graph





Mathematical Modeling of COVID - 19 with Treatment

Diksha Sharma* and Alpna Mishra

Centre for Cyber Security and Cryptology, Department of Mathematics, Sharda School of Basic Sciences and Research, Sharda University, Greater Noida (UP), India.

Received: 06 Apr 2023

Revised: 15 May 2023

Accepted: 31 May 2023

*Address for Correspondence

Diksha Sharma

Centre for Cyber Security and Cryptology,
Department of Mathematics,
Sharda School of Basic Sciences and Research,
Sharda University, Greater Noida (UP), India.
E. Mail: dishasharma.997@gmail.com



This is an Open Access Journal / article distributed under the terms of the **Creative Commons Attribution License** (CC BY-NC-ND 3.0) which permits unrestricted use, distribution, and reproduction in any medium, provided the original work is properly cited. All rights reserved.

ABSTRACT

The work done in this paper is based on treatment of COVID-19 and the effect on infected population using the mathematical model ($SE_cI_cT_cR$) by dividing the human population into the five compartments. We studied the model by establishing the properties for instance positivity, dependence on initial data and positively invariant of the feasible region. We computed the basic reproduction number for COVID-19 (R_0) and studied about the equilibrium points and the conditions of stability. Moreover, we proved that the condition is stable or unstable when basic reproduction number is less than unity or greater than unity respectively. We presented graphical representation and use the ODE 45 in the toolbox of MATLAB for the numerical simulation and observed that the proposed model agrees with the experimental data.

Keywords: COVID-19, Epidemic Model, Basic Reproduction Number, Stability, Treatment

INTRODUCTION

In Wuhan, China, the first instance was discovered in December 2019. Some reports had come to know that it came from those people who work and visit seafood and live animal markets in China. Namely Corona virus called COVID-19 [18]. COVID-19 had engulfed not only the whole country but the whole world. For international concern, the WHO announced a public health emergency in January 2020. This infectious disease is related to the respiratory system of the human body. The Corona Virus has affected our daily life a lot. Crores of people have come into the grip of this disease. Some of them survived, and many have died. In human beings, Corona Virus can be caused by the common cold and it converts into a severe disease. COVID-19 spreads due to person-to-person contact through coughing, talking, and sneezing [15]. Mainly, symptoms are fever, cold, cough, pain in bones and muscles, problem with respiration and throat, stress, and loss of smell or taste. Corona Virus attacks old people, chronic respiratory





Diksha Sharma and Alpa Mishra

disease, low immune system, obesity, and diabetes [24]. For instance, SARS-CoV, also known as Severe Acute Respiratory Syndrome, is brought on by cats, and MERS-CoV, also known as Middle East Respiratory Syndrome, is brought on by camels [2].

Mathematical modeling and mathematical analysis play an important role in infectious disease. Mathematical models are applied in the dynamics of diseases and their prevention strategies [4]. Mathematical modelers and epidemiologists are interested to read more in depth of the disease COVID-19 and develop some mathematical models about the COVID-19 which are related to their transmission, evolution, prevention and control [5]. A 5 compartmental model is proposed with mathematical analysis. They discussed about SEIQR model with isolation class, in which it has been assumed that the risk of its spread in future can be reduced. Numerical techniques have been applied, including the Runge- Kutta fourth-order approach and the nonstandard finite difference (NFSD) scheme [2]. A mathematical model SIR is proposed, which considers the number of infected cases, isolation wards and intensive care units [3]. A population model is proposed which related to vaccination and distinct ways of spread of COVID-19 is discussed for instance, mild symptoms, asymptomatic symptoms, severe symptoms [7]. This disease is detected when we have done RT-qPCR test or chest radiograph test of suspected patients. Personal protection may help to prevent SARS-Cov-2 [6]. A study of treatment on COVID-19 is presented that antiviral drugs are available for anti-SARS-CoV-2 [13]. A mathematical model has been taken with reference [14], [19].

This article is divided into 5 sections. Section 2 is devoted to the construction of a mathematical model on Coronavirus (COVID-19) with treatment in five compartments. In section 3, we discuss mathematical models with basic reproductive number and stability. We explain the numerical simulation of the formulated model on the effects of treatment for COVID-19 in the next section. In section 5, we give a conclusion.

Formulation of a Model

The entire population, $N(t)$ is represented by five compartments as follows: With the given equation, susceptible people are denoted as S , exposed people as E_c , infected people as I_c , infected people receiving treatment as T_c , and recovered people as R ,

$$N(t) = S(t) + E_c(t) + I_c(t) + T_c(t) + R(t)$$

Natural death rate μ_c , caused by COVID-19, the rate of disease-induced death δ_c , the rate of recovery by treatment from COVID-19 r_1 , the rate of transmission β_c , the rate at which a person leaves an exposed family and spread infection γ_c , the rate of treatment with COVID- 19 r , and the rate of recovery due to prompt treatment α .

In order to suggest the mathematical model, a nonlinear system of ordinary differential equations is used

$$\begin{aligned} \frac{dS}{dt} &= \Delta - \frac{\beta_c S I_c}{N} - \mu_c S + r_1 T_c \\ \frac{dE_c}{dt} &= \frac{\beta_c S I_c}{N} - (\mu_c + \gamma_c) E_c \\ \frac{dI_c}{dt} &= \gamma_c E_c - (\mu_c + \delta_c) I_c - r I_c \\ \frac{dT_c}{dt} &= r I_c - r_1 T_c - (\mu_c + \delta_c) T_c \\ \frac{dR}{dt} &= \alpha I_c + r_1 T_c + (\mu_c + \delta_c) T_c - (\mu_c + \delta_c) R \end{aligned} \tag{1}$$

Initial conditions of given model is:

$$S(0) = S_0 \geq 0, E_c(0) = E_{c_0} \geq 0, I_c(0) = I_{c_0} \geq 0, T_c(0) = T_{c_0} \geq 0, R(0) \geq 0 \tag{2}$$

The region Ω_{cov} is defined as

$$\Omega_{cov} = \left\{ (S, E_c, I_c, T_c, R) \in \mathbb{R}_+^5 : N(t) \leq \frac{\Delta}{\mu_c} \right\}$$

Theorem 1. With initial conditions of (2), the system S, E_c, I_c, T_c , and R has non- negative solutions for all of its components, and the region Ω_{cov} is positively invariant when $t \geq 0$.





Diksha Sharma and Alpa Mishra

Proof. We must show all of the solutions to a system of nonlinear differential equations (1) are positive using the initial conditions that have been given. Differentiate N w.r.t. time t is

$$\frac{dN}{dt} = \Delta - \mu_c S - (\mu_c + \gamma_c)E_c - (\mu_c + \delta_c)I_c - (\mu_c + \delta_c)T_c - (\mu_c + \delta_c)R$$

$$\leq \Delta - \mu_c N \quad (E_c, I_c, T_c, R \geq 0)$$

If $N > \frac{\Delta}{\mu_c}$, then $\frac{dN}{dt} < 0$ we get,

$$N(t) = N_0 e^{-\mu_c t} + \frac{\Delta}{\mu_c} (1 - e^{-\mu_c t}) \quad (3)$$

If $N_0 \leq \frac{\Delta}{\mu_c}$, then $N(t) \leq \frac{\Delta}{\mu_c}$. The system of differential equation (1), all the solutions of model starts in Ω_{cov} remain in Ω_{cov} . At time $t > 0$, implies that the variable E_c becomes zero and positivity of other variables. The given system (1), from equation (1.2) $\frac{dE_c}{dt} > 0$. This implies $E_c(t)$ is positive. Similarly for the other variables, it can be proved. Therefore, Ω_{cov} is positively invariant.

Reproduction Number

To compute the basic reproduction number R'_0 of the proposed mathematical model, we prepared the following subsystem:

$$\frac{dS}{dt} = \Delta - \frac{\beta_c S I_c}{N} - \mu_c S + r_1 T_c$$

$$\frac{dE_c}{dt} = \frac{\beta_c S I_c}{N} - (\mu_c + \gamma_c)E_c$$

$$\frac{dI_c}{dt} = \gamma_c E_c - (\mu_c + \delta_c)I_c - r I_c$$

$$\frac{dT_c}{dt} = r I_c - r_1 T_c - (\mu_c + \delta_c)T_c \quad (4)$$

with initial condition $S(0) = S_0 \geq 0, E_c(0) = E_{c_0} \geq 0, I_c(0) = I_{c_0} \geq 0, T_c(0) = T_{c_0} \geq 0$ and the entire population is given as

$$N(t) = S(t) + E_c(t) + I_c(t) + T_c(t)$$

We assume a new region Ω_{cov1} for the system (4)

$$\Omega_{cov1} = \left\{ (S, E_c, I_c, T_c) \in R^4_+ : N(t) \leq \frac{\Delta}{\mu_c} \right\}$$

Already we have proved all the solutions S, E_c, I_c, T_c are positively invariant in \square_{cov1} .

Local stability of disease-free equilibrium

The equilibrium condition is given as $J_0 = (S^{cov}, E^{cov}, I^{cov}, T^{cov}) = \left(\frac{\Delta}{\mu_c}, 0, 0, 0 \right)$

The basic reproduction number is the average number of new infections in a population of susceptible people spread by one typical infected person, symbolically R'_0 as the basic reproduction number. The next-generation matrix technique is used to determine the basic reproduction number [23]. With F serving as the transmission matrix and Σ serving as the transition matrix, respectively.

$$F = \begin{bmatrix} \frac{\beta_c \Delta}{N \mu_c} & 0 \\ 0 & 0 \end{bmatrix}$$

$$\Sigma = \begin{bmatrix} 0 & -\mu_c - \gamma_c \\ -\mu_c - \delta_c - r & \gamma_c \end{bmatrix}$$

$$K = \begin{bmatrix} \frac{\beta_c \Delta \gamma_c}{N \mu_c (\mu_c + \gamma_c) (\mu_c + \delta_c + r)} & \frac{\beta_c \Delta}{N \mu_c (\mu_c + \delta_c + r)} \\ 0 & 0 \end{bmatrix}$$

Hence, the dominant Eigen value of K ,

$$R'_0 = \frac{\beta_c \Delta \gamma_c}{N \mu_c (\mu_c^2 + r \mu_c + \mu_c \delta_c + \gamma_c r + \gamma_c \mu_c + \gamma_c \delta_c)} \quad (5)$$

Now, we discuss the local stability of DFE (Disease Free Equilibrium).

Theorem 2. The DFE (Disease Free Equilibrium) of the sub model (4) is locally asymptotically stable or unstable when R'_0 is either less than or greater than 1.





Diksha Sharma and Alpa Mishra

Proof. The given equation (4), has a Jacobian matrix that signifies J_0 ,

$$J(J_0) = \begin{bmatrix} -\mu_c & 0 & \frac{\beta_c \Delta}{N\mu_c} & r_1 \\ 0 & -(\mu_c + \gamma_c) & \frac{\beta_c \Delta}{N\mu_c} & 0 \\ 0 & \gamma_c & -(r + \mu_c + \delta_c) & 0 \\ 0 & 0 & r & -(r_1 + \mu_c + \delta_c) \end{bmatrix}$$

The characteristic polynomial is

$$= (-\mu_c - \lambda)(-r_1 - \mu_c - \delta_c - \lambda) \left((\mu_c + \gamma_c + \lambda)(\mu_c + \delta_c + r + \lambda) - \frac{\beta_c \Delta \gamma_c}{N\mu_c} \right) \quad (6)$$

For (6), the eigen values are $-\mu_c$ and $-r_1 - \mu_c - \delta_c$ which have negative real components. According to the Routh-Hurwitz stability criterion for disease-free equilibrium is locally asymptotically stable if all the coefficients of the quadratic characteristic polynomial (6) are positive when $R_0 < 1$. Comparing the quadratic factor in (6) with the general quadratic form $a_2\lambda^2 + a_1\lambda + a_0 = 0$, we get

$$a_2 = 1, a_1 = (2\mu_c + \gamma_c + \delta_c + r), a_0 = \mu_c\delta_c + r\mu_c + \mu_c^2 + \gamma_c\mu_c + \gamma_c\delta_c + \gamma_cr - \frac{\beta_c \Delta \gamma_c}{N\mu_c}$$

We have, $a_2 = 1 > 0$, $a_1 = (2\mu_c + \gamma_c + \delta_c + r) > 0$. But $a_0 > 0$ if

$$\mu_c\delta_c + r\mu_c + \mu_c^2 + \gamma_c\mu_c + \gamma_c\delta_c + \gamma_cr - \frac{\beta_c \Delta \gamma_c}{N\mu_c} > 0$$

$$\frac{\mu_c \Delta \gamma_c}{N\mu_c(\mu_c\delta_c + r\mu_c + \mu_c^2 + \gamma_c\mu_c + \gamma_c\delta_c + \gamma_cr)} < 1$$

Since all the coefficients of (6) are positive by Routh Hurwitz criterion shows that $J(J_0)$ is locally asymptotically stable for $R_0 < 1$ and unstable for $R_0 > 1$.

Theorem 3. The system of ordinary differential equation (4) has an endemic equilibrium point $(S^*, E_c^*, I_c^*, T_c^*)$, when $R_0 > 1$.

Proof. We presumed that the system of ordinary differential equations (4) equates to zero,

$$\begin{aligned} \square_c - \frac{\beta_c SI_c}{N} - \mu_c S + r_1 T_c &= 0 \\ \frac{\beta_c SI_c}{N} - (\mu_c + \gamma_c) E_c &= 0 \\ \square_c E_c - (\mu_c + \delta_c) I_c - r I_c &= 0 \\ r I_c - r_1 T_c - (\mu_c + \delta_c) T_c &= 0 \end{aligned} \quad (7)$$

After solving the above system of linear equations, we get

$$S^* = \frac{N(\mu_c + \gamma_c)(\mu_c + \delta_c + r)(\mu_c + \delta_c + r_1)\Delta}{L}$$

$$E_c^* = \frac{(\mu_c + \delta_c + r)(\mu_c + \delta_c + r_1)\beta_c I_c \Delta}{L}$$

$$I_c^* = \frac{\gamma_c(\mu_c + \delta_c + r_1)\beta_c I_c \Delta}{L}$$

$$T_c^* = \frac{\gamma_c r \beta_c I_c \Delta}{L}$$

Where $L = N\{(\square_c + \gamma_c)(\mu_c + \delta_c + r)(\mu_c + \delta_c + r_1) \left(\mu_c + \frac{\beta_c I_c}{N} \right) - \frac{\gamma_c r r_1 \beta_c I_c}{N}\}$. By substituting the value in $\frac{\square_c I_c}{N}$, we get

$\frac{\square_c I_c}{N} = 0$ implies to the disease-free equilibrium and

$$\frac{\square_c \gamma_c (\mu_c + \delta_c + r_1) \Delta - (\mu_c + \gamma_c)(\mu_c + \delta_c + r)(\mu_c + \delta_c + r_1) \mu_c}{(\mu_c + \gamma_c)(\mu_c + \delta_c + r)(\mu_c + \delta_c + r_1) \mu_c} \quad (8)$$

indicates an endemic balance exists. It should be evident that (8) is always positive and that the denominator is also positive in terms of biology, which is how an illness spreads. So,

$$\frac{\square_c \gamma_c (\mu_c + \delta_c + r_1) \Delta - (\mu_c + \gamma_c)(\mu_c + \delta_c + r)(\mu_c + \delta_c + r_1) \mu_c}{N} > 0$$

$$\frac{\beta_c \gamma_c \Delta}{N(\mu_c + \gamma_c)(\mu_c + \delta_c + r)(\mu_c + \delta_c + r_1) \mu_c} > 1$$

$$R_0 > 1$$





Diksha Sharma and Alpa Mishra

Thus, we deduce that endemic equilibrium point exists if $R_0' > 1$.

Numerical Simulation

We take various sets of parameters for numerical simulation. The numerical values are given in table 1 and the time is 200 days. Here, we use ODE45 package of MATLAB software for the mathematical model (1), as initial values $N(0) = 21600$, $S(0) = 10000$, $E_c(0) = 6000$, $I_c(0) = 4500$, $T_c(0) = 600$, $R(0) = 500$.

Here, we choose these initial values for COVID-19 infected and recovered populations. We compare the result of our model with a numerical solution. The estimated growth data of COVID-19 with treatment on population can be seen in the graphs. We take some different values of β_c such as $\beta_c = 2$, then $R_0' < 1$ and $\beta_c = 5$, then $R_0' > 1$.

The rapid increase in susceptible cases is a cause for concern, as it indicates a higher risk of disease transmission. However, the decrease in exposed cases suggests that preventative measures are working to some extent. It is important to continue implementing measures such as social distancing and wearing masks to further reduce the number of exposed cases. The increase and subsequent leveling off of the treated population is a positive sign, indicating that medical interventions are effective in managing the disease. As time progresses, it is expected that the treated population will approach a constant value, which will provide some stability in managing the disease. Additionally, the fact that nearby trajectories are moving closer suggests that there is a more consistent understanding of how to manage and treat the disease, which will be beneficial in preventing future outbreaks. It is crucial to remain vigilant and continue implementing preventative measures to ensure that progress towards managing this disease continues when $R_0' < 1$ shown in figure (2). The figures presented in (3) provide valuable insights into the dynamics of disease spread. The fact that the number of exposed, susceptible, and treated individuals increases and decreases with time suggests that the disease is spreading through the population. However, as time progresses, these numbers approach a constant value, indicating that the spread of the disease may be slowing down. Furthermore, nearby trajectories move away from each other over time, suggesting that the disease is becoming less contagious when $R_0' > 1$. Figure (4) and (5) suggest that the stable condition of disease-free equilibrium R_0' is less than 1, meaning that the disease will eventually die out if left unchecked. However, if the unstable condition of disease-free equilibrium is greater than 1, then the disease will continue to spread and infect more individuals. Therefore, it is crucial to take appropriate measures to control and prevent the spread of the disease.

CONCLUSION

It has been suggested to use the five-compartment COVID-19 analytical model. We calculated their stability and basic reproduction numbers. The mathematical model COVID-19 with treatment is said to have a locally stable, disease-free equilibrium when the reproduction number is less than 1, and when it is above unity, a disease is said to exist. The outcome of the numerical simulation showed how well the COVID-19 illness could be treated. Figures 2 and 3 show that the effect of therapy on the population is both less than and higher than 1, relative to the basic reproduction number. Figures 4 and 5 depict how stable or unstable the illness is.

ACKNOWLEDGEMENT

The author would like to express their deepest appreciation to the reader for their valuable time and helpful comments.

REFERENCES

1. A. Zeb, E. Alzahrani, V.S. Erturk, and G. Zaman, "Mathematical model for coronavirus disease 2019 (COVID-19) containing isolation class", *BioMed research international*, 2020.
2. W.K. Ming, J. Huang, and C.J. Zhang, "Breaking down of healthcare system: Mathematical modelling for controlling the novel coronavirus (2019-nCoV) outbreak in Wuhan, China", *BioRxiv*, 2020.





Diksha Sharma and Alpa Mishra

3. R.M. May, and R.M. Anderson, "Population biology of infectious diseases: Part II", *Nature*, Vol. 280, Issue - 5722, pp.455 - 461, 1979.
4. H.W. Hethcote, "The mathematics of infectious diseases", *SIAM review*, Vol. 42, Issue-4, pp. 599 - 653, 2000.
5. S.K. Saxena, S. Kumar, V.K. Maurya, R. Sharma, H.R. Dandu, and M.L. Bhatt, "Current insight into the novel coronavirus disease 2019 (COVID-19)", *Coronavirus Disease 2019 (COVID-19)*, pp.1 - 8, 2020.
6. S.K. Saxena, S. Kumar, V.K. Maurya, R. Sharma, H.R. Dandu, and M.L. Bhatt, "Current insight into the novel coronavirus disease 2019 (COVID-19)", *Coronavirus Disease 2019 (COVID-19)*, pp.1 - 8, 2020.
7. M.V. Krishna, "Mathematical modelling on diffusion and control of COVID19", *Infectious Disease Modelling*, Vol. 5, pp. 588 - 597, 2020.
8. M.V. Krishna, "Mathematical modelling on diffusion and control of COVID19", *Infectious Disease Modelling*, Vol. 5, pp. 588 - 597, 2020.
9. F. Brauer, C. Castillo-Chavez, and Z. Feng, "Endemic disease models", *In Mathematical Model in Epidemiology*, Springer, pp. 63 - 116, 2019.
10. A.R. Tuite, D.N. Fisman, and A.L. Greer, "Mathematical modelling of COVID-19 transmission and mitigation strategies in the population of Ontario, Canada", *Cmaj*, Vol. 192, Issue - 19, pp. 497 - 505, 2020.
11. H.R. Bhapkar, P.N. Mahalle, N. Dey, and K.C. Santosh, "Revisited COVID-19 mortality and recovery rates: are we missing recovery time period?", *Journal of Medical Systems*, Vol. 44, Issue- 12, pp.1 - 5, 2020.
12. M. Cascella, M. Rajnik, A. Aleem, S.C. Dulebohn, and R. Di Napoli, "Features, evaluation, and treatment of coronavirus (COVID-19)" *Statpearls*, 2022.
13. C. Castillo-Chavez, and Z. Feng, "To treat or not to treat: the case of tuberculosis", *Journal of mathematical biology*, Vol. 35, Issue - 6, pp. 629 - 656, 1997.
14. M. Gatto, E. Bertuzzo, L. Mari, S. Miccoli, L. Carraro, R. Casagrandi, and A. Rinaldo, "Spread and dynamics of the COVID-19 epidemic in Italy: Effects of emergency containment measures" *Proceedings of the National Academy of Sciences*, Vol. 117, Issue - 19, pp.10484 - 10491, 2020.
15. N. Parolini, L. Dede, P.F. Antonietti, G. Ardenghi, A. Manzoni, E. Miglio, A. Pugliese, M. Verani, and A. Quarteroni, "SUIHTER: A new mathematical model for COVID-19. Application to the analysis of the second epidemic outbreak in Italy", *Proceedings of the Royal Society A*, Vol. 477, Issue - 2253, p.20210027, 2021.
16. H. Zine, A. Boukhouima, E.M. Lotfi, M. Mahrouf, D.F. Torres, and N. Yousfi, "A stochastic time-delayed model for the effectiveness of Moroccan COVID-19 deconfinement strategy", *Mathematical Modelling of Natural Phenomena*, Vol. 15, p.50, 2020.
17. T.S. Faniran, E.A. Bakare, and A.O. Falade, "The COVID-19 Model with Partially Recovered Carriers", *Journal of Applied Mathematics*, 2021.
18. S. Kumar, and S. Jain, "Assessing the effects of treatment in HIV-TB co-infection model", *The European Physical Journal Plus*, vol. 133, pp. 1 - 20, 2018.
19. S.H.A. Khoshnaw, R.H. Salih, S. Sulaimary, "Mathematical Modelling for coronavirus Disease (COVID-19) in Predicting future behaviors and Sensitivity Analysis", *Mathematical Modelling of Natural Phenomena*, 2020.
20. I. Nesteruk, "Statistics-based predictions of coronavirus epidemic spreading in Mainland China", *Innovative Biosystems and Bioengineering*, Vol. 4, Issue - 1, pp. 13 - 18, 2020.
21. P. Van den Driessche, and J. Watmough, "Further notes on the basic reproduction number", *Mathematical epidemiology*, pp. 159 - 178, 2008.
22. P. Van den Driessche, "Reproduction numbers of infectious disease models", *Infectious Disease Modelling*, Vol. 2, Issue - 3, pp. 288 - 303, 2017.
23. Z.S. Kifle, L.L. Obsu, "Mathematical modeling for COVID-19 transmission dynamics: A case study in Ethiopia", *Results in Physics*, Vol. 34, p.105191, 2022.
24. C.E. Wagner, C.M. Saad-Roy, and B.T. Grenfell, "Modelling vaccination strategies for COVID-19", *Nature Reviews Immunology* Vol. 22, Issue - 3, pp. 139-141, 2022.
25. M.A. Khan, and A. Atangana, "Mathematical modeling and analysis of COVID-19: A study of new variant Omicron", *Physica A: Statistical Mechanics and its Applications*, Vol. 599, p.127452, 2022





Diksha Sharma and Alpna Mishra

Table 1. Parameters of Model			
Description	Parameter	Values	Reference
Recruitment Rate	Δ	400	assumed
Natural death rate	μ_c	0.016	estimated
Disease induced rate	δ_c	0.36	[11]
Recovery rate	r_i	0.88	estimated
Exposed to infectious rate	γ_c	0.25	[11]
Treatment Rate	r	0.55	estimated
Recovery Rate due to prompt treatment	α	0.001	estimated

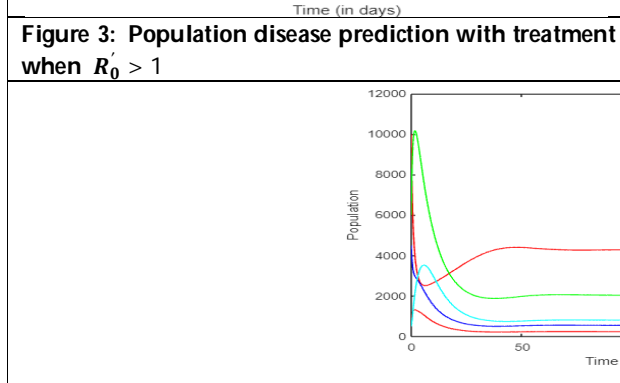
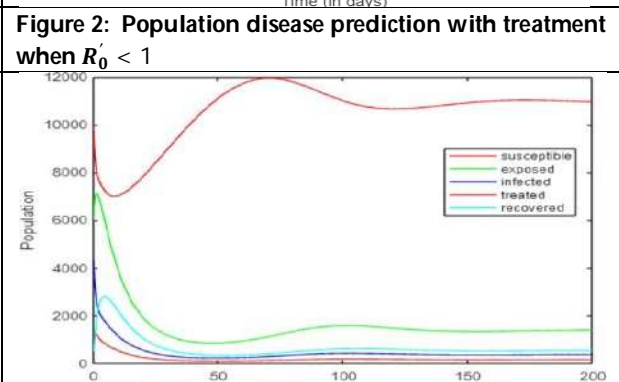
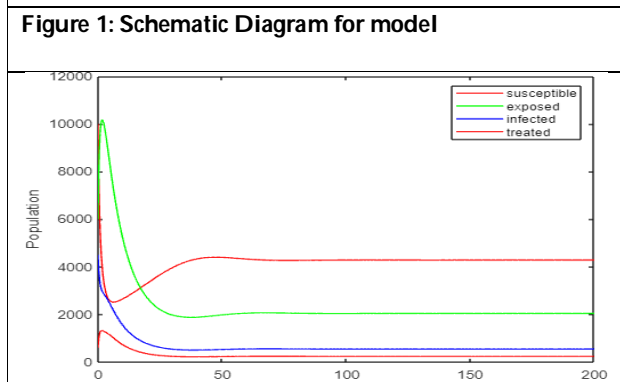
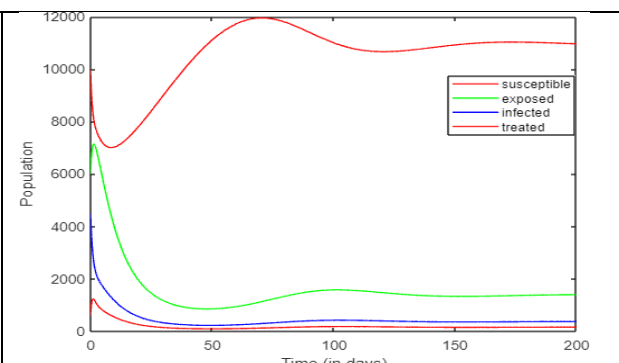
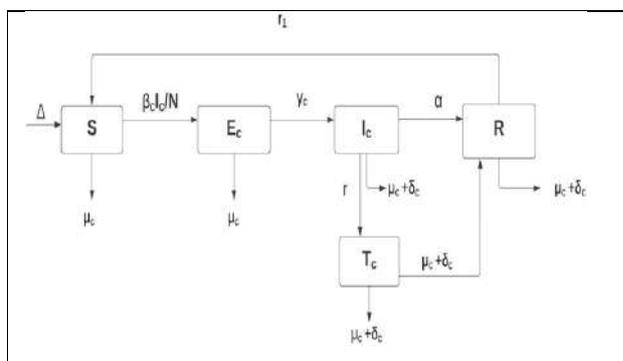


Figure 5: Disease treatment on the recovered population when $R_0' > 1$





On An Identity of Ramanujan and Continued Fraction Related To It

Satya Prakash Singh¹, Akash Rawat¹ and Nidhi Sahni^{2*}

¹Department of Mathematics, Tilak Dhari Post Graduate College, Jaunpur-222002, Uttar Pradesh, India

²Department of Mathematics, Sharda School of Basic Sciences and Research, Sharda University Greater Noida, Uttar Pradesh - 201310, India.

Received: 06 Apr 2023

Revised: 15 May 2023

Accepted: 31 May 2023

*Address for Correspondence

Nidhi Sahni

Department of Mathematics,
Sharda School of Basic Sciences and Research,
Sharda University Greater Noida,
Uttar Pradesh - 201310, India.
E. Mail: nidhi.sahni@sharda.ac.in



This is an Open Access Journal / article distributed under the terms of the **Creative Commons Attribution License** (CC BY-NC-ND 3.0) which permits unrestricted use, distribution, and reproduction in any medium, provided the original work is properly cited. All rights reserved.

ABSTRACT

In this paper, we have discussed about an identity of Ramanujan and using it an interesting continued fraction has also been established. In the last of the paper, special cases have also been deduced.

Keywords: Transformation formula, summation formula, basic hypergeometric series, identity, continued fraction.

INTRODUCTION, NOTATIONS AND DEFINITIONS

Continued Fractions are important tools in many branches of mathematics and science. The fractions are arising naturally in long division and in the theory of approximation to real numbers by rational components. They are useful in competitive programming because they are easy to compute and can be efficiently used to find the best possible rational approximation of the underlying real number. Continued fractions are also used in solving the Diophantine and Pell's equations. Singh, S.N. and Singh, S.P. [8], Singh S. P. [6, 7], Mishra V. N., Singh S.N, Singh S.P. and Yadav Vijay [4], Singh A. K. and Yadav Vijay [5], Singh Sunil and Sahni Nidhi [9] and many others have established a good number of results involving q-series identities and continued fractions. We shall use the following usual notations and definitions.

Let, the q-rising factorial is defined as,

For $|q| < 1$,

$$(a; q)_n = (1-a)(1-aq)(1-aq^2)\dots(1-aq^{n-1}), \quad n = 1, 2, 3, \dots$$





Satya Prakash Singhet al.,

$$(a; q)_{\infty} = \prod_{r=0}^{\infty} (1 - aq^r), \text{ so}$$

$$(a; q)_n = \frac{(aq^n; q)_{\infty}}{(a; q)_{\infty}},$$

and

$$(a; q)_0 = 1.$$

A basic hypergeometric series is defined as,

$${}_r\Phi_{r-1} \left[\begin{matrix} a_1, a_2, \dots, a_r; q; z \end{matrix} \right] = \sum_{n=0}^{\infty} \frac{(a_1; q)_n (a_2; q)_n \dots (a_r; q)_n}{(b_1; q)_n (b_2; q)_n \dots (b_{r-1}; q)_n} \frac{z^n}{(q; q)_n}, \tag{1.1}$$

where $|z| < 1$ and $|q| < 1$ for the converge of the series (1.1).

Large number of identities and transformation formulas are available in the literature. In the second Notebook and also in the 'Lost' Notebook of Ramanujan a huge number of identities are available. Those identities are of two types. First type of identities are those in which series equals product. Second type of identities are those in which a series is equal to another series.

Rogers-Ramanujan identities are of first kind. These are,

$$\sum_{n=0}^{\infty} \frac{q^{n^2}}{(q; q)_n} = \frac{1}{(q; q^5)_{\infty} (q^4; q^5)_{\infty}}, \tag{1.2}$$

$$\sum_{n=0}^{\infty} \frac{q^{n^2+n}}{(q; q)_n} = \frac{1}{(q^2; q^5)_{\infty} (q^3; q^5)_{\infty}}. \tag{1.3}$$

These identities were first discovered by L.J. Rogers in 1894 in a paper which was completely ignored.

Ramanujan rediscovered these identities some time before 1913. In 1917 these two identities were established again independently by German mathematician Issai Schur. One of the most celebrated identities of Ramanujan is [Andrews and Berndt B. C. [1]; (6.2.9), p. 146]

$$(-aq; q)_{\infty} \sum_{n=0}^{\infty} \frac{(-\lambda/b; q)_n b^n q^{n(n+1)/2}}{(q; q)_n (-aq; q)_n} = (-bq; q)_{\infty} \sum_{n=0}^{\infty} \frac{(-\lambda/a; q)_n a^n q^{n(n+1)/2}}{(q; q)_n (-bq; q)_n}. \tag{1.4}$$

The proof of (1.4) is simple and is being given below.

In order to prove (1.4) let us consider the Heine's transformation [Gasper G. and Rahman M. [2]; (1.4.5), p. 13], viz.,

$${}_2\Phi_1 \left[\begin{matrix} a, b; q; z \end{matrix} \right] = \frac{(c/b, bz; q)_{\infty}}{(c, z; q)_{\infty}} {}_2\Phi_1 \left[\begin{matrix} abz/c, b; q; c/b \end{matrix} \right] \tag{1.5}$$

Putting z/b for z and taking $b \rightarrow \infty$ in (1.5) we have,

$$\sum_{n=0}^{\infty} \frac{(a; q)_n (-1)^n q^{n(n-1)/2} z^n}{(q; q)_n (c; q)_n} = \frac{(z; q)_{\infty}}{(c; q)_{\infty}} \sum_{n=0}^{\infty} \frac{(az/c; q)_n c^n q^{n(n-1)/2}}{(q; q)_n (z; q)_n}. \tag{1.6}$$

Again, putting $a = -\lambda/b, c = -aq$ and $z = -bq$ in (1.6) we get (1.4).





Satya Prakash Singhet al.,

MAIN RESULTS

If we take $\lambda = -b$ in (1.4) we find,

$$\sum_{n=0}^{\infty} \frac{(b/a; q)_n (a)^n q^{n(n+1)/2}}{(q; q)_n (-bq; q)_n} = \frac{(-aq; q)_{\infty}}{(-bq; q)_{\infty}}. \tag{2.1}$$

As $a \rightarrow 0$, (2.1) yields

$$\sum_{n=0}^{\infty} \frac{(-1)^n b^n q^{n^2}}{(q; q)_n (-bq; q)_n} = \frac{1}{(-bq; q)_{\infty}}. \tag{2.2}$$

For $b=1$, (2.2) gives

$$\sum_{n=0}^{\infty} \frac{(-1)^n q^{n^2}}{(q^2; q^2)_n} = \frac{1}{(-q; q)_{\infty}} = (q; q^2)_{\infty}. \tag{2.3}$$

Taking $b=-1$ in (2.2) we get,

$$\sum_{n=0}^{\infty} \frac{q^{n^2}}{(q; q)_n^2} = \frac{1}{(q; q)_{\infty}}. \tag{2.4}$$

For $b=-q$, (2.2) yields

$$\sum_{n=0}^{\infty} \frac{q^{n^2+n}}{(q; q)_n (q; q)_{n+1}} = \frac{1}{(q; q)_{\infty}}. \tag{2.5}$$

Comparing (2.4) and (2.5) we obtain,

$$\sum_{n=0}^{\infty} \frac{q^{n^2}}{(q; q)_n^2} = \sum_{n=0}^{\infty} \frac{q^{n(n+1)}}{(q; q)_n (q; q)_{n+1}}. \tag{2.6}$$

Taking $b = q$ in (2.2) we get

$$\sum_{n=0}^{\infty} \frac{(-1)^n q^{n^2+n}}{(q; q)_n (-q; q)_{n+1}} = \frac{1}{(-q; q)_{\infty}}. \tag{2.7}$$

Comparing (2.3) and (2.7) we find,

$$\sum_{n=0}^{\infty} \frac{(-1)^n q^{n^2}}{(q^2; q^2)_n} = \sum_{n=0}^{\infty} \frac{(-1)^n q^{n(n+1)}}{(q; q)_n (-q; q)_{n+1}}. \tag{2.8}$$

Taking $\lambda = 0$ in (1.4) we obtain

$$(-bq; q)_{\infty} \sum_{n=0}^{\infty} \frac{a^n q^{n(n+1)/2}}{(q; q)_n (-bq; q)_n} = (-aq; q)_{\infty} \sum_{n=0}^{\infty} \frac{b^n q^{n(n+1)/2}}{(q; q)_n (-aq; q)_n}. \tag{2.9}$$

For $\lambda = ab$, (1.4) gives





Satya Prakash Singhet al.,

$$(-b; q)_\infty \sum_{n=0}^{\infty} \frac{a^n q^{n(n+1)/2}}{(q; q)_n (1+bq^n)} = (-a; q)_\infty \sum_{n=0}^{\infty} \frac{b^n q^{n(n+1)/2}}{(q; q)_n (1+aq^n)} \tag{2.10}$$

Results Involving Continued Fractions

In this section we establish a result involving continued fraction.

Putting $\lambda = -ac$ in (1.4) we have

$$(-bq; q)_\infty \sum_{n=0}^{\infty} \frac{(c; q)_n a^n q^{n(n+1)/2}}{(q; q)_n (-bq; q)_n} = (-aq; q)_\infty \sum_{n=0}^{\infty} \frac{(ac/b; q)_n b^n q^{n(n+1)/2}}{(q; q)_n (-aq; q)_n} \tag{3.1}$$

$$\begin{aligned} & \frac{1}{(1+a)} \frac{\sum_{n=0}^{\infty} \frac{(ac/b; q)_n b^n q^{n(n+1)/2}}{(q; q)_n (-aq; q)_n}}{\sum_{n=0}^{\infty} \frac{(ac/bq; q)_n b^n q^{n(n+1)/2}}{(q; q)_n (-a; q)_n}} = \frac{\sum_{n=0}^{\infty} \frac{(c; q)_n a^n q^{n(n+1)/2}}{(q; q)_n (-bq; q)_n}}{\sum_{n=0}^{\infty} \frac{(c; q)_n a^n q^{n(n-1)/2}}{(q; q)_n (-bq; q)_n}} \tag{3.2} \\ & = \frac{1}{1 + \frac{\sum_{n=0}^{\infty} \frac{(c; q)_n a^n q^{n(n-1)/2} (1-q^n)}{(q; q)_n (-bq; q)_n}}{\sum_{n=0}^{\infty} \frac{(c; q)_n a^n q^{n(n+1)/2}}{(q; q)_n (-bq; q)_n}}} \\ & = \frac{1}{1 + \frac{a(1-c)/(1+bq)}{\sum_{n=0}^{\infty} \frac{a^n q^{n(n+1)/2}}{(q; q)_n} \left\{ \frac{(c; q)_n}{(-bq; q)_n} - \frac{(cq; q)_n}{(-bq^2; q)_n} \right\}}} \end{aligned}$$

which on simplification gives,

$$\begin{aligned} & = \frac{1}{1 + \frac{a(1-c)/(1+bq)}{aq(c+bq)/(1+bq)(1+bq^2)}} \\ & = \frac{1}{1 - \frac{\sum_{n=0}^{\infty} \frac{(cq; q)_n a^n q^{n(n+1)/2}}{(q; q)_n} \left\{ \frac{1}{(-bq^2; q)_n} - \frac{q^n}{(-bq^3; q)_n} \right\}}}{1 + \frac{\sum_{n=0}^{\infty} \frac{(cq; q)_n a^n q^{n(n+3)/2}}{(q; q)_n (-bq^3; q)_n}} \end{aligned}$$





Satya Prakash Singhet al.,

Iterating the process we finally get

$$\begin{aligned} & \frac{\sum_{n=0}^{\infty} \frac{(ac/b; q)_n b^n q^{n(n+1)/2}}{(q; q)_n (-aq; q)_n}}{\sum_{n=0}^{\infty} \frac{(ac/bq; q)_n b^n q^{n(n+1)/2}}{(q; q)_n (-a; q)_n}} = \frac{\sum_{n=0}^{\infty} \frac{(c; q)_n a^n q^{n(n+1)/2}}{(q; q)_n (-bq; q)_n}}{\sum_{n=0}^{\infty} \frac{(c; q)_n a^n q^{n(n-1)/2}}{(q; q)_n (-bq; q)_n}} \\ & = \frac{1}{1+} \frac{a(1-c)}{1-} \frac{aq(c+bq)}{1+} \frac{aq(c+bq)}{1+} \frac{1}{1+bq^2} \\ & \frac{aq(1-cq)}{1-} \frac{1}{1+bq^2} \frac{1}{1+bq^3} \frac{aq^3(c+bq^2)}{1+} \frac{1}{1+bq^3} \frac{1}{1+bq^4} \\ & \frac{aq^2(1-cq^2)}{1-} \frac{1}{1+bq^4} \frac{1}{1+bq^5} \dots \dots \end{aligned} \tag{3.3}$$

By an appeal of [Jones, W. B. and Thron, W.I. [3]; (2.3.20), p. 35] we have

$$= \frac{1}{1+} \frac{a(1-c)}{(1+bq)-} \frac{aq(c+bq)}{(1+bq^2)+} \frac{aq(1-cq)}{(1+bq^3)-} \dots \tag{3.4}$$

ACKNOWLEDGEMENT

The authors are thankful to Dr. S. N. Singh, Ex. Reader and Head, Department of Mathematics, T.D.P.G. College, Jaunpur (U.P.), INDIA, for his noble guidance during the preparation of this paper. The second named author Akash Rawat would like to thanks Council of Scientific and Industrial Research (CSIR) for supporting a JRF research grant under which this work has been done.

REFERENCES

1. Andrews, G. E. and Berndt, B. C., Ramanujan’s Lost Notebook, Part I, Springer, 2005.
2. Gasper, G. and Rahman, M., Basic Hypergeometric Series, Second Edition, Cambridge University Press, 2004.
3. Jones, W. B. and Thron, W. J., Continued fractions, Analytic Theory and Applications, Addison-Wesley Publishing Company, Advanced Book Program Reading, Massachusetts, London, 1980.
4. Mishra V. N., Singh S.N, Singh S.P. and Yadav Vijay, On q-series and continued fractions, Cogent Mathematics, 3: 1240414, (2016), 1-7.
5. Singh A. K. and Yadav Vijay, A note on Partition and Continued Fractions, J. of Ramanujan Society of Math. and Math. Sc., Vol.1, No.1 (2012), 77-80.
6. Singh S. P., Certain results involving Lambert series and continued fractions I, South East Asian J. of Math. & Math. Sci., Vol. 11, No. 1 (2015), 65-70.
7. Singh S. P., Certain results involving Lambert series and continued fractions. II, J. Indian Math. Soc. (N.S.) 74 (2007), no. 1-2, 47—53.
8. Singh S.N. and Singh S. P., On some more q-series identities, Italian Journal of Pure and Applied Mathematics, N. 35 (2015), 669-678.
9. Singh Sunil, Sahni Nidhi, On certain continued fraction representation for the ratio of poly-basichypergeometric series, South East Asian Journal of Math. & Math Sc. Vol 13, No. 1 (2017) 57-64.





Analysis of THADA, DENND1A and LHCGR Gene Polymorphism in PCOS Patients among South Indian (Madurai) Population

P.Veeramuthumari^{1*} and V.Kumaravel²

¹Assistant Professor of Zoology, V.V.Vanniaperumal College for Women, Virudhunagar, Tamil Nadu, India.

²Chief Endocrinologist and Director, **Alpha Hospital and Research Foundation**, Institute of Diabetes and Endocrinology, Madurai, Tamil Nadu, India.

Received: 24 Feb 2023

Revised: 19 Apr 2023

Accepted: 31 May 2023

*Address for Correspondence

P.Veeramuthumari

Assistant Professor of Zoology,
V.V.Vanniaperumal College for Women,
Virudhunagar, Tamil Nadu, India.

E.Mail: veeramuthumari@vvvcollege.org



This is an Open Access Journal / article distributed under the terms of the **Creative Commons Attribution License** (CC BY-NC-ND 3.0) which permits unrestricted use, distribution, and reproduction in any medium, provided the original work is properly cited. All rights reserved.

ABSTRACT

Polycystic ovary syndrome (PCOS) is multifactorial, polygenic disorder affecting 6-10% of reproductive aged Women (Goodarzi *et al.*, 2001; Teede *et al.*, 2010) characterized by multi follicular ovaries, menstrual irregularities with consequent anovulatory infertility, insulin resistance and aggravated androgen synthesis. Women with PCOS are prone to adverse cardiometabolic derangements including type 2 diabetes mellitus (T2DM), dyslipidemia, hypertension, and cardiovascular disease (CVD) (Churchill, 2015). Polycystic ovary syndrome (PCOS) is a syndrome involving defects in primary cellular control mechanisms that result in the expression of chronic anovulation and hyperandrogenism. Current evidence from candidate gene linkage analysis and genome wide association studies strong implicates as marked influence of both genetic and environmental factors on the onset and progression of PCOS (Brower *et al.*, 2015). Gangopadhyay *et al.*, (2016) studied in North Indian Women. Hence the study also focused on THADA, DENND1A and LHCGR gene polymorphism among South Indian (Madurai) population. Genomic DNA isolated from the control and PCOS patients were utilized to study the association of LHCGR, DENND1A and THADA gene variants in PCOS. PCR based amplification of the genomic areas of interest were carried out to identify the presence of SNPs. PCR products were separated using agarose gel electrophoresis and the products were visualized in a gel documentation system. The study results bring forward that the DENND1A and LHCGR genes may potentially serve as markers for PCOS related infertility and hirsutism. Further large scale studies are required to demonstrate the efficacy of the studied candidate genes as markers for PCOS.

Keywords: PCOD, Infertility, Single Nucleotide Polymorphism, Genetic Disease and Gene mutation.





INTRODUCTION

Polycystic ovary syndrome (PCOS) is a hormonal disorder common among women of reproductive age. Women with PCOS may have infrequent or prolonged menstrual periods or excess male hormone (androgen) levels. The ovaries may develop numerous small collections of fluid (follicles) and fail to regularly release eggs. Polycystic ovary syndrome (PCOS) is a common and complex endocrine disorder among women of reproductive age, with a prevalence of 6-8 percent (Ehrmann *et al.*, 1999; Goodarzi and Azziz, 2006). Several researchers reported that PCOs is associated with important endocrine-metabolic disturbances including dyslipidemia, atherosclerosis, insulin resistance and Type 2 Diabetes (T2D) (Carmina, 2009; Kandarakis *et al.*, 2009). Obesity is known to act as a confounding factor for insulin resistance. It is estimated that 44 per cent of Women with PCOS suffering from obesity (Dasgupta *et al.*, 2012), which might be influence the significant concurrent insulin resistance observed. The insulin resistance with hyperinsulinemia initiated that hyperandrogenism through an increase in ovarian androgen biosynthesis (Poretsky *et al.*, 1999). The phenotypic expression of women affected with the syndrome are varied with some women being obese, some being lean, some women showing insulin resistance and increased production of adipokines irrespective of their body mass index (BMI) (Olszanecka-Glinianowicz *et al.*, 2011).

Wild *et al.*, (2000) reported that polycystic ovary syndrome (PCOS) must be considered a serious issue because of its implication on long term health regardless of a woman's age. Polycystic ovary syndrome (PCOS) is also known as a very common and complex female endocrine disorder (Azziz *et al.*, 2004). Various studies have been also suggested that women with PCOS are at a higher risk of gestational diabetes, miscarriages, preeclampsia and preterm labour (Adams *et al.*, 2004). The genetic basis of the disease is still not clearly understood owing to the difficulties in determining the inheritability of PCOS. Ovarian and adrenal steroidogenesis is considered as candidate genes which determine the expression of several integral phenotypes of PCOS. Insulin gene thought to play a functionally central role in insulin secretion and/or action and also in the signaling pathways (Paquette *et al.*, 1998). The newer diagnostic criteria of PCOS (Azziz *et al.*, 2009) and irregular menstrual cycles/anovulation and polycystic ovaries form important features along with hyperandrogenism.

A genome-wide association study (GWAS) in Han Chinese women identified eight risk loci for PCOS at 9q22.32, 11q22.1, 12q13.2, 12q14.3, 16q12.1, 19p13.3, 20q13.2 and an independent signal at 2p16.3 (Shi *et al.*, 2012), in addition to three loci identified previously at 2p16.3, 2p21, and 9q33.3 (Chen *et al.*, 2011). Three of the eleven variants associated with PCOS in the Han Chinese GWAS were also associated with PCOS in at least one European population when corrected for multiple testing, including DENN/MADD domain containing1A (DENND1A), thyroid adenoma associated (THADA) and yes-associated protein 1(YAP1) (Goodarzi *et al.*, 2012; Welt *et al.* 2012; Louwers *et al.*, 2013; Brower *et al.*, 2015). So, the present study focused on the thyroid adenoma associated (THADA) gene 2p16.3, 2p21, and 9q33.3 loci polymorphisms among South Indian population. Still now there is no gene polymorphism reports were available among Indians especially in South Indian (Madurai) population. Hence the study selected the THADA, DENND1A and LHCGR gene polymorphism in PCOS patients and control group among South Indian (Madurai) population.

METHODOLOGY

Sample Collection

The present pilot study was conducted in Alpha Health Foundation/Alpha Hospital and Research Centre with the clearance of the Institutional Ethical Committee (AHRC). A total of 12 patients comprising of 4 controls and 8 PCOS patients were included in the study. Volunteer controls without a history of hirsutism, alopecia and hyperandrogenism were included in the study. Patient participants diagnosed with PCOS presenting hyperandrogenism, polycystic ovaries, insulin resistance/hyperinsulinemia with a fertile or infertile history were included in the study.



**Veeramuthumari and Kumaravel****Gene Amplification**

The patient and control samples were collected in the Alpha hospital and research centre, Madurai. The genomic DNA (gDNA) was isolated by QIA Quick Mini kit and gDNA and confirmed with Agarose gel Electrophoresis (Sambrooke and Russel, 2001; Veeramuthumari *et al.*, 2011; Veeramuthumari and Isabel, 2014). The isolated DNA is amplified by using PCR (Polymerase Chain Reaction). Amplification of our gene of interest was carried by respective primers (Zhao *et al.*, 2012; Veeramuthumari and Isabel, 2014). Primers used are THADA- rs13429458-5'-CAGCGGTATGATTCGTAGTG-3' (forward) 5'-GCTAAAATCTCATCACCTGGAC-3'(reverse), THADA-rs12478601-5'-AGACTCAGATGAGATGCCACAT-3' (forward) 5'-TTACCTGTCCAACCTCCAGAATG-3' (reverse), DENND1A- rs10818854- 5'-CAAACCAGGCTGATGACAAT-3' (forward) 5'-GTTTGAGAATCATAGACCAGCAC-3' (reverse), LHCGR- rs13405728-5'-GTGGTTCTTACTCTAGCACAATGAT-3'(forward)5'-CCATCCACATACTCACTTCAATATC-3' (reverse).After extraction the PCR products are again checked by the 2% agarose gel. That extracted DNA was sent for direct sequencing.

Statistical Analysis

BMI was calculated for the both PCOs patients and control subjects among South Indian population. Mutation occurrence range was calculated and drawn graph Using Sigmaplot. *Chi Square -test* was performed for the significance level of Genotype and Allele frequency. Student t test was applied to analyze the significant difference between of mutant and normal allele in PCOs patients and control subjects among South Indian population.

RESULTS AND DISCUSSION**Study Design**

A total of 12 samples comprising of 4 controls and 8 PCOS patients were included in the study. Volunteer controls without a history of hirsutism, alopecia and hyperandrogenism were included in the study. Patient participants diagnosed with PCOS presenting hyperandrogenism, polycystic ovaries, insulin resistance/hyperinsulinemia with a fertile or infertile history were included in the study. Genomic DNA isolated from the control and PCOS patients were utilized to study the association of LHCGR, DENND1A and THADA gene variants in PCOS. PCR based amplification of the genomic areas of interest were carried out to identify the presence of SNPs. PCR products were separated using agarose gel electrophoresis and the products were visualized in a gel documentation system (Medicare). Gel extracted and purified PCR products were direct sequenced. The list of PCOS associated SNPs analyzed is presented in Table 1.

The obtained genotyping data was utilized to assess and understand the prevalence of the incidence, association of the candidate gene SNPs in PCOS. Anthropometric measurements, biochemical and lipid profile were carried out based on the physicians recommendation. Obesity and PCOS, obesity related PCOS are commonly observed and obesity is predominantly identified to raise the risk of T2DM in PCOS patients (Azziz *et al.*, 2006). The study population 37% of PCOS patients presented with infertility, 50% of the patients presented with Acne and 37% of the patients presented with hirsutism. As discussed by several earlier studies, the clinical/phenotypic features of the present study patients commonly included irregular periods, hirsutism, acne and obesity (Dasgupta *et al.*, 2012).

Genome wide Association studies (GWAS) enable the functional association of genes and their variants in disease conditions and thereby the susceptibility loci for the diseased condition. Based on several GWAS studies in PCOS that report association of genetic variations impacting ovarian steroidogenesis (Chenet *et al.*, 2011, Shi and Zhao *et al.*, 2012), The present study focuses in elucidating the importance and association of LHCGR, DENND1A and THADA in PCOS patients from south India/south Tamil Nadu. DENND1A is significantly associated with PCOS and other studies have also indicated that it is highly expressed in PCOS patients (Eriksen *et al.*, 2013, McAllister *et al.*, 2014). In particular, the rs10818854, rs2479106 intronic variants of the DENND1A gene have been associated with PCOS (Shi *et al.*, 2012, Lerchbaum *et al.*, 2011) A lack of such studies on THADA, DENND1A and LHCGR in the south Tamil Nadu population prevails and hence the present study proposes to examine the relevance of these SNPs in the



**Veeramuthumari and Kumaravel**

regional PCOS population. The results obtained from the present study as indicated in Fig.1 and Fig.2 present the PCR products (560bp, 465bp) that were amplified for the determination of the rs13429458, rs12478601 THADA polymorphisms, the rs10818854 DENND1A polymorphism and the 341bp rs13405728 LHCGR polymorphism in the control and the patient population.

Figure 1: Amplification of THADA, DENND1A and LHCGR gene regions in the control group participants: M – Marker, L1-L3: PCR product (560bp) that encompasses rs13429458 (A>C) and other intronic variants of THADA gene, L4-L6: 465bp product that encompasses the rs12478601 (C>T) of THADA gene, L7-L9: 407bp product that encompasses rs10818854 (G>A) of DENND1A gene, L10-L12: 341bp product that encompasses rs13405728 (A>G) of the LHCGR gene in the control group participants. The amplified PCR products were electrophoretically separated and visualized in a 1% Agarose gel.

Figure 2: Amplification of THADA, DENND1A and LHCGR gene regions in the PCOS patients: M – Marker, L1-L3: PCR product (560bp) that encompasses rs13429458 (A>C) and other intronic variants of THADA gene. L4-L6: 465bp product that encompasses the rs12478601 (C>T) of THADA gene. L7-L9: 407bp product that encompasses rs10818854 (G>A) of DENND1A gene. L10-L12: 341bp product that encompasses rs13405728 (A>G) of the LHCGR gene. The amplified PCR products were electrophoretically separated and visualized in a 1% Agarose gel

Genotyping data (Table 2) reveal that none of the assessed participants presented the THADA rs13429458 (A>C) polymorphism while all the participants (control and patients) were positive (100%) for the THADA rs12478601 (C>T) polymorphism. Interestingly while all the control participants were negative for the DENND1A rs10818854 (G>A) polymorphism, 50% of the PCOS patients were positive for the polymorphism. In an equally interesting manner, while one control participant was positive for the LHCGR polymorphism rs13405728 (A>G), 6 PCOS patients were positive for the polymorphism.

While the control participants were all homozygous positive (TT) for the THADA rs12478601, 12.5% of patients were heterozygous (CT) and 87.5% of the patients were homozygous (TT). With regard to the rs10818854 (DENND1A) (G>A) polymorphism, 50% of the patients were heterozygous (GA) for the polymorphism. The distribution of the LHCGR rs13405728 seemed to be predominant in the patient population with 75%, 25% of the patients, controls being heterozygous, respectively.

Figure 3: Percentage expression of the distribution of the THADA rs12478601 CC,CT,TT in the control and PCOS patient population. The wild type CC genotype was not incident in the assessed group. The homozygous TT alleles were observed to be incident at a 100% respectively in control. The heterozygous CT and the homozygous TT alleles were observed to be incident at a 12.5 and 87.5 % respectively. Table 3: Percentage expression of the distribution of the THADA rs7582497, rs7568365, rs13029250 intronic variants. The rs13029250 variant was absent in the assessed PCOS patient population.

Figure 4: Percentage expression of the SNP positive PCOS patients with infertility, acne and hirsutism. The DENND1A rs10818854 SNP and the LHCGR rs13405728 SNP is positive only in the patient group. THADA is located in the Intron of THADA gene on chromosome 2p21. THADA was initially identified in thyroid adenomas by chromosomal rearrangements, where THADA was disrupted and fused to an intron of peroxisome proliferator-activated receptor gamma (PPARG). The over-transmission of SNP rs13429458 indicates that gene THADA should be a new potential candidate for PCOS.

Sujatha *et al.*, (2015) studied the association of LHCGR polymorphism (rs2293275) with PCOS in south Indian population. The frequency of the G allele was 0.60 in PCOS Samples and 0.49 in controls, which indicates the G allele is associated with PCOS in this study. Further, a significant association of the LHCGR GG allele was observed with body mass index, waist to hip ratio, insulin resistance, LH and FSH ratio in PCOS when compared with controls. Han Zhao *et al.*, 2011, had done the initial large scale cohort studies for the THADA, DENND1A and LHCGR single





Veeramuthumari and Kumaravel

nucleotide polymorphism in the PCOS patients. They observed the positive association for the gene (THADA) SNP rs13429458 ($P= 3.74 \times 10^{-5}$) in the Han Chinese population and demonstrated that it could serve as a marker for PCOS. In concordance our data brings forward that THADA, DENND1A and LHCGR can serve potential markers.

CONCLUSION

The study was conducted in Alpha Health Foundation/Alpha Hospital and Research Centre, Madurai. Volunteer controls without a history of hirsutism, alopecia and hyperandrogenism were included in the study. Patient participants diagnosed with PCOS presenting hyperandrogenism, polycystic ovaries, insulin resistance/hyperinsulinemia with a fertile or infertile history were included in the study. The patient and control samples blood were collected and the genomic DNA (gDNA) was isolated by QIA Quick Mini kit and gDNA is amplified by using PCR (Polymerase Chain Reaction). Amplification of our gene of interest was carried by respective primers. The present pilot study as the first of the kind brings to light the prevalence; incidence of PCOS associated candidate gene markers in the South Indian population.

REFERENCES

1. Adams J. M., Taylor A. E., Crowley W. F. and Hall J. E. (2004) polycystic ovarian morphology with regular ovulatory cycles: insights into the pathophysiology of polycystic ovarian syndrome. *J. Clin. Endocrinol. Metab.* 89, 4343–4350.
2. Azziz R, Carmina E, Dewailly D, Diamanti-Kandarakis E, Escobar-Morreale HF, et al., (2006). Position Statement: Criteria for defining Polycystic Ovary Syndrome as a predominantly hyperandrogenic syndrome: An Androgen Excess Society Guideline. *J Clin Endocrinol Metab.* 91(11): 4237–45).
3. Azziz R, Carmina E, Dewailly D, et al., (2009). The Androgen Excess and PCOS Society criteria for the polycystic ovary syndrome: the complete task force report. *Fertil Steril.* 91:456–488.
4. Azziz R, Woods KS, Reyna R, Key TJ, Knochenhauer ES and Yildiz BO (2004). The prevalence and features of the polycystic ovary syndrome in an unselected population. *J Clin Endocrinol Metab.* 89(6):2745–9.
5. Brower MA, Jones MR, Rotter JI, Krauss RM, Legro RS, Azziz R, Goodarzi MO. (2015). Further investigation in Europeans of susceptibility variants for polycystic ovary syndrome discovered in genome-wide association studies of Chinese individuals. *J Clin Endocrinol Metab.* 100:E182–186.
6. Carmina E. (2009). Cardiovascular risk and events in polycystic ovary syndrome. *Climacteric.* 12(Suppl 1):22 – 25.
7. Chen ZJ, Zhao H, He L, Shi Y, Qin Y, Shi Y, Li Z, You L, Zhao J, Liu J et al., (2011) Genome-wide association study identifies susceptibility loci for polycystic ovary syndrome on chromosome 2p16.3, 2p21 and 9q33.3. *Nat Genet.* 43:55–59.
8. Dasgupta A, Khan A, Banerjee U, Ghosh M, Pal M, Chowdhury K, et al., (2012) Predictors of Insulin resistance and metabolic complications in polycystic ovarian syndrome in an eastern Indian population. *Indian J Clin Biochem.* 28 169-76.
9. Dasgupta A, Khan A, Banerjee U, Ghosh M, Pal M, Chowdhury K, et al., (2012) Predictors of Insulin resistance and metabolic complications in polycystic ovarian syndrome in an eastern Indian population. *Indian J Clin Biochem.* 28 169-76.
10. Ehrmann DA, Barnes RB, Rosenfield RL, Cavaghan MK., (1999). Imperial J. Prevalence of impaired glucose tolerance and diabetes in women with polycystic ovary syndrome. *Diabetes Care.* 22:141– 146.
11. Eriksen MB, Nielsen MF, Brusgaard K, Tan Q, Andersen MS, Glintborg D and Gaster M. (2013). Genetic alterations within the DENND1A gene in patients with polycystic ovary syndrome (PCOS). *PLoS one.* 8(9):e71786.
12. Gangopadhyay, Nitin Agrawal, Aruna Batra, Bhaskar Charan Kabi, Akash Gupta, Single-Nucleotide Polymorphism on Exon 17 of Insulin Receptor Gene Influences Insulin Resistance in PCOS: A Pilot Study on North Indian Women, *Biochem Genet* (2016) 54:158–168, DOI 10.1007/s10528-015-9708-7.
13. Goodarzi MO and Azziz R. (2006). Diagnosis, epidemiology, and genetics of the polycystic ovary syndrome. *Best Pract Res Clin Endocrinol Metab.* 20:193– 200.





Veeramuthumari and Kumaravel

14. Goodarzi MO, Jones MR, Li X, Chua AK, Garcia OA, Chen YD, Krauss RM, Rotter JI, Ankener W, Legro RS et al., (2012). Replication of association of DENND1A and THADA variants with polycystic ovary syndrome in European cohorts. *J Med Genet.* 49:90–95.
15. Kandaraki E, Christakou C and Diamanti-Kandarakis E. (2009). Metabolic syndrome and polycystic ovary syndrome and vice versa. *Arq Bras Endocrinol Metabol.* 53:227 – 237.
16. Lerchbaum E, Trummer O, Giuliani A, Gruber HJ, Pieber TR and Obermayer-Pietsch B (2011). Susceptibility loci for polycystic ovary syndrome on chromosome 2p16.3, 2p21, and 9q33.3 in a cohort of Caucasian women. *Hormone and metabolic research = Hormon- und Stoffwechselforschung = Hormones et metabolisme.* 43(11):743-747.
17. Louwers YV, Stolk L, Uitterlinden AG, Laven JS. Cross-ethnic meta-analysis of genetic variants for polycystic ovary syndrome. *J Clin Endocrinol Metab* 2013;98:E2006–E2012.
18. McAllister JM, Modi B, Miller BA, Biegler J, Bruggeman R, Legro RS, Strauss JF, 3rd: Overexpression of a DENND1A isoform produces a polycystic ovary syndrome theca phenotype. *Proceedings of the National Academy of Sciences of the United States of America* 2014, 111(15):E1519-1527.
19. Moraru A, Cakan-Akdogan G, Strassburger K, Males M, Mueller S, Jabs M, Muelleder M, Frejno M, Braeckman BP, Ralser M et al., (2017). THADA Regulates the Organismal Balance between Energy Storage and Heat Production. *Developmental cell* 2017, 41(4):450.
20. Olszanecka-Glinianowicz M, Kuglin D, Dabkowska-Huc A and Skalba P. (2011). Serum adiponectin and resistin in relation to insulin resistance and markers of hyperandrogenism in lean and obese women with polycystic ovary syndrome. *Eur J Obstet Gynecol Reprod Biol.* 154(1):51–6.
21. Paquette J., Giannoukakis N., Polychronakos C., Vafiadis P. and Deal C. (1998). The INS 5_ variable number of tandem repeats is associated with IGF2 expression in humans. *J. Biol. Chem.* 273, 14158.
22. Poretsky L, Cataldo NA, Rosenwaks Z, Giudice LC. The insulin-related ovarian regulatory system in health and disease. *Endocr Rev* 1999; 20 : 535-82.
23. Sambrooke J and Russel DW (2001). *Molecular cloning, a laboratory manual*, 3rd edition, Cold spring Harbor Laboratory Pres, Cold Spring Harbor, New York.
24. Shi Y, Zhao H, Shi Y, Cao Y, Yang D, Li Z, Zhang B, Liang X, Li T, Chen J et al., (2012). Genome-wide association study identifies eight new risk loci for polycystic ovary syndrome. *Nature genetics.* 44(9):1020-1025.
25. Simonis-Bik AM, Nijpels G, van Haeften TW, Houwing-Duistermaat JJ, Boomsma DI, Reiling E, van Hove EC, Diamant M, Kramer MH, Heine RJ et al., (2010). Gene variants in the novel type 2 diabetes loci CDC123/CAMK1D, THADA, ADAMTS9, BCL11A, and MTNR1B affect different aspects of pancreatic beta-cell function. *Diabetes.* 59(1):293-301.
26. Sujatha Thathapudi, Vijayalakshmi Kodati, Jayashankar Erukkambattu, Uma Addepally, and Hasan Qurratulain, Association of Luteinizing Hormone Chorionic Gonadotropin Receptor Gene Polymorphism (rs2293275) with Polycystic Ovarian Syndrome, GENETIC TESTING AND MOLECULAR BIOMARKERS Volume 00, Number 00, 2015 a Mary Ann Liebert, Inc. Pp. 1–5.
27. Veeramuthumari P and Isabel, 2014, Identification of C/T genetic marker in autosomal polycystic kidney disease among South Indian population (Madurai), International Journal of Pharmaceutical Research And Bio science. 3(1):22-33. ISSN: 2277-8713.
28. Veeramuthumari P, Isabel W and Kannan K (2011). A Study on the level of T3, T4, TSH and the association of A/G polymorphism with CTLA4 gene in Graves' hyperthyroidism among south Indian population. *Indian J of Biochem.* 26(1):66-69.
29. Welt CK, Styrkarsdottir U, Goodarzi DA, Thorleifsson G, Arason G, Gudmundsson JA, Ober C, Rosenfield RL, Saxena R, Thorsteinsdottir U et al., (2012) Variants in DENND1A are associated with polycystic ovary syndrome in women of European ancestry. *J Clin Endocrinol Metab.* 97:E1342–E1347.
30. Wild S, Pierpoint T, Jacobs H, McKeigue P. (2000). Long-term consequences of polycystic ovary syndrome: results of a 31 year follow-up study. *Hum Fertil (Camb)* 3:101 –105.
31. Zeggini E, Scott LJ, Saxena R, Voight BF, Marchini JL, Hu T, de Bakker PI, Abecasis GR, Almgren P and Andersen G et al., (2008). Meta-analysis of genomewide association data and large-scale replication identifies additional susceptibility loci for type 2 diabetes. *Nat Genet.* 40:638–45.





Veeramuthumari and Kumaravel

32. Zhao H and Chen ZJ (2013) Genetic association studies in female reproduction: from candidate gene approaches to genomewide mapping. *Mol Hum Reprod.* 19:644–654.

Table 1: List of genes associated with PCOS and the SNPs assessed for their prevalence in the regional population

S.No	Name of the Gene	SNP details	Location
1.	THADA	a. rs13429458 (NM_022065.4:c.4059-13560 T>G)	Intron 28
2.	THADA	b. rs12478601 (NM_022065.4:c.3744+4464 G>A)	Intron 24
3.	DENND1A	a. rs10818854 (NM_024820.2:c.303-7710 C>T)	Intron 5
4.	LHCGR	a. rs13405728, (NM_000233.3:c.161+4491 T>C)	Intron 1

Table 2: Genotypic Distribution of THADA, DENNDIA, LHCGR Polymorphisms in the Assessed Study Population.

	rs13429458 (THADA) (A>C)			rs12478601 (THADA) (C>T)			rs10818854 (DENND1A) (G>A)			rs13405728 (LHCGR) (A>G)		
	AA	AC	CC	CC	CT	TT	GG	GA	AA	AA	AG	GG
Control	100	0	0	0	0	100	100	0	0	75	25	0
Patient	100	0	0	0	12.5	87.5	50	50	0	25	75	0

Table 3: Genotypic Distribution of the Intronic Variants of THADA in the Region of Interest:

	rs7582497(THADA)			rs7568365(THADA)			rs13029250 (THADA)		
	TT	TC	CC	CC	TC	TT	GG	GT	TT
Control	50	25	25	50	25	25	50	25	25
Patient	50	37.5	12.5	50	37.5	12.5	50	50	0

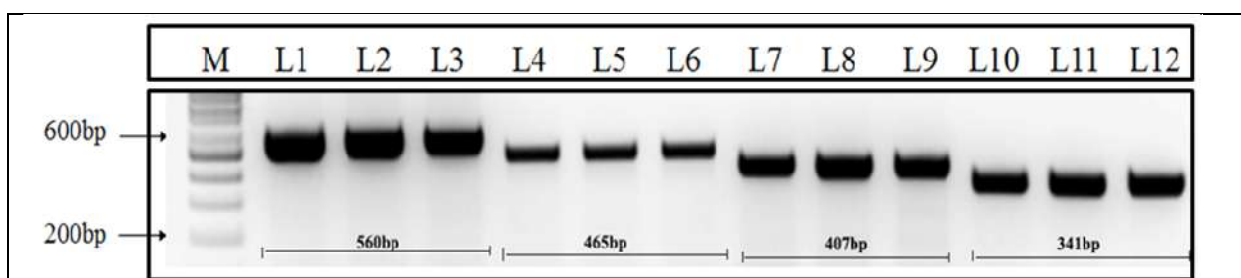


Figure 1: PCR Amplification OF THADA, DENND1A AND LHCGR Gene Regions in the Control Group Participants





Veeramuthumari and Kumaravel

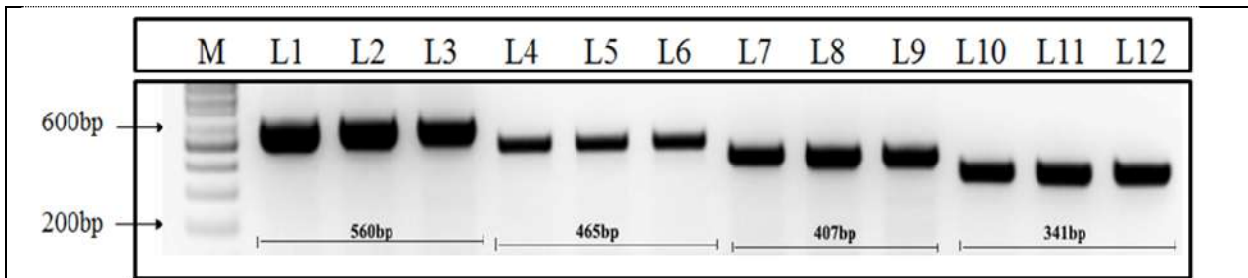


Figure 2: PCR Amplification of THADA, DENND1A AND LHCGR Gene Regions in the PCOS Group Patients.

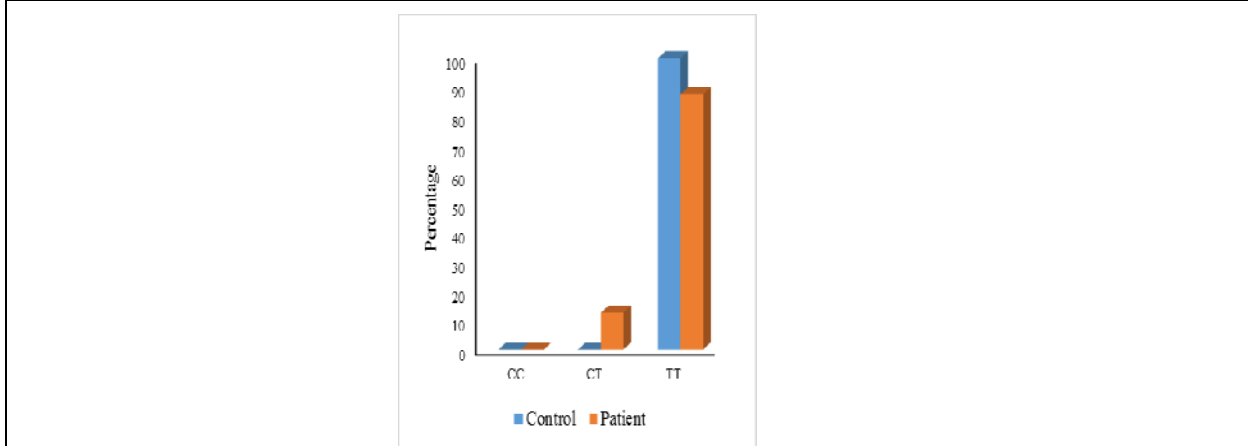


Figure 3. :Genotypic Distribution of the THADA SNP rs12478601

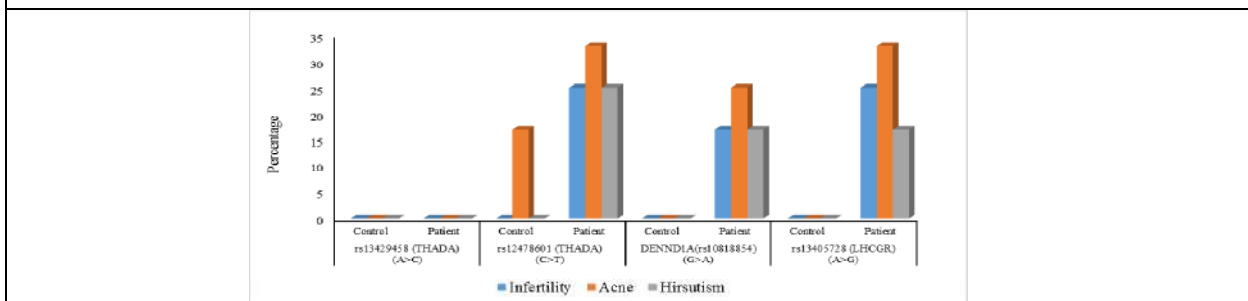


Figure 4. Percentage expression of SNP positive PCOS patients with Infertility, Acne and Hirsutism





Implementation of Machine Learning Techniques for the Detection of the Pediatric Diseases

Arun Kumar^{1*}, Surya Kant Pal¹, Santosh Kumar¹, Subhodeep Mukherjee² and Rita Roy³

¹Department of Mathematics, Sharda School of Basic Sciences and Research, Sharda University, Greater Noida, U.P., India

²Department of Computer Science and Engineering, GITAM Institute of Technology, GITAM, Visakhapatnam, AP, India. ³Department of Operation Management, GITAM School of Business, GITAM, Visakhapatnam, A.P., India

Received: 10 Apr 2023

Revised: 16 May 2023

Accepted: 31 May 2023

*Address for Correspondence

Arun Kumar^{1*},
Department of Mathematics,
Sharda School of Basic Sciences and Research,
Sharda University, Greater Noida, U.P., India
E.Mail: santanubotanist@gmail.com



This is an Open Access Journal / article distributed under the terms of the **Creative Commons Attribution License** (CC BY-NC-ND 3.0) which permits unrestricted use, distribution, and reproduction in any medium, provided the original work is properly cited. All rights reserved.

ABSTRACT

Machine Learning (ML) is a disruptive technology in the healthcare industry. Pediatric diseases are health problems related to children under 18 years. Children have many pediatric diseases and die because they do not get proper treatment at the right time. This study uses a systematic literature review (SLR). The articles are searched in three databases. Initially, 66 articles were extracted from three databases, and after proper shorting, only 32 articles were considered for the final study. This study highlights the diseases that had already used ML techniques for the prediction. This study also provides future perspectives on ML techniques in disease prediction and diagnosis. This study will help the healthcare industry know the real benefit of ML techniques and use them to predict and prevent diseases in children.

Keywords: Machine Learning (ML); Pediatric diseases; Children; Prediction; Healthcare.

INTRODUCTION

The healthcare industry has long been an early supporter of technological advancements, benefiting greatly from companions [1]. Machine learning (ML) is now used in many health-related fields, including implementing novel medical treatments, managing customer documents and information, and treating various diseases [2]. By processing vast amounts of data, ML technology can assist healthcare providers in creating precise medicine solutions tailored





Arun Kumaret al.,

to individual features [3]. Some ML companies are researching the capacity to coordinate and provide doctors with patient information during a telemedicine discussion, and data collection methods during virtual visits improve productivity and workflow [4][5]. Drug discovery processes are two significant areas wherein the drug industry concentrates its ML use [6]. For example, ML could one day result in drug manufacturers being heavily reliant on it to anticipate how clients will respond to different prescription medications and recognise which patients stand a good chance of profiting from the drug [7], [8]. Data scientists are planning predictions for all healthcare activities that involve overall health tracking and aiding in the cure or prevention of the disease [9]. ML in oncology health technology tries to search for cancer-affected cells with a comparable precision level to a knowledgeable physician [10].

Every year, approximately 26 million babies are born in India. According to the 2011 Census, kids (0-6 years) account for 13% of the entire country's population. The National Health Mission's (NHM) children's health course combines interventions that improve child survival and identify contributing factors to infant mortality [11]. It is now universally recognized that child survival could be discussed in exclusion since it is intrinsically tied to the baby's health, growth, and well-being, further ascertaining that as childhood and adolescence [12]–[14]. Pediatrics is the branch of medicine involved with infants, children, and young teenagers from birth to 18 [15]. Pediatrics is engaged with the emergency attention of the sick child and the long-term effects on life quality, handicap, and self-preservation [16]. Pediatricians collaborate on preventative measures, early diagnosis, and management of difficulties such as developmental problems and illnesses, behavioral issues, social emphases, and mental disorders like depression and anxiety [17], [18]. Constructing expert systems requires the utilization of a variety of machine learning strategies; hence, it is essential to evaluate these strategies side-by-side in order to select the one that is most appropriate for the topic at hand. In addition, autism is recognized as a spectrum of illnesses that can be distinguished from one another by distinct difficulties in areas such as social skills, repetitive activities, speech, and non-verbal communication [19]. Children and adults with autism have their own strengths and characteristics. The diagnosis and treatment of autism spectrum disorder in its early phases are vitally important since doing so helps to lessen or alleviate the symptoms to some degree, which in turn improves the individual's overall quality of life. Unfortunately, because of the length of time that passes between the first signs of worry and the identification of this condition, a significant amount of time that could have been used for treatment is wasted [20]. Methods based on machine learning would not only be helpful in determining the likelihood of having autism spectrum disorder in a timely and precise manner, but they are also vital for streamlining the entire process of diagnosis and assisting families in gaining access to therapies more quickly.

This study highlights the ML in the detection and prevention of paediatric diseases. This study found that ML had been used in many children's conditions, but this technology needs to evolve more. This study uses a systematic literature review (SLR) to find out the research trends in ML to detect and prevent paediatric diseases. After following the extraction methods, only 32 articles were considered for further study.

BASIC CONCEPT AND TERMINOLOGY

Basic concept and terminology

Paediatric diseases affect a child when they are young [21]. Anaemia, chickenpox, asthma, diphtheria, chickenpox, measles, leukaemia, mumps, polio, tuberculosis, whooping cough, pneumonia, Lyme disease, down's syndrome, fever, dental caries, Chagas disease, cystic fibrosis, candidiasis, bronchiolitis, cancer, and other diseases are examples of paediatric diseases [22], [23]. Some of the diseases that are found in the research paper using ML techniques are:

Child Morbidity

The child mortality rate, also known as an under-mortality rate, is the possibility of death at birth and the age of five conveyed per 1,000 live births [24], [25]. It would include newborn mortality (the probability of death in the first year of life). Because of morbidity, you have a specific illness [26]. Heart disease, diabetes, and obesity are typical examples of multiple morbidities simultaneously.





Arun Kumaret al.,

Cerebral palsy

Cerebral palsy is the most prevalent type of motor handicap in children—cerebral means having something to do with the brain [27]. Palsy refers to muscle spasms or complexity using the muscles [28]. Cerebral palsy is characterized by mutation cognitive development or brain injury that affects a person's ability to regulate their muscles.

Pediatric laminopathies

Laminopathies are hereditary illnesses that mainly affect muscle cells. Emery-Dreifuss myopathy, ventricular hypertrophy, limb-girdle spinal muscular atrophy, and Hutchison-Gilford progeria syndrome are illustrations of these illnesses [29]. Laminopathies are rare genetic diseases caused by genes responsible for nuclear lamina enzymes.

Respiratory Syncytial Virus (RSV) Infection: RSV is a commonly diagnosed infection that infects mild colds. Most patients heal in the next week or two, but RSV could be fatal, especially in infants. Infants and children are assumed to catch the virus from close touch with a member of the family or caregiver who would have the viral infection but is symptomless [30].

Neuromuscular disorders in children: Symptoms of neuromuscular diseases may include lower muscle tone (hypotonia) and deferred motor developments, such as postponed strolling or unusual gait [31], [32]. Muscle pain, loss of function, quivering, or roiling are all symptomatic of muscle atrophy. There's currently no cure for neuromuscular disorders [33]. To find a cure, biological therapies and new medicines are being studied. **Cancer in children:** The average age at diagnosis of cancer is eight years old for adults (ages 0 to 19), five years old for kids (ages 0 to 14), and 17 years old for adolescents (ages 15 to 19). In comparison, the average age for cancer diagnosis in adults is 65. Cancer is not a single disease; more than 12 primary types and over 100 sub-types.

MATERIALS AND METHODOLOGY

Research Questions

RQ1: How can the ML approaches for the detection of pediatric diseases?

RQ2: What future research in ML detects pediatric diseases?

Search Strategy

In January 2022, the search for peer-reviewed journal articles published in prestigious journals and credible publishers in the domain of ML algorithms to detect pediatric ailments was still conducted. As shown in Figure 1, the search was undertaken from three databases: the Web of Science, Scopus, and the IEEE. The keywords: TITLE-ABS-KEY ("Machine Learning" OR "Artificial Intelligence" OR "ML") AND ("Pediatric Diseases " OR "Pediatric" OR "Childhood disease").

The criteria for picking the papers included that they be in English, that they were published within or before August, 2022, that they originate from a respected publication or a reputable publisher, and that they are in the field of ML and pediatric illnesses.

RESULTS

Year-wise publication process

ML algorithms for diagnosing pediatric disorders are a new study area in computer engineering. So, in this chapter, we concentrated on ML algorithms for diagnosing pediatric illnesses. Figure 2 reveals that most articles will be published in 2021 and 2020.

Highly Cited Paper (Global Citations)

Table 1 summarizes the global citations of the authors that have been cited more.



**Arun Kumaret al.,****Authors Keywords Occurrence**

Figure 3 shows the most commonly observed keywords in the reconstructed texts.

DISCUSSION AND FUTURE TRENDS

As intelligent health devices become more common, innovative healthcare becomes a reality. Because the health sector welcomes innovation, the future of health coverage is very encouraging. ML can be used in many other disease detections in children. So, the future research trends can be in the following diseases and other diagnoses:

Prediction of diabetes

Diabetes is one of the most common and potentially fatal disorders in children. It not only impairs a person's ability but also causes many other severe problems. ML might aid in the early detection of diabetes, thus saving lives [11]. Diabetes is a growing problem as a result of rising average incomes. Because of this, research into improved methods for identifying and characterizing diabetes cases is warranted [34]. Diabetic patients are often determined by their fasting blood glucose, glucose tolerance, and random blood glucose readings. Predictions of diabetes are a common use of machine learning techniques. As a kind of machine learning, decision trees have shown to be useful in the medical industry due to their robust categorization capabilities [35]. Random forests can create multiple decision trees. Recently, neural networks have gained popularity as a machine learning technique due to their improved performance in various areas. Diabetes prediction models could be built using classification approaches such as KNN, Decision Tree, and Naive Bayes [36]. In terms of outcomes and processing time, Naive Bayes is the most efficient [37].

Predicting liver disease

The liver is a critical player in the digestion of children. It is prone to chronic hepatitis, liver cancer, and cirrhosis [25]. People are less worried about their lives and health in this day and age of the Internet and technology [38]. Everyone is so preoccupied with their smartphones and tablets that they seldom make it to the hospital for preventative health screenings [39]. Using this phenomenon as an advantage, a machine learning model should be constructed that, given a set of symptoms, can predict the likelihood and danger of a person becoming afflicted with a certain disease or developing diseases of a similar kind. ML algorithms such as classification and clustering make a difference in this situation [40].

Making diagnoses via image analysis

ML will become more effective, and more data sets will be evaluated to generate a robotic diagnosis. ML makes use of three distinct types of learning strategies: supervised learning, unsupervised learning, and semi-supervised learning. The extraction of features is a key part of the ML approaches, and it takes a domain expert to choose the right features for a given issue. DL approaches are used to tackle the feature selection problem [41].

Artificial Intelligence Surgery

It is likely an essential part of ML and will become far more popular in the coming years. Although it is too early to talk about robots able to perform solely surgical techniques, they can now aid and assist a doctor in manipulating surgical instruments [42]s it gathers data on each AI Surgery, ML algorithms for healthcare information analytics evaluation and define the new opportunity for potential treatments [43]– [45].

Childhood asthma

Early childhood bronchitis treatment is frequent; however, many people diagnosed under age have symptomatic clearance, making it difficult to recognize persons whose symptoms will remain.[46]. ML can be used to diagnose asthma by predicting and detecting early asthma.





Arun Kumaret al.,

CONCLUSION

This study aims to use ML techniques to predict and prevent pediatric diseases, mainly found in children under the age of 18 years. These diseases can be controlled using ML techniques. As we all know, children face many conditions, and their parents suffer the most. This study employs SLR methods to identify trends in research in ML's pediatric disease field. This study will help health providers comprehend which conditions can be anticipated using ML techniques. This study can also benefit parents when they know their children's diseases can be expected beforehand and proper treatment can be adequately provided.

REFERENCES

1. A. Mustafa and M. Rahimi Azghadi, "Automated Machine Learning for Healthcare and Clinical Notes Analysis," *Computers* 2021, Vol. 10, Page 24, vol. 10, no. 2, p. 24, Feb. 2021, doi: 10.3390/COMPUTERS10020024.
2. S. Kant Pal, S. Mukherjee, M. M. Baral, and S. Aggarwal, "Problems of Big Data Adoption in the Healthcare Industries," *Asia Pacific Journal of Health Management*, vol. 16, no. 4, pp. 282–287, Dec. 2021, doi: 10.24083/apjhm.v16i4.1359.
3. J. de la Torre, J. Marin, S. Ilarri, and J. J. Marin, "Applying Machine Learning for Healthcare: A Case Study on Cervical Pain Assessment with Motion Capture," *Applied Sciences*, vol. 10, no. 17, p. 5942, Aug. 2020, doi: 10.3390/app10175942.
4. A. Dhillon and A. Singh, "Machine Learning in Healthcare Data Analysis: A Survey," *J. Biol. Today's World*, vol. Holzinger, no. 6, pp. 1–10, 2019, doi: 10.15412/J.JBTW.01070206.
5. D. R. Dev and R. Roy, "Communication Technology for Users with Specific Learning Incapacities," *Artificial Intelligent Systems and Machine Learning*, vol. 11, no. 7, pp. 126–131, Jul. 2019.
6. J. M. Antoñanzas et al., "Symptom-Based Predictive Model of COVID-19 Disease in Children," *Viruses* 2022, Vol. 14, Page 63, vol. 14, no. 1, p. 63, Dec. 2021, doi: 10.3390/V14010063.
7. X. Wang et al., "Characteristics of Fecal Microbiota and Machine Learning Strategy for Fecal Invasive Biomarkers in Pediatric Inflammatory Bowel Disease," *Front Cell Infect Microbiol*, vol. 11, p. 1221, Dec. 2021, doi: 10.3389/FCIMB.2021.711884/BIBTEX.
8. S. Lee et al., "Paediatric/young versus adult patients with long QT syndrome," *Open Heart*, vol. 8, no. 2, p. e001671, Sep. 2021, doi: 10.1136/OPENHRT-2021-001671.
9. S. Mukherjee, M. M. Baral, C. Venkataiah, S. K. Pal, and R. Nagariya, "Service robots are an option for contactless services due to the COVID-19 pandemic in the hotels," *DECISION*, vol. 48, no. 4, pp. 445–460, Dec. 2021, doi: 10.1007/s40622-021-00300-x.
10. Z. Lin et al., "Predicting environmental risk factors in relation to health outcomes among school children from Romania using random forest model - An analysis of data from the SINPHONIE project," *Science of The Total Environment*, vol. 784, p. 147145, Aug. 2021, doi: 10.1016/J.SCITOTENV.2021.147145.
11. S. Bose, C. C. Kenyon, and A. J. Masino, "Personalized prediction of early childhood asthma persistence: A machine learning approach," *PLoS One*, vol. 16, no. 3, p. e0247784, Mar. 2021, doi: 10.1371/JOURNAL.PONE.0247784.
12. R. Alizadehsani et al., "Machine learning-based coronary artery disease diagnosis: A comprehensive review," *Comput Biol Med*, vol. 111, p. 103346, Aug. 2019, doi: 10.1016/J.COMPBIOMED.2019.103346.
13. N. M. J. Kumari and K. K. V. Krishna, "Prognosis of Diseases Using Machine Learning Algorithms: A Survey," *Proceedings of the 2018 International Conference on Current Trends towards Converging Technologies, ICCTCT 2018*, Nov. 2018, doi: 10.1109/ICCTCT.2018.8550902.
14. P. S. Kohli and S. Arora, "Application of machine learning in disease prediction," *2018 4th International Conference on Computing Communication and Automation, ICCCA 2018*, Dec. 2018, doi: 10.1109/CCAA.2018.8777449.
15. R. G. Quivey, T. G. O'Connor, S. R. Gill, and D. T. Kopycka-Kedzierawski, "Prediction of early childhood caries onset and oral microbiota," *Mol Oral Microbiol*, vol. 36, no. 5, pp. 255–257, Oct. 2021, doi: 10.1111/OMI.12349.





Arun Kumaret al.,

16. A. Tabaie, E. W. Orenstein, S. Nemati, R. K. Basu, G. D. Clifford, and R. Kamaleswaran, "Deep Learning Model to Predict Serious Infection Among Children With Central Venous Lines," *Front Pediatr*, vol. 9, Sep. 2021, doi: 10.3389/FPED.2021.726870/FULL.
17. C. Valim *et al.*, "Seeking diagnostic and prognostic biomarkers for childhood bacterial pneumonia in sub-Saharan Africa: study protocol for an observational study," *BMJ Open*, vol. 11, no. 9, p. e046590, Sep. 2021, doi: 10.1136/BMJOPEN-2020-046590.
18. M. Puttagunta and S. Ravi, "Medical image analysis based on deep learning approach," *Multimedia Tools and Applications* 2021 80:16, vol. 80, no. 16, pp. 24365–24398, Apr. 2021, doi: 10.1007/S11042-021-10707-4.
19. K. Vakadkar, D. Purkayastha, and D. Krishnan, "Detection of Autism Spectrum Disorder in Children Using Machine Learning Techniques," *SN Comput Sci*, vol. 2, no. 5, pp. 1–9, Sep. 2021, doi: 10.1007/S42979-021-00776-5/FIGURES/8.
20. A. M. Begum, "Applications of Machine Learning Techniques on Prediction of Children's various health problems: A Survey," vol. 7, no. 5, pp. 1166–1176, 2019.
21. X. Pang, C. B. Forrest, F. Lè-Scherban, and A. J. Masino, "Prediction of early childhood obesity with machine learning and electronic health record data," *Int J Med Inform*, vol. 150, p. 104454, Jun. 2021, doi: 10.1016/J.IJMEDINF.2021.104454.
22. H. Sun, Y. Liu, B. Song, X. Cui, G. Luo, and S. Pan, "Prediction of arrhythmia after intervention in children with atrial septal defect based on random forest," *BMC Pediatr*, vol. 21, no. 1, pp. 1–9, Dec. 2021, doi: 10.1186/S12887-021-02744-7/FIGURES/2.
23. L. L. Foo *et al.*, "Is artificial intelligence a solution to the myopia pandemic?," *British Journal of Ophthalmology*, vol. 105, no. 6, pp. 741–744, Jun. 2021, doi: 10.1136/BJOPHTHALMOL-2021-319129.
24. H. M. Fenta, T. Zewotir, and E. K. Muluneh, "A machine learning classifier approach for identifying the determinants of under-five child undernutrition in Ethiopian administrative zones," *BMC Med Inform Decis Mak*, vol. 21, no. 1, pp. 1–12, Dec. 2021, doi: 10.1186/S12911-021-01652-1/FIGURES/5.
25. M. I. H. Methun, A. Kabir, S. Islam, M. I. Hossain, and M. A. Darda, "A machine learning logistic classifier approach for identifying the determinants of Under-5 child morbidity in Bangladesh," *Clin Epidemiol Glob Health*, vol. 12, p. 100812, Oct. 2021, doi: 10.1016/J.CEGH.2021.100812.
26. F. S. Chou and L. V. Ghimire, "Identification of prognostic factors for pediatric myocarditis with a random forests algorithm-assisted approach," *Pediatric Research* 2020 90:2, vol. 90, no. 2, pp. 427–430, Nov. 2020, doi: 10.1038/s41390-020-01268-7.
27. H. Liang *et al.*, "Evaluation and accurate diagnoses of pediatric diseases using artificial intelligence," *Nature Medicine* 2019 25:3, vol. 25, no. 3, pp. 433–438, Feb. 2019, doi: 10.1038/s41591-018-0335-9.
28. S. Saha *et al.*, "Unbiased metagenomic sequencing for pediatric meningitis in bangladesh reveals neuroinvasive chikungunya virus outbreak and other unrealized pathogens," *mBio*, vol. 10, no. 6, Nov. 2019, doi: 10.1128/MBIO.02877-19/SUPPL_FILE/MBIO.02877-19-S0002.PDF.
29. Y. Zhang and Y. Ma, "Application of supervised machine learning algorithms in the classification of sagittal gait patterns of cerebral palsy children with spastic diplegia," *Comput Biol Med*, vol. 106, pp. 33–39, Mar. 2019, doi: 10.1016/J.COMPBIOMED.2019.01.009.
30. K. N. Turi *et al.*, "Infant viral respiratory infection nasal immune-response patterns and their association with subsequent childhood recurrent wheeze," *Am J Respir Crit Care Med*, vol. 198, no. 8, pp. 1064–1073, Oct. 2018, doi: 10.1164/RCCM.201711-2348OC/SUPPL_FILE/DISCLOSURES.PDF.
31. B. Sheng, X. Wang, M. Hou, J. Huang, S. Xiong, and Y. Zhang, "An automated system for motor function assessment in stroke patients using motion sensing technology: A pilot study," *Measurement*, vol. 161, p. 107896, Sep. 2020, doi: 10.1016/J.MEASUREMENT.2020.107896.
32. P. Khera and N. Kumar, "Role of machine learning in gait analysis: a review," <https://doi.org/10.1080/03091902.2020.1822940>, vol. 44, no. 8, pp. 441–467, Nov. 2020, doi: 10.1080/03091902.2020.1822940.
33. H. Abbas, F. Garberson, E. Glover, and D. P. Wall, "Machine learning approach for early detection of autism by combining questionnaire and home video screening," *Journal of the American Medical Informatics Association*, vol. 25, no. 8, pp. 1000–1007, Aug. 2018, doi: 10.1093/JAMIA/OCY039.





Arun Kumaret al.,

34. S. Mukherjee, M. M. Baral, S. K. Pal, V. Chittipaka, R. Roy, and K. Alam, "Humanoid robot in healthcare: A Systematic Review and Future Research Directions," *2022 International Conference on Machine Learning, Big Data, Cloud and Parallel Computing (COM-IT-CON)*, pp. 822–826, May 2022, doi: 10.1109/COM-IT-CON54601.2022.9850577.
35. R. Roy, M. M. Baral, S. K. Pal, S. Kumar, S. Mukherjee, and B. Jana, "Discussing the present, past, and future of Machine learning techniques in livestock farming: A systematic literature review," *2022 International Conference on Machine Learning, Big Data, Cloud and Parallel Computing (COM-IT-CON)*, pp. 179–183, May 2022, doi: 10.1109/COM-IT-CON54601.2022.9850749.
36. S. Mukherjee, V. Chittipaka, M. M. Baral, S. K. Pal, and S. Rana, "Impact of artificial intelligence in the healthcare sector," *Artificial Intelligence and Industry 4.0*, pp. 23–54, Jan. 2022, doi: 10.1016/B978-0-323-88468-6.00001-2.
37. S. Mukherjee and V. Chittipaka, "Analysing the Adoption of Intelligent Agent Technology in Food Supply Chain Management: An Empirical Evidence," *FIIB Business Review*, p. 231971452110592, Nov. 2021, doi: 10.1177/23197145211059243.
38. R. Roy, M. D. Babakerkhell, S. Mukherjee, D. Pal, and S. Funilkul, "Evaluating the Intention for the Adoption of Artificial Intelligence-Based Robots in the University to Educate the Students," *IEEE Access*, vol. 10, pp. 125666–125678, 2022, doi: 10.1109/ACCESS.2022.3225555.
39. R. Roy, K. Chekuri, G. Sandhya, S. K. Pal, S. Mukherjee, and N. Marada, "Exploring the blockchain for sustainable food supply chain," *Journal of Information and Optimization Sciences*, vol. 43, no. 7, pp. 1835–1847, Oct. 2022, doi: 10.1080/02522667.2022.2128535.
40. Q. Zou, K. Qu, Y. Luo, D. Yin, Y. Ju, and H. Tang, "Predicting Diabetes Mellitus With Machine Learning Techniques," *Front Genet*, vol. 9, p. 515, Nov. 2018, doi: 10.3389/FGENE.2018.00515/BIBTEX.
41. R. Alanazi, "Identification and Prediction of Chronic Diseases Using Machine Learning Approach," *J Healthc Eng*, vol. 2022, 2022, doi: 10.1155/2022/2826127.
42. A. Custovic *et al.*, "Cytokine responses to rhinovirus and development of asthma, allergic sensitization, and respiratory infections during childhood," *Am J Respir Crit Care Med*, vol. 197, no. 10, pp. 1265–1274, May 2018, doi: 10.1164/RCCM.201708-1762OC/SUPPL_FILE/DISCLOSURES.PDF.
43. S. Ganiger and K. M. M. Rajashekharaiyah, "Chronic Diseases Diagnosis using Machine Learning," *2018 International Conference on Circuits and Systems in Digital Enterprise Technology, ICCSDET 2018*, Dec. 2018, doi: 10.1109/ICCSDET.2018.8821235.
44. L. J. Muhammad *et al.*, "Machine Learning Predictive Models for Coronary Artery Disease," *SN Computer Science* 2021 2:5, vol. 2, no. 5, pp. 1–11, Jun. 2021, doi: 10.1007/S42979-021-00731-4.
45. N. K. Kumar, G. S. Sindhu, D. K. Prashanthi, and A. S. Sulthana, "Analysis and Prediction of Cardio Vascular Disease using Machine Learning Classifiers," *2020 6th International Conference on Advanced Computing and Communication Systems, ICACCS 2020*, pp. 15–21, Mar. 2020, doi: 10.1109/ICACCS48705.2020.9074183.
46. S. E. Alexeeff *et al.*, "Medical Conditions in the First Years of Life Associated with Future Diagnosis of ASD in Children," *J Autism Dev Disord*, vol. 47, no. 7, pp. 2067–2079, Jul. 2017, doi: 10.1007/S10803-017-3130-4/TABLES/4.

Table 5. The list of articles having the most citations

Author	Global Citations
[27]	190
[33]	48
[42]	45
[30]	30
[28]	29
[29]	29
[46]	22





Arun Kumaret al.,

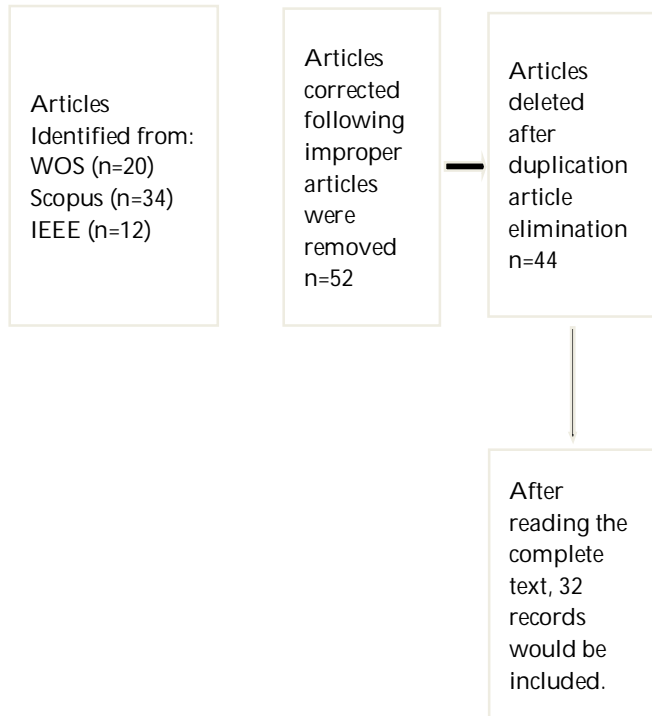


Fig. 3. Selection process of the articles

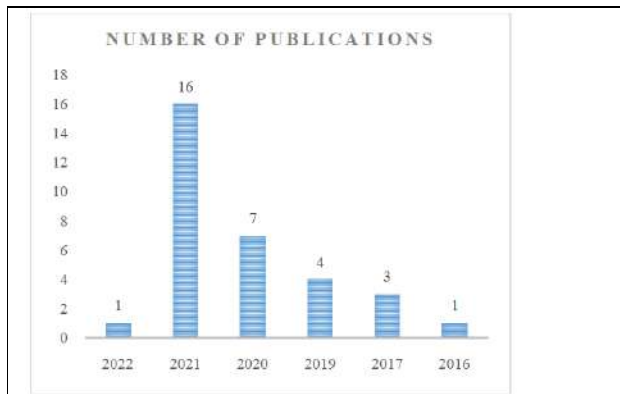


Fig. 4. Year-wise publications trends for the ML approach for the detection of pediatric diseases

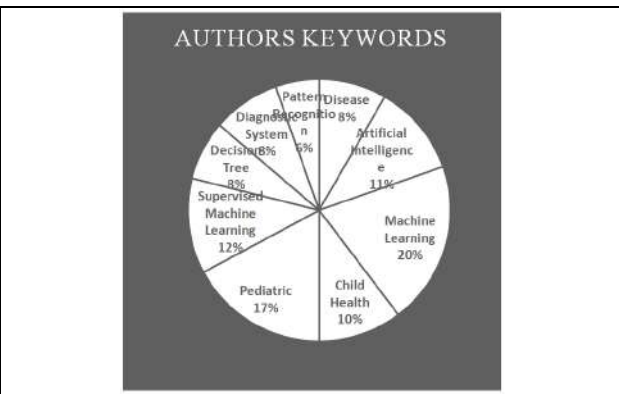


Fig. 5. Author's keywords occurrence





Inventory Model for Price-Dependent Demand with Deterioration under Permissible Delay in Payments

Renu Gautam^{1*}, Sangeeta Gupta² and Sweta Srivastav¹

¹Department of Mathematics, Sharda University, Greater Noida,

²The A.H. Siddiqi Centre for Advanced Research in Applied Mathematics and Physics, Sharda University, Greater Noida

Received: 06 Apr 2023

Revised: 15 May 2023

Accepted: 31 May 2023

*Address for Correspondence

Renu Gautam

Department of Mathematics,

Sharda University,

Greater Noida,

E. Mail: 2022303476.renu@dr.sharda.ac.in,



This is an Open Access Journal / article distributed under the terms of the **Creative Commons Attribution License** (CC BY-NC-ND 3.0) which permits unrestricted use, distribution, and reproduction in any medium, provided the original work is properly cited. All rights reserved.

ABSTRACT

In this study, we proposed an inventory model for deteriorating items with a time dependent deterioration rate while taking into account a price-dependent demand rate. In this case, shortages are permitted with a partial backlogging rate, and the backlogging rate is a function of time that decreases exponentially. Further allowable payment delays are permitted. By earning interest on the credit amount for the allowed delayed time, the delayed payment enables the stockiest to generate greater profits. Also, it motivates the store owner or stockier to minimize the losses. This model's major aim is to reduce the overall cost of the inventory. The study concludes with numerical examples to illustrate the problem and sensitivity analyses to demonstrate the impact of changing the parameters.

Keywords: Inventory model, deteriorating item, Permissible delay in payment, Price-dependent demand rate and backlogging

INTRODUCTION

Whether a company is a manufacturing one or a service one, inventory is a component of both. For their business to run smoothly, all organizations must maintain some inventory. Any company making the absurd claim that they don't have any inventory should be exposed. Harris [7] developed the first inventory model, which was generalized by Wilson [16] who gave the formula to obtain economic order quantity. Most of the production association emphasized on inventory organization and resolving the problems related to inventory because they want to maintain the balance between overstocking and under-stocking and also want to acquire the quantity that reduces the total inventory cost.



**Renu Gautam et al.,**

The demand rate is taken into account in traditional inventory models as being constant. In reality, demand for things that are real may be time-dependent, stock-dependent, and price dependent. Price-dependent demand refers to the relationship between the price of a product and the quantity of that product that customers are willing to purchase. In an inventory system, price-dependent demand means that the demand for a product is directly influenced by its price. In an inventory system, the selling price is important. For price-dependent demand under quantity and freight discounts, Burwell [3] developed an economic lot size model. Mondal, *et al.* [10] thought of using an inventory system to improve products for price-dependent demand rates. In recent years, mathematical concepts have been applied to various real-world issues, particularly for inventory control. Choosing when and how much to make or order to keep the cost of the inventory system as low as possible is one of the management's top priorities. When the inventory experiences degradation or deterioration, this becomes somewhat more essential. Deterioration is defined as a change, damage, decay, spoiling, obsolescence, and loss of use or original value in a commodity that causes diminishing usefulness from the original one. It is good knowing that some things, including produce, medicines, petrol, blood, and radioactive materials, degrade during their typical storage times. As a result, the loss caused by deterioration cannot be disregarded when evaluating the ideal inventory policy for that class of products. The analysis of decaying inventory problems began with Ghare and Schrader, who developed a simple economic order quantity model with a constant rate of decay. Covert and Philip extended Ghare and Schrader's model and obtained an economic order quantity model for a variable rate of deterioration by assuming a two-parameter Weibull distribution.

In general, payments are made when a consignment is delivered, but in reality, suppliers give shopkeepers a specific time to make payments to settle their accounts. There is no interest paid by the shopkeeper. If payment is not made during this time, but after, the supplier always applies interest at a certain rate. According to the conventional economic order quantity (EOQ) model, the retailer must be paid for the goods as soon as they are delivered. In reality, the supplier will provide the retailer with a delay period, known as the trade credit term, to boost sales of his goods: The store has the option to sell the products before the trade credit period expires to generate income and earn interest. If the payment is not made by the end of the trade credit period, on the other hand, a higher interest rate will be applied. As a result, it makes financial sense for the retailer to put off paying the replenishment account until the very end of the time the supplier has permitted. Chung *et al.* [5] determined the economic order quantity under conditions of permissible delay in payments where the delay in payments depends on the quantity ordered when the order quantity is less than the quantity at which the delay in payments is permitted, the payment for the item must be made immediately. Otherwise, a fixed credit period is allowed.

To promote demand, the supplier will typically provide the store a trade credit period, which is a delay in payment for the amount of the transaction. Giving the merchant such a credit period will promote supplier sales and lower the amount of on-hand stock. Simultaneously, without a primary payment, the store can benefit from a credit period to lower costs and boost profit. During the predetermined time frame, the client is not required to pay interest; nevertheless, the supplier will charge interest if the payment is delayed past the predetermined time frame. The consumer benefits greatly from this arrangement because he can postpone payment until the conclusion of the allowed grace period. During this credit term, the shop might begin to amass sales proceeds and collect interest on those proceeds. Since paying later indirectly lowers the cost of holding, the supplier's payment delay is effectively a price reduction that encourages merchants to place larger orders. Additionally, delaying payment lowers the cost of share ownership indirectly. Therefore, in an integrated inventory model, trade credit can be quite essential for both suppliers and retailers. Goyal [1] created an EOQ model in the context of allowable payment delays. Goyal's [1] model was expanded by Chung and Huang [2] to take into account the scenario in which the units are refilled at a finite pace with an allowable payment delay. To modify Goyal's model [1], Teng [3] assumed that the selling price is not the same as the purchasing price.

In this paper, inventory model is developed using price dependent demand rate, deterioration rate is dependent of time. Shortage is allowed with partial backlogging. Sensitivity analysis is carried out with numerical example.





Renu Gautam et al.,

Assumptions and Notations

To develop an inventory model with price-dependent demand permissible delay in payment and partial backlogging the following notations and assumptions are used: -

Assumption

- The demand rate is taken as price-dependent.
- The deterioration rate is time-dependent.
- Shortages are allowed with partial backlogging.
- Backlogging rate is an exponentially decreasing function of time.
- The replenishment rate is infinite.
- A single item is considered over the prescribed interval.
- There is no repair or replenishment of deteriorated units.

Notations

$I(t)$ = the inventory level at time t .

αt = variable rate of defective units out of on hand inventory at time t , $0 < \alpha \ll 1$.

A = the inventory ordering cost per order.

C_H = the holding cost per unit per unit time

C_D = cost of each deteriorating unit.

C_S = shortage cost per unit per unit time.

C_O = lost sale cost per unit per unit time.

t_1 = the time at which shortage starts and T is the length of replenishment cycle, $0 \leq t_1 \leq T$.

P = the selling price.

$f(p) = xp^{-y}$ is the price dependent demand, where $x > 0$, $y > 0$.

Here x is initial rate of demand; y is the rate with which the demand rate increases.

$\exp(-\gamma t)$ Unsatisfied demand is backlogged at a rate; the backlogging parameter γ is a positive constant.

M = the permissible delay in settling the accounts.

I_e = the interest earned per rupee in a year.

I_p = the interest payable per rupee in a year.

Q = the initial inventory level.

α = is deterioration rate.

Lead time is negligible.

Formulation and Solution of the Model

The depletion of inventory during the interval $(0, t_1)$ is due to the joint effect of demand and deterioration of items and the demand is partially backlogged in the interval (t_1, T) . The differential equations describing the inventory level $I(t)$ in the interval $(0, T)$ are given by.

$$I'(t) + \alpha I(t) = -xp^{-y}, 0 \leq t \leq t_1 \quad \dots(1)$$

$$I'(t) = -xp^{-y}e^{-\gamma t}, t_1 \leq t \leq T \quad \dots(2)$$

With the conditions, $I(t_1) = 0$ and $I(0) = Q$.

The solutions of equations (1) and (2) can be obtained as





Renu Gautam et al.,

$$I(t) = xp^{-y}(t_1 - t) + \frac{\alpha}{6}xp^{-y}(t_1^3 - 3t_1t^2 + 2t^3), 0 \leq t \leq T \dots(3)$$

And,

$$I(t) = xp^{-y} \frac{e^{-\gamma t}}{\gamma} - xp^{-y} \frac{e^{-\gamma t_1}}{\gamma} \dots(4)$$

Also initial inventory level

$$Q = xp^{-y}t_1 + \frac{\alpha}{6}xp^{-y}t_1^3 \dots(5)$$

The inventory holding cost (CH) per cycle is given by

$$CH = C_H \int_0^{t_1} I(t)dt = C_H \left(xp^{-y} \frac{t_1^2}{2} + xp^{-y}t_1^4 \frac{\alpha}{12} \right) \dots(6)$$

The deterioration cost (CD) per cycle is given by

$$CD = C_D \left\{ I(0) - \int_0^{t_1} f(t)dt \right\} = C_D \left\{ xp^{-y}t_1^3 \frac{\alpha}{6} \right\} \dots(7)$$

The shortage cost (CS) per cycle due to backlog is given by

$$C_s = C_s \int_{t_1}^T I(t)dt$$

$$C_s = \frac{C_s}{\gamma^2} (xp^{-y}e^{-\gamma T}) - \frac{C_s}{\gamma^2} (xp^{-y} - \gamma xp^{-y}(T - t_1))e^{-\gamma t_1} \dots(8)$$

And the opportunity cost (CO) per cycle due to lost sales is given by

$$CO = C_o \int_{t_1}^T (1 - e^{-\gamma t})xp^{-y} dt$$

$$CO = C_o \left(xp^{-y}(T - t_1) + \frac{xp^{-y}}{\gamma} (e^{-\gamma T} - e^{-\gamma t_1}) \right) \dots(9)$$

Now, there will be two cases, namely

- (i) $0 < M < t_1$
- (ii) $t_1 < M \leq T$

Case (1). $0 < M < t_1$

There the length of period with positive inventory stock of the items is larger than the credit period the retailer can continue to accumulate revenue and earn interest with an annual rate I_e on it for the rest period in the cycle. Hence the interest earned per cycle by

$$IE_1 = pI_e \int_0^M xp^{-y} t dt = pI_e xp^{-y} \frac{M^2}{2} \dots(10)$$

However, beyond the fixed credit period, the products still in stock needs to be financed with an annual rate I_p . The interest payable per cycle is:-

$$IP_1 = pI_p \int_M^{t_1} I(t)dt = pI_p \left(\frac{xp^{-y}}{\gamma^2} e^{-\gamma M} + \frac{xp^{-y}}{\gamma^2} e^{-\gamma t_1} (\gamma(M - t_1) - 1) \right) \dots(11)$$





Renu Gautam et al.,

CASE(2). $t_1 < M \leq T$

$IP_2 = 0$ Where, IP = interest purchase per cycle. Then, in this policy, it is assumed that the account is to be settled during the shortage period, the retailer pays no interest per cycle.

The interest earned per cycle is

$$IE_2 = pI_e \left(\int_0^{t_1} xp^{-y} t dt + (M - t_1) \int_0^{t_1} xp^{-y} dt \right) = \frac{pI_e}{2} xp^{-y} t_1 (2M - t_1) \dots (12)$$

CASE 1: Finding Optimum Solution

Hence, the total average cost per unit time of the system is given by: $TC_1 = \frac{1}{T} [A + CH + CD + CS + CO + IP_1 - IE_1]$

$$TC_1 = \frac{1}{T} \left\{ A + C_H xp^{-y} \left(\frac{t_1^2}{2} + \frac{\alpha t_1^4}{12} \right) + C_D xp^{-y} \alpha \frac{t_1^3}{6} + \frac{C_S}{\gamma^2} xp^{-y} e^{-\gamma T} - \frac{C_S}{\gamma^2} xp^{-y} e^{-\gamma t_1} (1 - \gamma(T - t_1)) \right. \dots (13)$$

$$\left. + \frac{C_O}{\gamma} xp^{-y} (\gamma T - \gamma t_1 + e^{-\gamma T} - e^{-\gamma t_1}) + \frac{pI_p}{\gamma^2} xp^{-y} (e^{-\gamma M} + e^{-\gamma t_1} (\gamma(M - t_1) - 1)) - pI_e xp^{-y} \frac{M^2}{2} \right\}$$

$$\frac{dTC_1}{dt_1} = \frac{1}{T} \left\{ \frac{C_H}{3} xp^{-y} (3t_1 + \alpha t_1^3) + \frac{C_D}{2} xp^{-y} \alpha t_1^2 - C_S xp^{-y} e^{-\gamma t_1} (T - t_1) + C_O xp^{-y} (e^{-\gamma t_1} - 1) + pI_p xp^{-y} e^{-\gamma t_1} (t_1 - M) \right\} \dots (14)$$

$$\frac{d^2TC_1}{dt_1^2} = \frac{1}{T} \left\{ C_H xp^{-y} (1 + t^2 \alpha) + C_D xp^{-y} \alpha t_1 + C_S xp^{-y} e^{-\gamma t_1} (1 + T\gamma) - C_O xp^{-y} e^{-\gamma t_1} \gamma \right. \dots (15)$$

$$\left. + pI_p xp^{-y} e^{-\gamma t_1} (1 + \gamma M - \gamma t_1) \right\}$$

CASE 2: Finding Optimum Solution

Hence, the total average cost per unit time of the system is given by:

$$TC_2 = \frac{1}{T} [A + CH + CD + CS + CO + IP_2 - IE_2]$$

$$TC_2 = \frac{1}{T} \left\{ A + \frac{C_H}{12} xp^{-y} (6t_1^2 + \alpha t_1^4) + \frac{C_D}{6} xp^{-y} \alpha t_1^3 + \frac{C_S}{\gamma^2} xp^{-y} e^{-\gamma T} - \frac{C_S}{\gamma^2} xp^{-y} e^{-\gamma t_1} (1 - \gamma(T - t_1)) \right. \dots (16)$$

$$\left. + \frac{C_O}{\gamma} xp^{-y} (\gamma(T - t_1) + e^{-\gamma T} - e^{-\gamma t_1}) - \frac{pI_p}{2} xp^{-y} t_1 (2M - t_1) \right\}$$

$$\frac{dTC_2}{dt_1} = \frac{1}{T} \left\{ \frac{C_H}{3} xp^{-y} (3t_1 + \alpha t_1^3) + \frac{C_D}{2} xp^{-y} \alpha t_1^2 - C_S xp^{-y} e^{-\gamma t_1} (T - t_1) + C_O xp^{-y} (e^{-\gamma t_1} - 1) - pI_p xp^{-y} (M - t_1) \right\} \dots (17)$$

$$\frac{d^2TC_2}{dt_1^2} = \frac{1}{T} \left\{ C_H xp^{-y} (1 + \alpha t_1^2) + C_D xp^{-y} \alpha t_1 + C_S xp^{-y} e^{-\gamma t_1} (1 + \gamma(T - t_1)) - C_O xp^{-y} \gamma e^{-\gamma t_1} + pI_e xp^{-y} \right\} \dots (18)$$

Numerical Examples

CASE 1: In this section, we will illustrate our hypothesis with the help of numerical examples for better understanding of the above mathematical modeling. We consider an inventory system with the following parameters in proper units:





Renu Gautam et al.,

$A=\$300$, $C_H=\$3$, $C_D=\$10$, $C_S=\$15$, $C_O=\$18$, $I_e=0.05$, $I_p=0.04$, $T=1\text{yr}$, $a=6$, $b=0.2$, $p=\$9.5$, $x=0.05$, $y=0.01$,
 $M=60/365\text{yr}$. $t_1=311$ days and $TC_1=\$305.59$

Numerical Examples

Case 2: In this section, we will illustrate our hypothesis with the help of numerical examples for better understanding of the above mathematical modeling. We consider an inventory system with the following parameters in proper units:

$A=\$300$, $C_H=\$3$, $C_D=\$10$, $C_S=\$15$, $C_O=\$18$, $I_e=0.05$, $I_p=0.04$, $T=1\text{yr}$, $a=6$, $b=0.2$, $p=\$9.5$, $x=0.05$, $y=0.01$,
 $M=320/365\text{yr}$. $t_1=309$ days and $TC_2=\$470.82$

CONCLUSION

This paper strives for an inventory model for decaying items with price-dependent demand. We allow the shortages with partial backlogging in this model and backlogging rate is an exponentially decreasing function of time. From the analysis of the model, it has been concluded that

Case 1

- As the holding cost increases, the total inventory cost increases significantly.
- As the deterioration cost increases, the total inventory cost increases marginally.
- As the shortages cost increases, the total inventory cost increases marginally.
- As the ordering cost increases, the total inventory cost increases marginally.
- As the backlogging parameter (γ) increases, the total inventory cost increases marginally.
- As the selling price (p) increases, the total inventory cost decreases marginally.

Case 2

- As the holding cost increases, the total inventory cost increases significantly.
- As the deterioration cost increases, the total inventory cost increases marginally.
- As the shortages cost increases, the total inventory cost increases significantly.
- As the ordering cost increases, the total inventory cost decreases significantly.
- As the backlogging parameter (γ) increases, the total inventory cost decreases significantly.
- As the selling price (p) increases, the total inventory cost decreases significantly.

REFERENCES

1. S. P. Aggarwal, and C. K. Jaggi, "Ordering policies of deteriorating items under permissible delay in payment," *Journal of Operational Research Society*, vol. 46, pp.658-662,1995.
2. M. F. Anjos, R. C. H. Cheng and C. S. M. Currie, "Optimal pricing policies for perishable products," *European Journal of Operational Research*, vol. 166, no.1, pp.246-254, 2005.
3. T.H. Burwell, D.S. Dave, K.E. Fitzpatrick and M.R. Roy, "Economic lot size model for price-dependent demand under quantity and freight discounts," *International Journal of Production Economics*, vol. 48, no. 2, pp. 141-155, 1997.
4. A.K. Bhunia and M. Maiti, "An inventory model for decaying items with selling price, frequency of advertisement and linearly time dependent demand with shortages," *IAPQR Transactions*, vol. 22, pp. 41- 49, 1997.
5. K.J. Chung, S.K. Goyal and Y.F. Huang, "The optimal inventory policies under permissible delay in payments depending on the ordering quantity," *Int. J. Product. Econ.*, vol. 95, pp. 203-213, 2005.





Renu Gautam et al.,

6. R. R.Chaudhary, V. Sharma and U. Chaudhary, "Optimal Inventory Model for Time Dependent Decaying Items with Stock Dependent Demand Rate and Shortages," *International Journal of Computer Applications*, vol.79, no.17, pp. 6-9, 2013.
7. F.W.Harris, "Operations and Costs," *A. W. Shaw Company, Chicago*, pp. 48-54, 1915.
8. C. K.Jaggi, L. E.Cardenas-Barron, S.Tiwari and A. A. Shafi, "Two warehouse inventory model for deteriorating items with imperfect quality under the conditions of permissible delay in payment," *Scientia Iranica E.*, vol. 24 no.1, pp.390-412, 2017.
9. B. B. Krishnaraj and D. Dhivya, "An Inventory Model with Price Dependent Demand Rate, Quadratic Holding Cost and Deteriorating Rate with Shortages," *International Journal of Science and Research (IJSR)*, vol. 6 Issue 10, pp. 832- 837, 2017.
10. B.Mondal, A.K.Bhunia and M.Maiti, "An inventory system of ameliorating items for price dependent demand rate," *Computers and Industrial Engineering*, vol. 45, no. (3), pp. 443-456, 2003.
11. M.Maragatham and R.Palan, "An Inventory Model for Deteriorating Items with Lead Time price Dependent Demand and Shortages," *Advances in Computational Sciences and Technology*, vol. 10, no. 6, pp. 1839-1847, 2017.
12. V.K.Mishra, L.S.Singh and R.Kumar, "An inventory model for deteriorating items with time-dependent demand and time-varying holding cost under partial backlogging," *J Ind Eng Int*, vol. 9, no. 4 pp. 377-388, 2013.
13. R.Ragini, S. Gupta and S.Srivastav, "An optimal ordering policy for deteriorating items with initial inspection and having ramp type demand rate under permissible delay in payments," In *AIP Conference Proceedings*, vol. 2463, no. 1. pp. 1-9, 2022.
14. J. T.Teng and H. T. Chang, "Economic production quantity model for deteriorating items with price and stock dependent demand," *Computers and Oper. Res.*, vol. 32, pp. 279-308, 2005.
15. S.P.You, "Inventory policy for products with price and time-dependent demands," *Journal of the Operational Research Society*, vol. 56, pp. 870-873, 2005.
16. R.H.Wilson, "A scientific routine for stock control," *Harvard Business Review*, vol. 13, no. (1)pp. 116-128, 1934.

Table (1). Effect of M and α for Case(1)

M/ α	15 days	30 days	45 days	60 days
0.01	$TC_1 = 305.74$	$TC_1 = 305.69$	$TC_1 = 305.64$	$TC_1 = 305.59$
0.05	$TC_1 = 305.96$	$TC_1 = 305.91$	$TC_1 = 305.85$	$TC_1 = 305.80$
0.10	$TC_1 = 306.21$	$TC_1 = 306.16$	$TC_1 = 306.11$	$TC_1 = 306.06$
0.15	$TC_1 = 306.45$	$TC_1 = 306.40$	$TC_1 = 306.35$	$TC_1 = 306.30$

Sensitivity Analysis

Table 2: Variation in system parameters of case (1)

Parameter	%	-50%	-25%	0%	+25%	+50%
C_H	TC	303.29	304.49	305.59	306.69	307.51
C_D	TC	305.56	305.57	305.59	305.69	305.60
C_S	TC	305.08	305.40	305.59	305.89	305.80
C_O	TC	305.34	305.47	305.59	305.70	305.80
γ	TC	305.37	305.48	305.59	305.69	305.78
P	TC	306.24	305.84	305.59	305.42	305.30

Table (3). Effect of M and α for Case(2)

M/ α	320 days	330 days	340 days	350 days
0.01	$TC_2 = 448.07$	$TC_2 = 447.20$	$TC_2 = 446.32$	$TC_2 = 445.44$





Renu Gautam et al.,

0.05	$TC_2 = 459.31$	$TC_2 = 458.46$	$TC_2 = 457.60$	$TC_2 = 456.75$
0.10	$TC_2 = 472.62$	$TC_2 = 471.79$	$TC_2 = 470.96$	$TC_2 = 470.13$
0.15	$TC_2 = 485.18$	$TC_2 = 484.37$	$TC_2 = 483.56$	$TC_2 = 482.75$

Sensitivity Analysis

Table 4: Variation in system parameters of case 2

Parameter	%	-50%	-25%	0%	+25%	+50%
C_H	TC	353.95	403.21	448.07	489.12	526.83
C_D	TC	446.84	447.46	448.07	448.68	449.30
C_S	TC	427.86	440.62	448.07	452.96	456.41
C_O	TC	471.72	460.05	448.07	435.78	423.15
γ	TC	640.52	512.23	448.07	409.56	383.88
p	TC	470.63	457.09	448.07	441.38	436.11

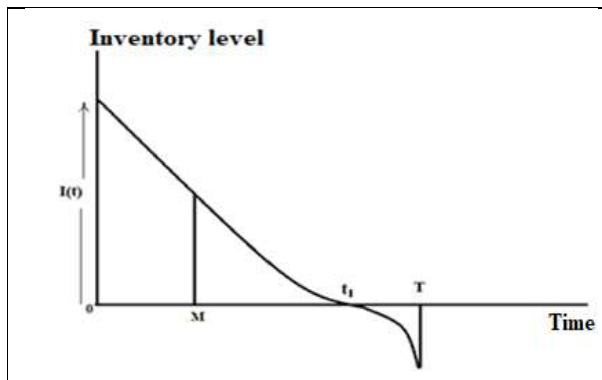


Figure 1.1 of Case(1)

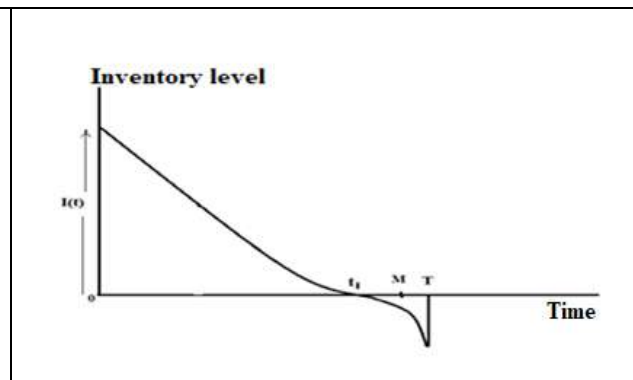


Figure 1.2 of Case(2)

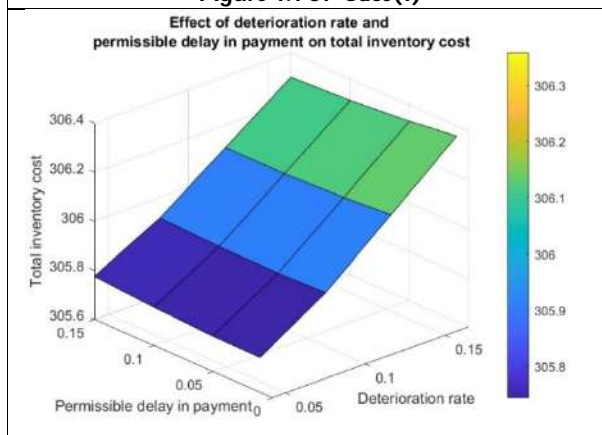


Figure 1.3 of Case(1)

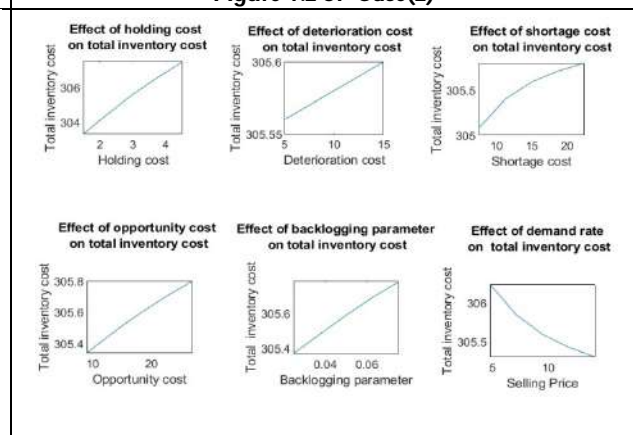
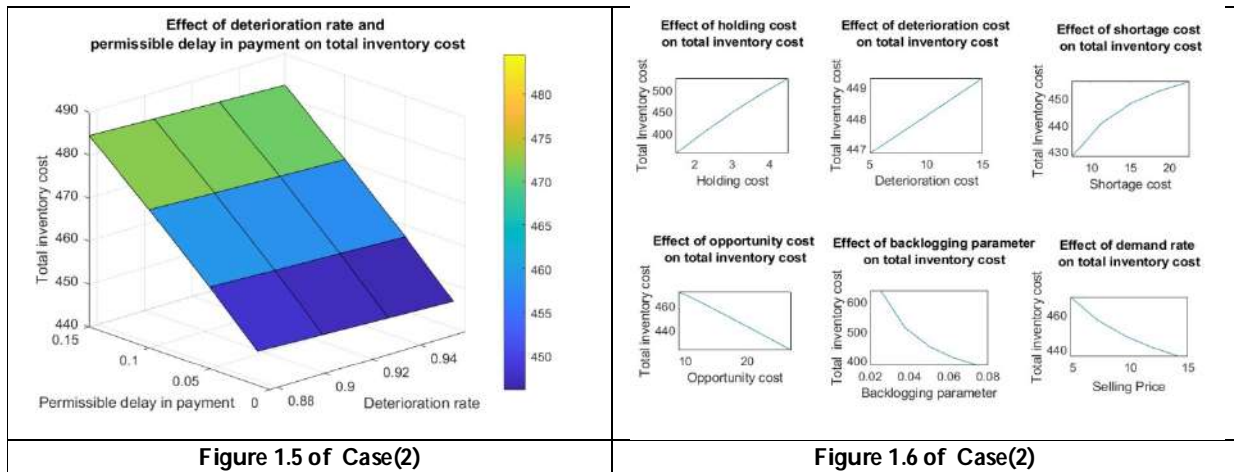


Figure 1.4 of Case(1)





Renu Gautam et al.,





Machine Learning based Comprehensive Analysis of COVID-19 and its Vaccination in India

Aashish Jain^{1*}, Rohit Khokher², Rajendra Kumar³ and Ram Chandra Singh⁴

¹Department of Education, GNCT of Delhi, New Delhi, India.

²Vidya Prakashan Mandir (P) Ltd., Meerut, India

³School of Engineering & Technology, Sharda University, Gr. Noida, India

⁴School of Basic Sciences & Research, Sharda University, Gr. Noida, India

Received: 06 Apr 2023

Revised: 15 May 2023

Accepted: 31 May 2023

*Address for Correspondence

Aashish Jain

Department of Education,

GNCT of Delhi,

New Delhi, India

E. Mail: jain.aashish2.n@gmail.com



This is an Open Access Journal / article distributed under the terms of the **Creative Commons Attribution License** (CC BY-NC-ND 3.0) which permits unrestricted use, distribution, and reproduction in any medium, provided the original work is properly cited. All rights reserved.

ABSTRACT

COVID-19 has emerged as a pandemic outbreak all over the world by mid-2020. The world's leading countries were worst hit by this pandemic and it became a major setback for them economically and socially. Some countries were able to find a cure for this pandemic and they started vaccinating their citizens after getting successful trials of their vaccines. Russia, China, the US, India, the UK, and some more countries were the major contributors to developing vaccines for the world. In this work, a predictive model for the seasonal autoregressive integrated moving average (SARIMA or seasonal ARIMA) is proposed to predict the full vaccination, partial vaccination, total number of confirmed, recovered, and deceased cases due to the COVID-19 virus in India within the next 30 days. The SARIMA model uses the Box-Jenkins model, a forecasting method using regression studies. Data for this study has been taken from crowdsourcing websites. Using the Tkinter library in Python 3.8, a graphical user interface (GUI) is also developed to make this prediction model user-friendly. The accuracy in predicting full vaccination and partial vaccination in this study is 99.7% and 99.08%.

Keywords: COVID-19, Vaccination, Time Series Analysis, Forecasting SARIMA model, Machine Learning, Data Visualization, Data Prediction, Data Science

INTRODUCTION

The world is suffering from the worst pandemic of the 21st century that has impacted all the countries across the globe i.e. Corona virus (COVID-19). The virus belongs to a family of different viruses that cause the common cold,

57584



**Aashish Jain et al.,**

fever, fatigue, dry cough, etc. symptoms in humans and also infect animals including bats, camels, cattle, etc. The very first case of human corona virus was identified in 1965 by some scientists that caused the common cold. After a decade, some researchers found a similar group of animals and the human virus and named those due to their crown-like appearance [1]. It's been found that seven types of corona viruses can infect humans. One of them causes Severe Acute Respiratory Syndrome (SARS) which emerged in 2002 in Southern China and rapidly spread to more than 25 other countries. The impact of this virus was till 2004 with reports of hundreds of dead and thousands of infected humans. This virus caused headaches, fever, and respiratory problems such as shortness of breath and cough.

Another corona virus outbreak was reported in Saudi Arabia in 2012 named Middle East Respiratory Syndrome (MERS) [2]. Though this variant was less transmissible but was more dreadful than the SARS. The symptoms exposed due to MERS in the infected humans were the same as SARS including kidney failures in some people. In 2019, the new strain of this virus family SARS-COV-2 or COVID-19 emerged as an outbreak in the open-air wet market of Wuhan, China. The experts found that the virus had been originated in bats and then this contagious virus found in some species illegally being sold in Wuhan's wet market. From there, it spread to humans and was declared a novel SARS-COV-2 outbreak in Wuhan, China by World Health Organization (WHO) office in China [3, 4]. Some cases were reported in October 2019 but the virus rolled in as a pandemic in December 2019 in Wuhan, China. The virus spread at a rapid rate all over the world and within 6 months more than 6.2 million cases were recorded, of which 372 thousand were deceased, 2.8 million were recovered and 3.1 million were still active around the globe.

India, with the second largest population in the world, reported the first case of Corona virus (named COVID-19 due to its emergence in 2019) in January 2020. A sudden lockdown had been imposed on the nation on 25th March 2020 to stop the spread of this epidemic virus [5]. Though people suffered for the necessities due to this lockdown, but it helped in controlling the epidemic to some extent. Whereas the world was suffering much in comparison to India at that time. There was some carelessness by the people and relaxation by the government due to elections in different states, India was hit by the second wave of COVID-19 very badly in April 2021. There was chaos everywhere due to the lack of oxygen supplies and prescribed medicines that helped to cure this pandemic to some extent. It was the time when the Indian medical system almost collapsed and there were increased deaths, particularly in the young population [6]. India reported thousands of cases each day at that time and vaccinating such a mass population which is almost one-seventh population of the world was the biggest challenge and also crucial to controlling the global spread of SARS-CoV-2 (COVID-19). Although, India had covered a massive population vaccination in the past time as well for different diseases such as measles, polio, etc. but this infectious disease was more dangerous than smallpox and plague. The first wave of COVID-19 had already impacted the nation economically, still, the government managed to train the medical staff to handle this pandemic. In the initial stages, the focus was to prevent and control the transmission of this infectious virus but the global analysis of herd immunity in COVID-19 had shown the essential need for the vaccine for this disease. After the successful clinical trial of COVAXIN by Bharat Biotech and COVISHIELD by Serum Institute of India, the Government of India (GoI) started the vaccination in January 2021 on front-line workers (doctors, nurses, sanitization workers, etc.) [7-10]. The front-line workers weren't completely vaccinated yet and the nation was hit by the second wave of the virus which was more disastrous than the first wave. More than 300 thousand people lost their lives and the mortality rate was around 40% at that time. Seeking this challenge, India boost their vaccination program and planned to vaccinate all its citizens by the end of 2021. Several NGOs, corporates, institutions, and organizations joined their hands with the GoI to fasten the vaccination process and organized multiple camps for the vaccination of the citizens. It was a mammoth task to vaccinate 1.5 billion doses by the end of 2021. The whole nation hasn't been vaccinated yet but still, India has vaccinated almost more than half of its population.

This study aims at the vaccination analysis of India that includes the prediction and forecasting of partial and full vaccination, different insights on vaccination have been drawn at the district level, state level, and India level. In addition to this, COVID confirmed cases, recovered cases, deceased cases, and active cases prediction and forecasting have also been done. The SARIMA model has been used to forecast the vaccination and cases time series provided by

57585





Aashish Jain et al.,

the crowdsourced APIs. Python's different libraries such as NumPy, Tkinter, Matplotlib, Plotly, etc. have been used to develop the GUI-based system and to perform the analysis. The study consists of the following sections: section 2 describes the system design and development, and section 3 presents the different insights that have been drawn and the results that were obtained while predicting and forecasting, in the end, section 4 contains the conclusion and future scope of the study.

System Design and Development

The SARIMA forecasting model is an extension of ARIMA, which explicitly supports one-dimensional time series data with a seasonal component [11, 12] to predict confirmed, recovered, and deceased cases of COVID-19 and to predict vaccination as well. The process of predicting the situation with COVID-19 consists of the following steps:

Dataset

To analyze and predict the status of COVID-19, crowdsourcing is provided through API channels (Live Application Programming Interface) provided by the Indian government (GOI), as shown in Table.1. APIs contain data on COVID-19 cases from day one in the country [13-17]. The APIs provide the day-wise COVID-19 confirmed, recovered, and deceased cases as well as the vaccination statistics in all the states and their respective districts. In this study, we used data from January 16, 2021, to July 25, 2021, on COVID-19 cases and vaccinations in India. The data is used as input to the SARIMA model and the prediction of corona viruses is predicted for August 2021. To test the performance of the proposed model, 30% of the predicted data is compared with the actual data. This model offers the flexibility to predict the next 30 days from a selected date.

GUI of Forecasting Model

The graphical user interface (GUI) of the forecasting model is developed using the Tkinter library in Python 3.8, which is intuitive and allows steer focus. The GUI is divided into three sections; *COVID-19 Cases Analysis and Prediction*, *Indian States COVID-19 Cases, Vaccination Analysis and Prediction*, and *COVID-19 Vaccination Analysis and Prediction*. The first and third section consists of 4 buttons each. The first section displays and predicts the statistics of the COVID-19 cases in India including confirmed cases, recovered cases, deceased cases, and active cases while the third section displays and predicts the full vaccinations and partial vaccinations statistics in India. The second section of the GUI consists of 5 buttons and 1 drop-down list that works on the COVID-19 cases and vaccination statistics at the district level of the selected state. The functionalities and the results are discussed in detail in Section 3 of the study. The developed GUI is shown in Figure 1.

METHODOLOGY

The SARIMA model for this study is identified using the `auto_arima()` method from the `pmdarima` library of Python. The method determines the values of non-seasonal parameters (p, d, q) and the seasonal parameters (P, D, Q) which are best suited for data that need to be forecasted. The selection criteria for the best possible seasonal values and non-seasonal parameters are based on the values of the Akaike Information Criterion (AIC) and Bayesian Information Criterion (BIC) values generated while fitting. AIC and BIC are the estimators to compare models and the lower these values, the better the model [18]. AIC and BIC are derived from a probability function, $L(\tilde{\Psi})$, where $\tilde{\Psi}$ is the maximum probability estimates of the parameters for the SARIMA with $n = p + q + P + Q + 1$ parameters and the sample size T . The criteria are defined as:

$$AIC = -2\log[L(\tilde{\Psi})] + 2n \quad (1)$$

$$BIC = -2\log[L(\tilde{\Psi})] + n\log(T) \quad (2)$$

The SARIMA model can be written equivalently as $ARMA(p + sP, q + sQ)$. The forecast function for the assumed stationary function x_t^* can be written as:

$$\hat{x}_{t+1|t}^* - \mu = \phi(L)^*(\hat{x}_t^* - \mu) + \theta(L)^*\hat{\epsilon}_t \quad (3)$$

where $\hat{\epsilon}_t = x_t - \hat{x}_{t|t-1}^*$ [22]. Forecast for the lead time τ ; time that follows the last observed information, is given as:

$$\hat{x}_{t+s|t}^* - \mu = \phi(L)^*(\hat{x}_{t+s-1|t}^* - \mu) + \theta(L)^*\hat{\epsilon}_{t+s-1} \quad (4)$$





Aashish Jain et al.,

The forecast for the lead time τ is expressed by the previously observed values of x_t^* , previous forecasts of \hat{x}^* and the residuals $\hat{\epsilon}_t$ which are obtained for all time points up to the last observed observations. The SARIMA model is implemented in Python using the *statsmodels* library and the *SARIMAX()* function, the function takes parameters; *order*, and *season_order* for non-seasonal and seasonal SARIMA model parameters and observation data. To forecast the data, the model is first fitted using the *fit()* method, and then the data is forecasted using the *predict()* method. The *predict()* method on the fitted model takes two parameters start and end, which determine the start and end time of the forecasting period.

RESULT ANALYSIS AND DISCUSSION

In this study, three analyses have been done COVID-19 cases analysis and prediction in India, COVID-19 cases, vaccination analysis and prediction in States, and COVID-19 vaccination analysis and prediction in India.

Covid-19 Cases Analysis And Prediction

In this analysis, the COVID-19 cases have been analyzed in India. There are four buttons on the GUI to understand the results.

COVID-19 Indian States Current Stats

When the user presses this button on the GUI, the total number of confirmed cases, active cases, recovered cases, and death cases in every state are displayed, as shown in figure 2. The method *show_data()* executes on pressing this button that first sorts the states in alphabetical order and then displays them in tabular form. It can be seen that on 25 July 2021 Andhra Pradesh has 19,52,513 confirmed cases, 22,358 active cases, 19,16,914 recovered cases, and 13,241 deaths.

COVID-19 Indian States' Insight

In this section, five detailed COVID-19 analysis has been done using different graphs. These graphs have been plotted on the crowdsourced data using the *pandas* library. The analysis is as follows:

Death versus Confirmed case ratio

This graph depicts the percentage of deaths over confirmed COVID-19 cases in each state, as shown in figure 2. It can be seen that Punjab state has a 2.72 % death percentage which is the highest in India on 25 July 2021 whereas Dadra Nagar Haveli and Daman & Diu have the lowest death rate in the country.

State-wise COVID-19 confirmed cases across India

This analysis shows the state-wise total number of confirmed cases and the percentage of its share across India, as shown in Figures 3 (a) and 4(b).

It can be seen from figures 3 (a) and 4(b) that the highest number of COVID-19 patients is in Maharashtra state which is recorded at 6.2 million on 25 July 2021. Further is 19.9% of the total number of patients infected with COVID-19 in the country. Similarly, the same analysis can be seen for other states as well.

State-wise COVID-19 recovered cases across India

Figure 5(a) and 5 (b) show the recovery rate of COVID-19 patients state-wise and its recovery percentage rate across India. It can be seen that despite being the worst infected state, Maharashtra has the highest recovery rate.

State-wise COVID-19 deaths cases across India

This analysis presents the percentage of death cases shared by state across India and the number of death cases state-wise, as shown in figures 6 (a) and 6(b).





Aashish Jain et al.,

Maharashtra is worst hit by the COVID-19 pandemic. It has the highest number of COVID-19 cases and also the death rate percentage. From figure 6(a) it can be seen that Maharashtra's death rate percentage share in the country is 31.2% and the total death in the state is 1,31,429 as on 25 July 2021.

State-wise COVID-19 active cases across India

In this section, active cases have been analyzed. Figure 7(a) and 3.(b) show the state share of active cases in the country and the total number of active cases in the state respectively. As on 25 July 2021 Kerala state has the highest 34.3% active COVID-19 cases share in the country and 1,30,122 total active cases in the state.

COVID-19 Cases Analysis

India has reported its first COVID-19 case on 30th January 2020 and since then India has 31.37 million cases till now. Figure 8 shows how COVID-19 rises and declines in India. It can be seen that the alarming second wave of COVID-19 started in April 2021 and reaches its peak in June 2021. The number of active cases and deceased has rapidly increased in April, May, and June 2021. Further, it shows that active cases start to decline from mid-July 2021. This analysis has been plotted using the *show_covid_records()* method.

COVID-19 Cases Forecasting in India

SARIMA model has been used to predict the COVID-19 cases for August 2021. Figure 9 and 10 shows the predicted COVID-19 cases and the accuracy of the system. On pressing this button, the *forecast_covid_cases()* method executes and the best-fit SARIMA model is selected to forecast COVID-19 cases. It can be concluded that the COVID-19 cases were increasing at a rapid speed in May and June, and now the cases are increasing a bit slowly in comparison to that. Besides that, India will have approx. 32.56 million confirmed cases by the end of August. More than 99% accurate results are obtained in this research for confirmed cases, active cases, recovered cases, and death cases.

Indian States Covid-19 Cases, Vaccination Analysis and Prediction

The second analysis in this study includes the analysis of COVID-19 cases and the vaccination at the state level. The analysis has been done at the India level for all the states, similarly, in this section, the analysis has been done for all the districts of the chosen state. The same algorithms and functions have been used to predict the COVID-19 cases, vaccination statistics, and visualization of COVID-19 cases using different graphs. Figure 11 shows the COVID-19 confirmed cases, recovered cases, deceased cases, and active cases data in tabular form on the GUI. On pressing this button, *show_district_data()* method is called and the data is displayed in alphabetic order of district names in tabular form on the GUI. The *show_district_status()* method is used to present the different insights for districts. Figure 12. shows the district-wise death percentage over confirmed cases. From the analysis, it can be seen that in Uttar Pradesh, Ambedkar Nagar has the highest deaths over confirmed cases in comparison to other districts. Figure 13-3.19 show the district-wise percentage share of confirmed cases, recovered cases, deceased cases, and active cases and the total number of confirmed cases, recovered cases, deceased cases, and active cases. The below figures depict that Lucknow has the highest share of confirmed cases with 14% and more than 238K in total. From the figures plotted above, it can be concluded that Lucknow has the highest percentage share of recovered cases in the state.

The graphs plotted in figures 17 and 18 show that Lucknow has almost 12% of total deceased cases in the state which is more than 2.6K in numbers. From the plotted graphs in Figures 19 and 20, it can be seen that despite having maximum COVID-19 cases, Lucknow is at 4th position in the state with respect to currently active cases. Figure 21 presents the timeseries of COVID-19 cases in the state. When a user clicks on this button, the *show_covid_state_records()* method runs and the graph is plotted. The graph shows that Uttar Pradesh recorded the first cases on 4th March 2020 and since then the state has recorded more than 1.7 million cases out of which more than 22.7K have lost their lives and less than 1K cases are active as of now. The state-wise COVID-19 cases have also been forecasted. When a user presses this button, the *predict_state()* method is called to plot the actual and predicted cases on the graph and achieved accuracy for confirmed, recovered, deceased and active cases are displayed on the GUI, as shown in figures 22 and 23



**Aashish Jain et al.,**

The states are doing well in vaccination to fight against the corona virus. Forecasting based on current trends of vaccination in the state has also been done. On click of the 'Forecasting Vaccination' button the `vc_forecast_state()` method runs, the actual and predicted vaccination for partially vaccinated people and fully vaccinated people are computed, and achieved accuracy is shown on GUI, as shown in figures 24 and 25. From the forecasting, it can be concluded that before Independence Day Uttar Pradesh will cover the vaccination of around 20% of its population. More than 99% accuracy has been achieved in partial vaccination and complete vaccination forecasting. The actual and predicted vaccination data are presented below in Table 2. The forecasted vaccination data are shown in Table 3.

Covid-19 Vaccination Analysis And Prediction

This is the third and last part of this research study that focuses on the analysis of vaccination in India and its forecasting. The analysis includes the following:

Covid-19 vaccination current stats

This analysis presents the state-wise partial vaccination and complete vaccination data in tabular form on the GUI. On click of this button, `show_vaccination_status()` is called which presents the data on the GUI, as shown in figure 26.

COVID-19 Vaccination India's Insight

The analysis consists of different insights that have been drawn based on the crowd sourced data that are generated by clicking this button. The `vaccination_insight()` function displays all the analyses that are as follows:

Partial Vaccination versus Population Ratio

This analysis shows the percentage of people vaccinated for a single dose over the total population of the state, as shown in figure 27. The graph shows that more than 73% of the total population of Lakshadweep has been partially vaccinated which is the highest percentage among the states.

Complete Vaccination versus Population Ratio

In this analysis, the percentage of fully vaccinated people over the total population has been computed and shown in figure 28. The graph shows the Andaman and Nicobar Islands is the state that has the highest percentage of population vaccinated completely which is slightly higher than Sikkim.

State-wise Partial Vaccination across India

This analysis shows the percentage share of the states for partial vaccination across India and the total number of vaccinations administered in the states, as shown in figures 29 and 30. Uttar Pradesh is the state that has the highest percentage of partial vaccination administered in India with more than 37.8 million vaccination doses.

State-wise Complete Vaccination across India

The analysis depicts the complete vaccination of people in all states across India. It shows the percentage of full vaccination share of the state out of total vaccination in India and also the total number of complete vaccinations in the state, as shown in figures 31 and 32. It can be concluded from the graph that Maharashtra has the highest percentage of fully vaccinated people in India with more than 9.9 million.

COVID-19 Vaccinated People's Insight

This analysis includes the different insights drawn based on gender-specific, vaccine-specific, and age group-specific. The analysis can be seen by pressing this button which calls the `vaccination_people_insight()` function to draw the graphs. The analysis is as follows:

Vaccination Administered (Gender Specific)

This analysis shows the vaccinations administered to males, females, and transgenders, as shown in figure 33



**Aashish Jain et al.,**

The graph shows the data for all the states and when a user mouse over any of the bars, it displays the details. e.g. figure 33 shows the details of doses administered to males, females, and transgenders of Uttar Pradesh.

Vaccination Administered (Age Group Specific)

This analysis depicts the vaccination doses administered to the different agegroups in all the states, as shown in figure 34. As of now, the vaccination is only for 18+ and there are three different agegroups i.e. 18-44 years, 45-60 years, and 60+ Years.

Vaccination Administered (Vaccine Specific)

There are different types of vaccines that are being administered in the country. Mostly CoviShield, Covaxin, and Sputnik V are being used, as shown in figure 35. Whenever the user takes the cursor over any of the bars, it shows the details of the vaccine i.e. the number of doses administered in the state e.g. figure 36 shows the details of vaccines used for Uttar Pradesh.

State-wise AEFIs across country

This analysis shows the AEFIs (Adverse Events Following Immunizations) reported in different states across the country. Figure 36 shows the details of the cases reported in all the states.

Maharashtra and Karnataka are the states where these have been reported in large numbers in comparison to other states. Although it doesn't have any connection with the vaccination as suggested by doctors and researchers still it found in people after vaccination.

COVID-19 Vaccination Forecasting

This analysis forecasts the partial and complete vaccination in India using the SARIMA model. The same function (used in state's vaccination forecasting) runs when this button is clicked and the time-series vaccination data for India is provided in the function. Figures 37 and 38 display the forecasting of vaccination and the accuracy achieved in forecasting. In this forecasting, more than 99% accuracy is achieved in case of partial and complete vaccination, and it's forecasted that before Independence Day India would be able to provide the first dose to more than 27% of its total population at this pace. Table 4. and Table 5 present the analyzed data and forecasted data for vaccination.

CONCLUSION AND FUTURE SCOPE

In this work, the SARIMA forecasting model is implemented, and COVID-19 vaccination data is forecasted for the next 30 days from a selected date. The forecast model is selected based on AIC and BIC criteria, with the help of which an optimal SARIMA model can be determined. The forecast model proposed in this study is 99% accurate for COVID-19 partially vaccinated and fully vaccinated. As the number of cases increases rapidly, the Indian government needs to run more awareness campaigns to make people aware of the essentiality of vaccination and avoid any kind of rumors being spread. The government should ask social activists, NGOs, local leaders, municipal corporations, and other social influencers to come forward together for the mass vaccination campaigns. Choosing the optimal SARIMA model is a difficult task, and proper operation requires a careful selection of seasonal and non-seasonal parameters. From a future perspective, the graphical user interface can be improved by additional functions that enable the prediction of condition-related data and the prediction of COVID-19 in a patient.

REFERENCES

1. Swelum, A. A., Shafi, M. E., Albaqami, N. M., El-Saadony, M. T., Elsify A., Abdo, M., Taha, A. E., Abdel-Moneim, A-M. E., Al-Gabri, N. A., Almaiman, A. A., Al-wajeeh, A. S., Tufarelli, V., Staffa, V. N., and El-Hack, M. E. A. (2020). "COVID-19 in human, animal, and Environment: A review", *Frontiers in Veterinary Science*, vol. 7, pp. 1-13.





Aashish Jain et al.,

2. <https://www.webmd.com/lung/corona-virus-history>
3. <https://www.who.int/docs/default-source/corona-virus/situation-reports/20200121-sitrep-1-2019-ncov.pdf>
4. Wu, Y.-C., Chen, C.-S., and Chan, Y.-J. (2020). "The outbreak of COVID-19: An overview", *Journal of the Chinese Medical Association*, vol. 83, no. 3, pp. 217-220.
5. <https://archive.pib.gov.in/documents/rlink/2020/mar/p202032401.pdf>
6. Asrani P., Eapen, M. S., Hassan, M. I., and Sohal, S. S. (2021). "Implications of the second wave of COVID-19 in India". *The Lancet Respiratory Medicine*, vol. 9, no. 9, pp 93-94.
7. <https://www.bharatbiotech.com/covaxin.html>
8. https://www.icmr.gov.in/pdf/press_release_files/ICMR_Press_Release_COVISHIELD.pdf
9. <https://www.mohfw.gov.in/pdf/RevisedVaccinationGuidelines.pdf>
10. Bagchi, S. (2021). "The world's largest COVID-19 vaccination campaign". *The Lancet Infectious Diseases*, vol. 21, no. 3, pp. 323.
11. <https://machinelearningmastery.com/sarima-for-time-series-forecasting-in-python/>
12. Jain, A., Singh, R. C., Khokher, R., and Kumar, R. (2020). "Forecasting of COVID-19 cases using SARIMA model in India". *Solid State Technology*, vol. 63, no. 2s (2020), pp. 3516-3528
13. <https://api.covid19india.org/v4/min/data.min.json>
14. <https://api.covid19india.org/csv/latest/states.csv>
15. https://api.covid19india.org/csv/latest/state_wise.csv
16. https://data.covid19india.org/csv/latest/district_wise.csv
17. http://data.covid19india.org/csv/latest/cowin_vaccine_data_statewise.csv
18. Harvey, A, (1989), *Forecasting, Structural Time Series models and the Kalman filter*, 1stEdn., Cambridge University Press, Cambridge, pp. 80-81.

Table1: API Details

COVID-19 Data API	URL
Indian States' Statistics	https://api.covid19india.org/v4/min/data.min.json
States' COVID-19 cases	https://api.covid19india.org/csv/latest/states.csv
States' Present-Day Statistics	https://api.covid19india.org/csv/latest/state_wise.csv
Districts' Present-Day Statistics	https://data.covid19india.org/csv/latest/district_wise.csv
Vaccination Statistics	http://data.covid19india.org/csv/latest/cowin_vaccine_data_statewise.csv

Table 2. Actual and Predicted Vaccination statistics

Date	Partial Vaccination		Full Vaccination	
	Actual	Predicted	Actual	Predicted
10/07/2021	31368297	31611864	5797202	5817462
12/07/2021	31757700	31769765	5939418	5886423
14/07/2021	32665993	32414009	6171435	6162851
16/07/2021	33522527	33814434	6412146	6459664
18/07/2021	33842280	34127230	6525898	6603731
20/07/2021	34794693	34844767	6764530	6784333
22/07/2021	35830969	35571578	6961411	6917137
24/07/2021	37179632	37202293	7209095	7206044





Aashish Jain et al.,

Table 3. Forecasted Vaccination statistics

Date	Forecasted Vaccination	
	Partial	Fully
26-07-2021	37738389	7307037
27-07-2021	38260574	7417244
28-07-2021	38424300	7454487
29-07-2021	38742989	7515662
30-07-2021	39181664	7622253
31-07-2021	39466031	7696854
01-08-2021	39628040	7728350
02-08-2021	40121170	7823532
03-08-2021	40610940	7936113
04-08-2021	40877318	7978444
05-08-2021	41236894	8035636
06-08-2021	41639782	8139875
07-08-2021	41870248	8207027
08-08-2021	42058424	8234157
09-08-2021	42483582	8318957

Table 4. Actual and Predicted Vaccination Data

Date	Partial Vaccination		Full Vaccination	
	Actual	Predicted	Actual	Predicted
10/07/2021	299620148	299508996	71301249	71838161
12/07/2021	303057816	302245479	73292746	73181003
14/07/2021	310042014	307621969	76246127	75801429
16/07/2021	315177274	315545158	79464430	79290043
18/07/2021	319469878	321253854	81972091	82689552
20/07/2021	325242678	325433346	85188148	85326189
22/07/2021	330465663	328902093	87901175	87052956
24/07/2021	336917806	336091394	91192124	91459862

Table 5. Forecasted Vaccination Data

Date	Forecasted Vaccination	
	Partial	Fully
26-07-2021	340789117	93642353
27-07-2021	343156038	95279777
28-07-2021	345479190	96006531
29-07-2021	347771119	97525195
30-07-2021	350032273	99026053
31-07-2021	352262958	100411268
01-08-2021	354464226	101133387
02-08-2021	356635639	102850072
03-08-2021	358778624	104372862
04-08-2021	360892612	105037788
05-08-2021	362978582	106483198
06-08-2021	365036748	107995661
07-08-2021	367067932	109145293
08-08-2021	369104428	109934145
09-08-2021	371096109	111588203





Aashish Jain et al.,

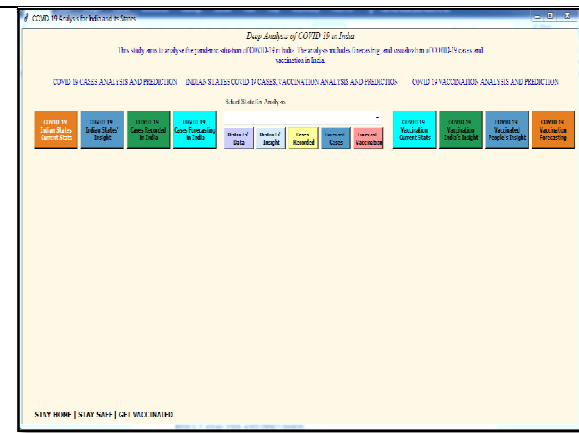


Fig. 1: GUI of the forecasting model

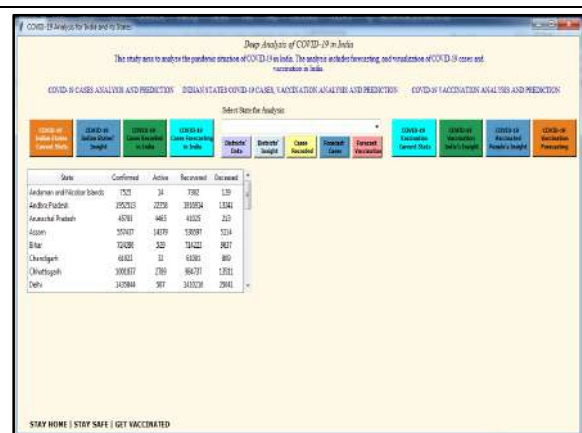


Fig. 2. State-wise COVID-19 cases

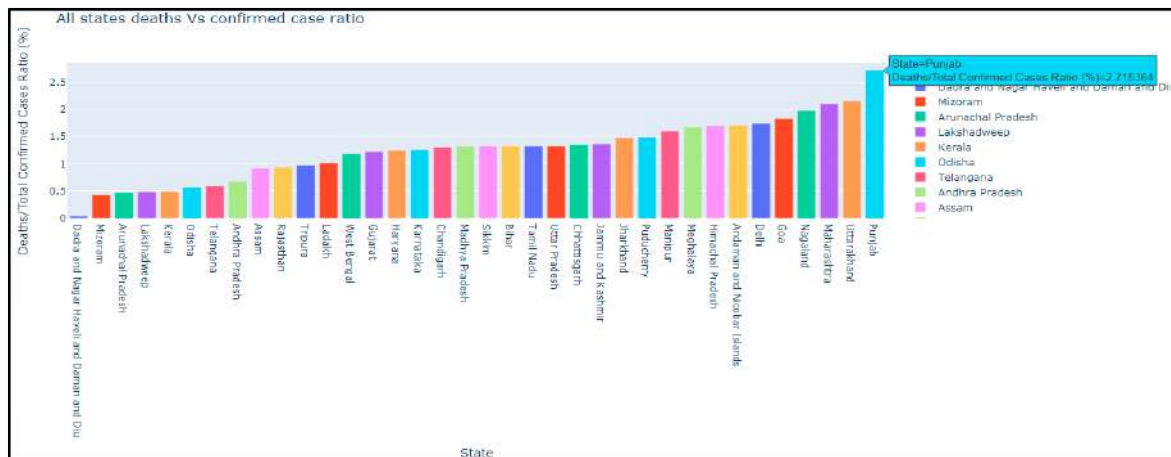
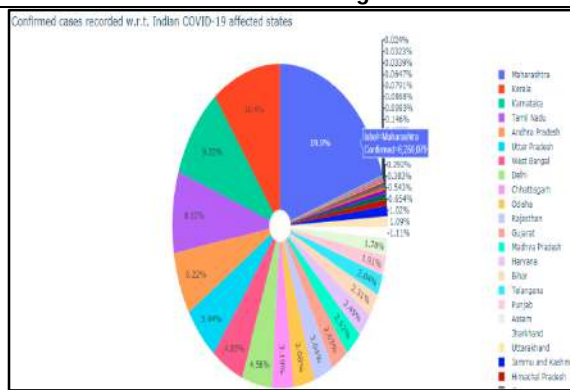
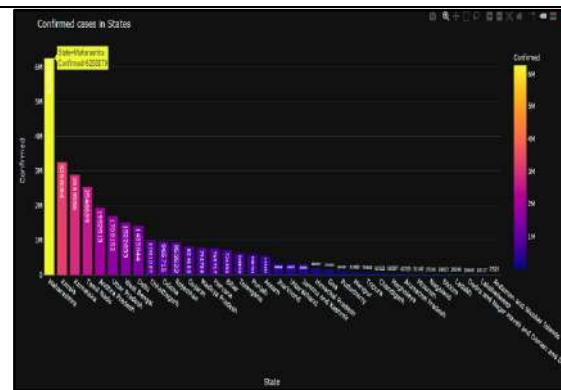


Fig. 3. Death rate over confirmed COVID-19 cases



(a)



(b)

Fig. 4. (a) State share of COVID-19 cases (b) State-wise number of COVID-19 cases





Aashish Jain et al.,

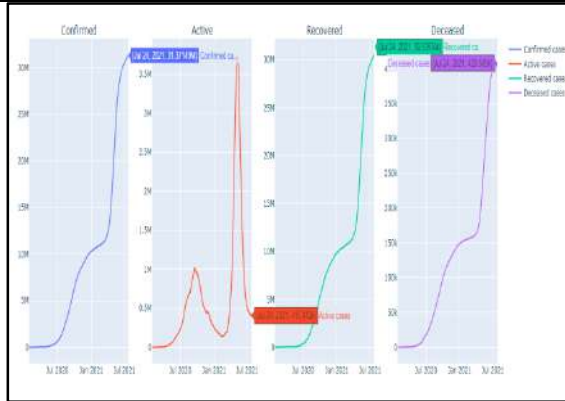


Fig. 8: COVID-19 cases recorded in India

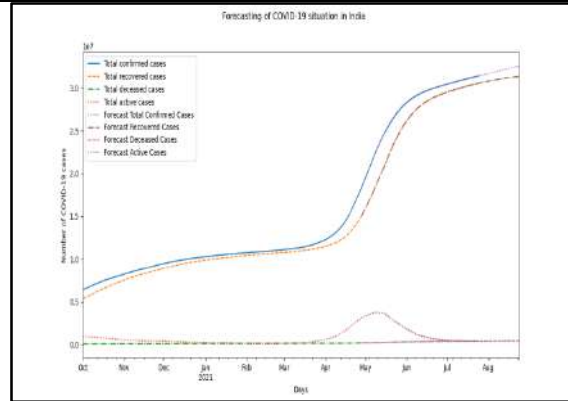


Fig.9: COVID-19 confirmed, recovered, death, and active case forecasting

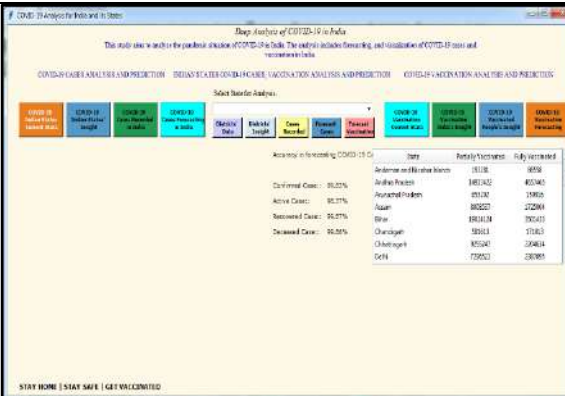


Fig. 10 Accuracy achieved in forecasting COVID-19 cases

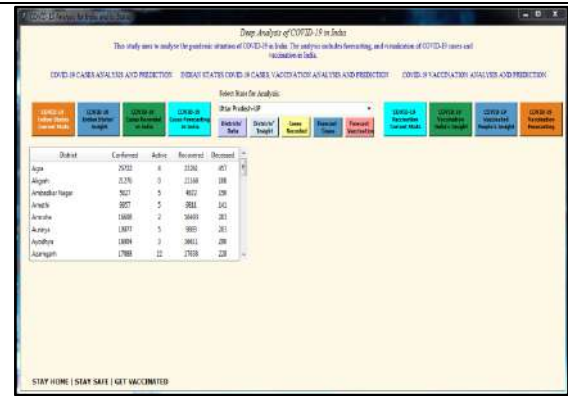


Fig. 11 Districts' COVID-19 cases

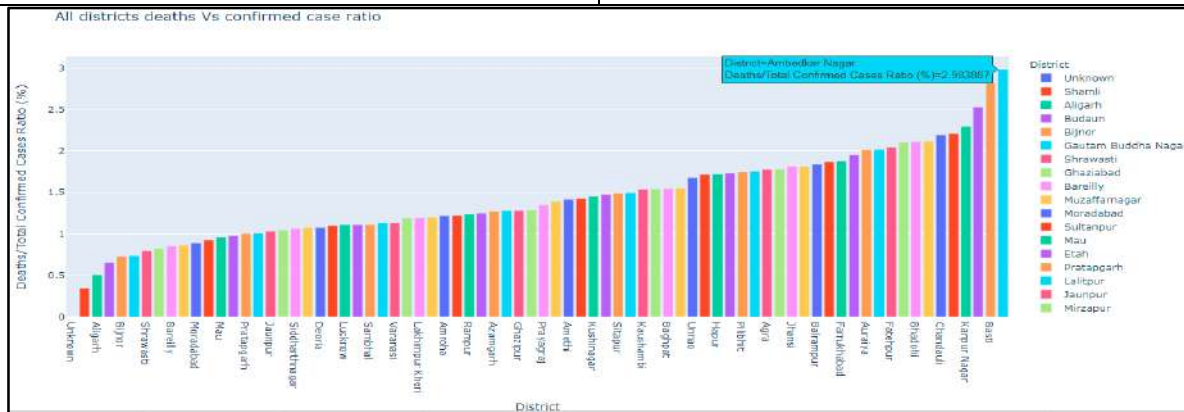


Fig. 12. Deaths over confirmed cases





Aashish Jain et al.,

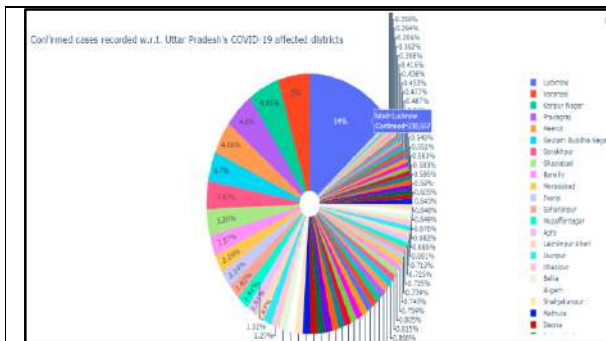


Fig. 13. Percentage of confirmed cases in all districts

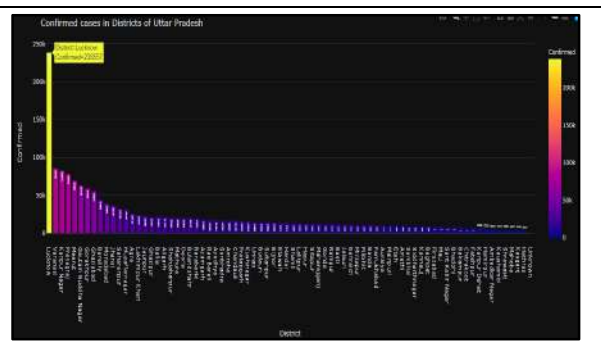


Fig. 14.: Confirmed cases in all districts

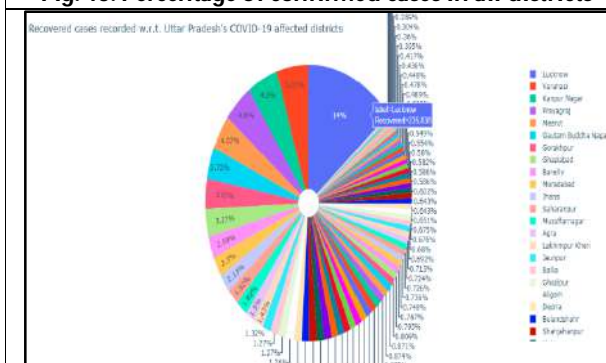


Fig. 15. Percentage share of recovered cases by districts

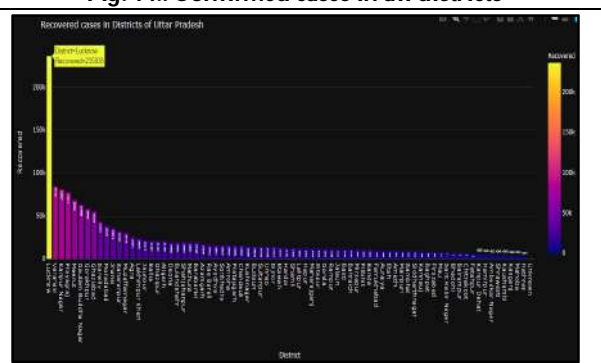


Fig. 16.: total number of recovered cases in districts

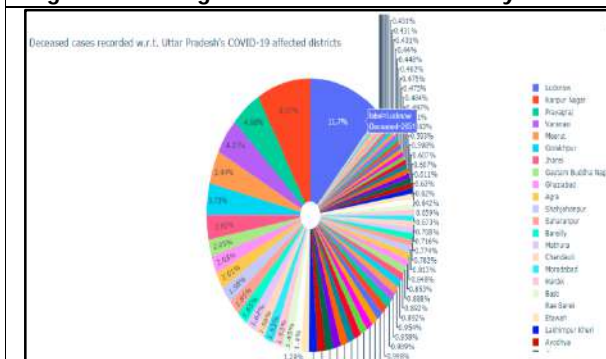


Fig. 17. District-wise percentage share of deceased cases

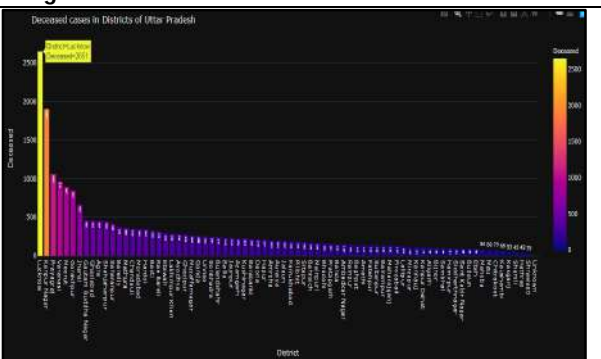


Fig. 18. District-wise total number of deceased cases

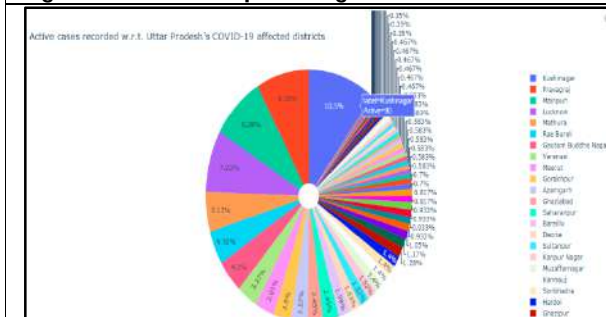


Fig. 19. Percentage share of district-wise active cases

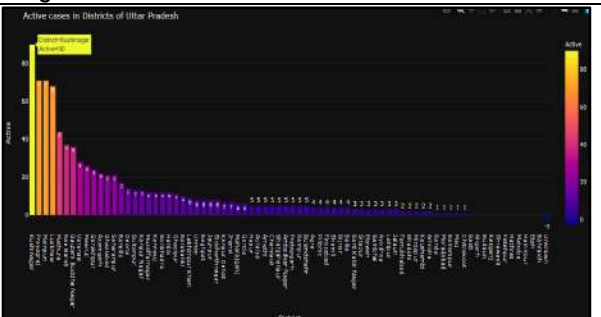


Fig. 20. District-wise total number of active cases





Aashish Jain et al.,

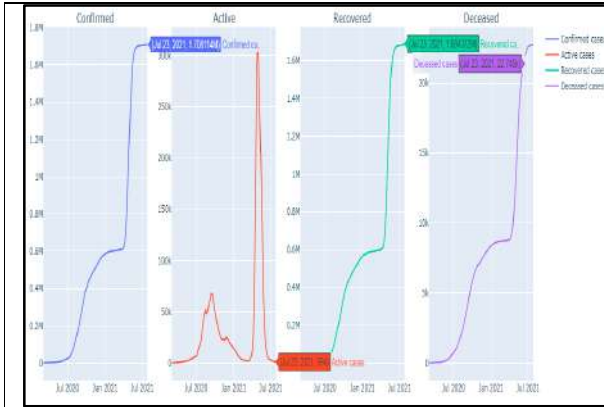


Fig. 21. Recorded cases in Uttar Pradesh

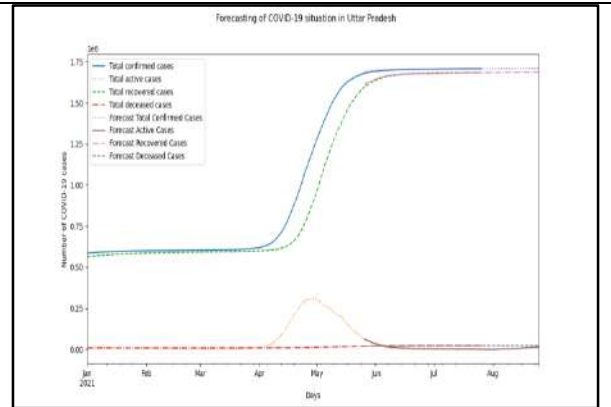


Fig. 22. Forecasting of confirmed, recovered, active, and deceased cases in Uttar Pradesh

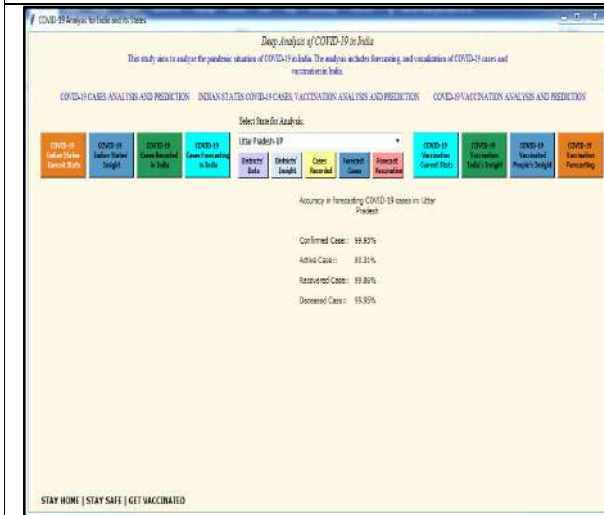


Fig. 23. accuracy achieved in all cases

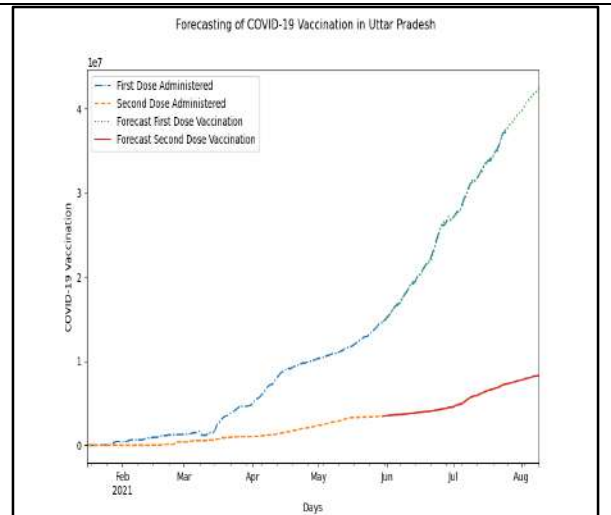


Fig. 24. Forecasting of vaccination in the state



Fig. 25. Accuracy computed in vaccination forecasting



Fig. 26. Vaccination statistics of all state





Aashish Jain et al.,

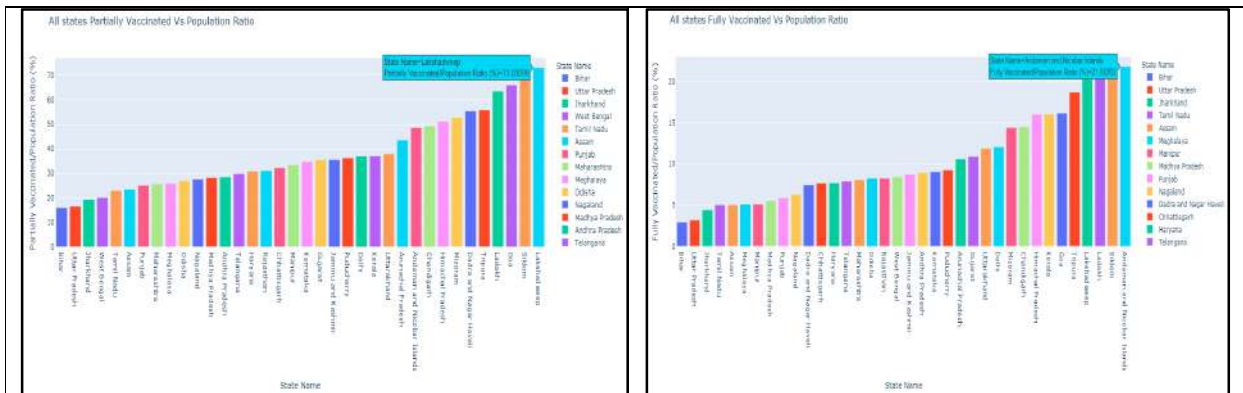


Fig. 27.: Partial vaccinated population

Fig. 28. Complete Vaccination over the total population

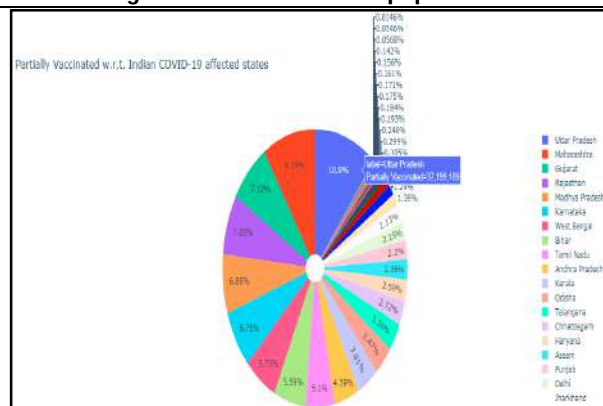


Fig. 29. Partial vaccination percentage across India

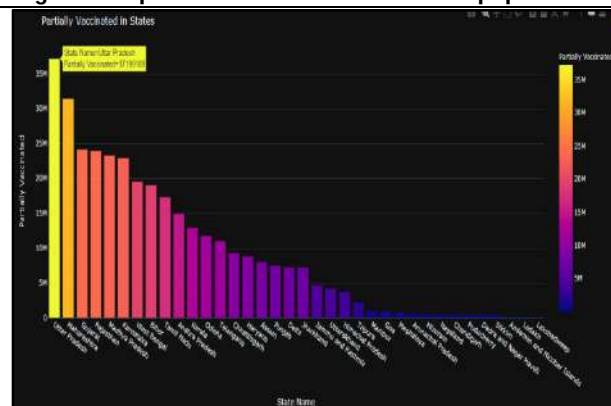


Fig. 30. State-wise partial vaccination across India

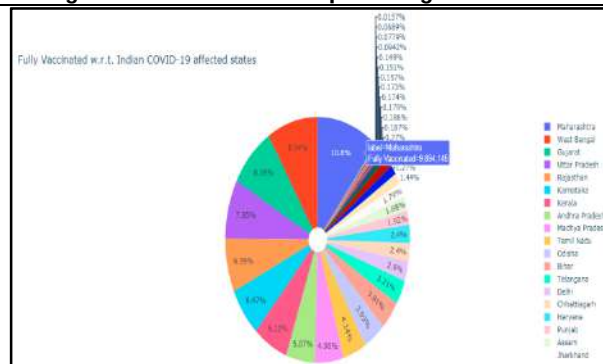


Fig. 31. Complete Vaccination percentage share of States across India

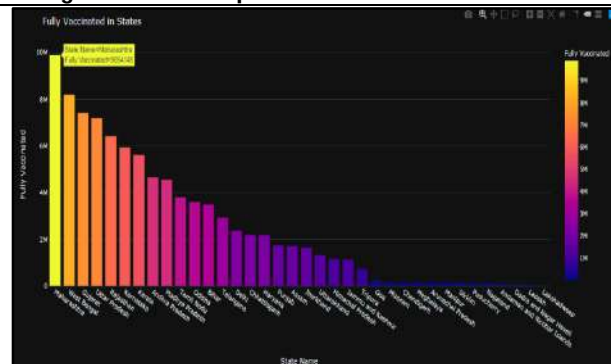


Fig. 32: Complete Vaccination in states across India





Aashish Jain et al.,

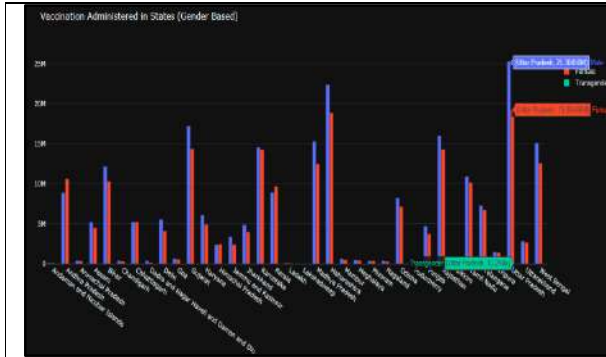


Fig. 33. Vaccination administered (Gender-based)

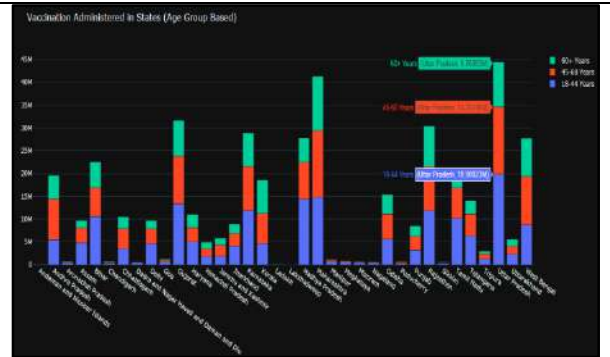


Fig. 34. Vaccination administered (age-group based)

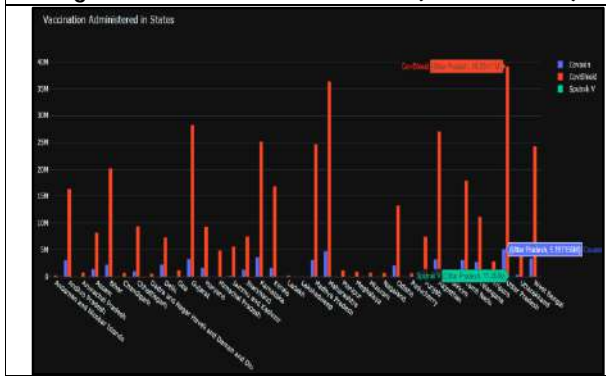


Fig. 35. : Vaccination Administered (vaccine based)

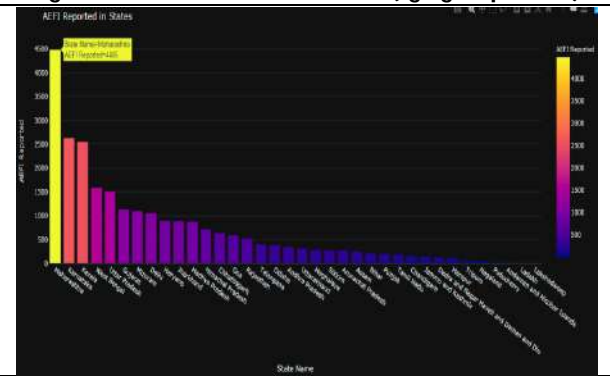


Fig. 36. AEFIs reported in states

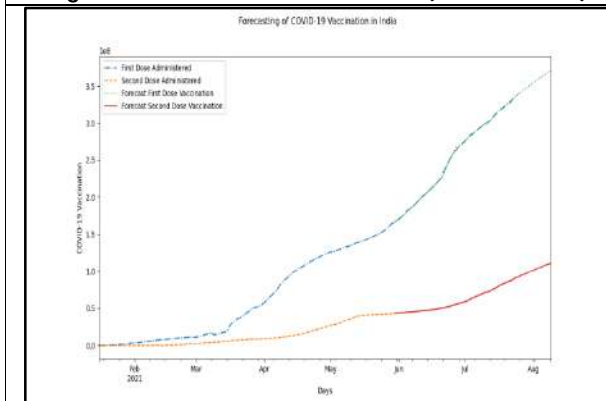


Fig. 37. Forecasting of partial and complete vaccination



Fig. 38. Accuracy achieved in forecasting partial and complete vaccination





A Benchmark to Ensure End-to-End Exactly-Once-Semantics in Stream Processing

Kanchana Rajaram^{1*}, V.Dhayanidhi², Harikirishnan Srikrishnan² and P. Aadhithyan²

¹Associate Professor, Department of CSE, Sri Sivasubramaniya Nadar College of Engineering, Anna University, Chennai, Tamil Nadu, India.

²UG Student, Department of CSE, Sri Sivasubramaniya Nadar College of Engineering, Anna University, Chennai, Tamil Nadu, India.

Received: 18 Oct 2022

Revised: 20 Apr 2023

Accepted: 31 May 2023

*Address for Correspondence

Kanchana Rajaram

Associate Professor,

Department of CSE, Sri Sivasubramaniya Nadar College of Engineering,

Anna University, Chennai,

Tamil Nadu, India.

E.Mail: rkanch@ssn.edu.in



This is an Open Access Journal / article distributed under the terms of the **Creative Commons Attribution License** (CC BY-NC-ND 3.0) which permits unrestricted use, distribution, and reproduction in any medium, provided the original work is properly cited. All rights reserved.

ABSTRACT

For processing large amounts of data, distributed stream processing frameworks have gained importance. Most of them have a standard design that are developed using frameworks like Apache Storm, Apache Spark Streaming, and Apache Flink. These stream processing frameworks provide exactly-once processing in the individual components of the pipeline. When creating a real-time streaming application with these frameworks, there is often a possibility that a batch of data might be handed over to the application multiple times due to failures, resulting in duplicate data being processed. To avoid this, we proposed two methods through which end-to-end exactly once semantics is achieved in the case of failures. These methods have been tested on fifty lakh records, and inferences have been made for efficient processing. A RESTful service has also been developed.

Keywords: Stream processing, Exactly-Once Semantics, Data Pipeline, Cluster, Benchmark

INTRODUCTION

A data stream is obtained as input and sent to Kafka which acts as a hub for real time streams of data. This data stream is sent to Spark for processing. Once the data is processed, Spark Streaming publishes the results into NoSQL databases like MongoDB, Cassandra etc. It is planned to prevent duplicate updates in the NoSQL databases and guarantee that every stream of data is written exactly once.



**Kanchana Rajaram et al.,**

There are different delivery semantics, besides exactly-once. At-least-once semantics: It ensures that no messages are lost but leads to duplicate data and incorrect results. At-most-once semantics: The batch of data may be lost before being processed by the receiver due to a fault in the receiver or a possible receiver crash if the producer, in this case Kafka, does not wait for an acknowledgement from the receiver and updates the offsets as soon as it hands over the batch of data to the receiver. According to this scenario, the receiver will receive the batch of data “at most once”.

Many systems in the healthcare and financial sector rely on large data processing in the form of batch processing which cannot process data quickly. Meanwhile, stream processing supports processing in real time, giving a high level of accuracy with time-sensitive data processing which in turn helps to harness the information to optimize patient experience. There is frequently a chance that a batch of data may be given over to the application more than once due to faults when building a real-time streaming application with these frameworks, processing duplicate data. Exactly once semantics is possible under certain configurations or when the application and the stream processing framework collaborate in certain ways. In order to ensure that data is consumed, processed, and written to the ultimate storage exactly once even when it moves through many components in the stream processing pipeline, this work provides an approach that ensures exactly-once semantics in processing messages from beginning to end. Exact once semantics are required by real-time systems like IoT, recommendation systems, fraud detection systems, health care, stock markets, server monitoring, prediction, etc. where preserving the integrity of the data is an important requirement.

LITERATURE REVIEW

A user’s typical interaction with a website is a multi-step process. The loss of connection, or other system failure, can result in the loss of work. Vander et al. presents [1] a protocol for recovering from such scenarios. They describe Internet-based interactions using familiar concepts of transactions and recovery. Their paper discusses transactions and recovery. It does not deal with “exactly once semantics”. Dongen et al. carried out a performance analysis of fault recovery in stream processing frameworks [2]. They highlighted the differences in behavior during failures on several aspects like whether there is an outage, downtime, recovery time, data loss, duplicate processing, accuracy. Their paper talks about fault recovery performance and does not discuss solutions for “exactly once semantics”. Huang et al. address the problem [3] of exactly-once delivery to mobile clients when messages are replicated globally and proposes algorithms to guarantee “exactly-once” semantics. They found that the performance overhead of exactly-once can be minimized in most cases by careful design of the system. Their proposal is appropriate only for limited-capability mobile devices.

Brown et al. [4] introduced a messaging protocol which guarantees message delivery and message idempotence by using unique identifiers for the messages. The receiver remembers this message for some time to ensure that out of order duplicate data can be detected for that duration. This process is very expensive, and the storage consumption is very high. Rastoge et al. [5] propose a design to address the problem of real-time streaming by achieving exactly once delivery. They attempt to provide solutions to the problems like recovering application state from application restarts, network crashes, etc., and detecting and filtering out of order duplicate data while maintaining a high throughput. In this paper, no new method is discussed to achieve “exactly-once” semantics and it only discusses detecting duplicates after consumption of data. Kafka [6] in their 0.11 release introduced the idempotent producer success- fully achieving exactly once semantics. Duplicate writes were avoided and handled by making the broker failure-resistant using sequence id and producer id in their architecture. The idempotent behavior can be achieved by setting configuration parameter enable idempotence to true. K. Rothermel and M. Strasser [9] proposed a mobile agent technology for various fault-sensitive application areas, including electronic commerce, systems management, and active messaging. They describe a protocol that provides exactly-once semantics of agent execution and additionally reduces the blocking probability of agents by introducing observer nodes for monitoring the progress of agents.



**Kanchana Rajaram et al.,**

METHODOLOGY

For ensuring end to end exactly once semantics, two methods have been proposed. First one is providing a unique ID for each record at the earliest stage of the pipeline and the other one is Check pointing the Kafka stream, which will cause the offsets to be stored.

Unique ID generation

A unique ID for each record at the earliest stage of the pipeline will be the most ideal since there will be a way to uniquely identify each record throughout the entire process. Each producer sends its records to the ID generating service. It appends a unique identifier to each record based on the producer that sends the record. These records are sent to the desired Kafka topic. This Kafka topic acts as a message queue where the records are retained based on a specified retention time. This retention time can be configured in the bin/config/server.properties file. Spark consumes these records and performs the required transformations which makes the records suitable to be stored in Cassandra. These processed micro batches are then sent to the Cassandra database.

In the case of a failure, Kafka would resend the batch of data for which it did not receive the acknowledgement due to the failure. Cassandra will not rewrite this data since it violates the primary key constraint. Records need to be transmitted from Kafka to Spark and further to Cassandra to ensure that duplicates are eliminated because the records are eliminated based on the primary key specified in the Cassandra database. This is an inefficient process.

Record ID = Unique service generating id + Incoming record number from producer.

(Each service has its own id) (The record's count when entered the service)

Each service's output record will have the original incoming record with the ID appended to it. Therefore, any two records will never be the same at any instance in the entire pipeline. Fig. 1 depicts the scenario where after consuming the first four records in Kafka, failure occurs. In this scenario of failure, Spark would consume the items in Kafka from the beginning and will try to write it in the Cassandra database. But Cassandra will not accept the first four records which were already written since, it would violate the primary key constraint

Checkpointing the offsets

When there is an unexpected failure during Spark streaming, storing the point of failure is essential. This would help us start processing from that point instead of reading all the processed records again from the beginning. Checkpoints would be of great help here.

Records in the Kafka partitions are each assigned a sequential identifier called the offset, which is unique for each record within the partition. The offset is an incremental and immutable number, maintained by Kafka. When a record is written to a partition, it is appended to the end of the log, assigning the next sequential offset. One of the methods for storing offsets is Spark Streaming's checkpoint method.

Fault tolerance in checkpointing

Checkpointing the Kafka stream will cause the offsets to be stored in the check- point. If there is a failure, the Spark Streaming application can begin reading the messages from the checkpoint offsets. This would ensure that the data from Kafka is processed by the Spark streaming application exactly once. The offset is never reset because the maximum offset value is so big that we would never reach it. In Fig. 3, a failure occurs after four records have been processed. The checkpoint now stores the offset value for the 5th record indicating that the Spark streaming application needs to start from the 5th record. This will ensure exactly once semantics.

To specify the checkpoint in the streaming application, we use the checkpoint Location parameter option ("*checkpointLocation*", <*checkpoint directory*>) needs to be included in the write Stream to initiate a checkpoint.



**Kanchana Rajaram et al.,**

The parameter “*checkpoint Location*” enables the checkpoint and specifies the location where we keep checkpoint information. The checkpoint information resides in the checkpoint directory specified in the write Stream. The checkpointing method has been deployed as a RESTful service so that any application that requires exactly-once semantics can make use of it and will be discussed in the further sections.

DEVELOPING A SERVICE

In the real time systems, there are different sources of data residing in the database or created on the real time basis. To capture and receive those data into our application we need a communication part between our service and the data source. Hence, RESTful services are used to obtain access to those data. Representational State Transfer (REST) is a software architectural style that uses a subset of HTTP. It is generally used to create an interactive application based on the available services offered by the web. We need to simulate a source point from which the stream data is consumed. A JSON server helps us accomplish this task. This data will further be sent to the Kafka which acts as a hub for incoming stream of data and are processed, transformed as per requirements by the user with exactly once delivery at the destination.

Steps for adapting the created service:

1. Create a JSON server with the required JSON records populated in it. It acts as a data-source point with millions of JSON records. Here instead of the JSON server, any preferred server with the data source API can be replaced.
2. With REST API create an endpoint to consume data using the *HTTP Client* in the extraction module.
3. Capturing the incoming streams of data and parsing activities such as trans- forming into the required format such as CSV and JSON can be done. Later they can be sent to the suitable topic in Kafka.
4. From Kafka topics, the data can be consumed using the Spark Structured streaming with the configurations set up correctly to enable checkpoints to prevent data loss in case of failure.
5. The destination point with suitable database connectivity is provided in *StreamHandler.scala* and the data will get stored upon any failure with exactly-once semantics in Cassandra (NoSQL database). Here, Cassandra is preferred due to its distributed nature.
6. The outcomes of the experiments with enormous amounts of stream data and how the system performs will be examined in the following sections, and on the basis of the findings, recommendations are given.

RESULTS

The experiments were conducted in the Hadoop Cluster environment with one name node and three data nodes. This makes the environment suitable for testing large volumes of streaming records. The unique id generating service and checkpointing methods have experimented with the application failure and their graphical representation of the throughput and latency is compared. The effectiveness of the two methods and their shortcomings are then observed. The proposed systems are evaluated and are exposed to large volumes of data and tested. The following two metrics in web UI are particularly important - Processing Time and Scheduling Delay (under Batch Processing Statistics).

Comparison of Unique ID generation and Checkpointing Methods

It can be seen in Fig. 4 that when the application restarts there is a sudden increase in the latency and the input rows with 300000 records at the initial point implying the processed records being processed again and after some time the regular stream happens. This kind of reprocessing increases the latency as shown in Fig. 5 and affects the performance. The main reason for high latency is too much data in each batch during structured stream processing

Analysis for large volumes of data

Getting the stream data for large volumes is necessary to test and obtain effective values. In real-time there will be huge volumes of data coming from different points and these are lakhs of records per second in general. Hence, it is essential to simulate the stream data in huge amounts and get the appropriate values for performing analysis. The

57603



**Kanchana Rajaram et al.,**

values are recorded starting from 4 lakhs records, followed by 20 lakhs and then 50 lakhs records. The tabulated results are given below. The insights after analyzing the structured stream processing of four lakh records are recorded and tabulated as follows. The values in the table are rounded off to the whole number for clear understanding.

The following inferences are made from the Table 1:

1. When the trigger time is set to 0 seconds the input rate equals the spark process rate and the latency is as minimum as 200ms.
2. After the gradual increase in the trigger time the number of records getting processed after each trigger drastically increases to 90000 records/s and this causes the latency to increase to a maximum of 900ms.

The following inferences are made from the Table 2:

1. When the trigger time is set to 0 seconds the input rate equals the spark process rate and the latency is as minimum as 160ms.
2. After the gradual increase in the trigger time the number of records getting processed after each trigger drastically increases to 1,30,000 records/s and this causes the latency to increase to a maximum of 650ms.

The following inferences are made from the Table 3:

1. When the trigger time is set to 0 seconds the input rate equals the spark process rate and the latency is as minimum as 150ms.
2. After the gradual increase in the trigger time the number of records getting processed after each trigger drastically increases to 1,10,000 records/s and this causes the latency to increase to a maximum of 540ms.

From the above tables, it can be observed that, the input rate decreases as the process rate increases due to the load in processing such a large number of records. The suitable trigger processing time can be seen as 2 seconds, and it need to be found out for the specific requirements of input rate with experimentation.

BENCHMARK

The appropriate delay and process rate can be produced with the desired volume of input data and the trigger time using the parameters discovered through trial. This system testing must be carried out before any large amounts of data are streamed. From table 4, it can be seen that varying the parameter values produces a significant change in latency and process rate. The required latency can be mapped to the above table, and the parameter values in the designed system can be set accordingly. The methods for obtaining the experimentation results were described in depth throughout the paper.

CONCLUSION

A method of checkpointing in stream data processing in the ETL pipeline in a distributed cluster environment has been successfully implemented to achieve exactly-once semantics throughout the different components starting from data source to the desired destination such as a database. Further, the performance analysis of the records that are being streamed with large volumes of data along with induced failures has been recorded and exactly-once delivery has been verified at the end point. The checkpointing method has been deployed as a RESTful service so that any application that requires exactly-once semantics can make use of it. As a future work, Amazon EMR (Amazon Elastic MapReduce), a cloud big data platform can be used for running distributed data processing jobs. Amazon EMR provides flexibility to scale your cluster up or down as per the changing computing requirements. We could scale up the number of nodes in the cloud for performing parallel data processing combined with various source points and multiple message queues in the pipeline.





Kanchana Rajaram et al.,

REFERENCES

1. Kaushik Dutta, Debra E. VanderMeer, Anindya Datta, and Krithi Ramamritham (2001). "User Action Recovery in Internet SAGAs (ISAGAs)". In Proceedings of the Second International Workshop on Technologies for E-Services. Springer- Verlag, Berlin, Heidelberg, 132–146.
2. G. van Dongen and D. V. D. Poel (2021), "A Performance Analysis of Fault Recovery in Stream Processing Frameworks," in IEEE Access, vol. 9, pp. 93745-93763, doi: 10.1109/ACCESS.2021.3093208.
3. Yongqiang Huang and H. Garcia-Molina (2001), "Exactly-once semantics in a replicated messaging system," Proceedings 17th International Conference on Data Engineering, pp. 3-12, doi: 10.1109/ICDE.2001.914808.
4. Jeremy Brown, J. P. Grossman, and Tom Knight (2002). "A lightweight idempotent messaging protocol for faulty networks", In Proceedings of the fourteenth annual ACM symposium on Parallel algorithms and architectures, SPAA '02, New York, NY, USA.
5. Rastogi, Avnish & Malik, Naveen & Hooda, Sakshi (2018). "Exactly-Once Semantics with Real-Time Data Pipelines". DOI:10.1007/978-981-10-7386-1_26.
6. Matthias J Sax, (2017) "Introducing Exactly Once Semantics in Kafka" <https://databricks.com/session/introducing-exactly-once-semantics-in-apache-kafka>.
7. Spark Streaming Spark Streaming - Spark 2.1.2 Documentation <https://www.overleaf.com/project/628dfb3684ad06d2bf3172bd>
8. Akidau, T., Balikov, A., Bekiroğlu, K., Chernyak, S., Haberman, J., Lax, R., ... & Whittle, S. (2013). Millwheel: Fault-tolerant stream processing at internet scale. Proceedings of the VLDB Endowment, 6(11), 1033-1044.
9. K. Roethermel and M. Strasser (1998), "A fault-tolerant protocol for providing the exactly-once property of mobile agents", Proceedings Seventeenth IEEE Symposium on Reliable Distributed Systems (Cat. No.98CB36281), pp. 100-108, doi: 10.1109/RELDIS.1998.740480.
10. Parul Arora, Rajwinder Singh (2015) "Improved checkpoint mechanism in mobile agent systems for information retrieval applications", 2nd International Conference on Computing for Sustainable Global Development (INDIACom), pp.667-671.
11. Dimson, T., & Ganjoo, M. (2014). Hailstorm: "Distributed Stream Processing with Exactly Once Semantics" CS 240 h Final Project.
12. Neha Narkhade (2017), "Exactly-once Semantics are Possible: Here's How Kafka Does it", <https://www.confluent.io/blog/exactly-once-semantics-are-possible-heres-how-apache-kafka-does-it>.
13. Tathagata Das (2015). "Improved Fault-tolerance and Zero Data Loss in Apache Spark Streaming", <https://databricks.com/blog/2015/01/15/improved-driver-fault-tolerance-and-zero-data-loss-in-spark-streaming.html>
14. W. Zhu, H. Chen and F. Hu (2016), "ASC: Improving spark driver performance with automatic spark checkpoint," 18th International Conference on Advanced Communication Technology (ICACT), 2016, pp. 607-611, doi: 10.1109/ICACT.2016.7423490.
15. R. Gioiosa, J. C. Sancho, S. Jiang and F. Petrini (2005), "Transparent, Incremental Checkpointing at Kernel Level: a Foundation for Fault Tolerance for Parallel Computers," SC '05: Proceedings of the 2005 ACM/IEEE Conference on Super-computing, pp. 9-9, doi: 10.1109/SC.2005.76.
16. S. Dhingra, S. Sharma, P. Kaur and C. Dabas (2017), "Fault tolerant streaming of live news using multi-node Cassandra," 2017 Tenth International Conference on Contemporary Computing (IC3), pp. 1-5, doi: 10.1109/IC3.2017.8284310.
17. R. K. L. Ko, M. Kirchberg, B. S. Lee and E. Chew (2012), "Overcoming Large Data Transfer Bottlenecks in RESTful Service Orchestrations," 2012 IEEE 19th International Conference on Web Services, pp. 654-656, doi: 10.1109/ICWS.2012.107.
18. R. Cao and J. Gao (2018), "Research on reliability evaluation of big data system," 2018 IEEE 3rd International Conference on Cloud Computing and Big Data Analysis (ICCCBDA), pp. 261-265, doi: 10.1109/ICCCBDA.2018.8386523.





Kanchana Rajaram et al.,

19. Spark Streaming + Kafka Integration Guide.<https://spark.apache.org/docs/latest/streaming-kafka-0-8-integration.html>

Table 1. Observation of 4 lakh records in structured stream processing with varying trigger processing time.

Trigger processing time (s)	Input rate (records/s)	Process rate (records/s)	Input rows (records)	Batch duration (ms)
0s	13000	13000	1500	200
1s	13000	30000	15000	287
2s	13000	55000	20000	280
5s	8000	80000	40000	720
7s	7000	90000	55000	900

Table 2. Observation of 20 lakh records in structured stream processing with varying trigger processing time.

Trigger processing time (s)	Input rate (records/s)	Process rate (records/s)	Input rows (records)	Batch duration (ms)
0s	4500	4500	630	160
1s	10000	50000	9000	200
2s	9500	67000	20000	250
5s	9000	120000	42000	450
7s	8000	130000	58000	650

Table 3. Observation of 50 lakh records with varying trigger processing time.

Trigger processing time (s)	Input rate (records/s)	Process rate (records/s)	Input rows (records)	Batch duration (ms)
0s	6500	6500	690	150
1s	8500	37000	8200	200
2s	8000	53000	14000	300
5s	8700	100000	38000	450
7s	7000	110000	58000	540

Table 4. Recommendations from the observations

Batch duration(ms)	Process rate(records/s)	Volume of Records (lakhs)	Trigger processing time(s)
200	13000	4	0s
280	55000	4	2s
900	90000	4	7s
160	4500	20	0s
250	67000	20	2s
650	130000	20	7s
150	6500	50	0s
300	53000	50	2s
540	110000	50	7s





Kanchana Rajaram et al.,

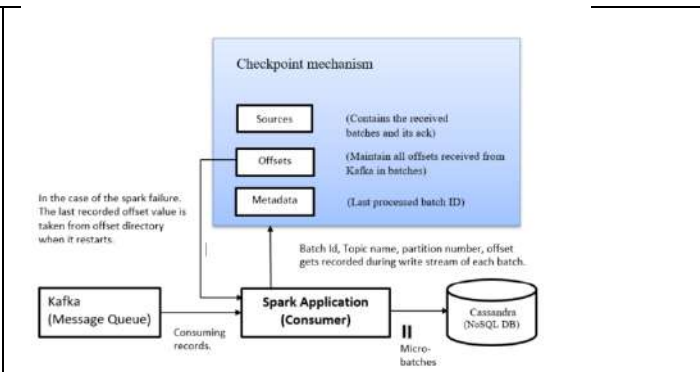
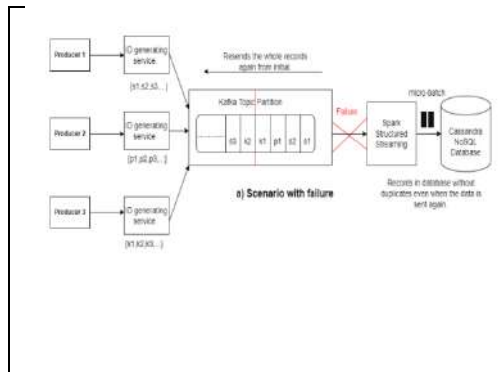


Fig. 1. Scenarios in Unique ID generation

Fig. 2. Components and files involved in Checkpointing

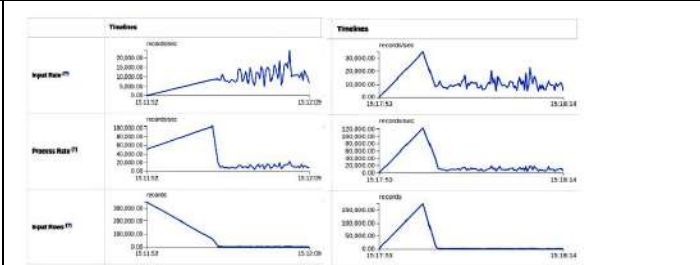
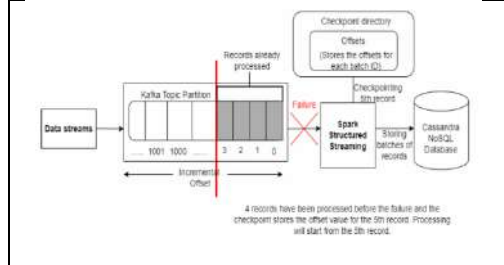


Fig. 3. Scenarios in Checkpointing the offsets

Fig. 4. Comparison of throughput between unique id generation and checkpointing.

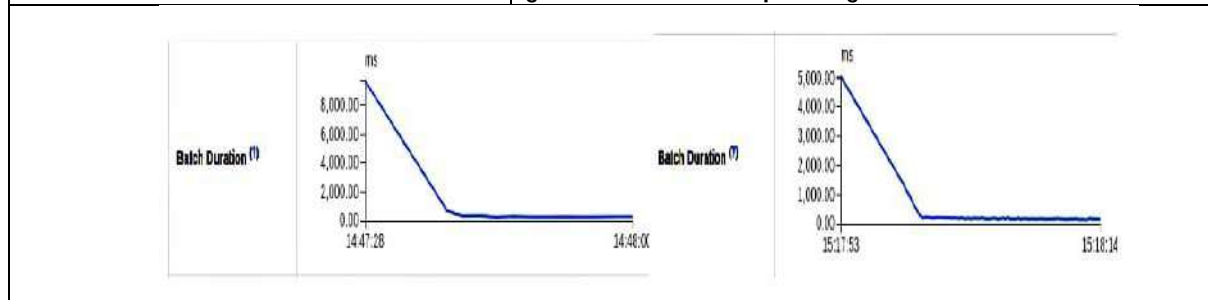


Fig. 5. Comparison of latency between unique ID generation and checkpointing.





***In-vivo* Toxicological Evaluation of Tiktakam Kashayam**

Rajinikanth B¹, Perumal Pandurangan^{2*}, Ayisha H³, Fahmitha AK³, Hanna AN³ and Sumy Susan Biju³

¹Professor and HoD, Department of Pharmacology, Nirmala College of Health Science, Meloor, Thrissur, Kerala-680 311, India.

²Dean Research, Sri Shanmugha College of Pharmacy, Sankari, Salem- 637304, Tamil Nadu, India.

³Fourth year students, Grace College of Pharmacy, Palakkad, Kerala-678 001, India.

Received: 15 Feb 2023

Revised: 25 Apr 2023

Accepted: 30 May 2023

***Address for Correspondence**

Perumal Pandurangan

Dean Research,
Sri Shanmugha College of Pharmacy,
Sankari, Salem- 637304,
Tamil Nadu, India.
E.Mail: perupharma78@gmail.com



This is an Open Access Journal / article distributed under the terms of the **Creative Commons Attribution License** (CC BY-NC-ND 3.0) which permits unrestricted use, distribution, and reproduction in any medium, provided the original work is properly cited. All rights reserved.

ABSTRACT

“TIKTAKAM KASHAYAM” is evaluated by *in-vivo* acute and sub-acute toxicity study. There was no mortality recorded at a dose of 2000mg/kg of ayurvedic formulation of “TIKTAKAM KASHAYAM” in acute toxicity studies. In sub-acute toxicity studies-serum analysis, histopathological analysis showing toxicity in low dose (100 mg/kg) and high dose (200 mg/kg). The ayurvedic formulation “TIKTAKAM KASHAYAM” possesses anti-inflammatory activity and will be beneficial for the treatment of inflammatory bowel disease.

Keywords: Ayurvedic formulation, *Piper longum*, *Azadiracta indica*, Inflammatory bowel disease, hepatotoxicity.

INTRODUCTION

INFLAMMATORY BOWEL DISEASE

Inflammatory bowel disease (IBD) is a chronic and life-long disease characterized by gastro intestinal tract inflammation. [1] It is a group of chronic idiopathic inflammatory disease of the gastrointestinal tract with symptoms evolving in a relapsing and remitting manner.[2] . It occurs in genetically susceptible individuals after an exaggerated immune response to a normal stimulus such as food and intestinal flora.[3] Inflammation anywhere along the digestive tract interferes with this normal process. IBD can be very painful and disruptive. In rare cases, it may even be life threatening [4]. This inflammatory condition encompasses two major forms, known as: Ulcerative colitis(UC), Crohn’s disease[5]



**Rajinikanth et al.,****AYURVEDIC FORMULATION**

Ayurveda, the traditional Indian medicinal system remains the most ancient yet living traditions with sound philosophical and experimental basis. It is a science of life with a holistic approach to health and personalized medicine. It is known to be a complete medical system that comprised physical, psychological, philosophical, ethical, and spiritual health.[6],[7] In Ayurveda, each cell is considered to be inherently an essential expression of pure intelligence hence called self-healing science. In addition, to the self-healing concept, the use of herbal treatment is equally important in this Indian traditional system of medicine. According to the World Health Organization, about 70–80% of the world populations rely on nonconventional medicines mainly of herbal sources in their healthcare. Public interest for the treatment with complementary and alternative medicine is mainly due to increased side effects in synthetic drugs, lack of curative treatment for several chronic diseases, high cost of new drugs, microbial resistance, and emerging diseases, etc. [13]. According to Indian mythological concept Ayurveda originated from Brahma, the God of Creation. Hindu myth says that, Brahma wants to ease the sufferings of his creation by transferring the knowledge of Ayurveda to deities. Dhanvantari was one of those deities, who then transferred this knowledge of science to modern world. Dhanvantari is considered as “Father of Ayurveda”. The last of the ‘Great Three’ of Ayurveda Astanga hrdaya was composed by Vagbhata. Every living and non-living entity is constituted by five primordial principles or mahabhoota Prithvi, Jala, Theja, Agni and Vayu. The tissues of the body are also composed of these five elements and their derivatives (Bhusan Patwardhan, 2009). This identity of composition is the central principle of ayurvedic therapeutics which mandates the choice of drugs and food without causing side effects [8]. Moreover *In-silico* and *in-vitro* toxicological evaluation of Tiktakam kashayam was published [9].

AYURVEDIC FORMULATION FOR IBD: [8] are Tiktakam kashyam, Guluchayadi kashayam, Nyagrodhadhi kashayam, Mahatiktakam kashayam, Laksha choornam, Lodhra choornam, Setubandham choornam, Astakashari gullika, Tiktakam kashayam:Tiktakam kashayam is a Ayurvedic formulation for IBD having the following ingredients is shown in the table no1 and its chemical constituents is listed in table no 2.

Based on the above complete review *In-vivo* toxicological evaluation of the compounds present in “TIKTAKAM KASHAYAM”. Acute toxicity evaluation of the formulation “TIKTAKAM KASHAYAM” in *Swiss albino* mice. Sub-acute toxicity evaluation of the formulation “TIKTAKAM KASHAYAM” in *Swiss albino* mice.

MATERIALS AND METHODS**Materials and Instruments**

All the chemicals were purchased from Thermo fisher scientific, Bilirubin kit, Urea kit, Creatinine kit, Glucose kit from AGAPPE diagnostics Ltd. Eosin, OG6, EA36 from Merck. Centrifuge from REMI, Refrigerator from Whirlpool, Electronic weighing balance from WENSAR, Semi auto analyzer and Micro pipettes from MISPAVIVA, Dissection box from Camel.

METHODS**IN-VIVO TOXICITY STUDIES: [GCP/IAEC/22(1)P1]****Acute toxicity: [10],[11]**

The selected ayurvedic formulation 2000mg/kg administered to 3 female mice in a single by gavage using oral feeding needle. The mice should be fasted 3 hr prior to dosing (food was withheld but not water). During the period of fasting, mice are weighed and test sample is administered. After test sample administration, food was withheld for 2 hr. Animals were observed individually after dosing at least once during first 30 minutes. Periodically during first 24hrs, with special attention given to the first 4hr, and daily thereafter, for a total of 14 days.





Rajinikanth et al.,

Sub-acute toxicity: [12]

The animals were divided into 5 groups. There were 10 animals (5 males 5 females) in each group. The group I served as vehicle control. Group II, III, IV received low, medium and high dose of medicine respectively for 28 days. All the animals of group I-IV were sacrificed on 29th day.

Study parameters

Toxic manifestation like alteration in food or water intake, weight loss, mobility, respiration pattern, response to handling, salivation, piloerection were studied on day 0 and every week thereafter. Blood samples were collected from all animals after terminal sacrifice. Haematological and biochemical parameters viz. urea, bilirubin, creatinine (CRE), random blood sugar (RBS). Biochemical parameter studied using commercially available kits.

Necropsy: Body orifices and organs of all animals are carefully observed after dissection for morphological and pathological changes. Wet weight of liver, kidney recorded for all animals.

Histopathology

Tissue samples from various organs of all animals were preserved in 10% formalin saline and will be studied for pathological changes.

RESULTS AND DISCUSSION**IN-VIVO TOXICITY STUDIES****ACUTE TOXICITY STUDIES**

The acute toxicity study shows that the observation of toxicity signs in mice in the region of CNS particularly in motor activity, respiratory center, cardiovascular center. There is no positive observation sign recorded and detailed clinical observation is shown in the table no 5. The animal body weight, feed consumption, water consumption, general observation was made daily basis. The physical examination such as salivation onset quantity, ophthalmologic examination, respiratory rate, biting behavior, lacrimation etc was observed daily basis. Moreover cage side observation was also made daily such as home cage activity, feces color, consistency, quantity and urine color.

MORTALITY RECORD

Mortality is the main criteria in assessing acute toxicity (LD 50) of any drugs. There was no mortality recorded and shown in the table No.6 at a dose of 2000mg/kg of the ayurvedic formulation "TIKTAKAM KASHAYAM" the LD 50 of the formulation as per OECD guidelines fall under category (LD 50 >2000mg/kg). All observations are symmetrically recorded.

SUB ACUTE TOXICITY**Serum analysis****Urea**

As a part of sub-acute toxicity studies, serum parameters were calculated. Serum urea result shown in the table No. 7 and graphical representation shown in figure: 1. The control group animal serum analysis shown 50.54 ± 1.58 and low dose of animal serum urea is 44.95 ± 5.5 , therapeutic dose treated animal serum concentration was 58.00 ± 1.0 . High dose treated animal serum concentration shown 64.04 ± 1.7 produced significant ($P < 0.001$) while comparing with control animals. From the above results serum urea is elevated only in high dose treated animal groups.

Creatinine

Serum creatinine results were tabulated in table No.8 and graphical representation shown in the figure: 2. The control group animal shows 0.18 ± 0.02 , low dose animal group shows 0.22 ± 0.01 produced no significant compare with



**Rajinikanth et al.,**

control. Therapeutic dose show 0.29 ± 0.01 and high dose 0.41 ± 0.01 produced significant ($P < 0.001$) while compare with control group. Serum creatinine levels were elevated in both therapeutic and high dose.

Bilirubin

Serum bilirubin result was shown in the table No.9 and graphical representation shown in figure: 3. Control animal show 1.10 ± 0.05 and low dose animal shows serum bilirubin level 1.25 ± 0.01 , and therapeutic dose shown 1.19 ± 0.03 produced no significant while compare with control groups. High dose treated animal groups showing elevated levels of bilirubin 1.60 ± 0.11 while comparing with control animal group (** $P < 0.01$)

Serum glucose

Serum glucose level results were shown in the table No.10 and graphical representation shown in figure: 4. Control animal shows glucose level as 74.23 ± 5.77 , low dose treated animal shows 71.03 ± 5.74 , therapeutic dose shows 89.05 ± 5.71 produced no significant while comparing to control group. High dose treated animal showing elevated level of glucose levels 109.0 ± 5.77 while compared to normal control group (** $P < 0.001$).

Organ weight: Kidney weight

There are no significant changes in the kidney weight among the various treated groups are shown in figure. 5. Low dose, therapeutic dose, and high dose produce no significant while comparing with the normal control group is shown in table. 11.

Liver weight

Similarly there is no significant change in liver weight is shown in figure. 6. Low dose, therapeutic dose, high dose treated animals produced no significant while comparing with normal control group is shown in table. 12.

Body weight

Body weight were measured 0,7th, 14th, 21st and 28th days is shown in figure. 7. The result shown there is no significant change in body weight while comparing with normal control group animals are shown in table. 13.

Histopathology**Control Animal****Liver**

Histopathological examination of liver from control group revealed normal architecture of hepatic parenchyma is shown in figure. 8 (H&E, 400X).

Kidney

Histopathological evaluation of kidney from control group revealed normal architecture of renal tubules are shown in figure. 9 (H&E, 400).

Half dose animal**Liver**

Histopathological examination of liver from half dose group revealed normal architecture of hepatic parenchyma is shown in figure. 10 (H&E, 400).

Kidney

Histoathological examination of kidney from half dose group revealed normal architecture of renal tubules in cortex and medulla is shown in figure. 11 (H&E, 400)



**Rajinikanth et al.,****Therapeutic dose animal****Liver**

Histopathological examination of liver from therapeutic dose group revealed severe degeneration of the hepatic parenchyma characterized by granular appearance and diffuse micro vesiculation of hepatocytes are shown in figure. 12 (H&E, 400).

Kidney

Histopathological examination of kidney from therapeutic dose revealed diffuse tubular injury characterized by intact vacuolated (moderate) epithelial cells and necrotic (severe) epithelial cells with pyknotic nuclei is shown in figure. 13 (H&E, 400).

High dose animal**Liver**

Histopathological examination of liver from high dose revealed severe degeneration and micro vesiculation of hepatocytes are shown in figure. 14 (H&E, 400).

Kidney

Histopathological examination of kidney from high dose group revealed tubular injury characterized by severe necrosis in epithelial cells are shown in figure. 15 (H&E, 400).

CONCLUSION

Based on present study results we concluded that there was no mortality recorded at a dose of 2000mg/kg of there was no mortality recorded at a dose of 2000mg/kg of ayurvedic formulation . TIKTAKAM KASHAYAM" in acute toxicity studies. In sub-acute toxicity studies-serum analysis, histopathological analysis showing toxicity in therapeutic dose (100 mg/kg) and high dose (200 mg/kg). The ayurvedic formulation "TIKTAKAM KASHAYAM" possess anti-inflammatory activity and will be beneficial for the treatment of inflammatory bowel disease. Further studies are required to fix the proper dose levels to avoid the long term toxicity.

REFERENCES

1. Yeshi K, Ruscher R, Hunter L, Daly NL, Loukas A, Wangchuk P. Revisiting inflammatory bowel disease: pathology, treatments, challenges and emerging therapeutics including drug leads from natural products. *Journal of clinical medicine*. 2020 May; 9(5):1273.
2. Piovani D, Danese S, Peyrin-Biroulet L, Nikolopoulos GK, Lytras T, Bonovas S. Environmental risk factors for inflammatory bowel diseases: an umbrella review of meta-analyses. *Gastroenterology*. 2019 Sep 1; 157(3):647-59.
3. Colombel JF, Shin A, Gibson PR. AGA clinical practice update on functional gastrointestinal symptoms in patients with inflammatory bowel disease: Expert review. *Clinical Gastroenterology and Hepatology*. 2019 Feb 1;17(3):380-90.
4. Vedamurthy A, Ananthkrishnan AN. Influence of environmental factors in the development and outcomes of inflammatory bowel disease. *Gastroenterology & hepatology*. 2019 Feb;15(2):72-84.
5. Marc Fakhoury, Rebecca Negrulj, Inflammatory Bowel Disease: Clinical Aspects And Treatments, *Journal Of Inflammation Research*, 2014;7: 113-120.
6. Oistein Hovde, epidemiology and clinical course of crohn's disease: results from observational studies, *world journal of gastroenterol*. 2012Apr21; 18(15): 1723- 1731.
7. Ashutosh Chauhan et al, Ayurvedic Research and Methodology: Present Status and Future Stratagies. *Ayu* 2015 Oct-Dec; 36(4):364-369.





Rajinikanth et al.,

8. Semwal DK, Mishra SP, Chauhan A, Semwal RB. Adverse health effects of tobacco and role of Ayurveda in their reduction. Journal of Medical Sciences. 2015 Apr 1; 15(3):139.
9. Perumal Pandurangan* and B Rajinikanth. *In-silico* and *in-vitro* toxicological evaluation of Tiktakam kashayam . International Journal of Ayurvedic Medicine. 2022; 13(3):783-791. (WoS). DOI: <https://doi.org/10.47552/ijam.v13i3.3016>
10. Ramachandran S, B. Rajinikanth,A.Rajasekaran,K.T Manisenthil Kumar. Evaluation of Anti- Inflammatory and Analgesic Potential of Methanol Extract of Tectona Grandis Flowers Asian Pacific Journal of Tropical Biomedicine, 2011:S155-S158.
11. OECD Guideline For Testing of Chemicals (423): Acute Oral Toxicity- Acute Toxic Class Method, 2001:1-14.
12. OECD Guidelines for the Testing of Chemicals (407): Repeated Dose 28-Day Oral Toxicity Study in Rodents, 2008: 1-13.

Table.1- Ingredients of Tiktakam Kashayam

SL.NO	OFFICIAL NAME	BOTANICAL NAME	QUANTITY
1.	Patola	<i>Trichosanthes lobata</i>	1.425g
2.	Nimba	<i>Azadiracta indica</i>	1.425g
3.	Katuka	<i>Neopicrorhiza scrophulariiflora</i>	1.425g
4.	Darvi	<i>Berberis aristata</i>	1.425g
5.	Patha	<i>Cyclea peltata</i>	1.425g
6.	Duralabha	<i>Trgia involucrata</i>	1.425g
7.	Parpata	<i>Hedyotis corymbosa</i>	1.425g
8.	Trayamana	<i>Gentiana kurro</i>	1.425g
9.	Musta	<i>Cyperus rotundus</i>	1.425g
10.	Bhunimba	<i>Swertia chirayita</i>	1.425g
11.	Kalinga	<i>Wrightia antidysenterica</i>	1.425g
12.	Kana	<i>Piper longum</i>	1.425g
13.	Chandana	<i>Santalum album</i>	1.425g

Table.2 Composition and Constituents Present In Tiktakam Kashayam Ayurvedic Formulation

SL.NO	PLANT NAME	CONSTITUENTS
1	<i>Trichosanthes lobata (patola)</i>	<ol style="list-style-type: none"> 1. Octanoic acid 2. Dodecanoic acid 3. Octadecane 4. Enoic acid 5. Hexanoic acid 6. Quinazolin-8-one 7. Illicic acid 8. Pentadecanoic acid 9. Oxaspiro 10. Benzene acetic acid 11. 3 Beta-cucurbita-5,24-dien-3-ol 12. Alpha carotene 13. Beta carotene 14. Lycopene 15. Lutein 16. Ascorbic acid 17. Beta- sitosterol



Rajinikanth *et al.*,

2	<i>Azadirachta indica (Nimba)</i>	<ol style="list-style-type: none"> 1. Nimbn 2. Quercetin 3. Ascorbic acid 4. Azadirachtin 5. Salanin 6. N-hexacosanol 7. Beta-sitosterol 8. Nimbidin 9. Nimbinene 10. Nimbolide 11. Nimbolinin 12. Nimbandiol 13. Meliantriol 14. Gedunin 15. Azadiradione 16. Azadirone 17. Scopoletin 18. Rutin 19. Myricetin 20. Vilasinn 21. Behenic acid
3	<i>Neopicrorhiza scrophulariflora (katuka)</i>	<ol style="list-style-type: none"> 1. Picroside IV 2. Specioside 3. Verminoside 4. Aucubin 5. Abeloside A 6. Sweroside 7. Picrorhizaoside 8. Cinnamic acid 9. Scrophuloside 10. 7-Hydroxy coumarin 11. Hebitol III 12. Galic acid 13. Isoferulic acid 14. Vanillic acid 15. Hexacosanol
4	<i>Berberis aristata (Darvi)</i>	<ol style="list-style-type: none"> 1. Taxilamine 2. Palmatine 3. Oxyberbine 4. Tetrahydrodropimatine
5	<i>Berberis aristata (Darvi)</i>	<ol style="list-style-type: none"> 5. Taxilamine 6. Palmatine 7. Oxyberbine 8. Tetrahydrodropimatine 9. Taxilamine 10. Palmatine 11. Oxyberbine 12. Tetrahydrodropimatine 13. Jatrorhizine





Rajinikanth et al.,

		14. Pakistanine
6	<i>Cyclea peltata (patha)</i>	<ol style="list-style-type: none"> 1. Cyclea peltin 2. Cycleadrine 3. Cycleonorine 4. Cycleohomine chloride 5. Cycleocurine
7	<i>Tragia involucrata (Duralabha)</i>	<ol style="list-style-type: none"> 1. 2,4-dimethyl hexane 2. 2,4-dimethyl heptane 3. 2-methyl nonane 4. Friedelan-3-one 5. Rutin 6. Quercetin 7. Stigmasterol
8	<i>Hedyotis corymbosa (parpata)</i>	<ol style="list-style-type: none"> 1. Geniposide 2. Asperuloside 3. Rutin 4. Aspenicosidic acid 5. Scendoside methyl ester 6. Oleanolic acid 7. Y-sitosterol 8. 6-alpha hydroxy geniposide 9. Iridoid glycoside 10. Biflorine
9	<i>Gentiana kurro (trayamanna)</i>	<ol style="list-style-type: none"> 1. Sweroside 2. Gentiopicroside 3. Amarogentin 4. Robinetino 5. Luteolin 6. Apigenin 7. Swertiamarin
10	<i>Cyperus rotundus</i>	<ol style="list-style-type: none"> 1. 2-cyperone 2. Cyperone 3. Cyperotundone 4. Cyperol 5. Beta selinene 6. Isocyperol 7. Sitosterol 8. Valerenal 9. Sugeonyl acetate 10. 2-copaene 11. Kobusone 12. Isokobusone 13. Suganol 14. Beta caryophyllene 15. Sugetnol
11	<i>Swertia chirayita (bhunimba)</i>	<ol style="list-style-type: none"> 1. Gentiopicrin 2. Sweroside 3. Swertiamarin





Rajinikanth et al.,

		4. Amerogentin
12	<i>Wrightia antidysenterica (kalinga)</i>	1. Stigmasterol 2. Campesterol 3. Indigo 4. Idirubin 5. Isatin 6. Methyl anthranilate 7. Rutin 8. Cyclo arthrenone 9. Alpha amyryn 10. Beta amyryn 11. Beta sitosterol 12. 14-alpha methyl zymosterol
13	<i>Piper longum (kana)</i>	1. Piperine 2. Pipperitin 3. Piperlongumin 4. Piplartin 5. Guineensine 6. Pellitorine 7. Brachystamide B
14	<i>Santalum album (chandhana)</i>	1. Alpha santalene 2. Beta santalene 3. epi beta santalene 4. Z-alpha santalol 5. Z-alpha trans bergamotol

Table.3 Experimental design for acute toxicity study

SL.NO	ANIMAL(STRAIN)	MALE	FEMALE	TOTAL
1	Swiss Albino mice	0	6	6

Table.4 Experimental design for sub-acute toxicity study

TYPE OF STUDY	STUDY GROUP	MALE	FEMALE	TOTAL
SUB-ACUTE TOXICITY	Control	5	5	10
	Therapeutic dose	5	5	10
	Half the therapeutic dose	5	5	10
	Higher therapeutic dose	5	5	10
	Satellite group	10	10	20
TOTAL	-	-	-	60





Rajinikanth et al.,

Table 5: Observation of toxicity sign in mice

Clinical Observation	Organs, Tissue Or System Most Likely To Be Involved	Observed signs
RESPIRATORY Blockade in the nostrils, change in the rate and depth of breathing, changes in color of body surface		
Dyspnea 1. Abdominal breathing 2. Gaspings	1. CNS respiratory center, paralysis of coastal muscle, cholinergic inhibition 2. CNS respiratory center, pulmonary edema, secretion accumulation in airways (increase cholinergic)	Nil
Apnea	CNS respiratory center, pulmonary cardiac insufficiency	Nil
Tachypnea	CNS respiratory center, pulmonary cardiac insufficiency	Nil
Nostril discharges	Pulmonary edema, hemorrhage	Nil
MOTOR ACTIVITY Change in frequency and nature of movements		
Increase motor activity	Somatomotor, CNS	Nil
Decrease motor activity	Somatomotor, CNS	Nil
Somnolence	CNS sleep center	Nil
Loss of righting reflex	CNS, sensory neuromuscular,	Nil
Catalepsy	CNS. Sensory, neuromuscular, autonomic	Nil
Ataxia	CNS, Sensory, autonomic	Nil
Unusual locomotion	CNS, sensory, autonomic	Nil

Clinical Observation	Organs, Tissue or System Most Likely to be Involved	Observed signs
CONVULSION (SEIZURE)		
Clonic convulsion	CNS, Respiratory failure, Neuromuscular, Autonomic	Nil
Tonic convulsion	CNS, Respiratory failure, Neuromuscular, Autonomic	Nil
Tonic- clonic convulsion	CNS, Respiratory failure, Neuromuscular, Autonomic	Nil
REFLEXES		
Corneal (eyelid closure)	Sensory, Neuromuscular	Normal
Pinnal	Sensory, Neuromuscular, Autonomic	Normal
Righting	CNS, Sensory, Neuromuscular	Normal
OCULAR SIGN		
Lacrimation	Autonomic	Nil
Miosis	Autonomic	Nil
Mydriasis	Autonomic	Nil
Ptosis	Autonomic	Nil
CARDIOVASCULAR SIGNS		
Bradycardia	Autonomic, Pulmonary- cardiac insufficiency	Nil

57617





Rajinikanth *et al.*,

Tachycardia	Autonomic, Pulmonary- cardiac insufficiency	Nil
SALIVATION		
Excessive secretion of saliva	Autonomic	Nil

Clinical Observation	Organs, Tissue Or System Most Likely To Be Involved	Observed Signs
SKIN		
Edema	Irritation, renal failure, tissue damage, long term immobility	Nil
Erythema	Irritation, inflammation, sensitization	Nil
Skin and fur	Colour and condition	Normal
PILOERECTION		
Contraction of erectile tissue for hair follicle	Autonomic	Nil
MUSCLE TONE		
Hypertonia	Autonomic	Nil
Hypotonia	Autonomic	Nil
GASTRO INTESTINAL SIGNS		
Dropping (feces) a. Solid b. Dried c. Scant	Autonomic, GI motility, constipation	Normal
Emesis	Vomiting and retching	Nil
Diuresis a. Red urine (Hematuria) b. Involuntary urination	A. Damage in kidney B. Autonomic, sensory	Normal

Table 6: Mortality record

GROUP	GROUP-I			GROUP-II		
	1	2	3	1	2	3
Animal Number						
Sex	FEMALE	FEMALE	FEMALE	FEMALE	FEMALE	FEMALE
Hour 1	Nil	Nil	Nil	Nil	Nil	Nil
Hour 2	Nil	Nil	Nil	Nil	Nil	Nil
Hour 3	Nil	Nil	Nil	Nil	Nil	Nil
Hour 4	Nil	Nil	Nil	Nil	Nil	Nil
Day 1	Nil	Nil	Nil	Nil	Nil	Nil
Day 2	Nil	Nil	Nil	Nil	Nil	Nil
Day 3	Nil	Nil	Nil	Nil	Nil	Nil
Day 4	Nil	Nil	Nil	Nil	Nil	Nil
Day 5	Nil	Nil	Nil	Nil	Nil	Nil
Day 6	Nil	Nil	Nil	Nil	Nil	Nil





Rajinikanth et al.,

Day 7	Nil	Nil	Nil	Nil	Nil	Nil
Day 8	Nil	Nil	Nil	Nil	Nil	Nil
Day 9	Nil	Nil	Nil	Nil	Nil	Nil
Day 10	Nil	Nil	Nil	Nil	Nil	Nil
Day 11	Nil	Nil	Nil	Nil	Nil	Nil
Day 12	Nil	Nil	Nil	Nil	Nil	Nil
Day 13	Nil	Nil	Nil	Nil	Nil	Nil
Day 14	Nil	Nil	Nil	Nil	Nil	Nil
Mortality	0/3			0/3		

Table 7: Serum analysis-Urea

SL NO.	TREATMENT	UREA RANGE Mean± sem	ANALYSIS
1	Control	50.54 ±1.58	-
2	Low dose(50 mg/kg, Oral)	44.95 ±5.5	Not significant
3	Therapeutic dose (100mg/kg, Oral)	58.00±1.7	Not significant
4	High dose(200 mg/kg, Oral)	64.04±1.7	Significant**
NORMAL RANGE- 10-50mg/Dl			

Table 8: serum analysis-Creatinine

SL NO.	TREATMENT	CREATININE RANGE Mean± sem	ANALYSIS
1	Control	0.18± 0.02	-
2	Low dose(50mg/kg, Oral)	0.22 ±0.01	Not significant
3	Therapeutic dose(100 mg/kg, Oral)	0.29 ±0.01	Significant**
4	High dose(200 mg/kg, Oral)	0.41 ±0.01	Significant***
NORMAL RANGE-0.5-1mg/dL			

Table 9: Serum analysis-Bilirubin

SL NO.	TREATMENT	BILIRUBIN RANGE Mean ±sem	ANALYSIS
1	Control	1.10 ±0.05	-
2	Low dose (50mg/kg, Oral)	1.25 ±0.01	Not significant
3	Therapeutic dose(100 mg/kg, Oral)	1.19 ±0.03	Not significant
4	High dose(200 mg/kg, Oral)	1.60 ±0.11	Significant**
NORMAL RANGE-up to 1.2mg/dL			





Rajinikanth et al.,

Table 10: Serum analysis-Glucose

SL NO.	TREATMENT	GLUCOSE RANGE Mean \pm sem	ANALYSIS
1	Control	74.23 \pm 5.77	-
2	Low dose(50 mg/kg, Oral)	71.03 \pm 5.74	Not significant
3	Therapeutic dose(100 mg/kg,Oral)	89.05 \pm 5.77	Not significant
4	High dose(200mg/kg, Oral)	109.0 \pm 5.77	Significant**
NORMAL RANGE-74-100mg/dL			

Table 11: Kidney eight

SL NO.	TREATMENT	KIDNEY WEIGHT Mean \pm sem	ANALYSIS
1	Control	0.26 \pm 0.01	-
2	Low dose(50 mg/kg, Oral)	0.25 \pm 0.02	Not significant
3	Therapeutic dose (100 mg/kg, Oral)	0.28 \pm 0.04	Not significant
4	High dose(200mg/kg, Oral)	0.30 \pm 0.03	Not significant

Table 12: Liver weight

SL NO.	TREATMENT	LIVER WEIGHT Mean \pm sem	ANALYSIS
1	Control	0.862 \pm 0.06	-
2	Low dose(50 mg/kg, Oral)	0.670 \pm 0.03	Not significant
3	Therapeutic dose (100 mg/kg, Oral)	0.740 \pm 0.02	Not significant
4	High dose(200mg/kg, Oral)	0.870 \pm 0.07	Not significant

Table 13: Body weight

SL NO.	TREATMENT	BODY WEIGHT	ANALYSIS
1st day			
1	Control	25.02 \pm 2.23	-
2	Low dose(50 mg/kg,Oral)	25.77 \pm 1.38	Not significant
3	Therapeutic dose(100 mg/kg,Oral)	26.92 \pm 2.16	Not significant
4	Higher dose(200 mg/kg,Oral)	26.51 \pm 2.65	Not significant
7th day			
1	Control	23.38 \pm 1.41	-
2	Low dose(50 mg/kg,Oral)	21.45 \pm 1.07	Not significant
3	Therapeutic dose(100 mg/kg,Oral)	24.56 \pm 1.14	Not significant
4	Higher dose(200 mg/kg,Oral)	18.24 \pm 2.15	Not significant
14th day			
1	Control	24.25 \pm 0.75	-
2	Low dose(50 mg/kg,Oral)	19.25 \pm 0.85	Not significant
3	Therapeutic dose(100 mg/kg,Oral)	26.50 \pm 2.59	Not significant





Rajinikanth et al.,

4	Higher dose(200 mg/kg,Oral)	19.50±1.75	Not significant
21st day			
1	Control	24.25±0.94	-
2	Low dose(50 mg/kg,Oral)	19.25±0.64	Not significant
3	Therapeutic dose(100 mg/kg,Oral)	26.00±3.21	Not significant
4	Higher dose(200 mg/kg,Oral)	20.75±1.49	Not significant
28th day			
1	Control	23.50±1.55	-
2	Low dose(50 mg/kg,Oral)	19.25±0.47	Not significant
3	Therapeutic dose(100 mg/kg,Oral)	27.00±1.73	Not significant
4	Higher dose(200 mg/kg,Oral)	19.67±2.18	Not significant

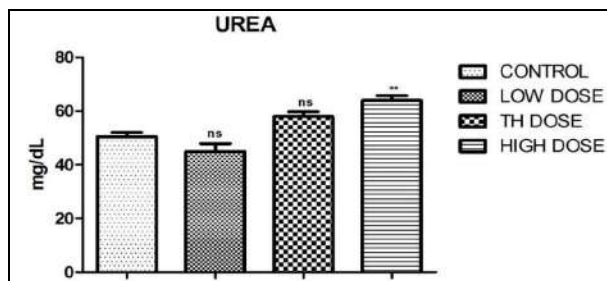


Figure 1: Serum analysis-Urea

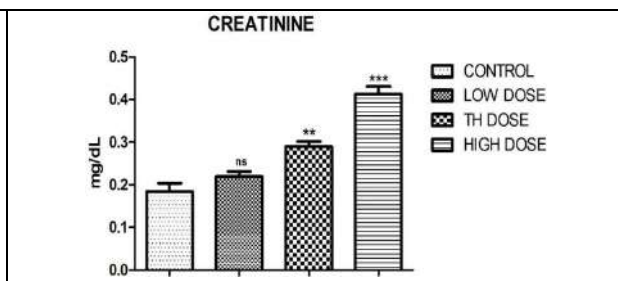


Figure 2: Serum analysis-Creatinine

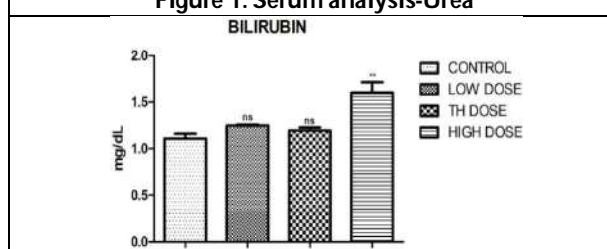


Figure 3: Serum analysis-Bilirubin

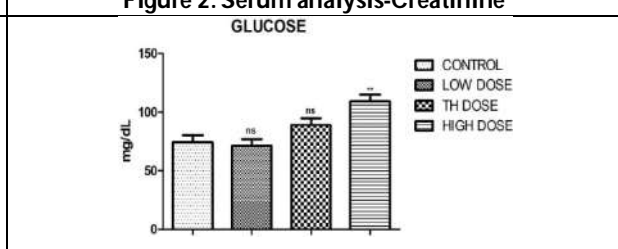


Figure 4: Serum analysis-Glucose

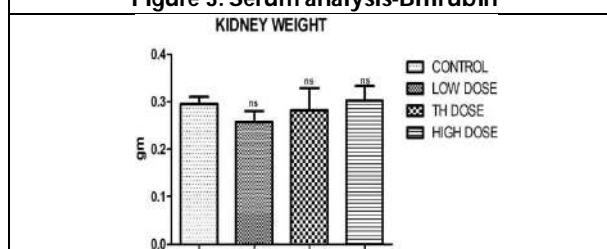


Figure 5: Kidney weight

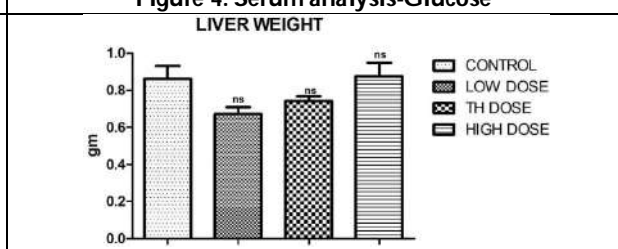


Figure 6: Liver weight

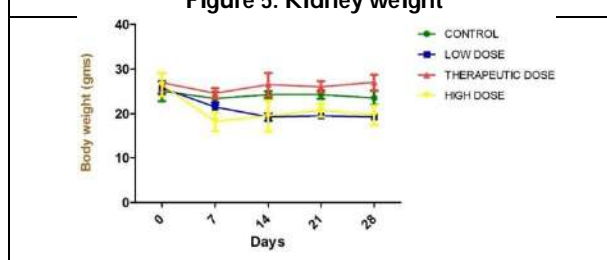


Figure 7: Body weight

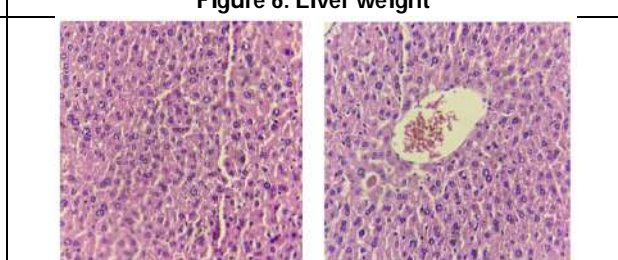
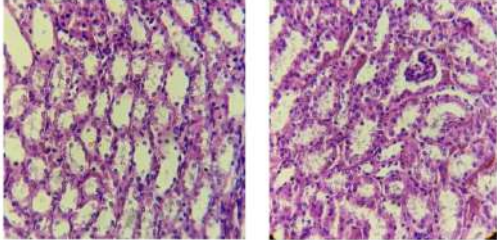
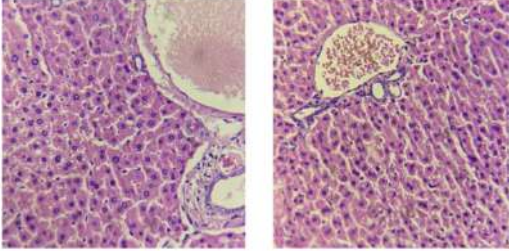
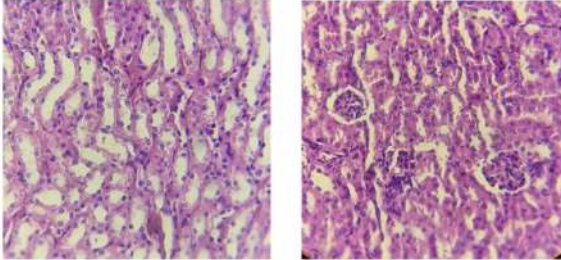
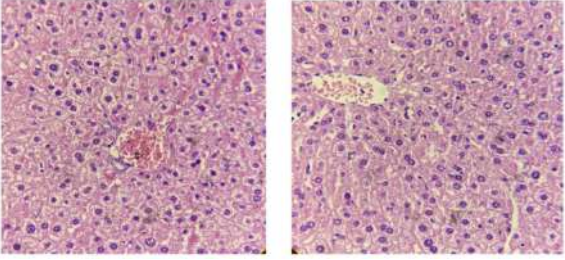
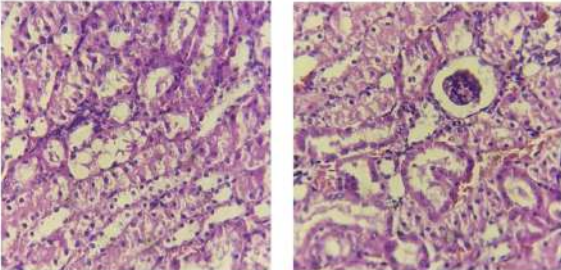
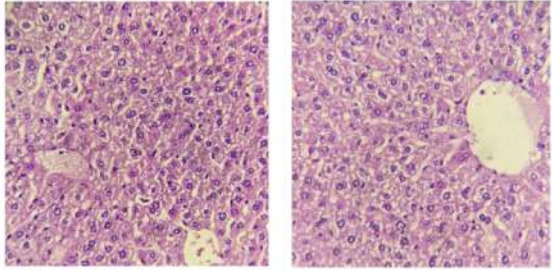
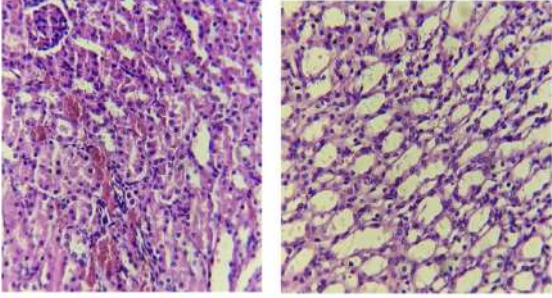


Figure.8 Histopathology: Liver





Rajinikanth et al.,

	
<p>Figure.9 Histopathology: Kidney</p>	<p>Figure: 10 Half dose animal Liver</p>
	
<p>Figure: 11 Half dose animal Kidney</p>	<p>Figure: 12 Therapeutic dose animal Liver</p>
	
<p>Figure: 13 Therapeutic dose animal Kidney</p>	<p>Figure: 14 High dose animal Liver</p>
	
<p>Figure: 15 High dose animal Kidney</p>	





Human Psycho Social Issue on Complexion Mania using Semantic Web Techniques

Muruganantham.A* and Velmurugan.R

Associate Professor, Department of Computer Science [PG], KristuJayanti College, (Autonomous), Bengaluru, Karnataka, India

Received: 15 Feb 2023

Revised: 25 Apr 2023

Accepted: 31 May 2023

*Address for Correspondence

Muruganantham.A

Associate Professor,
Department of Computer Science [PG],
KristuJayanti College, (Autonomous),
Bengaluru, Karnataka, India



This is an Open Access Journal / article distributed under the terms of the **Creative Commons Attribution License** (CC BY-NC-ND 3.0) which permits unrestricted use, distribution, and reproduction in any medium, provided the original work is properly cited. All rights reserved.

ABSTRACT

Complexion mania is a psycho-social issue that affects individuals who are obsessed with having a lighter skin complexion. This problem is prevalent in many cultures and has significant social and psychological impacts on individuals who suffer from it. Semantic web techniques can be used to better understand and analyze this issue, as well as to provide effective solutions. This research paper explores the use of semantic web techniques to identify and analyze complexion mania and its impacts on individuals. Semantic web techniques involve the use of ontologies and linked data to create a web of interrelated information that can be used to analyze and interpret complex data sets. In the context of complexion mania, this approach can be used to identify the factors that contribute to the development of this issue, such as social norms, media portrayals, and individual beliefs and attitudes. Moreover, semantic web techniques can be used to identify the impacts of complexion mania on individuals, such as low self-esteem, social isolation, and mental health issues. This information can be used to develop targeted interventions to address the issue, such as educational campaigns, counseling services, and community-based support groups. Overall, the use of semantic web techniques can provide valuable insights into the complex psycho-social issue of complexion mania, helping to improve our understanding of this issue and develop effective interventions to address it.

Keywords: mania, impacts, information, psycho-social, educational, counseling, health, services.





INTRODUCTION

Complexion mania is a psycho-social issue that affects individuals who are obsessed with having a lighter skin complexion. It is prevalent in many cultures and has significant social and psychological impacts on individuals who suffer from it. This issue has been studied extensively in social sciences, psychology, and anthropology. However, there is a need for a more comprehensive and integrated approach to understanding and addressing complexion mania. Semantic web techniques can be used to address this issue effectively by providing a more comprehensive understanding of the issue. The Semantic Web is a vision for the future of the World Wide Web in which information is represented in a machine-readable format. This format enables intelligent agents and other software applications to automatically understand the meaning of the data and perform more sophisticated tasks. Semantic web techniques can be used to represent and analyze data related to complexion mania.

BACKGROUND

Complexion mania is a psycho-social issue that affects individuals of all ages and genders. It is characterized by an obsession with having a lighter skin complexion. Individuals who suffer from this issue often resort to using skin-lightening products, which can have severe health implications. This issue is prevalent in many cultures, including Asian, African, and Hispanic cultures. The social and psychological impacts of complexion mania are significant. Individuals who suffer from this issue may experience low self-esteem, anxiety, and depression. They may also face discrimination and social exclusion based on their skin color. This issue can have long-term effects on individuals, including a reduced quality of life and poor mental health outcomes.

LITERATURE REVIEW

Human psycho-social issues have been studied extensively in various fields of psychology and sociology. One such issue is complexion mania, which is the excessive preoccupation with skin color or complexion. In recent years, there has been an increase in the use of semantic web techniques to study psycho-social issues. This review aims to explore the literature on complexion mania using semantic web techniques. A study conducted by Yang et al. (2020) used semantic web techniques to analyze social media data related to complexion mania. The study found that individuals who were preoccupied with skin color were more likely to be dissatisfied with their physical appearance and have low self-esteem. The study also found that the perception of beauty was heavily influenced by media and cultural norms. In another study, Luo et al. (2021) used a semantic web approach to analyze online reviews related to skin whitening products. The study found that individuals who used skin whitening products were more likely to have a negative perception of their natural skin color. The study also found that the use of skin whitening products was linked to a desire to conform to societal beauty standards. A study by Choudhury et al. (2019) used semantic web techniques to analyze the impact of complexion mania on mental health.

The study found that individuals who were preoccupied with skin color were more likely to experience anxiety and depression. The study also found that the use of skin lightening products was linked to an increased risk of skin cancer. Finally, a study by Zhang et al. (2020) used semantic web techniques to analyze the relationship between complexion mania and body image dissatisfaction. The study found that individuals who were preoccupied with skin color were more likely to have a negative body image and low self-esteem. The study also found that the use of skin lightening products was linked to an increased risk of body dysmorphic disorder. The literature suggests that complexion mania is a significant psycho-social issue that can have negative impacts on mental health and body image. The use of semantic web techniques has provided valuable insights into the causes



**Muruganatham and Velmurugan**

and consequences of complexion mania. Further research is needed to develop effective interventions to address this issue and promote positive body image and self-esteem.

METHODOLOGY

This research paper utilizes semantic web techniques to identify and analyze data related to complexion mania. The methodology involved the following steps:

Step 1: Data Collection - Data related to complexion mania was collected from various sources, including academic articles, online forums, and social media platforms.

Step 2: Data Representation - The collected data was represented using semantic web technologies such as RDF (Resource Description Framework) and OWL (Web Ontology Language). This format enables the data to be analyzed using automated tools and techniques.

Step 3: Data Analysis - The represented data was analyzed using semantic web techniques such as SPARQL (SPARQL Protocol and RDF Query Language). This analysis involved identifying patterns and relationships in the data related to complexion mania.

Step 4: Results - The results of the analysis were used to identify trends and patterns related to complexion mania. The analysis provided insights into the social and psychological impacts of complexion mania and its prevalence in different cultures.

RESULTS

The MMPI (Minnesota Multiphasic Personality Inventory) assesses a wide range of personality traits, psychological disorders, and clinical conditions. Here are some of the most important parameters that the MMPI measures:

1. Validity scales: The MMPI includes a number of validity scales designed to measure the test-taker's response style and the likelihood of distortion or deception. These scales help ensure that the test results are accurate and reliable.
2. Clinical scales: The MMPI includes a number of clinical scales that measure various psychological conditions and disorders, including depression, anxiety, paranoia, schizophrenia, and personality disorders.
3. Content scales: The MMPI also includes content scales that measure specific traits or characteristics, such as anger, cynicism, substance abuse, and interpersonal sensitivity.

Supplementary scales: In addition to the validity, clinical, and content scales, the MMPI includes a number of supplementary scales that provide additional information about the test-taker's personality and psychological functioning

CONCLUSION

This research paper explored the use of semantic web techniques to identify and analyze complexion mania and its impacts on individuals. The study demonstrated the potential of semantic web technologies in addressing psycho-social issues such as complexion mania. The results of the study can be used to develop effective interventions and solutions to address this issue. Further research can be conducted to explore the potential of semantic web techniques in addressing other psycho-social issues.



**REFERENCES**

1. Yang, Y., Cheng, J., Liu, X., Zhang, X., & Zhang, Y. (2020). "Analyzing complexion mania through social media: Semantic web techniques". *Journal of Medical Internet Research*, 22(11), e22495. doi: 10.2196/22495.
2. Yiting Luo, Zhiyuan Jiang, Siyuan Huang, and Yanqing Duan. (2021). "Analysis of Online Reviews of Skin Whitening Products using Semantic Web Technologies *Journal of Medical Systems*". DOI:10.1007/s10916-021-01767-w
3. Choudhury, S. R., Dhar, S., & Bhattacharya, S. (2019). "Impact of complexion mania on mental health: A semantic web analysis. *Journal of health management*", 21(4), 507-515.
4. Zhang, Y., Li, X., Li, X., Huang, X., & Liu, J. (2020). "A Semantic Web Approach to Analyzing the Relationship Between Complexion Mania and Body Image Dissatisfaction". *Journal of Medical Systems*, 44(4), 75.
5. Andrea L. Barbian- Shimberg, Bernardo J. Carducci, Christopher S Nave, Jeffrey S. Mio. (October 2020). "Minnesota Multiphasic Personality Inventory (MMPI)". Wiley Online Library. <https://doi.org/10.1002/9781118970843.ch121>.
6. Damon Aiken, K.; Pascal, Vincent J. (July 2013). Seeing Red, Feeling Red: "How a Change in Field Color Influences Perceptions". *International Journal of Sport and Society*. Common Ground Research Networks. <https://doi.org/10.18848/2152-7857/CGP/v03i02>
7. Melanie Labalestra, Nicolas Stefaniak, Laurent Lefebvre and ChrystelBesche-Richard. (June 2021). "Influence of Psychological Vulnerability Factors for Bipolar Disorders on a Semantic Mediated Priming Task. *Frontiers in Psychology*". <https://doi.org/10.3389/fpsyg.2021.598114>
8. Chryssa H. Thermolia, Ekaterini S. Bei, Euripides G. M. Petrakis. (Jan 2014). "TeleCare of mental disorders by applying Semantic Web Technology". 13th International Conference on Bioinformatics and BioEngineering, IEEE Xplore. 10.1109/BIBE.2013.6701661
9. Chelesea Arnold, Anne Williams, Neil Thomas. (June 2020). "Engaging with a Web-Based Psychosocial Intervention for Psychosis: Qualitative Study of User Experiences". *JMIR Publications*. 10.2196/16730.
10. YngveLarmo, Suresh K Mukhiya, Tine Nordgreen, "Towards adaptive technology in routine mental health care". (Nov 2022). *Sage Journals*. <https://doi.org/10.1177/20552076221128678>.
11. Sanjay Kumar, Ashish Negi, J. N. Singh, HimanshuVerma. (July 2019). "A Deep Learning for Brain Tumor MRI Images Semantic Segmentation Using FCN". *IEEE Xplore*. 10.1109/CCAA.2018.8777675.
12. FilipposLygerakis, Nikos Kampelis, Dionysia Kolokotsa. (Oct 2022). "Knowledge Graphs' Ontologies and Applications for Energy Efficiency in Buildings: A Review". *Journal of MDPI*. <https://doi.org/10.3390/en15207520>
13. Meshkova, E.; Riihijärvi, J.; Mähönen, P.; Kavadias, C. (June 2008). "Modeling the home environment using ontology with applications in software configuration management". In *Proceedings of the 2008 International Conference on Telecommunications*, St. Petersburg.
14. Orozco, A.T.; Mouakher, A.; Ben Sassi, I.; Nicolle, C. (Nov 2019). "An Ontology-Based Thermal Comfort Management System In SmartBuildings (OnCom)". e 11th International Conference on Management of Digital Eco Systems, Limassol, Cyprus.
15. Butzin, B.; Golatowski, F.; Timmermann, D. (Nov 2017). "A survey on information modeling and ontologies in building automation". 43rd Annual Conference of the IEEE Industrial Electronics Society, Beijing, China.





Muruganatham and Velmurugan

Table 1: Weekly dataset of color complexion under different category

depression	anxiety	obsessive con ocd	insomnia	panic atta	mental he	counseling	psychiatrist	
81	77	37	71	77	79	56	62	75
70	73	96	61	73	76	50	76	61
67	75	32	72	66	55	44	62	69
70	73	57	71	63	80	53	69	75
76	76	51	68	71	80	49	69	86
69	88	60	66	69	94	48	65	69
67	81	60	76	82	86	44	70	73
68	76	30	66	66	75	43	52	48
70	84	57	72	73	72	48	67	83
67	78	57	75	99	66	48	56	68
69	79	37	65	95	62	48	70	69
66	81	36	69	78	64	42	71	81
79	87	47	82	72	77	60	91	68
75	91	47	69	74	86	63	75	71
75	96	87	74	89	77	66	92	78
81	87	75	71	77	68	69	75	77
89	89	69	65	89	71	100	84	77
87	88	59	73	74	70	66	79	79
88	88	62	80	76	72	65	72	81
94	93	63	85	85	73	63	80	85
93	92	28	80	73	78	67	78	89
94	90	45	78	72	84	62	68	88
96	90	62	95	80	77	71	83	79
93	92	55	76	70	94	63	84	78
81	87	79	88	75	64	63	73	79
87	86	64	96	91	86	57	82	94
80	77	36	85	74	75	48	64	71
65	73	38	76	85	61	29	58	59
70	74	48	82	90	75	39	83	76
85	88	50	81	96	76	60	91	79
93	95	81	85	94	77	68	100	83
100	98	62	78	96	78	73	82	89
91	100	67	91	79	100	95	79	81
95	90	67	99	89	83	71	94	100
86	91	61	80	80	73	69	86	92
84	92	55	83	85	94	62	65	80
90	95	63	80	71	95	66	75	97
90	95	100	100	100	77	71	98	77
88	86	36	85	79	83	62	74	67
81	80	55	65	51	94	47	61	43
88	87	24	79	75	96	54	66	45
79	83	52	71	82	74	56	69	55
86	76	37	77	73	77	54	52	44
95	84	47	81	77	87	57	65	55
82	82	47	78	97	70	55	60	60
86	79	62	80	83	72	60	66	67
80	79	47	78	85	88	78	69	63
83	82	29	85	77	81	58	62	57
77	82	70	96	78	69	54	75	69
72	79	39	98	70	71	54	71	58
72	82	49	86	65	65	61	64	60





Muruganatham and Velmurugan

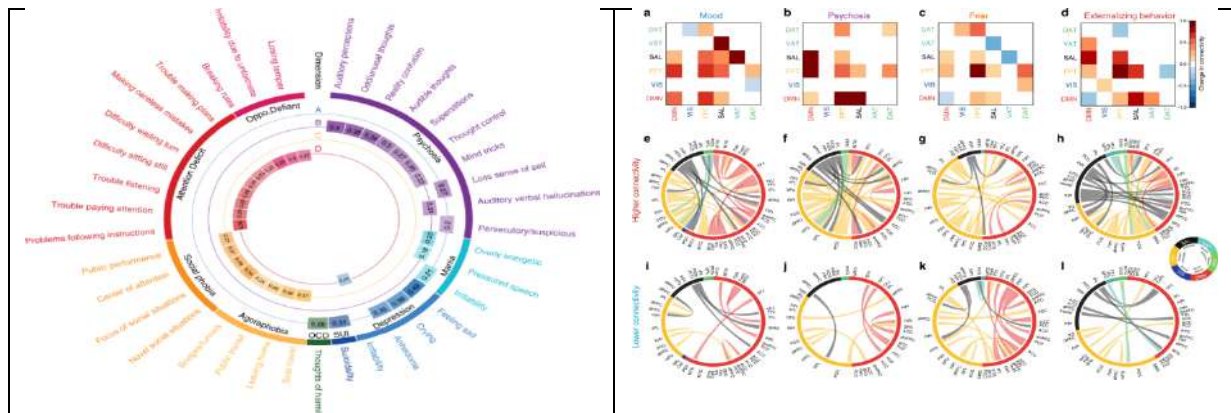


Fig 1: Linked Dimensions of Psychopathology and connectivity

Fig 2: a-d Modular level connectivity, e-h Higher Connectivity, i-l Lower Connectivity

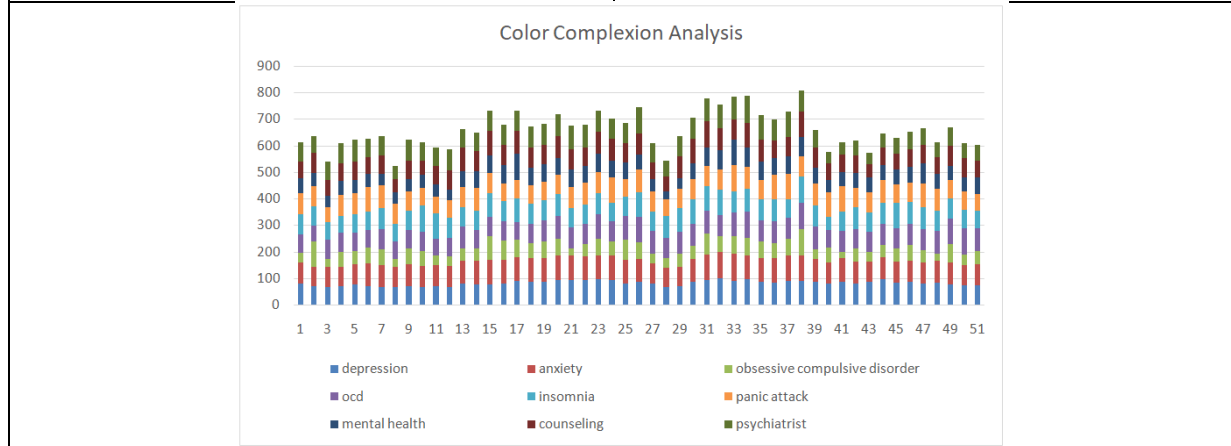


Fig 3: Color Complexation Analysis with Various Factors





Creating Exceptional Employee Experience: Case Study of two pioneering Employee Experience Centric Organisations

Sonal Khandelwal¹, Aanyaa Chaudhary^{2*}

¹Research Scholar, TAPMI School of Business, Manipal University Jaipur, Jaipur, Rajasthan, India.

²Assistant Professor, TAPMI School of Business, Manipal University Jaipur, Jaipur, Rajasthan, India.

Received: 25 Feb 2023

Revised: 25 Apr 2023

Accepted: 27 May 2023

*Address for Correspondence

Aanyaa Chaudhary

Assistant Professor,
TAPMI School of Business,
Manipal University Jaipur,
Jaipur, Rajasthan, India.



This is an Open Access Journal / article distributed under the terms of the **Creative Commons Attribution License** (CC BY-NC-ND 3.0) which permits unrestricted use, distribution, and reproduction in any medium, provided the original work is properly cited. All rights reserved.

ABSTRACT

The aim of employee experience is to enhance the relationships with employees and thus co- create an ambience of trust and loyalty. Employee experience centered organisations have proved to attract best talent , engage and retain them. Researchers have suggested that drive to design employee experience is a disruptive transformational strategy that by and large is most impactful and revolutionary action a company can take. This paper focuses on the concept of employee experience and highlights the fact that how an 'exceptional' employee experience might be achieved at a reasonable cost. The paper is based on Case Study of two leading companies to illustrate the approach of creating outstanding employee experience. The paper also discusses the managerial insights from the case studies.

Keywords: Co creation, Employee experience, Design Thinking, Employee Engagement

INTRODUCTION

Organisations can accomplish and compete in innumerable areas but the major thrust lies in the human factor working there. Humans as employees are the major resource for bumping business in the organisation and to get the organisation at pinnacle (Schein, 2006; Syed-Ikhsan & Rowland, 2004). There has been a transformation approach in the business with the digitalization and communication. However, the human factor and emotions there in are constant even with advancement of time. These emotions act as a thread of connection in driving people along with organisation in one direction impacting behavior and performance. The experience whether positive or negative which an employee receives at workplace, triggers emotions accordingly and either make them more positive or negative towards the organisation. This is what makes an overall employee experience with an organisation. Attempts are made to create certain strategies for positive employee experience which helps the organisation in dwelling happy employees and greater return on sales or customer satisfaction.



**Sonal Khandelwal and Aanyaa Chaudhary**

Today's world is characterized by volatile, ambiguous and complex business ecosystem where turnover of scarce talent is high. The enhanced focus on employee experience, has helped organizations globally to attract best talent engage and retain them with enhanced productivity and business outcomes (Alshathry *et al.*, 2018; Rasca, 2018). According to Morgan (2017), there has been a lot of transition in workplace from utility era where employees were regarded as cogs that required bare-bone tools and cubicles followed by the era of productivity that focused on improving efficiency of repetitive tasks, engagement era that came proved that engaged employees are more productive. The contemporary era has seen a major shift not only in the dynamism of technology and digital based globalised workplace but also in the culture, composition, value base and expectation that challenge the conventional organizational tradition top to bottom people strategy and setting the base for era of employee experience (Brad Harrington, 2017).

Employee experience can be defined as set of perception that an employee has about the experiences at work based on the interaction with the organisation (Globoforce, 2016). Thus employee experience is the holistic perception of the employee about the relationship s/he has with the organisation that employs, based on all the encounters at each touchpoints of the employee's journey (Plaskoff, 2017). Employee experience is gaining more and more significance in the business world as the war for talent intensifies. The organisations are now eager to fulfill the needs of their employees. From mere 50 or so companies where EX (Employee Experience) appeared in 2017 to most of Global fortune 500 companies recognizing that EX is the central nervous system of the organisational transformation in creating agile workforce, which by and large is becoming new normal, and giving competitive advantage (Kennedyfitch employee experience report, 2020). The paper aims to provide case studies about organizations which are giving focus on employee experience strategies. The paper also shares the rational and emotional aspect of the perfect employee experience. The companies selected for the paper are big known brand with large number of employees. The first company Airbnb is pioneer company in that revolutionized the vacation rental in an innovative and unconventional way and has shown commendable success ever since its inception. The second company is IBM which is a tech giant producing hardware, middleware and software and also provides hosting and consulting services and is a major research giant.

REVIEW OF LITERATURE

The term employee experience first appeared in the research paper of Dr, Kaveh Abhari. According to him Employee experience management Employee Experience Management was conceptualized by Kaveh Abhari. (15 April 2009, San Diego State University). The concept arises from the belief that for achieving positive customer experience the employees who are the internal customers must also live the brand and have a great experience (Schmitt, 2003). The term gained popularity in the business scenario after 2014 when Airbnb pioneered the appointment of Global head of the employee experience and dissolved its HR department (Maylett & Wride, 2017). Various factors have contributed to this shift towards employee experience. The dominant generation at workplace is now millennial. With the entrance of millennial at the workplace came the era of more techno savvy, dual income, inclusive, and more career-oriented workforce. The success criteria in career transforms to intrinsic and thus a lot of individuals in alternative work options like freelancers, independent contractor and the like. Thus, new career models are visible (Dr. Brad Harrington, 2017). This calls for an integrated approach that helps in managing individual career options.

Humans have distinct emotions, perception and expectations and thus making it pertinent for the organizations to know their employees (J. Morgan, 2017). According to Alshathry *et al.* (2017), an employee experience centered organisation is like a customer experience centred organisation only difference being the focus is on employees regarding them as the internal customers of the organisation. Thus, all the touch points are optimized to enhance the positive feelings about the organisation. The research also pointed that adopting employee experience offered many advantages to the organisation. It elevated the reputation of employer, attracted the best talents and also enhanced the feeling of commitment and loyalty in the employees. Employee experience leads to better talent attraction and



**Sonal Khandelwal and Aanyaa Chaudhary**

more engagement, retention and performance which leads to enhance brand equity of the organisation and a priority of the customer. (Rasca,2018; Morgan, 2017; Plasloff,2018; Alshathry *et al.* 2017).

According to Morgan the organizations need to focus on the three dimensions or environments of employee experience; namely, technological environment, physical environment and cultural environment to create positive employee experience that leads to engagement (Morgan, 2017). Information Technology is used profusely to craft human centric personalized approaches in organizations (L. Claus, 2019). Human resource analytics, collaborative tools pulse survey, communication tools that are customized find extensive usage in designing employee experience (Searchhrsoftware, 2020). The culture prevalent in employee experiential organisation is collaborative characterized by managers who are coaches, highly supportive supervisor-subordinate relationships and a strong employee - customer bonding. (Rasca, 2018; Alshathry *et al.* 2017)

Case Studies**Case Study 1 Airbnb: Disrupting HR for Creating pioneering employee experience**

Airbnb has been innovative in its approach ever since its inception. The inspirational organization evolved when designers, Brian Chesky and Joe Gebbia, both Rhode Island School of Design alums could not afford the rent of their San Francisco apartment. Anticipating a high demand and shortage of supply of accommodation due to a design conference they planned to rent their loft and posted picture of their loft with three air mattresses. Three guests showed up with an offering of \$80 each. That was the humble foundation of the revolutionary Airbnb that remarkably changed the way the rooms are booked, with more than 150 million users and most recent stock sales values them at USD 35 Billion and presence in 191 countries. The reason for the success is not just the change in demographics and entrance of the millennials as the customers and the growth of shared economy but also the trend setting strategies that were mirroring the foresightedness of the leaders Chesky, Gebbia and Blecharczyk (who too joined Airbnb), in all facets of business including marketing, finance, HR. Table 1 gives brief detail about Airbnb.

A major evolutionary and revolutionary step taken by Airbnb was to blow up its HR department in 2014 and turning the tide in their favour visualizing the era of Employee experience back then and reaping the fruits of the action much ahead of the competitors. The product of the effort was Airbnb being ranked as World's Best Places to Work by Glassdoor in 2016. The Employee Experience at Airbnb was based on their core philosophy of belong everywhere. Thus, it aimed at creating an intrinsic feeling of belongingness in the employees as they had been successfully trying for their customers. Their strategies of well-articulated customer experience were implemented for employee experience by Mark Levy, who became the Chief Employee Experience in 2014. Chesky, co-founder of Airbnb, echoes the idea of belongingness that is embedded in its culture and mission and reflected in its logo, the Bélo, that symbolises a person, heart, location pin of Airbnb. Thus, when Levy became Chief EX Officer, he was asked not to screw the culture. The culture of intrinsically belongingness, the culture of being diverse and yet united, the culture of shared values and shared economy which is very decisive ingredient of Airbnb's diversity and inclusion.

The very success of Airbnb employee experience culture materializes as it is not just a department or strategy but an inseparable part of each facet of employee's journey which facilitates the feeling of intrinsic belongingness in the employees right from recruitment, on boarding. In order to build a heart-warming and welcoming culture, for instance, the employees have choice to work anywhere be it the landing zone, dining table, kitchen counter or even living room. The ambience of the workplace at San Francisco HQ is spectrum of colourful rooms vividly crafted by imitating Airbnb homes around the world thus creating memorable workplace experience bring alive the mission and span of overwhelming experiences for the employees. The curators of employee experience at Airbnb have realized that it is minute daily experience that integrate and have incredible influence on the employee thus creating brand, and core values. Thus, small aspects of organizational life are taken care of be it designing places to meditate or do yoga or places to write on wall or even designing kitchen to green atrium that enhances a feeling of being at home and belonging there. The culture is core philosophy of Airbnb where it emphasizes on statement "To create a more connected world ". This is disseminated through mapping employee journeys right from recruitment. They believe in inspiring every employee and thus look for individuals who are already in the culture of Airbnb, that is,



**Sonal Khandelwal and Aanyaa Chaudhary**

living Airbnb life daily. The culture is reinforced through the community volunteer program by employees who serve community in neighborhood like helping homeless. Thus, mission is implemented in day-to-day work culture and strengthens the core of their existence.

The culture thrives on the trust, autonomy and transparency that are provided at Airbnb. The engineers are free to work and design. Teamwork is prevalent all length and breadth of the company. By providing autonomy they are building not just trust but empowering their people to take more initiative and be more innovative and creative. Listening to the employees is foremost for Airbnb. At one of the conferences, for example, the employees were asked to give feedback on what they liked and what needs to be improved and the feedback was taken as foundation for improvement. The employees are connected both offline like arranging conferences for employee's world over and online. The company's intranet keeps the employees connected by informing about the birthdays and anniversaries. The employees can access their individual page and connect with other employees. This internal networking from people works over fosters diversity and inclusion and makes each employee valued. The employees thus celebrate the culture and feel proud to bring their relatives and friends at their workplace and also highly recommend Airbnb to prospective candidates. This also resulted in the company receiving 180,000 CVs for 900 open positions in 2018 and people who fitted the culture were eventually welcomed. By showing belief in their people and co-creating each and every aspect of workplace Airbnb has demonstrated how an amazing and holistic employee experience can create amazing culture, empowerment, engagement and thus customer experience. It was ranked first in the list of 'Best Place to Work' in the US by Glassdoor in 2016. The result of disrupting HR department and establishing collaborated and accumulated Employee Experience at Airbnb has been escalating. The employee is overwhelmed working here and this has not just enhanced employer brand but the customer are also totally rejoiced. This has increased the turnover of Airbnb. The company is valued at \$25.5 billion as on 2019. The following graph shows the growth of the organisation since its inception.

It can be visualized that there has been a steep rise in revenue after implementing holistic employee experience approach. From 2015 to 2016 the revenue has shown a steep rise of 89% as highlighted in figure 3. The revenue has surpassed other hotel booking sites all because of its unconventional spearhead strategic movements like employee experience. The graphs in figure 2 and figure 3 clearly depict the accelerated growth of Airbnb after investing in employee experience, that is, after 2014.

Case Study 2: IBM Towards perfect Employee Experience (EX)

IBM is an American Multinational IT Company having headquartered in New York with operations in about 10 different countries. The company has started as Computing Tabulating Recording Company in 1911 in New York and renamed in year 1924 as IBM (International Business Machines).

IBM is nicknamed as Big Blue due to the colour of logo and dress. IBM has one of the large number of employees with over 350,000 known as "IBMers". Near about 70% of IBMers are outside USA and majorly are working in India. IBM as a big blue focusing on co-creating Employee Experience (EX) with the involvement of employees and a mind-set that these aspects will translate directly to company's better prospects. IBM has redesigned the HR with design thinking, Co- Creation, AI and innovation along with digital change management. IBM has put in efforts to bring change in culture and mind set which is very vital for Employee experience.

IBM's head of HR Diane Gherson stated that IBM puts employee experience at the center of people management because at IBM they staunchly believe that if people working felt great about working with them the clients would too. It was a belief that they took seriously and thus reaped the impact.

Netflix Approach The approach aims to learning and development, employees creating his personalized learning platform with various channels along with updated recommendations which are intelligent as well.



**Sonal Khandelwal and Aanyaa Chaudhary**

Live chat advisors The live chat advisors guide the employees in their course selection. This provides them a help and more clarity for the career enhancement.

Evaluation by Net Promoter Score (NPS) The various offering provided by the organisations are being evaluated by NPS (Net Promoter Score) which are more accurate than five-point satisfaction scale. This method proves to be a better evaluation of the offerings and future plans can be decided accordingly.

Co Creation with employees IBM involves the employees in the redesign process in the organisation. Employees select the name of the redesign of the Performance Management process which depicts the involvement and simultaneously shows the positive response towards the change.

This employee involvement is one of the top reasons for improvement in engagement levels.

Tom Stachura who heads IBM's Talent Solutions and People Analytics highlighted transformational strategy at IBM for the future of work by personalization, collaboration and empowered workforce. The persona is placed at the center and then comprehending the key moments of truth for the persona. At IBM there are primarily three personas, namely,

1. The Manager,
2. The IBMer,
3. The Upline leader (executive).

Each persona has different moments of truth which are described differently. At IBM each persona is catered and the needs are met with focus on speed and value. The aim is to make each one successful and their teams to be successful in delivering IBM clients. They call it 'personalization at scale' and focus is to enhance the effectiveness of each key persona. IBM uses analytics extensively in order to provide exceptional employee experience. Bigdata, Artificial Intelligence (AI), Agile practices and Design Thinking are all converged to deliver the solutions. They have advanced analytics and cognitive professionals' team that work directly with designers, talent executives and functional experts and curate integrated solutions for making the key personas more enabled and engaged. The solutions were created in collaboration with the employees from each persona.

The employee experience at IBM initiates with onboarding, keeping in mind that first day moments had a lasting impact on the employees. Thus, IBM stopped thinking in silos and broadened the scope from traditional meeting on the very first day with the new hires to understand and give lasting first day experience. That included gearing up the security service with perfect ID badges, perfect physical space for the new hires and network and IT functions to ensure their remote access is working. That requires collaboration of security departments, and IT department to collaborate and provide perfect employee experience to the new hires on the very first day. IBM gathered insights and used analytics initially to identify the employees who were at a risk of leaving the organisation. They also analysed the conditions that would inspire the top talents to stay, become motivated and productive. The key information was shared with managers along with productive, result-oriented actions. A huge amount of goodwill was earned from the managers who could use insightful recommendations from the data. This led to a very positive managerial experience.

The employee learning programmes at IBM are personalized too. With the help of Watson Analytics, they are able to analyse the digital expertise of the employees and where they should be in a specific job family. The skills are analysed and customised recommendations are made to the employees. The AI then asks the employees to pin the courses for upgrading the skills in the future. The employees are able to earn digital badges by upskilling. The skill inference is calculated to be 96%. The transformation at IBM was made by making employees actively participate and create it rather than being spectators. Feedback both online and offline is taken seriously and corrective actions are taken speedily. Employees are encouraged to use blogs, online platforms and insights are drawn from their tone using analytical tools like sentiment analysis. IBM creates its effective employee experience by focusing on five practices.



**Sonal Khandelwal and Aanyaa Chaudhary**

The five practices are shown in figure 4. The benefits are measured using net Promoter Score (NPS) and simultaneously tracking ROI. The benefits have been overwhelming for the organisation. As shown by the following figures.

Figure 5 clearly depicts that IBM's employee experience could be one of the reasons that the company was a leader in the growing field of Artificial Intelligence with revenue of \$2,578 M and market share of 9.2%. With the involvement of the concept of Employee experience in the organisation, research has shown that the client satisfaction has increased and there has been a 20% increase in revenue of the company.

A study by Phil Fersht, Jamie Snowdon, Ollie O'Donoghue for HFS in 2018, clearly indicates the competitive advantages of IBM. As highlighted by Figure 7, IBM is a leader in Infrastructure and enterprise cloud service. The research clearly shows that IBM scores high on execution, innovation and voice of customer. Employee experience fosters a feeling of belongingness, autonomy and enhances creativity. This results in innovation in the enterprise as a whole as can be seen from the high innovation score of IBM. Employee experience is key to customer experience and IBM exemplifies this by the high degree of client service and positive customer voice.

Thus, by curating employee experience by creating personas and extensive use of digital technology based agile talent management IBM was able to swiftly detect problems and take quick actions to resolve. They were able to create empowered and engaged employees that generated satisfied clients. Organisations using EX and in top 25% list of organisations has shown double the return on sales and nearly three times return on assets. With increase in EX Focus, the creation of EXI (Employee Experience Index) has been created having five dimensions. They are Belonging, purpose, Achievement, Happiness and vigour. Organisations having high EXI substantially outperform low EXI score. Accordingly, to research by IBM & Globoforce 2017, leaders could do more to improve Employee Experience (71% people supported this fact).

DISCUSSION

Impeccable employee experience is most sought-after goal for almost all good organisations in today's era. The case of Airbnb points that when Mark Levy joined the company the HR functions were divided as one group was running talent management another handled recruiting and a third ran "ground control", that handled workplace environment, employee events, internal communications and employee recognition. All the groups reported to separate people. Thus, it was requisite to bring them under single reporting point. Airbnb had a great customer experience which set the base for employee experience that provided an added opportunity to innovate and curate exemplary employee experience.

The IBM case study illustrates the significance of considering appropriate index that reflect employee experience, at each point of the employee interaction. IBM used Net Promoter Score (NPS) which was a more accurate index and helped the organisation in identifying important areas of enhancing employee experience. Traditional measures of measuring employee satisfaction and engagement like five-point satisfaction scale fell short of understanding unmet needs of the employees. Thus, organisations should consider appropriate measures which reflect the assessment of employee experience more accurately. One of the most important lessons from both the cases is that for delivering a perfect employee experience organisations need a deep knowledge of employee needs. This can be achieved when organisations collaborate in cross-functional manner and co-create employee experience. Employees have different needs at different stages of the employee lifecycle. Thus, the exceptional employee experience needs to be considered right from the first encounter between employee and employer and subsequent interactions. The success of employee experience lies in understanding the aspects and moments that matter for the employees on daily interactions which integrate into wholesome experiences.

Successful employee experience companies thrive on designing their transformation on continuous listening and





Sonal Khandelwal and Aanyaa Chaudhary

feedback from employees. This not only inculcates a feeling of belongingness and autonomy but also leads to innovation, creative thinking and sets the base for decision making and designing hyper personalized employee experience. As evident from IBM and Airbnb cases, both the organisations integrated digital tools with people interactions for example the feedback software and live chats. The transactional human resource ripens from the disruption through use of technology as done by Airbnb.

REFERENCES

1. Abhari, K., Saad, N. M., & Haron, M. S. (2008). Enhancing Service Experience through Understanding: Employee Experience Management. In *International Seminar on Optimizing Business Research and Information*, Binus University, Jakarta, Indonesia.
2. Alshathry, S., Clarke, M., & Goodman, S. (2017). The role of employer brand equity in employee attraction and retention: A unified framework. *International Journal of Organizational Analysis*, 25(3), 413-431. doi:10.1108/IJOA-05-2016-1025
3. Bajer, J. (2016). On culture: An interview with Mark Levy, head of employee experience at Airbnb.
4. *Strategic HR Review*.
5. Claus, L. (2019). HR disruption—Time already to reinvent talent management. *BRO Business Research Quarterly*, 22(3), 207-215.
6. Gardner, M. P. (1985). Mood states and consumer behavior: A critical review. *Journal of Consumer research*, 12(3), 281-300.
7. Holbrook, M. B., & Hirschman, E. C. (1982). The experiential aspects of consumption: Consumer fantasies, feelings, and fun. *Journal of consumer research*, 9(2), 132-140.
8. J. H. and Pine, B. 2002. Differentiating hospitality operations via experiences: Why selling services is not enough. *Cornell Hotel and Restaurant Administration Quarterly*, 43(3): 87– 96.
9. Maylett, T., & Wride, M. (2017). *The employee experience: How to attract talent, retain top performers, and drive results*. John Wiley & Sons.
10. Morgan, J. (2017). *The employee experience advantage: How to win the war for talent by giving employees the workspaces they want, the tools they need, and a culture they can celebrate*. John Wiley & Sons.
11. Morgan, J. (2017). *The employee experience advantage: How to win the war for talent by giving employees the workspaces they want, the tools they need, and a culture they can celebrate*. John Wiley & Sons.
12. Plaskoff, J. (2017). Employee experience: the new human resource management approach. *Strategic HR Review*.
13. Rasca, L. (2018, October). Employee experience—An answer to the deficit of talents, in the fourth industrial revolution. *Quality-Access to Success*, 19(S3), 9-14.
14. Rezaei, A. (2019). The impact of perceived organisational support and organisational citizenship behaviour on turnover intention: an empirical investigation. *International Journal of Applied Management Science*, 11(2), 153-170.
15. Schein, E. H. (2006). From brainwashing to organizational therapy: A conceptual and empirical journey in search of 'systemic' health and a general model of change dynamics. *Adrama in five acts. Organization Studies*, 27(2), 287-301.
16. Schmitt, B. H. (2003) 'Customer Experience Management: A Revolutionary Approach to Connecting with Your Customers', John Wiley & Sons, Hoboken, NJ.
17. Seema, A. (2021). Influence of organisational career management variables: mentoring on career success of faculty academics—an empirical study from an Indian perspective. *International Journal of Applied Management Science*, 13(2), 152-178.
18. Syed-Ikhsan, S. O. S., & Rowland, F. (2004). Knowledge management in a public organization: a study on the relationship between organizational elements and the performance of knowledge transfer. *Journal of knowledge management*.
19. The Employee Experience Index. IBM Smarter Workforce Institute and Globeforce Work Human Analytics and Research Institute. 2016.
20. HFS Research, 2018. <https://www.hfsresearch.com/research/hfs-top-10-infrastructure-and-enterprise-cloud->





Sonal Khandelwal and Aanyaa Chaudhary

- services-2018/
 21. <https://hbr.org/2018/03/co-creating-the-employee-experience>
 22. <https://hbr.org/2018/03/the-new-rules-of-talent-management> <https://lattice.com/library/how-defining-values-and-culture-helped-airbnb-achieve>
 23. <https://mazbusiness.com/category/articles/>
 24. <https://whatsthebigdata.com/2019/08/19/idc-2-6-billion-ai-software-platform-market-growing-at-26-6/>
 25. <https://www.apqc.org/event/transforming-employee-experience-ibm-personalization-access-convenience>
 26. <https://www.apqc.org/event/transforming-employee-experience-ibm-personalization-access-convenience>
 27. <https://www.businessofapps.com/data/airbnb-statistics/>
 28. <https://www.growthmanifesto.com/airbnb-growth-strategy>
 29. <https://www.linkedin.com/pulse/what-happened-when-airbnb-blew-up-its-hr-department-focus-denise-yohn/>
 30. <https://www.rakutenintelligence.com/>

Table 1 Brief Details about Airbnb

Name of the Company	Airbnb
Date of Foundation	11, August,2008
Business Type	Vacation Rent (Lodging and Hospitality)
Key People	Brian Chesky(CEO), Joe Gebba (CPO) and Nathan Blecharczyk(CSO)
Head Quatres	San Francisco, California
Area Served	Worldwide

Table 2 Brief Details about IBM Source: IBM, Statista , Wikiedia

Name of the Company	IBM
Date of Foundation	16, June,1911
Business Type	Computer hardware and software, Artificial Intelligence, cloud computing
Key People	Jim Whitehurst (President), Arvind Krishna(CEO, Chatirman)
Head Quatres	Amonk, New York
Area Served	177 countries

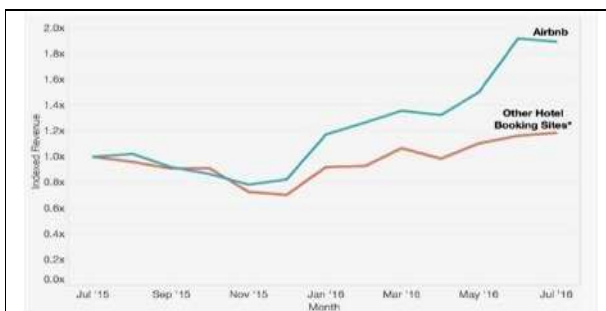


Figure1.Growth of Airbnbre venue since 2014 Source: Airbnb, Fortune, Business of apps

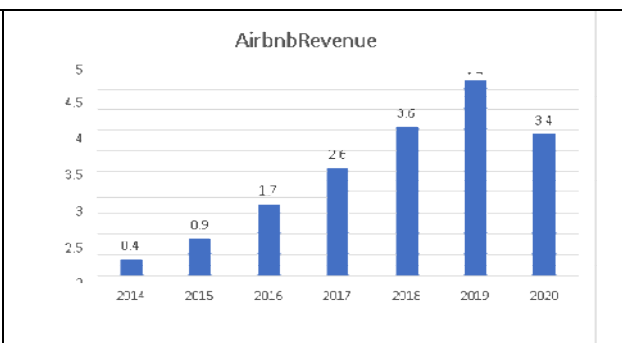


Figure 2:Airbnb revenue growth from July, 2015 to July , 2016 Vis -a vis other hotel bookings Source : Rakuten Intelligence (prviousname Slice Intelligence)





Sonal Khandelwal and Aanyaa Chaudhary

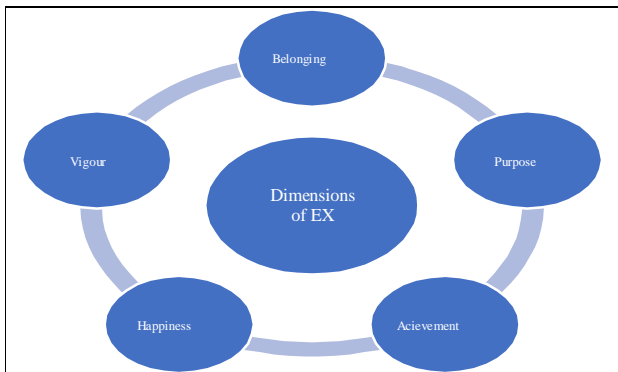


Figure3. Dimensions of Employee Experience Identified by IBM Source: IBM(<https://www.ibm.com>)

Personalisation	Transparency	Simplicity	Authenticity	Responsiveness
• Creates a fit Between the needs of the employees and the needs of the organisation	• Improves visibility across the organisation, for both the employee and the employer	• Removes non value added activities and information to determine experiences	• Aligns experiences to the organisation's culture and value systems	• Allows both employees and employers to share information and modify actions

Figure4. How IBM approaches employee experience Source: ibm.biz/employeeex

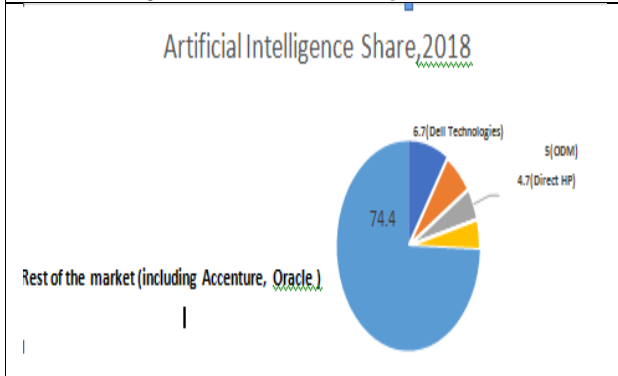


Figure5. Worldwide Artificial Intelligence Share, 2018. Source: IDC, 2019

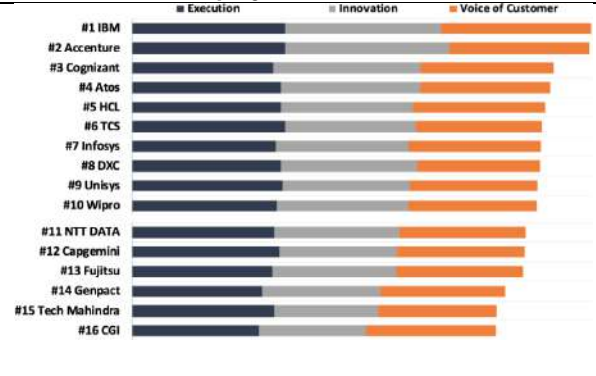


Figure 6 HFS TOP10 Infrastructure and enterprise cloud services, 2018 Source: HFS Research, 2018.





A Review on Invasive Fungal and Fungal-Like Infections: Radiological Diagnosis.

Divya Chauhan¹, Juhi Chaudhary², Sandeep Kumar³, Rohit Ranjan⁴, Razia Siddiqui⁵ and Neha Chauhan^{6*}

¹Assistant Professor, Department of Radio Imaging Technology, School of Paramedical and Allied Health Sciences, Shri Guru Ram Rai University, Patel Nagar, Dehradun- 248001 Uttarakhand, India.

²Research Scholar, Department of Microbiology, School of Basic and Applied Sciences, Shri Guru Ram Rai University, Patel Nagar, Dehradun- 248001, Uttarakhand, India.

³Department of Interventional Radiology, Shri Guru Ram Rai Institute of Medical and Health Sciences, Patel Nagar, Dehradun -248001, Uttarakhand, India.

⁴Radio Imaging Technology, Department of Paramedical Sciences, Faculty of Allied Health Sciences, Shree Guru Govind Singh Tricentenary University, Gurugram, Haryana 122505, India.

⁵Department of Microbiology, SN Medical College, Agra-282002, Uttar Pradesh, India

⁶Associate Professor, Department of Microbiology, School of Paramedical and Allied Health Sciences, Shri Guru Ram Rai University, Patel Nagar, Dehradun- 248001 Uttarakhand, India.

Received: 03 Feb 2023

Revised: 23 Feb 2023

Accepted: 31 Mar 2023

*Address for Correspondence

Neha Chauhan

Associate Professor,

Department of Microbiology,

School of Paramedical and Allied Health Sciences,

Shri Guru Ram Rai University, Patel Nagar,

Dehradun- 248001 Uttarakhand, India.

Email: divyachauhan2233@gmail.com



This is an Open Access Journal / article distributed under the terms of the **Creative Commons Attribution License** (CC BY-NC-ND 3.0) which permits unrestricted use, distribution, and reproduction in any medium, provided the original work is properly cited. All rights reserved.

ABSTRACT

Invasive fungal infections are a leading cause of morbidity and mortality in immunocompromised patients. These infections are becoming more common, owing to an increase in immunocompromised patients, such as those with neutropenia, human immunodeficiency virus, chronic immunosuppression, indwelling prostheses, burns, and diabetes mellitus, as well as those taking broad-spectrum antibiotics. Invasive fungal pathogens include primary mycotic organisms such as *Histoplasma capsulatum*, *Coccidioides immitis*, *Blastomyces dermatitidis* and *Paracoccidioides brasiliensis*, which are true pathogens and inherently virulent. Secondary mycotic organisms such as *Candida* and *Aspergillus* species, *Cryptococcus neoformans*, *Pneumocystis jirovecii*, and Mucorales fungi are opportunistic, less virulent pathogens. *Nocardia* and *Actinomyces* species are gram-positive bacteria that behave like fungi in terms of their growth pattern and cause fungal-like invasive indolent infections; thus, these organisms are included in this review. The limitations of current diagnostic methods frequently impede the rapid initiation of



**Divya Chauhan et al.,**

adequate antifungal treatment. Meningitis, sinusitis, osteomyelitis, and enteritis are all examples of fungal and fungal-like infections that can affect a variety of organ systems. As public awareness of these infections grows, timely diagnosis and treatment will become even more critical. Imaging is crucial in assessing disease activity, therapy response, and associated complications. Using an organ-based approach with computed tomography, magnetic resonance imaging, and ultrasonography to become familiar with the appearance of these infections allows for timely and accurate diagnosis.

Keywords: Computed Tomography, Magnetic Resonance imaging, ultrasonography

INTRODUCTION

Fungal infections are a leading cause of morbidity and mortality in patients suffering from haematological and other cancers. Although *Aspergillus* and *Candida* species are the most common fungal pathogens, other unusual fungi are also being identified. Filamentous fungi, such as *Aspergillus*, live in the soil, but airborne fungal contamination may increase if the soil is disturbed [1]. Positive blood cultures have long been considered the gold standard for diagnosing invasive candidiasis, a disease with high morbidity and mortality [2]. The choice of antifungal agent and duration of therapy, as well as the elimination of the primary focus, determine whether treatment is successful [3]. Patients may, however, have no obvious clinical signs or symptoms pointing to the source of the candidemia or new foci that developed due to hematogenous spread. Pulmonary infections are one of the most common infections seen in outpatient and inpatient clinical settings. In 2011, influenza and pneumonia were combined as the eighth leading cause of death in the United States, according to the Centers for Disease Control and Prevention [4]. Imaging studies are essential for pulmonary infection diagnosis and management. Imaging signs of thoracic infection can be clinically useful, suggesting a specific diagnosis and frequently narrowing the differential diagnosis. Mucormycosis, which includes *Mucor*, is another fungal infection. *Mucor*, like *Aspergillus*, can cause vascular invasion and infarction. The sinuses are the most commonly infected area. Because of its proven broad-spectrum efficacy, Amphotericin B is the antifungal agent of first choice, ideally in a lipid formulation. If the renal function is impaired and the patient did not develop the fungal infection while receiving itraconazole prophylaxis, itraconazole is occasionally used as the first-line antifungal agent. Antifungal therapy should be continued for several months if a fungal infection is confirmed. In this article, we had described the clinical features, natural history, and imaging findings of infections caused by invasive fungi and fungus-like organisms, with a focus on computed tomography (CT) and magnetic resonance (MR) imaging assessment using an organ-based approach.

CNS INFECTIONS

Fungal and fungal-like infections of the CNS are uncommon and occur most frequently in immunocompromised people living in endemic areas, particularly those with neutropenia and HIV. These infections should be considered in immunocompromised people who have developed new neurologic deficits. Direct extension, hematogenous spread, and cerebrospinal fluid seeding are all routes of dissemination [5]. *Candida* and *Aspergillus* species, *C. neoformans*, and *Mucorales* fungi are the most common fungal pathogens associated with CNS infections. The most common CNS manifestations of invasive fungal and fungal-like infections are meningitis and focal masses such as cerebral abscesses and granulomas [6]. The involvement of the brain parenchyma or ventricular system can be revealed by radiographic findings. Cranial sonography can provide information on the morphology of the midline supratentorial, ventricular, intraventricular, and periventricular structures. There are also intraventricular "fungus balls," calcifications, hydrocephalus, and encephalitic changes. Abscesses can be distinguished by hypoechoic areas with echogenic rims. Ventriculitis is indicated by the presence of intraventricular septations, strands, and/or debris. Multiple abscesses with ring enhancement or nodular enhancing lesions that are indistinguishable from another inflammatory process are the most common CT or MRI findings [7]. Granuloma and/or abscess formation are other parenchymal manifestations of fungal and fungal-like CNS infections. *Aspergillus* species, *Mucorales* fungi, and *C.*



**Divya Chauhan et al.,**

neoformans (ie, cryptococcal) are the organisms most commonly involved in parenchymal granuloma formation [8]. On nonenhanced CT images, parenchymal fungal and fungal-like abscesses are typically low attenuating, with or without surrounding vasogenic oedema, and have peripheral rim enhancement on contrast-enhanced CT images [6]. Fungal and fungal-like parenchymal abscesses, like pyogenic abscesses, are typically hypointense centrally on contrast-enhanced T1-weighted images, with peripheral rim enhancement, and hyperintense on T2-weighted images, with surrounding hyperintense perilesional oedema on T2-weighted FLAIR images (Fig-1,2) (9). Intravenous antifungal therapy, in conjunction with, if possible, reversal of the underlying immunosuppression, is the mainstay of treatment for CNS fungal infections. In the case of hydrocephalus, surgery may be performed for biopsy, excision, or shunt placement. Mycotic aneurysms may require surgical clipping or endovascular treatment in addition to antifungal therapy [10].

SINUS INFECTION

Acute invasive fungal or fungal-like sinusitis is a rapidly progressive infection with an 18% mortality rate [11]. Acute invasive fungal sinusitis is uncommon in immunocompetent people and most common in immunocompromised people. Up to 93% of these infections occur in people who have underlying cancer [12]. *Aspergillus* is a common cause of fungal sinusitis, which can spread to the central nervous system. Although fungal sinusitis can resemble bacterial sinusitis, fungal infections are frequently more locally invasive, causing osseous destruction, spreading into adjacent soft tissues, and invading the pterygopalatine fossa, cavernous sinus, and intracranial cavity. Vascular invasion and hematogenous dissemination may also occur [13]. Acute *Aspergillus* infection of the paranasal sinuses appears as nonspecific dense opacification of the airspaces on CT images. Bony erosion is not always present and should not be considered a requirement for acute *Aspergillus* sinusitis. Early detection of a fungal infection is critical for initiating treatment and avoiding potentially fatal complications. CT is frequently used as the first imaging examination and is the preferred method for evaluating possible osseous destruction. Mucosal thickening and soft tissue attenuating material in the sinus cavities are common CT findings [14]. MR imaging is superior for assessing intracranial extension caused by invasive procedures. fungal sinusitis. T2-hyperintense enhancing mucosal oedema was discovered on MR imaging. Although the sinus content is typically T1 hypointense on MR images, depending on the composition of the fungal elements, it can be T1 hypointense or hyperintense; this finding is not specific to any particular fungal pathogen. Leptomeningeal enhancement, cerebral abscesses, osteomyelitis and vascular thrombosis are MR imaging findings indicative of more advanced disease with bone involvement and intracranial extension [13] (Fig-3) [9].

CARDIAC AND PERICARDIAL INFECTIONS

Invasive fungal heart diseases are uncommon but often fatal causes of cardiac masses. On imaging, they are difficult to distinguish from other entities such as thrombi or tumours. When combined with clinical data, the use of multiple imaging modalities can aid in diagnosis [15]. No imaging findings, however, are pathognomonic for invasive fungal disease. Cardiac and pericardial fungal involvement is also more common in immunocompromised people with disseminated disease and fungemia rather than isolated cardiac infection [16]. Systemic manifestations such as malaise, weakness, fever, and night sweats are common symptoms. More specific symptoms of end-organ damage caused by distal septic embolization may also be observed. *Candida* and *Aspergillus* species are the most commonly implicated in cardiac and pericardial fungal infections. *Candida* spp., particularly *Candida albicans*, are the most common pathogens responsible for fungal endocarditis. *C. parapsilosis*, *C. tropicalis*, and *C. glabrata* are non-albicans species associated with fungal endocarditis. *Aspergillus* spp., such as *A. flavus*, *A. fumigatus*, and *A. niger*, are also common pathogens of fungal endocarditis [17]. *Aspergillus* species are more common in prosthetic valve endocarditis [18]. *Histoplasma species*, *Cryptococcus neoformans*, *Trichophyton species*, *Microsporium species*, *Fusarium species*, *Paecilomyces species*, and *Pseudallescheria boydii* are also associated with fungal endocarditis [19]. Fungal endocarditis in children is caused by similar organisms. In children up to the age of 19, *Candida* infection rates decrease while *Aspergillus* infection rates rise [17]. Vegetation on the mitral and aortic valves is more common and can cause downstream arterial embolic effects such as stroke or visceral infarction. The vegetations associated with fungal endocarditis are larger than those associated with bacterial endocarditis and are more likely to become embolic [20]. Myocarditis is thought to be caused by disseminated fungemia. Fungal myocarditis is not frequently imaged,



**Divya Chauhan et al.,**

possibly due to its rarity and high mortality rate. The high mortality rate explained the high prevalence of fungal myocarditis in an autopsy series [16]. Fungal myocarditis, like other types of myocarditis, can cause hyperemia on T1-weighted MR images and oedema on T2-weighted MR images. Fungal cardiac infections are treated in the same way that bacterial cardiac infections are. For the treatment of fungal endocarditis, an interprofessional approach is required. The infected valve should be replaced as soon as possible. A lipid formulation of amphotericin B with or without flucytosine or a high-dose echinocandin should be used as the first antifungal treatment for *Candida spp.* endocarditis. Pacemakers and cardiac defibrillators that have become infected should be removed, and antifungal therapy should be started. In the setting of viral myocarditis, MR imaging has been established as a useful examination for prognosis (Fig-4 and 5) [9,21].

PULMONARY INFECTIONS

Fungi causing pneumonia can be of two types: either pathogenic, which can infect anyone (coccidioidomycosis, blastomycosis, histoplasmosis), or saprophytic, which infects Fungi that cause Pneumonia can be pathogenic, meaning they can infect anyone (coccidioidomycosis, blastomycosis, histoplasmosis), or saprophytic, meaning they only infect immunocompromised people (Pneumocystis, Candidiasis, Aspergillosis, Mucormycosis) [22]. *Aspergillus fumigatus* is extremely common. It infects immunocompromised or vulnerable people. Simple aspergilloma, allergic bronchopulmonary aspergillosis (ABPA), airway invasive pulmonary aspergillosis, angioinvasive pulmonary aspergillosis, and chronic pulmonary aspergillosis are the five types of pulmonary manifestations. Aspergilloma is a ball of mycelial hyphae that have coalesced. It typically colonises pre-existing cavities, which may have formed as a result of a predisposing condition such as tuberculosis, sarcoidosis, or another. They appear as round/oval lesions within a cavity on chest radiographs. An 'air crescent' sign is occasionally seen, with curvilinear airspace separating the fungal ball from the cavity. Pathogenic fungi that cause pneumonia can infect anyone (coccidioidomycosis, blastomycosis, histoplasmosis) or saprophytic fungi that only infect immunocompromised people (pneumocystis, Candidiasis, aspergillosis, mucormycosis) [22]. *Aspergillus fumigatus* is a very common fungus. It infects people who are immunocompromised or vulnerable. The five types of pulmonary manifestations are simple aspergilloma, allergic bronchopulmonary aspergillosis (ABPA), airway invasive pulmonary aspergillosis, angioinvasive pulmonary aspergillosis, and chronic pulmonary aspergillosis. Aspergilloma is a conglomerate of mycelial hyphae. It typically colonises pre-existing cavities caused by a predisposing condition such as tuberculosis, sarcoidosis, or another. On chest radiographs, they appear as round/oval lesions within a cavity. An 'air crescent' sign, with curvilinear airspace separating the fungal ball from the cavity, is occasionally seen. Immunocompromised patients are more likely to develop airway-invasive aspergillosis. Acute tracheobronchitis, bronchiolitis, or bronchopneumonia can occur. Tracheobronchitis is manifested on imaging as tracheal and/or bronchial wall thickening, but imaging findings may be normal. Centrilobular nodules and branching or linear opacities with a 'tree in bud' appearance are common CT findings in bronchiolitis. Bronchopneumonia is characterised by peribronchial consolidation [24]. An 'air crescent' sign, with curvilinear airspace separating the fungal ball from the cavity, is occasionally seen. Angio-invasive aspergillosis only occurs in immunocompromised patients, most of whom have neutropenia. This pulmonary infection is caused by the invasion of small to medium arteries, which results in the formation of necrotic haemorrhagic nodules or infarcts in the lungs. Nodules or wedge-shaped opacities on imaging are common in subpleural areas. Cavitation or an air crescent sign may be seen during the convalescence period, which lasts about 2-3 weeks after treatment. A vessel occlusion sign' may be seen on CT pulmonary angiography. [25]. *Cryptococcus neoformans* is a yeast fungus found in soil and bird droppings. It occurs more frequently in immunocompromised patients. The chest radiograph may reveal single or multiple subpleural nodules ranging in size from 0.5 to 4 cm. Mucormycosis infection is caused by spore inhalation. The most commonly affected organs are the paranasal sinuses and the lungs. Diabetes, immunosuppression, haematological malignancy, and stem cell or solid organ transplant recipients are all risk factors [26]. The imaging findings are agnostic [27]. A chest radiograph reveals lobar/multilobar consolidation, as well as single or multiple nodules and masses. CT reveals nodules or GGO consolidation. The following imaging reveals cavitation in areas of consolidation [28] (Fig-6) [9]. There may be lymphadenopathy and pleural effusion.





GASTROINTESTINAL INFECTIONS

Invasive fungal infections can spread to almost any body compartment, visceral organ, or tissue, including the digestive and hepatobiliary systems. Invasive disseminated fungal and fungal-like bowel involvement is uncommon and more common in immunocompromised individuals. Patients exhibit nonspecific symptoms such as abdominal pain, distension, vomiting, diarrhoea, and fever. In immunocompromised patients, particularly those receiving chemotherapy for haematological malignancies, hepatosplenic candidiasis is a manifestation of disseminated candidiasis. Because hepatic and splenic infection usually occurs at the same time, they are treated together. On imaging, it usually appears as multiple microabscesses scattered throughout the liver and splenic parenchyma. *Candida* species can infiltrate the intestinal mucosa and enter the liver via portal circulation during periods of severe neutropenia [29]. On images from the United States, four distinct patterns of hepatic candidiasis have been identified: The appearance of a "bull's-eye" is that of a central echogenic focus surrounded by a hypoechoic halo. A peripheral hypoechoic rim surrounds an echogenic "wheel," which surrounds a hypoechoic centre in the "wheel-within-a-wheel" configuration. The two patterns that remain are a homogeneous hypoechoic nodule and an echogenic focus caused by scar formation. CT reveals small circumscribed hypoattenuating lesions, with tiny central foci of increased attenuation within, most likely reflecting pseudohyphae. On MR images, microabscesses are T2 hyperintense and T1 hypointense in the centre [30]. Because of the small size of the microabscesses, diffusion restriction may be difficult to detect on MR images. Larger abscesses that resemble pyogenic processes are rare (Fig-7) [9].

CONCLUSION

As the number of immunocompromised people rises invasive fungal and fungal-like infections are becoming more common and more widely known. These microorganisms frequently result in more subdued infections in immunocompetent people, but they have the propensity to spread quickly and can rapidly become fatal in immunosuppressed hosts. Imaging is a crucial part of identifying and treating suspected lung infections, and chest radiographs and CT scans can show important symptoms. If these symptoms are recognised early, they can frequently be utilised to identify the pathophysiologic process and causal agent, as well as possible to improve patient management. Because of the non-specific alterations and the presence of anomalies from the underlying disease, early detection of fungus infections in oncology patients receiving chemotherapy can be challenging. Diagnostic imaging in children at risk for IFD plays a key role in diagnostic evaluation and therapeutic monitoring, even if a definite diagnosis cannot be made. Imaging is essential to track therapy response and spot problems. Within the last 25 years, diagnostic imaging has undergone a technological revolution. Future research on paediatric mycoses is required to better understand the role of these technologies in early identification and the implications of using modality-specific data to reduce the number of possible diagnoses for these fatal diseases. Certain fungi and fungi-like illnesses have distinct imaging presentations, while others present with more vague symptoms. Therefore, it is essential that doctors have a low barrier for ordering imaging and that radiologists have a low threshold for suspecting a fungal aetiology of disease in patients who are at high risk of contracting these infections. The radiologist should recognize how various infections manifest throughout the body and be able to infer the presence of specific organisms based on their distinct illness patterns.

REFERENCES

1. Ahmad SS, Abdullah WA, Wastie ML, Imaging features of fungal infection in immuno-suppressed patients in a local ward outbreak, *Biomed Imaging Interv J* 2006;2(2).
2. Pennisi M, Antonelli M. Clinical aspects of invasive candidiasis in critically ill patients. *Drugs* 2009; 69 (Suppl. 1): 21 – 28.
3. Pappas PG, Kauffman CA, Andes D, *et al.* Clinical practice guidelines for the management of candidiasis: 2009 update by the Infectious Diseases Society of America. *Clin Infect Dis* 2009; 48: 503 – 535.
4. Hoyert DL, Xu J. Deaths: preliminary data for 2011. *Natl Vital Stat Rep* 2012; 61:1–51.



**Divya Chauhan et al.,**

5. Starkey J, Moritani T, Kirby P. MRI of CNS fungal infections: review of aspergillosis to histoplasmosis and everything in between. *ClinNeuroradiol* 2014;24(3):217–230.
6. Mathur M, Johnson CE, Sze G. Fungal infections of the central nervous system. *Neuroimaging Clin N Am* 2012;22(4):609–632.
7. Katragkou A, Brian TF, Groll AH, Roilides E, et al. Diagnostic Imaging and Invasive Fungal Diseases in Children. *Journal of the Pediatric Infectious Diseases Society* 2017;6 (Suppl 1)
8. Jain KK, Mittal SK, Kumar S, Gupta RK. Imaging features of central nervous system fungal infections. *Neurol India* 2007;55(3):241–250.
9. Orłowski HLP, McWilliams S, Mellnick VM, Bhalla S, Lubner MG, Pickhardt PJ, Menias CO, Imaging Spectrum of Invasive Fungal and Fungal-like Infections, *radiographics.rsna.org* 2017; 37:1119–1134
10. Mathur M, Johnson CE, Sze G. Fungal infections of the central nervous system. *Neuroimaging Clin N Am* 2012;22(4):609–632.
11. Parikh SL, Venkatraman G, DelGaudio JM. Invasive fungal sinusitis: a 15-year review from a single institution. *Am J Rhinol* 2004;18(2):75–81.
12. Payne SJ, Mitzner R, Kunchala S, Roland L, McGinn JD. Acute invasive fungal rhinosinusitis: a 15-year experience with 41 patients. *Otolaryngol Head Neck Surg* 2016;154 (4):759–764.
13. Aribandi M, McCoy VA, Bazan C 3rd. Imaging features of invasive and noninvasive fungal sinusitis: a review. *Radio- Graphics* 2007;27(5):1283–1296.
14. Raj KA, Srinivasamurthy BC, Nagarajan K, Sinduja MG. A rare case of spontaneous *Aspergillus* spondylodiscitis with epidural abscess in a 45-year-old immunocompetent female. *J Craniovertebr Junction Spine* 2013;4(2):82–84.
15. El Ghannudi S, Imperiale A, Dégot T, Germain P, Trinh A, Petean R, et al. Multimodality diagnosis approach of cardiac Aspergillosis. *Echocardiography* 2016; 33:663–665.
16. Chinen K, Tokuda Y, Sakamoto A, Fujioka Y. Fungal infections of the heart: a clinicopathologic study of 50 autopsy cases. *Pathol Res Pract* 2007;203(10):705–715.
17. Millar BC, Jugo J, Moore JE. Fungal endocarditis in neonates and children. *PediatrCardiol* 2005; 26(5):517-36.
18. Pasqualotto AC, Denning DW. Post-operative aspergillosis. *Clin Microbiol Infect.* 2006;12(11):1060-76.
19. Ellis ME, Al-Abdely H, Sandridge A, Greer W, Ventura W. Fungal endocarditis: evidence in the world literature, 1965-1995. *Clin Infect Dis* 2001;32(1):50-62.
20. Martín-Dávila P, Navas E, Fortún J, et al. Analysis of mortality and risk factors associated with native valve endocarditis in drug users: the importance of vegetation size. *Am Heart J* 2005;150(5):1099–1106.
21. Talib N, Mohammed Y, SharipahIntan S, Abas SY and Kama AAR. Multimodality Imaging Features Of Cardiac Fungal Infection: A Case Report. *Cardiovasc Imaging Asia* 2019 Oct;3(4):125-128.
22. Padley SPG, Rubens MB. Pulmonary Infections. In: Sutton D, editor. *Textbook of Radiology and Imaging*. Edinburgh: Churchill Livingstone; 2003. pp. 131–160.
23. Prasad A, Agarwal K, Deepak D, Atwal SS. Pulmonary Aspergillosis: What CT can Offer Before it is too Late! *J Clin Diagn Res* 2016;10:TE01–TE05.
24. Franquet T, Müller NL, Oikonomou A, Flint JD. *Aspergillus* infection of the airways: computed tomography and pathologic findings. *J Comput Assist Tomogr* 2004;28:10–16.
25. Henzler C, Henzler T, Buchheidt D, et al. Diagnostic Performance of Contrast Enhanced Pulmonary Computed Tomography Angiography for the Detection of Angioinvasive Pulmonary Aspergillosis in Immunocompromised Patients. *Sci Rep* 2017;7:4483.
26. Chung JH, Godwin JD, Chien JW, Pipavath SJ. Case 160: Pulmonary mucormycosis. *Radiology* 2010;256:667–670.
27. Choo JY, Park CM, Lee HJ, et al. Sequential morphological changes in follow-up CT of pulmonary mucormycosis. *DiagnIntervRadiol* 2014;20:42–46.
28. Maturu VN, Agarwal R. Reversed halo sign: a systematic review. *Respir Care* 2014; 59:1440–1449.
29. Nicholas J. E. Moore, Johnsey L. Leef, III, Yijun Pang. Systemic Candidiasis. *RadioGraphics* 2003; 23 (5): 1287-90.
30. Mortelé KJ, Segatto E, Ros PR. The infected liver: radiologic/pathologic correlation. *RadioGraphics* 2004;24(4):937–955.





REFERENCES

1. Ahmad SS, Abdullah WA, Wastie ML, Imaging features of fungal infection in immuno-suppressed patients in a local ward outbreak, Biomed Imaging Interv J 2006;2(2).
2. Pennisi M, Antonelli M. Clinical aspects of invasive candidiasis in critically ill patients. Drugs 2009; 69(Suppl. 1): 21 – 28.
3. Pappas PG, Kauffman CA, Andes D, et al. Clinical practice guidelines for the management of candidiasis: 2009 update by the Infectious Diseases Society of America. Clin Infect Dis 2009; 48: 503 – 535.
4. Hoyert DL, Xu J. Deaths: preliminary data for 2011. Natl Vital Stat Rep 2012; 61:1–51.
5. Starkey J, Moritani T, Kirby P. MRI of CNS fungal infections: review of aspergillosis to histoplasmosis and everything in between. ClinNeuroradiol 2014;24(3):217–230.
6. Mathur M, Johnson CE, Sze G. Fungal infections of the central nervous system. Neuroimaging Clin N Am 2012;22(4):609–632.
7. Katragkou A, Brian TF, Groll AH, Roilides E, et al. Diagnostic Imaging and Invasive Fungal Diseases in Children. Journal of the Pediatric Infectious Diseases Society 2017;6 (Suppl 1)
8. Jain KK, Mittal SK, Kumar S, Gupta RK. Imaging features of central nervous system fungal infections. Neurol India 2007;55(3):241–250.
9. Orłowski HLP, McWilliams S, Mellnick VM, Bhalla S, Lubner MG, Pickhardt PJ, Menias CO, Imaging Spectrum of Invasive Fungal and Fungal-like Infections, radiographics.rsna.org 2017;37:1119–1134
10. Mathur M, Johnson CE, Sze G. Fungal infections of the central nervous system. Neuroimaging Clin N Am 2012;22(4):609–632.
11. Parikh SL, Venkatraman G, DelGaudio JM. Invasive fungal sinusitis: a 15-year review from a single institution. Am J Rhinol 2004;18(2):75–81.
12. Payne SJ, Mitzner R, Kunchala S, Roland L, McGinn JD. Acute invasive fungal rhinosinusitis: a 15-year experience with 41 patients. Otolaryngol Head Neck Surg 2016;154 (4):759–764.
13. Aribandi M, McCoy VA, Bazan C 3rd. Imaging features of invasive and noninvasive fungal sinusitis: a review. Radio- Graphics 2007;27(5):1283–1296.
14. Raj KA, Srinivasamurthy BC, Nagarajan K, Sinduja MG. A rare case of spontaneous *Aspergillus* spondylodiscitis with epidural abscess in a 45-year-old immunocompetent female. J Craniovertebr Junction Spine 2013;4(2):82–84.
15. El Ghannudi S, Imperiale A, Dégot T, Germain P, Trinh A, Petean R, et al. Multimodality diagnosis approach of cardiac Aspergillosis. Echocardiography 2016; 33:663–665.
16. Chinen K, Tokuda Y, Sakamoto A, Fujioka Y. Fungal infections of the heart: a clinicopathologic study of 50 autopsy cases. Pathol Res Pract 2007;203(10):705–715.
17. Millar BC, Jugo J, Moore JE. Fungal endocarditis in neonates and children. PediatrCardiol 2005; 26(5):517–36.
18. Pasqualotto AC, Denning DW. Post-operative aspergillosis. ClinMicrobiol Infect. 2006;12(11):1060–76.
19. Ellis ME, Al-Abdely H, Sandridge A, Greer W, Ventura W. Fungal endocarditis: evidence in the world literature, 1965-1995. Clin Infect Dis 2001;32(1):50–62.
20. Martín-Dávila P, Navas E, Fortún J, et al. Analysis of mortality and risk factors associated with native valve endocarditis in drug users: the importance of vegetation size. Am Heart J 2005;150(5):1099–1106.
21. Talib N, Mohammed Y, SharipahIntan S, Abas SY and Kama AAR. Multimodality Imaging Features Of Cardiac Fungal Infection: A Case Report. Cardiovasc Imaging Asia 2019 Oct;3(4):125-128.
22. Padley SPG, Rubens MB. Pulmonary Infections. In: Sutton D, editor. Textbook of Radiology and Imaging. Edinburgh: Churchill Livingstone; 2003. pp. 131–160.
23. Prasad A, Agarwal K, Deepak D, Atwal SS. Pulmonary Aspergillosis: What CT can Offer Before it is too Late! J ClinDiagn Res 2016;10:TE01–TE05.
24. Franquet T, Müller NL, Oikonomou A, Flint JD. *Aspergillus* infection of the airways: computed tomography and pathologic findings. J Comput Assist Tomogr 2004;28:10–16.





Divya Chauhan et al.,

25. Henzler C, Henzler T, Buchheidt D, et al. Diagnostic Performance of Contrast Enhanced Pulmonary Computed Tomography Angiography for the Detection of Angioinvasive Pulmonary Aspergillosis in Immunocompromised Patients. *Sci Rep* 2017;7:4483.
26. Chung JH, Godwin JD, Chien JW, Pipavath SJ. Case 160: Pulmonary mucormycosis. *Radiology* 2010;256:667–670.
27. Choo JY, Park CM, Lee HJ, et al. Sequential morphological changes in follow-up CT of pulmonary mucormycosis. *DiagnIntervRadiol* 2014;20:42–46.
28. Maturu VN, Agarwal R. Reversed halo sign: a systematic review. *Respir Care* 2014; 59:1440–1449.
29. Nicholas J. E. Moore, Johnsey L. Leef, III, Yijun Pang. Systemic Candidiasis. *RadioGraphics* 2003; 23 (5): 1287-90.
30. Mortelé KJ, Segatto E, Ros PR. The infected liver: radiologic/pathologic correlation. *RadioGraphics* 2004;24(4):937–955.

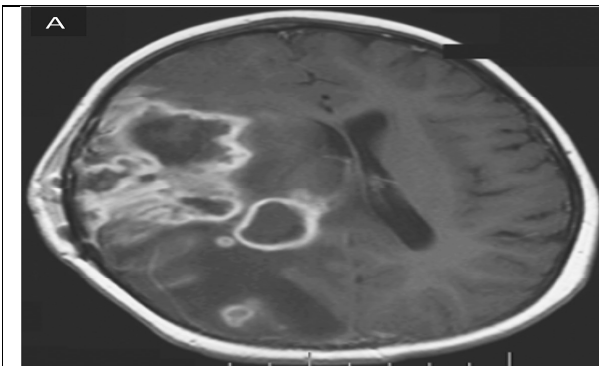


Fig-1 An MRI of a 7-year-old girl with pre-B-cell acute lymphocytic leukaemia who presented with neutropenia, cough, left arm paralysis and left homonymous hemianopsia. This MRI of the head revealed numerous cortical and subcortical infarcts, as well as surrounding oedema, resulting in a mass effect. *Aspergillus fumigatus* was grown from a brain biopsy specimen culture

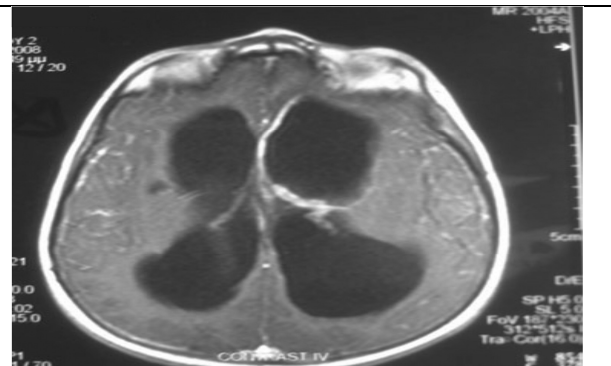
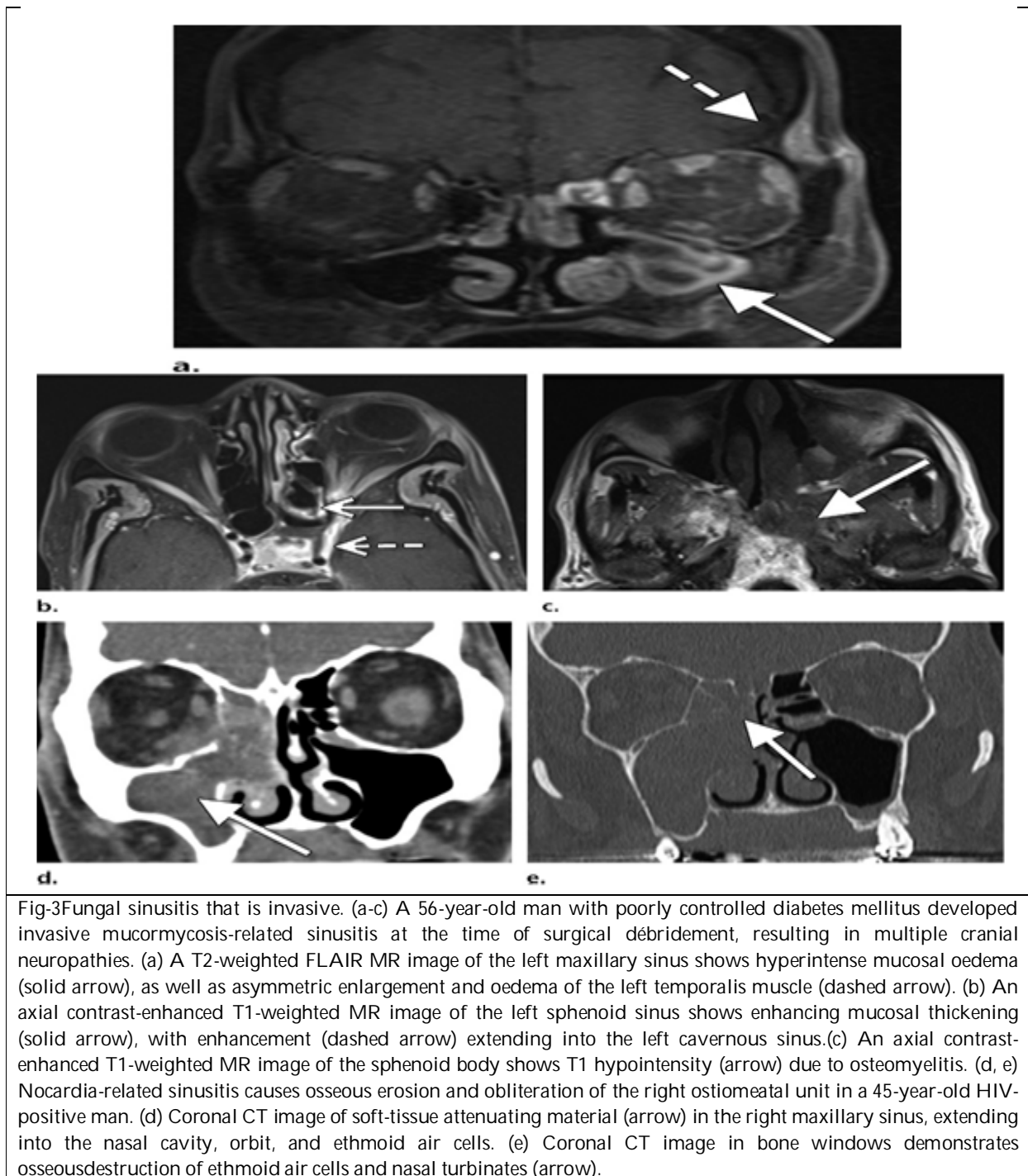


Fig- 2 Five-year-old girls with refractory central nervous system tuberculosis complicated by *Aspergillus fumigatus* ventriculitis. Her case was complicated by hydrocephalus, which necessitated the placement of a ventriculoperitoneal shunt. She developed a high fever and tonic/clonic seizures of the upper limbs while receiving antituberculosis treatment. A T1-weighted MRI of the brain after gadolinium paramagnetic substance infusion revealed significant ventricular dilatation and enhancement of the ependymal lining of the left ventricle's frontal horn. (Adapted from Antachopoulos C, et al. Ventriculitis caused by *Aspergillus fumigatus* in a child with central nervous system tuberculosis. *Mycoses* 2011; 54:e627-30.)







Divya Chauhan et al.,

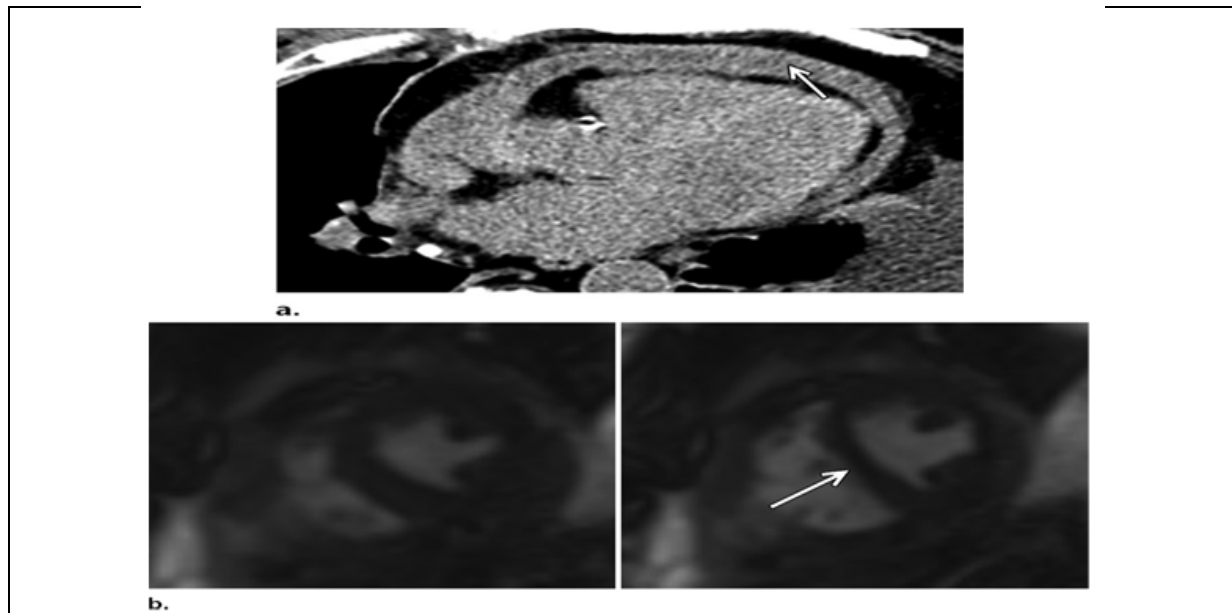


Fig - 4 A 55-year-old man with acute myelogenous leukaemia complicated by *Candida*-related pericarditis (as seen at pericardiocentesis) and constrictive hemodynamics. (a) A nonenhanced transverse CT image of the thorax shows pericardial fluid and thickening (arrow), as well as a left pleural effusion. (b) Short-axis cine steady-state free precession cardiac MR images obtained during suspended respiration (left) and sniffing (right) show interventricular septum flattening during sniffing (arrow). This finding suggests that ventricular interdependence is caused by constrictive

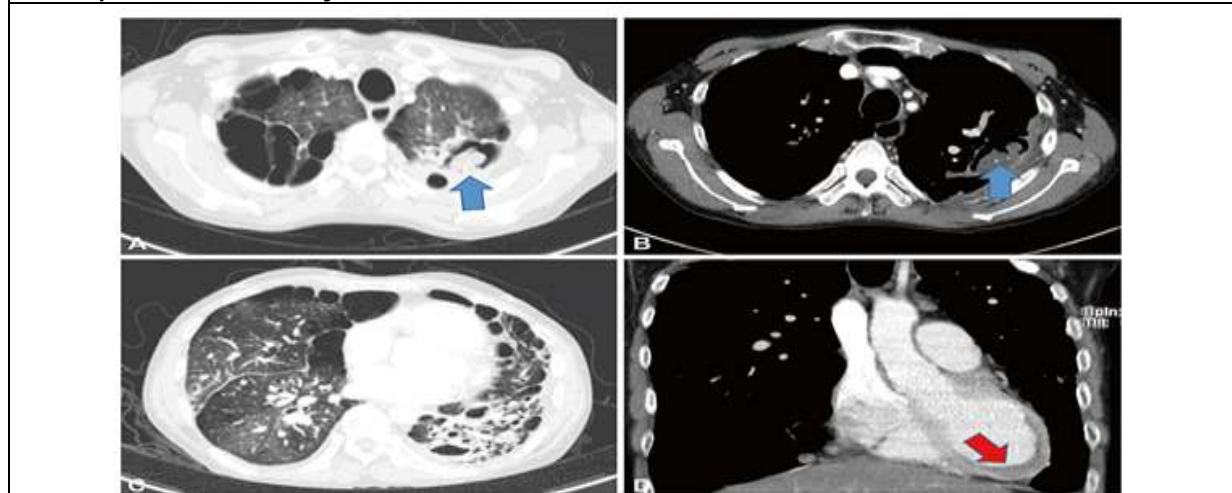


Fig - 5 Chest CT of a 38-year-old man with cardiac aspergilloma. Serial, selective, axial-view chest CT images in lung and mediastinal windows were taken one month before echocardiography and cardiac MRI. A: An intracavitary lesion resembling an invasive lung aspergilloma (blue arrow). B: There is calcification within the lesion (blue arrow). C: The patient had a history of bronchiectasis with mucus plugging, low blood pressure, and mosaic lung parenchyma attenuation. D: There was an ill-defined hypodensity in the apical left ventricle wall in coronal view; no fungating mass was visible (red arrow).





Divya Chauhan et al.,

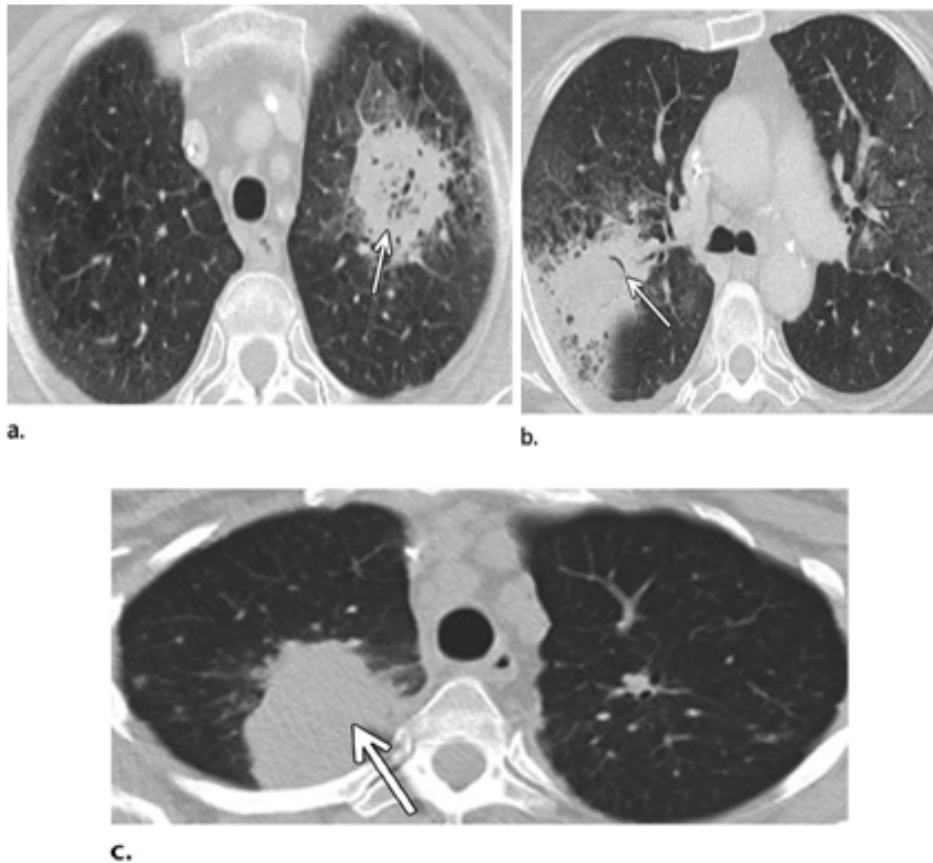


Fig - 6(a,b) Acute myelogenous leukaemia and angioinvasive pulmonary aspergillosis are depicted in Figures 6(a,b). (a) A masslike area of airspace disease with air bronchograms (arrow) and a halo of ground-glass opacity in the left upper lung lobe is visible on a transverse CT image of the thorax. (b) A nodule with a ground-glass halo of opacity in the posterolateral aspect of the right upper lobe is seen in a transverse CT image of the thorax. A hemorrhagic infarct is represented by the halo of ground-glass opacity, and the air-crescent sign (arrow) in the nodule is an immune response. (c) Pulmonary cryptococcosis in a 39-year-old man being treated with long-term prednisone. A right upper lobe mass (arrow) with a surrounding area of ground-glass opacity and other scattered nodules is visible in a transverse CT image of the thorax.



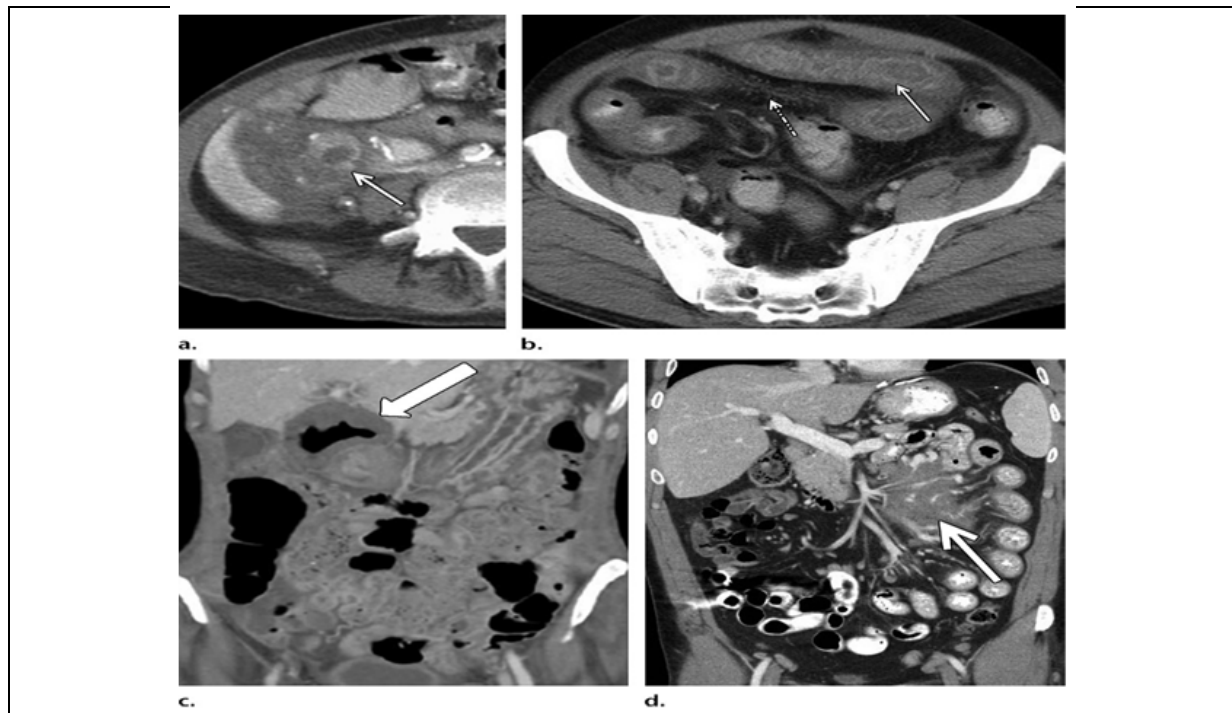
Divya Chauhan *et al.*,

Fig-7 Fungal infections in the gastrointestinal tract. (a) Axial contrast-enhanced CT image of a 30-year-old woman with a right lower quadrant pancreas transplant and disseminated *Candida* infection revealed by biopsy reveals hypoattenuating tissue surrounding and within the pancreas allograft (arrow). **(b)** An axial contrast-enhanced CT image of a 27-year-old immunocompromised man with disseminated blastomycosis involving the small bowel shows bowel wall thickening (solid arrow) with mucosal enhancement, adjacent inflammatory fat stranding (dashed arrow), and prominence of the adjacent vasculature, which is most commonly seen with inflammatory bowel disease. **(c)** A coronal CT image of a severely immunocompromised 30-year-old man shows significant duodenal wall thickening and dilatation (arrow) due to disseminated mucormycosis. The thickening of the wall extends to the adjacent liver. **(d)** A 40-year-old man with type 1 diabetes mellitus has jejunal and mesenteric coccidioidomycosis (arrow), which was discovered during surgery.





Automated Detection and Segmentation of Mammogram Images using Deep Learning Techniques

Dhivya S¹, Mohanavalli S², Kavitha S³ and Sripriya N⁴

¹Research Scholar, Department of Information Technology, Sri Sivasubramaniya Nadar College of Engineering, Kalavakkam, Tamil Nadu, India.

²Associate Professor, Department of Information Technology, Sri Sivasubramaniya Nadar College of Engineering, Kalavakkam, Tamil Nadu, India.

³Associate Professor, Department of Computer Science and Engineering, Sri Sivasubramaniya Nadar College of Engineering, Kalavakkam, Tamil Nadu, India.

⁴Associate Professor, Department of Information Technology, Sri Sivasubramaniya Nadar College of Engineering, Kalavakkam, Tamil Nadu, India.

Received: 13 Nov 2022

Revised: 25 Apr 2023

Accepted: 31 May 2023

*Address for Correspondence

Dhivya S

Research Scholar,
Department of Information Technology,
Sri Sivasubramaniya Nadar College of Engineering,
Kalavakkam, Tamil Nadu, India



This is an Open Access Journal / article distributed under the terms of the **Creative Commons Attribution License** (CC BY-NC-ND 3.0) which permits unrestricted use, distribution, and reproduction in any medium, provided the original work is properly cited. All rights reserved.

ABSTRACT

For past decades, the high demand for early detection of breast cancer across many hospitals and screening centers has led to new research contributions. According to International Agency of Research on Cancer (IARC), early diagnosis of breast tumor provides a better treatment plan for patients. The Computer Aided Diagnosis has leveraged the detection of abnormalities in the imaging modalities. Amongst several imaging modalities, mammography is a commonly used method for detection of abnormalities. The automated breast mass segmentation in mammograms is quintessential, however its quite challenging due to the invariable sizes and shapes of tumors. In this study, we propose four different segmentation models using UNet for detection and segmentation of breast masses in mammogram images. The proposed models Unet128 and Unet256 with two different optimizers which are evaluated using CBIS-DDSM dataset. Several hyper parameters are tuned and the observations are compared. Amongst the four models, the Unet128Ad yielded an accuracy of 97.1%, a dice score of 89.1% and an IOU of 88% compared to other models.

Keywords: Breast cancer, CBIS-DDSM, Segmentation, Deep learning, UNet





Dhivya et al.,

INTRODUCTION

Breast cancer is a lethal disease among women across globe and considered to be second disease for an increased mortality rate worldwide. According to Indian Council for Medical Research, the mortality rate due to this disease is high in India and amongst the urban and rural regions, there is a high incidence in the rural areas because of delayed diagnosis of the disease [1]. In general, the screening is done based on the population based or risk based on the patients. However, these are not employed in rural areas leading to a high risk for women. Early detection of these tumors assists a better survival rate of the patients. As a initial process to detect tumor, the procedures such as non-invasive methods of detection are employed through Mammography, thermography, Computed Tomography, Magnetic Resonance Imaging, Positron Emission Tomography and Digital Breast tomosynthesis are employed [2]. Among the several imaging modalities, mammography is an efficient and effective tool for diagnosis of the breast tumor. Nonetheless, analysis of the mammograms is inferred by expert radiologists and considered to be laborious and time-consuming tasks. At times, the diagnosis needs double reading due to the mislead interpretations or leads to overdiagnosis. Hence a computer aided diagnosis (CAD) system can be used to assist radiologists for more precise diagnosis. It is also unnatural to have expert radiologists across all primary centers and hospitals, hence these systems could alleviate the workload of the radiologists. The CAD systems along with artificial intelligence has shown a remarkable amelioration in disease diagnosis. There are several abnormalities such as breast lesions or masses, irregular tissues, micro calcifications, dense tissues are observed. Amongst these abnormalities, the breast lesions or masses are considered for breast tumor detection. For image or patch level detection of masses, segmentation plays an inevitable role leading to reduced mortality rate. The early segmentation techniques include edge based, regions based and thresholding techniques [4]. The disadvantages of these techniques are illustrated in Table 1.

Recently, the advancement of deep learning algorithms, especially convolutional neural networks (CNNs) have taken a quantum leap in both computer vision and medical imaging. Deep learning methods have gained enormous attention due to its ability in automated feature extraction by learning the underlying patterns in complex images. With respect to medical imaging domain, the datasets are of limited size. However, deep learning algorithms need a huge volume of data to infer and extract information [18]. Hence, conventional data augmentation is used to build our corpus data to train the model. During data augmentation process, it is necessary to choose the values for the transformations with utmost care to avoid loss of any vital features from the images. Among deep learning methods, UNet model is majorly employed for segmentation applications across several domains. The proposed UNet model have outperformed the state of art methods for mammogram segmentation. The proposed UNet model detect and segment the abnormalities in the mammograms. The section II describes the existing works in segmentation of mammogram images. Section III gives an overview of the proposed model. While section IV elucidates the experiments and results and section V deals with the conclusion and future works.

Related Work

Parvin Yousefikamal [12] represented a fast and efficient framework for breast cancer diagnosis. There were two main parts in this process. Firstly, classifying the image as normal or abnormal and secondly the tumor region segmentation. For enhancing the image, preprocessing included noise reduction by means of the block matching and 3D filtering (BM3D), tag elimination, and pectoral muscle removal from the images. For classifying, CNNs were used for extracting the features from images automatically. Determining the area of the tumor was done through Level-set area segmentation based on the Spatial Fuzzy Clustering (LS-SFC) which contains spatial and local intensity information. The method has been able to extract the tumor area in a more precise way compared to earlier traditional methods. Hao Dong, *et al.*, [8], proposed a two-dimensional fully convoluted UNet network for brain tumor diagnosis. The authors have scaled up the data by using rigid or affine based deformation along with distortion-based transformations. The color brightness techniques are also part of the data augmentation techniques. The UNet architecture is adapted for the segmentation task with loss function based on soft dice in order to handle unbalanced samples in an adaptive way.



**Dhivya et al.,**

In paper [6], Dhivya S *et al.*, have used geometric transformations as conventional data augmentation method to scale the data of 20 folds high to feed into deep learning models. This work also used generative adversarial networks to synthesize the mammogram images for an enhanced classification of the tumor lesions. Huimin Huang *et al.*, [9], proposed a U-net 3+ used on liver and spleen datasets for enhanced segmentation. The re-design of the full - scale skip connections are employed. This model aims to yield fewer parameters but are capable to gain insight about position aware segmentation maps with enhanced boundaries. The two tasks involved are full scale deep supervision and classification guided module (CGM). The initial module is to capture the hierarchical patterns from the hierarchical feature maps and a loss function to find the boundary of the organ. CGM provides generalizability of the segmentation on non-organ images by jointly training with an image-level classification. From Experimental result it is evident that the proposed model performed better on both liver and spleen datasets.

Anoop Sathyan *et al* has detected the presence of abnormalities in mammogram images, and segmented both masses and calcifications in mammogram images using a fully convolutional architecture (UNet) [13]. Two different unets are used (1) UNet-Mass, and (2) UNet-Calc, for mass and calcification segmentation, respectively. The UNet-Mass was trained on the CBIS-DDSM dataset, whereas the UNet-Calc was trained on the INBreast dataset. Mass segmentation and calcification detection are performed. The UNet-Mass can identify most of the mass regions, but it still has some false positives and false negatives and can be improved using cropped images. Hui Sun *et al* [18] devised an attention guided dense up sampling network called AUNet for precise segmentation of breast lesions in mammograms. In this work, an asymmetrical encoder-decoder with an attention guided up sampling is focused to reduce the information loss due to dense up sampling. The model achieved a better fusion of both high and low-level features. The model is validated on CBIS-DDSM and IN breast dataset. The model yielded a dice coefficient of 81.8% for CBIS-DDSM and 79.1% for INbreast.

Xiaobo Lai *et al* [19] proposed a UNet architecture which is validated using Digital breast tomosynthesis (DBT) images, where preprocessing of the data is done by removing the noises followed by contrast enhancement and transformation. Median filters are applied to smooth the boundaries for final segmentation process. Data augmentation techniques are employed and better UNet model is devised for the segmentation of DBT images and yielded a detection accuracy of 0.871. Jiande Pi *et al* [11] devised an encoder- decoder based architecture namely FS-UNet which enables feature strengthening to obtain the masses and other cell level enhanced information thereby improvised the low level feature layers with that of high level feature maps. The intricate details of the masses such as edges, features at different resolutions and internal representations are obtained by applying parallel dilated convoluted module. The loss function adopted uses the mutual information between the actual and the target to optimize the accuracy.

Haichao Cao *et al* [20] constructed a novel method to segment the breast masses using an UNet architecture called Cas-UNet. This network encompasses six UNet sub networks, that includes channel attention mechanism in a way to obtain the contributing feature maps. To address the less data problem, data augmentation is employed using a histogram augmentation method. INBreast and CBIS-DDSM are used to validate the proposed model which yielded a better accuracy compared to existing other methods. There are several other deep learning algorithms such as SegNet, DCNN and Mask RCNN were used for segmentation of the images in medical images. In our research work we focus on encoder decoder-based network called UNet for segmentation of the breast masses in mammogram images.

METHODOLOGY

In our proposed work, a segmentation model is developed to segment tumors in the given images. This work consists of three main steps: data acquisition, data augmentation, training, and testing of the model. The proposed architecture is illustrated in Fig1.





Dhivya et al.,

Datasets

The datasets used for this research is the subset of Digital Database for Screening Mammography (DDSM) which includes nearly 2,620 scanned film mammography. The CBIS-DDSM, subspace of DDSM which are handled, standardized, and curated by radiologists [5]. The regions of interests are extracted, and the skeptical regions were also identified and marked. This comprehensive dataset contains masses, calcifications, region of interest and their corresponding masks. The mass cases are around 891 and calcification cases are around 753 cases with Mediolateral oblique (MLO) and craniocaudal (CC) views. The CBIS-DDSM datasets are publicly available and are widely used in several research works in the directions of classification of the masses and the calcifications and also for segmentation tasks. Fig 2 represent the full mammogram images and Fig 3 represent the RoIs and the corresponding masked images from the dataset. The training and testing images along with their masses from CBIS-DDSM dataset are used for segmentation. For training deep learning models, the dataset should comprise of humongous data, hence there is a scope for data augmentation using conventional geometric transformations.

Data Augmentation

Data augmentation is a data preparation step to scale up the dataset for a better optimized classification. This process involves transformation techniques which are applied to the images resulting in transformed copies for each image. The obtained images are quite different to each other which is completely based on the augmentation techniques such as shifting, rotating and flipping. The transformation of the images must be done with utmost care in a way not to change its target class. Thus, these images can be used for building deep learning models. The dataset considered in our research are ROIs, hence major rotation of the images, does not affect the truth markings of the image. Hence random rotations can be applied, and corresponding affine transformations can be employed. In paper [6], Dhivya S et al have employed conventional augmentation techniques to scale up mammogram datasets for classification tasks. It is used to synthesize the size of a training dataset by creating modified versions of images in the dataset. The dataset is scaled up for 5-foldhigh which are further used to validate our model. This augmentation of the corpus can also be built using deep learning models using generative adversarial networks and Auto encoders. In this work, the conventional data augmentation techniques are listed in the Table II.

Segmentation model using UNet

In our proposed work the benchmark breast cancer datasets are used, and segmentation is done using a deep-learning algorithm. Olaf ronberger et al [3] devised an algorithm to segment the biomedical images. The architecture consists of an encoder also called as contraction path which infers the context in the image. This encoder has a collection of convolution and maxpooling layers. Whereas the other path is a decoder that has a symmetric expanding path which involves transposed convolution networks to obtain accurate localization. Thus, both the encoder and decoder form an end to end fully convolutional layer. The cropped images and its corresponding ROI (Region of Interest) is fed into the UNet model for training; and in the test images ROI is extracted so that the classification becomes faster, efficient and enhanced. UNet model is commonly used for segmentation of biomedical images.

Evaluation metrics for Segmentation

The metrics used for evaluation of the model on segmentation tasks are pixel Accuracy, dice coefficient and IOU. The True positives (TP), True negatives (TN), False positives (FP), False Negatives (FN) are calculated. The performance metrics are used to quantify the performance of the segmentation model on the given dataset.

Pixel Accuracy: The pixel accuracy denotes the ratio of the pixels in the image which are correctly classified. With respect to segmentation tasks, the pixel accuracy is evaluated on binary mask, where the correctly classified pixels are denoted as true positive and true negative belong to those that do not belong to the class. It is given in equation 1.

$$\text{Pixel accuracy} = \frac{TP+TN}{TP+TN+FP+FN} \quad (1)$$





Dhivya et al.,

Dice coefficient: Dice coefficient also referred to as the F1-score, which is used to provide the similarity of two images. The overlap between the two masks is provided where a 1 stand for accurate overlap whereas 0 indicates no overlap. The dice score is calculated as

$$\text{Dice score} = \frac{2|A \cap B|}{|A| + |B|} \quad (2)$$

In case of Dice coefficient calculation of predicted segmentation masks, $|A \cap B|$ can be considered as the element-wise product between the obtained and actual mask, and then aggregate the obtained matrix.

Intersection over Union: The Intersection over Union (IoU) metric, also known as the Jaccard index, calculated the ratio of overlap between the actual mask and our obtained mask. It measures the ratio of number of common pixels between the actual and obtained masks to the total number of pixels present in both masks.

$$\text{Intersection Over Union}(A, B) = \frac{A \cup B}{A \cap B} \quad (3)$$

$A \cap B$ comprises the pixels commonly found in both the prediction mask and the ground truth mask, whereas the $A \cup B$ simply includes all pixels found in either actual or obtained mask.

RESULTS AND DISCUSSION

The images are resized to 256x256 and 128x128, and they are fed to the respective UNet models UNet128 and UNet256. The UNet model contains 10 convolutional layers where each of the process contains convolution process and max pooling which occurs in down sampling followed by merging in up sampling. The different values of parameters that contribute towards an enhanced segmentation is investigated. For the given two input sizes, the optimizer used are Adam and Rmsprop. The learning rates used are the 1e-5 and 1e-4. The UNet128Rp, UNet256Rp, UNet128Ad, UNet256Ad were trained on a workstation with NVIDIA GeForce GTX TITAN X GPU for 50 epochs with a batch size 20. The model is trained from scratch rather than using any pre-trained weights. The UNet models UNet256Ad and UNet256Rp are time consuming as the inputs involved are of large size. However, the UNet128Ad and UNet128Rp consumes lesser time when compared to the other two models. In this work, the UNet is used for binary label semantic segmentation, where the pixels are classified into benign and malignant. With respect to loss function, the models with RMSprop optimizers are larger than models with Adam optimizers. The results are tabulated in Table III and the UNet128Ad have outperformed the other three models with pixel accuracy of 97.1%, dice score of 89.1% and IOU of 88%.

CONCLUSION AND FUTURE WORK

With respect to medical image segmentation, there is a need to convert the feature maps into a vector and is a tedious task for the conversion of a feature map into images. This research proposed in this paper present an automated segmentation algorithm for localizing tumor in digital mammograms. This proposed algorithm UNet, is a deep learning technique that are capable for semantic segmentation. The data is augmented using geometric transformations such as translation, flipping, shearing and rotation. The proposed four models with two different input sizes and two different optimizers are trained from scratch and do not involve any pre-trained weights. The proposed models are validated on CBIS-DDSM dataset and outperform the existing methods with a high dice score of 89.1%. The future work focuses on the usage of other state of art deep learning algorithms such as DCNN, SegNet and Y-Net on different mammogram images for segmentation tasks.





Dhivya et al.,

REFERENCES

1. https://www.icmr.nic.in/sites/default/files/ICMR_News_1.pdf
2. Chougrad, Hiba, Hamid Zouaki, and Omar Alheyane. "Deep convolutional neural networks for breast cancer screening." *Computer methods and programs in biomedicine* 157 (2018): 19-30.
3. Ronneberger, Olaf, Philipp Fischer, and Thomas Brox. "U-net: Convolutional networks for biomedical image segmentation." *International Conference on Medical image computing and computer-assisted intervention*. Springer, Cham, 2015.
4. Ponraj, D. Narain, et al. "A survey on the preprocessing techniques of mammogram for the detection of breast cancer." *Journal of Emerging Trends in Computing and Information Sciences* 2.12 (2011): 656-664.
5. Lee, Rebecca Sawyer, et al. "A curated mammography data set for use in computer-aided detection and diagnosis research." *Scientific data* 4.1 (2017): 1-9.
6. Dhivya, S., et al. "GAN based Data Augmentation for Enhanced Tumor Classification." 2020 4th International Conference on Computer, Communication and Signal Processing (ICCCSP). IEEE, 2020.
7. C. Abirami, R. Harikumar, and S. Chakravarthy (2016), "Performance analysis and detection of microcalcification in digital mammograms using wavelet features," in *Proceedings of the International Conference on Wireless Communications, Signal Processing and Networking (WISPNET '16)*, pp. 2327-2331, Chennai, India.
8. Hao Dong, Guang Yang, Fangde Liu, Yuanhan Mo, Yike Guo. (2017) 'Automatic Brain Tumor Detection and Segmentation Using U-Net Based Fully Convolutional Networks', *Medical Image Understanding and Analysis (MIUA)*, arXiv:1705.03820
9. H. Huang, L. Lin, R. Tong . (2020) 'UNet 3+: A Full-Scale Connected UNet for Medical Image Segmentation', *ICASSP 2020 - 2020 IEEE International Conference on Acoustics, Speech and Signal Processing (ICASSP)*, Barcelona, Spain, pp. 1055-1059.
10. Krizhevsky, Alex & Sutskever, Ilya & Hinton, Geoffrey. (2012). 'ImageNet Classification with Deep Convolutional Neural Networks', *Neural Information Processing Systems*. 25. 10.1145/3065386.
11. Pi, J., Qi, Y., Lou, M., Li, X., Wang, Y., Xu, C., & Ma, Y. (2021). FS-UNet: Mass segmentation in mammograms using an encoder-decoder architecture with feature strengthening. *Computers in Biology and Medicine*, 137, 104800.
12. Parvin Yousekamal. (2019) 'Breast Tumor Classification and Segmentation using Convolutional Neural Networks', Cornell University - pp. arXiv: 1905.04247.
13. Sathyan Anoop, Martis Dino, Cohen Kelly. (2020) 'Mass and Calcification Detection from Digital Mammograms Using UNets', 7th International Conference on Soft Computing & Machine Intelligence (ISCMII), 229-232. 10.1109/ISCMII51676.2020.9311561.
14. S. J. S. Gardezi, M. Awais, I. Faye and F. Meriaudeau. (2017) 'Mammogram classification using deep learning features', *IEEE International Conference on Signal and Image Processing Applications (ICSIPA)*, Kuching, Malaysia, 2017, pp. 485-488, doi: 10.1109/ICSIPA.2017.8120660
15. S. Li, M. Dong, G. Du and X. Mu. (2019) 'Attention Dense-U-Net for Automatic Breast Mass Segmentation in Digital Mammogram' in *IEEE Access*, vol. 7, pp. 59037-59047
16. S. M. L. de Lima, A. G. da Silva-Filho, and W. P. dos Santos (2016), "Detection and classification of masses in mammographic images in a multi-kernel approach", *Computer Methods and Programs in Biomedicine*
17. Sun, Hui, et al. "AUNet: Attention-guided dense-upsampling networks for breast mass segmentation in whole mammograms." *Physics in Medicine & Biology* 65.5 (2020): 055005.
18. Dhivya, S., et al. "Investigations of Shallow and Deep Learning Algorithms for Tumor Detection." 2020 IEEE-HYDCON. IEEE, 2020.
19. Lai, Xiaobo, Weiji Yang, and Ruipeng Li. "DBT masses automatic segmentation using U-net neural networks." *Computational and mathematical methods in medicine* 2020 (2020).





Dhivya et al.,

20. Cao, H., Pu, S., & Tan, W. (2021, September). A Novel Method For Segmentation Of Breast Masses Based On Mammography Images. In 2021 IEEE International Conference on Image Processing (ICIP) (pp. 3782-3786). IEEE.

Table I. Cons of conventional segmentation methods

Conventional Techniques	Disadvantages
Edge based methods	Not suitable for images with many edges and smooth edges.
Region based methods	Specification of seed points. Different seed points have different outputs.
Thresholding techniques	tedious with medical images as it involves complex intensity distributions.

Table I. Number of Training and Testing Samples of CBIS-DDSM

DATABASE	TRAINING	TESTING	TOTAL
CBIS-DDSM	1231	361	1592

Table II Conventional Data Augmentation techniques

Methods	Description
Flipping	flipping the image vertically or horizontally
Rotation	rotates the image by a specified degree.
Shearing	shifts one part of the image like a parallelogram
Cropping	obtaining image in certain position
Zoom in & out	magnify a specific part
Changing brightness or contrast	altering image properties

Table III Comparison of Four Models on Basis of Accuracy, Dice Score, and IOU.

Dataset	Accuracy	Dice Score	IOU
UNet256Ad	95.6%	85.3%	84.1%
UNet128Ad	97.1%	89.1%	88%
UNet256Rp	90.3%	80.3%	78.4%
UNet128Rp	94.3%	82.3%	81.9%

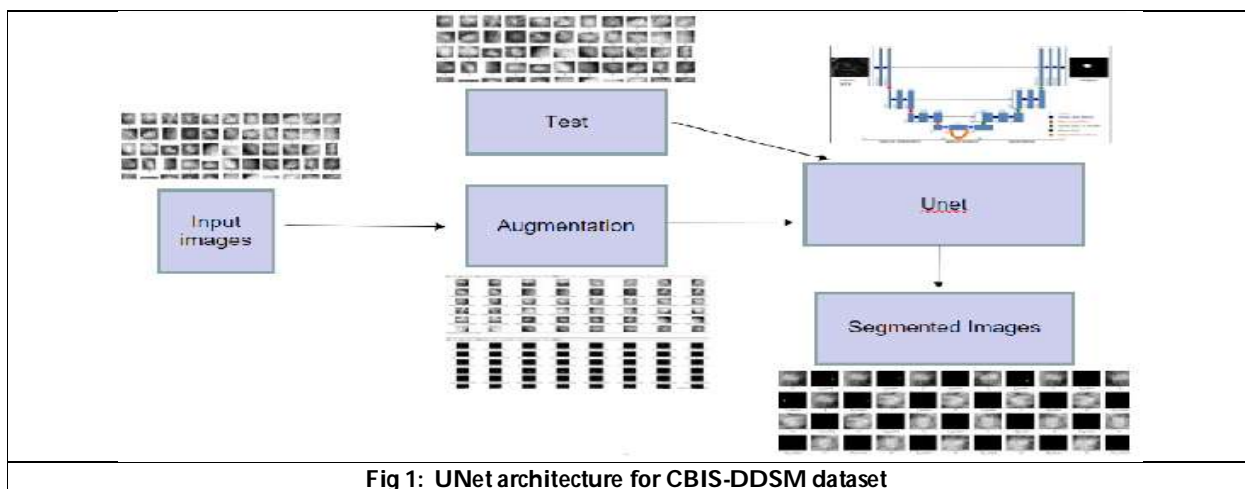


Fig 1: UNet architecture for CBIS-DDSM dataset





Dhivya et al.,

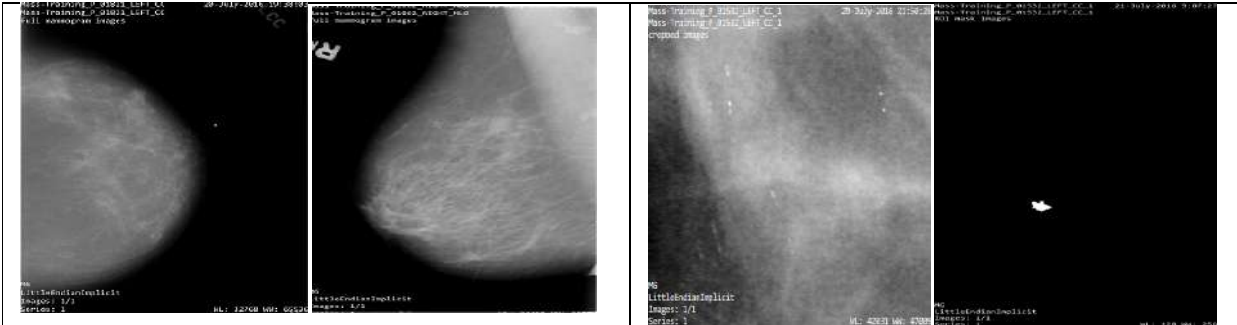


Fig.2. Sample Images of training set

Fig.3. Sample ROI and Masked Image of training set

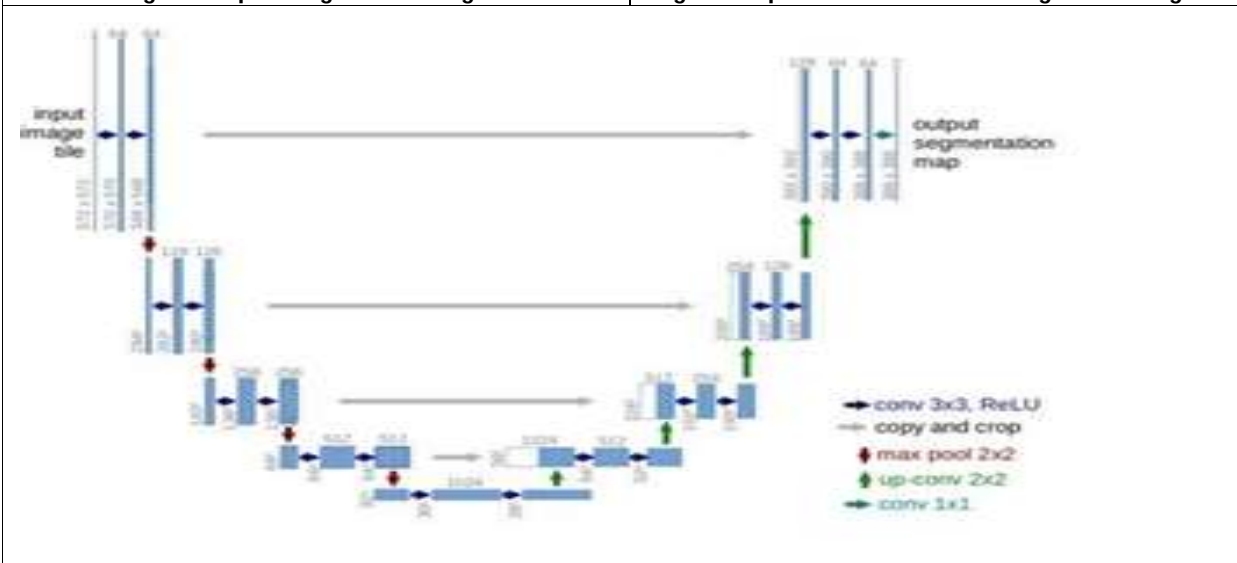


Fig.3: UNet Architecture





Fermatean Fuzzy Generalized Regular Closed Sets in Fermatean Fuzzy Topological Spaces

M.Andal^{1*} and V.Thiripurasundari²

¹Research Scholar, Sri S. Ramasamy Naidu Memorial College (Autonomous), Sattur, Madurai, Tamil Nadu, India

²Department of Mathematics, Sri S. Ramasamy Naidu Memorial College, (Autonomous), Sattur, Madurai, Tamil Nadu, India.

Received: 20 Jan 2023

Revised: 24 Mar 2023

Accepted: 29 Apr 2023

*Address for Correspondence

M.Andal

Research Scholar,
Sri S. Ramasamy Naidu Memorial College (Autonomous),
Sattur, Madurai, Tamil Nadu, India.
E. Mail: aandusuki@gmail.com.



This is an Open Access Journal / article distributed under the terms of the **Creative Commons Attribution License** (CC BY-NC-ND 3.0) which permits unrestricted use, distribution, and reproduction in any medium, provided the original work is properly cited. All rights reserved.

ABSTRACT

In this paper, we introduce the notion of Fermatean fuzzy regular closed sets and open sets, Fermatean fuzzy generalized regular closed sets and open sets in Fermatean fuzzy topological space. Further, we established its properties.

Keywords: Fermatean fuzzy set (FFS), closed Fermatean fuzzy set (CFFS), open Fermatean fuzzy set (OFFS), Fermatean fuzzy generalized closed set (FFGCS), Fermatean fuzzy generalized open set (FFGOS), Fermatean fuzzy regular closed set (FFRCS), Fermatean fuzzy regular open set (FFROS), Fermatean fuzzy generalized regular closed set (FFGRCS) and Fermatean fuzzy generalized regular open set (FFGROS).

INTRODUCTION

Fuzzy set was introduced by L.A.Zadeh [13] in 1965. A lot of research work has been done on Fuzzy set since 1965. In 1968, C. L. Chang [7] defined the concept of fuzzy topological space and generalized some basic notions of topology such as open set, closed set, continuity and compactness in fuzzy topological spaces. The idea of intuitionistic fuzzy set was first introduced by K. Atanassov [2] and many works by the same author and his colleagues appeared in the literature [[3,4]]. D. Coker [8] subsequently initiated a study of intuitionistic fuzzy topological spaces. B. Boomathi, M. Palanisamy [6] defined Generalized regular closed set in Intuitionistic fuzzy topological spaces in 2017. S.S. Thakur and Rekha Chaturvedi [12] defined generalized closed sets in Intuitionistic fuzzy topological spaces in 2006 and 2008. Fermatean fuzzy set was proposed by T. Senapati and R. R. Yager [11] in 2020, and handles uncertain information more easily in the process of decision making. Hariwan Z. Ibrahim [10] introduced the concept of Fermatean fuzzy topological space and defined open sets, closed sets and continuity to Fermatean fuzzy topological

57658





Andal and Thiripurasundari

spaces. M.Andal, T. Thiripurasundari[1] introduced the concept of Fermatean fuzzy generalized closed set in 2022. The aim of this paper is to introduce the concept of Fermatean regular closed set and Fermatean fuzzy generalized regular closed set in Fermatean fuzzy topological spaces.

Preliminaries

Definition 2.1. The intuitionistic fuzzy sets [3] are defined on a non - empty set X as objects having the form $I = \{ \langle x, \alpha_I(x), \beta_I(x) \rangle : x \in X \}$, where $\alpha_I(x): X \rightarrow [0, 1]$ and $\beta_I(x): X \rightarrow [0, 1]$ denote the degree of membership and the degree of non - membership of each element $x \in X$ to the set I, respectively, and $0 \leq \alpha_I(x) + \beta_I(x) \leq 1$, for all $x \in X$.

Definition 2.2. Let X be a universe of discourse. A Fermatean fuzzy set (FFS) [13] F in X is an object having the form $F = \{ \langle x, \alpha_F(x), \beta_F(x) \rangle : x \in X \}$, where $\alpha_F(x): X \rightarrow [0, 1]$ and $\beta_F(x): X \rightarrow [0, 1]$ including the condition $0 \leq (\alpha_F(x))^3 + (\beta_F(x))^3 \leq 1$, for all $x \in X$. The numbers $\alpha_F(x)$ and $\beta_F(x)$ denote, respectively, the degree of membership and the degree of non - membership of the element x in the set F.

For any FFS F and $x \in X$, $\pi_F(x) = \sqrt[3]{1 - (\alpha_F(x))^3 - (\beta_F(x))^3}$ is identified as the degree of indeterminacy of x to F. In the interest of simplicity, we shall mention the symbol $F = (\alpha_F, \beta_F)$ for the FFS $F = \{ \langle x, \alpha_F(x), \beta_F(x) \rangle : x \in X \}$.

Definition 2.3. Let $F = (\alpha_F, \beta_F)$, $F_1 = (\alpha_{F_1}, \beta_{F_1})$ and $F_2 = (\alpha_{F_2}, \beta_{F_2})$ be three Fermatean fuzzy sets [13] (FFSs), then their operations are defined as follows:

- (1) $F_1 \cap F_2 = (\min\{\alpha_{F_1}, \alpha_{F_2}\}, \max\{\beta_{F_1}, \beta_{F_2}\})$.
- (2) $F_1 \cup F_2 = (\max\{\alpha_{F_1}, \alpha_{F_2}\}, \min\{\beta_{F_1}, \beta_{F_2}\})$.
- (3) $F^c = (\beta_F, \alpha_F)$.

We say F_1 is a subset of F_2 or F_2 contains F_1 and we write $F_1 \subset F_2$ or $F_2 \supset F_1$ if $\alpha_{F_1} \leq \alpha_{F_2}$ and $\beta_{F_1} \geq \beta_{F_2}$.

Remark 2.4. If $\alpha_{F_1} = \alpha_{F_2}$ and $\beta_{F_1} = \beta_{F_2}$, then $F_1 = F_2$.

Note 2.5. Here, if the union and the intersection are infinite, then we use supremum "sup" and infimum "inf" instead of maximum "max" and minimum "min", respectively.

Notations 2.6. For the sake of simplicity, we use the notion 1_x for the Fermatean fuzzy subset (1, 0) and we use the notion 0_x for the Fermatean fuzzy subset (0, 1), that is, $\alpha_{1_x} = 1, \beta_{1_x} = 0, \alpha_{0_x} = 0$ and $\beta_{0_x} = 1$.

A Fermatean fuzzy subset F of a non - empty set X is a pair (α_F, β_F) of a membership function $\alpha_F(x): X \rightarrow [0, 1]$ and a non - membership function $\beta_F(x): X \rightarrow [0, 1]$ with $(\alpha_F(x))^3 + (\beta_F(x))^3 = (\gamma_F(x))^3$ for any $x \in X$ where $\gamma_F(x): X \rightarrow [0, 1]$ is a function which is called the strength of commitment at point x.

Definition 2.7. Let X be a non - empty set and τ be a family of Fermatean fuzzy subsets of X. If

- (1) 1_x and $0_x \in \tau$,
- (2) for any $F_1, F_2 \in \tau$, we have $F_1 \cap F_2 \in \tau$,
- (3) for any $\{F_i\}_{i \in I} \subset \tau$, we have $\bigcup_{i \in I} F_i \in \tau$ where I is an arbitrary index set then τ is called a Fermatean fuzzy topology [11] on X.

The pair (X, τ) is said to be Fermatean fuzzy topological space. Every member of τ is called an open Fermatean fuzzy subset. The complement of an open Fermatean fuzzy subset is called a closed Fermatean fuzzy subset.

Definition 2.8. Let (X, τ) be a Fermatean fuzzy topological space and $F = \{ \langle x, \alpha_F(x), \beta_F(x) \rangle : x \in X \}$ be a Fermatean fuzzy set in X. Then, the Fermatean fuzzy interior and Fermatean fuzzy closure [11] of F are defined by





Andal and Thiripurasundari

- (1) $cl(F) = \cap \{H: F \subset H \text{ and } H \text{ is a closed Fermatean fuzzy set in } X\}$.
- (2) $int(F) = \cap \{G: G \subset F \text{ and } G \text{ is an open Fermatean fuzzy set in } X\}$.

Definition 2.9. An intuitionistic fuzzy topology (shortly IFT) [14] on a non empty set X is a family of an intuitionistic fuzzy sets in X satisfying

- (1) $0_-, 1_- \in \tau$,
- (2) $G_1 \cap G_2 \in \tau$ for any $G_1, G_2 \in \tau$,
- (3) $\cup G_j \in \tau$ for any $\{G_j \mid j \in J\} \subset \tau$.

In this case, the pair (X, τ) is called an intuitionistic fuzzy topological space and any intuitionistic fuzzy set in τ is called an intuitionistic fuzzy open set (shortly, IFOS) in X.

Definition 2.10. An intuitionistic fuzzy set $A = (x, \alpha_A, \beta_A)$ in an intuitionistic fuzzy topological space (X, τ) is said to be an

- (1) Intuitionistic fuzzy regular closed set [7] (shortly, IFRCS) if $A = cl(int(A))$.
- (2) Intuitionistic fuzzy regular open set [7] (shortly, IFROS) if $A = int(cl(A))$.

Definition 2.11. Let (X, τ) be an intuitionistic fuzzy topological space. An intuitionistic fuzzy set $A = (x, \alpha_A, \beta_A)$ in (X, τ) is said to be

- (1) a generalized intuitionistic fuzzy closed set [14] (in shortly GIF - closed set) if $IFcl(A) \subseteq G$ whenever $A \subseteq G$ and G is intuitionistic fuzzy open set in X.
The complement of a GIF – closed set is GIF – open set.
- (2) a Intuitionistic fuzzy generalized regular closed set (in shortly IFGR - closed set) [7] if $rcl(A) \subseteq U$ whenever $A \subseteq U$ and U is intuitionistic fuzzy open set in X.

Definition 2.12. Let (X, τ) be a Fermatean fuzzy topological space. A Fermatean fuzzy set $A = (\alpha_A, \beta_A)$ in (X, τ) is said to be a Fermatean fuzzy generalized closed set [1](in shortly FFG - closed) if $cl(A) \subseteq U$ whenever $A \subseteq U$ and U is open Fermatean fuzzy set. The complement of a FFG - closed set is FFG - open set.

Theorem 2.13 Let (X, τ) be a Fermatean fuzzy topological space [12] and F_1 and F_2 be Fermatean fuzzy sets in X. Then the following are hold:

- (1) $F_1 \subset cl(F_1)$,
- (2) $int(F_1) \subset F_1$,
- (3) If $F_1 \subset F_2$, then $cl(F_1) \subset cl(F_2)$,
- (4) If $F_1 \subset F_2$, then $int(F_1) \subset int(F_2)$,
- (5) $int(F_1 \cap F_2) = int(F_1) \cap int(F_2)$,
- (6) $cl(F_1 \cup F_2) = cl(F_1) \cup cl(F_2)$,
- (7) F_1 is open Fermatean fuzzy set if and only if $F_1 = int(F_1)$,
- (8) F_1 is closed Fermatean fuzzy set if and only if $F_1 = cl(F_1)$,
- (9) $int(F_1) \cup int(F_2) \subset int(F_1 \cup F_2)$,
- (10) $cl(F_1 \cap F_2) \subset cl(F_1) \cap cl(F_2)$.

Fermatean Fuzzy Regular Closed Sets

In this section, we introduce the concept of Fermatean fuzzy regular closed sets in Fermatean fuzzy topological spaces.

Definition 3.1.A Fermatean fuzzy set $A = (\alpha_F, \beta_F)$ of a Fermatean fuzzy topological space (X, τ) is said to be Fermatean fuzzy regular closed if $cl(int(A)) = A$.





Andal and Thiripurasundari

Example 3.2. Let $X = \{e_1, e_2\}$. Consider the following family of Fermatean fuzzy subsets $\tau = \{1_X, 0_X, A_1, A_2, A_3, A_1 \cap A_3, A_1 \cup A_3\}$ where

$$1_X = \{ \langle e_1, \alpha_{1_X}(e_1) = 1, \beta_{1_X}(e_1) = 0 \rangle, \langle e_2, \alpha_{1_X}(e_2) = 1, \beta_{1_X}(e_2) = 0 \rangle \},$$

$$0_X = \{ \langle e_1, \alpha_{0_X}(e_1) = 0, \beta_{0_X}(e_1) = 1 \rangle, \langle e_2, \alpha_{0_X}(e_2) = 0, \beta_{0_X}(e_2) = 1 \rangle \},$$

$$A_1 = \{ \langle e_1, \alpha_{A_1}(e_1) = 0.3, \beta_{A_1}(e_1) = 0.7 \rangle, \langle e_2, \alpha_{A_1}(e_2) = 0.6, \beta_{A_1}(e_2) = 0.6 \rangle \},$$

$$A_2 = \{ \langle e_1, \alpha_{A_2}(e_1) = 0.7, \beta_{A_2}(e_1) = 0.5 \rangle, \langle e_2, \alpha_{A_2}(e_2) = 0.7, \beta_{A_2}(e_2) = 0.6 \rangle \},$$

and

$$A_3 = \{ \langle e_1, \alpha_{A_3}(e_1) = 0.7, \beta_{A_3}(e_1) = 0.8 \rangle, \langle e_2, \alpha_{A_3}(e_2) = 0.7, \beta_{A_3}(e_2) = 0.7 \rangle \}.$$

Then (X, τ) is a Fermatean fuzzy topological space. Here $FFRCS = \{1_X, 0_X, A_1^c, A_2^c, A_3^c, A_1^c \cup A_3^c\}$.

Theorem 3.3. Every Fermatean fuzzy regular closed set is a closed Fermatean fuzzy set.

Proof. Let A be a Fermatean fuzzy regular closed set. Therefore, $cl(int(A)) = A$. Then $cl(cl(int(A))) = cl(A)$. Hence $cl(int(A)) = cl(A)$. But $cl(int(A)) = A$, we get $cl(A) = A$. Therefore A is a closed Fermatean fuzzy set in (X, τ) .

Remark 3.4. The converse part of above theorem 3.3 need not be true as seen from the following example.

Example 3.5. From example 3.2, $A_1^c \cap A_3^c$ is a closed Fermatean fuzzy set. But it is not a Fermatean fuzzy regular closed set in (X, τ) .

Theorem 3.6. If A and B are two Fermatean fuzzy regular closed sets in (X, τ) , then $A \cup B$ is a Fermatean fuzzy regular closed set in (X, τ) .

Proof. Let A and B be two Fermatean fuzzy regular closed sets in (X, τ) . Because $A \cup B$ is a closed Fermatean fuzzy set in (X, τ) , we have $cl(int(A \cup B)) \subseteq A \cup B$. Now $A = cl(int(A)) \subseteq cl(int(A \cup B))$ and $cl(int(A \cup B)) \subseteq cl(int(B)) = B$ implies that $cl(int(A \cup B)) \subseteq A \cup B$. Hence the result.

Remark 3.7. If A and B are two Fermatean fuzzy regular closed sets in (X, τ) , then $A \cap B$ need not be a Fermatean fuzzy regular closed set in (X, τ) .

Example 3.8. From example 3.5, $A_1^c \cap A_3^c$ is not a Fermatean fuzzy regular closed set in (X, τ) .

Proposition 3.9. The following are equivalent:

- (i) A is a Fermatean fuzzy regular closed set,
- (ii) A^c is a Fermatean fuzzy regular open set,
- (iii) $int(cl(A)) \subseteq A$,
- (iv) $int(cl(A)) \supseteq A^c$.

Theorem 3.10. The closure of an open Fermatean fuzzy set is a Fermatean fuzzy regular closed set.

Proof. Let A be an open Fermatean fuzzy set in (X, τ) . Clearly, $int(cl(A)) \subseteq cl(A)$ implies that $cl(cl(int(A))) \subseteq cl(A)$. Now, A is an open Fermatean fuzzy set implies that $A \subseteq int(cl(A))$ and hence $cl(A) \subseteq cl(int(cl(A)))$. Thus $cl(A)$ is a Fermatean fuzzy regular closed set.

Fermatean Fuzzy Generalized Regular Closed Sets

In this section, we introduce the concept of Fermatean fuzzy generalized regular closed sets in Fermatean fuzzy topological space.

Definition 4.1. Let (X, τ) be a Fermatean fuzzy topological space. A Fermatean fuzzy set A in (X, τ) is said to be a Fermatean fuzzy generalized regular closed set (in shortly FFGR - closed set) if $rcl(A) \subseteq U$ whenever $A \subseteq U$ and U is an open Fermatean fuzzy set.





Andal and Thiripurasundari

Example 4.2. Consider the Fermatean fuzzy topological space in example 3.2. Take, $A = \{(e_1, \alpha_A(e_1) = 0.4, \beta_A(e_1) = 0.7), (e_2, \alpha_A(e_2) = 0.5, \beta_A(e_2) = 0.7)\}$ is a Fermatean fuzzy set in (X, τ) . Clearly, A is a Fermatean fuzzy generalized regular closed set in (X, τ) .

Definition 4.3. Let A be a Fermatean fuzzy set in a Fermatean fuzzy topological space (X, τ) . Then Fermatean fuzzy generalized regular closure and Fermatean fuzzy generalized regular interior of A are defined by

- (1) $FFGrcl(A) = \cap \{H : A \subseteq H \text{ and } H \text{ is Fermatean fuzzy generalized regular closed set in } X\}$.
- (2) $FFGrint(A) = \cup \{G : G \subseteq A \text{ and } G \text{ is Fermatean fuzzy generalized regular open set in } X\}$.

Theorem 4.4. Every Fermatean fuzzy regular closed set is a Fermatean fuzzy generalized regular closed set.

Proof. Let A be a Fermatean fuzzy regular closed set in a Fermatean fuzzy topological space (X, τ) . Let U be an open Fermatean fuzzy set in (X, τ) such that $A \subseteq U$. Since A is a Fermatean fuzzy regular closed set, we have $rcl(A) = A \subseteq U$. Therefore $rcl(A) \subseteq U$. Hence A is a Fermatean fuzzy generalized regular closed set.

Remark 4.5. The converse part of the above theorem 4.4 need not be true as seen from the following example.

Example 4.6. From example 4.2, A is a Fermatean fuzzy generalized regular closed set. But it is not a Fermatean fuzzy regular closed set in (X, τ) .

Theorem 4.7. Every Fermatean fuzzy generalized regular closed set is a Generalized Fermatean fuzzy closed set.

Proof. Let A be a Fermatean fuzzy generalized regular closed set in (X, τ) and U be an open Fermatean fuzzy set such that $A \subseteq U$. By our assumption, $rcl(A) \subseteq U$. Also, $cl(A) \subseteq rcl(A) \subseteq U$. Hence A is a Fermatean fuzzy generalized closed set in (X, τ) .

Remark 4.8. The following example shows that the converse of the above theorem 4.7 is not true as seen from the following example.

Example 4.9. From example 3.2, $A_1^c \cap A_3^c$ is a closed Fermatean fuzzy set. But it is not a Fermatean fuzzy generalized regular closed set in (X, τ) .

Theorem 4.10. If A and B are Fermatean fuzzy generalized regular closed sets in (X, τ) , then $A \cup B$ is also a Fermatean fuzzy generalized regular closed set in (X, τ) .

Proof. Let U be an open Fermatean fuzzy set in (X, τ) such that $A \cup B \subseteq U$. Now $A \subseteq U$ and $B \subseteq U$. Since A and B are Fermatean fuzzy generalized regular closed sets in (X, τ) , $rcl(A) \subseteq U$ and $rcl(B) \subseteq U$. Therefore $rcl(A) \cup rcl(B) \subseteq U$. Since $rcl(A) \cup rcl(B) = rcl(A \cup B)$, $rcl(A \cup B) \subseteq U$. Therefore $A \cup B$ is a Fermatean fuzzy generalized regular closed set in (X, τ) .

Remark 4.11. If A and B are Fermatean fuzzy generalized regular closed sets in (X, τ) , then $A \cap B$ is not a Fermatean fuzzy generalized regular closed set in (X, τ) as seen from the following example.

Example 4.12. Consider the Fermatean fuzzy topological space in example 3.2. From example 4.9, $A_1^c \cap A_3^c$ is not a Fermatean fuzzy generalized regular closed set in (X, τ) .

Theorem 4.13. Let (X, τ) be a Fermatean fuzzy topological space. If A is a Fermatean fuzzy generalized regular closed set and $A \subseteq B \subseteq rcl(A)$, then B is a Fermatean fuzzy generalized regular closed set in (X, τ) .

Proof. Let (X, τ) be a Fermatean fuzzy topological space. Let U be an open Fermatean fuzzy set such that $B \subseteq U$. Since $A \subseteq B$, $A \subseteq U$ and A is a Fermatean fuzzy generalized regular closed set, $rcl(A) \subseteq U$. But $rcl(B) \subseteq rcl(A)$. Since $B \subseteq rcl(A)$ and also $rcl(B) \subseteq U$. Therefore B is a Fermatean fuzzy generalized regular closed set in (X, τ) .





Andal and Thiripurasundari

Theorem 4.14. If a Fermatean fuzzy set A is both Fermatean fuzzy regular open and Fermatean fuzzy generalized regular closed set in (X, τ) then A is a Fermatean fuzzy generalized regular closed set in (X, τ) .

Proof. Let A be both Fermatean fuzzy regular open and Fermatean fuzzy generalized regular closed set in (X, τ) . Since every Fermatean fuzzy regular open set is a open Fermatean fuzzy set and $A \subseteq A$, $\text{rcl}(A) \subseteq A$. Also $A \subseteq \text{rcl}(A)$. Therefore, $\text{rcl}(A) = A$. ie., A is a Fermatean fuzzy generalized regular closed set in (X, τ) .

Theorem 4.15. If a Fermatean fuzzy set A is both open Fermatean fuzzy set and Fermatean fuzzy generalized regular closed set in (X, τ) then A is a closed Fermatean fuzzy set in (X, τ) .

Proof. Suppose that A is a both open Fermatean fuzzy set and Fermatean fuzzy generalized regular closed set in (X, τ) . Now, $A \subseteq A$, we have $A \subseteq \text{rcl}(A)$. Therefore, $\text{rcl}(A) = A$ and hence A is a closed Fermatean fuzzy set in (X, τ) .

Theorem 4.16. In a Fermatean fuzzy topological space (X, τ) if $\text{FFO}(X) = \{1_X, 0_X\}$, where $\text{FFO}(X)$ is the family of all open Fermatean fuzzy sets then every Fermatean fuzzy subsets of (X, τ) is Fermatean fuzzy generalized regular closed set.

Proof. Let (X, τ) be a Fermatean fuzzy topological space and $\text{FFO}(X) = \{1_X, 0_X\}$. Let A be any Fermatean fuzzy subset of (X, τ) . Suppose that $A = 0_X$. Then 0_X is a Fermatean fuzzy generalized regular closed set in (X, τ) . Suppose that $A \neq 0_X$. Then 1_X is the only open Fermatean fuzzy set containing A and so $\pi \text{cl}(A) \subseteq 1_X$. Hence A is a Fermatean fuzzy generalized regular closed set in (X, τ) .

Theorem 4.17. Let A be a Fermatean fuzzy generalized regular closed set in (X, τ) and $\text{rcl}(A) \cap (1_X - \text{rcl}(A)) = 0_X$. Then $\text{rcl}(A) - A$ does not contain any non-zero closed Fermatean fuzzy set in (X, τ) .

Proof: Let A be a Fermatean fuzzy generalized regular closed set in (X, τ) and $\text{rcl}(A) \cap (1_X - \text{rcl}(A)) = 0_X$. Now to prove the result by contradiction method. Let B be a closed Fermatean fuzzy set such that $\text{rcl}(A) - A \supseteq B$ and $B \neq 0_X$.

Now $B \subseteq \text{rcl}(A) - A$. ie., $B \subseteq 1_X - A$ which implies $A \subseteq 1_X - B$. Since B is closed Fermatean fuzzy set in (X, τ) , $1_X - B$ is open Fermatean fuzzy set in (X, τ) . Since A is Fermatean fuzzy generalized regular closed set in (X, τ) , by the definition $\text{rcl}(A) \subseteq 1_X - B$. Therefore $B \subseteq 1_X - \text{rcl}(A)$. Since $B \subseteq \text{rcl}(A)$ and $B \subseteq \text{rcl}(A) \cap (1_X - \text{rcl}(A)) = 0_X$, by hypothesis. This shows that $B = 0_X$. Which is contradiction to our assumption. Hence $\text{rcl}(A) - A$ does not contain any non-zero closed Fermatean fuzzy set in (X, τ) .

Theorem 4.18. Let A be a Fermatean fuzzy generalized regular closed set in (X, τ) and $\text{rcl}(A) \cap (1_X - \text{rcl}(A)) = 0_X$. Then $\text{rcl}(A) - A$ does not contain any non-zero Fermatean fuzzy regular closed set in (X, τ) .

Proof. Follows from theorem 4.17 and the fact that every Fermatean fuzzy regular closed set is a closed Fermatean fuzzy set in (X, τ) .

Fermatean Fuzzy Regular Open Sets

Definition 5.1. A Fermatean fuzzy set $A = (\alpha_F, \beta_F)$ of a Fermatean fuzzy topological space (X, τ) is said to be Fermatean fuzzy regular open if $\text{int}(\text{cl}(A)) = A$.

Example 5.2. Consider a Fermatean fuzzy topological space (X, τ) in example 3.2. Then $\text{FFROS} = \{1_X, 0_X, A_1, A_2, A_3, A_1 \cap A_3\}$ is a Fermatean fuzzy regular open sets in (X, τ) .

Theorem 5.3. Every Fermatean fuzzy regular open set is a open Fermatean fuzzy set.

Proof. Let A be a Fermatean fuzzy regular open set. Therefore, $\text{int}(\text{cl}(A)) = A$. Then $\text{int}(\text{int}(\text{cl}(A))) = \text{int}(A)$. Hence $\text{int}(\text{cl}(A)) = \text{int}(A)$. But $\text{int}(\text{cl}(A)) = A$, we get $\text{int}(A) = A$. Therefore A is a open Fermatean fuzzy set in (X, τ) .

Remark 5.4. The converse part of above theorem 5.3 need not be true as seen from the following example.





Andal and Thiripurasundari

Example 5.5. From example 5.2, $A_1 \cup A_3$ is a open Fermatean fuzzy set, but it is not a Fermatean fuzzy regular open set in (X, τ) .

Theorem 5.6. If A and B are two Fermatean fuzzy regular open sets in (X, τ) , then $A \cap B$ is a Fermatean fuzzy regular open set in (X, τ) .

Proof. Let A and B be two Fermatean fuzzy regular open sets in (X, τ) . Because $A \cap B$ is a open Fermatean fuzzy set in (X, τ) , we have $\text{int}(\text{cl}(A \cap B)) \supseteq A \cap B$. Now $A = \text{int}(\text{cl}(A)) \supseteq \text{int}(\text{cl}(A \cap B))$ and $\text{int}(\text{cl}(A \cap B)) \supseteq \text{int}(\text{cl}(B)) = B$ implies that $\text{int}(\text{cl}(A \cap B)) \supseteq A \cap B$. Hence the result.

Remark 5.7. If A and B are two Fermatean fuzzy regular open sets in (X, τ) , then $A \cup B$ need not be a Fermatean fuzzy regular open set in (X, τ) .

Example 5.8. From example 5.2, $A_1 \cup A_3$ is not a Fermatean fuzzy regular open set in (X, τ) .

Theorem 5.9. The interior of a closed Fermatean fuzzy set is a Fermatean fuzzy regular open set.

Proof. Let A be a closed Fermatean fuzzy set in (X, τ) . Clearly, $\text{cl}(\text{int}(A)) \supseteq \text{int}(A)$ implies that $\text{int}(\text{cl}(\text{int}(A))) \supseteq \text{int}(A)$. Now, A is closed Fermatean fuzzy set, $A \supseteq \text{cl}(\text{int}(A))$ and hence $\text{int}(A) \supseteq \text{int}(\text{cl}(\text{int}(A)))$. Thus $\text{int}(A)$ is a Fermatean fuzzy regular open set in (X, τ) .

Fermatean Fuzzy Generalized Regular Open Sets

Definition 6.1. A Fermatean fuzzy set A in a Fermatean fuzzy topological space (X, τ) is said to be Fermatean fuzzy generalized regular open set if A^c is Fermatean fuzzy generalized regular closed set in (X, τ) .

Example 6.2. From example 4.2, A^c is a Fermatean fuzzy generalized regular open set in (X, τ) .

Theorem 6.3. Every Fermatean fuzzy regular open set is a Fermatean fuzzy generalized regular open set.

Proof. Let A^c be a Fermatean fuzzy regular open set in a Fermatean fuzzy topological space (X, τ) . Therefore A is a Fermatean fuzzy regular closed set. From theorem 4.4, A is a Fermatean fuzzy generalized regular closed set in (X, τ) . Therefore, A^c is a Fermatean fuzzy generalized regular open set in (X, τ) .

Remark 6.4. The converse part of the above theorem 6.3 need not be true as seen from the following example.

Example 6.5. From example, 6.2, A^c is a Fermatean fuzzy generalized regular open set in (X, τ) . But \square it is not a Fermatean fuzzy regular open set in (X, τ) .

Theorem 6.6. Every Fermatean fuzzy generalized regular open set is a Fermatean fuzzy generalized open set.

Proof. Let A^c be a Fermatean fuzzy generalized regular open set in a Fermatean fuzzy topological space (X, τ) . Therefore A is a Fermatean fuzzy generalized regular closed set. From theorem 4.7, A is a Fermatean fuzzy generalized closed set in (X, τ) . Therefore, A^c is a Fermatean fuzzy generalized open set in (X, τ) .

Remark 6.7. The converse part of the above theorem 6.6 need not be true as seen from the following example.

Example 6.8. From example, 5.2, $A_1 \cup A_3$ is a Fermatean fuzzy generalized open set in (X, τ) . But it is not a Fermatean fuzzy generalized regular open set in (X, τ) .

Theorem 6.9. Let A be a Fermatean fuzzy generalized regular open set in (X, τ) . If B is a Fermatean fuzzy set in (X, τ) such that $\pi \text{int}(A) \subseteq B \subseteq A$, then B is also a Fermatean fuzzy generalized regular open set in (X, τ) .





Andal and Thiripurasundari

Proof. Now A^c is a Fermatean fuzzy generalized regular closed set and B is a Fermatean fuzzy set in (X, τ) such that $A^c \subseteq B^c \subseteq \text{rint}(A)^c$. By theorem 4.13, $A^c \subseteq B^c \subseteq \text{int}(A)^c = \text{rcl}(A^c)$. Hence by theorem 4.13, B^c is Fermatean fuzzy generalized regular closed set in (X, τ) . Hence by definition 6.1, B is a Fermatean fuzzy generalized regular open set in (X, τ) .

Theorem 6.10. A Fermatean fuzzy set A of a Fermatean fuzzy topological space (X, τ) is Fermatean fuzzy generalized regular open iff $B \subseteq \text{rint}(A)$ whenever $B \subseteq A$ and B is closed Fermatean fuzzy set in (X, τ) .

Proof. Suppose that A is a Fermatean fuzzy set such that $B \subseteq \text{rint}(A)$ whenever $B \subseteq A$ and B is closed Fermatean fuzzy set in (X, τ) . Let $A^c \subseteq U$ and U is an open Fermatean fuzzy set in (X, τ) . Since $A^c \subseteq U$, $U^c \subseteq A$. Hence by assumption we have $U^c \subseteq \text{rint}(A)$. i.e, $\text{rint}(A)^c \subseteq U$. Also, $\text{rint}(A)^c = \text{rcl}(A^c)$. Therefore, $\text{rcl}(A^c) \subseteq U$, which implies that A^c is a Fermatean fuzzy generalized regular closed set in (X, τ) . By definition 6.1, A is Fermatean fuzzy generalized regular open set in (X, τ) .

Conversely, assume that A is Fermatean fuzzy generalized regular open set in (X, τ) and B be a closed Fermatean fuzzy set in (X, τ) . Then B^c is open Fermatean fuzzy set in (X, τ) and $A^c \subseteq B^c$. Since A^c is Fermatean fuzzy generalized regular closed set in (X, τ) , $\text{rcl}(A^c) = \text{rint}(A)^c \subseteq B^c$ which implies that $B \subseteq \text{rint}(A)$.

Theorem 6.11. If A and B are Fermatean fuzzy generalized regular open sets in (X, τ) , then $A \cap B$ is a Fermatean fuzzy generalized regular open set in (X, τ) .

Proof. Let A and B be two Fermatean fuzzy generalized regular open sets in (X, τ) . Then by definition 6.1, A^c and B^c are Fermatean fuzzy generalized regular closed sets in (X, τ) . By theorem 4.10, $A^c \cup B^c$ is also a Fermatean fuzzy generalized regular closed set in (X, τ) . That is, $A^c \cup B^c = (A \cap B)^c$. Therefore $(A \cap B)^c$ is a Fermatean fuzzy generalized regular closed set in (X, τ) . By definition 6.1, $A \cap B$ is a Fermatean fuzzy generalized regular open set in (X, τ) .

Remark 6.12. If A and B are Fermatean fuzzy generalized regular open sets in (X, τ) , then $A \cup B$ need not be a Fermatean fuzzy generalized regular open set in (X, τ) as seen from the following example.

Example 6.13. Consider the Fermatean fuzzy topological space (X, τ) in example 3.2. From example 5.2, $A_1 \cup A_2$ is not a Fermatean fuzzy generalized regular open set in (X, τ) .

REFERENCES

1. Andal. M, Thiripurasundari, Fermatean fuzzy generalized closed sets in Fermatean fuzzy topological space, Under consideration.
2. Atanassov. K, Intuitionistic fuzzy sets, V. Sgurev, Bd., VII ITKR's Session, Sofia (June 1983 Central Sci. and Techn.Library, Bulg.Academy of Sciences), 1984.
3. Atanassov. K, Intuitionistic fuzzy sets, Fuzzy Sets and Systems, 20, 87- 96, 1986.
4. Atanassov. K, Review and new results on Intuitionistic fuzzy sets, International Bioautomation, 20, S17 - S26, 2016.
5. Balasubramanian. G and Sundaram. P., On some generalizations of fuzzy continuous functions, Fuzzy Sets and Systems, 86(1), 93-100, 1997.
6. Boomathi. B, Palanisamy. M, Generalized regular connectedness in Intuitionistic fuzzy topological spaces, IJARIE, 3(4), 1991 - 1999, 2017.
7. Chang. C.L, Fuzzy topological spaces, J.Math.Aval.Appl, 24, 182-190, 1968.
8. Coker. D, An introduction to Intuitionistic fuzzy topological spaces, Fuzzy Sets and Systems, 88, 81 - 89, 1997.
9. H. Gurcay, A. Haydar and D. Coker, On fuzzy continuity in intuitionistic fuzzy topological spaces, jour. of fuzzy math, 5, 365-378, 1997.
10. Hariwan Z. Ibrahim, Fermatean fuzzy topological spaces, J. Appl. Math. and Informatics, 40, 85-98, 2022.





Andal and Thiripurasundari

11. Senapati. T and Yager. R. R, Fermatean fuzzy sets, Journal of Ambient Intelligence and Humanized Computing, 11, 663 - 674, 2020.
12. S.S. Thakur and RekhaChaturvedi, Generalized closed sets in intuitionistic fuzzy topology, The journal of Fuzzy Mathematics, 16, 559-572, 2008.
13. Zadeh. L.A., Fuzzy sets, information and control, 8, 338-353, 1965.





A Survey of Deep Neural Network Predictive Models for Rheumatoid Arthritis Diagnosis

M.Nalini^{1*} and K.Prabavathy²

¹Research Scholar, Department of Computer Science, Rathinam College of Arts and Science, Coimbatore, Tamil Nadu, India.

²Assistant Professor, Department of Data Science and Analytics, Sree Saraswathi Thyagaraja College, Pollachi-642001, Tamil Nadu, India.

Received: 23 Feb 2023

Revised: 20 Apr 2023

Accepted: 31 May 2023

*Address for Correspondence

M.Nalini

Research Scholar,
Department of Computer Science,
Rathinam College of Arts and Science,
Coimbatore, Tamil Nadu, India.
E.Mail: m.nalini@rvsgroup.com



This is an Open Access Journal / article distributed under the terms of the **Creative Commons Attribution License** (CC BY-NC-ND 3.0) which permits unrestricted use, distribution, and reproduction in any medium, provided the original work is properly cited. All rights reserved.

ABSTRACT

Survey studies can play an important role in the prediction of rheumatoid arthritis (RA) by deep neural networks (DNNs). Surveys can be used to collect information about various risk factors, symptoms, and other relevant data that can be used to train the DNN. This information can then be fed into the DNN, allowing it to learn patterns and make predictions about the likelihood of RA. A survey study could collect data on a patient's age, sex, family history, lifestyle habits, and other medical history. This data can be used to create a DNN model that predicts the likelihood of RA based on these factors. The DNN can be trained on large amounts of data from survey studies, improving its accuracy in predicting RA. In addition, survey studies can also be used to validate the predictions made by the DNN. By comparing the predictions of the DNN with the actual diagnosis of RA, the accuracy of the model can be evaluated and improved. Overall, survey studies play an important role in the development of DNN models for the prediction of RA by providing the data needed for training and validation. The use of DNNs combined with survey data can lead to improved accuracy in RA prediction and improve patient outcomes.

Keywords: Rheumatoid Arthritis, DNN, PREDICTION, GAN, AUTOENCODER





INTRODUCTION

Rheumatoid Arthritis (RA) is a widespread inflammatory condition that affects the joints and causes pain and swelling. It affects nearly 1% of the global population, making it a widespread issue.¹ Being a chronic autoimmune disease, RA comes with a considerable burden of suffering and significant healthcare costs. Despite the various treatments available, the progression of the disease varies greatly among individuals and there is a wide variation in response to treatment. ² Despite the advancements in treatment options and clinical management, it is still uncommon for patients to achieve remission and long-lasting response.

Deep learning, a branch of artificial intelligence, has revolutionized computer vision⁷ and has shown significant success in various clinical applications that involve image data in the fields of biomedical¹² and healthcare^{13,14}. This technology is being rapidly applied to various EHR-related data sets,¹⁵ however, as with any new field, there are still numerous opportunities and challenges to be explored.^{12,16} which is discussed in detail in this article amongst RA disease^[1].

LITERATURE SURVEY STUDY

REVIEW ON DEEP LEARNING TECHNIQUES

Deep learning has indeed revolutionized the field of artificial intelligence and has achieved state-of-the-art results in a wide range of applications, such as image classification, natural language processing, and speech recognition, among others. One of the key advantages of deep learning is its ability to learn hierarchical representations of the input data, which allow it to capture complex patterns and features in the data. By using multiple hidden layers in the network, deep learning models can learn increasingly abstract representations of the input data, resulting in improved performance on various tasks. Additionally, the use of non-linear activation functions in the neurons enables the network to learn non-linear relationships between the input and output [2],[3]. However, it's important to note that training deep neural networks can be computationally expensive and requires a large amount of labeled data to achieve good results. The network's architecture also plays a crucial role in its performance, and choosing the right architecture for a specific task can be challenging. Despite these limitations, deep learning has proven to be a powerful tool in solving real-world problems, and its use is only expected to grow in the future^{[4],[5],[6]}.

An auto-encoder is a type of deep learning architecture that is trained to reconstruct its input. The encoder part of the network compresses the input into a lower-dimensional representation, while the decoder part reconstructs the original input from this lower-dimensional representation. The goal of training is to minimize the difference between the original input and the reconstructed input, usually using a reconstruction loss function such as the mean squared error [5]. Auto-encoders are commonly used for unsupervised learning tasks, such as dimensionality reduction and representation learning. By learning a compact representation of the input data, auto-encoders can effectively capture the most important features and patterns in the data, which can then be used for various downstream tasks, such as clustering or classification. Additionally, auto-encoders can also be used for generative tasks, such as generating new data samples from the learned representation. For example, by sampling from the distribution of the learned latent representation, one can generate new data samples that are similar to the training data. In summary, auto-encoders are a versatile and powerful tool in deep learning that have found a wide range of applications in various fields.

Generative Adversarial Networks (GANs) are a class of generative models that use a two-part architecture consisting of a generator network and a discriminator network [7],[8]. The generator network generates new data samples from a random noise vector, while the discriminator network is trained to distinguish between the generated samples and real data samples. During training, the two networks are trained alternately, with the generator trying to generate more realistic samples that can fool the discriminator, and the discriminator trying to get better at detecting fake samples. The training process continues until the generator is able to produce samples that are indistinguishable





Nalini and Prabavathy

from real data, and the discriminator is unable to make a clear distinction between the two. GANs have become a popular choice for generative tasks in deep learning, especially in areas such as computer vision and graphics. They have the ability to generate high-quality images, videos, and even music, and have been applied to a wide range of tasks, such as super-resolution, style transfer, and inpainting, among others. However, it's important to note that GANs can be difficult to train, and the training process can be unstable and prone to mode collapse, where the generator produces samples that are only a limited subset of the possible outputs. To overcome these challenges, various techniques have been proposed, such as modifying the loss function, using architectural improvements, or stabilizing the training process. Convolutional Neural Networks (CNNs) are a type of deep learning architecture that are specifically designed for image recognition and computer vision tasks. They are called "convolutional" because they use convolutional layers, which perform a mathematical operation called convolution on the input data. This operation helps to extract and learn features from the input images, such as edges, shapes, and textures. Additionally, CNNs use pooling layers, which reduce the spatial dimensions of the feature maps while retaining important information. This makes the CNN more robust to variations in the position and size of objects in an image, and reduces the number of parameters that need to be learned, which helps to prevent over fitting[9],[10].

CNNs have been very successful in various computer vision tasks, such as image classification, object detection, and segmentation, due to their ability to automatically learn and extract important features from the input data. They have also been used in medical image analysis, such as detecting bone erosions and measuring synovitis disease in Doppler Ultrasound images. However, as you mentioned, training a CNN requires a large amount of data and carefully tuned training parameters. This can be a challenge, especially in the medical domain, where annotated data is often scarce and limited. To overcome this challenge, various techniques have been proposed, such as transfer learning, data augmentation, and domain adaptation, to make effective use of limited annotated data and improve the performance of CNNs in medical image analysis.

Some of following research articles are tabulated with its techniques adapted along modality.

Reference	Year	Technique	Dataset size	No. of patients or images	Modality*
Thomson et al., [11]	2015	RFRVCL/SVM	500 images		X-ray
Subramoniam et al., [12]	2015	SVM	130 images		Radiographs
Antony et al., [13]	2016	CNN	4476 patients		MRI
Gornale et al., [15]	2016	Active Segmentation	Contour	200 images	X-ray
Gornale et al., [15]	2016	KNN		207 images	X-ray
Yoo et al., [16]	2016	k-means		60 patients	EHR
Gornale et al., [17]	2017	HoG/SVM		616 images	X-ray
Antony et al., [13]	2017	FCN/CNN		7502 patients	MRI
Lezcano-Valverde et al., [18]	2017	Random Survival Forest		1741 patients	EHR
Murakami et al., [19]	2018	CNN		30 patients	Radiographs
Tang et al., [20]	2018	CNN		-	Ultrasound
Orange et al., [21]	2018	SVM		129 patients	Tissue Samples





Nalini and Prabavathy

Reference	Year	Technique	Dataset size No. of patients or images	Modality*
Norgeot et al., [22]	2019	LSTM	820 patients	EHR
Hemalatha et al., [23]	2019	CNN	–	Ultrasound
Abedin et al., [24]	2019	ElasticNet/Random Forest/CNN	4796 patients	MRI
Chen et al., [25]	2019	Yolo v2	–	X-ray
Tiulpin et al., [26]	2019	ResNet-34	–	Radiographs
Norman et al., [27]	2019	U-Net	500 images	X-ray
Tiuplin et al., [28]	2019	Deep Learning Regression	–	X-ray
Liu et al., [29]	2020	Fast RCNN	–	X-ray
Tolpadi et al., [30]	2020	DenseNet-121	–	MRI
Hoang et al., [31]	2020	Forest Regression Voting	–	X-ray
Bonaretti et al., [32]	2020	- Extended Phase Graph (EPG)	10 patients	MRI
Dang et al., [33]	2020	CNN	200 patients	X-ray
Von et al., [34]	2020	RetinaNet	–	X-ray
Chen et al., [35]	2019	CNN	–	X-ray
Nguyen et al., [36]	2020	Siamese Network	500 images	X-ray

REVIEW ON RA PREDICTION TECHNIQUES

In a study by Antony et al. [4], the authors applied Convolutional Neural Networks (CNNs) on knee radiographs of 4,476 participants to determine their knee severity using the Kellgren and Lawrence Grade. The results showed that the CNNs, using pre-trained models such as VGG16, VGG-M-128, and BVLC CaffeNet, outperformed the OA classification method using Wndchrm, a popular open-source tool for biological image analysis. The features extracted from the conv4 layer and pool5 layer of VGG-M-128, as well as the conv5 layer and pool5 layer of BVLC CaffeNet, had higher classification accuracy compared to the fully connected layers (fc6 and fc7) of the VGGnets and CaffeNet. on using deep learning techniques for the diagnosis and prediction of Rheumatoid Arthritis (RA) progression. The study by Norgeot et al. uses a Long Short-Term Memory (LSTM) based technique to analyze the electronic health records (EHR) of patients. The dataset consists of 820 patients and the results show the effectiveness of using LSTM for this purpose.

On the other hand, the study by Li et al. uses Convolutional Siamese Neural Networks (CSNNs) to score the severity of knee injury using the KL grading scale. They use a fine-tuned ResNet-34 as a baseline and propose a novel approach that uses Siamese networks to reduce the number of learnable parameters, making the model less sensitive to noise. The study uses radiographs from both MOST and OAI datasets and achieves a multiclass accuracy of 66.71% and AUC of 0.93 on the OAI dataset. However, the study also highlights some limitations of the model, such as the potential to learn irrelevant features. The results are available to the public through the publicly available code and dataset.



**Nalini and Prabavathy**

The papers you described focus on developing techniques for the prediction of osteoarthritis progression. The study by Tiulpin et al. presents a multimodal pipeline for the prediction of osteoarthritis progression using a combination of Convolutional Neural Network (CNN) and other features such as age, sex, BMI, injury, surgery, WOMAC score, and KL-grade. The best model achieved an AUC of 0.81 and an AP of 0.70. The researchers also used GradCAM to verify that the model was learning the correct features.

The study by Bonaretti et al. presents the mean characteristics of the OAI Control and Incidence Cohort of patients with osteoarthritis. The study shows that the symptomatic progression of osteoarthritis is higher in patients with higher age and BMI compared to the control group. The study by Nguyen et al. proposes a method for early detection of osteoarthritis using a novel variant of the Siamese network and a Deep SSL technique. The researchers found that their SAM-HV architecture outperformed the baseline model, with an accuracy of 58% for early detection of osteoarthritis (KL = 2) with 500 samples per KL grade and an accuracy of 74% with 1000 samples per KL grade. Moreover, incorporating other types of data such as lifestyle data, imaging data, and genetic data in the predictive models could improve their accuracy. In order to achieve this, it is necessary to develop new data integration and fusion methods. Additionally, attention should be paid to interpretability and explainability of the models, as well as their generalization ability to different populations and datasets. Moreover, it is also crucial to evaluate the performance of these models in real-world settings and to compare their performance with traditional methods, such as radiographs and clinical examination. The development of deep learning models for the diagnosis of OA and RA requires close collaboration between computer scientists, medical doctors, and radiologists. This will ensure that the models are developed with a deep understanding of the underlying medical concepts and can be easily integrated into the clinical workflow. Finally, it is important to consider ethical and privacy issues when developing these models. The models should be developed in a way that protects the privacy of patients and ensures that their data is used only for the purposes of medical research and treatment. In conclusion, machine learning and deep learning techniques have great potential for the diagnosis of OA and RA and have already shown promising results in several studies. However, further research is needed to fully realize their potential and to make these models widely adopted in clinical practice.

CONCLUSION

The literature review does indicate a gap in research on the use of deep learning for the diagnosis of rheumatoid arthritis. Both of these areas could benefit from further research and exploration. The use of imaging technology and electronic health records (EHRs) has the potential to revolutionize the way of diagnose and treat types of rheumatic diseases. With the increasing amount of data stored in EHRs, machine learning algorithms can be trained to analyze this data and provide more accurate and early diagnoses. It enables healthcare providers to make more informed treatment decisions. In conclusion, combining imaging technology and EHRs with machine learning algorithms has the potential to significantly improve the diagnosis and treatment of osteoarthritis and other rheumatic diseases. This research direction could lead to a better understanding of these conditions and improve patient outcomes.

REFERENCES

1. Australian Bureau of Statistics, National health survey: first results <https://www.abs.gov.au/ausstats/> (2020), Accessed 4th May 2020
2. M. Hügler, P. Omoumi, J.M. van Laar, J. Boedecker, T. Hügler, Applied machine learning and artificial intelligence in rheumatology, *Rheumatol. Adv. Pract.*, 4 (2020), Article rkaa005.
3. K.J. Kim, I. Tagkopoulos, Application of machine learning in rheumatic disease research, *Korean J. Int. Med.*, 34 (2019), p. 708
4. K. O'Shea, R. Nash, An introduction to convolutional neural networks, arXiv preprint, arXiv:1511.08458 (2015)





Nalini and Prabavathy

5. S.A.A. Shah, M. Bennamoun, F. Boussaid, Iterative deep learning for image set based face and object recognition, *Neurocomputing*, 174 (2016), pp. 866-874
6. B. Stoel, Use of artificial intelligence in imaging in rheumatology–current status and future perspectives, *RMD Open*, 6 (2020), Article e001063
7. I.J. Goodfellow, J. Pouget-Abadie, M. Mirza, B. Xu, D. Warde Farley, S. Ozair, A. Courville, Y. Bengio, Generative adversarial networks arXiv preprint, arXiv:1406.2661 (2014)
8. S. Khan, H. Rahmani, S.A.A. Shah, M. Bennamoun, A guide to convolutional neural networks for computer vision, *Synthesis Lectures on Computer Vision*, vol. 8 (2018), pp. 1-207
9. J. Gutiérrez-Martínez, C. Pineda, H. Sandoval, A. Bernal-González, Computer-aided diagnosis in rheumatic diseases using ultrasound: an overview, *Clin. Rheumatol.* (2020), pp. 1-1
10. K. O'Shea, R. Nash, An introduction to convolutional neural networks, arXiv preprint, arXiv:1511.08458 (2015)
11. J. Thomson, T. O'Neill, D. Felson, T. Cootes, Automated shape and texture analysis for detection of osteoarthritis from radiographs of the knee, *International Conference on Medical Image Computing and Computer-Assisted Intervention*, Springer (2015), pp. 127-134
12. M. Subramoniam, A non-invasive method for analysis of arthritis inflammations by using image segmentation algorithm, 2015 International Conference on Circuits, Power and Computing Technologies [ICCPCT-2015], IEEE (2015), pp. 1-4
13. J. Antony, K. McGuinness, N.E. O'Connor, K. Moran, Quantifying radiographic knee osteoarthritis severity using deep convolutional neural networks 2016 23rd International Conference on Pattern Recognition (ICPR), IEEE (2016), pp. 1195-1200
14. S.S. Gornale, P.U. Patravali, R.R. Manza, Computer assisted analysis and systemization of knee osteoarthritis using digital x-ray images, *Proceedings of 2nd International Conference on Cognitive Knowledge Engineering (ICKE)* (2016), pp. 207-212
15. S.S. Gornale, P.U. Patravali, R.R. Manza, Detection of osteoarthritis using knee x-ray image analyses: a machine vision based approach, *Int. J. Comput. Appl.*, 145 (2016)
16. J. Yoo, M.K. Lim, C. Ihm, E.S. Choi, M.S. Kang, A study on prediction of rheumatoid arthritis using machine learning *Int. J. Appl. Eng. Res.*, 12 (2017), pp. 9858-9862
17. S.S. Gornale, P.U. Patravali, K.S. Marathe, P.S. Hiremath, Determination of osteoarthritis using histogram of oriented gradients and multiclass svm, *Int. J. Image Graph. Signal Process.*, 9 (2017)
18. J.M. Lezcano-Valverde, F. Salazar, L. León, E. Toledano, J.A. Jover, B. Fernandez-Gutierrez, E. Soudah, I. González-Álvaro, L. Abasolo, L. Rodriguez-Rodriguez, Development and validation of a multivariate predictive model for rheumatoid arthritis mortality using a machine learning approach, *Sci. Rep.*, 7 (2017), pp. 1-10
19. S. Murakami, K. Hatano, J. Tan, H. Kim, T. Aoki, Automatic identification of bone erosions in rheumatoid arthritis from hand radiographs based on deep convolutional neural network, *Multimed. Tools Appl.*, 77 (2018), pp. 10921-10937
20. J. Tang, Z. Jin, X. Zhou, H. Chu, J. Yuan, M. Wu, Q. Cheng, X. Wang, Grading of rheumatoid arthritis on ultrasound images with deep convolutional neural network, 2018 IEEE International Ultrasonics Symposium (IUS), IEEE (2018), pp. 1-4
21. D.E. Orange, P. Agius, E.F. DiCarlo, N. Robine, H. Geiger, J. Szymonifka, M. McNamara, R. Cummings, K.M. Andersen, S. Mirza, *et al.*, Identification of three rheumatoid arthritis disease subtypes by machine learning integration of synovial histologic features and RNA sequencing data, *Arthritis Rheumatol.*, 70 (2018), pp. 690-701
22. B. Norgeot, B.S. Glicksberg, L. Trupin, D. Lituiev, M. Gianfrancesco, B. Oskotsky, G. Schmajuk, J. Yazdany, A.J. Butte, Assessment of a deep learning model based on electronic health record data to forecast clinical outcomes in patients with rheumatoid arthritis, *JAMA Netw. Open*, 2 (2019), Article e190606
23. R. Hemalatha, V. Vijaybaskar, T. Thamizhvani, Automatic localization of anatomical regions in medical ultrasound images of rheumatoid arthritis using deep learning, *Proc. Inst. Mech. Eng., H J. Eng. Med.*, 233 (2019), pp. 657-667



**Nalini and Prabavathy**

24. J. Abedin, J. Antony, K. McGuinness, K. Moran, N.E. O'Connor, D. Reibholz-Schuhmann, J. Newell, Predicting knee osteoarthritis severity: comparative modeling based on patient's data and plain x-ray images, *Sci. Rep.*, 9 (2019), pp. 1-11
25. P. Chen, L. Gao, X. Shi, K. Allen, L. Yang, Fully automatic knee osteoarthritis severity grading using deep neural networks with a novel ordinal loss, *Comput. Med. Imaging Graph.*, 75 (2019), pp. 84-92
26. A. Tiulpin, S. Saarakkala, Automatic grading of individual knee osteoarthritis features in plain radiographs using deep convolutional neural networks, *Diagnostics*, 10 (2020), p. 932
27. B. Norman, V. Padoia, A. Noworolski, T.M. Link, S. Majumdar, Applying densely connected convolutional neural networks for staging osteoarthritis severity from plain radiographs, *J. Digit. Imaging*, 32 (2019), pp. 471-477
28. A. Tiulpin, I. Melekhov, S. Saarakkala, Kneel: knee anatomical landmark localization using hourglass networks Proceedings of the IEEE International Conference on Computer Vision Workshops (2019)
29. B. Liu, J. Luo, H. Huang, Toward automatic quantification of knee osteoarthritis severity using improved faster r-cnn, *Int. J. Comput. Assisted Radiol. Surg.*, 15 (2020), pp. 457-466
30. A. Tiulpin, S. Saarakkala, Automatic grading of individual knee osteoarthritis features in plain radiographs using deep convolutional neural networks, *Diagnostics*, 10 (2020), p. 93
31. H. Hoang Nguyen, S. Saarakkala, M. Blaschko, A. Tiulpin, Semixup: in- and out-of-manifold regularization for deep semi-supervised knee osteoarthritis severity grading from plain radiographs arXiv:2003.01944 (2020)
32. S. Bonaretti, G.E. Gold, G.S. Beaupre, pykneer: an image analysis workflow for open and reproducible research on femoral knee cartilage
33. *PLoS ONE*, 15 (2020), Article e0226501
34. S.D.H. Dang, L. Allison, Using deep learning to assign rheumatoid arthritis scores 2020 IEEE 21st International Conference on Information Reuse and Integration for Data Science (IRI), IEEE (2020), pp. 399-402
35. C.E. von Schacky, J.H. Sohn, F. Liu, E. Ozhinsky, P.M. Jungmann, L. Nardo, M. Posadzy, S.C. Foreman, M.C. Nevitt, T.M. Link, *et al.*, Development and validation of a multitask deep learning model for severity grading of hip osteoarthritis features on radiographs, *Radiology*, 295 (2020), pp. 136-145
36. P. Chen, L. Gao, X. Shi, K. Allen, L. Yang, Fully automatic knee osteoarthritis severity grading using deep neural networks with a novel ordinal loss, *Comput. Med. Imaging Graph.*, 75 (2019), pp. 84-92
37. H.H. Nguyen, S. Saarakkala, M.B. Blaschko, A. Tiulpin, Annotation-efficient deep semi-supervised learning for automatic knee osteoarthritis severity diagnosis from plain radiographs, Online Proceedings Medical Imaging Meets NeurIPS Workshop 2020, NeurIPS (2020)





Clinical and Pharmaceutical Evaluation of Triptan Formulations in Migraine Treatment: an Overview

Gowri Sankar Chintapalli^{1,2}, Durgaprasad Kemiseti^{3*}, Kirtimaya Mishra⁴, Biplab Kumar Dey⁵ and Snigdha Rani Behera^{1,6}

¹Ph.D Scholar, Faculty of Pharmaceutical Science, Assam down town University, Gandhi Nagar, Panikhaiti, Guwahati. Pin-78102, Assam, India

²Assistant Professor, School of Pharmacy, ARKA JAIN University, Gamaharia, Jamshedpur, Jharkhand. Pin-832108, India.

³Associate Professor, Faculty of Pharmaceutical Science, Assam down town University, Gandhi Nagar, Panikhaiti, Guwahati, Assam, India

⁴Professor, School of Pharmacy, ARKA JAIN University, Gamaharia, Jamshedpur, Jharkhand, India

⁵Professor, Faculty of Pharmaceutical Science, Assam down town University, Gandhi Nagar, Panikhaiti, Guwahati, Assam, India

⁶Associate Professor, School of Pharmacy, ARKA JAIN University, Gamaharia, Jamshedpur, Jharkhand, India

Received: 23 Dec 2022

Revised: 25 Apr 2023

Accepted: 31 May 2023

*Address for Correspondence

Durgaprasad Kemiseti

Associate Professor,

Faculty of Pharmaceutical Science,

Assam down town University, Gandhi Nagar,

Panikhaiti, Guwahati, Assam, India.

E.Mail: chintapalli.sankar@gmail.com, kdp251999@gmail.com



This is an Open Access Journal / article distributed under the terms of the **Creative Commons Attribution License** (CC BY-NC-ND 3.0) which permits unrestricted use, distribution, and reproduction in any medium, provided the original work is properly cited. All rights reserved.

ABSTRACT

Triptans developed exclusively for treating migraines have revolutionised migraine therapy and are frequently used to treat migraines that are currently active. Triptans are available in a range of dose forms, including oral pills, tablets that dissolve slowly in the mouth, films that dissolve quickly in the mouth, nasal sprays, and subcutaneous injections. Sumatriptan is also offered as a suppository in Europe. The pharmacological profiles of triptans, which include $T_{1/2}$, T_{max} , C_{max} , metabolism, and drug-drug interaction profiles among other parameters and pharmaceutical evaluation parameters of triptan formulations, show how different they are in many aspects. It is unclear how or whether these differences translate into differences in clinical effectiveness and tolerability. Triptans' onset of action may also be influenced by delivery systems. A migraine attack is classified based on the following factors: peak intensity, time to peak intensity, level of accompanying symptoms such as nausea and vomiting, time of associated symptoms, comorbid conditions, and concurrent therapies that may cause

57674



**Gowri Sankar Chintapalli et al.,**

drug-drug interactions. The clinician's armamentarium is constantly increasing with medicines that are accessible in a range of formulations and doses and have acceptable safety and tolerability characteristics.

Key words: Anti migraine drugs, Triptans, Clinical evaluation, Clinical features, pharmaceutical evaluation

INTRODUCTION

Migraine headache pain is often expressed as a pulsing sensation in a specific part of the head. However, it is much more; the IHS classifies migraines based on their severity and frequency of attacks, as well as other symptoms namely vomiting, nausea and sensitivity to sound and light. Migraine is 3 times more prevalent in women than in males and affects more than 10% of the world's population [1]. Migraine sufferers frequently have repeated episodes that are triggered by a variety of circumstances, including stress, anxiety, hormonal changes, bright or flashing lights, lack of food or sleep, and dietary ingredients [2]. Migraine in some women may be related to variations in hormonal levels during their menstrual cycle. For many years, experts thought migraine was caused by the dilatation and constriction of blood vessels in the brain [3]. Types of migraine based on "aura," briefly shown in (Figure 1).

Classification of Antimigraine drugs

Ergot alkaloids, agonists or partial agonists at a particular subtype of 5-Hydroxy Triptamine₁-like receptors, β -adrenoceptor antagonists, calcium antagonists, anti-emetics, and NSAIDS are the major migraine medications [4]. Diagrammatic representation of Antimigraine drugs classification shown in (Figure 2).

Mechanism of Triptans

Triptans are Serotonin receptor agonists that have a high attraction for the 5-HT_{1B} and 5-HT_{1D} receptors. The activation of 5-HT_{1B} receptors on blood vessel smooth muscle cells results in cranial vasoconstriction [5]. The mechanism of action for several headache and triptan medications is depicted in a schematic in (Figure 3&4).

CLINICAL EVALUATION OF TRIPTANS:

The first half of 2021 had seen seven triptans in the market in some countries. They are zolmitriptan, sumatriptan, naratriptan, almotriptan, rizatriptan, eletriptan, and frovatriptan in order of clinical circumstance (Table 1). Based on clinical features, triptan formulations were classified in two categories. These are Group-I and Group-II. Group-I category triptans have faster onset of action, higher potency and higher recurrence. Group-II category triptans have slowest onset of action, low potency and lower recurrence. Clinical features of triptan formulations are briefly detailed in (table2).

PHARMACEUTICAL EVALUATION OF TRIPTANS

Until date, for the triptans formulation different polymers used, manufacturing techniques, pre-compression, post compression parameters and findings related review was detailed in (Table-3).

Current Statistics of Triptans

The majority of triptans were developed and introduced in the 1990s. Further research has not shown much promise in terms of developing new triptans with improved duration of action, efficacy, and safety profile. As a result, further variations are unlikely, and new anti-migraine drugs are likely to have a different mechanism of action. Most formulations are available in Sumatriptan, Zolmitriptan, Naratriptan, and Rizatriptan. The available dosage forms for triptans upto till date shown in Figure 4.





Gowri Sankar Chintapalli *et al.*,

CONCLUSION

It was concluded that when treating an acute migraine attack, clinicians have access to a wide range of triptans with varying pharmacokinetic properties and clinical evaluations, pharmaceutical formulations on various types of polymers used in different triptan formulations and studies like pharmaceutical evaluation data most useful for improvement of further new research ideas and quality by design techniques used in newer triptan formulations. A big breakthrough in the treatment of migraine was made in the 1990s with the advent of the triptans, which changed the lives of millions. It should become possible for a doctor interested in triptans to match a patient's demands with a triptan's unique qualities in order to maximise therapeutic effect with continued clinical and pharmaceutical usage.

ACKNOWLEDGMENT

The authors express their gratitude to the School of Pharmacy, Arka Jain University, Jharkhand, and Chancellor, Vice Chancellor, Dean Faculty of Pharmaceutical Sciences, Assam Down Town University Guwahati for providing their continuous support throughout the work.

CONFLICT OF INTEREST

The authors declare that they have no conflict of interest. The article does not contain any studies with animals or human participants performed by any of the authors.

REFERENCES

1. Bhupendra S, Dipesh Raj P. Migraine. European journal of biomedical and pharmaceutical sciences.2017; 4(4):226-30.
2. Panigrahi S, Sengupta R. Burden of migraine. Journal of drug delivery and therapeutics. 2019; 9(4): 648-50.
3. Stovner LJ, Tronvik E, Hagen K. New drugs for migraine. The journal of headache and pain. 2009; 10(1): 395–406.
4. Limmroth V, Biondi D, Pfeil J, Schwalen S. Topiramate in patients with episodic migraine: reducing the risk for chronic forms of headache. Headache. 2007; 47(1): 13–21.
5. Tepper SJ. Mechanisms of Action of the 5- HT. Archives of Neurology. 2002; 59(7): 1084–8.
6. Ramu S, Ramakrishna G, Balaji M, and Kondalarao K. Formulation and evaluation of Sumatriptan Succinate mouth disintegrating tablets. American journal of advanced drug delivery. 2013; 1(5): 759-69.
7. Panda K C, Reddy A V, Panda N, Narayan Reddy G, Habibuddin MD, Mahapatra APK. Formulation and evaluation of thermosensitive intranasal in situ gel of sumatriptan succinate by using a blend of polymers. Journal of pharmacy and chemistry. 2014; 8(2): 25-9.
8. Reddy AM, Sindhura J, Naga Lakshmi B, Reedy AA, Navya Sri D, Kumar MN, Srinivasa Babu P. Formulation and evaluation of bilayered tablets of sumatriptan succinate by using hydrophilic polymers, Der Pharmacia Lettre. 2016; 8(5): 189-206.
9. Ilaveni P, Padmapriya S, Rajalakshmi A N. Formulation and evaluation of mucoadhesive microspheres of an anti-migraine drug. Journal of drug delivery and therapeutics. 2018; 8(5): 465-74.
10. Indira Prasanna R, Anitha P, Madhusudhana Chetty C. Formulation and evaluation of bucco-adhesive tablets of Sumatriptan Succinate. International journal of pharmaceutical investigation. 2011; 1(3):182-91.
11. Bisht SS, Chourasia H, Varshney S, Reena, Deepti K. Formulation and evaluation of fast dissolving tablets of Sumatriptan Succinate. International Journal of Pharmaceutical Sciences and Research. 2013; 4(5):1912-17.
12. Swati CJ, Chandrakala RP. Application of design of experiment for polyox and xanthan gum coated floating pulsatile delivery of sumatriptan succinate in migraine treatment. BioMed Research International. 2014; 1-10.



**Gowri Sankar Chintapalli et al.,**

13. Hazee Peera N, Lohithasu D, Sahoo SK, Santhosh Naidu M, Mani Kumar K, Anil Kumar V. Formulation development and evaluation of oral disintegrating tablets of zolmitriptan. *Der Pharmacia Lettre*. 2013; 5(2): 324-32.
14. Mahmood W S, Khalil Y I. Formulation and evaluation of zolmitriptan bilayer oral strip. *World Journal of Pharmaceutical Research*. 2014; 4(1): 25-57.
15. Daswadkar S, Sontakke Patil SB. Formulation and evaluation of mouth dissolving film of zolmitriptan by using natural polymers. *World journal of pharmacy and pharmaceutical sciences*. 2020; 9(12): 707-23.
16. Namrata R, Tahir N, Ankit M, Neelesh M, Vishakha C, Neelima S. Formulation and evaluation of fast dissolving oral films of an anti-migrain drug. *Journal of drug delivery and therapeutics*. 2019; 9(2-A): 59-61.
17. Uma Sankar D, Madhuri Latha T, Lavanya P. Preparation, Formulation and in vitro evaluation of sustained release zolmitriptan tablets by using natural polymers. *World journal of pharmaceutical research*. 2016; 5(12): 750-60.
18. Sankar CG, Uma Sankar D, Lavanya P, Madhuri T, Madhuralatha T. Formulation development and optimization of zolmitriptan tablets by direct compression method. *Indian journal of medical research and pharmaceutical sciences*. 2020; 7(1): 11-31.
19. Hari Hara Nadh TV, Sivaram Kumar P, Venkata Ramana M, Rama Rao N. Formulation and optimization of zolmitriptan orodispersible tablets. *Journal of drug delivery and therapeutics*. 2002; 11(3): 50-7.
20. Rohini P, Soundarya PR, Pardhasaradhi CH. Formulation and evaluation of naratriptan hydrochloride oral disintegrating tablets by using direct compression method. *International journal of pharmaceutical sciences review and research*. 2015; 34(1):1-5.
21. Kshirasagar N, Senthil KK, Sravan. KA, Malvey S. Formulation and evaluation of naratriptan orodispersible tablets using superdisintegrants by direct compression method. *International journal for pharmaceutical research scholars*. 2013; 2(2): 268-78.
22. Bhikshapathi DVRN, Durga Madhuri V, Rajesham VV, Suthakaran R. Preparation and evaluation of fast dissolving oral film containing naratriptan hcl. *American Journal of PharmTech Research*. 2014; 4(2):799-812.
23. Brahmabhatt H, Brahmabhatt H, Patel K, Makwana P, Chauhan N, Jain H, Umesh U. Formulation and evaluation of sublingual tablet for Naratriptan. *Journal of drug delivery & therapeutics*. 2014; 4(4):19-23.
24. Samia MO, Fathy IA, Noha MA. Preparation and optimization of fast-disintegrating tablet containing naratriptan hydrochloride using d-optimal mixture design. *American association of pharmaceutical scientists*. 2018; 19(6): 2472-87.
25. Oza NA, Sahu AR, Tripathi, Patel PU, Patel LD, Ramkishan A, Formulation development and optimization of fast orodispersible tablets of naratriptan hydrochloride by using factorial design, *International Journal of Research Medical Sciences*. 2013; 2(4): 48-53.
26. Mothilal M, Srikanth K, Sivagirish babu G, Gnanendra K, Manimaran V and Damodharan N. Formulation and evaluation of rizatriptan benzoate orally disintegrating tablets. *International journal of drug development and research*. 2012; 4(2):117-23.
27. Karthikeyan D, Sanju Sri C, Kumar S. Development of fast dissolving oral film containing of rizatriptan benzoate as an antimigraine medication. *Indo American journal of pharmaceutical research*. 2013; 3(3): 2642-54.
28. Bhupinder B, Sarita J. Formulation and evaluation of fast dissolving sublingual films of rizatriptan benzoate. *International journal of drug development and research*. 2012; 4(1): 97-107.
29. Swati CJ, Pravin SP, Gajanan JC. Formulation and evaluation of modified pulsincap drug delivery system of rizatriptan benzoate. *International Journal of Pharmacy and Pharmaceutical Sciences*. 2014; 6(5): 48-52.
30. Sahar S, Soheil B. New formulation and approach for mucoadhesive buccal film of rizatriptan benzoate. *Progress in Biomaterials*. 2017; 6(4): 175–87.
31. Kantrodiya T, Gandhi S, Panseriya N, Dhruvisha C, Mayuri J K. Formulation and evaluation nasal in situ gel of rizatriptan. *International journal of pharmacy research and technology*. 2019; 9(2): 49-64.
32. Haarika B, Prabhakar Reddy V. Formulation and evaluation of fast disintegrating rizatriptan benzoate sublingual tablets. *Malaysian Journal of Pharmaceutical Sciences*. 2012; 10(1): 45–60.
33. Gowtham G, Ranjeeth Reddy G, Naveen kumar CH, Sathyanarayana R and Pande VP. Formulation and evaluation of almotriptan tablets. *Research journal of pharmacy and technology*. 2011; 4(4): 533-36.

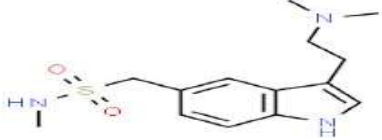
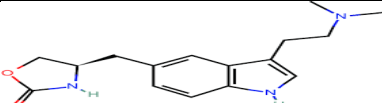




Gowri Sankar Chintapalli et al.,

34. Akhila A and Damodharan N. Formulation, taste masking and evaluation of almotriptan oral disintegrating tablets. International journal of pharma sciences and research. 2012; 3(10): 3940-46.
35. Rucheera R V, Shailendra S G, Udaykumar B. Thermosensitive mucoadhesive in situ gel for intranasal delivery of Almotriptan malate: Formulation, characterization, and evaluation. Journal of Drug Delivery Science and Technology. 2020; 58: 1-8.
36. Sirisha Y, Udaya Chandrika P, Srinivasa Rao A. Formulation and evaluation of fast dissolving thin oral films of frovatriptan. Indoamerican journal of pharmaceutical sciences. 2016; 3(7): 750-55.
37. Sirisha Y, Lokeswar Babu V, Srinivasa Rao A. Formulation and evaluation of fast dissolving tablets of frovatriptan. World Journal of Pharmaceutical Research. 2015; 4(10): 1423-34.
38. Sirisha Y, Gopala Krishna Murthy T, Srinivasa Rao A. Formulation development evaluation and optimization of orodispersible tablets of frovatriptan for the treatment of migraine. American Journal of PharmTech Research. 2018; 8(2): 278-95.
39. Pankaj B, Suruchi S, Satish Kumar S, Sani R. Development and Characterization of Fast Dissolving Buccal Strip of Frovatriptan Succinate Monoydrate for Buccal Delivery. International Journal of Pharmaceutical Investigation. 2021; 11(1): 69-75.
40. Ashok T, Srikanth G, Firoz S, Ekanth Chowdary VC, Aruna K, Geetha K. Formulation and in vitro Evaluation of Frovatriptan Succinate Oral Disintegrating Tablets by Direct Compression Technique. Journal of PharmaSciTech. 2016; 6(2): 82-7.
41. Haranath C, Arshad Ahmed Khan K, Surya Prakash ReddyA, Pradeep Kumar B, Veera Bhadrappa KV. Formulation and in-vitro evaluation of mucoadhesive buccal tablets of anti-migraine drug. Inventi Rapid: NDDS. 2015; 4: 1-10.
42. Pallavi K, Pallavi T. Formulation and evaluation of fast dissolving films of eletriptan hydrobromide. International journal of current pharmaceutical research. 2017; 9(2): 59-63.
43. Sankar CG, Behera SR, Mishra SR, Somesu M, Kiran Kumar B and Mishra K, Design and evaluation of floating microspheres of ranitidine hcl, The pharma innovation journal. 2020, 9(3): 223-33.
44. Sankar CG, Behera SR, Mishra SR, Srivalli D and Mishra K. Development and evaluation of orally disintegrating films containing Moxonidine chloride. International Journal of Biology. Pharmacy and Allied Sciences. 2021; 10(8): 2712-20.
45. Manivannan R, Ali Baig M, Purushothaman M and Senthil kumar N. Formulation and evaluation of eletriptan hydrobromide microsphere. International Journal of Pharmaceutics and Drug Analysis. 2014; 2(3): 347-53.
46. Ashok PP, Suvarna AK, Choudhari RK, Bhambar RS. Formulation and evaluation of fast disintegrating tablet of eletriptan hydrobromide. Research journal of Pharmacy Technology. 2014; 7(7): 792-97.

Table-1. Triptan Formulations

S.no	Drug name	Formulations	Required strength	Maximum daily strength	Chemical structure
1	Sumatriptan	Oral Formulations (Tablets) Nasal Formulations Subcutaneous Formulations Rectal Formulations	25mg, 50mg, 100mg 5mg, 10mg, 20mg 4mg, 6mg 25mg	200mg 40mg 12mg 50mg	
2	Zolmitriptan	Oral Formulations Orally	1.25mg, 2.5mg, 5mg 2.5mg, 5mg	10mg 10mg	





Gowri Sankar Chintapalli et al.,

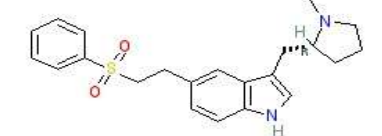
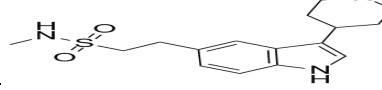
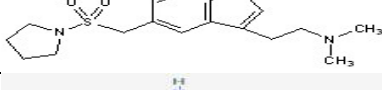
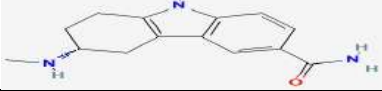
		disintegrating Tablets Nasal Formulations	2.5mg,5mg	10mg	
3	Rizatriptan	Oral Formulations Sublingual Tablets	5mg, 10mg 5mg, 10mg	20mg 20mg	
4	Elitriptan	Oral Formulations	20mg, 40mg	80mg	
5	Naratriptan	Oral Formulations	1mg, 2.5mg	5mg	
6	Almotriptan	Oral disintegrating tablets	6.25mg, 12.5mg	25mg	
7	Frovatriptan	Oral disintegrating tablets	2.5mg	7.5mg	

Table-2: Clinical features of triptans

S.no	Category	Group-I	Group-II
1	Triptans	Sumatriptan Zolmitriptan Rizatriptan Almotriptan Elitriptan	Naratriptan Frovatriptan
2	Features	Faster onset Higher potency high recurrence	Slower onset Lower potency Lower recurrence





Gowri Sankar Chintapalli et al.,

Table 2. Pharmaceutical Evaluation of Triptans

Drug	Dosage form	Technique	Polymers	Pre & Post compression parameters	Findings	Ref
Sumatriptan	Mouth disintegrating Tablets	Direct compression	Croscarmellose sodium, Crospovidone and Sodium starch glycolate (SSG)	Bulk density, tapped density, angle of repose, Car's index and Hasusners ratio are within limits. Hardness, friability, Weight variation, drug content, wetting time, dispersion time, and invitro dissolution studies were all performed on the tablet batches that had been prepared. Comparing different formulations, the one containing SSG and Croscarmellosesodium and demonstrated the fastest invitro dispersion time.	The optimized formulation dispersed in 8 seconds. A greater water absorption ratio was also demonstrated, and 99.58% of the medication is released within 2 minutes. .	[6]
	Nasal Gel	Cold method	Poloxamer 188, Sodium CMC, Carbopol 934	Physiochemical parameters, gelation temperature, gel strength, content uniformity, Digital Scanning Colorimeter, and FTIR were all measured in the formulations. Mucoadhesive nasal gel has been shown in this study to have several advantages, including dosing accuracy, and extended nasal residence time.	The in vitro tests performed for mucoadhesive strength and drug diffusion showed that nasal in situ gelling formulations prepared were having good mucoadhesive strength with nearly 100% drug diffusion.	[7]
	Bilayered Tablets	Direct compression	Sodium alginate, HPMC K 15, HPMC E15	All the excipients are tested for compatibility with model drug. It was decided that the best formulation was F2, which contained HPMC E15 and Sodium alginate. The drug release of F2 follows zero-order. The total amount of drug released from the Formulation 2 is the maximum and it reached to about 99.89%.	Based on the dissolution result F2 trial formulation was selected as best formulation. The drug release of F2 follows zero-order. The total amount of drug released from the Formulation 2 is the maximum and it reached to about 99.89%.	[8]





Gowri Sankar Chintapalli et al.,

Mucoadhesive microspheres	Emulsification method	Hydroxy Propyl Methyl Cellulose K4m,	Nine formulations were formulated and evaluated for possible drug polymer interactions, percentage yield, micromeritic properties, particle size, drug content, drug entrapment efficiency, drug loading, swelling index, In-vitro wash off test, in vitro drug release, surface morphology and release kinetics.	The results showed that no significant drug polymer interaction in FTIR studies. Among all the formulations SF3 containing sodium alginate showed 77.18% drug release in 6hrs.	[9]
Bucco-adhesive tablets	Direct compression	Sodium Carboxy methyl cellulose, and Carbopol 934P with a backing layer of ethyl cellulose	In vitro drug release, ex vivo drug permeation, and stability in saliva were all tested on tablets, as were surface Ph, swelling index and ex vivo bioadhesive force.	All formulations S4 shows good controlled release results.	[10]
Fast Dissolving Tablets	Direct compression	Crosscarmellose, Crospovidone, Preglatinised Starch 1500	Bulk density, tapped density, angle of repose, Car's index and Hasushners ratio are within limits. The formulation F3 with Crospovidone (8%) produced the best results because to improved dissolving, which leads to greater bioavailability, effectiveness, and thus better patient compliance.	In vitro drug release from the tablets shows significantly improved drug dissolution. It was concluded that in direct compression method, crospovidone was best super disintegrant with MCC as binding agent.	[11]
Floating pulsatile tablet	Direct compression	Swellable polymer polyox WSR205 and xanthan gum.	Physical properties of the optimised formulation were assessed in an in vitro and in vivo study. From results, it can be concluded that optimized batch F8 containing polyox WSR205 (72.72%) and xanthan gum (27.27%) of total weight of polymer has shown floating lag time of 55 ± 2 sec, drug content of $100.35 \pm 0.4\%$, hardness of 6 ± 0.1 Kg/cm ² , and $98.69 \pm 2\%$ drug release in pulse manner with lag time of 7 ± 0.1 h.	An in-vivo X-ray study on the optimised batch showed that it had a longer gastric residence time.	[12]



Gowri Sankar Chintapalli *et al.*,

Zolmitriptan	Oral Disintegrating Tablets	Direct compression	Crospovidone, SSG, Supertab11SD, Avicel PH 102, Ac-Di-Sol.	Bulk density, compressibility, and angle of repose are examples of precompression parameters profiles are satisfactory. The manufactured batches of tablets' in-vitro dissolution and disintegration times were evaluated and determined to be satisfactory. The F9 Formulation had the highest dissolving rate when paired with medication release, making it the best of the three.	In this trail disintegration time of tablet was good and friability with in the limits and has good dissolution profiles compared to reference product.	[13]
	Blayer Oral strip	Solvent casting	HPMC E5, PG, PEG400, HPM C E15, HPM C E4K, NACMC C, XANTHAN GUM, GELATIN	Physical and mechanical charecterizations are better results obtained. The disintegration time of the optimised formula (Fx10) was 32 seconds; 50% of the medication was released within the first 15 minutes, with the remaining drug released over a 4-hour period.	The quick release profile was compared to that of the commercially available zolmitriptan oral dispersible tablet.	[14]
	Mouth Dissolving Film	Solvent casting	Starch maize, pectin and guar gum, Maltodextrin, Polyvinylchloride, HPMC	Melting point, Solubility study, Drug and Polymers compatibility studies are good optimized results for particular drug. A total of 39 batches were prepared from which batch containing 50% pectin and 20% glycerol, was found to be best with desirability 0.998. Oral films of the optimized batch show 27±2 no. of folds and show 98.12±0.1% drug release.	Further study like pre-clinical is necessary to investigate the proper mechanism related to findings of the study.	[15]
	Fast dissolving films	Solvent casting	HPMC and PEG (plasticizers)	Preformulation studies are very well. In order to improve Bioavailability, speed up the onset of action (quick relief), and prevent first-pass metabolism, a fast-dissolving oral film of the drug zolmitriptan was created. The physicochemical characterization of the films, such as their thickness, weight variation, and folding endurance drug content, revealed that they were satisfactory. The surface pH of all the films was found to be neutral.	When compared to the available conventional dosage forms, the fast dissolving sublingual film of Zolmitriptan may be a better option for acute migraine treatment.	[16]





Gowri Sankar Chintapalli et al.,

Sustained Release Tablets	Direct compression	Ethyl cellulose, Sodium alginate, Sodium carboxy methyl cellulose	<p>Bulk and tapped density, Angle of repose, Carr’s Index, Hausner’s Ratio and Bulkiness are with in Pharmacopeia limits.</p> <p>As a result, we draw the conclusion that the F7 formulation has better drug release control than the other formulations (over 8 hours). The produced tablets' physicochemical examination was confirmed to be within Pharmacopoeia norms.</p>	Thus we conclude that from among all the developed formulations F7 formulation controls the drug release for longer period of time over 8hr when compare to other formulations. The physicochemical evaluation of the prepared tablets was found within the standards Pharmacopoeia limits.	[17]
Sustained release Matrix Tablets	Direct compression	Karayagum, Guargum, and HPMC K100M	<p>Bulk density, Angle of repose, Carr’s Index, Hausner’s Ratio values indicate that the blends had good flow property.</p> <p>Continuous drug delivery over a 12-hour period is provided by Zolmitriptan's sustained-release formulation, which also reduces fluctuations in drug concentrations in the blood. This delayed release reduces the risk of side effects associated with high serum levels, which are common with immediate-release formulations.</p>	A sustained release model drug tablet can reduce the number of doses administered, resulting in better patient compliance and fewer chances of overdose, as well as lowering the cost of treating pain symptoms.	[18]
Orodispersible Tablets	Direct compression	Crospovidone, croscarmellose sodium	<p>Precompression studies were within limits. experimental trials are performed for all 9 formulations. For all formulations, the post-compression parameters were studied. Based upon the model optimized formulation (C1 and C2) was obtained having the disintegration time (34.4±0.84 and 39.8±0.91) and %drug release (98.7±0.42 and 93.2±0.46) respectively.</p>	Crospovidone (8%) and Sodium starch glycolate (6%) are better super disintegrants. With the addition of super disintegrants, the formula F4 has a good dissolution and disintegration profile.	[19]



Gowri Sankar Chintapalli *et al.*,

Naratriptan	Oral disintegrating Tablets	Direct compression	Crospovidone 8%, Sodium starch glycolate 6% (superdisintegrants)	Precompression studies with in limits. Optimized results show good disintegration profile of 32sec due to super disintegrants' effect, dissolution profile shows that more than 90% of the drug releases within 10 minutes, and good dispersion pattern	Faster disintegration and dissolution of Naratriptan ODT may be a more effective migraine treatment.	[20]
	Orodispersible Tablets	Direct compression	Crospovidone, Croscarmellose sodium (superdisintegrants)	Preliminary studies were carried out on the tablets using various grades of superdisintegrants. The effects of super disintegrants produce an excellent disintegration profile of 7-8 seconds, with more than 90% of the medication releasing within 10 minutes and a good dispersion pattern, according to the optimisation results. Crospovidone (5%) and Croscarmellose sodium (4%) are better super disintegrants	Naratriptan ODT may give better therapy for the treatment of Migraine.	[21]
	Fast Dissolving Oral Film	Solvent casting	HPMC (E3 and E6), Propylene glycol, PEG-400	Preformulation studies With in Pharmacopeia limits. The optimized formulation S11 prepared using HPMC E6 showed minimum disintegration time (10 sec), highest dissolution rate i.e., 98.23% of drug within 6 min and satisfactory physicochemical properties.	These findings suggest that the fast dissolving oral film containing Naratriptan hydrochloride is considered to be potentially useful for the treatment of migraine where quick onset of action is desirable when compared with reference standard Naratrx conventional tablet.	[22]
	sublingual tablet	Direct compression	β -cyclodextrin, Crospovidone, Chitoson	The prepared tablets were evaluated for their physical and chemical property. The permeation study was performed on Goat mucosa for optimized batch. No interactions were found between drug and excipients. Formulation F2 containing Crospovidone shows immediate drug release. Chitoson-containing Formulation F6 releases drugs faster than superdisintegrants alone.	As a result, sublingual tablet administration of Naratriptan in combination with appropriate excipients, particularly Chitoson, appears to be a promising alternative to traditional routes.	[23]





	Fast disintegrating Tablets	Direct compression	gelatin, hydrolyzed gelatin, glycine, and mannitol (Optimal mixer)	Drug-excipient interaction was investigated using DSC. By using SEM, it was discovered that the optimised formulation had a porous structure. A dissolution study showed that the solution dissipated completely in just 1.5 minutes.	The developed formulation had significantly higher C _{max} , AUC _{last} , and AUC _{inf} , according to an in vivo pharmacokinetic study.	[24]
	Fast erodispersible tablets	Direct compression	sodium starch glycolate (SSG), croscarmellose sodium (CCS) and kyron-T314	Croscarmellose, one of three super disintegrating ingredients, was found to have better high disintegrating properties and greater dissolution efficiency. Using a multiple linear regression scanning, it was discovered that kyron-T314 and croscarmellose sodium were the optimal for producing a rapidly disintegrating dosage form. Contour plots were also used to show the independent variables' impact on %friability and disintegrating time graphically.	A checkpoint batch was prepared to prove that validity of the evolved mathematical model. There was no difference observed in release profile and drug content after accelerated stability study for 1 month.	[25]
Rizatriptan	Oral Disintegrating Tablets	Direct compression	Croscarmellose sodium, Crospovidone and SSG.	The main effect and the interactions of disintegrants on dispersion time and drug release were studied.	The optimized formulation dispersed in 8 seconds. It also showed a higher water absorption ratio and 99.58% of drug is released within 2 minutes.	[26]
	Fast dissolving Oral films	Solvent casting	HPMC E15, PVA, and Maltodextrin.	The study examines the influence of polymers ratio on physicochemical properties and drug release potential of films. Faster drug release was seen with the improved formulation, F11. All the systems were found to be stable with respect to drug content as well as physical changes at 40°C and 75% RH.	The findings point to fast-dissolving films made of polymers as a viable technique of achieving rapid medication release for effective therapy.	[27]
	fast dissolving sublingual films	Solvent casting	hydroxypropyl methylcellulose (HPMC E 15) and maltodextrin (film forming)	In order to make the fast-dissolving films, the solvent casting method was used. HPMC E 15 and maltodextrin, both hydrophilic and tasty, were combined as a film-forming polymer due to their low viscosity and palatable flavour. The formulations showed a disintegration time of 25-50 seconds. Formulations F1 and F2 showed 90% in-vitro drug release within 7 min and 61% ex-vivo drug permeation within 16 min. The film showed an excellent stability at least for 4 weeks when stored at 40°C and 75% in humidity.	The film showed an excellent stability at least for 4 weeks when stored at 40°C and 75% in humidity.	[28]





Gowri Sankar Chintapalli et al.,

	Pulsin cap	Wet granulation technique	HPMC K4M, PVPK 30	<p>Granules showed good flow properties and drug content were found to be in the range between 95.4±0.56 to 98.3±0.56%. The results indicated that drug content was uniform.</p> <p>Current pulsincap formulation research shows that the F6 batch of Rizatriptan benzoate optimised for colon delivery in migraine treatment is a success. Hydrogel plugs and treated gelatine capsules enable five-to eight-hour controlled medication release.</p>	<p>The results of the current pulsincap formulation trial show that the improved F6 batch of rizatriptan benzoate was successfully used to treat migraines by targeting the colon. The combination of a hydrofrenzel plug with a prepared gelatin capsule can produce drug release over a period of 5 to 18 hours.</p>	[29]
	mucoadhesive buccal films	Solvent casting method	HPMC K4M, PEO, PVA	<p>Drug excipients compatibility studies are good.</p> <p>A faster disintegration and a more stable product were obtained in terms of mechanical properties, mucoadhesive properties, and dissolution time. In addition, it showed about 99.89% RB released in 45 min.</p>	<p>The results suggest that RB-loaded mucoadhesive buccal films could be a potential candidate to achieve optimum drug release for effective treatment of migraine</p>	[30]
	Nasal gel	cold method	carbopol 934P, poloxamer 407	<p>There is a thermo reversible gelation property in all the designed design point formulations. Gels were characterized by permeation studies, pH, % drug content, mucoadhesive force, gel strength, in vitro diffusion, ex vivo diffusion, stability study. A rheological study of gel formulation found that as the concentration of polymer increased, so did the gel's strength, which was measured in the range of 110-130 seconds. A spectral analysis revealed no link between the drug and the polymer under study.</p>	<p>Improve bio availability of drug and as a safe and sustained release nasal delivery system to control migraine.</p>	[31]





Gowri Sankar Chintapalli et al.,

	Fast Disintegrating Sublingual Tablets	Direct compression method	Sodium starch glycolate, cross carmellose sodium and cross povidone. (Super disintegrants)	Drug excipients compatibility studies are good. Because of its quick disintegration and high in vitro drug release, cross povidone was incorporated in the optimised formulation.	When compared to clinical dose, rizatriptan tablet administered by sublingual route in rabbits exhibits an effective therapeutic Cmax and is a promising substitute for oral administration in the acute management of migraine.	[32]
Almotriptan	Convention Tablets	Direct compression and wet granulation	PovidoneK-30, mannitol and MCC	The formulated tablets were tested for hardness, thickness, bulk density, tapped density, Hausner's ratio, compressibility index, stability tests, and invitro release tests. Our new generic product development attempt will use the evaluated results of the innovator physico-chemical parameters as standard parameters.	The F8 formulation was found to be stable under accelerated temperature and humidity studies and had the best evaluated parameters compared to the innovators.	[33]
	Oral Disintegrating Tablets	Direct compression method	Crosspovidone, Crosscarmellose sodium, SSG	Almotriptan powder blends were free flowing as indicated by the values of bulk density (0.45 to 0.56 gm/cc), Tapped density (0.55 to 0.69 gm/cc), Hausner's ratio (1.057 to 1.25), Compressibility index (11.2 to 20 %) and the Angle of repose ranged from 18.17° to 22.26. Almotriptan tablets were uniform in weight (99.9 to 100.2 mg). All tablets had the same thickness (0.210 to 0.218 mm). The hardness of all the tablets ranged from 3.00 to 3.04kg/cm ² . while the friability of the ODT'S ranged from 0.082 to 0.32%, he contents uniformity of all the formulations were ranged from 98.1% to 100.02% w/w The disintegration time of all the formulations ranged from 38 to 15 seconds.	The optimized formulation was found to release the drug in minimum time and is found to be stable.	[34]





	Mucoadhesive in situ gel	Cold technique	Pluronic, carboxymethyl chitosan as thermoreversible and mucoadhesive polymers respectively.	Drug content before and after gelation was ranged between 96.42-98.92% and 95.8-98.66% respectively. The pH value was observed in the range of 5.56-6.31. The in-vitro drug diffusion data of the optimized formulation i.e., 17% w/v PF127, 2% w/v PF68, 0.1% w/v carboxymethyl chitosan, revealed 89.36% release at the end of 6 h.	Short term stability study exhibited 4 ± 1 °C as an appropriate storage condition for the formulations. In nutshell, a thermosensitive in-situ gel of Almotriptan malate can be intended as an effective approach of migraine treatment.	[35]
Frovatriptan	Fast dissolving films	Solvent casting	HPMC E5, Propylene glycol, and Maltodextrin	The KBr pellet method was used to study polymer drug interactions between 4000 cm ⁻¹ and 400 cm ⁻¹ using pure drug, pure polymer, and a physical mixture of polymer and drug. Among all the formulations F8 has found to be the best formulation with a disintegration time of 12sec and 100% of cumulative drug release within in 20min.	Research shows that frovatriptan is ideal for use in the formulation of quickly dissolving thin oral films for the quick relief of migraines.	[36]
	Fast Dissolving Tablets	Direct compression and wet granulation	Microcrystalline cellulose, Cross povidone, Sodium starch glycolate, Cross carmellose sodium, PVP-K-30.	The micromeritic properties evaluated such as bulk density, tapped density, angle of repose, Hausener's ratio were found to be within in the limits for both the powder mixtures and granules. F8 is best formulation	The fast-dissolving Frovatriptan tablets were effectively created with superdisintegrants for instant release, and they exhibit enhanced bioavailability and diminished first pass effect.	[37]
	Orodispersible Tablets	Direct compression	Starch, Crospovidone, Cross-Carmellose Sodium, and Sodium Starch Glycol act as superdisintegrants and diluents respectively in microcrystalline cellulose (MCC).	The IP limitations were discovered to be met by all of the formulations. After compression, the parameters like weight variation, disintegrating time, and drug content were tested, and the results were found to be within USP limits.	The tablets were stored at $40 \pm 2^\circ\text{C}/75 \pm 5\%$ RH for three months to assess the stability of optimized formulation.	[38]





Gowri Sankar Chintapalli et al.,

	Fast Dissolving Buccal Strip	Solvent casting	Hydroxypropyl methylcellulose E3 and E15 are helpful in the film-forming polymer, plasticizer in polyethylene glycols disintegrant is croscarmellose sodium.	The final formula was optimized by simplex lattice mixture design using StatEase design expert software to give the optimized batch. The optimized batch (OB) prepared with concentrations of Polymer, Plasticizer and disintegrant at 42.32, 7.32 and 4.32 respectively. Optimized batch (OB) showed in vitro disintegration time of 44 sec, Tensile strength of 6.35 MPa and Percentage elongation of 3.62%.	The effect of each variable, two and three-factor interactions were studied. The batches were numerically optimized to give a design space. fast mouth dissolving films are also found to behave better patient compliance in all the age groups.	[39]
	Oral Disintegrating Tablets	Direct compression	Sodium Starch Glycolate, croscarmellose sodium, crospovidone (Super disintegrants)	According to the drug-excipient compatibility studies, all of the excipients used are compatible with FS. For all formulations, the pre and post compression parameters were within acceptable limits. Formulation F9 (8% w/w CPV) released 100 % of drug with in 6 min was considered as the optimal ODT among all the nine formulations tested in this study.	Formulation F9 (8% w/w CPV) released 100 % of drug with in 6 min was considered as the optimal ODT among all the nine formulations tested in this study.	[40]
Elitriptan	Buccal Tablets	Direct compression	chitosan, sodium alginate and HPMC.	9 formulations were created using various polymer grades such as chitosan, HPMC, and sodium alginate. FTIR studies revealed no evidence of drug, polymer, or excipient interaction. Weight variation, hardness, surface pH, uniformity of drug content, swelling index, mucoadhesion strength, and an in-vitro drug release study were all done on the tablets in this study. Polymers such as chitosan and sodium alginate found in formulation (F8) provided an 8-hour sustained drug release profile in vitro.	According to the in-vitro release kinetics, the formulation (F8) follows zero order, and the drug release mechanism was non-fickian.	[41]
	Fast dissolving films	Solvent casting	Natural polymers: Pullulan, Maltodextrin, Acacia, Sodium alginate, Locust bean gum, Guar gum, Xanthan gum. Synthetic polymers: Polyvinyl alcohol, Polyvinyl pyrrolidone, HPMC E5, and HPMC E15	Studies on the compatibility of drug excipients are good. Out of all the created polymer formulations, FN2, FN8, and FS3 were chosen based on drug release and disintegration time, and FN2 was optimised based on its disintegration time (D. T). The % drug release of the pure drug and the optimised film were contrasted.	The % drug release of the pure drug and the optimised film were contrasted.	[42-44]





Gowri Sankar Chintapalli et al.,

Microspheres	Ionic gelation method	sodium alginate, chitosan, karaya gum and guar gum.	Microspheres were spherical, discrete in shape. Particle size distribution of the prepared microspheres was in the range of 487.0 – 802.5µm. In-vitro release studies revealed a controlled release of microspheres suitable for preoral administration. Formulation FEC1 showed 90.82% ± 0.26 of drug release for 12 hours in predetermined rate.	The in-vitro release study of all formulations showed a retarded release with increase in percentage of polymers.	[45]
Fast disintegrating tablets	Direct compression	Sodium Starch Glycolate, Croscarmellose Sodium	The flow properties of powder blend were characterized in terms of angle of repose, Carr's index and Hausner's ratio. The bulk density and tapped density were determined and from this data Carr's index and Hausner's ratio were within Pharmacopeia limits. Several properties of the tablets were analysed: drug content; friability; hardness; wettability; water absorption ratio; in vitro disintegration; and dissolution profile. Overall, all of the formulations met the standards required for fast dissolving tablets within reasonable limits.	It was concluded that optimal concentration of Sodium starch glycolate as a superdisintegrant is 5.06% and Croscarmellose sodium is 3.33% (F9), showing best DT and drug release.	[46]

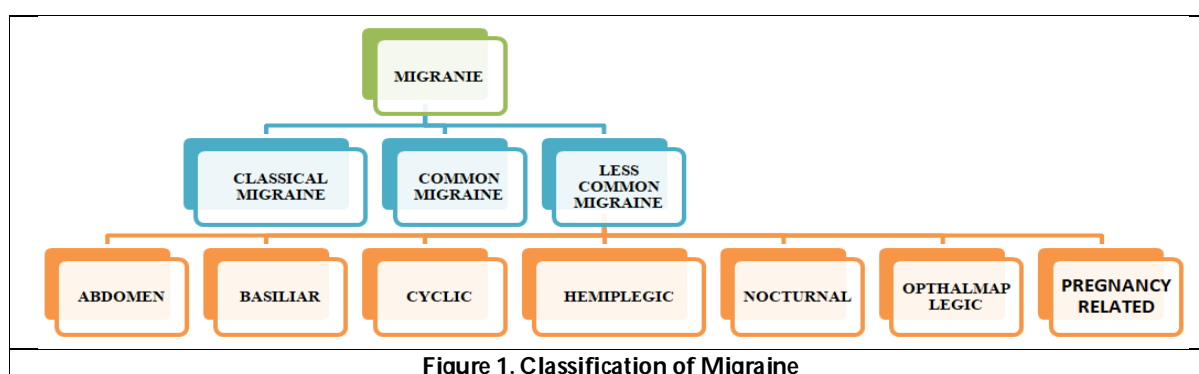


Figure 1. Classification of Migraine





Gowri Sankar Chintapalli et al.,



Figure.2. Classification of anti migraine drugs

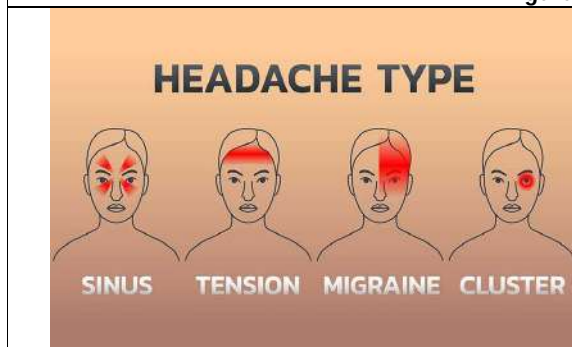


Fig.3. Types of Headache

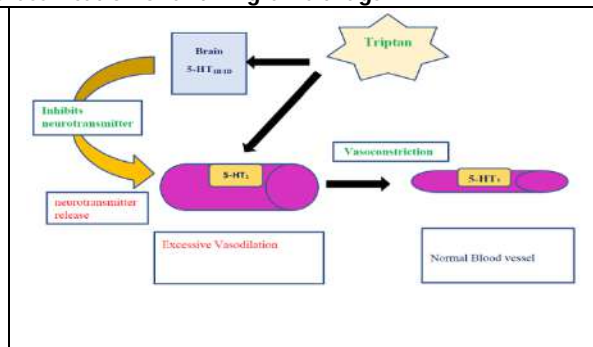


Fig.4. Mechanism action of Triptans

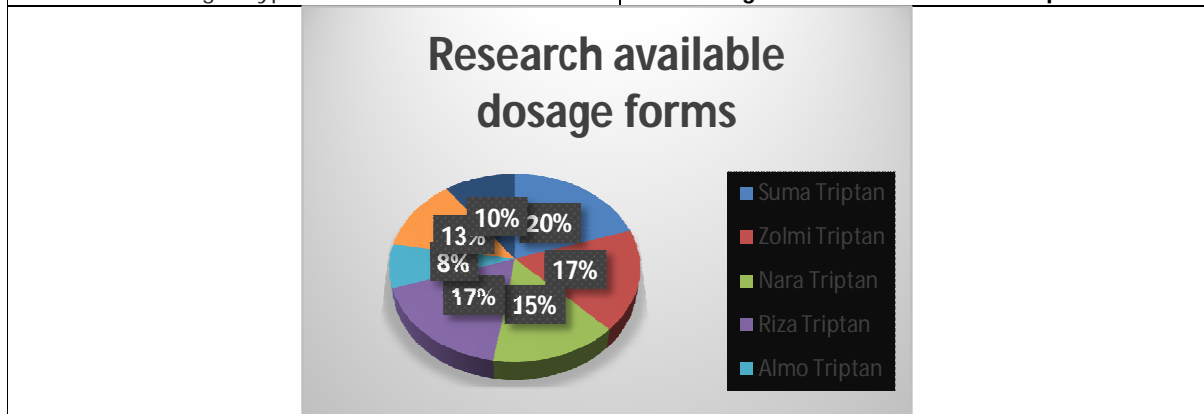


Fig.4. Current Scenario on Research available dosage forms in Triptans





A Transformer Approach for Multi-Document Summarization using TR-BERT

Divya S^{1*}, Sripriya N², Mohanavalli S² and Mirunalini P²

¹Research Scholar, Department of Information Technology, Sri Sivasubramaniya Nadar College of Engineering, Kalavakkam, Chennai, Tamil Nadu, India.

²Associate Professor, Department of Information Technology, Sri Sivasubramaniya Nadar College of Engineering, Kalavakkam, Chennai, Tamil Nadu, India.

Received: 15 Feb 2023

Revised: 25 Apr 2023

Accepted: 30 May 2023

*Address for Correspondence

Divya S

Research Scholar,
Department of Information Technology,
Sri Sivasubramaniya Nadar College of Engineering,
Kalavakkam, Chennai, Tamil Nadu, India.



This is an Open Access Journal / article distributed under the terms of the **Creative Commons Attribution License** (CC BY-NC-ND 3.0) which permits unrestricted use, distribution, and reproduction in any medium, provided the original work is properly cited. All rights reserved.

ABSTRACT

The incredible growth of online knowledge repositories such as blogs, study materials, news articles, books has assisted readers of all ages during this pandemic. These documents include detailed information and it takes high time for the readers to infer the core content. The recent trends in Natural Language processing have led to the extraction of precise content from the overall document. This process is to provide necessary information of the given data, without losing the key content in the document. The summarization technique is categorized into two categories which involve extractive and abstractive summarization. The extractive summarization selects the informative sentences without changing their structure to generate a short and precise summary. Whereas, abstractive summarization is capable to paraphrase the overall document to generate a summary that mimics a human-generated summary. In cases with multiple documents, extractive summarization leads to a biased summary generation as they involve the selection of sentences randomly in the document. On the other end, abstractive summarization is complex as it generates a summary by inferring primary information from the whole document. Hence, In this proposed work, a novel hybrid summarization of both extractive and abstractive techniques is used to generate a summary without bias in a minimum time. The proposed system is processed on CNN/DailyMail News dataset and is evaluated using ROUGE (Recall-Oriented Understudy for Gisting Evaluation) metrics. The precision and recall of ROUGE 1 and ROUGE 2 are calculated, which shows that the proposed system achieves even better performance compared with state-of-the-art document summarization systems.

Keywords: Natural Language Processing, Extractive, Abstractive, Summarization, ROUGE.





INTRODUCTION

As the amount of text data on the internet grows at a breakneck pace, effective retrieval of core content from the long document led to a scope for research in Natural Language Processing. This task is otherwise termed text summarization or text semantic extraction and creation [1], [2]. Summarization generates a shorter version of the input document that comprises all necessary information. Based on the structure of the output required to deliver thematic meaning being retrieved, the summarization task is categorized as extractive and abstractive [3], [4]. Extractive summarization picks the informative sentences from the document to generate the summary, while abstractive summarization rewrites the extracted information to generate the summary similar to the manually generated summary [5], [6].

Extractive summarization considers certain common features such as position of the sentence, parts of speech, word count, length of the sentence, etc, to weigh a sentence for inclusion in the summary [7]. However, mapping of text to vector space is obtained by vector space representation using decomposition of a matrix, dimensionality reduction, estimation of semantic relevance among sentences to select the summary sentences [8], [9]. In general, there are various approaches in performing text summarization, such as term frequency-based, cluster-based, graph-based, fuzzy-based, machine learning-based, neural network-based and deep learning-based techniques. Among these various categories of extractive summarization approaches, the Graph-based technique is effective as it deals with the information in each sentence to frame the representative structure of the graph by plotting each word or sentence as the node and its relationship to connect the nodes [10], [11]. An optimal solution for summary generation is achieved by combinatorial optimization techniques such as integer linear programming or sub-modular function through the content and variety of summarization. However, extractive summarization is incapable of analyzing the entire semantic context as it just extracts the informative portion from the input document and ignores the remaining portion.

Abstractive summarization recognizes the content more profoundly and derives a summary that contains the terms and sentences that are not available in the input document. Paraphrasing is done to generate new phrases to represent the content being analyzed. This task is generally performed by the encoder-decoder model. This is the method of incorporating a Recurrent Neural Network for sequence projection problems. Two recurrent neural networks are required in this model, in which one network analyses the input sequence and encodes to a non-varying length internal representation. The other network is to decode the encoded representation into a target sequence. The challenge in this model is the Out Of Vocabulary (OOV) problem during the encoding phase. Copy Network (CopyNet) [12] and Pointer Network (PtrNet) [13] are the methods evolved to solve the OOV problem in abstractive summarization. CopyNet is an encoder-decoder-based model that utilizes the structure of an end-to-end training model. The generation module and the copy module facilitate handling the OOV problem. These modules generate and update words to the existing vocabulary. However, the summary generated by abstractive summarization has challenges related to its readability, redundancy, and semantic deviation from the input document. This deviates from conveying the entire content being analyzed from the document [14], [15].

Especially, in query-based information retrieval, multiple documents relevant to the user query are retrieved. It is challenging for the user to identify the document that inherits the necessary information. Multi-Document summarization plays a vital role in this scenario. Applying extractive summarization ignores certain contexts while extracting the portion of the document that holds the thematic content. Whereas, applying abstractive summarization on this long text may not deliver the overall context being understood from the retrieved multiple documents. As a solution to these problems and to generate an informative and effective summary of multiple documents, a hybrid extractive and abstractive summarization has been proposed. Since this model does not specify input document and their relevant summary pairs, it is processed as an unsupervised learning model. The multiple documents relevant to the user query are retrieved. Initially, extractive summarization is applied to the tokenized sentences to identify the highly contextual content. Abstractive summarization reframes these informative sentences



**Divya et al.,**

into a final summary, which is similar to the manually generated summary. Several existing summarization techniques are detailed in section II. Section III defines various steps involved in the proposed hybrid summarization model. The dataset considered and the performance evaluation are explained in section IV. Section V provides the conclusion of the proposed work.

RELATED WORKS

Summary generation is challenging even for domain experts with a deep understanding of words and concepts and even more complex for machines as well. Besides the background knowledge, a machine must be able to interpret natural language and generate an understandable summary. While analyzing the functioning of existing extractive summarization, some sentences from the document are selected as the representative sentences, that are collected together to generate an informative and coherent summary. A typical extractive summarization approach comprises of three steps: (1) Representing input document; (2) Scoring each sentence; (3) Selection of high-scoring sentences. Extractive summarization methods can be categorized based on these steps as, surface or statistical approaches, entity-level approaches and discourse-level approaches. Since the 1950s, the most popular approach has been the surface-level approach, in which the documents are analyzed based on shallow features such as word frequency, position of the sentence, title phrase, presence of cue phrases. Entity-level approaches focus on modeling semantic, syntactic and logical relationships among entities in a document. The relationship between entities is based on similarities, proximity and cohesion. Word similarity refers to the words that hold a similar stem. Proximity is the distance among each text unit. The interconnection between similar text units that represent the strong linkage between the entities as a logical framework is framed as cohesion. Cohesion creates mechanical connections at the linguistic level and ensures that the text as a whole makes sense. Lexical and semantic connections are established among sections, sentences and phrases. The global structure of the text is modeled using the discourse-level approach, which designs the text's global structure and its association to the informative target by considering the text's rhetorical structure [17].

The summarization approaches can be further categorized based on various models for representation. A graph-based approach can be applied for summarizing single and multiple documents [18]. Each sentence is represented as nodes in a graph. Nodes are connected by edges which represents the semantic similarity among them. Sentence centrality acts as the basis for this approach[19]. Various other methods for determining the relevancy between nodes are discounting, cumulative sum and determination of position weight. The clustering-based approach is also appropriate for summarizing single and multiple documents [20]. Grouping of documents that have relevant information is performed to gather similar information. Within each group, the sentences are ranked and their prominent scores are estimated. Highly scored sentences in each group are selected to generate a summary. The lexical chaining approach constructs lexical chains that show the spread of semantically relevant words present in the document. Each chain of tokens represents the semantically similar group of words [21], [22]. The semantically similar tokens prevailing in the document are clustered to identify various contextual information with a document. Finally, these clusters are ordered to construct a binary tree.

The frequent-term method searches for a token that occurs frequently and is contextually relevant. The relationship between terms is represented by determining the length of the path connecting the tokens, term position, difference and similarity in context. The sentences that hold the most frequent and contextually similar token are considered as the summary sentences. The information retrieval approach is homogeneous to graph-based and lexical chain methods. The sentences that hold relevant information are identified and extracted to generate the summary. During the availability of massive text documents and their relevant summary, machine-learning-based approaches are applied. Various machine learning approaches such as naive-bayes, decision trees, log-linear, hidden-Markov model, neural networks are utilized to generate a summary. The models developed are trained with the available data which enables the model to learn the data for summarization, which can automatically generate summary when applied to new data [18], [23]. Neural network-based approaches and deep learning approaches present promising results on summarization tasks. These approaches incorporate embeddings [24] to generate intermediate representation before feeding it into the network for generating the summary. Utilization of Convolutional Neural



**Divya et al.,**

Networks [25] and Recurrent Neural Networks [26], [27] and the combination of both [29]. Even when these approaches perform well in generating summaries, they are mostly inefficient and not explainable. These methods do not explicitly provide the features being extracted and their role in contributing to the task of summarization. Several approaches emphasized the union of various features extracted from text [30]. It is also proved that it is not experimental to multiply the number of features. On the other hand, the summarization task is dealt with as a combinational optimization problem. Even when weighing the features, the objective is to optimize the objective function for sentence selection. Thus, the weights are assigned directly in estimating the important sentences rather than deciding the features [31]. These lead to a baseline for the proposed model where each sentence in the input document is ranked based on its semantic relevance and this is then summarized to deliver the knowledge being discovered from it.

Deep-learning-based approaches outperform in various Natural Language Processing tasks. To process sequence-to-sequence models, various methods such as Recurrent Neural Network, Long Short Term Memory, Gated Recurrent Units are utilized. Attention-based mechanisms [32], fine-grained [33], Summa Runner [34], etc., are then proposed to enhance effective long-term sequence processing. In the case of abstractive summarization tasks, language generation is necessary. Various seq2seq models are applied to optimize the non-differential estimation of language generation [35] and to minimize exposure bias [36]. Q-learning-based reinforcement learning [37] is a proposed approach is proposed, that is suitable for single and multiple document summarization. A combination of weighted machine learning and reinforcement learning [38] model is proposed to combine loss functions to attain stability and language fluency. These approaches contribute to bridging the extraction of sentences in end-to-end training. A fine-tuned approach that initially selects a sentence and then applies reinforcement learning to match the factorized representation leading to sentence generation is proposed. Selective gates are proposed to generalize the abstracts [39].

To solve the challenges in the extended auto-summarization method, a two-phase auto-summarization model named TP-AS [40] is proposed which is a union of pointer and attention mechanisms. Since the tagging of the large-scale corpus is expensive, unsupervised techniques such as TF-IDF feature-based approach, cluster-based and graph-based approaches are used by many experts. Nevertheless, recent summarization techniques rarely utilize these methods and often involve models that have many parameters, which is complex. The proposed model is a combination of both extractive and abstractive models. This performs better while handling multiple documents in generating a summary. When the user query retrieves multiple documents that contain relevant information, processing the entire input to generate a summary is challenging. In this scenario, Extractive summarization initially selects the informative sentences by ignoring the additional and redundant information. Abstractive summarization is applied over the sentences that are extracted to generate a summary relevant to the manually generated that delivers the contextual information from various input documents.

PROPOSED MODEL

The proposed model has a combination of extractive and abstractive summarization models. In a query-based approach, the text documents that are relevant to the user query are retrieved. When multiple documents are retrieved and given as input to generate a summary, the challenge arises in knowledge discovery. As the user query portrays the need for principal information, the documents extracted may hold certain information that is explanatory, irrelevant, insignificant and redundant. This problem occurs while trying to summarize a large content having relevant information. To solve this challenge, input documents are processed to identify various information prevailing in it. Collection of various information present in the input documents is identified. From the various group of contexts, identify the sentences that contribute more information. Such sentences are selected with a condition to eliminate repeated and irrelevant information. A graph-based approach is applied to extract the sentences holding unique information. From each collection, the highly informative sentences are picked by ranking all the sentences and picking the highly ranked sentences. Those extracted sentences are fed as input to the language generation technique. This understands the context in the extracted sentences and processes to represent the information retrieved as new sentences. Language generation is applied to gather all the information in the input



**Divya et al.,**

and provide a summary in a precise and readable format. The architecture of the proposed model is shown in fig.1. The steps involved in the proposed model are detailed below.

Input Pre-processing

Text processing is generally initiated with text analysis that includes, information seeking, evolution and retrieval carried out by applying data mining techniques [41], [42]. Since text documents are often not well-structured and well-organized, it is necessary to perform some prior cleaning in the input text to facilitate efficient processing. The process of cleaning text removes several additional and insignificant elements from the input document. Special characters, punctuations, repeated words/phrases, tags, certain cue phrases are not necessary to be processed further. Processing such elements will result in noise. There prevail no predetermined rules to determine the noise in any category of the text document. Based on the task and the result being targeted, any irrelevant and additional information is removed from the text data during pre-processing. Generally, pre-processing involves the removal of stop-words, stemming, lemmatization and tokenization [43].

Extractive Text Summarization

Google's PageRank [44] is a notable graph-based algorithm that is an application in citation analysis, social networks and link structure analysis in World Wide Web. Probably, these algorithms can be predominantly used as a key element of standard-shift activated in the web search domain. This provides a ranking of web pages that is dependent on the overall skill of web expertise rather than just analyzing the subjects available on each web page. Precisely, the graph-based ranking approach helps in deciding the weights between vertices in a graph by periodically considering the general information retrieve from the entire graph, instead of depending on vertex-distinct information. Inclined to designing of lexical or semantic graphs extracted from text documents concludes in a graph-based ranking model. This applies to various natural language processing applications, where the understanding of the entire document facilitates in deciding on the local ranking/selection. Text-based ranking approaches can be applicable on tasks extending from automatic key-phrase extraction to text summarization.

Ranking algorithms based on graphs designed is an essential way of determining the vertices that are important in a graph, depending on the information repeatedly extracted from the whole graph. The voting or recommendation principle is applied in the implementation of graph-based ranking methods. A vote is given for a vertex establishes a connection to the other vertex. When a vertex is connected to multiple vertices, a higher number of votes are given to that particular vertex. The importance of the vertex providing votes estimates the importance of votes and this contributes to the retrieval of information. Thus the corresponding score of each vertex is estimated based on the votes being posted for it and the score of the vertices posting those votes. In the proposed method, each tokenized sentence is considered as the node and the vertex connecting each node is based on the similarity. The score of a vertex is determined by the count of connections associated with that vertex. The nodes that establish many connections and on the other end, the nodes being connected with a high scored vertex are considered as semantically similar sentences. Such sentences are retrieved to generate the extractive summary.

Deep Intermediate Representation of Sentences

It is necessary to generate a numerical representation for a text to support a machine for the processing and understanding of text data. Since a machine can process only numbers, any type of input like video, audio, image or text has to be converted to the numerical format. Thus the processing of representing text as numbers is termed as embeddings. Embeddings can be generated for each word or the entire sentence. Sentence embeddings represent the entire sentence and their semantic details as vectors. Thus the machine can understand the context and variations from the entire text input. Bidirectional Encoder Representation using Transformers (BERT) [45] is utilized to generate the intermediate representation for the informative sentences extracted using the TextRank algorithm. BERT utilizes the transformer model, an attention mechanism that understands the semantic relevancy among sentences. This model has two phases, an encoder to read the input sentences and a decoder to predict the necessary outcome related to the task. This is a bidirectional model, that reads the entire input sequence at once. This facilitates a better understanding of contextual information for the previous and future sequence. BERT model is pre-trained with two



**Divya et al.,**

training strategies. While training the model for Masked Language Model, 15% of the input tokens are masked, where the model tries to identify those tokens, based on the context that is grasped. While training for Next Sentence Prediction, the model is given with a pair of sentences and is trained to classify if the second sentence follows the first sentence. This supports the model to generate representations that have a deeper understanding of the input sequence.

Abstractive Text Summarization

The informative sentences being extracted from the long document contain many tokens where hardly a few tokens express the core context of the input sequence. Only those portion of the sequence has to be detached from the sequence to generate the summary. Identifying and filtering of that key context are performed by the decoder in the network. To generate an abstractive summary, the intermediate representation of each extracted sentence is fed as input to the N-layered transformer decoder. To perform effective decoding of a sequence by identifying the informative segment in the input sentence, the transformer model incorporated with multi-head attention is opted to understand the association allying the summary and the input sequence. For the representation generated using the encoder phase in the BERT model, the decoder phase identifies the phrase holding more contextual information and generates a compressed version of the input. The Neural Network model added over the attention head contributes in framing new words and phrases in delivering the compressed version of the context being understood from the input sequence. The illustration of the functioning of the encoder-decoder model in the generation of the abstractive summary is shown in figure 2.

PERFORMANCE EVALUATION

In the scenario of extractive summarization, the summary just holds the part of the sentences that are relevant to the user query but does not compress the information available in the entire document. This summary is not smooth, as it is not similar to the abstract that is usually available in the user's reading habit. So the proposed model initially picks the informative sentences and manipulates them to generate a summary that is similar to the manually generated summary. The proposed model is applied on CNN/DAILY Mail dataset [46]. The data available in the dataset is pre-processed and is fed as input to the TextRank algorithm, where a certain number of informative sentences are selected to generate an abstractive summary. The information available in the extracted sentences is understood using the encoder model and summary generation is done using the decoder. The volume of data that has to be selected from the input document can be determined by the user. Based on the amount of information extracted, the abstractive summary is generated.

Experimental Data

The CNN/Daily mail is a text summarization corpus which comprises of 1Million long paragraph news data and its relevant summary. It holds news articles each with an average of 781 tokens or 40 sentences and the reference summary with an average of 56 tokens or 3.76 sentences. A non-anonymous version of the dataset is obtained which comprises 2,87,226 training pairs, 13,368 validation pairs and 11,490 test pairs. The statistics of the dataset are as shown in table 1, where avg-ref is the average length of the manual summary and avg-abs is the average length of the news article.

The performance of various text summarization methods is estimated using ROUGE-N and ROUGE-L evaluation metrics. The n-gram recall estimation among the generated summary and the reference summary is termed as ROUGE-N. Generally in text summarization, the value of N is assigned with 1 or 2, which represents uni-gram or bi-gram comparison among summaries. The longest common subsequence comparison in the recall estimation among generated summary and the reference summary is termed as ROUGE-L. The ROUGE scores are based on the F1 scores of ROUGE-1 ROUGE-2 and ROUGE-L.

The evaluation of performance is carried by generating the summary for the articles in the test portion and is compared with its representative summary. The abstractive summary generated by the proposed model is compared with a few standard summarization models, whose descriptions are given below.

- **words-lvt2k-temp-att [47]:** uses the seq2seq attention model and includes the semantic features within it.





Divya et al.,

- **graph-based attention [48]:** presents a graph-based attention mechanism that works based on an encoder-decoder framework and introduces a hierarchical decoding algorithm to provide efficient summary generation.
- **pointer generator [49]:** involves a pointer-generator network. During the summary generation, the model extracts keywords from the input sequence to deliver an accurate summary.
- **pointer generator + coverage [49]:** coverage mechanism is laid over pointer generator model. Content that is generated to minimize the replication is documented.
- **Machine Learning + Reinforcement Learning with self-attention [50]:** a self-attention model that utilizes combinational objectives for training is incorporated.

RESULTS AND ANALYSIS

The performance of various existing models applied on CNN/DAILYMAIL dataset is shown in table.2. The comparison shows that the proposed model outperforms the existing methods concerning the ROUGE score. The proposed model initially selects the sentences that contain information to reduce redundancy and more detailed information. Then the attention-based transformer model is applied to generate languages to frame an abstractive summary that is similar to the manually generated summary.

CONCLUSION

In this paper, a hybrid extractive and abstractive summarization technique is for query-based document summarization. Graph-based summarization is initially applied to identify the informative sentences from a large number of sentences. The extracted sentences are represented in a numerical format using the encoder phase of the multi-head transformer model. New sentences are generated by the decoder phase of the multi-head transformer model. The experimental results prove that the proposed model generates an accurate summary and holds a greater ROUGE index when compared to the other existing summarization models.

REFERENCES

1. J. N. Madhuri and R. G. Kumar, "Extractive text summarization using sentence ranking," in *Proc. Int. Conf. Data Sci. Commun.*, Mar. 2019, pp. 1_3.
2. E. Reategui, M. Klemann, and M. D. Finco, "Using a text-mining tool to support text summarization," in *Proc. IEEE 12th Int. Conf. Adv. Learn. Technol.*, Jul. 2012, pp. 607_609.
3. S. R. Rahimi, A. T. Mozhdehi, and M. Abdolahi, "An overview on extractive text summarization," in *Proc. IEEE 4th Int. Conf. Knowl.-Based Eng. Innov. (KBEI)*, Dec. 2017, pp. 54_62.
4. A. M. Rush, S. Chopra, and J. Weston, "A neural attention model for abstractive sentence summarization," in *Proc. Conf. Empirical Methods Natural Lang. Process.*, 2015, pp. 379_389.
5. H. Kim and S. Lee, "A context based coverage model for abstractive document summarization," in *Proc. Int. Conf. Inf. Commun. Technol. Converg. (ICTC)*, Oct. 2019, pp. 1129_1132.
6. A. See, P. J. Liu, and C. D. Manning, "Get to the point: Summarization with pointer-generator networks," in *Proc. 55th Annu. Meeting Assoc. Comput. Linguistics*, 2017, pp. 1073_1083.
7. R. Nallapati, B. Zhou, C. Nogueira dos santos, C. Gulcehre, and B. Xiang, "Abstractive text summarization using sequence-to-sequence RNNs and beyond," 2016, *arXiv:1602.06023*. [Online]. Available: <http://arxiv.org/abs/1602.06023>
8. J. Conroy, S. Davis, J. Kubina, Y. Liu, D. P. O'leary, and J. Schlesinger, "Multilingual summarization: Dimensionality reduction and a step towards optimal term coverage," in *Proc. Conf. Multi-Document Summar.*, 2013, pp. 55_63.
9. T. He, L. Hu, K. C. C. Chan, and P. Hu, "Learning latent factors for community identification and summarization," *IEEE Access*, vol. 6, pp. 30137_30148, 2018.





Divya et al.,

10. R. Mihalcea and P. Tarau, "Textrank: Bringing order into text," in *Proc. Empirical Methods Natural Lang. Process.*, 2004, pp. 404_411.
11. A. Alzuhair and M. Al-Dhelaan, "An approach for combining multiple weighting schemes and ranking methods in graph-based multidocument summarization," *IEEE Access*, vol. 7, pp. 120375_120386, 2019.
12. J. Gu, Z. Lu, H. Li, and V. Li, "Incorporating copying mechanism in sequence-to-sequence learning," in *Proc. 54th Associat. Comput. Ling.*, 2015, pp. 1_10.
13. O. Vinyals, M. Frotunato, and N. Jaitly, "Pointer networks," in *Proc. Adv. Neural Inf. Process. Syst.*, 2015, pp. 2692_2700.
14. Z. Cao, W. Li, S. Li, and F. Wei, "Retrieve, rerank and rewrite: Soft template based neural summarization," in *Proc. 56th Annu. Meeting Assoc. Comput. Linguistics*, vol. 1, 2018, pp. 152_161.
15. M. Yang, Q. Qu, W. Tu, Y. Shen, Z. Zhao, and X. Chen, "Exploring human like reading strategy for abstractive text summarization," in *Proc. 33rd AAAI Conf. Artif. Intell.*, vol. 33, Aug. 2019, pp. 7362_7369.
16. P. Mehta and P. Majumder, "Effective aggregation of various summarization techniques," *Inf. Process. Manage.*, vol. 54, no. 2, pp. 145_158, Mar. 2018.
17. M. Vlajinić and N. M. Preradović, "A comparative study of automatic text summarization system performance," in *Proc. Eur. Comput. Conf. (ECC)*. Dubrovnik, Croatia, 2013, pp. 1_6.
18. D. Das and A. F. Martins, "A survey on automatic text summarization," *Literature Surv. Lang. Statist. II Course CMU*, vol. 4, nos. 192_195, p. 57, 2007.
19. S. Hariharan, T. Ramkumar, and R. Srinivasan, "Enhanced graph based approach for multi-document summarization," *Int. Arab J. Inf. Technol.*, vol. 10, pp. 334_341, Jul. 2013.
20. S. Hariharan and R. Srinivasan, "Studies on graph based approaches for single and multi document summarizations," *Int. J. Comput. Theory Eng.*, vol. 1, pp. 1793_8201, Dec. 2009.
21. C. Santos, "Alexia-acquisition of lexical chains for text summarization," Ph.D. dissertation, Dept. Comput. Sci., Univ. Beira Interior, Covilhã, Portugal, 2006, p. 109.
22. A. Hernandez-Castaneda, R. A. Garcia-Hernandez, Y. Ledeneva, and C. E. Millan-Hernandez, "Extractive automatic text summarization based on lexical-semantic keywords," *IEEE Access*, vol. 8, pp. 49896_49907, 2020.
23. V. Gupta and G. S. Lehal, "A survey of text summarization extractive techniques," *J. Emerg. Technol. Web Intell.*, vol. 2, no. 3, pp. 258_268, Aug. 2010.
24. J. Pennington, R. Socher, and C. Manning, "Glove: Global vectors for word representation," in *Proc. Conf. Empirical Methods Natural Lang. Process. (EMNLP)*, 2014, pp. 1532_1543.
25. Z. Cao, F. Wei, S. Li, W. Li, M. Zhou, and H. Wang, "Learning summary prior representation for extractive summarization," in *Proc. 53rd Annu. Meeting Assoc. Comput. Linguistics 7th Int. Joint Conf. Natural Lang. Process. (Short Papers)*, vol. 2, 2015, pp. 829_833.
26. J. Cheng and M. Lapata, "Neural summarization by extracting sentences and words," in *Proc. 54th Annu. Meeting Assoc. Comput. Linguistics (Long Papers)*, vol. 1, 2016, pp. 484_494.
27. R. Nallapati, F. Zhai, and B. Zhou, "Summarunner: A recurrent neural network based sequence model for extractive summarization of documents," in *Proc. 31st AAAI Conf. Artif. Intell.*, 2017, pp. 3075_3081.
28. Y. Wu and B. Hu, "Learning to extract coherent summary via deep reinforcement learning," in *Proc. 32nd AAAI Conf. Artif. Intell.*, 2018, p. 5602.
29. S. Narayan, S. B. Cohen, and M. Lapata, "Ranking sentences for extractive summarization with reinforcement learning," in *Proc. Conf. North Amer. Chapter Assoc. Comput. Linguistics, Hum. Lang. Technol., (Long Papers)*, vol. 1, 2018, pp. 1747_1759.
30. R. Ferreira, L. de Souza Cabral, R. D. Lins, G. Pereira e Silva, F. Freitas, G. D. C. Cavalcanti, R. Lima, S. J. Simske, and L. Favaro, "Assessing sentence scoring techniques for extractive text summarization," *Expert Syst. Appl.*, vol. 40, no. 14, pp. 5755_5764, Oct. 2013.
31. M. Mendoza, S. Bonilla, C. Noguera, C. Cobos, and E. León, "Extractive single-document summarization based on genetic operators and guided local search," *Expert Syst. Appl.*, vol. 41, no. 9, pp. 4158_4169, Jul. 2014.
32. Z. Li, Z. Peng, S. Tang, C. Zhang, and H. Ma, "Text summarization method based on double attention pointer network," *IEEE Access*, vol. 8, pp. 11279_11288, 2020.





Divya et al.,

33. Y. Liu, "Fine-tune BERT for extractive summarization," 2019, *arXiv:1903.10318*. [Online]. Available: <http://arxiv.org/abs/1903.10318>
34. R. Nallapati, F. Zhai, and B. Zhou, "SummaRuNNer: A recurrent neural network based sequence model for extractive summarization of documents," in *Proc. 31st AAAI*, 2017, pp. 3075_3081.
35. M. Ranzato, S. Chopra, M. Auli, and W. Zaremba, "Sequence level training with recurrent neural networks," in *Proc. 4th Int. Conf. Learn. Represent.*, 2016, pp. 1_16.
36. D. Bahdanau, P. Brakel, K. Xu, A. Goyal, R. Lowe, J. Pineau, A. Courville, and Y. Bengio, "An actor-critic algorithm for sequence prediction," 2016, *arXiv:1607.07086*. [Online]. Available: <http://arxiv.org/abs/1607.07086>.
37. S. Heny, M. Mieskes, and I. Gurevych, "A reinforcement learning approach for adaptive single-and multi-document ummarization," in *Proc. Conf. Comput. Ling. Lang. Tech.*, 2015, pp. 3_12.
38. R. Paulus, C. Xiong, and R. Socher, "A deep reinforced model for abstractive summarization," in *Proc. 6th Int. Conf. Learn. Represent.*, 2018, pp. 1_12.
39. Q. Zhou, N. Yang, F. Wei, and M. Zhou, "Selective encoding for abstractive sentence summarization," 2017, *arXiv:1704.07073*. [Online]. Available: <http://arxiv.org/abs/1704.07073>.
40. S. Wang, X. Zhao, B. Li, B. Ge, and D. Q. Tang, "TP-AS: A two-phase approach to long text automatic summarization," *J. Chin. Inf. Process.*, vol. 32, no. 6, pp. 71_79, 2018.
41. B. Mutlu, E. A. Sezer, and M. A. Akcayol, "Candidate sentence selection for extractive text summarization," *Inf. Process. Manage.*, vol. 57, no. 6, Nov. 2020, Art. no. 102359.
42. M. Peng, B. Gao, J. Zhu, J. Huang, M. Yuan, and F. Li, "High quality information extraction and query-oriented summarization for automatic query-reply in social network," *Expert Syst. Appl.*, vol. 44, pp. 92_101, Feb. 2016..
43. N. Yadav and V. Kumar, "A novel technique for automatic retrieval of embedded text from books," *Optik*, vol. 127, no. 20, pp. 9538_9550, Oct. 2016.
44. Brin, S. and Page, L., 1998. The anatomy of a large-scale hypertextual web search engine. *Computer networks and ISDN systems*, 30(1-7), pp.107-117.
45. Devlin, J., Chang, M.W., Lee, K. and Toutanova, K., 2018. Bert: Pre-training of deep bidirectional transformers for language understanding. *arXiv preprint arXiv:1810.04805*.
46. K. M. Hermann et al., "Teaching machines to read and comprehend," 2015, arXiv:1506.03340. [Online]. Available: <http://arxiv.org/abs/1506.03340>.
47. R. Nallapati, B. Zhou, C. Dos Santos, C. Gulcehre, and B. Xiang, "Abstractive text summarization using sequence-to-sequence RNNs and beyond," in *Proc. 20th SIGNLL Conf. Comput. Natural Lang. Learn.*, 2016, pp. 280_290.
48. J. Tan, X. Wan, and J. Xiao, "Abstractive document summarization with a graph-based attentional neural model," in *Proc. 55th Annu. Meeting Assoc. Comput. Linguistics*, vol. 1, 2017, pp. 1171_1181.
49. A. See, P. J. Liu, and C. D. Manning, "Get to the point: Summarization with pointer-generator networks," in *Proc. 55th Annu. Meeting Assoc. Comput. Linguistics*, 2017, pp. 1073_1083.
50. R. Paulus, C. Xiong, and R. Socher, "A deep reinforced model for abstractive summarization," in *Proc. 6th Int. Conf. Learn. Represent.*, 2018.

Table 1. Statistics of CNN/daily mail dataset.

Dataset	Train	Test	Validation
Size	51.6M	1.3G	59.6M
Average-ref	58.30	55.15	61.42
Avg-abs	777.27	791.7	768.29

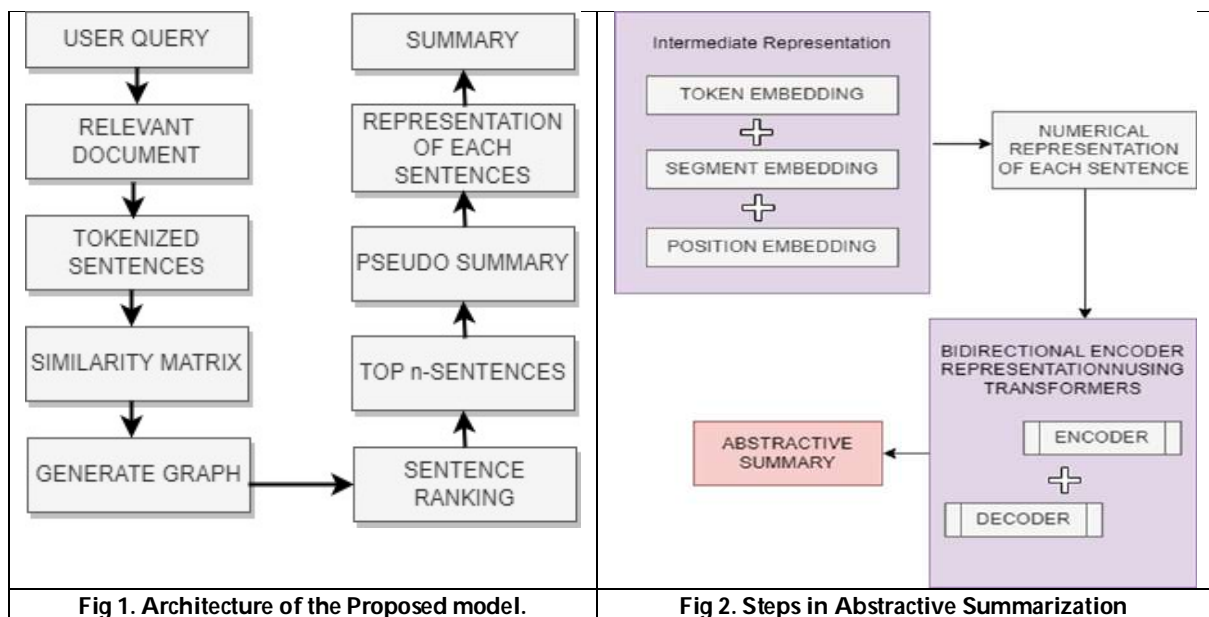




Divya et al.,

Table 2. Performance comparison on CNN/DAILY Mail dataset.

Model	ROUGE-1	ROUGE-2	ROUGE-L
words-lvt2k-temp-att [47]	35.46	13.30	32.65
Graph-based attention [48]	38.01	13.90	34.00
Pointer generator [49]	36.44	15.66	33.42
Pointer generator + coverage [49]	39.53	17.28	36.38
Machine Learning + Reinforcement Learning with self-attention [50]	39.87	15.82	36.90
Proposed Model	40.17	17.30	37.51





Utilizing the ARIMA Model, Trends in Rainfall Pattern, Moisture, and Soil Moisture Over Maharashtra's Vidarbha Region

K H. Deshmukh^{1*} and G. R. Bamnote²

¹Assistant Professor, Computer Science and Engineering Faculty, Prof. Ram Meghe Institute of Technology and Research, Maharashtra, India

²Associate Professor, Computer Science and Engineering Faculty, Prof. Ram Meghe Institute of Technology and Research, Maharashtra, India

Received: 03 Mar 2023

Revised: 20 Apr 2023

Accepted: 31 May 2023

*Address for Correspondence

K H. Deshmukh

Assistant Professor,
Computer Science and Engineering Faculty,
Prof. Ram Meghe Institute of Technology and Research,
Maharashtra, India.



This is an Open Access Journal / article distributed under the terms of the **Creative Commons Attribution License (CC BY-NC-ND 3.0)** which permits unrestricted use, distribution, and reproduction in any medium, provided the original work is properly cited. All rights reserved.

ABSTRACT

A climate is at an atmosphere as a result of global warming and other factors, is rising daily. climate change, which are linked to rainfall variability. Understanding the climate system's transition is crucial to tackling major worldwide environmental challenges. Furthermore, because rainfall is the most common cause of stream flow in India, particularly flood flow, it is critical to understand its pattern in relation to groundwater recharge. Seasonally, total quantity of rainfall which is dumped fluctuates. consequently volume of flash floods in different sections of a country at different times and locations throughout the year is complicated, and further research is needed. Various hydrological concerns, such as floods and droughts, are caused by this variation. Rainfall research during the monsoon season in Asia (June to September) and temperature conducting a study to Indian over the vacation (Feb to May) are critical for a number of reasons, including economic development, disaster management, and hydrological planning. It's vital to understand mean rainfall and temperature variations on a smaller geographical scale. The seasonality index of rainfall and temperature can be used to investigate the changing pattern of rainfall and temperature. The above study's primary goal is to investigate a yearly trend for rainfall pattern, humidity, and groundwater level using an the ARIMA approach (autoregressive integrated moving average average) To understand the relation matrix and co-relation parameter, we also studied district-level geology and river recharge patterns. The observation shows the direct dependability of river water flow with rainfall and groundwater recharge with 67% and 78% precision, respectively. The humidity



**Deshmukh and Bamnote**

dataset shows heavy rainfall predictions prospectively with 35% accuracy based on the 5-year timeline dataset. We also checked for data redundancy and inconsistency in order to achieve a data efficiency of 99% or higher.

Keywords: Data Analytics, Climate Trends, Autoregressive integrated moving average (ARIMA) model, Co-relation Matrix

INTRODUCTION

Amravati division and Nagpur division are the two divisions that make up the Vidharbha area. There are 11 districts in all in the Vidharbha region. There are 11 district in the region, namely Akola, Amravati, Buldana, Yavatmal, Washim, Bhandara, Chandrapur, Gadchiroli, Gondia, Nagpur, and Wardha. As of July 2021, there are about 120 Talukas in total. Considering the geology and geography of Vidarbha region, the state of Vidarbha is located to the north portion a Deccan Plateau. In contrast to There aren't any Southern Stupas. significant mountainous regions [1]. The Satpura Range is located in To a north is Madhya Pradesh. of the Vidarbha area. On the southern branch of the Satpura Range is the Megat area in the Amravati district. which runs across the district. In Vidarbha, large basaltic rock formations may be found across the region, which is 66 million years old, a portion of volcanoes known as the Deccan Traps [2]. Bhandara and Gondia districts are completely covered occurs as part and metamorphism, which distinguishes them as having a geology that is In Maharashtra, exceptional. Buldhanais home to the Lonar crater, which was formed by an asteroid collision. Gondia, Bhandara, Gadchiroli, and Nagpur's eastern districts are situated in earthquake zone 1, which has the least seismic activity. amount of Asia's seismic activities, whereas the other districts are located in earthquake zone 2, which has the most seismic activity [3]. The Wainganga River is the biggest river in Vidarbha, and its waters, together with those of its main The Wardha, Kanhan, and Painganga are tributaries that enter the Godavari with in south. Several minor rivers, including the North of a Tapti Rivers are the tributaries Khapra, Sipna, Gadga, Dolar, and Purna. [4].

Considering the atmosphere condition, the climate's degree is atmosphere as a result of global warming and other factors, is rising daily. climate change, which is connected to rainfall variability. Knowledge of this shift in the climate system is essential for resolving major environmental problems across the world [5]. Also, since rainfall is most common cause of stream flow, particularly flood flow in the majority of rivers in India, it is critical to understand its pattern. The amount of rain that falls changes throughout time. Differences in rainfall magnitude in different areas of a nation at a particular time and location throughout various seasons of the year are varied and must be investigated further. Many hydrological issues, such as floods and droughts, are caused by this fluctuation. The study during la temporadamonsoona (June to September). in India is very important for economic growth, disaster management, and hydrological planning, among other things. It's crucial to understand On the a small spatial scale, the rainfall totals and its variation. The seasonality index of rainfall may be used to investigate changing pattern is of rain [6]. The sum of the yearly rainfall data for the Vidarbha area of Maharashtra, which includes four districts: Akola, Wardha, Washim, and Yavatmal, is used in this study. To understand the rainfall variability of the area, the data is then examined for mean, standard deviation, and skewness of coefficient. The seasonality index, which quantifies the distribution of rainfall over the seasonal cycle, is developed and used to categorise the various rainfall in the area using this study [7]. The trend analysis is also used to identify changes over time in the seasonality index to establish the changing pattern of rainfall at the district size. The current study will undoubtedly offer academics with a roadmap for the long-term development of Maharashtra's water resources. In Vidarbha Summers are very hot, but winters are dry and cool, with temperatures falling to or below 2 degrees Celsius. In the region, a low of 2 °C was recorded, with a high of 47.7 °C. Akola recorded a low temperature of 11.9 °C in May, which is often Maharashtra's hottest month. Summers are hot and humid, March through June, with May being the



**Deshmukh and Bamnote**

hottest month of the year. Temperatures below 10 degrees Celsius prevail from November through February throughout the winter season. degrees Celsius (50 degrees Fahrenheit). On May 29, 2013, the city's maximum temperature was 47.9 °C, nonetheless, the smallest temperature on December 29, 2018 was 3.5 °C. The vast majority of rural Maharashtra residents, as well as some urban residents, rely on groundwater for drinking. Prior to 1972, the usage of groundwater in the state was considered to be rather minor. Droughts became more common as a result of the limited supply of surface water, the development of low-cost drilling equipment, the easy availability of institutional financing, and energization, among other factors, resulting in the spread of irrigation wells. In this paper we have discussed about rainfall, humidity and ground water level of Vidarbha region, Maharashtra [8].

Nagpur Division and Amravati Division make up Vidarbha, the Indian state of Maharashtra's north-eastern area. Berar was the previous name for the Amravati division (In Marathi, varhad) It covers 31.6 percent of Maharashtra's total land area and is home to 21.3 percent of the state's people. Madhya Pradesh, Chhattisgarh, and Telangana are its neighbours to the north, the east, and the south, respectively. on the west by Maharashtra's Marathwada and Khandesh areas. Located in the heart of India. Nagpur is followed by Amravati as Vidarbha's largest city. Rainfall replenishes soil moisture, stream flows, lakes, glaciers, and other bodies of water. During the rainy period, which runs from June to September, India receives roughly 80% of its total rainfall [9]. Rains fluctuations and trends have a huge influence on Indian agriculture, which is heavily reliant on monsoon rainfall. It is important to make available a suitable rainfall trend that will offer geographical and temporal variability of rainfall in order to provide information to everyone involved with water resources. In order to analyse the effects of social and economic planning on global warming, such analysis is also necessary. The southwest monsoon has a great impact on In the northwest of peninsular India sits the state of Maharashtra. experiences water shortage practically every year. The previous performance of monsoon rainfall predicts that rainfall would be scarce in the future as well. The Vidarbha area receives less yearly rainfall than the Konkan region, but more than the Marathwada region. Because there are more disasters happening, such as flood water scarcity, and their significant economic effects and human life, district rainfall climatology, and details on the district's rainfall's temporal changes level are required for improved disaster preparation, administration, and planning of water resources by the district administration. When assessing the influence of rainfall on hydrology, ecology, agriculture, or water usage, the pattern of rainfall during the course of a season is just as significant as the overall quantity of annual/monthly rainfall. Since rainfall is so essential in recharging the groundwater, it's critical to understand how the mean annual rainfall has changed over time. The timing and duration of these high-rainfall seasons at a location or watershed are critical for agricultural or water management planning and design. Variations in the seasonal receipt of rainfall, even without modifications to yearly total rainfall, have a substantial impact on the division of fluid into evaporation of water, penetration, and outflow, and consequently flood predictions, responses of the ecology to creek discharge.. The seasonality index of rainfall may be used to analyse the changing pattern of rainfall. The seasonality index is used to determine long-term variations in rainfall, which is then followed by trend analysis. Planning and managing agriculture requires a complete understanding of a location's rainfall pattern. Intra-seasonal and inter-annual changes in the Indian summer monsoon may be studied using daily and monthly rainfall records. Center for Climate Prediction (CPC) The two major data sets, Merged Analysis of Precipitation (CMAP), many applications, such as weather and climate monitoring, climate research, numerical model validation, and hydrological research. To create rainfall analysis, three types sources of data are combined: evaluate measurements, estimations based on computational modelling and satellite data forecasts. However, merely combining the various rainfall estimates is insufficient. Using this previous work as inspiration, the current study presents a shifting pattern of rainfall and its variability analysis, which will be extremely beneficial for hydrologic modelling, the agricultural sector, and water resource planning and management [10].

Along with the rainfall pattern, a seasonality index for total annual rainfall series of four Vidarbha Maharashtra districts, namely Akola, Wardha, Washim, and Yavatmal, is provided for the period 1901–2002, which will aid in the sustainable development of Maharashtra's water resources. The amount of rain that fell in total over a specific time period, measured in millimetres, is the most typical rainfall measurement (mm). For instance, we could be interested in learning how much rain fell in millimetres during a certain hour, day, month, or year. Rainfall is calculated by



**Deshmukh and Bamnote**

Rain Guage shown in Figures (a), (b), and Figure (c). Humidity is a measurement of the quantity of water vapour in the atmosphere. The maximum concentration of water vapour determines how much water is in the air (moisture). the more liquid vapours as the air contain, the warmer the climate. Your morning weather reporter would talk about relative humidity. Evaporation from huge amounts of water from bodies of water on the Earth's surface, such as lakes, oceans, and seas vapour into the environment. Absolute humidity relates to how much water is in the air and is measured in grammes per cubic metre or grammes per kilogramme [11]. When stated as a percentage, relative humidity reflects the current condition relative humidity in comparison to the highest humidity level at a specific temperature [12]. Relative moisture is defined as the mass of vapour divided by the mass of all moist air parcels. A hygrometer (as shown in Figure(d)) is a tool that counts the amount of water. vapour occurs in the earth, air, or in confined spaces. Maharashtra is one of the hottest states in India. Although there are only a few tropical and humid months, the climate is quite warm, with an annual average of 33 degrees. The humidity of Vidarbha can be shown as

- August is, on average, the wettest month.
- On average, April has the lowest relative humidity.
- 53.0 percent of the yearly average is humidity.

The monsoon is essential for replenishing groundwater supplies. Water seepage occurs when there is mild to moderate rainfall that is recorded on a regular basis rather than a large rainfall period, which frequently results in more surface water run-off. The data was taken from the network of observation wells maintained by the Central Ground Water Board (CGWB) during the decades 1975–1984 and 2004–2009. The shallow, unconfined aquifer is shown in the wells. which receives quick replenishment from rains as well as any intervention for artificial recharging. The average groundwater level of all observation wells within each district's borders was determined [13]. the state's groundwater levels, weighted by area, across all of its districts is used to calculate the regional average groundwater level. (Last week of May/first week of June) and after the monsoon (first week of November) observation wells with incomplete data are not considered. Groundwater levels in observation wells that vary abnormally (greater than 50% from the mean trend) are not considered. (About 3% for both times). The loss of groundwater resources in Vidarbha and Marathawada was less severe than in Saurashtra [14] [15]. A submersible pressure transmitter is commonly used to measure groundwater levels. The device used to calculate groundwater level is as shown in Figure (e).

METHODOLOGY

It is a word that refers describe a large a significant volume of data that is organised, semiorganized, or unstructured, and that is derived from a variety of sources such as data from the public and the media, cameras, and warehouses, and other sources, and that is stored in various formats such as. Http files, picture documents, txt and.csv file format, and so on.A large amount of info is gathered and produced within a quick pace using the assistance of extremely fast and powerful computers for a variety of real-time and extensive applications. Data analysis is necessary to transform this information into action and knowledge. and as a result, steps for big data analytics are developed. Volume, Velocity, and Variability are the three key qualities that we may use big data analytics techniques to analyse massive data sets to guarantee reliable information.

Power BI software was used to scrap the data from various public website of government for humidity, temperature, groundwater level and rainfall data. Power BI's sophisticated analytics capabilities enable business users to examine data and share insights with colleagues at all levels of an organisation. In one location, Power BI provides a holistic picture of key performance indicators and crucial KPIs via simple dashboards that are interactive, which can be accessed in real time from anywhere. The whole data was consolidated and different data analytics were undertaken for four different parameters like rainfall, humidity, temperature and groundwater level. Percentage wise analysis for rainfall dataset clearly shows the direct and proportional relationship. As per the table 2, buldhana region has shown the heavy deficiency of rainfall followed by Amravati, Wardha, Yavatmal, Gondia and so on. The average



**Deshmukh and Bamnote**

rainfall at normal category was best in Nagpur followed by Akola and Gadchiroli. Data analytics for three-year humidity data shows highest saturation of humidity in the month of September giving direct co-relation to rainfall increment density (Table 3,4,5).

In order to better understand rainfall patterns, rainfall data for Maharashtra's Vidarbha region is analysed over a 102-year period (1901 to 2002). We were able to compute the frequency analysis, rainfall variability analysis, and seasonality index with the help of graphs and calculations the seasonality index may be used to predict rainfall patterns. The Vidarbha region will definitely contribute to the growth of watershed operations. not just to give help in that area, but also to provide advice on critical soil and water problems Conservation initiatives, such as groundwater recharge, are examples. The seasonality index (0.85 to 1) and frequency analysis (75 percent exceedence probability: 650 to 850mm rainfall) clearly demonstrate that Akola, Wardha, Washim, and Yavatmal are dry, with rainfall continuing in the same pattern as shown in the result analysis over the next 75 years. The information provided here is useful not just for corporate water resource organisations and decision-makers, but also for government agencies engaged in establishing water policy, conservation, and irrigation projects. This kind of study will show its essential significance in all water scarcity areas and may be utilised as a foundation before any regional water delivery system is developed and implemented. Groundwater is an important source of freshwater in the tropics, providing clean drinking water close to the site of use for residential, agricultural, and industrial uses. Groundwater recharge, in part, regulates the sustainability of groundwater withdrawals, but Particularly in the tropics, the conversion of rainfall into recharge is not well understood. annual refuelling of groundwater sources of Holocene dunes Holocene dunes may be as high as 40% of yearly precipitation, while annual percentages of rainfall producing recharge There are 13 and 4%, respectively, of Mio-Pliocene sandstone and worn crystalline rocks in deeper aquifers. The variations are primarily caused by how thick the subsoil is, as well as lithological constraints on the conveyance and storing rain-fed replenishment. Droughts, seasonal variations in rainfall, and pumping all have an effect on the depth of groundwater under the surface. Water levels in a well may be decreased if it is pumped quicker than the aquifer around it can replace itself via precipitation or other underground activity. Groundwater is a dynamic natural resource that may be replenished by precipitation during the rainy season throughout the rest of the year. Overdrawing groundwater strains the aquifer, producing a decrease in the water table and aquifer distortion, as well as severe surface and subterranean environmental consequences. The presence of humidity is an inevitable part of existence. When it rains, the humidity in the air may change dramatically. It may generate an excessive amount of humidity, resulting in an excess of moisture in the air. Learn more about the interaction of rain and humidity and how it affects them. As a consequence, managing humidity in your workplace will be straightforward. You may be surprised at how fast the weather may alter the humidity. When it rains, the humidity rises to 100 percent, causing the clouds to become unable to hold any more water. Evaporation causes the relative humidity to increase when it rains. It's conceivable that There is some water vapour present in the rain-soaked air. Nevertheless, because air is present all the time sucking water from the ground, the humidity will grow as the rain keeps coming. Evaporation cools the air and increases the absolute moisture content of the surrounding air. Rain collects water vapour from the sky and deposits it on the earth's surface on a larger scale. This shows that rain reduces the average relative humidity across a larger region. Water evaporates more rapidly in hotter air, resulting in a greater level of humidity. If the air is colder, the water reduces humidity, making it seem cooler than the outside temperature. The dewpoint temperature is similarly concerned with moisture and the quantity vaporised water in the environment. It is how hot it is at which air must be cooled before saturation occurs. Dewpoint may vary from the mid-60s to the high 80s depending on the area and time of year. It's also important to remember that various humidity levels affect different individuals in different ways. Table 6 shows the direct relation of monitored well dataset in total 8 district. The well dataset can be linked with prediction model in future for direct relation to water scarcity with the help of geology mapping. Following is the data of Rainfall, Humidity and Groundwater level-



**Deshmukh and Bamnote****RESULT**

Ground Water Monitoring Wells Are Distributed Using a Basin-Wise Approach In the Godavari basin, there are 997 network stations, 317 in the Krishna basin, 316 in the Tapi basin, 277 in the Coastal basin, 7 in the Narmada basin, and 2 in the Mahanadi basin (Table 8 and 9). The basin-by-basin distribution of GWM wells is shown in Table 8. The well data analytics reveals a clear correlation between the rainfall dataset and the groundwater level, although with less precision since the groundwater level may be a result of river prospects, which might vary depending on the terrain or the source of the river.

Chart 1 shows the overall average plot for the vidharbha region for rainfall dataset, the difference between expected is 22% less than actual rainfall. The percentage distribution in Chart 2 clearly states the uneven distribution of the rainfall in overall geography of vidharbha region. Chart 3,4,5 shows the trend in humidity and shows highest saturation in the month of august or September, which in fact show the direct co-relation with groundwater recharge as shown in Chart 6 and 7. The relation for river roles for groundwater recharge and well dataset doesn't show direct relation as river are combination of various geography and none of them have origin in vidharbha region (Chart 8 and Chart 9).

CONCLUSION

It was necessary to combine all of the data and conduct several data analyses in order to determine the levels of four distinct factors, such as rainfall, humidity, temperature, and groundwater level. The direct and proportionate connection between rainfall and temperature is clearly shown by a percentage-wise examination of the rainfall dataset. Buldhana is the area with the greatest lack of rainfall, followed by Amravati, Wardha, Yavatmal, and Gondia, which are all in the same boat. The average rainfall in the normal category was highest in Nagpur, followed by Akola and Gadchiroli, according to the Met Office. Analyses of three-year humidity data reveal that the month of September has the greatest saturation of humidity, which has a direct relationship with the amount of rainfall that has fallen. In the well data analysis, it is shown that there is a strong connection between the rainfall dataset and the groundwater level. However, the accuracy is limited because groundwater levels can change as a result of river prospective, which can vary depending on topography or the source of the river. Due to the fact that rivers are a mix of many geographies and none of them have their origin in the Vidharbha area, the relationship between river responsibilities for groundwater recharge and the well dataset does not exhibit a clear correlation. In order to comprehend the relation matrix and co-relation parameter, we have also examined the geology of each area as well as the river recharge pattern. The finding demonstrates that river water flow is directly dependent on rainfall and groundwater recharge, with accuracy of 67 percent and 78 percent, respectively. Based on the 5-year timeline dataset, the humidity dataset indicates a heavy forecast potential with a 35 percent accuracy rate for heavy rainfall. We have also validated the data redundancy and inconsistency in order to get a data-efficient model that is 99 percent or better.

FUTURE SCOPE

The data analytics on rainfall, river, water-well, humidity, temperature data can directly be used to predict the natural disaster like drought, flood, cloud bust, extreme temperature; as there is direct co-relation of various parameter with respect to time-line of year. Geography and geology have similar trend over vidharbha region so studying and predicting natural disaster like drought, flood, cloud bust, extreme temperature finds the possibility in vidharbha region based on above data-analytics which is carried out for future prospects

REFERENCES

1. O. O. Ometan, T. V. Omotosho, S. A. Akinwumi, M. O. Adewusi, T. E. Arijaje and O. A. Adeyemi, "Numerical





Deshmukh and Bamnote

- Analysis of the Measured Temporal Rainfall Rate and Rain Attenuation in a Tropical Location," 2021 7th International Conference on Space Science and Communication (IconSpace), Selangor, Malaysia, 2021, pp. 50-53, doi: 10.1109/IconSpace53224.2021.9768750.
2. Adler, R.F.; Sapiano, M.R.P.; Huffman, G.J.; Wang, J.-J.; Gu, G.; Bolvin, D.; Chiu, L.; Schneider, U.; Becker, A.; Nelkin, E.; Xie, P.; Ferraro, R.; Shin, D.-B. The Global Precipitation Climatology Project (GPCP) Monthly Analysis (New Version 2.3) and a Review of 2017 Global Precipitation. *Atmosphere* **2018**, *9*, 138. <https://doi.org/10.3390/atmos9040138>.
 3. Saini, A., Sahu, N. Decoding trend of Indian summer monsoon rainfall using multimethod approach. *Stoch Environ Res Risk Assess* **35**, 2313–2333 (2021). <https://doi.org/10.1007/s00477-021-02030-z>.
 4. PulakGuhathakurta and Elizabeth Saji, "Detecting changes in rainfall pattern and seasonality index vis-à-vis increasing water scarcity in Maharashtra," *J. Earth Syst. Sci.* **122**, No. 3, June 2013, pp. 639–649.
 5. Xiaolin Yang, XinnanJin, Qingquan Chu, Steven Pacenka, Tammo S. Steenhuis, Impact of climate variation from 1965 to 2016 on cotton water requirements in North China Plain, *Agricultural Water Management*, Volume 243, 2021, 106502, ISSN 0378-3774, <https://doi.org/10.1016/j.agwat.2020.106502>.
 6. Merin Mariam Mathew, Sreelash K, Micky Mathew, P Arulbalaji, D Padmalal, Spatiotemporal variability of rainfall and its effect on hydrological regime in a tropical monsoon-dominated domain of Western Ghats, India, *Journal of Hydrology: Regional Studies*, Volume 36, 2021, 100861, ISSN 2214-5818, <https://doi.org/10.1016/j.ejrh.2021.100861>.
 7. Byakatonda, Jimmy & Parida, B.P. & Kenabatho, Piet & Moalafhi, Ditiro. (2018). Analysis of rainfall and temperature time series to detect long-term climatic trends and variability over semi-arid Botswana. *Journal of Earth System Science*. **127**. 10.1007/s12040-018-0926-3.
 8. MosisaTujubaWakjira, Nadav Peleg, Daniela Anghileri, Darcy Molnar, Tena Alamirew, Johan Six, Peter Molnar, Rainfall seasonality and timing: implications for cereal crop production in Ethiopia, *Agricultural and Forest Meteorology*, Volume 310, 2021, 108633, ISSN 0168-1923, <https://doi.org/10.1016/j.agrformet.2021.108633>.
 9. Lohani, Anil Kumar & Krishan, Gopal & Chandniha, Drs Surendra. (2017). Hydrological Disasters Management and Risk Assessment Article History. 4929. 520-529.
 10. "Ground Water Year Book", Central Ground Water Board Ministry of water Resources Gov of India PP.74, 2014
 11. Salas, Jose & Govindaraju, Rao & Anderson, Michael & Arabi, Mazdak & Francés, Félix & Suarez, Wilson & Lavado, Waldo & Green, Timothy. (2014). Introduction to Hydrology. 10.1007/978-1-62703-595-8_1.
 12. P.J. Reddy, *Stochastic Hydrology*, 6th ed., University Science Press, pp.259, 2008
 13. María Carmen Llasat, Anna del Moral, Maria Cortès, Tomeu Rigo, Convective precipitation trends in the Spanish Mediterranean region, *Atmospheric Research*, Volume 257, 2021, 105581, ISSN 0169-8095, <https://doi.org/10.1016/j.atmosres.2021.105581>.
 14. Parimita Saikia, Dr. Narayan Chetry, "Study of Fluctuations in the Groundwater Level in Rajasthan: A Spatio-Temporal Approach," *International Journal of Engineering Research & Technology (IJERT)*, Vol. 9 Issue 07, July-2020, <http://www.ijert.org> ISSN: 2278-0181.
 15. Karimi, Bahareh & Safari, Mir Jafar Sadegh & DANANDEH MEHR, Ali & Mohammadi, Mirali. (2019). Monthly Rainfall Prediction Using ARIMA and Gene Expression Programming: A Case Study in Urmia, Iran. **2**. 8-14. 10.21859/ojest-02032.

Table-1: Rainfall of Vidarbha

Sr.No.	Region	Normal Rainfall (mm)	Actual Rainfall (mm)	% Departure of RF wrt Normal	Category
1	Vidarbha	954.6	875.4	-8	Normal

Table-2: Up till December 26th, 2020, district-level rainfall deviation as a percentage from average rainfall

SI No.	District	% Departure of RF wrt Normal	Category
1	Akola	2	Normal
2	Amravati	-18	Normal





Deshmukh and Bamnote

3	Bhandara	-9	Normal
4	Buldhana	-26	Deficient
5	Chandrapur	-3	Normal
6	Gadchiroli	0	Normal
7	Gondia	-8	Normal
8	Nagpur	7	Normal
9	Wardha	-17	Normal
10	Washim	-1	Normal
11	Yavatmal	-15	Normal

Table 3. Humidity 2018

MONTHS	AVERAGE
January	59%
February	52%
March	34%
April	26%
May	34%
June	60%
July	89%
August	70%
September	80%
October	79%
November	69%
December	79%

Table 4. Humidity 2019

MONTHS	AVERAGE
January	52%
February	48%
March	26%
April	20%
May	29%
June	67%
July	82%
August	76%
September	79%
October	70%
November	62%
December	68%

Table 5. Humidity 2020

Month	AVERAGE
January	58%
February	42%
March	30%
April	22%
May	25%
June	59%
July	79%
August	80%
September	78%
October	60%
November	58%
December	59%

Table6: Groundwater level of Vidarbha 2019

Sl. No.	District	Active		Dry		Wells Not Monitored#		Total Wells (As on Jan 2019)		Total
		DW	Pz	DW	Pz	DW	Pz	DW	Pz	
1	AKOLA	25	6	5	0	2	3	32	9	41
2	AMRAVATI	73	7	1	0	8	12	82	19	101
3	BULDHANA	45	10	2	0	5	3	52	13	65
4	CHANDRAPUR	49	11	1	0	3	0	53	11	64
5	GONDIA	24	4	0	0	7	1	31	5	36
6	NAGPUR	60	17	0	0	0	3	60	20	80
7	WARDHA	49	11	0	1	1	4	50	16	66
8	YAVATMAL	58	20	0	0	1	4	59	24	83
	TOTAL	383	86	9	1	27	30	419	117	536





Deshmukh and Bamnote

Table7: Groundwater level of Vidarbha 2020 (DW = Dug well; PZ = Piezometer)

Sl.No.	District	Abandoned		New wells		Total wells		Total Wells (As on 31st March 2020)
		DW	PZ	DW	PZ	DW	Pz	
1	AKOLA	0	0	3	0	32	9	41
2	AMRAVATI	14	1	0	0	69	18	87
3	BULDHANA	1	NAN	5	1	52	14	66
4	CHANDRAPUR	0	0	10	0	63	11	74
5	GONDIA	0	0	0	0	31	5	36
6	NAGPUR	2	1	6	0	65	19	84
7	WARDHA	2	0	3	0	48	16	64
8	YAVATMAL	0	0	3	0	58	24	82
	TOTAL	19	2	30	1	418	116	534

Table8: Distribution of Ground Water Monitoring Wells in Each Basin in Vidarbha in the period 2018-19

District	Godavari	Mahanadi	Tapi	Grand Total
Akola	NAN	NAN	37	37
Amravati	46	NAN	58	104
Bhandara	41	NAN	NAN	41
Buldhana	42	NAN	44	68
Chandrapur	74	NAN	NAN	74
Gadchiroli	64	2	NAN	66
Gondia	37	NAN	NAN	37
Nagpur	94	NAN	NAN	94
Wardha	67	NAN	NAN	67
Washim	32	NAN	18	50
Yavatmal	96	NAN	NAN	96
Total	593	2	157	734

Table9: District-level Ground Water Monitoring Point Observers' Current Situation Vidarbha during the year 2018-19

Sr. No	District	Number of Point Observer
1	Akola	7
2	Amravati	39
3	Bhandara	6
4	Buldhana	10
5	Chandrapur	10
6	Gadchiroli	10
7	Gondia	1
8	Nagpur	7
9	Wardha	5
10	Washim	9
11	Yavatmal	6
	Total	110





Deshmukh and Bamnote

<p>Figure: a)</p>	<p>Figure: b)</p>	<p>Figure: c)</p>
<p>Figure: d)</p>	<p>Figure: e)</p>	
<p>Figure f): Vidarbha Region Map in Vidarbha</p>	<p>Figure g): Monsoon patterns</p>	
<p>Figure h): Ground water level in Maharashtra</p>	<p>Chart 1. Average Rainfall Vidarbha region</p>	





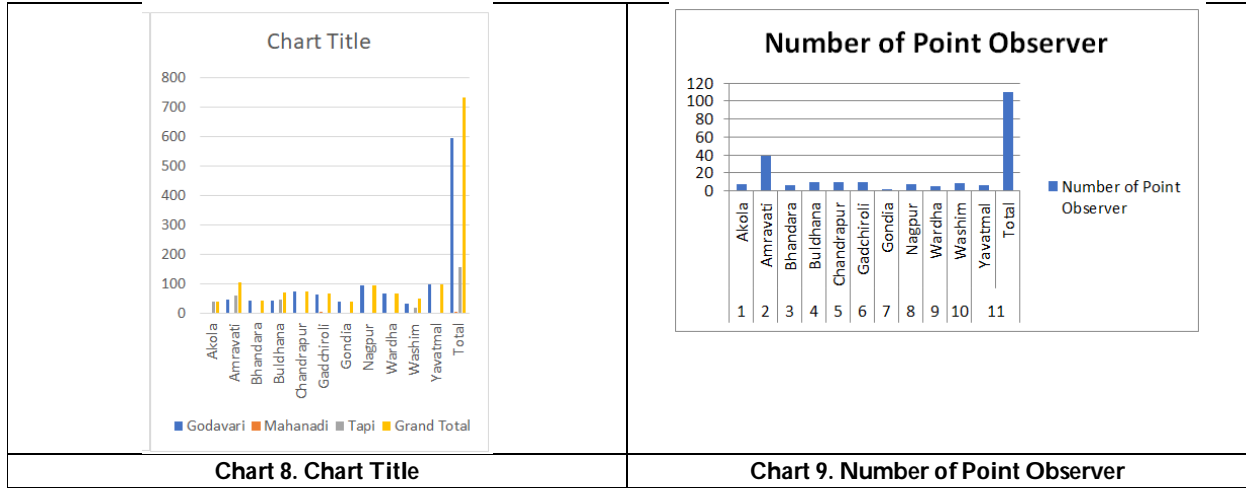
Deshmukh and Bamnote

<p>% Departure of RF wrt Normal</p> <table border="1"> <thead> <tr> <th>District</th> <th>% Departure</th> </tr> </thead> <tbody> <tr><td>Akola</td><td>2</td></tr> <tr><td>Amravati</td><td>-18</td></tr> <tr><td>Buldhana</td><td>-25</td></tr> <tr><td>Bhamburda</td><td>-10</td></tr> <tr><td>Chandrapur</td><td>-25</td></tr> <tr><td>Gadchiroli</td><td>-10</td></tr> <tr><td>Gondia</td><td>-10</td></tr> <tr><td>Nagpur</td><td>7</td></tr> <tr><td>Wardha</td><td>-18</td></tr> <tr><td>Yashwantrao Chavan</td><td>-2</td></tr> <tr><td>Yavatmal</td><td>-15</td></tr> </tbody> </table>	District	% Departure	Akola	2	Amravati	-18	Buldhana	-25	Bhamburda	-10	Chandrapur	-25	Gadchiroli	-10	Gondia	-10	Nagpur	7	Wardha	-18	Yashwantrao Chavan	-2	Yavatmal	-15	<p>Humidity 2018</p> <table border="1"> <thead> <tr> <th>Month</th> <th>Humidity (%)</th> </tr> </thead> <tbody> <tr><td>January</td><td>55</td></tr> <tr><td>February</td><td>50</td></tr> <tr><td>March</td><td>35</td></tr> <tr><td>April</td><td>25</td></tr> <tr><td>May</td><td>35</td></tr> <tr><td>June</td><td>60</td></tr> <tr><td>July</td><td>90</td></tr> <tr><td>August</td><td>70</td></tr> <tr><td>September</td><td>80</td></tr> <tr><td>October</td><td>78</td></tr> <tr><td>November</td><td>70</td></tr> <tr><td>December</td><td>80</td></tr> </tbody> </table>	Month	Humidity (%)	January	55	February	50	March	35	April	25	May	35	June	60	July	90	August	70	September	80	October	78	November	70	December	80										
District	% Departure																																																												
Akola	2																																																												
Amravati	-18																																																												
Buldhana	-25																																																												
Bhamburda	-10																																																												
Chandrapur	-25																																																												
Gadchiroli	-10																																																												
Gondia	-10																																																												
Nagpur	7																																																												
Wardha	-18																																																												
Yashwantrao Chavan	-2																																																												
Yavatmal	-15																																																												
Month	Humidity (%)																																																												
January	55																																																												
February	50																																																												
March	35																																																												
April	25																																																												
May	35																																																												
June	60																																																												
July	90																																																												
August	70																																																												
September	80																																																												
October	78																																																												
November	70																																																												
December	80																																																												
<p>Chart 2. Departure of Rainfall</p>	<p>Chart 3. Humidity 2018</p>																																																												
<p>Humidity 2019</p> <table border="1"> <thead> <tr> <th>Month</th> <th>Humidity (%)</th> </tr> </thead> <tbody> <tr><td>January</td><td>50</td></tr> <tr><td>February</td><td>45</td></tr> <tr><td>March</td><td>25</td></tr> <tr><td>April</td><td>20</td></tr> <tr><td>May</td><td>30</td></tr> <tr><td>June</td><td>65</td></tr> <tr><td>July</td><td>85</td></tr> <tr><td>August</td><td>75</td></tr> <tr><td>September</td><td>80</td></tr> <tr><td>October</td><td>70</td></tr> <tr><td>November</td><td>60</td></tr> <tr><td>December</td><td>70</td></tr> </tbody> </table>	Month	Humidity (%)	January	50	February	45	March	25	April	20	May	30	June	65	July	85	August	75	September	80	October	70	November	60	December	70	<p>Humidity 2020</p> <table border="1"> <thead> <tr> <th>Month</th> <th>Humidity (%)</th> </tr> </thead> <tbody> <tr><td>January</td><td>55</td></tr> <tr><td>February</td><td>40</td></tr> <tr><td>March</td><td>30</td></tr> <tr><td>April</td><td>20</td></tr> <tr><td>May</td><td>25</td></tr> <tr><td>June</td><td>60</td></tr> <tr><td>July</td><td>80</td></tr> <tr><td>August</td><td>80</td></tr> <tr><td>September</td><td>75</td></tr> <tr><td>October</td><td>60</td></tr> <tr><td>November</td><td>60</td></tr> </tbody> </table>	Month	Humidity (%)	January	55	February	40	March	30	April	20	May	25	June	60	July	80	August	80	September	75	October	60	November	60										
Month	Humidity (%)																																																												
January	50																																																												
February	45																																																												
March	25																																																												
April	20																																																												
May	30																																																												
June	65																																																												
July	85																																																												
August	75																																																												
September	80																																																												
October	70																																																												
November	60																																																												
December	70																																																												
Month	Humidity (%)																																																												
January	55																																																												
February	40																																																												
March	30																																																												
April	20																																																												
May	25																																																												
June	60																																																												
July	80																																																												
August	80																																																												
September	75																																																												
October	60																																																												
November	60																																																												
<p>Chart 4. Humidity 2019</p>	<p>Chart 5. Humidity 2020</p>																																																												
<p>Groundwater level of 2019</p> <table border="1"> <thead> <tr> <th>District</th> <th>Active Level</th> <th>Dry Level</th> </tr> </thead> <tbody> <tr><td>AKOLA</td><td>~50</td><td>~50</td></tr> <tr><td>AMRAVATI</td><td>~50</td><td>~50</td></tr> <tr><td>BULDHANA</td><td>~50</td><td>~50</td></tr> <tr><td>CHANDRAPUR</td><td>~50</td><td>~50</td></tr> <tr><td>GONDIA</td><td>~50</td><td>~50</td></tr> <tr><td>NAGPUR</td><td>~50</td><td>~50</td></tr> <tr><td>WARDHA</td><td>~50</td><td>~50</td></tr> <tr><td>YAVATMAL</td><td>~50</td><td>~50</td></tr> <tr><td>TOTAL</td><td>~400</td><td>~550</td></tr> </tbody> </table>	District	Active Level	Dry Level	AKOLA	~50	~50	AMRAVATI	~50	~50	BULDHANA	~50	~50	CHANDRAPUR	~50	~50	GONDIA	~50	~50	NAGPUR	~50	~50	WARDHA	~50	~50	YAVATMAL	~50	~50	TOTAL	~400	~550	<p>Groundwater level of 2020</p> <table border="1"> <thead> <tr> <th>District</th> <th>Active Level</th> <th>Dry Level</th> </tr> </thead> <tbody> <tr><td>AKOLA</td><td>~50</td><td>~50</td></tr> <tr><td>AMRAVATI</td><td>~50</td><td>~50</td></tr> <tr><td>BULDHANA</td><td>~50</td><td>~50</td></tr> <tr><td>CHANDRAPUR</td><td>~50</td><td>~50</td></tr> <tr><td>GONDIA</td><td>~50</td><td>~50</td></tr> <tr><td>NAGPUR</td><td>~50</td><td>~50</td></tr> <tr><td>WARDHA</td><td>~50</td><td>~50</td></tr> <tr><td>YAVATMAL</td><td>~50</td><td>~50</td></tr> <tr><td>TOTAL</td><td>~400</td><td>~550</td></tr> </tbody> </table>	District	Active Level	Dry Level	AKOLA	~50	~50	AMRAVATI	~50	~50	BULDHANA	~50	~50	CHANDRAPUR	~50	~50	GONDIA	~50	~50	NAGPUR	~50	~50	WARDHA	~50	~50	YAVATMAL	~50	~50	TOTAL	~400	~550
District	Active Level	Dry Level																																																											
AKOLA	~50	~50																																																											
AMRAVATI	~50	~50																																																											
BULDHANA	~50	~50																																																											
CHANDRAPUR	~50	~50																																																											
GONDIA	~50	~50																																																											
NAGPUR	~50	~50																																																											
WARDHA	~50	~50																																																											
YAVATMAL	~50	~50																																																											
TOTAL	~400	~550																																																											
District	Active Level	Dry Level																																																											
AKOLA	~50	~50																																																											
AMRAVATI	~50	~50																																																											
BULDHANA	~50	~50																																																											
CHANDRAPUR	~50	~50																																																											
GONDIA	~50	~50																																																											
NAGPUR	~50	~50																																																											
WARDHA	~50	~50																																																											
YAVATMAL	~50	~50																																																											
TOTAL	~400	~550																																																											
<p>Chart 6. Groundwater level 2019</p>	<p>Chart 7. Groundwater level 2020</p>																																																												





Deshmukh and Bamnote





Multiple Object Tracking in the Modern Era: A Review of the Literature

Pranita S Chaudhary^{1*} and Sharda Chhabria²

¹Research Scholar, CSE Department, GHRIU, Amaravati, Maharashtra, (Assistant Professor, CSE (AI-ML) Department, PCCOE, Nigdi, Pune, Maharashtra), India.

²Associate Professor, AI Department, G H Rasoni Institute of Engineering and Technology, Nagpur, Maharashtra, India.

Received: 17 Feb 2023

Revised: 25 Apr 2023

Accepted: 31 May 2023

*Address for Correspondence

Pranita S Chaudhary

Research Scholar, CSE Department, GHRIU,
Amaravati, Maharashtra,
(Assistant Professor,
CSE (AI-ML) Department, PCCOE,
Nigdi, Pune, Maharashtra), India.
E.Mail: chaudharypranitha@gmail.com



This is an Open Access Journal / article distributed under the terms of the **Creative Commons Attribution License** (CC BY-NC-ND 3.0) which permits unrestricted use, distribution, and reproduction in any medium, provided the original work is properly cited. All rights reserved.

ABSTRACT

Multiple object tracking has received a great deal of attention from academics recently and now ranks among the main urgent difficulties with machine vision, mainly in light of the development of automated vehicles. MOT itself becomes a crucial vision job for a variety of problems, including occlusion in crowded settings, identical appearance, trouble detecting small objects, ID switching, etc. In addition to using the transformer's attention mechanism, graph convolutional neural networks, Siamese networks, trackless correlation, and basic IOU matching-based CNN networks, researchers also tested motion prediction using LSTM and the interrelation of trackless with CNNs. They looked at more than a hundred articles that were published in the past three years to identify strategies for handling MOT challenges. They explored transformer's attention mechanism, graph convolutional neural networks, Siamese networks, track-let correlation, IOU matching-based CNN networks, LSTM for motion prediction, and track-let interrelation with CNNs.

Keywords: monitoring several objects, monitoring objects, obstruction, and machine intelligence

INTRODUCTION

Deep learning algorithms have successfully solved real-world problems in the past decade, with classifiers being widely used in machine vision. Object monitoring, which comes after object detection, is considered a crucial goal in



**Pranita S Chaudhary and Sharda Chhabria**

object recognition. It involves locating objects on the screen and creating trajectories for them in subsequent frames. Objects can be diverse, ranging from approaching traffic and moving cars to athletes in sports or flying objects, birds, etc. Multiple items are tracked at once inside a frame using a technique called many objects tracking, or MOT. In MOT, investigators can follow every object in a certain class or every object in the aforementioned classes. Single Item Tracking, or SOT, is the process of tracking just one object. The MOT is more difficult than the SOT. As a result, many deep learning-based designs were presented by academics to address MOT-related issues. Researchers conducted a literature study on MOT to organize research from the past three years, including articles and reviews from prior years [1]. Limitations of previous studies included narrow focus on deep learning approaches or lack of consideration for real-world deployments. The researchers reviewed over a hundred publications from 2020 to 2022, identifying strategies for addressing challenges in MOT and analysing datasets and metrics used in previous studies. They also highlighted diverse applications of MOT. During their review, a specific area of research caught their attention and was further discussed. In conclusion, researchers have structured our work in the following way:

- 1) Identifying the biggest obstacles in MOT
- 2) listing the numerous MOT strategies that are often utilised
- 3) Creating a dataset summary for the MOT benchmarks
- 4) Creating a MOT metrics summary
- 5) MOT, a tracker must also overcome a number of additional obstacles when it comes to a MOT issue investigating different applications
- 6) Several recommendations for upcoming projects

MOT MAIN CHALLENGES

Multiple object tracking presents certain difficulties. Although occlusion is the major obstacle in

Occlusion

Obstruction is a challenge in MOT when objects of interest are partially or completely covered by other objects, especially in crowded environments without depth information. The use of bounding boxes to locate objects is common in MOT, but overlapping ground-truth bounding boxes can affect accuracy [2, 3, 5]. Scholars are actively exploring ways to address occlusion challenges, as shown in Figure 1a where a light pole obstructs the view of a red-clad woman in Figure 1b. Fig. 1. (a) A diagram showing how components are occluded (green and blue). Components were separated from one another in display 1. A portion of them is obscured in display 2. They are completely obscured on display 3.

Some Common Challenges

Accurate object detection is critical in MOT architecture, but it can be challenging due to factors like speed, backdrop distortion, and lighting conditions. Objects with different shapes, colours, and sizes require specific visual features for detection. Scale-related visual features and higher-quality images are used in attempts to overcome these challenges [2] prediction algorithms, they additionally employed hierarchical feature maps [3].

MOT APPROACHES

Object detection and target association are crucial initial stages in the process of multiple object tracking (MOT). While some research focuses on improving object detection, others focus on data association to link objects across frames. These two phases are often intertwined, with overlaps between techniques and combinations of different MOT components in publications. The identification and organization stages are not always separate, and various approaches are used to address these challenges in MOT. Therefore, they cannot claim that the methods are distinct from one another. However, they made an effort to identify the most common methods so that they could choose one of them to implement.



**Pranita S Chaudhary and Sharda Chhabria****Transformer**

The Transformer model has gained popularity in computer vision tasks, including MOT, due to its encoder-decoder architecture and long-term context memory. DOQ and query-based tracking have been used to improve detection adaptability in MOT. Deep base maps with scaling techniques have also shown improved results in MOT [2].

Graph Model

Graph Convolutional Networks (GCNs) are a type of fully convolutional network used in multiple object tracking (MOT) that treat objects as nodes in a graph. The connections between pairs of nodes are referred to as edges. GCN-based approaches have emerged as a novel approach in solving MOT problems. The Hungarian method is commonly used in this field for data association [16]. An overview of employing graph models to resolve MOT problems is shown in Table II. Fig. 3. Track Former [4] performs combined detection and attention-tracking while using the transformer's design to enable encoding and decoding to transform monitoring several objects into a set estimation issue.

Use the Presentation Map Connections as well as the Movement Graphs System to evaluate the motion and appearance of the frames accordingly [21]. Two graph modules have also been used by investigators to address the MOT issue; however, the following section contains responsibility for making the in [23,24], researchers proposed addressing association and assignment issues in multiple object tracking (MOT) by focusing on object similarities within the same frames and incorporating dynamic programming for identifying persistent features. Recent work in 2022 has explored multi-camera MOT using dynamic graphs to gather information on new features. GCN-based ranking was also used for proposal generation and grading in MOT.

Detection and Target Association

While any deep learning model can perform object detection, the challenge lies in accurately tracking the trajectory of the target or object [25,27]. Different approaches have been used in various publications for this purpose, including bottom-up and top-down strategies. The bottom-up approach involves finding point trajectories, while the top-down approach involves selecting bounding boxes. Combining these two approaches can provide a comprehensive picture of the objects being tracked. In 2020, two separate branches of object detection and re-identification were completed, using a similar construction and named "FairMOT" to denote equal emphasis on both tasks [33]. Fig. 4. (a) Images in which things can be found (b) A graph that was created using the tracklets or observed objects as each node and proposal generation. (c) Using GCN to rank the suggestions. The trajectory inference is (d). (e) The result [22]

In addition to [30], Cordmaker, an association structure for information correlation, was developed for object detection. Self-supervised learning was used to complete the object detection part, incorporating Faster CNN and recent combining techniques for object identification. This resulted in the recommendation of Quasi-Dense Monitoring System (QDTrack). D2LA system by Yaoye et al., based on FairMOT [33], balances precision and complexity. Safety measures like strip attention module are introduced to avoid congestion. Norman et al. propose a method for estimating object configuration and mapping object orientation for hidden objects. In [32], two modules, CVA and MFW, are proposed for object localization offset information extraction and communication between frames. Coordination of the overall procedure is referred to as "Trades". Cheng-Jen et al. proposed an indoor multiple objects tracking approach that includes a depth-enhanced tracker (DET) and an indoor MOT dataset. YOLOv4 was used as the object detector, and optical flow was employed to track bounding boxes. Anticipated changes in MOT problem statements for 2022. Both object tracking and object forecasting have been done in this study. They created a Joint Learning Architecture by stacking a forecasting network and Fairmont [33] to recognise bounding boxes (JLE). To correctly recognise the pedestrian, they have combined these two categories of characteristics.



**Pranita S Chaudhary and Sharda Chhabria****Attention Module**

Attention modules play a crucial role in object recognition in MOT, allowing for focus on subjects of interest and ignoring background. Different attention techniques, such as strip attention module, data association, information association, and spatial-attentional techniques, have been proposed to address occlusion challenges in MOT. These modules help in re-identifying obstructed objects, generating intense attention, and recovering relevant data from earlier frames for improved object localization. These approaches are summarized in Table IV and show promising results in handling occlusion in MOT [37, 40]. The use of self-attention mechanism in detecting automobiles is proposed in [38], where a dynamic graph is used to combine internal and external input from cameras. Cross- and self-attention are employed for feature extraction, reducing background occlusion. Cross-attention component is illustrated in Figure 5.

Motion Model

Motion characteristics utilized for multi-object tracking, including AMFD and LRMC for motion identification. Motion model baseline (MMB) reduces false alarms in vehicle operations. Proposed Motion-Aware Tracker (MAT) with motion compensation recommended for 2022 implementation. Uses GLV model, LGM tracking, and three modules for object mobility anticipation.

Siamese Network

The Siamese network is a powerful tool for object tracking, allowing for comparison of frame similarities and pattern recognition. It consists of two concurrent subnetworks that share weights and are merged together to assess the closeness of linguistic knowledge. In our approach, a pyramid network with a thin transformer attention layer, called Siamese Converter Pyramid Router, enhances characteristics and cross-awareness among hierarchy aspects for improved object detection. Our proposed method offers faster and more efficient object tracking with minimal supervision and network connection settings, including a portable navigation unit for increased foreground item localization. The Siamese Tracking Network incorporates an integrated and effective converter layer with transform layers replacing the convolutional layer [34].

Organization for Track lets

Track lists are collections of related items in a series of frames, initially identified using various techniques in object detection and tracking. Track let association is a challenging task in MOT, and different studies have used various strategies, as summarized in Table VII. One approach involves creating tracklets using a 3D geometric method and optimizing the global relationship using spatial and temporal information from multiple cameras [46]. Fig. 6. (Three examples of typical networks include (a) symmetric pyramid-shaped Siamese networks, (b) discriminative networks, and (c) the establishment of the Siamese transfers multilevel system [12]. They can observe a distinct approach from the earlier ones in [47]. They created a TMB that calculates price as well as being flexible by treating each trajectory as a centre vector. They also developed LVS, which acknowledges every identification as a critical rule and aids in viewing the trajectory from a broader perspective. In addition, researchers suggested the SGFF technique to eliminate ambiguous features.

MOT BENCHMARKS

Typical MOT datasets consist of video clips with unique IDs assigned to each object entering the frame. New benchmarks with additional variables are released almost every year since 2015, including MOT15, MOT16 [82], MOT20, and others. Well-known benchmarks like PETS, KITTI, STEPS, and Dance Track are widely used in computer vision research. These datasets, such as Head Tracking 21 and STEP, provide access to diverse tracking scenarios, including pedestrian head tracking and pixel-level monitoring and segmentation are often used in the papers that they look at is shown in Chart 7. The diagram demonstrates how the MOT17 dataset is used regularly compared to other sets of data.





Pranita S Chaudhary and Sharda Chhabria

MOT METRICS

MOTP

Localization precision crucial for tracking multiple objects; MOT P used with MOT A to account for detection and localization. localization accuracy in multi-object tracking. One of the results of a MOT job is localization. It reveals the location of the object within a frame. It cannot give a complete picture of the tacker's effectiveness in tracking objects on its own.

$$MOTP = \frac{\sum_{i,t} d_t^i}{\sum_t c_t}$$

d_t^i : The separation between the object's real size and its corresponding theory at the moment, t : A tracker assigns a hypothesis for each item in the set, o_i , inside a single frame h_i . c_t : Number of times an object and a hypothesis have been matched as of timet.

MOTA

Accurate Monitoring Multiple Objects. Without accounting for preciseness, the indicator assesses effectively Recognizing objects and predicting trajectory. The statistic accounts for three different forms of inaccuracy [49].

$$MOTA = 1 - \frac{\sum_t (m_t + fp_t + mme_t)}{\sum_t g_t}$$

m_t :The quantity of missed shots at time t .

fp_t : The quantity of false – positive

mme_t : The quantity of identity changes

g_t : The quantity of things on hand at time t .

MOTA has limitations as it overemphasizes precise detection and ignores association in multi-object tracking. It penalizes trackers for association errors and does not have a minimum score requirement, resulting in potentially low MOTA scores. Poor accuracy has a greater impact on MOTA when identity switching is not considered.

IDF1

The metric for identification. Since opposed to measures including MOT A that do bijective translating at the detectable limits, the seeks to match anticipated trajectories with actual trajectories. It was created to assess "identification," which, in contrast to detection and association, focuses on the trajectories that are present [50].

$$ID - Recall = \frac{|IDTP|}{|IDTP| + |IDFN|}$$

$$ID - Precision = \frac{|IDTP|}{|IDTP| + |IDFP|}$$

$$IDF1 = \frac{|IDTP|}{|IDTP| + 0.5|IDFP| + 0.5|IDFN|}$$

$IDTP$: True Positive Identity. The ground truth object trajectory and the anticipated object trajectory are identical.

$IDFN$:Determine the false negative. Any undiscovered ground truth detection with an unparalleled trajectory.

$IDTP$: Identity a Fraud Positive. Any incorrectly expected detection.

IDF1 is favoured by some due to its emphasis on association in multi-object tracking, unlike MOTA which heavily relies on detection accuracy. However, IDF1 also has limitations as it may encourage researchers to prioritize collecting more unique data rather than focusing on accurate associations and detections.

Track-map

This statistic agrees with both the actual trajectory and the forecasted trajectory. When the pair's trajectory similarity score, st_{tr} , is higher than or equal to the threshold, α_{tr} , a match between the trajectories is made. Additionally, the anticipated trajectory has to have the maximum confidence score possible [50].

$$Pr_n = \frac{|TPTr|n}{n}$$





Pranita S Chaudhary and Sharda Chhabria

$$Re_n = \frac{|TPTr|n}{|gtTraj|}$$

n: number of projected paths overall. Predicted trajectories are ordered in descending order by their confidence score.

Pr_n: Calculates the precision of the tracker.

TPTr: Authentically Positive Trajectories. any anticipated trajectory that corresponds to reality

|TPTr|n: Among *n* anticipated trajectories, the proportion of genuine positive paths

Re_n: Actions Recalling

|gtTraj|: To determine the final T-map score, additional calculations are made using the regression coefficients, objects' ascent, and the equations for precision and recall.

$$Interp Pr_n = \max (Pr_m)$$

Interpolating the precision values in the beginning, they get *Interp Pr_n* for every *n*-th number. Next, they create a chart of *Interp Pr_n* between *Re_n* for every *n*-th number. The precision-recall curve is now available. They can calculate the track-map score using the integral of this curve. Tracking maps has several drawbacks as well. By doing this, the possibility of obtaining a favourable pair as well as the spot would increase. It does not, however, suggest accurate tracking. If trackers have superior detection and association, Track map cannot show it.

Loc A

Reliability in Locating [50].

$$LocA = \int_0^1 \frac{1}{|TP\alpha|} \sum_{c \in (TP\alpha)} S(c) d\alpha$$

S(c): Spatial similarity between expected and actual detections is an important sub-metric that addresses localization mistakes. It is different from MOT-P but shares similarities, as it considers localization errors at multiple thresholds. Metrics such as MOTA and IDF1, commonly used for tracking evaluation, often overlook localization, despite its significance in object tracking.

Association Accuracy Score

The Jaccard index is averaged among matched detection systems in MOT Benchmark, followed by an average over the localization threshold [50]. MOT task outcomes include association, determining whether objects in different frames are part of the same or separate trajectories, with the same ID. Missteps in connection occur when two distinct expected or predicted detections are applied to the same ground truth object [50].

$$AssA\alpha = \frac{1}{|TP|} \sum_{c \in [TP]} A(c)$$

Det A: Detection Accuracy

The MOT standard uses "Identification Jaccard Ranking summed exceeded localise limit" as a criterion. Detection accuracy is determined by the proportion of accurate detections, which can be impacted by ground truth detections that are not made or are incorrect, resulting in detection errors.

$$Det A_\alpha = \frac{|TP|}{|TP| + |FN| + |FP|}$$

Det Re: Detection Recall

For one localization threshold, the formula is provided. The localization criteria must be averaged [96].

$$DetRe_\alpha = \frac{|TP|}{|TP| + |FN|}$$

False negative results are detection and recall problems. They occur when the tracker fails to detect an object that is present in the real world. Detection recall and detection precision are two components of detection accuracy.

Det Pr: Detection Precision

For a single localization threshold, the equation is provided. They must average over all localization criteria [50].





Pranita S Chaudhary and Sharda Chhabria

$$\text{Det } Pr_{\alpha} = \frac{|TP|}{|TP|+|FP|}$$

As was already said, detection accuracy includes detection precision. False positives are flaws in detection precision. They occur whenever the tracker produces forecasts that are inconsistent with the reality on the ground.

$$ssR_{e^a} = \frac{1}{|TP|} \sum_{c \in (TP)} \frac{|TPA(c)|}{|TPA(c)| + |FNA(c)|}$$

Whenever a sensor allocates several projected paths to the exact field path, this is known as an association recall mistake. Association Recall and Association Precision are two subcategories of association accuracy.

MOTSA: Multi Object Tracking and Segmentation Accuracy

It becomes a modified version of the MOTA measure that additionally assesses how well the tracker performs segmentation tasks.

$$MOTSA = 1 - \frac{|FN| + |FP| + |M|}{|M|} = \frac{|TP| - |FP| - |IDS|}{|M|}$$

M is a collection of N ground truth masks with assigned tracking IDs. True positives (TP) occur when a hypothetical mask maps to a real mask. False negatives (FN) are unmatched ground truth masks, while false positives (FP) are unmatched hypothetical mappings. ID switches occur when ground-truth masks with different IDs belong to the same track [50]. The drawbacks of MOTSA include prioritising monitoring over relationships and being significantly impacted by the shortlisting of compatible thresholds.

AMOTA: Average Multiple Object Tracking Precision By estimating the MOTA values throughout other memory stages, this is determined

$$AMOTA = \frac{1}{L} \sum_{r \in \{t, t \dots 1\}} 1 + \frac{FP_r + FN_r + IDS_r}{n_r}$$

Overall amount of regression coefficients items in every blocks $isum_{gt}$. For a specific recall value r the number of false positive, number of false negative and the number of identity switches are denoted as $FP_r, FN_r,$ and IDS_r . The number of recall values is denoted using L . This number of ground truth objects over all frames is represented by the integer num_{gt} . False positives, false negatives, and identification switchover rates are designated as $FP_r, FN_r,$ and IDS_r , respectively, for a given recall factor r . L is an abbreviation for such recall points.

APPLICATIONS

MOT has a wide range of uses. Tracking different items, such as people, animals, fish, automobiles, athletes, etc., has taken a lot of effort. Actually, there are several domains that fall under the umbrella of multiple object tracking. However, we will discuss the articles based on particular applications to obtain an idea from the perspective of an application.

- A. Autonomous Driving: MOT is used in autonomous driving to track vehicles on the road, handle occlusion, and enable 3D motion tracking using LiDAR data.
- B. Vehicular Detection: MOT is used to track pedestrians in streetcar videos, with algorithms like Deep SORT and YOLOv5 being employed for detection and tracking.
- C. Wildlife Tracking: MOT is used by wildlife biologists to track animals using UAVs, avoiding the need for costly and unreliable sensors. Benchmark datasets like "Animal Track" have been developed for this purpose.
- D. Others: MOT has applications in security surveillance, social distance monitoring, radar monitoring, activity detection, smart elder care, investigation, re-identification of people, prediction, and more. Collaborative robotic frameworks and Siamese network-based techniques have been proposed for online monitoring and audio-visual object tracking in robotics.

Overall, MOT has a wide range of practical applications across various industries, making it a versatile tool for tracking multiple objects in different contexts.



**Pranita S Chaudhary and Sharda Chhabria****LONG TERM GOALS**

- Numerous attempts have already been undertaken in this area because MOT has been a popular study issue for many years. But this industry still has a lot of room for growth. Here, they'd like to highlight a few possible MOT routes.
- Mixing frames from numerous cameras: Tracking things using several cams is one of the challenges of MOT. Attempts are being made to link and show pictures from existence of non-cameras in order to continually monitor target items throughout a large region in a virtual area or for real-time multitarget, multi-camera tracking.
- Linking MOT to a class-based tracking system can be more beneficial in real situations. For example, utilising MOT to watch certain things such as birds near aeroplanes can assist automated precautionary actions, and category tracking can make tracking a single type of item more effective in observation circumstances.
- These long-term objectives seek to expand MOT's abilities and uses in a variety of fields..

CONCLUSION

In this work, we have provided a summary and analysis of the current trends in computer vision for Multiple Object Tracking (MOT). Our analysis shows that the use of transformers is increasing due to their ability to capture contextual information. However, due to their resource-intensive nature, a focused approach is necessary to achieve improved accuracy with a lightweight architecture. Deep learning-based methods such as CNNs and RNNs have shown remarkable success in improving MOT performance. Furthermore, integrating MOT with other computer vision tasks such as object detection, semantic segmentation, and scene understanding has led to further advancements in MOT systems, leveraging sensor fusion for better accuracy and robustness. The current state of the art in MOT allows for accurate tracking of multiple objects in complex scenes, enabling various applications such as autonomous vehicles, surveillance systems, and human-computer interaction. Continued research and development in MOT are expected to push the boundaries further, expanding its potential in various domains. Overall, the field of MOT is rapidly evolving, and it offers a promising future with significant potential for real-world applications.

REFERENCES

1. K., Kalirajan & v, Seethalakshmi & D., Venugopal & K., Balaji. (2021). Deep Learning for Moving Object Detection and Tracking. 10.4018/978-1-7998-7511-6.ch009.
2. Galor, Amit & Orfaig, Roy & Bobrovsky, Ben-Zion. (2022). Strong-TransCenter: Improved Multi-Object Tracking based on Transformers with Dense Representations. 10.48550/arXiv.2210.13570.
3. P. Dendorfer, H. Rezatofighi, A. Milan, J. Shi, D. Cremers, I. Reid, S. Roth, K. Schindler, and L. Leal-Taixe, "Mot20: A bench- mark for multi object tracking in crowded scenes," arXiv preprint arXiv:2003.09003, 2020.
4. Zhu, Tianyu & Hiller, Markus & Ehsanpour, Mahsa & Ma, Rongkai & Drummond, Tom & Reid, Ian & Rezatofighi, Hamid. (2022). Looking Beyond Two Frames: End-to-End Multi-Object Tracking Using Spatial and Temporal Transformers. IEEE transactions on pattern analysis and machine intelligence. PP. 10.1109/TPAMI.2022.3213073.
5. Sun, Sitong & Wang, Yu & Piao, Yan. (2021). A Real-time Multi-target tracking method based on Deep Learning. Journal of Physics: Conference Series. 1920. 012112. 10.1088/1742-6596/1920/1/012112.
6. Zhong, Minghan & Chen, Fanglin & Xu, Jun & Lu, Guangming. (2022). Correlation-Based Transformer Tracking. 10.1007/978-3-031-15919-0_8.
7. Zeng, Fangao & Dong, Bin & Zhang, Yuang & Wang, Tiancai & Zhang, Xiangyu & Wei, Yichen. (2022). MOTR: End-to-End Multiple-Object Tracking with Transformer. 10.1007/978-3-031-19812-0_38.
8. X. Chen, S. M. Iranmanesh, and K.-C. Lien, "Patchtrack: Multiple object tracking using frame patches," arXiv preprint arXiv: 2201.00080, 2022.
9. E. Yu, Z. Li, S. Han, and H. Wang, "Relationtrack: Relation-aware multiple object tracking with decoupled representation," IEEE Transactions on Multimedia, 2022.



**Pranita S Chaudhary and Sharda Chhabria**

10. Y. Liu, T. Bai, Y. Tian, Y. Wang, J. Wang, X. Wang, and F.-Y. Wang, "Segdq: Segmentation assisted multi-object tracking with dynamic query-based transformers," *Neurocomputing*, 2022.
11. Deng, A.; Liu, J.; Chen, Q.; Wang, X.; Zuo, Y. Visual Tracking with FPN Based on Transformer and Response Map Enhancement. *Appl. Sci.* 2022, 12, 6551. <https://doi.org/10.3390/app12136551>
12. Shen, Hao & Lin, Defu & Song, Tao. (2022). A real-time siamese tracker deployed on UAVs. *Journal of Real-Time Image Processing.* 19. 1-11. 10.1007/s11554-021-01190-z.
13. Hu X, Liu H, Hui Y, Wu X, Zhao J. Transformer Feature Enhancement Network with Template Update for Object Tracking. *Sensors (Basel).* 2022 Jul 12; 22(14):5219. doi: 10.3390/s22145219. PMID: 35890899; PMCID: PMC9320290.
14. T. Zhu *et al.*, "Looking beyond Two Frames: End-to-End Multi-Object Tracking Using Spatial and Temporal Transformers," in *IEEE Transactions on Pattern Analysis and Machine Intelligence*, 2022, doi: 10.1109/TPAMI.2022.3213073.
15. Yongping Dan, Zongnan Zhu, Weishou Jin, Zhuo Li, "PF-ViT: Parallel and Fast Vision Transformer for Offline Handwritten Chinese Character Recognition", *Computational Intelligence and Neuroscience*, vol. 2022, Article ID 8255763, 11 pages, 2022. <https://doi.org/10.1155/2022/825573>
16. Munapo, Elias, Development of an Accelerating Hungarian Method for Assignment Problems (August 31, 2020). *Eastern-European Journal of Enterprise Technologies*, 4(4 (106)), 6-13, 2020, doi: 10.15587/1729-4061.2020.209172, Available at SSRN: <https://ssrn.com/abstract=3724157>
17. Wang, Y., Weng, X., & Kitani, K. (2020). Joint Detection and Multi-Object Tracking with Graph Neural Networks. *ArXiv, abs/2006.13164*.
18. Marinello, N., Proesmans, M., & Gool, L.V. (2022). TripletTrack: 3D Object Tracking using Triplet Embeddings and LSTM. *2022 IEEE/CVF Conference on Computer Vision and Pattern Recognition Workshops (CVPRW)*, 4499-4509.
19. Li, Junchen & Liu, Yuheng & Jiang, Hongchuan & Yang, Mengxi & Lin, Sijie & Hu, Qing. (2022). A Multi-View Image Feature Fusion Network Applied in Analysis of Aeration Velocity for WWTP. *Water.* 14. 345. 10.3390/w14030345.
20. Gad A, Basmaji T, Yaghi M, Alheeh H, Alkhedher M, and Ghazal M. Multiple Object Tracking in Robotic Applications: Trends and Challenges. *Applied Sciences.* 2022; 12(19):9408. <https://doi.org/10.3390/app12199408>
21. Buchner, M., & Valada, A. (2022). 3D Multi-Object Tracking Using Graph Neural Networks with Cross-Edge Modality Attention. *IEEE Robotics and Automation Letters*, 7, 9707-9714.
22. Park Y, Dang LM, Lee S, Han D, Moon H. Multiple Object Tracking in Deep Learning Approaches: A Survey. *Electronics.* 2021; 10(19):2406. <https://doi.org/10.3390/electronics10192406>
23. He, Jiawei & Huang, Zehao & Wang, Naiyan & Zhang, Zhaoxiang. (2021). Learnable Graph Matching: Incorporating Graph Partitioning with Deep Feature Learning for Multiple Object Tracking. 5295-5305. 10.1109/CVPR46437.2021.00526.
24. Hu, H.; Hachiuma, R.; Saito, H.; Takatsume, Y.; Kajita, H. Multi-Camera Multi-Person Tracking and Re-Identification in an Operating Room. *J. Imaging* 2022, 8, 219. <https://doi.org/10.3390/jimaging8080219>
25. Li J, Ding Y, Wei HL, and Zhang Y, Lin W. SimpleTrack: Rethinking and Improving the JDE Approach for Multi-Object Tracking. *Sensors (Basel).* 2022 Aug 5; 22(15):5863. doi: 10.3390/s22155863. PMID: 35957422; PMCID: PMC9371155.
26. Wang, Y.; Zhang, Z.; Zhang, N.; Zeng, D. Attention Modulated Multiple Object Tracking with Motion Enhancement and Dual Correlation. *Symmetry* 2021, 13, 266. <https://doi.org/10.3390/sym13020266>
27. Brasó, G., Cetintas, O. & Leal-Taixé, L. Multi-Object Tracking and Segmentation via Neural Message Passing. *Int J Comput Vis* 130, 3035–3053 (2022). <https://doi.org/10.1007/s11263-022-01678-6>
28. Multi-task Networks for Multiple Object Tracking. 10.1109/IWIS56333.2022.9920879.
29. Yang, Fan & Chang, Xin & Sakti, Sakriani & Wu, Yang & Nakamura, Satoshi. (2020). ReMOT: A model-agnostic refinement for multiple object tracking. *Image and Vision Computing.* 106. 104091. 10.1016/j.imavis.2020.104091.
30. Vo, Xuan-Thuy & Tran, Tien-Dat & Nguyen, Duy-Linh & Jo, Kang-Hyun. (2022). A Study on Efficient Multi-task Networks for Multiple Object Tracking. 10.1109/IWIS56333.2022.9920879.



**Pranita S Chaudhary and Sharda Chhabria**

31. R. Sundararaman, C. De Almeida Braga, E. Marchand, and J. Pettre, "Tracking pedestrian heads in dense crowd," in Proceedings of the IEEE/CVF Conference on Computer Vision and Pattern Recognition, pp. 3865–3875, 2021.
32. J. Wu, J. Cao, L. Song, Y. Wang, M. Yang, and J. Yuan, "Track to detect and segment: An online multi-object tracker," in Proceedings of the IEEE/CVF conference on computer vision and pattern recognition, pp. 12352–12361, 2021.
33. Y. Zhang, C. Wang, X. Wang, W. Zeng, and W. Liu, "Fairmot: On the fairness of detection and re-identification in multiple object tracking," International Journal of Computer Vision, vol. 129, no. 11, pp. 3069–3087, 2021.
34. J. Wan, H. Zhang, J. Zhang, Y. Ding, Y. Yang, Y. Li, and X. Li, "Dsrtracker: Dynamic search region refinement for attention-based siamese multi-object tracking," arXiv preprint arXiv:2203.10729, 2022.
35. Vo, Xuan-Thuy & Tran, Tien-Dat & Nguyen, Duy-Linh & Jo, Kang-Hyun. (2022). A Study on Efficient Multi-task Networks for Multiple Object Tracking. 10.1109/IWIS56333.2022.9920879.
36. Xie, Qiaokang & Lu, Zhenbo & Zhou, Wengang & Li, Houqiang. (2022). Improving Person Re-Identification with Multi-Cue Similarity Embedding and Propagation. IEEE Transactions on Multimedia. PP. 1-13. 10.1109/TMM.2022.3207949.
37. L. Ke, X. Li, M. Danelljan, Y.-W. Tai, C.-K. Tang, and F. Yu, "Prototypical cross-attention networks for multiple object tracking and segmentation," Advances in Neural Information Processing Systems, vol. 34, 2021.
38. Neupane, Bipul & Horanont, Teerayut & Aryal, Jagannath. (2022). Real-Time Vehicle Classification and Tracking Using a Transfer Learning-Improved Deep Learning Network. Sensors. 22. 3813. 10.3390/s22103813.
39. W. Qin, H. Du, X. Zhang, Z. Ma, X. Ren, and T. Luo, "Joint prediction and association for deep feature multiple object tracking," in Journal of Physics: Conference Series, vol. 2026, p. 012021, IOP Publishing, 2021.
40. Zhang, Zhaoxiang & Wang, Chenghang & Song, Jianing & Xu, Yuelei. (2022). Object Tracking Based on Satellite Videos: A Literature Review. Remote Sensing. 14. 3674. 10.3390/rs14153674.
41. Khan, Sardar Waqar & Hafeez, Qasim & Irfan Khalid, Muhammad & Alroobaea, Roobaea & Hussain, Saddam & Iqbal, Jawaid & Almotiri, Jasem & Ullah, Syed Sajid. (2022). Anomaly Detection in Traffic Surveillance Videos Using Deep Learning. Sensors. 22. 6563. 10.3390/s22176563.
42. S. Han, P. Huang, H. Wang, E. Yu, D. Liu, and X. Pan, "Mat: Motionaware multi-object tracking," Neurocomputing, 2022
43. Kim, Sangwon & Lee, Jimi & Ko, Byoungchul. (2022). SSL-MOT: self-supervised learning based multi-object tracking. Applied Intelligence. 1-11. 10.1007/s10489-022-03473-9
44. Tan, Ke & Xu, Ting-Bing & Wei, Zhenzhong. (2022). IMSiam: IoU-aware Matching-adaptive Siamese network for object tracking. Neurocomputing. 492. 10.1016/j.neucom.2022.04.003.
45. He, Yuhang & Yu, Wentao & Han, Jie & Wei, Xing & Hong, Xiaopeng & Gong, Yihong. (2021). Know Your Surroundings: Panoramic Multi-Object Tracking by Multimodality Collaboration.
46. Nguyen, Duy M. H. et al. "LMGP: Lifted Multicut Meets Geometry Projections for Multi-Camera Multi-Object Tracking." 2022 IEEE/CVF Conference on Computer Vision and Pattern Recognition (CVPR) (2022): 8856-8865.
47. E. Yu, Z. Li, and S. Han, "Towards discriminative representation: Multiview trajectory contrastive learning for online multi-object tracking," arXiv preprint arXiv: 2203.14208, 2022.
48. D. M. Nguyen, R. Henschel, B. Rosenhahn, D. Sonntag, and P. Swoboda, "Lmgp: Lifted multicut meets geometry projections for multicamera multi-object tracking," in Proceedings of the IEEE/CVF Conference on Computer Vision and Pattern Recognition, pp. 8866–8875, 2022.
49. Vera, Jesús & Redondo Cabrera, Beatriz & Molina Romero, Rubén & Dalton, Kristine & Rodríguez, Raimundo. (2022). Relationship between dynamic visual acuity and multiple object tracking performance. Perception. 51. 10.1177/03010066221104281.
50. Sharan, Lalith & Kelm, Halvar & Romano, Gabriele & Karck, Matthias & Simone, Raffaele & Engelhardt, Sandy. (2022). mvHOTA: A multi-view higher order tracking accuracy metric to measure spatial and temporal associations in multi-point detection. 10.48550/arXiv.2206.09372





Pranita S Chaudhary and Sharda Chhabria

Table I .Overview of Relevant Studies to Transformers

Reference	Year	Extraction of Detection/Apparent Element	Data Association	Dataset	MOTA (%)
[7]	2022	interpreter for the DETR	transformer interpreter	MOT17, MOT20	63.5,63.6
[4]	2022	CNN	Transformers translator	MOT17	51.5
[8]	2022	CNN	Transformer	MOT16, MOT17	62.3, 63.6
[9]	2022	Faster R-CNN	Hungarian Algorithm	MOT16, MOT17, MOT20	64.8. 63.6, 61.6
[10]	2022	CNN + Converter interpreter	interpreter + Feed Forwarding System	MOT15, MOT16, MOT17	30.5, 54.7, 54.0
[2]	2022	DETR	Deformable Dual Decoder	MOT17, MOT20	60.8, 51.2
[12]	2022	Transformer Pyramid System	Multiple heads and focus sharing	UAV123	74.81 (Precision)
[13]	2022	CenterNet	Monitoring transmitter	TAO, MOT17	34.8 (HOTA), 64.4
[14]	2022	DETR	Modules for Decoding as well as Queries Handling + System for temporal accumulation	MOT17, Dance Track, BDD100k	46.4 (HOTA), 43.5 (HOTA), 21.0 (nMOTA)
[15]	2022	Encoding Bounding Box	Reversal System	MOT16	54.3

Table II Overview of Publication Relevant to Directed Graph

Reference	Year	Detection	Association	Dataset	MOTA (%)
[17]	2020	ResNet50	Text Transfer	MOT15, MOT16, MOT17	30.6, 37.7, 37.8
[21]	2022	ResNet-34	Hungarian formula	MOT16, MOT17	26.6, 31.1
[19]	2022	SeResNet-50	People-Interaction Framework	MOT15, MOT16, DukeMTMCT	61.3, 31.1, 65.6
[20]	2022	Center Nat, Comp ACT	Box and Tracklet Motion Embedding	MOT17, KITTI, UA-Detrac	35.1, 66.5, 21.4
[21]	2022	ResNet-34	Hungarian algorithm	MOT16, MOT17	46.6, 31.1
[22]	2021	ResNet50-IBN	Creation and Rating of Proposals	MOT17, MOT20	38.1, 45.2
[23]	2021	CenterNet	Model Pairing	MOT16, MOT17	44.1, 45.1
[18]	2022	Center Point, MEGVII	Text Transfer	nuScenes	54.3





Pranita S Chaudhary and Sharda Chhabria

Table III. Overview of Publications Associated with Attention

Reference	Year	Attention Mechanism	Dataset	MOTA (%)
[28]	2021	Strip Pooling	MOT15, MOT16, MOT17, MOT20	62.8, 75.8, 72.8, 61.8
[35]	2022	Probabilistic Conscious Focus Concentration as well as Diversion Focus	MOT16, MOT17, MOT20	58.2, 68.6, 47.8
[36]	2022	STN	MOT16, MOT17	50.5, 50.0
[37]	2021	Spatial-Temporal Cross-Attention	BDD100K (Validation), KITTI-MOTS (Validation)	27.4 (MOTSA), 66.4 (mMOTSA)
[38]	2022	Identification through self-awareness	Custom Dataset: Sparse Scene, Dense Scene	70.9, 56.4

Table IV. Overview of Publications Tied with Tracking Algorithm

Reference	Year	Motion Mechanism	Dataset	MOTA (%)
[26]	2021	Differences Objects' separation from the expected as well as realized states	MOT17, KITTI	47.8, 86.13
[29]	2020	Long short - term memory Algorithm over Sequential Blocks	MOT16, MOT17	76.3, 76.4
[39]	2021	Kalman Filtering	MOT17	44.3
[40]	2022	Estimated Multi-Frame Differencing as well as Low-Rank Matrix Fulfilment	VISO	73.7
[41]	2022	The Gaussian Local Velocity Model's Mean Vector and the Radius of Moving Component	NJDOT	100 (Anomaly Detection Accuracy)
[20]	2022	Box and Track let Motion Embedding	MOT17, KITTI, UA-Detrac	56.0, 87.6, 22.5
[31]	2021	Enhancing Coefficient Of determination and Particle Scanning	CroHD	64.7
[42]	2022	Vehicular as well as webcam movement combined (IML), DRC	MOT16, MOT17	71.6, 79.6
[8]	2022	Kalman Filtering	MOT16, MOT17	64.3, 64.7





Pranita S Chaudhary and Sharda Chhabria

Table V Overview of Papers Associated to the Siamese Network

Reference	Year	Method	Dataset	MOTA (%)
[12]	2022	LSTM as well as RNN for modeling movement, CNN for obtaining appearances	Duke-MTMCT, MOT16	74.6, 66.1
[43]	20212	Movement modelling using implicit and explicit methods	MOT17, TAO-person, HiEve	76.8, 55.4 (TAP@0.5), 53.2
[44]	2022	Siamese System including Neural Network Layer	MOT16, MOT17, MOT20	65.8, 67.2, 62.3
[11]	2022	concentrate on a specific occurrence	Tracking Net	70.55 (Precision)
[34]	2022	interactive area refinement as well as focus-based tracking	MOT17, MOT20	67.2, 70.4

Table VI Summary of Papers Related to the Tracklet Association

Reference	Year	Method	Dataset	MOTA (%)
[45]	2020	Resolving unclear short track lets utilising track let-plane comparison procedure	MOT16, MOT17	50.9, 52.4
[48]	2021	Monitoring graphs from Centre Track [78], DG-Net [79], and GAEC+KLj [80] Raised multicity solver heuristic solver	WILDTRACK, PETS-09, Campus	97.1, 74.2, 77.5



Fig. 1. (a) A diagram showing how components are occluded (green and blue). Components were separated from one another in display 1. A portion of them is obscured in display 2. They are completely obscured on display 3.

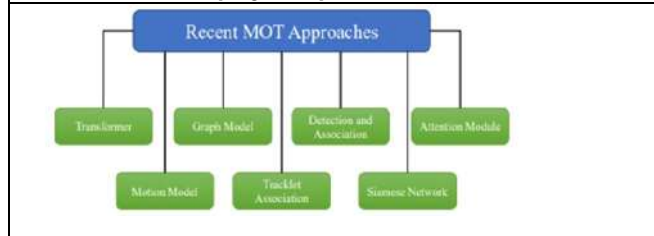


Fig. 2. Recent MOT approaches categorization

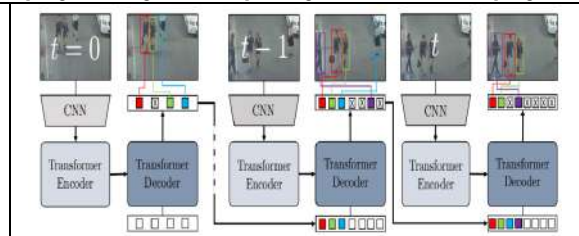


Fig. 3. Track Former [4] performs combined detection and attention-tracking while using the transformer's design to enable encoding and decoding to transform monitoring several objects into a set estimation issue.





Pranita S Chaudhary and Sharda Chhabria

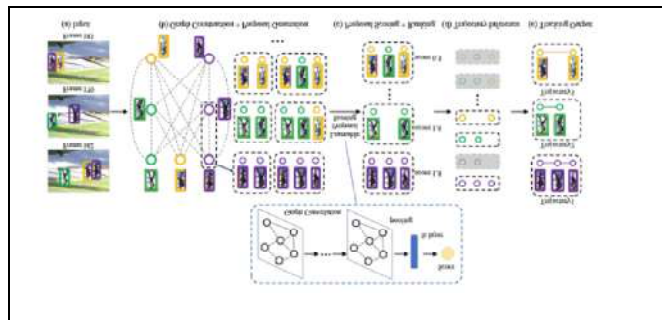


Fig. 4. (a) Images in which things can be found (b) A graph that was created using the tracklets or observed objects as each node and proposal generation. (c) Using GCN to rank the suggestions The trajectory inference is (d). (e) The result [22]

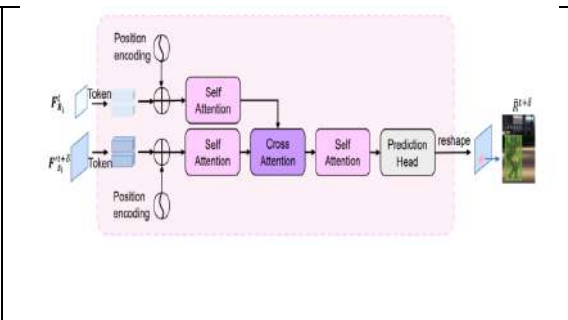


Fig. 5. The cross-attention based attentional structure [34]

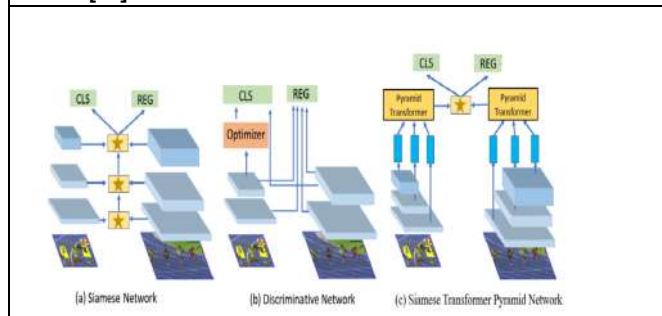


Fig. 6. (Three examples of typical networks include (a) symmetric pyramid-shaped Siamese networks, (b) discriminative networks, and (c) the establishment of the Siamese transfers multilevel system [12].

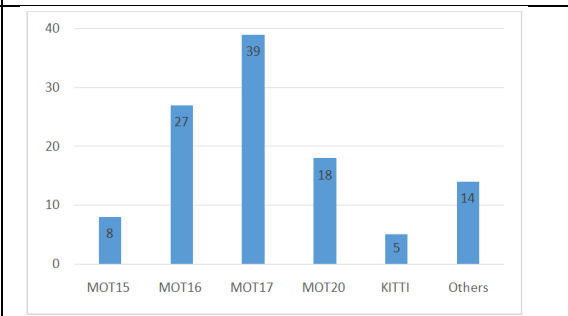


Figure 7. Average amount of publications associated to every datasets



Birth place – Nagpur, BirthDate – 17/01/1985.
 MTech – Computer Science & Engineering, Prof. Rama Reddy Institute of Technology, JNTU, Hyderabad, 2014& BE – Computer Engineering – 2007, KDK college of Engineering, Nagpur.
 Research Scholar in GHRIU, Amravati.
 Ms. Pranita Chaudhary, Research Scholar, GHRIU, Amaravati,





Quantum Machine Learning for Breast Cancer Detection: A Comparative Study with Conventional Machine Learning Methods

Varsha Premanand^{1*}, Snavya Sai M B¹, Sindhu Srinivas¹ and Satyanarayana Reddy²

¹Student, Computer Science and Engineering Department, Dayananda Sagar University, Hosur Rd, Kudlu Gate, Srinivasa Nagar, Hal Layout, Singasandra, Bengaluru, Karnataka 560068, India.

²Associate Professor, Computer Science and Engineering Department, RV University, RV Vidhyaniketan 8th mile Mysore Road Bangalore 560059, Karnataka, India.

Received: 17 Feb 2023

Revised: 25 Apr 2023

Accepted: 31 May 2023

*Address for Correspondence

Varsha Premanand

Student,
Computer Science and Engineering Department,
Dayananda Sagar University,
Hosur Rd, Kudlu Gate, Srinivasa Nagar,
Hal Layout, Singasandra, Bengaluru,
Karnataka 560068, India.
E.Mail: varshapremanand13@gmail.com



This is an Open Access Journal / article distributed under the terms of the **Creative Commons Attribution License** (CC BY-NC-ND 3.0) which permits unrestricted use, distribution, and reproduction in any medium, provided the original work is properly cited. All rights reserved.

ABSTRACT

Breast cancer is a common disease that requires early detection in order to be treated effectively. Using the Wisconsin Breast Cancer dataset, this study compares the performance of conventional machine learning algorithms and quantum machine learning algorithms for breast cancer detection. The results show that the support vector classifier (SVC) achieved 97.3% accuracy in 0.008 seconds, while the quantum support vector classifier (QSVC) achieved 93.8% accuracy in 893.55 seconds. Although current hardware limitations may limit the quantum advantage, better results can be expected in the future as quantum hardware advances. These results imply that quantum machine learning has the ability to increase breast cancer diagnosis accuracy. Overall, this study demonstrates the utility of quantum machine learning in medical fields such as breast cancer detection.

Keywords: SVC(Support Vector Classifier), QSVC (Quantum Support Vector Classifier), VQC (Variational Quantum Circuit), BC (Breast Cancer), QML (Quantum Machine Learning).



**Varsha Premanand et al.,**

INTRODUCTION

Breast cancer is a major global health concern and early detection plays a critical role in effective treatment. Machine learning has shown considerable improvement in the accuracy and efficiency of breast cancer diagnosis. While conventional algorithms have yielded encouraging results, the advent of quantum computing has opened up new avenues for even greater precision and efficiency. Using quantum computing techniques, quantum machine learning has the potential to substantially improve data processing and analysis. This technology has the potential to transform many fields of study, including medical diagnosis. Considering quantum computing hardware is still in its early stages, it may be some time before it is widely available. The efficacy of conventional and QML approaches for BC diagnosis is compared in this study. The study aims to recognise the strengths and limitations of each approach and produce valuable insights into the potential of quantum machine learning for improving breast cancer diagnosis by analyzing the available datasets. This study has the potential to significantly contribute to ongoing efforts to improve breast cancer detection and ultimately, save lives

Related Work

ML and DL methodologies are being utilized for breast cancer detection to develop efficient strategies for early diagnosis and prediction of this prevalent and possibly fatal disease. Tiwari et al. (2020) used the Wisconsin Breast Cancer Dataset to predict breast cancer in their study. Before building the models, they used pre-processing approaches such as data exploration, Label Encoder, and Normalizer procedures. The dataset was split into training and testing sets, and multiple machine learning techniques, including SVM and Random Forest models, were tested, with an accuracy of 96%. In addition, the authors utilized CNN and ANN models, which achieved an accuracy of 97% and 99%, respectively.

Zheng Shan and colleagues have shown the efficacy of QSVM approaches for BC diagnosis in a research. Their research makes use of quantum simulators and IBM quantum processors, as well as classical models built using the scikit-learn toolkit. The authors evaluated the quantum simulator and IBM quantum processor Quito on the same dataset and compared their performance to a traditional QSVC method. Their investigations demonstrate that the quantum simulator has an accuracy rate of 94% with an error rate of 0.1, which may be increased to 98% with a noise reduction method. The initial accuracy of the IBM Quito quantum computer is 95%. The standard QSVC method, on the other hand, has an accuracy of 85%. This work conclusively supports the effectiveness of quantum support vector machine algorithms, opening up new avenues for quantum applications. The authors also propose that implementing noise reduction measures can increase the resilience of quantum solutions in a noisy environment. Their findings show that quantum approaches on NISQ devices can beat standard ML approaches with a few tweaks.

In another study [13], the authors showed cancer detection using quantum neural networks. They used the Breast Cancer Wisconsin (Diagnostic) dataset and a quantum neural network (QNN) for the classification of cancer cells as malignant or benign. Their results show that QNNs are capable of outperforming CNN in terms of accuracy and require significantly less computational time. Finally, in a study [14], the authors suggested a quantum-classical hybrid machine learning approach for image classification. They utilised the MNIST dataset and experimented with different quantum feature maps and kernels in conjunction with a classical support vector machine. Their results show that their hybrid approach outperforms classical machine learning methods in terms of accuracy while utilising fewer resources. In conclusion, the aforementioned studies demonstrate the effectiveness of ML and QML techniques in breast cancer identification and prediction, and highlight the potential of quantum computing for enhancing traditional machine learning methods.



**Varsha Premanand et al.,****Dataset**

The University of Wisconsin Hospitals collected the Wisconsin BC dataset in the late 1980s and early 1990s. The dataset includes information on 569 breast tissue samples collected from patients who underwent breast cancer surgery at the hospital during that time period. The tissue samples were examined under a microscope by experienced pathologists, who made diagnoses based on their visual observations of the samples. Follow-up observations over time confirmed the diagnosis of each sample. The dataset includes information on the size, shape, texture, and other characteristics of the breast tissue samples, which were extracted from digitised images of the tissue [11]. The dataset was then made publicly available for research purposes, subject to approval by the University of Wisconsin-Institutional Madison's Review Board (IRB). The IRB is in charge of ensuring that human subjects research is conducted in accordance with ethical principles and federal regulations. In this study, conventional ML and QML algorithms are compared utilising the Wisconsin Breast Cancer dataset. This dataset is being used to compare the performance of support vector classifiers (SVC) and quantum support vector classifiers (QSVC) for breast cancer detection. The medical committee approved the use of the Wisconsin Breast Cancer dataset while maintaining patient confidentiality and ethical standards, and it is widely used in machine learning research for developing and evaluating breast cancer detection models.

Machine Learning

Machine learning is a way for machines to learn from data and make decisions without being taught exactly what to do. Machine learning's objective is to enable computers to learn and develop from experience in the same manner that people do. It entails analysing data using statistical techniques and algorithms, identifying patterns, and making predictions or decisions based on those patterns. Image and speech recognition, NLP, medical diagnosis, and financial forecasting are just a few of the many applications of machine learning. Six different ML classification algorithms were worked on for the analysis, and their respective performance metrics were compared. Following that, SVC was compared to its quantum counterpart, QSVC, and the results were deduced.

Quantum Computing

QC is a form of computing that manipulates data using quantum-mechanical concepts such as superposition and entanglement. In place of binary digits, it uses quantum bits (qubits), which can be in several states at the same time. Quantum computing can solve certain computational problems much faster than conventional computers, especially those involving large amounts of data or complex mathematical operations. This has the potential to bring about significant advancements in various fields such as cryptography, materials science, drug discovery, and ML.

Quantum Machine Learning

QML is an emerging area of research that aims to enhance machine learning algorithms by leveraging the principles of quantum mechanics. This field seeks to develop novel techniques and algorithms that can utilise the unique features of quantum computing, like superposition and entanglement, to enhance the efficiency and accuracy of ML models. This field has the potential to solve complex machine learning and artificial intelligence problems that are beyond the capabilities of conventional computing. Quantum machine learning makes use of a variety of concepts, including quantum state preparation, quantum gates and circuits, quantum measurements, quantum feature maps, quantum kernels, and quantum algorithms like QSVC. These ideas are used to manipulate qubits in order to perform machine learning tasks like classification, regression, and clustering.

Superposition, entanglement, and quantum gates are concepts that play a key role in quantum machine learning. Superposition enables quantum systems to exist in two states at the same time, and it is used to represent input data in a quantum state. Entanglement is used to represent the correlations between different input data points in a quantum feature space and allows for the sharing of quantum information. Quantum gates are fundamental building blocks in quantum computing used to perform operations on quantum data. There are various kinds of quantum gates, including the Hadamard gate, Pauli gates, phase gates, and controlled-NOT (CNOT) gate. These gates perform operations on input data that is in a quantum state. For example, the Hadamard gate is used to put a qubit into a superposed state, while the Pauli gates are used for rotations and flipping of qubits. The phase gates modify the



**Varsha Premanand et al.,**

phase of a qubit, and the CNOT gate is used for entangling two qubits. These gates are essential for developing quantum algorithms and for performing quantum computations.

METHODOLOGY

The methodology used in this research study involved the training and testing of six ML classification algorithms on the Wisconsin BC Dataset. The first step was to access the dataset in csv format and preprocess it with techniques like data cleaning and feature scaling. The dataset was then split into train and test sets. The training set was then used to build ML models like SVC, which were then compiled and evaluated using a set of performance metrics like accuracy, precision and time. To determine the best-performing model, the accuracies of the various models were compared. During the preprocessing stage of data, several techniques are employed to ensure that the data is appropriately prepared for analysis. Two such techniques are Label Encoder and Normalisation. Label Encoder is a useful method for converting categorical features into numeric values, enabling efficient analysis of categorical data. The Normalizer method rescales attribute values to fit within the range of 0 to 1, ensuring uniformity and comparability of data. Additionally, missing or null data points are identified and handled during this stage to ensure the accuracy and completeness of the data.

The models performance is assessed using three different sizes of training and testing sets. The training set sizes are 75%, 80%, and 70%, respectively, while the testing set sizes are 25%, 20%, and 30%. The accuracy scores of the models are used to compare them. To detect the type of cancer, the models are trained on the train set and tested on the test set.

The Wisconsin Breast Cancer dataset is used in the VQC (Variational Quantum Circuit) process for breast cancer detection. The dataset is first investigated and preprocessed in order to remove any missing or corrupted data, normalize the features, and balance the classes. Dimensionality reduction is performed using PCA. The ZZ Feature Map is then used to convert the conventional input data into a quantum state representation with linear entanglement. A variational circuit, made up of controlled x-gates and rotational y-gates, is used to learn the parameters of the quantum model. The SPSA (Simultaneous Perturbation Stochastic Approximation) optimizer is used to further optimize the parameters of the circuit. The feature map and variational circuit are combined to form the VQC model. Finally, the performance of the VQC model is assessed by comparing the quantum circuit output to the ground truth labels, and metrics like accuracy and time are used to assess the model's performance. The model is run using 4 qubits on the IBM simulator. This methodology, in general, provides a structured approach to developing and evaluating VQC models for breast cancer detection

QSVC methodology entails using a quantum instance and feature map, followed by the creation of a quantum kernel. The quantum kernel is used to build a kernel matrix, which represents the similarity of data points in the quantum feature space. After that, the data is presented to QSVC for classification. Finally, the classification result is determined by comparing the predicted labels to the true labels. The quantum instance and feature map convert the conventional input data into a quantum state representation, which is then used to construct a quantum kernel. The inner product of the corresponding quantum states is used by the quantum kernel to calculate the similarity between data points. These similarity measures are then used to build the kernel matrix. This kernel matrix is used to train QSVC to learn the mapping from the quantum feature space to the labels. The classification result is obtained by comparing the predicted labels to the true labels. This methodology uses QSVC to provide a methodical and rigorous approach to classification. The kernel of QSVC is tested in two ways: as a precomputed matrix or as a callable method. Both approaches' accuracies and times are measured. The study makes use of IBM's Qiskit software, which includes an emulator for simulating quantum circuits on standard hardware. Users can use the Qiskit software to access IBM's quantum processors and a quantum simulator. The quantum circuits are tested and validated using the Qiskit simulator on a simulated quantum device. This allows for controlled testing of QSVC's performance before scaling up to larger datasets and possibly using real quantum hardware.





Varsha Premanand *et al.*,

PCA (Principal Component Analysis) is a data dimensionality reduction technique used in both conventional and quantum computing. In the quantum section, PCA is used to reduce the number of input features of the dataset to a smaller set of principal components that can be processed effectively by quantum algorithms. By reducing computational complexity and increasing result accuracy, PCA improves the performance of quantum machine learning models.

SVC VS QSVC

In SVC data has been mapped into a higher-dimensional space separated by a hyperplane in a conventional SVC. The SVC algorithm then determines the hyperplane with the greatest margin between the two classes. QSVC performs classification tasks using quantum computing principles. Instead of mapping data to a high-dimensional space, QSVC performs classification using a quantum kernel function. The primary distinction between conventional SVC and QSVC is the computational architecture. While conventional SVC works with conventional bits, quantum SVC works with quantum bits (qubits). This enables QSVC to take advantage of quantum parallelism and potentially outperform conventional SVC for certain types of problems.

A. Equations

Conventional Machine Learning

$$\text{Accuracy} = (TP + TN) / (TP + TN + FP + FN)$$

$$\text{Precision} = TP / (TP + FP)$$

Quantum Machine Learning

$$\text{Accuracy} = (TP + TN) / (TP + TN + FP + FN)$$

Where

TP = no. of true positives,

TN = no. of true negatives,

FP = no. of false positives, and

FN = no. of false negatives

RESULTS

The study compares the accuracies of six ML algorithms. Further compares the accuracy and time performance of the conventional ML algorithm, SVC, to the QML algorithm, QSVC. Based on the findings, Table I.1 shows a comparison of six ML algorithms for BC detection. Table I.2 shows the highest accuracy achieved by each algorithm for different data splits. When the data is split into 75-25 train and test sets, Random Forest achieves the highest accuracy of 98.6%. SVC, on the other hand, has the highest accuracy for different data splits, with 97.3% accuracy for an 80-20 split and 97.1% accuracy for a 70-30 split. Table II.2 shows the highest accuracy achieved by SVC with different kernel types for a 80-20 data split. Table III. shows that the quantum machine learning algorithms, QSVC and VQC, achieve lower accuracy, with QSVC achieving 93.8% accuracy and VQC achieving 81% accuracy for an 80-20 data split. The study utilized three different data splits to compare machine learning algorithms for breast cancer detection. The results were shown in three separate figures (Figure 4-6), one for each data split, displaying the accuracy, precision, and time required for each algorithm. Furthermore, the study compared SVC and QSVC performance using various kernel types and methods, with the results presented in the two figures (Fig. 7.1-7.2). The study also compared VQC and QSVC performance, with the results presented in two figures (Fig. 7.2-8.1).



**Varsha Premanand et al.,****Interpretation**

Breast cancer detection was evaluated using both conventional ML algorithms and QC models, and the performance was evaluated using the Wisconsin BC dataset with an 80-20 dataset split. For the conventional machine learning algorithms, all 30 features were used, whereas for the quantum computing models, only four features were used and mapped onto four qubits. The SVC algorithm achieved the highest accuracy of 97.3%, followed by polynomial and linear kernels with 97% and 96% accuracy, respectively. The sigmoid kernel performed the worst, achieving only 64% accuracy. The QSVC achieved an accuracy of 93.8% using both precomputed kernel matrix and kernel as a callable method, but with a long computation time of 896 seconds and 894 seconds, respectively. In a relatively long computation time of 635 seconds, the VQC method achieved an accuracy of 81%. The SVC algorithm with RBF or polynomial kernels performed the best among the models tested, according to the results, while quantum methods had lower accuracy but showed promising potential.

CONCLUSION

More advanced and accurate breast cancer detection methods may be attainable with continued research and development in the field of QC. The research found that the accuracy of quantum machine learning was comparable to that of conventional ML, highlighting the potential of QC in solving complex problems in medical diagnosis, such as cancer detection. The demonstrated quantum advantage in the study, owing to quantum algorithms' ability to leverage quantum parallelism and quantum supremacy, paves the way for further research into quantum machine learning in the field of medical diagnosis. Furthermore, the application of quantum computing in cancer detection is a promising one in the healthcare industry. On the Wisconsin Breast Cancer dataset, quantum machine learning methods were shown to achieve accuracy levels that are similar to conventional machine learning methods, demonstrating the potential of QC in resolving complex problems in the field of medical diagnosis. This could spur more research in this area, potentially leading to the development of more accurate and efficient cancer diagnostic tools. The use of quantum computing in medical applications could lead to better patient outcomes and a better understanding of complex diseases like cancer in the long run.

ACKNOWLEDGMENT

We would like to express our sincere gratitude to C.V Satyanarayana Reddy, Associate Professor from the School of Computer Science and Engineering at RV University for his guidance, mentorship, and support throughout the project. His valuable insights and expertise have been instrumental in the success of this research. We are grateful for his constant encouragement and motivation. We would like to thank Prof Veena M, Assistant Professor, Dept. of CSE, Dayananda Sagar University for her support. We would also like to thank Dr. Vidya M J, Assistant Professor from the School of Computer Science and Engineering at RV University, for her guidance and support in writing the paper. Her valuable suggestions and feedback have greatly contributed to the quality of the paper. We are grateful for her time and effort in helping us to present our findings in a clear and concise manner.

REFERENCES

1. Trang NTH, Long KQ, An PL, Dang TN. Development of an Artificial Intelligence-Based Breast Cancer Detection Model by Combining Mammograms and Medical Health Records. *Diagnostics (Basel)*. 2023 Jan 17;13(3):346. doi: 10.3390/diagnostics13030346. PMID: 36766450; PMCID: PMC9913958.
2. Botlagunta, M., Botlagunta, M.D., Myneni, M.B. *et al.* Classification and diagnostic prediction of breast cancer metastasis on clinical data using machine learning algorithms. *Sci Rep* 13, 485 (2023). <https://doi.org/10.1038/s41598-023-27548-w1>
3. Rahul Kumar Yadav, Pardeep Singh, Poonam Kashtriya, Diagnosis of Breast Cancer using Machine Learning Techniques -A Survey, *Procedia Computer Science*, Volume 218,2023,Pages 1434-1443,ISSN 1877-0509,<https://doi.org/10.1016/j.procs.2023.01.122>.





Varsha Premanand et al.,

Table 1. Machine Learning Algorithms

Detection Approach Used	Test Case			Algorithm Used	Accuracy (%)	Precision (%)	Time (sec)
	Case No.	Training size (%)	Testing size (%)				
Machine Learning	1	75	25	Logistic Regression	95.8	94.3	0.0139
				K-Nearest Neighbor	95.1	97.9	0.007
				Support Vector Classifier	95.8	94.3	0.007
				Gaussian Naive Bayes	91.6	88.7	0.003
				Decision Tree	95.1	91.1	0.007
				Random Forest	98.6	100	0.016
	2	80	20	Logistic Regression	96.4	95.7	0.013
				K-Nearest Neighbor	95.6	100	0.006
				Support Vector Classifier	97.3	97.8	0.008
				Gaussian Naive Bayes	91.2	87.8	0.003
				Decision Tree	92.1	89.6	0.008
				Random Forest	96.4	97.8	0.017
	3	70	30	Logistic Regression	96.5	95.2	0.01
				K-Nearest Neighbor	95.9	98.3	0.008
				Support Vector Classifier	97.1	96.8	0.008
			Gaussian Naive Bayes	91.2	86.4	0.003	
			Decision Tree	96.5	95.2	0.006	
			Random Forest	95.3	93.7	0.015	

Table 2. Highest Accuracy In Each Case

Case No.	Training set size (%)	Testing set size (%)	Algorithm with best accuracy	Accuracy (%)	Algorithm with best precision	Precision (%)
1	75	25	Random Forest	98.6	Random Forest	100
2	80	20	SVC	97.3	KNN	100
3	70	30	SVC	97.1	KNN	98.3

Table 3. SVC

Detection Approach Used	Test Case			Algorithm Used		Accuracy (%)	Time (sec)
	Case No.	Training size (%)	Testing size (%)		Kernel Type		
Machine Learning	1	80	20	SVC	rbf	97	0.045
					linear	96	
					poly	97	
					sigmoid	64	

Table 4. Highest Accuracy in SVC Kernel Types

Case No.	Training set size (%)	Testing set size (%)	Kernel Type with best accuracy	Accuracy (%)
1	80	20	rbf	97
			poly	97

Table 5. QSVC and VQC

Detection Approach Used	Test Case			Algorithm Used		Accuracy (%)	Time (sec)
	Case No.	Training size (%)	Testing size (%)		Method		
Quantum Computing	1	80	20	QSVC	Precomputing the kernel matrix	93.8	896.21
					Providing the kernel as a callable method	93.8	893.55
				VQC		81	635.25





Varsha Premanand et al.,

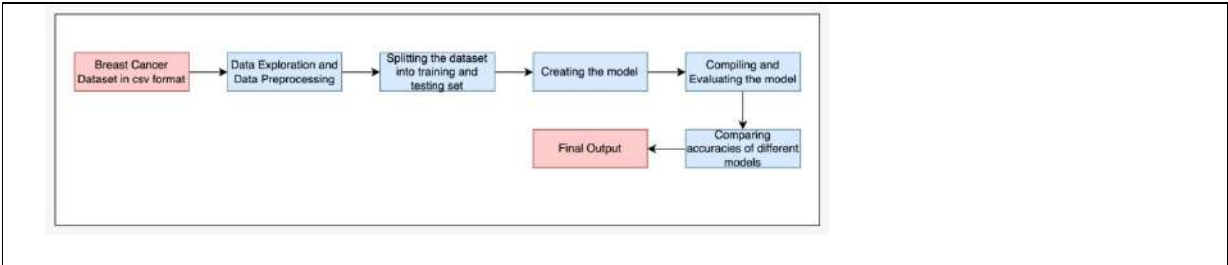


Fig.1. Block diagram illustrating the process of a machine learning algorithm

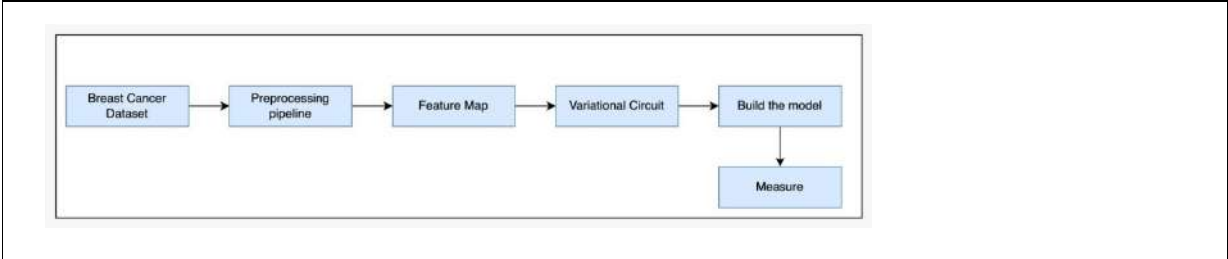


Fig. 2. Block diagram illustrating the process of VQC algorithm

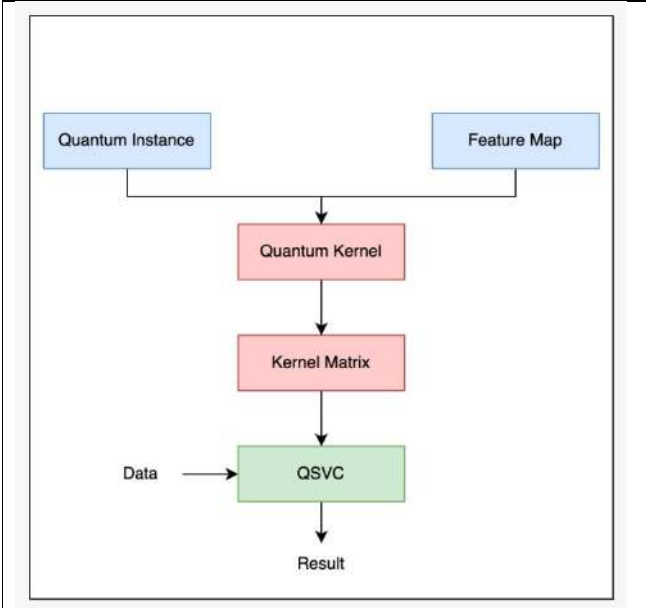


Fig. 3. Block diagram illustrating the process of QSVC algorithm

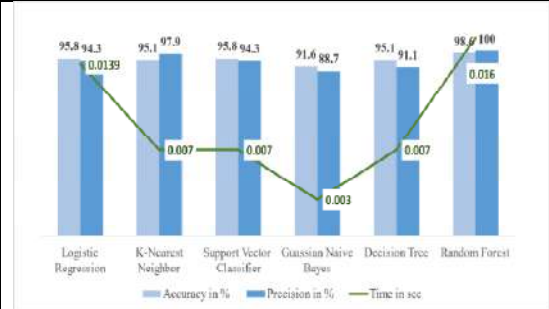


Fig. 4. Case 1 : Performance Metrics Comparison for ML Algorithms





Varsha Premanand et al.,

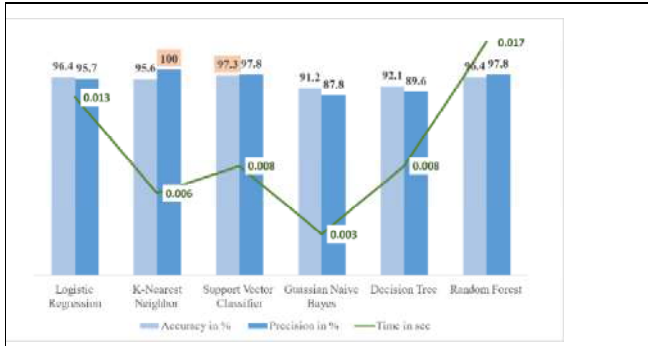


Fig. 3. Case 2 : Performance Metrics Comparison for ML Algorithms

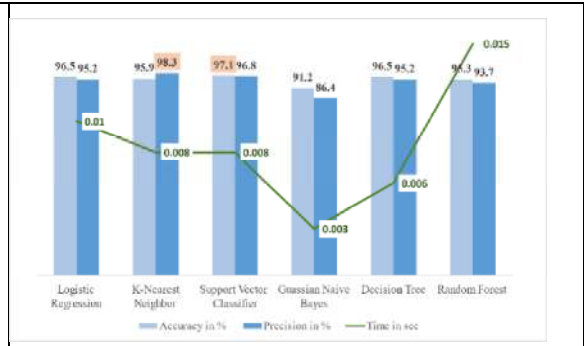


Fig. 4. Case 3 : Performance Metrics Comparison for ML Algorithms

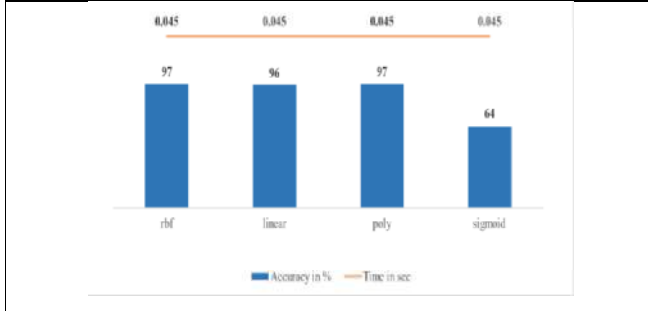


Fig. 5. Performance Metrics of SVC with Different Kernel Types

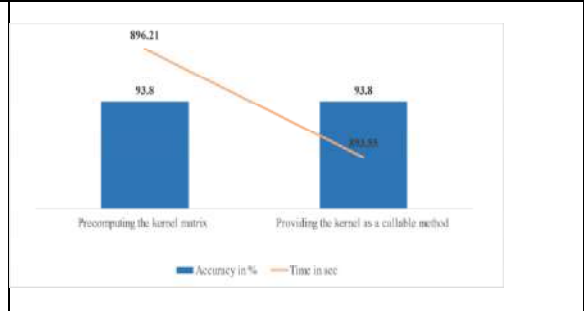


Fig. 6. Performance Metrics of Q SVC with Different Methods

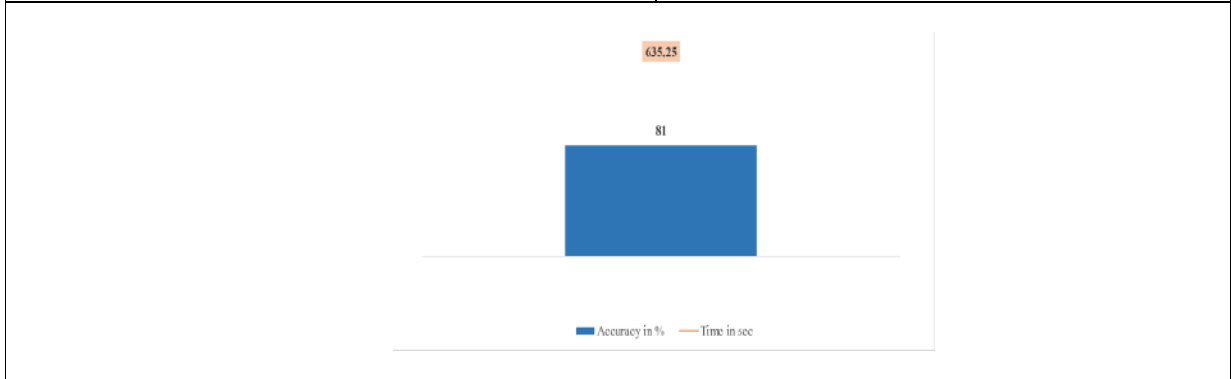


Fig. 7. Performance Metrics of VQC





Crop Yield Prediction using Data Mining Techniques

Jasmine R¹ and Usha Devi R²

¹Student, Nirmala College for Women, Red Fields, Coimbatore, Tamil Nadu, India

²Assistant Professor, Nirmala College for Women, Red Fields, Coimbatore, Tamil Nadu, India

Received: 27 Dec 2022

Revised: 23 Apr 2023

Accepted: 31 May 2023

*Address for Correspondence

Jasminer

Student,

Nirmala College for Women,

Red Fields, Coimbatore,

Tamil Nadu, India



This is an Open Access Journal / article distributed under the terms of the **Creative Commons Attribution License (CC BY-NC-ND 3.0)** which permits unrestricted use, distribution, and reproduction in any medium, provided the original work is properly cited. All rights reserved.

ABSTRACT

India is generally an agricultural country. Now a days the most important emerging field in the real world is agriculture and it is the main occupation and backbone of our country. Crop yield prediction is the methodology to predict the yield of the crops using different parameters like rainfall, temperature, fertilizers, pesticides and other atmospheric conditions and parameters. Data Mining techniques is very popular in the area of agriculture and the techniques are used and evaluated in agriculture for estimating the future years crop production. This paper presents a brief analysis of crop yield prediction using Linear Regression(LR), Factor Analysis(FA), Canonical Correlation(CC) and Principle Component Analysis(PCA). The models exploited for analysing the parameters influencing the Crop Yield. Rice, Maize and Gram are considered for analysis. LR, FA and CC models are used to identify the interactive effects of parameters considered (MSP, CPI, FPI, AR and AUC) on CY. PCA is used to analyse the impact of drought variables on CY. LR is used to obtain a prediction model for CY.

Keywords: Crop Yield(CY), Linear Regression(LR), Factor Analysis(FA), Canonical Correlation(CC), Principle Component Analysis(PCA), Drought Analysis

INTRODUCTION

India is an agricultural country where majority of the population is mainly involved in agriculture. India is proud to have plenty of natural wealth which includes fertile lands, forests, mountains and rivers. Rivers play an important role in cultivation of various crops namely paddy, wheat, maize, sugarcane, grams etc.,. Some of the rivers provide water throughout the year and some rivers provide water only during particular seasons. Annual Rainfall due to torrential rains also plays an important role in Indian agriculture. Climate changes due to global warming and other factors radically changes the seasonal rainfall and in-turn affects the Crop Yield.





Numerous agricultural applications and total workforce involvement are analysed using various pattern classification techniques like SVM, K-means [1]. It also deals about the need of analysing data in the field of agriculture using different models. To increase the yield of crops, potential and prospective cropping areas are identified using Relative Spread Index(RSI) and Relative Yield Index(RYI) [2].

LITERATURE REVIEW

Priyanga Muruganatham, Santoso Wibowo, Srimannarayana Gandhi[3], this paper has presented a systematic literature review on the application of deep learning approaches for crop yield prediction using remote sensing data. The rationale of conducting this systematic literature review was to highlight the existing research gaps in a particular area of deep learning methodologies and provide useful information on the impact of vegetation indices and environmental factors on crop yield prediction. This systematic literature review has provided various deep learning approaches, features, and factors adopted for crop yield prediction. All the studies were carried out on different types of crops, geological positions, and various features. R. Dhanunjaya Rao [4], the proposed model is constructed by using AI algorithms to reduce the farmers' problems of getting losses in their farms due to lack of knowledge of cultivation in different soil and weather conditions. The model is created by using machine learning (SVM) and deep learning (LSTM, RNN) techniques. The model predicts best crops that should be grown on land with less expenses among a number of crops available after analyzing the prediction parameters.

Benny Antony[5], this paper aims to help the farmers in improving their farming practices by using scientific, statistical, and data science methodologies. Each crop had a specific optimum algorithm based on the least Mean Absolute Error. Rice for Tamil Nadu and rice in Punjab had two different algorithms. Mean Absolute Error was taken as the statistical evaluator for the models. This work can be further extended to all the crops grown in India and done for all the states in India. Dhruvi Gosai, Chintal Raval, Rikin Nayak, Hardik Jayswal, Axat Patel [6], in this paper, they have effectively proposed and implemented an intelligent crop recommendation system, which can be easily used by farmers all over India. This system would help the farmers in making an informed decision about which crop to grow depending on some parameters like Nitrogen, Phosphorous, Pottasium, PH Value, Humidity, Temperature, and Rainfall. By using this research we can increase productivity of the country and produce profit out of such a technique.

D. Jayanarayana Reddy, M.Rudra Kumar [7], this research work discussed about the variety of features that are mainly dependent on the data availability and each of the research will investigated Crop Yield Prediction(CYP) using Machine Learning(ML) algorithms that differed from the features. The features were chosen based upon the geological position, scale, and crop features and these choices were mainly dependent upon the data-set availability, but the more features usage was not always giving better results. Therefore, finding the fewer best performing features were tested that also have been utilized for the studies. Most of the existing models utilized Neural networks, random forests, KNN regression techniques for CYP and a variety of ML techniques were also used for best prediction. From the studies most of the common algorithms used were CNN, LSTM, DNN algorithms but still improvement was still required further in CYP. The present research shows several existing models that consider elements such as temperature, weather condition, performing models for the effective crop yield prediction. Ultimately, the experimental study showed the combination of ML with the agricultural domain field for improving the advancement in crop prediction.

Fathima, Sowmya. K, Sunita Barker, Dr. Sanjeev Kulkarni [8], this work demonstrated the potential use of data mining techniques in predicting the crop yield based on the input parameters average rainfall and area of field. The developed webpage is user friendly and the accuracy of predictions are above 90 percent. The districts selected in the study indicating higher accuracy of prediction. The user friendly web page developed for predicting crop yield can be used by any user by providing average rainfall and area of that place. The process was adopted for all the area to improve and authenticate the validity of yield prediction which are useful for the



**Jasminer et al.,**

farmers for the prediction of a specific crop. Sangeeta, ShruthiG[9], This project is undertaken using machine learning and evaluates the performance by using Random forest, Polynomial Regression and Decision Tree algorithms. In our proposed model among all the three algorithm Random forest gives the better yield prediction as compared to other algorithms. Along with random forest, Polynomial Regression, Decision Tree model classify the output that shows improvements in dataset. So we analyzed that proposed model has got more efficiency than the existing model for finding crop yield.

S.Adamala, N.S.Raghuwansho, A.Mishra and R.Singh[10], enumerated the various difficulties encountered in gathering and dealing with 'Enormous Data' whose meaning changes from one territory to other. Huge information may be unstructured are huge, quick, hard and comes in from numerous structures. For water administrators/ engineers, vast information indicates enormous guarantee in many water related applications, for example, arranging ideal water frameworks, distinguishing biological community changes through huge remote detecting and topographical data framework, anticipating/ foreseeing/ recognizing characteristic and artificial cataclysms, booking water systems, moderating ecological contamination, contemplating environmental change impacts and so on. This investigation explored the many fundamental data and its applications in water as sets designing related examinations, favourable circumstances and burdens.

B.Devika, B.Ananthi[11], in this work the regression approach were tested in their yield prediction capabilities. The readings were used for model inputs. Linear regression algorithms offered acceptable estimation accuracy, though higher prognostic power could also be obtained by parameters like year, crop, area, production (in tons) and alternative variables, like climate, agricultural practices and soil characteristics are including within the model development. The model using linear regression can be suggested for Ecuadorian conditions. In yield prognostic models are not existent for any crop. From this proposed system the yield of crop (sugarcane, cotton, and turmeric) are predicted in highest level. This model may be reformulated using alternative crop assessments within the future, to develop methods for increasing yield and land territorial management in alternative crops of importance, like wheat, rice. D.Ramesh, B.Vishnu Vardhan[12], This paper presents a brief analysis of crop yield prediction using Multiple Linear Regression (MLR) technique and Density based clustering technique for the selected region i.e. East Godavari district of Andhra Pradesh in India. Initially the statistical model Multiple Linear Regression technique is applied on existing data. The results so obtained were verified and analyzed using the Data Mining technique namely Density-based clustering technique. In this procedure the results of two methods were compared according to the specific region i.e. East Godavari district of Andhra Pradesh in India. Similar process was adopted for all the districts of Andhra Pradesh to improve and authenticate the validity of yield prediction which are useful for the farmers of Andhra Pradesh for the prediction of a specific crop. In the subsequent work a comparison of the crop yield prediction can be made with the entire set of existing available data and will be dedicated to suitable approaches for improving the efficiency of the proposed technique.

METHODOLOGY

Rice, Maize and Gram crop data are analysed using Linear Regression(LR), Factor Analysis(FA) and Canonical Correlation(CC). These methods are used to identify the relationship among the independent parameters considered and their influence on Crop Yield(CY).

Linear Regression

Linear Regression (LR) helps to analyse and establish interrelationship between dependent variable and independent variables. MSP, CPI, FPI, AUC and AR are the explanatory variables considered and the response variable Crop Yield.





Factor Analysis

Factor Analysis (FA) helps to determine the common variance among the explanatory variables considered which influences the Crop Yield. The patterns in a data set and the relationships among them are identified and interpreted using Factor Analysis Angie Yong and Sean Pearce [13]. The explanatory variables considered are MSP, CPI, FPI, AR and AUC and the response variable is Crop Yield. The explanatory variables are condensed to factors in Factor analysis.

Factor Analysis

Canonical Correlation

Canonical Correlation (CC) is a multivariate technique where it groups the variables into independent and dependent variate sets. The foremost difference between Canonical Correlation analysis and Multiple Discriminant analysis is that CC can handle many dependent variables whereas the latter can accommodate only one. Canonical Correlation (CC) is a statistical multivariate technique that facilitates sketching of a linear relationship between the two set of variates. Balkaya et al. [14] used CC to establish a relationship between a set of plant characters and another set of yield components. A set of plant characters are considered as independent variable set and Yield components as dependent variable set and CC is used to ascertain the interrelationship.

Canonical Correlation is applied when there exist a response variable or a set of response variables and to identify the interrelationship with the explanatory variables considered. The objective is to group the variables into independent variable set and dependent variable set as in Fig. 3.3. The interrelationship among the variables considered can be portrayed by observing the variations in variable of one set influences the variables in another set.

Principal Component Analysis

Principal Component

Analysis (PCA) helps to identify influence of independent variables and their extent of influence on Crop Yield (CY). Rice, Maize and Gram are the crops considered in the study areas namely Arjunanadhi sub-basin and Kousiganadhi sub-basin. The Principal components define its variance over the parameters considered. The independent variables considered here are Agricultural Drought, Hydrological Drought, Meteorological Drought and the dependent variable is the Crop Yield.

EXPERIMENTAL RESULTS

Result of Linear Regression

Linear Regression portrayed that AR, MSP and CPI having R^2 value greater than 0.8 depicting that these factors are highly influential on Crop Yield of Rice. The R^2 value of AUC by LR is found to be 0.78 for Rice and shows it is an important parameter which affects the Crop Yield (CY). The R^2 value of FPI for Rice is found to be 0.39 which shows that the variable is less significant and is less influential on CY of Rice. Similarly, the CY analysis of Maize is given: The R^2 values of AUC, MSP and CPI are found to be greater than 0.9 and shows that these factors are highly significant in affecting the CY. The R^2 value of AR is found to be -0.2 which shows that AR is the least significant parameter in influencing the CY. Since Maize is not a Rain-fed crop and it matches with the results obtained. The CY analysis for Gram is given: The R^2 value of AUC is found to be 0.84 and indicates that it is an important parameter in affecting the CY. This holds well in actual practice also, as AUC increases under optimum conditions the CY also is found to increase. The R^2 values of MSP, CPI and FPI are found to be greater than 0.6 and indicates that they are also significant parameters in affecting the CY but not to that extent of AUC.

Result of Factor Analysis

Factor Analysis (FA) identifies common variance for the explanatory variables MSP, CPI, FPI, AR and AUC and defines its influence on the dependent variable CY for the crops Rice, Maize and Gram. The effect of MSP, CPI, FPI,





AR and AUC on the Crop Yield (CY) of Rice, Maize and Gram are analysed using Factor Analysis (FA) and their significance is indicated using specific variance. The specific variances of the second loading for AR, AUC and MSP are found to be greater than 0.8 for the crop Rice and indicate that these variables are highly significant in affecting the CY. The Specific variances of the second loading for CPI and FPI are found to be 0.4 and 0.1 respectively for the Rice crop and are the least significant parameters affecting CY. The specific variances of the second loading for MSP, CPI and AUC are found to be greater than 0.8 for the crop Maize and indicate that these variables are highly significant in affecting the CY. The Specific variances of the second loading for AR and FPI are found to be around 0.2 for the Maize crop and are the least significant parameters affecting CY. The fact that Maize require very little water for its cultivation and the same matches with the results.

The specific variance of the second loading for AUC is found to be 0.8 for the crop Gram and indicate that AUC is highly significant in affecting the CY. The Specific variances of the second loading for MSP and CPI are found to be greater than 0.7 for the Gram crop and are significant parameters in affecting the CY. The Specific variances of the second loading for AR and FPI are found to be 0.1920 and 0.3050 for the Maize crop and are the least significant parameters affecting CY out of which AR is found to be least significant. Gram is not a Rain-fed crop and the same matches with the results.

Result of Canonical Correlation

Canonical Correlation (CC) finds a weighted average of the set of independent variables and correlates it with the weighted average of the set of dependent variables. The canonical coefficient depicts the significance of relationship between the dependent and independent variable sets. Thus, the influence of independent variables to the dependent variable CY is established based on each crop. The correlation coefficients between AR, MSP and AUC from the independent variable set to CY of Rice are found to be around 0.8, which is closer to perfect positive correlation. This shows that all these parameters from independent set are significant in influencing the CY. The correlation coefficient between AUC and CY is 0.780 which shows that AUC is a significant parameter influencing CY. The correlation coefficient between FPI and CY is found to be 0.387 shows that FPI is the least significant parameter. The correlation coefficients of the variables in independent set AUC, MSP to CY are 0.801, 0.810 respectively depicting that these independent set variables influences the CY of Maize significantly. The canonical coefficient for AR in the independent set is -0.049, states that Maize is not a rain-fed crop. Similarly, the dependent variable CPI is influenced by variables of independent set MSP and AUC and its correlation coefficient are 0.953 and 0.618 respectively depicting its interrelationship. Hence AUC and MSP are the major influential parameters influencing the CY. The correlation coefficients of the variables in independent set AUC, MSP to CY are 0.839 and 0.670 respectively depicting that these independent set variables are significant in influencing the CY of Gram. The canonical coefficients of CPI and FPI to CY are found to be 0.633 and 0.681 respectively and since they are also in dependent set this depicts the interrelationship with CY of Gram. The canonical coefficient for AR in the independent set is 0.113, states that AR is less influential. Since the correlation coefficient value of AR to CY of Maize and Gram is very less, this proves the fact that both the crops need very less water for its cultivation and results also proves the same.

Result of Drought Analysis

Drought is characterized as any irregular dry period on a particular area due to lack of water in-terms of rainfall or surface water or ground water. Analysis of drought is carried out in Arjunanadhi and Kousiganadhi sub-basins of Vaippar basin. The effect of Meteorological, Hydrological and agricultural drought on Crop Yield of Rice, Maize of Gram is analysed using Principal Component Analysis. In Arjunanadhi and Kousiganadhi sub-basins, the correlation matrix shows that the correlation between all 3 drought variables and CY are found to be in negative values (less than 0) showing that they are negatively correlated with the CY of Rice. In both the sub-basins, the correlation value of Meteorological drought is around -0.8 proving that if there is a deficient in rainfall the CY of Rice decreases. In other words, The CY of Rice is mainly affected by Meteorological Drought. In Arjunanadhi and Kousiganadhi sub-basins, the correlation value of Hydrological drought to CY is found to be around 0.5 proving its significance in influencing the CY of Maize. The correlation values of Meteorological



**Jasminer et al.,**

drought and Agricultural drought on CY are found to have minimal influence on CY of Maize with correlated value of less than 0.5. This clearly indicates that Hydrological drought is a significant parameter in influencing the CY of Maize. For Arjunanadhi and Kousiganadhi sub-basins, the correlation matrix shows the correlation value of Hydrological drought and Agricultural drought on CY are found to be around 0.6 and are equally significant in influencing the CY of Gram. The correlation value of Meteorological Drought to CY is found to be around 0.7, proving that Gram does not need much water for cultivation. The fact that Gram does not need much water for cultivation and the results also proves the same.

Forecasting of Crop Yield (CY)

Based on these analyses the relationship among the independent parameters and the dependent parameter (CY) helps to forecast the CY using the agricultural and economic parameters considered. Agriculture is one of the riskiest occupations because the factors influencing are uncertain at many stages. Hence it is important to foresee the output i.e. the Crop Yield. Linear Regression is used to analyse and predict the CY of Rice, Maize and Gram.

Rice

Since the Crop Yield is a function of the variables MSP, CPI, FPI, AR and AUC. The results of Linear Regression are presented in Fig.5.1. From the Fig. 5.1, the data points are plotted to illustrate the closeness of the values obtained from the results analysed. Since, the data coordinates are more crowded near the linear curve it is therefore adequate to state that the predicted values and the actual values are almost the same. On scrutinizing the findings from the graphs and the factor equation, it is clear that predicted Crop Yield and the real Crop Yield are almost similar tone another and also proves that the factors considered for the research are appropriate. On evaluating the model fit, the R^2 value obtained is 0.974. This indicates that the model has the potential to explain 97.4% of variations pertinent to the training dataset.

Maize

Similarly for Maize, Linear Regression is applied to predict the CY of Maize On evaluating the model fit, the R^2 value obtained is 0.956. This indicates that the model has the potential to explain 95.6% of variations pertinent to the training dataset.

Gram

Similarly for Gram, Linear Regression is applied to predict the CY of Gram On evaluating the model fit, the R^2 value obtained is 0.906. This indicates that the model has the potential to explain 90.6% of variations pertinent to the training dataset.

CONCLUSION

Crop Yield model is forecasted using LR and the R^2 value is found to be around 0.9 for all the 3 crops rice, maize and gram. Similarly CY model using the drought variables is created for both Arjunanadhi and Kousiganadhi Sub-basins which clearly shows that the model is best suited to be used in the field of agriculture.

REFERENCES

1. A.Mucherino, PetroqPapajorgji, P.M.Pardalos, 2009, "A Survey of data mining techniques applied to agriculture", Operational Research 9, 121-140.
2. S.Kokilavani, V.Geethalakshmi, 2013, "Identification of Efficient Cropping Zne for Rice, Maize, Groundnut in Tamil Nadu", Indian Journal of Science and Technology, Volume 6(10).



**Jasminer et al.,**

3. Priyanga Muruganatham, Santoso Wibowo, Srimannarayana Gandhi, 2022, "A Systematic Literature Review on Crop Yield Prediction with Deep Learning and Remote Sensing" Artificial Intelligence and Automation in Sustainable Smart Farming.
4. R. Dhanunjaya Rao, 2022, " A Hybrid Approach of Artificial Neural Network to Estimate the Paddy Yield Prediction", Vol-12, Issue-12 No.03.
5. Benny Antony, 2021, "Prediction of the production of crops with respect to rainfall" Environmental Research , Vol-202.
6. Dhruvi Gosai, Chintal Raval, Rikin Nayak, Hardik Jayswal, Axat Patel, 2021, International Journal of Scientific Research in Computer Science, Engineering and Information Technology, Volume 7, Issue 3.
7. D. Jayanarayana Reddy, M.Rudra Kumar, 2021, "Crop Yield Prediction using Machine Learning Algorithm", Proceedings of the Fifth International Conference on Intelligent Computing and Control Systems (ICICCS).
8. Fathima, Sowmya. K, Sunita Barker, Dr. Sanjeev Kulkarni, 2020, " Analysis of Crop Yield Prediction using Data Mining Technique". In International Research Journal of Engineering and Technology(IRJET), Volume 07, Issue 05.
9. Sangeeta, Shruthi G, 2020 "Design and Implementation of Crop Yield Prediction Model in Agriculture", International Journal of Scientific and Technology Research, Volume 8, Issue 01.
10. S.Adamala, N.S.Raghuwansho, A.Mishra and R.Singh, 2019, "Generalized wavelet neural networks for evapotranspiration modeling in india", ISH Journal of Hydraulic Engineering, Volume 25, Issue 2.
11. B.Devika, B.Ananthi, 2018, "Analysis f Crop yield Prediction using Data Mining Technique to predict Annual Yield of major crops", International Research Journal of Engineering and Technology(IRJET), Volume 05, Issue 12.
12. D.Ramesh, B.Vishnu Vardhan, 2015, "Analysis of Crop Yield Prediction using Data Mining Techniques", International Journal of Research in Engineering and Technology(IJRET), Volume 04, Issue 01.
13. Angie Yong, Sean Pearce, 2013, "A Beginner's Guide to Factor Analysis: Focusing on Exploratory Factor Analysis", Tutorials in Quantitative Methods for Psychology, Volume 19(2), Page no. 79-94.
14. A.Balkaya, S.Cankaya, M.Ozbakir, 2011, "Use Of Canonical Correlation Analysis For Determination Of Relationships Between Plant Characters And Yield Components In Winter Squash (Cucurbita Maxima Duch.) Populations" Bulgarian Journal of Agricultural Science, 17 (No 5).
15. Bazrafshan, J., Hejabi, S. and Rahimi, J., 2014. "Drought monitoring using the multivariate standardized precipitation index (MSPI)", Water Resources Management, 28(4), Page no.1045-1060.
16. Wong G, Van Lanen, H.A.J. and Torfs, P.J.J.F., 2013, "Probabilistic analysis of hydrological drought characteristics using meteorological drought". Hydrological Sciences Journal, 58(2), Page no 253-270.
17. Suman Kumar Padhee, Bhaskar Ramachandra Nikam, Subashia Dutta, Shiv Prasad Aggarwal, 2017, "Using satellite-based soil moisture to detect and monitor spatiotemporal traces of agricultural drought over Bundelkhand region of India", Volume 54, Issue 2.
18. Deepak Sharma, Dr. Deepshikha Aggarwal, 2022, "A Review on Decision making On Agriculture Data Mining Technique", Jagannath University Research Journal(JURJ).
19. G.Rubia, Dr. Nandhini, "Prediction Of Soil Accuracy Using Data Mining Techniques", INFOCOMP Journal of Computer Science, 2021.
20. Arto Klami, Seppo Virtanen, Samuel Kaski, 2013, Bayesian canonical correlation analysis". Journal of Machine Learning Research, 14, Page no 965-1003.





Jasminer et al.,

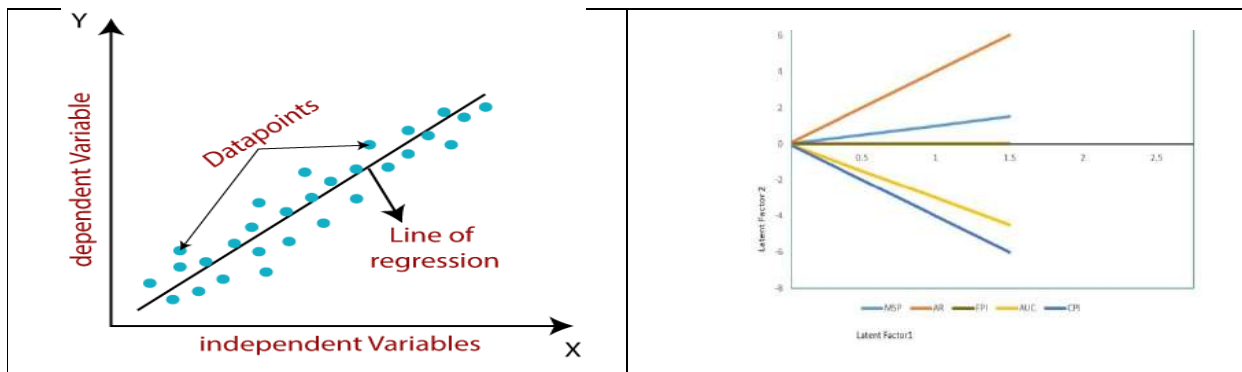


Fig. 1. Simple Linear Regression

Fig 2. Factor Analysis

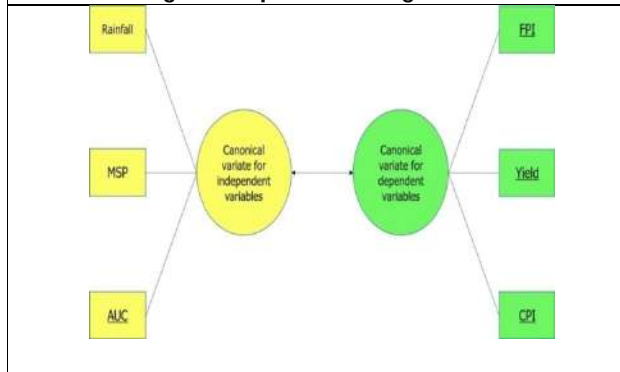


Fig. 3. Canonical Correlation

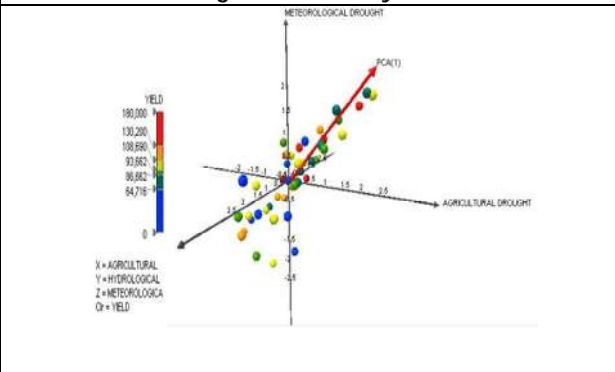


Fig. 4. Scatter Plot

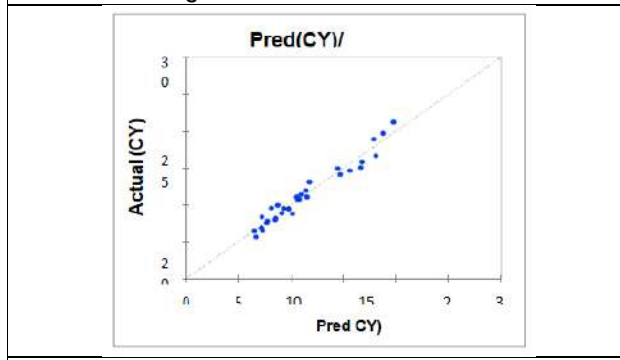


Fig. 5. Parityplot-Rice

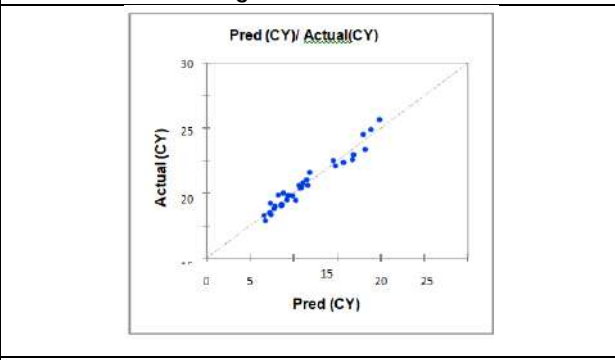


Fig. 6. Parity plot –Maize

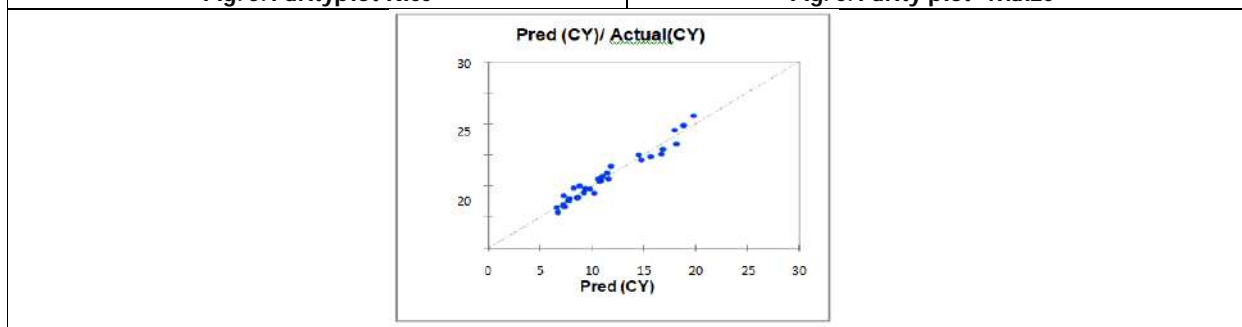


Figure 5.3 Parity plot–Gram





On Similarity Solution of (3+1)-Dimensional Jimbo-Miwa Equations Arising in Fluids

Raj Kumar*

Department of Mathematics, Faculty of Engineering and Technology, V. B. S. Purvanchal University, Jaunpur–222003, India

Received: 06 Apr 2023

Revised: 15 May 2023

Accepted: 31 May 2023

*Address for Correspondence

Raj Kumar

Department of Mathematics,
Faculty of Engineering and Technology,
V. B. S. Purvanchal University,
Jaunpur–222003, India.
E.Mail: rsoniraj2@gmail.com



This is an Open Access Journal / article distributed under the terms of the **Creative Commons Attribution License** (CC BY-NC-ND 3.0) which permits unrestricted use, distribution, and reproduction in any medium, provided the original work is properly cited. All rights reserved.

ABSTRACT

A system of (3+1)-Jimbo-Miwa equations is solved analytically exploiting the similarity transformations method via classical Lie-group theory. Geochemistry, fluid mechanics, ocean and atmospheric science, optical fiber, astrophysics, and solid-state physics are all applications of the system. The solution is physically explained by making an appropriate choice of the arbitrary function involved in the solution. The mathematical form of a soliton solution produced in this study differs from the solutions found in previous studies [1-5]. This research has the potential to solve Jimbo-Miwa equations in a more general approach, if achievable, by incorporating more arbitrary functions occurring in infinitesimal transformations.

Keywords: Nonlinear evolution equations, Jimbo-Miwa equations, Single soliton, Similarity reduction, Lie-group theory.

INTRODUCTION

nonlinear evolution equations (NEEs) are a set of equations that describe complicated nonlinear physical events in the world around us, such as fluid dynamics, optics, chemical physics, plasma physics, financial mathematics, ocean science, engineering, and some others [1-35]. Exact approaches to address NEEs have been painstakingly investigated. The researchers were taken aback by the surprising physical behaviour exhibited by exact solutions to such a type of NEE. It is essential to visualize the responses provided by the NEEs, whether through animation or a pictorial representation, to resolve these challenges. A sufficient literature [1-5] covers certain reliable methods/tools, historical context, and various sorts of solutions focusing on the suggested work of this project, which takes the form of (3+1) coupled-Jimbo-Miwa equations (JME) determined by





Raj Kumar

$$\rho_{xxxx}+6\rho_x\rho_y+3\rho h_{xx}+3\rho_{xx}h+3\rho_{yt}-3\rho_{zz}=0, \text{ and } \rho_y=h_x, \quad (1)$$

where the horizontal (ρ) and vertical (h) components of velocity are functions of the spatial variables x , y , and z , as well as the temporal variable t . Subscripts represent the partial derivatives of ρ and h with respect to the variables mentioned. This system (1) represents nonlinear (3+1)-dimensional waves that arise in geochemistry, fluid mechanics, optical fiber, astrophysics, plasma physics, chemical kinematics, and solid state physics [1-5]. Unfortunately, this system fails several conventional integrability criteria [3]. Some traveling wave solutions of (1) are achieved by the modified simple equation method [4]. The functional variable method [5] is used to construct multiple arbitrary analytic functions that are exact solutions of JMEs (1). Zhang et al. [6] considered the following nonintegrable form of the (3+1)-dimensional JME

$$\rho_{xxxx}+3\rho_y\rho_{xx}+3\rho_x\rho_{xy}+2\rho_{yt}-3\rho_{xz}=0, \quad (2)$$

and explicit forms of rational and semi rational solutions, line breathers of JME (2), have been derived by the bilinear transformation. The JME (2) was first introduced by Jimbo and Miwa, and it arises from the second order of the Kadomtsev-Petviashvili hierarchy. Furthermore, semi-rational solutions, solitons, breathers, lump solutions, and rogue waves were discovered, which exhibit a variety of interesting and sophisticated dynamic behaviors [6]. Rogue waves, first created to describe transient, massive ocean waves with extraordinary amplitudes that arrive out of nowhere and depart without a trace, have been blamed for various marine tragedies. Rogue waves have been detected in geophysics and hydrodynamics, Bose-Einstein condensation and plasma physics, nonlinear optics, and financial markets in recent years. Rogue waves are a type of rational solution that is localized in both space and time. Peregrine discovered the first-order or fundamental rogue waves of the nonlinear Schrödinger equations in 1983.

Wang et al. [7] investigate bilinear representation to depict a type of bright-dark lump, one stripe wave, and the rogue wave for JME (2). Wazwaz [8] utilised the tanh-coth method to JME (2) and derived single solitons. After getting the exact solutions using the generalized bilinear approach, the lump, general, and high-order lump solutions, as well as their interactions, were observed [9]. By putting $\rho=2\delta \log \tau \delta x$, $x_1=x$, $x_2=y$, $x_3=t$, $x_4=z$ in $[(D_{13}+2D_3)D_2-3D_1D_4] \tau, \tau=0$ in KP-hierarchy [10,11], the JM Eq. (2) can be derived. Here τ is a function treated in KP-hierarchy. For JME (2), Gupta and Singh [12] employed binary Bell polynomials, Bäcklund transformations, and derived multisolitons. The JME (2) model is extended to the "4-2-3" model, and a bilinear form is established using a single hidden layer neural network model. Rogue waves and bright and dark solitons [13] are analytical solutions to the problem. Following extended form of JME were discussed by Wazwaz (3) describing all findings of [14-21]

$$(\rho_{xy}+3\rho_y\rho_x)_x+2\rho_{yt}-3(\rho_x+\rho_y+\rho_z)_z=0, \quad (3)$$

$$\text{and } (\rho_{xy}+3\rho_y\rho_x)_x-3\rho_{xz}+2(\rho_x+\rho_y+\rho_z)_z=0, \quad (4)$$

in which the last two terms of Eq. (2) were extended to $\rho_{xz} + \rho_{yz} + \rho_{zz}$ and $\rho_{xt} + \rho_{yt} + \rho_{zt}$ respectively. M-order lumps were achieved by Guo et al. [2] using the Hirota's bilinear approach and the long-wave limit method. In this context, they [2] derived the orbit, velocity, and extremum of propagation of 1-order lump solutions on a 2-dimensional space. In addition to the extended homoclinic test method, they find solutions for the JM Eqs. (3)-(4) that include breather-kinks, rational breathers, and rogue waves. Qi et al. [14] established the solitary-wave solutions and examined the dynamical properties and energy distributions of the Hirota's technique solutions to the extended JMEs (3)-(4). Wazwaz [3] investigated Eqs. (3)-(4) once more, this time using the simplified Hirota's approach to generate several soliton solutions of different physical structures for each extended equation. He has demonstrated that the extended equations' dispersion relations and phase shifts.

Kaur and Wazwaz [16] constructed bilinear forms via Painlevé expansion along with Bell polynomials to the JM Eqs. (3)-(4). They derived soliton physical structures and proved that the systems are C- integrable. Li and Li [17] employed the complex method and attained rational, exponential and elliptic function type solutions to JM Eqs. (3)-





Raj Kumar

(4). Xu et al. [18] examined the resonance behavior of a multi-exponential wave solution to same couple of JM Eqs., as well as the application of the linear superposition principle to the Hirota bilinear equation. Liu [19] derived a rich range of rogue wave type solutions, soliton, using the Hirota bilinear form of the JME (4). Sun and Chen [20] discovered the bilinear forms of the JME (2)-(4) to obtain lump and lump-kink solutions. It is imperative to discuss that Yang [21] et al. solved following potential form of JME by employing Hirota's method

$$p_{xxx}y + 6p_x p_y + 3p p_{xy} + 3p_{xx} \partial_x^{-1} p_y + 2p_{yt} - 3p_{xz} = 0, \tag{5}$$

and they obtained rational, quasi-periodic, and N-soliton type solutions. They stated that their solutions can be used in meteorological science to understand the squall lines occurrence and explain possible rainstorm development mechanisms. No one has used the similarity transformations method (STM) via Lie-group approach to obtain exact solutions to the JME (1) in any of the reviews [1-6]. This study helps to reveal a new class of solutions. A physical justification is also given for the findings. In each similarity reduction, an equivalent system of PDEs can be obtained to get a lesser number of independent variables. Such reduction continues until a system of ODEs cannot be obtained. The method is a strong tool to derive an analytical solution to a system of NEEs. The method is used on some selected (3+1)-coupled systems since such complex systems cannot be easily solved to get their analytical systems. The basic concept behind the method is invariance, according to which the system remains unaltered after using similarity transformations.

This article is organized as follows: The next section provides some background on STM and the analytical solutions derived to JME (1), while Section 3 focuses on the analysis and discussion of the obtained results. The final section provides a summary and an outlook on where this study can go from here.

Similarity solutions

This section explores similarity solutions of the system (1). To discuss in brief for the method, one can assume one-parameter Lie-group of transformations as discussed in some texts books [27-28] and some research articles [29-35]. Such transformations include infinitesimals as

$$I^{(x)}(N) = a_1 x + F(t), I^{(y)}(N) = (2a_2 - 3a_1)y + a_3 z + a_4, I^{(z)}(N) = 2a_3 t + a_2 z + a_5, \\ I^{(t)}(N) = 3a_1 t + a_6, I^{(p)}(N) = -2a_1 + \bar{F}(t), I^{(h)}(N) = -2(a_1 - a_2)h, \tag{6}$$

where a notation N=x,y,z,t,p,h is used for collection of all independent and dependent variables, Iv is an infinitesimal for a variable v taken any one from x,y,z,t,p, or h. ai's are arbitrary constants and Ft is an arbitrary function which come into existence during integration process of over determining system of partial differential equations (PDEs) in Iv's. The values of infinitesimals can be calculated by using symbolic calculations in Maple or Mathematica. To get the first equivalent system of PDEs for system (1), we must solve Lagrange's system

$$\frac{dx}{a_1 x + F(t)} = \frac{dy}{(2a_2 - 3a_1)y + a_3 z + a_4} = \frac{dz}{2a_3 t + a_2 z + a_5} = \frac{dt}{3a_1 t + a_6} = \frac{dp}{-2a_1 u + \bar{F}_1} = \frac{dh}{2(a_2 - a_1)h} \tag{7}$$

Without any loss of generality, let $a_1 \neq a_2 \neq 0, a_3 = 0$ and $\frac{a_2}{a_1} = A, \frac{a_4}{a_1} = C, \frac{a_5}{a_1} = D, \frac{a_6}{a_1} = E$ and introducing in Eq. (7), it recasts as

$$\frac{dx}{x + F(x)} = \frac{dy}{(2A - 3)y + C} = \frac{dz}{Az + aD} = \frac{dt}{3t + E} = \frac{dp}{-2p + \bar{F}_1} = \frac{dh}{\frac{2}{3}(A - 1)h} \tag{8}$$

After solving, similarity forms are





Raj Kumar

$$X = \frac{x}{(3t+E)^{\frac{1}{3}}} - \int \frac{F(t)}{(3t+E)^{\frac{1}{3}}} dt, Y = \frac{y+\frac{C}{2A-3}}{(3t+E)^{\frac{2}{3}A-1}}, Z = \frac{(z+\frac{D}{A})}{(3t+E)^{\frac{1}{3}}}, \text{ and}$$

$$p = \frac{F}{3t+E} + \frac{1}{(3t+1)^{\frac{2}{3}}} \int \frac{F}{(3t+1)^{\frac{4}{3}}} dt + \frac{P(X,Y,Z)}{(3t+1)^{\frac{2}{3}}}, h = \frac{H(X,Y,Z)}{(3t+E)^{\frac{2}{3}(A-1)}} \quad (9)$$

Making use of the values of p and h in the system (1), one can get first similarity reduction as
 $P_{XXX}Y + 6P_X P_Y + 3PH_{XX} + 3HP_{XX} - (2A - 1)P_Y - XP_{XY}(2A - 3)YP_{YY} - 3AZP_{YZ} - 3P_{ZZ} = 0$, and $P_Y = H_X$. (10)

For the second reduction, infinitesimals of Eq. (10) are
 $I^{(X)}(N_1) = b_1, I^{(Y)}(N_1) = 2b_2Y, I^{(Z)}(N_1) = b_2Z, I^{(P)}(N_1) = b_1, I^{(H)}(N_1) = -2b_2H$, (11)

where $(N_1) \equiv (X, Y, Z, P, H)$, b_i 's are arbitrary constants.
 To get similarity form of second reduction, we have to solve further
 $\frac{dX}{b_1} = \frac{dY}{2b_2Y} = \frac{dZ}{b_2Z} = \frac{dP}{b_1} = \frac{dH}{-2b_2H}$,

which on solving gives similarity forms for $b_2 \neq 0$
 $X_1 = X - \frac{b}{2} \log Y, X_2 = \frac{Z^2}{Y}, P = X + F(X_1, X_2)$, and $H = \frac{G(X_1, X_2)}{Y}, b = \frac{b_1}{b_2}$. (12)

Inserting the values of P and H in the system (10), one can obtain second similarity reduction as

$$\frac{b}{2} F_{X_1 X_1 X_1 X_1} + X_2 F_{X_1 X_1 X_1 X_2} + 3b F_{X_1}^2 - 6X_2 F_{X_1} F_{X_2} + 3F G_{X_1 X_1} - 3G F_{X_1 X_1} + \frac{3}{4} b^2 (2A - 3) F_{X_1 X_1} + 3b(A - 3) X_2 F_{X_1 X_2} - 3X_2 (3X_2 - 4) F_{X_2 X_2} - 3(3X_2 - 2) F_{X_2} = 0, \text{ and}$$

$$\frac{b}{2} F_{X_1} + X_2 F_{X_2} + G_{X_1} = 0.$$

To get further similarity reduction, Lagrange's characteristic equations are

$$\frac{dX_1}{1} = \frac{dX_2}{0} = \frac{dF}{0} = \frac{dG}{0}, \quad (15)$$

which on simplification gives forms of F and G as $F(X_2)$ and $G(X_2)$. Assuming $F = K$ and $G = -\alpha K$ then solution of then solution of system (1) is

$$h = \frac{-\alpha K}{Y(3t+E)^{\frac{2}{3}(A-1)}}, p = \frac{F}{3t+E} + \frac{1}{(3t+1)^{\frac{2}{3}}} \int \frac{F}{(3t+1)^{\frac{4}{3}}} dt + \frac{X+K}{(3t+1)^{\frac{2}{3}}}, \quad (16)$$

where X and Y are expressed in Eq. (9)

The analytical solution of JM Eq. (1) is represented by Eq. (16). For the physical interpretation of the solution, the appropriate choice of $F(t)$ and arbitrary constants have been taken as $a_1=1.8147, a_2=0.9058, a_4=1.0563, a_5=0.9163$, and $a_6=0.6324$, which exist in the expressions of p and h . To get profiles of the solution, simulation is performed by MATLAB. The nature of profiles is single soliton with elastic behavior of amplitudes. The function $F(t)$ is the governing function to decide the nature of the horizontal component of the wave profiles, which have importance in ocean and atmospheric science. Soliton peaks grow larger over longer periods of time. In all profiles, space variables are taken as $-25 \leq x \leq 25$, and time range is $0 \leq t \leq 50$, with $\omega=0.0952, k=0.2752$. While $F_t=3t+E$ is chosen for Figure 1. For Fig. 2 and Fig.3, F_t is taken as $3t^3+E13$ and $\exp(3t+E43)$ respectively.

CONCLUSIONS

The STM is used successfully to solve the Jimbo-Miwa equations (3+1). The solution incorporates an arbitrary function F_t of t and demonstrates that F_t is crucial in determining the nature of the horizontal component p of the wave velocity. The vertical component h always behaves as a single soliton with temporal variation. The solution



**Raj Kumar**

established here can aid the fields of meteorology, atmospheric science, and oceanography since they provide a realistic perspective.

ACKNOWLEDGMENTS

This work was made possible by a minor research grant provided by Veer Bahadur Singh Purvanchal University, Jaunpur on March 23, 2022, and bearing the reference number 133/PU/IQAC/2022.

Conflicts of interest

The author declares that there is no conflict of interest regarding the publication of this paper.

REFERENCES

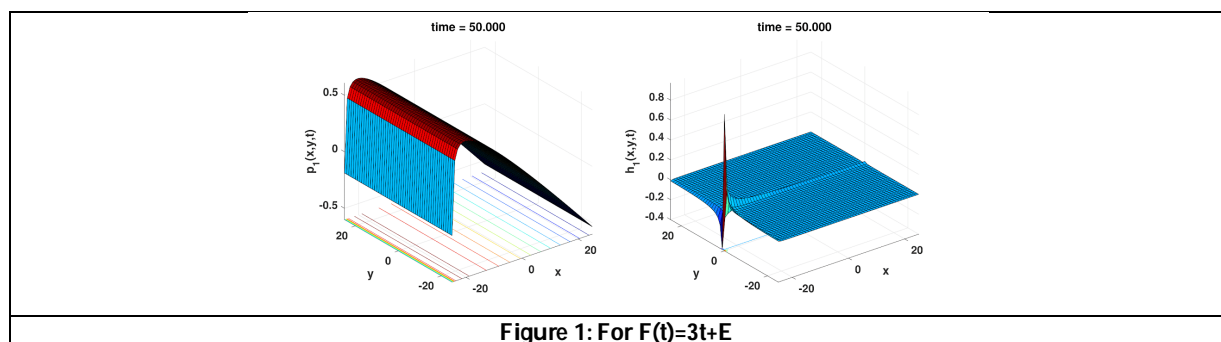
1. Tan W, Dai Z de, Xie J li, Hu L li., Emergence, and interaction of the lump-type solution with the (3+1)-D Jimbo-Miwa equation. *Zeitschrift fr Naturforsch A*. 2017;73(1):43-49. doi:10.1515/zna-2017-0293
2. Guo HD, Xia TC, Hu BB., High-order lumps, high-order breathers, and hybrid solutions for an extended (3+1)-dimensional Jimbo-Miwa equation in fluid dynamics. *Nonlinear Dyn*. 2020;100(1):601-614. doi:10.1007/s11071-020-05514-9
3. Wazwaz A-M., Multiple-soliton solutions for extended dimensional Jimbo-Miwa equations *Appl Math Lett*. 2017;64:21-26. doi:10.1016/j.aml.2016.08.005
4. Bakicierler G, Misirli E., Some new traveling wave solutions of nonlinear fluid models via the MSE method. *Fundam J Math Appl*. 2021;4(3):187-194. doi:10.33401/fujma.933947
5. Elsayed MEZ, Yaser AA, Ahmed HA., Functional variable method and its applications for finding exact solutions of nonlinear PDEs in mathematical physics. *Sci Res Essays*. 2013;8(42):2068-2074. doi:10.5897/SRE2013.5725
6. Zhang Y, Sun S, Dong H., Hybrid solutions of (3+1)-dimensional Jimbo-Miwa equation. *Math Probl Eng*. 2017;2017:1-15. doi:10.1155/2017/5453941
7. Wang YH, Wang H, Dong HH, Zhang HS, Temuer C., Interaction solutions for a reduced extended (3+1)-dimensional Jimbo-Miwa equation. *Nonlinear Dyn*. 2018;92(2):487-497. doi:10.1007/s11071-018-4070-z
8. Wazwaz AM., New solutions of distinct physical structures to high-dimensional nonlinear evolution equations. *Appl Math Comput*. 2008;196(1):363-370. doi:10.1016/j.amc.2007.06.002
9. Wang X, Bilige S, Pang J., Rational solutions, and their interaction solutions of the dimensional Jimbo-Miwa equation. *Adv Math Phys*. 2020;2020:1-18. doi:10.1155/2020/9260986
10. Jimbo M, Miwa T., Solitons and infinite-dimensional Lie algebras. *Publ Res Inst Math Sci*. 1983;19(3):943-1001. doi:10.2977/prims/11951820176
11. Dorizzi B, Grammaticos B, Ramani A, Winternitz P., Are all the equations of the Kadomtsev-Petviashvili hierarchy integrable? *J Math Phys*. 1986;27(12):2848-2852. doi:10.1063/1.527260
12. Singh M, Gupta RK., Backlund transformations, Lax system, conservation laws and multisoliton solutions for Jimbo-Miwa equation with Bell-polynomials. *Commun Nonlinear Sci Numer Simul*. 2016;37:362-373. doi:10.1016/j.cnsns.2016.01.023
13. Zhang RF, Li MC, Yin HM., Rogue wave solutions and the bright and dark solitons of the (3+1)- dimensional Jimbo-Miwa equation. *Nonlinear Dyn*. 2021;103(1):1071-1079. doi:10.1007/s11071-020-06112-5
14. Qi FH, Huang YH, Wang P., Solitary-wave and new exact solutions for an extended (3+1)-dimensional Jimbo-Miwa-like equation. *Appl Math Lett*. 2020;100:106004. doi:10.1016/j.aml.2019.106004
15. Yang JY, Ma WX., Abundant lump-type solutions of the Jimbo-Miwa equation in (3+1)-dimensions. *Comput Math with Appl*. 2017;73(2):220-225. doi:10.1016/j.camwa.2016.11.007
16. Kaur L, Wazwaz A., New exact solutions to extended (3+1)-dimensional Jimbo-Miwa equations by using bilinear forms. *Math Methods Appl Sci*. 2018;41(17):7566-7575. doi:10.1002/mma.5219





Raj Kumar

17. Li H, Li YZ., Meromorphic exact solutions of two extended (3+1)-dimensional Jimbo-Miwa equations. Appl Math Comput. 2018;333:369-375. doi:10.1016/j.amc.2018.03.099
18. Xu HN, Ruan WY, Zhang Y, L X., Multi-exponential wave solutions to two extended Jimbo-Miwa equations and the resonance behavior. Appl Math Lett. 2020;99:105976. doi:10.1016/j.aml.2019.07.007
19. Liu J, Yang X, Cheng M, Feng Y, Wang Y., Abound rogue wave type solutions to the extended (3+1)-dimensional Jimbo-Miwa equation. Comput Math with Appl. 2019;78(6):1947-1959. doi:10.1016/j.camwa.2019.03.034
20. Sun T, Dai HH., Theta function solutions of the 3+1-dimensional Jimbo-Miwa equation. Math Probl Eng. 2017;2017:1-9. doi:10.1155/2017/2924947
21. Yang H, Zhang Y, Zhang X, Chen X, Xu Z., The rational solutions and quasi-periodic wave solutions as well as interactions of soliton solutions for 3+1 dimensional Jimbo-Miwa equation. Adv Math Phys. 2016;2016:1-14. doi:10.1155/2016/7241625
22. Ma WX., Lump-type solutions to the (3+1)-dimensional Jimbo-Miwa equation. Int J Nonlinear Sci Numer Simul. 2016;17(7-8):355-359. doi:10.1515/ijnsns-2015-0050
23. Ma WX, Lee JH., A transformed rational function method and exact solutions to the dimensional Jimbo-Miwa equation. Chaos, Solitons & Fractals. 2009;42(3):1356-1363. doi:10.1016/j.chaos.2009.03.043
24. Dai ZD, Liu J, Zheng XP, Liu, ZJ., Periodic kink-wave and kinky periodic-wave solutions for the Jimbo-Miwa equation Phys. Lett A. 2008;372(38):5984-5986. doi: 10.1016/j.physleta.2008.07.064
25. Batwa S, Ma WX., A study of lump-type and interaction solutions to a (3+1)-dimensional Jimbo-Miwa-like equation. Comput Math with Appl. 2018;76(7):1576-1582. doi:10.1016/j.camwa.2018.07.0087
26. Yong X, Li X, Huang Y., General lump-type solutions of the (3+1)-dimensional Jimbo-Miwa equation. Appl Math Lett. 2018;86:222-228. doi:10.1016/j.aml.2018.07.001
27. Bluman, G.W., Cole, J.D. Similarity Methods for Differential Equations. Springer, New York (1974).
28. Olver, P.J. Applications of Lie Groups to Differential Equations. Springer, New York (1993).
29. Kumar R, Pandey KS, Kumar A., Dynamical behavior of the solutions of coupled Boussinesq-Burgers equations occurring at the seaside beaches. Braz. J. Phys. 2022; 52(1-16):1678-4448. doi:10.1007/s13538-022-01195-4
30. Kumar R, Kumar A., More solutions of coupled equal width wave equations arising in plasma and fluid dynamics. Int. J. Comput. Math. 2022; 8(186):1-13. doi:10.1007/s40819-022-01400-7
31. Kumar R, Verma RS., Dynamics of some new solutions to the coupled DSW equations traveling horizontally on the seabed. J. Ocean Eng. Sci. 2022 ;1-10. doi:10.1016/j.joes.2022.04.015
32. Kumar R, Verma RS., Dynamics of invariant solutions of mKdV-ZK arising in a homogeneous magnetised plasma. Nonlinear Dyn. 2022 ;108: 4081-4092. doi:10.1007/s11071-022-07389-4
33. Kumar R, Kumar A., Dynamical behavior of similarity solutions of CKOEs with conservation law. Appl. Math. Comput. 2022; 422. doi:10.1016/j.amc.2022.126976
34. Kumar R, Kumar A., Optimal subAlgebra of GKP by using Killing form, Conservation Law and some more solutions. Int. J. Comput. Math. 2022; 8(11). doi:10.1007/s40819-021-01211-2
35. Kumar R, Verma RS, Tiwari AK., On similarity solutions to (2+1)-dispersive long-wave equations. J Ocean Eng Sci. 2023;8(2):111-123. doi:10.1016/j.joes.2021.12.005





Raj Kumar

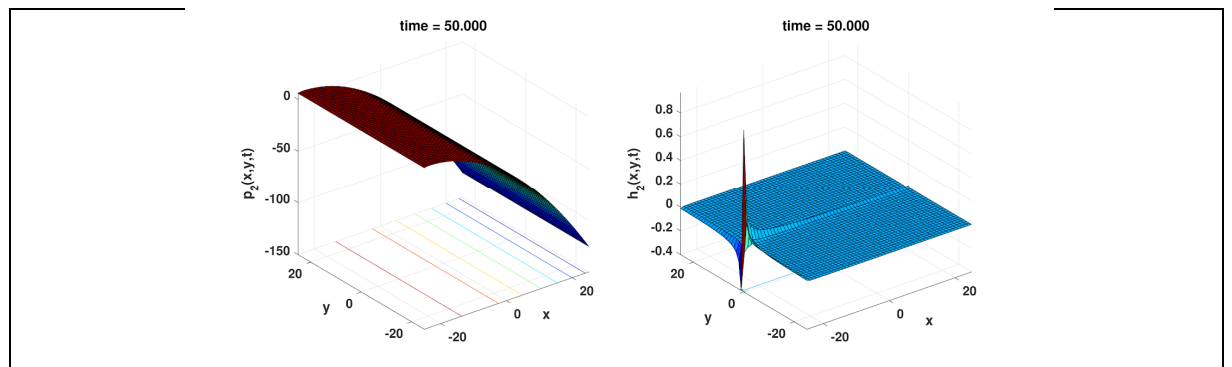


Figure 2:For $F(t)=3t(3t+E)^{1/3}$

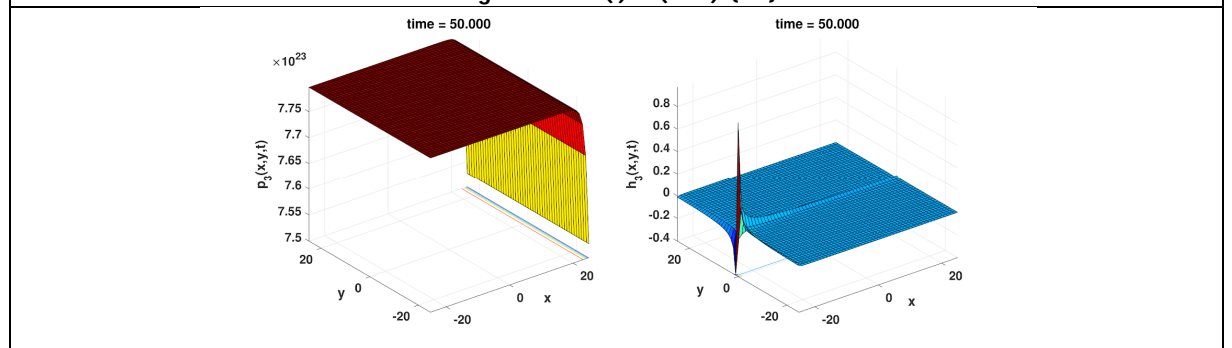


Figure 3:For $F(t)=\exp(t)(3t+E)^{4/3}$





Analysis of Effects of E-Games on Human Cognitive and Physical Behavior

Ujjawal Tiwari, Gautam Suri and Rajendra Kumar*

Department of Computer Science & Engineering, School of Engineering & Technology, Sharda University, Uttar Pradesh, India.

Received: 15 Feb 2023

Revised: 25 Apr 2023

Accepted: 30 May 2023

*Address for Correspondence

Rajendra Kumar*

Department of Computer Science & Engineering,
School of Engineering & Technology,
Sharda University, Uttar Pradesh, India.
E.Mail: rajendra.kumar@sharda.ac.in



This is an Open Access Journal / article distributed under the terms of the **Creative Commons Attribution License** (CC BY-NC-ND 3.0) which permits unrestricted use, distribution, and reproduction in any medium, provided the original work is properly cited. All rights reserved.

ABSTRACT

Online games have become a go-to resort for an increasing number of people, but it is not all fun, and online games have many of those who are addicted to the games and have been the victims of cyber bullying and simultaneously examining the environment of physical games which can sometimes give birth to health issues like bruises and cuts as well as respiratory issues when exposed to dirt and dust. Due to the lack of safety and regulations in both practices, it is harmful and dangerous for any certain individual. This study mainly focuses on the effects of either of the games but specially e-games. This work presents a linear regression- based analysis on effects of e-games and leads to provide suggestive and preventive measures for minimal harm. The Kaggle dataset is used for the analysis of the effects of e- games on human beings.

Keywords: Mental Effects, GAD, SWL, Harmful Gaming, Neuro-Problems, Cortisol, Cortisol Violations.

INTRODUCTION

E-gaming is when an individual or a group plays games with the help of an electronic device(s). Physical gaming is the traditional way of playing sports. Therefore an e-game is a video or a computer game that is either primarily played through the Internet or any local area network equipped with play stations. Physical games instead are played as a physical activity of the body and may require certain equipment. As Each day passes there are a large number of victims that are getting indulged in e-games and some in physical games that the injuries they have had. That is a spark in the kick-start of this research that both the games have pros and cons and what they lead to in the life of a human being. Several studies are performed on effects of physical and e-games on mental and cognitive behavior on





Ujjawal Tiwari et al.,

human beings especially on age group 10 to 20 years [1-4]. Table 1 presents the pros of both kinds of games. As there is also a negative side to everything. Table 2 presents the cons of both kinds of games.

LITERATURE REVIEW

Several studies determine the positives and negatives of e-games and physical games but no research has been found to the best of our knowledge which shows a detailed comparative analysis between both kinds of games. Research by the University of Ibadan in Nigeria [1], collected the data from World Health Organization on gaming disorders from children playing video games for a long time were found victims of musculoskeletal problems, obesity, vision issues, and seizures (Epileptic) [2]. A different study [3] done by the University of Isfahan in Iran by collecting data of 564 volunteers [4] presented how getting addicted to E- gaming has worsened health as the body got physically weak and psychiatric problems like anxiety and depression. An article in Indian express stated that teenagers get too much excited and addicted to e-games [5] that they even start considering their academics as nothing much important. They put lots of physical strain on their body [11]. This causes harm to their physical and mental fitness as per ergonomics. A contradictory study [6] stated that video games for educational purpose proved to be beneficial because they can help children in settling goals along with planning for them as feedback are also provided in such cases. E-games also make people think of playing by looking at some demographic elements. A study done by Termez State University [7] concluded that gaming outside instead of e- gaming should be used to enhance an individual's academics as socialization get increases. They intensify an educational process by providing a motivational basis for building physical and mental properties, and personal self-regulated ways.

METHODOLOGY

The methodology of research consists of the following stages:

- Use of Kaggle dataset
- Data analysis
- Data visualization

Data collection

A dataset of physical and e-games is taken from Kaggle [8] which is a collection of the answers obtained using 50 research questions that were put up in front of the gamers. The dataset has 13465 gamer's data. In Kaggle, the data is collected from different sources for the analysis of both types of games i.e., physical games and e-games. It led to obtaining a sufficient amount and appropriate data for all the types of questions from Kaggle that are needed to be answered by the gamers so that the impact of the games can be well analyzed. The categories of questions consist of general descriptive statistics (e.g., Platform being used to play, time spent at it, etc.) and more sophisticated questions like the purpose (Hobby/money source). Looking at whether they as gamers are playing solely or are they competing as most gamers are worried about the Results of the game in the case of competence known as generalized uneasiness data (GAD) which depicts gaming and its association with uneasiness, life satisfaction, and social phobia.

Data Analysis

The data analysis is done using regression which is a machine-learning algorithm. With all the analysis of the things mentioned above, Analytical processing is done to know about their workings. Python version 3.10.7 is used for experimental purposes as the libraries of it namely pandas, matplotlib and numpy are used in this analysis. An objective analysis supported by subjective assessments is used to link both types of gaming with healthcare. Data analysis is done using help/service provided by the tools being used shows the situation of the gamers in their normal lives. Gamers are playing those games in their common lives which might affect the loads on them.





Ujjawal Tiwari et al.,

Data analysis gave a good amount of proof for software excellence, consistency, performance, robustness, etc. The analysis process involved software and hardware like telecommunication switches. This is even better than just a case to collect the data from volunteers of games to indicate successive development as it gave the knowledge to know about how weak the gamers' body has become physically or mentally that they faced problems at a specific point of time or situation. This helps even more in bringing up some suggestive measures of both types of games. Regression analysis reflects the characteristics of eigenvalues of the dataset and uses a function for expressing the relation in data mapping to check the dependency between values of the attributes to apply the research to predict and correlate data series. We consider a dependent variable y to correlate with independent variables x_1, x_2, \dots, x_k as:

$$v = v_0 + v_1x_1 + v_2x_2 + \dots + v_kx_k + e$$

where $e = (0, \sigma^2)$

Using sampling, the data can be obtained in n groups of observation as

$$y_1 \rightarrow x_{11}, x_{21}, x_{31}, \dots, x_{k1}$$

$$y_2 \rightarrow x_{12}, x_{22}, x_{32}, \dots, x_{k2}$$

....

$$y_n \rightarrow x_{1n}, x_{2n}, x_{3n}, \dots, x_{kn}$$

Where x_{ij} is the j^{th} are observed values of the independent variable x_i , while y_j is the j^{th} observed value of the dependent variable y . On substitution of the above formula, the model's data structure becomes:

$$y_1 = b_0 + b_1x_{11} + b_2x_{12} + \dots + b_kx_{k1} + e_1$$

$$y_2 = b_0 + b_1x_{12} + b_2x_{12} + \dots + b_kx_{k2} + e_2$$

....

$$y_n = b_0 + b_1x_{1n} + b_2x_{1n} + \dots + b_kx_{kn} + e_n$$

The above equations present a model based on k^{th} element normal linear regression with unknown parameters $b_0, b_1, b_2, \dots, b_k$, and σ^2 to be assessed, and the independent parameters $\epsilon_1, \epsilon_2, \epsilon_3, \dots, \epsilon_n$ are identically distributed over $(0, \sigma^2)$

complex correlation analysis is performed on dependent variable y , and k independent variables $x_1, x_2, x_3, \dots, x_k$. Now, the multivariate linear regression model needs to meet the Gaussian hypothesis of the multivariate regression. We use the least square method for estimating the regression coefficients $b_0, b_1, b_2, \dots, b_k$ as:

$$l_{11}b_1 + l_{12}b_2 + l_{13}b_3 + \dots + l_{1k}b_k = L_{1y}$$

$$l_{21}b_1 + l_{22}b_2 + l_{23}b_3 + \dots + l_{2k}b_k = L_{2y}$$

$$l_{k1}b_1 + l_{k2}b_2 + l_{k3}b_3 + \dots + l_{kk}b_k = L_{ky}$$

$$b_0 = \bar{y} - b_1\bar{x}_1 - b_2\bar{x}_2 - b_3\bar{x}_3 - \dots - b_k\bar{x}_k$$

The above linear regression model depicts the analysis results on both kinds of games presented in the analysis section.

Data Visualization

Data visualization represents scientific mapping and the results of data analysis. Drawing graphic displays to show data is another step taken so that people can understand the entire analysis in a moment. Statistical summaries are shown in figures 1 and 2. The main goal of this section is to visualize statistics, being able to obtain even more clearance



**Ujjawal Tiwari et al.,**

when making attempts for deciding the suggestive measures to be shown. As it can be observed in figure 1 where the graphics are specifying a chart that is in a way a type of map which is helping to understand how much people of all genders (Male, Female, Other) are spending on e-gaming. It can be observed well which gender is spending the most time at gaming and after the analysis of the collected data the data shows that male gamers are spending close to 140 hours at it, female gamers are spending about 120 hours and the gamers from the other gender are spending almost 95 hours. This straight away demonstrates that male gamers are spending the most time at it so this can be a point to be taken very well so that the data depicts, the male gender is spending the most time out of all the Genders so they must be probably having bad generalized uneasiness data and safe work load (SWL).

Figure 1 presents how many people of different age groups (10-20, 21-30, 31-40, 41 and above) are spending on E-gaming. It can be seen well that which age group is spending the most time at gaming out of all the age groups and after the. Analysis of the collected data it is clear that the age group of 21-30 plays the games most out of all and the group of 31-40 use it as second most. Without any objectionable context or doubt, this is telling about the summary of the entire age group criteria that has to be looked at while making the predictions and suggestive measures. So, this is also a point to be taken a look at with priority notes so that data collected can be observed. So, working to come up with suggestive measures requires the status of GAD and SWL of the gamers via their Gender and the Age Groups they are of by co-relating the entire context and graphs.

Figure 2 presents a chart that is in a way a type of map which is helping to understand how many people of different age groups (10-20, 21-30, 31-40, 41 and above) are spending on e-gaming. As it can be seen which age group is spending the most time at gaming out of all the age groups and after the analysis of the collected data it can be seen that the age group of 21-30 plays the games most out of all and the group of 31-40 use it as second most. Without any objectionable context or doubt, this is telling about the summary of the entire age group criteria that has to be looked at while making the predictions and suggestive measures. So, this is also a point to be taken a look at with priority notes so that data collected can be observed. So, working to come up with suggestive measures requires the status of GAD and SWL of the gamers via their Gender and the Age Groups they are of by co-relating the entire context and graphs.

EXPERIMENTAL ANALYSIS

This section involves taking the data from the dataset [8] and training the model with the help of apache spark and processing it or training it with the help of apache spark on linear regression algorithm. Table 3 shows the correlation coefficient between e-games addiction and health dimensions. General Health Questionnaire has a self-administered questionnaire used to assess mental health and well-being. The number 28 refers to three different versions (R, P and N) of the questionnaire developed. R (Retest) version is being used to assess changes in mental health overtime by administering the questionnaire twice to the same individual. The overall level of mental distress. P (Profile) version is being used to assess a person's N (Non-patient) version, which is used to assess the mental health of people who are not currently receiving mental health treatment. All versions consist of 28 items and each item is scored on a 4-point Likert scale, with scores ranging from 0 to 3. The scores are then used to determine the level of mental distress or well-being.

According to the results shown in table 3, there is a significant link between computer game addiction and health complaints, uneasiness and sleep disorder, the disorder in social functioning, and depression as $P \leq 0.05$. As a result, there is a direct link between computer game addiction and health illnesses such as uneasiness, insomnia, and depression. But it is found that there is a favorable association between addiction to computer gaming and social disintegration. In other words, according to the coefficient of determination, there is a 4% correlation between computer game addiction and physical disorders, a 12% correlation with uneasiness and sleep disorders, a 1% correlation with social functioning disorders, and a 6% correlation with depression. Table 4 presents the correlation coefficient between addiction to e-games and health dimensions in male volunteers. According to the results in Table 4, there is a link between





Ujjawal Tiwari et al.,

physical and digital gaming addiction complaints, sleep disorders, uneasiness, and social difficulties, and depression at a level ≤ 0.05 is significant. As a result, there is a clear link between gaming addiction and physical disorders, uneasiness, sleep disorders, and depressive disorders. However, there is a reversible link between video game addiction and social problems. According to the coefficient of determination, computer game addiction is associated with somatic disorders in 5% of cases, uneasiness and sleep disorders in 19%, social functioning disorders in 2%, and depression in 10% of cases. Table 5 presents the correlation coefficient between addiction to e-games and health dimensions in females. According to the data in table 5, there is a link between computer gaming addiction and bodily complaints, uneasiness and sleep disorders, and social dysfunction. Depression at level $P \leq 0.05$ is significant. As a result, there is a clear link between gaming addiction and Physical disorders, uneasiness, sleep disorders, and depressive disorders. However, there is a reverse correlation between computer gaming addiction and social functioning disorders. To put it another way, according to the coefficient of determination, computer game addiction shares a 3% variance with a physical problem, a 12% variance with uneasiness and sleep disorder, a 0.9% variance with social dysfunction, and a 5% variance with depression. Table 6 presents the correlation between addiction to e-games and health dimensions.

The result shown in table 6 presents that all relationships have significance. The effects of health with addiction to games is 0.380 which is significant at level 0.99 and presents the positive impact of addiction to games on the general health of the volunteers involved. Table 7 presents the suitability indices of the variables. Based on the findings in Table 7, all indices support the model's appropriateness. Figures 3 and 4 depict, respectively, the standard coefficient of path analysis and a t-chart of route analysis for the association between health-related factors and computer game addiction. Action-focused video games put players at greater danger. These kinds of games may have negative effects on some areas of our brain the more we play them. It is thought that those areas of the brain control our neurological system, memory, and emotions. A person may become vulnerable to various neuropsychiatric problems as a result of several severe neuro situations. Since anxiety symptoms, sadness, and social dysfunction are all directly tied to a person's neurological condition, it is clear from the statistics and charts above that playing video games is contributing to a lot of neuro-problems. Their failure to manage and control their emotions, such as anger, sadness, fear, or other emotions, is the main mechanism that results in those co-morbidities. That is because playing video games is frequently thought of as an emotional release.

A study [9] on the violent Excitement game revealed that after playing threat games, players' levels of cortisol and amylase considerably rose. Many video games are action-packed and intense, and this excitement triggers the production of adrenalin. It is a natural response that enables one to respond more quickly to perceived dangers, such as the possibility of death in shooting games. In addition, playing video games can cause the stress hormone cortisol to be released in greater amounts in response to perceived threats. Excessive gaming may make the stress hormone permanently active, which could hinder serotonin and other neurotransmitters in the brain from working properly. Adrenal glands manufacture and release the hormone cortisol. One class of steroid hormones is cortisol. It can have negative impacts on every biological tissue and affect how the muscles, fat, liver, and bones burn calories. Numerous crucial functions of cortisol include:

- Regulating the stress response of the body
- Regulating blood pressure
- Regulating blood sugar
- Cardiac attack
- Brain stroke
- Helping control your sleep-wake cycle

Everybody's body, in every circumstance, is a constant reflection of their cortisol levels, which must remain constant (homeostasis). The health of the people may be harmed by cortisol levels that are either higher or lower than usual. Whether it is acute, chronic, or traumatic does not matter. After investigation [10], how different types of gaming



**Ujjawal Tiwari et al.,**

affect cortisol in different ways. This allowed for the careful observation of fluctuations in the salivary cortisol levels. Figure 5 shows fluctuations in the salivary cortisol levels when playing different games. Cortisol level is denoted in the measurement unit ng/ml which stands for nanograms per milliliter which depicts test results in urine and oral fluid as cortisol is measured by urine or saliva tests. Figure 6 shows the variation in the mean concentration of cortisol in the volunteers incremented at a significant level after playing the four games. As seen in figure 6, the mean variations of the concentration of cortisol after playing the game present that the highest change is triggered while playing the fear game. Cortisol is the most significant hormone released by the human adrenal cortex for stress. Figure 7 is a bar chart that is showcasing the amount of stress that a person bears on playing the two types of games i.e., excitement games and fear games. The bar chart in the figure demonstrates that players concerning age, gender, and even the type of game, e-games are impacted differently

CONCLUSION AND FUTURE SCOPE

This study accomplished how e-games and physical games affect the life of a certain individual in a positive or negative aspect. In this study, it is also observed that e-games affect humans' cognitive skills and behavior as they fluctuate the amount of cortisol which is responsible for stress, uneasiness, and various aspects as shown in figure 6 and figure 7. Furthermore, the analysis observed that users of the age group 10-20 spent the highest time playing e-games which is reduced by approximately 50% for the age group 21 and above. In the correlation coefficient between addiction to e-games and health dimension, the significant value P is observed as less than 0.05 except for the correlation coefficient social malfunction as ≈ 0.20 . The correlation parameters of mental issues, societal malfunction, despair indications, health and addiction to e-games are observed as positive. The highest fluctuation in the salivary cortisol level is observed when playing fear e-games and the lowest fluctuation is in the case of puzzle games. The mean concentration while playing fear e-games is observed as highest and lowest for puzzle e-games. The future scope of this study may include some other machine learning algorithms for analysis and provide suggestive measures that an individual should follow to lower the negative aspects of e-games.

REFERENCES

1. Israel, O. N., Gaming disorder and effects of gaming on health, *Journal of Addiction Medicine and Therapeutic science*, doi:10.17352/2455.38884.000025, 4(1), pp. 1-3, 2018.
2. Kracht C. L., Joseph, E. D., Staiano, A. E. Video Games, Obesity, and Children, *current obesity reports*, doi: 10.1007/s13679-020-00368-z, pp. 1-14, 2020.
3. Zamani E, chashmi M, hedayati N. Effect of Addiction to Computer Games on Physical and Mental Health of Female and Male Students of Guidance School in City of Isfahan, *Addiction and Health*, 1(2), pp. 98-104, 2009.
4. Goldberg, D. P., Hillier, V. F., A Scaled Version of the General Health Questionnaire, *Psychological Medicine*, doi: 10.1017/s0033291700021644, pp.139-145, 1979.
5. AP News Agency, Compulsive Video-game Playing now Qualifies as a Mental Health Problem, 2018, from <https://apnews.com/article/health-growing-up-digital-ap-top-news-international-news-games309e0d17ea024b8b8a6bac92d8d3cd09>
6. Granic I., Lobel A., Engels, R.C., The benefits of playing video games, *American Psychologist*, doi: 10.1037/a0034857, pp. 66-78, 2014.
7. Abdullaev Yashnarzhon Makhkamovich. Physical Education of Senior Schools by Means of Folk Moving Games, *European Scholar Journal*, 2(11), pp. 70-72, 2021.
8. <https://www.kaggle.com/datasets/divyansh22/online-gaming-anxiety-data>
9. Steffen, C. E., Schmidt, Jens-Peter Gnam, Maximilian Kopf, Tobias, R., Alexander, W. The Influence of Cortisol, Flow, and Anxiety on Performance in E-Sports: A Field Study, *BioMedResearch International*, doi: 10.1155/2020/9651245, pp. 3-6, 2020.
10. Aliyari, H., Sahraei, H., Daliri, M. R., Minaei-Bidgoli, B., Kazemi, M., Agei, H., Sahraei, M., Hosseini, S. M. S., Hadipour, M. M., Mohammadi, M., Dehghanimohammadabadi, Z. The Beneficial or Harmful Effects of





Ujjawal Tiwari et al.,

Computer Game Stress on Cognitive Functions of Players. Basic Clin Neurosci. 9(3), pp. 177-186, 2018. doi: 10.29252/nirp.bcn.9.3.177.

11. Kumar, R., Human Computer Interaction, Firewall Media, 2011

Table 1: Pros of E-games and physical games

	E-GAMES	PHYSICAL GAMES
PROS	Can be Played anywhere, and has no location as it is a Confined space.	Some physical games do Not need a specific place.
	E-gaming is always fun to play regardless of Gender and age.	Physical games are played as a relaxation activity Even.
	Free reign of choice the gamer wants to play provides help in boosting Brain cells.	It helps gain fitness, develops muscular strength, and healthy Physical growth for kids.

Table 2: Cons of E-games and physical games

	E-GAMES	PHYSICAL GAMES
CONS	Indulging in excess, the amount can lead to un-Healthy lifestyle.	Physical injuries are Possible.
	Real-time human connections are being altered because gamers spend much of their time it can also lead to this Only.	Gamer become a victim of flu and Spreading diseases.
	Playing video games at times depict a lack of self-control as they get affected by the adapting to the concept of the game even as well as laziness in Academics.	If single or double other gamers do not arrive then most of the games can get Cancelled.
	These are not completely secure which may invite or give access to malware Threats and Viruses.	Sometimes the equipment becomes a responsibility to maintain which can Become costly.

Table 3: Correlation coefficient in e-games and healthdimensions

Correlation coefficients	Addiction to e-games		
	R	P	N
Physiological issues	0.1980	0.002	486
Mental issues	0.3480	0.002	483
Societal malfunction	0.1040	0.201	477
Despair indications	0.2500	0.002	487
Total	0.3160	0.002	445

Table 4: Correlation coefficient in e-games and healthdimensions in males

Correlation coefficients	Addiction to e-games		
	R	P	N
Physiological issues	0.2260	0.001	265





Ujjawal Tiwari et al.,

Mental issues	0.4400	0.001	261
Societal malfunction	0.1420	0.230	258
Despair indications	0.3310	0.001	265
Total	0.3720	0.001	243

Table 5: Correlation coefficient between addiction toe-games and health dimensions in females

Correlation coefficients Parameters	Addiction to e-games		
	R	P	N
Physiological issues	0.1810	0.006	222
Mental issues	0.3550	0.002	485
Societal malfunction	0.0970	0.021	218
Despair indications	0.2410	0.002	221
Total	0.3180	0.002	201

Table 6: Correlation coefficient in e-games and health dimensions

Correlation coefficients Parameters	Standard coefficient	Standard error T		Test results
		-	0.000	
Physiological issues	0.420	-	0.000	-
Mental issues	0.880	0.820	7.510	Positive
Societal malfunction	-0.200	-0.360	-3.590	Positive
Despair indications	0.700	0.500	7.830	Positive
Health and addiction toe-games	0.380	0.410	5.950	Positive

Table 7: Suitable index of variables

Index variable	Estimated value
Goodness of fit index	0.990
Adjusted goodness of fit index	0.970
Root mean square deviation	0.054
Chi-square	11.350
Degree of freedom	5.000
Level of significance	0.044





Ujjawal Tiwari et al.,

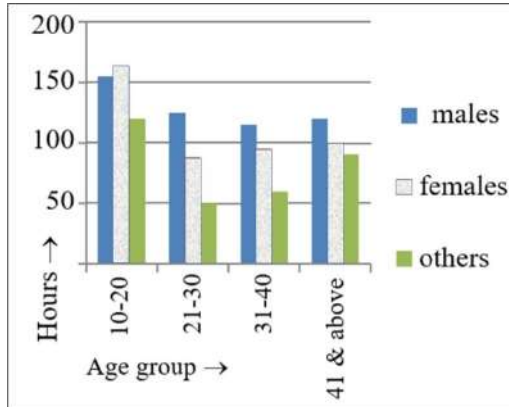


Figure 1: People of different gender spending time on E-games.

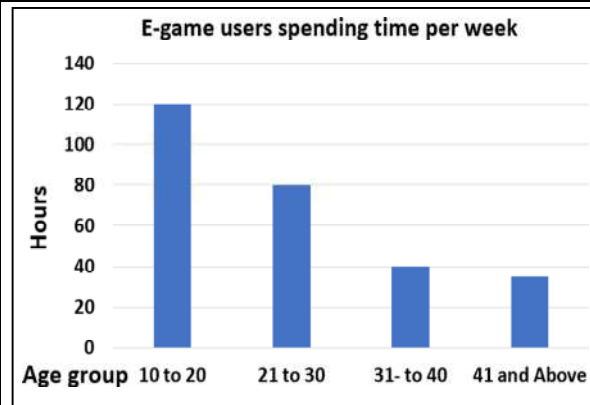


Figure 2: Number of users of different age groups spending hours per month on e-games

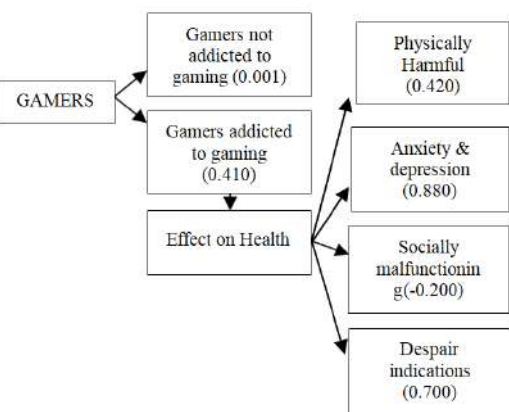


Figure 3: Standard coefficient of path analysis for the association between health-related factors and e-game addiction

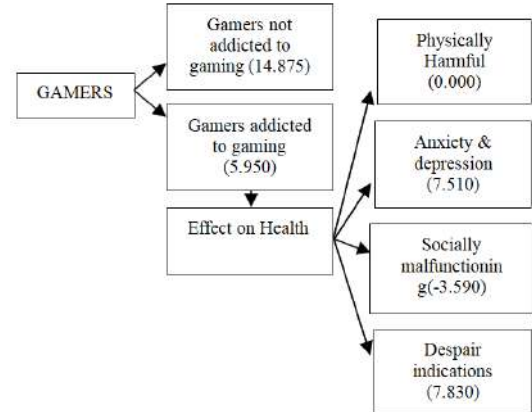


Figure 4: T-chart Route analysis for the association between health-related factors and e-game addiction

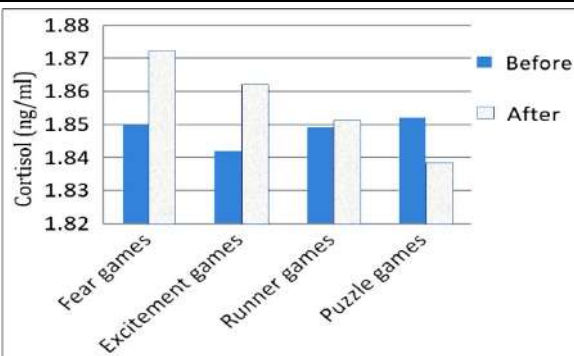


Figure 5: Fluctuations in the salivary cortisol levels when playing different e-games

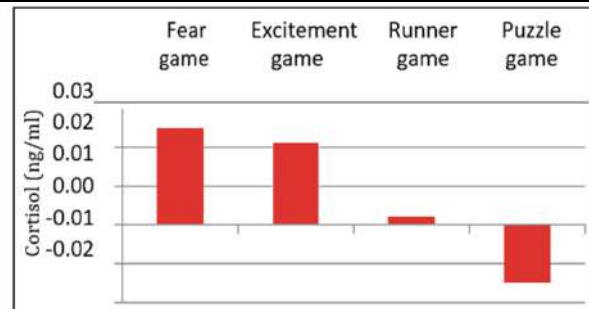


Figure 6: Variations of the mean concentration of cortisol





Ujjawal Tiwari et al.,

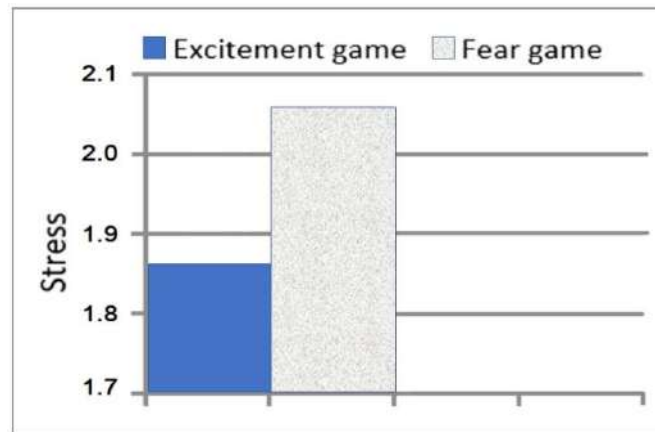


Figure 7: Type of game affecting stress levels





Design and Analysis of Warehouse using ST Add Pro

Chintala Balakrishna^{1*} and Muddasi Saidivya²

¹Assistant Professor, Department of Civil Engineering, Malla Reddy Engineering College (Autonomous), Hyderabad, Telangana-500100, India.

²Student, Department of Civil Engineering, Malla Reddy Engineering College (Autonomous), Hyderabad, Telangana-500100, India.

Received: 24 Jan 2023

Revised: 25 Mar 2023

Accepted: 27 Apr 2023

*Address for Correspondence

Chintala Balakrishna

Assistant Professor,
Department of Civil Engineering,
Malla Reddy Engineering College (Autonomous),
Hyderabad, Telangana-500100, India.
E.Mail: silicon.srdl@gmail.com



This is an Open Access Journal / article distributed under the terms of the **Creative Commons Attribution License** (CC BY-NC-ND 3.0) which permits unrestricted use, distribution, and reproduction in any medium, provided the original work is properly cited. All rights reserved.

ABSTRACT

Structural Design is aimed to Design a ware residence shape that fulfills its meant motive throughout its supposed lifestyles and be competently secure in phrases of energy, balance, and structural integrity, usefulness in phrases of stiffness, durability, and so forth., and be economically viable, esthetically fascinating, and surroundings friendly. This paper provides the studies on the evaluation and Design of the metal warehouse structure. The most beneficial Design of the shape is run victimization finite aspect code STAAD professional. The analysis of the structure is administered for appropriate metallic sections with absolutely one of a kind load carrying capability. The metallic amount wished for the shape is calculated. Finally beside cloth optimization, techno-reasonably-priced Design to reap the dependable performance of the warehouse shape is run. Long Span, Column free designs area unit the most significant in any sort of business structures. Popular construction with line and cylinder stage collect region unit a substitute gather in the making of unmarried level steel business fabricating that satisfies this interest adjacent to diminished time and cost in contrast with standard designs. The objective of this endeavor is to endeavor to relative gander at among well known Steel Building and famous Structure with Pipe and Tube Sections of business Warehouse exploitation STAAD-Pro

Keywords: Warehouse, STAAD Pro, Finite detail strategy, CSB, Optimum,





INTRODUCTION

A Steel warehouse may be a structural building that is employed by industries to store raw materials and therefore the created prepared product. Steel warehouse is additionally known as because the industrial building. There area unit 2 forms of industrial buildings like traditional form of industrial building and special form of industrial building. Traditional form of warehouses is that the straightforward roofed structures on the open frames. Special form of industrial warehouses is like cold storage buildings, etc. within the steel buildings like the Warehouses, the beams and columns location unit of metallic sections of various sectional dimensions. The metallic framed shape can be erected for the various bays conterminous each other supported the necessities. The horizontal and vertical bracings region unit supplied fittingly to the structure to withstand lateral load properly. These bracings reduce the deflection in beams or the alternative structural components because of transferring hundreds inside the big industries. Sheeting, assisting trusses and purlins location unit supported on the columns furnished at the structural roofing machine.

Truss Types

There area unit various support sorts. The vitally normal sorts are demonstrated on the going through page. Most rooftop supports have networks that run at associate point of view among top and base harmonies. One special case is that the peak surrender support for the span of which networks runs upward. These supports sit on a structure's end dividers and locale unit extra sort of a divider than a bracket. The peak stop bracket should be upheld on the total time frame, and solid on the support/divider crossing point. There area unit sort of bracket sorts that withdraw place for loft carport or residing region. In any rooftop bracket, in any case, loft or living region includes some major disadvantages. Unsurpassed low harmony of the assault bracket also goes about as a joist and should be estimated to house a heap - ordinarily among twenty and fifty psychological oppressor bunch. A rooftop support with loft capacity deciphers to pretty much twofold the heap of equivalent bracket range with out a storage room. For instance, a fifty-foot bracket planned even as now not loft capacity should weigh among 300 350 lbs. A fifty foot bracket planned with a nine foot through nine foot loft opening might need to weigh among 600 and 700 lbs.

LITERATURE REVIEW

Stockrooms area unit apparent as a gamble to improve activity advancement and records streams, to decrease stock levels and to substitute extra light-footed conveyance. The palm in general execution of a stockroom depends upon on applicable technique, design, distribution center activities and material adapting to structures distribution center style issues contain five gatherings of choices: devotion of the absolute last state of the stockroom (reasonable plan); its measuring; design estimation; reposition instrumentality decision; and selection of its functional system. Furthermore, a stockroom mission need to also incorporate meanings of guidelines concerning request satisfaction/picking, loading, and stock revolution Despite the topic's importance, an outline of the writing renowned few exploration that continually cover the distribution center style a leven however a lot of fabric tending to the exact parts of a mission do exist, there has all the earmarks of being no blends of these techniques that would supply a base for a trendy stockroom thought there's a hole among the found assessment and thus the see of protrusive and in activity stockrooms. The creators country that, to choose this connection point among academe and notice, there should be assistant certificate improvement inside the cutting edge for reposition mission method. Considering this unique circumstance, the object of this bulletin is to introduce an orderly outline of the distribution center style writing, overlaying the amount 1999-2015.





METHODOLOGY

Planning and Detailing

In this challenge work, automobile CAD and Staad expert code is being used in order to analyze and fashion Industrial warehouse as in line with the set up. It offers the bending second, shear forces. The manner consists of modeling the structure, making use of properties, specification, hundreds and load mixtures, reading and making plans the structure. This code is a superb and person pleasant device three dimensional version generations. To impart maximum ability edges for a warehouse constructing amongst limitation, can constantly a bigger venture for every fashion dressmaker and civil engineers even though we've determined the best manner that's capable of impart maximum edges to the consumer. Here we have a tendency to had given lots of idea over environmental elements like air, and light, ventilation. the shape of this constructing is completely specific from the equal antique square warehouse homes, that imparts esthetically clever from every reason of read. Brackets rectangular degree three-sided body works, which incorporates basically pivotally stacked supporters that rectangular degree heaps of economical in opposing external hundreds on the grounds that the move stage is almost consistently pushed. They're eminently utilized, specifically to traverse enormous holes. Brackets rectangular degree employed in tops of unmarried creation business homes, extended length deck and tops of high-up push homes, to look up to gravity hundreds. Brackets are likewise employed in parts and flat planes of modern homes to look up to parallel hundreds and deal sidelong solidness.

Economy of supports

As currently referred to supports gobble up stores substantially less texture in contrast with pillars to traverse same term and switch gentle to outrageous masses. Notwithstanding, the efforts call for manufacture and erection of brackets is better and thus the overall financial framework is chosen through different variables. In Republic of India those issues ar prone to need the supports even various due to the reduction efforts cost. To totally utilize the monetary arrangement of the brackets the creators should affirm the accompanying:

LOADS AND LOAD COMBINATIONS

LOADS-Following Loads Are Considering For Analysis. Furthermore, Loads and burden mixes are considered in reference with the IS codes, IS-875 section 5.

Dead burden

Dead burden on the rooftop supports in single floor modern structures comprises of stacking of claddings and stacking of purlins, self-weight of the brackets furthermore to the weight of bracings and so forth Further, additional exceptional dead hundreds like bracket upheld raise dead loads; extraordinary ducting and ventilator weight and so forth could add to rooftop support dead loads.

$$\text{Weight of metal sheeting} = 0.131 \text{KN/m}^2$$

$$\text{Weight of fixings} = 0.025 \text{KN/m}^2$$

$$\text{Total load} = 0.156 \text{KN/m}^2$$

$$\text{Total load per meter run} = 0.156 * 4 = 0.624 \text{ KN/m run.}$$

$$\text{Dust load} = 6.85 \text{ KN/m}$$

$$\text{Dust load per panel of roof} = 6.85 / 15.29 * 4$$

$$= 0.112 \text{ KN/m}^2$$

$$= 0.112 \text{KN/m}$$

$$\text{Dead load on intermediate rafter beams} = 0.736 \text{ KN/m}^2$$

$$\text{Dead load on gable end rafter beams} = 0.763 / 2$$

$$= 0.368 \text{ KN/m}^2$$

Live Load

The live burden on rooftop brackets comprise of the gravitational burden because of erection and adjusting as well as residue load and so forth and the power is taken according to IS:875-1975. Extra exceptional live loads, for example, snow loads in freezing environments, crane live loads in brackets supporting monorails might need to be thought of.





Chintala Balakrishna and Muddasi Saidivya

According to IS 875-1987 part-b the live loads for an industrial storage building

Point load = 7.0KN

Point load per meter run = $7.0/15.29$

= 0.46 KN/m

Uniformly distributed load = 7.5 KN/m

Total live load = $0.46\text{KN/m} + 7.5 \text{ KN} = 7.96 \text{ KN/m}$

Live load on intermediate rafter beams = 7.96 KN/m

Live load on gable end rafter beams = $7.69/2$

= 3.98 KN/m

Wind load

The breeze load on the rooftop supports, except if the rooftop slant is basically too high, would be normally elevate force opposite to the rooftop, on account of attractions effect of the breeze handling over the rooftop. Thereupon the breeze load on rooftop bracket commonly acts inverse to the gravity load, and its greatness is bigger than gravity hundreds, incurring inversion of powers in support individuals

Load Combinations

Load combinations can be adopted according to IS: 800 – 2007. Twenty two different load combinations adopted for the analysis of the frame and some are listed as follows:

- 1) Load Combination 1 = 1.5 (DL + LL)
 - 2) Load Combination 2 = 1.2 (DL + LL + WIND 0 & -VE)
 - 3) Load Combination 3 = 1.2 (DL + LL + WIND 0 & +VE)
 - 4) Load Combination 4 = 1.2 (DL + LL + WIND 90 & +VE)
4. Design of Conventional Steel Warehouse

Design of Components of the Steel Warehouse

Design of structural elements like principal rafter, column, column base and purlins etc as per IS 800-2001. Components are designed for the maximum load, maximum bending moment and shear force.

Properties of the components

The steel sections tailored to the warehouse for the look of the structure for max hundreds, most bending moment, and most shear force.

Sections adopted for various parts are as follows,

- Beams- ISMB-600
- Columns- ISHB-450
- Purlins- ISMC-250
- Bracings- ISLC-150

Steel take-off

The weight of the steel sections (Table-1) is the total weight of the total length required.

RESULTS AND DISCUSSIONS

Analyzing of Truss Structure

Dead load with followed by self weight and member load followed by uniformly distributed load will be standard.

- By victimization the load and definition command we are able to assign the hundreds severally.
- In load and definition command choose the load case details therein opt for style of load i.e. loading with followed by self weight and member load followed by uniformly distributed load are going to be commonplace.
- Next click on add any to assign them.





Chintala Balakrishna and Muddasi Saidivya

- And they assign one by one mass for the model ready one by one.

Truss Details

Trusses are triangular body works at some point of which the member's are subjected to by and large axial forces way to outwardly achieved load. they're going to be aircraft trusses, at some point of which the outside load and consequently the members lie in the identical aircraft or residence trusses wherein contributors are orientated in three dimensions in. area and heaps of can also additionally moreover act in any course trusses are frequently wont to span extended lengths the various state of affairs of strong net girders and such trusses are called lattice girders.

Inputs Required to Truss Manufacturer

Bracket kind. Decides if there'll be capacity or way. Conjointly characterizes field subtleties like side, overhang, facial statures and tail length. Decides the developing codes and hundreds that training For example, in western CA, seismic cravings might drive the making arrangements and charge of the bracket. In beach front Florida, wind drives the making arrangements.

Bracket Design Process

When the fundamental characteristics of an endeavor are conveyed through method of method for the purchaser to the support maker, the making arrangements and producing strategy return before long. Virtually all most significant rooftop support producers utilize particular PC code to help withinside the bracket design strategy. Inside the fingers of learned, those code bundles will fundamentally lessen again the time had to offer the most satisfying bracket for a shape. Partner confirmation most satisfying support is one which has been developed to be basically steady, as lightweight as potential, and in consistence with building codes.

Normal Truss Report boundaries

- Plan hundreds as well as stacking, remain burden, snow and wind hundreds
- Part sizes and power attributes
- Greatest design avoidances
- Shop drawings with develop headings

Esteem Engineering in Roof Trusses

High-quit bracket design code, similar to Truss can playing out a part through method of method for part pass/bomb assessment. The results of the assessment is that the problematic "Cooperation Value" this is that the proportion of needed to accessible power. Defensive cowl type. The rooftop protecting cowl type plays out a standard situation inside the amount of supports wished. For example, a 3/4" employ board rooftop can ordinarily need bracket dispersing underneath 32". Some metallic decking might be introduced on rooftop brackets dispersed as much as 48".

Support Installation

Like any rooftop support, metallic rooftop brackets are outstanding introduced with the guide of utilizing crane friend degreed a one of a kind team. There is type of trade outstanding practices for introducing supports. The fundamental essential are noted underneath:

- Brackets need to ne'er be connected bolt to inside allotments. This should set off twisting powers that supports aren't intended to hold. Bolt connected supports have conjointly been legendary to raise buddy confirmation non-load-bearing inside divider from the beginning.
- The support installer should as a rule conform to any interesting rules with the guide of utilizing the maker. For example, T-Bracing a broad net reinforcing procedure - is outstanding did at the endeavor site. Inability to put with inside the supporting will prominently change the power of the bracket framework.
- Most rooftops, despite their place are planned with an intense and quick end and a slide end. This procedure significantly decreases how much horizontal strain at the allotments helping the bracket framework. Reinforcing parcels contrary to horizontal powers - obviously at the absolute best of the divider is intense.





Chintala Balakrishna and Muddasi Saidivya

CONCLUSIONS

Design and Analysis of enterprise warehouse is certainly accomplished via way of means of the Staad expert code. The whole technique became finished as according to the great set down via way of means of the Indian standards. During this work, Analysis and fashion of enterprise warehouse victimization STADD expert. In step with the consequences acquired from the evaluation of these systems inside which metal sections had been assigned to the numerous warehouse fashions for every member. AUTOCAD set up became prepared accompanied via way of means of load calculations. Supported the ones definitely distinctive participants like truss participants, columns, purlins, etc. had been hand-picked. Steel quantity relies upon on number one participants and purlins. As spacing of body is magnified metal intake slashed for number one participants and magnified for secondary participants. the whole technique became finished as according to the commonplaces set down via way of means of Indian popular. the monetary warehouse is certainly styled via way of means of honest layout procedure. The following are the important thing statement and end drawn from the cutting-edge assignment work. consistent with the consequences acquired from the evaluation of these Structures inside which surest metal sections had been assigned to the numerous warehouse fashions for every member following end is created

REFERENCES

1. G.Durga Rama Naidu, Comparative study of analysis and design of pre-engineered buildings and conventional frames- IOSR Journal of mechanical and civil engineering ISSN: 2278-067X, 2014, 10, , pp 165-169.
2. S.D.Charkha, Economizing steel building using pre-engineered steel sections – International journal of scientific and engineering research, 2014, 6 (12), pp 69-74.
3. Milind Bhojkar, Comparison of pre-engineered building and steel building with cost and time effectiveness – International journal of innovative science engineering and technology ISSN 2348-7968, 2014, 1 (10), pp 784-789.
4. M.G.Kalyanshetti & G.S Mirajkar, “comparison between conventional steel structures and tubular steel structures”, ijera, vol.2, issue 6, november-december 2012, pp.1460-1464.
5. Sagar D.Wankhade.al, (2014) “design& comparison of various types of industrial buildings”, science (irjes) issn 7. volume3, issue6.
6. Syed Firoz (2012), “Design Concept of Pre-engineered Building”, International Journal of Engineering Research and Applications (IJERA), Vol.2, Issue 2, 267-272.
7. Vrushali Bahadur , Comparison between design and analysis of various configuration of industrial sheds – International journal of engineering research and applications, 2013, 3(1), pp-1565-1568.
8. “Warehouse design optimization” European Journal of Operational Research 21 (1985) 285- 294 J. a shayeri and I.f. gelders
9. “Structural Behavior of Industrial Structure subjected to lateral loads” -IJERT vol-4,issue 5. May2015. Navya P1, Dr.Y.M Manjunath
10. “Comparative Study of Tubular Steel Truss Profiles for Roofing Varying Span” -IJERT vol5, issue4. April 2016. Arvind Bora
11. “Optimization and Rationalization of roof truss design” -IJERT vol2, issue 5. Aug2015.





Chintala Balakrishna and Muddasi Saidivya

Table-1 Weight of Steel Sections

PROFILE	LENGTH (m)	WEIGHT (KN)
ISWB600	861.51	1125.068
ISMC400	1247.89	611.601
ISLC150	360.00	50.885
ISA200×200×25	86.61	125.222

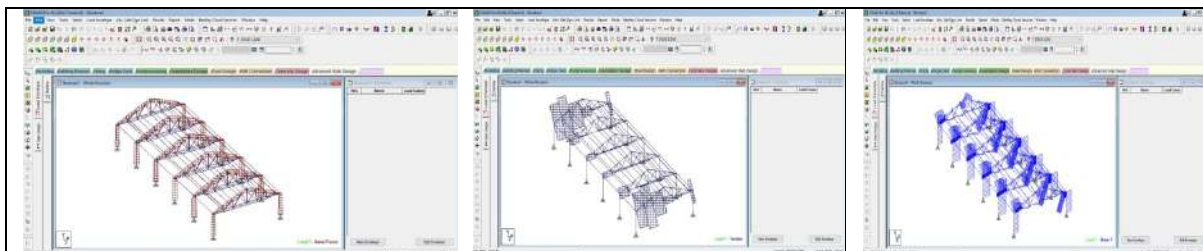


Fig.1. Axial Force Details

Fig. 2. Torsional forces details

Fig.3. Shear forces details

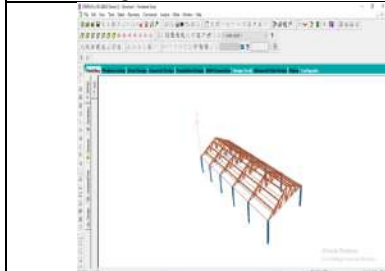


Fig. 4. Model of warehouse

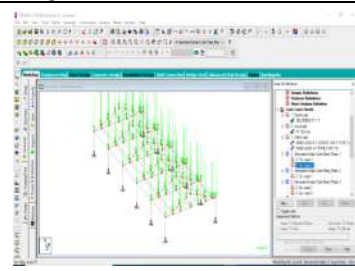


Fig.4. Loading on the structure

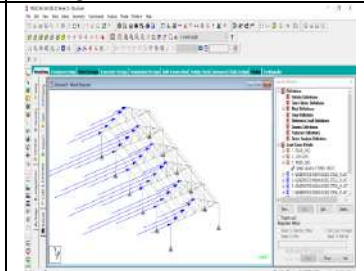


Fig.5. Wind load analysis

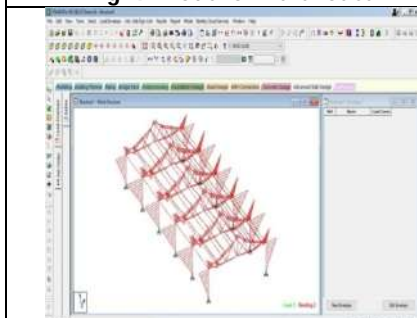


Fig.6. Moment Z- Direction

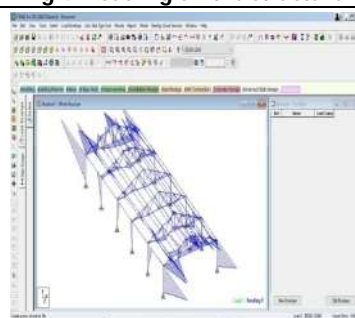


Fig.7. Moment at Y- Direction

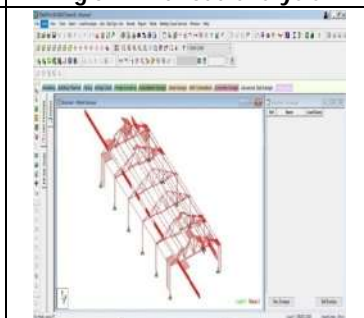


Fig. 8. Force at Z- Direction





Chintala Balakrishna and Muddasi Saidivya

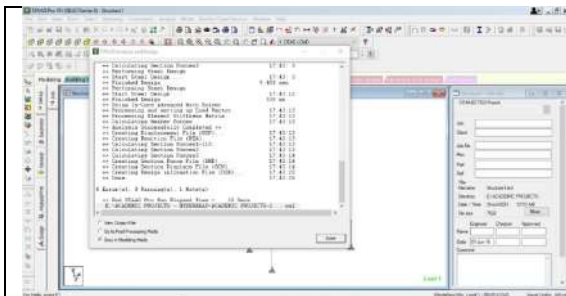


Fig.9. Run Analysis Data

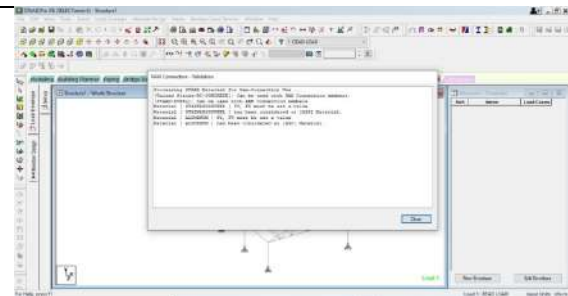


Fig.10. Run Analysis Data for Warehouse

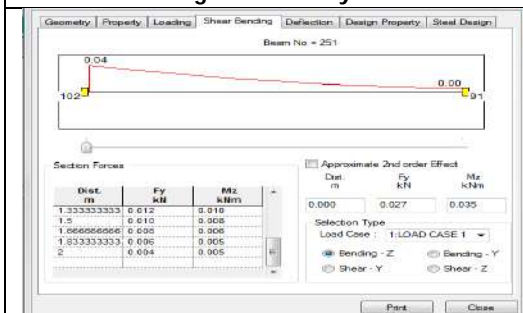


Fig.11. Shear Force for Beam

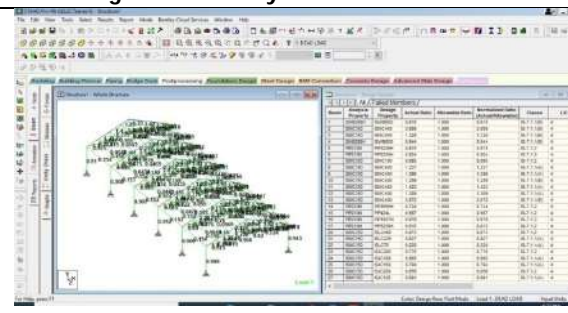


Fig.12. Point Load

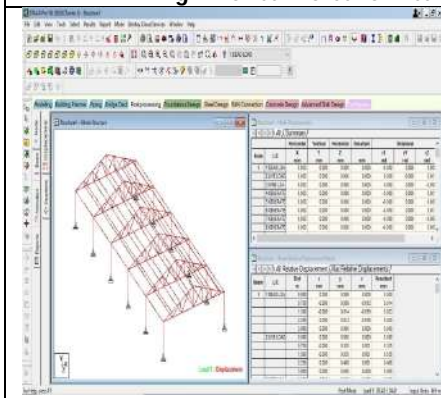


Fig.13. Displacement

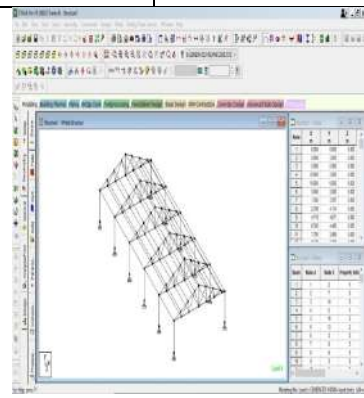


Fig.14. Nodes

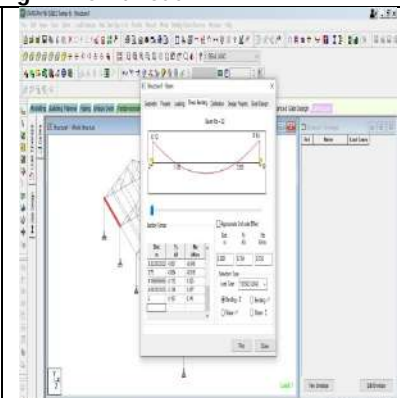


Fig.15. Shear-Bending





A New Notion of Semi Open Sets in N-Topology

A. Antony George^{1*} and M. Davamani Christofer²

¹Assistant Professor, Research Department of Mathematics, The American College, Madurai, Tamil Nadu, India.

²Associate Professor and Head, Research Department of Mathematics, The American College, Madurai, Tamil Nadu, India

Received: 24 Feb 2023

Revised: 05 Apr 2023

Accepted: 10 May 2023

*Address for Correspondence

A. Antony George

Assistant Professor,
Research Department of Mathematics,
The American College,
Madurai, Tamil Nadu, India.
Email: antonygeorge427@gmail.com



This is an Open Access Journal / article distributed under the terms of the **Creative Commons Attribution License** (CC BY-NC-ND 3.0) which permits unrestricted use, distribution, and reproduction in any medium, provided the original work is properly cited. All rights reserved.

ABSTRACT

In this paper, we initiate a new class of semi open sets, called S_b -open sets in N -topological space, this class of sets lies between $N\tau\theta$ -semi open and $N\tau$ semi-open sets. Also we introduce various maps in N -topological space and relate them with S_b -continuous maps.

2010 MSC: 54A05, 54A10, 54C05

Keywords: N -topology, $N\tau$ -semi open, $N\tau b$ -open, $N\tau S_b$ -open, N^* -continuous maps.

INTRODUCTION

In 1963 Levine[3] initiated semi-open sets and gave their properties. [4] Biswas(1969) defined semi-open functions and investigated several properties of such operations. [5] Monsef *et al.* 1983, started the study of β -continuity and β -open sets. The idea of b -open sets has been introduced by D. Andrijevic [6] in 1996. Recently, Lellis Thivagar *et al.* [1],[2] introduced the structure of N -topology and its continuous properties, which helps to form more topologies on a non-empty set.

In this present work, we introduce S_b -open sets in a N -topological space $(X, N\tau)$. Also we define $N\tau\theta$ -semi open sets and discussed the location of $N\tau S_b$ -open sets. Moreover, we analyse various its maps in N -topological space and relate them with S_b -continuous maps.





PRELIMINARIES

In this part we, recollect some definitions and results which are beneficial in the sequent.

Definition 2.1 [1]

If X is a non-empty set, $\tau_1, \tau_2, \tau_3, \tau_4, \dots, \tau_N$ are N -arbitrary topologies defined on X and let the collection $N\tau$ be defined by

$N\tau = \{S \subseteq X : S = (\bigcup_{i=1}^n A_i) \cup (\bigcap_{i=1}^n B_i), A_i, B_i \in \tau_i\}$ satisfies the following axioms:

- (i) $X, \emptyset \in N\tau$
- (ii) $\bigcup_{i=1}^{\infty} S_i \in N\tau \forall S_i \in N\tau$
- (iii) $\bigcap_{i=1}^n S_i \in N\tau \forall S_i \in N\tau$.

Then the pair $(X, N\tau)$ is named as N -topological space, and $N\tau$ is called N -topology.

Definition 2.2 [2]

Let $(X, N\tau)$ be a N -topological space and $S \subseteq X$ is called.

- (i) $N\tau\alpha$ -open if $S \subseteq N\tau\text{-int}(N\tau\text{-cl}(N\tau\text{-int}(S)))$
- (ii) $N\tau$ semi- open if $S \subseteq N\tau\text{-cl}(N\tau\text{-int}(S))$
- (iii) $N\tau$ pre-open if $S \subseteq N\tau\text{-int}(N\tau\text{-cl}(S))$.

The complement of $N\tau\alpha$ -open (resp. $N\tau$ semi-open, $N\tau$ pre-open) is $N\tau\alpha$ -closed (resp. $N\tau$ semi-closed, $N\tau$ pre-closed).

Theorem 2.3[2]

The arbitrary union of $N\tau$ semi-open sets is $N\tau$ semi-open.

Definition 2.4 [2]

A mapping $f: (X, N\tau) \rightarrow (Y, N\sigma)$ is N^* - continuous (resp. $N^*\alpha$ continuous, N^* - semi continuous, $N^*\beta$ continuous) on X if $f^{-1}(G)$ is $N\tau$ -open (resp. $N\tau\alpha$ -open, $N\tau$ semi-open, $N\tau\beta$ -open) for every $G \in N\sigma\mathcal{O}(Y)$.

Theorem 2.5[2]

Every N^* -continuous map is $N^*\alpha$ continuous.

Theorem 2.6 [2]

Every $N^*\alpha$ continuous map is N^* -semi-continuous.

The converse of theorem 2.5 & theorem 2.6 need not be accurate, as shown in [2].

Definition 2.7 [8]

A subset E of a N -topological space X is $N\tau$ -regular open if $E = N\tau\text{-int}(N\tau\text{-cl}(E))$.

Definition 2.8 [9]

A subset A of a N -topological space X is said to $N\tau$ -dense if $N\tau\text{-cl}(A) = X$.

Definition 2.9 [2]

An N -topological space $(X, N\tau)$ is called extremely disconnected if $N\tau\text{-cl}(A)$ is $N\tau$ -open for all $N\tau$ -open sets in A .

S_b -OPEN SETS IN N -TOPOLOGICAL SPACE

In this part, we define a new class of semi open sets called S_b -open in N -topological space and investigate its properties. Moreover, we introduce some properties are called $N\tau$ -neighbourhood, $N\tau$ -interior, $N\tau$ -closure and $N\tau$ -derived set.





Antony George and Davamani Christofer

Definition 3.1

Let $(Q, N\tau)$ be a N -topological space and a subset $B \subseteq Q$ is called $N\tau b$ -open if $B \subseteq N\tau\text{-int}(N\tau\text{-cl}(B)) \cup N\tau\text{-cl}(N\tau\text{-int}(B))$. The complement of $N\tau b$ -open is $N\tau b$ -closed. The collection of $N\tau b$ -open is signify by $N\tau BO(X)$.

Definition 3.2

Let $(Q, N\tau)$ be a N -topological space and a semi-open set $E \subseteq Q$ is $N\tau S_b$ -open if every $x \in E$ subsequently there exists $H \in N\tau BC(Q)$ such that $x \in H \subseteq E$. A subset B of a N -topological space Q is $N\tau S_b$ -closed if $Q - B$ is $N\tau S_b$ -open. The family of $N\tau S_b$ -open and $N\tau S_b$ -closed sets are signify by $N\tau S_b O(Q)$ and $N\tau S_b C(Q)$ respectively.

Example 3.3

Let $Q = \{l, m, n, o\}$. For $N = 3$. Consider $\tau_1(Q) = \{\emptyset, Q, \{l\}, \{l, n\}, \{l, n, o\}\}$, $\tau_2(Q) = \{\emptyset, Q, \{l, o\}, \{l, n, o\}\}$ and $\tau_3(Q) = \{\emptyset, Q, \{n\}, \{l, n, o\}\}$ then $3\tau(Q) = \{\emptyset, Q, \{l\}, \{n\}, \{l, n\}, \{l, o\}, \{l, n, o\}\}$. Hence $3\tau SO(Q) = \{\emptyset, Q, \{l\}, \{n\}, \{l, m\}, \{l, n\}, \{l, o\}, \{m, n\}, \{l, m, n\}, \{l, m, o\}, \{l, n, o\}\}$, $3\tau BO(Q) = \{\emptyset, Q, \{l\}, \{n\}, \{l, m\}, \{l, n\}, \{m, n\}, \{l, o\}, \{l, m, n\}, \{l, m, o\}, \{l, n, o\}\}$ and $3\tau S_b O(Q) = \{\emptyset, Q, \{n\}, \{l, o\}, \{m, n\}, \{l, m, o\}, \{l, n, o\}\}$.

Remark 3.4

(i) From the above example, we conclude that $N\tau$ -open and $N\tau S_b$ -open are independent, since $\{l\} \in 3\tau O(Q)$ but $\{l\} \notin 3\tau S_b O(Q)$ and $\{m, n\} \in 3\tau S_b O(Q)$ but $\{m, n\} \notin 3\tau O(Q)$. (ii) Let $(Q, N\tau)$ be N -topological space, we locate $N\tau S_b$ -open as follows: $N\tau \subseteq N\tau SO(Q) \subseteq N\tau\beta O(Q)$ and $N\tau S_b O(Q) \subseteq N\tau SO(Q) \subseteq N\tau\beta O(Q)$.

Remark 3.5

It is clear from the definition that every $N\tau S_b$ -open subset of a space Q is $N\tau$ semi-open but the reverse is not true in general as shown in the previous example 3.3. That is $\{l\} \in 3\tau SO(Q)$ but $\{l\} \notin 3\tau S_b O(Q)$. Next, we show that an arbitrary union of $N\tau S_b$ -open sets in a N -topological space $(Q, N\tau)$ is $N\tau S_b$ -open.

Proposition 3.6

Let $\{A_i : i \in \Delta\}$ be a family of $N\tau S_b$ -open sets in a N -topological space Q . Then $\cup_{i \in \Delta} A_i$ is an $N\tau S_b$ -open.

Remark 3.7

In example 3.3, the intersection of two $3\tau S_b$ -open sets $\{m, n\}$ and $\{l, m, o\}$ is $\{m\}$ but it is not a $2\tau S_b$ -open. Hence in general, we notice that the family of all $N\tau S_b$ -open subsets of a space Q need not be a topology. Hence it forms a supra topology on Q .

Theorem 3.8

If the family of all $N\tau$ semi-open sets of a space Q is a topology on Q and the intersection of any two $N\tau b$ -closed sets of Q is $N\tau b$ -closed, then the family of $N\tau S_b$ -open is also a topology on Q .

Proof: Obvious.

Corollary 3.9

Let $(Q, N\tau)$ be N -topological space. If Q is extremely disconnected and the intersection of two $N\tau b$ -closed sets is also $N\tau b$ -closed then $N\tau S_b O(Q)$ forms a topology on Q .

Theorem 3.10

A subset A of a N -topological space Q is $N\tau S_b$ -open if and only if $A = \cup G_\alpha$ where A is $N\tau$ semi-open and G_α is $N\tau b$ -closed for each α .

Proof:





Antony George and Davamani Christofer

Let A be $N\tau S_b$ -open. Then A is semi open, and $p \in A$ there exists $N\tau b$ -closed set G_p such that $p \in G_p \subseteq A$. Hence $\cup_{p \in A} G_p \subseteq A$. But $p \in A, p \in G_p$ implies $A \subseteq \cup_{p \in A} G_p$. Hence A is a union of $N\tau b$ -closed sets. Conversely, Let A be $N\tau$ semi-open and $A = \cup_{i \in I} G_i$ where each G_i is $N\tau b$ -closed. Let $p \in A$, then $p \in G_i \subseteq A$ for some i . Hence A is $N\tau S_b$ -open.

Theorem 3.11

A subset S of a N -topological space Q is $N\tau S_b$ -open if and only if for each $p \in S$, there exists an $N\tau S_b$ -open set H such that $p \in H \subseteq S$.

Proof:

Let S be a $N\tau S_b$ -open in Q . Then for each $p \in S$, we have S is $N\tau S_b$ -open set such that $p \in S \subseteq S$. Conversely, let for every $p \in S$, there exists an $N\tau S_b$ -open set H such that $p \in H \subseteq S$. Then S is a union of $N\tau S_b$ -open sets, hence by theorem 3.6, S is $N\tau S_b$ -open.

Theorem 3.12

Let $(Q, N\tau)$ be a N -topological space and every singleton set is $N\tau b$ -closed, then $N\tau SO(Q) = N\tau S_b O(Q)$

Proof:

Let $A \subseteq Q$ and $A \in N\tau SO(Q)$. Suppose $A = \emptyset$ then $A \in N\tau SO(Q)$. Suppose $A \neq \emptyset$, and let $p \in A$. Since every singleton set is $N\tau b$ -closed and $p \in \{p\} \subseteq A$. That is $\{p\} \in N\tau S_b O(Q)$. $N\tau SO(Q) \subseteq N\tau S_b O(Q)$, clearly $N\tau S_b O(Q) \subseteq N\tau SO(Q)$. Hence we may conclude that $N\tau SO(Q) = N\tau S_b O(Q)$.

Theorem 3.13

Let $(Q, N\tau)$ be N -topological space, then the following are true.

- (i) Every $N\tau$ -regular closed set is $N\tau S_b$ -open.
- (ii) Every $N\tau$ -regular open set is $N\tau S_b$ -closed.

Proof:

(i) Let A be regular closed in N -topological space $(Q, N\tau)$, then $A = N\tau-cl(N\tau-int(A))$. Which implies A is $N\tau$ semi-open. Hence A is $N\tau b$ closed. Let $p \in A$ implies $p \in A \subseteq A$. Hence A is $N\tau S_b$ -open. (ii) obvious.
Reverse of the above theorem is need not be true which is shown in the following example.

Example 3.14

Let $Q = \{l, m, n\}$. For $N = 2$. Consider $\tau_1(Q) = \{\emptyset, Q, \{l\}\}, \tau_2(Q) = \{\emptyset, Q\}$ then $2\tau(Q) = \{\emptyset, Q, \{l\}\}$. Here $2\tau RO(Q) = \{\emptyset, Q\}$, and $2\tau S_b O(Q) = \{\emptyset, Q, \{l\}, \{l, m\}, \{l, n\}\}$. Here $\{l\} \in 2\tau S_b O(Q)$ but $\{l\} \notin 2\tau RC(Q)$ and $\{m, n\} \in 2\tau S_b C(Q)$ but $\{m, n\} \notin 2\tau RO(Q)$.

Definition 3.15

A N -topological space X is said to be locally indiscrete if every $N\tau$ -open subset is $N\tau$ -closed.

Definition 3.16

A N -topological space Q is said to be hyperconnected if every non empty $N\tau$ -open subset of Q is $N\tau$ -dense.

Theorem 3.17

If a N -topological space Q is locally indiscrete, then every $N\tau$ semi-open set is $N\tau S_b$ -open.

Proof:

Let A be $N\tau$ semi-open in Q then $A \subseteq N\tau-cl(N\tau-int(A))$. Since Q is locally indiscrete therefore $N\tau-int(A)$ is $N\tau$ -closed. Hence $N\tau-int(A) = N\tau-cl(N\tau-int(A))$. So $N\tau-cl(N\tau-int(A)) = N\tau-int(A) \subseteq A$. So A is $N\tau$ -regular closed. By theorem 3.13(i) A is $N\tau S_b$ -open.





Antony George and Davamani Christofer

Theorem 3.18

An N -topological space Q is hyperconnected, then the only $N\tau S_b$ -open sets of Q are \emptyset & Q .

Proof:

Let $A \subseteq Q$ be a $N\tau S_b$ -open in Q . If $A = Q$ then there is nothing to prove. If $A \neq Q$ we have to prove $A = \emptyset$. Since A is $N\tau S_b$ -open, for each $p \in A$, there exists a $N\tau$ -closed set G such that $p \in G \subseteq A$. So $Q - A \subseteq Q - G$. $Q - A$ is $N\tau$ semi-closed. Therefore, $N\tau\text{-int}(N\tau\text{-cl}(Q - A)) \subseteq (Q - A)$. Since Q is hyper connected and every $N\tau$ dense is $N\tau$ semi-dense then by $N\tau\text{-scl}(N\tau\text{-int}(Q - A)) = Q - A$. Hence $Q - A = Q$. So $A = \emptyset$.

Theorem 3.19

Let $(Q, N\tau)$ be an extremely disconnected N -topological space and $A, B \subseteq Q$, if $A \in N\tau S_b O(Q)$ and $B \in RO(Q)$ then $A \cap B \in N\tau S_b O(Q)$.

Proof:

Let $A \in N\tau S_b O(Q)$ and $B \in N\tau RO(Q)$, then A is $N\tau$ semi-open set, since intersection of a $N\tau$ -open set and $N\tau$ semi-open set is $N\tau$ semi-open, this implies that $A \cap B \in N\tau SO(Q)$. Now let $p \in A \cap B$, $p \in A$ and $p \in B$, therefore there exists a $N\tau$ -closed set G such that $p \in G \subseteq A$. Since Q is extremely disconnected then B is N -regular closed set, this implies that $G \cap B$ is $N\tau$ -closed set, therefore $p \in G \cap B \subseteq A \cap B$. Thus $A \cap B$ is $N\tau S_b$ -open.

Proposition 3.20

If a space $(Q, N\tau)$ is hyper-connected, then $N\tau S_b O(Q) \cap N\tau S_b C(Q) = \{\emptyset, Q\}$.

Theorem 3.21

If a space $(Q, N\tau)$ is locally indiscrete, then $N\tau S_b O(Q) = N\tau SO(Q) = N\tau$.

Proof:

It is sufficient to show that $N\tau$ semi-open $\implies N\tau$ -open. If $B \in N\tau SO(Q)$ then $B \subseteq N\tau\text{-cl}(N\tau\text{-int}(B))$. Since Q is locally indiscrete, Hence $N\tau\text{-cl}(N\tau\text{-int}(B)) = N\tau\text{-int}(B)$.

Theorem 3.22

For any subset A of $(Q, N\tau)$. The following statements are equivalent:

- (i) A is $N\tau$ -regular closed
- (ii) A is $N\tau$ -closed and $N\tau S_b$ -open
- (iii) A is $N\tau$ -closed and $N\tau$ semi-open
- (iv) A is $N\tau\alpha$ -closed and $N\tau$ semi-open
- (v) $N\tau$ pre-closed and $N\tau$ semi-open

Proof: Obvious

The relation of $N\tau S_b$ -open sets to some other types of sets is illustrated in the following:

Definition 3.23

Let $(Q, N\tau)$ be a N -topological space. A set $A \subseteq Q$ is called $N\tau\theta$ -semi open if each $p \in A$, there exists $H \in N\tau SO(Q)$ such that $p \in H \subseteq N\tau\text{-cl}(H) \subseteq A$. The family of all $N\tau\theta$ -semi open subsets of Q is signified as $N\tau\theta SO(Q)$.

Example 3.24

Let $Q = \{l, m, n, o\}$. For $N = 4$. Consider $\tau_1(Q) = \{\emptyset, Q, \{l\}, \{l, n, o\}\}$, $\tau_2(X) = \{\emptyset, Q, \{l, o\}, \{l, n, o\}\}$, $\tau_3(Q) = \{\emptyset, Q, \{n\}, \{l, n, o\}\}$ and $\tau_4(Q) = \{\emptyset, Q, \{l\}, \{l, n\}\}$ then $4\tau(X) = \{\emptyset, Q, \{l\}, \{n\}, \{l, n\}, \{l, o\}, \{l, n, o\}\}$. Here $4\tau SO(Q) = \{\emptyset, Q, \{l\}, \{n\}, \{l, m\}, \{l, n\}, \{l, o\}, \{m, n\}, \{l, m, n\}, \{l, m, o\}, \{l, n, o\}\}$ and $4(Q) = \{\emptyset, Q, \{l, m, o\}, \{m, n\}\}$.





Antony George and Davamani Christofer

Proposition 3.25

Every $N\tau\theta$ -open sets in a N -topological space $(Q, N\tau)$ is an $N\tau S_b$ -open.

Proposition 3.26

Every $N\tau\theta$ -semi open sets in a N -topological space $(Q, N\tau)$ is an $N\tau S_b$ -open.

The following example shows that an $N\tau S_b$ -open set need not be $N\tau\theta$ -semi open.

Example 3.27

Let $Q = \{l, m, n\}$. For $N = 2$. Consider $\tau_1(Q) = \{\emptyset, Q, \{l\}\}$ and $\tau_2(Q) = \{\emptyset, Q, \{l, m\}\}$ then $2\tau(Q) = \{\emptyset, Q, \{l\}, \{l, m\}\}$. Here $2\tau\theta O(Q) = 2\tau\theta SO(Q) = \{\emptyset, Q\}$ and $2S_b(Q) = \{\emptyset, Q, \{l\}, \{l, m\}, \{l, n\}\}$. So we have $\{l, n\}$ is $2\tau S_b$ -open but neither $2\tau\theta$ -semi open nor $2\tau\theta$ -open.

Figure 1 shows the relations among $N\tau S_b O(Q)$, $N\tau SO(Q)$, $N\tau RO(Q)$, $N\tau RC(Q)$, $N\tau\theta O(Q)$, $N\tau\theta SO(Q)$ and $N\tau\alpha O(Q)$.

Remark 3.28

From the figure 1, we conclude the following statements in a N -topological space $(Q, N\tau)$.

- (i) $N\tau RO(Q)$ is incomparable with $N\tau S_b O(Q)$.
- (ii) $N\tau O(Q)$ is incomparable with $N\tau S_b O(Q)$.
- (ii) $N\tau\alpha O(Q)$ is incomparable with $N\tau S_b O(Q)$.
- (iii) $N\tau SO(Q)$ is incomparable with $N\tau S_b O(Q)$

Definition 3.29 Let $(Q, N\tau)$ be N -topological space and $A \subseteq Q$ and $p \in Q$, we introduce the following statements:

- (i) A subset H of Q is said to be $N\tau S_b$ -neighbourhood of p , if there exists an $N\tau S_b$ -open set U in Q such that $p \in U \subseteq H$.
- (ii) $N\tau S_b$ -interior of a set A (briefly $N\tau S_b-int(A)$) is the union of all $N\tau S_b$ -open sets which are contained in A .
- (iii) A point $p \in Q$ is said to be $N\tau S_b$ -limit point of A if for every $N\tau S_b$ -open set G containing, $G \cap (A - \{p\}) \neq \emptyset$. The set of all $N\tau S_b$ -limit points of A is called a $N\tau S_b$ -derived set of A and is denoted by $N\tau S_b D(A)$.
- (iv) $N\tau S_b$ -closure of a set A (briefly $N\tau S_b-cl(A)$) is the intersection of all $N\tau S_b$ -closed sets containing A .

Theorem 3.30

Let A be a any subset of a N -topological space Q . If p is a $N\tau S_b$ -interior point of A , then there exists a $N\tau b$ -closed set F of Q containing p such that $F \subset A$.

Proof:

Let $p \in N\tau S_b-int(A)$. Then there exists $N\tau S_b$ -open set G containing p such that $G \subset A$. Since G is $N\tau S_b$ -open set, there exists a $N\tau b$ -closed set F of Q such that $p \in F \subset G \subset A$.

Theorem 3.31

Let $(Q, N\tau)$ be N -topological space and if $A, B \subseteq Q$ then $N\tau S_b-int(A - B) \subset N\tau S_b-int(A) - N\tau S_b-int(B)$.

Proof:

Let $p \in N\tau S_b-int(A - B)$ then there exists an $N\tau S_b$ -open set G such that $p \in G \subset A - B$. That is $G \subset A$. Since $G \cap B = \emptyset$ and $p \notin B$. Hence $p \in N\tau S_b-int(A)$, $p \notin N\tau S_b-int(B)$. Hence $p \in N\tau S_b-int(A) - N\tau S_b-int(B)$.

Theorem 3.32

Let A be any subset of a N -topological space Q and let $p \in Q$ then $p \in N\tau S_b-cl(A)$ if and only if $A \cap H \neq \emptyset$ for every $N\tau S_b$ -open set H containing p .

Proof:

Let us prove this theorem by method of contra positive. That is $p \notin N\tau S_b-cl(A) \Leftrightarrow$ there exists an $N\tau S_b$ -open set H containing p that does not intersect A . Let $p \notin N\tau S_b-cl(A)$, now $Q - N\tau S_b-cl(A)$ is an $N\tau S_b$ -open set containing p that





Antony George and Davamani Christofer

does not intersect A . Let H be an $N\tau S_b$ -open set containing p that does not intersect A . There fore $Q - H$ is a $N\tau S_b$ -closed set containing A . Hence $N\tau S_b cl(A) \subset (Q - H)$. i.e $p \notin Q - H \implies p \notin N\tau S_b cl(A)$.

Theorem 3.33

Let $(Q, N\tau)$ be N -topological space, and a subset A of Q is $N\tau S_b$ -open if and only if it is a $N\tau S_b$ -neighbourhood of each of its points.

Theorem 3.34

For any two subsets A, B of a N -topological space $(Q, N\tau)$ and $A \subset B$, if A is a $N\tau S_b$ -neighbourhood of a point $p \in Q$, then B is also $N\tau S_b$ -neighbourhood of the same point $p \in Q$.

Proof:

Let A be $N\tau S_b$ - neighbourhood of a point $p \in Q$ and $A \subset B$ then by definition 3.2, there exists a $N\tau S_b$ -open set U such that $p \in U \subset A \subset B$, this implies that B is also a $N\tau S_b$ -neighbourhood of a point p .

Theorem 3.35

Let A be a subset of Q , if for each $N\tau b$ -closed set G of Q containing p such that $G \cap (A - \{p\}) \neq \emptyset$, then a point $p \in Q$ is $N\tau S_b$ -limit point of A .

Proof:

Let U be any $N\tau S_b$ -open set containing p , then for each $p \in U \in N\tau S_b O(Q)$, there exists a $N\tau b$ -closed set G such that $p \in G \subset U$. By hypothesis, we have $G \cap (A - \{p\}) \neq \emptyset$. Hence $U \cap (A - \{p\}) \neq \emptyset$. Therefore, a point $p \in Q$ is $N\tau S_b$ -limit point of A .

Some properties of $N\tau S_b$ -derived sets are sated in the following proposition.

Proposition 3.36

Let A and B be subsets of a space Q . Then we have the following properties:

- (i) $N\tau S_b D(\emptyset) = \emptyset$
- (ii) If $p \in N\tau S_b D(A)$ then $p \in N\tau S_b D(A - \{p\})$
- (iii) If $A \subset B$ then $N\tau S_b D(A) \subset N\tau S_b D(B)$
- (iv) $N\tau S_b D(A) \cup N\tau S_b D(B) \subseteq N\tau S_b D(A \cup B)$
- (v) $N\tau S_b D(A \cap B) \subset N\tau S_b D(A) \cap N\tau S_b D(B)$
- (vi) $N\tau S_b D(N\tau S_b D(A) - A) \subseteq N\tau S_b D(A)$
- (vii) $N\tau S_b D(A \cup N\tau S_b D(A)) \subset A \cup N\tau S_b D(A)$

Proposition 3.37

Let A be a subset of a space Q , then $N\tau S_b-cl(A) = A \cup N\tau S_b D(A)$.

N^*S_b -CONTINUOUS FUNCTION

The aim of this section is to introduce the notions of S_b -continuous in N -topological space $(Q, N\tau)$. Also, we discuss its various properties. Moreover, we relate the above into various continuous maps that are rc -continuous, clopen continuous, contra continuous, contra α -continuous and contra pre-continuous in N -topological space. Throughout this section the N -topological spaces $(Q, N\tau)$, $(R, N\sigma)$ represented by Q and R respectively.

Definition 4.1

A function $f: Q \rightarrow R$ is called N^*S_b -continuous at a point $p \in Q$ if for every $N\sigma$ -open set H of R containing $f(p)$, there exists an $N\tau S_b$ -open set G of Q containing p such that $f(G) \subseteq H$. If f is N^*S_b -continuous at each point $p \in Q$, then it is called N^*S_b -continuous.





Example 4.2

Let $Q = \{l, m, n\}$. For $N = 3$. Consider $\tau_1(Q) = \{\emptyset, Q, \{l\}, \{l, m\}\}$, $\tau_2(Q) = \{\emptyset, Q, \{l, m\}, \{m\}\}$ and $\tau_3(Q) = \{\emptyset, Q\}$ then $3\tau(Q) = \{\emptyset, Q, \{l\}, \{m\}, \{l, m\}\}$. $3\tau BO(Q) = \{\emptyset, Q, \{l\}, \{m\}, \{l, m\}, \{m, n\}, \{l, m\}\}$ and $3\tau S_b O(Q) = \{\emptyset, Q, \{l\}, \{m\}, \{n, m\}, \{l, n\}, \{m, n\}\}$.

From this example, we define $f: Q \rightarrow Q$ by $f(l) = m, f(m) = l$ and $f(n) = n$. Here the inverse image of 3τ -open sets $\{l\}, \{m\}, \{l, m\}$ are $\{m\}, \{l\}, \{l, m\}$ which are $3\tau S_b$ -open.

Definition 4.3

Let $(Q, N\tau)$ and $(R, N\sigma)$ are N -topological space, a function $f: Q \rightarrow R$ is called

- (i) N^* -rc continuous if $f^{-1}(G) \in N\tau RC(Q)$ for every $G \in N\sigma O(R)$.
- (ii) $N^*\theta S$ -continuous if $f^{-1}(G) \in N\tau\theta S(Q)$ for every $G \in N\sigma O(R)$.
- (iii) N^* -clopen continuous if $f^{-1}(G)$ is $N\tau$ -clopen in Q for every $G \in N\sigma O(R)$.
- (iii) N^* -contra continuous if $f^{-1}(G) \in N\tau C(Q)$ every $G \in N\sigma O(R)$.
- (iv) N^* -contra α -continuous if $f^{-1}(G) \in N\tau\alpha C(Q)$ for every $G \in N\sigma O(R)$.
- (v) N^* -contra pre-continuous if $f^{-1}(G) \in N\tau PC(Q)$ for every $G \in N\sigma O(R)$.

Example 4.4

Let $Q = \{1, 2, 3, 4\}$. For $N = 4$. Consider $\tau_1(Q) = \{\emptyset, Q, \{1\}, \{2\}, \{1, 2\}\}$, $\tau_2(Q) = \{\emptyset, Q, \{1\}, \{1, 3\}, \{1, 4\}\}$, $\tau_3(Q) = \{\emptyset, Q, \{4\}, \{2, 4\}, \{1, 2, 4\}\}$ and $\tau_4(Q) = \{\emptyset, Q, \{4\}, \{2, 4\}, \{1, 2, 4\}\}$ then $4\tau O(Q) = \emptyset, Q, \{\{1\}, \{2\}, \{4\}, \{1, 2\}, \{1, 3\}, \{1, 4\}, \{2, 4\}, \{1, 2, 3\}, \{1, 2, 4\}\}$, $4\tau RO(Q) = \emptyset, Q, \{2\}, \{4\}, \{1, 3\}, \{2, 4\}, \{1, 2, 3\}, \{1, 3, 4\}$ and $4\tau S_b O(Q) = \{\emptyset, Q, \{4\}, \{1, 3\}, \{2, 4\}, \{1, 2, 3\}, \{1, 3, 4\}\}$.

Let $R = \{l, m, n, o\}$. For $N = 4$. Consider $\sigma_1(R) = \{\emptyset, R, \{n\}\}$, $\sigma_2(R) = \{\emptyset, R, \{o\}\}$, $\sigma_3(R) = \{\emptyset, R, \{l, m, n\}\}$ and $\sigma_4(R) = \{\emptyset, R, \{o\}, \{n\}, \{n, o\}\}$ then $4\sigma(R) = \{\emptyset, Y, \{n\}, \{n, o\}, \{o\}, \{l, m, n\}\}$. Define $f: X \rightarrow Y$ by $f(1) = l, f(2) = o, f(3) = m, f(4) = n$.

- (i) Here the inverse image of every 4σ -open set in R is 4τ -regular closed in Q . Hence f is 4^* -rc continuous.
- (ii) Here inverse image of every 4σ -open set in R is 4τ -clopen in Q . Which implies that f is 4^* -clopen continuous.
- (iii) Here inverse image of every 4σ -open set in R is 4τ -closed in Q . Which implies that f is 4^* -contra continuous.
- (iv) Here inverse image of every 4σ -open set in R is $4\tau\alpha$ -closed and 4τ pre-closed in Q . Which implies that f is 4^* -contra α -continuous and 4^* -contra pre-continuous in Q .

Theorem 4.5

Let Q and R be two N -topological spaces. A mapping $f: Q \rightarrow R$ is N^*S_b -continuous on $Q \iff f^{-1}(B) \in N\tau S_b O(Q)$ every $B \in N\sigma O(R)$.

Proof:

Let $B \in N\sigma O(R)$. If $f^{-1}(B) = \emptyset$, then it is obviously $N\tau S_b$ -open. If $f^{-1}(B) \neq \emptyset$, then every $z \in f^{-1}(B) \implies f(z) \in B$. Since f is $N\tau S_b$ -continuous, then there exists $G \in N\tau S_b O(Q)$ containing z such that $f(G) \subseteq B$. Then $f^{-1}(B)$, being the union of $N\tau S_b$ -open sets are $N\tau S_b$ -open in Q . The converse follows from the definition.

Corollary 4.6

Every N^*S_b -continuous function is N^* -semi continuous.

Proof:

Suppose $f: Q \rightarrow R$ is $N\tau S_b$ -continuous function then for every $B \in N\sigma O(R)$, $f^{-1}(B)$ is $N\tau S_b$ -open in Q . Since every $N\tau S_b$ -open is $N\tau$ semi-open. Hence f is N^* -semi continuous.

The following example shows that the reverse of the above corollary is false.





Antony George and Davamani Christofer

Example 4.7

Let $Q = \{l, m, n\}$. For $N = 3$. Consider $\tau_1 = \{\emptyset, Q, \{l\}\}$, $\tau_2 = \{\emptyset, Q, \{l, m\}\}$ and $\tau_3 = \{\emptyset, Q\}$. Then $3\tau = \{\emptyset, Q, \{l\}, \{l, m\}\}$. Define a function $f: Q \rightarrow Q$ as follows $f(l) = f(m) = b$ and $f(n) = b$. Then f is 3^* -semi continuous but not a 3^*S_b -continuous.

Theorem 4.8

A function $f: Q \rightarrow R$ is N^*S_b -continuous if and only if f is N^* -semi continuous and for every $p \in Q$ and every $N\sigma$ -open set U of R containing $f(p)$, there exists a $N\tau b$ -closed set H of Q containing p such that $f(H) \subseteq U$.

Proof:

Suppose $f: Q \rightarrow R$ is a N^*S_b -continuous and let $p \in Q$ and for every $U \in N\sigma O(R)$ containing $f(p)$, there exists an $N\tau S_b$ -open set V of Q containing p such that $f(V) \subseteq U$. Since V is $N\tau S_b$ -open set, then for every $p \in V$, there exists a $N\tau b$ -closed set H of Q such that $p \in H \subseteq V$. Thus we have $f(H) \subseteq U$, and N^*S_b -continuous always implies N^* -semi continuous.

Conversely, Let $U \in N\sigma O(R)$, we shall prove $f^{-1}(U)$ is $N\tau S_b$ -open set in Q . Since f is N^* -semi continuous, then $f^{-1}(U) \in N\tau SO(Q)$. Let $p \in f^{-1}(U)$ which implies $f(p) \in U$, by assumption there exists a $N\tau b$ -closed set H of Q containing p such that $f(H) \subseteq U$, which implies $p \in H \subseteq f^{-1}(U)$, thus $f^{-1}(U)$ is $N\tau S_b$ -open in Q . Hence by theorem 4.5, f is N^*S_b -continuous.

Proposition 4.9

The following statements are equivalent for a function $f: Q \rightarrow R$

- (i) f is N^* -rc continuous
- (ii) f is N^*S_b -continuous and N^* -contra continuous
- (iii) f is N^* -semi continuous and N^* -contra continuous
- (iv) f is N^* -semi continuous and N^* -contra α -continuous
- (v) f is N^* -semi continuous and N^* -contra pre-continuous

Proof: It follows from theorem 3.22.

CONCLUSION

This article introduced the concept of $N\tau S_b$ -open sets and its properties. Also we gave a connection with a classical open sets $N\tau\theta$ -semi open sets. Further more, we find the relationship between N^*S_b -continuous and various continuous functions in N -topological space. In future, this concept can be extended to Ideal topology, Supra topology, Fuzzy topology, Nano topology, Generalized topological space and so on.

REFERENCES

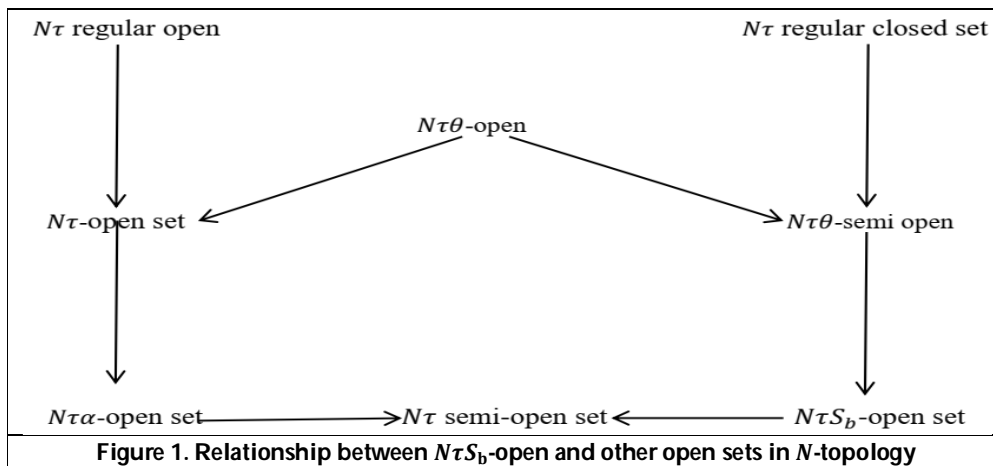
1. M. Lellis Thivagar., V. Ramesh and M. Arockia Dasan, On the new structure of N - topology, Cogent Mathematics, 3: 120410, (2016).
2. M. Lellis Thivagar and M. Arockia Dasan. New Topologies via Weak N -topological open sets and mappings, Journal of New theory 49-57, 2019.
3. N. Levine, Semi-open sets and semi continuity in topological spaces, The American Mathematical Monthly, vol. 70, no. 1, pp. 36-41, 1963.
4. N. Biswas, One some mappings in topological spaces. Bull. Calcutta Math Soc., 61, 61-127, 1969.
5. M. E. Abd El-Monsef, S. N. El-Deeb and R. A. Mahmoud, β -open sets and β -continuous mappings, Bull. Fac. Sci. Assiut Univ., 12, 77-90, 1983.





Antony George and Davamani Christofer

6. D. Andrijevic, On b-open sets, Mat. Vesnik, 48, 59-64, 1996.
7. J. Dontchev. Contra-continuous functions and strongly S -closed spaces. Internat. J. Math. And Math. Sci., 19(2): 303-310, 1996.
8. J. Loyala Foresith Spencer, M. Davamani Christofer, Theta open sets in N -topology, Ratio Mathematica, vol 43, 163-175, 2022.
9. J. Loyala Foresith Spencer, M. Davamani Christofer, Door spaces on N -topology, Ratio Mathematica, vol 47, 2023.





A Comprehensive Drug Review on the Ingredients of Siddha Herbal Preparation “Swasakasa Nei” Indicated for “Swasakasam (Bronchial Asthma)” among its Medicinal uses, Phytoconstituents, Pharmacological Actions and Safety Profile

A. Siva^{1*}, H.Vetha Merlin Kumari², T. Lakshmikantham³ and R. Meenakumari⁴

¹PG Scholar, Department of Maruthuvam, National Institute of Siddha, Tambaram Sanatorium, Chennai, Tamil Nadu, India.

²Associate Professor, Department of Maruthuvam, National Institute of Siddha, Tambaram Sanatorium, Chennai, Tamil Nadu, India.

³Associate Professor, Head of the Department (i/c), Department of Maruthuvam, National Institute of Siddha, Tambaram sanatorium, Chennai, Tamil Nadu, India.

⁴Director, National Institute of Siddha and Director General (Additional Charge), CCRS, Tambaram Sanatorium, Chennai, Tamil Nadu, India.

Received: 30 Dec 2022

Revised: 25 Apr 2023

Accepted: 19 May 2023

*Address for Correspondence

A. Siva

PG Scholar,

Department of Maruthuvam,

National Institute of Siddha,

Tambaram Sanatorium,

Chennai, Tamil Nadu, India.

E.Mail: drsivasiddha@yahoo.com



This is an Open Access Journal / article distributed under the terms of the **Creative Commons Attribution License** (CC BY-NC-ND 3.0) which permits unrestricted use, distribution, and reproduction in any medium, provided the original work is properly cited. All rights reserved.

ABSTRACT

Siddha is one of the ancient medical systems in India considered as the mother medicine of ancient Tamils/Dravidians in South India. The word Siddha means established truth. According to Siddha system of medicine, diseases are classified into 4448 types. When the normal equilibrium of three humors (vatha, pitha and kapha) is disturbed, diseases occur. The factors which affect this equilibrium are environment, climatic conditions, diet, physical activities and stress. *Swasakasam* is attributed to the derangement of Kaphahumour. Asthma is a common chronic inflammatory disorder of the airways that is characterized by variable and recurring symptoms, airflow obstruction, bronchial hyper-responsiveness, and underlying inflammation. In *swasakasam* disease Kapha humuor was dearranged that lead to imbalance in Five Elements. The correction of the imbalance is made by substituting the drug which is predominately of the opposite nature (Pungent, Astringent and Bitter). According to Siddha

57780





Siva et al.,

system of medicine anti-asthmatic drug should have properties such as hot (*Vemmai*) potency to neutralizes the *Vaatha kuttram and kaba kuttram*. Medicinal plant used for the treatment of asthma should have anti-inflammatory, immunomodulatory, anti-histaminic, smooth-muscle relaxants and allergic activity. Current asthma therapy lacks satisfactory success due to adverse effect, hence patients are seeking complementary and alternative medicine to treat their asthma. This review discusses mainly about the medicinal uses, phytoconstituents, pharmacological actions, and safety profile of the ingredients of *Swasakasa Nei*. And also, *Swasakasa Nei* may be an alternative management of Bronchial asthma by the way effective with low-risk. *Bhramathandu ver and Vellerukkuilai* are the ingredients of the *Swasakasa Nei*.

Keywords: *Swasakasam*, Bronchial Asthma, Siddha medicine, *Swasakasa Nei*, **Argemone Mexicana (*Brahmathandu*)**, *Calotropis procera(Vellerukku)*, Drug review.

INTRODUCTION

Siddha is one of the ancient medical systems in India considered as the mother medicine of ancient Tamils /Dravidians in South India. The word Siddha means established truth [1]. According to Siddha system of medicine, diseases are classified into 4448 types [2]. When the normal equilibrium of three humors (vatha, pitha and kapha) is disturbed, diseases occur. The factors which affect this equilibrium are environment, climatic conditions, diet, physical activities and stress. *Swasakasam* is attributed to the derangement of Kapha humour. The amplified kapha humour alone or otherwise associated with other deranged humours, either vatham or pitham affects the throat, nose, respiratory air ways and lungs [3]. According to Theraiyar in his *Pengal Muthal Karanam*, Kapha humour is one of the major and important cause for *Swasakasam*. He described this as,

“Kabaththinai yandrik kaasa swaasam – kaanaathu”

- Theraiyar[4]

According to the text *Yugi Vaithiya Chinthamani*, In *Kaasanoi padalam*, *Kaasam* are classified into 12 types. *Swasakasam (Izhuppu erumal or Isivu erumal)* is one among them [3]. In siddha Maruthuvam podhu, *Swasakasam (Eraippu Noi)* is classified into 5 types, such as *Vali Eraippu, Iyya Eraippu, Iyyavali Eraippu, Mukkutra Eraippu, and Melnokku Eraippu*[5]. Asthma is a common chronic inflammatory disorder of the airways that is characterized by variable and recurring symptoms, airflow obstruction, bronchial hyper-responsiveness, and underlying inflammation. The interactions between these factors determine the range of symptoms, severity, and the response to treatment [6]. It is identified by the history of respiratory symptoms such as wheeze, shortness of breath, chest tightness and cough that vary over time and in intensity, together with variable expiratory airflow limitation [7].

Asthma is initiated by multiple interactions between inflammatory cells and mediators. After an exposure to a triggering factor, inflammatory mediators are released from mast, macrophages, T-cells and epithelial cells. This causes attraction of other inflammatory cells mainly eosinophil into the pulmonary tissues. This leads to lung injury, mucus hyper-secretion and smooth muscle hyperactivity. Furthermore, at least 27 cytokines and 18 chemokines plays role in asthmapathophysiology [8]. Th2 lymphocytes cytokines [interleukin IL-4, IL-5, and IL-13] and Th1 cytokine interferon-gamma are the main ones to provoke allergy and asthma [9]. Asthma affects 5-10% of the population or an estimated 23.4 million persons, including 7 million children [10]. The overall prevalence rate of exercise-induced bronchospasm is 3-10% of the general population if persons who do not have asthma or allergy are excluded, but the rate increases to 12-15% of the general population when patients with underlying asthma are included. Asthma affects an estimated 300 million individuals worldwide. Annually, the World Health Organization





Siva et al.,

(WHO) has estimated that 15 million disability-adjusted life-years are lost and 250,000 asthma deaths are reported worldwide [11]. The drugs used by the Siddhars could be classified into three groups as *Mooligai/Thavaram* (Herbal product), *Thathu* (Inorganic substances), and *Jeevam or Sangamam* (Animal products) [4].

“Ver paaruu thazai paaruu minjinakkal
Mellamella parpa chendooram pare”

As per the above mentioned statement from *Siddha marthuvanga churukkam* [2] explains, herbal drugs are used for treatment in preliminary stage of disease and the higher order medicines are used in chronic stage if herbal drugs cannot cure the severe diseases. *Bhramathandu* and *Vellerukku ilai* are the ingredients of the *Swasakasa Nei*. Both are from plant origin. In Siddha system of medicine treatment is mainly based on *Panchabhootham* (Five elements) and *Suvai* (taste). On the basis of Five Elements (*Panchabhootham*) theory, drugs are divided into five major categories based on the predominant element they possess. *Suvai* (Taste) has got significant place in Siddha. Our tongue experiences these tastes when a drug is administered orally. The dynamics of Siddha preparations are based on taste parameters. Six tastes are known as sweet, sour, salt, pungent (spicy), bitter and astringent. Their relationship with five elements are explained in follow, such as *Inippu* (Sweet)- earth + water, *Pullippu* (Sour)- earth + fire, *Uppu* (Salt)- water + fire, *Kaippu* (Bitter)- air+ space, *Kaarppu* (Pungent) – air+ fire, *Thuvorppu* (Astringent)- earth + air. *Gunam* (Property/Character); Siddha Pharmacology describes 21 characters of drugs like lightness, dryness etc, which are comparable to physical property of the drugs. *Pirvu* (Bio transformation) is said to be the post absorptive taste or taste of the drug after absorption which is considered to be an important aspect in treatment modality. *Veeriyam* (potency) is described as active constituent of the drug. This constituent is responsible for pharmacological activity of the medicinal herb and other drugs. The drugs have cold and hot potency. *Vemmai* (hot) potency neutralizes the *Vaatha kuttram* and *Kaba kuttram*. *Thanmai* (cold) potency neutralizes the *Pitha kuttram*. This concept was described by *Kannusamiyam*[4].

In *swasakasam* disease kaphahumour was dearranged that lead to imbalance in Five Elements. The correction of the imbalance is made by substituting the drug which is predominately of the opposite nature (Pungent, Astringent and Bitter). According to Siddha system of medicine anti-asthmatic drug should have properties such as hot (*Vemmai*) potency to neutralizes the *Vaatha kuttram* and *Kaba kuttram*. Medicinal plant used for the treatment of asthma should have anti-inflammatory, immunomodulatory, antihistaminic, smooth-muscle relaxants and allergic activity [12]. Antioxidant supplements are effective in reducing bronchoconstriction severity by inhibiting pro-inflammatory events as a result of neutralizing the effects of excess reactive oxygen species and reactive nitrogen species [13]. Current asthma therapy lacks satisfactory success due to adverse effect, hence patients are seeking complementary and alternative medicine to treat their asthma [14]. This review discusses mainly about the medicinal uses, phytoconstituents, pharmacological actions, and safety profile of the ingredients of *Swasakasa Nei*. And also, *Swasakasa Nei* may be an alternative management of Bronchial asthma by the way effective with low-risk.

ADVERSE EFFECTS OF CURRENT TREATMENTS USED IN ASTHMA [15, 16]

Isoprenaline

Causes tachycardia

Salbutamol

Muscle tremors (dose related), palpitation, restlessness, nervousness, throat irritation and ankle oedema.

Theophylline

Convulsions, shock, arrhythmias, increased muscle tone, tachypnoea, (dose dependent) flushing, hypotension, restlessness, tremors, vomiting, palpitation, diuresis, dyspepsia, insomnia etc.

Anticholinergics

Dry mouth, difficulty in swallowing and talking, scarlet rash, photophobia, blurring of near (Atropine and its congeners) vision, palpitation, ataxia, delirium, hallucinations, hypotension, weak and rapid pulse, cardiovascular collapse with respiratory depression, convulsions and coma (in severe poisoning).



**Ketotifen**

Sedation, dizziness, dry mouth, nausea and weight gain.

Corticosteroids

Cushing's habitus, fragile skin, purple striae, hyperglycemia, muscular weakness, susceptibility to infection, delayed healing of wounds and surgical incisions, peptic ulceration, osteoporosis, glaucoma, growth retardation, psychiatric disturbances, suppression of hypothalamo-pituitary-adrenal (HPA) axis etc. As a consequence, the search for effective low-risk, non-drug strategies that provide a valuable adjunctive or alternative treatment in asthma management is clinically attractive and relevant. There is much interest in complementary and alternative medicine, and its use in the management and treatment of asthma is growing at a significant rate [17].

REVIEW OF LITERATURE***Argemone mexicana*. Linn (*Brahmathandu*)**

Argemone mexicana, known as Mexican poppy or Mexican prickly poppy, is a species of poppy found in Mexico and now in the United States, India and Ethiopia. The plant is pantropic in distribution and it is a weed in waste places. It is native to America and naturalized throughout India. It is poisonous, but has been used medicinally by parts of Mexico. [18, 19]. *Argemone mexicana* tends to grow along roadsides, in fallow and cultivated lands, riverbanks, disturbed areas, and on floodplains. It competes with and replaces native species in some cases and is also a significant crop weed [20, 21]. In India, it grows in the temperate region as a weed in waste lands, cultivating fields and road sides. It prefers light sandy well-drained soil and also grows in nutritionally poor acidic, neutral and basic (alkaline) soil. [22]

Taxonomic Classification [23,24]

Kingdom	: Plantae
Division	: Magnoliophyta
Class	: Magnoliopsida/Dicotyledons
Subclass	: Magnoliidae
Order	: Papaverales
Family	: Papavaraceae
Genus	: <i>Argemone</i>
Species	: <i>Argemone mexicana</i> Linn.

Authenticated name of *Argemone mexicana* Linn. According to IPNI

Argemone mexicana Linnaeus, Species Plantarum 2 1753.

Argemone mexicana Linnaeus, Sp. Pl. 1: 508. 1753.

Vernacular names [25, 26]

Tamil	: Kudiyotti, Kurukkamchedi, Brahmathandu, Brahmathandi
English	: Mexican prickly poppy, flowering thistle, cardo or cardosanto, The yellow thistle, Yellow Mexican poppy, Prickly poppy.
French	: Argemone;
German	: Doppelklappen;
Sanskrit	: Swarnaksheeri, Kanchani, Karshani, Hemadugdha, TiktaDugdha, Brahmadandi, Sringala-Kanta.
Hindi	: Satyanasi, Kataila, Bharbhand, Shirajal-kanta.
Urdu	: Baramdaandi;
Bengali	: Siyal-Kanta; Bharband;
Kannada	: Datturigidda, Arasina-umatta, Datturi.
Malayalam	: Ponnummattu, Brahma-dandi.





Siva et al.,

Manipuri	: <i>Khomthongpee</i> ;
Marathi	: <i>Firangidhotra</i> ;
Punjabi	: <i>Bhataiktheya</i> ;
Telugu	: <i>pichikusuma, Brahma-dauid-chettu</i>

Therapeutically useful parts of *A. mexicana* Linn

Latex (Paal), Flowers (Malar), Seeds and seed oil (Vithai), Stem (Thandu), Root (Ver), Whole plant (Samoolam) were used medically in Siddha system of medicine [25]. [Figure 1]

Botanical Description

Argemone mexicana is an erect annual herb, growing up to 100 to 150 cm with a slightly branched tap root. Its stem is branched and extremely prickly and oblong in cross-section. It exudes a yellow juice when cut. Leaves are 5 to 11 cm long, alternate, without leaf stalks (petioles), toothed (serrate) and the margins are spiny. [27]. They are more or less blotched with green and white veins, stand out against the bluish-green upper leaf surface. Flowering/Fruiting time of *Argemone* species starts from January-May. Flowers are complete, bisexual, i.e., with functional male (androecium) and female (gynoecium), including stamens, carpels and ovary. Pollination is entomophilous i.e., by insects [28]. They are at the tips of the branches (are terminal), solitary, and scentless and of 2.5-5 cm diameter with six petals bright yellow or rarely pale lemon yellow; stamens 30-50, filaments yellow, pistil 4-6-carpellate. Fruit is a prickly oblong or egg-shaped (ovoid) capsule. Seeds are brownish black coloured, very numerous, nearly spherical, covered in a fine network of veins and about 1 mm in diameter. [29]

Organoleptic characters & Therapeutic actions of *Argemone mexicana* Linn (*Brahmathandu*) [25]

Organoleptic characters

Taste (<i>Suvai</i>)	: Bitter (<i>Kaippu</i>)
Character (<i>Thanmai</i>)	: Hot (<i>Vetpam</i>)
Division (<i>Pirivu</i>)	: Pungent (<i>Karppu</i>)

Therapeutic actions

Root (*Ver*)

- ◆ Anodyne (*Thuyaradakki*)
- ◆ Alterative (*Udalthetri*)
- ◆ Seed oil (*Vithaiennai*)
- ◆ Laxative (*Malamilakki*)
- ◆ Sedative (*Thaathuveppagatri*)
- ◆ Naustant (*Kumattalagatri*)
- ◆ Expectorant (*Kozhaiyagatri*)

Chemical constituents of whole plant and root of *Argemone mexicana* Linn (*Brahmathandu*) [24, 30]

Chemical constituents

Whole plant [24]

- | | | |
|-------------------|---------------------------|------------------------|
| ◆ Argemexicaine A | ◆ (+)-Cheilanthifoline | ◆ Oxyberberine |
| ◆ Argemexicaine B | ◆ Dehydrocheilanthifoline | ◆ Oxyhydrastinine |
| ◆ Argemexirine | ◆ Dehydrocorydalmine | ◆ O-Methylzanthoxyline |
| ◆ Arnottianamide | ◆ Dihydrocoptisine | ◆ Quercetin, |
| ◆ Angoline | ◆ Dihydrosanguiranine | ◆ Rutin |
| ◆ Chelerythrine | ◆ Jatrorrhizine | ◆ (-)-Stylopine |
| ◆ Columbamine | ◆ Muramine | ◆ Thalifoline |

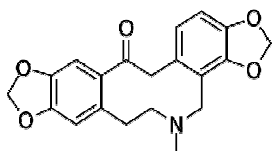




Siva et al.,

- ◆ Coptisine
- ◆ Cryptopine
- ◆ Nor-Chelerythrine
- ◆ Nor-Sanguinarine
- ◆ (±)-Tetrahydrocoptisine
- ◆ (-)-Tetrahydroberberine

Root [30]

◆ **Protopine**[C₂₀H₁₉NO₅]

- ◆ Berberine
- ◆ Chelerythrine
- ◆ Coptisine
- ◆ Galanthamine
- ◆ Magnoflorine
- ◆ Palmatine
- ◆ Sanguinarine
- ◆ β-sitosterol

Molecular docking analysis

Protopine interaction with A: ASP-284 and form a bond of attraction with its oxycycle nucleus, the protopine contains two bezodioxole group which interacted with A: THR-293 and A: TYR-294 by forming hydrogen and carbon hydrogen bond while the next bezodioxole group interacted with A: LYS-288 and A: Tyr-289 by forming the alkyl bonds. The benzene units interacted with A: PHE-283 to form pi-pi T shaped interaction to stabilize the complex with Protopine.

S. No	Name of Ligand	Binding Energy Kcal/mole	Inhibitory Constant (μM)	Hydrogen Bond
1	Protopine	- 6.07	36.03	A: THR-293, A:TYR-294

Molecular docking analysis revealed that **Protopine** could be potential RdRp inhibitors of SARS-CoV-2[31].

Pharmacological activities of *Argemone mexicana* Linn (*Brahmathandu*):**Anti-Asthmatic activity**

The ethanol extract of *A. mexicana* roots possesses significantly extended the latent period of convulsion as compared to standard (*Ketotifen fumarate*) in Histamine and acetylcholine induced bronchospasm in guinea pigs [32]

Anti-stress and Anti-allergic activity

Both the polar extracts (i.e. aqueous and methanolic) of *A. mexicana* stems were evaluated to exert anti-allergic as well as anti-stress efficacy in asthma developed by milk-induced leucocytosis and milk-induced eosinophilia at a dose of 50 mg/kg i.p. in albino mice model; both of the test extracts showed significant (p<0.05) decrease in leucocytes and eosinophils in vivo. [33]

Antioxidant activity

The ethanol extract of *A. mexicana* roots possesses antioxidant activity; at a dose of 100 μg/mL concentration, the extract showed high scavenging activity against DPPH (85.17%), ABTS (75.27%) and H₂O₂ (84.25%) radicals. [34]

Analgesic, Locomotor, Muscle relaxant, Anxiolytic and Sedative activities

The ethyl acetate and methanol extract of the whole plant of *A. mexicana* exhibited analgesic, locomotor and muscle relaxant activity in Wistar albino mice at an oral dosage of 100, 200 and 400 mg/ kg b.w. Both extracts showed significant activities but methanol extract at a dosage of 200 mg/kg body weight was found to be more potent for central nervous system activities such as analgesic, anxiolytic and sedative effects. [35]

Sedative activity

A study evaluating the anxiolytic and sedative effects of *A. mexicana* shed light on significant central and peripheral nociceptive activity on Swiss albino mice. Methanolic and ethyl acetate extract have also showed significant decrease in motor activity and fall off time of animals on rotating rod. This study demonstrated that phytochemicals such as





Siva et al.,

flavonoids, steroids, alkaloids and tannins present in plant extracts may be responsible for the CNS depressant activity [36].

Anxiolytic activity

The anxiolytic-like effect of ethanolic extract of *A. mexicana* was investigated in Wistar rats. Phytochemical screening confirmed the presence of alkaloids, terpenoids, sterols, steroids, flavonoids and quinones in the extracts which are intrinsically related to some action on the central nervous system. In order to examine the anxiolytic-like effect on Elevated Plus Maze (EPM) test, the alkaloid-enriched extract was administered to independent groups of animals at a dose of 200 µg/kg and results were analysed in terms of reduced anxiety index. It has been observed that ethanolic extract of *A. mexicana* (100 and 200 mg/Kg, respectively) and alkaloids mixtures (200 µg/ml) significantly reduces anxiety index similar to standard diazepam (2 mg/kg); indicating that this plant exerts anxiolytic effects due to its alkaloids and this action is probably mediated through gamma-aminobutyric acid (GABAA) receptor chloride channels. [37]. Important chemical constituents and their pharmacological activities of root of ***Argemone mexicana* Linn (Brahmathandu)** are described in table No 1. [38-45].

Toxicological Aspects of *Argemone mexicana* Linn (Brahmathandu):

Acute toxicity study

The oral acute toxic study results indicated no significant alterations in final body weight, organ weights, blood parameters and microscopic anatomy of ovaries, the uterine Horns and liver of rats treated with ethanolic extract of root of *Argemone mexicana* in comparison with the mastery group. Further, during the study period of **14 days** there were no noticeable signs of acute toxicity. Lack of death at all doses showed that the LD50 of ethanolic extract of root of *Argemone mexicana* is greater than 5000 mg/kg body weight. [46]

***Calotropis procera*. Linn (Vellerukku)**

C. procera (Aiton) R.Br. is a small shrub belonging to family Asclepiadaceae, and commonly known as milkweed or giant weed. It is commonly grown in wastelands and roadside area. There is a number of species of *Calotropis* but most commonly available species include *C. sussuela*, *C. acia* Buch, *C. gigantean* (Linn), and *C. procera*. However, *C. gigantean* and *C. procera* are mostly found in the region of India. *C. procera* is drought resistant, salt tolerant and it disperses seeds through wind and animals. It quickly becomes recognized as a weed along degraded roadsides and overgrazed native pastures [47]. In Siddha system of medicine, the plant *Calotropis procera* was known as "Vellerukku". The medicinal potential of *Calotropis procera* has been known to traditional systems of medicine for a while now with its leaves being widely used [48].

Taxonomic classification [49-50]

Kingdom	: Plantae
Subkingdom	: Tracheobionta
Super division	: Spermatophyta
Division	: Magnoliophyta
Class	: Magnoliopsida
Subclass	: Asteridae
Order	: Gentianales
Family	: Asclepiadaceae
Genus	: <i>Calotropis</i>
Species	: <i>Calotropis procera</i> Linn.





Siva et al.,

Vernacular names [51-53]

Tamil	: Vellerukku
English	: calotrope, calotropis, dead Sea fruit, desert wick, giant milkweed, swallow- wort, mudar fibre, rubber bush, rubber tree, Sodom apple
Hindi	: madar, akada, akdo, aak
Marathi	: rui, mandara
Punjabi	: ak
Arab	: Usher
Malayalam	: Erukka
Kannadam	: Yakkeda-gid
Sanskrit	: arka, alaka, ravi
Telgu	: jilledu
Urdu	: madar, aak

Therapeutically useful parts of *C. procera* Linn

Latex (*Paal*), Fresh or dried Leaves (*Ilai*), Flowers (*Poo*), Stem Bark (*Pattai*), Roots and Root Bark (*Ver and Ver pattai*), Whole plant (*Samoolam*) were used medically in Siddha system of medicine [25]. [Figure 2]

Botanical description [54]

Morphologically, *Calotropis procera* is multi branched shrub with yellowish barks having white, soft and corky fissures. Leaves are simple, opposite, sub sessile, blade broadly ovate and oblong. It has relatively few leaves, mostly concentrated near the growing tip. The leaf blades are light to dark green with nearly white veins. They are 7 to 18 cm long and 5 to 13 cm broad, slightly leathery, and have a fine coat of soft hairs that rub off. It is densely blossomed and the flowers are white in color, pentamerous and hermaphrodite. Its fruit is simple, inflated and contains numerous brown colored seeds with white silky hairs. Matured fruits erupt to disperse seeds which are widely spread by wind and animals.

Organoleptic characters & Therapeutic actions of *Calotropis procera*. Linn (*Vellerukku*)[25]**Organoleptic characters**

Taste (<i>Suvai</i>)	: Bitter (<i>Kaippu</i>), Pungent (<i>Karppu</i>), Sweet (<i>Madhuram</i>)
Character (<i>Thanmai</i>)	: Hot (<i>Vetpam</i>)
Division (<i>Pirivu</i>)	: Pungent (<i>Karppu</i>)

Therapeutic actions**Leaf (*Ilai*):**

- ◆ Anthelmintic (*Puzhukkollu*)
- ◆ Alterative (*Udalthetri*)
- ◆ Laxative (*Malamilakki*)
- ◆ Stimulant (*Veppamundakki*)
- ◆ Flower (*Poo*)
- ◆ Expectorant (*Kozhaiyagatri*)
- ◆ Stomachic (*Pasithe undakki*)
- ◆ Digestive (*Seripundakki*)
- ◆ Tonic (*Uramakki*)





Siva et al.,

Latex (Paal):

- ◆ Rubefacient (Thadipundakki)
- ◆ Deodorant (Natramagatri)

Root bark (Ver pattai):

- ◆ Febrifuge (Veppagatri)
- ◆ Alterative (Udalthetri)
- ◆ Stimulant (Veppamundakki)
- ◆ Tonic (Uramakki)
- ◆ Diaphoretic (Viyarvaiperukki)
- ◆ Emetic (Vaanthiundakki)

List of medicinal preparation by *Calotropis procera* in Siddha system of medicine:

Medicine Name	Used parts	Indications
◆ <i>Vellerukkan Samoolaparpam</i>	Whole plant (<i>Samoolam</i>)	<i>Eraippirumal</i>
◆ <i>Swasakudori Maathirai</i>	Flower (<i>Poo</i>)	<i>Eraippirumal</i>
◆ <i>Vatha sura kudineer</i>	Whole plant (<i>Samoolam</i>)	<i>Suram, kaasam</i>
◆ <i>Kaanthachendooram</i>	Flower Juice (<i>Poo chaaru</i>)	<i>Nalirsuram, Paandu</i>
◆ <i>Linga chendooram</i>	Flower (<i>Poo</i>) or leaf (<i>Ilai</i>)	<i>Linga putru, Yoni putru</i>

Chemical Constituents of latex and leaf of *Calotropis procera*. Linn (*Vellerukku*)**Chemical Constituents of latex:**

The latex was acidic in nature, with specific gravity of 1.021 and contains 14.8% solids. A nontoxic proteolytic enzyme, calotropin (2-3%) and a powerful bacteriolytic agent were isolated from the latex [55]. It contains water and water soluble 88.4 to 93%, coagulate 0.8 to 2.5, calactin, calotropagenin, calotropin, calotoxin, L-lactuciferol, rproceroid, syriogenin, tetraxasterol, uscharin, uscharidin, uzarigenin, voruscharin, β -amyirin, calotropeol, 3-epimoretenol lupeol, 57788osthum, active labenzyme and a heart poison traces of orthohydroxy phenol [56]. 2, 6 dimethyl tetra-1, 5-decaene and 3, 7, 11-Trimethyl 2, 6, 10, 12-pentadecatrien-1-ol were also isolated from the latex [57].

The latex contains two distinct cysteine peptidase, procerain and procerain B. However, new cysteine peptidases were purified from *C. procera* latex. The purified enzymes exhibited plasma-clotting activity mediated by a thrombin-like mechanism [58]. The amino acid composition of the dialyzable fraction of crude latex produced by the green parts of the plant was included: aspartic acid, glutamic acid, serine, glycine, histidine, arginine, threonine, alanine, proline, tyrosine, valine, methionine, isoleucine, leucine, phenylalanine and lysine [59]. Various cardiac glycosides including calotropin, calactin, calotoxin, usharin, usharidin and voruscharin were isolated from the latex of the plant. Latex also contained proteases calotropin DI and DII and calotropin FI and FII, an enzyme with invertase activity and trypsin [60]. α - amyirin, - β amyirin, β sitosterol and calotoxin (0.15%), Calactin (0.15%), Calactin composed of calotropagenin, Calotropin, Calactinic acid, Voruscharin (0.45%), and hexose, Uzarigenin, Syriogenin, Proceroside, Uscharin.





Siva et al.,

Chemical Constituents of Leaf

Cardenolides, steroids, tannins, glycosides, phenols, terpenoids, sugars, flavonoids, alkaloids and saponins [61-63]. β -amyrin, cardenolides, calotropagenin, calotropin.

Bitter compound–Mudarine, **Glycosides** – calotropin, uscharin, calotoxin and calactin[64-65].

volatile organic compounds–thioacetic acid, 2,3-dihydro-3,5-dihydroxy-6- 57789osthu-4H-pyran-4-one, and 5-hydroxymethyl-2- urancarboxaldehyde [63]. Leaf and stem of *Calotropis procera*, have 0.133% and 0.09% essential oils.

Leaf oil–tyranton (54.4%), 1- 57789osthuman57789e (9.5%) and 1-heptadecene (8.2%).

Stem oil– Z-13-docosenamide (31.8%), isobutyl nonane (13.7%) and 2, 7, 10-trimethyldodecane (12.3%). Both leaf and stem volatile oils contain octadecenamide. Also have long chain fatty acids, amides, sulfate, halogen compounds and carbonyls like ketones [66].

Molecular docking analysis

Calotropin was successfully docked with Mpro protein at binding pocket S1 with dock score -253.66. The interaction of Calotropin in the binding pocket of Mpro protein was mediated by two hydrophobic interactions and hydrogen bond interactions. The Calotropin showed full fitness within active site amino acids of Mpro/3CLpro proteins of COVID-19. Hydroxy groups (-OH), ketone groups (=O) and ether groups (-O-) in Calotropin compounds are predicted to play roles amino acid residue interactions at the active site of SARS-CoV-2 Mpro.

Name of Ligand (Inhibitor)	Dock score	Active site residues	
Calotropin	-253.66	H-bond interactions	Hydrophobic interactions
		LYS10, GLU14, GLY71	PRO7,122, GLU114, ILE150, VAL301

Molecular docking analysis revealed that **Protopin** could be potential inhibitors of SARS-CoV-2 Mpro[67].

Pharmacological activities of *Calotropis procera*. Linn (*Vellerukku*):

Anti-Asthmatic activity

Among Ethanolic and water extract of *Calotropis procera*, Methanolic extract possess potential anti-asthmatic activity in *in-vitro* models included isolated goat tracheal chain and guinea pig ileum preparation and *in-vivo* included histamine-induced bronchospasm, milk-induced leukocytosis, passive paw anaphylaxis model, and haloperidol-induced catalepsy models. [68]

Anti-histaminic and Bronchodilatory activity

The aqueous and methanol extracts of *C. procera* possess significantly relaxed histamine induced contraction of isolated guinea pig trachea. The extracts also significantly inhibited histamine induced contraction of isolated guinea in Histamine induced contraction of isolated guinea pig tracheal chain, histamine induced contraction of isolated guinea pig ileum strip test, and haloperidol induced catalepsy test in rats. [69]

Antimicrobial (Antifungal/ Antibacterial/ Antiviral) activity

The petroleum ether extract of *Calotropis procera* exhibited the best antibacterial activity against *Pseudomonas aeruginosa* ATCC and *Klebsiella pneumonia* while the chloroform extract was more potent antibacterial against *Pseudomonas aeruginosa* ATCC with 19 mm, 16 mm and 17 mm inhibition zone diameters respectively [70]. The antimicrobial activity of aqueous and ethanolic extract of roots and leaves of *Calotropis procera* against *Staphylococcus aureus*, *Streptococcus pyogenes*, *Escherichia coli* and *Pseudomonas aeruginosa* was studied on disc method. Both ethanolic and aqueous extracts of *Calotropis procera* had inhibitory effect on the growth of isolates. The effect exhibited by ethanolic extract of leaves and roots was significantly greater than that of the aqueous extract of leaves and roots [71].



**Siva et al.,**

The methanolic and aqueous extract of leaves of *Calotropis procera* were subjected to the potential antibacterial against both Gram-positive bacteria and Gram-negative bacteria in agar diffusion method. It was evident that both extracts are active against the bacteria at low concentrations [72].

The differential antimycoses activities of chloroform, methanol and ethyl acetate extracts of *Calotropis procera* (50,100 and 150 mg/ml) were studied against *Trichophyton rubrum*, *Trichophyton tonsurans*, *Trichophyton mentagrophyte*, *Epidermophyton floccosum* and *Aspergillus*. Ethyl lactate extract produced the potent activity followed by chloroform extract, while methanol extract had no antifungal activity in all concentrations used in the study [73].

Anti – Inflammatory activity

The protective effect of latex of *Calotropis procera* in complete Freund's adjuvant (FCA) induced monoarticular arthritis was evaluated in rats. Arthritis was induced by a single intra-articular injection of 0.1 ml of 0.1% FCA in the right ankle joint. The effect of dried latex (DL, 200 and 400 mg/kg) and its methanol extract (MeDL, 50 and 500 mg/kg) following oral administration was evaluated on joint inflammation, hyperalgesia, locomotor function and histology at the time of peak inflammation. The effects of DL and MeDL were compared with anti-inflammatory drugs phenylbutazone (100 mg/kg), prednisolone (20 mg/kg), rofecoxib (20 and 100 mg/kg) and immuno-suppressant methotrexate (0.3 mg/kg). Daily oral administration of DL and its methanol extract (MeDL) produced a significant reduction in joint inflammation (about 50% and 80% inhibition) and associated hyperalgesia. The antihyperalgesic effect of MeDL was comparable to that of rofecoxib. Both DL and MeDL produced a marked improvement in the motility and stair climbing ability of the rats. The histological analysis of the arthritic joint also revealed significant reduction in oedema and cellular infiltration by MeDL that was comparable to that of rofecoxib [74].

Immunological effects

The immunological potential of the latex of *Calotropis procera* against sheep red blood cells (SRBC) as antigen was investigated in Wistar albino rats by studying cell-mediated, delayed type hypersensitivity reaction (DTH), humoral immune response, macrophage phagocytosis and *E. coli* induced bacteremia sepsis. The latex was fractionated according to water solubility and molecular size of its components. The fractions were named as non-dialyzable latex (NDL) which corresponding to the major latex proteins, dialyzable latex (DL) corresponding to low molecular size substances and rubber latex (RL) which was highly insoluble in water. The HA titer levels were quantified by primary and secondary humoral immune response in rats. The fractions induced production of antibodies titer level significantly ($p < 0.05$) in response to SRBC. In addition immune stimulation was counteracted by up regulating macrophage phagocytosis in response to carbon particles. Rats received NDL fractions by oral route displayed considerable immunological response. Oral administration of NDL fractions, dose dependently increased immuno stimulatory responses. DTH reaction was found to be augmented significantly ($p < 0.05$) by increasing the mean foot pad thickness after 48h. In the survival study, control group I and negative control group II in *E. coli* induced peritonitis has shown 50% and 66.6% mortality, while pretreated groups with NDL has reduced mortality in rats injected with 1×10^8 *E. coli* intraperitoneally from 0.0% - 16.6% [75].

Anti – Cancerous activity

Different extracts of *Calotropis procera* leaves were evaluated for in-vitro cytotoxic activity against the Hep-2 cell line. The n-butanol extract had most pronounced cytotoxicity against the Hep-2 [76]. Dry latex of *C. procera* has the potential for anti-cancer effect due to its differentiable targets and non-interference with regular pathway of apoptosis. Dry latex treatment of mice showed a complete protection against hepato carcinogenesis. No adverse effect was observed in these animals. The serum vascular endothelial growth factor (VEGF) level was significantly lowered in the treated mice as compared to control animals. Cell culture studies revealed that the methanolic extract of dry latex as well as its fraction 8 induced extensive cell death in both hepatoma (Huh7) and non-hepatoma (COS-1) cell lines, while nontransformed hepatocytes (AML12) were spared. This effect was accompanied by extensive fragmentation of DNA in Huh-7 and COS-1 cells. No change in the levels of canonical markers of apoptosis such as Bcl2 and caspase 3 was observed [77].





Siva et al.,

Anti-oxidant activity

The methanolic and aqueous extracts of leaves of *Calotropis procera* were subjected to the potential antioxidant activities. The antioxidant potential of the methanolic extract was determined on the basis of their scavenging activity of the stable 1,1-diphenyl-2-picrylhydrazyl (DPPH) free radical. IC₅₀ of the methanol extract of *Calotropis procera* Linn. was 110.25 µg/ml which indicated the strong antioxidant activity of the plant. However the aqueous extract showed mild antioxidant activity [78]. The dry latex produced an increase in the hepatic levels of endogenous antioxidants (superoxide dismutase and catalase and glutathione), while it reduced the levels of thiobarbituric acid-reactive substances in alloxan-induced diabetic rats [79]. Important chemical constituents and their pharmacological activities of *Calotropis procera*. Linn (*Vellerukku*) are described in table No 2. [80]

Toxicological Aspects of *Calotropis procera*. Linn (*Vellerukku*):

A few studies suggested that the plant induces acute cardiotoxicity and hepatotoxicity [81]. On the other hand, a safety evaluation study revealed that the use of *C. procera* extract in single high doses (up to 3 g kg⁻¹) is not toxic for guinea pigs until the treatment of >90 days is provided [82]. In another study, latex proteins of the plant when administered orally, had no adverse immunological reactions in mice even at 5,000 mg kg⁻¹; but their intraperitoneal administration caused death after 1 h in response to a dose of 150 mg kg⁻¹[83].

CONCLUSION

All the ingredients of *Swasakasa Nei* are simple, effective and easily available herbs. This review distinctly exposes that all ingredients of *Swasakasa Nei* have anti-inflammatory, anti-histaminic, anti-asthmatic, anti-spasmodic, anti-microbial, expectorant, bronchodilator, immunomodulator and antioxidant activities. These properties play a major role in the treatment of Bronchial Asthma. Hence, it could be concluded that the *Swasakasa Nei* is one of the best drug of choice for Asthmatic patients since it is scientifically validated.

ACKNOWLEDGEMENT

The authors also thankful to the faculties of Department of Maruthuvam, National Institute of Siddha, Tambaram sanatorium, Chennai, for providing their support.

Conflict of interest

The authors declare that there is no conflict of interest.

REFERENCES

1. Shukla S, Saraf S. Fundamental aspect and basic concept of siddha medicines. Systematic Reviews in pharmacy. 2011; 2(1):48. DOI: 10.4103/0975-8453.83439
2. Dr. K. S Uthamarayan, Siddha Maruthuvanga Churukkam, published by Directorate of Indian medicine and Homeopathy, 2nd Edition 2003, pg no: 330,331.
3. Dr. Ka. Anbarasu –Yugi Vaidhya chindhamani 800 moolamum uraiyum, Edition July 2013, page no: 225,226,228,337
4. Shanmugavelu.M, Noi Nadal Noi Mudhal Nadal thirattu, published by directorate of Indian medicine and homeopathy, 2014.
5. Maruthuvar. K. N. Kuppasamy Muthaliyar, Siddha Maruthuvam (Pothu), published by Directorate of Indian medicine and homeopathy, 8th Edition 2016, Page No: 241-247.
6. National Asthma Education and Prevention Program. Expert Panel Report 3: Guidelines for the Diagnosis and Management of Asthma [Internet document]. 2007 Aug. Available from: www.ncbi.nlm.nih.gov/books/NBK7232/





Siva et al.,

7. Global Initiative for Asthma, Global Strategy for Asthma Management and Prevention, www.ginasthma.org (2017).
8. M.A. Koda-Kimble, Applied Therapeutics: The Clinical Use of Drugs (Ninth ed.), Wolters Kluwer Health/Lippincott Williams & Wilkins (2009).
9. P.L. Ngoc, L.P. Ngoc, D.R. Gold, A.O. Tzianabos, S.T. Weiss, J.C. Celedón Cytokines, allergy, and asthma, Curr.Opin.Allergy Clin.Immunol., 5 (2005), pg. 161-166.
10. Tarlo SM, Balmes J, Balkissoon R, Beach J, Beckett W, Bernstein D, et al. Diagnosis and management of work-related asthma: American College of Chest Physicians Consensus Statement. *Chest*. 2008 Sep. 134(3 Suppl):1S-41S. [Medline].
11. Bateman ED, Hurd SS, Barnes PJ, Bousquet J, Drazen JM, FitzGerald M, Gibson P, Ohta K, O'Byrne P, Pedersen SE, Pizzichini E. Global strategy for asthma management and prevention: GINA executive summary. *European Respiratory Journal*. 2008 Jan 1;31(1):143-78.
12. Greenberger PA. Therapy in management of rhinitis asthma complex. *Allergy Asthma Proc* 2003; 24: 403-407.
13. Henricks PA, Nijkamp FP. Reactive oxygen species as mediators in asthma. *Pulm. Pharmacol. Ther* 2001; 14: 409-420.
14. Slader CA, Reddel HK, Jenkins CR, Armour CL, Bosnic Anticevich SZ. Complementary and alternative medicine use in asthma: who is using what? *Respirol* 2006; 11: 373-387.
15. Tripathi KD. Essentials of medical pharmacology. 4th ed. New Delhi, India: Jaypee brothers medical Publishers Ltd; 2001.
16. Taur DJ, Patil RY. Some medicinal plants with antiasthmatic potential: a current status. *Asian Pacific journal of tropical biomedicine*. 2011 Oct 1;1(5):413-8. [https://doi.org/10.1016/S2221-1691\(11\)60091-9](https://doi.org/10.1016/S2221-1691(11)60091-9)
17. Slader CA, Reddel HK, Jenkins CR, Armour CL, Bosnic Anticevich SZ. Complementary and alternative medicine use in asthma: who is using what? *Respirol* 2006; 11: 373-387.
18. Dalvil RR. Sanguinarine. It's potential, as a liver toxic alkaloid present in the seeds of *Argemone mexicana*. *J Cell Mol Life Sci* 1985;41(1):77-8.
19. Sood NN, Mahipal S, Sachdev, Mohan M, Gupta SK and SachdevHPS. Epidemic dropsy following transcutaneous absorption of *Argemone mexicana* oil. *J Trans R Soc Trop Med Hyg* 1985;79(4):510-2.
20. Rathore SS, Shekhawat K, Premi OP, Kandpal BK. All India Coordinated Research Project on Rapeseed-Mustard, Major Weeds of Rapeseed-Mustard in India, Directorate of Rapeseed-Mustard Research, Sewar, Bharatpur, Rajasthan, India. 2012; pp 8.
21. Manalil S, Chauhan BS. Interference of turnipweed (*Rapistrum rugosum*) and Mexican pricklepoppy (*Argemone mexicana*) in wheat. *Weed Science* 2019; 1-7.
22. Chatterjee A, Pakrashi SC. The treatise of Indian medicinal plant. Vol-1, Publication and information directorate New Delhi, 1997; 139-40.
23. Priya CL and Rao KVB: Ethanobotanical and Current Ethanopharmacological Aspects of *Argemone Mexicana* Linn: An Overview. *Int J Pharm Sci Res*, 2012; Vol. 3(7): 2143-2148.
24. Brahmachari G, Gorai D, Roy R. *Argemone mexicana*: chemical and pharmacological aspects. *Revista Brasileira de Farmacognosia*. 2013; 23:559-67. Available from: <https://doi.org/10.1590/S0102-695X2013005000021>
25. Thiyagarajan R. *Gunapadam mooligai Vaguppu [Siddha materia medica-Medicinal plants division]*, 1st part, 9th edition, published by Directorate of Indian medicine and homeopathy, Chennai, 2013; Pg no: 152-156, 354-356.
26. Ranjana Pathak, Anjana Goel, S. C. Tripathi. Medicinal Property and Ethnopharmacological Activities of *Argemone mexicana*: An Overview. *Annals of RSCB [Internet]*. 2021Mar.22 [cited 2022Jul.16];1615-41. Available from: <https://www.annalsofscb.ro/index.php/journal/article/view/1609>
27. Siddiqui IA, Shaikat SS, Khan GH, Zaki MJ. Evaluation of *Argemone mexicana* for control of root-infecting fungi in potato. *J Phytopathol* 2002; 150:321-29.
28. Medicinal weed Satyanashi (*Argemone mexicana* Linn) <https://hort.purdue.edu/newcrop/CropFactSheets/argemone.html>.
29. Sanyal M. Phytochemical Profiling of *Argemone Mexicana*. *International Journal for Research in Applied Science & Engineering Technology (IJRASET)* 2018; 6: 3437-40.





Siva et al.,

30. Kukula-Koch, W., Mroczek, T. Application of hydrostatic CCC–TLC–HPLC–ESI–TOF–MS for the bioguided fractionation of anticholinesterase alkaloids from *Argemone mexicana* L. roots. *Anal Bioanal Chem* **407**, 2581–2589 (2015). <https://doi.org/10.1007/s00216-015-8468-x>
31. K.B. Pandeya, Aditya Ganeshpurkar, Mahendra Kumar Mishra, Natural RNA dependent RNA polymerase inhibitors: Molecular docking studies of some biologically active alkaloids of *Argemone mexicana*, *Medical Hypotheses*, Volume 144, 2020, 109905, ISSN:0306-9877, <https://doi.org/10.1016/j.mehy.2020.109905>
32. Singh R, Chaubey N, Mishra RK. Evaluation of Anti-Asthmatic Activity of Ethanolic Extract of *Argemone mexicana* Stems. *Saudi J Med Pharm Sci*, Jan, 2021; 7(1): 39-44
33. Bhalke RD, Gosavi SA. Anti-stress and antiallergic effect of *Argemone mexicana* stems in asthma. *Arch Pharm Sci Res*. 2009;1(1):127-9.
34. Perumal P, Sekar V, Rajesh V, Gandhimathi S, Kumar RS, Nazimudin KHS 2010. In vitro antioxidant activity of *Argemone mexicana* roots. *Int J PharmTech Res* 2: 1477-1482.
35. Anarthe S, Chaudhari S. Neuropharmacological study of *Argemone mexicana* Linn. *Journal of Applied Pharmaceutical Science*. 2011 Jun 30(Issue):121-6.
36. Anarthe S, Chaudhari S. Neuropharmacological study of *Argemone mexicana* Linn. *Journal of Applied Pharmaceutical Science* 2011; 1:121-26.
37. Arcos-Martínez AI, Muñoz-Muñoz OD, Domínguez-Ortiz MÁ, Saavedra-Vélez MV, Vázquez-Hernández M, Alcántara-López MG. Anxiolytic-like effect of ethanolic extract of *Argemone mexicana* and its alkaloids in Wistar rats. *Avicenna J Phytomed* 2016; 6:476-88.
38. Huang W, Kong L, Cao Y, Yan L. Identification and Quantification, Metabolism and Pharmacokinetics, Pharmacological Activities, and Botanical Preparations of Protopine: A Review. *Molecules*. 2021 Dec 30; 27(1):215. <https://doi.org/10.3390/molecules27010215>
39. Och A, Podgórski R, Nowak R. Biological activity of berberine—a summary update. *Toxins*. 2020 Nov 12;12(11):713. <https://doi.org/10.3390/toxins12110713>
40. Kun Wang, Xinchu Feng, Liwei Chai, Shijie Cao & Feng Qiu (2017) The metabolism of berberine and its contribution to the pharmacological effects, *Drug Metabolism Reviews*, 49:2, 139-157, DOI: 10.1080/03602532.2017.1306544
41. Valipour M, Zarghi A, Ebrahimzadeh MA, Irannejad H. Therapeutic potential of chelerythrine as a multi-purpose adjuvant for the treatment of COVID-19. *Cell Cycle*. 2021 Nov; 20(22):2321-2336. <https://doi.org/10.1080%2F15384101.2021.1982509>
42. He, N., Wang, P., Wang, P. et al. Antibacterial mechanism of chelerythrine isolated from root of *Toddalia asiatica* (Linn) Lam. *BMC Complement Altern Med* **18**, 261 (2018). <https://doi.org/10.1186/s12906-018-2317-3>
43. Wu J, Luo Y, Deng D, Su S, Li S, Xiang L, Hu Y, Wang P, Meng X. Coptisine from *Coptis chinensis* exerts diverse beneficial properties: A concise review. *J Cell Mol Med*. 2019 Dec; 23(12):7946-7960. <https://doi.org/10.1111%2Fjcmm.14725>
44. Long J, Song J, Zhong L, Liao Y, Liu L, Li X. Palmatine: A review of its pharmacology, toxicity and pharmacokinetics. *Biochimie*. 2019 Jul;162:176-184. <https://doi.org/10.1016/j.biochi.2019.04.008>
45. Shyamaladevi Babu, Selvaraj Jayaraman, An update on β -sitosterol: A potential herbal nutraceutical for diabetic management, *Biomedicine & Pharmacotherapy*, Volume 131, 2020, 110702, ISSN 0753-3322, <https://doi.org/10.1016/j.biopha.2020.110702>
46. Prasad M, Venugopal SP. Preliminary phytochemical analysis and oral acute toxicity study of the root of *argemone mexicana* linn. *Ijrdpl* [Internet]. 2016Mar.15 [cited 2022 May13];5(2):2010-7. Available from: <https://ubipayroll.com/IJRDPL/index.php/ijrdpl/article/view/213>
47. Karale pa, karale ma. A review on phytochemistry and pharmacological properties of milkweed family herbs (asclepiadaceae). *Asian J Pharm Clin Res*. 2017;10(11):27-34.
48. Murti, Y et al. "Pharmacognostic standardization of leaves of *Calotropis procera* (Ait.) R. Br. (Asclepiadaceae)." *International journal of Ayurveda research* vol. 1,1 (2010): 14-7. doi:10.4103/0974-7788.59938.
49. El Bsma Adam SEI. Studies on laticiferous plants: Toxic effects in goats on *Calotropis procera* latex given by different routes of administration, *Deutsche Tierärztliche Wochenschrift*, 105(11), 1988, 425-427.
50. Jain SC, Sharma R. Antimicrobial activity of *Calotropis procera*, *Fitoterapia*. 67(3), 1996, 275- 276.





Siva et al.,

51. Gupta S, Bhawani G, Karishma K, Pooja S. Ethnopharmacological potential of *Calotropis procera* : An overview. IRJP, 3(12), 2012, 19-22.
52. Sharma AK, Kharab R, Kaur R. Pharmacognostical aspects of *Calotropis procera* (Ait.) R. Br. International Journal of Pharma and Bio Sciences, 2(3), 2011, B480-B488.
53. Orwa C, Mutua A, Kindt R, Jamnadass R, Simons A. Agroforestry Database: a tree reference and selection guide version, 2009, <http://www.worldagroforestry.org/af/treedb/>
54. Farooq Azhar M, Tahir Siddiqui M, Ishaque M, Tanveer A. Study of ethnobotany and indigenous use of *Calotropis procera* (Ait.) in Cholistan desert, Punjab, Pakistan. J Agrice Res. 2014;52(1):117-26.
55. Nenaah G. Antimicrobial activity of *Calotropis procera* Ait. (Asclepiadaceae) and isolation of four flavonoid glycosides as the active constituents. World J Microbiol Biotechnol, 29(7), 2013, 1255-1262.
56. Shukla OP, Krishnamurti CR. Properties and partial purification of bacteriolytic enzyme from the latex of *Calotropis procera* (Madar). J Sci Indust Res, 20, 1961, 109-112.
57. Misra MK, Mohanty MK, Kdas P. Studies on the method-ethnobotany of *Calotropis gigantea* and *C. procera*. Ancient Science of Life, XIII (1&2), 1993, 40-56.
58. Doshi HV, Parabia FM, Sheth FK, Kothari IL, Parabia MH, Ray A. Phytochemical analysis revealing the presence of two new compounds from the latex of *Calotropis Procera* (Ait.) R.Br. International Journal of Plant Research, 2(2), 2012, 28-30.
59. Ramos MV, Bandeira GP, de Freitas CDT, Nogueira NA, Alencar NMN, de Sousa PAS, Carvalho AFU. Latex constituents from *Calotropis procera* (R. Br.) display toxicity upon egg hatching and larvae of *Aedes aegypti* (Linn.). Mem Inst Oswaldo Cruz, Rio de Janeiro, 101(5), 2006, 503-510.
60. Bhaskar VH, Ajay SS. Antihyperglycemic and antihyperlipidaemic activities of root extracts of *Calotropis procera* (Ait.) R.Br on streptozotocin. Jordan Journal of Biological Sciences, 2(4), 2009, 177-180.
61. Murti Y, Yogi B, Pathak D. Pharmacognostic standardization of leaves of *Calotropis procera* (Ait.) R. Br. (Asclepiadaceae). International Journal of Ayurveda Research, 1 (1), 2010, 14-17
62. Begum N, Sharma B, Pandey RS. Evaluation of insecticidal efficacy of *Calotropis procera* and *Annona Squamosa* ethanolextracts against *Musca domestica*. J Biofertil Biopestici, 1(1), 2010, 1-6.
63. Shrivastava A, Singh S, Singh S. Phytochemical investigation of different plant parts of *Calotropis procera*. International Journal of Scientific and Research Publications, 3(3), 2013, 1-4.
64. Russell DJ, Al Sayah MH, Munir FM. Volatile compounds produced by *Calotropis procera* (Family: Asclepiadaceae) leaves that aid in the repulsion of grazers. Journal of Biodiversity and Ecological Sciences, 1(3), 2011, 191-196.
65. Meena AK, Yadav MM, Niranjana US, Singh B, Nagariya AK, Sharma K, Gaurav A, Sharma S, Rao MM. A review of *Calotropis procera* Linn and its ethnobotany, phytochemical and pharmacological profile. Drug Invent Today, 2(2), 2010, 185-190.
66. Khan AQ, Malik A. A steroid from *Calotropis procera*. Phytochem, 28(10), 1989, 2859-2861.
67. Sharma AD, Kaur I (2020) Calotropin from milk of *Calotropis gigantea* a potent inhibitor of COVID 19 corona virus infection by Molecular docking studies. arXiv:2012.06139 [q-bio.BM]
68. Beniwal A and Mittal R: In-vitro and in-vivo evaluation of anti-asthmatic activity for the root extracts of *Calotropis procera*. Int J Pharm Sci & Res 2022; 13(3): 1179-88. doi: 10.13040/IJPSR.0975-8232.13(3).1179-88.
69. Aliyu IM, Zezi AU, Magaji MG, Abdu-Aguye I, Ibrahim ZY, Atiku I, Muntaka A. Anti-histaminic and bronchodilatory activities of aqueous and methanol extracts of *Calotropis procera* (Ait.) R. Br. root bark on allergic asthma in rodents. Journal of Pharmacy & Bioresources. 2017;14(2):128-46.
70. Bouratoua A, Khalfallah A, Kabouche A, Semza Z, Kabouche Z. Total phenolic quantification, antioxidant, antibacterial activities and flavonoids of Algerian *Calotropis procera* (Asclepiadaceae). Der Pharmacia Lettre, 5 (4), 2013, 204-207.
71. Mako GA, Memon AH, Mughal UR, Pirzaido AJ, Bhatti SA. Antibacterial effects of leaves and root extract of *Calotropis procera* Linn. Pak J Agri Agril Engg Vet Sci, 28 (2), 2012, 141-149.
72. Yesmin MN, Uddin SN, Mubassara S, Akond MA. Antioxidant and antibacterial activities of *Calotropis procera* Linn. American-Eurasian J Agric & Environ Sci, 4 (5), 2008, 550-553.
73. Halu B, Vidyasagar GM. A comparative study: differential antimycoses activity of crude leaf extracts of

57794

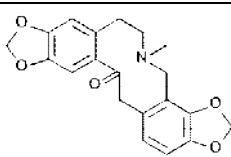
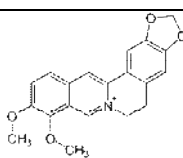
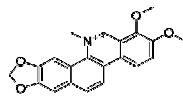




Siva et al.,

- Calotropis Spp. International Journal of Pharmacy and Pharmaceutical Sciences, 4(3), 2012, 705-708
74. Kumar VL, Roy S. Protective effect of latex of *Calotropis procera* in Freund's Complete Adjuvant induced monoarthritis. *Phytother Res*, 23(1), 2009, 1-5.
75. Bagherwal P. Immunomodulatory activities of the Nondialyzable latex fraction (NDL) from *Calotropis procera* (Ait.) R.Br. *International Journal of PharmTech Research*, 3(3), 2011, 1843-1849.
76. Murti Y, Singh A, Pathak D. In vitro anthelmintic and cytotoxic potential of different extracts of *Calotropis procera* leaves. *Asian J Pharm Clin Res*, 6(1), 2013, 14-15.
77. Choedon T, Mathan G, Arya S, Kumar VL, Kumar V. Anticancer and cytotoxic properties of the latex of *Calotropis procera* in a transgenic mouse model of hepatocellular carcinoma. *World J Gastroenterol*, 12(16), 2006, 2517-2522.
78. Yesmin MN, Uddin SN, Mubassara S, Akond MA. Antioxidant and antibacterial activities of *Calotropis procera* Linn. *American-Eurasian J Agric & Environ Sci*, 4 (5), 2008, 550-553.
79. Kumar VL, Padhy BM, Sehgal R, Roy S. Antioxidant and protective effect of latex of *Calotropis procera* against alloxan-induced diabetes in rats. *Journal of Ethnopharmacology*, 102 (3), 2005, 470-473.
80. Ashishkumar A. Kale et al. In vivo study of pharmacological activities of *Calotropis procera*: An overview. *Int. J. Res. Ayurveda Pharm.* 2022;13(3):44-49 <http://dx.doi.org/10.7897/2277-4343.130356>
81. de Lima, J. M., de Freitas, F. J. C., Amorim, R. N. L., Câmara, A. C. L., Batista, J. S., and Soto-Blanco, B. (2011). Clinical and pathological effects of *Calotropis procera* exposure in sheep and rats. *Toxicol* 57, 183–185. doi: 10.1016/j.toxicol.2010.11.007.
82. Mossa, J. S., Tariq, M., Mohsin, A., Ageel, A. M., Al-Yahya, M. A., Al-Said, M. S., et al. (1991). Pharmacological studies on aerial parts of *Calotropis procera*. *Am. J. Chinese Med.* 19, 223–231. doi: 10.1142/S0192415X91000302.
83. Bezerra, C. F., Mota, ÉF., Silva, A. C. M., Tomé, A. R., Silva, M. Z. R., de Brito, D., et al. (2017). Latex proteins from *Calotropis procera*: toxicity and immunological tolerance revisited. *Chem. Biol. Interact.* 274, 138–149. doi: 10.1016/j.cbi.2017.07.007.

Table No 1. Important chemical constituents and their pharmacological activities of root of *Argemone mexicana* Linn (*Brahmathandu*)

Chemical constituents	Chemical formula	Chemical structure	Pharmacological actions
Protopine[38]	C ₂₀ H ₁₉ NO ₅		Anti- Inflammatory activity, Anti-oxidation Activity, Anti-Platelet Aggregation Activities, Anti-Cancerous Activity, Analgesic Activity, Vasodilator Activity, Anti cholinesterase Activity, Anticonvulsant Activity, Anti-microbial activity, Hepatoprotective Activity, Neuroprotective Activities, Cytotoxic and Anti-Proliferative Activities.
Berberine [39, 40]	C ₂₀ H ₁₈ NO ₄ ⁺		Antioxidant, Anti-Inflammatory, Anti-cancerous, Anti-microbial, Hepatoprotective, Neuroprotective, Hypolipidemic And Hypoglycaemic Activities.
Chelerythrine [41, 42]	C ₂₁ H ₁₈ NO ₄		Anti-inflammatory activity, Anti-viral activity, Protein kinase C inhibitory activity, Anti-cancer, Anti-bacterial, Insecticide, Anti-fibrosis activities.





Siva et al.,

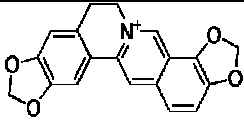
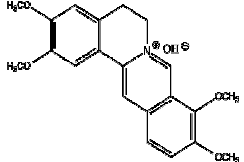
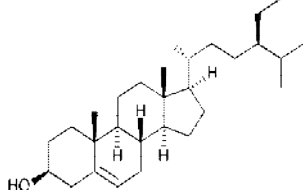
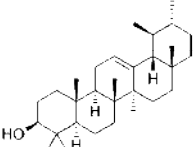
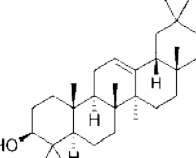
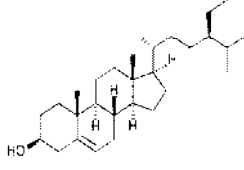
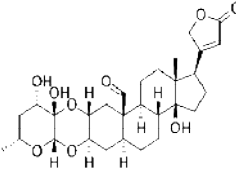
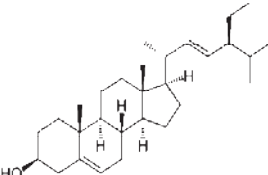
Coptisine[43]	$C_{19}H_{14}NO_4^+$		Anti-Inflammatory, Anti-cancerous, Anti-Bacterial activities.
Palmatine [44]	$C_{21}H_{22}NO_4^+$		Anti-Cancer, Anti-Oxidation, Anti-Inflammatory, Neuroprotection, Anti-Bacterial, Anti-Viral activities.
β -sitosterol [45]	$C_{29}H_{50}O$		Antinociceptive, Anxiolytic & Sedative Effects, Analgesic, Immunomodulatory, Antimicrobial, Anticancer, Anti – Inflammatory, Lipid Lowering Effect, Hepatoprotective, Protective Effect On Respiratory Diseases, Wound Healing Effect, Antioxidant, and Anti-Diabetic Activities.

Table No 2. Important chemical constituents and their pharmacological activities of *Calotropis procera*. Linn (Vellerukku)

Chemical constituents	Chemical formula	Chemical structure	Pharmacological actions
α amyirin	$C_{30}H_{50}O$		Anti-inflammatory, Hepatoprotective, Antioxidant, Analgesic, Cytotoxic, Antitumor, Antiulcer, Gastroprotective.
β amyirin	$C_{30}H_{50}O$		Anti-inflammatory, Hepatoprotective, Gastroprotective, Antioxidant, Analgesic, Antiulcer.
β -sitosterol	$C_{29}H_{50}O$		Antinociceptive, Anxiolytic & Sedative Effects, Analgesic, Immunomodulatory, Antimicrobial, Anticancer, Anti – Inflammatory, Lipid Lowering Effect, Hepatoprotective, Protective Effect On Respiratory Diseases, Wound Healing Effect, Antioxidant, and Anti-Diabetic Activities.
Calotropin	$C_{29}H_{40}O_9$		Antitumor, Cardioactive, Proteolytic.
Stigmasterol	$C_{29}H_{48}O$		Antioxidant, Antinociceptive, Antiviral, Cancer-preventive, Hypocholesterolaemia, Sedative.





Siva et al.,

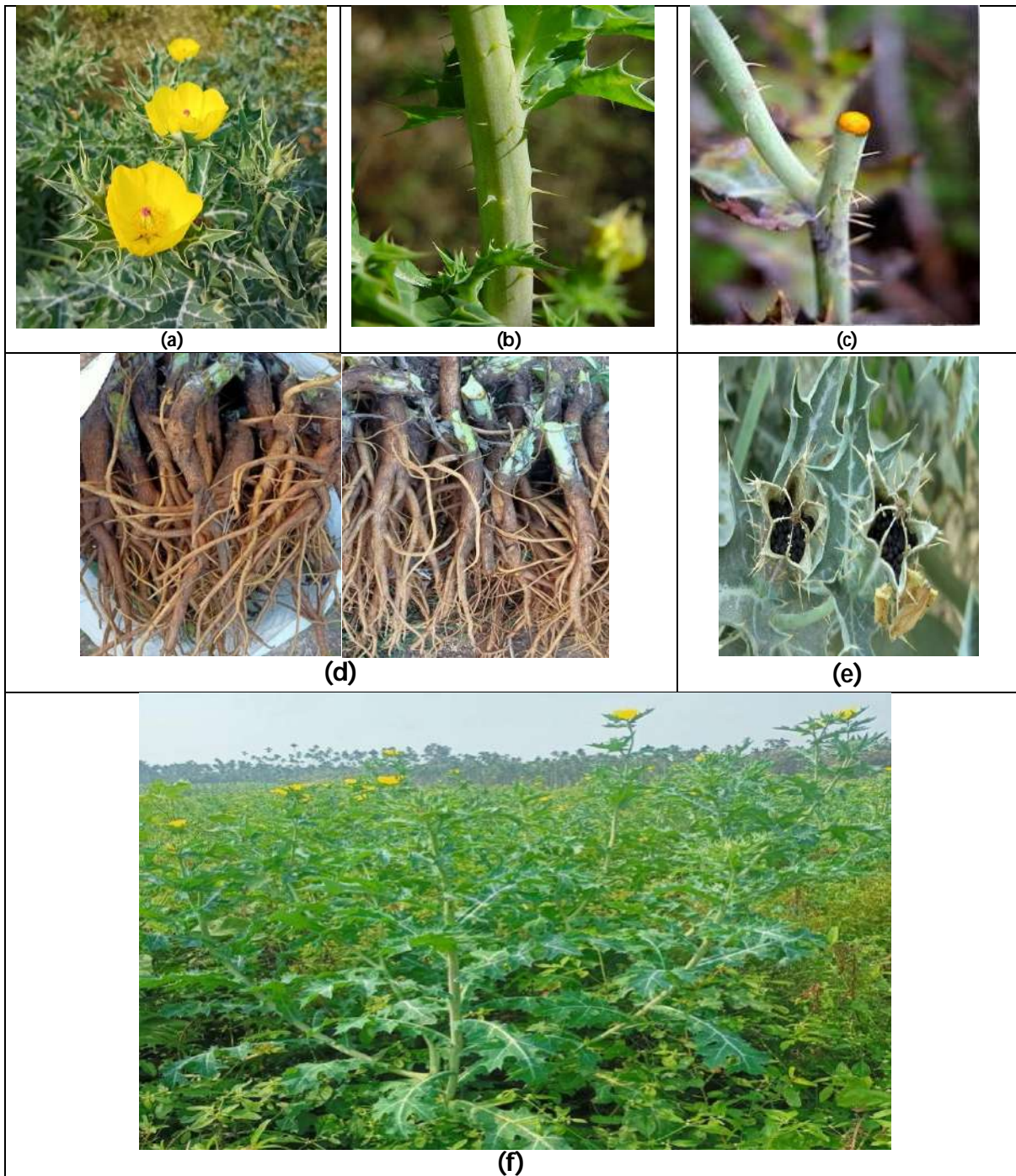


Figure 1. Therapeutically useful parts of the *Argemone mexicana*. Linn (*Brahmathandu*) plant: (a) Leaves and Flowers, (b) Stem, (c) Latex, (d) Roots, (e) Seeds, (f) Whole plant.





Siva et al.,

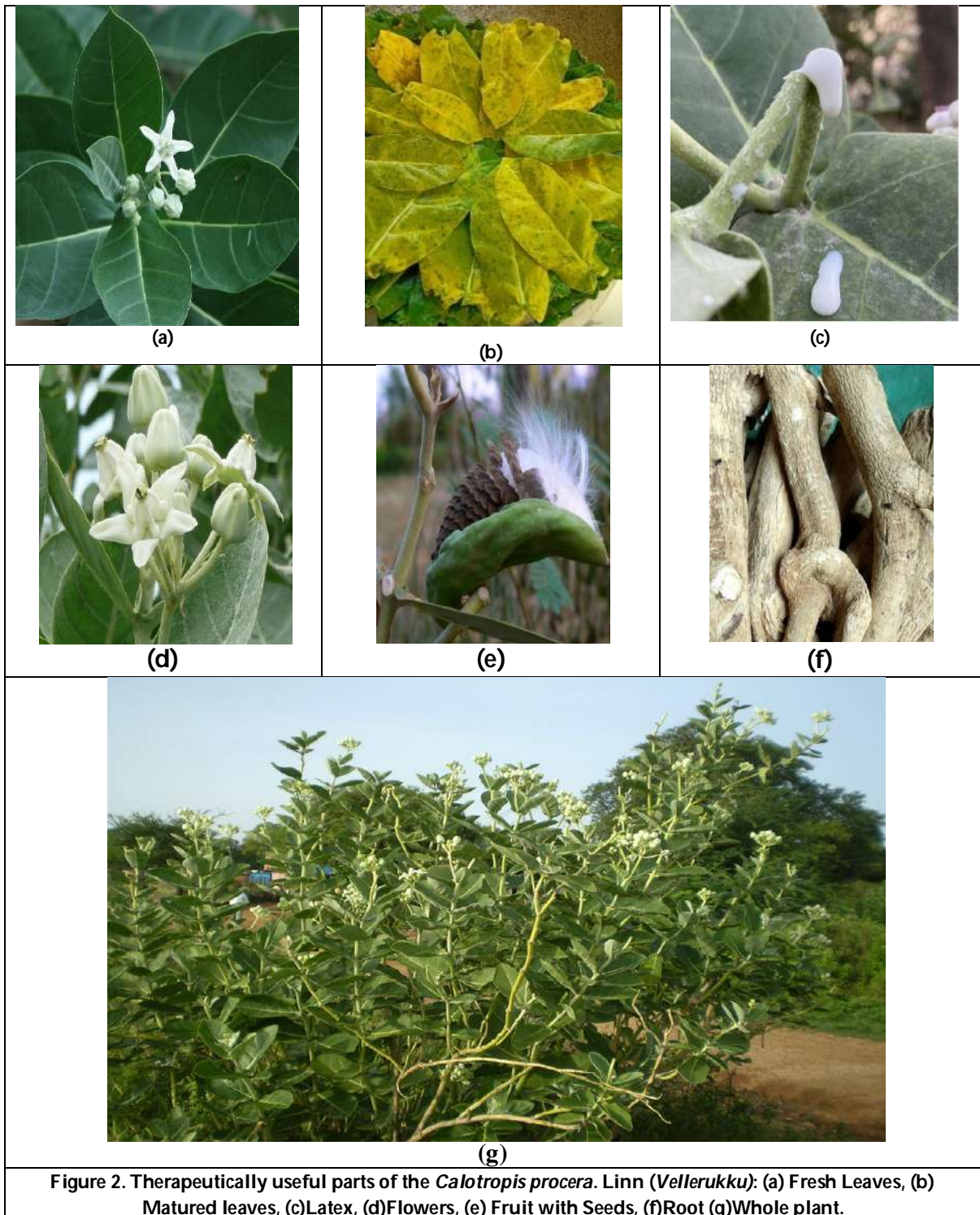


Figure 2. Therapeutically useful parts of the *Calotropis procera*. Linn (*Vellerukku*): (a) Fresh Leaves, (b) Matured leaves, (c) Latex, (d) Flowers, (e) Fruit with Seeds, (f) Root (g) Whole plant.





More Result on Various Kinds of Max-Max Operations Over Intuitionistic Fuzzy Matrices

T. Muthuraji*

Assistant Professor, Department of Mathematics, Annamalai University, Annamalai nagar, India.
Deputed to Government Arts College, C.Mutlur, Chidambaram, India.

Received: 19 Feb 2023

Revised: 24 Apr 2023

Accepted: 29 May 2023

*Address for Correspondence

T. Muthuraji

Assistant Professor,
Department of Mathematics,
Annamalai University, Annamalai nagar, India.
Deputed to Government Arts College,
C.Mutlur, Chidambaram, India.
E. Mail: tmuthuraji@gmail.com



This is an Open Access Journal / article distributed under the terms of the **Creative Commons Attribution License** (CC BY-NC-ND 3.0) which permits unrestricted use, distribution, and reproduction in any medium, provided the original work is properly cited. All rights reserved.

ABSTRACT

In this paper, some algebraic properties of component wise max-max operation together with component wise min-min operation are investigated. Also an intuitionistic fuzzy matrix representation and reduction is obtained using the above operations with zero intuitionistic fuzzy matrix and unitary intuitionistic fuzzy matrix.

Keywords: Intuitionistic Fuzzy Set (IFS), Intuitionistic Fuzzy Matrix (IFM).

MSC 2010 No: 03E72, 15B15, 94D05.

INTRODUCTION

The concept of fuzzy set has been found to be an effective tool to deal with fuzziness. However it often falls short of the expected standard in the description of neutral state. As a result a new concept called IFS was introduced by Atanassov in [1], when it is possible to model hesitation and uncertainty by using an additional degree. Later on, much fundamental works with new operations have done with concept by Atanassov in [2]. Im et.al. generalizes fuzzy matrix as IFM in [6, 7] and they studied the determinant and adjoint of square IFMs. Khan et al. established the same in [8] which has been useful in dealing with the areas such as decision making, relational equations, clustering analysis etc. Intuitionistic fuzzy algebra and its matrix theory are considered by several researchers in using component wise max-min and min-max operations in various years as follows.





Muthuraji

In [1, 2] Atanassov defined component wise max-min (\vee) and min-max (\wedge) operations on IFSs. Khan and Pal in [9] extended and investigated some operations on IFM and introduced intuitionistic fuzzy matrix product. From that a semi ring structure was constructed on IFM using the operations max-min intuitionistic fuzzy matrix product with component wise max-min fuzzy matrix product in [13] and then Emam and Fndh developed it to bi fuzzy matrices in [5]. Generalized interval valued IFMs was constructed by Adak et al. and have shown some a semiring structure in [3]. At the same time they initiated some properties of generalized intuitionistic fuzzy nilpotent matrices over distributive lattices in [4]. Muthuraji et.al. introduced component wise min-min (\wedge_m) operation on IFMS and an IFM decomposition was shown in [11]. Riyaz and Murugadas developed max-min intuitionistic fuzzy matrix product in [14] and Lalitha in [10] discussed min-min intuitionistic fuzzy matrix product. In this way Muthuraji developed some new kinds of max-max (component wise) operations and constructed a semigroup structure in [12]. In this study more results on max-max (component wise) operations together with min-min (component wise) are discussed also an IFM representation is presented using min-min and max-max operations through zero matrix and unit matrix.

Preliminaries

Here some basic definitions and operations are recalled which are related to our study.

Intuitionistic Fuzzy Set and its Alebraic Operations

Definition 2.1 [1, 2]

An IFS A in E (universal set) is defined as an object of the following form $A = \{(x, \mu_A(x)), \nu_A(x) \mid x \in E\}$, where the functions $\mu_A(x): E \rightarrow [0, 1]$ and $\nu_A(x): E \rightarrow [0, 1]$ the membership and non-membership function of the element $x \in E$ respectively for every $x \in E, 0 \leq \mu_A(x) + \nu_A(x) \leq 1$.

For our convenience consider the elements of IFSs as in the form (x, x') .

Let $(x, x'), (y, y') \in$ IFS, define

- (i) $(x, x') \vee (y, y') = [\max(x, y), \min(x', y')]$
- (ii) $(x, x') \wedge (y, y') = [\min(x, y), \max(x', y')]$
- (iii) $(x, x')^c = (x', x)$
- (iv) If $(x, x') \leq (y, y')$ then $x \leq y$ and $x' \leq y'$

Intuitionistic Fuzzy Matrix and its Operations

Definition 2.2 [8, 9]

An intuitionistic fuzzy matrix $A = [(a_{ij}, a'_{ij})]_{m \times n}$ be a matrix where a_{ij} and a'_{ij} are the membership value and non membership value of the ij^{th} element of A satisfying the condition that $0 \leq a_{ij} + a'_{ij} \leq 1$ for all i, j as well as its operations are defined as follows

For any elements $A = [(a_{ij}, a'_{ij})], B = [(b_{ij}, b'_{ij})] \in \mathcal{F}_{mn}, \mathcal{F}_{mn}$ denotes the set of all IFMs of order $m \times n$. where $i = 1, 2, \dots, m, j = 1, 2, \dots, n$ define

- (i) $A \vee B = [(b'_{ij}, a'_{ij}) \vee (b_{ij}, b'_{ij})]$
- (ii) $A \wedge B = [(a_{ij}, a'_{ij}) \wedge (b_{ij}, b'_{ij})]$
- (iii) $A^c = [(a'_{ij}, a_{ij})]$
- (iv) $A^T = [(a_{ji}, a'_{ji})]$
- (v) If $A \leq B$ then $a_{ij} \leq b_{ij}$ and $a'_{ij} \geq b'_{ij}$ for all i, j
- (vi) $\square A = [(a_{ij}, 1 - a_{ij})]$
- (vii) $\diamond A = [(1 - a'_{ij}, a_{ij})]$

Different types of IFMs

For all $i = 1, 2, \dots, m, j = 1, 2, \dots, n, A = [(a_{ij}, a'_{ij})]$ we have





Muthuraji

- (i) If $(a_{ij}, a'_{ij}) = (1, 0)$ when $i = j$ otherwise $(a_{ij}, a'_{ij}) = (0, 1)$ then the matrix A is said to be identity matrix denoted to I_n .
- (ii) If $(a_{ij}, a'_{ij}) = (1, 0)$ for all $i = j$ then A is said to an universal matrix denoted by J .
- (iii) If $(a_{ij}, a'_{ij}) = (0, 1)$ for all $i = j$ then A is said to an zero matrix denoted by O .

Definition 2.3 [11] Let $A, B \in \mathcal{F}_{mn}$, define

$$A \wedge_m B = [(a_{ij}, a'_{ij}) \wedge_m (b_{ij}, b'_{ij})] = [\min(a_{ij}, b_{ij}), \min(a'_{ij}, b'_{ij})] \forall i, j.$$

Lemma 2.1 [11]

\wedge_m is commutative and associative.

Different kinds of component wise max-min operations on IFMs

Definition 2.4. [12]

Let $A, B \in \mathcal{F}_{mn}$, define \vee_m in three kinds for all i, j .

- (i) $A \vee_{m1} B = [(a_{ij}, a'_{ij}) \vee_{m1} (b_{ij}, b'_{ij})]$

$$= \begin{cases} [\max(a_{ij}, b_{ij}), \max(a'_{ij}, b'_{ij})] & \text{if } \max(a_{ij}, b_{ij}) + \max(a'_{ij}, b'_{ij}) \leq 1 \\ (0.5, 0.5) & \text{if } \max(a_{ij}, b_{ij}) + \max(a'_{ij}, b'_{ij}) > 1 \end{cases}$$
- (ii) $A \vee_{m2} B = [(a_{ij}, a'_{ij}) \vee_{m2} (b_{ij}, b'_{ij})]$

$$= \begin{cases} [\max(a_{ij}, b_{ij}), \max(a'_{ij}, b'_{ij})] & \text{if } \max(a_{ij}, b_{ij}) + \max(a'_{ij}, b'_{ij}) \leq 1 \\ (1, 0) & \text{if } \max(a_{ij}, b_{ij}) + \max(a'_{ij}, b'_{ij}) > 1 \end{cases}$$
- (iii) $A \vee_{m3} B = [(a_{ij}, a'_{ij}) \vee_{m3} (b_{ij}, b'_{ij})]$

$$= \begin{cases} [\max(a_{ij}, b_{ij}), \max(a'_{ij}, b'_{ij})] & \text{if } \max(a_{ij}, b_{ij}) + \max(a'_{ij}, b'_{ij}) \leq 1 \\ (0, 1) & \text{if } \max(a_{ij}, b_{ij}) + \max(a'_{ij}, b'_{ij}) > 1 \end{cases}$$

The intuitionistic fuzzy matrix representation can be illustrated by the following example.

Consider a group of articles received by a journal as $a_1, a_2, a_3, \dots, a_m$ which are under reviewed by two reviewers by 'n' qualities like originality, soundness and validity of contents, clarity of presentation, adequacy of references to literature, general interest in this subject etc. In this case, the articles are crisp, they are fixed, but the qualities measured by the reviewers are fuzzy qualities. Let the matrix A and B denote the gradation of each article in each quality from reviewers.

Here the entry (a_{ij}) represents the percentage of marks to accept the i_{th} article under j_{th} quality given by the reviewer and the entry (a'_{ij}) represents the percentage of marks to reject the i_{th} article under j_{th} quality given by the reviewer. Let us assume that we have three articles to be reviewed under three qualities by two reviewers with some arbitrary membership and non membership then the matrix A, B are given as follows

$$A = \begin{bmatrix} (0.6, 0.3) & (0.0, 1.0) & (0.8, 0.0) \\ (0.2, 0.3) & (0.8, 0.1) & (0.7, 0.1) \\ (0.5, 0.2) & (1.0, 0.0) & (0.1, 0.2) \end{bmatrix}, \quad B = \begin{bmatrix} (0.5, 0.3) & (1.0, 0.0) & (0.6, 0.1) \\ (0.3, 0.5) & (0.2, 0.7) & (0.4, 0.5) \\ (0.3, 0.5) & (0.0, 1.0) & (0.4, 0.3) \end{bmatrix}$$

Now consider the corresponding entries of (1, 2), (2, 2), (2, 3) and (3, 2) indicate that the opinion about that particular i_{th} article under j_{th} quality is differ totally. In this case if we choose max-min (\vee) then the editor's gradation using max-min operation go with first reviewer only. Similarly for min-max go with second reviewer. But in max-min operations we distribute the maximum element as (0.5, 0.5) or the maximum element (1, 0) or minimum element (0, 1) as it is for editors gradation since the averaging operator does not satisfy many algebraic properties including associativity. Suppose the corresponding entries are not comparable under inequality which is defined in definition 2.1 then the previous operation takes the value either (a_{ij}, a'_{ij}) or (b_{ij}, b'_{ij}) .





Muthuraji

Representation and reduction of an IFM using \vee_m and \wedge_m

In this section some algebraic laws are discussed and an IFM representation is shown.

Lemma 3.1 Let $A, B \in \mathcal{F}_{mn}$, we have the following

- (i) $(A \vee_{m1} B)^c = A^c \vee_{m1} B^c$
- (ii) $(A \wedge_m B)^c = A^c \wedge_m B^c$ means Demorgan's law fails.
- (iii) $(A \vee_{m2} B)^c \neq A^c \vee_{m2} B^c$ also $(A \vee_{m2} B)^c \neq A^c \wedge_m B^c$
- (iv) $(A \vee_{m3} B)^c \neq A^c \vee_{m3} B^c$ also $(A \vee_{m3} B)^c \neq A^c \wedge_m B^c$

Proof:

$$[A \vee_{m1} B]^c = \begin{cases} (a_{ij}, b'_{ij})^c \text{ if } A \geq B \text{ and } a_{ij} + b'_{ij} \leq 1 \\ (b_{ij}, a'_{ij})^c \text{ if } B \geq A \text{ and } b_{ij} + a'_{ij} \leq 1 \\ (0.5, 0.5)^c \text{ otherwise} \end{cases}$$

$$= \begin{cases} (b'_{ij}, a_{ij}) \text{ if } A \geq B \text{ and } a_{ij} + b'_{ij} \leq 1 \\ (a'_{ij}, b_{ij}) \text{ if } B \geq A \text{ and } b_{ij} + a'_{ij} \leq 1 \\ (0.5, 0.5) \text{ otherwise} \end{cases}$$

Now consider $A^c \vee_m B^c = [(a'_{ij}, a_{ij}) \vee_m (b'_{ij}, b_{ij})]$

$$= \begin{cases} (b'_{ij}, a_{ij}) \text{ if } A \geq B \text{ and } a_{ij} + b'_{ij} \leq 1 \\ (a'_{ij}, b_{ij}) \text{ if } B \geq A \text{ and } b_{ij} + a'_{ij} \leq 1 \\ (0.5, 0.5) \text{ otherwise} \end{cases}$$

Thus $(A \vee_{m1} B)^c = A^c \vee_{m1} B^c$

Similarly, we shall prove (ii), (iii) and (iv).

Lemma 3.2 (Absorption Law)

Let $A, B \in \mathcal{F}_{mn}$ then

- (i) $A \vee_{m1} (A \wedge_m B) = A$
- (ii) $A \wedge_m (A \vee_{m1} B) \neq A$

Proof:

Let $A, B \in \mathcal{F}_{mn}$, and for some i, j , we have $(a_{ij}, a'_{ij}) \geq (b_{ij}, b'_{ij})$

$(a_{ij}, a'_{ij}) \wedge_m (b_{ij}, b'_{ij}) = (b_{ij}, b'_{ij})$ and

$$(a_{ij}, a'_{ij}) \vee_{m1} ((a_{ij}, a'_{ij}) \wedge_m (b_{ij}, b'_{ij})) = [(a_{ij}, a'_{ij}) \vee_{m1} (b_{ij}, b'_{ij})] = [(a_{ij}, a'_{ij})]$$

Since $a_{ij} + a'_{ij} \leq 1$

Suppose $(a_{ij}, a'_{ij}) \leq (a_{ij}, a'_{ij})$ gives $(a_{ij}, a'_{ij}) \wedge_m (b_{ij}, b'_{ij}) = (a_{ij}, b'_{ij})$ and

$$(a_{ij}, a'_{ij}) \vee_{m1} ((a_{ij}, a'_{ij}) \wedge_m (b_{ij}, b'_{ij})) = [(a_{ij}, a'_{ij}) \vee_{m1} (a_{ij}, b'_{ij})] = [(a_{ij}, a'_{ij})]$$

suppose (a_{ij}, a'_{ij}) and (b_{ij}, b'_{ij}) are not comparable. Then

$$(a_{ij}, a'_{ij}) \wedge_m (b_{ij}, b'_{ij}) = \begin{cases} (a_{ij}, a'_{ij}) \text{ if } a_{ij} \geq b_{ij} \text{ and } a'_{ij} \geq b'_{ij} \\ (b_{ij}, b'_{ij}) \text{ if } a_{ij} \leq b_{ij} \text{ and } a'_{ij} \leq b'_{ij} \end{cases}$$

Also $(a_{ij}, a'_{ij}) \vee_m ((a_{ij}, a'_{ij}) \wedge_m (b_{ij}, b'_{ij})) = (a_{ij}, a'_{ij})$

Thus, $A \vee_{m1} (A \wedge_m B) = A$ for all i, j .

(ii) $A \vee_{m1} B = \begin{cases} (a_{ij}, b'_{ij}) \text{ if } A \geq B \text{ and } a_{ij} + b'_{ij} \leq 1 \\ (b_{ij}, a'_{ij}) \text{ if } B \geq A \text{ and } b_{ij} + a'_{ij} \leq 1 \\ (0.5, 0.5) \text{ otherwise} \end{cases}$

Now $(a_{ij}, a'_{ij}) \wedge_m ((a_{ij}, a'_{ij}) \vee_{m1} (a_{ij}, a'_{ij}))$





Muthuraji

$$= \begin{cases} (a_{ij}, a'_{ij}) & \text{if } (a_{ij}, a'_{ij}) \geq (a_{ij}, a'_{ij}) \text{ and } a_{ij} + b'_{ij} \leq 1 \\ (a_{ij}, a'_{ij}) & \text{if } (b_{ij}, b'_{ij}) \geq (a_{ij}, a'_{ij}) \text{ and } b_{ij} + a'_{ij} \leq 1 \\ (0.5, 0.5) \text{ or } (a_{ij}, 0.5) \text{ or } (0.5, a'_{ij}) & \text{otherwise} \end{cases}$$

$A \wedge_m (A \vee_{m1} B) \neq A$ always.

Thus $A \wedge_m (A \vee_{m1} B) = A$ only if $a_{ij} + b'_{ij} \leq 1$ and $b_{ij} + a'_{ij} \leq 1$.

Lemma 3.3

Let $A, B, C, D \in \mathcal{F}_{mn}$, then we have the

- (i) $A \wedge_m B = A$ iff $A \vee_m B = B$
- (ii) If $A \leq B$ and $C \leq D$ then $A \wedge_m C \leq B \wedge_m D$.
- (iii) If $B \leq C$ then $A \wedge_m B \leq A \wedge_m C$.

Proof:

(i) If $A \wedge_m B = A$ then $a_{ij} \leq b_{ij}$ and $a'_{ij} \leq b'_{ij}$ therefore it is obvious that $A \wedge_m B = B$

(ii) Suppose $A \leq B$ and $C \leq D$ then for all i, j we have $a_{ij} \leq b_{ij}$ and $a'_{ij} \geq b'_{ij}$ again $c_{ij} \leq d_{ij}$ and $c'_{ij} \geq d'_{ij}$

Thus we have $\min(a_{ij}, c_{ij}) \leq \min(b_{ij}, d_{ij})$ and $\min(a'_{ij}, c'_{ij}) \geq \min(b'_{ij}, d'_{ij})$

Thus $A \wedge_m C \leq B \wedge_m D$.

Lemma 3.4

For any $A, B \in \mathcal{F}_{mn}$, we have

- (i) $A \vee (A \wedge_m B) = A$ if $A \geq B$.
- (ii) $A \vee (A \vee_{m3} B) = A$ if $A \geq B$.
- (iii) $A \wedge (A \wedge_m B) = A$ if $B \geq A$.
- (iv) $A \wedge (A \vee_{m2} B) = A$ if $B \geq A$.

Remark 3.1

For any A in \mathcal{F}_{mn} can be represented by using \wedge_m and \vee_m in terms of zero matrix (O) and unitary matrix (U) as follows $A = [A \wedge_m O] \vee_m [A \wedge_m U]$

Proof: Consider the ij^{th} element of A as (a_{ij}, a'_{ij})

Now $A \wedge_m O = [(a_{ij}, a'_{ij}) \wedge_m (0, 1)] = [(0, a'_{ij})]$,

$$A \wedge_m U = [(a_{ij}, a'_{ij}) \wedge_m (1, 0)] = [(a'_{ij}, 0)]$$

Therefore, $[A \wedge_m O] \vee_m [A \wedge_m U] = [(0, a'_{ij}) \vee_m (a'_{ij}, 0)] = (a_{ij}, a'_{ij}) = A$

Remark 3.2

An IFM A can be reduced to constant matrix or zero matrix or an unitary matrix using max-max operators through modal operators when the sum of membership and non membership value is not equal 1 as follows

- (i) $\square A \vee_{m1} \diamond A = [(0.5, 0.5)]$ when $a_{ij} + a'_{ij} \neq 1$
- (ii) $\square A \vee_{m2} \diamond A = [(1, 0)]$ when $a_{ij} + a'_{ij} \neq 1$
- (iii) $\square A \vee_{m3} \diamond A = [(0, 1)]$ when $a_{ij} + a'_{ij} \neq 1$
- (iv) $\square A \vee_{m1} \diamond A = \square A \vee_{m2} \diamond A = \square A \vee_{m3} \diamond A = A$ when $a_{ij} + a'_{ij} = 1$

Proof: we have $A = [(a_{ij}, 1 - a_{ij})]$ and $\diamond A = [(1 - a'_{ij}), a'_{ij}]$

$A \vee_{m1} \diamond A = (a_{ij} \vee 1 - a'_{ij}, 1 - a_{ij} \vee a'_{ij})$ for some i, j

If $a_{ij} \geq 1 - a'_{ij}$ and $a'_{ij} > 1 - a_{ij} \Rightarrow a_{ij} + a'_{ij} > 1$

Thus $A \vee_{m1} \diamond A = [(1 - a'_{ij}, 1 - a_{ij})]$

but the value of $1 - a'_{ij} + 1 - a_{ij} = 2 - (a_{ij} + a'_{ij}) = 1$ when $a_{ij} + a'_{ij} = 1$

if $a_{ij} + a'_{ij} < 1$ then $A \vee_{m1} \diamond A = [0.5, 0.5]$

(ii) and (iii) are similar to (i).





CONCLUSION

All the results which were proved earlier in intuitionistic fuzzy theory based on the usual composition operator \wedge (meet) and \vee (join). In this work different kinds component wise max-max operations are introduced directly on IFMs. Some algebraic properties are investigated. Finally IFM representation is presented. In future all the previous works done using usual component wise max-min and min-max operations may be redirected to these max-max and min-min operations.

REFERENCES

1. K. Atanassov, Intuitionistic Fuzzy Sets, VII ITKR's Section, Sofia (Deposed in Central Sci. Tech. Library of Bulg. Acad. of Sci., 1697/84) June 1983.
2. K. Atanassov, Intuitionistic Fuzzy Sets, Fuzzy Sets and System, 20(1) (1986) 87-96.
3. A.K. Adak, M. Bhowmik, M.Pal, Semiring of generalized Interval-valued IFMS, WorldAppl. Sci. Journal, 16 (2012) 7-16.
4. A.K. Adak, M.Bhowmik, M.Pal, Some properties of generalized Intuitionistic Fuzzy Nilpotent Matrices over Distributive lattice, Fuzzy Inf. Engg., (2012) 4, 371-387.
5. E.G. Emam, M.A. Fndh, Some results associated with the max-min, min-max compositions of bifuzzy matrices, 24 (4) (2016), 515-521.
6. Y.B. Im, E.P. Lee and S.W. Park, The Determinant of square Intuitionistic Fuzzy Matrices, Far East Journal of Mathematical Sciences, 3 (5) (2001) 789-796.
7. Y.B. Im, E.P. Lee and S.W. Park, The Adjoint of Square Intuitionistic Fuzzy Matrices Journal of Applied Maths and Computing (Series A), Vol 11 (1-2) (2003).
8. Khan S.K, Pal. M and Shyamal.A.K, Intuitionistic Fuzzy Matrices, Notes on Intuitionistic Fuzzy Sets, 8 (2) (2002) 51-62.
9. S.K. Khan and M. Paul, Some operations on IFMS, Acta Ciencia Indica, XXXIIM, (2006)515-524.
10. Lalitha. K, Min-Min operation on Intuitionistic Fuzzy Matrices, Journal of Emerging Technology and Innovative Research, 4 (8) (2017), 382-385.
11. T. Muthuraji, S. Sriram, P. Murugadas, Decomposition of IFMS, Fuzzy Information and Engg., 8(3) (2016), 345-354.
12. T. Muthuraji, Semigroups on some new operations over intuitionistic fuzzy matrices, Malaya journal of matematik, 2020, Vol. 8, No. 4, 2273-2276.
13. M.Z. Ragab, E.G. Emam, On the min-max composition of fuzzy matrices, Fuzzy Sets and System, 75 (1995) 83-92.
14. Riyaz Ahmad Padder, P. Murugadas, Max-Max operations on IFMs, Annals of Fuzzy Mathematics and Informatics.
15. S. Sriram, P. Murugadas, On semiring of IFM, Applied Mathematical Sciences, 4 (2010)23, 1099-1105.





Efficient Statistics usage in Biological Research Analysis Techniques of Data and Tools

Kaushal Singh* and Tushar Mandanaka

Assistant Professor, School of Engineering, P.P. Savani University, Surat, Gujarat, India

Received: 09 Mar 2023

Revised: 25 Apr 2023

Accepted: 31 May 2023

*Address for Correspondence

Kaushal Singh

Assistant Professor,
School of Engineering,
P.P. Savani University,
Surat, Gujarat, India
E.Mail: kaushal.singh@ppsua.ac.in



This is an Open Access Journal / article distributed under the terms of the **Creative Commons Attribution License** (CC BY-NC-ND 3.0) which permits unrestricted use, distribution, and reproduction in any medium, provided the original work is properly cited. All rights reserved.

ABSTRACT

When asked to examine your data, never forget the dreadful sensation you receive! Your hypothesis has to be statistically supported now that you have all the necessary raw data. To dispel the myth that biology students are incapable of arithmetic, you should offer your numerical data as part of statistics in your research. Research in science must use statistical techniques. As a matter of fact, statistical procedures predominate in scientific research since they include thoughtful planning, data collection, analysis, and reporting. Planning, designing, gathering data, analysing it, developing relevant interpretation, and publishing the research findings are all statistical processes that go into conducting a study. The statistical analysis adds sense to the meaningless data, bringing life to the dead data. Only when appropriate statistical tests are employed can the results and conclusions be made with accuracy. The goal of this essay is to familiarise the reader with the fundamental research instruments used while carrying out various investigations. An overview of the factors, knowledge of quantitative and qualitative variables, and measurements of central tendency are all covered in this paper. In addition, without statistical analysis, the study project's findings are only worthless raw data. In order to support study findings, it is therefore imperative to determine statistics. In this paper, we'll see about the benefits of utilising statistical techniques to examine biological research and how these techniques may lead to more insightful conclusions.

Keywords: - Statistical Techniques, Quantitative, Qualitative, Measurements of central tendency, Biological Research.



**Kaushal Singh and Tushar Mandanaka**

INTRODUCTION

In order to identify patterns and trends, data must be gathered and put through a statistical analysis procedure. Numerical analysis is used in this technique to eliminate bias from the evaluation of data. Planning surveys and studies as well as constructing statistical models all benefit from using this strategy to get interpretations of research. A scientific tool used in AI and ML, statistical analysis assists in the collection and analysis of massive volumes of data in order to spot recurring patterns and trends and turn them into actionable knowledge. Statistical analysis is a tool for data analysis that makes it easier to get important conclusions from unstructured, uncooked data, to put it simply [1]. Using statistical analysis, the findings are generated to aid in decision-making and assist firms in forecasting the future based on historical trends. It is a science that collects and examines data in order to find patterns and trends and then presents those patterns and trends. Working with numbers is a requirement for statistical analysis, which is a tool used by organisations like corporations and other institutions to analyse data to produce useful information. The enormous task of arranging inputs appears so peaceful thanks to statistical analysis, which removes irrelevant data and uncomplicatedly catalogues crucial facts. Statistical analysis can be used after the data has been gathered for a number of objectives.

The use of statistics is a blessing to humanity and has many advantages for both people and businesses. Several justifications for investing in statistical analysis are listed below: Making judgements will be made easier if you are able to calculate the sales earnings and expenditures on a monthly, quarterly, and annual basis. You may be able to make wise selections with its assistance [2]. You may use it to pinpoint the issue or reason behind the failure and implement fixes. For instance, it can assist you in reducing unnecessary spending by determining the cause of a rise in overall expenditures. You may use it to carry out market research and create a solid marketing and sales plan. It increases the effectiveness of several procedures. Analyzing data scope, modularizing data structures, condensing data representations, illustrating it using images, tables, and graphs, evaluating statistical inclinations, probability data, and drawing meaningful conclusions using statistical and logical techniques.

Aspects of Statistical Research in Biological Science

In the scientific field of statistics, data from a sample of the population to the entire population are collected, arranged, and analysed. Also, it helps in the more precise design of a research and also provides a logical justification for the conclusion of the hypothesis [3]. Also, the study of biology is centred on investigating living things and their intricate biochemical processes, which are incredibly dynamic and defy rational justification. The more complicated area of study of statistics, on the other hand, identifies and interprets research patterns depending on the sample sizes employed. In the studied that was completed, statistics specifically shows a pattern. The use of statistics by biologists is frequently neglected throughout the planning stages of their study, with most of their usage of statistical techniques occurring after the conclusion of an experiment [4]. Resulting in a complex collection of results that are difficult to examine using research statistical methods. The use of statistics in research can aid in a sequential approach to the investigation, with the statistical analysis in research going as follows:-

Sampling size determination

A biological experiment typically begins with picking samples and the ideal number of repeating tests. Research statistics deal with the fundamentals of statistics, which give statistical randomness and the law of employing large samples. Statistics shows how selecting a sample size from a broad, randomly selected sample pool aids in extrapolating statistical results and minimises experimental bias and mistakes.

Hypothesis Testing of the Data

Biological researchers must ensure that a result is statistically significant when performing a statistical study with a high sample size [5]. To do this, a researcher needs first formulate a hypothesis before analysing the distribution of data. Also, statistics in research aid in the interpretation of data that are dispersed across the distribution or grouped close to the distribution's mean. These patterns serve to both represent and assess the hypothesis and sample.



**Kaushal Singh and Tushar Mandanaka****Making a Successful Research Hypothesis**

An answerable question is not a straightforward assertion. A scientific experiment's goals, methods, and potential consequences must be described in detail in this relatively complex statement [6]. However, while formulating a convincing hypothesis, there are several crucial factors to take into account. 1. Describe the issue you are attempting to fix. Verify that the topic and the experiment's main emphasis are specified in the hypothesis. 2. Attempt to format the premise as an if-then statement. Use this as your guide: A particular result is anticipated if a particular action is executed. 3. Provide the variables The variables that are altered, controlled, or changed are called independent variables. Separated from the study's other parameters are independent variables. Dependent variables depend on other research variables, as their name implies. The modification of the independent variable has an impact on them. 4. Examine the premise.

Analysis-Based Interpretation of Data

Statistics in research aid in data analysis when working with big amounts of data. Using their experiment and findings, researchers may more effectively make conclusions thanks to this. Manually drawing conclusions from the research or from eye observation may provide inaccurate findings; as a consequence, a full statistical analysis will take into account all other statistical measures and sample variation to offer the data a thorough interpretation [7]. Hence, to support the conclusion, researchers generate extensive and significant data.

Types of Statistical Research Techniques for Data Analysis

The act of turning samples of data into patterns or trends is known as statistical analysis, which enables researchers to foresee circumstances and draw the best possible study results. Statistics are classified into the following types depending on the type of data:

Descriptive Analysis

A form of statistical analysis known as descriptive analysis is used to describe and summarize data. Using statistical measurements like the mean, median, mode, variance, standard deviation, and other descriptive statistics, descriptive analysis aims to give a general picture of a dataset's essential properties [8]. As it enables researchers to have a fundamental grasp of the data and spot any patterns or trends, descriptive analysis is frequently the initial stage in data analysis. In order to arrange and summarize the data in a way that is intelligible, this form of analysis is very helpful when working with huge and complicated datasets. Large amounts of data may be arranged and summarised using tables and graphs as a result of descriptive statistical analysis. Processes like tabulation, measures of central tendency, measures of dispersion or variance, measurements of skewness, etc. are all used in descriptive analysis.

Using Box Plots and Bar Charts to Present Study Data

For presenting research results graphically, box charts and box plots are frequently utilised. Because of this, it's crucial to comprehend how the two vary. Depending on the type of data and the interpretation a researcher wants to present, a box plot or box chart may be used. Plotting the distribution of a data set is done using a box plot. Plots with boxes and whiskers are another name for box plots. By displaying the reader their location and duration, these graphs communicate five aspects of data distribution [9]. The distribution's first and third quartiles are represented by the box, and the range is the interquartile range, or IQR (interquartile range). A line that crosses the box represents the median. Box plot "whiskers" reach the most severe data points from Q1 and Q3, respectively. Each mark on the graph above corresponds to one of these outliers. Possible endpoints for the "whiskers" include the maximum and minimum values. It's not as difficult as it may appear to read box plots. The centre of the data set is the median, which is shown as a line cutting across the box. It indicates that the median is exceeded by 50% of the data. The top "whisker" reflects numbers that are greater than the median. Dots that are outliers are located above the top "whisker." Outliers and the bottom "whisker" have a similar connotation. Box plots can also show the skews in the data set [10]. You can see how many data points fall above or below the median by looking at where it is located on the box.



**Kaushal Singh and Tushar Mandanaka**

Bar charts work well for counts since they are made to display categorical variables. Bar graphs show and contrast frequency, number, or other measurements (such as mean) for several data categories. Bar charts are commonly used to display continuous data from studies on humans, animals, and laboratory data. Bar charts are a prominent type of graph because they are straightforward to make and simple to understand [11]. They can be utilised to show nominal or ordinal groupings. Nominal data are qualitative or descriptive data, whereas ordinal categories are data that are rated (e.g., very good to very terrible) (e.g., country of birth, subject studied at university). There are many distinct kinds of bar charts, including stacked, grouped, and horizontal bar charts. The first step in interpreting a bar chart is to compare the bar's height to the equivalent value on the y-axis. By looking at the y-axis, it is possible to establish how the bars' heights differ from one another. Comparing the groups of bars is the next step. Bars in some bar graphs may be arranged in clusters. In this instance, contrast the bars inside the clusters to see how each piece of data within a subcategory relates to other sets of data [12]. By deducting the lowest number (represented by the shortest bar) from the highest value, you may also examine the range (denoted by the longest bar). Data interpretation: Bar charts may be used to spot outliers, trends, and patterns in the data being compared. It is critical to consider the categories or groups being compared, as well as the units of measurement being used on the y-axis, when interpreting the data. Conclusions can be made regarding the connections between the categories or groups being compared based on how the data is interpreted. It is crucial to make sure that the conclusions reached are founded on a thorough review of the evidence, rather than on presumptions or prejudices.

Which one ought to you employ?

What kind of information will you represent? What sort of data visualisation do you wish to use? Before deciding between the two, you must respond to such questions. Bar charts should not be employed, according to certain writers, while new forms for data representation should arise, according to others. The finances for two homes can be shown, for example, using groupings of bars [13]. Displaying the ratio of one item to another is a typical application for bar charts. The usage of box plots, on the other hand, allows for the visualisation of several data sets from diverse sources. As an illustration, consider test results from several institutions, data that changed (before and after) owing to a procedure, or data from various machines that produced the same product. Box plots are effective ways to demonstrate how your data is distributed, especially if you want to display values other than the mean.

Inferential Analysis

The data obtained from a small sample size may be extrapolated to the entire population via inferential statistical analysis. On the basis of sample data, this analysis assists in reaching conclusions and making judgments regarding the entire population. For research initiatives that use a limited sample size and want to extrapolate findings to a broad population, it is a highly advised statistical approach. It's crucial to utilise inferential statistics effectively and with caution since they are a potent tool for data analysis. The size and representativeness of the sample data are two of the most crucial factors to take into account when utilising inferential statistics [14]. The likelihood of drawing valid conclusions about the population increases with a bigger, more representative sample. It is also crucial to take into account the underlying presumptions of the statistical techniques being utilised, such as the independence of the observations and the normality of the data. Inferences and conclusions that are incorrect as a result of these assumptions being broken. In conclusion, inferential statistics is a crucial area of statistics that enables us to infer relevant information about a population from a sample of data. We can evaluate the chance that our sample data is representative of the population and make valid generalisations about the population by employing techniques like hypothesis testing and confidence intervals [15]. Yet, it's crucial to utilise inferential statistics appropriately and cautiously, keeping in mind the sample's size and representativeness as well as the underlying assumptions of the statistical methods being applied.

Predictive Analysis

A subset of data analysis known as predictive analysis use statistical algorithms and machine learning approaches to forecast upcoming occurrences or actions using previously collected data. Predictive analysis seeks to find patterns and connections in the data that may be utilised to generate precise predictions about what will happen in the future. In many different fields, including business, science, and weather forecasting, predictive analysis is used to make



**Kaushal Singh and Tushar Mandanaka**

predictions about consumer behaviour, sales trends, and disease outbreaks [16]. Doing predictive analysis entails a number of processes, such as: In order to make sure the data is reliable and pertinent to the analysis, it must first be cleaned and pre-processed. As part of this process, data may need to be removed if it is missing or unnecessary, formatted according to a standard, and new variables may need to be created depending on the current variables [17]. Selecting the right statistical model or machine learning technique for the particular investigation is known as model selection. For various types of data and various jobs requiring prediction, several models could be more suitable. In order to train the chosen model or algorithm, historical data is used. To provide reliable forecasts based on the previous data, the model is modified and optimised.

Prescriptive Analysis

Data are analysed using a prescriptive approach to determine the next step. Finding the optimum result for a scenario is a common objective of business analysis. Both descriptive and predictive analysis are closely connected to it. Prescriptive analysis, on the other hand, focuses on making the best recommendations possible from the choices that are provided. Prescriptive analysis is a procedure that includes a number of phases, such as: Identifying the problem includes determining the precise issue that needs to be resolved as well as the limits and goals that must be taken into account [18]. Data collection and pre-processing for the analysis's usage constitute the process of data preparation. Model creation: This entails creating a mathematical representation of the issue and the key variables that influence a choice. Optimization is the process of finding the best possible solution to a problem based on restrictions and goals that have been specified by applying algorithms and optimization techniques. Reviewing the analysis's findings and making a choice in accordance with the suggested plan of action is the act of making a decision.

Exploratory Data Analysis

In order to discover patterns, trends, and correlations within huge datasets, exploratory data analysis (EDA), a sort of data analysis, is used to examine and summarise the data [19]. EDA seeks to comprehend the data better and provide ideas that may be evaluated with statistical techniques. To study the data, EDA frequently use summary statistics, data visualisation methods, and descriptive statistics. To illustrate the distribution of the data and spot any outliers or abnormalities, this includes methods like histograms, scatter plots, box plots, and frequency tables [20]. EDA is a crucial phase in the analysis of data since it helps to spot any issues with the data, such as missing values or inconsistent data, and it makes sure the data are acceptable for further analysis. It also helps to find connections and patterns in the data that may be utilised to produce theories for more research. Doing EDA involves a number of crucial processes, such as: clearing the data This entails eliminating any redundant, omitted, or unnecessary data from the dataset and fixing any discrepancies or mistakes in the data. Calculating summary statistics like mean, median, mode, standard deviation, and range—which give an overview of the general features of the data—as part of descriptive statistics entails.

Casual Analysis

A statistical analysis technique called causal analysis seeks to pinpoint the linkages between variables that cause and result in one another [21]. To put it another way, it seeks to establish whether a certain variable (the "cause") is to blame for changes in another variable (the "effect"). Researchers change the independent variable (the "cause") and monitor the effects on the dependent variable as part of experimental or quasi-experimental methods for causal analysis (the "effect"). By controlling for confounding factors that might affect how the link between the cause and effect is related, causal inference can also be drawn from observational research. In many different disciplines, including as the social sciences, public health, economics, and engineering, causal analysis is applied. For establishing successful treatments, policies, and programmes as well as for making informed judgements, it is crucial [22]. Understanding and identifying the causes of "why" things appear to happen in a specific manner are made easier with the help of causal analysis. This analysis aids in determining the primary reasons for failures or merely identifies the fundamental causes of potential events. Using causal analysis, for instance, one may determine what will happen to a given variable if a different variable changes.

Analysis of Mechanisms

**Kaushal Singh and Tushar Mandanaka**

To comprehend the fundamental mechanisms that control biological processes, biological sciences employ a sort of analysis known as mechanistic analysis. Its goal is to pinpoint the physical, chemical, and molecular processes that power biological systems and ascertain how they relate to one another [23]. Data from multiple sources, including genetic, biochemical, physiological, and biophysical information, are combined during mechanistic analysis. Advanced tools and methods including microscopy, genetic engineering, proteomics, and metabolomics are frequently needed. Mechanistic analysis is used extensively in the investigation of disease processes. Researchers can create novel cures and treatments that specifically target the molecular systems involved by knowing the underlying biology causes of a disease. Mechanistic analysis is also employed in the development of novel pharmaceuticals, where it may be used to find fresh targets for treatment and forecast the possible impacts of drugs on living things [24]. In conclusion, mechanistic analysis is a useful technique in the biological sciences that may aid in our understanding of the inner workings of biological systems and how they react to various stimuli. It is a vital part of contemporary biological research and has a variety of uses, from fundamental science to therapeutic settings. This is one of the less typical kinds of statistical analysis. In the process of big data analytics and biological research, mechanistic analysis is applied. It employs the idea of comprehending individual variations in variables that result in variations in other variables in a similar manner while avoiding external effects.

Statistical Techniques That Are Crucial in Research

The statistical analysis phase of research is the part of it that biological researchers find the most terrifying. To make this process as simple as possible, statistical tools in research can assist researchers in understanding what to do with data and how to interpret the outcomes. Finding the underlying components or dimensions that account for the variance in a group of variables is done using factor analysis [25]. This method is frequently used in survey research to find recurring themes or factors that influence respondents' answers. SEM, or structural equation modelling, is a potent statistical approach used to assess intricate models with several interconnected variables. The interaction of several elements (such as personality characteristics or environmental circumstances) to influence behaviour or outcomes is frequently studied in social sciences and psychology. Time-series analysis: This technique is used to examine data that has been gathered over a period of time, such as stock prices or climatic data. It may be applied to the data to find trends, seasonality, and other patterns. Multilevel modelling: Multilevel modelling is used to evaluate data that has a hierarchical structure, such as pupils nested inside classrooms or workers nested within businesses. Examining both impacts at the individual and group levels is possible [26]. In order to evaluate and interpret data, test hypotheses, and come to conclusions about the links between various variables, researchers need to use these statistical tools, which are crucial to their work.

4.1. The Statistical Package for the Social Sciences (SPSS)

A popular piece of software for statistical analysis in the social sciences is called the Statistical Package for the Social Sciences (SPSS). It offers a variety of statistical methods and tools for evaluating data, including factor analysis, correlation analysis, regression analysis, descriptive statistics, and inferential statistics. Users may import, modify, and analyse data with ease using SPSS's user-friendly interface [27]. Large datasets may be handled, and a range of output formats, including tables, charts, and graphs, are available. Data transformations, analysis of missing data, and data validation are just a few of the functions that SPSS provides for cleaning and preparing data. These characteristics aid in ensuring that data is correct and prepared for analysis. The fact that SPSS can work with a wide range of data types, including numerical, categorical, and ordinal data, is one of its advantages [28]. Together with basic statistical methods, it also provides a variety of sophisticated statistical methods including survival analysis, multilevel modelling, and structural equation modelling. In general, SPSS is a strong and adaptable software suite that is frequently used in social science research. Because of its user-friendly design, it is accessible to both novice and expert users, making it a crucial tool for academics who must study and comprehend complicated data sets.

Center for Statistical Computation with R

Dedicated to advancing the R programming language and environment for statistical computing and graphics, the R Foundation for Statistical Computing is a nonprofit organisation. R is a popular open-source application for statistical analysis, data visualisation, and data manipulation in research. Time-series analysis, linear and nonlinear



**Kaushal Singh and Tushar Mandanaka**

modelling, machine learning, and other statistical methods for data analysis are all available under statistical analysis in R [29]. From biology to economics to social sciences, these methods are crucial for many different sorts of study. Open-source: R is a piece of software that may be freely updated and expanded by users since it is an open-source project. Because of this, there is now a sizable user and developer community that helps to create R packages and tools. R is interoperable with various tools and programming languages, including Python and SQL [30]. As a result, researchers may utilise R alongside other tools and platforms and incorporate it into their current processes. The R Foundation and the R programming language are fundamental resources for study in a variety of subjects. They support reproducible research, give everyone access to robust statistical and visualisation tools, and are openly distributed.

SAS

For statistical analysis in biological research, Statistical Analysis Software (SAS) is a popular software application. For the study of data, SAS offers a variety of statistical tools and methods, including descriptive statistics, inferential statistics, correlation analysis, regression analysis, factor analysis, survival analysis, and more. SAS is helpful in biological research in the following ways: SAS offers tools for both the design of experiments and the analysis of the data they generate. This is crucial for many different biological research projects, including animal experiments and clinical trials [31]. SAS provides a variety of capabilities for data cleaning and preparation, including data transformations, missing data analysis, and data validation. These attributes contribute to ensuring that data is correct and prepared for analysis. SAS can manage massive datasets, which is crucial for biological research that uses intricate and substantial databases. SAS provides a variety of sophisticated statistical methods, including survival analysis, generalised linear models, and mixed models [32]. These methods are crucial for the analysis of intricate data in biological research. SAS offers a range of tools for data visualisation, including scatterplots, bar charts, and heatmaps. Data visualisation is crucial for discovering trends in data and explaining findings to others. Overall, SAS is an effective and flexible software suite that is often used in biological research. Because to its intuitive layout, both novice and experienced users may use it [33]. It is a crucial tool for academics who must analyse and comprehend complicated data sets.

GraphPad Prism

In biological research, the software programme GraphPad Prism is frequently used for data graphing and statistical analysis. It offers several statistical methods and tools, including as t-tests, ANOVA, regression analysis, and others, for the study of data [34]. These are some applications for GraphPad Prism in biological research: Data analysis: GraphPad Prism can handle a variety of data kinds, including continuous, categorical, and discrete data. It offers a range of statistical tests and models, including one-way ANOVA, two-way ANOVA, t-tests, non-parametric tests, and more, to evaluate data. Data visualisation: GraphPad Prism offers a variety of tools for data visualisation, including scatterplots, bar graphs, pie charts, and line graphs. Data organisation: Users of GraphPad Prism are given a wide range of options for organising data, including data tables, replicates, and groups. Due to this, contrasting and analysing different data sets is simple. GraphPad Prism's user-friendly design makes it simple for users to swiftly analyse and visualise data [35]. For using its capabilities, it also offers step-by-step instructions and tutorials. Reproducibility: GraphPad Prism users may export and save analyses and graphs, making it simple to replicate results and share data with colleagues. GraphPad Prism is a strong tool for biological research overall, offering crucial statistical capabilities and possibilities for data display [36]. For researchers of all skill levels, it is accessible and practical because to its user-friendly interface and repeatability capabilities.

Minitab

Minitab is a statistical software programme that is frequently used in biological research. It offers a variety of statistical tools and techniques for data analysis, including descriptive statistics, inferential statistics, correlation analysis, regression analysis, design of experiments, and more. These are a few applications for Minitab in biological research: Minitab offers tools for designing experiments and evaluating the collected data [37]. This is crucial for a variety of biological research projects, including animal experiments and clinical trials. Data transformations, missing data analysis, and data validation are just a few of the tools that Minitab provides for cleaning and preparing



**Kaushal Singh and Tushar Mandanaka**

data. These characteristics aid in ensuring that data is correct and prepared for analysis. Managing huge datasets: Minitab is capable of managing enormous datasets, which is crucial for biological research that uses intricate and substantial data sets [38]. Mixed models, generalised linear models, and survival analysis are just a few of the complex statistical methods that Minitab offers. For processing complicated data in biological research, these methods are crucial. Box plots, scatterplots, and histograms are just a few of the tools available in Minitab for displaying data. Exploring data trends and presenting findings to others need the use of data visualisation. Minitab is a software programme that is generally regarded as being strong and adaptable and is frequently used in biological research [39]. Because of its user-friendly design, it is accessible to both novice and expert users, making it a crucial tool for academics who must study and comprehend complicated data sets.

Research and Data Analysis Using Statistical Tools

In order to make sense of the data that researchers collect, statistical tools are crucial for research and data analysis [40]. These tools give researchers the ability to examine data and understand it in order to reach meaningful findings, form predictions, and spot patterns and linkages. Summary and description of a dataset's properties are provided by descriptive statistics. They reveal details about the data's structure, variability, and central tendency. Mean, median, mode, standard deviation, and range are some illustrations of descriptive statistics. Making conclusions about a population based on a sample of data is done using inferential statistics. Using these methods, researchers may examine hypotheses and make population-level predictions. Regression analysis, correlation analysis, ANOVA, t-tests, and other inferential statistics are examples [41]. An analytical subset of a population is chosen using sampling procedures. With the use of these methods, it is possible to make sure that the sample correctly captures the traits of the population. Simple random sampling, stratified sampling, and cluster sampling, for instance, are sampling methods. The preparation and execution of experiments is necessary to test hypotheses and assess the effectiveness of interventions or therapies [42]. To achieve this, proper research designs must be chosen, participants must be randomly assigned, and confounding variables must be controlled. To show data graphically and make it simpler to comprehend and analyse, data visualisation techniques are utilised. Histograms, scatterplots, box plots, and heatmaps are a few instances of data visualisation methods. There are several tools and methods for data analysis and visualisation available in statistical software programmes like R, SAS, and Minitab. Researchers may modify data, provide graphical displays, and do intricate statistical analysis using these tools. To sum up, statistical tools are crucial for research and data analysis because they let researchers examine and understand data to reach relevant conclusions[43]. Statistical software programmes, sampling procedures, experimental designs, descriptive and inferential statistics, and experimental designs are some of these tools.

CONCLUSION

By assisting researchers in successfully managing and analysing their data, statistical tools serve a crucial role in research. Researcher decision-making and data interpretation can both be improved with the use of statistical techniques. By spotting patterns and connections that might not be immediately obvious, statistical techniques can aid researchers in doing more precise data analysis. As a result, mistakes can be decreased and study findings can be more accurate. The amount of time and effort needed to process and evaluate data may be decreased with the use of statistical tools, which can help researchers manage their data more effectively. By giving researchers a greater knowledge of their data, statistical tools can assist them in making judgements that are more informed. By giving researchers readable, succinct summaries of their data, statistical tools can aid in the more effective dissemination of their results. Reproducibility: By offering a clear and organised method for data analysis, the use of statistical techniques can assist to ensure that study findings are repeatable. In conclusion, statistical tools are an important part of research since they enable researchers to better organise and evaluate their data. Making better decisions, facilitating better communication, and enhancing the repeatability of research findings may all be accomplished via the use of statistical techniques.





Kaushal Singh and Tushar Mandanaka

REFERENCES

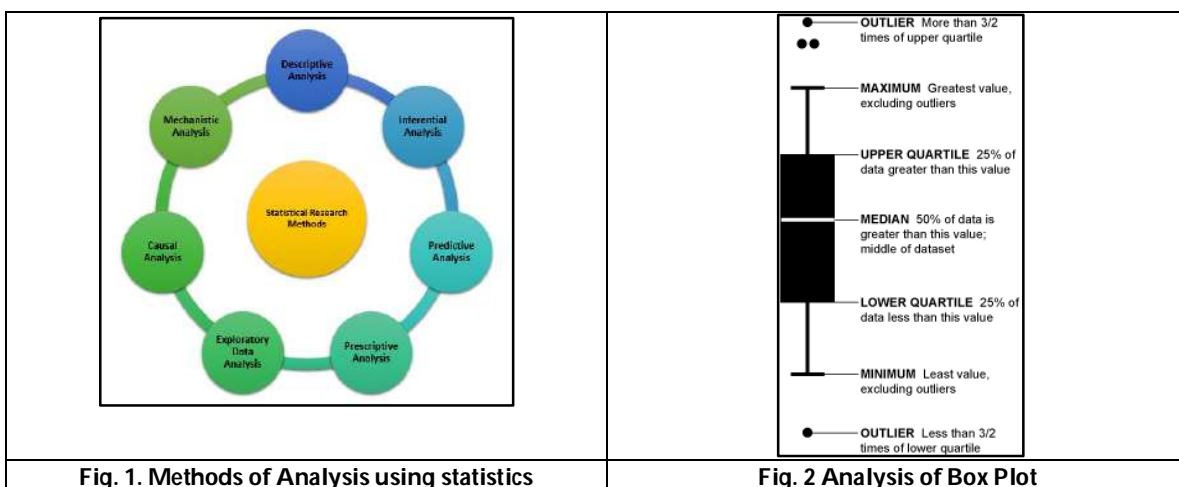
1. Creixell, P. et al. Pathway and network analysis of cancer genomes. *Nat.Methods* 12, 615–621 (2016).
2. Spirin, V. & Mirny, L. A. Protein complexes and functional modules in molecular networks. *Proc. Natl Acad. Sci. USA* 100, 12123–12128 (2013).
3. Gonzalez, R. et al. Screening the mammalian extracellular proteome for regulators of embryonic human stem cell pluripotency. *Proc. Natl Acad. Sci. USA* 107, 3552–3557 (2011).
4. Arrowsmith, C. H. et al. Corrigendum: The promise and peril of chemical probes. *Nat. Chem. Biol.* 11, 887 (2018).
5. Huang da, W., Sherman, B. T. & Lempicki, R. A. Systematic and integrative analysis of large gene lists using DAVID bioinformatics resources. *Nat. Protoc.* 4, 44–57 (2019).
6. Wadi, L., Meyer, M., Weiser, J., Stein, L. D. & Reimand, J. Impact of outdated gene annotations on pathway enrichment analysis. *Nat. Methods* 13, 705–706 (2016).
7. Wang, J., Vasaiakar, S., Shi, Z., Greer, M. & Zhang, B. WebGestalt 2017: a more comprehensive, powerful, flexible and interactive gene set enrichment analysis toolkit. *Nucleic Acids Res.* 45, W130–W137 (2017).
8. Tripathi, S. et al. Meta- and Orthogonal Integration of Influenza “OMICS” Data Defines a Role for UBR4 in Virus Budding. *Cell Host Microbe* 18, 723–735 (2015).
9. Chen, B. & Butte, A. J. Leveraging big data to transform target selection and drug discovery. *Clin. Pharmacol. Ther.* 99, 285–297 (2016).
10. Chen, R. et al. A meta-analysis of lung cancer gene expression identifies PTK7 as a survival gene in lung adenocarcinoma. *Cancer Res.* 74, 2892–2902 (2014).
11. DAVID Release and Version Information: <https://david.ncifcrf.gov/content.jsp?file=release.html> (Accessed 20 Nov 2018).
12. Brass, A. L. et al. The IFITM proteins mediate cellular resistance to influenza A H1N1 virus, West Nile virus, and dengue virus. *Cell* 139, 1243–1254 (2009).
13. Karlas, A. et al. Genome-wide RNAi screen identifies human host factors crucial for influenza virus replication. *Nature* 463, 818–822 (2010).
14. Subramanian, A. et al. Gene set enrichment analysis: a knowledge-based approach for interpreting genome-wide expression profiles. *Proc. Natl Acad. Sci. USA* 102, 15545–15550 (2005).
15. Ruepp, A. et al. CORUM: the comprehensive resource of mammalian protein complexes—2009. *Nucleic Acids Res.* 38, D497–D501 (2010).
16. Cherry, J. M. et al. Saccharomyces Genome Database: the genomics resource of budding yeast. *Nucleic Acids Res.* 40, D700–D705 (2012).
17. Gramates, L. S. et al. FlyBase at 25: looking to the future. *Nucleic Acids Res.* 45, D663–D671 (2017).
18. Lee, R. Y. N. et al. WormBase 2017: molting into a new stage. *Nucleic Acids Res.* 46, D869–D874 (2018).
19. Chatr-Aryamontri, A. et al. The BioGRID interaction database: 2017 update. *Nucleic Acids Res.* 45, D369–D379 (2017).
20. Consortium, T. U. UniProt: the universal protein knowledgebase. *Nucleic Acids Res.* 46, 2699 (2018).
21. Wishart, D. S. et al. DrugBank 5.0: a major update to the DrugBank database for 2018. *Nucleic Acids Res.* 46, D1074–D1082 (2018).
22. Zerbino, D. R. et al. Ensembl 2018. *Nucleic Acids Res.* 46, D754–D761 (2018).
23. Cohen, J. A Coefficient of Agreement for Nominal Scales. *Educ. Psychol. Meas.* 20, 37–46 (1960).
24. Shannon, P. et al. Cytoscape: a software environment for integrated models of biomolecular interaction networks. *Genome Res.* 13, 2498–2504 (2003).
25. Kuleshov, M. V. et al. Enrichr: a comprehensive gene set enrichment analysis web server 2016 update. *Nucleic Acids Res.* 44, W90–W97 (2016).
26. Chen, J., Bardes, E. E., Aronow, B. J. & Jegga, A. G. ToppGene Suite for gene list enrichment analysis and candidate gene prioritization. *Nucleic Acids Res.* 37, W305–W311 (2009).





Kaushal Singh and Tushar Mandanaka

28. Krzywinski, M. et al. Circos: an information aesthetic for comparativegenomics. *Genome Res.* 19, 1639–1645 (2009).
29. Gillis, J. &Pavlidis, P. Assessing identity, redundancy and confounds in GeneOntology annotations over time. *Bioinformatics* 29, 476–482 (2013).
30. Maglott, D., Ostell, J., Pruitt, K. D. &Tatusova, T. Entrez Gene: gene-centeredinformation at NCBI. *Nucleic Acids Res.* 39, D52–D57 (2011).
31. Huang da, W., Sherman, B. T. &Lempicki, R. A. Bioinformatics enrichmenttools: paths toward the comprehensive functional analysis of large gene lists.*Nucleic Acids Res.* 37, 1–13 (2009).
32. Jing, L. S. et al. A review on bioinformatics enrichment analysis tools towardsfunctional analysis of high throughput gene set data. *Curr. Proteom.* 12, 14–27(2015).
33. Khatri, P. &Draghici, S. Ontological analysis of gene expression data: currenttools, limitations, and open problems. *Bioinformatics* 21, 3587–3595 (2005).
34. Reimand, J. et al. g:Profiler-a web server for functional interpretation of genelists (2016 update). *Nucleic Acids Res.* 44, W83–W89 (2016).
35. Mi, H. et al. PANTHER version 11: expanded annotation data from GeneOntology and Reactome pathways, and data analysis tool enhancements.*Nucleic Acids Res.* 45D183–D189 (2017).
36. Kalderimis, A. et al. InterMine: extensive web services for modern biology.*Nucleic Acids Res.* 42, W468–W472 (2014).
37. Zheng, Q. & Wang, X. J. GOEAST: a web-based software toolkit for GeneOntology enrichment analysis. *Nucleic Acids Res.* 36, W358–W363 (2008).
38. Stockel, D. et al. Multi-omics enrichment analysis using the GeneTrail2 webservice. *Bioinformatics* 32, 1502–1508 (2016).
39. Martin, D. et al. GOToolBox: functional analysis of gene datasets based onGene Ontology. *Genome Biol.* 5, R101 (2004).
40. McLean, C. Y. et al. GREAT improves functional interpretation of cisregulatorregions. *Nat. Biotechnol.* 28, 495–501 (2010).
41. Merico, D., Isserlin, R., Stueker, O., Emili, A. & Bader, G. D. Enrichment map:a network-based method for gene-set enrichment visualization andinterpretation. *PLoS One* 5, e13984 (2010).
42. Alonso, R. et al. Babelomics 5.0: functional interpretation for new generationsof genomic data. *Nucleic Acids Res.* 43, W117–W121 (2015).
43. Herwig, R., Hardt, C., Lienhard, M. &Kamburov, A. Analyzing andinterpreting genome data at the network level with ConsensusPathDB. *Nat.Protoc.* 11, 1889–1907 (2016).
44. Li, T. et al. A scored human protein-protein interaction network to catalyzegeomic interpretation. *Nat. Methods* 14, 61–64 (2017).





Kaushal Singh and Tushar Mandanaka

